CFD Flame Spread Model Validation: Multi-Component Data Set Framework

By

William Chiu-Kit Wong

A Thesis

Submitted to the Faculty

of the

WORCESTER POLYTECHNIC INSTITUTE

in partial fulfillment of the requirements for the

Degree of Master of Science

in

Fire Protection Engineering

August 2012

APPROVED:

Professor Nicholas A. Dembsey, Major Advisor

Jarrod Alston, Co-Advisor

Andrew Coles, Co-Advisor

Dr. Christopher Lautenberger, Co-Advisor

Professor Kathy A. Notarianni, Head of Department

Abstract

Review of the literature shows that the reported correlation between predictions and experimental data of flame spread vary greatly. The discrepancies displayed by the models are generally attributed to inaccurate input parameters, user effects, and inadequacy of the model. In most experiments, the metric to which the model is deemed accurate is based on the prediction of the heat release rate, but flame spread is a highly complex phenomenon that should not be simplified as such. Moreover, fire growth models are usually made up of distinctive groups of calculation on separate physical phenomena to predict processes that drive fire growth. Inaccuracies of any of these "sub-models" will impact the overall flame spread prediction, hence identifying the sources of error and sensitivity of the subroutines may aid in the development of more accurate models.

Combating this issue required that the phenomenon of flame spread be decomposed into four components to be studied separately: turbulent fluid dynamics, flame temperature, flame heat transfer, and condensed phase pyrolysis. Under this framework, aspects of a CFD model may be validated individually and cohesively. However, a lack of comprehensive datasets in the literature hampered this process. Hence, three progressively more complex sets of experiments, from free plume fires to fires against an inert wall to combustible wall fires, were conducted in order to obtain a variety of measurements related to the four inter-related components of flame spread. Multiple permutations of the tests using different source fuels, burner size, and source fire heat release rate allowed a large amount of comparable data to be collected for validation of different fire configurations.

FDS simulations using mostly default parameters were executed and compared against the experimental data, but found to be inaccurate. Parametric study of the FDS software shows that there are little definitive trends in the correlation between changes in the predicted quantities and the modeling parameters. This highlights the intricate relationships shared between the subroutines utilized by FDS for calculations related to the four components of flame spread. This reveals a need to examine the underlying calculation methods and source code utilized in FDS.

Acknowledgment

This research wouldn't have been possible without the guidance from Professor Nick Dembsey, Andrew Coles, Dr. Chris Lautenberger and Jarrod Alston. My thanks go to them for presenting me with this challenge but also providing me with all the tools I needed to overcome it. They showed me how a great investigator of sciences would think and act, while ceaselessly prompting me to learn to do the same. I'm forever indebted to my mentors for their tremendous patience and guidance.

I could not have completed the experiments without Randy Harris and Ryan Hartwell at the WPI Fire Safety Laboratory. Their experience and insights helped pulled me out of a lot of tough spots over the years; and I am grateful for the many candid conversations we had during some of the mundane, but very tranquil fire tests. It was my pleasure and privilege to have worked with both of these gentlemen.

I would like to thank Arup and University of California, Berkeley for their generous sponsorships for this research.

This research was supported in part by the National Science Foundation through TeraGrid resources provided by Purdue University under grant number TG-CTS090062.

Jillian, thank you for believing in me and putting up with me all these years, I can't wait to see where our lives will take us in the future.

爸爸,媽媽, 對您們多年來養育我,栽培我的恩典,我真的感激不盡,
我只有希望將來可以好好孝敬您們.

Preface

In order to address the shear amount of data generated in the current research, the thesis is divided into separate parts such that representative data from the experiments was featured prominently, yet the full dataset may still be presented with some comparisons against other data and predictions from FDS.

The first section presents a consolidated review of the issues facing flame spread modeling, the availability of fire growth data in a very piecemeal format, the steps taken to decompose the complex phenomena, and descriptions of the experiments designed to capture a comprehensive dataset for the analysis of flame spread under this framework. Data from the current experiments formed the basic of a validation dataset against which FDS simulations were compared, and found to be in need of improvement.

Appendices A to E summarized various faucets of the experimental designs and featured the detailed analysis of the experimental data. The free plume, inert wall, and combustible wall flame spread datasets are presented in Appendix F.

Appendices G to I outline the sensitivity analyses performed on the FDS simulations in the areas of material properties and grid resolution. Some sample FDS input files are provided in Appendix J for references.

A selection of FDS parameters were systematically changed in order to determine their effect on the different configuration of the simulations, and are presented in Appendices K to M.

An expanded summary of the research is provided in Appendix N that contains the complete literature review, experimental setup descriptions, experimental data presentation and analysis, and the examination of FDS results and parametric study.

Contents

List of Appendices

Table of Tables

Table of Figures

Nomenclature

Symbol		Unit		Quantity
$A_{burning}$		m^2		Burning area
c_{TS}		J/kg-K		Metal calorimeter specific heat
D_h		m		Hydraulic diameter
$\frac{dT_s}{dt}$		K/s		Thin skin calorimeter back surface temperature change rate
FH		m		Mean flame height
FSR		m^2/s		Flame spread rate
h_{conv}		W/m^2K		Convective heat transfer coefficient
h_{cr}		W/m^2K		Contract resistance heat transfer coefficient
HF				Non-dimensional heat flux
H_{f100}		m		100% intermittency flame height
HRR_{rad}		kW		Radiative heat release rate
HRRPUA		kW/m^2		Heat release rate per unit area
HRR_{rad}		kW		Radiative heat release rate
$\dot{q}_i''$		kW/m^2		Incident heat flux
$\dot{q}_{lat}''$		kW/m^2		Lateral conduction rate
t		sec		Time
TSC				Thin-skin calorimeter
T_0		K		Ambient temperature
T_1		K		Thin skin calorimeter substrate front surface temperature
T_g		K		Gas temperature
T_s		K		Metal calorimeter temperature
$Z_{0.5}$		m		50% intermittency mean flame height
α_s				Metal calorimeter front-face absorptivity
δ_{TS}		m		Metal calorimeter thickness
$\rho_{TS}\rho_{TS}$		kg/m^3		Metal calorimeter density
ϵ_b				Metal calorimeter back-face emissivity
ϵ_s				Metal calorimeter front-face emissivity
σ		W/m^2K		Stefan-Boltzmann constant

Introduction

Fire tests are used by building products manufacturers to demonstrate that their products meet various safety regulations. However, testing can be cost-prohibitive during early research and development when tests of multiple permutations of the products are necessary. With advances in computational capabilities, manufacturers and engineers have begun to pursue fire modeling as a complement to traditional fire testing.

Computational fluid dynamics (CFD) fire modeling has been used to simulate large-scale fire development since the mid 1990's. A recent review of the literature suggests that there remains considerable uncertainty associated with large scale fire development (fire growth) modeling using CFD[1]: comparisons between experimental data and model calculations have exhibited various amount of discrepancy. To improve current predictive capabilities, additional verification and validation of the models is necessary to identify the source of discrepancy between model and experiment.

Traditionally, experimentally-measured heat release rate (HRR) is used as the primary metric against which a fire model's predictive capabilities are judged. However, a good correlation between a modeled heat release rate curve and its experimental counterpart does not necessarily mean that the model accurately simulated the physics of fire growth due to compensating effects.

The complexity of fire growth makes it difficult to isolate factors that contribute to the discrepancy between model calculations and experimental data. The overall flame spread process can be simplified by decoupling and studying four major components that contribute to fire development:

1. Turbulent buoyant fluid flow
2. Gas phase kinetics
3. Flame heat transfer to burning and unburned fuel
4. Condensed-phase pyrolysis

By breaking down fire growth development into these components and assessing a fire model against each component, the model's predictive capabilities can be evaluated. This requires a comprehensive and self-consistent set of data containing information related to all four areas of fire growth.

Although such a data set would be of great value for improving the predictive capabilities of fire growth models, to the best of the authors' knowledge, such a data set is not currently available. There is a lack of comprehensive fire growth data in the literature that contains information on all four components[2]: most experiments only deal with one or two components of fire development, which limits the usefulness of these datasets in a complete validation of a flame spread model.

Review of Available Flame Spread Datasets

Experimental flame spread datasets from the literature contain various amount and types of data that fall within the four components of flame spread. In theory, data from similar experiments could be combined into a coherent dataset; however, this requires much interpretation and interpolation, which reduces the dataset's overall applicability and may lead to internal inconsistencies.

Review of flame spread datasets in the literature shows that the emphasis is typically on turbulence and flame heat transfer together, or flame heat transfer with condensed phase pyrolysis. The turbulence and flame heat transfer-oriented experiments collected velocity and temperature data around the test compartment and wall surface temperature distribution, while some collected heat flux distribution or flame height data as well[3-6]. The majority of flame heat transfer and condensed phase pyrolysis experimental data were reported in the form of heat flux distribution, pyrolysis progression, and wall surface temperature[7-13]. Some works also presented gas phase kinetics data such as flame temperature, with pyrolysis data[14-16]. Experiments that report three of the four component of flame spread are rare, with one example being Walmerdahl and Werling's[17] series of flame spread experiments in a compartment. Other flame spread research in the literature has various amounts of data useful for model validation[18-23]. Further details can be found in Section N.1 of Wong's thesis[24].

Overview of CFD Models' Current Capabilities for Fire Growth Modeling

Several CFD models have been used in fire engineering practices, and they may be grouped based on their underlying simulation principles and capabilities. One standout characteristic of the general purpose CFD models is that they may use one of the three turbulence solvers in the calculations: Reynolds-Averaged-Navier-Stokes (RANs), Large Eddy Simulation (LES), and Direct Numerical Simulation (DNS). However, the use of DNS solver is, thus far, generally impractical in fire engineering applications due to its requirement for highly resolved mesh in order to achieve accurate solutions. Most of the CFD models developed specifically for fire modeling use the RANS approach for turbulence resolution, except for FDS which uses the LES and DNS solvers. Similar to the general purpose CFD models, OpenFOAM and its derivative model FireFOAM have the capabilities of using all three types of turbulence solvers. Table 1 presents the types of turbulence solver utilized in several commonly used CFD models.

Table 1 - Sample CFD models used in practical fire protection engineering

	Turbulence Solver		
General Purpose CFD Codes	**RANS**	**LES**	**DNS**
ANSYS CFX	X	X	X
ANSYS Fluent	X	X	X
PHOENICS	X	X	X
CD-adapco STAR-CCM	X	X	X
Specific Fire Field CFD Models	**RANS**	**LES**	**DNS**
FDS	--	X	X
JASMINE	X	--	--
FireFOAM	--	X	--
SMARTFIRE	X	--	--
SOFIE	X	--	--

General purpose CFD codes

ANSYS CFX is a general purpose CFD software that can utilize one of multiple solver routines in a simulation, as well as highly unstructured and non-uniform meshes. There is no inherent pyrolysis model in the base code; however, the software allows custom models to be implemented, such that the user has the ability to calculate for pyrolysis in a flame spread simulation. This technique was employed in the modeling of cable trays fire spread conducted by the Gesellschaft für Anlagen –und Reaktorsicherheit mbH (GSR) as a benchmarking exercise[25]. Additional validation works on CFX had been undertaken on unconfined pool fires and compartment fires[26-28].

ANSYS Fluent is a popular general purpose CFD software package that is capable of solving models with a high degree of customization in the computational domains and solution methods. Fluent allows the user to specify solvers for phenomena such as turbulence and radiation separately. In actual fire engineering practice, Fluent was not use extensively for flame spread simulation because, similar to CFX, a pyrolysis model is not included in the base Fluent code. However, researchers have circumvented this shortcoming by coupling solid-state pyrolysis calculations with the Fluent solution[29, 30]. Some validation works on Fluent used for fire modeling have been carried out, with focus placed on the areas of turbulence and temperature in the region around a fire[31-33].

PHOENICS (Parabolic Hyperbolic Or Elliptic Numerical Integration Code Series) is another general purpose CFD code package used in fire engineering. Similar to the other general purpose CFD codes, PHOENICS may utilize a large variety of turbulence models for solution, but custom functions are required for any pyrolysis calculation. Validation work on the PHOENICS code was undertaken for compartment fires, focusing on experimentally determined temperature and velocity near the fire[27, 34, 35].

CD-adapco distributes STAR-CD and, more recently, STAR-CCM+. While STAR-CCM+ includes several fire-specific phenomena, it does not include a pyrolysis model. Consequently, we are unaware of any uses of STAR-CCM+ for simulating fire development.

Specific fire field CFD models

Fire Dynamics Simulator (FDS) is a CFD modeling tool with both the LES and DNS solvers that is under active development the National Institute of Standards and Technology (NIST). It is a full-package fire simulation software where turbulence, combustion, radiation, pyrolysis, and water spray can be modeled. Furthermore, the FDS+Evac module may be used to simulate evacuation with agent behaviors changing based on smoke spread predicted in the base FDS model[36, 37]. A large variety of fire experiments at different scales, and in all areas of fire development including turbulence, heat transfer, and solid state pyrolysis have been used in the validation of the software[38-40].

JASMINE (Analysis of Smoke Movement In Enclosure) model was developed by Building Research Establishment Ltd (BRE) for the solution of fire and smoke movement. The software utilizes the 3D transient RANS equations for solution. Although multiple solvers are available for combustion and radiation modeling, in JASMINE, turbulence is calculated using the standard two-equation k-ε model with buoyancy modification. A pyrolysis model is not incorporated into the base code. JASMINE has been validated against a large series of fire experiments including balcony spill plume, tunnel fires, and compartment fires. Metrics used in the validation exercises included velocity and temperature in a compartment, as well as heat flux to the wall[41-43].

FireFOAM is developed by FM Global based on the open source CFD package OpenFOAM (Open Source Field Operation and Manipulation) and uses a LES solver. Turbulence, combustion, thermal radiation, solid state pyrolysis, soot, water spray, and surface film flow models are all incorporated in the base code. It is a relatively new software package that is being actively validated against available experimental data in the areas of turbulence, heat flux, soot generation, and flame spread in of small- to full-scale fire experiments[39, 44-47].

SMARTFIRE is developed by the Fire Safety Engineering Group at the University of Greenwich[48, 49]. A variety of solvers and models are available for the combustion and radiation components of fire and smoke spread, but for turbulence, SMARTFIRE utilizes the 3D transient RANS equations for solution. Results from fire simulations can be incorporated as inputs in the evacuation model EXODUS. Currently, solid state pyrolysis modeling is not available, but is under development[50]. Validation of SMARTFIRE had been completed on wood crib and compartment fires experiments. Temperatures in the plume and around the compartment, as well as velocity profiles in the doorway, were used as metrics in the validation exercises[51, 52].

SOFIE (Simulation of Fires in Enclosures) is a CFD field model originally developed at the University of Cranfield. Official development of the code ceased in 2009. Simulations in SOFIE are based on the solution of the RANS equations with a finite volume approach. Similar to other CFD codes, multiple models are used for turbulence and combustion calculations. Thermal radiation in SOFIE is simulated via a discrete transfer radiation model only. A number of flame spread models are available for use in the code that relates cone calorimeter data, rate of volatile release to heat flux, and pyrolysis front tracking through energy balance. Validation works for SOFIE ranged from small- to full-scale experiments, involving soot formation, radiation transport, turbulence and temperatures within the compartment, and generation of toxic combustion products[53-56].

Scope of current research

The lack of datasets with comprehensive flame spread data prompted the design of experiments with a focus on decoupling the four components that contribute to fire growth. The basic experiments involve a combustible vertical wall within a compartment where ignition of the combustible wall panel is achieved with an area source fire.

The combustible wall panel scenario may be deconstructed into the following three components:

1. The fuel: a combustible wall covering;
2. The environment: a vertical wall;

3. The ignition source: an area gas burner.

The process in which the combustible wall panel breaks down and burns is called condensed phase pyrolysis, whereas the interactions of the wall panel with the source fire plume are controlled by flame heat transfer, gas phase kinetics, and fluid mechanics. Without the solid fuel, the base scenario devolves into a fire against an inert wall, whose interactions are through flame heat transfer and turbulent fluid mechanics. Furthermore, if the wall is absent, the scenario becomes a free plume fire defined through its fluid turbulence and combustion characteristics only. Figure 1 presents the breakdown from a combustible wall, to an inert wall, to a free plume fire scenario.

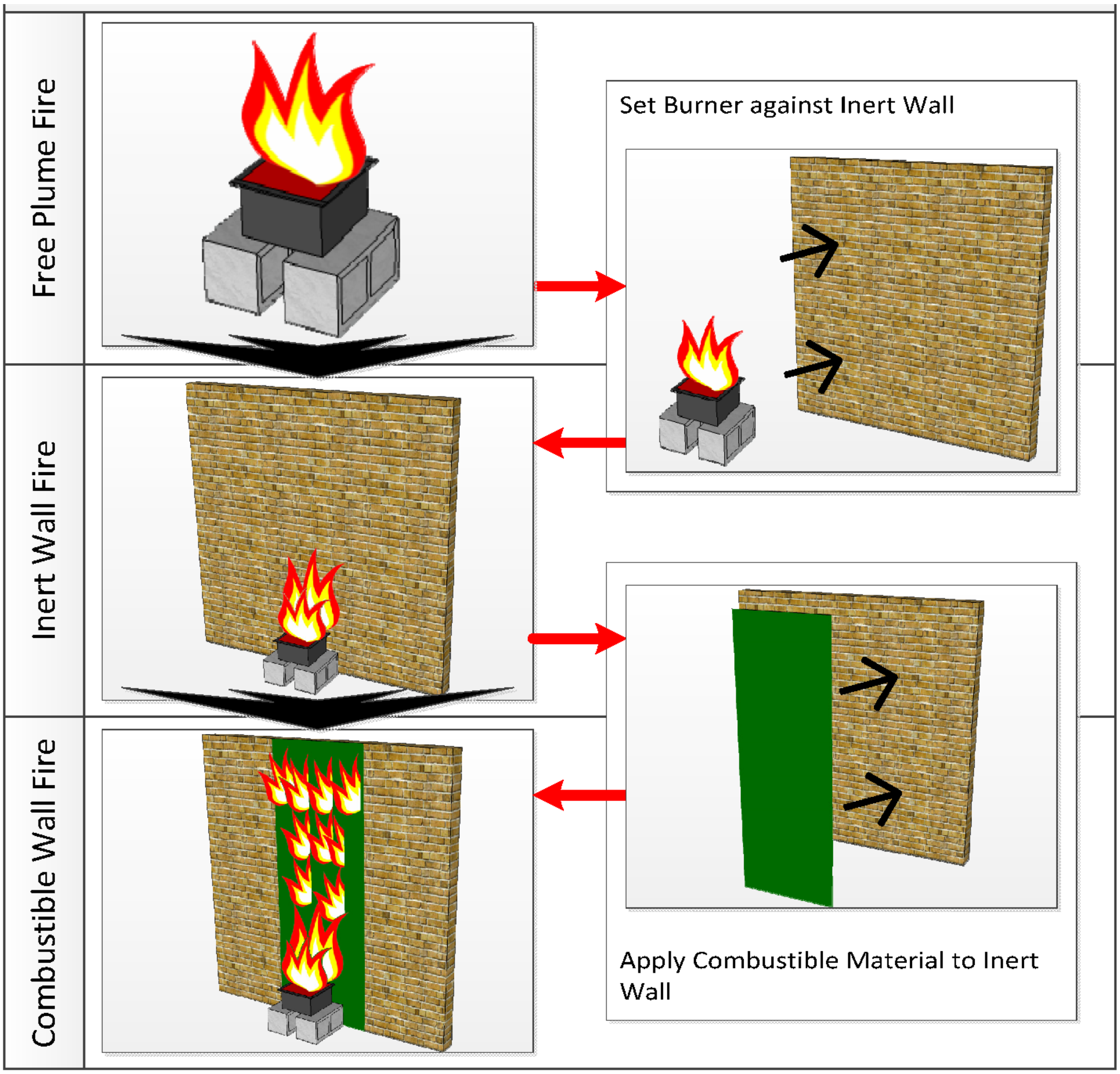

Figure 1 - Evolution of free plume to combustible wall scenarios

These three different, but related, experimental configurations allowed in-depth examination of the components of flame spread and collection of a comprehensive set of fire growth data. In order to provide comparable data, the three series of experiments were conducted under similar configurations. The wall material used in the combustible tests was a commercially available fiber-reinforced plastic (FRP).

Along with the condensed-phase decomposition (pyrolysis) information, the generated dataset may be used in engineering calibration works on different fire models in a structured fashion. By using multiple measured quantities as metrics against which a model's predictions are compared, different facets of the decomposed flame spread process can be modeled and validated individually, allowing compensating effects to be more easily identified. This process can potentially lead to a logically and progressively built fire model that is also physically accurate.

Experimental setup and procedure

From simple free plume fires, to inert wall fires, to combustible wall fires, three progressively complex series of tests were conducted. All experiments were designed so that data related to the four major flame spread components may be collected. Although the three experimental configurations differed significantly, some characteristics, such as the source fire HRRs, burner sizes, and measurement locations were retained across the test series so that trends in the data could be analyzed. Further information on the experimental setup may be found in Section N.2 of Wong's thesis[24].

Test Environment and Primary Conditions

All tests were conducted inside a standard room fire testing compartment, modified to have dimensions of 2.4 m x 2.4 m x 2.4 m (W x D x H) with an opening of 2.4m x 2.0 m (W x H). A large scale hood (2.4 m x 2.4 m) was located adjacent to the test compartment for the collection of combustion products and connected to a Large Oxygen Depletion System (LODS) for gas species analysis.

Source fires

A 0.3 m Square and a 0.6 m by 0.3 m Rectangle gas burner were used; both burners' top surfaces were located 0.4 m above the compartment floor. Both burners were fitted with a 25 mm wide flange welded around the top edges. A 12 mm thick ceramic fiber blanket was installed at each burner's top surface to act as a diffuser. Three fuels were used in the study: natural gas (generalized as methane), propane, and propylene.

Two source fire sizes were utilized: 50 kW or 75 kW - whose generated heat were high enough to be above the critical heat flux needed for ignition of the FRP specimen, but with low enough such that the time available for potential flame spread is sufficiently long to allow for meaningful data acquisition.

Free Plume Fire Test Experimental Setup and Procedure

In the free plume fire tests, the source burner was centered in the compartment. Centerline plume velocity and temperature were measured using bi-directional probes and thermocouples installed on two support rakes. After ignition, the source fire outputs a steady HRR for five minutes, which was sufficient to achieve a quasi-steady environment based on the resulting data. Figure 2 shows a schematic of the free plume fire test configuration.

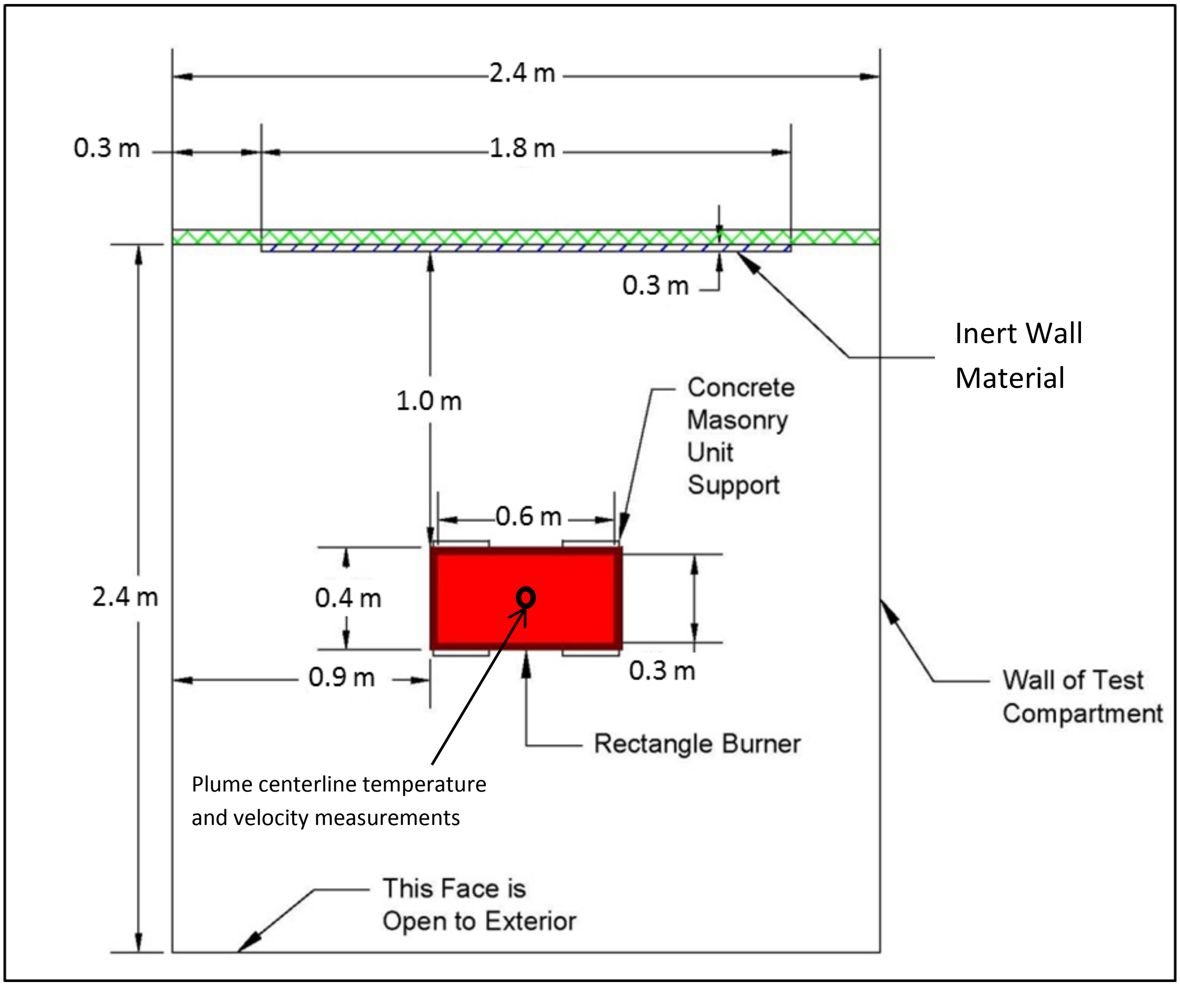

Figure 2 - Free plume fire test configuration - plan view

Inert Wall Fire Test Experimental Setup and Procedure

In the inert wall experiments, the burner was positioned centrally and flush against the wall (along the 0.6 m-side for the Rectangle burner). Heat flux to the wall and near-wall temperature measurements were made in addition to the plume-specific and HRR-related measurements. Experiments were run for five minutes to achieve quasi-steady state conditions.

The inert wall used in the test was constructed with two layers of 12 mm thick Kaowool®HT ceramic fiberboards[57] over a drywall and plywood support structure. The Kaowool® fiberboards measured 1.8 m wide by 2.4 m high, centered on a2.4 m by2.4 m support structure near the back of the compartment. Figure 3 shows the orientation of the burner in relation to the wall in the inert wall fire test configuration.

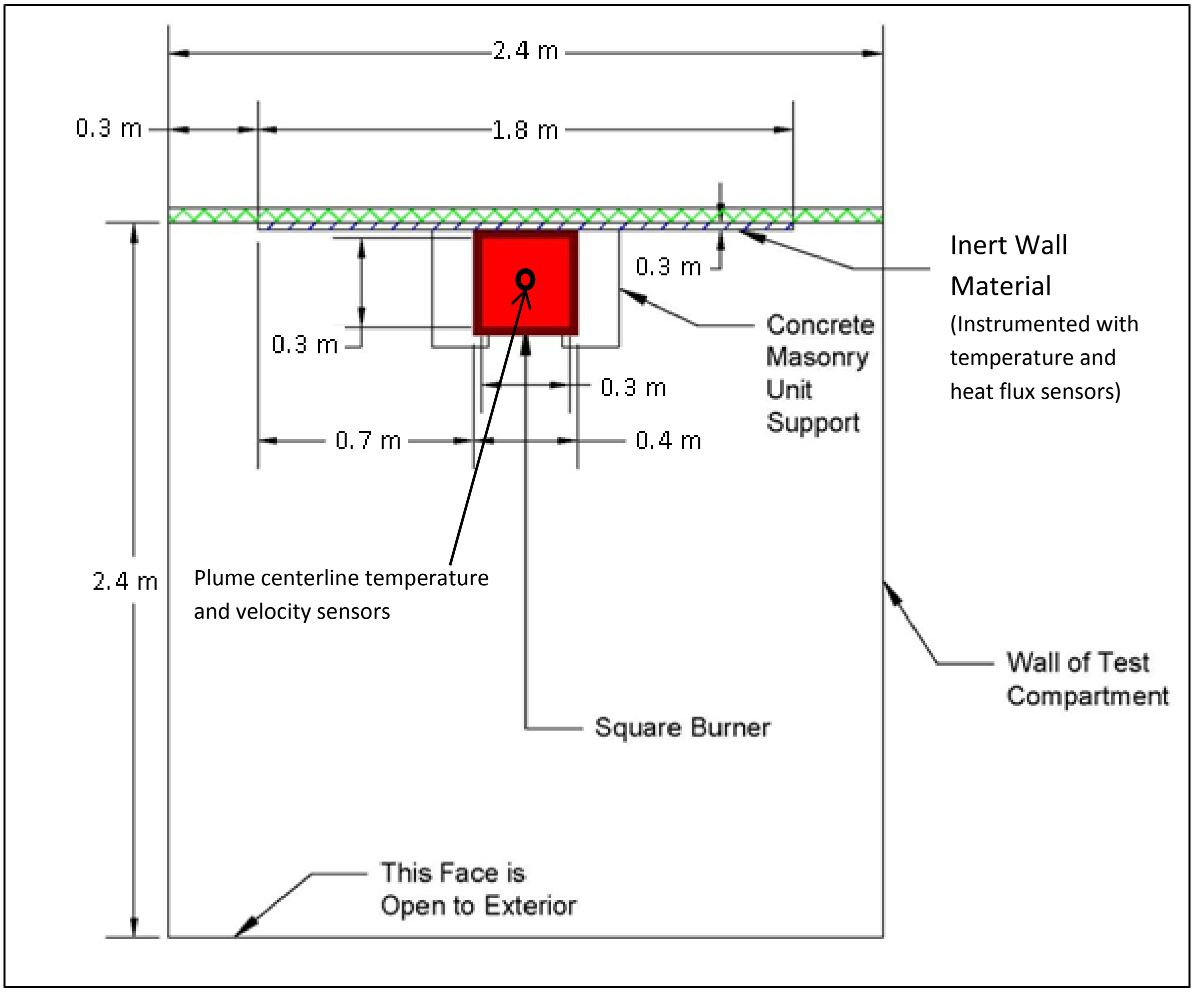

Figure 3 – Inert wall fire test configuration - plan view

Table 2 lists the various permutations of the free plume and inert wall experiments.

Table 2 – Specifications of free plume and inert wall experiments

Source Fuel	**Source Fire HRR (kW)**	**Burner Size (m x m)**
Methane	50	0.3 x 0.3
Methane	75	0.3 x 0.3
Propane	50	0.3 x 0.3
Propane	75	0.3 x 0.3
Propane	50	0.6 x 0.3
Propane	75	0.6 x 0.3
Propylene	50	0.3 x 0.3
Propylene	75	0.3 x 0.3
Propylene	50	0.6 x 0.3
Propylene	75	0.6 x 0.3

Combustible Wall Fire Test Experimental Setup and Procedure

Combustible wall experiments were similar to the inert wall experiments except that a combustible wall finish material was installed over the inert wall structure. The specimen was a FRP panel with a Class C (ASTM E84) flame spread rating. The material's resin base is a modified polyester copolymer and inorganic fillers, reinforced with a weave of chopped fiberglass. The panel's thickness is 2 mm nominal, with a smooth back-face and a pebbled, embossed white front surface. The width of the panel was 1.2 m and its height was 2.4 m. A 0.1 m by 0.1 m grid was drawn on the panel to aid flame and burning area tracking. Small openings were cut into the FRP panel to expose the wall-mounted heat flux and temperature measuring instruments. All specimens were fastened onto the inert wall with approximately 30 mechanical fasteners in no fixed pattern, with special care to ensure a tight-fit.

Two different types of flame spread tests were conducted: 1) initiating source fire terminated upon panel ignition, and, 2) initializing fire HRR maintained constant throughout the test, as shown in Table 3.

Table 3 - FRP combustible wall fire test specifications

Test Name	Source Fire Fuel	Source Fire HRR (kW)	Source Burner Shape	Time of Source Fire Reaches 50/75 kW (sec)	Source Fire Duration (sec)	Constant Source fire
A1*	Propylene	>75	Rectangle			
A2**	Propylene	75	Rectangle			
A3**	Propane	50	Rectangle			
A4	Propane	75	Rectangle	15	115	
A5	Propane	50	Square	15	98	
A6	Propane	75	Square	15	84	
A7	Propylene	50	Square	15	65	
A8	Propylene	75	Square	15	60	
A9	Propylene	50	Rectangle	12	68	
A10	Propylene	75	Rectangle	12	55	
A11	Propylene	50	Rectangle	12	68	
A12	Propylene	50	Rectangle	12	900	✓
A13	Propylene	50	Square	12	900	✓
A14	Propylene	75	Square	15	66	
A15	Propane	50	Square	15	85	
A16	Propane	75	Square	20	900	✓
A17	Propane	75	Rectangle	23	900	✓
A18	Propane	50	Rectangle	15	82	

* Test A1's source fire was not consistent

** Water was applied after flashover in Tests A2 and A3

Figure 4 presents a schematic of the combustible wall fire experiment configuration.

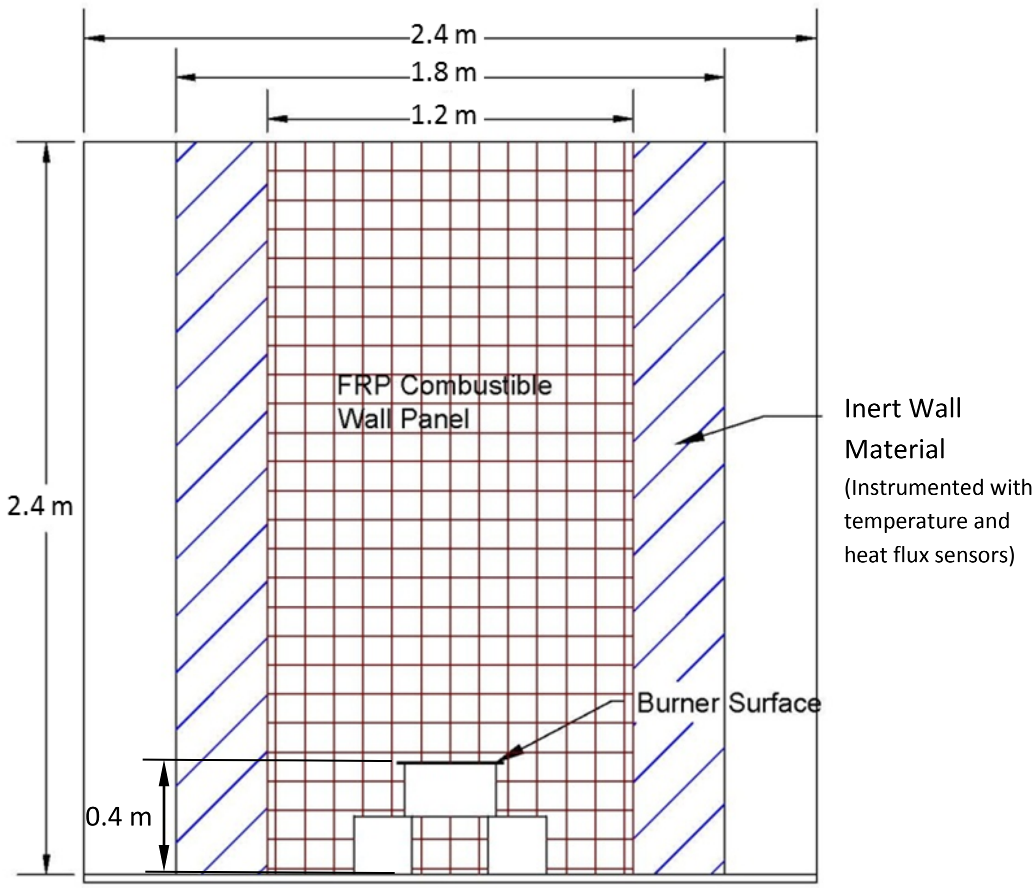

Figure 4 – Combustible wall fire test configuration - front view

The various measurements taken during each type of experiment, including their associated instruments and locations, are summarized in Table 4.

Table 4 –Fire test measurements for different experiment types

			Measurement	Instruments	Locations
FREE FIRE PLUME EXPERIMENTS	INERT WALL FIRE EXPERIMENTS	COMBUSTIBLE WALL EXPERIMENTS	Heat release rate	• Fuel flowmeter (source fire only) • LODS oxygen consumption • LODS CO/CO_2 generation	N/A
			Plume centerline velocity	• Bi-directional probe, pressure transducer and thermocouple set	10 locations along burner centerline, 0.2 m, and 0.5 to 1.7 m above burner
			Plume centerline temperature	• Welded K-type thermocouple wire (24 AWG) • 20, 24, 28, 30 AWG welded K-type thermocouples used in six Isotherm stations for radiation correction	13 locations along burner centerline, from 0.05 m to 1.85 m above burner
			Flame height	• Digital video camcorder	Camcorder positioned head-on outside of the compartment
			Heat flux to wall	• Thin skin calorimeter (TSC) • Schmidt-Boelter water-cooled heat flux gauge (combustible wall tests only)	TSCs at six different elevations along centerline, and three at 0.3 m , three at 0.6 m left of centerline, three at 0.3 m , three at 0.6 m right of centerline Schmidt-Boelter heat flux gauges, at six elevations and 0.3 m away from centerline
			Near-wall temperature	• Welded 20 AWG thermocouple wire	18 total, in three groups at three elevations on both side of centerline, and at different perpendicular distances to the wall
			Flame spread	• Digital video camcorders • Post-burn damage index • Mass load cell (Pre- and post-test)	First camcorder positioned head-on outside of the compartment Another video was filmed from the corner of the compartment opening

Heat Release Rate Measurement

HRR of each test was determined in multiple ways. The fuel flow rate through the mass flow controller provides a flow-based HRR of the source fire for propane and propylene source fires only. For all tests, HRR was also calculated by oxygen consumption calorimetry following the ASTM E-1354 methodology, and from CO/CO_2 generation rates [58-60].

Uncertainty of the flow-based HRR was determined to be ±13 kW based on the reported accuracy of the flowmeter. The uncertainty of the O_2-based HRR was established to be approximately ±25 kW from calibration tests. Given the greater uncertainty associated with the O_2-based HRR, the flow-based HRR was used in the reporting and analysis of the source fire HRR.

In the combustible wall fire experiments, the source fire HRRs were characterized based on the flow-based HRR, but the global HRR, which constitutes a summation of HRRs from both the source burner and the burning wall panel, was calculated based on oxygen consumption. Uncertainty in the HRR of the combustible wall panel fire was calculated to be ±28 kW.

Plume Temperature

Plume centerline temperature measurements were made with thermocouples constructed from welded 24-AWG thermocouple wires. Six Isotherm stations, necessary for radiation correction of the temperature measurements, were also installed and were consisted of additional thermocouples made from 20-, 28-, and 30-AWG wires. All of the thermocouple wires were K type with Special Limits of Error (SLE) with an uncertainty of 0.4% of full scale. Figure 5 shows the thermocouple locations on the two rakes.

Accuracy of the K-type thermocouples used in the plume centerline temperature measurements is on the order of ±5°C based on their specifications. However, this inherent uncertainty of the equipment is negligible when the thermocouples were used inside a fire plume: due to heat transfer (loss) over the thermocouple bead, the recorded temperature must be radiation-corrected to estimate the true gas temperature. The correction is assumed to yield the highest possible true gas temperature at the thermocouple location; hence, the uncertainty in the temperature measurement is represented by the range between the corrected temperature (maximum limit) and uncorrected/recorded temperature (minimum limit).

Radiation correction of thermocouple measurement

In close proximity to a fire, a thermocouple's bead temperature differs from the true gas temperature due to radiative and convective heat transfers. Estimation of the actual gas temperature was based on temperature recorded at the various isotherm stations. Due to the quasi-steady conditions established in the free plume and inert wall experiments, temperature correction of data from those tests was based on Blevins and Pitts' methodology[61]. For data from the combustible wall fire experiments, Young's method[62] was found to be more applicable. Details of the thermocouple radiation correction methods are found in Appendix C in Wong[24].

Plume Velocity

A total of 10 bi-directional probe and transducer pairs were used for plume velocity measurement, they were located at 0.2 m, and 0.5 to 1.7 m above the centerline of the burner at 0.15 m intervals. The probe's dimensions were based on Newman's design[63]. The bi-directional probes were oriented along the centerline axis of the burner. Pressure differential between the two ends of a probe was measured using a pressure transducer with range of ±12.5 Pa and a sensitivity of ±0.25 Pa[64, 65]. The locations of the temperature and velocity-sensing instruments along the burner centerline are presented in Figure 5.

Height above Burner (m)	24-AWG Thermocouple	Isotherm Station	Bi-Directional Probe
1.85	✓		
1.7	✓	✓	✓
1.55	✓	✓	✓
1.4	✓		✓
1.25	✓		✓
1.1	✓	✓	✓
0.95	✓	✓	✓
0.8	✓		✓
0.65	✓		✓
0.5	✓	✓	✓
0.35	✓	✓	
0.2	✓		✓
0.05	✓		

Figure 5 – Plume centerline instrumentations

The calibration constant for the bi-directional probe design was reported to be 1.18[63]. Flow inside the fire plume was assumed to be composed of air only, under ideal gas conditions. Ambient pressure before and after the tests were averaged over 3-minute periods for use to scale the measurements. Velocity is calculated from the pressure and temperature measurements using Heskestad's method[66].

Plume centerline velocity from the free plume and inert wall tests was normalized using the convective HRR of the source fire in order to compensate the data for the varying radiation component of the different source fuels. The experimental data is compared against McCaffrey's correlation[67], generated from data from natural gas fires with a square burner with similar dimensions to the one used in the current research. Normalization of the velocity using the mean flame height was also performed, with details in Section N in the thesis[24]. The uncertainties of the velocity measured for each free plume fire and inert wall fire test configuration are calculated based on the maximum standard deviation of the data, shown in Table 4.

Table 5 - Velocity data uncertainties based on different factors

Burner Size	Experimental Configuration	Uncertainty in velocity ($m\ s^{-1}\ kW^{1/5}$)
Square	Free plume	0.28
Rectangle	Free plume	0.28
Square	Inert wall	0.23
Rectangle	Inert wall	0.40

Velocity measured during the combustible wall fire experiments were not normalized due to the highly transient nature of the fire growth. Additionally, based on the observed data-drift and the characteristics of the velocity sensing equipment, the uncertainty of the velocity measurements for the periods of time before the sample HRR peaked is assumed to be approximately ±0.7 m/s for bi-directional probes located less than 1.0 m above the source burner surface, and ±1 m/s for probes at least 1.0 m above the burner surface.

Flame Height

Digital videos of the fire experiments were recorded at 30 frames per second (fps) by a camcorder located outside the compartment. Motion tracking software was used to track the flame tip height in frames extracted from the videos. The mean flame height was defined based on the 50% intermittency.

Based on the distance of the digital camcorder from the fire, resolution of the video recording, sensitivity of the tracking software, and human errors in the manual flame tip tracking procedure; the uncertainty associated with the native flame height data was estimated to be ±0.05 m.

In free plume experiments by other researchers, different normalization methods were utilized[66, 68-70]. Normalization was necessary to allow comparison of data from different source fire scenarios (fuel type, HRR, and burner size). In this paper, flame heights were normalized with Heskestad's method using the nondimensional HRR parameter, N[71].

Near-wall Temperature

Near-wall temperature was measured by welded 20-AWG (0.81 mm) thermocouples offset from the inert wall surface at various distances. A total of 18 thermocouples were used, grouped into three groups of six installed at 0.35 m, 0.95 m, and 1.55 m above the burner surface. Within each group, the thermocouples were located at 2.5 cm, 5 cm, and 7.5 cm away from the centerline on both sides. The near-wall temperature data were radiation-corrected similarly to the centerline temperature data, the uncertainty of the data is also represented by the range between the corrected and uncorrected values. The location of the near-wall thermocouples are presented in Table 6.

Only the near-wall temperature data from a combustible wall fire test are reported here, the full analysis and data from the inert wall fire tests are available in Section N.4 of Wong[24].

Table 6 - Locations of near-wall thermocouples

		Distance from centerline					
		-7.5 cm	**-5.0 cm**	**-2.5 cm**	**2.5 cm**	**5.0 cm**	**7.5 cm**
		Perpendicular distance from wall (mm)					
Height above burner	**155 cm**	15	20	25	30	35	40
	95 cm	35	30	25	20	15	10
	35 cm	0	5	10	15	20	25

Incident Heat Flux to Wall

Heat flux to the wall was measured using 18 thin-skin calorimeters (TSCs) installed along the centerline, and at 0.3 m and 0.6 m away on both sides of the centerline at six elevations of 0.2, 0.5, 0.8, 1.1, 1.4, and 1.7 m above the burner. The TSCs were designed based on ASTM E459[72] and previous research at the WPI Fire Lab[73, 74]; they were constructed as part of the inert wall structure, using the two layers of 12 mm thick refractory ceramic fiberboards as the substrate. The “thin skin” of the devices was made of a 5 cm x 5 cm, Inconel 718 plate. An AWG 20 thermocouple wire was welded intrinsically to the center-back of the Inconel plate while a second thermocouple was sandwiched between two substrate layers.

Six water-cooled Schmidt-Boelter (S-B) heat flux gauges installed at 0.3 m from each side of the centerline at the same heights as the TSC groups were utilized only in the combustible wall fire tests. Locations of the TSCs, S-B heat flux gauges, and near-wall thermocouples installed on the inert wall are shown in Figure 6.

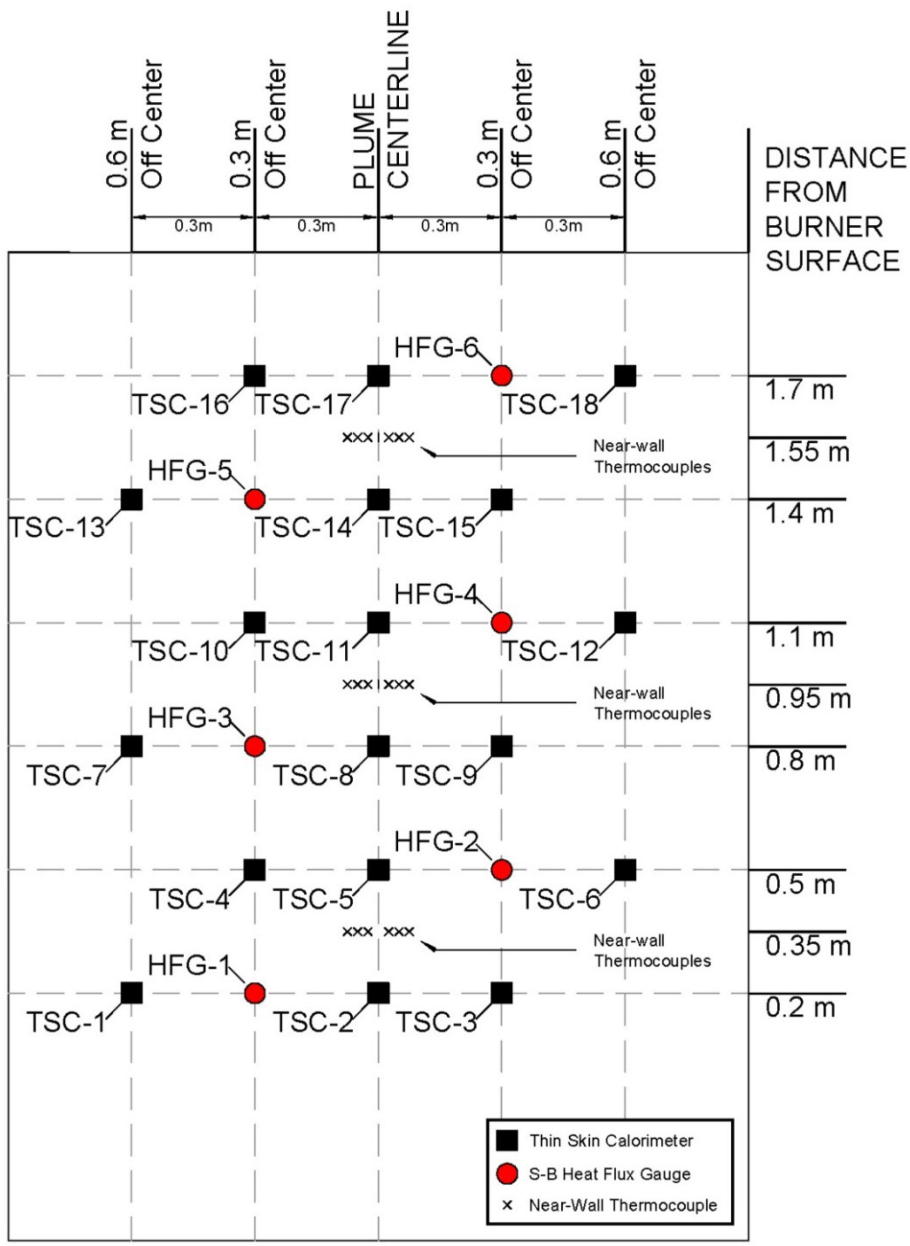

Figure 6 - Inert wall instrumentations

A one-dimensional heat transfer process was assumed for the TSC measurements. Since the metal calorimeter plate of the TSC is thin and is of a metal with known properties and thickness, a lumped thermal capacity analysis was employed in determining the net heat flux. The various heat transfer routes through the Inconel plate are shown in Figure 7, with the incident heat (cold wall) flux is found using Equation (1):

$$\dot{q}_i^{"} = \frac{\rho_{TS} c_{TS} \delta_{TS} \dfrac{dT_s}{dt} + \varepsilon_s \sigma (T_s^4 - T_0^4) + h_{conv}(T_s - T_g) + (4\varepsilon_b \sigma T_s^3 + h_{cr})(T_s - T_1)}{\alpha_s} \quad (1)$$

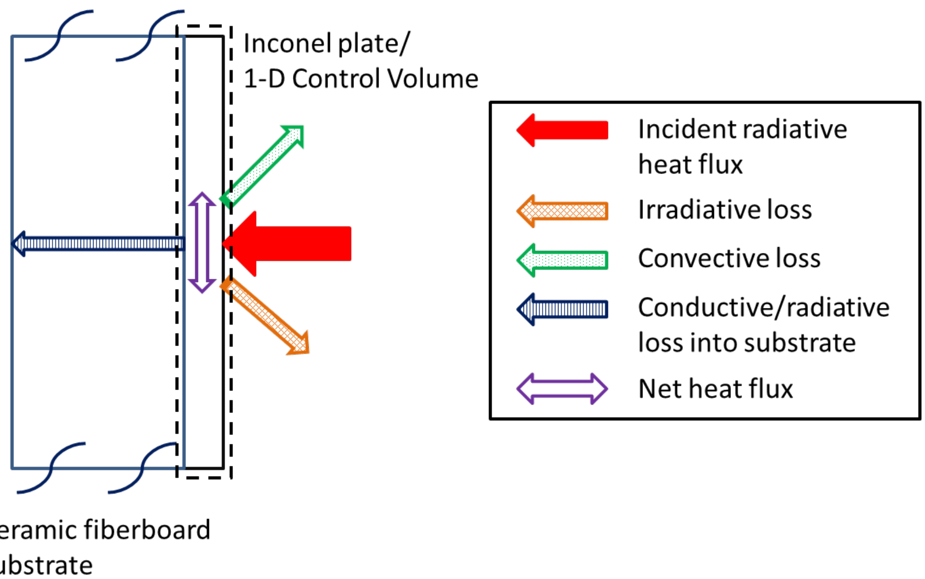

Figure 7 - Heat transfer balance model of TSC

The uncertainty of the heat flux measurement using TSCs was found to be approximately ±2.6 kW/m^2 through calibration experiments using the cone calorimeter. However, the TSCs were only subjected to radiative heat flux insult in such an environment: there was no flame impingement or forced flow over the plate. In actual experiments, the uncertainty is assumed to be twice the cone case at about ±5.2 kW/m^2. Additionally, research had suggested that the uncertainty may be as large as 10% of the measurement[73], so the uncertainty of the TSC is at defined here as ±5.2 kW/m^2, or ±10% of the measurement, whichever is greater.

The incident heat flux measured during the combustible wall fire experiments were not time-averaged or normalized due to their non-steady state nature. Furthermore, since the flame spread over the wall panel created flow over the TSCs with time-varying velocities, which was not measured, hence, the convective heat transfer component of Equation (1) $h_{conv}(T_s - T_g)$, was not determined in the incident radiative heat flux calculation. To account for this this omission, the uncertainty of the measured incident radiative heat flux for the combustible wall tests is defined to be twice the uncertainty determined for the steady case: ±10.4 kW/m^2, or ±10% of the measurement, whichever is greater.

Flame Spread Measurements

Mass loss was calculated based on the initial and final mass of the panel. The final burn pattern was constructed based on values of percentage-damaged assigned to each cell on the drawn grid. Two cameras were used to collect video data of the tests for burn area tracking: one camera was located directly in front of the sample on the inert wall, while the other was positioned at the compartment opening at a diagonal to the sample. The test videos were digitized for burning area tracking.

Flame spread rate based on HRR time history

HRR of the burning wall panel and heat flux to wall were used to estimate the spread rate of the fire on the combustible wall panel. Time-averaged heat release rate per unit area (HRRPUA) of the FRP specimen under different external heat fluxes were determined from the cone test data. A burning area time-history of the FRP specimen was determined for each of the combustible wall fire tests by using a constant HRRUPA as in Equation (2):

$$A_{burning}(t) = \frac{HRR(t)}{HRRPUA} \tag{2}$$

The burning area change history was then calculated using Equation (3):

$$\frac{dA_{burning}}{dt} = A_{burning}(t) - A_{burning}(t-1) \tag{3}$$

Assuming that the flame spread rate (FSR) takes the form of area per unit time, its calculation is the same as Equation (3), but only considering positive or zero values since it is physically impossible to have negative flame spread, as shown in Equation (4):

$$FSR(t) = A_{burning}(t) - A_{burning}(t-1) \quad \text{,only positive, otherwise, zero} \tag{4}$$

The total burnt area of each FRP panel specimen was measured using the 0.1m x 0.1m grid drawn on the panel as a guide to gauge the fire damage to the cell. A rod was used to probe the various cells post-burn; damage to the cell could be determined by observing the amount of resin left. All cells were assigned a damage index, and the subtotals for each damage range were found. The final burnt area was estimated based on the damage index, and is assumed to be the sum of the product of the percentage damage and the damage area, as shown in Equation (5):

$$\text{Total burnt area} = \sum(\text{Burn area} * \%damage) \tag{5}$$

As an example, details of the bunt area, with a breakdown showing the extents of various degree of damages, from Experiment A4 (Rectangle burner, 75 kW, propane, terminated source) is presented in Table 7.

Table 7 – Fire damage assessment of Experiment A4

Damage to Resin	# of cells	Area (m^2)
Up to 100% damage	109	1.09
Up to 75% damage	78	0.78
Up to 50% damage	9	0.09
Up to 25% damage	0	0
no damage	92	0.92
Total Burnt Area		1.72

In terms of flame spread, the total burnt area may be approximated as the summation of the FSR over time, as shown in Equation (6):

$$\text{Total burnt area} = \sum(\text{FSR}(t) * dt) \tag{6}$$

In order to relate the cone calorimeter tests with the full-scale tests, the HRRPUA of the FRP specimen generated during a full-scale test is desired. Using an iterative method and assuming that the HRRPUA during the full-scale test is constant, its value can be found by equating both Equations (5) and (6) to form Equation (7):

$$\sum(\text{FSR}(t) * dt) = \sum(\text{Burn area} * \% damage) \tag{7}$$

$$HRRPUA_{Iterative} = \frac{\sum(HR\text{R}(t) * dt)}{\sum(FS\text{R}(t) * dt)}$$

From calculations, it was observed that the iterative HRRPUA value is approximately 300 kW/m^2 for the FRP material, which is similar to the 90th percentile cone-based HRRPUA value under 75 kW/m^2 of external cone heat flux. This is supported by the fact that centerline wall heat flux measurements made during the full-scale FRP tests approached 80 kW/m^2 to 100 kW/m^2 at the height of flame spread. It must be noted that a constant HRRPUA served only as an approximation since the FRP panel's HRRUPA varied with time and imposed heat flux. Under this method, the uncertainty of the estimated FSR is significant, at approximately ±0.01 m^2/s. Additional information on the derivation of this flame spread estimation is presented in Section N.4 of Wong[24].

The flame spread rate estimate method using the HRR time history does not provide a sense of the direction of the burn (straight up or skewed), nor the shape of the burning areas. For these details, additional information was required.

Flame spread rate based on burning progression

To track the flame spread movement over the combustible wall panels, video footage of each tests was analyzed. Images extracted from the video files were used to track the flame spread by visually identifying the outline of the burning areas. Due to the volume of images and software limitations, the process was performed for every 2 seconds of recorded data.

It was assumed that the burning areas may be approximated by rectangular shapes and the burning progression was separated into three distinct phases as shown in Figure 8. The burning area time-history was developed from the total burning areas based on the rectangle area estimation method over a minimum of 180 seconds, starting from the point when flame attachment was visible on the FRP panel. The burning area was found to increase from Stage 1 until the end of Stage 2, then decreased in Stage 3, and afterward, any burning that remained took on the shape of lines.

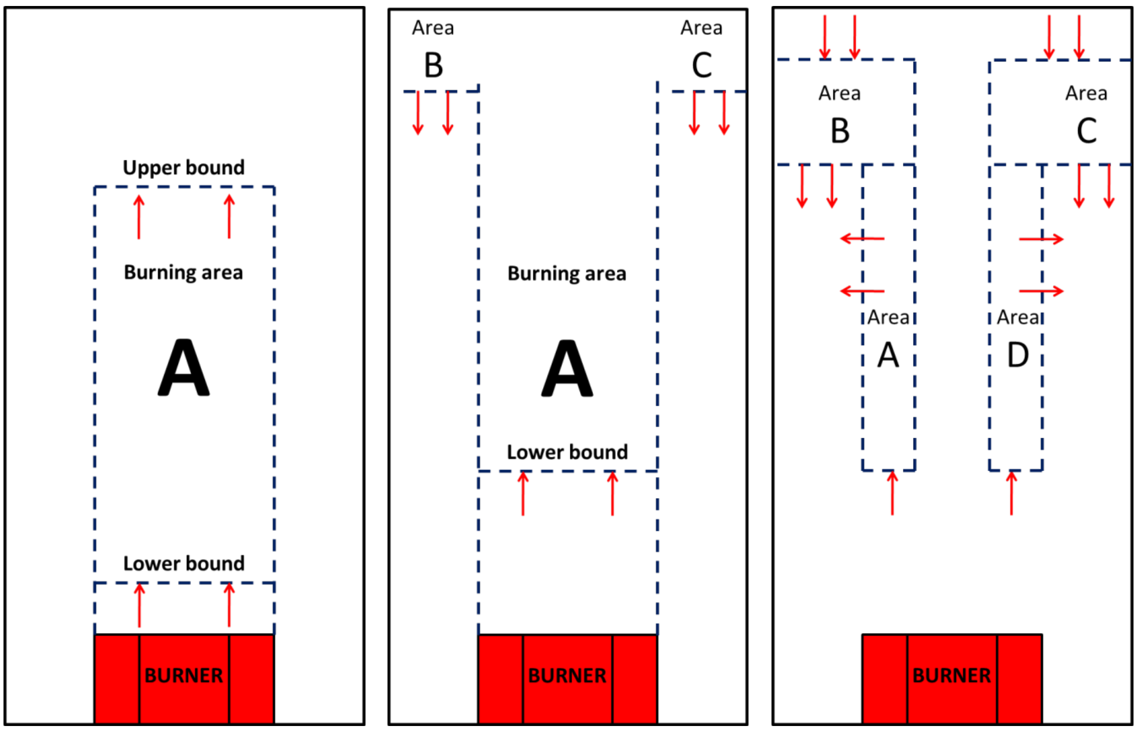

Figure 8 - Burning area progression, early to late stages (from left to right)

Although this method of flame spread may be used to compliment the HRRPUA method, however, there are some limitations. First of all, the quality of the video footage dictated the quality of the data. The 0.1m x 0.1m square grid drawn on the wall panel aided the tracking process, and the resulting uncertainty based on the grid could be estimated to be four grid spaces at 0.04 m^2.

FRP specimen cone calorimeter tests

A series of bench-scale cone calorimeter (ASTM E1354 [59], ISO 5660 [75]) tests were conducted with the FRP specimen at external heat fluxes of 25, 50, and 75 kW/m^2. Figure 9 shows the HRRPUA of the FRP materials in the six cone calorimeter tests at the three external fluxes. Thermocouples were attached to the front and back surfaces of the FRP sample in the center to collect temperature-time histories for thermal property estimations. The full cone test data are collected in Appendix F, and discussed in additional details in Appendix A in the thesis[24].

Figure **9** - Cone test heat release rates per unit area of wall panel

Experimental data

The free plume fire tests were designed to collect data only related to the fluid dynamics/turbulence and gas phase kinetics. Measurements made in the inert wall fire scenario of the full-scale tests are related to the fluid dynamics/turbulence, gas phase kinetics, as well as heat transfer to environment. Combustible wall tests allowed collection of all data relevant to all four components of flame spread. In general, due to their quasi-steady nature, experimental data from the free plume and inert wall tests were time-averaged and normalized to eliminate fuel source effects.

For combustible wall experiments, only the data from a representative experiment conducted using a terminated 75 kW propane fire with the Rectangle burner (Experiment A4) is presented here. Complete analysis of the experimental data is presented in Section N.4, and the full dataset from each test is available in Appendix F of the complete thesis[24].

Free Plume Fire tests Data

Heat release rate

All tests were conducted with a 75 kW or a 50 kW source fire; the average calculated HRR values based on the fuel flow and oxygen consumption were within the uncertainties.

Plume centerline temperature rise

The corrected plume centerline temperatures from the free plume tests conducted with a Square burner are presented in Figure 10. The temperatures have been normalized using the convective HRRs and burner hydraulic diameter, then compared to McCaffrey's correlation[67].

The uncorrected temperatures were approximately 25% lower than their corrected counterparts at normalized heights below 0.05 m/kW$^{0.4}$ regardless of test types; however, the correction significantly decreases at higher elevations. McCaffrey's correlation was found to lie between the corrected and uncorrected temperature measurements.

It is noted that the centerline temperatures from a Rectangle burner fire were much lower than those recorded in the tests using the Square burner above a normalized height of 0.05 m/kW$^{0.4}$. This is likely due to the shorter flames generated by the Rectangle burner at the comparable HRRs.

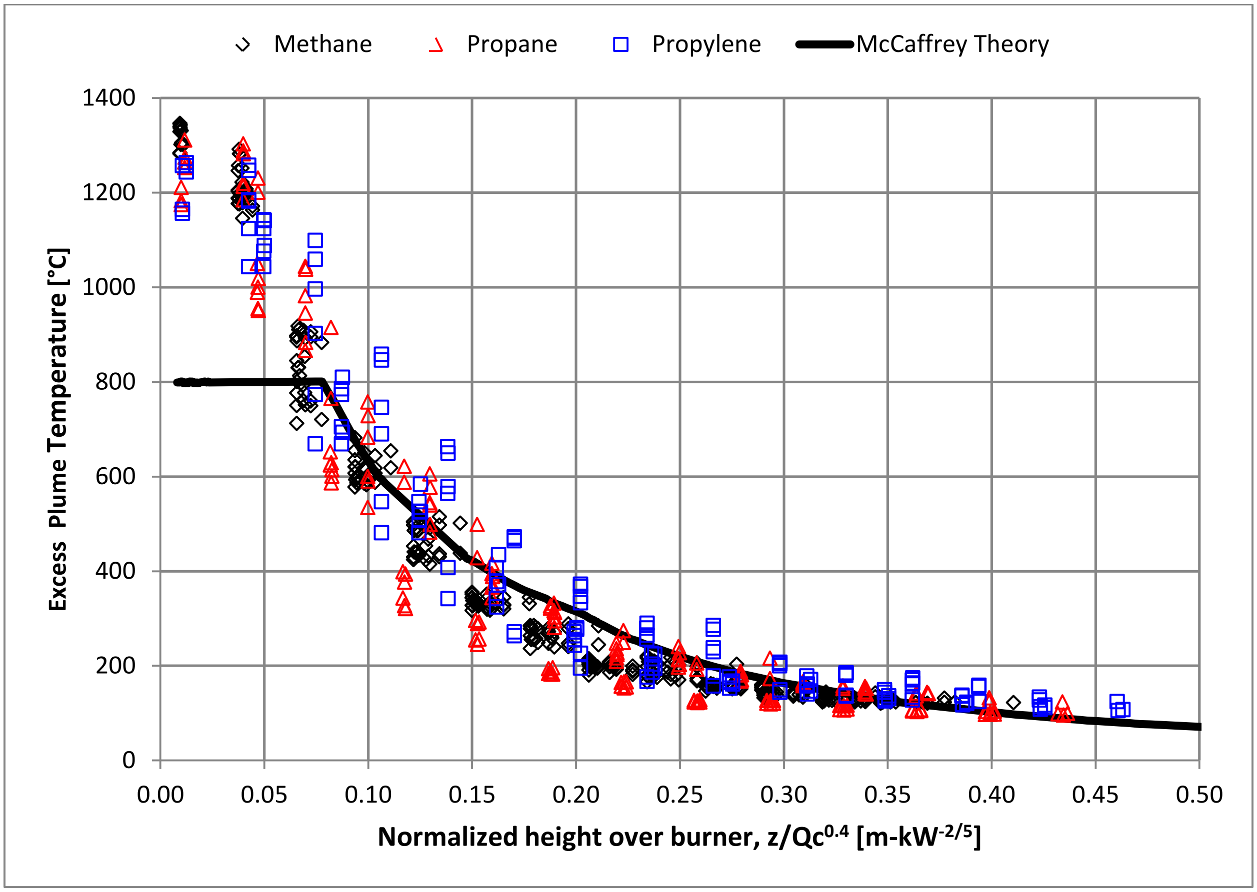

Figure 10 - Plume centerline temperature rise from free **p**lume **fire** tests using Square **b**urner

Complete analysis of the plume temperature including those obtained in tests conducted with the Rectangle burner, and data normalized using the mean flame height is available in Section N.4 of the thesis[24].

Plume centerline velocity

Figure 11 shows the measured centerline plume velocity from the tests conducted with a Square burner. McCaffrey's correlation is also provided for comparison. The height and velocity were been normalized against a fire's convective HRR. Complete analysis of the velocity measured in tests conducted with a Rectangle burner and data normalized using the mean flame height may be found in Section N.4 of the thesis[24].

The velocities measured in the current experiments were only within range of McCaffrey's uncertainty at a normalized height between 1.5 to 2 $m/kW^{0.4}$; outside of this range, the measurements were outside of McCaffrey's data spread. The uncertainty of the measured velocities is estimated to be as high as 1 m/s.

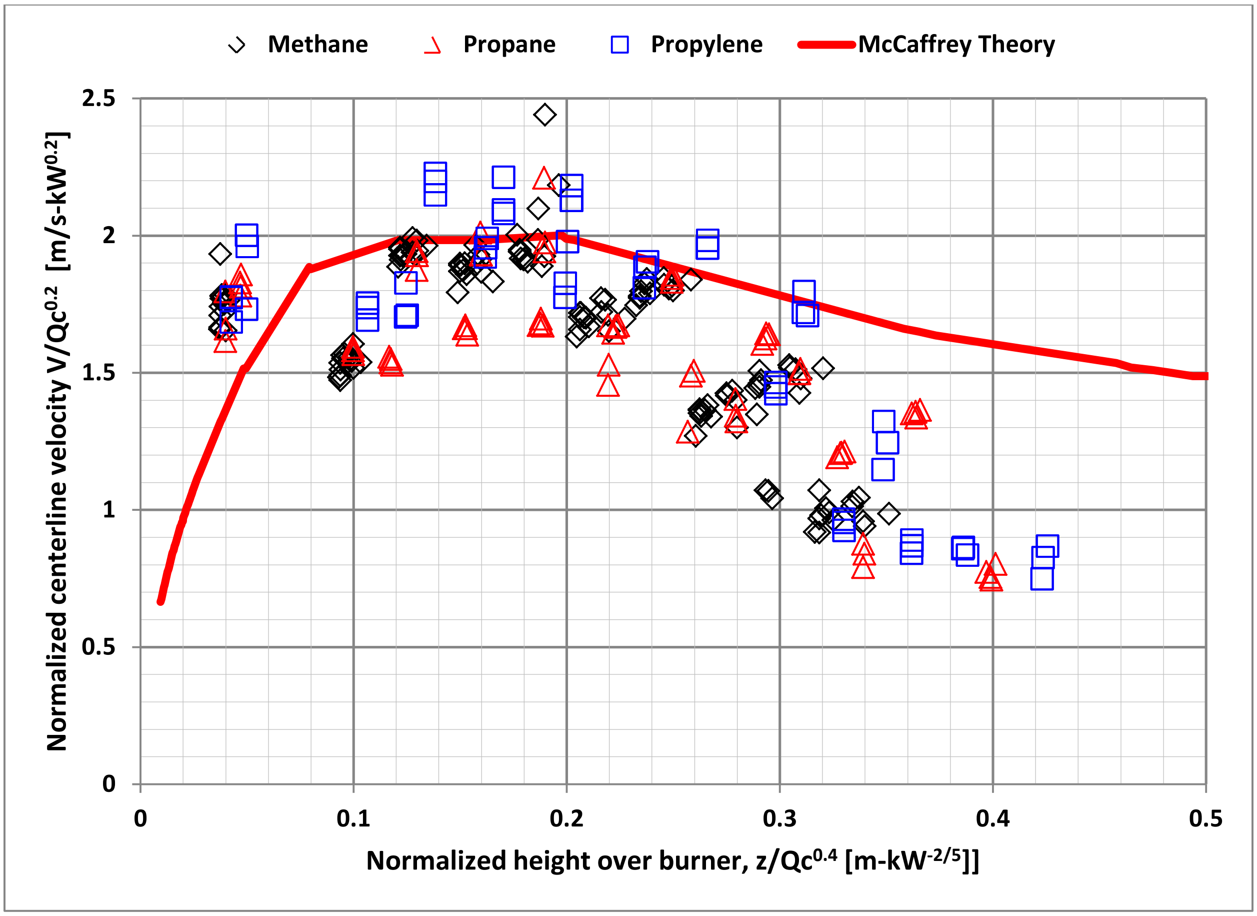

Figure 11 – Plume centerline velocity from free plume fire tests using Square burner

Flame height

The measured flame heights from the free plume tests are normalized based on the method used by Heskestad[71] in Figure 12. Using the total heat release rates of methane, propane, and propylene, Heskestad's correlation suggests that the propylene flame height should be taller than the propane and the methane flame heights, which is also observed in the current dataset. The uncertainty of Heskestad's correlation was reported to be 15-20%[76], so the current data falls within range of the uncertainties, except for the methane fire flame heights. Flame height data comparisons made using additional normalization methods may be found in Section N.4 of Wong[24].

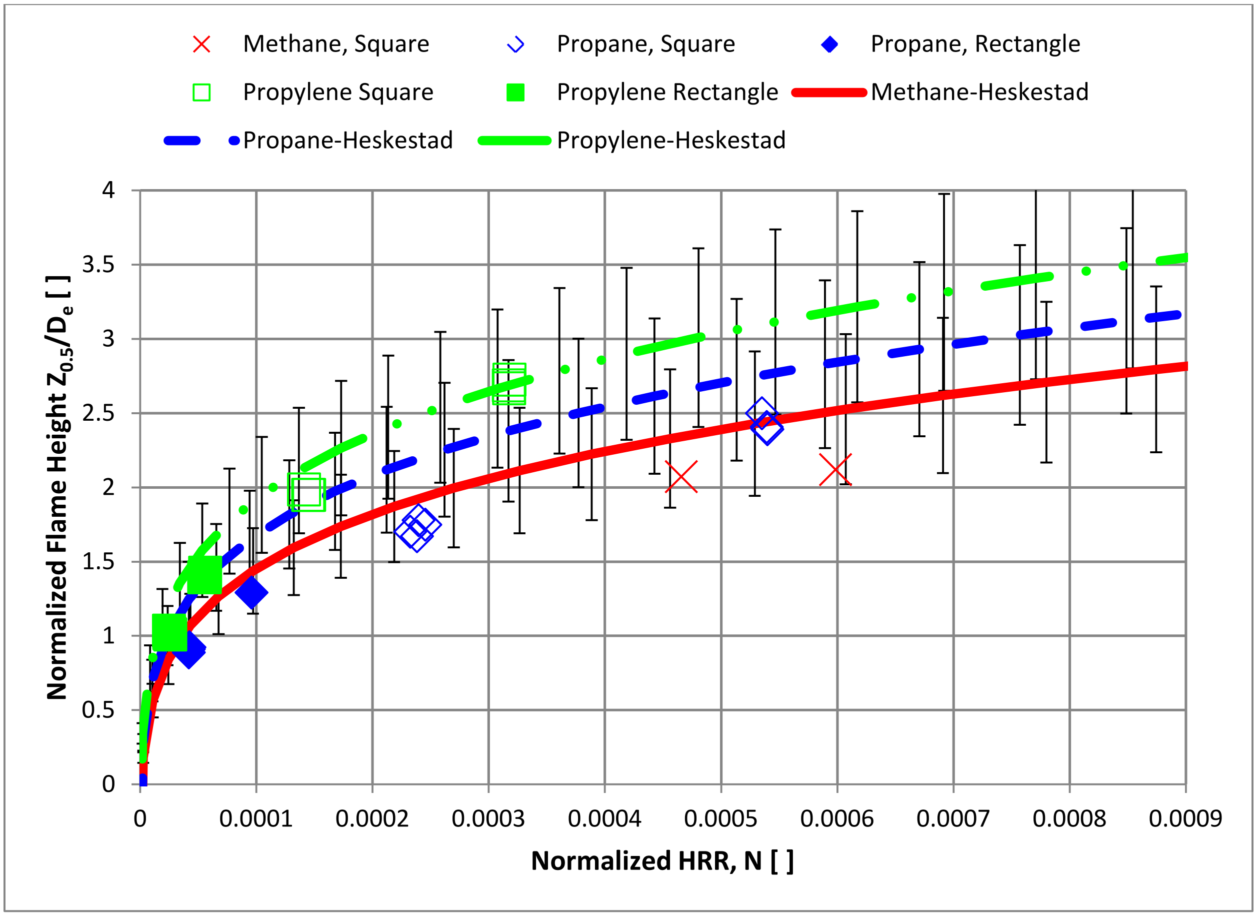

Figure 12 - Comparison of flame height data from free plume fire tests with Heskestad's correlations

Inert Wall Fire Tests Data

Heat release rate

All tests were conducted with a 75 kW or a 50 kW source fire, and the calculated HRR values based on the fuel flow and oxygen consumption were within the uncertainties. Additionally, the uncertainties of all measured HRRs fell within their intended HRR level.

Plume centerline temperature rise

The corrected plume centerline temperatures from the inert wall tests conducted with a Square burner are presented in Figure 13. Again, the temperatures have been normalized using the convective HRR of the fires and compared to McCaffrey's correlation[67].

Similar to the free plume centerline temperature rise, the uncorrected temperatures from the inert wall cases were approximately 25% lower than their corrected counterparts at normalized heights below 0.05 $m/kW^{0.4}$ regardless of test types; however, the correction significantly decreases with height. McCaffrey's correlation was found to lie between the corrected and uncorrected temperature measurements. Compared to the data from the free plume fire tests, the centerline temperatures of the inert wall fire were slightly lower, likely due to the fire leaning against the inert wall, causing the thermocouples to be misaligned with the centerline of the plume.

Centerline temperatures from a Rectangle burner fire were noted to be much lower than from a Square burner fire above a normalized height of 0.05 $m/kW^{0.4}$. This is likely due to the shorter flames generated by the Rectangle burner.

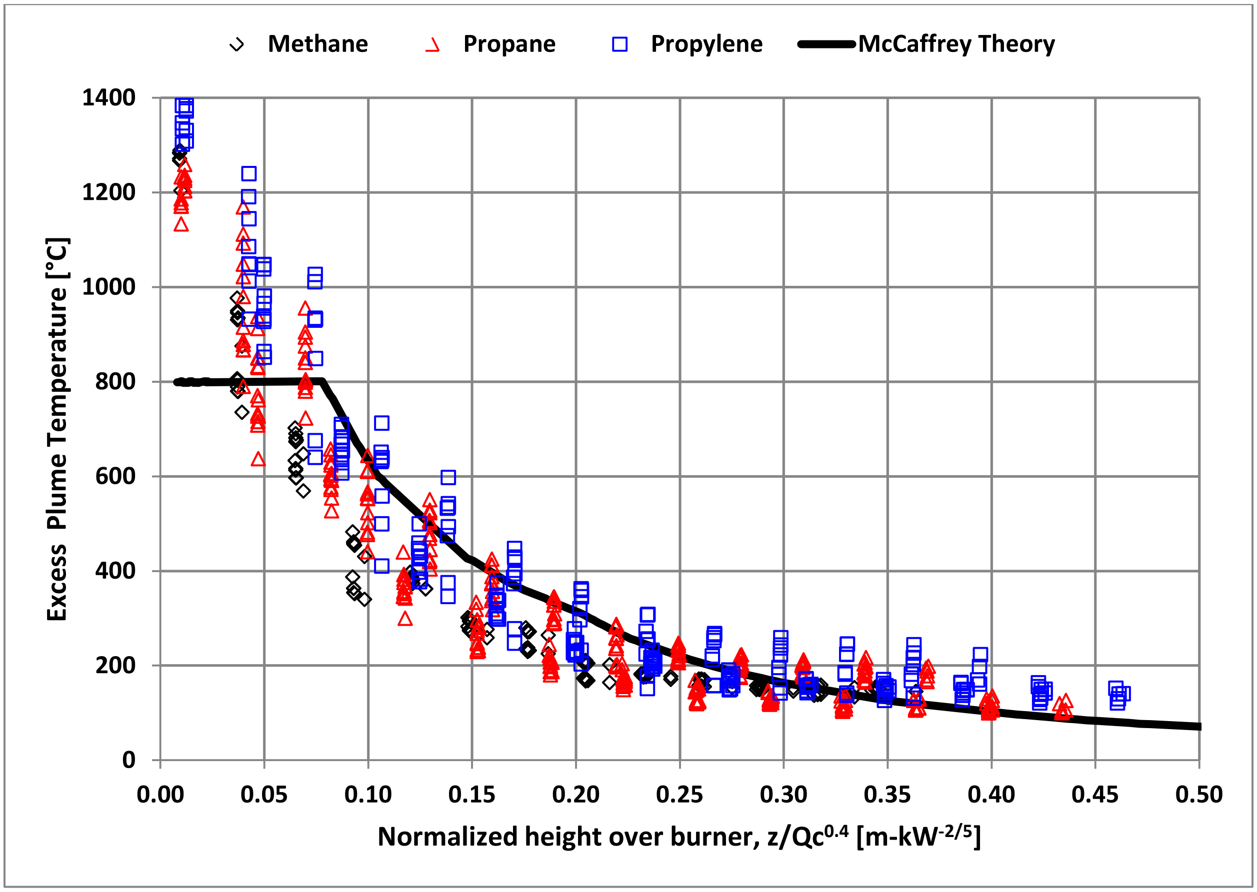

Figure 13 - Plume centerline temperature rise from inert wall fire tests using Square burner

Section N.4 of the thesis[24] contains the complete analysis of the plume temperature including those obtained in tests conducted with the Rectangle burner, as well as data normalized with the mean flame height.

Plume centerline velocity

Figure 14 presents the centerline plume velocity from the inert wall tests conducted with a Square burner, shown against McCaffrey's correlation. The height and velocity have been normalized against

the convective HRR. Complete analysis of the velocity measured in tests conducted with a Rectangle burner and normalization against mean flame height may be found in Section N.4 of the thesis[24].
The velocity measured in the inert wall tests is generally lower than that from the free plume tests, most likely due to the flame and plume leaning against the wall, disengaging the plume centerline away from the bi-directional probes. This effect also caused additional data scatter, reflected in the differing uncertainty from 0.23 m s^{-1} $kW^{1/5}$ to 0.40 m s^{-1} $kW^{1/5}$ for tests with the Square and the Rectangle burner, respectively.

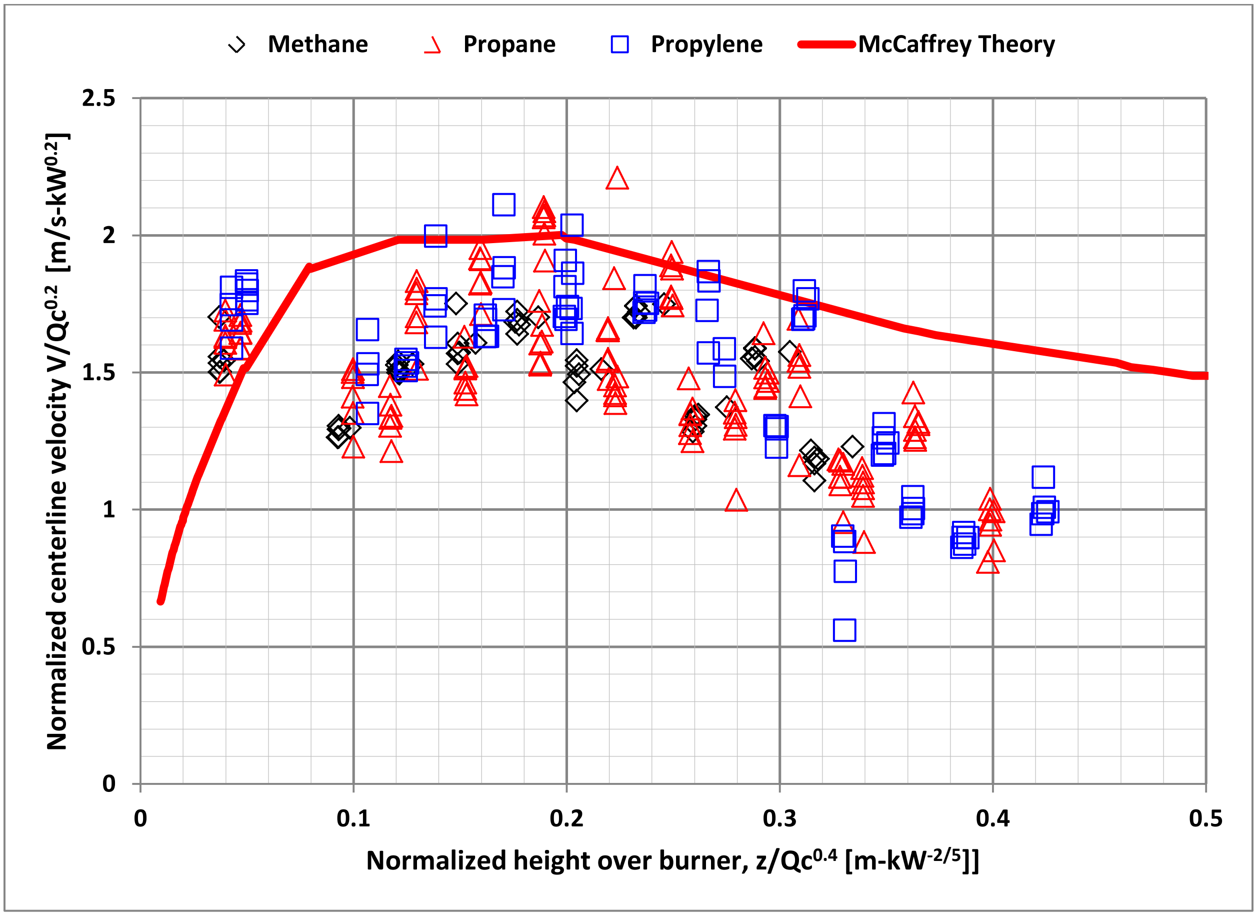

Figure 14 – Plume centerline velocity from inert wall fire tests using Square burner

Flame height

Flame height data from the inert wall tests are compared to Heskestad's correlation in Figure 15. The uncertainty of the Heskestad's correlation was reported to be 15-20%[76], so the current data falls within range of the uncertainties, except for the methane flame heights. Presence of the inert wall decreased the flame heights because the flame leaned toward the wall, which also reduced the plume temperature and velocity slightly. Flame height data normalized using different methods may be found in Section N.4 of the thesis[24].

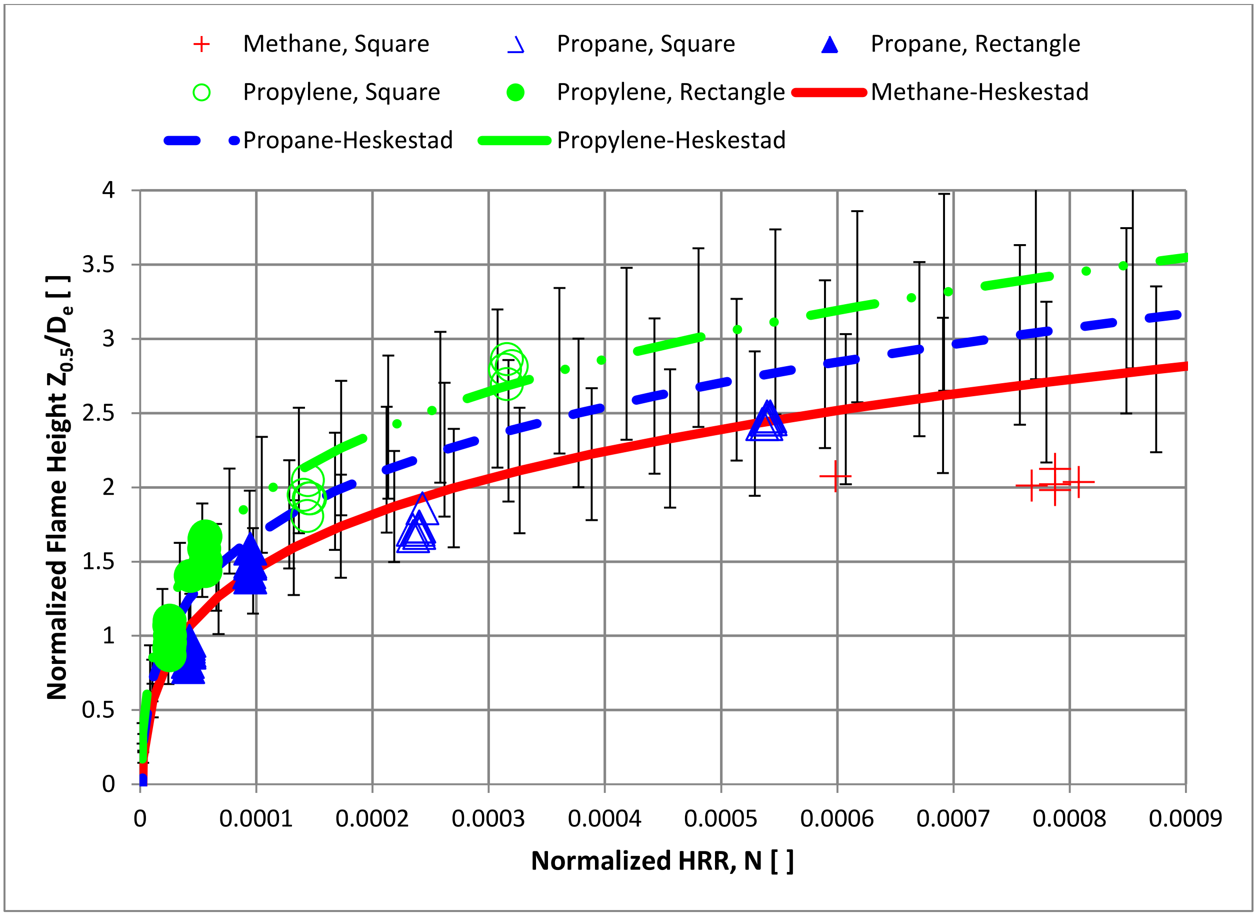

Figure 15 - Comparison of flame height data from inert wall fire tests with Heskestad's correlations

Incident heat flux to wall

In the Inert wall fire experiments, heat flux to the wall measured by the TSCs was normalized using the 100% intermittency flame height and the radiative HRR of the fire. It was assumed that the fire may be represented by a cylinder with a hot surface that output heat at a constant HRRPUA. The diameter of the cylindrical fire was taken as the hydraulic diameter of the source burner, and the 100% intermittency flame height was used as the cylinder's height. The 100% intermittency flame height was calculated as 3/5th of the 50% intermittency mean flame height, and the circular area is found using Equation (8):

$$A_{fire} = \pi D_h H_{f100} \tag{8}$$

The HRRUPA on the surface of the cylindrical fire can then be determined from the radiative component of the HRR using Equation (9):

$$HRRPUA_{fire} = \frac{HRR_{rad}}{A_{fire}} \tag{9}$$

Finally, the incident heat flux measured at the TSCs was normalized against the HRRPUA of the fire cylinder using Equation (10):

$$HF = \frac{\dot{q}_i^{"}}{HRRPUA_{fire}} \tag{10}$$

It was assumed that the source fires were symmetrical such that heat fluxes measured on both sides of the centerline were always equal. TSC elevations were normalized against the 100% intermittency flame height as well. This normalization method allows collapse of data for all TSCs at different heights and distances from the centerline.

The normalized heat flux recorded in the experiments using the Square burner is presented in Figure 16. The highest heat fluxes were recorded at the centerline. Data from the Square burner fire tests show that the heat flux decreases with height and horizontal distance from the centerline, however, in the Rectangle burner data, there was little variation in the heat flux measured at 0.3 m or 0.6 m away from centerline. The measured heat fluxes in the Square burner tests were generally greater than those measured using the Rectangle burner.

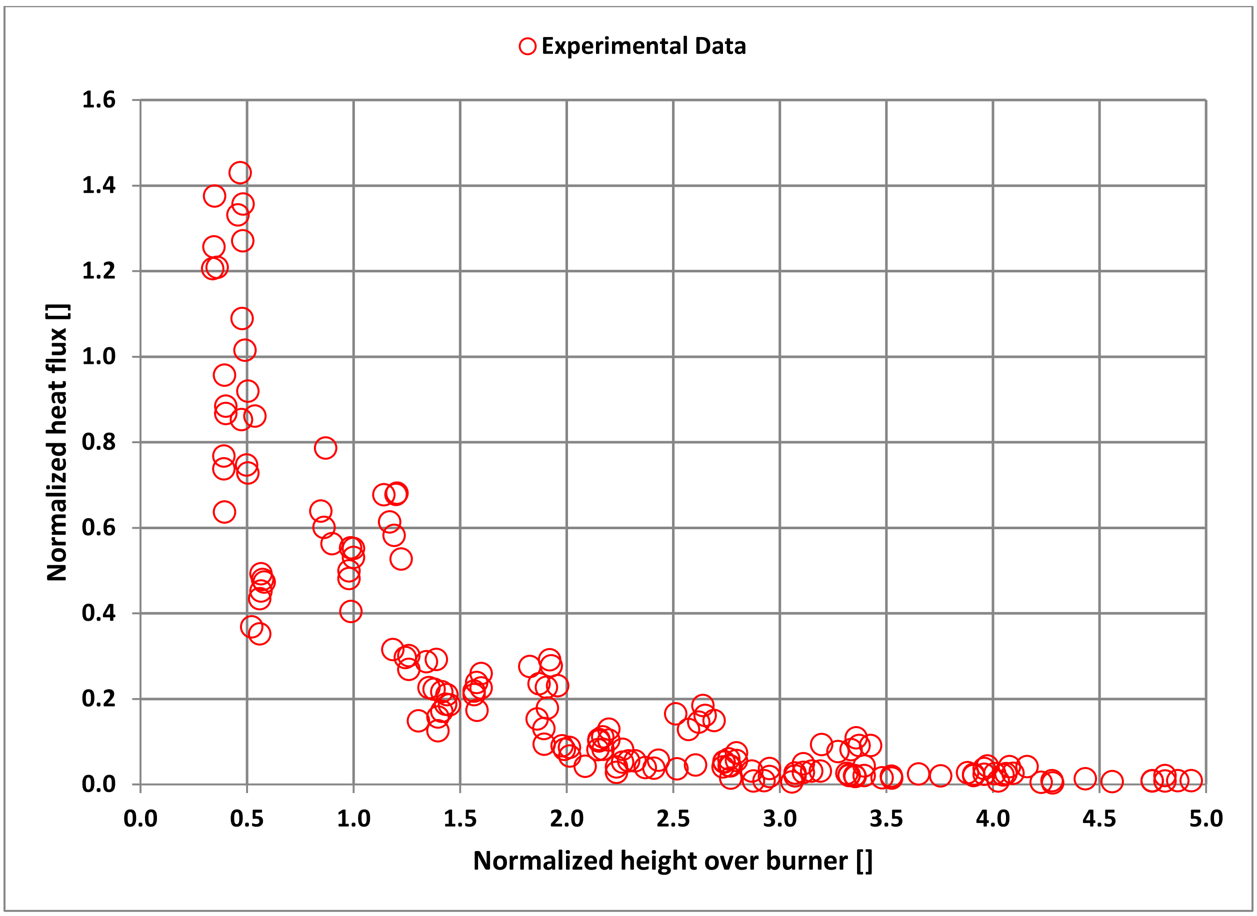

Figure 16 – Centerline normalized wall heat flux with the Square burner

In Figure 17, elevations of the measurements were normalized with the measured mean flame height; the heat flux was not normalized.

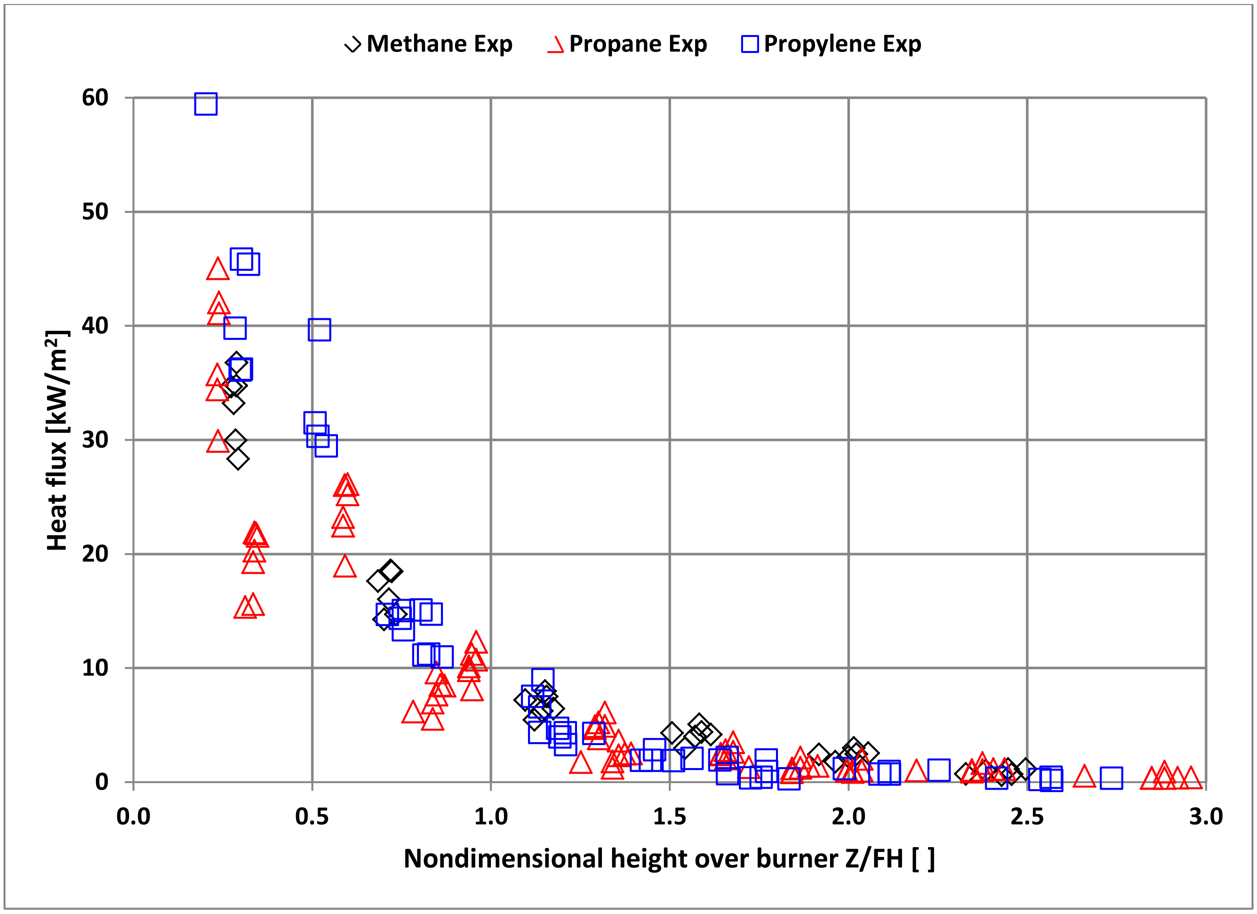

Figure 17 – Centerline non-normalized wall heat flux on inert wall with the Square burner

Combustible Wall Fire Tests Data

Data from only one out of the 18 combustible wall experiments are analyzed and presented in this paper, a complete analysis of additional experiments may be found in Section N.4, and the complete sets of data from all tests are available in Appendix F of the thesis[24].

Heat release rate

Although the FRP panel generally burned for more than 20 minutes during the tests, only the HRR during first 10 minutes of the tests was reported because the majority of flame spread occurred within this period. A discrepancy in the HRR that reflects the termination of fuel gas flow is evident in the HRR curves of most tests soon after ignition, when the burning panel's fire decreased momentarily and then increased until its peak, which always corresponds with "rollover" (ignition of hot combustion gases) under the ceiling.

Table 8 presents a summary of the time to peak and peak HRR values from the combustible wall fire tests. Regardless of experiment configurations, a propylene source fire tended to cause earlier times to peak (rollover under ceiling) than the propane experiments at the same source fire size. In the experiments where the source fire was continuous, the total heat released (THR) was also the highest. Additionally, it is observed that a source fire at the higher HRR correlates with a shorter time to peak.

Table 8 - FRP combustible wall fire tests HRR summary

Test Name	Source Fire Fuel	Source Fire HRR (kW)	Source Burner Shape	Time at Peak HRR (sec)	Peak HRR (kW)	End Test Time (sec)
A1*	Propylene	>75	Rectangle	N/A	N/A	N/A
A2**	Propylene	75	Rectangle	N/A	N/A	N/A
A3**	Propane	50	Rectangle	233	255	3,215
A4	Propane	75	Rectangle	181	370	2,120
A5	Propane	50	Square	234	250	1,685
A6	Propane	75	Square	168	275	1,390
A7	Propylene	50	Square	190 - 204	290	1,845
A8	Propylene	75	Square	120	315	1,195
A9	Propylene	50	Rectangle	167	300	1,488
A10	Propylene	75	Rectangle	132	380	1,225
A11	Propylene	50	Rectangle	162	320	1,288
A12	Propylene	50	Rectangle	119	540	1,092
A13	Propylene	50	Square	121	530	710
A14	Propylene	75	Square	155	290	1,131
A15	Propane	50	Square	205	260	1,105
A16	Propane	75	Square	131	565	1,380
A17	Propane	75	Rectangle	113	615	942
A18	Propane	50	Rectangle	196 - 210	250	1,055

Figure 18 and Figure 19 show the HRR time histories from the tests using the Rectangle burner with a 75 kW source fire, and those from tests with a Square burner at 50 kW, respectively. HRR histories of experiments under other configurations are compared in Section N.4 of the thesis[24].

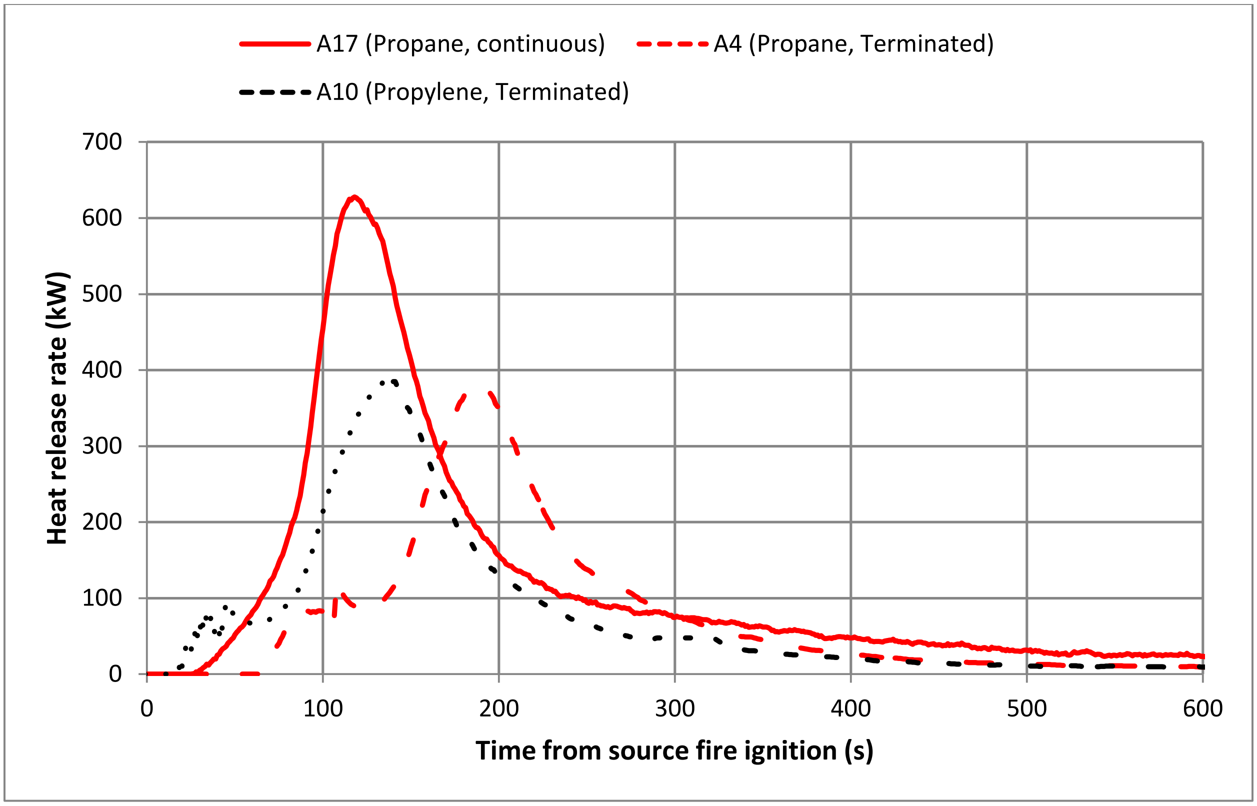

Figure 18 - HRR time histories for Rectangle burner with a 75 kW source fire

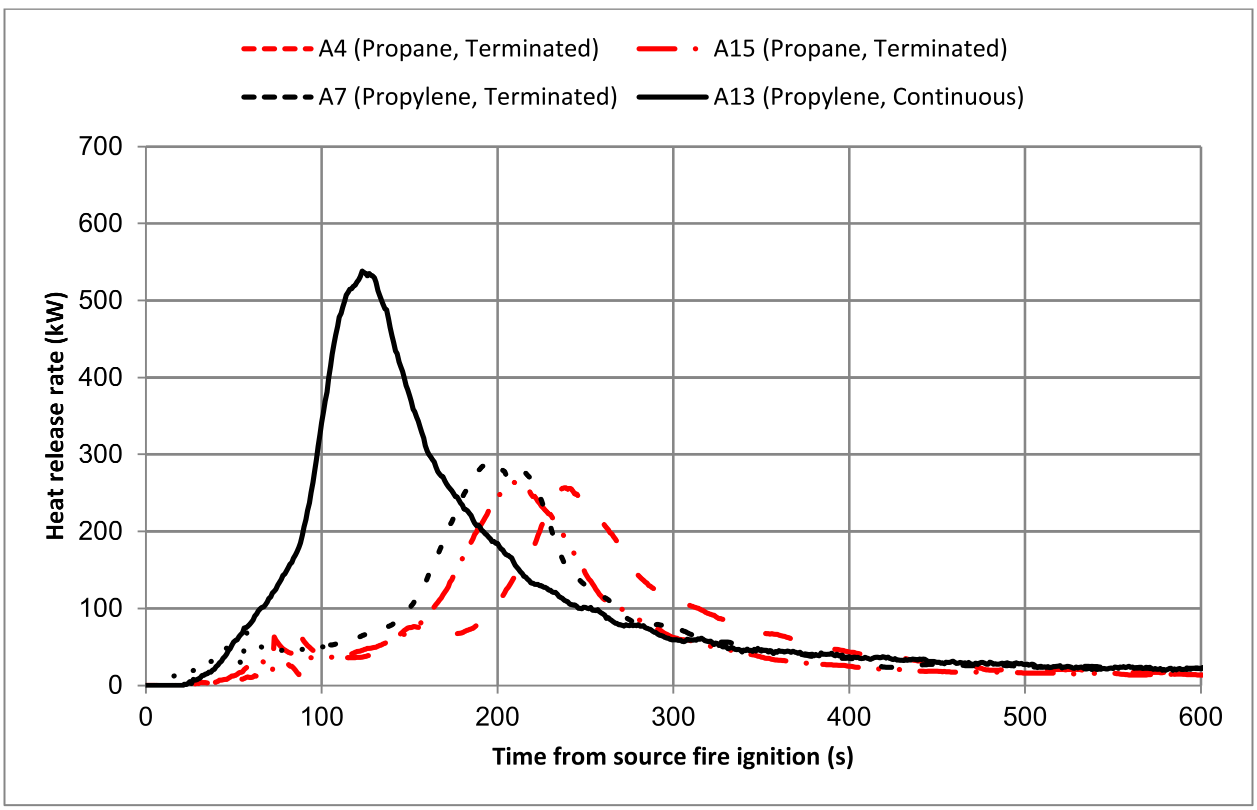

Figure 19 - HRR time histories for Square burner with a 50 kW source fire

The HRR data have shown that the peak HRR was approximately 300 kW ±40 kW for experiments where the source fire was terminated upon flame attachment on the FRP. For the experiments where the source fire was continuous throughout, the FRP's HRR peaked at 580 kW ±50 kW. The difference in the peak HRR may be attributed to the heat from the source fire continuously driving the flame spread on the FRP so that more area was ignited continuously, and higher pyrolysis and mass loss rates in those area under high external heat flux insults.

Experiments with one of the following conditions: a terminated source fire, using propylene source fuel, or a source fire at the higher HRR at 75 kW, were found to exhibit shorter times to panel ignition and peak HRR, higher peak HRRs and total mass lost were also observed. A comparison of tests with different burner sizes shows that the Rectangle burner tests exhibited longer times to panel ignition than from the Square burner. The effect on time to peak HRR due to burner size was less significant, but the Rectangle burner generally yielded higher peak HRRs, and greater overall mass lost.

A spike is shown in each of the combustible panel HRR time histories for tests with a terminated source fire. The spike is present at the time when the source burner was shut off, and is generated as an artifact in the calculations of the panel HRR. In actuality the FRP HRR at that point of fire growth does not decrease or increase sharply, but is relatively constant. For completeness of the data, the HRR curves presented here are not modified.

Plume centerline temperature

The corrected centerline temperature rises from Experiment A4 are presented in Figure 20 and Figure 21. For thermocouples up to 1 m above the burner surface, temperatures were highest when the source burner outputs 75 kW, but reduced as the source fire was terminated and the FRP began to burn, suggesting that these thermocouples were not significantly affected by the wall panel fire. At elevations above 1.10 m, the thermocouples were above the source fire's flame region, such that the temperature increases were low before the FRP started to burn. However, as the fire spread along the center of the panel, the temperature along this portion of the centerline rapidly increased until the FRP's HRR peaked. Finally, at the peak HRR, the highest centerline temperature was registered at the highest thermocouple due to flame rollover under the ceiling.

For the thermocouples near the burner surface, the radiation correction process yielded a "correction" of approximately 400 K to 500 K, which corresponded to approximately 50% of the recorded temperature; this large correction factor was due to the presence of higher-speed flow and flames. At 0.35 m to 0.65 m above the burner surface, the temperature increase due to correction drastically dropped off to an order of 100 K. At 1.10 m to 1.85 m, the thermocouples were inside the buoyant plume above the source flame and had relatively small correction on the order of 50 K to 100 K. However, the correction at the highest thermocouple was larger at around 200 K when the HRR of the FRP fire was at its peak and rollover occurred under the ceiling. After the initial fire has shut off, the dominant plume no longer exists, and the "plume centerline" temperatures recorded should be considered "burner centerline" temperatures only.

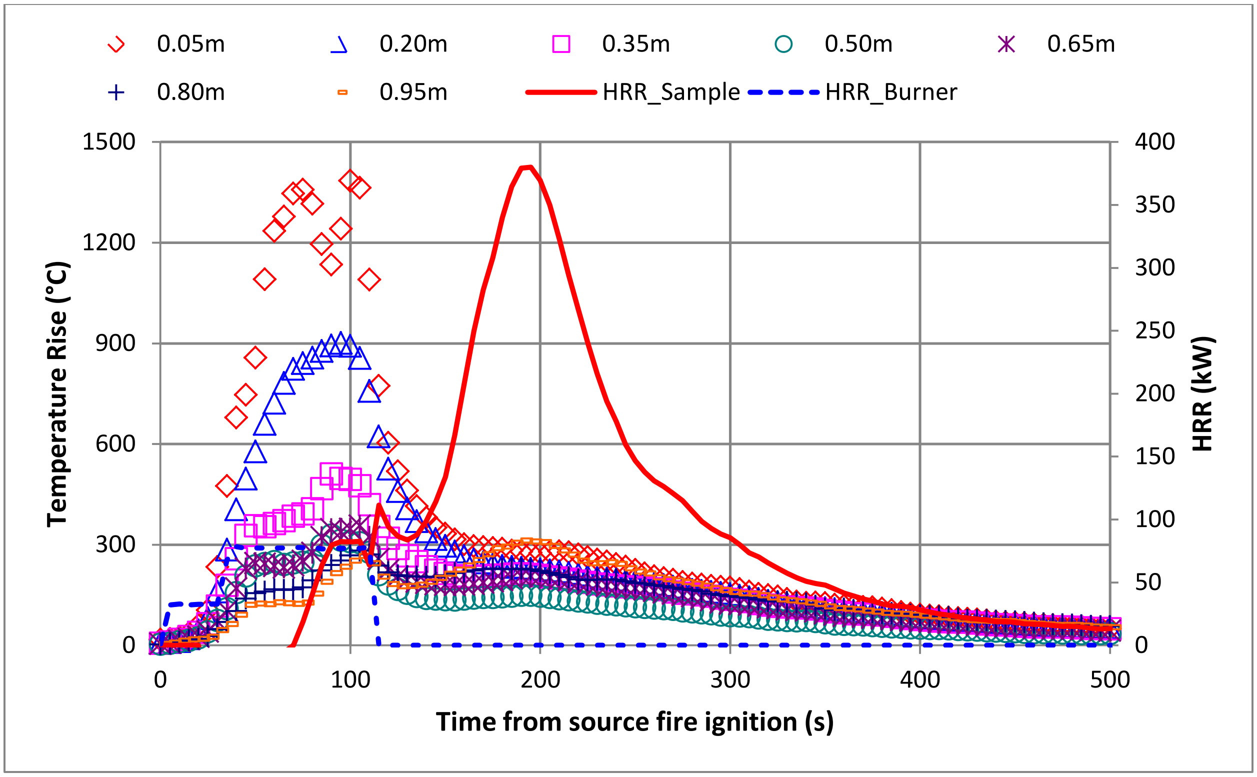

Figure 20 – Corrected plume/burner centerline temperature rise (< 1 m above burner) in Experiment A4 (Rectangle burner, 75 kW, propane, terminated source)

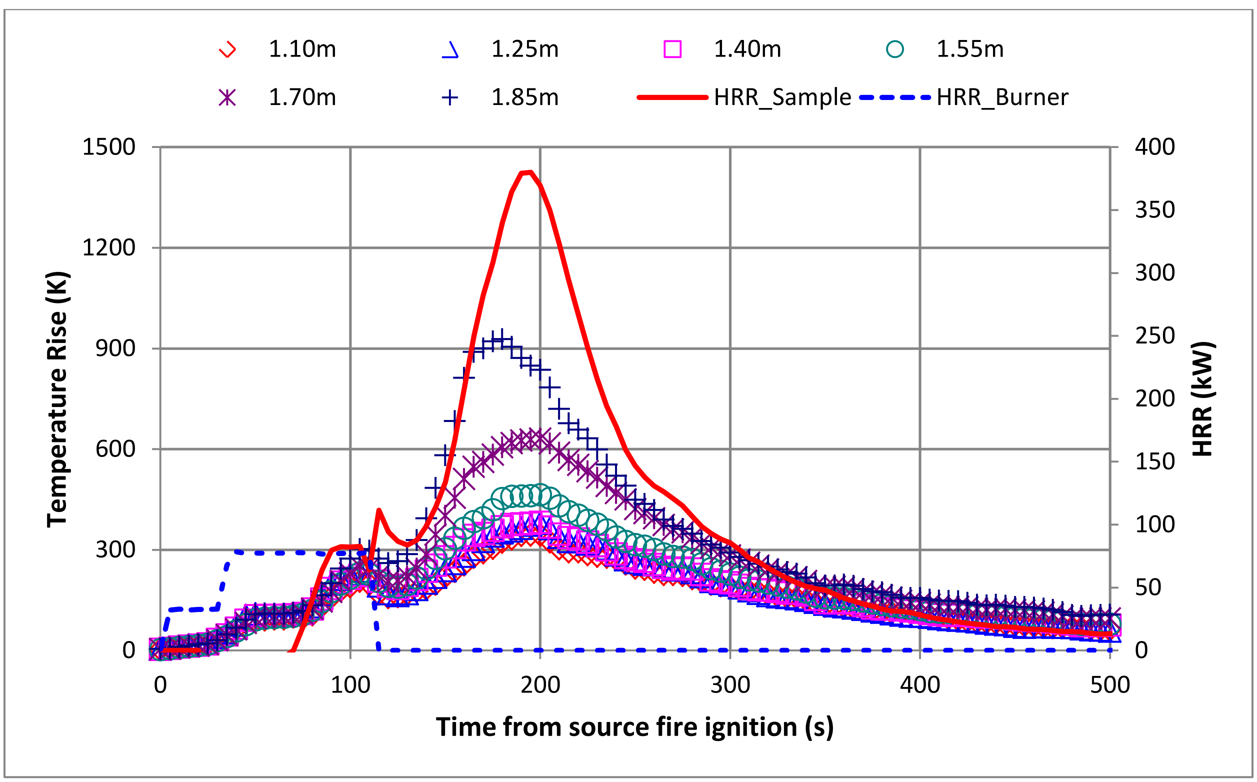

Figure 21 - Corrected centerline/burner centerline temperature rise (> 1 m above burner) in Experiment A4 (Rectangle burner, 75 kW, propane, terminated source)

Plume centerline velocity

Thermal effects from the fires on the velocity-measurement equipment were significant in the combustible wall tests. It is cautioned that the data be ignored after the peak HRR due to adverse thermal effects on the transducers. Although the velocity measurements may be inaccurate at this stage, the flow's measured directionality was found to still be valid.

Due to data-drift and the characteristics of the velocity sensing equipment, the uncertainty of the velocity measurements for the period of times before the sample HRR peaked is assumed to be approximately ±0.7 m/s for probes less than 1.0 m above the source burner surface, and ±1.0 m/s for probes at least 1.0 m above the burner surface.

Figure 22 presents the upward vertical velocity recorded in Test A4 at elevations from 0.20 m to 0.95 m above the source burner surface. The velocity in this range was driven mostly by the source fire plume. At the peak HRR, the velocity increased at the locations between 0.20 m to 0.80 m above the burner surface. However, the probe located at 0.95 m registered a negative flow over the same period of time. Velocity measurements at 1.10 m to 1.70 m are presented in Figure 23. The velocity recorded at 1.25 m to 1.70 m became negative during peak HRR most likely due to the pressure generated by the descending smoke layer at this stage of fire growth. Due to the proximity to the ceiling, the magnitude of the downward flow was largest at the highest probe. Because of thermal effects on the instruments, significant drift is observed for all the probes after peak HRR.

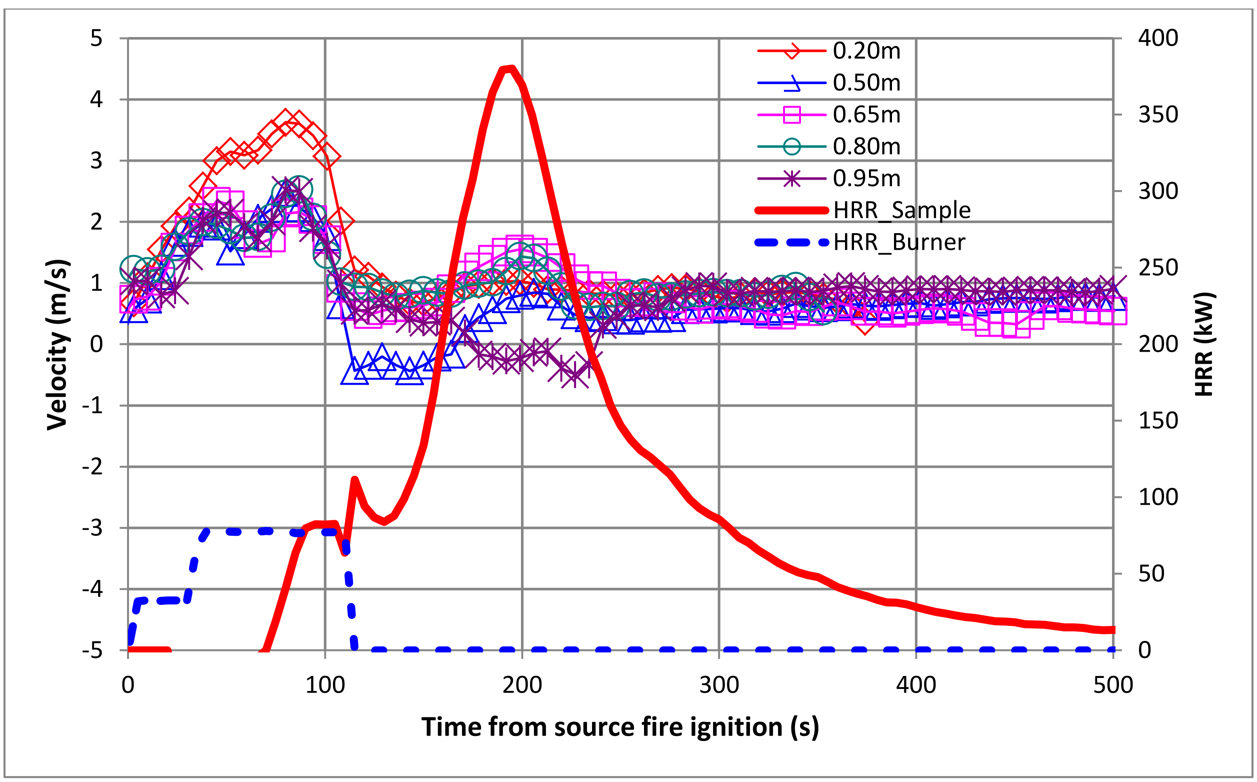

Figure 22 – Plume/burner centerline velocity (<1 m above burner) in Experiment A4 (Rectangle burner, 75 kW, propane, terminated source)

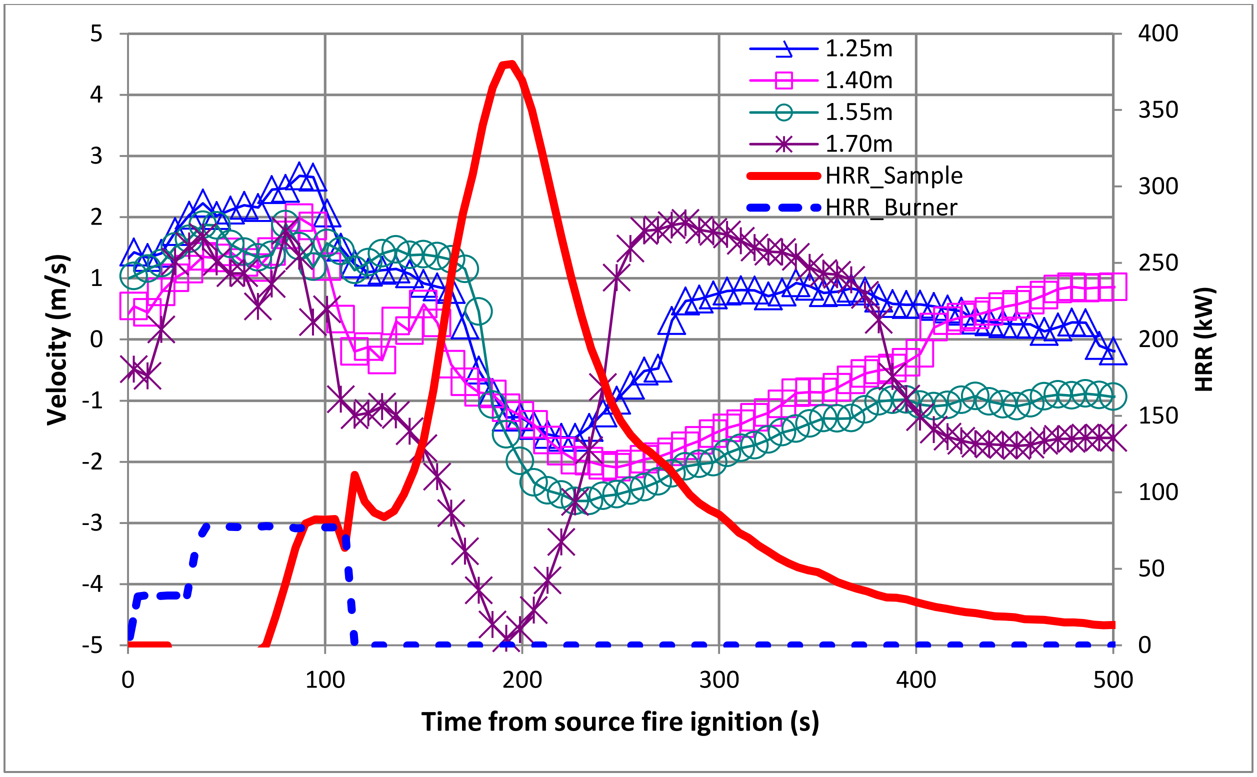

Figure 23 – Plume/burner centerline velocity (>1 m above burner) in Experiment A4 (Rectangle burner, 75 kW, propane, terminated source)

Incident heat flux to wall

The heat flux measured at the highest and lowest elevations during Test A4 are presented in Figure 24 and Figure 25, respectively. At 0.2 m above the burner surface, the centerline heat flux reached 40 kW/m^2 when the source fire was ignited, and then rose to 70 kW/m^2 when the panel was ignited. Before the specimen's HRR peaked, the centerline heat flux at this height sharply reduced, indicating that the fire on the panel had moved away from this location. At 1.7 m above the burner surface, the heat fluxes measured before the FRP specimen ignited was under 5 kW/m^2; the fluxes at all locations along this height increased concurrently to a range of 55 to 65 kW/m^2 when the HRR peaked. A notable exception is the gauge located 0.6 m to the right of the centerline, for which the heat flux increased as the HRR reduced. This behavior suggests that, during the period of the peak HRR at the location just below this elevation, flame spread across the entire panel almost simultaneously, resulting in the concurrent increase of heat flux.

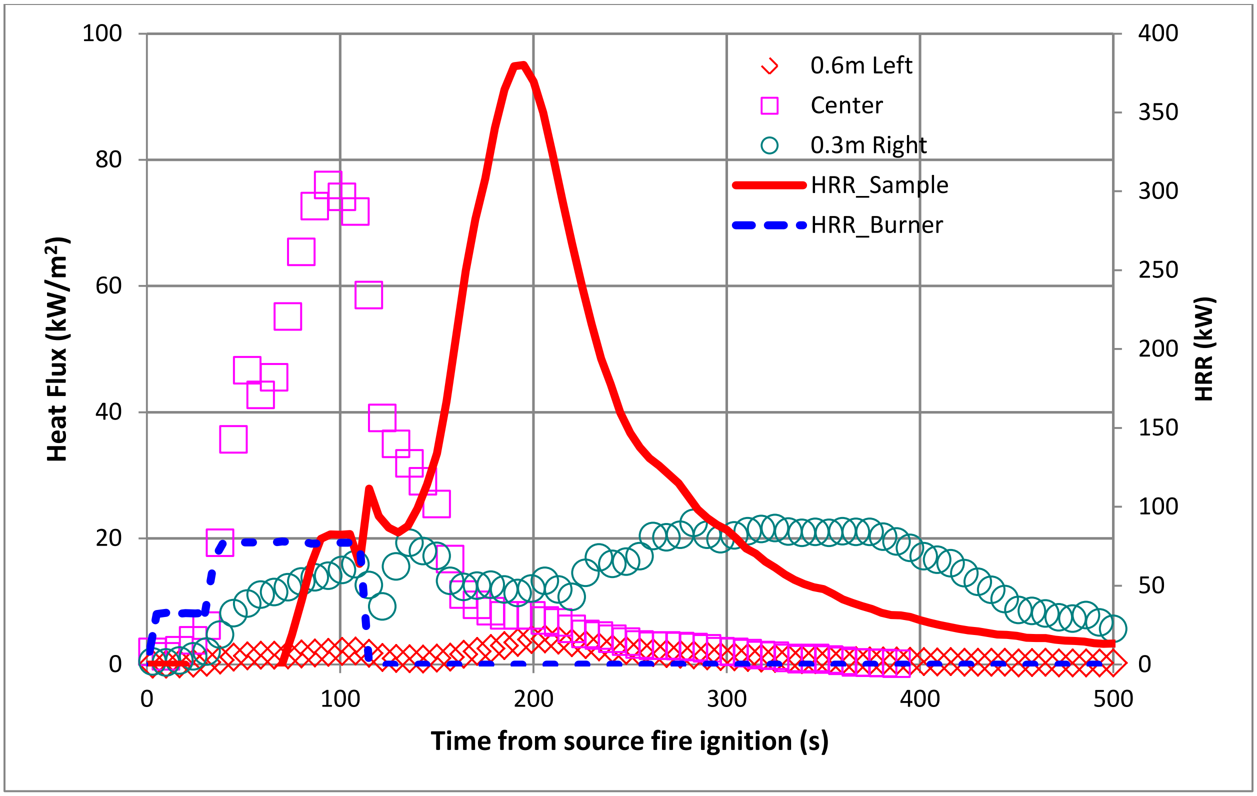

Figure 24 – Heat flux (0.2 m over burner) in Experiment A4 (Rectangle burner, 75 kW, propane, terminated source)

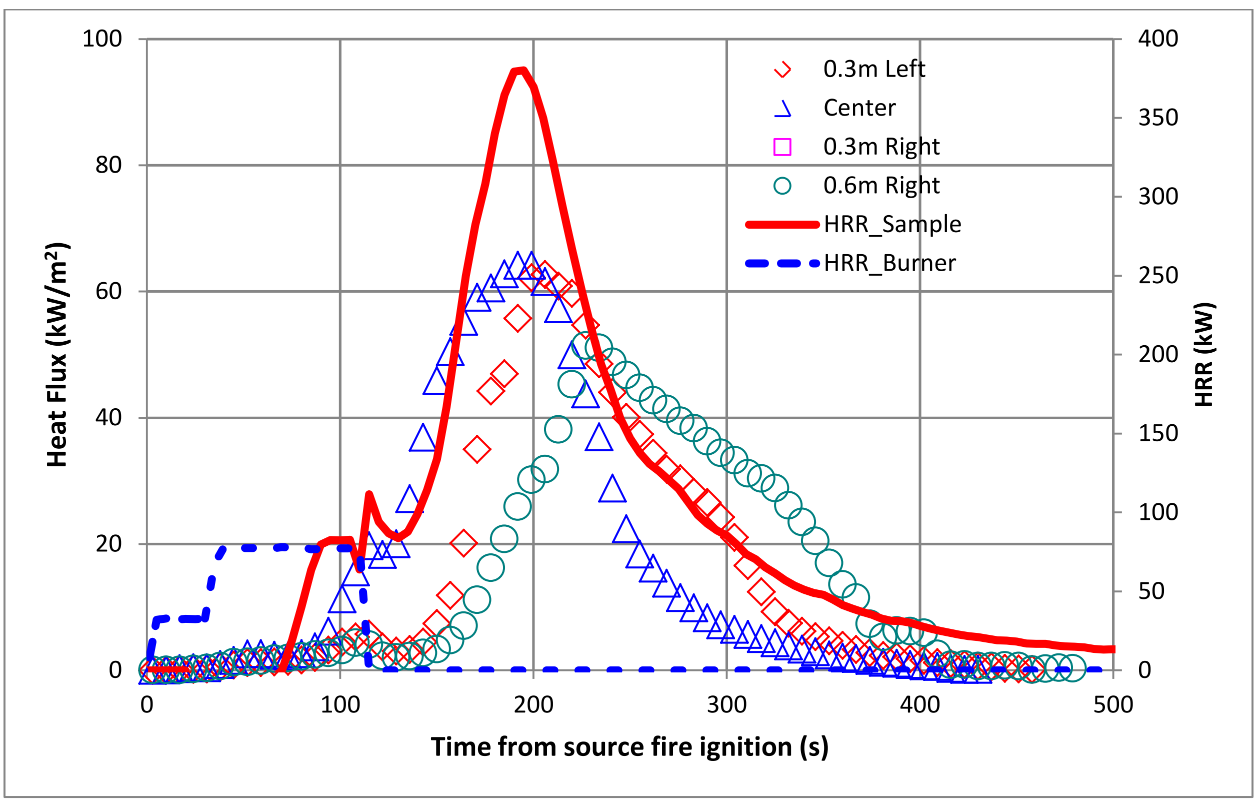

Figure 25 - Heat flux (1.7 m over burner) in Experiment A4 (Rectangle burner, 75 kW, propane, terminated source)

Flame spread rate

Flame spread rate calculated for Experiment A4 is presented in Figure 26. The initial flame spread was slow because of the source HRR was terminated upon panel ignition. The highest peak in the FSR corresponds to the point when rollover occurred under the ceiling accompanied by a rapid increase of the flame spread rate due to increases in lateral spread and downward spread. After the initial peak, the FSR gradually increases again into another peak then decreases and becomes insignificant for the remainder of the experiment.

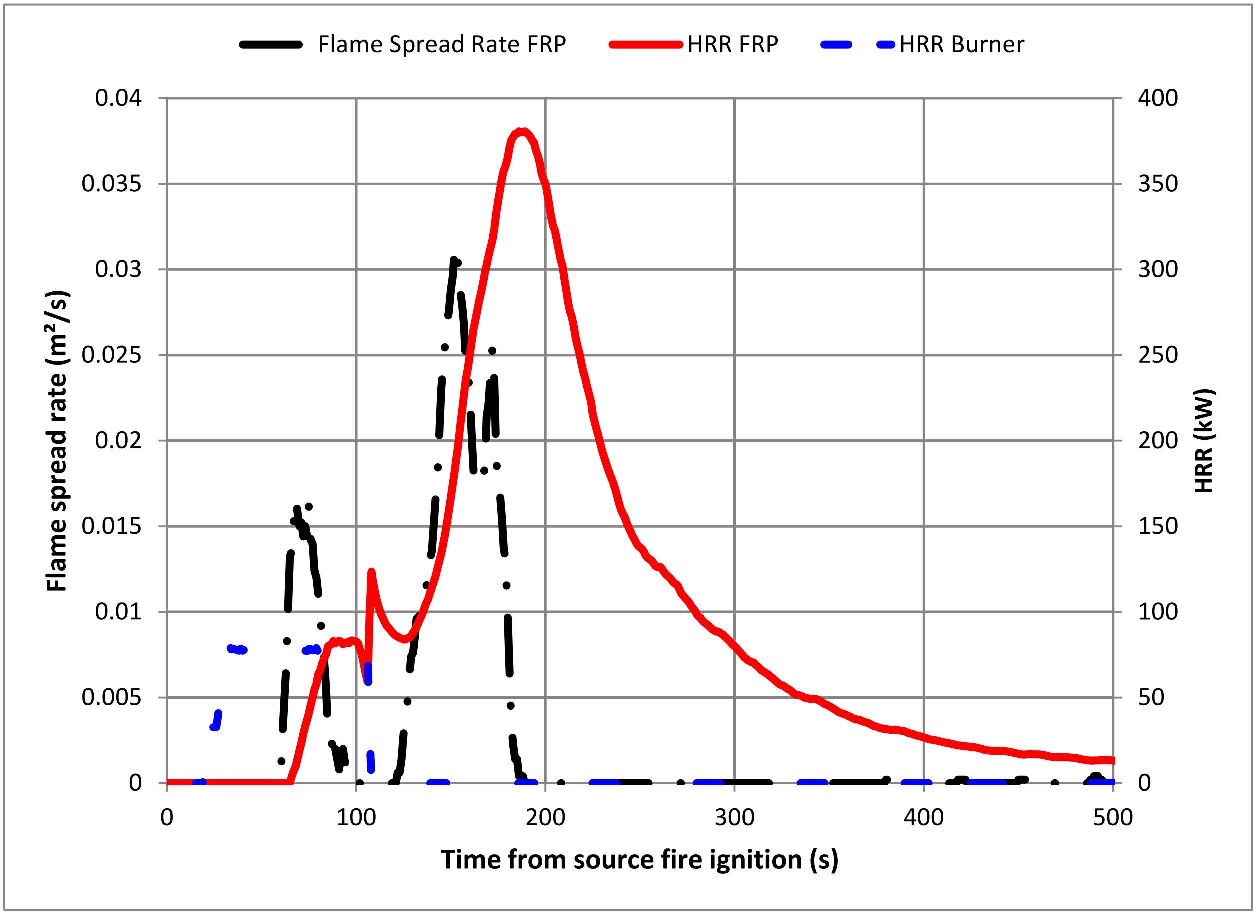

Figure 26 - Flame spread rates and HRRs comparison of Experiment A4

The FRP burning area history, showing the position and dimensions of the panel burning in relation to the burner's top edge (y-axis) and centerline (x-axis), of Experiment A4 is presented in Table 9 to Table 11. These time-history charts have been time-shifted to begin when the source fire was extinguished. For the first 70 seconds of fire growth, Stage 1 burning, as defined previously as mostly upward only, commenced. After that, Stage 2 burning lasted for approximately 40 seconds where the burning area progressed downward away from the center and continued to move upward from the bottom. The downward spread was caused by flame impingement under the ceiling. Peak HRR was measured during Stage 2 burning. At Stage 3, the central area of the panel was burnt out, and the burning area was spilt into two sections. Both burn areas progressed downward and toward the outside edge of the panel until total burnout. After this stage of fire growth, only several short, linear areas remained burning.

Table 9 – Stage 1 burning flame spread progression in Experiment A4

Stage 1 Burning

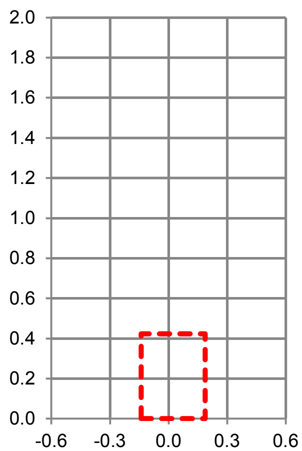

0 sec

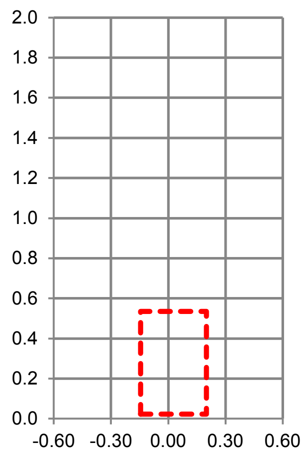

10 sec

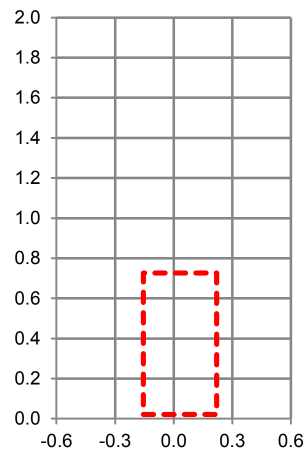

20 sec

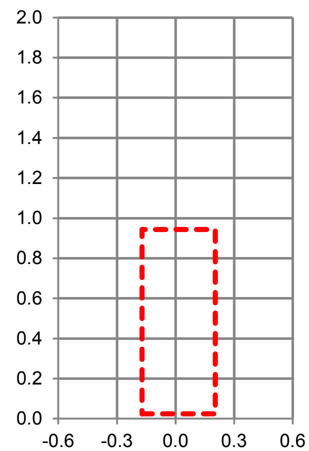

30 sec

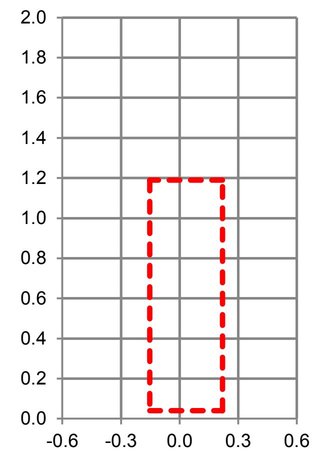

40 sec

Stage 1 Burning

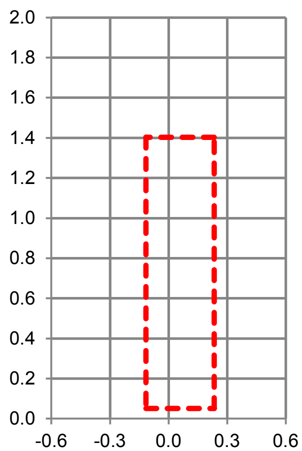

50 sec

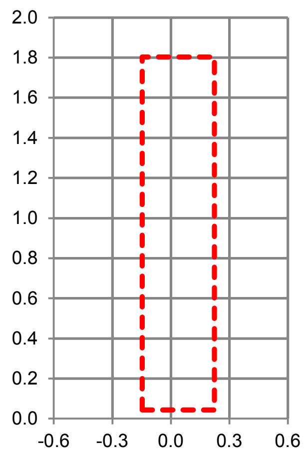

60 sec

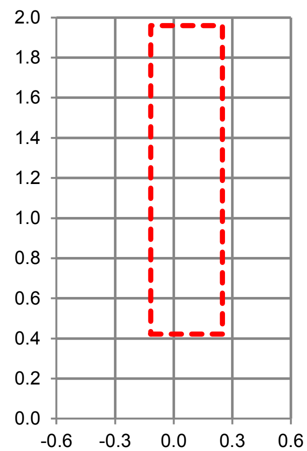

70 sec

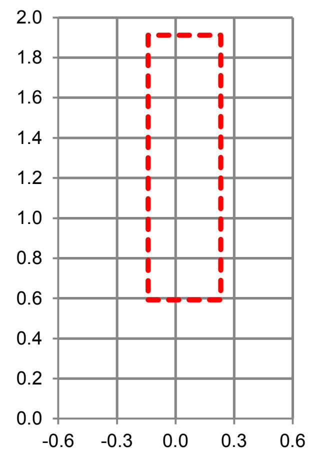

80 sec

*Dimensions are in meters

Table 10 - Stage 2 burning flame spread progression in Experiment A4

Stage 2 Burning	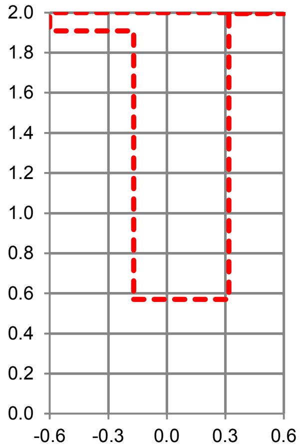	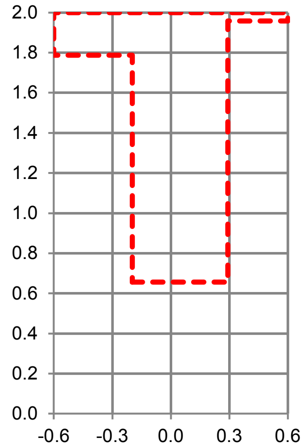	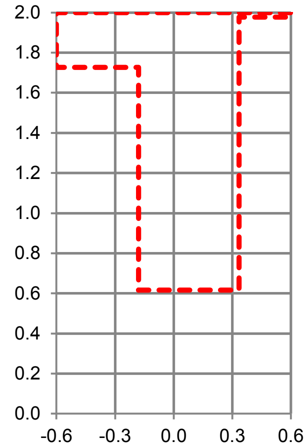	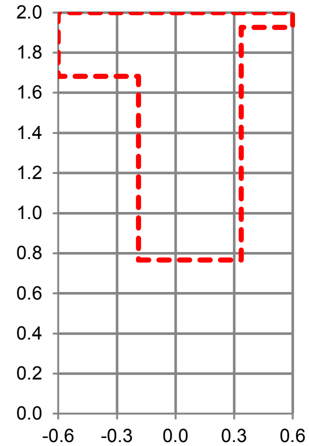	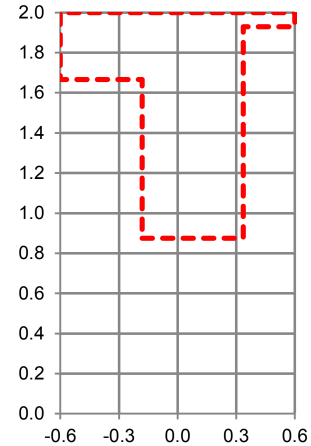
	85 sec	90 sec	95 sec	100 sec	105 sec
Stage 2 Burning	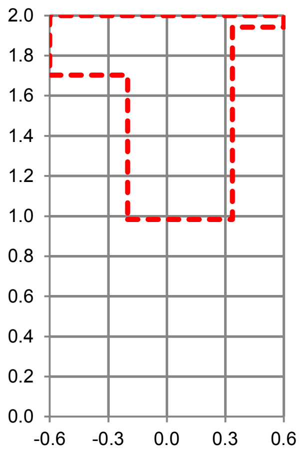	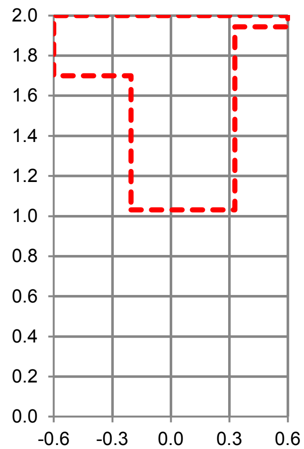	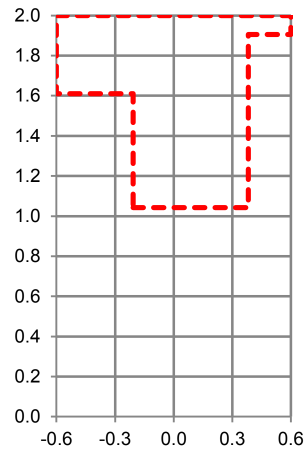	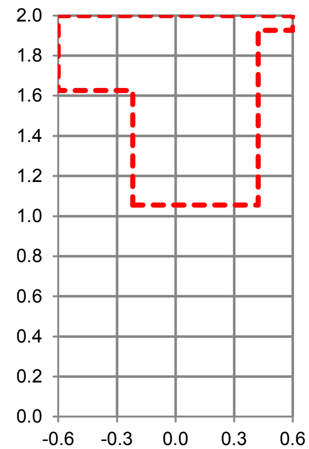	
	110 sec	115 sec	120 sec	125 sec	

*Dimensions are in meters

Table 11 - Stage 3 burning flame spread progression in Experiment A4

Stage 3 Burning

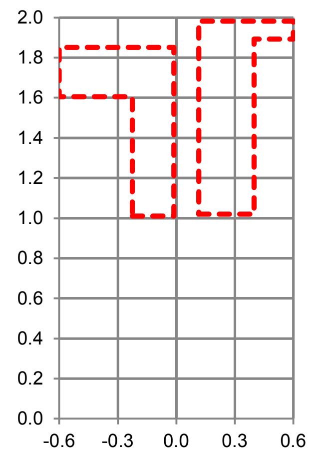

130 sec

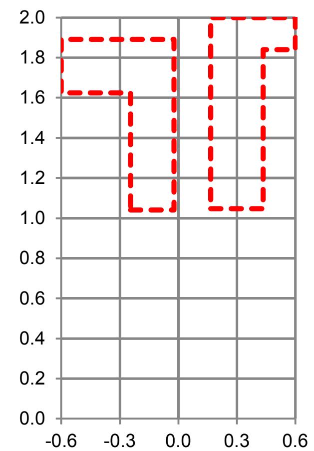

140 sec

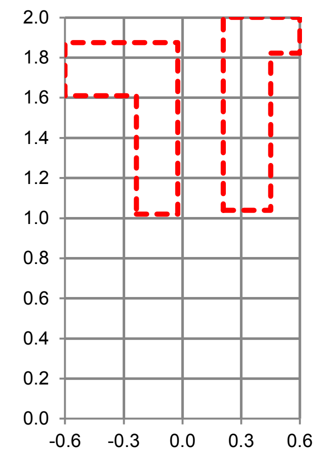

150 sec

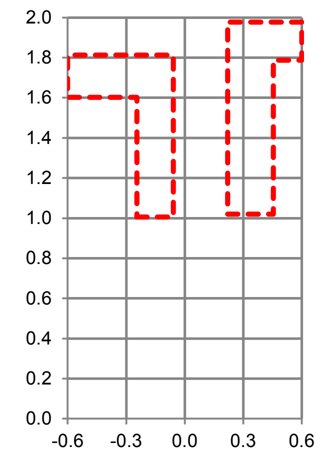

160 sec

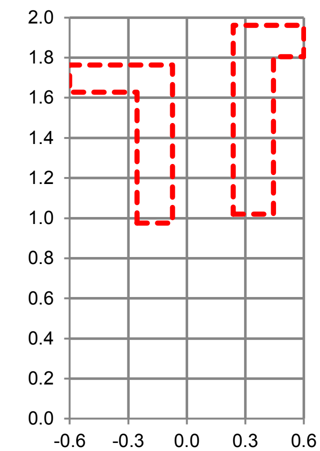

170 sec

Stage 3 Burning

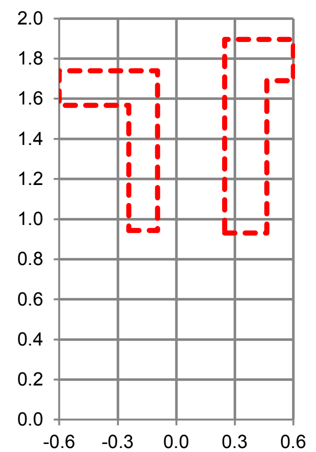

180 sec

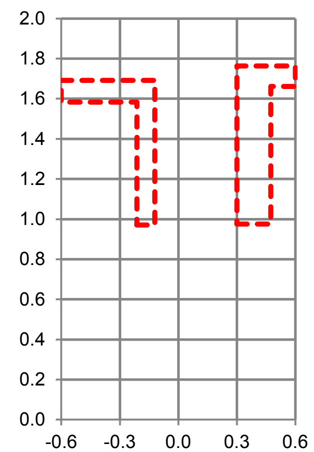

190 sec

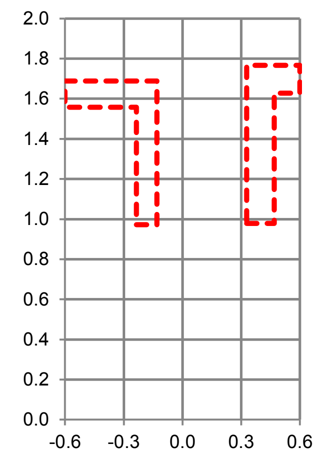

200 sec

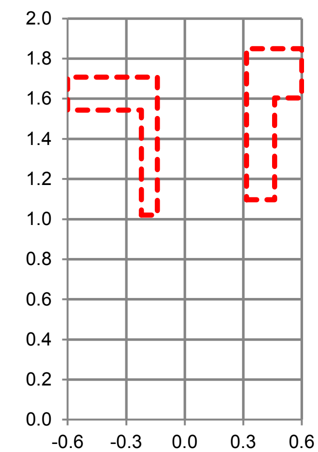

210 sec

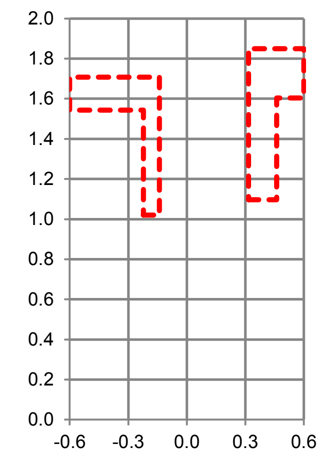

220 sec

*Dimensions are in meters

Conclusion

A framework to analyze flame spread and to validate a CFD flame spread model by decomposing the complex process into several inter-related components has been presented. The four flame spread components are classified as:

1. Turbulent buoyant fluid flow
2. Gas phase kinetics
3. Flame heat transfer
4. Condensed-phase pyrolysis.

Based on this framework, three progressively complex experiments, from free plume, to inert wall fires, to combustible wall flame spread were carried out to enable collection of data relevant to each component of flame spread. Similar characteristics such as fuel, burner shape and source fire HRR were preserved between sets of experiment to show the interconnectivity of those flame spread components, resulting in a comprehensive set of flame spread data. Measurements made in the experiments include HRR, plume centerline temperature and velocity, heat flux to wall, near-wall temperature, flame height, flame spread progression, mass loss, and burn pattern.

Many CFD fire simulation calibration exercises are judged based on a single global metric such as HRR, which can lead to a failure to identify compensating effects from the various contributing phenomena and components of flame spread. The decomposition framework and data presented in this paper allows a user to build and validate a model in a logical, progressive, and piecewise fashion, thereby achieving suitable validation of constituent components of a fire growth model as well as the model as a whole. Through this process of data verification and validation, a physically more accurate model may potentially be developed.

Recommendations for future work

Experimental data from the three series of fire tests are intended to be used in future validation and verification for the development of fire models. A user of the dataset can choose different fire experiments to model and compare the results with real experimental data, or use the current data with other researchers' results to deduce correlations that describe free plume fires, inert wall fires, and combustible wall fires.

Review of the collected data shows that there are large uncertainties in the velocity and temperature measurements. The data measurement was limited, in part, by the equipment available. Although bi-directional probes have been proved to be extremely reliable in many different research projects, the pressure transducers necessary to accurately measure the relatively small pressure differential inside a low-HRR fire plume can be cost-prohibitive. Thermal effects from the fire on the transducers, gas sample lines, and electrical wires also contributed to the high uncertainty. Other methods of measuring fire plume velocity that reduces uncertainty should be considered, such as using laser Doppler techniques, installing transducers with higher sensitivity, and different mounting options for the equipment. Thermocouple measurements are inherently inaccurate because of the need for radiation correction, but they may also be complimented by other temperature measurement methods such as using infrared cameras or aspirated thermocouples. In addition, video camera with a higher resolution can also improve the accuracy of the flame height and flame spread progression measurements.

Some supplementary quantities that can expand the dataset may include additional wall-surface and near-wall temperatures embedded in the wall, as well as post-burn cooling of the inert wall measured using thermocouples or with a high-resolution infrared camera. Both of these quantities will aid in the understanding of the flame heat transfer to its surrounding, as well as provide another means to track the progression of flame spread. Measurements of gas temperature and velocity away from the centerline can also be made to better describe the environment within and around the fire plume.

Expansion of the dataset may also include additional configurations of the source fire such as additional fuels, burner sizes, and HRRs. The types of wall lining materials used in the combustible wall fire tests may also be expanded to include materials of different characteristics as well, such as different types of plastic and wood paneling commonly used in the built environment. However, it is cautioned that the critical source fire HRR should be found that correlates with the minimal heat flux needed to ignite the paneling.

References

1. Lautenberger C and Hostikka S. Large Scale Fire Modeling. In: Wilkie CA, Morgan AB and Dekker M, (eds.). *Flame Retardancy of Polymeric Materials, 2nd ed*. Boca Raton, FL: Taylor and Francis, 2009.
2. Lautenberger C, Wong W, N. Dembsey, Coles A and Fernadez-Pello C. Large-Scale Turbulent Flame Spread Modeling with FDS5 on Charring and Noncharring Materials. In: *Fire and Materials 2009*, San Francisco, CA, 2009. London, UK: Interscience Communications, Ltd.
3. Verification and Validation of Selected Fire Models for Nuclear Power Plant Applications. NUREG-1824. Washington, DC: U.S. Nuclear Regulatory Commission, 2006.
4. Shields TJ, Silcock GWH, Moghaddam AZ and Azhakesan MAZ, J. A Comparison of Fire Retarded and Non-Fire Retarded Wood-Based Wall Linings Exposed to Fire in an Enclosure. *Fire and Materials*. 1999; 23: pp.17-25.
5. Yan Z and Holmstedt G. CFD and Experimental Studies of Room Fire Growth on Wall Lining Materials. *Fire Safety Journal*. 1996; 27: pp.201-38.
6. Peacock RD, Davis S and Babrauskas V. Data for Room Fire Model Comparisons. *Journal of Research of the National Institute of Standards and Technolog*. 1991; 96: pp.411-62.
7. Qian C, Ishida H and Saito K. Upward Flame Spread Along the Vertical Corner Walls. NIST-GCR-94-648. Gaithersburg, MD: National Institute of Standards and Technology, 1993.
8. Brehob EG, Kim CI and Kulkarni AK. Numerical Model of Upward Flame Spread on Practical Wall Materials. *Fire Safety Journal*. 2006; 36: pp.225-40.
9. Mitler HE and Steckler KD. Comparison of Wall-Fire Behavior with and without a Ceiling. NISTIR 5380. Gaithersburg, MD: National Institute of Standards and Technology, 1993.
10. Consalvi JL, Pizzo Y and Porterie B. Numerical Analysis of the Heating Process in Upward Flame Spread Over Thick PMMA Slabs. *Fire Safety Journal*. 2008; 43: pp.351-62.
11. Ohlemiller TJ and Cleary TG. Upward Flame Spread on Composite Materials. In: *Fire and Polymers II: Materials and Test for Hazard Prevention, American Chemical Society, ACS Symposium Series 599*, Washington, DC, 1994.
12. Ohlemiller T, Cleary T and Shields J. Effect of Ignition Conditions on Upward Flame Spread on a Composite Material in a Corner Configuration. *Fire Safety Journal*. 1998; 31: pp.331-44.
13. Wu PK, Orloff L and Tewarson A. Assessment of Material Flammability with the FSG Propagation Model and Laboratory Test Methods. In: *Thirteenth Joint Panel Meeting of the UJNR Panel of Fire Research and Safety*, Gaithersburg, MD, 1996. Gaithersburg, MD: NIST.
14. Kokkala M, Goransson U and Soderbom J. EUREFIC - Large Scale Fire Experiments in a Room with Combustible Linings. SP Report 1990:41. Boras: Swedish National Testing and Research Institute, 1990.
15. Kokkala M, Goransson U and Soderbom J. Five Large_Scale Room Fire Experiments: Project 3 of the EUREFIC Fire Research Programee. Espoo: Technical Research Centre of Finland, 1992.
16. Wu KK, Fan WF, Chen CH, Liou TM and Pan IJ. Downward Flame Spread Over a Thick PMMA Slab in an Opposed Flow Environment: Experiment and Modeling. *Combustion and Flame* 2003; 132: pp.697-707.
17. Walmerdahl P and Werling P. Fire Growth and Spread - An Experimental Study in Model-Scale. FOI-R--0907--SE. Stockholm: Swedish Defence Research Agency, 2003.
18. Wu PK and Bill RG. Laboratory Tests for Flammability Using Enhanced Oxygen. *Fire Safety Journal*. 2003; 38: pp.203-17.
19. Rangwala AS, Buckley SG and and Torero JL. Upward Flame Spread on a Vertically Oriented Fuel Surface: The Effect of Finite Width. *Proceedings of the Combustion Institute*. 2007; 31: pp.2607-15.
20. Hietaniemi J, Hostikka S and Vaari J. FDS Simulation of Fire Spread - Comparison of Model Results with Experimental Data. VTT Working Papers 1459-7683. Finland: VTT Building and Transport, 2004.

21. Hostikka S and McGrattan KB. Large Eddy Simulation of Wood Combustion. In: *International Interflam Conference*, Edinburgh, Scotland, 2001. London, UK: Interscience Communications, Ltd.
22. Stroup DW, Delauter L, Lee J and Roadarmel G. Upholstered Chair Fire Tests Using a California Technical Bulletin 133 Burner Ignition Source. Gaithersburg, MD: National Institute of Standards and Technology, 2001.
23. Lattimer BY, Hunt SP, Wright M and Sorathia U. Modeling Fire Growth in a Combustible Corner. *Fire Safety Journal*. 2003; 38: pp.771-96.
24. Wong W. *CFD Flame Spread Model Validation: Multi-component Data Set Framework.* MS Thesis, Worcester Polytechnic Institute, Worcester, MA, 2012.
25. Evaluation of Fire Models for Nuclear Power Plant Applications - Flame Spread in Cable Tray Fires Benchmark Exercise No. 5. SR 2491. Gesellschaft fur Anlagen-und Reaktorsicherheit (GRS) mbH, 2006.
26. Combustion Science & Engineering, Inc. CFX. Computer Models For Fire and Smoke - International Survey of Computer Models for Fire and Smoke, http://www.firemodelsurvey.com/pdf/cfx_2001.pdf (2008, accessed July 1, 2012).
27. Liu Y, Moser A and Sinai Y. Comparison of a CFD Fire Model Against Ventilated Fire Experiment in an Enclosure. *International Journal of Ventilation*. 2004; 3: pp.169-82.
28. Wen J, Huang L, AMIN E and Nolan P. Modeling Sooting Jet Fires in a Large-Scale Offshore Compartment. *Twenty-Seventh Symposium (International) on Combustion/The Combustion Institute*. 1998: pp.2881-6.
29. Rauwoens P, Degroote J, Wasan S, Vierendells J and Merci B. Simulations of Upward Flame Spread by Coupling a Pyrolysis Model with a CFD Calculation. In: *V European Conference on Computational Fluid Dynamics ECCOMAS CFD 2010*, Lisbon, Portugal, 2010.
30. Papadikis K, Gu S, Bridgewater A and Gerhauser H. Application of CFD to Model Fast Pyrolysis of Biomass. *Fuel Processing Technology*. 2009; 90: pp.504-12.
31. Gutiérrez-Montesa C, Sanmiguel-Rojasa E, Kaiserb A and Viedma A. Numerical Model and Validation Experiments of Atrium Enclosure Fire in a New Fire Test Facility. *Building and Environment*. 2008; 43: pp.1912-28.
32. Kang K. Verification of CFD Modeling for Smoke Control Using Two Compartment Fire Experiments. *ASHRAE Transactions*. 2009; 115: pp.254.
33. Zhang J, Ji J, Huo R, Yuan H and Yang R. A Comparison of Simulation and Experiment on Stack Effect in Long Vertical Shaft. *Journal of Fire Sciences*. 2006; 24: pp.121-35.
34. Combustion Science & Engineering, Inc. PHOENICS. Computer Models For Fire and Smoke - International Survey of Computer Models for Fire and Smoke, http://www.firemodelsurvey.com/pdf/PHOENICS_2001.pdf (2008, accessed July 1, 2012).
35. Mawhinney R, Galea E, Hoffmann N and Patel M. A Critical Comparison of a PHOENICS Based Fire Field Model with Experimental Compartment Fire Data. *Journal of Fire Protection Engineering*. 1994; 6: pp.137-52.
36. McGrattan KB, McDermott R, Hostikka S and Floyd JE. Fire Dynamics Simulator (Version 5) User's Guide. NIST Special Publication 1019-5. Gaithersburg, MD: National Institute of Standards and Technology, 2010.
37. McGrattan KB, Hostikka S, Floyd JE, et al. Fire Dynamics Simulator (Version 5) Technical Reference Guide Volume 1: Mathematical Model. NIST Special Publication 1018-5. Gaithersburg, MD: National Institute of Standards and Technology, 2010.
38. Combustion Science & Engineering, Inc. FDS. Computer Models For Fire and Smoke - International Survey of Computer Models for Fire and Smoke, http://www.firemodelsurvey.com/pdf/FDS_2007.pdf (2008, accessed July 1, 2012).

39. Maragkos G, Rauwoens P and Merci B. Application of FDS and FireFOAM in Large Eddy Simulations of a Turbulent Buoyant Helium Plume. In: *7th Mediterranean Combustion Symposium (MCS-7)*, Cagliari, Sandinia, Italy, 2011.
40. Smardz P. *Validation of Fire Dynamics Simulator (FDS) for Forced and Natural Convection Flows.* MS Thesis, University of Ulster, Londonberry, UK, 2006.
41. Combustion Science & Engineering, Inc. JASMINE. Computer Models For Fire and Smoke - International Survey of Computer Models for Fire and Smoke, http://www.firemodelsurvey.com/pdf/JASMINE_2007.pdf (2008, accessed July 1, 2012).
42. Evaluation of Fire Models for Nuclear Power Plant Applications: Cable Tray Fire - Appendix G. NISTIR 6872. Baltimore, MD: National Institute of Standards and Technology, 2002.
43. Cavity Barriers: Final Factual Report of the Experimental Programme: Annex D - CFD Modelling of Cavity Barrier Scenarios. Building Research Establishment Ltd., 2005.
44. Wang Y, Meredith K, Chatterjee P, Krishnamoorthy N, Zhou XC and Dorofeev S. Status of FireFOAM Development and Future Plan. In: *3rd FM Global Open Source CFD Fire Modeling Workshop*, Norwood, MA, 2011. FM Global.
45. Chaos M, Khan M, Krishnamoorthy N, De Ris JL and Dorofeev S. Evaluation of Optimization Schemes and Determination of Solid Fuel Properties for CFD Fire Models using Bench-Scale Pyrolysis Tests. *Proceedings of the Combustion Institute*. 2011; 33: pp.2599-606.
46. Krishnamoorthy N, Chaos M, Khan M, Chatterjee P, Wang Y and Dorofeev S. Experimental and Numerical Study of Flame Spread in the Parallel Panel Geometry. In: *6th International Seminar on Fire and Explosion Hazard*, Leeds, UK, 2010.
47. Wang Y, Chatterjee P and De Ris JL. Large Eddy Simulation of Fire Plumes. *Proceedings of the Combustion Institute*. 2011; 33: pp.2473-80.
48. Ewer J, Galea E, Patel M, Taylor S, Knight B and Petridis M. SMARTFIRE: An Intelligent CFD Based Fire Model. *Journal of Fire Protection Engineering*. 1999; 10: pp.13-27.
49. Ewer J, Galea E, Patel M, Jia F, Grandison A and Wang Z. SMARTFIRE - The Fire Field Modelling Environment. In: *V European Conference on Computational Fluid Dynamics ECCOMAS CFD 2010*, Lisbon, Portugal, 2010.
50. Fire Safety Engineering Group, University of Greenwich. SMARTFIRE Future Developments. SmartFire, (2012, accessed July 19, 2012).
51. Ewer J, Jia F, Grandison A and Galea E. SMARTFIRE Verification and Validation Report. Report Version 4.1.1. CMS, University of Greenwich, 2008.
52. Combustion Science & Engineering, Inc. SMARTFIRE. Computer Models For Fire and Smoke - International Survey of Computer Models for Fire and Smoke, http://www.firemodelsurvey.com/pdf/SMARTFIRE_2007.pdf (2008, accessed July 1, 2012).
53. Combustion Science & Engineering, Inc. SOFIE. Computer Models For Fire and Smoke - International Survey of Computer Models for Fire and Smoke, http://www.firemodelsurvey.com/pdf/SOFIE_2007.pdf (2008, accessed July 1, 2012).
54. Bressloff N, Moss J and Rubini P. CFD Predictions of Coupled Radiation Heat Transfer and Soot Production in Turbulent Flames. *Twenty-Sixth Symposium (International) on Combustion*. 1996: pp.2379-86.
55. Welch S. Development and Validation of a Comprehensive Model for Flame Spread and Toxic Products in Full-Scale Scenarios. SP 998. Baltimore, MD: National Institute of Standards and Technology, 2003.
56. Tuovinen H, Van Hees P and Axelsson A. Implementation of a Physical Flame Spread Model in the SOFIE CFD Model. SP Report 1999:32. Boras, Sweden: SP Swedish National Testing and Research Institute, 1999.
57. Kaowool High Temperature Boards Product Information. Product Literature No: 06.06/5 14-715.

58. Parker W. Calculations of the Heat Release Rate by Oxygen Consumption for Various Applications. NBSIR 81-2427-1. Washington, DC: National Bureau of Standards, Center for Fire Research, 1982.
59. ASTM Standard E1354-04a, "Standard Test Method for Heat and Visible Smoke Release Rates for Materials and Products Using an Oxygen Consumption Calorimeter". West Conshochocken, PA: ASTM International, 2004.
60. Janssens M. Calorimetry. *The SFPE Handbook of Fire Protection Engineering, 3rd ed*. Quincy, MA: NFPA, 2002.
61. Blevins L and Pitts W. Modeling of Bare and Aspirated Thermocouples in Compartment Fires. NISTIR 6310. Gaithersburg, MD: National Institute of Standards and Technology, 1999.
62. Young CN. *Thermocouple Compensation.* MS Thesis, University of Waterloo, Waterloo, ON, 1998.
63. Newman JS. Multi-Directional Flow Probe Assembly for Fire Application. *Journal of Fire Sciences*. 1987; 5: pp.50-6.
64. Omega Engineering, Inc. Differential Pressure Transducer with Field Selectable Range, PX277. http://www.omega.com/Pressure/pdf/PX277.pdf (2012, accessed July 15, 2012).
65. Low Pressure Transducer PX274, PX275, PX277, and PX278 Instruction Sheet. Product Literature No: M2759-0305.
66. Heskestad G. Bidirectional Flow Tube for Fire-Induced Vent Flows. FMRC Serial Number 21011.4. Factory Mutual Research Corporation, 1974.
67. McCaffrey BJ. Purely Buoyant Diffusion Flames: Some Experimental Results. NBSIR 79-1910. Washington, D.C.: Center for Fire Research, National Engineering Laboratory, 1979.
68. Zukoski E, T. Kubota and B. Cetegen. Entrainment in Fire Plumes. *Fire Safety Journal*. 1981; 3: pp.107-22.
69. Quintiere J and Grove B. Correlations for Fire Plumes. NIST-GCR-98-744. Gaithersburg, MD: National Institute for Standards and Technology, 1998.
70. Alston J and Dembsey N. Evaluation of Dimensionless Flame Height Parameters to Account for Fuel Source Effects. In: *Fire Safety Science-Proceedings of the Seventh International Symposium*, Worcester, MA, 2002. London, UK: Interscience Communications, Ltd.
71. Heskestad G. On Q* and the Dynamics of Turbulent Diffusion Flames. *Fire Safety Journal*. 1998; 30: pp.215-27.
72. ASTM Standard E459-05, "Standard Test Method for Measuring Heat Transfer Rate using a Thin-Skin Calorimeter". West Conshochocken, PA: ASTM International, 2005.
73. Alston J. *Room/Corner Fire Calibration Data: Marine Composite Screening Specimens.* MS Thesis, Worcester Polytechnic Institute, Worcester, MA, 2004.
74. Kwon JW. *Evaluating FDSv4 Upward Flame Spread.* M.S. Thesis, Worcester Polytechnic Insitute, Worcester, MA, 2006.
75. ISO 5660-1:2002 "Reaction-to-fire tests -- Heat release, smoke production and mass loss rate -- Part 1: Heat release rate (cone calorimeter method)". Geneva Switzerland: International Organization for Standardization, 2002.
76. Anderson SK. *Qualitative Study of the Effect of a Compartment Enclosure on Fire Plume Entrainment.* MS Thesis, Worcester Polytechnic Institute, Worcester, MA, 1998.

Appendix A Combustible wall material selection process

To measure an adequate amount of flame spread data in the combustible wall fire test, it was necessary to identify a material that readily ignites and supports self-propagating fires in realistic situations. Both of these criteria are essentially the properties of any ASTM-E84 Class C combustible material. Moreover, the specimen needs to be structurally sound during testing. Based on these criteria a selection process took place to identify, rigid, combustible, and commercially available wall panel. Specimens of thermoplastics and a fiber-reinforced plastic (FRP) were tested, and the FRP panel was chosen to be used in the full-scale test series.

A.1 Thermoplastics selection process

The first round of the material selection process looked at the thermoplastics polypropylene (PP) and high-density polyethylene (HDPE). These plastics are versatile in their compositions and applications; they are used in the manufacturing of stationary items to decorative wall or ceiling panels. The generic PP and HDPE materials are combustible, but chemicals can be applied during the manufacturing/ formulation process to make the end-product flame-retarded. Moreover, the plastics are commercially available as rigid rectangular panels of different dimensions and transparency, which is ideal for cone testing or mounted vertically for wall fire tests. For the current study, sheets of ½" thick, 2 ft by 4 ft panels were used in the preliminary cone and wall testing. A black PP panel was used, and sheets of black and white HDPE panels were tested, all materials were opaque. Originally it was planned to test a white PP panel as comparison, but it was not available from the manufacturer at the time of the material selection process, so it was scrapped.

Since the plastics come in different color based on their formulas, this presented an opportunity to test the essentially the same material with different radiative properties: a black material may react differently than a white material because of different reflectivity, absorptivity, or transmittance. Although these properties were not directly measured in the current study, however, by measuring fire-related quantities such as time to ignition, one can qualitatively relate the radiative properties to material behaviors.

A.1.1 Cone calorimeter testing

Nine cone calorimeter tests were conducted on the three specimens, each under 50 kW/m2 heat flux insult. For each specimen, 1 test was run without any thermocouple implementation, but in 2 two tests thermocouples were bonded to the top and bottom surfaces and inside the sample's center at the 1/3 and 2/3 depths. These thermocouples were intended to give sample heating history for material properties estimation. For each test, the heat release rate history, heat of combustion history (HoC) times to ignition and extinction were recorded and presented in and Figure 1.

Table 1 - HDPE and Polypropylene samples cone test results

Test Number	Material	Color	Thermocouples?	Density (kg/m3)	Time to Ignition (sec)	Time to Extinction (sec)	Peak HRR (kW/m2)	Peak HoC (kJ/g)
1	HDPE	White	No	976	77	944	1700	100
2	HDPE	White	Yes	975	97	1004	1490	100
3	HDPE	White	Yes	965	91	1311	1462	80
4	HDPE	Black	No	962	46	1180	989	140
5	HDPE	Black	Yes	965	56	1199	969	100
6	HDPE	Black	Yes	961	56	1131	1066	80
7	Polypropylene	Black	No	918	22	1210	751	120
8	Polypropylene	Black	Yes	923	25	1106	873	80
9	Polypropylene	Black	Yes	918	21	1268	683	80

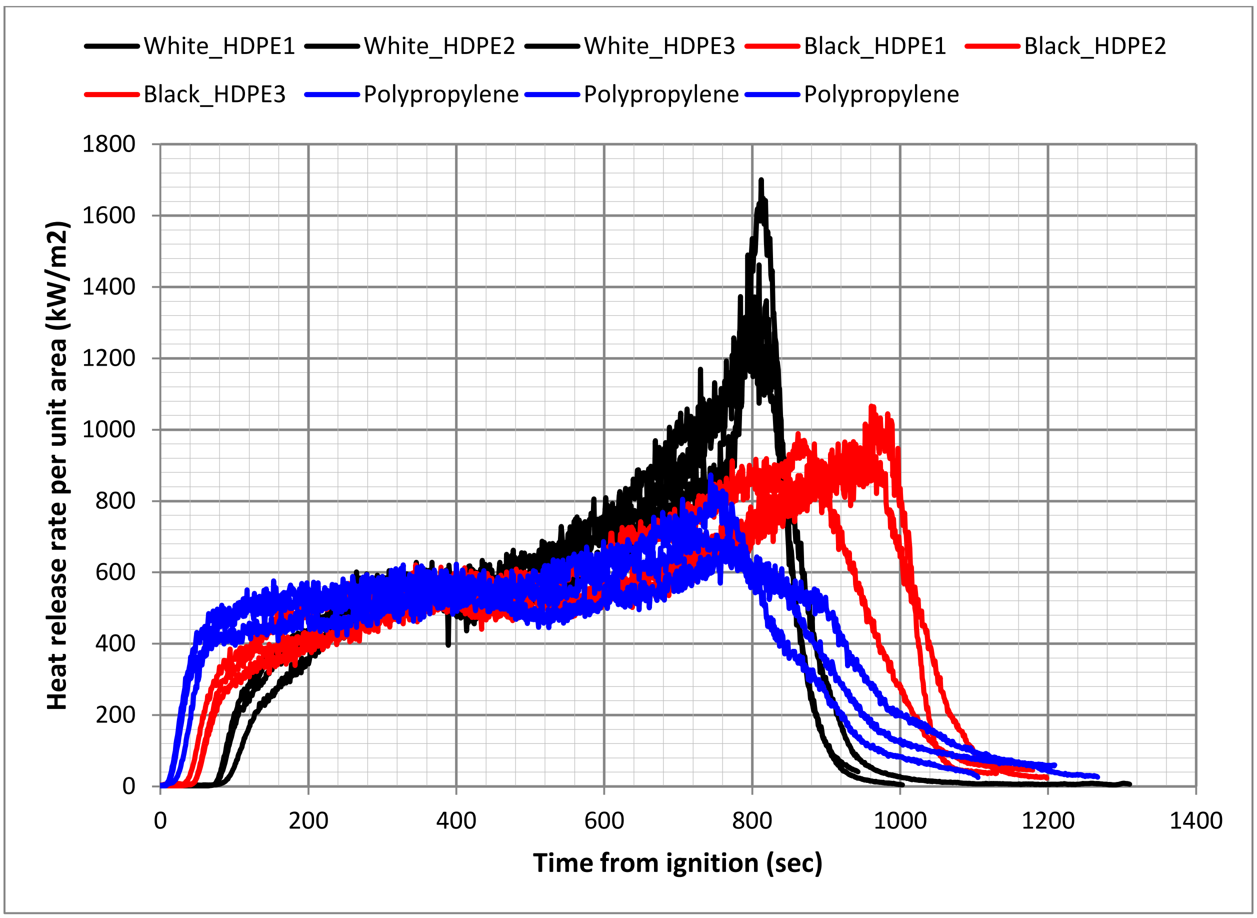

Figure 1 - HDPE and PP cone test HRR time history

Comparing the times to ignition between the three specimens during cone testing, it appears that the black PP sample ignited quicker than the black HDPE and white HDPE samples. Also, between the two

HDPE specimens, the black HDPE ignited before the white did, which suggests that the black HDPE acted more as blackbody and absorbed more radiation from the cone heater than the white HDPE samples.

The bench-scale cone testing on the PP and HDPE specimens also revealed that upon the application of high heat flux, both plastics readily soften, melted, boiled, and then ignited. During the fire, char formed early on, but soon became broken up and moved around the surface by the boiling liquid plastic. The heat and soot released during the cone tests also were atypically high; in some cases melting the silicone tubing that transports the gas sample from the cone calorimeter's ductwork to the gas analyzers. Additionally, as the sample melted, droplets of molten plastics were leaked through the aluminum foil that wrapped around the sample onto the cone test platform; these droplets were collected and used in the mass loss calculation.

A.1.2 Half-scale wall panel testing

To simulate a full-scale wall panel test, a series of half scale tests were conducted using single sheet of the 2" x 4" thermoplastic panel mounted vertically. These preliminary half-scale tests were not instrumented with temperature, velocity, or heat flux measuring devices, nor were the HRRs measured. The goal of these qualitative experiments was merely to display the fire behaviors of the thermoplastics in order to determine whether they exhibit the material selection criteria needed for testing in the main series. Both the Square and the Rectangular burners were used to determine whether the flame spread will be essentially one-dimensional and upward. The burner was placed against the panel in the center, with the burning surface 3.5" away from the bottom edge of the panel. After the first test with the black polypropylene panel, a water basin was placed under the wall panel in order to collect and extinguish any burning droplets to prevent a pool fire.

Upon ignition of the source fire, the surfaces of the thermoplastics quickly soften, started to flow downward, and soon ignited. After flame attachment was achieved on the panel, the source burner was turned off, and moved away to prevent contamination of the burner surface with molten plastic. Initially, the fires seem to slow down, but as more area of the panel soften and melted, the fire quickly spread to the rest of the panel. It was observed that as the fire progressed, the dripping intensified and also the panel became sagged and wrapped, causing empty space between the panel and the support wall that flames could easily spread to. Large crumbs of droplets also continued to burn when floating in the water path, creating a pool fire-like problem. The amount of soot and heat released during the half-scale tests was also large, and as the panel became fully involved, the tests were terminated due to safety reasons. Afterward, the unburnt mass was determined from the mass of the panel still on the wall and the droplets in the water bath and it was found that about 20% of the pre-burn panel mass was lost to dripping. Section 0 presents the experiment notes and photographs of the four half-scale panel tests.

Due to the high rate of heat and soot released during the fire, the lack of rigidity during testing, and the melting-dripping effects, both the PP and HDPE panels were determined to be unsuitable for the main series of combustible wall experiments since FDS cannot, at its current stage, model such behaviors. Another material was used instead.

A.2 FRP selection

At an unrelated burn demonstration conducted at the WPI Fire Lab, a commercially available, 0.09”-thick FRP panel with a smooth back-face and a pebbled, embossed white front surface was used. The FRP sheet consisted of modified polyester copolymer and inorganic fillers as the resin base and reinforced with a weave of random chopped fiberglass. The panel was available as an ASTM-E84 Class A or a Class C panel, and similar products are commonly used in construction projects where moisture and mold protection on walls or ceilings are desired. The Class A and Class C specimens were ignited together with the Rectangular burner to show the different flame spread properties between the classifications.

During the test, although the Class A panel was ignited, the flame quickly self-extinguished with little flame spread. However, the Class C panel continued to spread until fully involved, but was structurally rigid throughout. The Class C specimen exhibited all of the criteria established in the material selection process and was thus chosen to be used in the full-scale combustible wall experiments.

The rigid FRP panel chosen for use in full-scale testing is commercially available and advertised for use as ceiling and wall linings in environments designed to be moisture- and mold-free. The panel has a Class C (ASTM E84) flame spread rating. It is consisted of modified polyester copolymer and inorganic fillers as the resin base and reinforced with a weave of random chopped fiberglass. The panel’s thickness is 0.09” (2.3 mm) nominal, with a smooth backface and a pebbled, embossed white front surface. The dimensions of the panel in the full-scale experiments were to be 1.2 m in width and 2.4 m in height.

A.2.1 Cone calorimeter tests

Seven cone calorimeter tests were conducted on the three specimens, under external heat fluxes of 25, 50, and 75 kW/m^2. Equipment malfunctions during Test 4 caused a failed test and so it was repeated as Test 7. Two tests were run at each external heat flux insult, and in one of each similar tests thermocouples were glued to the top and bottom center of the specimen, the tests with thermocouples are Tests 3, 6, and 7. A thermal compound was used to bond the thermocouples to the surfaces. It was observed that in the 25 kW/m^2 and 75 kW/m^2 instrumented tests, the thermocouple lost contact with the specimen surfaces within 30 seconds of the cone shutter opening, but during the 50 kW/m^2 test the thermocouple remained on the specimen surface for the duration of the test.

In all tests, once the cone shutter opened, white smoke was released from the specimen and crackling noises were heard. Then flashes of flame occurred and followed with cellular flames that spread to all 4 edges. All tests ended with edge burning and then corner burning. Table 2 presents the cone calorimeter test configurations and pre-burn information as well as test results.

Table 2 – Class C FRP Test Schedule

FRP Sample	Thickness [mm]	Volume [mm³]	Weight [g]	Density [kg/m³]	External Flux [kW/m²]	Time to Ignition [sec]	Time to Extinction [sec]	Peak HRR [kW/m²]	Peak HoC [kJ/g]	Avg HRR [kW/m2]	Avg HoC [kJ/g]
1	1.93	19949	29.42	1474.7	25	106	462	233	160	73	20
2	1.95	20034	29.35	1464.9	50	37	359	279	105	88	19
3	1.93	20268	29.30	1445.4	25	117	457	244	151	82	19
4	1.91	19671	29.01	1475.0	50	37	290	N/A	N/A	N/A	N/A
5	1.96	19836	29.56	1490.3	75	24	210	366	119	146	21
6	1.96	20961	30.73	1466.1	75	25	227	357	84	134	20
7	1.92	19601	28.72	1465.3	50	39	288	294	74	113	20

Figure 2 presents the HRRPUA time-history of the six FRP cone calorimeter tests. In the figure, time-zero corresponds to the time when the shutter opens. It is shown that the magnitude and the timing of the peak HRRPUA value are inversely proportional to the magnitude of the external heat flux. The data from each test at identical heat flux are relatively consistent.

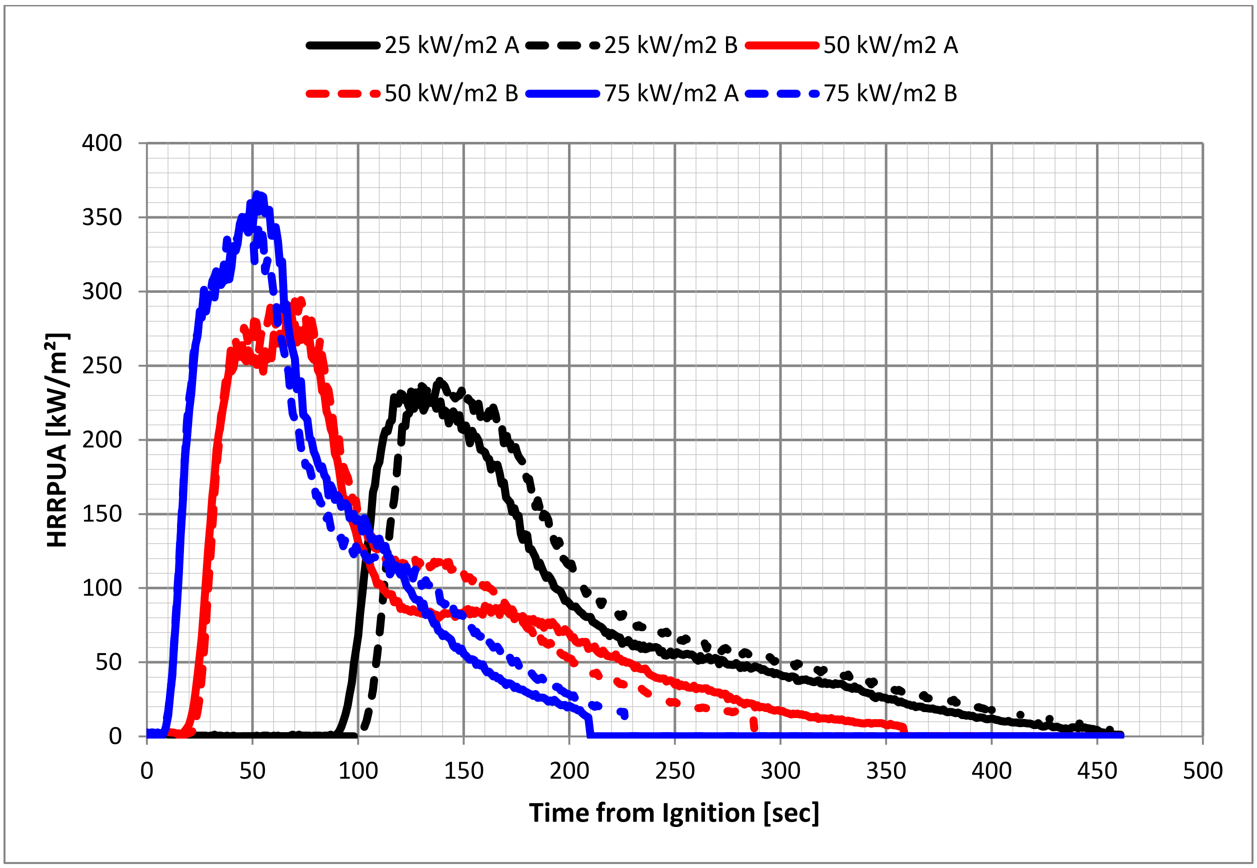

Figure 2 - Cone test heat release rates per unit area

Figure 3 presents the heat of combustion time-history of the six FRP cone calorimeter tests. In the figure, time-zero corresponds to the time when the shutter opens. It is shown that the timing of the peak heat of combustion value is inversely proportional to the magnitude of the external heat flux. However, the magnitude at the peak heat of combustion has a similar trend except for the ones associated with the 50 kW/m^2 tests where the values of the HoC are the highest in all cases. The data from each test at identical heat flux are relatively consistent.

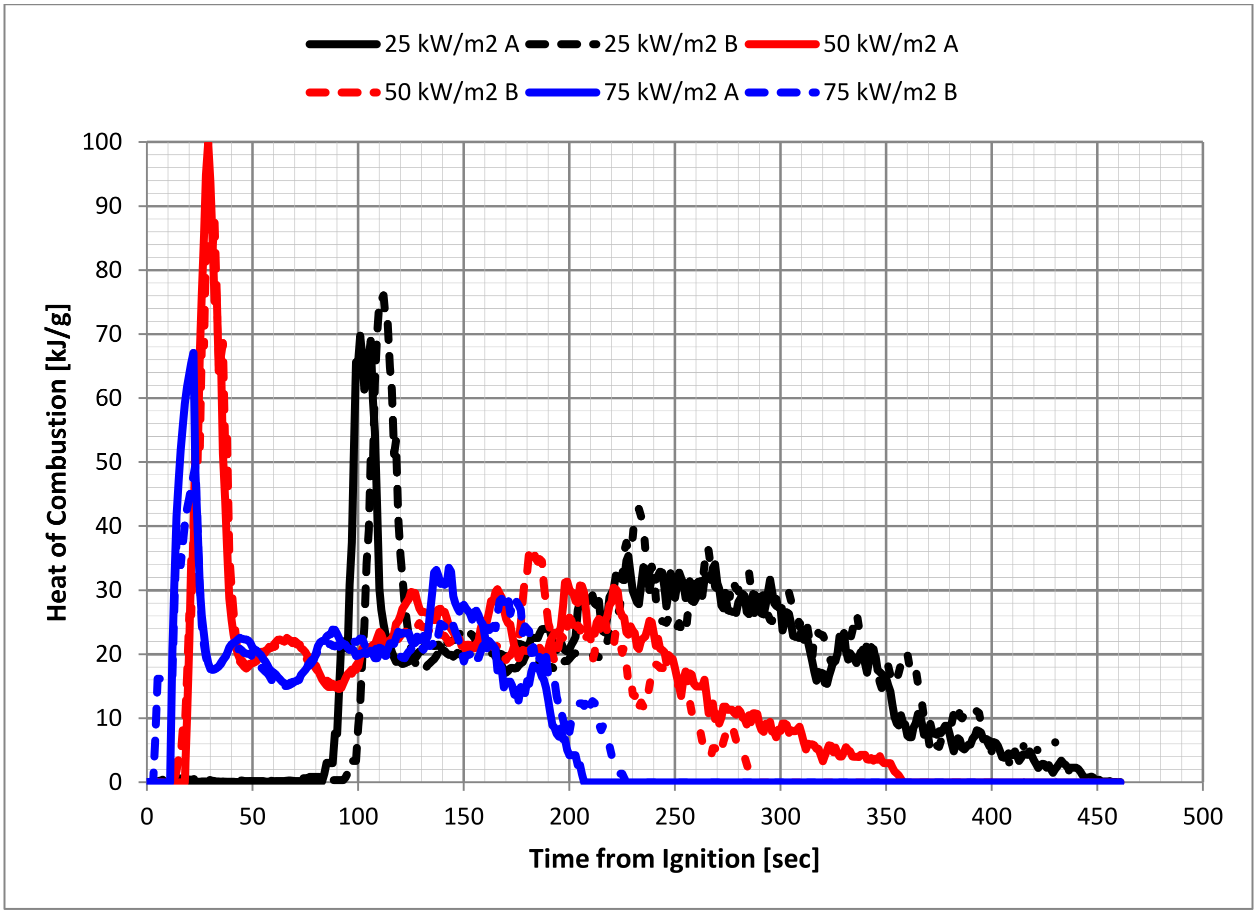

Figure 3 - Cone test heat of combustions

Figure 4 to Figure 6shows the HRRPUA time history and the top and backface temperatures collected during the instrumented 25, 50, and 75 kW/m^2 cone tests. In all cases, the temperature recorded on both surfaces grew exponentially as the specimen became ignited, identified by the sharp increase of the HRRPUA value. The surface and backface temperatures also tracked closely together, suggesting that the specimens may be considered thermally-thin.

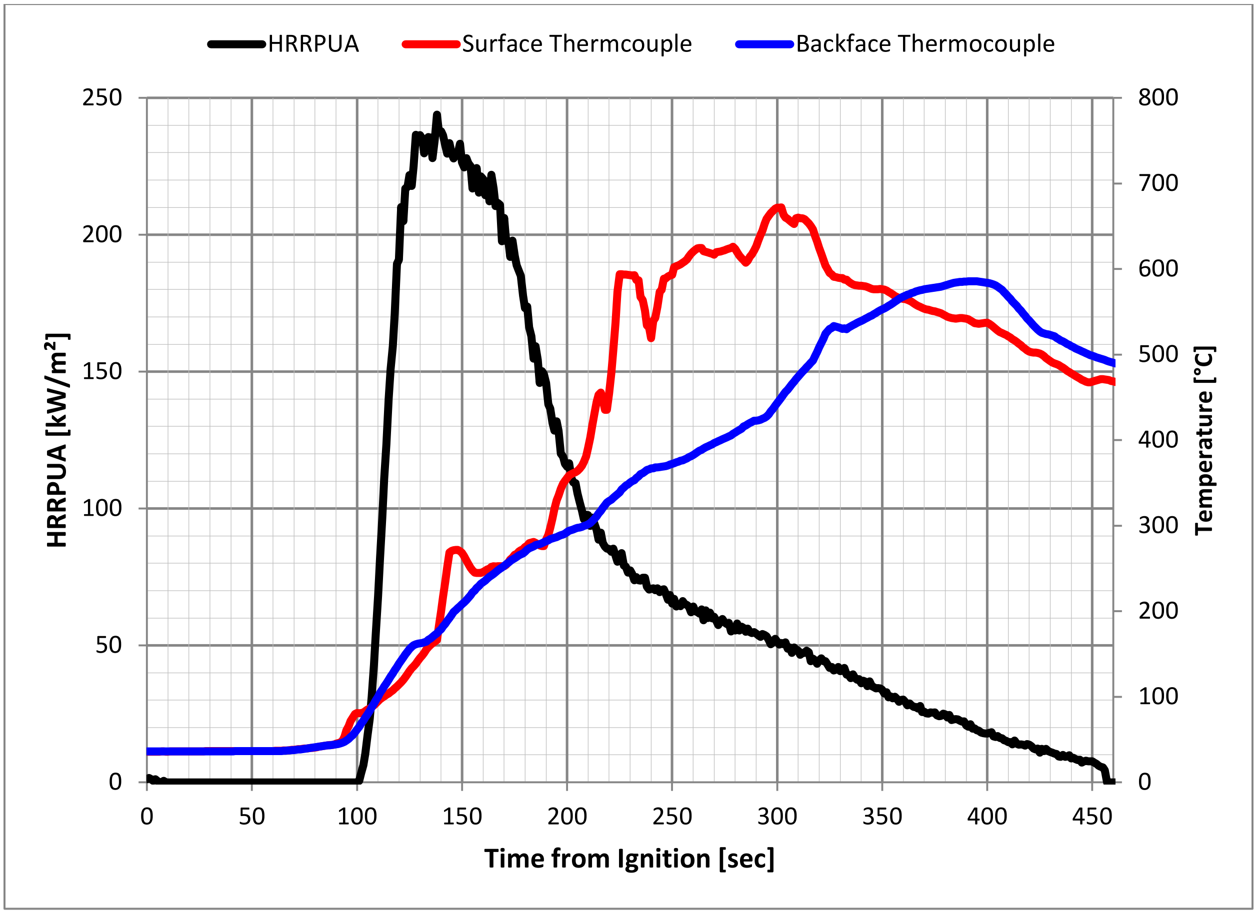

Figure 4 - Instrumented cone test at 25 kW/m2 HRRPUA and temperatures

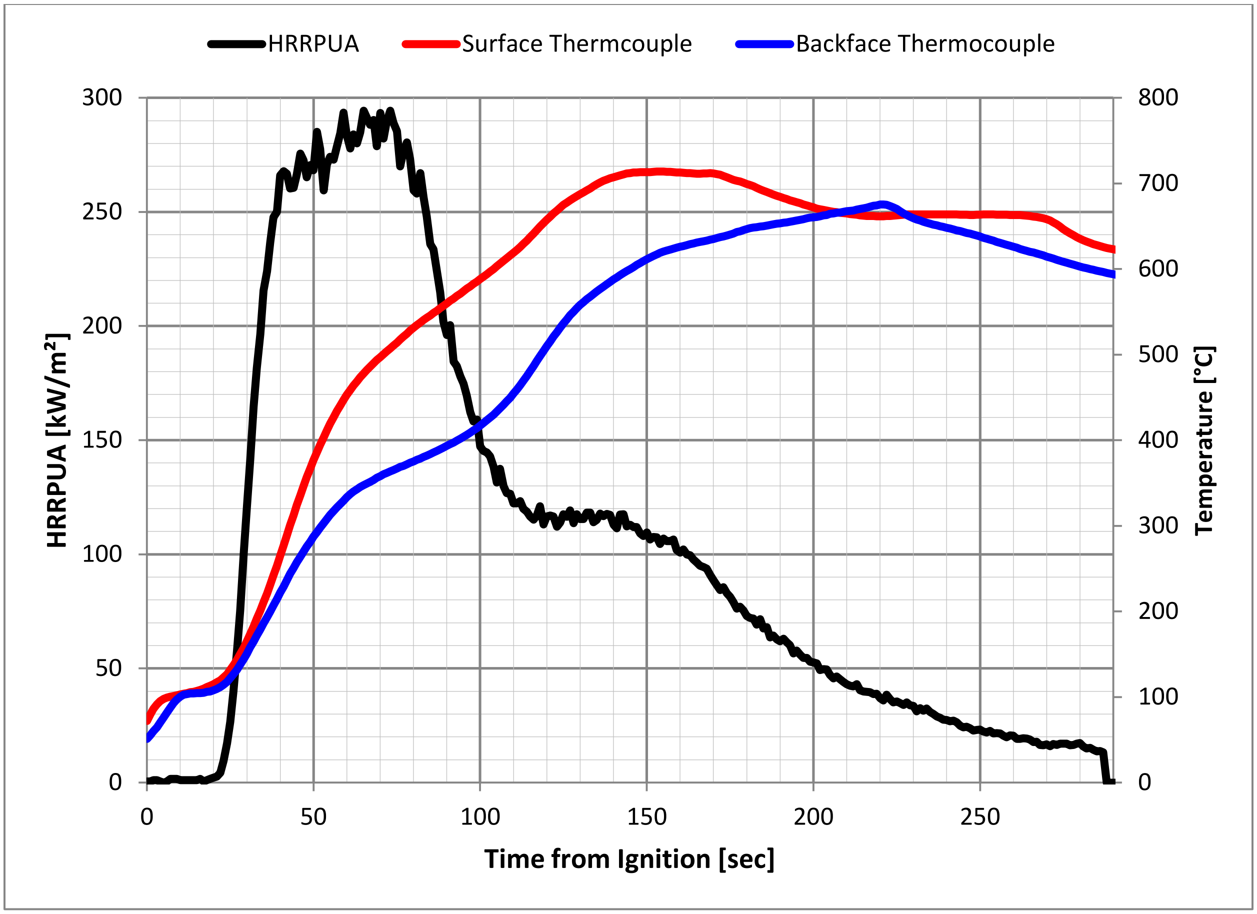

Figure 5 - Instrumented cone test at 50 kW/m2 HRRPUA and temperatures

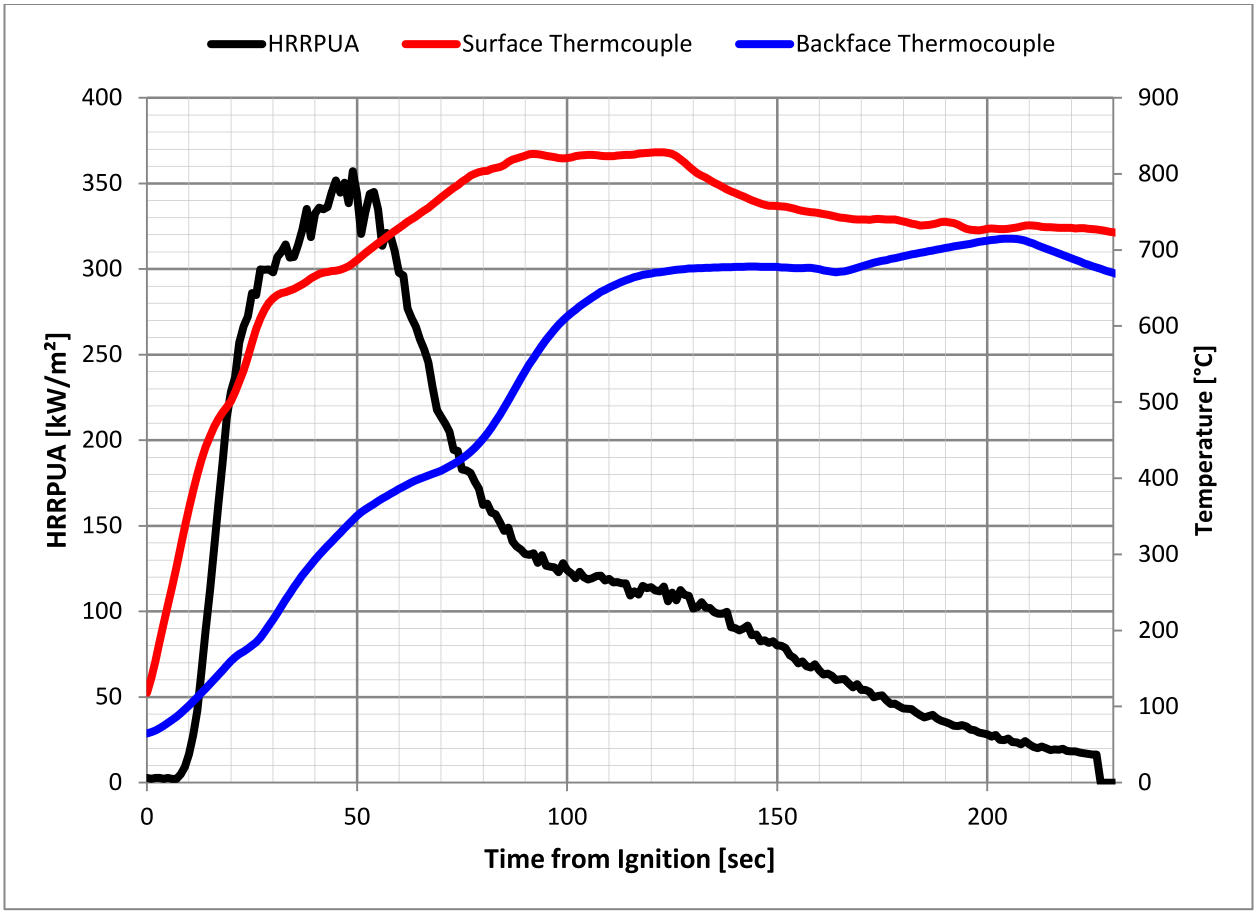

Figure 6 - Instrumented cone test at 75 kW/m2 HRRPUA and temperatures

A.3 Conclusion

To identify suitable material for full-scale combustible wall testing, a set of material selection criteria were established: the material must be readily ignited, supports self-propagating fires in realistic situations, and stay rigid when burnt. Three thermoplastics: polypropylene and high-density polyethylene with different colors were tested and was found to be unsuitable due to its high heat content and melting behaviors. The final selection was a thin, commercially available FRP panel consisted of a polyester resin reinforced with fiberglass.

A.4 Thermoplastics half-scale wall experiment notes

A.4.1 Black polypropylene

- Polypropylene, ½” thick panel, test conducted on 7/07/09
- Original dimension, 2 ft x 3.6 ft
- Pre-burnt mass: 8.54 kg
- 1’x1’ Square burner, with a surface 3-4” above the bottom surface of the panel
- Burner is set adjacent to panel without gap, centered
- Burner fuel: natural gas

- After ignition, source fuel flow was adjusted to create a flame at about 1-2’ height
- Burner was left on for 11 minutes
- Burner was not moved for the duration of the test
- The wall panel catches on fire at the bottom area adjacent to the flame, the initial burn area was triangular in shape
- At the beginning of burning, a lot of white smoke was generated

- As the wall burns and melts, liquefied materials were collected on the flange of the burner
- The melted material then dripped on both side of the burner and continued burning
- As the wall fire increased in size, the droplets burnt more readily and created a stream of fire from the base of the burner to the wall

- The lower portion of the wall panel bowed out and sagged (about 2’ above burner surface)
- Wall surface was mostly liquefied wherever there was flame attachment
- The burning pool on the side of the burner caused the bottom edge to start burning, so flame spread was not really in the downward direction for the area below the burner surface

- A large hole near the burner was burnt through the panel, flame entered the cavity and the flame spread rate increased
- Flame entering through the bottom of the panel caused flame spread on the back of the panel while front surface was also burning
- Structural failure of the panel was imminent
- Decision was made to knock down the fire before panel collapses

- After the fire on the surface was knocked down with water spray, the fire on the back surface continued to burn
- Flame spread at the back was quick
- The panel appeared to be sagging and failing quickly again

- Side of the panel was ripped off to allow total extinguishment
- After extinguishment, polypropylene panel hardened quickly
- Maintenance was performed on the burner by replacing the Kaowool® blanket because it was covered with melted plastic
- Recognized the need to extinguish the wall fire early for safety reasons, and the need to collect droplets for further analysis

A.4.2 White HDPE

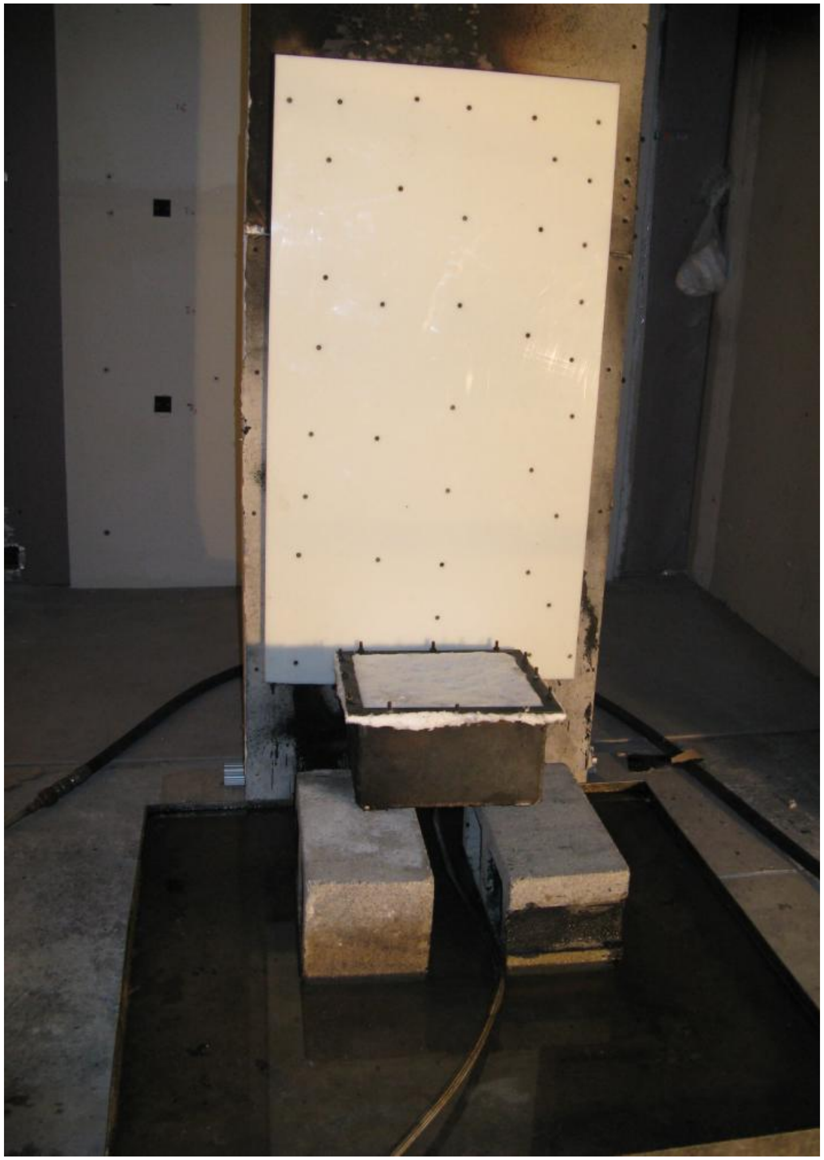

- White HDPE, ½" thick panel, test conducted on 7/09/09
- Original dimension, 2' x 3.6'
- Pre-burn mass: 8.06 kg
- 1'x1' Square burner, with a surface 3-4" above the bottom surface of the panel
- Burner was set adjacent to panel without gap, centered
- Source fuel: natural gas
- Water basin was set in underneath the burner and wall panel to catch and extinguish droplets
- Applied more screws than first test to secure panel onto support wall

- 0:00 – Source burner ignition
- 1:30 – Source flame to 1’-2’ high
- 6:30 – Screw holes near bottom began to soften
- Increased source fire height to about 2’-3’,since the wall panel did not catch on fire with the smaller fire
- 15:50 – Burner moved to about 6” away from panel; melted material on burner continues to burn, little burning on the wall, source burner shut off
- 19:17 – Liquid dripping, and burning seemed to move downward from the initial area
- 25:00 – Translucent layer formed at the burn area
- 19:17 – Liquid dripping, and continued downward
- 25:00 – Translucent layer formed at the burn area
- 26:00 – Bottom edge started to burn

- 26:55 – Significant dripping continued, droplets burned and extinguished quickly
- 28:00 – Significant dripping, now the droplets burn readily and continuously
- 30:00 – Molten plastic adhered to wall, burning below bottom edge
- 32:00 – Domed burning area on surface popped open
- 33:00 – Steady stream of burning liquid hit water level, keep burning
- 34:00 – Multiple streams of burning liquid formed along bottom edge

- 44:20 – Burner was ignited again, moved to about 1’ away from wall panel because fire on wall panel had reduced significantly
- 47:46 – Significant amount of white smoke was produced, moved in a vortex around the plume
- 48:51 – Large bubbles formed on several areas of the panel
- From around this point on, flamed spread occurred in a upward direction but skewed to the left

- 50:23 – wall panel became warped, smoke and flames came out of the back of the wrapped portions on the left edge
- 53:15 – Source burner shut down again

- 54:11 – Significant wall burning
- 58.40 – Burning portion of the left side of the wall acquired the appearance and movement of molten glass

- 1:46:00 – Wood on the back of the wall started smoking
- 1:48:15 – Fire extinguished; wood on the back wall still burning

- Observations:
- The 1'x1' burner may not adequately start the panel burning to allow it to achieve a 1-D upward flame spread characteristic due to the fact that turbulence can affect the verticalness of the source burner flame
- Upon inspection and salvage of the wall, it was found that the long burn time caused the back wall to be completely burnt through, so a new wall with Kaowool® insulation boards was constructed for future testing

- Significant amount of the HDPE was melted and dropped to the ground, which would’ve created a substantial pool fire if not extinguished during the test
- Remaining mass: 3.43 kg
- Mass lost/dripped: 1.58 kg
- Mass burnt: 3.05 kg
- % Dripped to pre-burn: 20%
- % Dripped to burnt: 52%
- Moving the burner away and keeping the dropped material from burning seemed to slow the flame spread because the ignited molten materials didn’t cause additional flame to impinge nor attach onto new area of the wall

A.4.3 Black HDPE

- Black HDPE ½” thick panel, test conducted on 7/13/09
- Original dimension, 2’ x 3.6’
- Pre-burnt mass: 8.3 kg
- 2’ Rectangular burner, with a surface 3-4” above the bottom surface of the panel (A larger burner was used to test whether flame spread would proceed mostly in the upward direction
- Burner is set adjacent to panel without gap, centered
- Source fuel: natural gas
- New support wall, reinforced with Kaowool® insulation boards, was built for mounting the combustible wall panel
- Water basin in place below the burner and wall panel to catch droplets

- 1:33 – Flame about 1’-2’ high at burner
- 3:30 – Small area of liquefied surface near burner surface; triangular in shape, peaked near the centerline
- 6:30 – Numerous small cracks in the triangular burn area formed

- 7:00 – Wall panel on fire in the middle, starts to melt
- 7:45 – Burner moved to 3” away from wall; panel bows out at the bottom-center area; dripping intensify
- 14:00 – Burner turned off, moved away; flame on wall smoky and small

- 15:00 – Few sections on wall bowed out; areas that were burning earlier became charred
- 21:00 – Burning concentrated in a 6” section of the bottom edge near the center

- 24:00 – Fire size on wall increased
- 26:00 – Molten material clinged onto the support wall area below the panel and continued to burn
- 28:30 – Significant dripping of molten materials started

- 30:00 – Flame increased in size; significant dripping, forming pool fires on top of the water in the basin
- 31:45 – Large hole burnt through the wall panel near bottom

- 32:30 - Large dripping fire that generated little smoke
- 38:00 – Flame moved behind pockets created by the bowed-out areas on the wall
- 47:00 – Smoke escaped through the back of the panel
- Form this point on, the flame spread became more 1-D, direction of flame spread/pyrolysis was mostly upward only

- 56:00 – Some smoke escaped out of back of the panel at the top
- 57:20 – Molten pool of plastic formed at the side of the support wall on the water surface, not burning

- 1:02:00 – Smoke from top/back part of wall caught on fire
- 1:03:14 – Whole wall panel covered in flame
- 1:06:00 – Large amount of small droplets being “ejected” away from the wall, did not burn on the way down, just emitted smoke
- 1:07:00 – Large pieces near the top of wall fell into the water basin

- 1:10:00 – Pool fire on water extinguished; little burning on the wall; lots of white smoke generated
- 1:23:00 – Fire self-extinguished
- Residue left on wall is powdery, probably charred material; basically a complete burn with insignificant amount of remaining material on the wall

- Observations:
- Remaining mass: 0 kg
- Mass lost/dripped: 4.22 kg
- Mass burnt: 4.08 kg
- % Dripped to pre-burn: 51%
- % Dripped to burnt: 103%
- Using a 1x2 burner allows for more 1-D upward flame spread, although the center/bottom usually caught on fire first
- The melting and dripping characteristics suggested that the material is not suitable for further study since FDS cannot predict these behaviors.

A.4.4 Polypropylene 2

- Polypropylene, ½" thick panel, test conducted on 7/14/09
- Original dimensions: 2' x 4'
- Pre-burnt mass: 8.54 kg
- 2 ft Rectangular burner, with a surface 3-4" above the bottom surface of the panel
- Burner is set adjacent to panel without gap, centered
- Source fuel: natural gas
- From previous experience, the 2' wide burner will give a more uniform flame spread once the panel catches on fire

- 0:00 – Ignition of source burner
- 0:49 – Source burner flame was at 1’-2’ in height
- 2:30 – Small triangular area at the bottom of the wall panel caught on fire, the area was liquidly, but not running down the wall surface
- 5:30 – Burner was moved to approximately 9” away from the panel; a larger triangular area on panel (1.5 ft wide at bottom, which is near the burner) was on fire; panel started dripping; flame was spreading downward from melted material

- 6:30 – Surface of burning triangular area began to bow out; significant melting and run-off occurred
- 8:40 – Burner turned off; fire sustaining by itself, a lot of white smoke was generated

- 10:10 – Bottom edge of the panel caught on fire
- 10:55 – Dripping became significant; molten material on the surface moved downward and spread the flame

- 12:30 – Additional areas on surface bowed out; some became raised domes, and some folded and collapsed upon themselves

- 19:45 – Large area near the bottom burnt through, created a large hole in middle of panel; flame went into the space between the wall panel and backboard
- Flame spread was fast, but still no 1-D upward effect, burning area enlarged in a triangular shape

- Significant dripping at this stage of burning, large pieces of wall melted and landed in water still burning, hard to extinguished due to the heat
- 22:00 – Flame wrapped around the right side of the support wall structure
- 22:45 – Wall panel ejected burning droplet outside of water basin
- 23:00 – Ceiling jet formed, room filled with smoke
- Fire size was significant and had to be reduced with water application multiple times; the large burning pool at the base of the wall contributes to the size of the wall fire

- Only a small portion of wall panel was burnt during the 25 min test
- The surface of the partially burnt portion is bumpy with lots of small holes that didn’t penetrate the sample
- The remaining sample was mostly warped

- Observations
- Remaining mass: 4.70 kg
- Mass lost/dripped: 1.11 kg
- Mass burnt: 2.73 kg
- % Dripped to pre-burn: 13%
- % Dripped to burnt: 41%
- Based on the size of the burnt remain, it appears that about 30% of original panel is burnt/dripped, and out of that about 50% had been melted and dripped
- It may be concluded that the polypropylene panel has a fast flame spread rate, and melts extensively/quickly
- The melting and dripping characteristics suggested that the material is not suitable for further study since FDS cannot predict these behaviors

Appendix B Velocity measurement optimization

Many different types of instrumentations had been developed for velocity measurement in various situations. For fire research, some examples of flowfield measurements include the hot-wire anemometer, vane anemometer, pitot-static tube, bi-directional probe, five point probe, laser Doppler anemometry, laser Doppler velocimetry, particle image velocimetry[1, 2]. In the current research, the goal was to measure the velocity at different heights above the burner inside a fire plume inside a compartment, in the center, and against a wall.

The laser-based flowfield measurement methods are the most advanced and accurate, but the cost was prohibitive with the budget of the current research. Hot-wire anemometry was not suitable for measuring extremely heated gases such as those found in a fire plume. There was also no vane anemometer that can measure the low velocity flow inside the plume of a low HRR fire that is also rated for high temperature use and within budget. Within the other three choices, the bi-directional probe was commonly viewed as the cheapest, the most rugged, and proven in previous research such as those conducted by McCaffrey and Heskestad[3, 4]. Bases on these advantages, the velocity measurement in the current research was conducted with bi-directional probes and pressure transducers, as mentioned in greater details in Section 2 of this report. The following provides a quick summary of the process and changes made to the hardware in order to improve the velocity measurement.

B.1 Original bi-directional probe setup

The original setup of the bidirectional probes were different from the one used in the fire tests. In the old setup, each probe was connected to two Swagelok reducing unions and a pair of silicon tubings. Silicon tubings were chosen due to their flexibility (so that rakes holding the probes could be moved) and high temperature rating (the probes were in the fire and tubing would be heated. Strips of Kaowool® ceramic paper were wrapped around the Swagelok and the first 18” of the tubings to provide additional insulation; the ceramic paper was held together by heat-resistant aluminum tape. Each probe was paired with a pressure transducer with a range of ±62.5 Pa; the transducers were mounted on the wall outside of the test compartment, at the same heights as the probes to reduce hydrostatic difference that could affect the readings. The transducers were the same model as the ones later use, but with a wider range of operation. The silicon tubings were run from the rakes down to the ground, then to the opening of the compartment, then upward to the corresponding sensing ports of the transducers. This caused the tubings to have different lengths from 20’ to 40’. The ten transducers were connected to a power supply in series, so that a failed connection would not affect the other transducers. The transducers were also connected to the data-acquisition (DAC) system

B.2 Debugging the original setup

A series of inert wall and free plume fire tests using different fuels and different source burner HRRs was run, and the velocity data were compared with plume correlations. It was found that the velocity measured was too scattered and too low overall. Then a series of tests was conducted using an inert plume created by an industrial size fan pointing upward, and a heated plume created by a heat-gun. The bi-directional probe readings in these tests were compared to readings taken from a hot-wire anemometer. The comparisons of the measurements showed that the readings were comparable at higher velocity but there was a mismatch at the lower velocities found in plume. This suggested that the transducers were not sensitive enough to pick up the small pressure change created by the low-velocity flow. To combat this effect, new transducers with a smaller range ±12.5 Pa were installed, as well as shielded wires between the transducers and the DAC system.

The inert and heated inert plume tests were conducted again, this time with better comparisons between the bi-directional probe and the anemometer readings. Some fire tests were run again, and the bi-directional probe readings were less scattered, but still lower than the expected velocity based on plume correlation and previously published data. In light of this, it was theorized that the long silicon tubing may have stretched or otherwise deformed in the hot environment around the fire and caused the pressure readings to deteriorate over long transport distance.

To reduce the distance while maintaining the mobility of the rakes, some transducers were removed from the wall outside and installed directly on the rakes behind the probes. Some inert plumes and fire plume tests were conducted and the readings between the bi-directional probes, anemometer readings, and plume correlations were much improved at the locations where the transducers were installed on the rake. This confirmed that the long length of the tubings were problematic and needed to be corrected.

B.3 Redesigned bi-directional probe setup

As presented in Section 2 of the report, the final design of the bi-directional probe setup consisted of a probe connected to two copper tubings via the Swagelok reducing unions. The transducers with a range of ±12.5 Pa were connected to the tubings and all were wrapped with ceramic paper or ceramic blanket for insulation against temperature rise. Connecting between the transducers and the DAC system were shielded wires that powered the transducers and transmitted the signals. The wires were then wrapped with ceramic paper and put into a ceramic-weave sleeve for additional protection against heated gases.

B.4 Conclusion

A lot of the choices made in the original design of the bi-directional setup had to be changed to improve the velocity readings. Although most of the hardware alterations made were minor, they could've been avoided if better information regarding the use of bi-directional probes in a fire plume was available. There were some valuable research on the probe designs, but it was difficult to find information related to the supporting instruments to be used with the probes. This short summary of long works may serves as a guide to using and debugging bi-directional probes in extreme situations, and the lessons learnt should also applied to other near-fire instrumentation.

B.5 References

1. Schulz JK. Measurement of Magnitude and Direction of Hot Gas Flow in a Fire Compartment with a Five-Hole Probe. Christchurch, New Zealand: School of Engineering, University of Canterbury, 2002.
2. Tieszen SR. On the Fluid Mechanics of Fires. *Annual Review of Fluid Mechanics*. 2001; 33: pp.67-95.

3. Heskestad G. Bidirectional Flow Tube for Fire-Induced Vent Flows. FMRC Serial Number 21011.4. Factory Mutual Research Corporation, 1974.
4. Newman JS. Multi-Directional Flow Probe Assembly for Fire Application. *Journal of Fire Sciences*. 1987; 5: pp.50-6.

Appendix C Thermocouple Radiation Correction

Bare-bead thermocouples are widely used in fire studies because they are cheap and easy to set up, however, the temperature reported by thermocouples in close proximity to a fire may differs from the true gas temperature because they have an actual body and are subjected to radiative and convective heat transfers that are not easily quantified.

In a fire situation, radiation is exchanged between a thermocouple and the enclosure walls, the hot gases, and the ambient environment. Heat can also be exchanged via convection to and from the thermocouples. Additionally, the heating time lag of a thermocouple can also cause misrepresentation of the true temperature. These effects are extremely hard to be addressed during a fire test, so a temperature correction may be performed after data have been collected in order to determine the true gas temperature from the bead temperature. The experimental setup had been designed with this in mind, allowing the plume velocity measurements to be used as part of the convective heat transfer correction for the plume temperature.

Two methods of correction have been tested with some minor variations to determine the most applicable corrective method for the current tests data. The approaches used in this study were based on the methodologies of Blevins and Pitts, and Young.

Blevins and Pitts' steady state thermocouple compensation methodology

Blevins and Pitts' method of thermocouple compensation assumes a steady state heat transfer between the thermocouple and its environment. The enclosure was assumed to be a graybody, where all surfaces are surfaces opaque and isothermal, with abosroptivities and emissivities independent of wavelength and temperature. Additionally, it is assumed that all transferred radiation has the same intensity in all directions. Moreover, for the idealized form of heat transfer equation to hold true, the surrounding environment is assumed to have a constant temperature.

The model used by Blevins and Pitts assumes that heat is transferred to and from the bare-bead thermocouple through convection and radiation only. The energy balance equation is reported in equation [1].

$$T_b^{\ 4}[\varepsilon_b \sigma] + \mathrm{T}_b[h_{bU}] - [\varepsilon_b \sigma T_\infty^{\ 4} + h_{bU} T_g] = 0 \qquad [1]$$

Where:

$T_b = Bare - bead\ thermocouple\ temperature$

$T_g = True\ gas\ temperature$

$T_\infty = Surrounding\ environment\ (radiating)\ temperature$

$h_{bU} = Average\ convective\ heat\ transfer\ coefficient\ over\ the\ thermocouple$

$\epsilon_b = Emissivity\ of\ thermocouple$

$\sigma = Stefan - Boltzmann\ constant$

The bare-bead thermocouple temperature is the temperature recorded by the thermocouple; the surrounding temperature is the graybody enclosure temperature, assumed to be the ambient temperature of the test compartment ~25°C. The emissivity of the thermocouple is assumed to be 0.80, typical for a dull, oxidized metal. The convective heat transfer coefficient is calculated using equation [2].

$$h_{bU} = \frac{Nu_D k}{D} \quad [2]$$

Where:

$Nu_D = Nusselt\ number\ of\ external\ flow\ over\ sphere$
$k = Thermal\ conductivity\ of\ air\ at\ thermocouple$
$D = Bead\ diameter$

The Nusselt number takes into consideration of the external flow's turbulence (Reynolds number) and thermal diffusivity (Prandtl number), as suggested by Whitaker's correlation in equation [3].

$$\overline{Nu_D} = 2 + (0.4\,\mathrm{Re}_D{}^{0.5} + 0.06\,\mathrm{Re}_D{}^{2/3})\,\mathrm{Pr}^{0.4}\left(\frac{\mu_\infty}{\mu_\omega}\right)^{0.25} \quad [3]$$

Where:

$\mu_\infty = Visocity\ evalucated\ at\ the\ free\ stream\ temperature$
$\mu_w = Visocity\ evaluated\ at\ the\ thermocouple\ surface$

In Whitaker's correlation, physical properties are evaluated at the true gas temperature, except for μ_w. However, since the true gas temperature is not known, the physical properties are evaluated at the bare-bead thermocouple temperature instead by assuming that the thermocouple temperature is sufficiently close to the true gas temperature.

Assuming a steady state condition, the thermocouple correction under Blevins and Pitts' method was carried out using the recorded time-averaged temperature for T_b. The Reynolds number was calculated using the velocity recorded by the bi-directional probes at the corresponding heights, or interpolated with neighboring measurements. The physical properties needed were calculated or interpolated from published correlations.

It has been observed that at the isotherm stations nearest to the burner base, the temperature variations over the 4 different-sized thermocouples increased greatly from under 50K to over 100K, these variations were much decreased at locations away from the burner. The corrected temperature appears to rise significantly near the burner, but was similar to the recorded temperature further away along the centerline.

Young's transient thermocouple compensation methodology

Another method of thermocouple correction was developed by Young that take into account the response time of the thermocouples and the use of multiple thermocouples at a single location as an isotherm station in a transient analysis. As established previously, the thermocouple temperature is not the true gas temperature because of radiative heat losses from the thermocouple body. So theoretically if a thermocouple does not have a body (infinitely small), then there will be no losses and its recorded temperature will be the true gas temperature. Although an infinitely small thermocouple cannot be constructed physically, it may be modeled based on thermocouples of varying sizes, as in an isotherm station.

Young's correlation assumes that the different thermocouples in an isotherm station will response to temperature change in the environment differently because of their various time constants, and that each thermocouple has a different radiative heat transfer rate based on their sizes. A heat balance equation that describes the various heat transfers of a thermocouple is presented in equation [4], which is a form of equation [1] but with consideration of the thermocouple's response time.

$$\rho_b c p_b d_b \frac{dT_b}{dt} = h_{bU}(T_g - T_b) + \varepsilon_b \sigma (T_\infty{}^4 - T_b{}^4) \quad [4]$$

Where:

$cp_b = Thermocopule\ specific\ heat$
$d_b = Thermocopule\ characteristic\ dimension$
$\rho_b = Thermocopule\ density$
$\frac{dT_b}{dt} = Thermocopule\ temperature\ change\ rate$
$T_b = Bare - bead\ thermocouple\ temperature$
$T_g = True\ gas\ temperature$
$T_\infty = Surrounding\ environment\ (radiating) temperature$
$h_{bU} = Average\ convective\ heat\ transfer\ coefficient\ over\ the\ thermocouple$
$\epsilon_b = Emissivity\ of\ thermocouple$
$\sigma = Stefan - Boltzmann\ constant$

The characteristic dimension d_b was reported to be the wire diameter in the heating phase due to a lag in temperature rise at the bead since it is larger than the wire diameter. This results in a temperature discrepancy across the bead that is not recordable with the instruments. Hence, the Young's correlation method is only valid for the heating and steady phase of a fire in an enclosure.

The average convective heat transfer coefficient at the thermocouple in Young's correlation is calculated using the Nusselts number correlation developed by Collis and Williams for flow over wires. Compared to equation [3], the Collis and Williams' Nusselts number is only related to the Reynolds number and the gas properties were simplified to a temperature loading function, as shown in equation [5].

$$Nu = \frac{0.24 + 0.56\,\mathrm{Re}^{0.45}}{\left(\frac{T_m}{T_g}\right)^{-0.17}} \quad [5]$$

Where:

$T_m = Film\ temperature\ (averaged\ between\ T_b\ and\ T_g)$

The temperature loading function uses the average temperature between the bead temperature and the gas temperature, which is not known. As previously mentioned, the true gas temperature may be measured by an infinitely small thermocouple, and that its value may be interpolated from the 4 thermocouple temperatures within an isotherm station. Hence, an assumed true gas temperature is used in the Nusselts number calculation in order to facilitate the additional corrective calculations needed. The Reynolds number was calculated using the velocity recorded by the bi-directional probes at the corresponding heights, or interpolated with neighboring measurements. The physical properties were calculated or interpolated from published correlations. The non-dimensional parameters and the average convective heat transfer coefficient were found for every thermocouple in each isotherm station, the variables were then used in the solution for the corrected true gas temperature for all thermocouples on the two rakes.

Ideally, all four thermocouple wire gages in each isotherm station can be used together for temperature correction, however, it was determined that the results would be inconsistent with large uncertainty, most likely due to the sensitivity of the thermocouples to the changing conditions of the fire plume. It was simpler to develop equations to find the true gas temperature using only pairs of two thermocouples. The heat balance equation was expanded to pairs of thermocouples in equation [6].

$$T_g = \left(\frac{1}{h_{b2U} - h_{b1U}}\right)\left(\rho_b c p_b \left(d_{b2}\frac{dT_{b2}}{dt} - d_{b1}\frac{dT_{b1}}{dt}\right) + h_{b2U}T_{b2} - h_{b1U}T_{b1} - \varepsilon\sigma({T_{b2}}^4 - {T_{b1}}^4)\right) \qquad [6]$$

Six pairings are possible with four thermocouples resulting in six calculated true gas temperature values per isotherm station. The values were then averaged to determine the pairing with the most consistent results and low error, which turn out to be between the AWG 30 and AWG 20 thermocouples. The correction factor was then determined by dividing the average temperature with the original measured temperature from the AWG 24 thermocouple. The factor was then applied to other thermocouples at the same height and neighboring thermocouples by interpolation. It was reported in previous studies that the consistency of the corrected results varies greatly in regions where the temperature change is drastic, such as inside the flame region and at the upper/lower layers interface. The Young's method predicts a lower temperature than the method used by Blevins and Pitts near the burner in the flame region, but greatly exaggerated the temperature away in the buoyant plume.

Young's steady state thermocouple compensation methodology

As a comparison, the Young's thermocouple compensation method was also applied to the data in a steady state setting where the response and heating lag of the thermocouples were not considered. Equation [6] was modified into equation [7].

$$T_g = \left(\frac{1}{h_{b2U} - h_{b1U}}\right)\left(h_{b2U}T_{b2} - h_{b1U}T_{b1} - \varepsilon\sigma({T_{b2}}^4 - {T_{b1}}^4)\right) \qquad [7]$$

The goal of this analysis was to test whether a hybrid correction method that takes into account of the various isotherm stations could be used on the time-averaged temperature in a steady-state correction analysis. This method consistently predicts a lower temperature, which seems to suggest an incompatibility for our application because the temperature was supposed to be raised in the correction process.

Comparison between three thermocouple compensation methodologies

The original temperature data are plotted against the corrected data in the following charts. Only the 24 AWG thermocouple time-averaged readings were included. There is a trend that the Young's steady state method consistently underpredicts the centerline temperature, while the Young's transient method appears to overpredict especially in region away from the burner. Additionally, Young's transient correction method appear to produce inconsistent temperature readings at locations where there were two thermocouples, which reaches up to 200°C near the burner. Blevins and Pitts' method seems to produce the most reasonable prediction where the temperature near the burner is raised, yet in the buoyant plume the corrected temperature is close to the original readings.

The same trends hold for both propylene and methane fires at different burner sizes and under free plume and inert wall configurations. The charts are presented in Figure 1 to Figure 6.

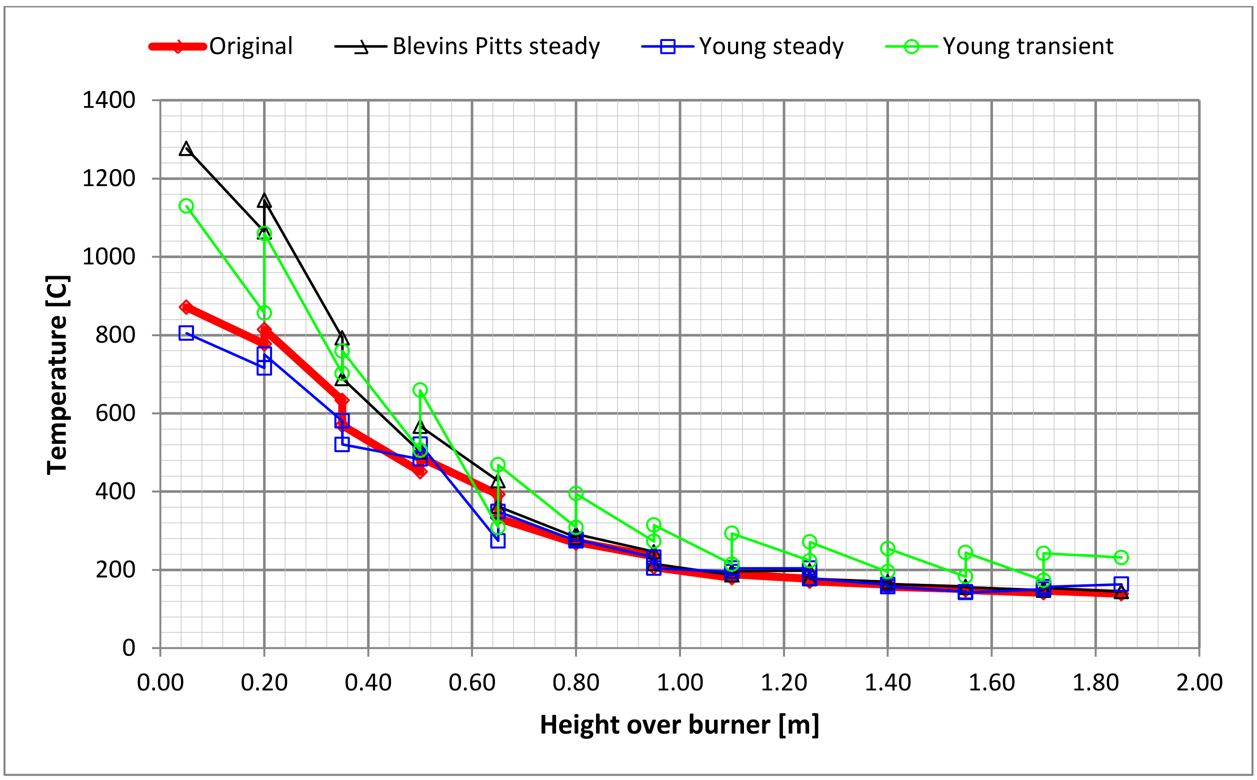

Figure 1 - Temperature corrections vs. original for 50kW propylene 1ft free plume fire

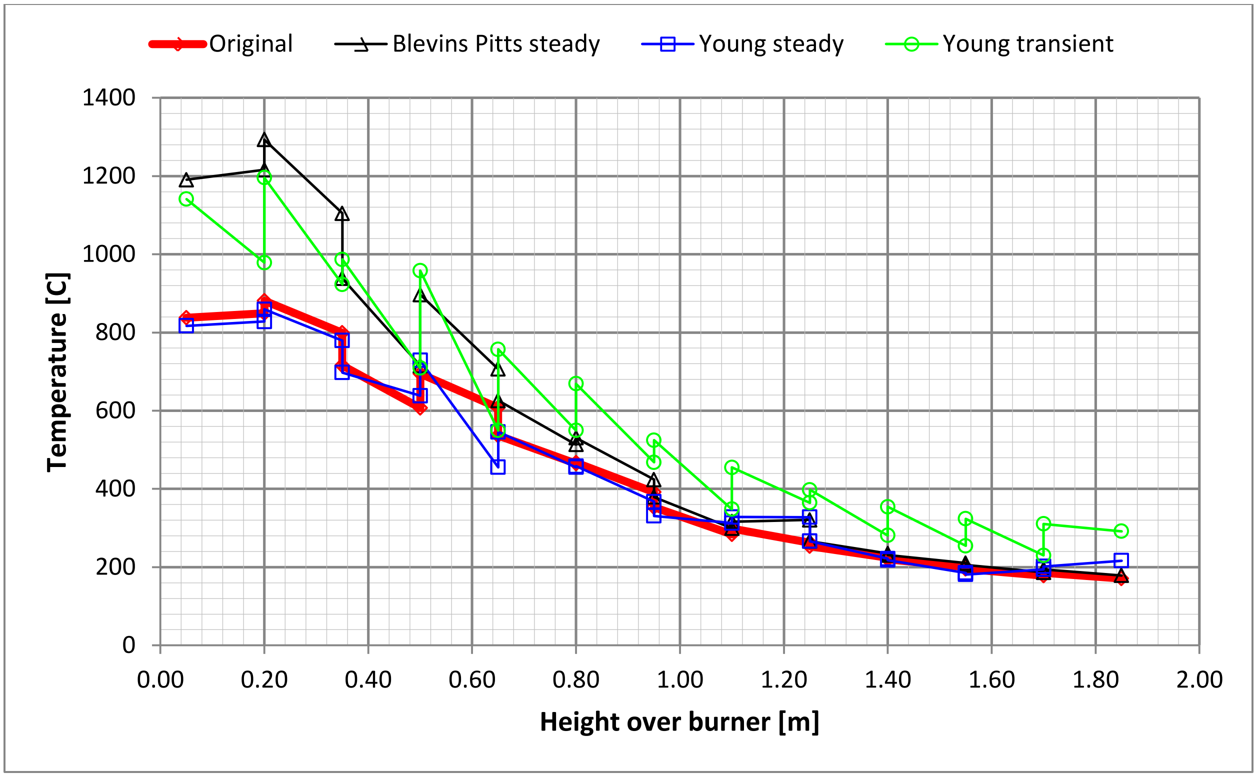

Figure 2 - Temperature corrections vs. original for 75kW propylene 1ft free plume fire

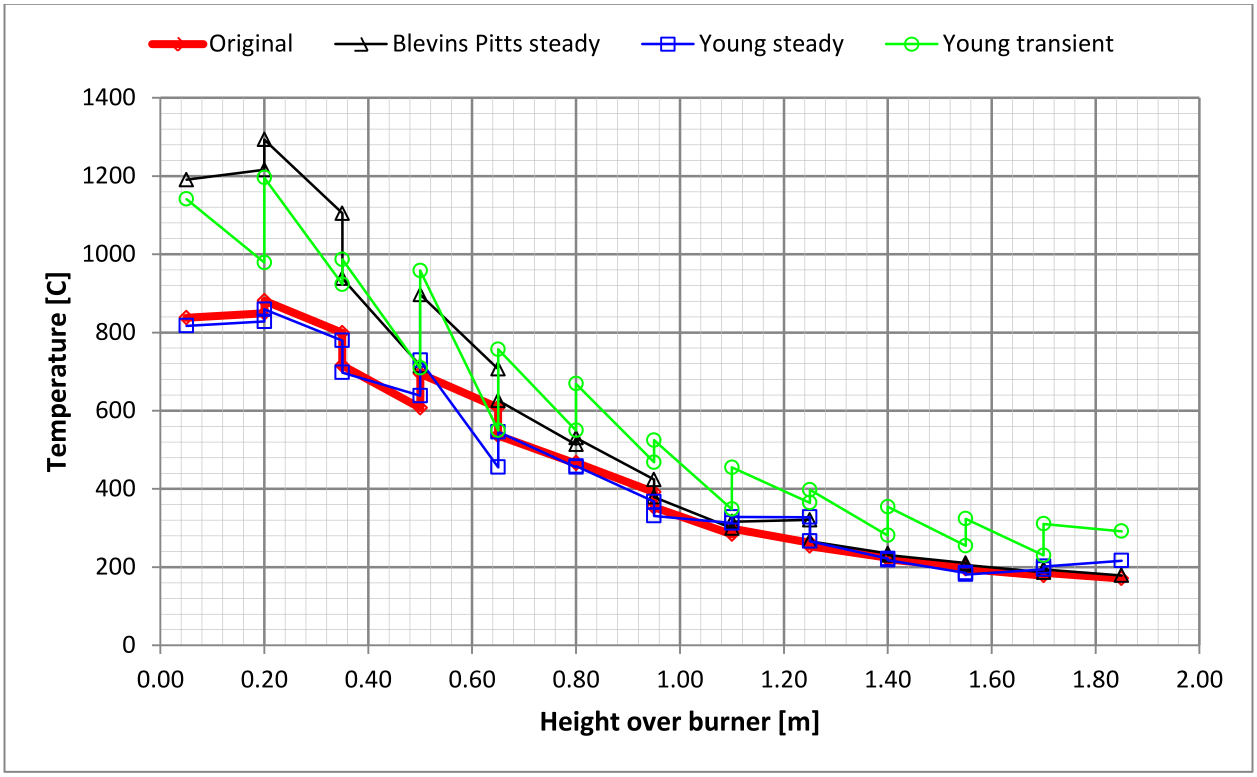

Figure 3 - Temperature corrections vs. original for 50kW propylene 2ft free plume fire

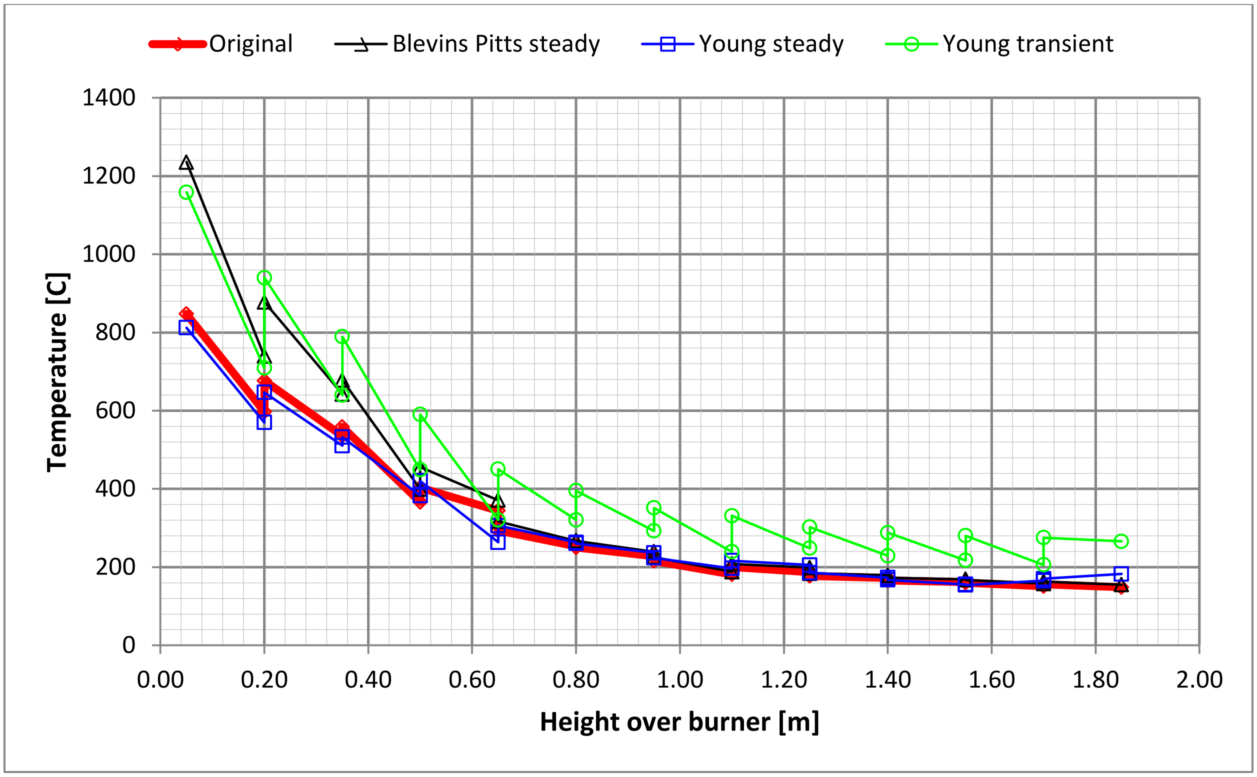

Figure 4 - Temperature corrections vs. original for 75kW propylene 2ft free plume fire

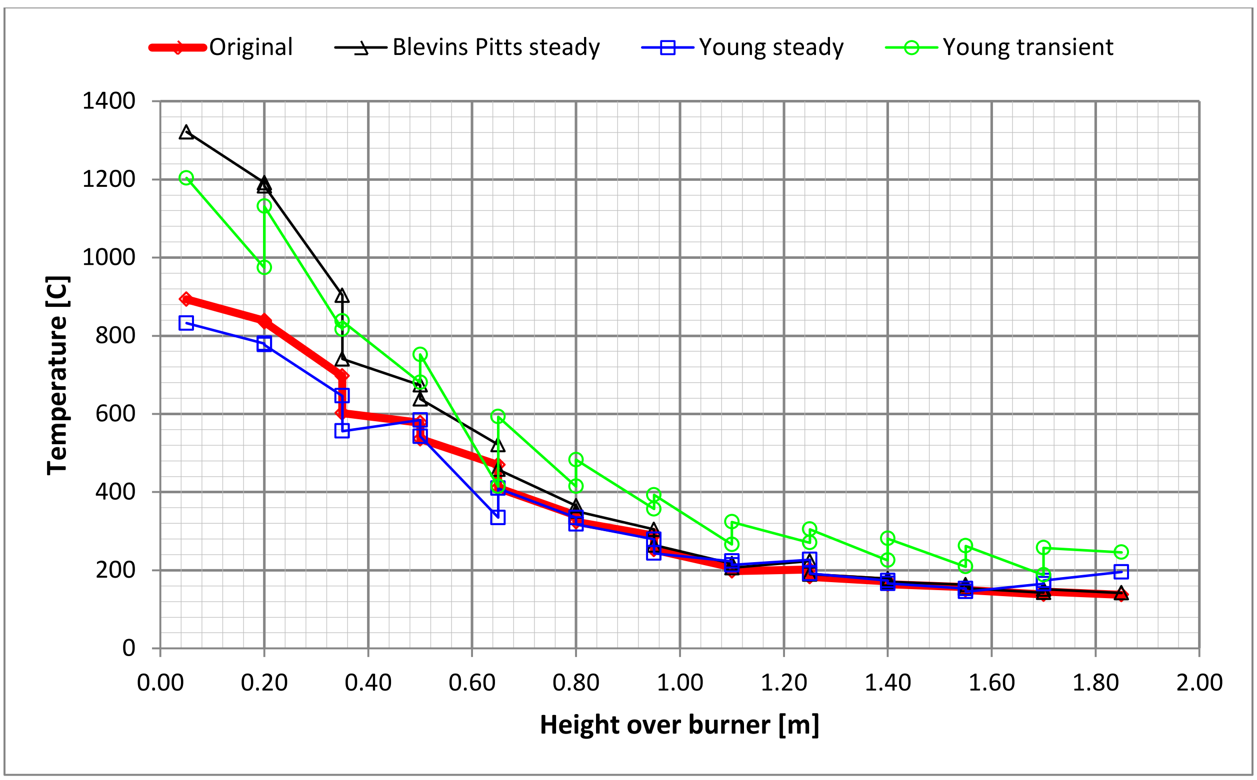

Figure 5 - Temperature corrections vs. original for methane 1ft free plume fire

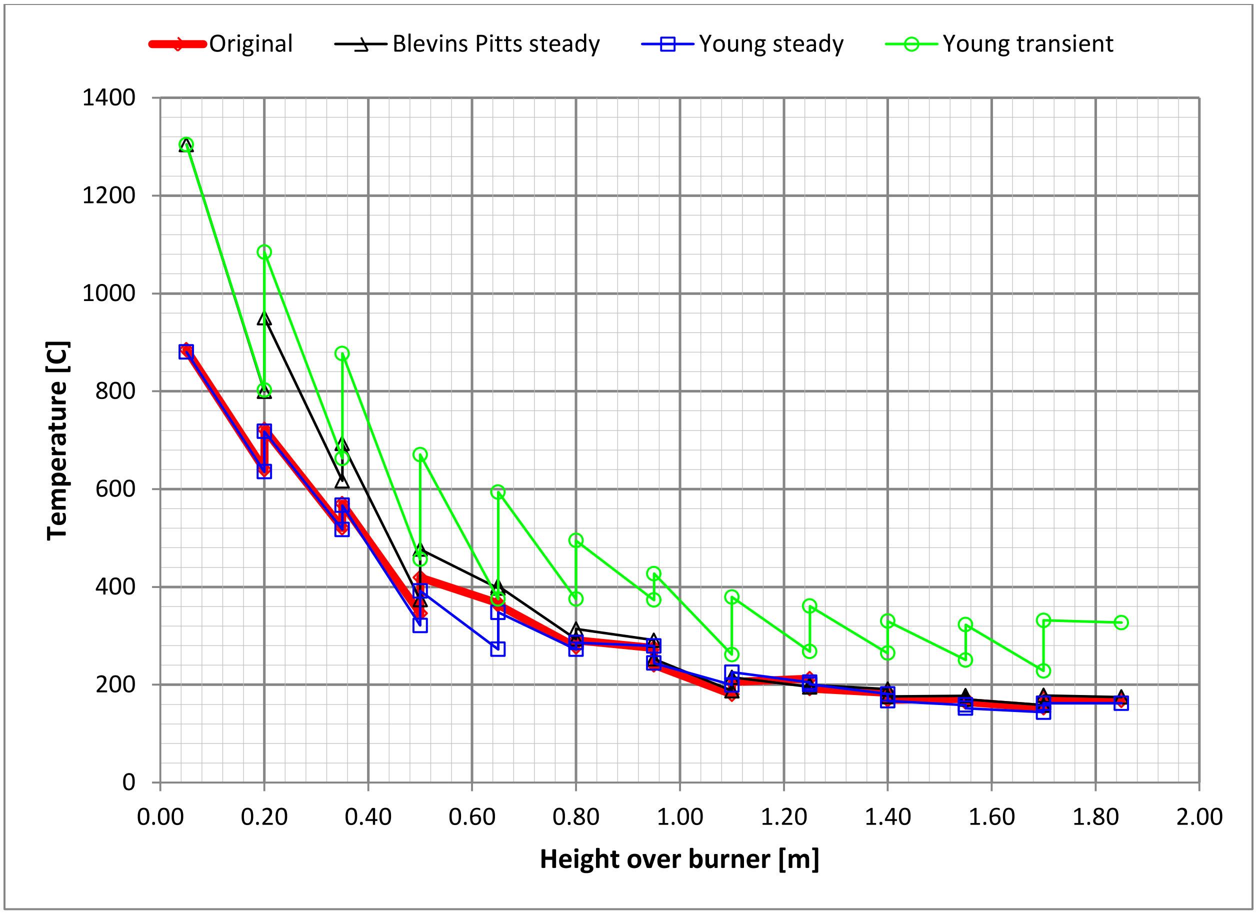

Figure 6 - Temperature corrections vs. original for methane 1ft inert wall fire

Appendix D Fire Experiment Data Analysis Reports

Detailed data summary reports on the collected data are presented in this section. Information presented here are complimentary to those in the main report.

D.1 Heat Release Rate

D.1.1 Oxygen Consumption Calorimetry Systems Calibration and Uncertainty Analysis

An HRR analysis using mass loss data in addition to the usual O2, CO/CO2 and flow rate data has been performed. 4 tests have been conducted at 100 kW according to the flow meter. The weight of the propane gas was measured using a load cell throughout each test for accurate mass loss data after some smoothing. A time averaged mass loss rate can also be found with the before and after weight of the propane gas cylinder. It should be noted that the load cell has a stated uncertainty of +/-0.1 full-scale at 250 kg, which is about 25 grams. The calibration of the load cell with calibrated weights also confirms the noise of the signal to be represents around 25 grams, which correlates well with the manufacturer stated uncertainty.

Based on the data from the SFPE HB, 3rd, the chemical heat of combustion for propane is 43.7 kJ/g, and for a 100 kW fire, this translates to about a mass loss rate of 2.28 g/s.

Since the uncertainty of the load cell is about 25 grams, a smoothing of the data over 30 second (or about 68.4 g of propane lost at 100 kW), has been applied. The chemical het of combustion is then used to find the HRR based on each mass loss data point. Then the mass loss data and HRR data is averaged. Also, the HRR rate is also found by calculating the total mass loss for each test (before/after mass value). These are presented in the table below.

Table 1 - HRR from Mass Loss

	MLR	MLR (before/after)	HRR	HRR (before/after)
Test 1	2.035	2.03	88.9	88.7
Test 2	2.01	2	87.8	87.4
Test 3	2.02	2	88.3	87.4
Test 4	2.01	2.05	87.7	89.6
Test 5	2.37	2.4	103.58	105.3
Test 6	2.35	2.35	102.6	103.1
Test 7	1.92	2.16	83.7	94.5

Table 2 shows the various calculated HRR from the mass loss calibration tests.

Table 2 - Mass Loss HRR compared to other HRR calculations

	HRR	HRR (before/after)	O2 HRR	Correct O2	CO/CO2	Flow
Test 1	88.9	88.7	124.7	96.1	127.1	103.1
Test 2	87.8	87.4	129.8	99.9	121.7	102.8
Test 3	88.3	87.4	130.8	100.7	121.2	103.0
Test 4	87.7	89.6	131.7	101.4	122.6	102.7
Test 5	103.58	105.3	138.3	106.5	123.3	103.0
Test 6	102.6	103.1	135.4	104.2	120.9	103.3
Test 7	83.7	94.5	136.4	105.0	122.9	102.7

As can be seen, the HRR calculated based on the mass loss are lower than the expected 100 kW (represented by the Flow HRR) and also the O2 and CO/CO2 HRR.

The uncertainty in the mass data is about 25 grams, the following calculation shows its corresponding uncertainty in the HRR calculation.

The HRR can be found as: $HRR = \Delta H_{ch} * \frac{mass\ loss}{time}$

The uncertainty of the HRR from mass loss is $\delta HRR_{mass} = \left|\frac{\partial HRR}{\partial mass\ loss}\right| * \delta mass$

Where $\delta mass$ is the uncertainty of the load cell. The uncertainty of the heat of combustion and time are insignificant and so they are not included in the calculations.

So the uncertainty of the HRR is found to be:

$$\delta HRR_{mass} = \left|\frac{\partial HRR}{\partial mass\ loss}\right| * \delta mass$$

$$\delta HRR_{mass} = \left|\frac{\Delta H_{ch}}{time}\right| * 25\ grams$$

The chemical heat of combustion is 43.7 kJ/g, and for most of the tests the total time used per test is about 990 sec.

$$\delta HRR_{mass} = \left|\frac{44.7\ kJ/g}{990\ sec}\right| * 25\ grams$$

And the uncertainty amounts to about 1.1 kW.

Figure 1 shows that the mass loss HRR generally fall just outside of the error bars from the O2 HRR, CO/CO2 HRR, and the Flow HRR, but within bound of the corrected O2 HRR. Though it should be noted that there are slight overlaps for the Flow HRR and the mass loss HRR within their error bars. Tests 5 to

7 are performed the day after Tests 1 to 4 were conducted, and it can be seen that in Test 5 and 6, the mass loss HRRs correlate well with the Flow HRR, but then in Test 7, the mass loss HRR is again lower than the Flow HRR.

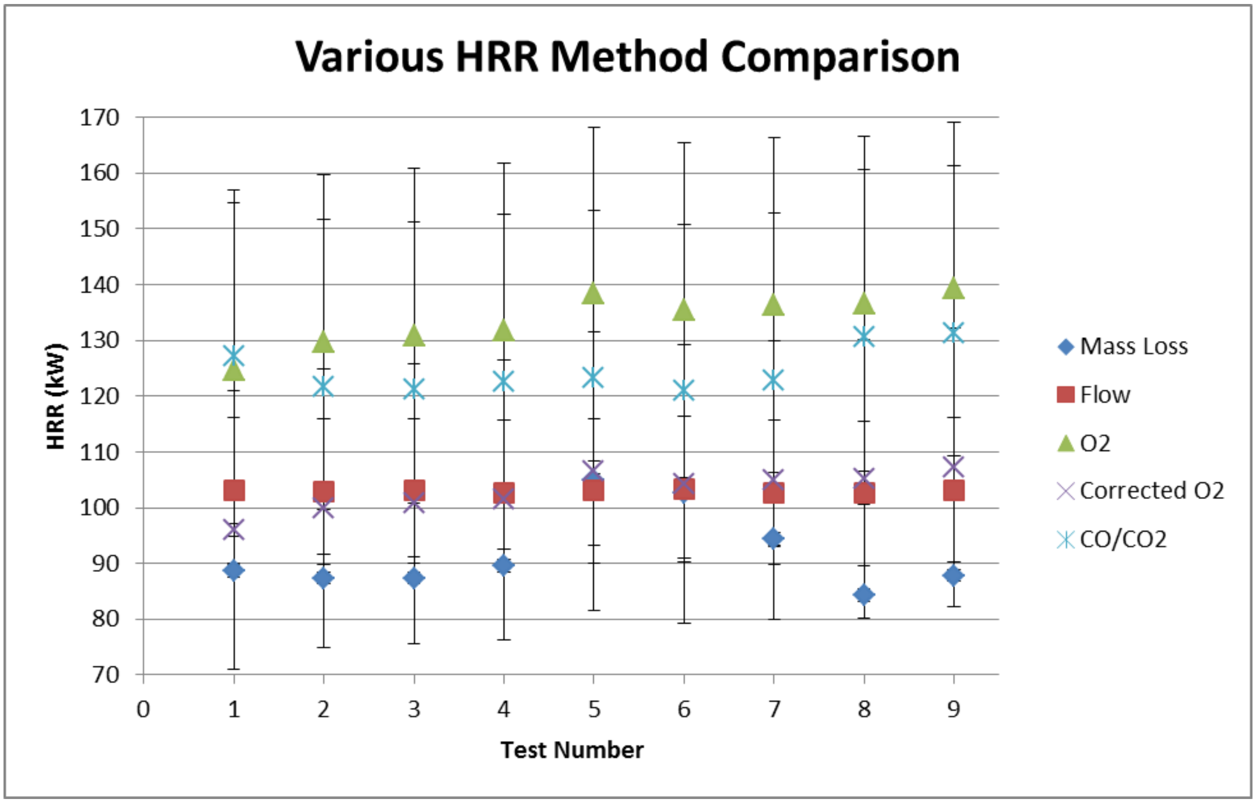

Figure 1 - HRR comparison

The heat release rate of a fire in the LODS can be approximated in three different ways, through the estimated fuel flow rate, oxygen consumption calorimetry, and CO/CO_2 generation calorimetry. Calibration for the LODS calorimetry systems is achieved by burning natural gas while monitoring the flow rate to find an average HRR that is then compared with the HRR calculated through oxygen consumption. In the calibration, it has been assumed that the flow rate HRR is more accurate and there will always be a correction factor needed in the oxygen consumption HRR.

Table 3 shows the HRR calculated through flow rate measurements and oxygen consumption calorimetry. Four calibrations using natural gas has been performed, and during each calibration the flow rate of the gas was changed 3 or 4 times in order to cover a range of different HRR fires. It is found that the O2 HRR is constantly higher than the flow HRR, and the average ratio of $\frac{Flow\ HRR}{O2\ HRR}$ is about 0.77, hence if the flow HRR is deemed more accurate, a correction factor of 0.77 is used on the measured O2 HRR to reduce it by 77% to get the “true” HRR of the experimental fires. This technique has been used since the inception of the experiments but upon closer inspection this shift in HRR does not show up in most of the inert wall propane test HRR measurements, and the shift is not of the same value for the inert wall propylene test HRR measurements. These points raise the question of whether the correction is needed and whether the natural gas flow rate from the gas meter is accurate.

Table 3 - Methane Calibration Data

Methane Calibration Data

Corrected by taking 77% of the O2 HRR

Calibration 1

	Flow_HRR	O2_HRR	Ratio flow/O2	% difference	O2_HRR	%Difference
A	39.49	47.18	0.84	19.47	36.33	-8.01
B	210.35	296.20	0.71	40.81	228.07	8.42
C	261.13	370.97	0.70	42.07	285.65	9.39

Calibration 2

	Flow_HRR	O2_HRR	Ratio flow/O2	% difference	O2_HRR	%Difference
A	42.28	50.78	0.83	20.09	39.10	-7.53
B	57.00	69.62	0.82	22.14	53.61	-5.95
C	61.83	76.48	0.81	23.70	58.89	-4.75

Calibration 3

	Flow_HRR	O2_HRR	Ratio flow/O2	% difference	O2_HRR	%Difference
A	47.07	58.94	0.80	25.22	45.38	-3.58
B	119.55	153.91	0.78	28.74	118.51	-0.87
C	198.96	251.73	0.79	26.52	193.83	-2.58
D	260.29	337.94	0.77	29.83	260.21	-0.03

Calibration 4

	Flow_HRR	O2_HRR	Ratio flow/O2	% difference	O2_HRR	%Difference
A	57.35	76.70	0.75	33.75	59.06	2.99
B	119.08	159.09	0.75	33.60	122.50	2.87
C	214.28	281.49	0.76	31.36	216.75	1.15
D	261.06	345.02	0.76	32.16	265.67	1.76

Figure 2 shows HRR measured from the four calibrations, each calibration was performed over 3 or 4 separate fire sizes. Calibrations 2, 3, and 4 show similar trends with similar linear regression line slopes and y-intercepts. The data from Calibration 1 shows that the disparity between the O2 and flow rate HRR is even higher.

Figure 3 shows the O2 HRR gathered as one group and also the comparison between the corrected (77%) and original measured HRR. The uncorrected O2 HRR shows a linear regression slope of 1.3 and a y-intercept of -6.7 kW. Whereas the corrected O2 HRR shows a linear regression slope of 1.05 and a y-intercept of -5.1 kW, this shows that applying the correction factor at 77%, produce a good correlation between the flow rate and O2 HRR.

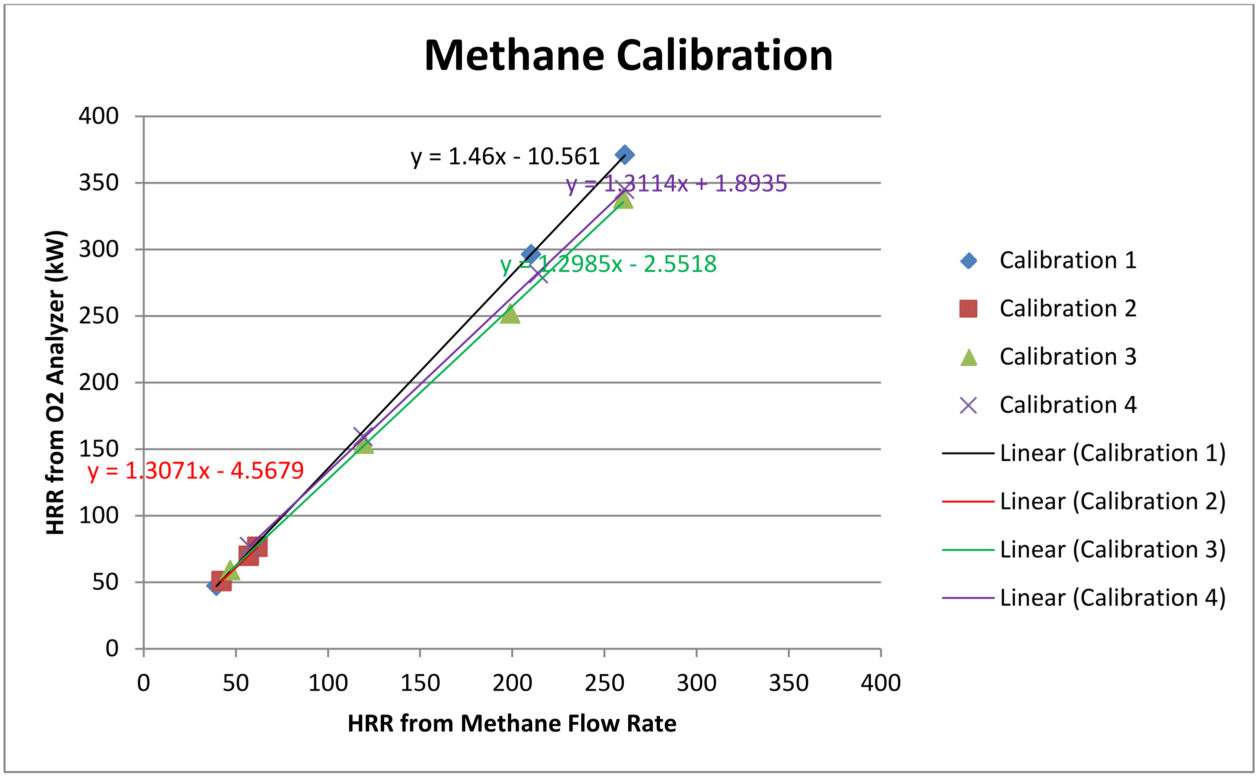

Figure 2 - Individual Methane Calibration HRR

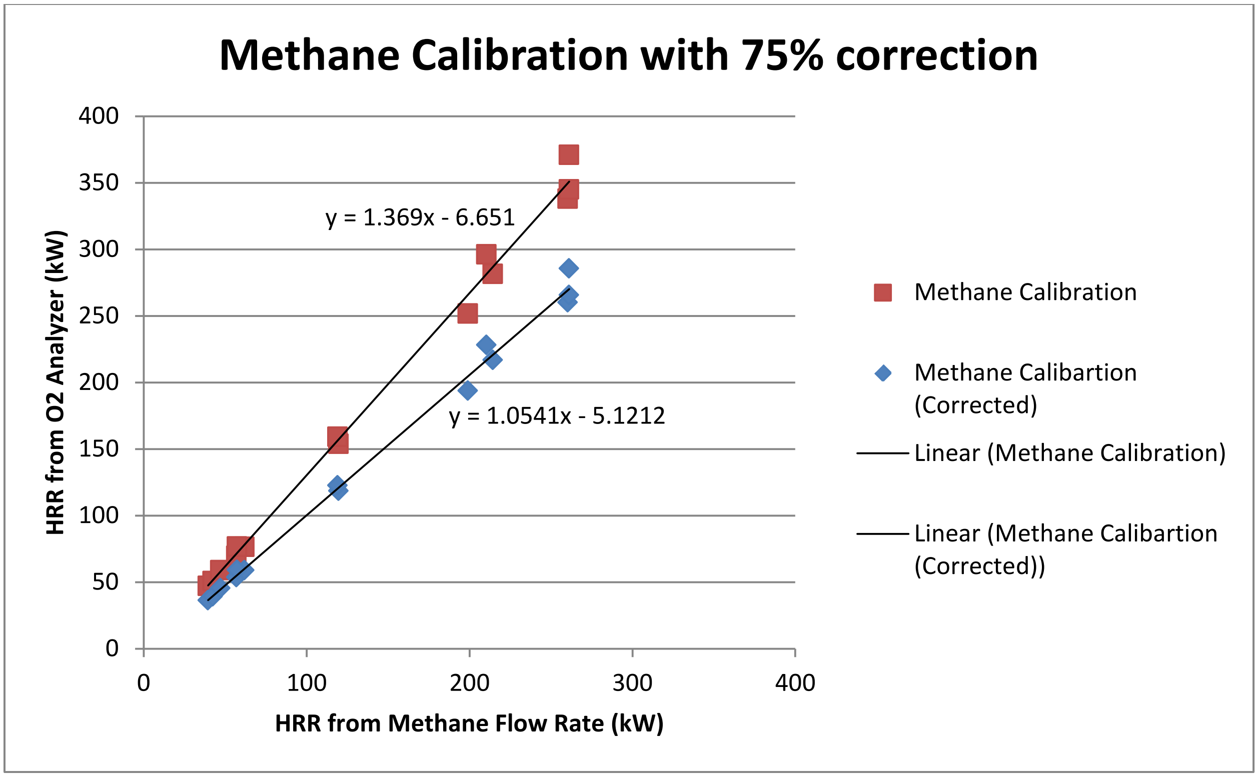

Figure 3 - Methane Calibration HRR Corrected

The average HRR of the inert wall fire tests are recorded in Table 4. The ratios $\frac{Flow\ HRR}{O2\ HRR}$ for propane fires are quite good, at about 0.94; the ratios $\frac{Flow\ HRR}{O2\ HRR}$ for propylene fires are on average 0.88, which suggests a bigger difference. If the flow rate data from the mass flow controller can be trusted, then it appears that the correlation between the O2 HRR and the flow rate HRR are better than the methane calibration and the correction factor described earlier may be inaccurate. Table 4 also shows the ratio $\frac{Flow\ HRR}{O2\ HRR\_corrected}$ if the O2 HRR has been corrected by 77%, and this causes it to drop to 0.73 for propane and 0.68 for propylene, which means that the correction may not be applied correctly. It should also be noted for larger fire sizes, the O2 HRR tends to be over-estimated.

The standard deviations for the HRR are calculated based on different "dial-in"/flow HRR. For propane, Tests 1, 4, 6, and 7 are grouped as the "100 kW" fires, and Tests 2, 3, 5 are grouped as the "250 kW" fires with the standard deviation found for each group separately. For propylene, Tests 8, 9, and 10 are grouped as the "85 kW" fires, and Tests 8 and 12 are grouped as the "210 kW" fires. These were meant to be set to 100 kW and 250 kW respectively but the flow setting were not correct during the fire tests. For propane, the standard deviation for O2 HRR of the 100 kW fires is found to be 6.1 kW and 3.5 kW for 250 kW fires. For propylene, the standard deviation for O2 HRR of the 85 kW fires is found to be 3.6 kW and 12.5 kW for the 210 kW fires.

The accuracy of the flow controller is reported to be at 1% full scale over 875 slpm, which in this case corresponds to 8.75 slpm and about 12.5 kW for both fuel. The standard deviations found of the O2 HRR all fall below or around this value, which suggests that the O2 HRRs are reasonably accurate.

Table 4 - Inert Wall Fire Test HRRs

Inert Test HRR Data Propane					
	O2_HRR	O2_HRR (corrected 77%)	Flow_HRR	Ratio O2/Flow	Ratio O2/Flow corrected
Test 1	84.4	65.0	102.5	0.82	0.63
Test 2	256.4	197.4	251.8	1.02	0.78
Test 3	250.6	193.0	252.0	0.99	0.77
Test 4	89.6	69.0	102.4	0.87	0.67
Test 5	257.0	197.9	251.8	1.02	0.79
Test 6	94.3	72.6	102.5	0.92	0.71
Test 7	98.6	75.9	102.7	0.96	0.74
				Standard Error	
Standard Deviation from ~100 kW fires			6.1	3.53	
Standard Deviation from ~250 kW fires			3.5	2.03	
Propylene					
	O2_HRR	O2_HRR (modified 77%)	Flow_HRR	Ratio O2/Flow	Ratio O2/Flow corrected
Test 8	226.2	174.2	210.4	1.08	0.83
Test 9	61.8	47.6	85.7	0.72	0.56
Test 10	64.0	49.3	86.3	0.74	0.57
Test 11	68.8	53.0	84.9	0.81	0.62
Test 12	208.5	160.6	210.8	0.99	0.76
Test 13	324.2	249.7	302.3	1.07	0.83
Test 14	101.4	78.0	121.7	0.83	0.64
Test 15	71.0	54.7	91.6	0.78	0.60
				Standard Error	
Standard Deviation from ~85 kW fires			3.6	2.5	
Standard Deviation from ~210 kW fires			12.5	8.8	

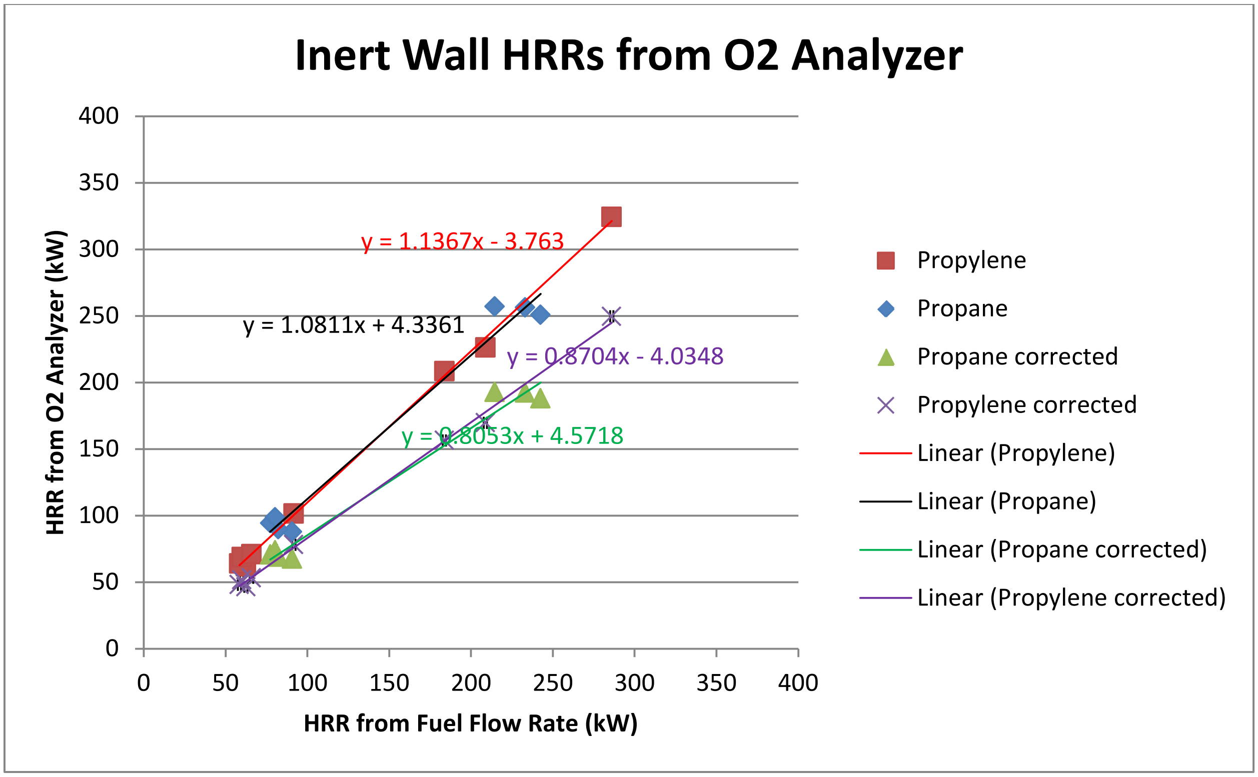

Figure 4 shows the inert wall test O2 and flow rate HRRs comparison as separated by fuel type and correction. One can see that the original O2 HRRs for propane correlates well with flow rate HRR, but varies for propylene. The corrected O2 HRRs under-estimate for both fuel gases.

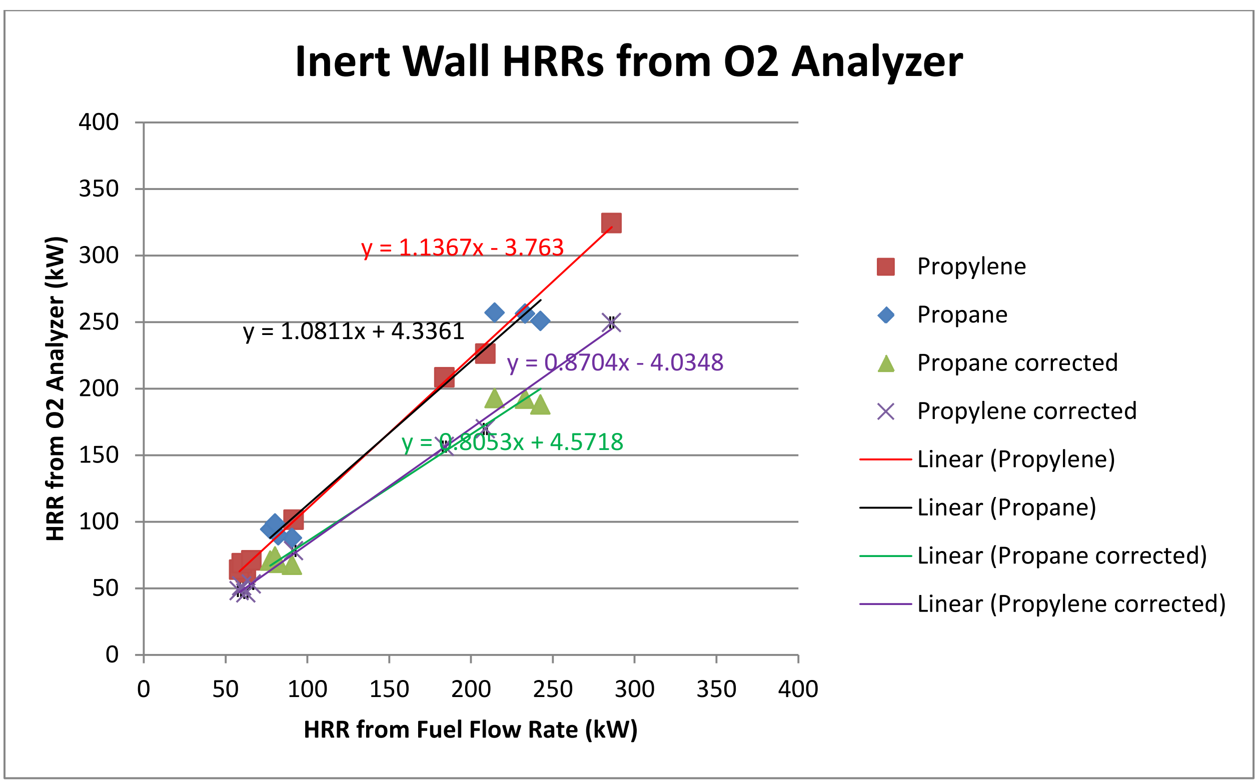

Inert Wall HRRs from O2 Analyzer
HRR from O2 Analyzer (kW)
HRR from Fuel Flow Rate (kW)
0
50
100
150
200
250
300
350
400
y = 1.1367x - 3.763
y = 1.0811x + 4.3361
y = 0.8704x - 4.0348
y = 0.8053x + 4.5718
Propylene
Propane
Propane corrected
Propylene corrected
Linear (Propylene)
Linear (Propane)
Linear (Propane corrected)
Linear (Propylene corrected)

Figure 4 – Inert Test HRRs by Fuel Type

Figure 5 shows the inert wall test HRRs collected as one group and calculates the linear regression line for both the original values and the corrected values. The linear regression lines suggest an over-estimation of the original value and an under-estimation of the corrected values. Again, the over estimation most likely stem from the tests with the larger fire sizes.

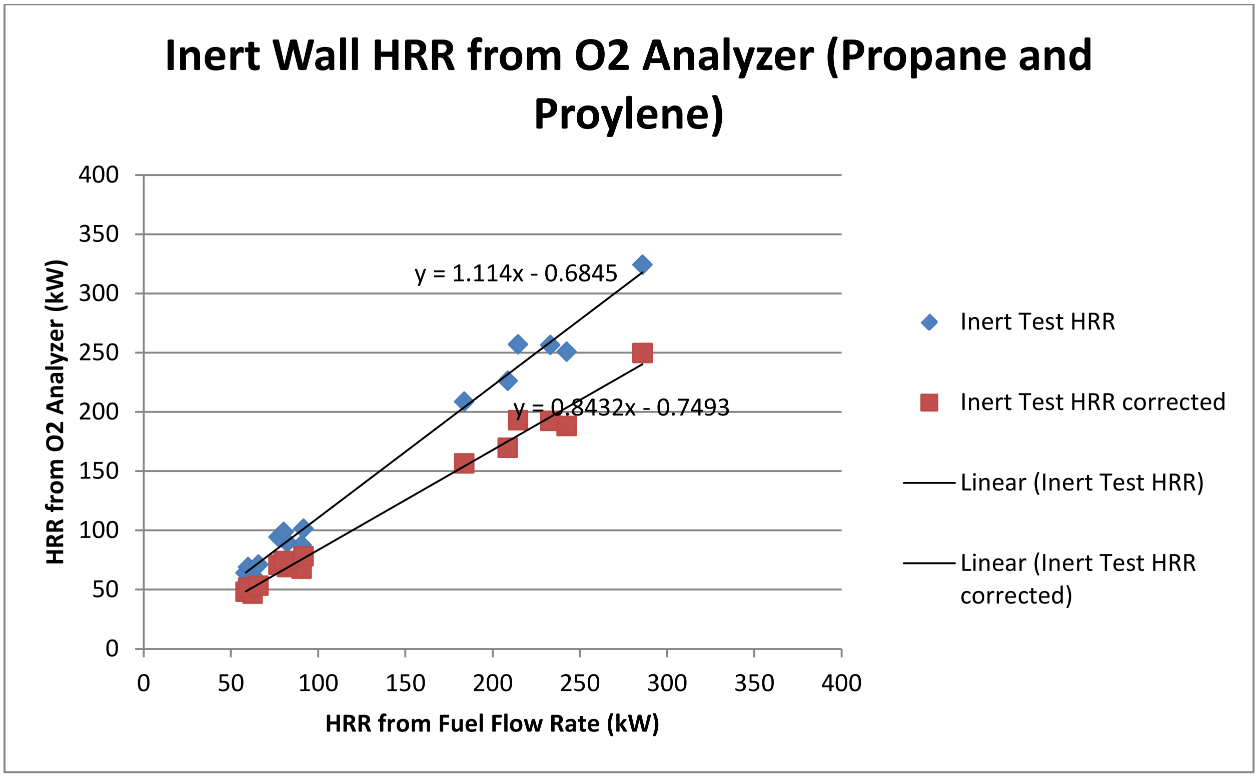

Figure 5 - Inert Test HRRs (collected)

Figure 6 shows the methane calibration HRRs vs the inert wall HRRs, we can see 2 distinct trendlines, with the one for methane calibration having a larger slope over 1, but the one for the inert wall HRRs has a larger y-intercept in magnitude. Given the data reported here, the correction factor needed for the methane calibration may not apply to the propane and propylene tests: there might be a slight offset in the natural gas flow meter that causes the large discrepancy.

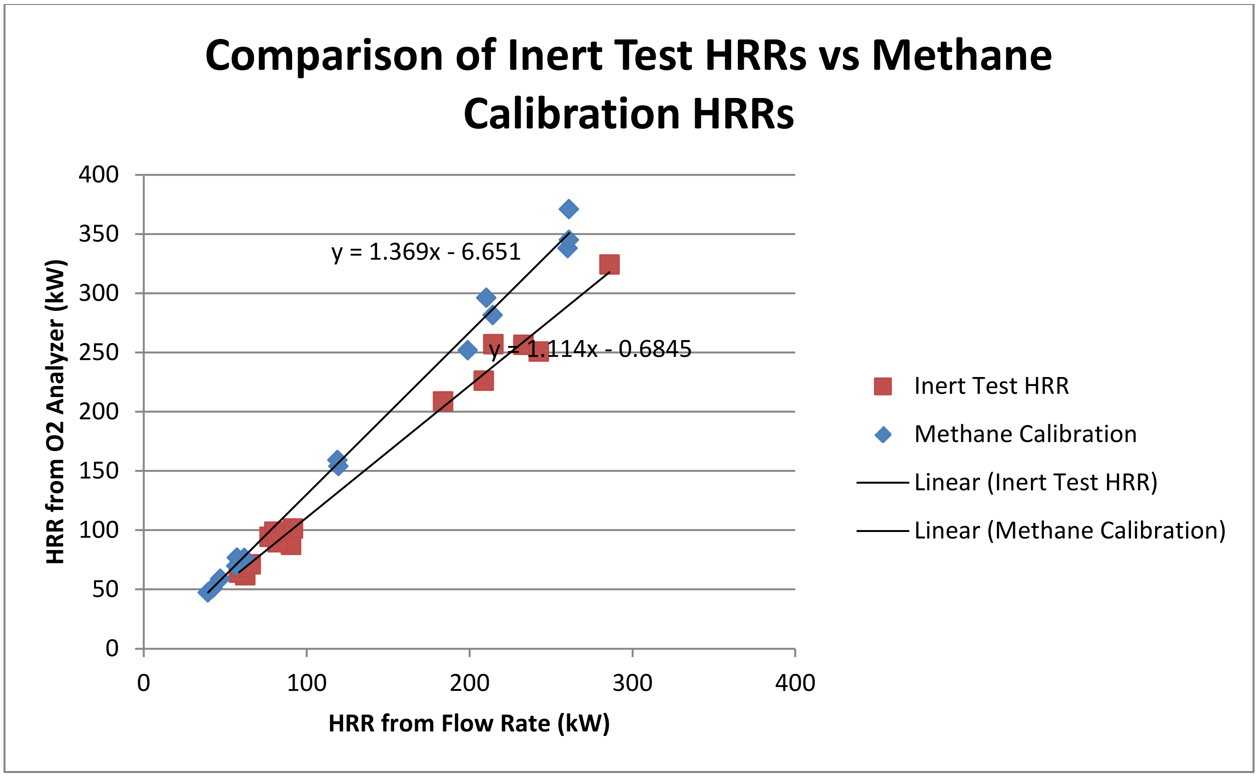

Figure 6 - Inert Wall HRRS vs Methane Calibration

The heat release rate data from the inert wall tests and various propane plume and mass flow controller flow tests have been complied into one dataset. Also, the HRR based on CO/CO2 generation has been calculated based on equations presented by Marc Janssens in the Calorimetry chapter of the SFPE Handbook.

Table 5 shows the various method of calculating the HRR for each test: oxygen consumption, corrected oxygen consumption based on methane calibration data (77% of O2 consumption), CO/CO2 generation, and HRR based on flow rate measured by the mass flow controller. Note that 2 major events dealing with the collection of data had occurred during testing, first is that the O2 analyzer on the LODS was repaired and re-calibrated after Test 12 of the Inert wall test series, and second is that the mass flow controller has been sent out and re-calibrated after Test 15 of the Inert wall test series. So based on these events, the propane fire data can be separated into pre- and post- “O2 analyzer fixed and MFC recalibrated” groups, and the propylene fire data can be separated into pre- and post- “O2 analyzer recalibrated” groups.

In the O2 HRR and the CO/CO2 HRR, the water vapor molar fraction of the combustion has been assumed to be very small (~ a few %), since the fire lab is climate controlled, and has been ignored in the calculations. This might need to be considered further since the water vapor concentration can have some impact on the HRR.

Table 5- Inert Test HRR Data

Inert Test HRR Data

Propane

	O2_HRR	O2_HRR (corrected 77%)	CO_CO2 HRR	Flow_HRR	Ratio O2/Flow	Ratio O2/Flow corrected	Ratio CO/Flow
Test 1	87.6	67.5	77.2	102.5	0.85	0.66	0.75
Test 2	256.4	192.3	229.2	251.8	1.02	0.76	0.91
Test 3	250.6	188.0	222.3	252.0	0.99	0.75	0.88
Test 4	89.6	69.0	80.1	102.4	0.87	0.67	0.78
Test 5	257.0	192.8	232.1	251.8	1.02	0.77	0.92
Test 6	94.3	70.7	85.4	102.5	0.92	0.69	0.83
Test 7	98.6	73.9	89.3	102.7	0.96	0.72	0.87

O2 HRR

Standard Deviation from ~100 kW fires	4.9
Standard Deviation from ~250 kW fires	3.5

Propylene

	O2_HRR	O2_HRR (modified 77%)	CO_CO2 HRR	Flow_HRR	Ratio O2/Flow	Ratio O2/Flow corrected	Ratio CO/Flow
Test 8	226.2	169.7	199.9	210.4	1.08	0.81	0.95
Test 9	61.8	46.4	54.0	85.7	0.72	0.54	0.63
Test 10	64.0	48.0	58.5	86.3	0.74	0.56	0.68
Test 11	68.8	51.6	60.0	84.9	0.81	0.61	0.71
FROM THIS POINT ON THE O2 ANALYZER HAD BEEN RE-CALIBRATED							
Test 12	208.5	156.4	183.8	210.8	0.99	0.74	0.87
Test 13	324.2	249.7	286.0	302.3	1.07	0.83	0.95
Test 14	101.4	78.0	91.8	121.7	0.83	0.64	0.75
Test 15	71.0	53.2	65.8	91.6	0.78	0.58	0.72

O2 HRR

Standard Deviation from ~85 kW fires	3.6
Standard Deviation from ~210 kW fires	12.5

FROM THIS POINT ON THE MASS FLOW CONTROLLER HAS BEEN CALIBRATED

Propane Plume Data							
	O2_HRR	O2_HRR (modified 77%)	CO_CO2 HRR	Flow_HRR	Ratio O2/Flow	Ratio O2/Flow corrected	Ratio CO/Flow
Test 7_A	67.4	51.9	59.8	53.1	1.27	0.98	1.13
Test 7_B	101.0	77.8	90.7	78.7	1.28	0.99	1.15
Test 7_C	133.1	102.5	107.5	102.4	1.30	1.00	1.05
Test 7_D	202.6	156.0	180.8	155.8	1.30	1.00	1.16
Test 8_A	57.1	44.0	49.2	50.2	1.14	0.88	0.98
Test 8_B	95.4	73.4	84.1	78.0	1.22	0.94	1.08
Test 8_C	130.5	100.5	115.4	102.8	1.27	0.98	1.12
Test 8_D	172.5	132.9	153.5	129.2	1.34	1.03	1.19
Test 8_E	207.7	159.9	184.9	154.9	1.34	1.03	1.19
Test 8_F	281.7	216.9	251.0	204.2	1.38	1.06	1.23
Test 9_A	67.3	51.8	54.2	52.8	1.27	0.98	1.03
Test 9_B	138.8	106.9	124.4	103.0	1.35	1.04	1.21
Test 9_C	103.4	79.6	96.4	52.8	1.96	1.51	1.83
Test 9_D	163.3	125.7	149.9	103.0	1.59	1.22	1.46

The errors/uncertainties in the HRR calculations have been considered as followed. For the Flow HRR, accuracy of the flow meter is about 1% full-scale and translates to 13 kW. For the O2 and the CO/CO2 HRR, accuracy of the oxygen analyzer is 0.1%, it dominates and translates to 30 kW. For the corrected O2 HRR, the accuracy of the oxygen analyzer again dominates, and translates to 25 kW. These have been used in the following diagrams where applicable.

Uncertainties:

Flow HRR uncertainty	13	kW
O2 HRR uncertainty	30	kW
CO/CO2 HRR uncertainty	30	kW
Corrected O2 HRR uncertainty	25	kW
Mass Loss uncertainty	1.1	kW

Figure 7 shows the different HRR values calculated for all the inert wall and free plume tests. There is a wide spread of data and it can be seen that the CO/CO2 HRR generally is lower than the O2 HRR.

- Tests 1 to 7 (propane inert wall test before analyzer repair and MFC calibration) shows good correlation between the Flow HRR and the O2 HRR at high HRR, but at low HRR, the O2 HRR tends to underestimates.
- Tests 8 to 12 (propylene inert wall test before analyzer repair) show that the O2 HRR overestimate over the Flow HRR for 250 kW fires, but underestimates for smaller fire size.
- Tests 13 to 15 (propylene inert wall test after analyzer repair) shows the same trend as the earlier propylene test.
- Tests 16 to 29 (propane plume test after analyzer repair and MFC calibration) shows generally good correlation between various HRRs for small fires, but there is obvious overestimation of O2 HRR over Flow HRR whereas the CO/CO2 HRR is close to the Flow HRR.

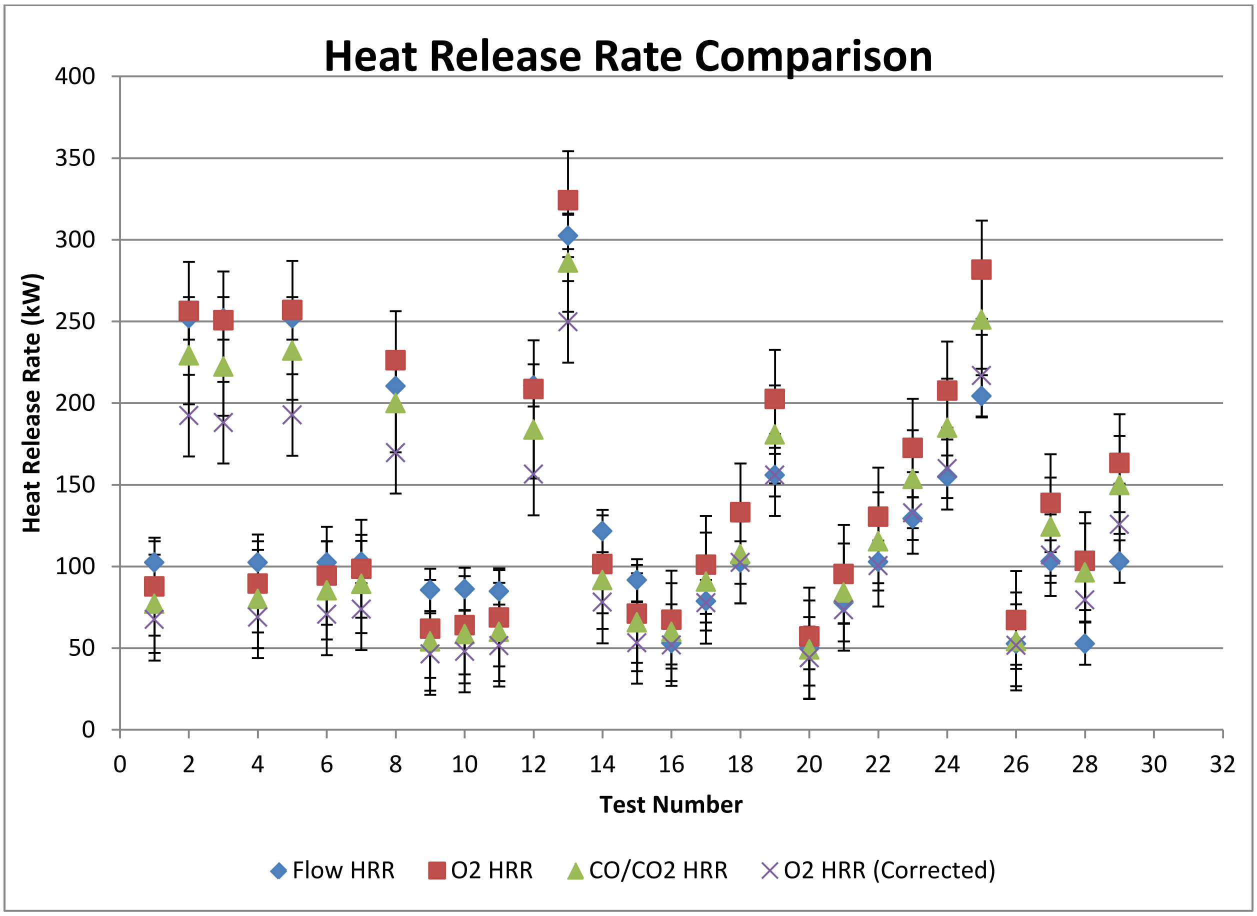

Figure 7 - HRRs of all tests

Figure 8 shows the comparison between O2 and Flow HRRs. Before the MFC calibration (Tests 1 to 15), their values generally over laps within their errors, but afterward the discrepancy between the 2 series of data widen.

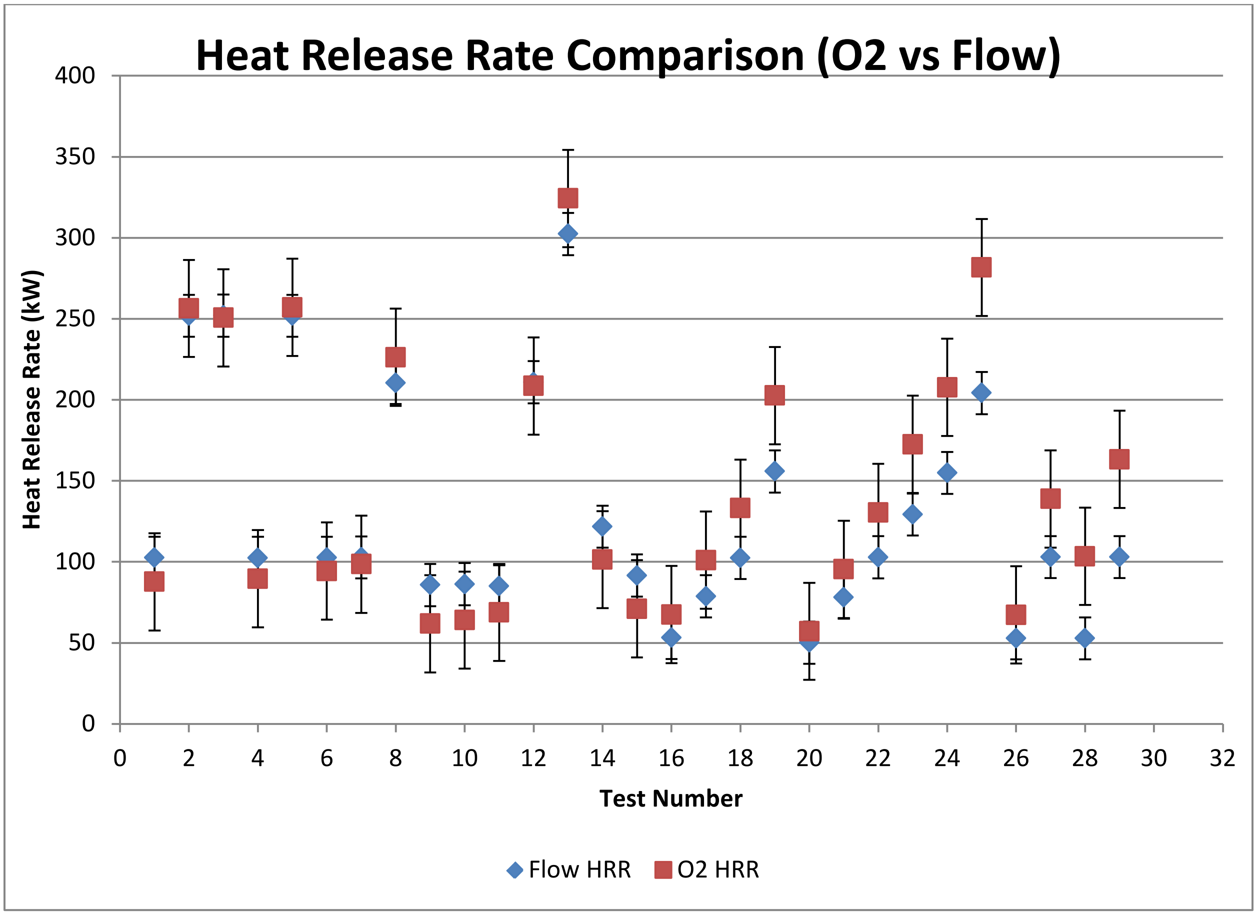

Figure 8 - O2 vs Flow HRRs of all tests

Figure 9 shows the comparison between the CO/CO2 and Flow HRR. The values generally overlaps throughout all tests except for those after Test 15 and the MFC has been calibrated, where the discrepancy deepens.

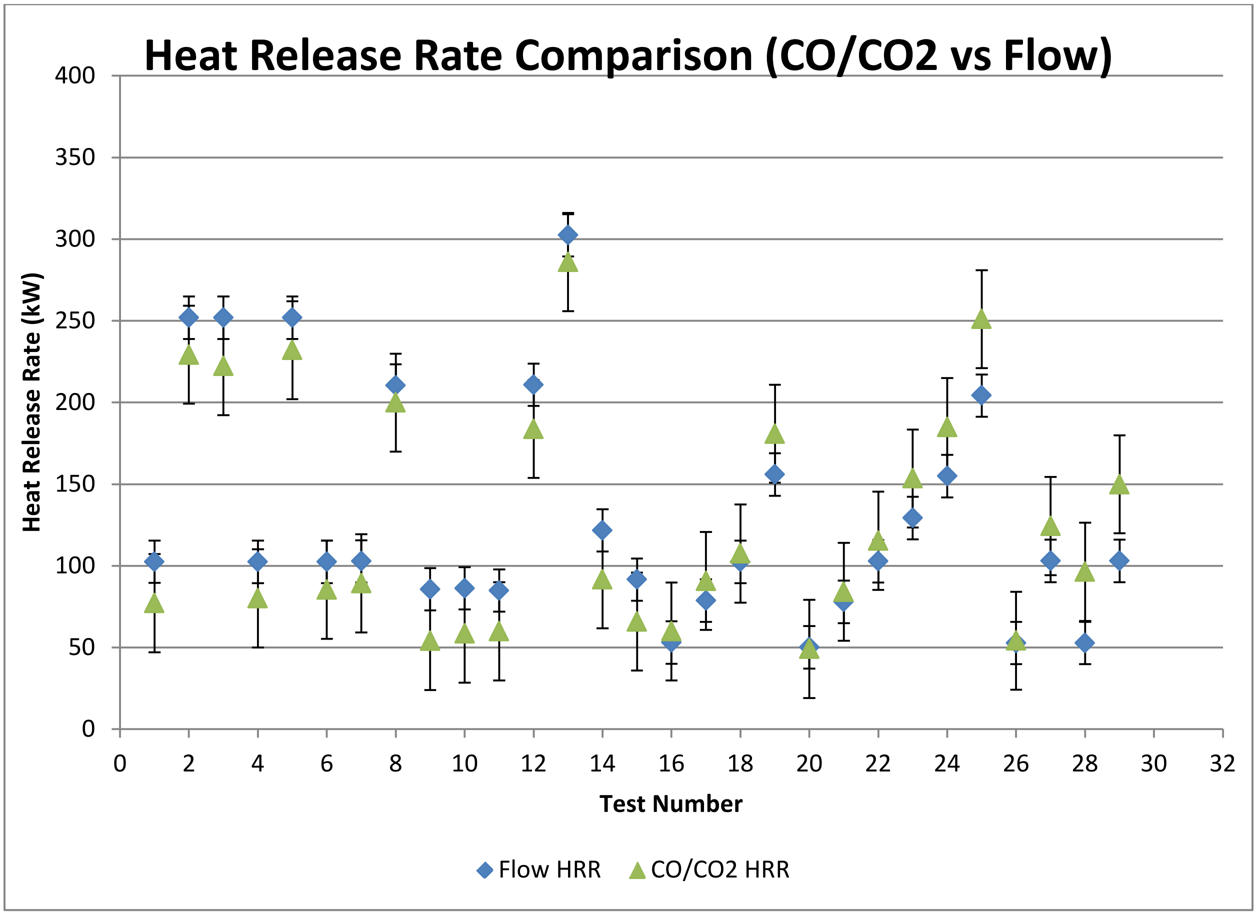

Figure 9 - CO/CO2 vs Flow HRR of all tests

Figure 10 shows the comparison between the corrected O2 HRR (77% of O2 HRR per methane calibration data) vs Flow HRR. For the values before Test 16 (before MFC calibration), their values generally are outside of each other's errors, but they are much better correlated after the MFC is calibrated.

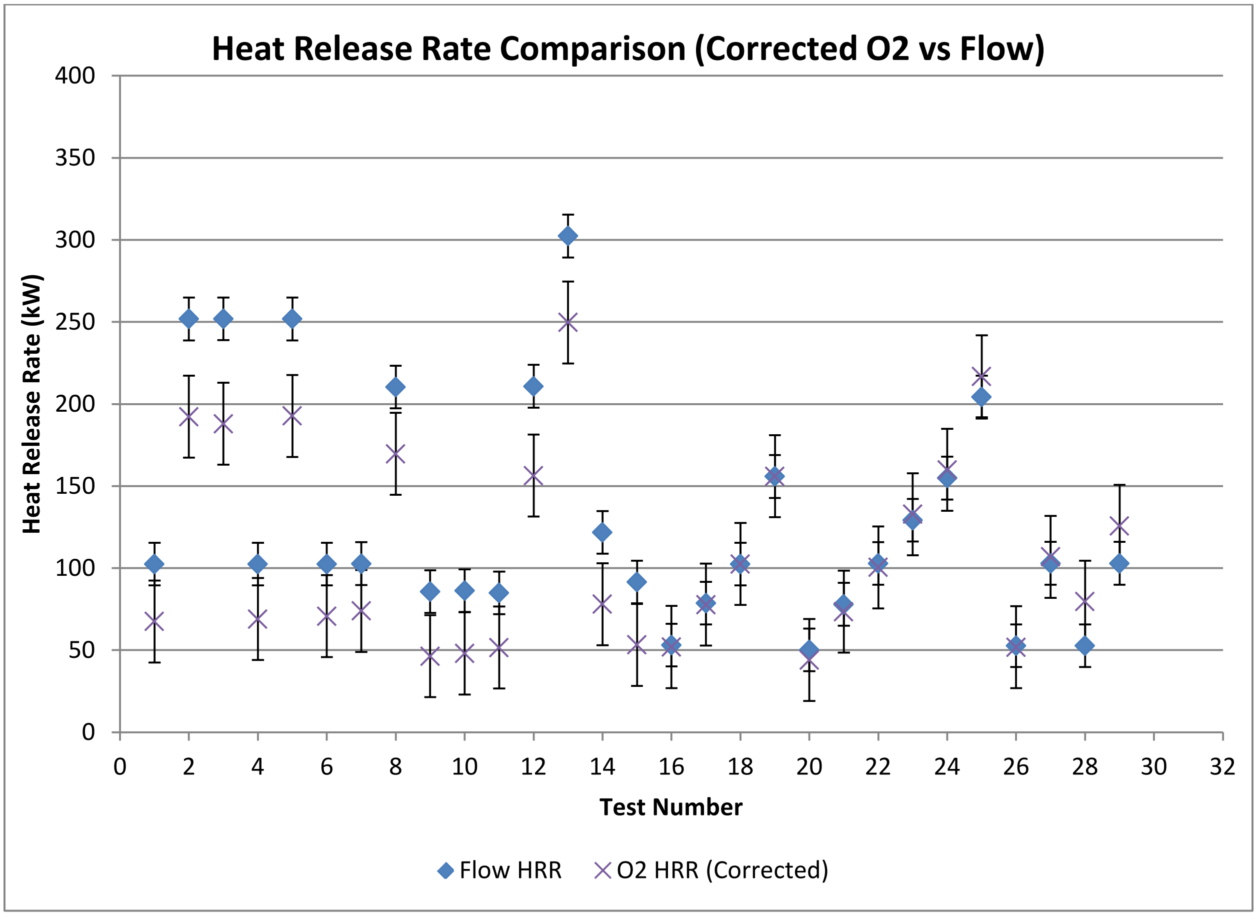

Figure 10 - Corrected O2 vs Flow HRR of all tests

To see the correlation between the O2 HRR and the Flow HRR, they are graphed together on Figure 11. The slope of the trendline shows an overestimation in part of the O2 HRR. The data spread is quite wide.

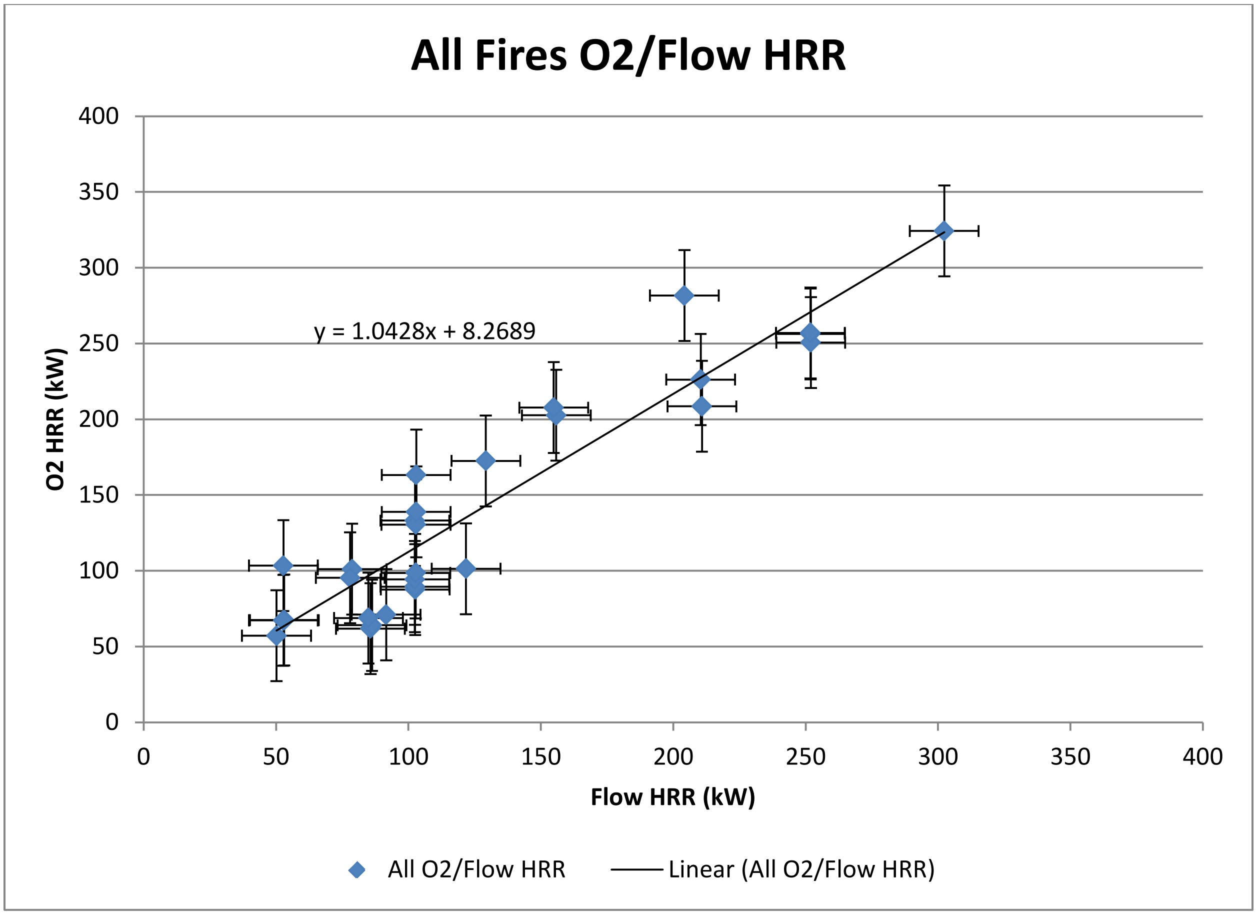

Figure 11 – O2 and Flow HRR correlation

To see the correlation between the CO/CO2 HRR and the Flow HRR, they are graphed together on Figure 12. The slope of the trendline shows an underestimation on the part of the CO/CO2 HRR. Again, the data spread is quite wide.

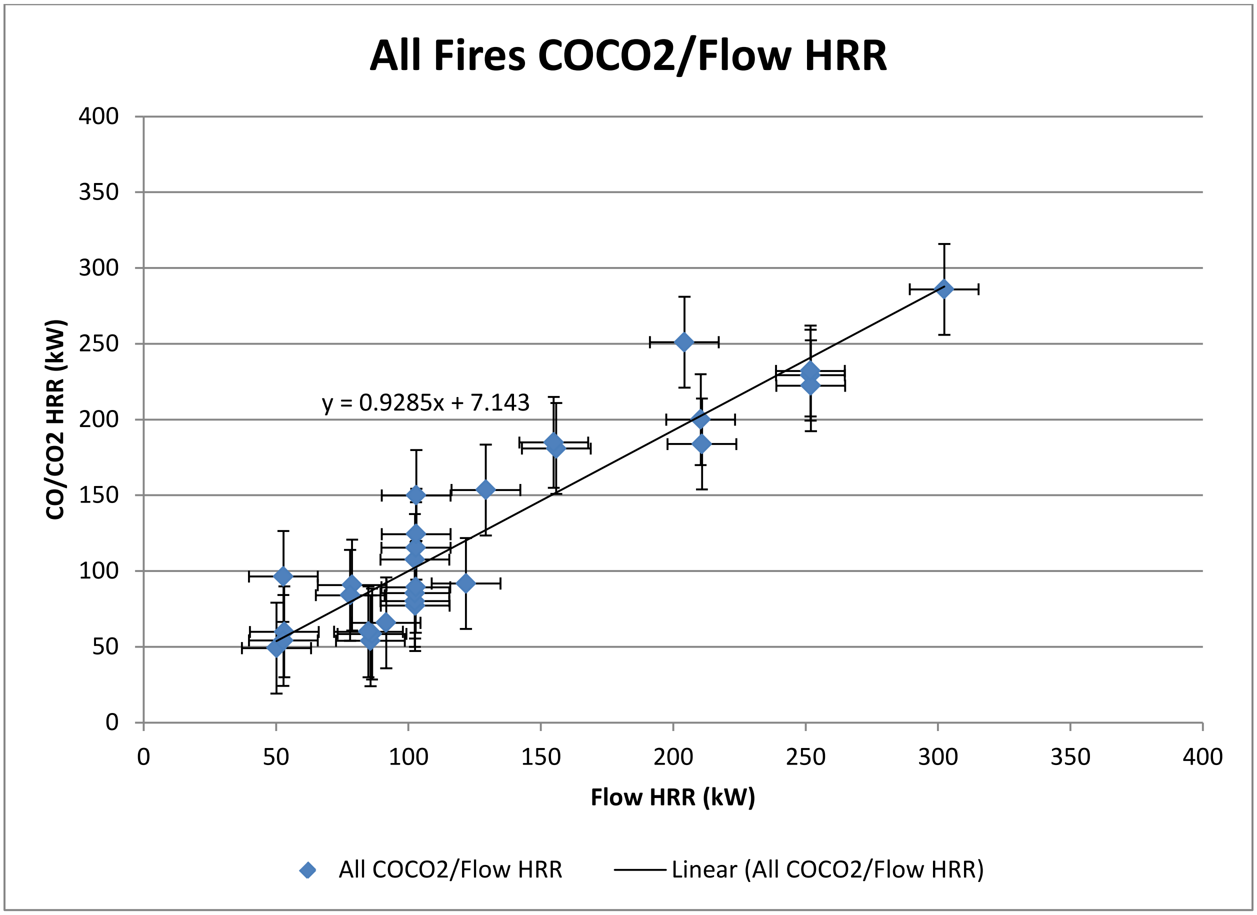

Figure 12 – CO/CO2 and Flow HRR correlation

To see the correlation between the corrected O2 HRR and the Flow HRR, they are graphed together on Figure 13. The slope of the trendline shows an underestimation on the part of the corrected O2 HRR. Again, the data spread is quite wide.

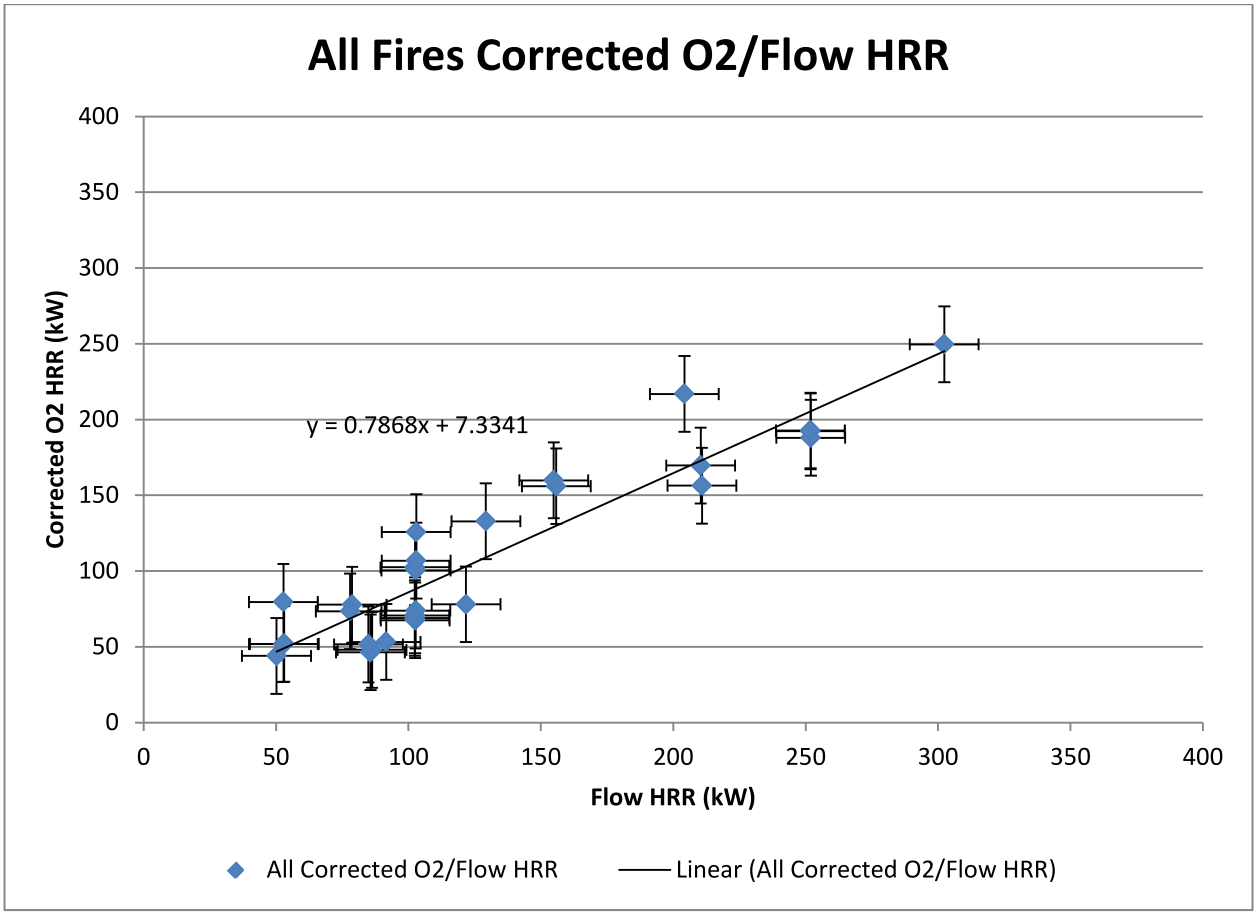

Figure 13 – Corrected O2 and Flow HRR correlation

To see the correlation between the corrected O2 HRR and the CO/CO2 HRR, they are graphed together on Figure 14. The slope of the trendline shows an overestimation on the part of the O2 HRR, however, the data spread is quite tight, meaning a good correlation between these 2 sets of data.

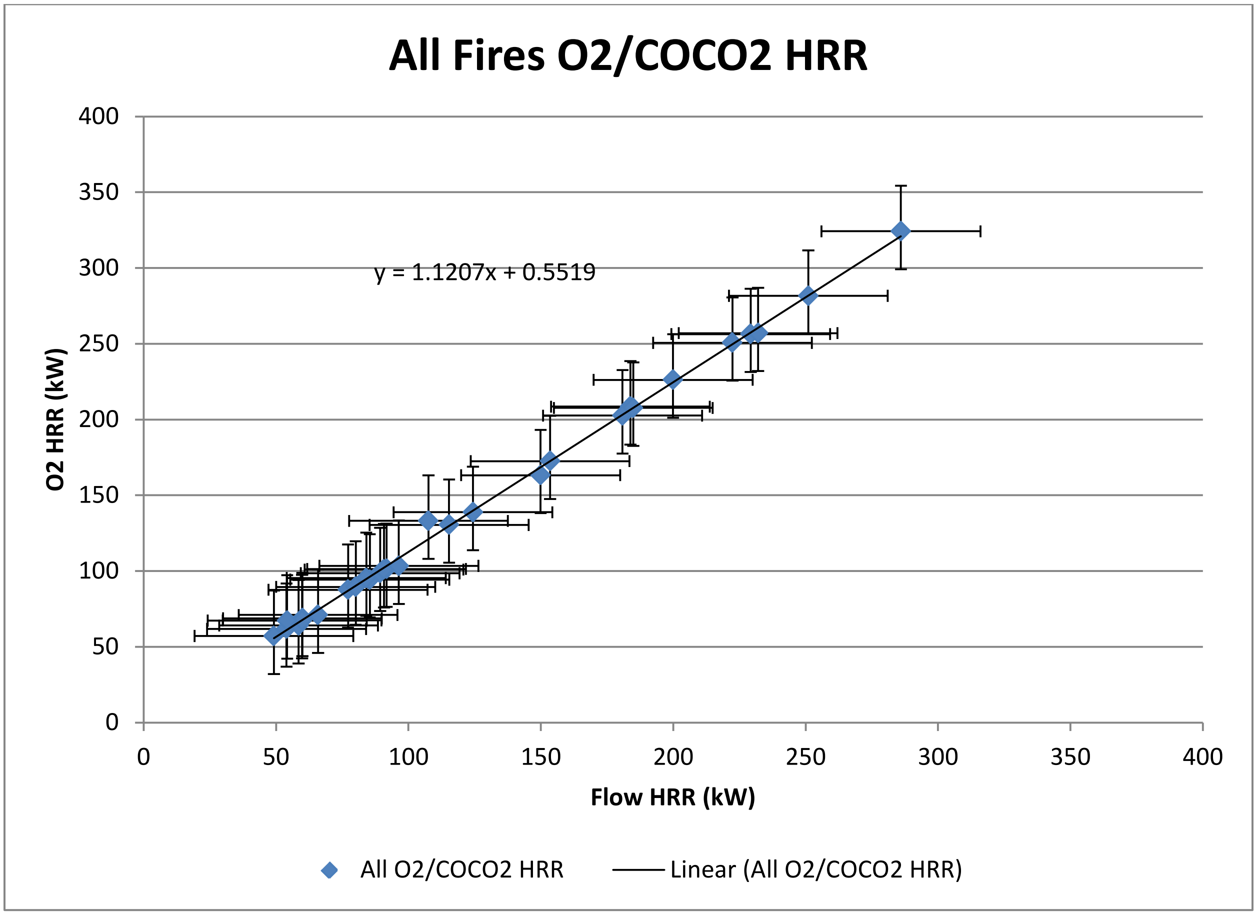

Figure 14 – O2 and CO/CO2 HRR correlation

Correlation between the corrected O2 HRR and the CO/CO2 HRR is shown in Figure 15. The slope of the trendline shows an underestimation on the part of the corrected O2 HRR, however, the data spread is quite tight, meaning a good correlation between these two sets of data.

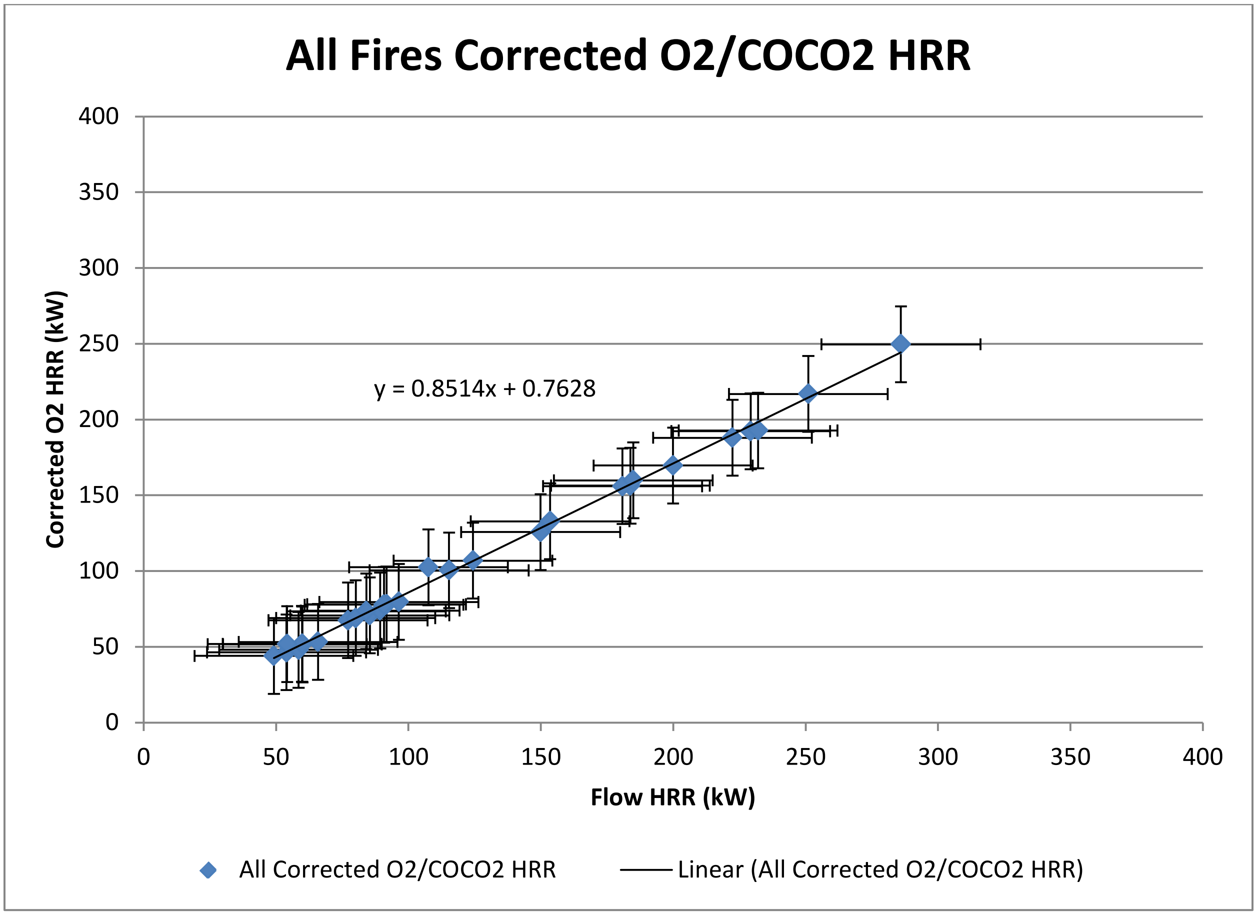

Figure 15 – Corrected O2 and CO/CO2 HRR correlation

Based on the presentation of data from Figure 7 to Figure 10, there seem to be a major difference between the HRR data from before and after the MFC calibration. Though repairing the O2 analyzer might also have an effect, it is hard to see it because of the smaller number of comparable tests available for analysis. So based on these events, the propane fire data can be separated into pre- and post- “O2 analyzer fixed and MFC recalibrated”groups, and the propylene fire data can be separated into pre- and post- “O2 analyzer recalibrated” groups.

Figure 16 to Figure 18 shows the before and after “O2 analyzer fix and MFC recalibrated” groups of the propane fire data. The “before” data shows good correlation for the O2 and CO/CO2 vs Flow HRR, the “after” data shows good correlation for the corrected O2 vs Flow HRR. The effect of having the analyzer fixed and MFC calibrated seems to cause overestimation of the LODS-measured HRR over the calculated Flow HRR.

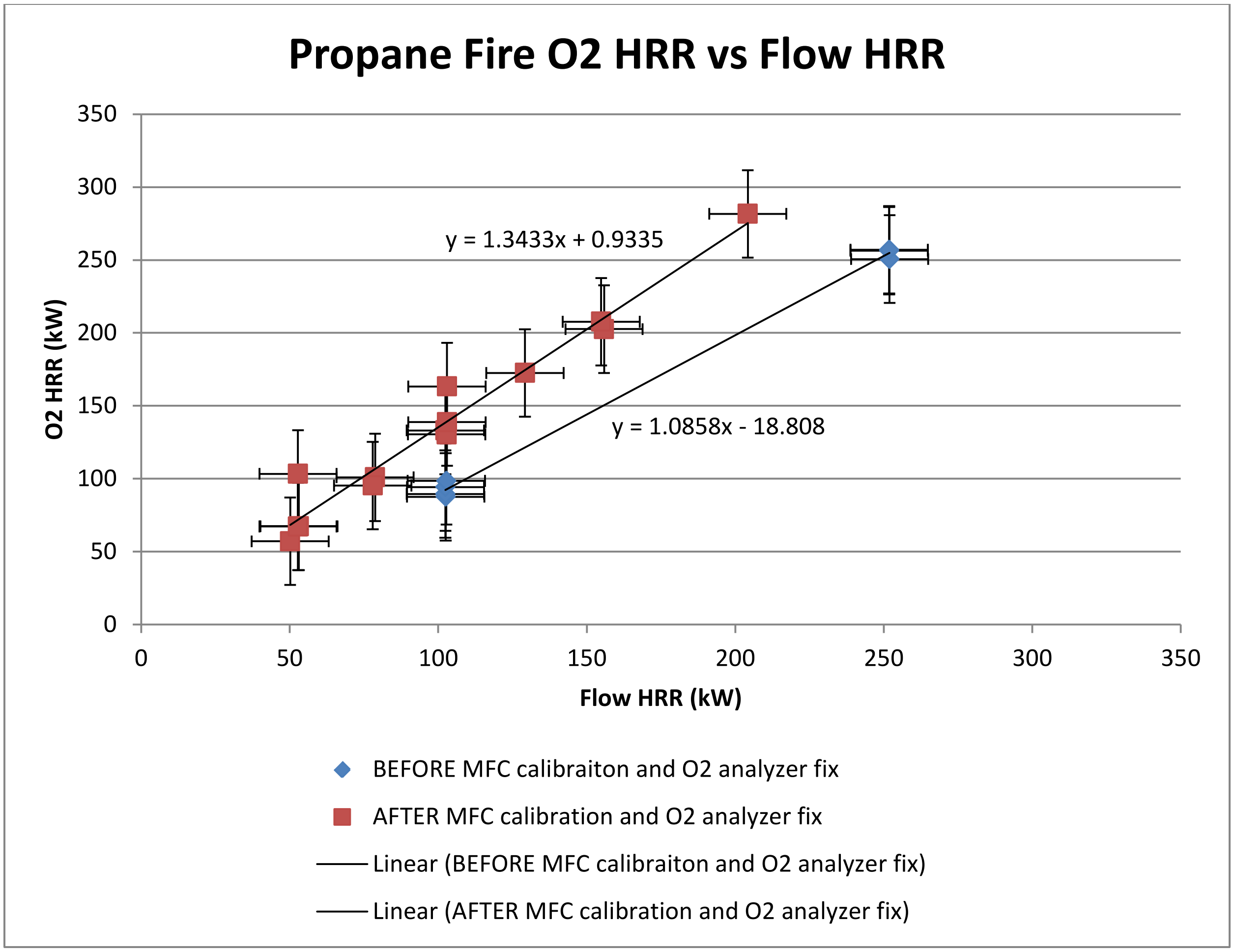

Figure 16 - Propane fires O2 vs Flow HRR

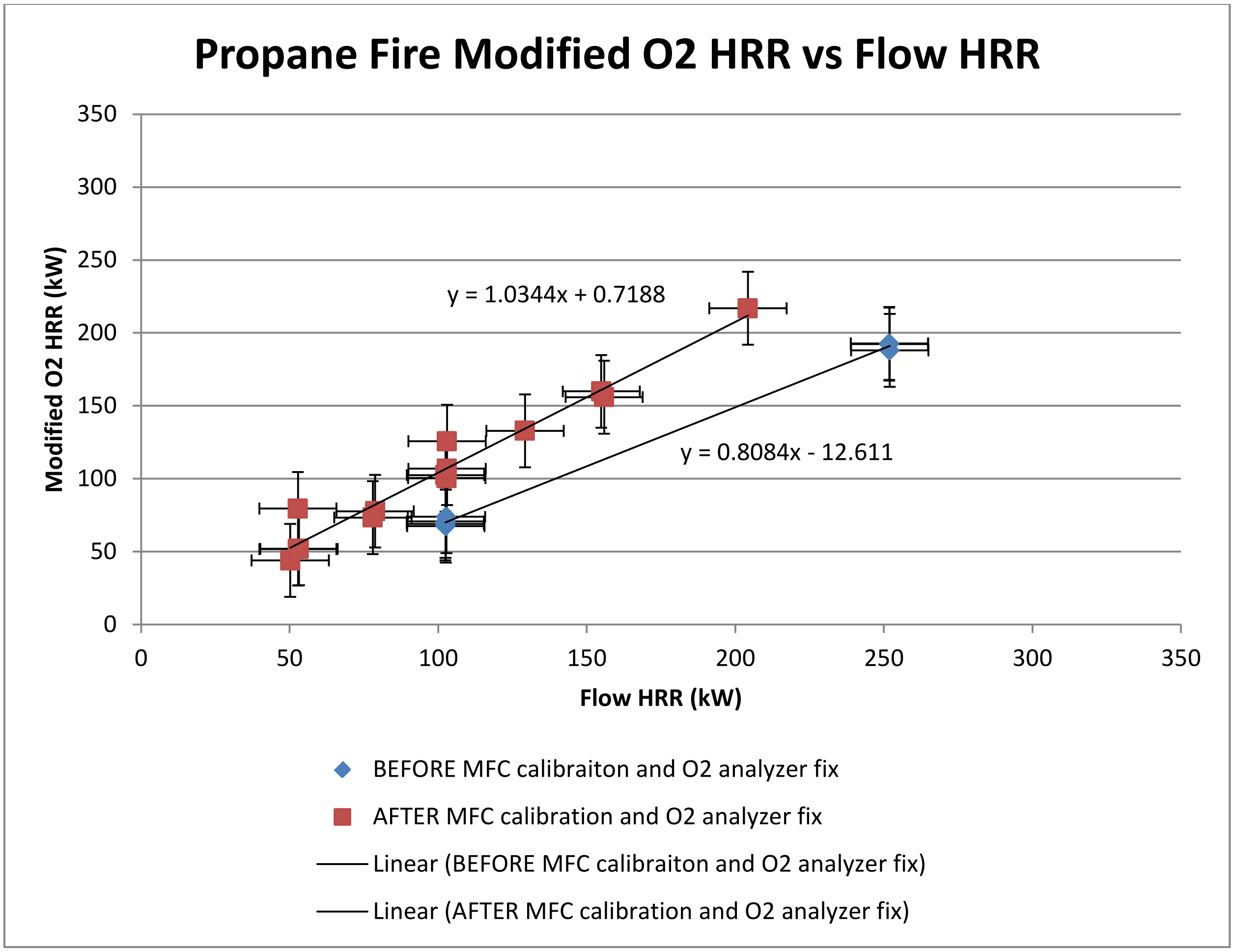

Figure 17 - Propane fires corrected O2 vs Flow HRR

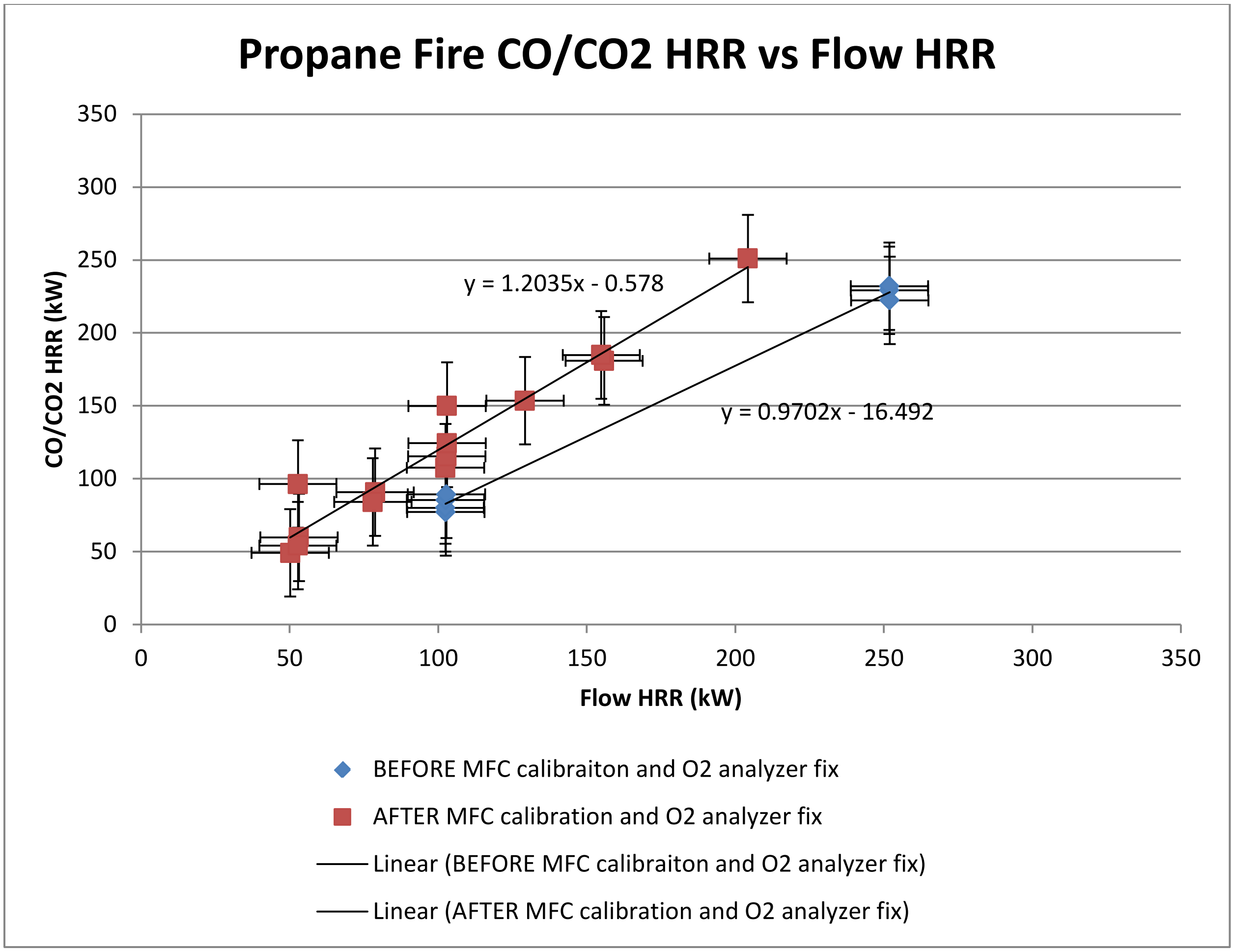

Figure 18 - Propane fires CO/CO2 vs Flow HRR

Figure 19 and Figure 20 shows the O2 and corrected O2 HRR vs CO/CO2 HRR. The spread of the data is tight, and the repair and recalibration did not seem to have an effect here, most likely due to the fact that the calculation of these HRRs are largely affected by the amount of oxygen measured.

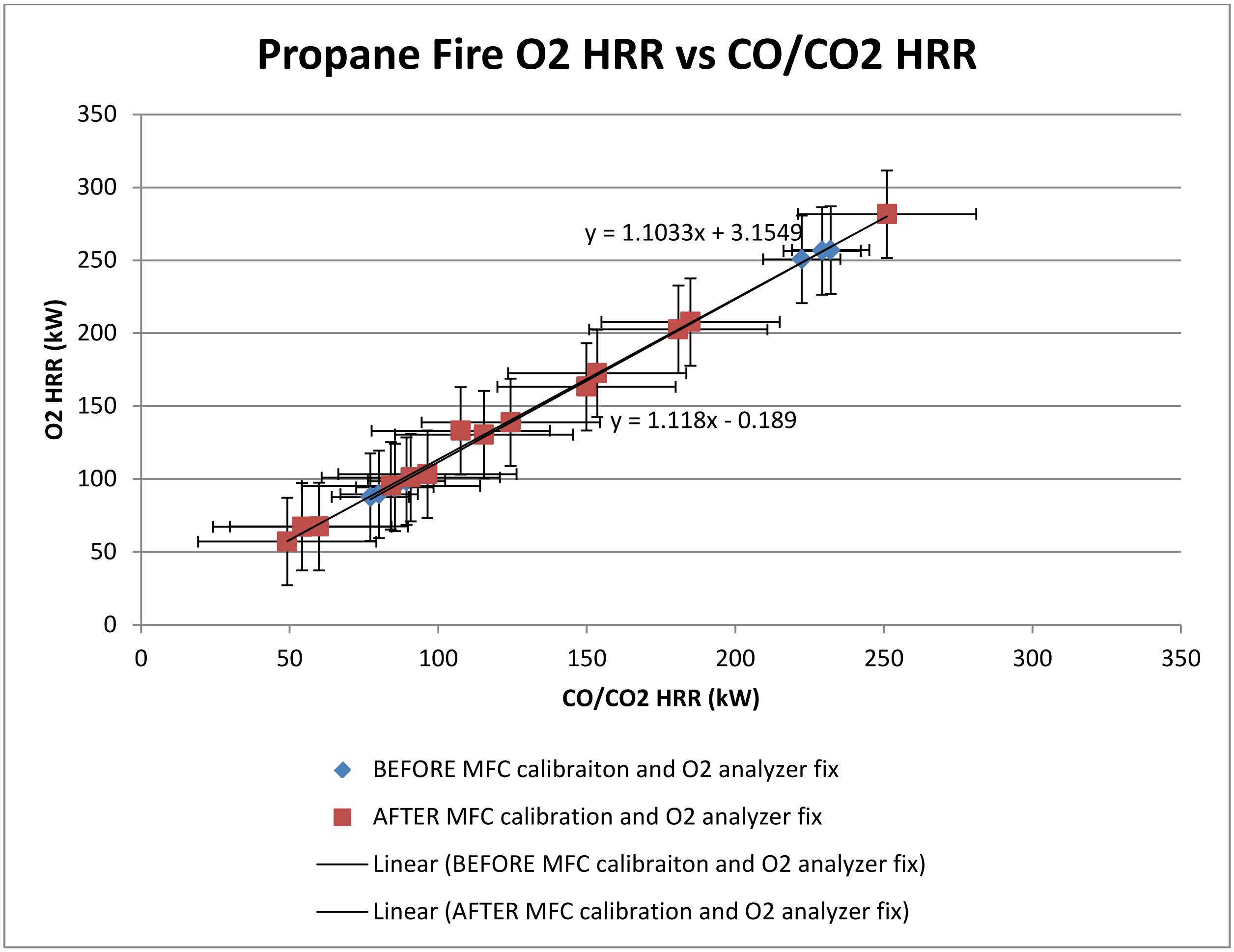

Figure 19 - Propane fires O2 vs CO/CO2 HRR

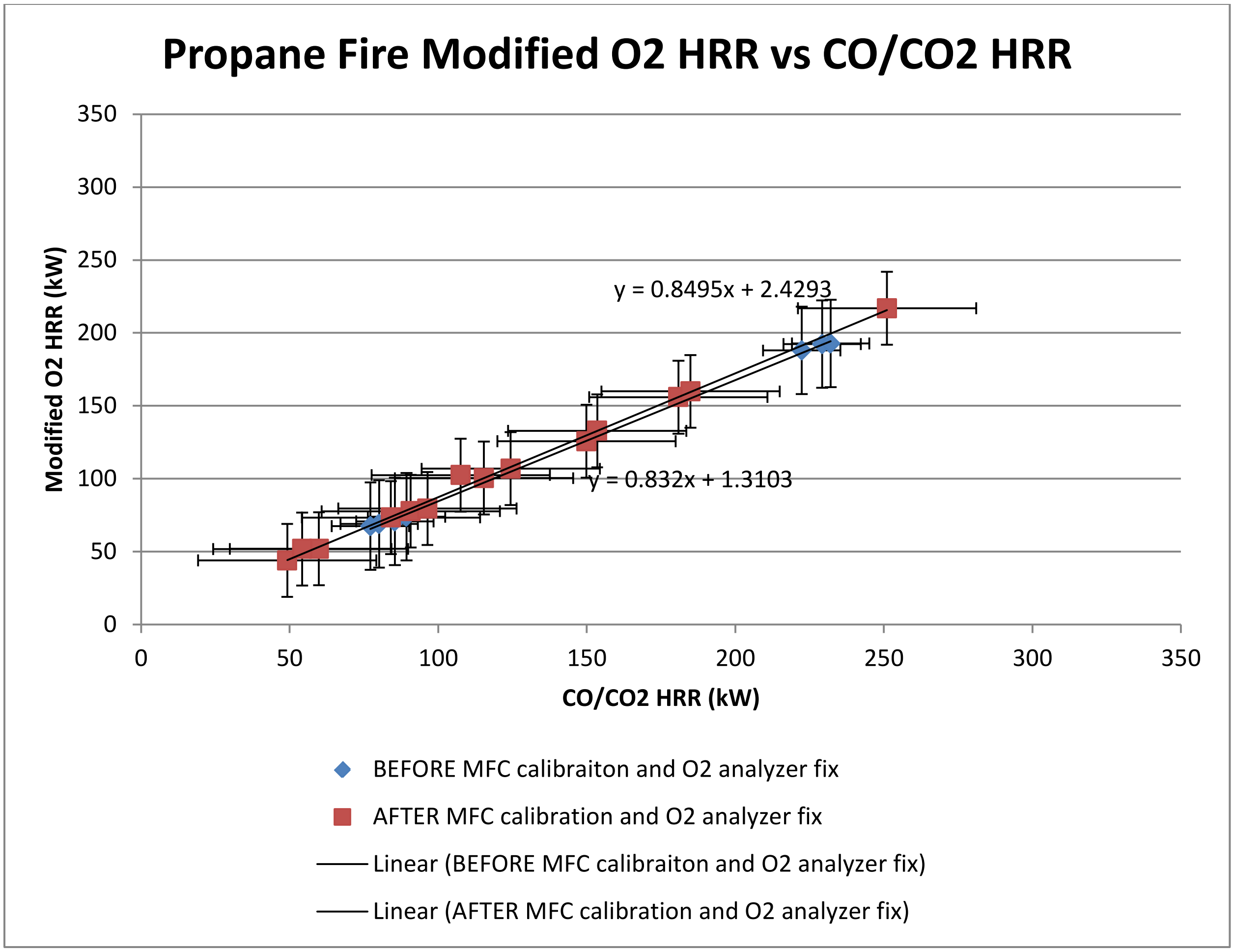

Figure 20 - Propane fires corrected O2 vs CO/CO2 HRR

Figure 21 to Figure 23 shows the before and after "O2 analyzer fixed" groups of the propylene fire data. The "before" and "after" data both show good correlation and there are little changes in the slope of the trendlines. This suggests that just fixing the O2 analyzer did not altered the behavior of the measured HRR much.

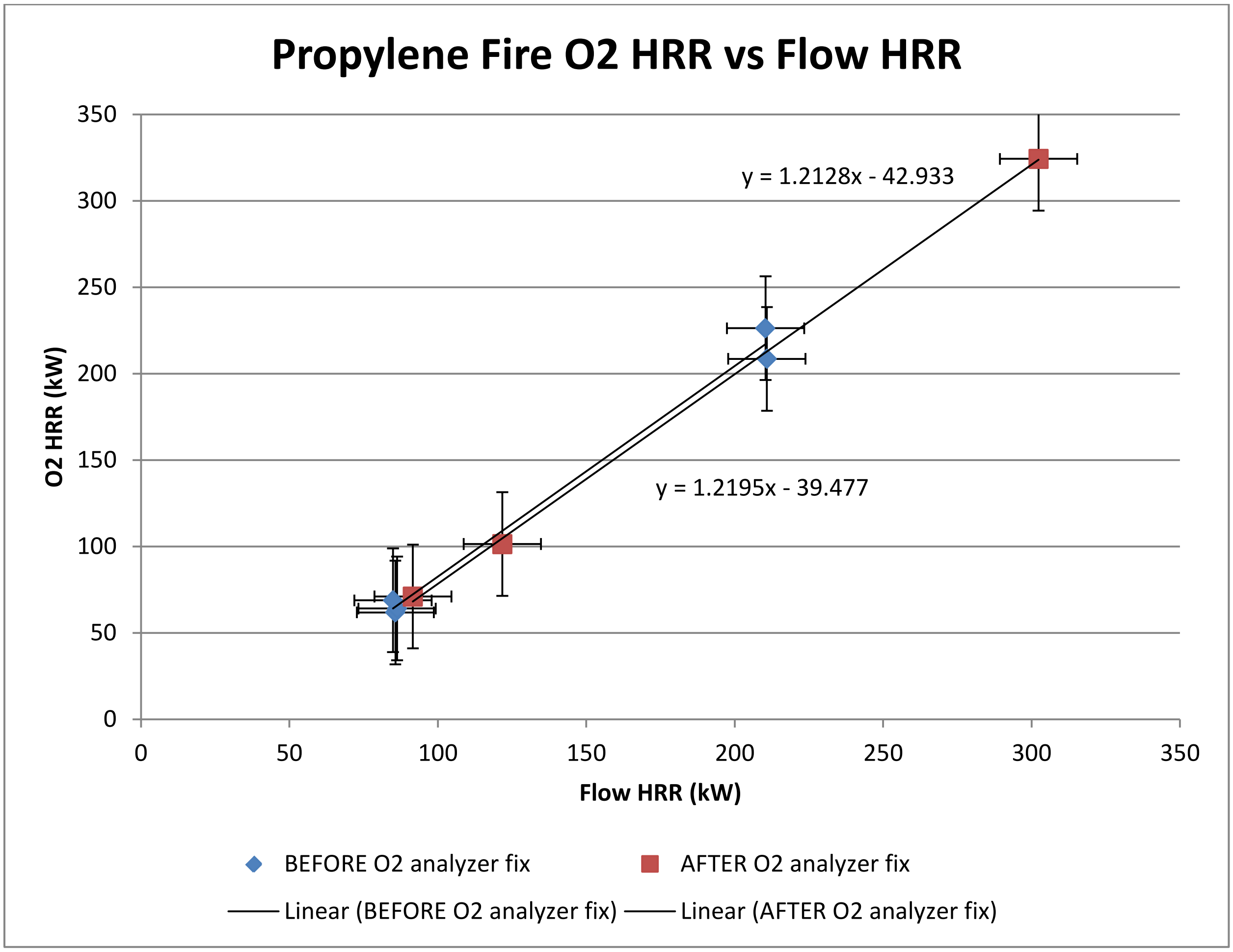

Figure 21 – Propylene fires O2 vs Flow HRR

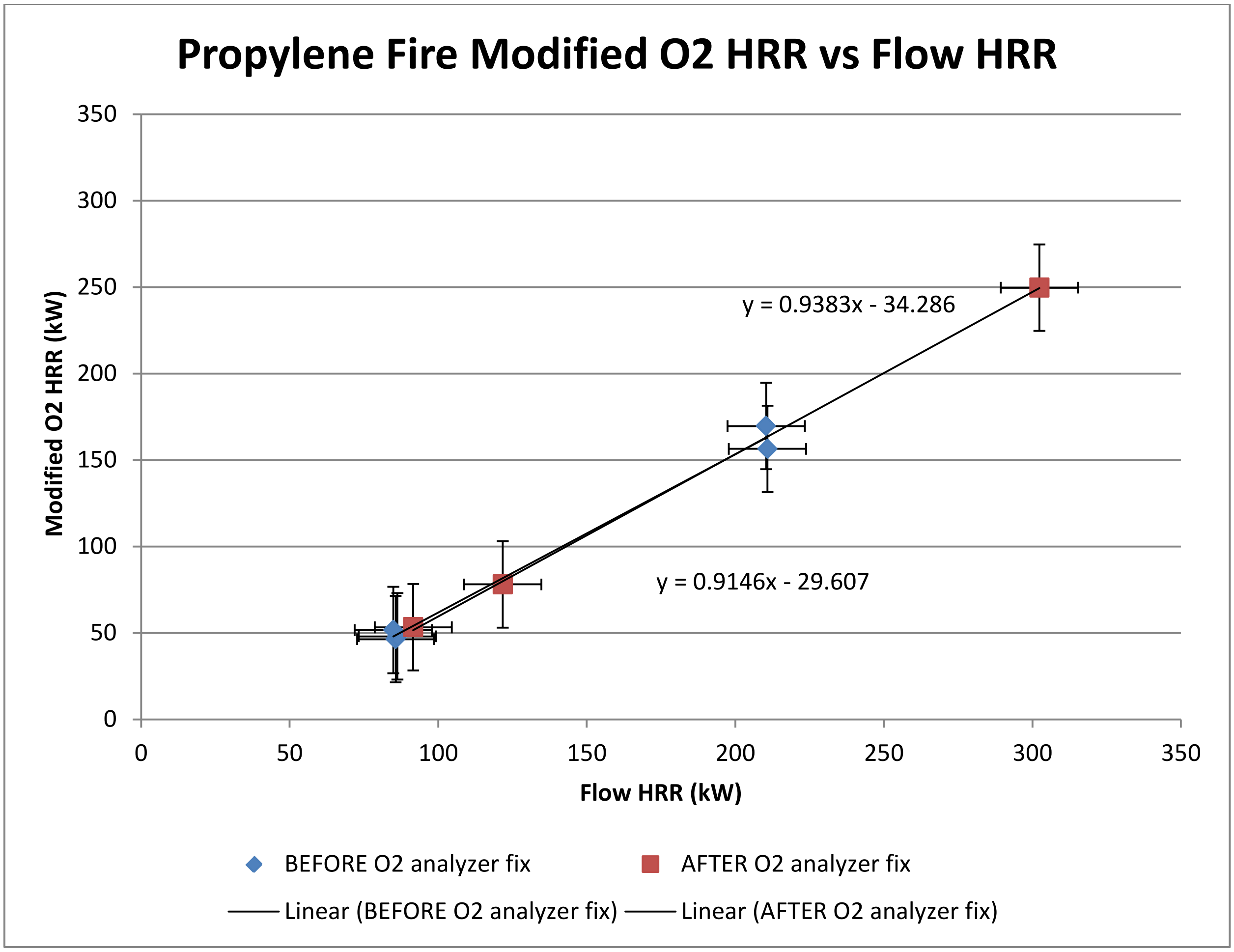

Figure 22 - Propylene fires corrected O2 vs Flow HRR

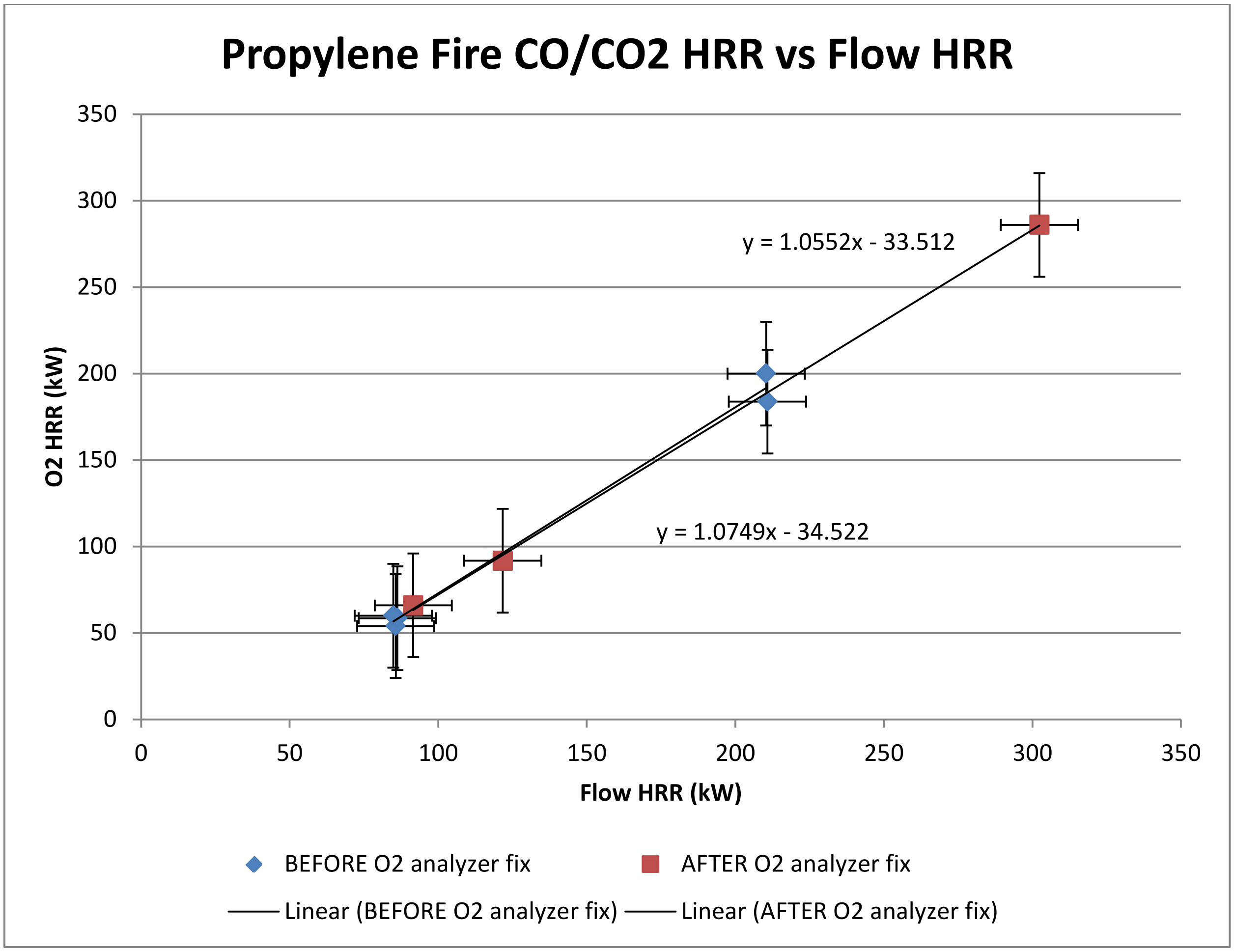

Figure 23 - Propylene fires CO/CO2 vs Flow HRR

Figure 24 and Figure 25 shows the O2 and corrected O2 HRR vs CO/CO2 HRR for the propylene fires.

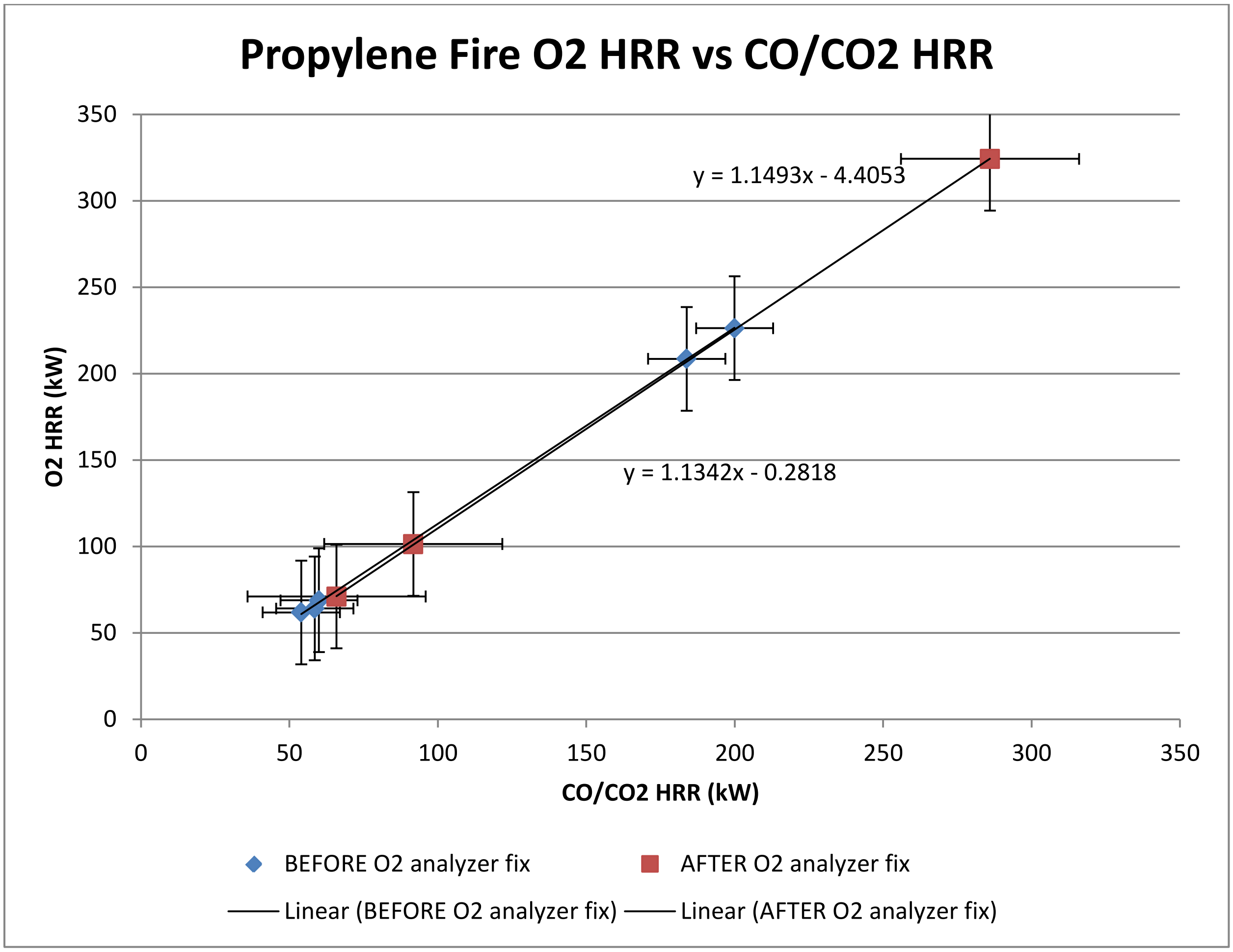

Figure 24 - Propylene fires O2 vs CO/CO2 HRR

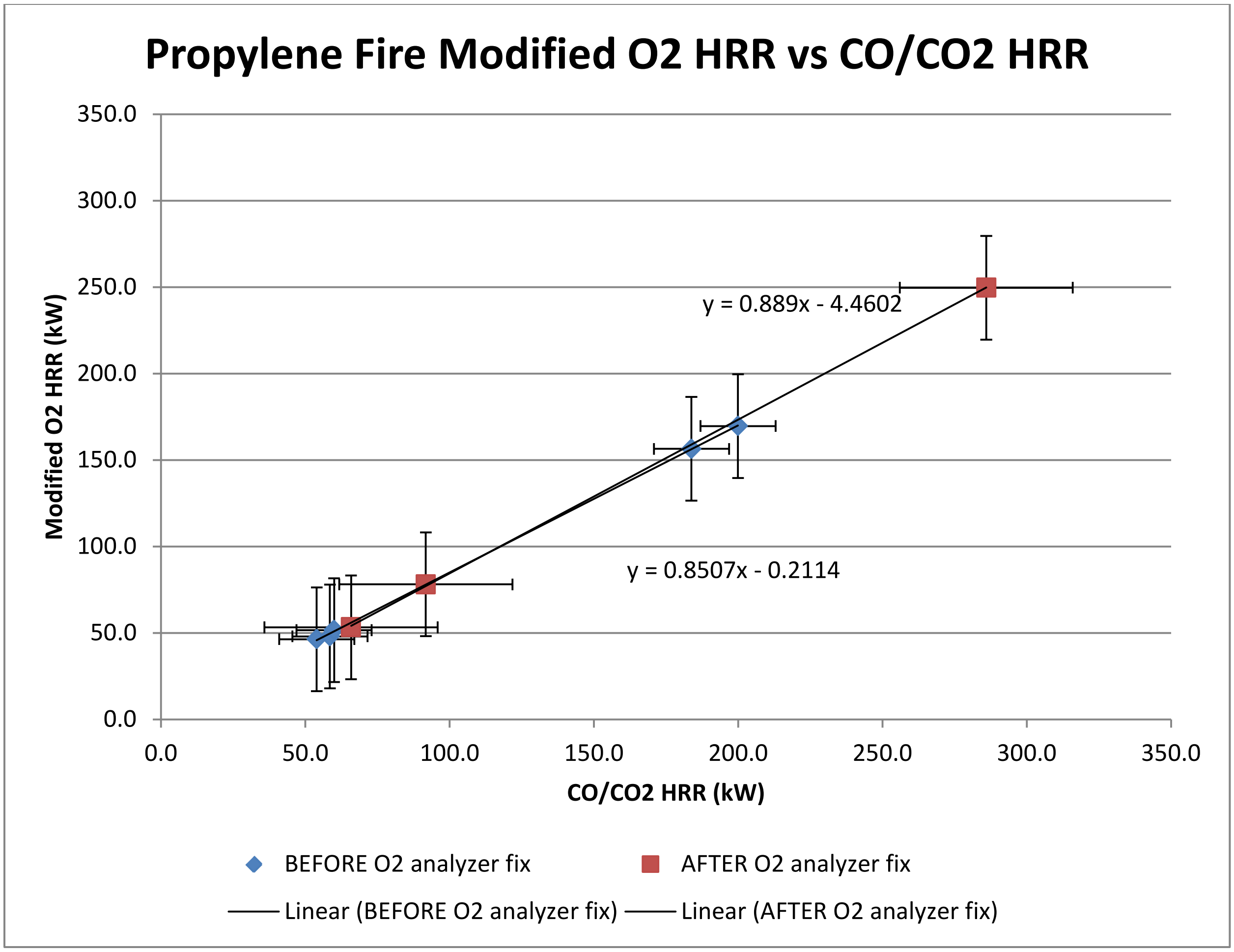

Figure 25 - Propylene fires corrected O2 vs CO/CO2 HRR

D.1.2 Free Plume and Inert Wall Experiment HRR Analysis

In the plume and inert wall fire tests, the heat release rates were measured via the fuel flow controller, oxygen consumption calorimetry, and carbon monoxide/carbon dioxide generation calorimetry. In the combustible wall fire tests, the HRR of the source fire was calculated from the measured mass flow rate, whereas the overall fire HRR was measured through oxygen consumption calorimetry.

The mass flow rate through the flow controller was recorded during each test and used to calculate the HRR, it is assumed to be the most accurate method available in the lab because the system was recently factory-calibrated. A correction factor of 77% was applied to the O_2-based HRR as previously established via methane calibration and propane flow calibration. Details of the calibration are shown in Section D.1.1.

The HRR measurement uncertainties were established for the different HRR measurement methods, and are presented in Table 6. The details of the uncertainty calculations are presented in D.1.1.

Table 6 - Heat release rate uncertainties

HRR Method	Uncertainty [kW]
Flow	13.0
O2 Corrected	25.0
CO/CO2	30.0
Mass Loss	1.1
O2, no correction	30.0

The following data are taken in the recent baseline test series. Experiments were conducted using an 1 ft Square burner and a 2 ft x 1 ft Rectangle burner. The burners were located centrally in the compartment for plume tests, and against the false wall for the inert wall tests. Propane and propylene were used and were set to produce fires at approximately 50 to 75 kW. A total of 70 tests were conducted and their HRRs are presented in Figure 26. The Flow HRRs are close to the 50 and 75 kW marks, the O_2 HRRs sometimes predict higher and other time lower, but all of the CO/CO_2 HRRs are higher than the other two sets of HRR.

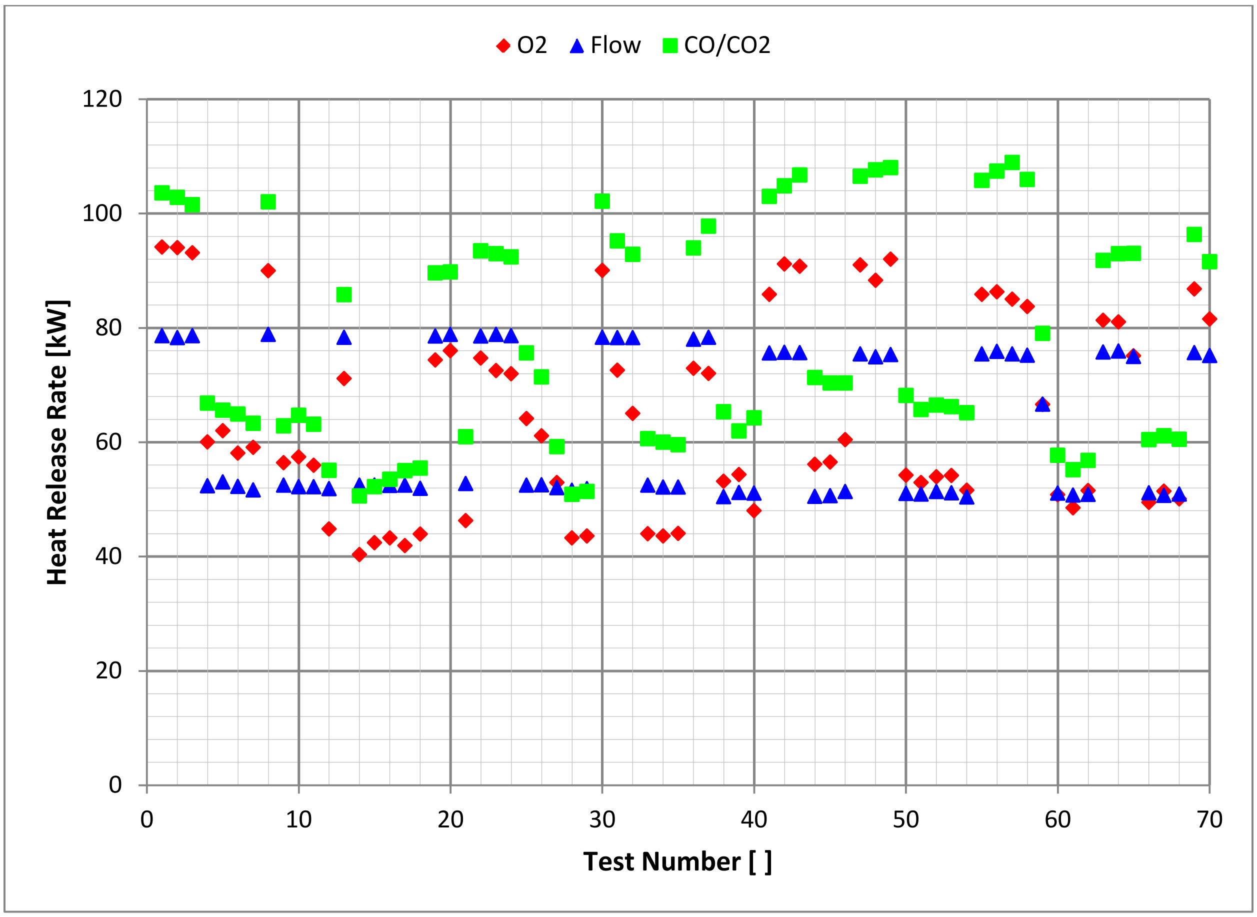

Figure 26 - Recorded HRRs from all three methods

Figure 27 shows the O_2 and Flow HRR graphed with uncertainties. The Flow HRRs are all close to the intended 50 and 75 kW, however, there are more variation in the O_2 HRRs. This is not surprising since the uncertainty of the O_2 HRR is almost twice as large as the Flow HRRs. Nonetheless, the values are all within each other's uncertainties and should both be valid.

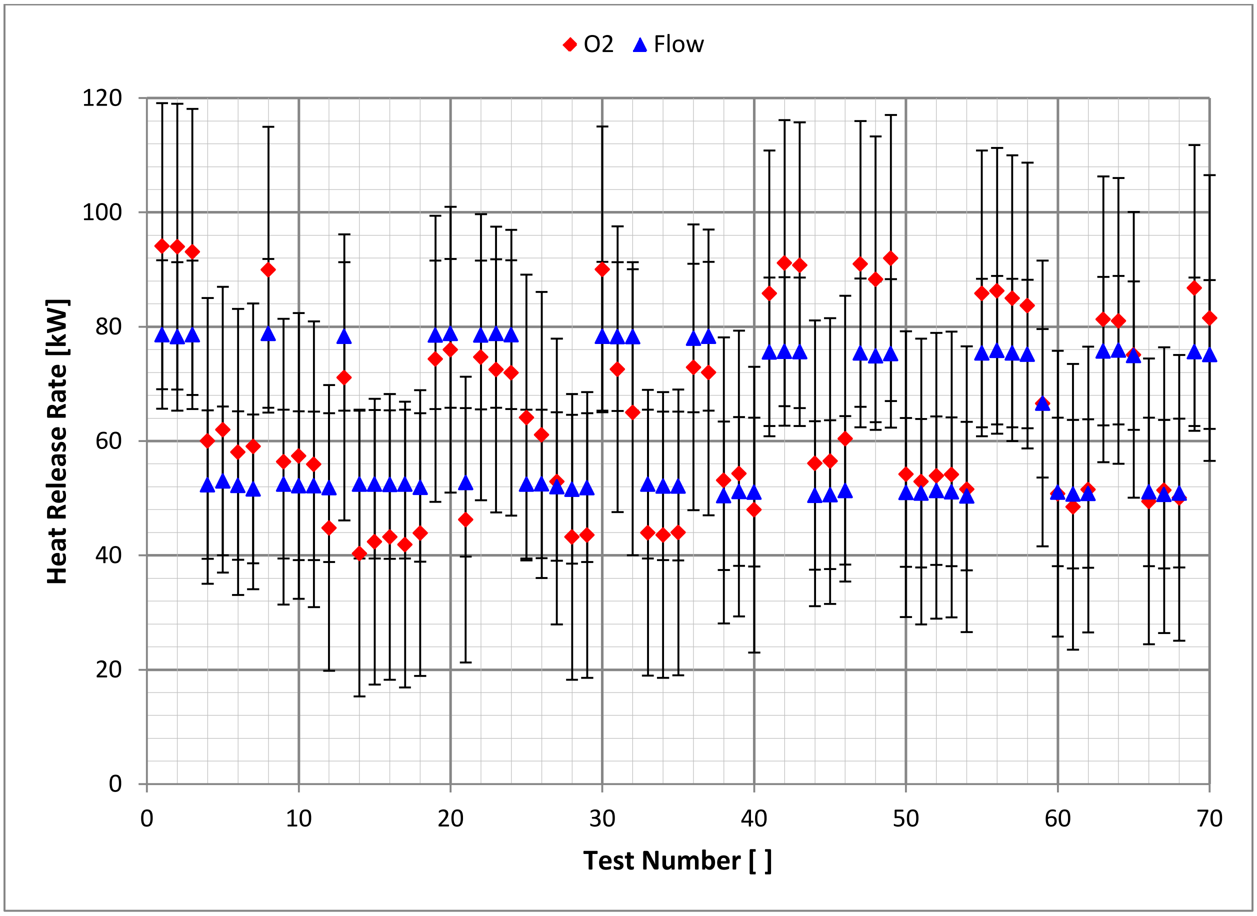

Figure 27 - O2-based and Flow-based HRR comparisons, with uncertainties

The ratio between the O_2 and Flow HRR is presented in Figure 28. The O_2 HRRs are within ±21% of the true (flow) HRRs. The average ratio across all tests is about 1.03, meaning that the O_2 HRRs can be expected to be at least 3% over the Flow HRRs.

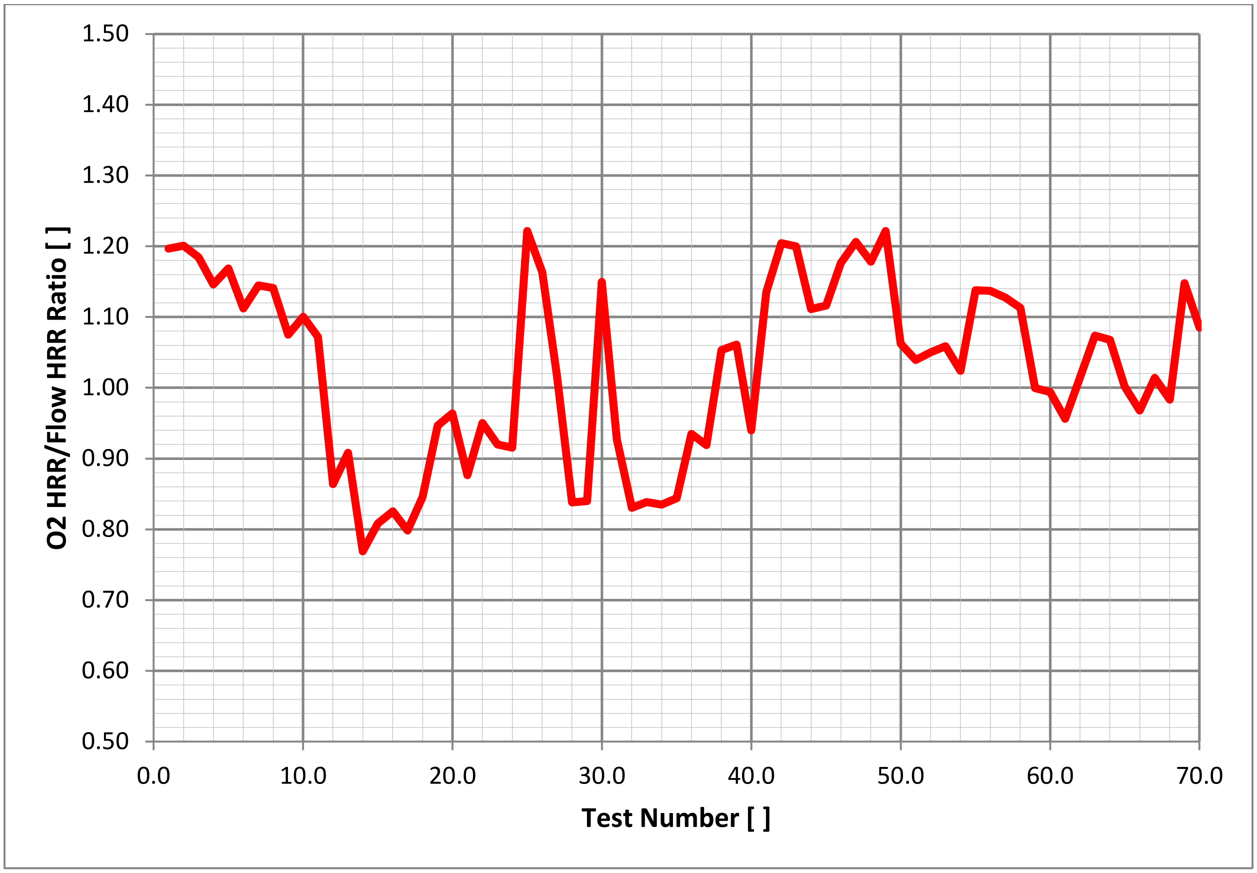

Figure 28 - O2/Flow HRR Ratio

The O_2 HRRs are plotted against the Flow HRRs along with a fitted line in Figure 29, all of the data falls within range of the error bars and the fitted line, which suggests a good correlation of the data.

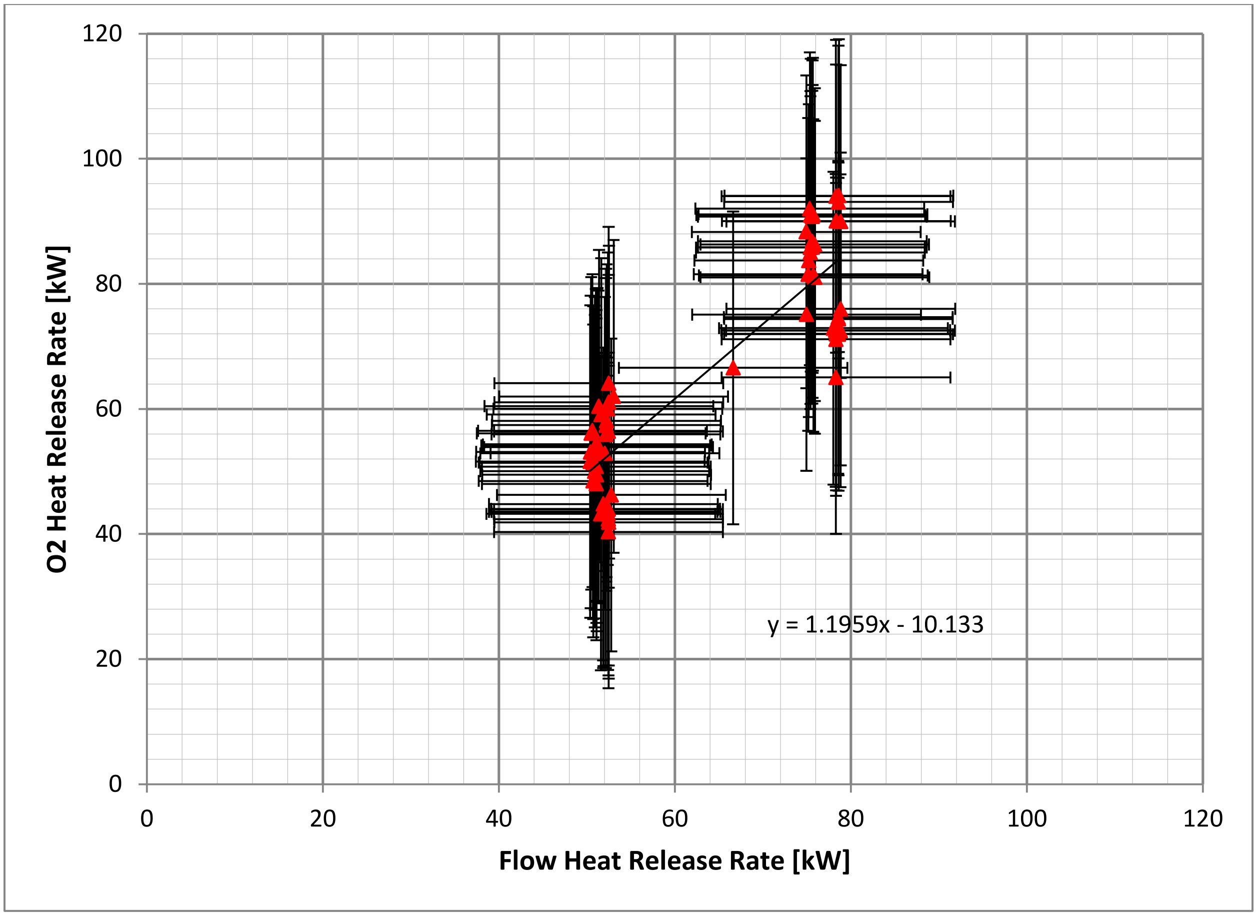

Figure 29 - O2-based HRR vs Flow-based HRR, with uncertainties

Figure 30 shows that the CO/CO_2 and the Flow HRRs all fall within each other's uncertainty. Most of the CO/CO_2 HRRs over-predict by a relatively large margin with the exceptions of a few tests at 50 kW where the deviation is very small.

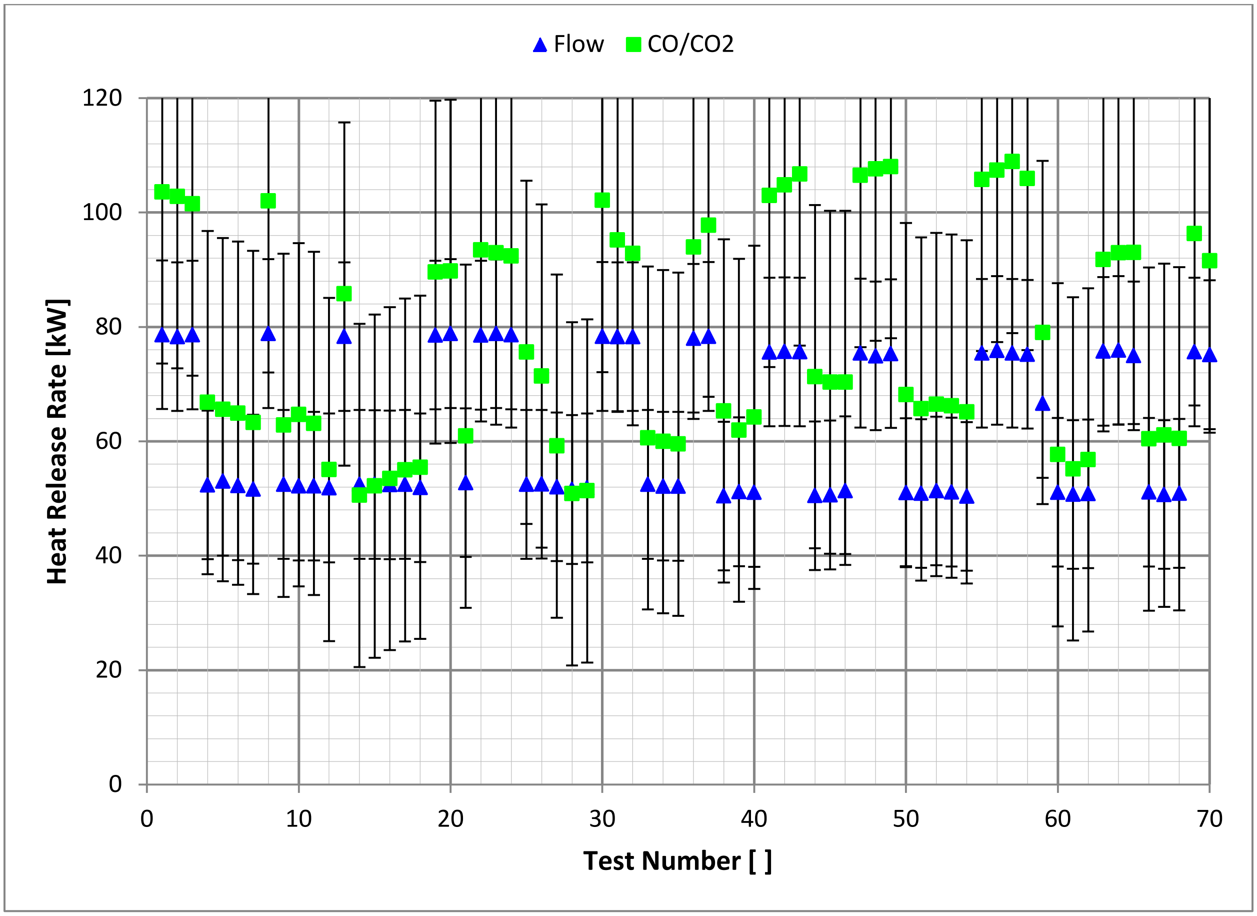

Figure 30 - CO/CO2-based and Flow-based HRR comparisons, with uncertainties

The ratio between the CO/CO_2 and Flow HRR is presented in Figure 31. The CO/CO_2 HRRs over-predict the true (Flow) HRRs by up to 45% in a few instances. There are only 3 cases of under-prediction by the CO/CO_2 by a few percents. The average ratio across all tests is about 1.23, meaning that the CO/CO_2 HRRs can be expected to be at least 23% over the Flow HRRs. This suggests that there might be a systematic error in the CO/CO_2 HRR measurements and they should not be used without further analysis.

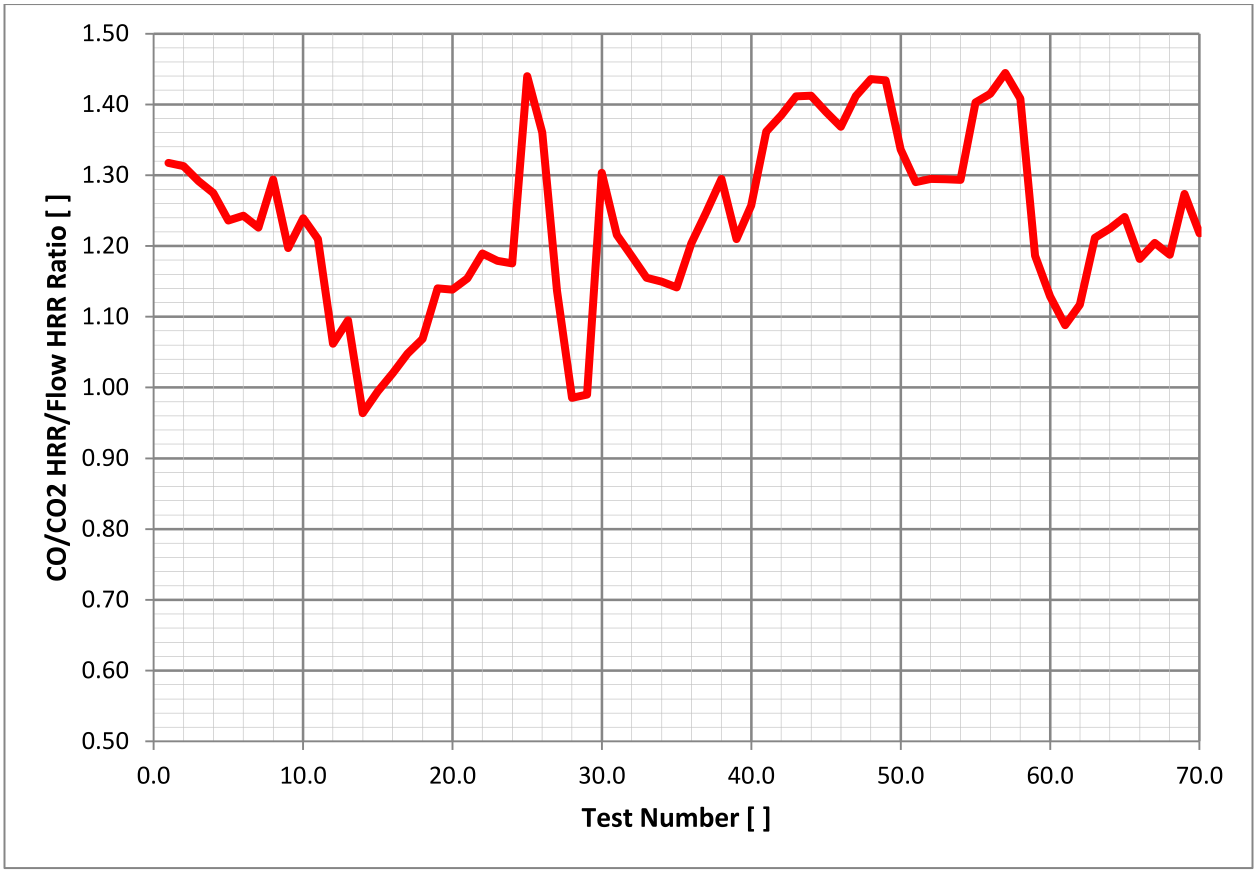

Figure 31 - CO2/Flow HRR Ratio

The CO/CO_2 HRRs are plotted against the Flow HRRs along with a fitted line in Figure 32, all of the data falls within range of the error bars and the fitted line, which suggests a good correlation of the data.

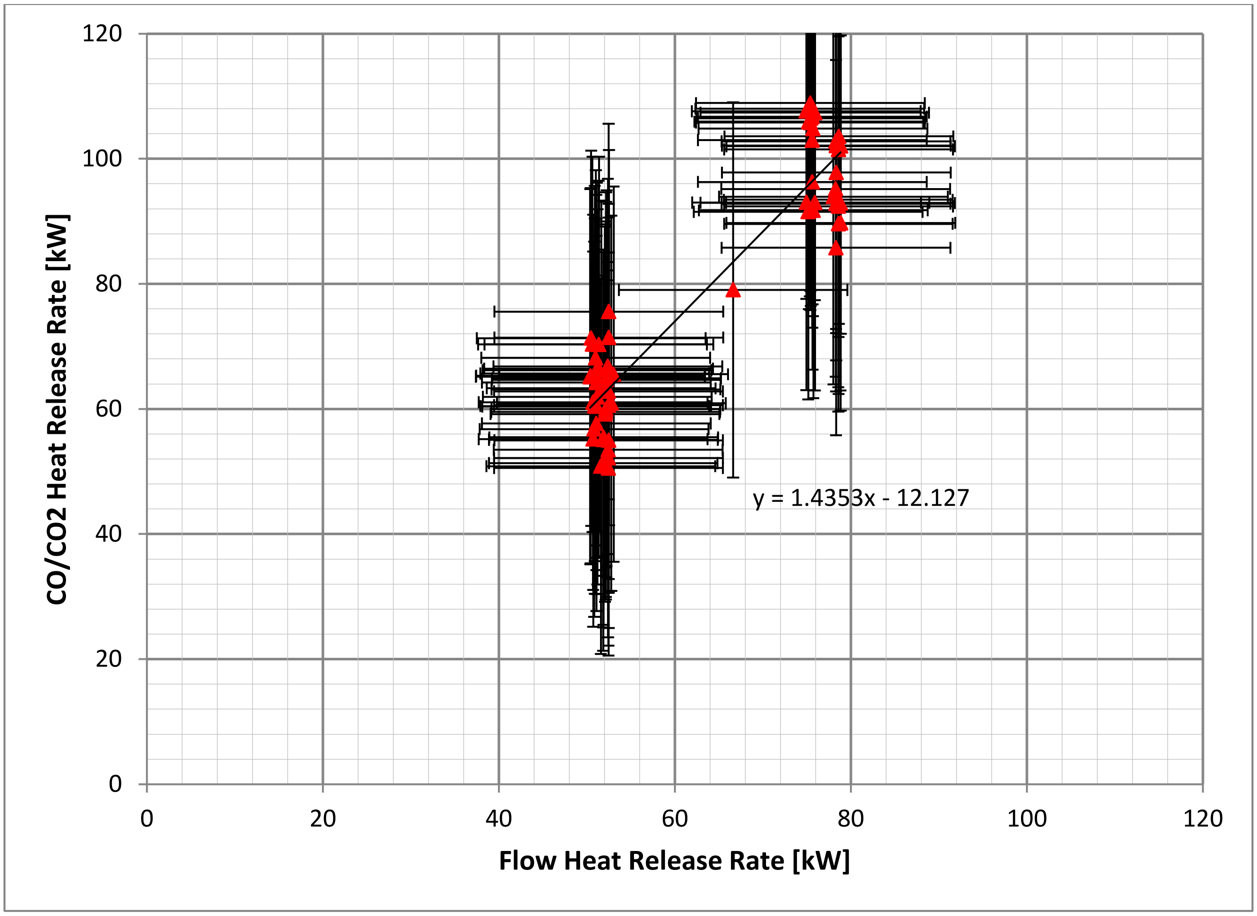

Figure 32 - CO/CO2-based HRR vs Flow-based HRR, with uncertainties

Figure 33 shows that the CO/CO_2 and the O_2 HRRs all fall within each other's uncertainty. All of the CO/CO_2 HRRs over-predict by a relatively large margin with the exceptions of a few tests at 50 kW where the deviation is very small.

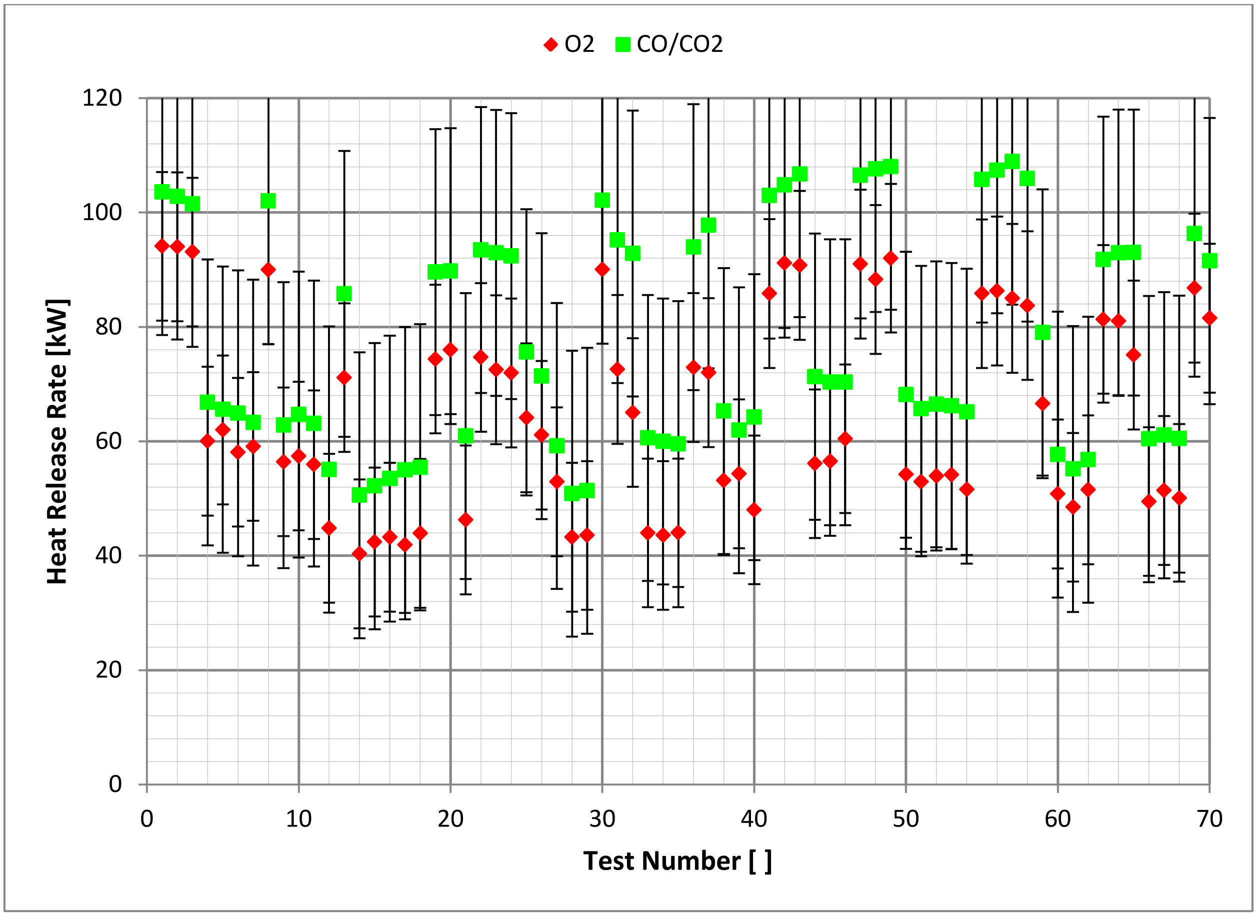

Figure 33 - O2-based and Flow-based HRR comparisons, with uncertainties

The ratio between the O_2 and CO/CO_2 HRR is presented in Figure 34. The average ratio is about 0.83, meaning that the O_2 HRRs are lower than the CO/CO_2 HRRs by about 27%.

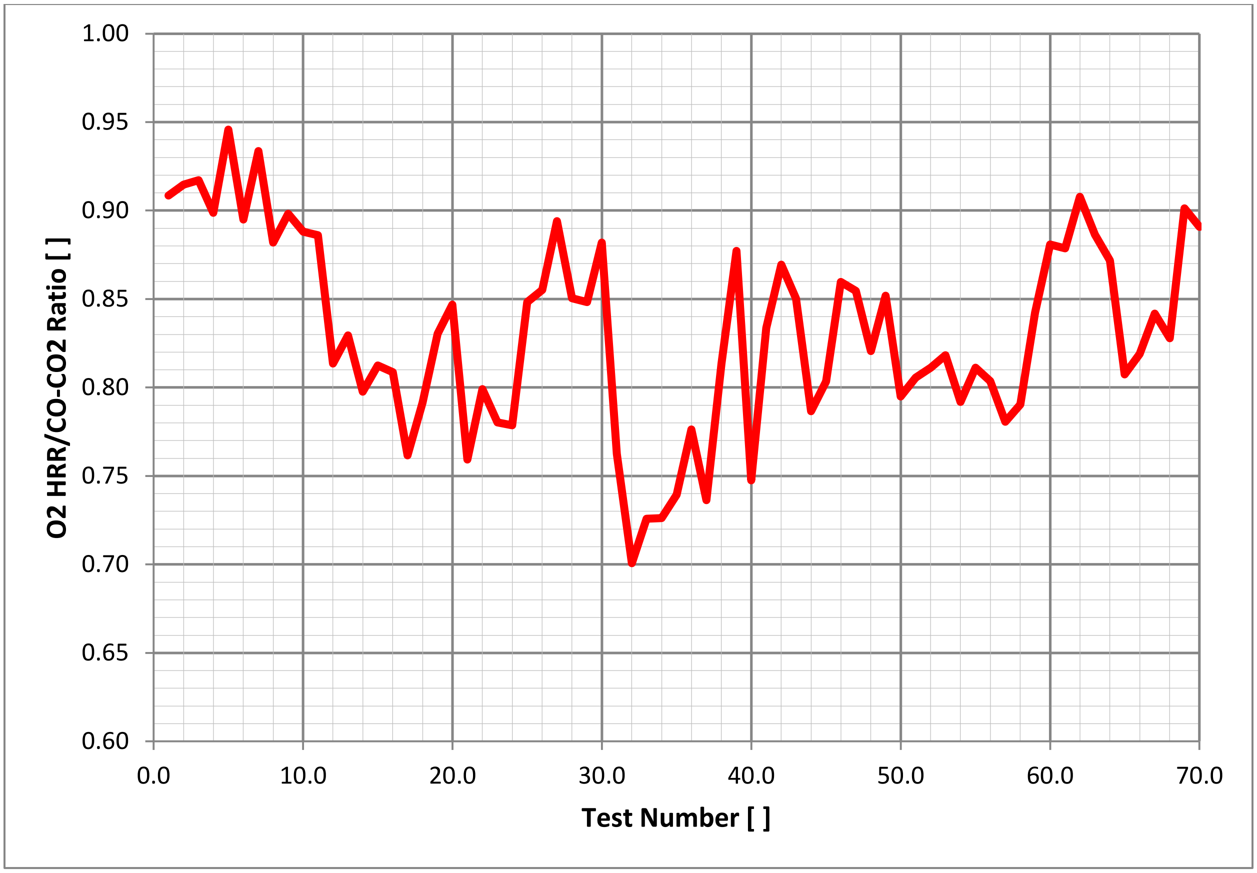

Figure 34 - CO-CO2/O2 HRR Ratio

The O_2 HRRs are plotted against the CO/CO2 HRRs along with a fitted line in Figure 35, all of the data falls within range of the error bars and the fitted line, which suggests a good correlation of the data.

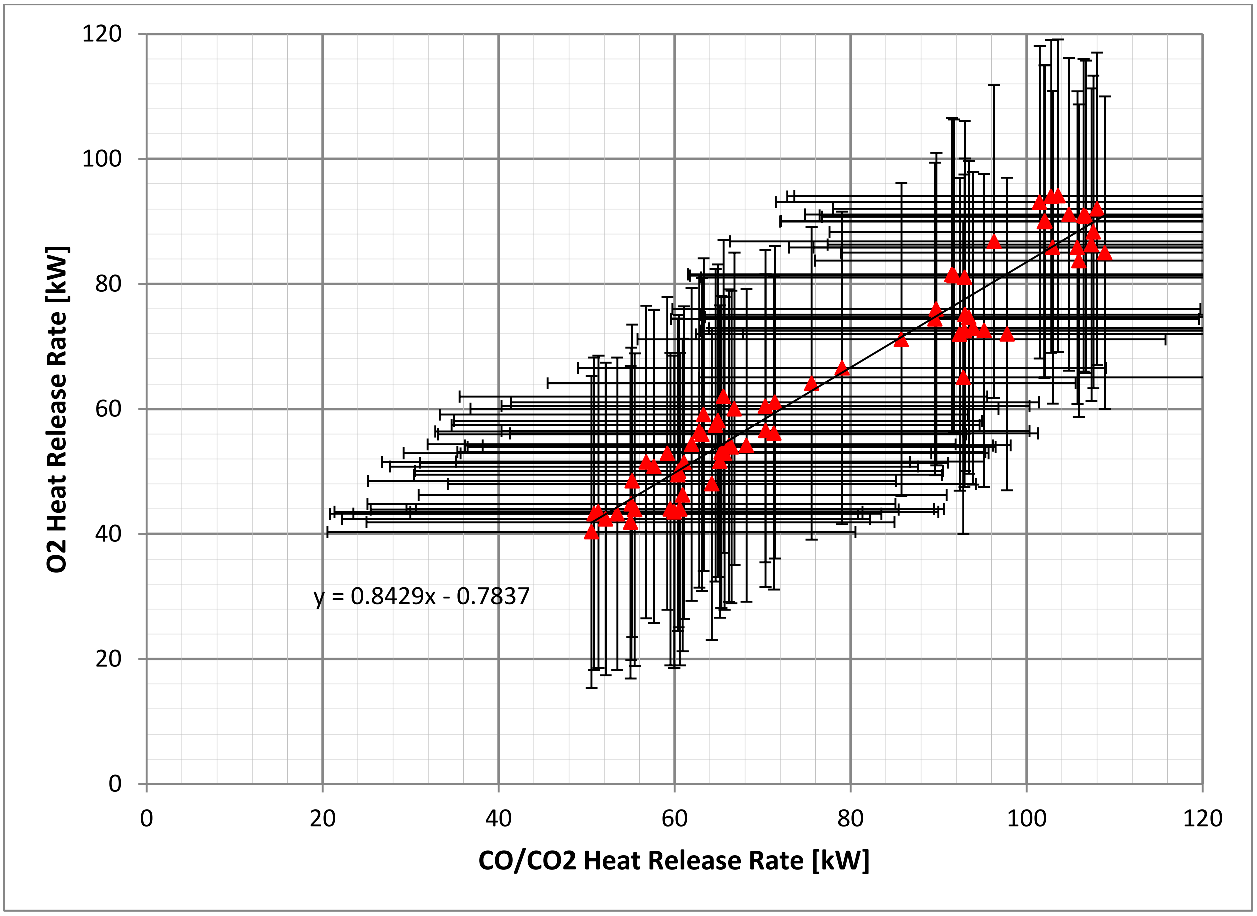

Figure 35 - O2-based HRR vs CO/CO2-based HRR, with uncertainties

This analysis suggests that the most reasonable HRR to use for further analysis is the Flow HRR since it is more consistent than the other HRR calculation method and has lower uncertainty.

D.1.3 Combustible Wall Experiment HRR

The heat release rate of a fire gives information about the energy output of the burning material. In the FRP panel full-scale tests, the total heat release rate of each test was measured using the LODS, which was made up of the source fire HRR and the FRP fire HRR. Most of the tests were conducted with the burner fuel turned off after ignition on the panel was achieved, but in four tests the burner was kept on.

To find the burning FRP HRR, the source fire HRR was calculated based on flow rate at the flowmeter and subtracted from the total heat release rate. Any discrepancy in the burning panel HRR was then smoothed out, and presented in Figure 36 to fig Figure 40, grouped based on burner size and source fire HRR.

It is noted that the time zero in the charts represent the time at which the source fire reached the desired HRR.

Figure 36 shows the HRR time histories from the 1 ft Square burner with 50 kW source fire. The propylene tests had quicker times to peak (rollover under ceiling) than the propane test at the same source fire size. However, the test where the source fire was kept on for the whole test had the quickest time to peak, and also the most heat generated. The small discrepancies at the HRR curves of the tests occur when the burner was turned off, where the burning panel's fire usually decreased in size momentarily then increases until rollover.

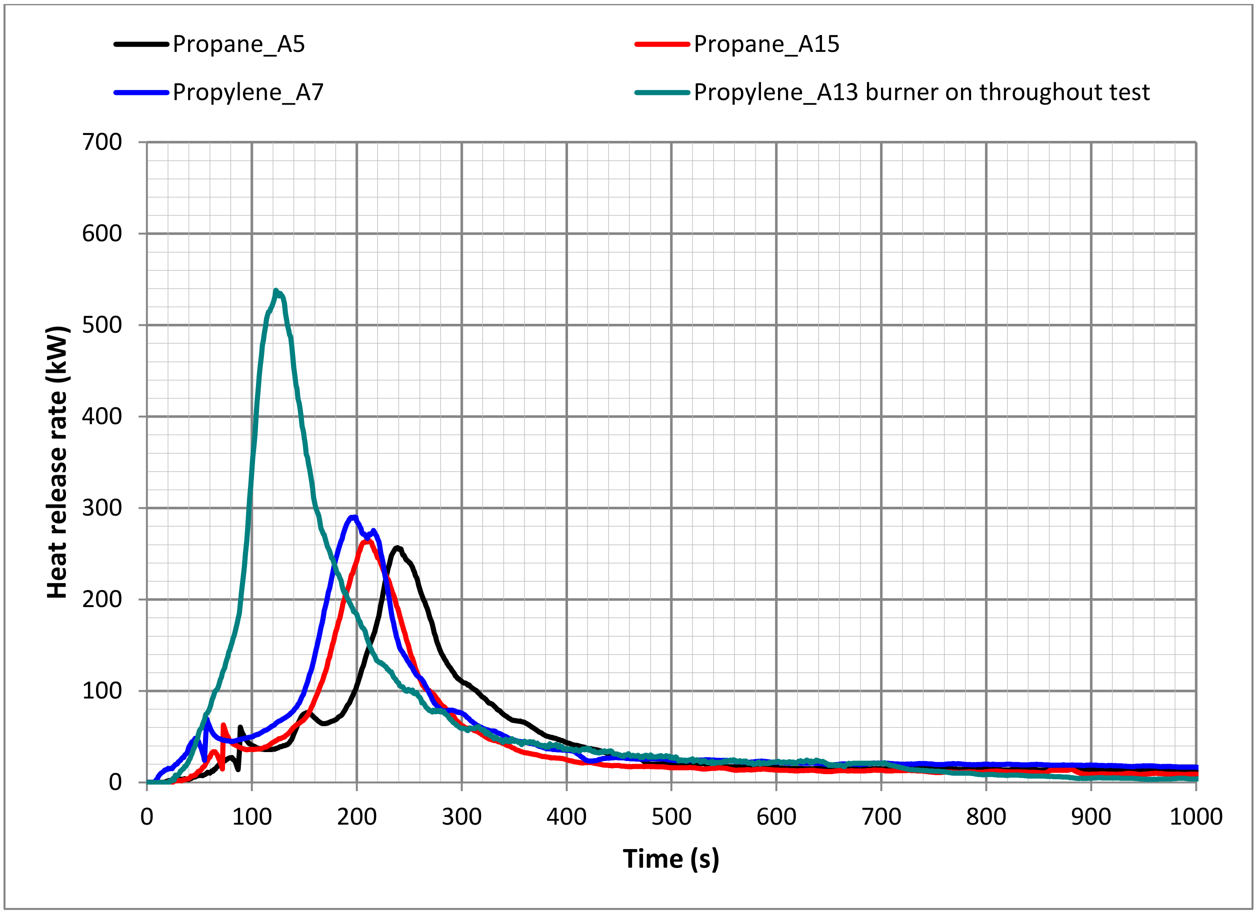

Figure 36 - HRR time histories for 1ft Square burner with 50 kW source fire

Figure 37 shows the HRR time histories from the 1 ft Square burner with 75 kW source fire. The propylene tests had quicker times to peak (rollover under ceiling) than the propane test at the same source fire size. In test where the source fire was kept on for the whole test the most heat was generated. Compared to the cases using the same burner but at 50 kW source fire size, the times to peak was shorter in the 75 kW cases where the burner fuel was shut off.

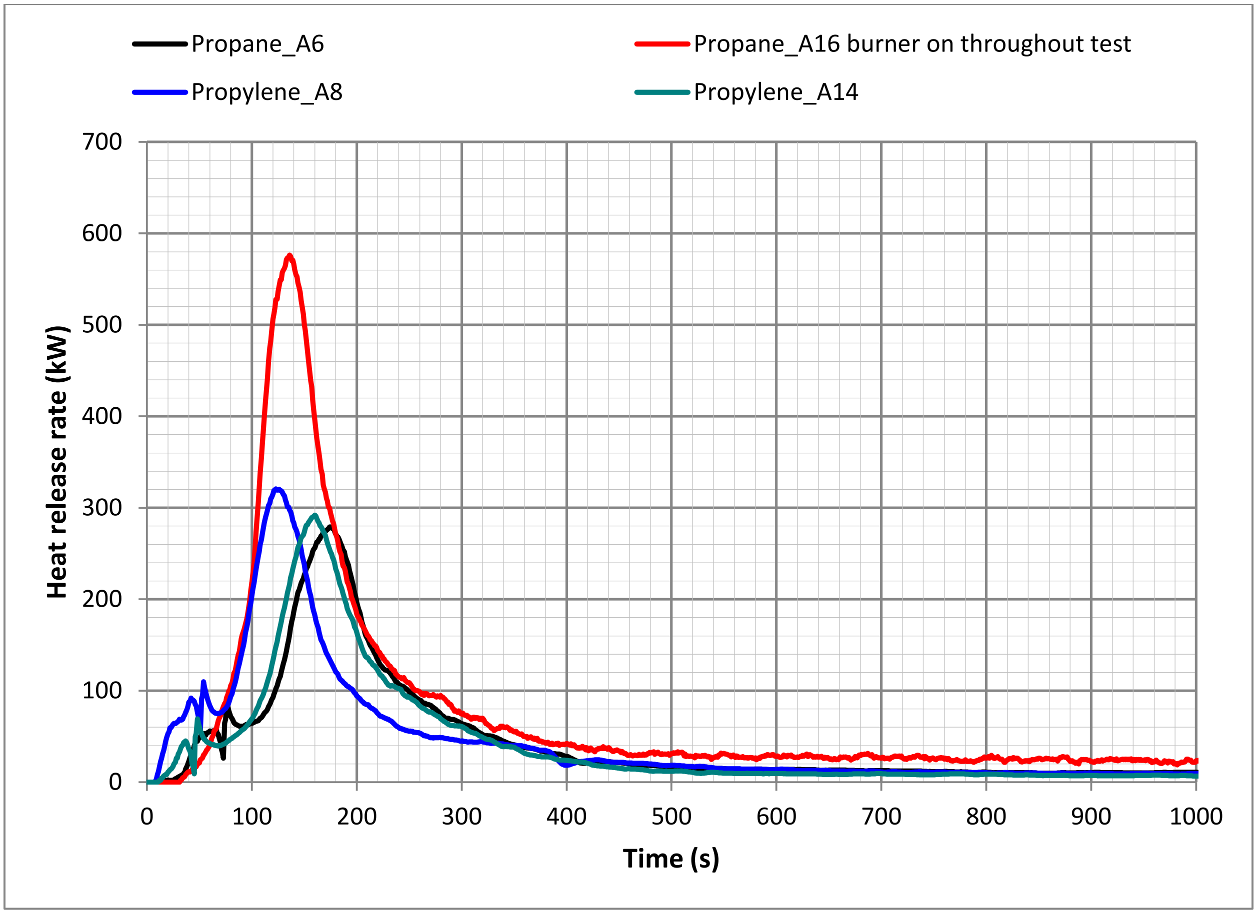

Figure 37 - HRR time histories for 1ft Square burner with 75 kW source fire

Figure 38 shows the HRR time histories from the 2 ft Rectangle burner with 50 kW source fire. The propylene tests had quicker times to peak (rollover under ceiling) than the propane test at the same source fire size. However, the test where the source fire was kept on for the whole test had the quickest time to peak, and also the most heat generated. These trends are similar to the 50 kW cases with the 1 ft Square burner.

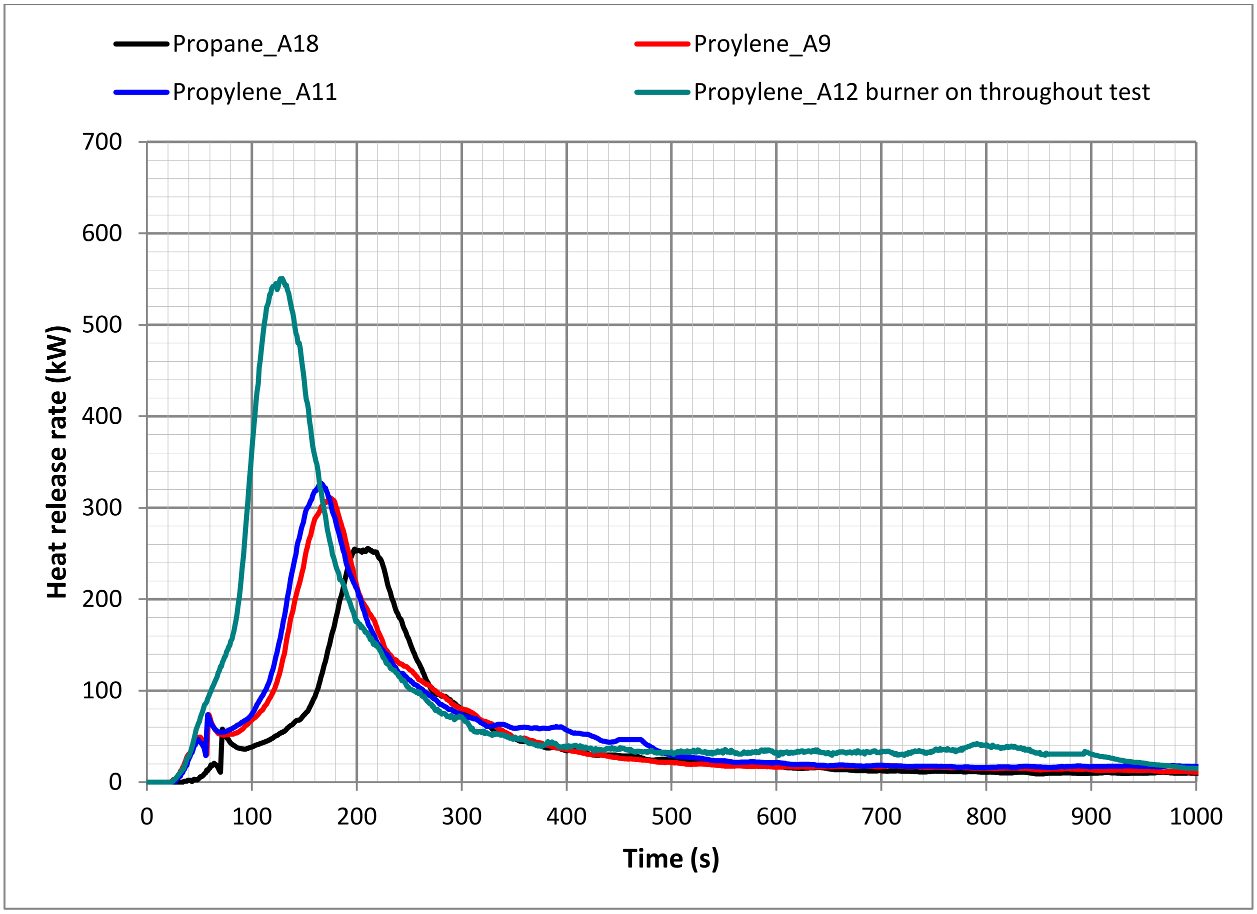

Figure 38 - HRR time histories for 2ft Rectangle burner with 50 kW source fire

Figure 39 shows the HRR time histories from the 2 ft Rectangle burner with 75 kW source fire. The propylene tests had quicker times to peak (rollover under ceiling) than the propane test at the same source fire size. In test where the source fire was kept on for the whole test the most heat was generated. Compared to the cases using the same burner but at 50 kW source fire size, the times to peak was shorter in the 75 kW cases where the burner fuel was shut off.

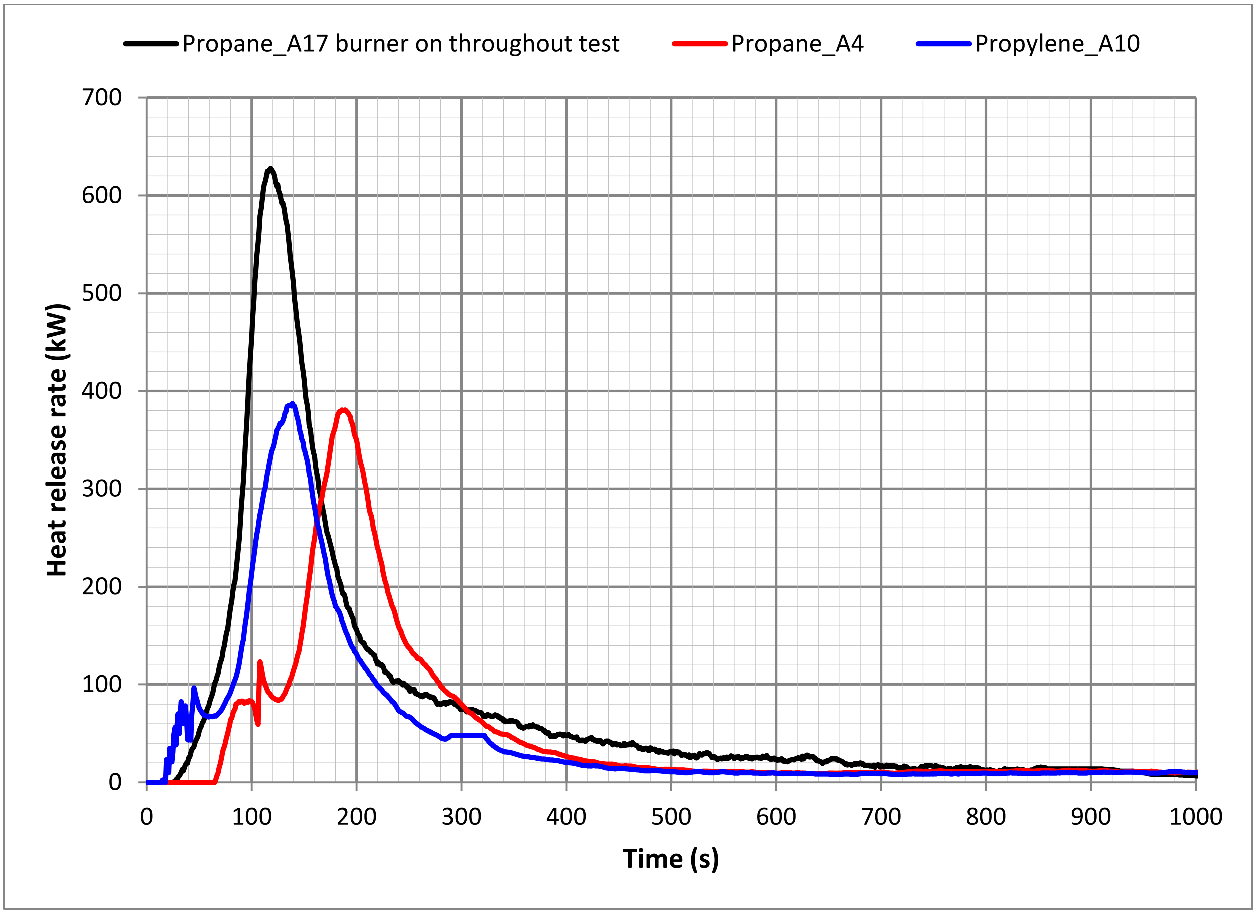

Figure 39 - HRR time histories for 2ft Rectangle burner with 75 kW source fire

Figure 40 shows the HRR time histories from the 2 ft Rectangle burner with different source fire HRRs. The tests recorded here had water application to cool the fire to prevent flashover as the side walls and ceiling was burning. Also in Test A1 and A2 the source fire flared up over the desired constant HRR.

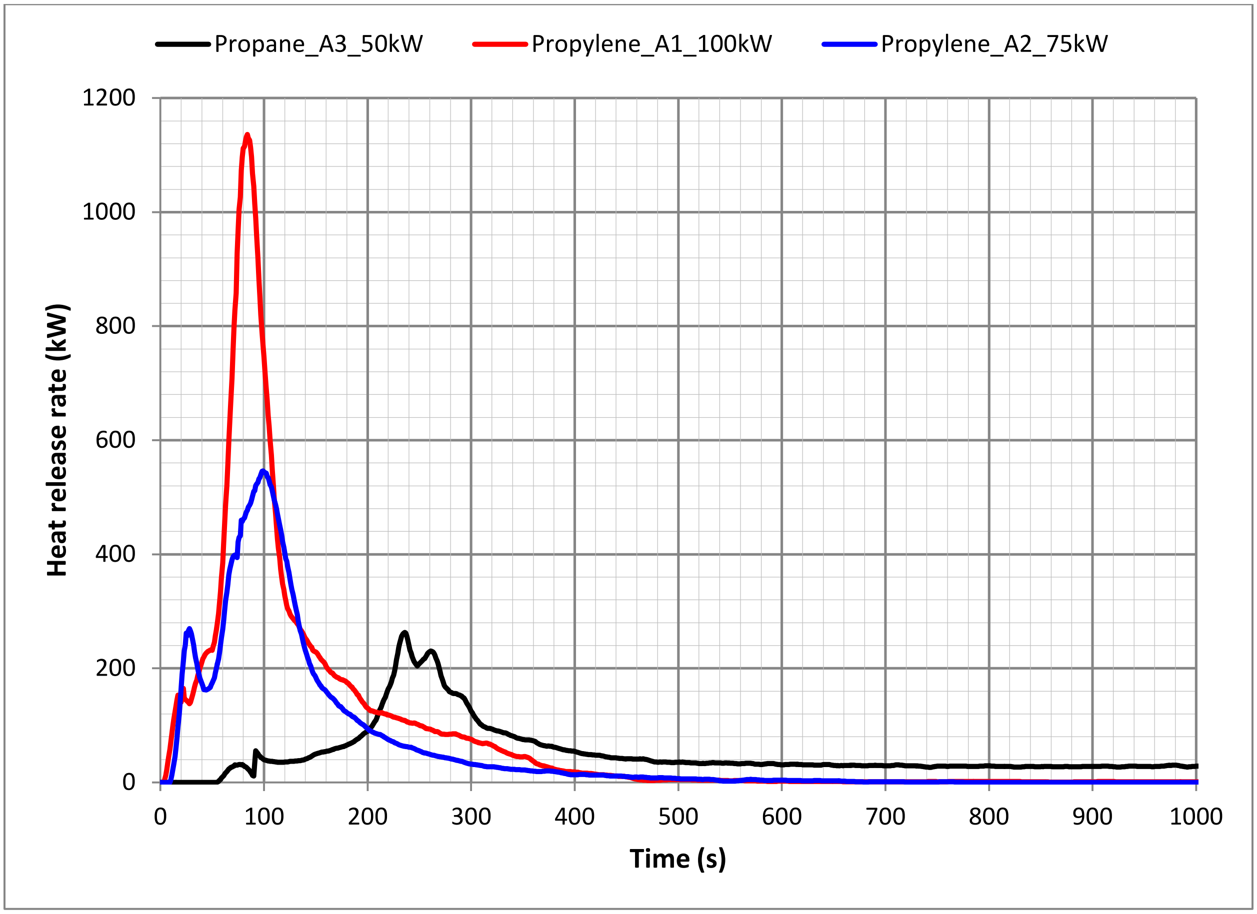

Figure 40 - HRR time histories for 2ft Rectangle burner with various source fire

D.2 Plume Centerline Temperature

The centerline temperature is a characteristic of the fire plume and is an important variable in the study of flame turbulence study. The temperature varies drastically over height because the plume is made up of 2 distinctive sections: the flame region, and the un-combusted buoyant plume.

Temperature measuring instruments were installed onto two rakes. The majority of the centerline temperature measurements were made via 24-AWG thermocouple wires with welded bead-ends at 15 cm intervals. Six Isotherm stations, consisting of three welded thermocouple wires using 20 AWG, 28 AWG, and 30 AWG wires were installed at varying intervals alongside with the 24-AWG thermocouples. Some of the thermocouples located below a height of 0.8 m over the burner were consisted of pre-made 24-AWG thermocouple with a larger diameter than the welded 24-AWG thermocouple wires. These wires were protected with a ceramic fiber weave against fire damage; the thermocouple wires elsewhere on the rakes were coated with a fiberglass weave that provides less protection against fire. Figure 41 shows the instrumentation locations on the two rakes.

CENTERLINE RAKE 1 INSTRUMENTATION

Height above Ground (m)	Height above Burner (m)	Thermocouple	Isotherm
2.25	1.85	CTC-7	
2.1	1.7	BDTC-6	
1.95	1.55	CTC-6	CISO-3
1.8	1.4	BDTC-5	
1.65	1.25	CTC-5	
1.5	1.1	BDTC-4	
1.35	0.95	CTC-4	CISO-2
1.2	0.8	BDTC-3	
1.05	0.65	CTC-3	
0.9	0.5	BDTC-2	
0.75	0.35	CTC-2	CISO-1
0.6	0.2	BDTC-1	
0.45	0.05	CTC-1	

CENTERLINE RAKE 2 INSTRUMENTATION

Height above Ground (m)	Height above Burner (m)	Thermocouple	Isotherm
2.1	1.7	PTC-7	PISO-3
1.95	1.55	BDTC-10	
1.8	1.4	PTC-6	
1.65	1.25	BDTC-9	
1.5	1.1	PTC-5	PISO-2
1.35	0.95	BDTC-8	
1.2	0.8	PTC-4	
1.05	0.65	BDTC-7	
0.9	0.5	PTC-3	PISO-1
0.75	0.35	PTC-2	
0.6	0.2	PTC-1	

Figure 41 - Rake Instrumentations

All of the thermocouple wires were of K type with Special Limits of Error (SLE) with an uncertainty of ±1°C or 0.4% full scale. The operable range of the K type thermocouples is between 0°C to 1250°C, and given our application to locate the thermocouples inside the hot fire plume, it is assumed that the uncertainty of the thermocouples will be at the higher limit, at 0.4% = 5°C. The following analysis of the centerline plume temperature data shows that this deviation is insignificant inside the fire plume.

McCaffrey's [1] and Hasemi's [2] plume data had been used for comparison. It has been reported that McCaffrey's thermocouples are about 1.0 mm in diameter, and Hasemi's thermocouples are about 0.1 mm in diameter. The thermocouples used in the WPI experiments are from welded 24 AWG thermocouple wires, and have an approximate diameter of 1.2 mm. Hence there may be a need of performing radiation correction to our data in order to compare different datasets effectively.

McCaffrey's plume temperature data is composed of data from 5 different fire sizes using a 1 ft x 1 ft square sand burner with methane in the open. McCaffrey's data was normalized with $Z/Q^{2/5}$ with Z being the height above burner surface and Q as the HRR of the fire. The data from all fire tests were accumulated on the same chart, and a clear trend is shown. Hasemi's plume temperature data is composed of data from 6 different fuel sizes using a 0.2, 0.3, and 0.5 diameter circular burner with propane in the open. The temperature was recorded along the centerline and was normalized using the product of the non-dimensional HRR, $Q^{*2/5}$, commonly found by using equation [1], and the diameter of burner.

$$Q^* = \frac{Q}{\rho_\infty c_p T_\infty g^{0.5} D^{2.5}} \qquad [1]$$

In the current study, the centerline plume temperature was measured in fires with the burner in the open and against an inert wall. Three types of fuel were used: methane, propane, and propylene, along with two burners sized at 1 ft Square and a 1 ft x 2 ft Rectangle. The fuel sizes were between 50 and 75 kW, chosen to represent a building fire at the early stage of development. Flame height of each fire was also measured to be used as a normalization agent.

Since different fuels were used between the three studies and datasets, the normalization using HRR has been corrected by using the convective HRR rather than the reported, chemical HRR of the fuel. Hence, the main differentiating characteristic of the fuels, their radiative fraction, was taken out of the comparison and a more generalized comparison could be made. Plume temperature data from all three studies were normalized mainly with the convective HRR to the 2/5th power, similar to McCaffrey.

Note that the temperature presented in this section has not been corrected.

To calculate the standard deviation of the data and to measure the spread, the following reduction had been performed:

The data from different fire tests was grouped as one, and sorted by the value of the normalized height, rounded to 2 decimal points after zero. This way, the measurements with similar normalized height value were singularized, then the average and the standard deviation were found within each group. The maximum difference between the highest and lowest values in each group is found and halved to find the spread also. Table 7 shows an example of McCaffrey's data with the data singularization and reduction.

Table 7 - Example McCaffrey data reduction

$Z/Q^{2/5}$	$Z/Q^{2/5}$	ΔT		$Z/Q^{2/5}$	ΔT	ΔT	ΔT	ΔT	ΔT
($m*kW^{2/5}$)	($m*kW^{2/5}$)	(°C)		Average	Average	Std Dev	Max diff/2	Avg+Diff	Avg-Diff
x	x	(z/Q⅖)^η		x					
0.01	0.01	581.08		0.01	659.87	67.70	78.02	737.90	581.85
0.01	0.01	632.60							
0.01	0.01	688.69							
0.01	0.01	737.12							
0.02	0.02	752.95		0.02	735.05	50.46	85.66	820.71	649.38
0.02	0.02	757.76							
0.02	0.02	638.00							
0.02	0.02	674.22							
0.02	0.02	701.98							
0.02	0.02	794.01							
0.02	0.02	707.97							
0.02	0.02	751.35							
0.02	0.02	744.99							
0.02	0.02	809.33							

Using the above procedure, the largest standard deviation of temperature in the McCaffrey data was found to be 87.7°C. The largest spread, which denotes the largest difference between the highest/lowest values of temperature at each normalized height, is found to be approximately 85.7°C. Figure 42 shows the average temperature rise vs. normalized height in blue, whereas the error bar represents the average standard deviation of 35.5°C; the dashed red and green lines signify the higher and lower end of the temperature rise data, and the purple line shows the centerline plume temperature profile as suggested by using McCaffrey's plume theory and equations.

It should be noted that this analysis of McCaffrey's data is based not on actual data, but based on the data-points that are approximated based on the figures included in his report.

To better understand the correlation between the methane plume data by McCaffrey and our data with propane and propylene fire plumes, the normalization using HRR has been corrected by using the convective HRR rather than the chemical HRR, this way, the main differentiating characteristic of the fuels, radiative fraction, is taken out of the equation and a more accurate comparison can be made.

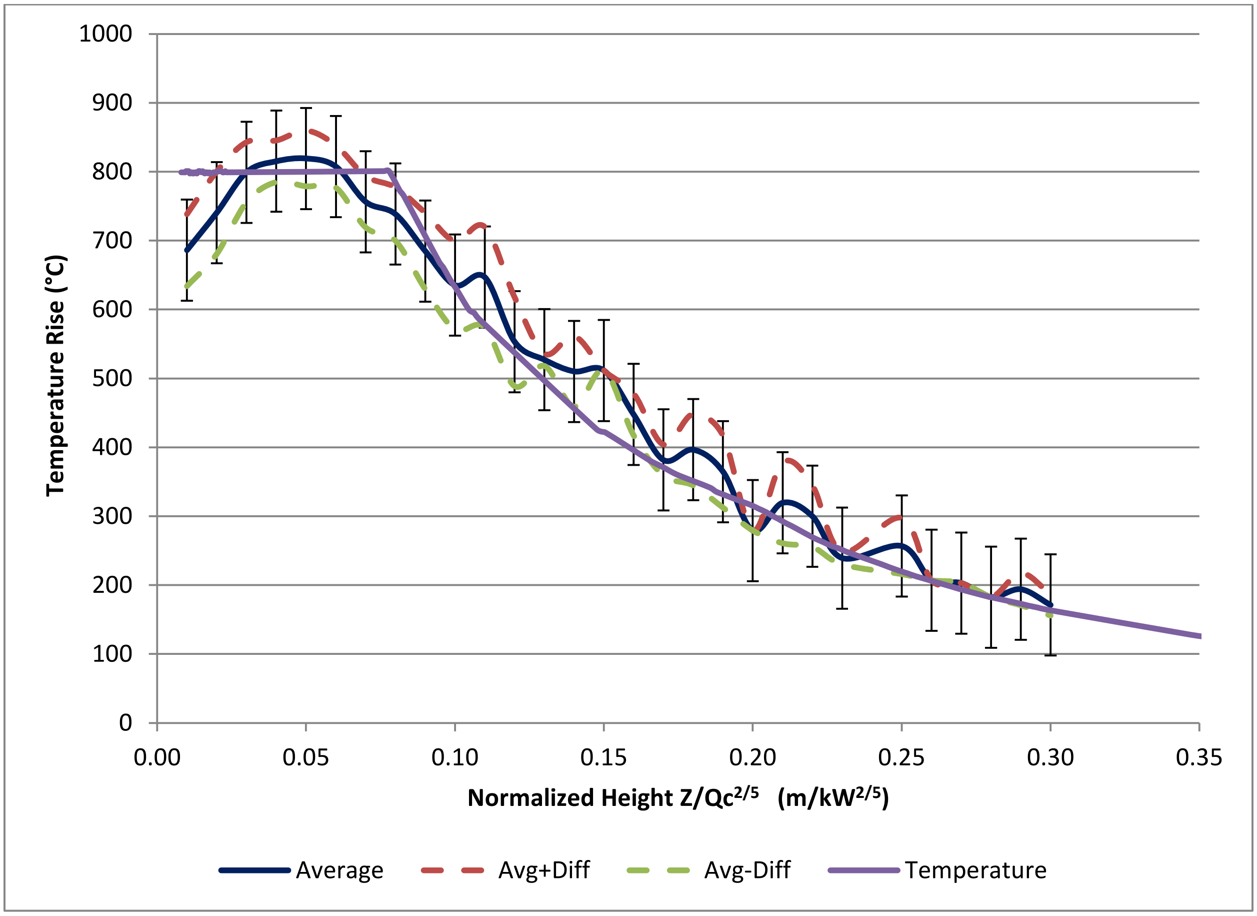

Figure 42 - McCaffrey's plume temperature rise data showing spread and normalized with convective HRR

Figure 43 shows the methane free plume centerline temperature vs. McCaffrey's and Hasemi's data. The error in our measurements is relatively small, and they are generally lower than the reported measurements until at the far-plume region. One possibility for the lower temperature is that our measurements have not yet been radiation corrected. The tests were conducted with netting installed at the test compartment to smooth out the flow near the fire plume (a pervious test was conducted without netting and the plume was tilted, causing much lower "centerline" temperature).

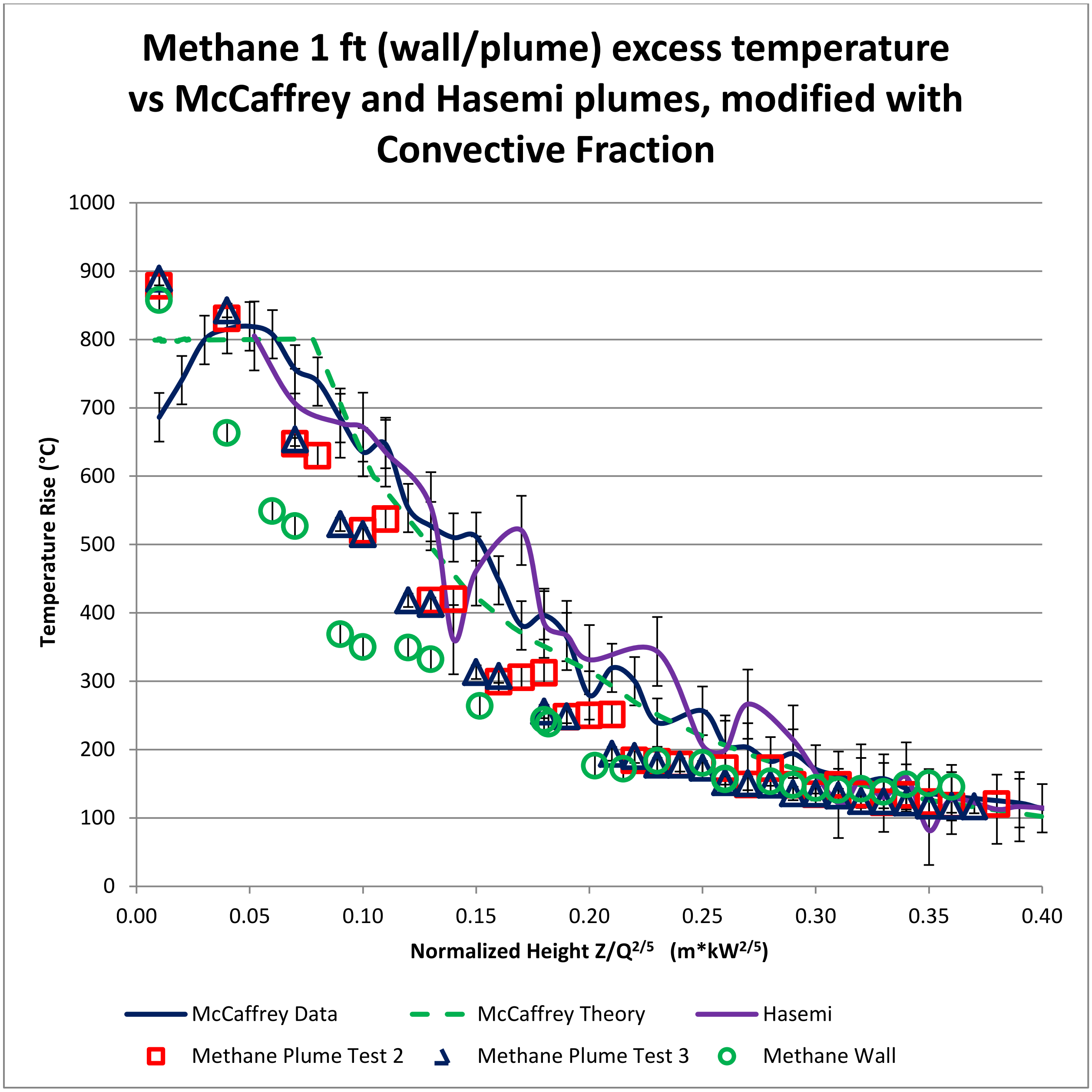

Figure 43 - Natural gas plume test vs McCaffrey

Additional inert wall fire tests using propane at 50 kW and 75 kW are conducted with the netting in-place. The results are collected into 2 series and plotted in Figure 44. The temperature shows the same trend with our free plume data and McCaffrey's and Hasemi's plume data but are slightly lower than the free plume data, especially in the 1 ft square burner case (shown in Figure 45 and Figure 46). This can be an effect of the plume "climbing the wall". The plume vs inert wall centerline temperature data varies little for the 2 ft burner.

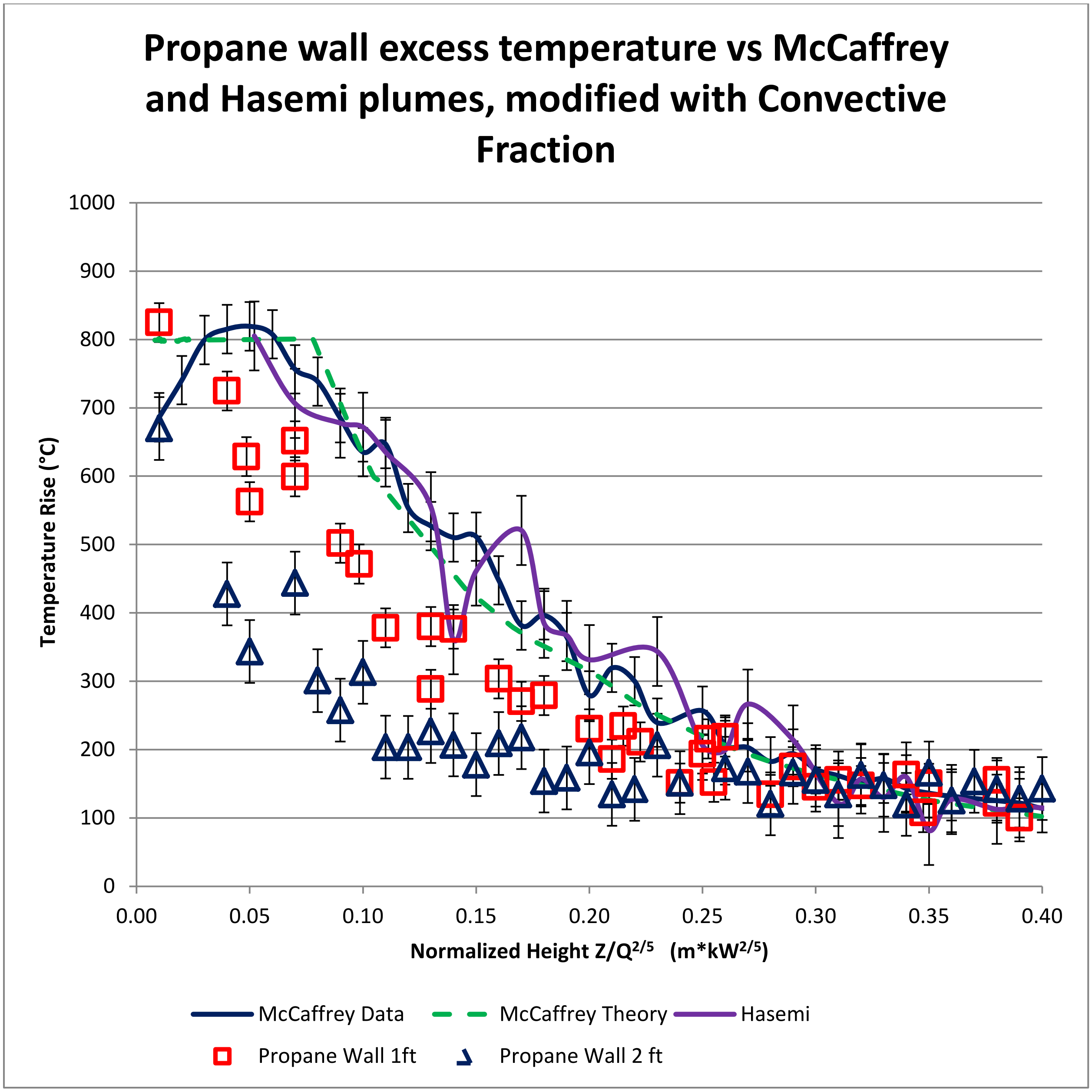

Figure 44 - Propane Wall Tests vs. McCaffrey and Hasemi

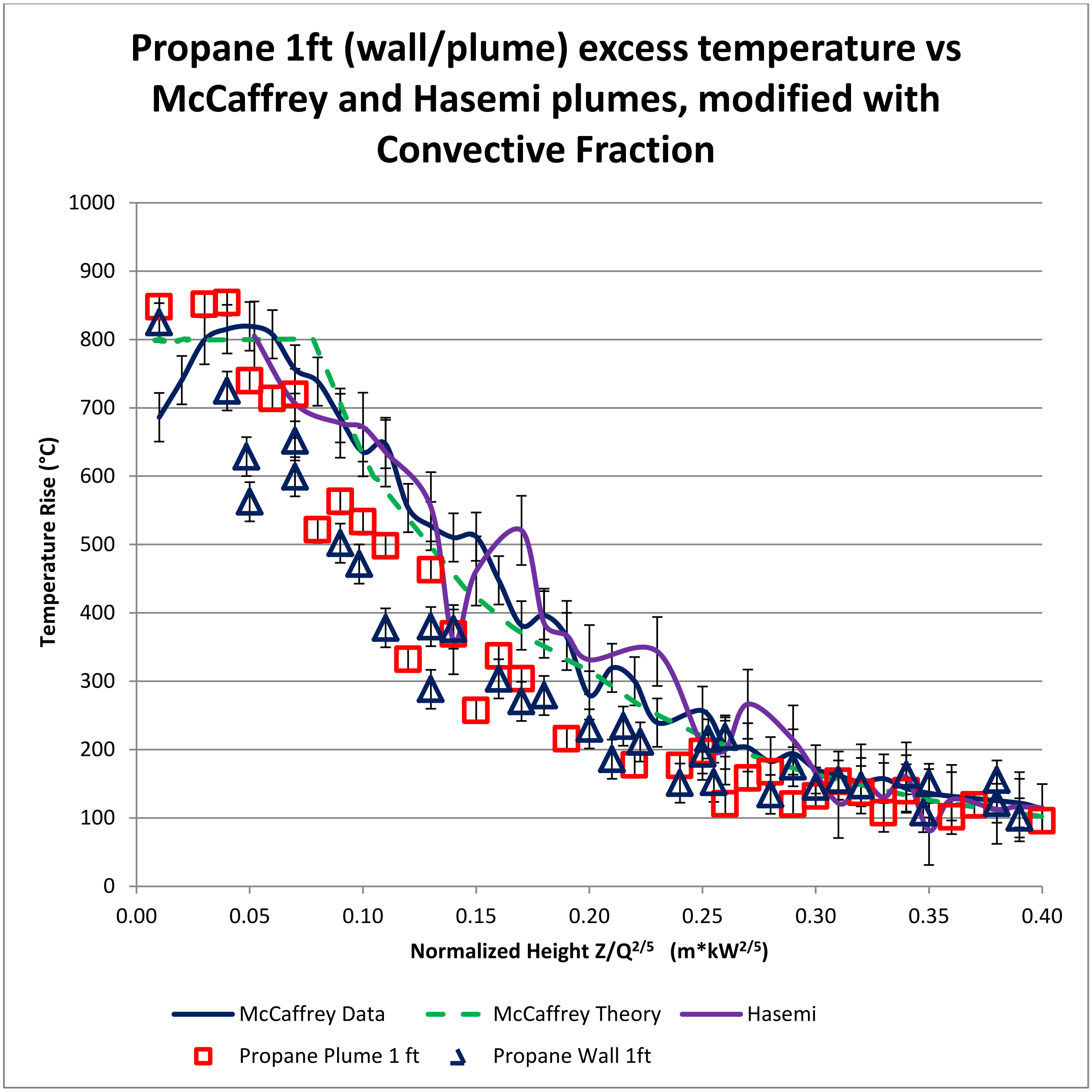

Figure 45 - Propane 1 ft Burner vs McCaffrey and Hasemi

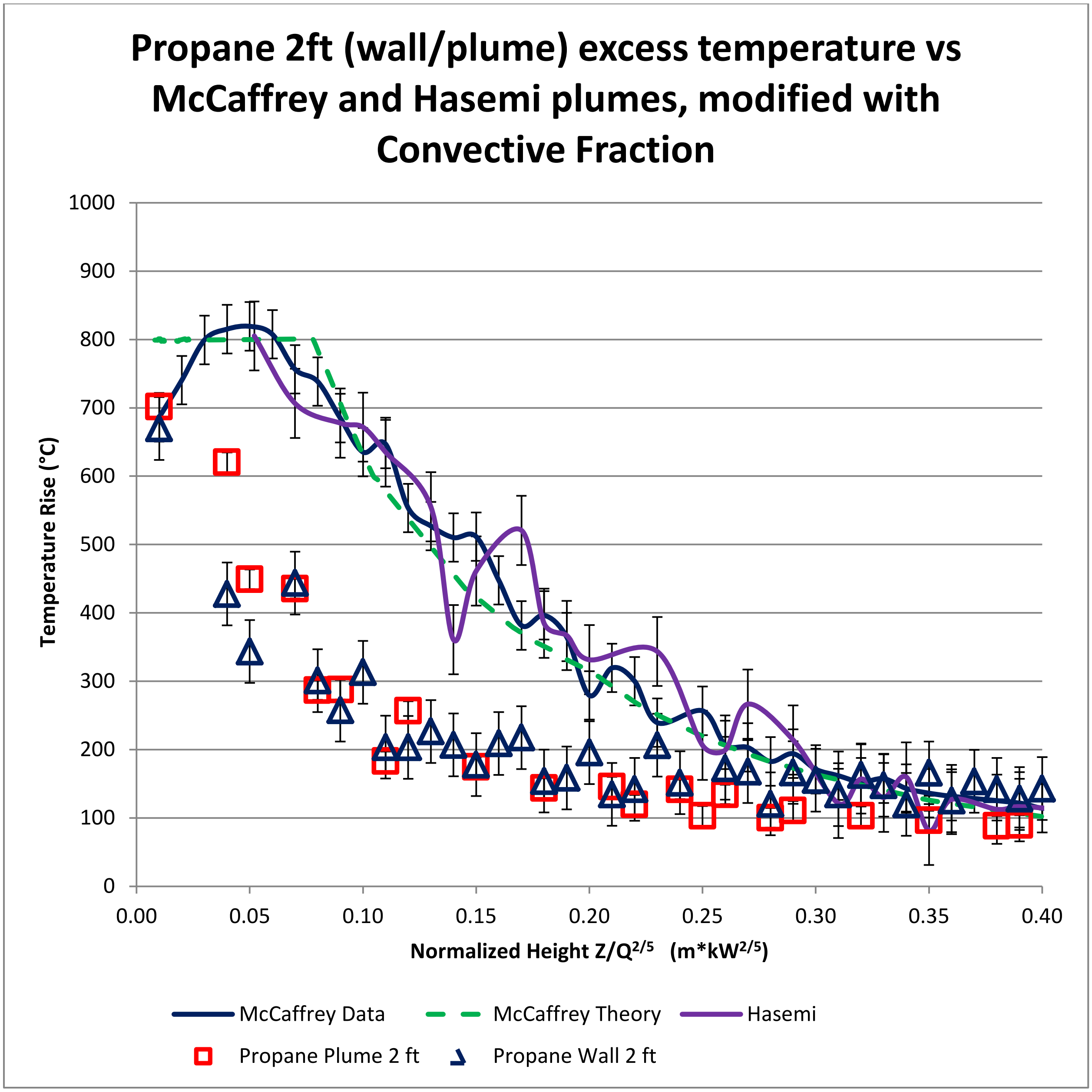

Figure 46 - Propane 2 ft Burner vs McCaffrey and Hasemi

A series of test with propylene at 50 kW and 75 kW was conducted and the centerline temperature is presented in Figure 47. The normalization of the x axis was again normalized using the convective HRR for each fire. The data from the 1 ft burner is very compatible to the McCaffrey's and Hasemi's data, likely due to the shape of the burner being either a square or a circle. The 2 ft burner's temperature is lower, most likely due to the geometry of the burner.

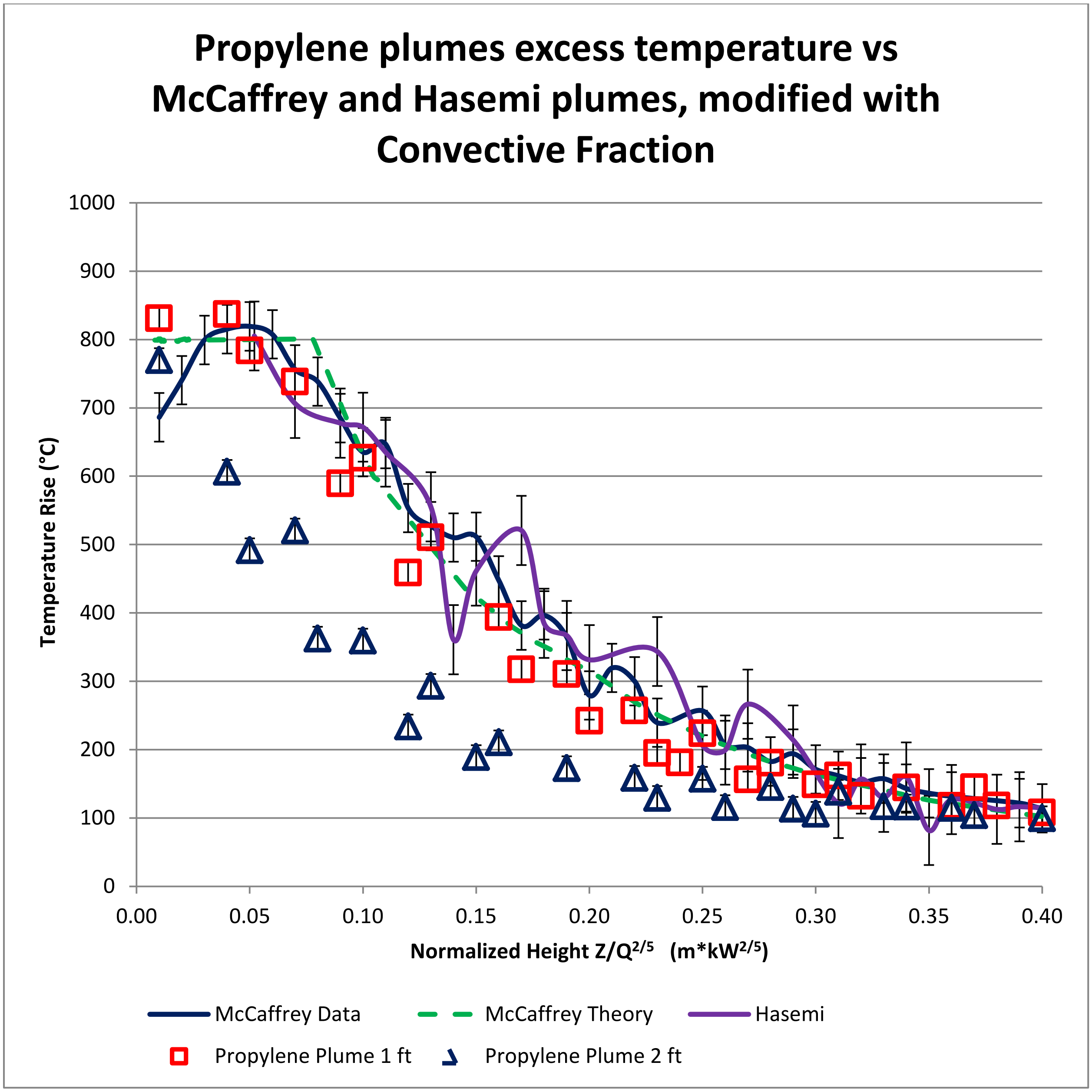

Figure 47 - Propylene Plume Tests vs. McCaffrey and Hasemi

Additional inert wall fire tests using propylene at 50 kW and 75 kW are conducted with the netting in-place. The results are collected into 2 series and plotted in Figure 48. The temperature shows the same trend with our free plume data and McCaffrey's and Hasemi's plume data but are slightly lower than the free plume data, especially in the 1 ft square burner case (shown in Figure 49 and Figure 50). This can be an effect of the plume "climbing the wall". Again, the plume vs inert wall centerline temperature data varies little for the 2 ft burner.

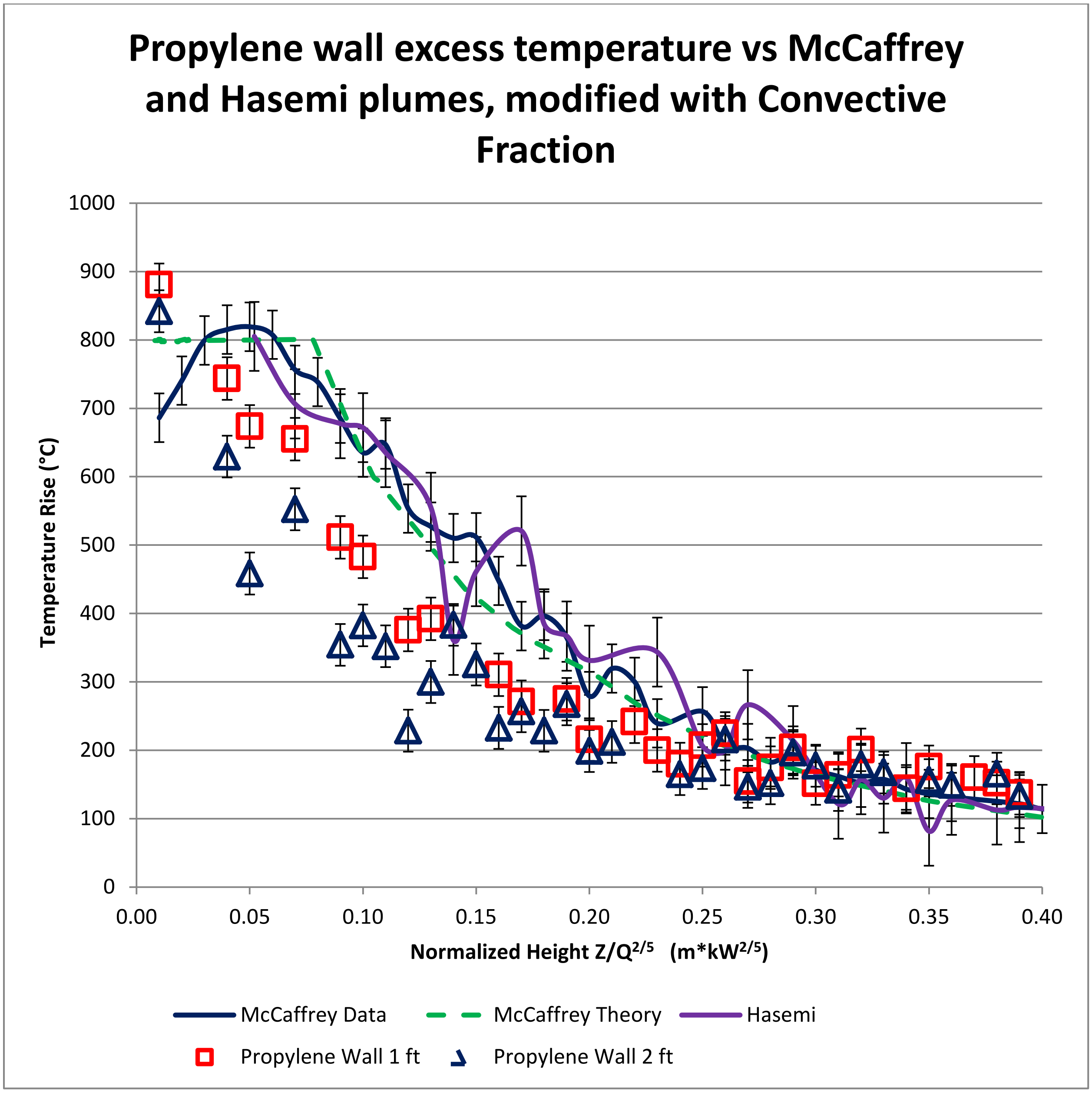

Figure 48 - Propylene Wall Tests vs. McCaffrey and Hasemi

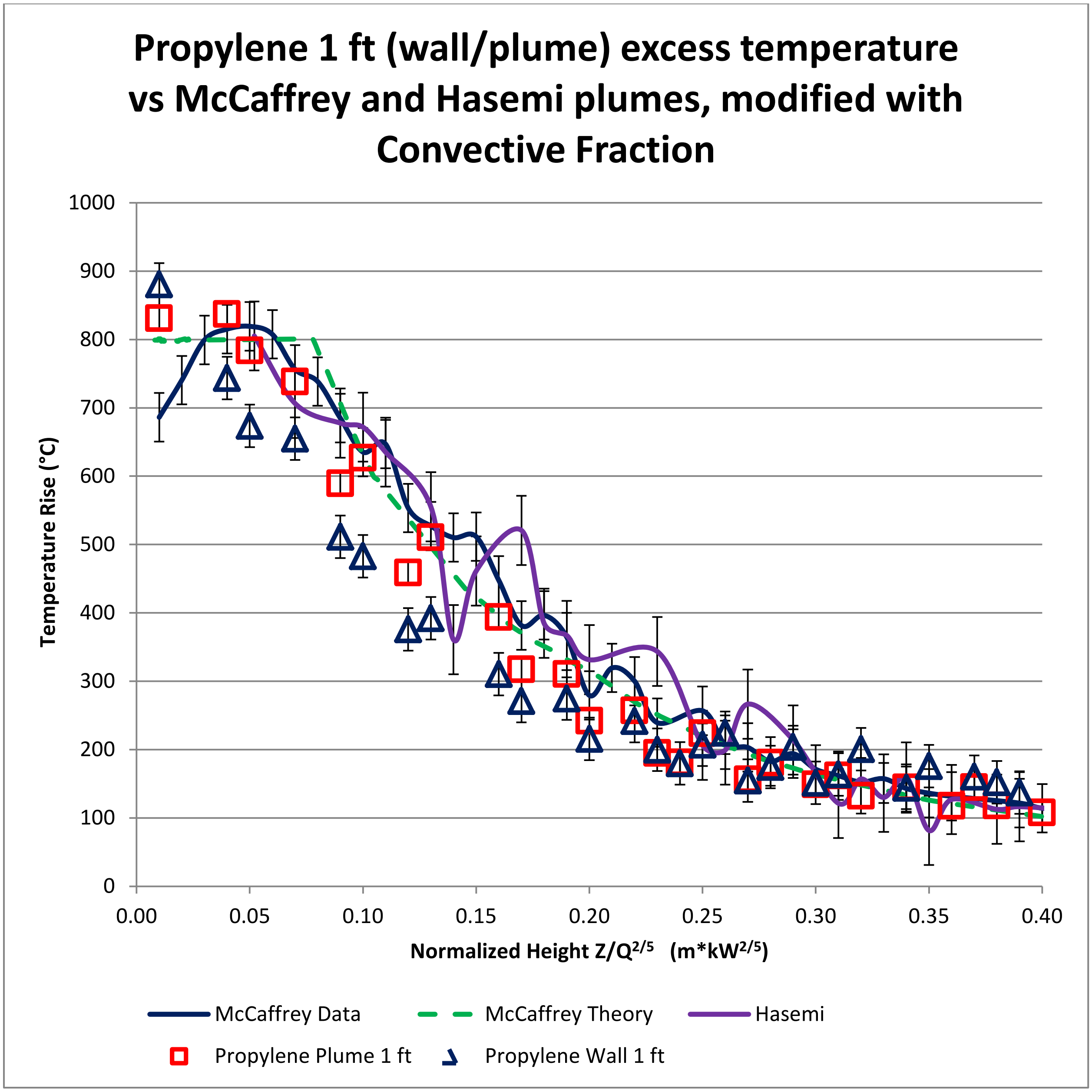

Figure 49 - Propylene 1 ft Burner vs McCaffrey and Hasemi

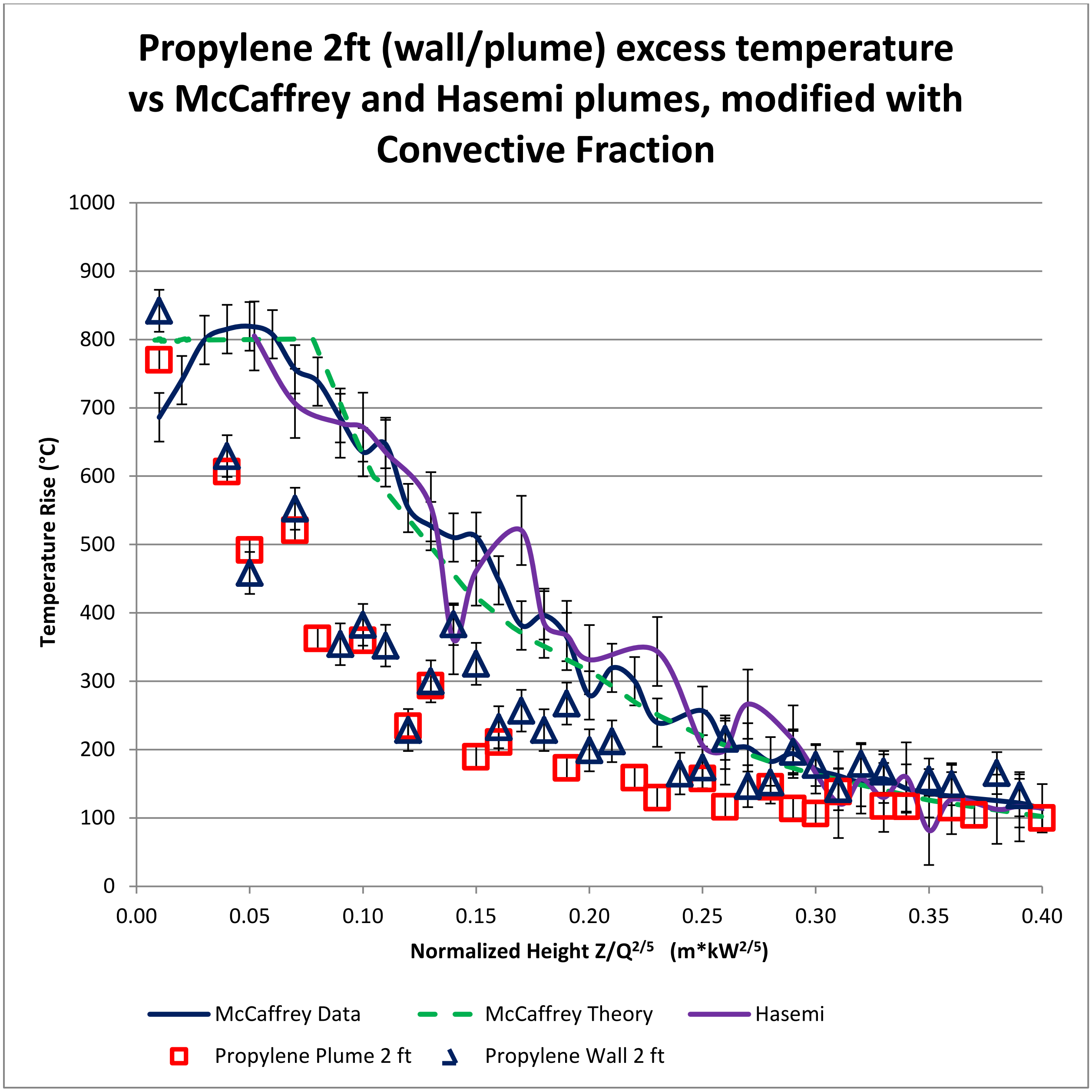

Figure 50 - Propylene 2 ft Burner vs McCaffrey and Hasemi

Another normalization method for the data is to use the 50% intermittency mean flame height to normalize the height. The following charts Figure 51to Figure 54 show the full temperature dataset normalized with flame height. The mean flame height appears to be a very effect normalizing agent for the free plume temperature data, allowing the different fuels to be collapsed tightly. For the inert wall fires, the spread of the data appears to be larger, due to additional turbulence stemming from the bisection of the plume by the inert wall.

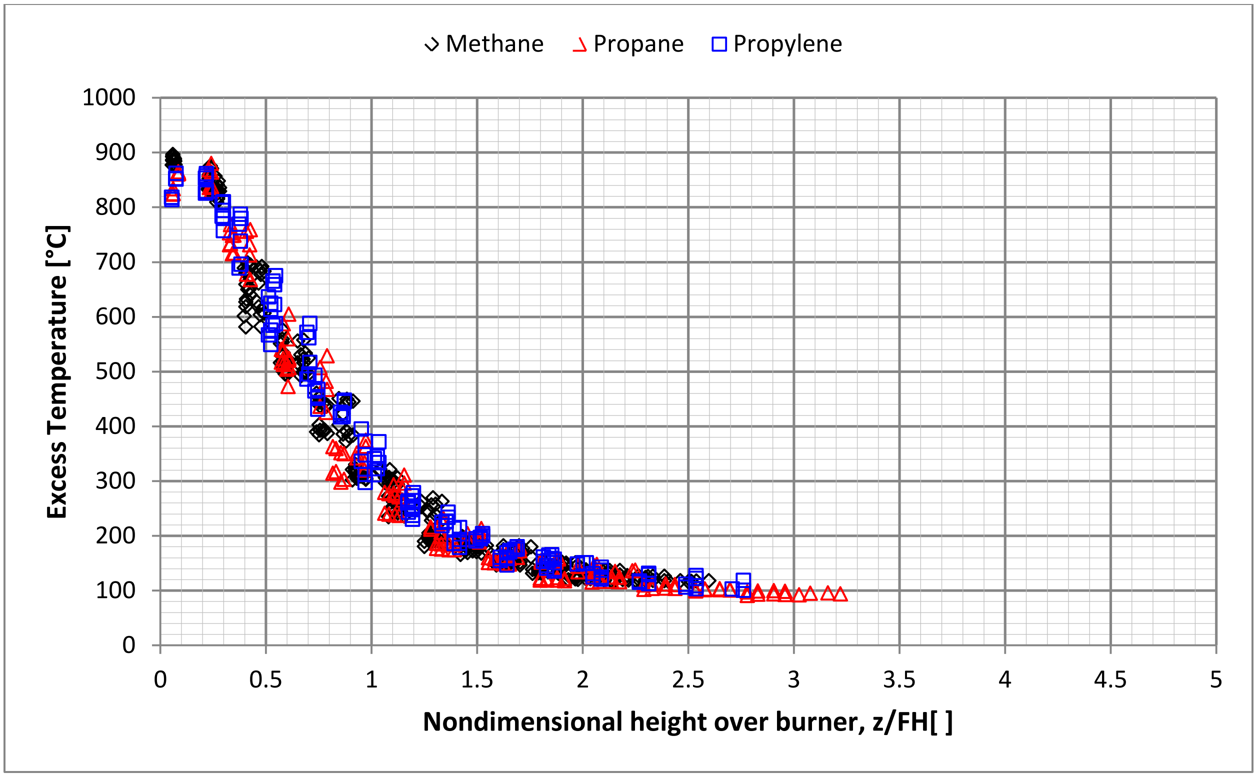

Figure 51 - Excess temperature vs normalized height using flame height for 1ft free plume Square burner

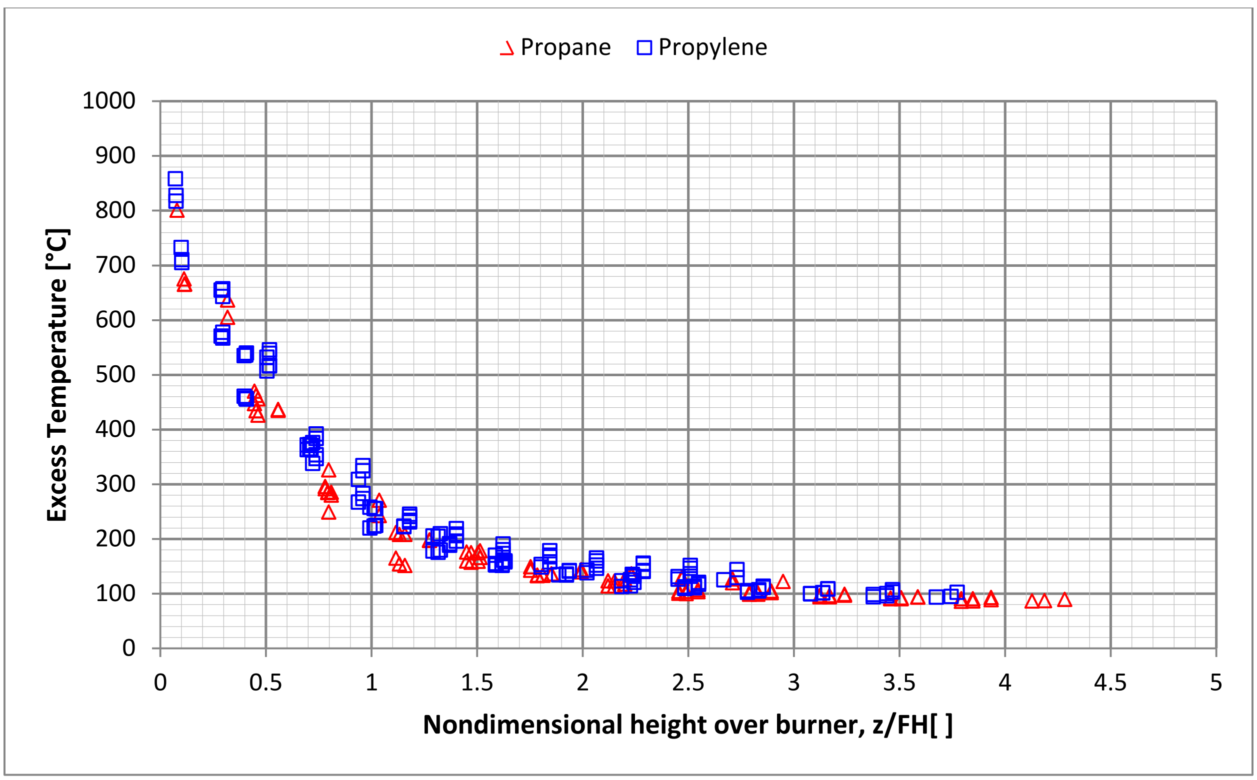

Figure 52 - Excess temperature vs normalized height using flame height for 2ft free plume Rectangle burner

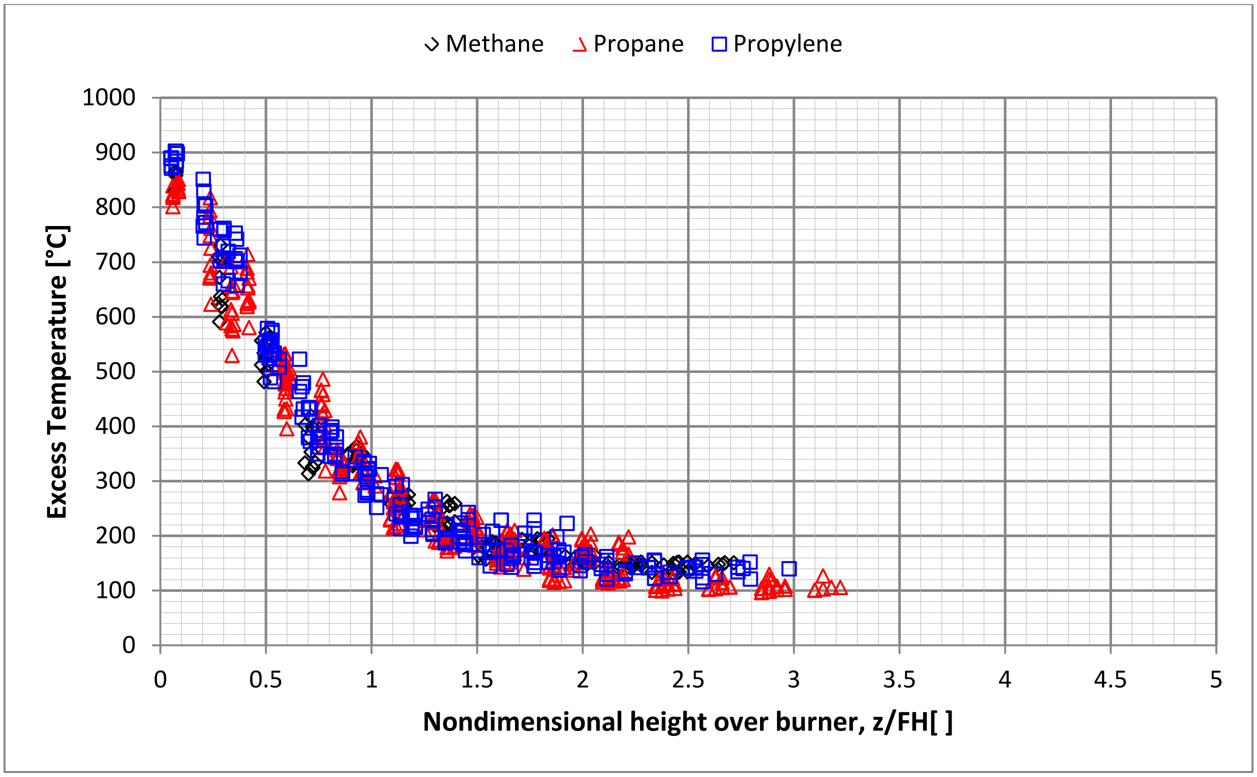

Figure 53 - Excess temperature vs normalized height using flame height for 1ft inert wall Square burner

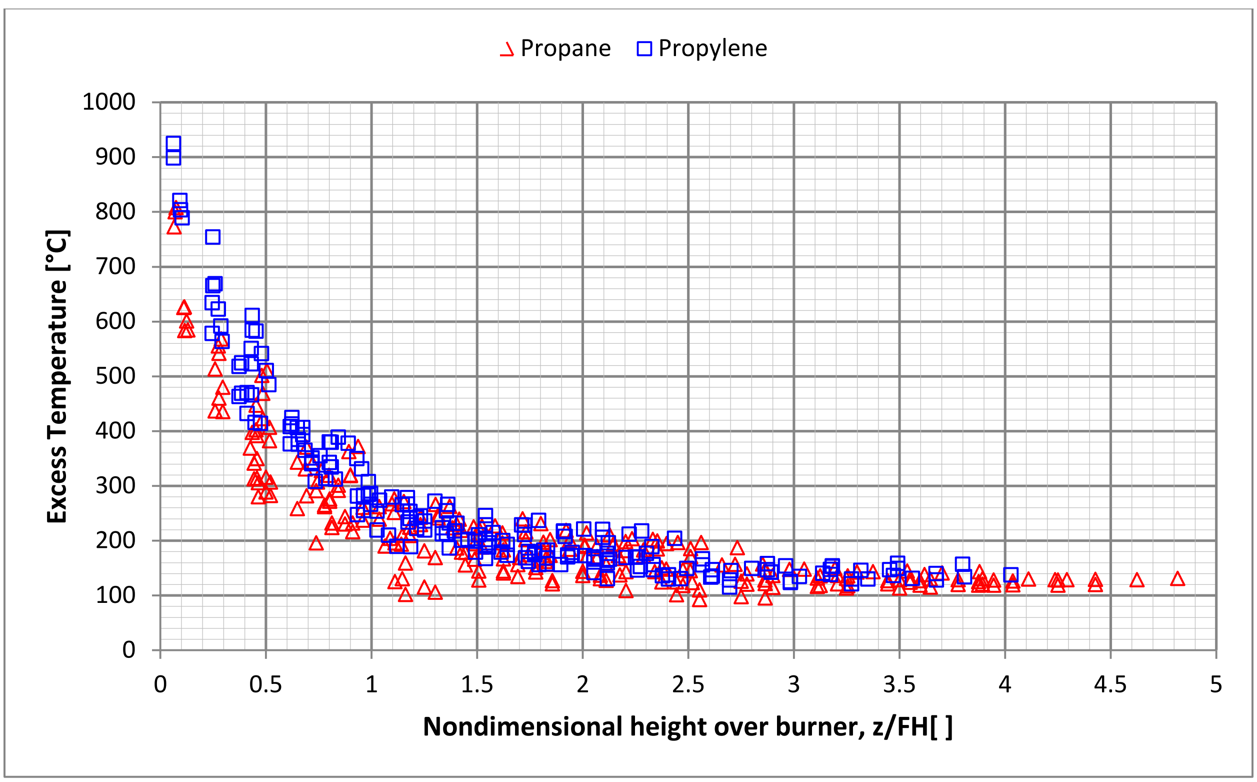

Figure 54 - Excess temperature vs normalized height using flame height for 2ft inert wall Rectangle burner

D.2.1 Plume Centerline Temperature from Free Plume and Inert Wall Fires (Corrected)

The corrected centerline temperature of the plume and inert wall fires are collected in this section. The correction method used for the free plume and inert wall experiments was developed by Blevin and Pitts, and it was applied to the time-averaged centerline temperature data measured during the tests.

Figure 55 shows the temperature of methane free plume fires from the 1 ft Square burner as compared to the McCaffrey data and theory. The comparison here is made between fires using the same type and sized burners. The height over the burner had been normalized with the convective HRR. For the region close to the burner surface up to 0.05, the measured and corrected temperature were greater McCaffrey's data and theory, however between 0.05 and 0.15, the corrected temperature were in line with McCaffrey's data and theory. After 0.15, the corrected temperature is within the distribution of the McCaffrey data although the uncorrected temperature is lower.

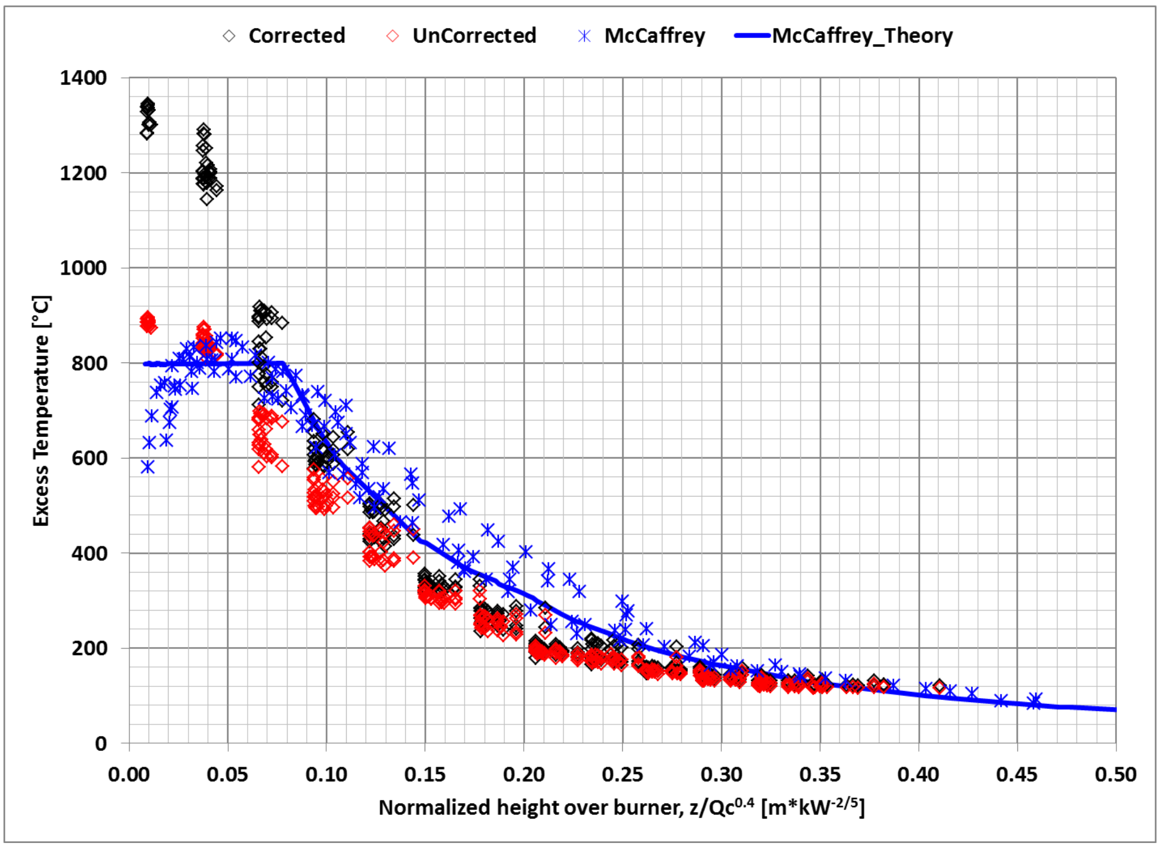

Figure 55 – Centerline temperature of methane fires using 1 ft Square burner, normalized with convective HRR

A comparison between the 1 ft Square methane free plume fire centerline temperature and McCaffrey's data normalized against the flame heights is presented in Figure 56. The same trends are noted as in the comparison using the other normalization method.

This suggests that the current methane centerline temperature data relates well with McCaffrey's data within a reasonable range.

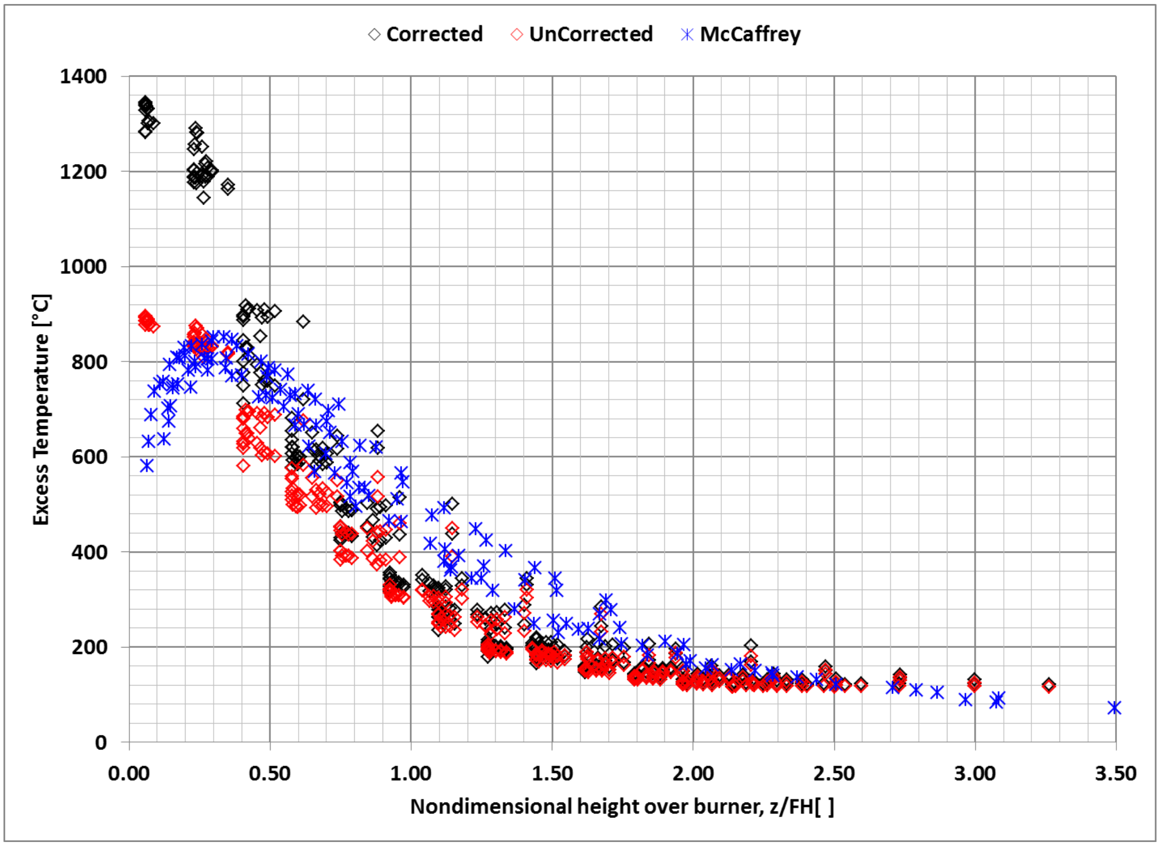

Figure 56 - Centerline temperature of methane fires using 1 ft Square burner, normalized with mean flame height

Figure 57 shows the centerline temperature of all free plume fires using the 1 ft Square burner normalized with convective HRR. Both corrected and uncorrected temperatures are plotted, and the real gas temperature should be within these two sets of values. The correction often increased the measured temperature by 50% for z < 0.05, but it significantly decreases as z increased. It can be observed that the McCaffrey's theory cut between the two bands of data.

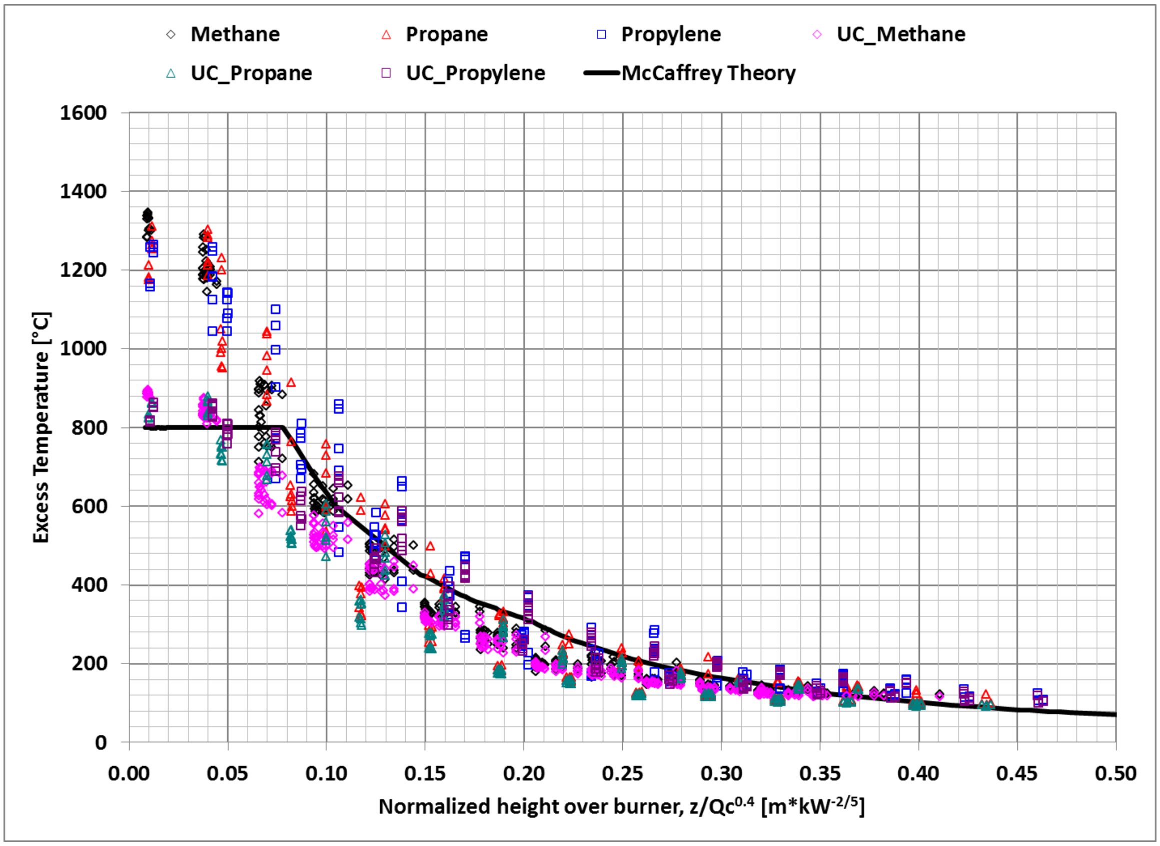

Figure 57 - Centerline temperature of all free plume fires using 1 ft Square burner, normalized with convective HRR

Figure 58 shows the centerline temperature of all free plume fires using the 2 ft Rectangle burner normalized with convective HRR. Both corrected and uncorrected temperatures are plotted, and the real gas temperature should be within these two sets of values. The correction often increased the measured temperature by 50% for z < 0.05, but it significantly decreases as z increased. It is observed that compared to the centerline temperature of the 1 ft Square burner fires and McCaffrey's theory, the temperature generated using the 2 ft Rectangle burner was much lower starting from z = 0.05. This is reasonable because of the shorter flames from the Rectangle burner.

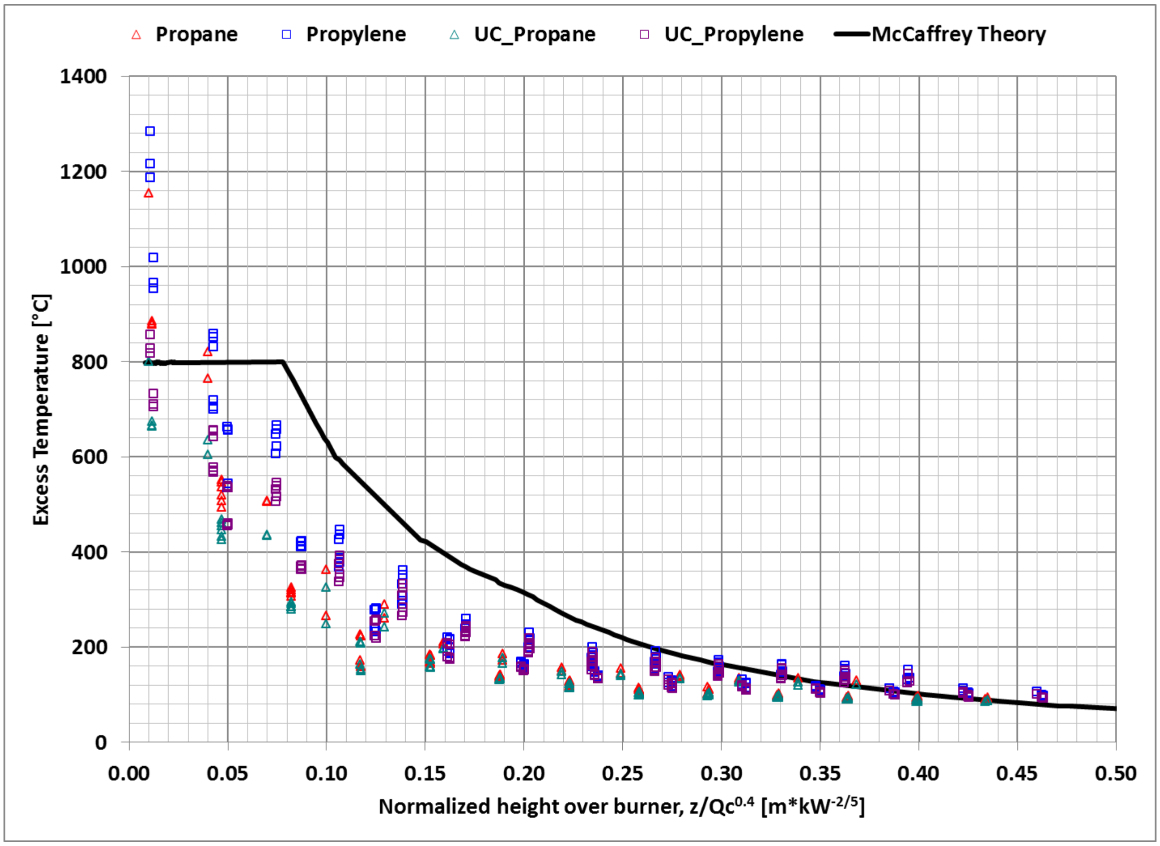

Figure 58 - Centerline temperature of all free plume fires using 2 ft Rectangle burner, normalized with convective HRR

Figure 59 shows the centerline temperature of all inert wall fires using the 1 ft Square burner normalized with convective HRR. Both corrected and uncorrected temperatures are plotted, and the real gas temperature should be within these two sets of values. Compared to the temperature from the comparable free plume fires, the centerline temperature of the inert wall fire is lower, most likely due to the fact that the fire plume leans against the wall. The correction often increased the measured temperature by 50% for z < 0.05, but it significantly decreases as z increased. It can be observed that the McCaffrey's theory still fits reasonable well in the inert wall data.

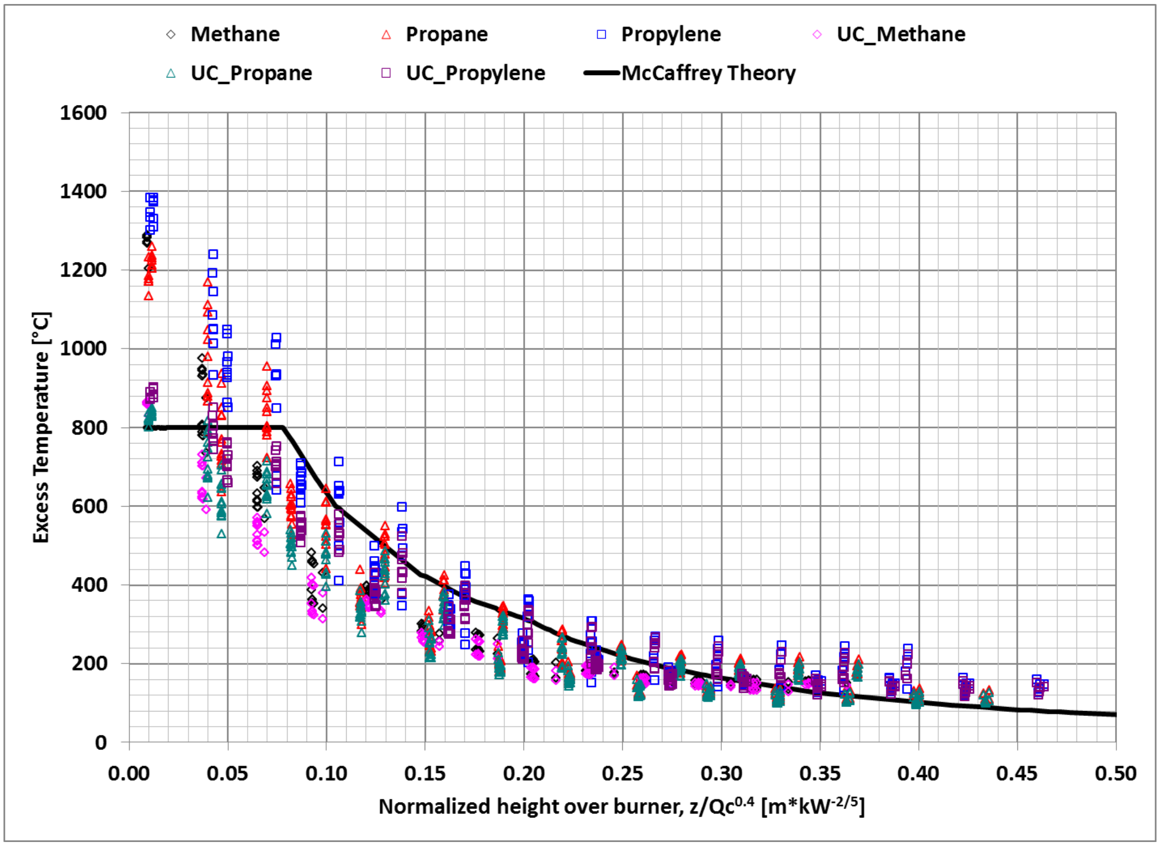

Figure 59 - Centerline temperature of all inert wall fires using 1 ft Square burner, normalized with convective HRR

Figure 60 shows the centerline temperature of all inert wall fires using the 2 ft Rectangle burner normalized with convective HRR. Both corrected and uncorrected temperatures are plotted, and the real gas temperature should be within these two sets of values. The correction often increased the measured temperature by 50% for z < 0.05, but it significantly decreases as z increased. It is observed that compared to the centerline temperature of the 1 ft Square burner inert wall fires and McCaffrey's theory, the temperature generated using the 2 ft Rectangle burner was much lower starting from z = 0.05. This is reasonable because of the shorter flames from the Rectangle burner. The temperature here is also lower than that recorded during the free plume 2 ft burner fires, most likely due to flame lean against the wall.

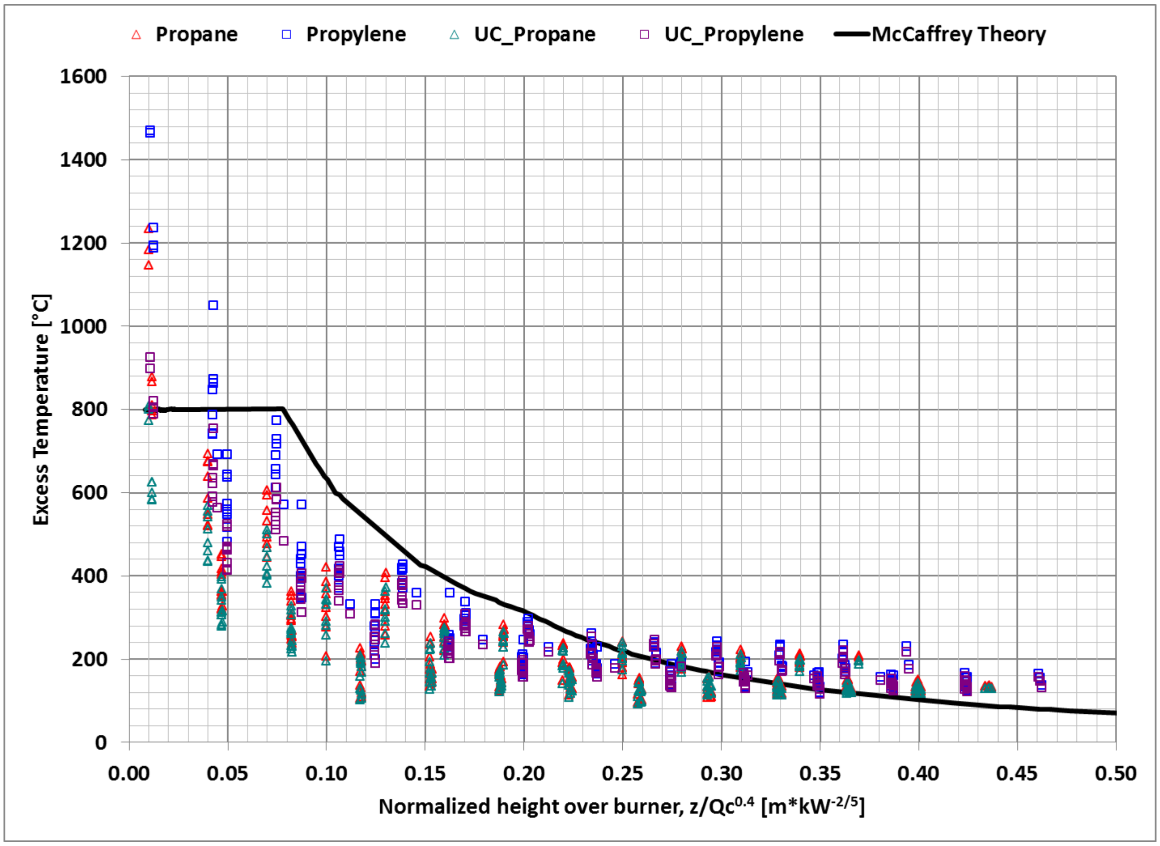

Figure 60 - Centerline temperature of all inert wall fires using 2 ft Rectangle burner, normalized with convective HRR

The fire tests data presented in Figure 57 to Figure 60 are normalized using the mean flame height and presented in Figure 61 to Figure 64. The two different sets of corrected and uncorrected data still formed two bands of temperature “limits” but overall the temperature distribution is tighter when normalized against mean flame height.

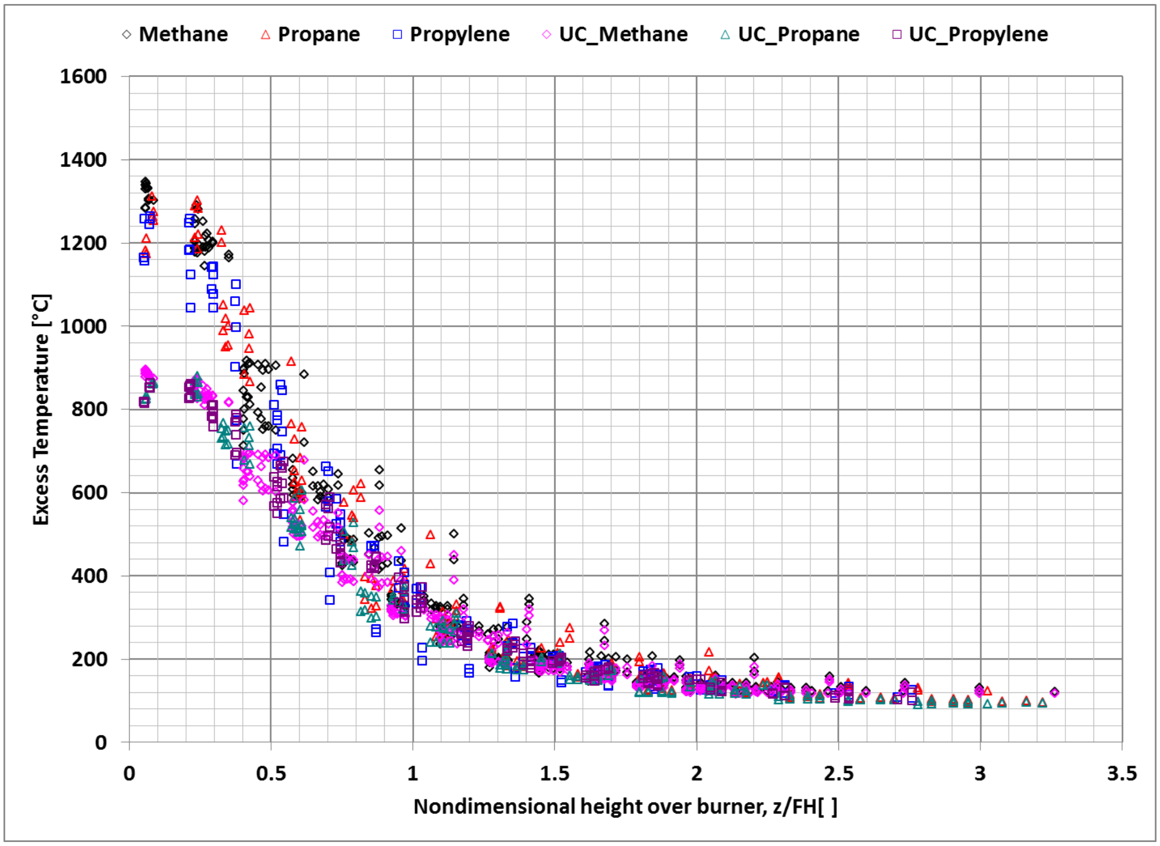

Figure 61 - Centerline temperature of all free plume fires using 1 ft Square burner, normalized with mean flame height

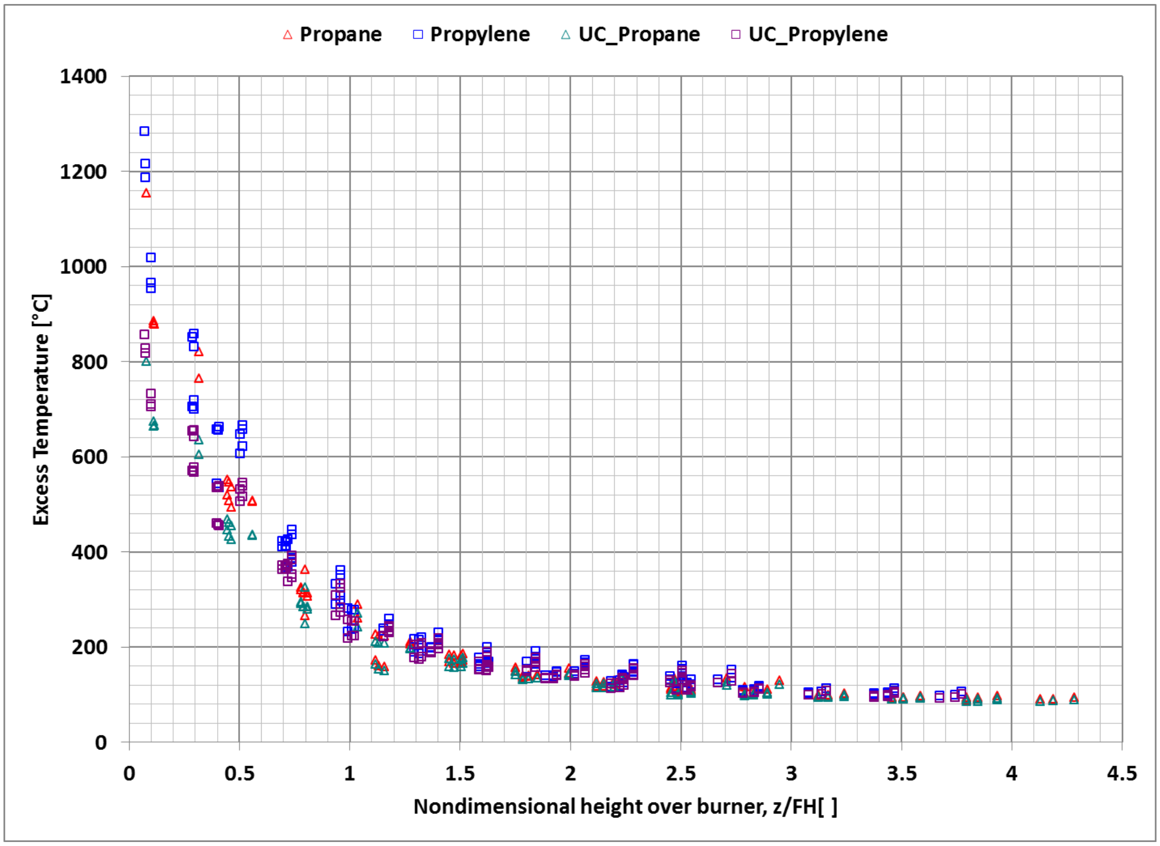

Figure 62 - Centerline temperature of all free plume fires using 2 ft Rectangle burner, normalized with mean flame height

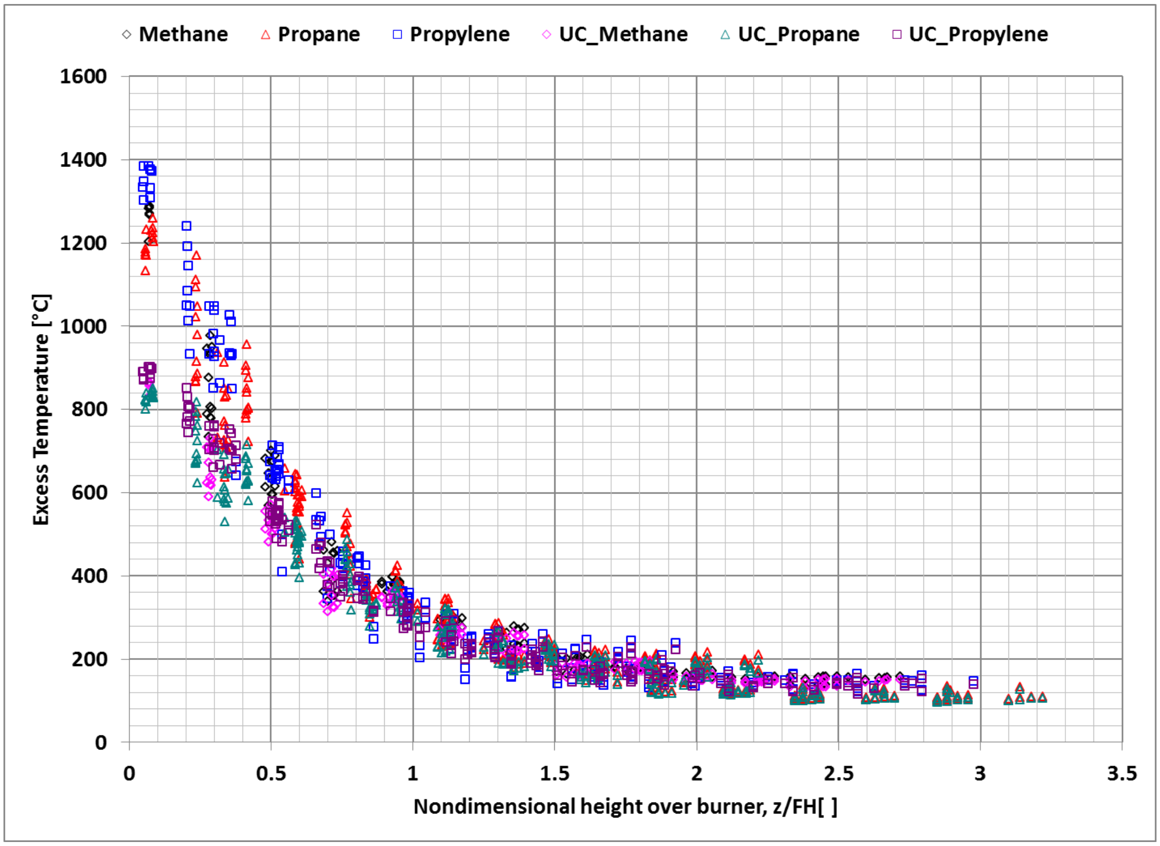

Figure 63 - Centerline temperature of all inert wall fires using 1 ft Square burner, normalized with mean flame height

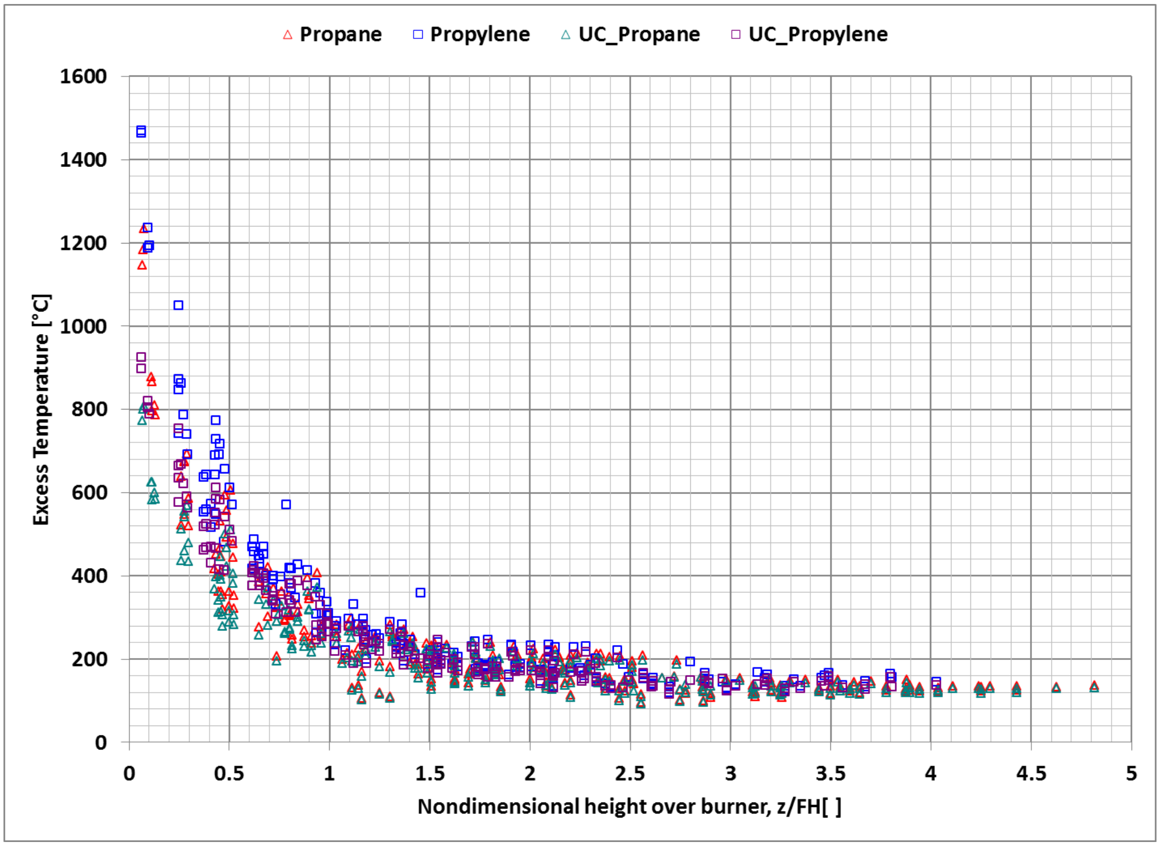

Figure 64 - Centerline temperature of all inert wall fires using 2 ft Rectangle burner, normalized with mean flame height

D.3 Plume Centerline Velocity

Centerline velocities inside a fire plume from three different fuels: propane, propylene, and natural gas (methane) at various HRRs have been measured and collated. Similar data had been collected by McCaffrey [1] and by Hasemi and Tokunaga [2]. In the previous studies, the data, as presented in the literature, had been normalized in two different methods using a form of the fire's heat release rate. The same normalization methods were applied to the current data for comparisons. Additionally, it was found that velocity data can also be normalized using the mean flame height, allowing similar data to be collapsed and compared.

Velocity measuring methods ranged from simple vane anemometer to sophisticated laser Doppler velocimeter (LDV). To measure the velocity inside a fire plume with accuracy repeatedly and economically, a cheap and rugged approach was needed. Bi-directional probes had been proven in other studies over the years to satisfy these criteria. In the current study, bi-directional probes and thermocouples were used to measure the pressure differential and temperature at different heights along the centerline of the fire plume; the velocity was then calculated based on the pressure differential and air properties at the recorded temperature.

The bi-directional probe's design was based on Newman [3], which was in turn based on Heskestad's original design [4]. A bi-directional velocity probe is a short metal pipe with a diaphragm that bisects the tube over a circular plane; a pair of long pipes with small diameter are attached and opened to the two halves of the larger cylinder. The probe is positioned with an open end perpendicular to the measured flow; in the current research, the probes were oriented vertically along the centerline of the plume using two rakes, and the lower section of a probe is the front end where the other section is the back end. The back end of the velocity probe is assumed to remain close to static pressure. When flow is introduced into the front end, it results in a pressure difference between the two tail ends of the thinner pipes, measureable with a pressure transducer.

The pressure transducers were initially installed outside of the burn room and were connected to the two thin pipes of the bi-directional probes via pairs of long (>15 ft) silicone tubing. However, early data suggested that the long tubing was susceptible to pressure loss and hence the transducers were then installed on the rakes and connected to the bi-directional probes with rigid copper tubing. Kaowool blankets were used to insulate the transducers and tubing against heat and fire damage. The transducers used in the current research have a range of ±12.5 Pa and a sensitivity of ±1% over 10 V, about 0.1 V. A voltage change from ambient indicates a pressure difference and a flow. Although the instruments were well insulated, high temperature generated during a fire test can offset the transducers. Hence, the ambient pressures before and after a fire tests were averaged over 3 minutes and used to scale the readings during each test.

Heskestad developed a formula to reduce the pressure and temperature data by using equation [1].

$$U = C * \sqrt{2\Delta P / \rho} \qquad [1]$$

Where:

$U = Velocity$
$C = Calibration\ constant$
$\Delta P = Pressure\ differential$
$\rho = Fluid\ density$

The calibration constant for the specific design of the bi-directional probe was determined to be 1.18 by Newman. The flow was assumed to be made up of air only, and the fluid density was determined based on the temperature of the thermocouple installed in the proximity of the bi-directional probe. The velocity data was then smoothed out and averaged over the time where the source fire was steady.

In the current study, normalization has been applied to the data in the two different ways used by McCaffrey and by Hesemi. They are of similar format, but with McCaffrey relying on the measured HRR, where Hasemi used a characteristic HRR, the hydraulic diameter of the burner, and the virtual origin. Both methods had been applied to the current data, McCaffrey's data, and some of Hasemi's data where possible. (In his article, Hasemi had reported data under both normalization methods; however, some of the data were reported without the necessary information to deconstruct the data to be transformed for different ways of comparisons).

A drawback to directly compare the current dataset with McCaffrey's and Hasemi's is that the fuels of the source fire were different: McCaffrey used methane and Hasemi used propane exclusively, and loose correlation between the datasets could be due to fuel effects. To combat this, an equalization method was applied to the data by finding the convective HRR from each test and from the dataset (where possible) and back-calculating the reported normalizations through the use of the convective HRR. This way, the most significant differing feature of the fire based on the fuels, the radiative heat output, was taken out of consideration and the data can be compared on equal grounds.

Note that the McCaffrey's data is from a series of tests using a 1' x 1' Square burner; Hesami's data is from tests using dia=0.2 m, 0.3 m, 0.5 m circular burner and square burner with sides at 0.2 m, .3 m, and .5 m.

Since McCaffrey reported the mean flame height recorded during his fire tests along with the velocity data, an attempt was made to use the mean flame height as a means for normalization. In this method, the heights of the bi-directional probe were normalized against the mean flame heights. The non-dimensional height was found using equation [2]:

$$Z_{FH} = Z / FH \qquad [2]$$

Where:

$$Z_{FH} = Non - dimensional\ height$$
$$Z = Height\ of\ bi - directional\ probe\ above\ burner$$
$$FH = mean\ flame\ height\ of\ source\ fire$$

In this normalization, the velocity was not non-dimensionalized, but is reported in unit of m/s. Both the current data and McCaffrey's data were normalized using this method for comparison. Similar to the normalizing of McCaffrey's data to account for the convective heat released, his plume centerline velocity data from fires with different HRR was back-calculated to instrument height [m] and velocity [m/s], then equation [2] was used to normalize the height.

To find the uncertainty in McCaffrey's dataset normalized with the convective HRR, velocity data at similar normalized height (0.01 m/kW$^{0.4}$) were grouped together and the standard deviation within each group was found. A similar approach was used to find the uncertainty in the flame height normalized dataset, but an interval of the nondimensional height at 0.05 was used instead. It is assumed that the largest standard deviation value should sufficiently represent the uncertainty in McCaffrey's data. The uncertainty in McCaffrey's velocity, normalized with the convective HRR was found to be about 0.13 m s^{-1} kW$^{1/5}$, and is about 0.72 m/s when normalized with the mean flame height.

The uncertainties in the current dataset were found using the above methods, an uncertainty is associated with each burner size and test type and shown in Table 8.

Table 8 - Velocity data uncertainties based on different factors

Burner Size	Test Type	Uncertainty in velocity
Convective HRR Normalization		
1 ft Square	Free plume	0.28 m s^{-1} kW$^{1/5}$
2 ft Rectangle	Free plume	0.28 m s^{-1} kW$^{1/5}$
1 ft Square	Inert wall	0.23 m s^{-1} kW$^{1/5}$
2 ft Rectangle	Inert wall	0.40 m s^{-1} kW$^{1/5}$
Flame Height normalization		
1 ft Square	Free plume	0.84 m/s
2 ft Rectangle	Free plume	0.94 m/s
1 ft Square	Inert wall	1.33 m/s
2 ft Rectangle	Inert wall	1.42 m/s

Centerline velocity of the free plume fire tests conducted with the 1 ft Square burner, with the mean flame height normalization is presented in Figure 65. The current data falls mostly within the uncertainty of McCaffrey's data for the velocity measured up to 2.5 times the mean flame height. At 1.5 to 3 times of the mean flame height, velocity of the propane and propylene fires falls out of the uncertain range of McCaffrey's data. It is noted that the current data from methane fires correlate quite well with McCaffrey's data from methane fires since both study used same-sized burner and fuel.

The uncertainty of the measured data is about 0.84 m/s.

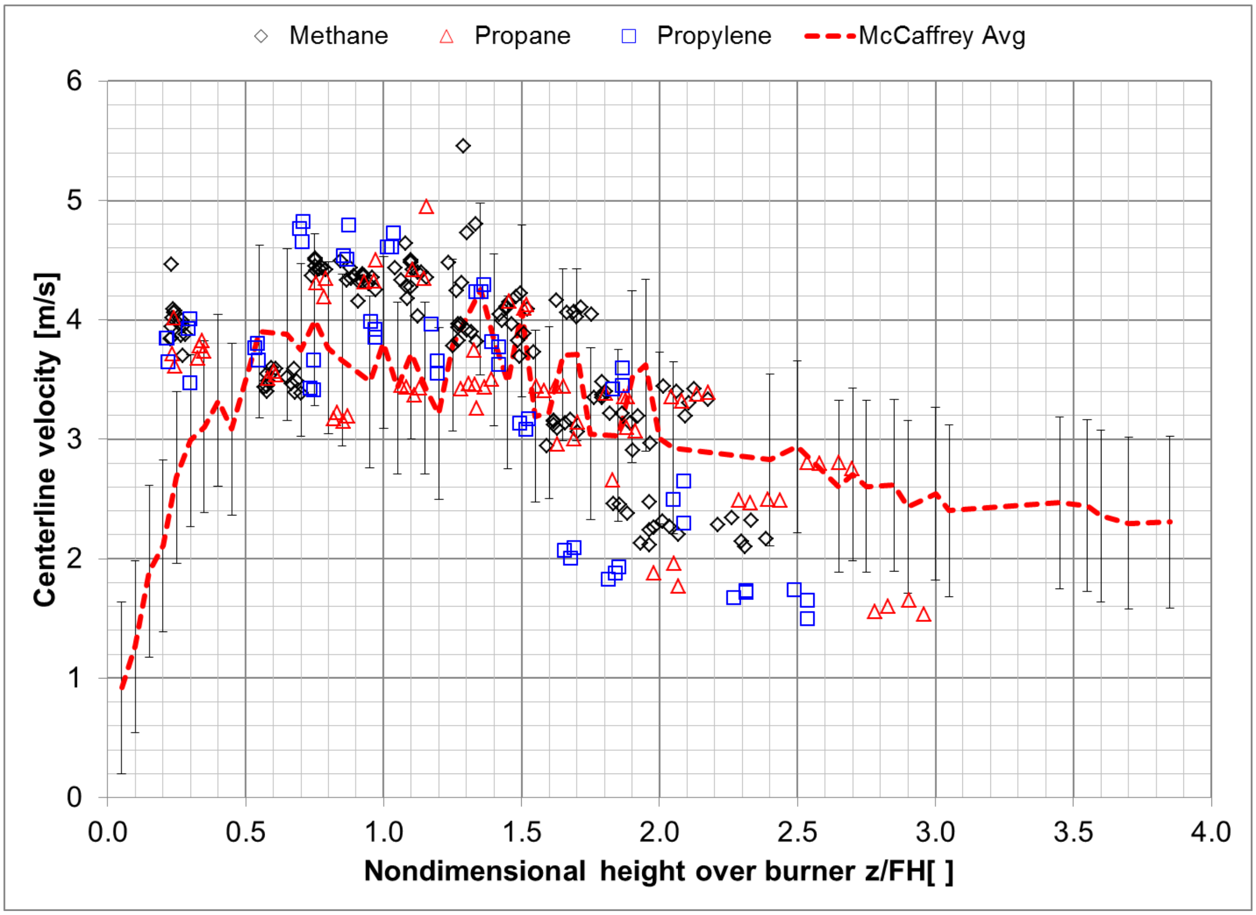

Figure 65 – Free plume fire test centerline velocity, 1 ft Square burner, normalized with mean flame height

Centerline velocity of the free plume fire tests conducted with the 1 ft Square burner, normalized with the convective HRR is presented in Figure 66. The current data generally falls out of the range of McCaffrey's data with uncertainty, although some good correlation is observed in the methane test data. At the normalized height above 2.5, the measured velocity falls below that of McCaffrey's data.

The uncertainty of the measured data is about 0.28 m s^{-1} $kW^{1/5}$, more than twice that of McCaffrey's.

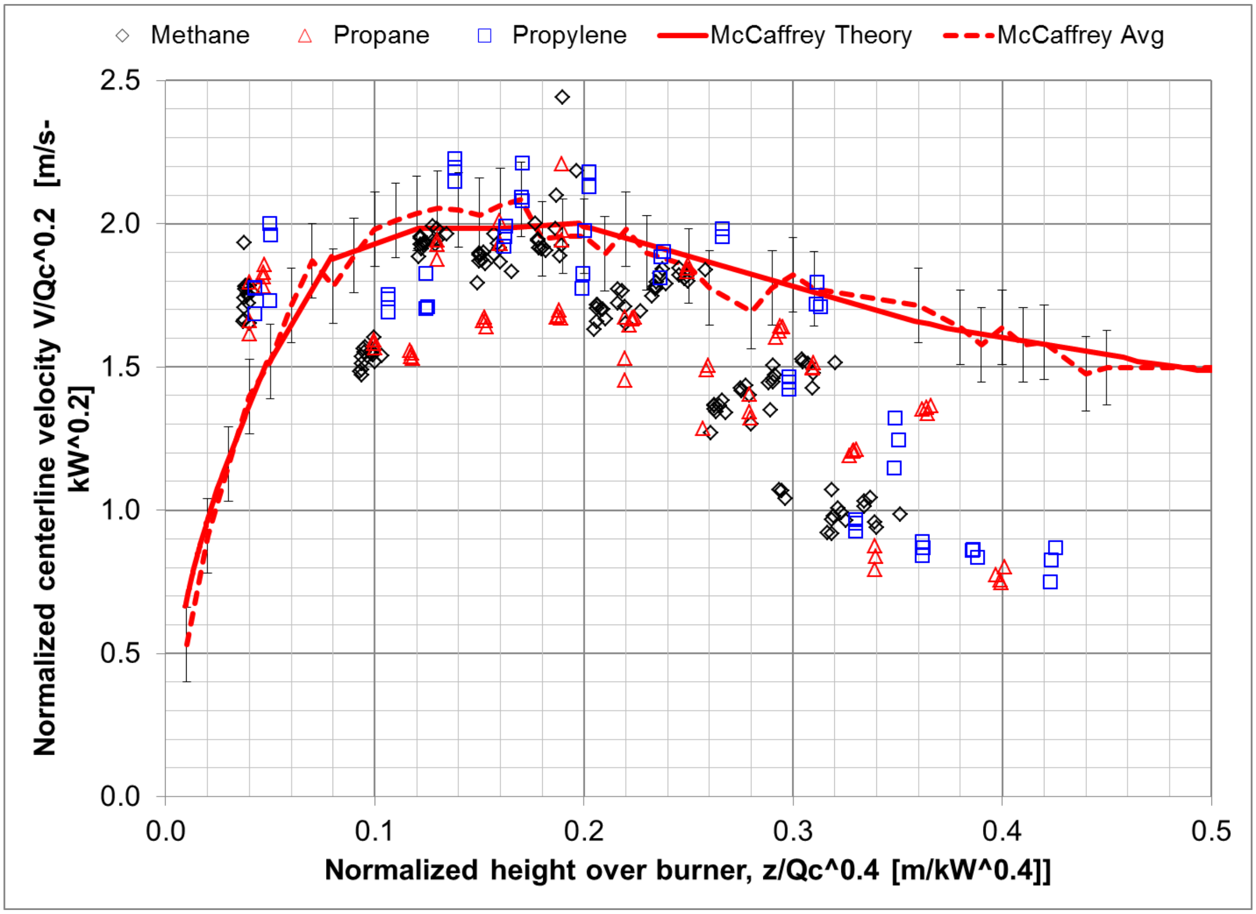

Figure 66 – Free plume fire test centerline velocity, 1 ft Square burner, normalized with convective HRR

Figure 67 presents the centerline velocity from the free plume tests conducted with the 2 ft Rectangle burner, as normalized with mean flame height. The current data falls mostly within the uncertainty of McCaffrey's data. But at over 2 times the mean flame height, some of the measured velocity falls below McCaffrey's uncertainty.

The uncertainty of the measured data is about 0.94 m/s, higher than that of the free plume using 1 ft Square burner. This is reasonable since the plume above the Rectangle burner was observed to fluctuate more.

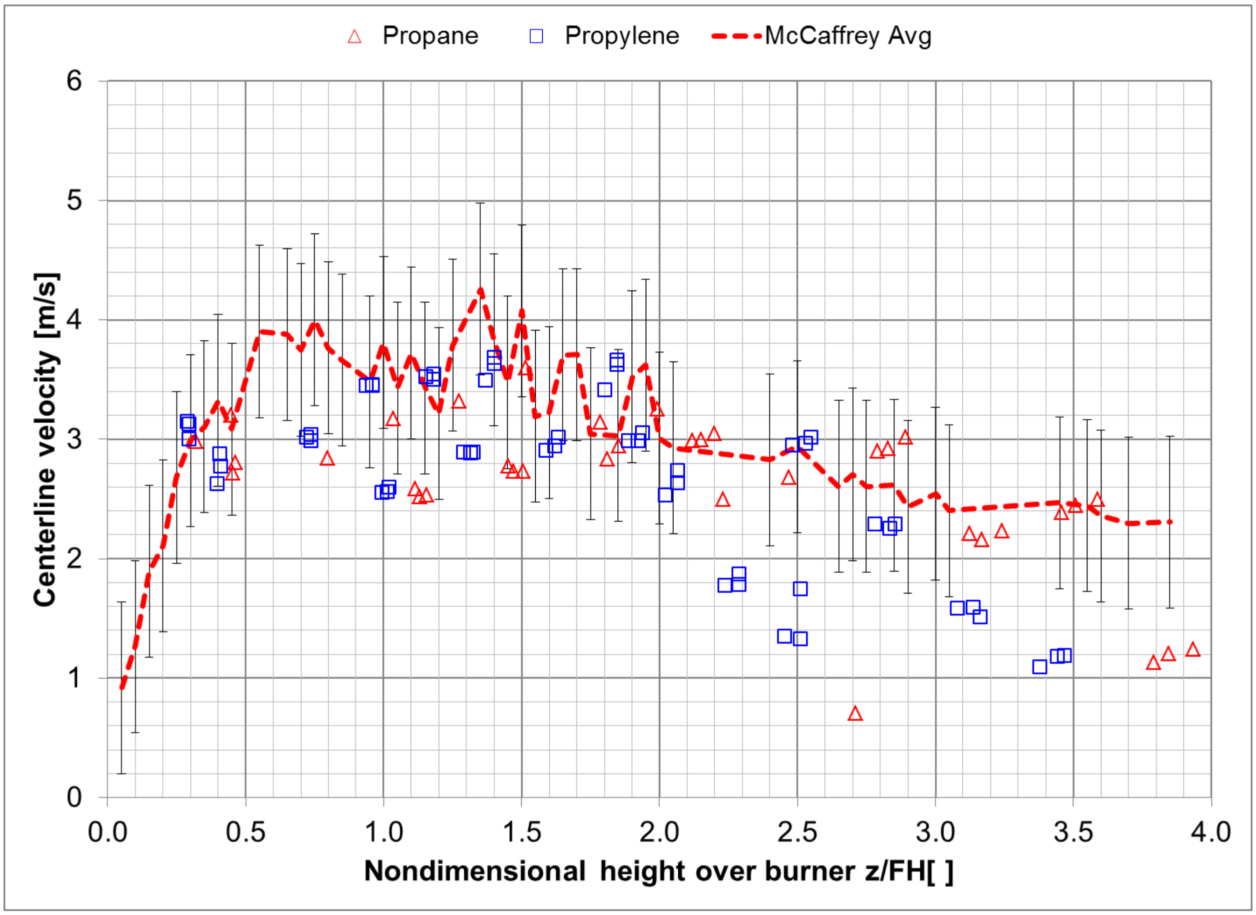

Figure 67 - Free plume fire test centerline velocity, 2 ft Rectangle burner, normalized with mean flame height

Figure 68 presents the centerline velocity from the free plume tests conducted with the 2 ft Rectangle burner, as normalized with the convective HRR. The current data falls mostly below the uncertainty of McCaffrey's data except for the velocity measured at normalized height at 0.05 m/kW$^{0.4}$.

The uncertainty of the measured data is about 0.28 m s^{-1} kW$^{1/5}$, more than twice that of McCaffrey's.

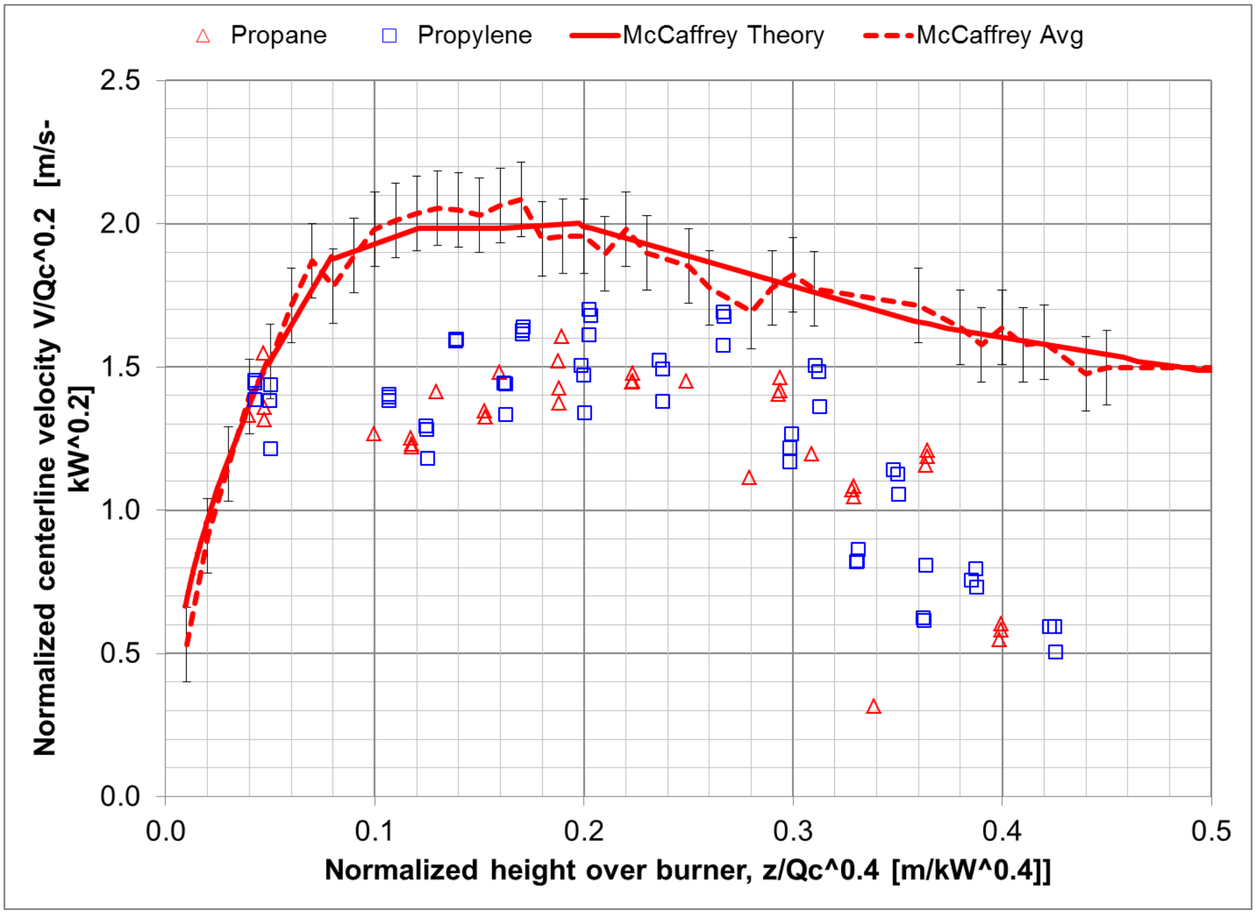

Figure 68 - Free plume fire test centerline velocity, 2 ft Rectangle burner, normalized with convective HRR

Centerline velocity of the inert wall fire tests conducted with the 1 ft Square burner, with the mean flame height normalization is presented in Figure 69. The current data falls mostly within the uncertainty of McCaffrey's data for the velocity measured up to 1.5 times the mean flame height. At 1.5 to 3 times of the mean flame height, velocity of the propane and propylene fires falls out of the uncertain range of McCaffrey's data. It is noted that the current data from methane fires correlate quite well with McCaffrey's data from methane fires since both study used same-sized burner and fuel. The measured velocity in the inert wall tests is generally lower than that from the free plume tests, most likely due to the fact that the plume leans against the inert wall and its centerline no longer corresponds to the bi-directional probes' centerline.

The uncertainty of the measured data is about 1.33 m/s, greater than that from the free plume tests, most likely due to the plume's leaning tendency as previously mentioned.

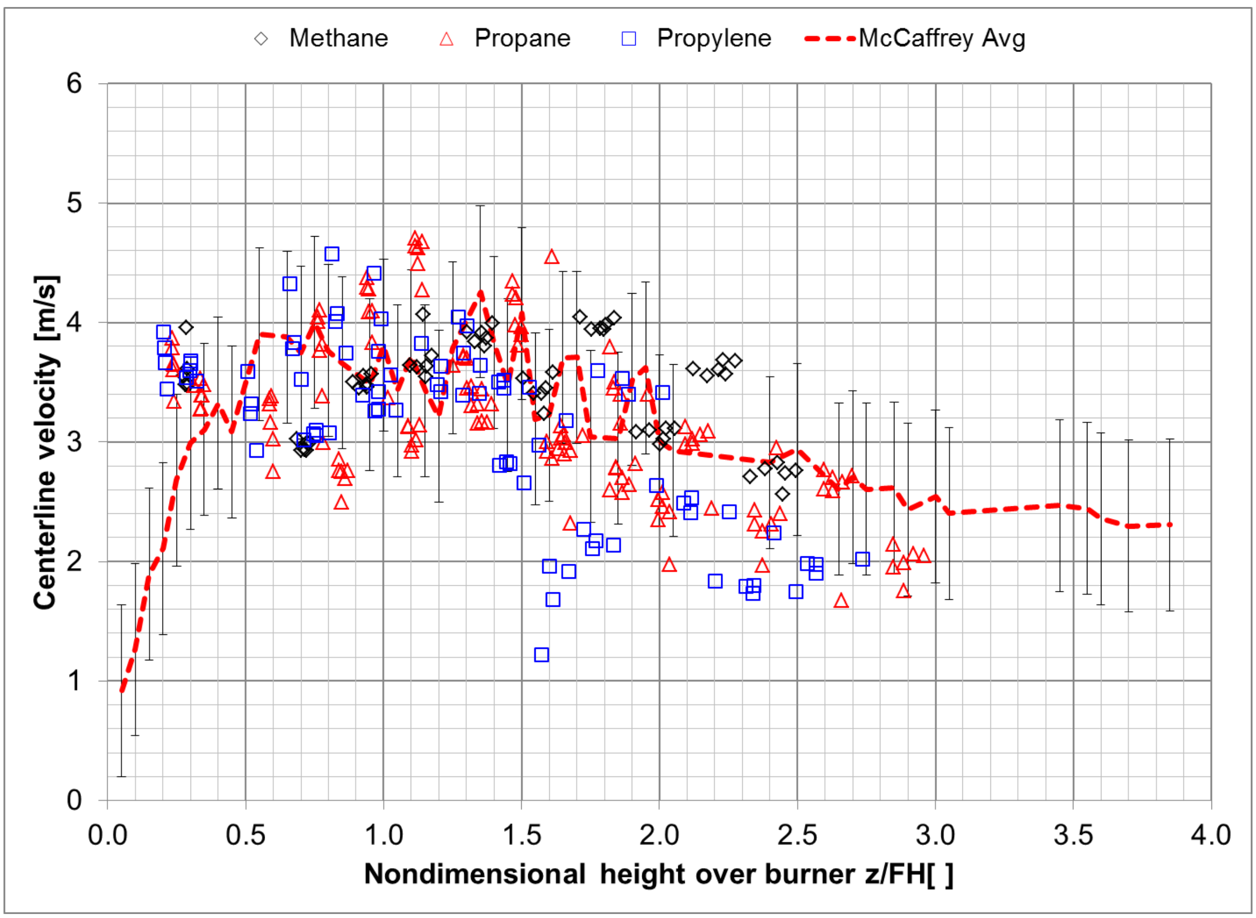

Figure 69 – Inert wall fire test centerline velocity, 1 ft Square burner, normalized with mean flame height

Centerline velocity of the inert wall fire tests conducted with the 1 ft Square burner, with the convective HRR normalization is presented in Figure 70. The current data generally falls out of the range of McCaffrey's data with uncertainty, which is to be expected due to the plume's leaning against the wall and out of the centerline.

The uncertainty of the measured data is about 0.22 m s^{-1} $kW^{1/5}$, about twice that of McCaffrey's.

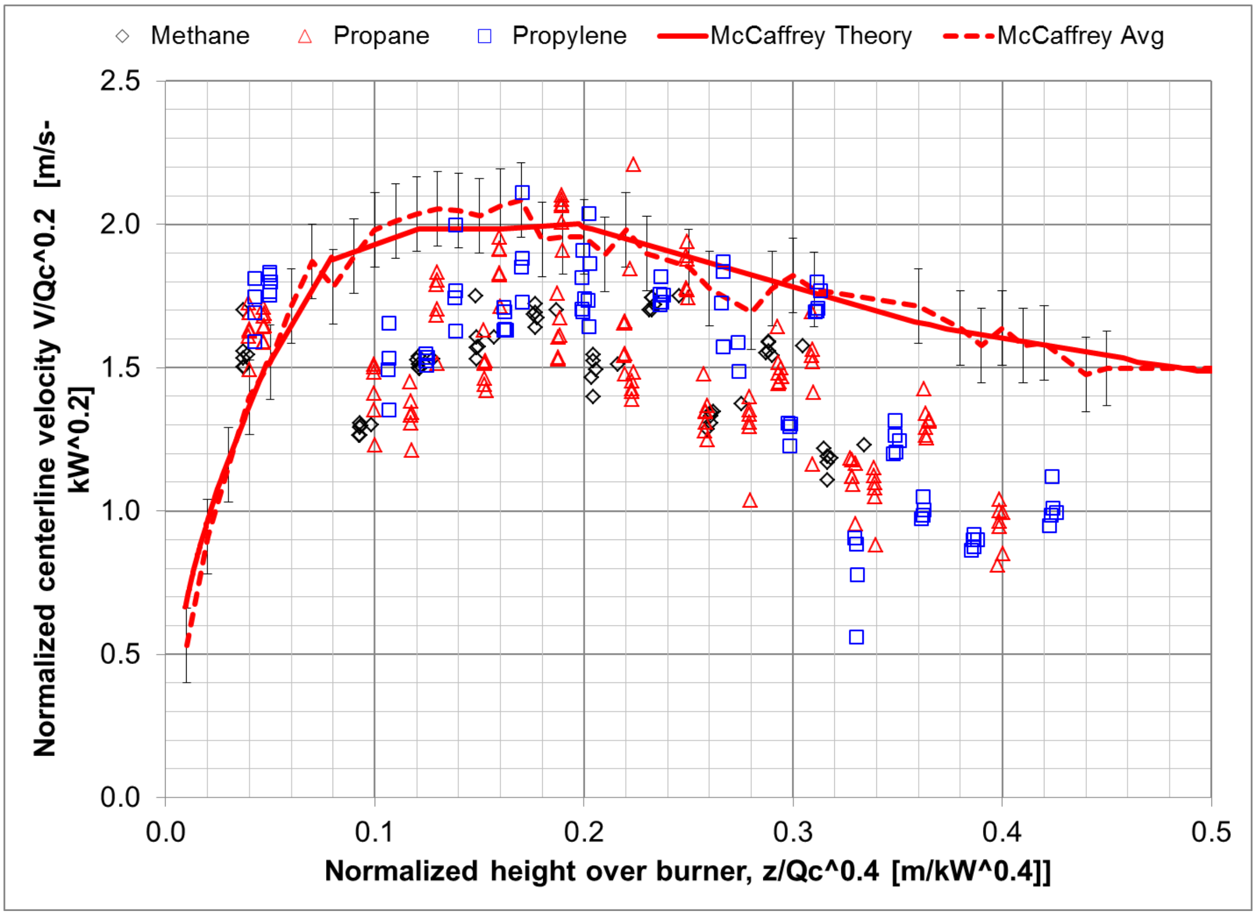

Figure 70 – Inert wall fire test centerline velocity, 1 ft Square burner, normalized with convective HRR

Figure 71 presents the centerline velocity from the inert wall tests conducted with the 2 ft Rectangle burner, as normalized with mean flame height. There is significantly greater scatter in this data than the velocity data generated in other test configurations, due to the larger burner used and the wall leaning tendencies common in inert wall fire tests.

The uncertainty of the measured data is about 1.42 m/s, highest of all.

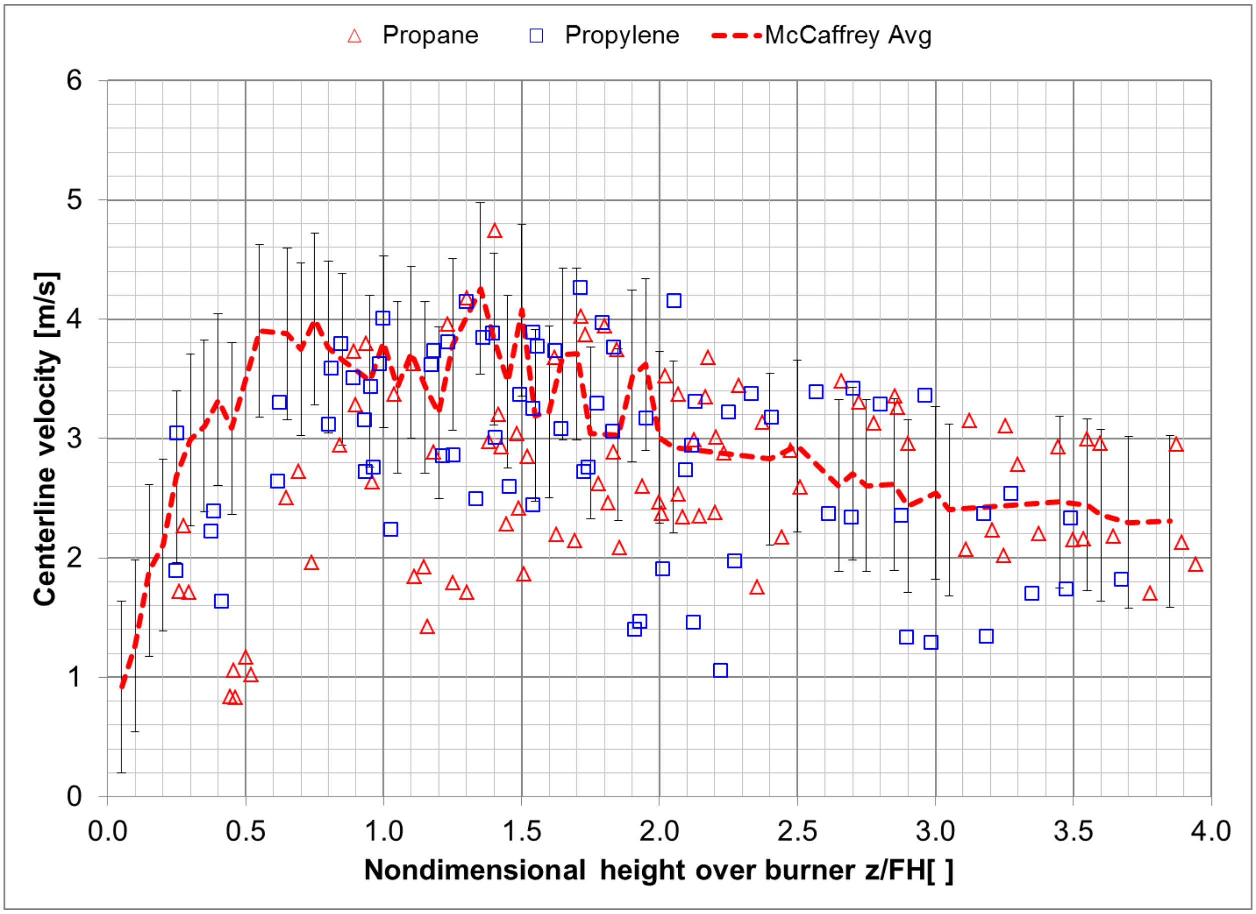

Figure 71 – Inert wall fire test centerline velocity, 2 ft Rectangle burner, normalized with mean flame height

Centerline velocity of the inert wall fire tests conducted with the 2 ft Rectangle burner, with the convective HRR normalization is presented in Figure 72. The current data generally falls out of the range of McCaffrey's data with uncertainty, which is to be expected due to the larger burner used and the fire plume's leaning against the wall and out of the centerline.

The uncertainty of the measured data is about 0.40 m s^{-1} $kW^{1/5}$, about three times that of McCaffrey's.

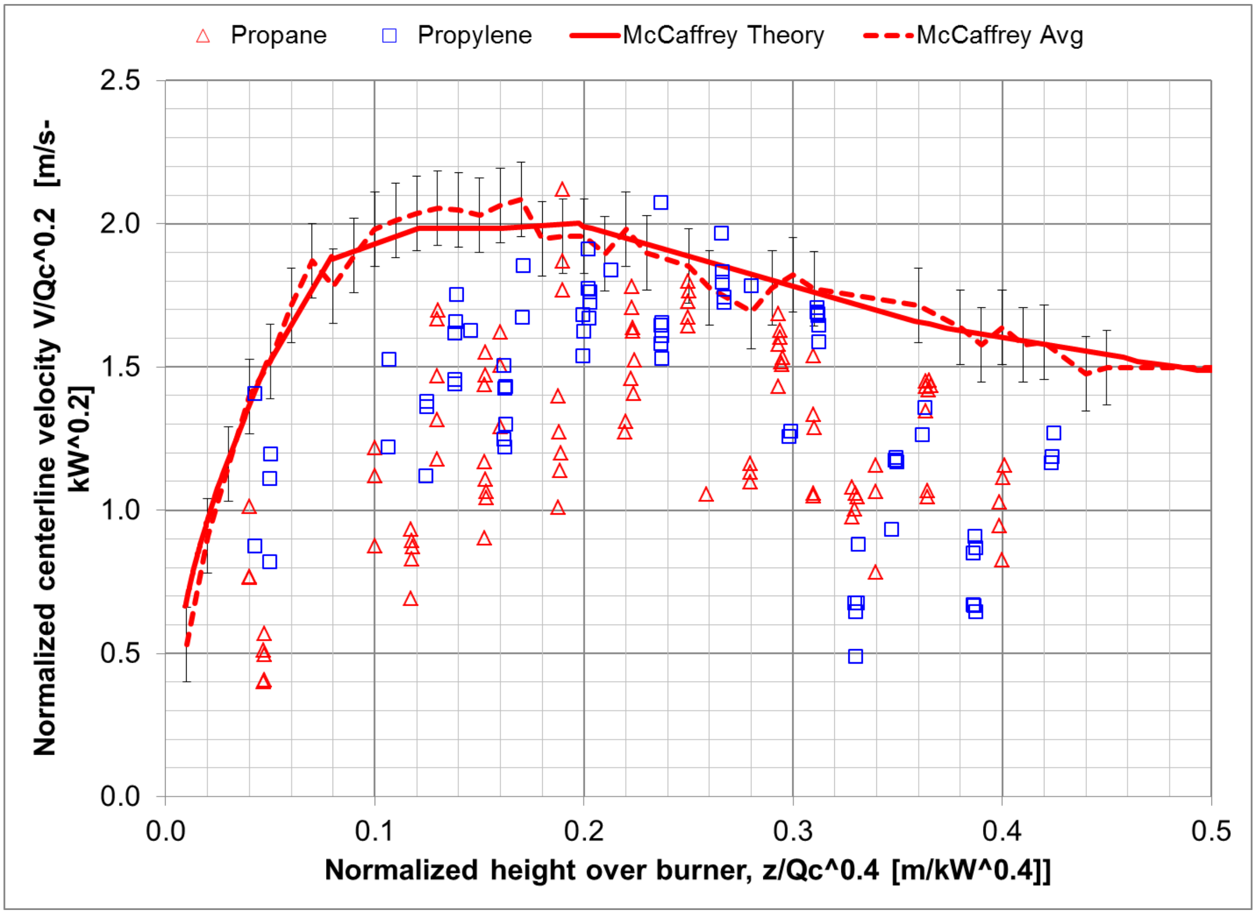

Figure 72 – Inert wall fire test centerline velocity, 2 ft Rectangle burner, normalized with convective HRR

To present the current velocity data in the same format used by Hasemi, the velocity probe's height was normalized using equation [3], and the measured velocity is normalized using equation [4].

$$\frac{Z + dZ}{Q*^{\frac{2}{5}} D_h} = \text{non-dimensoinal height} \quad [3]$$

$$\frac{U}{\sqrt{Q*^{\frac{2}{5}} D_h}} = \text{non-dimensoinal velocity} \quad [4]$$

Where:

$dZ = distance\ to\ virtual\ origin$
$Q* = non - dimensional\ HRR$
$D_h = hydraulic\ diameter\ of\ burner$

And the characteristic HRR Q* is defined by:

$$Q* = \frac{Q}{\rho_\infty cp T_\infty g^{0.5} D_h^{2.5}} \quad [5]$$

McCaffrey's data was deconstructed into the empirical height and velocity, and then normalized accordingly to Hasemi's method. It is noted that Hasemi's velocity data was presented in the paper in the already-normalized format without specific information to the HRR of the tests, thus it was not possible to correct the non-dimensional HRR convectively.

The comparison between the current 1 ft Square free plume fire velocity data, McCaffrey's, and Hasemi's data is presented in Figure 73. It should be noted that the current data has the most similarity with McCaffrey's and Hasemi's Square burner test data. The methane free plume data appears to follow the trend of McCaffrey's data at normalized height value from 1 to 4, and the propane free plume data appears to follow the trend of Hasemi's data at normalized height value from 0 to 4. At normalized height > 4, the current velocity data seem to fall below the other datasets. Overall, the current data appears to be within the bands of data set by McCaffrey and Hasemi.

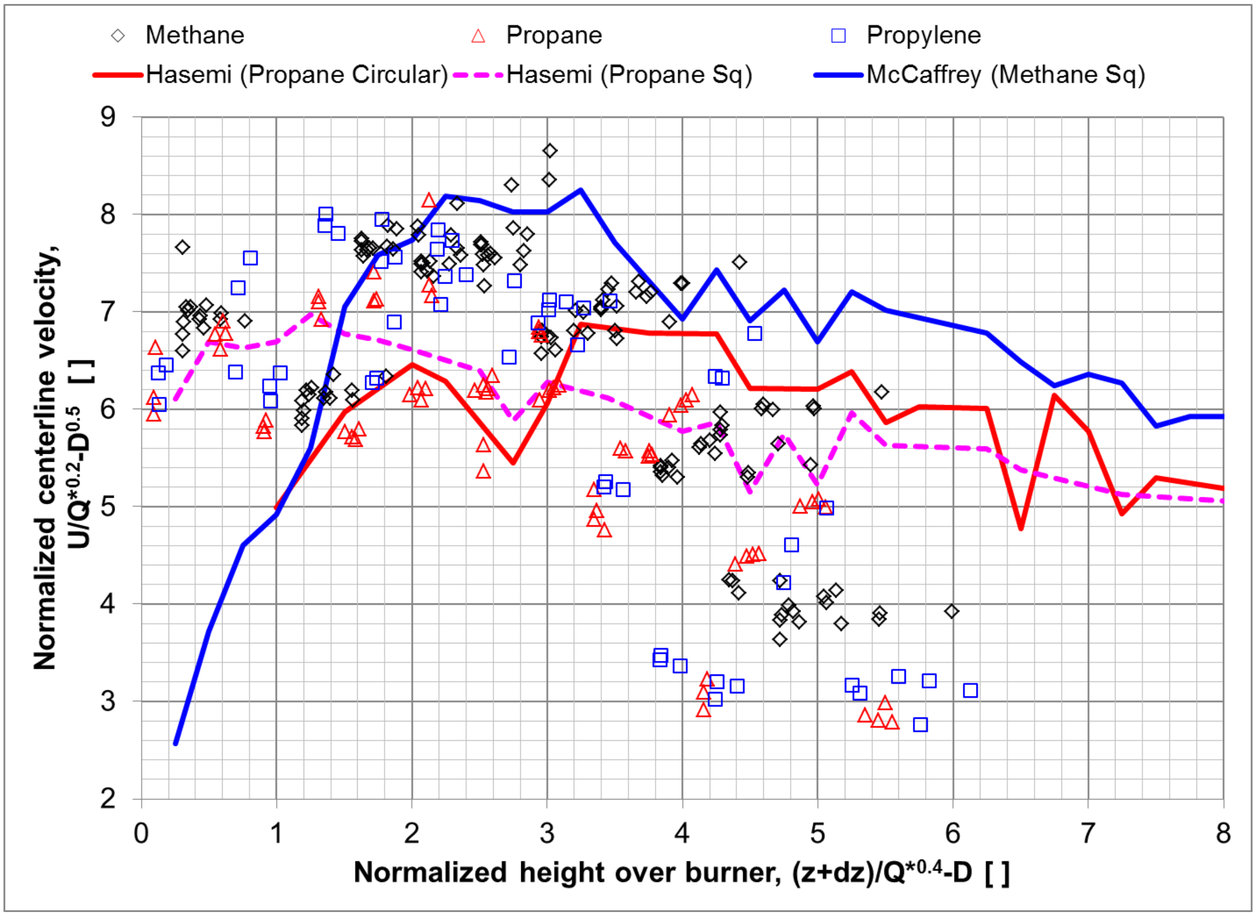

Figure 73 -1 ft Square burner velocity comparison with Hasemi, no convective correction

Figure 74 presents the current free plume fire centerline velocity using the 2 ft Rectangle burner as compared to the McCaffrey and Hasemi datasets. Both the propane and propylene free plume centerline velocity appears to follow the trend set by Hasemi's dataset but has a lower value overall. This is expected as the burner shape and size between the current data and the compared data were different.

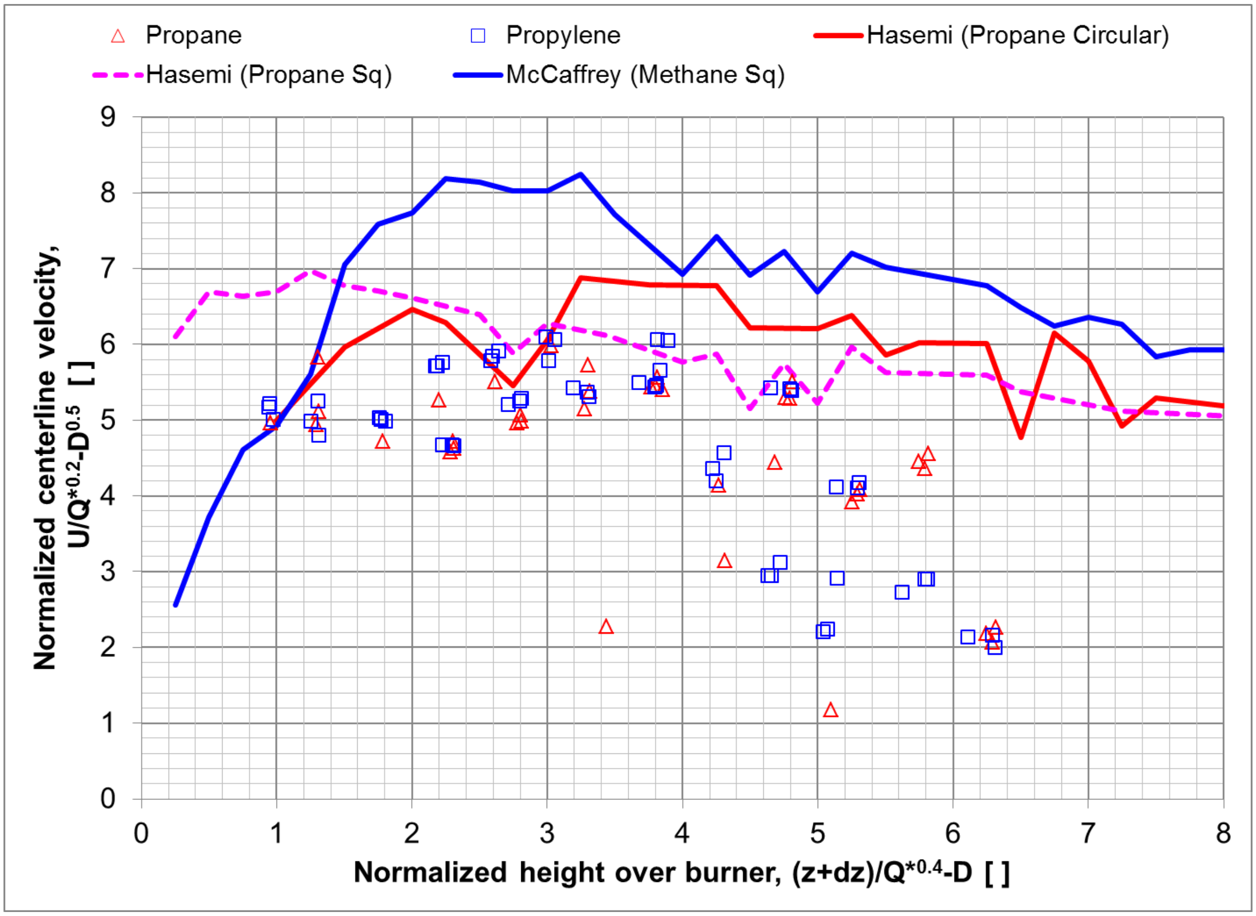

Figure 74 - 2 ft Rectangle burner velocity comparison with Hasemi, no convective correction

D.4 Wall Heat Flux

Heat flux is one of the major driving forces behind flame spread, this energy imposed on the combustible material by a base fire may be used to preheat additional fuel and provide the necessary energy for pyrolysis and combustion.

Thin-skin calorimeters were used to measure heat flux on the inert wall. In the combustible wall experiments, several water-cooled heat flux gauges were installed to compliment the thin skin calorimeters.

The thin skin calorimeters are constructed using square Inconel plates (5.0 cm x 5.0 cm), painted black, mounted on 2 layers of Kaowool ceramic fiber boards. A thermocouple wire was welded to the back center of the Inconel plate and another thermocouple was sandwiched between the two Kaowool boards. Temperature data was gathered from each test, and the temperature differential between the two thermocouples was used to calculate the heat flux at the thin skin calorimeters. Heat transfer from the calorimeters by radiation, convection, and conduction were considered.

The water-cooled heat flux gauges used in the experiments were of the Schmidt-Boelter thermopile type sensor. The heat flux is absorbed at the surface and transferred to the back water-cooled surface, where temperature differential between the surfaces is a function of the absorbed heat flux and the emf output is generated by a thermopile.

A total of 18 thin skin calorimeters were installed on the wall, they were located along the centerline, at 1 ft and 2 ft left/right of the centerline, at different height. In the combustible wall experiments, the heat flux gauges were installed 1 ft off of the centerline at various heights. Figure 75 shows the locations of the thin skin calorimeters (as numbers) and heat flux gauges (as letters).

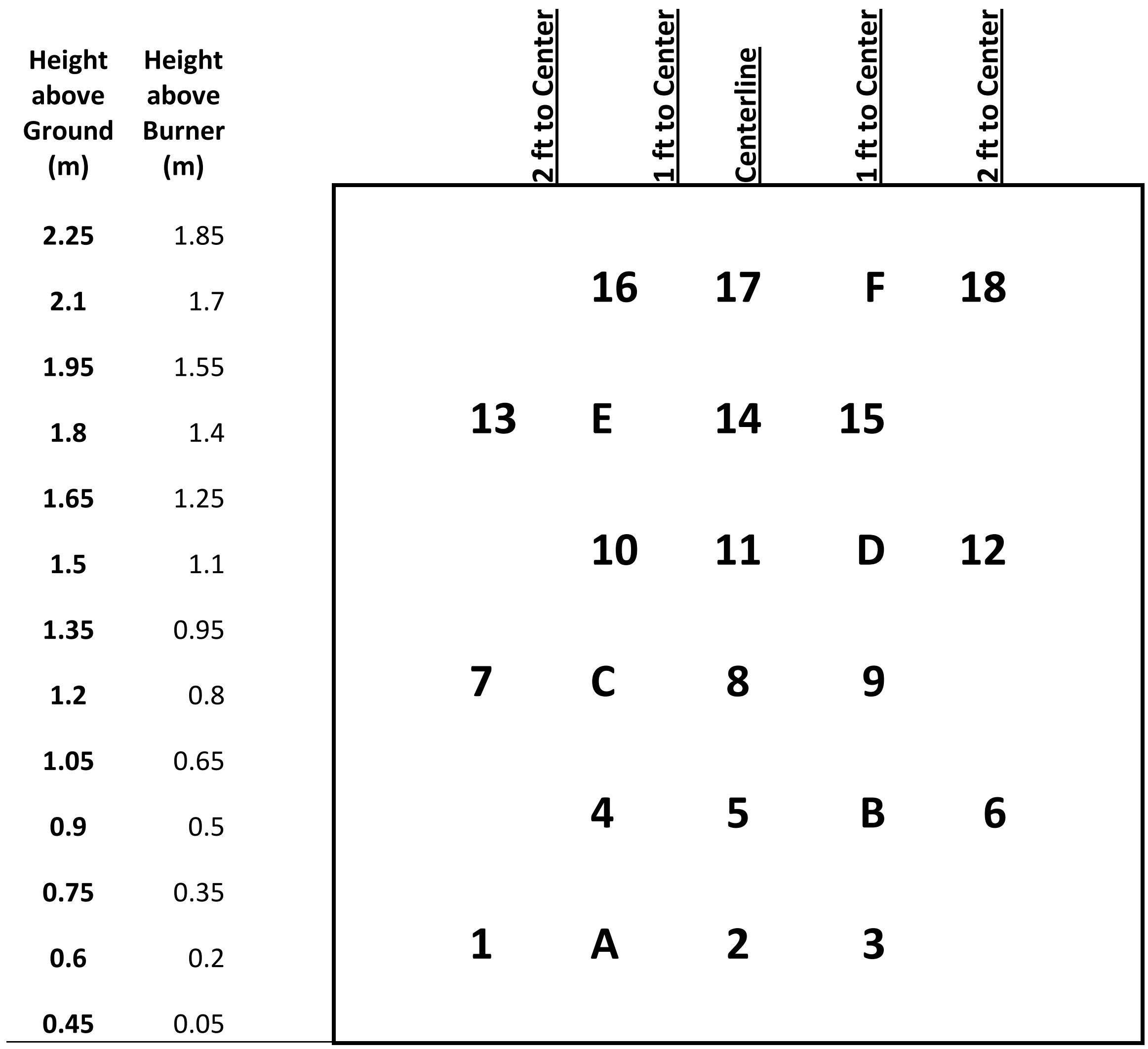

Figure 75 - Thin skin calorimeter locations on wall

The design of the thin skin calorimeters was completed before the full-scale fire tests, they are tested in the cone calorimeter as standalone units under different heat fluxes measured with a calibrated water-cool Schmidt Boelter heat flux gauge that has an uncertainty of about 2% full range of 100 kW/m^2 = 2 kW/m^2. Two identical thin skin calorimeter units (TSC_Unit A and TSC_Unit B) are tested for consistency.

Table 9 and Table 10 show the data used for the calibration of the thin skin calorimeters. There are about 150 readings per TSC unit per heat flux, and the standard deviation of the sample and the standard deviation of the mean of the measurements are found. For both units, the standard deviation was largest when the heat flux was large, and the heat fluxes measured are lower than the "true" heat fluxes. The largest standard deviation is 2.60 kW, and it is show in both Figure 76 and Figure 77. Figure 76 shows the calibration data as two separate datasets and Figure 77 shows the calibration data as a single dataset with an "averaged" regression line.

Table 9 - TSC Unit A Calibration Data

	(kW)	(kW)	(kW)	(kW)	(kW)	(kW)	(kW)
Heat Flux Gauge	100	84.8	75.5	50.8	30.1	21.3	10.5
TSC Mean	87.80	77.32	68.28	49.47	29.21	20.72	10.15
Std Dev Sample	2.60	1.41	1.12	1.72	0.59	0.36	0.18

Table 10 - TSC Unit B Calibration Data

	(kW)	(kW)	(kW)	(kW)	(kW)	(kW)	(kW)
Heat Flux Gauge	100	84.8	75.5	50.8	30.1	21.3	10.5
TSC Mean	88.82	77.93	69.99	50.65	29.36	20.62	11.19
Std Dev Sample	2.59	1.40	0.99	2.00	0.97	0.34	0.54

Considering how the orientation and the construction of the TSCs are different than from the units used in the cone calibration, the correction factor deduced from the calibration may not be applicable for the full-scale TSC data. Perhaps it is more reasonable to show the full-scale test mean heat flux data with error bars of 2.6 kW/m^2 (one standard deviation).

Figure 76 - TSC Calibration at various heat fluxes, separate datasets for both TSCs

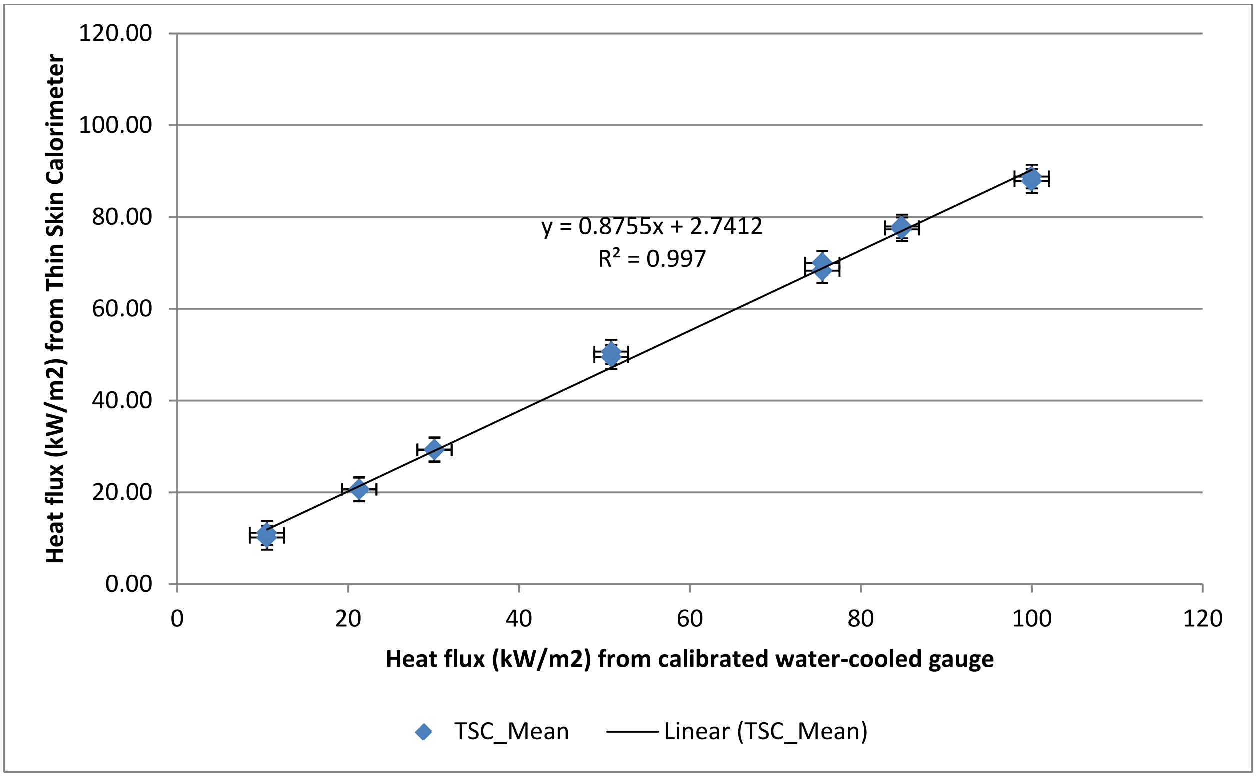

Figure 77 - TSC Calibration at various heat fluxes, single dataset for both TSCs

In the full-scale inert wall test series, the heat flux data was calculated from the thin skin calorimeter's temperature data, and then averaged to find a mean heat flux at each location for when the fire had achieved a steady HRR. The temperature differential between the front- and the back-face thermocouples was converted to absorbed heat flux based on the material properties of the Inconel plate and the ceramic fiber board substrate. The calculated absorbed heat flux was corrected with heat transfer losses such as conduction into the substrate, convective losses over the plate, and radiative losses on the surface of the Inconel plate.

The conductive loss into the surrounding substrate was calculated using a finite difference scheme using the temperature measured at the two thermocouples; the calculations assume a constant loss through the substrate.

Convective heat transfer at the thin skin calorimeter mainly consists of the heat transfer between the flow and the Inconel plate. Along the centerline, the flow is nominally upward and hot, which adds heat into the TSCs. But away from the centerline, the flow conditions are more complicated, as the TSCs may be inside the heated plume, but also may be cooled off by entrained cool air. Hence, the velocity of the flow over the plate is a significant factor. In the present analysis, the convective heat loss at the TSCs along the centerline was calculated using the velocity measured at the centerline, and for the TSCs that were 2 ft away from the centerline, which are outside of the plume, the velocity was assumed to be 0.5 m/s, which had been estimated by other researchers for flow around the compartment. For the TSCs 1 ft away from the centerline, a velocity of 0.5 m/s was used for tests with the 1 ft Square burner, with the assumption that these TSCs were outside of the plume. In some tests using the 2 ft Rectangle burner, the velocity near the plates had been recorded at about 5 cm away from the plates; these measurements were used in similar tests with corresponding HRRs for the convective heat transfer calculations. Table 11 shows the different velocity measurements used in convective heat loss calculations for the wall heat flux.

Table 11 - Velocity for convective heat transfer calculation in heat flux calculations

	Velocity at TSCs		
	TSCs on centerline	TSCs 1 ft away	TSCs 2 ft away
Square	plume centerline	0.5 m/s	0.5 m/s
Rectangle	plume centerline	measured at plate	0.5 m/s

The radiative heat transfer (irradiation) was calculated using the temperature at the plate and the ambient gas temperature over the plate. The ambient gas temperature over all TSCs was assumed to be the plate temperature before burner ignition.

The previously calculated uncertainty in the heat flux measurement should be increased on account of the various heat loss corrections applied to the measurements since the calculations involved other measured quantities during the experiments. These quantities such as temperature and velocity have their inherent uncertainties and are to be considered in the heat flux measurement's uncertainties. Of the three corrections, the largest uncertainty came from the convective correction where the velocity uncertainty was large. For now it is assumed that the uncertainty was twice the uncertainty determined during calibration at 5.2 kW/m^2. Alston suggested that the uncertainty may be as great as 10% of the measurement.

Figure 78 to Figure 80 show the heat flux of the 1ft Square burner tests using methane, propane, and propylene at various HRRs. Figure 81 and Figure 82 show the heat flux of the 2ft Rectangle burner tests using propane and propylene at 50 kW and 75 kW. The height of the TSCs had been normalized using the 50% intermittency flame height from each test. No normalization for the heat flux had been done at this point. Data from all fires were stable without tilt or flame detachment, so the 1ft and 2ft left/right heat fluxes were collapsed onto 2 sets of data labeled as 2ft from centerline and 1ft from centerline.

The centerline heat flux greatly exceeds the heat flux measured at the other positions in all cases. Heat fluxes from the propylene tests were generally greater than the other two fuels for the corresponding heights. These trends are consistent for the heat fluxes measured for the 2ft Rectangle burner tests for propane and propylene as well.

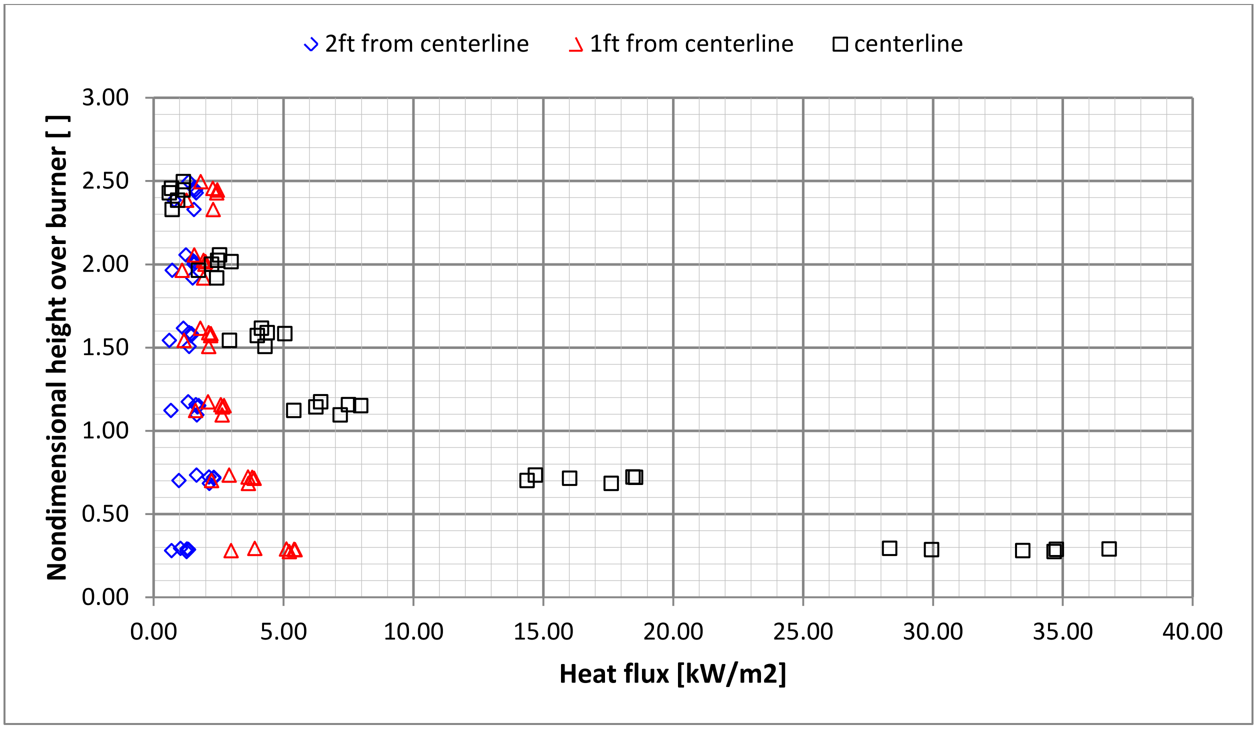

Figure 78 - Heat flux from Methane 1ft Square burner tests

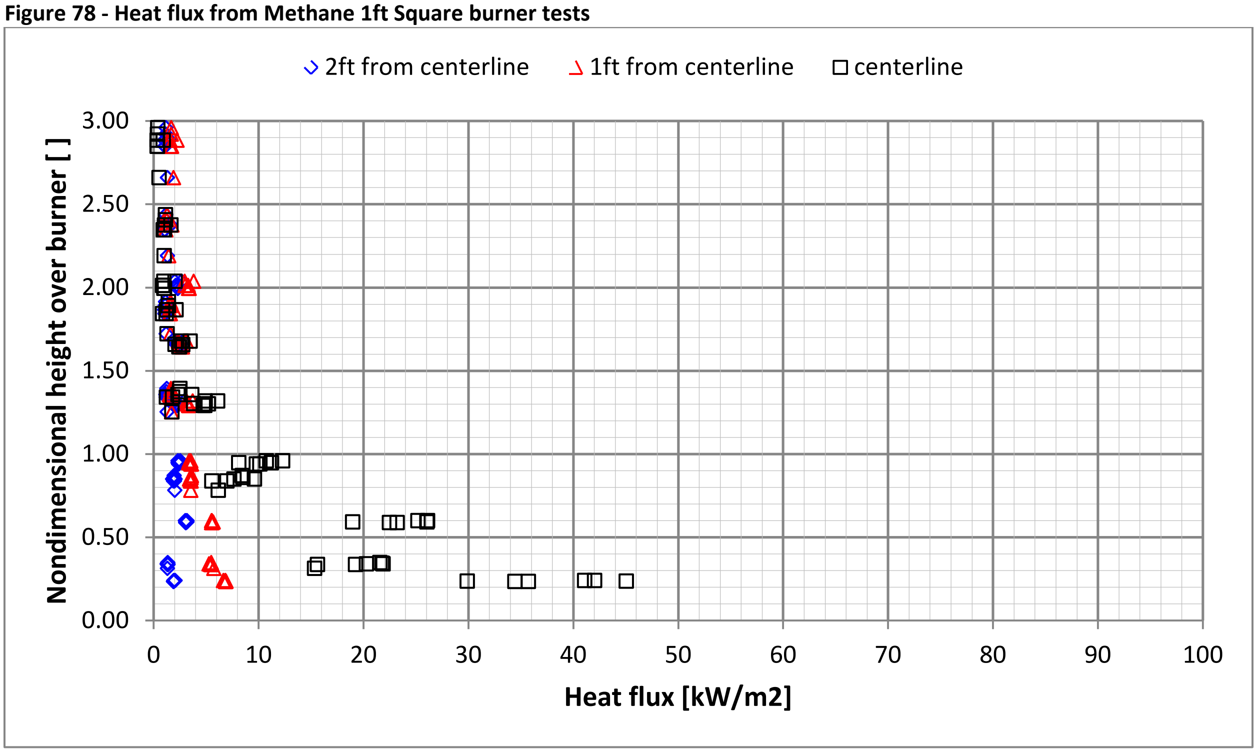

Figure 79 - Heat flux from Propane 1ft Square burner tests

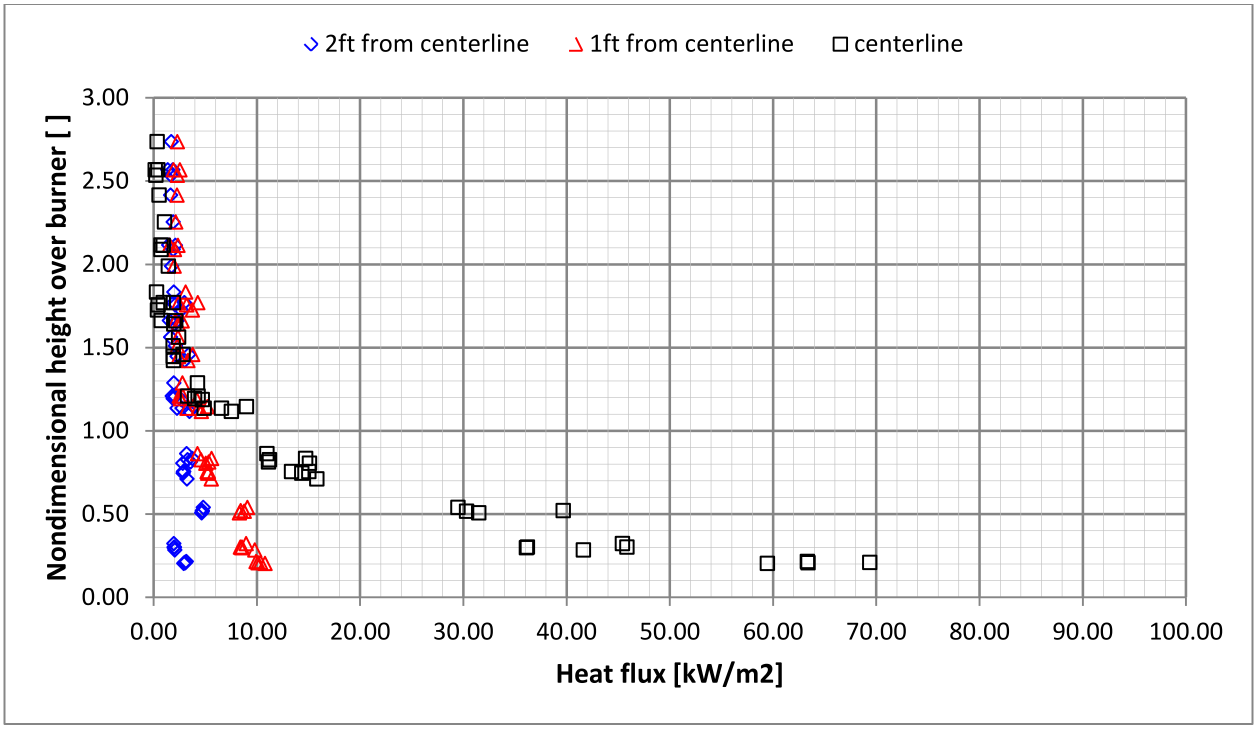

Figure 80 - Heat flux from Propylene 1ft Square burner tests

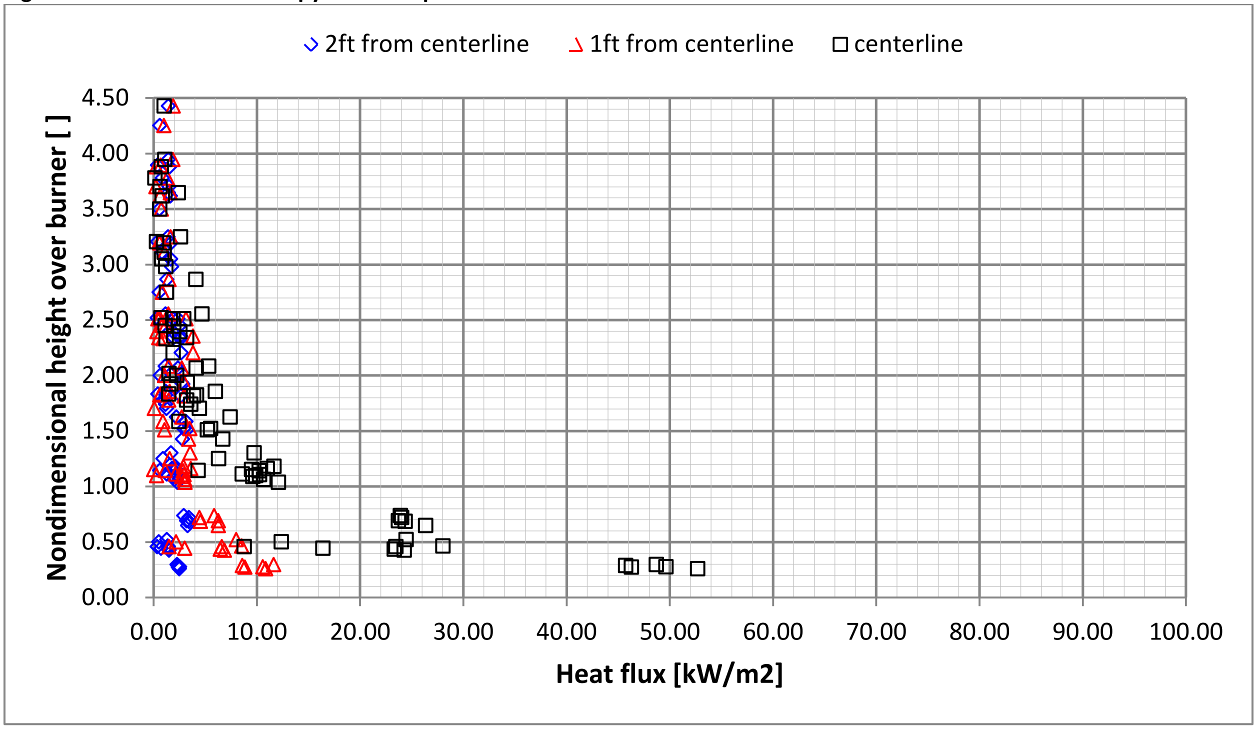

Figure 81 - Heat flux from Propane 2ft Rectangle burner tests

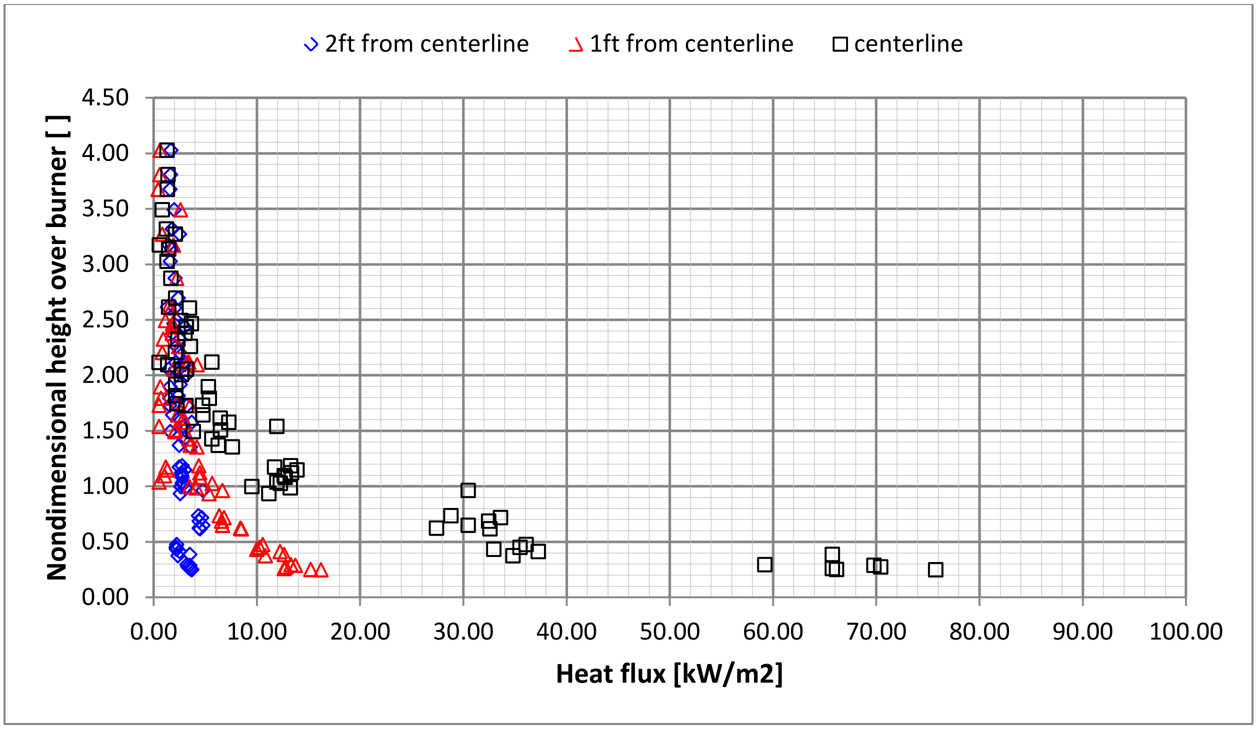

Figure 82 - Heat flux from Propylene 2ft Rectangle burner tests

D.4.1 Wall Heat Flux Normalization with the Source Convective Heat Release Rate

A method to normalize the heat flux based on the convective heat release rate of the tests was explored. The results from the 1ft Square burner test are presented in Figure 83 to Figure 85. Results from the 2ft Rectangle burner are presented in Figure 86and Figure 87. The heat flux was divided by the convective heat release rate of the fire based on fuel type and the flow-based HRR (for propane and propylene) and O2-based HRR (for the methane).

Normalization with the convective HRR does not seem to have a large effect on the appearance of the data. The same trends from the un-normalized data still hold true.

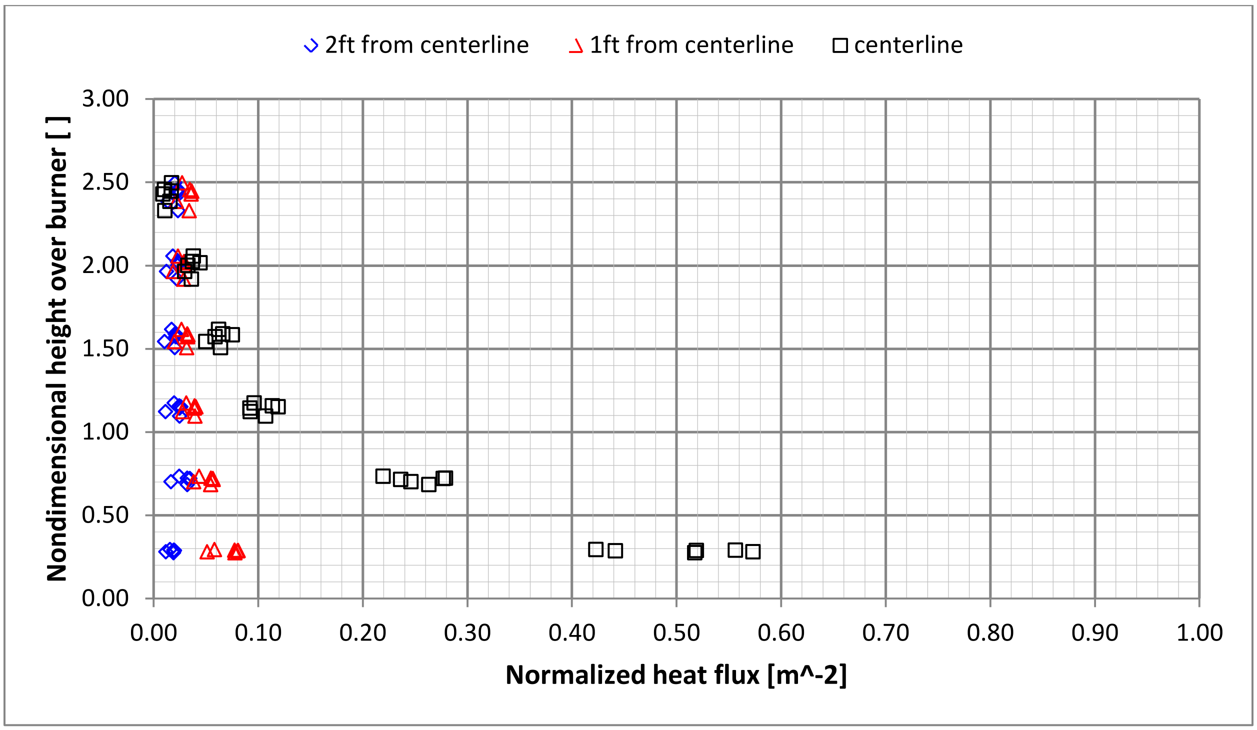

Figure 83 - Heat flux (normalized with convective HRR) from Methane 1ft Square burner tests

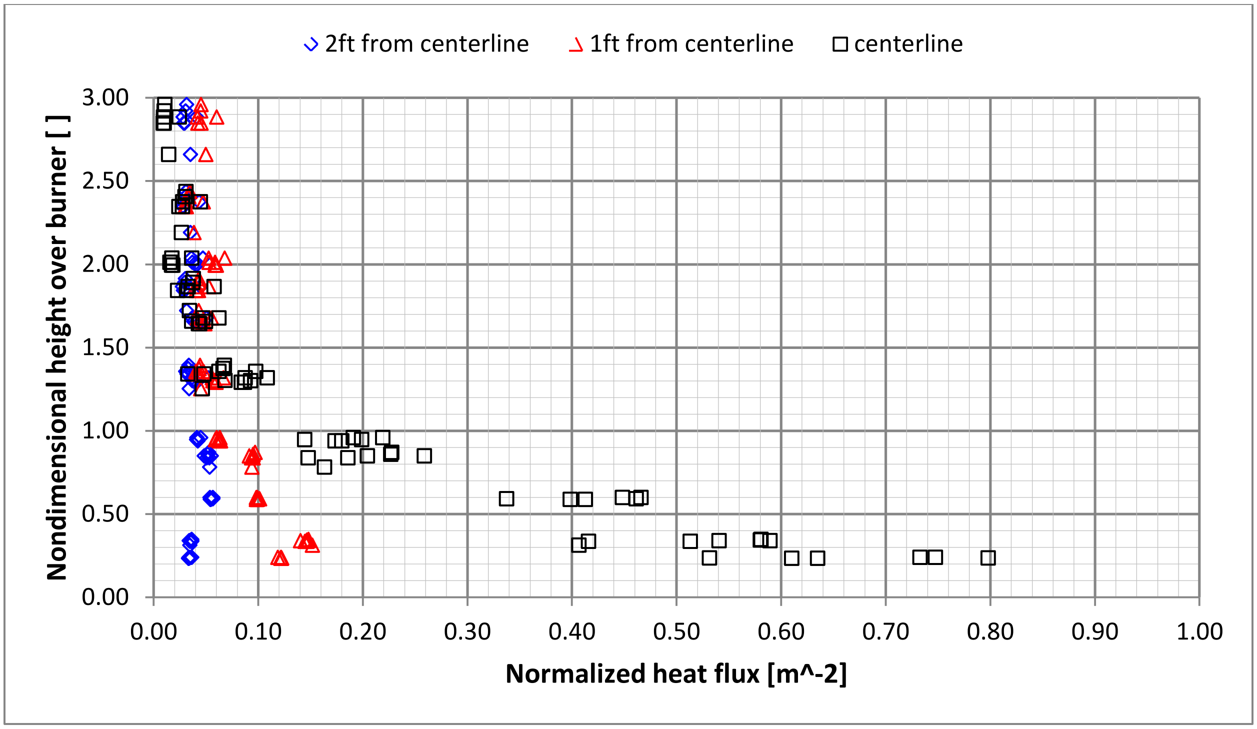

Figure 84 - Heat flux (normalized with convective HRR) from Propane 1ft Square burner tests

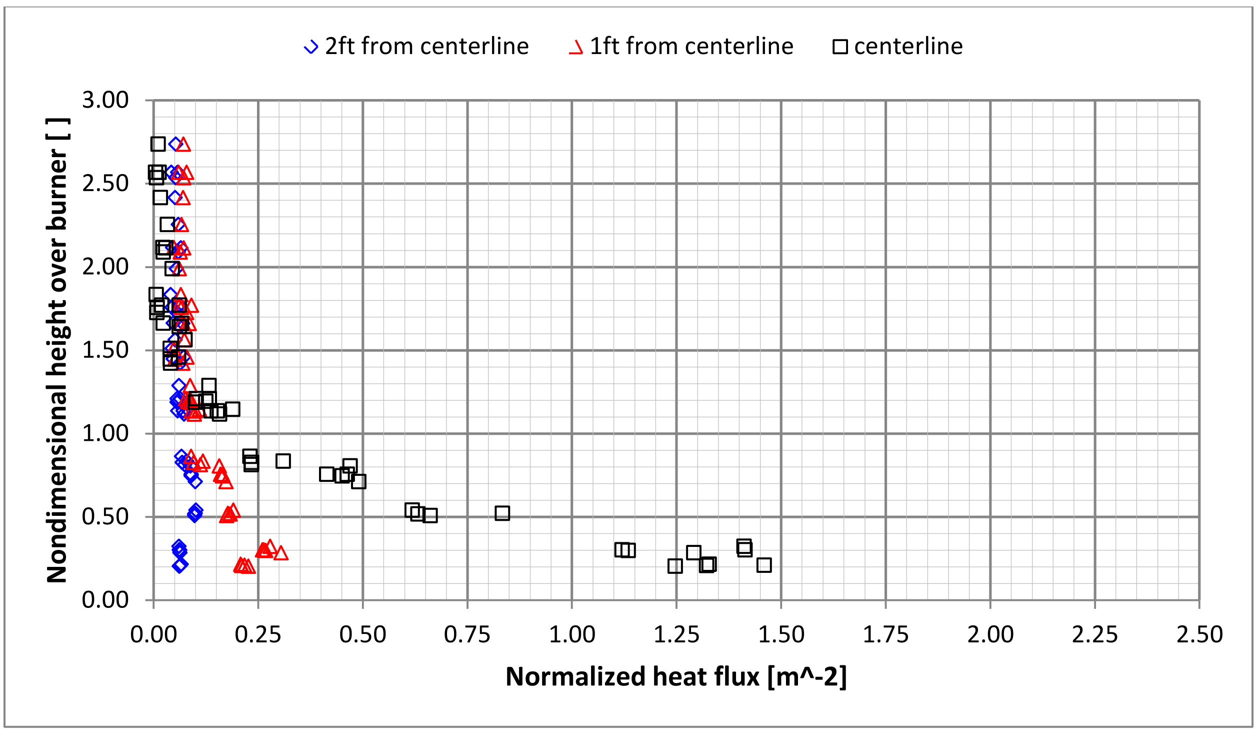

Figure 85 - Heat flux (normalized with convective HRR) from Propylene 1ft Square burner tests

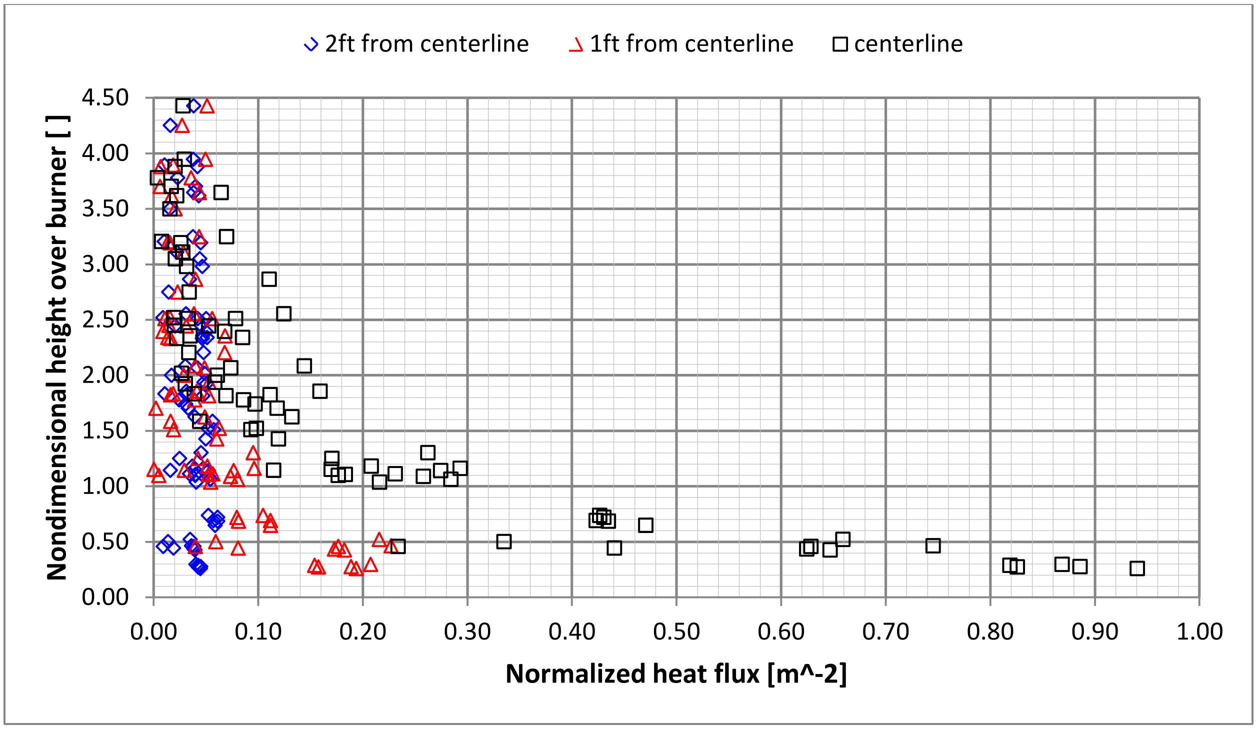

Figure 86 - Heat flux (normalized with convective HRR) from Propane 2ft Rectangle burner tests

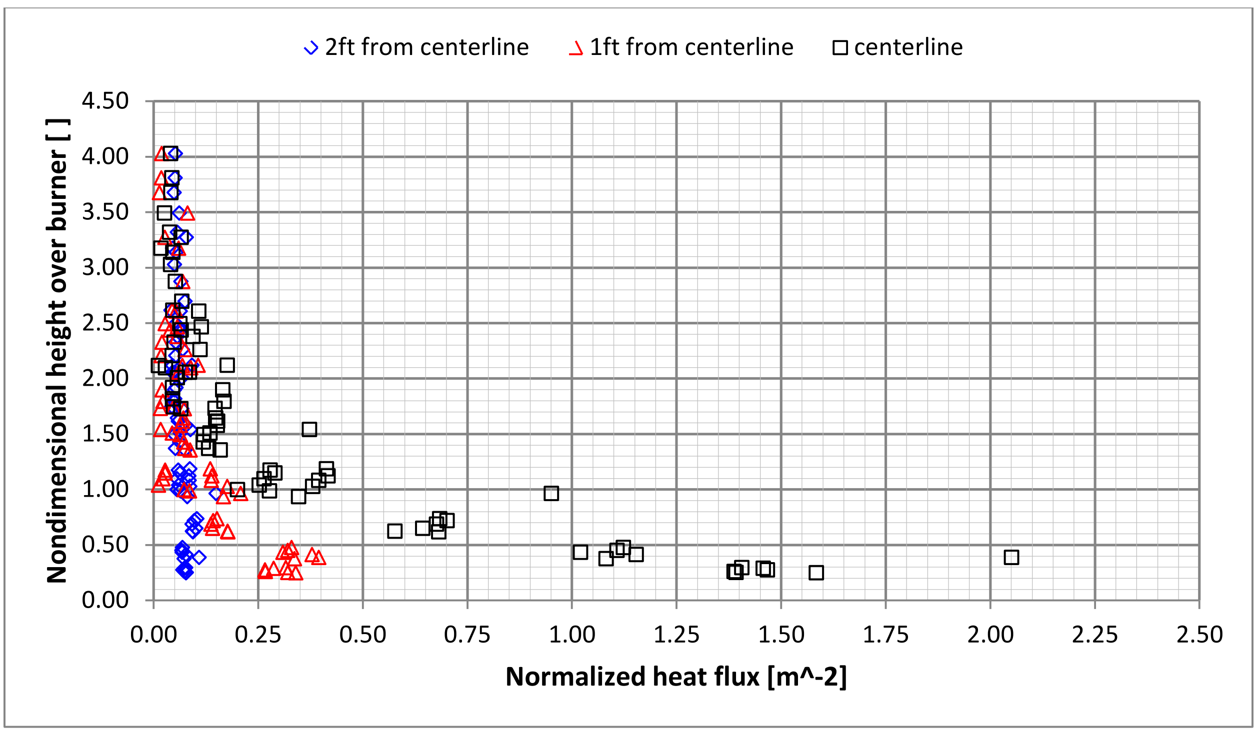

Figure 87 - Heat flux (normalized with convective HRR) from Propylene 2ft Rectangle burner tests

Another normalization method was applied to both the height of the TSCs and the heat flux by dividing the height with the convective HRR. The results from the 1ft Square burner test are presented in Figure 88 to Figure 90. Results from the 2ft Rectangle burner are presented in Figure 91 and Figure 92. The heat flux was divided by the convective heat release rate of the fire based on fuel type and the flow-based HRR (for propane and propylene) and O2-based HRR (for the methane).

Normalization with the convective HRR does not seem to have a large effect on the appearance of the data. The same trends from the un-normalized data still hold true. So it makes more sense to normalize the height using the mean flame height than the convective HRR.

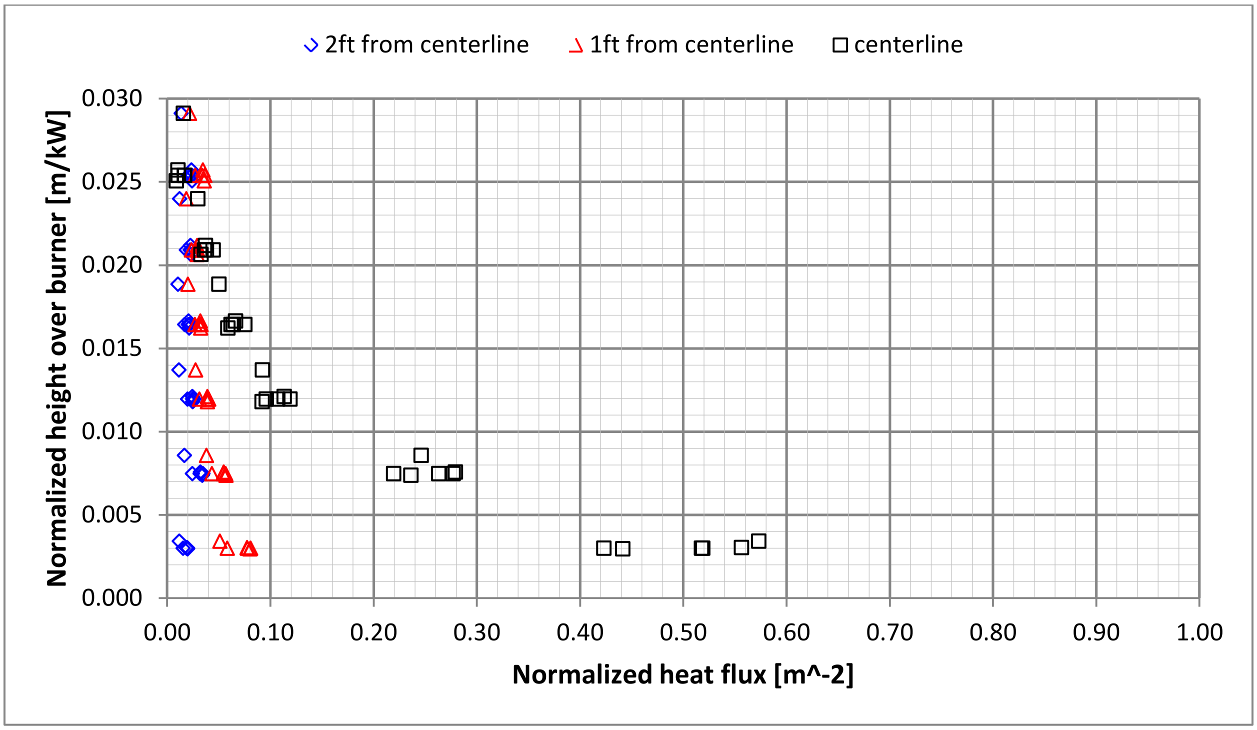

Figure 88 - Heat flux and height both normalized with convective HRR from Methane 1ft Square burner tests

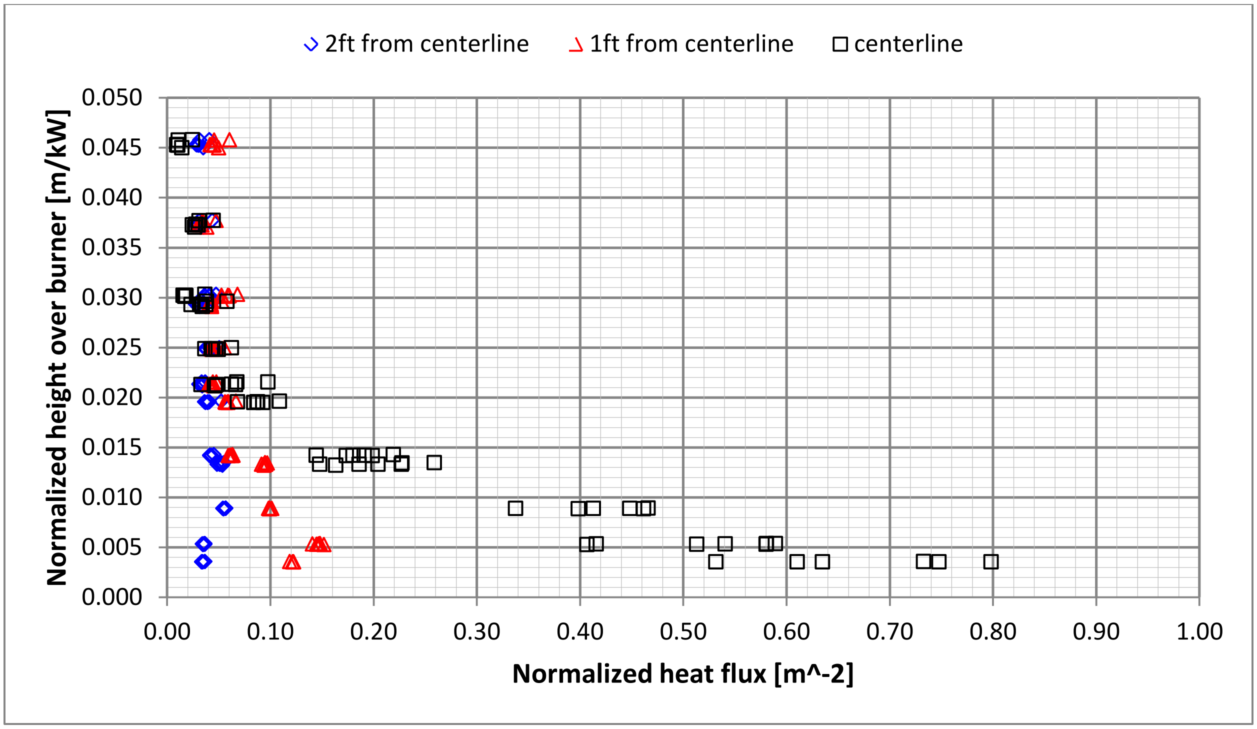

Figure 89 - Heat flux and height both normalized with convective HRR from Propane 1ft Square burner tests

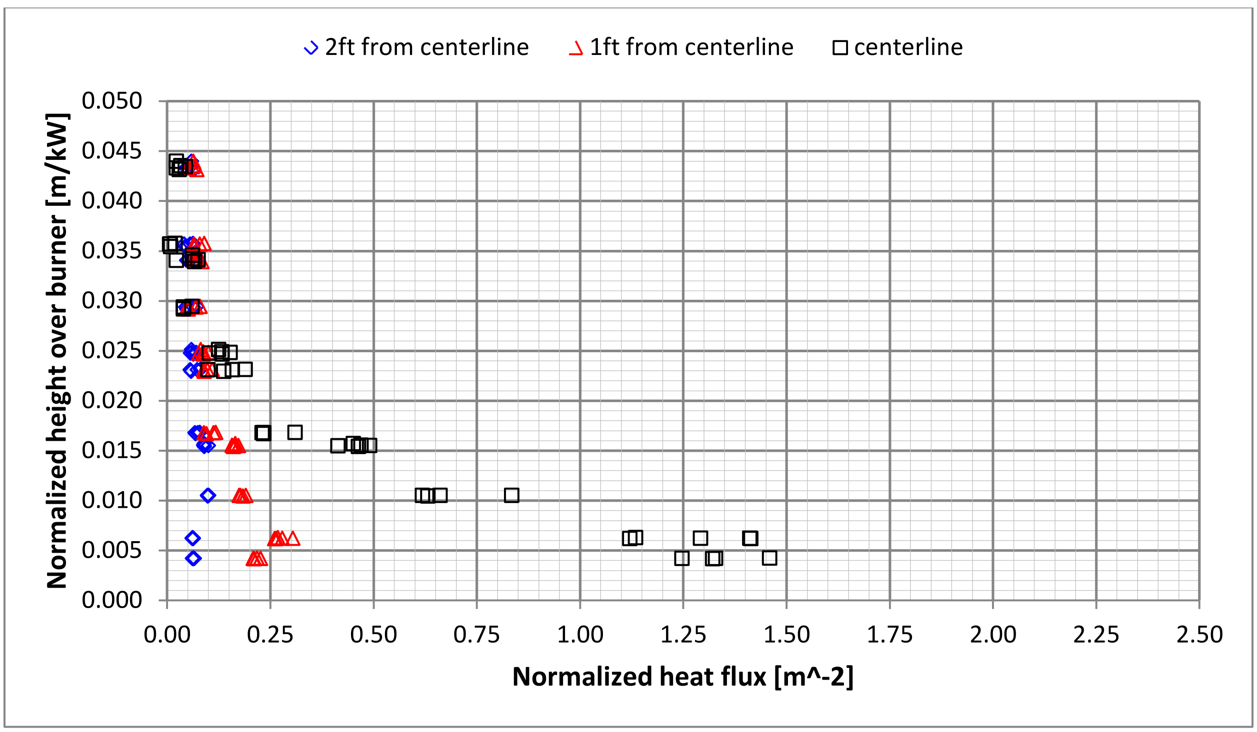

Figure 90 - Heat flux and height both normalized with convective HRR from Propylene 1ft Square burner tests

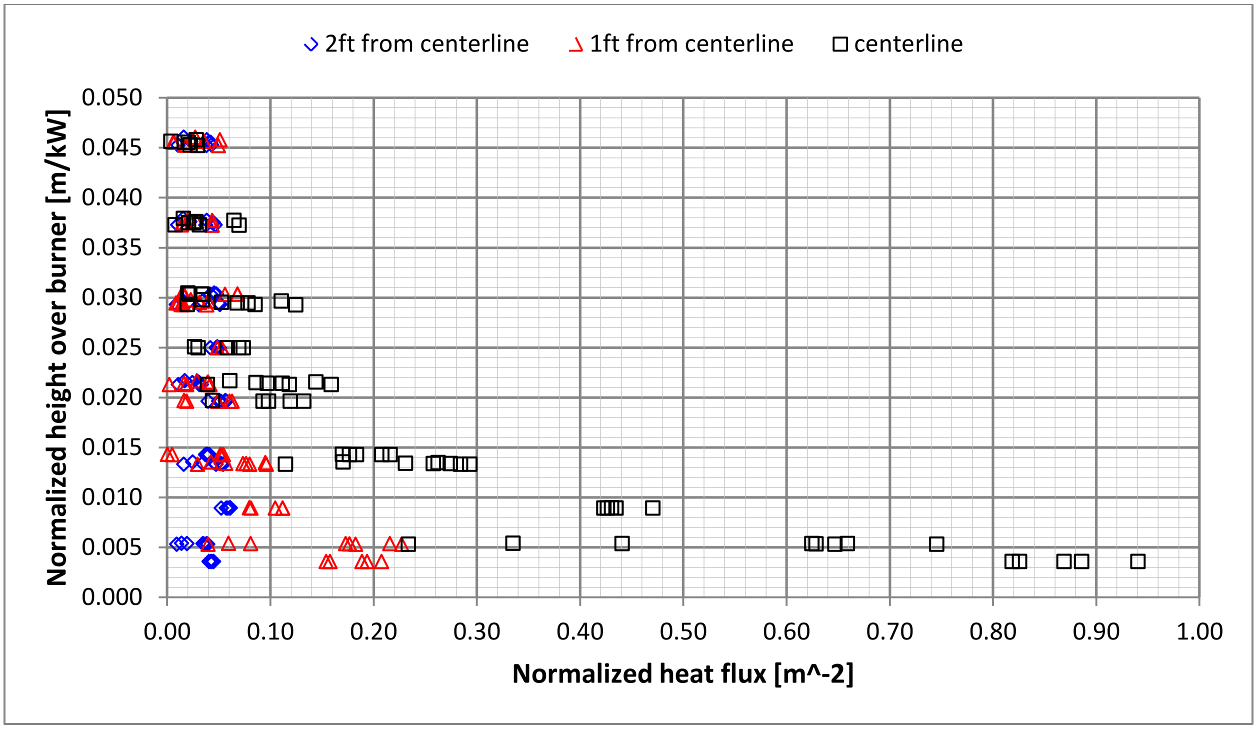

Figure 91 - Heat flux and height both normalized with convective HRR from Propane 2ft Rectangle burner tests

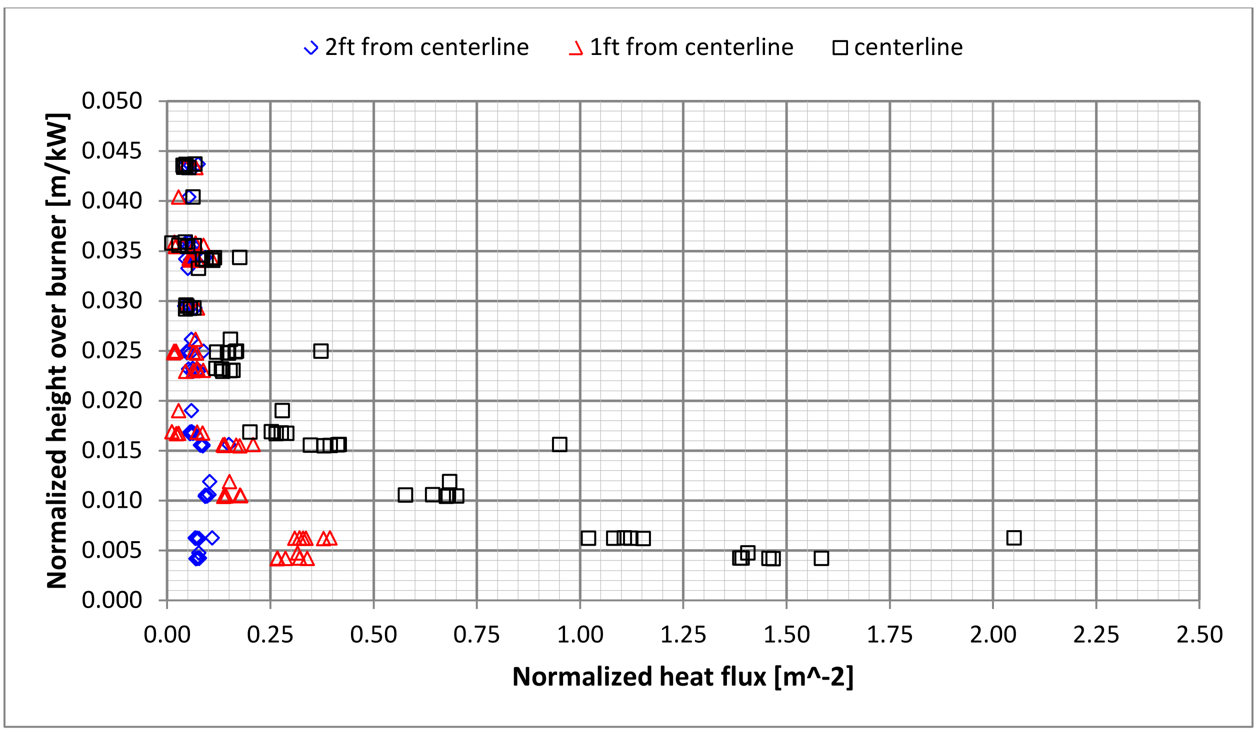

Figure 92 - Heat flux and height both normalized with convective HRR from Propylene 2ft Rectangle burner tests

D.4.2 Wall Heat Flux Normalization based on Fire Cylinder Assumption

In previous graphing exercises, the wall heat flux in the inert wall tests was normalized against the convective heat release rate, and the height of the TSCs was normalized with 50% intermittency mean flame height as well as the convective heat release rate. In the graphs below, however, the wall heat flux is normalized against an HRRPUA value based on the radiative heat release rate, and the height is normalized against 100% intermittency flame height.

The HRRPUA value used for normalization was determined by assuming that the fire plume has a cylindrical shape with a surface area of that of an open cylinder, A:

$$A = \pi * D_h * FH$$

Where D_h is the hydraulic diameter of the burner, and FH is the 100% intermittency flame height.
In this exercise, the 100% intermittency flame height was determined as the 60/100 value of the 50% mean flame height.

The HRRPUA of the fire is then found to be:

$$HRRPUA = \frac{HRR_{rad}}{A}$$

The heat flux is then normalized as:

$$HF\,[\,] = \frac{HF[\frac{kW}{m^2}]}{HRRPUA[\frac{kW}{m^2}]}$$

Figure 93 shows the normalized heat flux of all tests, regardless of fire size, fuel type, and burner size. As expected, the heat flux along the centerline was larger than the heat flux recorded 1 ft and 2 ft away from the centerline.

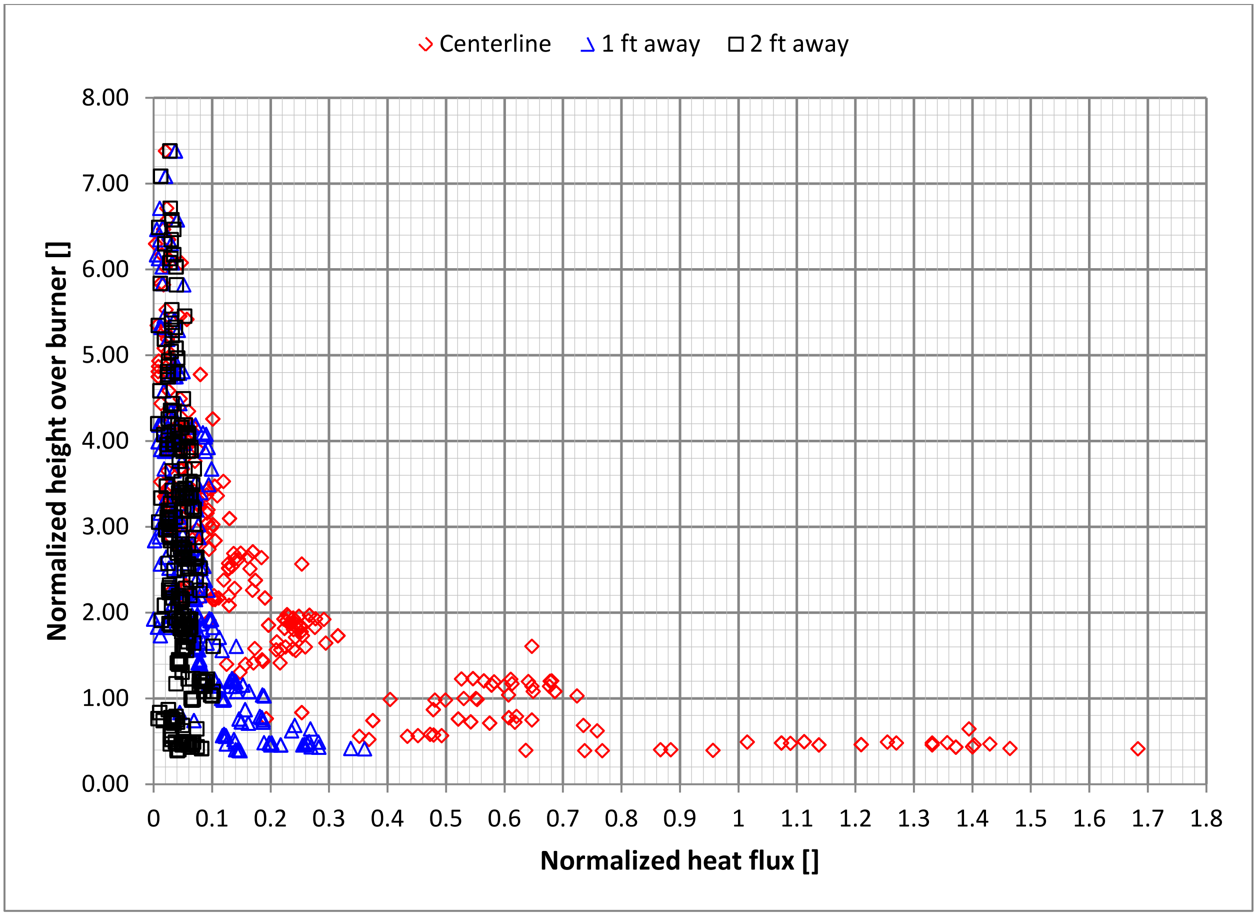

Figure 93 - Normalized heat flux of all tests

Figure 94 shows the heat flux recorded at the tests using the 1 ft Square burner. The highest heat flux again was measured along the center, but not over 60% of the HRRPUA of a fire. It is also shown that the heat flux measured 1 ft away from centerline was greater than the heat flux measured at 2 ft away from centerline.

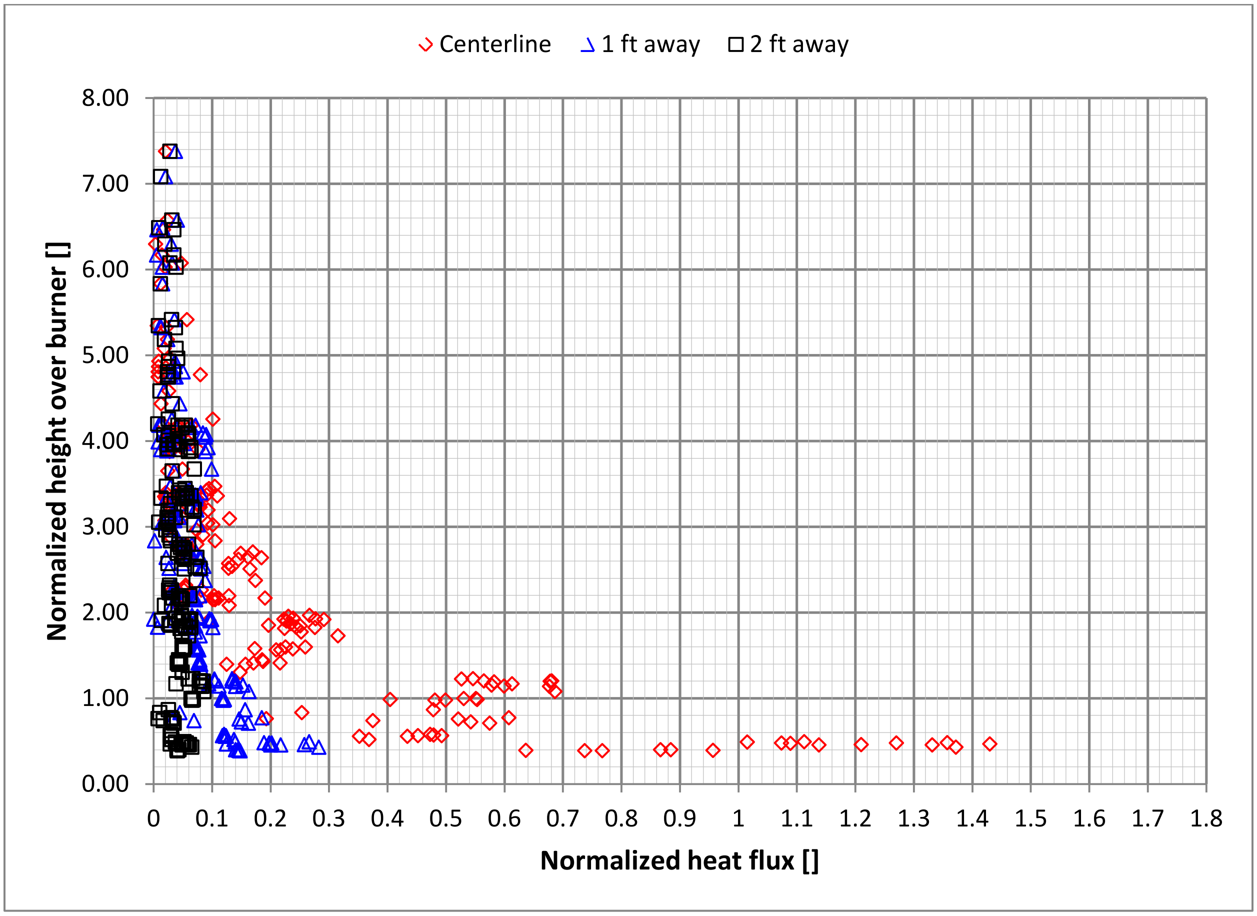

Figure 94 - Normalized heat flux of all 1 ft Square burner tests

Figure 95 shows the heat flux measured at the 2 ft Rectangle burner tests. Compared to the 1 ft burner case, the heat flux along the centerline is greater, almost reaching 100% of HRRPUA. However, the heat flux measured at the TSCs 1 ft and 2 ft away are smaller.

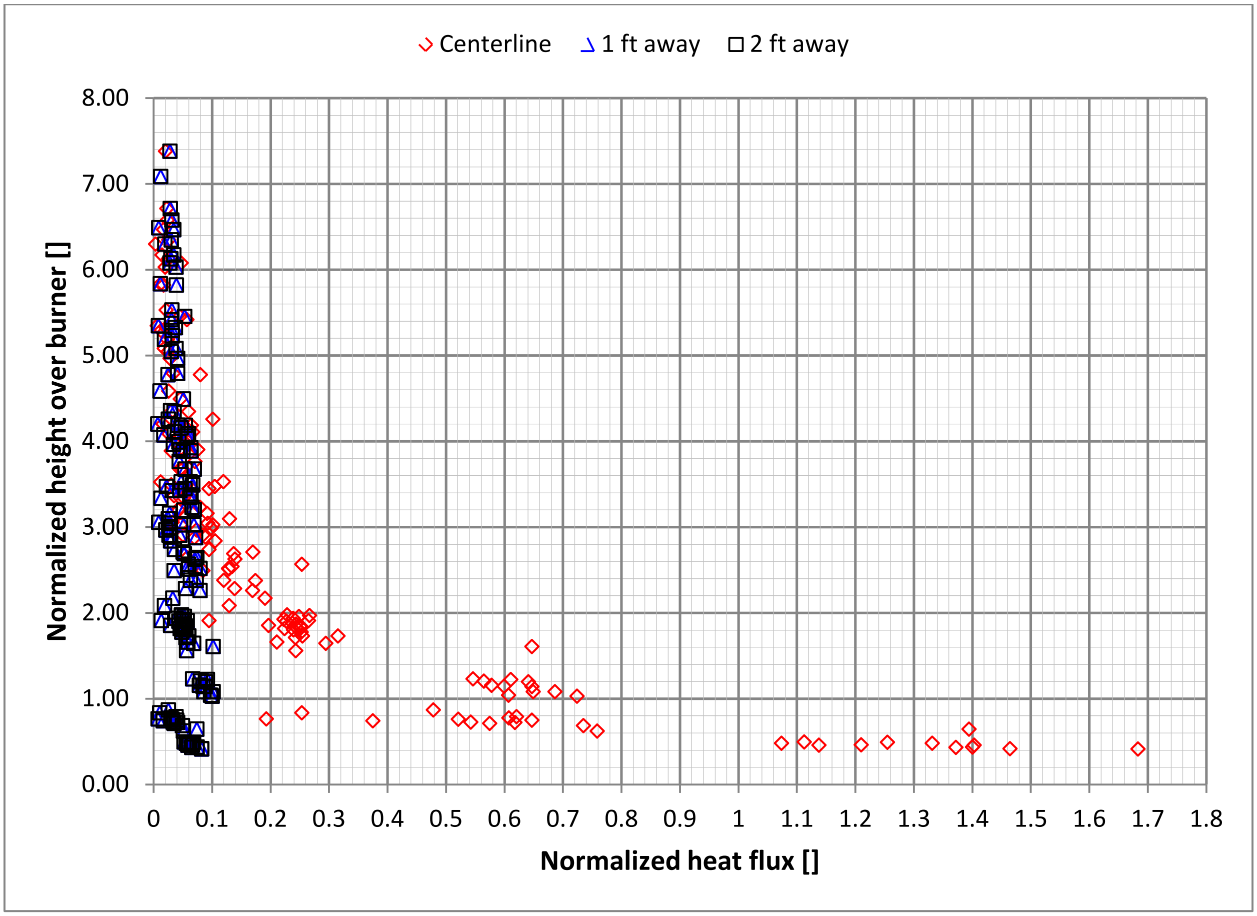

Figure 95 - Normalized heat flux of all 2 ft Rectangle burner

The heat flux on the inert wall was also normalized against an assumed cylindrical fire with a height same as the 50% intermittency mean flame height. The height of the TSCs was normalized with the mean flame height. Using the mean flame height stretched the flame cylinder and increased the normalized heat flux values.

Figure 96 shows the normalized heat flux of all tests, regardless of fire size, fuel type, and burner size. As expected, the heat flux along the centerline was larger than the heat flux recorded 1 ft and 2 ft away from the centerline.

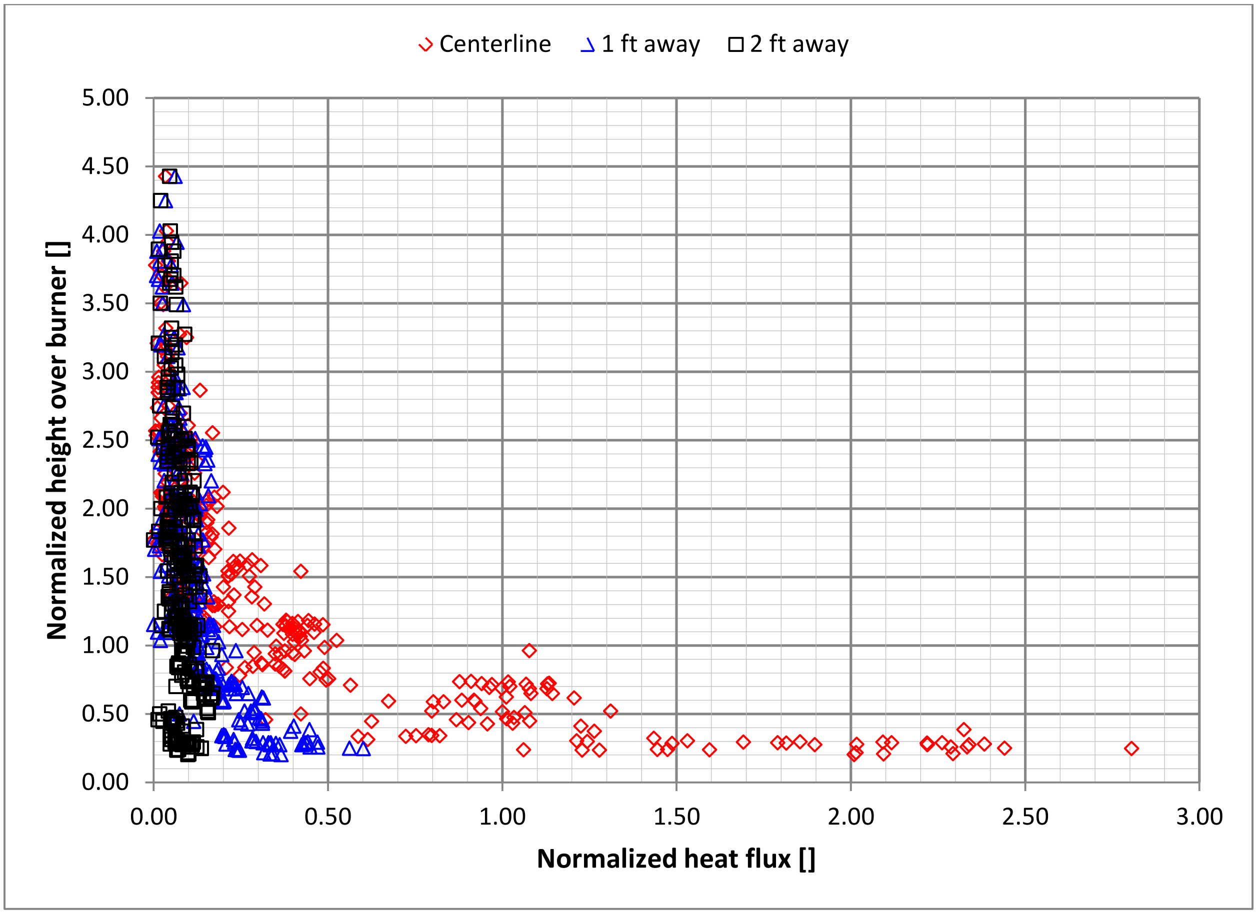

Figure 96 - Normalized heat flux (using mean flame height) of all tests

Figure 97 shows the heat flux recorded at the tests using the 1 ft Square burner. The highest heat flux again was measured along the center, but not over 60% of the HRRPUA of a fire. It is also shown that the heat flux measured 1 ft away from centerline was greater than the heat flux measured at 2 ft away from centerline.

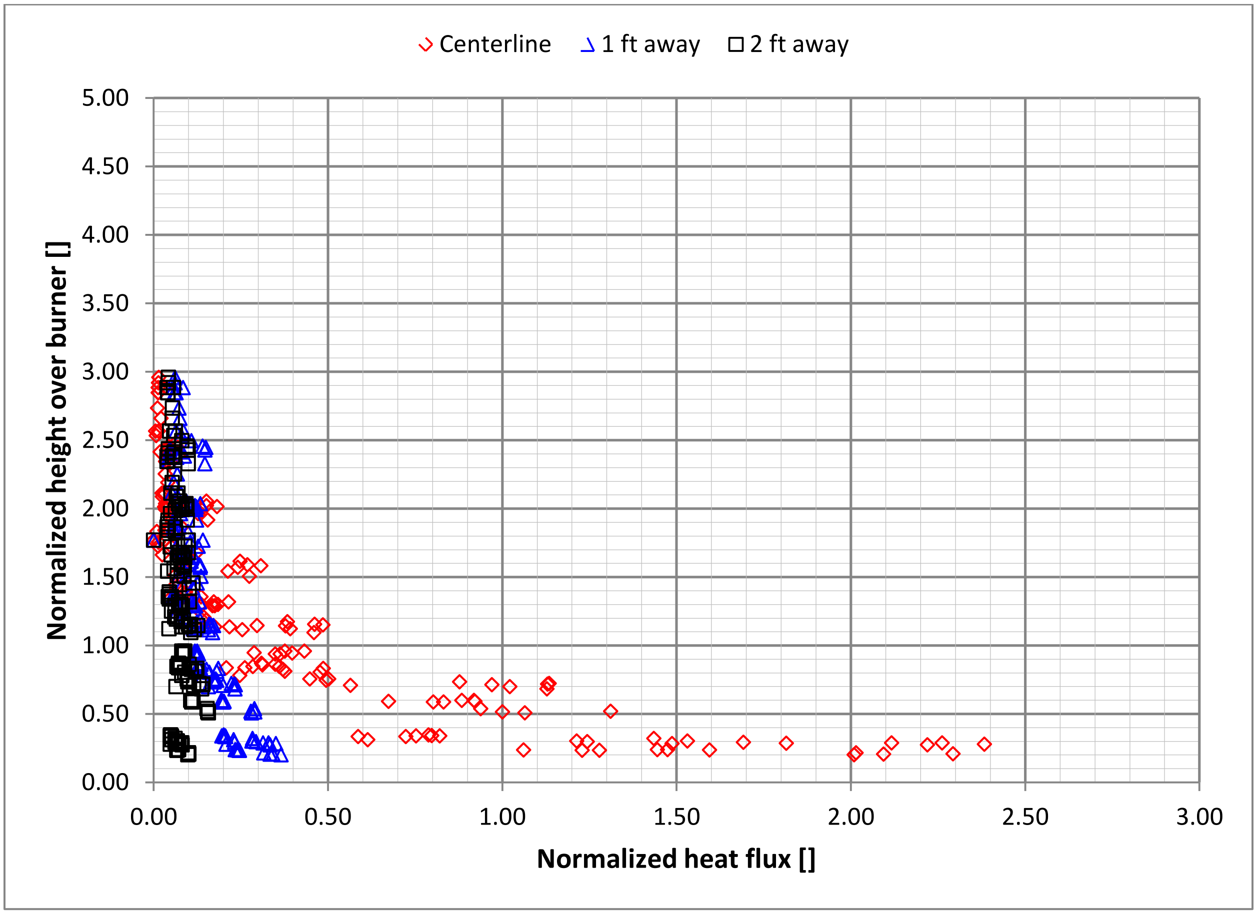

Figure 97 - Normalized heat flux (using mean flame height) of all 1 ft Square burner tests

Figure 98 shows the heat flux measured at the 2 ft Rectangle burner tests. Compared to the 1 ft burner case, the heat flux along the centerline is greater, almost reaching 100% of HRRPUA. However, the heat flux measured at the TSCs 1 ft and 2 ft away are smaller.

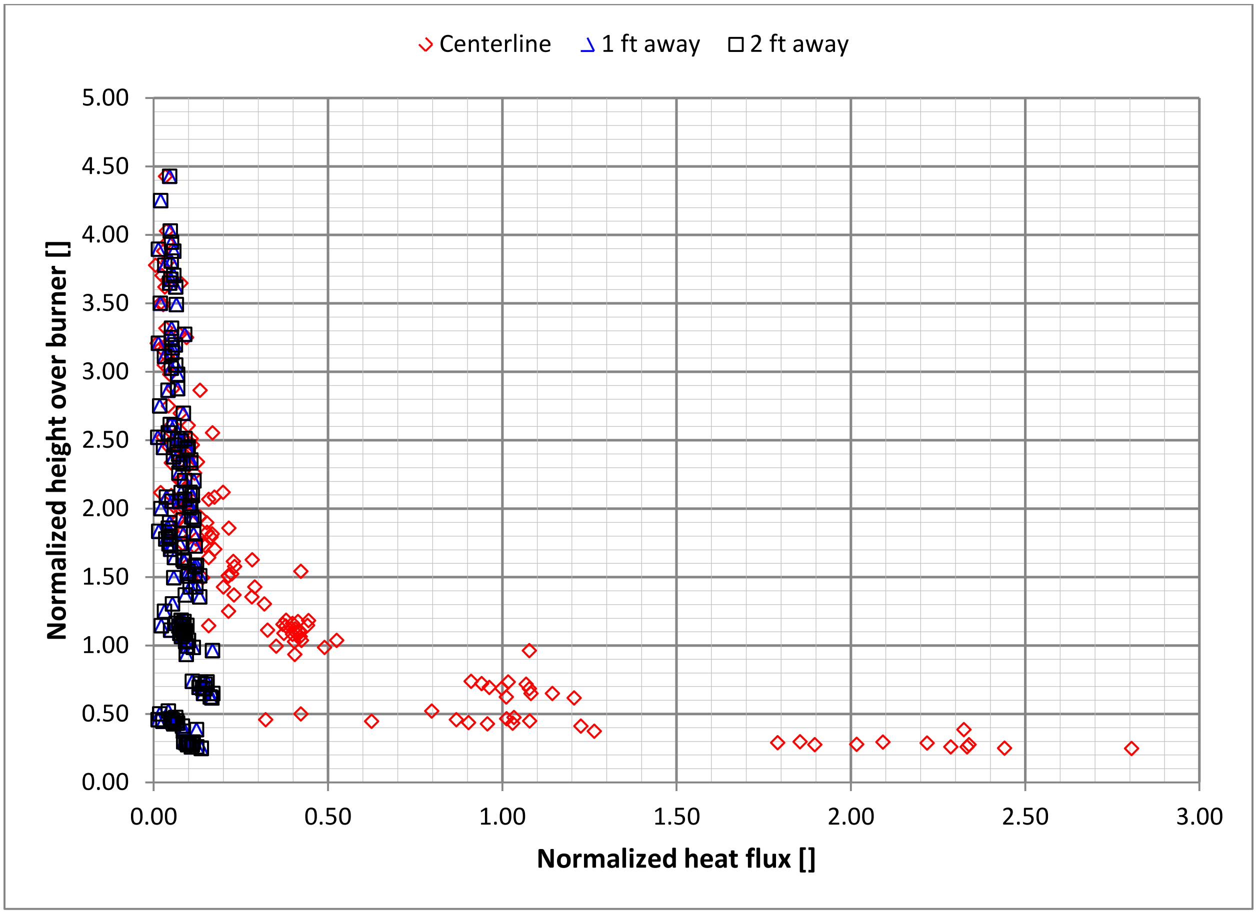

Figure 98 - Normalized heat flux (using mean flame height) of all 2 ft Rectangle burner

D.5 Near-Wall Temperature

Temperature measurements taken near a burning, combustible wall may be used as a means to track the fire progression over the burning surface. On an inert wall with an adjacent burner, however, the temperatures can lead to a description of the upward flow boundary layer. In the current inert and combustible wall experiments, near-wall temperature was measured by thermocouples installed on the wall at regular intervals close to the centerline.

Welded 20 AWG (0.81 mm) thermocouple wires were used as the thermocouples; they are installed through the back of the false wall and were offseted from the wall's front surface at various distances from 0 mm to 40 mm perpendicular to the wall. A series of 18 thermocouples were used, grouped into 3 groups of six and installed at 0.35 m, 0.95 m, and 1.55 m from the burner surface. The thermocouples are located at 2.5 cm, 5 cm, and 7.5 cm away from the centerline. Table 12 shows the locations of the thermocouples.

Table 12 - Locations of near-wall thermocouples

		Distance from centerline					
		-7.5 cm	**-5.0 cm**	**-2.5 cm**	**2.5 cm**	**5.0 cm**	**7.5 cm**
		Perpendicular distance from wall [mm]					
Height above burner	**155 cm**	15	20	25	30	35	40
	95 cm	35	30	25	20	15	10
	35 cm	0	5	10	15	20	25

With this thermocouple grid, a partial map of the wall boundary layer may be obtained based on temperature readings. An upward thermal boundary layer is created on the inert wall by the fire plume adjacent to the wall. The plume and boundary layer differs in size, temperature, and velocity based on the burning area and fire size, which are all properties that drives flame spread on a vertical wall. The boundary layer is assumed to be one-dimensional and points vertically upward, and its thickness is defined as the interface where the temperature is the highest. By tracking the highest temperature from each group of six thermocouples at different heights, the layer thickness at that height will be the thermocouple's distance from centerline.

A time-averaged temperature reading was found for each station over the steady-state period of the fire. Also note that the temperature reported in this section have not been radiation corrected.

Corrected temperature is presented in the main report, and it is assumed that the uncorrected and corrected near-wall temperature represents the lower and upper bounds, respectively, of the true temperature at that location.

The temperature was plotted against the non-dimensional convective HRR parameter N, as suggested by Heskestad. The pattern visible in Figure 99 suggests that there might be a correlation that may be used to predict the near-wall temperature based on the parameter N.

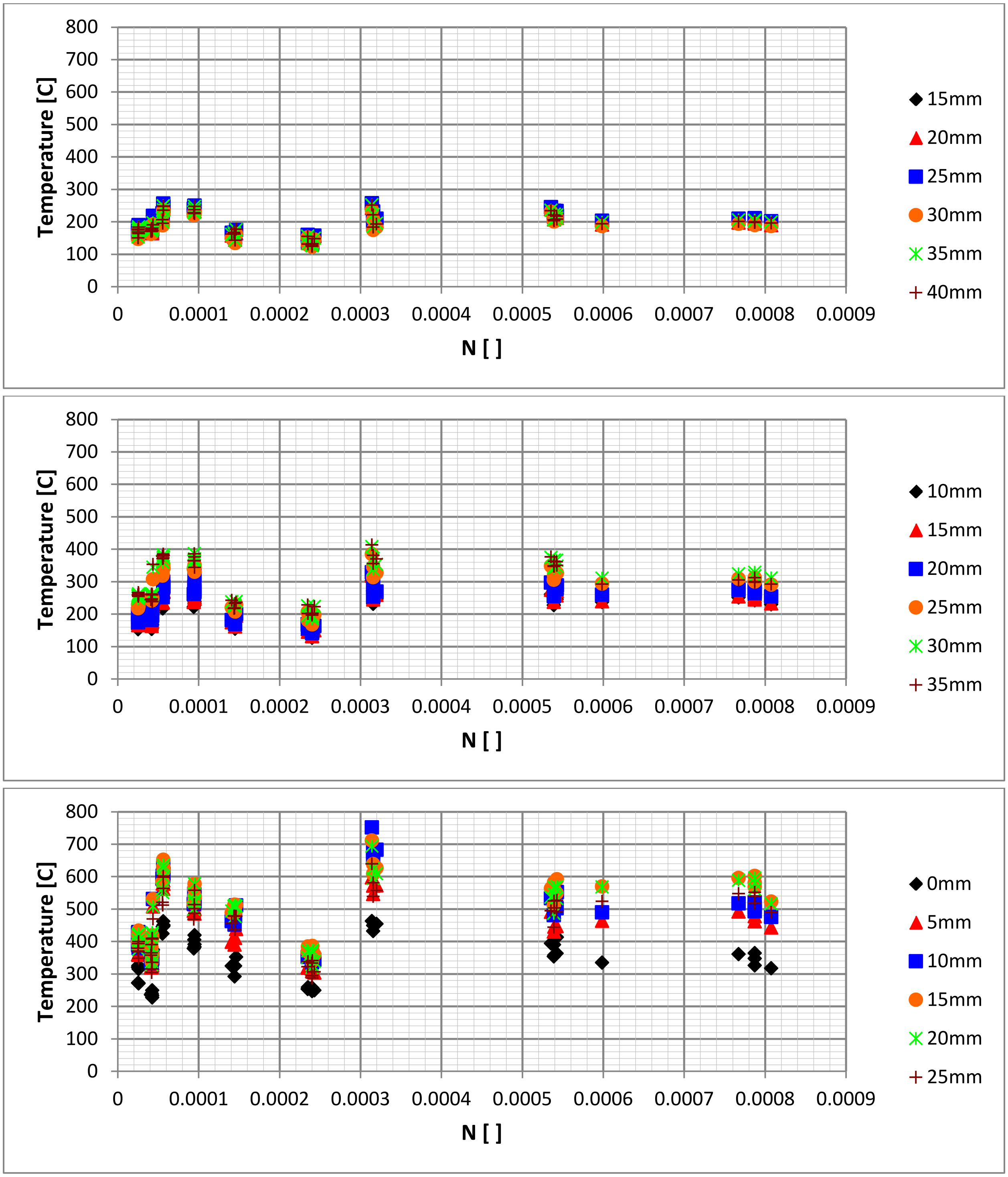

Figure 99 - Inert wall fires near-wall temperature against N (Top=1.55m, middle=0.95m, bottom=0.35m above burner)

The temperature is also plotted against the non-dimensional convective HRR parameter Q_c^* based on the HRR and the hydraulic diameter of the burner in Figure 100. When plotted against Q_c^*, the data appears to be more clustered together and this format is used for other charts.

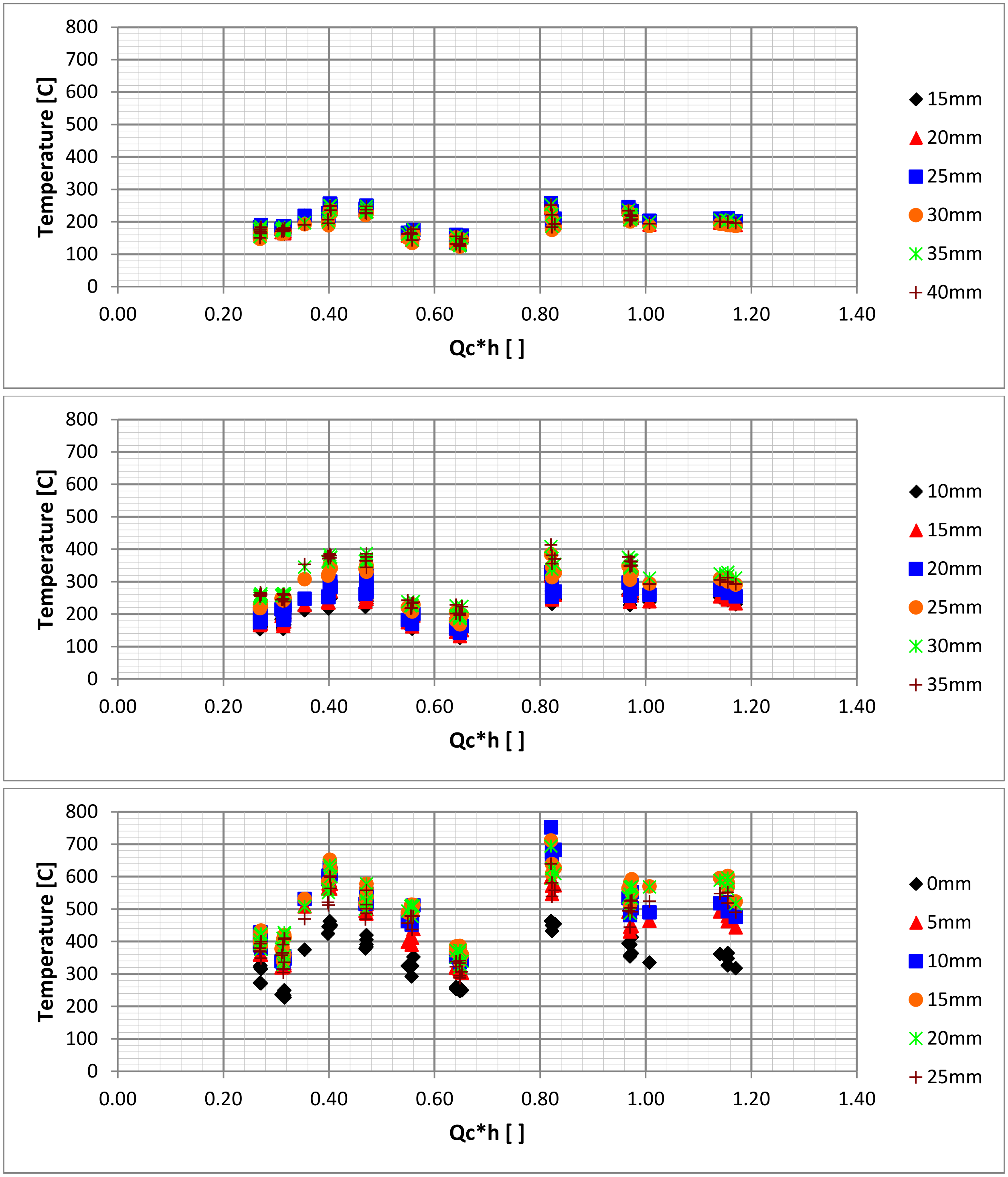

Figure 100 - Inert wall fires near-wall temperature against Q_c^* (Top=1.55m, middle=0.95m, bottom=0.35m above burner)

D.5.1 Approximate Thermal Boundary Layer Thickness

By separately plotting the temperature by fuel type and burner size, better observations can be made. For methane, only the 1 ft Square burner was used. Figure 101 shows that the at the height z=0.35 m above the burner, the temperature is lowest at the wall's surface and rises until y=15~20 mm (away from wall surface), then drops lower at y=25 mm. This suggests that the boundary layer thickness is between 15 and 20 mm. The unitless number next to the test designation in the legend denotes the non-dimensional HRR Q_c^*.

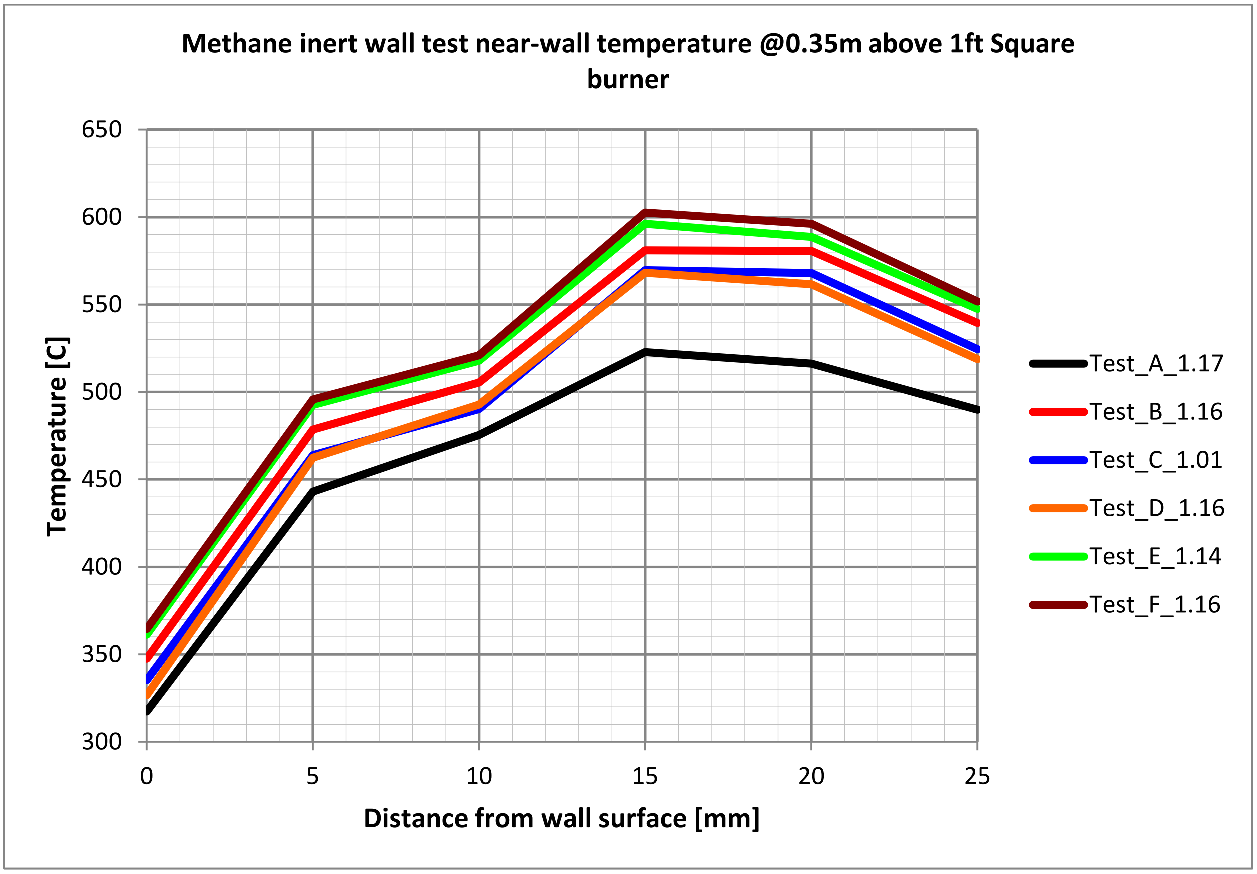

Figure 101 - Methane 1 ft Square burner near-wall temperature at 0.35 m above burner surface

At z=0.95 m above the burner, the highest temperature was recorded at 30 mm, as shown in Figure 102. This suggests that the boundary layer thickness is between 30 and 35 mm at this height.

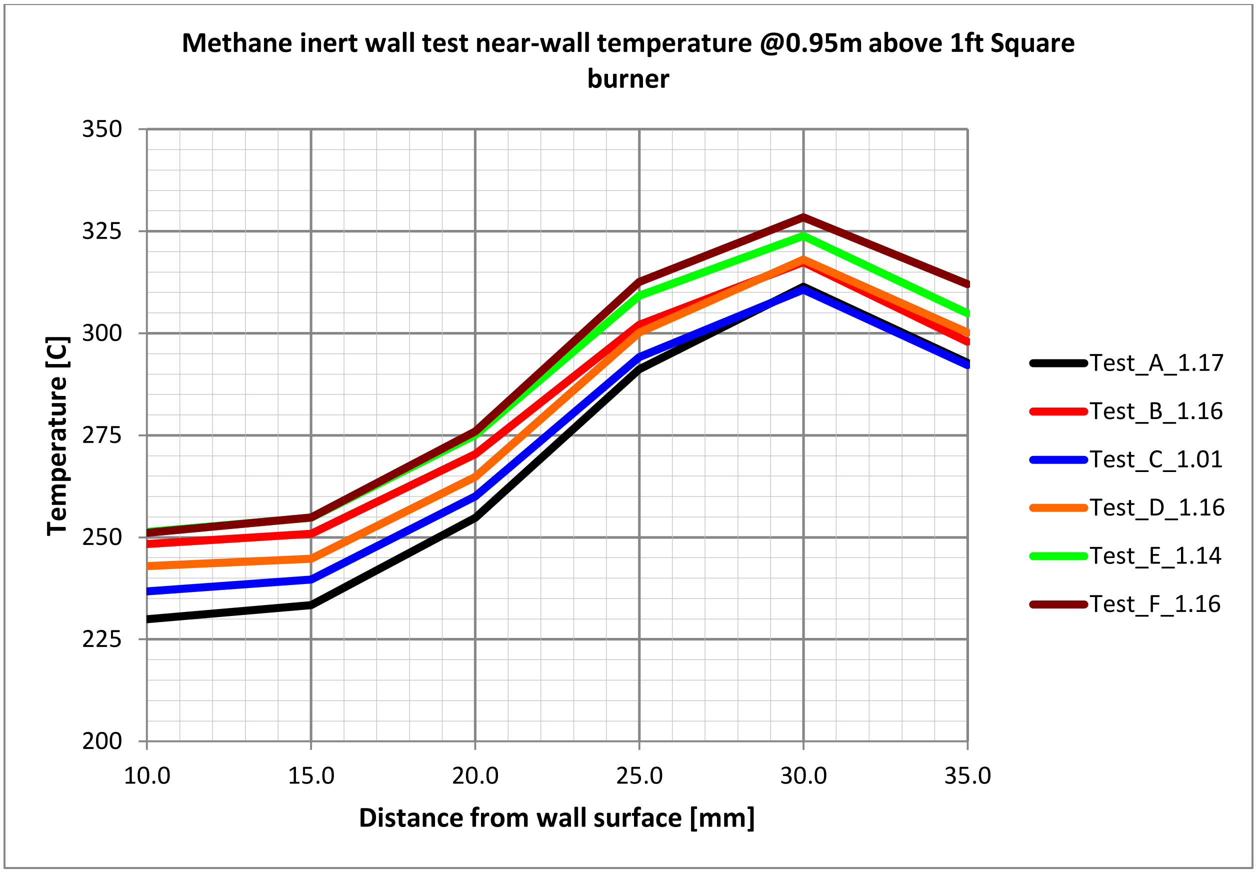

Figure 102 - Methane 1 ft Square burner near-wall temperature at 0.95 m above burner surface

At z=1.55 m above the burner, the highest temperature was recorded at 25 mm, as shown in Figure 103. This suggests that the boundary layer thickness is between 25 and 35 mm at this height.

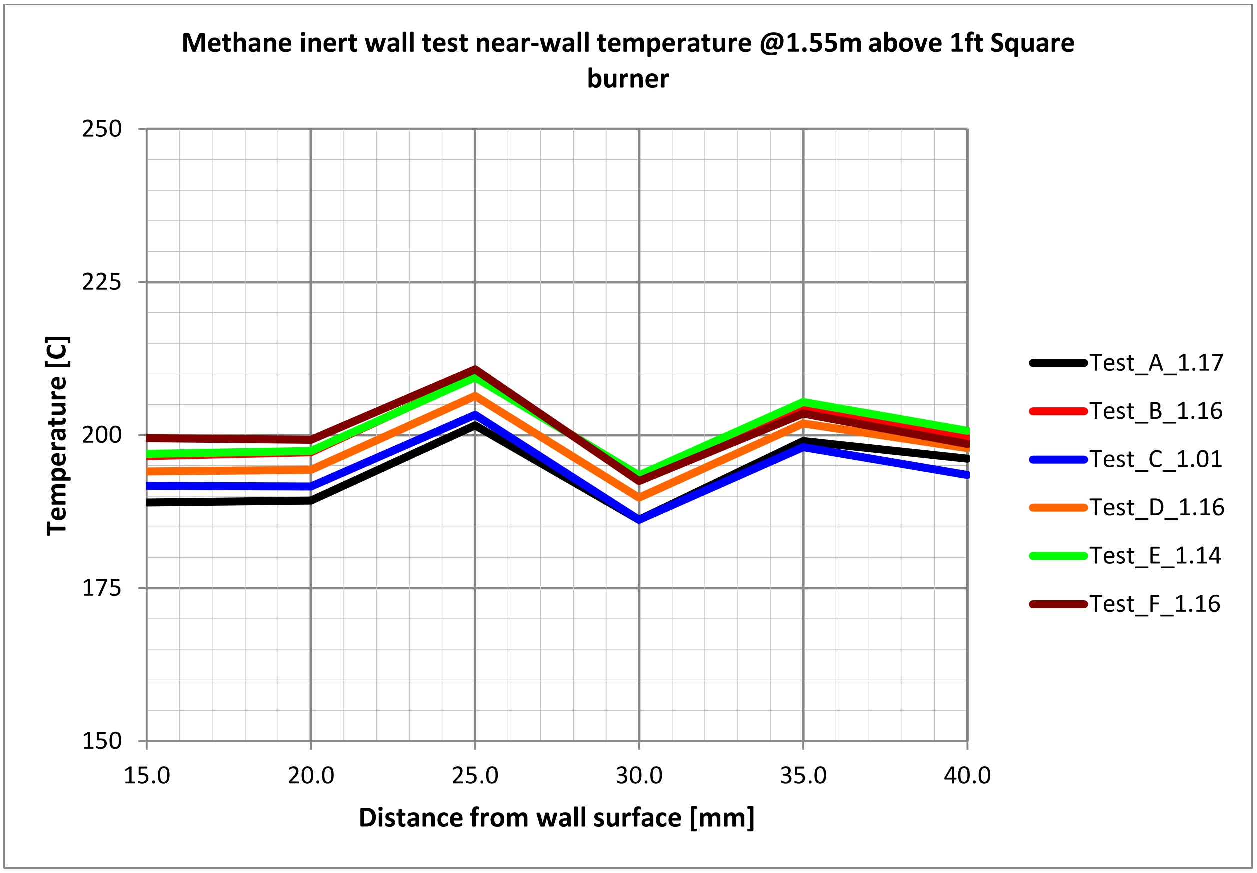

Figure 103 - Methane 1 ft Square burner near-wall temperature at 1.55 m above burner surface

Near-wall temperature from fries with propane and the 1 ft Square burner at 50 kW with z=0.35 m above the burner is plotted in Figure 104. The highest temperature is recorded at y=15mm, and the boundary layer thickness is about 15 and 20 mm.

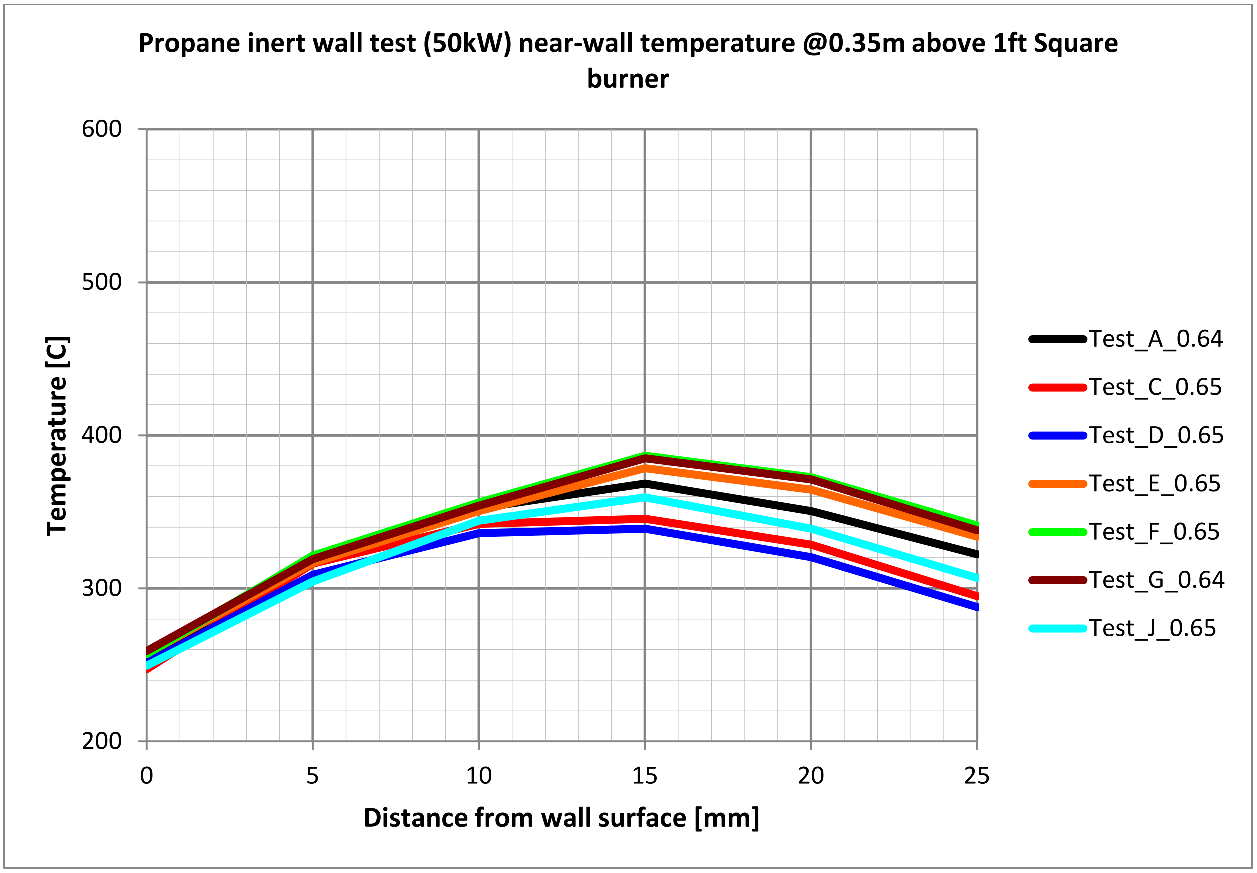

Figure 104 - Propane 1 ft Square burner near-wall temperature at 0.35 m above burner surface

At z=0.95 m above the burner, the highest temperature was recorded at 35 mm, as shown in Figure 105. This suggests that the boundary layer thickness is at least 35 mm.

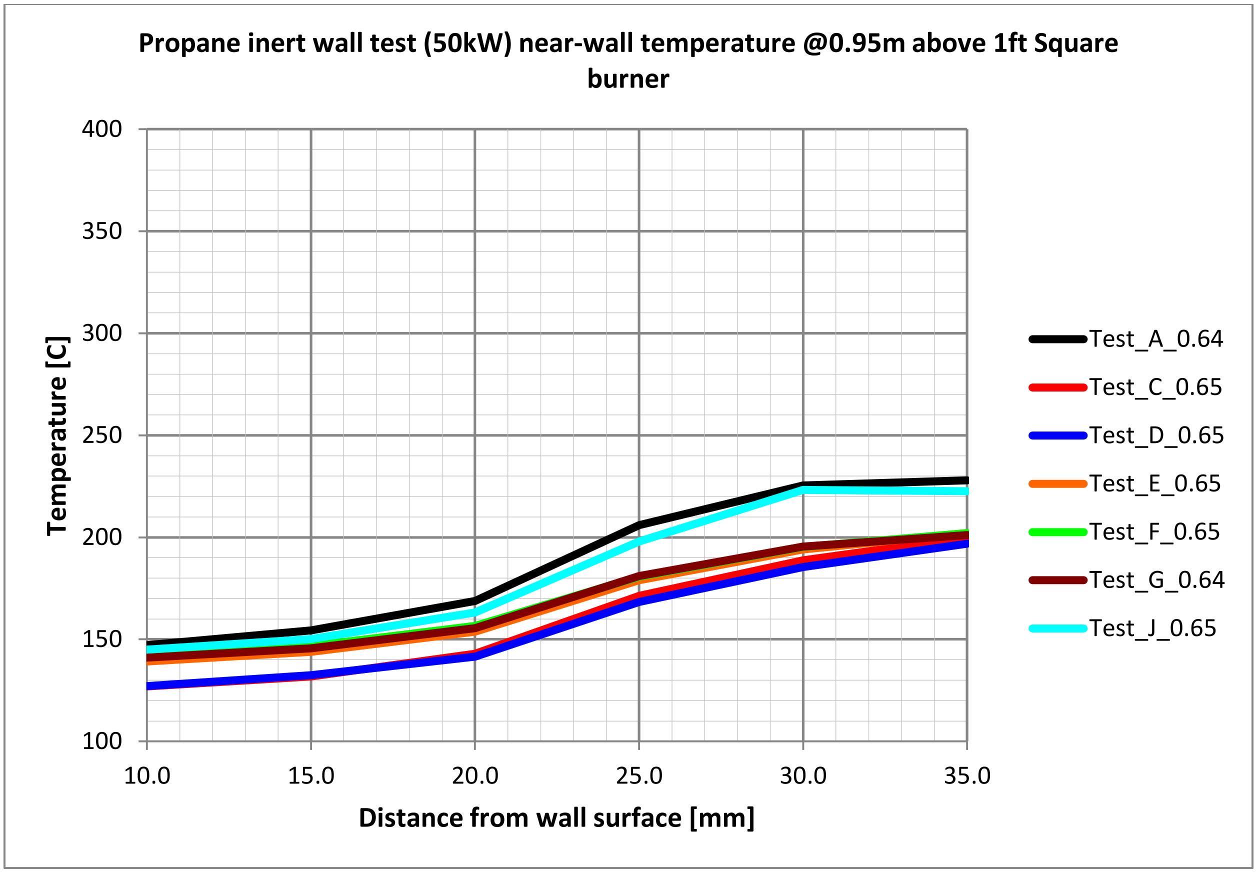

Figure 105 - Propane 1 ft Square burner near-wall temperature at 0.95 m above burner surface

At z=1.55 m above the burner, the highest temperature was recorded at 25 mm, as shown in Figure 106. This suggests that the boundary layer thickness is between 25 and 30 mm at this height.

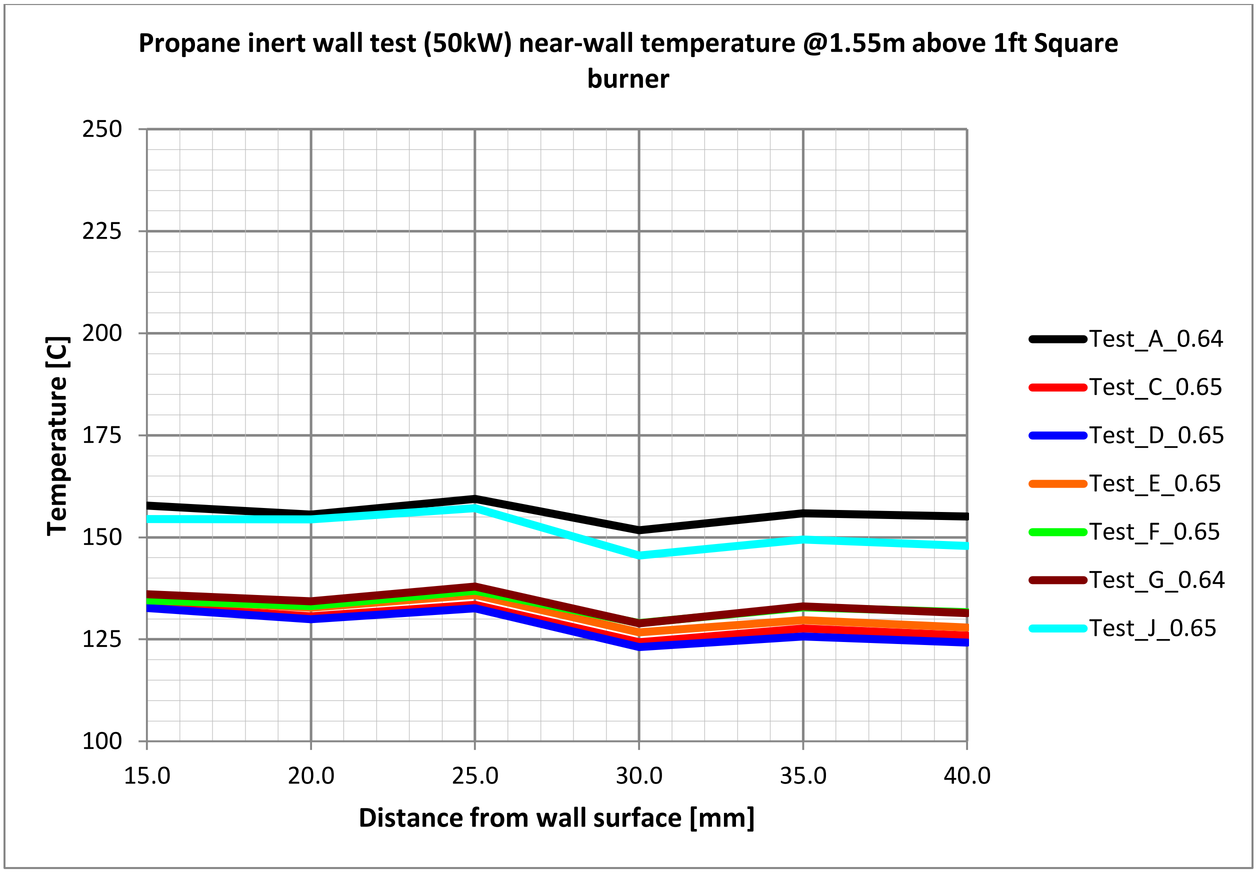

Figure 106 - Propane 1 ft Square burner near-wall temperature at 1.55 m above burner surface

Near-wall temperature from fries with propane and the 1 ft Square burner at 75 kW with z=0.35 m above the burner is plotted in Figure 107. The highest temperature is recorded at y=15mm, and the boundary layer thickness is about 15 and 20 mm.

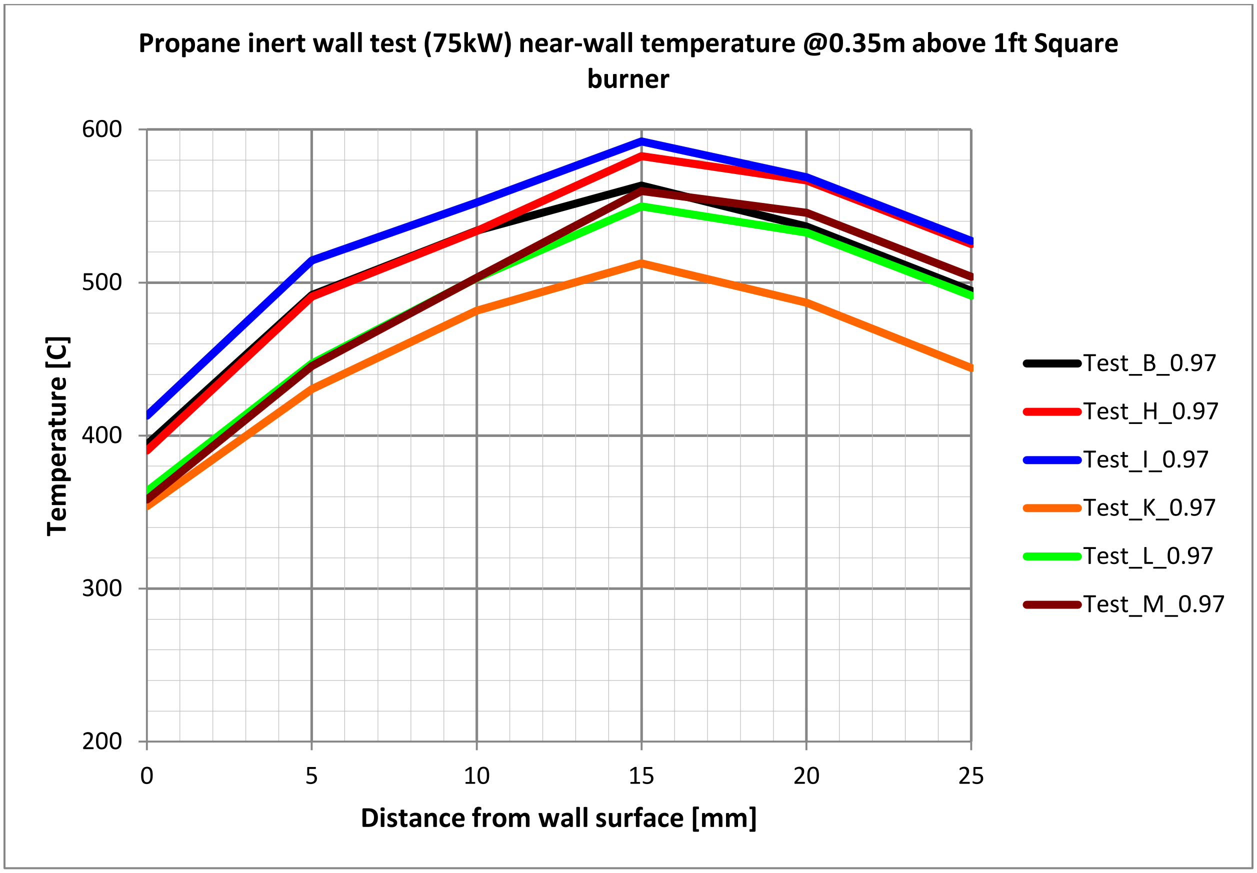

Figure 107 - Propane 1 ft Square burner near-wall temperature at 0.35 m above burner surface

At z=0.95 m above the burner, the highest temperature was recorded at 35 mm, as shown in Figure 108. This suggests that the boundary layer thickness is at least 35 mm.

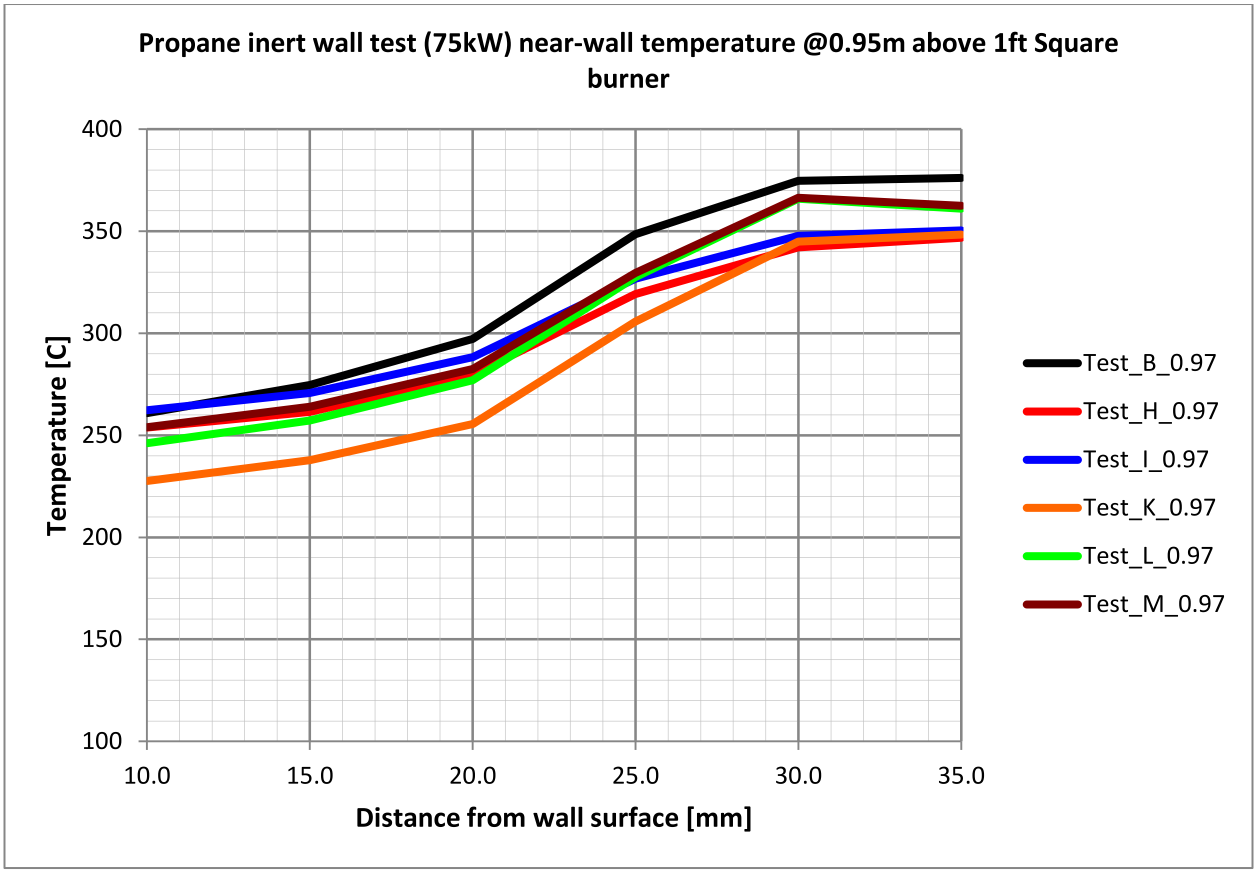

Figure 108 - Propane 1 ft Square burner near-wall temperature at 0.95 m above burner surface

At z=1.55 m above the burner, the highest temperature was recorded at 25 mm, as shown in Figure 109. This suggests that the boundary layer thickness is between 25 and 30 mm at this height.

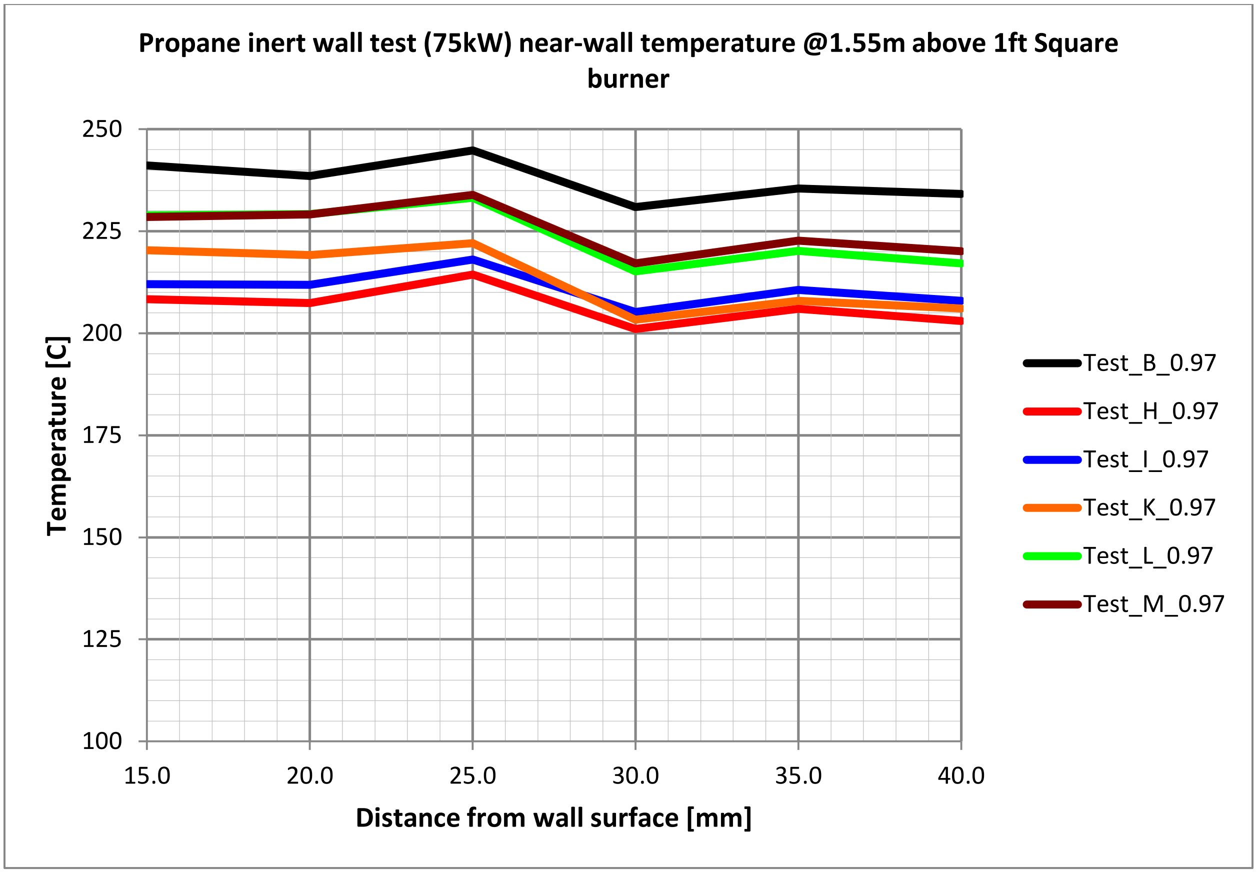

Figure 109 - Propane 1 ft Square burner near-wall temperature at 1.55 m above burner surface

The boundary layers of the 50 kW fires and the 75 kW fires seem to have the same general shape but the temperatures recorded are higher for the 75 kW fires.

Near-wall temperature from fries with propane and the 2 ft Rectangle burner with 50 kW at z=0.35 m above the burner is plotted in Figure 110. The highest temperature is recorded at y=20mm, and the boundary layer thickness is about 20 and 25 mm.

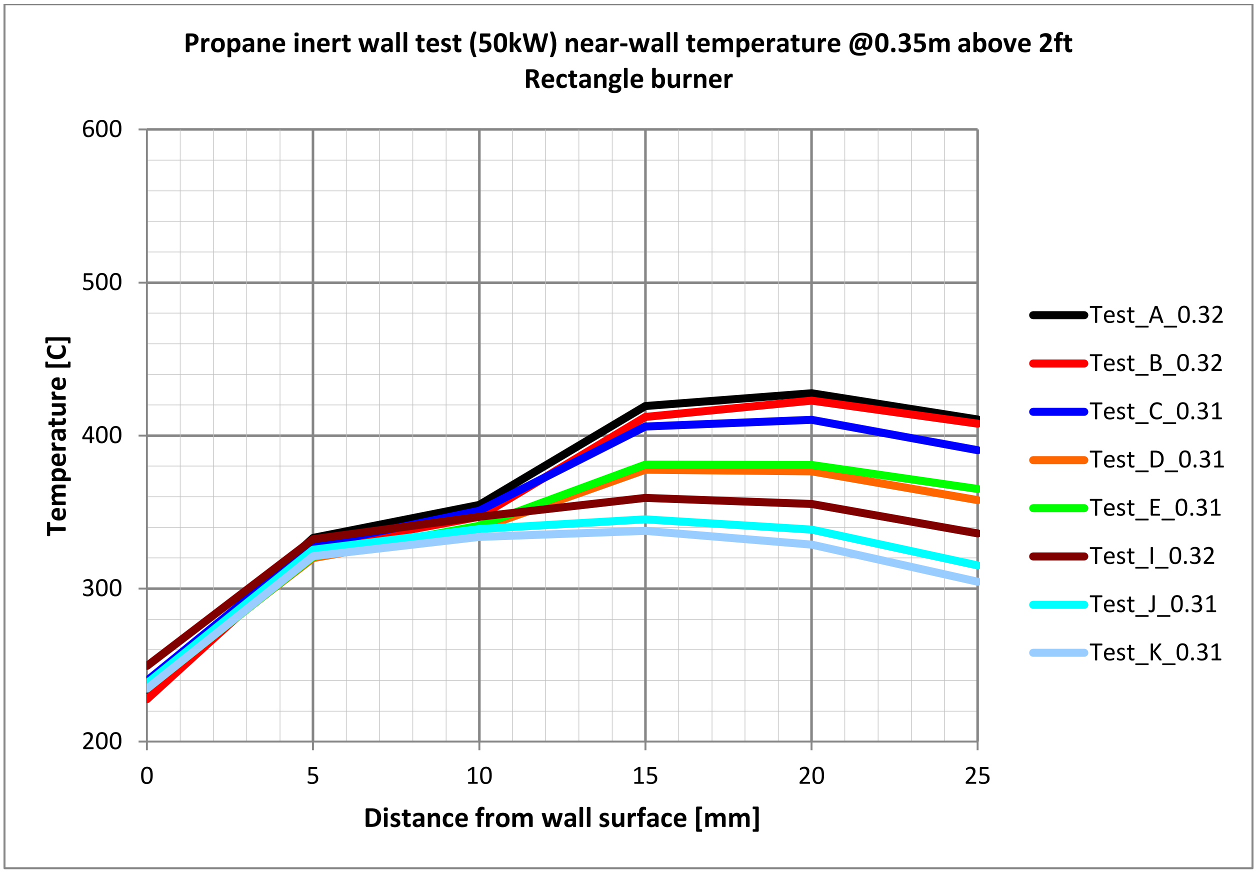

Figure 110 - Propane 2 ft Rectangle burner near-wall temperature at 0.35 m above burner surface

At z=0.95 m above the burner, the highest temperature was recorded at 35 mm, as shown in Figure 111. This suggests that the boundary layer thickness is at least 35 mm.

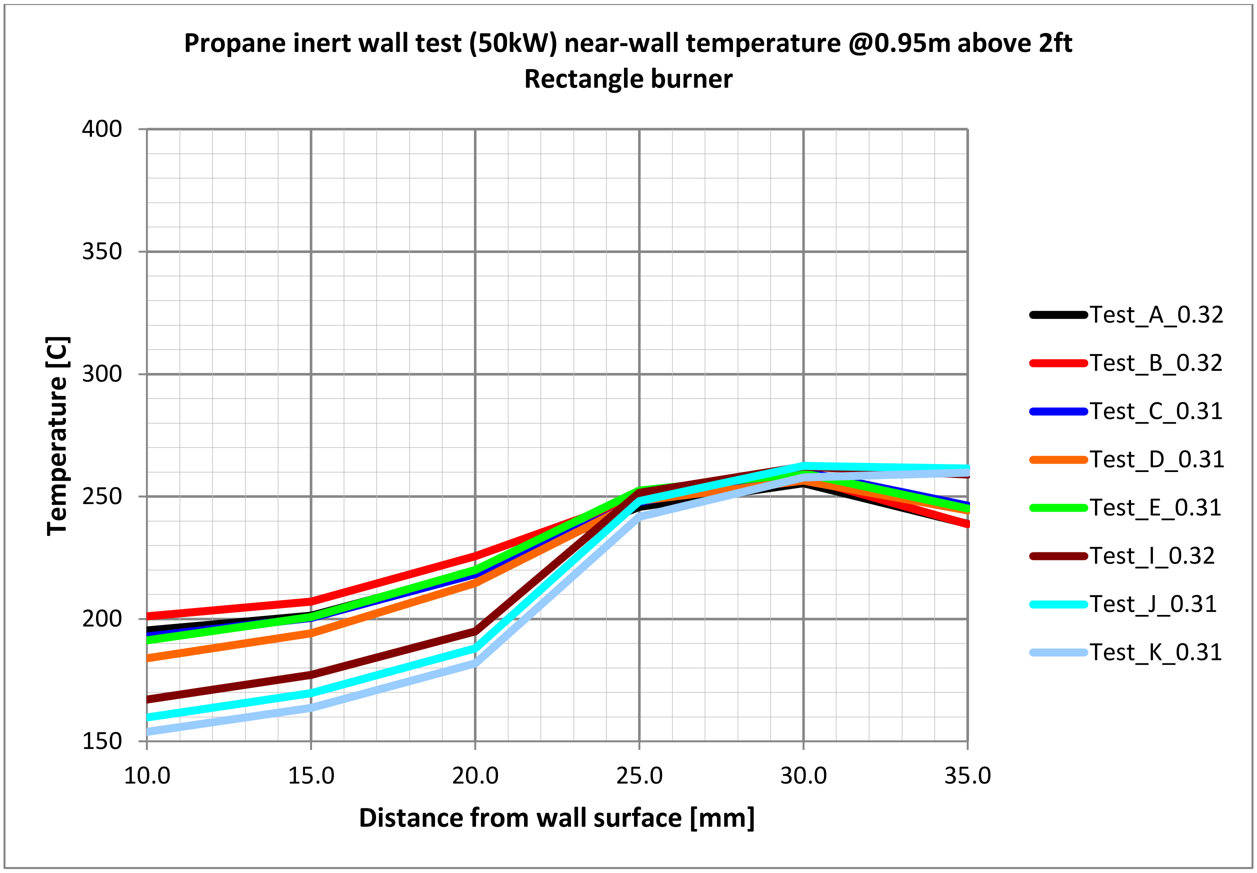

Figure 111 - Propane 2 ft Rectangle burner near-wall temperature at 0.95 m above burner surface

At z=1.55 m above the burner, the highest temperature was recorded at 25 mm, as shown in Figure 112. This suggests that the boundary layer thickness is between 25 and 30 mm at this height.

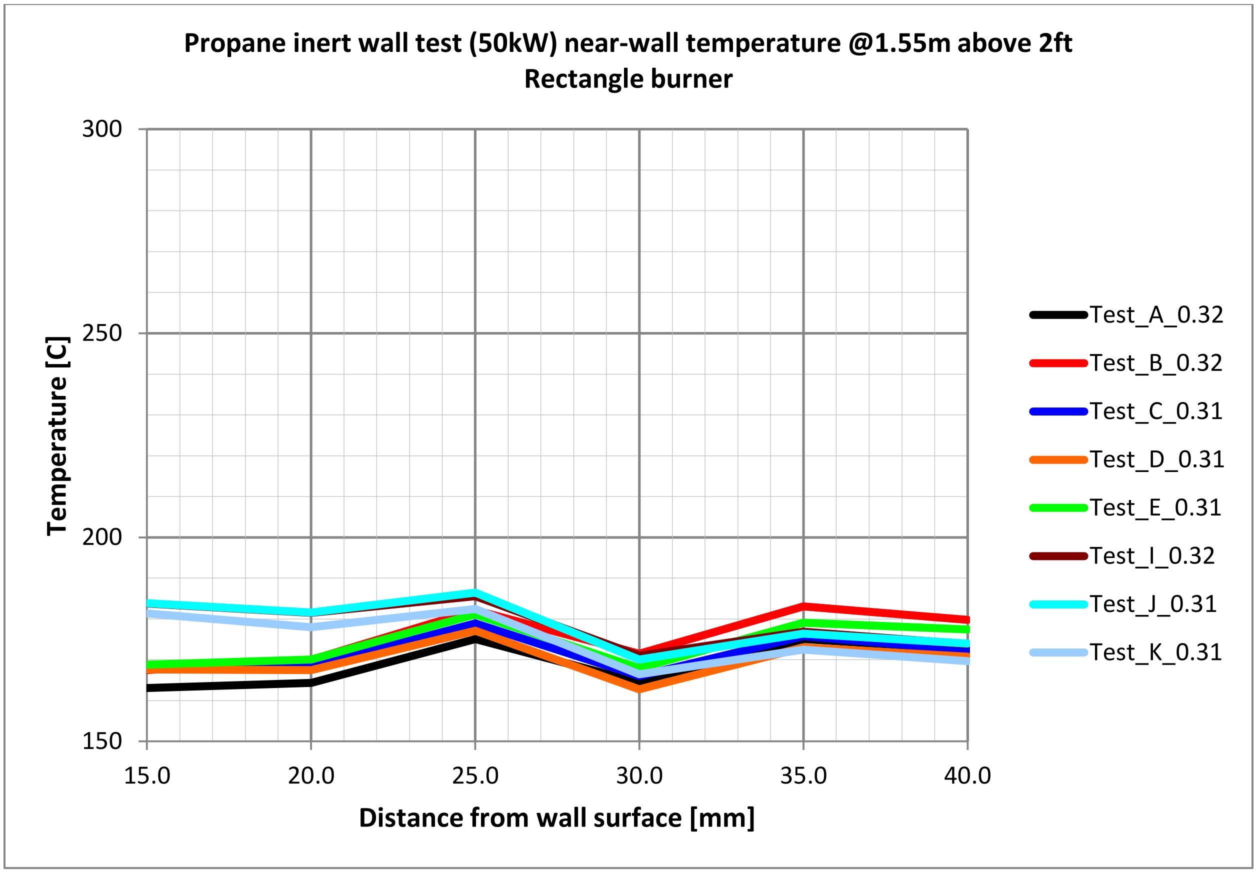

Figure 112 - Propane 2 ft Rectangle burner near-wall temperature at 1.55 m above burner surface

Near-wall temperature from fries with propane and the 2 ft Rectangle burner with 75 kW at z=0.35 m above the burner is plotted in Figure 116. The highest temperature is recorded at y=20mm, and the boundary layer thickness is about 20 and 25 mm.

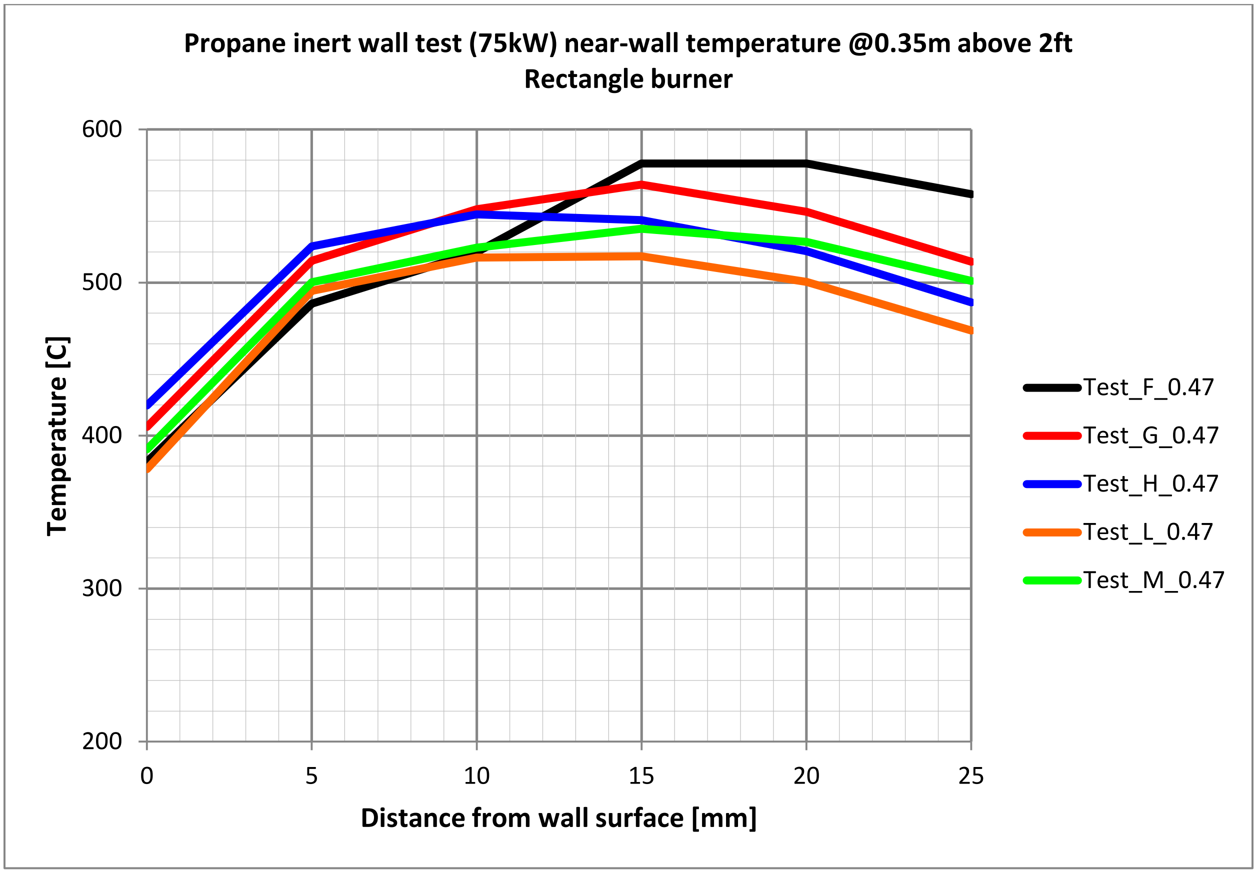

Figure 113 - Propane 2 ft Rectangle burner near-wall temperature at 0.35 m above burner surface

At z=0.95 m above the burner, the highest temperature was recorded at 35 mm, as shown in Figure 114. This suggests that the boundary layer thickness is at least 35 mm.

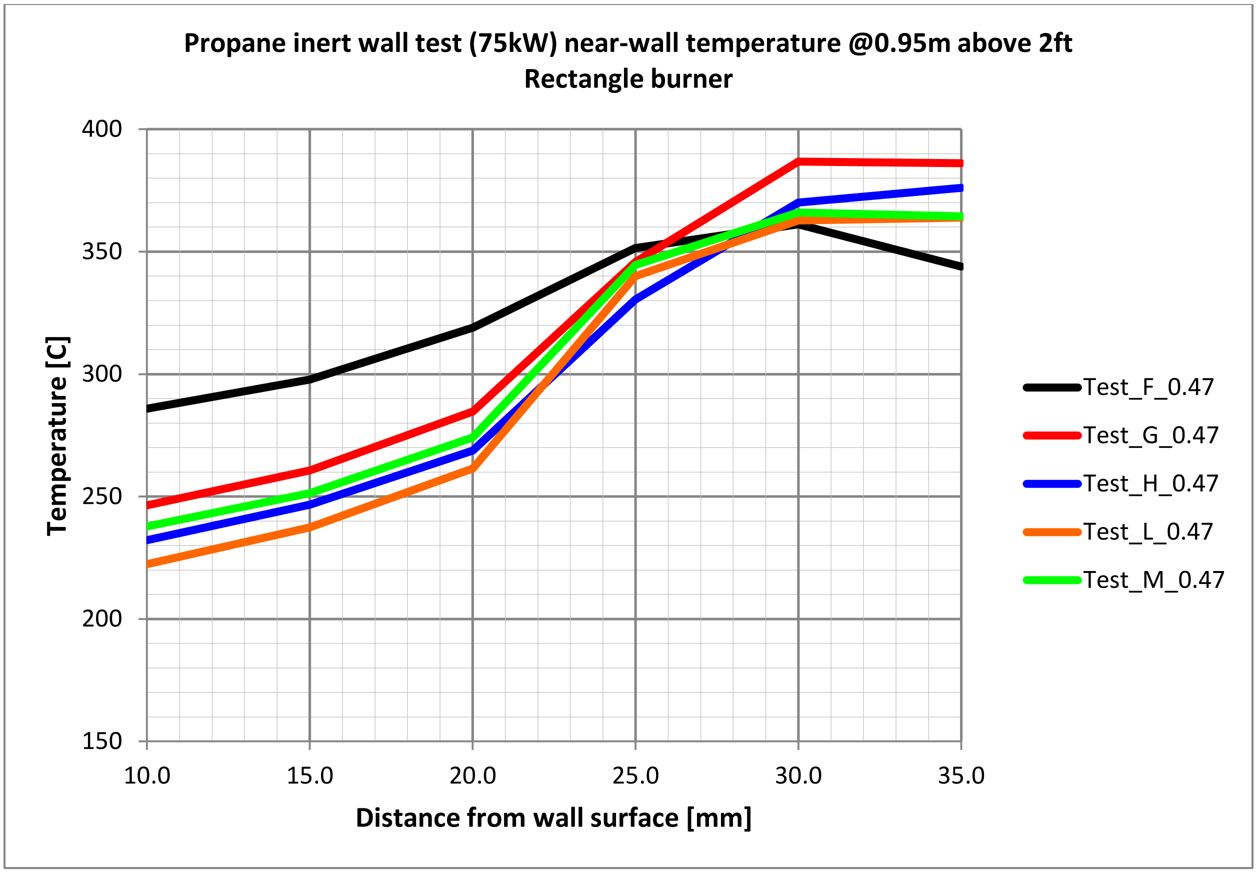

Figure 114 - Propane 2 ft Rectangle burner near-wall temperature at 0.95 m above burner surface

At z=1.55 m above the burner, the highest temperature was recorded at 25 mm, as shown in Figure 115. This suggests that the boundary layer thickness is between 25 and 30 mm at this height.

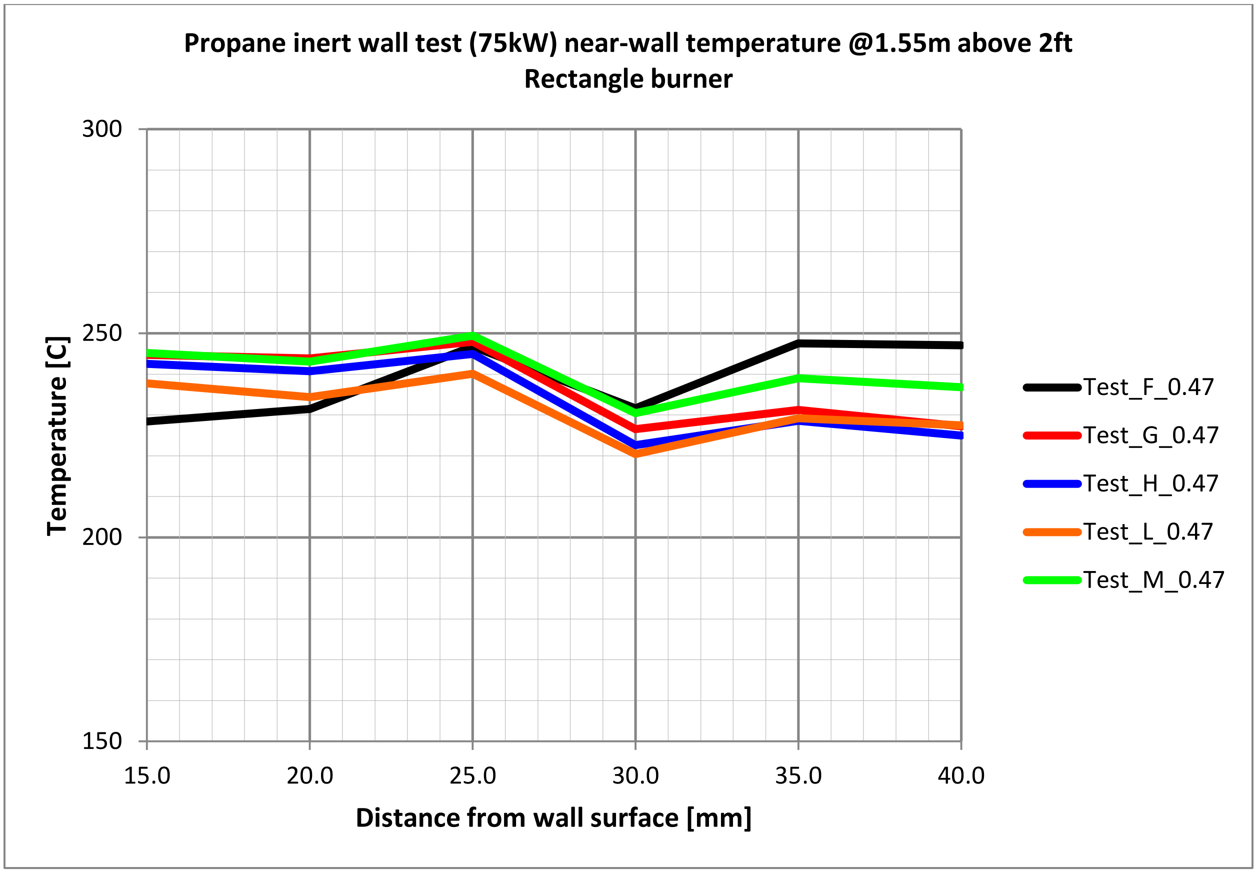

Figure 115 - Propane 2 ft Rectangle burner near-wall temperature at 1.55 m above burner surface

Same as with the 1 ft burner, the boundary layers of the 50 kW and 75 kW fires have the same profile, but higher temperatures for the 75 kW cases.

Near-wall temperature from fries with propylene and the 1 ft Square burner with 50 kW at z=0.35 m above the burner is plotted in Figure 116. The highest temperature is recorded at y=20mm, and the boundary layer thickness is about 20 and 25 mm.

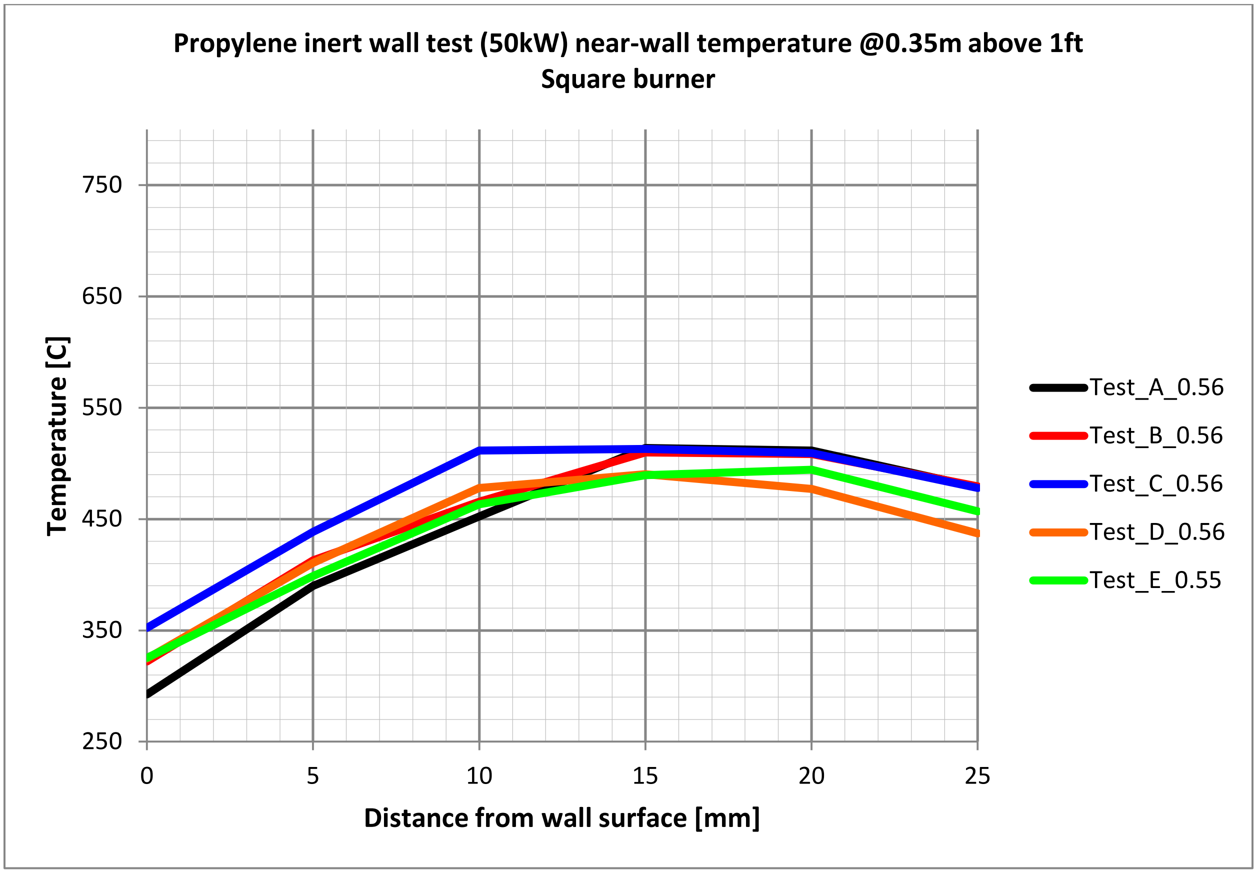

Figure 116 - Propylene 1 ft Square burner near-wall temperature at 0.35 m above burner surface

At z=0.95 m above the burner, the highest temperature was recorded at 35 mm, as shown in Figure 117. This suggests that the boundary layer thickness is at least 35 mm.

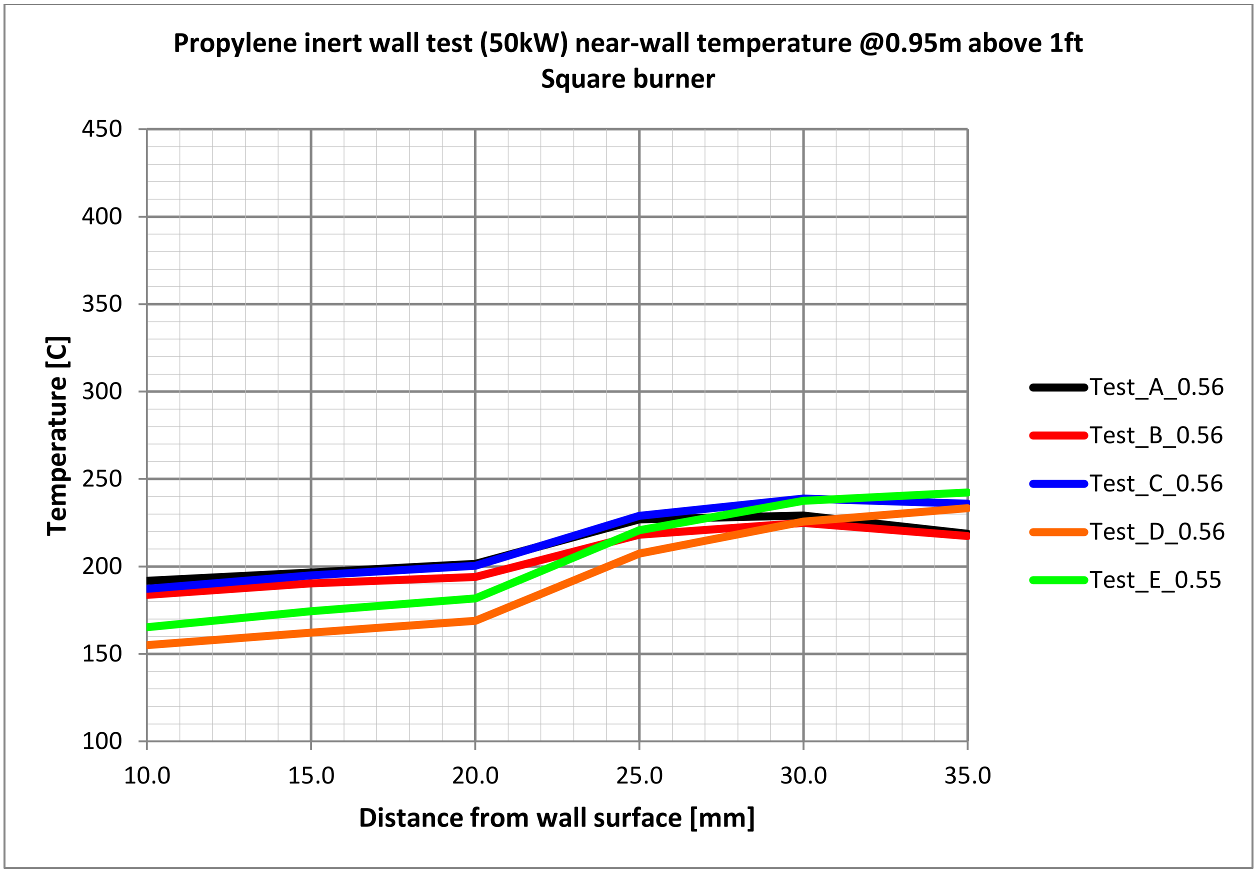

Figure 117 - Propylene 1 ft Square burner near-wall temperature at 0.95 m above burner surface

At z=1.55 m above the burner, the highest temperature was recorded at 40 and 35 mm, as shown in Figure 118. This suggests that the boundary layer thickness is between 35 and 40 mm at this height.

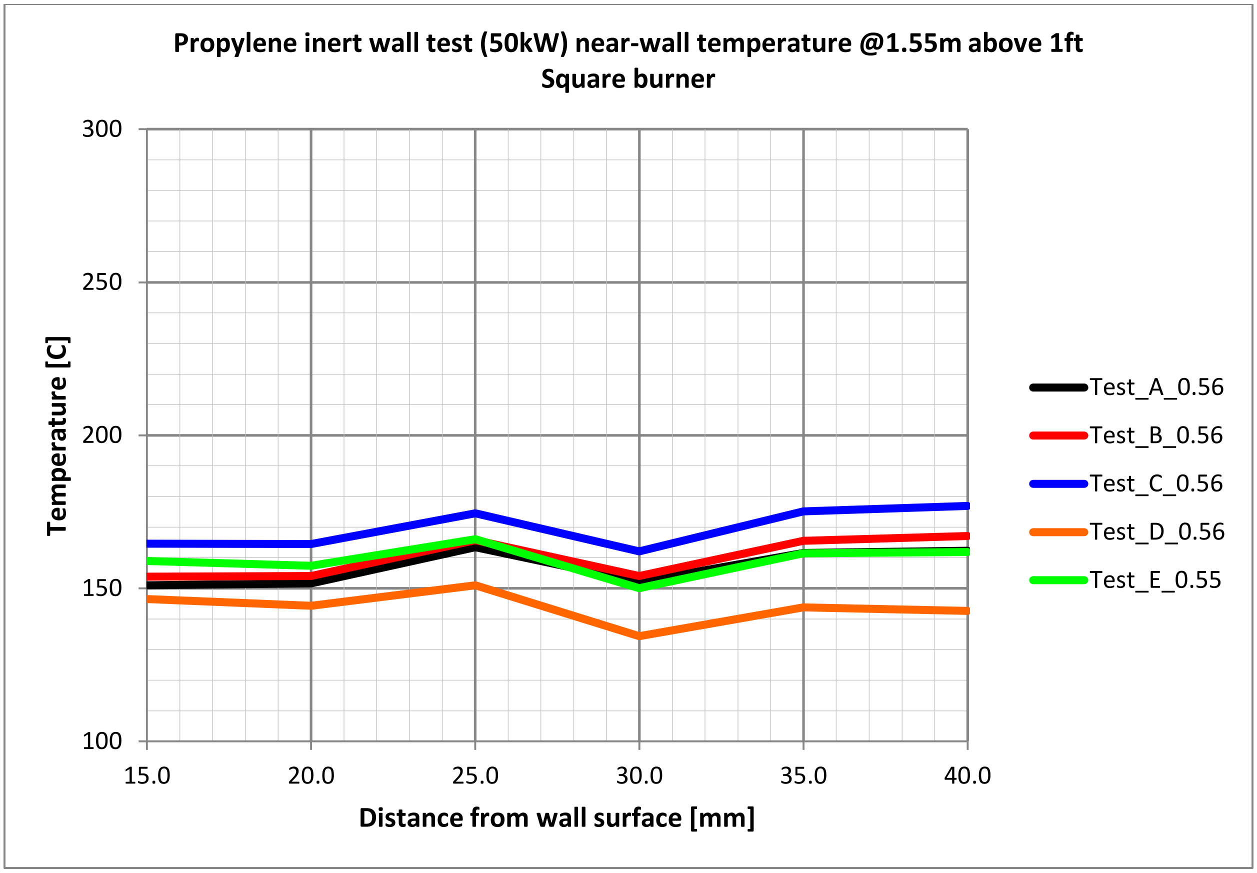

Figure 118 - Propylene 1 ft Square burner near-wall temperature at 1.55 m above burner surface

Near-wall temperature from fries with propylene and the 1 ft Square burner with 75 kW at z=0.35 m above the burner is plotted in Figure 119. The highest temperature is recorded at y=20mm, and the boundary layer thickness is about 20 and 25 mm.

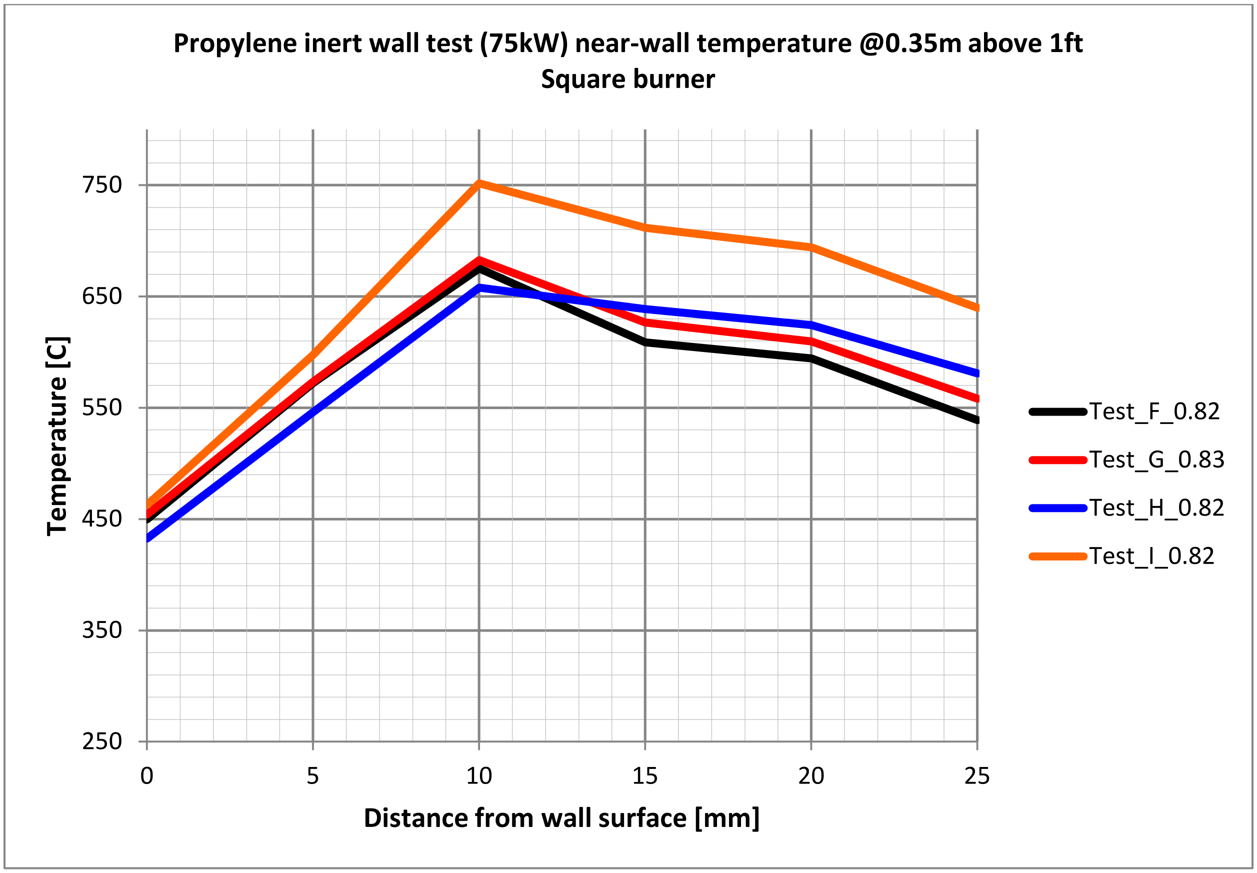

Figure 119 - Propylene 1 ft Square burner near-wall temperature at 0.35 m above burner surface

At z=0.95 m above the burner, the highest temperature was recorded at 35 mm, as shown in Figure 120. This suggests that the boundary layer thickness is at least 35 mm.

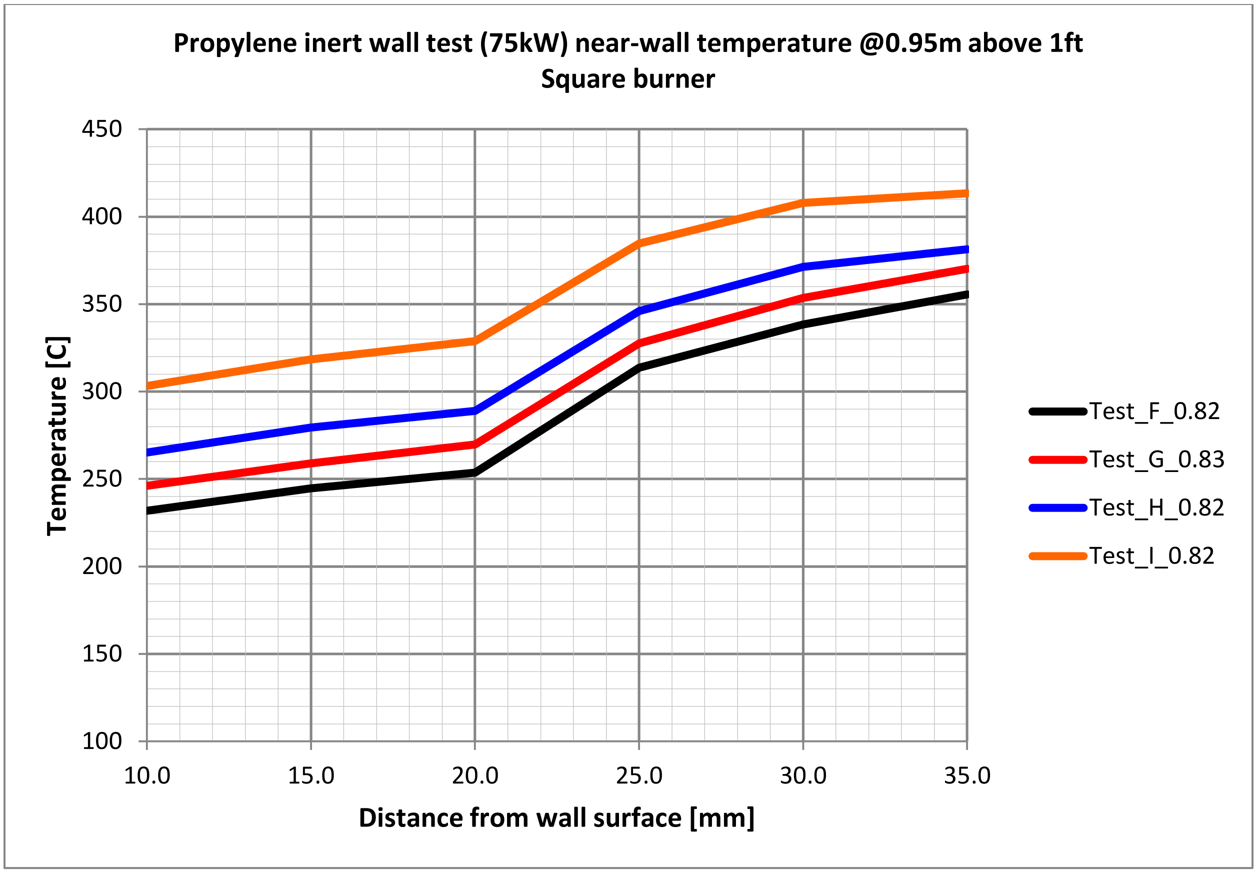

Figure 120 - Propylene 1 ft Square burner near-wall temperature at 0.95 m above burner surface

At z=1.55 m above the burner, the highest temperature was recorded at 40 and 35 mm, as shown in Figure 121. This suggests that the boundary layer thickness is between 35 and 40 mm at this height.

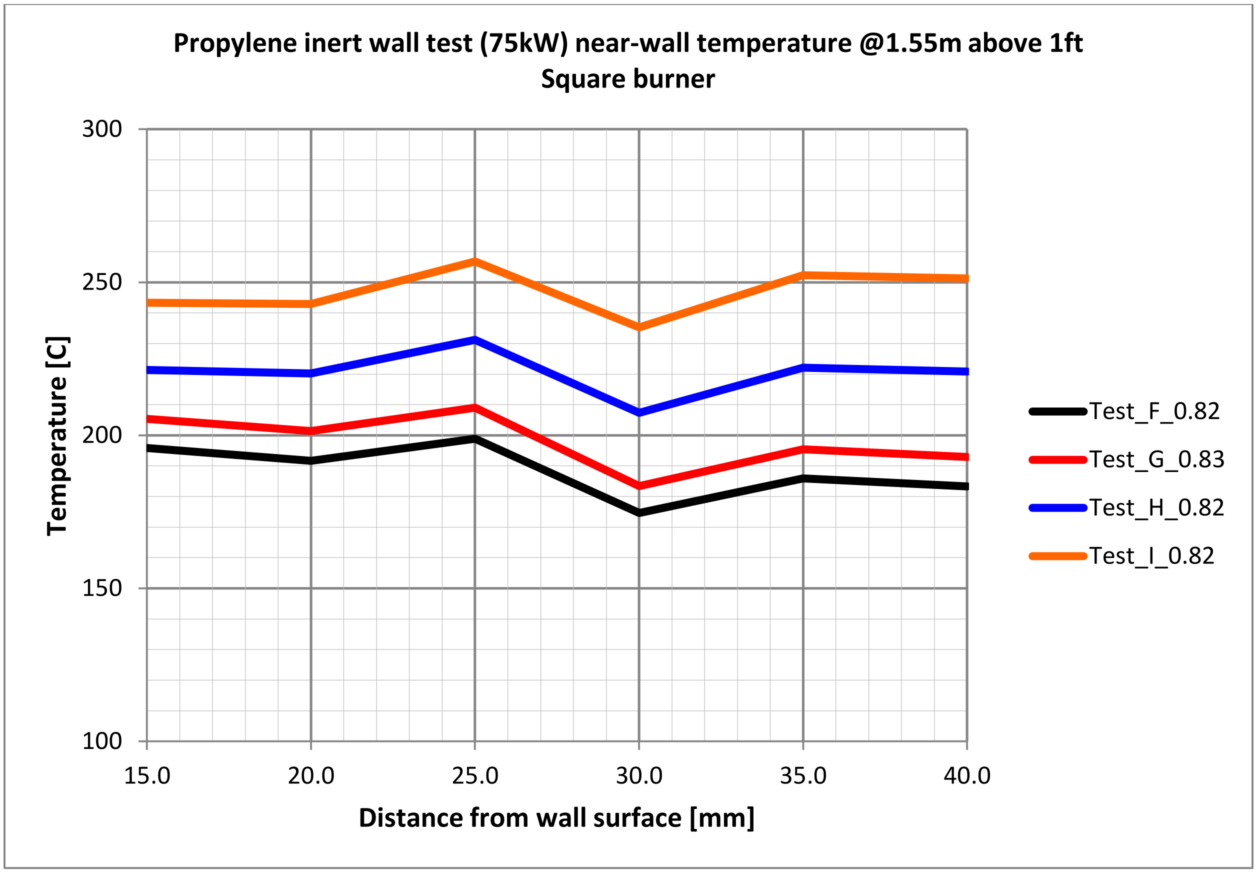

Figure 121 - Propylene 1 ft Square burner near-wall temperature at 1.55 m above burner surface

Near-wall temperature from fries with propylene and the 2 ft Rectangle burner with 50 kW at z=0.35 m above the burner is plotted in Figure 122. The highest temperature is recorded at y=15mm, and the boundary layer thickness is about 15 and 20 mm.

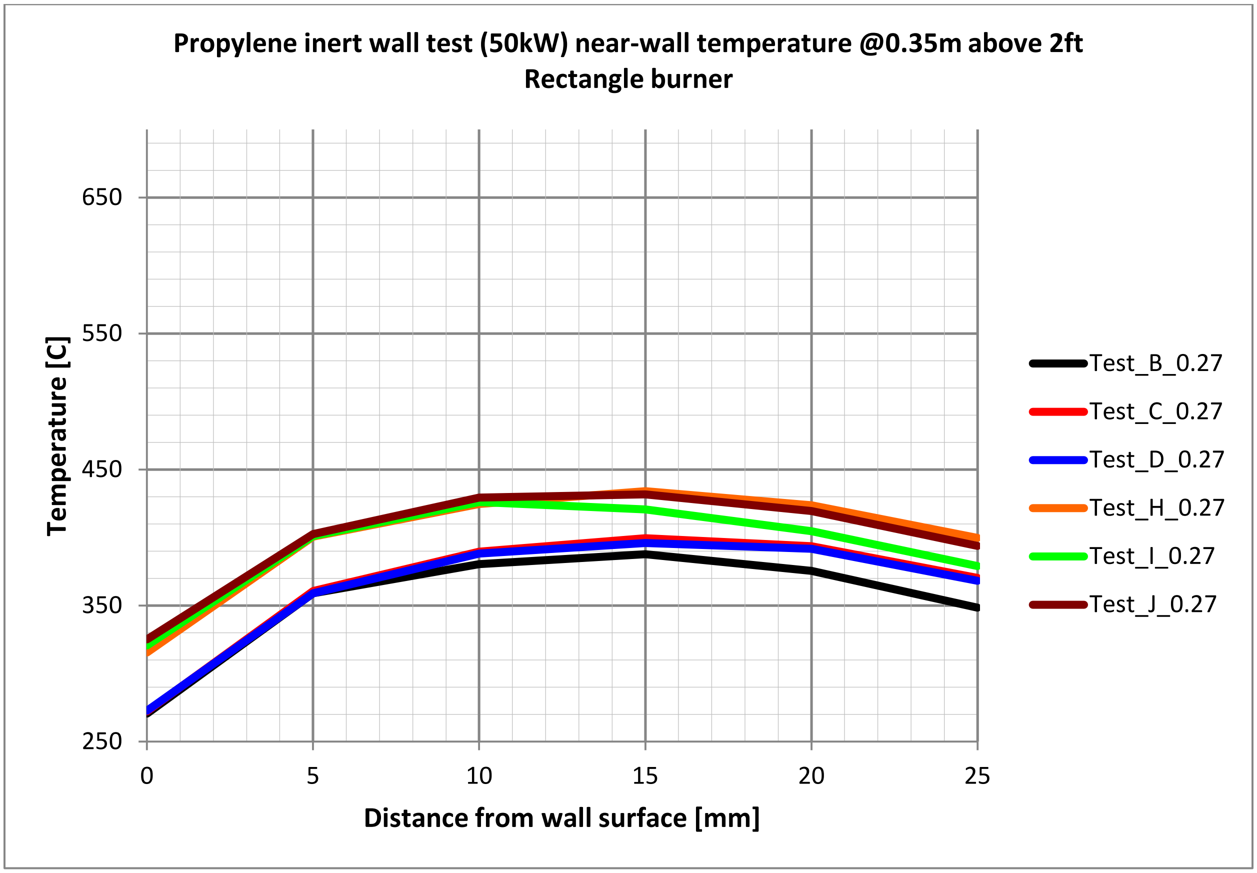

Figure 122 - Propylene 2 ft Square burner near-wall temperature at 0.35 m above burner surface

At z=0.95 m above the burner, the highest temperature was recorded at 35 mm, as shown in Figure 123. This suggests that the boundary layer thickness is at least 35 mm.

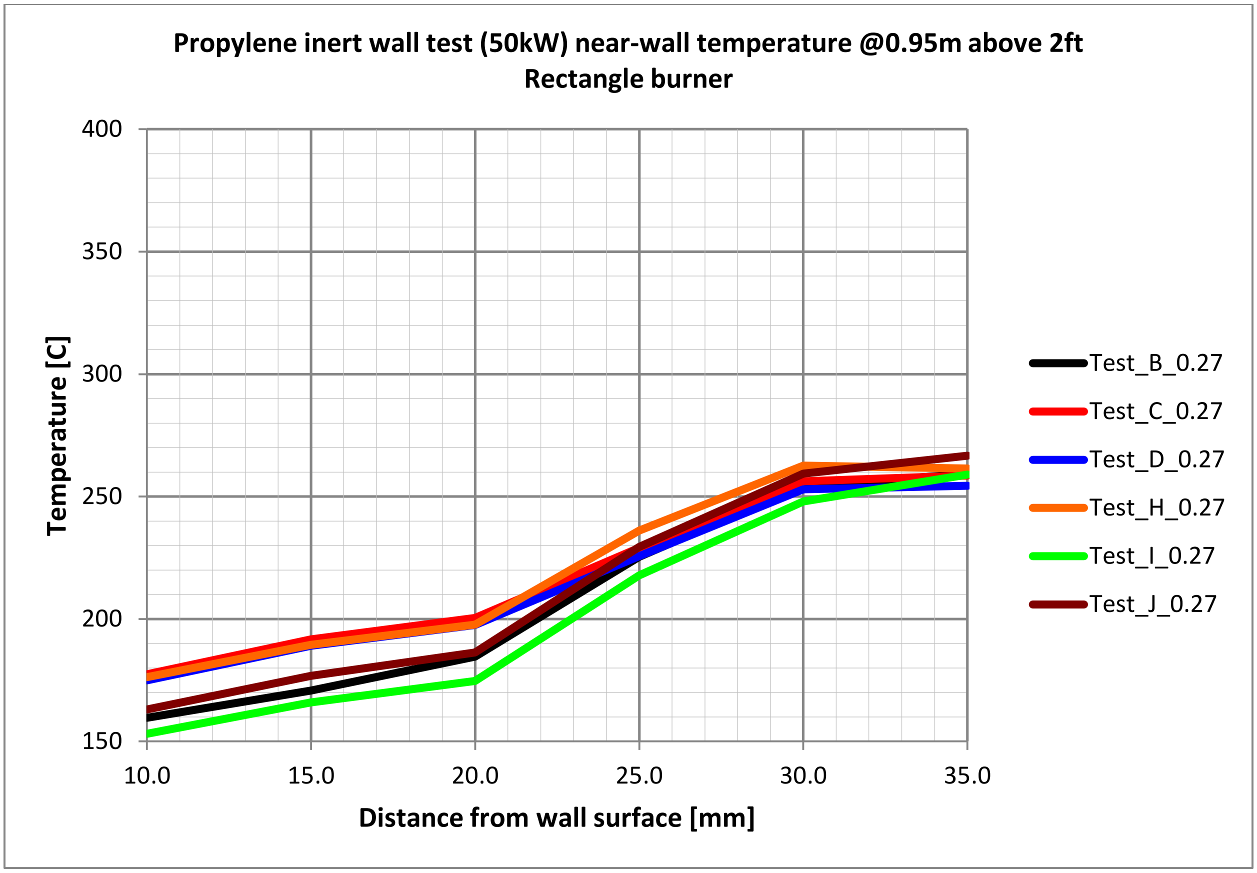

Figure 123 - Propylene 2 ft Square burner near-wall temperature at 0.95 m above burner surface

At z=1.55 m above the burner, the highest temperature was recorded at 25 mm, as shown in Figure 124. This suggests that the boundary layer thickness is between 25 and 30 mm at this height.

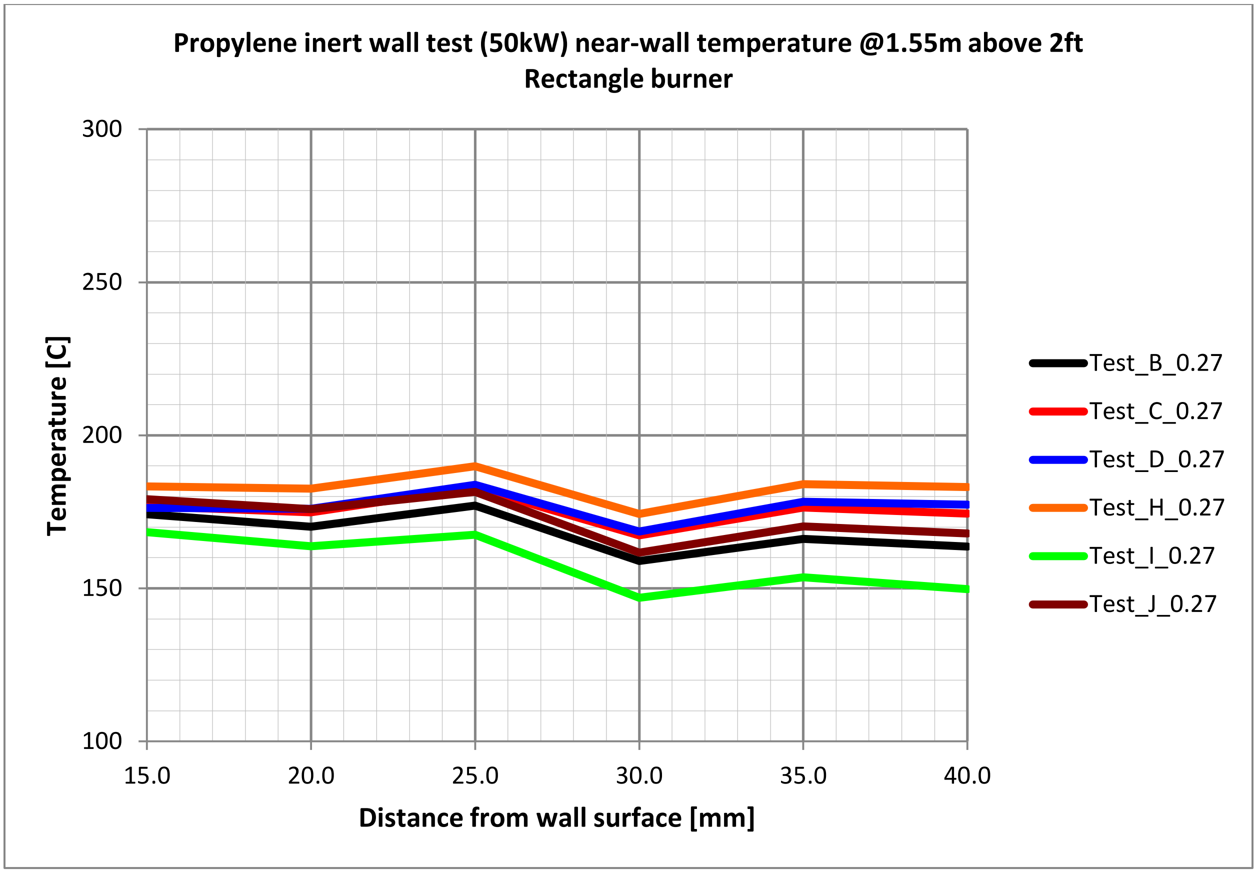

Figure 124 - Propylene 2 ft Square burner near-wall temperature at 1.55 m above burner surface

Near-wall temperature from fries with propylene and the 2 ft Rectangle burner with 75 kW at z=0.35 m above the burner is plotted in Figure 125. The highest temperature is recorded at y=15mm, and the boundary layer thickness is about 15 and 20 mm.

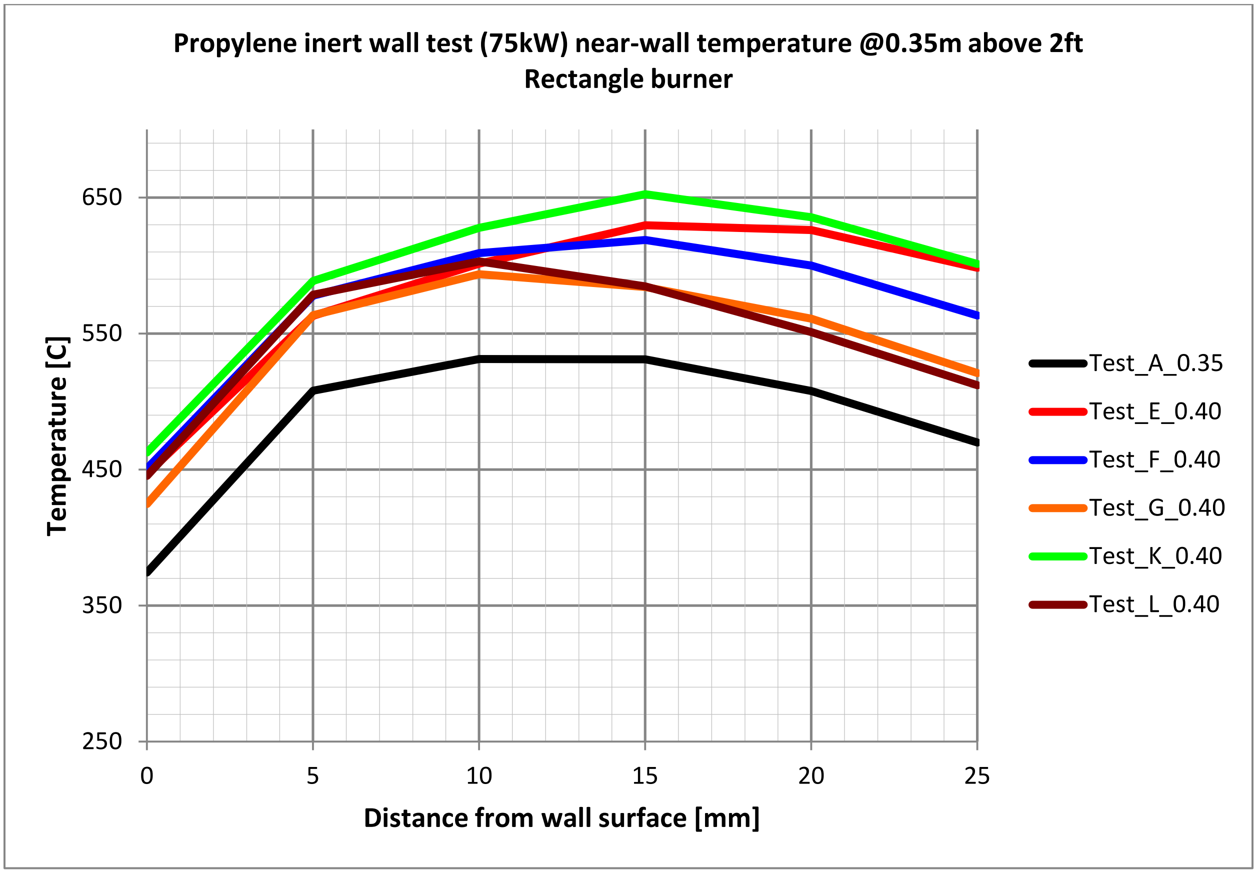

Figure 125 - Propylene 2 ft Square burner near-wall temperature at 0.35 m above burner surface

At z=0.95 m above the burner, the highest temperature was recorded at 35 mm, as shown in Figure 126. This suggests that the boundary layer thickness is at least 35 mm.

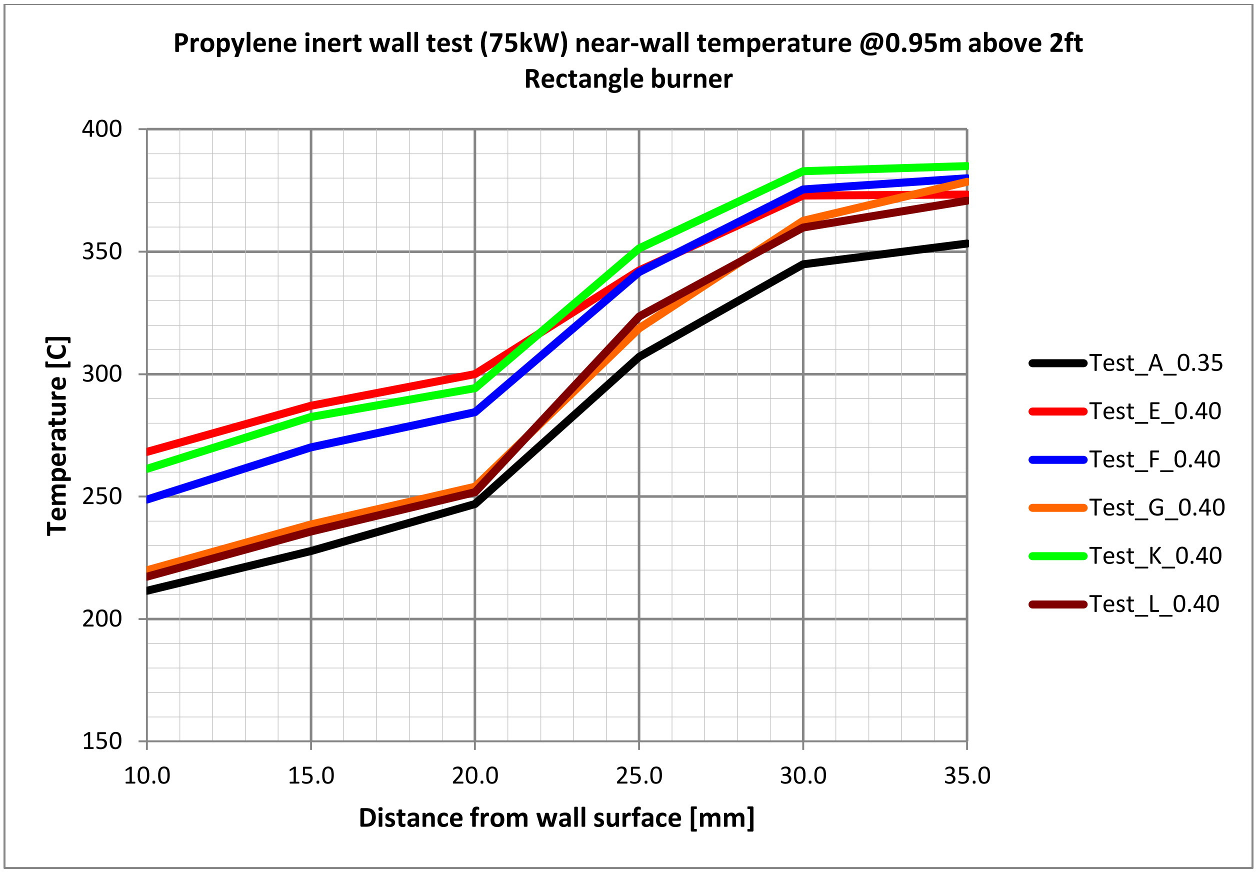

Figure 126 - Propylene 2 ft Square burner near-wall temperature at 0.95 m above burner surface

At z=1.55 m above the burner, the highest temperature was recorded at 25 mm, as shown in Figure 127. This suggests that the boundary layer thickness is between 25 and 30 mm at this height.

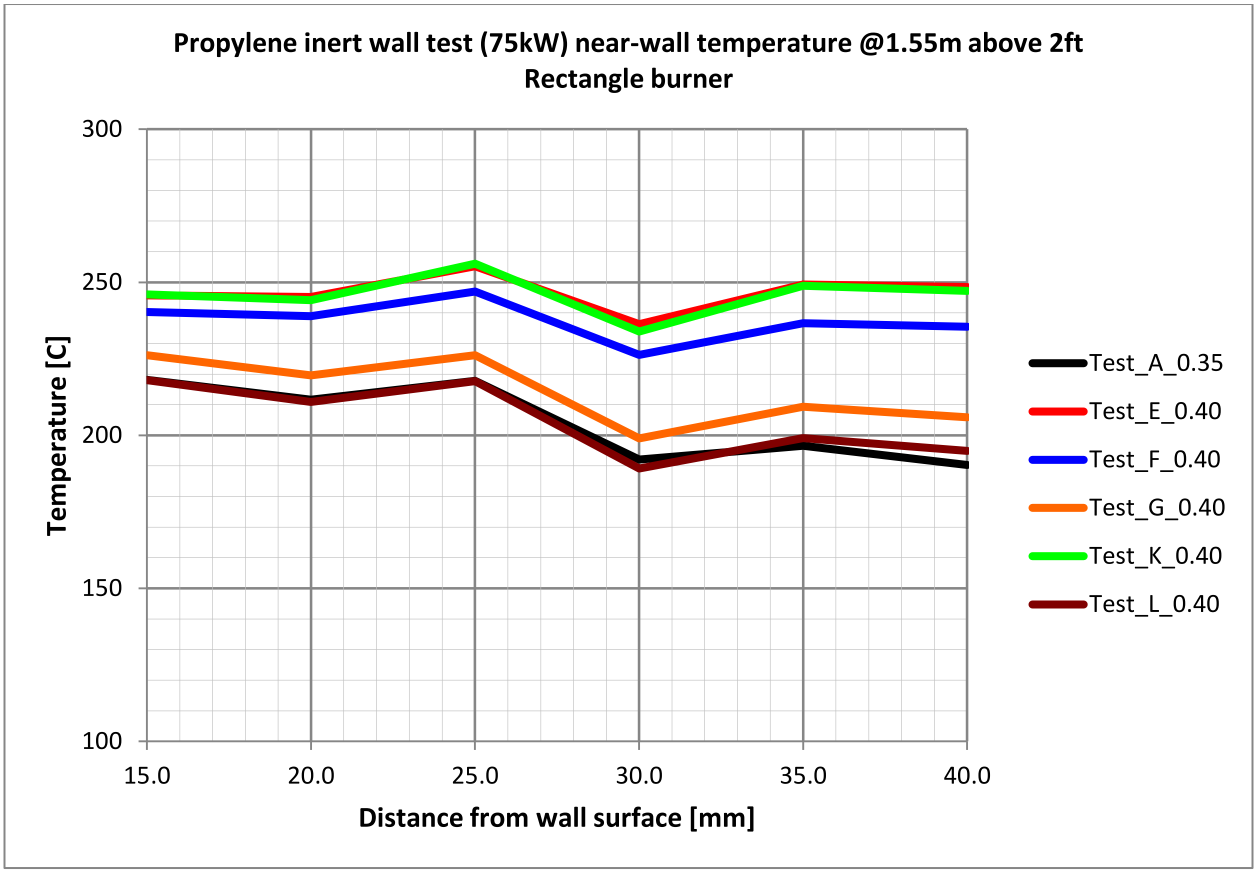

Figure 127 - Propylene 2 ft Square burner near-wall temperature at 1.55 m above burner surface

Figure 128 to Figure 136 present the layer of the different test based on fuel type and burner size.

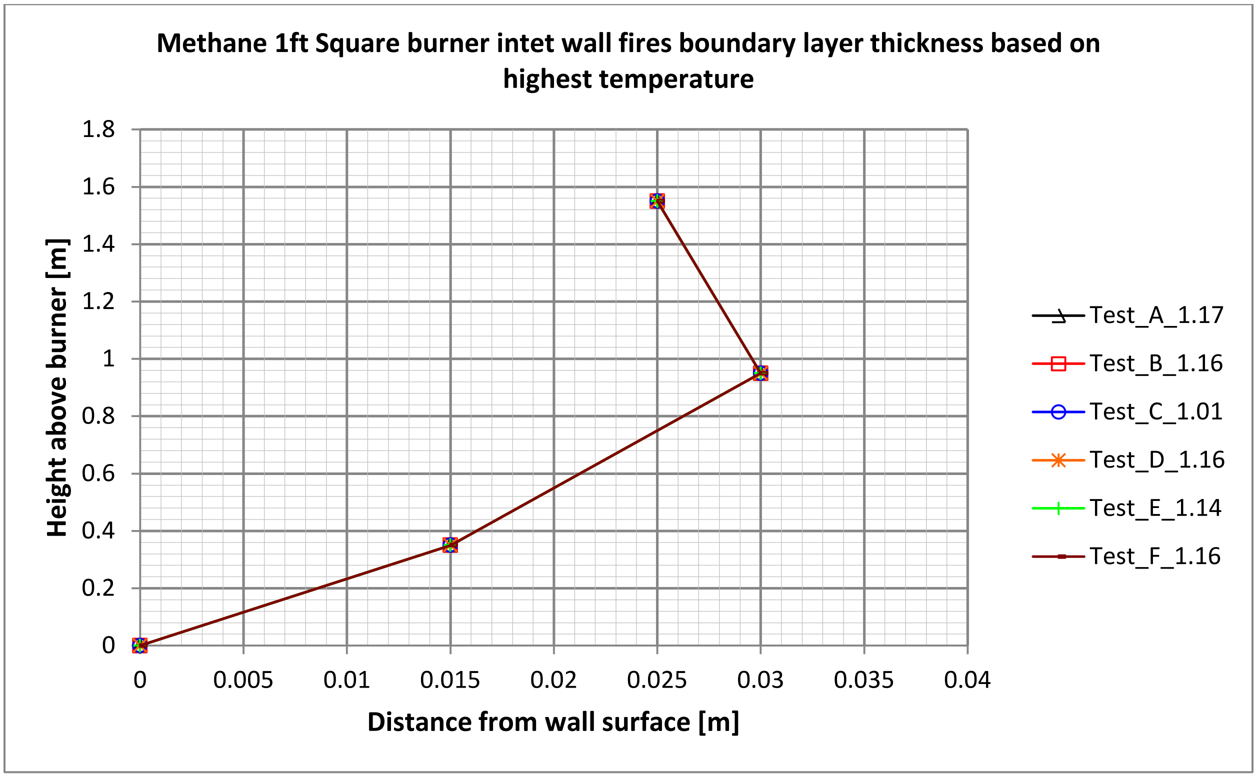

Figure 128 - Methane Square burner 50 kW boundary layers

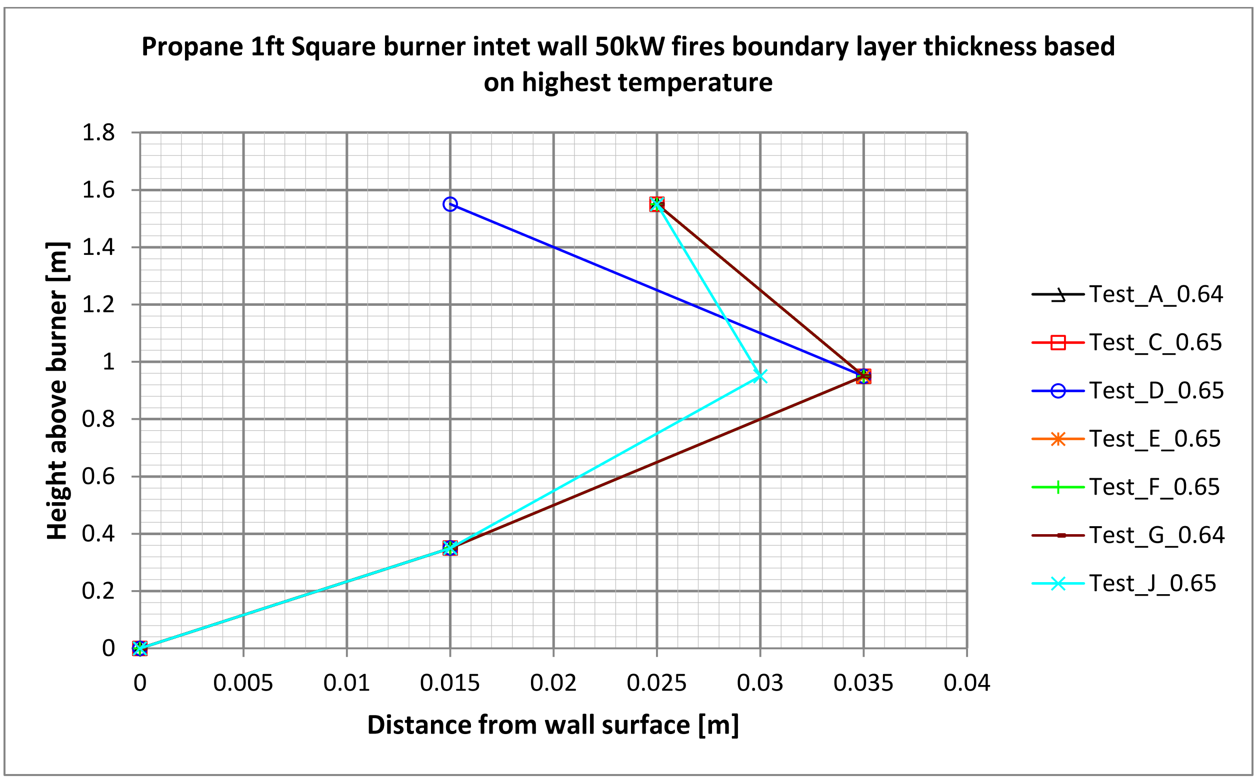

Figure 129 - Propane Square burner 50 kW boundary layers

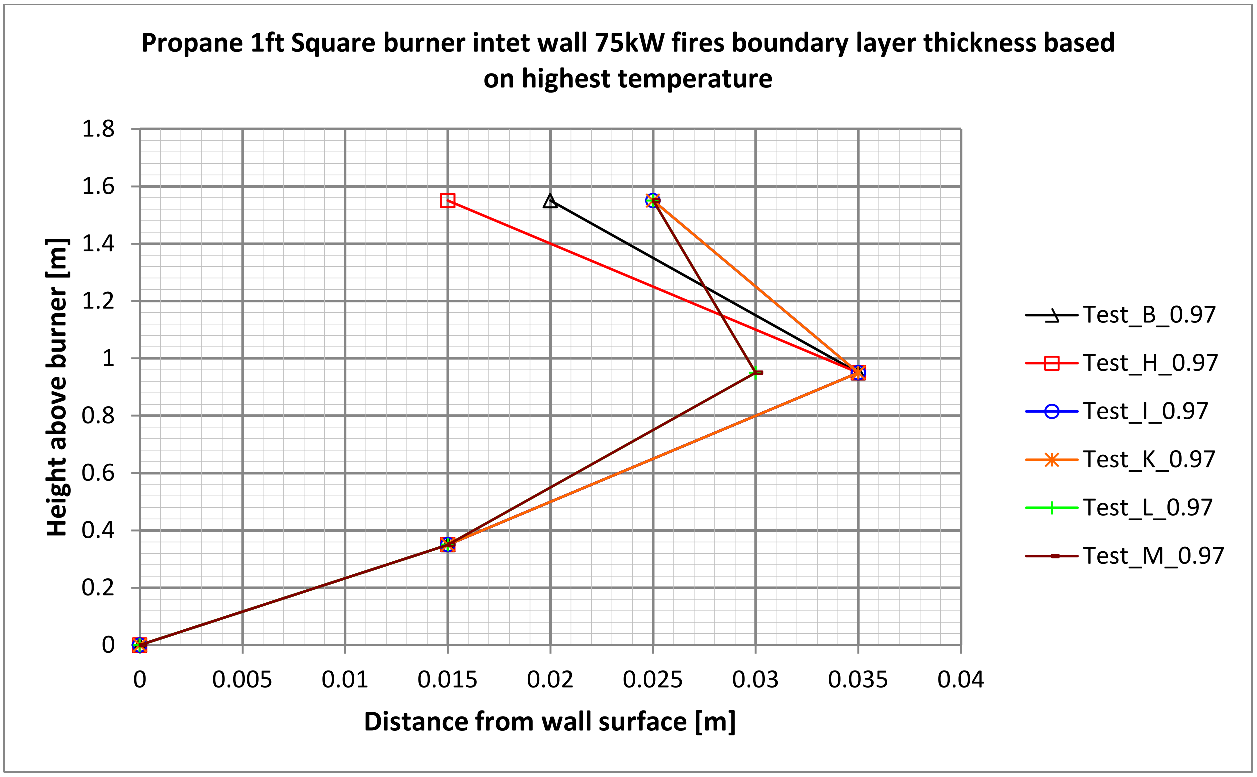

Figure 130 - Propane Square burner 75 kW boundary layers

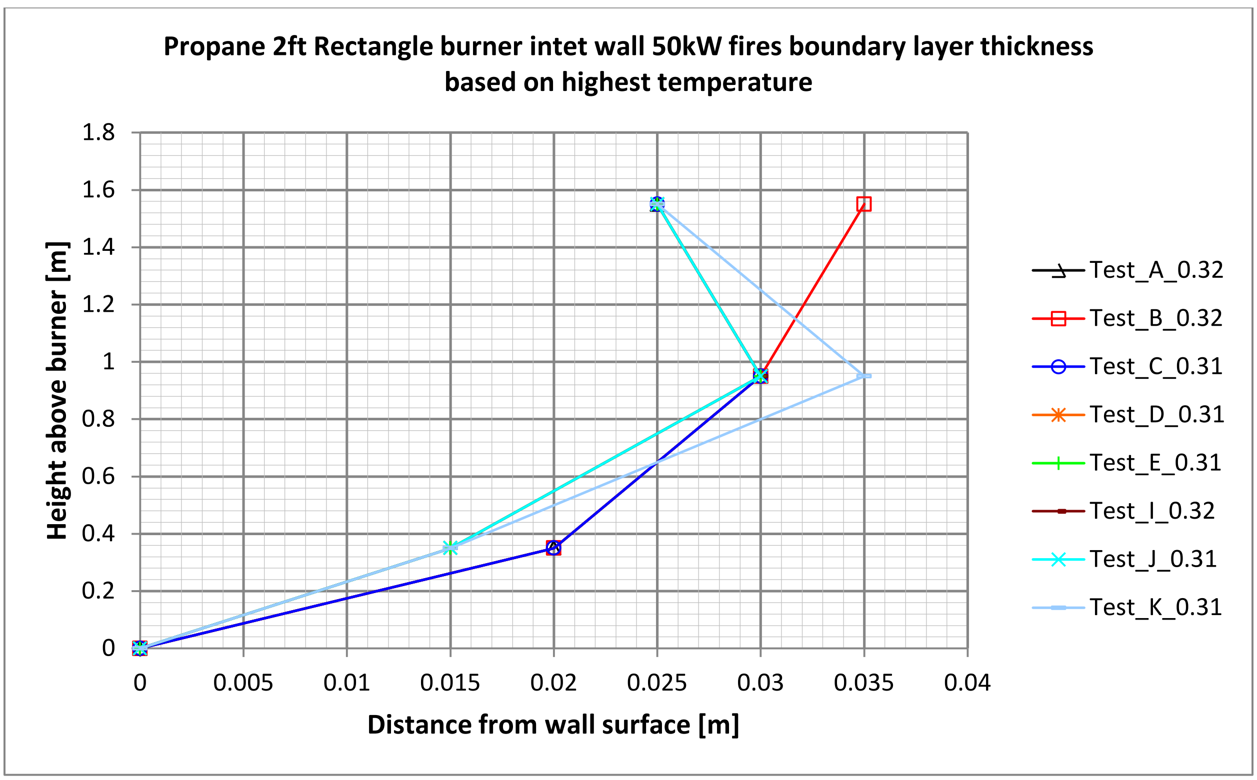

Figure 131 - Propane Rectangle burner 50 kW boundary layers

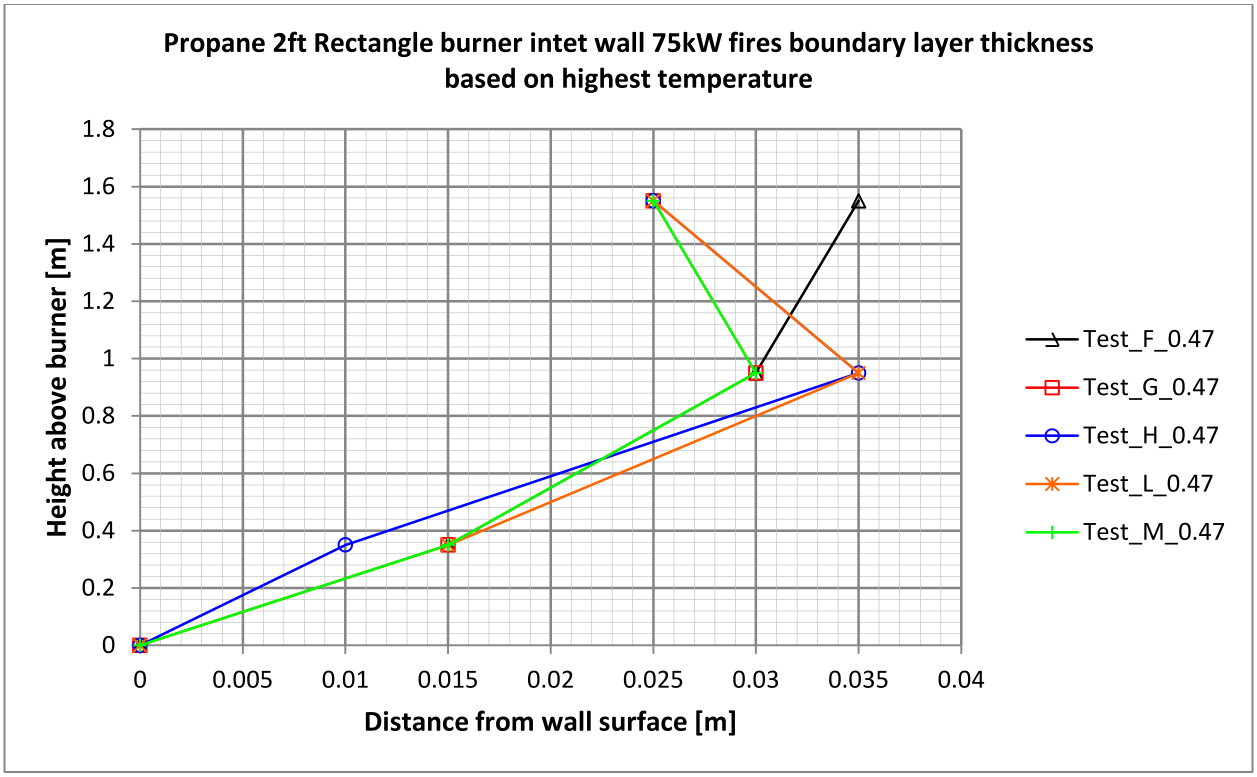

Figure 132 - Propane Rectangle burner 75 kW boundary layers

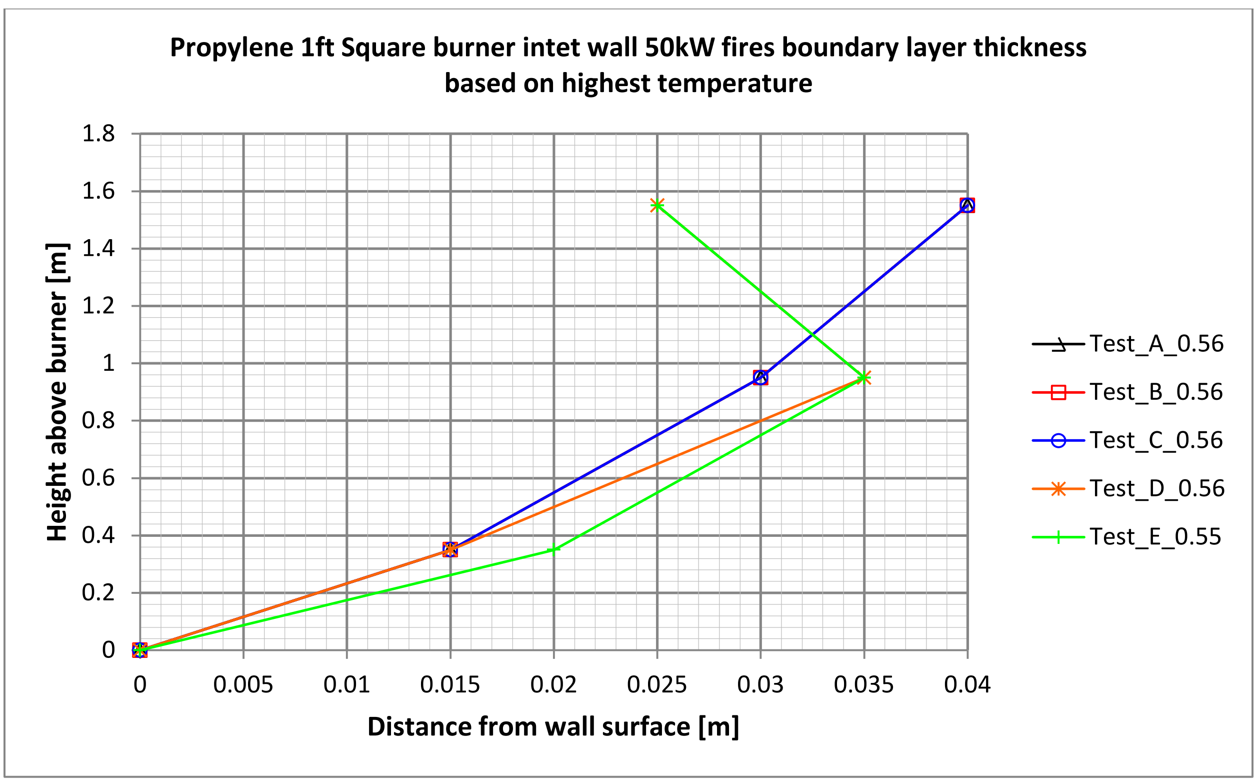

Figure 133- Propylene Square burner 50 kW boundary layers

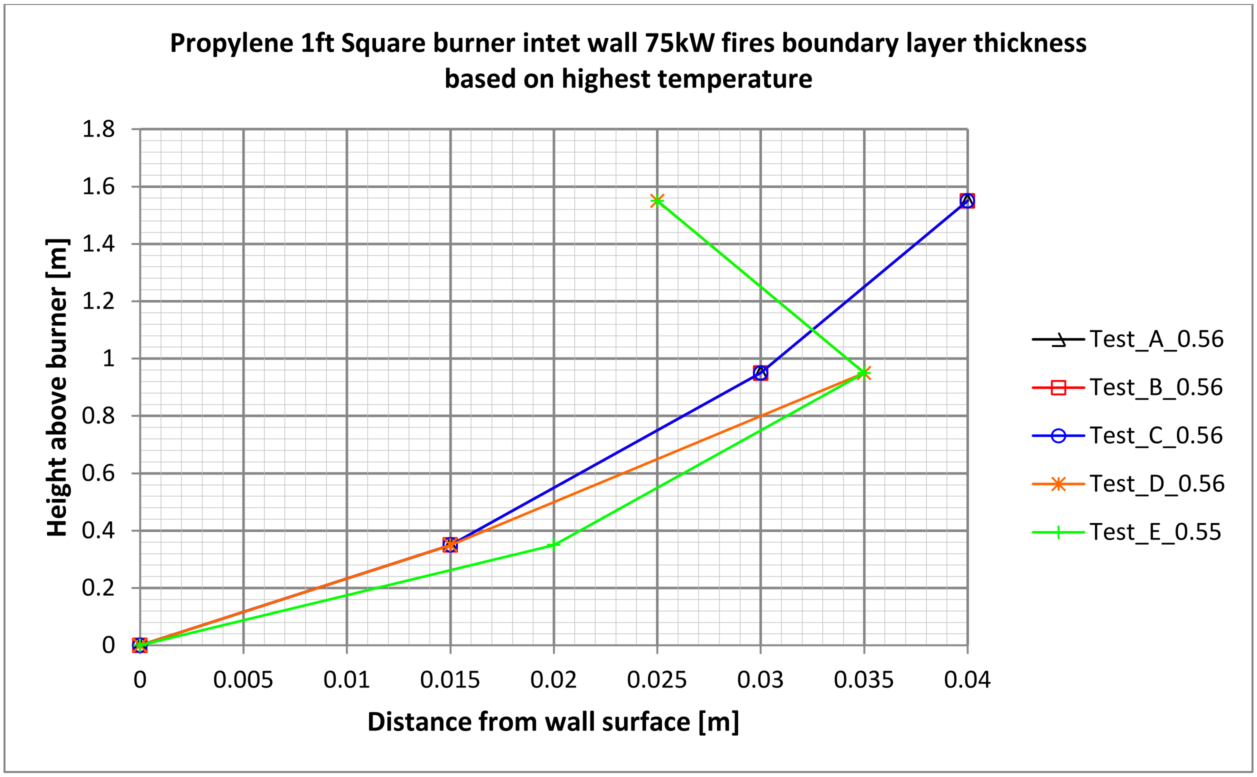

Figure 134 - Propylene Square burner 75 kW boundary layers

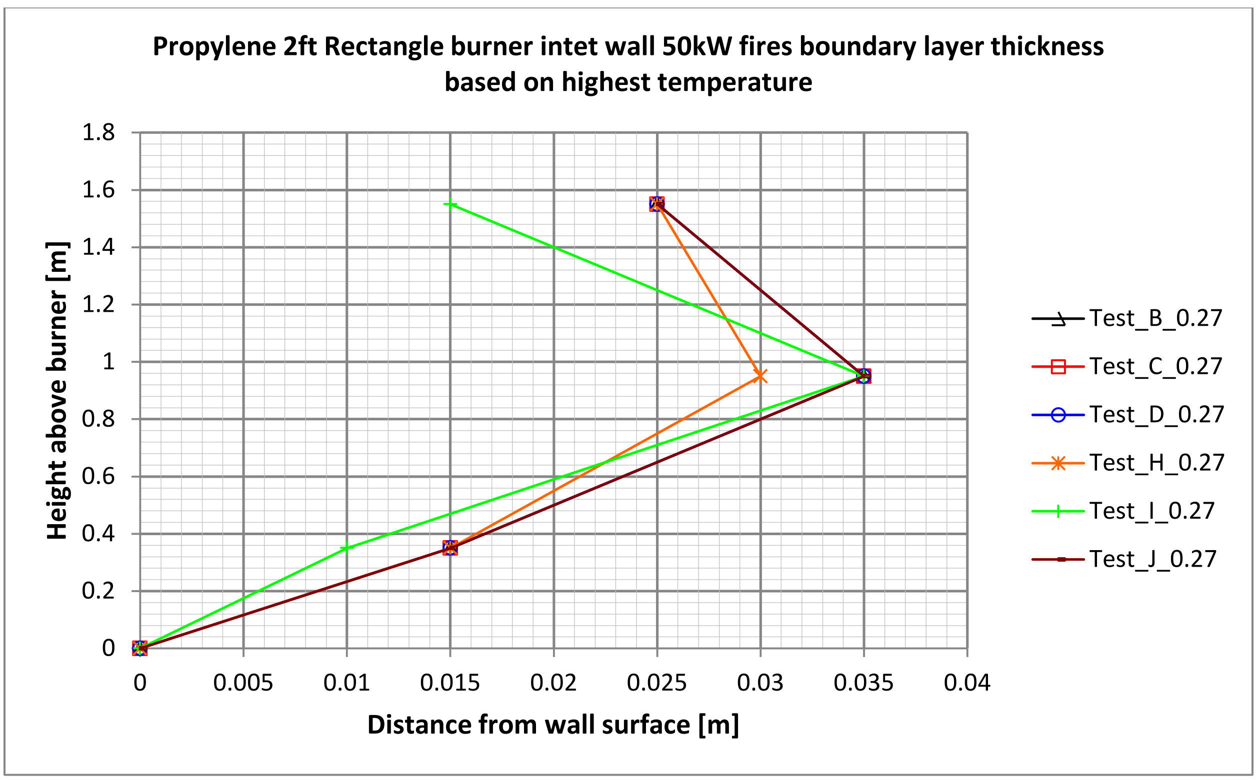

Figure 135 - Propylene Rectangle burner 50 kW boundary layers

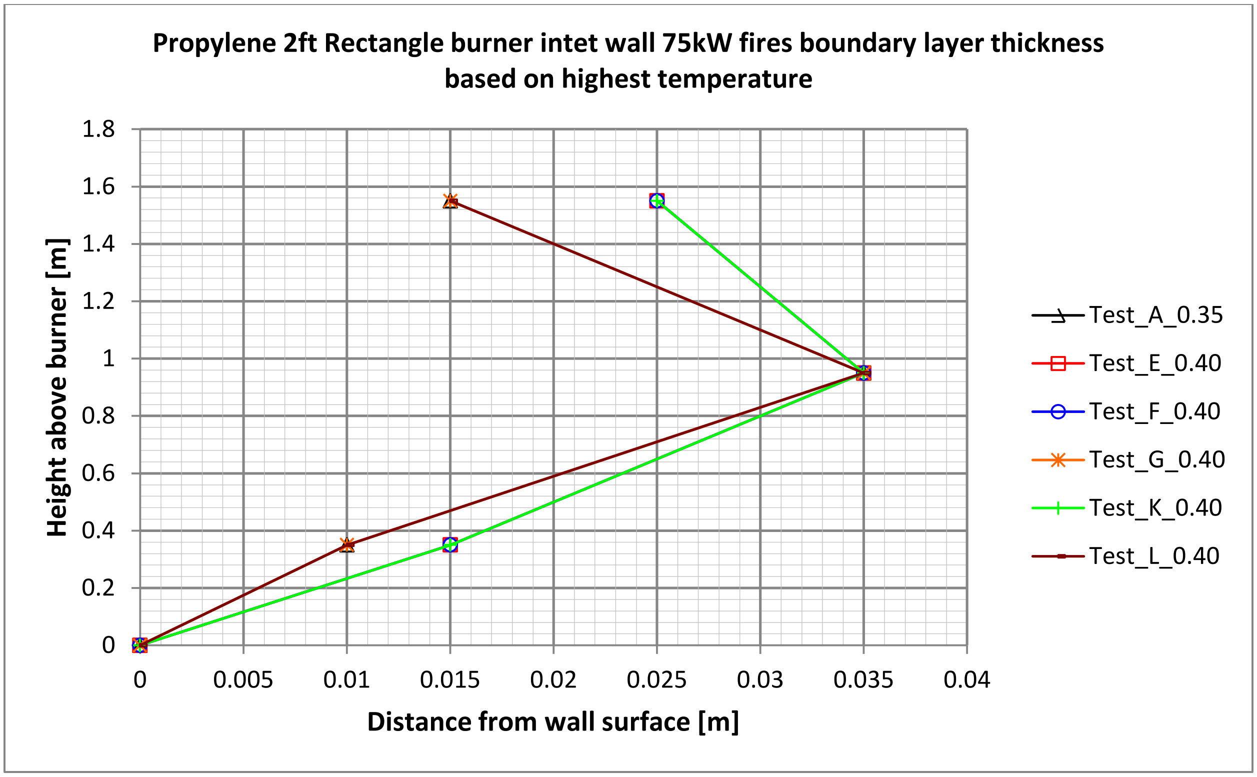

Figure 136 - Propylene Rectangle burner 75 kW boundary layers

D.6 Flame Height

The shape and size of the heating area imposed by an initializing fire on a combustible material can affect its flame spread and pyrolysis just as the starting fire's HRR, heat flux, and velocity. For this flame spread study, it is important to characterize the various starting fire conditions so that correlations can be made with established theories, previous experimental data, and computer simulation results.

Experiments of free plume and inert wall fire using propane and propylene as fuels, two different burners, and two different HRRs were conducted. The propane and propylene gases were sent through the gas delivery system with a mass flow controller at rates equivalent to 50 kW and 75 kW fires. Only these two HRRs were considered as they have been proven enough to ignite the combustible FRP specimen and provide adequate flame spread data. A few tests were also conducted using natural gas (98% methane) at 60 kW to 70 kW in order to provide additional data for comparison. Some thermophysical properties of the various fuels are listed in Table 13.

Table 13 - Fuel Properties

Fuel	Heats of Combustion [MJ/kg]				Stoich. Air/Fuel ratio
	Total	Chemical	Convective	Radiative	
Methane (98% pure)	50.1	49.6	42.6	7.0	17.16
Propane	46.0	43.7	31.2	12.5	15.60
Propylene	46.4	40.5	25.6	14.9	14.70

The burners used in the study are Square (1 ft x 1 ft) and Rectangular (1 ft x 2 ft) with 1 inch flange around the perimeter. An 1 in thick Kaowool ceramic fiber blanket was installed at the surface of each burner to act as a diffuser for even gas flow on the surface. In the free plume tests, the burner was located in the center of the test compartment; in the inert wall tests, the burner was set centrally against the wall (the long side of the 1 ft x 2 ft burner was parallel to the wall).

The flow conditions in the compartment during an experiment had been observed to disturb the fire plume under both free plume/inert wall situations. To minimize the disturbance, a sheet of aluminum screen mesh was installed at the opening of the compartment, and another sheet was installed around the burner at the front. Entrainment conditions around the plume were stabilized resulting in straight and undisturbed fire plumes.

A total of 77 fire tests were conducted, each condition was repeated at least once for repeatability. Each fire was run for minimum 5 minutes and video data was captured using a Canon digital camcorder at a rate of 30 frames per second in the high-definition MTS format. The videos are then converted into jpeg images using Virtualdub-1.9.9. Each video was decimated by 30 frames so that an extraction was taken per second. 300 frames from each test were then imported into Tracker 3.0, a software for motion tracking, and the positions of the flame tips were tracked and then exported to Excel for further analysis. The 0%, 10%, 50%, 90% and 100% intermittency flame heights were found and the mean flame heights (50% intermittency) are plotted.

Previous works by fire researchers such as Zukoski[5], Heskestad[6], Quintiere and Grove[7], and Alston [8] presented mean flame height data as normalized by the burner's dimension vs. a non-dimensional heat release rate.

The non-dimensional HRR is commonly found by using [1].

[1] $$Q^* = \frac{Q_c}{\rho_\infty c_p T_\infty g^{0.5} D^{2.5}}$$

Q_c is the convective heat release rate of the fire based on the total heat of combustion; it is calculated using the flow-metered HRR by multiplying it with the convective fraction. It should be noted that it has been reported by Alston [8] and Anderson [9] that Zukoski's method of normalization uses the total heat release rate, although Drysdale suggests that the convective HRR was used in the reporting of flame height data. This discrepancy needs additional investigation, however, the convective HRR was used to in the normalization of the current data because it seems to provide better correlation to established theories and data.

Although it has been suggested that the Q* parameter neglect fuel properties and may not predict flame height accurately without some refinement, most correlations uses this basic form of normalization so the same treatment was applied to the current data.

Zukoski suggests that the non-dimensional flame height correlates to Q* as equation [2]

[2] $$\frac{z_f}{D_h} = \gamma Q^{*n}$$

Where γ=3.3, and n=2/3 for $Q^* \leq 1$ and n=2/5 for $Q^* > 1$. The Q* here is calculated using the hydraulic diameter of the fire, D_h where D_h=4A/P and using the total heat release rate of the fuel. A similar correlation was developed by Anderson [9] using propane and a square burner, with a modification of γ=2.5, which has a 25% decrease of flame height. This may be explained by the different fuel (propane) and different burner shape (circular) used in Zukoski's study.

The comparison between current data and Zukoski's and Anderson's correlation is presented in Figure 137. Current data falls between Anderson's and Zukoski's correlations and it is shown that Propylene fires seem to have a higher non-dimensional flame height than propane fires, which is in turn higher than methane fires. This is expected because of the fuels' properties. There does not seem to be a difference between plume and wall effect on flame height, however, it is noted that in inert wall tests, the flame plume tends to lean back and hug the wall regardless of burner size or HRR.

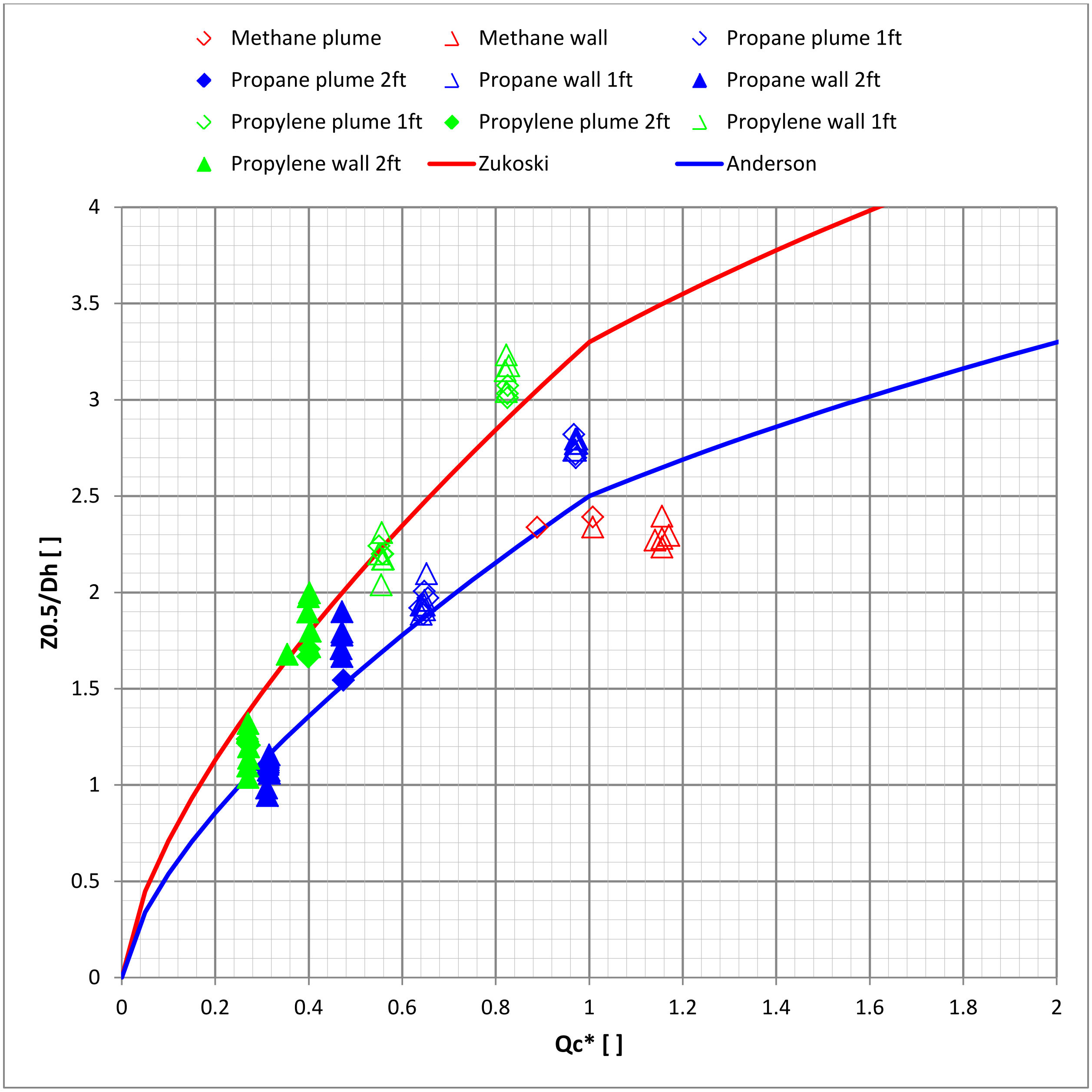

Figure 137 - Comparison of current flame height data with Zukoski's and Anderson's correlations

Alston and Dembsey [8] conducted similar experiments using methane, propane, and propylene and 0.3 m Square and 0.3 m Circle burners. The flame heights were normalized with the burner's hydraulic diameter and the HRR was normalized with total HRR. Their data suggested that there is little distinction in flame height between similar sized square and circle burner, but propane fires had taller flame than propylene fires which are similar to methane fires, as shown in Figure 138. The uncertainty of their data is reported to be about ±5 cm/± 0.2 in non-dimensional term, which overlaps the current data (with normalized convective HRR) for Q* < 0.6 only.

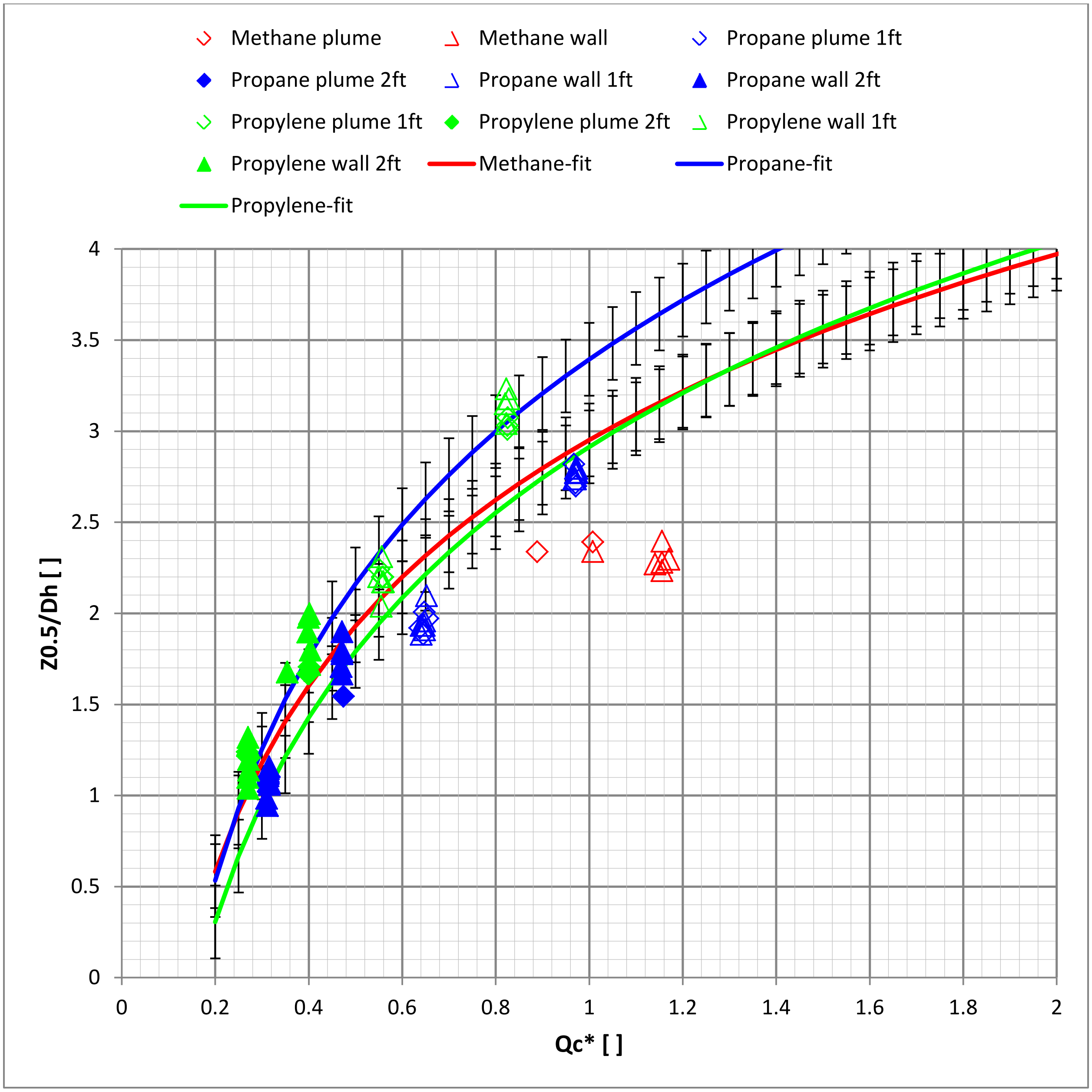

Figure 138 - Comparison of current flame height data with Alston's data-fitted lines

Heskestad [6] developed another flame height correlation based on a wide range of experiments of different fuels as shown in equation [3]

[3] $$\frac{Z_{50}}{D_e} = -1.02 + 15.6N^{\frac{1}{5}}$$

$$N = \left[\frac{c_p T_\infty}{\frac{H_T}{r}}\right]^3 Q^{*2}$$

In this case, the length the flame height is normalized to is the equivalent fire diameter, $D_e=(4A/\pi)^{0.5}$. The non-dimensional parameter N (based on the convective HRR) was determined for the current data to be plotted against the measured flame height in Figure 139. Using the total heat release rates of methane, propane, and propylene, Heskestad's correlation suggests that the propylene flame height is taller than the propane and the methane flame heights, which is also shown in current data. The uncertainty of the Heskestad's correlation is reported by Anderson to be about 15-20%, making the current data falls within range of the uncertainties.

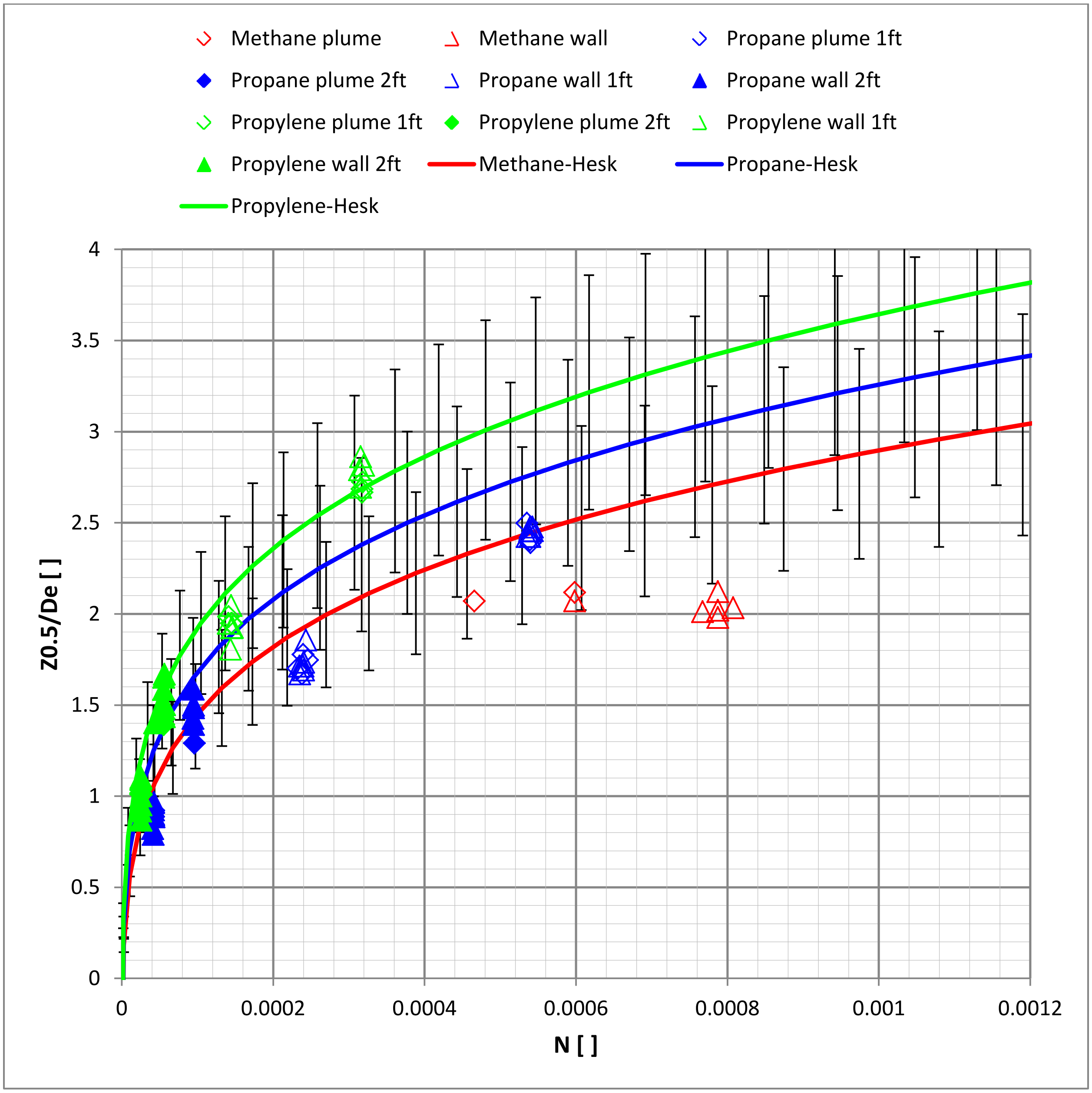

Figure 139 - Comparison of current flame height data with Heskestad's correlation

Quintiere and Grove [7] developed a flame height correlation based on the convective fraction of the heat release rate, thereby taking combustion efficiency and plume buoyance into consideration. The original Quintiere and Grove flame height correlation, which uses the chemical heat of combustion in the calculation of Q*, was modified by Alston to use the total heat of combustion in its formulation so that comparison can be made. The modified flame height correlation is show in [4]

$$Q^* = 0.00590 \frac{\Psi^{\frac{3}{2}}}{(\chi_{ch} - \chi_{rad})} \left(\frac{z_f}{D}\right)^{\frac{1}{2}} \left(1 + C_1 \left(\frac{z_f}{D}\right)\right)^m \left(1 + C_1 a \left(\frac{z_f}{D}\right)\right)^n \qquad [4]$$

$$where\ \Psi = \frac{(\chi_{ch} - \chi_{rad}) \left(\frac{H_T}{r}\right)}{c_p T_\infty}$$

Where shape aspect ratio, a, is the burner's short dimension divided by the long, D is the fire characteristic dimension, and C_1, m, and n are coefficients based on burner shape as shown below.

Table 14 - Quintiere and Grove flame height correlation coefficients

	C_1	m	n	D
Axisymmetric	0.357	1	1	Hydraulic diameter
Rectangle	0.398	1	1	Short side
Infinite line	0.888	1	0	Line width

For the Square burner, D=0.304m (hydraulic diameter = edge length), and for the Rectangle burner D=0.304m (short side length).

The correlation is produced by predetermining a series of Z_f/D ratios and calculating the corresponding Q*. To allow comparison with this correlation, the current data's HRRs were corrected to a convective HRR only then non-dimensionalized. This is achieved by using [5] and the D value prescribed above

[5]

$$Q_c = Q * \left(\frac{H_{Tot}}{H_{ch}}\right) * \left(\frac{H_{cov}}{H_{Tot}}\right)$$

$$Q^* = \frac{Q_c}{\rho_\infty c_p T_\infty g^{0.5} D^{2.5}}$$

Error! Reference source not found. shows that the correlation makes no distinction between the flame heights of a propane or propylene fire and that curiously the flame height from the Rectangle burner is higher than the Square burner. The correlation for the Rectangle was supported by data from Hasemi and Nishihata[10], which might warrants further investigation.

However, contrary to the correlation, in the current data the propylene fires had taller flame heights than propane fires and so did the Square burner over Rectangle burner fires. It should be noted that the propane Square burner flame heights correlate very well with the Q+G correlation for propane and propylene fires.

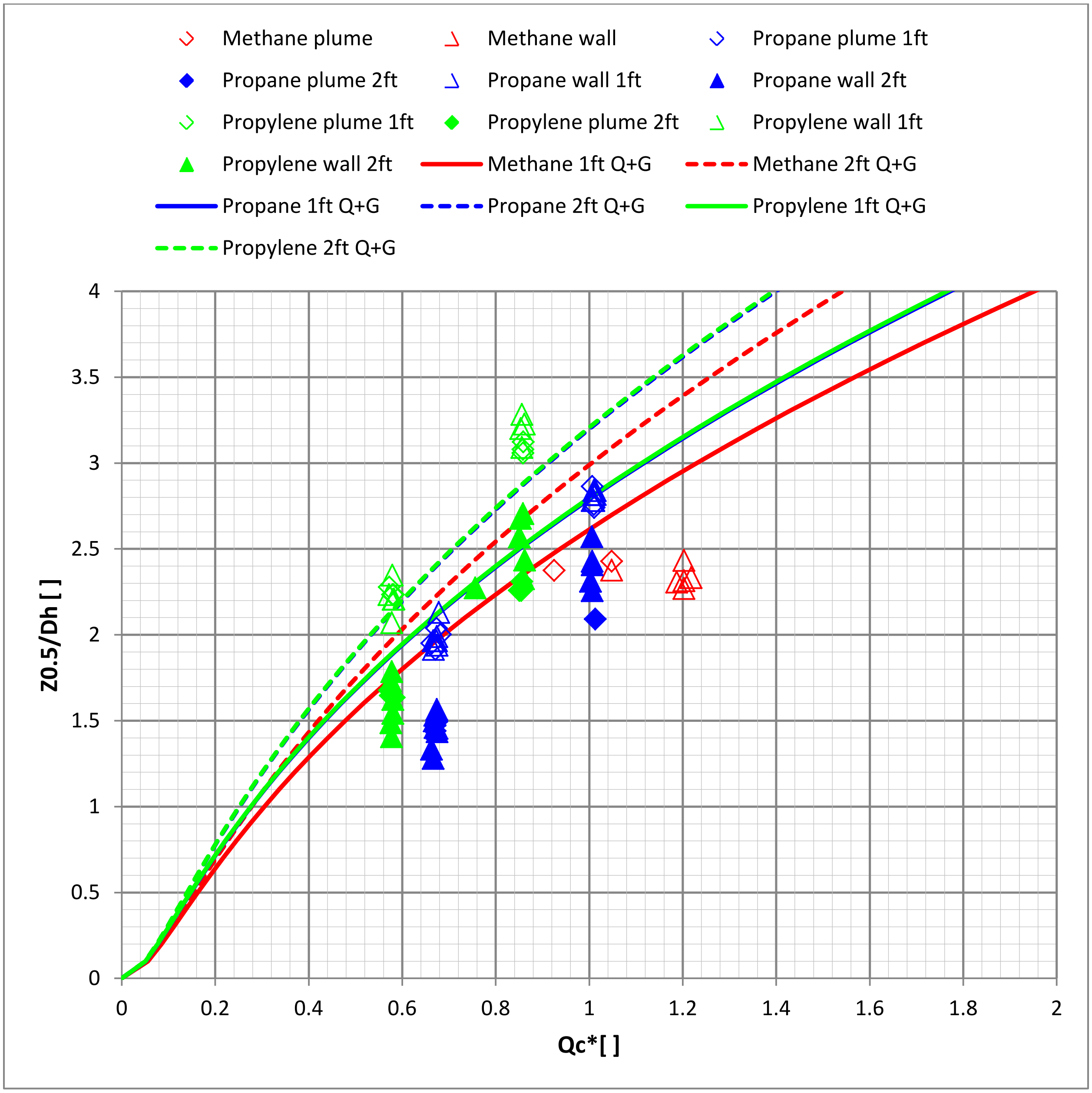

Figure 140 - Comparison of current flame height data with Quintiere and Grove's correlation

D.7 Flame Spread

Wall flame spread tests were conducted with a commercially available Class C fiber-reinforced plastic (FRP) material. Each specimen measures 2.4 m high by 1.2 m wide, and was mounted on an inert wall constructed of ceramic fiberboards. Holes were cut into the FRP sheets so that wall mounted instruments, such as thermocouples, thin skin calorimeters, and water-cooled heat flux gauges, could protrude from the specimen and measure surface flame spread properties such as temperature and heat flux. At a minimum, 30 drywall screws were used to mount the FRP panel onto the back-wall in order to ensure the surface was flat and minimize the chance for edge burning.

Two burners were used as the ignition source: the 1ft Square and the 2ft x 1ft Rectangle burner. During a test, the burner was positioned with the long side flush against the FRP panel and centered along the centerline of the panel. Although flame spread was not directly measurable, the spread rate can be estimated from the HRR, wall temperature, heat flux, and video footage data from a test.

The majority of the fire spread in the beginning of a test was upward wall spread, but as the test continued, concurrent/lateral and downward spreads were also observed.

D.7.1 Flame spread rate calculated from full scale HRR based on HRRPUA from cone data

Cone calorimeter experiments were performed with the FRP panel at three different heat flux levels: 25 kW/m^2, 50 kW/m^2, and 75 kW/m^2 for two tests each. The pair of tests consisted of one with embedded and surface thermocouples on the specimen and one without. The fire properties of the specimen were collected, including the heat release rate per unit area (HRRPUA).

In the cone tests, the HRRPUA was determined as a function of time, and its time-averaged value was found. It was determined that the HRRPUA of the FRP specimens had a range of values as determined from the different tests. Table 15 shows the average as well as the 50% to 100% percentiles, of the time-averaged HRRPUA from the tests, averaged with all 6 tests in the first column, and averaged between tests with similar heat flux levels in the second to fourth column.

Table 15 - Time-averaged HRRPUA values from cone tests

	Overall	25kW Avg	50kW Avg	75kW Avg
Average	110.1	96.5	95.6	138.2
50%	84.7	63.6	76.8	113.7
60%	104.4	80.8	97.2	135.1
70%	132.3	120.2	102.4	174.2
80%	203.7	184.2	161.7	265.3
90%	267.8	219.3	261.6	322.5
100%	295.5	238.3	286.8	361.4

According to Table 15, the HRRPUA of the FRP appears to increase with imposed heat flux. The average across all six tests was found to be about 110 kW/m^2, with a low at about 96 kW/m^2 at imposed 25 kW/m^2 and 50 kW/m^2 heat fluxes, and a high at 138 kW/m^2 at imposed 75 kW/m^2 heat flux. The time-averaged HRRPUA may be misleading because the typical HRRPUA curves of the sample had a high peak soon after ignition but tail off for a long duration during subsequent burning. Since the major flame spread of the full-sized FRP panels occurred quickly after ignition, the representative HRRPUA of the sample should be higher than the time-based averages, and more likely in the 70-80 percentiles of the value, which will ranges from 100 kW/m^2 for imposed heat flux at 25 kW/m^2 to 270 kW/m^2 for imposed heat flux at 75 kW/m^2.

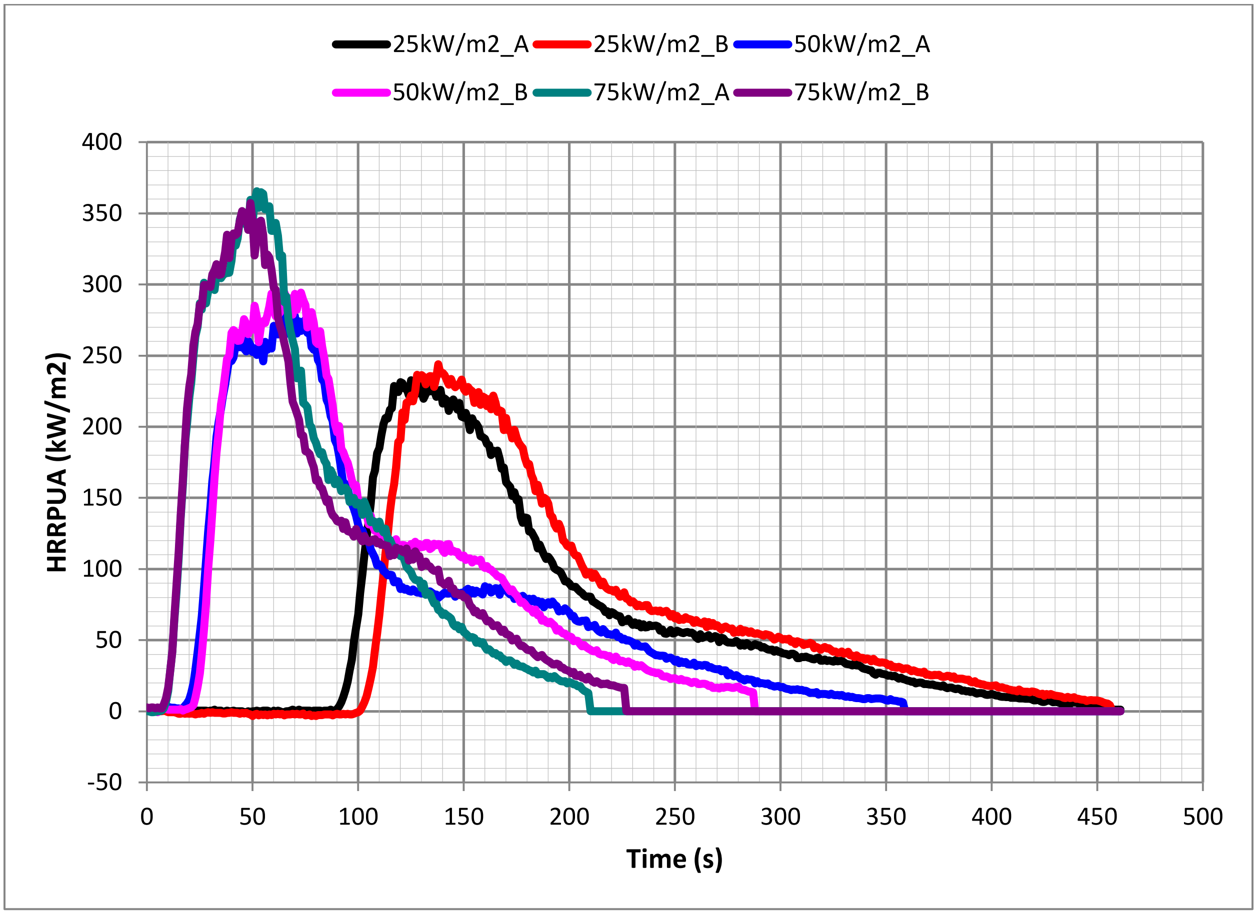

Figure 141 - Cone tests HRRPUA time history

Based on the wall heat flux measurements made during the full-scale FRP tests, the centerline heat flux reached up to 80 kW/m^2 to 100 kW/m^2, it may be assumed that the specimen's HRRPUAs in these cases could be upward of the 270 kW/m^2 found previously in the cone tests (80 percentiles of the 75 kW/m^2 tests). It must be cautioned that using a constant HRRPUA served only as an approximation since the FRP panel's HRRUPA can vary with time and imposed heat flux.

A burning area time-history could be determined from the full-scale FRP panel tests with a constant HRRUPA using [1].

$$A_{burning}(t) = \frac{HRR(t)}{HRRPUA} \qquad [1]$$

The burning area change history would then be calculated as the change in the burning area using [2].

$$\frac{dA_{burning}}{dt} = A_{burning}(t) - A_{burning}(t-1) \qquad [2]$$

Assuming that flame spread rate (FSR) takes the form of area per unit time, its calculation is the same as equation [2], but only with consideration to the positive or zero values since it is not physically possible to have negative flame spread. So the flame spread rate is of the FRP panel is represented in [3].

$$FSR(t) = A_{burning}(t) - A_{burning}(t-1) \quad \text{,only positive, otherwise, zero} \qquad [3]$$

A way to ground the FSR calculations was to utilize the final burnt area as an upper bound: total burning area cannot be larger than the final burnt area. The final burnt area of each FRP panel specimen was measured using the 0.1m x 0.1m grid drawn on the panel as a guide to gauge the fire damage to the cell. A rod was used to poke the various cells and the damage to the cell could be determined by observation of the amount of resin left. 100% damage means all resin burnt off, only fiberglass weave left behind, 75% damage suggests only some resin left, mostly fiberglass, 50% damage is where half of the cell's resin remains, 25% damage means most resin survives, and 0% means no fire damage. All cells were assigned a damage index, and the subtotals for each damage range were found, and the total is always 2.88 m^2. Table 16 shows a sample damage index summary.

Table 16 - Sample damage summary from Test A5

# of cell	Damage to Resin	Area (m2)
56	up to 100% damage	0.56
77	up to 75% damage	0.77
15	up to 50% damage	0.15
4	up to 25% damage	0.04
136	no damage	1.36

The total burnt area is assumed to be summation of the products between percentage damage and the associated areas, as shown in [4].

$$\text{Total burnt area} = \sum(\text{Burn area} * \%damage) \qquad [4]$$

Since the definition of flame spread means that only spreads to new area were counted ([3]), the summation of the FSR equates to adding up the new spread area over time until the total burnt area was reached. So, in terms of flame spread, the total burnt area also equals to the summation of the products between FSR per unit time, as shown in [5].

$$\text{Total burnt area} = \sum(\text{FSR}(t)) \qquad [5]$$

Using [5] and the constant HRRPUAs found as the overall average between all cone tests (110 kW/m^2), average between cone tests with at 25 kW/m^2 heat flux (96.5 110kW/m^2), and average between cone tests with heat flux at 75 kW/m^2 (138.2 kW/m^2), it was found that these HRRPUA values were too low and produces a total burnt area much larger than the true burnt area found using [4]. This holds true for all 18 FRP panel tests, hence, these time-averaged HRRPUA values from the cone tests were most likely too low to be used in the flame spread calculation in the full-scale tests.

In light of the discrepancy with the low HRRPUA values, an iterative method to find an assumed constant HRRPUA value for each FRP full scale test that equates both [4] and [5] into [6] was created.

$$\sum(\mathrm{FSR}(t)) = \sum(\mathrm{Burn\ area} * \%damage) \quad [6]$$

The resulting, corrected HRRPUA values for the full-scale tests were all larger than the time-averaged values, and were plotted in Figure 142. The similar trend of increasing heat flux to the wall (increasing HRR of burner fire) leading to an increased in the assumed constant HRRPUA is evident.

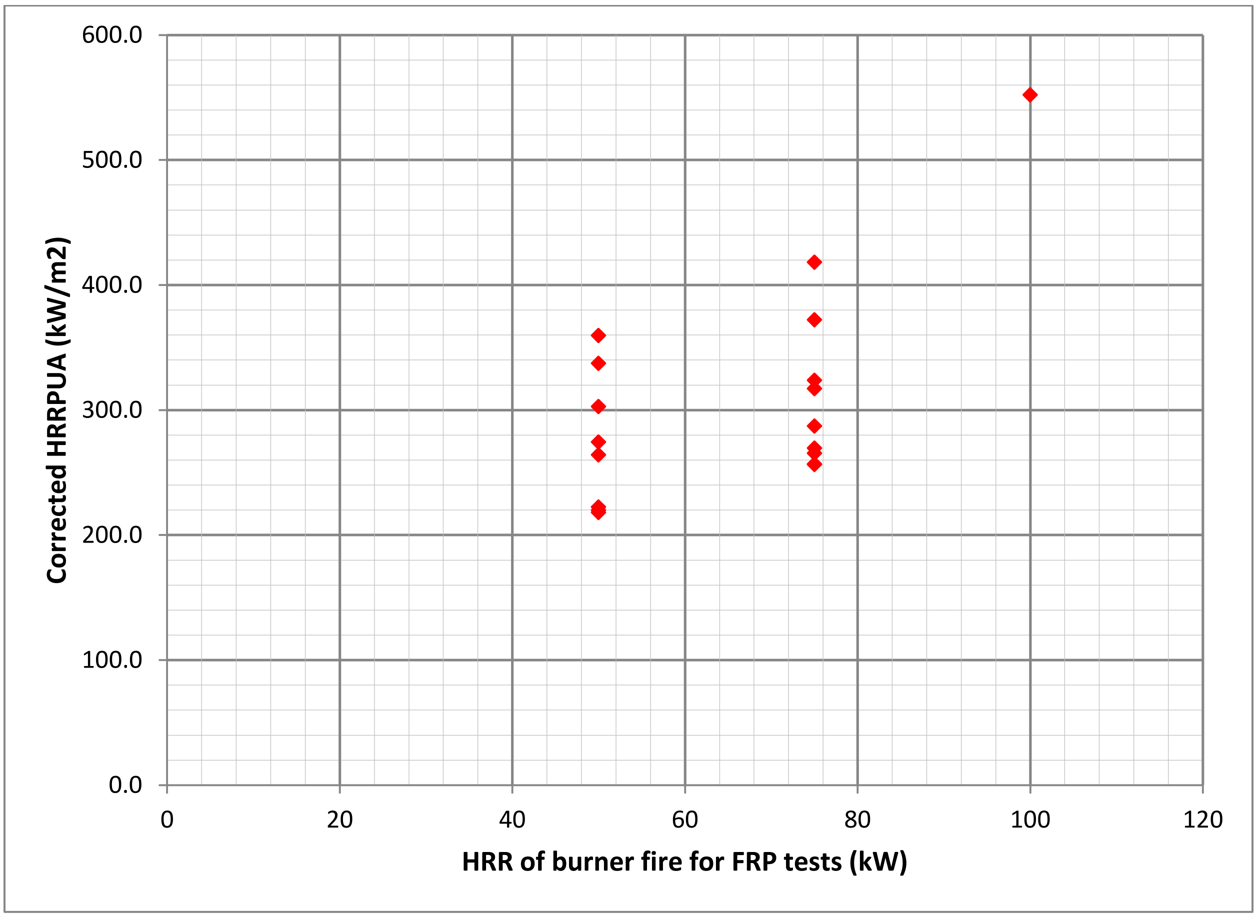

Figure 142 - Corrected HRRPUA for 18 full-scale FRP panel tests

Compared to the average cone HRRPUA, the iterative HRRPUA from the wall tests were higher. However, as stated previously, the average cone HRRPUA would be an estimate on the low end since heat fluxes to the wall during the fire reaches upward of 80 kW/m^2 to 100 kW/m^2. A more reasonable comparison should be made with the 80th to 90th percentiles cone HRRPUA data from the tests with 75 kW/m^2 heat flux insult cases. The ratio between the cone HRRPUA and the iterative HRRPUA values are plotted in Figure 143, which shows the comparison with the 75 kW/m^2 heat flux tests' average, 70 percentile, 80th percentile, and 90th percentile HRRPUA values. The ratios were calculated using [7].

$$Ratio = \frac{\text{Iterative HRRPUA - Cone HRRPUA}}{\text{Cone HRRPUA}} \quad [7]$$

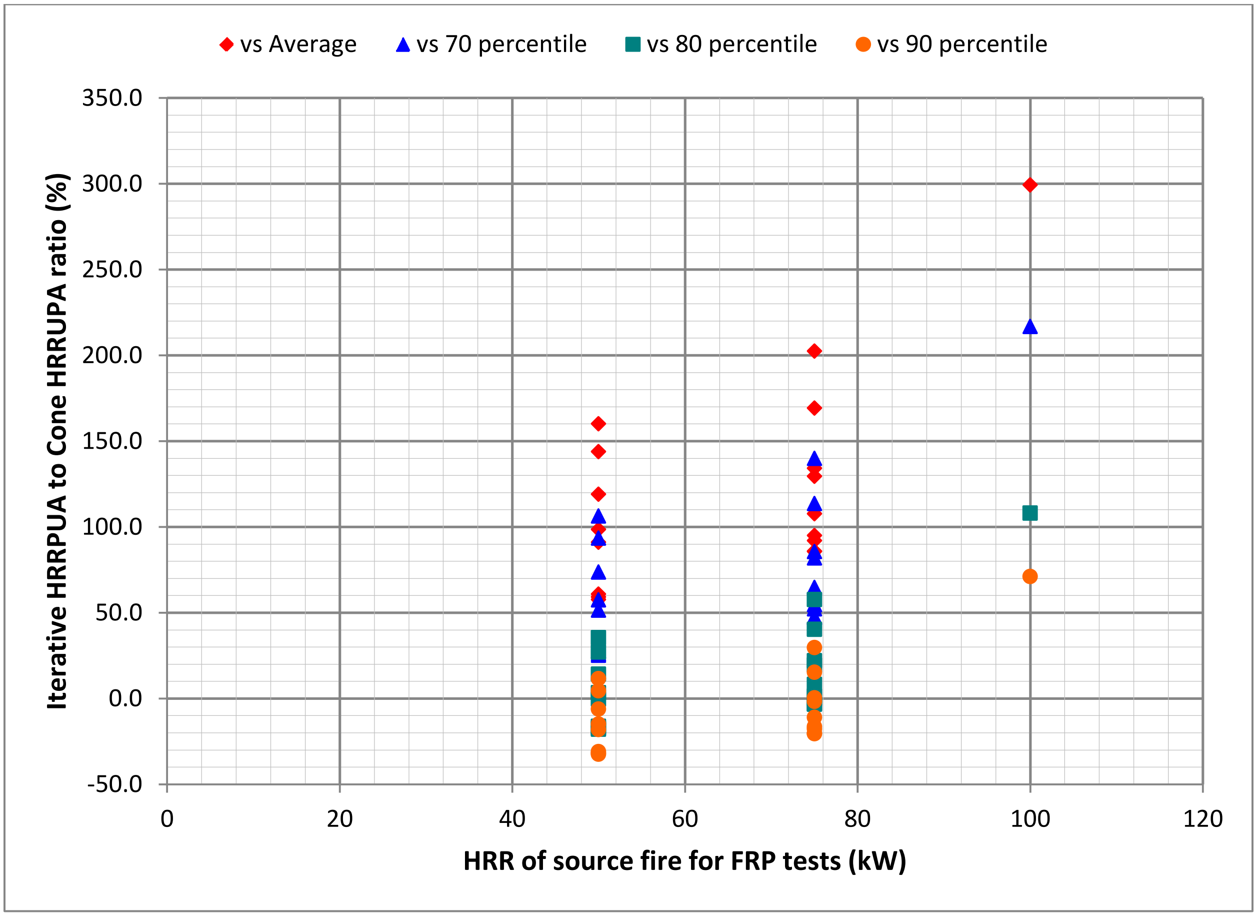

Figure 143 - Iterative HRRPUA vs Cone HRRPUA ratios

It is shown that the iterative HRRPUA values correspond well with the cone HRRPUA value at 75 kW/m^2 incident heat flux at the 90th percentile. The differences were at most at +15%/-50% for the FRP tests with 50 kW source fire, and at +30%/-20% for those tests using a 75 kW source fire, which are reasonable. The iterative HRRPUA from the 100 kW source fire test should be considered an outlier since that corresponding FRP test had a faulty ignition fire and had to be suppressed with water spray. This method of estimating flame spread rate appears to be reasonable and the flame spread rate time histories for the 18 tests are plotted in Figure 144 to Figure 148 - Flame spread rate of tests conducted with 2ft Rectangle burner at 75 kW, separated into different groups based on burner size and burner HRR. It should be noted that the time zero in the following charts was set to the time when the source burner reached the designated HRRs.

Figure 144 shows the flame spread rate of tests using the 1 ft Square burner at 50 kW source fire. All of the curves show a gradual increase in FSR, then three of the four FSR curves have a large spike, which correspond to the point where rollover occurred under the ceiling. At this point there was a rapid increase of the flame spread rate due to increase in lateral spread and downward spread. The Test A13 using Propylene did not have such a spike because the burner was on throughout the test and the flame spread rate peaked over ~10 sec rather than spiking almost instantaneously. After the peaking/spiking, the FSR gradually increases again into a peak then decreases and becomes insignificant for the remaining of the test.

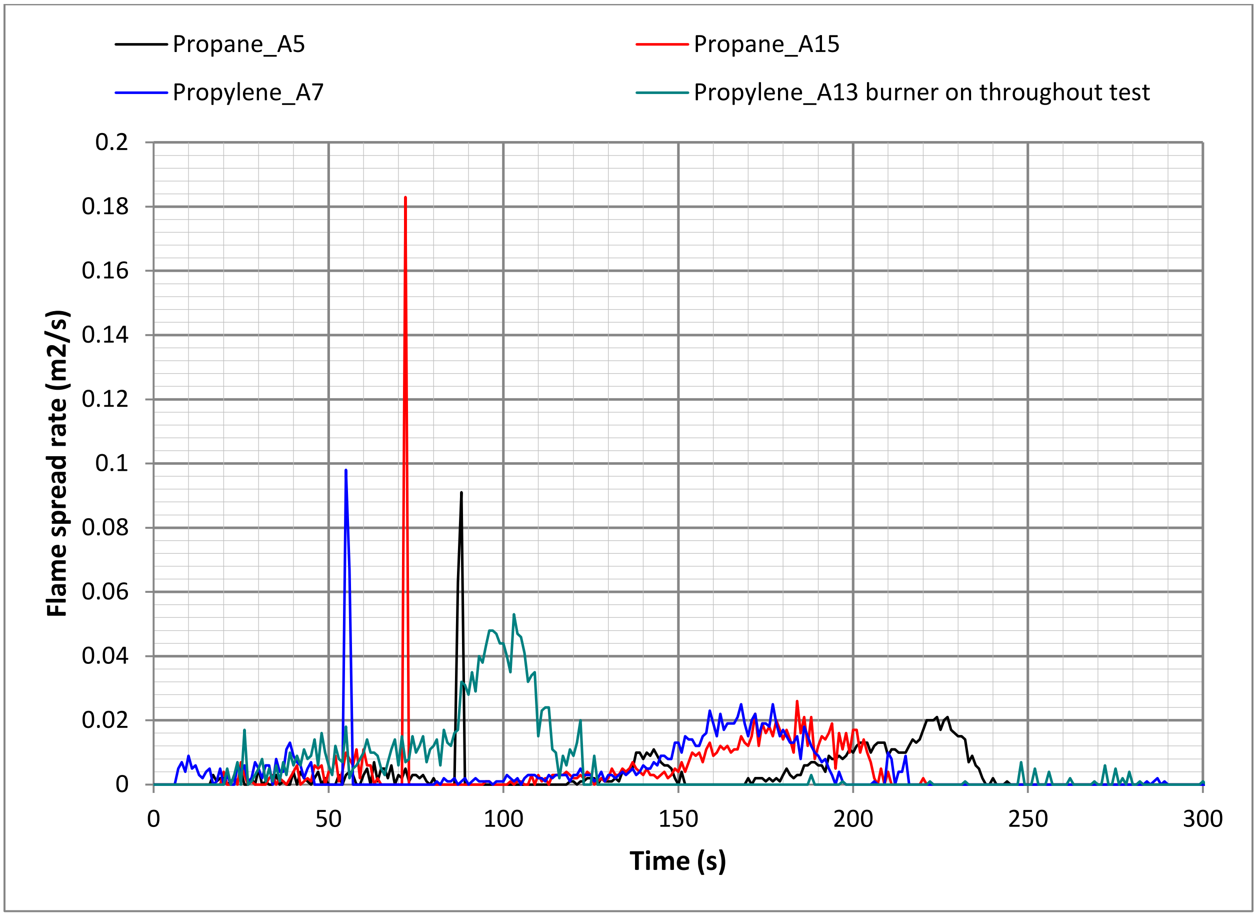

Figure 144 - Flame spread rate of tests conducted with 1ft Square burner at 50 kW

Figure 145 shows the flame spread rate of tests using the 1 ft Square burner at 75 kW source fire. All of the curves show a gradual increase in FSR, then three of the four FSR curves have a large spike, which correspond to the point where rollover occurred under the ceiling. At this point there was a rapid increase of the flame spread rate due to increase in lateral spread and downward spread. The Test A16 using Propane did not have such a spike because the burner was on throughout the test and the flame spread rate peaked over ~10 sec rather than spiking almost instantaneously. After the peaking/spiking, the FSR gradually increases again into a peak then decreases and becomes insignificant for the remaining of the test. This is similar to the Square burner with 50 kW cases, but the FSRs here were generally higher, and the total burn times are shorter.

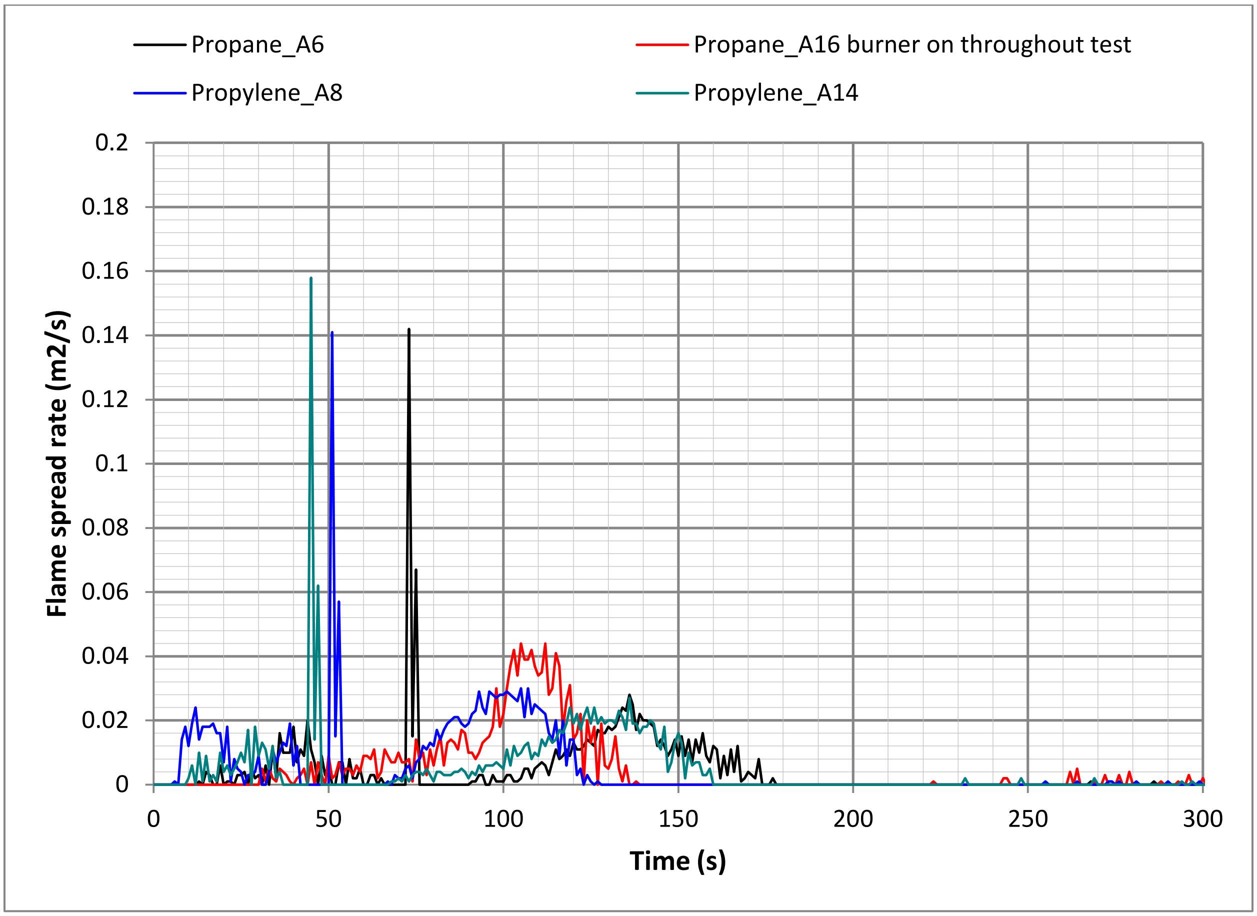

Figure 145 - Flame spread rate of tests conducted with 1ft Square burner at 75 kW

Figure 146 shows the flame spread rate of tests using the 2 ft Rectangle burner at 50 kW source fire. All of the curves show a gradual increase in FSR, then three of the four FSR curves have a large spike, which correspond to the point where rollover occurred under the ceiling. At this point there was a rapid increase of the flame spread rate due to increase in lateral spread and downward spread. The Test A12 using Propylene did not have such a spike because the burner was on throughout the test and the flame spread rate peaked over ~10 sec rather than spiking almost instantaneously. After the peaking/spiking, the FSR gradually increases again into a peak then decreases and becomes insignificant for the remaining of the test.

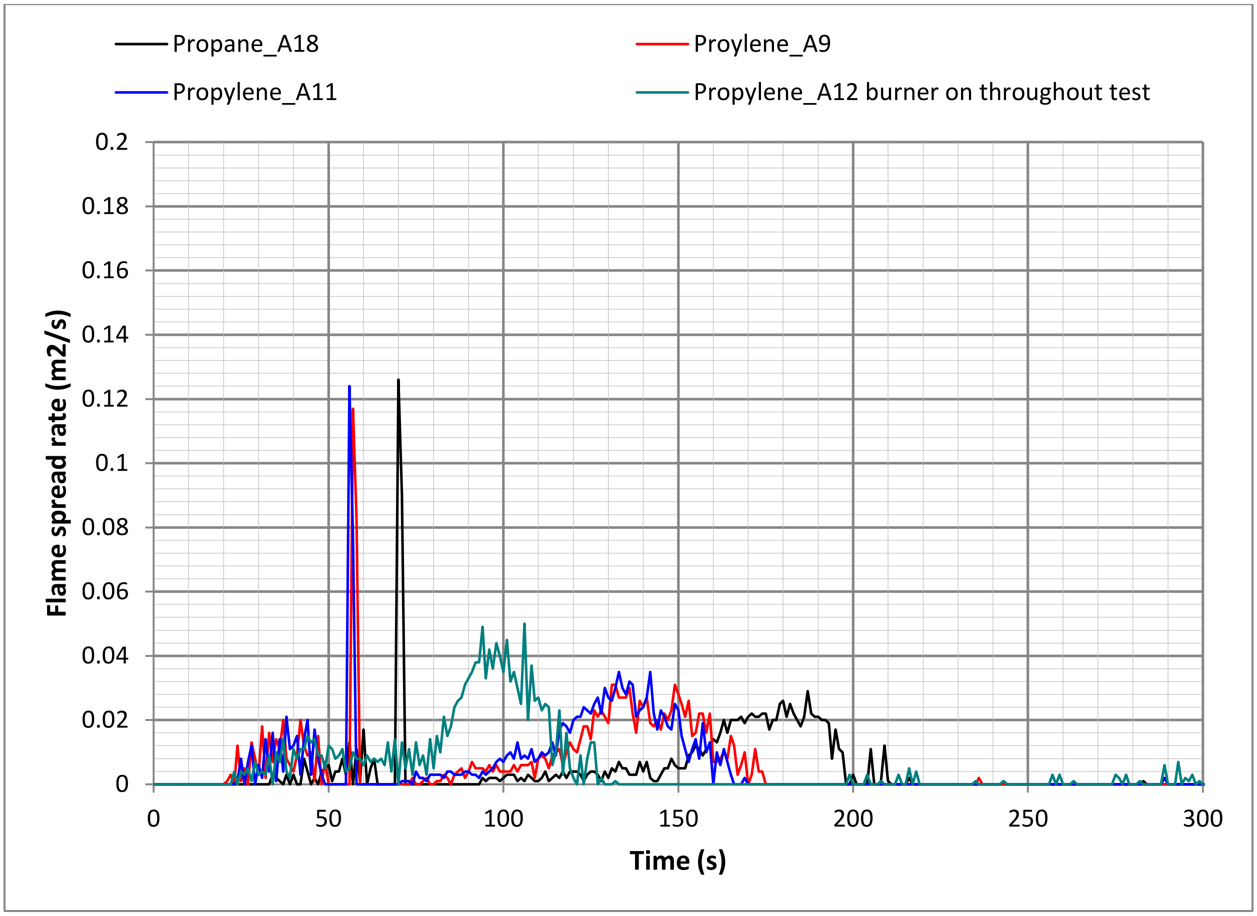

Figure 146 - Flame spread rate of tests conducted with 2ft Rectangle burner at 50 kW

Figure 147 shows the flame spread rate of tests using the 2 ft Rectangle burner at 75 kW source fire. All of the curves show a gradual increase in FSR, then three of the four FSR curves have a large spike, which correspond to the point where rollover occurred under the ceiling. At this point there was a rapid increase of the flame spread rate due to increase in lateral spread and downward spread. The Test A17 using Propane did not have such a spike because the burner was on throughout the test and the flame spread rate peaked over ~10 sec rather than spiking almost instantaneously. Also, the Propylene A10 test had a series of chaotic spikes, most likely due to sensitivity in the HRR curve. After the peaking/spiking, the FSR gradually increases again into a peak then decreases and becomes insignificant for the remaining of the test. This is similar to the Rectangle burner with 50 kW cases.

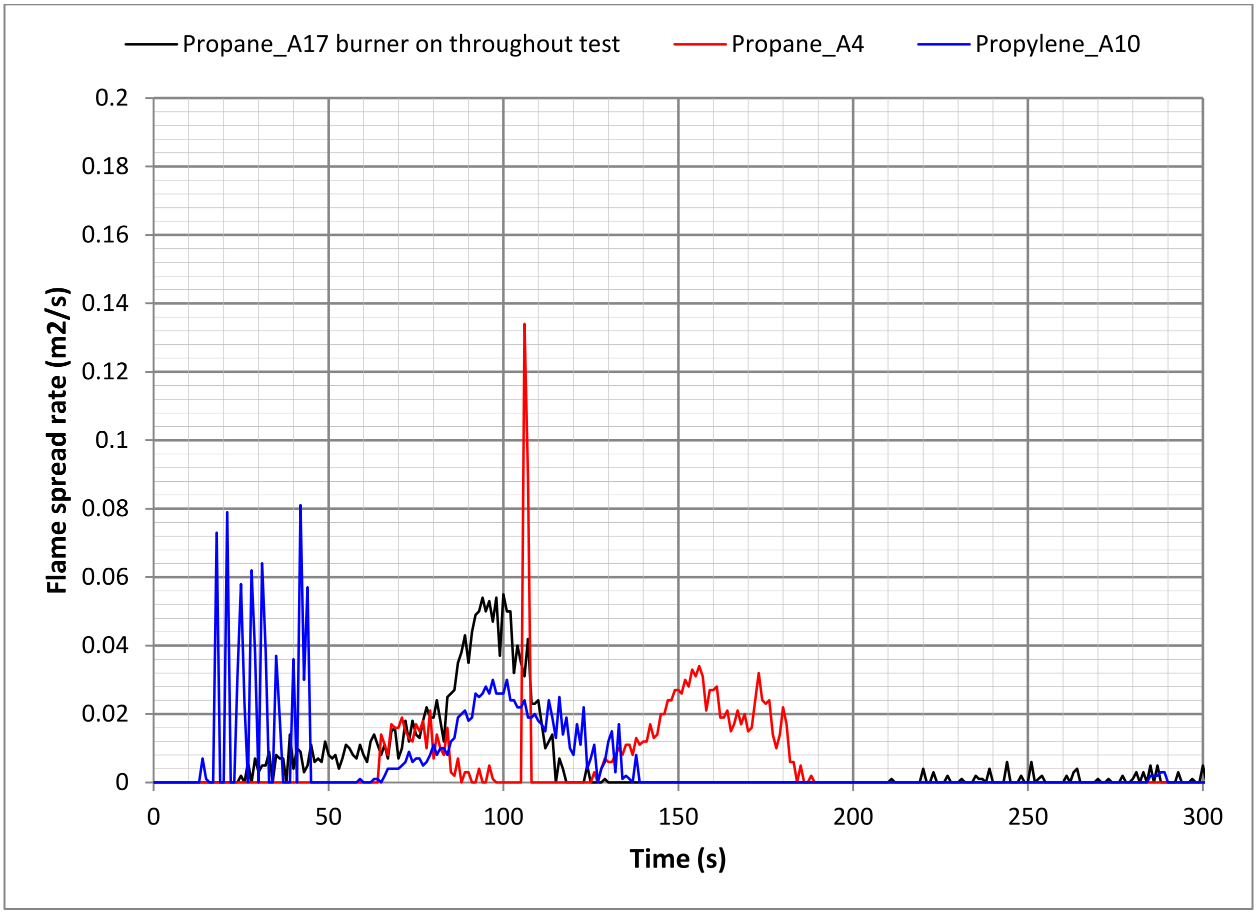

Figure 147 - Flame spread rate of tests conducted with 2ft Rectangle burner at 75 kW

Figure 148 shows the flame spread rate of tests using the 2 ft Rectangle burner at different source fire sizes. These tests are singled out because water was applied during the all three tests and they have more unique source heat release rate (Test A1 and A2 had flare up above 100 kW and 75 kW). These resulted in more chaotic heat release curve that translated into chaotic FSR curves.

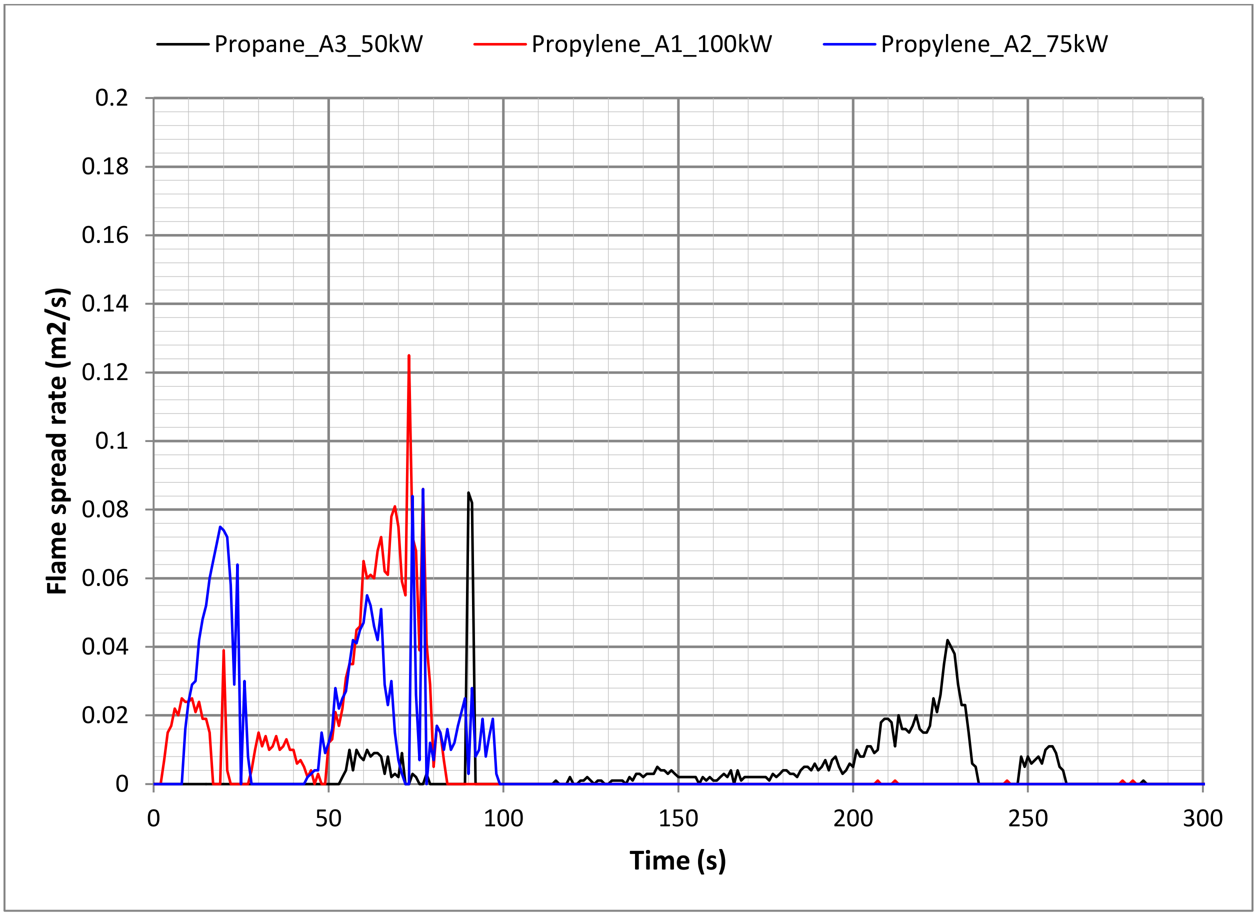

Figure 148 - Flame spread rate of tests conducted with 2ft Rectangle burner at 75 kW

The tests using propane as the source fire fuel appear to ignite the panel slower than the propylene cases at the same source HRRs. The differences in total burn time appear to be related to burner source fire HRR, where the higher HRR relates to a shorter burn time.

D.7.2 Flame spread rate calculated from video data and observations

Another method to determine flame spread of the FRP wall panel used the video recordings for analysis. Each burn test was filmed with two digital video cameras usually, head-on, and at an angle to the side of the burn compartment. It was determined that the angled video camera captured the better footage since smoke often obscured the top of the burning panel in the footage from the head-on camera. As such, the footage from the angled video camera was used as the primary source for the flame spread analysis with the other footage and notes made during the test as compliment.

The angled camera's output was converted from MiniDV into the Windows Media Video (WMV) format, and the other camera's output was recorded in the high-definition MTS format; both cameras recorded at 30 frames per seconds (fps). Virtualdub-1.9.9 (with plug-ins) was used to pull image sequences from the videos at 1 fps. The images were then imported into the software Tracker-3.10 to track the flame spread by pinpointing the outline of burning areas. Due to the amount of images and limitation of software, the process was performed for every 2 seconds from the video; moreover, it was found that tracking the burning areas every 2 seconds was sufficient because of the slow spread rate.

In order to track the flame spread using video data, it was assumed that the burning areas may be represented by rectangular shapes and the progression was separated into 3 phases as shown in Figure 149 from left to right. In the early phase of the wall panel fires, the burning area may be summarized as a centered rectangle A that was bounded at the burner's edge at the bottom with an upper bound that traveled upward; but as the panel burn, the lower bound of the rectangular area also moved up.

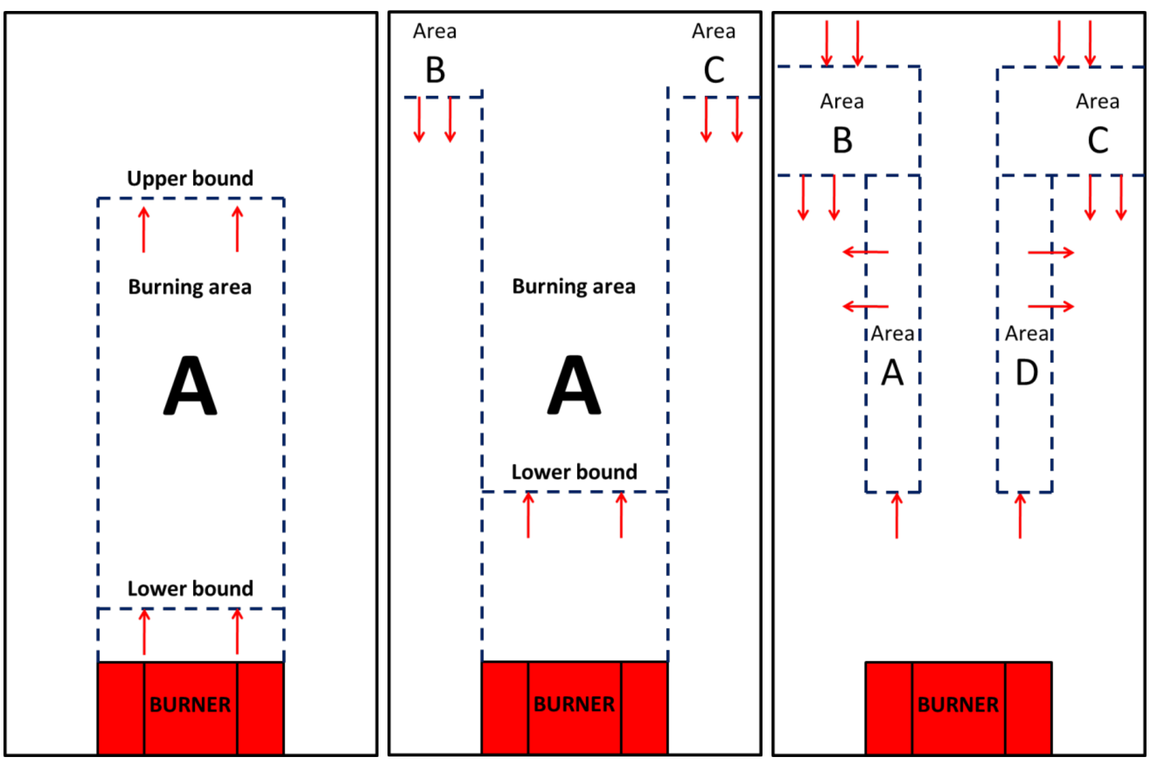

Figure 149 - Burning area progression, from left to right (early to late stages)

After the initial burn period, flames reached and became bent at the ceiling and the fire spread to the edges of the wall panel and the burning area, obtaining a “T” shape with a downward-moving horizontal top-bar. At this period the burning area may be approximated by three rectangles A, B and C, all bounded at the top by the top edge of the wall panel. The central rectangle A shrunk from the bottom edge but the vertical length of the flange rectangles B and C increases downward. At this stage there was usually little lateral spread to the vertical sides of rectangle A.

At the later stage of major flame progression, the area along the center was burnt out and the burning area could be described by Areas A, B, C and D. The Areas A and D regress upward and outward, whereas the horizontal edges of Areas B and C continued moving downward. After this stage of flame spread, the remaining burning was in the form of line fires where the burning area cannot be accurately measured given the resolution of the video footage.

In the tracking process, the positions of the corners of the fire were recorded using Tracker. Since the edges of the fire were not straight, some post-processing, such as averaging the x- or y- coordinates at certain points, was performed to the location data to create straight rectangular shapes that conform to those presented in Figure 149.

Although this method of flame spread measurement was reasonably accurate and may be used to compliment the HRRPUA method, there are many limitations to this method of flame spread analysis, however. First of all, the quality of the video footage dictated the quality of the base data. The high-definition video data recorded high quality image but the top of the wall panel image was obscured by smoke; the standard-definition video from the angled camera recorded more details, such as flame attachment, that made burn area tracking easier than from the front-view HD video, although at a lower resolution. The 0.1m x 0.1m square grid drawn on the wall panel aided in the tracking process, and the resulting largest uncertainties could be estimated to be about 0.2 m or 0.04 m^2.

The burning area time-history was developed from the total burning areas based on the rectangle area estimation method over a minimum of 180 seconds, starting from distinguishable FRP panel ignition. There were some scatters in the area data mainly due to the sensitivity of the manual tracking method. The burning area was found to increase in Stage 1 until the end of Stage 2 progression, then decreased in Stage 3 and the subsequent line burning.

2ft Rectangle burner @ 50 kW source fire flame spread

The tests A9, A11, A12 and A18 used the 2ft Rectangle burner with 50 kW and different source fire gases. Test A9 and A11 uses propylene, Test A18 uses propane, Test A12 uses propylene with burner on throughout test. The burning area charts show the progression of the burning area based on time history starting from noticeable burning of the FRP panel.

Figure 150 and Figure 151 show the Stages 1 to 3 burning area of Test A9 and also the final damage chart. The burning area charts show the progression of the burning area based on time history. The final burn area shows the damage on the FRP panel due to fire spread with different colors showing the amount of damage to the resin base as shown in Table 17. Each cell represents a 0.1m x 0.1m square.

Table 17 - Damage summary of Test A9

# of cell	Damage to Resin	Area (m2)
134	**up to 100% damage**	1.34
51	**up to 75% damage**	0.51
9	**up to 50% damage**	0.09
8	**up to 25% damage**	0.08
86	**no damage**	0.86

Figure 152 and Figure 153 show the Stages 1 to 3 burning area of Test A11 and also the final damage chart. The final burn area shows the damage on the FRP panel due to fire spread with different colors showing the amount of damage to the resin base as shown in Table 18.

Table 18 - Damage summary of Test A11

# of cell	Damage to Resin	Area (m2)
135	**up to 100% damage**	1.35
60	**up to 75% damage**	0.6
4	**up to 50% damage**	0.04
5	**up to 25% damage**	0.05
84	**no damage**	0.84

Test A9 and A11 were identical tests. The sizes of the burning areas were very similar with slight difference in timing of the progression. The final burn area and damage between the two tests were almost identical. The shift of the damage to the right of the panel could be attributed to the flow environment of the test compartment.

Figure 154 and Figure 155 show the Stages 1 to 3 burning area of Test A18 and also the final damage chart. The burning area charts show the progression of the burning area based on time history. The final burn area shows the damage on the FRP panel due to fire spread with different colors showing the amount of damage to the resin base as shown in Table 19. Each cell represents a 0.1m x 0.1m square.

Table 19 - Damage summary of Test A18

# of cell	Damage to Resin	Area (m2)
104	**up to 100% damage**	1.04
51	**up to 75% damage**	0.51
7	**up to 50% damage**	0.07
8	**up to 25% damage**	0.08
118	**no damage**	1.18

The difference between Test A18 and Tests A9/A11 were the source burner fuel used. The sizes of the burning areas were very similar with slight difference in timing of the progression; the final burn patterns were also similar. The slight shift of the damage to the right of the panel could be attributed to the flow environment of the test compartment.

Test A12 was different from the A9, A11, and A18 because the source fire remained at 50 kW throughout the test, which affected the combustible wall flame spread greatly in speed and also intensity. Figure 156 and Figure 157 show the Stages 1 to 3 burning area of Test A12 and also the final damage chart. The final burn area shows the damage on the FRP panel due to fire spread with different colors showing the amount of damage to the resin base as shown in Table 20.

Table 20 - Damage summary of Test A12

# of cell	Damage to Resin	Area (m2)
193	**up to 100% damage**	1.93
42	**up to 75% damage**	0.42
1	**up to 50% damage**	0.01
1	**up to 25% damage**	0.01
51	**no damage**	0.51

Compared to Tests A9, A11, and A18 where the source fire was turned off after panel ignition, the burning speed of the combustible panel in Test A12 was much faster and the burning area was larger due to the presence of the source fire. The source fire provided a turbulent environment and energy that accelerated the upward and lateral spread of the fire such that most of the panel above the burner level was completely burnt out.

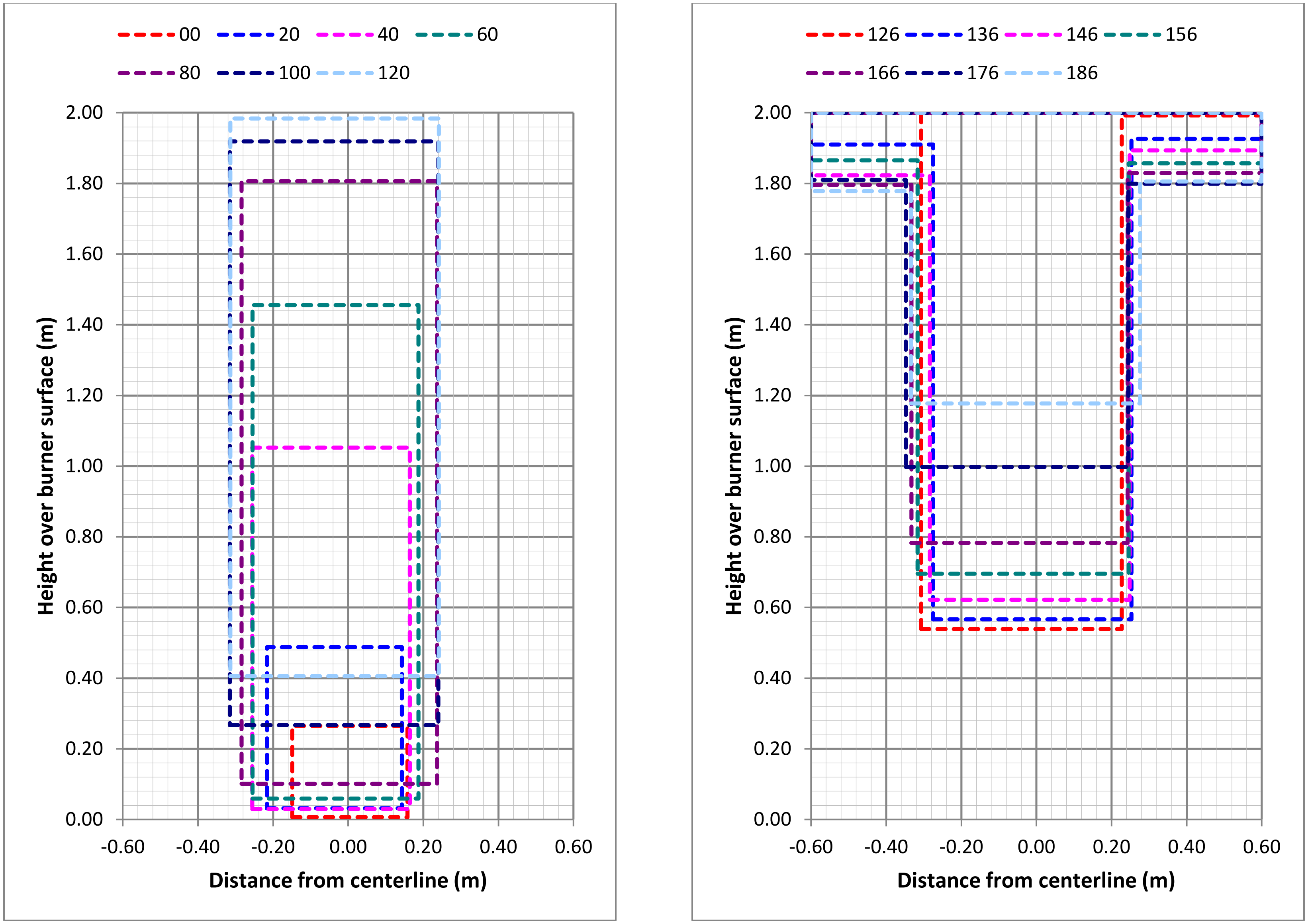

Figure 150 – Stages 1 and 2 burning areas in Test A9 (2ft Rectangle burner, Propylene, 50 kW source)

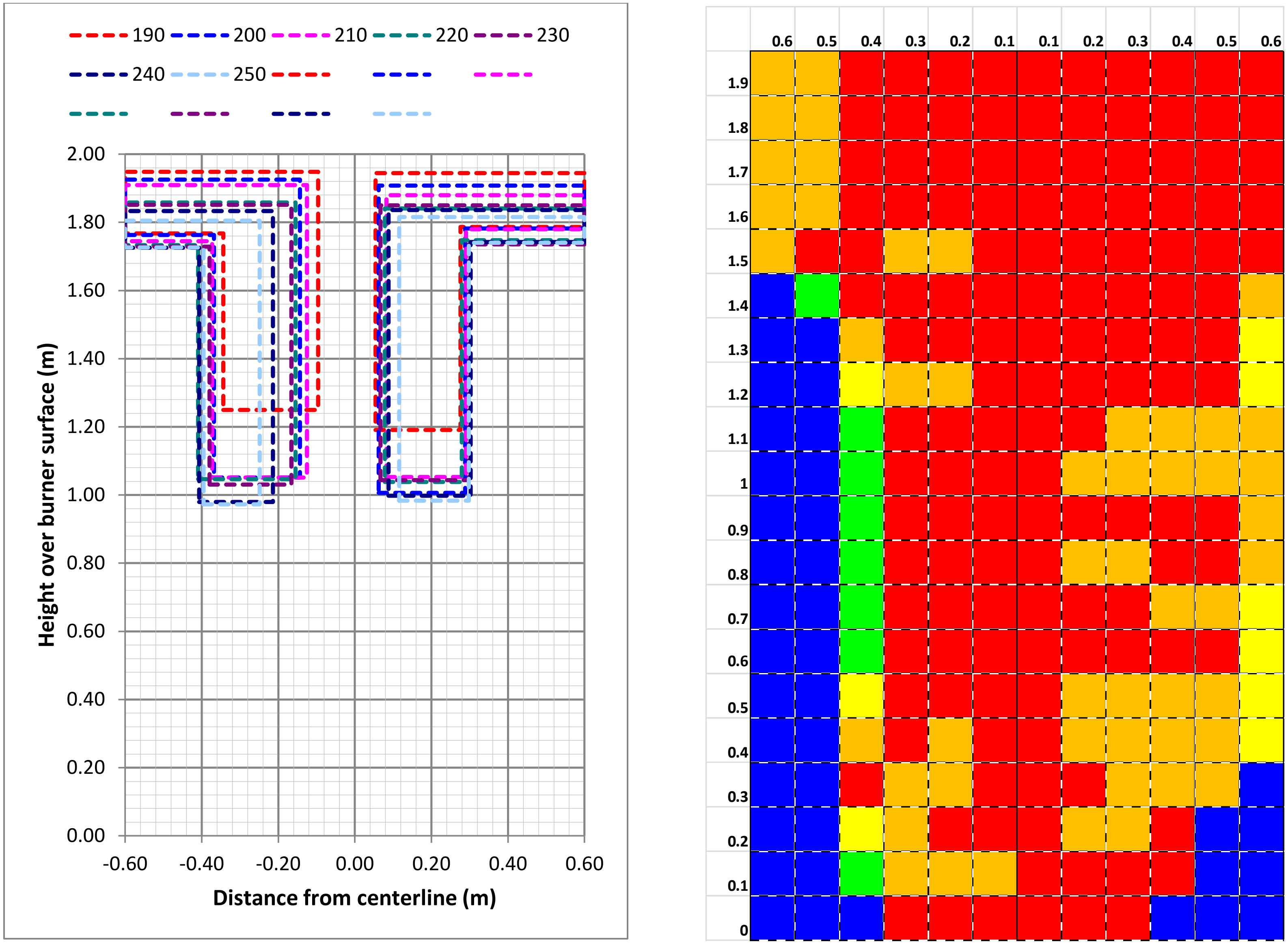

Figure 151 - Stage 3 burn area and final damage chart of Test A9 (2ft Rectangle burner, Propylene, 50 kW source)

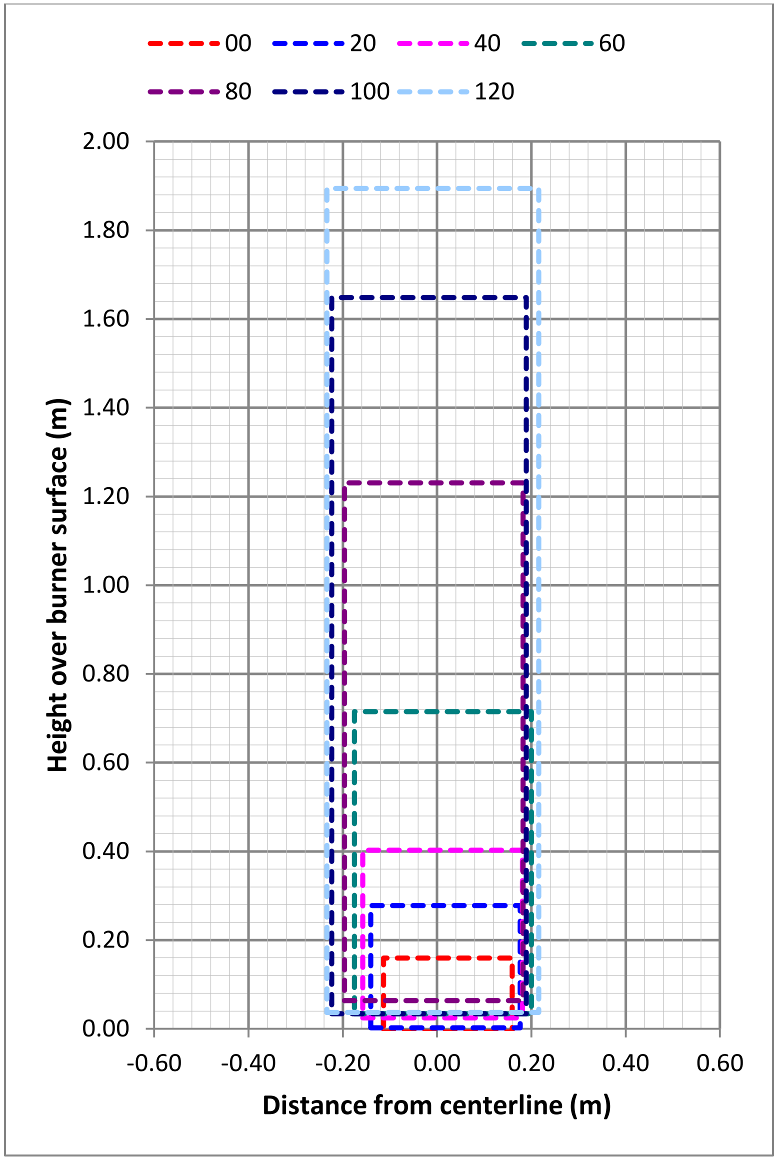

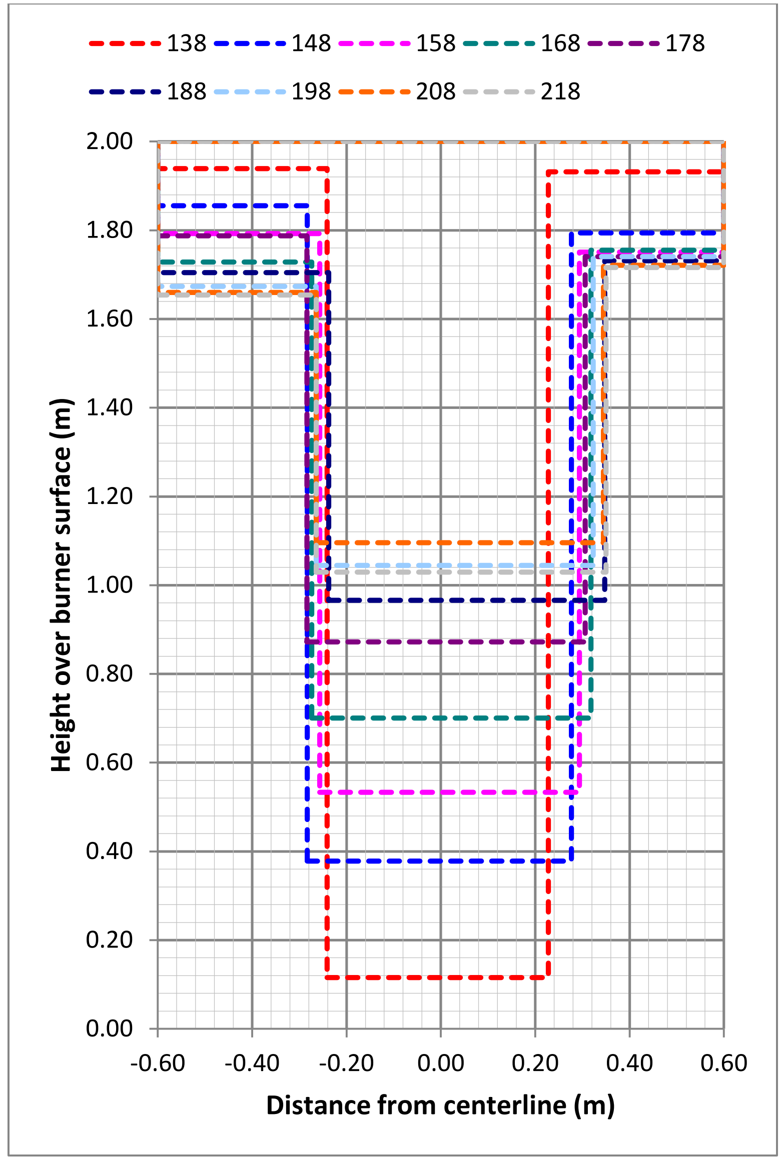

Figure 152 – Stages 1 and 2 burning areas in Test A11 (2ft Rectangle burner, Propylene, 50 kW source)

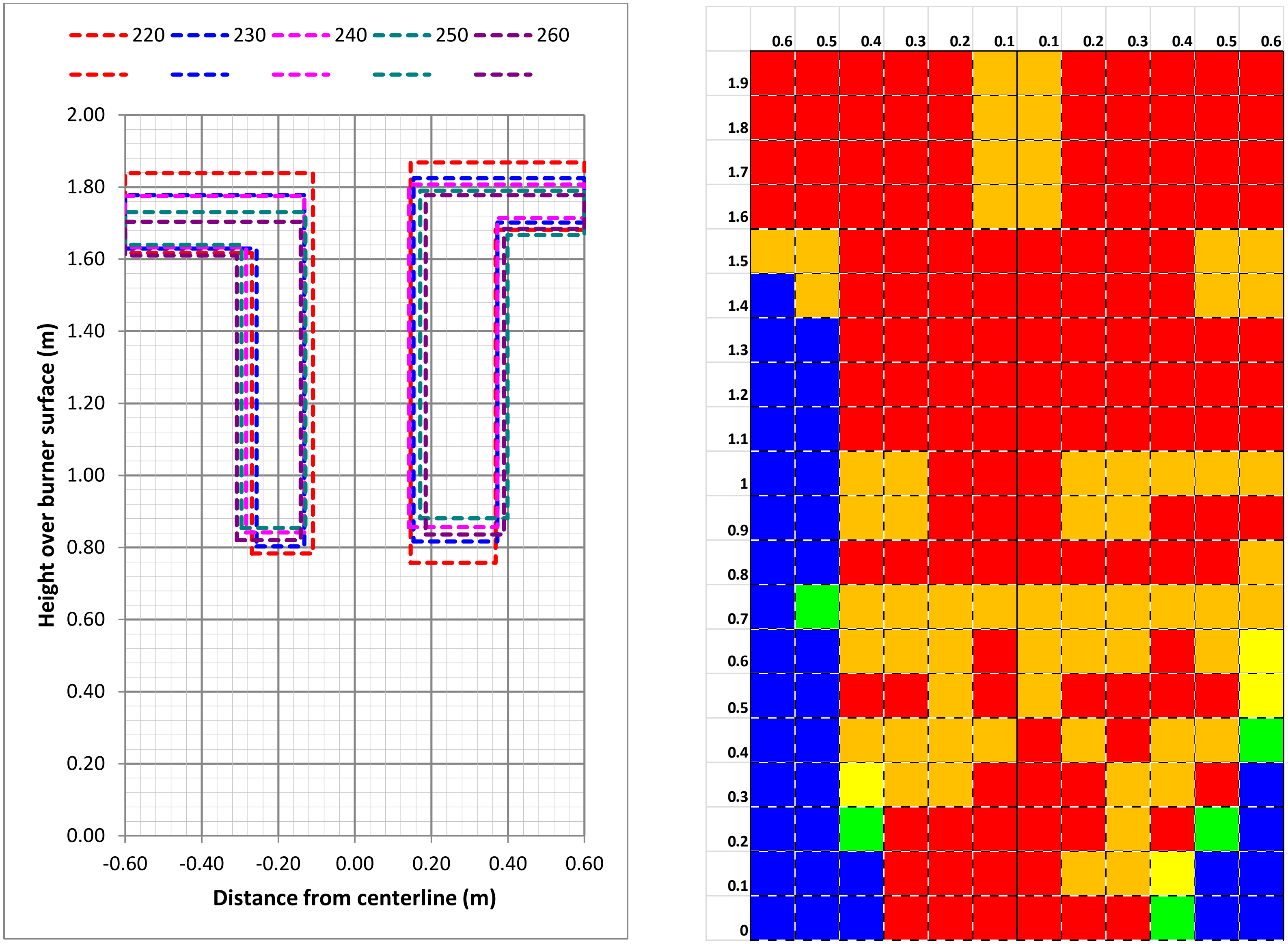

Figure 153 - Stage 3 burn area and final damage chart of Test A11 (2ft Rectangle burner, Propylene, 50 kW source)

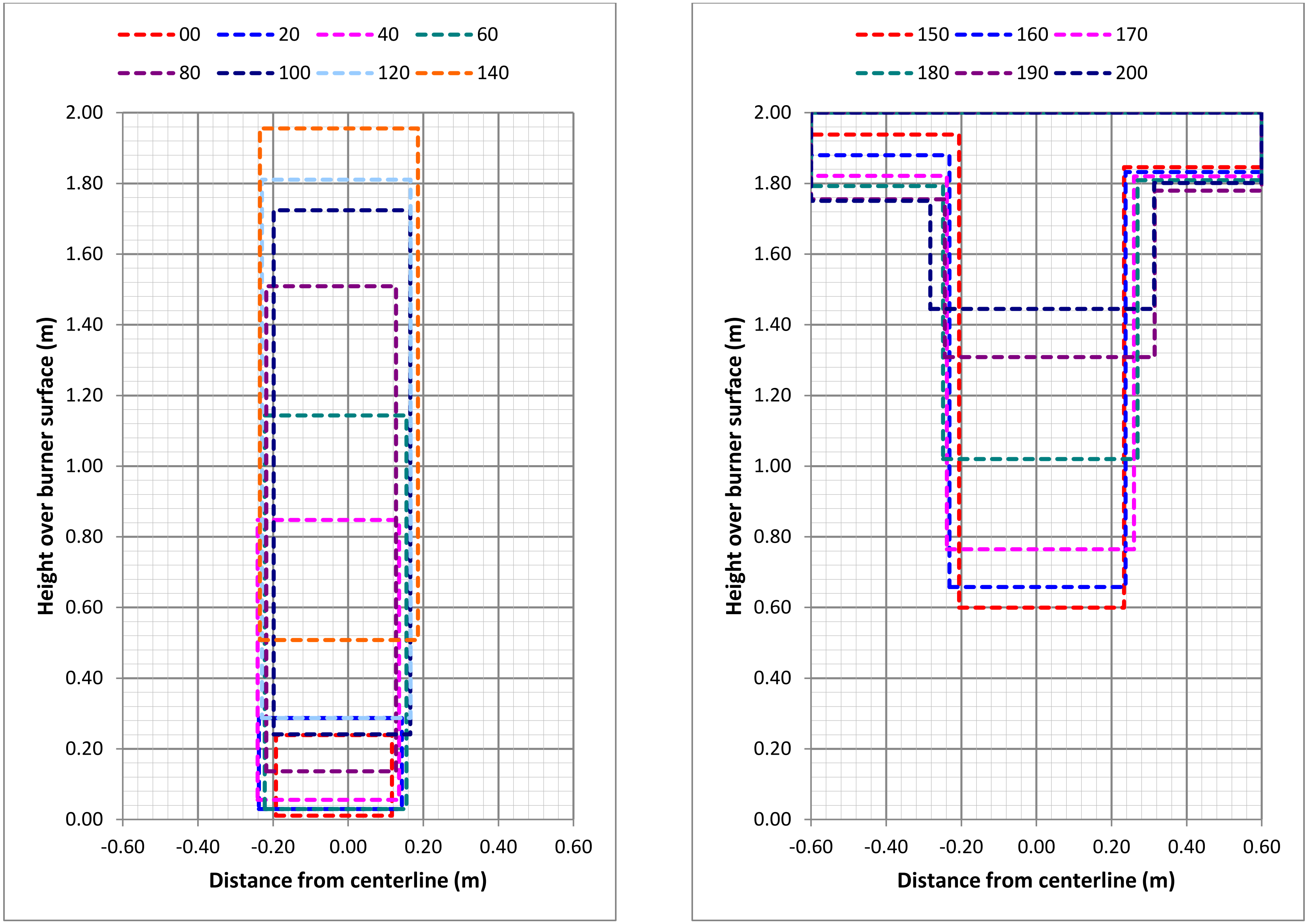

Figure 154 – Stages 1 and 2 burning areas in Test A18 (2ft Rectangle burner, Propane, 50 kW source)

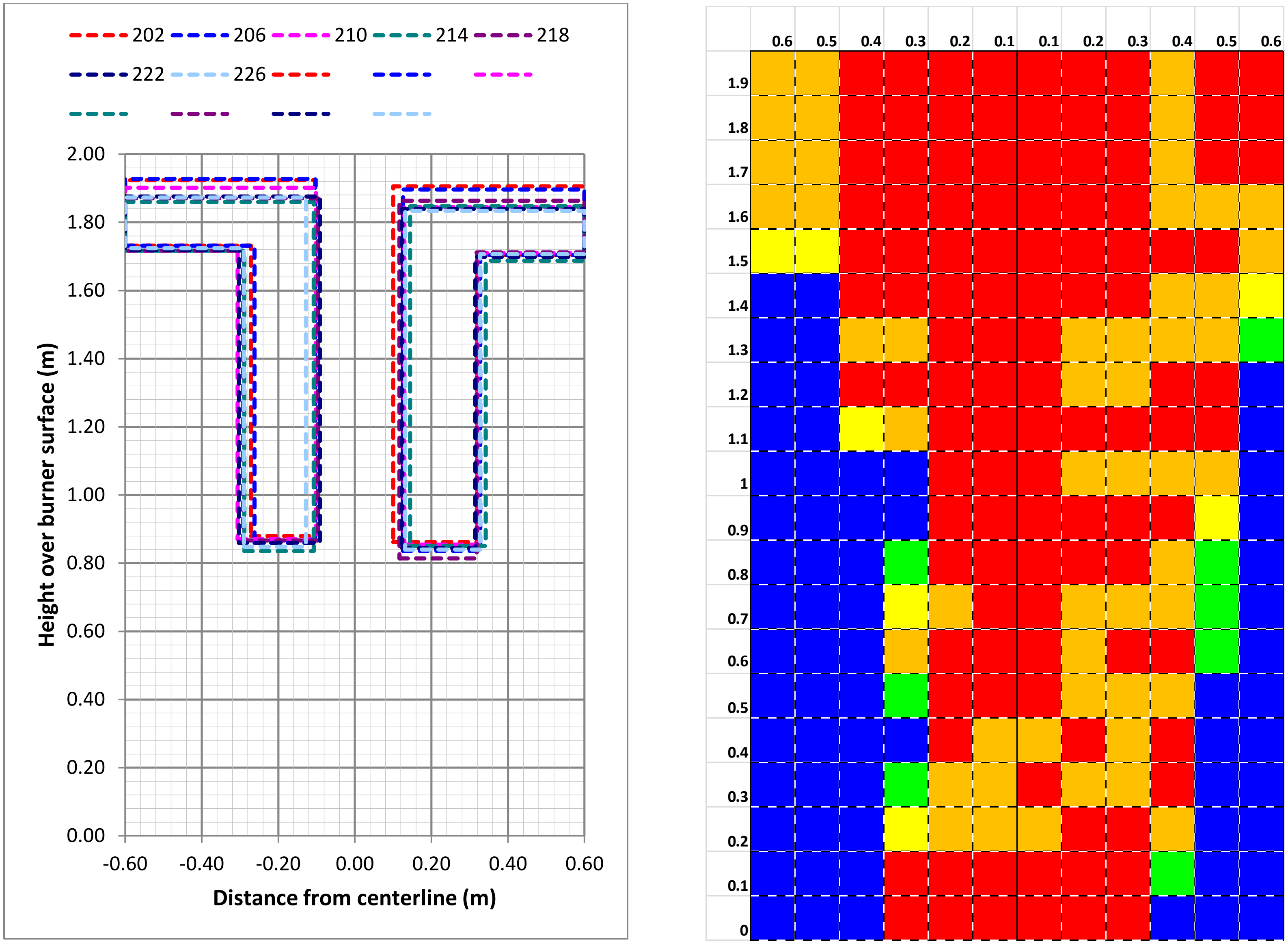

Figure 155 - Stage 3 burn area and final damage chart of Test A18 (2ft Rectangle burner, Propane, 50 kW source)

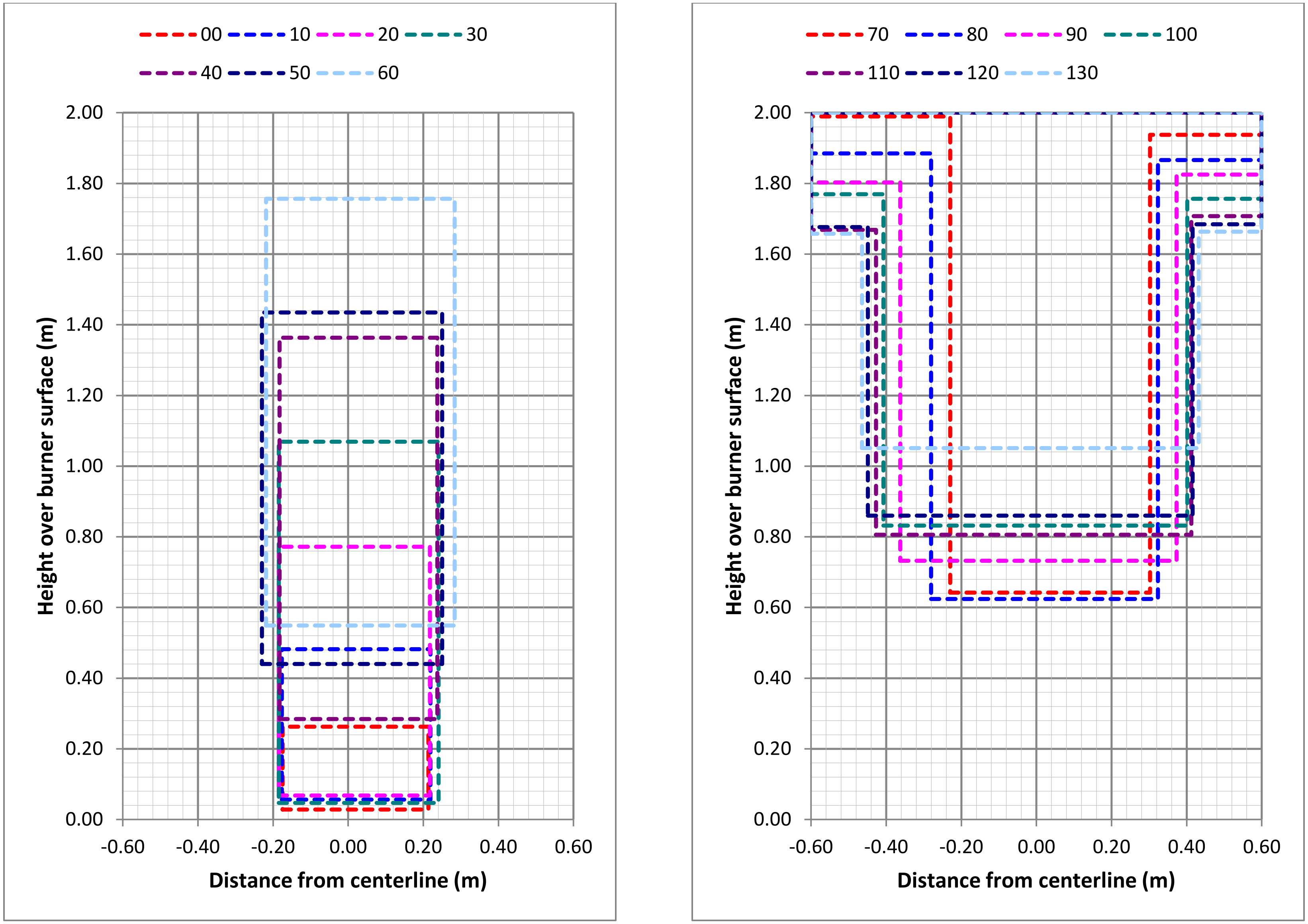

Figure 156 – Stages 1 and 2 burning areas in Test A12 (2ft Rectangle burner, Propylene, 50 kW source on throughout test)

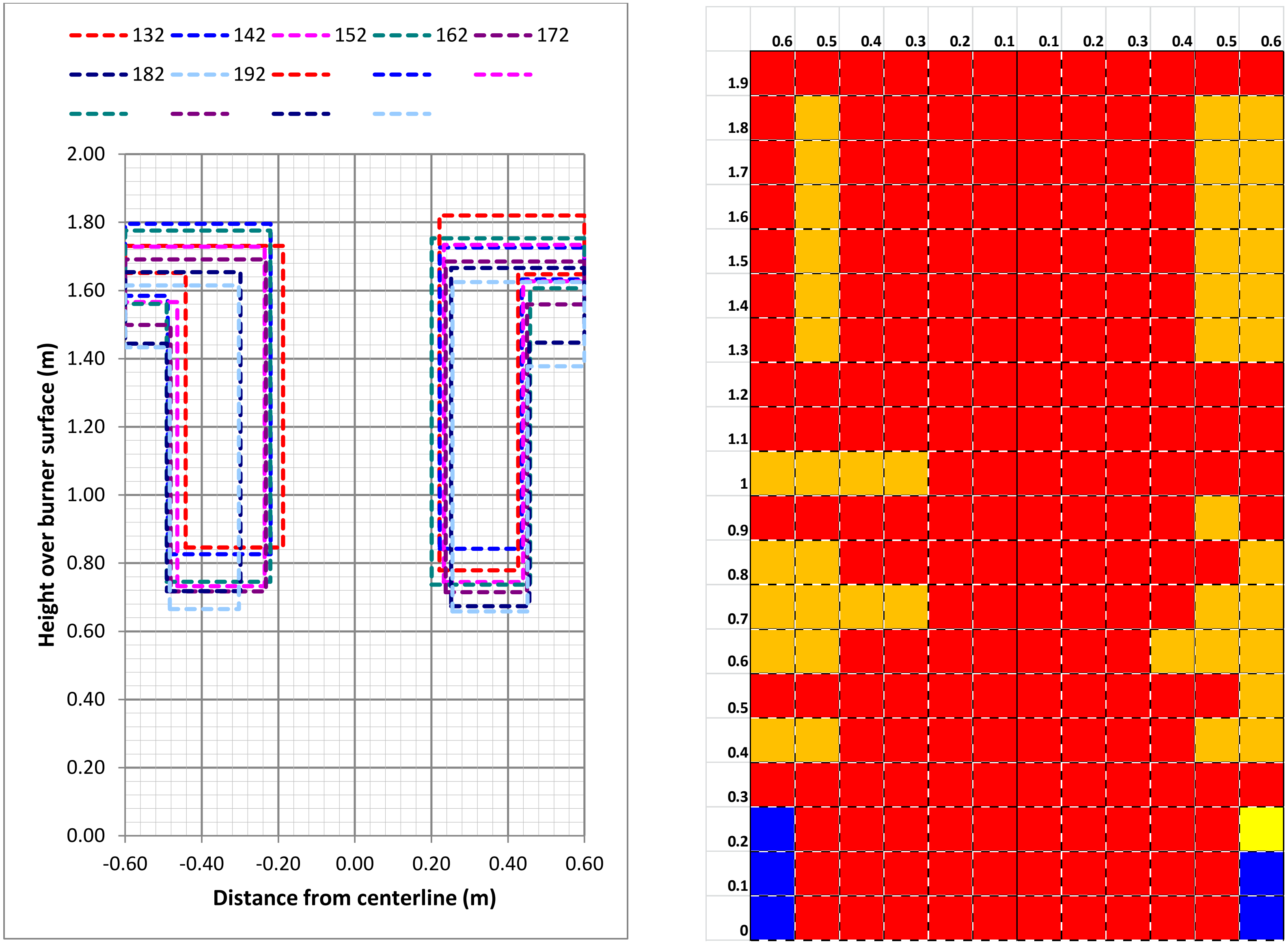

Figure 157 - Stage 3 burn area and final damage chart of Test A12 (2ft Rectangle burner, Propylene, 50 kW source on throughout test)

2ft Rectangle burner @ 75 kW source fire flame spread

The following tests A4, A10, and A17 used the 2ft Rectangle burner with 75 kW and different source fire gases. Test A4 uses propane, Test A10 uses propylene, Test A17 uses propane with burner on throughout test. The burning area charts show the progression of the burning area based on time history starting from noticeable burning of the FRP panel.

Figure 158 and Figure 159 show the Stages 1 to 3 burning area of Test A4 and also the final damage chart. . The final burn area shows the damage on the FRP panel due to fire spread with different colors showing the amount of damage to the resin base as shown in Table 21. Each cell represents a 0.1m x 0.1m square.

Table 21 - Damage summary of Test A4

# of cell	Damage to Resin	Area (m2)
109	up to 100% damage	1.09
78	up to 75% damage	0.78
9	up to 50% damage	0.09
0	up to 25% damage	0
92	no damage	0.92

Figure 160 and Figure 161 show the Stages 1 to 3 burning area of Test A10 and also the final damage chart. The final burn area shows the damage on the FRP panel due to fire spread with different colors showing the amount of damage to the resin base as shown in Table 22.

Table 22 - Damage summary of Test A10

# of cell	Damage to Resin	Area (m2)
129	up to 100% damage	1.29
70	up to 75% damage	0.7
3	up to 50% damage	0.03
4	up to 25% damage	0.04
82	no damage	0.82

Test A4 and A10 were identical except for the source burner fuel. The sizes of the burning areas and their rate of progression were also similar. The final burn area and damage between the two tests were also comparable.

Test A17 was different from the A4 and A10 because the source fire remained at 75 kW throughout the test, which affected the combustible wall flame spread greatly in speed and also intensity. Figure 162 and Figure 163 show the Stages 1 to 3 burning area of Test A10 and also the final damage chart. The final burn area shows the damage on the FRP panel due to fire spread with different colors showing the amount of damage to the resin base as shown in Table 23.

Table 23 - Damage summary of Test A17

# of cell	Damage to Resin	Area (m2)
214	**up to 100% damage**	2.14
18	**up to 75% damage**	0.18
2	**up to 50% damage**	0.02
3	**up to 25% damage**	0.03
51	**no damage**	0.51

Compared to Test A4 and A10 where the source fire was turned off after panel ignition, the burning speed of the combustible panel in Test A17 was much faster and the burning area was larger due to the presence of the source fire. The source fire provided a turbulent environment and energy that accelerated the upward and lateral spread of the fire such that most of the panel above the burner level was completely burnt out.

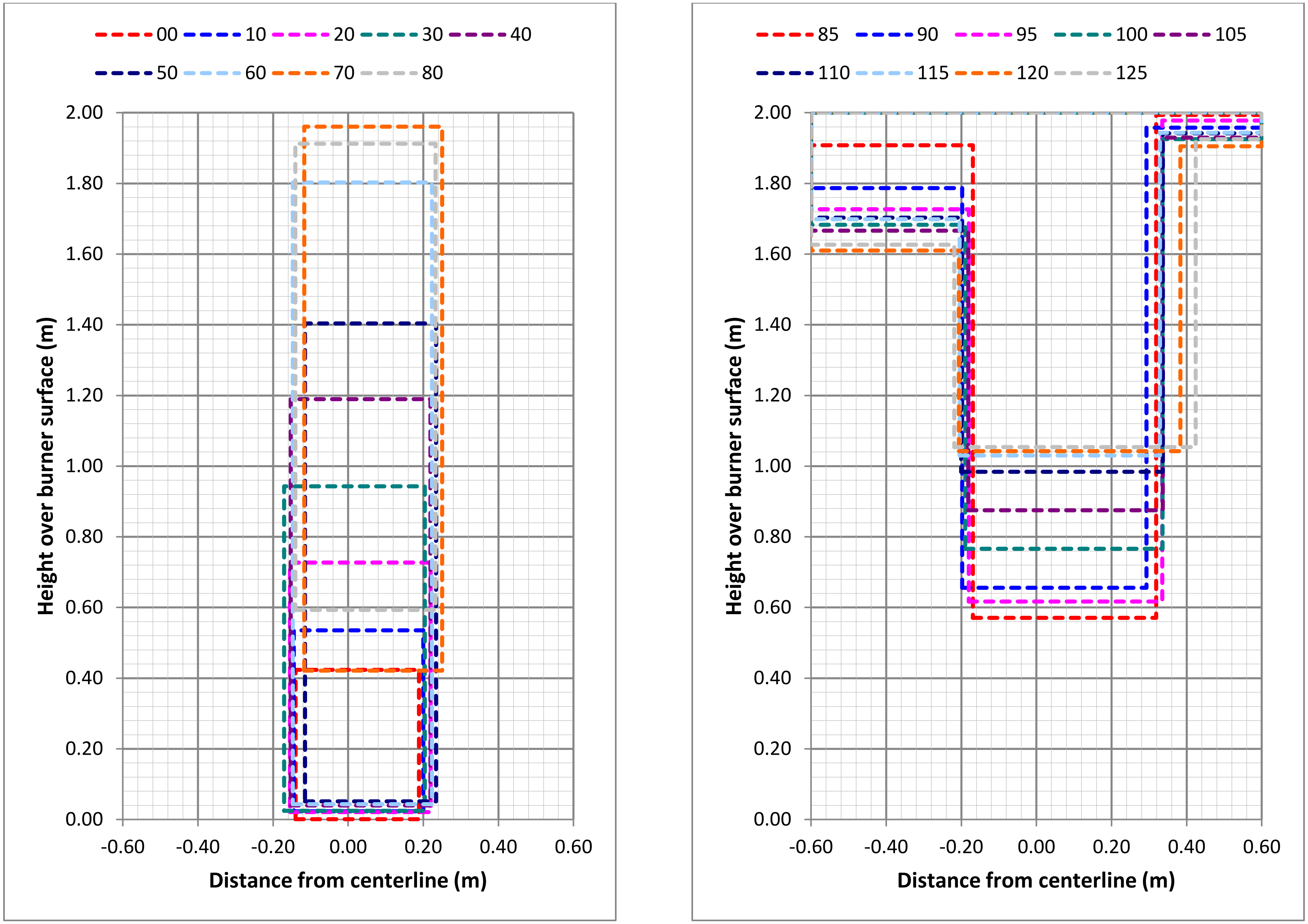

Figure 158 – Stages 1 and 2 burning areas in Test A4 (2ft Rectangle burner, Propane, 75 kW source)

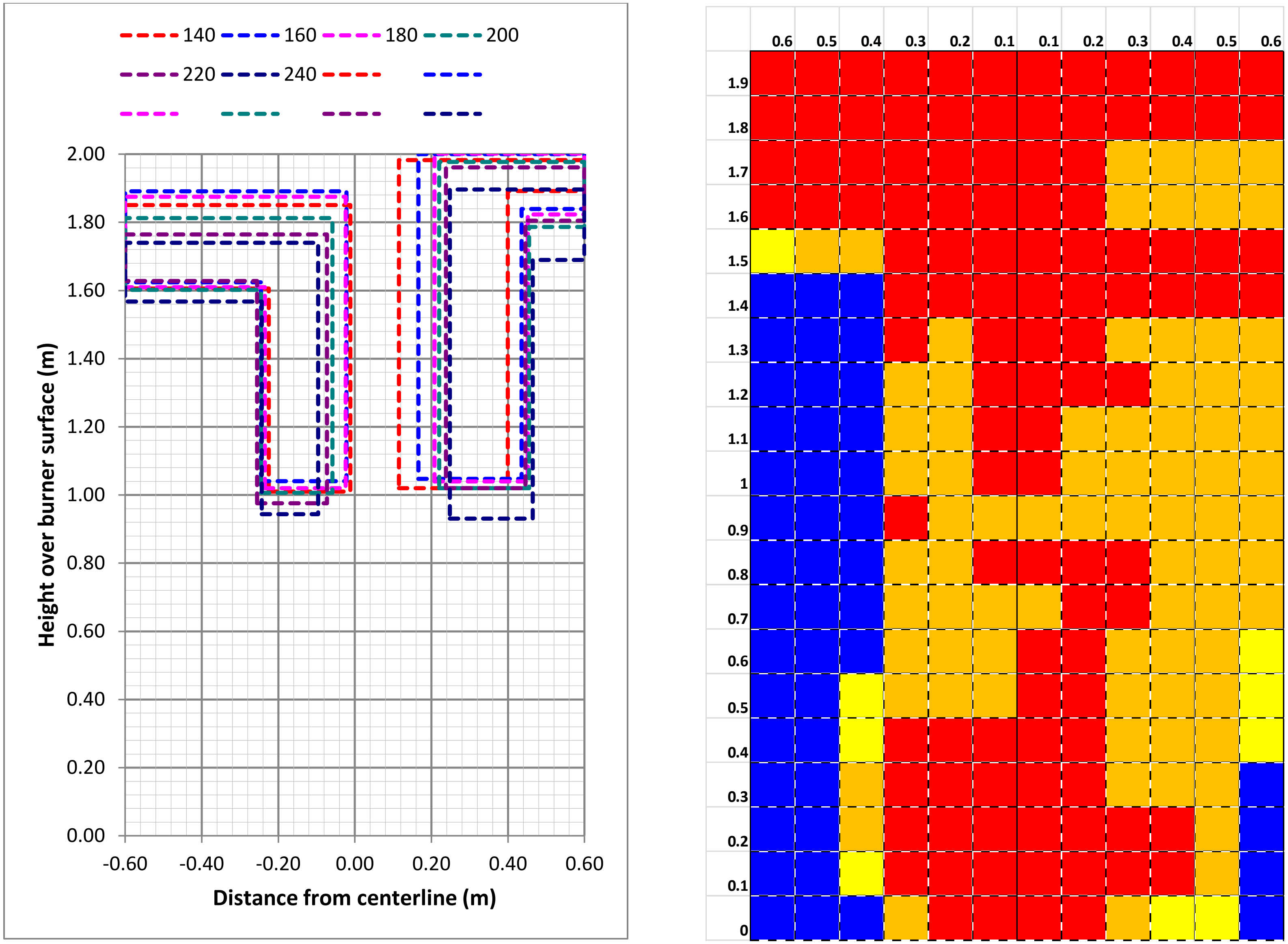

Figure 159 - Stage 3 burn area and final damage chart of Test A4 (2ft Rectangle burner, Propane, 75 kW source)

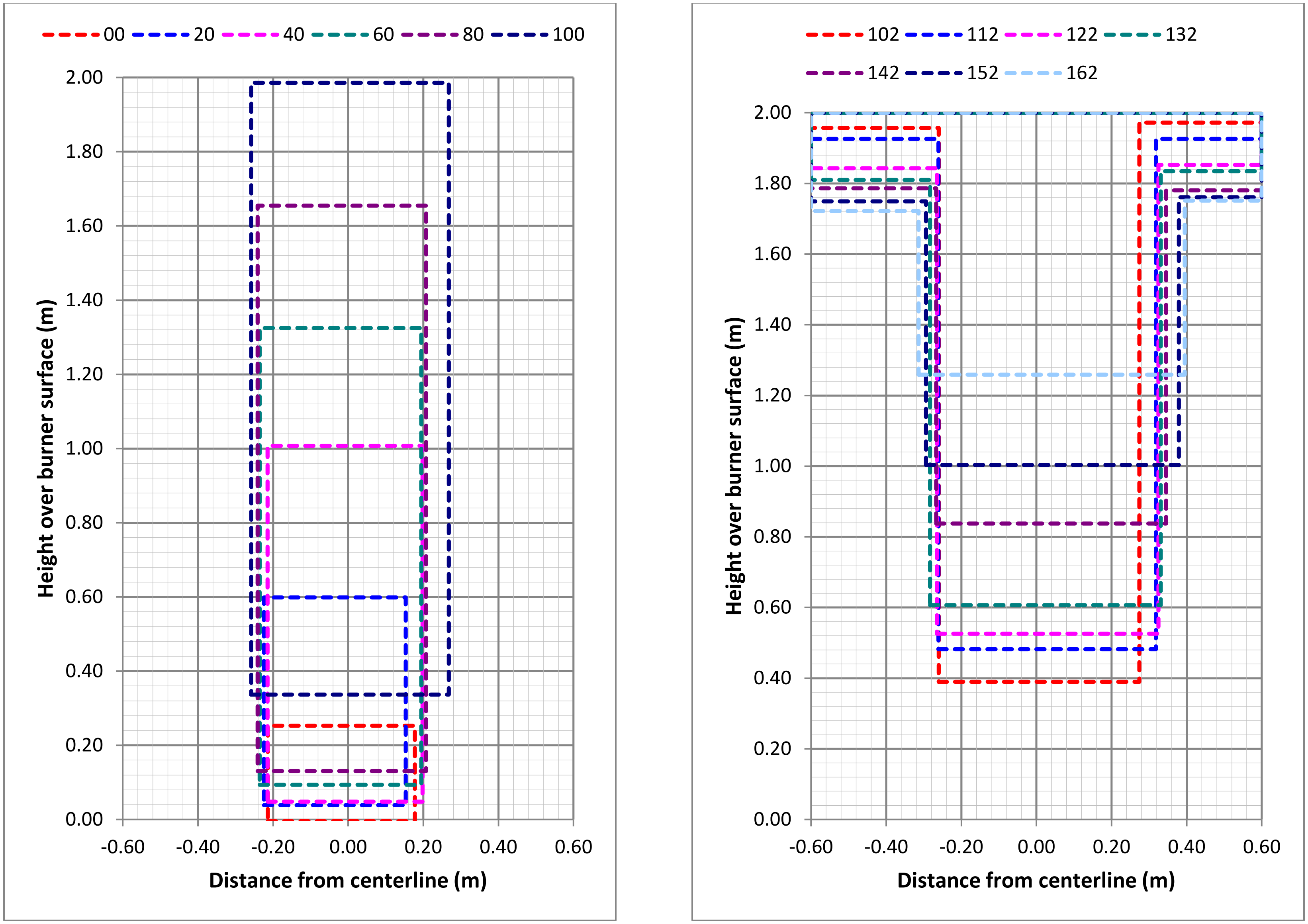

Figure 160 - Stages 1 and 2 burning areas in Test A10 (2ft Rectangle burner, Propylene, 75 kW source)

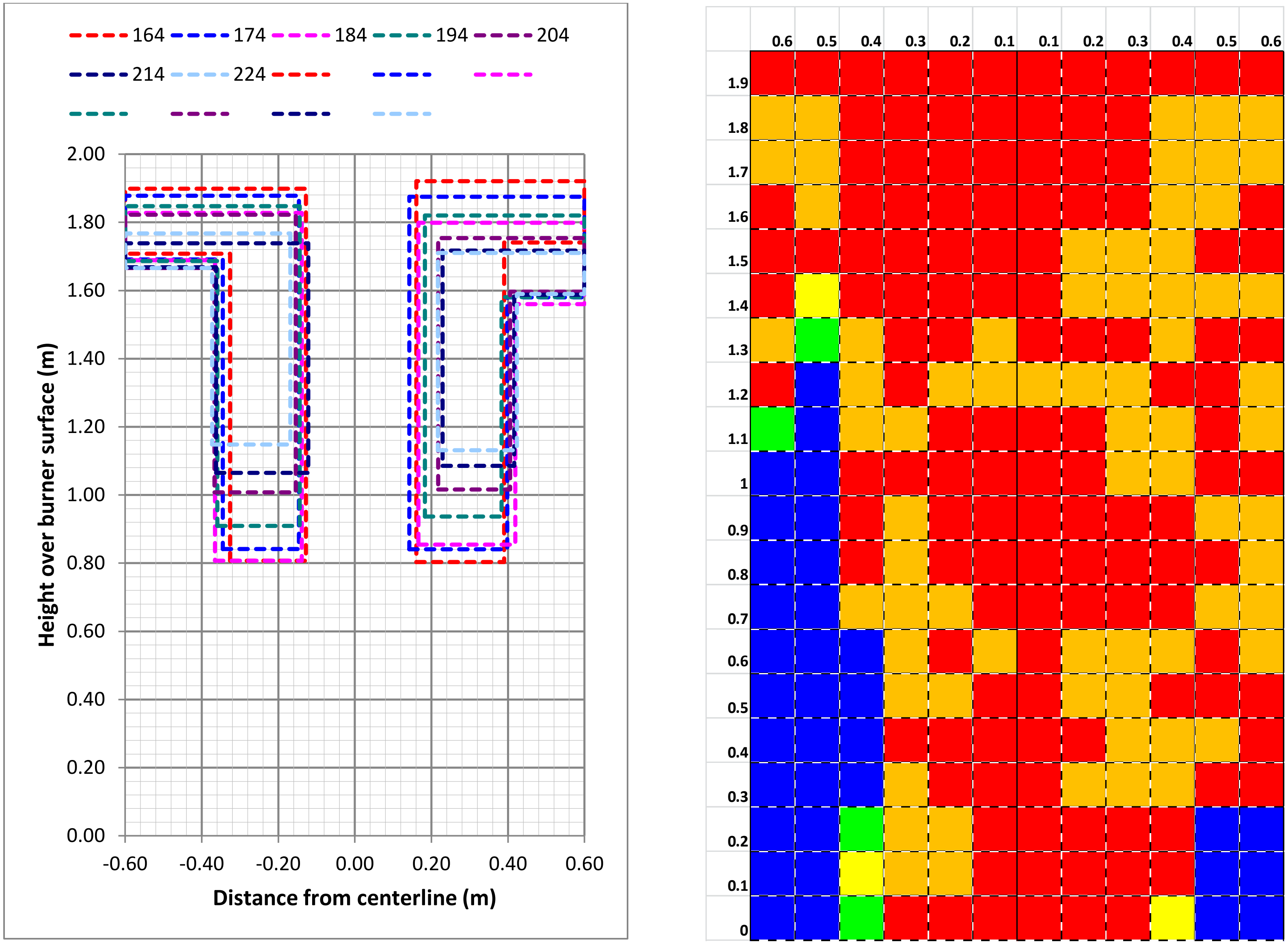

Figure 161 - Stage 3 burn area and final damage chart of Test A10 (2ft Rectangle burner, Propylene, 75 kW source)

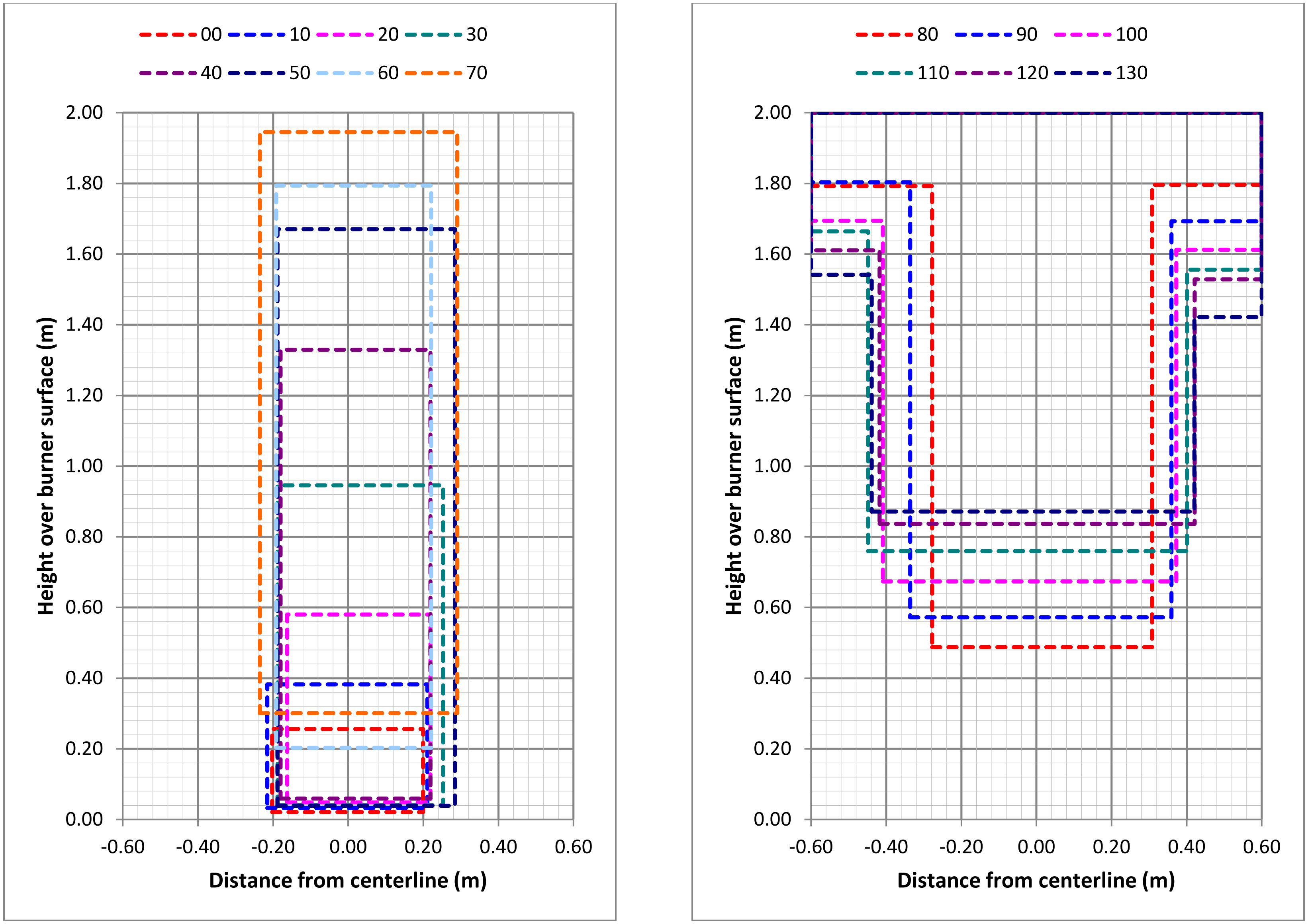

Figure 162 - Stages 1 and 2 burning areas in Test A17 (2ft Rectangle burner, Propane, 75 kW source on throughout test)

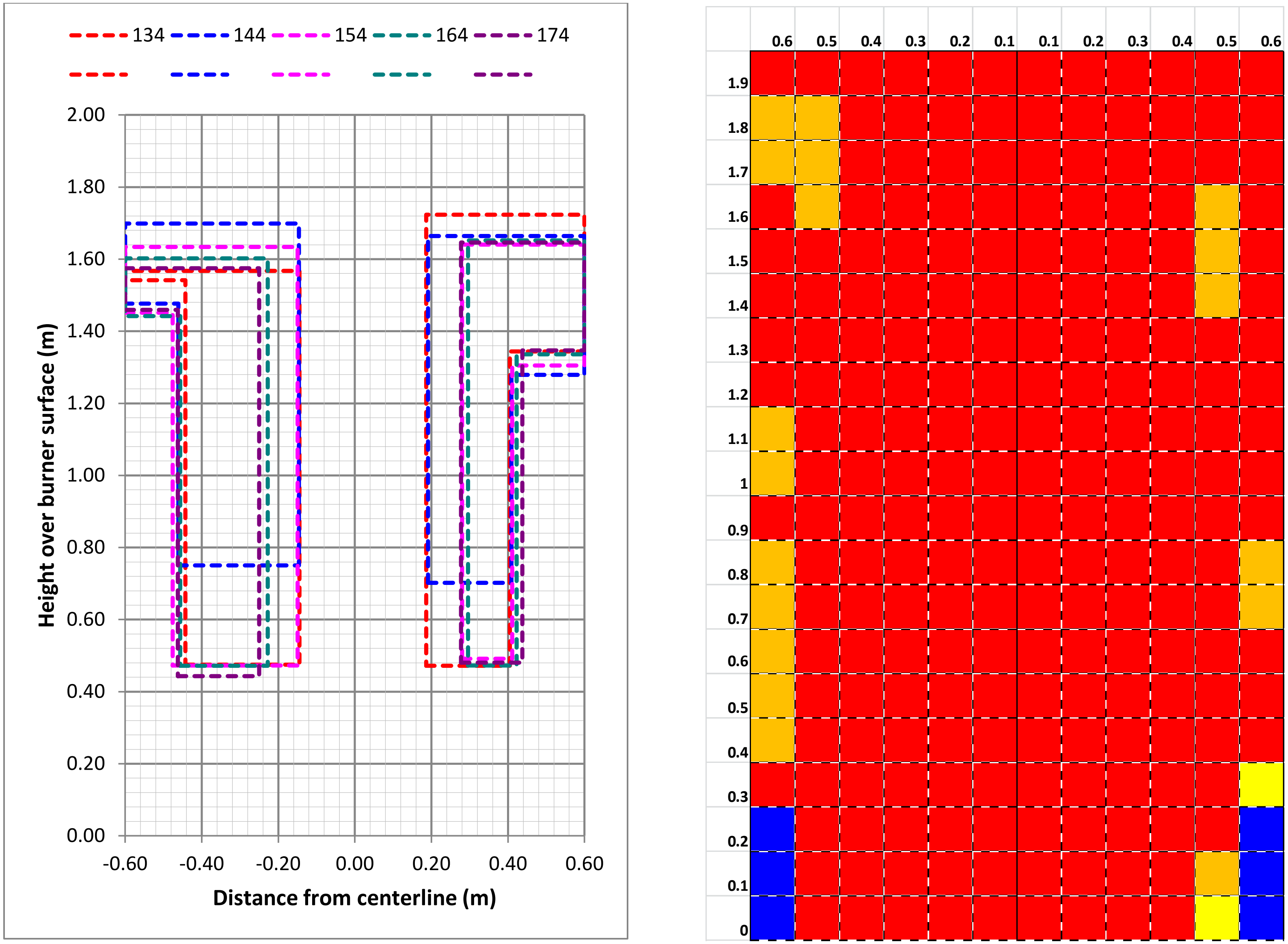

Figure 163 - Stage 3 burn area and final damage chart of Test A17 (2ft Rectangle burner, Propane, 75 kW source on throughout test)

1ft Square burner @ 50 kW source fire flame spread

The following tests A5, A7, A13 and A15 used the 1ft Square burner with 50 kW and different source fire gases. Tests A5 and A15 uses propane, Test A7 uses propylene, Test A13 uses propylene with burner on throughout test. The burning area charts show the progression of the burning area based on time history starting from noticeable burning of the FRP panel.

Figure 164 and Figure 165 show the Stages 1 to 3 burning area of Test A5 and also the final damage chart. The burning area charts show the progression of the burning area based on time history. The final burn area shows the damage on the FRP panel due to fire spread with different colors showing the amount of damage to the resin base as shown in Table 24. Each cell represents a 0.1m x 0.1m square.

Table 24 - Damage summary of Test A5

# of cell	Damage to Resin	Area (m2)
56	**up to 100% damage**	0.56
77	**up to 75% damage**	0.77
15	**up to 50% damage**	0.15
4	**up to 25% damage**	0.04
136	**no damage**	1.36

Figure 166 and Figure 167 show the Stages 1 to 3 burning area of Test A15 and also the final damage chart. The final burn area shows the damage on the FRP panel due to fire spread with different colors showing the amount of damage to the resin base as shown in Table 25.

Table 25 - Damage summary of Test A15

# of cell	Damage to Resin	Area (m2)
57	**up to 100% damage**	0.57
88	**up to 75% damage**	0.88
13	**up to 50% damage**	0.13
9	**up to 25% damage**	0.09
121	**no damage**	1.21

Test A5 and A15 were identical tests. The sizes of the burning areas were very similar with slight difference in timing of the progression. The final burn area and damage between the two tests were almost identical. The shift of the damage to the right of the panel could be attributed to the flow environment of the test compartment.

Figure 168 and Figure 169 show the Stages 1 to 3 burning area of Test A7 and also the final damage chart. The burning area charts show the progression of the burning area based on time history. The final burn area shows the damage on the FRP panel due to fire spread with different colors showing the amount of damage to the resin base as shown in Table 26. Each cell represents a 0.1m x 0.1m square.

Table 26 - Damage summary of Test A7

# of cell	Damage to Resin	Area (m2)
81	**up to 100% damage**	0.81
85	**up to 75% damage**	0.85
16	**up to 50% damage**	0.16
0	**up to 25% damage**	0
106	**no damage**	1.06

The difference between Test A7 and Tests A5/A15 were the source burner fuel used. The sizes of the burning areas were very similar with slight difference in timing of the progression; the final burn patterns were also similar. The shift of the damage to the right of the panel could be attributed to the flow environment of the test compartment.

Test A13 was different from the A5, A7, and A15 because the source fire remained at 50 kW throughout the test, which affected the combustible wall flame spread greatly in speed and also intensity. Figure 170 and Figure 171 show the Stages 1 to 3 burning area of Test A13 and also the final damage chart. The final burn area shows the damage on the FRP panel due to fire spread with different colors showing the amount of damage to the resin base as shown in Table 27.

Table 27 - Damage summary of Test A13

# of cell	Damage to Resin	Area (m2)
173	**up to 100% damage**	1.73
37	**up to 75% damage**	0.37
18	**up to 50% damage**	0.18
3	**up to 25% damage**	0.03
57	**no damage**	0.57

Compared to Tests A5, A7, and A15 where the source fire was turned off after panel ignition, the burning speed of the combustible panel in Test A13 was much faster and the burning area was larger due to the presence of the source fire. The source fire provided a turbulent environment and energy that accelerated the upward and lateral spread of the fire such that most of the panel above the burner level was completely burnt out.

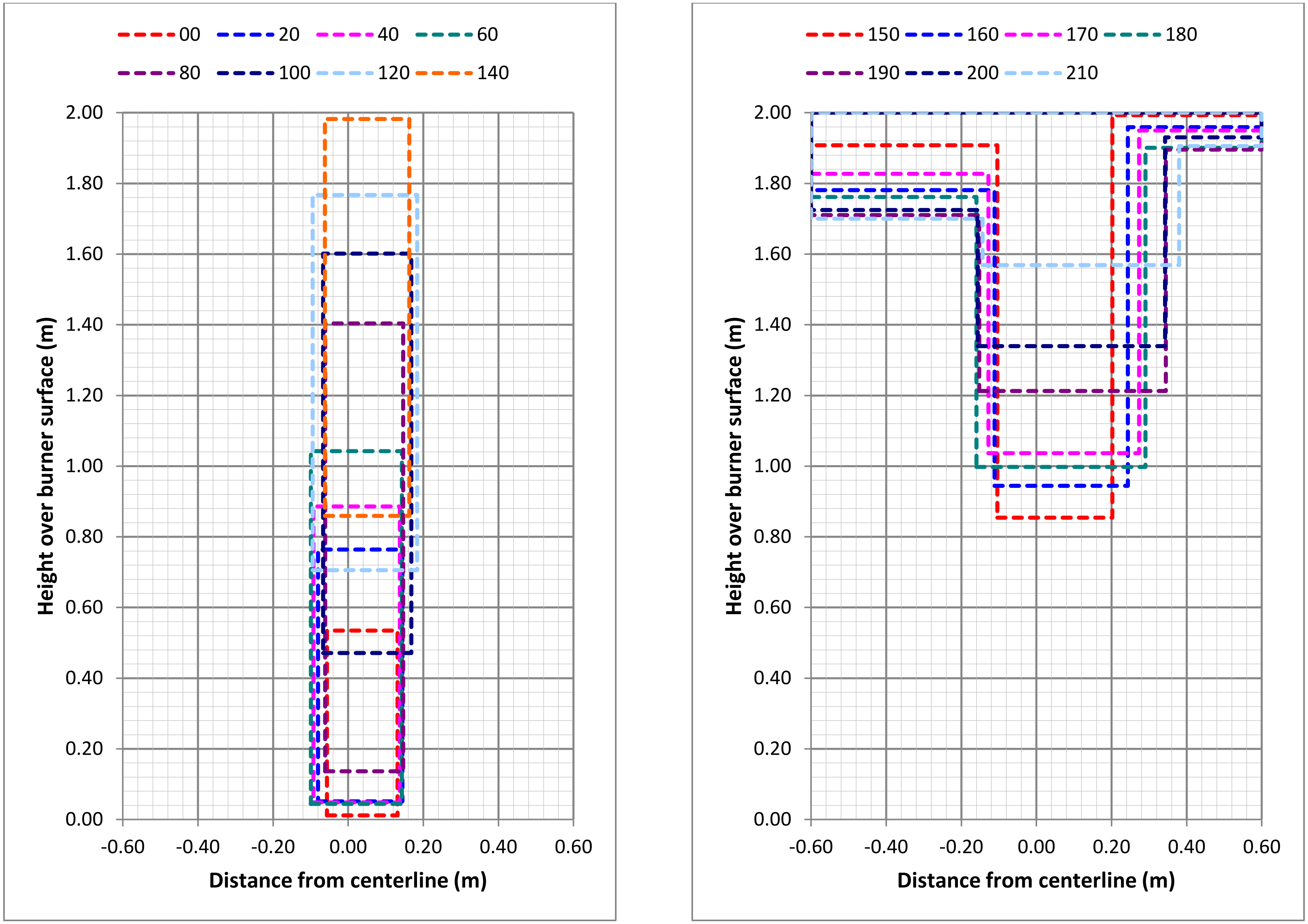

Figure 164 – Stages 1 and 2 burning areas in Test A5 (1ft Square burner, Propane, 50 kW source)

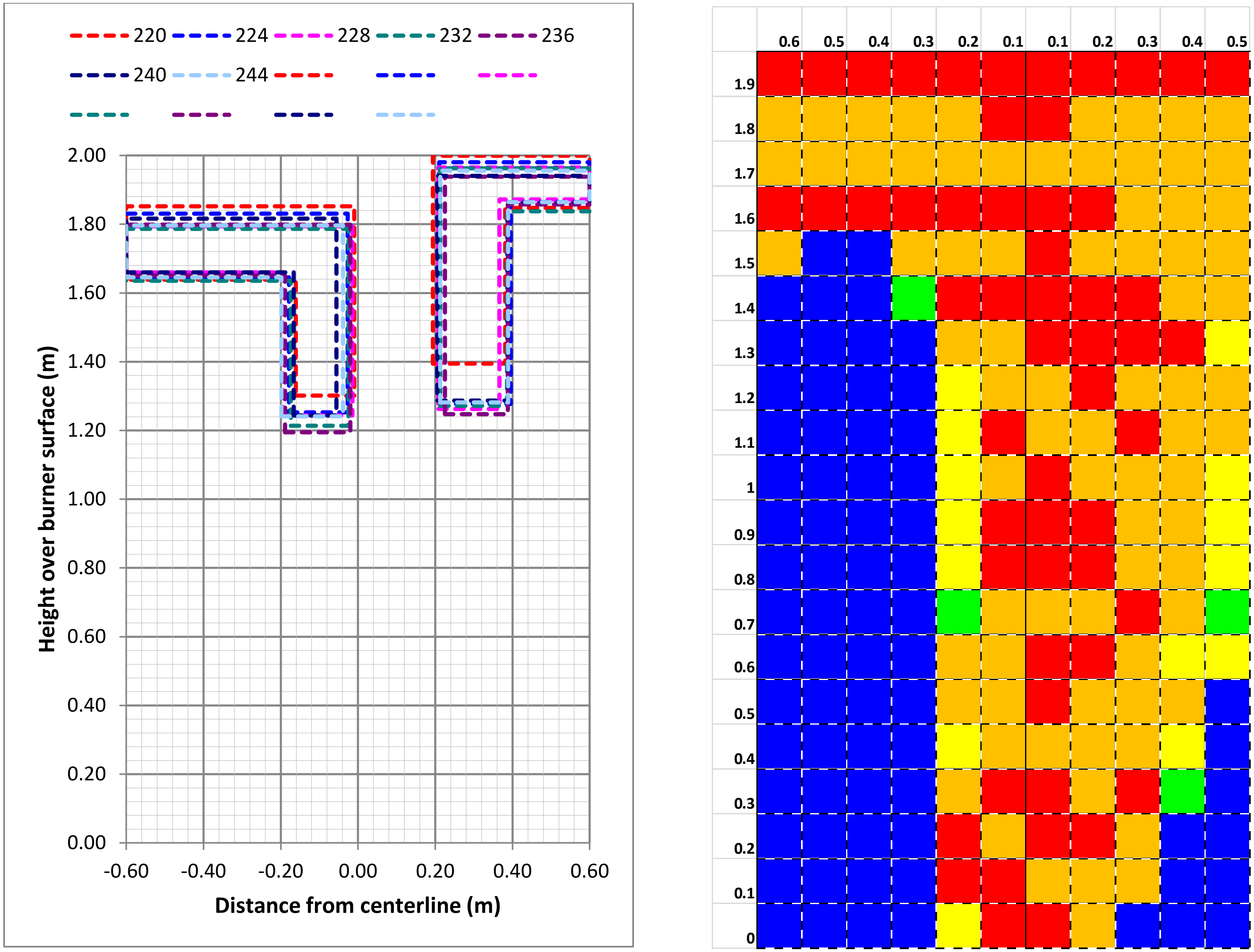

Figure 165 - Stage 3 burn area and final damage chart of Test A5 (1ft Square burner, Propane, 50 kW source)

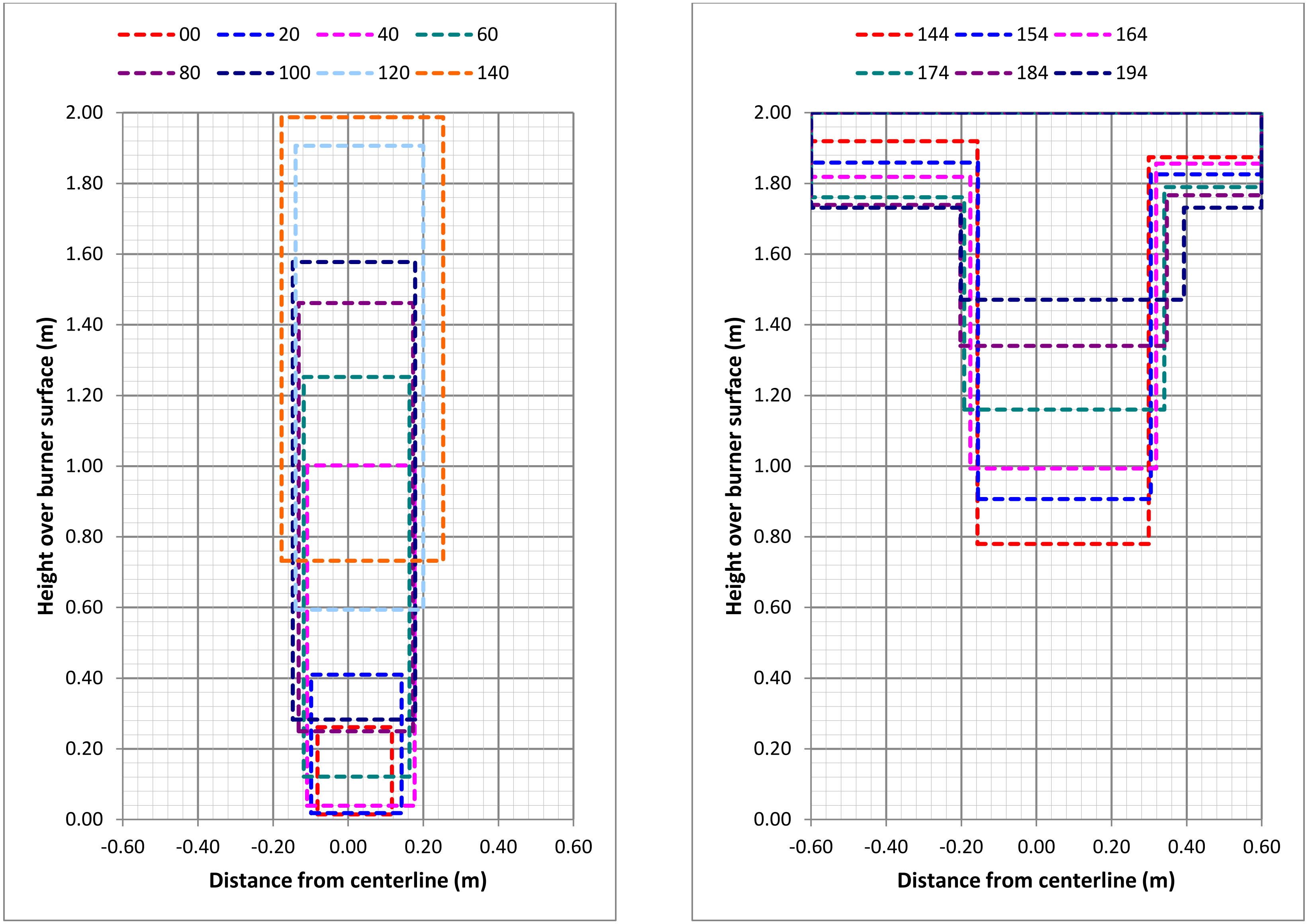

Figure 166 – Stages 1 and 2 burning areas in Test A15 (1ft Square burner, Propane, 50 kW source)

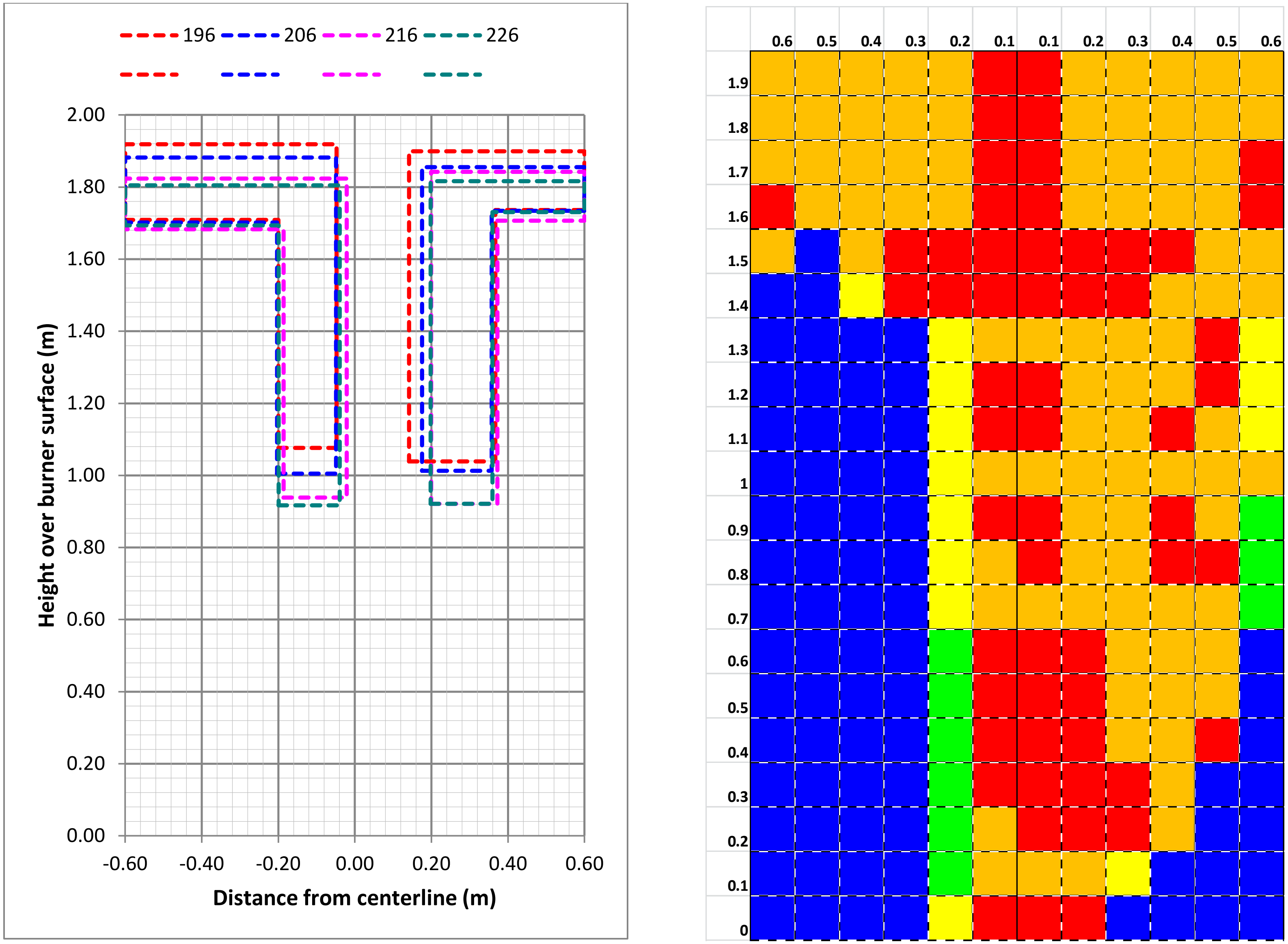

Figure 167 - Stage 3 burn area and final damage chart of Test A15 (1ft Square burner, Propane, 50 kW source)

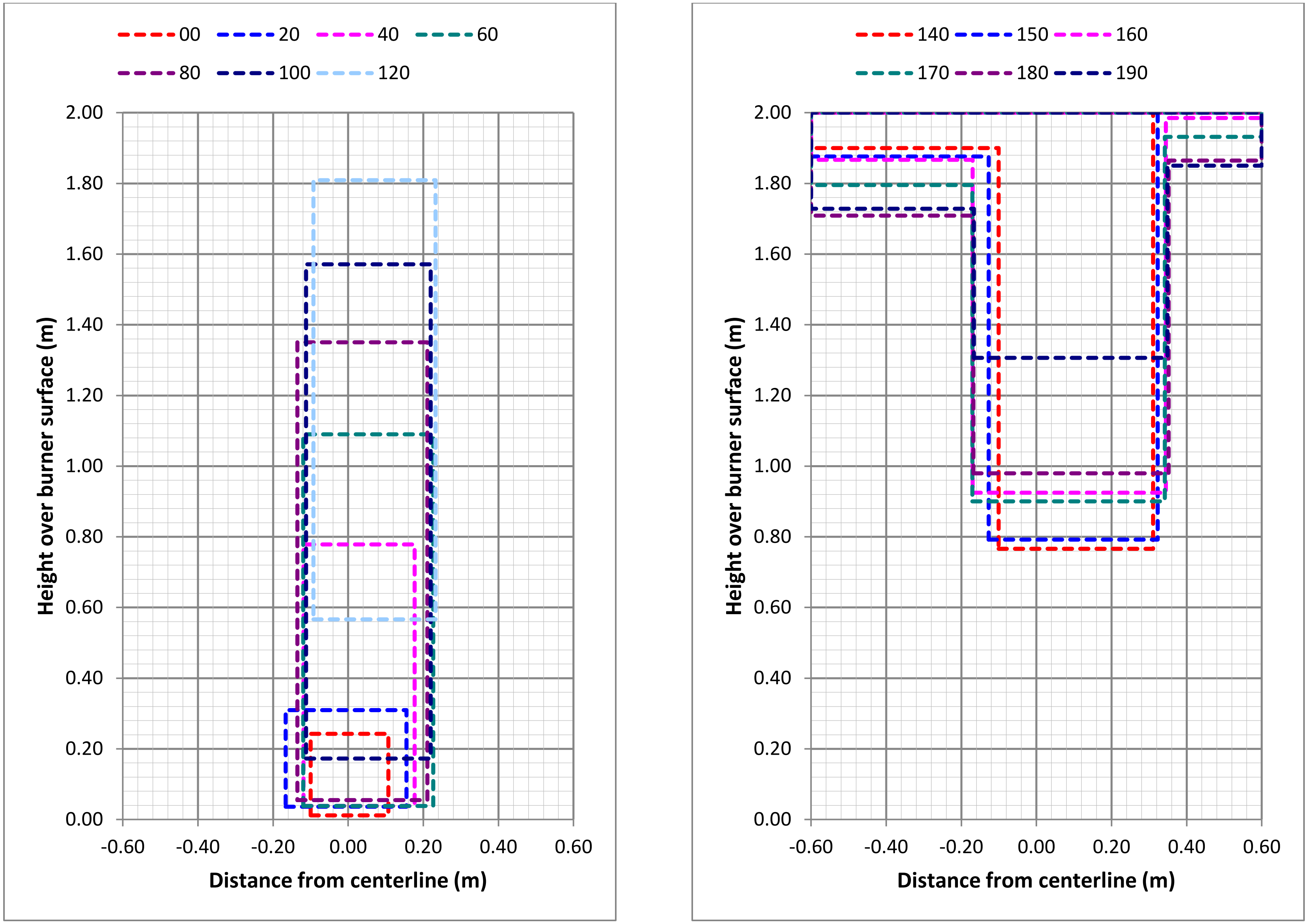

Figure 168 – Stages 1 and 2 burning areas in Test A7 (1ft Square burner, Propylene, 50 kW source)

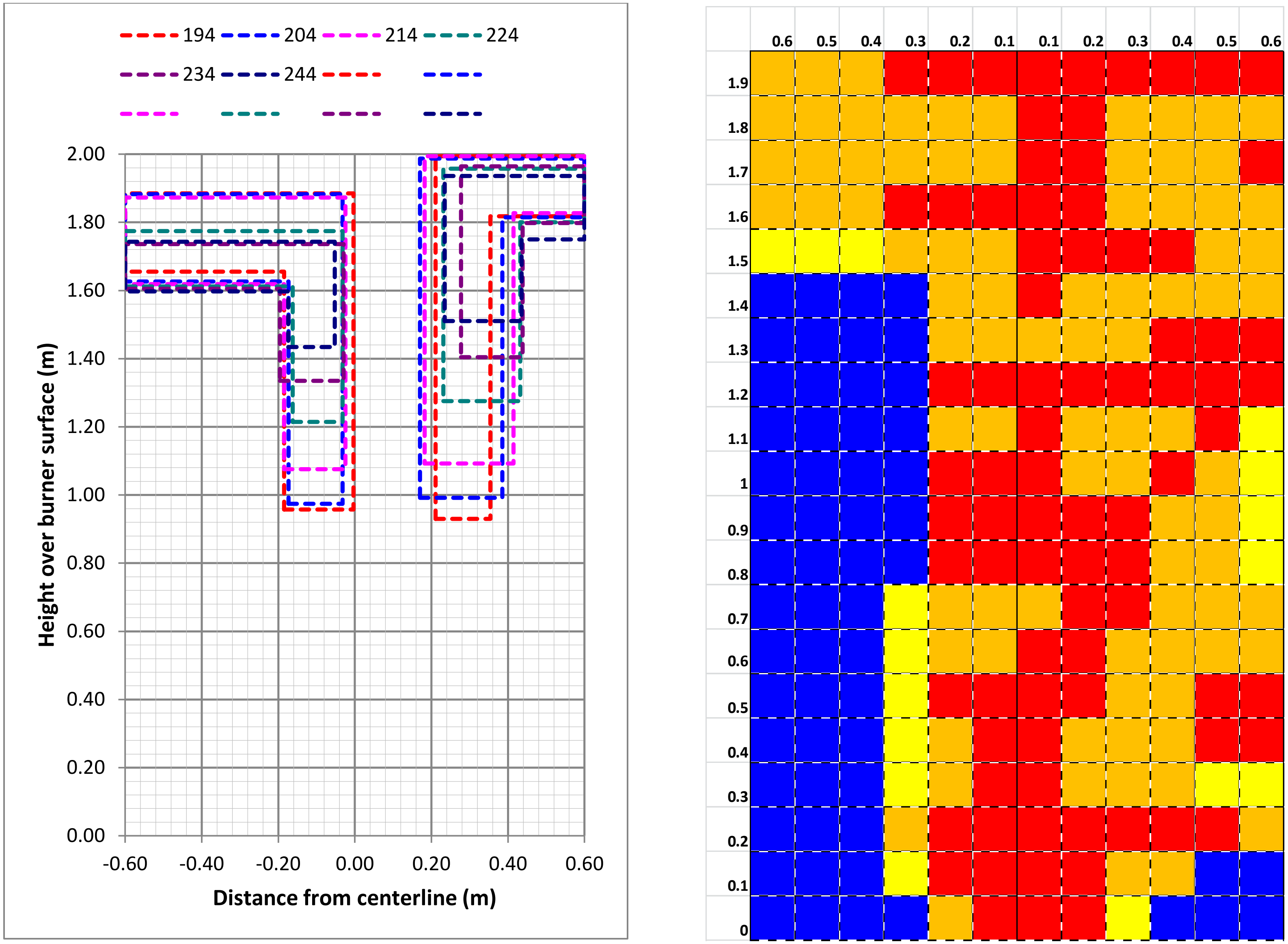

Figure 169 - Stage 3 burn area and final damage chart of Test A7 (1ft Square burner, Propylene, 50 kW source)

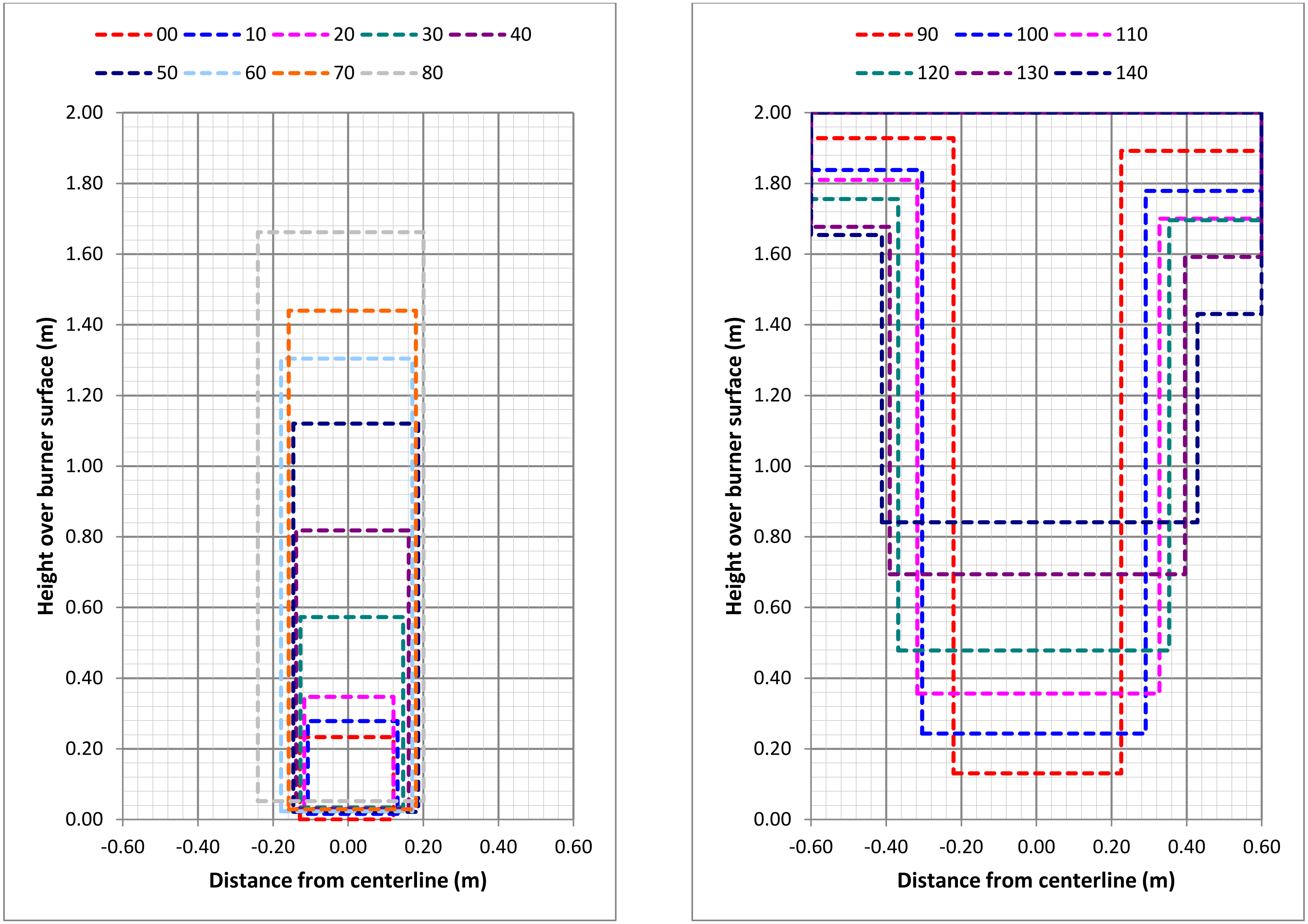

Figure 170 – Stages 1 and 2 burning areas in Test A13 (1ft Square burner, Propylene, 50 kW source on throughout test)

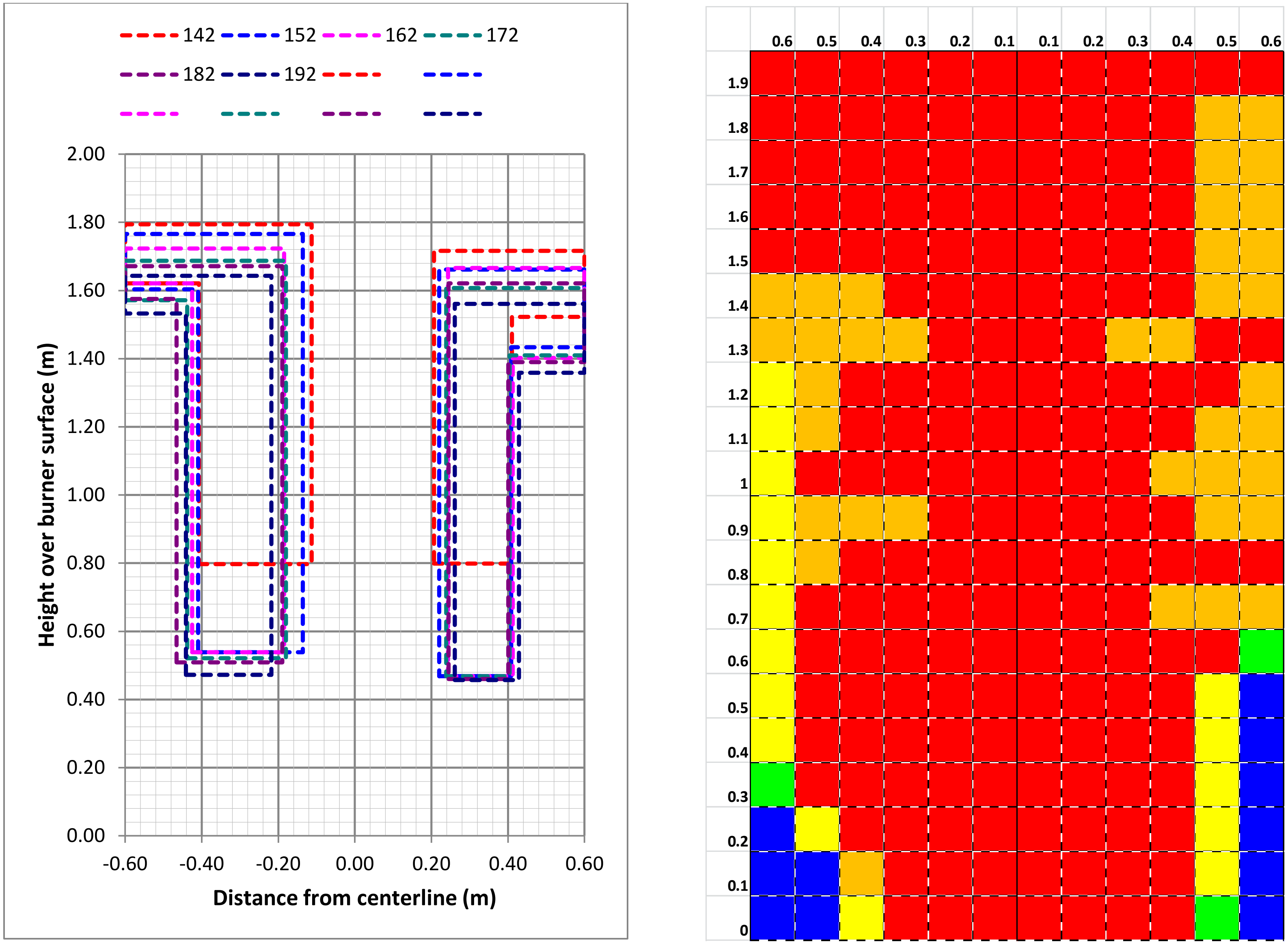

Figure 171 - Stage 3 burn area and final damage chart of Test A13 (1ft Square burner, Propylene, 50 kW source on throughout test)

1ft Square burner @ 75 kW source fire flame spread

The following tests A6, A8, A14 and A16 used the 1ft Square burner with 75 kW and different source fire gases. Test A6 used propane, Tests A8 and A14 used propylene, Test A16 uses propane with burner on throughout test. The burning area charts show the progression of the burning area based on time history starting from noticeable burning of the FRP panel.

Figure 172 and Figure 173 show the Stages 1 to 3 burning area of Test A6 and also the final damage chart. The burning area charts show the progression of the burning area based on time history. The final burn area shows the damage on the FRP panel due to fire spread with different colors showing the amount of damage to the resin base as shown in Table 28. Each cell represents a 0.1m x 0.1m square.

Table 28 - Damage summary of Test A6

# of cell	Damage to Resin	Area (m2)
56	**up to 100% damage**	0.56
77	**up to 75% damage**	0.77
15	**up to 50% damage**	0.15
4	**up to 25% damage**	0.04
136	**no damage**	1.36

Figure 174 and Figure 175 show the Stages 1 to 3 burning area of Test A8 and also the final damage chart. The final burn area shows the damage on the FRP panel due to fire spread with different colors showing the amount of damage to the resin base as shown in Table 29 - Damage summary of Test A8.

Table 29 - Damage summary of Test A8

# of cell	Damage to Resin	Area (m2)
109	**up to 100% damage**	1.09
64	**up to 75% damage**	0.64
18	**up to 50% damage**	0.18
0	**up to 25% damage**	0
97	**no damage**	0.97

Figure 176 and Figure 177 show the Stages 1 to 3 burning area of Test A14 and also the final damage chart. The burning area charts show the progression of the burning area based on time history. The final burn area shows the damage on the FRP panel due to fire spread with different colors showing the amount of damage to the resin base as shown in Table 30. Each cell represents a 0.1m x 0.1m square.

Table 30 - Damage summary of Test A14

# of cell	Damage to Resin	Area (m2)
96	up to 100% damage	0.96
56	up to 75% damage	0.56
17	up to 50% damage	0.17
7	up to 25% damage	0.07
112	no damage	1.12

Test A8 and A14 were identical tests. The sizes of the burning areas were very similar with slight difference in timing of the progression. The final burn area and damage between the two tests were almost identical. The shift of the damage to the right of the panel could be attributed to the flow environment of the test compartment.

The difference between Test A6 and Tests A8/A14 were the source burner fuel used. The sizes of the burning areas were very similar with slight difference in timing of the progression; the final burn patterns were also similar. The shift of the damage to the right of the panel was less significant as compared to the 1ft Square burner at 50 kW cases because the larger source fire size was more stable and vertical.

Test A16 was different from the A6, A8, and A14 because the source fire remained at 50 kW throughout the test, which affected the combustible wall flame spread greatly in speed and also intensity. Figure 178 and Figure 179 show the Stages 1 to 3 burning area of Test A16 and also the final damage chart. The final burn area shows the damage on the FRP panel due to fire spread with different colors showing the amount of damage to the resin base as shown in Table 31.

Table 31 - Damage summary of Test A16

# of cell	Damage to Resin	Area (m2)
219	up to 100% damage	2.19
25	up to 75% damage	0.25
0	up to 50% damage	0
0	up to 25% damage	0
44	no damage	0.44

Compared to Tests A6, A8, and A14 where the source fire was turned off after panel ignition, the burning speed of the combustible panel in Test A16 was much faster and the burning area was larger due to the presence of the source fire. The source fire provided a turbulent environment and energy that accelerated the upward and lateral spread of the fire such that most of the panel above the burner level was completely burnt out.

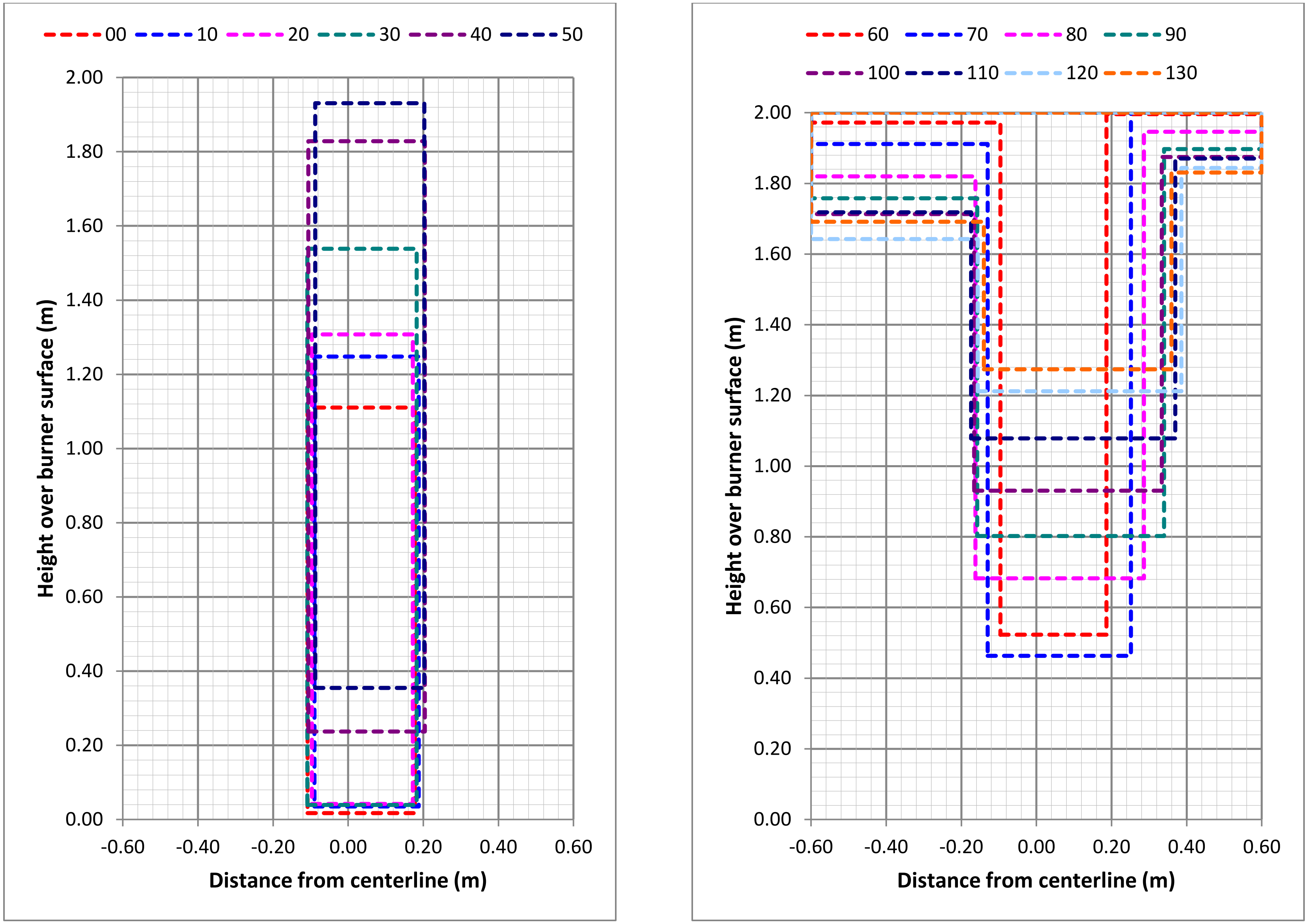

Figure 172 – Stages 1 and 2 burning areas in Test A6 (1ft Square burner, Propane, 75 kW source)

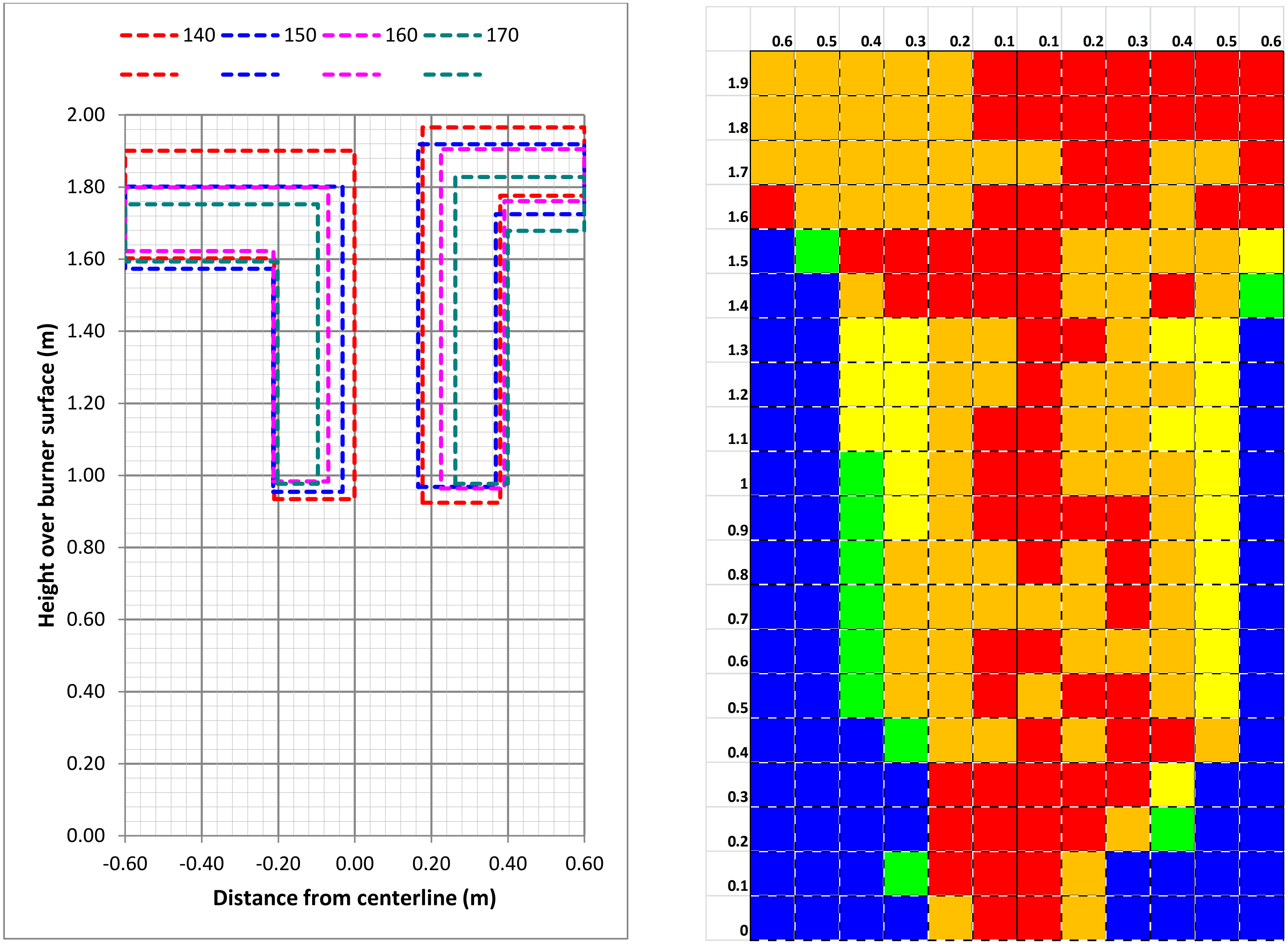

Figure 173 - Stage 3 burn area and final damage chart of Test A6 (1ft Square burner, Propane, 75 kW source)

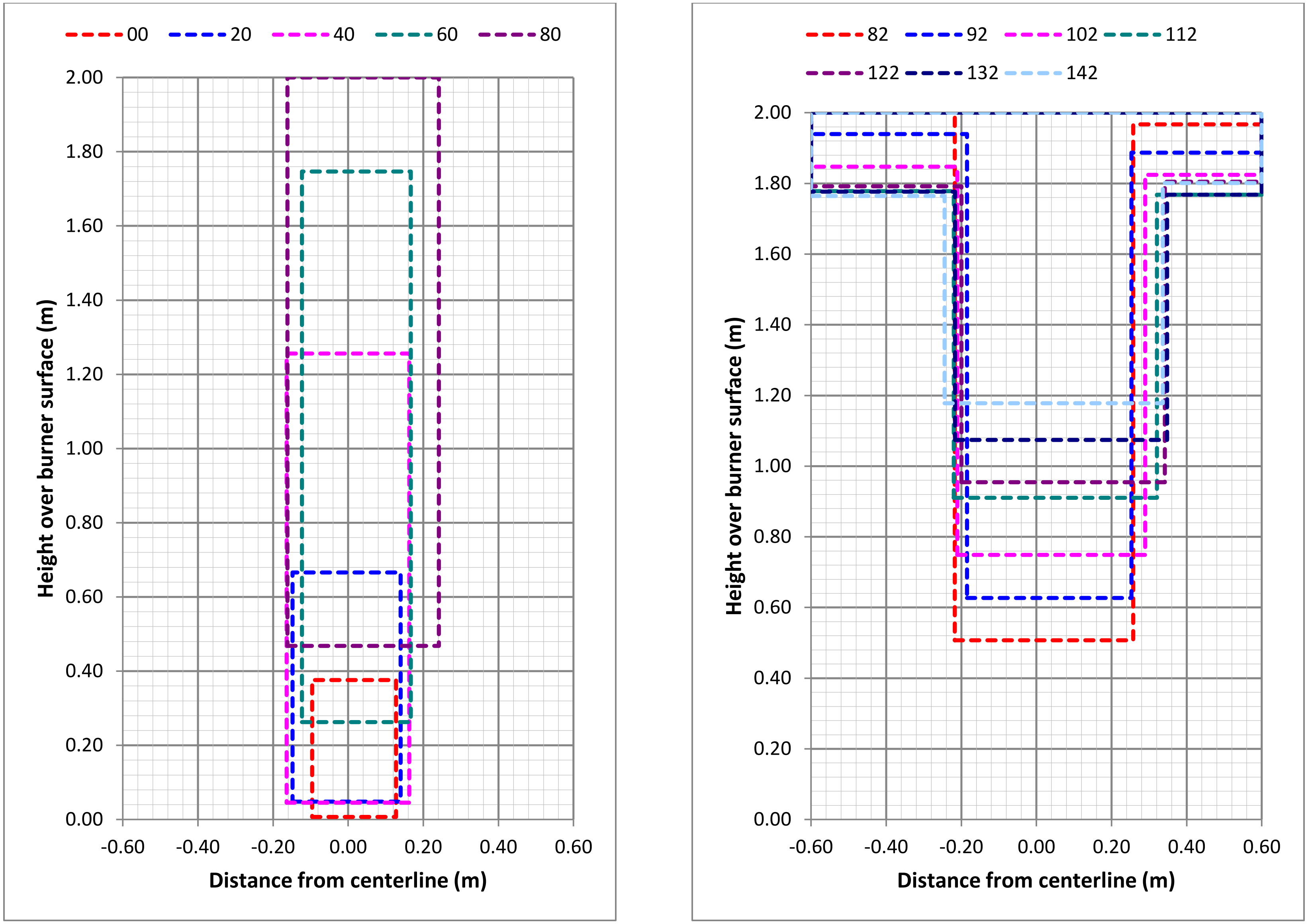

Figure 174 – Stages 1 and 2 burning areas in Test A8 (1ft Square burner, Propylene, 75 kW source)

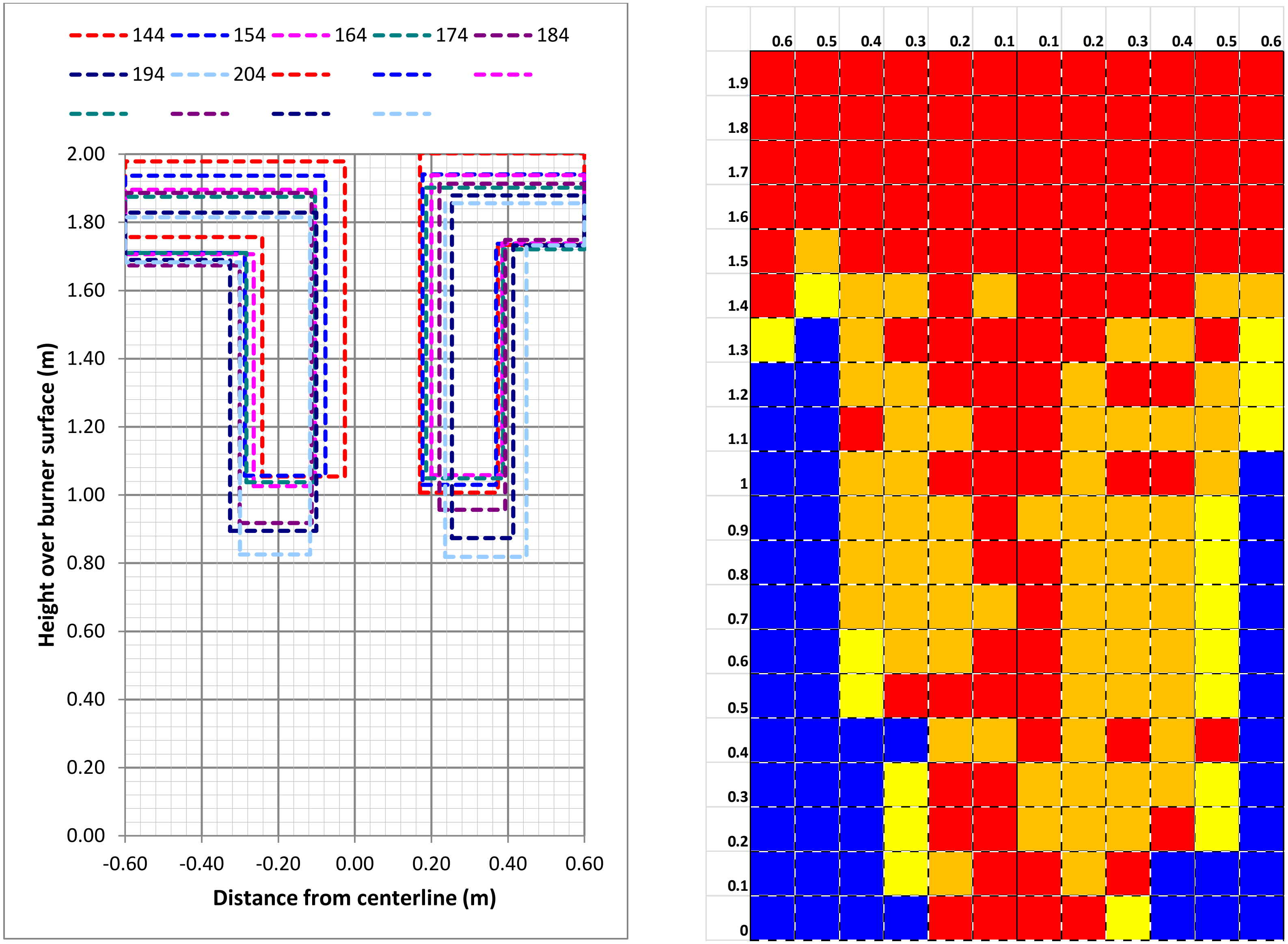

Figure 175 - Stage 3 burn area and final damage chart of Test A8 (1ft Square burner, Propylene, 75 kW source)

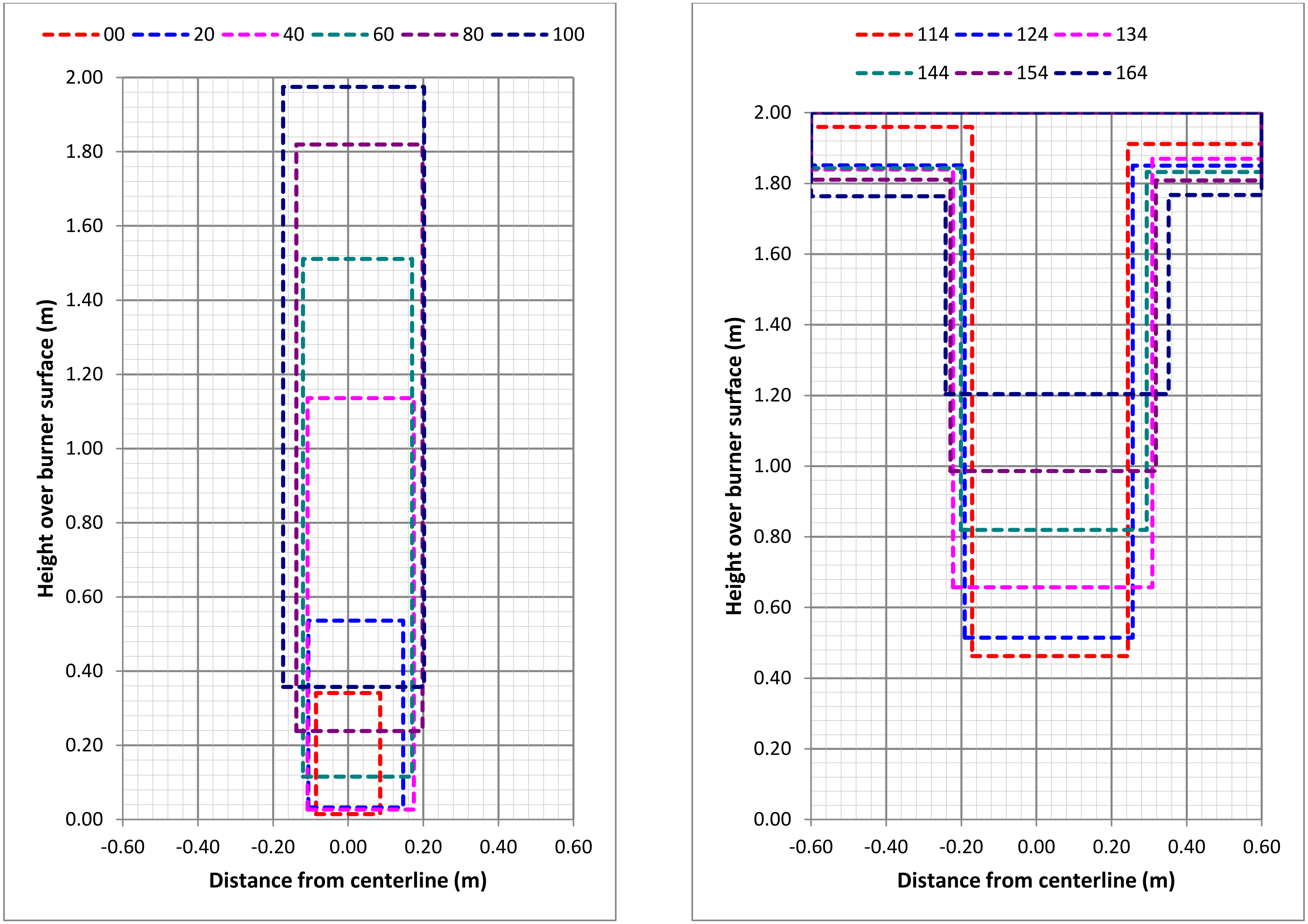

Figure 176 – Stages 1 and 2 burning areas in Test A14 (1ft Square burner, Propylene, 75 kW source)

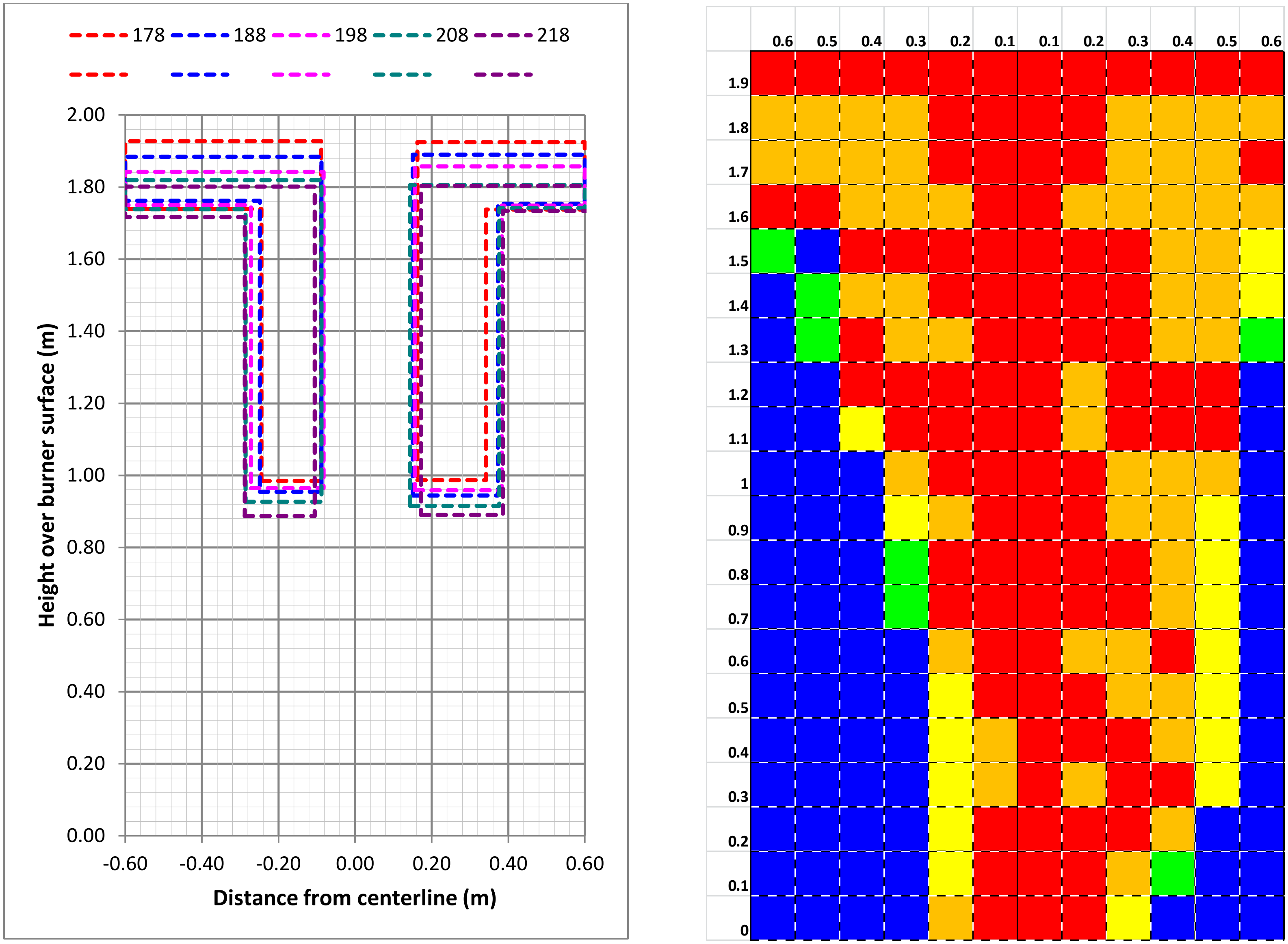

Figure 177 - Stage 3 burn area and final damage chart of Test A14 (1ft Square burner, Propylene, 75 kW source)

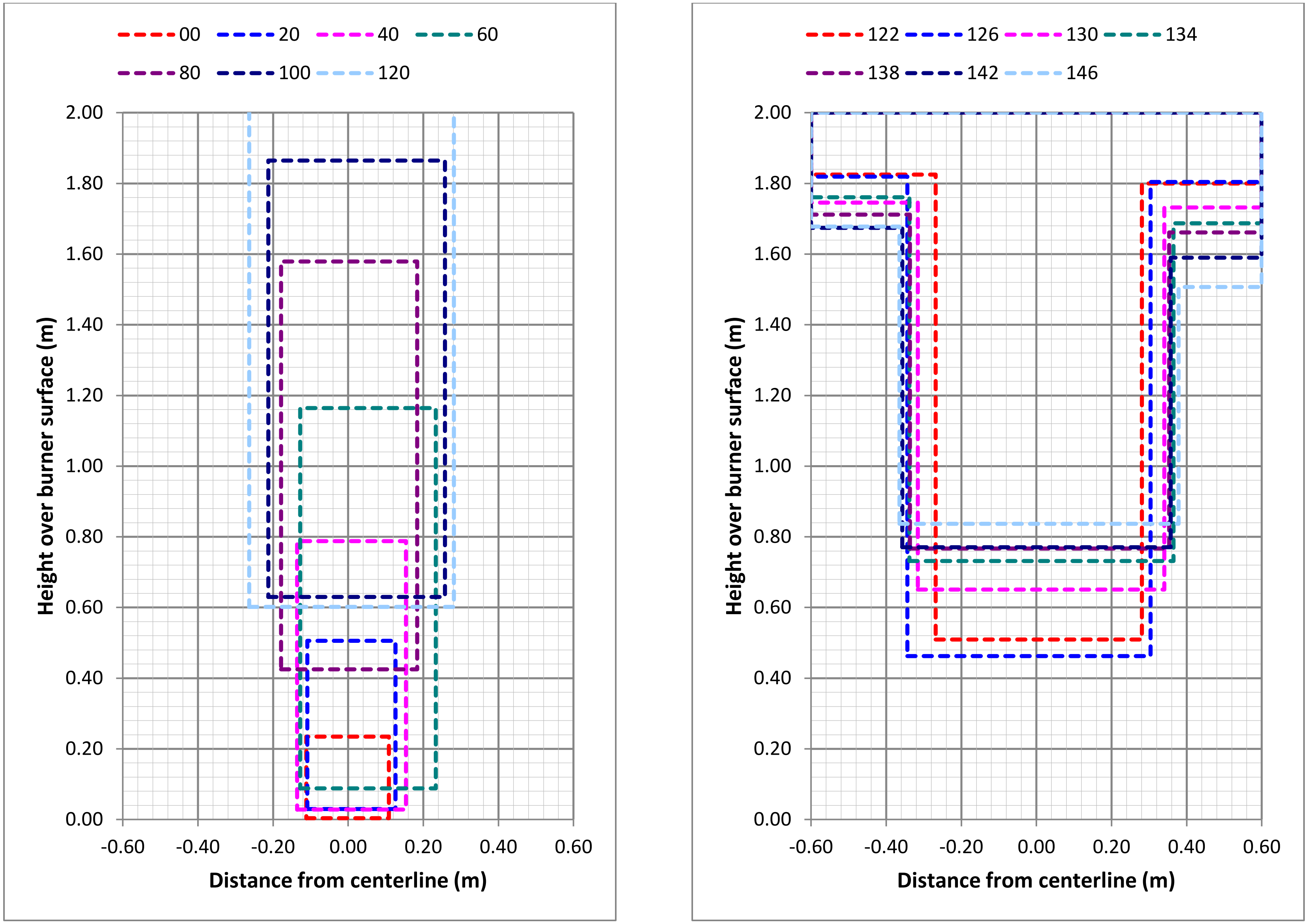

Figure 178 – Stages 1 and 2 burning areas in Test A16 (1ft Square burner, Propane, 75 kW source on throughout test)

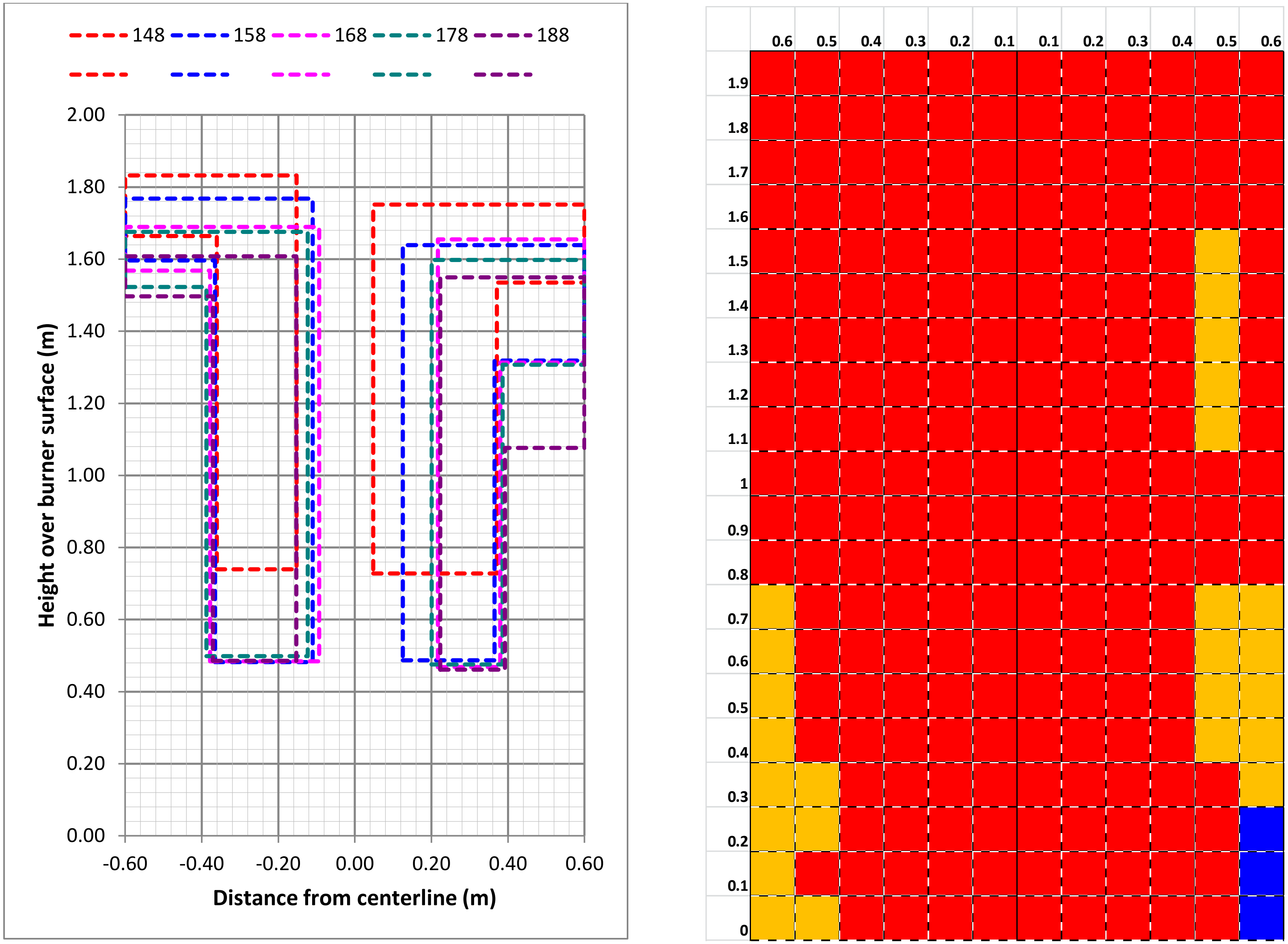

Figure 179 - Stage 3 burn area and final damage chart of Test A16 (1ft Square burner, Propane, 75 kW source on throughout test)

D.7.3 Combustible Wall Tests FRP Wall Panel Total Burnt Area

The total burn area of the FRP panel after a test was found using [4] based on the damage grid produced for each test. Most of the wall panel tests have a T-shape burn pattern, where the horizontal bar of the "T" is usually about 0.5 m to 0.6 m, but the vertical column of the "T" differs between the 1 ft burner cases and the 1 ft burner cases with the Square burner producing a thinner column than the Rectangle burner. The size of the source fire appears to have little to no effect on the size of the final burn area.

Figure 180 shows the total burnt areas of each of the FRP tests. For the same burner size and HRR, the propylene tests had generally larger total burnt areas than the propane tests. The largest total burnt areas were recorded for the tests where the source fire was on throughout. There also appears to be a trend where the higher HRRs resulted in larger burnt areas, although the differences were slight.

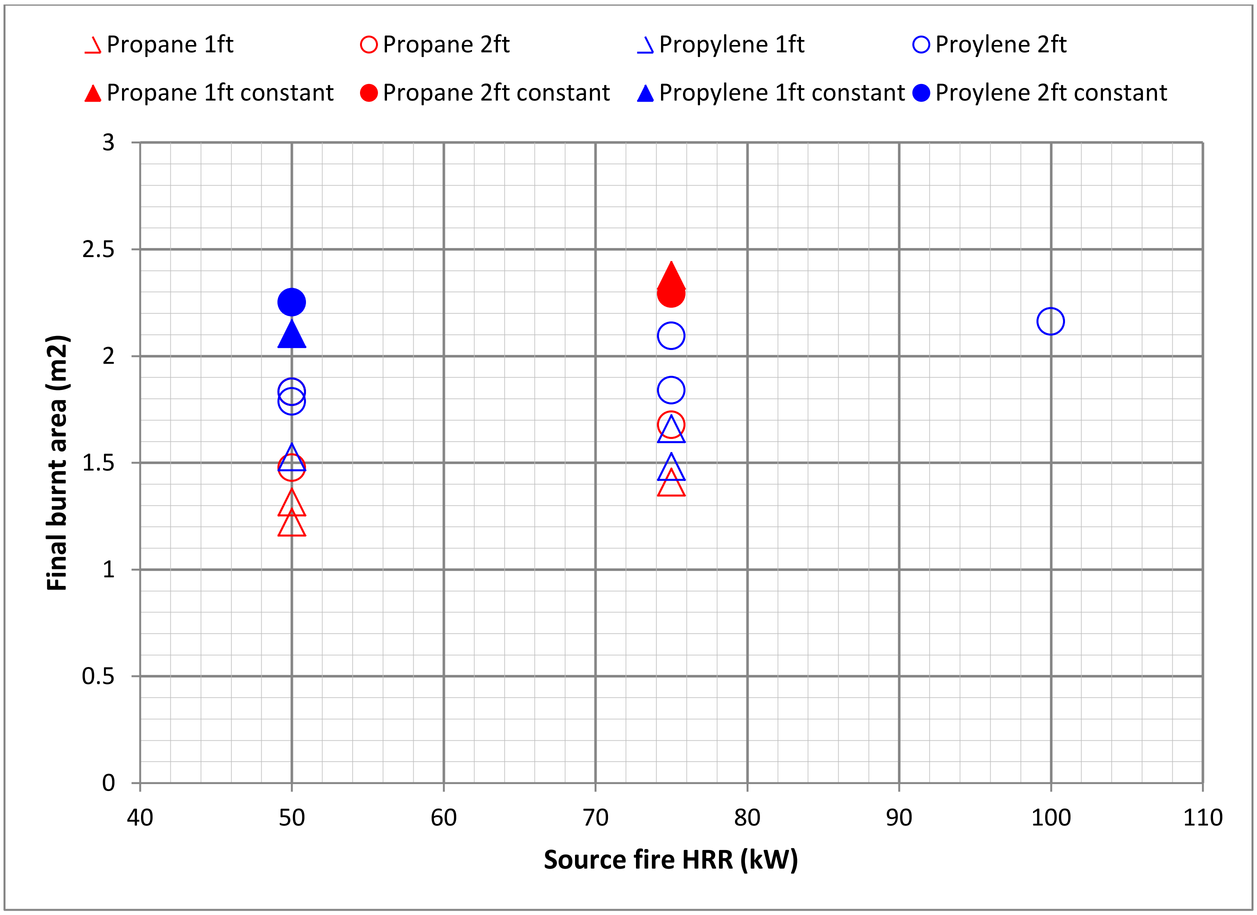

Figure 180 - Total burnt area comparisons

D.9 References

1. McCaffrey BJ. Purely Buoyant Diffusion Flames: Some Experimental Results. NBSIR 79-1910. Washington, D.C.: Center for Fire Research, National Engineering Laboratory, 1979.
2. Hasemi Y and Tokunaga T. Flame Geometry Effects on the Buoyant Plumes from Turbulent Diffusion Flames. *Fire Science and Technology*. 1984; 4: pp.15-6.
3. Newman JS. Multi-Directional Flow Probe Assembly for Fire Application. *Journal of Fire Sciences*. 1987; 5: pp.50-6.
4. Heskestad G. Bidirectional Flow Tube for Fire-Induced Vent Flows. FMRC Serial Number 21011.4. Factory Mutual Research Corporation, 1974.
5. Zukoski E, T. Kubota and B. Cetegen. Entrainment in Fire Plumes. *Fire Safety Journal*. 1981; 3: pp.107-22.
6. Heskestad G. On Q* and the Dynamics of Turbulent Diffusion Flames. *Fire Safety Journal*. 1998; 30: pp.215-27.
7. Qintiere JaBG. Correlations for Fire Plumes. 1998.
8. Alston JaND. Evaluation of Dimensionless Flame Height Parameters to Account for Fuel Source Effects. In: 2007. proceedings of thhe Seventh International Symposium.
9. Anderson SKaND. Qualitative Study of the Effect of a Compartment Enclosure on Fire Plume Entrainment. Worcester, MA: Worcester Polytechnic Institute, 1998.
10. Hasemi YaMN. Fuel Shape Effect on the Deterministic Properties of Turbulent Diffusion Flames. In: *Fire Safety Science - Proceedings of the Second International Symposium, International Association for Fire Safety Science*, New York, 1988. Washington, DC: Hemisphere Publishing Corporation.

Appendix E Cone Test Summary Sheets

This section presents the cone calorimeter test data for each of the tests run during the combustible material selection process detailed in Appendix A.

E.1 Thermoplastic Test 1 – White HDPE Sample 1

Cone Calorimeter Test Run Data

Dept. of Fire Protection Engineering

100 Institute Road
Worcester, MA 01609
Phone: (508) 831-5628
Fax: (508) 831-5862

Test Information

Test Number:	Test 01A
Specimen Identification:	White High Density Polyethylene Sample 01A
Material Name:	White HDPE 01A
Manufacturer/Submitter:	Not Reported
Sample Description:	White half-inch thick panel, no TCs
Raw Data File Name:	Test_01A_White_HDPE_01A.txt
Reduced Data File Name:	Test_01A_White_HDPE_01A.xls
Date of Test:	6/18/2009
Tester:	Will Wong

Test Parameters

Ambient Temperature:	75	F
Relative Humidity:	41	%
Heat Flux:	50	kW/m^2
Exhaust Duct Flow Rate:		30 g/s
Orientation:		Horizontal
Specimen Holder:		TRUE
Specimen Preparation:		2 layer foil
Notes:		1" Separation

Specimen Information

Specimen Color:	[]	White
Specimen Thickness:	[mm]	12.3
Specimen Test Area:	[m^2]	0.0088
Specimen Initial Mass:	[g]	117.1
Specimen Final Mass:	[g]	3.1
Specimen Density:	[g/cm^3]	1.0
Mass Lost:	[g]	113.9
Total Heat Evolved:	[kJ]	4211

Test Times [s]

Shutter Open:	183
Time to Ignition:	260
Flameout:	1127
Clean Air/End of Test:	1136

Daily C-Factor

0.050

The Peak, Average and Total parameters are computed over the test period ignition to flame out. There are 4 exceptions. The first three involve initial heat release rate averages for periods after ignition of 60, 180 and 300 seconds. The final involves the average mass loss rate which is computed over the time period from 10% mass loss to 90% mass loss.

Parameter	Unit	Value
Heat Release		
Peak Heat Release Rate	[kW/m^2]	1700
Average Heat Release Rate	[kW/m^2]	550
Total Heat Release	[MJ/m^2]	477
Average HRR for the first 60s	[kW/m^2]	105
Average HRR for the first 180s	[kW/m^2]	268
Average HRR for the first 300s	[kW/m^2]	361
Peak Heat of Combustion	[kJ/g]	678
Average Heat of Combustion	[kJ/g]	48
Smoke Obscuration		
Peak SEA	[m^2/g]	1.197
Average SEA	[m^2/g]	0.369
Peak Smoke Yield	[g/g]	0.141
Average Smoke Yield	[g/g]	0.043
Peak Smoke Production Rate	[m^2/s]	0.122
Average Smoke Production Rate	[m^2/s]	0.051
Total Smoke Release	[m^2]	48.584
Gas Production Rates		
Peak Carbon Monoxide	[g/s]	0.009
Average Carbon Monoxide	[g/s]	0.002
Peak Carbon Dioxide	[g/s]	4.333
Average Carbon Dioxide	[g/s]	1.292
Mass Loss		
Peak Mass Loss Rate	[g/s]	0.380
Average Mass Lass Rate	[g/s]	0.168
Initial Mass	[g]	117.1
Final Mass	[g]	3.1
Mass Loss Fraction	[]	0.97
Burn Time		
Time to Ignition	[s]	77
Duration of Flaming	[s]	867
Duration of Test	[s]	953

Observations

Time	Observation
	Replaced HEPA filter
	Replaced gas sample tubing from gas sample ring to cold trap
228	Trace amount of white smoke
237	A lot of white smoke
244, 251, 253	flashes
265	Surface boils, char on most of surface, surface liquidly with char bubbles
300	cellular turbulent flame cone
340	Liquid creeps down the frame sides
440	Char pieces pushed to edges and corners
540	Flame cringes above frame
	bright yellow flame with little white smoke
578	Droplet dripped
800	Flame outside of cone
867	Flame noted in the duct over the hood
950	A lot of flame outside of cone, heavy noise
990	Flame shrinks
1019	Flame becomes cellular, lots of black smoke, edge burning only
1053	White powder left on the foil
1075	Corner burning only
	Droplet mass at 5.6220 g

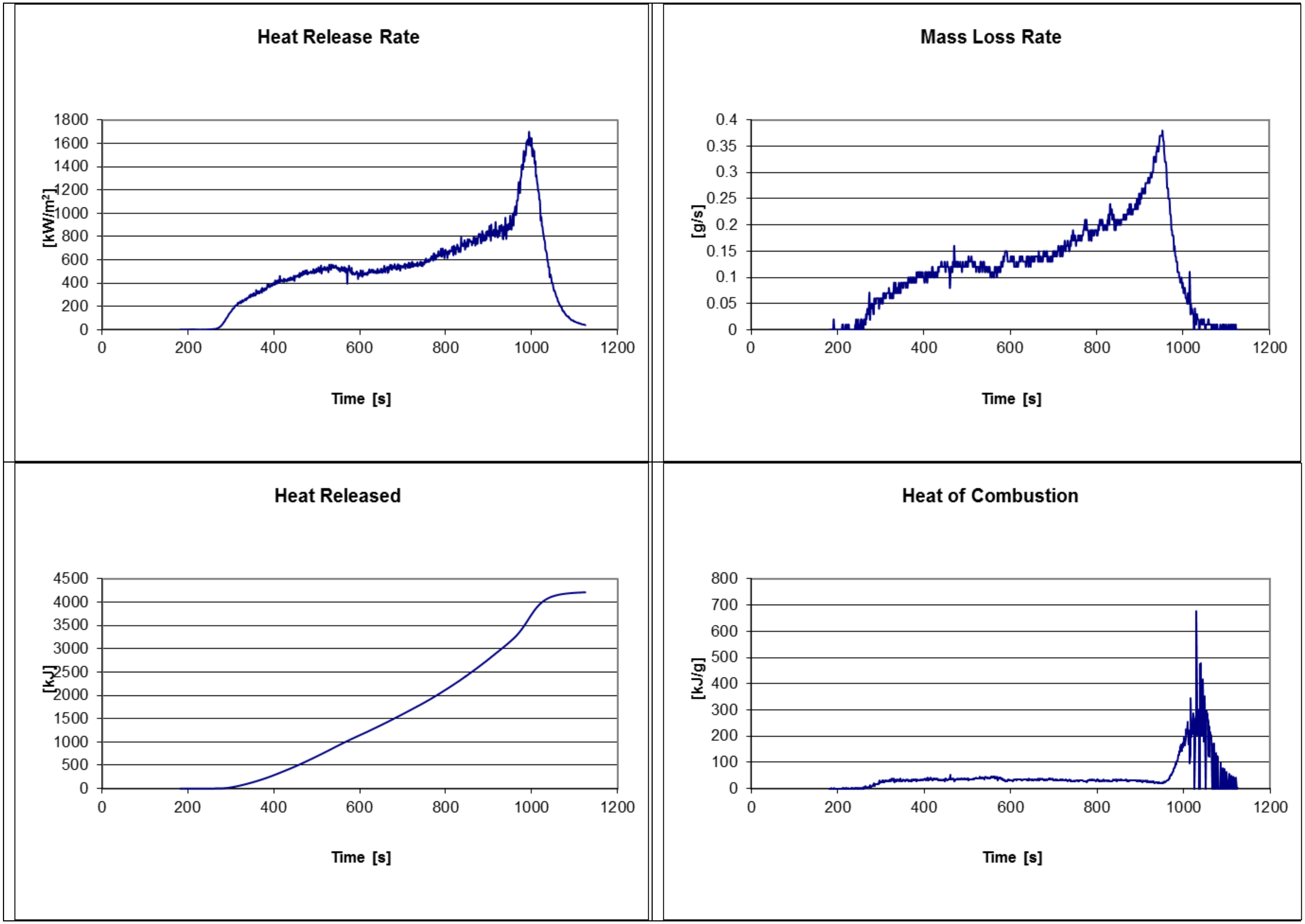
Heat Release Rate
[kW/m2]
1800
1600
1400
1200
1000
800
600
400
200
0
0
200
400
600
800
1000
1200
Time [s]
Mass Loss Rate
[g/s]
0.4
0.35
0.3
0.25
0.2
0.15
0.1
0.05
0
0
200
400
600
800
1000
1200
Time [s]
Heat Released
[kJ]
4500
4000
3500
3000
2500
2000
1500
1000
500
0
0
200
400
600
800
1000
1200
Time [s]
Heat of Combustion
[kJ/g]
800
700
600
500
400
300
200
100
0
0
200
400
600
800
1000
1200
Time [s]

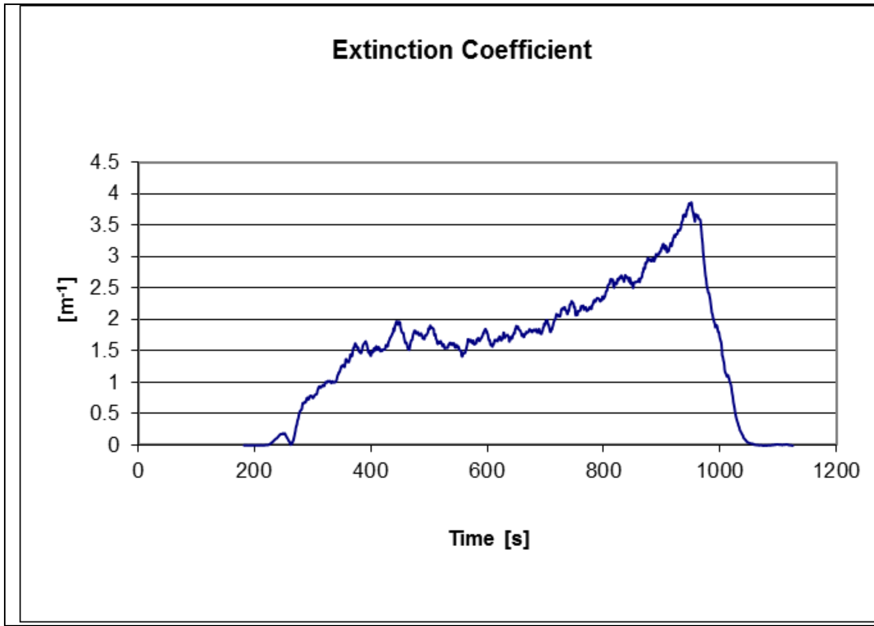
Extinction Coefficient
4.5
4
3.5
3
2.5
2
1.5
1
0.5
0
[m-1]
0
200
400
600
800
1000
1200
Time [s]

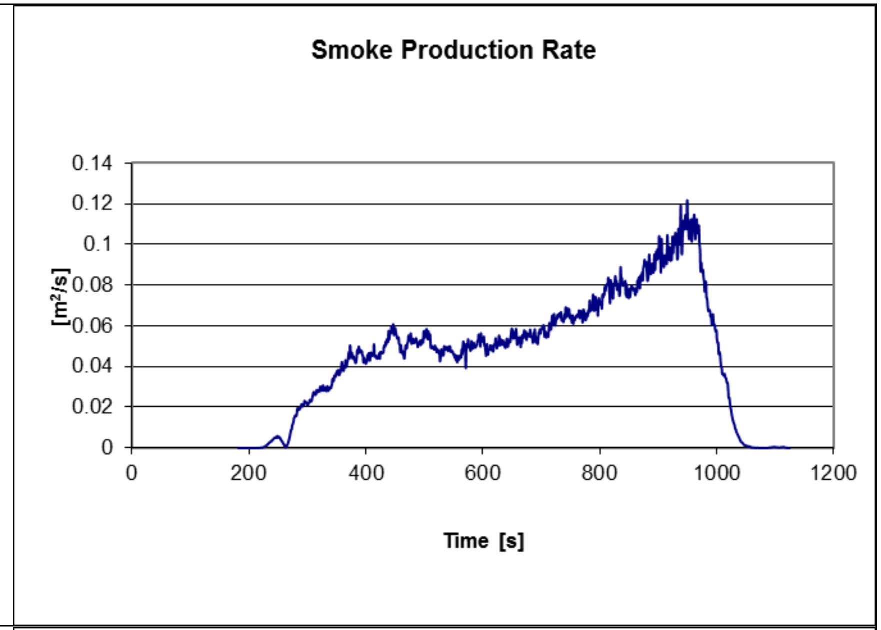
Smoke Production Rate
0.14
0.12
0.1
0.08
0.06
0.04
0.02
0
[m2/s]
0
200
400
600
800
1000
1200
Time [s]

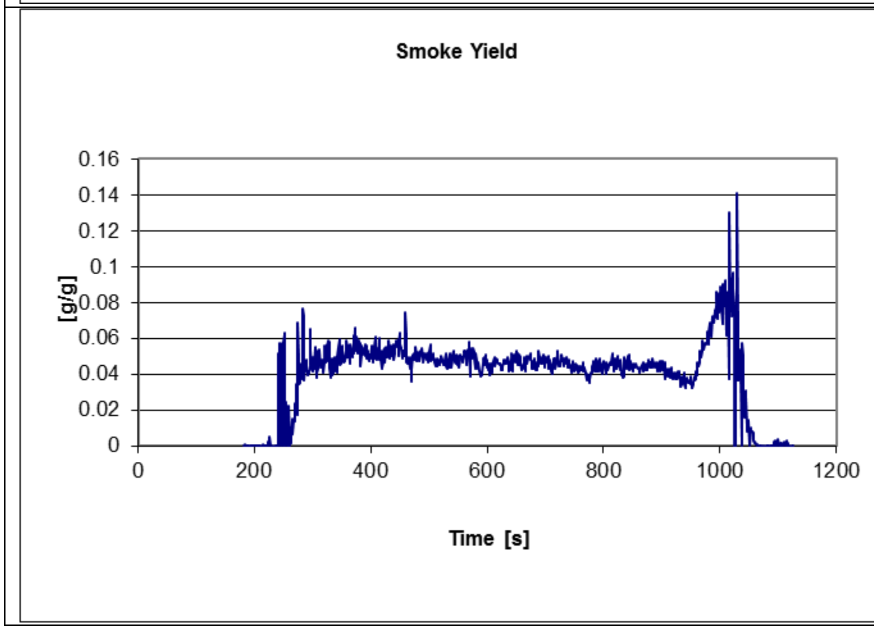
Smoke Yield
0.16
0.14
0.12
0.1
0.08
0.06
0.04
0.02
0
[g/g]
0
200
400
600
800
1000
1200
Time [s]

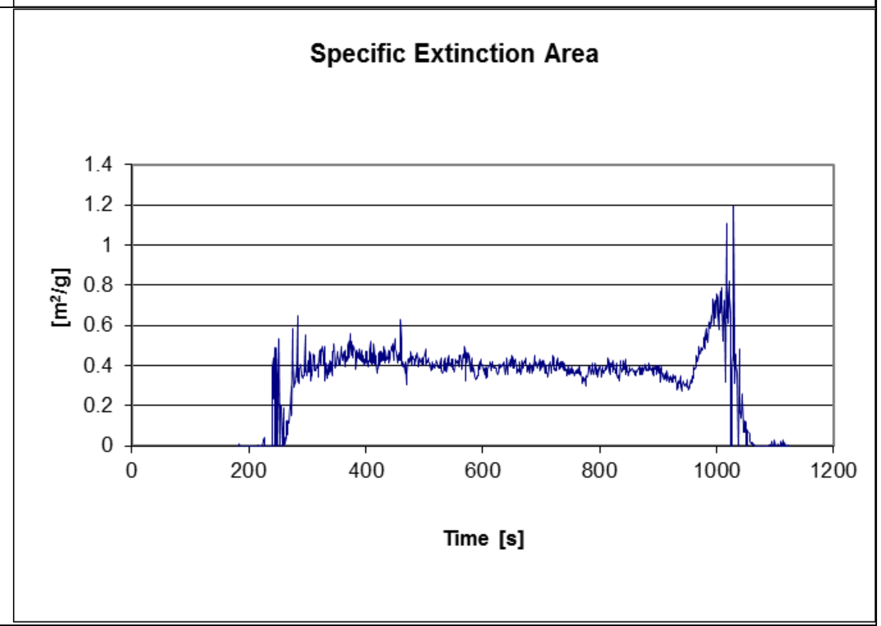
Specific Extinction Area
1.4
1.2
1
0.8
0.6
0.4
0.2
0
[m2/g]
0
200
400
600
800
1000
1200
Time [s]

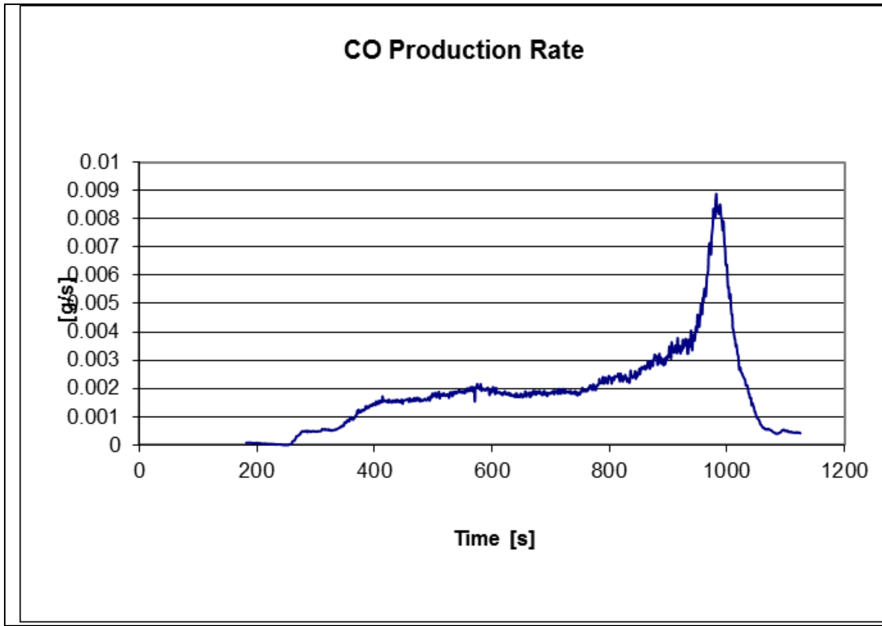
CO Production Rate
0.01
0.009
0.008
0.007
0.006
0.005
0.004
0.003
0.002
0.001
0
[g/s]
0
200
400
600
800
1000
1200
Time [s]

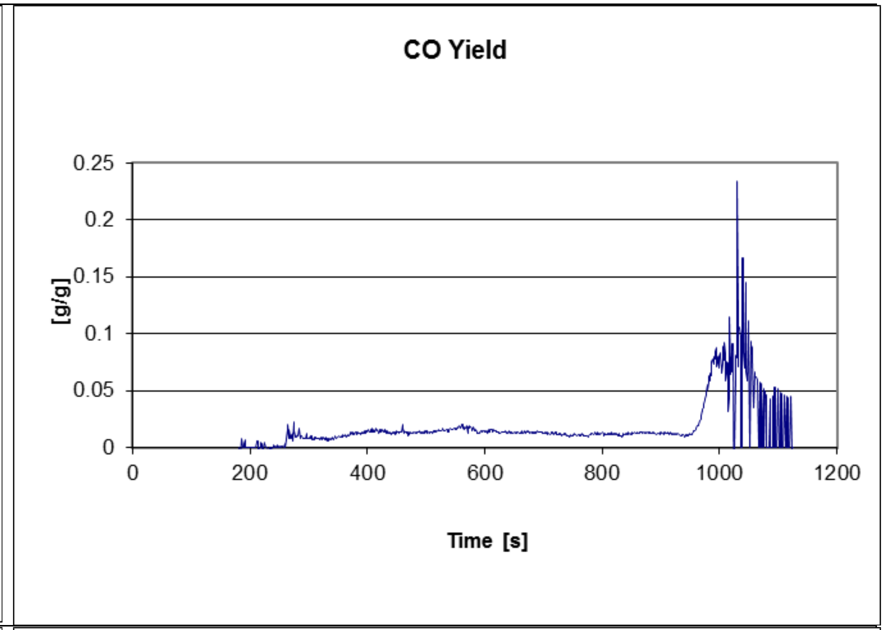
CO Yield
0.25
0.2
0.15
0.1
0.05
0
[g/g]
0
200
400
600
800
1000
1200
Time [s]

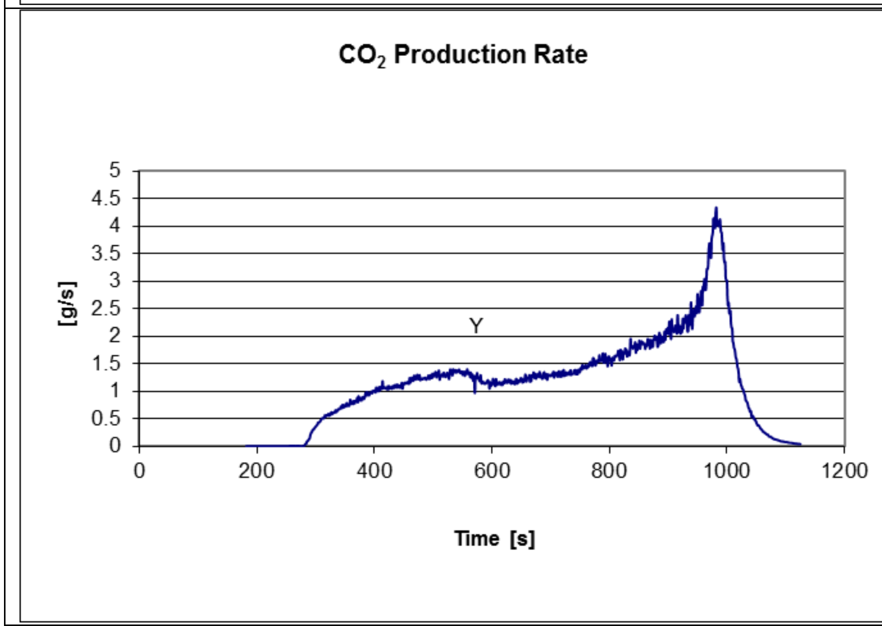
CO_2 Production Rate
5
4.5
4
3.5
3
2.5
2
1.5
1
0.5
0
[g/s]
Y
0
200
400
600
800
1000
1200
Time [s]

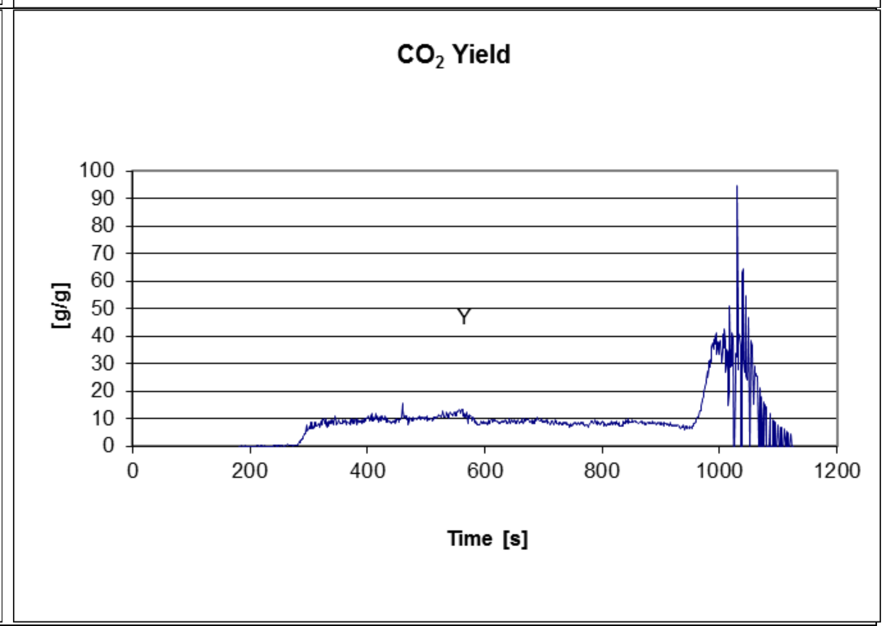
CO_2 Yield
100
90
80
70
60
50
40
30
20
10
0
[g/g]
Y
0
200
400
600
800
1000
1200
Time [s]

E.2 Thermoplastic Test 5 – White HDPE Sample 2

Cone Calorimeter Test Run Data

Dept. of Fire Protection Engineering

100 Institute Road
Worcester, MA 01609
Phone: (508) 831-5628
Fax: (508) 831-5862

Test Information

Test Number:	Test 05
Specimen Identification:	White High Density Polyethylene Sample 02
Material Name:	White HDPE 02
Manufacturer/Submitter:	Not Reported
Sample Description:	White half-inch thick panel, 4 TCs
Raw Data File Name:	Test_05_White_HDPE_02.txt
Reduced Data File Name:	Test_05_White_HDPE_02.xls
Date of Test:	6/30/2009
Tester:	Will Wong

Test Parameters

Ambient Temperature:	76	F
Relative Humidity:	49	%
Heat Flux:	50	kW/m^2
Exhaust Duct Flow Rate:		30 g/s
Orientation:		Horizontal
Specimen Holder:		TRUE
Specimen Preparation:		2 layer foil
Notes:		1" Separation

Specimen Information

Specimen Color:	[]	White
Specimen Thickness:	[mm]	12.3
Specimen Test Area:	[m^2]	0.0088
Specimen Initial Mass:	[g]	121.3
Specimen Final Mass:	[g]	13.2
Specimen Density:	[g/cm^3]	1.0
Mass Lost:	[g]	108.1
Total Heat Evolved:	[kJ]	4733

Test Times [s]

Shutter Open:	198
Time to Ignition:	289
Flameout:	1509
Clean Air/End of Test:	1523

Daily C-Factor		
		0.041

The Peak, Average and Total parameters are computed over the test period ignition to flame out. There are 4 exceptions. The first three involve initial heat release rate averages for periods after ignition of 60, 180 and 300 seconds. The final involves the average mass loss rate which is computed over the time period from 10% mass loss to 90% mass loss.

Parameter	Unit	Value
Heat Release		
Peak Heat Release Rate	[kW/m^2]	1462
Average Heat Release Rate	[kW/m^2]	439
Total Heat Release	[MJ/m^2]	536
Average HRR for the first 60s	[kW/m^2]	247
Average HRR for the first 180s	[kW/m^2]	369
Average HRR for the first 300s	[kW/m^2]	440
Peak Heat of Combustion	[kJ/g]	112
Average Heat of Combustion	[kJ/g]	30
Smoke Obscuration		
Peak SEA	[m^2/g]	0.513
Average SEA	[m^2/g]	0.125
Peak Smoke Yield	[g/g]	0.060
Average Smoke Yield	[g/g]	0.015
Peak Smoke Production Rate	[m^2/s]	0.055
Average Smoke Production Rate	[m^2/s]	0.017
Total Smoke Release	[m^2]	13.967
Gas Production Rates		
Peak Carbon Monoxide	[g/s]	0.006
Average Carbon Monoxide	[g/s]	0.002
Peak Carbon Dioxide	[g/s]	3.540
Average Carbon Dioxide	[g/s]	1.019
Mass Loss		
Peak Mass Loss Rate	[g/s]	1.240
Average Mass Lass Rate	[g/s]	0.163
Initial Mass	[g]	121.3
Final Mass	[g]	13.2
Mass Loss Fraction	[]	0.89
Burn Time		
Time to Ignition	[s]	91
Duration of Flaming	[s]	1220
Duration of Test	[s]	1325

Observations

Time	Observation
205	White smoke
260	Surface blackens
280	Bubbling starts
285	Real ignition
303	Bright yellow uniform flame cone, little smoke, surface boiling with
	some charred pieces
365	Surface TC sort of off the surface, but touching the pool
390	Some flame over frame
506	Droplet drips
540	Boiling over most of surface, some char remains afloat
650	1 embedded TC moved
700	Flame over whole surface
770	Some flame outside of cone
930	Lots of dripping at thermocouple location
1000	Lots of side burning
1030	Bottom foil visible
1070	Some pool burning on edge
1100	Flame more turbulent/cellular, more black smoke
1139	Edge burning only
1160	White/Black residue
	Droplet mass at 2.3751g

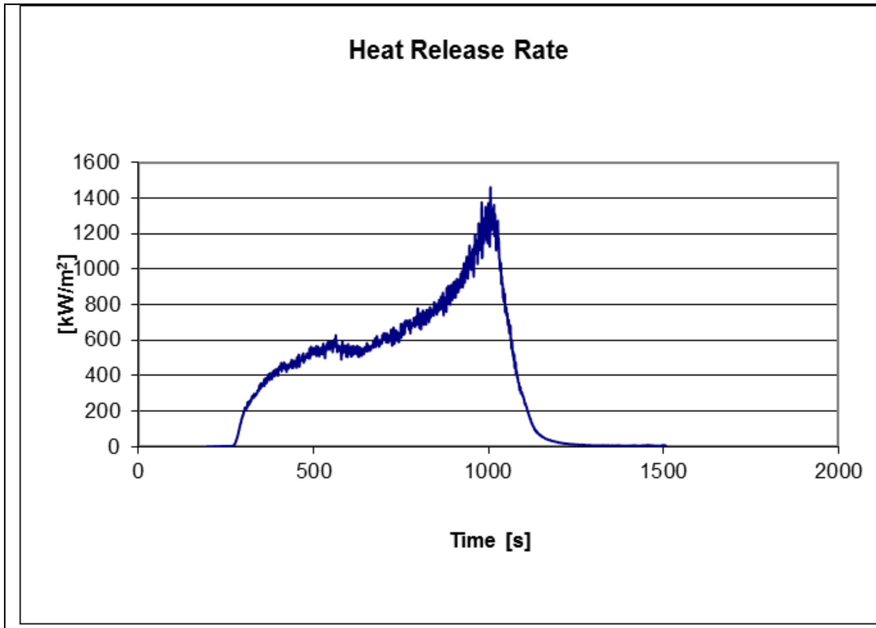
Heat Release Rate
[kW/m²]
1600
1400
1200
1000
800
600
400
200
0
0
500
1000
1500
2000
Time [s]

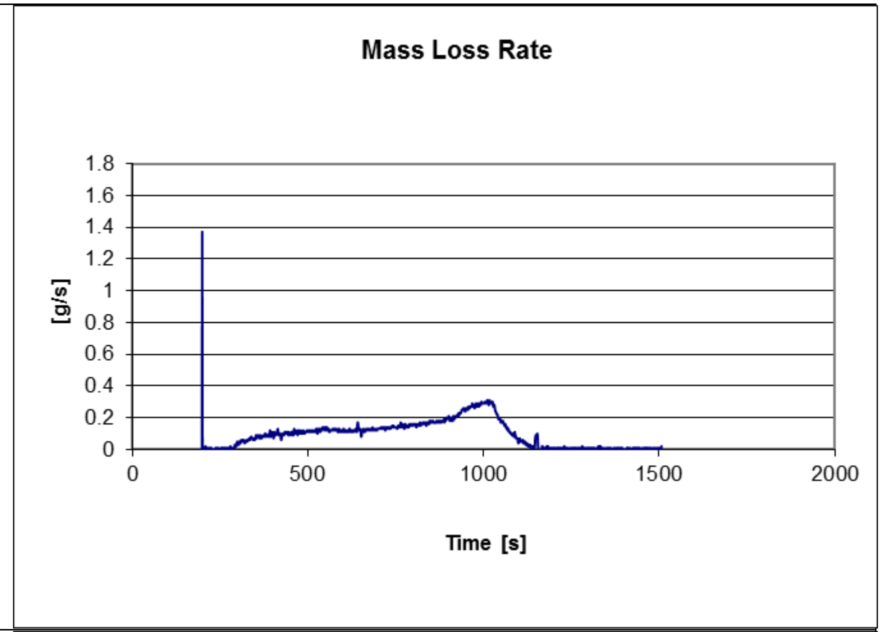
Mass Loss Rate
[g/s]
1.8
1.6
1.4
1.2
1
0.8
0.6
0.4
0.2
0
0
500
1000
1500
2000
Time [s]

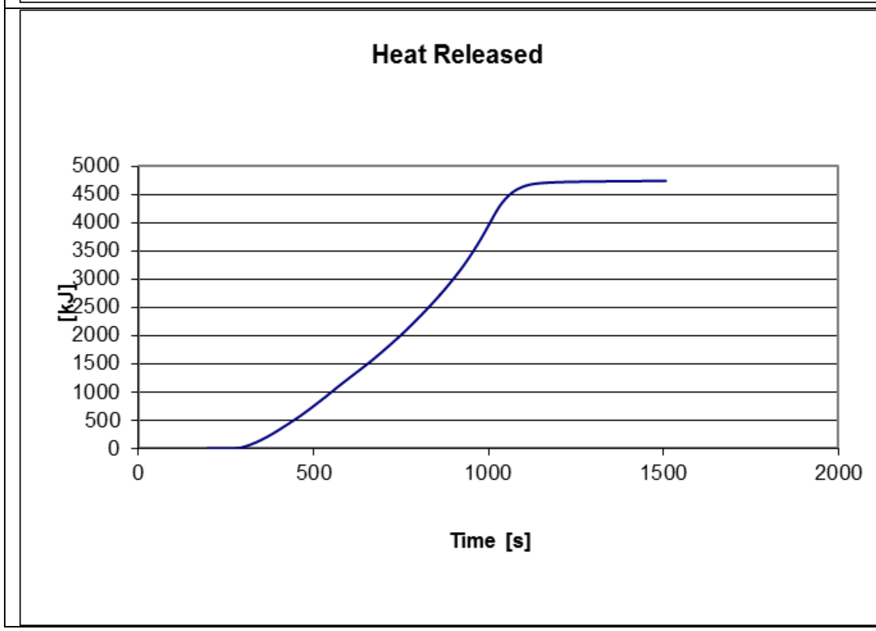
Heat Released
[kJ]
5000
4500
4000
3500
3000
2500
2000
1500
1000
500
0
0
500
1000
1500
2000
Time [s]

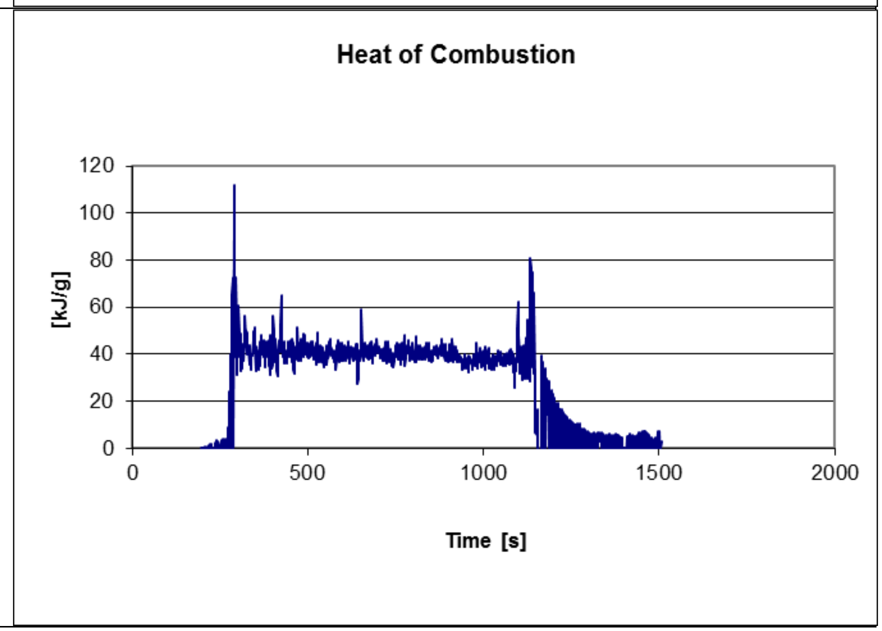
Heat of Combustion
[kJ/g]
120
100
80
60
40
20
0
0
500
1000
1500
2000
Time [s]

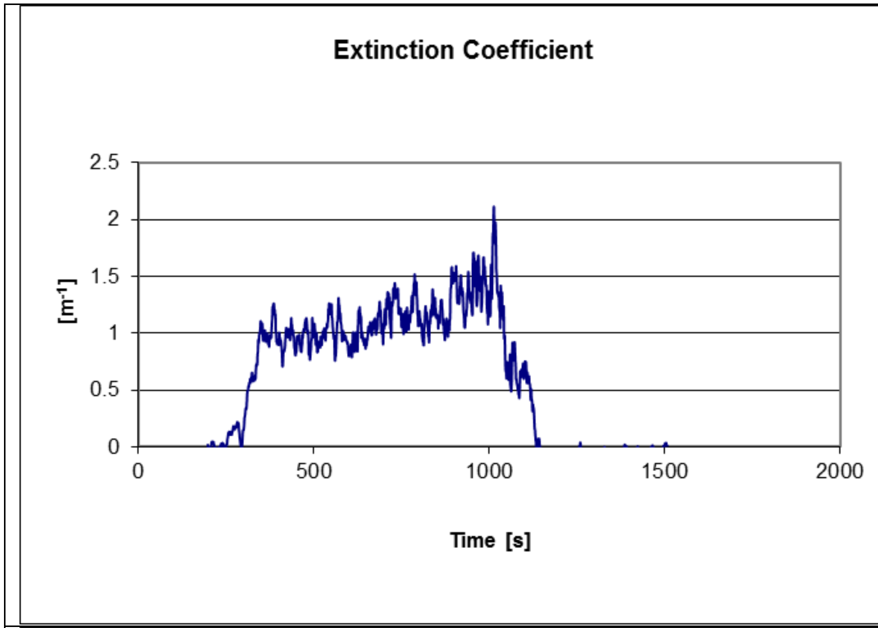
Extinction Coefficient
2.5
2
1.5
1
0.5
0
[m-1]
0
500
1000
1500
2000
Time [s]

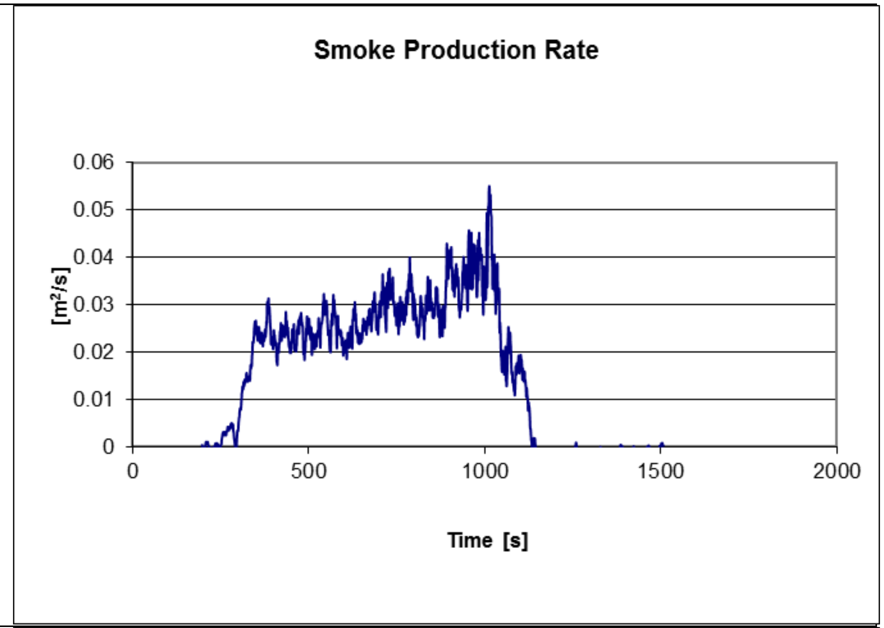
Smoke Production Rate
0.06
0.05
0.04
0.03
0.02
0.01
0
[m2/s]
0
500
1000
1500
2000
Time [s]

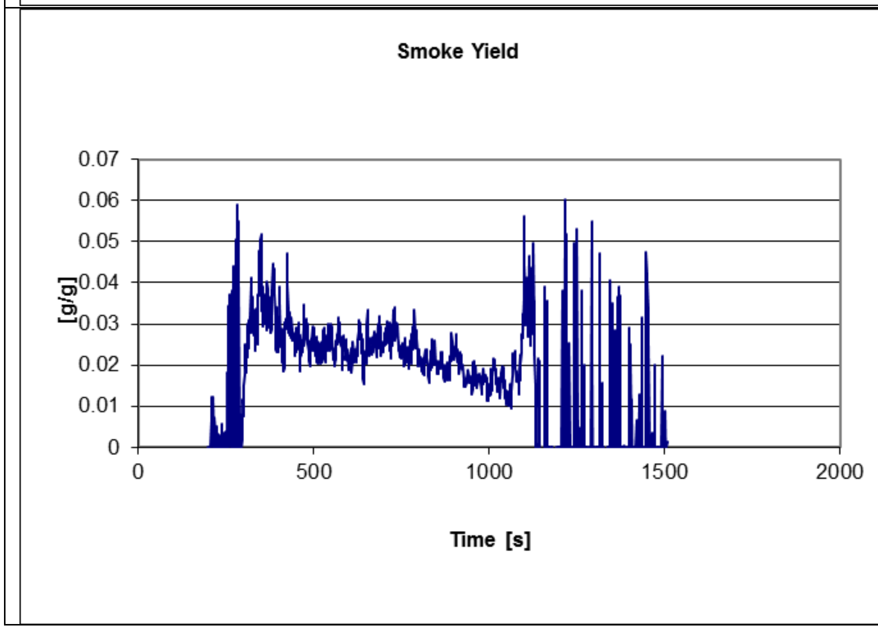
Smoke Yield
0.07
0.06
0.05
0.04
0.03
0.02
0.01
0
[g/g]
0
500
1000
1500
2000
Time [s]

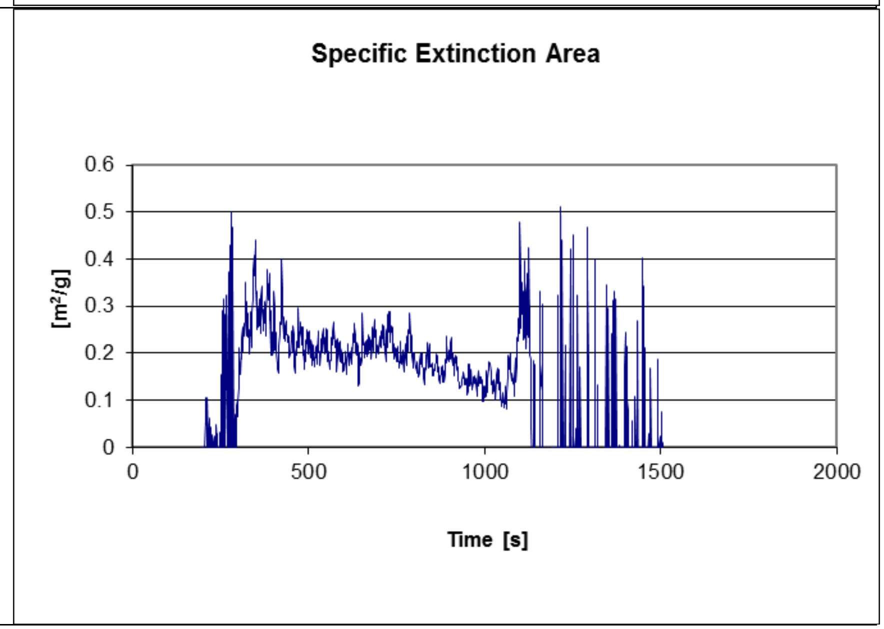
Specific Extinction Area
0.6
0.5
0.4
0.3
0.2
0.1
0
[m2/g]
0
500
1000
1500
2000
Time [s]

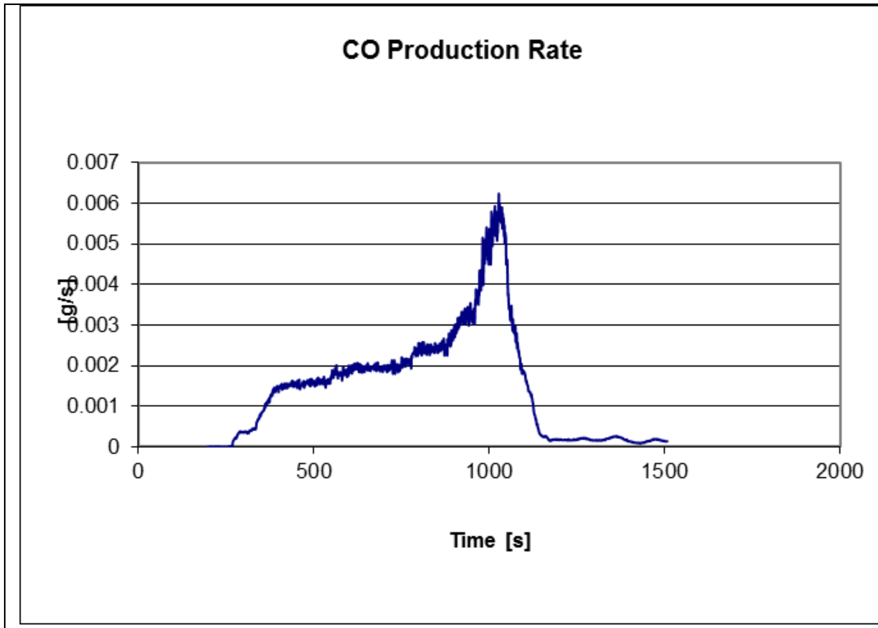

CO Production Rate
0.007
0.006
0.005
0.004
0.003
0.002
0.001
0
[g/s]
0
500
1000
1500
2000
Time [s]

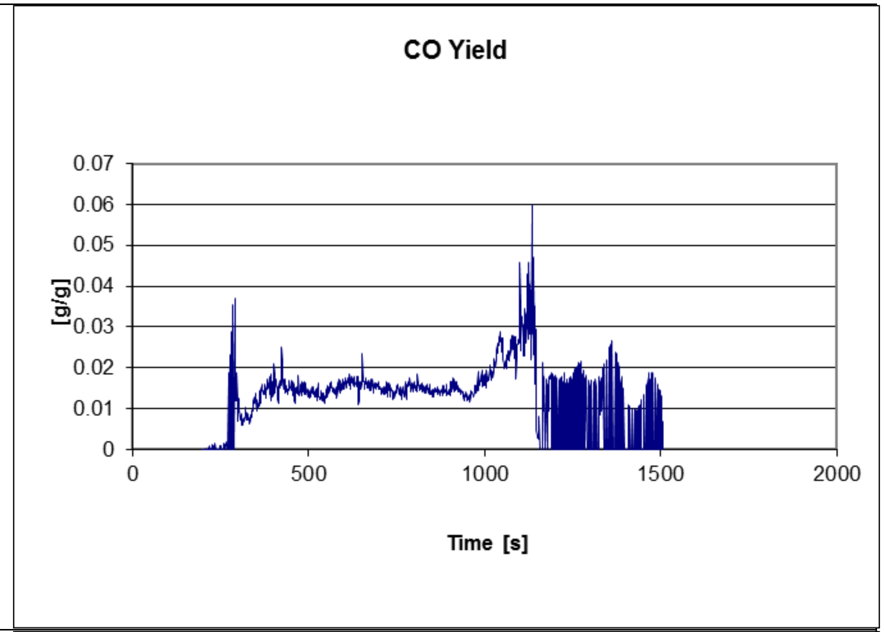

CO Yield
0.07
0.06
0.05
0.04
0.03
0.02
0.01
0
[g/g]
0
500
1000
1500
2000
Time [s]

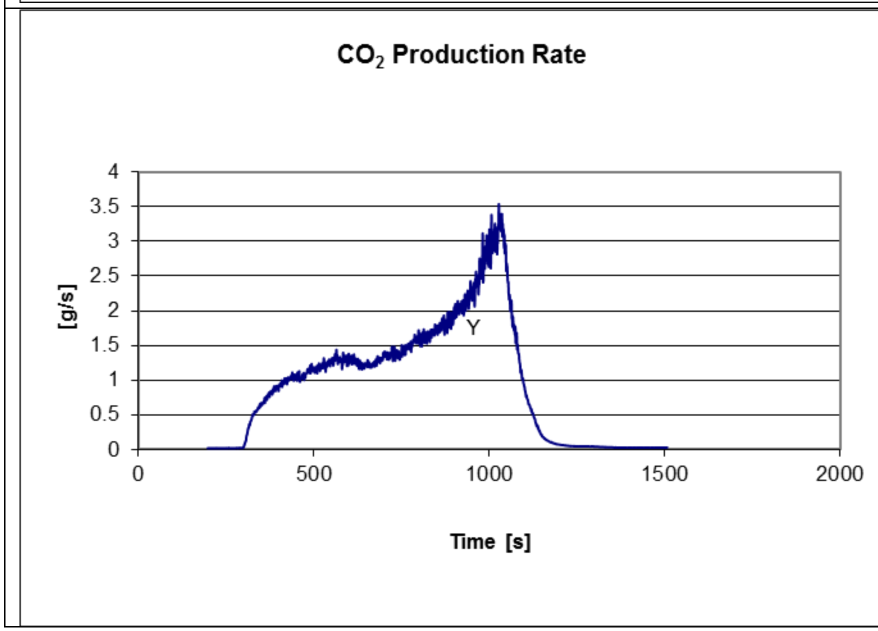

CO2 Production Rate
4
3.5
3
2.5
2
1.5
1
0.5
0
[g/s]
Y
0
500
1000
1500
2000
Time [s]

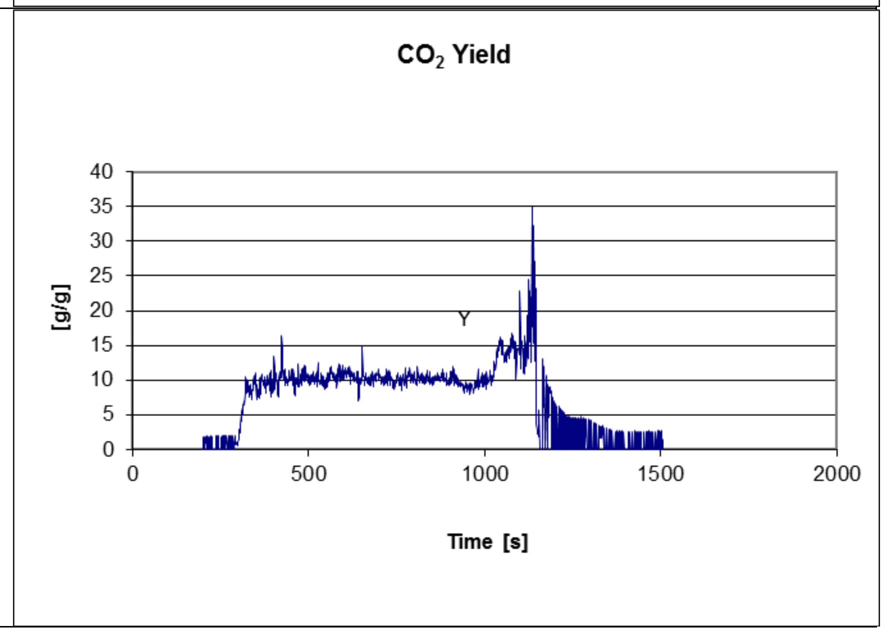

CO2 Yield
40
35
30
25
20
15
10
5
0
[g/g]
Y
0
500
1000
1500
2000
Time [s]

TC Locations

	Depth from side		Height from bottom
1	40mm	←	8.5mm
2	40.5mm	←	2.5mm

From Left Side

101mm

50.5mm	x 1
50mm	x 2

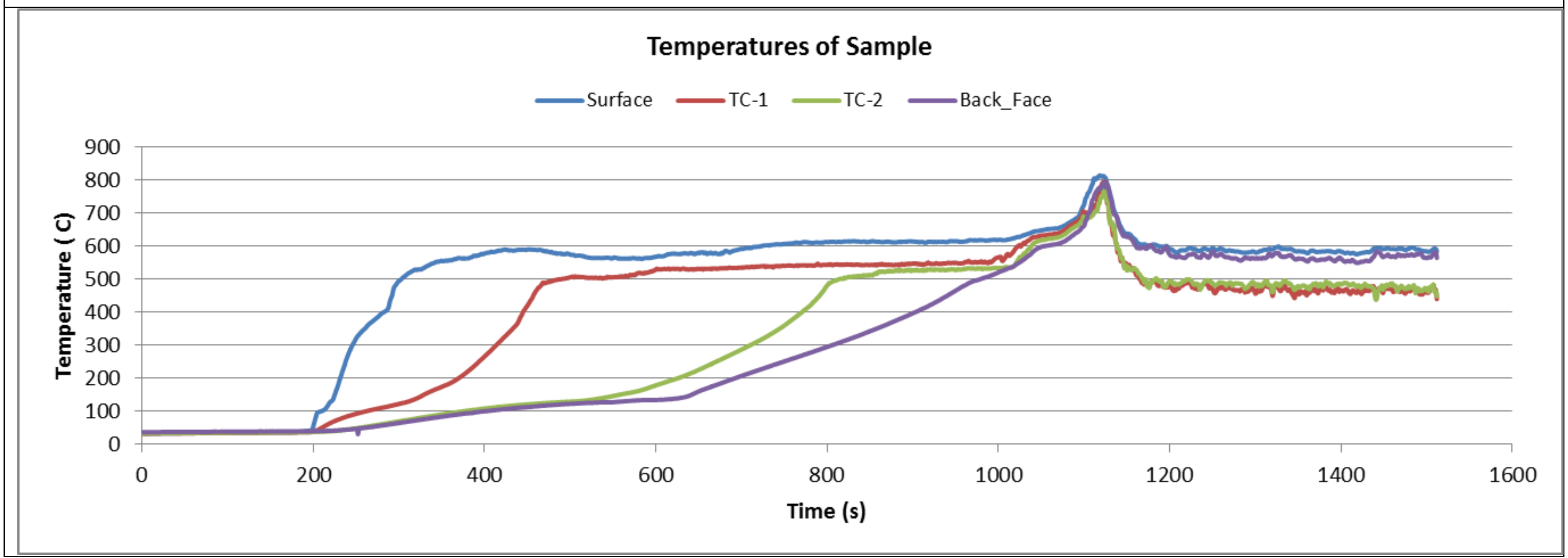

E.3 Thermoplastic Test 4 – White HDPE Sample 3

Cone Calorimeter Test Run Data

Dept. of Fire Protection Engineering

100 Institute Road
Worcester, MA 01609
Phone: (508) 831-5628
Fax: (508) 831-5862

Test Information

Test Number:	Test 04
Specimen Identification:	White High Density Polyethylene Sample 03
Material Name:	White HDPE 03
Manufacturer/Submitter:	Not Reported
Sample Description:	White half-inch thick panel, 4 TCs
Raw Data File Name:	Test_04_White_HDPE_03.txt
Reduced Data File Name:	Test_04_White_HDPE_03.xls
Date of Test:	6/30/2009
Tester:	Will Wong

Test Parameters

Ambient Temperature:	74	F
Relative Humidity:	50	%
Heat Flux:	50	kW/m^2
Exhaust Duct Flow Rate:		30 g/s
Orientation:		Horizontal
Specimen Holder:		TRUE
Specimen Preparation:		2 layer foil
Notes:		1" Separation

Specimen Information

Specimen Color:	[]	White
Specimen Thickness:	[mm]	12.3
Specimen Test Area:	[m^2]	0.0088
Specimen Initial Mass:	[g]	121.2
Specimen Final Mass:	[g]	-2.4
Specimen Density:	[g/cm^3]	1.0
Mass Lost:	[g]	123.6
Total Heat Evolved:	[kJ]	4740

Test Times [s]

Shutter Open:	186
Time to Ignition:	283
Flameout:	1190
Clean Air/End of Test:	1200

Daily C-Factor

	0.041

The Peak, Average and Total parameters are computed over the test period ignition to flame out. There are 4 exceptions. The first three involve initial heat release rate averages for periods after ignition of 60, 180 and 300 seconds. The final involves the average mass loss rate which is computed over the time period from 10% mass loss to 90% mass loss.

Parameter	Unit	Value
Heat Release		
Peak Heat Release Rate	[kW/m^2]	1490
Average Heat Release Rate	[kW/m^2]	592
Total Heat Release	[MJ/m^2]	536
Average HRR for the first 60s	[kW/m^2]	301
Average HRR for the first 180s	[kW/m^2]	409
Average HRR for the first 300s	[kW/m^2]	473
Peak Heat of Combustion	[kJ/g]	97
Average Heat of Combustion	[kJ/g]	37
Smoke Obscuration		
Peak SEA	[m^2/g]	0.401
Average SEA	[m^2/g]	0.144
Peak Smoke Yield	[g/g]	0.047
Average Smoke Yield	[g/g]	0.017
Peak Smoke Production Rate	[m^2/s]	0.051
Average Smoke Production Rate	[m^2/s]	0.023
Total Smoke Release	[m^2]	17.520
Gas Production Rates		
Peak Carbon Monoxide	[g/s]	0.006
Average Carbon Monoxide	[g/s]	0.002
Peak Carbon Dioxide	[g/s]	3.266
Average Carbon Dioxide	[g/s]	1.312
Mass Loss		
Peak Mass Loss Rate	[g/s]	0.580
Average Mass Lass Rate	[g/s]	0.167
Initial Mass	[g]	121.2
Final Mass	[g]	-2.4
Mass Loss Fraction	[]	1.02
Burn Time		
Time to Ignition	[s]	97
Duration of Flaming	[s]	907
Duration of Test	[s]	1014

Observations

Time	Observation
190	White Smoke
210	Surface with big bubble
250	Char on surface is black
265	Flame flash
279	Ignition, real time
306	Big bubbles boiling over whole surface
357	Surface TC still "touching" surface
400	1 TC from depth sticking out over the top of sample, about 1.5 cm
460	Surface boiling, less char than before
502	flame is bright yellow, tall, little black smoke
561	Surface TC still near surface
607	One droplet
775	Flame is over frame
825	Surface TC still near surface, but surrounded by char pieces
849	Some flame outside of cone
890	Melted material on sides of frame
935	Lots of dripping on side of frame
960	Big flame outside of cone
1015	Bottom of tin foil can be seen
1051	Almost no material left, flame is dark yellow, smaller
1097	Edge burning only
1112	White/black powdery residue noted
1140	one flamelet on edge
	Droplet mass at 2.0662g
	Post fire analysis Some thermal compound is found between TC and surface of the sample

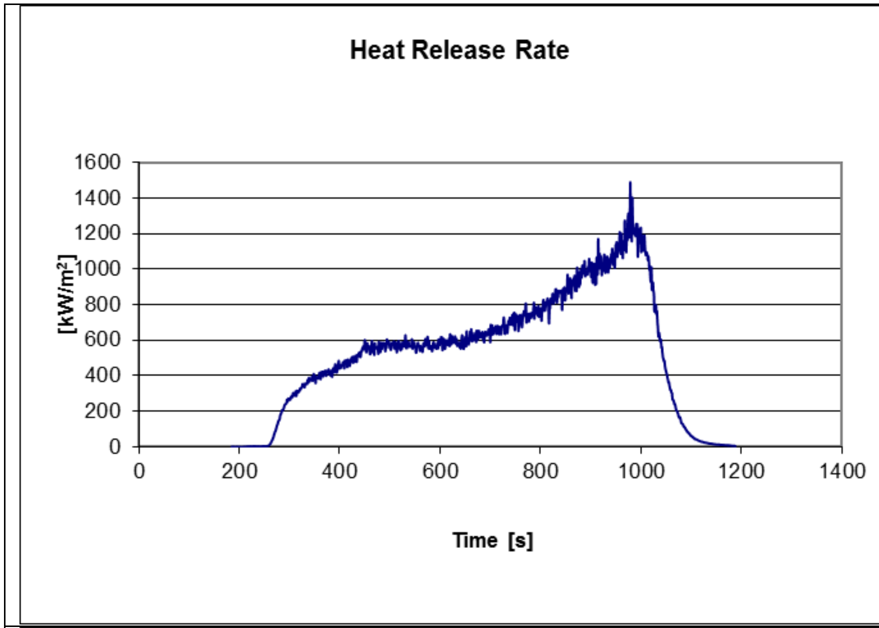
Heat Release Rate
[kW/m2]
1600
1400
1200
1000
800
600
400
200
0
0
200
400
600
800
1000
1200
1400
Time [s]

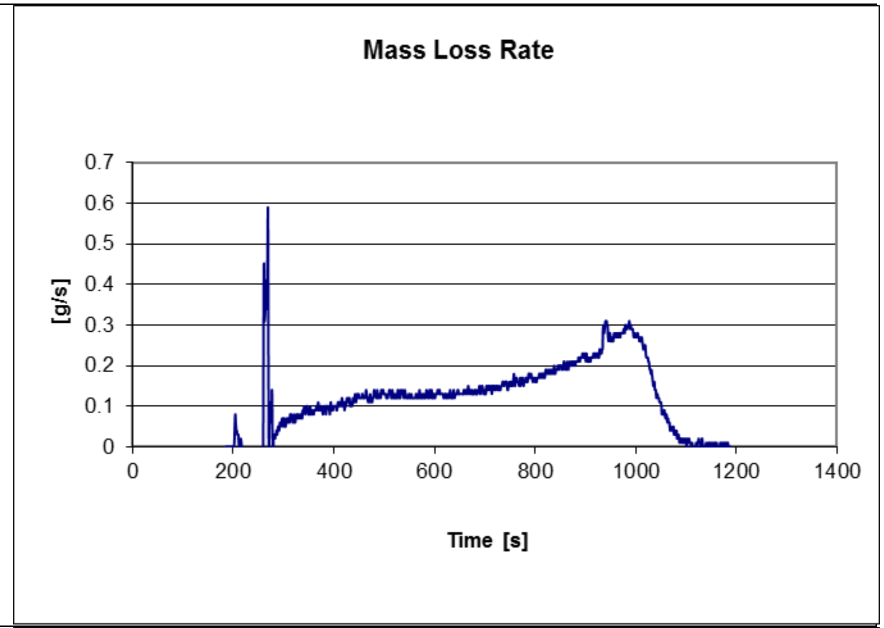
Mass Loss Rate
[g/s]
0.7
0.6
0.5
0.4
0.3
0.2
0.1
0
0
200
400
600
800
1000
1200
1400
Time [s]

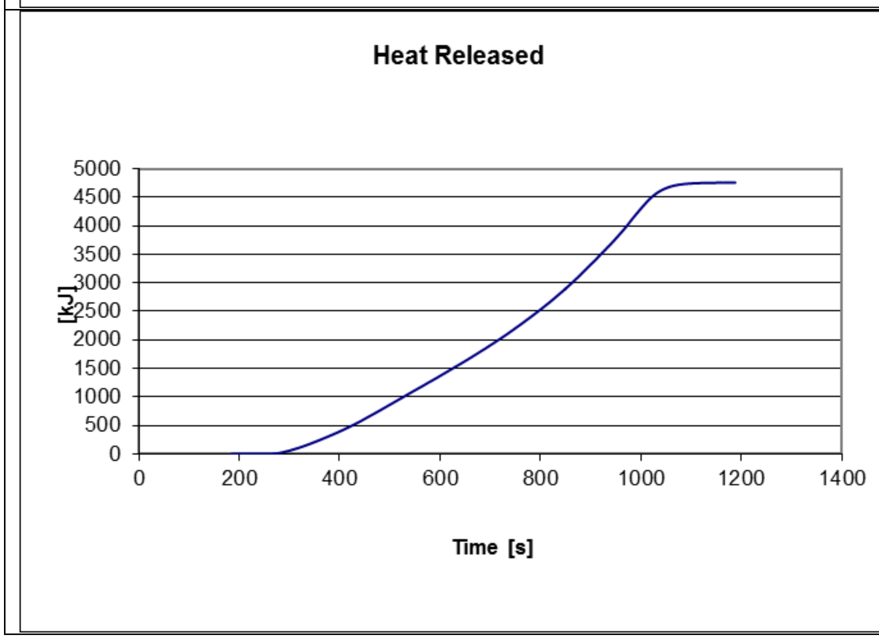
Heat Released
[kJ]
5000
4500
4000
3500
3000
2500
2000
1500
1000
500
0
0
200
400
600
800
1000
1200
1400
Time [s]

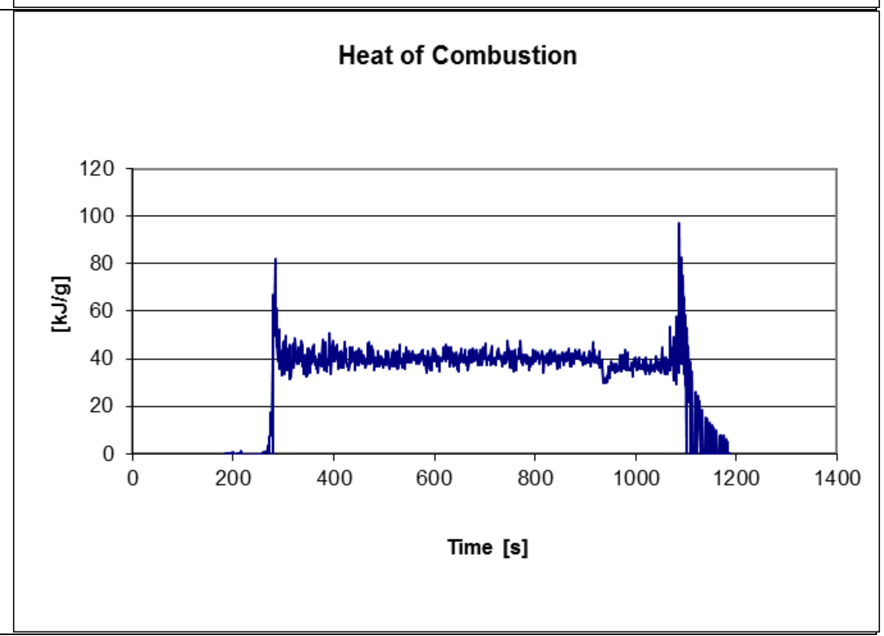
Heat of Combustion
[kJ/g]
120
100
80
60
40
20
0
0
200
400
600
800
1000
1200
1400
Time [s]

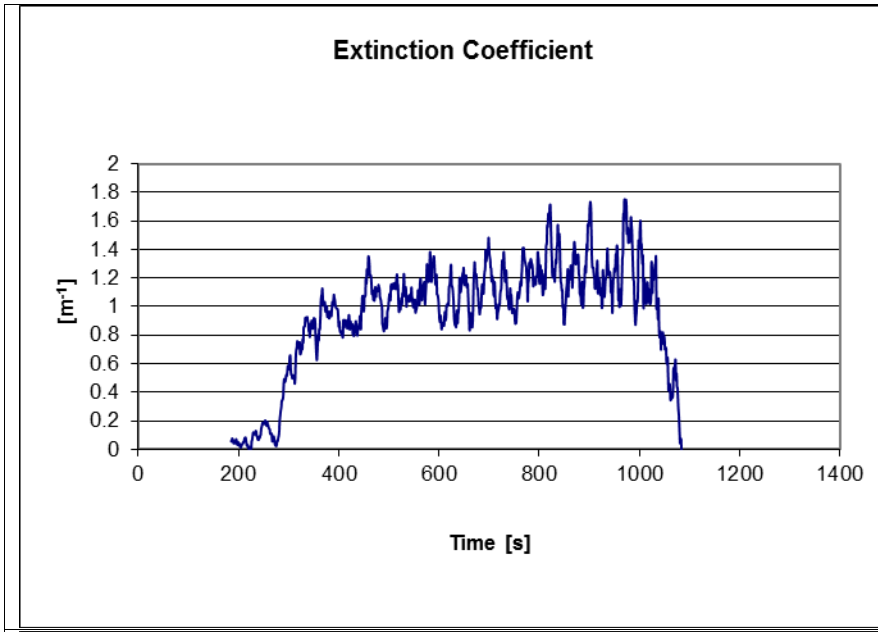
Extinction Coefficient
[m-1]
2
1.8
1.6
1.4
1.2
1
0.8
0.6
0.4
0.2
0
0
200
400
600
800
1000
1200
1400
Time [s]

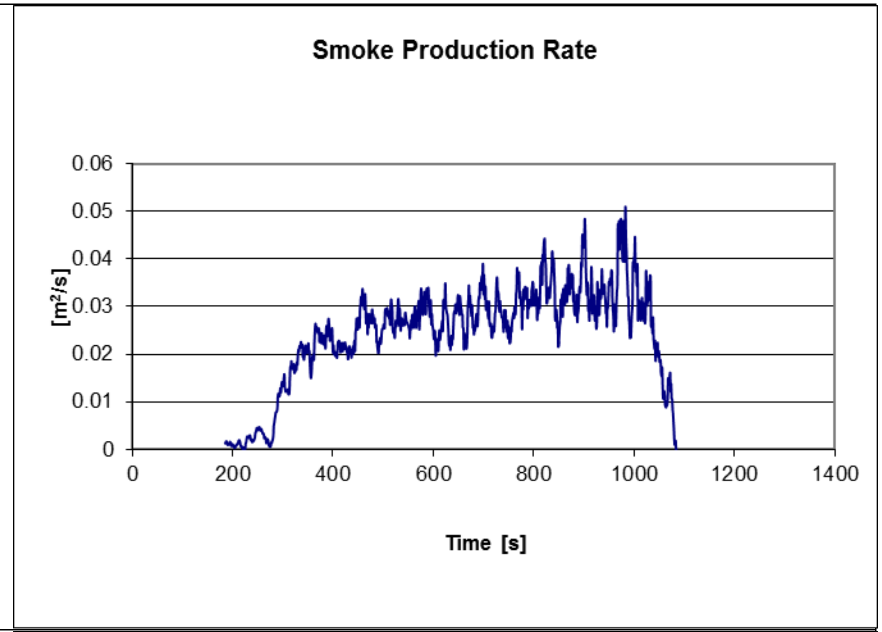
Smoke Production Rate
[m2/s]
0.06
0.05
0.04
0.03
0.02
0.01
0
0
200
400
600
800
1000
1200
1400
Time [s]

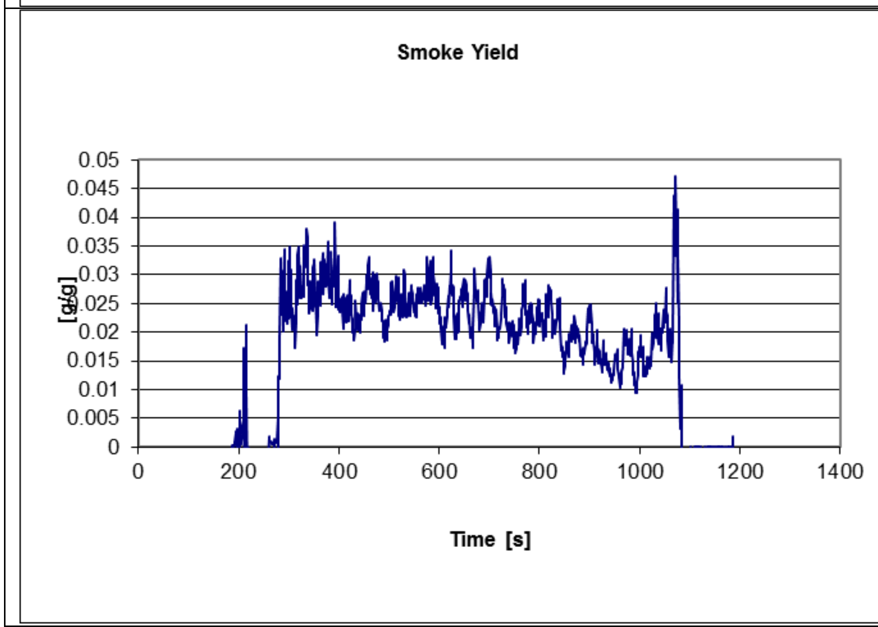
Smoke Yield
[g/g]
0.05
0.045
0.04
0.035
0.03
0.025
0.02
0.015
0.01
0.005
0
0
200
400
600
800
1000
1200
1400
Time [s]

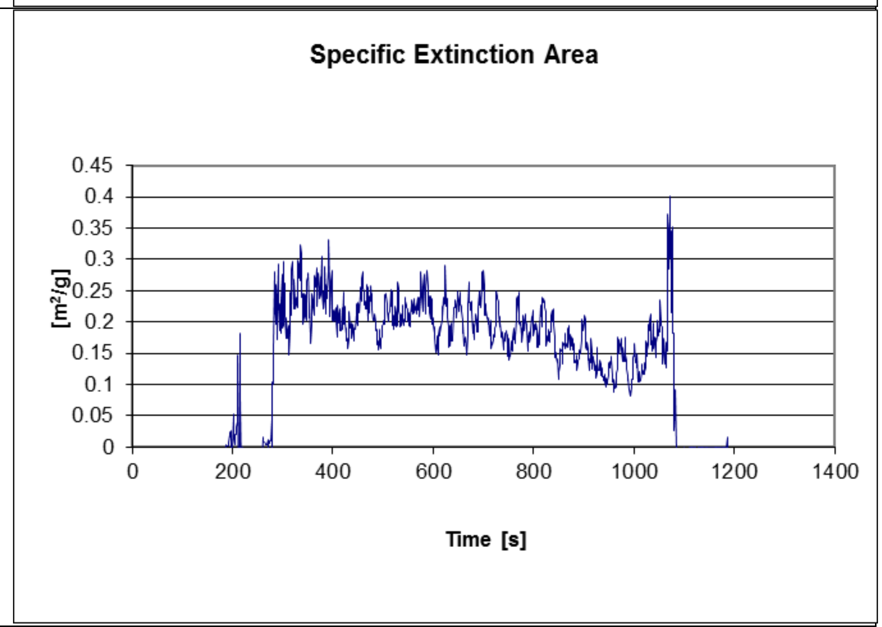
Specific Extinction Area
[m2/g]
0.45
0.4
0.35
0.3
0.25
0.2
0.15
0.1
0.05
0
0
200
400
600
800
1000
1200
1400
Time [s]

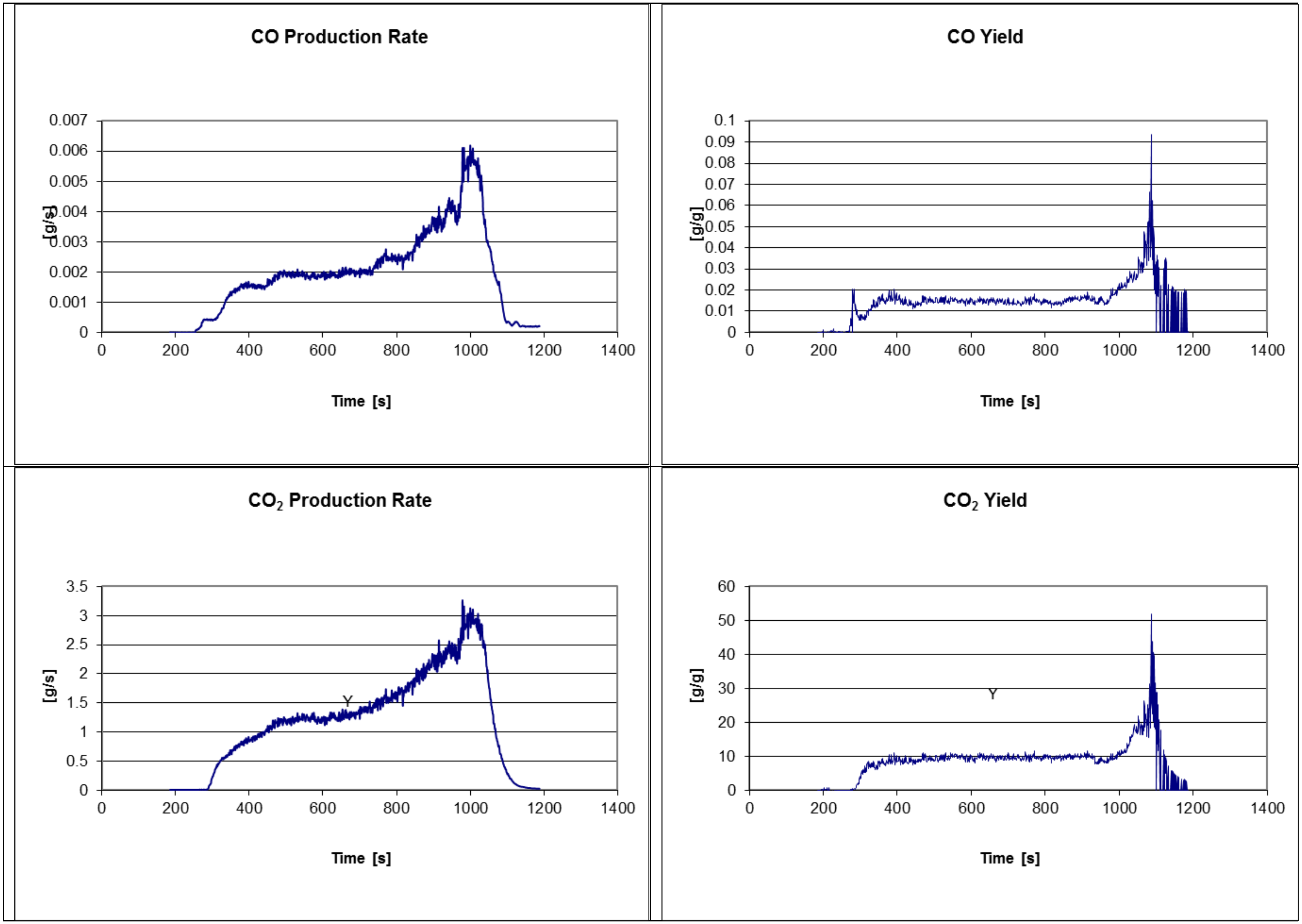

CO Production Rate
[g/s]
Time [s]
CO Yield
[g/g]
Time [s]
CO_2 Production Rate
[g/s]
Time [s]
CO_2 Yield
[g/g]
Time [s]

TC Locations

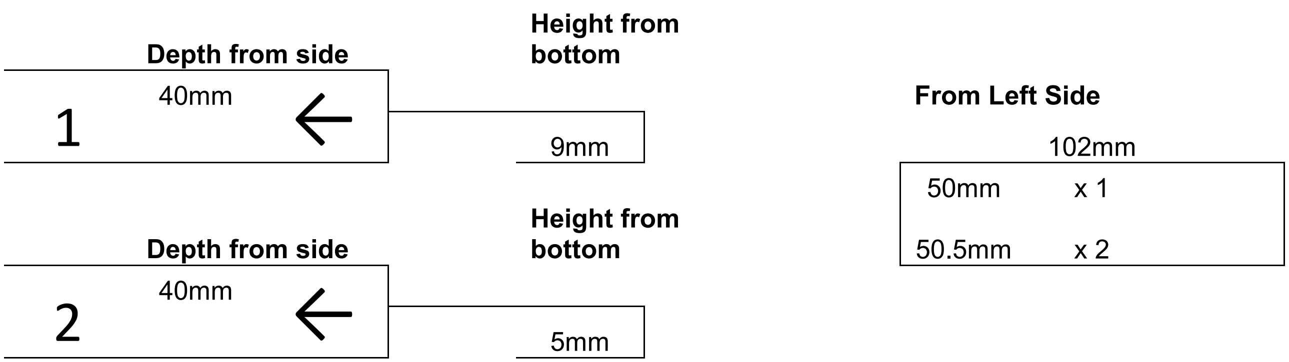

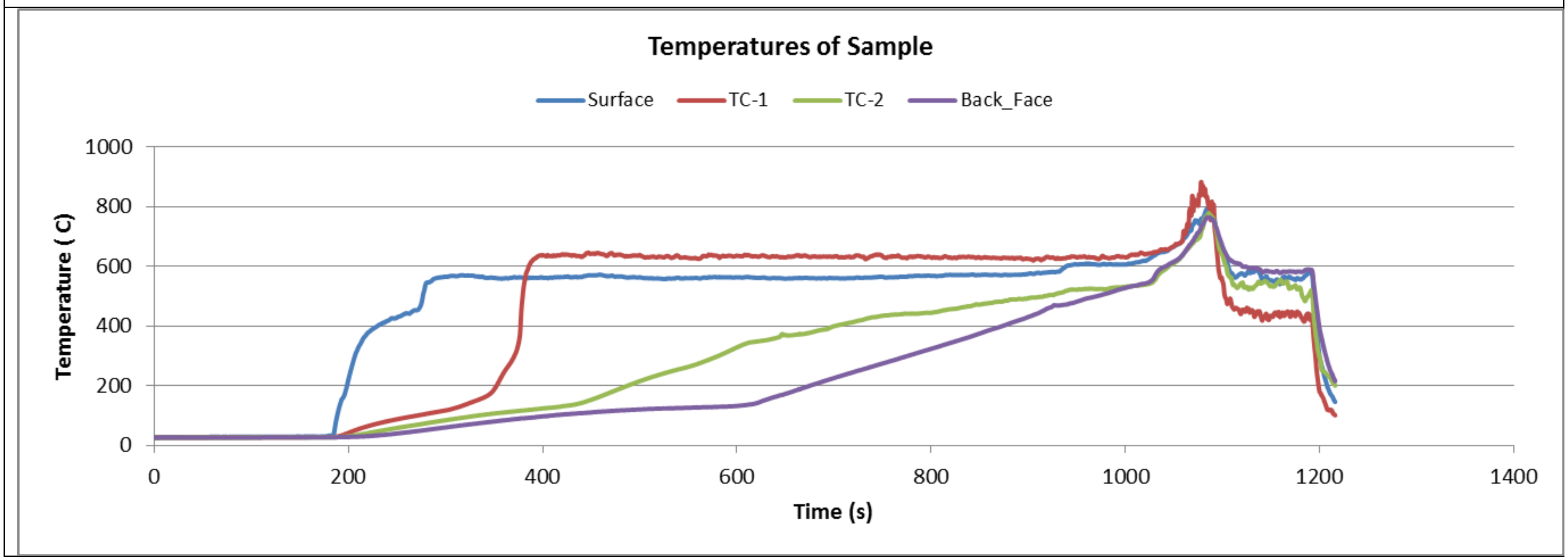

E.4 Thermoplastic Test 2 – Polypropylene Sample 1

Cone Calorimeter Test Run Data

Dept. of Fire Protection Engineering

100 Institute Road
Worcester, MA 01609
Phone: (508) 831-5628
Fax: (508) 831-5862

Test Information

Test Number:	Test 02A
Specimen Identification:	Black Polypropylene 01A
Material Name:	Polypropylene 01A
Manufacturer/Submitter:	Not Reported
Sample Description:	Black half-inch thick panel, no TCs
Raw Data File Name:	Test_02A_PolyP_01A.txt
Reduced Data File Name:	Test_02A_PolyP_01A.xls
Date of Test:	6/18/2009
Tester:	Will Wong

Test Parameters

Ambient Temperature:	74	F
Relative Humidity:	41	%
Heat Flux:	50	kW/m^2
Exhaust Duct Flow Rate:		30 g/s
Orientation:		Horizontal
Specimen Holder:		TRUE
Specimen Preparation:		2 layer foil
Notes:		1" Separation

Specimen Information

Specimen Color:	[]	Black
Specimen Thickness:	[mm]	12.3
Specimen Test Area:	[m^2]	0.0088
Specimen Initial Mass:	[g]	115.4
Specimen Final Mass:	[g]	3.4
Specimen Density:	[g/cm^3]	0.9
Mass Lost:	[g]	112.0
Total Heat Evolved:	[kJ]	4497

Test Times [s]

Shutter Open:	183
Time to Ignition:	205
Flameout:	1393
Clean Air/End of Test:	1406

Daily C-Factor

	0.050

The Peak, Average and Total parameters are computed over the test period ignition to flame out. There are 4 exceptions. The first three involve initial heat release rate averages for periods after ignition of 60, 180 and 300 seconds. The final involves the average mass loss rate which is computed over the time period from 10% mass loss to 90% mass loss.

Parameter	Unit	Value
Heat Release		
Peak Heat Release Rate	[kW/m^2]	751
Average Heat Release Rate	[kW/m^2]	428
Total Heat Release	[MJ/m^2]	509
Average HRR for the first 60s	[kW/m^2]	287
Average HRR for the first 180s	[kW/m^2]	426
Average HRR for the first 300s	[kW/m^2]	462
Peak Heat of Combustion	[kJ/g]	152
Average Heat of Combustion	[kJ/g]	43
Smoke Obscuration		
Peak SEA	[m^2/g]	1.543
Average SEA	[m^2/g]	0.576
Peak Smoke Yield	[g/g]	0.182
Average Smoke Yield	[g/g]	0.068
Peak Smoke Production Rate	[m^2/s]	0.114
Average Smoke Production Rate	[m^2/s]	0.062
Total Smoke Release	[m^2]	78.067
Gas Production Rates		
Peak Carbon Monoxide	[g/s]	0.004
Average Carbon Monoxide	[g/s]	0.002
Peak Carbon Dioxide	[g/s]	1.622
Average Carbon Dioxide	[g/s]	0.884
Mass Loss		
Peak Mass Loss Rate	[g/s]	0.170
Average Mass Lass Rate	[g/s]	0.130
Initial Mass	[g]	115.4
Final Mass	[g]	3.4
Mass Loss Fraction	[]	0.97
Burn Time		
Time to Ignition	[s]	22
Duration of Flaming	[s]	1188
Duration of Test	[s]	1223

Observations

Time	Observation
197	Smoke
197-205	Series of flashes
220	Black smoke, yellow/orange flame
240	Boiling surface/bubbling
367	Most of surface charred, bumpy
550	Smoke out of hood
715	Most of boiling occuring at edges, some in between the bumps over the surface
755	Center rose up, small popping noises, then center sunken
990	Flame cone becomes more turbulent, shrinks
1115	Mostly edge burning only, cellular flames, surface bumpy, mostly char left
1286	Corner burning only, smoke is black, remaining residue is black, but white near center
	Droplet mass at 0.0191g

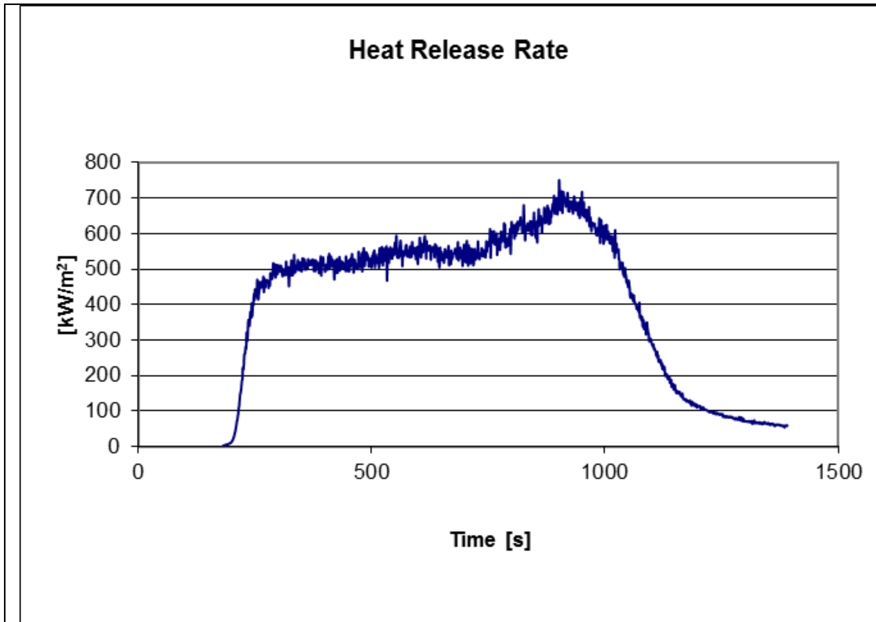

Heat Release Rate
800
700
600
500
400
300
200
100
0
[kW/m²]
0
500
1000
1500
Time [s]

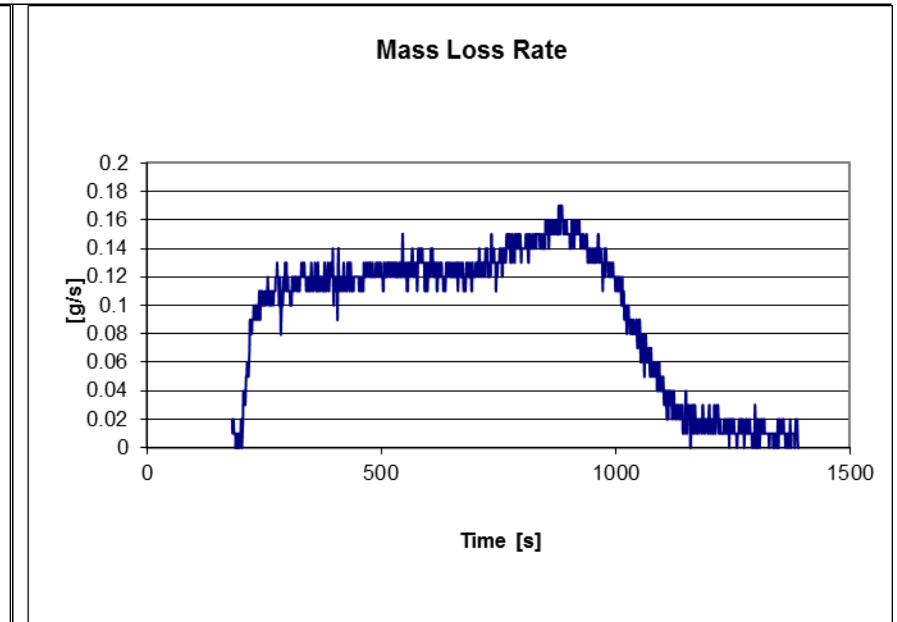

Mass Loss Rate
0.2
0.18
0.16
0.14
0.12
0.1
0.08
0.06
0.04
0.02
0
[g/s]
0
500
1000
1500
Time [s]

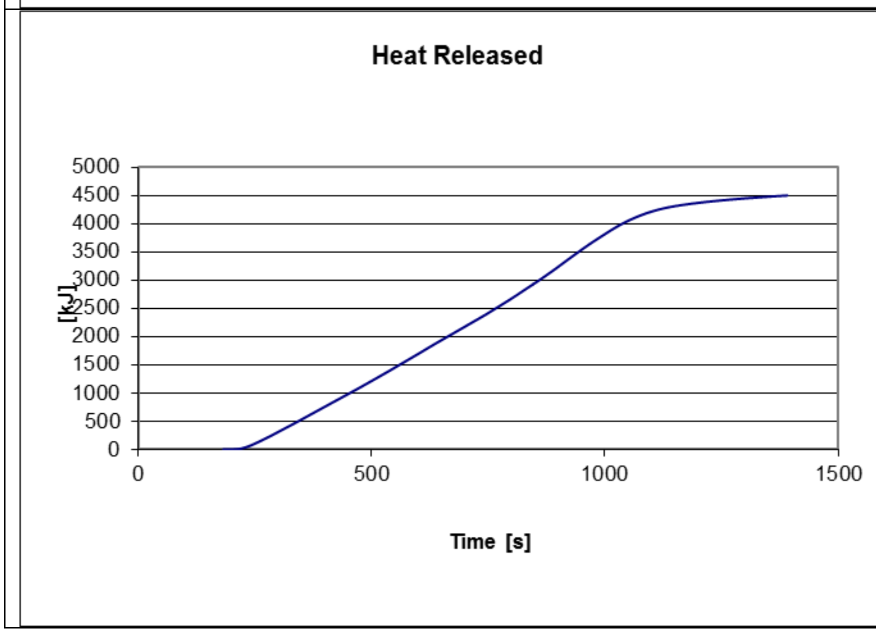

Heat Released
5000
4500
4000
3500
3000
2500
2000
1500
1000
500
0
[kJ]
0
500
1000
1500
Time [s]

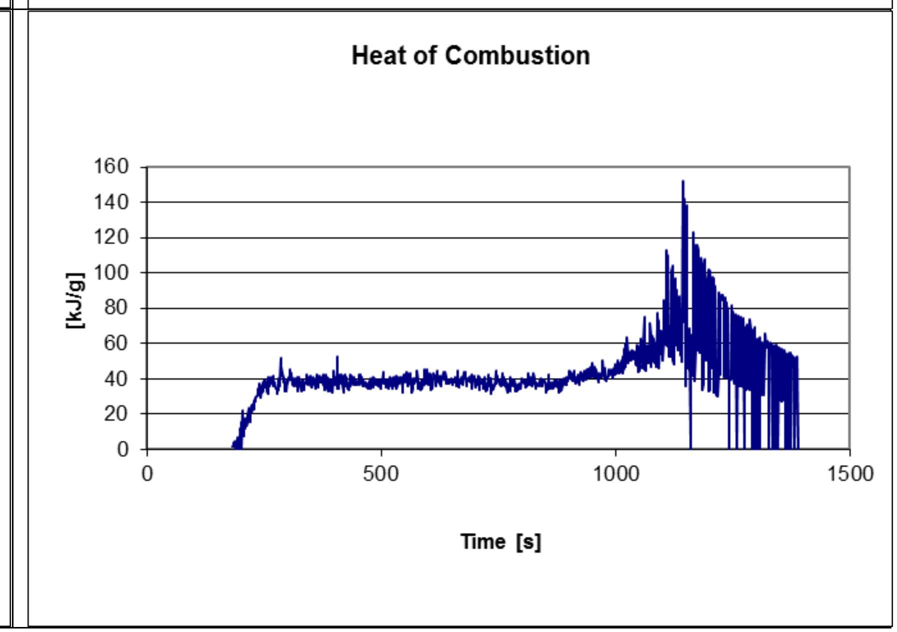

Heat of Combustion
160
140
120
100
80
60
40
20
0
[kJ/g]
0
500
1000
1500
Time [s]

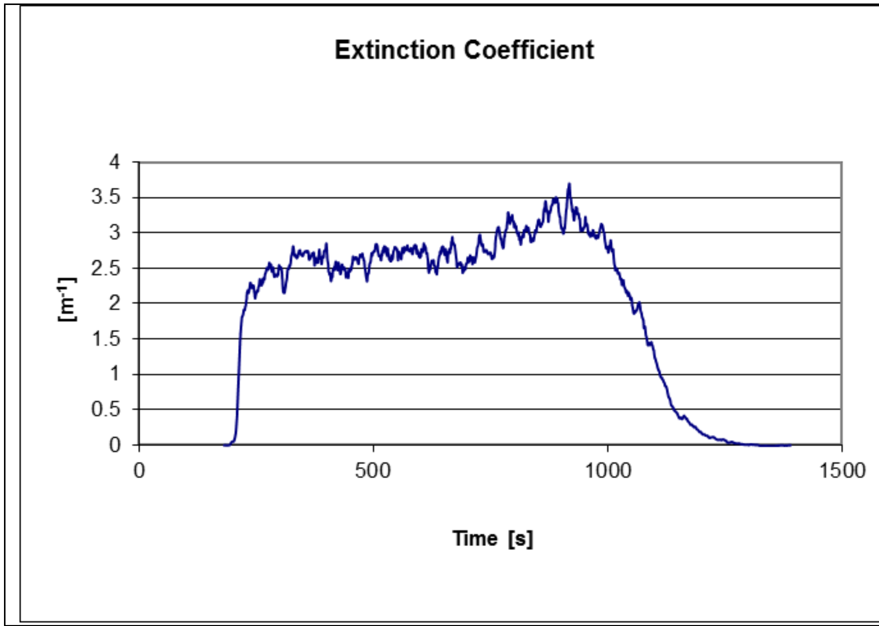
Extinction Coefficient
[m-1]
4
3.5
3
2.5
2
1.5
1
0.5
0
0
500
1000
1500
Time [s]

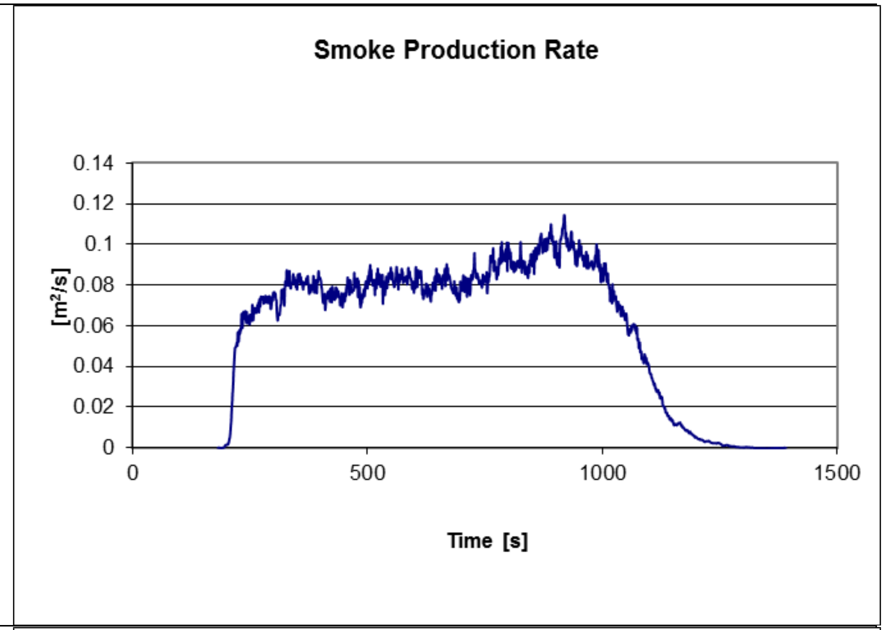
Smoke Production Rate
[m2/s]
0.14
0.12
0.1
0.08
0.06
0.04
0.02
0
0
500
1000
1500
Time [s]

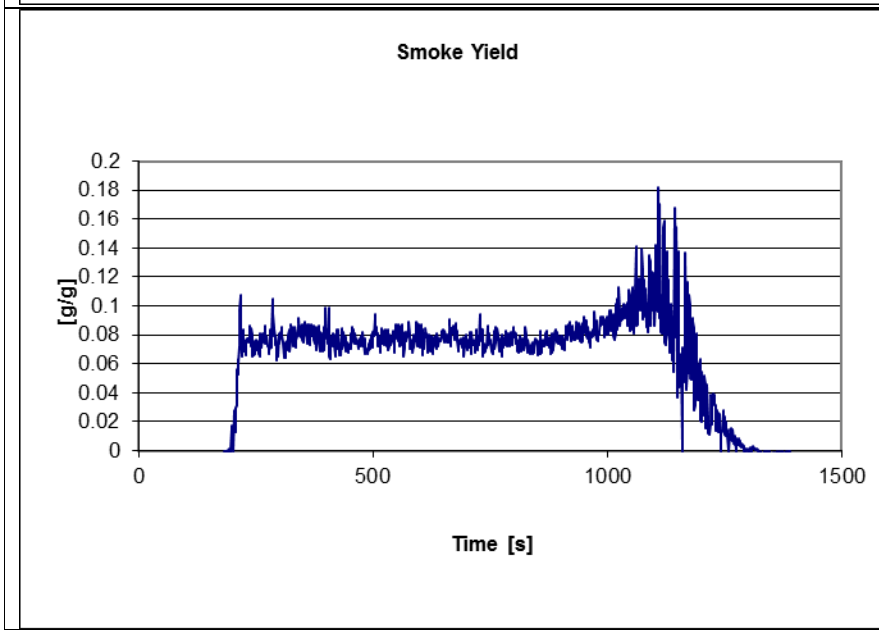
Smoke Yield
[g/g]
0.2
0.18
0.16
0.14
0.12
0.1
0.08
0.06
0.04
0.02
0
0
500
1000
1500
Time [s]

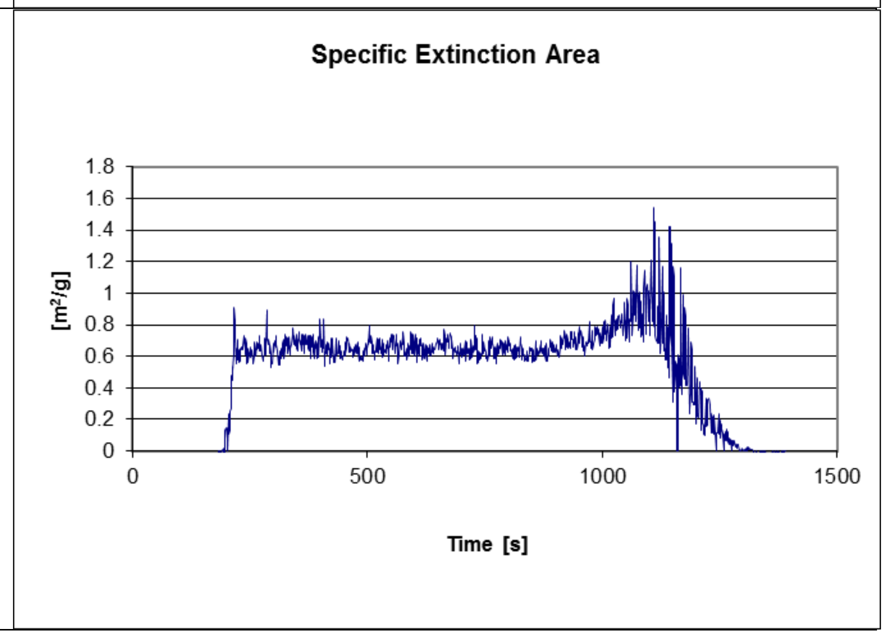
Specific Extinction Area
[m2/g]
1.8
1.6
1.4
1.2
1
0.8
0.6
0.4
0.2
0
0
500
1000
1500
Time [s]

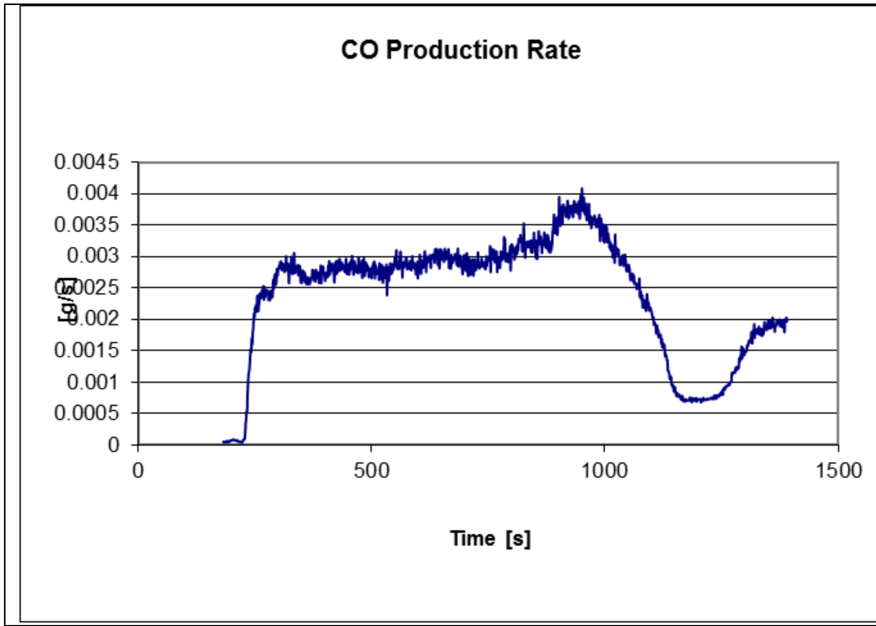
CO Production Rate
0.0045
0.004
0.0035
0.003
0.0025
0.002
0.0015
0.001
0.0005
0
[g/s]
0
500
1000
1500
Time [s]

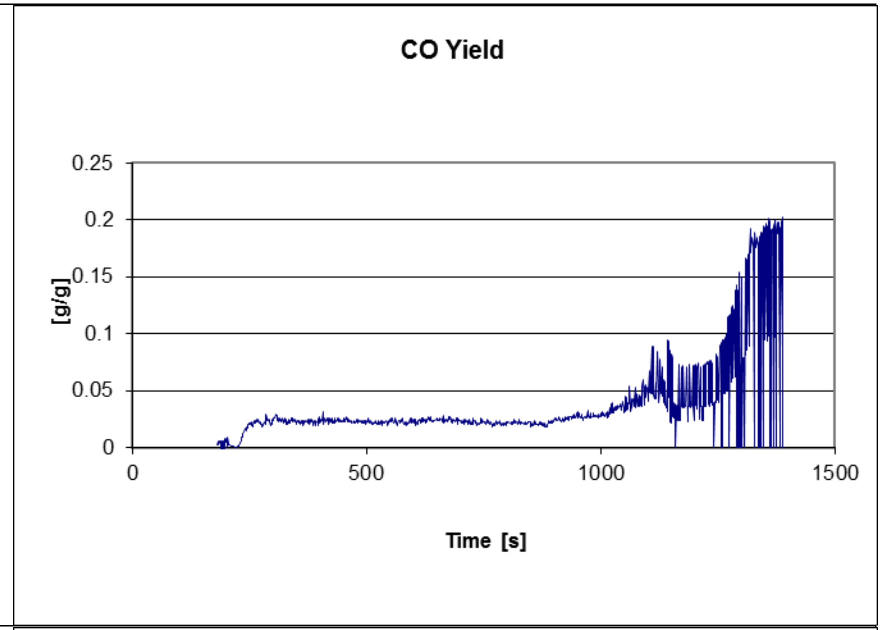
CO Yield
0.25
0.2
0.15
0.1
0.05
0
[g/g]
0
500
1000
1500
Time [s]

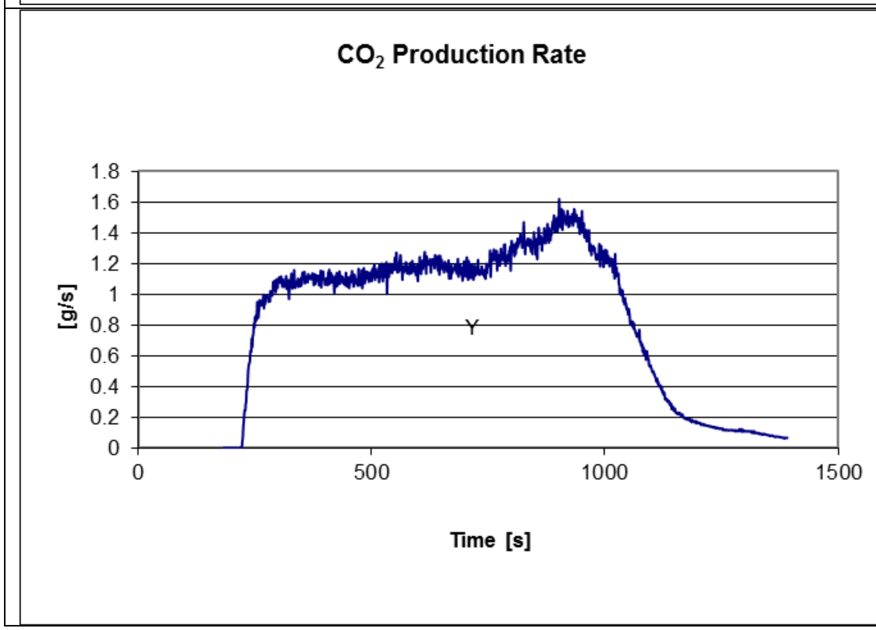
CO_2 Production Rate
1.8
1.6
1.4
1.2
1
0.8
0.6
0.4
0.2
0
[g/s]
Y
0
500
1000
1500
Time [s]

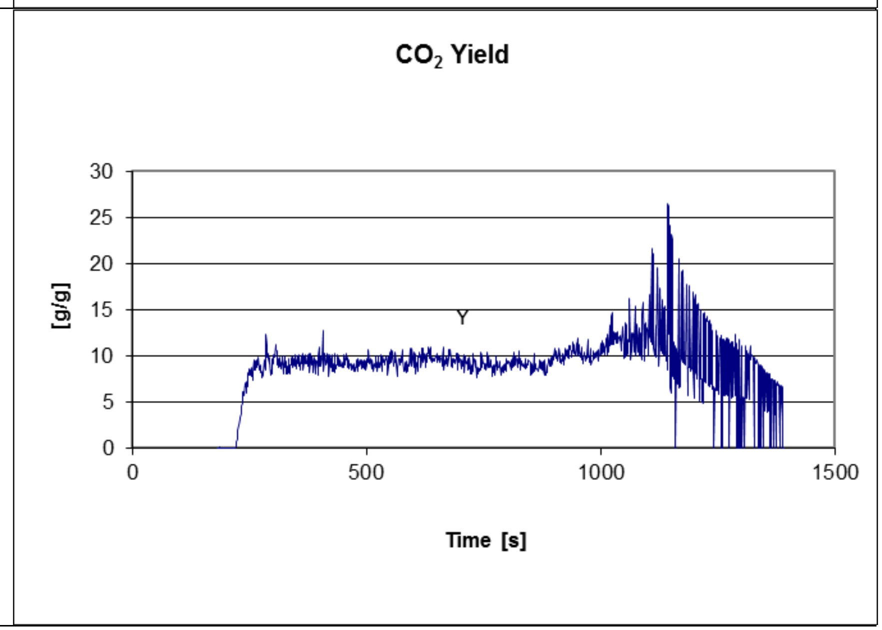
CO_2 Yield
30
25
20
15
10
5
0
[g/g]
Y
0
500
1000
1500
Time [s]

E.5 Thermoplastic Test 6 – Polypropylene Sample 2

Cone Calorimeter Test Run Data

Dept. of Fire Protection Engineering

100 Institute Road
Worcester, MA 01609
Phone: (508) 831-5628
Fax: (508) 831-5862

Test Information

Test Number:	Test 06
Specimen Identification:	Black Polypropylene Sample 02
Material Name:	Black Polypropylene 02
Manufacturer/Submitter:	Not Reported
Sample Description:	Black half-inch thick panel, 4 TCs
Raw Data File Name:	Test_06_PolyP_02.txt
Reduced Data File Name:	Test_06_PolyP_02.xls
Date of Test:	6/30/2009
Tester:	Will Wong

Test Parameters

Ambient Temperature:	77	F
Relative Humidity:	47	%
Heat Flux:	50	kW/m^2
Exhaust Duct Flow Rate:		30 g/s
Orientation:		Horizontal
Specimen Holder:		TRUE
Specimen Preparation:		2 layer foil
Notes:		1" Separation

Specimen Information

Specimen Color:	[]	Black
Specimen Thickness:	[mm]	12.3
Specimen Test Area:	[m^2]	0.0088
Specimen Initial Mass:	[g]	116.5
Specimen Final Mass:	[g]	0.2
Specimen Density:	[g/cm^3]	0.9
Mass Lost:	[g]	116.3
Total Heat Evolved:	[kJ]	4545

Test Times [s]

Shutter Open:	196
Time to Ignition:	221
Flameout:	1302
Clean Air/End of Test:	1316

Daily C-Factor

0.041

The Peak, Average and Total parameters are computed over the test period ignition to flame out. There are 4 exceptions. The first three involve initial heat release rate averages for periods after ignition of 60, 180 and 300 seconds. The final involves the average mass loss rate which is computed over the time period from 10% mass loss to 90% mass loss.

Parameter	Unit	Value
Heat Release		
Peak Heat Release Rate	[kW/m^2]	873
Average Heat Release Rate	[kW/m^2]	476
Total Heat Release	[MJ/m^2]	514
Average HRR for the first 60s	[kW/m^2]	403
Average HRR for the first 180s	[kW/m^2]	480
Average HRR for the first 300s	[kW/m^2]	509
Peak Heat of Combustion	[kJ/g]	138
Average Heat of Combustion	[kJ/g]	39
Smoke Obscuration		
Peak SEA	[m^2/g]	1.244
Average SEA	[m^2/g]	0.323
Peak Smoke Yield	[g/g]	0.146
Average Smoke Yield	[g/g]	0.038
Peak Smoke Production Rate	[m^2/s]	0.066
Average Smoke Production Rate	[m^2/s]	0.037
Total Smoke Release	[m^2]	32.304
Gas Production Rates		
Peak Carbon Monoxide	[g/s]	0.005
Average Carbon Monoxide	[g/s]	0.002
Peak Carbon Dioxide	[g/s]	1.954
Average Carbon Dioxide	[g/s]	1.086
Mass Loss		
Peak Mass Loss Rate	[g/s]	0.290
Average Mass Lass Rate	[g/s]	0.137
Initial Mass	[g]	116.5
Final Mass	[g]	0.2
Mass Loss Fraction	[]	1.00
Burn Time		
Time to Ignition	[s]	25
Duration of Flaming	[s]	1081
Duration of Test	[s]	1120

Observations

Time	Observation
213	Lots of smoke, surface TC came off surface by a little
220	Real Ignition
240	Boiling over surface with many small bubbles, flame uniform, orange/yellow
290	Surface TC no longer touching surface
370	Some area on surface charred
380	Droplet
430	Most of surface charred
460	1 embedded TC moved to position above surface
540	2nd embedded TC moved above surface
560	Central area and edges boil, where other areas are charred
740	Some smoke escapes out of hood
960	Only edges boiling
1010	Flame cone shrinks
1120	Flame becomes cellular
1150	Only edge burning, dark smoke
	Droplet mass at 0.0165g

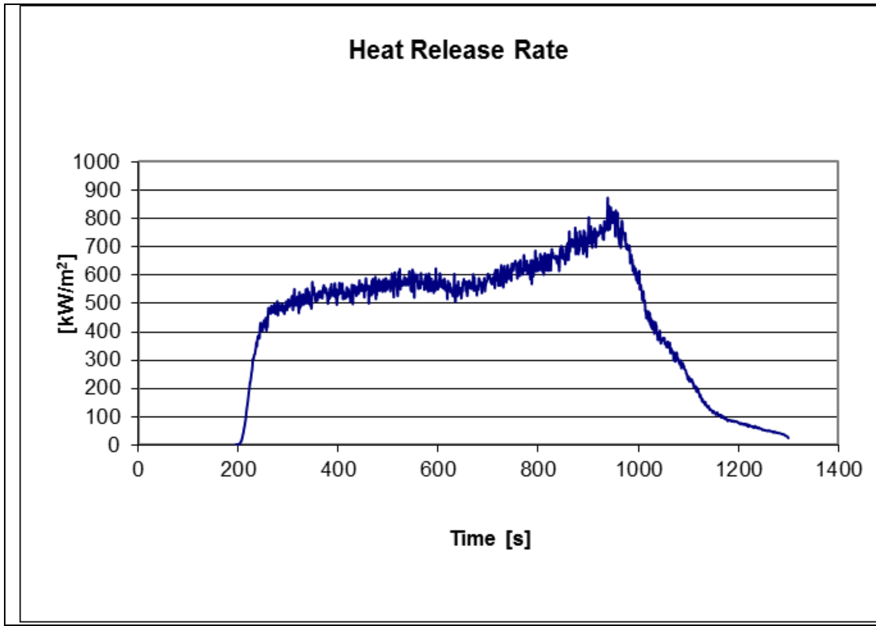
Heat Release Rate
[kW/m²]
1000
900
800
700
600
500
400
300
200
100
0
0
200
400
600
800
1000
1200
1400
Time [s]

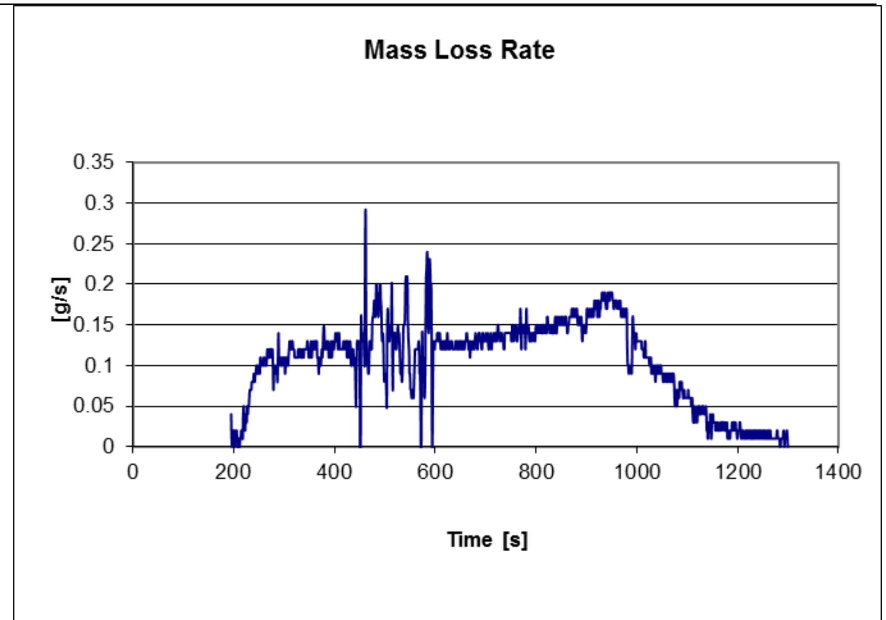
Mass Loss Rate
[g/s]
0.35
0.3
0.25
0.2
0.15
0.1
0.05
0
0
200
400
600
800
1000
1200
1400
Time [s]

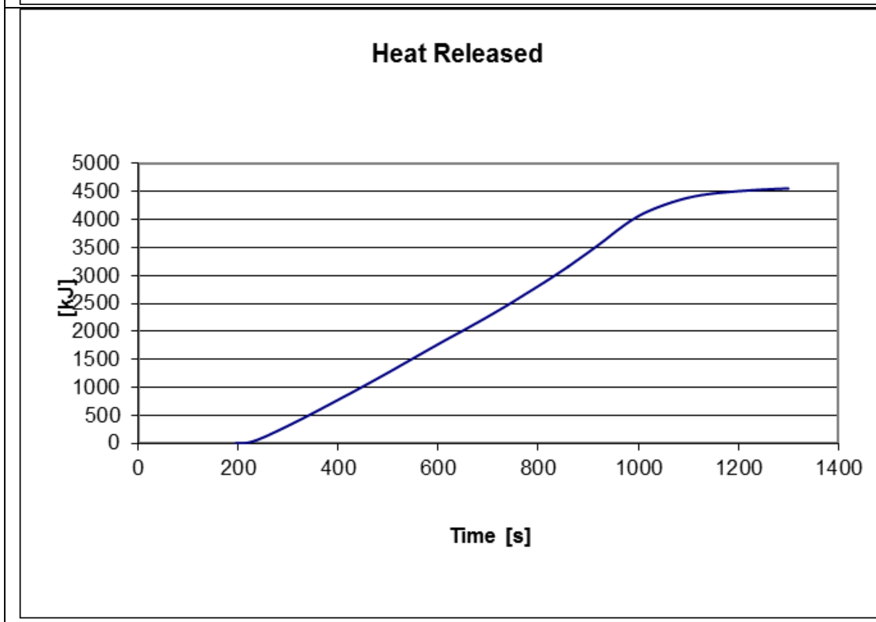
Heat Released
[kJ]
5000
4500
4000
3500
3000
2500
2000
1500
1000
500
0
0
200
400
600
800
1000
1200
1400
Time [s]

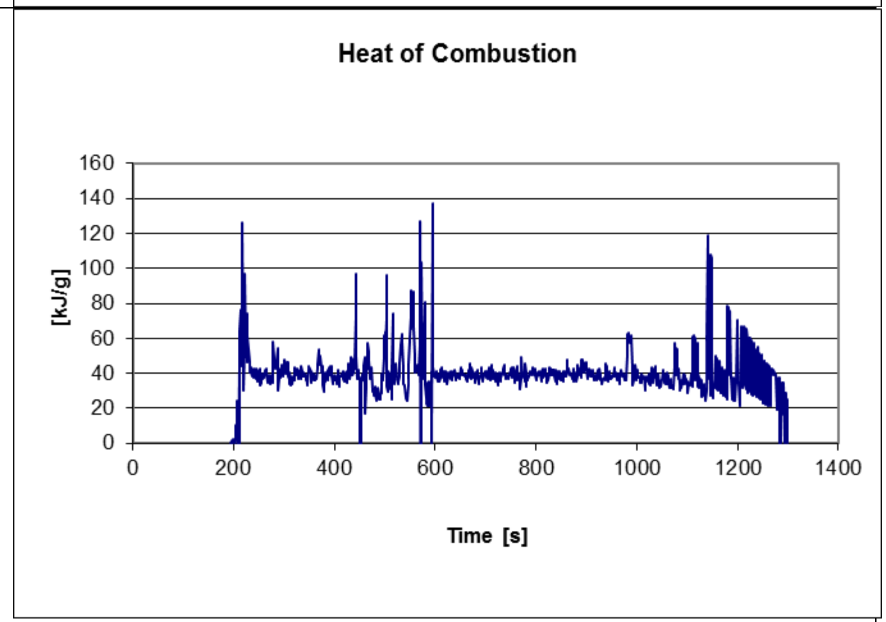
Heat of Combustion
[kJ/g]
160
140
120
100
80
60
40
20
0
0
200
400
600
800
1000
1200
1400
Time [s]

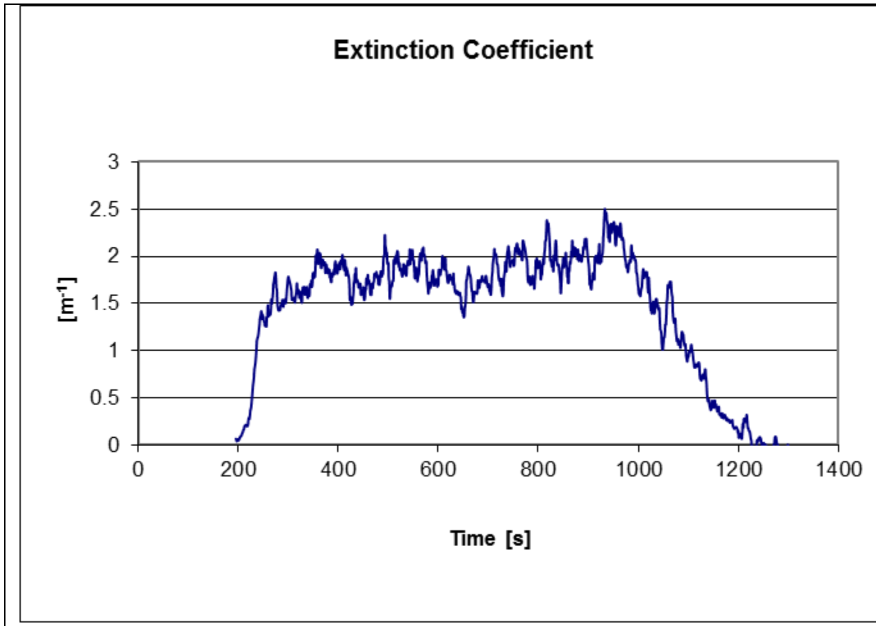
Extinction Coefficient
[m-1]
3
2.5
2
1.5
1
0.5
0
0
200
400
600
800
1000
1200
1400
Time [s]

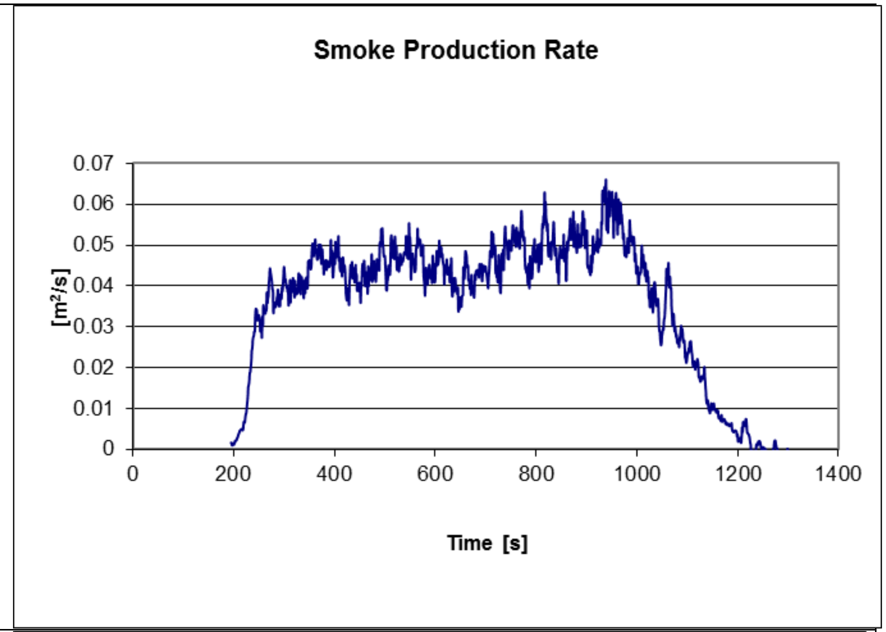
Smoke Production Rate
[m2/s]
0.07
0.06
0.05
0.04
0.03
0.02
0.01
0
0
200
400
600
800
1000
1200
1400
Time [s]

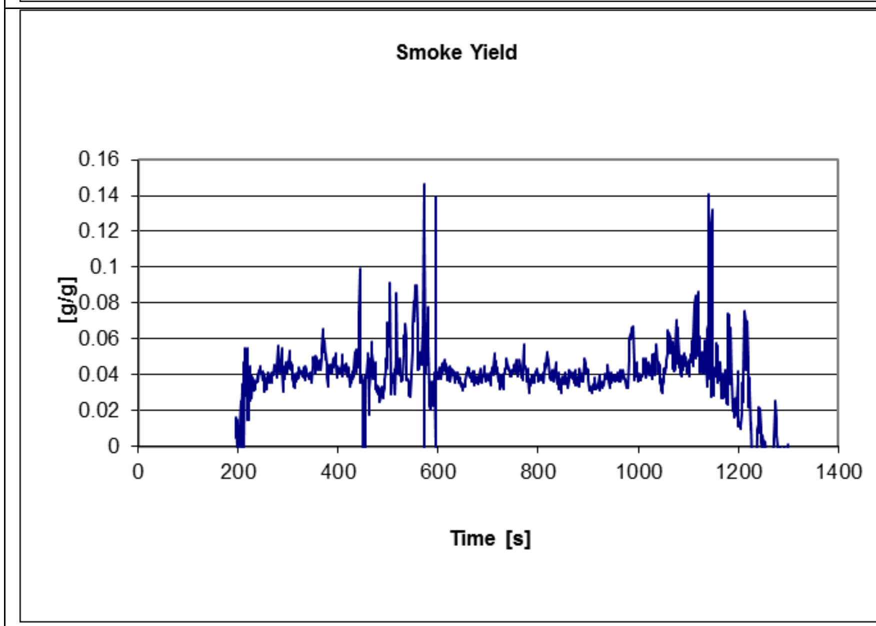
Smoke Yield
[g/g]
0.16
0.14
0.12
0.1
0.08
0.06
0.04
0.02
0
0
200
400
600
800
1000
1200
1400
Time [s]

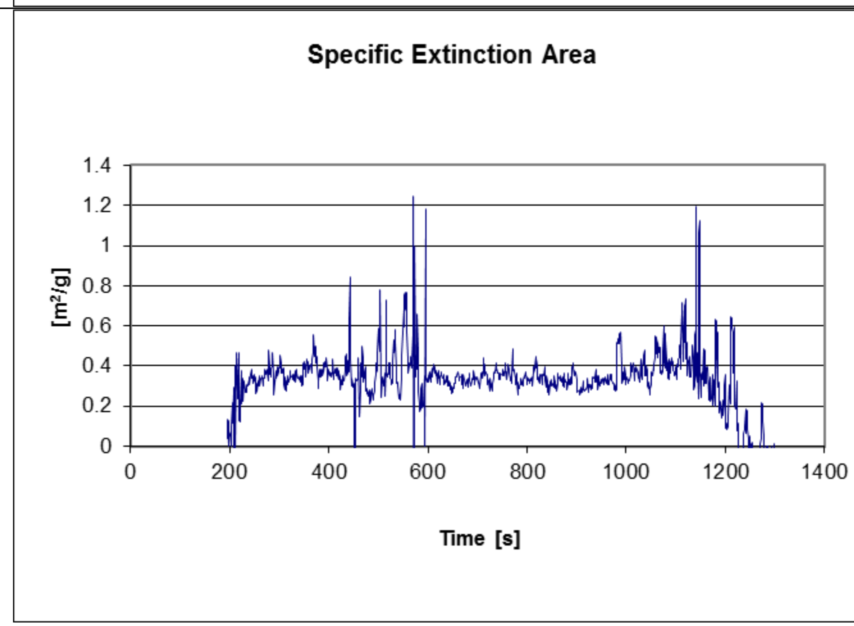
Specific Extinction Area
[m2/g]
1.4
1.2
1
0.8
0.6
0.4
0.2
0
0
200
400
600
800
1000
1200
1400
Time [s]

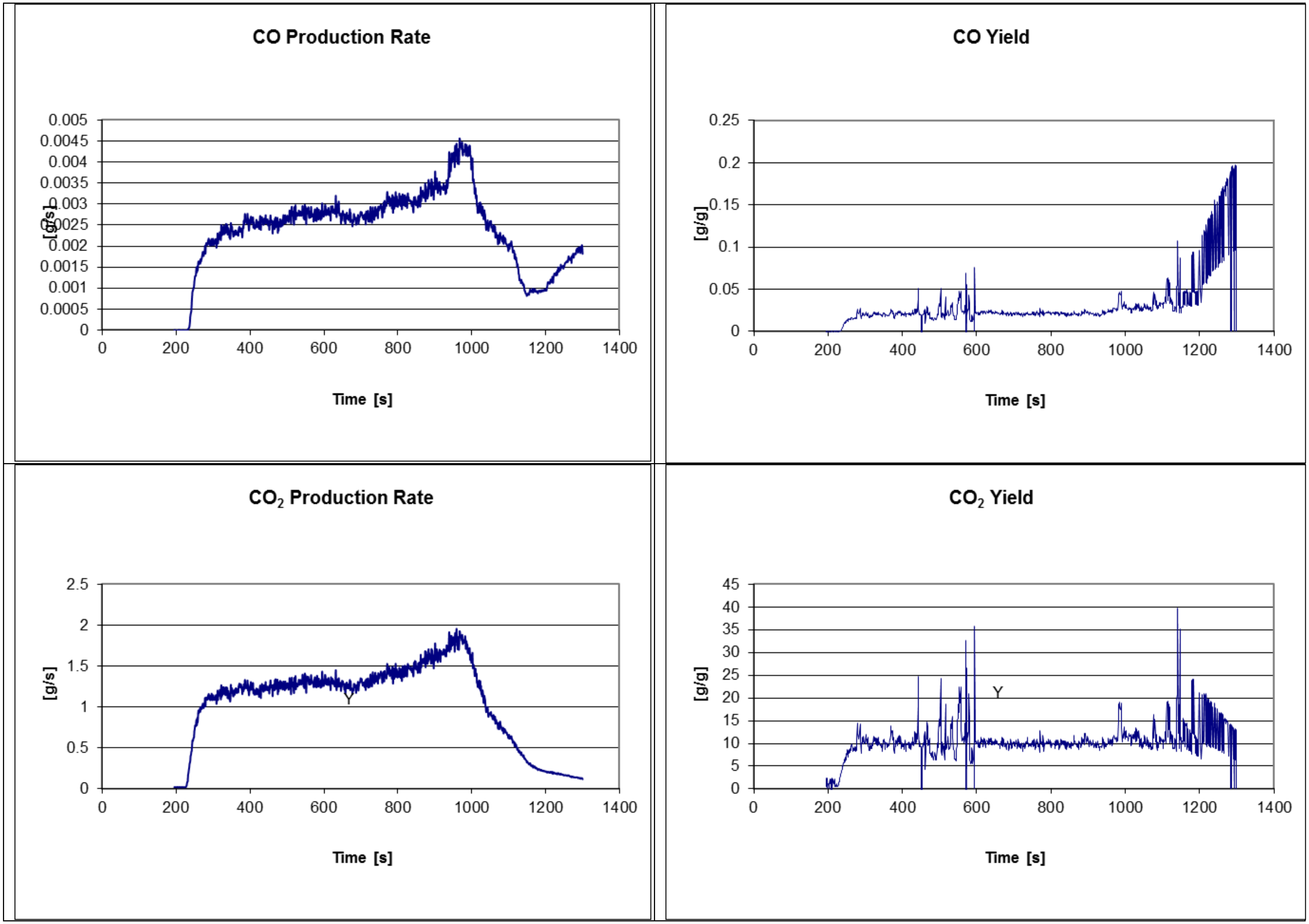

CO Production Rate
[g/s]
Time [s]
CO Yield
[g/g]
Time [s]
CO_2 Production Rate
[g/s]
Y
Time [s]
CO_2 Yield
[g/g]
Y
Time [s]

TC Locations

	Depth from side		Height from bottom
1	38mm	←	8.68mm
2	40.5mm	←	6.5mm

From Left Side

100mm	
50mm	x 1
50mm	x 2

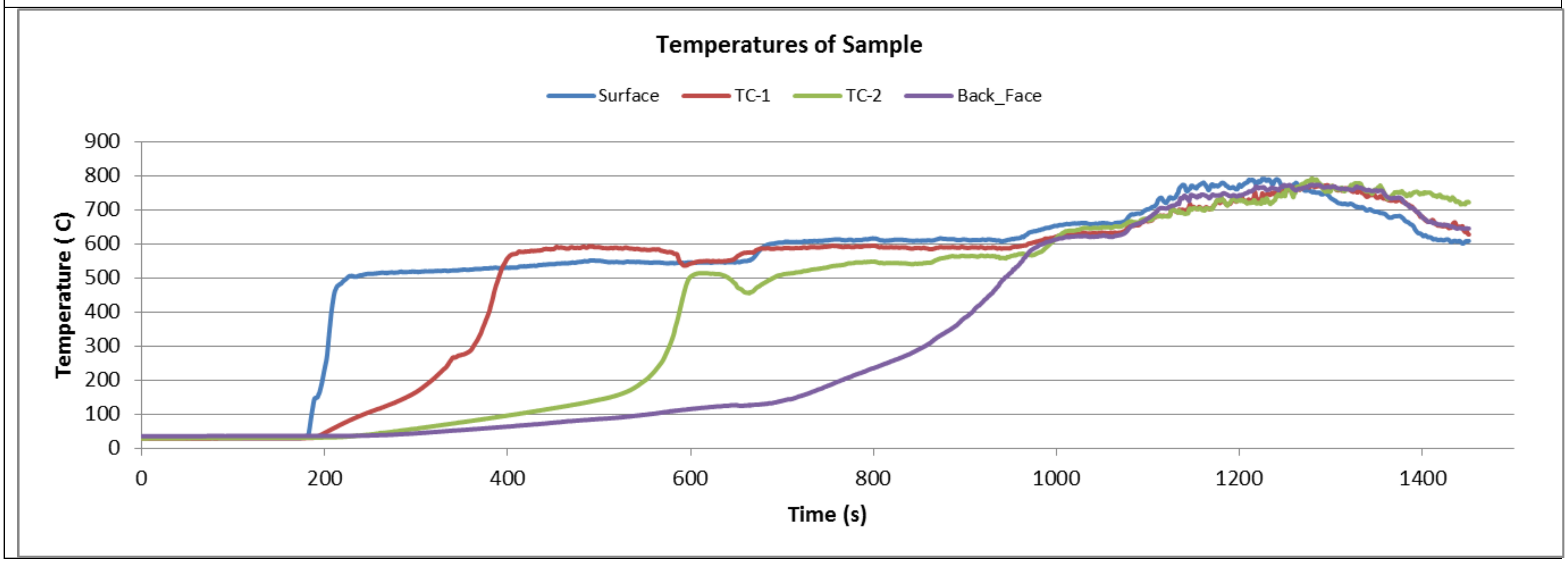

E.6 Thermoplastic Test 7 – Polypropylene Sample 3

Cone Calorimeter Test Run Data

Dept. of Fire Protection Engineering

100 Institute Road
Worcester, MA 01609
Phone: (508) 831-5628
Fax: (508) 831-5862

Test Information

Test Number:	Test 07
Specimen Identification:	Black Polypropylene Sample 03
Material Name:	Black Polypropylene 03
Manufacturer/Submitter:	Not Reported
Sample Description:	Black half-inch thick panel, 4 TCs
Raw Data File Name:	Test_07_PolyP_03.txt
Reduced Data File Name:	Test_07_PolyP_03.xls
Date of Test:	6/30/2009
Tester:	Randy Harris

Test Parameters

Ambient Temperature:	77	F
Relative Humidity:	47	%
Heat Flux:	50	kW/m^2
Exhaust Duct Flow Rate:		30 g/s
Orientation:		Horizontal
Specimen Holder:		TRUE
Specimen Preparation:		2 layer foil
Notes:		1" Separation

Specimen Information

Specimen Color:	[]	Black
Specimen Thickness:	[mm]	12.3
Specimen Test Area:	[m^2]	0.0088
Specimen Initial Mass:	[g]	111.9
Specimen Final Mass:	[g]	-0.1
Specimen Density:	[g/cm^3]	0.9
Mass Lost:	[g]	112.0
Total Heat Evolved:	[kJ]	4392

Test Times [s]

Shutter Open:	181
Time to Ignition:	202
Flameout:	1449
Clean Air/End of Test:	1467

Daily C-Factor

0.041

The Peak, Average and Total parameters are computed over the test period ignition to flame out. There are 4 exceptions. The first three involve initial heat release rate averages for periods after ignition of 60, 180 and 300 seconds. The final involves the average mass loss rate which is computed over the time period from 10% mass loss to 90% mass loss.

Parameter	Unit	Value
Heat Release		
Peak Heat Release Rate	[kW/m^2]	683
Average Heat Release Rate	[kW/m^2]	399
Total Heat Release	[MJ/m^2]	497
Average HRR for the first 60s	[kW/m^2]	325
Average HRR for the first 180s	[kW/m^2]	404
Average HRR for the first 300s	[kW/m^2]	432
Peak Heat of Combustion	[kJ/g]	131
Average Heat of Combustion	[kJ/g]	38
Smoke Obscuration		
Peak SEA	[m^2/g]	1.066
Average SEA	[m^2/g]	0.302
Peak Smoke Yield	[g/g]	0.125
Average Smoke Yield	[g/g]	0.036
Peak Smoke Production Rate	[m^2/s]	0.053
Average Smoke Production Rate	[m^2/s]	0.030
Total Smoke Release	[m^2]	30.012
Gas Production Rates		
Peak Carbon Monoxide	[g/s]	0.004
Average Carbon Monoxide	[g/s]	0.002
Peak Carbon Dioxide	[g/s]	1.555
Average Carbon Dioxide	[g/s]	0.920
Mass Loss		
Peak Mass Loss Rate	[g/s]	0.190
Average Mass Lass Rate	[g/s]	0.118
Initial Mass	[g]	111.9
Final Mass	[g]	-0.1
Mass Loss Fraction	[]	1.00
Burn Time		
Time to Ignition	[s]	21
Duration of Flaming	[s]	1247
Duration of Test	[s]	1286

Observations

Time	Observation
198	White smoke Thick black smoke after ignition No dripping Glowing combustion after flameout

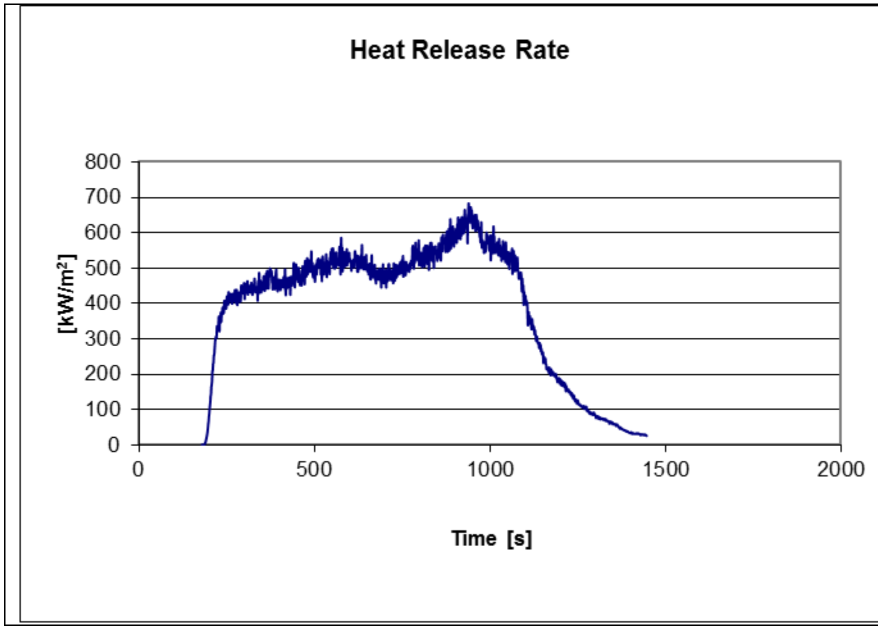

Heat Release Rate
800
700
600
500
400
300
200
100
0
[kW/m²]
0
500
1000
1500
2000
Time [s]

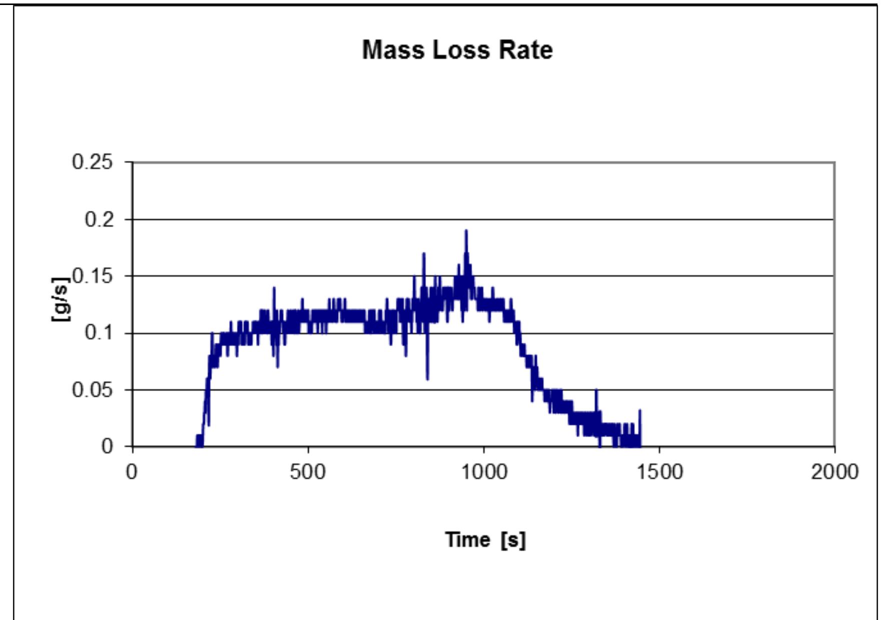

Mass Loss Rate
0.25
0.2
0.15
0.1
0.05
0
[g/s]
0
500
1000
1500
2000
Time [s]

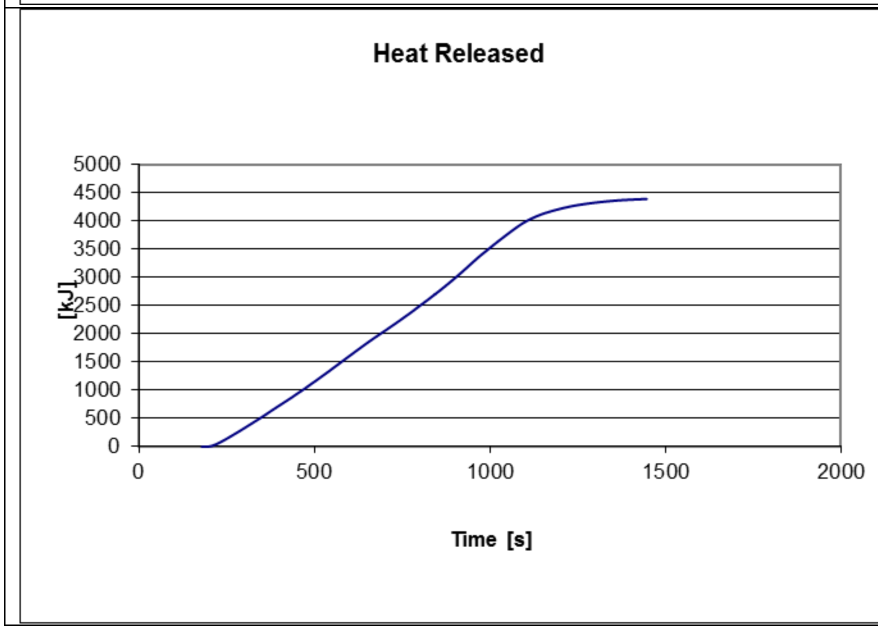

Heat Released
5000
4500
4000
3500
3000
2500
2000
1500
1000
500
0
[kJ]
0
500
1000
1500
2000
Time [s]

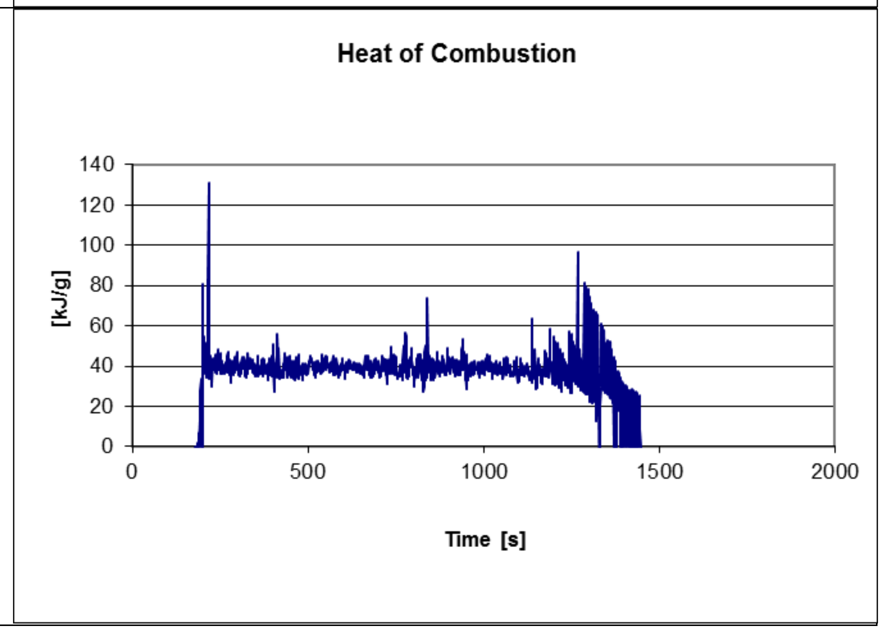

Heat of Combustion
140
120
100
80
60
40
20
0
[kJ/g]
0
500
1000
1500
2000
Time [s]

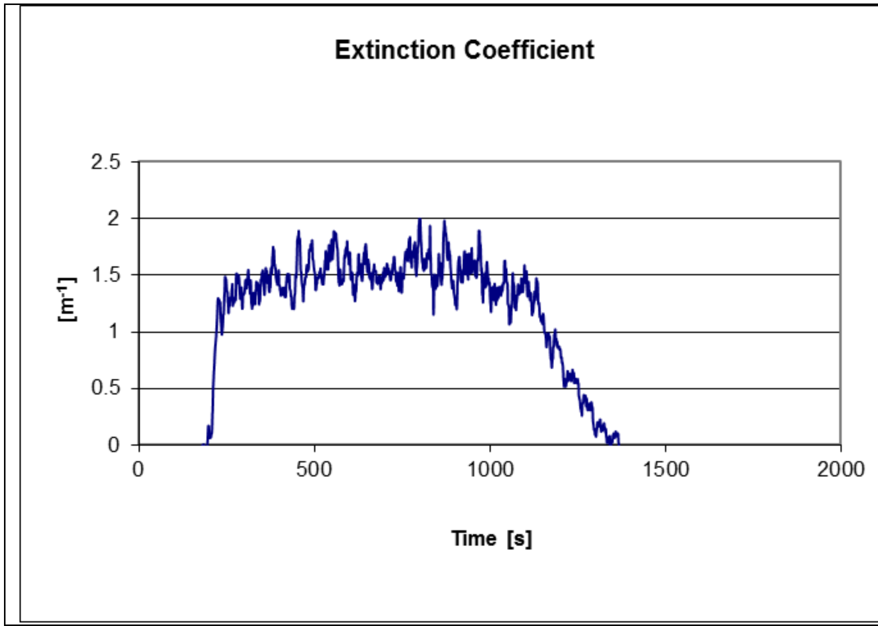
Extinction Coefficient
[m-1]
2.5
2
1.5
1
0.5
0
0
500
1000
1500
2000
Time [s]

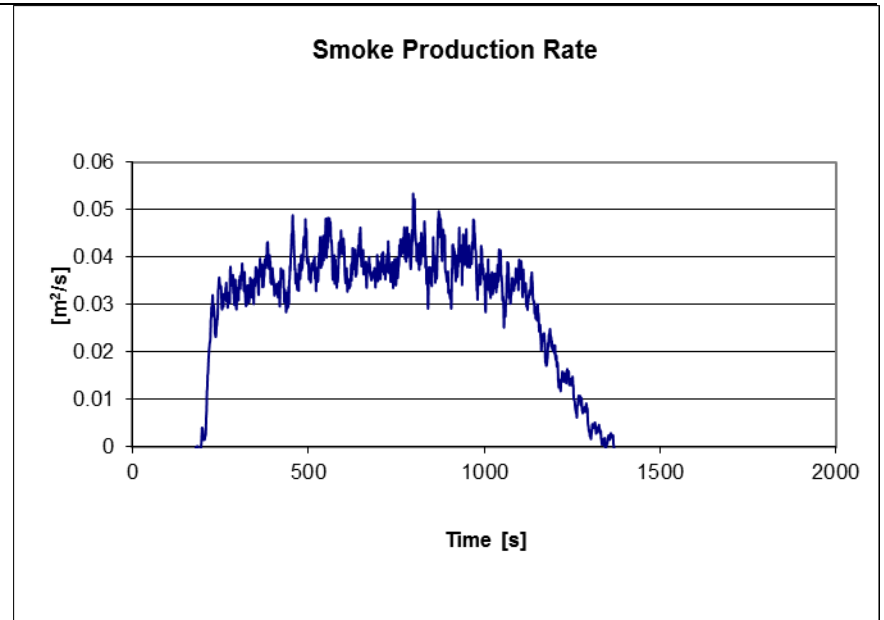
Smoke Production Rate
[m2/s]
0.06
0.05
0.04
0.03
0.02
0.01
0
0
500
1000
1500
2000
Time [s]

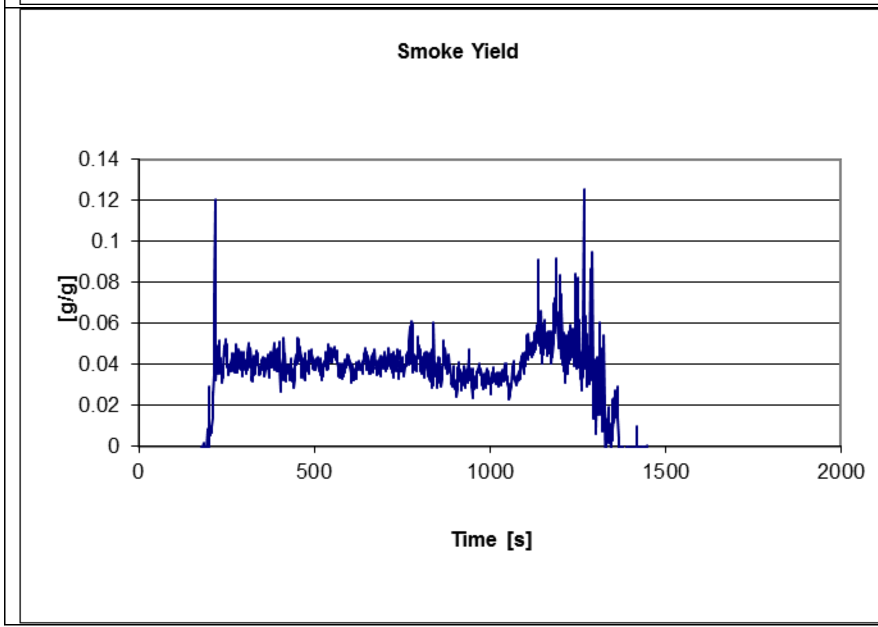
Smoke Yield
[g/g]
0.14
0.12
0.1
0.08
0.06
0.04
0.02
0
0
500
1000
1500
2000
Time [s]

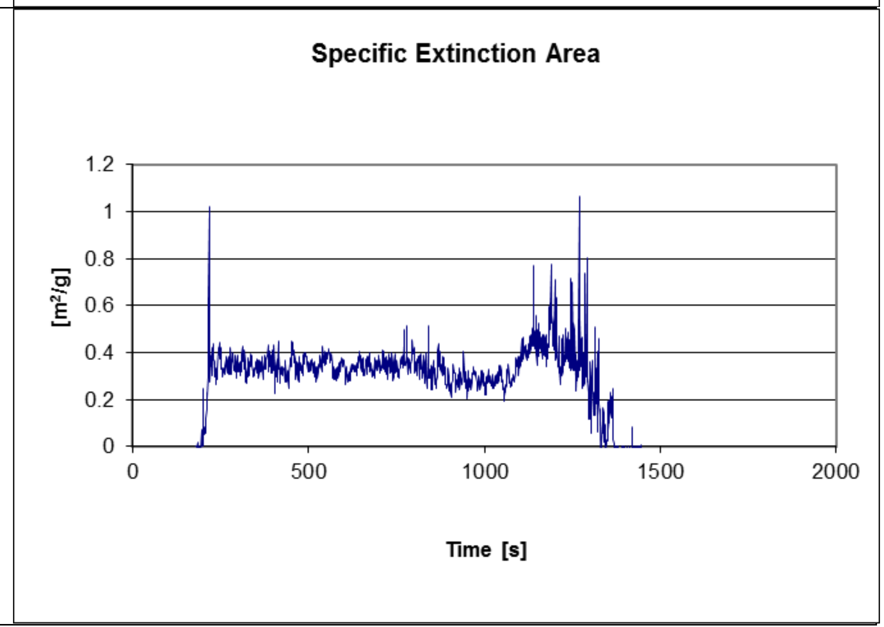
Specific Extinction Area
[m2/g]
1.2
1
0.8
0.6
0.4
0.2
0
0
500
1000
1500
2000
Time [s]

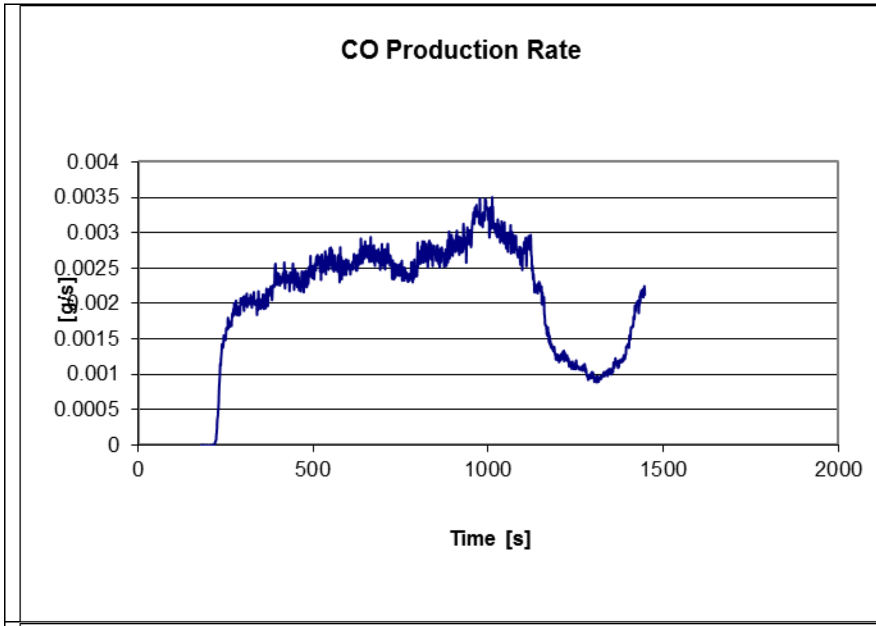
CO Production Rate
0.004
0.0035
0.003
0.0025
0.002
0.0015
0.001
0.0005
0
[g/s]
0
500
1000
1500
2000
Time [s]

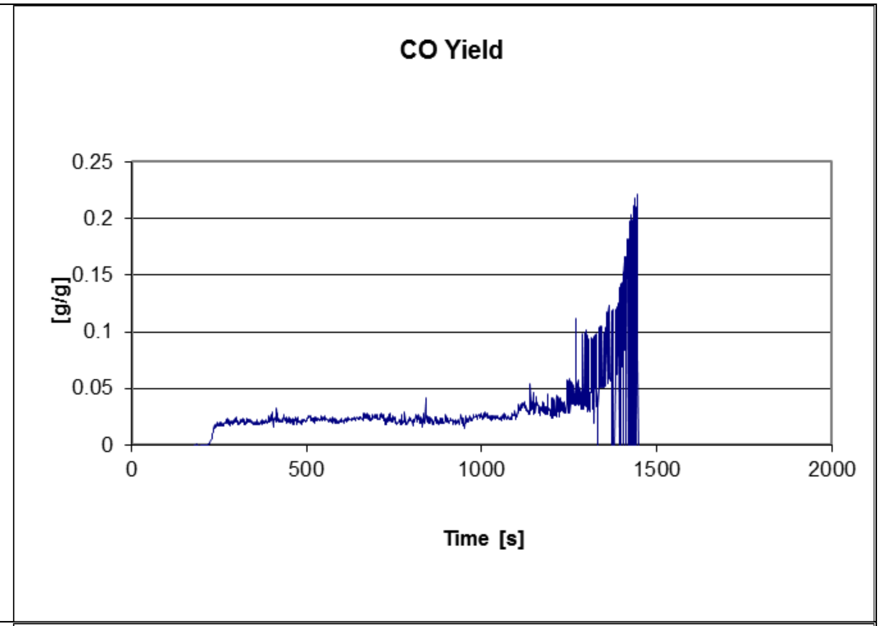
CO Yield
0.25
0.2
0.15
0.1
0.05
0
[g/g]
0
500
1000
1500
2000
Time [s]

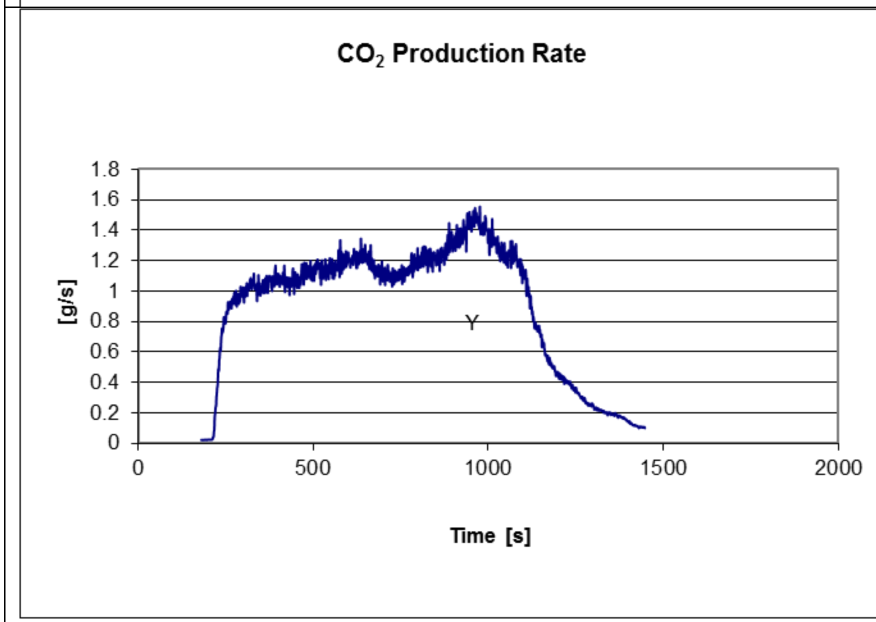
CO_2 Production Rate
1.8
1.6
1.4
1.2
1
0.8
0.6
0.4
0.2
0
[g/s]
Y
0
500
1000
1500
2000
Time [s]

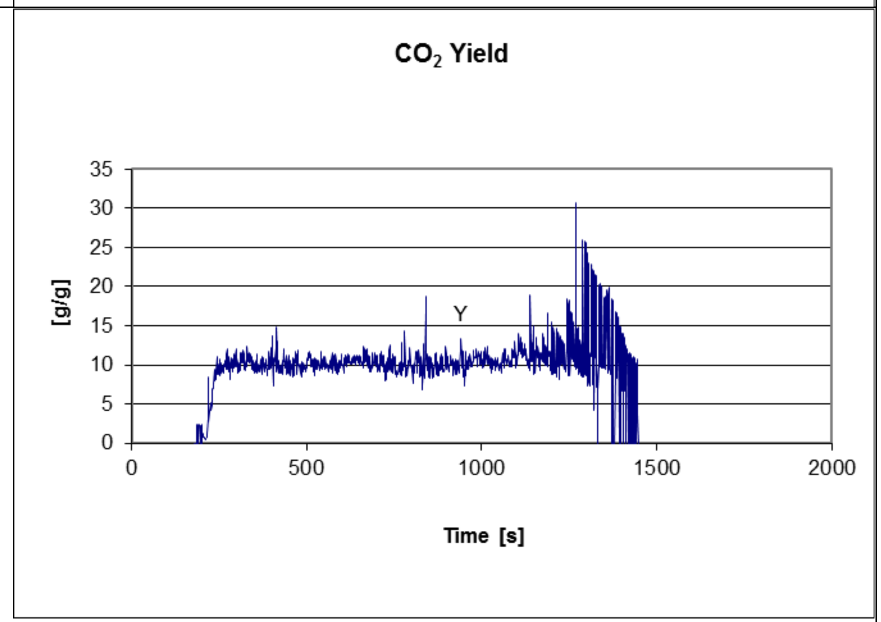
CO_2 Yield
35
30
25
20
15
10
5
0
[g/g]
Y
0
500
1000
1500
2000
Time [s]

TC Locations

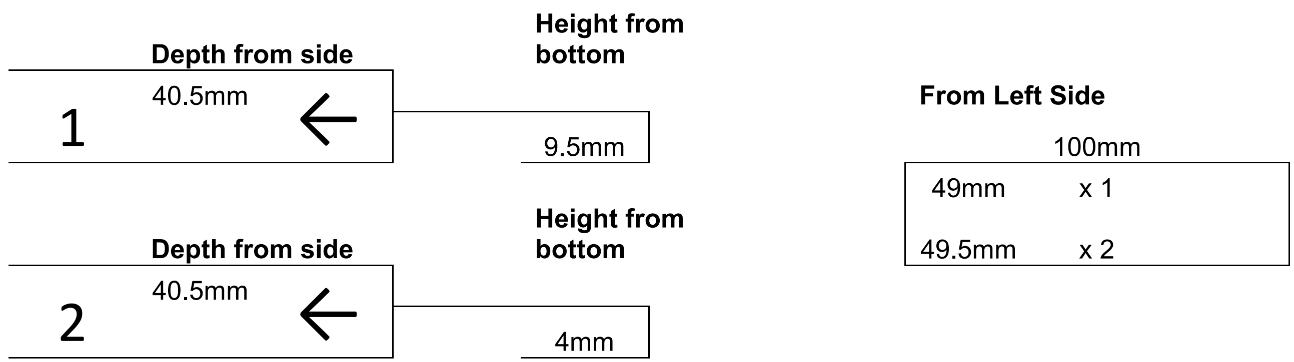

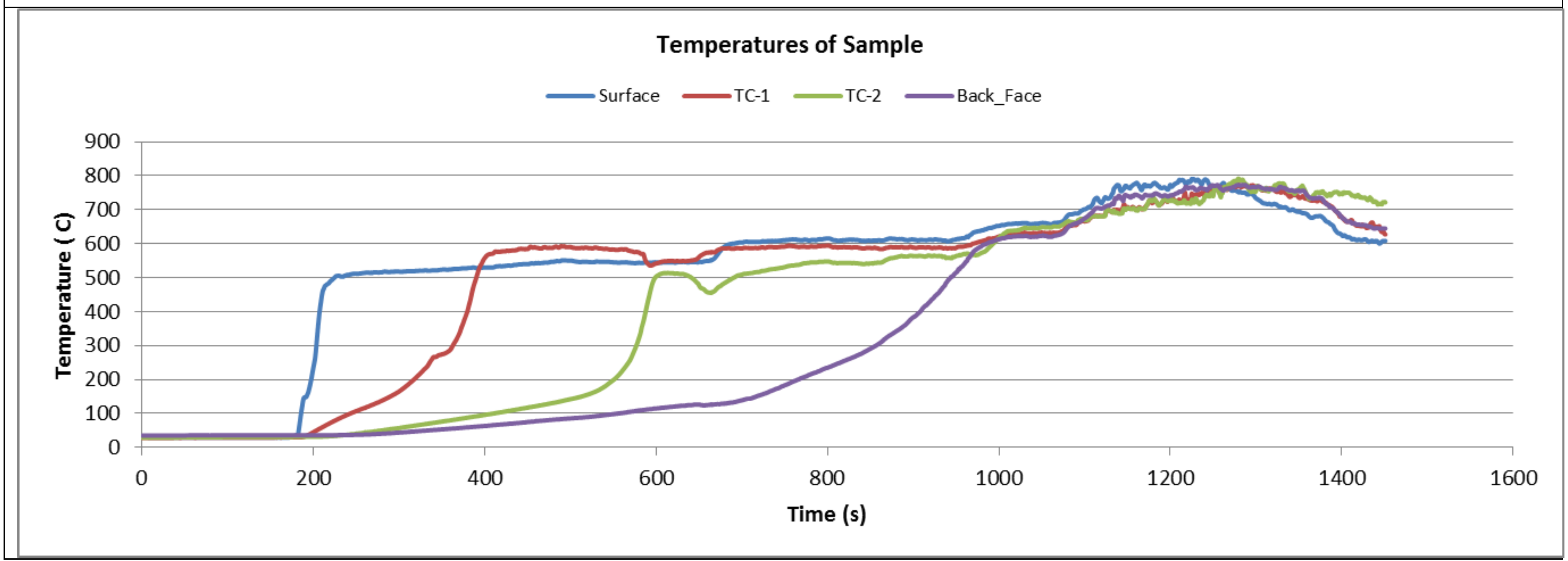

E.7 Thermoplastic Test 3 – Black HDPE Sample 1

Cone Calorimeter Test Run Data

Dept. of Fire Protection Engineering

100 Institute Road
Worcester, MA 01609
Phone: (508) 831-5628
Fax: (508) 831-5862

Test Information

Test Number:	Test 03
Specimen Identification:	Black High Density Polyethylene Sample 01
Material Name:	Black HDPE 01
Manufacturer/Submitter:	Not Reported
Sample Description:	Black half-inch thick panel, no TCs
Raw Data File Name:	Test_03_Black_HDPE_01.txt
Reduced Data File Name:	Test_03_Black_HDPE_01.xls
Date of Test:	6/18/2009
Tester:	Will Wong

Test Parameters

Ambient Temperature:	74	F
Relative Humidity:	41	%
Heat Flux:	50	kW/m^2
Exhaust Duct Flow Rate:		30 g/s
Orientation:		Horizontal
Specimen Holder:		TRUE
Specimen Preparation:		2 layer foil
Notes:		1" Separation

Specimen Information

Specimen Color:	[]	Black
Specimen Thickness:	[mm]	12.6
Specimen Test Area:	[m^2]	0.0088
Specimen Initial Mass:	[g]	121.0
Specimen Final Mass:	[g]	0.2
Specimen Density:	[g/cm^3]	1.0
Mass Lost:	[g]	120.8
Total Heat Evolved:	[kJ]	5250

Test Times [s]

Shutter Open:	202
Time to Ignition:	248
Flameout:	1382
Clean Air/End of Test:	1396

Daily C-Factor

0.050

The Peak, Average and Total parameters are computed over the test period ignition to flame out. There are 4 exceptions. The first three involve initial heat release rate averages for periods after ignition of 60, 180 and 300 seconds. The final involves the average mass loss rate which is computed over the time period from 10% mass loss to 90% mass loss.

Parameter	Unit	Value
Heat Release		
Peak Heat Release Rate	[kW/m^2]	989
Average Heat Release Rate	[kW/m^2]	524
Total Heat Release	[MJ/m^2]	594
Average HRR for the first 60s	[kW/m^2]	281
Average HRR for the first 180s	[kW/m^2]	400
Average HRR for the first 300s	[kW/m^2]	456
Peak Heat of Combustion	[kJ/g]	165
Average Heat of Combustion	[kJ/g]	45
Smoke Obscuration		
Peak SEA	[m^2/g]	1.016
Average SEA	[m^2/g]	0.363
Peak Smoke Yield	[g/g]	0.120
Average Smoke Yield	[g/g]	0.043
Peak Smoke Production Rate	[m^2/s]	0.093
Average Smoke Production Rate	[m^2/s]	0.046
Total Smoke Release	[m^2]	54.481
Gas Production Rates		
Peak Carbon Monoxide	[g/s]	0.004
Average Carbon Monoxide	[g/s]	0.002
Peak Carbon Dioxide	[g/s]	1.974
Average Carbon Dioxide	[g/s]	0.931
Mass Loss		
Peak Mass Loss Rate	[g/s]	0.240
Average Mass Lass Rate	[g/s]	0.140
Initial Mass	[g]	121.0
Final Mass	[g]	0.2
Mass Loss Fraction	[]	1.00
Burn Time		
Time to Ignition	[s]	46
Duration of Flaming	[s]	1134
Duration of Test	[s]	1194

Observations

Time	Observation
226	White smoke
242	3-4 flashes
261	Surface bumpy, melted, and boiling
295	Flame cone is yellow/bright orange, and uniform
430	Surface bumpy, looks like charred bubbles
457	Little smoke, black and gray
642	Most bubbling on edges, and some bubbling in center
764	Pool burning on right edge, instead of charring
911	Some flame outside of cone
942	Left edge turn into pool, charred material seem to be pushed into center
1068	Most surface charred, left edge bubbling, flame still over all of surface
1147	Flame cone shrinks, more turbulent
1206	Some edge burning only, cellular flames
1256	1 droplet
1280	Corner burning, some flashes dance on surface
	black flakey residue
	Droplet mass 0.0475g

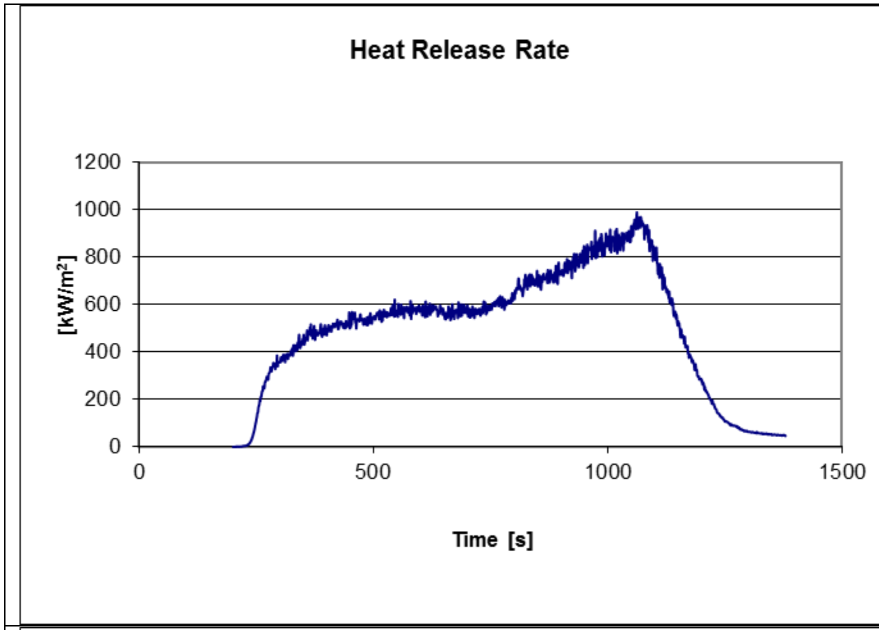
Heat Release Rate
[kW/m²]
1200
1000
800
600
400
200
0
0
500
1000
1500
Time [s]

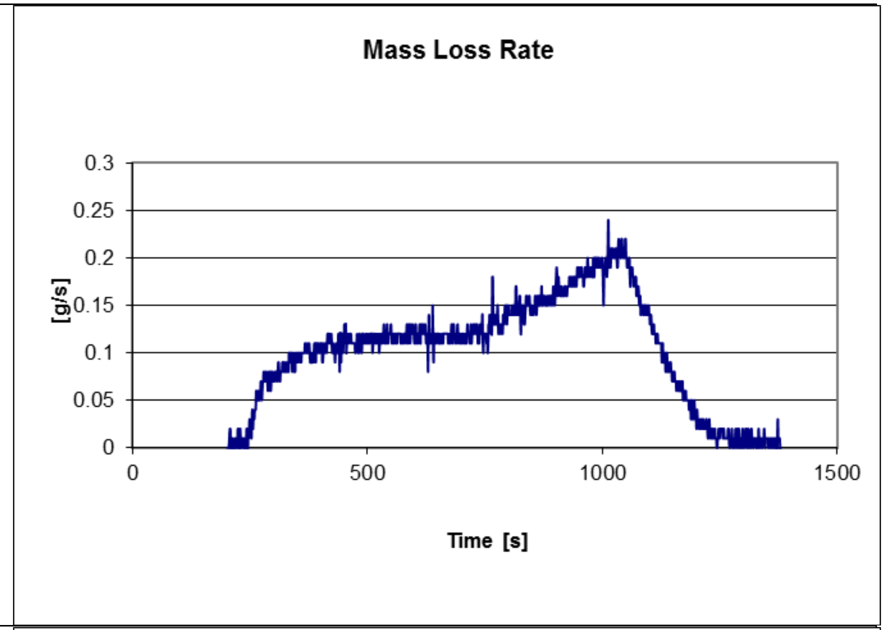
Mass Loss Rate
[g/s]
0.3
0.25
0.2
0.15
0.1
0.05
0
0
500
1000
1500
Time [s]

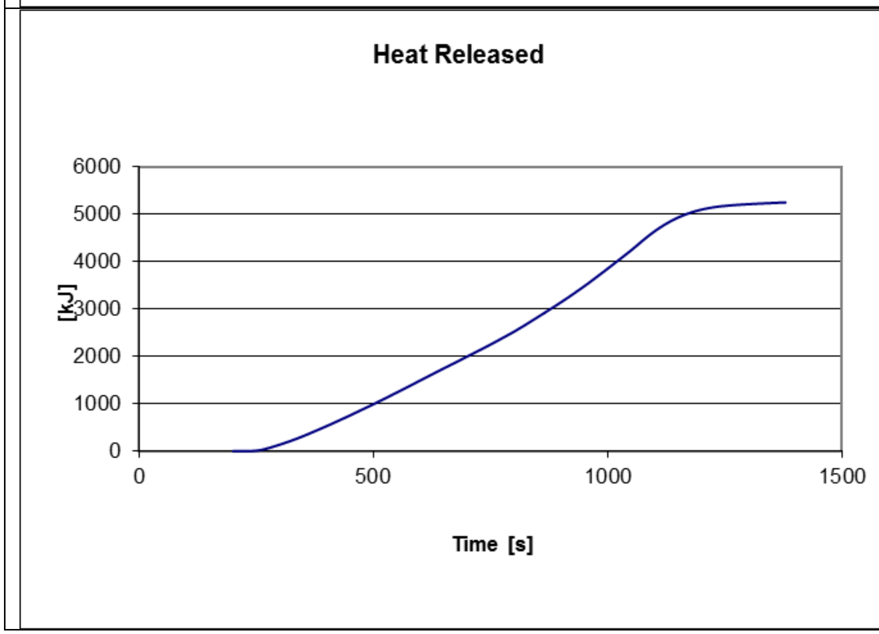
Heat Released
[kJ]
6000
5000
4000
3000
2000
1000
0
0
500
1000
1500
Time [s]

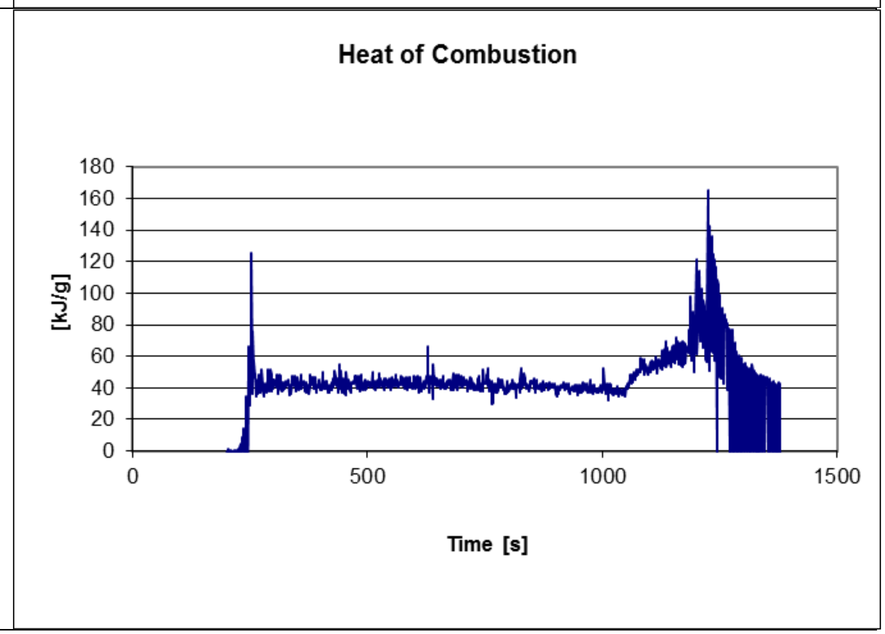
Heat of Combustion
[kJ/g]
180
160
140
120
100
80
60
40
20
0
0
500
1000
1500
Time [s]

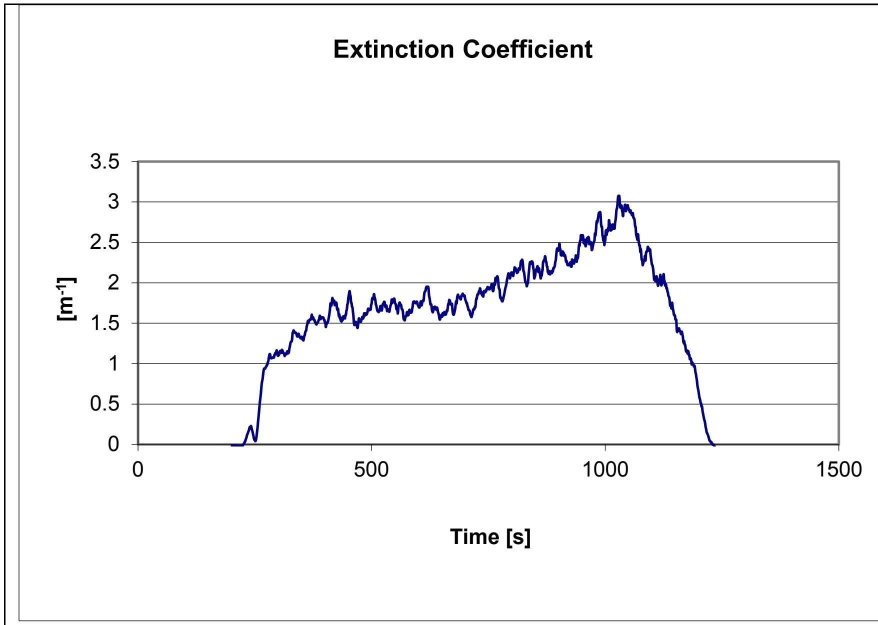
Extinction Coefficient
3.5
3
2.5
2
1.5
1
0.5
0
[m-1]
0
500
1000
1500
Time [s]

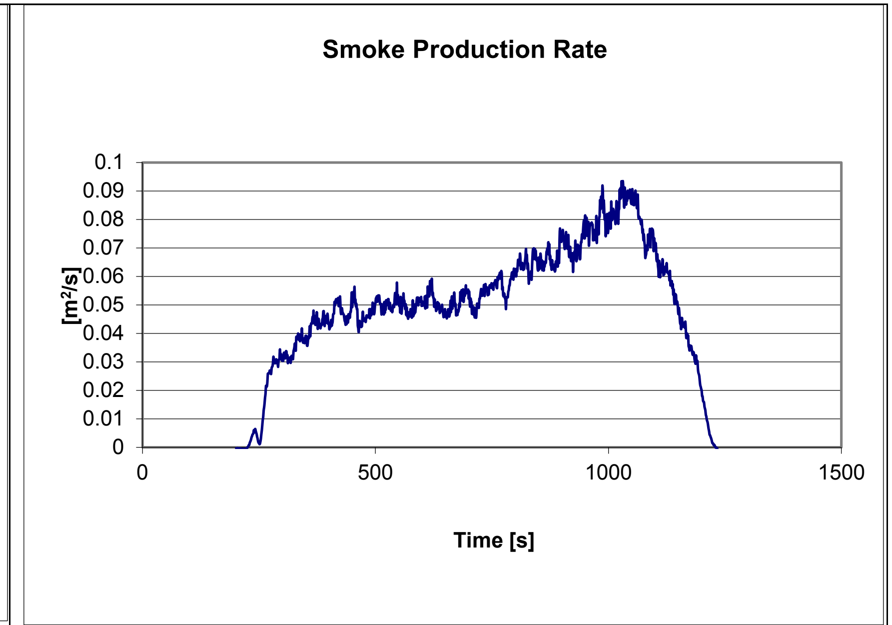
Smoke Production Rate
0.1
0.09
0.08
0.07
0.06
0.05
0.04
0.03
0.02
0.01
0
[m²/s]
0
500
1000
1500
Time [s]

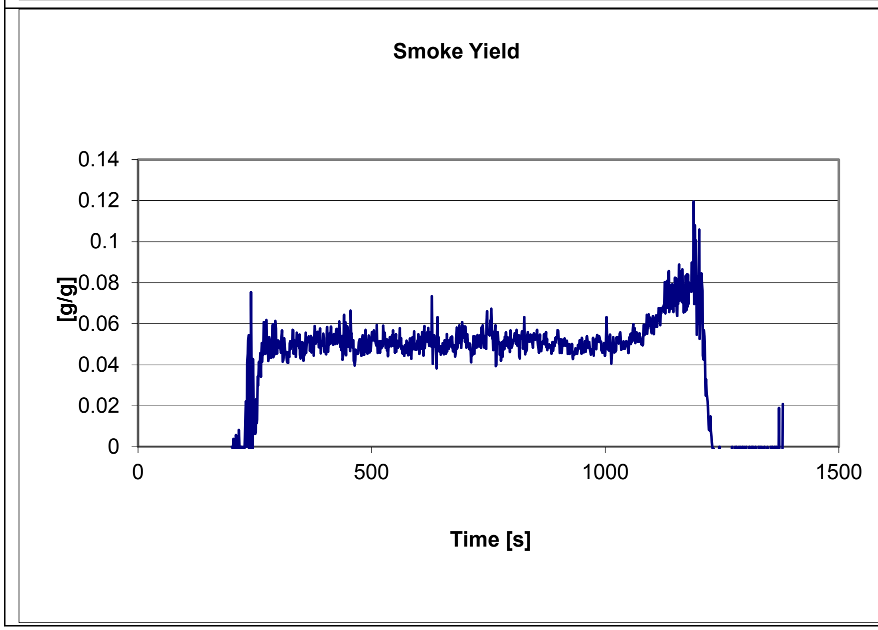
Smoke Yield
0.14
0.12
0.1
0.08
0.06
0.04
0.02
0
[g/g]
0
500
1000
1500
Time [s]

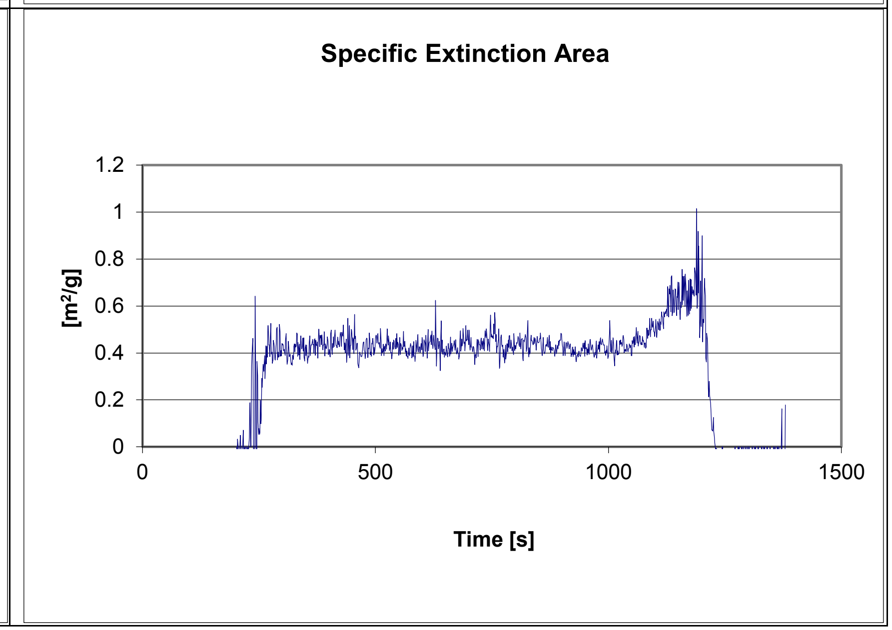
Specific Extinction Area
1.2
1
0.8
0.6
0.4
0.2
0
[m²/g]
0
500
1000
1500
Time [s]

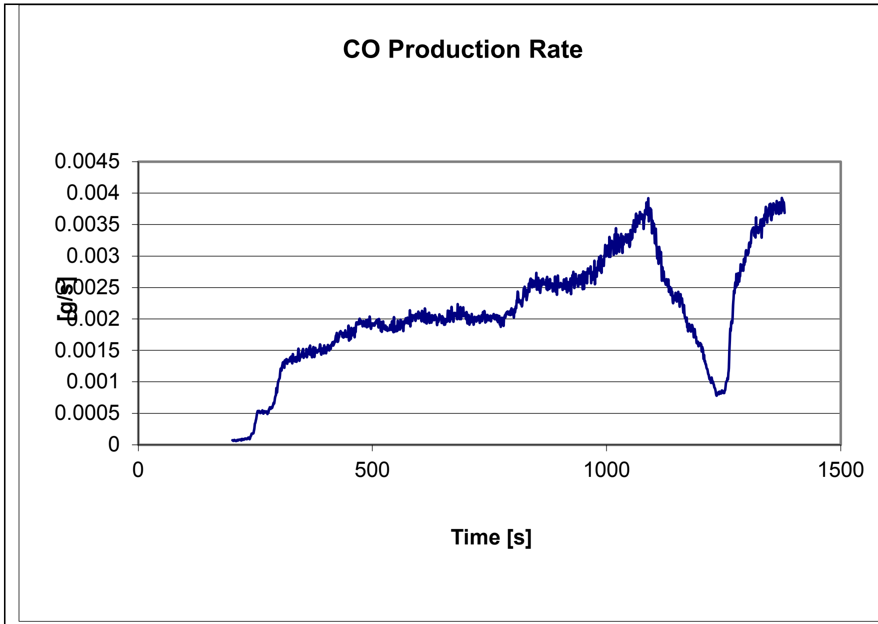
CO Production Rate
[g/s]
0.0045
0.004
0.0035
0.003
0.0025
0.002
0.0015
0.001
0.0005
0
0
500
1000
1500
Time [s]

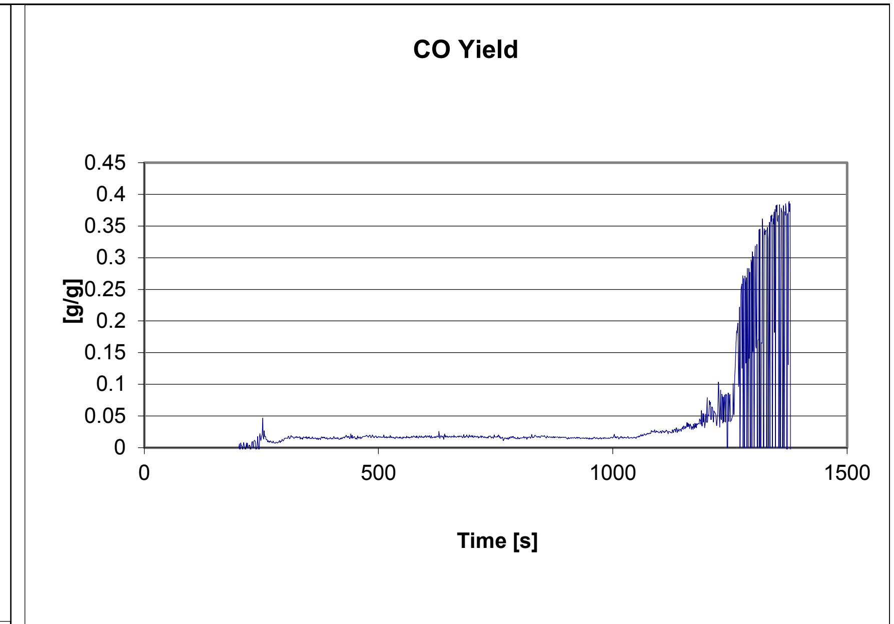
CO Yield
[g/g]
0.45
0.4
0.35
0.3
0.25
0.2
0.15
0.1
0.05
0
0
500
1000
1500
Time [s]

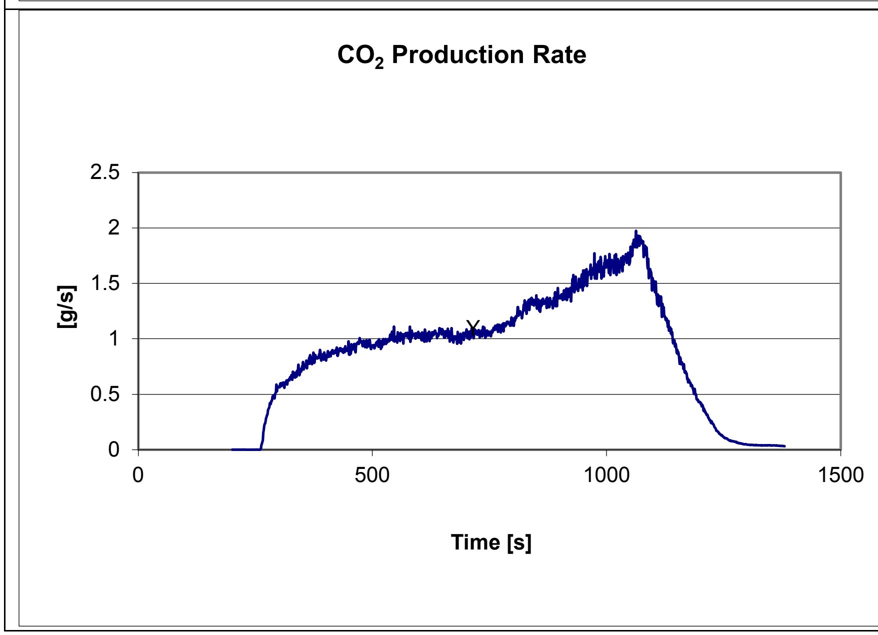
CO_2 Production Rate
[g/s]
2.5
2
1.5
1
0.5
0
0
500
1000
1500
X
Time [s]

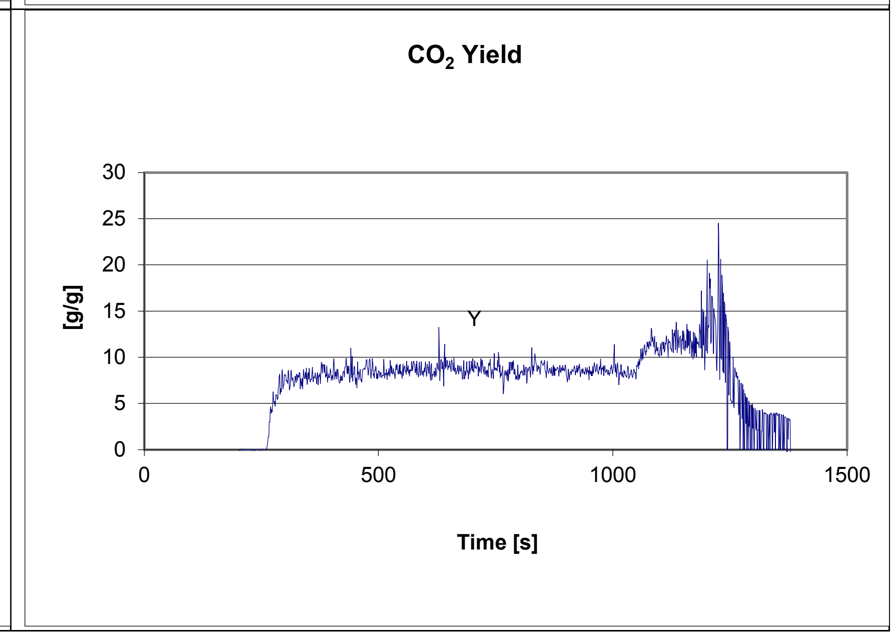
CO_2 Yield
[g/g]
30
25
20
15
10
5
0
0
500
1000
1500
Y
Time [s]

E.8 Thermoplastic Test 8 – Black HDPE Sample 2

Cone Calorimeter Test Run Data

Dept. of Fire Protection Engineering

100 Institute Road
Worcester, MA 01609
Phone: (508) 831-5628
Fax: (508) 831-5862

Test Information

Test Number:	Test 08
Specimen Identification:	Black High Density Polyethylene Sample 02
Material Name:	Black HDPE 02
Manufacturer/Submitter:	Not Reported
Sample Description:	Black half-inch thick panel, 4 TCs
Raw Data File Name:	Test_08_Black_HDPE_02.txt
Reduced Data File Name:	Test_08_Black_HDPE_02.xls
Date of Test:	6/30/2009
Tester:	Randy Harris

Test Parameters

Ambient Temperature:	76 F
Relative Humidity:	49 %
Heat Flux:	50 kW/m^2
Exhaust Duct Flow Rate:	30 g/s
Orientation:	Horizontal
Specimen Holder:	TRUE
Specimen Preparation:	2 layer foil
Notes:	1" Separation

Specimen Information

Specimen Color:	[]	Black
Specimen Thickness:	[mm]	12.6
Specimen Test Area:	[m^2]	0.0088
Specimen Initial Mass:	[g]	124.9
Specimen Final Mass:	[g]	1.1
Specimen Density:	[g/cm^3]	1.0
Mass Lost:	[g]	123.9
Total Heat Evolved:	[kJ]	5044

Test Times [s]

Shutter Open:	242
Time to Ignition:	298
Flameout:	1441
Clean Air/End of Test:	1459

Daily C-Factor

0.041

The Peak, Average and Total parameters are computed over the test period ignition to flame out. There are 4 exceptions. The first three involve initial heat release rate averages for periods after ignition of 60, 180 and 300 seconds. The final involves the average mass loss rate which is computed over the time period from 10% mass loss to 90% mass loss.

Parameter	Unit	Value
Heat Release		
Peak Heat Release Rate	[kW/m^2]	969
Average Heat Release Rate	[kW/m^2]	499
Total Heat Release	[MJ/m^2]	571
Average HRR for the first 60s	[kW/m^2]	273
Average HRR for the first 180s	[kW/m^2]	358
Average HRR for the first 300s	[kW/m^2]	400
Peak Heat of Combustion	[kJ/g]	121
Average Heat of Combustion	[kJ/g]	39
Smoke Obscuration		
Peak SEA	[m^2/g]	1.965
Average SEA	[m^2/g]	0.132
Peak Smoke Yield	[g/g]	0.231
Average Smoke Yield	[g/g]	0.016
Peak Smoke Production Rate	[m^2/s]	0.092
Average Smoke Production Rate	[m^2/s]	0.020
Total Smoke Release	[m^2]	11.760
Gas Production Rates		
Peak Carbon Monoxide	[g/s]	0.004
Average Carbon Monoxide	[g/s]	0.002
Peak Carbon Dioxide	[g/s]	2.297
Average Carbon Dioxide	[g/s]	1.169
Mass Loss		
Peak Mass Loss Rate	[g/s]	0.230
Average Mass Lass Rate	[g/s]	0.131
Initial Mass	[g]	124.9
Final Mass	[g]	1.1
Mass Loss Fraction	[]	0.99
Burn Time		
Time to Ignition	[s]	56
Duration of Flaming	[s]	1143
Duration of Test	[s]	1217

Observations

Time	Observation
265	White Smoke Surface very fluid after ignition

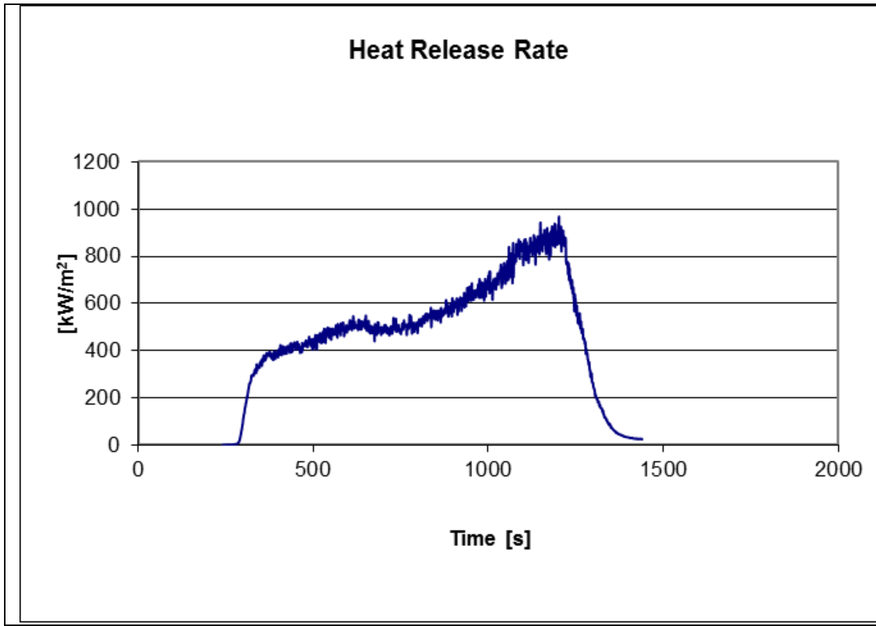
Heat Release Rate
1200
1000
800
600
400
200
0
[kW/m²]
0
500
1000
1500
2000
Time [s]

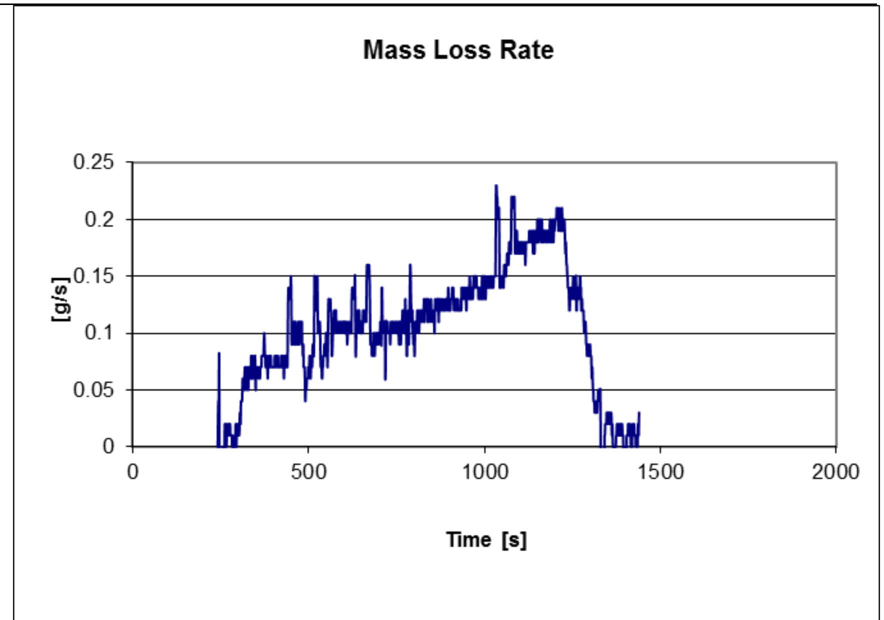
Mass Loss Rate
0.25
0.2
0.15
0.1
0.05
0
[g/s]
0
500
1000
1500
2000
Time [s]

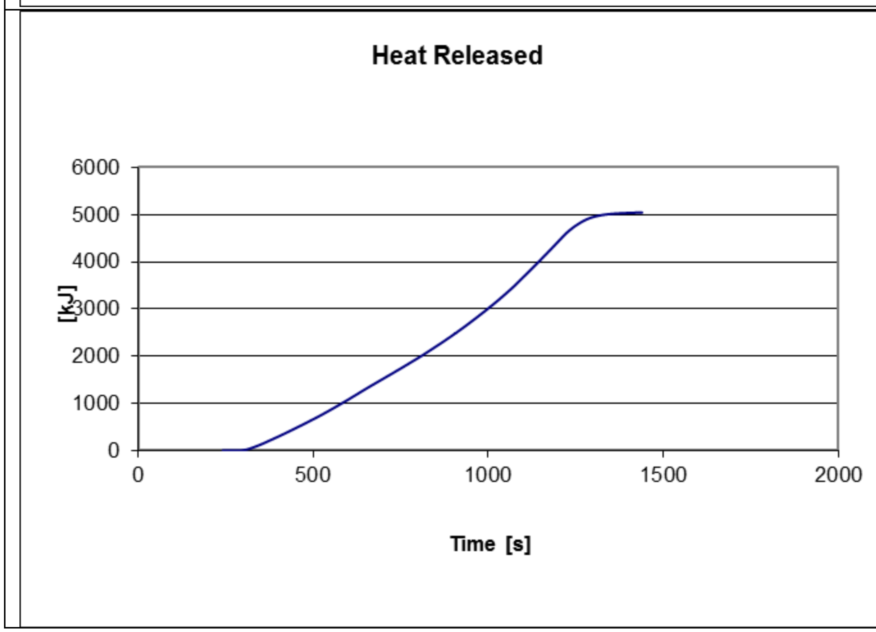
Heat Released
6000
5000
4000
3000
2000
1000
0
[kJ]
0
500
1000
1500
2000
Time [s]

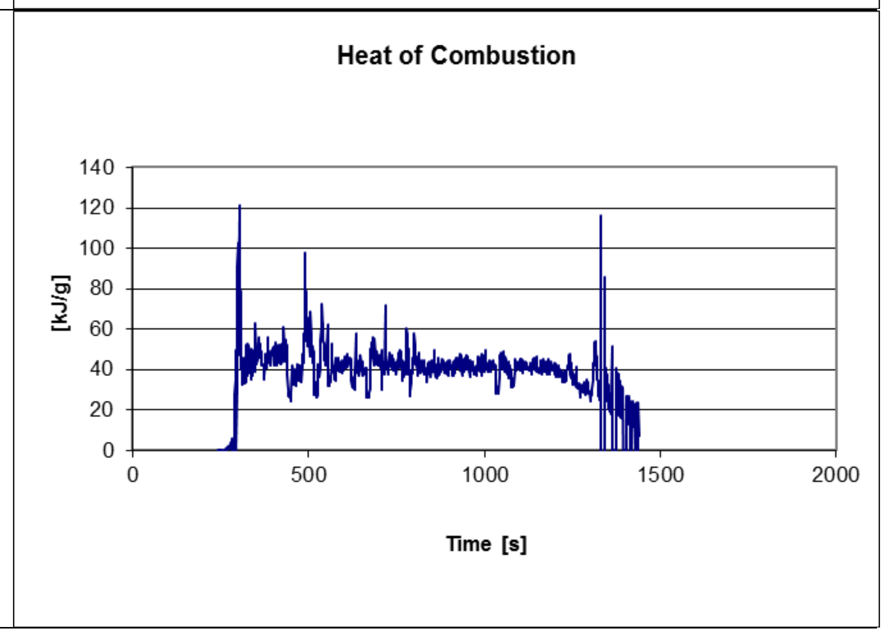
Heat of Combustion
140
120
100
80
60
40
20
0
[kJ/g]
0
500
1000
1500
2000
Time [s]

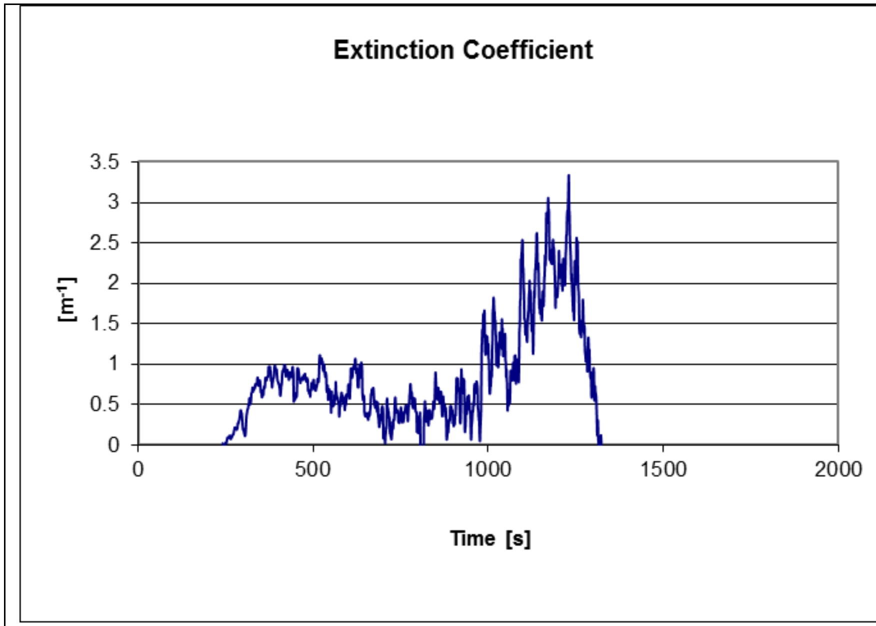
Extinction Coefficient
3.5
3
2.5
2
1.5
1
0.5
0
[m-1]
0
500
1000
1500
2000
Time [s]

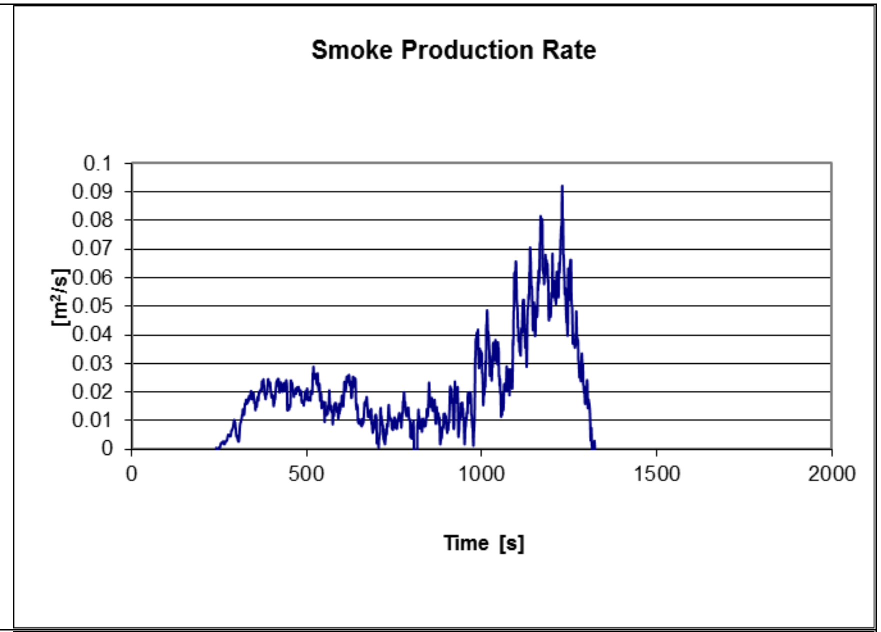
Smoke Production Rate
0.1
0.09
0.08
0.07
0.06
0.05
0.04
0.03
0.02
0.01
0
[m2/s]
0
500
1000
1500
2000
Time [s]

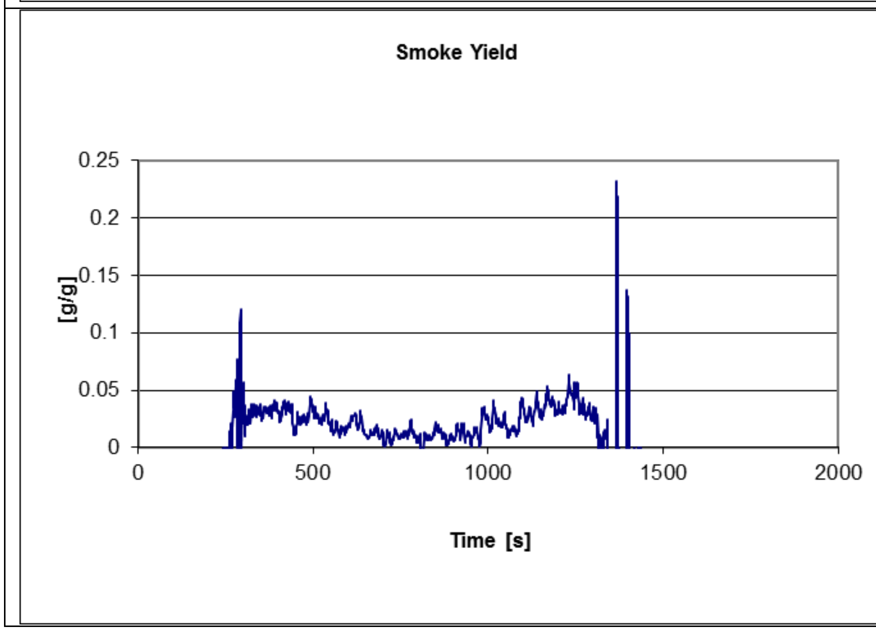
Smoke Yield
0.25
0.2
0.15
0.1
0.05
0
[g/g]
0
500
1000
1500
2000
Time [s]

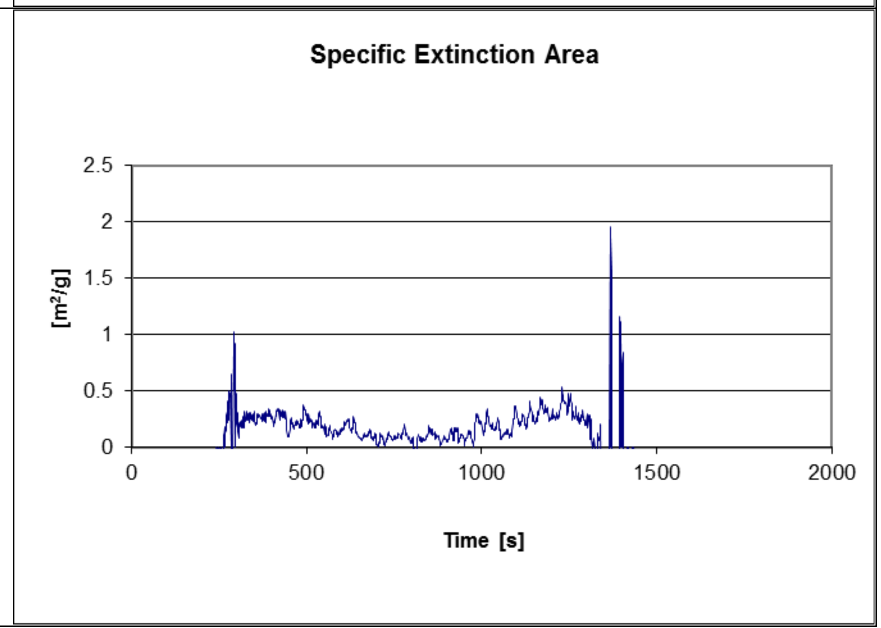
Specific Extinction Area
2.5
2
1.5
1
0.5
0
[m2/g]
0
500
1000
1500
2000
Time [s]

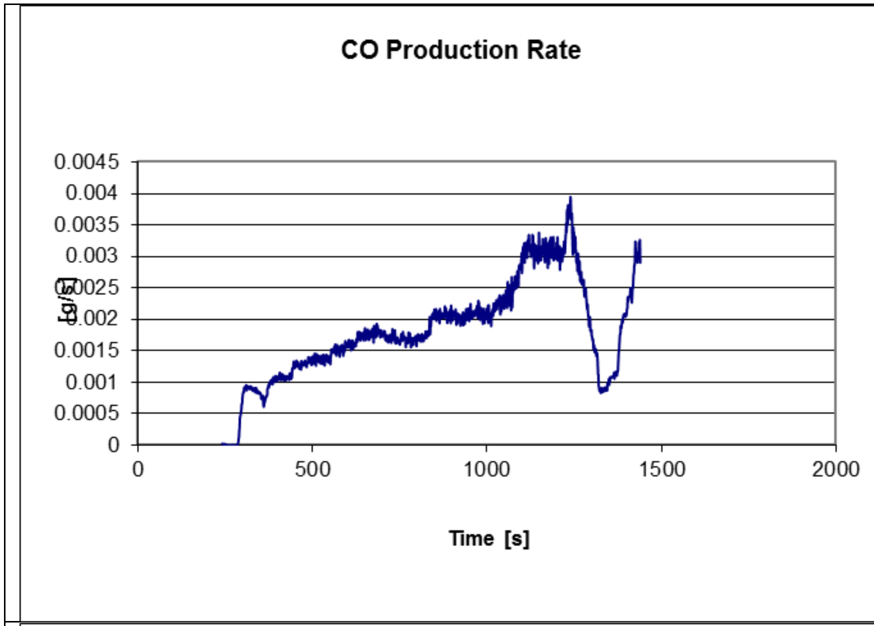
CO Production Rate
[g/s]
0.0045
0.004
0.0035
0.003
0.0025
0.002
0.0015
0.001
0.0005
0
0
500
1000
1500
2000
Time [s]

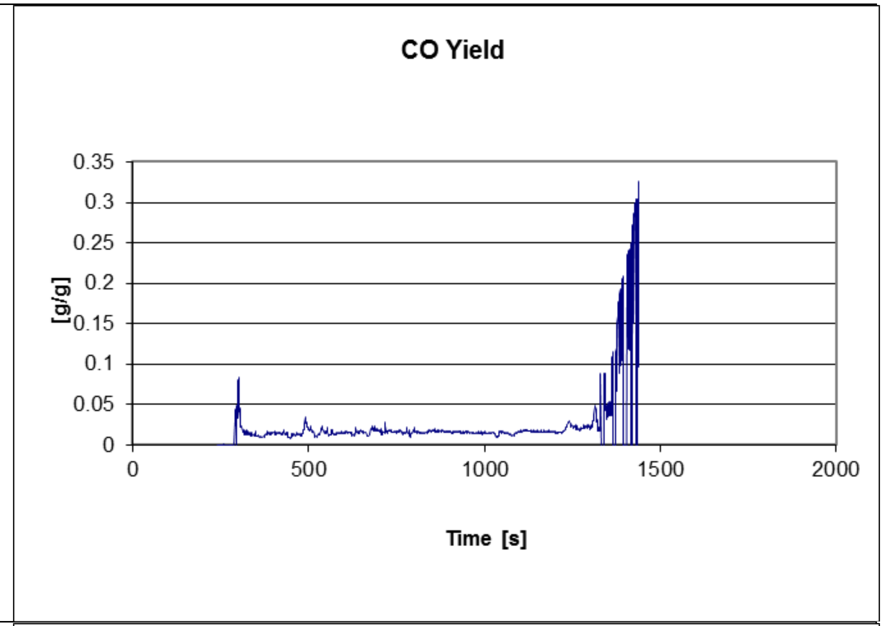
CO Yield
[g/g]
0.35
0.3
0.25
0.2
0.15
0.1
0.05
0
0
500
1000
1500
2000
Time [s]

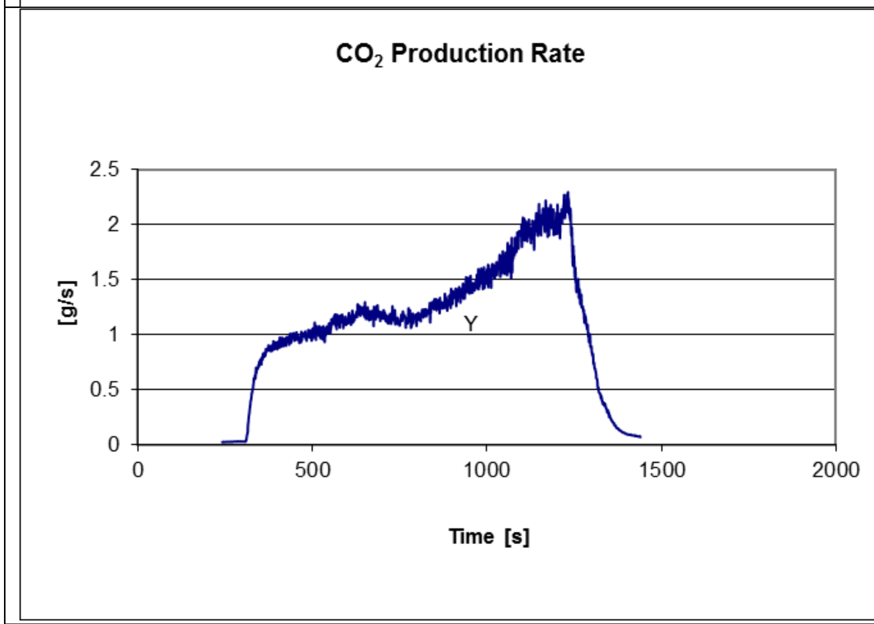
CO_2 Production Rate
[g/s]
2.5
2
1.5
1
0.5
0
Y
0
500
1000
1500
2000
Time [s]

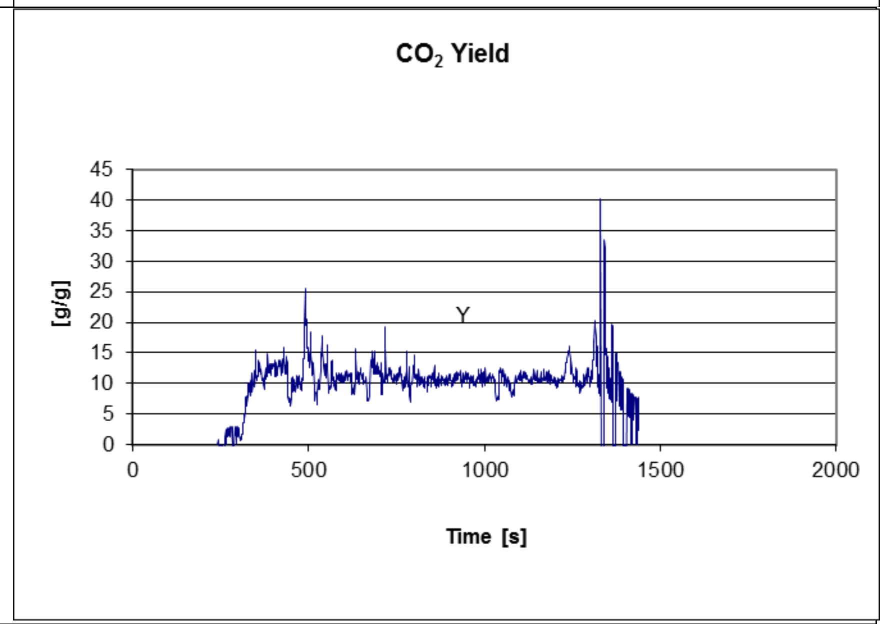
CO_2 Yield
[g/g]
45
40
35
30
25
20
15
10
5
0
Y
0
500
1000
1500
2000
Time [s]

TC Locations

	Depth from side	Height from bottom
1	40.5mm	9.5mm
2	40.5mm	4.5mm

From Left Side

102mm

50mm	x 1
50.5mm	x 2

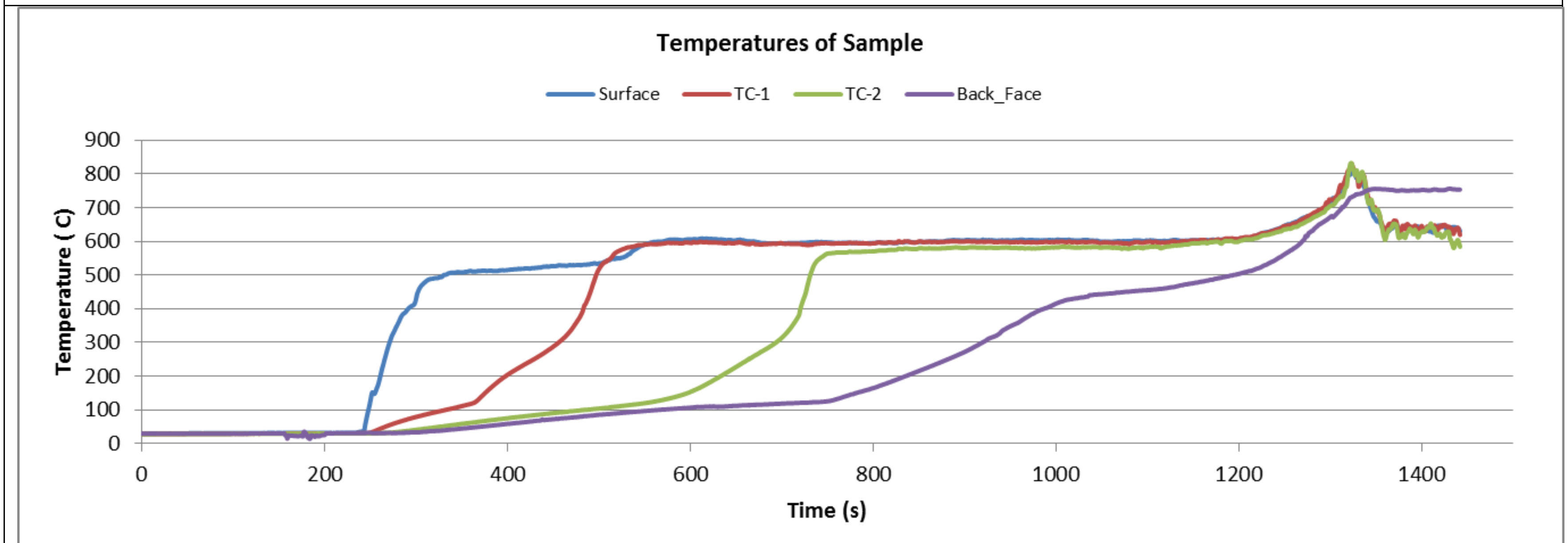

E.9 Thermoplastic Test 9 – Black HDPE Sample 3

Cone Calorimeter Test Run Data

Dept. of Fire Protection Engineering

100 Institute Road
Worcester, MA 01609
Phone: (508) 831-5628
Fax: (508) 831-5862

Test Information

Test Number:	Test 09
Specimen Identification:	Black High Density Polyethylene Sample 03
Material Name:	Black HDPE 03
Manufacturer/Submitter:	Not Reported
Sample Description:	Black half-inch thick panel, 4 TCs
Raw Data File Name:	Test_09_Black_HDPE_03.txt
Reduced Data File Name:	Test_09_Black_HDPE_03.xls
Date of Test:	6/30/2009
Tester:	Randy Harris

Test Parameters

Ambient Temperature:	76	F
Relative Humidity:	48	%
Heat Flux:	50	kW/m^2
Exhaust Duct Flow Rate:		30 g/s
Orientation:		Horizontal
Specimen Holder:		TRUE
Specimen Preparation:		2 layer foil
Notes:		1" Separation

Specimen Information

Specimen Color:	[]	Black
Specimen Thickness:	[mm]	12.6
Specimen Test Area:	[m^2]	0.0088
Specimen Initial Mass:	[g]	122.0
Specimen Final Mass:	[g]	0.1
Specimen Density:	[g/cm^3]	1.0
Mass Lost:	[g]	122.0
Total Heat Evolved:	[kJ]	4989

Test Times [s]

Shutter Open:	284
Time to Ignition:	340
Flameout:	1415
Clean Air/End of Test:	1149

Daily C-Factor

	0.041

The Peak, Average and Total parameters are computed over the test period ignition to flame out. There are 4 exceptions. The first three involve initial heat release rate averages for periods after ignition of 60, 180 and 300 seconds. The final involves the average mass loss rate which is computed over the time period from 10% mass loss to 90% mass loss.

Parameter	Unit	Value
Heat Release		
Peak Heat Release Rate	[kW/m^2]	1066
Average Heat Release Rate	[kW/m^2]	525
Total Heat Release	[MJ/m^2]	565
Average HRR for the first 60s	[kW/m^2]	240
Average HRR for the first 180s	[kW/m^2]	327
Average HRR for the first 300s	[kW/m^2]	388
Peak Heat of Combustion	[kJ/g]	107
Average Heat of Combustion	[kJ/g]	39
Smoke Obscuration		
Peak SEA	[m^2/g]	7.609
Average SEA	[m^2/g]	-0.241
Peak Smoke Yield	[g/g]	0.895
Average Smoke Yield	[g/g]	-0.028
Peak Smoke Production Rate	[m^2/s]	0.040
Average Smoke Production Rate	[m^2/s]	-0.008
Total Smoke Release	[m^2]	12.734
Gas Production Rates		
Peak Carbon Monoxide	[g/s]	0.004
Average Carbon Monoxide	[g/s]	0.002
Peak Carbon Dioxide	[g/s]	2.650
Average Carbon Dioxide	[g/s]	1.231
Mass Loss		
Peak Mass Loss Rate	[g/s]	0.230
Average Mass Lass Rate	[g/s]	0.133
Initial Mass	[g]	122.0
Final Mass	[g]	0.1
Mass Loss Fraction	[]	1.00
Burn Time		
Time to Ignition	[s]	56
Duration of Flaming	[s]	1075
Duration of Test	[s]	865

Observations

Time	Observation
295	Surface TC lost contact
1320	Cellular flame

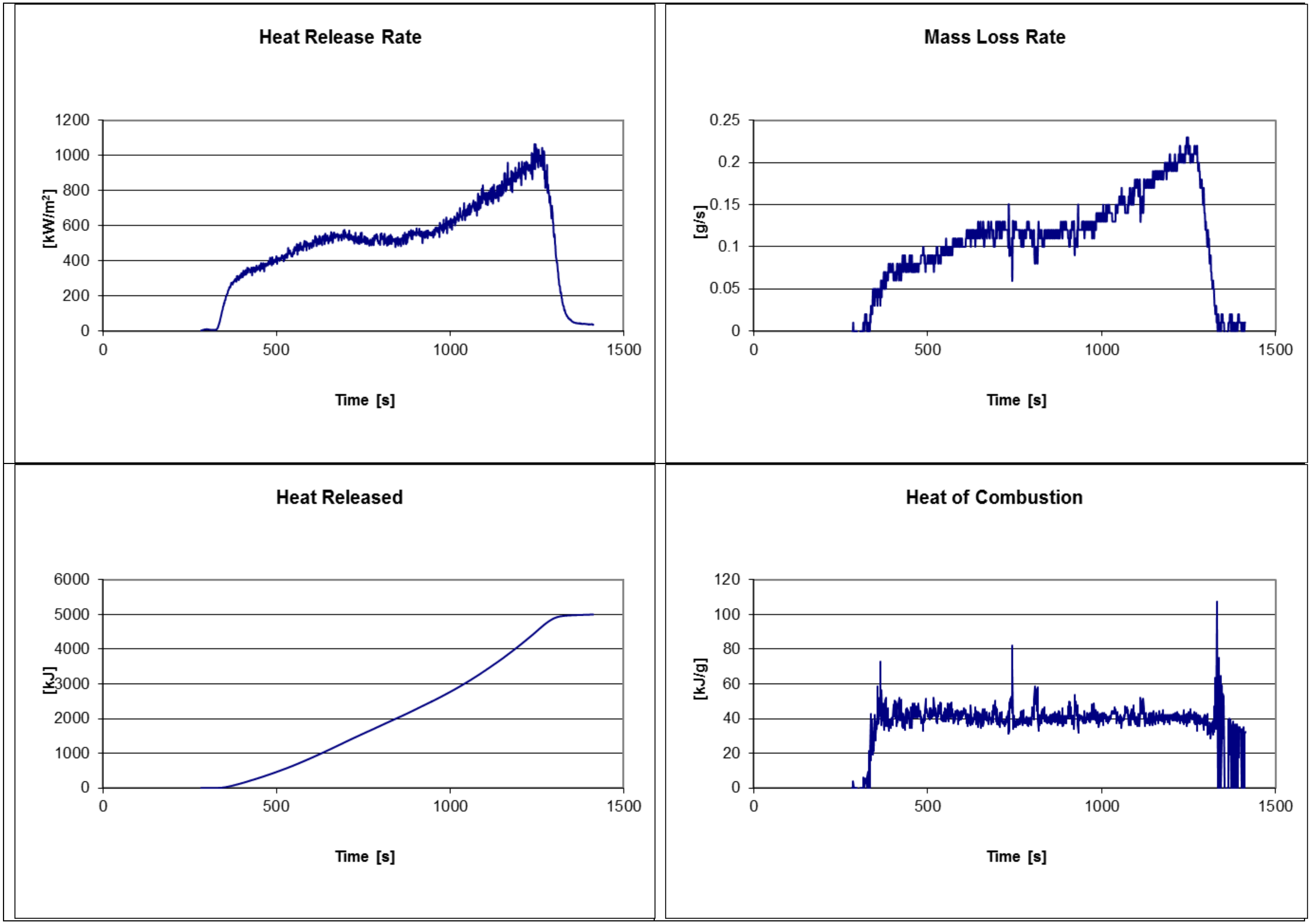
Heat Release Rate
[kW/m²]
1200
1000
800
600
400
200
0
0
500
1000
1500
Time [s]
Mass Loss Rate
[g/s]
0.25
0.2
0.15
0.1
0.05
0
0
500
1000
1500
Time [s]
Heat Released
[kJ]
6000
5000
4000
3000
2000
1000
0
0
500
1000
1500
Time [s]
Heat of Combustion
[kJ/g]
120
100
80
60
40
20
0
0
500
1000
1500
Time [s]

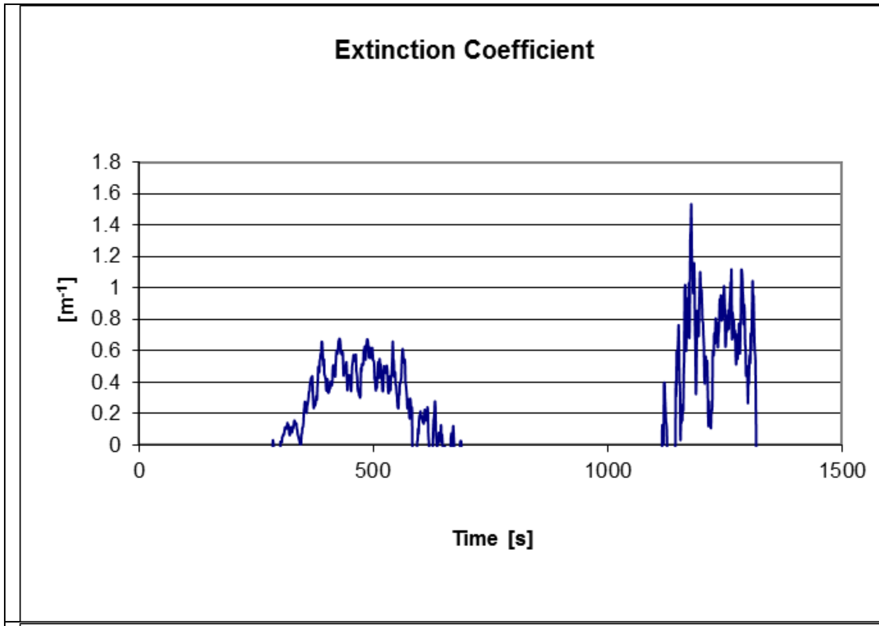
Extinction Coefficient
[m-1]
1.8
1.6
1.4
1.2
1
0.8
0.6
0.4
0.2
0
0
500
1000
1500
Time [s]

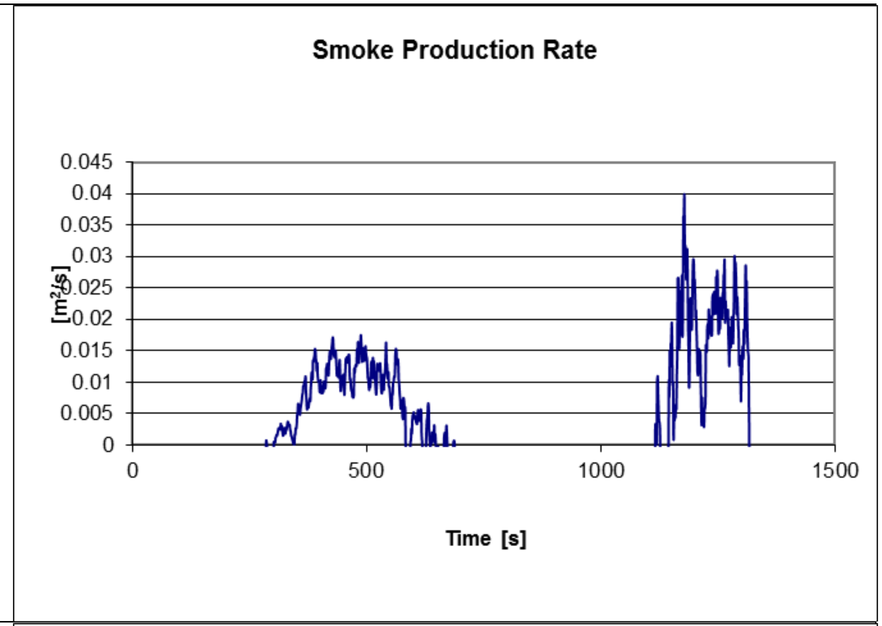
Smoke Production Rate
[m2/s]
0.045
0.04
0.035
0.03
0.025
0.02
0.015
0.01
0.005
0
0
500
1000
1500
Time [s]

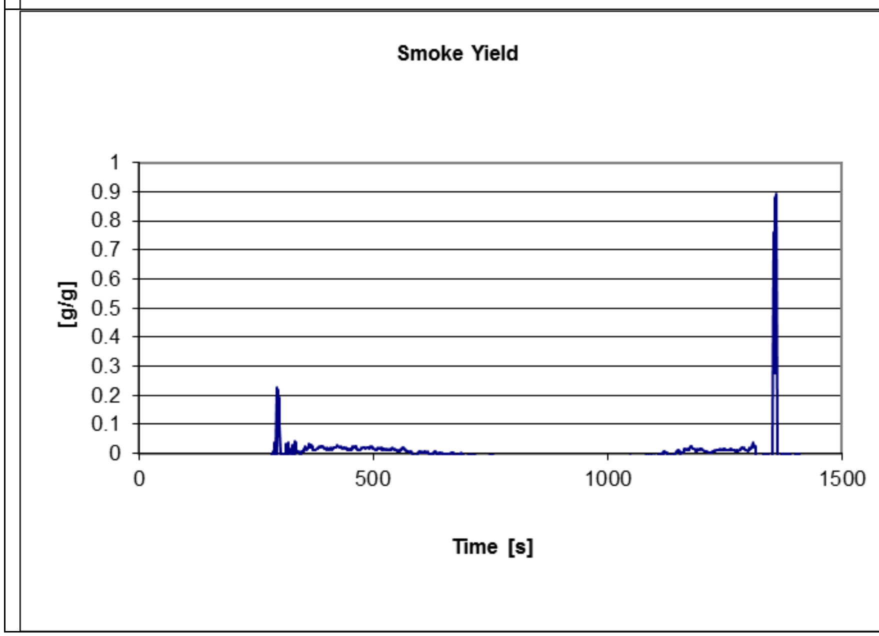
Smoke Yield
[g/g]
1
0.9
0.8
0.7
0.6
0.5
0.4
0.3
0.2
0.1
0
0
500
1000
1500
Time [s]

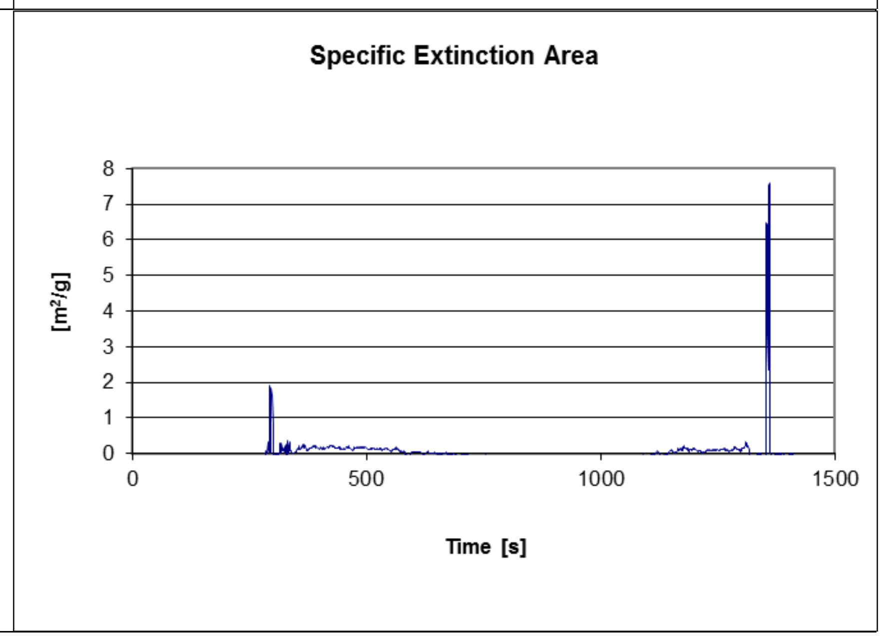
Specific Extinction Area
[m2/g]
8
7
6
5
4
3
2
1
0
0
500
1000
1500
Time [s]

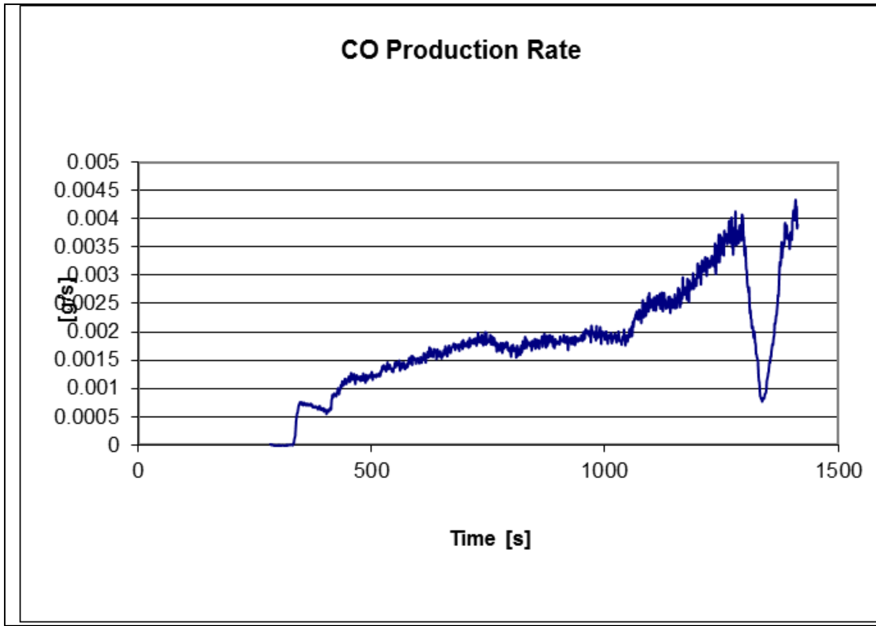
CO Production Rate
[g/s]
0
0.0005
0.001
0.0015
0.002
0.0025
0.003
0.0035
0.004
0.0045
0.005
0
500
1000
1500
Time [s]

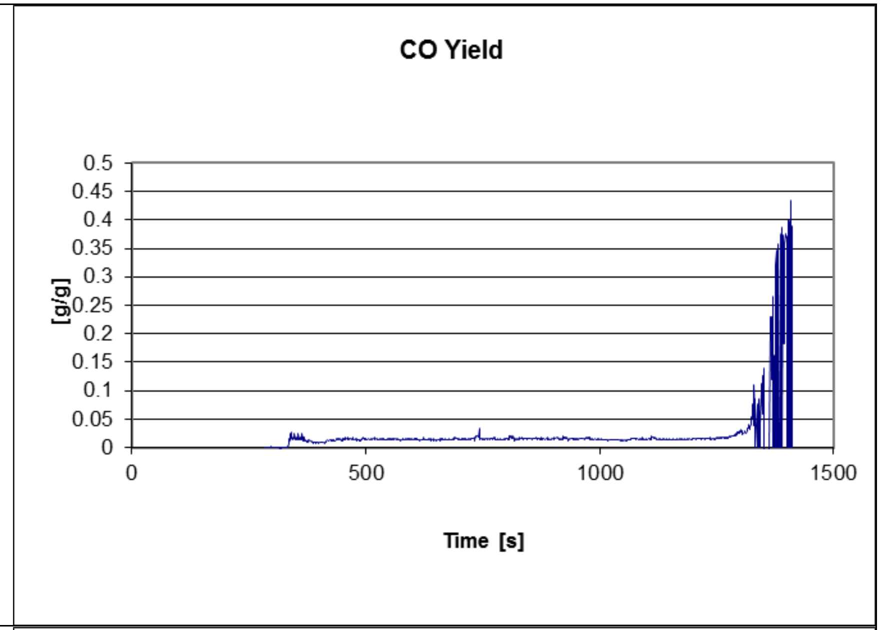
CO Yield
[g/g]
0
0.05
0.1
0.15
0.2
0.25
0.3
0.35
0.4
0.45
0.5
0
500
1000
1500
Time [s]

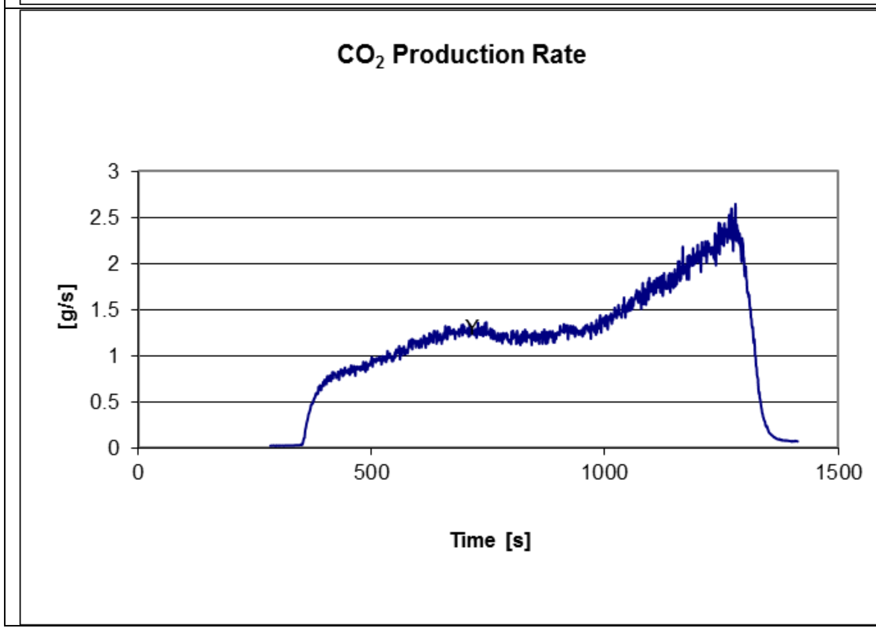
CO_2 Production Rate
[g/s]
0
0.5
1
1.5
2
2.5
3
0
500
1000
1500
Time [s]

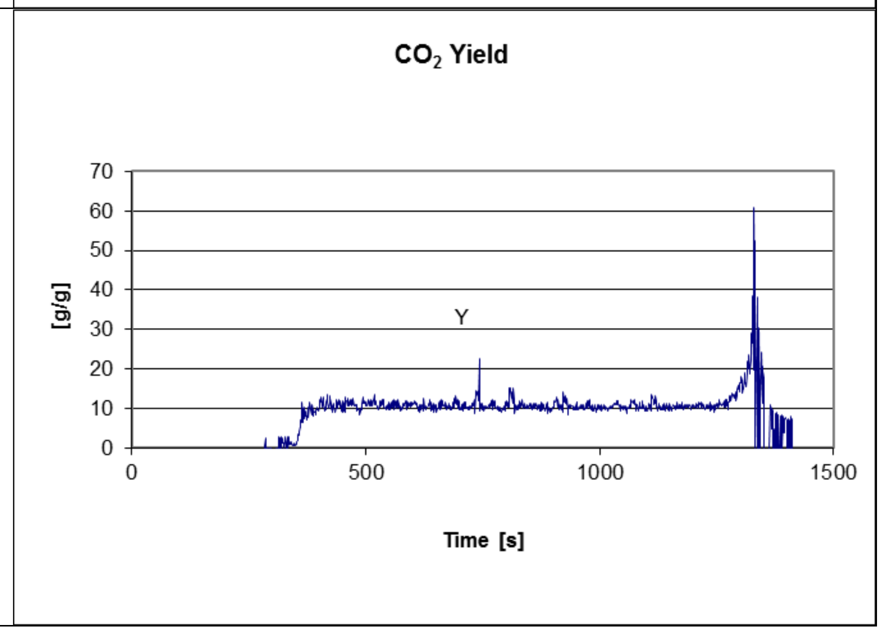
CO_2 Yield
[g/g]
Y
0
10
20
30
40
50
60
70
0
500
1000
1500
Time [s]

TC Locations

	Depth from side		Height from bottom
1	40.5mm	←	10mm
2	40.5mm	←	4.5mm

From Left Side

100mm	
51mm	x 1
50.5mm	x 2

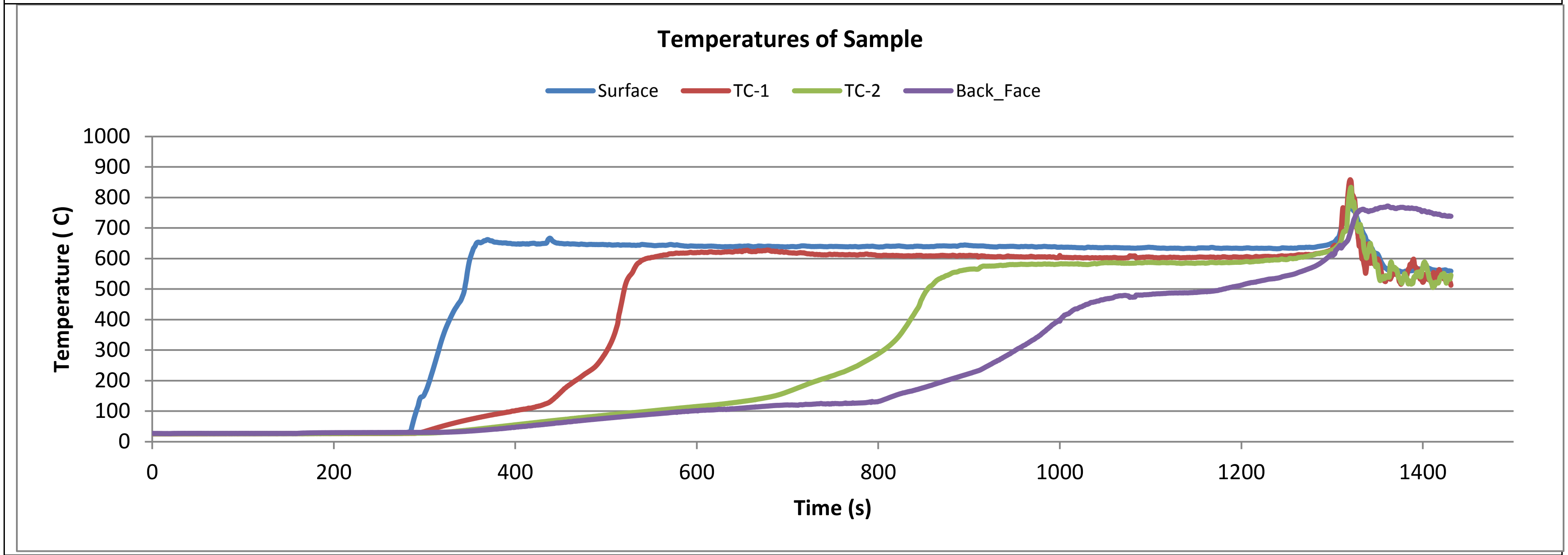

E.10 FRP Test 1 – External Flux at 25 kW/m², un-instrumented

Cone Calorimeter Test Run Data

Dept. of Fire Protection Engineering

100 Institute Road
Worcester, MA 01609
Phone: (508) 831-5628
Fax: (508) 831-5862

Test Information

Test Number:	3/5/2010 - 1
Specimen Identification:	FRP Specimen 1
Material Name:	Class C FRP
Manufacturer/Submitter:	Not Reported
Sample Description:	White, FRP panel
Raw Data File Name:	030410sample01.txt
Reduced Data File Name:	FRP Sample 01
Date of Test:	3/5/2010
Tester:	R. Hartwell

Test Parameters

Ambient Temperature:	70	F
Relative Humidity:	25	%
Heat Flux:	25	kW/m^2
Exhaust Duct Flow Rate:	30 g/s	
Orientation:	Horizontal	
Specimen Holder:	TRUE	
Specimen Preparation:	2 layer foil	
Notes:	1" Separation	

Specimen Information

Specimen Color:	[]	White
Specimen Thickness:	[mm]	1.9
Specimen Test Area:	[m^2]	0.0088
Specimen Initial Mass:	[g]	29.4
Specimen Final Mass:	[g]	15.9
Specimen Density:	[g/cm^3]	1.5
Mass Lost:	[g]	13.5
Total Heat Evolved:	[kJ]	228

Test Times [s]

Shutter Open:	191
Time to Ignition:	297
Flameout:	653
Clean Air/End of Test:	659

Daily C-Factor

	0.045

The Peak, Average and Total parameters are computed over the test period ignition to flame out. There are 4 exceptions. The first three involve initial heat release rate averages for periods after ignition of 60, 180 and 300 seconds. The final involves the average mass loss rate which is computed over the time period from 10% mass loss to 90% mass loss.

Parameter	Unit	Value
Heat Release		
Peak Heat Release Rate	[kW/m^2]	233
Average Heat Release Rate	[kW/m^2]	73
Total Heat Release	[MJ/m^2]	26
Average HRR for the first 60s	[kW/m^2]	212
Average HRR for the first 180s	[kW/m^2]	124
Average HRR for the first 300s	[kW/m^2]	85
Peak Heat of Combustion	[kJ/g]	160
Average Heat of Combustion	[kJ/g]	20
Smoke Obscuration		
Peak SEA	[m^2/g]	1.668
Average SEA	[m^2/g]	0.362
Peak Smoke Yield	[g/g]	0.196
Average Smoke Yield	[g/g]	0.043
Peak Smoke Production Rate	[m^2/s]	0.093
Average Smoke Production Rate	[m^2/s]	0.020
Total Smoke Release	[m^2]	7.349
Gas Production Rates		
Peak Carbon Monoxide	[g/s]	0.003
Average Carbon Monoxide	[g/s]	0.001
Peak Carbon Dioxide	[g/s]	0.499
Average Carbon Dioxide	[g/s]	0.209
Mass Loss		
Peak Mass Loss Rate	[g/s]	0.120
Average Mass Lass Rate	[g/s]	0.045
Initial Mass	[g]	29.4
Final Mass	[g]	15.9
Mass Loss Fraction	[]	0.46
Burn Time		
Time to Ignition	[s]	106
Duration of Flaming	[s]	356
Duration of Test	[s]	468

Observations

Time	Observation
230	white smoke
246	crackling
290	flashes
300	cellular flame in center, then spread to 4 edges
400	edge burning
550	corner burning
	After test, center of surface in a circular pattern, is white. specimen surface outside of center is black

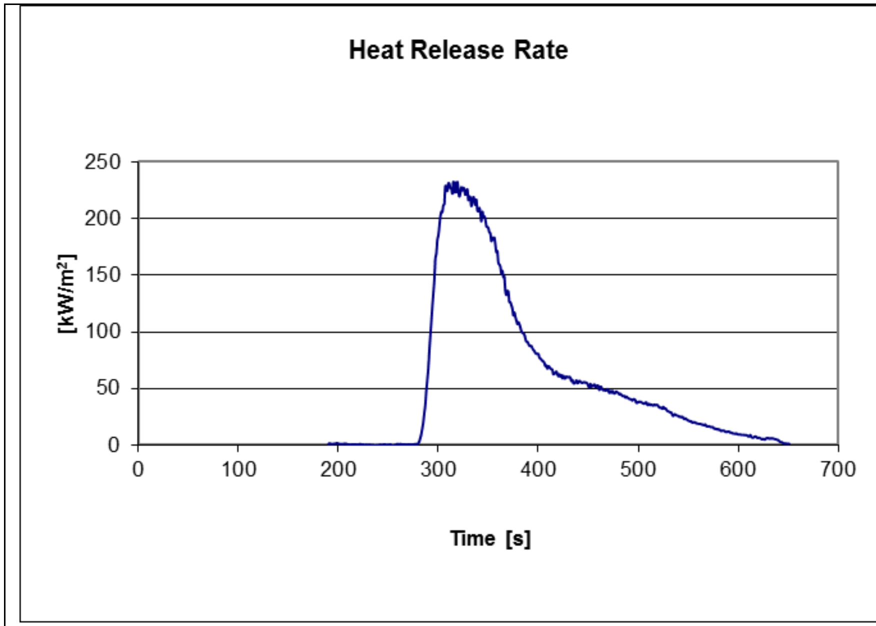
Heat Release Rate
[kW/m²]
250
200
150
100
50
0
0
100
200
300
400
500
600
700
Time [s]

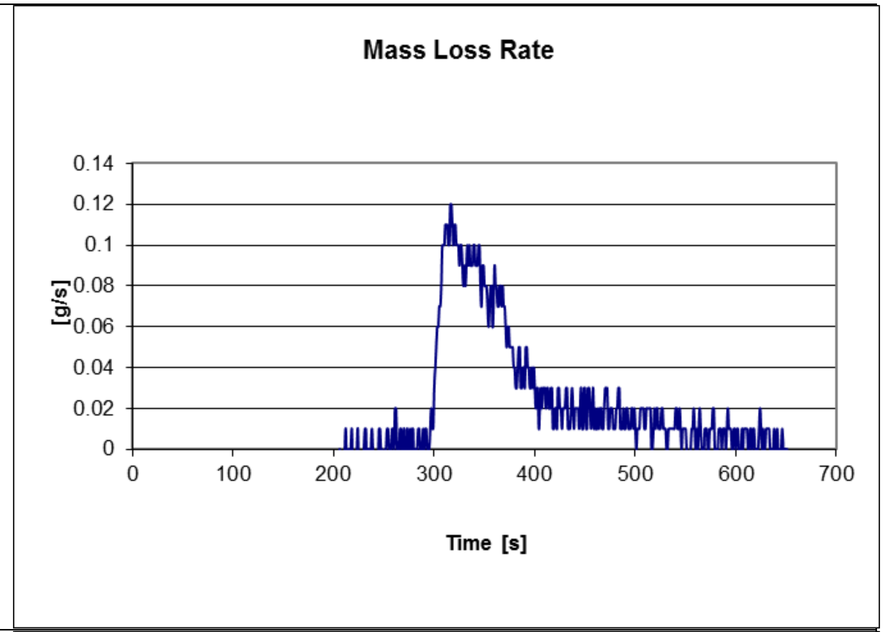
Mass Loss Rate
[g/s]
0.14
0.12
0.1
0.08
0.06
0.04
0.02
0
0
100
200
300
400
500
600
700
Time [s]

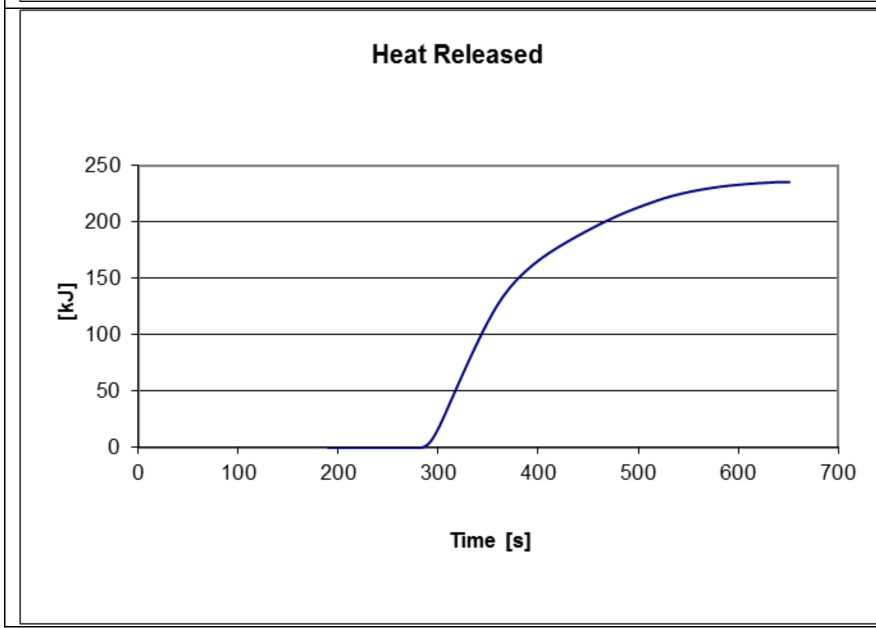
Heat Released
[kJ]
250
200
150
100
50
0
0
100
200
300
400
500
600
700
Time [s]

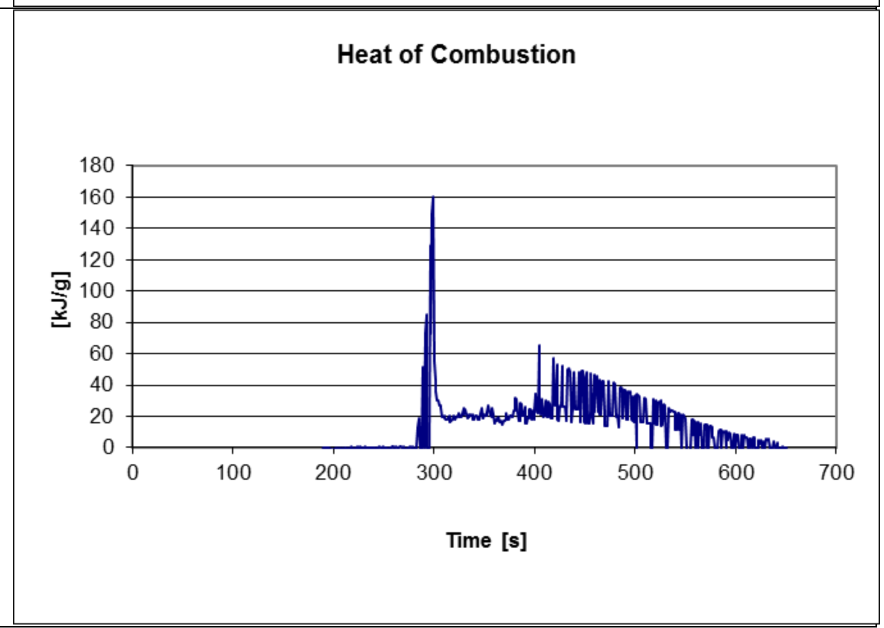
Heat of Combustion
[kJ/g]
180
160
140
120
100
80
60
40
20
0
0
100
200
300
400
500
600
700
Time [s]

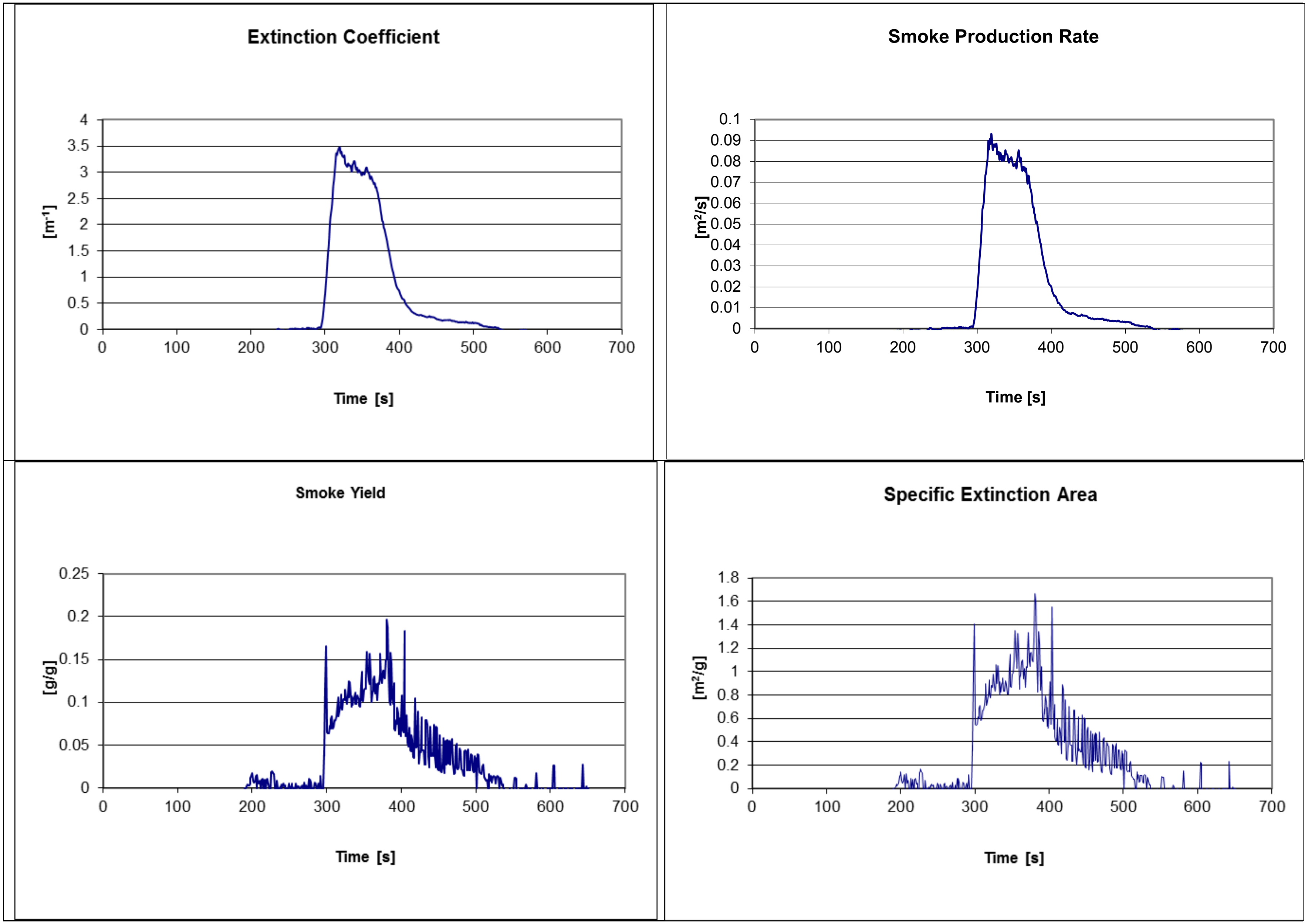

Extinction Coefficient
[m-1]
Time [s]
Smoke Production Rate
[m2/s]
Time [s]
Smoke Yield
[g/g]
Time [s]
Specific Extinction Area
[m2/g]
Time [s]

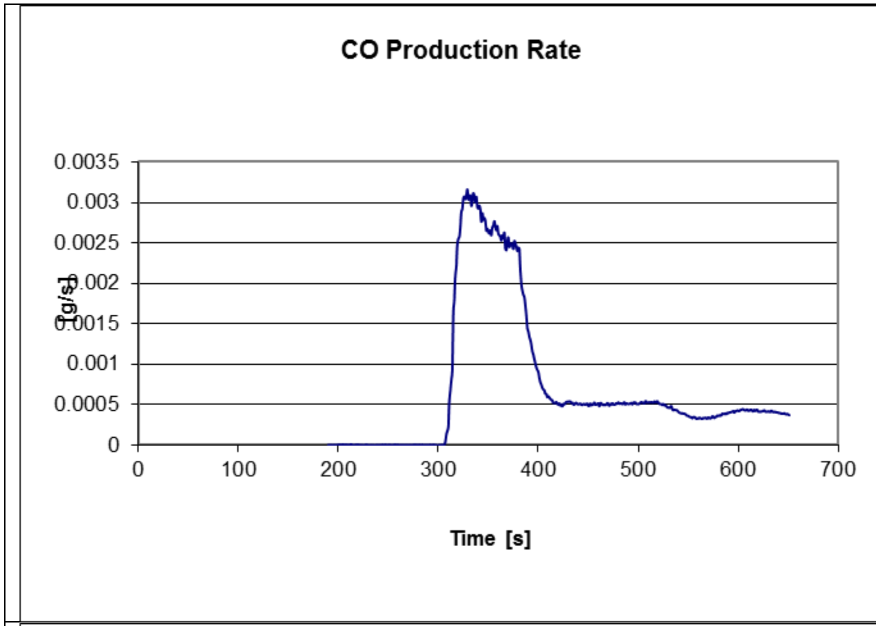
CO Production Rate
0.0035
0.003
0.0025
0.002
0.0015
0.001
0.0005
0
[g/s]
0
100
200
300
400
500
600
700
Time [s]

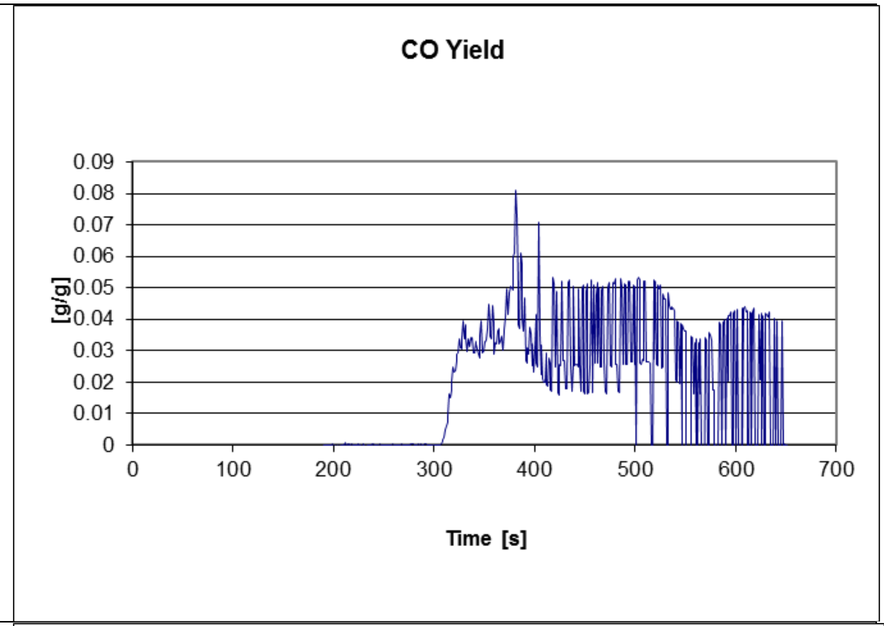
CO Yield
0.09
0.08
0.07
0.06
0.05
0.04
0.03
0.02
0.01
0
[g/g]
0
100
200
300
400
500
600
700
Time [s]

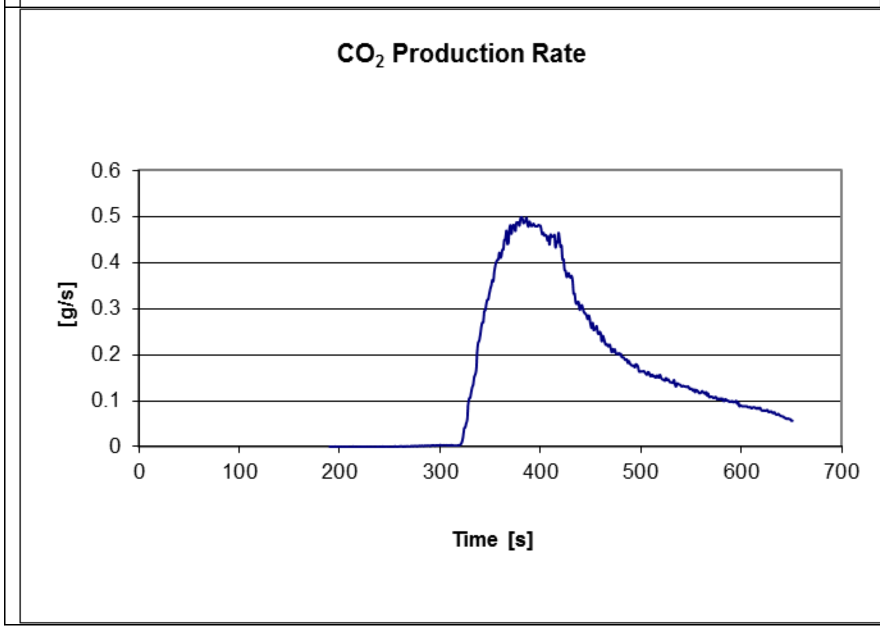
CO_2 Production Rate
0.6
0.5
0.4
0.3
0.2
0.1
0
[g/s]
0
100
200
300
400
500
600
700
Time [s]

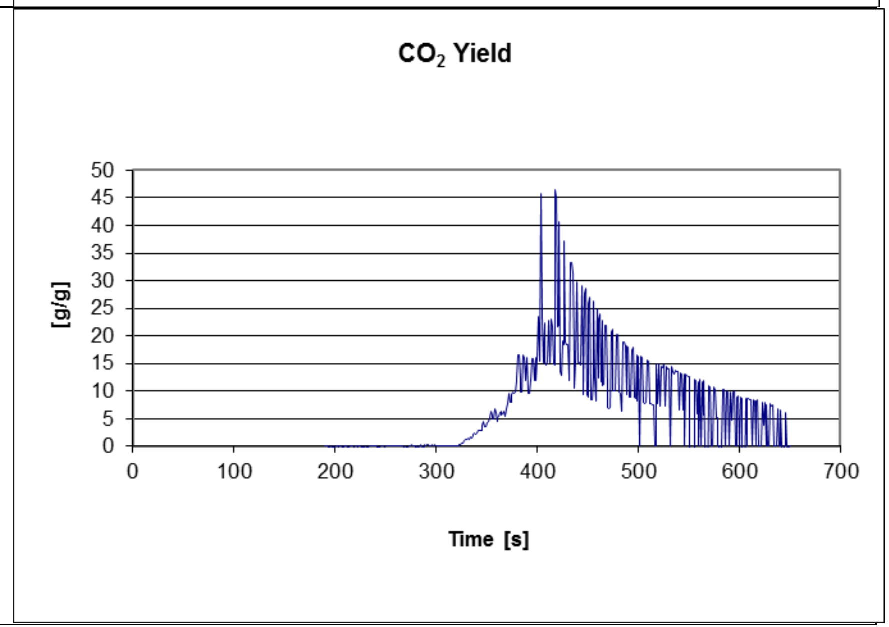
CO_2 Yield
50
45
40
35
30
25
20
15
10
5
0
[g/g]
0
100
200
300
400
500
600
700
Time [s]

E.11 FRP Test 3 – External Flux at 25 kW/m², instrumented

Cone Calorimeter Test Run Data

Dept. of Fire Protection Engineering

100 Institute Road
Worcester, MA 01609
Phone: (508) 831-5628
Fax: (508) 831-5862

Test Information

Test Number:	3/5/2010 - 2
Specimen Identification:	FRP Specimen 3, 2 TCs
Material Name:	Class C FRP
Manufacturer/Submitter:	Not Reported
Sample Description:	White, FRP panel
Raw Data File Name:	030410sample03.txt
Reduced Data File Name:	FRP Sample 03
Date of Test:	3/5/2010
Tester:	R. Hartwell

Test Parameters

Ambient Temperature:	70	F
Relative Humidity:	25	%
Heat Flux:	25	kW/m^2
Exhaust Duct Flow Rate:		30 g/s
Orientation:		Horizontal
Specimen Holder:		TRUE
Specimen Preparation:		2 layer foil
Notes:		1" Separation

Specimen Information

Specimen Color:	[]	White
Specimen Thickness:	[mm]	1.9
Specimen Test Area:	[m^2]	0.0088
Specimen Initial Mass:	[g]	29.3
Specimen Final Mass:	[g]	18.0
Specimen Density:	[g/cm^3]	1.5
Mass Lost:	[g]	11.3
Total Heat Evolved:	[kJ]	245

Test Times [s]

Shutter Open:	211
Time to Ignition:	328
Flameout:	668
Clean Air/End of Test:	684

Daily C-Factor

0.045

The Peak, Average and Total parameters are computed over the test period ignition to flame out. There are 4 exceptions. The first three involve initial heat release rate averages for periods after ignition of 60, 180 and 300 seconds. The final involves the average mass loss rate which is computed over the time period from 10% mass loss to 90% mass loss.

Parameter	Unit	Value
Heat Release		
Peak Heat Release Rate	[kW/m^2]	244
Average Heat Release Rate	[kW/m^2]	82
Total Heat Release	[MJ/m^2]	28
Average HRR for the first 60s	[kW/m^2]	221
Average HRR for the first 180s	[kW/m^2]	131
Average HRR for the first 300s	[kW/m^2]	91
Peak Heat of Combustion	[kJ/g]	151
Average Heat of Combustion	[kJ/g]	19
Smoke Obscuration		
Peak SEA	[m^2/g]	1.322
Average SEA	[m^2/g]	0.457
Peak Smoke Yield	[g/g]	0.155
Average Smoke Yield	[g/g]	0.054
Peak Smoke Production Rate	[m^2/s]	0.102
Average Smoke Production Rate	[m^2/s]	0.024
Total Smoke Release	[m^2]	8.814
Gas Production Rates		
Peak Carbon Monoxide	[g/s]	0.004
Average Carbon Monoxide	[g/s]	0.001
Peak Carbon Dioxide	[g/s]	0.528
Average Carbon Dioxide	[g/s]	0.230
Mass Loss		
Peak Mass Loss Rate	[g/s]	0.130
Average Mass Lass Rate	[g/s]	0.047
Initial Mass	[g]	29.3
Final Mass	[g]	18.0
Mass Loss Fraction	[]	0.39
Burn Time		
Time to Ignition	[s]	117
Duration of Flaming	[s]	340
Duration of Test	[s]	473

Observations

Time	Observation
255	white smoke
265	Top TC loses contact
270	crackling
320	flashes
	cellular flame in center, then spread to 4 edges
400	some smoke outside of hood
463	edge burning
560	corner burning

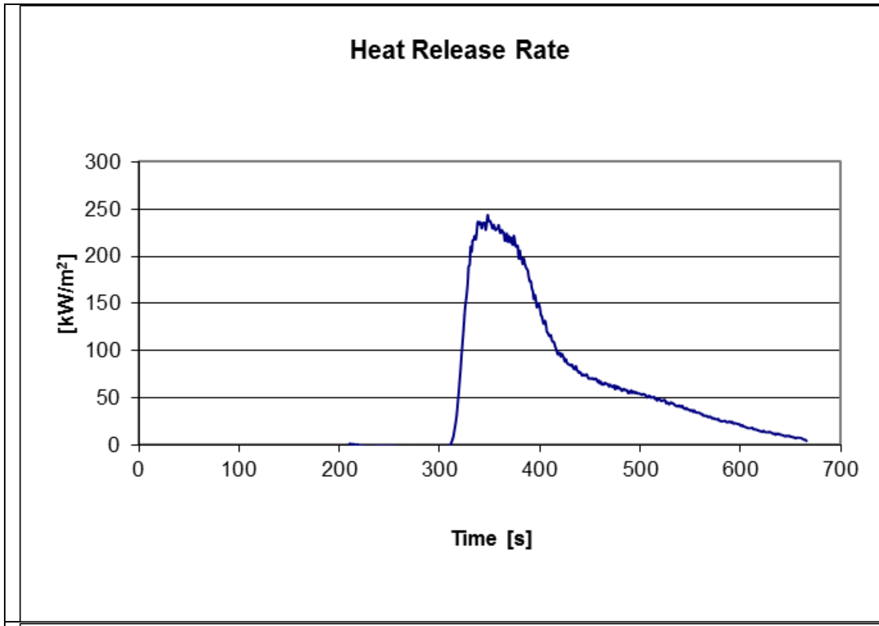
Heat Release Rate
300
250
200
150
100
50
0
[kW/m2]
0
100
200
300
400
500
600
700
Time [s]

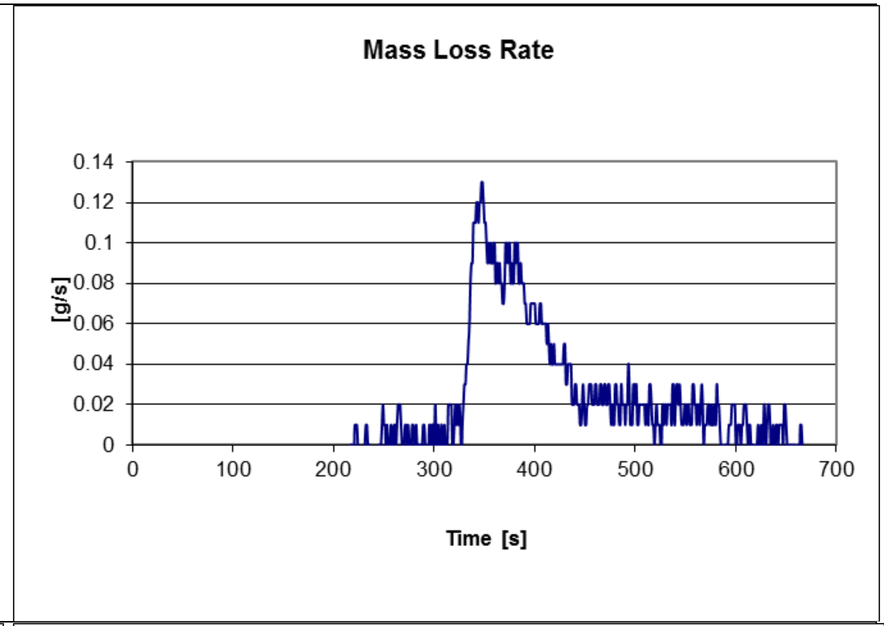
Mass Loss Rate
0.14
0.12
0.1
0.08
0.06
0.04
0.02
0
[g/s]
0
100
200
300
400
500
600
700
Time [s]

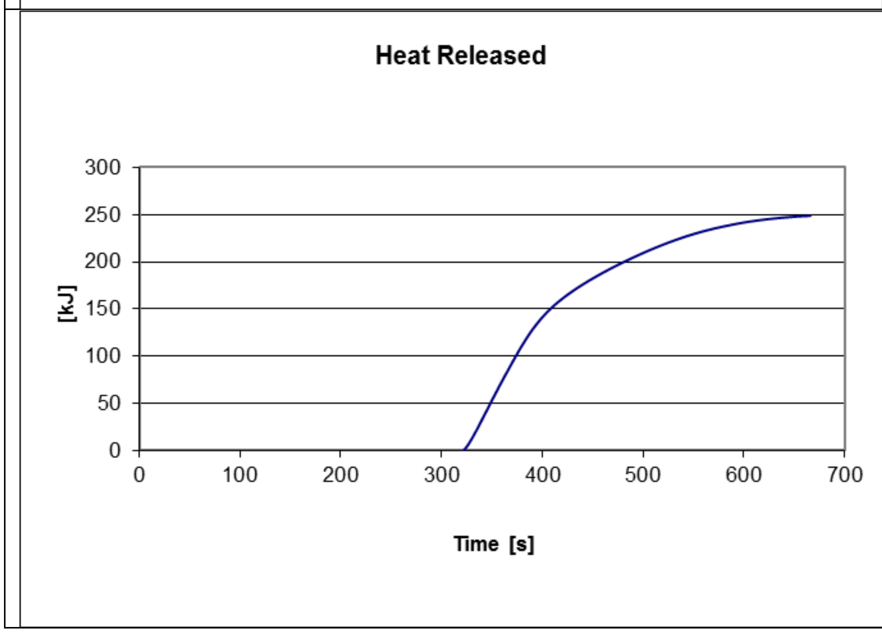
Heat Released
300
250
200
150
100
50
0
[kJ]
0
100
200
300
400
500
600
700
Time [s]

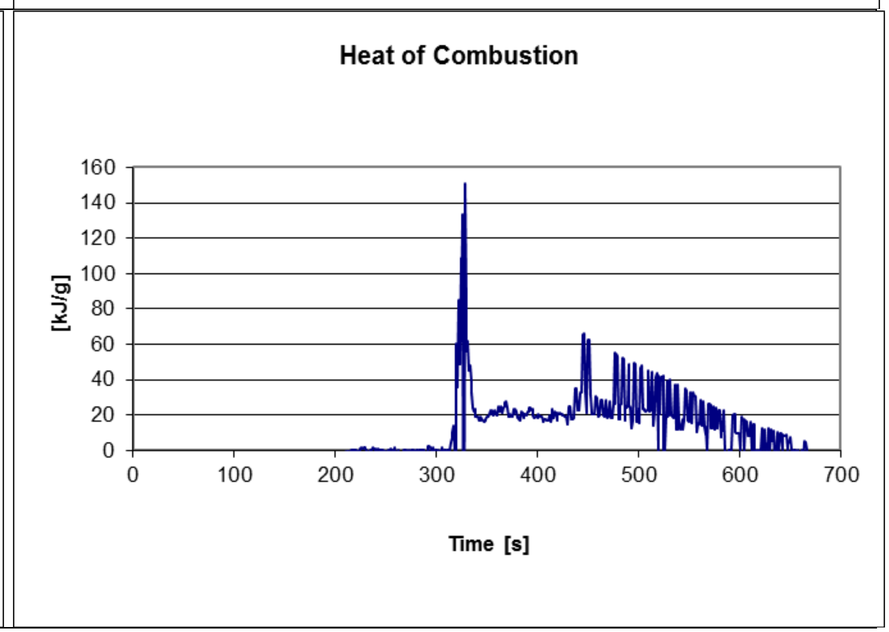
Heat of Combustion
160
140
120
100
80
60
40
20
0
[kJ/g]
0
100
200
300
400
500
600
700
Time [s]

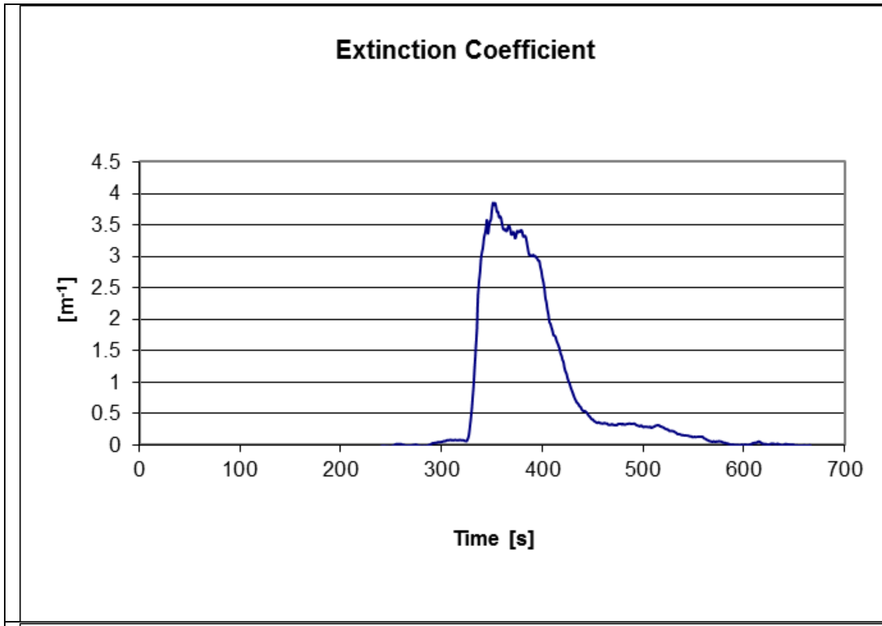
Extinction Coefficient
[m-1]
4.5
4
3.5
3
2.5
2
1.5
1
0.5
0
0
100
200
300
400
500
600
700
Time [s]

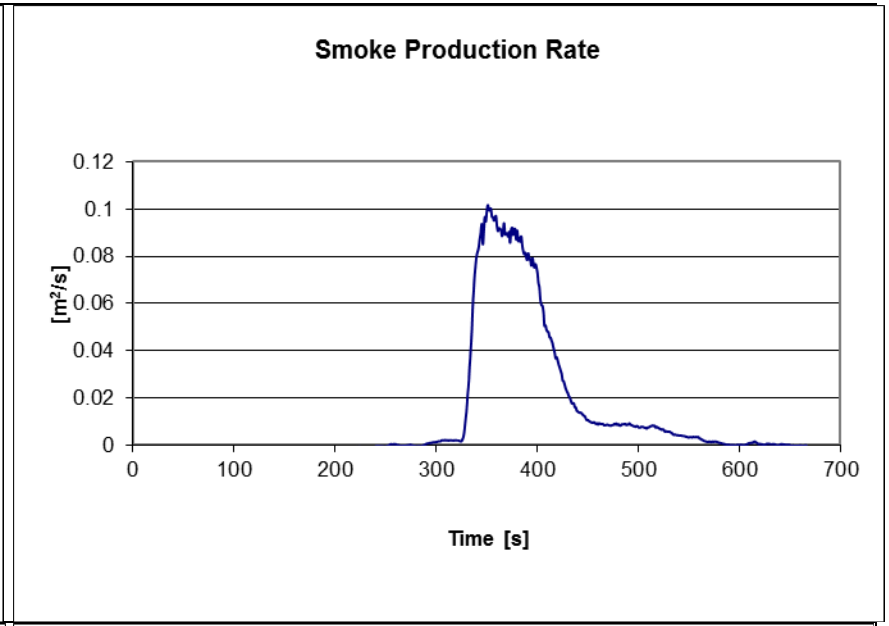
Smoke Production Rate
[m2/s]
0.12
0.1
0.08
0.06
0.04
0.02
0
0
100
200
300
400
500
600
700
Time [s]

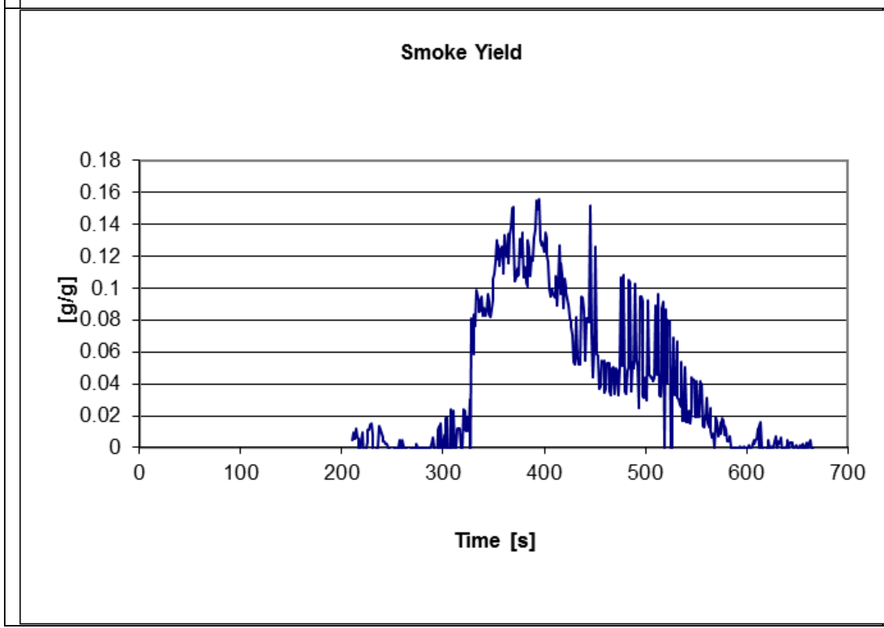
Smoke Yield
[g/g]
0.18
0.16
0.14
0.12
0.1
0.08
0.06
0.04
0.02
0
0
100
200
300
400
500
600
700
Time [s]

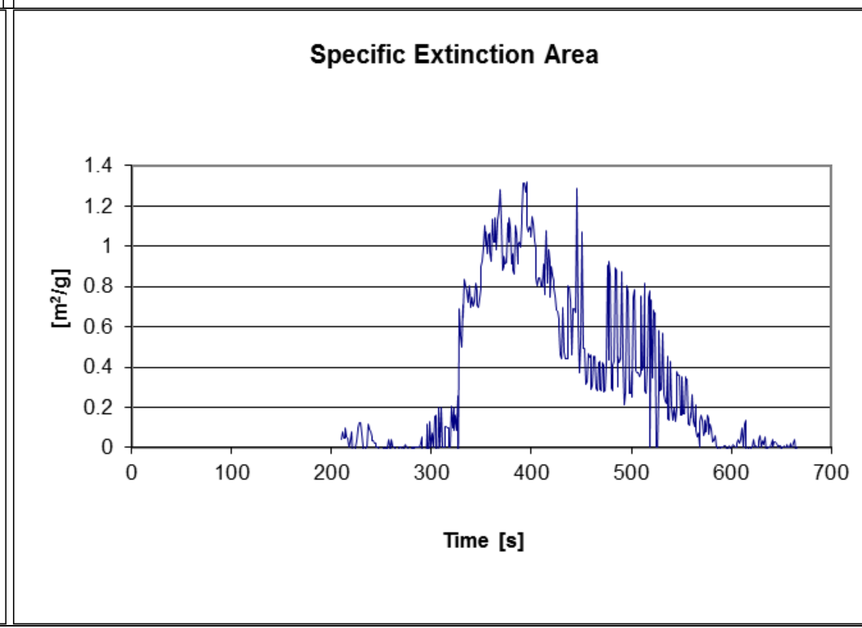
Specific Extinction Area
[m2/g]
1.4
1.2
1
0.8
0.6
0.4
0.2
0
0
100
200
300
400
500
600
700
Time [s]

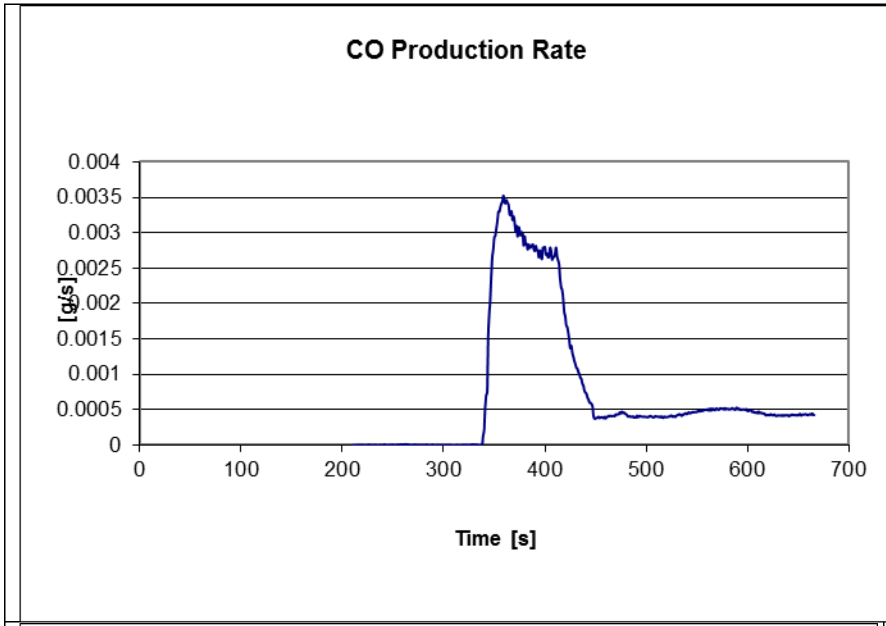
CO Production Rate
[g/s]
0.004
0.0035
0.003
0.0025
0.002
0.0015
0.001
0.0005
0
0
100
200
300
400
500
600
700
Time [s]

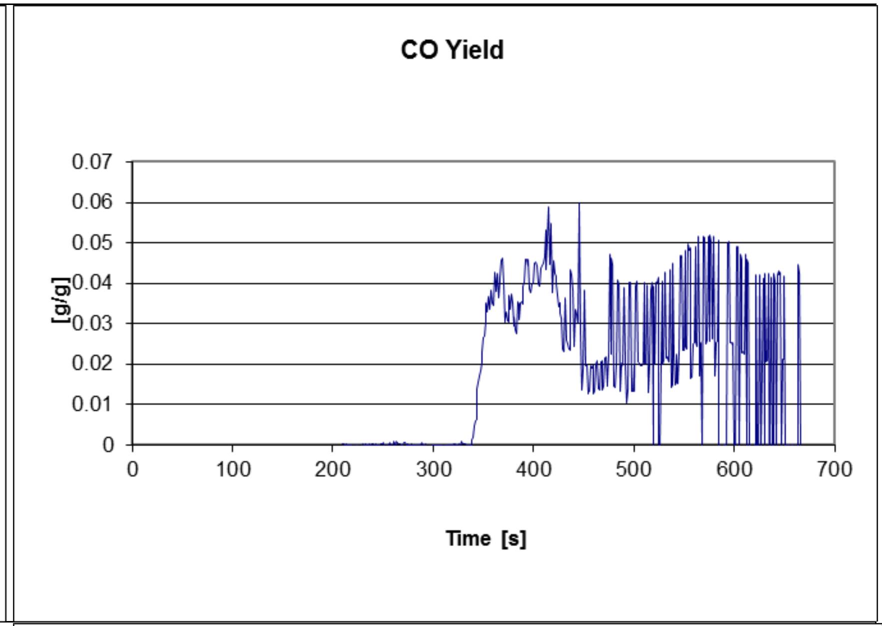
CO Yield
[g/g]
0.07
0.06
0.05
0.04
0.03
0.02
0.01
0
0
100
200
300
400
500
600
700
Time [s]

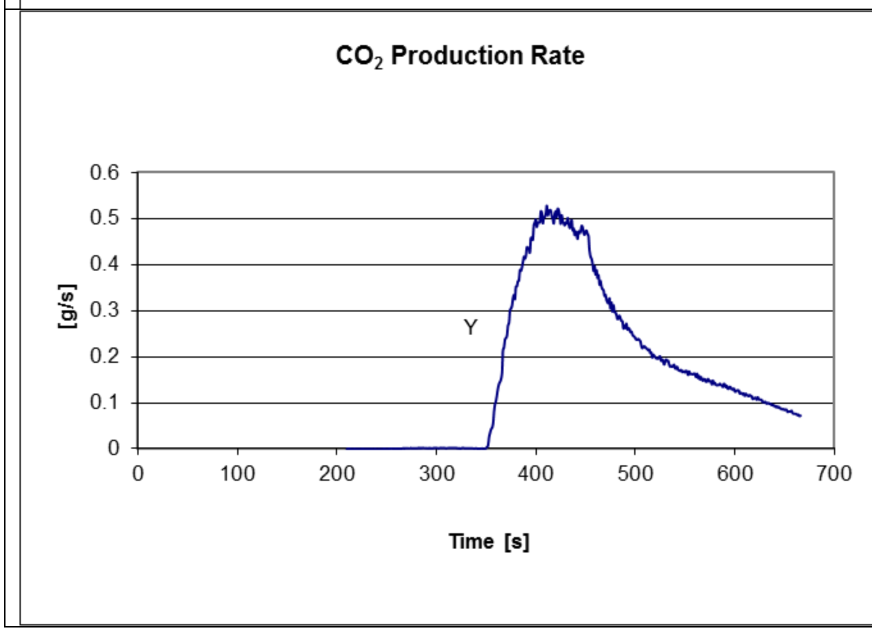
CO2 Production Rate
[g/s]
0.6
0.5
0.4
0.3
0.2
0.1
0
Y
0
100
200
300
400
500
600
700
Time [s]

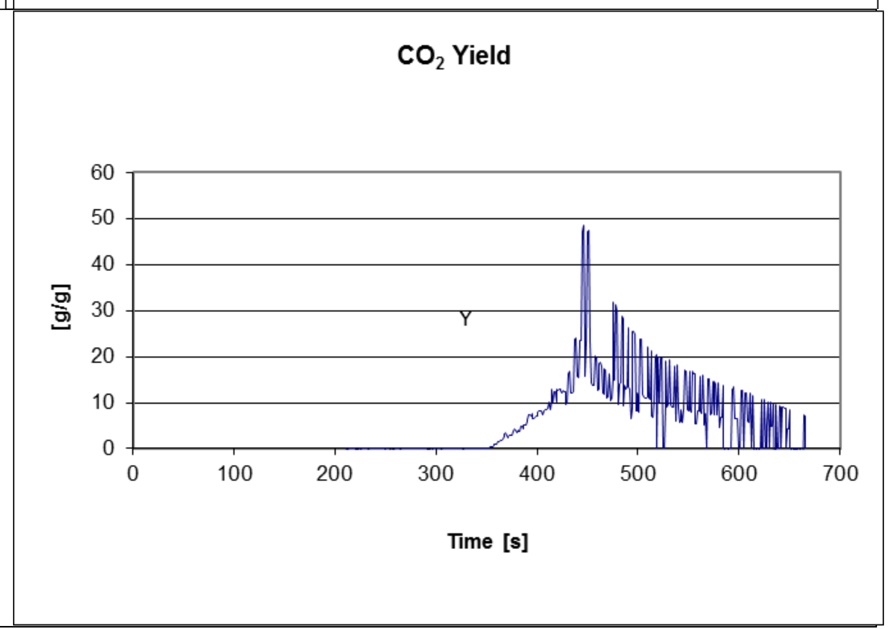
CO2 Yield
[g/g]
60
50
40
30
20
10
0
Y
0
100
200
300
400
500
600
700
Time [s]

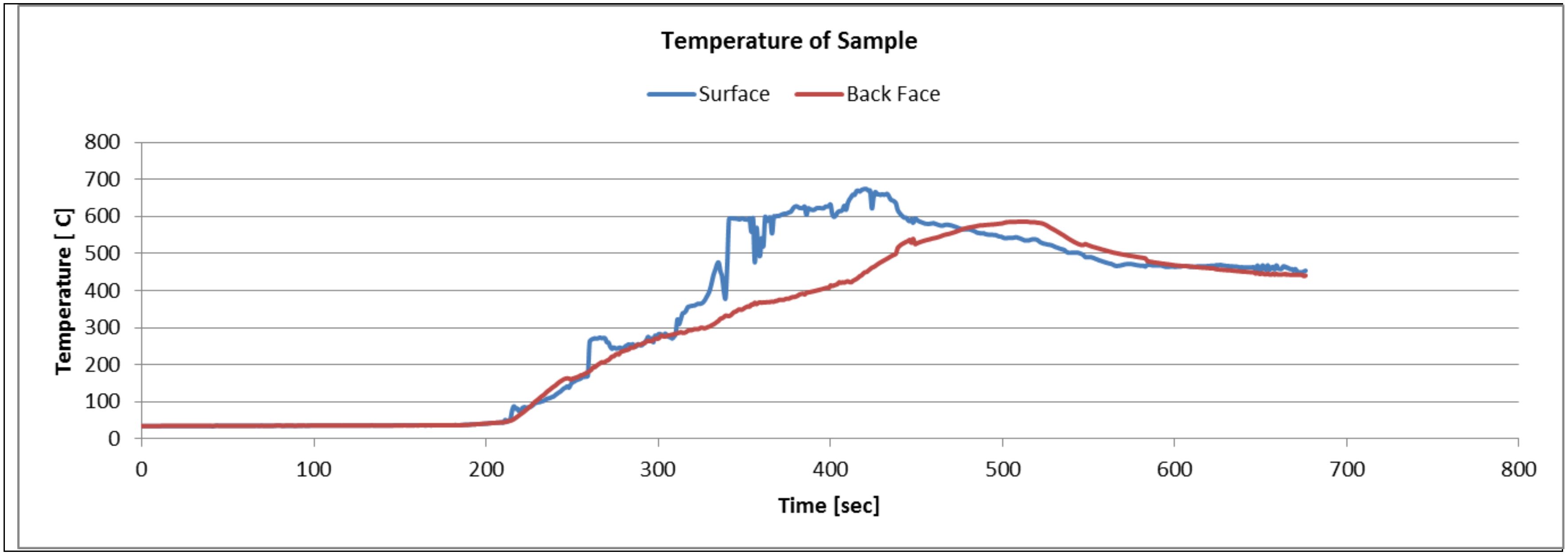
Temperature of Sample
Surface
Back Face
Temperature [C]
Time [sec]
0
100
200
300
400
500
600
700
800

E.12 FRP Test 2 – External Flux at 50 kW/m², un-instrumented

Cone Calorimeter Test Run Data

Dept. of Fire Protection Engineering

100 Institute Road
Worcester, MA 01609
Phone: (508) 831-5628
Fax: (508) 831-5862

Test Information

Test Number:	3/4/2010 - 1
Specimen Identification:	FRP Specimen 2
Material Name:	Class C FRP
Manufacturer/Submitter:	Not Reported
Sample Description:	White, FRP panel
Raw Data File Name:	030410sample02.txt
Reduced Data File Name:	FRP Sample 02
Date of Test:	3/4/2010
Tester:	R. Hartwell

Test Parameters

Ambient Temperature:	83	F
Relative Humidity:	20	%
Heat Flux:	50	kW/m^2
Exhaust Duct Flow Rate:		30 g/s
Orientation:		Horizontal
Specimen Holder:		TRUE
Specimen Preparation:		2 layer foil
Notes:		1" Separation

Specimen Information

Specimen Color:	[]	White
Specimen Thickness:	[mm]	1.9
Specimen Test Area:	[m^2]	0.0088
Specimen Initial Mass:	[g]	29.3
Specimen Final Mass:	[g]	32.5
Specimen Density:	[g/cm^3]	1.5
Mass Lost:	[g]	-3.2
Total Heat Evolved:	[kJ]	249

Test Times [s]

Shutter Open:	189
Time to Ignition:	226
Flameout:	548
Clean Air/End of Test:	579

Daily C-Factor
0.044

The Peak, Average and Total parameters are computed over the test period ignition to flame out. There are 4 exceptions. The first three involve initial heat release rate averages for periods after ignition of 60, 180 and 300 seconds. The final involves the average mass loss rate which is computed over the time period from 10% mass loss to 90% mass loss.

Parameter	Unit	Value
Heat Release		
Peak Heat Release Rate	[kW/m^2]	279
Average Heat Release Rate	[kW/m^2]	88
Total Heat Release	[MJ/m^2]	28
Average HRR for the first 60s	[kW/m^2]	246
Average HRR for the first 180s	[kW/m^2]	138
Average HRR for the first 300s	[kW/m^2]	94
Peak Heat of Combustion	[kJ/g]	105
Average Heat of Combustion	[kJ/g]	19
Smoke Obscuration		
Peak SEA	[m^2/g]	2.004
Average SEA	[m^2/g]	0.594
Peak Smoke Yield	[g/g]	0.236
Average Smoke Yield	[g/g]	0.070
Peak Smoke Production Rate	[m^2/s]	0.128
Average Smoke Production Rate	[m^2/s]	0.031
Total Smoke Release	[m^2]	7.402
Gas Production Rates		
Peak Carbon Monoxide	[g/s]	0.004
Average Carbon Monoxide	[g/s]	0.001
Peak Carbon Dioxide	[g/s]	0.754
Average Carbon Dioxide	[g/s]	0.259
Mass Loss		
Peak Mass Loss Rate	[g/s]	0.140
Average Mass Lass Rate	[g/s]	0.055
Initial Mass	[g]	29.3
Final Mass	[g]	32.5
Mass Loss Fraction	[]	-0.11
Burn Time		
Time to Ignition	[s]	37
Duration of Flaming	[s]	322
Duration of Test	[s]	390

Observations

Time	Observation
208	white smoke
220	crackling
	after ignition, cellular flame then uniform flame cone, surface charr right after ignition
290	cellular flame again
330	edge burning only

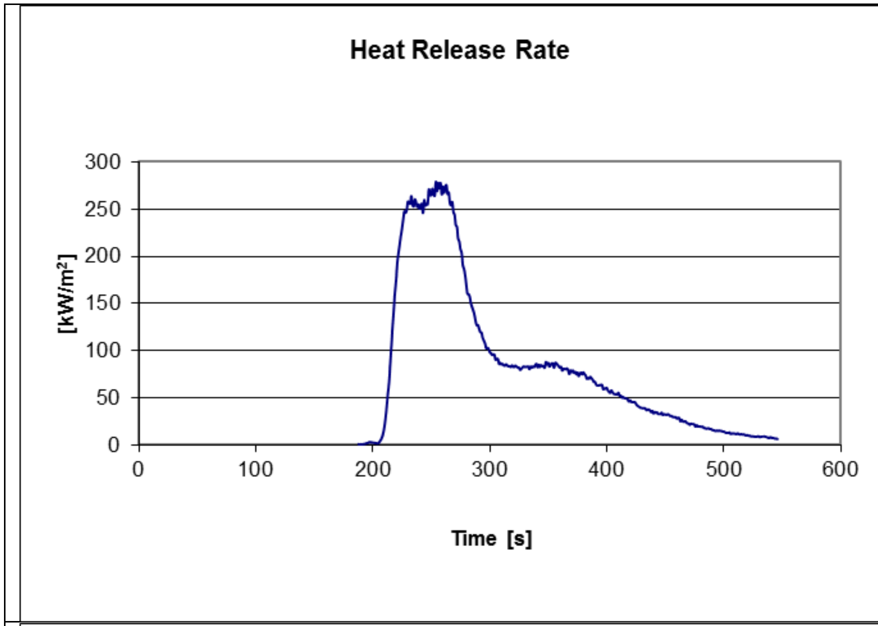
Heat Release Rate
[kW/m²]
300
250
200
150
100
50
0
0
100
200
300
400
500
600
Time [s]

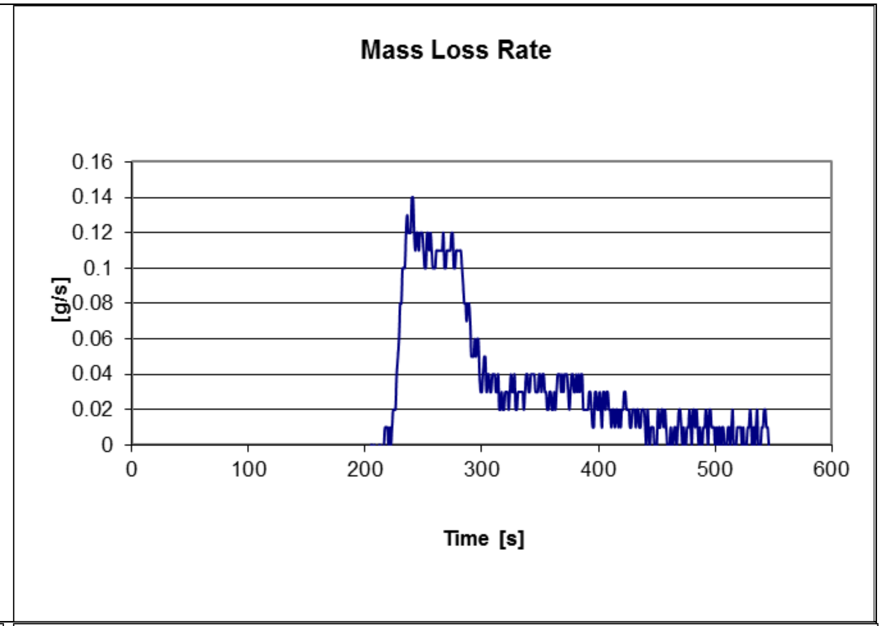
Mass Loss Rate
[g/s]
0.16
0.14
0.12
0.1
0.08
0.06
0.04
0.02
0
0
100
200
300
400
500
600
Time [s]

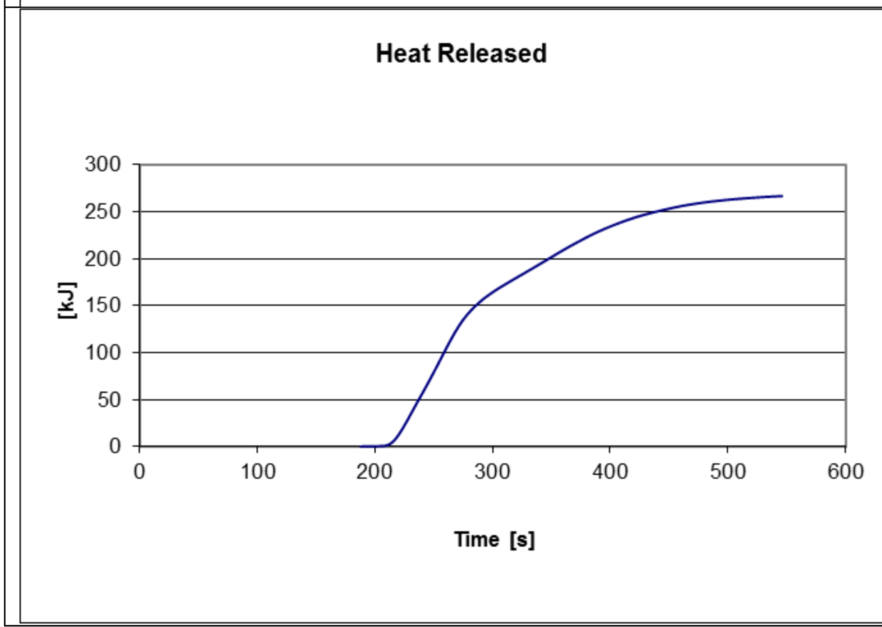
Heat Released
[kJ]
300
250
200
150
100
50
0
0
100
200
300
400
500
600
Time [s]

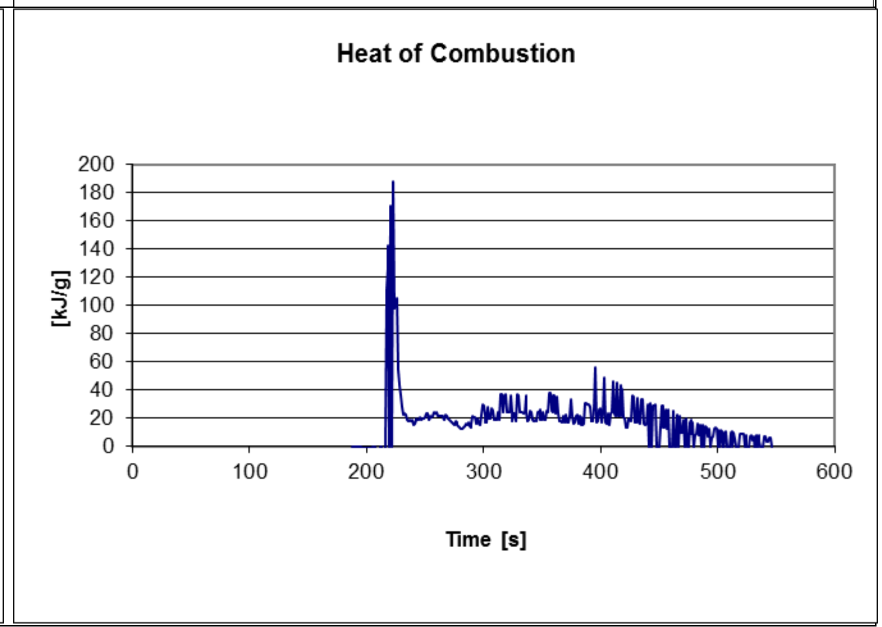
Heat of Combustion
[kJ/g]
200
180
160
140
120
100
80
60
40
20
0
0
100
200
300
400
500
600
Time [s]

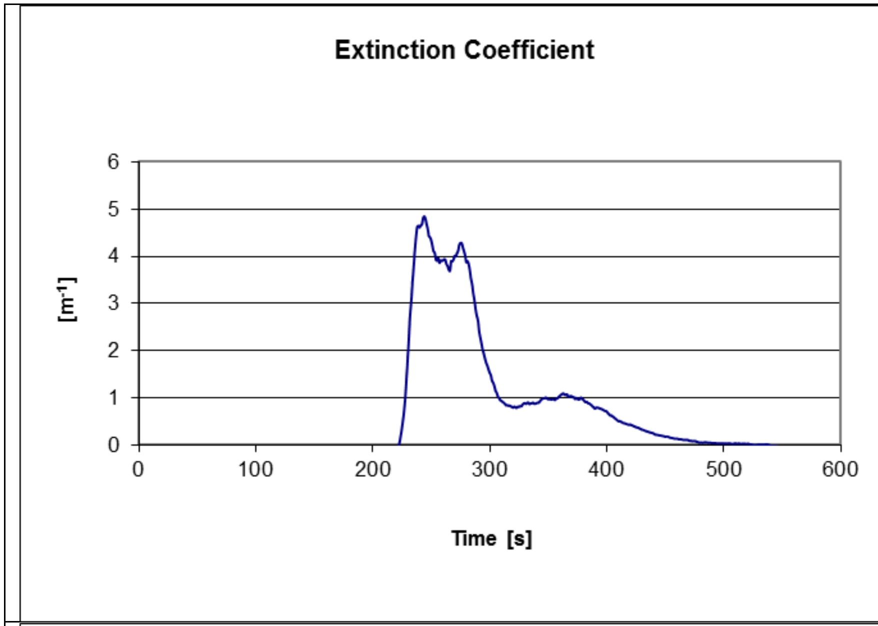
Extinction Coefficient
[m-1]
Time [s]

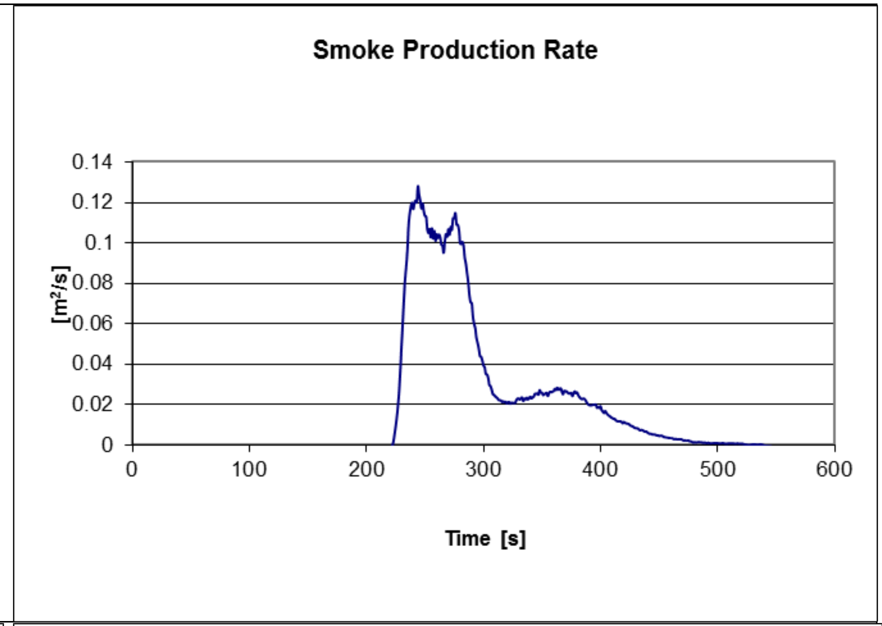
Smoke Production Rate
[m2/s]
Time [s]

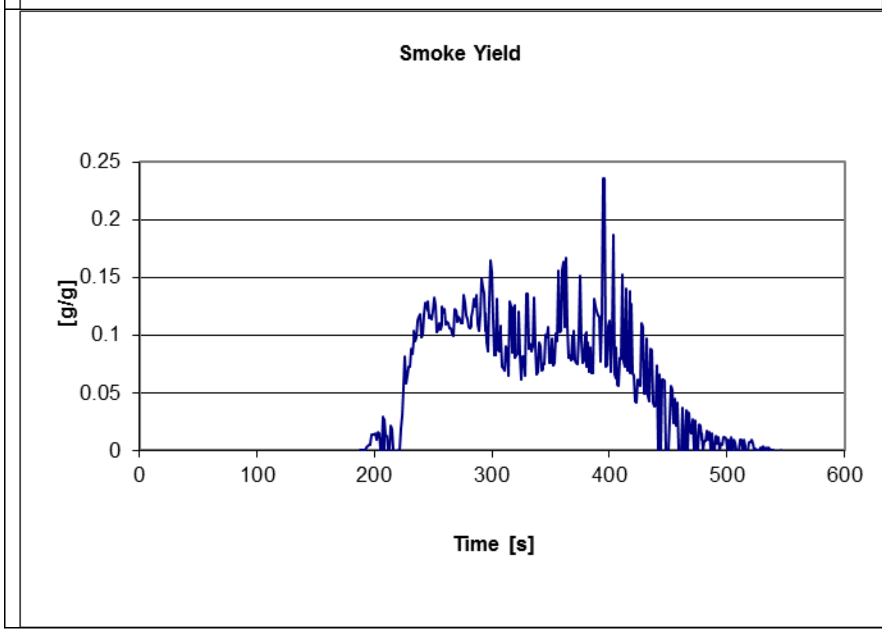
Smoke Yield
[g/g]
Time [s]

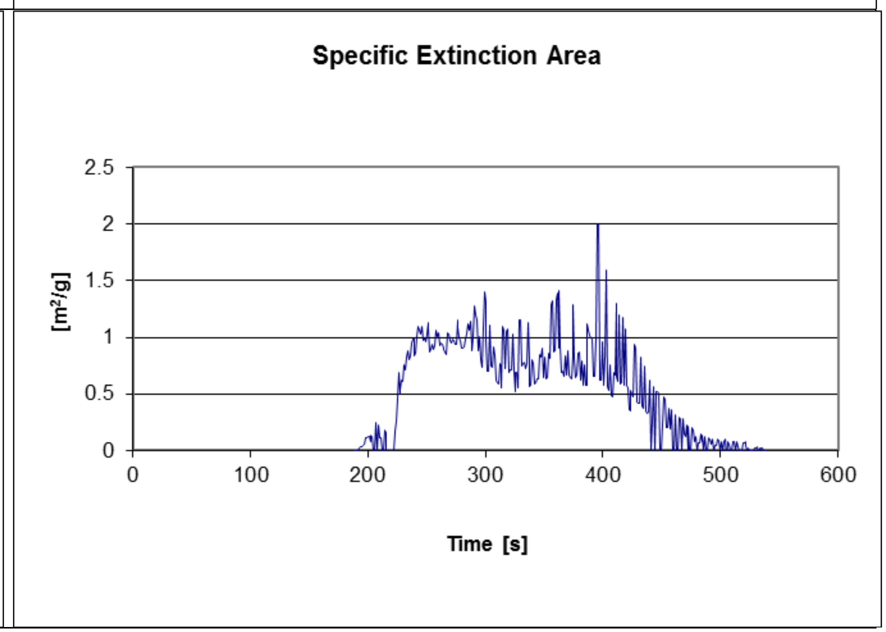
Specific Extinction Area
[m2/g]
Time [s]

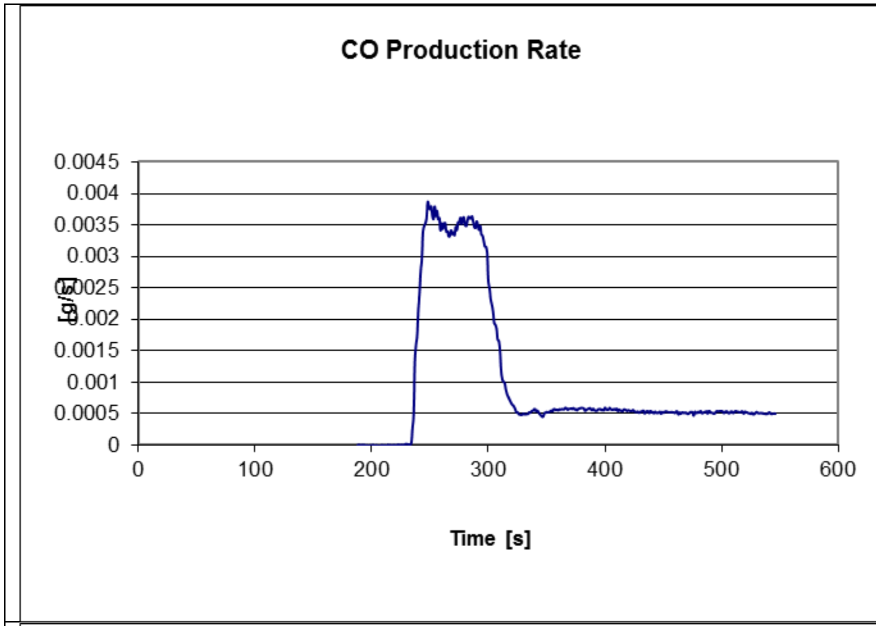

CO Production Rate
[g/s]
Time [s]

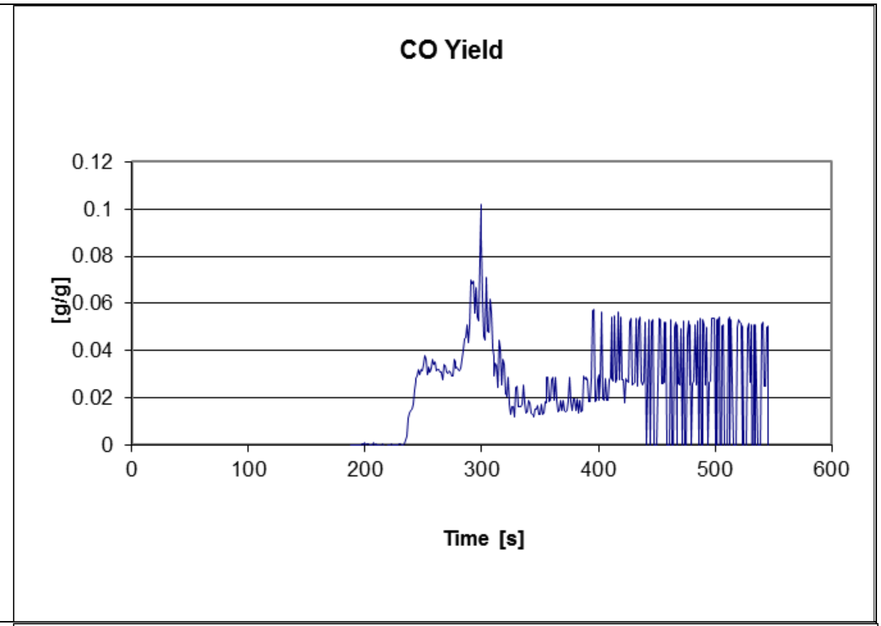

CO Yield
[g/g]
Time [s]

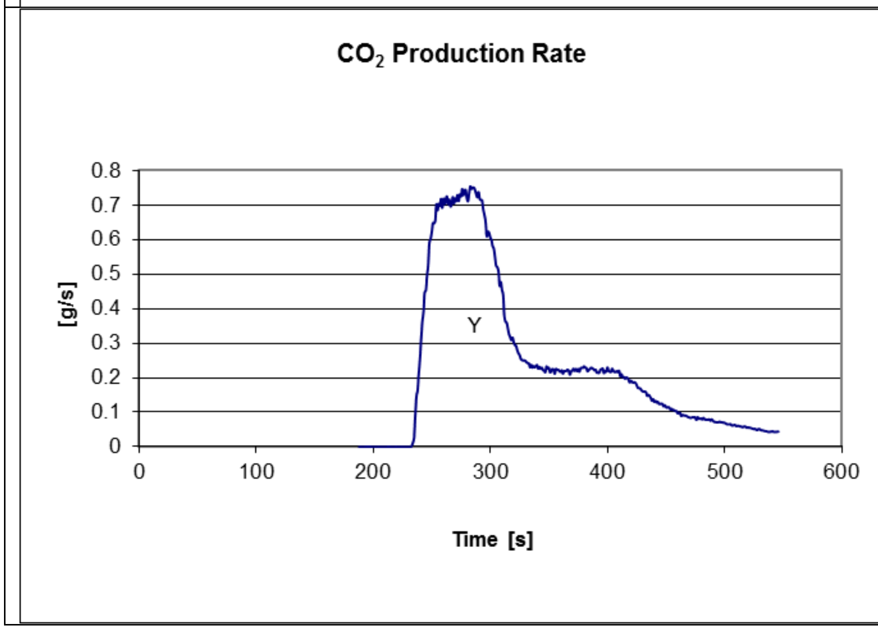

CO2 Production Rate
[g/s]
Y
Time [s]

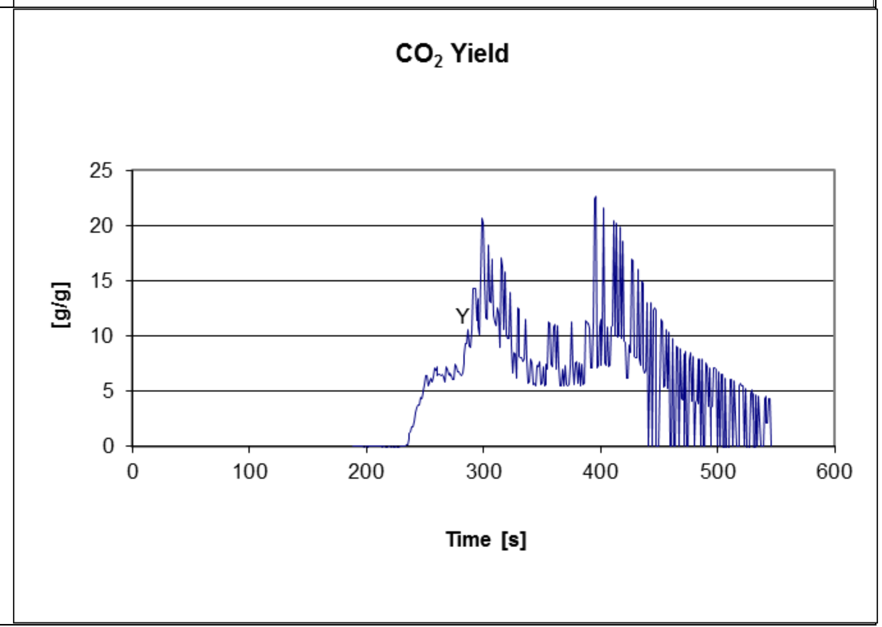

CO2 Yield
[g/g]
Y
Time [s]

E.13 FRP Test 7 – External Flux at 50 kW/m^2, instrumented

Cone Calorimeter Test Run Data

Dept. of Fire Protection Engineering

100 Institute Road
Worcester, MA 01609
Phone: (508) 831-5628
Fax: (508) 831-5862

Test Information

Test Number:	3/4/2010 - 5
Specimen Identification:	FRP Specimen 7, 2 TCs
Material Name:	Class C FRP
Manufacturer/Submitter:	Not Reported
Sample Description:	White, FRP panel
Raw Data File Name:	030410sample07.txt
Reduced Data File Name:	FRP Sample 07
Date of Test:	3/4/2010
Tester:	R. Hartwell

Test Parameters

Ambient Temperature:	83	F
Relative Humidity:	20	%
Heat Flux:	50	kW/m^2
Exhaust Duct Flow Rate:		30 g/s
Orientation:		Horizontal
Specimen Holder:		TRUE
Specimen Preparation:		2 layer foil
Notes:		1" Separation

Specimen Information

Specimen Color:	[]	White
Specimen Thickness:	[mm]	1.9
Specimen Test Area:	[m^2]	0.0088
Specimen Initial Mass:	[g]	28.7
Specimen Final Mass:	[g]	18.2
Specimen Density:	[g/cm^3]	1.5
Mass Lost:	[g]	10.5
Total Heat Evolved:	[kJ]	248

Test Times [s]

Shutter Open:	212
Time to Ignition:	251
Flameout:	500
Clean Air/End of Test:	521

Daily C-Factor

0.044

The Peak, Average and Total parameters are computed over the test period ignition to flame out. There are 4 exceptions. The first three involve initial heat release rate averages for periods after ignition of 60, 180 and 300 seconds. The final involves the average mass loss rate which is computed over the time period from 10% mass loss to 90% mass loss.

Parameter	Unit	Value
Heat Release		
Peak Heat Release Rate	[kW/m^2]	294
Average Heat Release Rate	[kW/m^2]	113
Total Heat Release	[MJ/m^2]	28
Average HRR for the first 60s	[kW/m^2]	259
Average HRR for the first 180s	[kW/m^2]	148
Average HRR for the first 300s	[kW/m^2]	94
Peak Heat of Combustion	[kJ/g]	74
Average Heat of Combustion	[kJ/g]	20
Smoke Obscuration		
Peak SEA	[m^2/g]	1.894
Average SEA	[m^2/g]	0.680
Peak Smoke Yield	[g/g]	0.223
Average Smoke Yield	[g/g]	0.080
Peak Smoke Production Rate	[m^2/s]	0.129
Average Smoke Production Rate	[m^2/s]	0.042
Total Smoke Release	[m^2]	8.588
Gas Production Rates		
Peak Carbon Monoxide	[g/s]	0.004
Average Carbon Monoxide	[g/s]	0.001
Peak Carbon Dioxide	[g/s]	0.826
Average Carbon Dioxide	[g/s]	0.333
Mass Loss		
Peak Mass Loss Rate	[g/s]	0.140
Average Mass Lass Rate	[g/s]	0.073
Initial Mass	[g]	28.7
Final Mass	[g]	18.2
Mass Loss Fraction	[]	0.37
Burn Time		
Time to Ignition	[s]	39
Duration of Flaming	[s]	249
Duration of Test	[s]	309

Observations

Time	Observation
	Similar condition to the other 50 kW/m2 heat flux test
	Top thermocouple stays on surface for most of the test

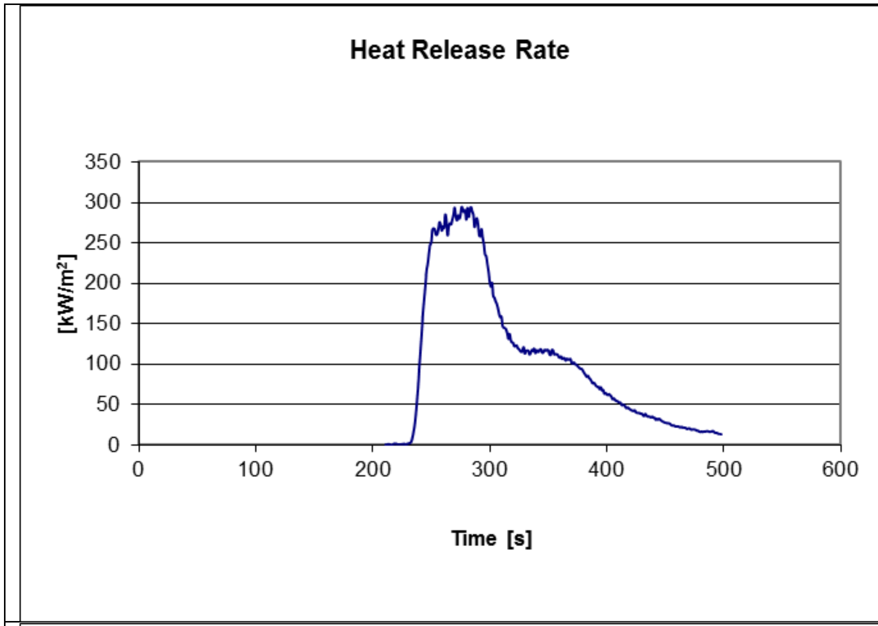
Heat Release Rate
[kW/m²]
0
50
100
150
200
250
300
350
0
100
200
300
400
500
600
Time [s]

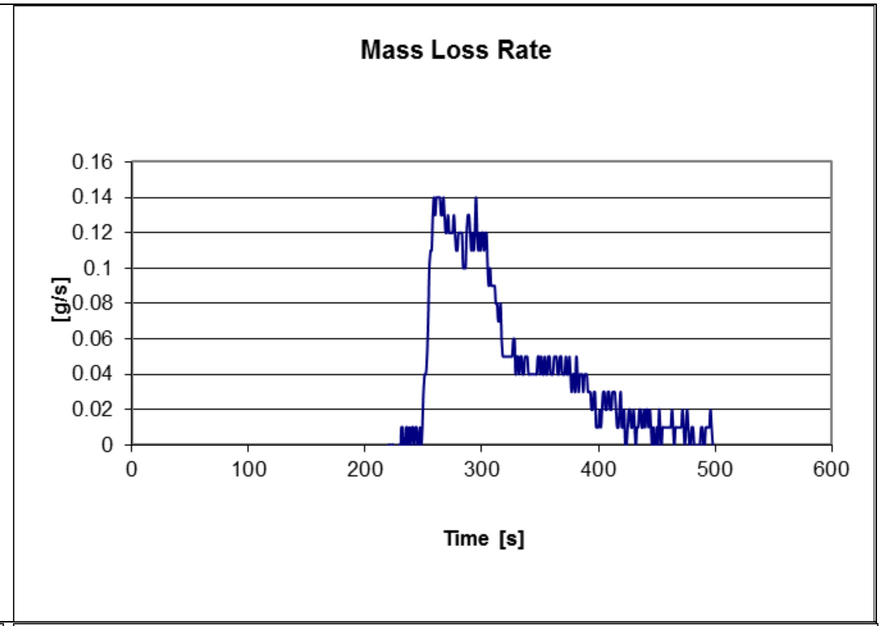
Mass Loss Rate
[g/s]
0
0.02
0.04
0.06
0.08
0.1
0.12
0.14
0.16
0
100
200
300
400
500
600
Time [s]

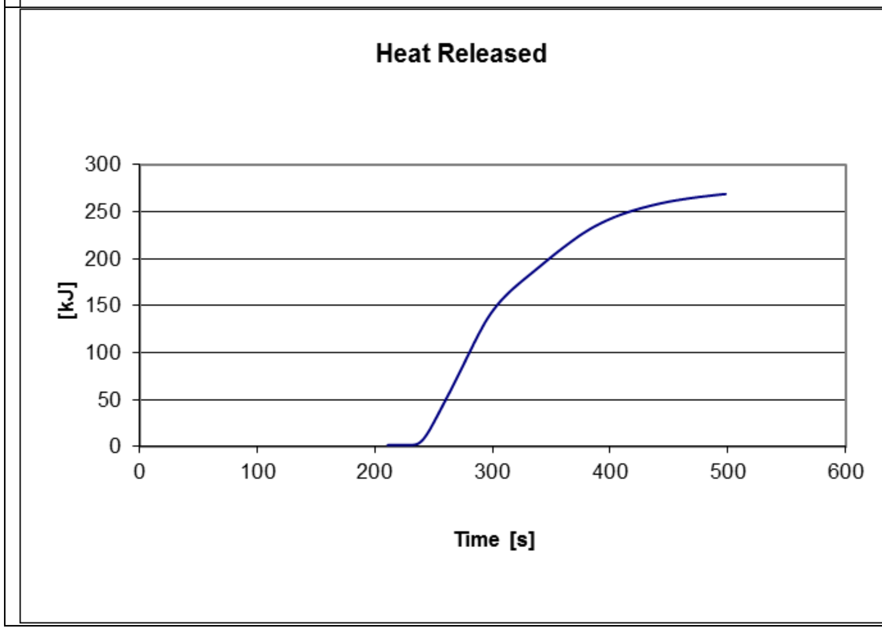
Heat Released
[kJ]
0
50
100
150
200
250
300
0
100
200
300
400
500
600
Time [s]

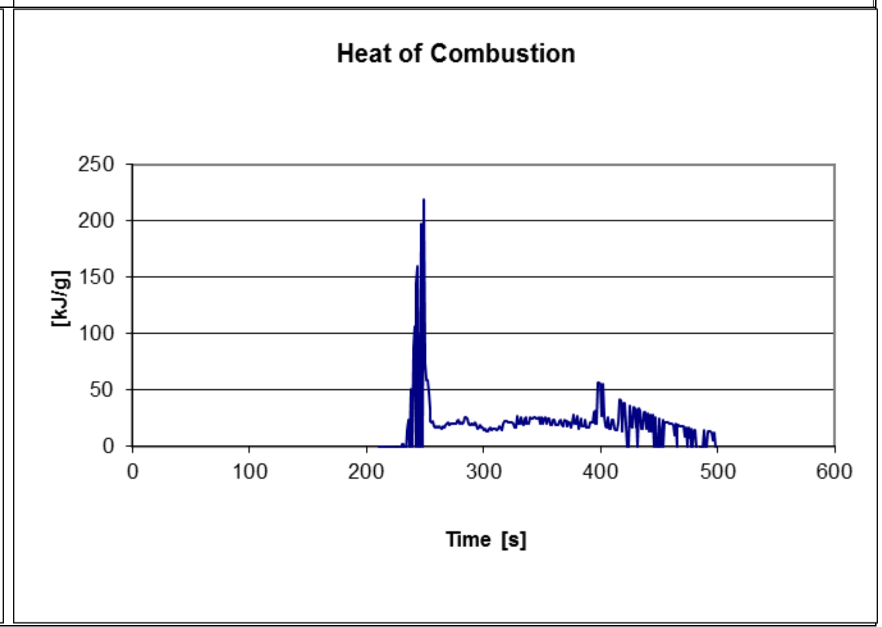
Heat of Combustion
[kJ/g]
0
50
100
150
200
250
0
100
200
300
400
500
600
Time [s]

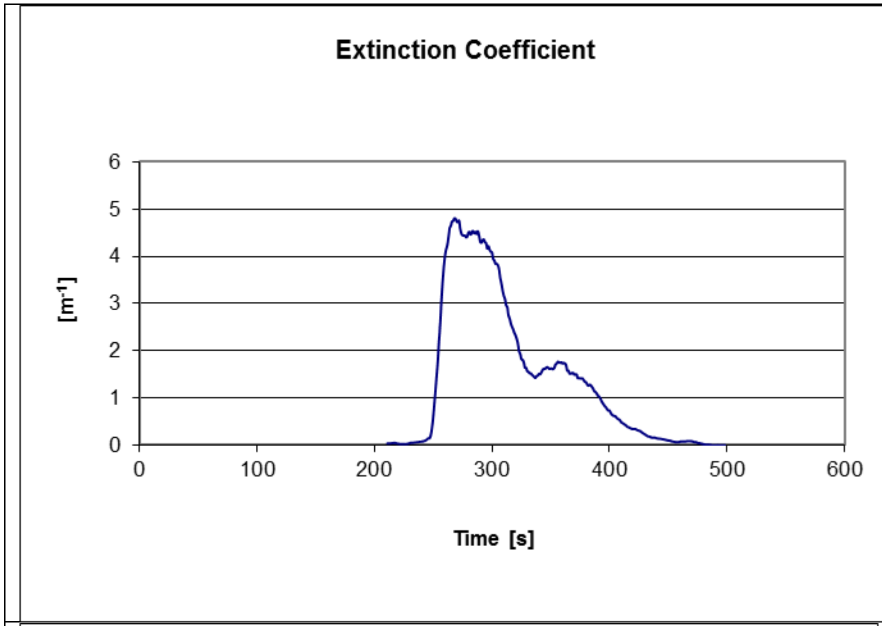
Extinction Coefficient
6
5
4
3
2
1
0
[m-1]
0
100
200
300
400
500
600
Time [s]

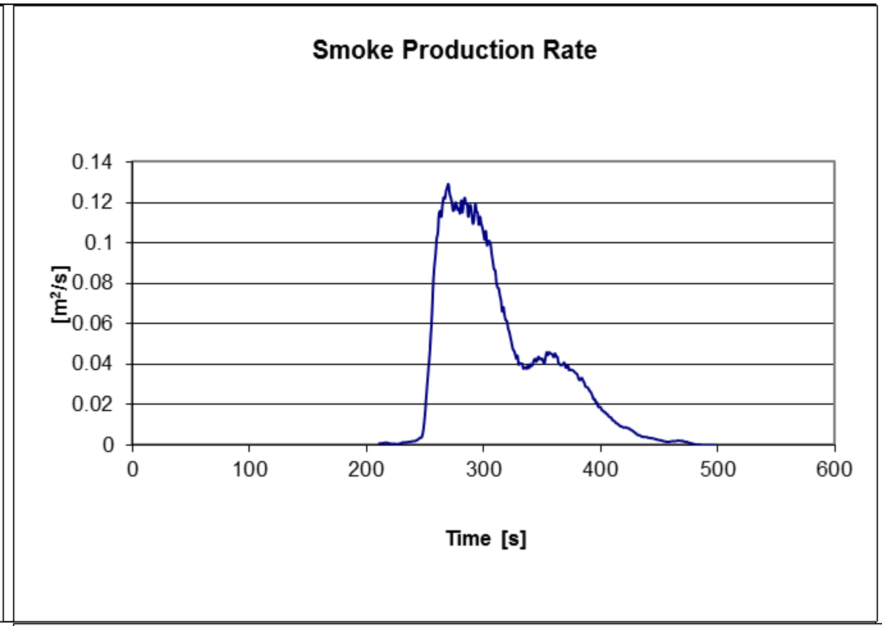
Smoke Production Rate
0.14
0.12
0.1
0.08
0.06
0.04
0.02
0
[m²/s]
0
100
200
300
400
500
600
Time [s]

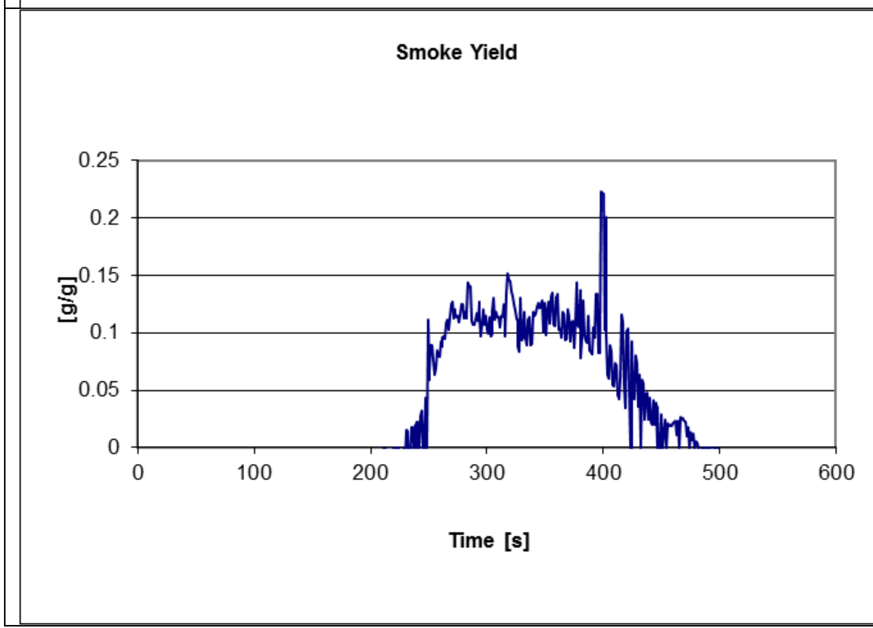
Smoke Yield
0.25
0.2
0.15
0.1
0.05
0
[g/g]
0
100
200
300
400
500
600
Time [s]

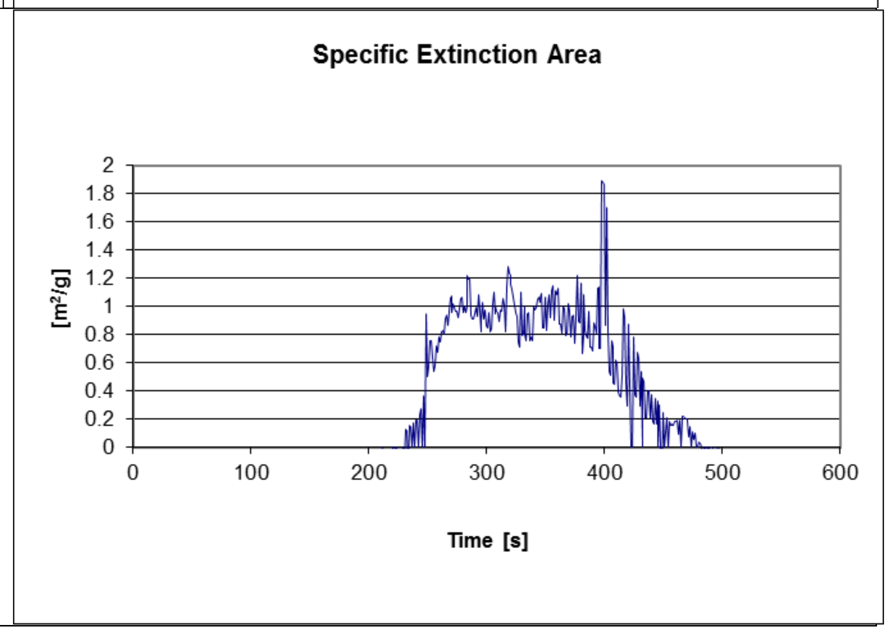
Specific Extinction Area
2
1.8
1.6
1.4
1.2
1
0.8
0.6
0.4
0.2
0
[m²/g]
0
100
200
300
400
500
600
Time [s]

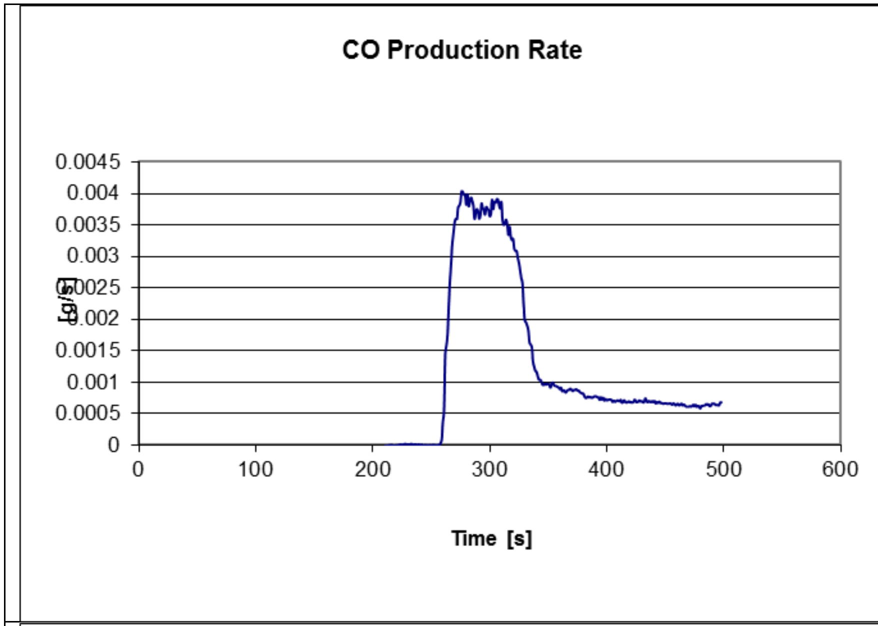
CO Production Rate
[g/s]
0.0045
0.004
0.0035
0.003
0.0025
0.002
0.0015
0.001
0.0005
0
0
100
200
300
400
500
600
Time [s]

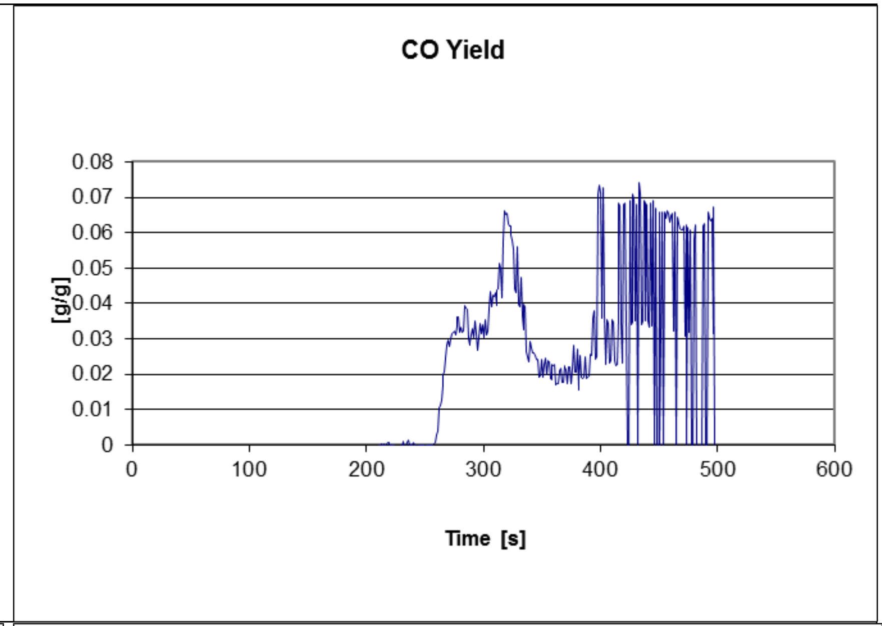
CO Yield
[g/g]
0.08
0.07
0.06
0.05
0.04
0.03
0.02
0.01
0
0
100
200
300
400
500
600
Time [s]

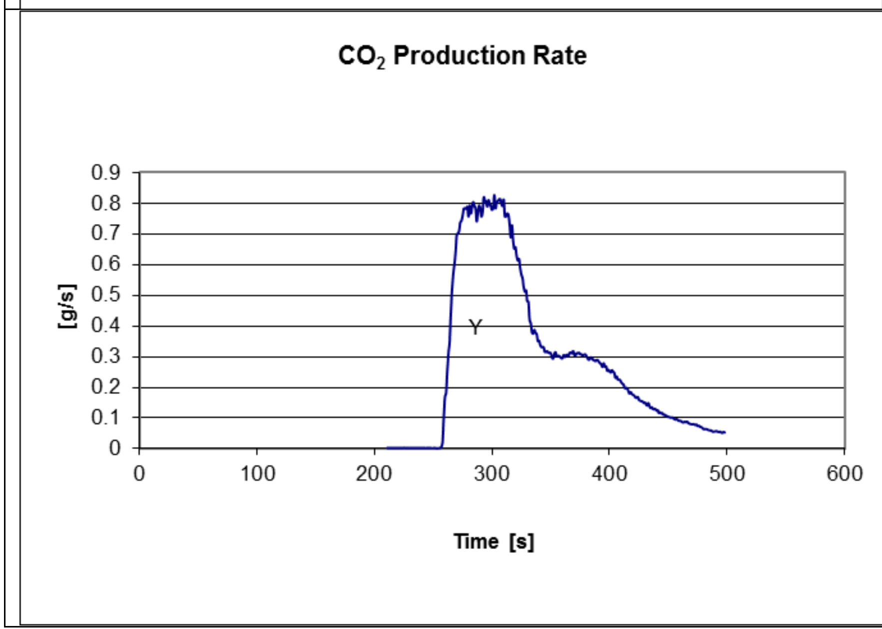
CO_2 Production Rate
[g/s]
0.9
0.8
0.7
0.6
0.5
0.4
0.3
0.2
0.1
0
Y
0
100
200
300
400
500
600
Time [s]

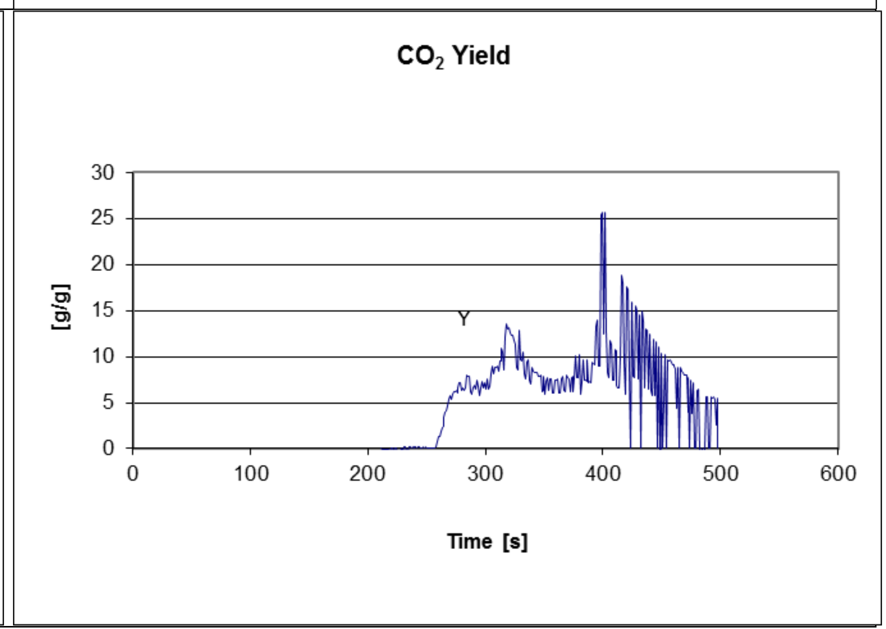
CO_2 Yield
[g/g]
30
25
20
15
10
5
0
Y
0
100
200
300
400
500
600
Time [s]

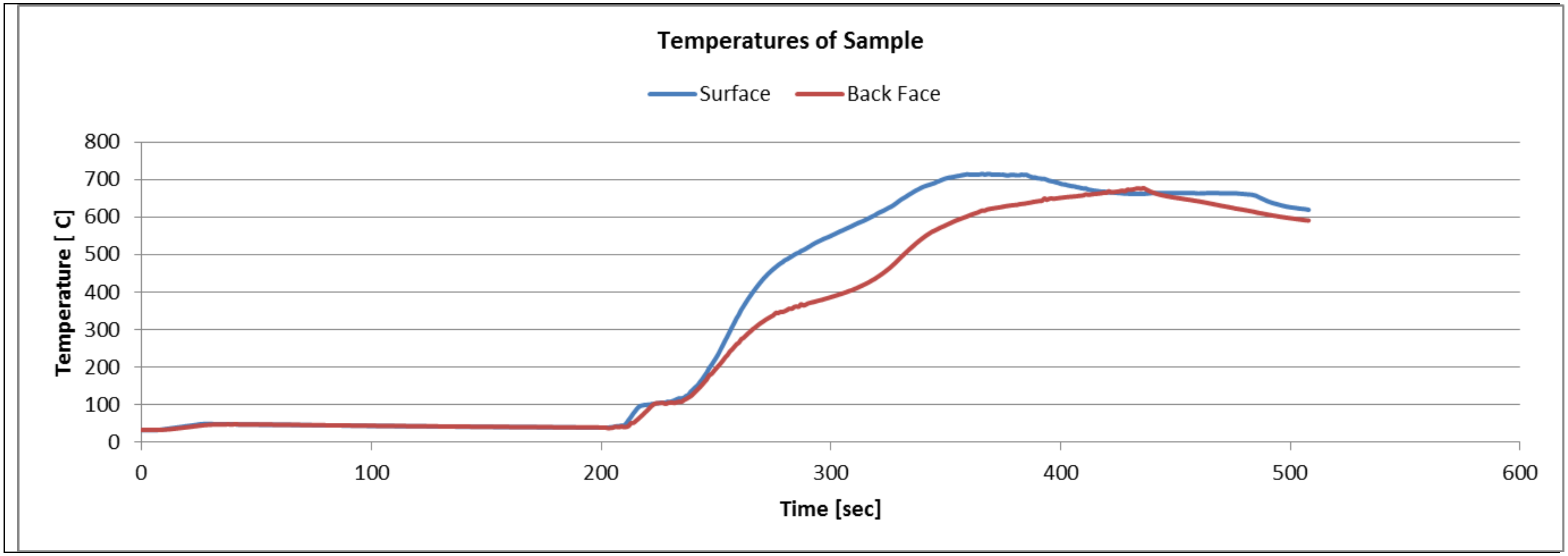
Temperatures of Sample
Surface
Back Face
800
700
600
500
400
300
200
100
0
Temperature [C]
0
100
200
300
400
500
600
Time [sec]

E.14 FRP Test 5 – External Flux at 75 kW/m², un-instrumented

Cone Calorimeter Test Run Data

Dept. of Fire Protection Engineering

100 Institute Road
Worcester, MA 01609
Phone: (508) 831-5628
Fax: (508) 831-5862

Test Information

Test Number:	3/4/2010 - 3
Specimen Identification:	FRP Specimen 5
Material Name:	Class C FRP
Manufacturer/Submitter:	Not Reported
Sample Description:	White, FRP panel
Raw Data File Name:	030410sample05.txt
Reduced Data File Name:	FRP Sample 05
Date of Test:	3/4/2010
Tester:	R. Hartwell

Test Parameters

Ambient Temperature:	83	F
Relative Humidity:	20	%
Heat Flux:	75	kW/m^2
Exhaust Duct Flow Rate:	30 g/s	
Orientation:	Horizontal	
Specimen Holder:	TRUE	
Specimen Preparation:	2 layer foil	
Notes:	1" Separation	

Specimen Information

Specimen Color:	[]	White
Specimen Thickness:	[mm]	2.0
Specimen Test Area:	[m^2]	0.0088
Specimen Initial Mass:	[g]	29.6
Specimen Final Mass:	[g]	29.7
Specimen Density:	[g/cm^3]	1.5
Mass Lost:	[g]	-0.1
Total Heat Evolved:	[kJ]	239

Test Times [s]

Shutter Open:	317
Time to Ignition:	341
Flameout:	527
Clean Air/End of Test:	541

Daily C-Factor

0.045

The Peak, Average and Total parameters are computed over the test period ignition to flame out. There are 4 exceptions. The first three involve initial heat release rate averages for periods after ignition of 60, 180 and 300 seconds. The final involves the average mass loss rate which is computed over the time period from 10% mass loss to 90% mass loss.

Parameter	Unit	Value
Heat Release		
Peak Heat Release Rate	[kW/m^2]	366
Average Heat Release Rate	[kW/m^2]	146
Total Heat Release	[MJ/m^2]	27
Average HRR for the first 60s	[kW/m^2]	298
Average HRR for the first 180s	[kW/m^2]	151
Average HRR for the first 300s	[kW/m^2]	91
Peak Heat of Combustion	[kJ/g]	119
Average Heat of Combustion	[kJ/g]	21
Smoke Obscuration		
Peak SEA	[m^2/g]	2.122
Average SEA	[m^2/g]	0.836
Peak Smoke Yield	[g/g]	0.250
Average Smoke Yield	[g/g]	0.098
Peak Smoke Production Rate	[m^2/s]	0.178
Average Smoke Production Rate	[m^2/s]	0.065
Total Smoke Release	[m^2]	10.060
Gas Production Rates		
Peak Carbon Monoxide	[g/s]	0.005
Average Carbon Monoxide	[g/s]	0.002
Peak Carbon Dioxide	[g/s]	0.729
Average Carbon Dioxide	[g/s]	0.392
Mass Loss		
Peak Mass Loss Rate	[g/s]	0.170
Average Mass Lass Rate	[g/s]	0.097
Initial Mass	[g]	29.6
Final Mass	[g]	29.7
Mass Loss Fraction	[]	0.00
Burn Time		
Time to Ignition	[s]	24
Duration of Flaming	[s]	186
Duration of Test	[s]	224

Observations

Time	Observation
330	white smoke
334	crackling
	ignition then cellular flame then flame cone
360	surface charred after ignition
450	edge burning
490	corner burning

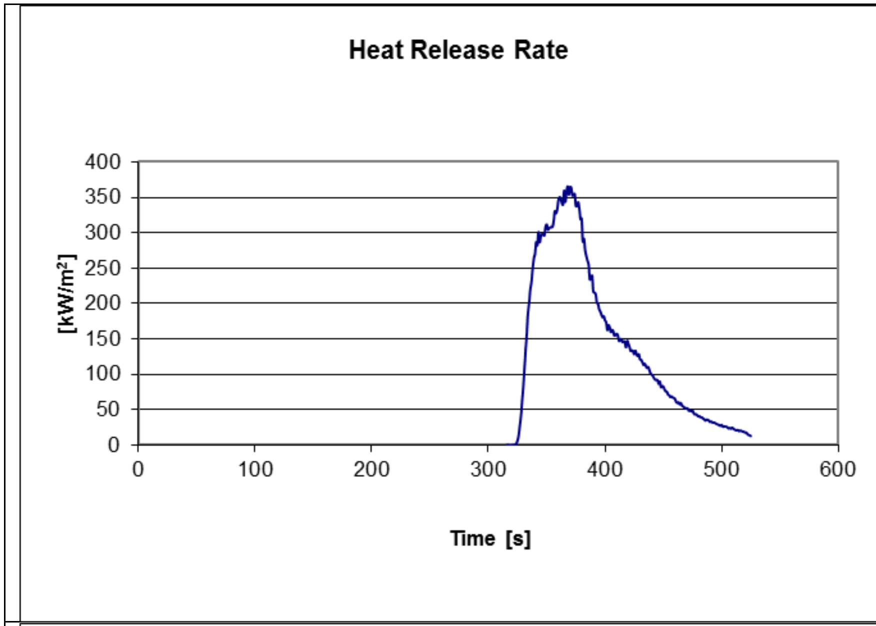
Heat Release Rate
400
350
300
250
200
150
100
50
0
[kW/m²]
0
100
200
300
400
500
600
Time [s]

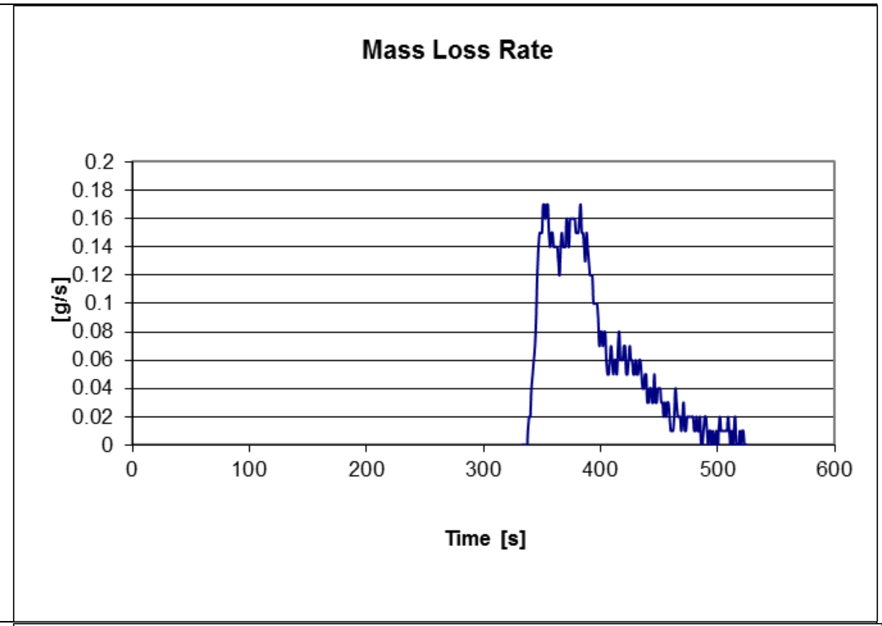
Mass Loss Rate
0.2
0.18
0.16
0.14
0.12
0.1
0.08
0.06
0.04
0.02
0
[g/s]
0
100
200
300
400
500
600
Time [s]

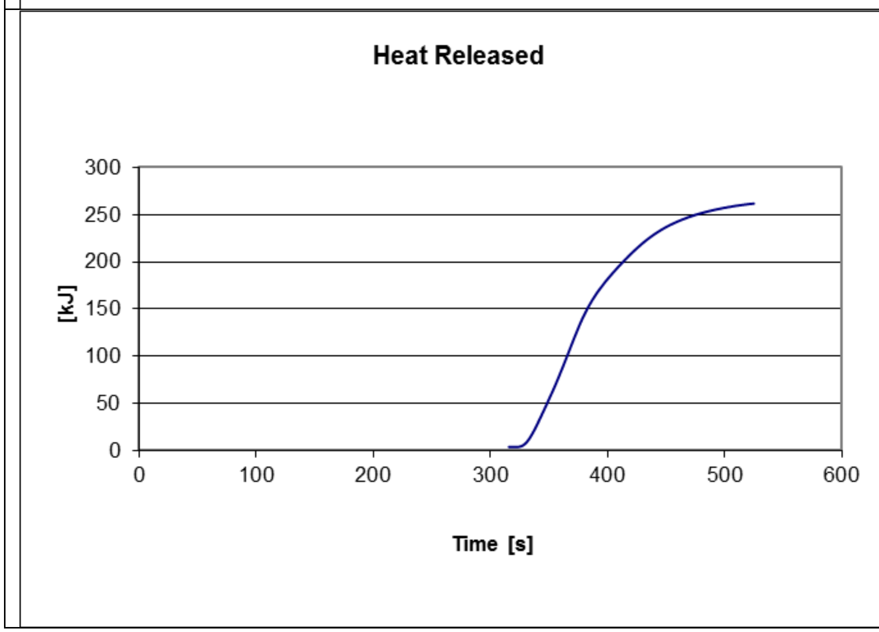
Heat Released
300
250
200
150
100
50
0
[kJ]
0
100
200
300
400
500
600
Time [s]

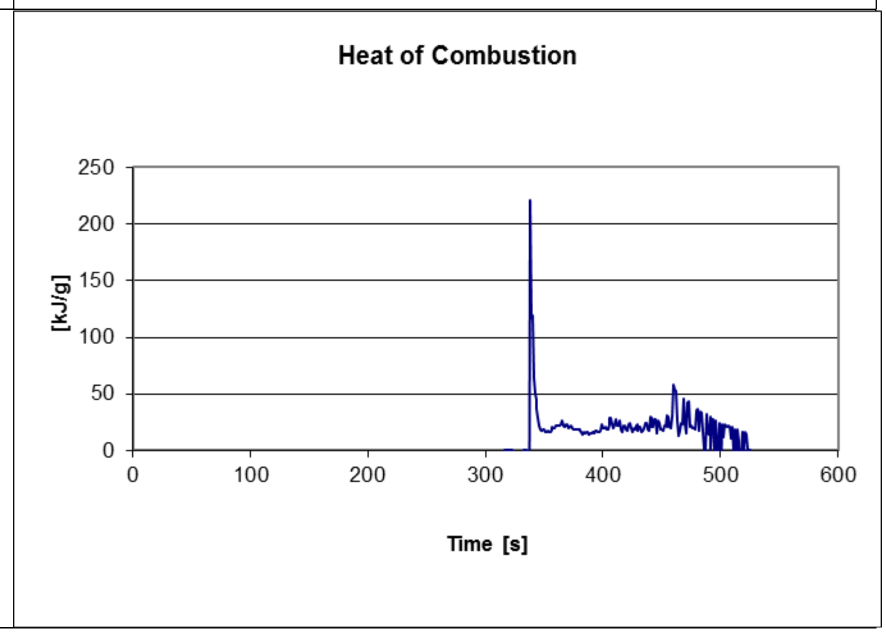
Heat of Combustion
250
200
150
100
50
0
[kJ/g]
0
100
200
300
400
500
600
Time [s]

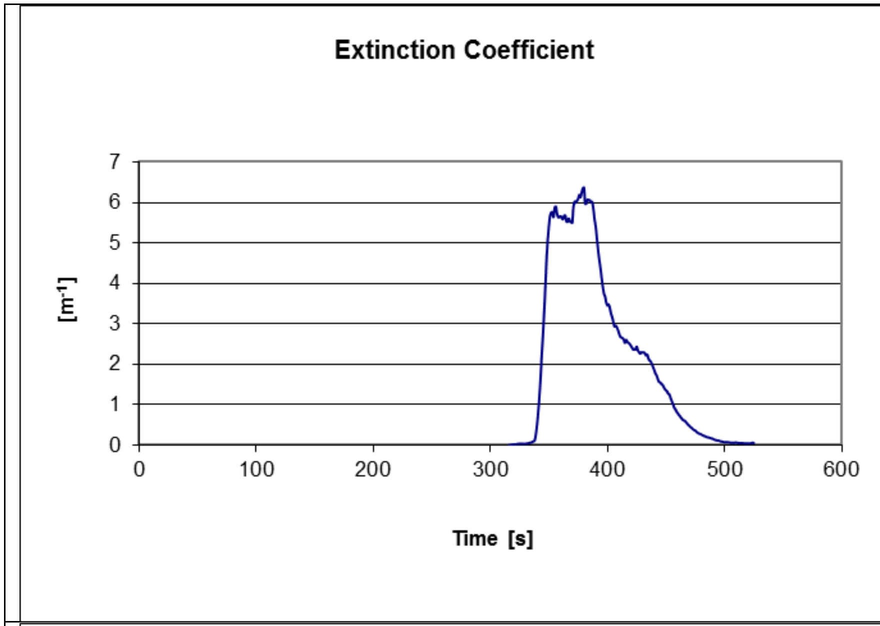
Extinction Coefficient
[m-1]
0
1
2
3
4
5
6
7
0
100
200
300
400
500
600
Time [s]

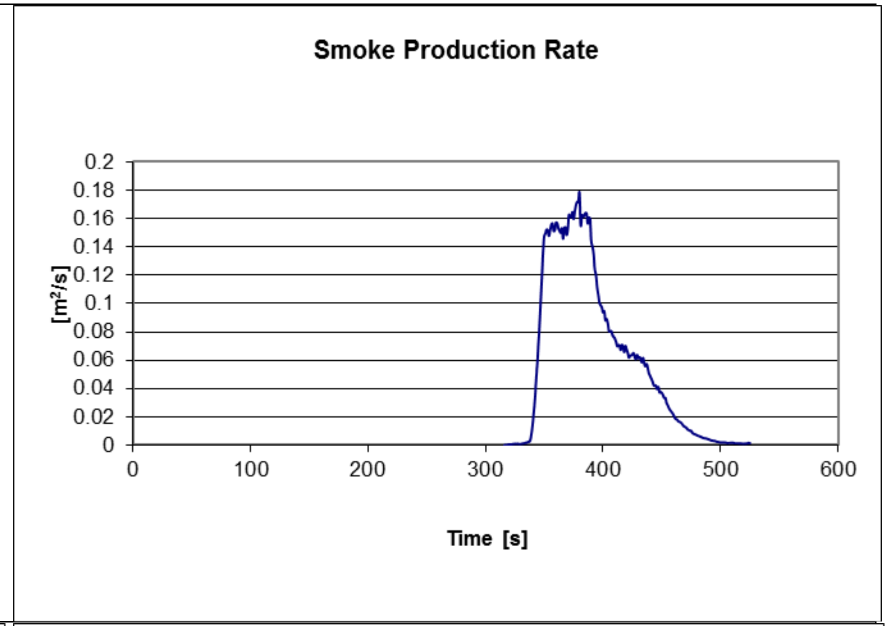
Smoke Production Rate
[m2/s]
0
0.02
0.04
0.06
0.08
0.1
0.12
0.14
0.16
0.18
0.2
0
100
200
300
400
500
600
Time [s]

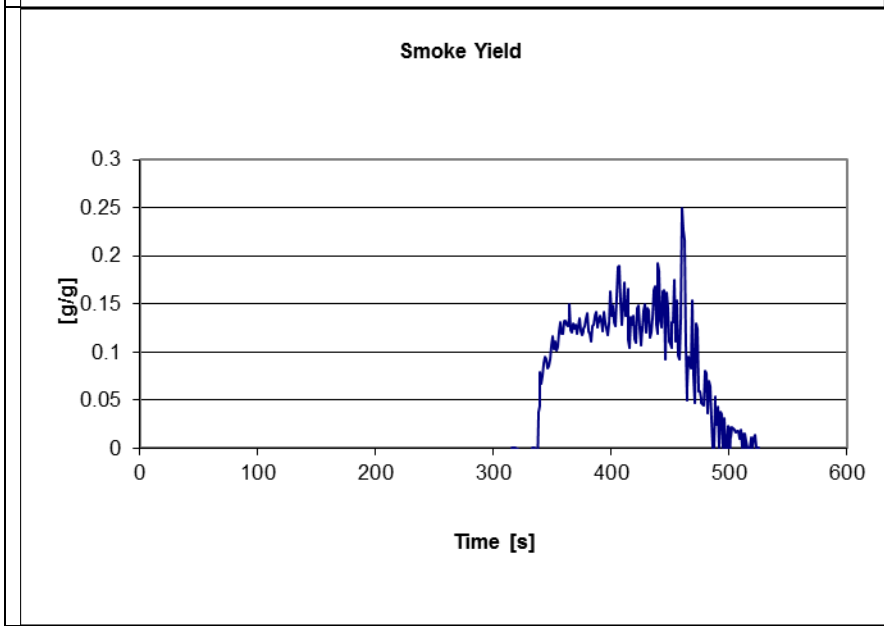
Smoke Yield
[g/g]
0
0.05
0.1
0.15
0.2
0.25
0.3
0
100
200
300
400
500
600
Time [s]

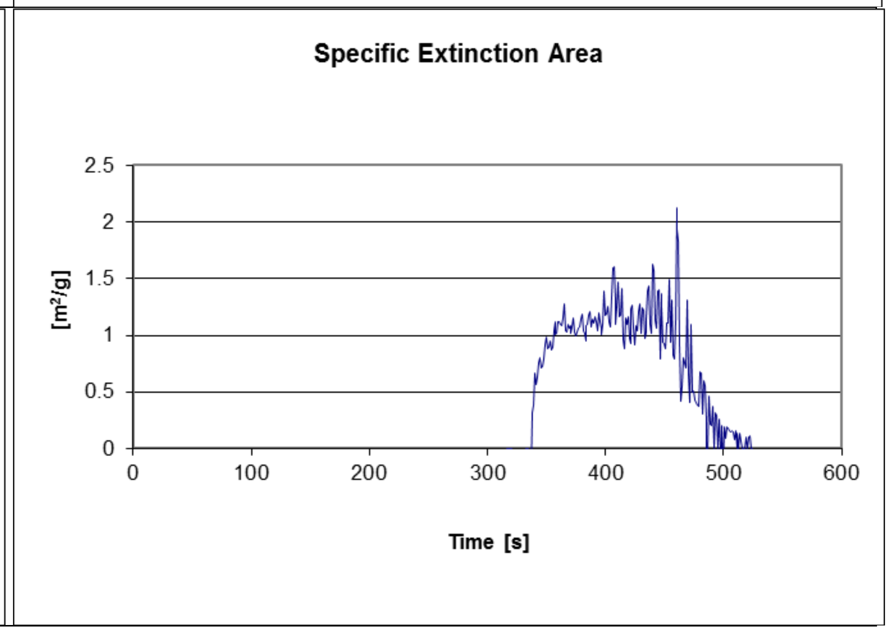
Specific Extinction Area
[m2/g]
0
0.5
1
1.5
2
2.5
0
100
200
300
400
500
600
Time [s]

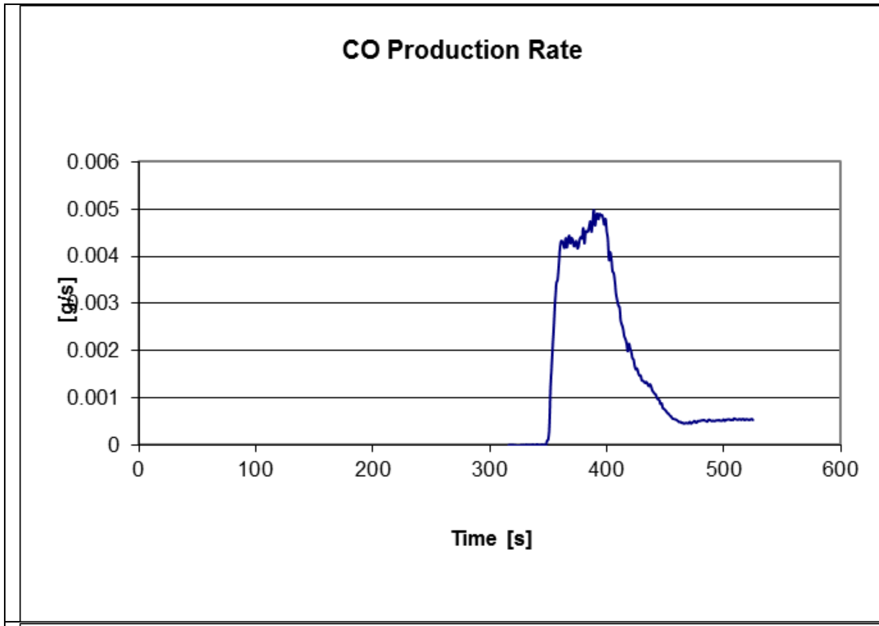
CO Production Rate
0.006
0.005
0.004
0.003
0.002
0.001
0
[g/s]
0
100
200
300
400
500
600
Time [s]

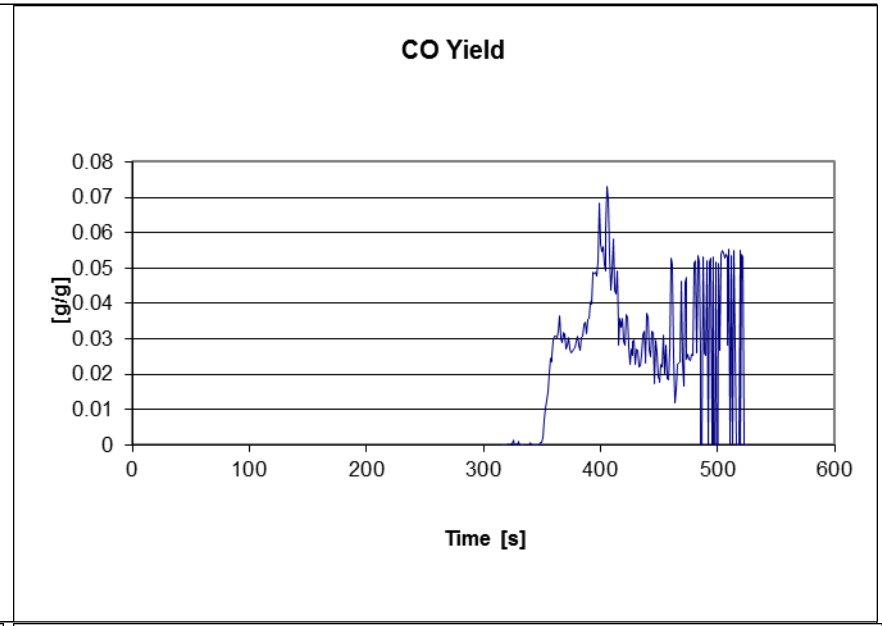
CO Yield
0.08
0.07
0.06
0.05
0.04
0.03
0.02
0.01
0
[g/g]
0
100
200
300
400
500
600
Time [s]

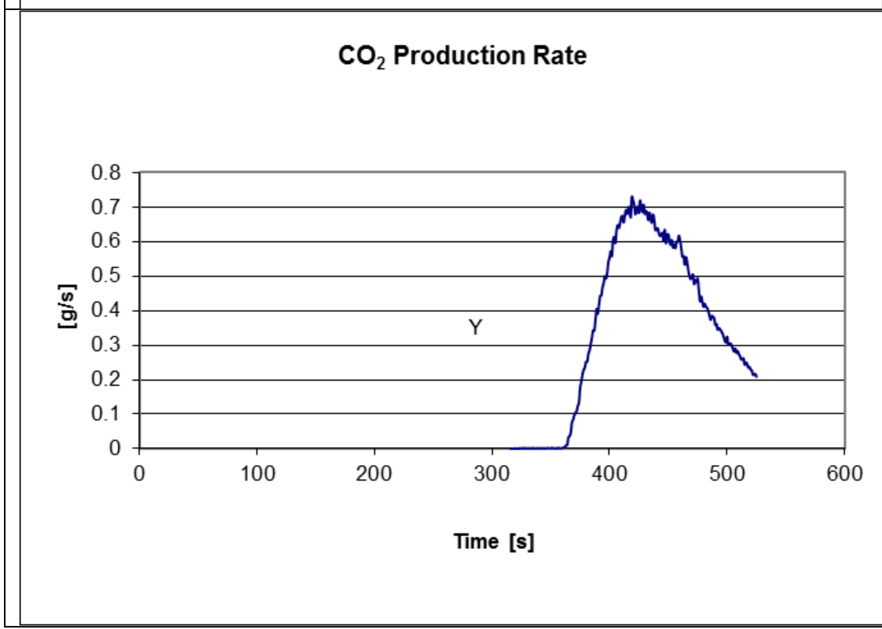
CO2 Production Rate
0.8
0.7
0.6
0.5
0.4
0.3
0.2
0.1
0
[g/s]
Y
0
100
200
300
400
500
600
Time [s]

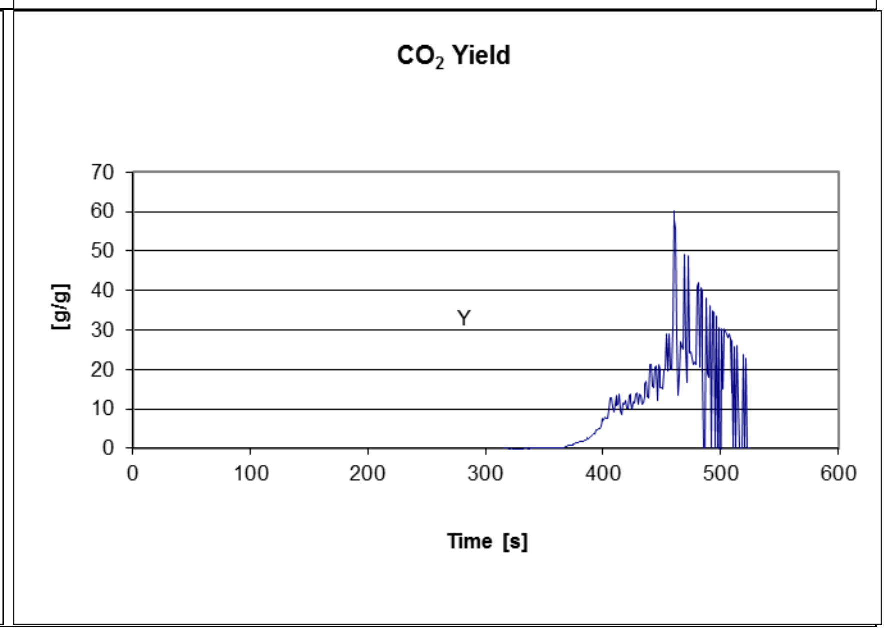
CO2 Yield
70
60
50
40
30
20
10
0
[g/g]
Y
0
100
200
300
400
500
600
Time [s]

E.15 FRP Test 6 – External Flux at 75 kW/m^2, instrumented

Cone Calorimeter Test Run Data

Dept. of Fire Protection Engineering

100 Institute Road
Worcester, MA 01609
Phone: (508) 831-5628
Fax: (508) 831-5862

Test Information

Test Number:	3/4/2010 - 4
Specimen Identification:	FRP Specimen 6, with 2 TCs
Material Name:	Class C FRP
Manufacturer/Submitter:	Not Reported
Sample Description:	White, FRP panel
Raw Data File Name:	030410sample06.txt
Reduced Data File Name:	FRP Sample 06
Date of Test:	3/4/2010
Tester:	R. Hartwell

Test Parameters

Ambient Temperature:	83	F
Relative Humidity:	19	%
Heat Flux:	75	kW/m^2
Exhaust Duct Flow Rate:		30 g/s
Orientation:		Horizontal
Specimen Holder:		TRUE
Specimen Preparation:		2 layer foil
Notes:		1" Separation

Specimen Information

Specimen Color:	[]	White
Specimen Thickness:	[mm]	2.0
Specimen Test Area:	[m^2]	0.0088
Specimen Initial Mass:	[g]	30.7
Specimen Final Mass:	[g]	31.3
Specimen Density:	[g/cm^3]	1.5
Mass Lost:	[g]	-0.6
Total Heat Evolved:	[kJ]	238

Test Times [s]

Shutter Open:	216
Time to Ignition:	241
Flameout:	443
Clean Air/End of Test:	466

Daily C-Factor

	0.045

The Peak, Average and Total parameters are computed over the test period ignition to flame out. There are 4 exceptions. The first three involve initial heat release rate averages for periods after ignition of 60, 180 and 300 seconds. The final involves the average mass loss rate which is computed over the time period from 10% mass loss to 90% mass loss.

Parameter	Unit	Value
Heat Release		
Peak Heat Release Rate	[kW/m^2]	357
Average Heat Release Rate	[kW/m^2]	134
Total Heat Release	[MJ/m^2]	27
Average HRR for the first 60s	[kW/m^2]	280
Average HRR for the first 180s	[kW/m^2]	148
Average HRR for the first 300s	[kW/m^2]	90
Peak Heat of Combustion	[kJ/g]	84
Average Heat of Combustion	[kJ/g]	20
Smoke Obscuration		
Peak SEA	[m^2/g]	1.598
Average SEA	[m^2/g]	0.781
Peak Smoke Yield	[g/g]	0.188
Average Smoke Yield	[g/g]	0.092
Peak Smoke Production Rate	[m^2/s]	0.161
Average Smoke Production Rate	[m^2/s]	0.057
Total Smoke Release	[m^2]	9.960
Gas Production Rates		
Peak Carbon Monoxide	[g/s]	0.005
Average Carbon Monoxide	[g/s]	0.002
Peak Carbon Dioxide	[g/s]	0.684
Average Carbon Dioxide	[g/s]	0.368
Mass Loss		
Peak Mass Loss Rate	[g/s]	0.180
Average Mass Lass Rate	[g/s]	0.085
Initial Mass	[g]	30.7
Final Mass	[g]	31.3
Mass Loss Fraction	[]	-0.02
Burn Time		
Time to Ignition	[s]	25
Duration of Flaming	[s]	202
Duration of Test	[s]	250

Observations

Time	Observation
230	top TC came off of surface
	after ignition, cellular flame then flame cone
353	one drip, falme outside of specimen holder
403	corner burning

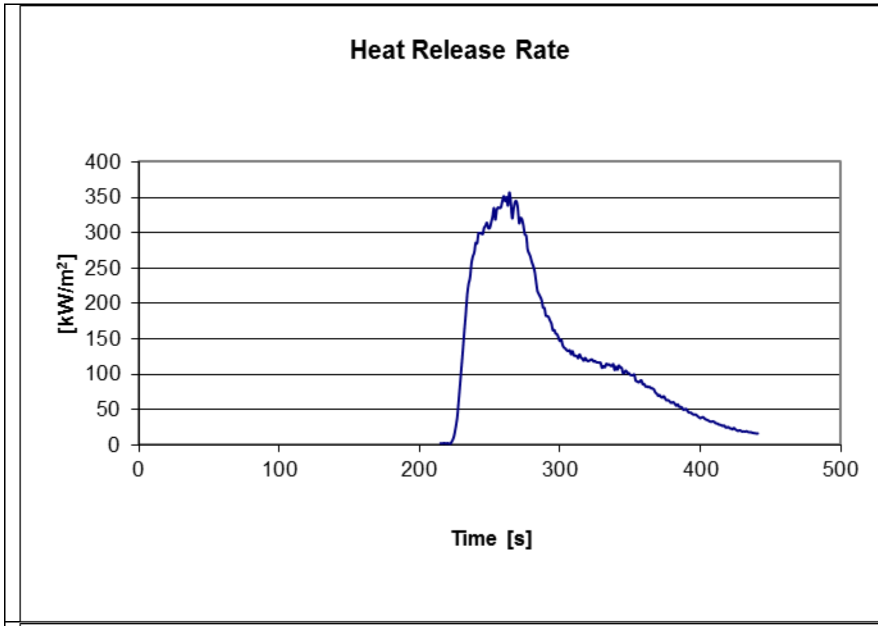
Heat Release Rate
[kW/m²]
400
350
300
250
200
150
100
50
0
0
100
200
300
400
500
Time [s]

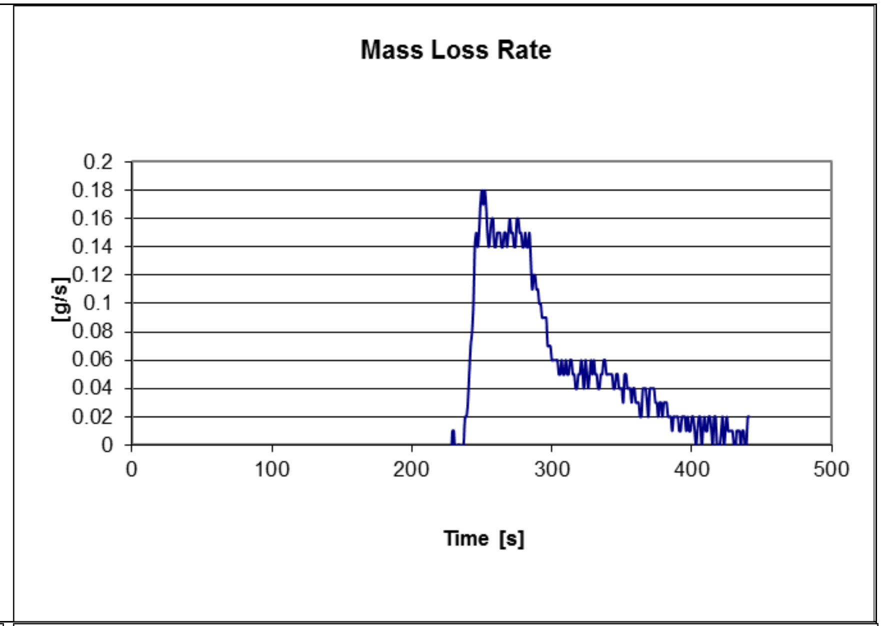
Mass Loss Rate
[g/s]
0.2
0.18
0.16
0.14
0.12
0.1
0.08
0.06
0.04
0.02
0
0
100
200
300
400
500
Time [s]

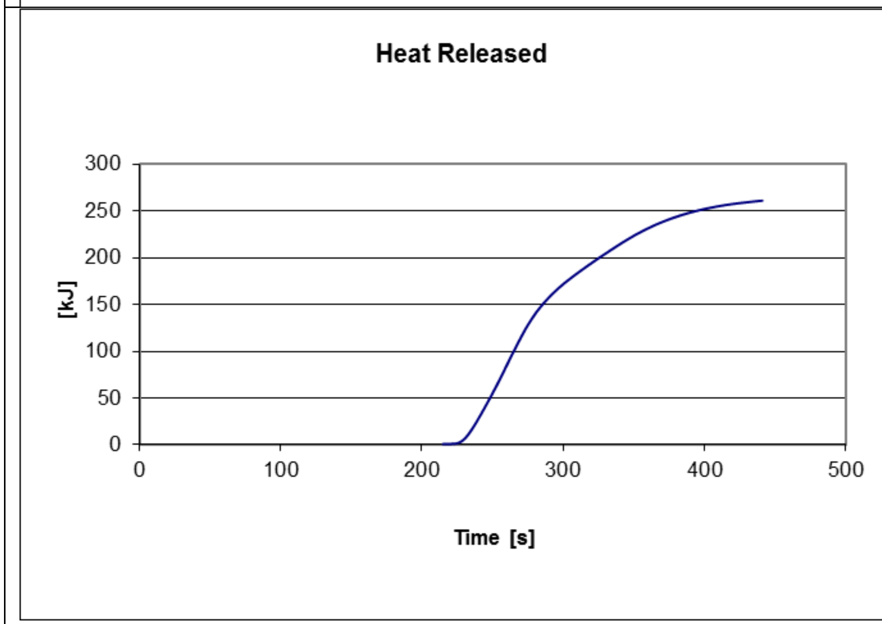
Heat Released
[kJ]
300
250
200
150
100
50
0
0
100
200
300
400
500
Time [s]

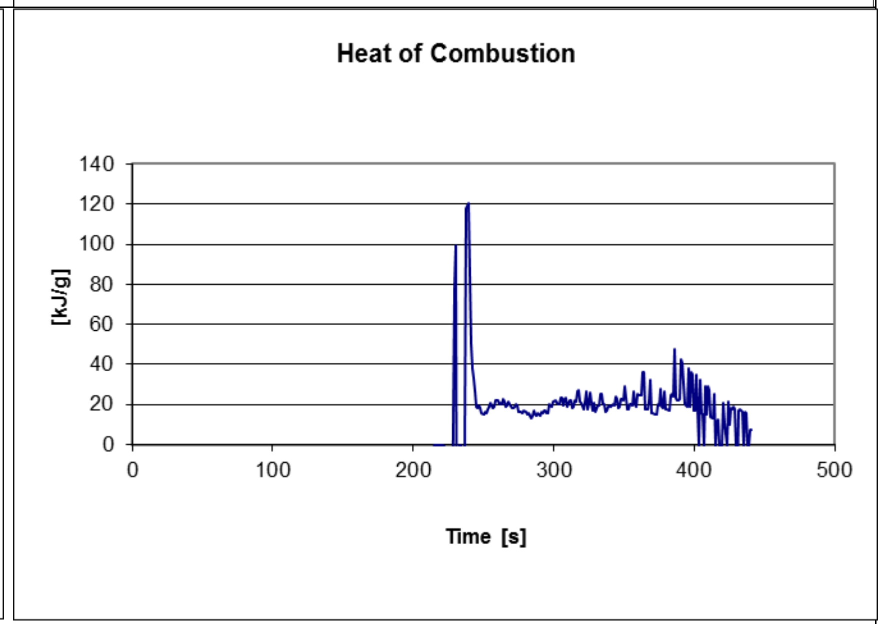
Heat of Combustion
[kJ/g]
140
120
100
80
60
40
20
0
0
100
200
300
400
500
Time [s]

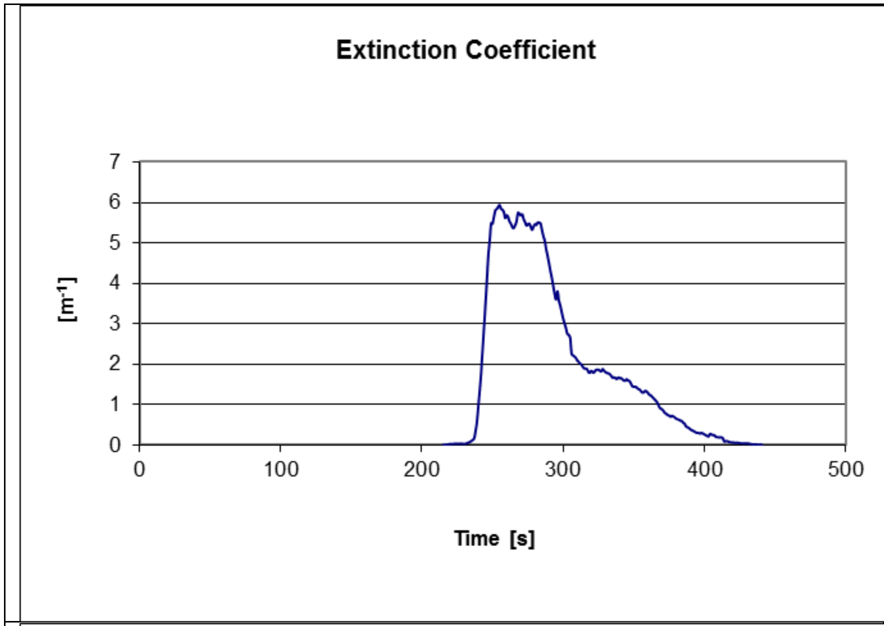
Extinction Coefficient
[m-1]
Time [s]

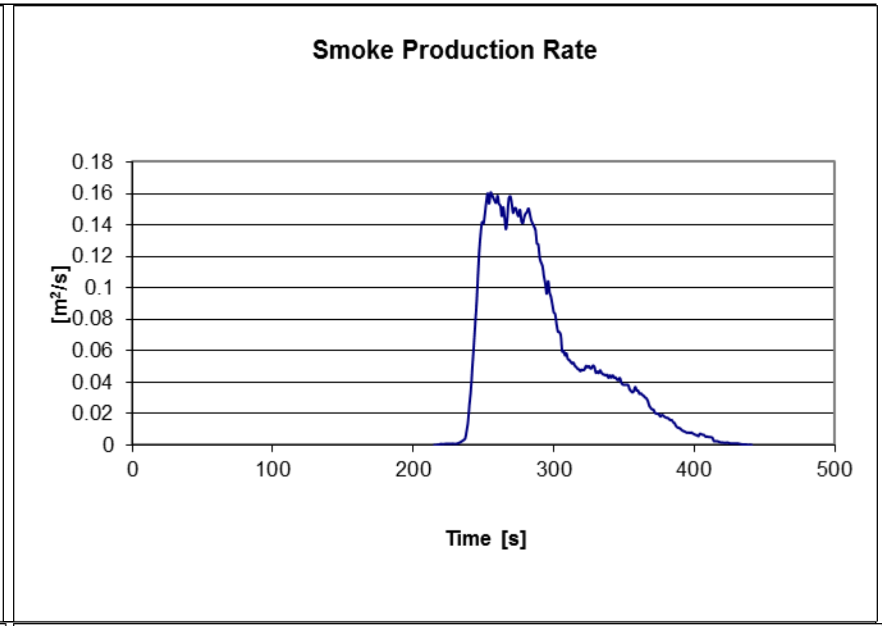
Smoke Production Rate
[m2/s]
Time [s]

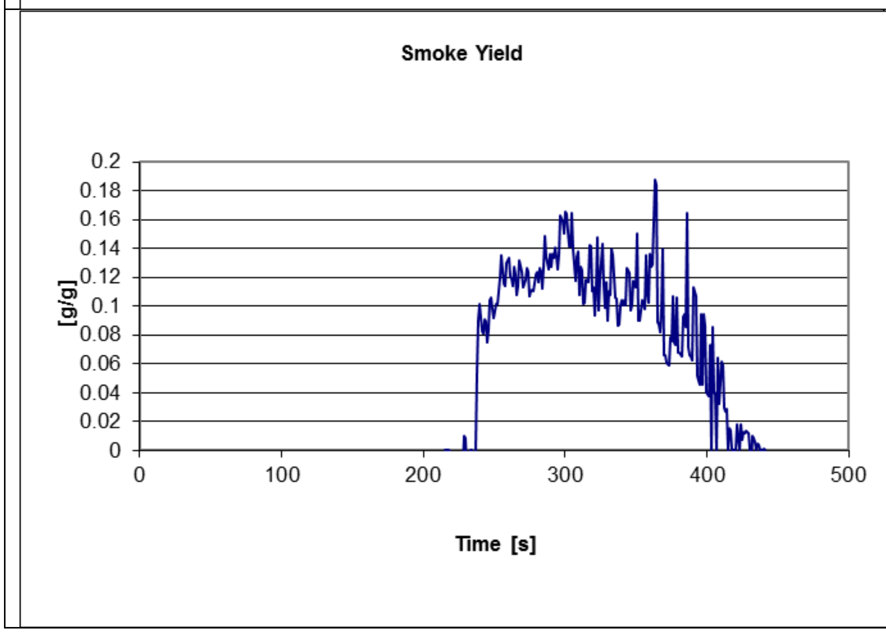
Smoke Yield
[g/g]
Time [s]

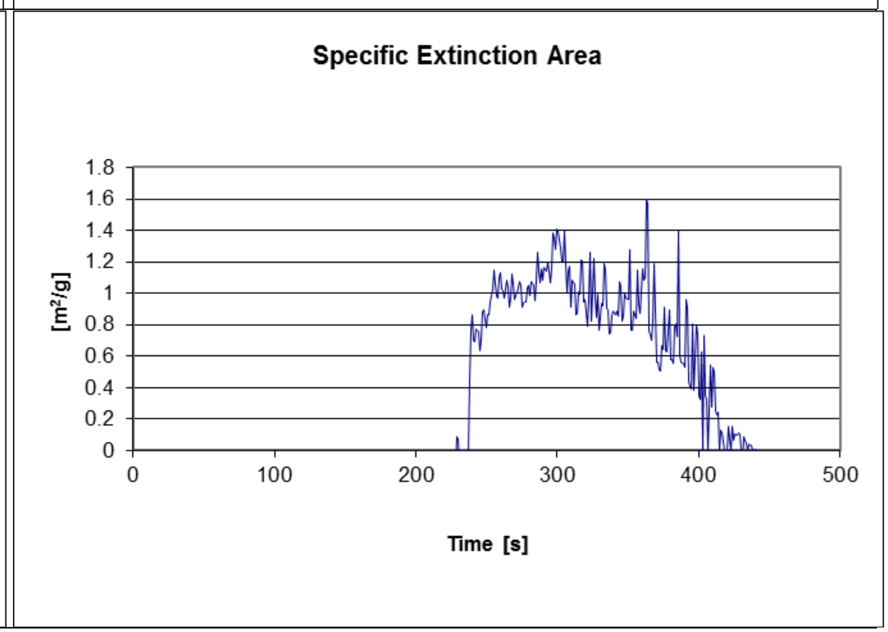
Specific Extinction Area
[m2/g]
Time [s]

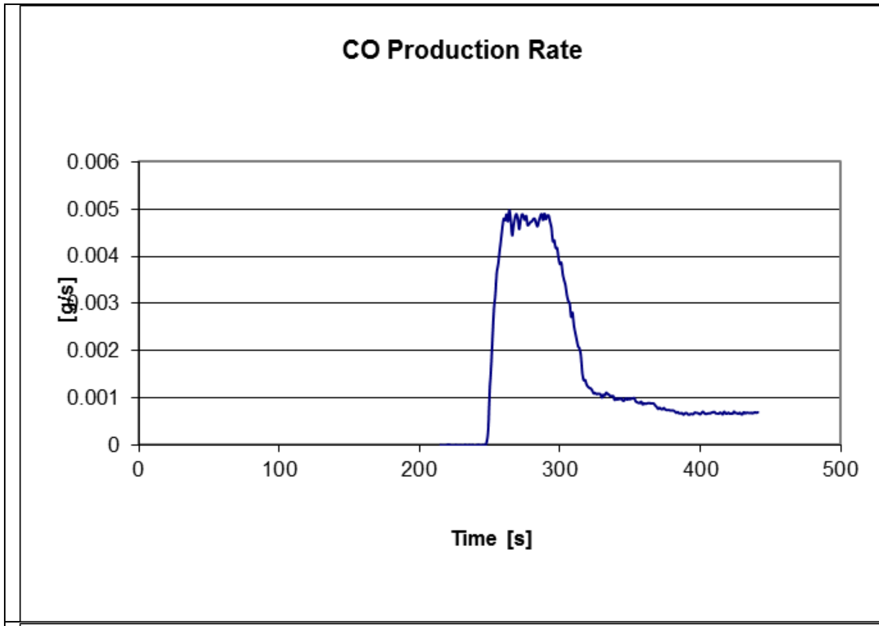
CO Production Rate
[g/s]
Time [s]

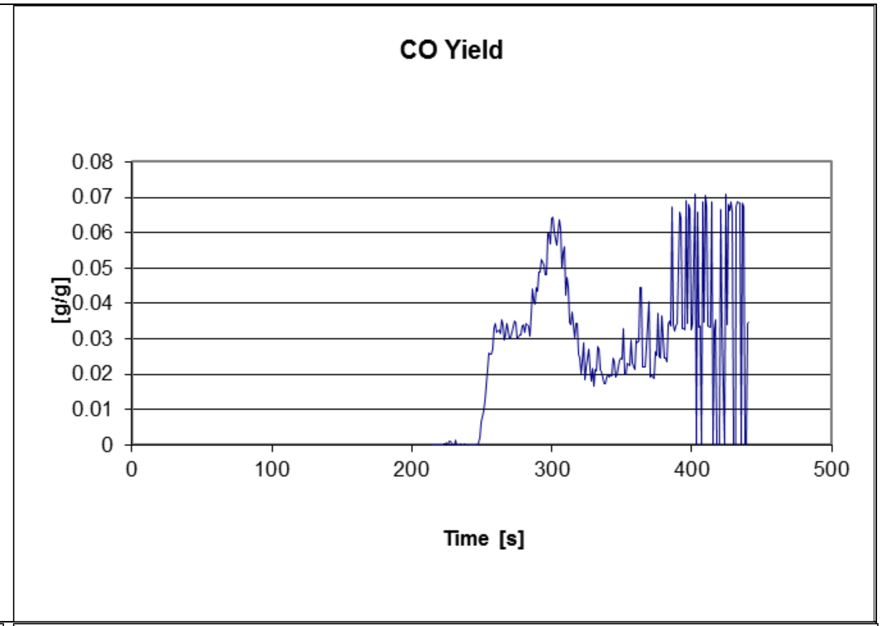
CO Yield
[g/g]
Time [s]

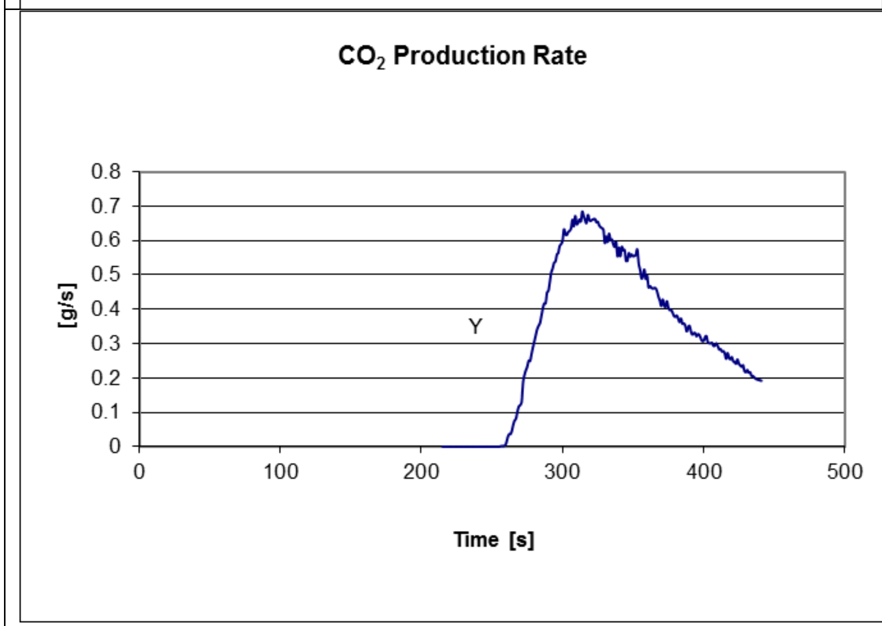
CO_2 Production Rate
[g/s]
Y
Time [s]

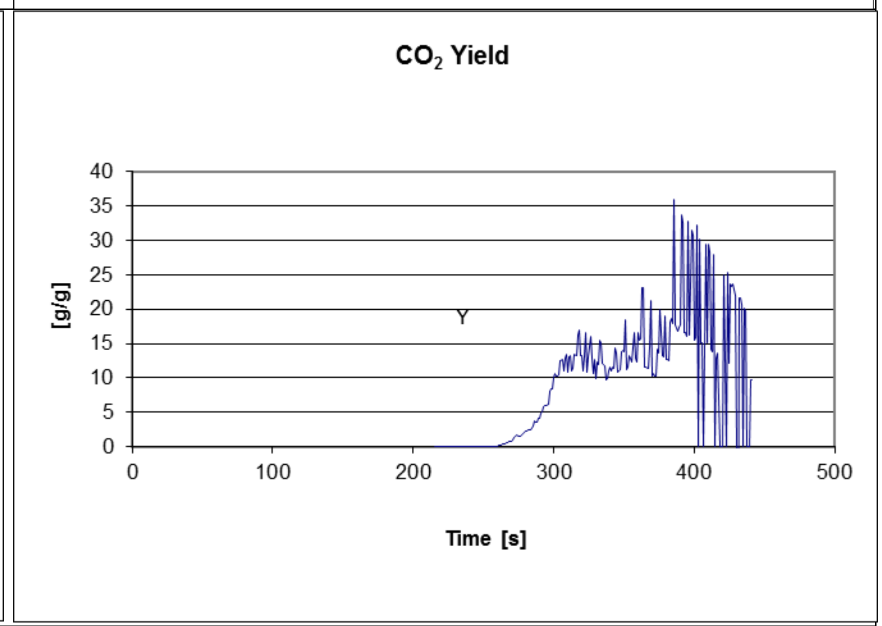
CO_2 Yield
[g/g]
Y
Time [s]

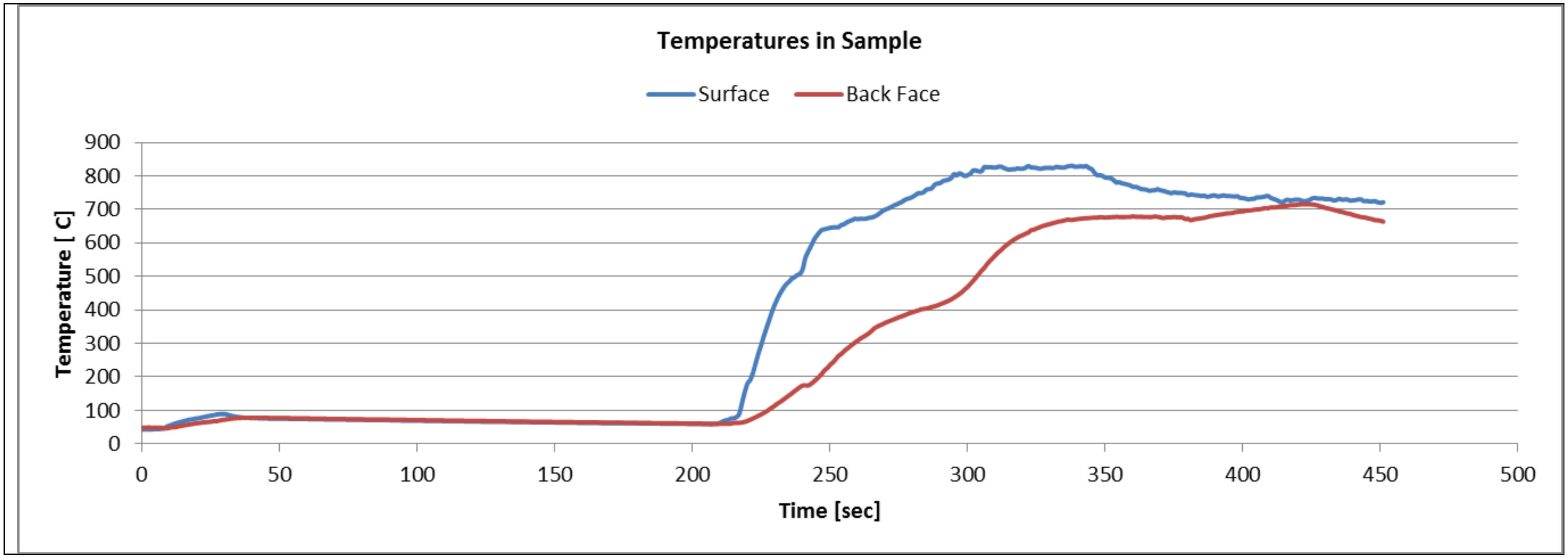
Temperatures in Sample
Surface
Back Face
Temperature [C]
900
800
700
600
500
400
300
200
100
0
0
50
100
150
200
250
300
350
400
450
500
Time [sec]

Appendix F Test Data Summary

This sections contains the test data from the three test series

1. Free plume fire tests
2. Inert wall fire tests
3. Combustible wall fire tests

F.1 Free Plume Fire Tests Data Summary

This Section collects the data from the free plume fire tests in the area of:

- Plume centerline temperature
- Plume centerline velocity
- Mean flame height (50% intermittency)

All data presented in this section have been time-averaged. Additionally, the temperature data have been radiation corrected.

The various testing scenarios are outlined in Table 1

Table 1 – Free plume fire test specifications

Test Name	Source Fire Fuel	Source Fire HRR (kW)	Source Burner Size (ft x ft)
1	Methane	30	1 x 1
2	Methane	50	1 x 1
3	Methane	60	1 x 1
4	Methane	70	1 x 1
5	Methane	75	1 x 1
6	Propane	50	1 x 1
7	Propane	75	1 x 1
8	Propane	50	2 x 1
9	Propane	75	2 x 1
10	Propylene	50	1 x 1
11	Propylene	75	1 x 1
12	Propylene	50	2 x 1
13	Propylene	75	2 x 1

PLUME CENTERLINE TEMPERATURE																	
FUEL	**Name**	**Burner**	**HRR**	**CTC-1**	**BDTC-1**	**CTC-2**	**BDTC-2**	**CTC-3**	**BDTC-3**	**CTC-4**	**BDTC-4**	**CTC-5**	**BDTC-5**	**CTC-6**	**BDTC-6**	**CTC-7**
			[kW]	**[K]**	**[K]**	**[K]**	**[K]**	**[K]**	**[K]**	**[K]**	**[K]**	**[K]**	**[K]**	**[K]**	**[K]**	**[K]**
Methane	P1A	Square	50	1594	1456	1014	911	731	624	537	479	463	444	427	424	415
Methane	P1B	Square	60	1598	1496	1043	911	730	622	540	481	466	446	429	426	417
Methane	P1C	Square	60	1599	1501	1053	881	723	613	533	475	461	441	426	424	416
Methane	P1D	Square	68	1595	1515	1053	878	717	613	541	479	465	444	429	424	416
Methane	P2A	Square	77	1577	1470	1005	928	723	637	557	499	473	452	431	425	414
Methane	P2B	Square	77	1622	1539	1070	913	746	644	556	496	473	450	431	425	415
Methane	P2C	Square	77	1575	1481	1043	871	717	610	529	473	459	440	426	424	416
Methane	P2D	Square	68	1624	1545	1086	909	746	644	561	497	475	451	432	426	416
Methane	P2E	Square	67	1625	1472	1070	876	725	627	552	489	471	446	432	425	416
Methane	P2F	Square	76	1632	1550	1094	887	734	631	548	491	469	447	430	425	416
Methane	P2G	Square	66	1624	1509	1044	884	708	615	533	485	464	444	427	422	414
Methane	P2H	Square	74	1636	1576	1123	878	734	630	550	492	471	449	432	427	417
Methane	P2I	Square	73	1629	1575	1106	882	726	624	542	488	468	446	430	426	417
Methane	P2J	Square	75	1639	1584	1123	880	733	631	549	493	473	450	434	428	418
Propane	P-1ft-1A	Square	79	1505	1575	1160	1050	833	710	609	541	506	474	457	449	437
Propane	P-1ft-1B	Square	78	1476	1581	1176	1022	792	682	589	521	496	463	452	445	434
Propane	P-1ft-1C	Square	79	1468	1596	1239	977	776	659	574	510	490	461	451	445	436
Propane	P-1ft-1D	Square	52	1605	1524	1058	881	721	615	542	486	466	445	429	425	416
Propane	P-1ft-1E	Square	53	1557	1344	918	692	548	487	449	420	414	400	398	396	391
Propane	P-1ft-1F	Square	52	1546	1293	880	670	538	481	446	419	412	400	396	394	389
Propane	P-1ft-1G	Square	52	1568	1311	894	687	550	489	448	422	414	402	398	397	392
Propane	P-2ft-1A	Rectangle	79	1448	1115	799	656	555	504	466	450	439	432	426	428	423
Propane	P-2ft-1B	Rectangle	52	1179	845	614	521	462	434	411	408	395	390	387	388	384
Propane	P-2ft-1C	Rectangle	52	1173	840	608	517	460	433	411	404	395	390	387	388	384
Propane	P-2ft-1D	Rectangle	52	1172	829	607	517	462	436	415	405	398	393	390	390	387
Propylene	P-1ft-A	Square	50	1537	1434	986	877	664	573	487	461	440	423	413	410	400
Propylene	P-1ft-B	Square	51	1550	1417	962	840	635	565	489	470	450	437	428	427	418
Propylene	P-1ft-C	Square	51	1556	1436	998	820	617	548	480	458	434	418	411	407	398
Propylene	P-1ft-D	Square	76	1449	1551	1289	1139	871	765	639	583	531	498	478	467	452
Propylene	P-1ft-E	Square	76	1458	1540	1195	1151	857	765	626	572	523	493	473	463	449
Propylene	P-1ft-F	Square	76	1550	1417	962	840	635	565	489	470	450	437	428	427	418
Propylene	P-2ft-A	Rectangle	50	1311	951	716	574	482	457	433	421	406	399	397	396	391
Propylene	P-2ft-B	Rectangle	51	1246	949	716	571	479	454	434	423	408	401	399	398	392
Propylene	P-2ft-C	Rectangle	51	1259	955	713	571	484	462	440	429	414	408	406	405	400
Propylene	P-2ft-D	Rectangle	75	1578	1144	940	718	583	532	491	471	447	437	435	431	424
Propylene	P-2ft-E	Rectangle	75	1508	1151	951	729	590	540	499	481	457	446	440	436	428
Propylene	P-2ft-F	Rectangle	75	1480	1124	960	740	602	552	509	493	471	460	455	453	445

PLUME CENTERLINE TEMPERATURE (CONT.)														
FUEL	Name	Burner	HRR	PTC-1	PTC-2	PTC-3	BDTC-7	PTC-4	BDTC-8	PTC-5	BDTC-9	PTC-6	BDTC-10	PTC-7
			[kW]	[K]	[K]	[K]	[K]	[K]	[K]	[K]	[K]	[K]	[K]	[K]
Methane	P1A	Square	50	1464	1176	947	794	638	577	490	496	451	436	416
Methane	P1B	Square	60	1493	1199	937	808	638	582	492	499	453	437	418
Methane	P1C	Square	60	1481	1188	900	790	621	571	484	491	451	435	416
Methane	P1D	Square	68	1485	1202	912	787	618	565	491	498	450	435	417
Methane	P2A	Square	77	1496	1138	975	798	649	578	508	514	454	437	420
Methane	P2B	Square	77	1498	1190	948	797	637	577	503	510	452	436	420
Methane	P2C	Square	77	1481	1188	900	790	621	571	484	491	451	435	416
Methane	P2D	Square	68	1483	1201	943	795	635	572	501	510	452	437	420
Methane	P2E	Square	67	1438	1147	908	761	610	553	495	501	447	432	419
Methane	P2F	Square	76	1481	1180	913	779	620	570	494	502	451	436	418
Methane	P2G	Square	66	1482	1186	895	784	622	565	487	495	448	434	417
Methane	P2H	Square	74	1469	1203	894	778	623	575	495	503	454	439	420
Methane	P2I	Square	73	1491	1205	892	780	620	571	491	499	452	437	419
Methane	P2J	Square	75	1481	1211	890	784	624	578	495	504	455	440	421
Propane	P-1ft-1A	Square	79	1513	1337	893	898	688	625	529	533	482	459	438
Propane	P-1ft-1B	Square	78	1506	1331	883	870	663	606	517	520	474	455	434
Propane	P-1ft-1C	Square	79	1478	1275	828	838	637	596	502	508	474	454	434
Propane	P-1ft-1D	Square	52	1494	1208	915	791	620	567	499	509	450	435	417
Propane	P-1ft-1E	Square	53	1282	945	636	589	477	458	417	420	409	400	390
Propane	P-1ft-1F	Square	52	1248	922	620	582	476	459	415	419	408	399	390
Propane	P-1ft-1G	Square	52	1244	908	614	586	476	459	416	420	410	400	391
Propane	P-2ft-1A	Rectangle	79	1059	801	559	583	500	479	444	449	435	428	421
Propane	P-2ft-1B	Rectangle	52	814	619	466	478	431	421	404	410	393	388	383
Propane	P-2ft-1C	Rectangle	52	800	607	455	476	432	420	400	405	393	388	383
Propane	P-2ft-1D	Rectangle	52	787	600	452	476	435	424	401	404	396	391	386
Propylene	P-1ft-A	Square	50	1381	1102	818	727	570	518	454	464	429	416	404
Propylene	P-1ft-B	Square	51	1337	1066	774	700	556	519	460	471	442	431	421
Propylene	P-1ft-C	Square	51	1369	1079	800	671	536	496	445	455	423	411	401
Propylene	P-1ft-D	Square	76	1478	1392	1039	943	758	666	558	578	501	478	456
Propylene	P-1ft-E	Square	76	1475	1352	983	956	763	661	550	570	498	475	455
Propylene	P-1ft-F	Square	76	1337	1066	774	700	556	519	460	471	442	431	421
Propylene	P-2ft-A	Rectangle	50	837	704	526	510	452	433	410	417	402	397	392
Propylene	P-2ft-B	Rectangle	51	830	706	530	509	451	432	411	418	404	399	394
Propylene	P-2ft-C	Rectangle	51	828	705	532	514	458	441	418	424	411	406	401
Propylene	P-2ft-D	Rectangle	75	999	900	661	625	527	493	452	462	442	434	425
Propylene	P-2ft-E	Rectangle	75	1012	915	672	644	540	512	461	472	452	442	431
Propylene	P-2ft-F	Rectangle	75	994	915	681	655	553	523	474	485	466	457	447

PLUME CENTERLINE VELOCITY													
FUEL	**Name**	**Burner**	**HRR**	**BD-1**	**BD-2**	**BD-3**	**BD-4**	**BD-5**	**BD-6**	**BD-7**	**BD-8**	**BD-9**	**BD-10**
			[kW]	**[m/s]**	**[m/s]**	**[m/s]**	**[m/s]**	**[m/s]**	**[m/s]**	**[m/s]**	**[m/s]**	**[m/s]**	**[m/s]**
Methane	P1A	Square	50	3.7	3.4	4.2	3.7	2.9	2.1	4.3	5.5	4.0	3.3
Methane	P1B	Square	60	3.8	3.4	4.2	3.8	2.9	2.1	4.4	4.6	4.0	3.3
Methane	P1C	Square	60	3.9	3.4	4.0	3.7	3.0	2.2	4.3	4.8	4.0	3.3
Methane	P1D	Square	68	3.9	3.5	4.3	3.9	3.2	2.3	4.4	4.7	4.1	3.4
Methane	P2A	Square	77	4.5	3.4	4.3	3.9	3.1	2.5	4.5	4.5	4.1	3.3
Methane	P2B	Square	77	3.8	3.5	4.4	3.8	3.1	2.1	4.5	4.5	4.1	3.4
Methane	P2C	Square	77	3.9	3.4	4.4	4.0	3.2	2.2	4.5	4.5	4.1	3.5
Methane	P2D	Square	68	4.0	3.5	4.4	4.0	3.2	2.3	4.5	4.5	4.2	3.4
Methane	P2E	Square	67	3.9	3.5	4.3	4.0	3.2	2.3	4.3	4.2	4.1	3.4
Methane	P2F	Square	76	4.0	3.5	4.4	4.0	3.1	2.3	4.4	4.4	4.1	3.4
Methane	P2G	Square	66	4.0	3.6	4.3	3.8	3.1	2.1	4.4	4.3	4.1	3.2
Methane	P2H	Square	74	4.1	3.6	4.4	3.9	3.2	2.3	4.4	4.4	4.2	2.5
Methane	P2I	Square	73	4.1	3.6	4.2	3.8	3.1	2.2	4.4	4.4	4.1	2.4
Methane	P2J	Square	75	4.1	3.6	4.3	3.9	3.1	2.3	4.4	4.4	4.2	2.5
Propane	P-1ft-1A	Square	79	3.6	3.5	4.5	3.3	3.1	1.8	4.4	4.9	4.1	3.4
Propane	P-1ft-1B	Square	78	3.7	3.5	4.3	3.4	3.0	1.9	4.3	4.4	4.2	3.4
Propane	P-1ft-1C	Square	79	4.0	3.6	4.3	3.7	3.0	2.0	4.2	4.3	4.1	3.4
Propane	P-1ft-1D	Square	52	3.7	3.2	3.5		2.5	1.6	3.5	3.4	3.4	2.8
Propane	P-1ft-1E	Square	53	3.8	3.2	3.5	2.7	2.5	1.6	3.4	3.4	3.3	2.8
Propane	P-1ft-1F	Square	52	3.7	3.2	3.5	3.1	2.5	1.5	3.4	3.4	3.4	2.8
Propane	P-1ft-1G	Square	52	3.8	3.1	3.4	3.1	2.5	1.7	3.4	3.4	3.4	2.8
Propane	P-2ft-1A	Rectangle	79	3.0	2.8	3.3	1.4	2.5	0.7	3.2	3.6	3.3	2.7
Propane	P-2ft-1B	Rectangle	52	3.2	2.6	3.1		2.2	1.1	2.8	3.0	2.9	2.4
Propane	P-2ft-1C	Rectangle	52	2.7	2.5	2.8		2.2	1.2	2.7	3.0	2.9	2.4
Propane	P-2ft-1D	Rectangle	52	2.8	2.5	2.9	1.7	2.2	1.2	2.7	3.0	3.0	2.5
Propylene	P-1ft-A	Square	50	3.9	3.4	4.0		2.5	1.7	4.0	3.8	3.4	1.7
Propylene	P-1ft-B	Square	51	3.5	3.4	3.6		2.3	1.5	3.9	3.6	3.4	1.7
Propylene	P-1ft-C	Square	51	4.0	3.7	3.7		2.6	1.7	3.9	3.8	3.6	1.7
Propylene	P-1ft-D	Square	76	3.8	3.8	4.5		3.1	1.9	4.7	4.6	4.2	2.0
Propylene	P-1ft-E	Square	76	3.8	3.8	4.5		3.1	1.8	4.8	4.6	4.2	2.1
Propylene	P-1ft-F	Square	76	3.7	3.7	4.8		3.2	1.9	4.8	4.7	4.3	2.1
Propylene	P-2ft-A	Rectangle	50	2.6	2.6	2.9		2.3	1.1	2.9	3.0	3.0	1.6
Propylene	P-2ft-B	Rectangle	51	2.9	2.6	2.9		2.3	1.2	2.9	3.0	3.0	1.6
Propylene	P-2ft-C	Rectangle	51	2.8	2.6	3.0		2.3	1.2	2.9	3.1	3.0	1.5
Propylene	P-2ft-D	Rectangle	75	3.1	3.0	3.5		2.5	1.4	3.4	3.5	3.4	1.8
Propylene	P-2ft-E	Rectangle	75	3.0	3.0	3.5		2.7	1.7	3.5	3.6	3.6	1.9
Propylene	P-2ft-F	Rectangle	75	3.5	3.7	1.8	3.0		1.3	3.7	3.1	3.5	2.6

MEAN FLAME HEIGHT				
FUEL	Name	Burner	HRR	Flame Height
			[kW]	[m]
Methane	P1A	Square	50	0.6
Methane	P1B	Square	60	0.7
Methane	P1C	Square	60	0.7
Methane	P1D	Square	68	0.7
Methane	P2A	Square	77	0.9
Methane	P2B	Square	77	0.9
Methane	P2C	Square	77	0.9
Methane	P2D	Square	68	0.8
Methane	P2E	Square	67	0.8
Methane	P2F	Square	76	0.9
Methane	P2G	Square	66	0.7
Methane	P2H	Square	74	0.8
Methane	P2I	Square	73	0.8
Methane	P2J	Square	75	0.8
Propane	P-1ft-1A	Square	79	0.8
Propane	P-1ft-1B	Square	78	0.9
Propane	P-1ft-1C	Square	79	0.8
Propane	P-1ft-1D	Square	52	0.6
Propane	P-1ft-1E	Square	53	0.6
Propane	P-1ft-1F	Square	52	0.6
Propane	P-1ft-1G	Square	52	0.6
Propane	P-2ft-1A	Rectangle	79	0.6
Propane	P-2ft-1B	Rectangle	52	0.4
Propane	P-2ft-1C	Rectangle	52	0.4
Propane	P-2ft-1D	Rectangle	52	0.4
Propylene	P-1ft-A	Square	50	0.7
Propylene	P-1ft-B	Square	51	0.7
Propylene	P-1ft-C	Square	51	0.7
Propylene	P-1ft-D	Square	76	0.9
Propylene	P-1ft-E	Square	76	0.9
Propylene	P-1ft-F	Square	76	0.9
Propylene	P-2ft-A	Rectangle	50	0.5
Propylene	P-2ft-B	Rectangle	51	0.5
Propylene	P-2ft-C	Rectangle	51	0.5
Propylene	P-2ft-D	Rectangle	75	0.7
Propylene	P-2ft-E	Rectangle	75	0.7
Propylene	P-2ft-F	Rectangle	75	0.7

F.2 Inert Wall Fire Tests Data Summary

This Section collects the data from the inert wall fire tests in the area of:

- Plume centerline temperature
- Plume centerline velocity
- Heat flux to wall
- Near-wall Temperature
- Mean flame height (50% intermittency)

All data presented in this section have been time-averaged. Additionally, the temperature data have been radiation corrected.

The various testing scenarios are outlined in Table 1

Table 2 - Inert wall fire test specifications

Test Name	Source Fire Fuel	Source Fire HRR (kW)	Source Burner Size (ft x ft)
1	Methane	70	1 x 1
2	Methane	75	1 x 1
3	Methane	80	1 x 1
4	Propylene	50	1 x 1
5	Propylene	75	1 x 1
6	Propylene	50	2 x 1
7	Propylene	75	2 x 1
8	Propane	50	1 x 1
9	Propane	75	1 x 1
10	Propane	50	2 x 1
11	Propane	75	2 x 1

PLUME CENTERLINE TEMPERATURE

FUEL	Name	Burner	HRR	CTC-1	BDTC-1	CTC-2	BDTC-2	CTC-3	BDTC-3	CTC-4	BDTC-4	CTC-5	BDTC-5	CTC-6	BDTC-6	CTC-7
			[kW]	[K]	[K]	[K]	[K]	[K]	[K]	[K]	[K]	[K]	[K]	[K]	[K]	[K]
Methane	W1A	Square	79	1560	1269	995	775	690	595	528	500	475	451	442	450	441
Methane	W1B	Square	78	1576	1239	974	754	679	587	523	498	474	450	442	451	442
Methane	W1C	Square	68	1497	1169	941	724	655	569	518	495	470	446	439	446	438
Methane	W1D	Square	78	1577	1223	966	750	675	587	526	498	473	449	443	451	448
Methane	W1E	Square	77	1582	1228	970	747	674	586	524	498	472	448	443	452	444
Methane	W1F	Square	78	1565	1242	983	752	680	592	531	504	477	449	445	452	444
Propane	W-1ft-1A	Square	52	1552	1055	847	636	525	500	460	450	429	419	422	429	419
Propane	W-1ft-1B	Square	78	1526	1273	1097	795	697	650	583	558	518	497	501	510	491
Propane	W-1ft-1C	Square	52	1518	1143	923	676	540	509	466	444	414	397	399	401	394
Propane	W-1ft-1D	Square	52	1529	1205	939	685	542	510	469	447	414	398	400	401	394
Propane	W-1ft-1E	Square	52	1505	1123	888	646	523	493	459	441	411	396	401	403	396
Propane	W-1ft-1F	Square	52	1496	1126	887	650	527	500	463	444	414	400	403	406	398
Propane	W-1ft-1G	Square	52	1497	1143	899	661	532	502	464	444	415	401	404	406	399
Propane	W-1ft-1H	Square	79	1464	1341	1169	860	716	669	591	550	499	468	469	473	459
Propane	W-1ft-1I	Square	79	1479	1315	1143	856	712	667	590	552	502	471	474	477	463
Propane	W-1ft-2A	Square	53	1523	1230	951	733	612	537	484	462	436	418	419	423	413
Propane	W-1ft-2B	Square	79	1426	1462	1248	937	822	718	629	580	526	491	489	489	471
Propane	W-1ft-2C	Square	79	1464	1405	1198	905	800	706	621	575	525	493	493	496	488
Propane	W-1ft-2D	Square	79	1471	1386	1187	903	795	705	621	578	529	498	499	500	481
Propane	W-2ft-1A	Rectangle	52	1159	703	602	520	470	464	436	444	426	419	422	429	422
Propane	W-2ft-1B	Rectangle	53	1090	648	550	464	429	427	406	409	411	411	416	427	422
Propane	W-2ft-2A	Rectangle	52	1172	696	589	505	458	453	424	422	418	414	418	428	422
Propane	W-2ft-2B	Rectangle	52	1104	655	563	488	446	445	422	421	415	411	416	426	421
Propane	W-2ft-2C	Rectangle	52	1081	646	550	474	435	437	416	417	415	413	417	428	424
Propane	W-2ft-2D	Rectangle	78	1528	879	770	617	551	535	487	484	474	469	473	489	480
Propane	W-1ft-3A	Rectangle	78	1440	932	825	679	625	577	534	520	498	483	493	502	488
Propane	W-1ft-3B	Rectangle	78	1477	968	851	713	646	592	546	531	505	487	497	505	490
Propane	W-1ft-3C	Rectangle	52													
Propane	W-1ft-3D	Rectangle	52													
Propane	W-1ft-3E	Rectangle	52													
Propane	W-1ft-3F	Rectangle	78													
Propane	W-1ft-3G	Rectangle	78													
Propylene	W-1ft-A	Square	51	1676	1340	933	792	639	570	496	471	450	435	430	432	422
Propylene	W-1ft-B	Square	51	1665	1258	900	735	592	540	485	468	452	442	440	442	433
Propylene	W-1ft-C	Square	51	1670	1340	939	740	597	548	497	484	465	455	455	457	445
Propylene	W-1ft-D	Square	51	1624	1331	1002	752	602	543	491	465	436	419	421	422	414
Propylene	W-1ft-E	Square	50	1601	1274	976	724	591	541	492	476	452	440	442	443	433
Propylene	W-1ft-F	Square	75	1676	1340	933	792	639	570	496	471	450	435	430	432	454

PLUME CENTERLINE TEMPERATURE

FUEL	Name	Burner	HRR	CTC-1	BDTC-1	CTC-2	BDTC-2	CTC-3	BDTC-3	CTC-4	BDTC-4	CTC-5	BDTC-5	CTC-6	BDTC-6	CTC-7
			[kW]	[K]	[K]	[K]	[K]	[K]	[K]	[K]	[K]	[K]	[K]	[K]	[K]	[K]
Propylene	W-1ft-G	Square	76	1595	1484	1304	924	768	680	613	565	506	474	478	475	463
Propylene	W-1ft-H	Square	75	1627	1533	1320	1006	828	740	653	600	546	515	517	510	491
Propylene	W-1ft-I	Square	75	1640	1437	1225	933	786	719	638	601	560	536	539	537	516
Propylene	W-2ft-A	Rectangle	67													
Propylene	W-2ft-B	Rectangle	51													
Propylene	W-2ft-C	Rectangle	51													
Propylene	W-2ft-D	Rectangle	51													
Propylene	W-2ft-E	Rectangle	76													
Propylene	W-2ft-F	Rectangle	76													
Propylene	W-2ft-G	Rectangle	75													
Propylene	W-2ft-H	Rectangle	51	1487	866	693	571	522	498	473	464	455	446	455	459	450
Propylene	W-2ft-I	Rectangle	51	1480	936	762	603	529	495	469	453	428	413	425	428	429
Propylene	W-2ft-J	Rectangle	51	1529	929	734	601	532	504	479	464	446	434	444	447	440
Propylene	W-2ft-K	Rectangle	76	1762	1140	982	764	675	630	577	554	534	516	525	527	510
Propylene	W-2ft-L	Rectangle	75	1758	1342	1066	780	664	604	562	530	490	463	478	478	469

PLUME CENTERLINE TEMPERATURE

FUEL	Name	Burner	HRR	PTC-1	PTC-2	PTC-3	BDTC-7	PTC-4	BDTC-8	PTC-5	BDTC-9	PTC-6	BDTC-10	PTC-7
			[kW]	[K]	[K]	[K]	[K]	[K]	[K]	[K]	[K]	[K]	[K]	[K]
Methane	W1A	Square	79	1100	926	680	690	575	572	466	474	464	451	430
Methane	W1B	Square	78	1082	906	656	674	567	565	463	471	463	450	432
Methane	W1C	Square	68	1028	862	633	655	552	557	457	464	459	446	427
Methane	W1D	Square	78	1073	890	647	670	566	564	461	469	464	450	431
Methane	W1E	Square	77	1072	890	645	667	564	565	461	469	463	450	432
Methane	W1F	Square	78	1096	909	657	675	569	568	467	474	464	451	433
Propane	W-1ft-1A	Square	52	931	820	593	573	480	469	418	427	430	425	419
Propane	W-1ft-1B	Square	78	1083	1016	734	738	611	602	495	514	516	505	491
Propane	W-1ft-1C	Square	52	1020	895	668	589	491	456	416	420	406	399	393
Propane	W-1ft-1D	Square	52	1064	917	685	589	491	450	419	423	405	400	394
Propane	W-1ft-1E	Square	52	1009	870	645	561	473	442	413	417	405	400	396
Propane	W-1ft-1F	Square	52	1001	865	648	567	480	449	415	419	408	403	398
Propane	W-1ft-1G	Square	52	1020	884	659	578	483	452	416	420	409	403	399
Propane	W-1ft-1H	Square	79	1180	1095	846	770	635	584	490	505	483	471	457
Propane	W-1ft-1I	Square	79	1172	1092	847	762	630	581	493	508	488	476	462
Propane	W-1ft-2A	Square	53	1026	897	639	627	515	497	438	440	429	421	414
Propane	W-1ft-2B	Square	79	1208	1134	816	844	681	637	535	540	507	491	471
Propane	W-1ft-2C	Square	79	1161	1081	775	817	666	637	530	536	511	495	478

PLUME CENTERLINE TEMPERATURE														
FUEL	**Name**	**Burner**	**HRR**	**PTC-1**	**PTC-2**	**PTC-3**	**BDTC-7**	**PTC-4**	**BDTC-8**	**PTC-5**	**BDTC-9**	**PTC-6**	**BDTC-10**	**PTC-7**
			[kW]	**[K]**	**[K]**	**[K]**	**[K]**	**[K]**	**[K]**	**[K]**	**[K]**	**[K]**	**[K]**	**[K]**
Propane	W-1ft-2D	Square	79	1160	1073	770	816	666	639	529	536	515	500	481
Propane	W-2ft-1A	Rectangle	52	655	597	429	499	457	467	434	447	435	428	419
Propane	W-2ft-1B	Rectangle	53	613	541	399	445	419	442	389	401	430	425	417
Propane	W-2ft-2A	Rectangle	52	657	585	424	481	442	454	398	410	431	425	418
Propane	W-2ft-2B	Rectangle	52	621	546	413	468	435	450	395	403	427	423	416
Propane	W-2ft-2C	Rectangle	52	615	531	404	457	429	446	392	400	429	424	418
Propane	W-2ft-2D	Rectangle	78	814	737	501	572	514	534	441	455	493	485	472
Propane	W-1ft-3A	Rectangle	78	815	761	570	607	546	550	480	484	502	496	485
Propane	W-1ft-3B	Rectangle	78	841	785	596	638	560	552	491	496	505	498	489
Propane	W-1ft-3C	Rectangle	52	710	632	493	530	469	473	442	447	446	442	437
Propane	W-1ft-3D	Rectangle	52	739	646	497	531	467	473	444	449	448	444	443
Propane	W-1ft-3E	Rectangle	52	746	657	508	547	475	471	447	451	447	443	441
Propane	W-1ft-3F	Rectangle	78	987	899	663	700	575	565	527	532	518	508	500
Propane	W-1ft-3G	Rectangle	78	968	887	651	689	577	575	526	535	523	515	506
Propylene	W-1ft-A	Square	51	1225	968	703	668	540	526	444	451	445	435	424
Propylene	W-1ft-B	Square	51	1156	922	670	629	516	506	444	447	450	443	434
Propylene	W-1ft-C	Square	51	1232	961	691	633	520	510	460	464	463	457	448
Propylene	W-1ft-D	Square	51	1220	996	721	642	524	486	442	440	428	421	414
Propylene	W-1ft-E	Square	50	1144	947	675	631	516	502	450	453	448	442	435
Propylene	W-1ft-F	Square	75	1225	968	703	668	540	526	444	451	445	435	424
Propylene	W-1ft-G	Square	76	1378	1223	944	826	666	590	517	513	489	475	461
Propylene	W-1ft-H	Square	75	1342	1227	927	891	722	655	547	552	530	517	495
Propylene	W-1ft-I	Square	75	1306	1142	851	835	687	652	549	558	552	539	519
Propylene	W-2ft-A	Rectangle	67	984	865	625	651	540	522	480	486	461	453	450
Propylene	W-2ft-B	Rectangle	51	841	691	514	538	468	466	434	438	433	429	427
Propylene	W-2ft-C	Rectangle	51	984	865	625	651	540	522	480	486	461	453	450
Propylene	W-2ft-D	Rectangle	51	774	641	492	507	456	471	431	438	445	440	437
Propylene	W-2ft-E	Rectangle	76	1034	905	664	675	575	576	518	529	525	522	513
Propylene	W-2ft-F	Rectangle	76	1079	949	692	707	590	582	514	523	510	502	495
Propylene	W-2ft-G	Rectangle	75	1156	1010	742	720	584	553	503	509	484	475	471
Propylene	W-2ft-H	Rectangle	51	809	684	527	530	474	480	445	445	459	456	449
Propylene	W-2ft-I	Rectangle	51	852	745	565	544	468	457	428	425	426	423	419
Propylene	W-2ft-J	Rectangle	51	846	722	557	551	480	475	440	438	447	443	437
Propylene	W-2ft-K	Rectangle	76	1035	936	710	711	597	590	518	522	535	527	510
Propylene	W-2ft-L	Rectangle	75	1165	1022	752	709	575	548	488	482	482	474	464

PLUME CENTERLINE VELOCITY													
FUEL	**Name**	**Burner**	**HRR**	**BD-1**	**BD-2**	**BD-3**	**BD-4**	**BD-5**	**BD-6**	**BD-7**	**BD-8**	**BD-9**	**BD-10**
			[kW]	**[m/s]**	**[m/s]**	**[m/s]**	**[m/s]**	**[m/s]**	**[m/s]**	**[m/s]**	**[m/s]**	**[m/s]**	**[m/s]**
Methane	W1A	Square	79	4.0	2.9	4.1	3.4	3.0	2.8	3.6	3.9	4.0	3.6
Methane	W1B	Square	78	3.6	3.0	3.6	3.5	3.1	2.7	3.5	3.9	4.0	3.6
Methane	W1C	Square	68	3.5	2.9	3.6	3.4	3.1	2.8	3.5	3.9	3.9	3.5
Methane	W1D	Square	78	3.6	2.9	3.5	3.2	3.0	2.6	3.5	3.8	3.9	3.7
Methane	W1E	Square	77	3.5	3.0	3.6	3.5	3.1	2.7	3.5	3.9	4.0	3.6
Methane	W1F	Square	78	3.5	3.0	3.7	3.6	3.1	2.8	3.6	4.0	4.0	3.7
Propane	W-1ft-1A	Square	52	3.4	2.5	3.4	2.6	2.0	1.8	2.9	4.6	3.0	2.7
Propane	W-1ft-1B	Square	78	3.3	2.8	3.8	3.3	2.3	2.0	3.4		3.9	3.2
Propane	W-1ft-1C	Square	52	3.3	2.8	3.2	2.8	2.4	2.1	3.1	3.0	3.1	2.8
Propane	W-1ft-1D	Square	52	3.5	2.9	3.3	2.8	2.3	2.0	3.1	2.9	3.0	2.6
Propane	W-1ft-1E	Square	52	3.3	2.8	3.2	2.7	2.3	2.0	3.0	2.9	3.0	2.6
Propane	W-1ft-1F	Square	52	3.4	2.7	3.2	2.6	2.3	2.1	3.0	2.9	3.1	2.7
Propane	W-1ft-1G	Square	52	3.5	2.8	3.3	2.8	2.4	2.0	3.1	3.1	3.1	2.7
Propane	W-1ft-1H	Square	79	3.6	3.0	4.1	3.5	2.9	2.4	3.8	4.7	4.0	3.4
Propane	W-1ft-1I	Square	79	3.6	3.2	4.1	3.5	2.9	2.6	3.8	4.6	4.0	3.5
Propane	W-1ft-2A	Square	53	3.5	3.0	3.6	3.1	2.4	1.7	3.4	3.8	3.4	2.9
Propane	W-1ft-2B	Square	79	3.7	3.4	4.3	3.7	3.0	2.5	4.1	4.5	4.2	3.5
Propane	W-1ft-2C	Square	79	3.9	3.4	4.3	3.7	3.0	2.5	4.0	4.7	4.2	3.8
Propane	W-1ft-2D	Square	79	3.8	3.3	4.4	3.7	3.1	2.4	4.0	4.6	4.3	2.6
Propane	W-2ft-1A	Rectangle	52	1.1	1.9	2.9		2.2	2.1	2.4	3.7	3.3	3.0
Propane	W-2ft-1B	Rectangle	53	0.8	1.4	2.1	2.1	2.0	1.9	1.9	3.0	3.0	3.0
Propane	W-2ft-2A	Rectangle	52	0.8	1.8	2.6	2.2	2.1	1.7	2.3	6.8	3.1	2.9
Propane	W-2ft-2B	Rectangle	52	1.2	1.8	2.5	1.7	2.2	2.4	2.2	3.1	3.2	3.0
Propane	W-2ft-2C	Rectangle	52	1.0	1.7	2.3	1.6	2.2	2.3	2.1	2.9	3.1	3.0
Propane	W-2ft-2D	Rectangle	78	1.7	2.0	2.9	1.8	2.5	2.6	2.6	4.7	3.7	3.4
Propane	W-1ft-3A	Rectangle	78	2.9	4.0	2.4	2.5	2.9	2.4	3.7	1.7	3.4	2.5
Propane	W-1ft-3B	Rectangle	78	3.3	5.7	2.3	2.7	2.8	1.8	3.9	2.3	3.6	2.6
Propane	W-1ft-3C	Rectangle	52							3.0	3.5	3.5	2.8
Propane	W-1ft-3D	Rectangle	52							3.0	3.3	3.4	2.2
Propane	W-1ft-3E	Rectangle	52							3.2	3.4	3.3	2.2
Propane	W-1ft-3F	Rectangle	78							3.8	13.9	3.9	2.9
Propane	W-1ft-3G	Rectangle	78							3.7	4.2	4.0	3.0
Propylene	W-1ft-A	Square	51	3.5	3.0	3.8	3.0	2.6	2.2	3.4	3.6	3.6	1.8
Propylene	W-1ft-B	Square	51	3.5	3.1	3.4	2.4	2.4	2.0	3.3	3.5	3.4	1.8
Propylene	W-1ft-C	Square	51	3.7	3.1	3.4	1.6	2.4	1.9	3.3	3.4	3.4	1.7
Propylene	W-1ft-D	Square	51	3.7	3.1	3.6	3.2	2.5	2.0	3.4	3.5	3.4	1.8
Propylene	W-1ft-E	Square	50	3.6	3.1	3.5	1.1	2.5	2.0	3.3	3.5	3.5	1.8
Propylene	W-1ft-F	Square	75	3.4	2.9	3.7		2.7	2.1	3.5	3.6	3.4	1.9

PLUME CENTERLINE VELOCITY													
FUEL	**Name**	**Burner**	**HRR**	**BD-1**	**BD-2**	**BD-3**	**BD-4**	**BD-5**	**BD-6**	**BD-7**	**BD-8**	**BD-9**	**BD-10**
			[kW]	**[m/s]**	**[m/s]**	**[m/s]**	**[m/s]**	**[m/s]**	**[m/s]**	**[m/s]**	**[m/s]**	**[m/s]**	**[m/s]**
Propylene	W-1ft-G	Square	76	3.8	3.2	4.0		2.8	2.1	3.8	3.8	3.7	2.0
Propylene	W-1ft-H	Square	75	3.9	3.6	4.6		2.8	2.3	4.3	4.4	4.0	1.2
Propylene	W-1ft-I	Square	75	3.7	3.3	4.1		2.8	2.2	3.8	4.0	4.0	1.7
Propylene	W-2ft-A	Rectangle	67							3.4	3.9	3.8	2.0
Propylene	W-2ft-B	Rectangle	51							3.0	4.2	3.4	1.7
Propylene	W-2ft-C	Rectangle	51							2.6	3.3	3.3	1.7
Propylene	W-2ft-D	Rectangle	51							2.4	3.2	3.4	1.8
Propylene	W-2ft-E	Rectangle	76							3.2	3.8	4.0	1.1
Propylene	W-2ft-F	Rectangle	76							3.5	4.1	4.3	1.5
Propylene	W-2ft-G	Rectangle	75							3.8	3.8	3.7	1.9
Propylene	W-2ft-H	Rectangle	51	1.6	2.2	3.1		2.4	2.3	2.5	3.2	3.4	1.3
Propylene	W-2ft-I	Rectangle	51	2.4	2.8	3.3		2.3	2.5	2.9	3.1	3.2	1.3
Propylene	W-2ft-J	Rectangle	51	2.2	2.7	3.4		2.4	2.4	2.9	3.3	3.4	1.3
Propylene	W-2ft-K	Rectangle	76	1.9	2.6	3.6		2.7	2.7	3.1	3.6	3.9	1.4
Propylene	W-2ft-L	Rectangle	75	3.0	3.3	4.0		2.8	2.9	3.6	3.7	3.8	1.5

HEAT FLUX TO WALL																					
FUEL	**Name**	**Burner**	**HRR**	**TSC-1**	**TSC-2**	**TSC-3**	**TSC-4**	**TSC-5**	**TSC-6**	**TSC-7**	**TSC-8**	**TSC-9**	**TSC-10**	**TSC-11**	**TSC-12**	**TSC-13**	**TSC-14**	**TSC-15**	**TSC-16**	**TSC-17**	**TSC-18**
			[kW]	**[kW/m2]**	**[kW/m2]**	**[kW/m2]**	**[kW/m2]**	**[kW/m2]**	**[kW/m2]**	**[kW/m2]**	**[kW/m2]**	**[kW/m2]**	**[kW/m2]**	**[kW/m2]**	**[kW/m2]**	**[kW/m2]**	**[kW/m2]**	**[kW/m2]**	**[kW/m2]**	**[kW/m2]**	**[kW/m2]**
Methane	W1A	Square	79	1	30	5	4	16	2	2	6	3	2	4	1	2	2	2	2	1	2
Methane	W1B	Square	78	1	35	5	4	18	2	2	7	3	2	4	1	2	2	2	2	1	2
Methane	W1C	Square	68	1	33	3	2	14	1	1	5	2	1	3	1	1	2	1	1	1	1
Methane	W1D	Square	78	1	35	5	4	19	2	2	8	3	2	5	1	2	3	2	2	1	2
Methane	W1E	Square	77	1	37	5	4	18	2	2	8	3	2	4	1	2	2	2	2	1	2
Methane	W1F	Square	78	1	28	4	3	15	2	1	6	2	2	4	1	1	3	2	2	1	1
Propane	W-1ft-1A	Square	52	1	22	5	4	10	2	1	4	2	2	2	2	2	2	2	2	1	2
Propane	W-1ft-1B	Square	78	2	41	7	6	26	3	3	12	4	4	6	3	3	3	3	4	2	3
Propane	W-1ft-1C	Square	52	1	19	5	4	7	2	1	2	2	2	1	1	1	1	1	2	0	1
Propane	W-1ft-1D	Square	52	1	16	6	4	6	2	1	1	2	2	1	1	1	1	1	2	0	1
Propane	W-1ft-1E	Square	52	1	20	5	3	8	2	1	2	2	2	1	1	1	1	1	2	0	1
Propane	W-1ft-1F	Square	52	1	22	6	4	9	2	1	2	2	2	1	1	1	1	1	2	0	1
Propane	W-1ft-1G	Square	52	1	22	6	4	8	2	1	3	2	2	1	1	1	1	1	2	0	1
Propane	W-1ft-1H	Square	79	2	42	7	6	25	3	2	11	3	3	5	2	2	3	2	3	1	2
Propane	W-1ft-1I	Square	79	2	45	7	6	26	3	2	11	3	3	5	2	2	3	2	3	1	2
Propane	W-1ft-2A	Square	53	1	15	6	4	6	2	1	2	2	2	1	1	1	1	1	2	1	1
Propane	W-1ft-2B	Square	79	2	30	7	6	19	3	2	8	3	3	4	2	2	2	3	3	1	2
Propane	W-1ft-2C	Square	79	2	34	7	6	22	3	2	10	4	3	5	2	2	2	3	3	1	2

HEAT FLUX TO WALL																					
FUEL	**Name**	**Burner**	**HRR**	**TSC-1**	**TSC-2**	**TSC-3**	**TSC-4**	**TSC-5**	**TSC-6**	**TSC-7**	**TSC-8**	**TSC-9**	**TSC-10**	**TSC-11**	**TSC-12**	**TSC-13**	**TSC-14**	**TSC-15**	**TSC-16**	**TSC-17**	**TSC-18**
			[kW]	**[kW/m2]**	**[kW/m2]**	**[kW/m2]**	**[kW/m2]**	**[kW/m2]**	**[kW/m2]**	**[kW/m2]**	**[kW/m2]**	**[kW/m2]**	**[kW/m2]**	**[kW/m2]**	**[kW/m2]**	**[kW/m2]**	**[kW/m2]**	**[kW/m2]**	**[kW/m2]**	**[kW/m2]**	**[kW/m2]**
Propane	W-1ft-2D	Square	79	2	36	7	6	23	3	2	10	4	3	5	2	2	2	3	3	1	2
Propane	W-2ft-1A	Rectangle	52	0	9	1	1	4	1	0	1	1	1	1	0	0	0	1	1	0	0
Propane	W-2ft-1B	Rectangle	53	1	28	9	4	11	2	1	6	2	1	5	1	1	3	2	2	1	1
Propane	W-2ft-2A	Rectangle	52	1	16	3	2	9	1	1	3	1	1	2	1	1	1	1	1	0	1
Propane	W-2ft-2B	Rectangle	52	1	12	2	2	6	1	1	2	1	1	1	1	1	1	1	1	0	1
Propane	W-2ft-2C	Rectangle	52	1	24	8	4	10	2	1	5	1	1	4	1	1	2	2	2	1	1
Propane	W-2ft-2D	Rectangle	78	2	49	12	6	24	3	2	12	3	3	7	2	2	4	3	3	2	2
Propane	W-1ft-3A	Rectangle	78	3	53	11	6	26	3	2	12	3	3	7	3	3	4	3	4	2	3
Propane	W-1ft-3B	Rectangle	78	3	50	11	6	24	3	2	10	3	4	6	3	3	3	3	4	2	3
Propane	W-1ft-3C	Rectangle	52	1	24	7	3	11	2	1	4	0	1	3	2	2	1	0	1	1	2
Propane	W-1ft-3D	Rectangle	52	1	23	7	3	10	2	1	4	1	0	3	2	2	1	1	0	1	2
Propane	W-1ft-3E	Rectangle	52	1	23	6	3	10	2	1	4	0	0	3	2	2	1	-1	0	1	1
Propane	W-1ft-3F	Rectangle	78	2	46	9	4	24	3	2	9	0	1	2	3	3	1	-1	1	1	3
Propane	W-1ft-3G	Rectangle	78	2	46	9	5	24	3	2	10	0	1	5	3	3	2	-1	1	1	3
Propylene	W-1ft-A	Square	51	2	42	10	6	16	3	2	5	3	2	2	2	2	1	2	2	1	2
Propylene	W-1ft-B	Square	51	2	45	9	5	15	3	2	4	3	2	2	2	2	1	2	2	0	2
Propylene	W-1ft-C	Square	51	2	46	9	5	15	3	2	4	3	3	2	2	2	1	2	3	0	2
Propylene	W-1ft-D	Square	51	2	36	8	5	13	3	2	3	2	2	1	2	1	1	2	2	0	1
Propylene	W-1ft-E	Square	50	2	36	9	5	14	3	2	4	3	2	2	2	2	1	2	2	0	2
Propylene	W-1ft-F	Square	75	3	63	10	9	29	5	3	11	4	4	5	3	2	2	2	3	0	2
Propylene	W-1ft-G	Square	76	3	63	10	9	30	5	3	11	5	4	7	3	2	2	2	3	0	2
Propylene	W-1ft-H	Square	75	3	59	11	8	32	5	4	11	5	5	8	3	3	2	3	4	0	3
Propylene	W-1ft-I	Square	75	3	69	10	8	40	5	4	15	6	5	9	4	3	3	4	4	1	3
Propylene	W-2ft-A	Rectangle	67	3	59	13	6	29	4	2	12	1	3	6	2	2	3	-1	1	3	2
Propylene	W-2ft-B	Rectangle	51	2	33	10	4	13	3	2	5	1	2	3	2	2	1	-1	0	1	2
Propylene	W-2ft-C	Rectangle	51	2	36	10	4	13	3	2	5	1	2	4	2	2	1	0	1	1	2
Propylene	W-2ft-D	Rectangle	51	2	36	11	4	13	3	2	5	1	2	3	2	2	1	0	1	1	2
Propylene	W-2ft-E	Rectangle	76	4	70	14	7	34	5	3	14	1	3	7	4	3	3	0	2	3	3
Propylene	W-2ft-F	Rectangle	76	3	70	13	7	32	4	3	13	1	2	6	3	3	2	-1	1	2	3
Propylene	W-2ft-G	Rectangle	75	3	66	13	7	30	5	3	12	1	3	6	3	2	2	-1	1	2	3
Propylene	W-2ft-H	Rectangle	51	3	37	12	6	12	3	2	5	2	2	4	2	2	2	2	3	1	2
Propylene	W-2ft-I	Rectangle	51	3	66	13	7	30	5	3	12	1	3	6	3	2	2	-1	1	2	3
Propylene	W-2ft-J	Rectangle	51	2	35	11	5	11	3	2	4	2	2	3	1	1	1	1	2	1	1
Propylene	W-2ft-K	Rectangle	76	4	76	16	9	33	5	3	13	4	4	8	4	3	3	4	4	1	3
Propylene	W-2ft-L	Rectangle	75	4	66	15	8	27	4	3	10	3	4	6	2	2	2	2	3	1	2

NEAR-WALL TEMPERATURE																					
FUEL	**Name**	**Burner**	**HRR**	**WTC-1**	**WTC-2**	**WTC-3**	**WTC-4**	**WTC-5**	**WTC-6**	**WTC-7**	**WTC-8**	**WTC-9**	**WTC-10**	**WTC-11**	**WTC-12**	**WTC-13**	**WTC-14**	**WTC-15**	**WTC-16**	**WTC-17**	**WTC-18**
			[kW]	**[K]**	**[K]**	**[K]**	**[K]**	**[K]**	**[K]**	**[K]**	**[K]**	**[K]**	**[K]**	**[K]**	**[K]**	**[K]**	**[K]**	**[K]**	**[K]**	**[K]**	**[K]**
Methane	W1A	Square	79	619	778	823	891	881	843	588	611	586	545	520	517	471	472	485	468	482	479
Methane	W1B	Square	78	656	829	868	982	981	917	594	618	600	563	540	537	480	480	494	476	489	483
Methane	W1C	Square	68	637	805	842	961	959	892	587	609	589	550	526	523	474	474	487	468	481	477
Methane	W1D	Square	78	631	807	849	962	952	887	597	619	597	556	533	531	477	477	491	472	486	481
Methane	W1E	Square	77	674	849	886	1007	995	930	603	625	608	568	545	541	480	481	494	476	490	484
Methane	W1F	Square	78	678	853	891	1019	1007	936	611	630	612	569	545	540	483	483	496	475	488	482
Propane	W-1ft-1A	Square	52	545	626	664	684	661	627	514	511	489	449	433	425	438	436	440	432	436	436
Propane	W-1ft-1B	Square	78	716	849	912	958	916	853	688	686	654	593	567	551	530	527	535	519	524	522
Propane	W-1ft-1C	Square	52	537	619	650	655	634	593	484	472	453	422	410	405	412	409	412	402	406	404
Propane	W-1ft-1D	Square	52	542	610	642	646	623	584	481	468	450	420	411	405	411	408	411	401	404	402
Propane	W-1ft-1E	Square	52	549	619	661	696	679	640	487	478	461	434	423	418	414	411	415	405	408	406
Propane	W-1ft-1F	Square	52	549	625	668	706	689	649	487	479	463	437	426	422	413	412	416	407	411	410
Propane	W-1ft-1G	Square	52	551	622	665	704	687	645	485	479	463	436	425	420	415	413	417	407	412	410
Propane	W-1ft-1H	Square	79	709	845	908	984	959	895	650	645	618	572	551	542	493	492	500	485	491	487
Propane	W-1ft-1I	Square	79	739	880	937	998	962	898	655	652	627	582	562	552	497	497	504	490	496	493
Propane	W-1ft-2A	Square	53	540	604	652	671	646	607	509	509	481	443	429	424	435	435	437	425	429	427
Propane	W-1ft-2B	Square	79	663	761	831	876	838	779	653	649	603	545	524	513	506	505	508	488	493	491
Propane	W-1ft-2C	Square	79	675	782	861	929	904	844	668	674	627	569	546	533	515	516	520	500	506	502
Propane	W-1ft-2D	Square	79	669	781	862	946	924	863	670	675	630	575	554	543	517	518	523	504	511	508
Propane	W-2ft-1A	Rectangle	52	527	649	677	765	777	753	527	546	535	505	485	478	444	445	457	445	457	454
Propane	W-2ft-1B	Rectangle	53	522	644	671	762	777	755	528	550	540	513	492	485	449	451	465	453	466	462
Propane	W-2ft-2A	Rectangle	52	535	644	673	749	755	727	532	547	533	501	481	473	449	450	461	447	458	454
Propane	W-2ft-2B	Rectangle	52	530	632	657	708	706	681	534	548	538	501	478	466	449	449	459	444	455	452
Propane	W-2ft-2C	Rectangle	52	529	635	660	714	713	693	535	552	544	507	485	475	450	451	464	449	461	460
Propane	W-2ft-2D	Rectangle	78	711	857	909	1004	1004	971	647	668	656	617	592	579	516	519	536	519	537	536
Propane	W-1ft-3A	Rectangle	78	739	895	947	974	945	894	701	702	651	579	551	535	536	535	540	516	521	516
Propane	W-1ft-3B	Rectangle	78	754	904	935	930	899	849	683	676	629	558	533	517	534	532	537	511	518	514
Propane	W-1ft-3C	Rectangle	52	540	639	657	672	667	643	550	554	541	478	459	448	469	466	471	455	461	458
Propane	W-1ft-3D	Rectangle	52	527	630	646	654	646	618	554	555	538	471	451	440	468	466	471	453	460	457
Propane	W-1ft-3E	Rectangle	52	523	624	640	644	633	604	551	549	531	464	444	434	466	462	467	449	456	453
Propane	W-1ft-3F	Rectangle	78	692	847	879	880	855	811	659	657	631	545	519	503	529	525	531	509	519	517
Propane	W-1ft-3G	Rectangle	78	708	855	888	906	894	856	674	676	649	566	540	525	538	535	542	521	531	528
Propylene	W-1ft-A	Square	51	589	710	793	880	877	829	504	516	513	485	480	474	432	433	446	434	444	445
Propylene	W-1ft-B	Square	51	625	740	811	874	872	830	503	512	504	477	473	466	436	436	449	436	448	450
Propylene	W-1ft-C	Square	51	662	773	876	878	873	827	524	527	516	484	478	470	447	447	458	445	459	461
Propylene	W-1ft-D	Square	51	628	736	827	844	826	771	521	512	492	450	442	435	427	425	432	414	424	423
Propylene	W-1ft-E	Square	50	629	721	807	843	850	799	531	526	507	464	456	446	441	439	449	431	444	444
Propylene	W-1ft-F	Square	75	789	970	1144	1030	1005	918	665	644	614	544	534	519	482	477	485	458	471	468

NEAR-WALL TEMPERATURE																					
FUEL	**Name**	**Burner**	**HRR**	**WTC-1**	**WTC-2**	**WTC-3**	**WTC-4**	**WTC-5**	**WTC-6**	**WTC-7**	**WTC-8**	**WTC-9**	**WTC-10**	**WTC-11**	**WTC-12**	**WTC-13**	**WTC-14**	**WTC-15**	**WTC-16**	**WTC-17**	**WTC-18**
			[kW]	**[K]**	**[K]**	**[K]**	**[K]**	**[K]**	**[K]**	**[K]**	**[K]**	**[K]**	**[K]**	**[K]**	**[K]**	**[K]**	**[K]**	**[K]**	**[K]**	**[K]**	**[K]**
Propylene	W-1ft-G	Square	76	794	967	1151	1053	1026	944	683	662	630	562	550	535	493	488	497	468	481	478
Propylene	W-1ft-H	Square	75	762	922	1104	1070	1046	976	694	681	650	583	572	556	514	513	525	498	515	513
Propylene	W-1ft-I	Square	75	805	1005	1282	1206	1172	1076	736	729	699	631	619	601	537	537	554	528	548	546
Propylene	W-2ft-A	Rectangle	67	689	870	904	903	870	815	661	650	606	536	514	496	507	499	506	477	482	475
Propylene	W-2ft-B	Rectangle	51	565	672	699	708	693	658	549	544	511	466	451	439	458	453	461	441	449	446
Propylene	W-2ft-C	Rectangle	51	689	870	904	903	870	815	661	650	606	536	514	496	507	499	506	477	482	475
Propylene	W-2ft-D	Rectangle	51	569	675	712	722	717	687	546	544	513	481	472	457	460	460	469	452	463	462
Propylene	W-2ft-E	Rectangle	76	785	956	1016	1064	1059	1011	686	686	648	597	582	560	540	540	552	529	544	543
Propylene	W-2ft-F	Rectangle	76	788	974	1025	1041	1009	952	693	687	646	578	562	537	532	530	540	516	528	526
Propylene	W-2ft-G	Rectangle	75	752	949	995	981	945	885	693	673	619	544	526	505	515	508	515	484	496	492
Propylene	W-2ft-H	Rectangle	51	623	733	767	780	765	732	554	555	525	481	472	458	469	469	477	459	470	469
Propylene	W-2ft-I	Rectangle	51	626	728	762	755	734	700	551	538	504	456	447	433	453	448	452	429	436	432
Propylene	W-2ft-J	Rectangle	51	632	732	768	771	754	720	560	551	517	469	458	444	465	461	467	445	455	452
Propylene	W-2ft-K	Rectangle	76	816	1012	1080	1125	1093	1032	701	699	659	591	577	553	542	540	554	528	545	543
Propylene	W-2ft-L	Rectangle	75	783	980	1020	989	936	878	683	670	625	541	523	503	509	501	509	476	487	482

MEAN FLAME HEIGHT				
FUEL	**Name**	**Burner**	**HRR**	**Mean Flame Height**
			[kW]	**[m]**
Methane	W1A	Square	79	0.7
Methane	W1B	Square	78	0.7
Methane	W1C	Square	68	0.7
Methane	W1D	Square	78	0.7
Methane	W1E	Square	77	0.7
Methane	W1F	Square	78	0.7
Propane	W-1ft-1A	Square	52	0.6
Propane	W-1ft-1B	Square	78	0.8
Propane	W-1ft-1C	Square	52	0.6
Propane	W-1ft-1D	Square	52	0.6
Propane	W-1ft-1E	Square	52	0.6
Propane	W-1ft-1F	Square	52	0.6
Propane	W-1ft-1G	Square	52	0.6
Propane	W-1ft-1H	Square	79	0.8
Propane	W-1ft-1I	Square	79	0.8
Propane	W-1ft-2A	Square	53	0.6
Propane	W-1ft-2B	Square	79	0.8
Propane	W-1ft-2C	Square	79	0.9
Propane	W-1ft-2D	Square	79	0.9
Propane	W-2ft-1A	Rectangle	52	0.4
Propane	W-2ft-1B	Rectangle	53	0.4
Propane	W-2ft-2A	Rectangle	52	0.5
Propane	W-2ft-2B	Rectangle	52	0.4
Propane	W-2ft-2C	Rectangle	52	0.4
Propane	W-2ft-2D	Rectangle	78	0.7
Propane	W-1ft-3A	Rectangle	78	0.8
Propane	W-1ft-3B	Rectangle	78	0.7
Propane	W-1ft-3C	Rectangle	52	0.5
Propane	W-1ft-3D	Rectangle	52	0.4
Propane	W-1ft-3E	Rectangle	52	0.5
Propane	W-1ft-3F	Rectangle	78	0.7
Propane	W-1ft-3G	Rectangle	78	0.7
Propylene	W-1ft-A	Square	51	0.7
Propylene	W-1ft-B	Square	51	0.6
Propylene	W-1ft-C	Square	51	0.7
Propylene	W-1ft-D	Square	51	0.7

MEAN FLAME HEIGHT

FUEL	Name	Burner	HRR	Mean Flame Height
			[kW]	[m]
Propylene	W-1ft-E	Square	50	0.7
Propylene	W-1ft-F	Square	75	0.9
Propylene	W-1ft-G	Square	76	1.0
Propylene	W-1ft-H	Square	75	1.0
Propylene	W-1ft-I	Square	75	1.0
Propylene	W-2ft-A	Rectangle	67	0.7
Propylene	W-2ft-B	Rectangle	51	0.5
Propylene	W-2ft-C	Rectangle	51	0.4
Propylene	W-2ft-D	Rectangle	51	0.4
Propylene	W-2ft-E	Rectangle	76	0.7
Propylene	W-2ft-F	Rectangle	76	0.7
Propylene	W-2ft-G	Rectangle	75	0.8
Propylene	W-2ft-H	Rectangle	51	0.5
Propylene	W-2ft-I	Rectangle	51	0.5
Propylene	W-2ft-J	Rectangle	51	0.5
Propylene	W-2ft-K	Rectangle	76	0.8
Propylene	W-2ft-L	Rectangle	75	0.8

F.3 Combustible Wall Fire Tests Data Summary

This section presents the results of the various combustible wall tests, where their configurations are shown in Table 2.

The data presented for each test are:

1. Heat Release Rate
2. Plume centerline velocity
3. Plume centerline temperature rise (corrected based on methods detailed in Appendix C)
4. Wall temperature rise at different perpendicular distances from wall surface (corrected based on methods detailed in Appendix C)
5. Wall heat flux
6. Flame spread progression
7. Final burn pattern

Refer to Appendix N for the details of the experimental setup and instrumentation. Refer to Appendices D and N for data analysis and reduction explanations.

Although the instruments were routinely maintained, but due to the time and budgetary constraints, malfunctioning units are not necessarily replaced. Where the data is incomplete or requires special attentions, notes are provided in the charts.

Table 3 - Combustible Wall Test Configurations

Test Name	Source Fire Fuel	Source Fire HRR (kW)	Source Burner Size (ft x ft)	Constant Source HRR
A1	Propylene	100	2 x 1	
A2	Propylene	75	2 x 1	
A3	Propane	50	2 x 1	
A4	Propane	75	2 x 1	
A5	Propane	50	1 x 1	
A6	Propane	75	1 x 1	
A7	Propylene	50	1 x 1	
A8	Propylene	75	1 x 1	
A9	Propylene	50	2 x 1	
A10	Propylene	75	2 x 1	
A11	Propylene	50	2 x 1	
A12	Propylene	50	2 x 1	✓
A13	Propylene	50	1 x 1	✓
A14	Propylene	75	1 x 1	
A15	Propane	50	1 x 1	
A16	Propane	75	1 x 1	✓

Test Name	Source Fire Fuel	Source Fire HRR (kW)	Source Burner Size (ft x ft)	Constant Source HRR
A17	Propane	75	2 x 1	✓
A18	Propane	50	2 x 1	

F.3.1 Test A1

LODS Test Run Data

100 Institute Road
Worcester, MA 01609
Phone: (508) 831-5628
Fax: (508) 831-5680

Test Information

Test Number:	A1
Specimen Identification:	FRP 1, 100 kW initial Propylene fire, 1 x 2 burner
Material Name:	Class C FRP panel
Manufacturer/Submitter:	Not Reported
Raw Data File Name:	Test A1 - FRP_Propylene_100kW_2ft.txt
Reduced Data File Name:	Test A1 - FRP_Propylene_100kW_2ft_reduced_xlsx
Date of Test:	19-Mar-2010
Tester:	W. Wong

Test Parameters

Ambient Temperature:	N/A
Relative Humidity:	N/A

Specimen Information

Specimen Initial Mass:	[kg]	8.8
Specimen Final Mass:	[kg]	5.8
Mass Lost:	[kg]	3.0
Heat Evolved (net):	[kJ]	0

Parameter	Unit	Value
Mass Loss		
Initial Mass	[kg]	8.8
Final Mass	[kg]	5.8
Mass Loss	[%]	34.11

LODS Test Run Data

Center for Firesafety Studies

100 Institute Road
Worcester, MA 01609
Phone: (508) 831-5628
Fax: (508) 831-5680

Test Notes

Test Number:	0
Date:	03/19/10
Material:	Class C FRP panel
Specimen Identification:	FRP 1, 100 kW initial Propylene fire, 1 x 2 burner

Observations

Time	Observation
00:00	Start VI
10:15	Ignition of Burner
10:25	Start Video Camera
10:35	100 kW
10:35	Crackling noise from FRP sheet
10:45	Flame reaches ceiling
11:15	Backface burning seen near right edge near a thin-skin calorimeter
11:20	Source fire off
11:20	Flame spread to both edges of panel under ceiling
11:40	Rollover of ceiling layer
11:45	Paper layer of sheetrocks on both sides of room burning
12:05	Water jet applied for a few seconds to extinguish side burning of sheetrock
13:00	Centerline 2 ft of panel mostly charred, sides have reversed V-pattern char
14:00	Still some backface burning at around 1.5 m height on the right edge
14:30	Flame is confined to a V-shaped line on both sides, highest point at around
	0.5-0.6 m, and about 0.2 m width, spreading downward slowly
23:00	Smoke coming out of the holes cut out for the thin skin calorimeters
	numbered (1-6) bottom 2 rows
35:30	IR camera started, still small flames on panel
43:45	No Flame
44:00	Clean air started

There is a short in the circuit of the centerline rake at around 11:30, so all bi-directional probe data will be off after that.

	Post burn analysis shows that the short occurred at transducer 6, the line has been replaced. Transducer 4's voltage out is inconsistent, it needs to be checked out, transducers may have been damaged Unburnt mass left: 1.742 kg, burnt mass left: 4.022 kg

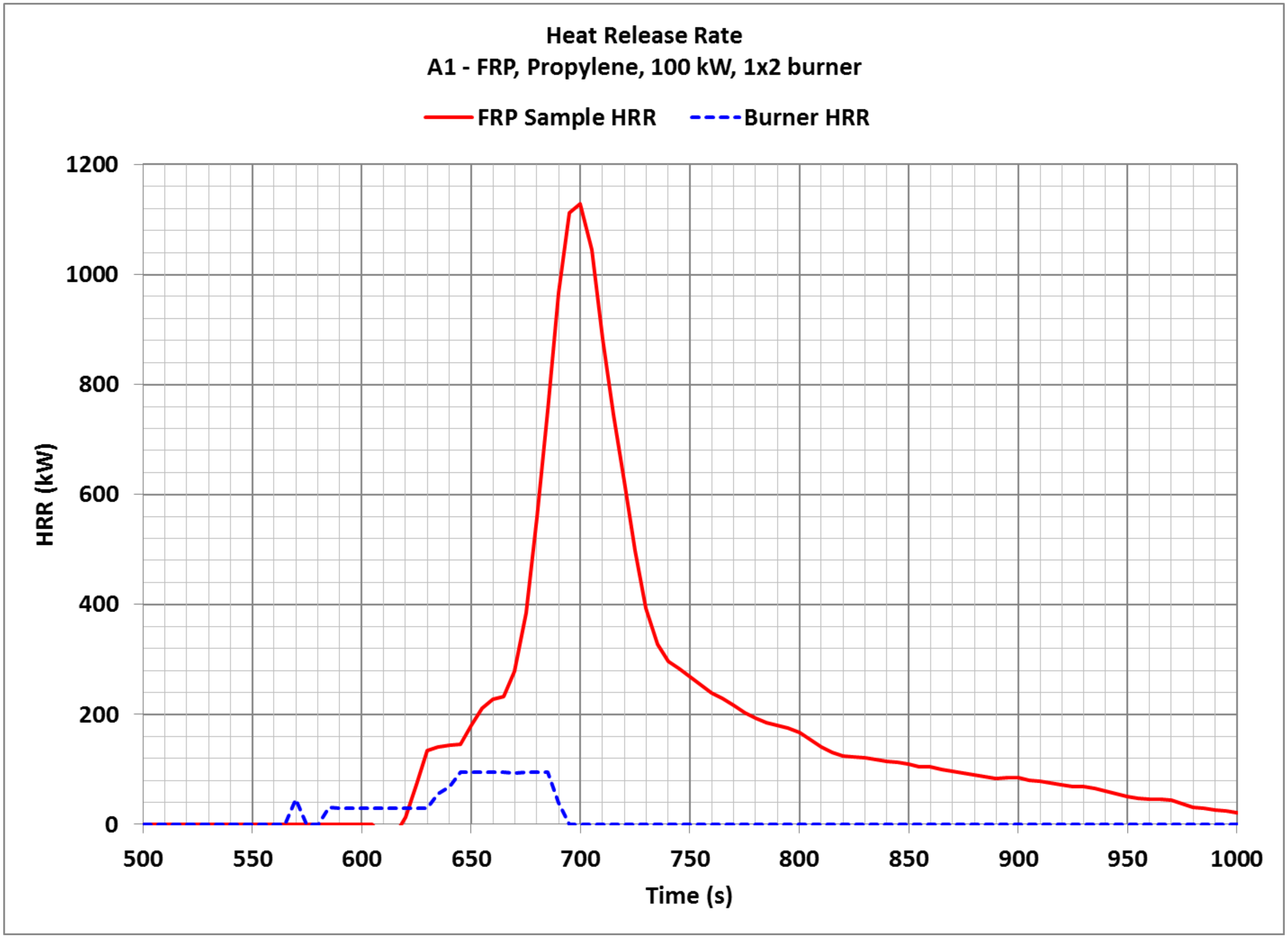

Heat release ratesof the source burner fire and of the specimen fire measured during test

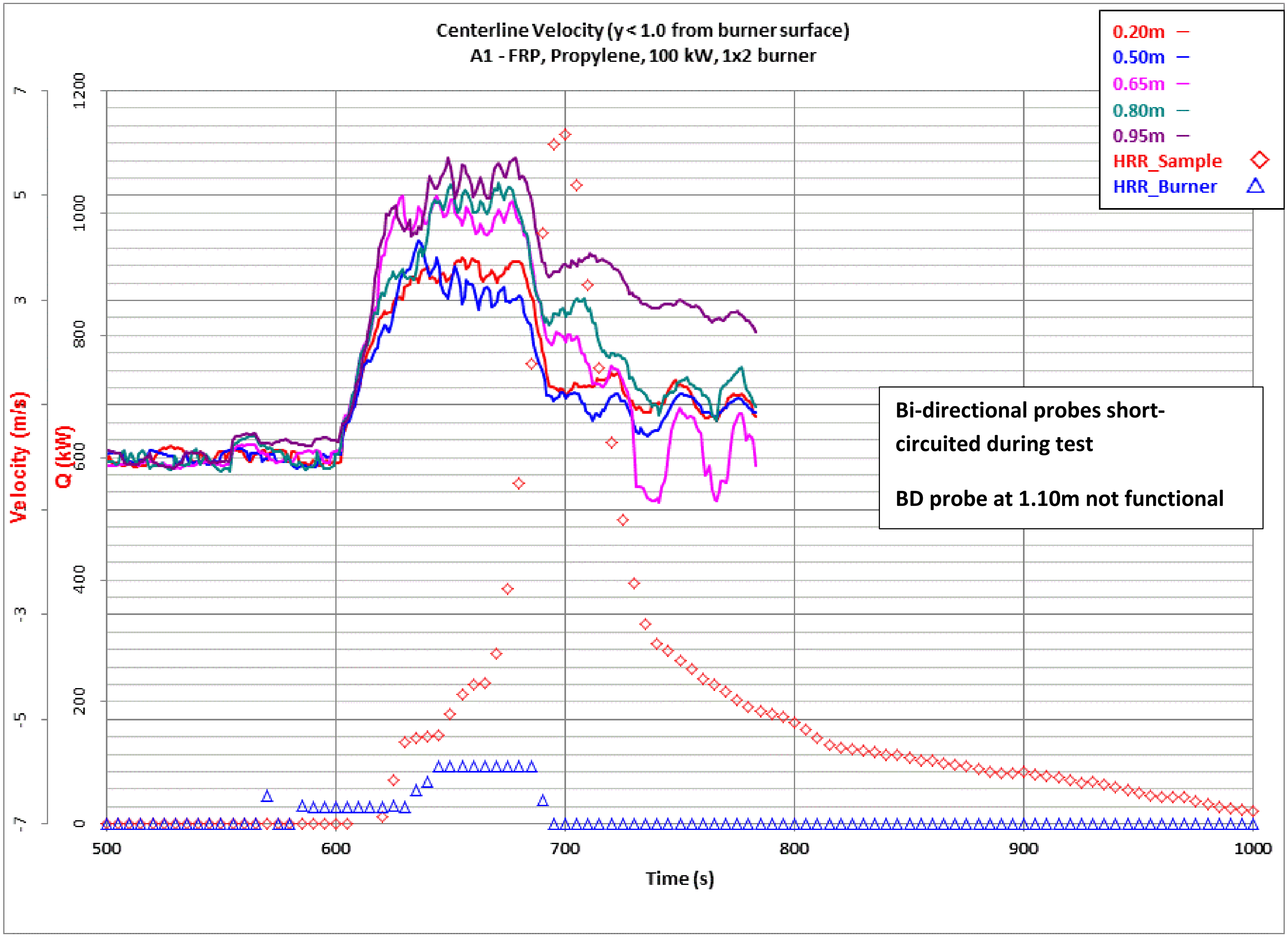

Centerline plume velocities measured from 0.2m to 0.95m above the burner surface

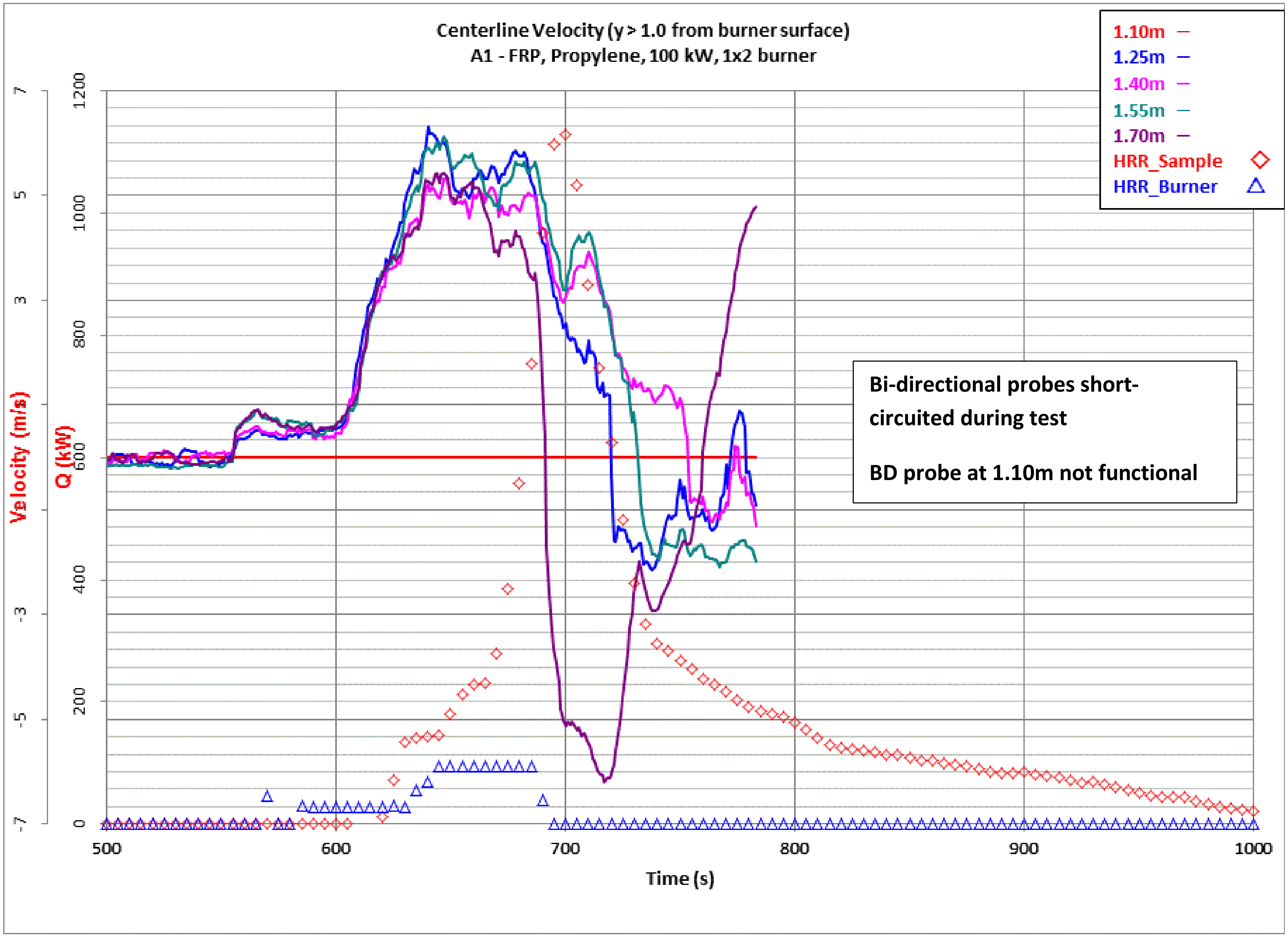

Centerline plume velocities measured from 1.1m to 1.7m above the burner surface

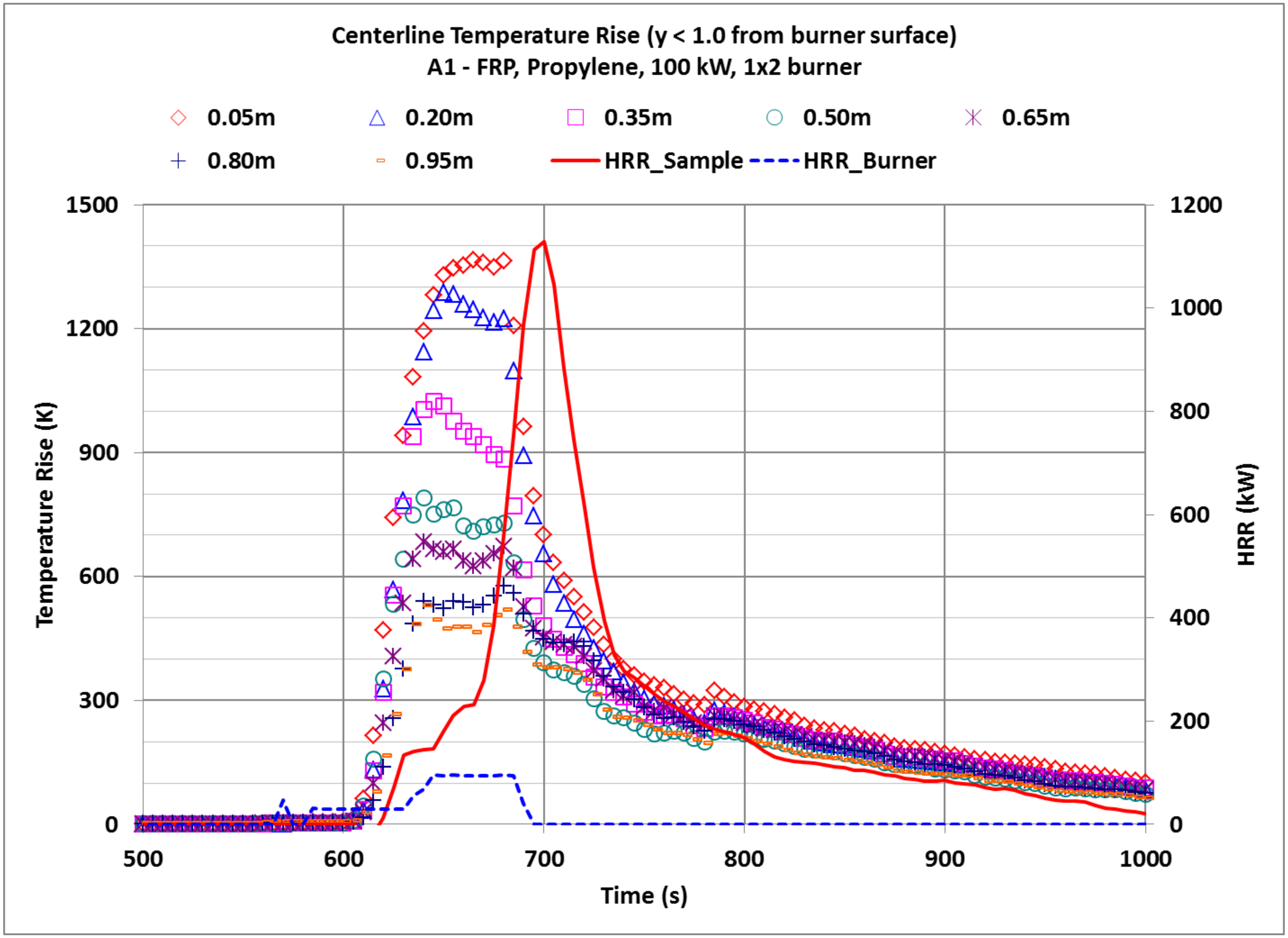

Centerline plume temperature rise measured from 0.05m to 0.95m above the burner surface

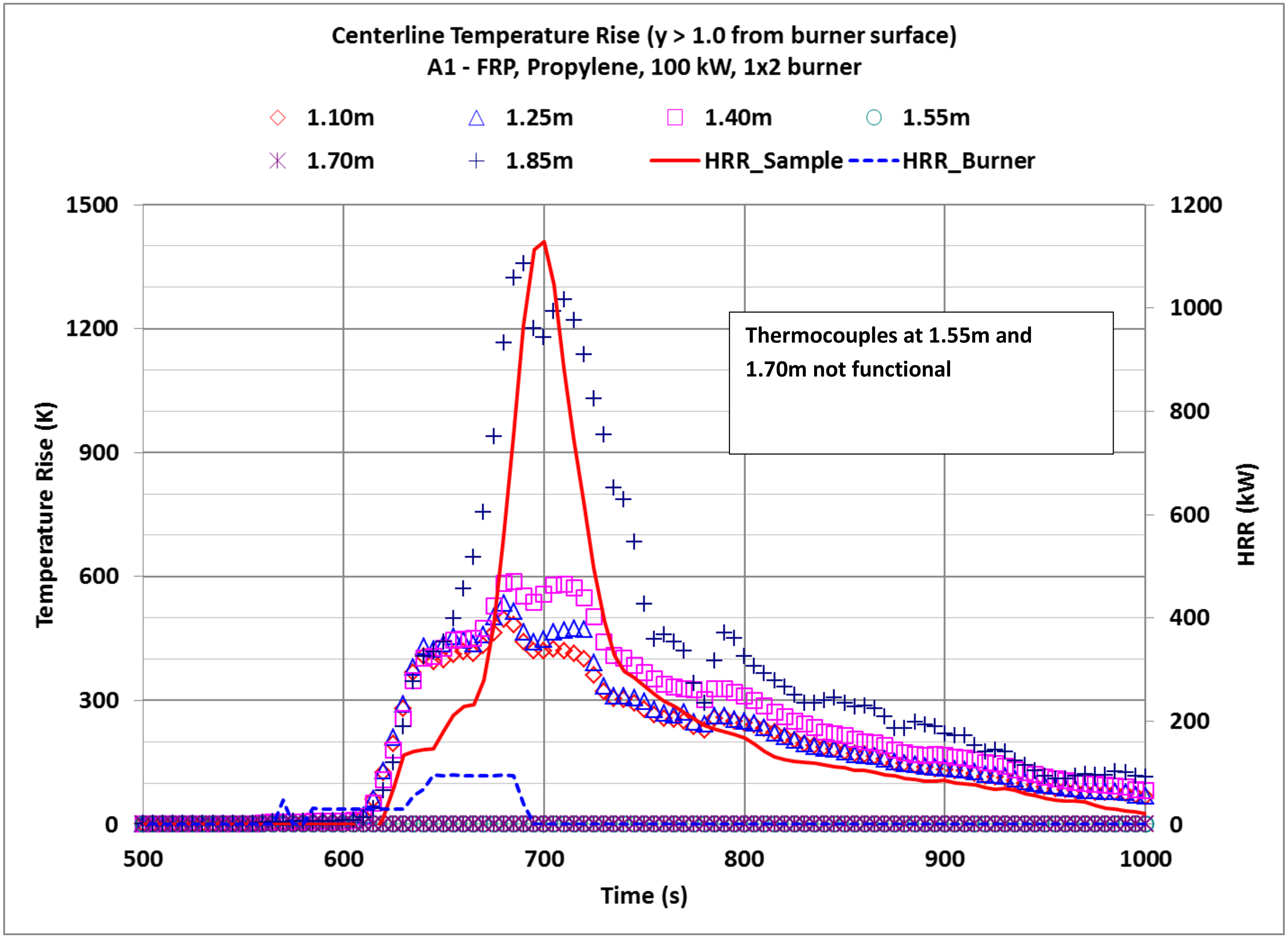

Centerline plume temperature rise measured from 1.10m to 1.85m above the burner surface

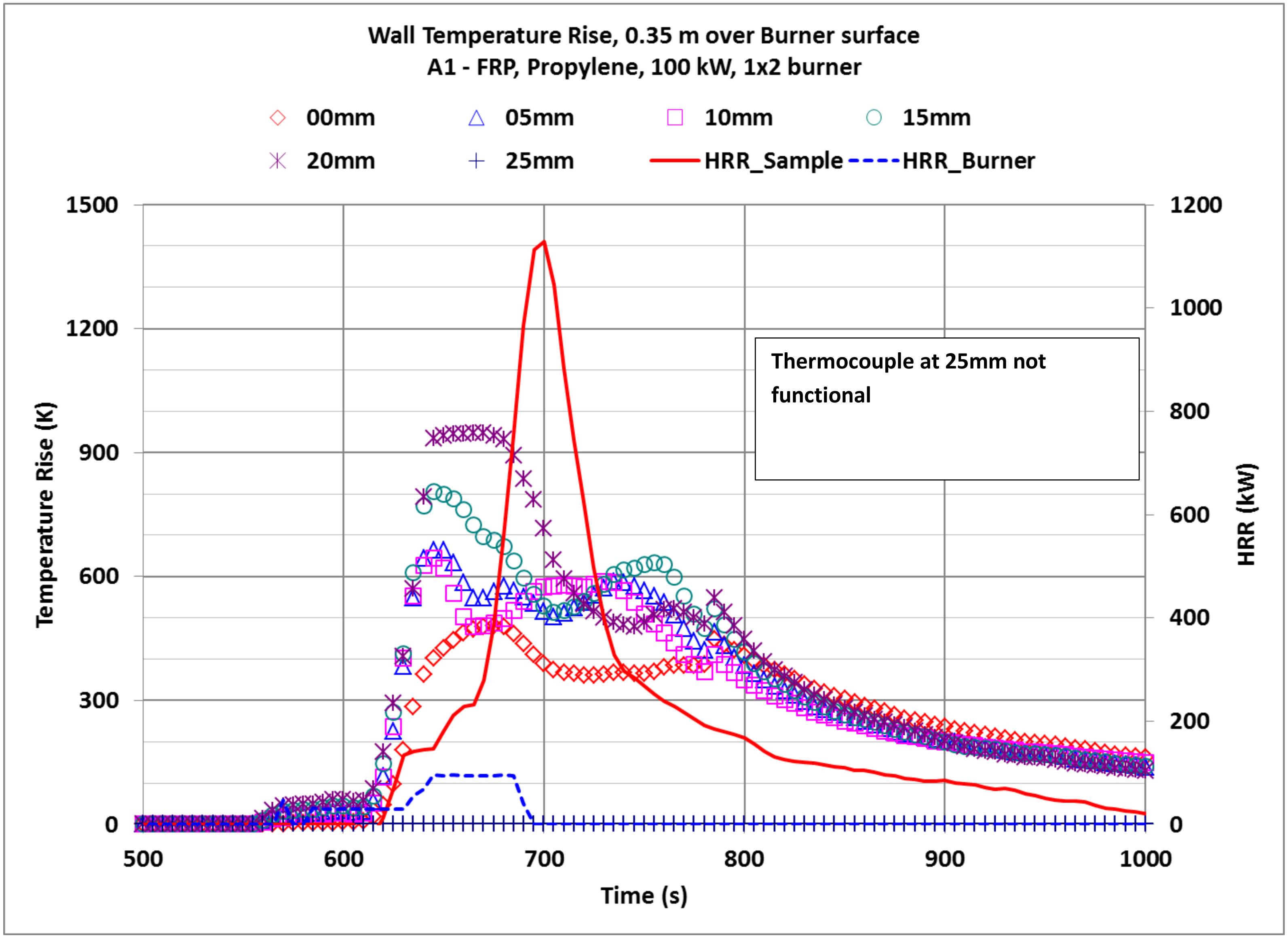

Temperature rise along the wall’s centerline at 0.35m over the burner surface, measured at different perpendicular distances to as indicated

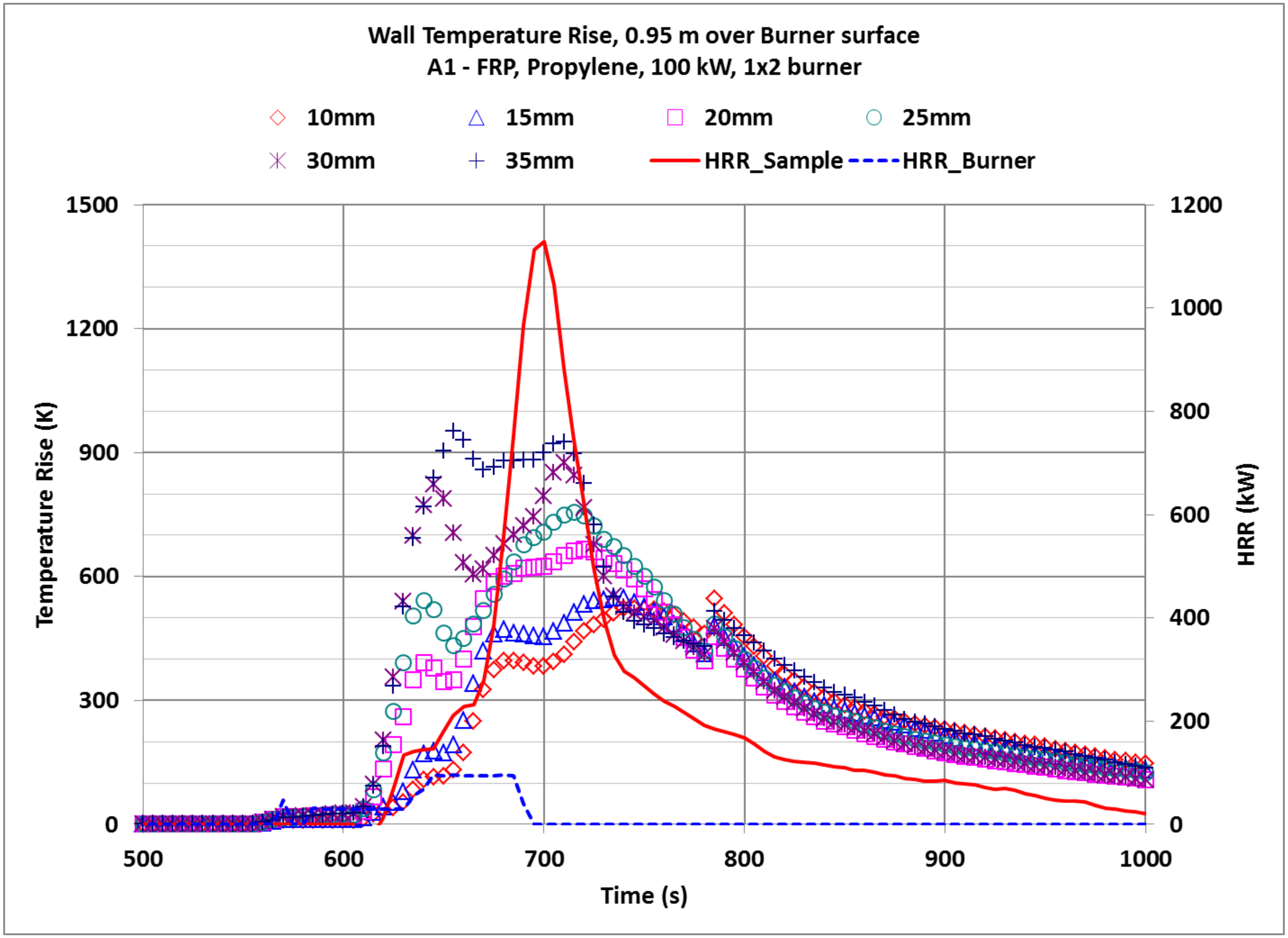

Temperature rise along the wall's centerline at 0.95m over the burner surface, measured at different perpendicular distances to as indicated

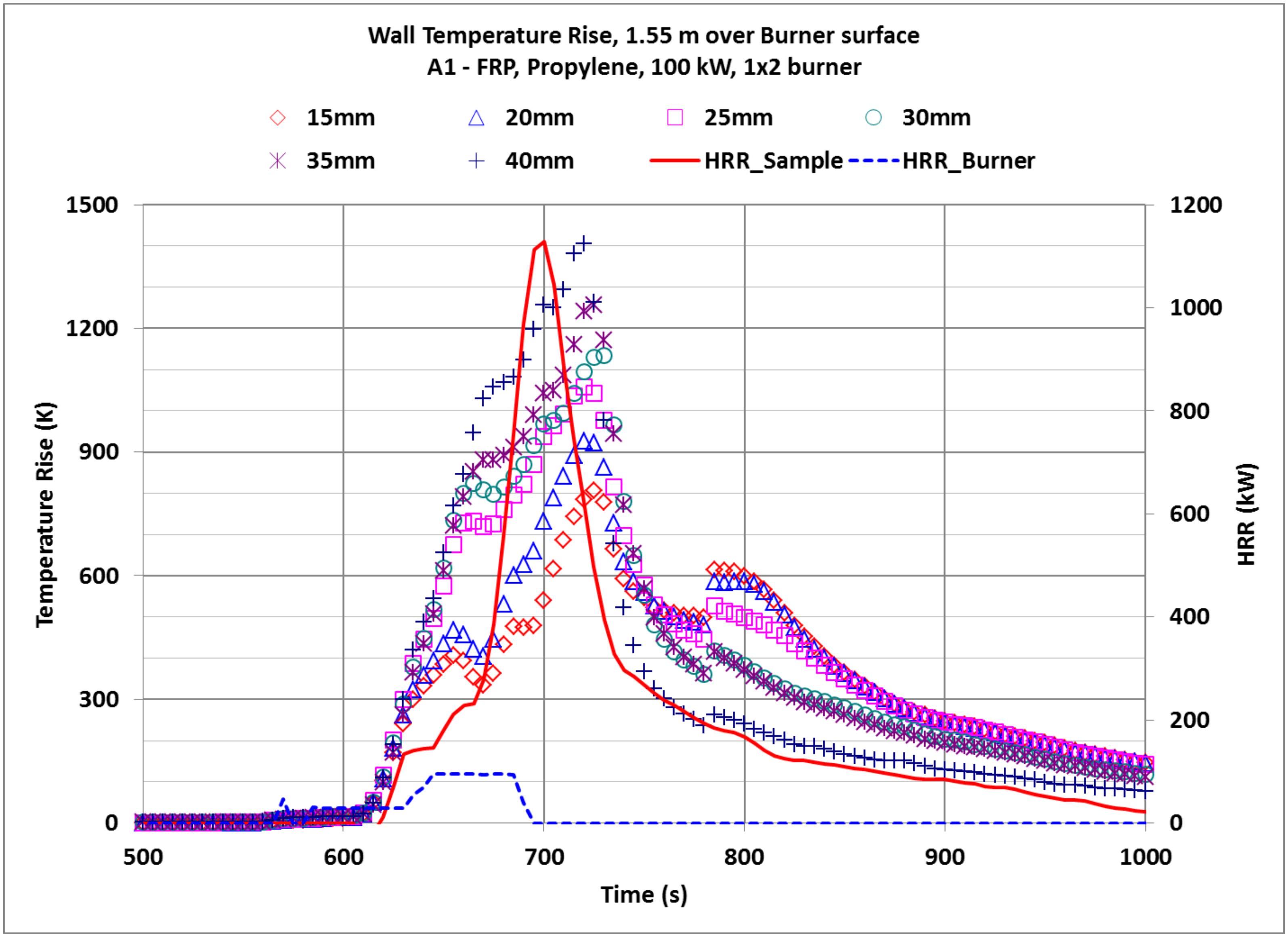

Temperature rise along the wall's centerline at 1.55m over the burner surface, measured at different perpendicular distances to as indicated

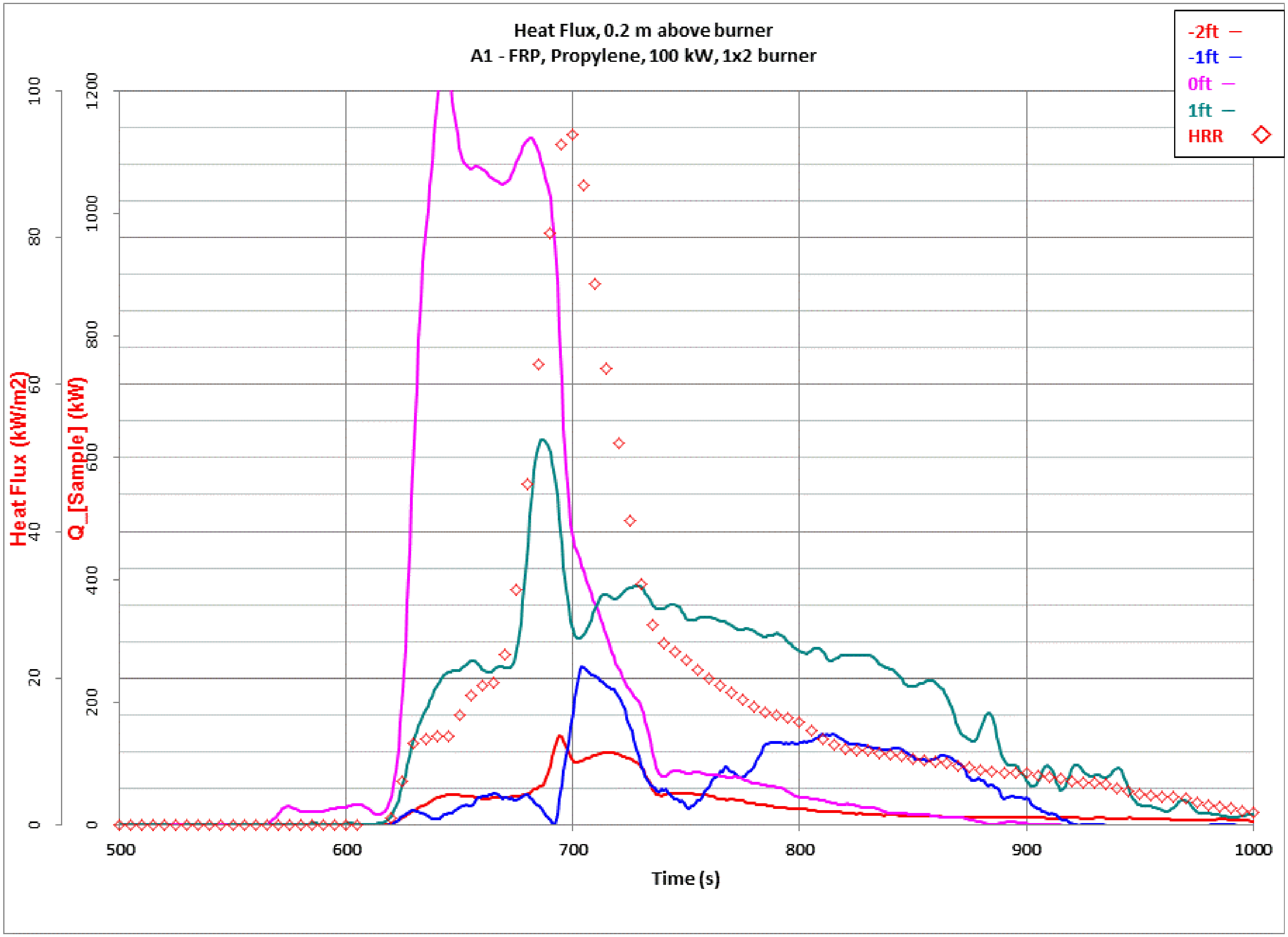

Heat flux measured at various distances from the centerline (negative indicates left of centerline), 0.2m vertically from burner surface

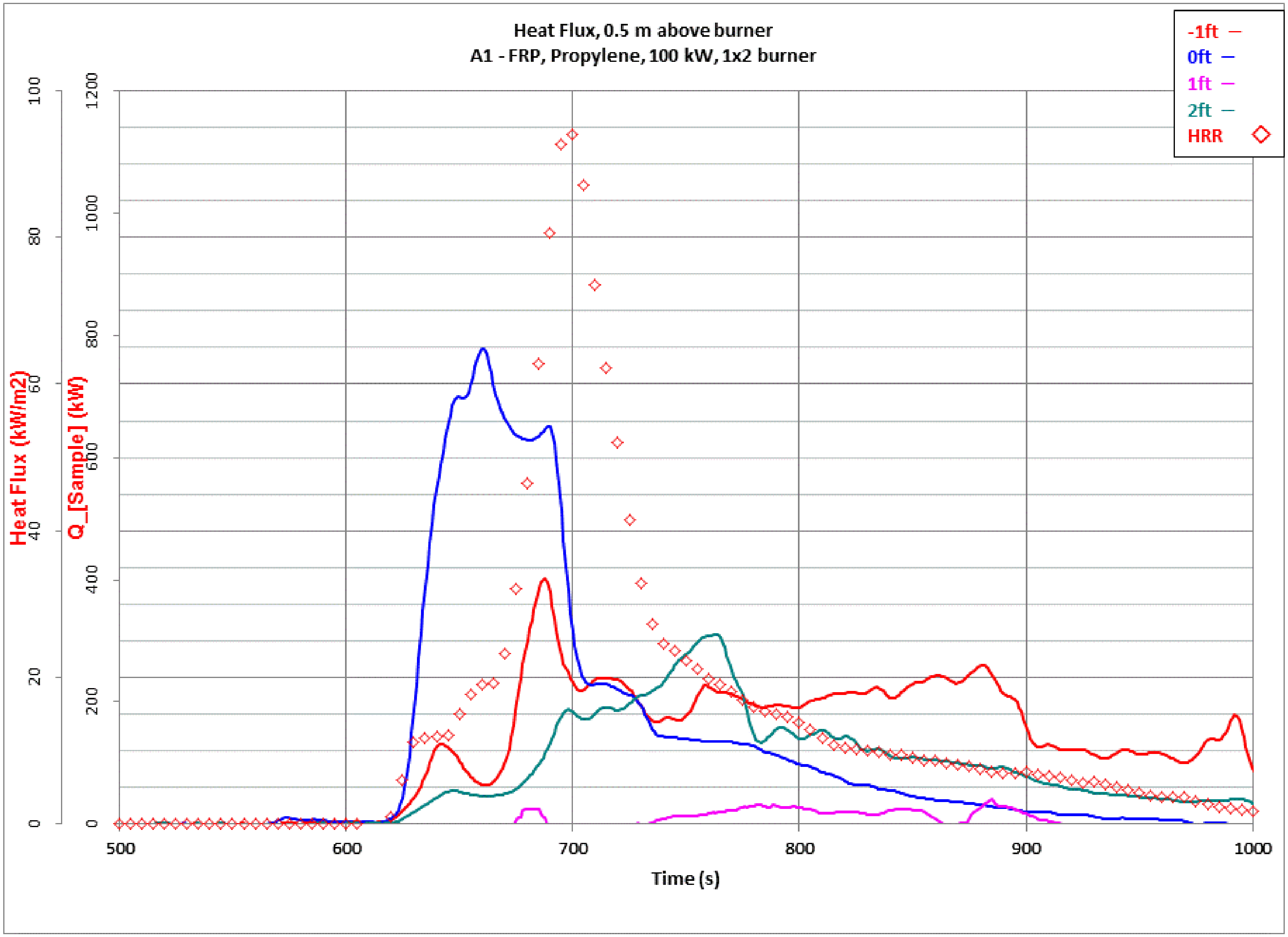

Heat flux measured at various distances from the centerline (negative indicates left of centerline), 0.5m vertically from burner surface

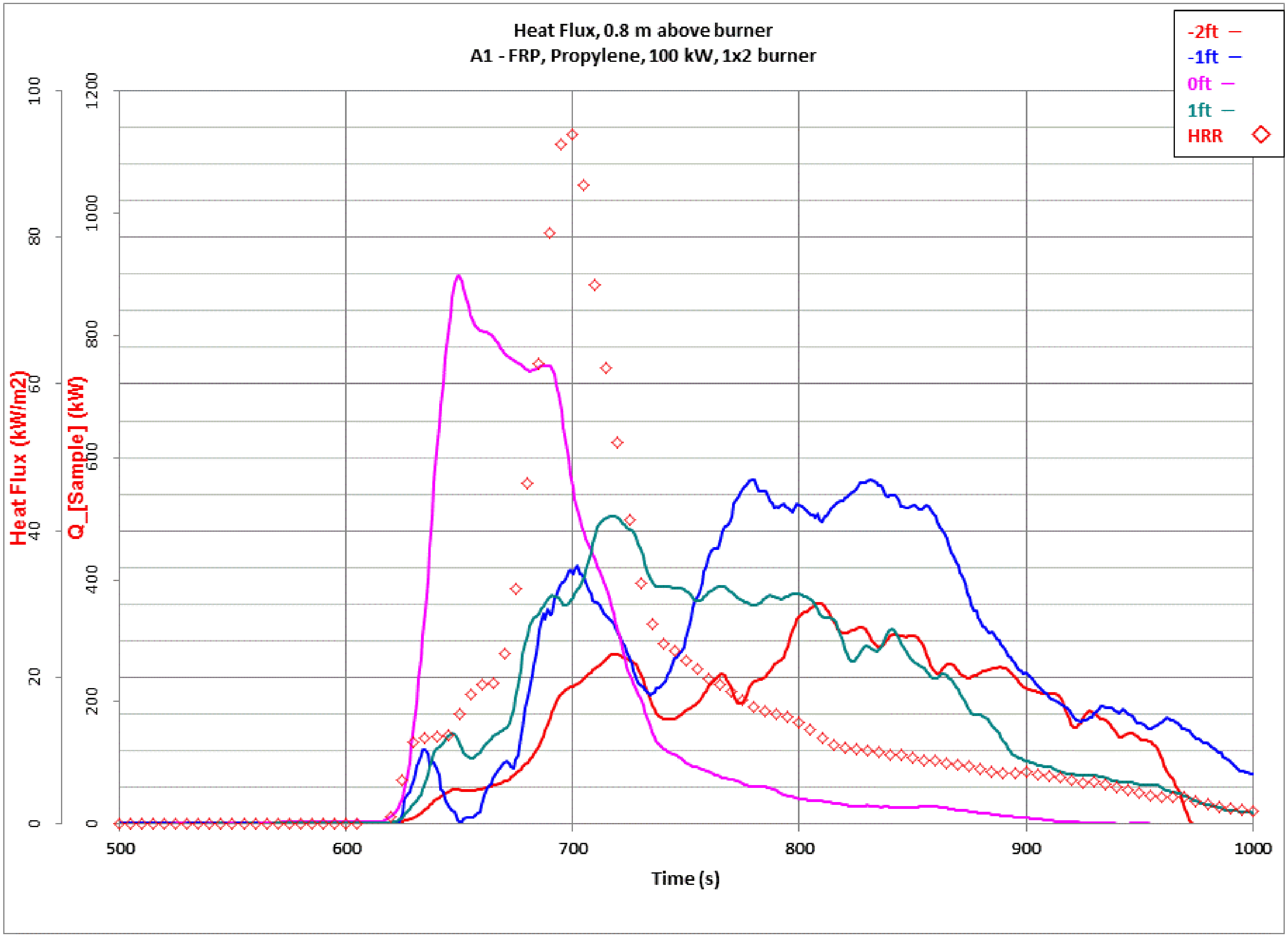

Heat flux measured at various distances from the centerline (negative indicates left of centerline), 0.8m vertically from burner surface

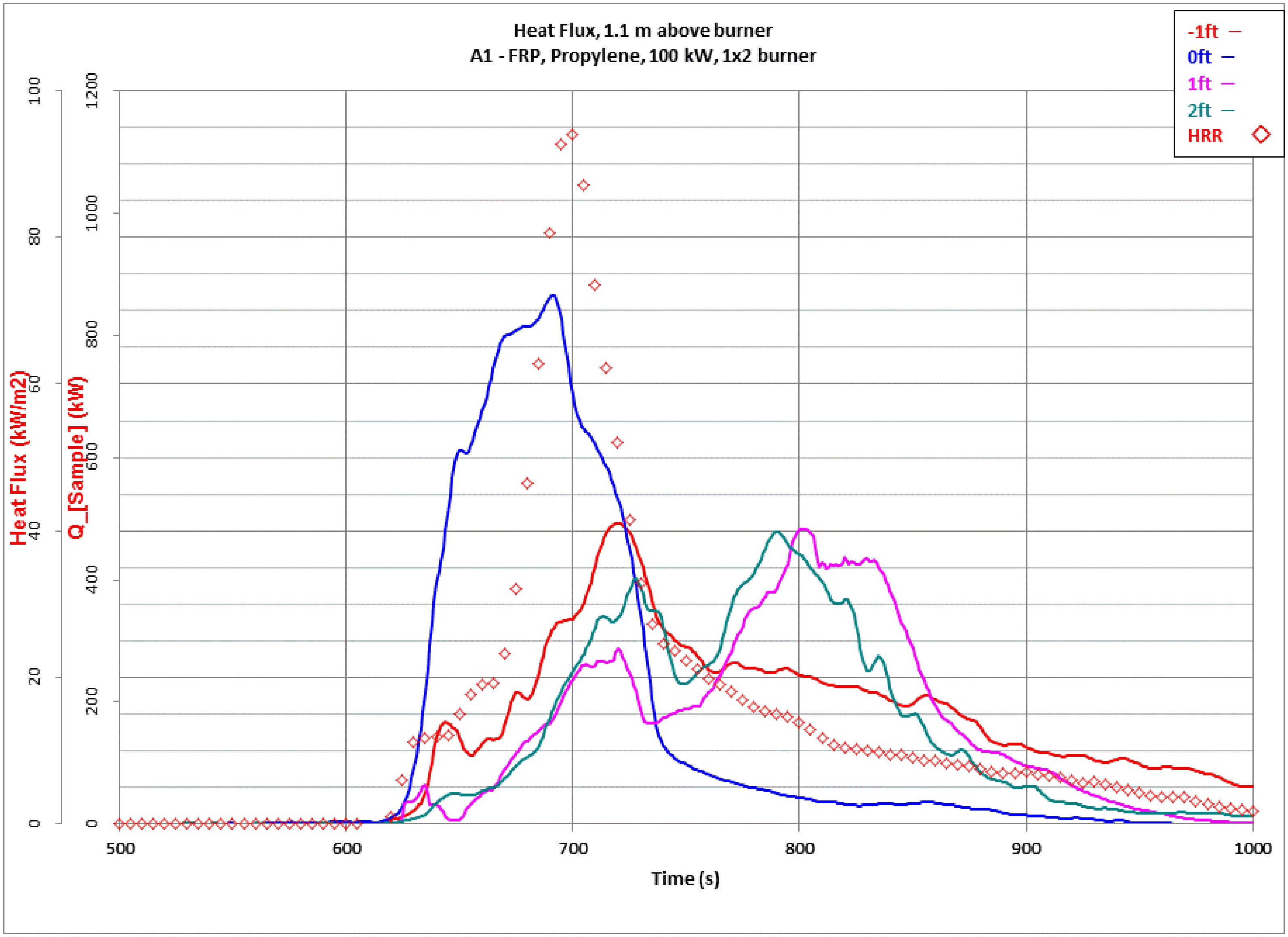

Heat flux measured at various distances from the centerline (negative indicates left of centerline), 1.1m vertically from burner surface

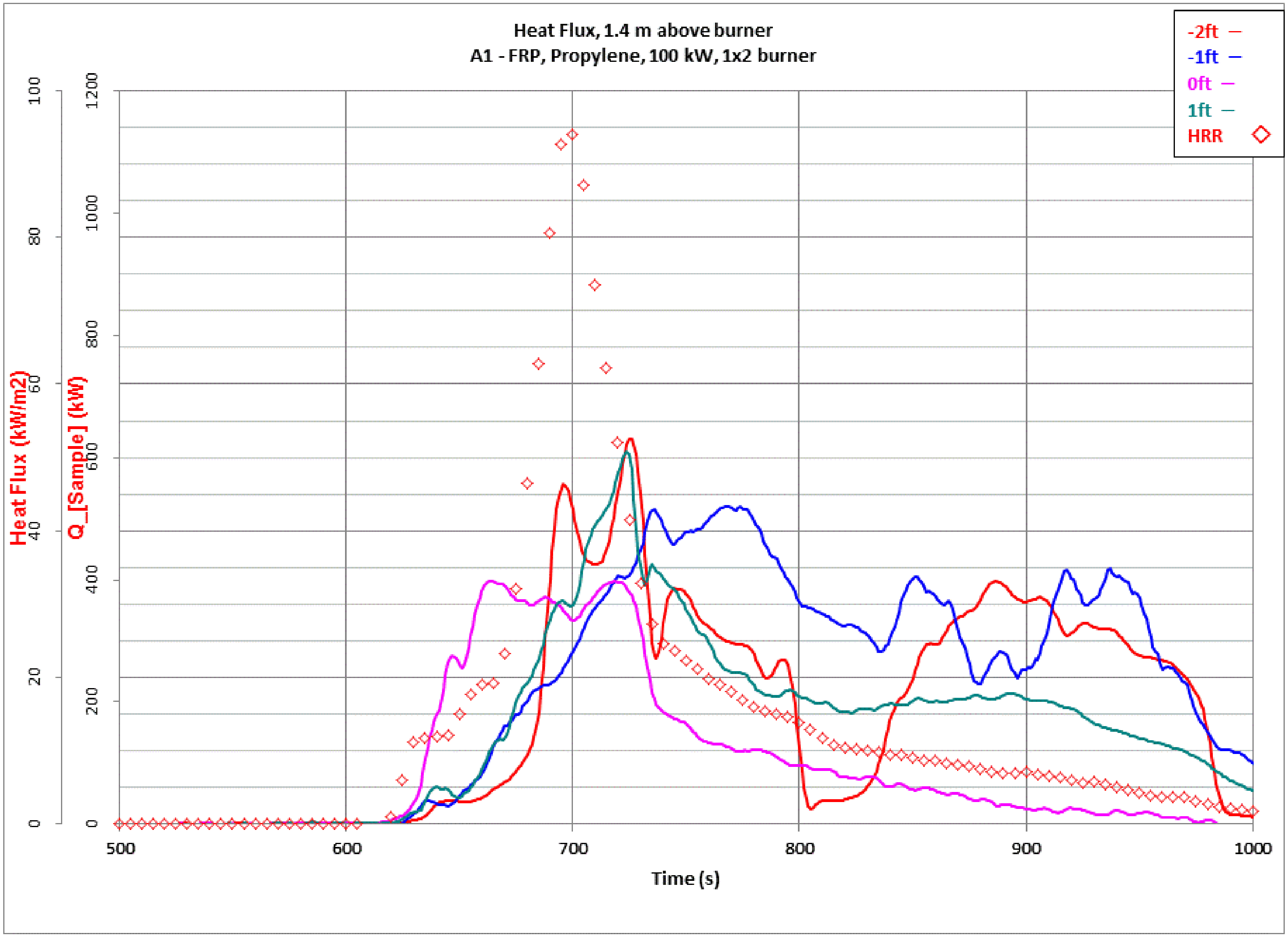

Heat flux measured at various distances from the centerline (negative indicates left of centerline), 1.4m vertically from burner surface

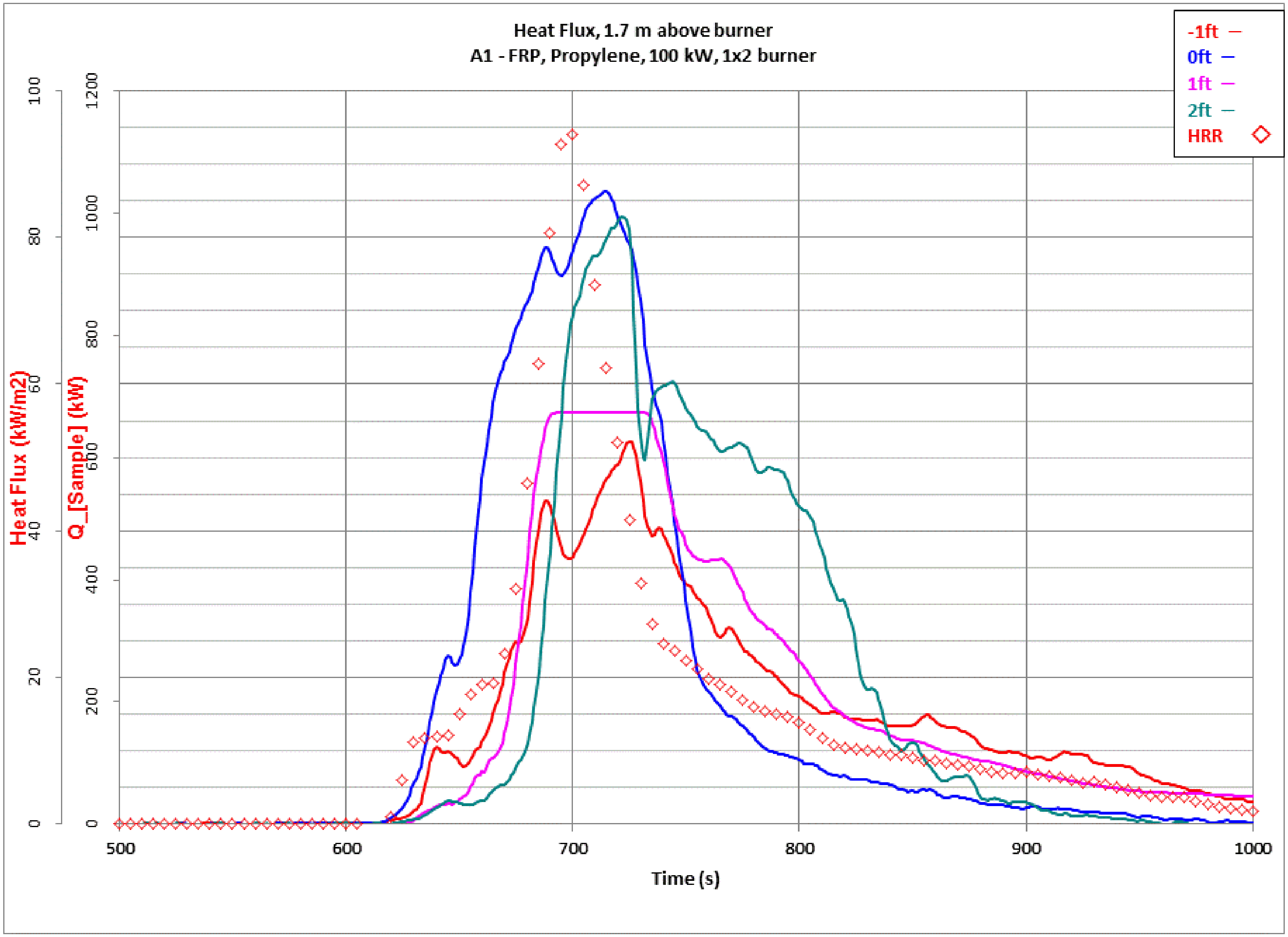

Heat flux measured at various distances from the centerline (negative indicates left of centerline), 1.7m vertically from burner surface

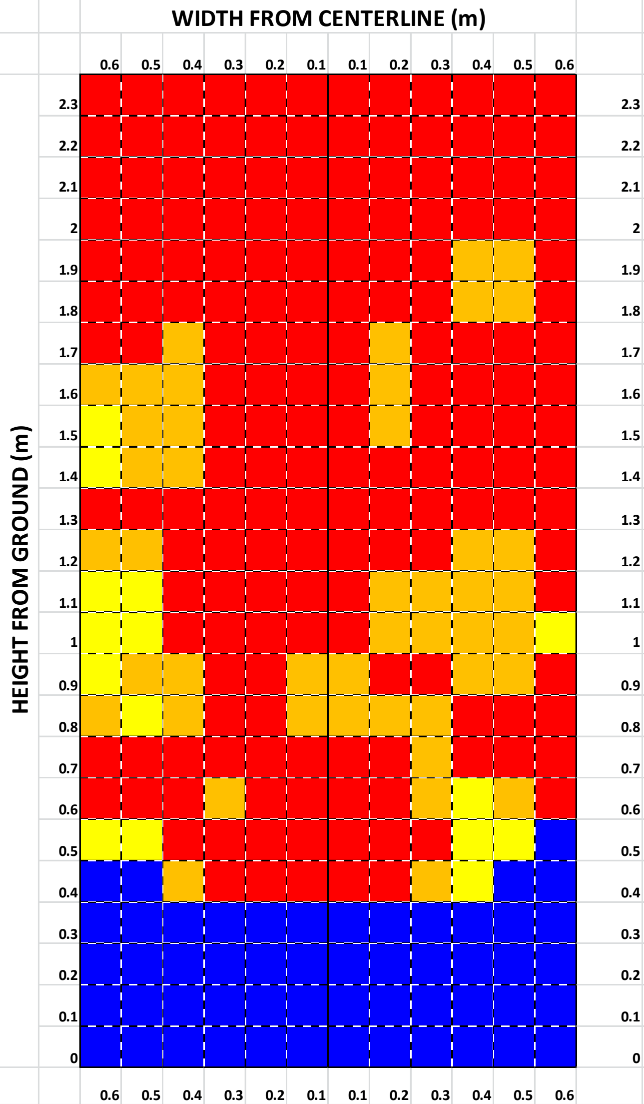

# of cell	Damage to Resin	Area (m2)
175	up to 100% damage	1.75
45	up to 75% damage	0.45
15	up to 50% damage	0.15
0	up to 25% damage	0
53	no damage	0.53

Initial mass:	8.75	kg
Final unburnt mass:	1.742	kg
Final burnt mass:	4.022	kg
Total mass loss during fire	2.986	kg

Burn damage pattern observed after fire test

F.3.2 Test A2

LODS Test Run Data

Center for Firesafety Studies

100 Institute Road
Worcester, MA 01609
Phone: (508) 831-5628
Fax: (508) 831-5680

Test Information

Test Number:	A2
Specimen Identification:	FRP 2, 75 kW initial Propylene fire, 1 x 2 burner
Material Name:	Class C FRP panel
Manufacturer/Submitter:	Not Reported
Raw Data File Name:	Test A2 - FRP_Propylene_75kW_2ft.txt
Reduced Data File Name:	Test A2 - FRP_Propylene_75kW_2ft_reduced.xlsx
Date of Test:	23-Mar-2010
Tester:	W. Wong

Test Parameters

Ambient Temperature:	N/A
Relative Humidity:	N/A

Specimen Information

Specimen Initial Mass:	[kg]	8.7
Specimen Final Mass:	[kg]	6.1
Mass Lost:	[kg]	2.6
Heat Evolved (net):	[kJ]	0

Parameter	Unit	Value
Mass Loss		
Initial Mass	[kg]	8.7
Final Mass	[kg]	6.1
Mass Loss	[%]	30.08

LODS Test Run Data

Center for Firesafety Studies

100 Institute Road
Worcester, MA 01609
Phone: (508) 831-5628
Fax: (508) 831-5680

Test Notes

Test Number:	0
Date:	03/23/10
Material:	Class C FRP panel
Specimen Identification:	FRP 2, 75 kW initial Propylene fire, 1 x 2 burner

Observations

Time	Observation
00:00	Start VI
07:15	Start Video Camera
12:25	Ignition of Burner
12:30	Flare up of the source fire, then slows down
12:35	Flow set to 75 kW
12:50	Crackling noise from panel, panel ignites
13:05	Smoke coming out from back of panel on right edge
	Back-face burning at TSC-10 on the right edge of panel
13:40	Burner turned off
13:45	No flame at burner
13:48	Rollover of top layer
14:10	Left edge on fire from 1.5 m to 2.5 m
14:30	Back-face burning at TSC-8 (on centerline)
15:13	Charred area along centerline extends to 0.3 m on both sides, no flame here
16:00	Reverse V burning pattern on both sides
16:53	Smoke coming out of TSC-7 on left edge
17:18	Backface burning at the hole for WTC-7
23:00	IR Camera turned on
31:49	Smoke coming out of TSC-3 on right edge
38:00	TSC-10 is impinged by fire on the left side
39:00	On the right there is a burning line fire from (0.2, 0.8) to (0.3, 1.6) on grid
40:35	TSC-10's left side has back-face burning
43:00	No more back-face burning at TSC-10
54:00	Smoke coming out of 0.45 m on the right edge

55:55	Back-face burning at TSC-6, cased by small vertical line fire at underneath
1:16:30	Terminated test
	The rollover cased little burning on the new ceiling drywalls, no burning on sidewalls
	A lot of damage at the line between unburnt and burnt area due to length of burning there
	Initial source fire tilts to the right at about 5-10deg
	Unburnt mass left: 2.232 kg, burnt mass left: 3.872 kg

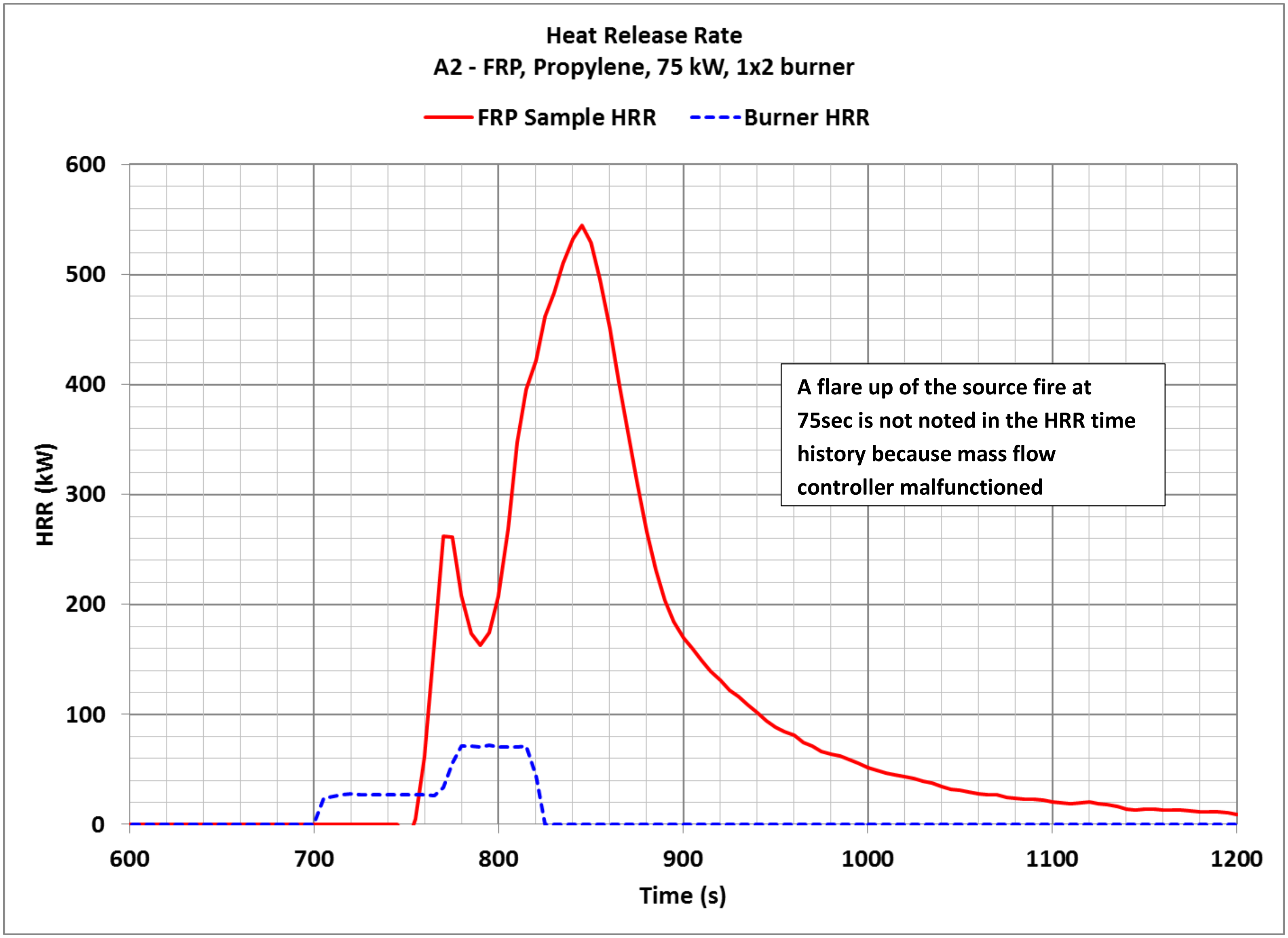

Heat release ratesof the source burner fire and of the specimen fire measured during test

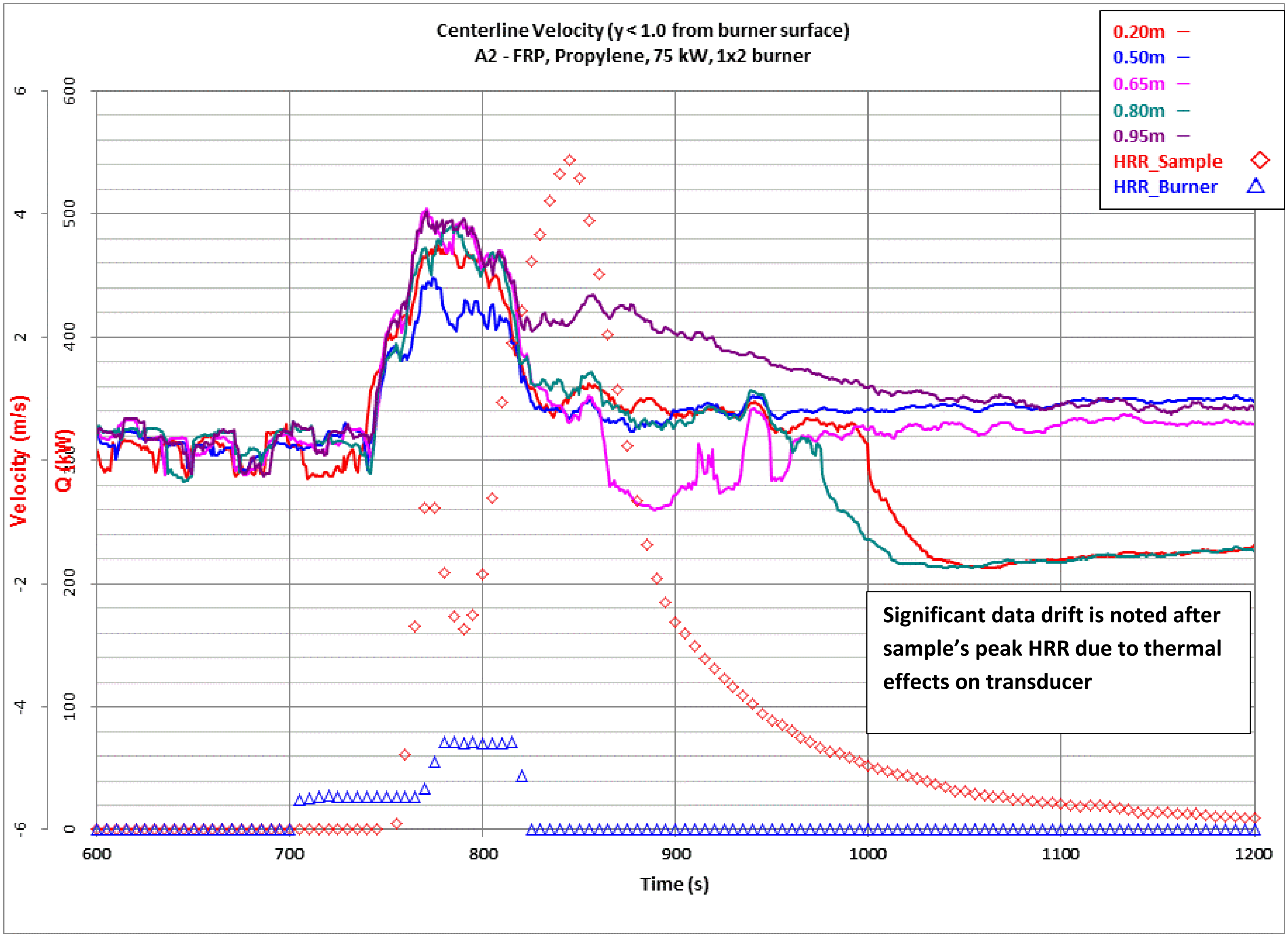

Centerline plume velocities measured from 0.2m to 0.95m above the burner surface

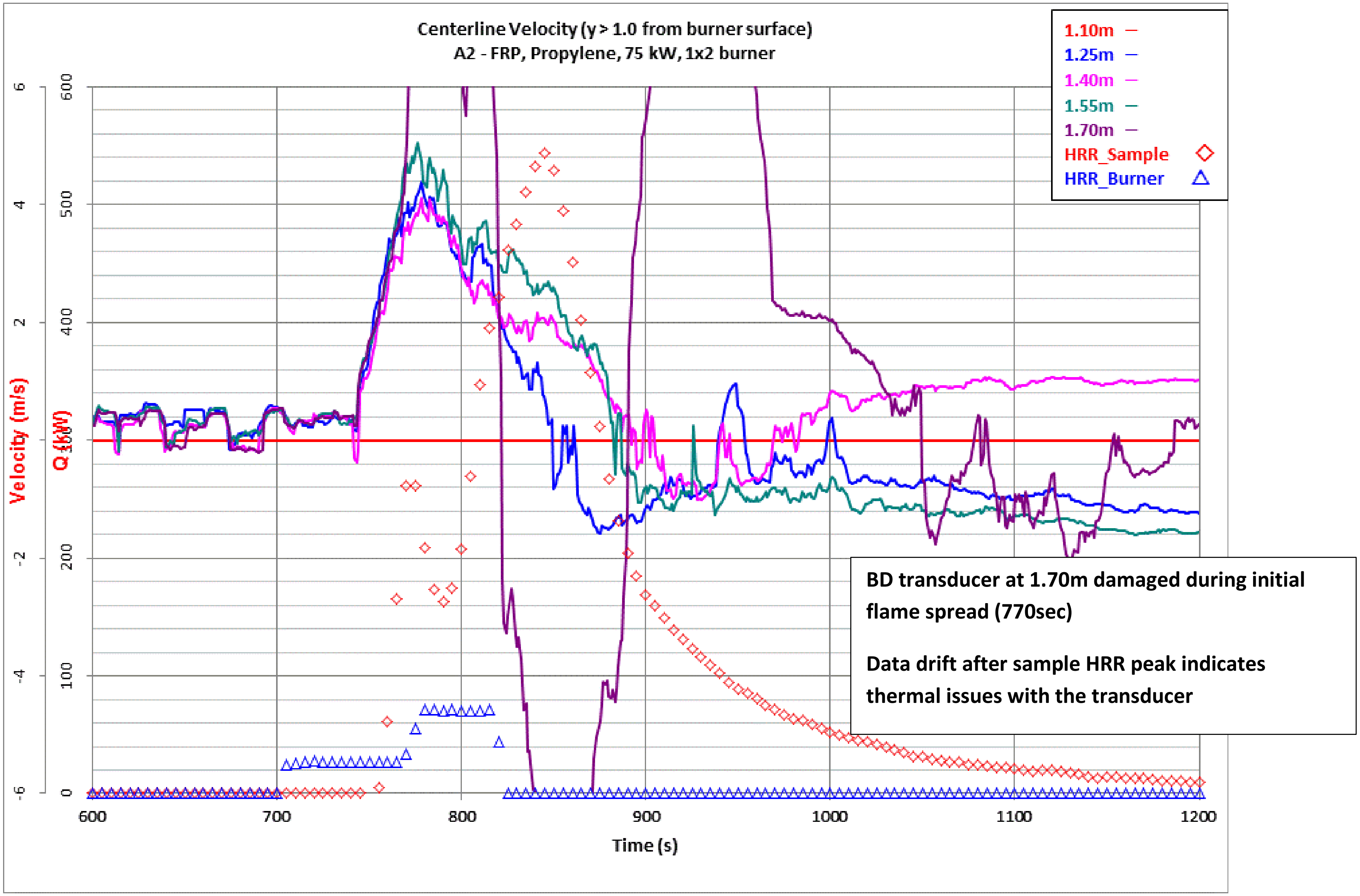

Centerline plume velocities measured from 1.1m to 1.7m above the burner surface

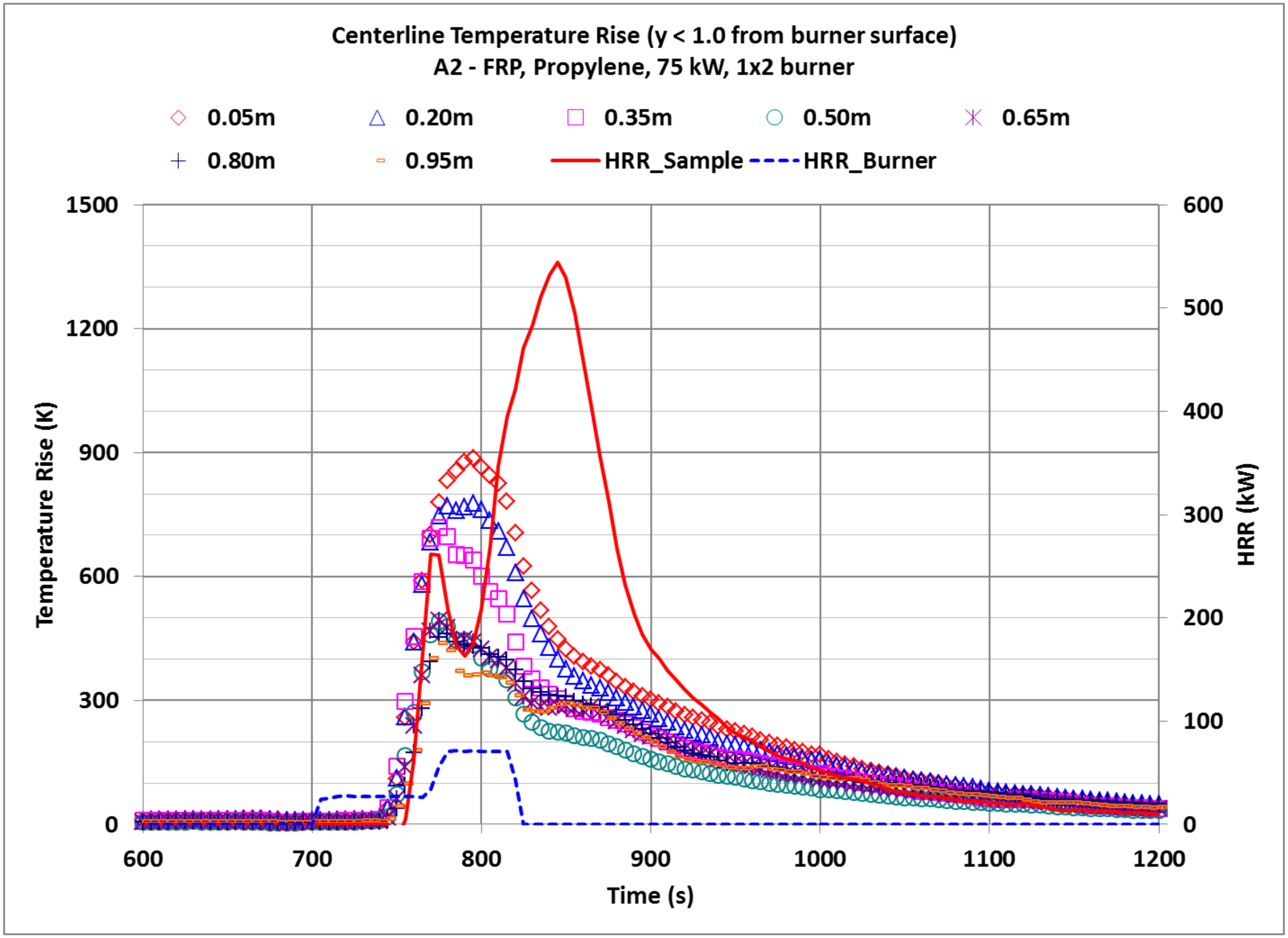

Centerline plume temperature rise measured from 0.05m to 0.95m above the burner surface

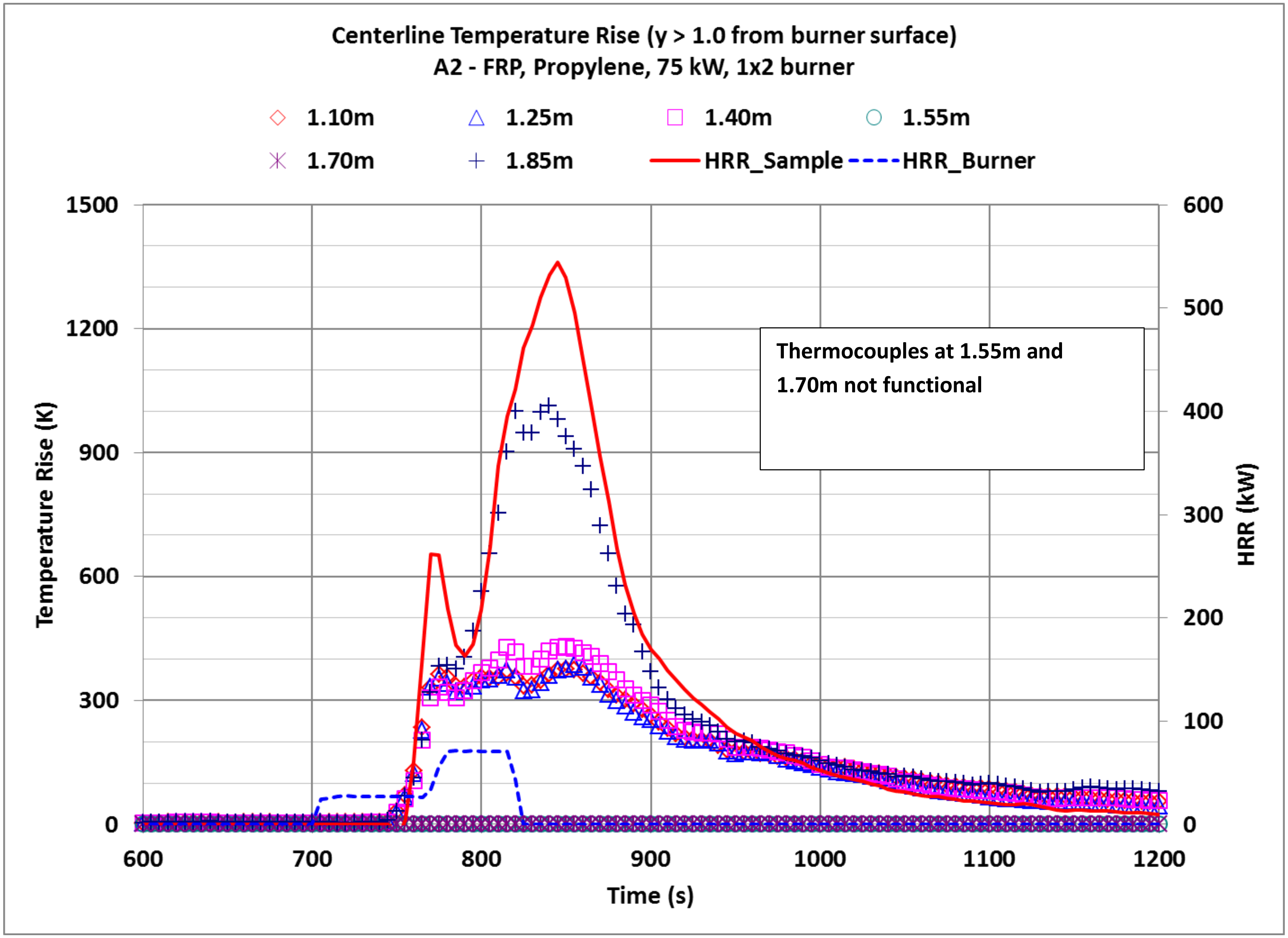

Centerline plume temperature rise measured from 1.10m to 1.85m above the burner surface

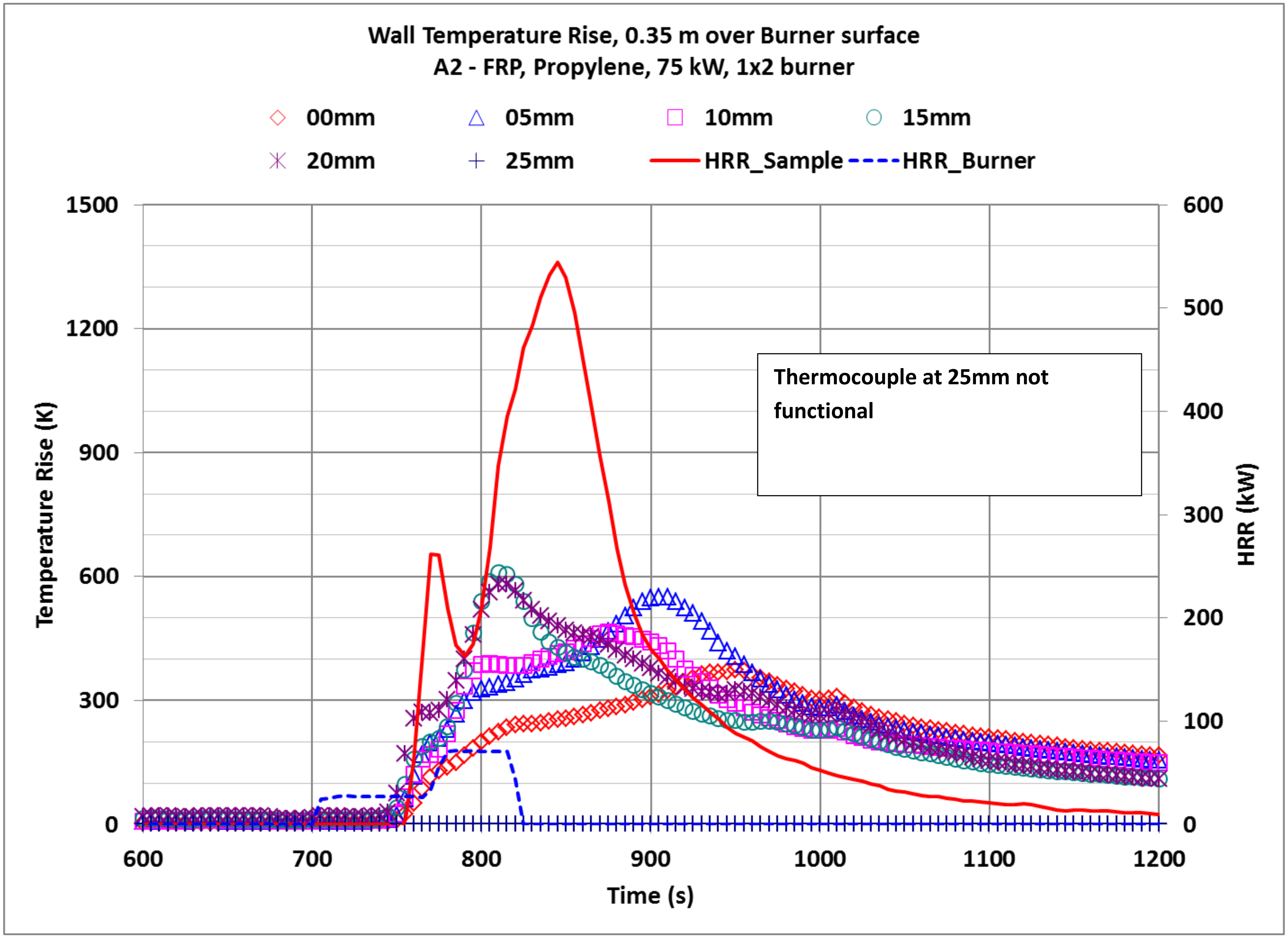

Temperature rise along the wall's centerline at 0.35m over the burner surface, measured at different perpendicular distances to as indicated

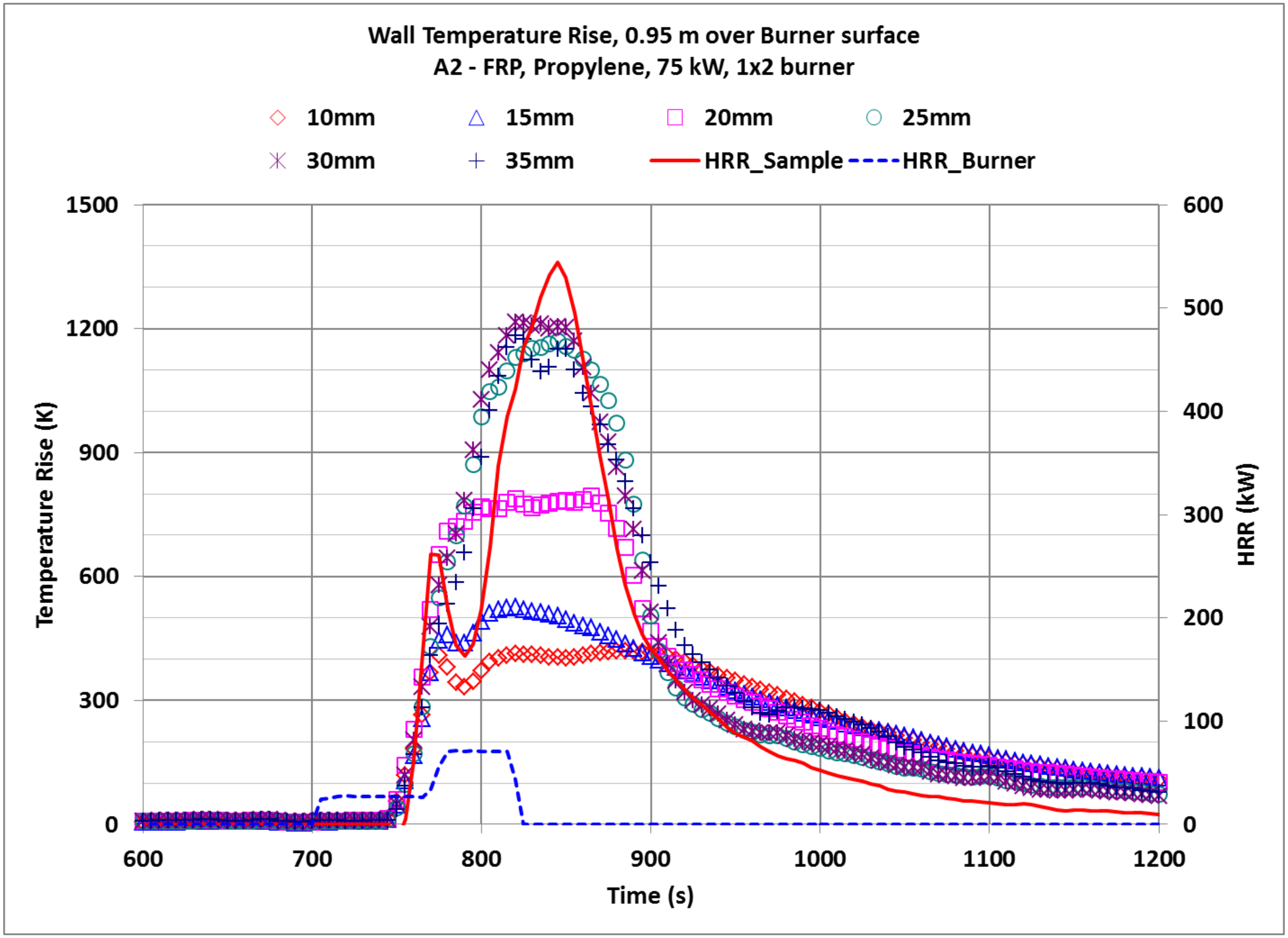

Temperature rise along the wall's centerline at 0.95m over the burner surface, measured at different perpendicular distances to as indicated

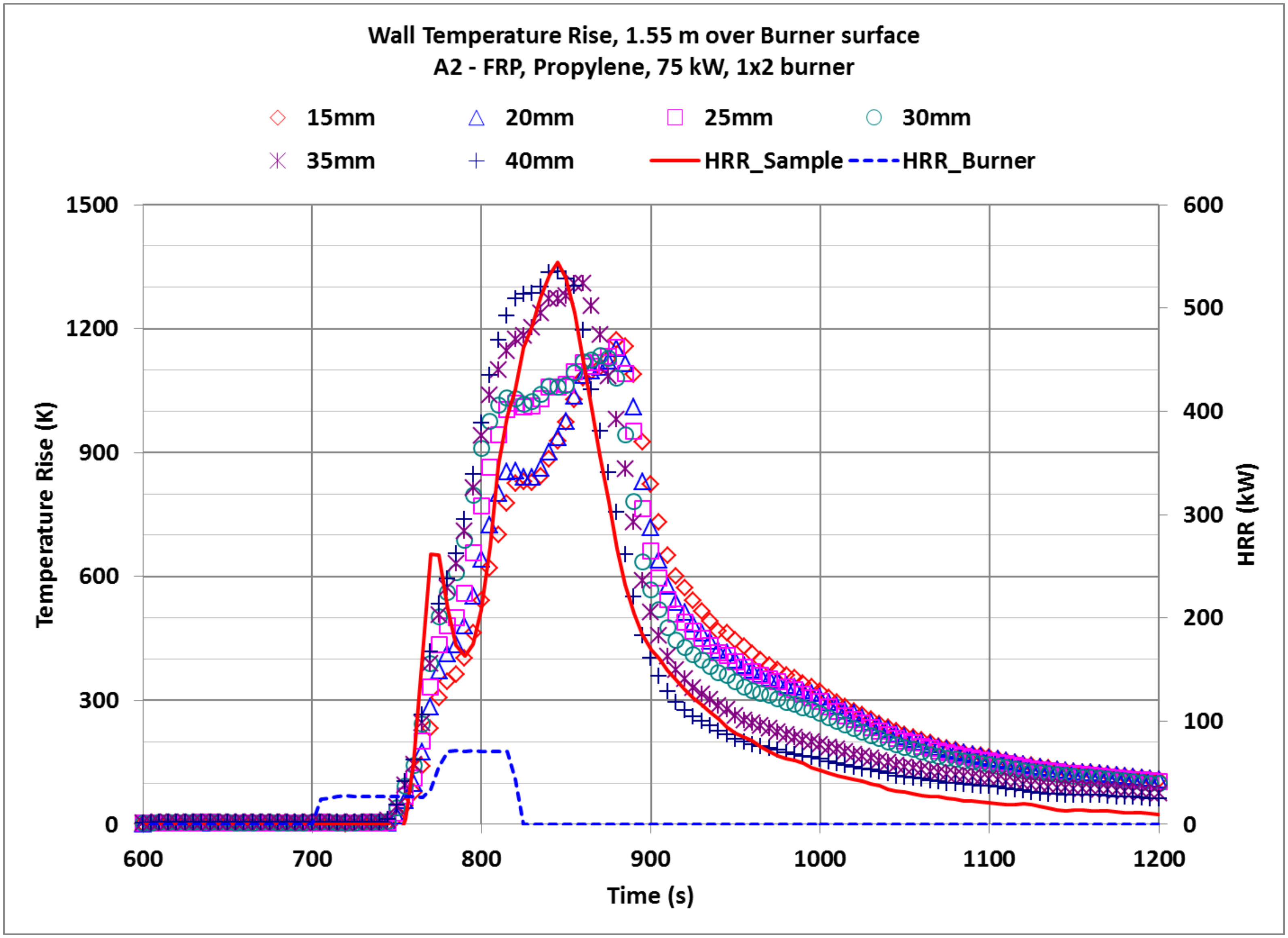

Temperature rise along the wall's centerline at 1.55m over the burner surface, measured at different perpendicular distances to as indicated

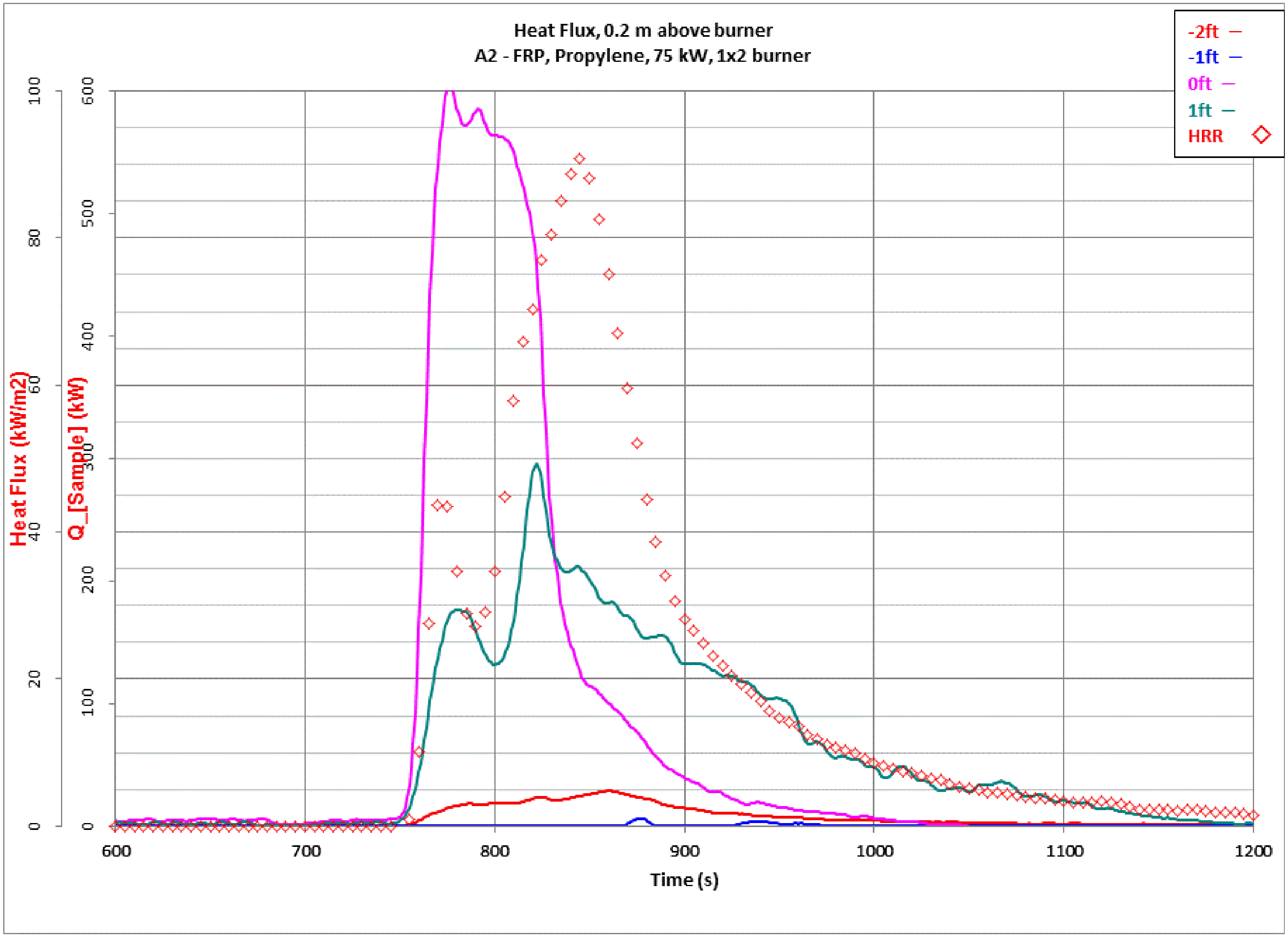

Heat flux measured at various distances from the centerline (negative indicates left of centerline), 0.2m vertically from burner surface

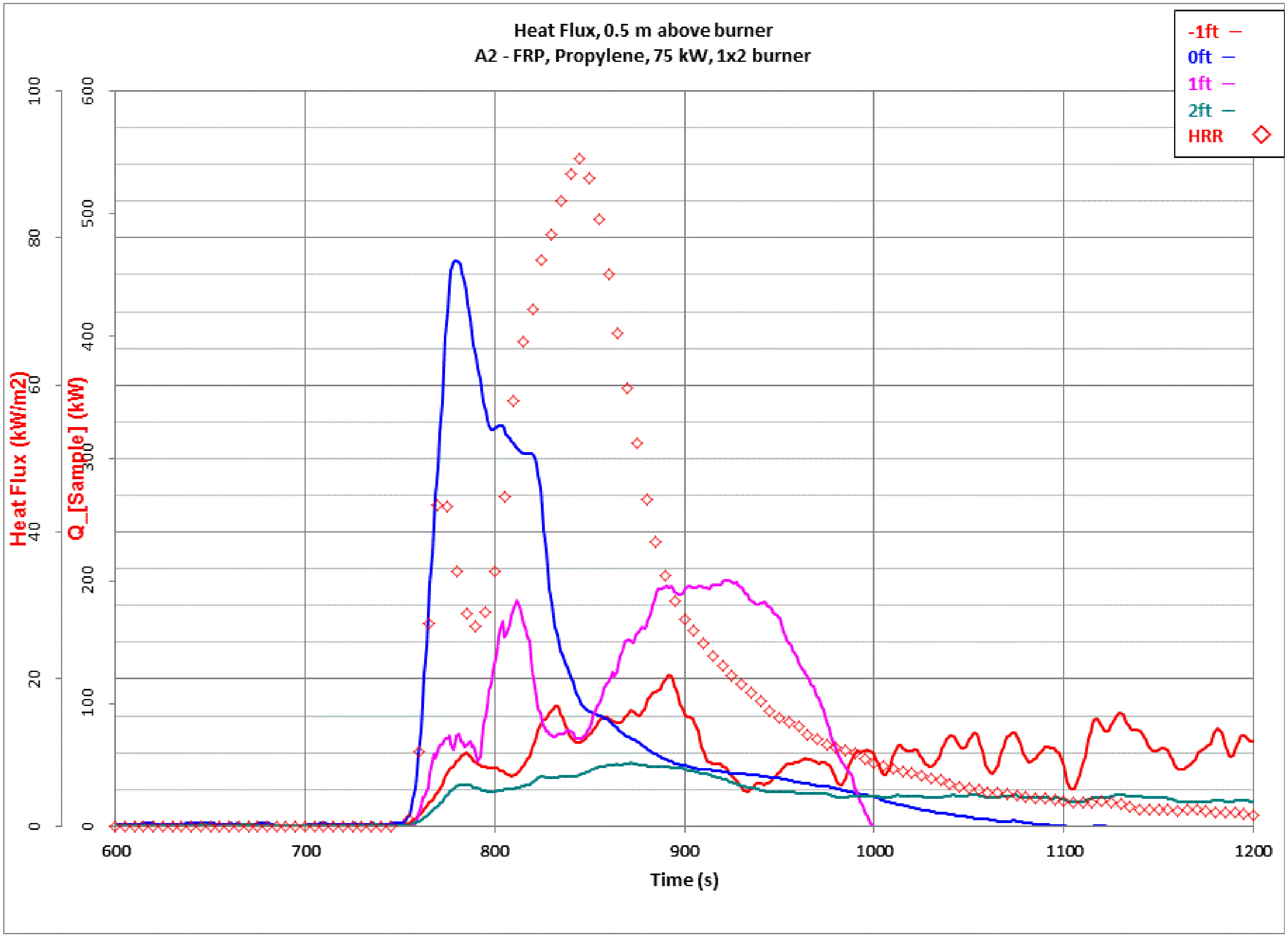

Heat flux measured at various distances from the centerline (negative indicates left of centerline), 0.5m vertically from burner surface

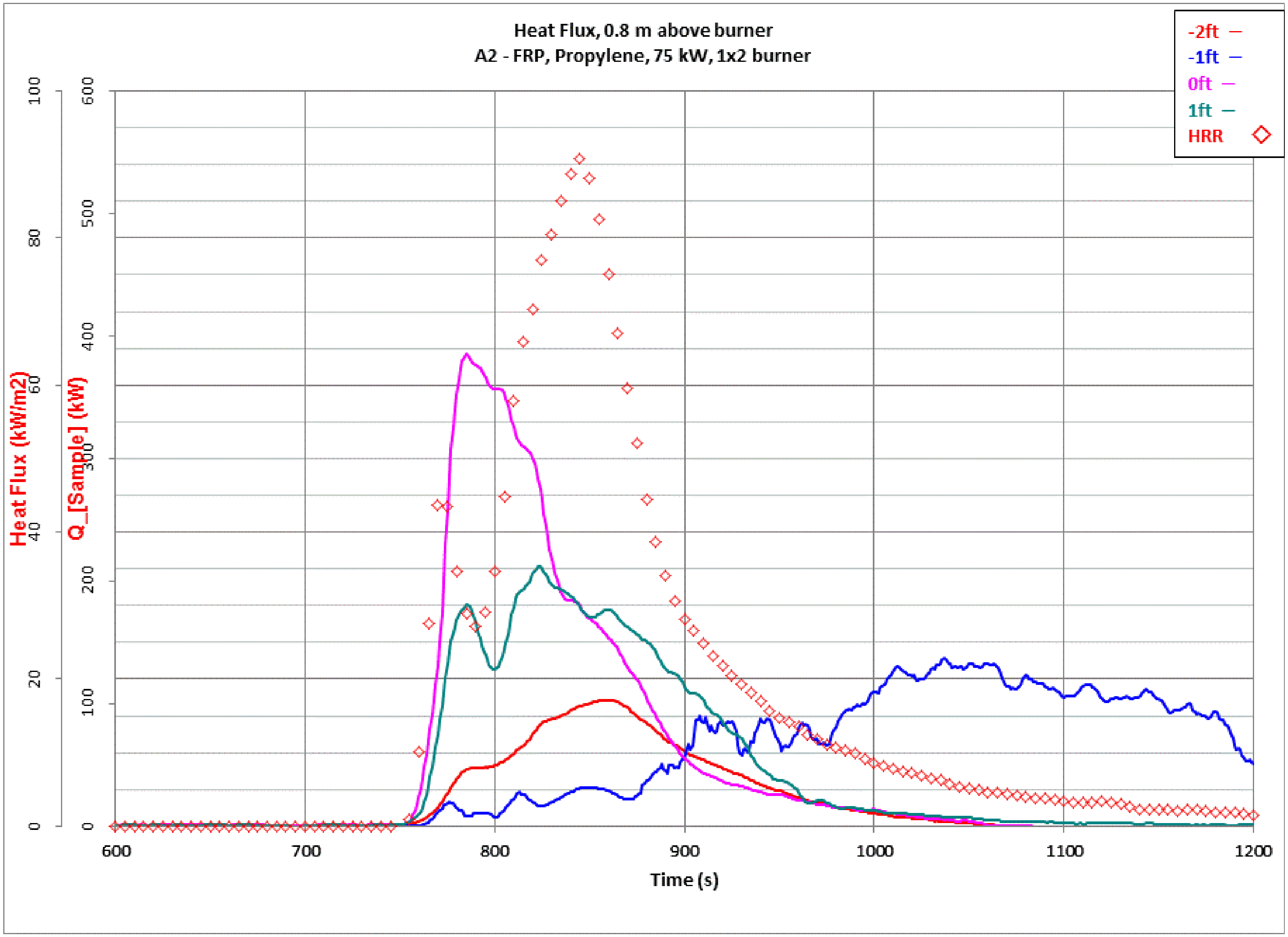

Heat flux measured at various distances from the centerline (negative indicates left of centerline), 0.8m vertically from burner surface

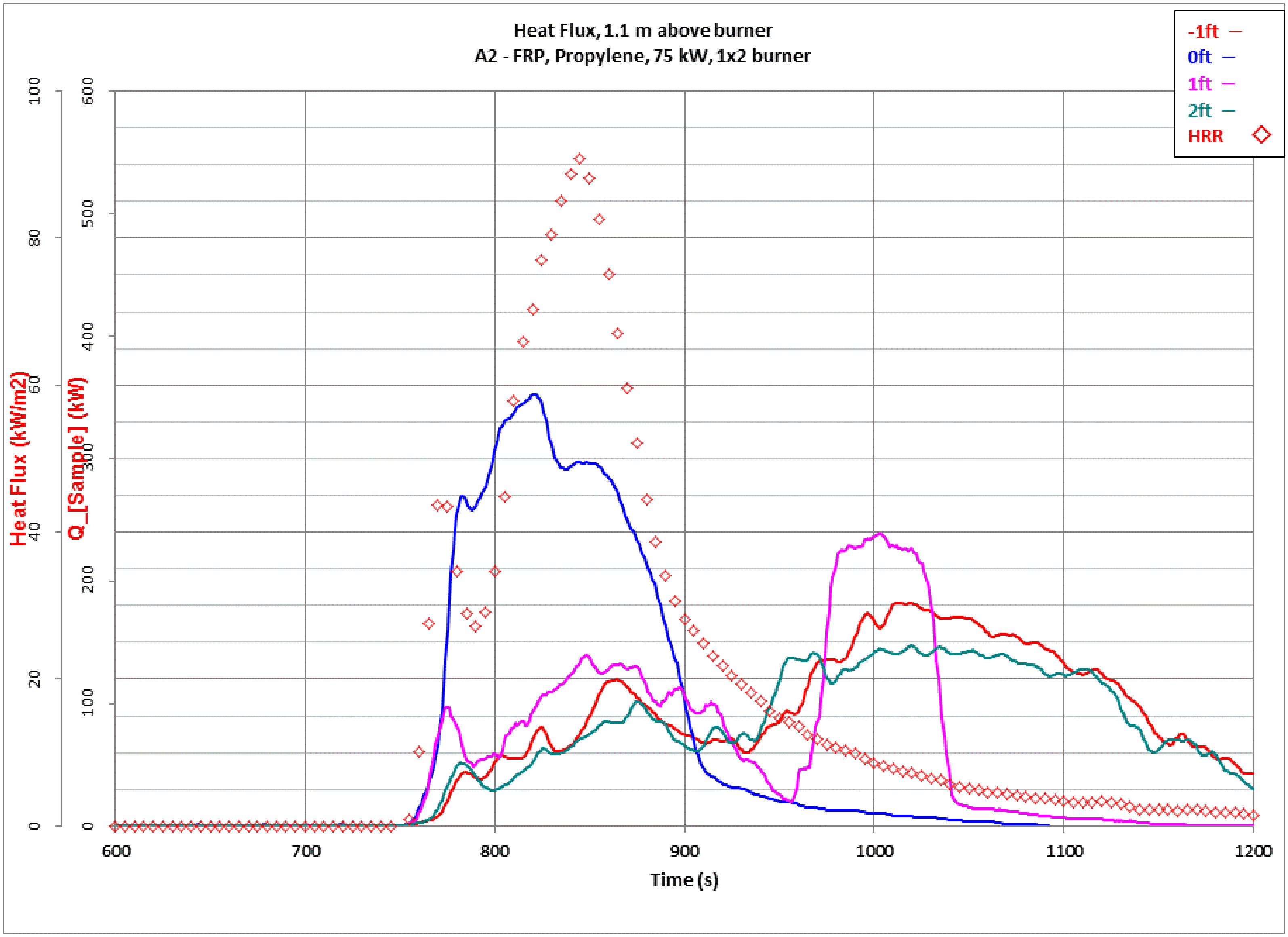

Heat flux measured at various distances from the centerline (negative indicates left of centerline), 1.1m vertically from burner surface

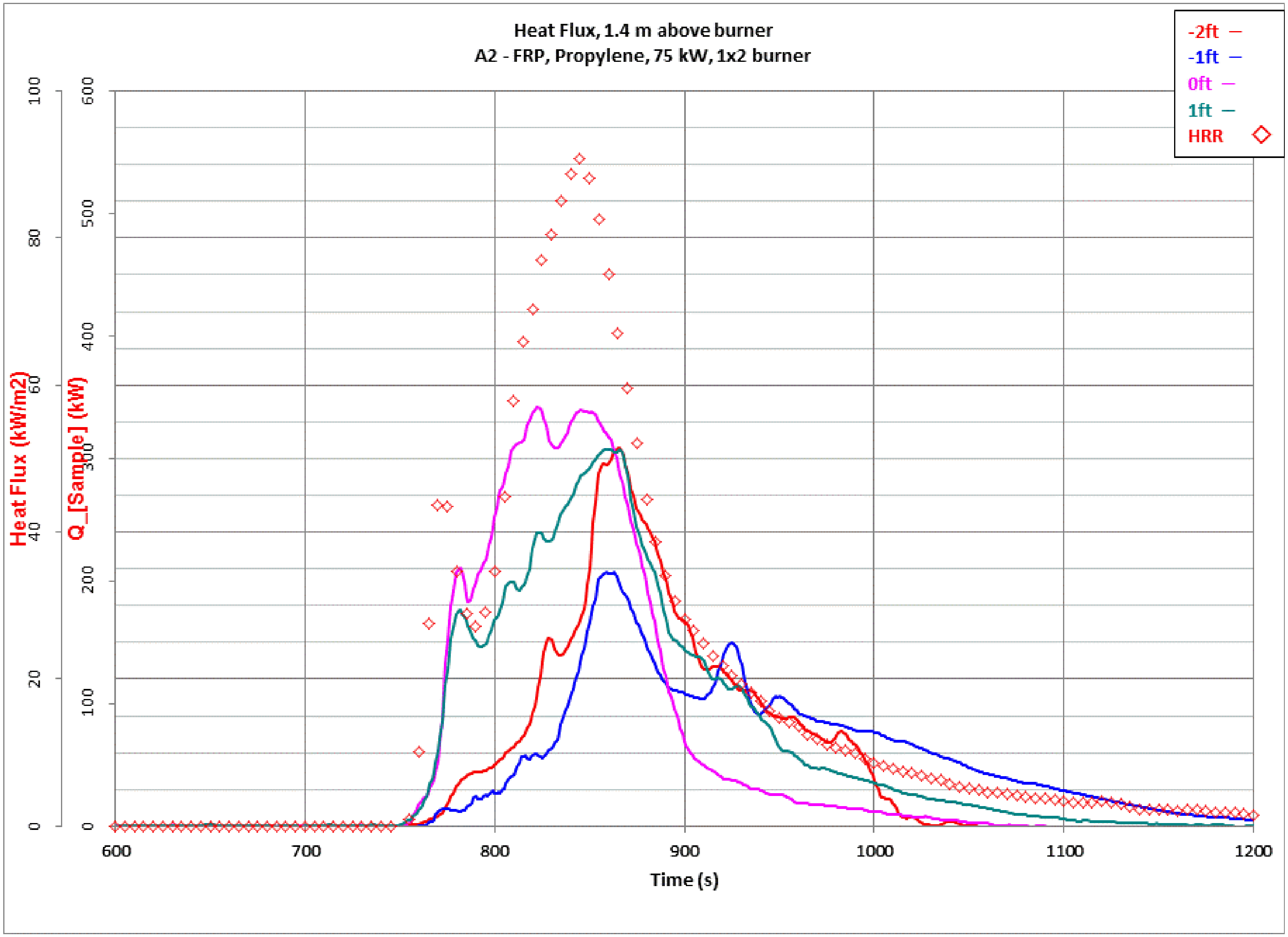

Heat flux measured at various distances from the centerline (negative indicates left of centerline), 1.4m vertically from burner surface

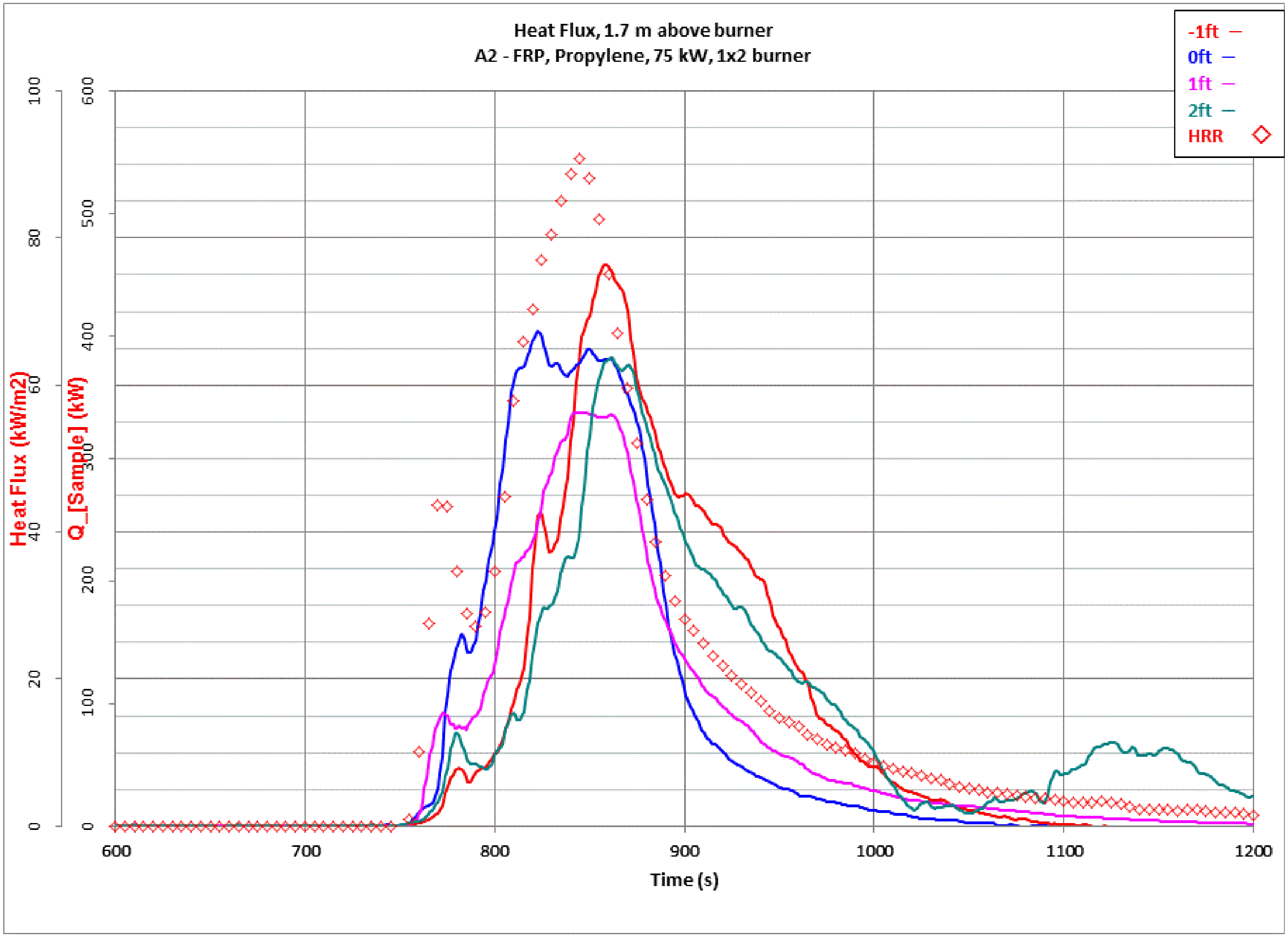

Heat flux measured at various distances from the centerline (negative indicates left of centerline), 1.7m vertically from burner surface

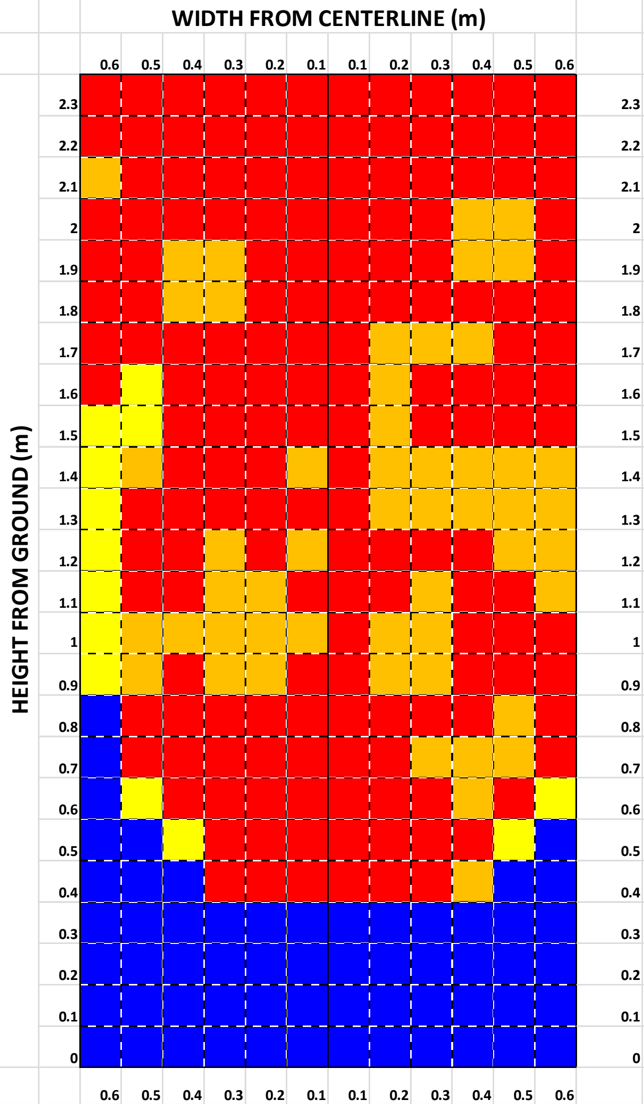

# of cell	Damage to Resin	Area (m2)
164	up to 100% damage	1.64
52	up to 75% damage	0.52
13	up to 50% damage	0.13
0	up to 25% damage	0
59	no damage	0.59

Initial mass:	8.73	kg
Final unburnt mass:	2.232	kg
Final burnt mass:	3.872	kg
Total mass loss during fire	2.626	kg

Burn damage pattern observed after fire test

F.3.3 Test A3

LODS Test Run Data

Center for Firesafety Studies

100 Institute Road
Worcester, MA 01609
Phone: (508) 831-5628
Fax: (508) 831-5680

Test Information

Test Number:	A3
Specimen Identification:	FRP 3, 50 kW initial Propane fire, 1 x 2 burner
Material Name:	Class C FRP panel
Manufacturer/Submitter:	Not Reported
Raw Data File Name:	Test A3 - FRP_Propane_50kW_2ft.txt
Reduced Data File Name:	Test A3 - FRP_Propane_50kW_2ft_reduced.xlsx
Date of Test:	7-Sep-2010
Tester:	W. Wong

Test Parameters

Ambient Temperature:	N/A
Relative Humidity:	N/A

Specimen Information

Specimen Initial Mass:	[kg]	8.7
Specimen Final Mass:	[kg]	6.6
Mass Lost:	[kg]	2.1
Heat Evolved (net):	[kJ]	0

Parameter	Unit	Value
Mass Loss		
Initial Mass	[kg]	8.7
Final Mass	[kg]	6.6
Mass Loss	[%]	23.94

LODS Test Run Data

Center for Firesafety Studies

100 Institute Road
Worcester, MA 01609
Phone: (508) 831-5628
Fax: (508) 831-5680

Test Notes

Test Number:	0
Date:	09/07/10
Material:	Class C FRP panel
Specimen Identification:	FRP 3, 50 kW initial Propane fire, 1 x 2 burner

Observations

Time	Observation
00:00	Start VI
04:00	Start Camera 1
04:15	Start Camera 2
07:15	Burner ignition
07:30	Reach target HRR @ 50 kW
08:08	Crackling noise
08:25	Panel ignition
08:42	Burner turned off
09:30	Remote area smoking @ TSC-4, HFG-2, and TSC-10
09:44	Flame hit ceiling
10:18	Burning reaches left and right edges, T burning starts
10:25	Rollover under ceiling, flame layer about 30 cm deep
	Flame spread down to y=2m on the left side, higher on the right side
12:30	Little ignition at TSC-10
25:05	Terminate test by little water application

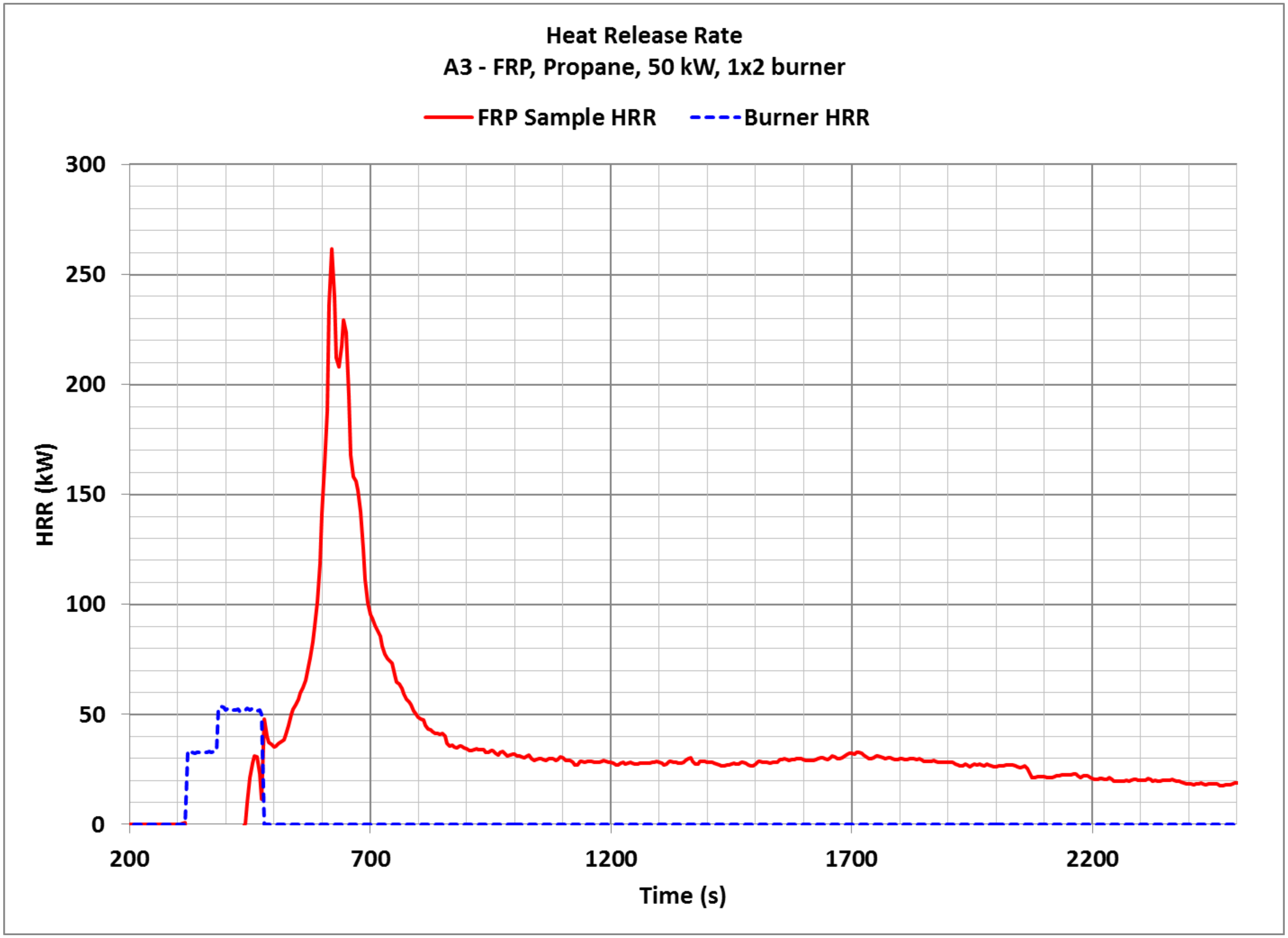

Heat release ratesof the source burner fire and of the specimen fire measured during test

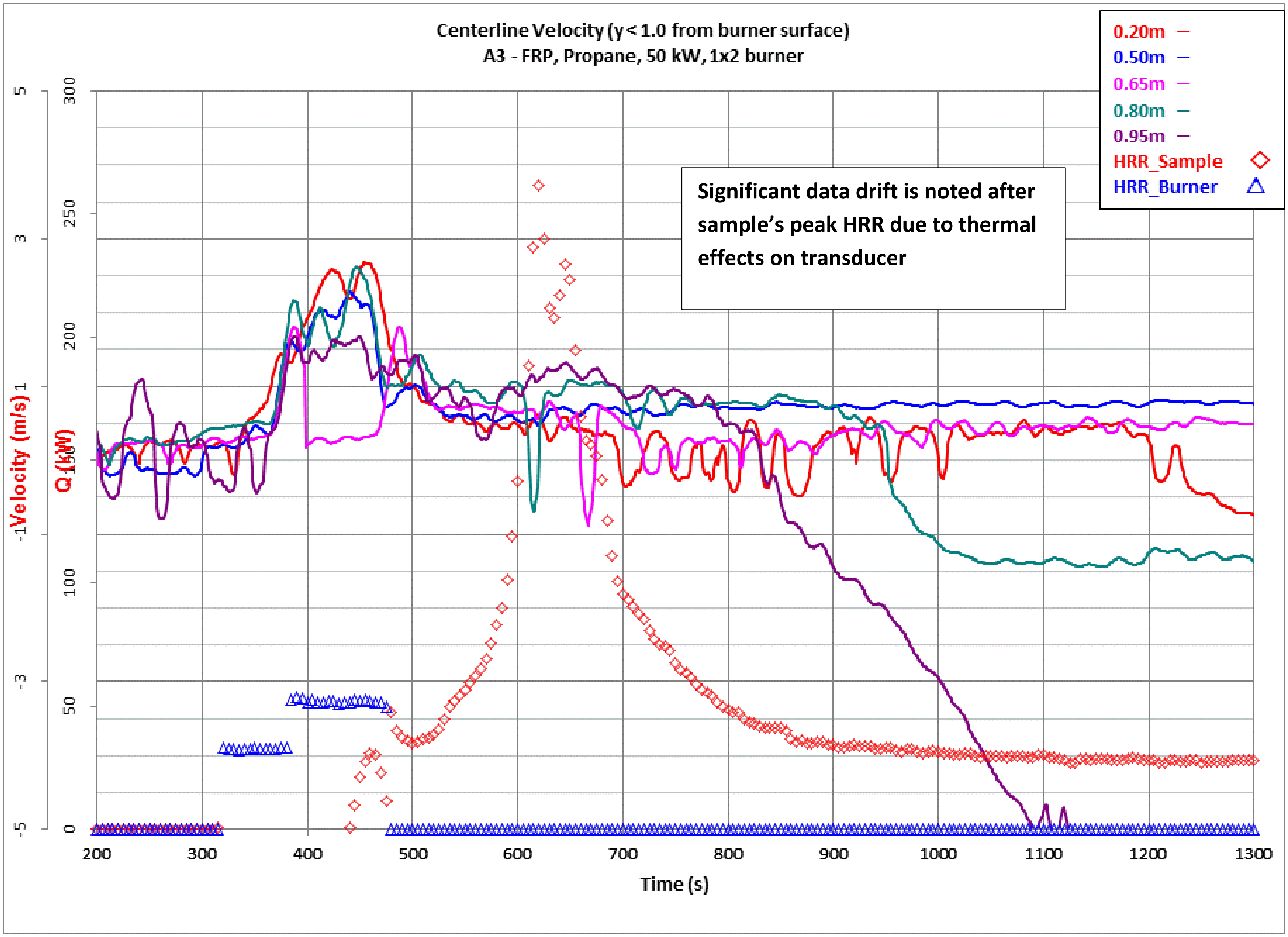

Centerline plume velocities measured from 0.2m to 0.95m above the burner surface

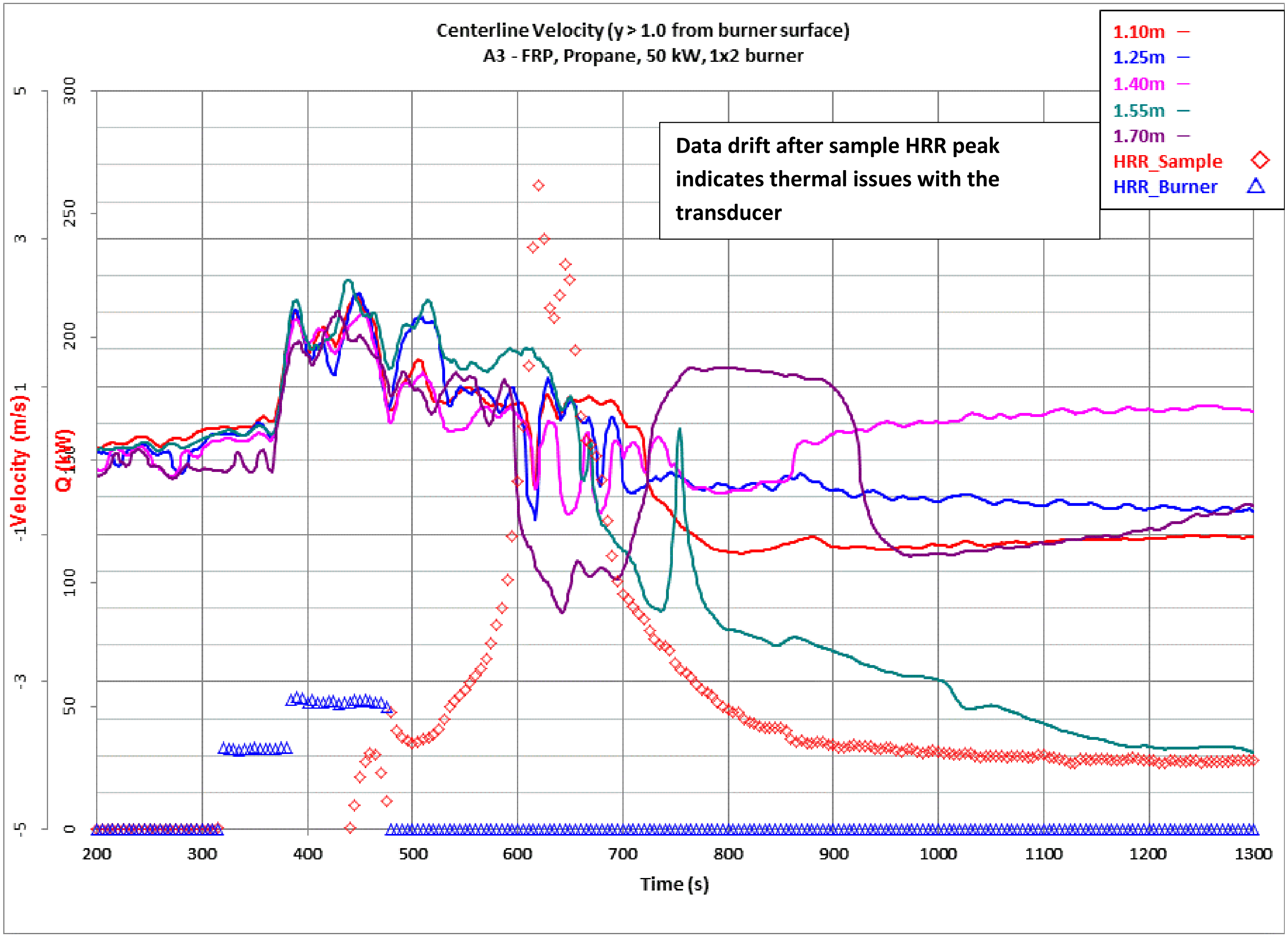

Centerline plume velocities measured from 1.1m to 1.7m above the burner surface

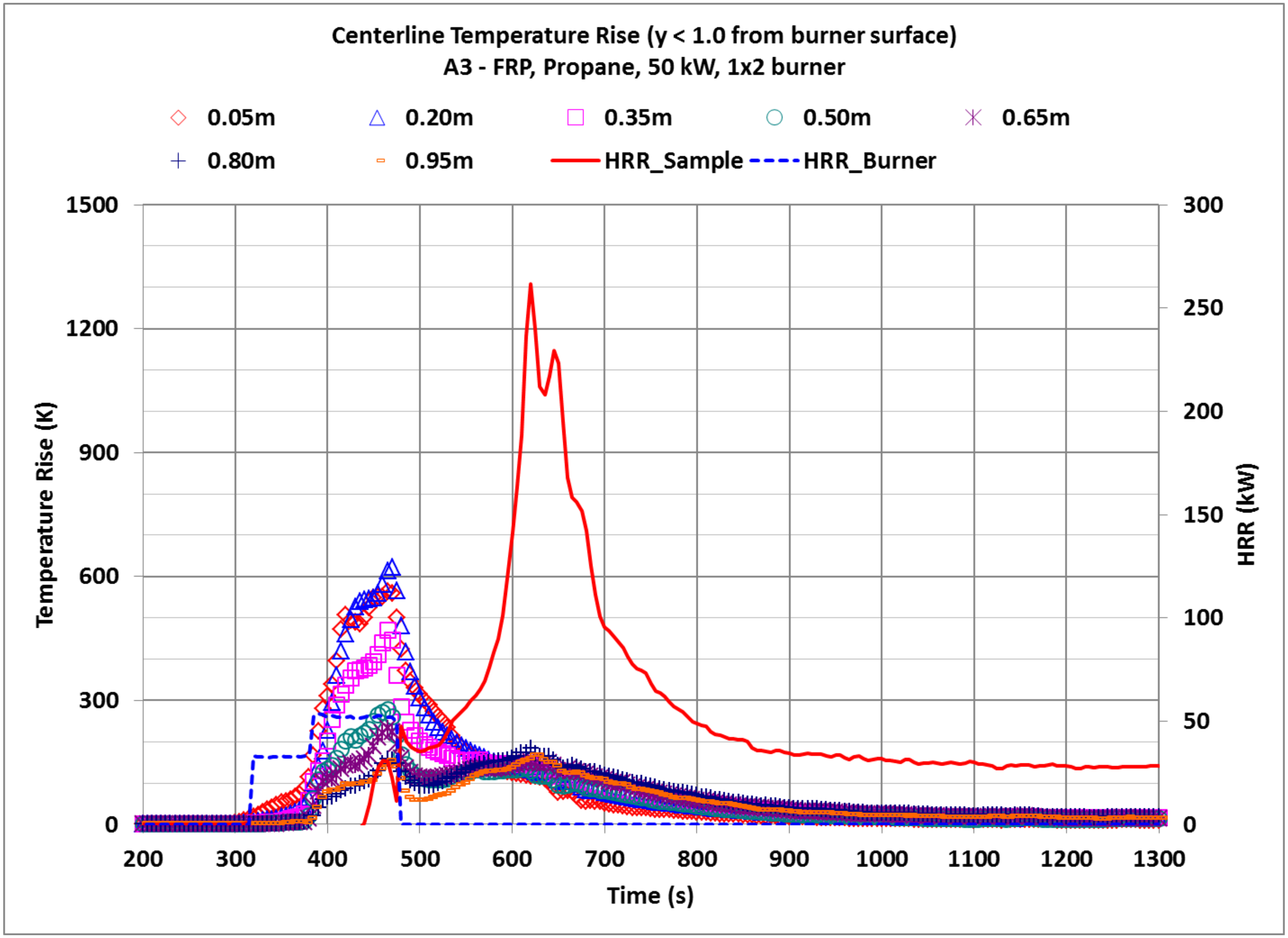

Centerline plume temperature rise measured from 0.05m to 0.95m above the burner surface

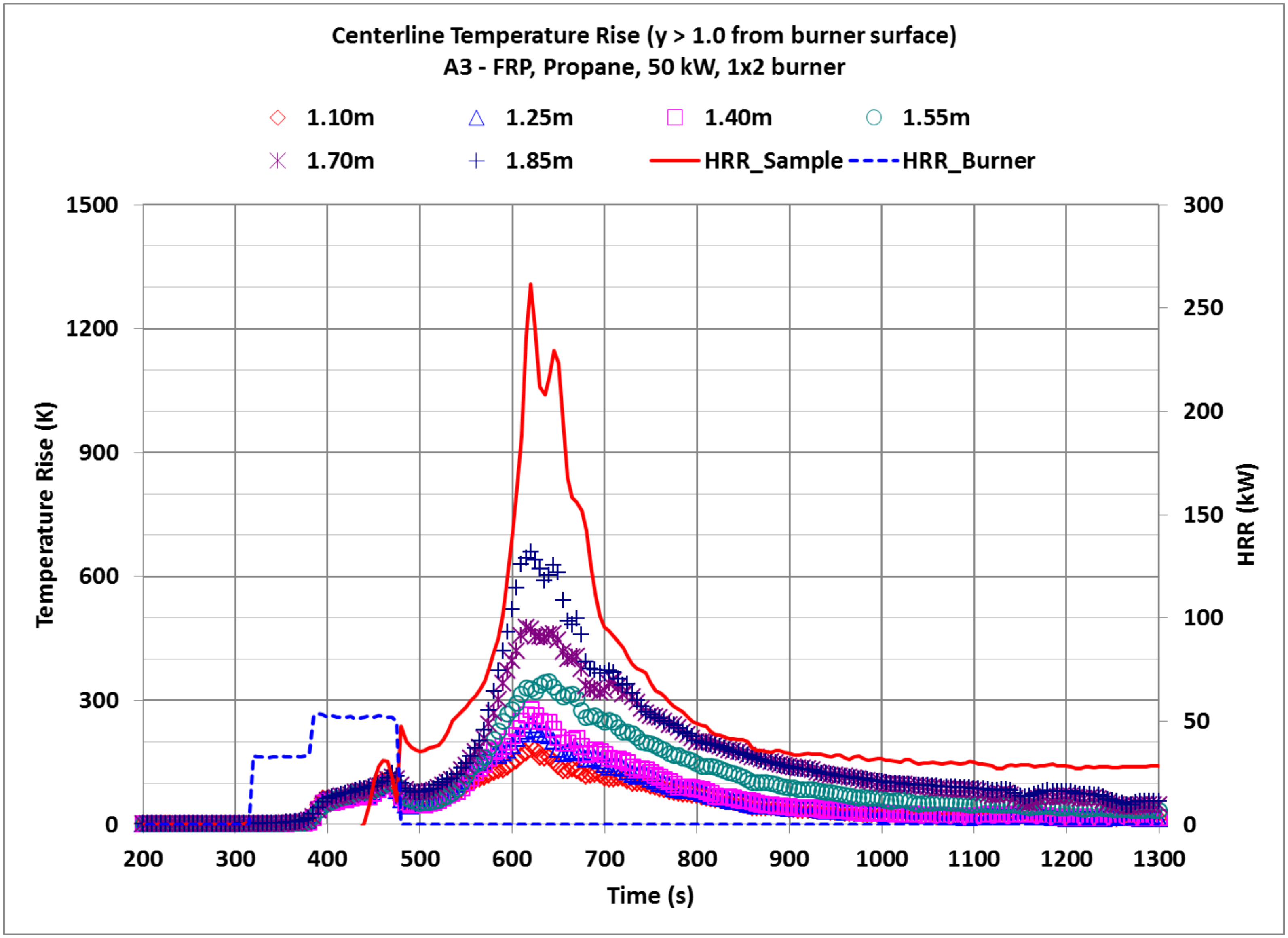

Centerline plume temperature rise measured from 1.10m to 1.85m above the burner surface

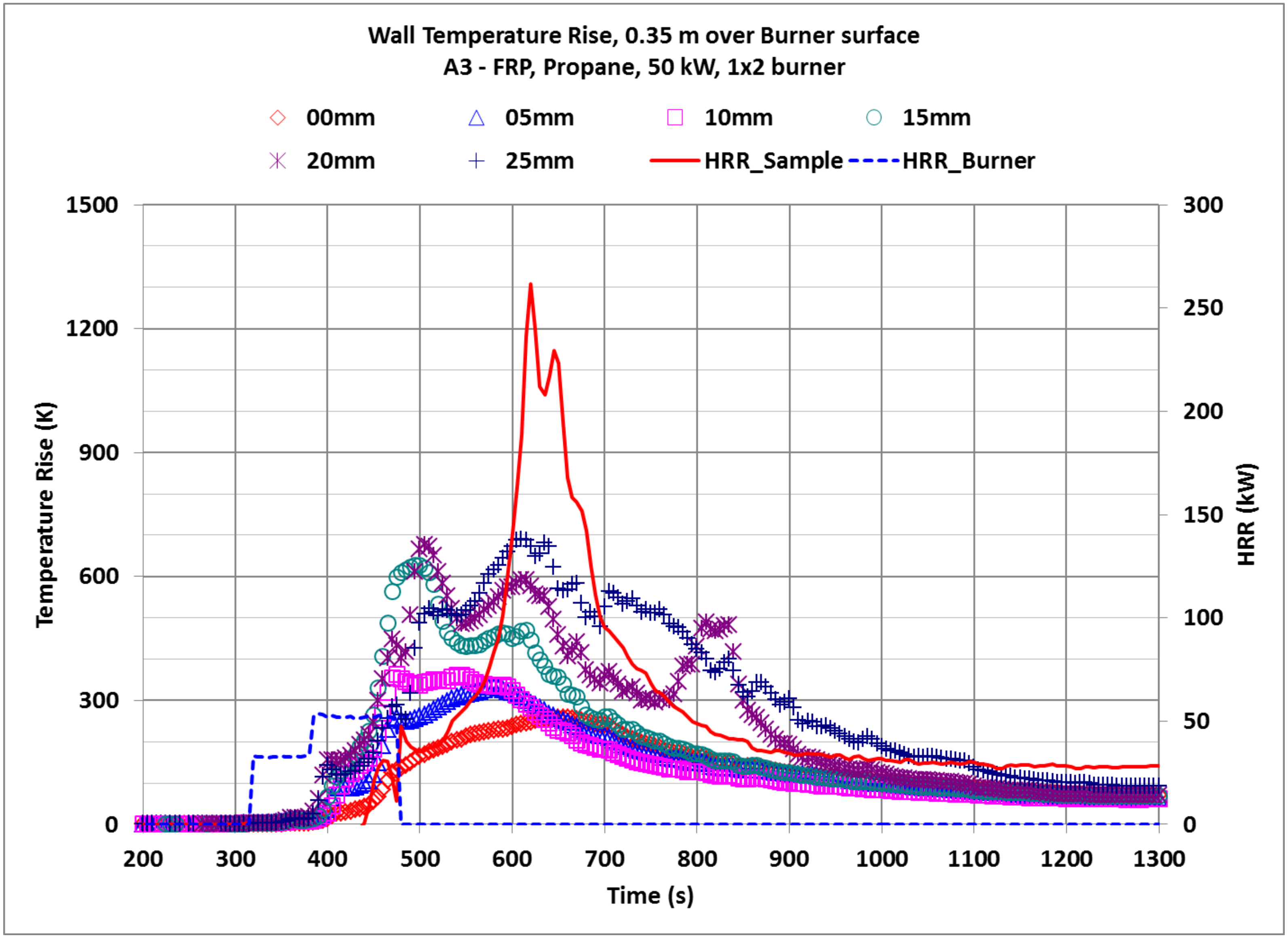

Temperature rise along the wall's centerline at 0.35m over the burner surface, measured at different perpendicular distances to as indicated

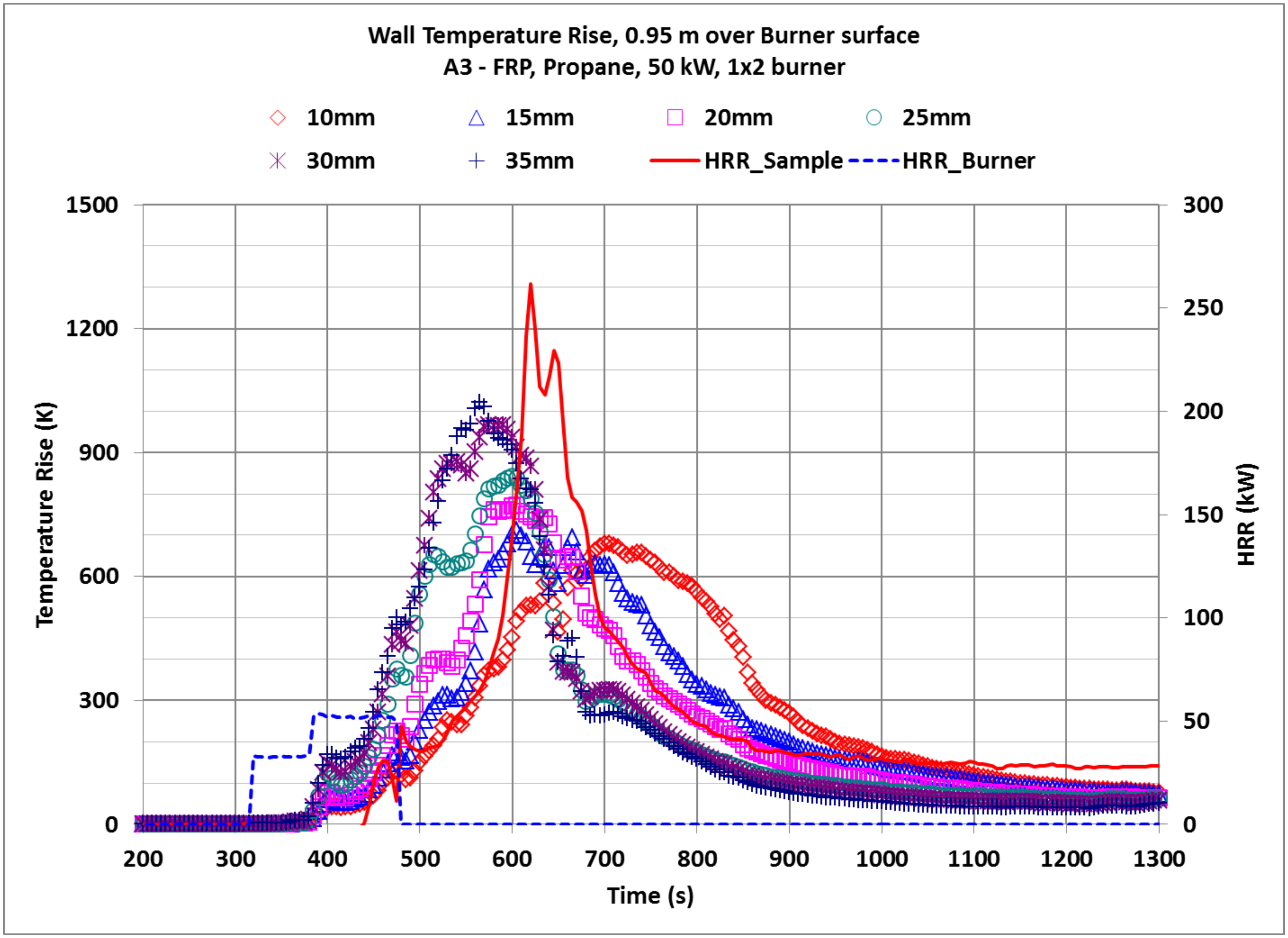

Temperature rise along the wall's centerline at 0.95m over the burner surface, measured at different perpendicular distances to as indicated

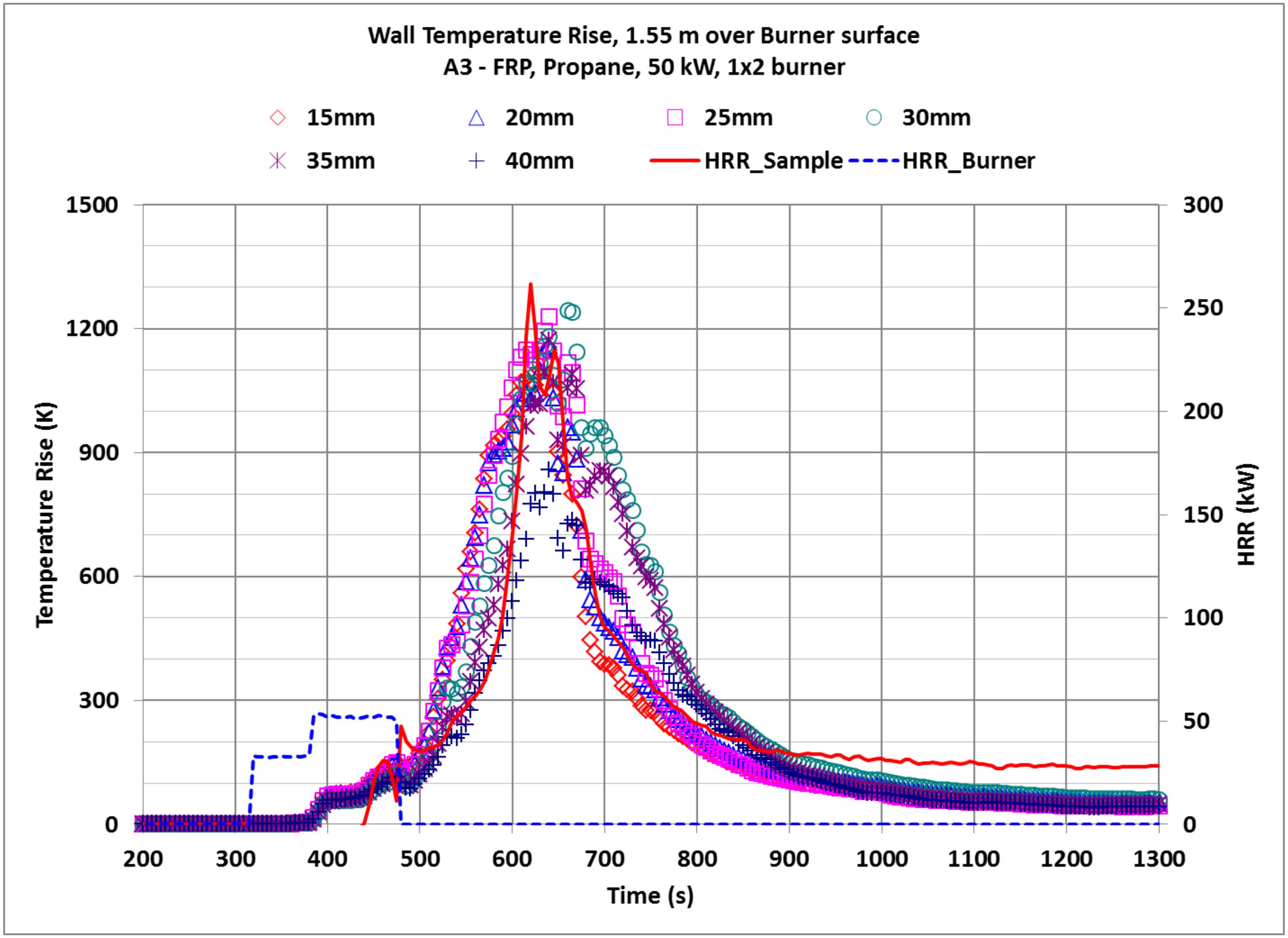

Temperature rise along the wall's centerline at 1.55m over the burner surface, measured at different perpendicular distances to as indicated

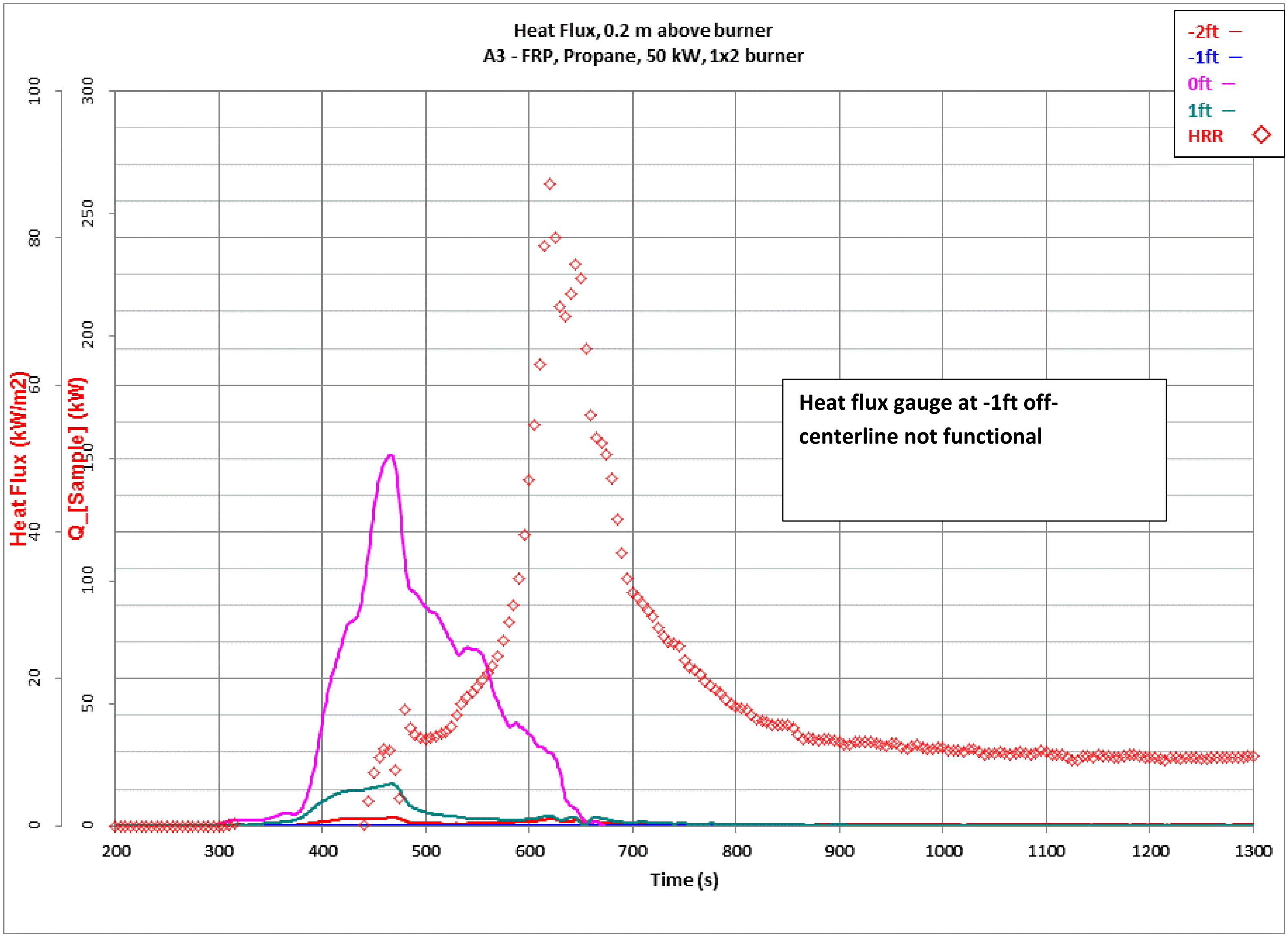

Heat flux measured at various distances from the centerline (negative indicates left of centerline), 0.2m vertically from burner surface

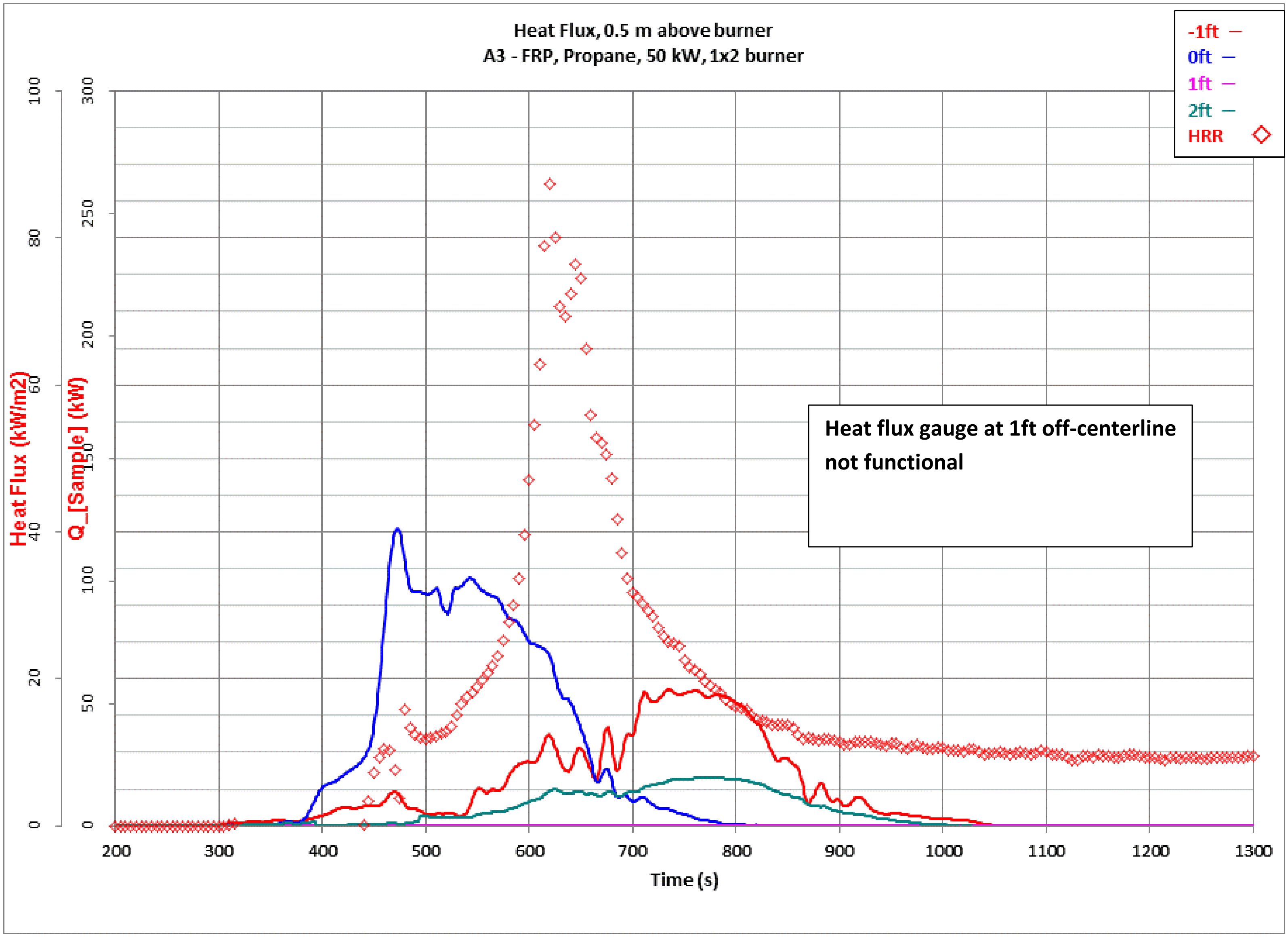

Heat flux measured at various distances from the centerline (negative indicates left of centerline), 0.5m vertically from burner surface

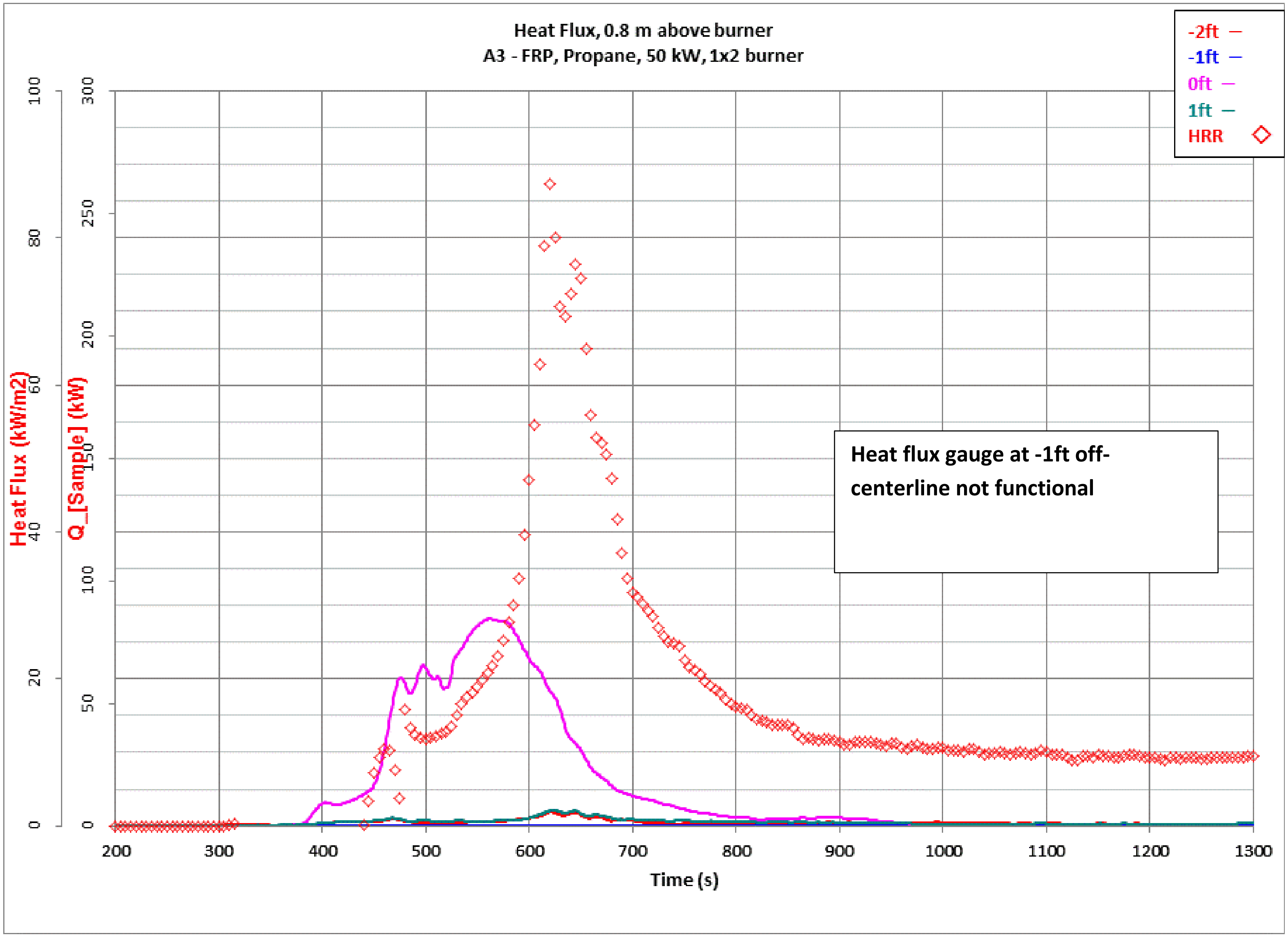

Heat flux measured at various distances from the centerline (negative indicates left of centerline), 0.8m vertically from burner surface

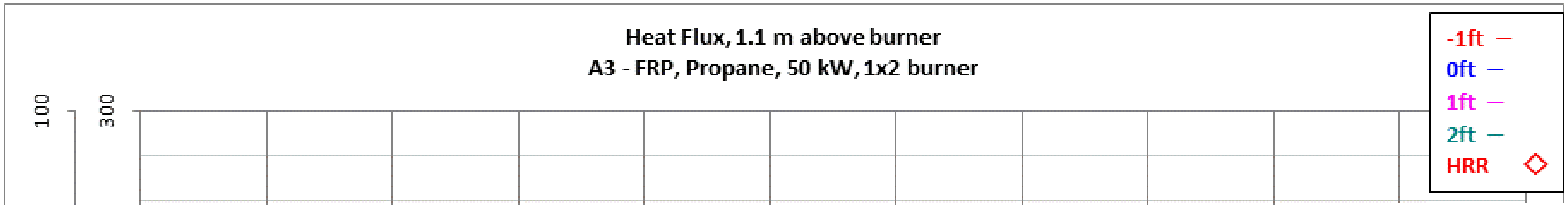

Heat flux gauge at 1ft off-centerline not functional

Heat flux measured at various distances from the centerline (negative indicates left of centerline), 1.1m vertically from burner surface

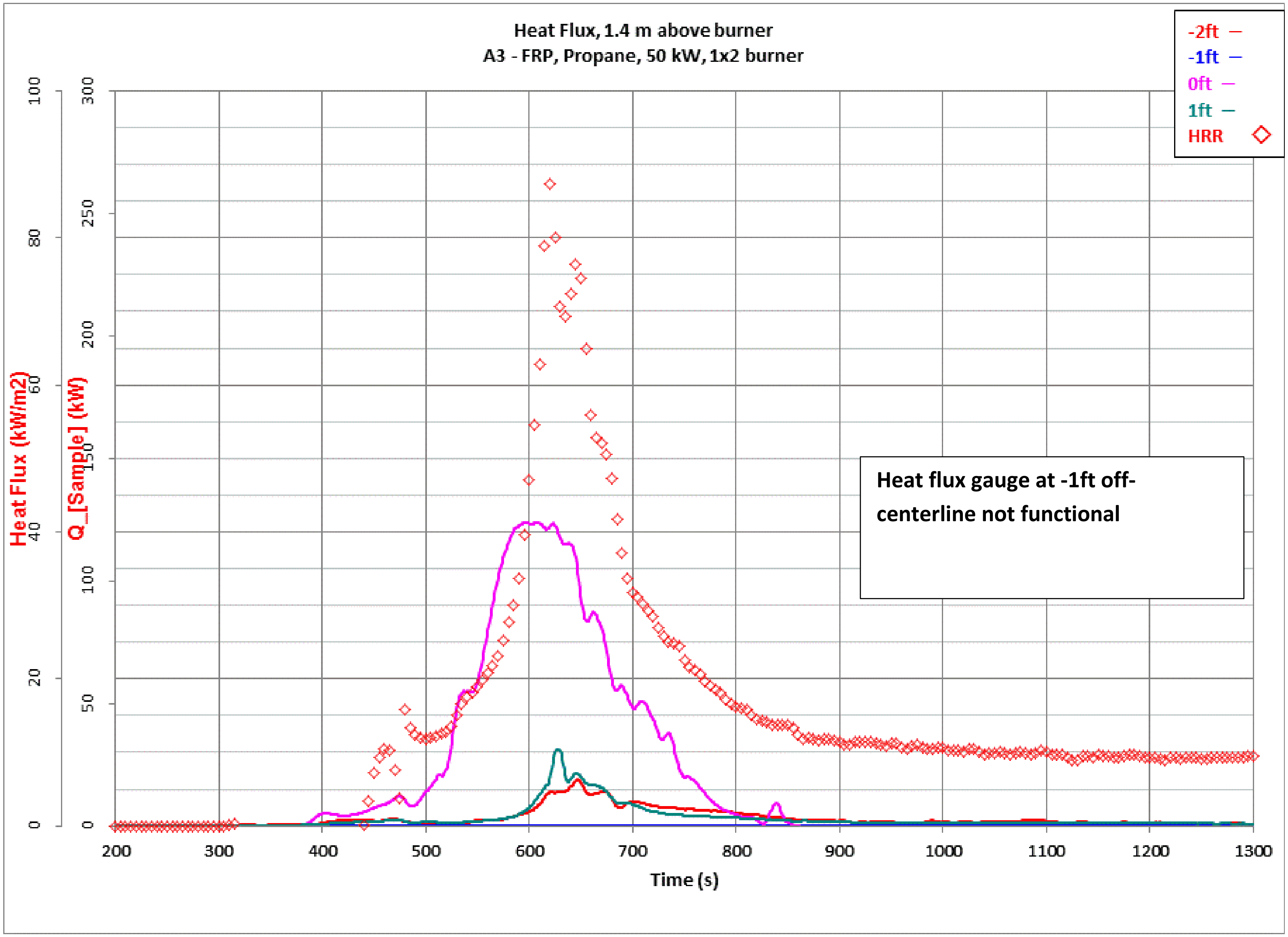

Heat flux measured at various distances from the centerline (negative indicates left of centerline), 1.4m vertically from burner surface

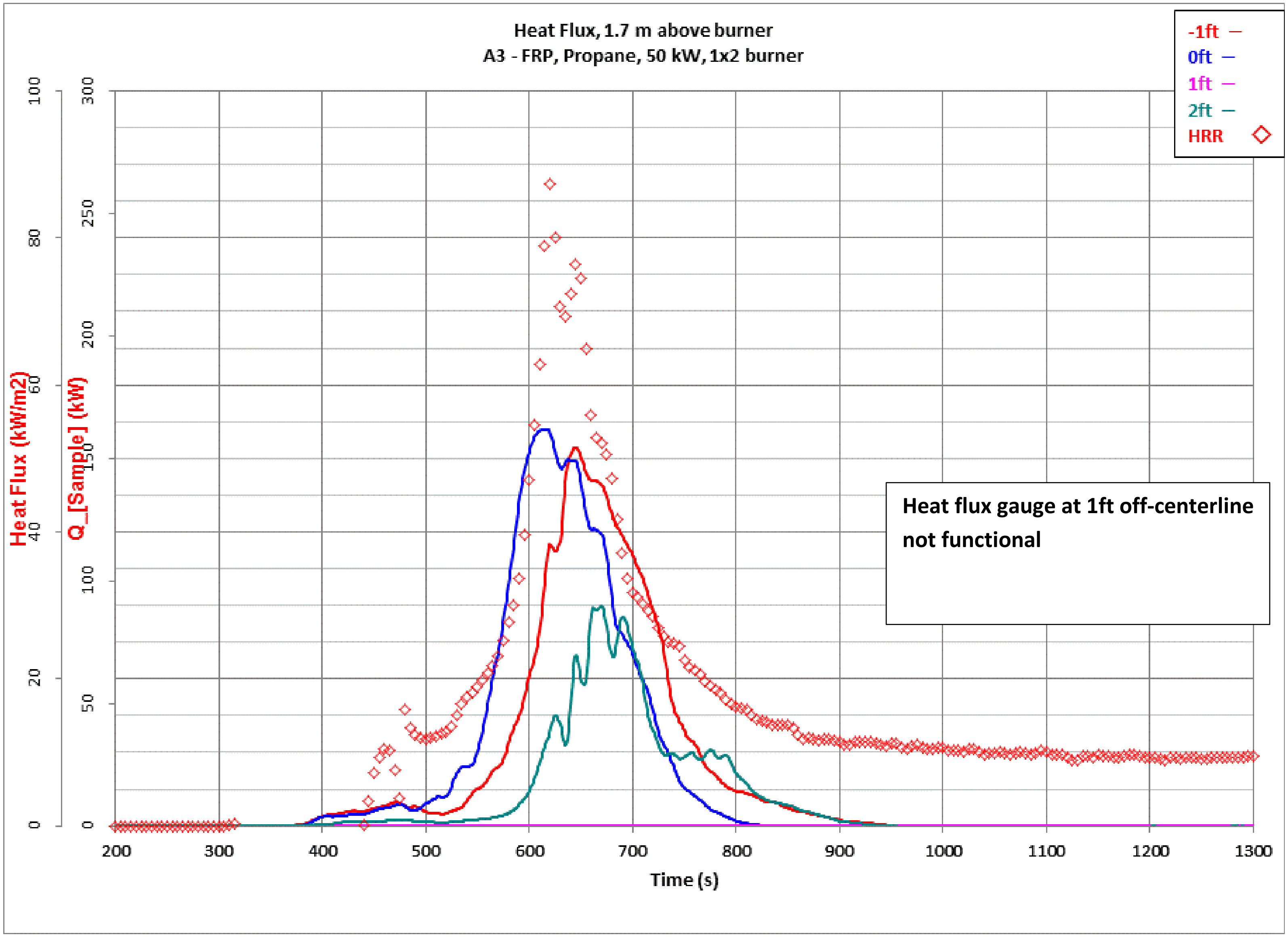

Heat flux measured at various distances from the centerline (negative indicates left of centerline), 1.7m vertically from burner surface

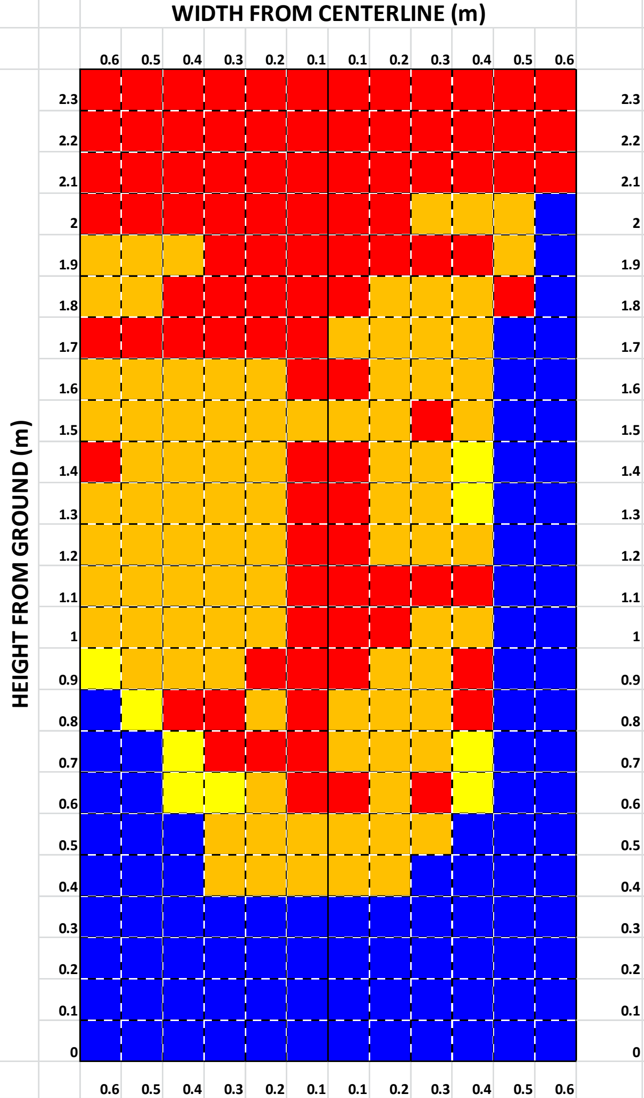

# of cell	Damage to Resin	Area (m2)
95	up to 100% damage	0.95
91	up to 75% damage	0.91
9	up to 50% damage	0.09
0	up to 25% damage	0
93	no damage	0.93

Initial mass:	8.73	kg
Final unburnt mass:	3.38	kg
Final burnt mass:	3.26	kg
Total mass loss during fire	2.09	kg

Burn damage pattern observed after fire test

F.3.4 Test A4

LODS Test Run Data

Center for Firesafety Studies

100 Institute Road
Worcester, MA 01609
Phone: (508) 831-5628
Fax: (508) 831-5680

Test Information

Test Number:	A4
Specimen Identification:	FRP 4, 75 kW initial Propane fire, 1 x 2 burner
Material Name:	Class C FRP panel
Manufacturer/Submitter:	Not Reported
Raw Data File Name:	Test A4 - FRP_75kW_Propane_2ft.txt
Reduced Data File Name:	Test A4 - FRP_75kW_Propane_2ft_reduced.xlsx
Date of Test:	3-Nov-2010
Tester:	W. Wong

Test Parameters

Ambient Temperature:	N/A
Relative Humidity:	N/A

Specimen Information

Specimen Initial Mass:	[kg]	8.7
Specimen Final Mass:	[kg]	6.4
Mass Lost:	[kg]	2.3
Heat Evolved (net):	[kJ]	0

Parameter	Unit	Value
Mass Loss		
Initial Mass	[kg]	8.7
Final Mass	[kg]	6.4
Mass Loss	[%]	25.98

LODS Test Run Data

WPI Center for Firesafety Studies

100 Institute Road
Worcester, MA 01609
Phone: (508) 831-5628
Fax: (508) 831-5680

Test Notes

Test Number:	0
Date:	11/03/10
Material:	Class C FRP panel
Specimen Identification:	FRP 4, 75 kW initial Propane fire, 1 x 2 burner

Observations

Time	Observation
00:00	Start VI
11:00	Start Camera 1
11:05	Start Camera 2
16:00	Burner ignition
16:15	Reach target HRR @ 75 kW
17:05	Crackling noise
16:41	Panel ignition
18:00	Burner off
18:00	Flame hit ceiling
	T pattern soon after flame hit ceiling
18:45	Rollover under ceiling
19:00	Some burning of sidewalls
20:30	line fires only
22:00	Remote area burning @ TSC-9, HFC-2, HFC-4, insignificant
25:20	Remote area burning @ HFG-1, near line fire
28:40	Remote area burning @ TSC-4, HFG-5, both near line fires
33:30	Remote area burning @ TSC-12, insignificant
51:35	Terminate test by little water application

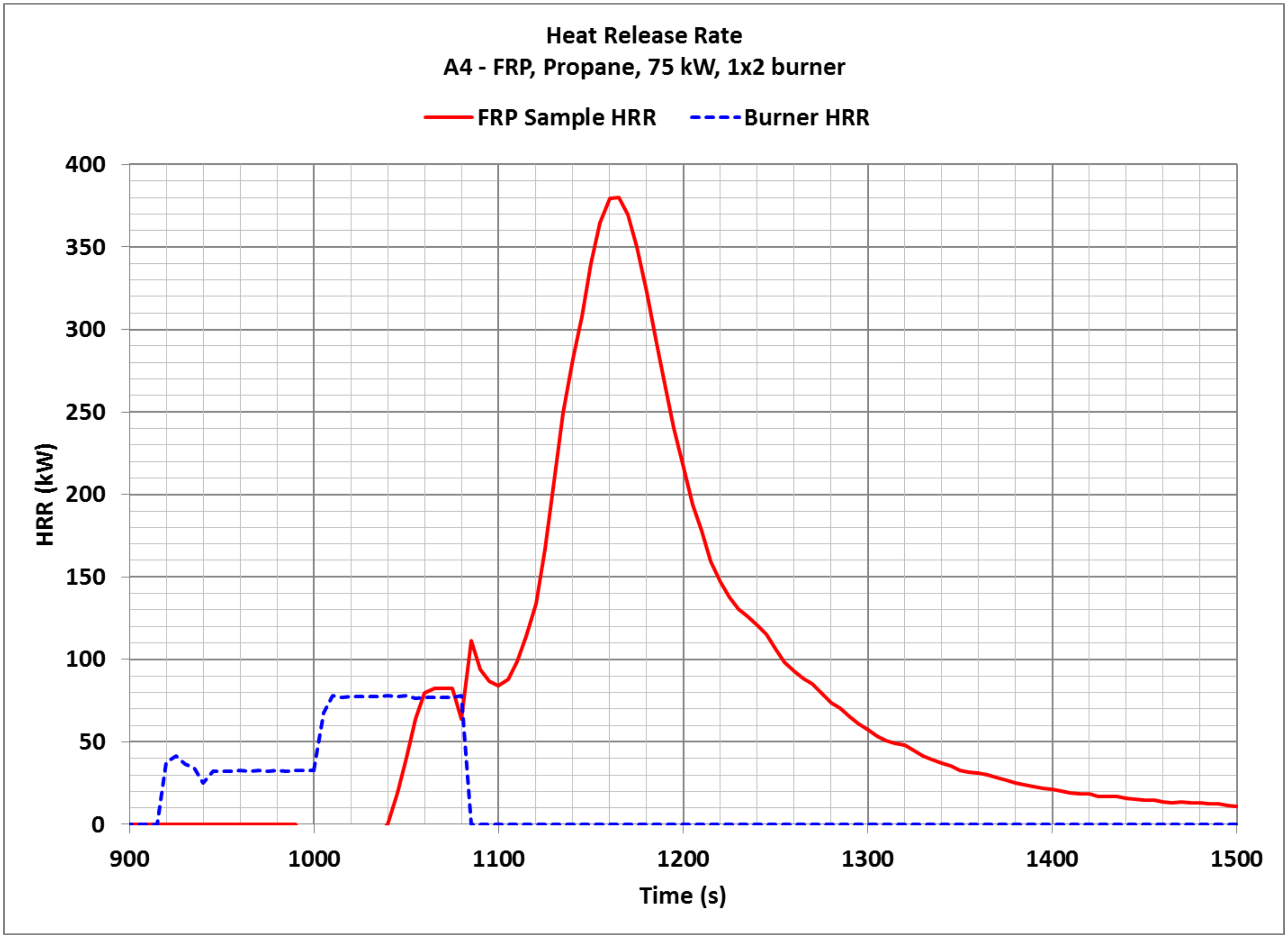

Heat release ratesof the source burner fire and of the specimen fire measured during test

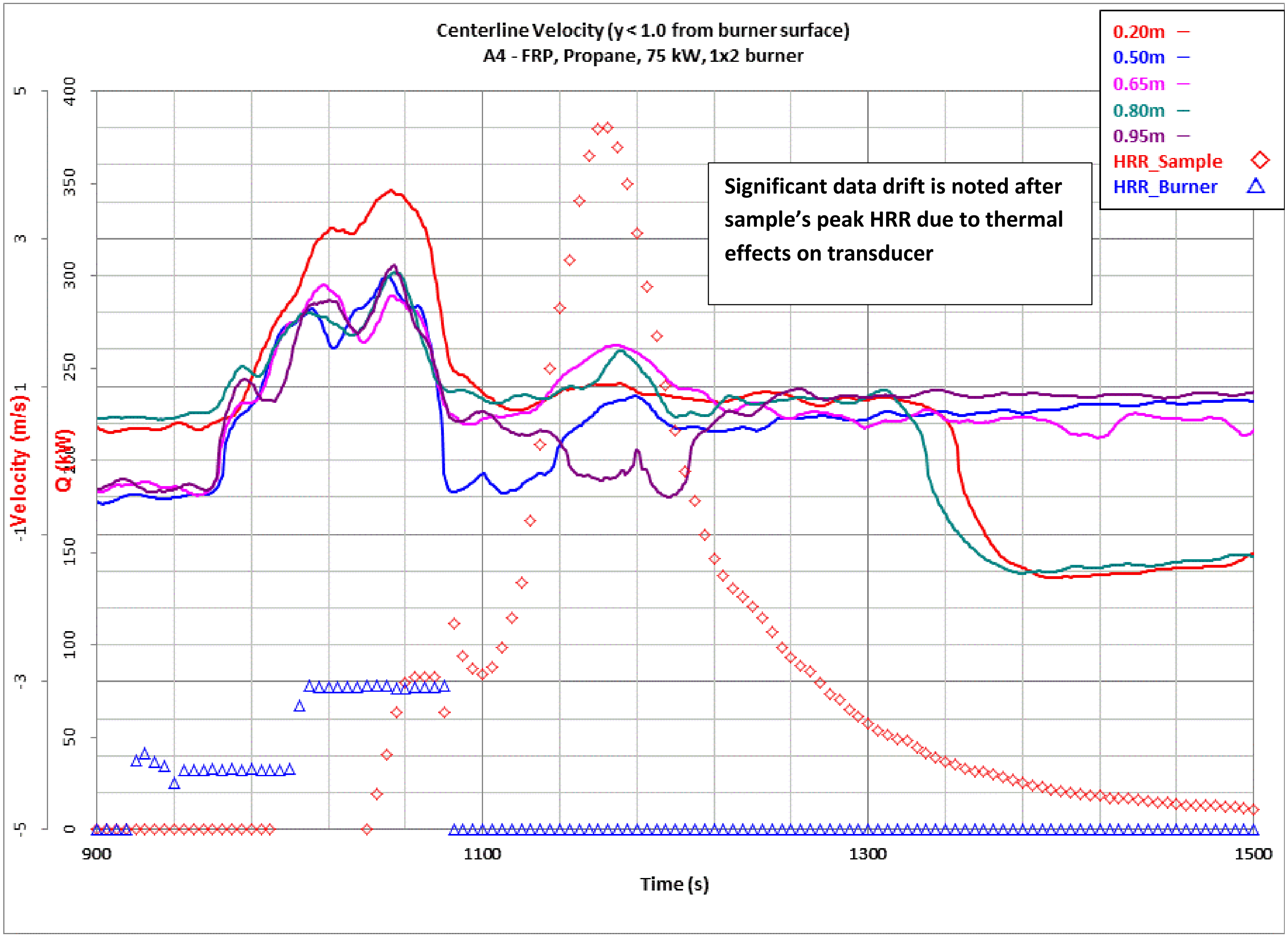

Centerline plume velocities measured from 0.2m to 0.95m above the burner surface

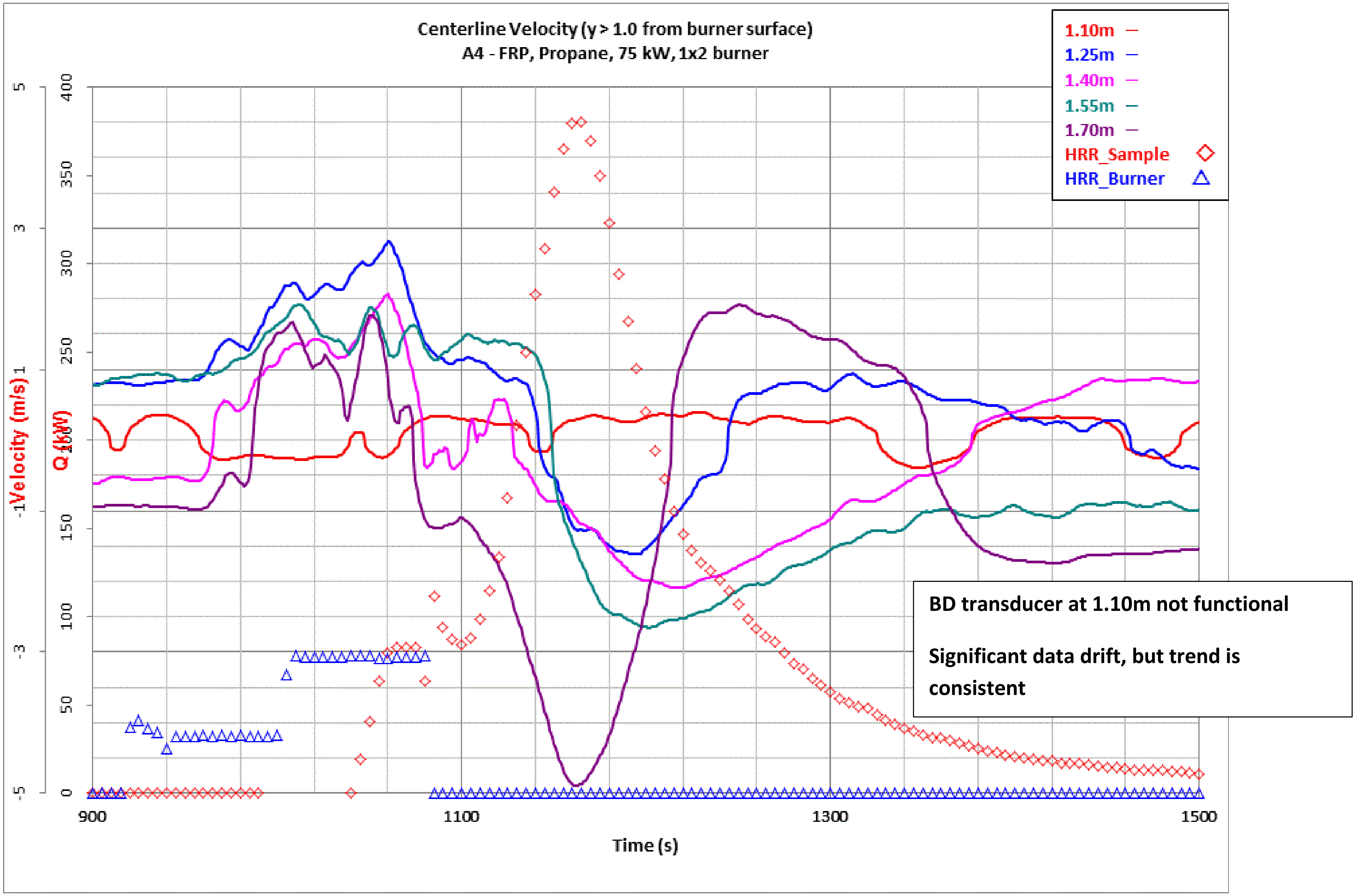

Centerline plume velocities measured from 1.1m to 1.7m above the burner surface

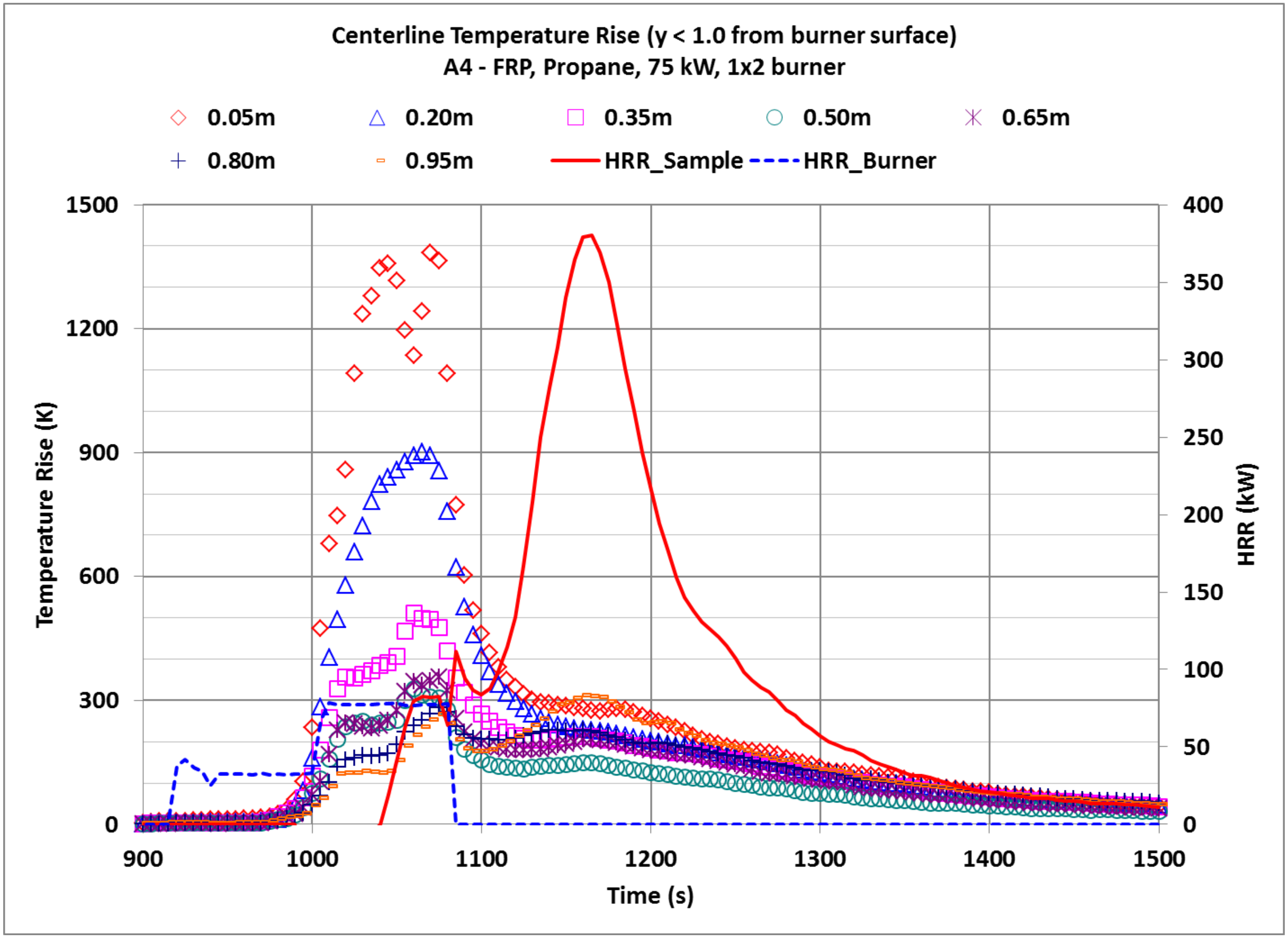

Centerline plume temperature rise measured from 0.05m to 0.95m above the burner surface

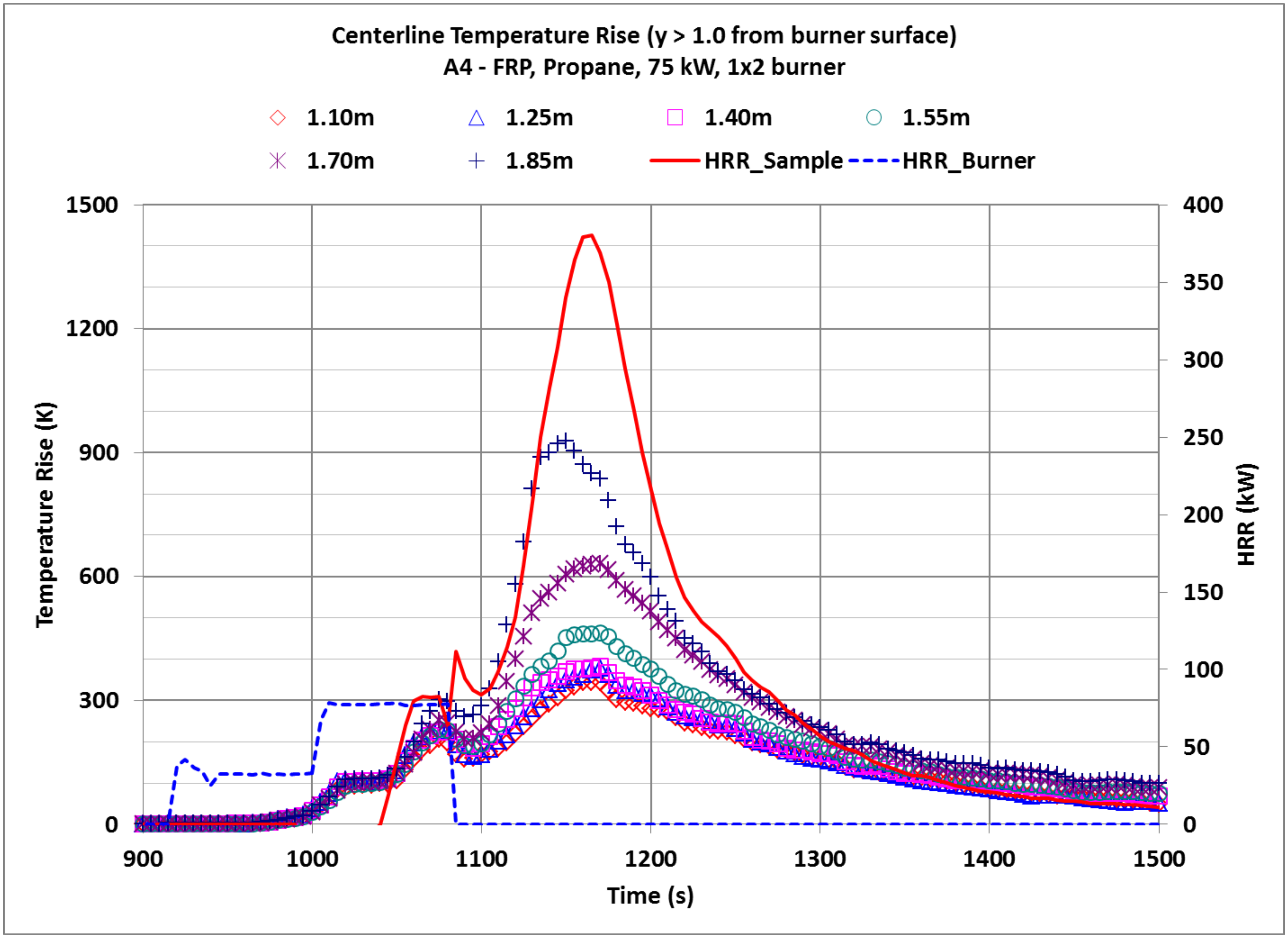

Centerline plume temperature rise measured from 1.10m to 1.85m above the burner surface

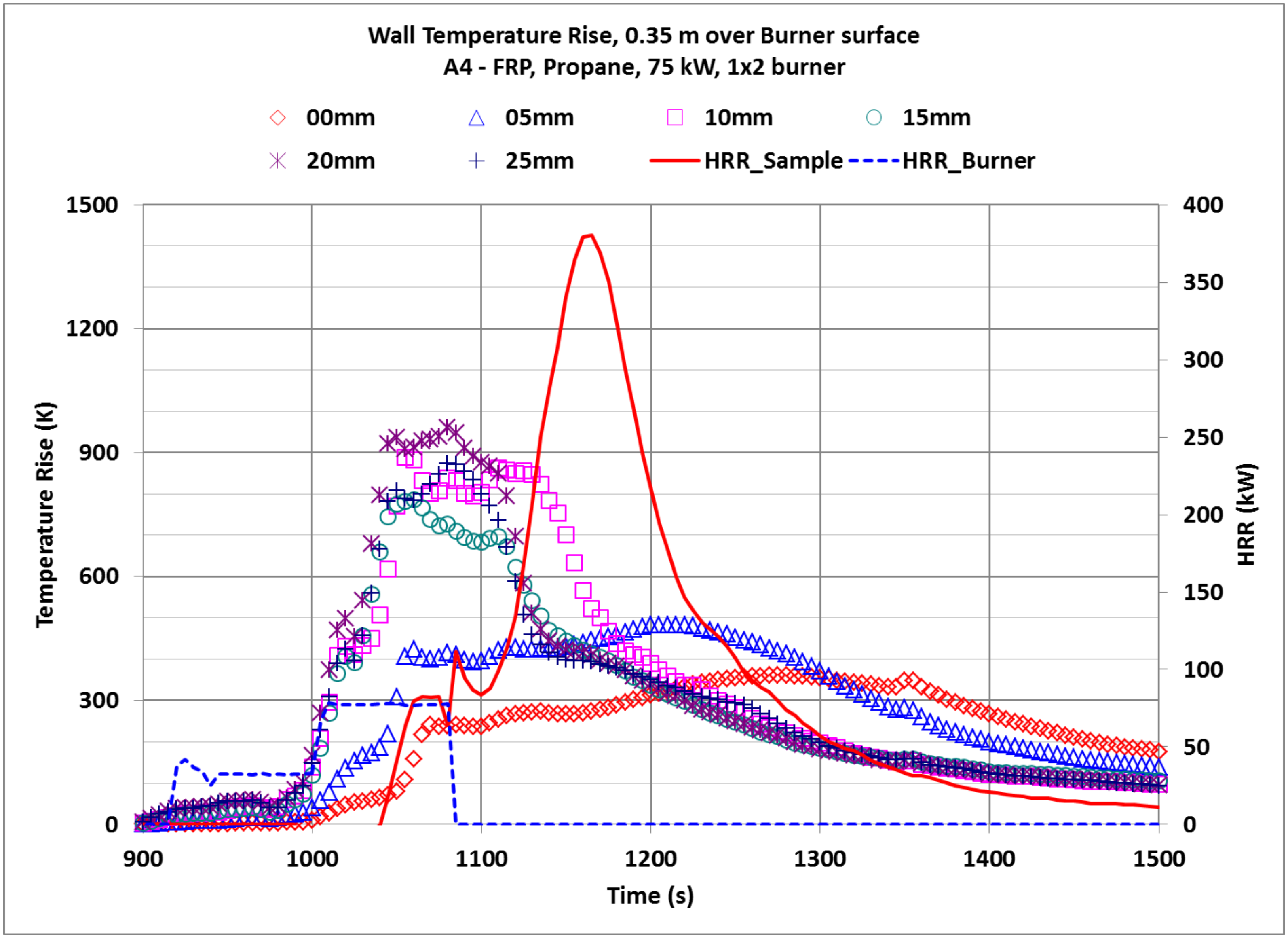

Temperature rise along the wall's centerline at 0.35m over the burner surface, measured at different perpendicular distances to as indicated

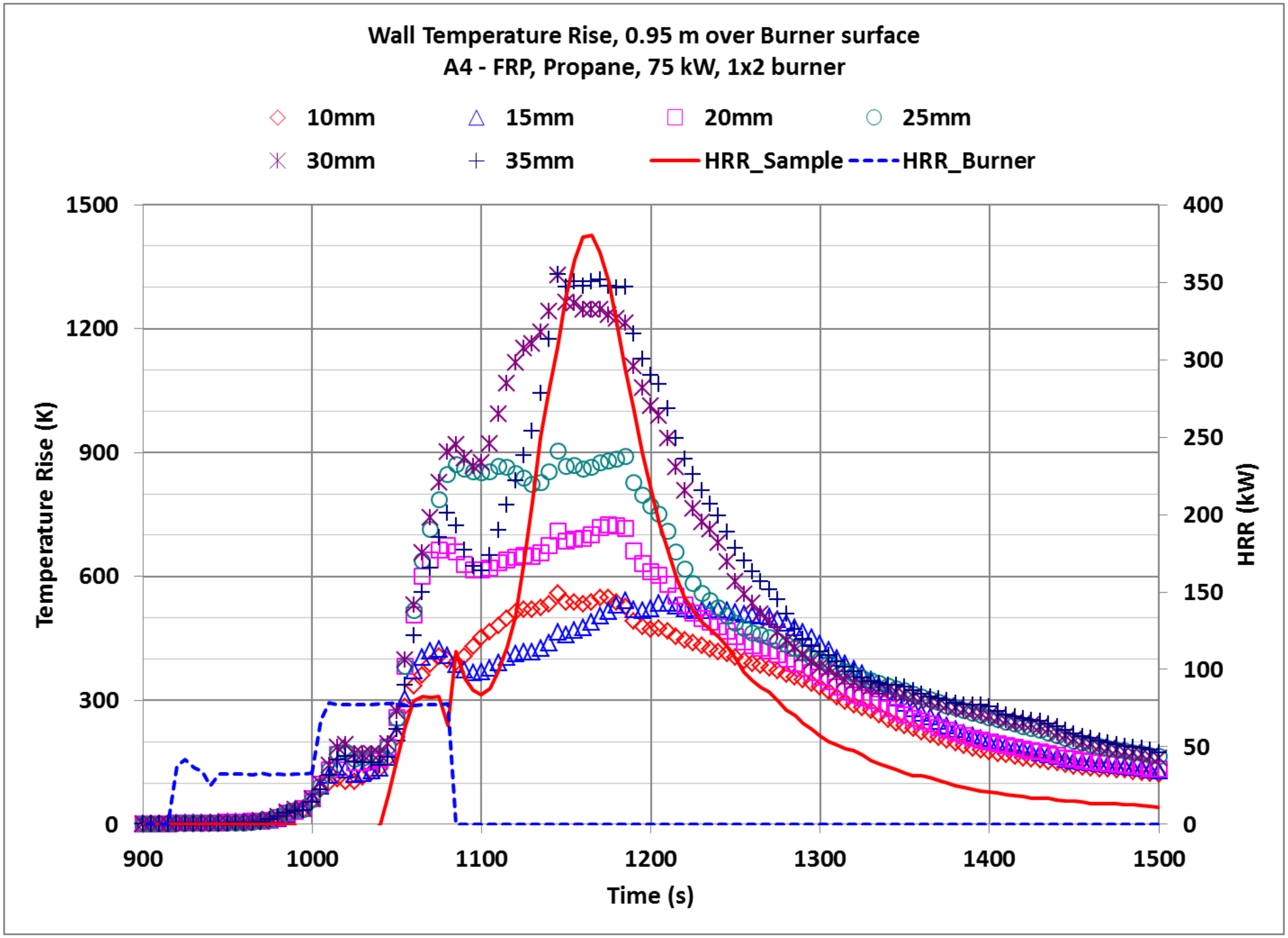

Temperature rise along the wall's centerline at 0.95m over the burner surface, measured at different perpendicular distances to as indicated

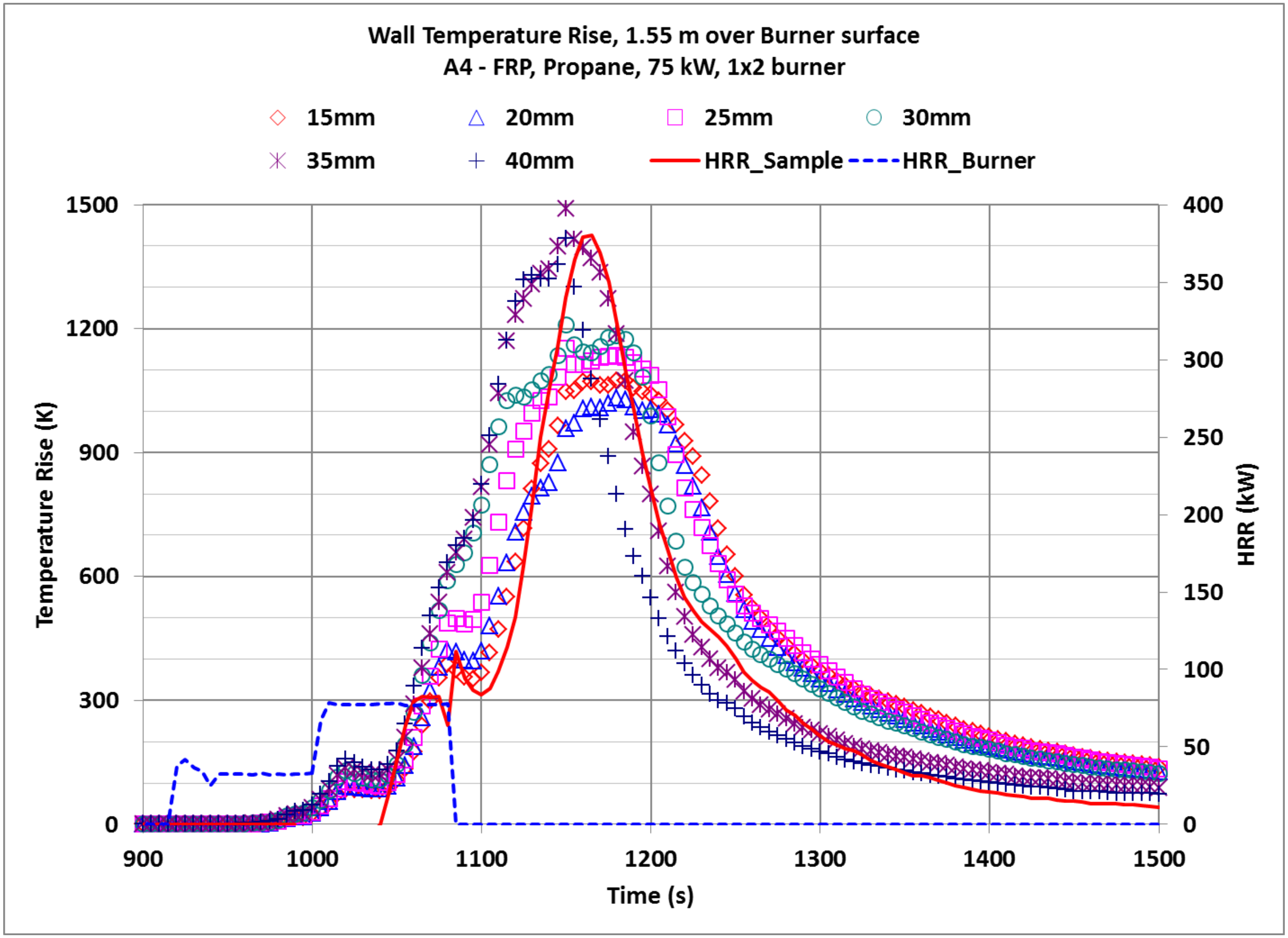

Temperature rise along the wall's centerline at 1.55m over the burner surface, measured at different perpendicular distances to as indicated

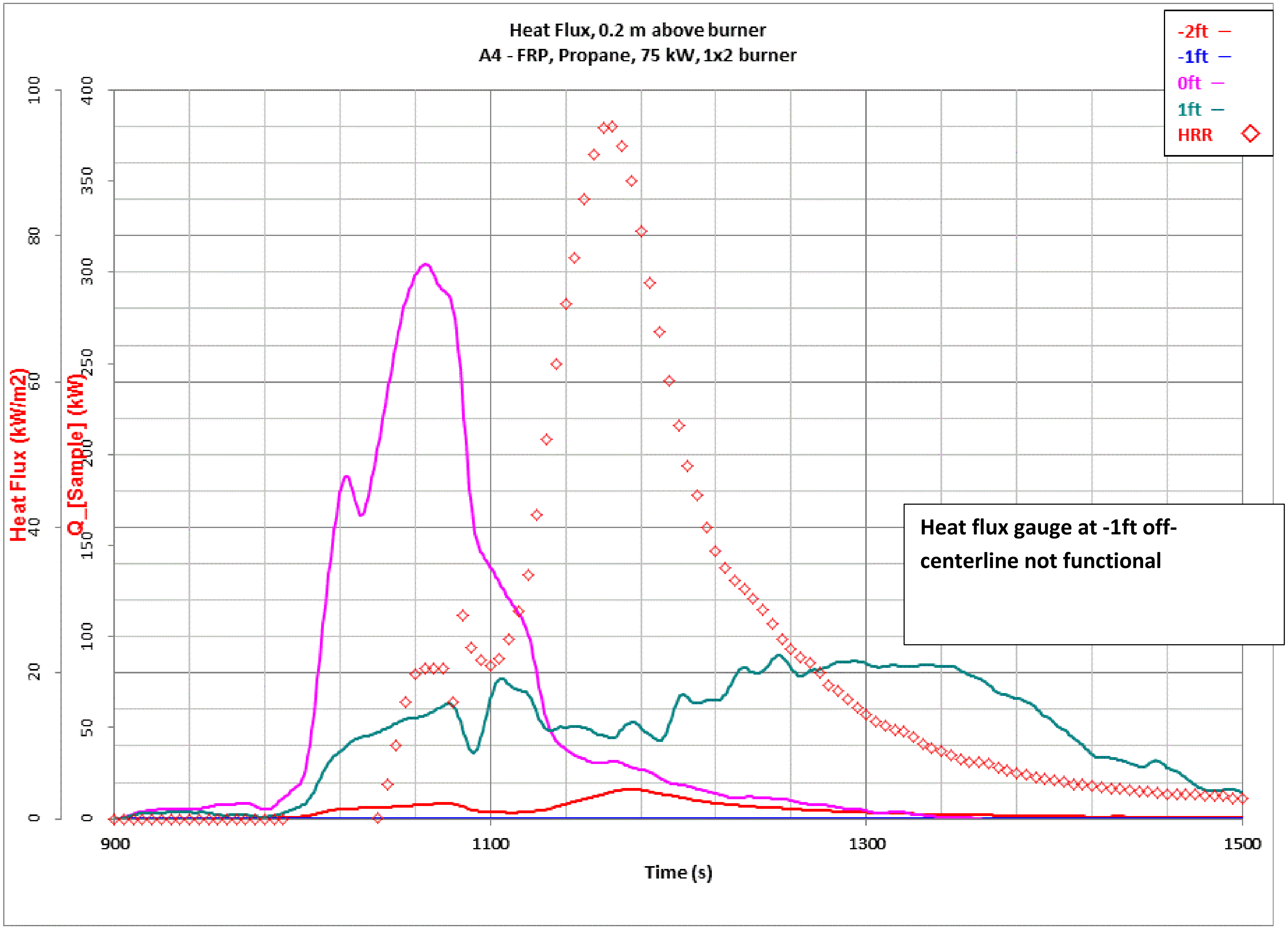

Heat flux measured at various distances from the centerline (negative indicates left of centerline), 0.2m vertically from burner surface

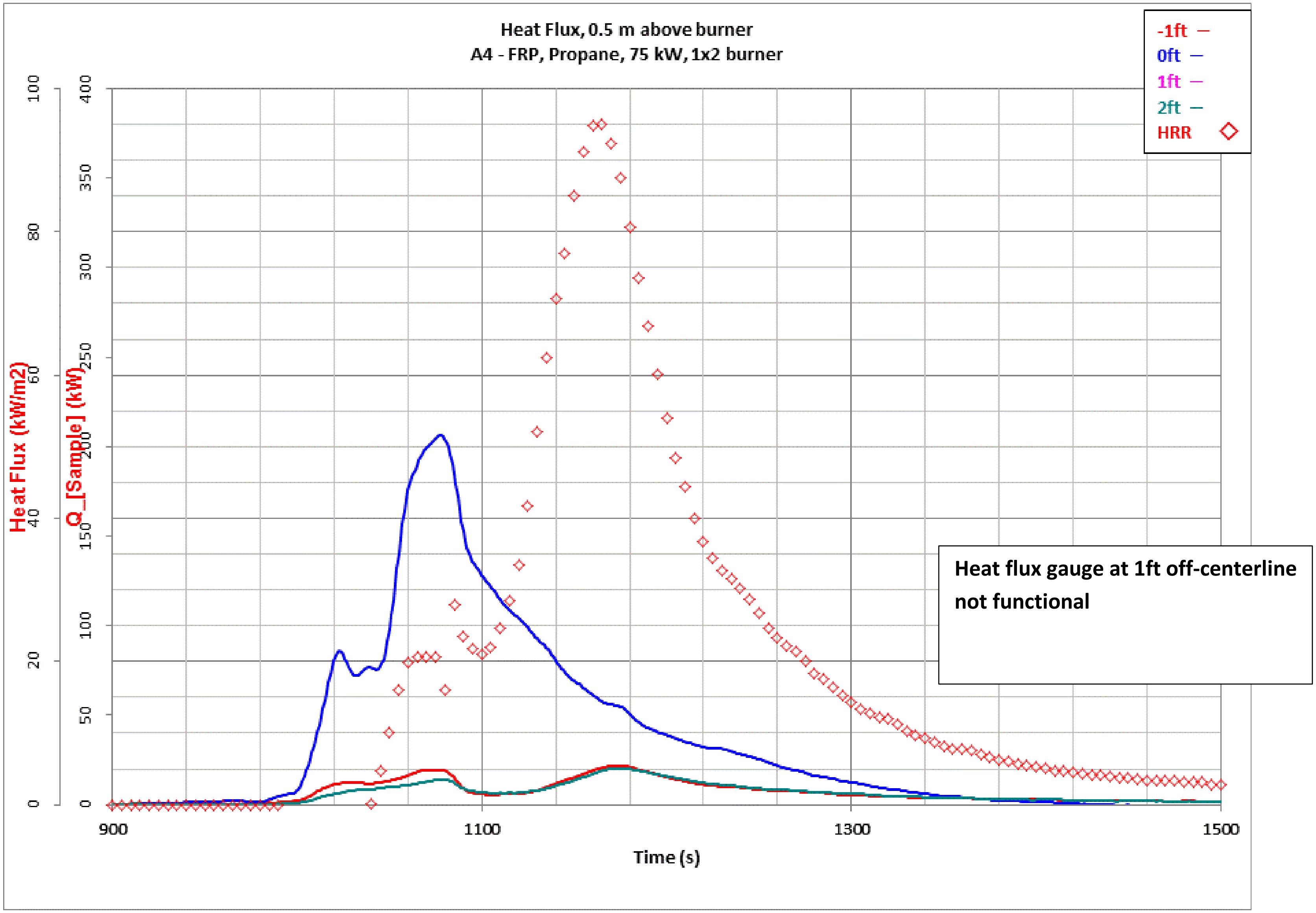

Heat flux measured at various distances from the centerline (negative indicates left of centerline), 0.5m vertically from burner surface

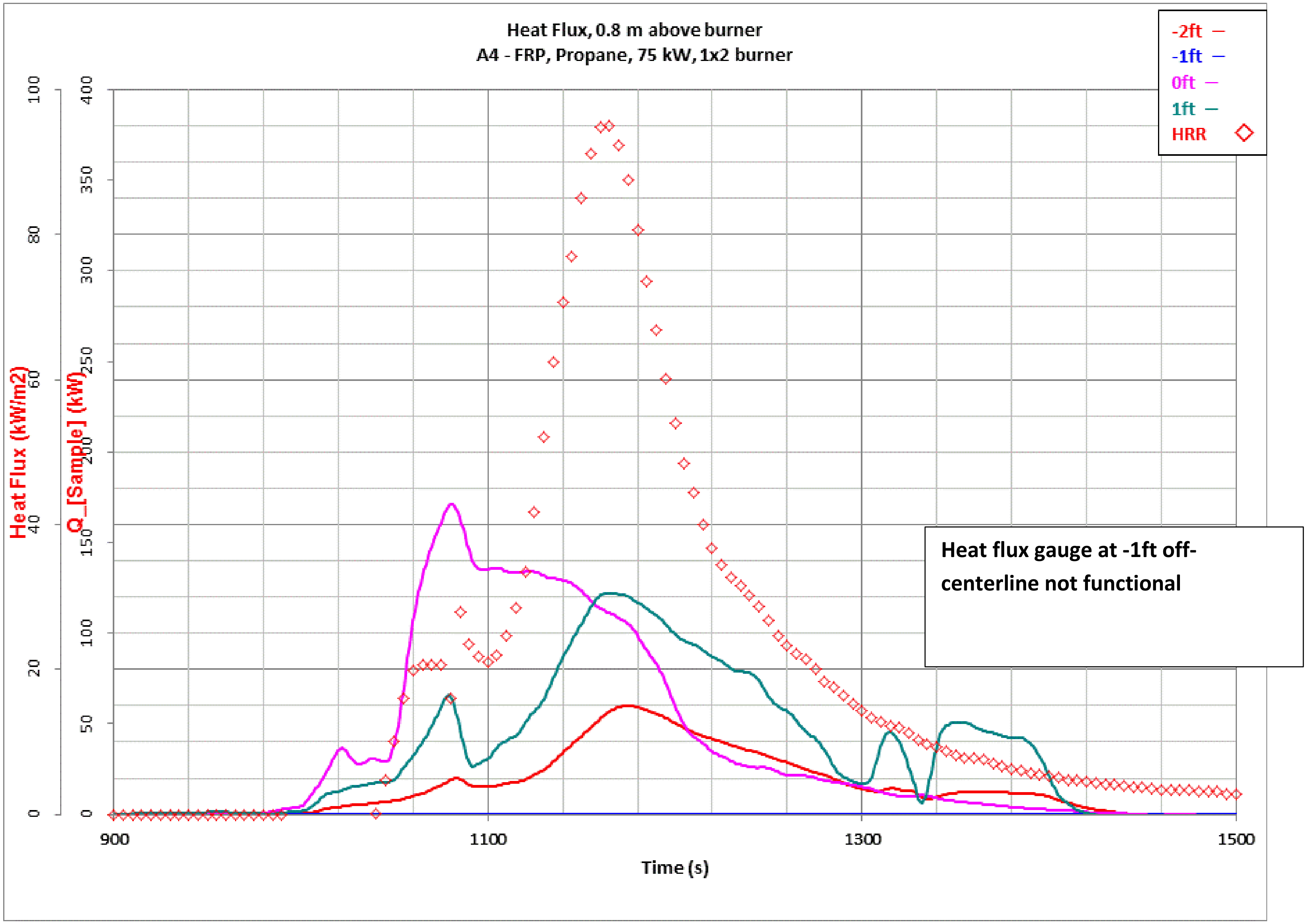

Heat flux measured at various distances from the centerline (negative indicates left of centerline), 0.8m vertically from burner surface

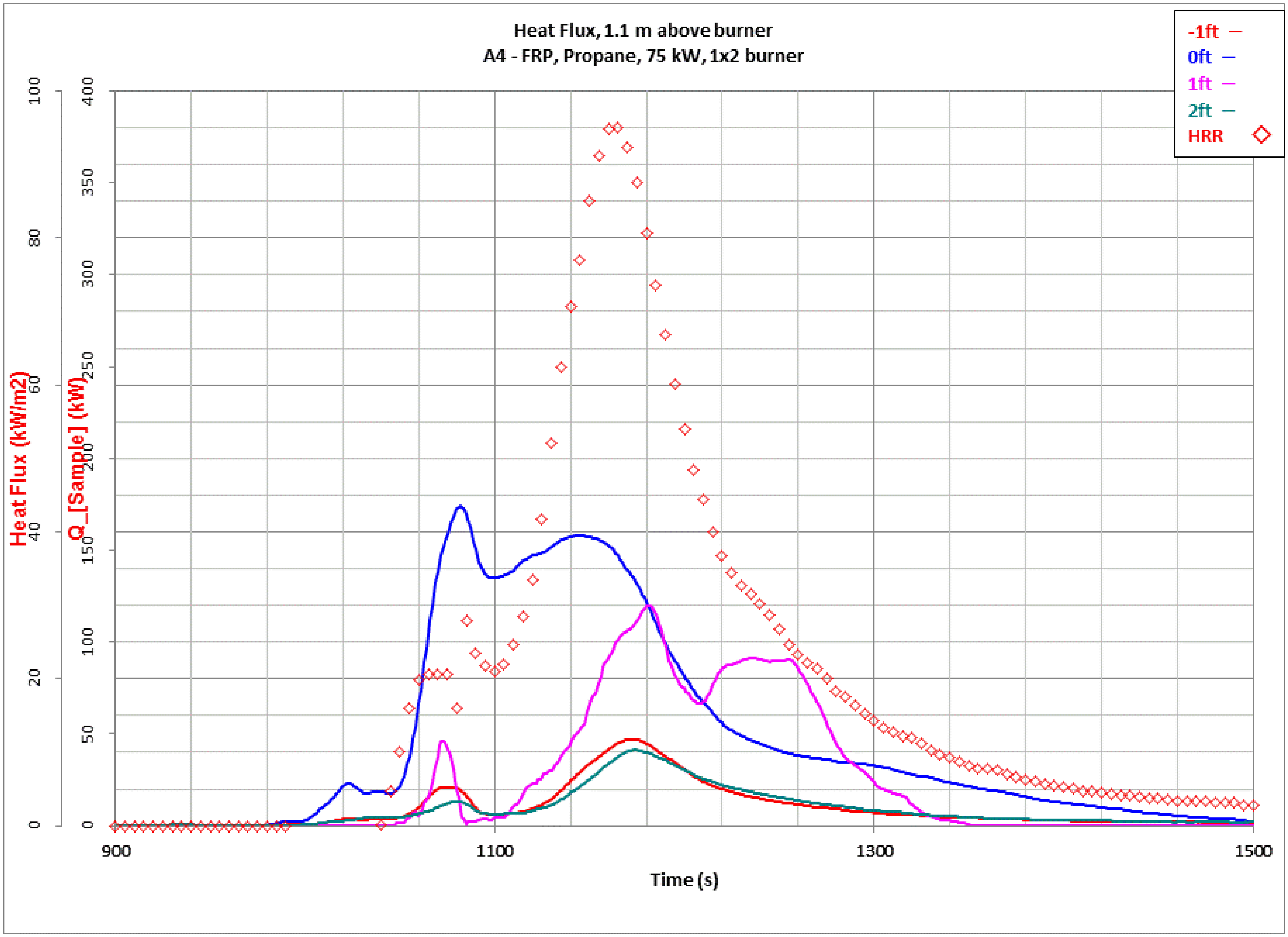

Heat flux measured at various distances from the centerline (negative indicates left of centerline), 1.1m vertically from burner surface

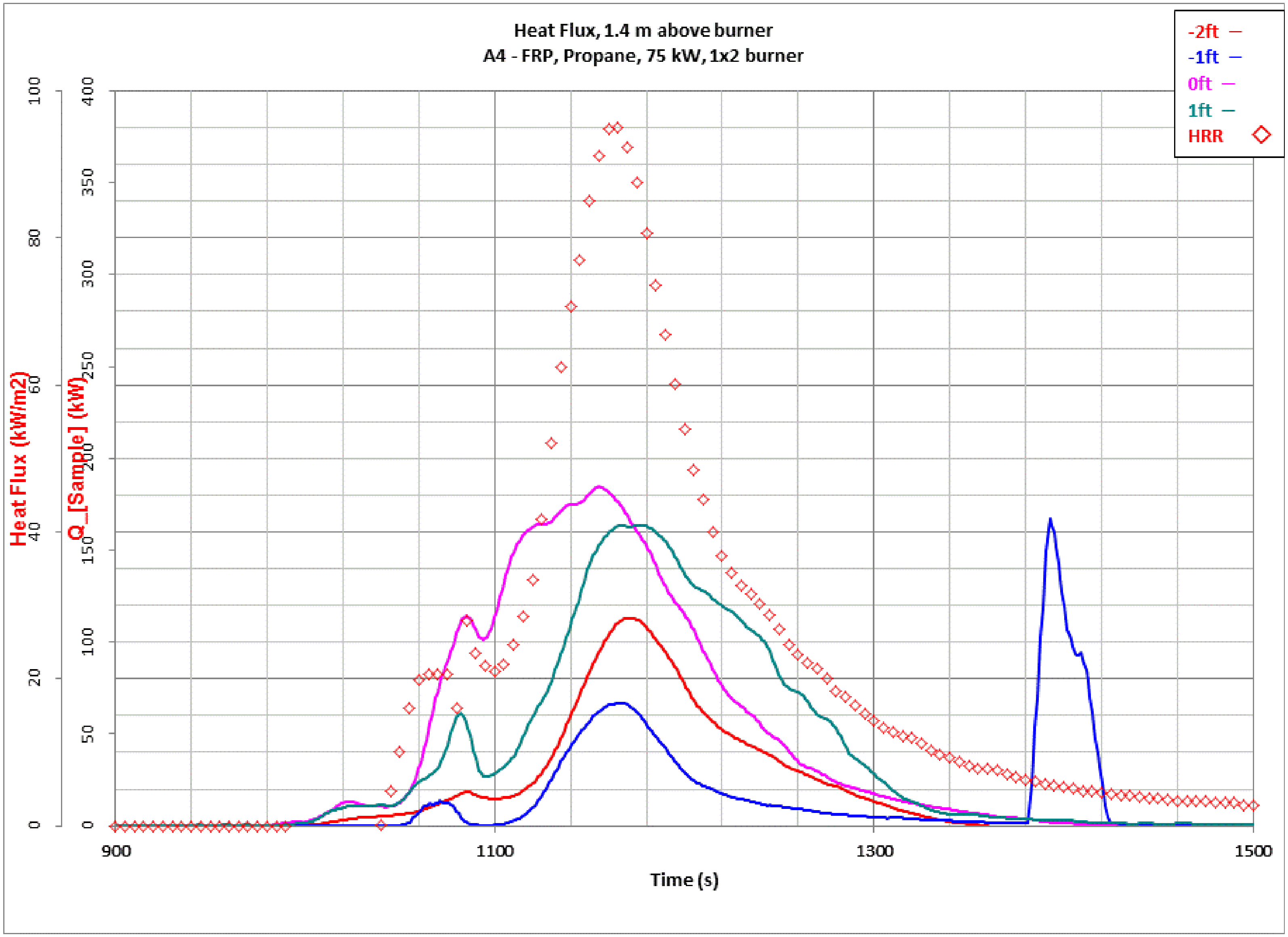

Heat flux measured at various distances from the centerline (negative indicates left of centerline), 1.4m vertically from burner surface

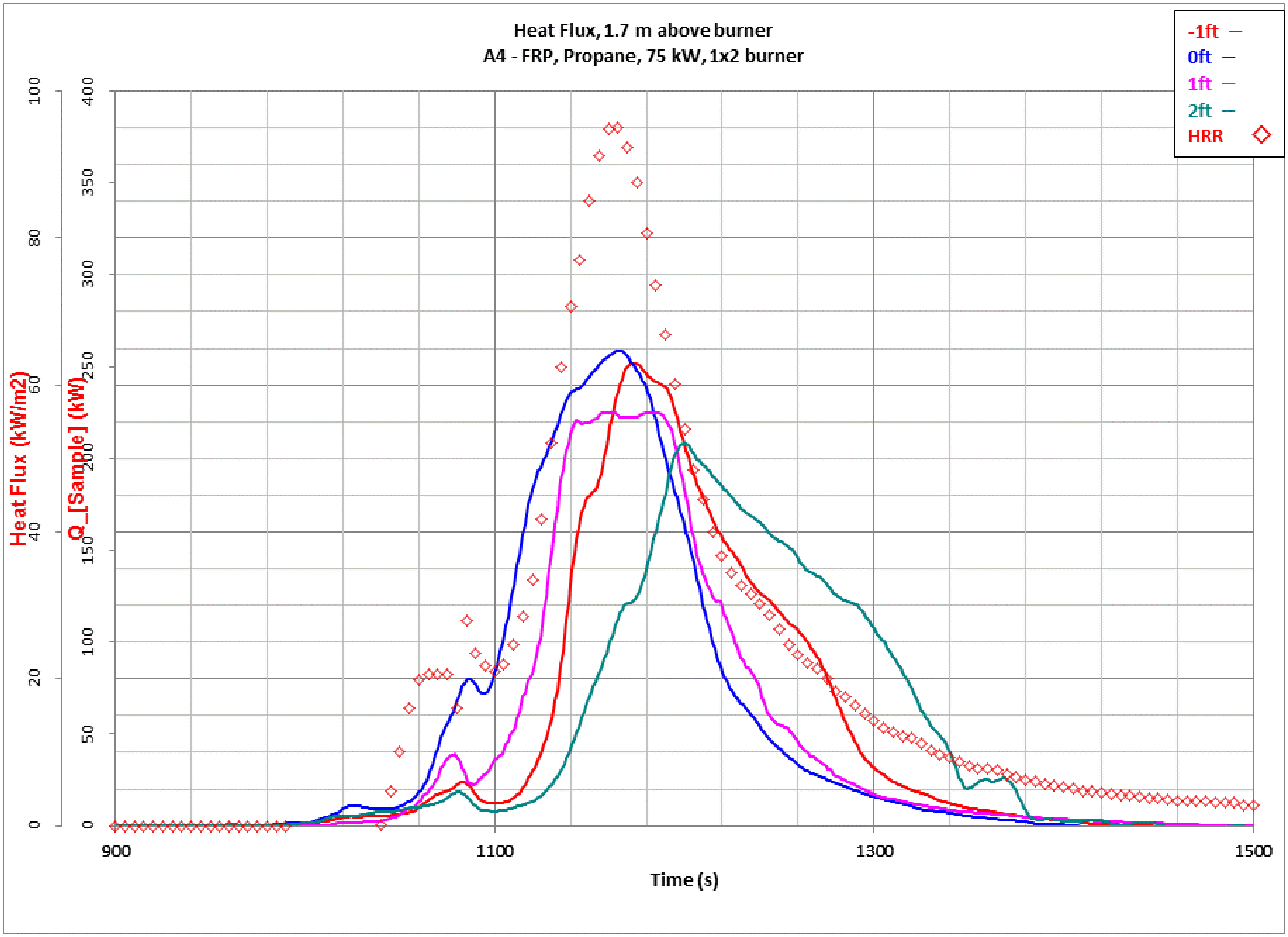

Heat flux measured at various distances from the centerline (negative indicates left of centerline), 1.7m vertically from burner surface

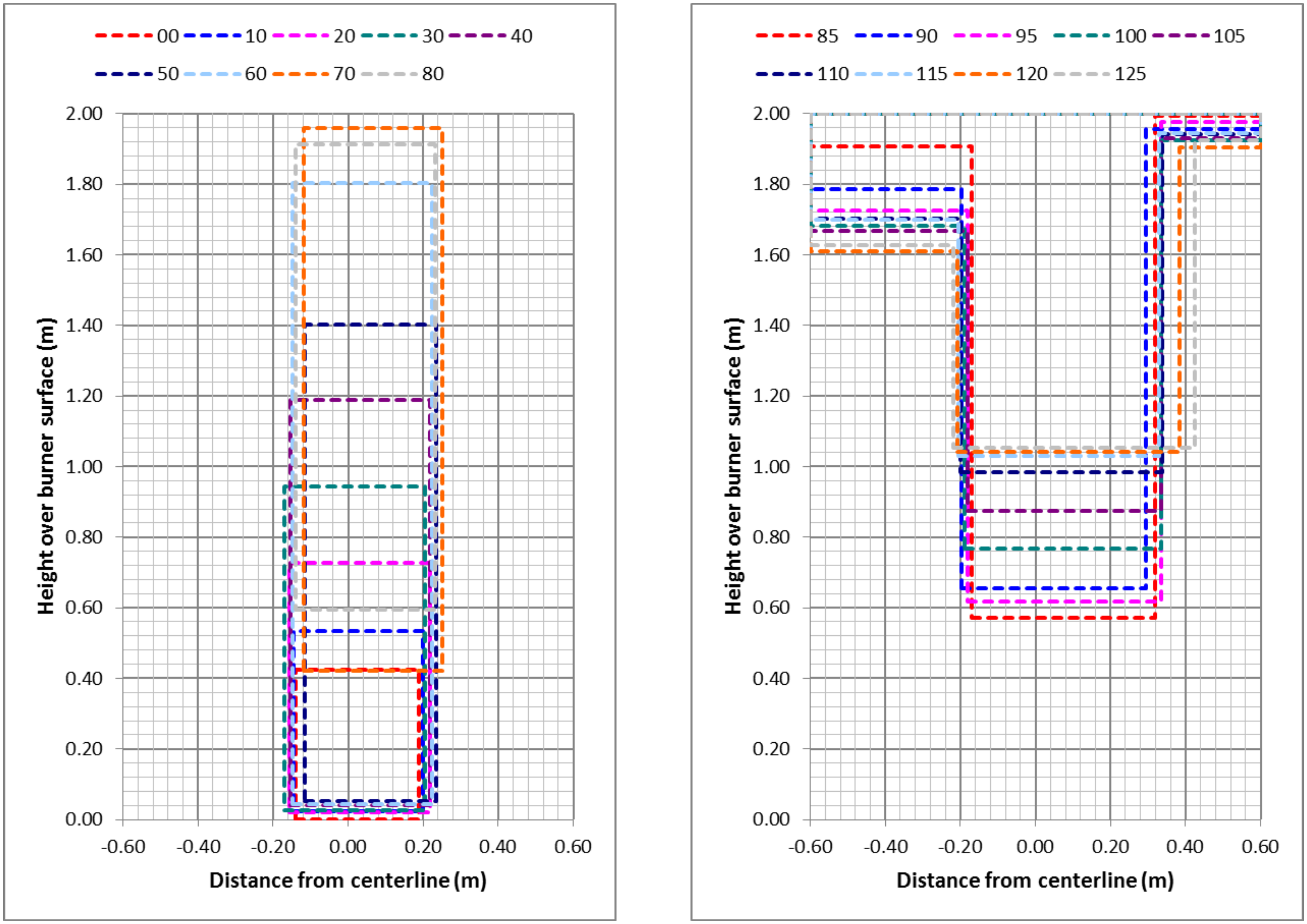

Stages 1 and 2 burning areas in Test A4 (2ft Rectangle burner, Propane, 75 kW source)

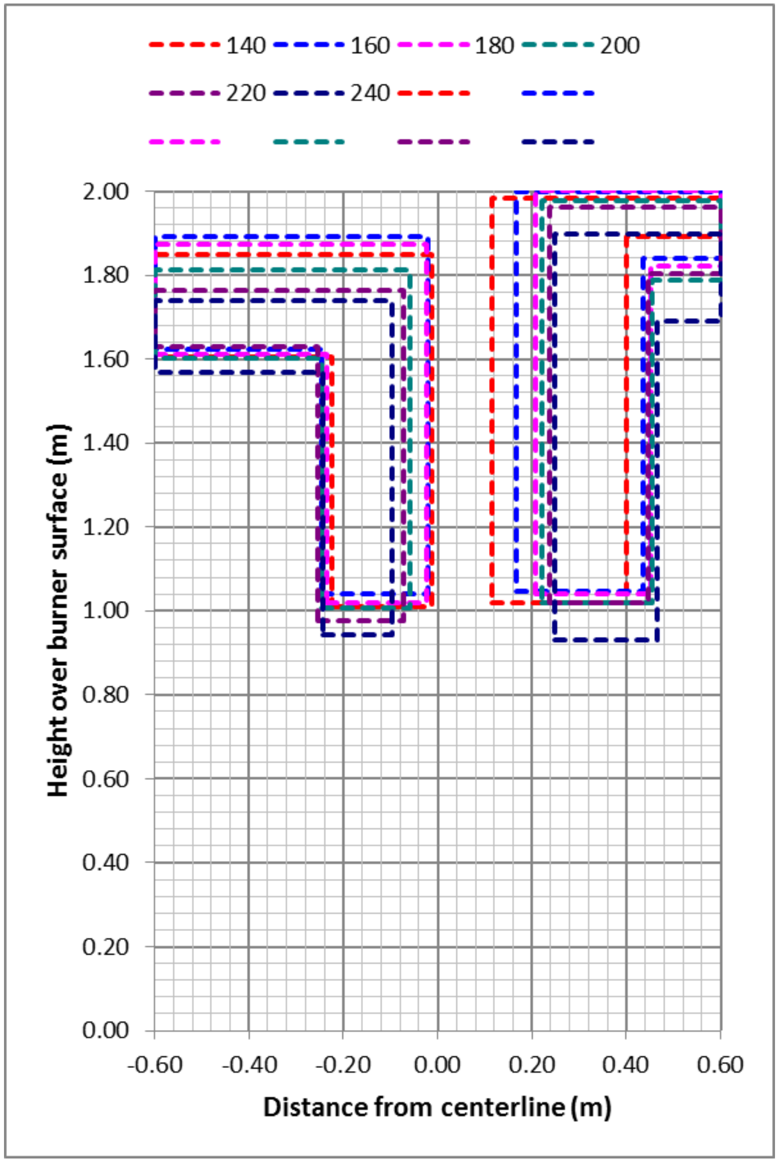

Stage 3 burn area and final damage chart of Test A4 (2ft Rectangle burner, Propane, 75 kW source)

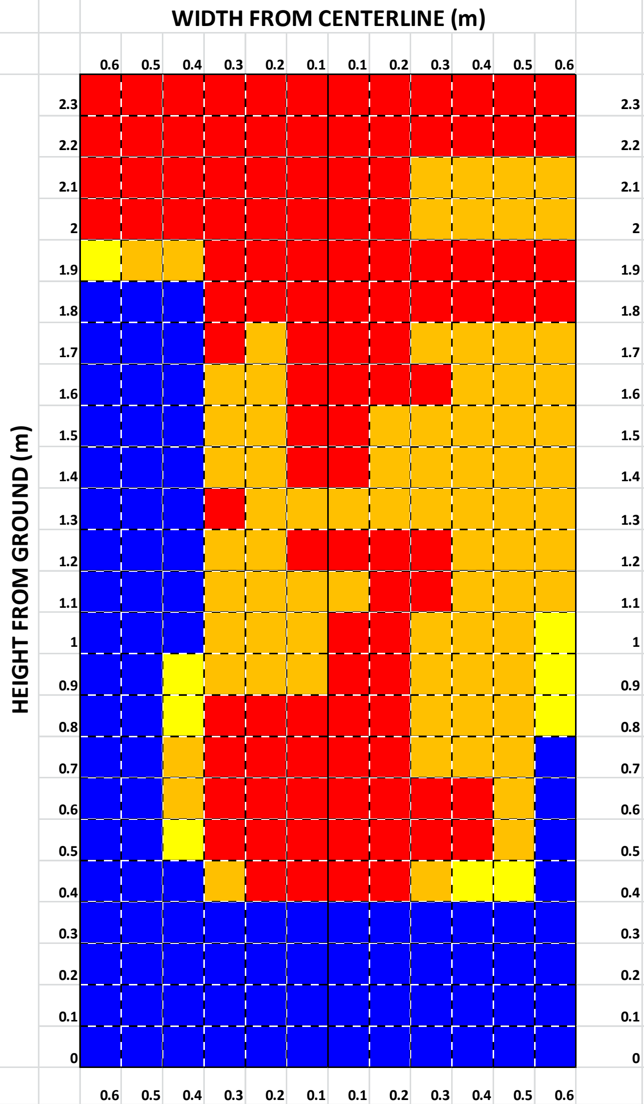

# of cell	Damage to Resin	Area (m2)
109	up to 100% damage	1.09
78	up to 75% damage	0.78
9	up to 50% damage	0.09
0	up to 25% damage	0
92	no damage	0.92

Initial mass:	8.7	kg
Final unburnt mass:	3.24	kg
Final burnt mass:	3.26	kg
Total mass loss during fire	2.2	kg

Burn damage pattern observed after fire test

F.3.5 Test A5

LODS Test Run Data

Center for Firesafety Studies

100 Institute Road
Worcester, MA 01609
Phone: (508) 831-5628
Fax: (508) 831-5680

Test Information

Test Number:	A5
Specimen Identification:	FRP 5, 50 kW initial Propane fire, 1 x 1 burner
Material Name:	Class C FRP panel
Manufacturer/Submitter:	Not Reported
Raw Data File Name:	Test A15 - FRP_Propane_50kW_1ft.txt
Reduced Data File Name:	Test A15 - FRP_Propane_50kW_1ft_reduced.xlsx
Date of Test:	4-Nov-2010
Tester:	W. Wong

Test Parameters

Ambient Temperature:	N/A
Relative Humidity:	N/A

Specimen Information

Specimen Initial Mass:	[kg]	8.7
Specimen Final Mass:	[kg]	7.1
Mass Lost:	[kg]	1.6
Heat Evolved (net):	[kJ]	0

Parameter	Unit	Value
Mass Loss		
Initial Mass	[kg]	8.7
Final Mass	[kg]	7.1
Mass Loss	[%]	18.81

LODS Test Run Data

Center for Firesafety Studies

100 Institute Road
Worcester, MA 01609
Phone: (508) 831-5628
Fax: (508) 831-5680

Test Notes

Test Number:	0
Date:	11/04/10
Material:	Class C FRP panel
Specimen Identification:	FRP 5, 50 kW initial Propane fire, 1 x 1 burner

Observations

Time	Observation
00:00	Start VI
14:50	Start Camera 1
15:00	Start Camera 2
17:49	Burner ignition
18:05	Reach target HRR @ 50 kW
18:39	Crackling noise
19:10	Panel ignition, mainly at area under TSC-2 to above burner
19:33	Burner off
20:40	Flame hit ceiling
21:30	Burning reaches left and right edges, T-pattern start
21:40	Rollover
	Remote area burning @ TSC-9, insignificant
	The burner flame was tilted
24:10	Remote area smoking on right edge @ y = 1 m
24:00	Only line fires remain
46:10	Terminate test with little water application

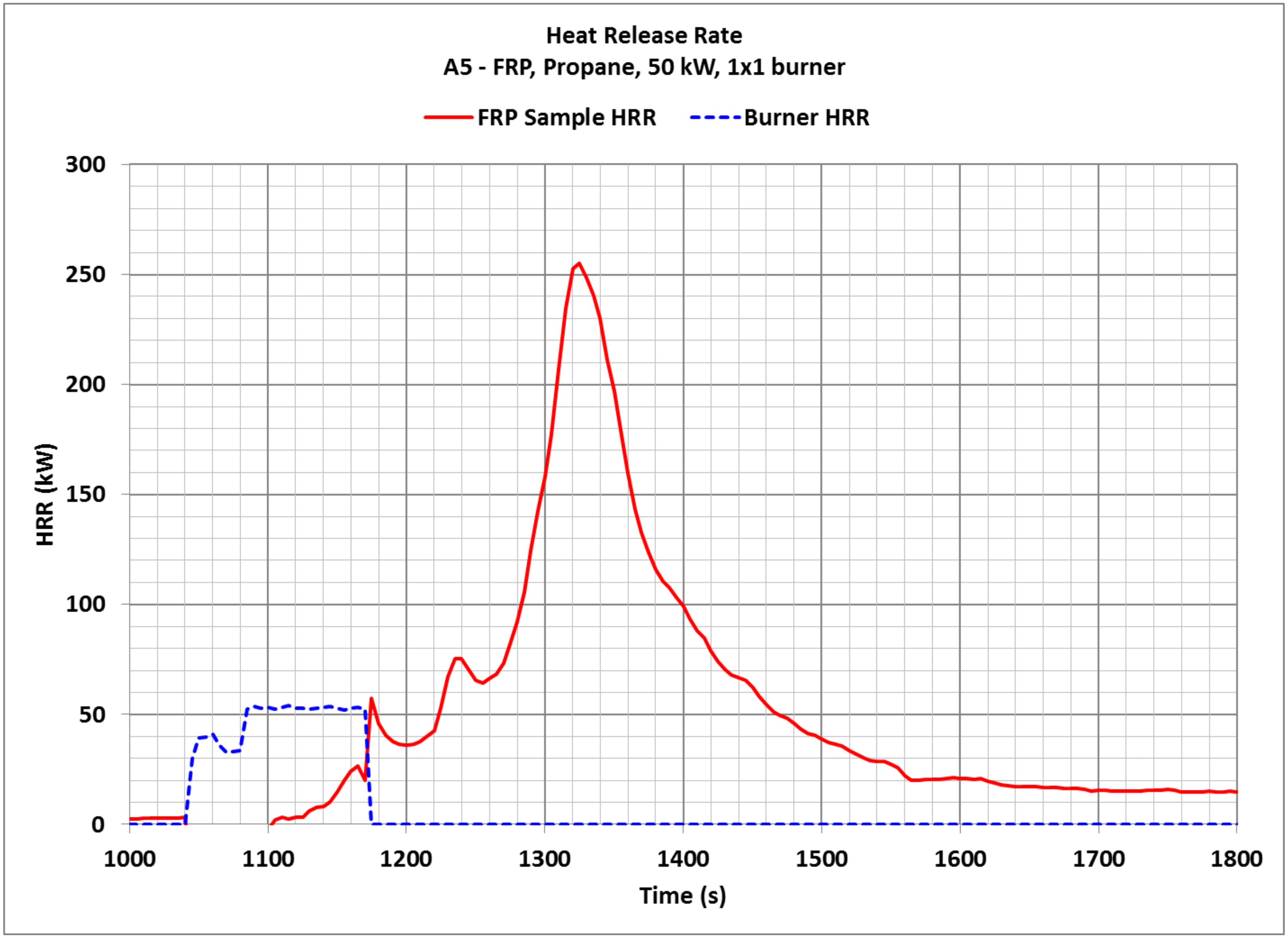

Heat release ratesof the source burner fire and of the specimen fire measured during test

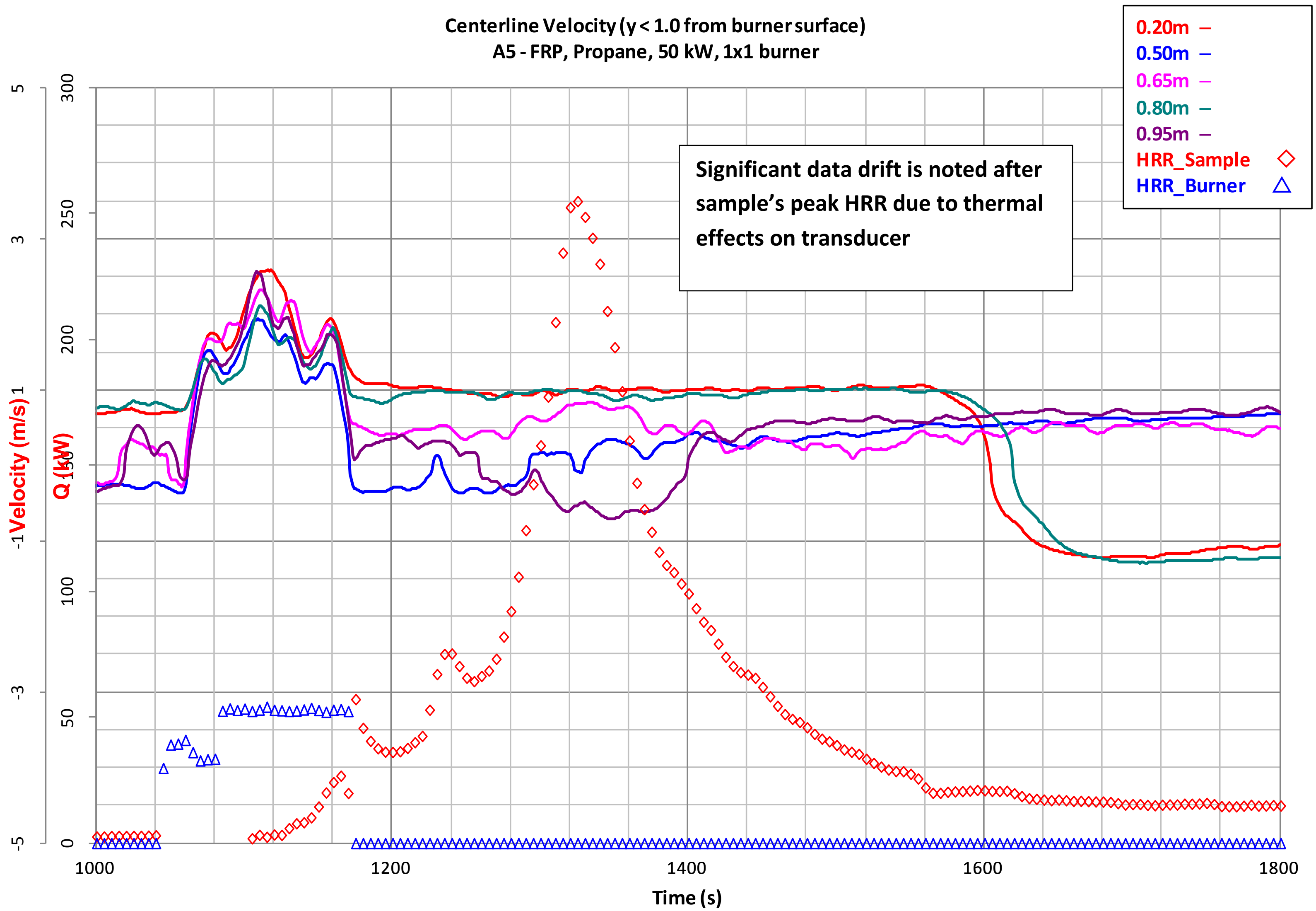

Centerline plume velocities measured from 0.2m to 0.95m above the burner surface

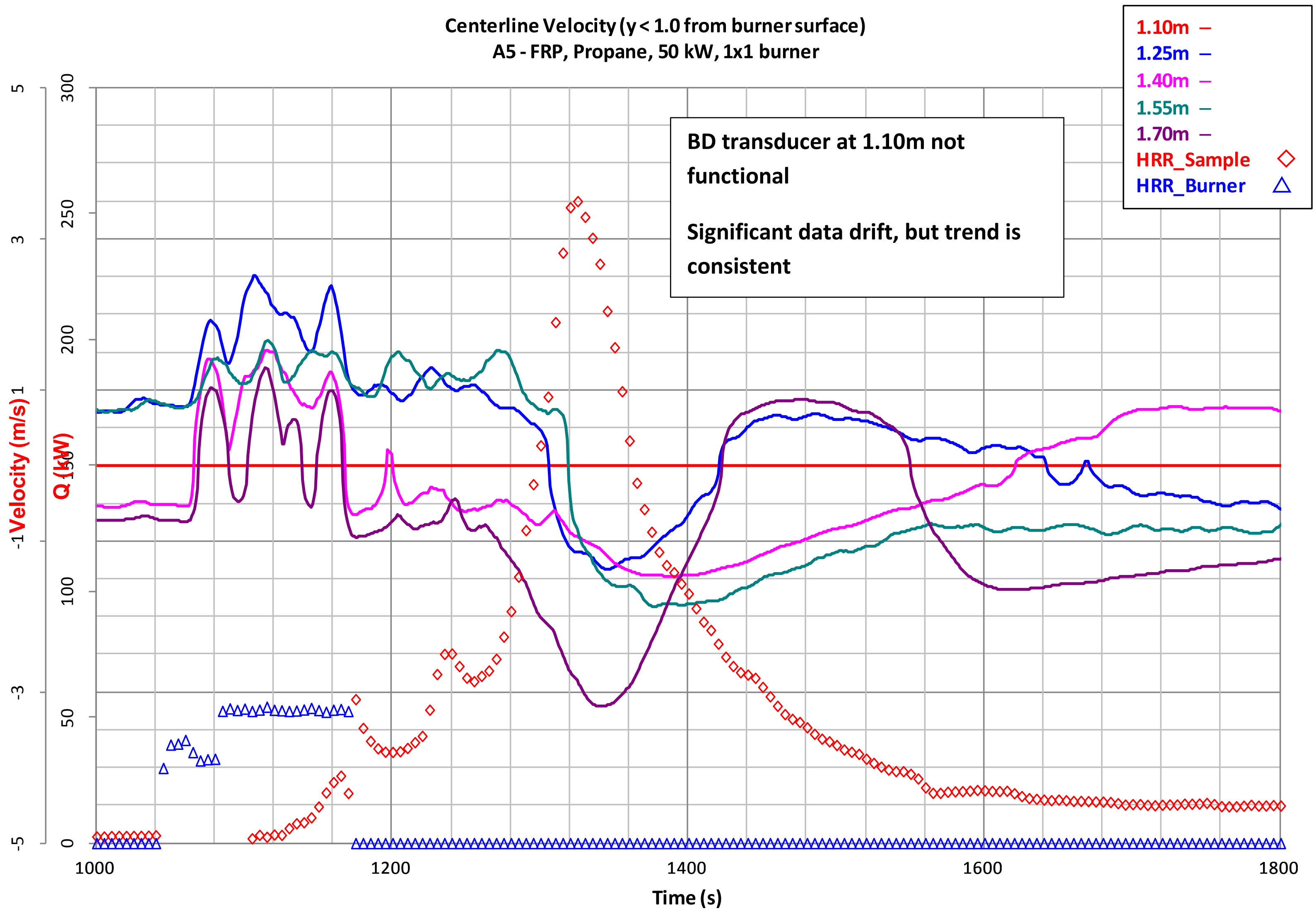

Centerline plume velocities measured from 1.1m to 1.7m above the burner surface

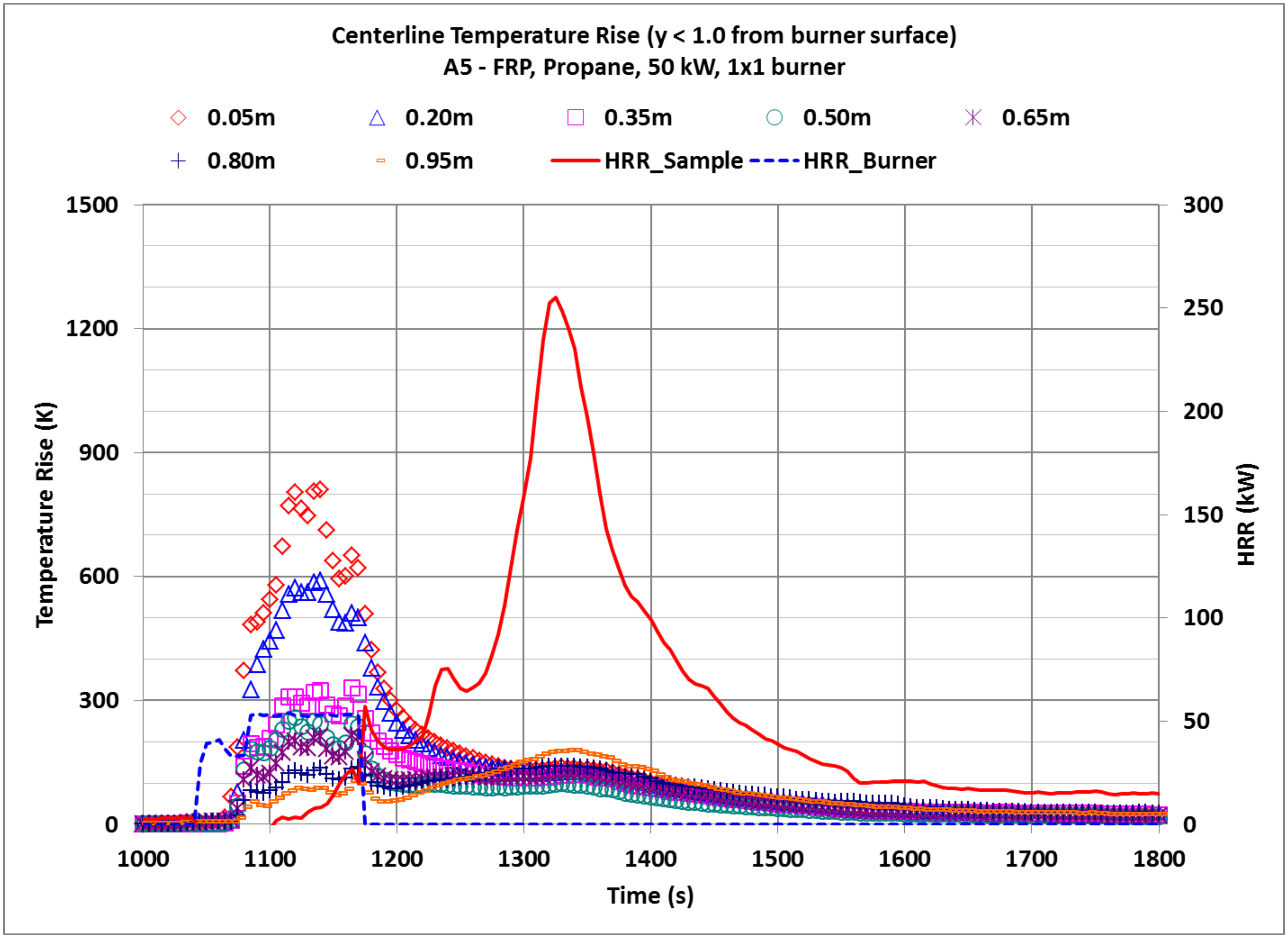

Centerline plume temperature rise measured from 0.05m to 0.95m above the burner surface

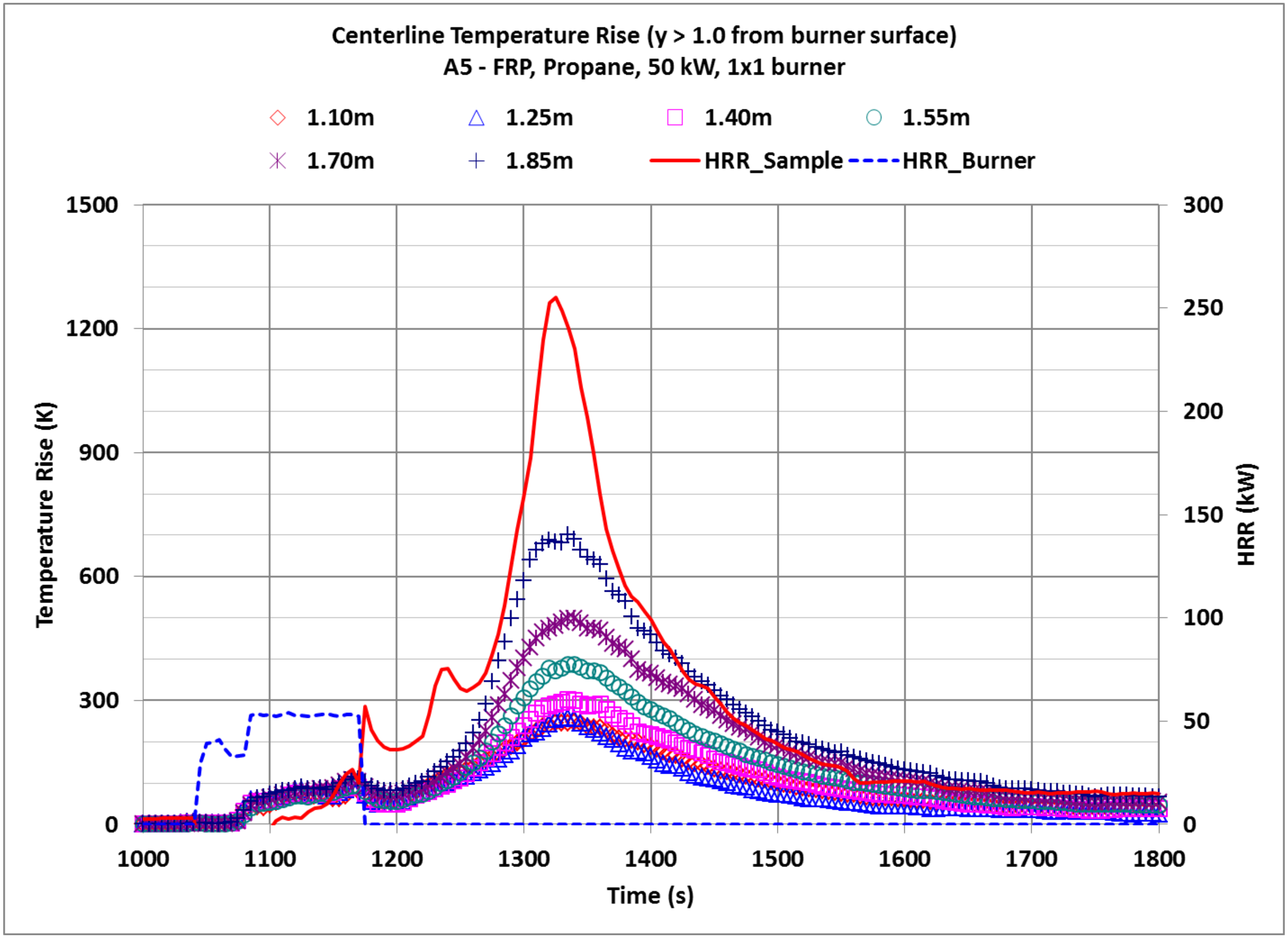

Centerline plume temperature rise measured from 1.10m to 1.85m above the burner surface

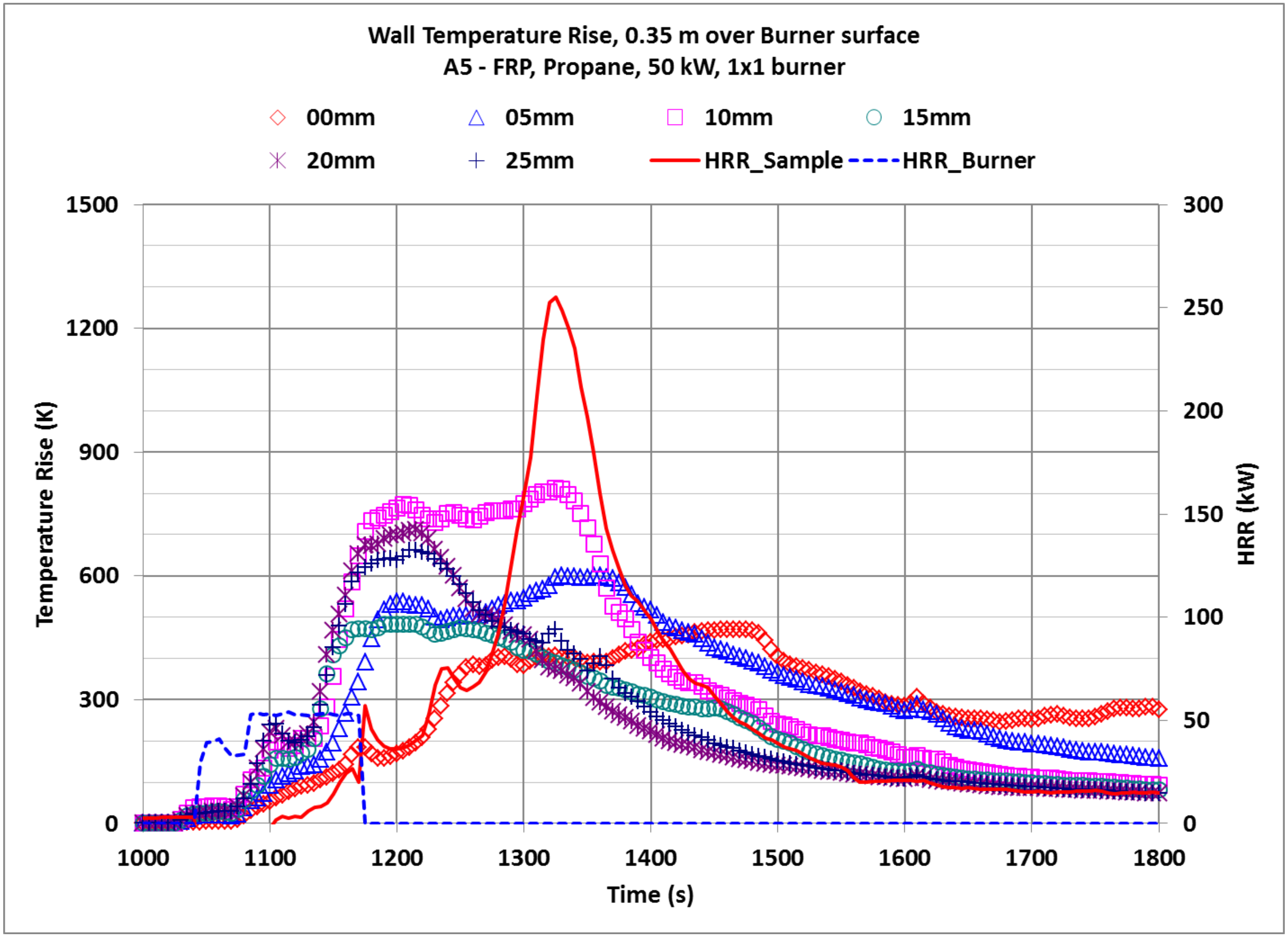

Temperature rise along the wall's centerline at 0.35m over the burner surface, measured at different perpendicular distances to as indicated

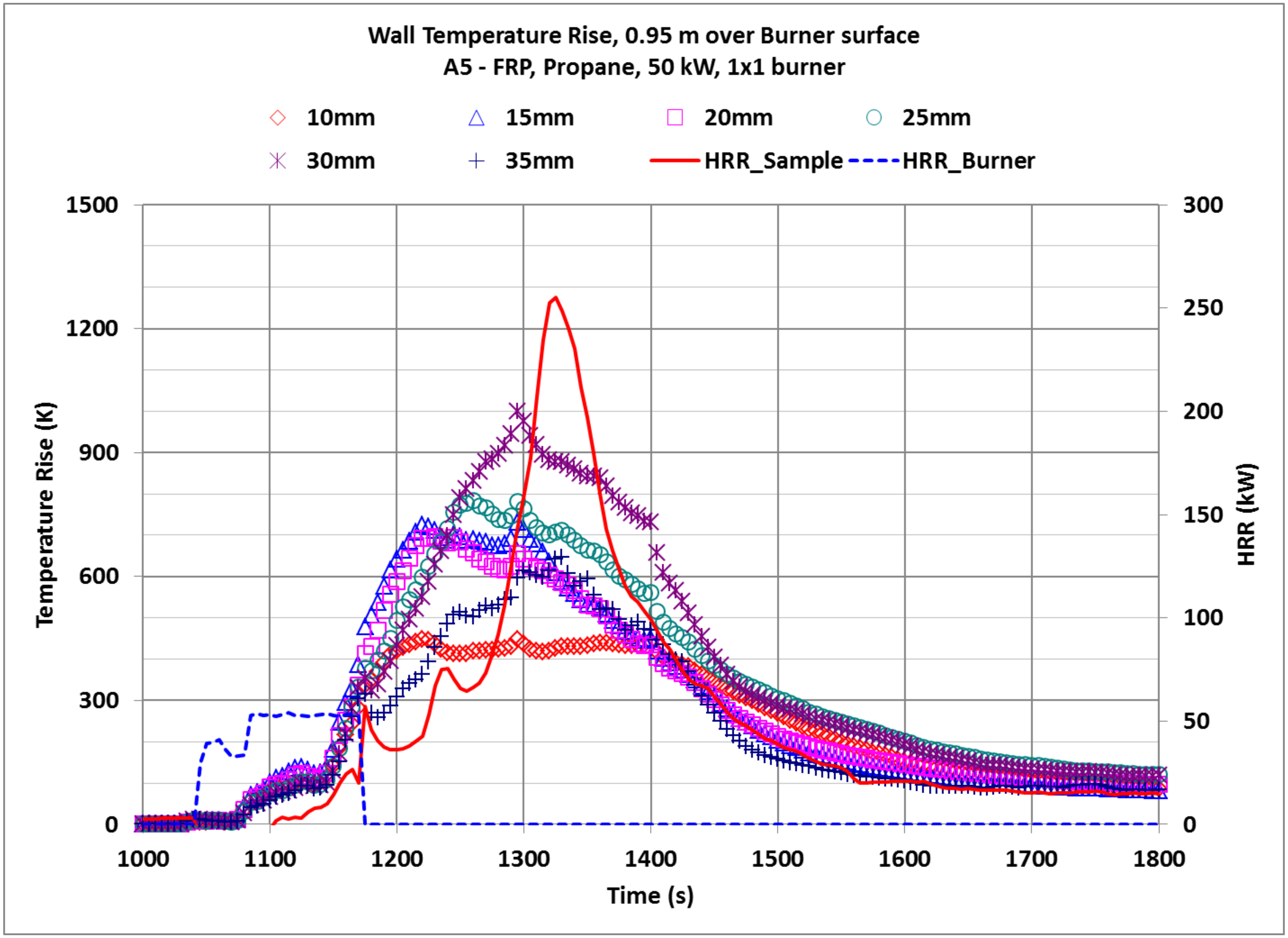

Temperature rise along the wall's centerline at 0.95m over the burner surface, measured at different perpendicular distances to as indicated

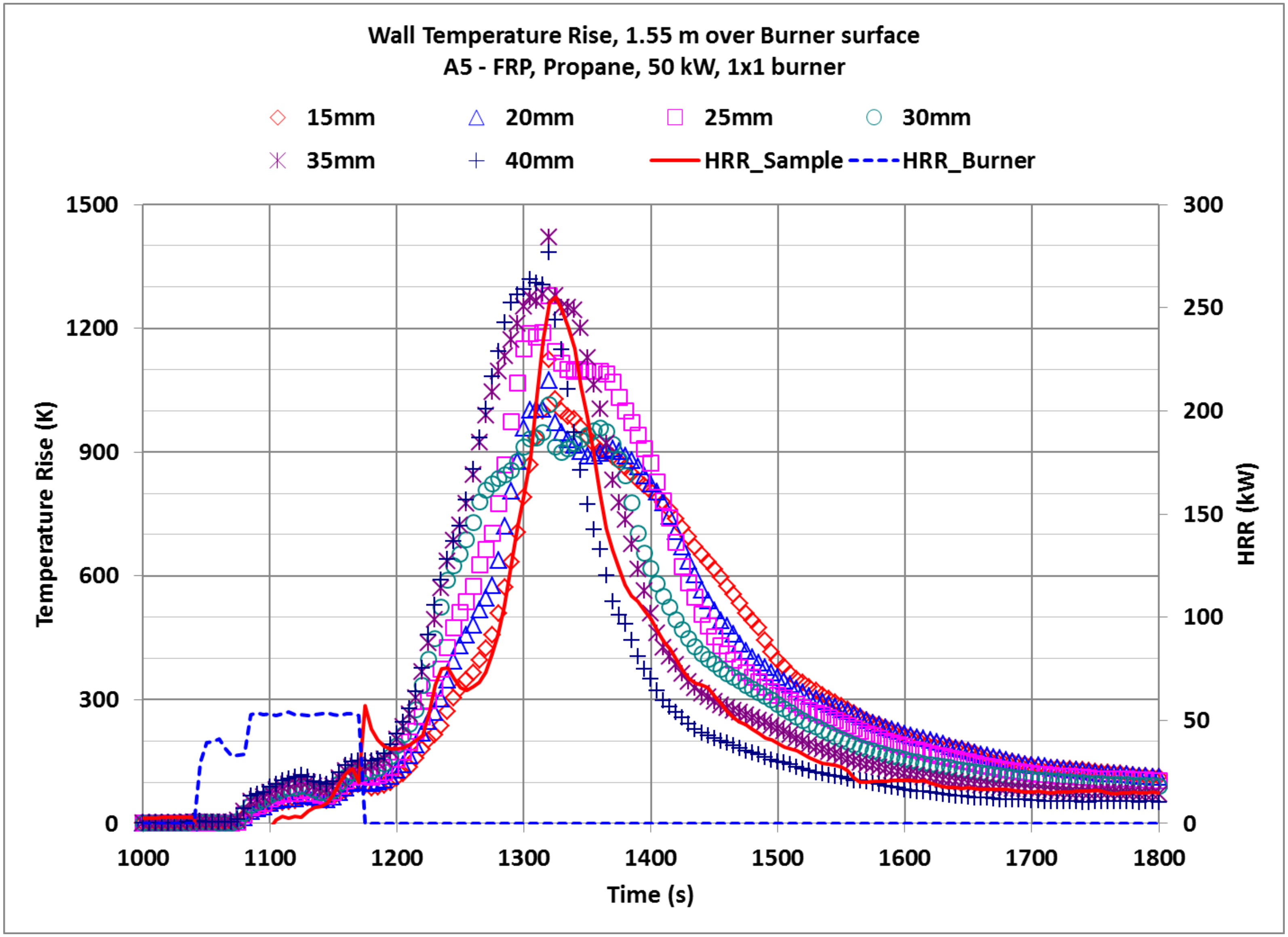

Temperature rise along the wall's centerline at 1.55m over the burner surface, measured at different perpendicular distances to as indicated

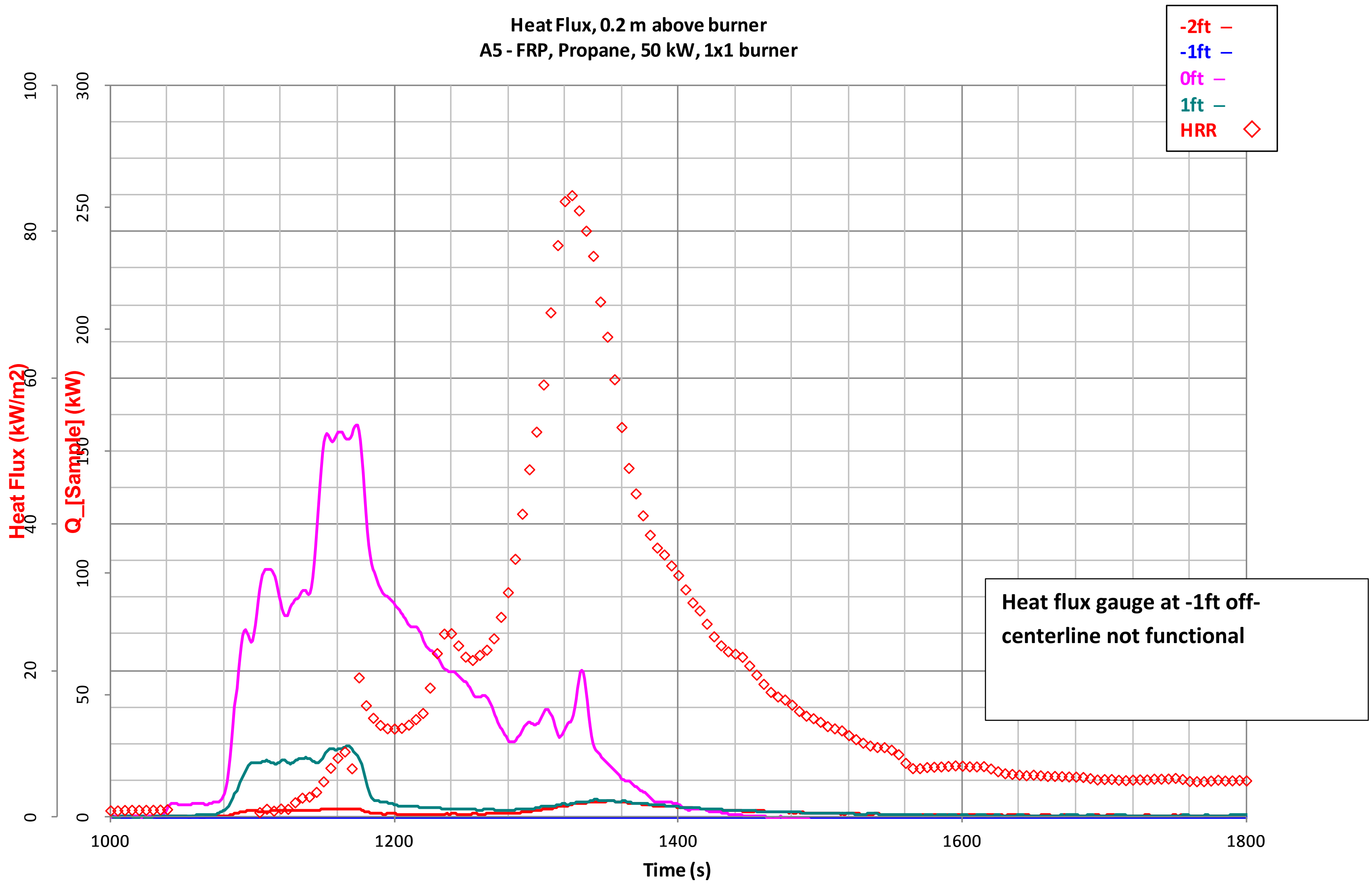

Heat flux measured at various distances from the centerline (negative indicates left of centerline), 0.2m vertically from burner surface

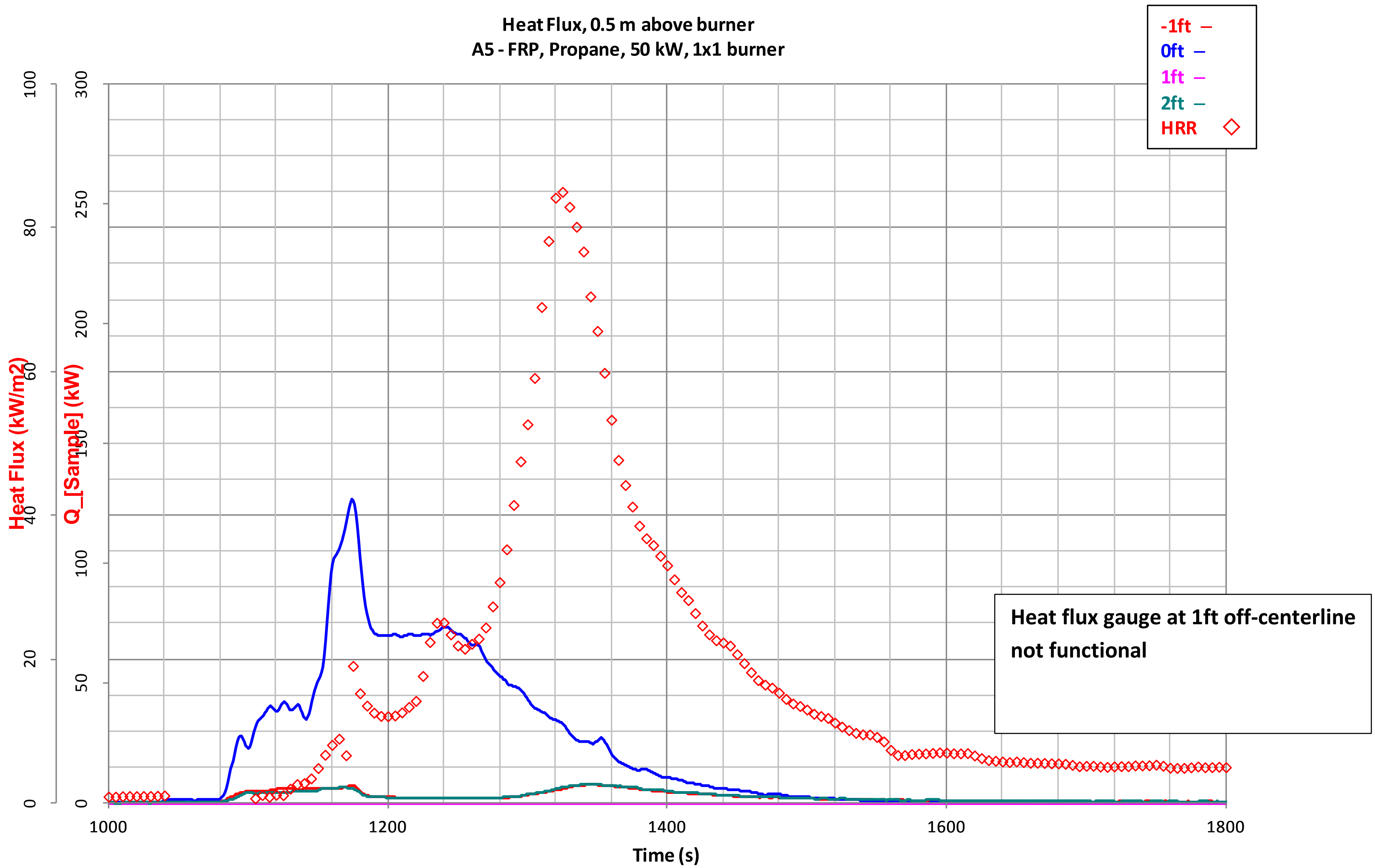

Heat flux measured at various distances from the centerline (negative indicates left of centerline), 0.5m vertically from burner surface

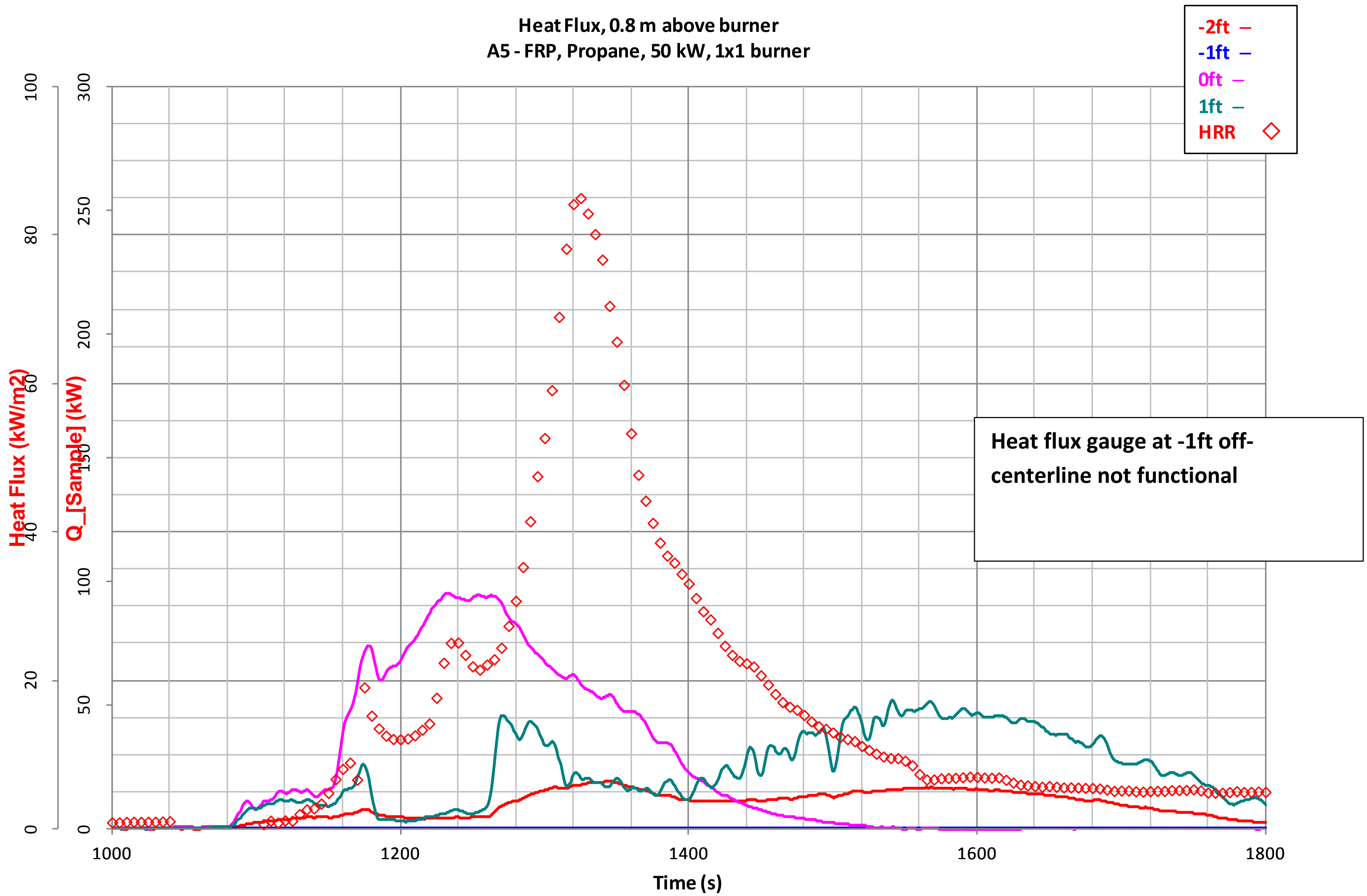

Heat flux measured at various distances from the centerline (negative indicates left of centerline), 0.8m vertically from burner surface

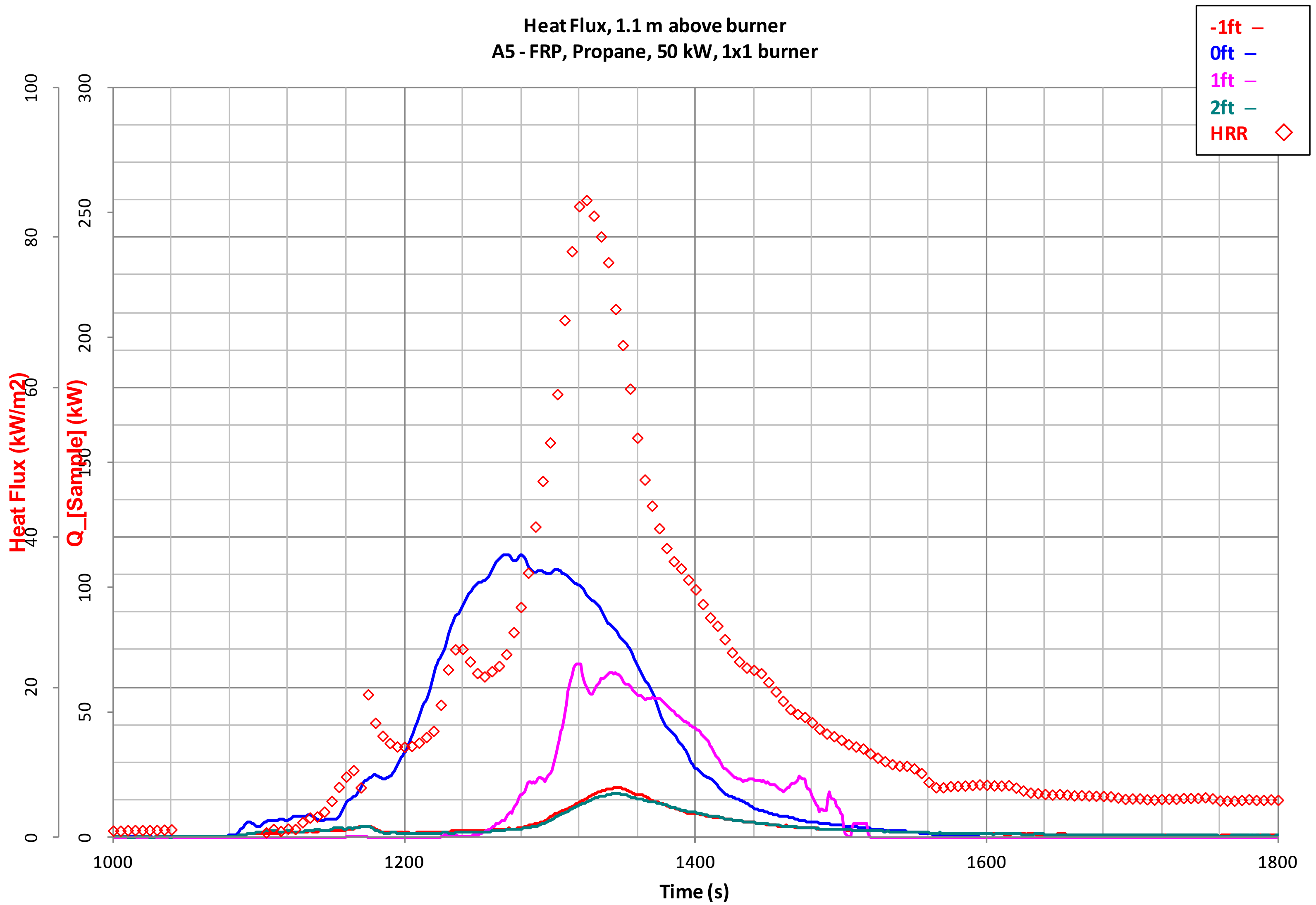

Heat flux measured at various distances from the centerline (negative indicates left of centerline), 1.1m vertically from burner surface

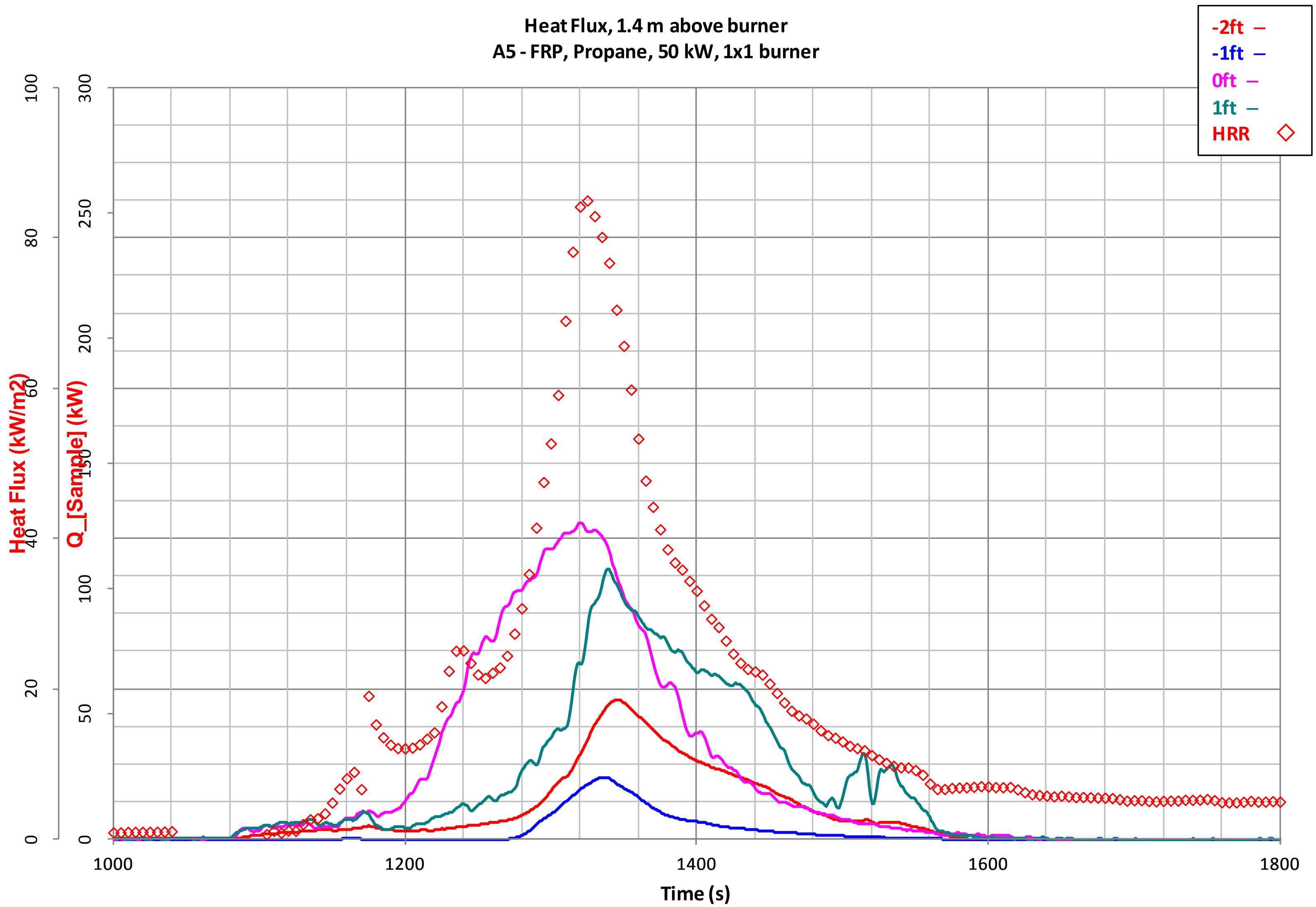

Heat flux measured at various distances from the centerline (negative indicates left of centerline), 1.4m vertically from burner surface

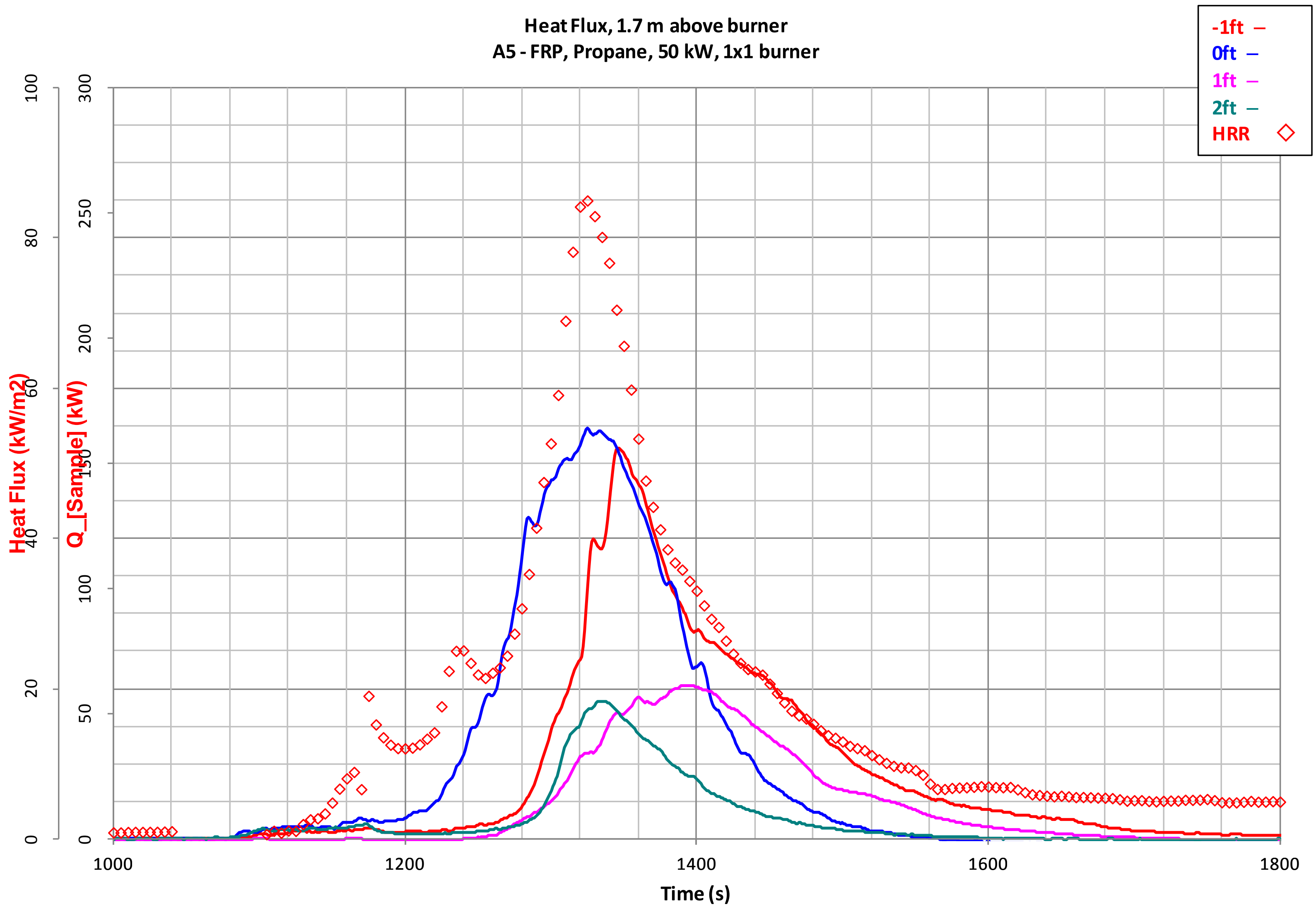

Heat flux measured at various distances from the centerline (negative indicates left of centerline), 1.7m vertically from burner surface

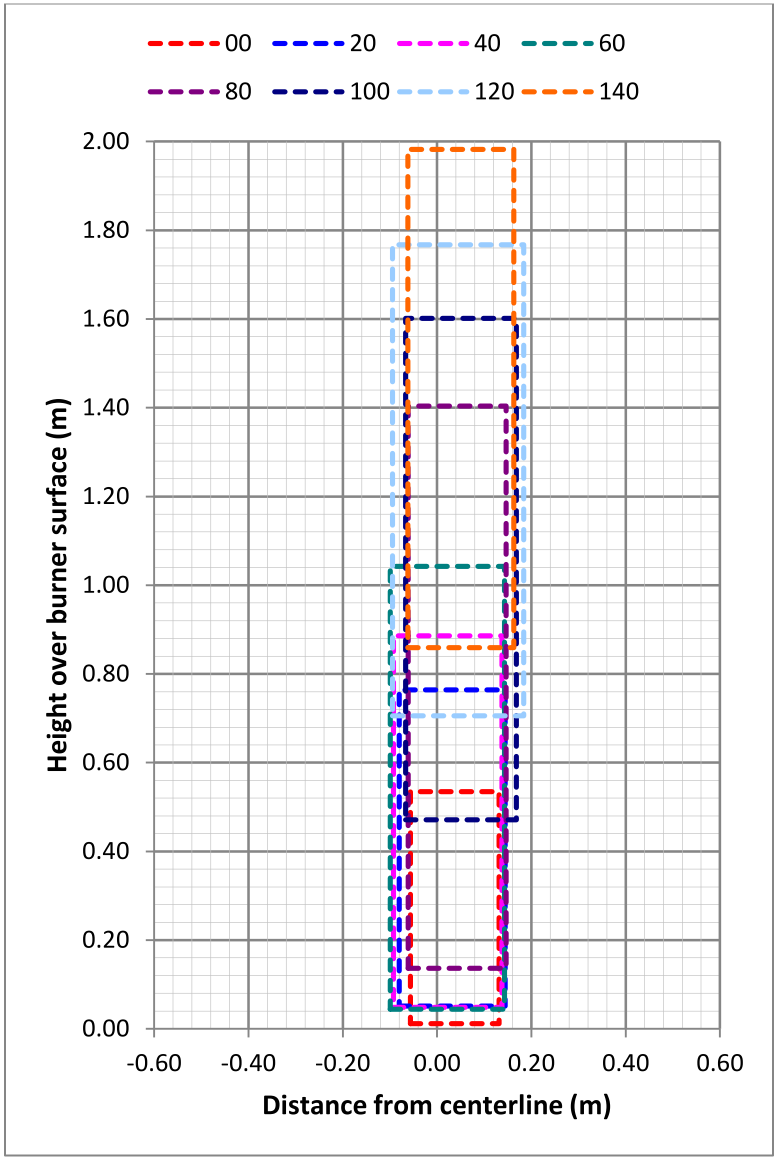

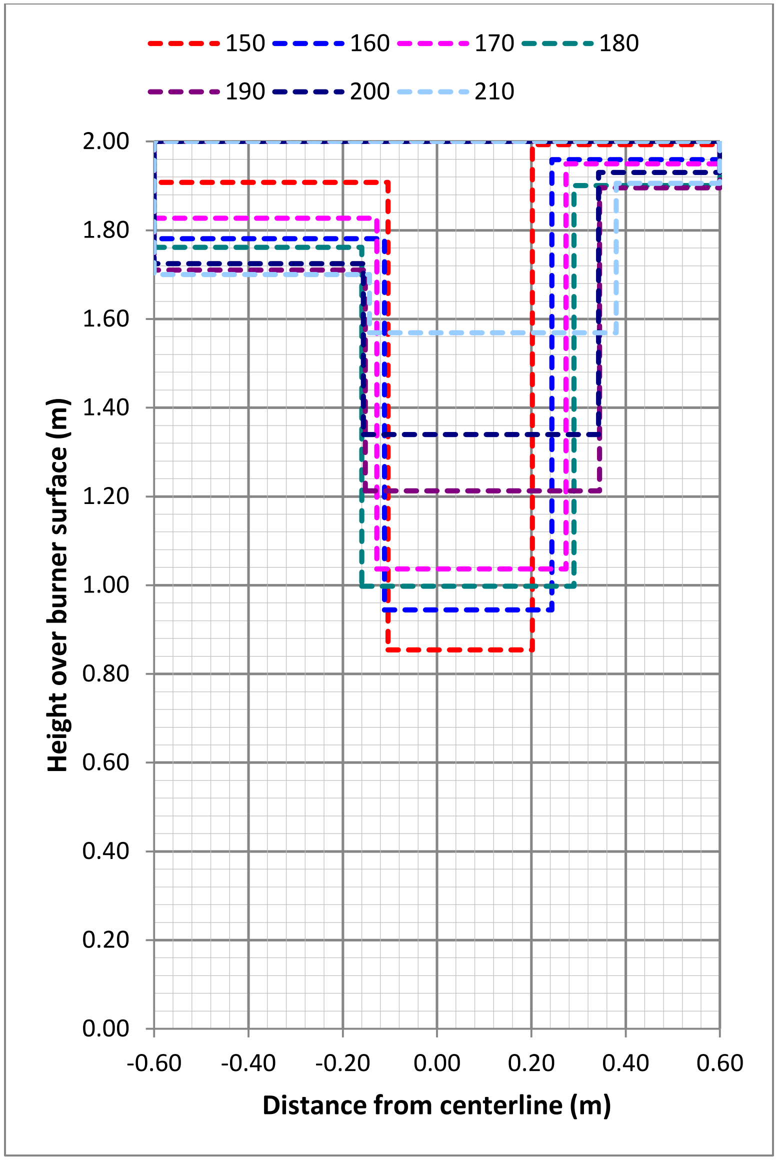

Stages 1 and 2 burning areas in Test A5 (1ft Square burner, Propane, 50 kW source)

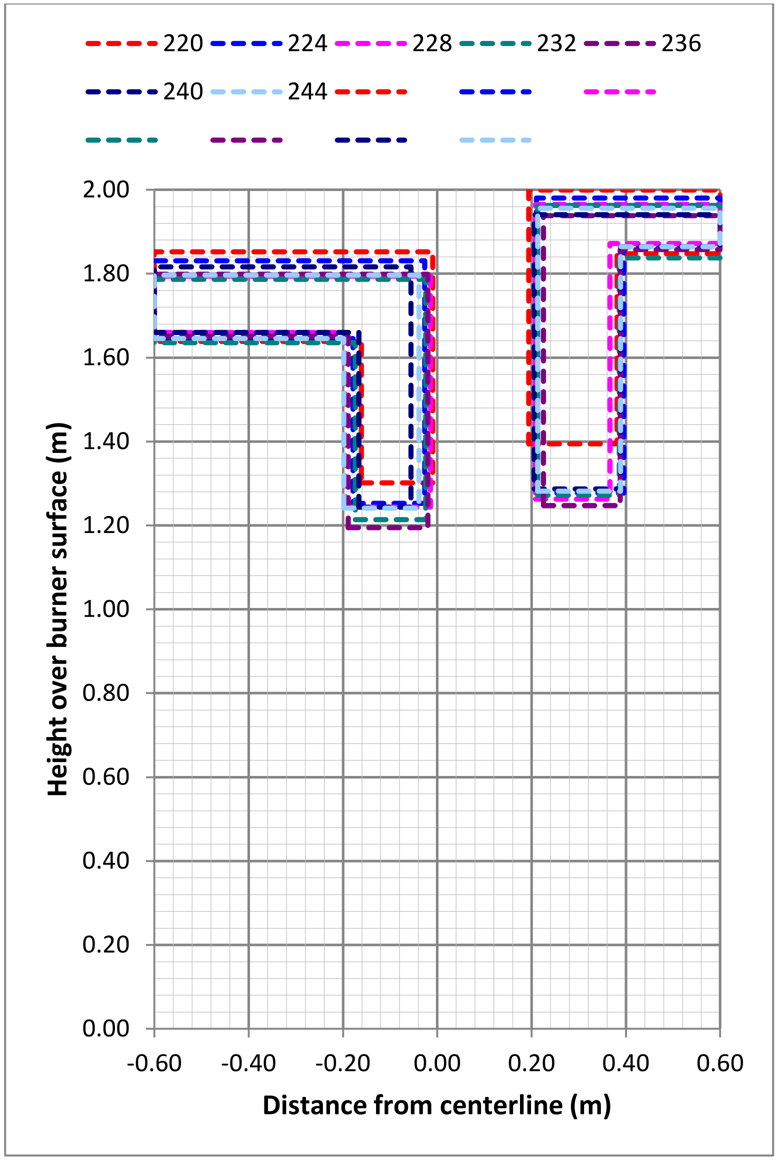

Stage 3 burn area and final damage chart of Test A5 (1ft Square burner, Propane, 50 kW source)

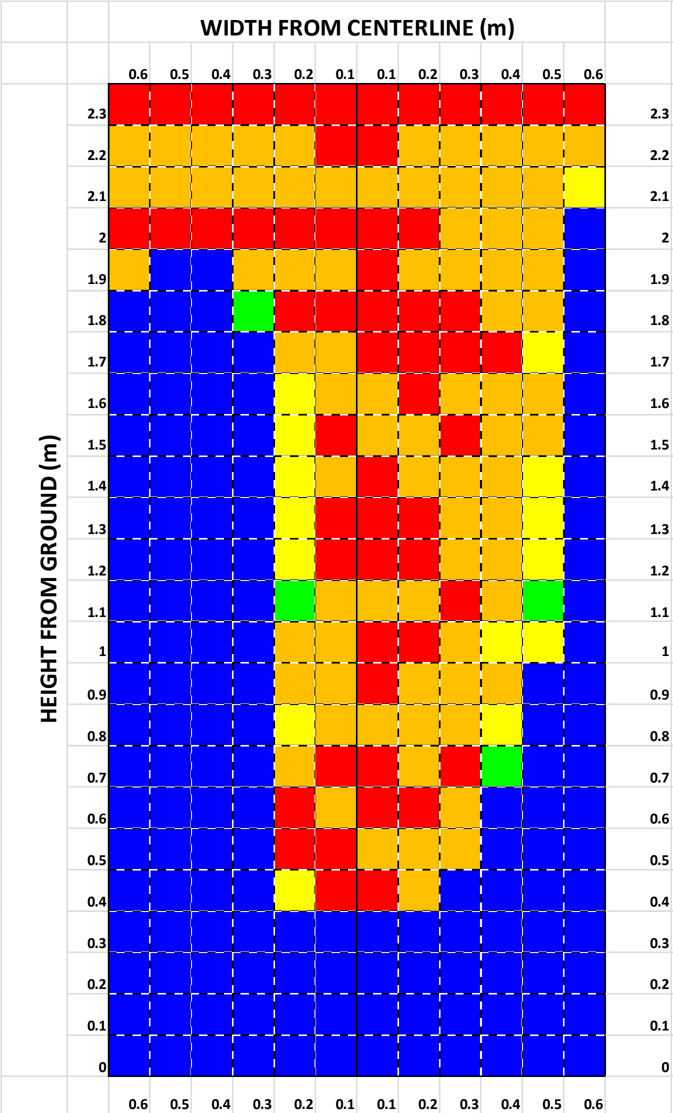

# of cell	Damage to Resin	Area (m2)
56	up to 100% damage	0.56
77	up to 75% damage	0.77
15	up to 50% damage	0.15
4	up to 25% damage	0.04
136	no damage	1.36

Initial mass:	8.72	kg
Final unburnt mass:	4.82	kg
Final burnt mass:	2.26	kg
Total mass loss during fire	1.64	kg

Burn damage pattern observed after fire test

F.3.6 Test A6

LODS Test Run Data

Center for Firesafety Studies

100 Institute Road
Worcester, MA 01609
Phone: (508) 831-5628
Fax: (508) 831-5680

Test Information

Test Number:	A6
Specimen Identification:	FRP 6, 75 kW initial Propane fire, 1 x 1 burner
Material Name:	Class C FRP panel
Manufacturer/Submitter:	Not Reported
Raw Data File Name:	Test A6 - FRP_75kW_Propane_1ft.txt
Reduced Data File Name:	Test A6 - FRP_75kW_Propane_1ft_reduced.xlsx
Date of Test:	5-Nov-2010
Tester:	W. Wong

Test Parameters

Ambient Temperature:	N/A
Relative Humidity:	N/A

Specimen Information

Specimen Initial Mass:	[kg]	8.3
Specimen Final Mass:	[kg]	6.5
Mass Lost:	[kg]	1.8
Heat Evolved (net):	[kJ]	0

Parameter	Unit	Value
Mass Loss		
Initial Mass	[kg]	8.3
Final Mass	[kg]	6.5
Mass Loss	[%]	22.12

LODS Test Run Data

Center for Firesafety Studies

100 Institute Road
Worcester, MA 01609
Phone: (508) 831-5628
Fax: (508) 831-5680

Test Notes

Test Number:	0
Date:	11/05/10
Material:	Class C FRP panel
Specimen Identification:	FRP 6, 75 kW initial Propane fire, 1 x 1 burner

Observations

Time	Observation
00:00	Start VI
05:45	Start Camera 1
06:00	Start Camera 2
08:44	Burner ignition
09:00	Reach target HRR @ 75 kW
09:25	Crackling noise
09:43	Panel ignition, mainly at area under TSC-2 to above burner
10:14	Burner off
10:30	Remote area smoking @ HFG-2, TSC-8
10:30	Remote area burning @ TSC-3, which is close to the burning V pattern
10:30	Flame hit ceiling
10:45	Burning T-pattern
10:45 to 12:30	Rollover under ceiling
	Remote area smoking @ TSC-4
21:30	Some insignificant burning @ TSC-4, which is close to the line fire
24:45	Some insignificant burning @ HFG-3, which is close to the line fire
32:10	Terminate test with little water application

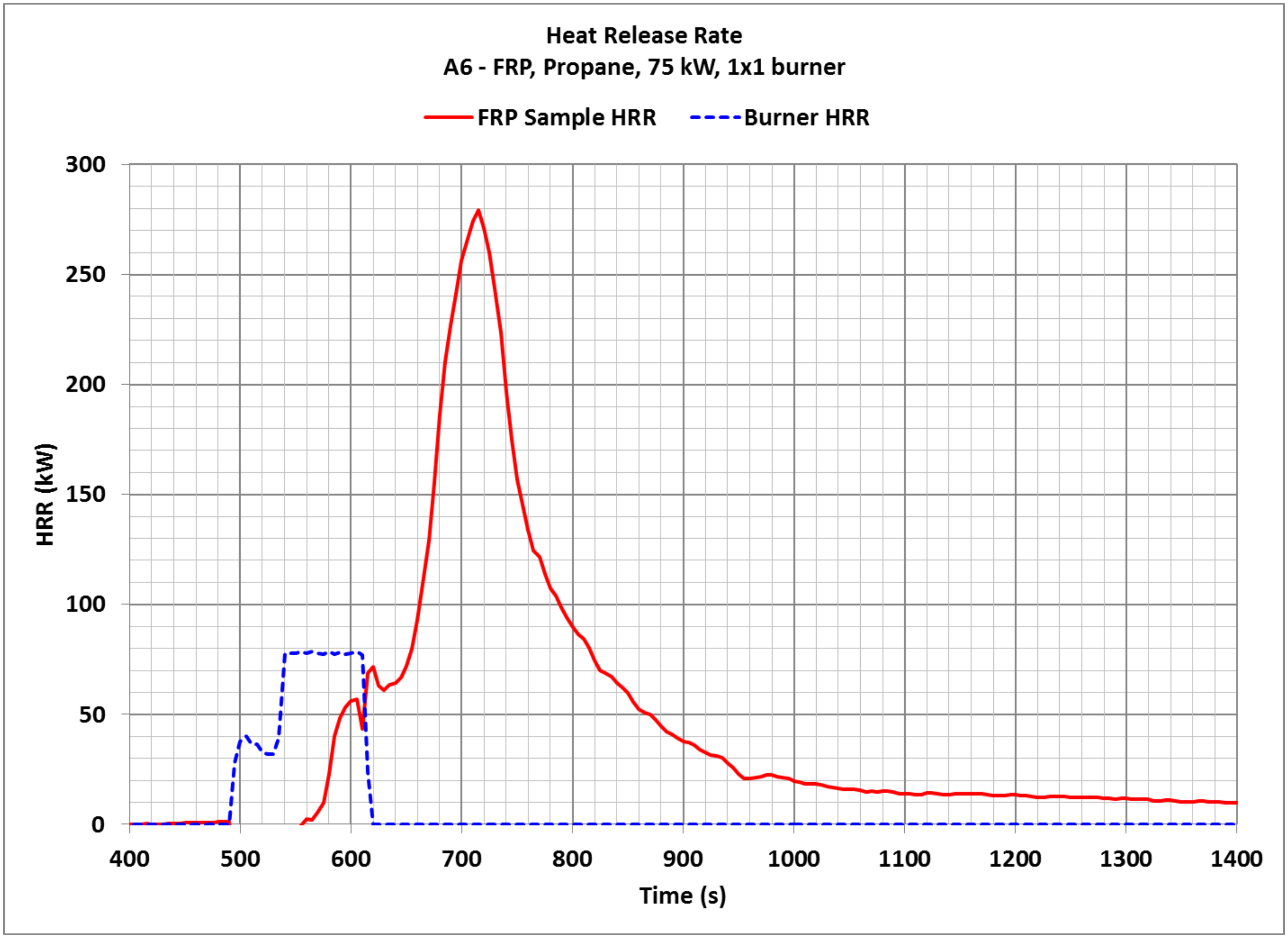

Heat release ratesof the source burner fire and of the specimen fire measured during test

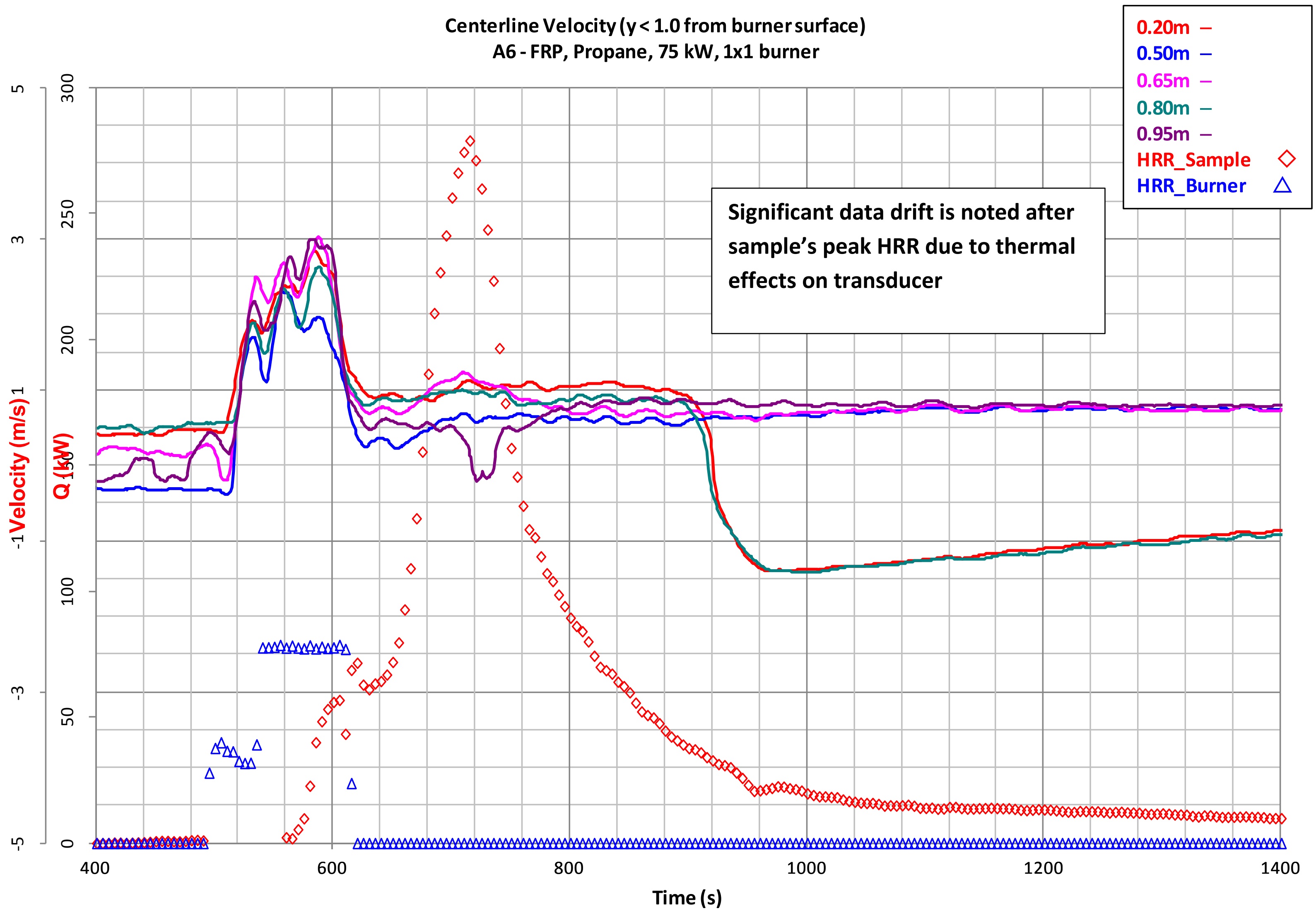

Centerline plume velocities measured from 0.2m to 0.95m above the burner surface

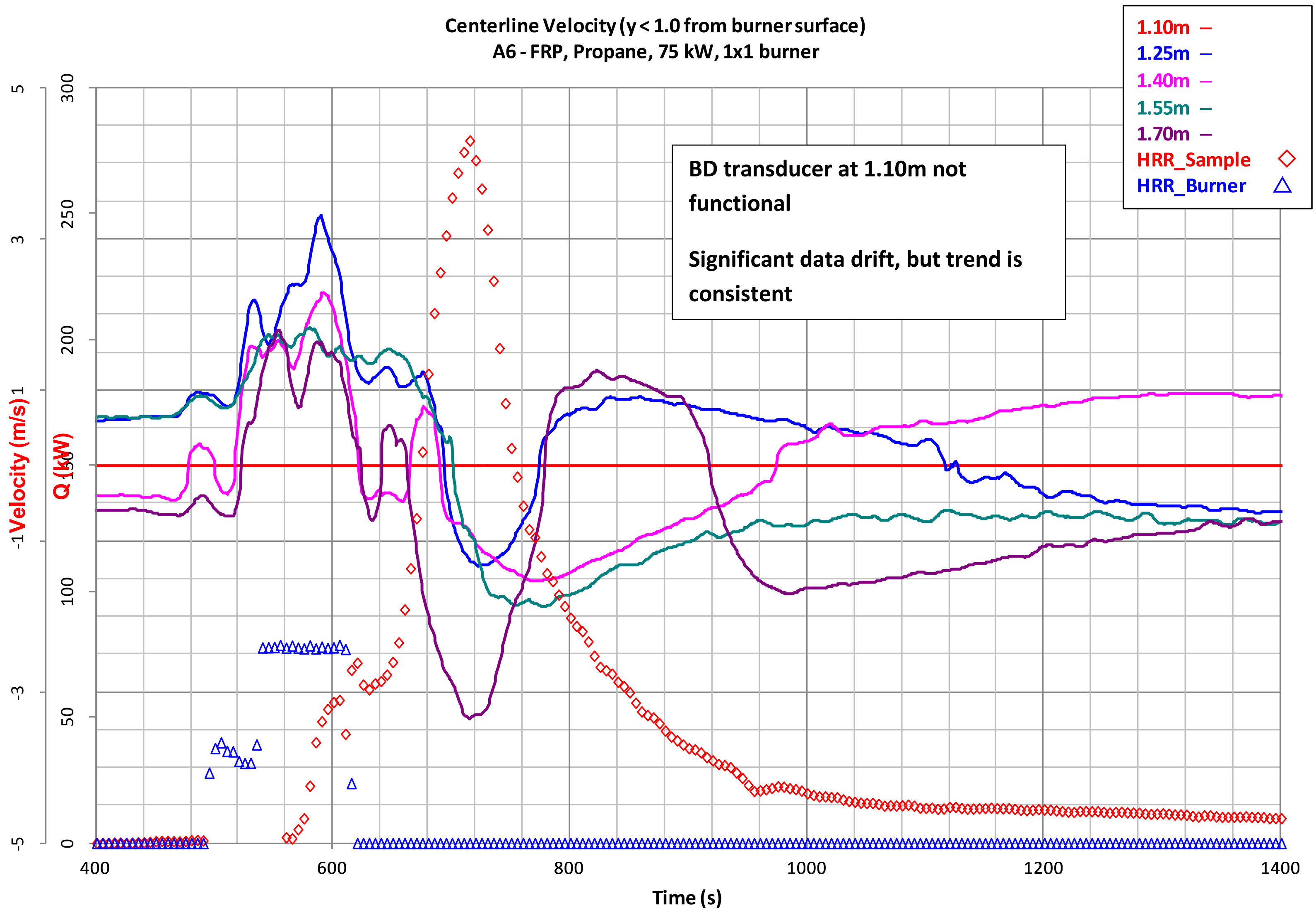

Centerline plume velocities measured from 1.1m to 1.7m above the burner surface

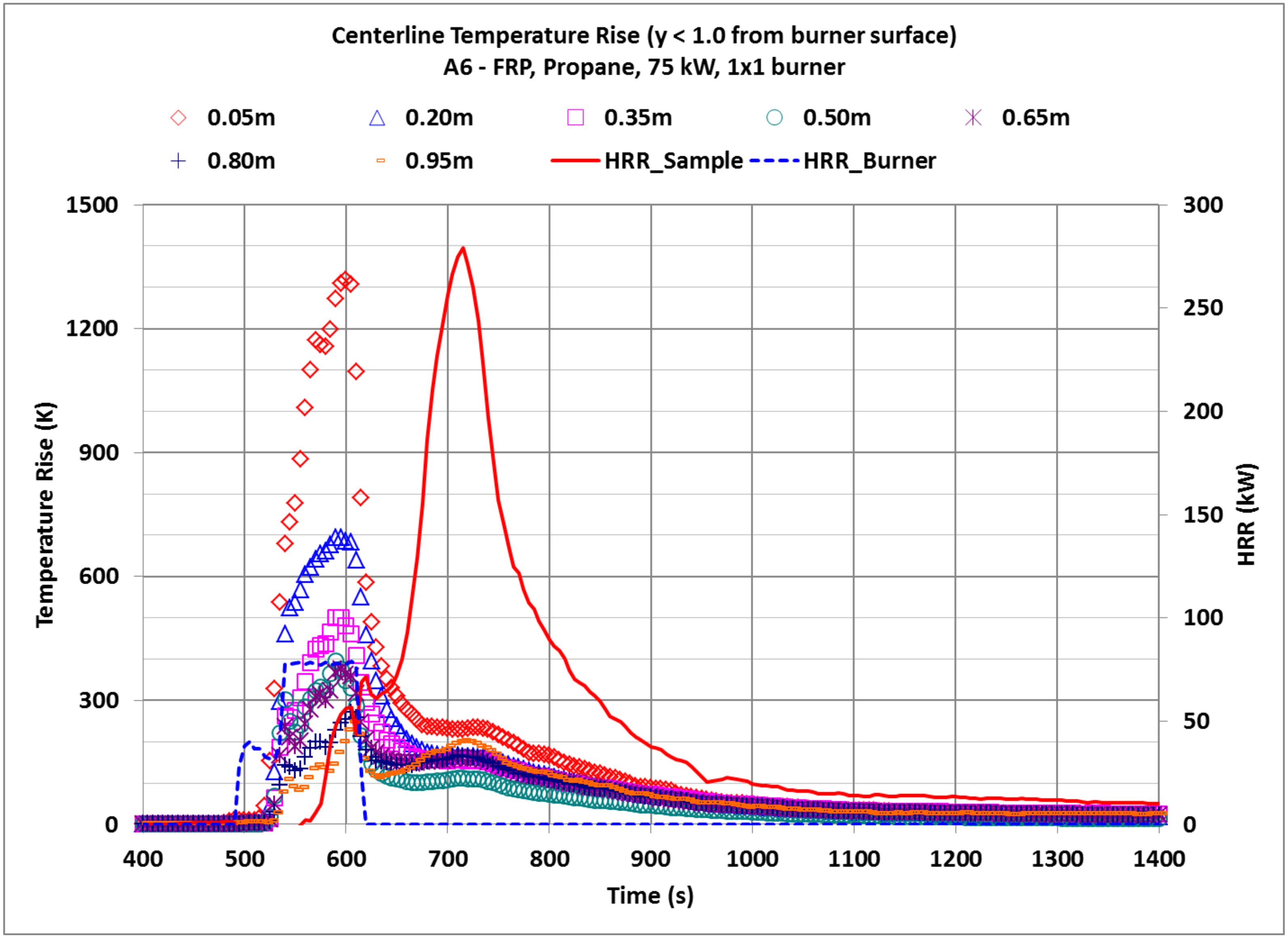

Centerline plume temperature rise measured from 0.05m to 0.95m above the burner surface

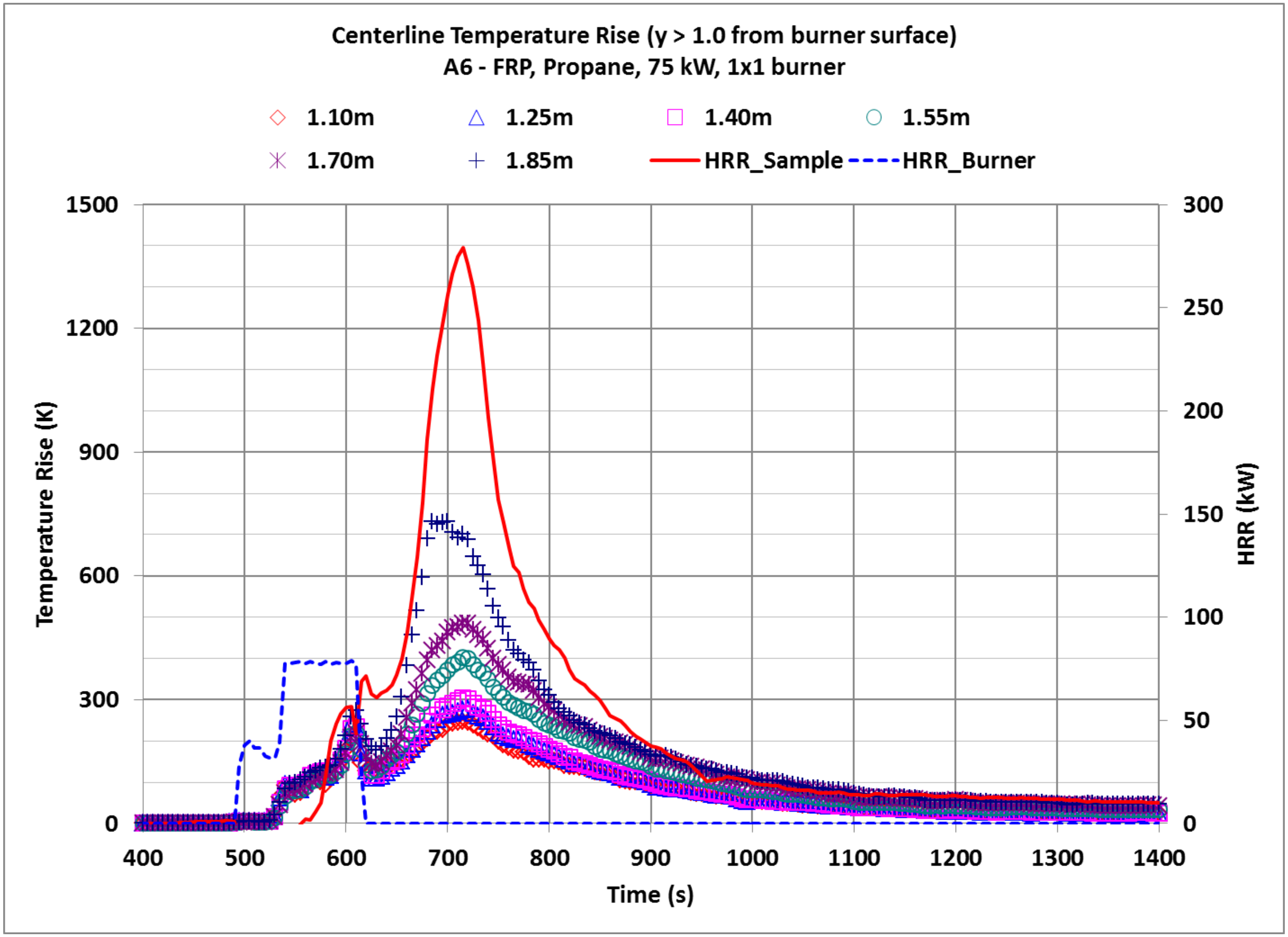

Centerline plume temperature rise measured from 1.10m to 1.85m above the burner surface

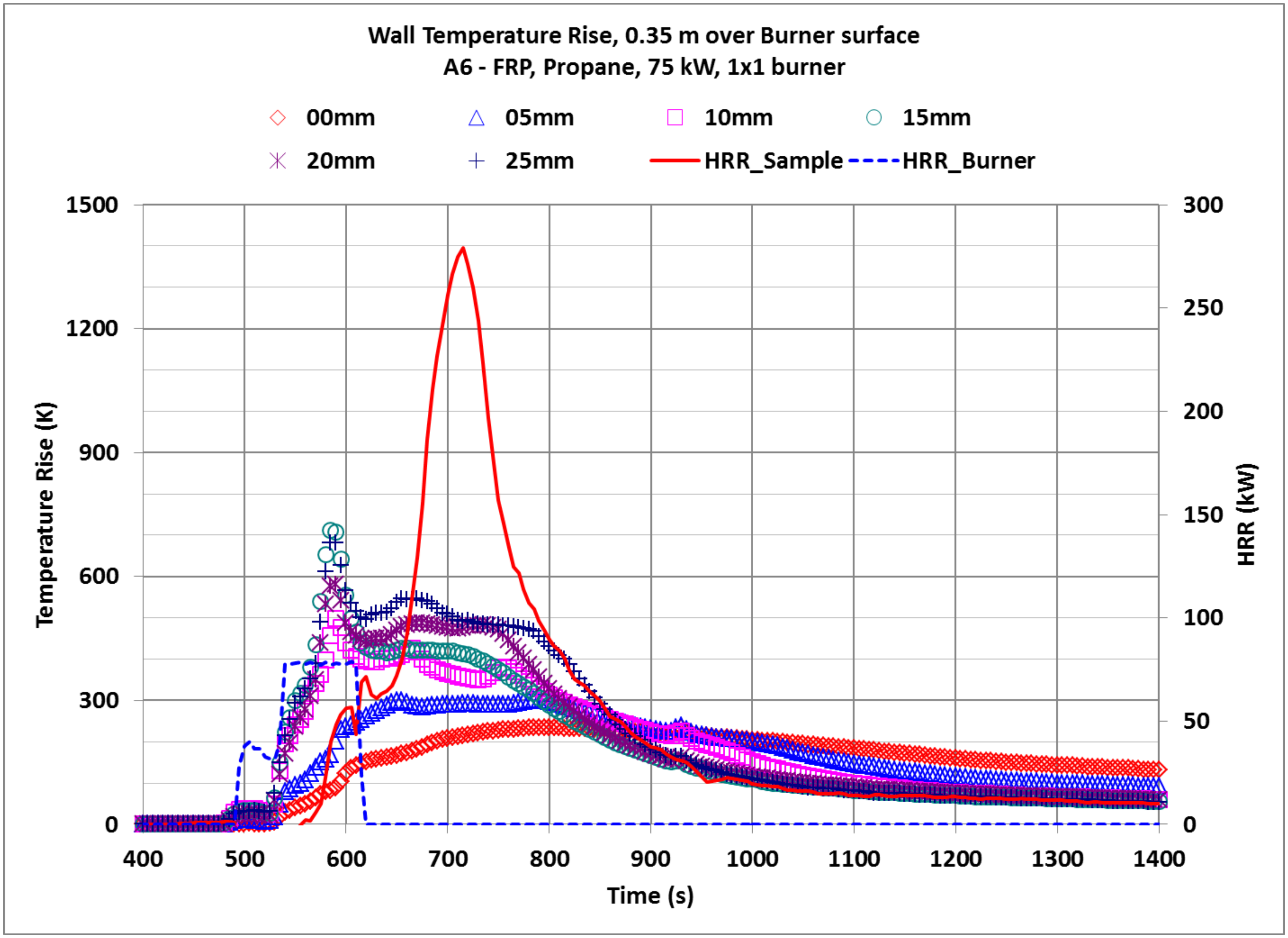

Temperature rise along the wall's centerline at 0.35m over the burner surface, measured at different perpendicular distances to as indicated

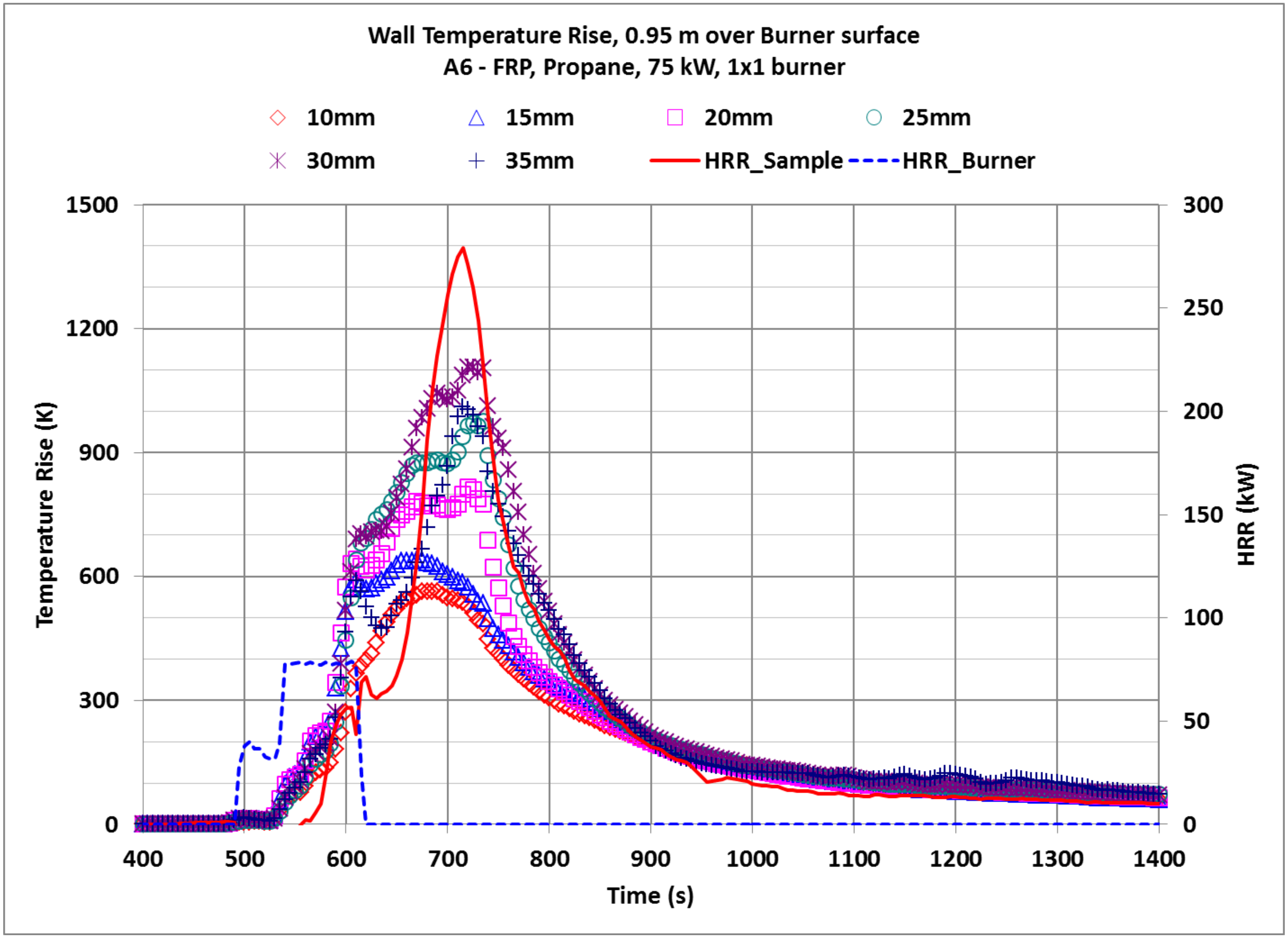

Temperature rise along the wall's centerline at 0.95m over the burner surface, measured at different perpendicular distances to as indicated

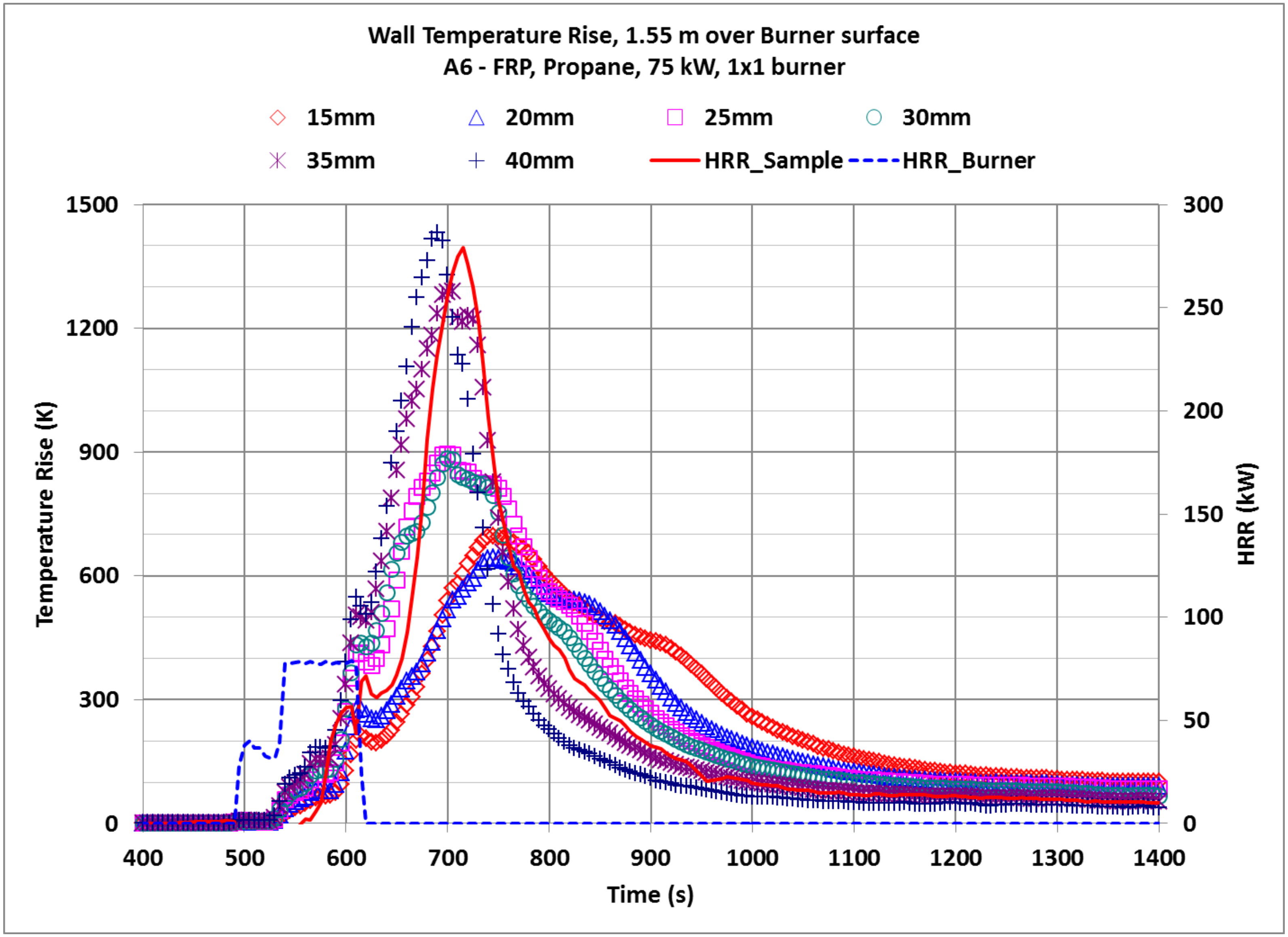

Temperature rise along the wall's centerline at 1.55m over the burner surface, measured at different perpendicular distances to as indicated

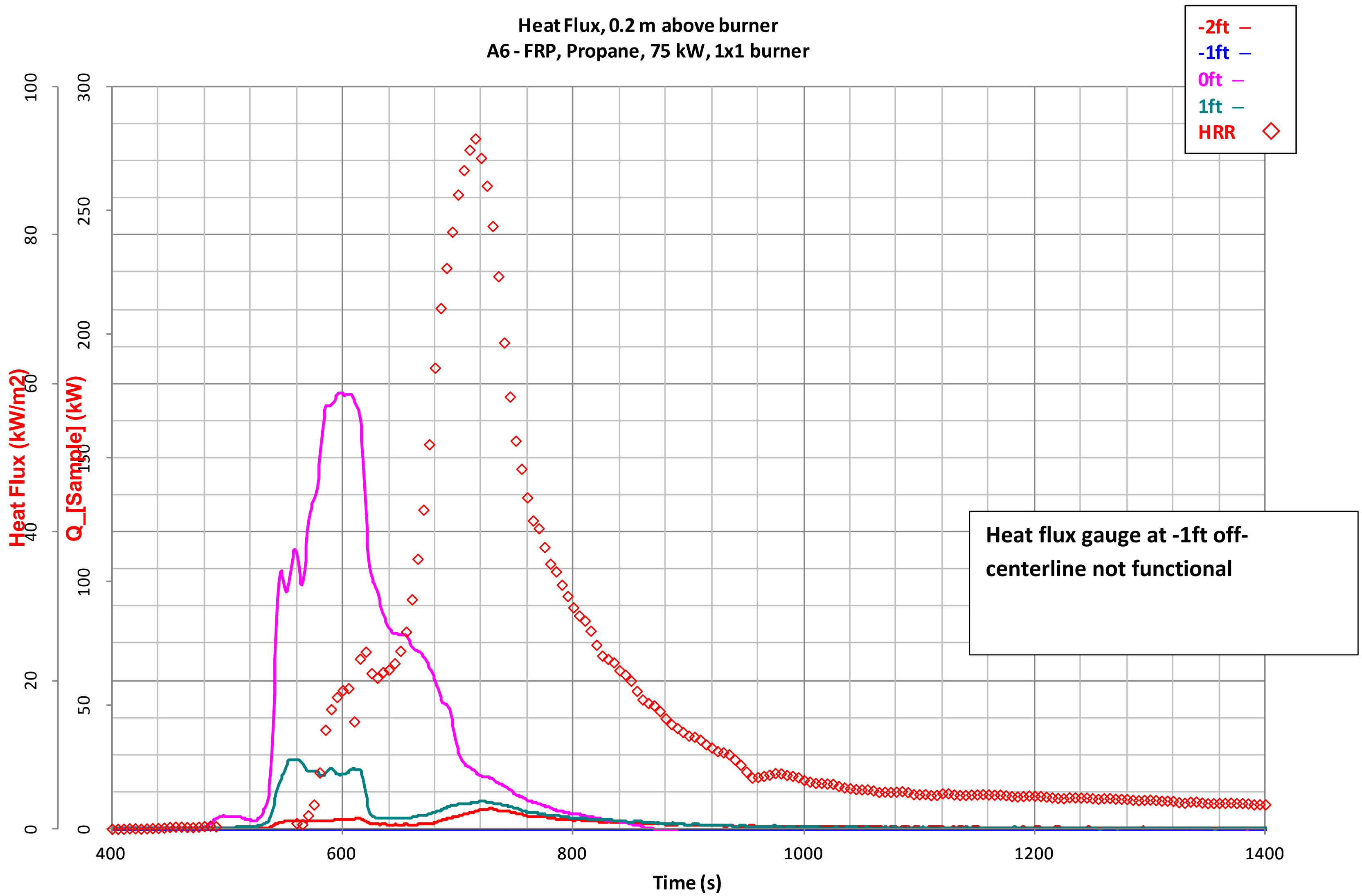

Heat flux measured at various distances from the centerline (negative indicates left of centerline), 0.2m vertically from burner surface

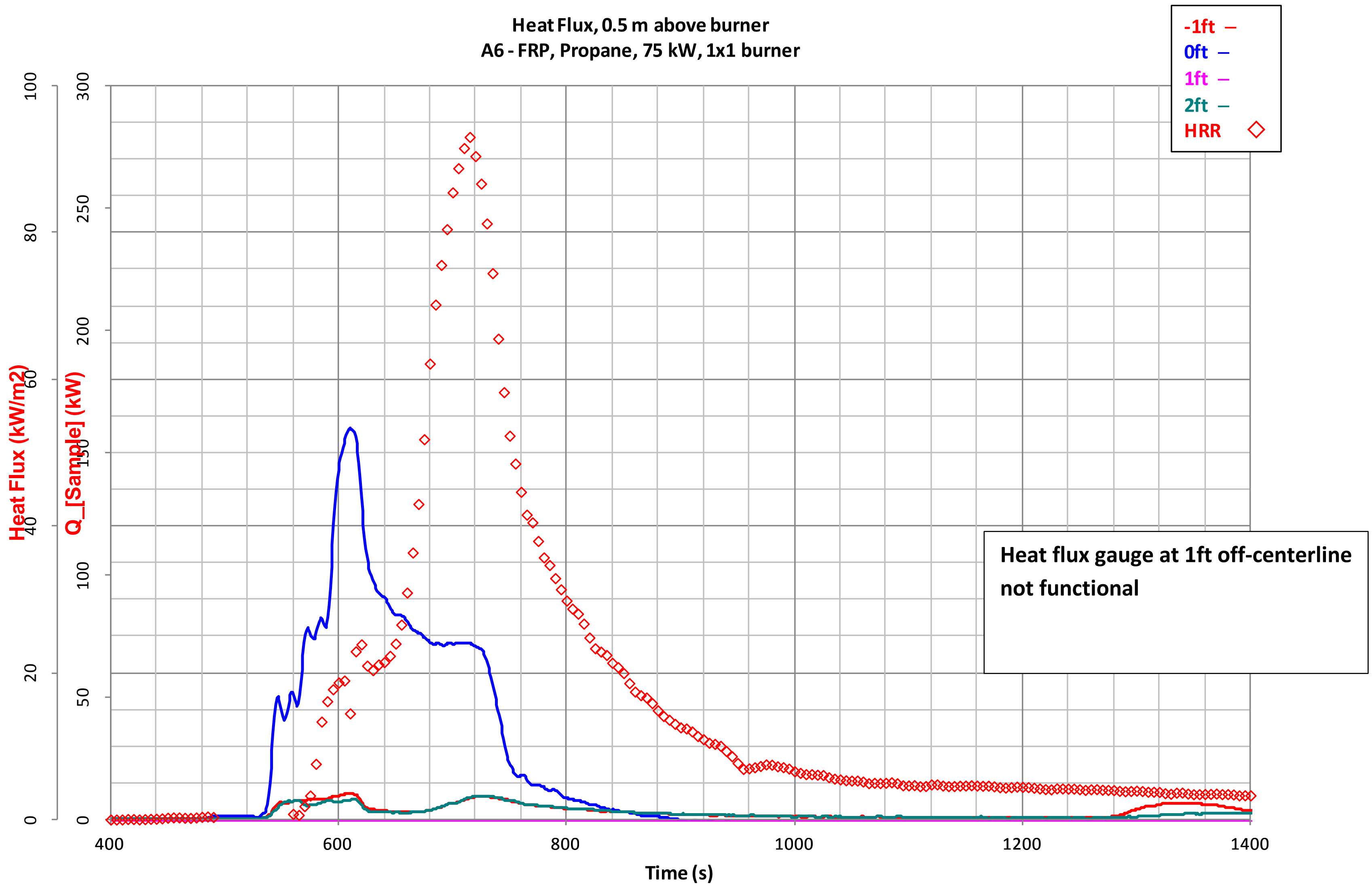

Heat flux measured at various distances from the centerline (negative indicates left of centerline), 0.5m vertically from burner surface

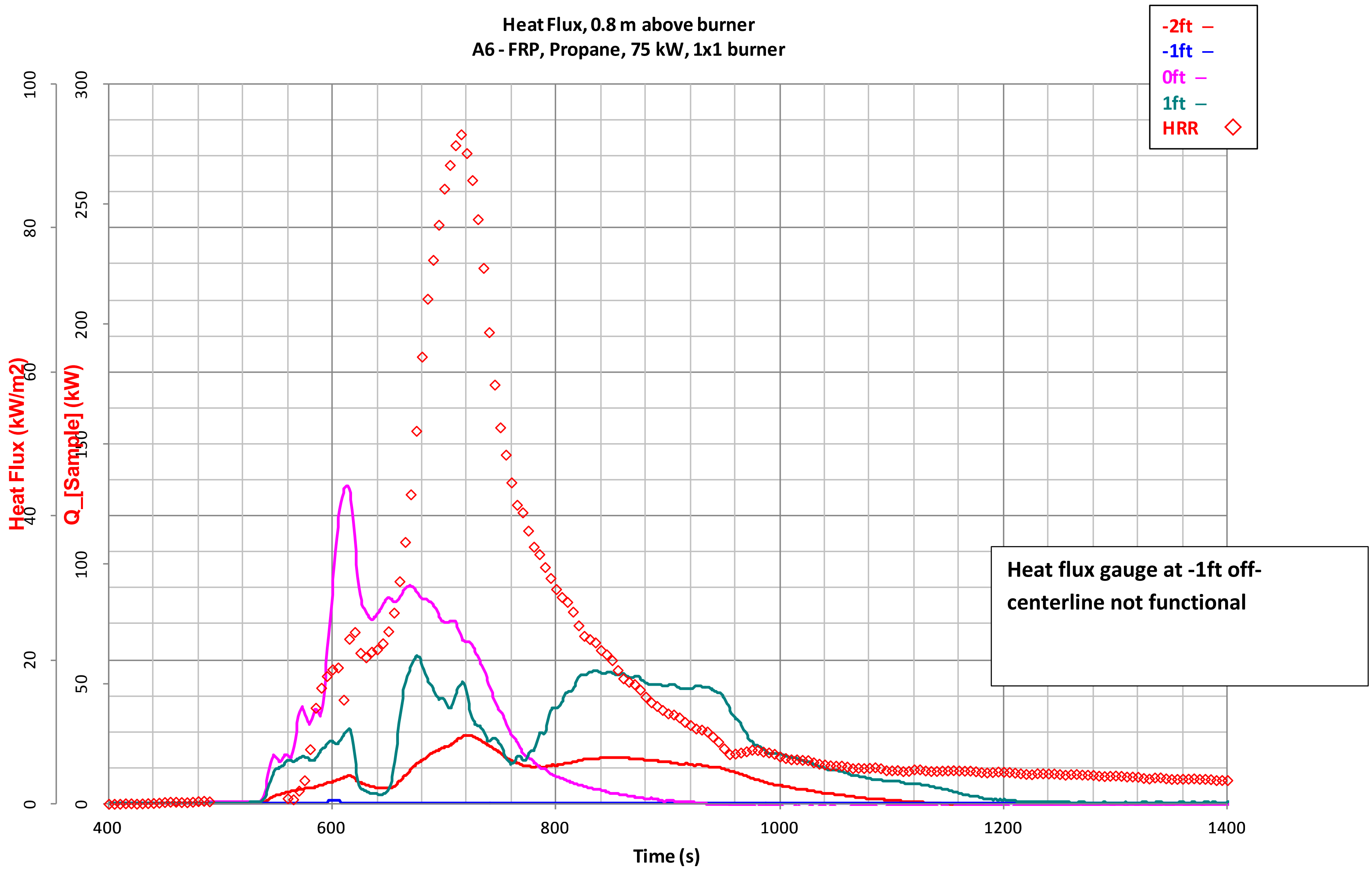

Heat flux measured at various distances from the centerline (negative indicates left of centerline), 0.8m vertically from burner surface

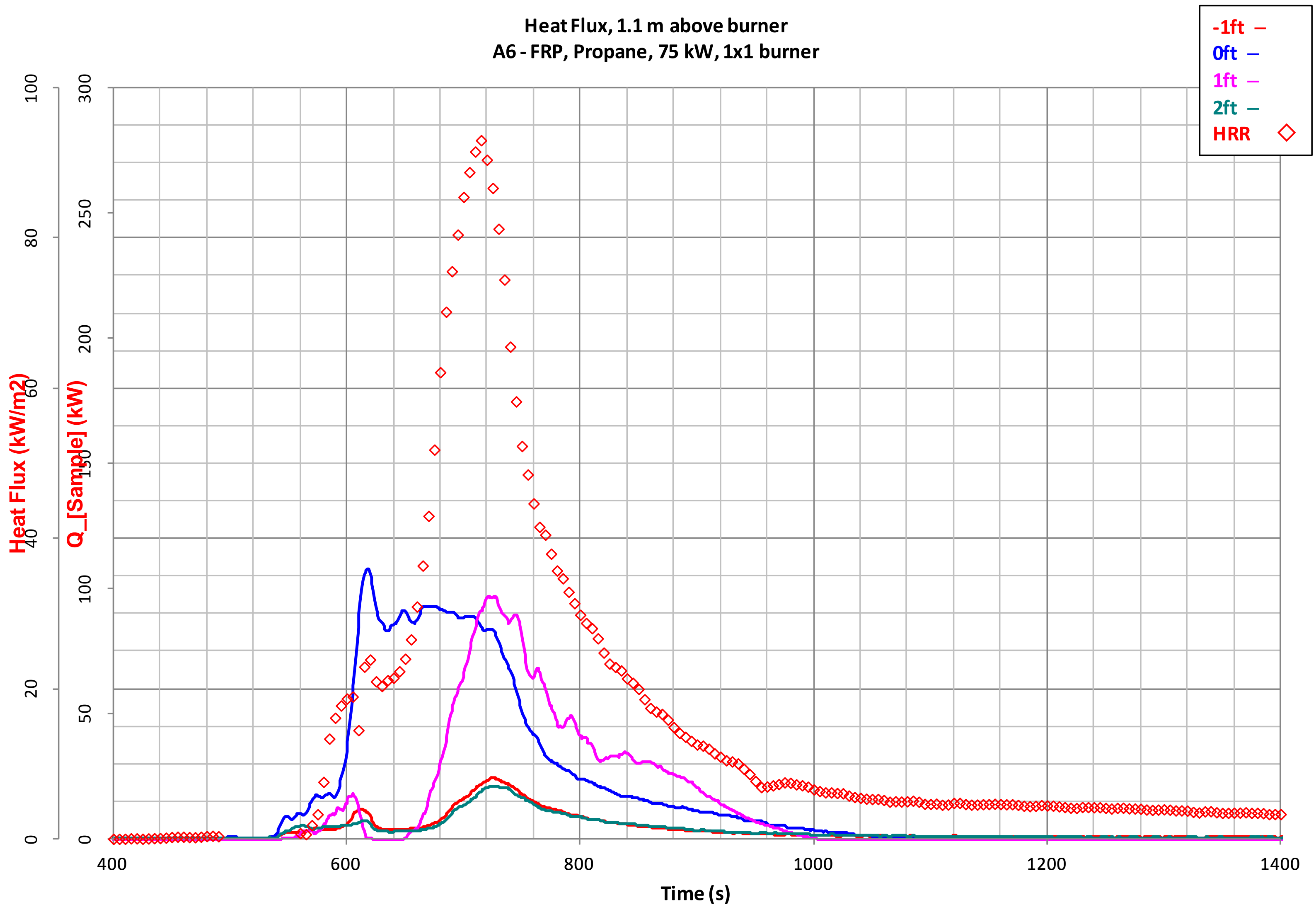

Heat flux measured at various distances from the centerline (negative indicates left of centerline), 1.1m vertically from burner surface

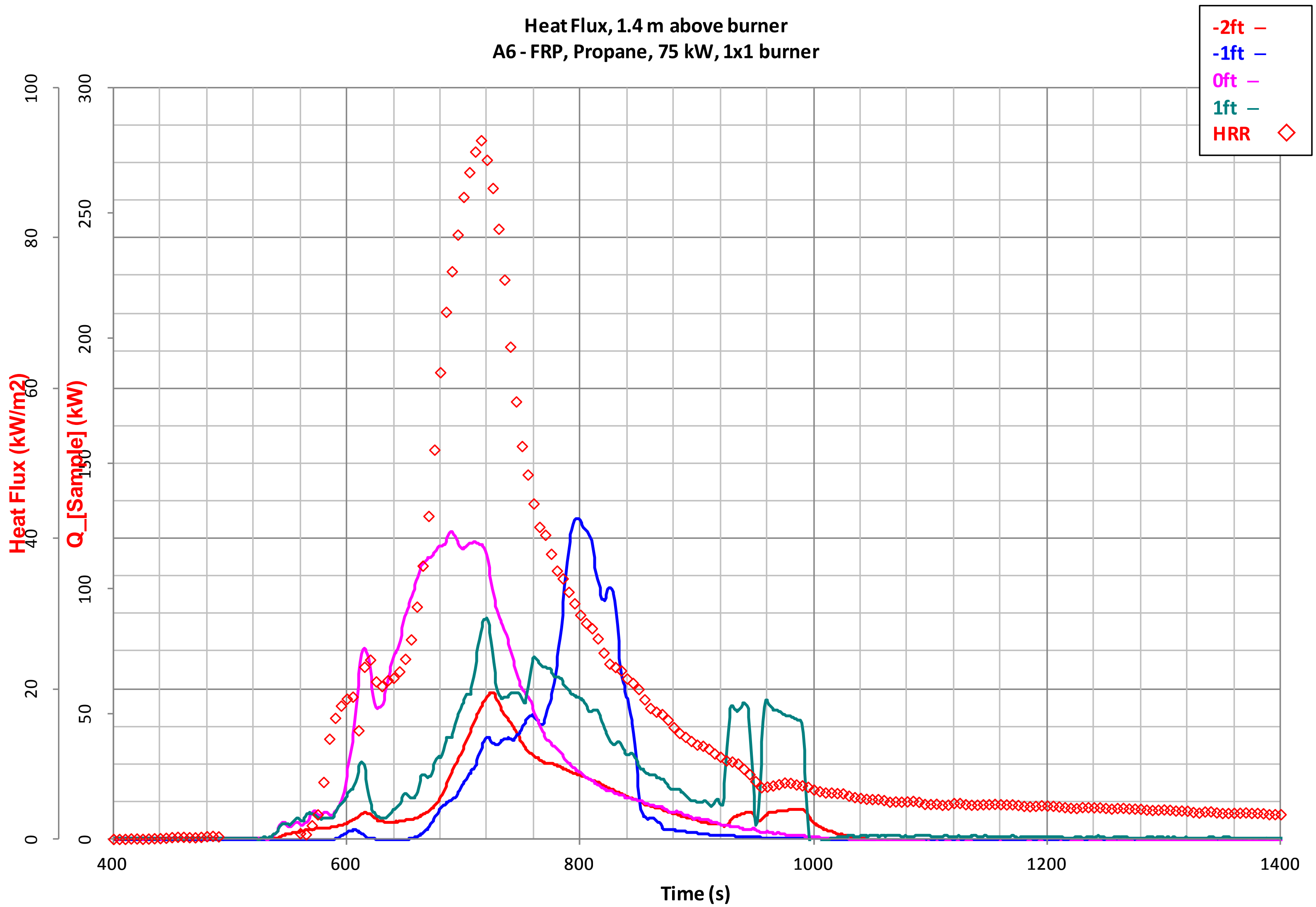

Heat flux measured at various distances from the centerline (negative indicates left of centerline), 1.4m vertically from burner surface

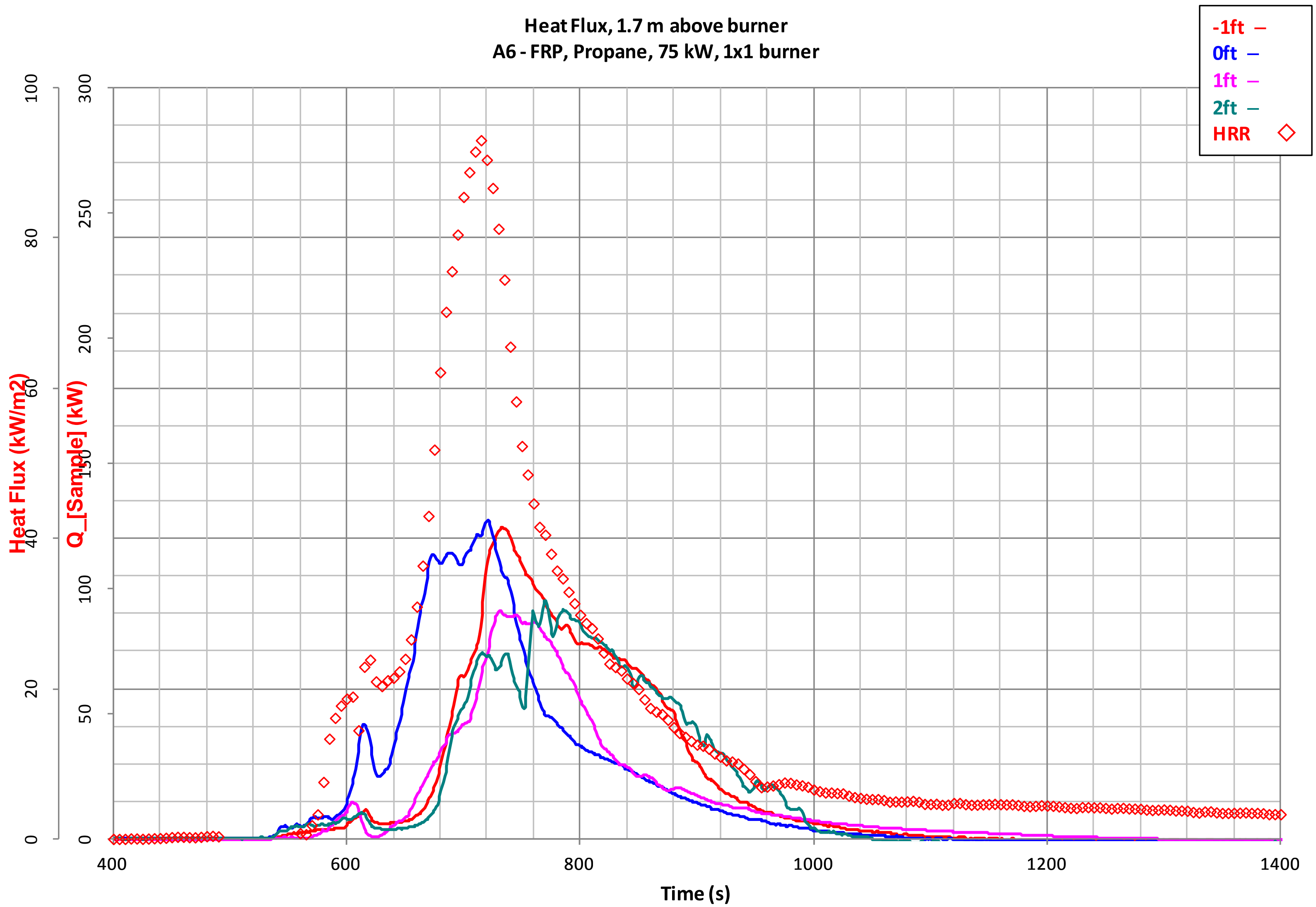

Heat flux measured at various distances from the centerline (negative indicates left of centerline), 1.7m vertically from burner surface

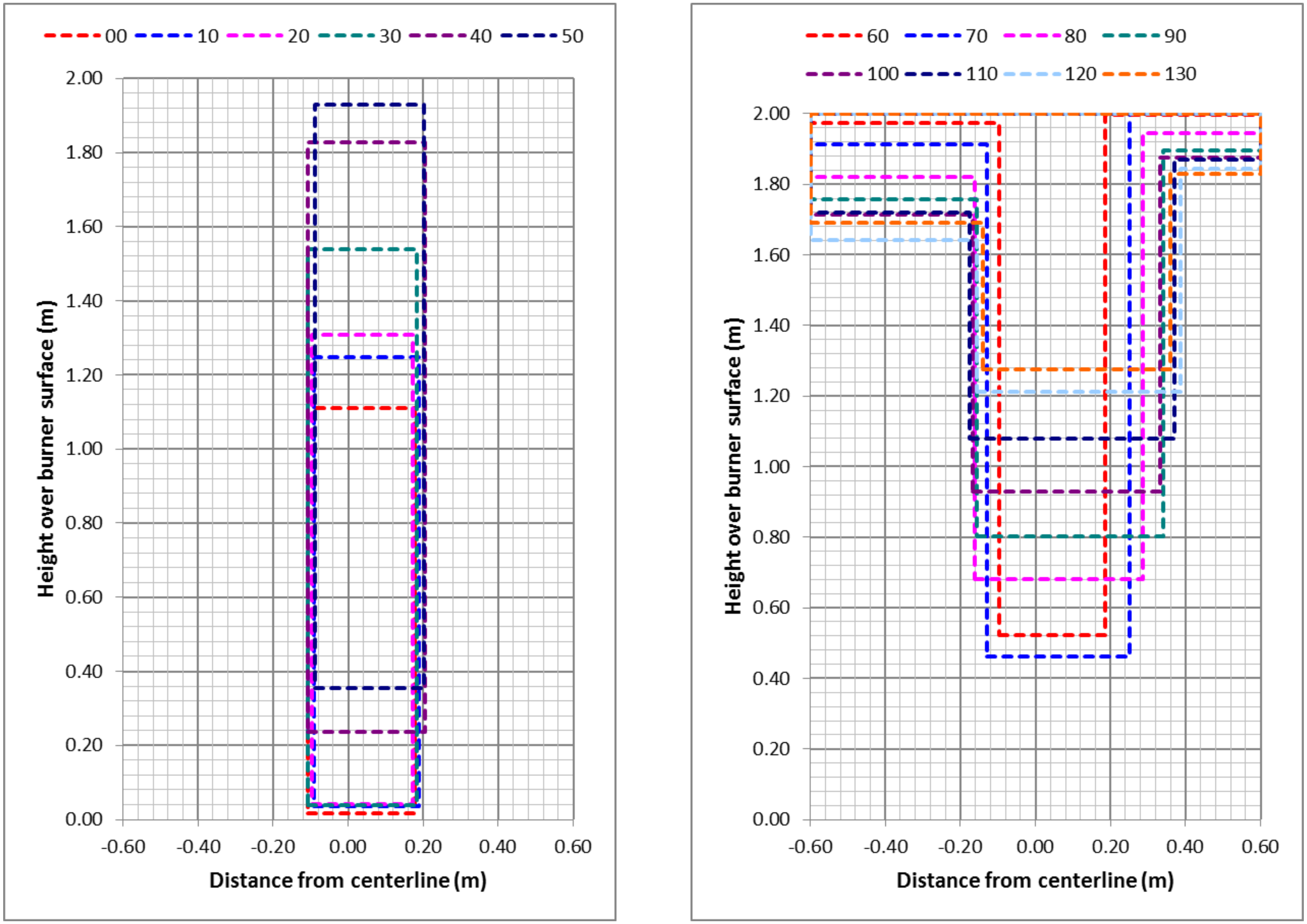

Stages 1 and 2 burning areas in Test A6 (1ft Square burner, Propane, 75 kW source)

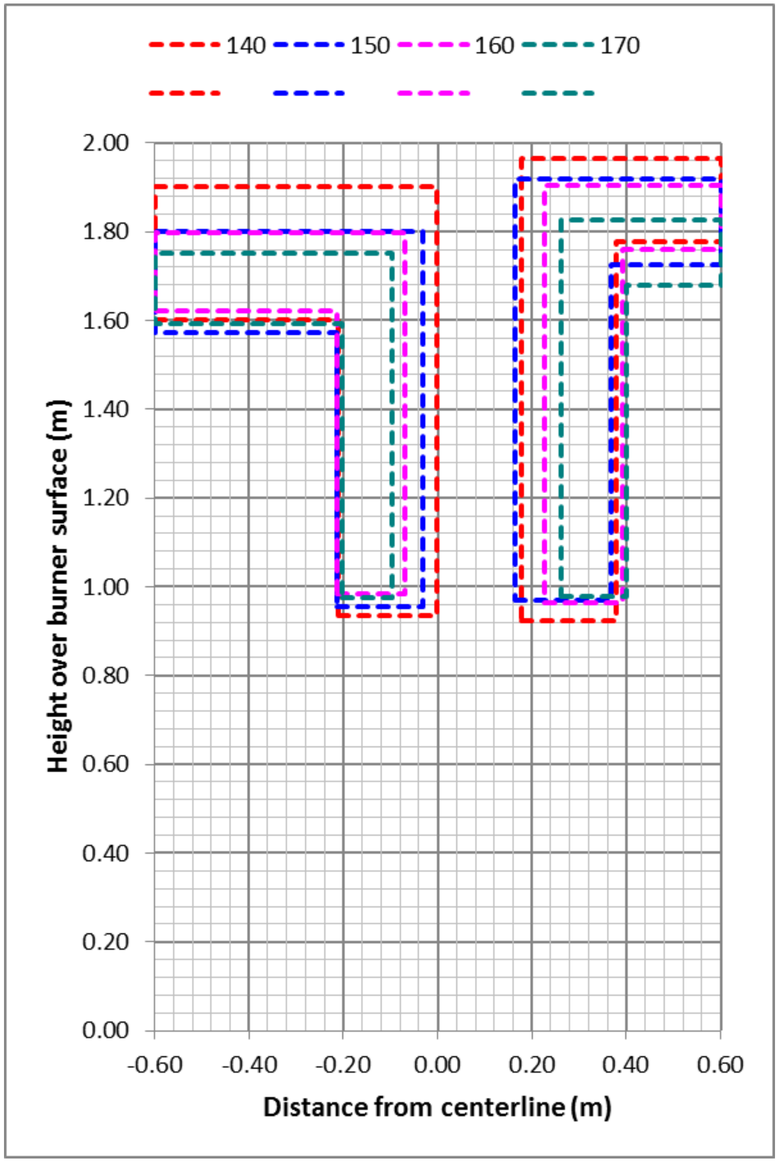

Stage 3 burn area and final damage chart of Test A6 (1ft Square burner, Propane, 75 kW source)

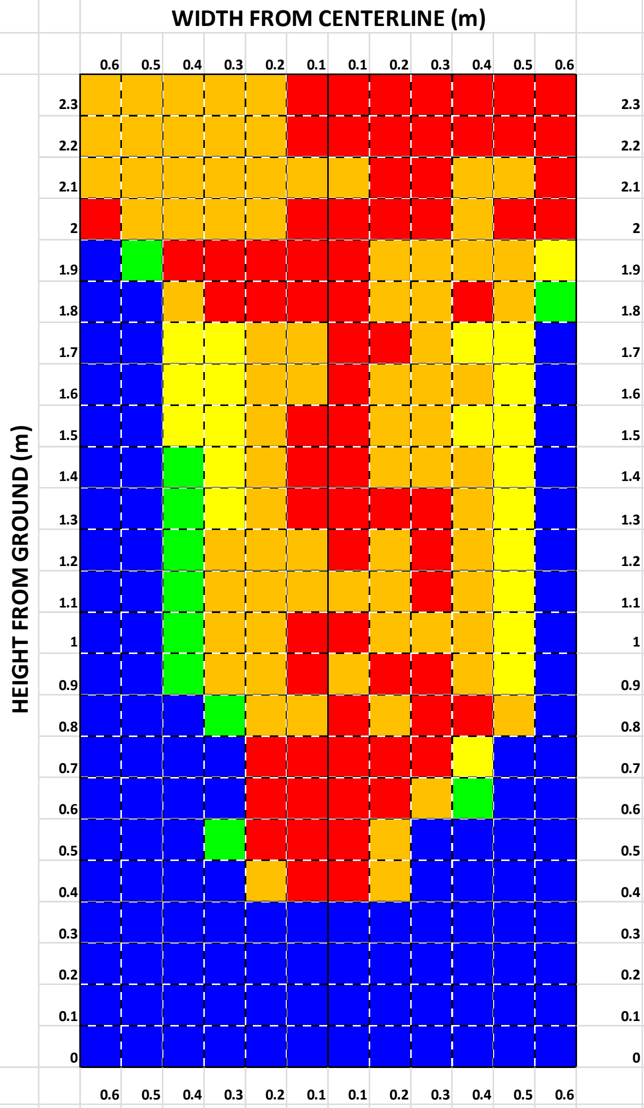

# of cell	Damage to Resin	Area (m2)
70	up to 100% damage	0.7
77	up to 75% damage	0.77
21	up to 50% damage	0.21
11	up to 25% damage	0.11
109	no damage	1.09

Initial mass:	8.32	kg
Final unburnt mass:	3.94	kg
Final burnt mass:	2.54	kg
Total mass loss during fire	1.84	kg

Burn damage pattern observed after fire test

F.3.7 Test A7

LODS Test Run Data

Center for Firesafety Studies

100 Institute Road
Worcester, MA 01609
Phone: (508) 831-5628
Fax: (508) 831-5680

Test Information

Test Number:	A7
Specimen Identification:	FRP 7, 50 kW initial Propylene fire, 1 x 1 burner
Material Name:	Class C FRP panel
Manufacturer/Submitter:	Not Reported
Raw Data File Name:	Test A7 - FRP_50kW_Propylene_1ft.txt
Reduced Data File Name:	Test A7 - FRP_50kW_Propylene_1ft_reduced.xlsx
Date of Test:	8-Nov-2010
Tester:	W. Wong

Test Parameters

Ambient Temperature:	N/A
Relative Humidity:	N/A

Specimen Information

Specimen Initial Mass:	[kg]	8.2
Specimen Final Mass:	[kg]	6.2
Mass Lost:	[kg]	2.0
Heat Evolved (net):	[kJ]	0

Parameter	Unit	Value
Mass Loss		
Initial Mass	[kg]	8.2
Final Mass	[kg]	6.2
Mass Loss	[%]	23.96

LODS Test Run Data

Center for Firesafety Studies

100 Institute Road
Worcester, MA 01609
Phone: (508) 831-5628
Fax: (508) 831-5680

Test Notes

Test Number:		0
Date:	11/08/10	
Material:	Class C FRP panel	
Specimen Identification:	FRP 7, 50 kW initial Propylene fire, 1 x 1 burner	

Observations

Time	Observation
00:00	Start VI
05:30	Start Camera 1
05:40	Start Camera 2
08:00	Burner ignition
08:15	Reach target HRR @ 50 kW
08:33	Crackling noise
08:48	Panel ignition
09:10	Burner off
09:46	Remote area ignition @ TSC-3, TSC-9, insignificant, intermittent
	Remote area smoking @ TSC-4 until after rollover
	Remote area smoking on right edge @ y = 0.5m, TSC-6 for 7 min
10:15	Flame hit ceiling
10:50	T-pattern burning under ceiling
11:15	Rollover
11:16	Some edge burning on right edge @ 1.6m, ignited by rollover
36:00	Only burning is on right edge @ y = 1.0m to 1.7 m
39:00	Terminate test with little water application

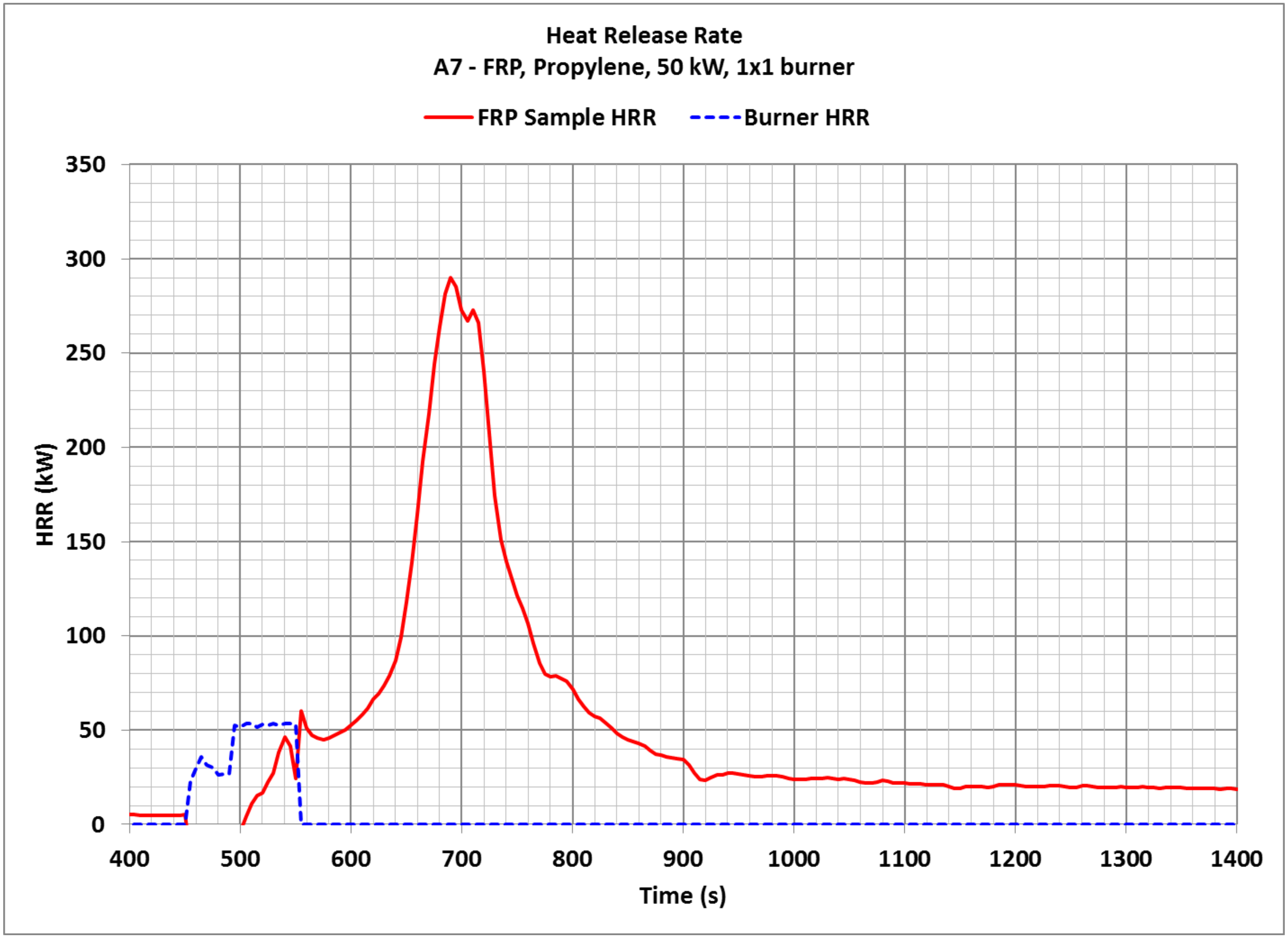

Heat release ratesof the source burner fire and of the specimen fire measured during test

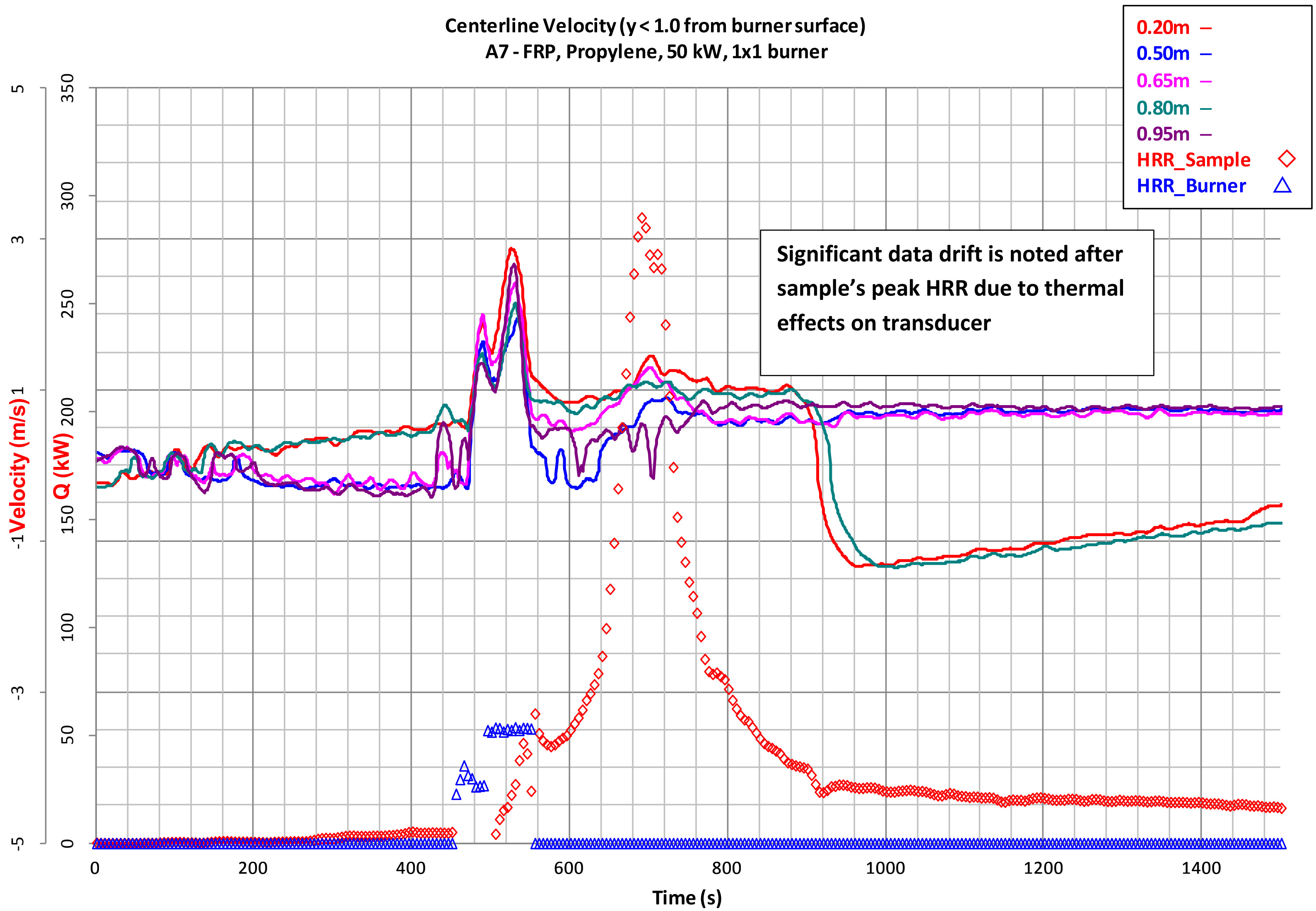

Centerline plume velocities measured from 0.2m to 0.95m above the burner surface

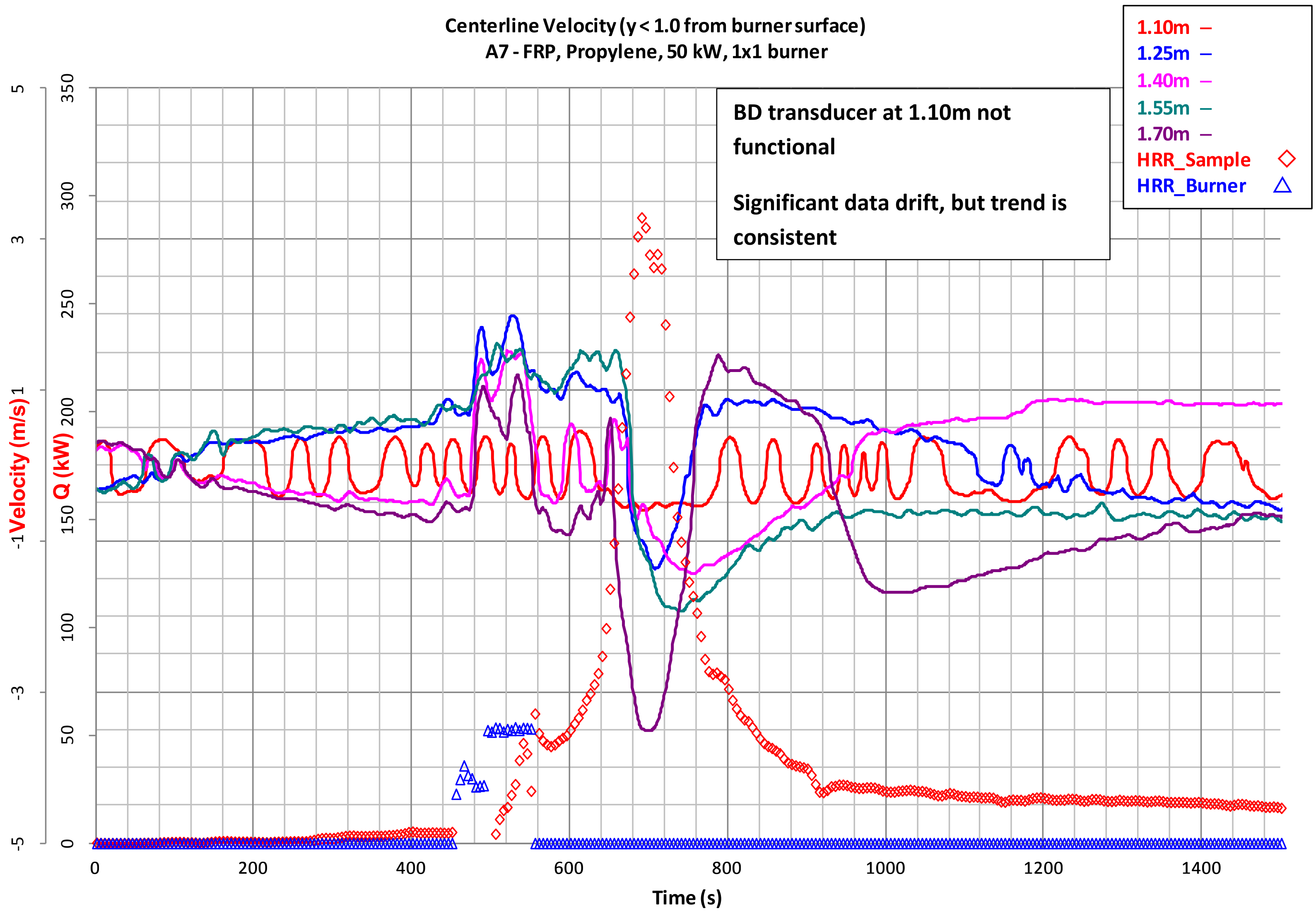

Centerline plume velocities measured from 1.1m to 1.7m above the burner surface

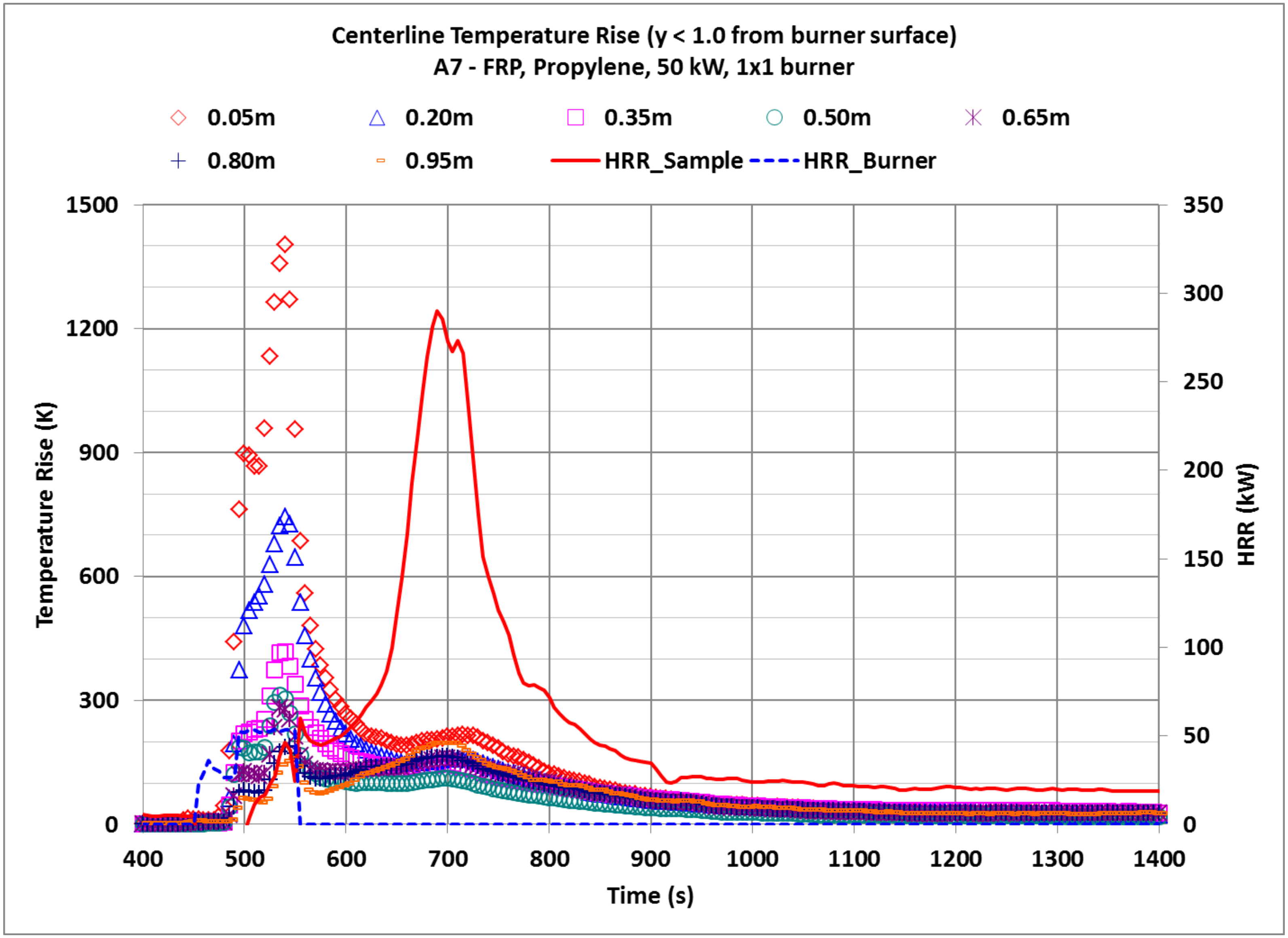

Centerline plume temperature rise measured from 0.05m to 0.95m above the burner surface

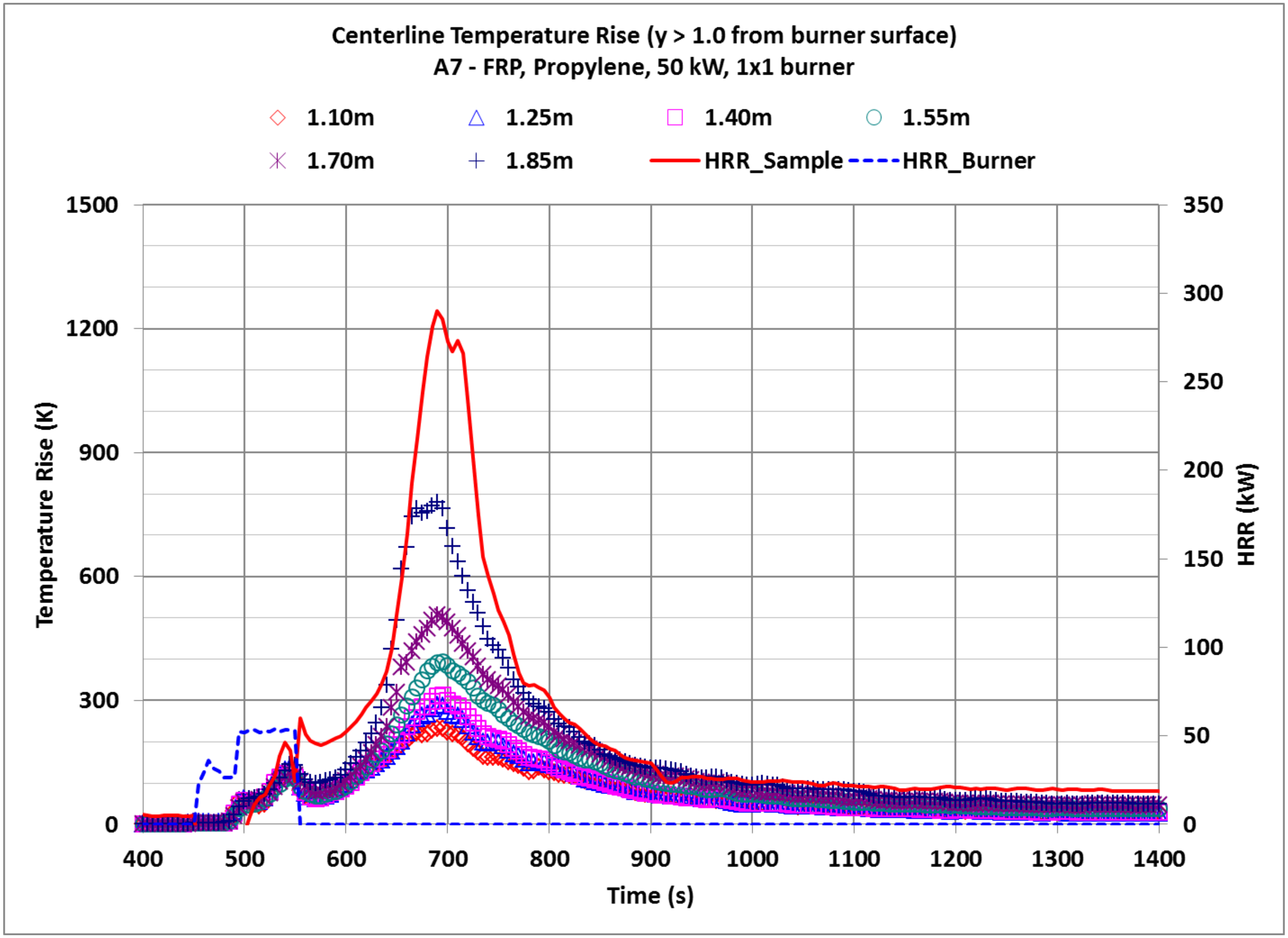

Centerline plume temperature rise measured from 1.10m to 1.85m above the burner surface

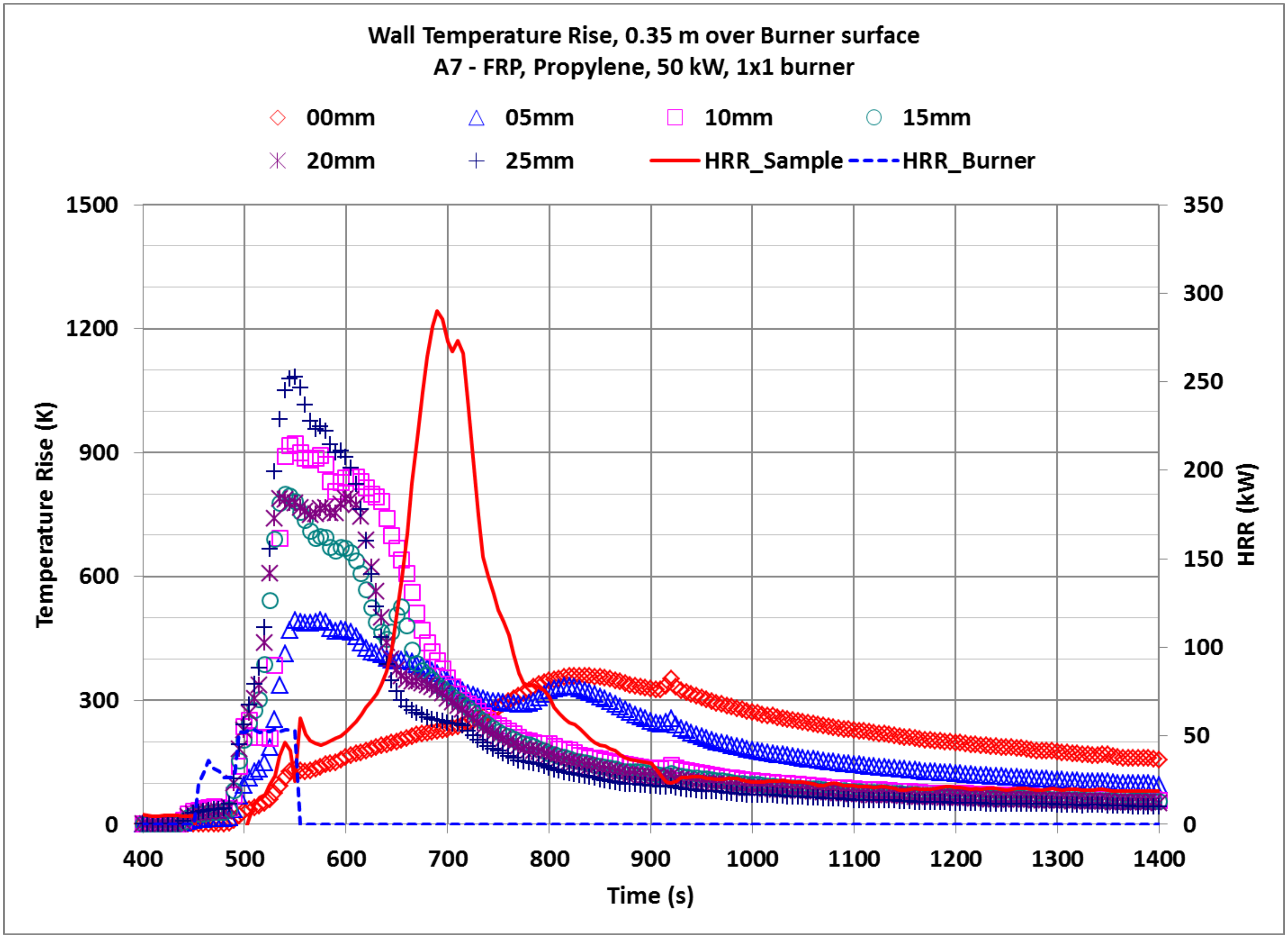

Temperature rise along the wall’s centerline at 0.35m over the burner surface, measured at different perpendicular distances to as indicated

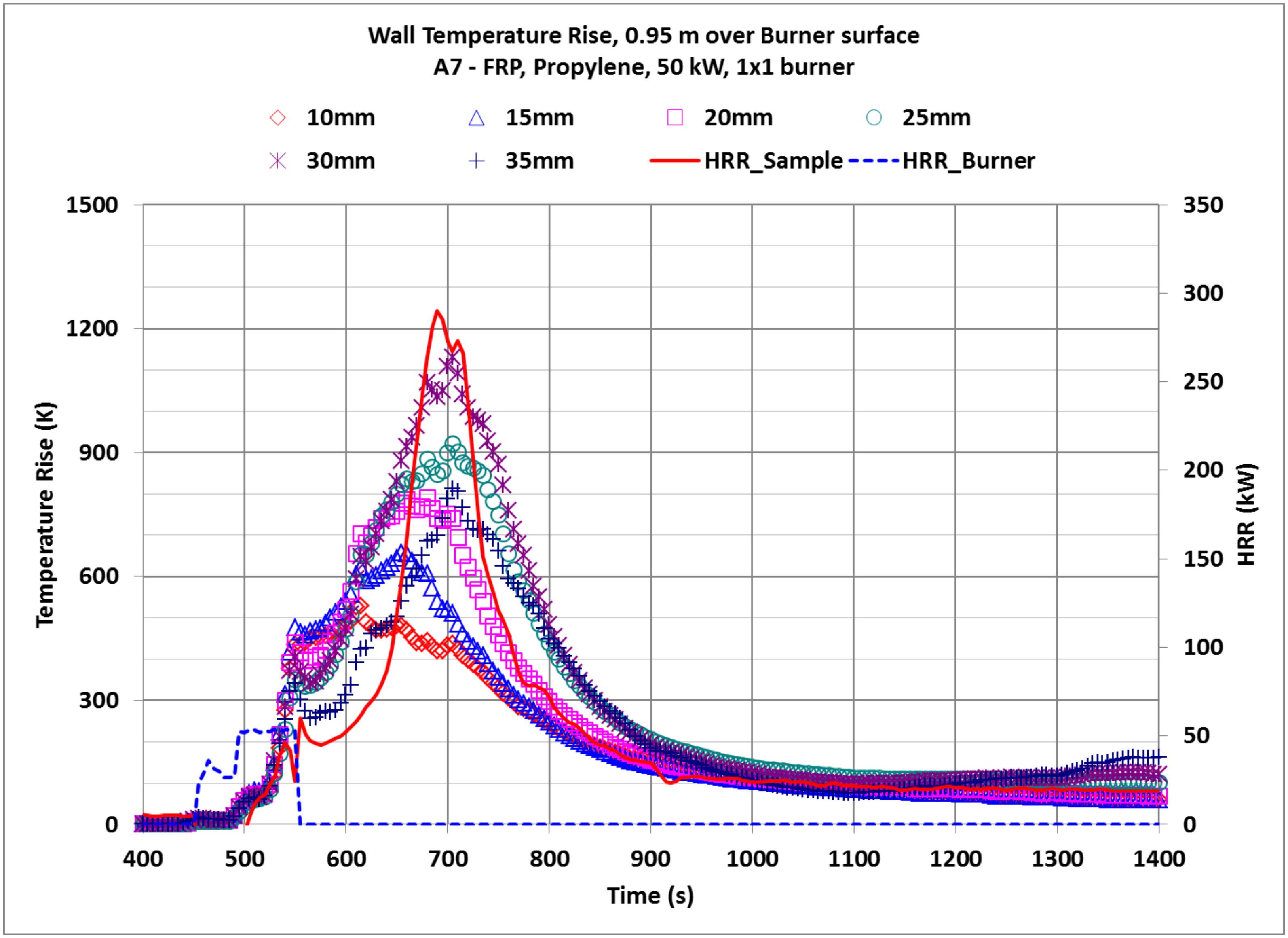

Temperature rise along the wall's centerline at 0.95m over the burner surface, measured at different perpendicular distances to as indicated

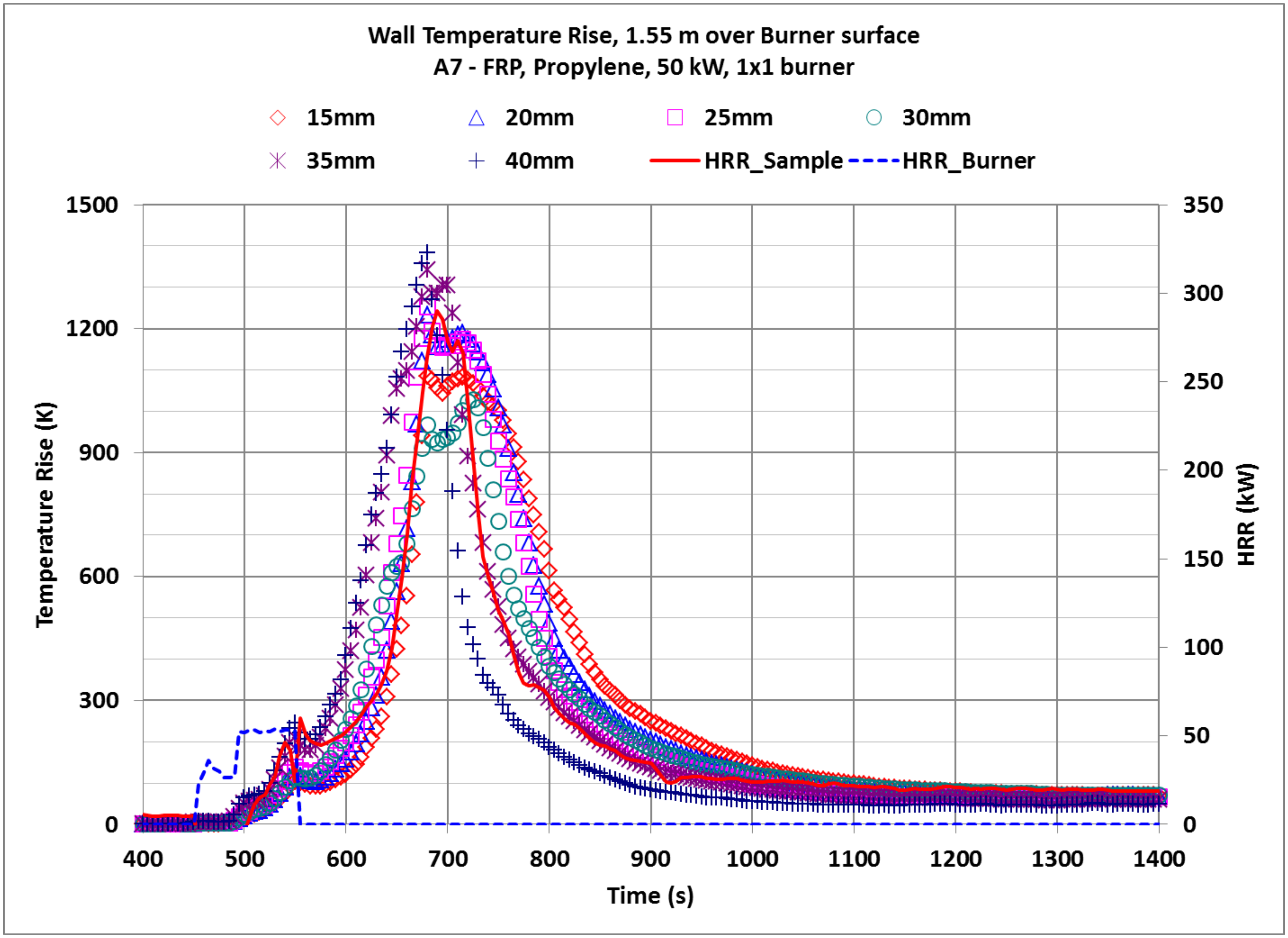

Temperature rise along the wall's centerline at 1.55m over the burner surface, measured at different perpendicular distances to as indicated

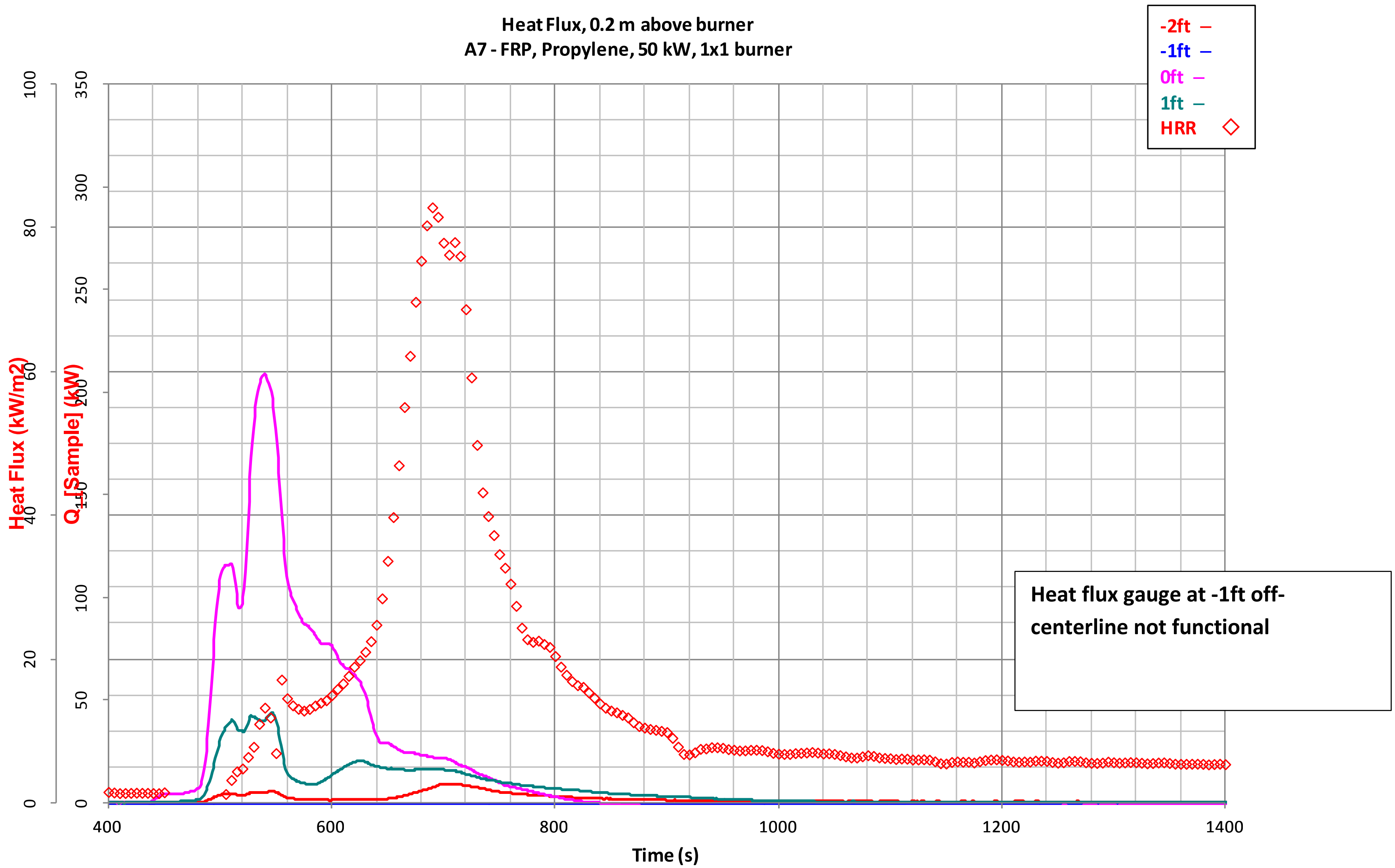

Heat flux measured at various distances from the centerline (negative indicates left of centerline), 0.2m vertically from burner surface

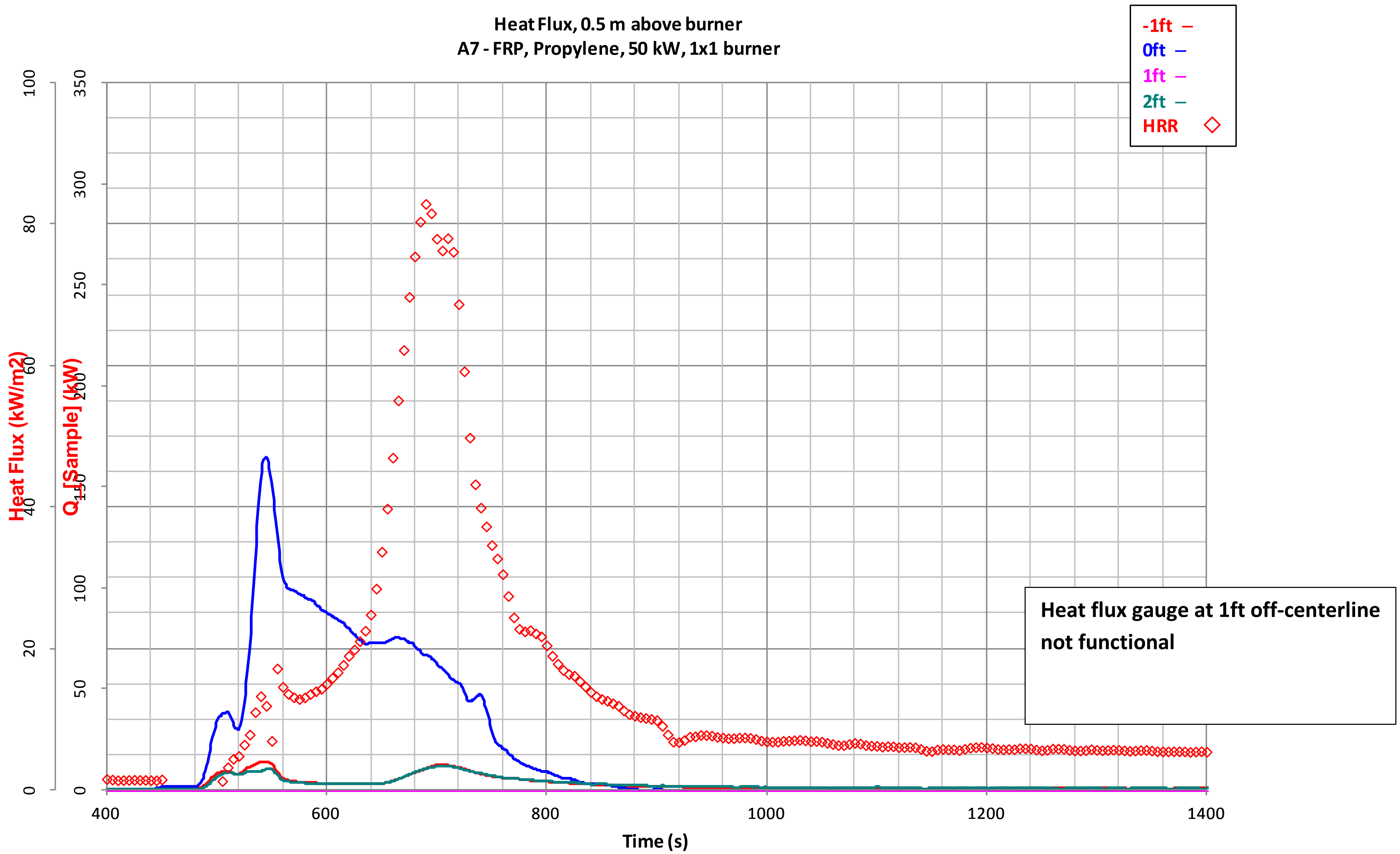

Heat flux measured at various distances from the centerline (negative indicates left of centerline), 0.5m vertically from burner surface

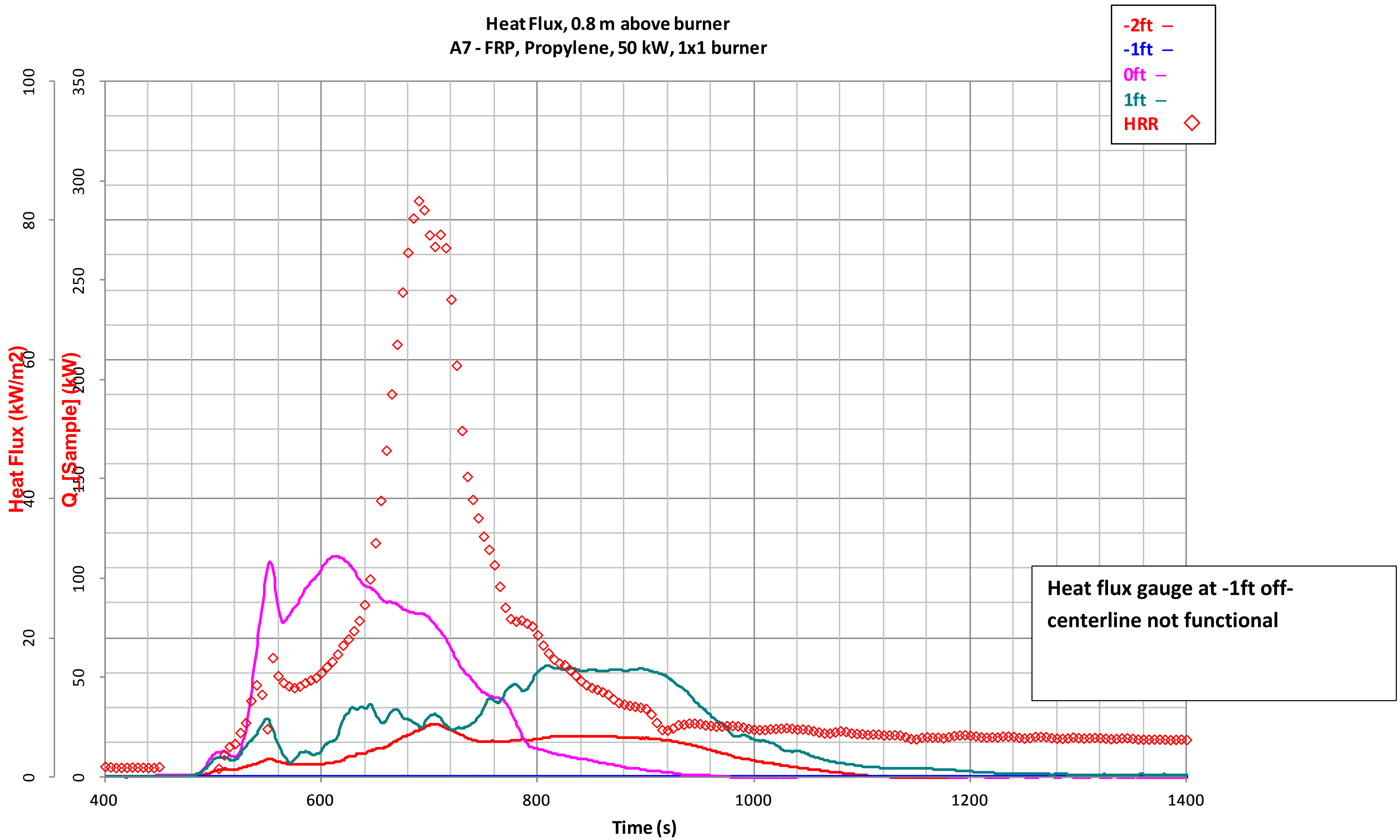

Heat flux measured at various distances from the centerline (negative indicates left of centerline), 0.8m vertically from burner surface

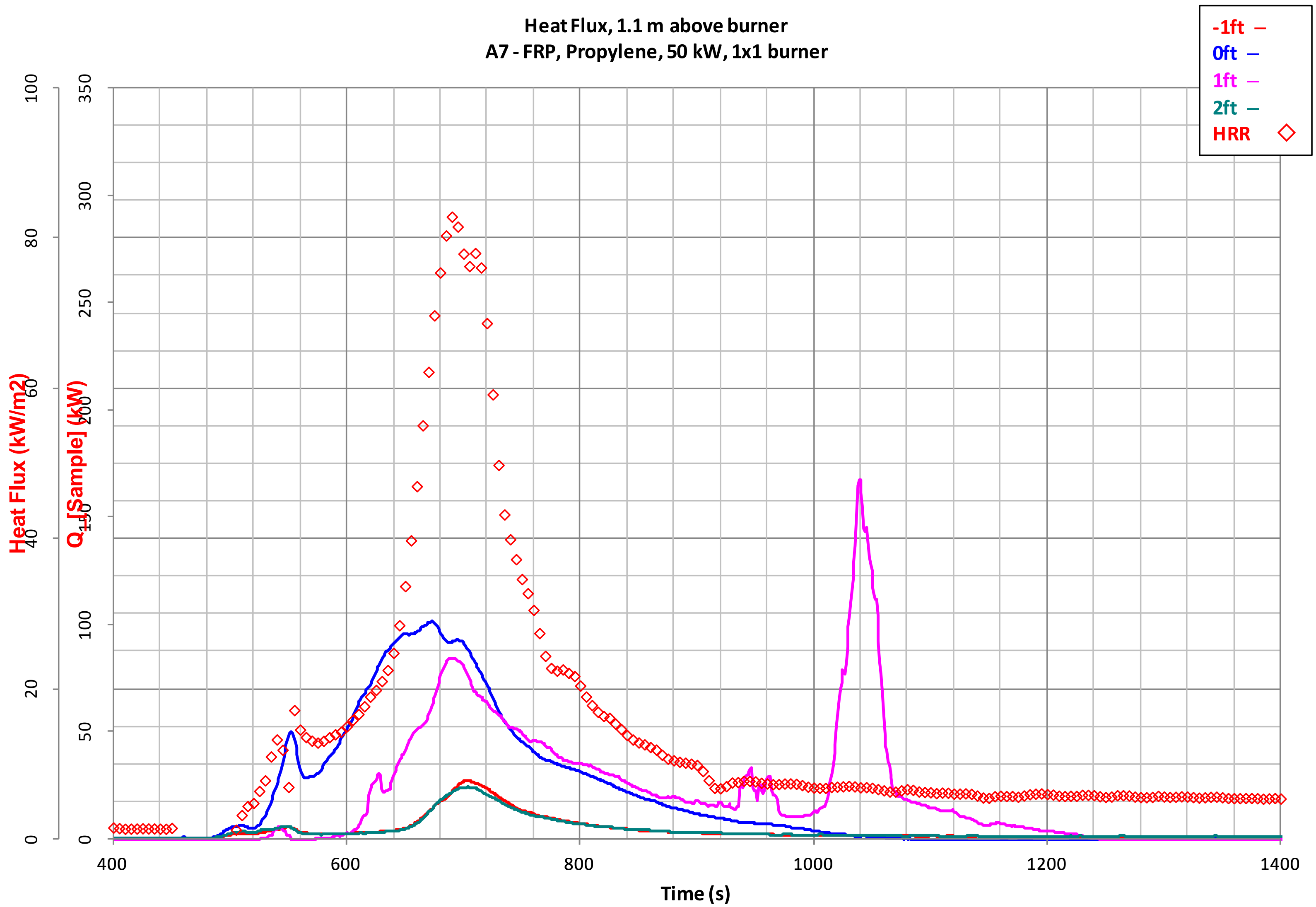

Heat flux measured at various distances from the centerline (negative indicates left of centerline), 1.1m vertically from burner surface

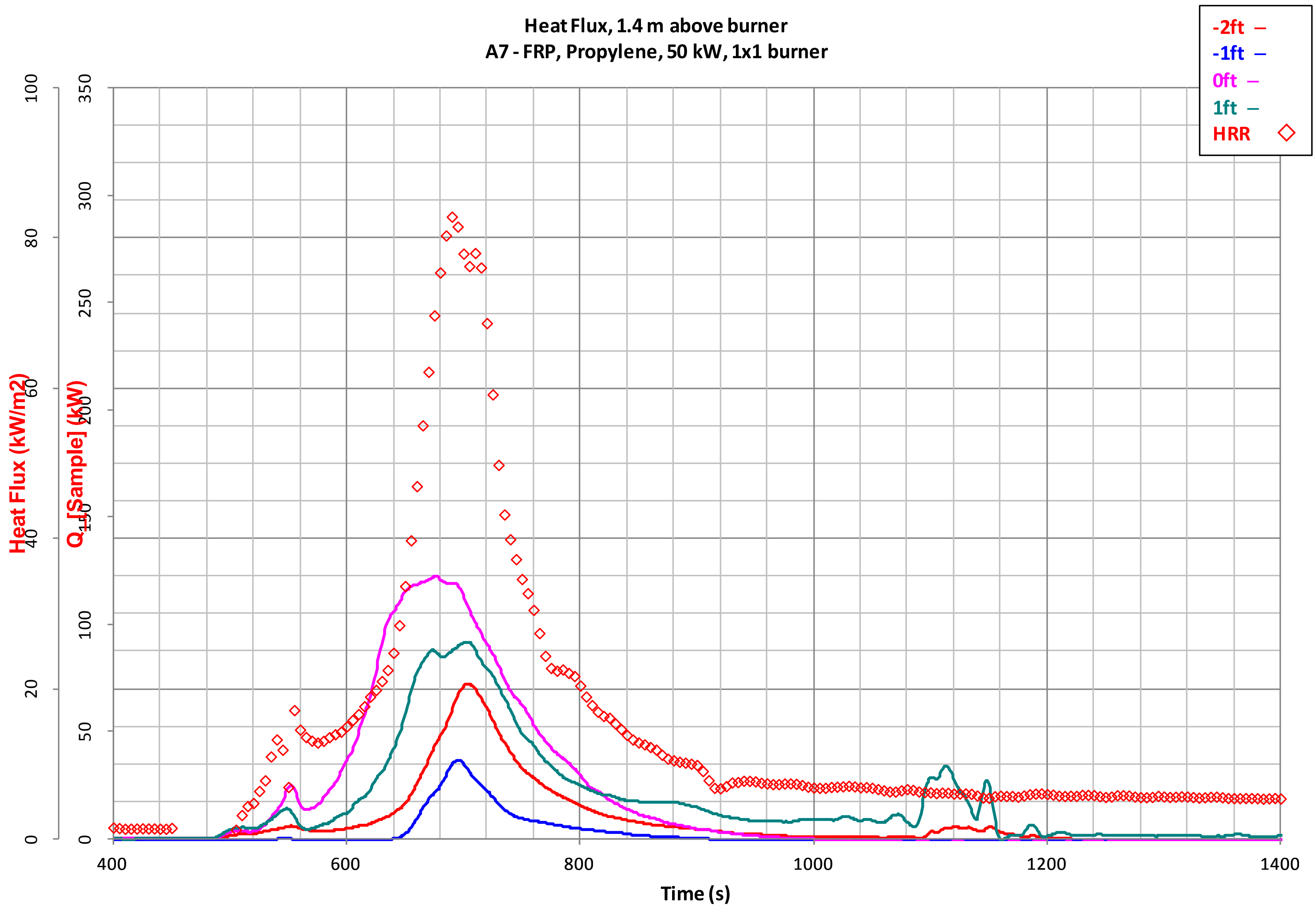

Heat flux measured at various distances from the centerline (negative indicates left of centerline), 1.4m vertically from burner surface

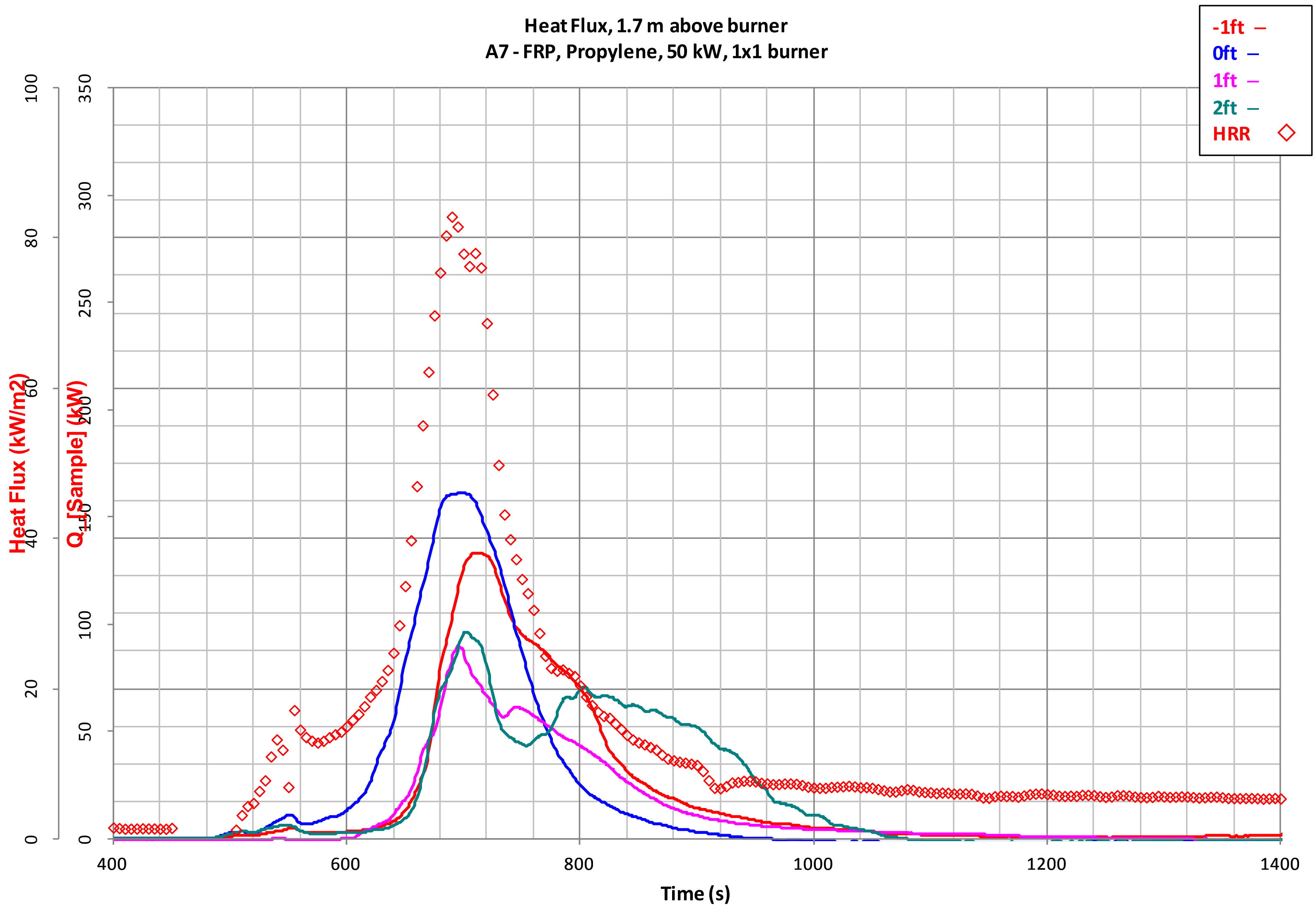

Heat flux measured at various distances from the centerline (negative indicates left of centerline), 1.7m vertically from burner surface

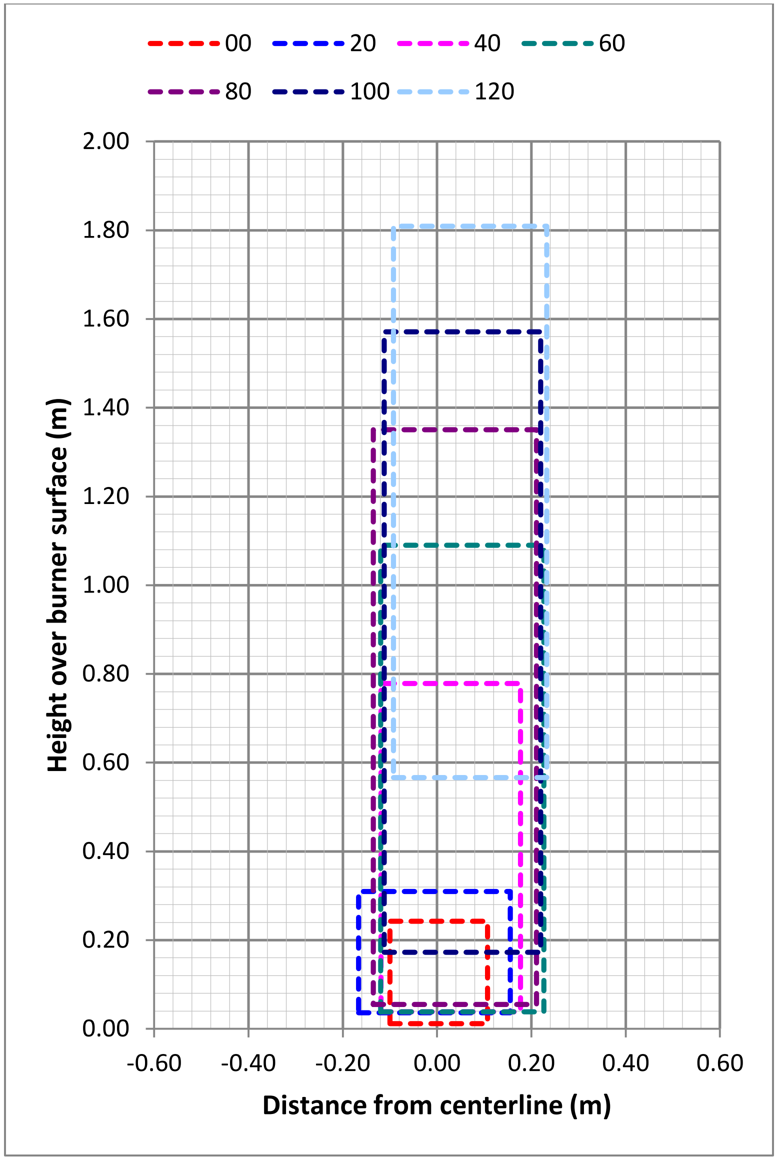

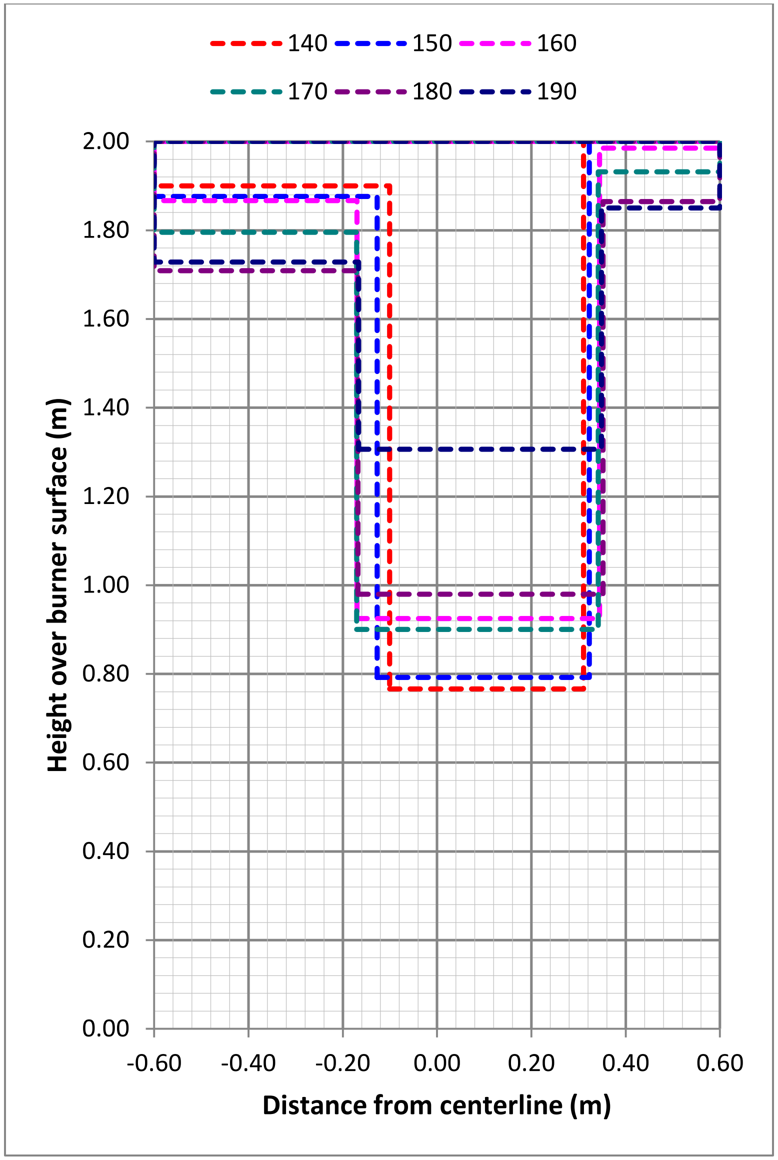

Stages 1 and 2 burning areas in Test A7 (1ft Square burner, Propylene, 50 kW source)

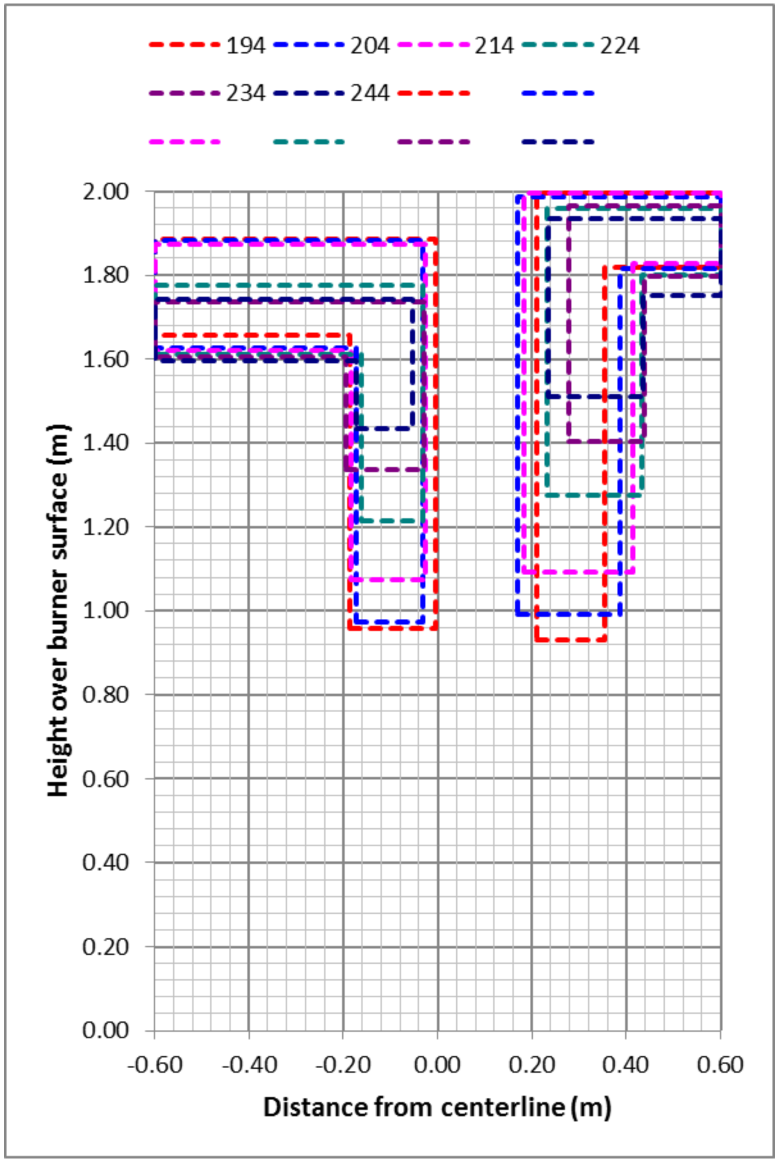

Stage 3 burn area and final damage chart of Test A7 (1ft Square burner, Propylene, 50 kW source)

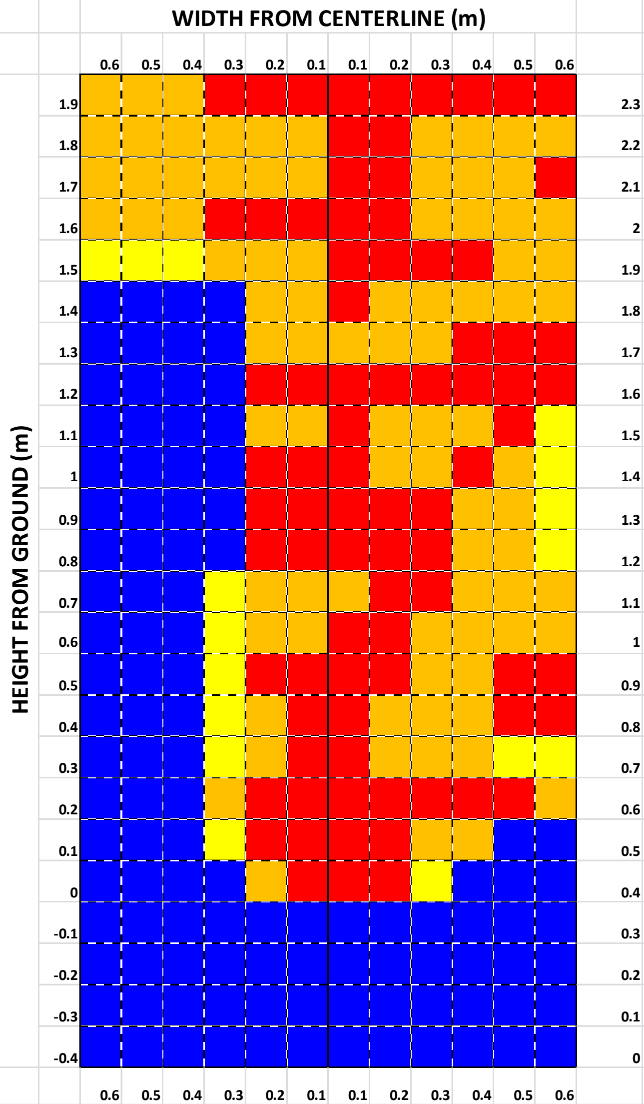

# of cell	Damage to Resin	Area (m2)
81	up to 100% damage	0.81
85	up to 75% damage	0.85
16	up to 50% damage	0.16
0	up to 25% damage	0
106	no damage	1.06

Initial mass:	8.18	kg
Final unburnt mass:	3.44	kg
Final burnt mass:	2.78	kg
Total mass loss during fire	1.96	kg

Burn damage pattern observed after fire test

F.3.8 Test A8

LODS Test Run Data

Center for Firesafety Studies

100 Institute Road
Worcester, MA 01609
Phone: (508) 831-5628
Fax: (508) 831-5680

Test Information

Test Number:	A8
Specimen Identification:	FRP 8, 75 kW initial Propylene fire, 1 x 1 burner
Material Name:	Class C FRP panel
Manufacturer/Submitter:	Not Reported
Raw Data File Name:	Test A8 - FRP_75kW_Propylene_1ft.txt
Reduced Data File Name:	Test A8 - FRP_75kW_Propylene_1ft_reduced.xlsx
Date of Test:	9-Nov-2010
Tester:	W. Wong

Test Parameters

Ambient Temperature:	N/A
Relative Humidity:	N/A

Specimen Information

Specimen Initial Mass:	[kg]	8.1
Specimen Final Mass:	[kg]	6.2
Mass Lost:	[kg]	1.9
Heat Evolved (net):	[kJ]	0

Parameter	Unit	Value
Mass Loss		
Initial Mass	[kg]	8.1
Final Mass	[kg]	6.2
Mass Loss	[%]	23.95

LODS Test Run Data

Center for Firesafety Studies

100 Institute Road
Worcester, MA 01609
Phone: (508) 831-5628
Fax: (508) 831-5680

Test Notes

Test Number:	0
Date:	11/09/10
Material:	Class C FRP panel
Specimen Identification:	FRP 8, 75 kW initial Propylene fire, 1 x 1 burner

Observations

Time	Observation
00:00	Start VI
04:15	Start Camera 1
04:30	Start Camera 2
07:36	Burner ignition
07:50	Reach target HRR @ 75 kW
08:05	Crackling noise
08:13	Panel ignition, mainly at area under TSC-2 to above burner
08:40	Burner off
08:45	Flame hit ceiling
09:00	Small remote area ignition @ TSC-4, HFG-2, TSC-9, all close to wall fire
09:20	T pattern under ceiling
09:25 to 10:00	Rollover under ceiling
10:25	Remote area ignition on right edge @ y = 1.6 m to ceiling
11:20	Remote area ignition @ TSC-3
27:45	Terminate test with little water application

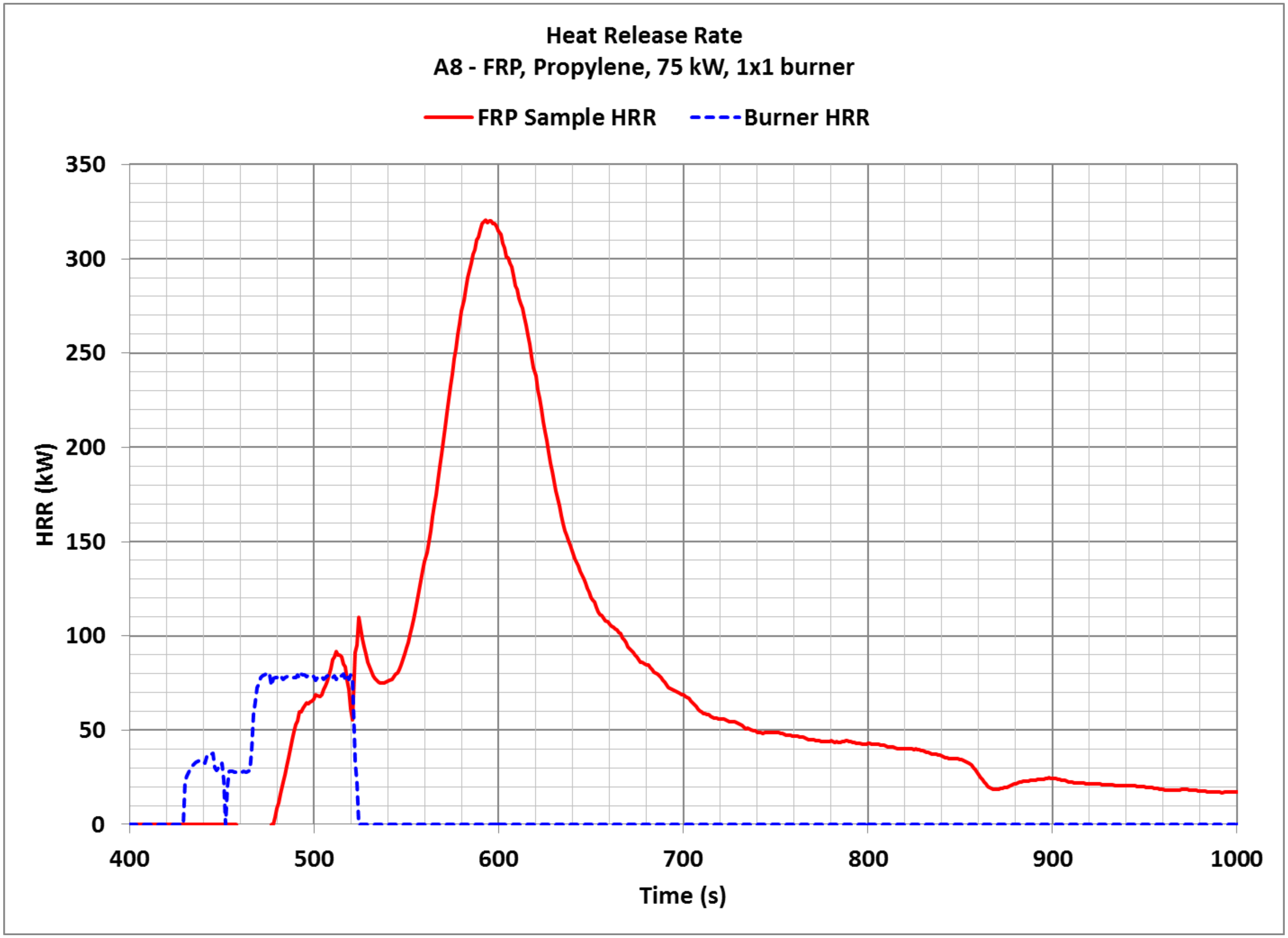

Heat release ratesof the source burner fire and of the specimen fire measured during test

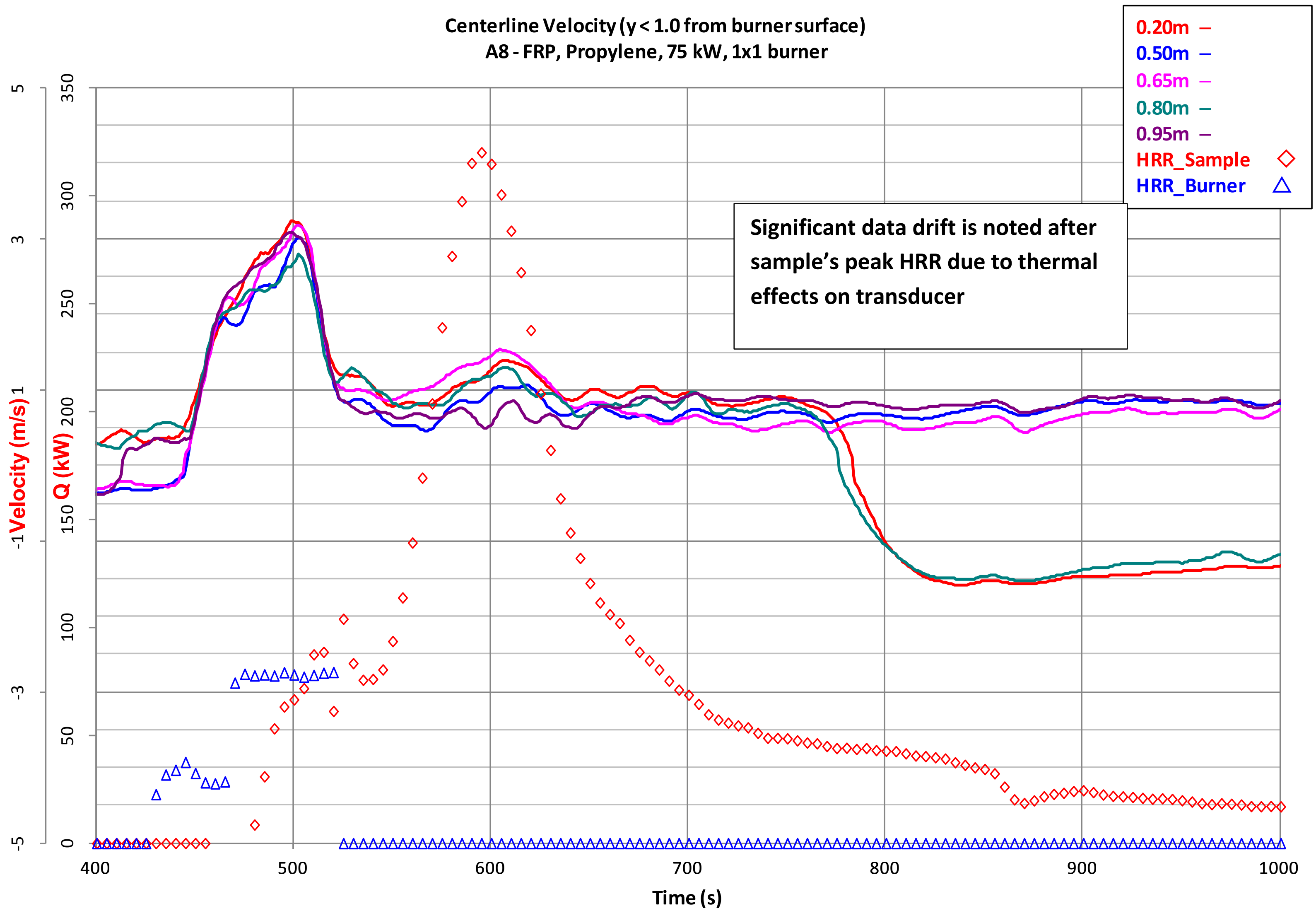

Centerline plume velocities measured from 0.2m to 0.95m above the burner surface

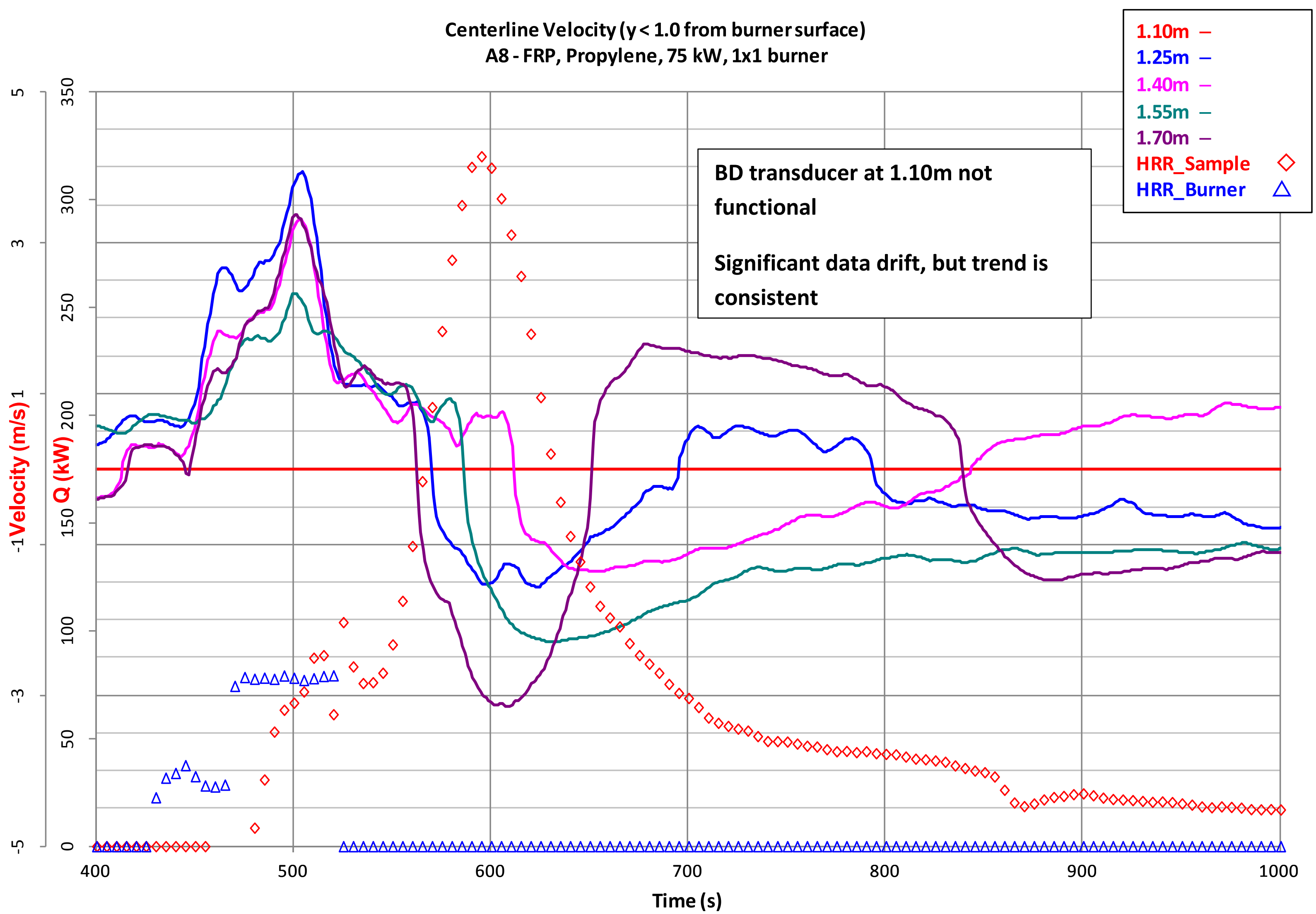

Centerline plume velocities measured from 1.1m to 1.7m above the burner surface

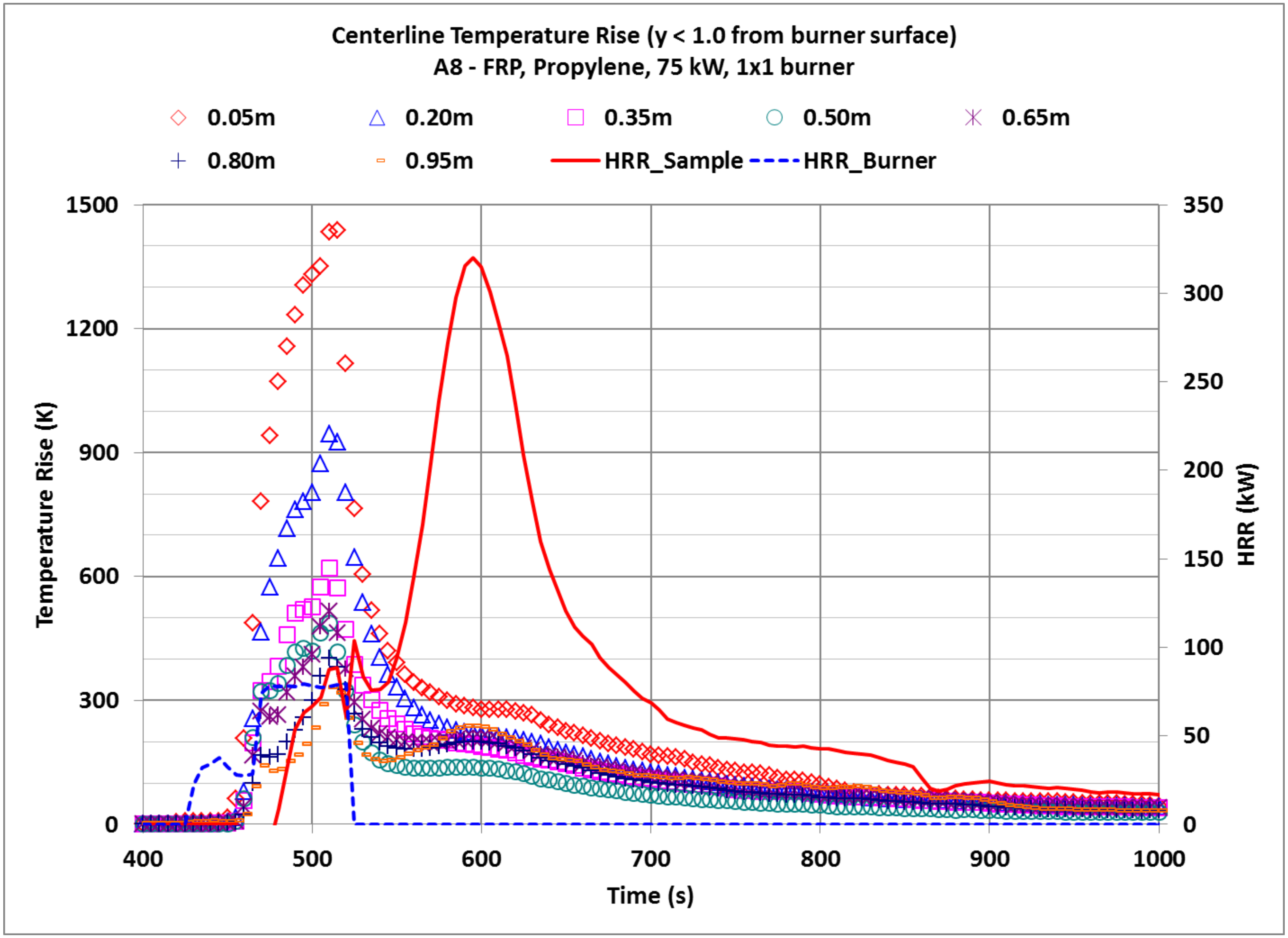

Centerline plume temperature rise measured from 0.05m to 0.95m above the burner surface

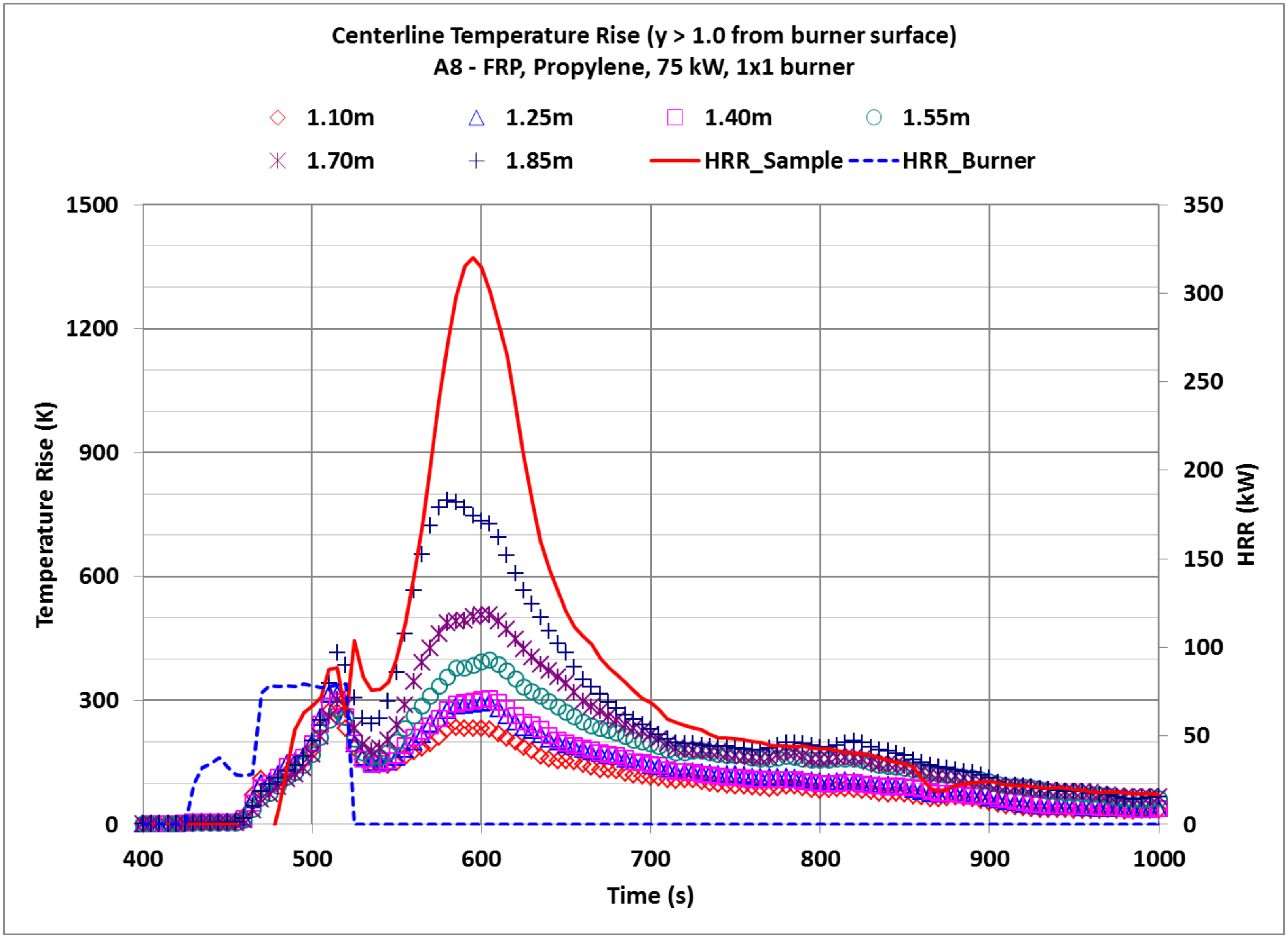

Centerline plume temperature rise measured from 1.10m to 1.85m above the burner surface

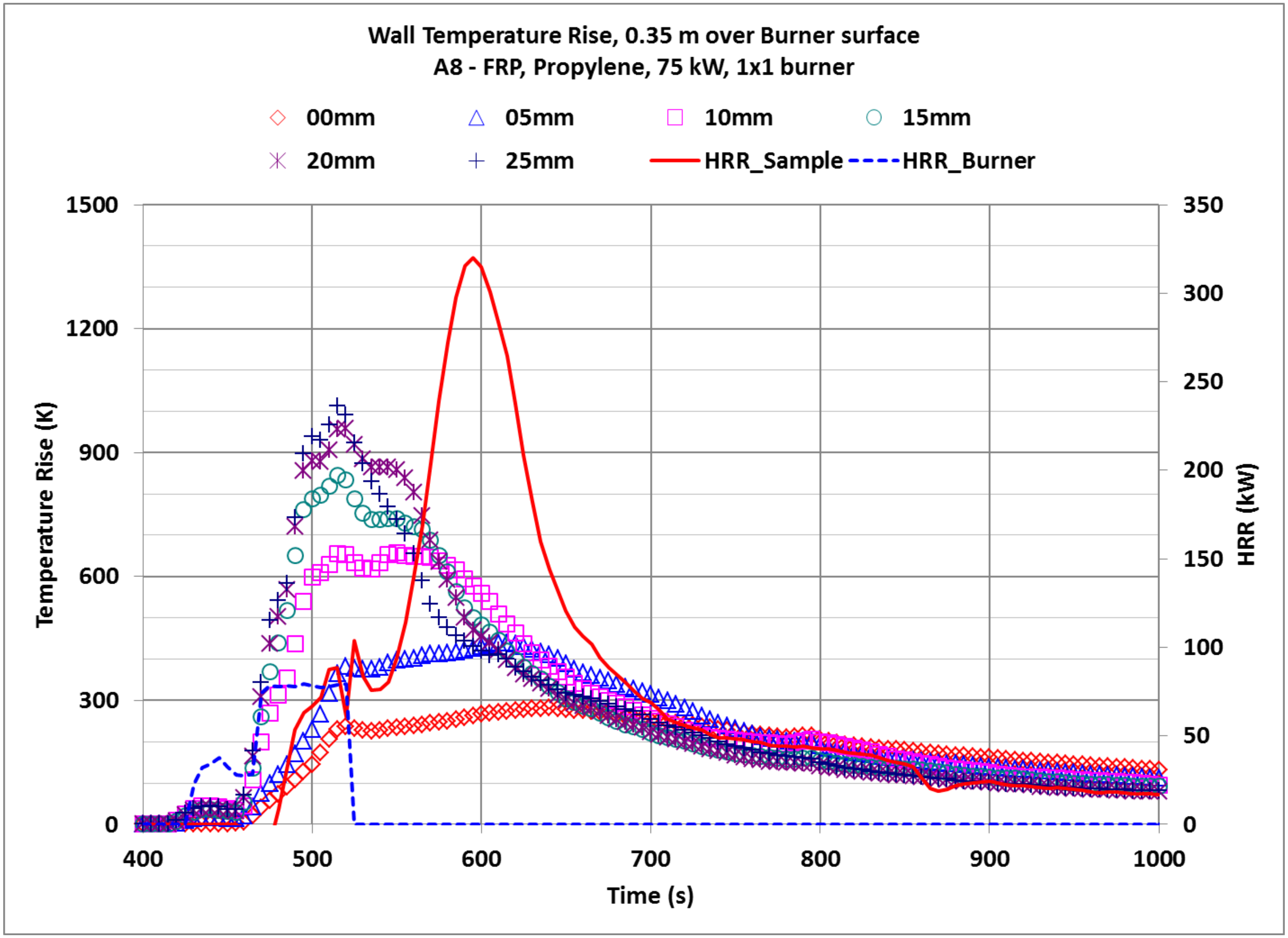

Temperature rise along the wall's centerline at 0.35m over the burner surface, measured at different perpendicular distances to as indicated

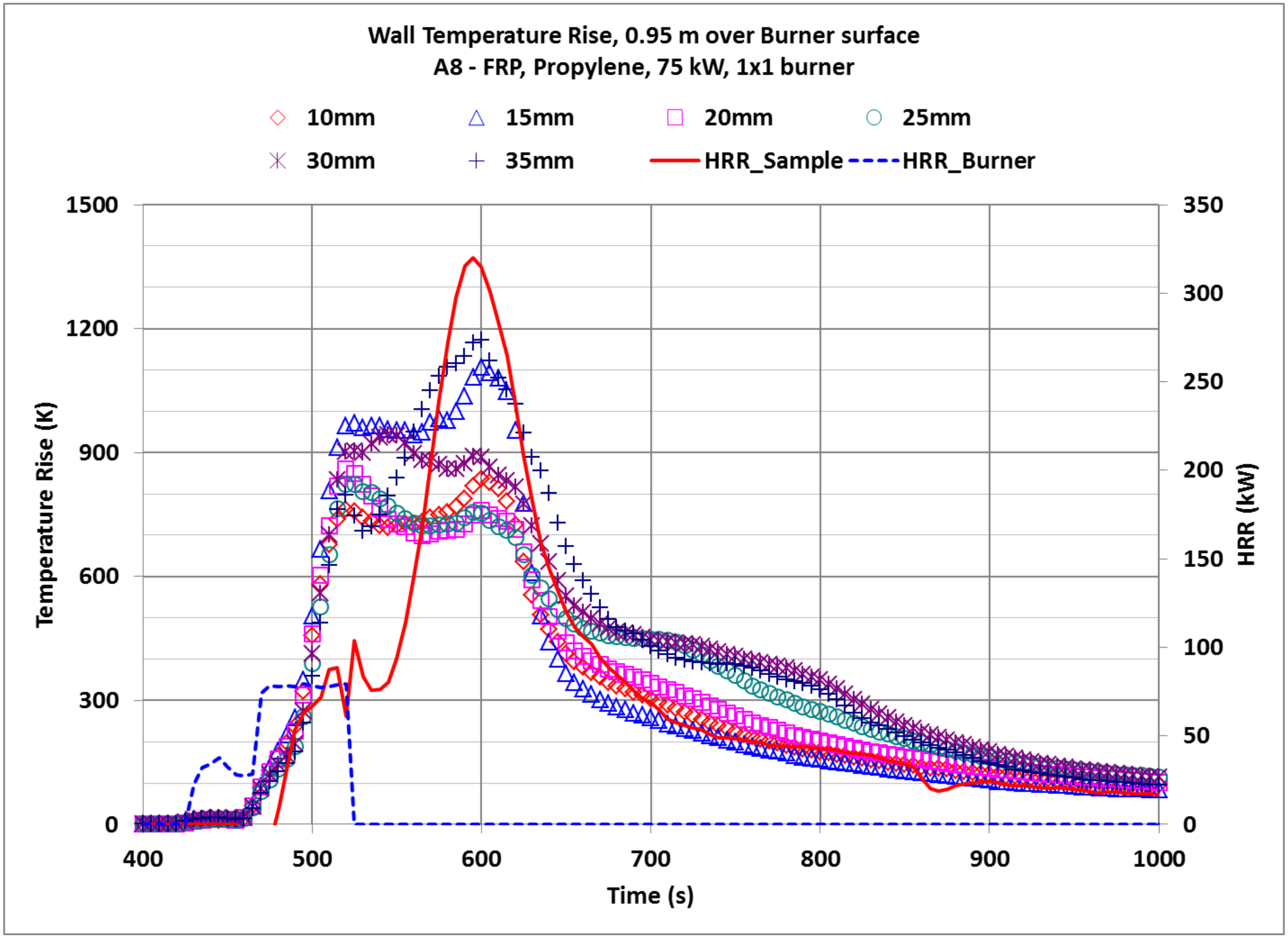

Temperature rise along the wall's centerline at 0.95m over the burner surface, measured at different perpendicular distances to as indicated

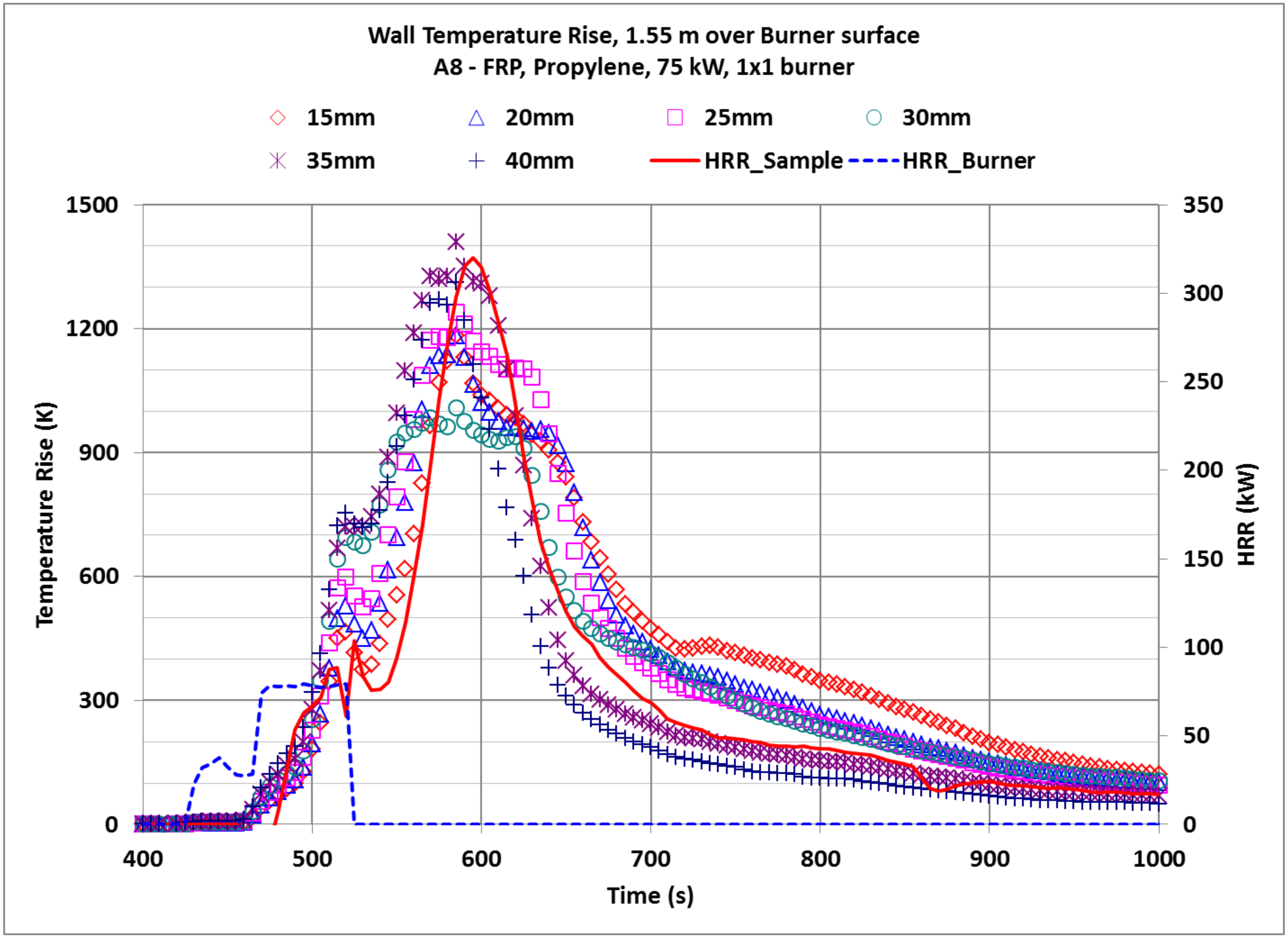

Temperature rise along the wall's centerline at 1.55m over the burner surface, measured at different perpendicular distances to as indicated

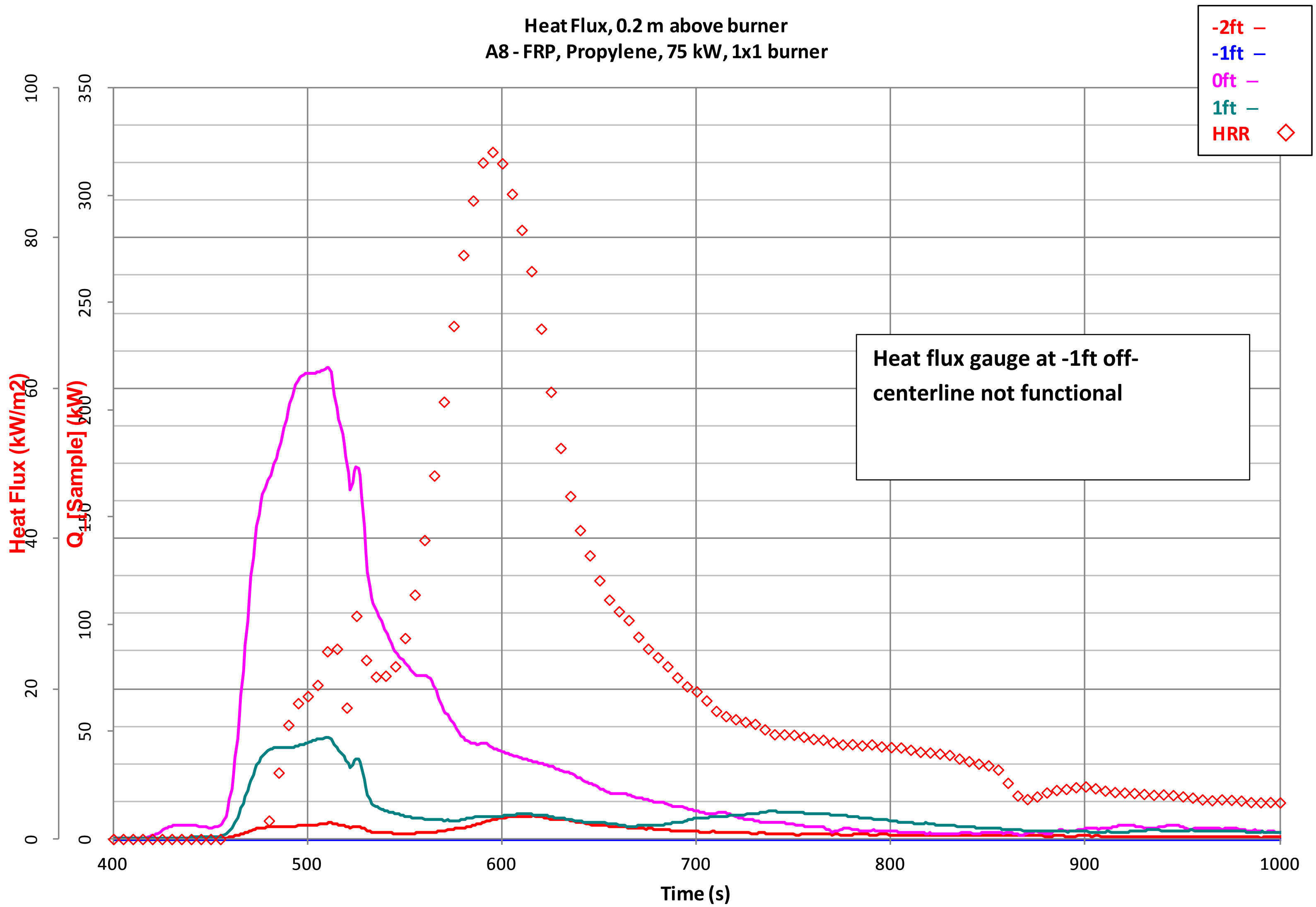

Heat flux measured at various distances from the centerline (negative indicates left of centerline), 0.2m vertically from burner surface

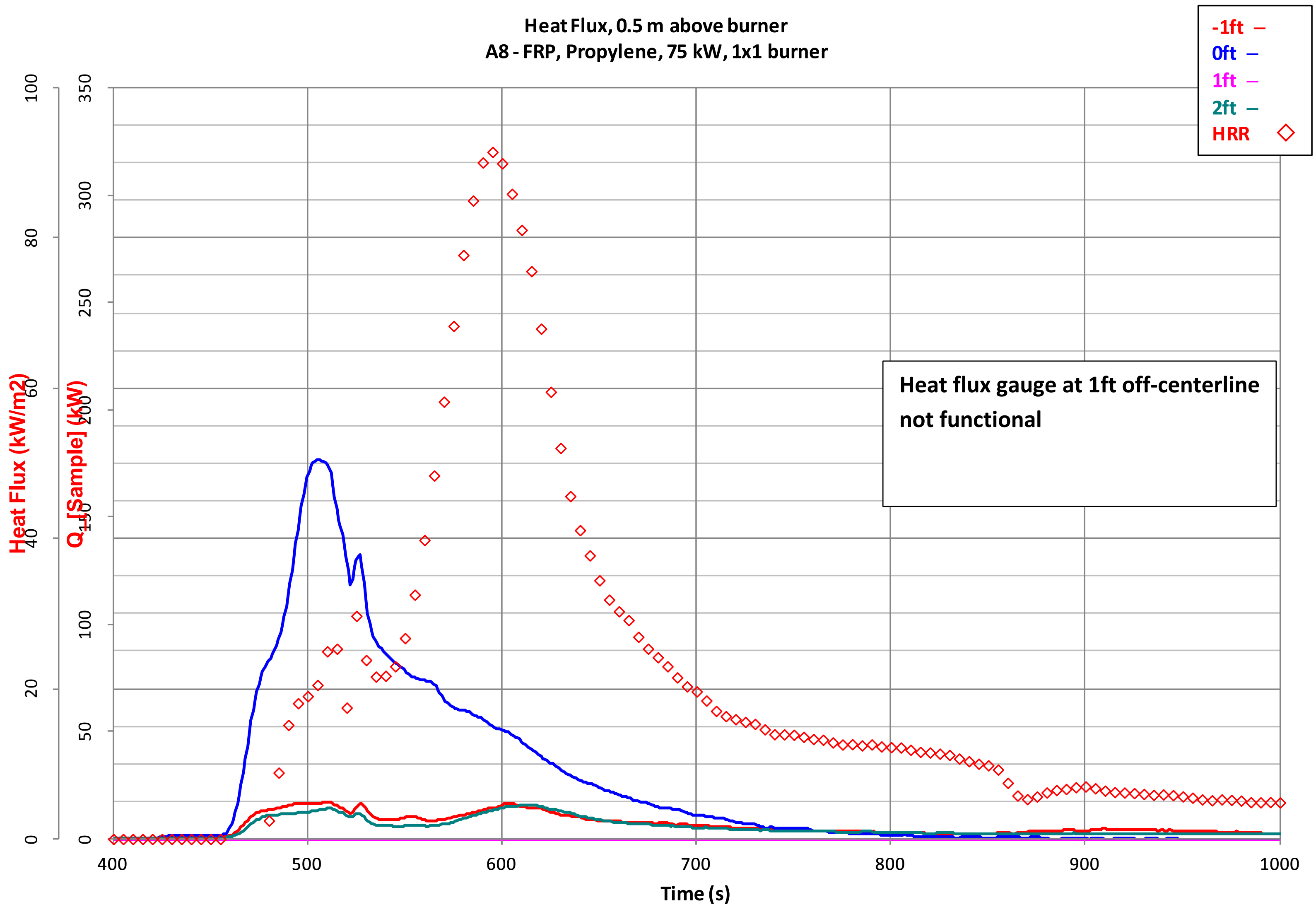

Heat flux measured at various distances from the centerline (negative indicates left of centerline), 0.5m vertically from burner surface

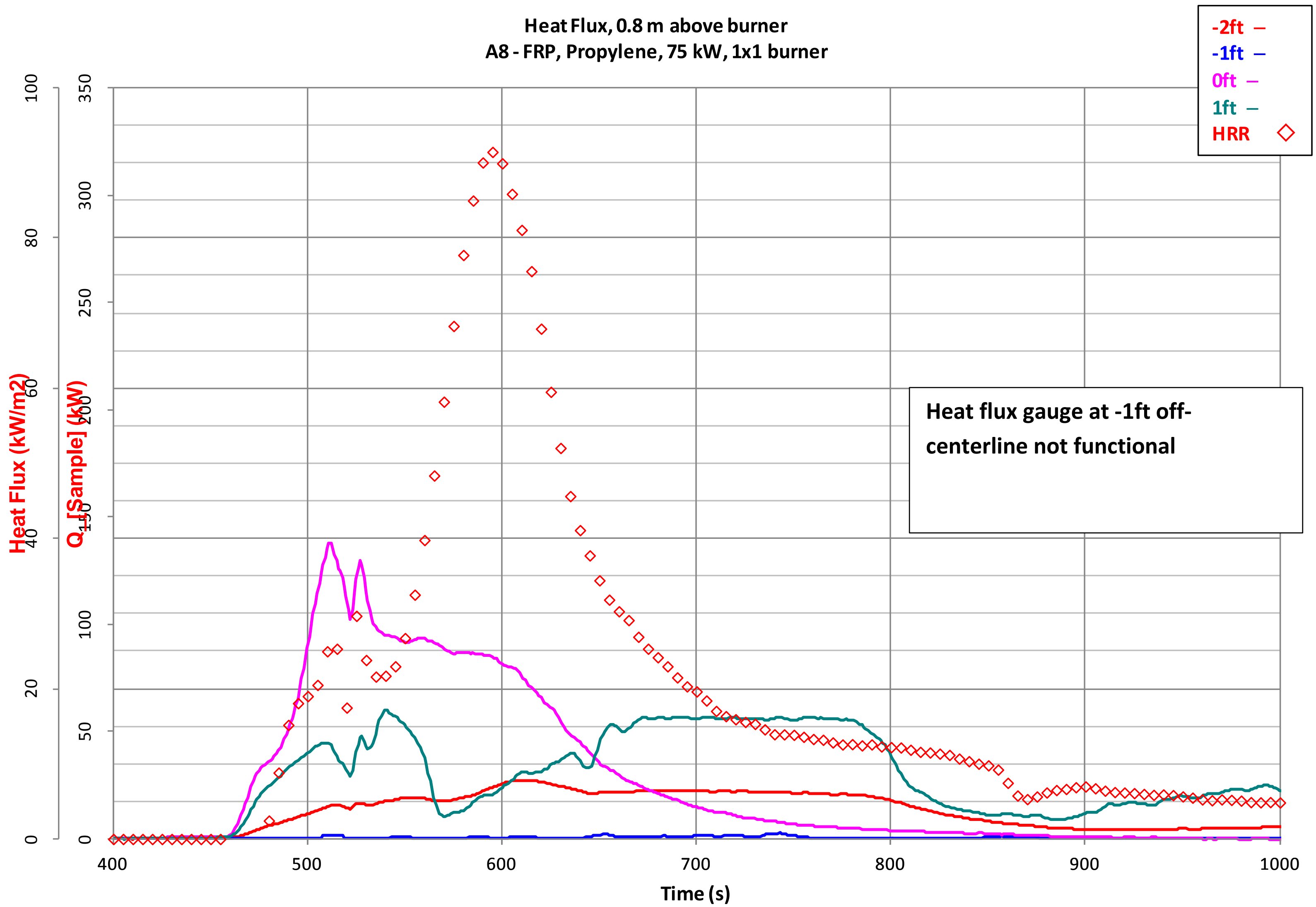

Heat flux measured at various distances from the centerline (negative indicates left of centerline), 0.8m vertically from burner surface

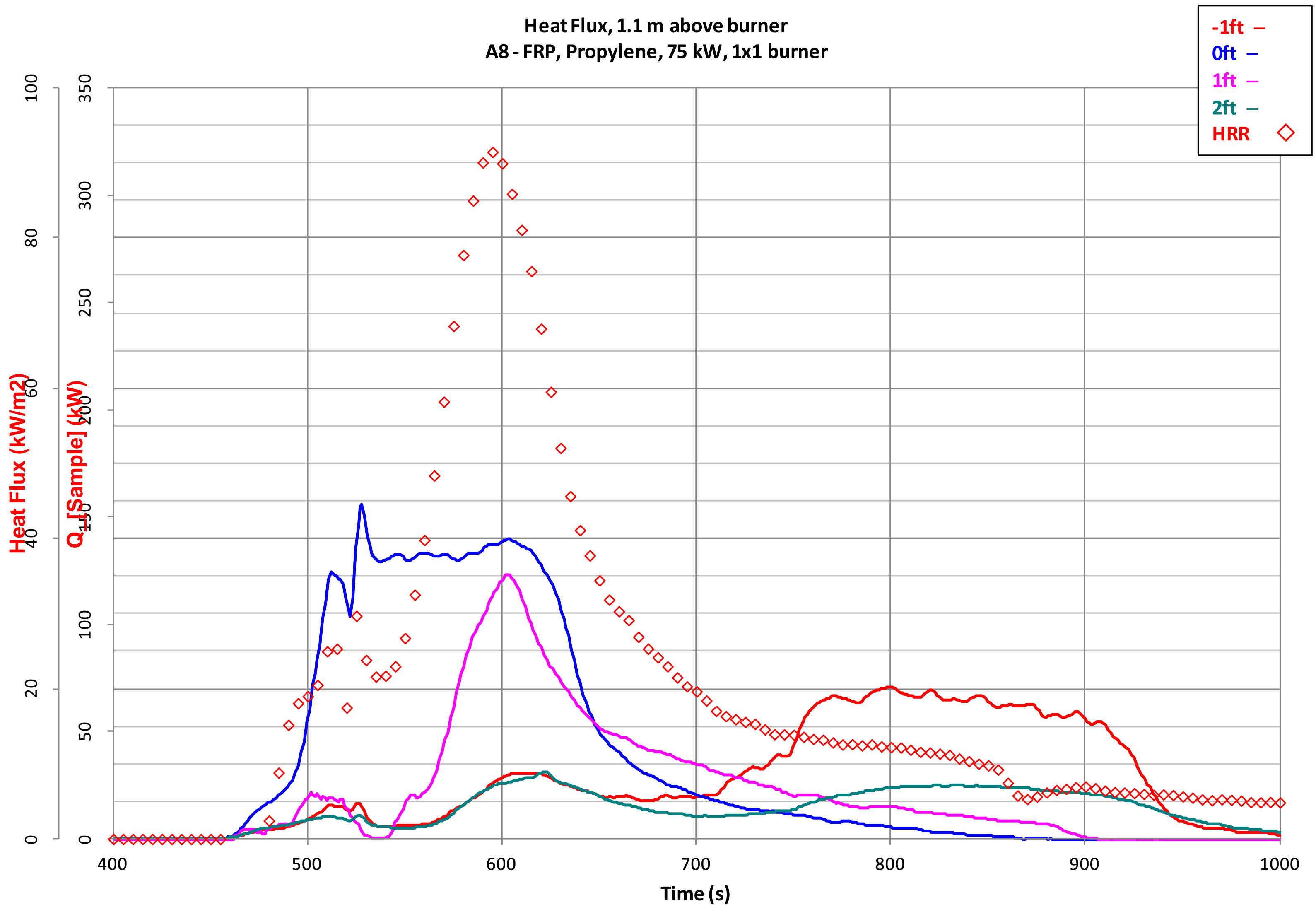

Heat flux measured at various distances from the centerline (negative indicates left of centerline), 1.1m vertically from burner surface

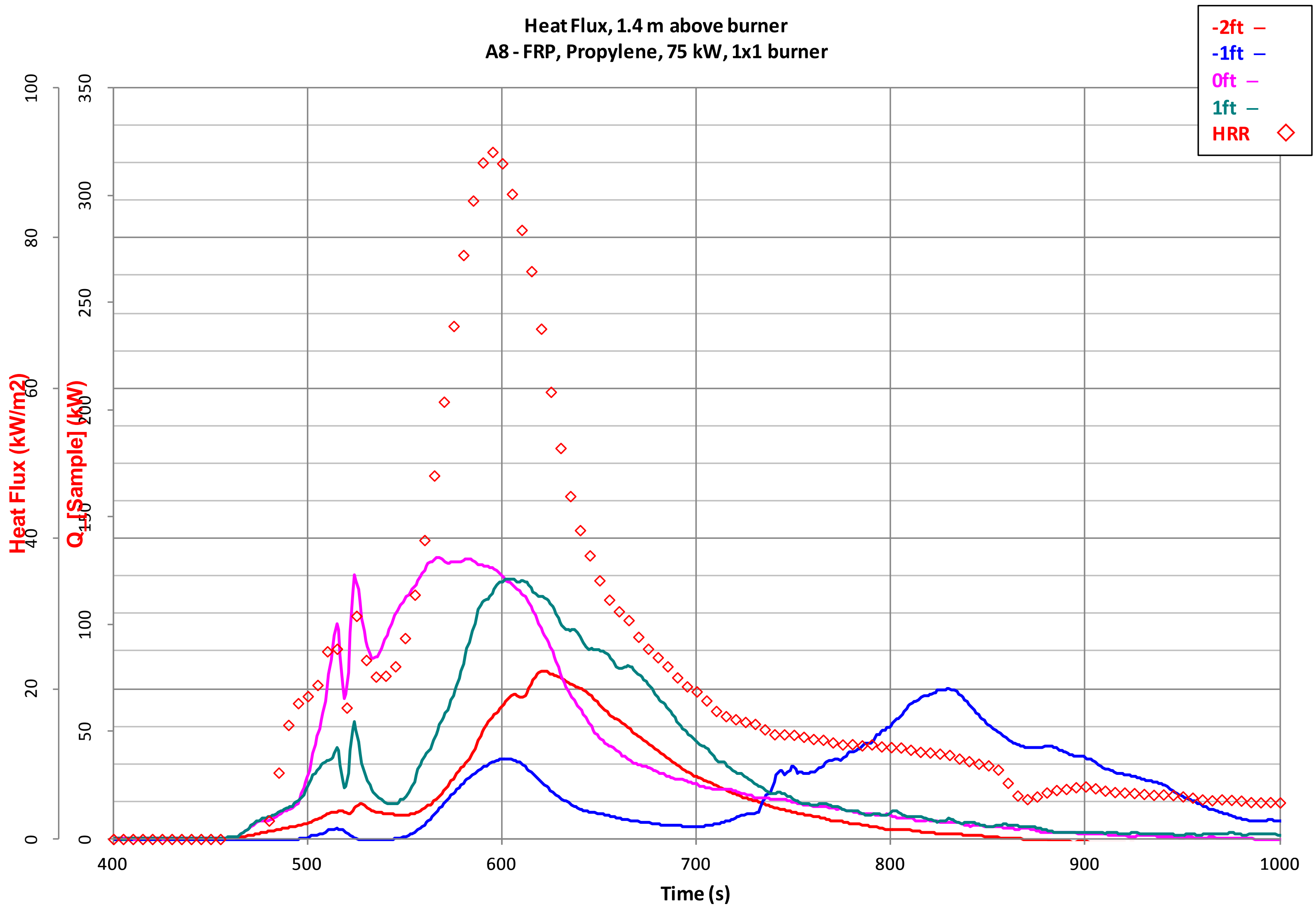

Heat flux measured at various distances from the centerline (negative indicates left of centerline), 1.4m vertically from burner surface

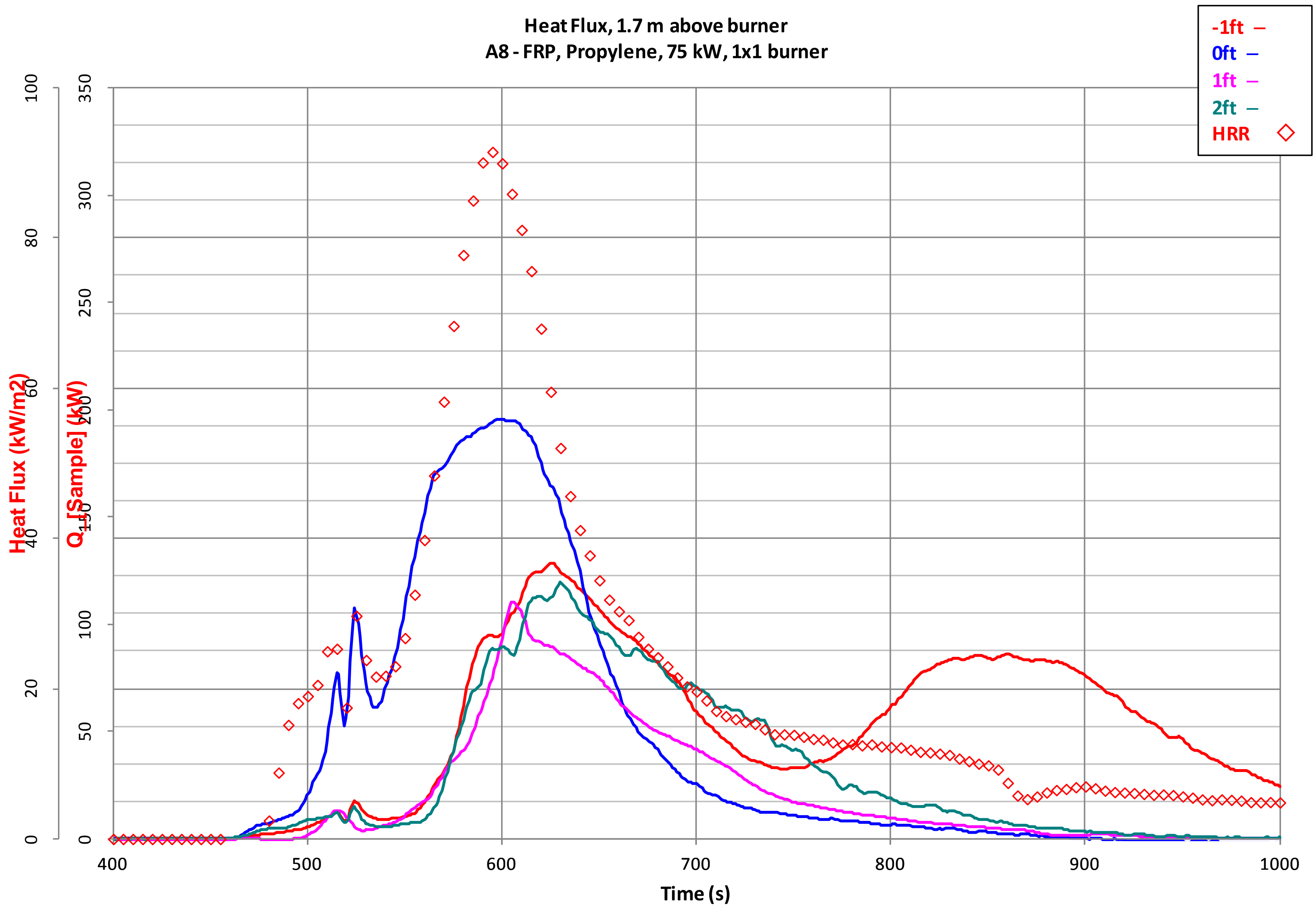

Heat flux measured at various distances from the centerline (negative indicates left of centerline), 1.7m vertically from burner surface

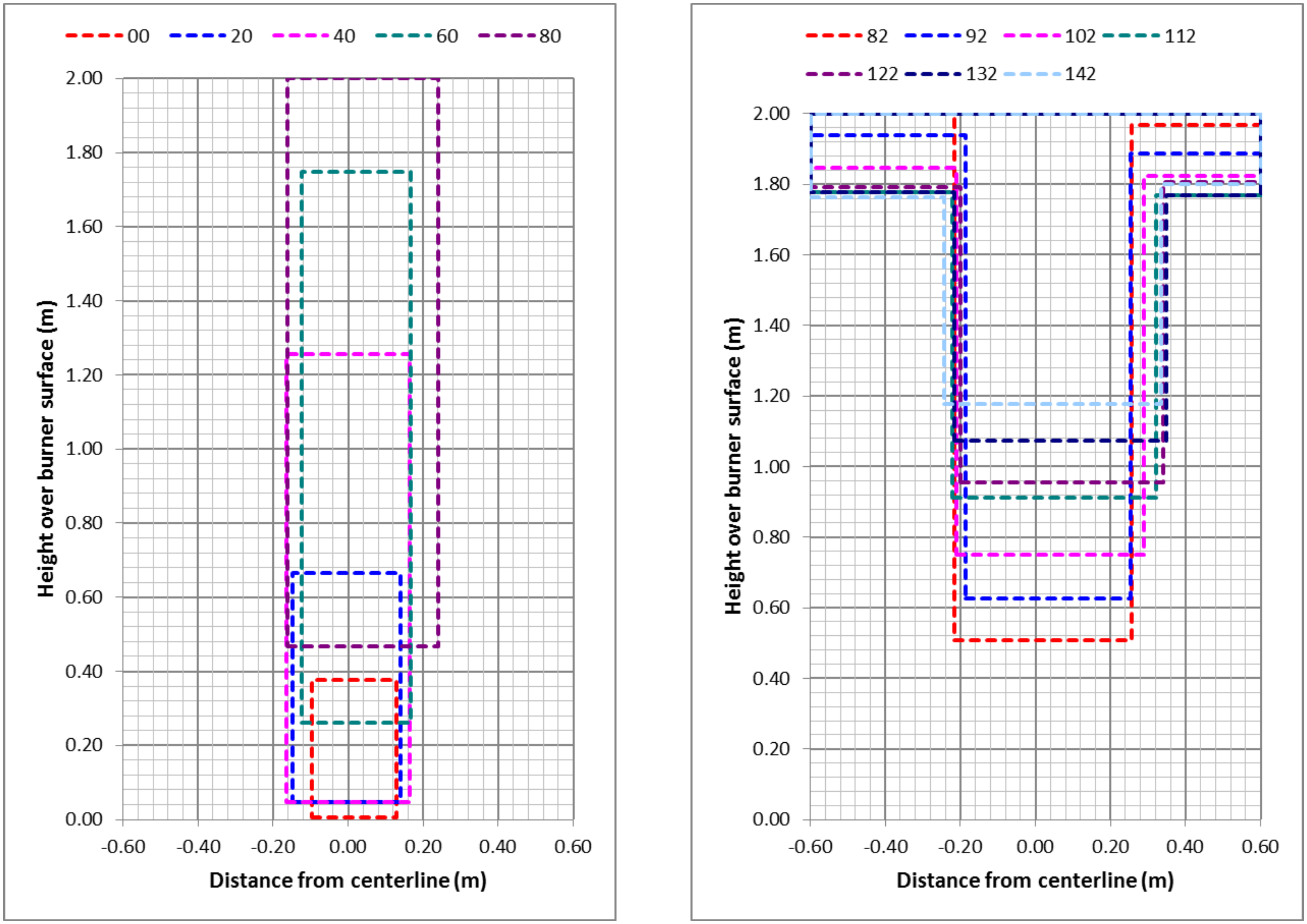

Stages 1 and 2 burning areas in Test A8 (1ft Square burner, Propylene, 75 kW source)

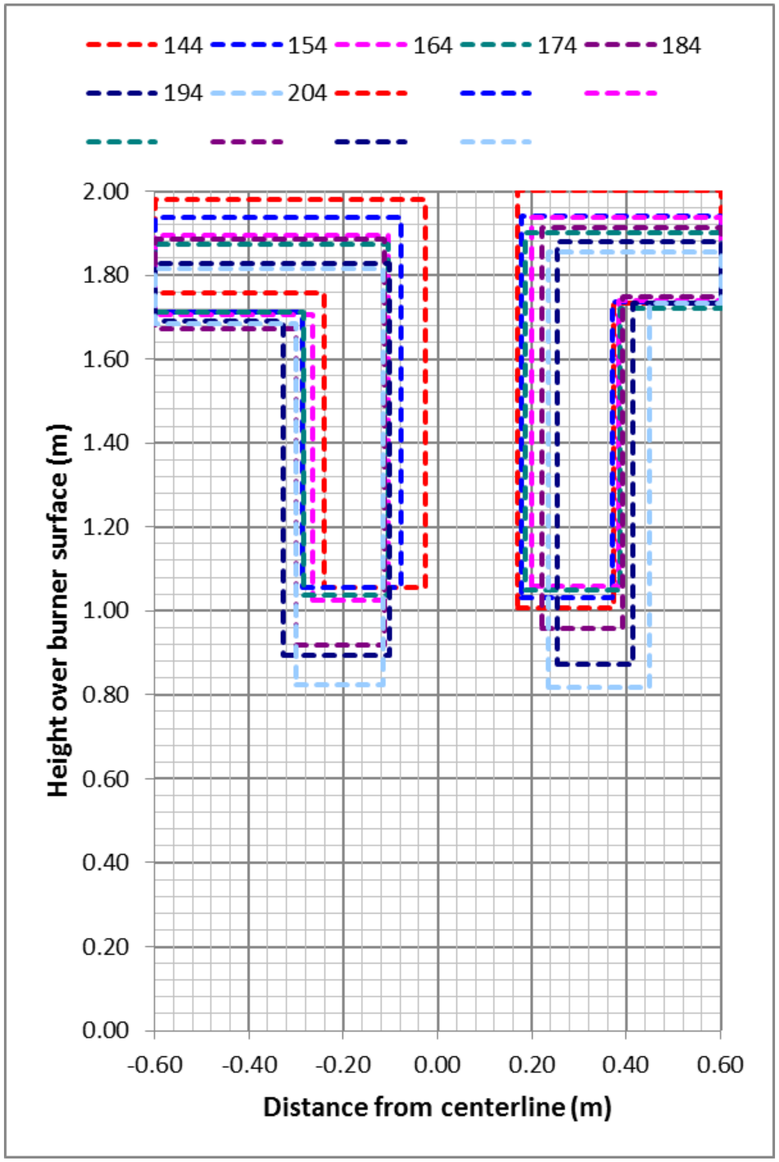

Stage 3 burn area and final damage chart of Test A8 (1ft Square burner, Propylene, 75 kW source)

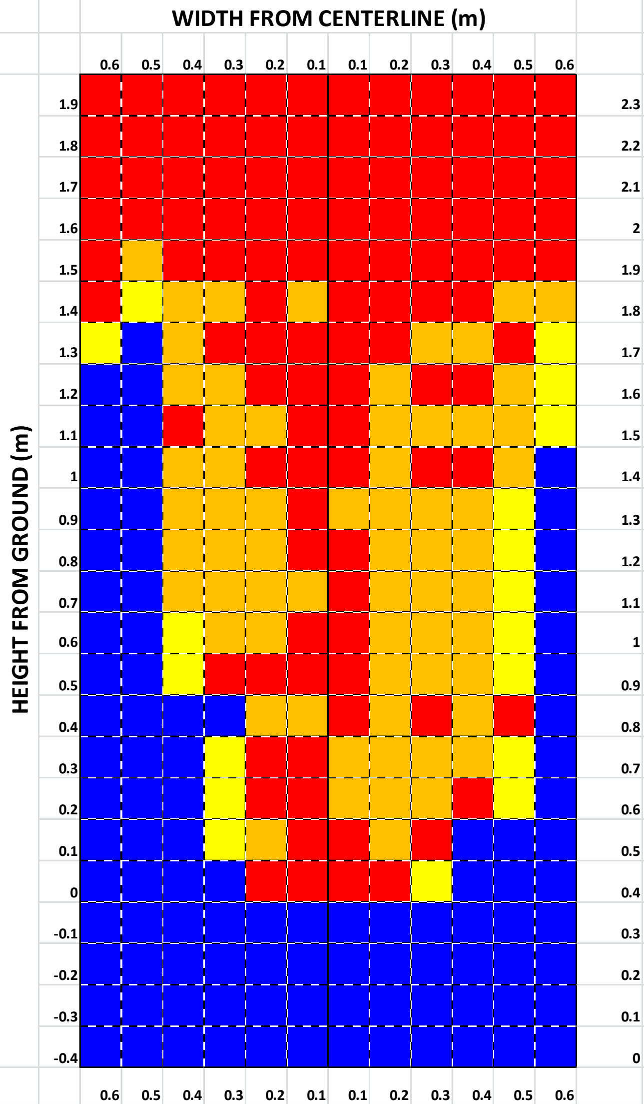

# of cell	Damage to Resin	Area (m2)
109	**up to 100% damage**	1.09
64	**up to 75% damage**	0.64
18	**up to 50% damage**	0.18
0	**up to 25% damage**	0
97	**no damage**	0.97

Initial mass:	8.1	kg
Final unburnt mass:	3.56	kg
Final burnt mass:	2.6	kg
Total mass loss during fire	1.94	kg

Burn damage pattern observed after fire test

F.3.9 Test A9

LODS Test Run Data

Center for Firesafety Studies

100 Institute Road
Worcester, MA 01609
Phone: (508) 831-5628
Fax: (508) 831-5680

Test Information

Test Number:	A9
Specimen Identification:	FRP 9, 50 kW initial Propane fire, 1 x 2 burner
Material Name:	Class C FRP panel
Manufacturer/Submitter:	Not Reported
Raw Data File Name:	Test A9 - FRP_50kW_Propylene_2ft.txt
Reduced Data File Name:	Test A9 - FRP_50kW_Propylene_2ft_reduced.xlsx
Date of Test:	10-Nov-2010
Tester:	W. Wong

Test Parameters

Ambient Temperature:	N/A
Relative Humidity:	N/A

Specimen Information

Specimen Initial Mass:	[kg]	8.3
Specimen Final Mass:	[kg]	6.0
Mass Lost:	[kg]	2.3
Heat Evolved (net):	[kJ]	0

Parameter	Unit	Value
Mass Loss		
Initial Mass	[kg]	8.3
Final Mass	[kg]	6.0
Mass Loss	[%]	27.88

LODS Test Run Data

Center for Firesafety Studies

100 Institute Road
Worcester, MA 01609
Phone: (508) 831-5628
Fax: (508) 831-5680

Test Notes

Test Number:	0
Date:	11/10/10
Material:	Class C FRP panel
Specimen Identification:	FRP 9, 50 kW initial Propane fire, 1 x 2 burner

Observations

Time	Observation
00:00	Start VI
06:30	Start Camera 1
06:40	Start Camera 2
09:00	Burner ignition
09:12	Reach target HRR @ 50 kW
09:38	Crackling noise
09:40	Panel ignition, mainly at area under TSC-2 to above burner
10:10	Burner off
11:32	T-pattern burning under ceiling Remote area smoking @ right edge @ y = 0.5 m and y = 1.2 m Remote area ignition @ TSC-10, not significant, near main wall fire
11:38 to 12: 38	Rollover under ceiling
16:00	Line fires on both side of burner only
34:00	Terminate test with little water application

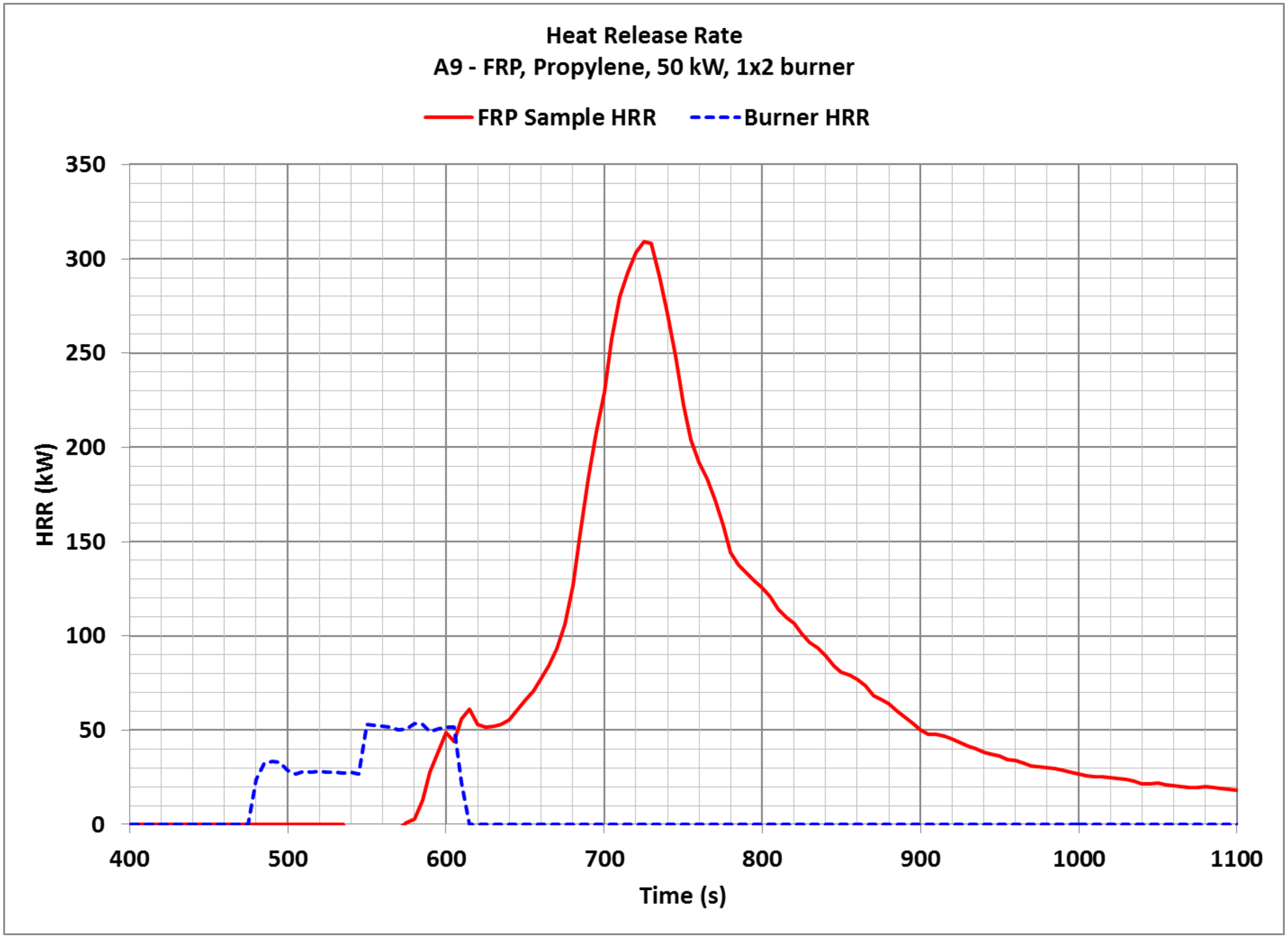

Heat release ratesof the source burner fire and of the specimen fire measured during test

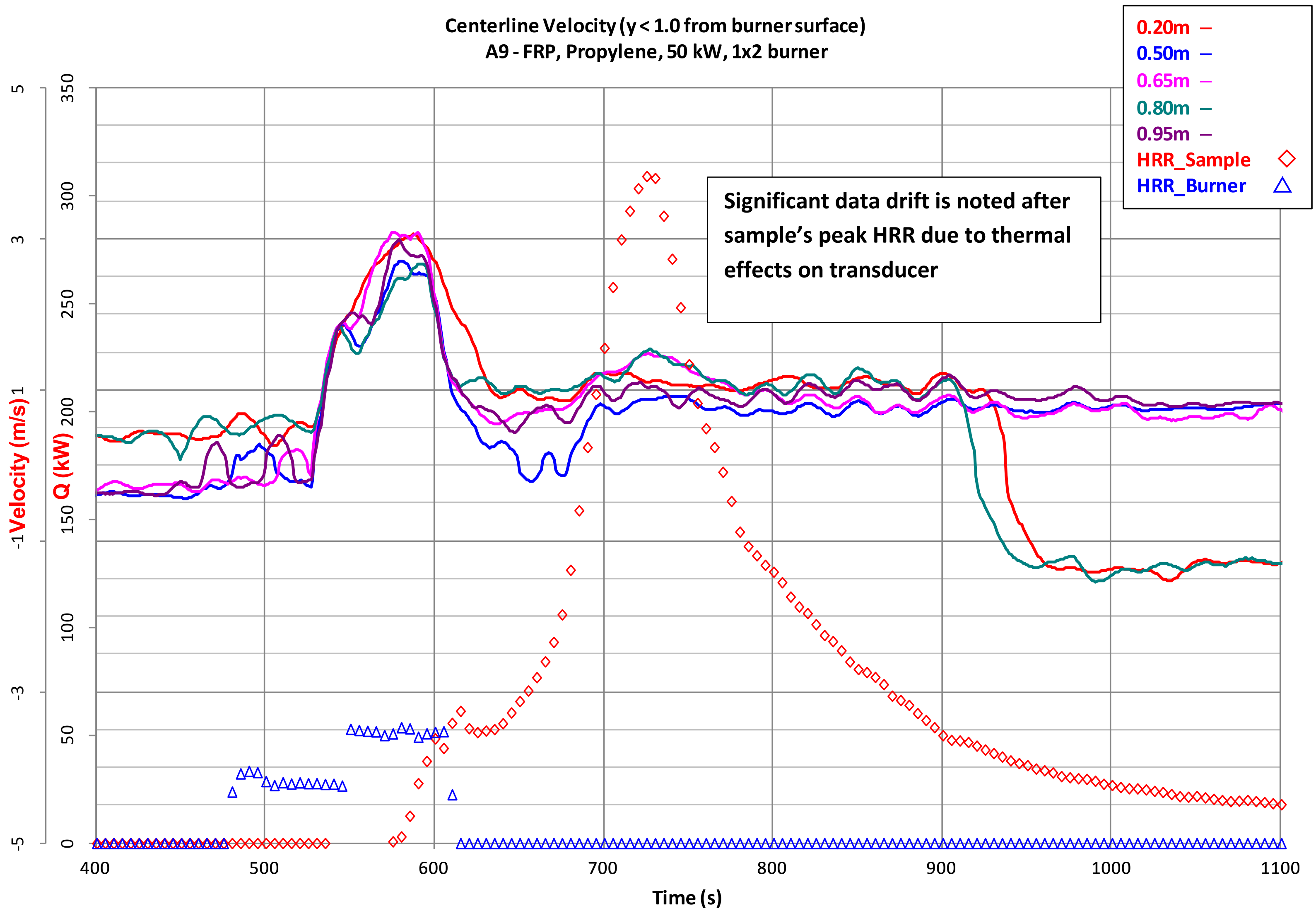

Centerline plume velocities measured from 0.2m to 0.95m above the burner surface

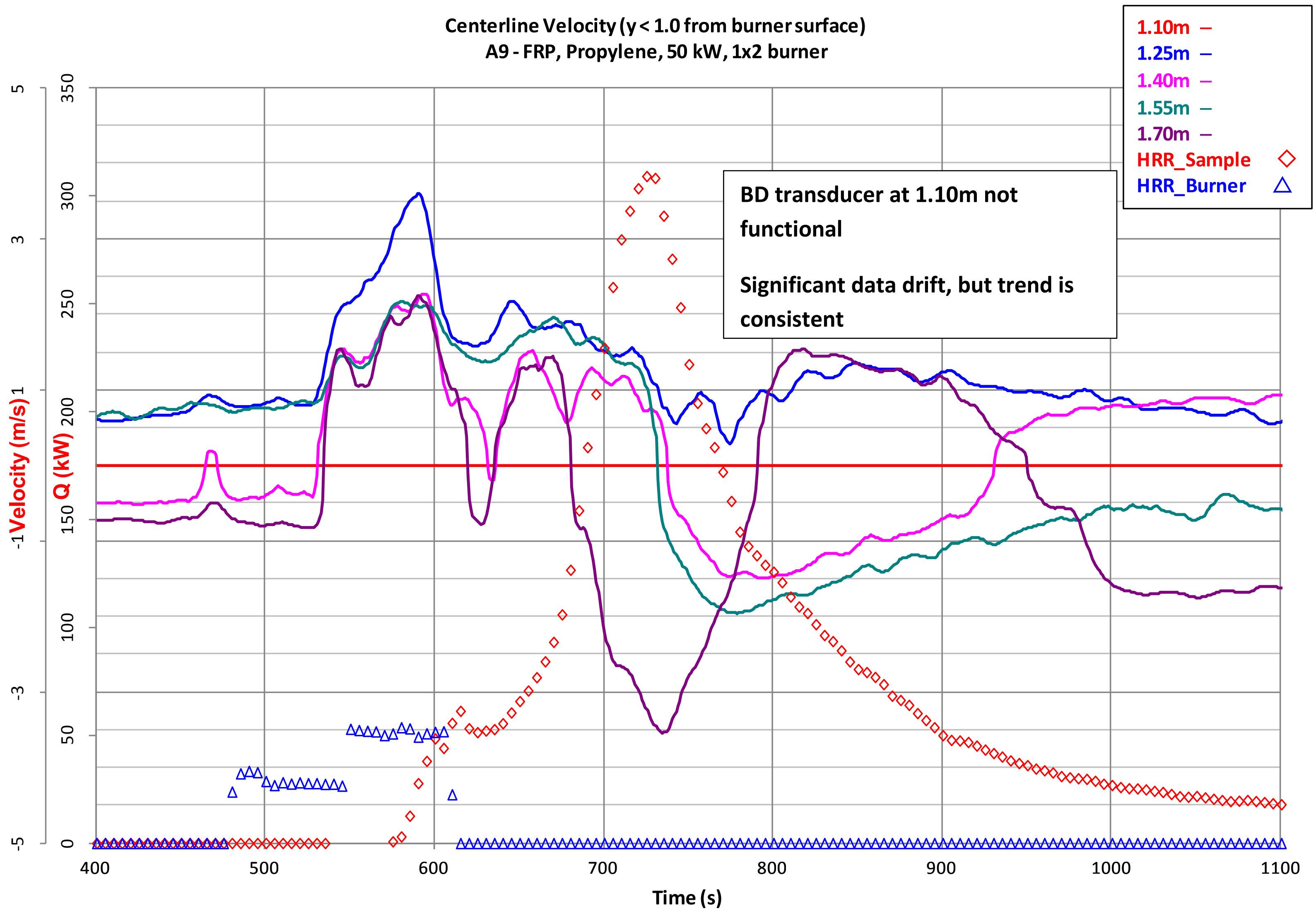

Centerline plume velocities measured from 1.1m to 1.7m above the burner surface

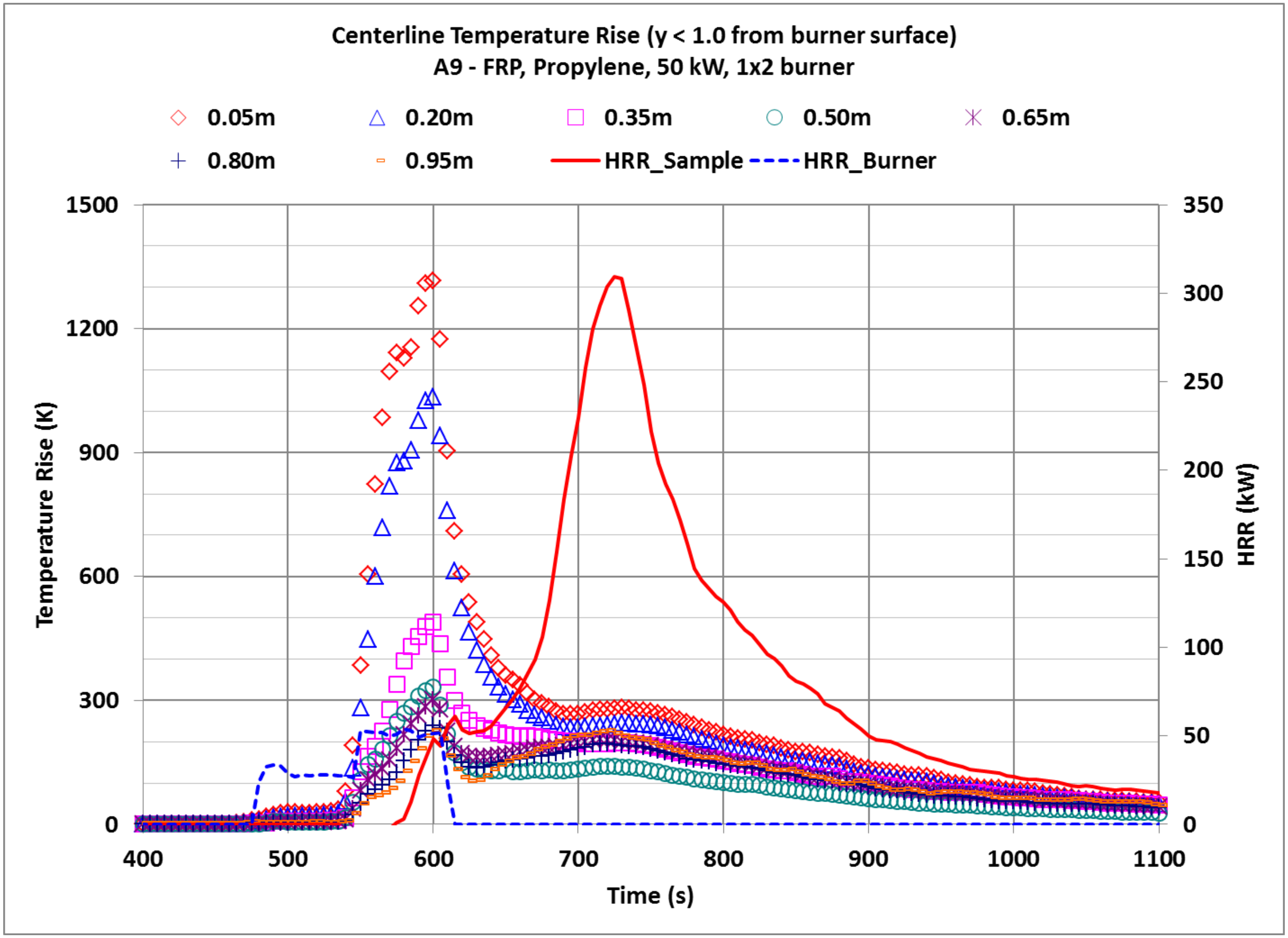

Centerline plume temperature rise measured from 0.05m to 0.95m above the burner surface

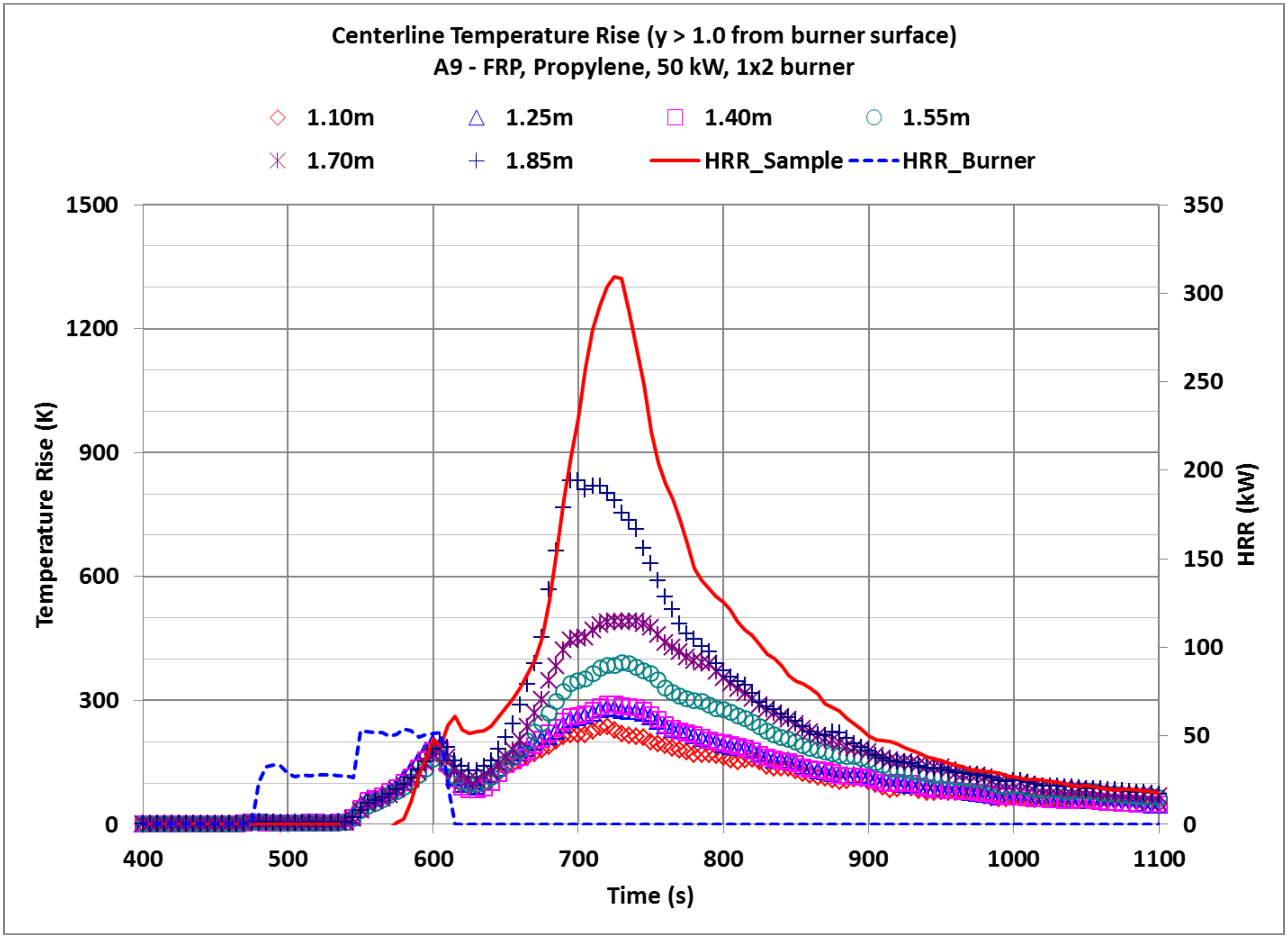

Centerline plume temperature rise measured from 1.10m to 1.85m above the burner surface

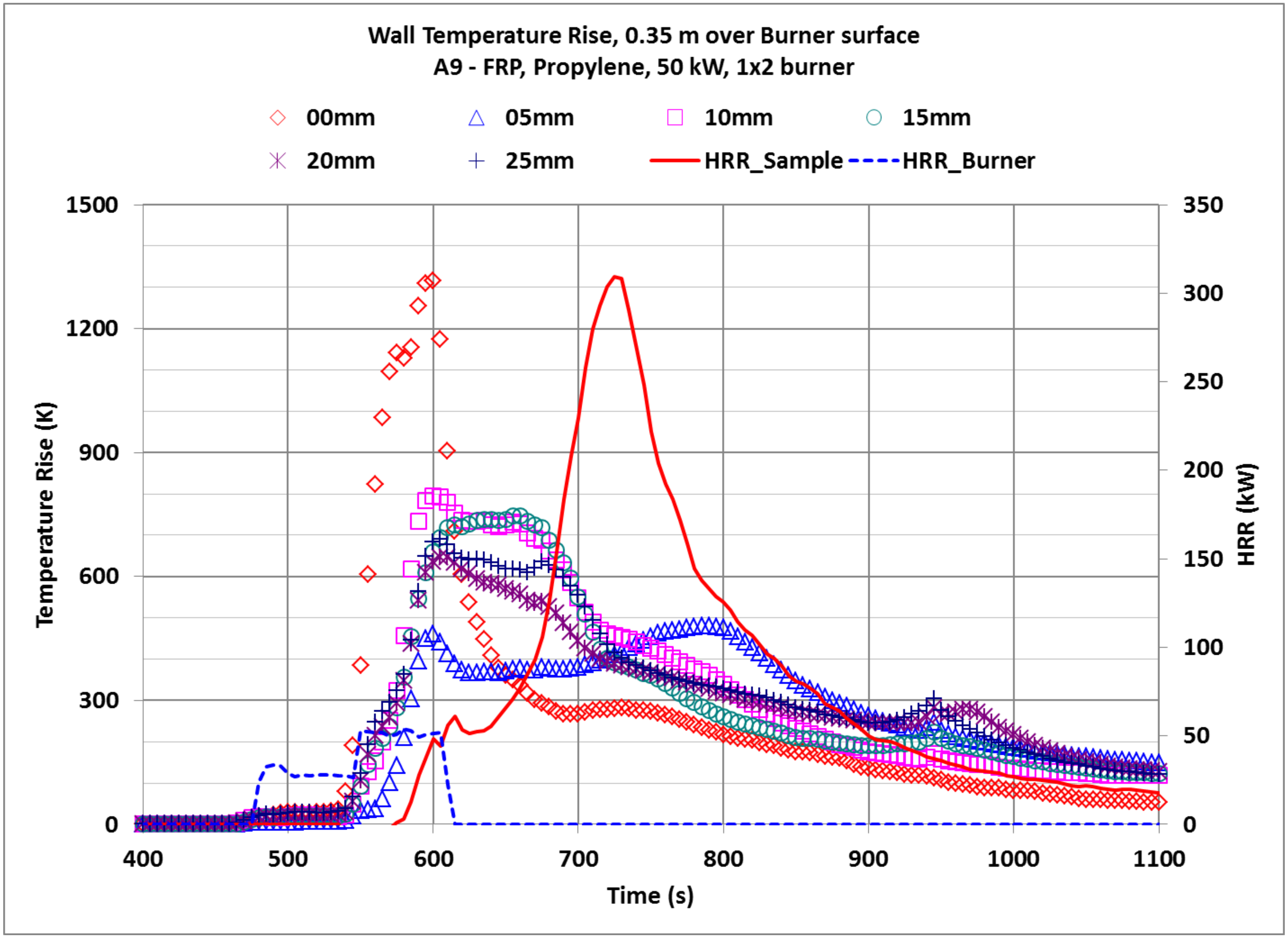

Temperature rise along the wall's centerline at 0.35m over the burner surface, measured at different perpendicular distances to as indicated

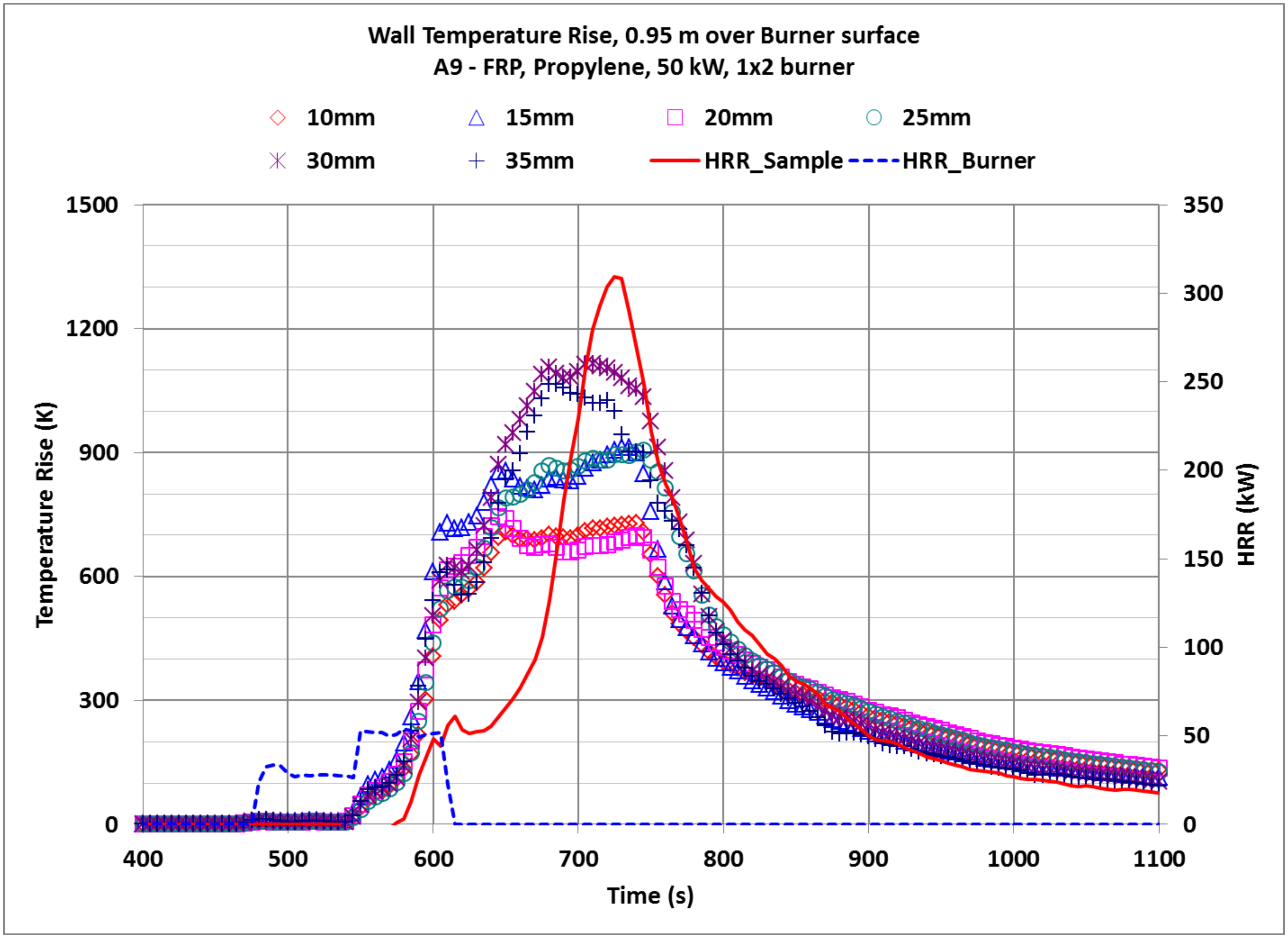

Temperature rise along the wall's centerline at 0.95m over the burner surface, measured at different perpendicular distances to as indicated

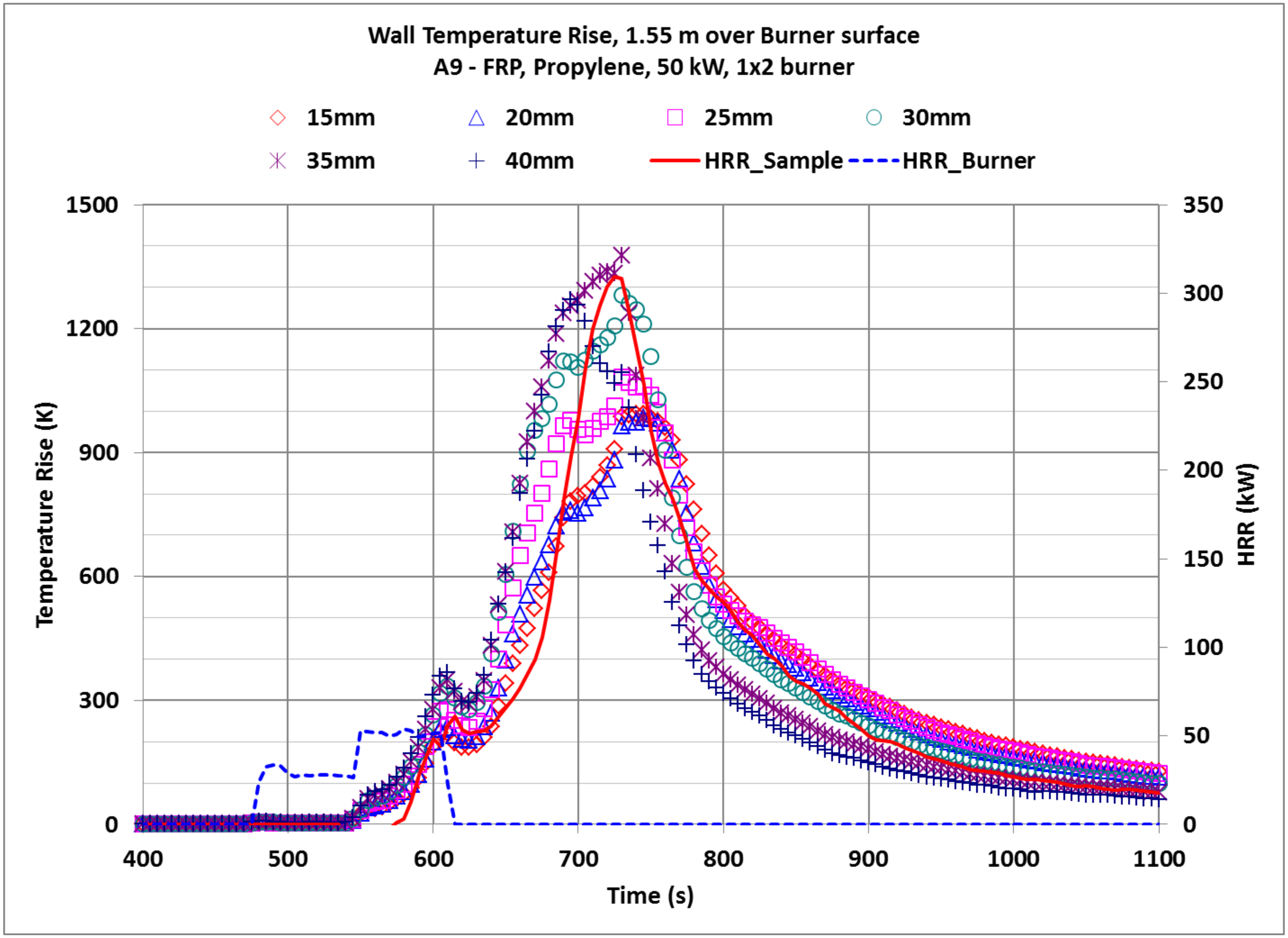

Temperature rise along the wall's centerline at 1.55m over the burner surface, measured at different perpendicular distances to as indicated

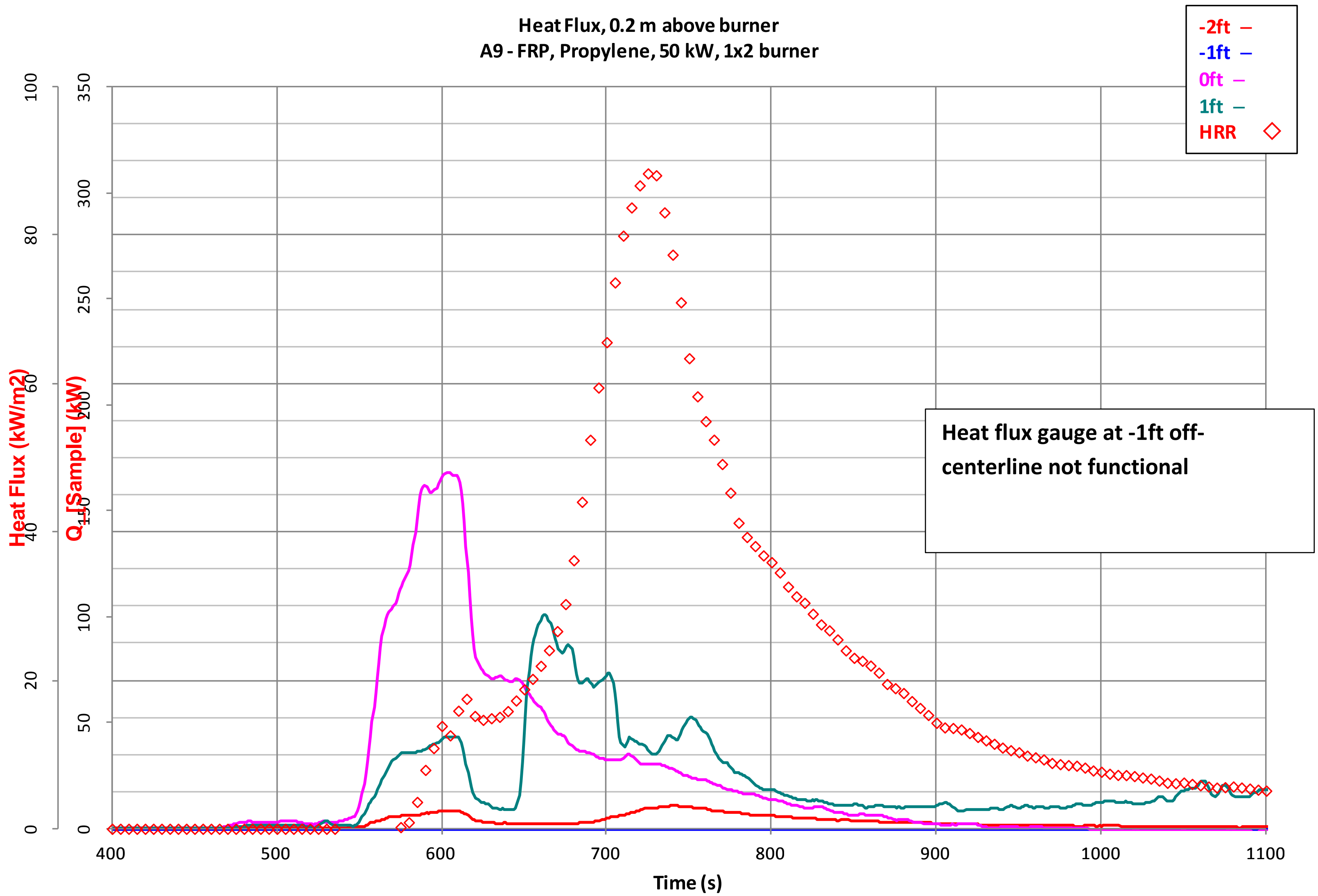

Heat flux measured at various distances from the centerline (negative indicates left of centerline), 0.2m vertically from burner surface

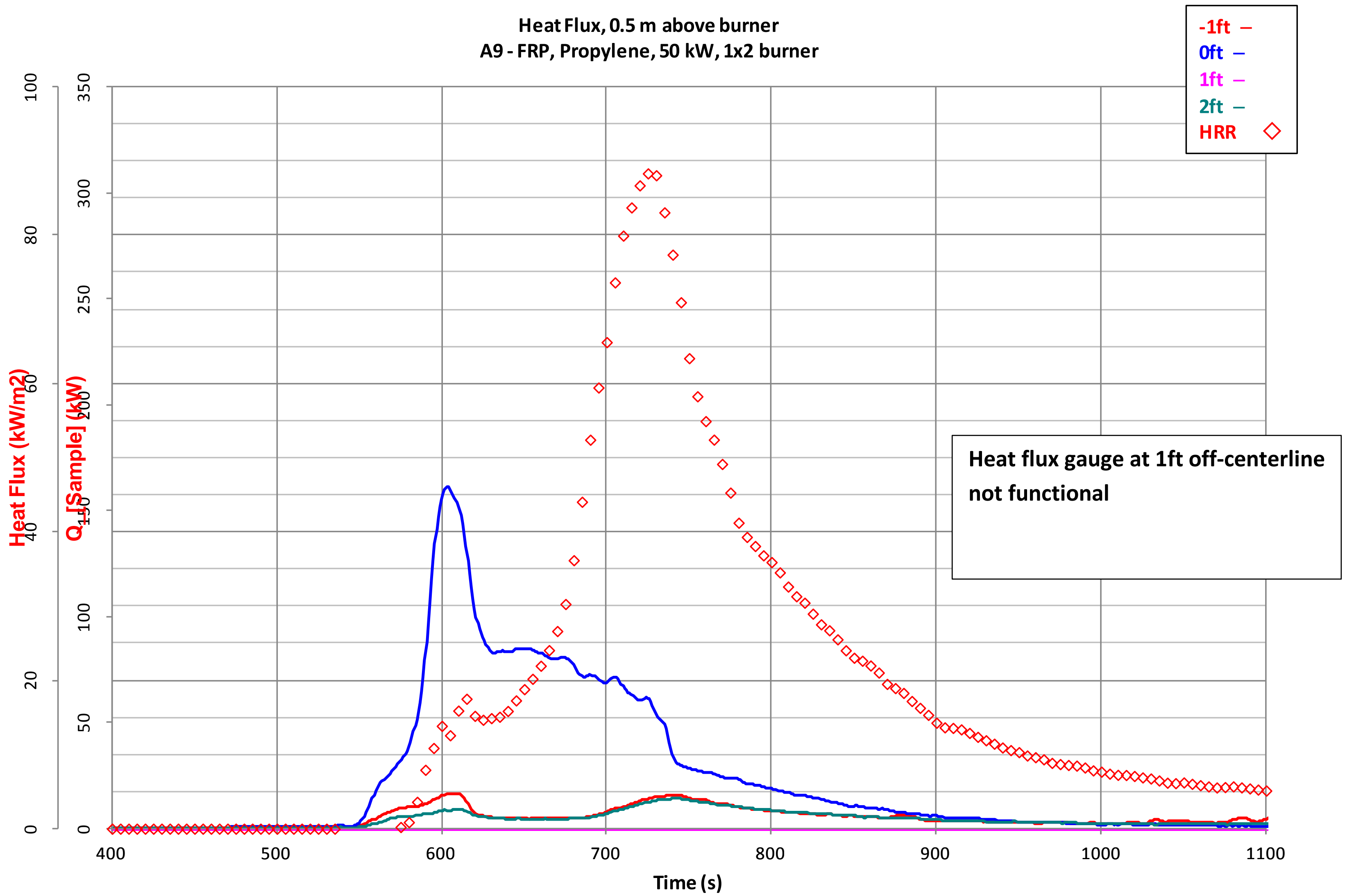

Heat flux measured at various distances from the centerline (negative indicates left of centerline), 0.5m vertically from burner surface

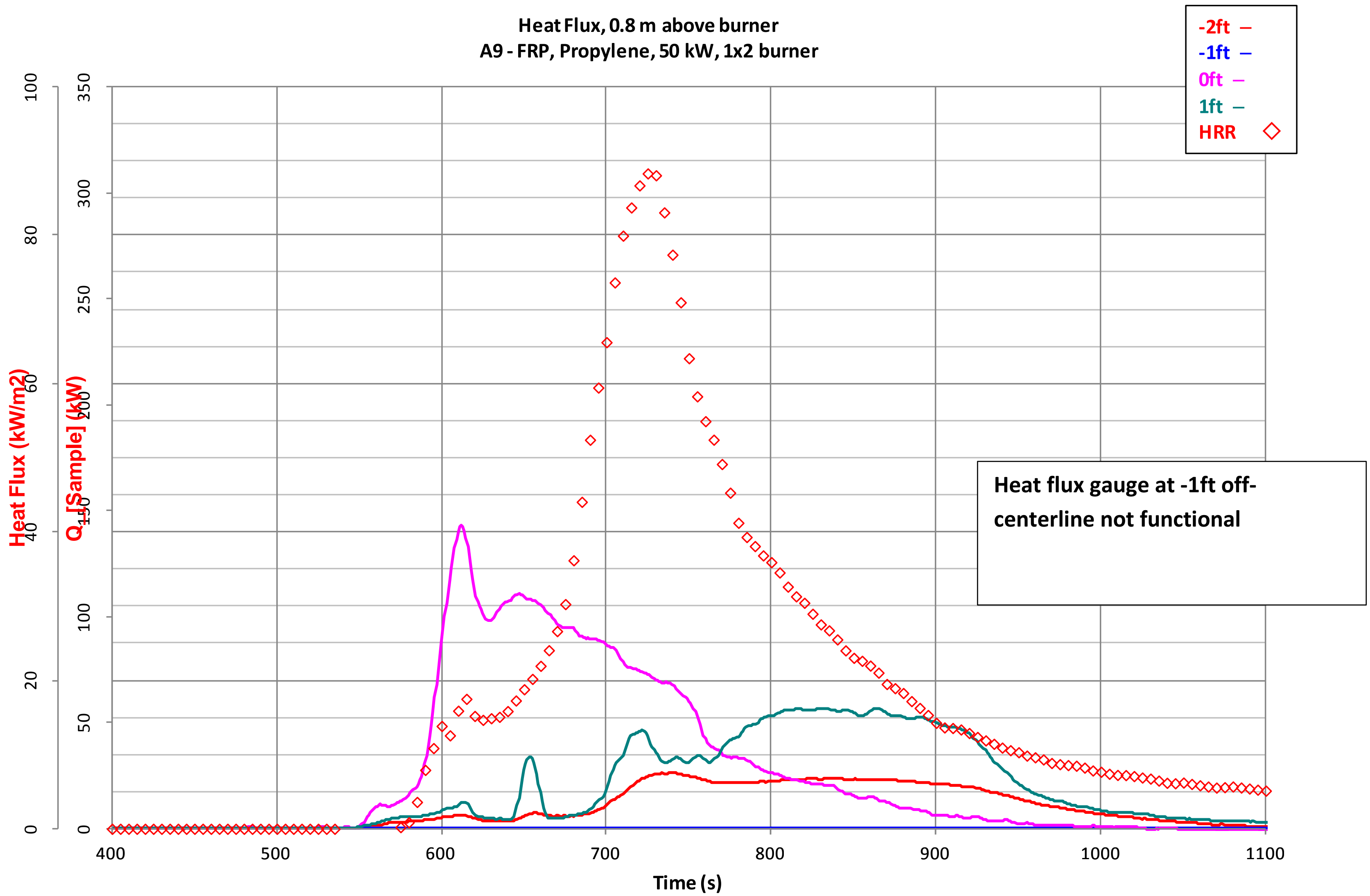

Heat flux measured at various distances from the centerline (negative indicates left of centerline), 0.8m vertically from burner surface

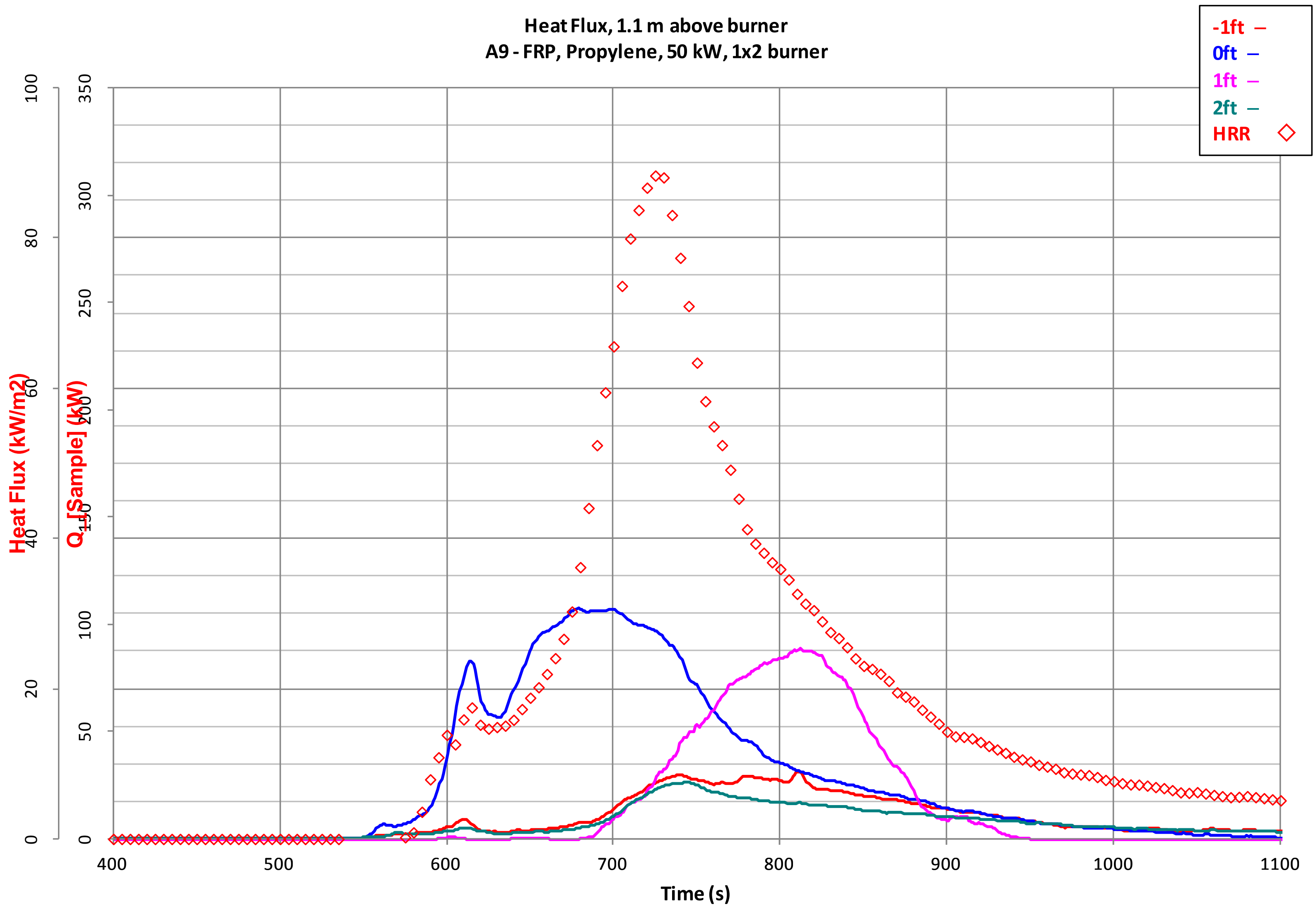

Heat flux measured at various distances from the centerline (negative indicates left of centerline), 1.1m vertically from burner surface

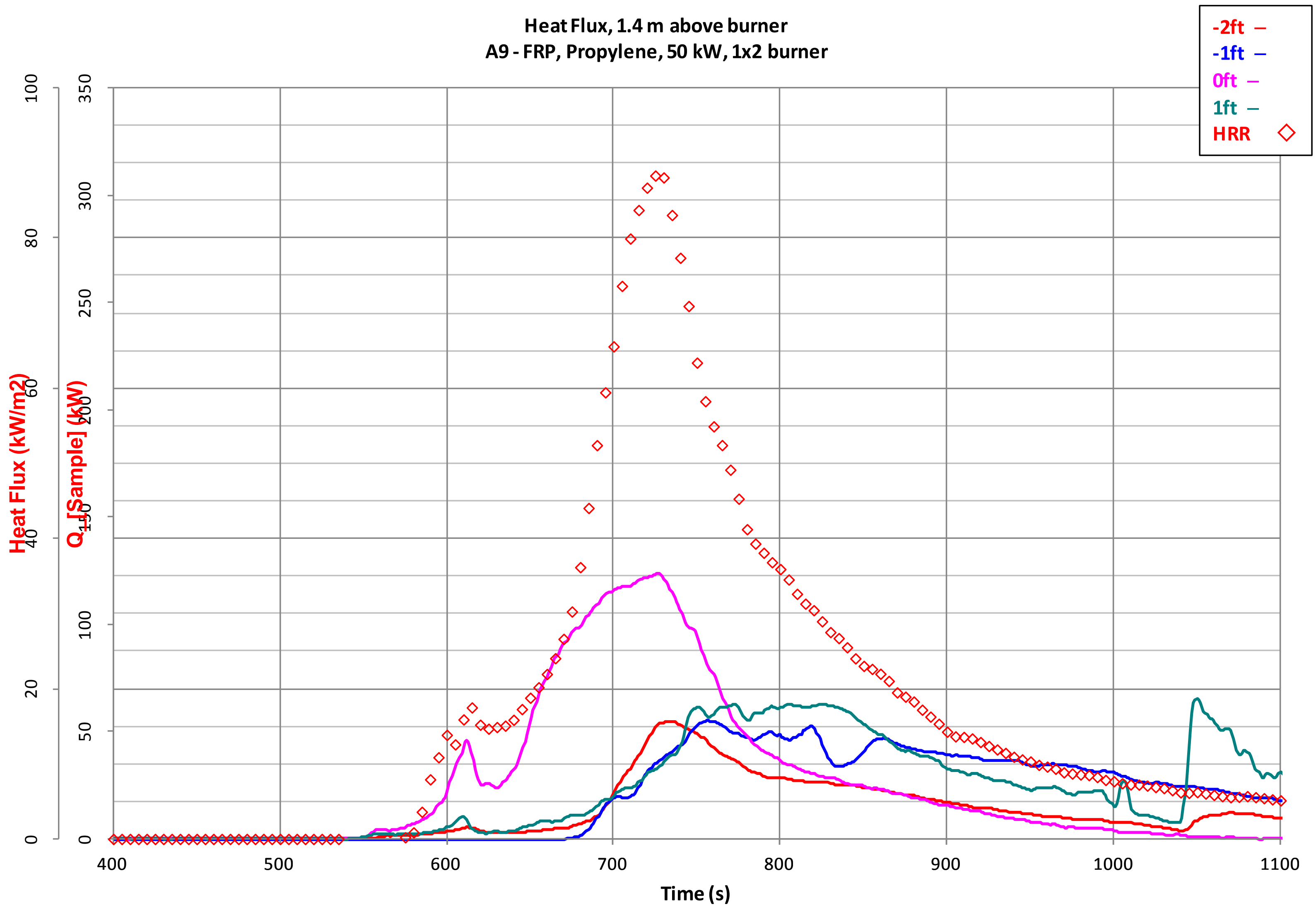

Heat flux measured at various distances from the centerline (negative indicates left of centerline), 1.4m vertically from burner surface

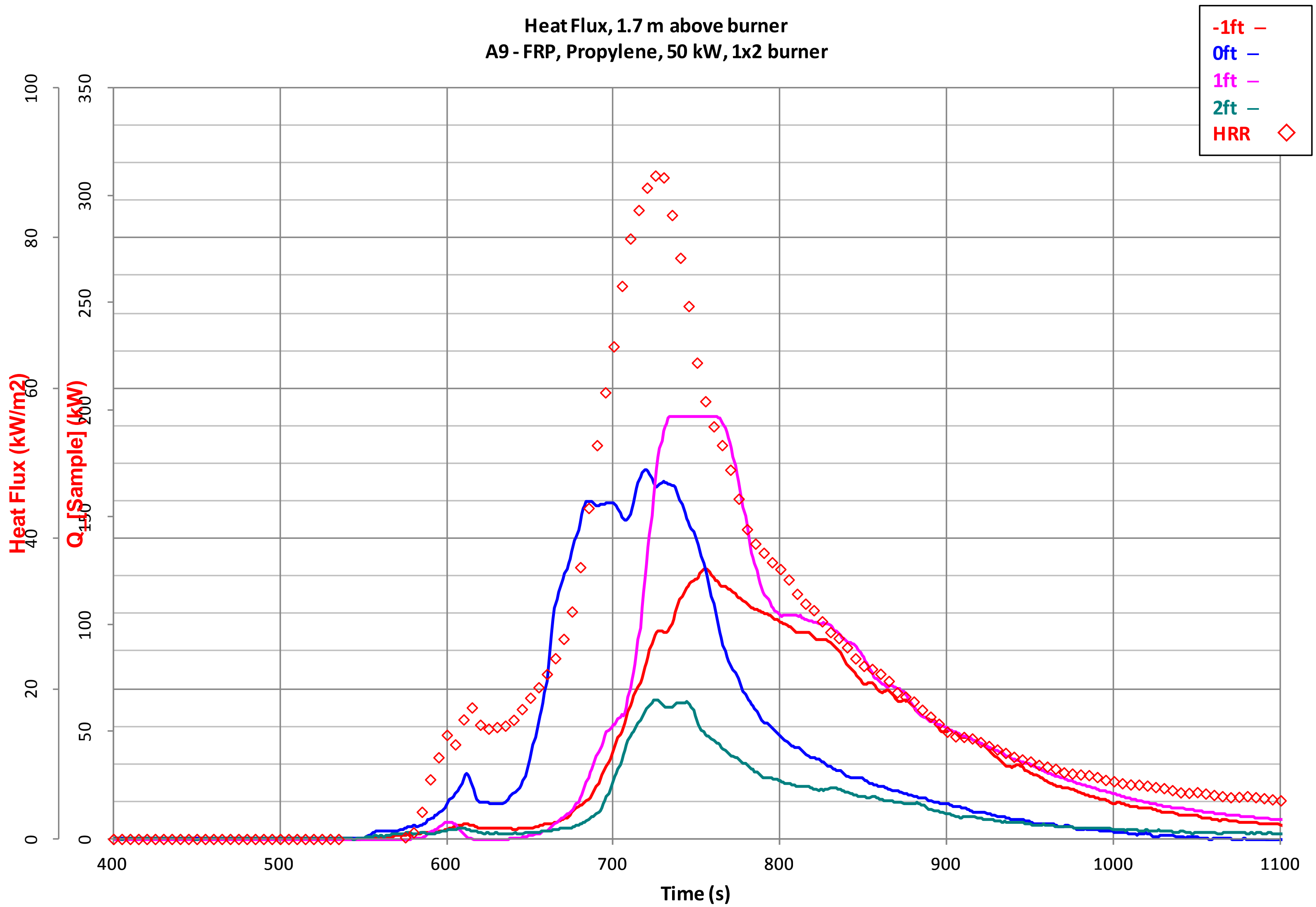

Heat flux measured at various distances from the centerline (negative indicates left of centerline), 1.7m vertically from burner surface

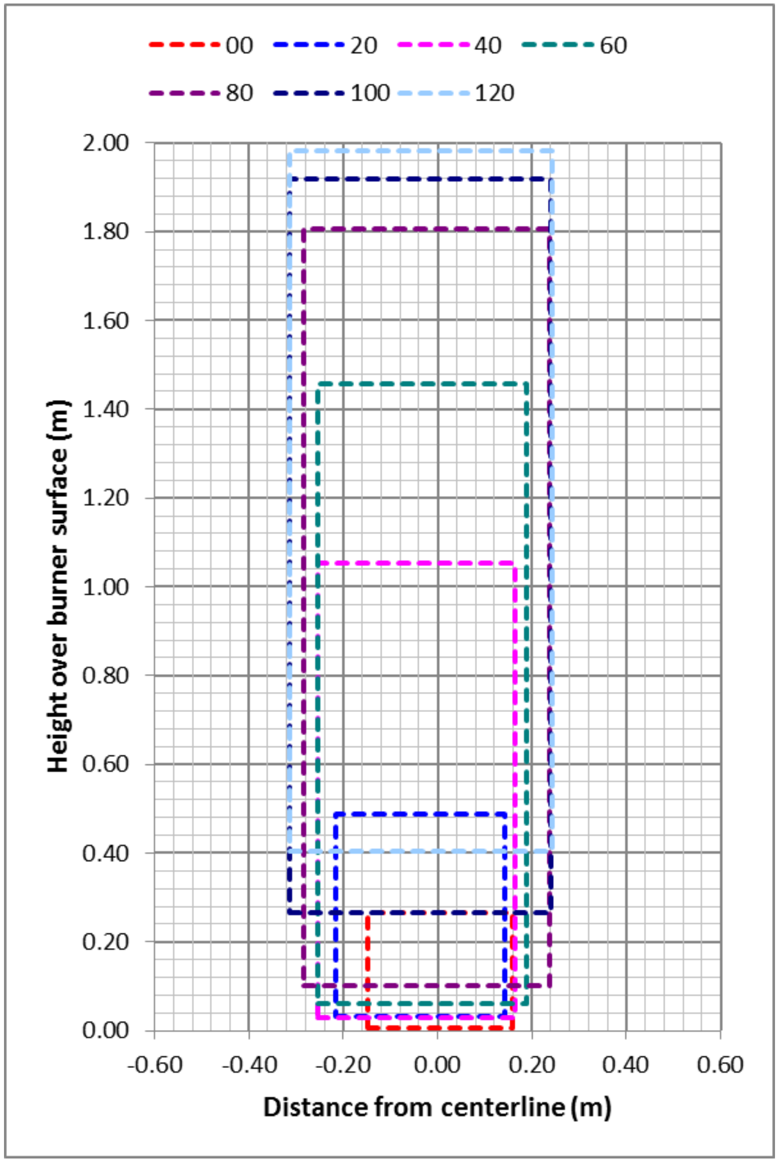

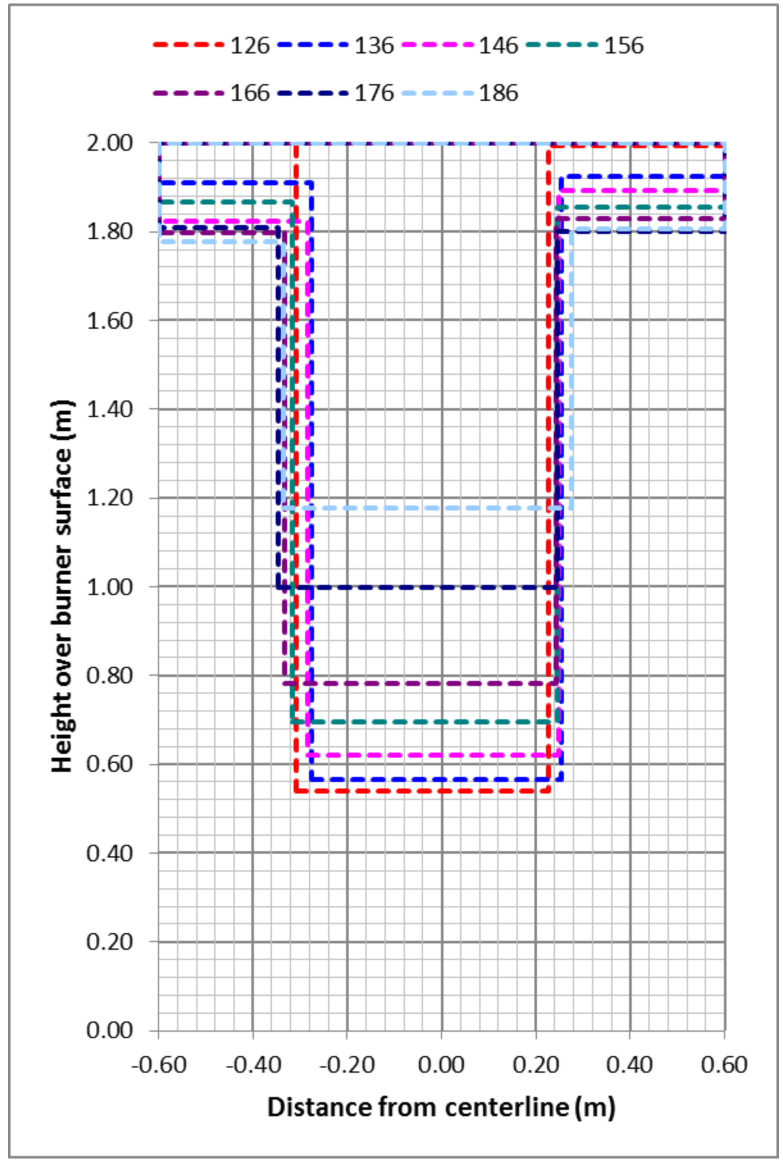

Stages 1 and 2 burning areas in Test A9 (2ft Rectangle burner, Propylene, 50 kW source)

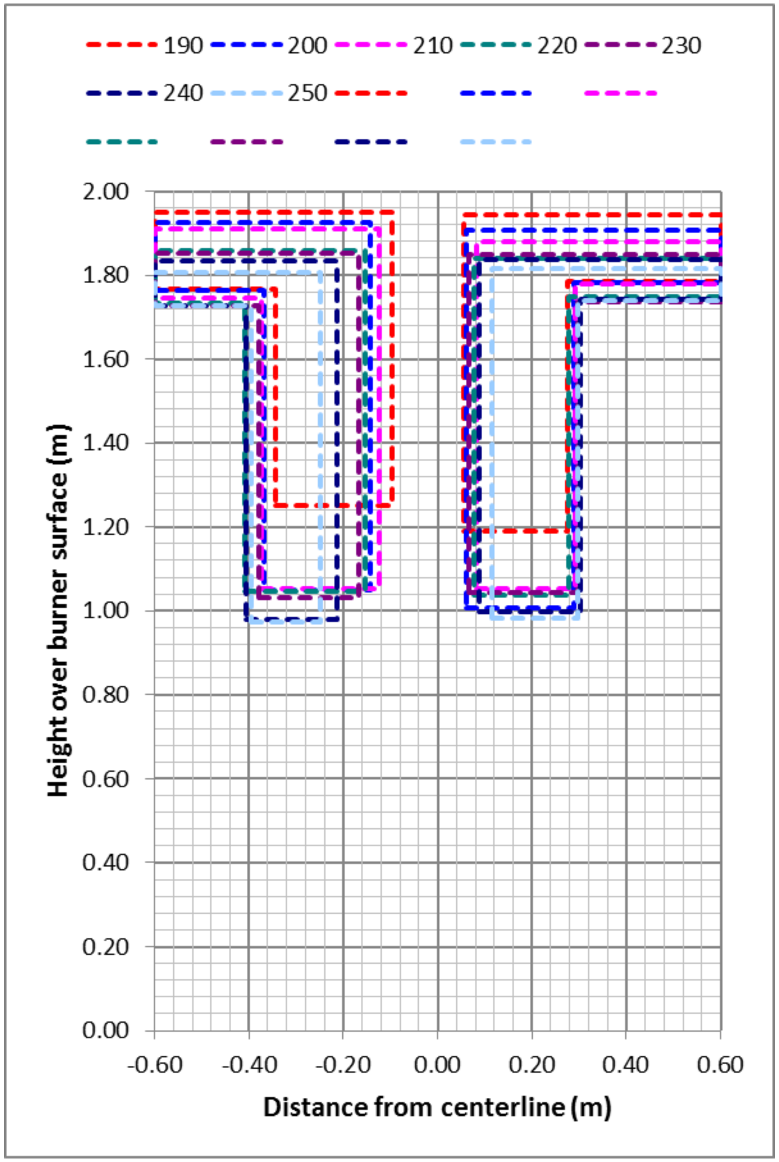

Stage 3 burn area and final damage chart of Test A9 (2ft Rectangle burner, Propylene, 50 kW source)

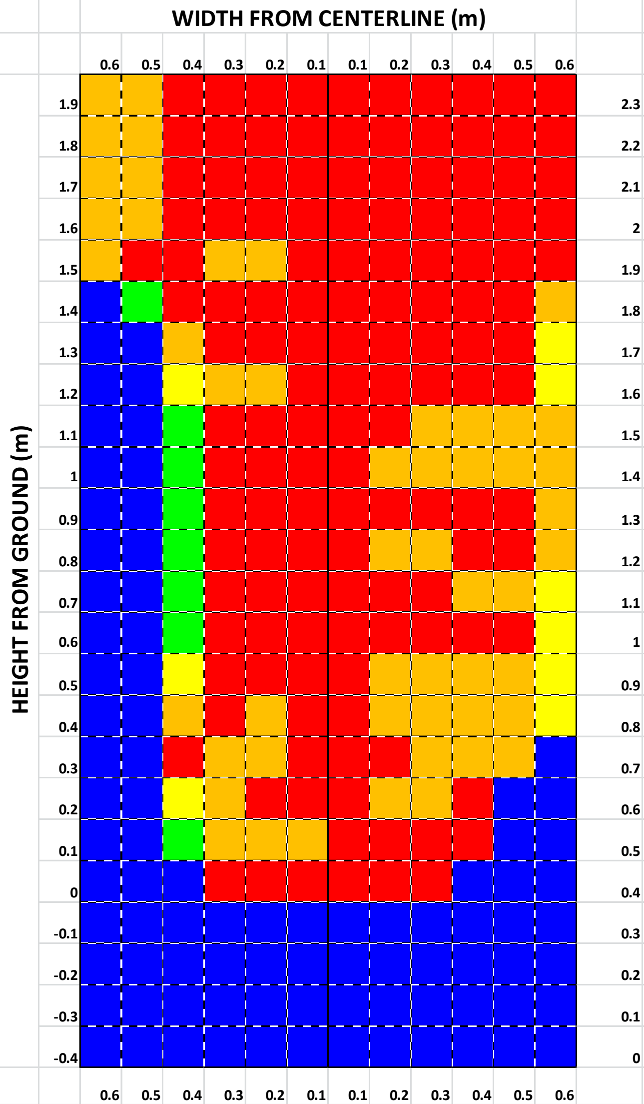

# of cell	Damage to Resin	Area (m2)
134	up to 100% damage	1.34
51	up to 75% damage	0.51
9	up to 50% damage	0.09
8	up to 25% damage	0.08
86	no damage	0.86

Initial mass:	8.32	kg
Final unburnt mass:	3.08	kg
Final burnt mass:	2.92	kg
Total mass loss during fire	2.32	kg

Burn damage pattern observed after fire test

F.3.10 Test A10

LODS Test Run Data

Center for Firesafety Studies

100 Institute Road
Worcester, MA 01609
Phone: (508) 831-5628
Fax: (508) 831-5680

Test Information

Test Number:	A10
Specimen Identification:	FRP 10, 75 kW initial Propylene fire, 1 x 2 burner
Material Name:	Class C FRP panel
Manufacturer/Submitter:	Not Reported
Raw Data File Name:	Test A10 - FRP_75kW_Propylene_2ft.txt
Reduced Data File Name:	Test A10 - FRP_75kW_Propylene_2ft_reduced.xlsx
Date of Test:	11-Nov-2010
Tester:	W. Wong

Test Parameters

Ambient Temperature:	N/A
Relative Humidity:	N/A

Specimen Information

Specimen Initial Mass:	[kg]	8.3
Specimen Final Mass:	[kg]	5.8
Mass Lost:	[kg]	2.5
Heat Evolved (net):	[kJ]	0

Parameter	Unit	Value
Mass Loss		
Initial Mass	[kg]	8.3
Final Mass	[kg]	5.8
Mass Loss	[%]	29.88

LODS Test Run Data

Center for Firesafety Studies

100 Institute Road
Worcester, MA 01609
Phone: (508) 831-5628
Fax: (508) 831-5680

Test Notes

Test Number:	0
Date:	11/11/10
Material:	Class C FRP panel
Specimen Identification:	FRP 10, 75 kW initial Propylene fire, 1 x 2 burner

Observations

Time	Observation
00:00	Start VI
05:10	Start Camera 1
01:20	Start Camera 2
07:24	Burner ignition
07:40	Reach target HRR @ 75 kW
07:53	Crackling noise
08:15	Panel ignition
08:25	Burner off
08:50	Flame hit ceiling
09:09	T-pattern burning
09:35 to 10:50	Rollover under ceiling
10:50	Little burning of the wall paper on the right for 30 sec
	Remote area ignition @ TSC-3, but close to main wall fire
	Remote area smoking @ TSC-4, TSC-9, and HFG-2
12:00	Little edge burning @ y - 1.5 m on both side, caused by rollover and
	escaping gas from panel on the edges
28:05	Terminate test with little water application

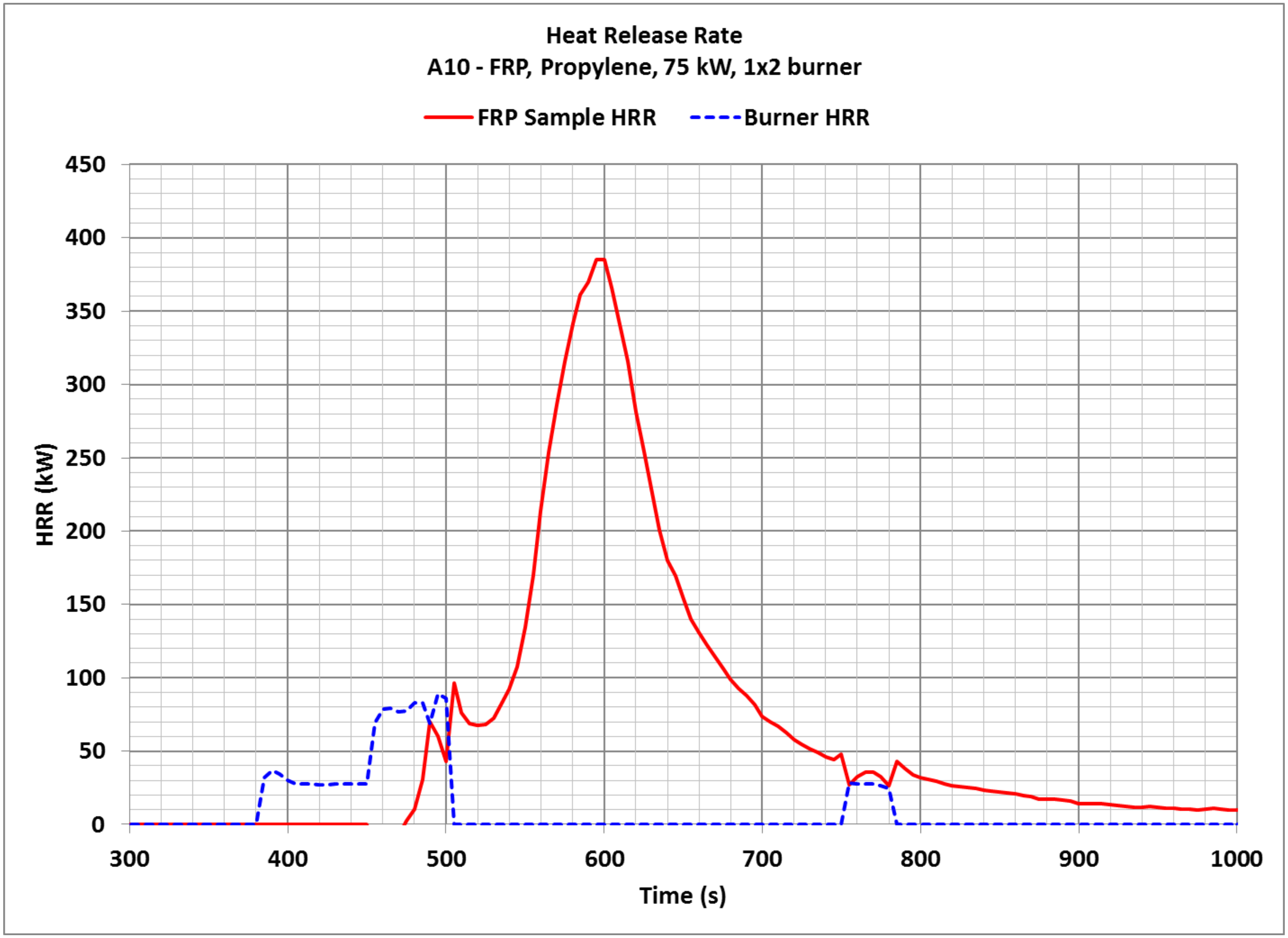

Heat release ratesof the source burner fire and of the specimen fire measured during test

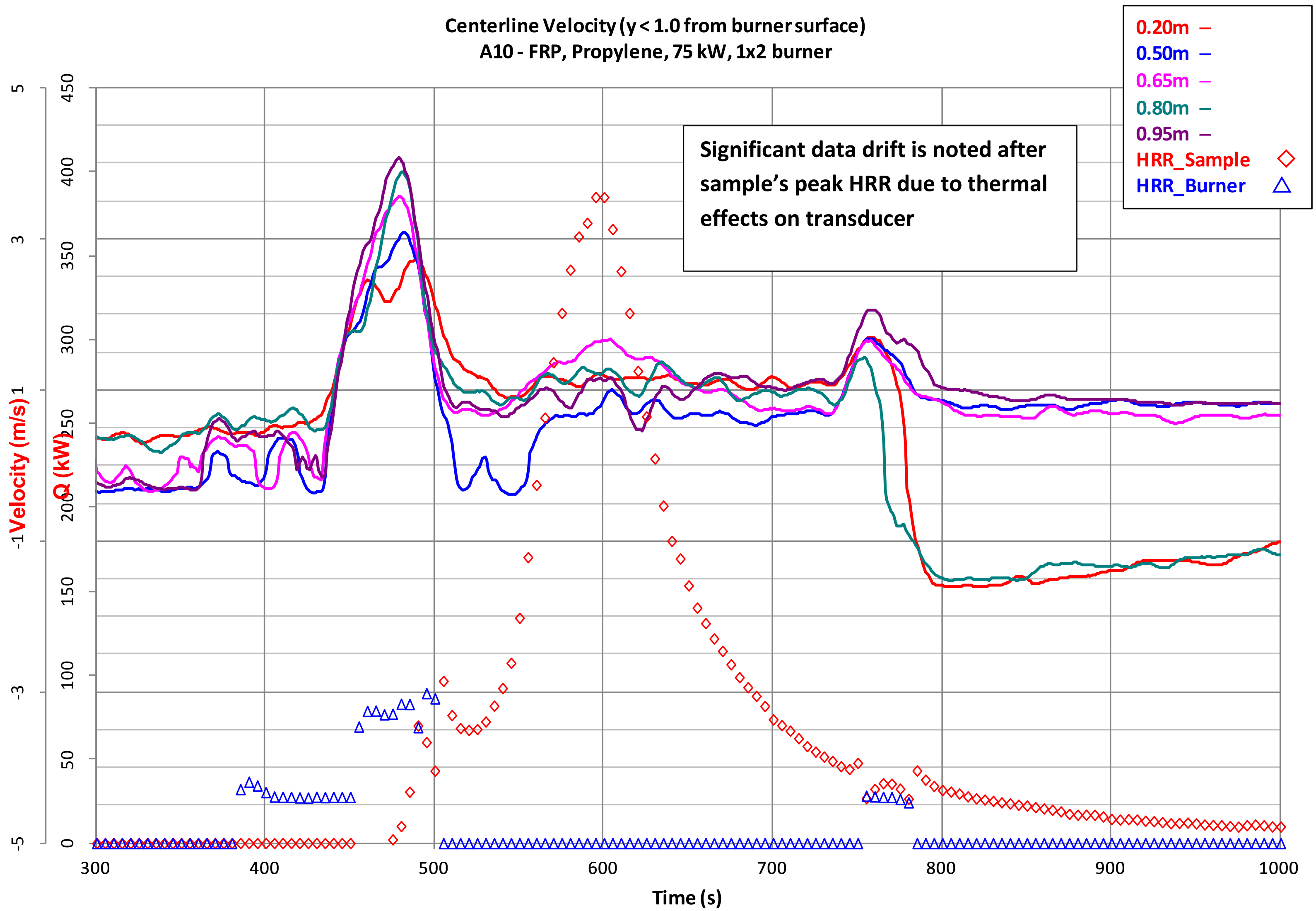

Centerline plume velocities measured from 0.2m to 0.95m above the burner surface

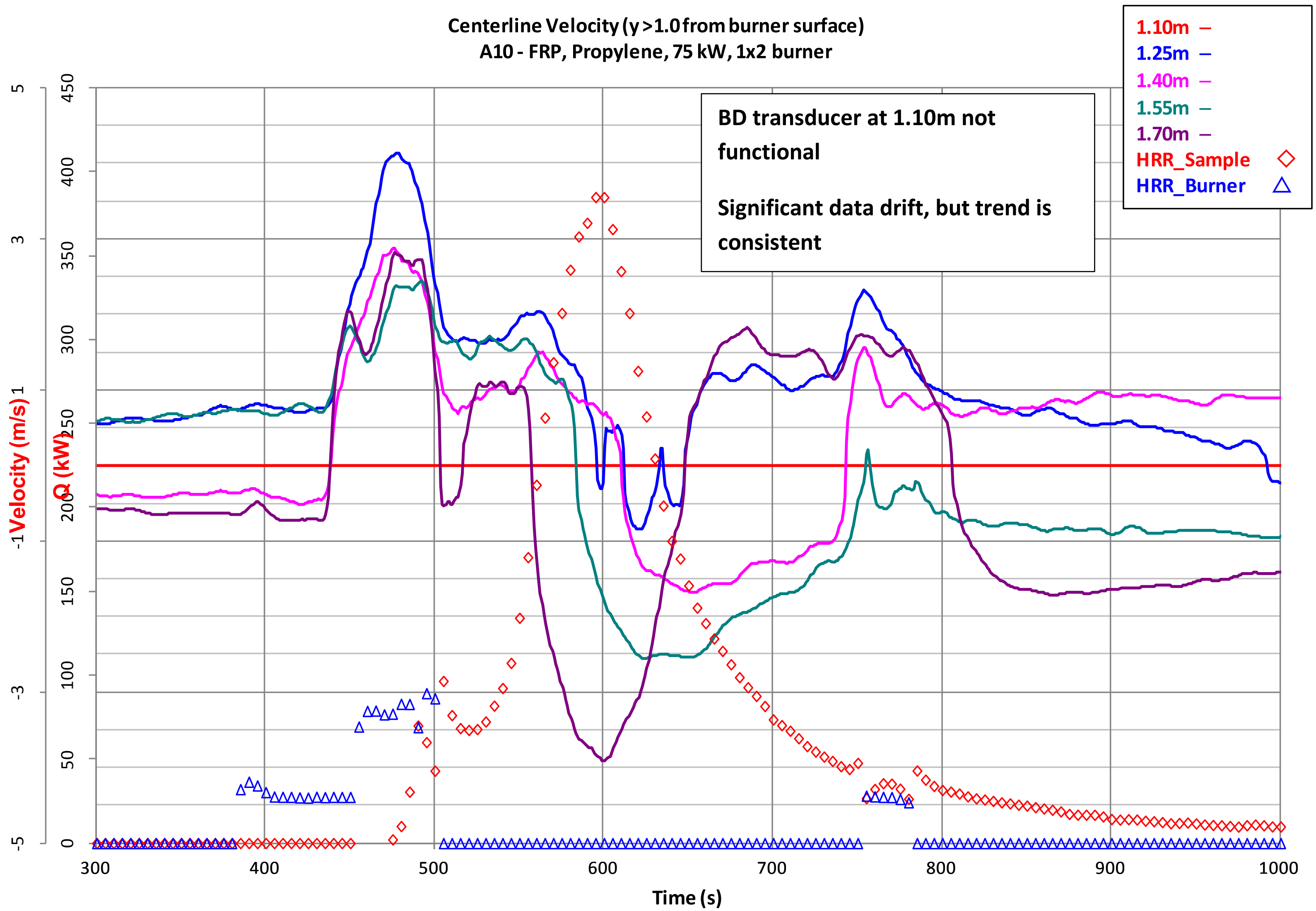

Centerline plume velocities measured from 1.1m to 1.7m above the burner surface

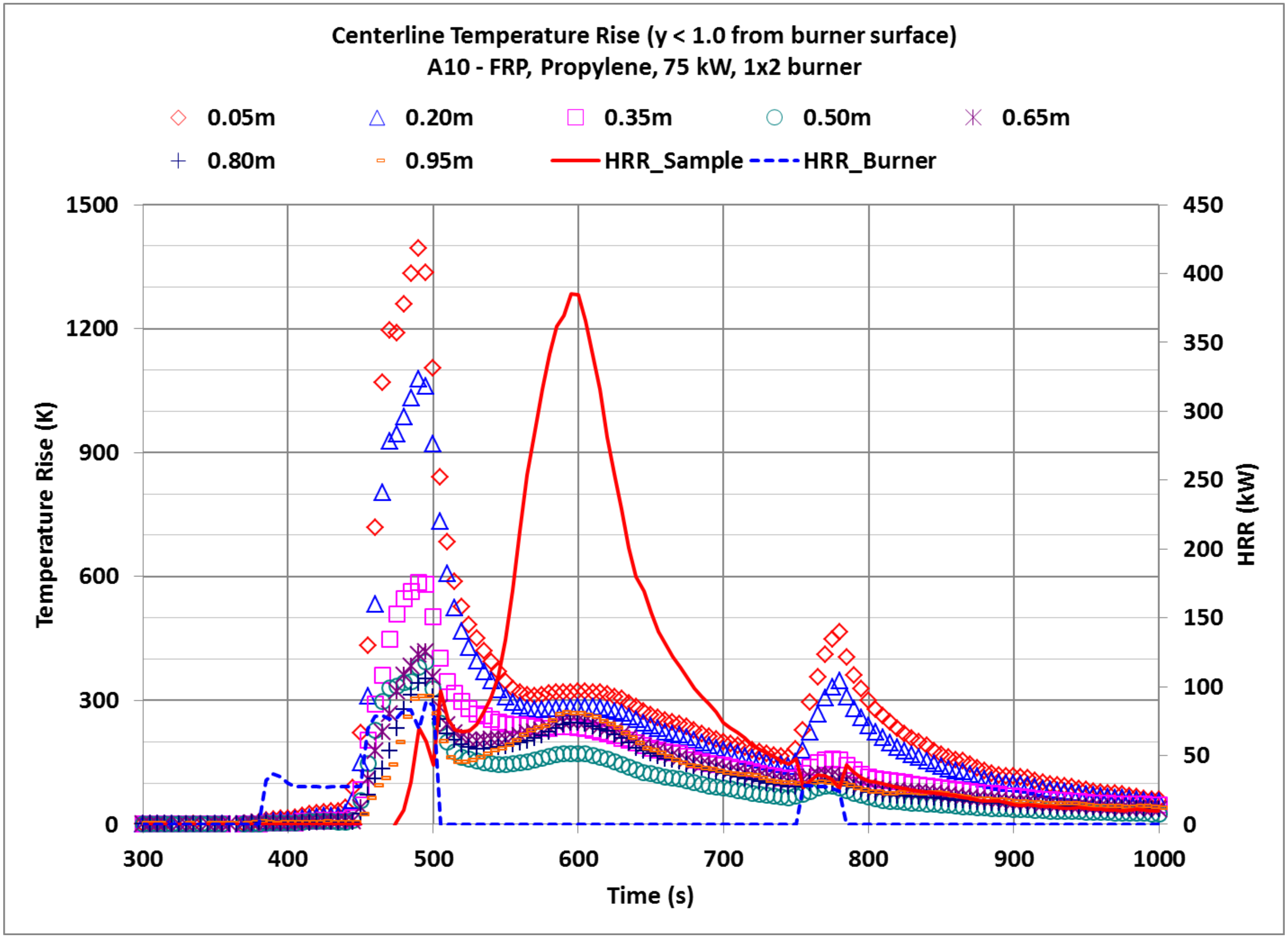

Centerline plume temperature rise measured from 0.05m to 0.95m above the burner surface

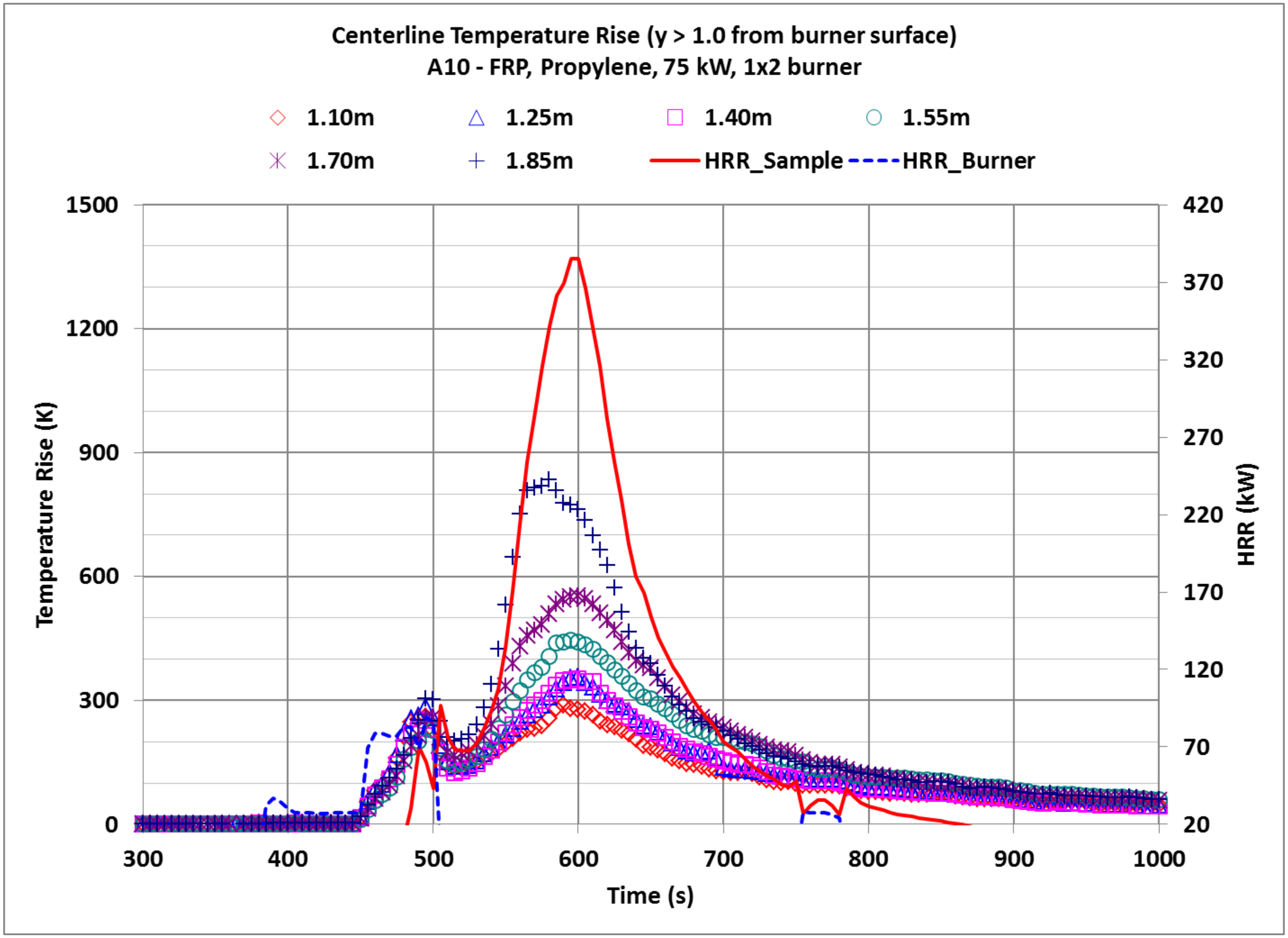

Centerline plume temperature rise measured from 1.10m to 1.85m above the burner surface

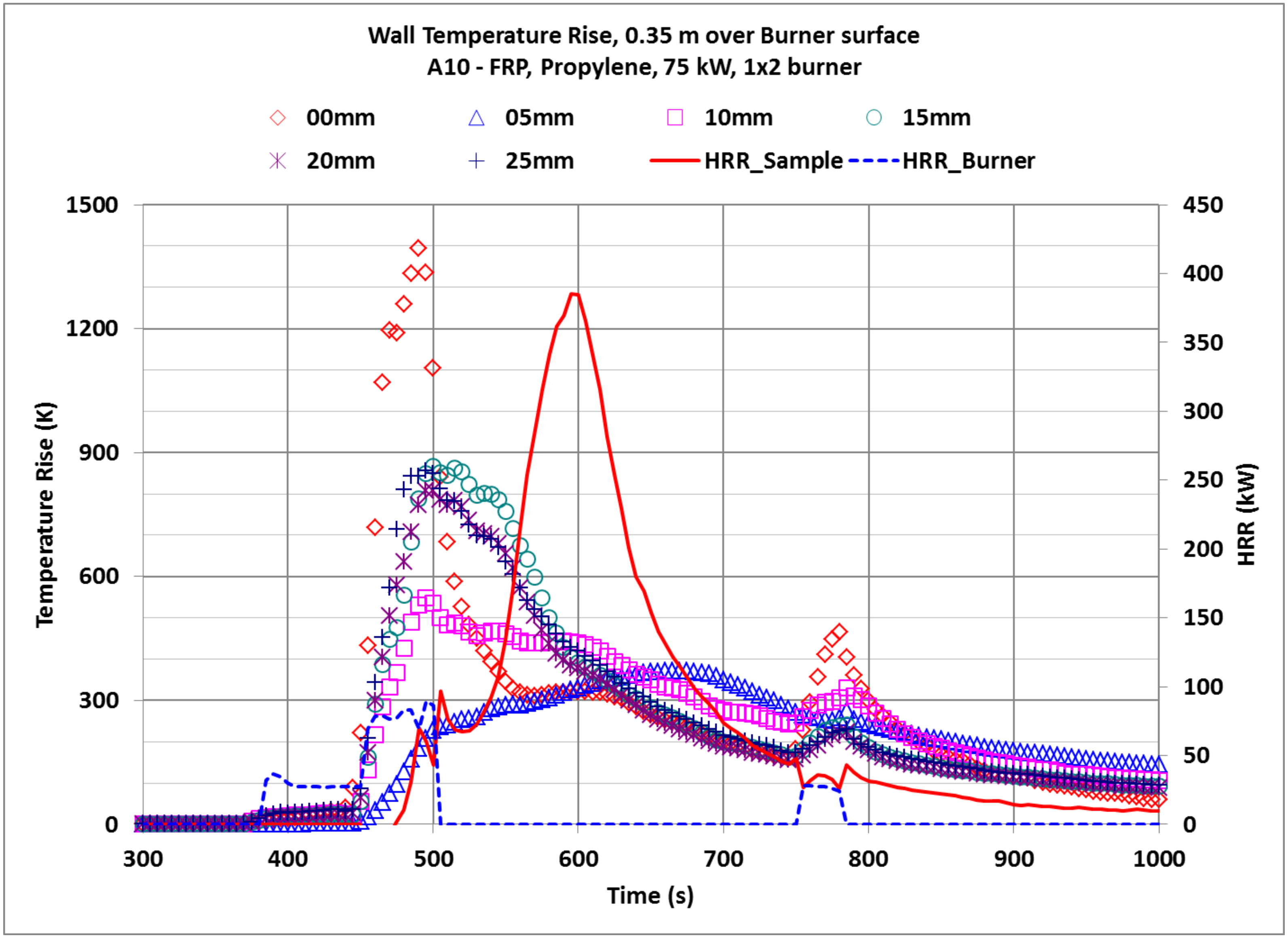

Temperature rise along the wall's centerline at 0.35m over the burner surface, measured at different perpendicular distances to as indicated

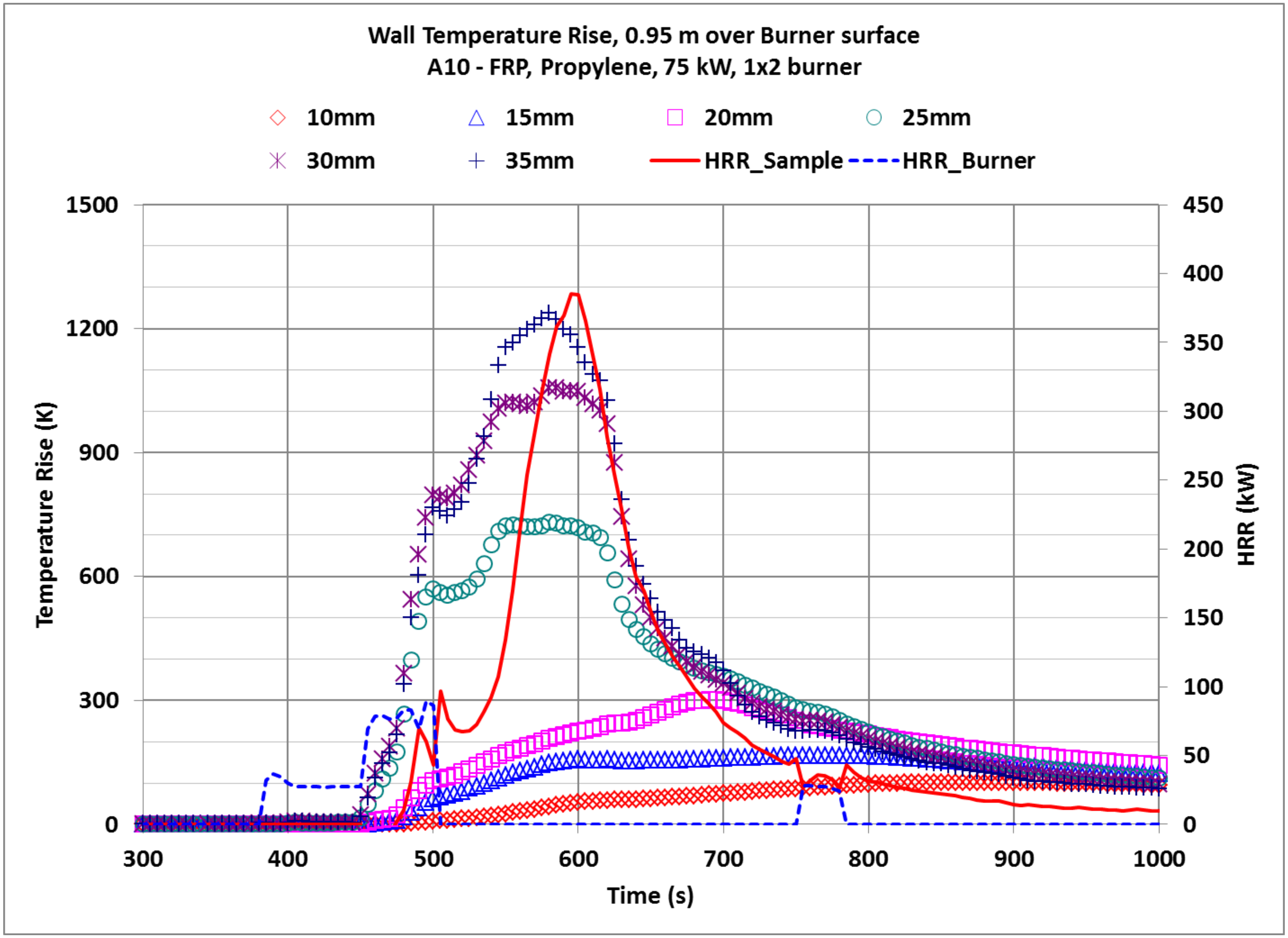

Temperature rise along the wall's centerline at 0.95m over the burner surface, measured at different perpendicular distances to as indicated

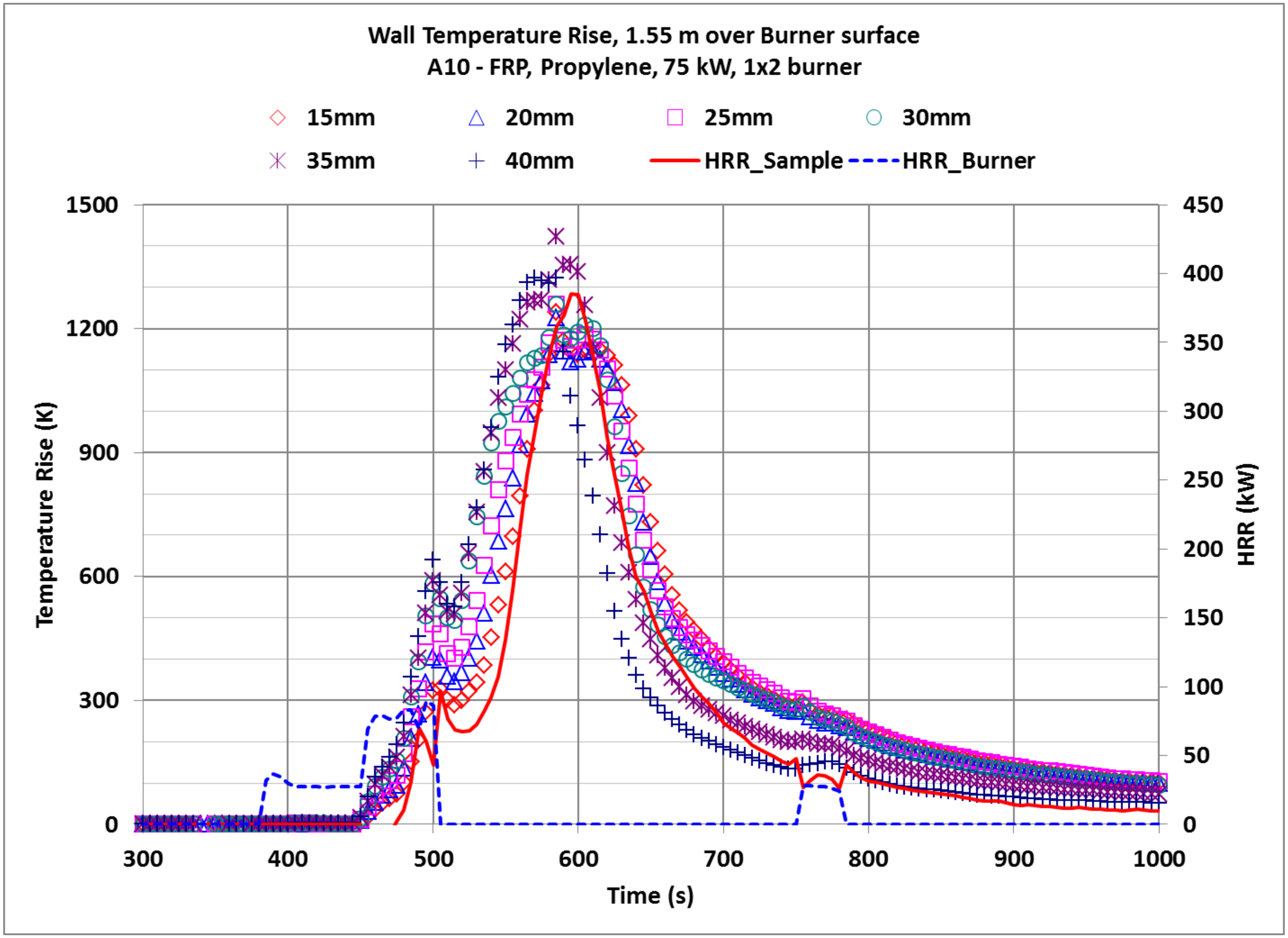

Temperature rise along the wall's centerline at 1.55m over the burner surface, measured at different perpendicular distances to as indicated

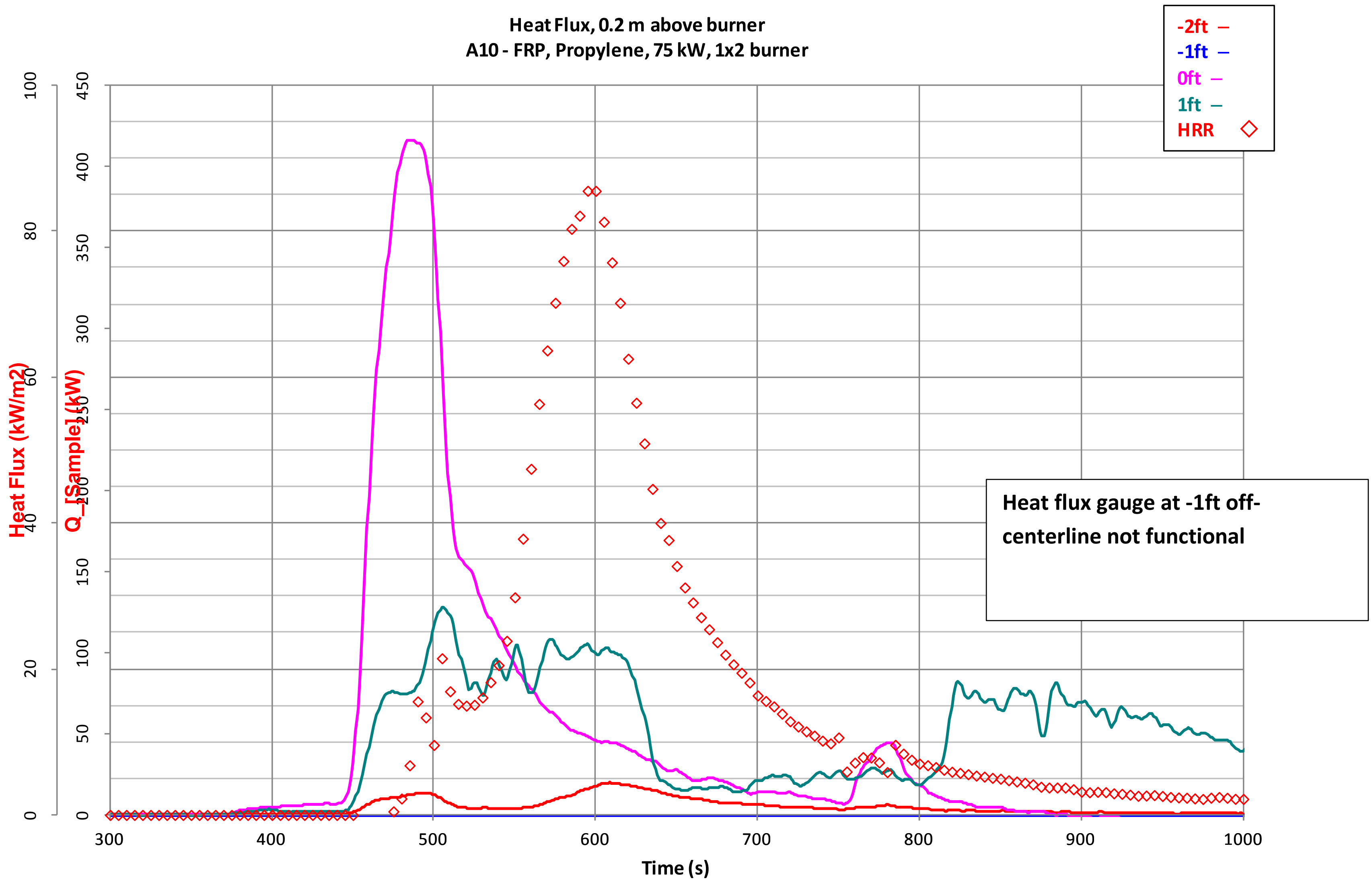

Heat flux measured at various distances from the centerline (negative indicates left of centerline), 0.2m vertically from burner surface

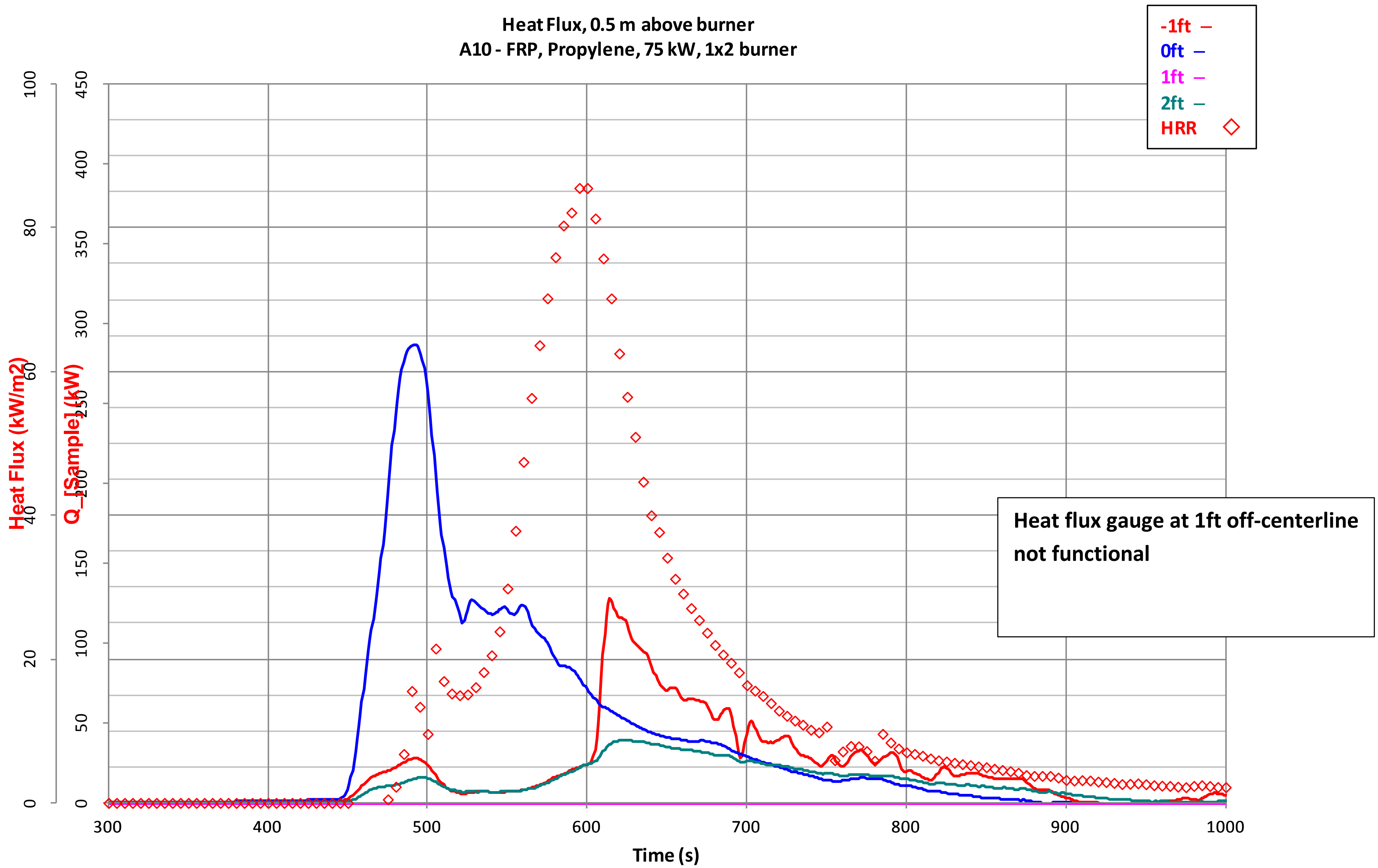

Heat flux measured at various distances from the centerline (negative indicates left of centerline), 0.5m vertically from burner surface

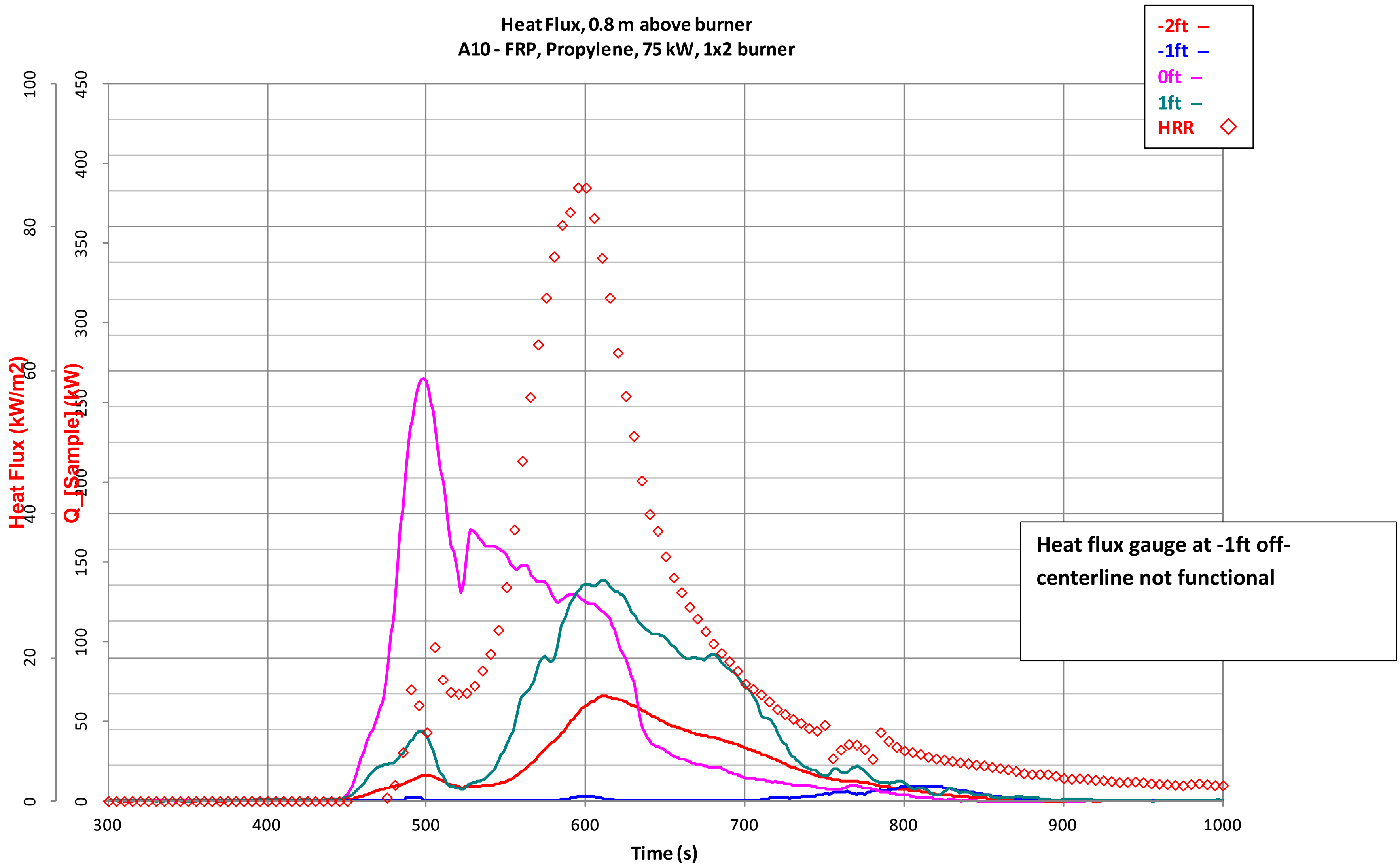

Heat flux measured at various distances from the centerline (negative indicates left of centerline), 0.8m vertically from burner surface

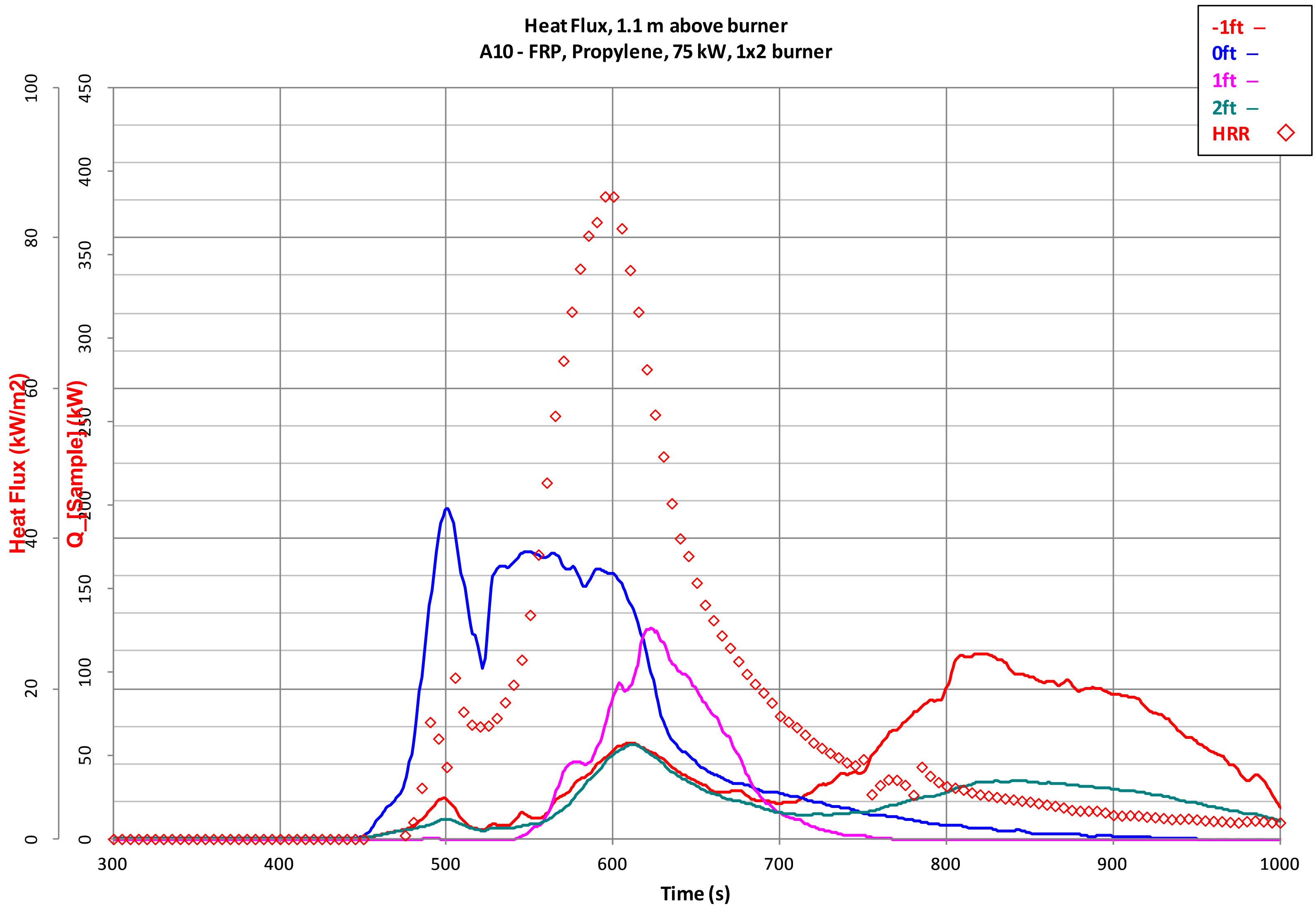

Heat flux measured at various distances from the centerline (negative indicates left of centerline), 1.1m vertically from burner surface

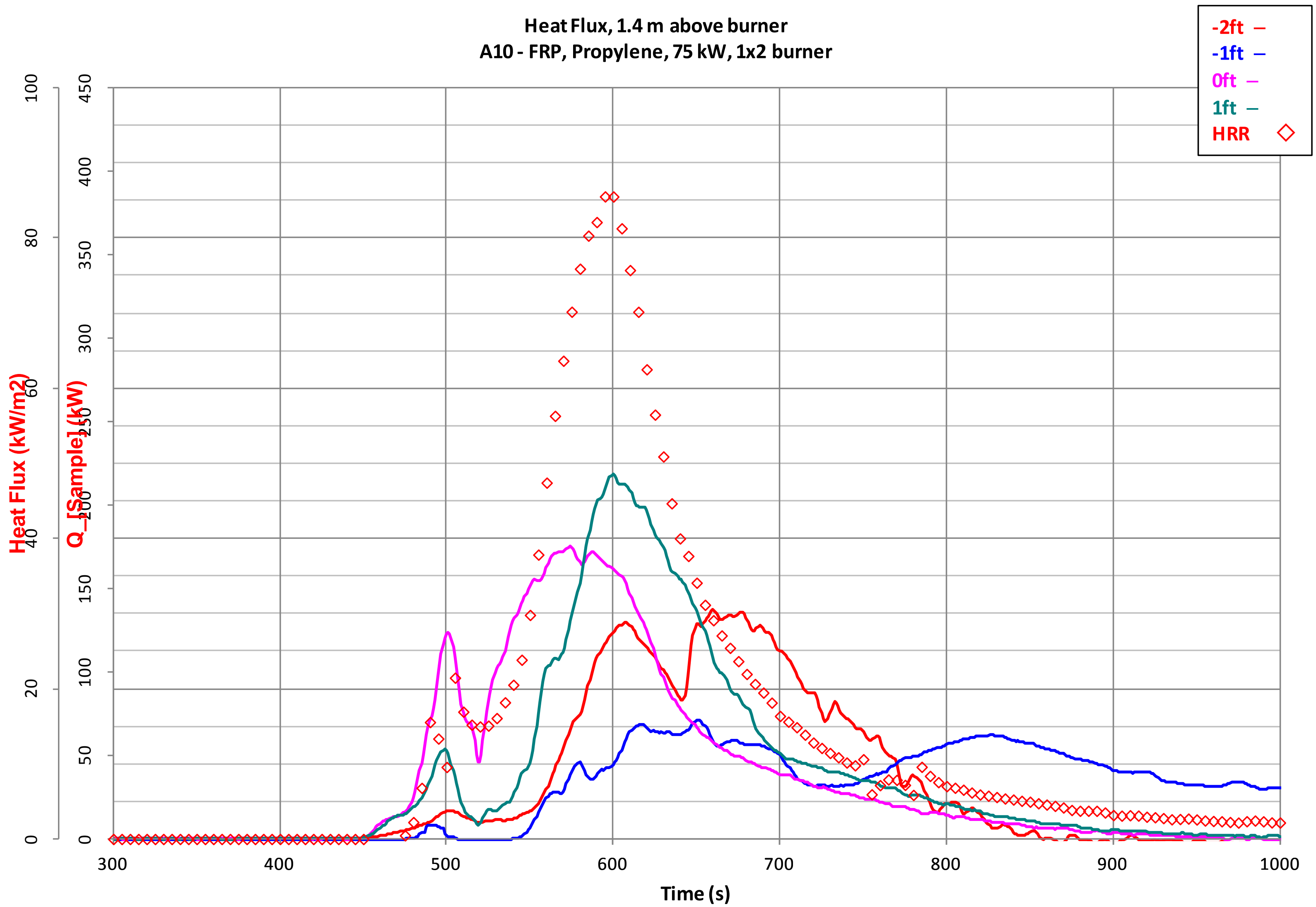

Heat flux measured at various distances from the centerline (negative indicates left of centerline), 1.4m vertically from burner surface

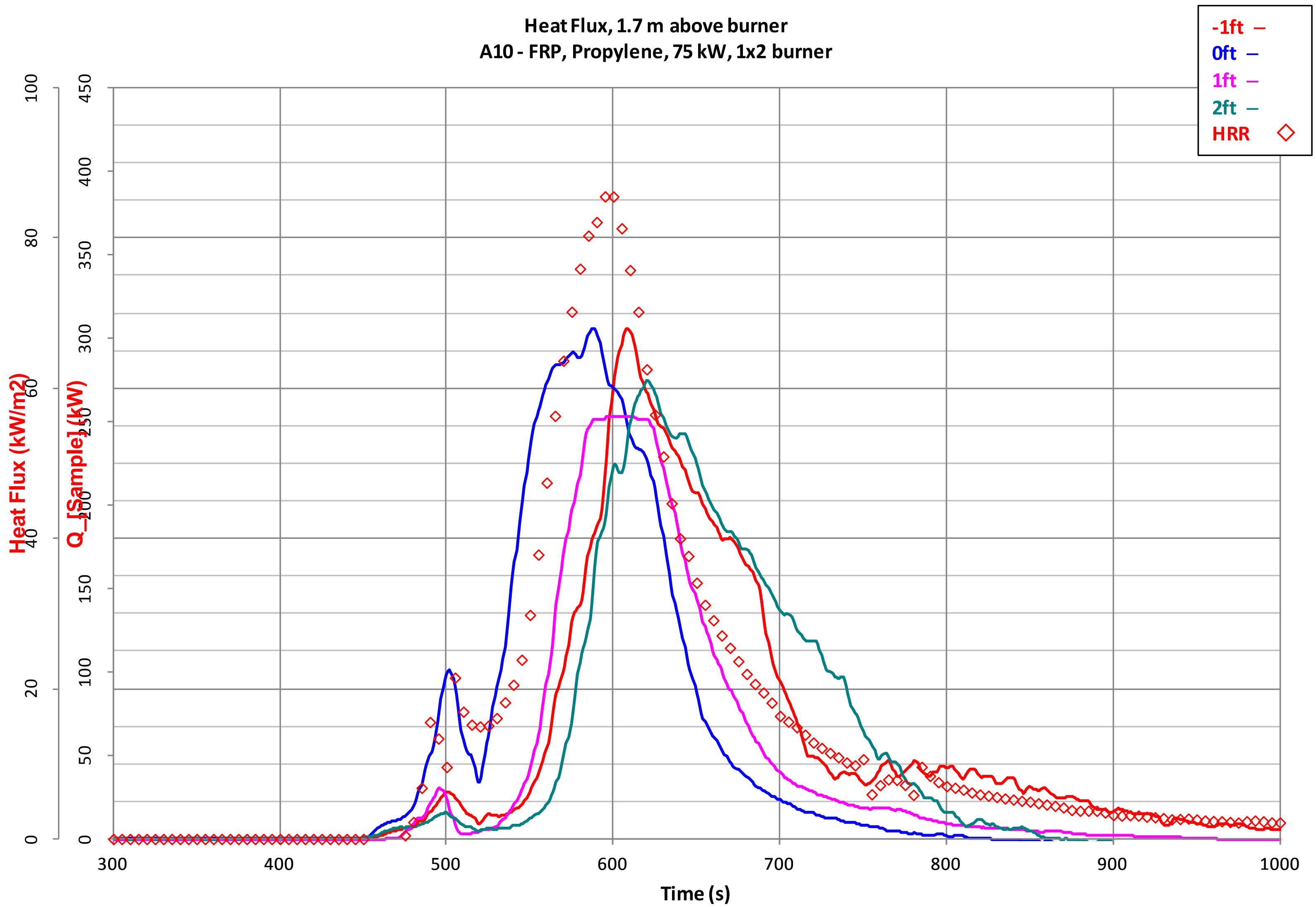

Heat flux measured at various distances from the centerline (negative indicates left of centerline), 1.7m vertically from burner surface

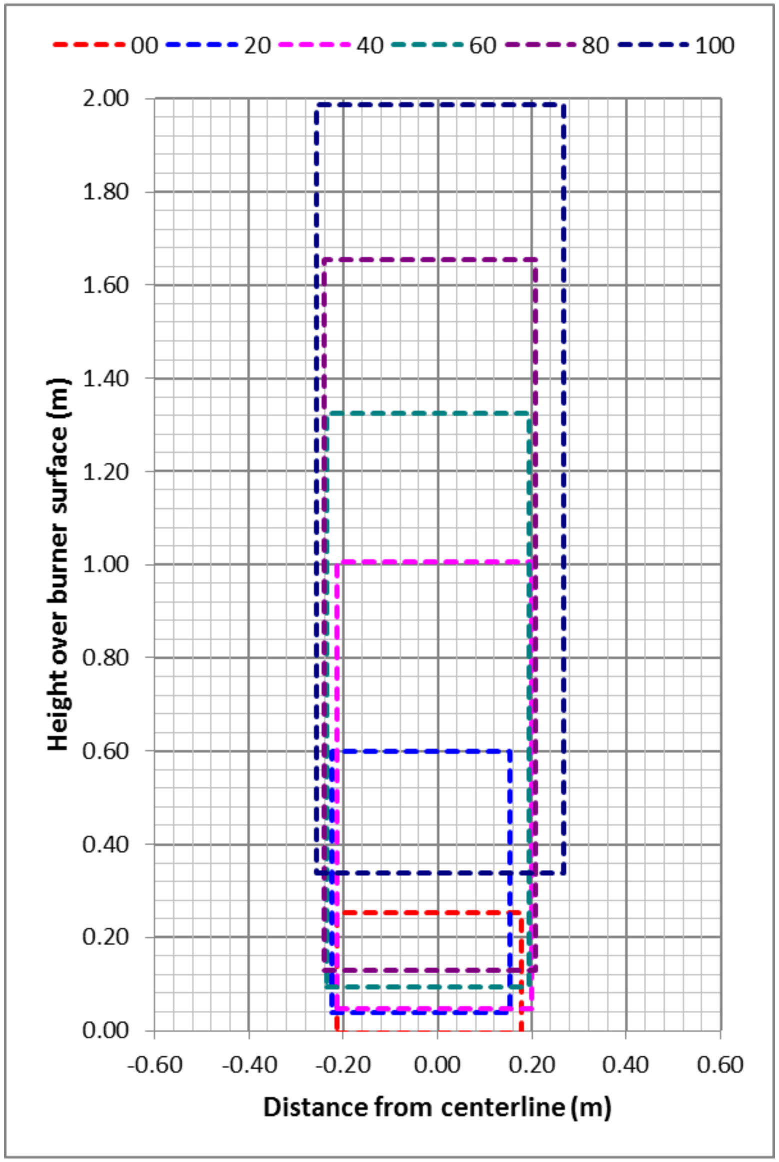

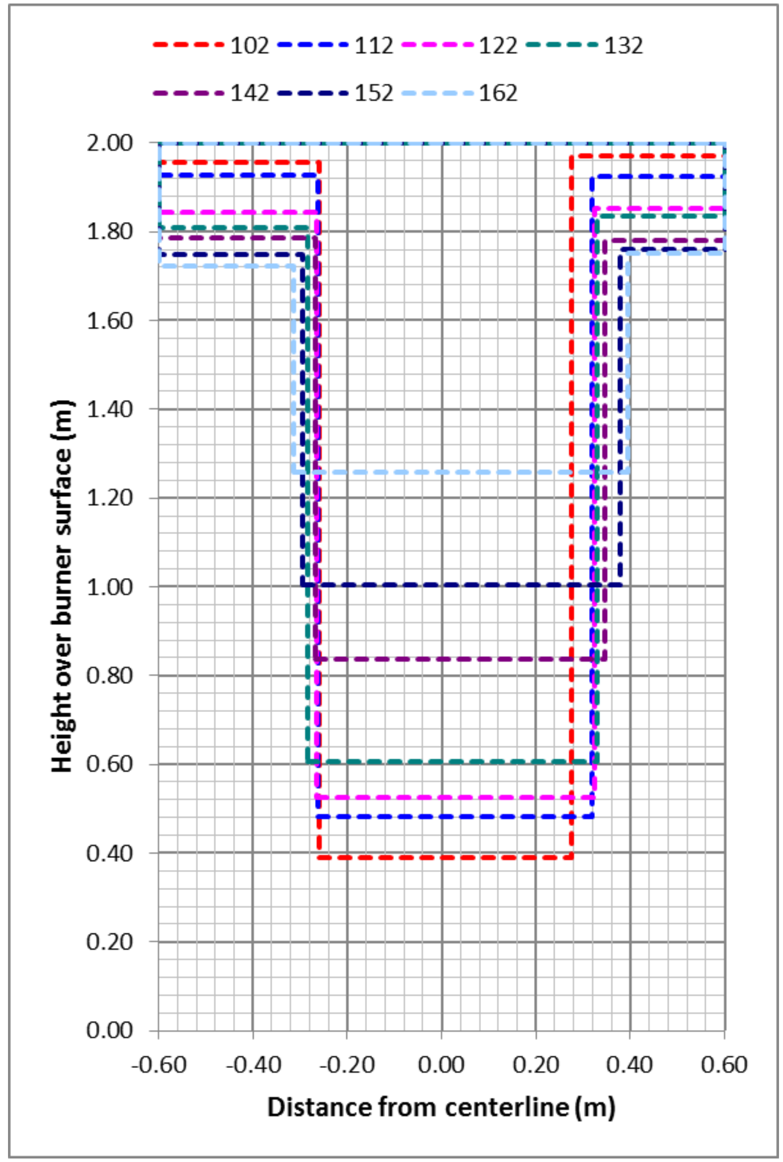

Stages 1 and 2 burning areas in Test A10 (2ft Rectangle burner, Propylene, 75 kW source)

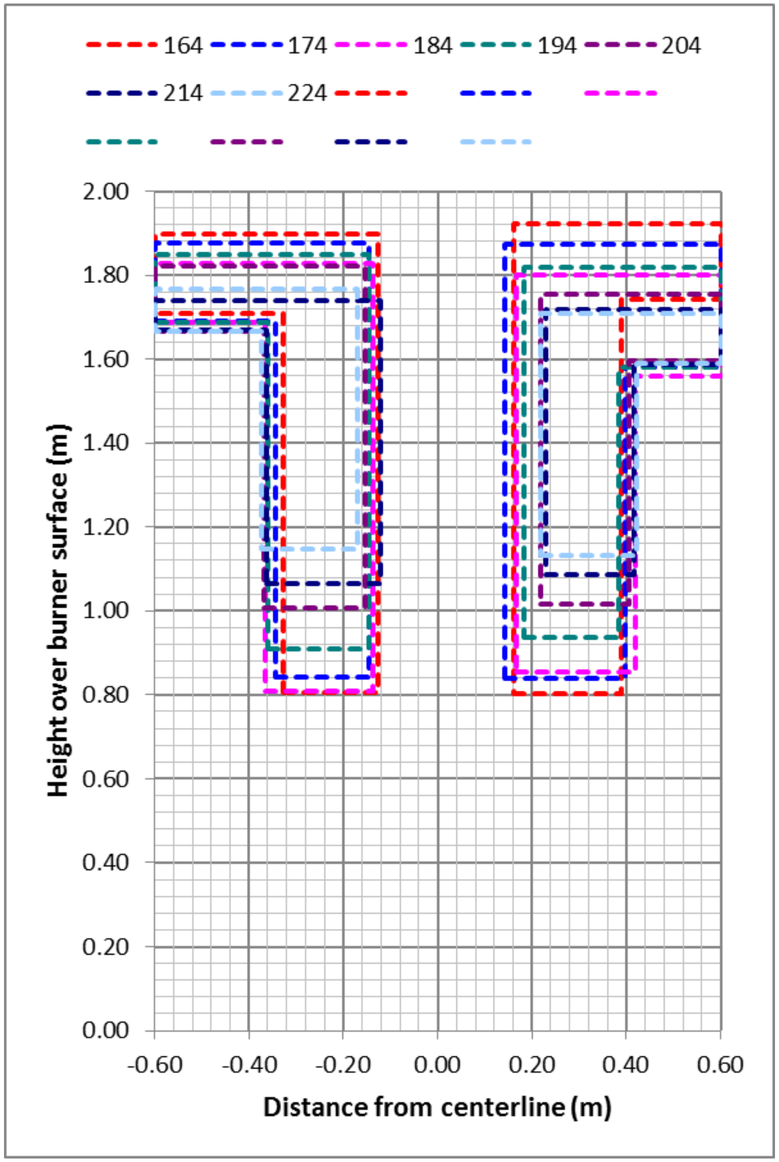

Stage 3 burn area and final damage chart of Test A10 (2ft Rectangle burner, Propylene, 75 kW source)

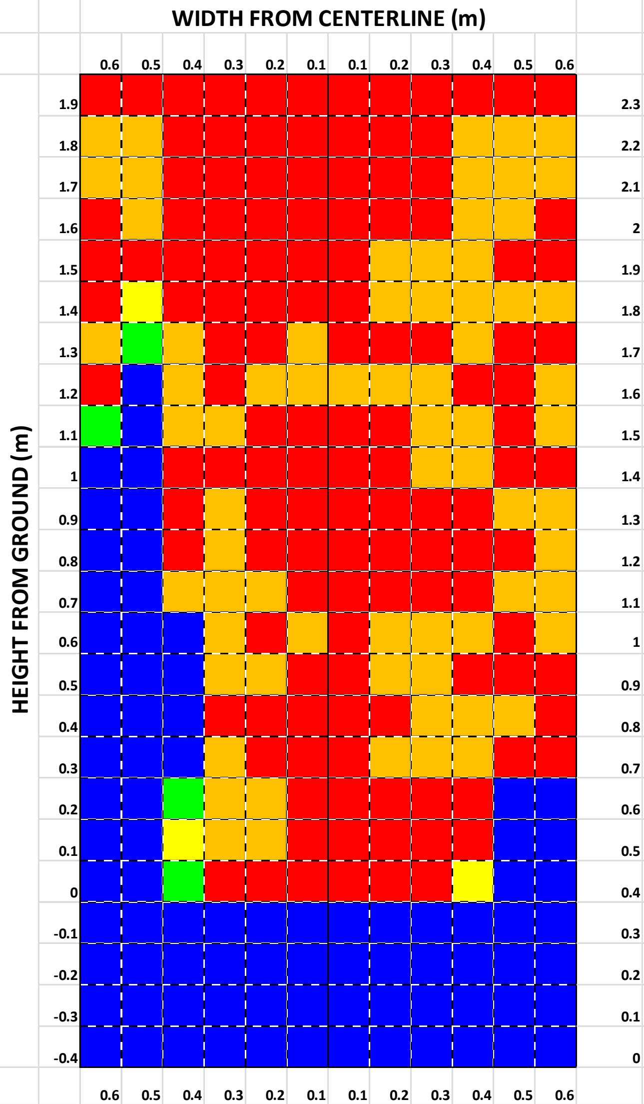

# of cell	Damage to Resin	Area (m2)
129	up to 100% damage	1.29
70	up to 75% damage	0.7
3	up to 50% damage	0.03
4	up to 25% damage	0.04
82	no damage	0.82

Initial mass:	8.3	kg
Final unburnt mass:	2.72	kg
Final burnt mass:	3.1	kg
Total mass loss during fire	2.48	kg

Burn damage pattern observed after fire test

F.3.11 Test A11

LODS Test Run Data

Center for Firesafety Studies

100 Institute Road
Worcester, MA 01609
Phone: (508) 831-5628
Fax: (508) 831-5680

Test Information

Test Number:	A11
Specimen Identification:	FRP 11, 50 kW initial Propylene fire, 1 x 2 burner
Material Name:	Class C FRP panel
Manufacturer/Submitter:	Not Reported
Raw Data File Name:	Test A11 - FRP_50kW_Propylene_2ft.txt
Reduced Data File Name:	Test A11 - FRP_50kW_Propylene_2ft_reduced.xlsx
Date of Test:	15-Nov-2010
Tester:	W. Wong

Test Parameters

Ambient Temperature:	N/A
Relative Humidity:	N/A

Specimen Information

Specimen Initial Mass:	[kg]	8.4
Specimen Final Mass:	[kg]	5.9
Mass Lost:	[kg]	2.5
Heat Evolved (net):	[kJ]	0

Parameter	Unit	Value
Mass Loss		
Initial Mass	[kg]	8.4
Final Mass	[kg]	5.9
Mass Loss	[%]	29.83

LODS Test Run Data

Center for Firesafety Studies

100 Institute Road
Worcester, MA 01609
Phone: (508) 831-5628
Fax: (508) 831-5680

Test Notes

Test Number:	0
Date:	11/15/10
Material:	Class C FRP panel
Specimen Identification:	FRP 11, 50 kW initial Propylene fire, 1 x 2 burner

Observations

Time	Observation
00:00	Start VI
08:00	Start Camera 1
03:30	Start Camera 2
09:35	Burner ignition
09:52	Reach target HRR @ 50 kW
10:18	Crackling noise
10:30	Panel ignition, mainly at area under TSC-2 to above burner
10:50	Burner off
	Remote area smoking @ HFG-5
11:42	Flame hit ceiling
11:55	Remote area ignition @ HFG-5, insignificant
12:10	Burning reaches left and right sides
12:20	T pattern started
12:20	Rollover under ceiling TSC-10, HFG-5 ignited contributed to sustained burning around rollover time
14:00	Remote smoking at right edge @ TSC-3 to y = 2.0, not ignited
15:00	Remote ignition @ HFG-1, TSC-4, TSC-10, HFG-5, makes line fires on the left edge more prominent, but individually insignificant
21:00	Some insignificant back face burning @ HFG-3
31:20	Terminate test with little water application

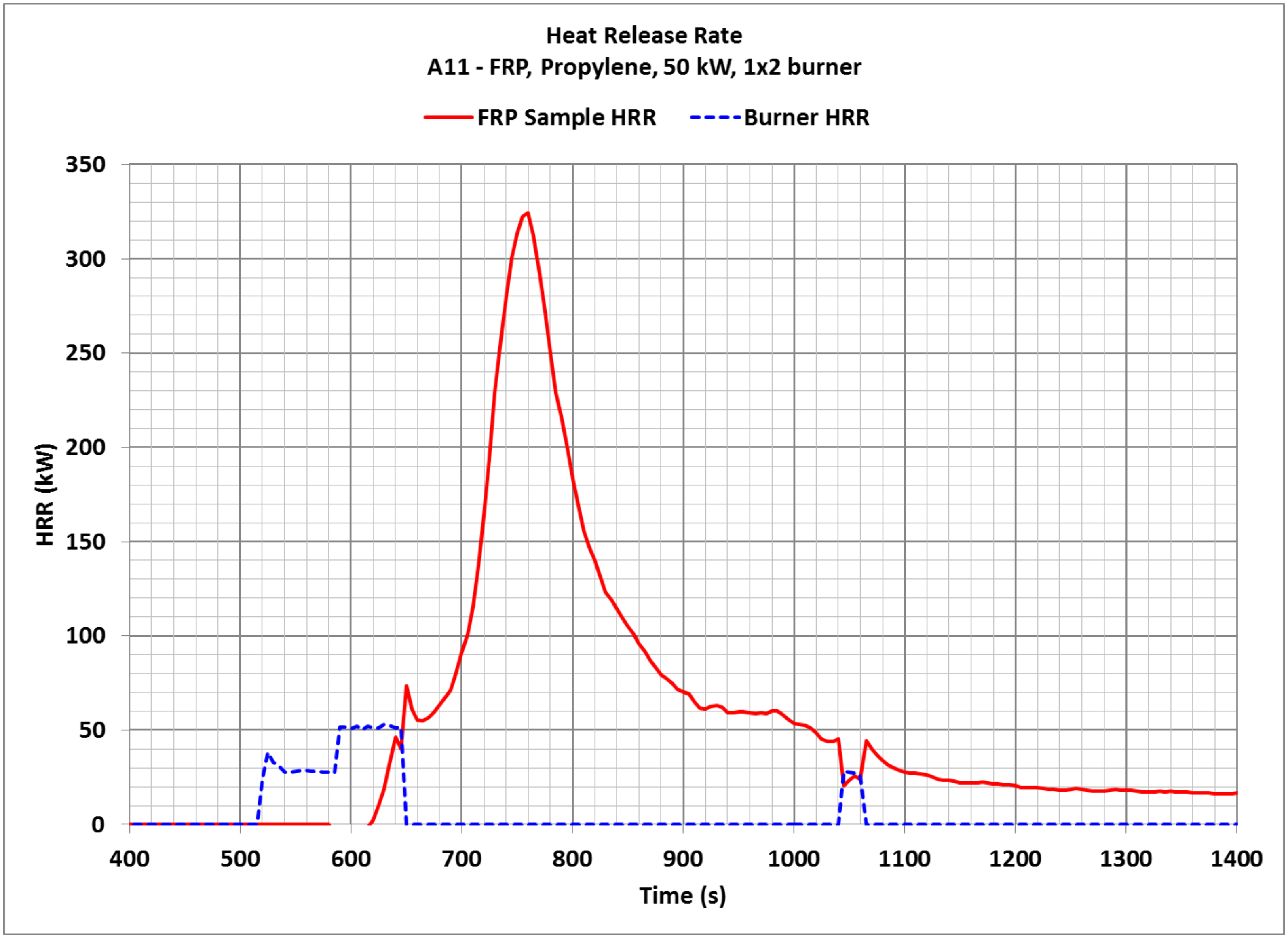

Heat release ratesof the source burner fire and of the specimen fire measured during test

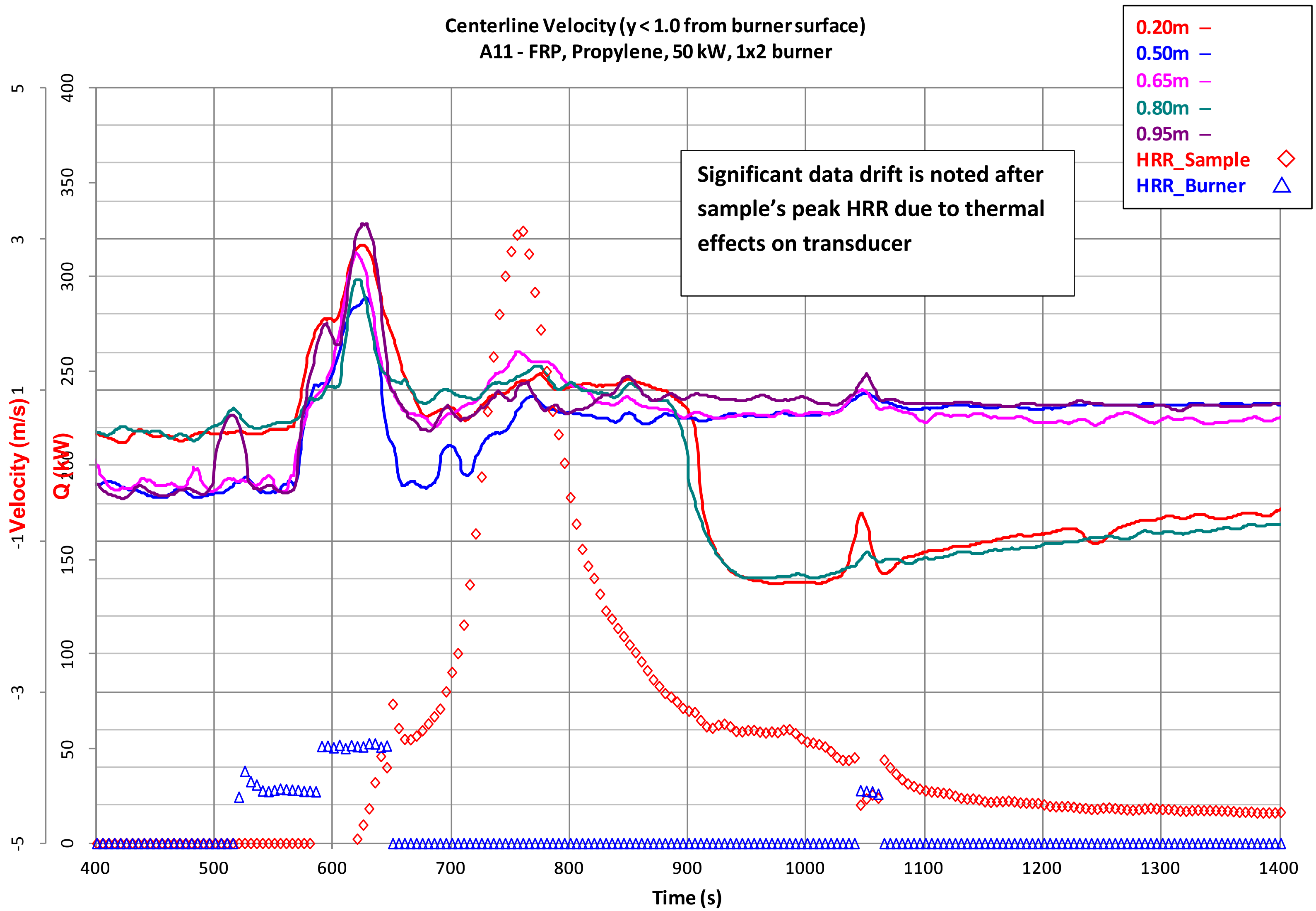

Centerline plume velocities measured from 0.2m to 0.95m above the burner surface

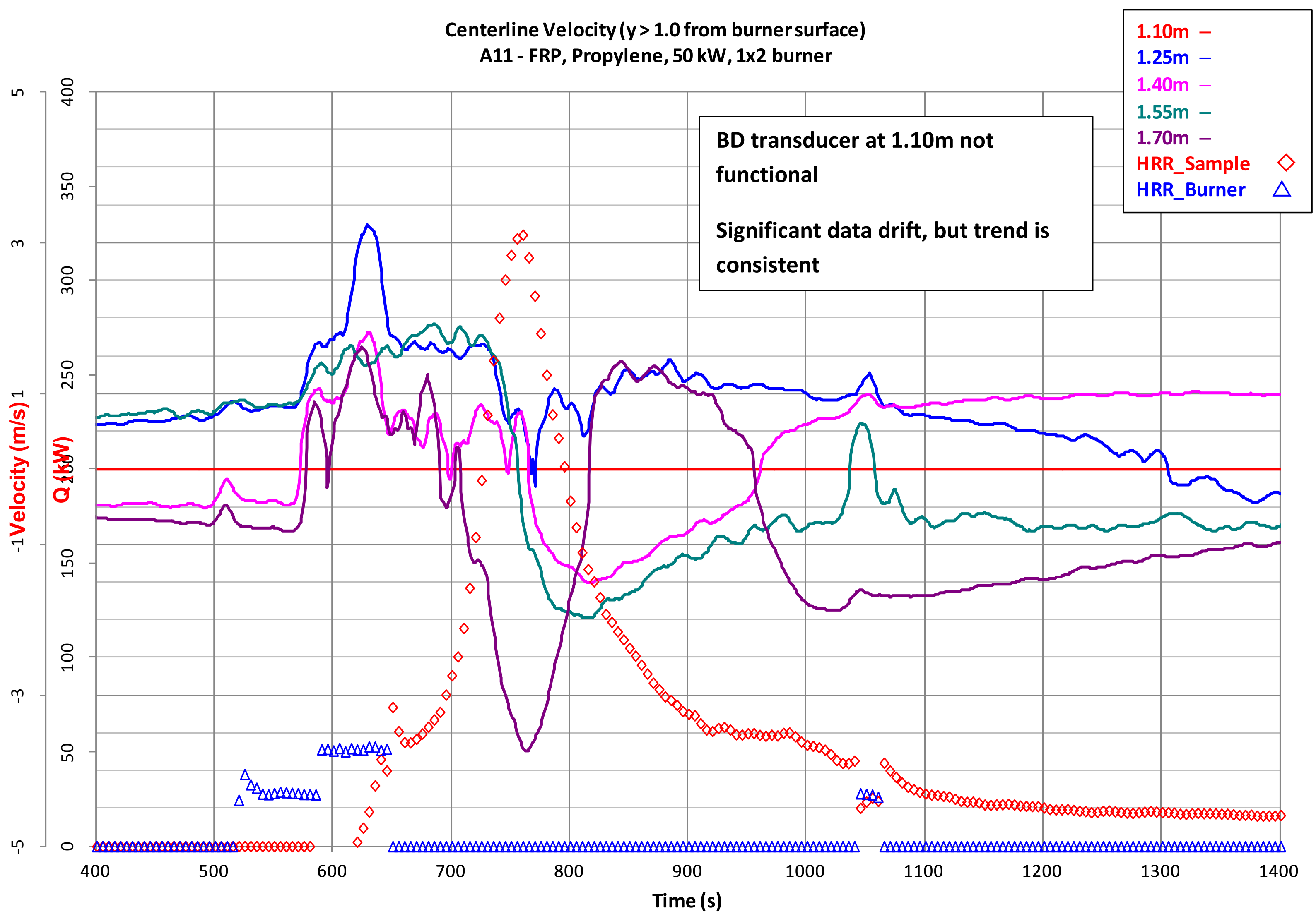

Centerline plume velocities measured from 1.1m to 1.7m above the burner surface

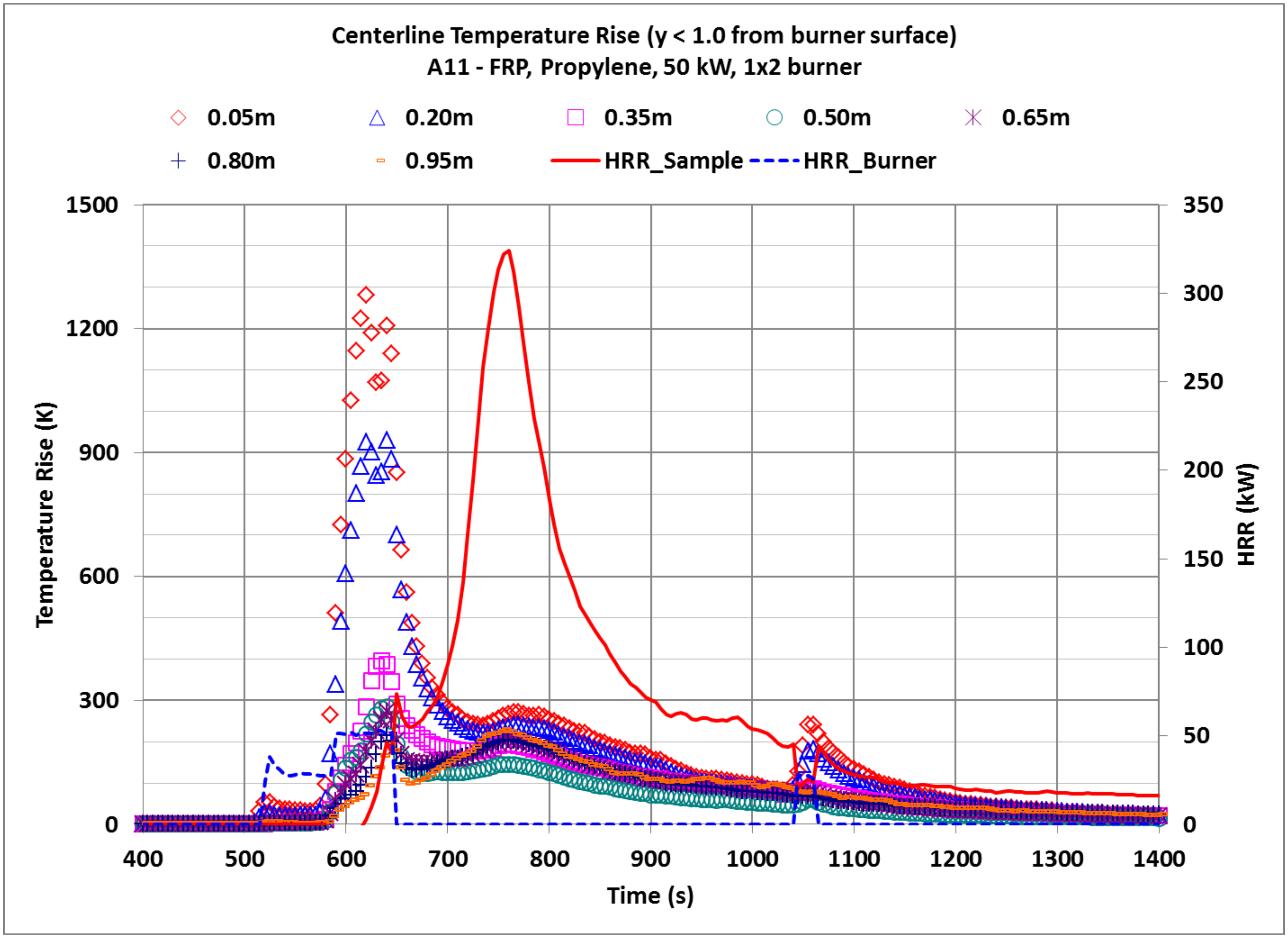

Centerline plume temperature rise measured from 0.05m to 0.95m above the burner surface

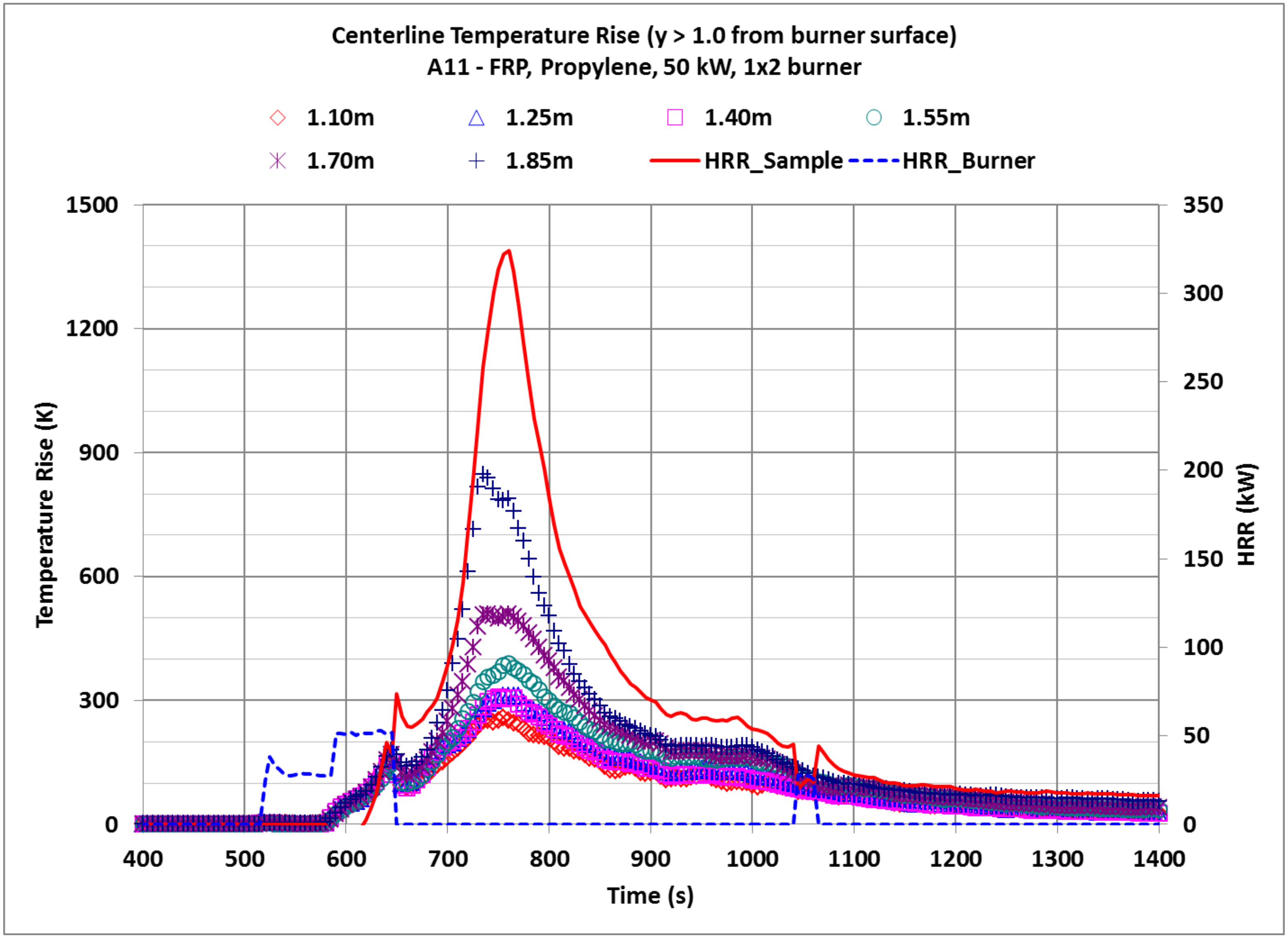

Centerline plume temperature rise measured from 1.10m to 1.85m above the burner surface

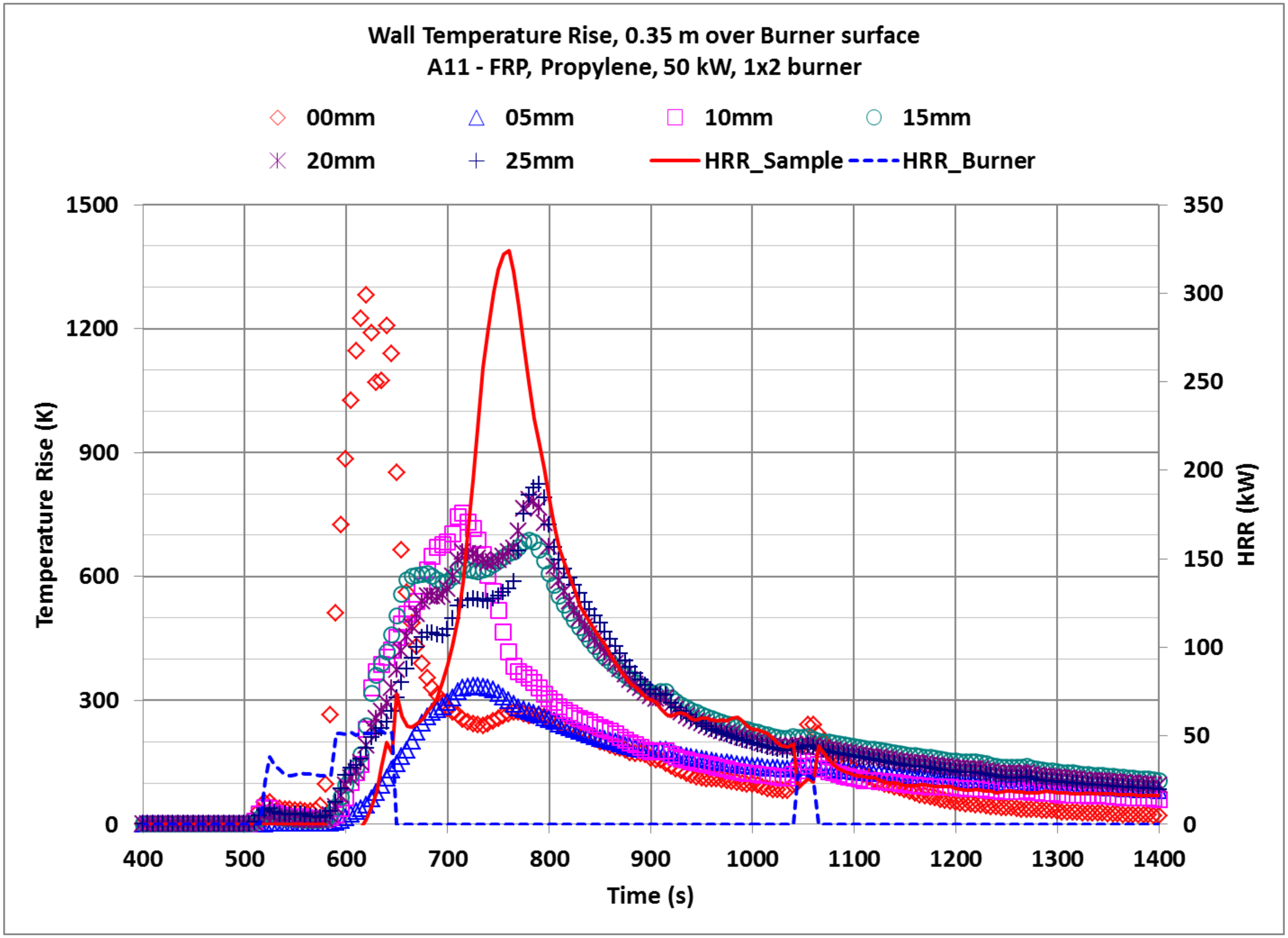

Temperature rise along the wall's centerline at 0.35m over the burner surface, measured at different perpendicular distances to as indicated

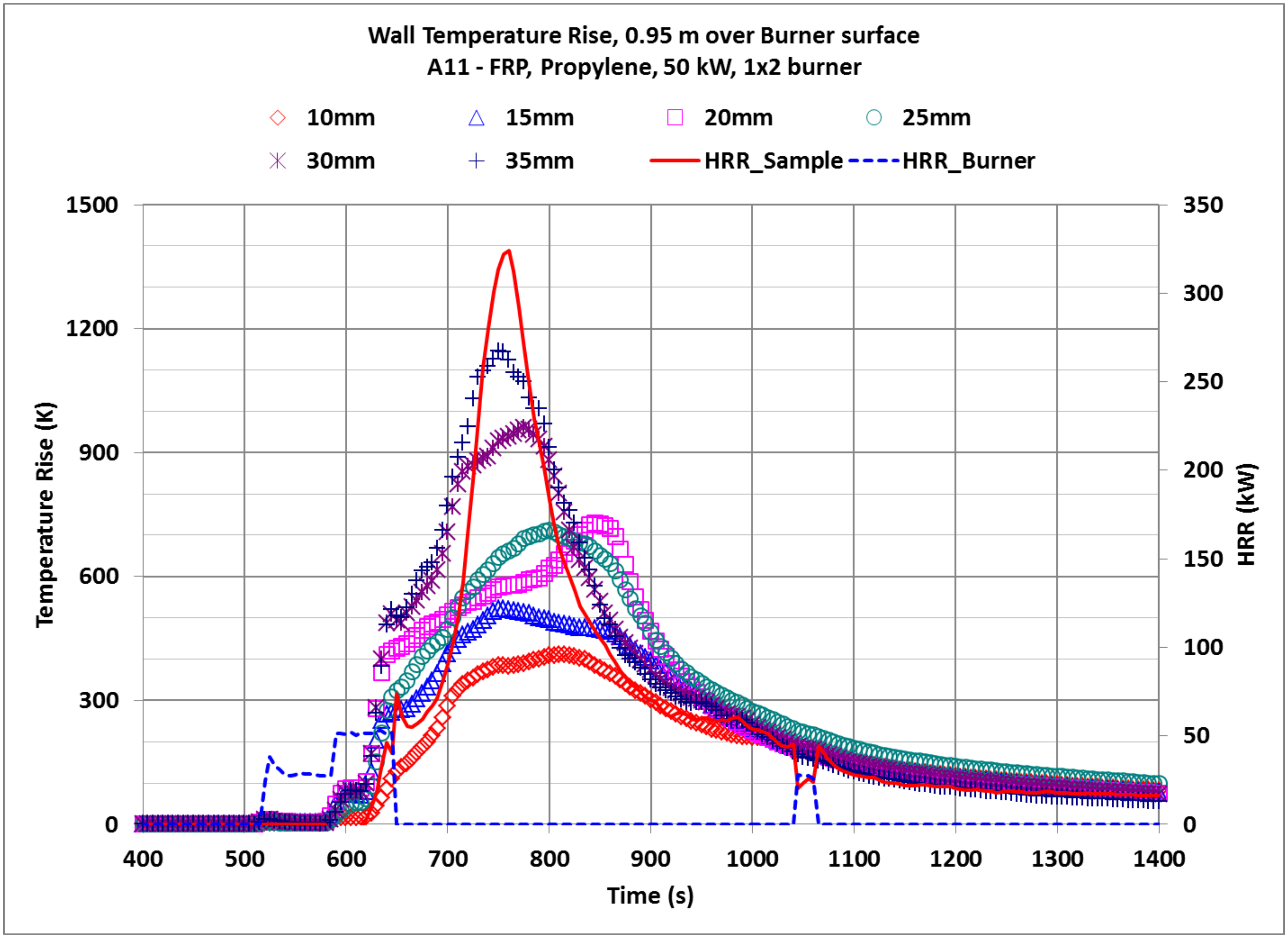

Temperature rise along the wall's centerline at 0.95m over the burner surface, measured at different perpendicular distances to as indicated

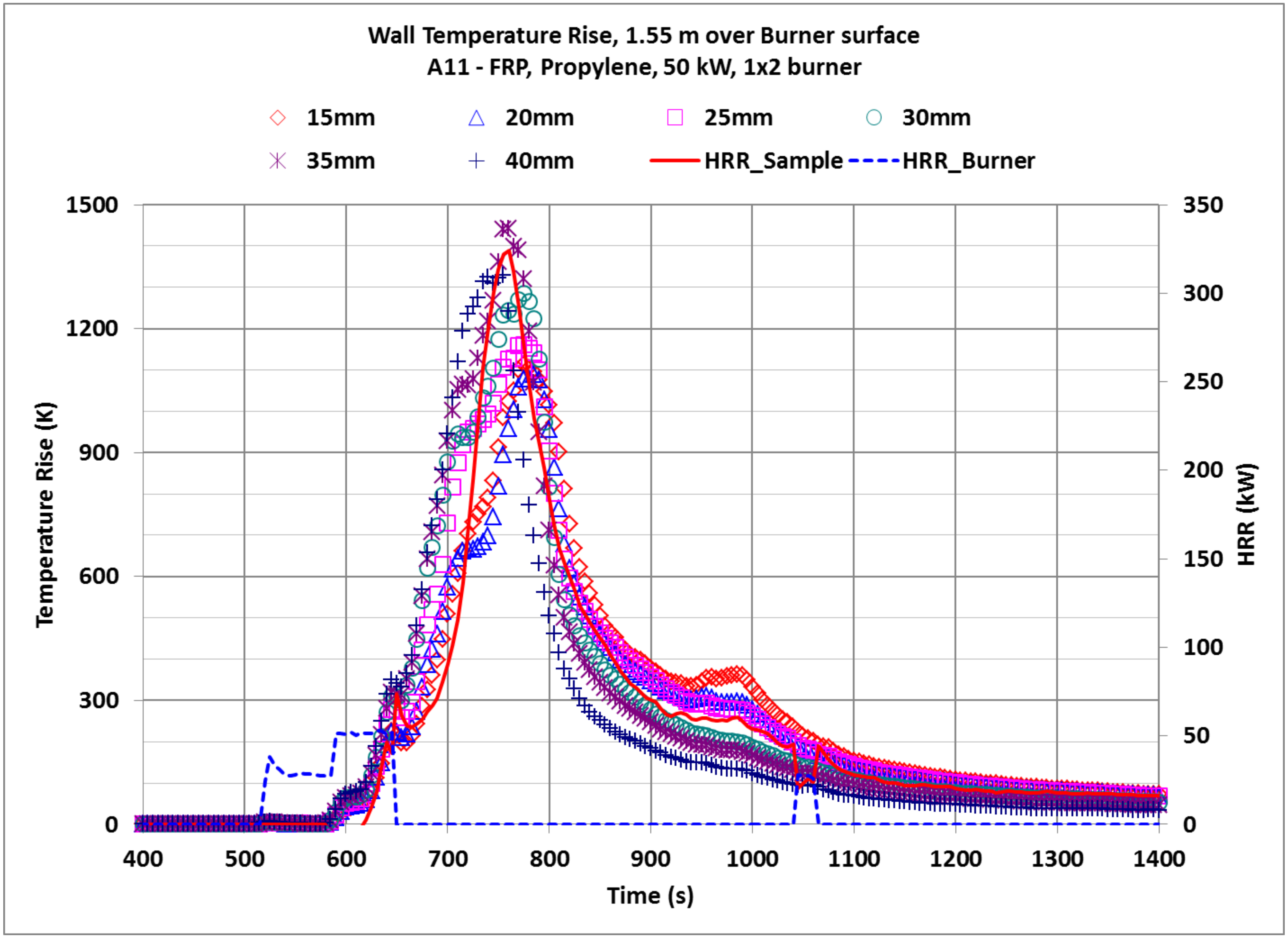

Temperature rise along the wall's centerline at 1.55m over the burner surface, measured at different perpendicular distances to as indicated

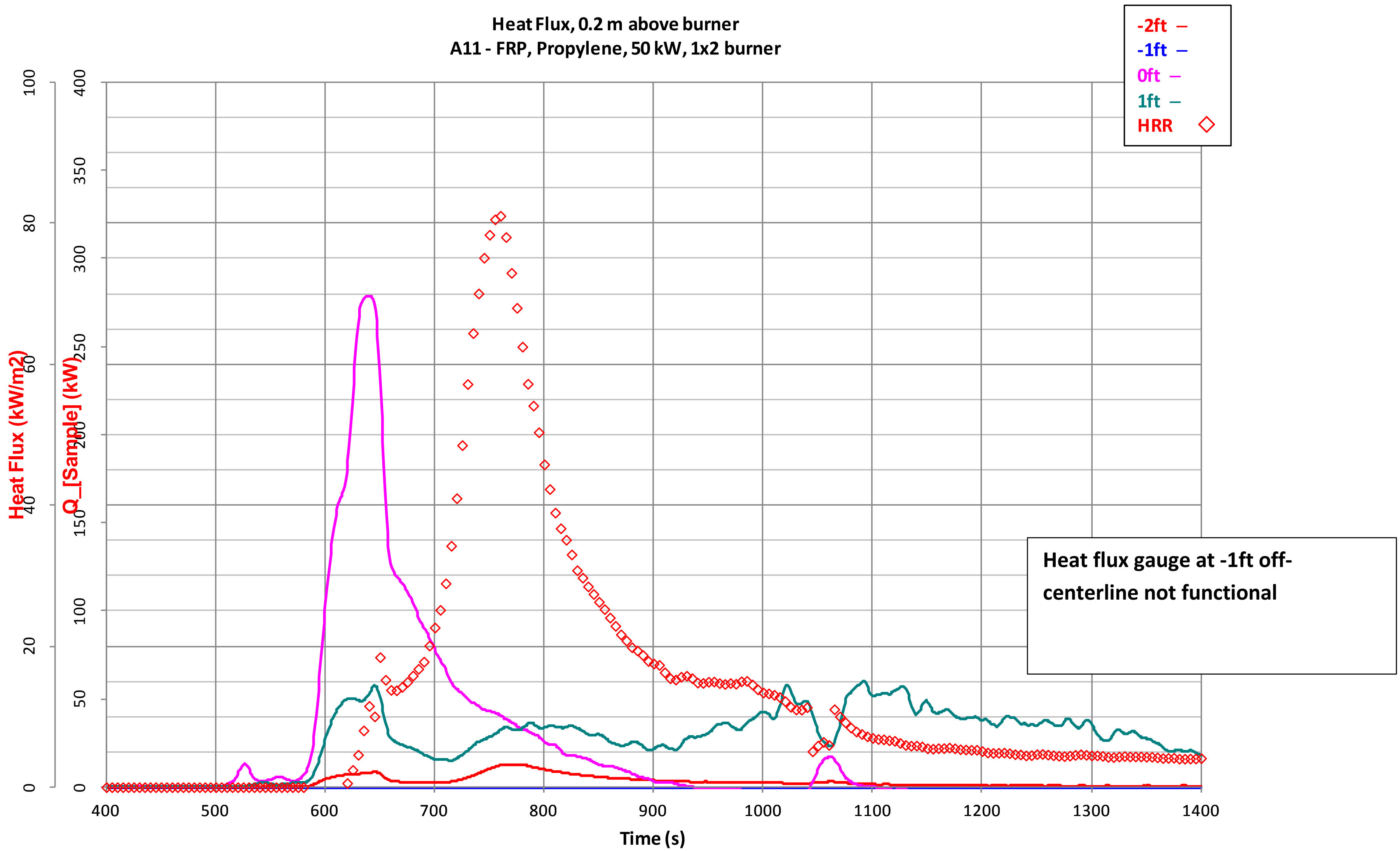

Heat flux measured at various distances from the centerline (negative indicates left of centerline), 0.2m vertically from burner surface

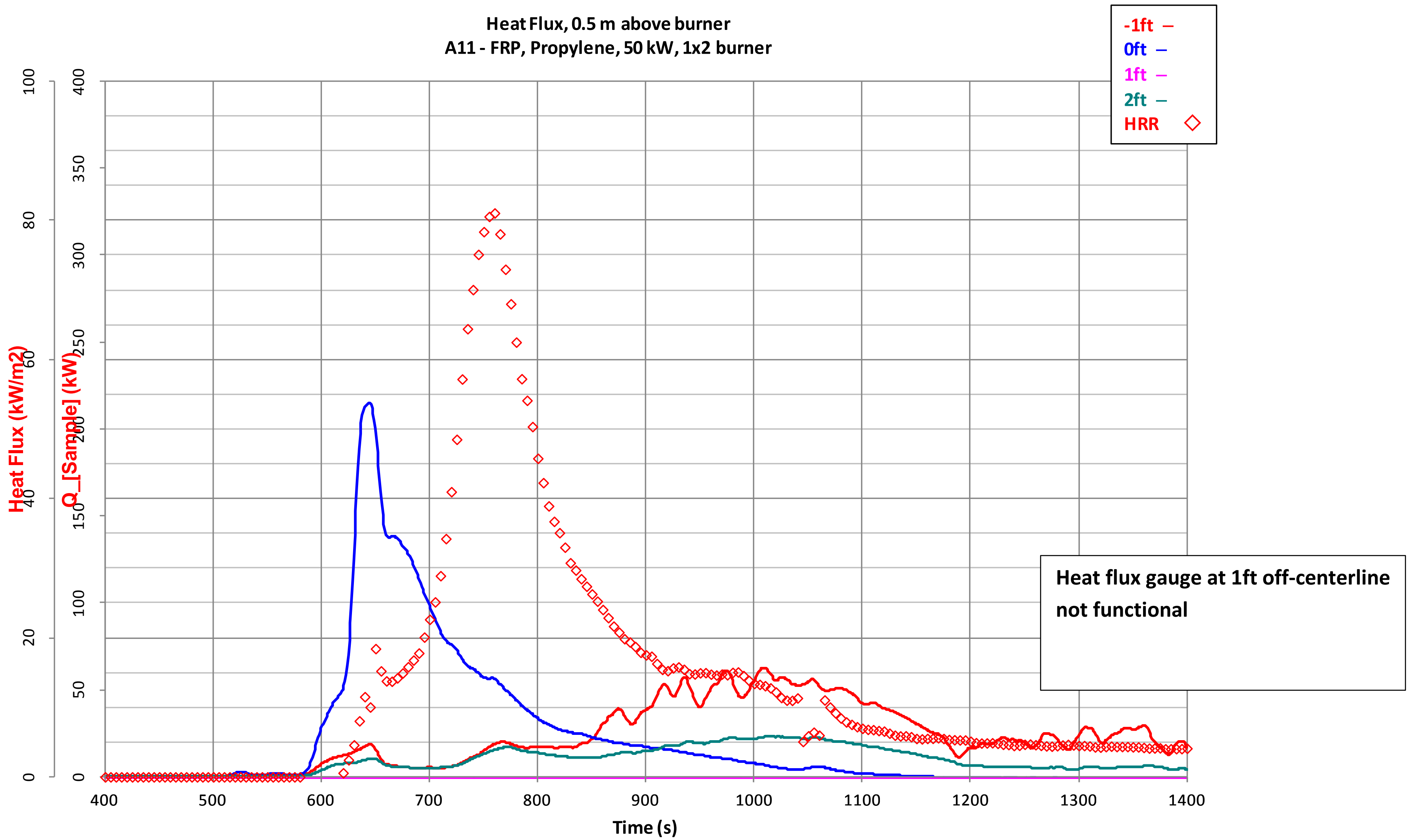

Heat flux measured at various distances from the centerline (negative indicates left of centerline), 0.5m vertically from burner surface

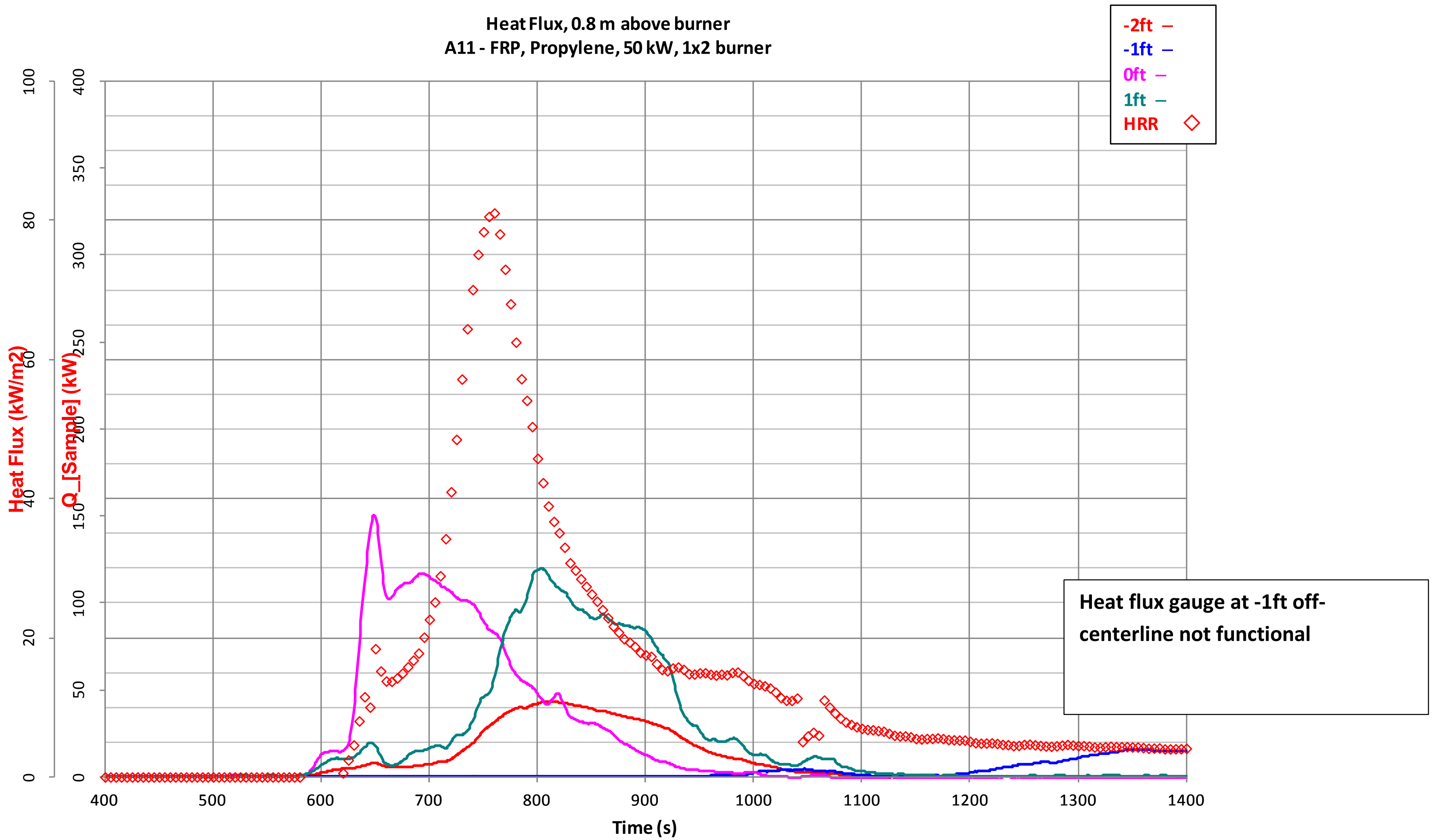

Heat flux measured at various distances from the centerline (negative indicates left of centerline), 0.8m vertically from burner surface

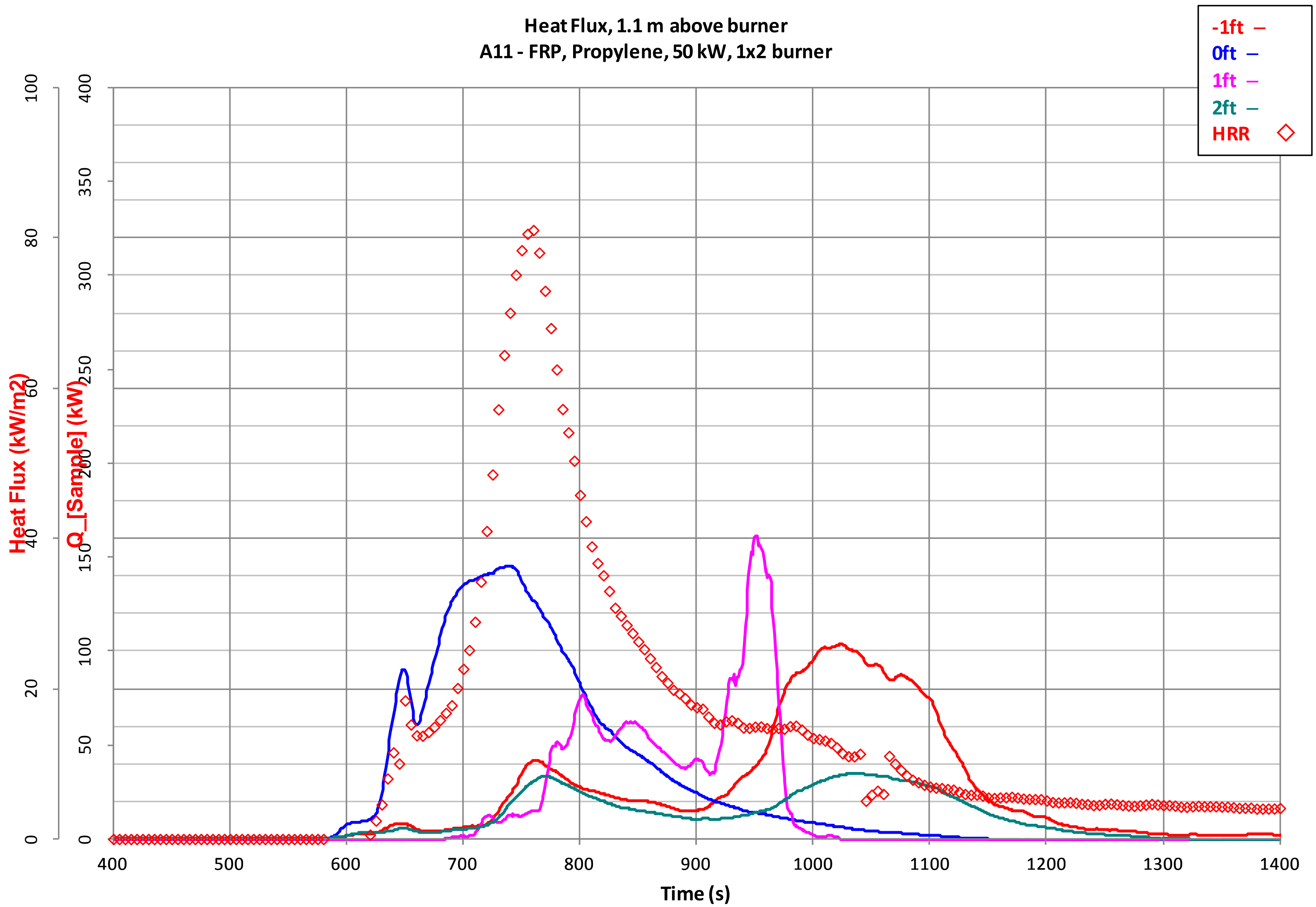

Heat flux measured at various distances from the centerline (negative indicates left of centerline), 1.1m vertically from burner surface

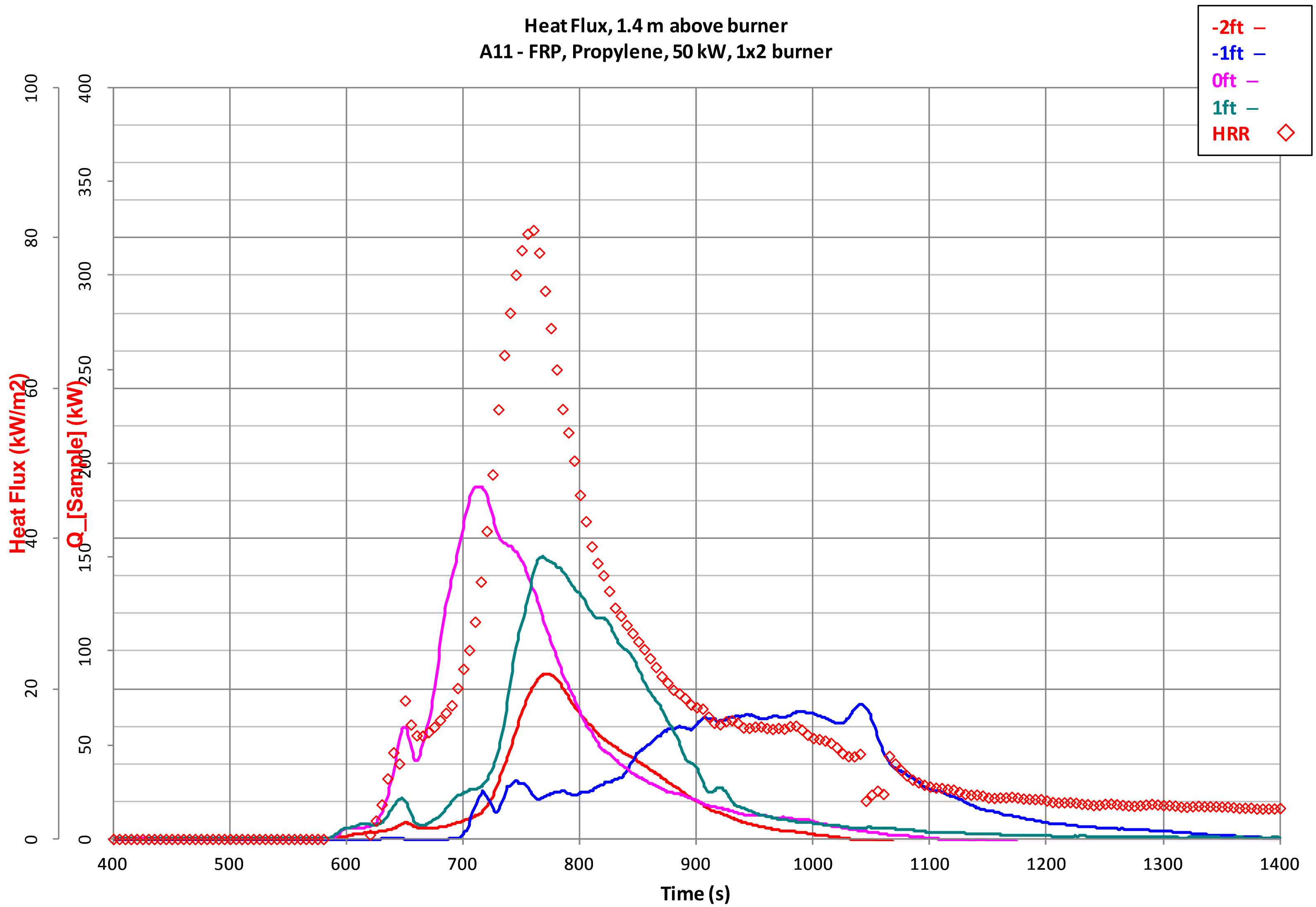

Heat flux measured at various distances from the centerline (negative indicates left of centerline), 1.4m vertically from burner surface

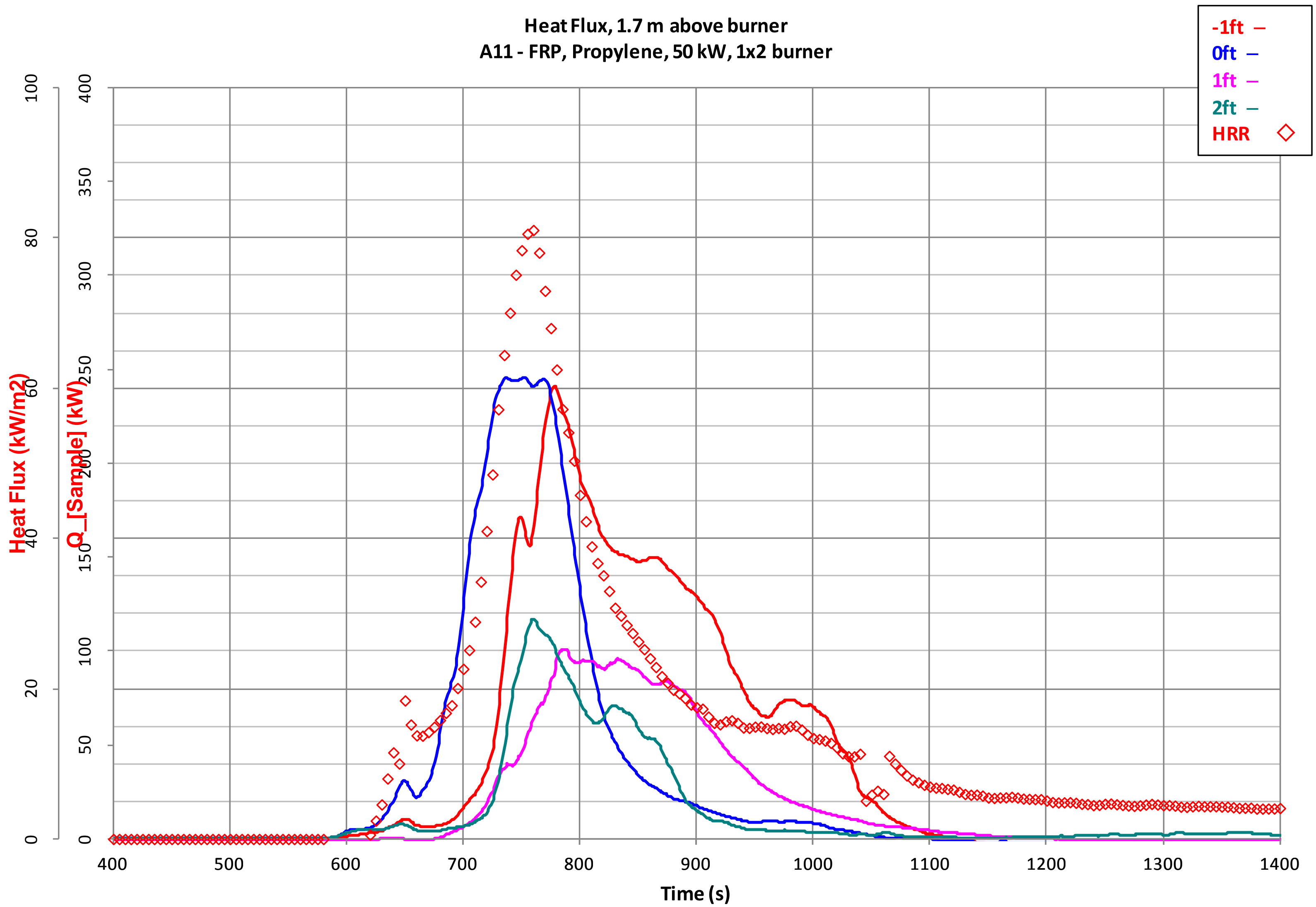

Heat flux measured at various distances from the centerline (negative indicates left of centerline), 1.7m vertically from burner surface

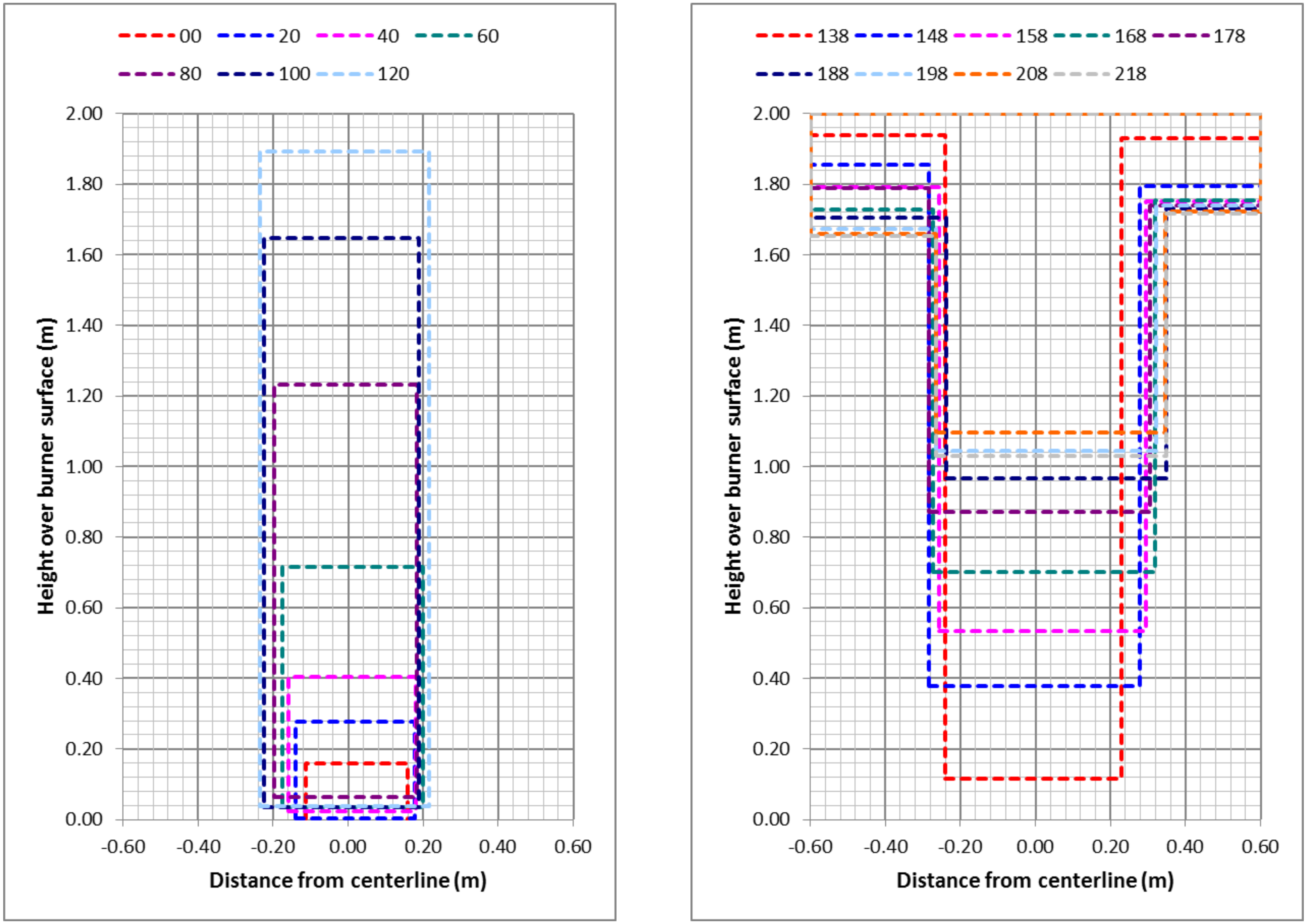

Stages 1 and 2 burning areas in Test A11 (2ft Rectangle burner, Propylene, 50 kW source)

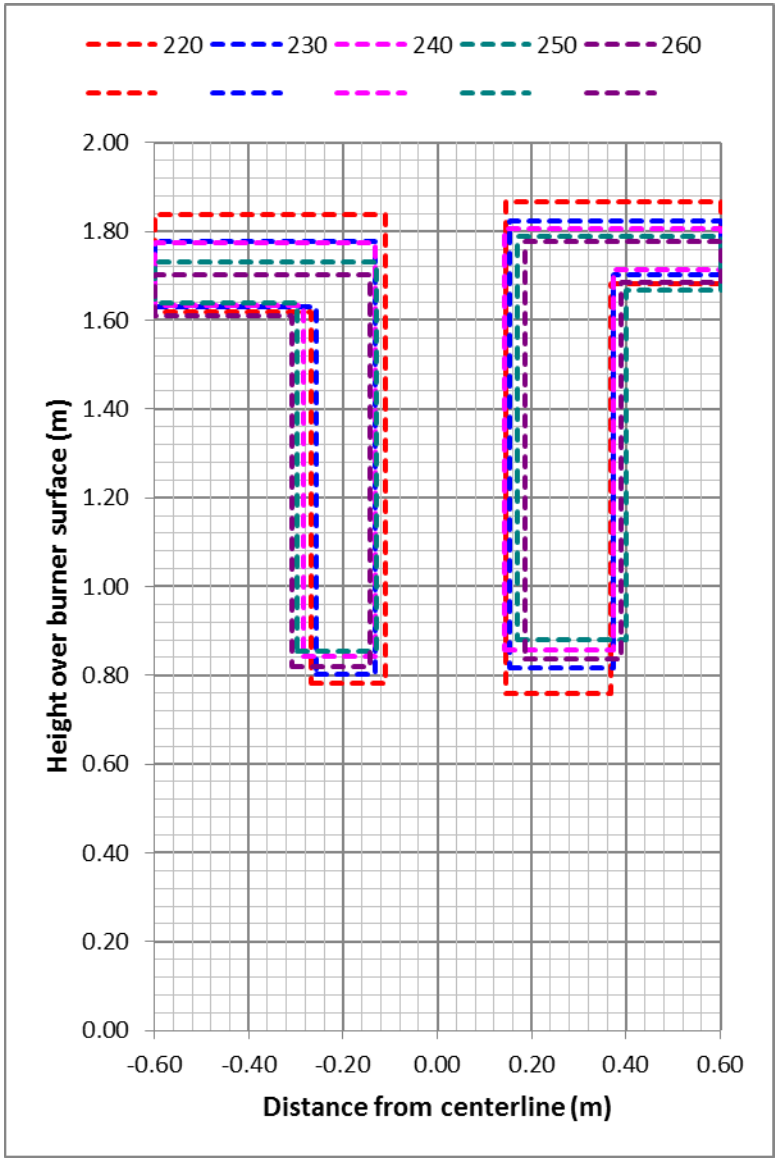

Stage 3 burn area and final damage chart of Test A11 (2ft Rectangle burner, Propylene, 50 kW source)

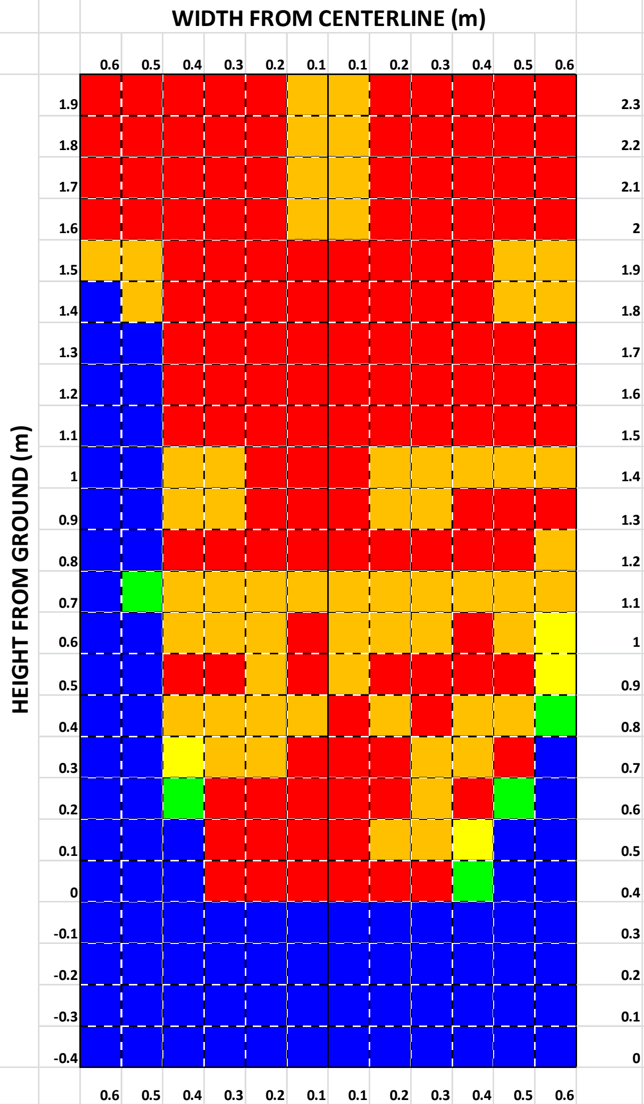

# of cell	Damage to Resin	Area (m2)
135	up to 100% damage	1.35
60	up to 75% damage	0.6
4	up to 50% damage	0.04
5	up to 25% damage	0.05
84	no damage	0.84

Initial mass:	8.38	kg
Final unburnt mass:	2.96	kg
Final burnt mass:	2.92	kg
Total mass loss during fire	2.5	kg

Burn damage pattern observed after fire test

F.3.12 Test A12

LODS Test Run Data

Center for Firesafety Studies

100 Institute Road
Worcester, MA 01609
Phone: (508) 831-5628
Fax: (508) 831-5680

Test Information

Test Number:	A12
Specimen Identification:	FRP 12, 50 kW continuous Propylene fire, 1 x 2 burner
Material Name:	Class C FRP panel
Manufacturer/Submitter:	Not Reported
Raw Data File Name:	Test A12 - FRP_Propylene_50kW_2ft.txt
Reduced Data File Name:	Test A12 - FRP_Propylene_50kW_2ft_reduced.xlsx
Date of Test:	16-Nov-2010
Tester:	W. Wong

Test Parameters

Ambient Temperature:	N/A
Relative Humidity:	N/A

Specimen Information

Specimen Initial Mass:	[kg]	8.1
Specimen Final Mass:	[kg]	5.1
Mass Lost:	[kg]	3.1
Heat Evolved (net):	[kJ]	0

Parameter	Unit	Value
Mass Loss		
Initial Mass	[kg]	8.1
Final Mass	[kg]	5.1
Mass Loss	[%]	37.68

LODS Test Run Data

Center for Firesafety Studies

100 Institute Road
Worcester, MA 01609
Phone: (508) 831-5628
Fax: (508) 831-5680

Test Notes

Test Number:	0
Date:	11/16/10
Material:	Class C FRP panel
Specimen Identification:	FRP 12, 50 kW continuous Propylene fire, 1 x 2 burner

Observations

Time	Observation
00:00	Start VI
04:30	Start Camera 1
03:30	Start Camera 2
07:46	Burner ignition
07:58	Reach target HRR @ 50 kW
08:23	Crackling noise
08:32	Panel ignition, mainly at area under TSC-2 to above burner, 0.2 m wide
08:55	Flame hit ceiling
09:15	Remote area ignition @ HFG-1, TSC-3, insignificant, but next to burner plume
	Remote area smoking on left and right edge
09:30	Burning reaches left and right edges
09:40	Rollover of ceiling layer, some edge burner near ceiling
10:25	Little wall paper burning on both sidewalls
11:45 to 11:55	Right edge @ y = 1.0 to 1.8 m burn for 10 seconds
14:30	Line fires only
15:00	Remote area smoking on both edges at y = 0.6 m
18:10	Left edge has some remote ignition at y = 1.1 to 1.3 for 45 sec
22:37	Burner turned off, small flashes
23:30	Small flashes at burner, some smoke out of right edge at y = 0.1 to 0.3 m
26:10	Terminate test with little water application, burner still flashes

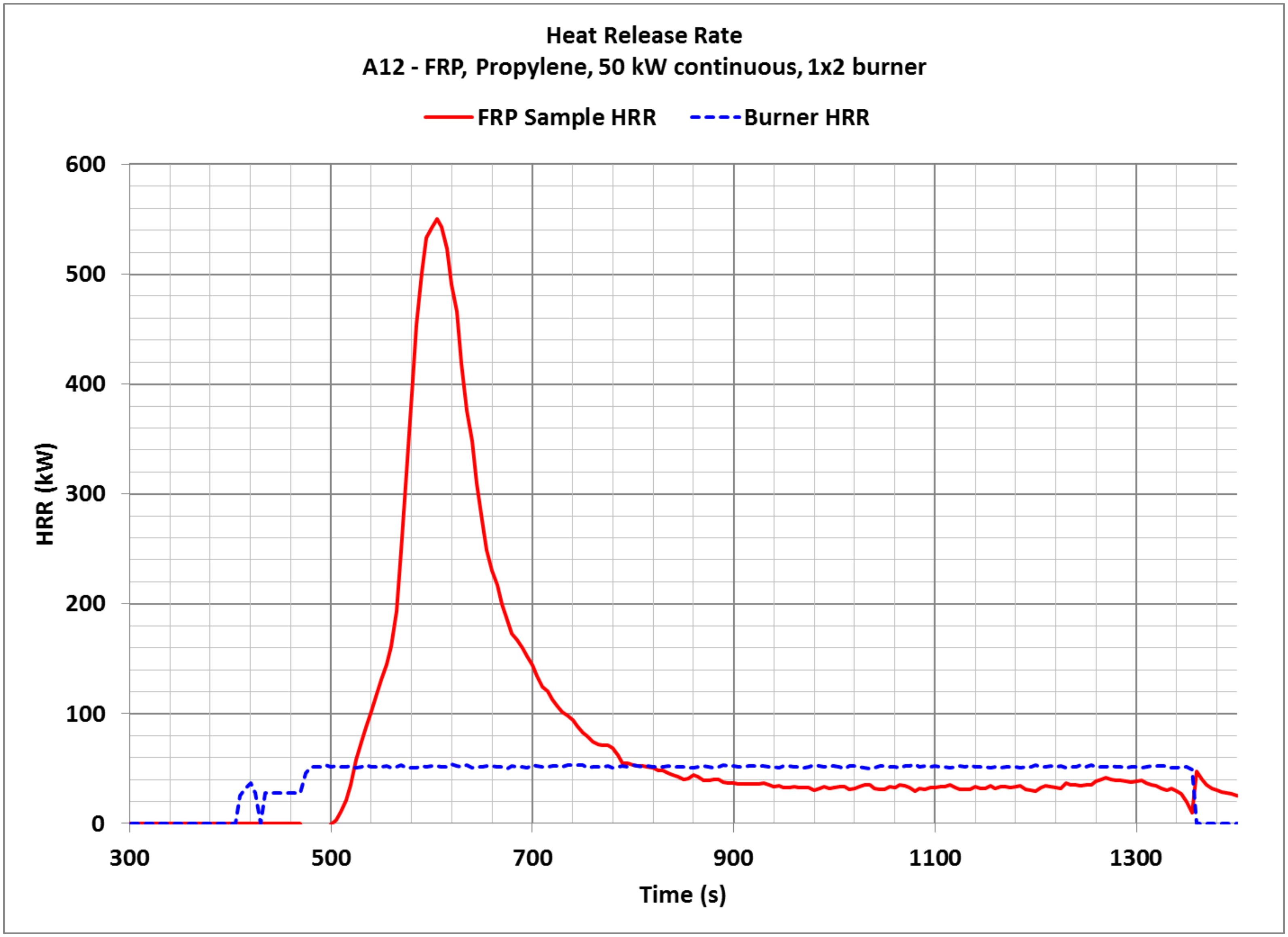

Heat release ratesof the source burner fire and of the specimen fire measured during test

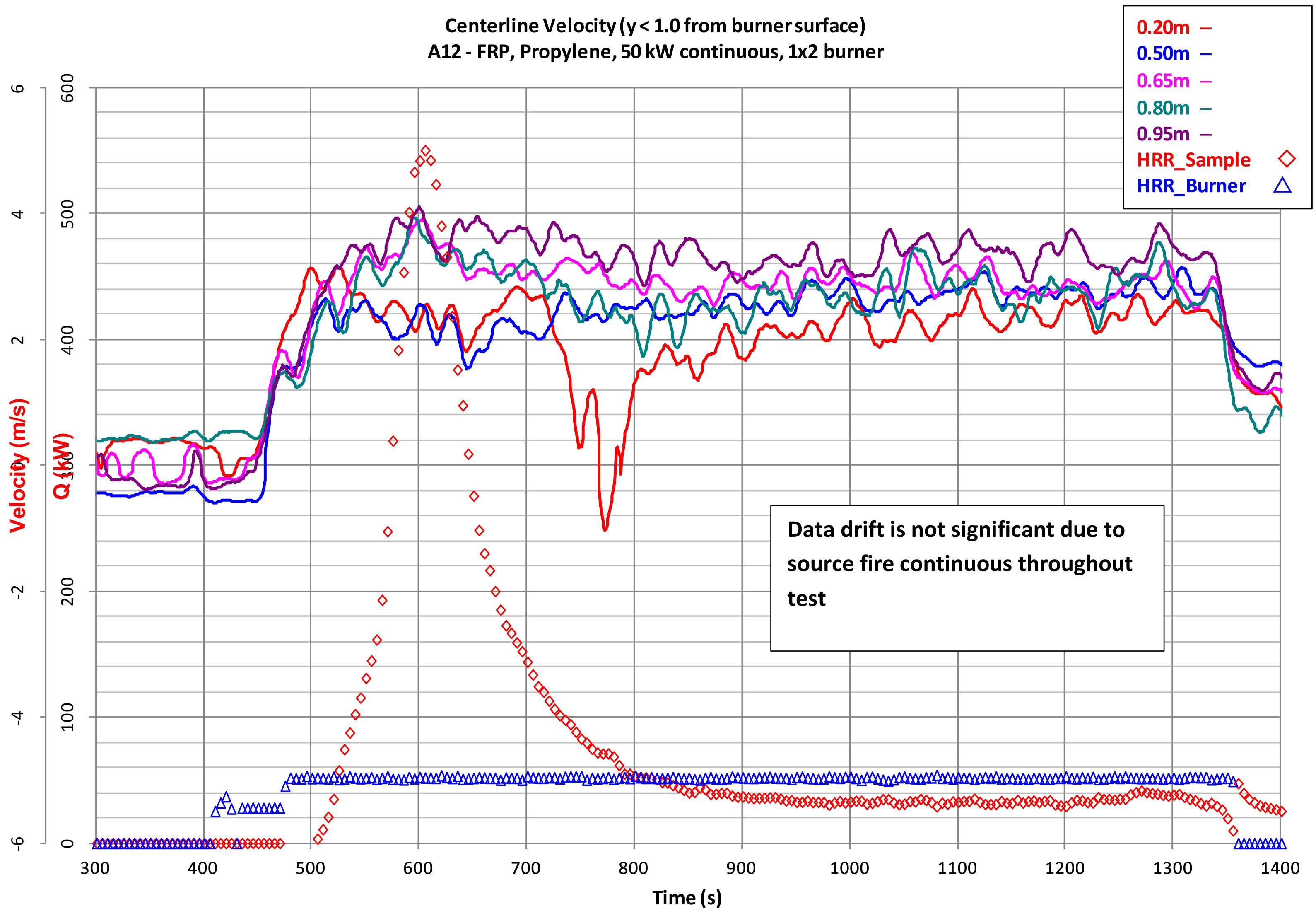

Centerline plume velocities measured from 0.2m to 0.95m above the burner surface

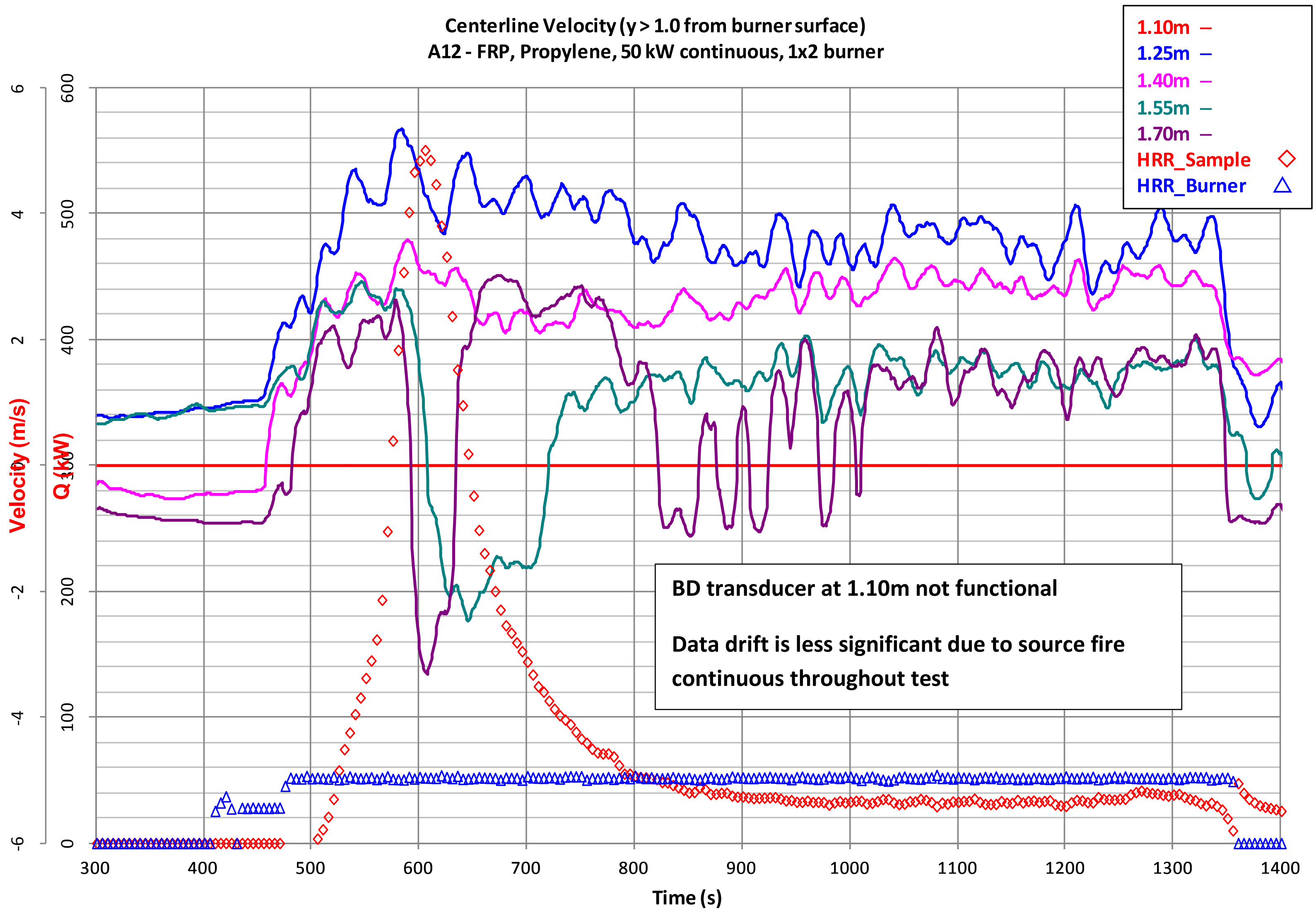

Centerline plume velocities measured from 1.1m to 1.7m above the burner surface

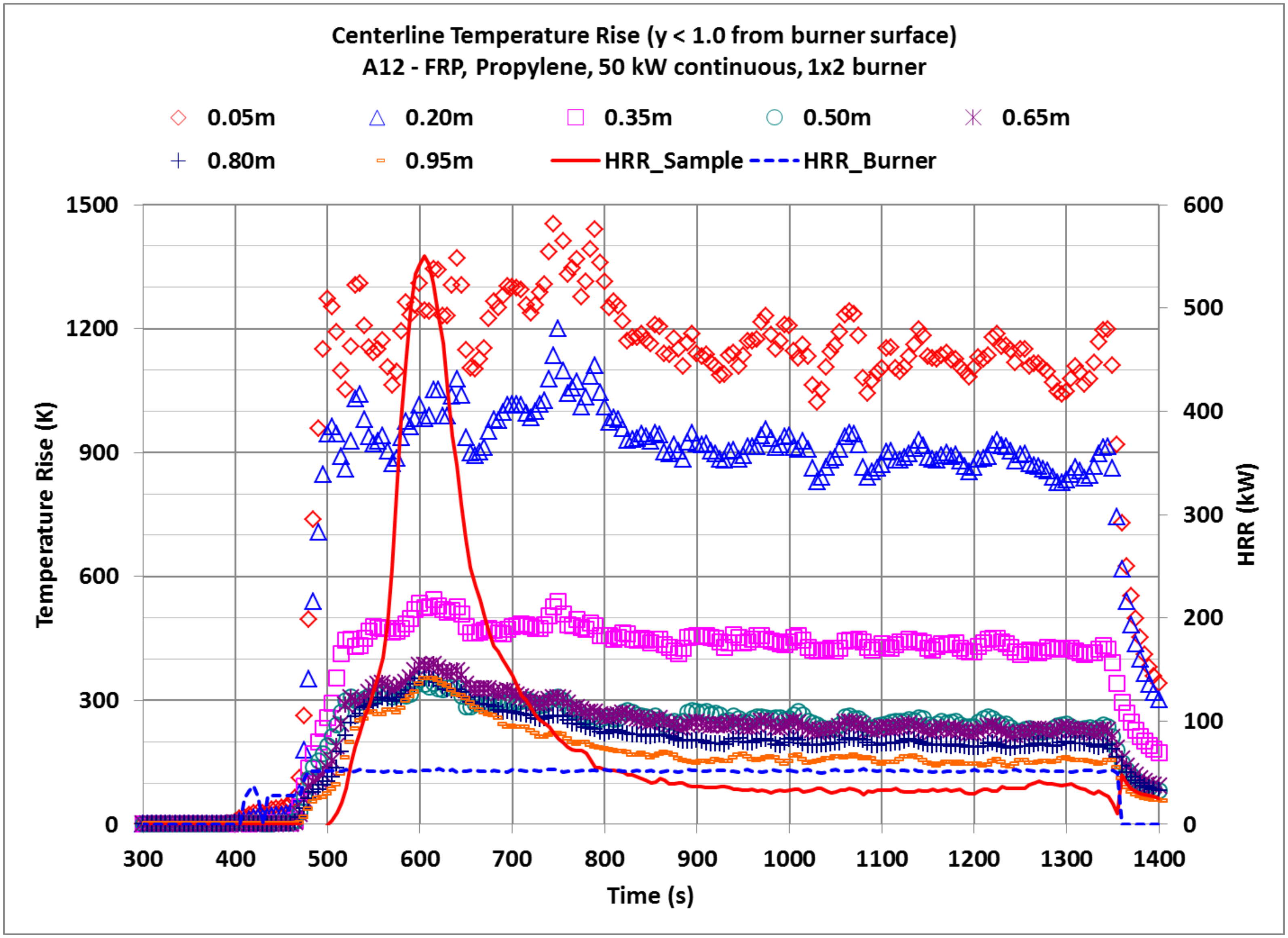

Centerline plume temperature rise measured from 0.05m to 0.95m above the burner surface

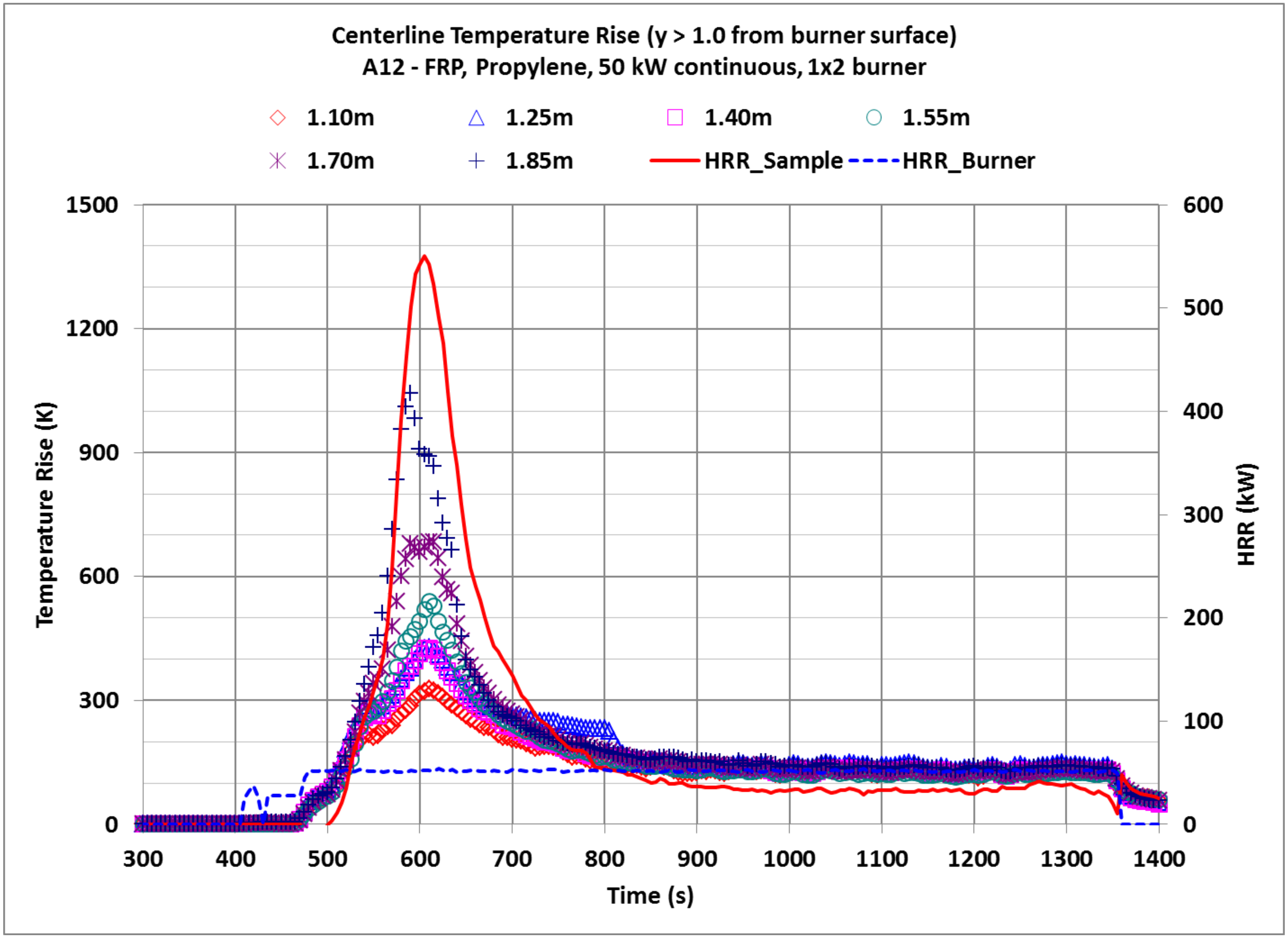

Centerline plume temperature rise measured from 1.10m to 1.85m above the burner surface

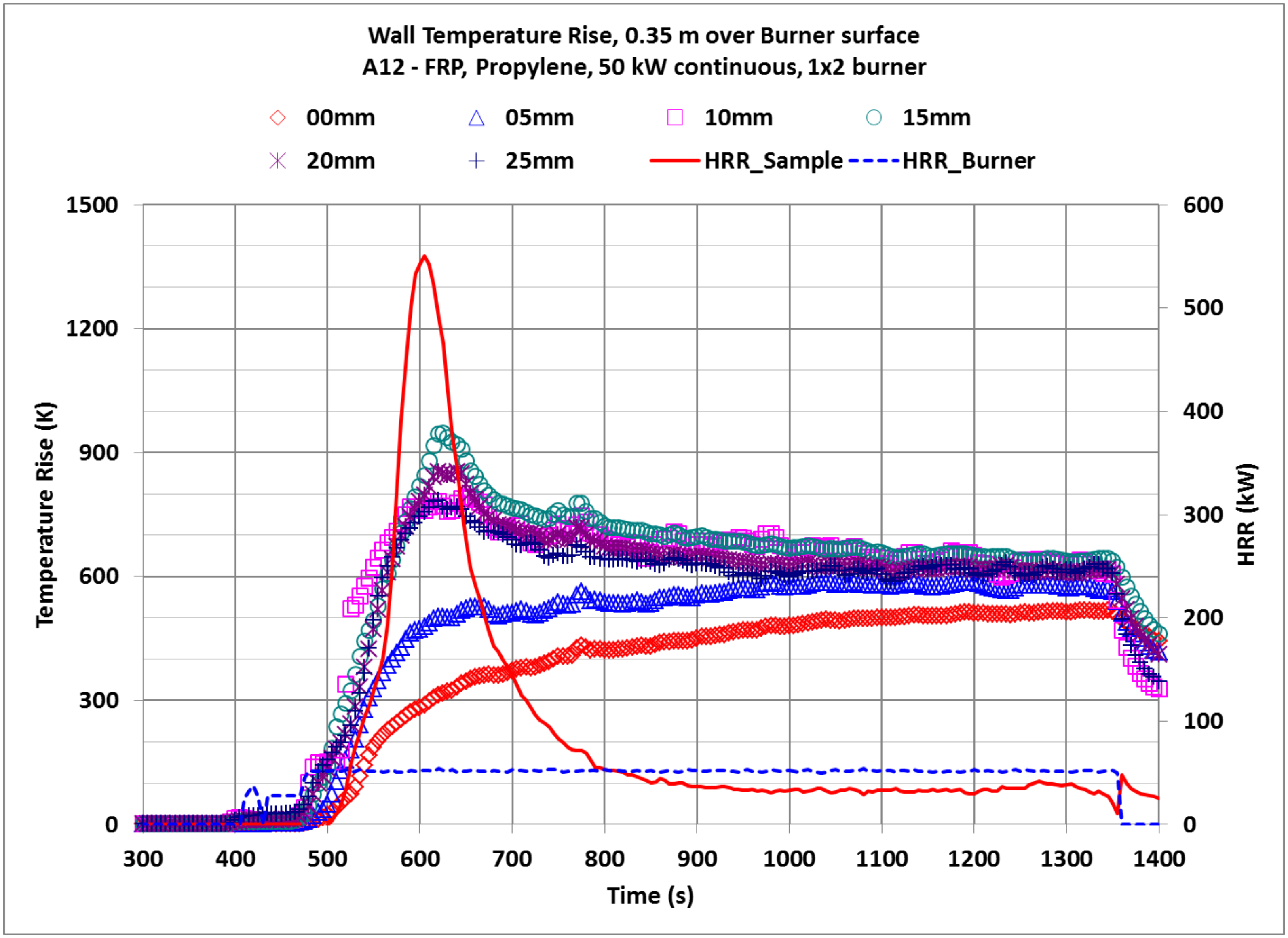

Temperature rise along the wall's centerline at 0.35m over the burner surface, measured at different perpendicular distances to as indicated

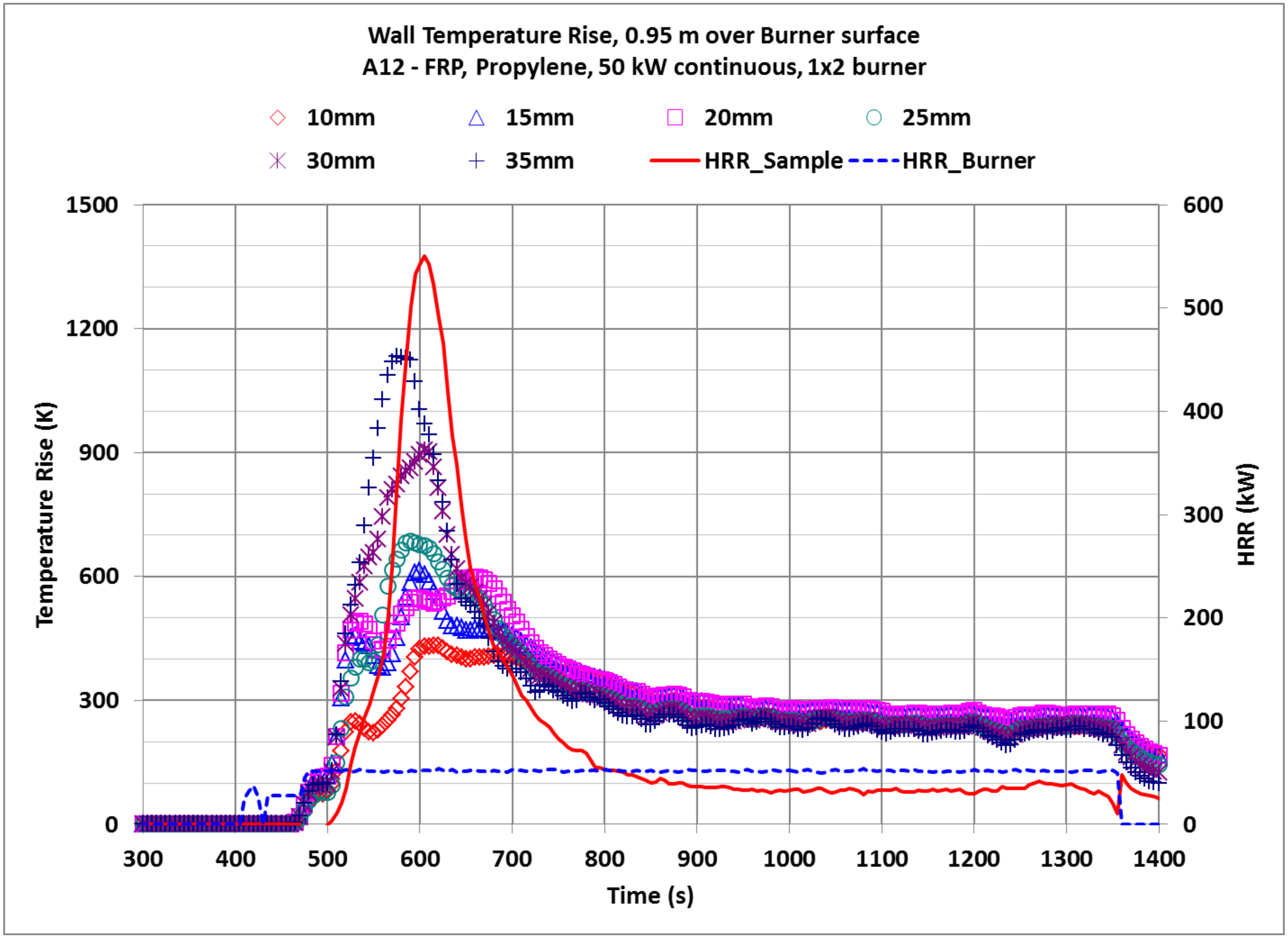

Temperature rise along the wall's centerline at 0.95m over the burner surface, measured at different perpendicular distances to as indicated

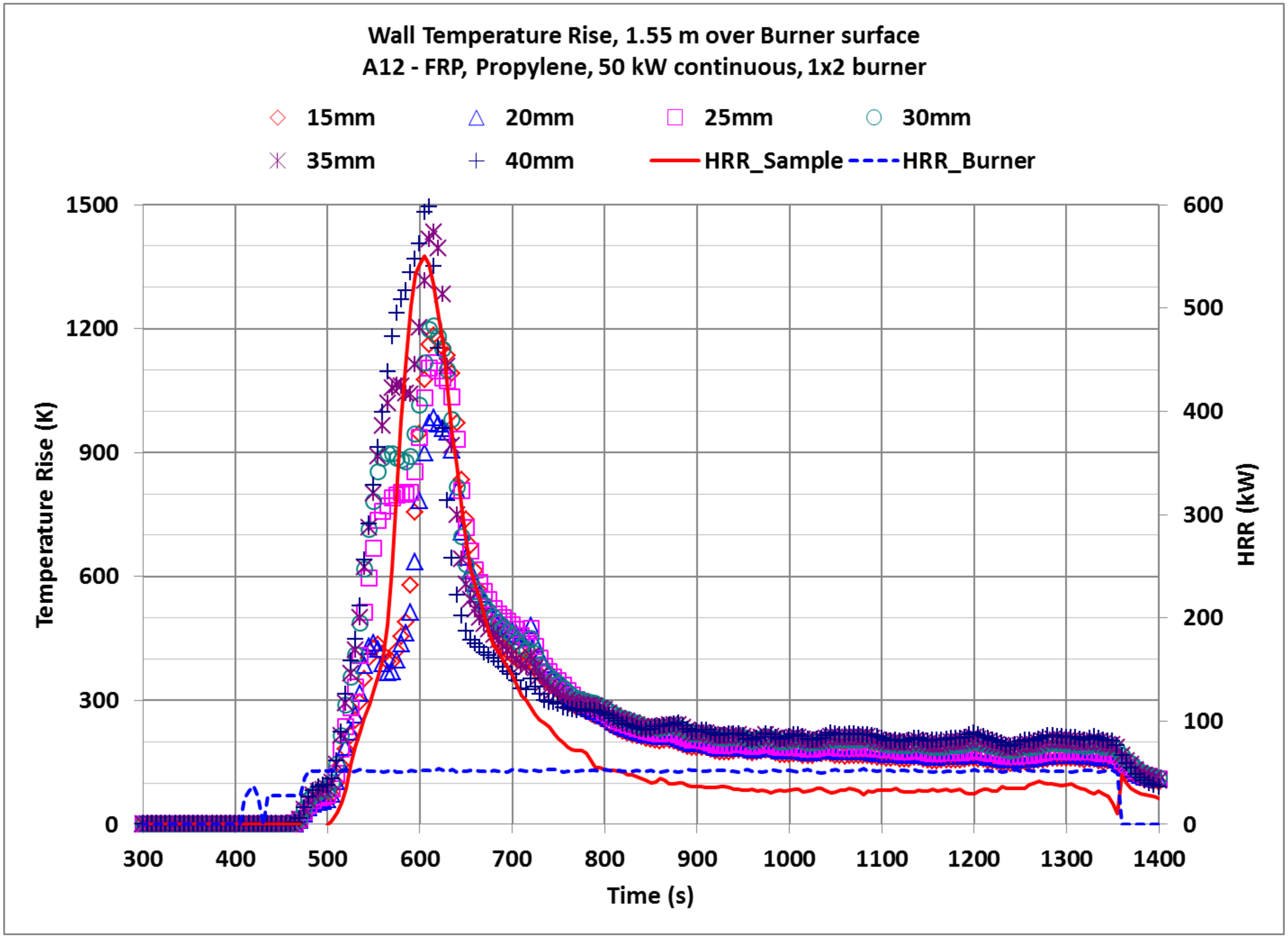

Temperature rise along the wall's centerline at 1.55m over the burner surface, measured at different perpendicular distances to as indicated

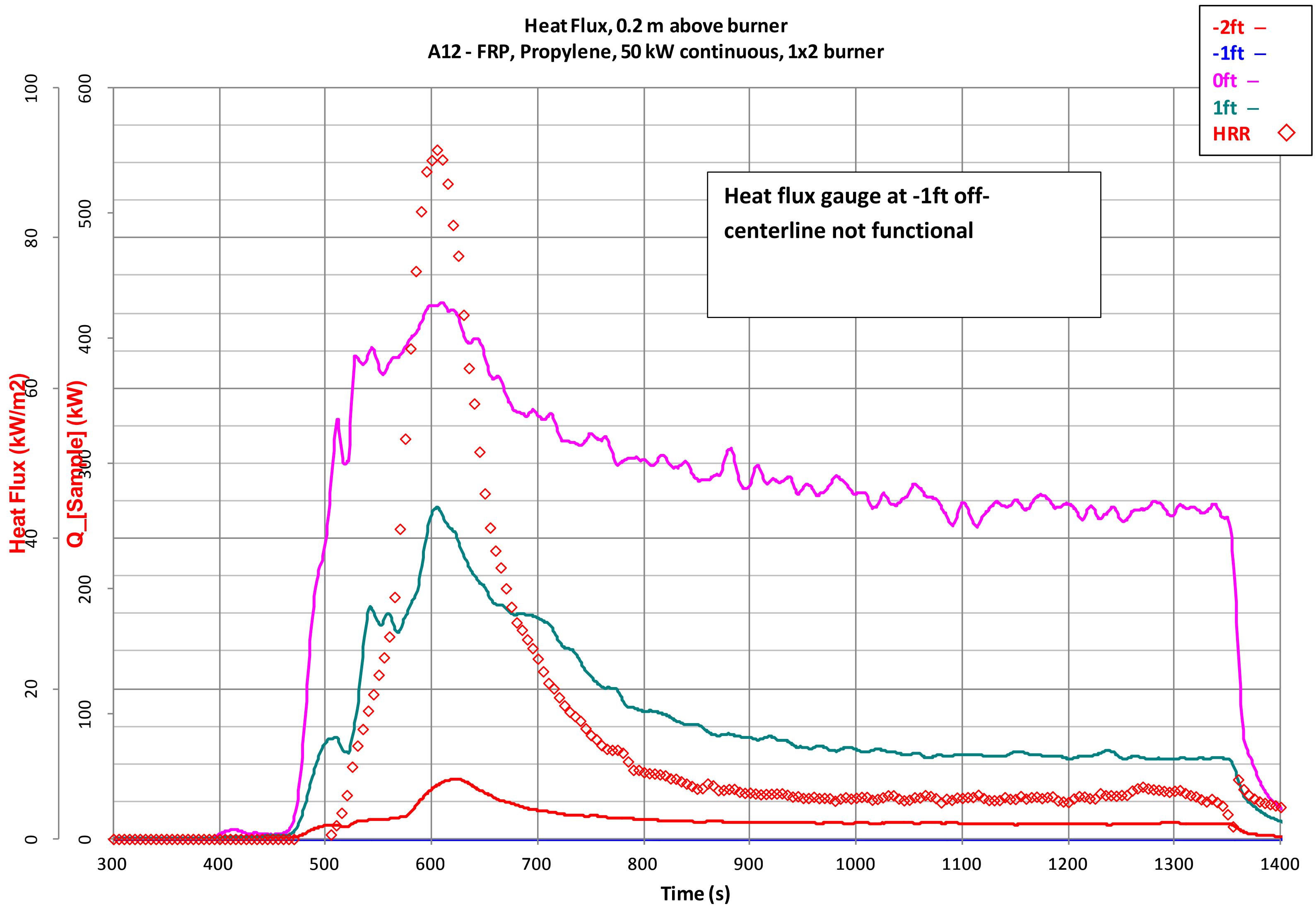

Heat flux measured at various distances from the centerline (negative indicates left of centerline), 0.2m vertically from burner surface

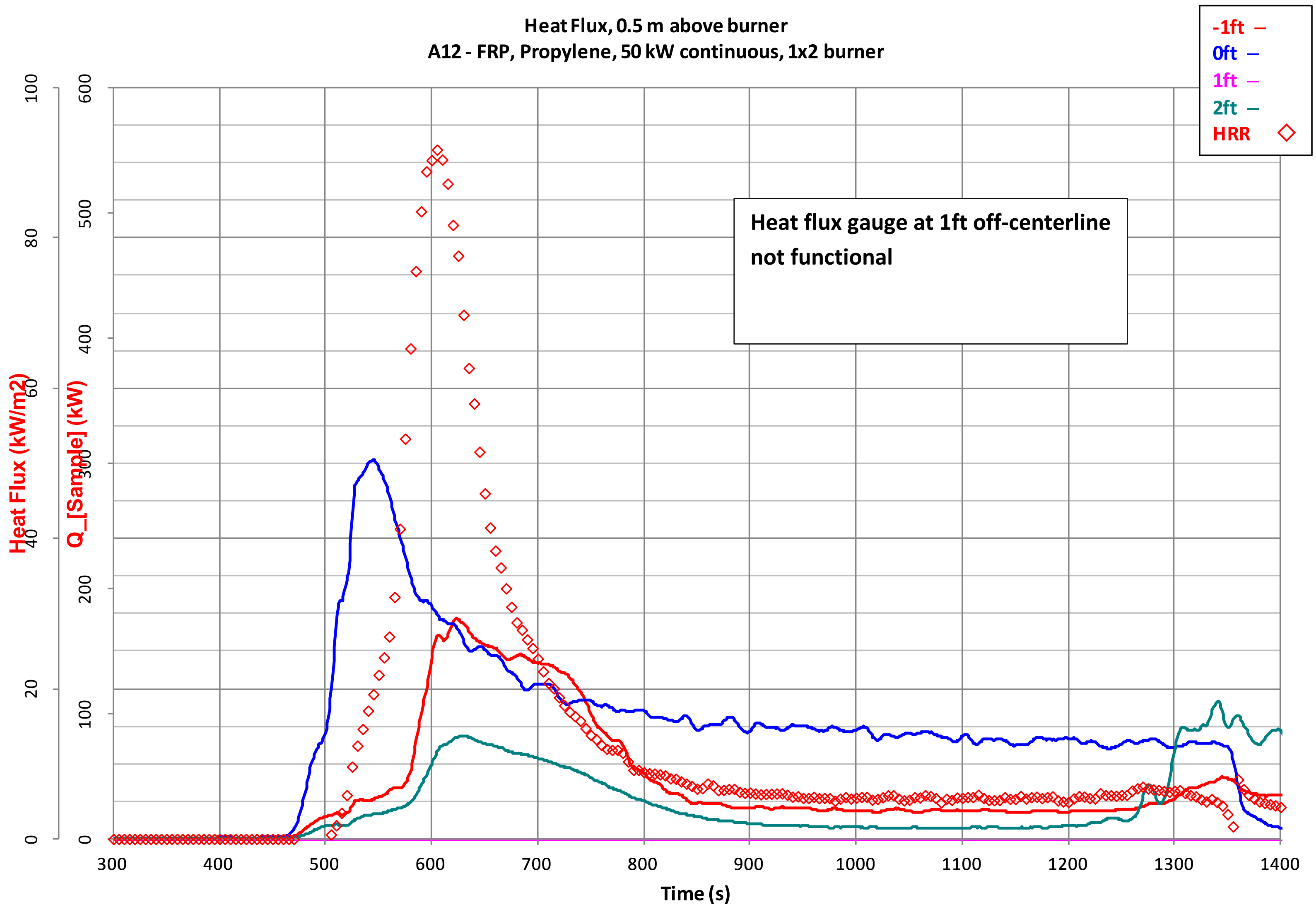

Heat flux measured at various distances from the centerline (negative indicates left of centerline), 0.5m vertically from burner surface

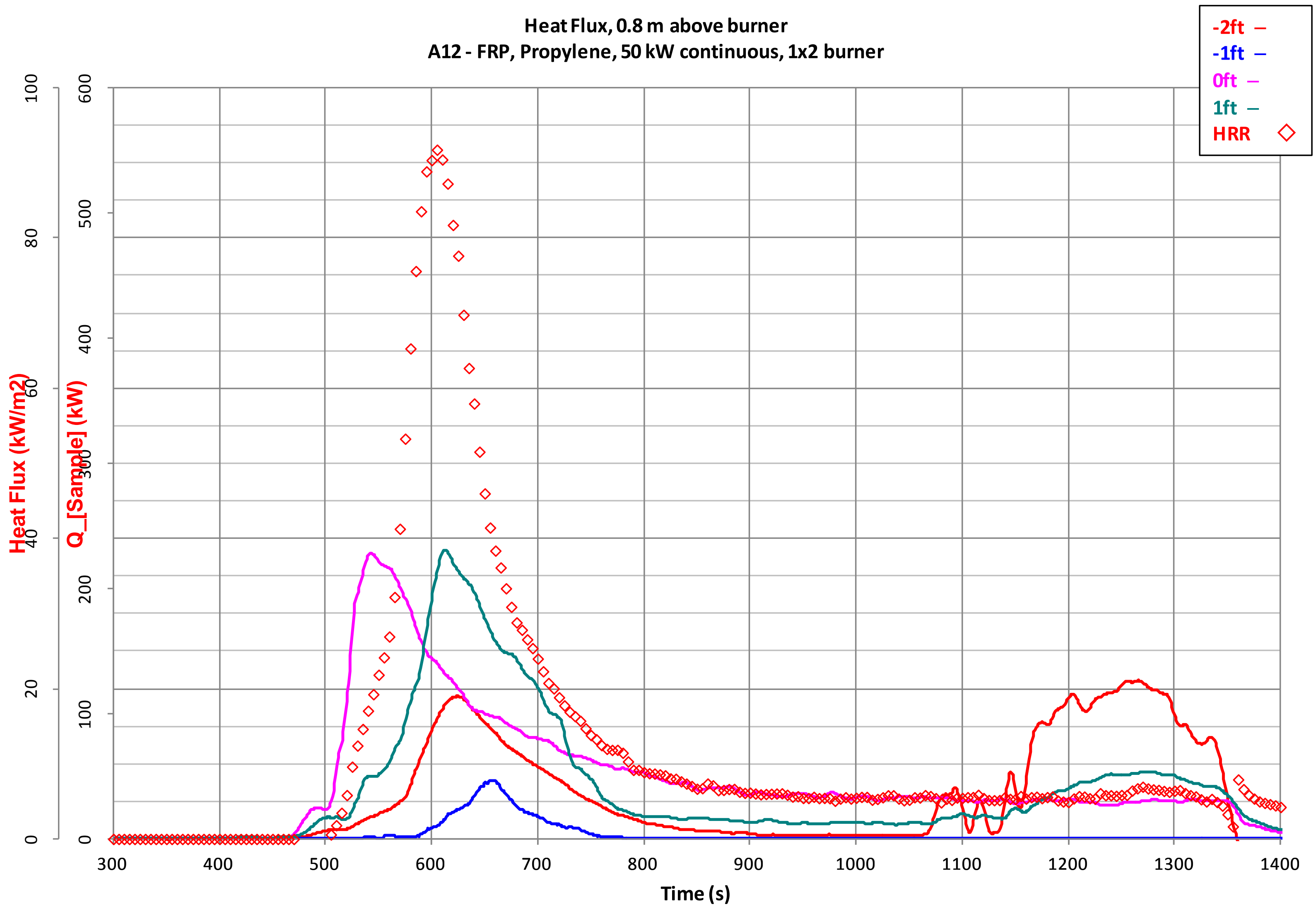

Heat flux measured at various distances from the centerline (negative indicates left of centerline), 0.8m vertically from burner surface

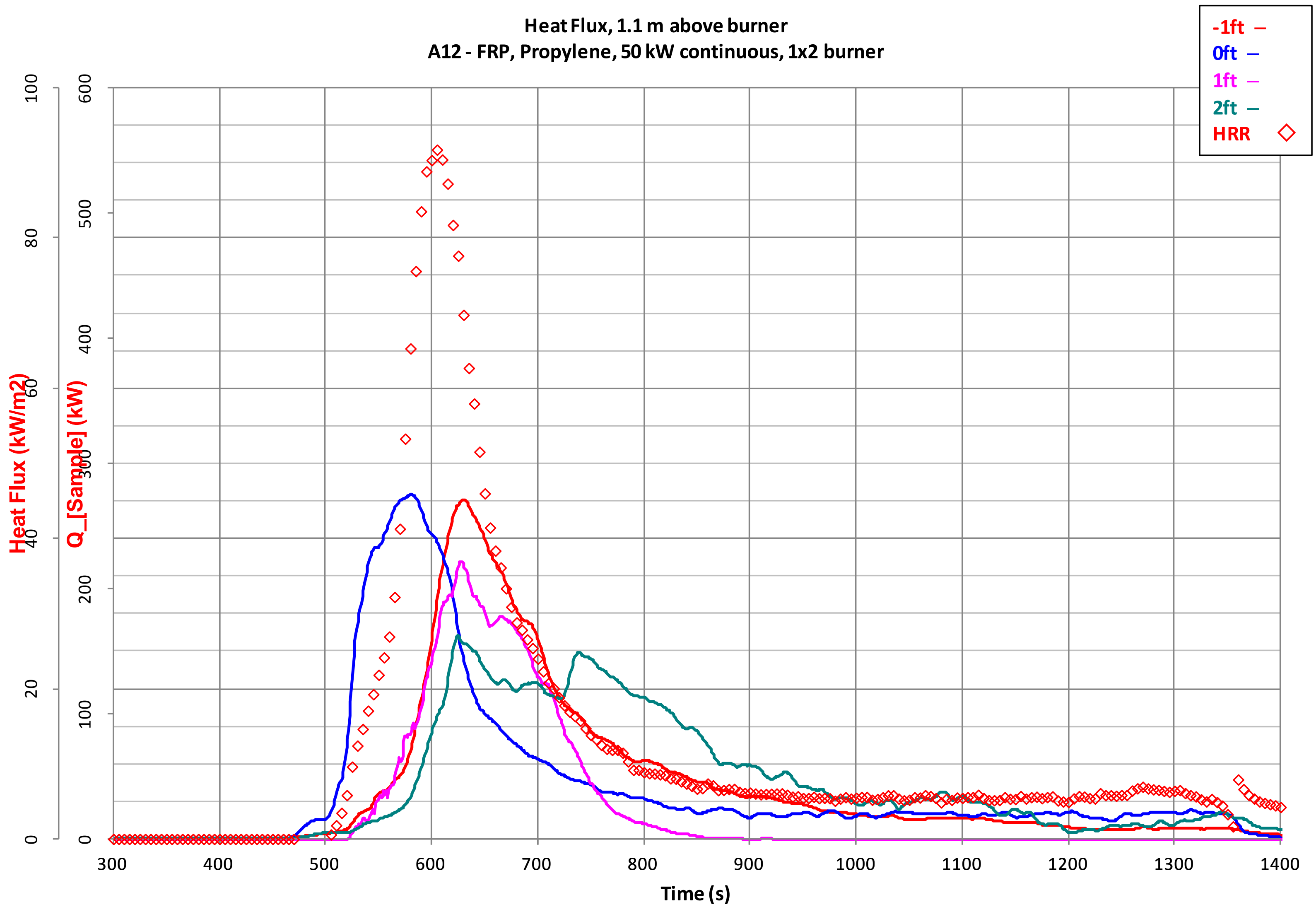

Heat flux measured at various distances from the centerline (negative indicates left of centerline), 1.1m vertically from burner surface

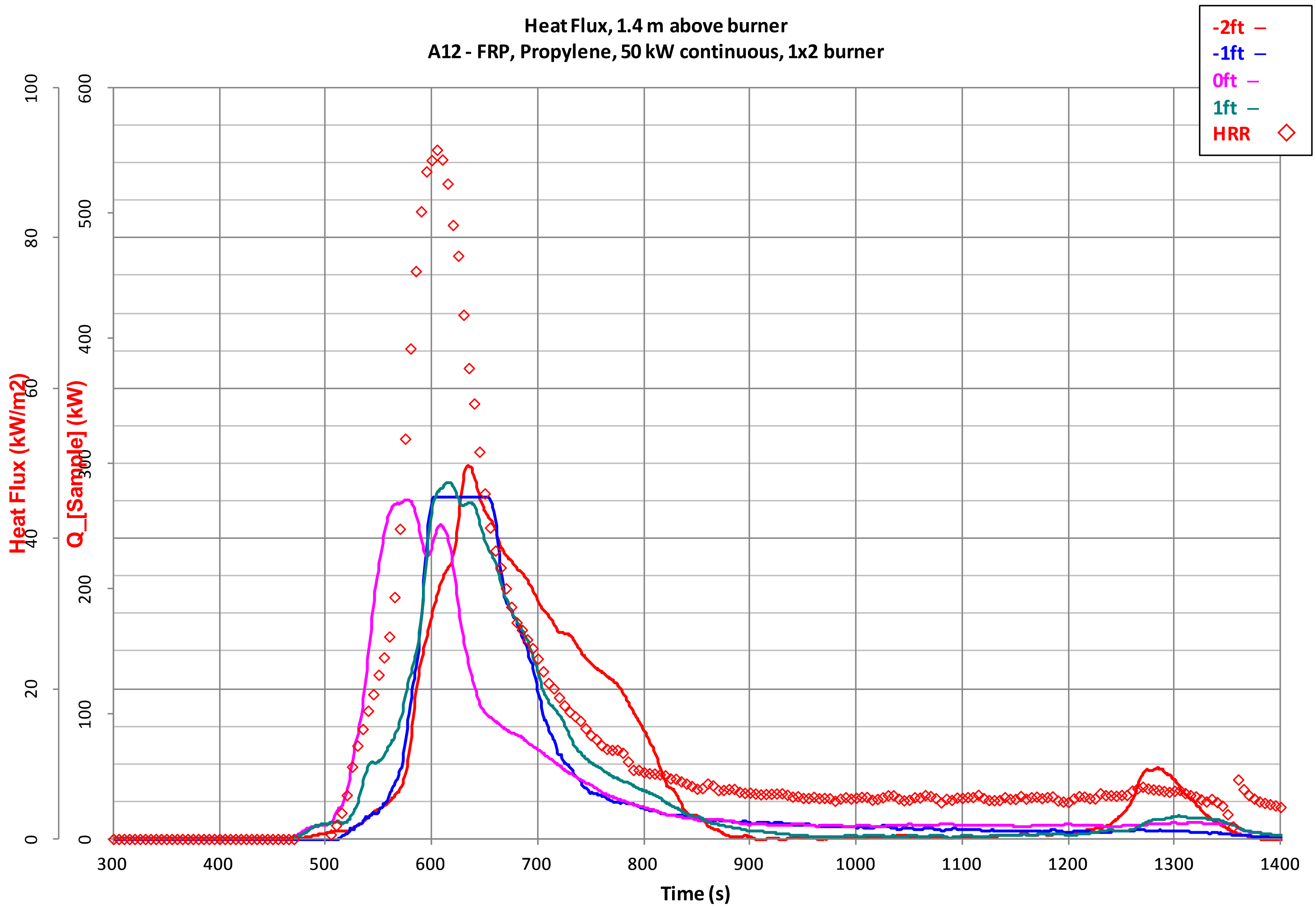

Heat flux measured at various distances from the centerline (negative indicates left of centerline), 1.4m vertically from burner surface

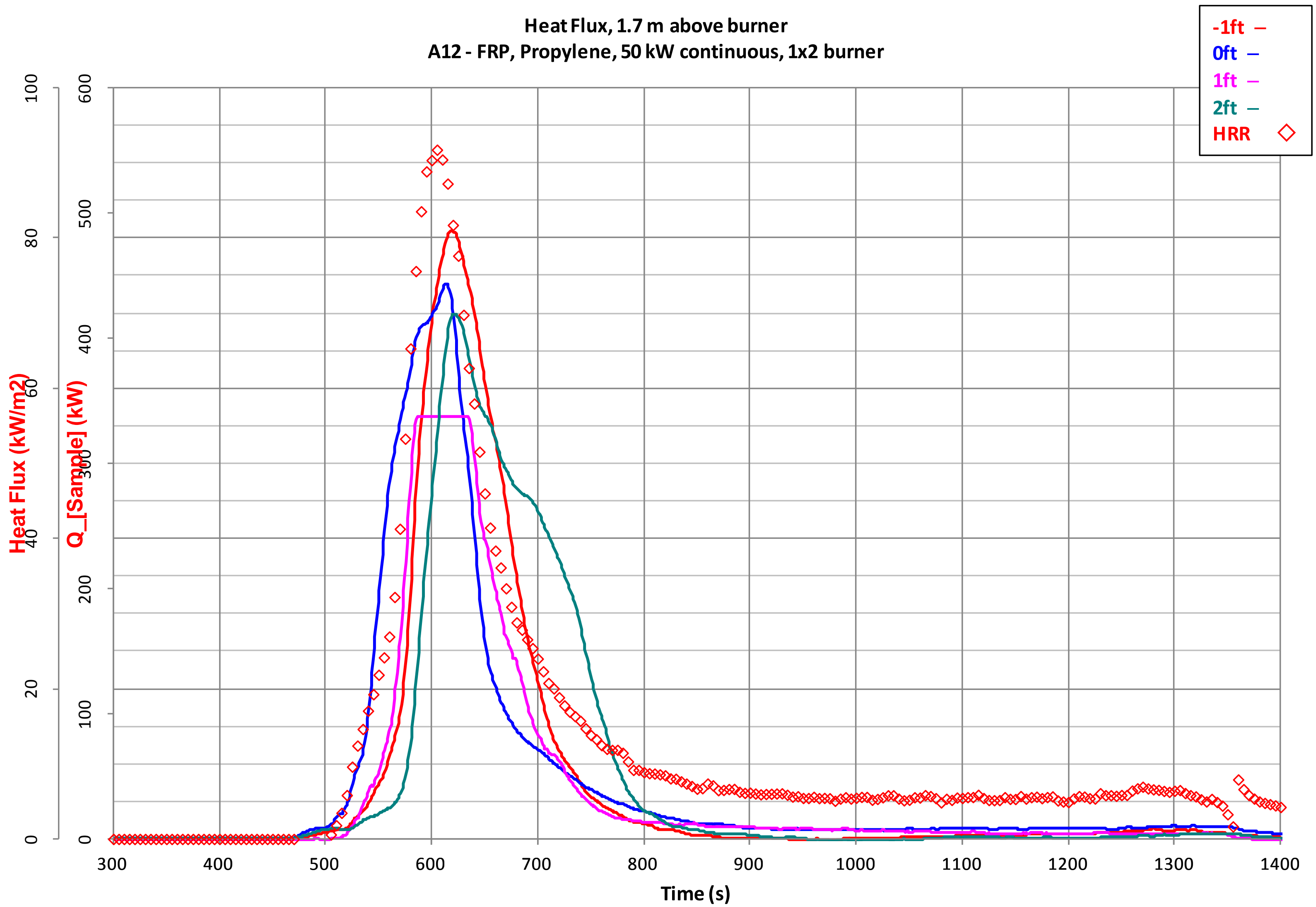

Heat flux measured at various distances from the centerline (negative indicates left of centerline), 1.7m vertically from burner surface

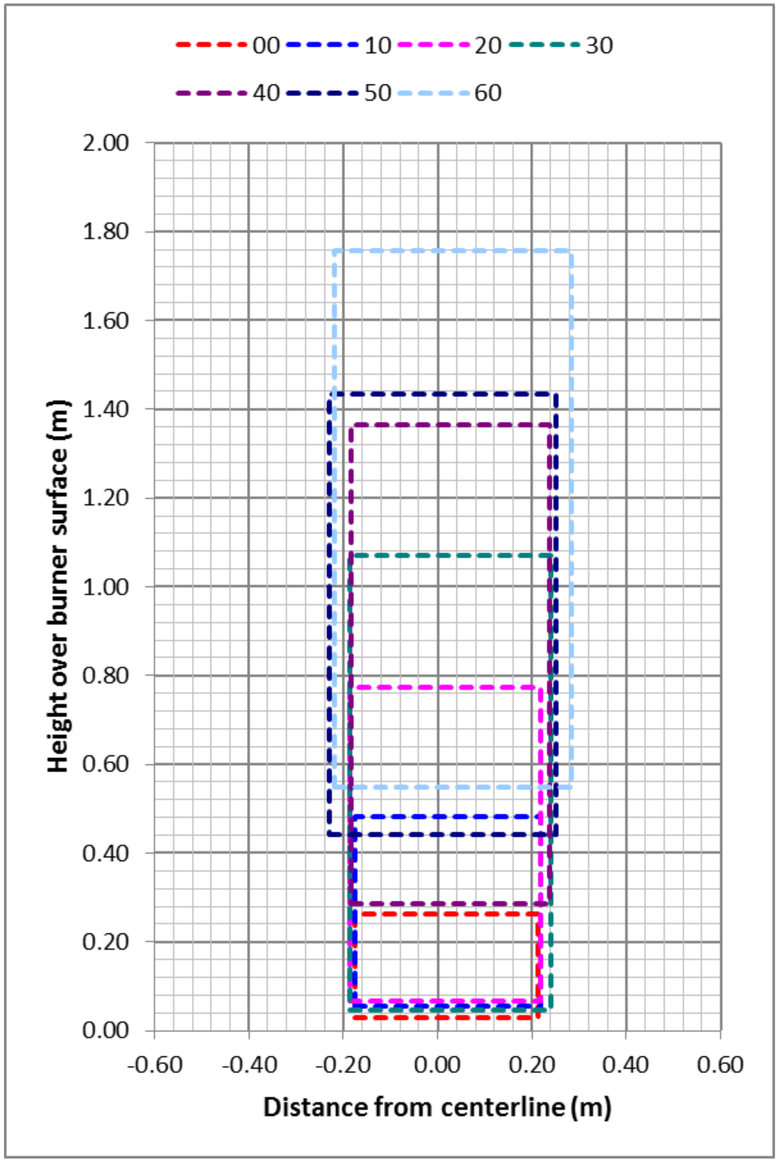

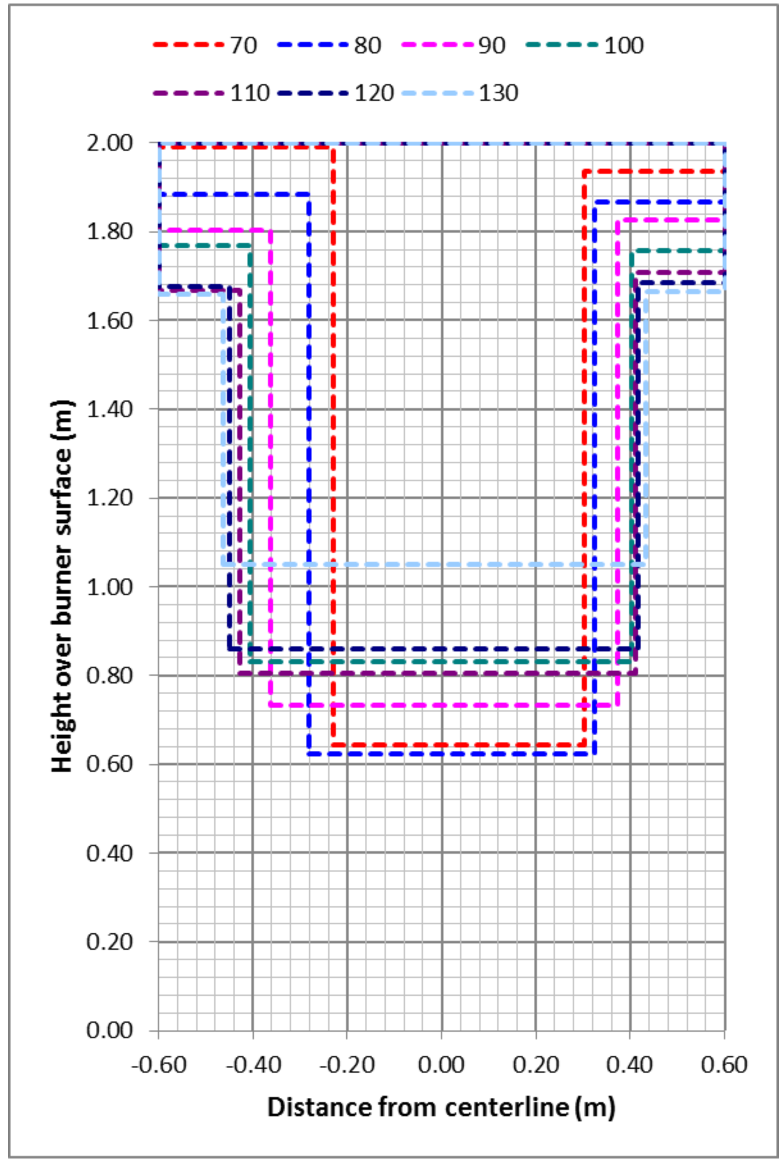

Stages 1 and 2 burning areas in Test A12 (2ft Rectangle burner, Propylene, 50 kW source on throughout test)

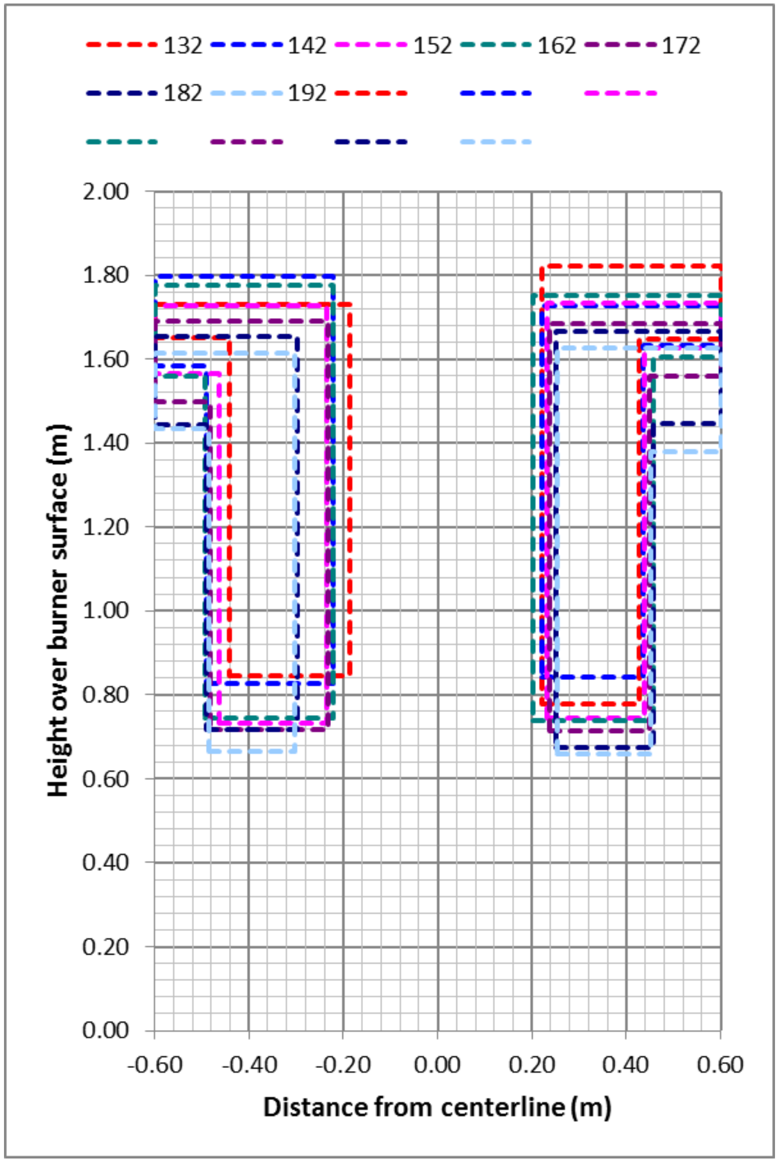

Stage 3 burn area and final damage chart of Test A12 (2ft Rectangle burner, Propylene, 50 kW source on throughout test)

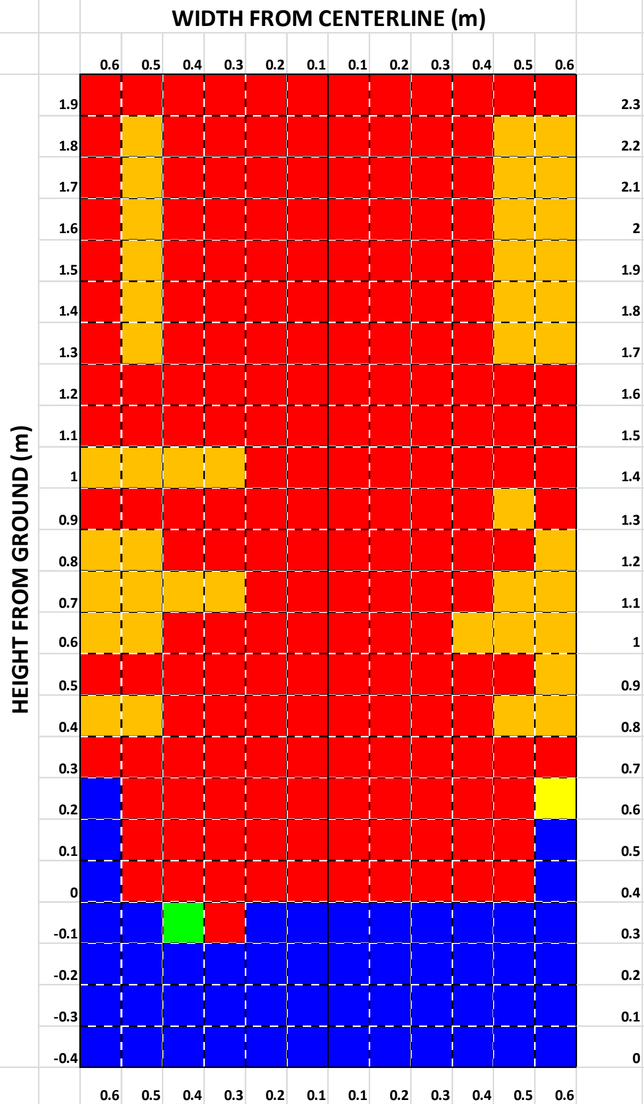

# of cell	Damage to Resin	Area (m2)
193	up to 100% damage	1.93
42	up to 75% damage	0.42
1	up to 50% damage	0.01
1	up to 25% damage	0.01
51	no damage	0.51

Initial mass:	8.12	kg
Final unburnt mass:	1.48	kg
Final burnt mass:	3.58	kg
Total mass loss during fire	3.06	kg

Burn damage pattern observed after fire test

F.3.13 Test A13

LODS Test Run Data

Center for Firesafety Studies

100 Institute Road
Worcester, MA 01609
Phone: (508) 831-5628
Fax: (508) 831-5680

Test Information

Test Number:	A13
Specimen Identification:	FRP 13, 50 kW continuous Propylene fire, 1 x 1 burner
Material Name:	Class C FRP panel
Manufacturer/Submitter:	Not Reported
Raw Data File Name:	Test A13 - FRP_Propylene_50kW_1ft.txt
Reduced Data File Name:	Test A13 - FRP_Propylene_50kW_1ft_reduced_xlsx
Date of Test:	17-Nov-2010
Tester:	W. Wong

Test Parameters

Ambient Temperature:	N/A
Relative Humidity:	N/A

Specimen Information

Specimen Initial Mass:	[kg]	8.2
Specimen Final Mass:	[kg]	5.4
Mass Lost:	[kg]	2.8
Heat Evolved (net):	[kJ]	0

Parameter	Unit	Value
Mass Loss		
Initial Mass	[kg]	8.2
Final Mass	[kg]	5.4
Mass Loss	[%]	34.07

LODS Test Run Data

Center for Firesafety Studies

100 Institute Road
Worcester, MA 01609
Phone: (508) 831-5628
Fax: (508) 831-5680

Test Notes

Test Number:	0
Date:	11/17/10
Material:	Class C FRP panel
Specimen Identification:	FRP 13, 50 kW continuous Propylene fire, 1 x 1 burner

Observations

Time	Observation
00:00	Start VI
03:20	Start Camera 1
03:10	Start Camera 2
06:10	Burner ignition
06:25	Reach target HRR @ 50 kW
	Burner flame plume tilts to right at 5-10 deg
07:05	Panel ignition, mainly at area under TSC-2 to above burner
07:35	Flame hit ceiling
07:50	Remote ignition @ HFG-1, TSC-3, insignificant
08:00	T pattern under ceiling
08:15 to 09:10	Rollover under ceiling
08:50	Rollover layer about 40 to 50 cm thick
09:00	Remote area smoking at right edge @ y = 1.2 m
10:00	Small remote area flaming at right edge @ y = 1.2 m
10:40	Burner flame plume starts to lean left or straight up, corrected the initial lean right behavior
15:00	Only line fires on both side (~40 cm away) of the burner remaining, the source fire is about 0.6 m high, and doesn't seem to affect the wall line fires
17:45	Burner turned off
18:15	Terminate test with little water application, burner still flashes insignificantly

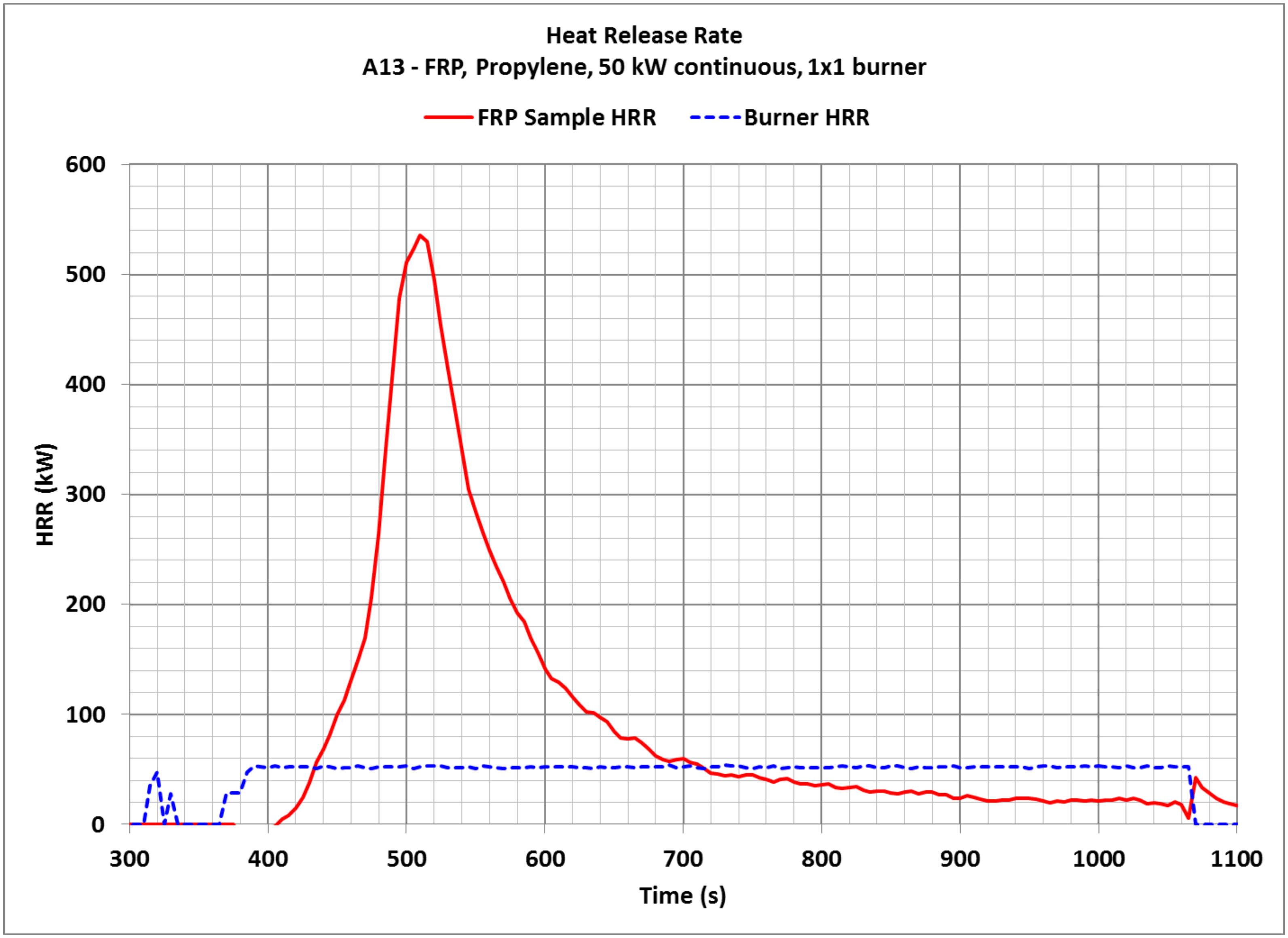

Heat release ratesof the source burner fire and of the specimen fire measured during test

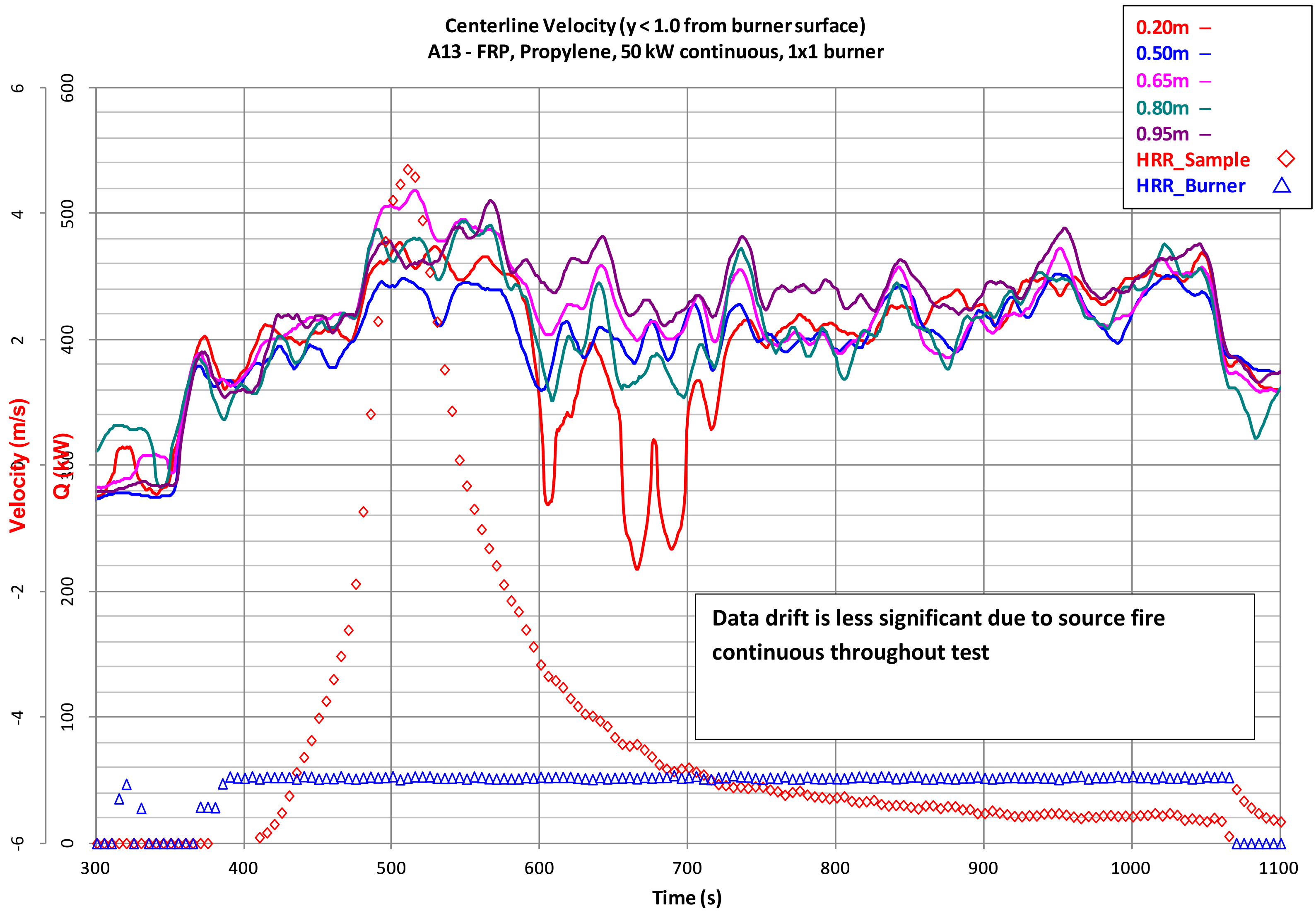

Centerline plume velocities measured from 0.2m to 0.95m above the burner surface

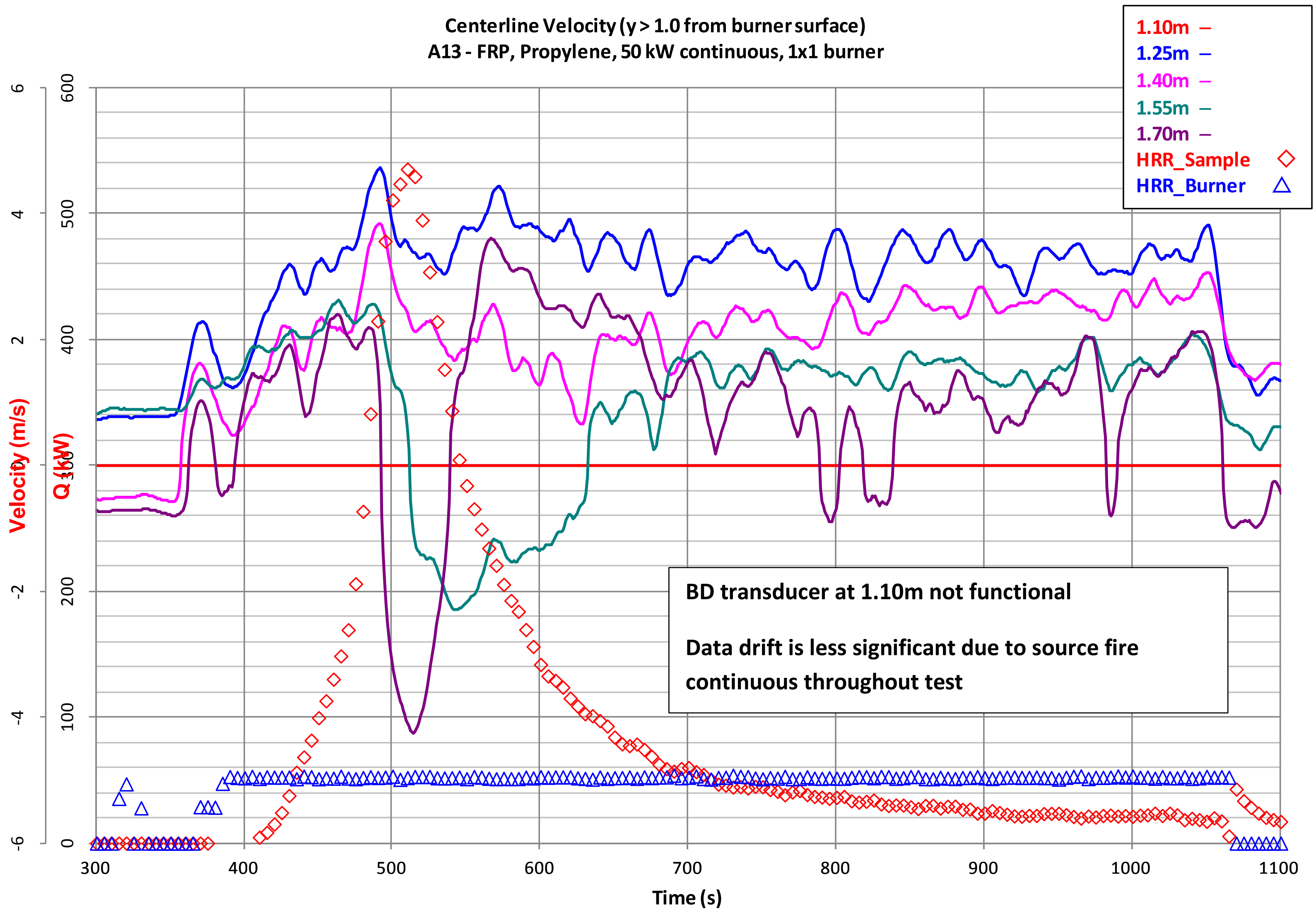

Centerline plume velocities measured from 1.1m to 1.7m above the burner surface

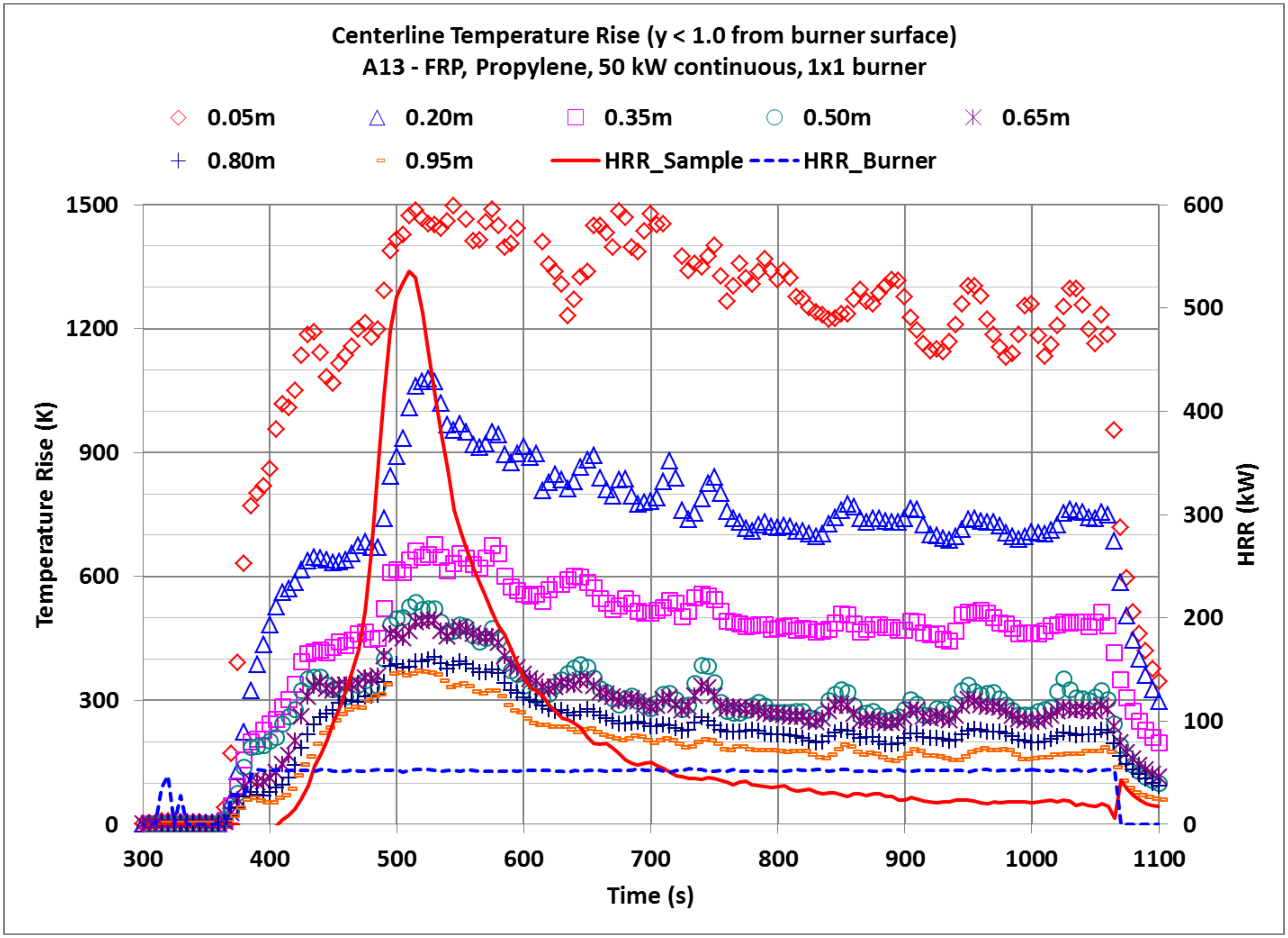

Centerline plume temperature rise measured from 0.05m to 0.95m above the burner surface

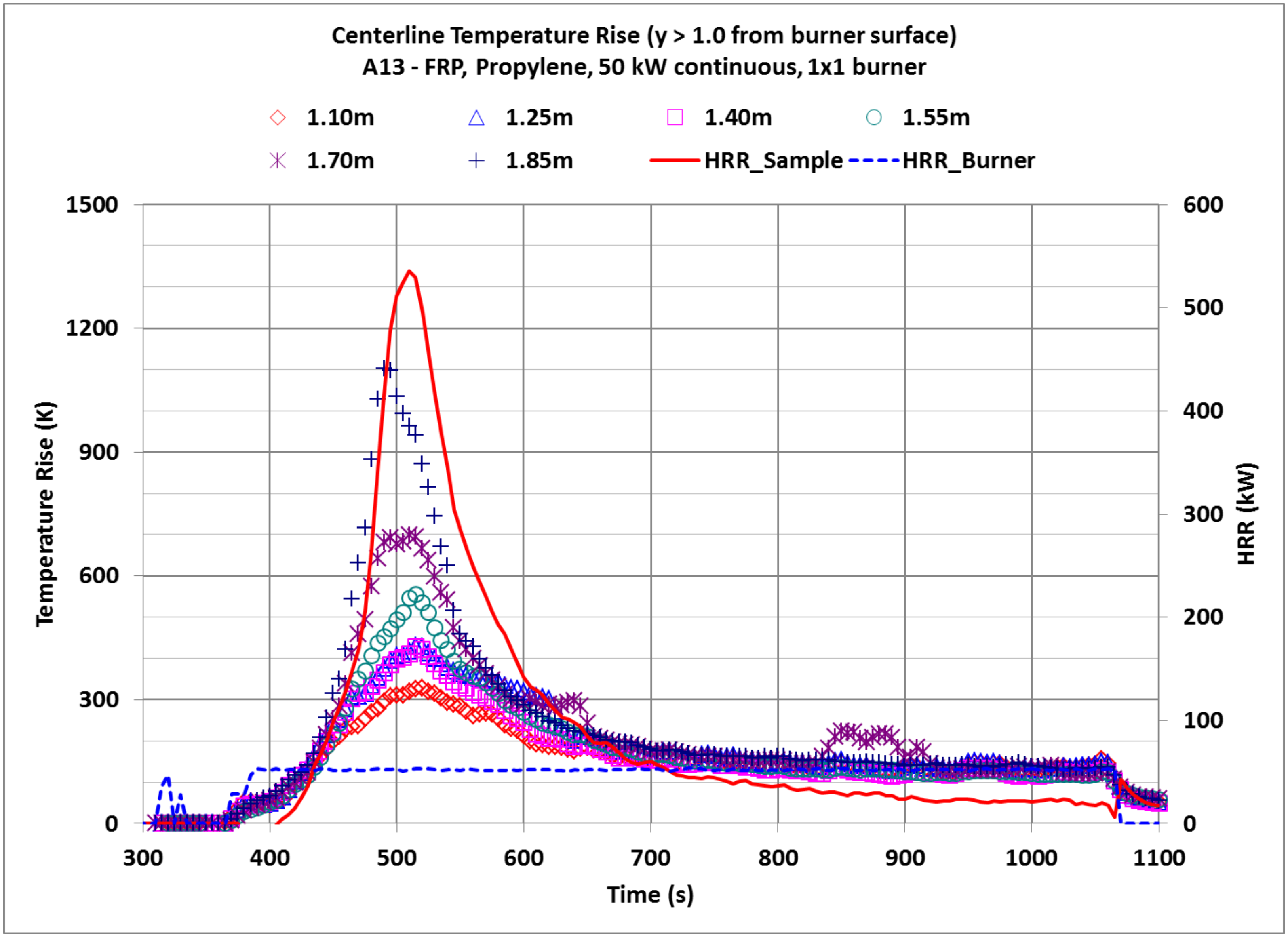

Centerline plume temperature rise measured from 1.10m to 1.85m above the burner surface

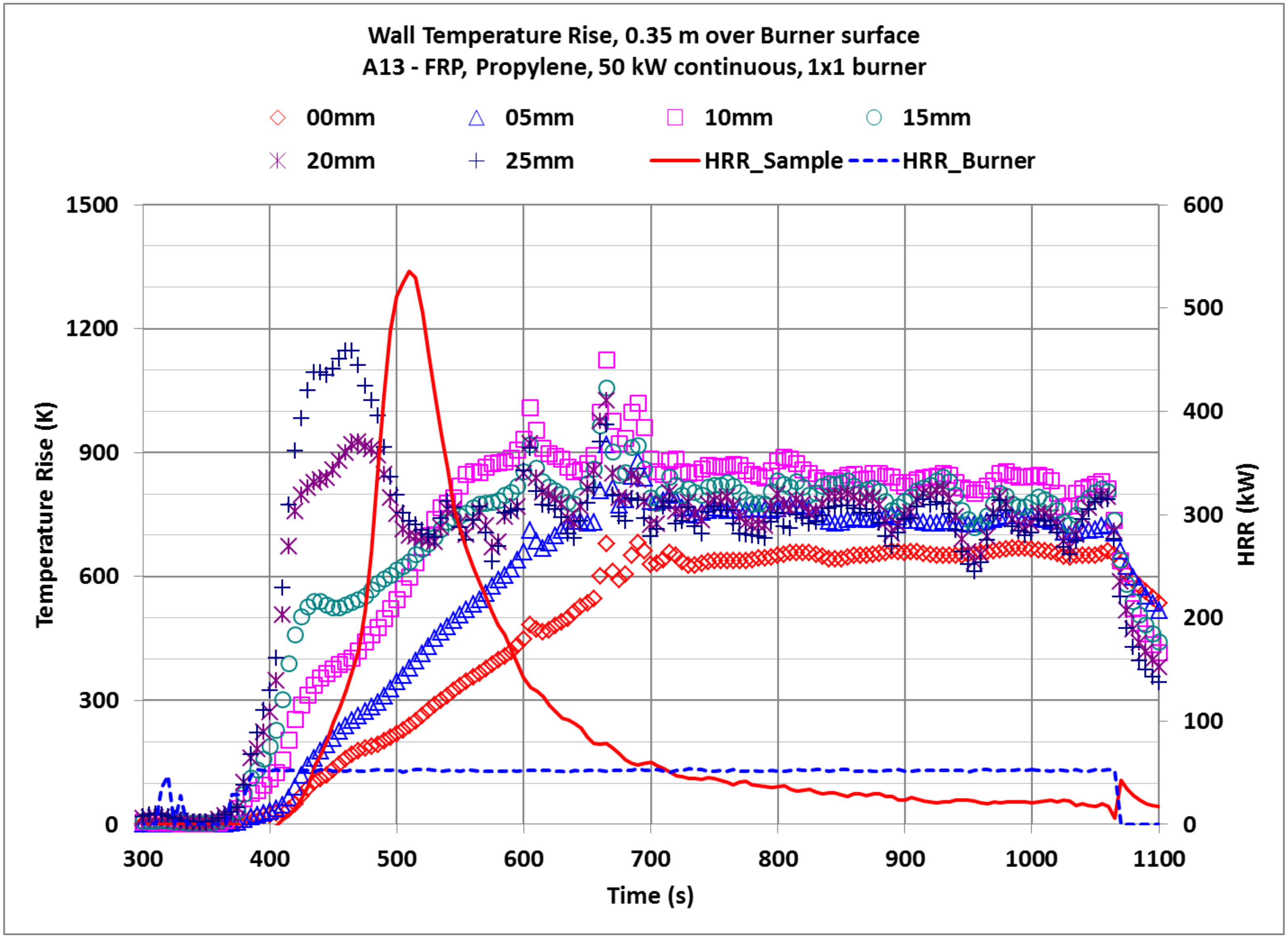

Temperature rise along the wall's centerline at 0.35m over the burner surface, measured at different perpendicular distances to as indicated

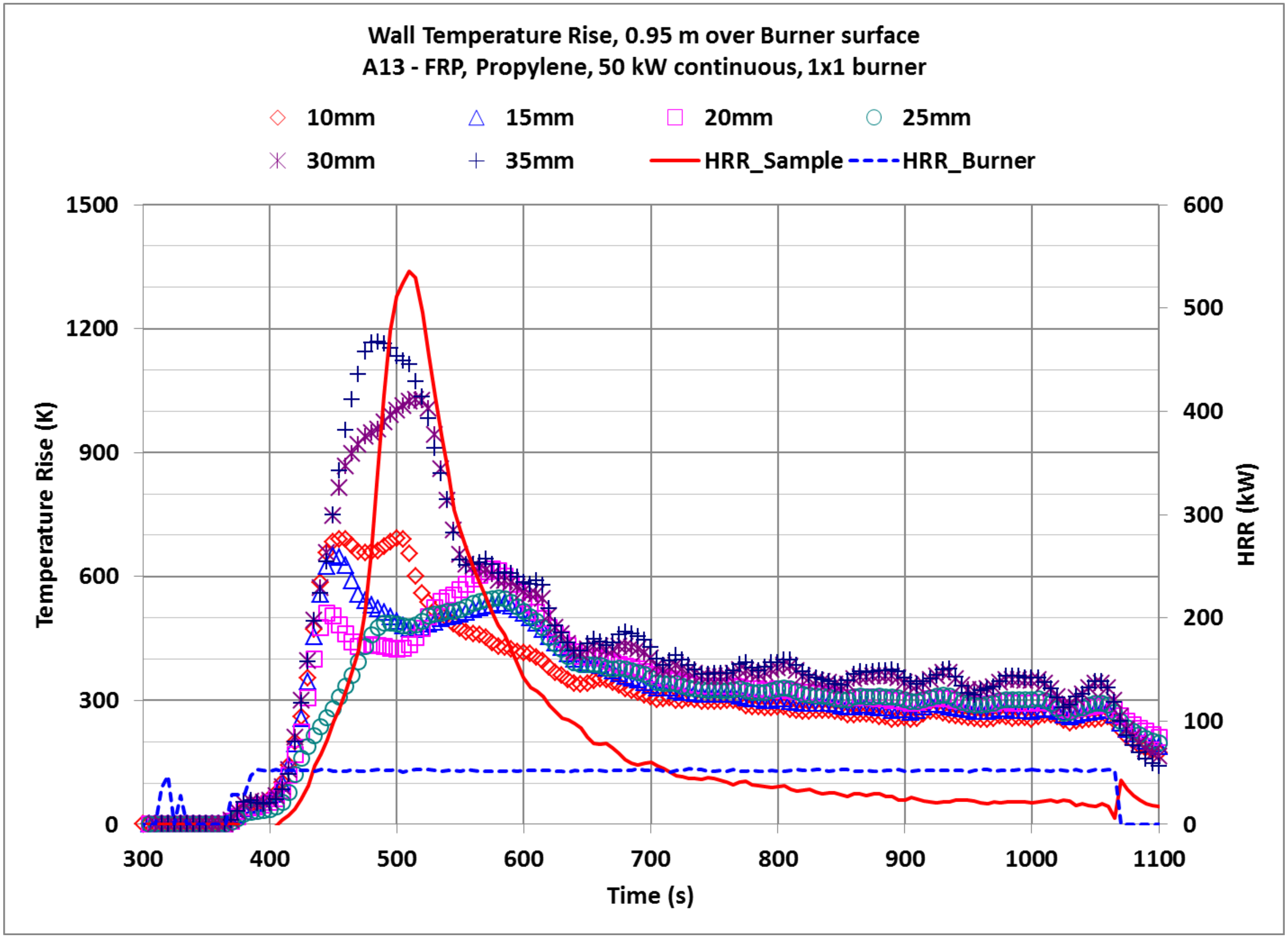

Temperature rise along the wall's centerline at 0.95m over the burner surface, measured at different perpendicular distances to as indicated

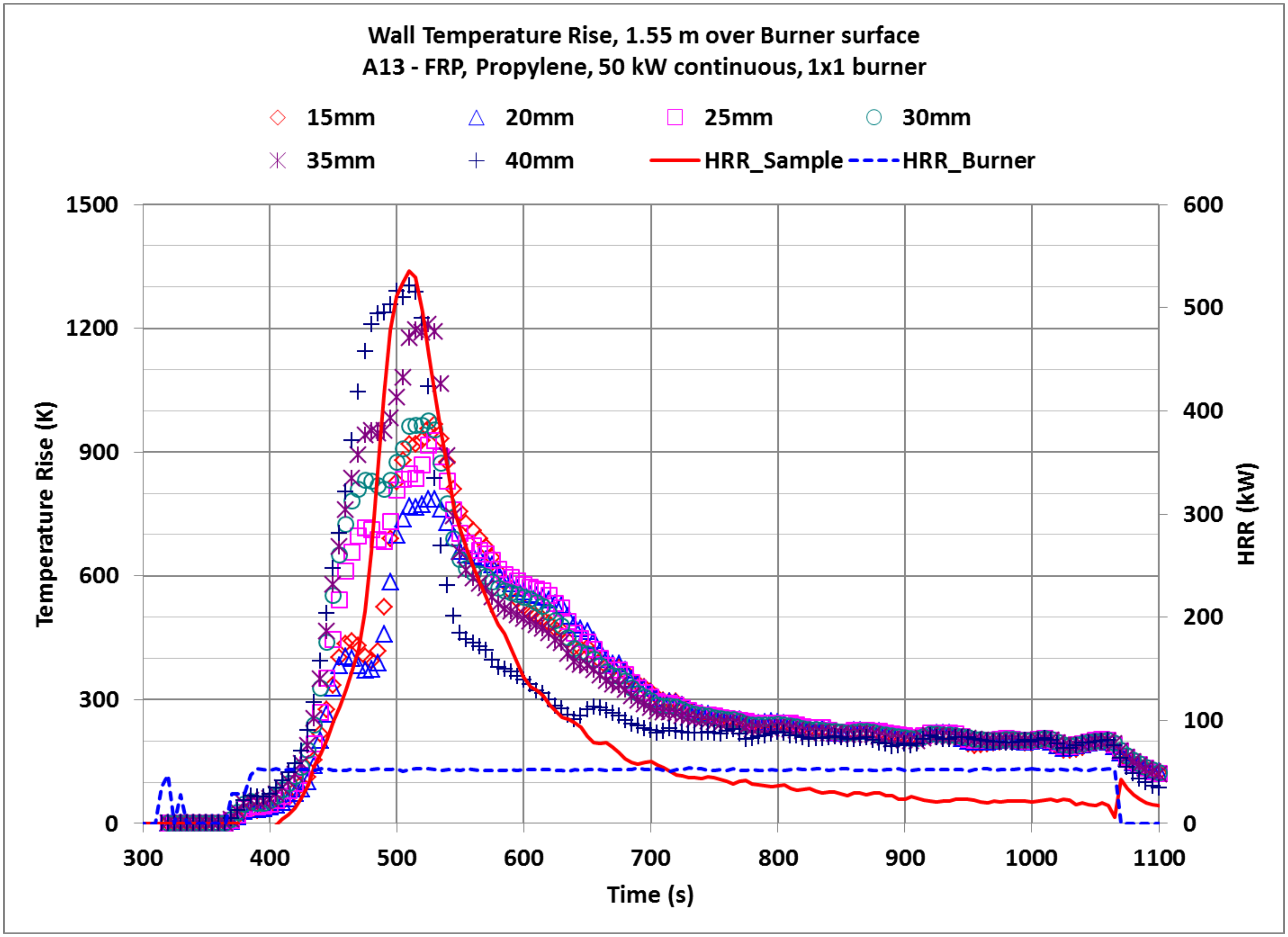

Temperature rise along the wall's centerline at 1.55m over the burner surface, measured at different perpendicular distances to as indicated

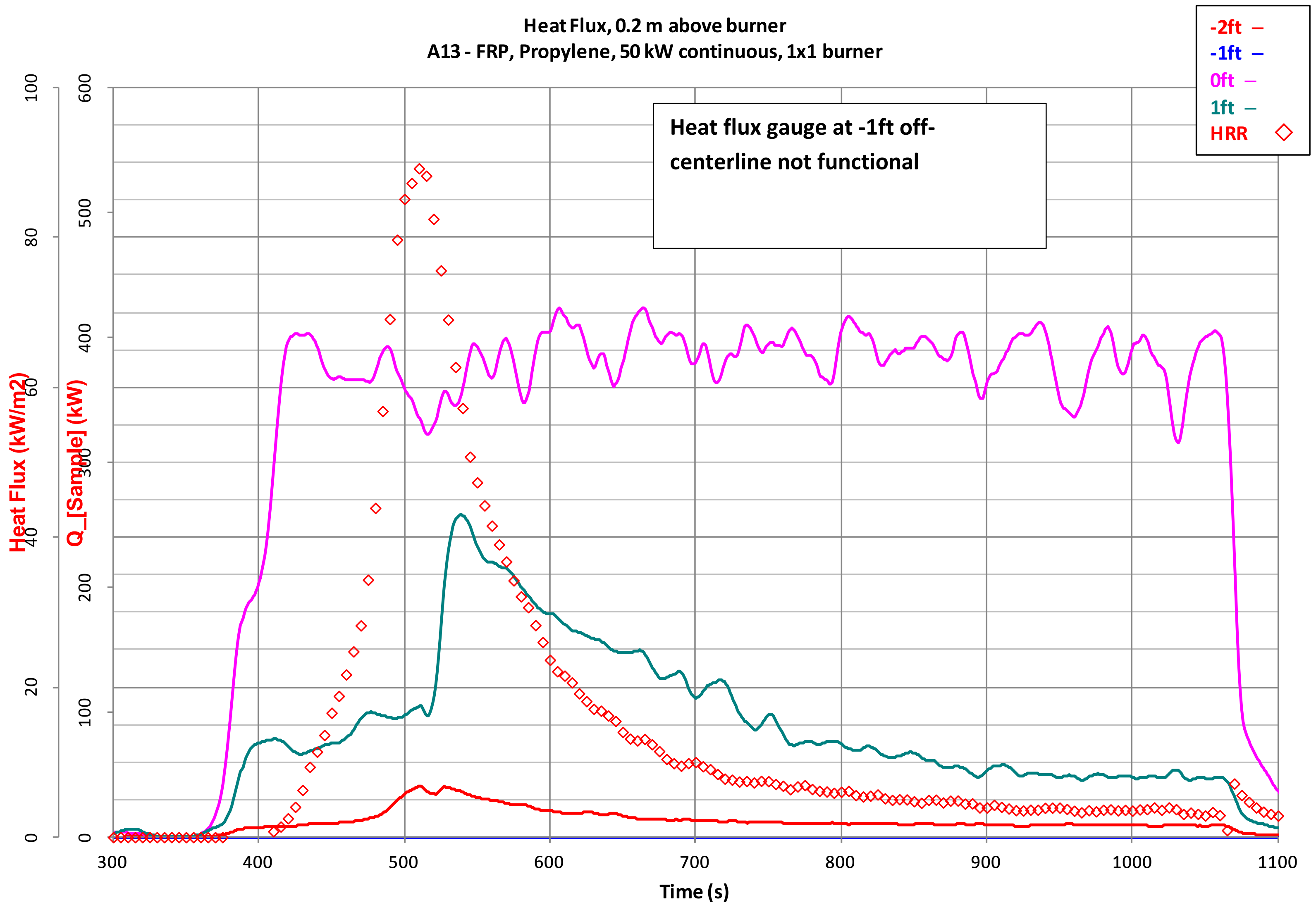

Heat flux measured at various distances from the centerline (negative indicates left of centerline), 0.2m vertically from burner surface

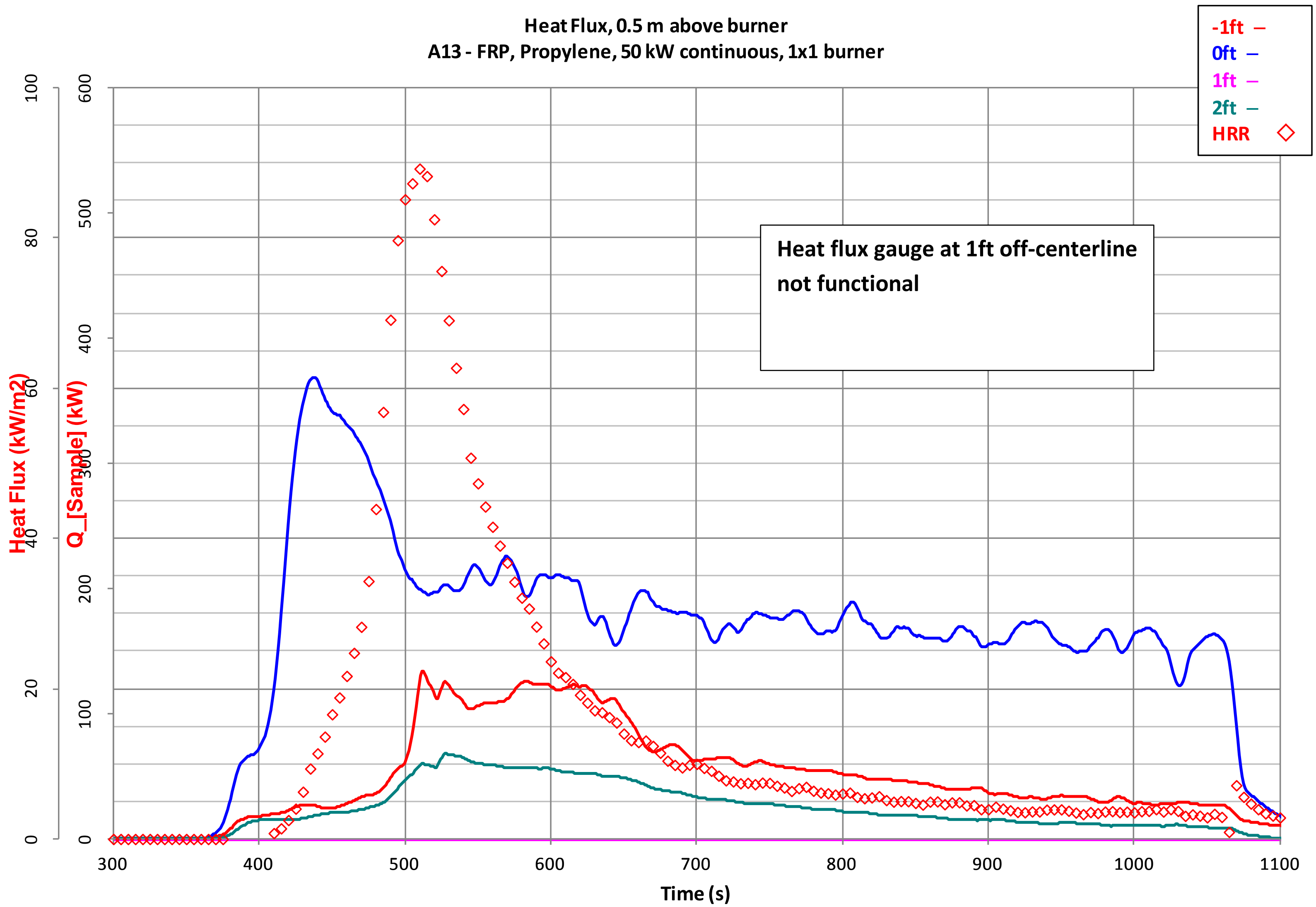

Heat flux measured at various distances from the centerline (negative indicates left of centerline), 0.5m vertically from burner surface

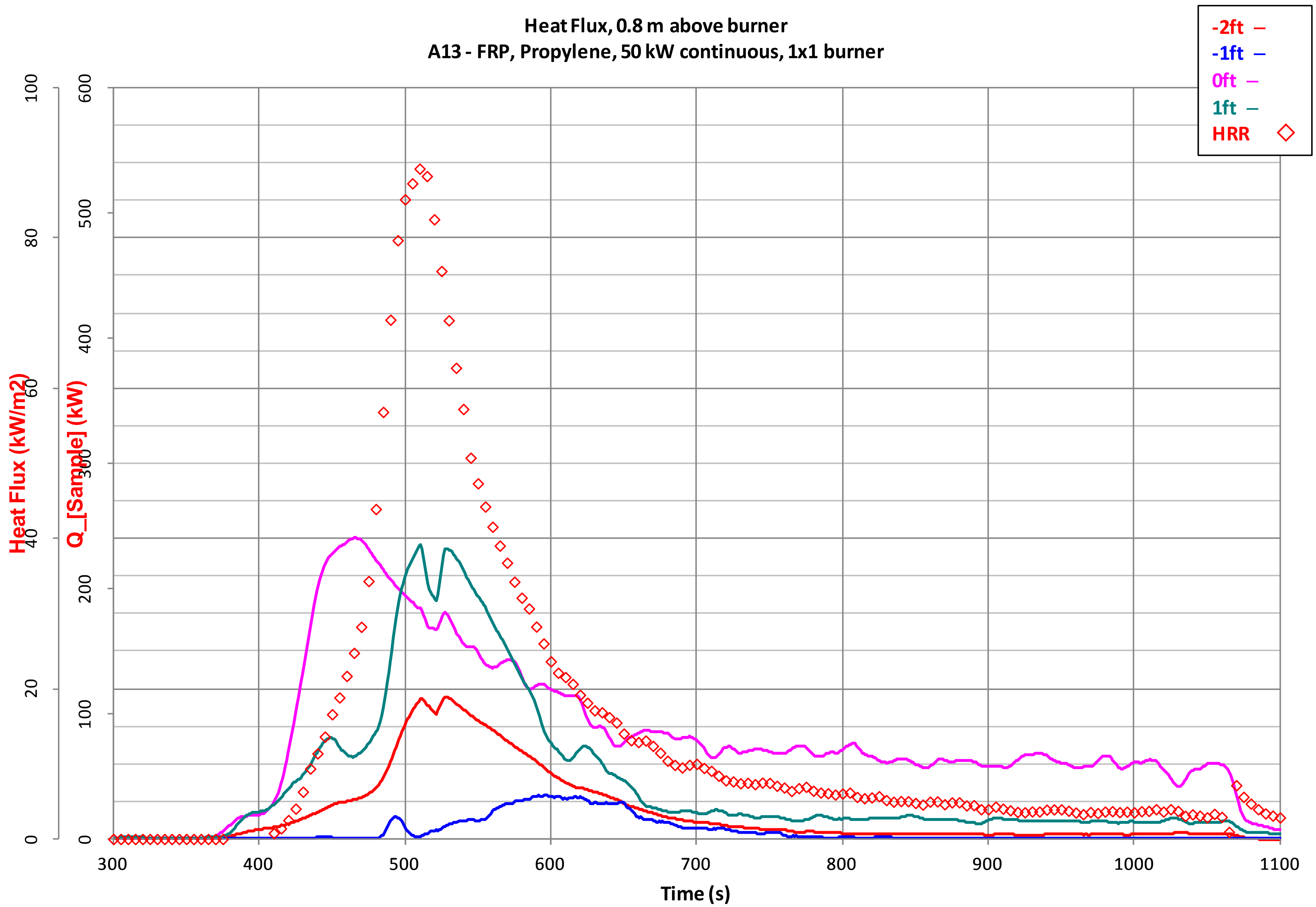

Heat flux measured at various distances from the centerline (negative indicates left of centerline), 0.8m vertically from burner surface

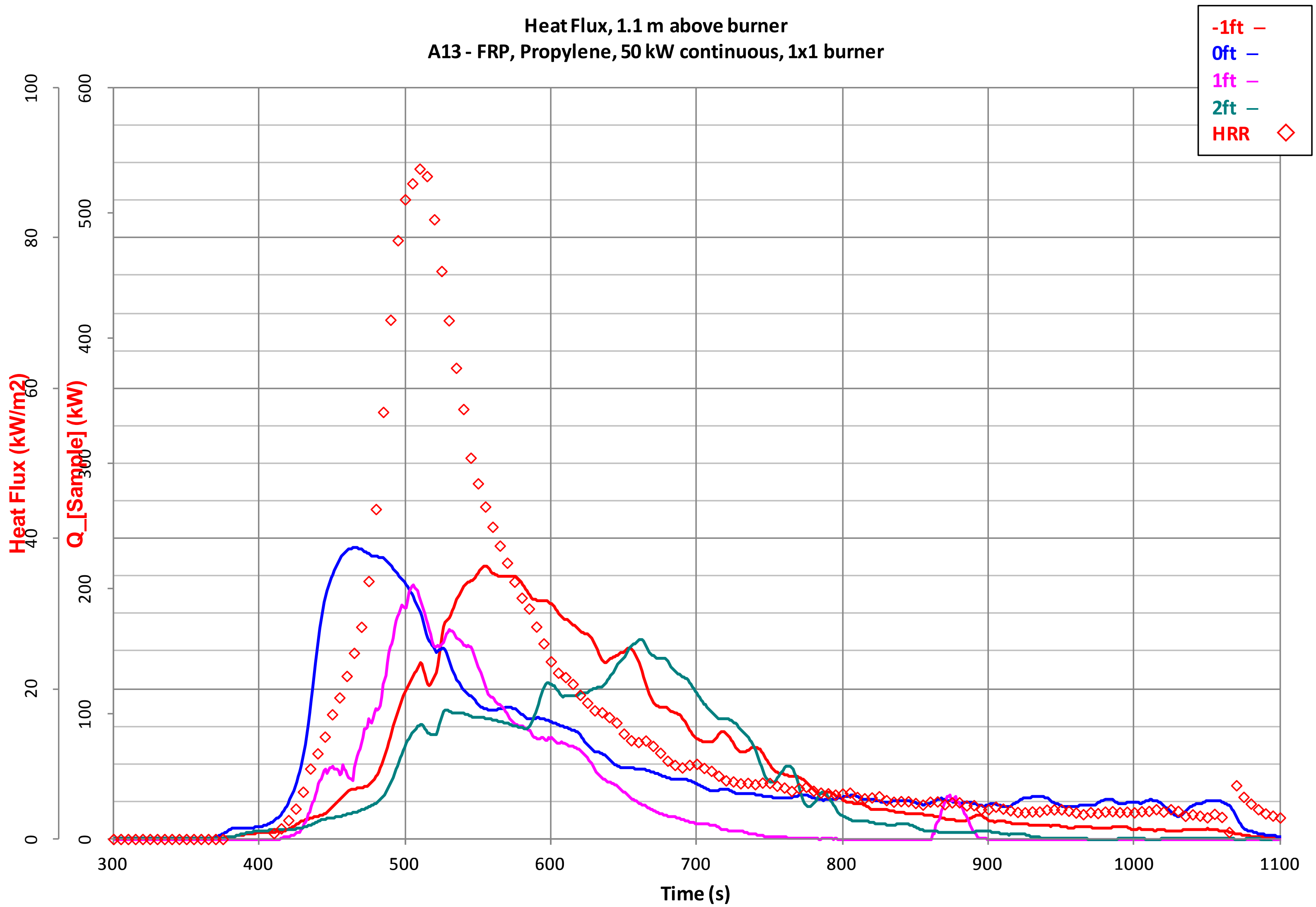

Heat flux measured at various distances from the centerline (negative indicates left of centerline), 1.1m vertically from burner surface

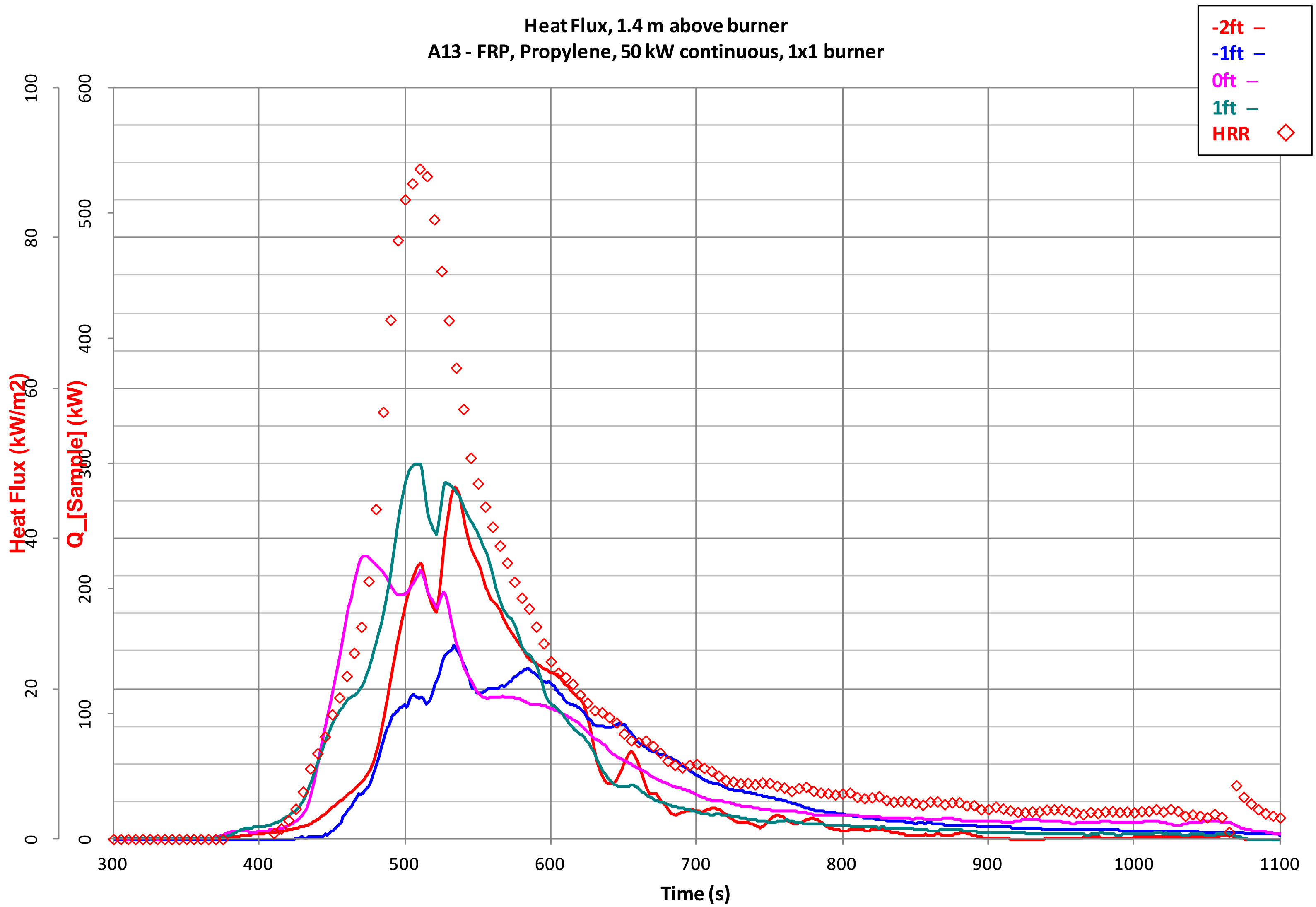

Heat flux measured at various distances from the centerline (negative indicates left of centerline), 1.4m vertically from burner surface

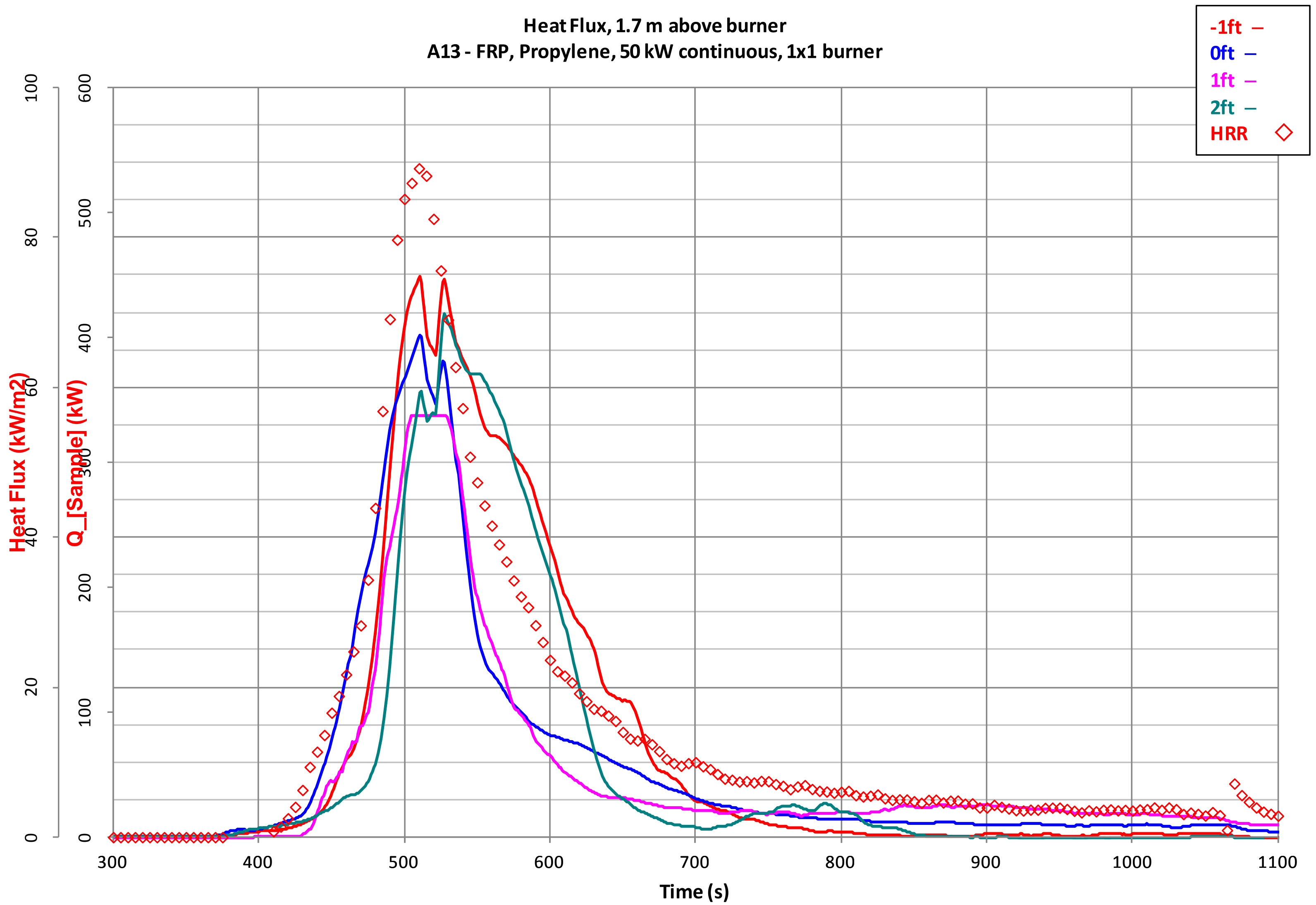

Heat flux measured at various distances from the centerline (negative indicates left of centerline), 1.7m vertically from burner surface

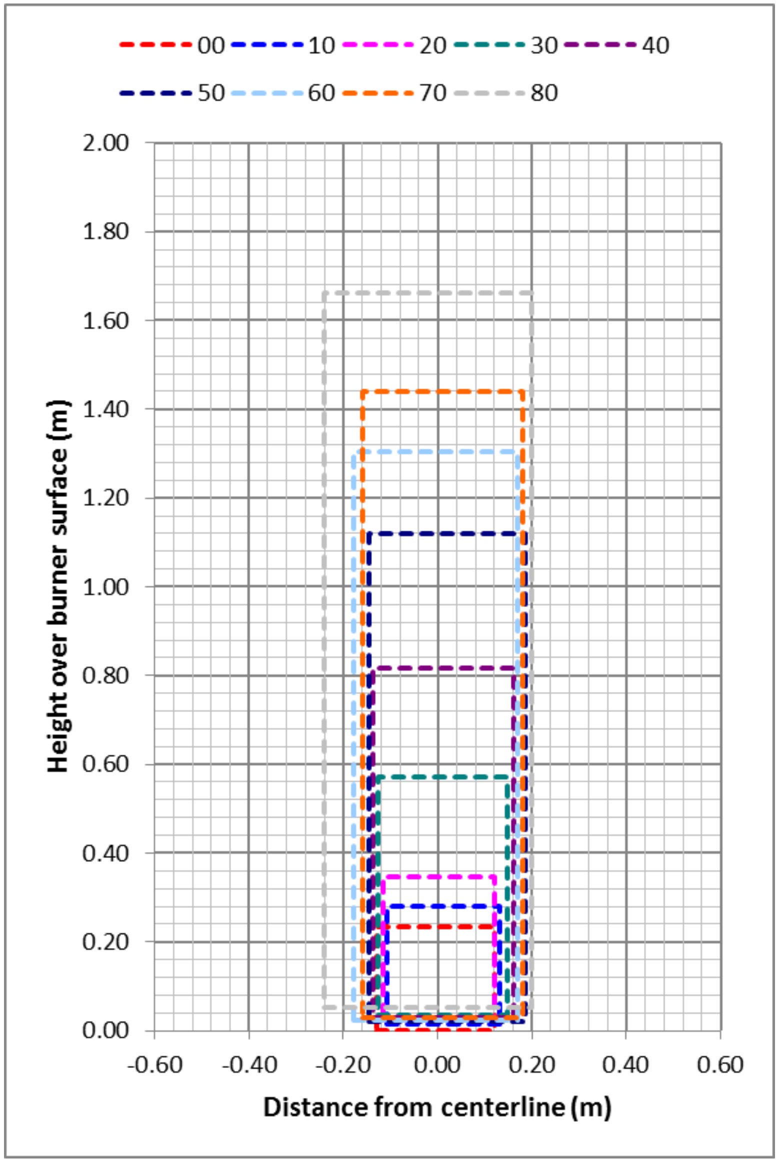

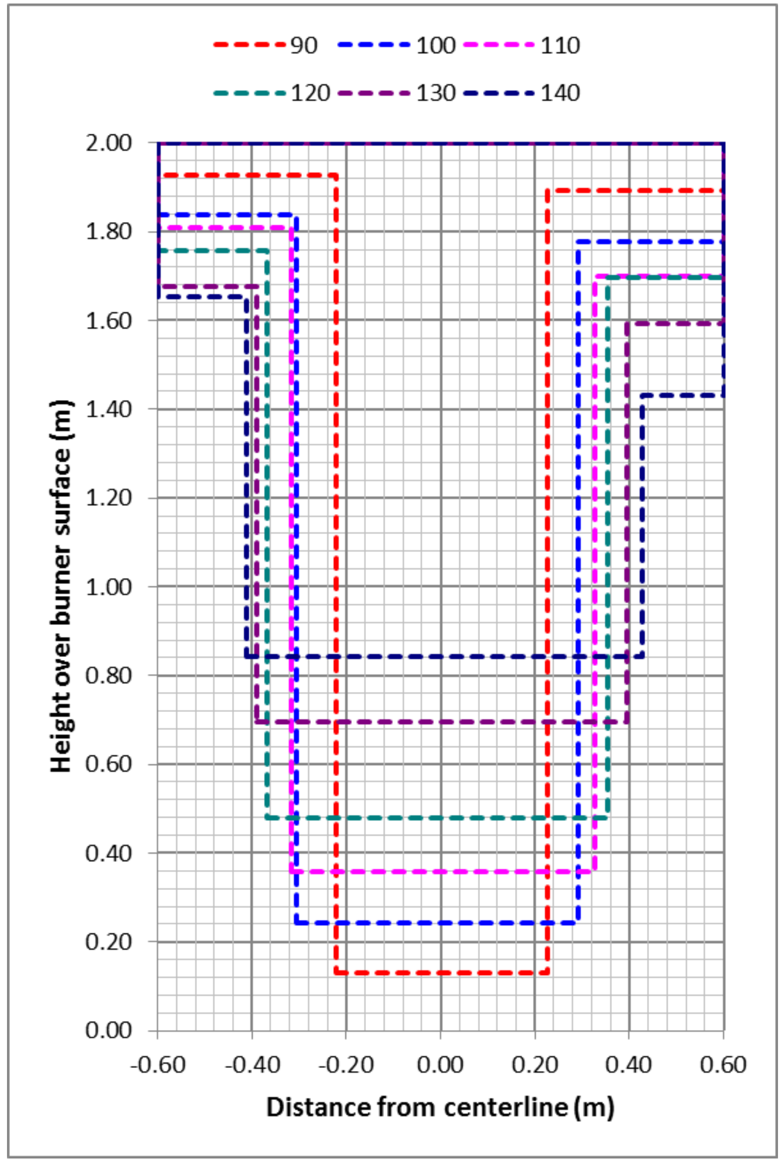

Stages 1 and 2 burning areas in Test A13 (1ft Square burner, Propylene, 50 kW source on throughout test)

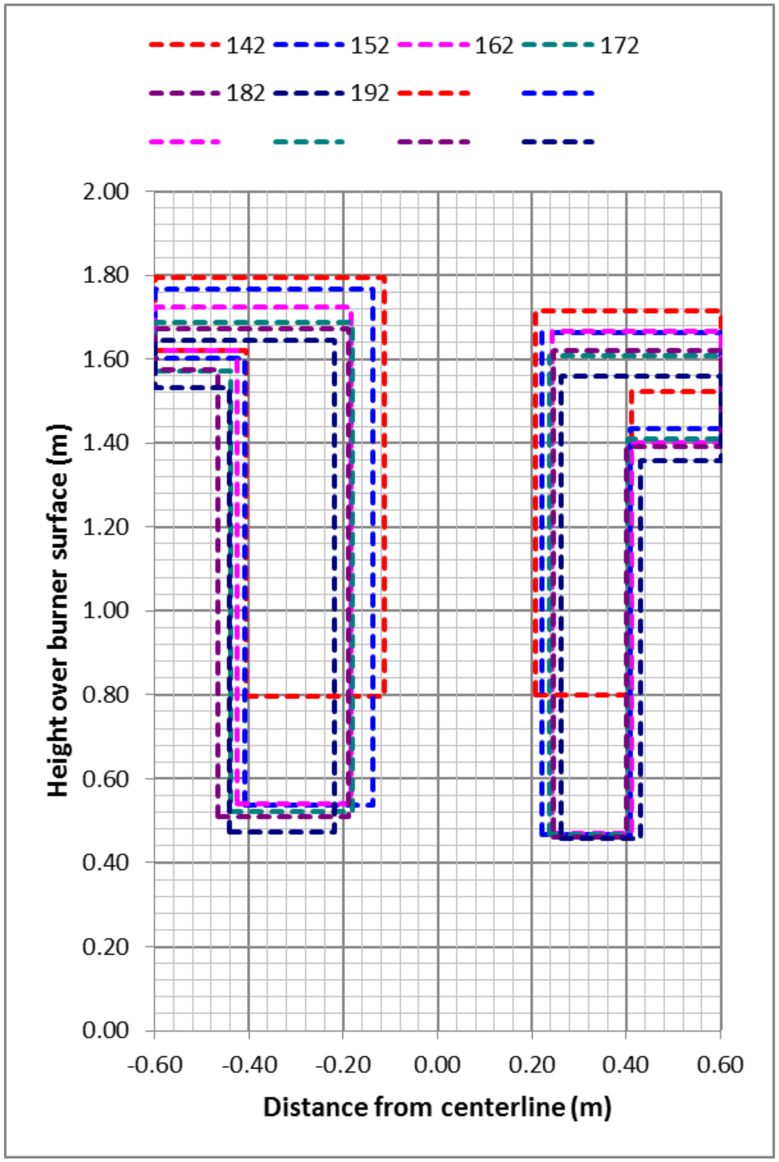

Stage 3 burn area and final damage chart of Test A13 (1ft Square burner, Propylene, 50 kW source on throughout test)

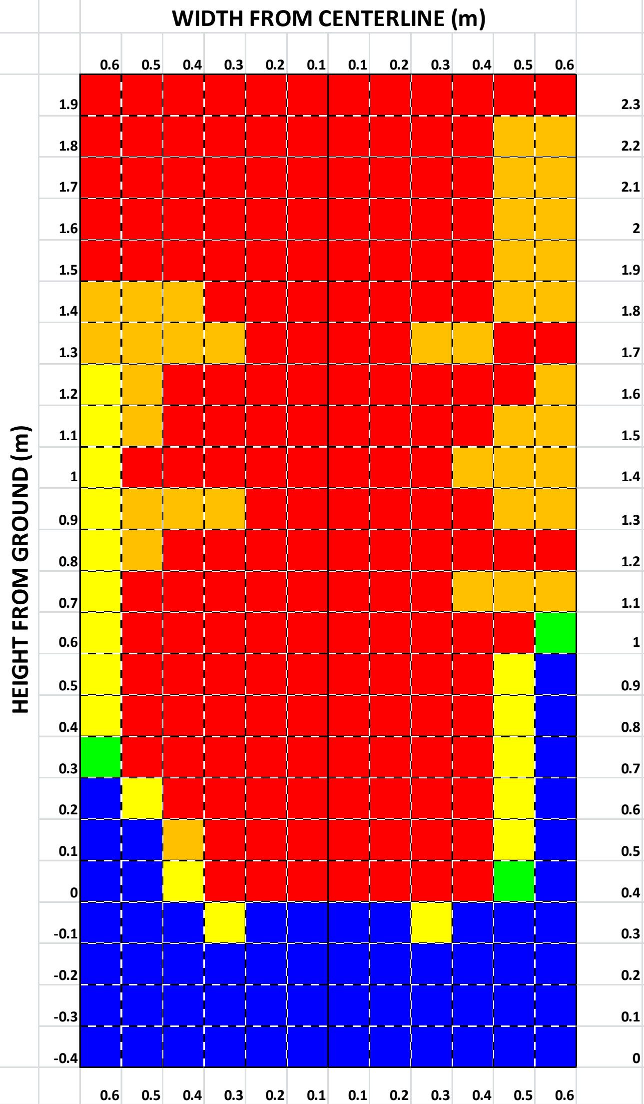

# of cell	Damage to Resin	Area (m2)
173	up to 100% damage	1.73
37	up to 75% damage	0.37
18	up to 50% damage	0.18
3	up to 25% damage	0.03
57	no damage	0.57

Initial mass:	8.16	kg
Final unburnt mass:	2.16	kg
Final burnt mass:	3.22	kg
Total mass loss during fire	2.78	kg

Burn damage pattern observed after fire test

F.3.14 Test A14

LODS Test Run Data

Center for Firesafety Studies

100 Institute Road
Worcester, MA 01609
Phone: (508) 831-5628
Fax: (508) 831-5680

Test Information

Test Number:	A14
Specimen Identification:	FRP 14, 75 kW initial Propylene fire, 1 x 1 burner
Material Name:	Class C FRP panel
Manufacturer/Submitter:	Not Reported
Raw Data File Name:	Test A14 - FRP_Propylene_75kW_1ft.txt
Reduced Data File Name:	Test A14 - FRP_Propylene_75kW_1ft.txt_reduced.xlsx
Date of Test:	18-Nov-2010
Tester:	W. Wong

Test Parameters

Ambient Temperature:	N/A
Relative Humidity:	N/A

Specimen Information

Specimen Initial Mass:	[kg]	8.5
Specimen Final Mass:	[kg]	6.6
Mass Lost:	[kg]	1.9
Heat Evolved (net):	[kJ]	0

Parameter	Unit	Value
Mass Loss		
Initial Mass	[kg]	8.5
Final Mass	[kg]	6.6
Mass Loss	[%]	22.35

LODS Test Run Data

WPI Center for Firesafety Studies

100 Institute Road
Worcester, MA 01609
Phone: (508) 831-5628
Fax: (508) 831-5680

Test Notes

Test Number:	0
Date:	11/18/10
Material:	Class C FRP panel
Specimen Identification:	FRP 14, 75 kW initial Propylene fire, 1 x 1 burner

Observations

Time	Observation
00:00	Start VI
06:15	Start Camera 1
06:00	Start Camera 2
11:18	Burner ignition
11:34	Reach target HRR @ 75 kW
11:45	Crackling noise
12:00	Panel ignition, mainly at area under TSC-2 to above burner
12:20	Burner off
13:20	Remote area smoking @ TSC-3, TSc-10, HFG-2, TSC-9, smoke small flashes
13:20	Flame hit ceiling
13:32	Burning reaches left and right edges, T-pattern starts
13:38 to 14:50	Rollover of ceiling layer, thickness of flame is about 30 cm, down to y = 2 m
30:25	fire extinguished with little water application

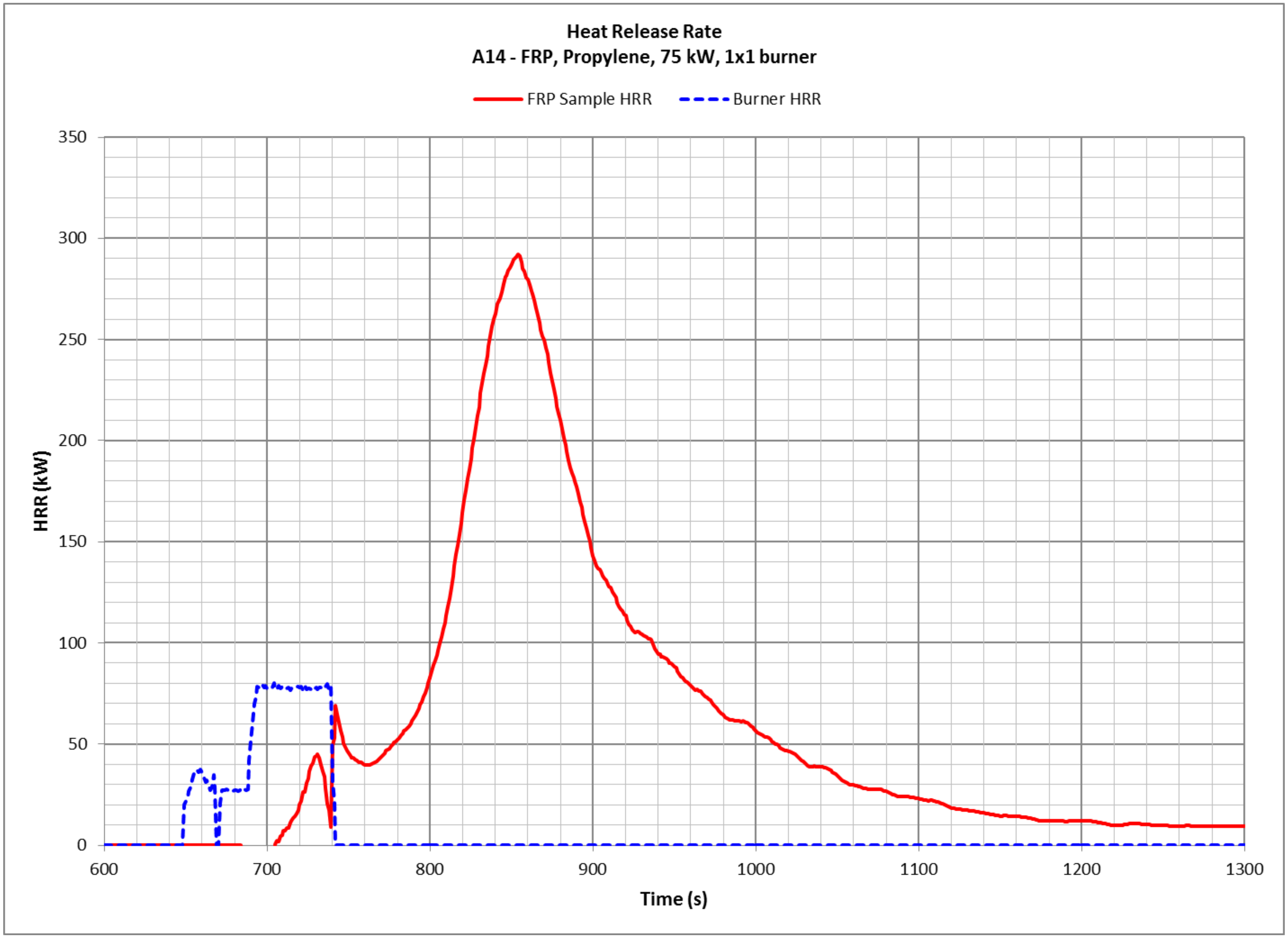

Heat release ratesof the source burner fire and of the specimen fire measured during test

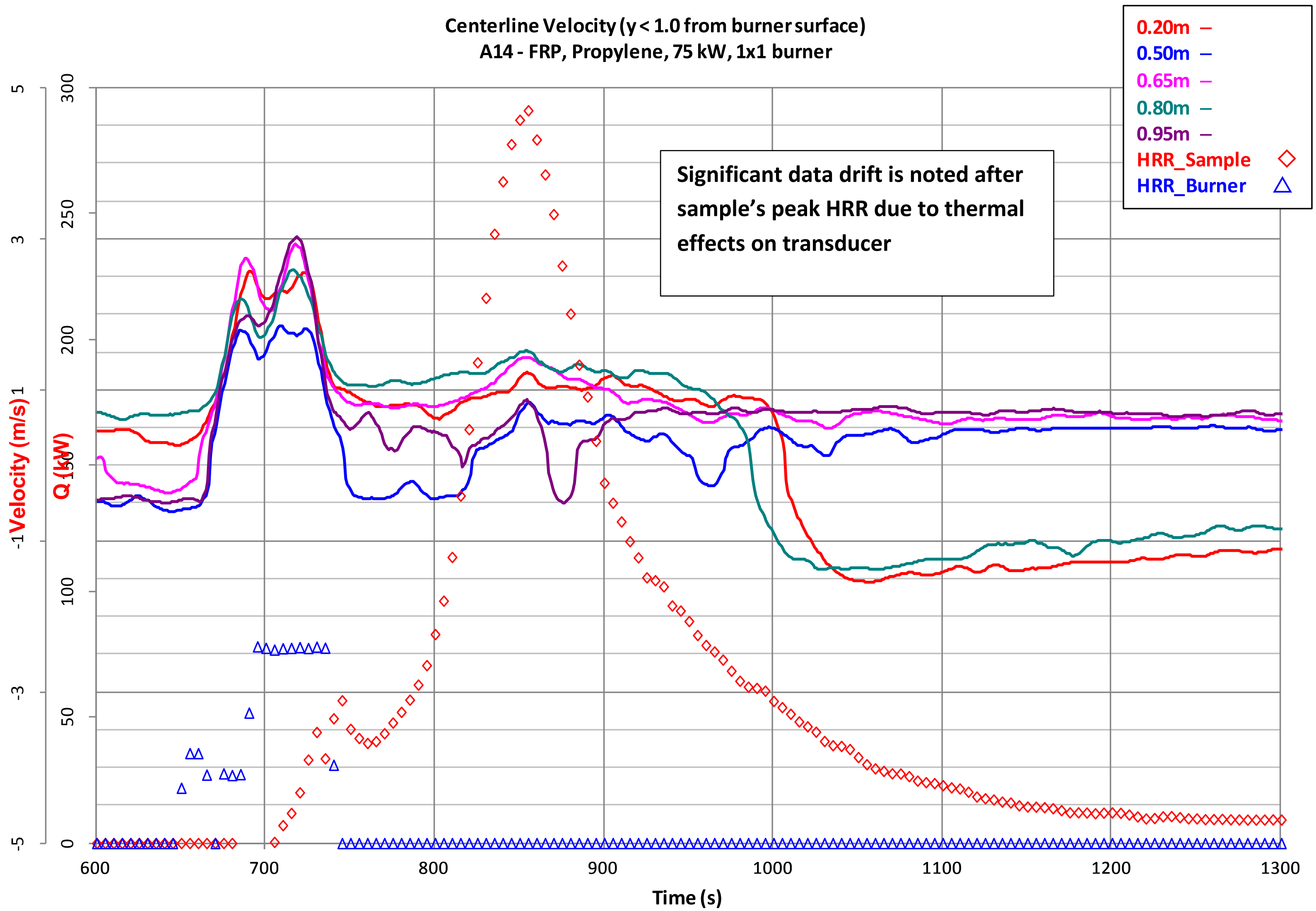

Centerline plume velocities measured from 0.2m to 0.95m above the burner surface

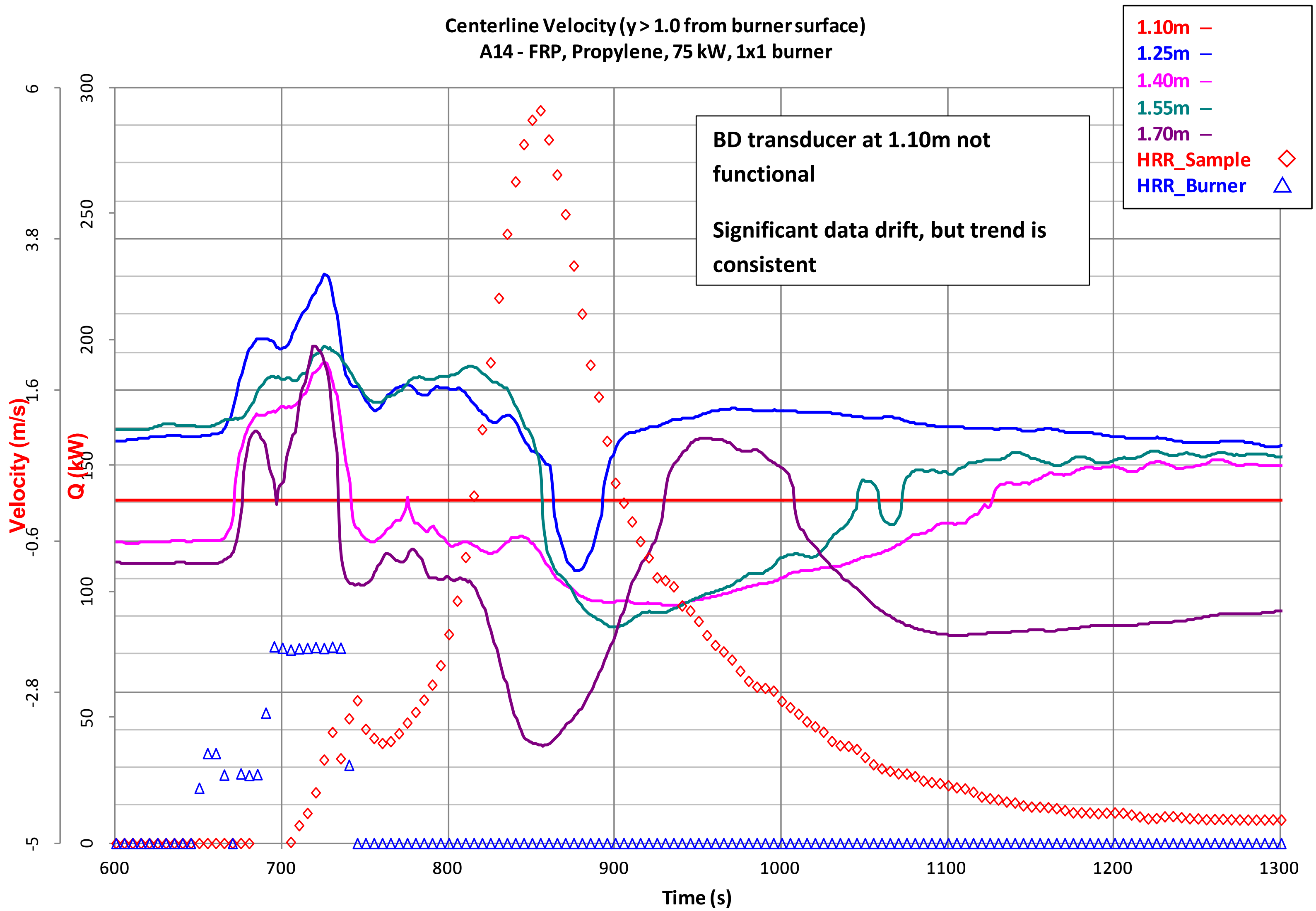

Centerline plume velocities measured from 1.1m to 1.7m above the burner surface

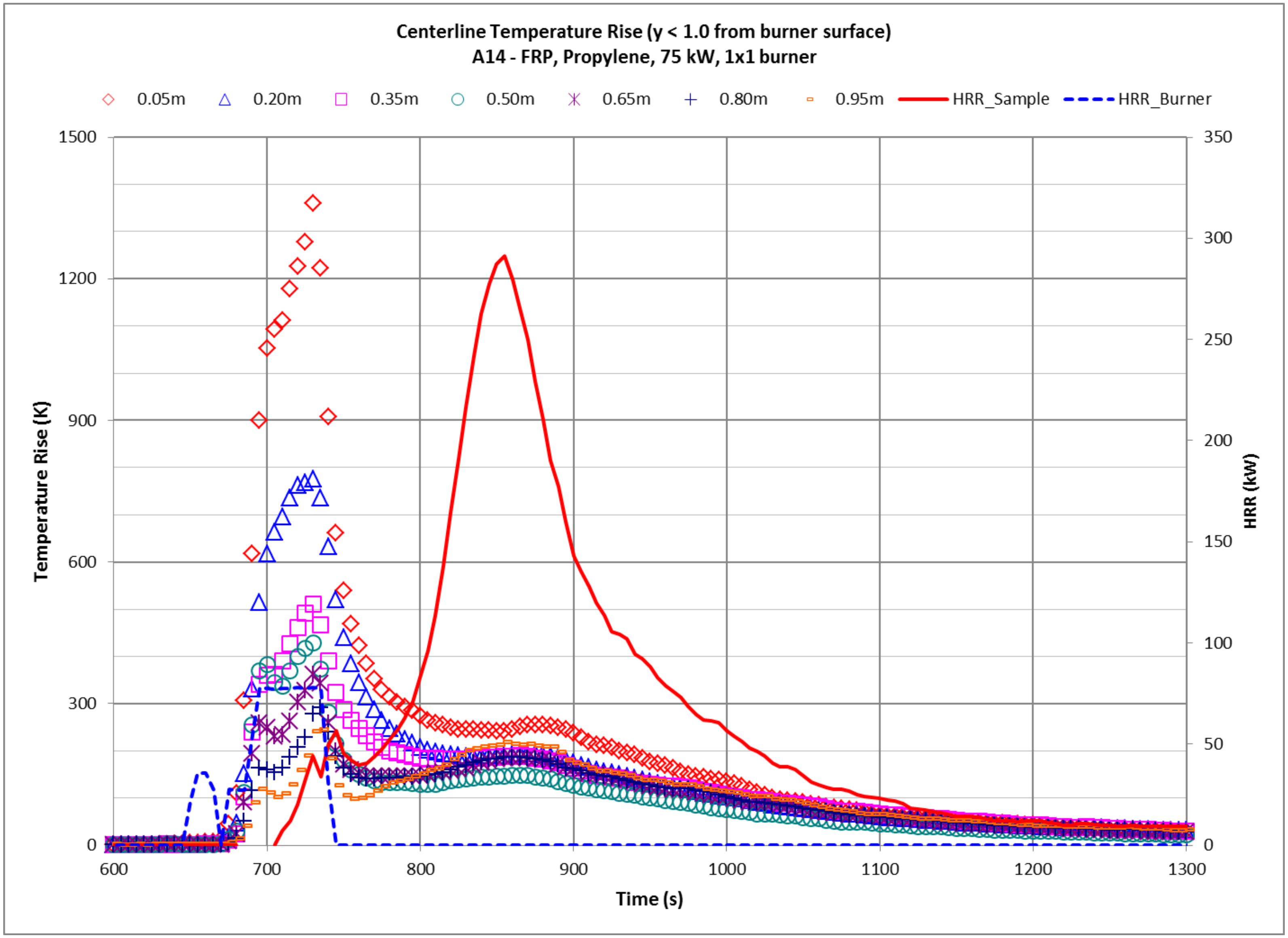

Centerline plume temperature rise measured from 0.05m to 0.95m above the burner surface

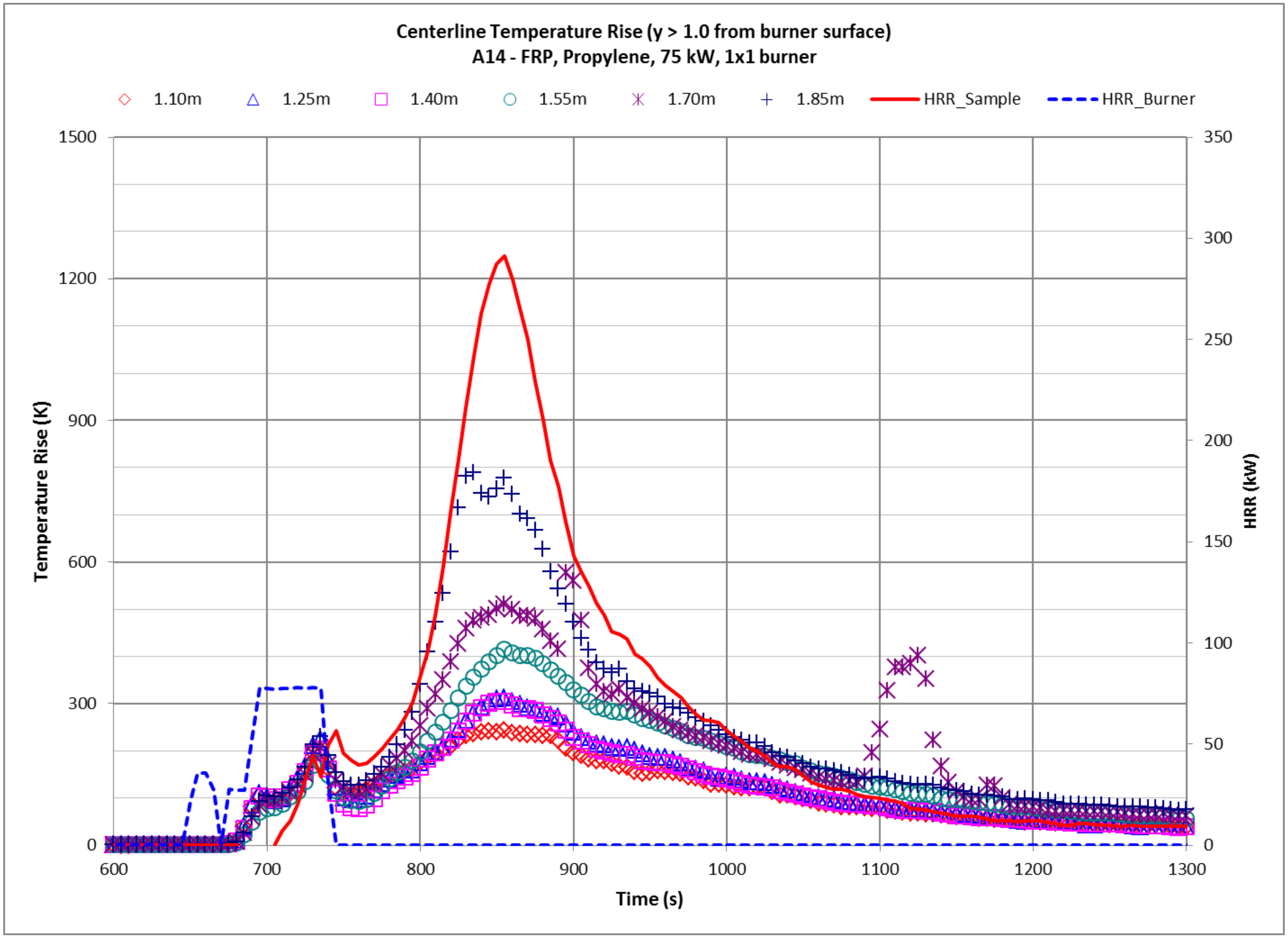

Centerline plume temperature rise measured from 1.10m to 1.85m above the burner surface

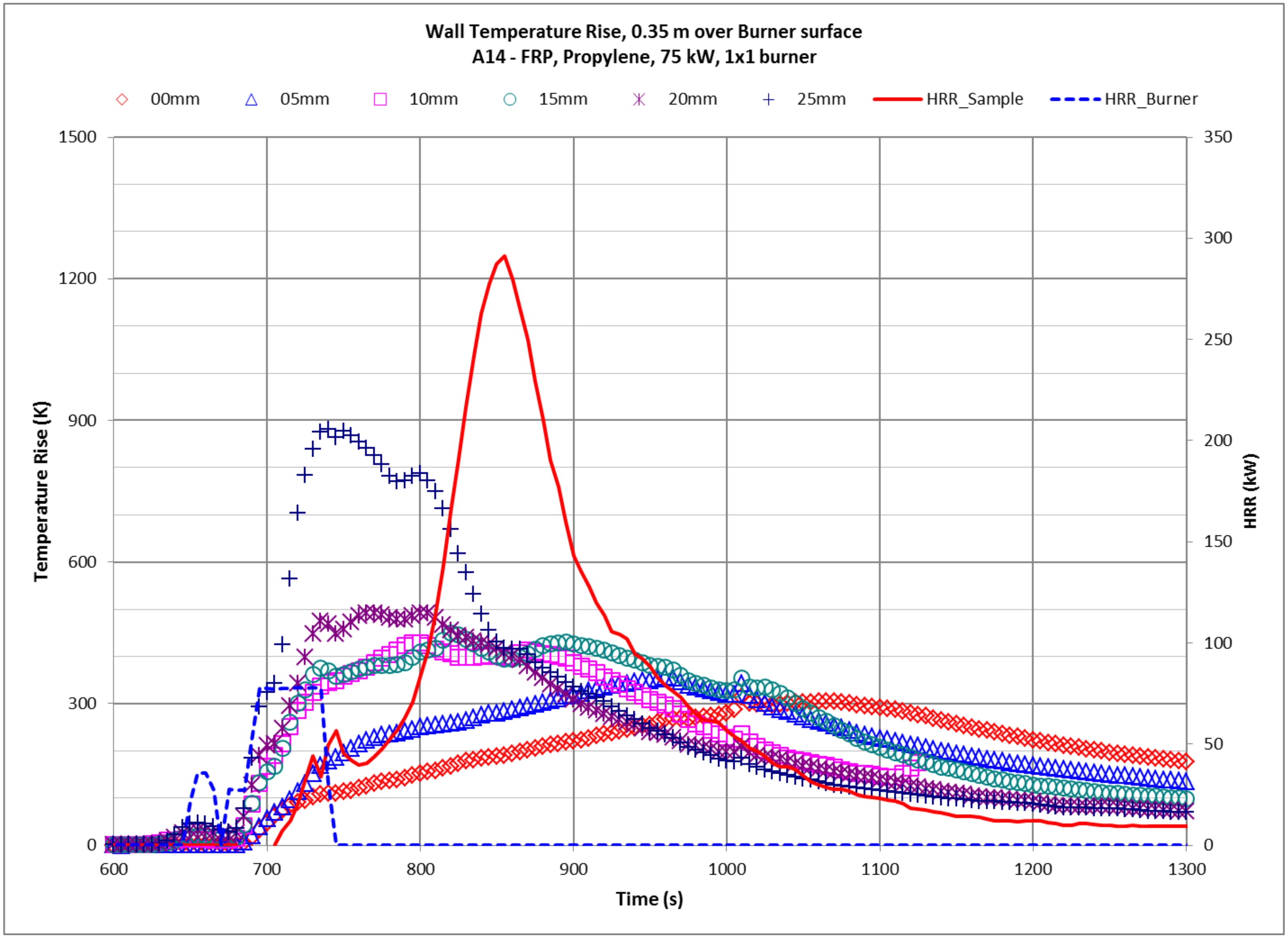

Temperature rise along the wall's centerline at 0.35m over the burner surface, measured at different perpendicular distances to as indicated

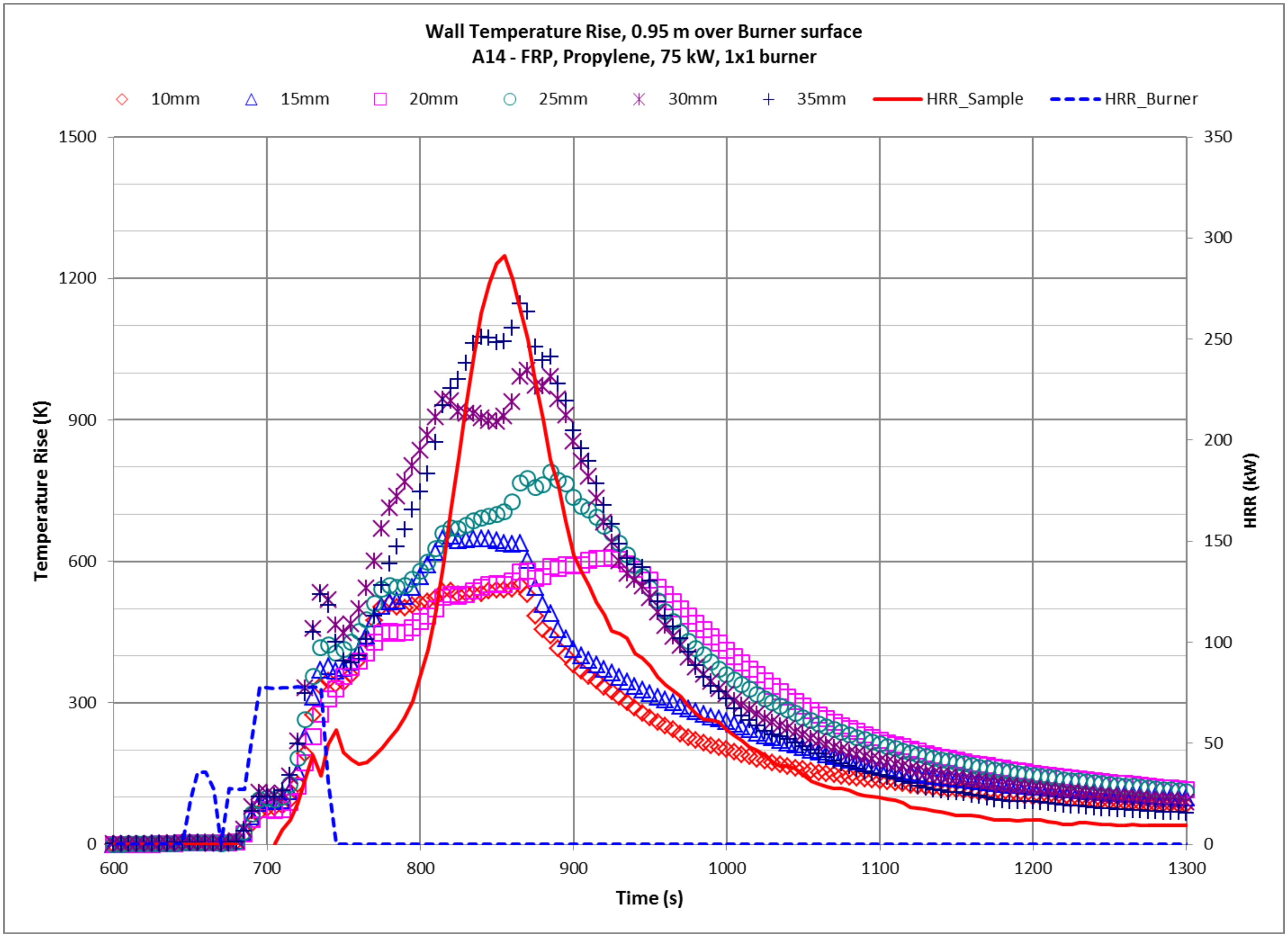

Temperature rise along the wall's centerline at 0.95m over the burner surface, measured at different perpendicular distances to as indicated

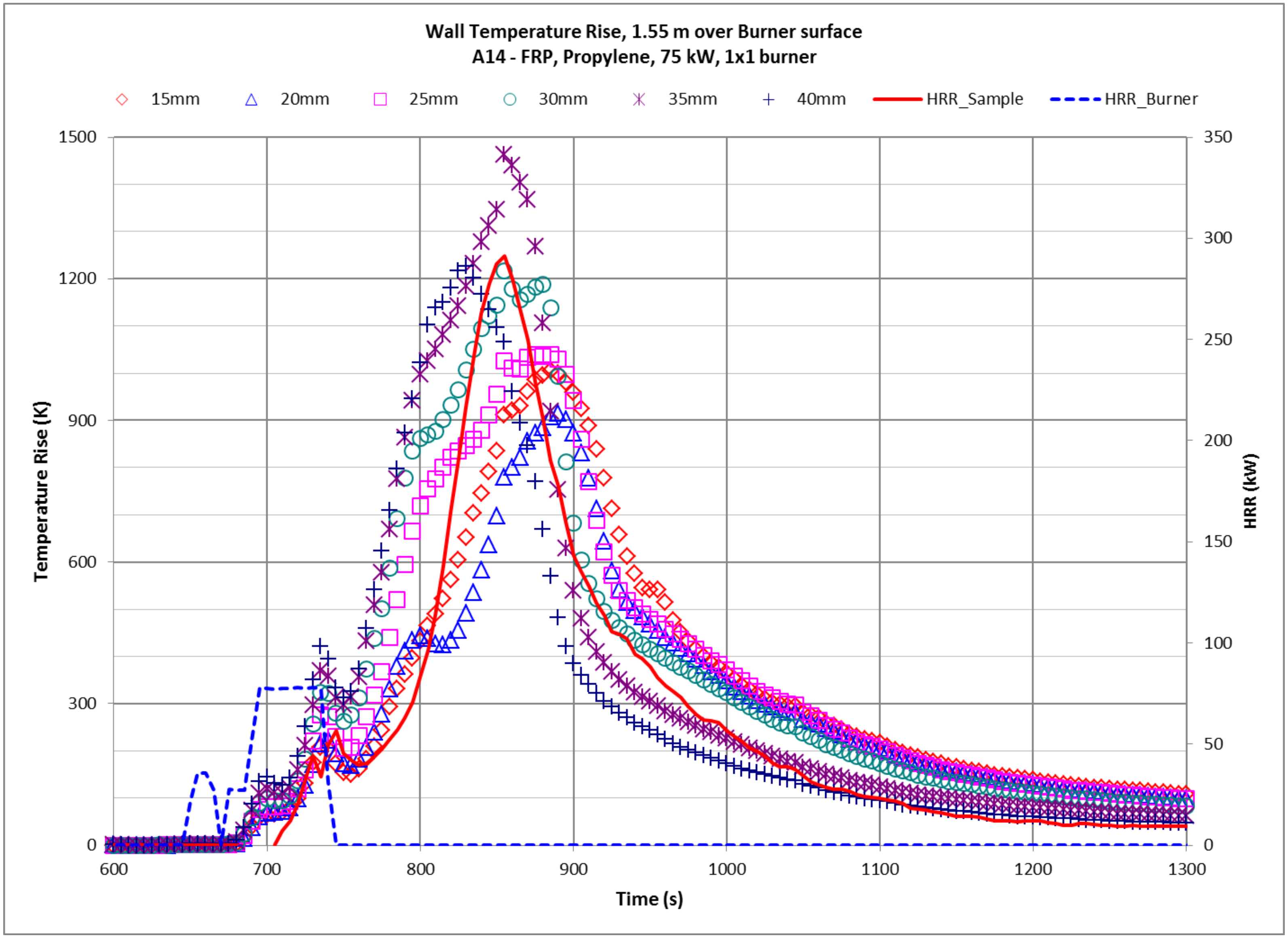

Temperature rise along the wall's centerline at 1.55m over the burner surface, measured at different perpendicular distances to as indicated

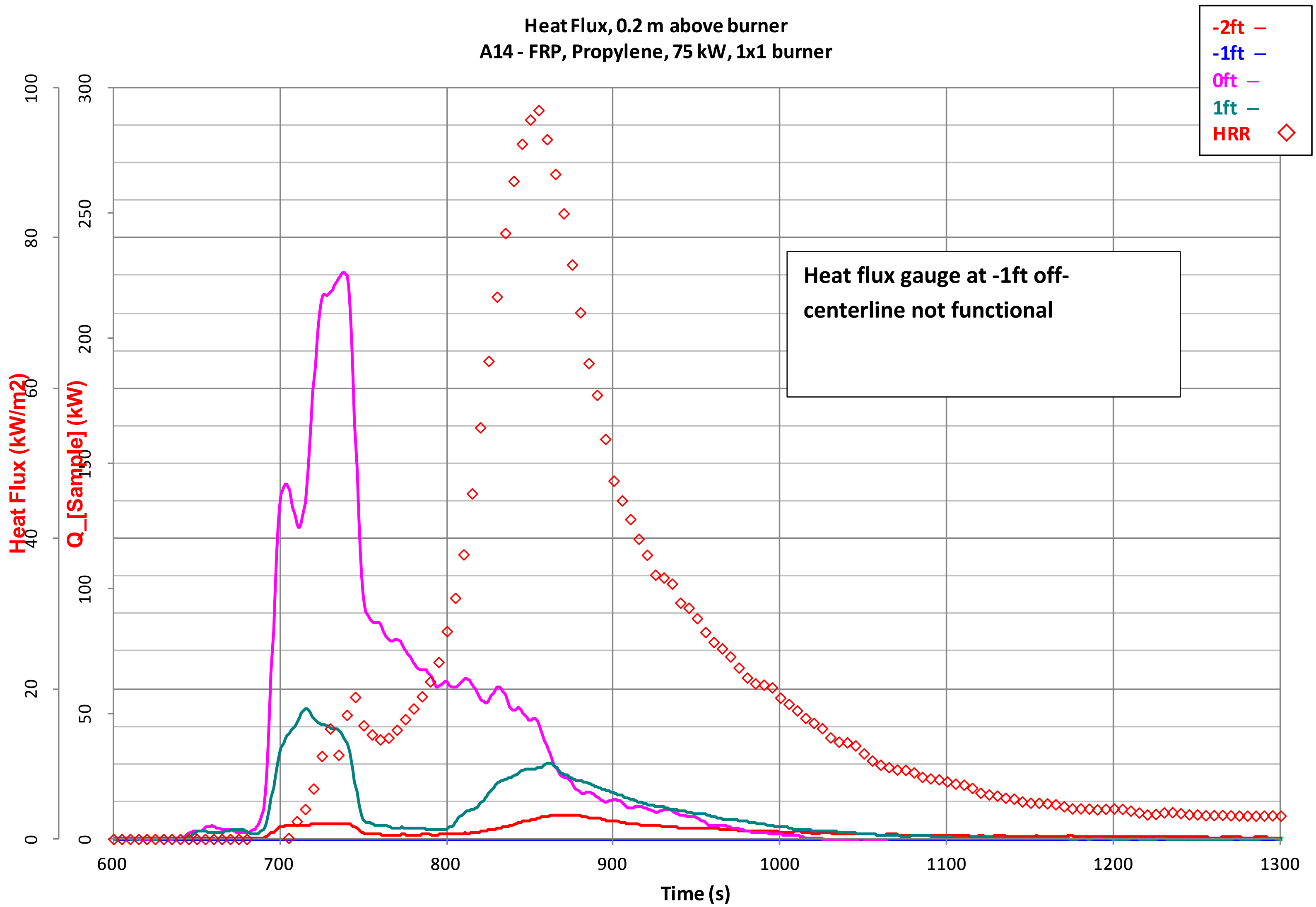

Heat flux measured at various distances from the centerline (negative indicates left of centerline), 0.2m vertically from burner surface

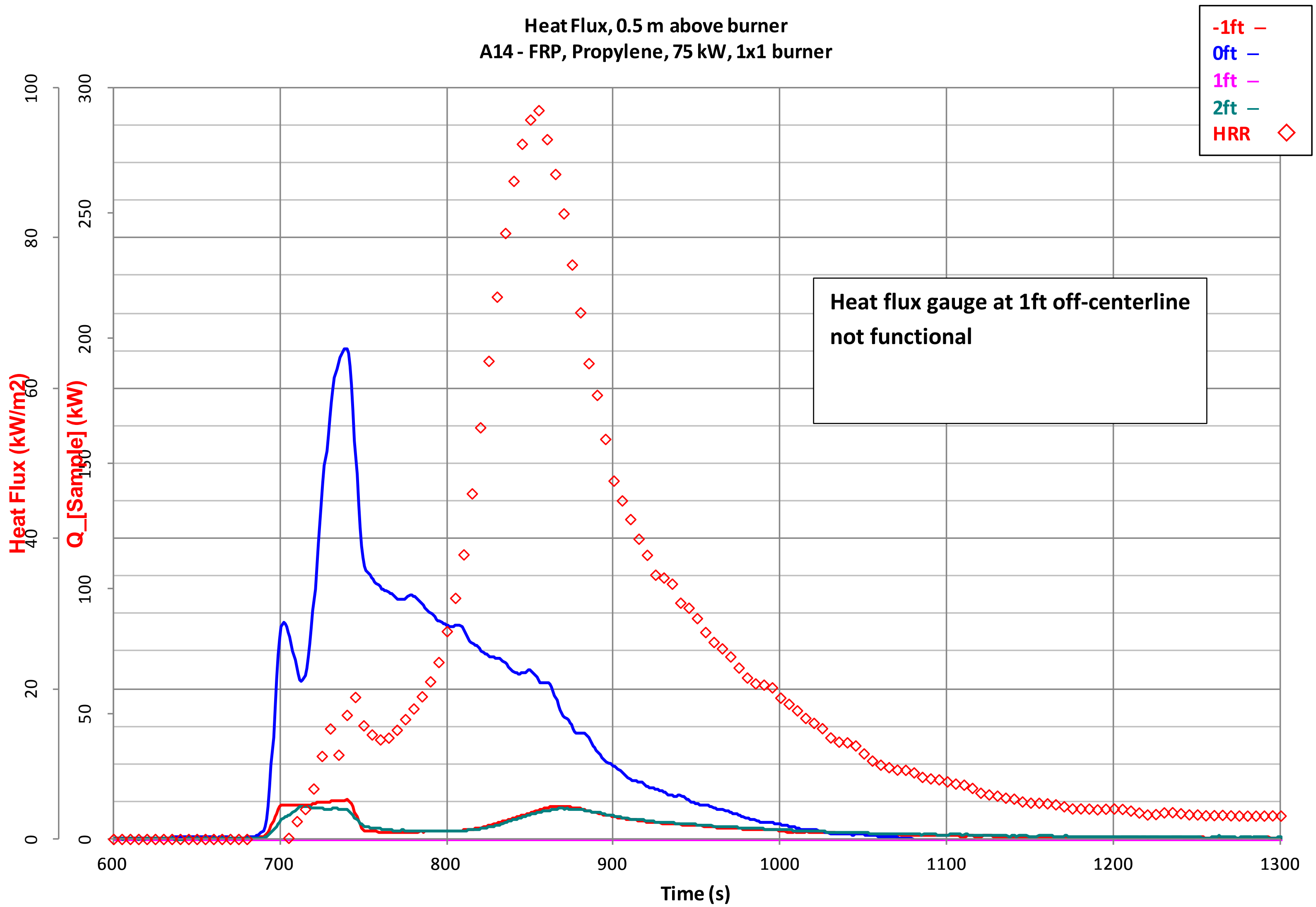

Heat flux measured at various distances from the centerline (negative indicates left of centerline), 0.5m vertically from burner surface

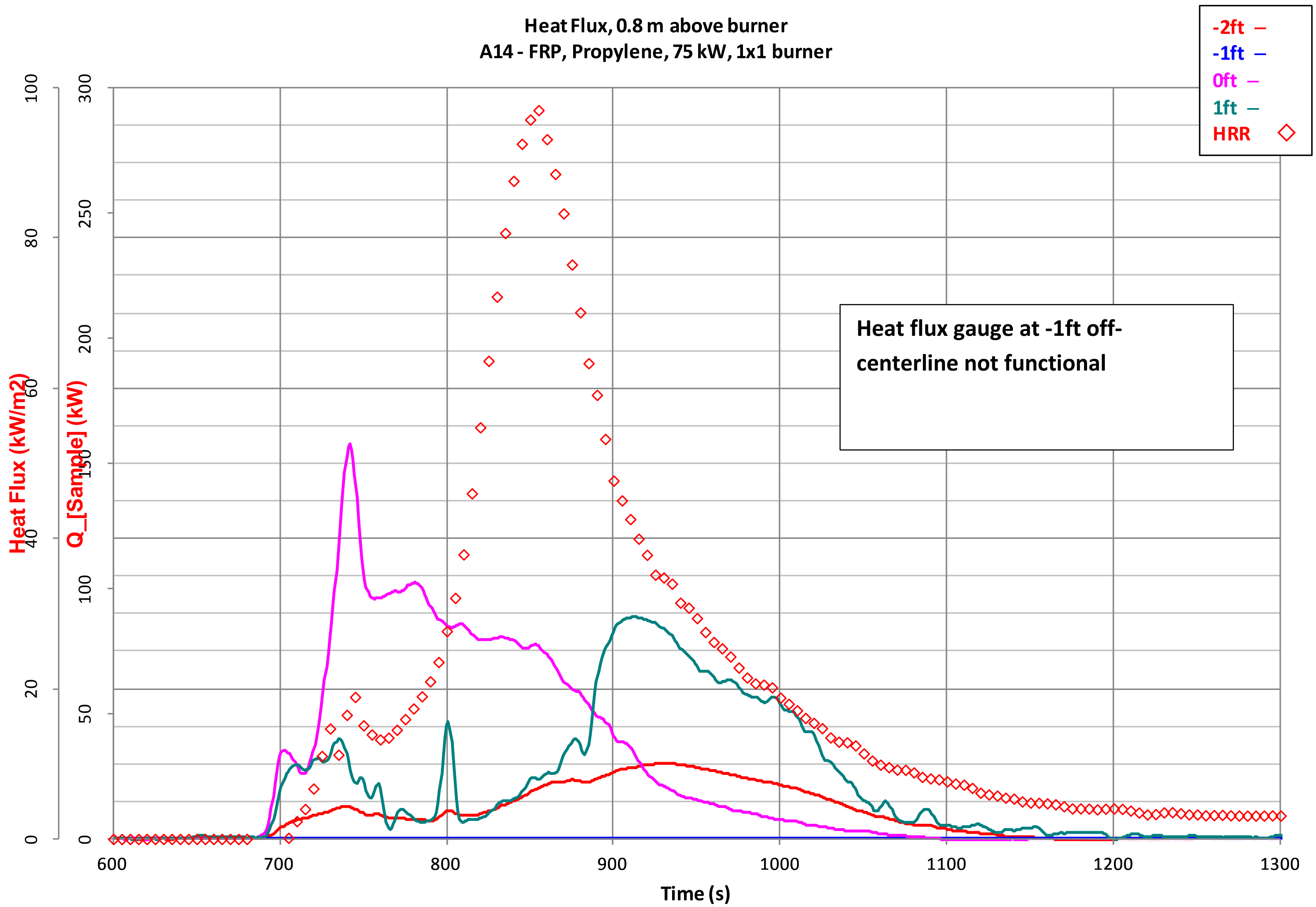

Heat flux measured at various distances from the centerline (negative indicates left of centerline), 0.8m vertically from burner surface

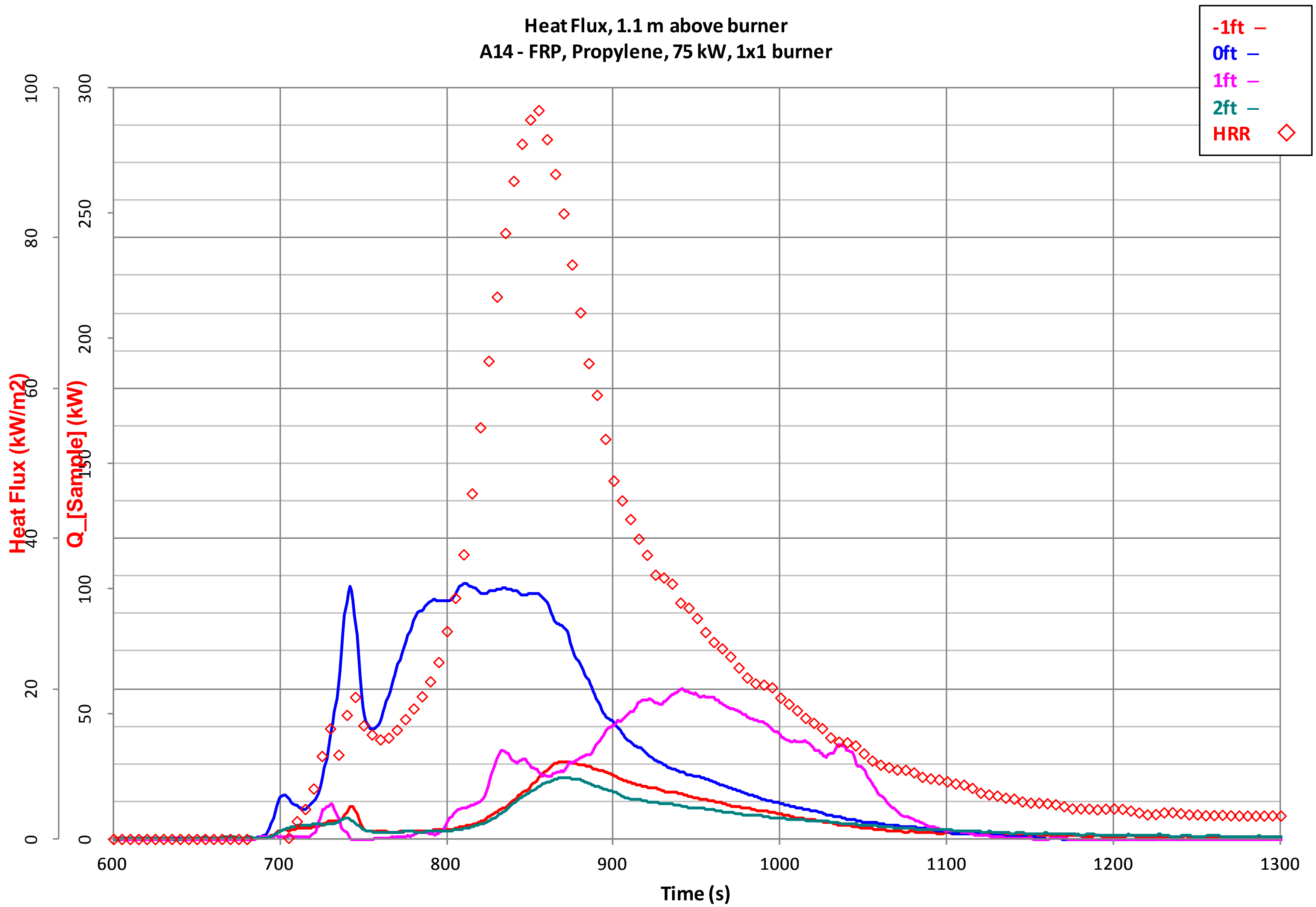

Heat flux measured at various distances from the centerline (negative indicates left of centerline), 1.1m vertically from burner surface

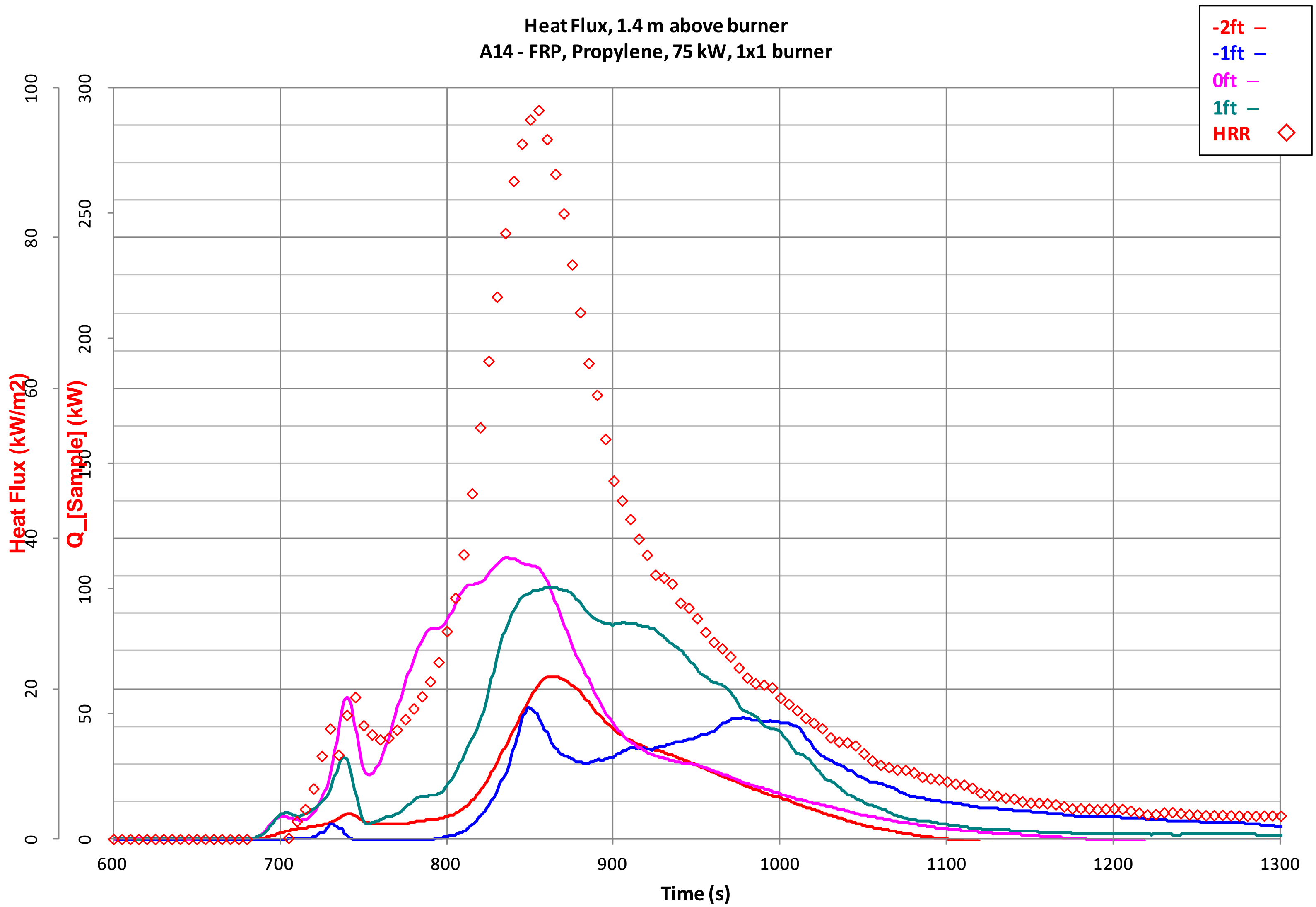

Heat flux measured at various distances from the centerline (negative indicates left of centerline), 1.4m vertically from burner surface

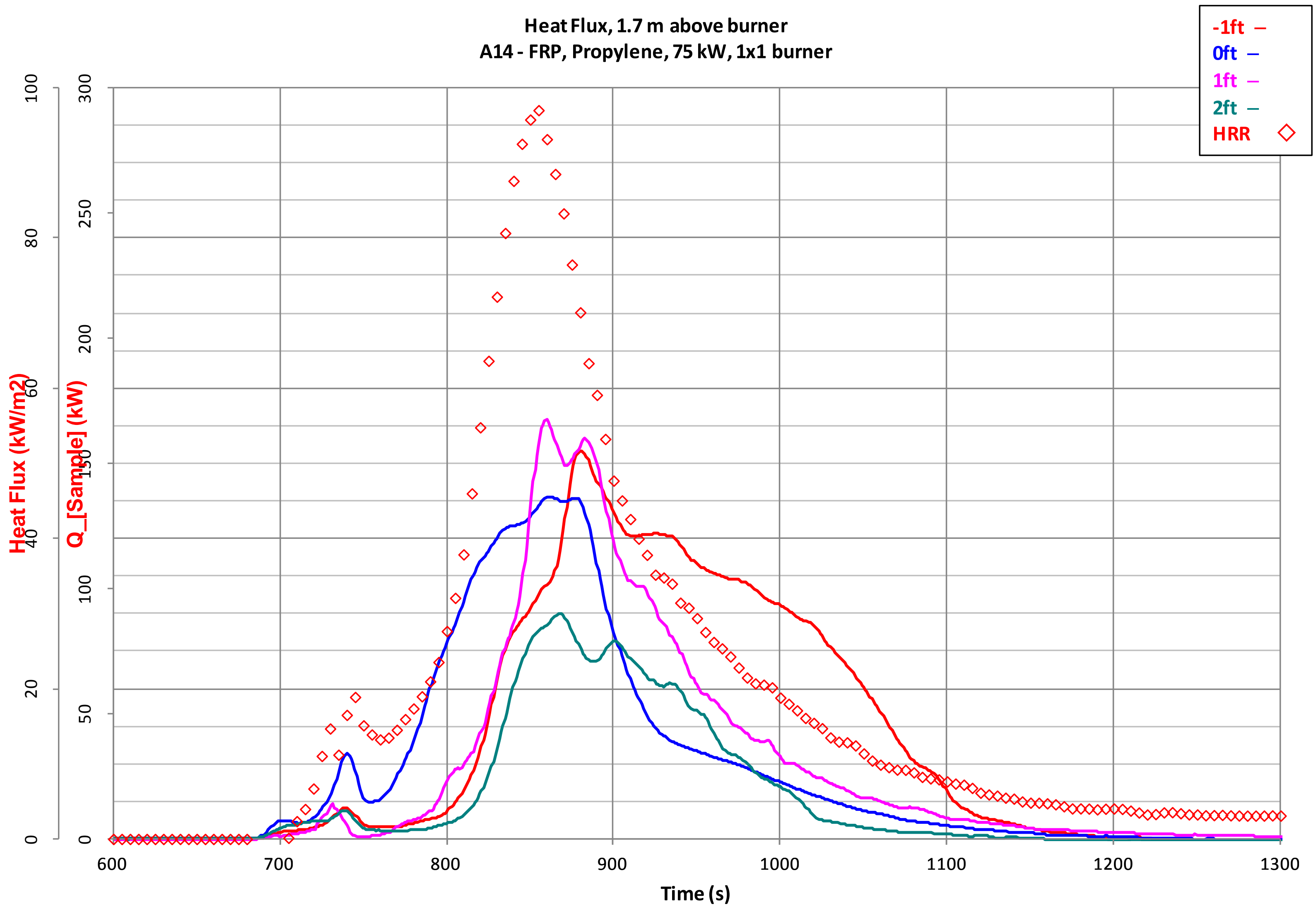

Heat flux measured at various distances from the centerline (negative indicates left of centerline), 1.7m vertically from burner surface

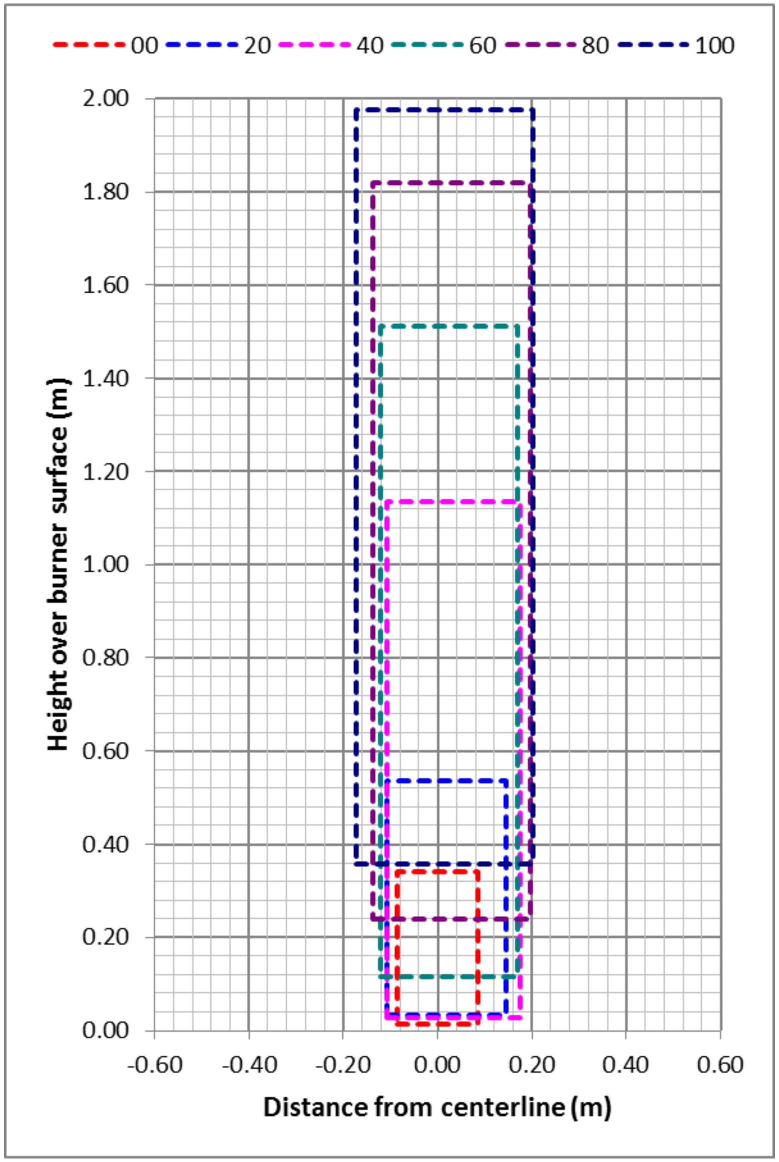

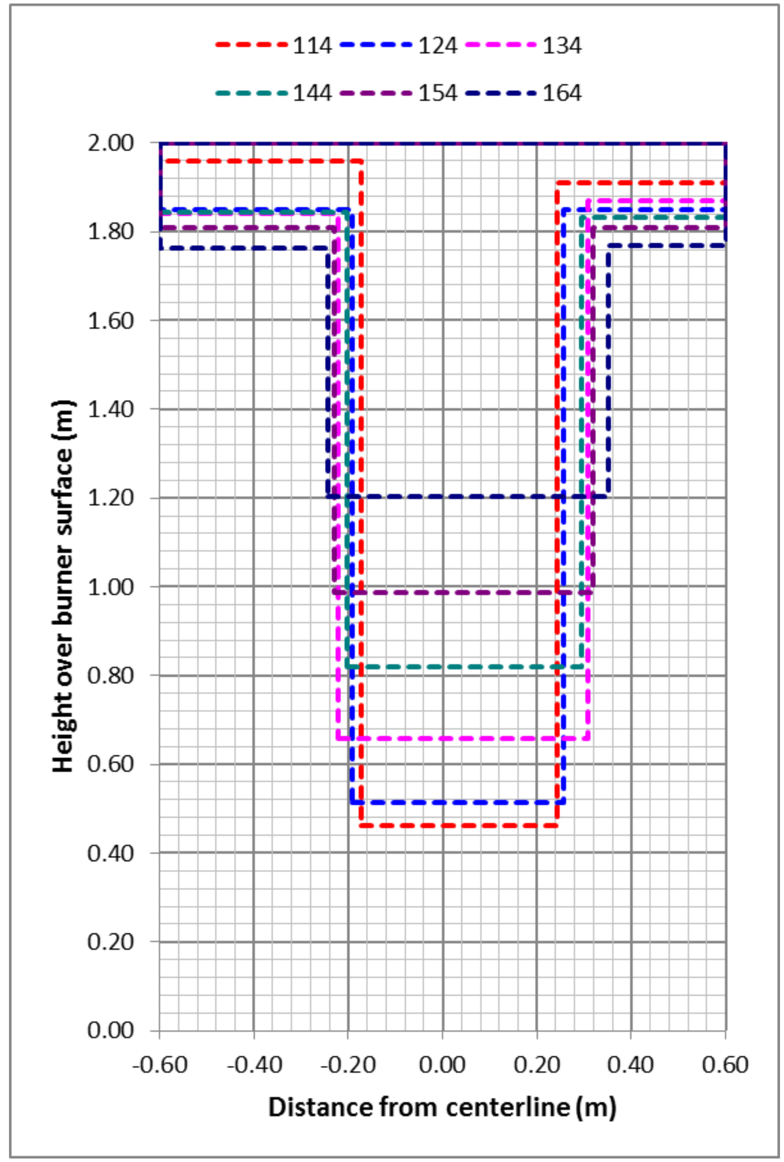

Stages 1 and 2 burning areas in Test A14 (1ft Square burner, Propylene, 75 kW source)

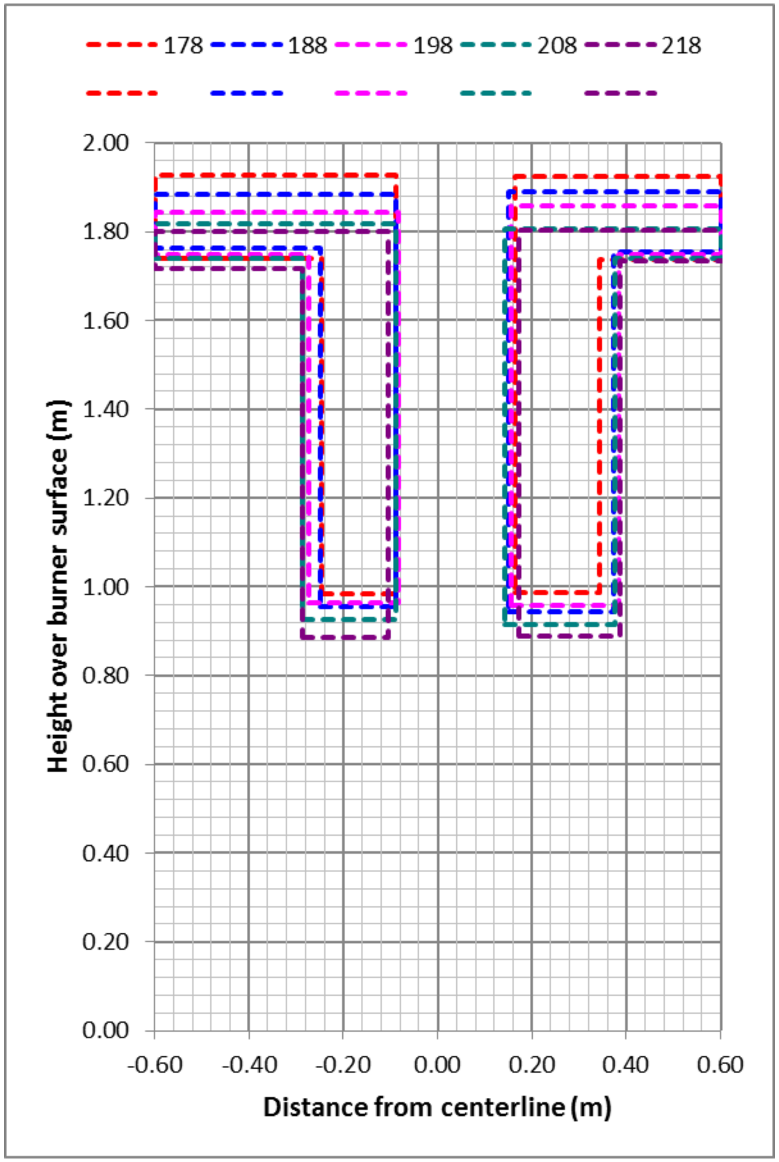

Stage 3 burn area and final damage chart of Test A14 (1ft Square burner, Propylene, 75 kW source)

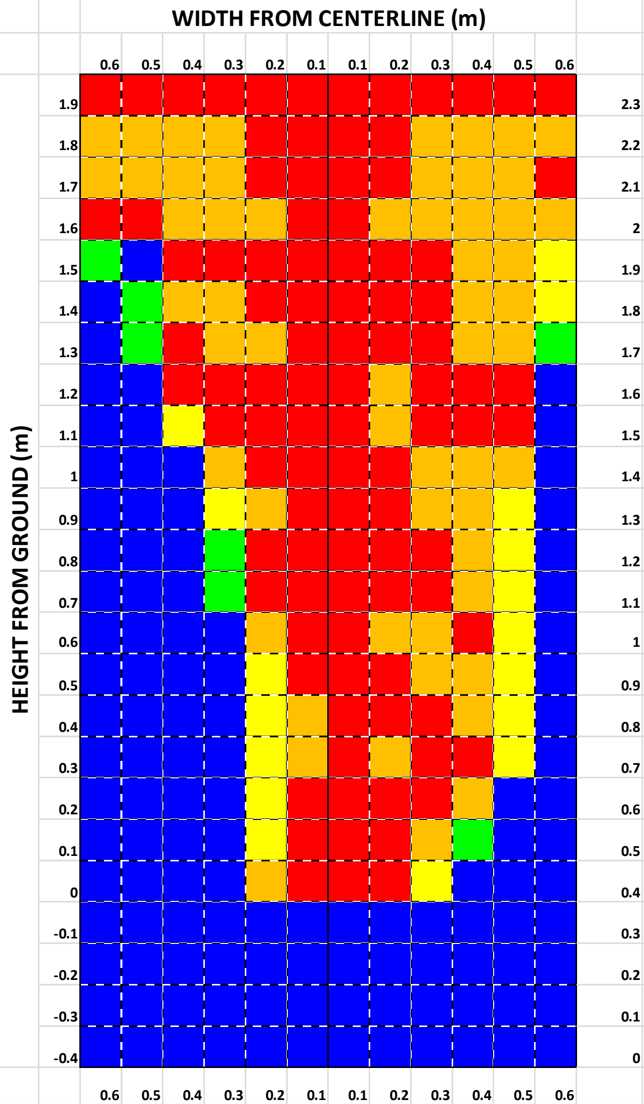

# of cell	Damage to Resin	Area (m2)
96	up to 100% damage	0.96
56	up to 75% damage	0.56
17	up to 50% damage	0.17
7	up to 25% damage	0.07
112	no damage	1.12

Initial mass:	8.5	kg
Final unburnt mass:	4	kg
Final burnt mass:	2.46	kg
Total mass loss during fire	2.04	kg

Burn damage pattern observed after fire test

F.3.15 Test A15

LODS Test Run Data

Center for Firesafety Studies

100 Institute Road
Worcester, MA 01609
Phone: (508) 831-5628
Fax: (508) 831-5680

Test Information

Test Number:	A15
Specimen Identification:	FRP 15, 50 kW initial Propane fire, 1 x 1 burner
Material Name:	Class C FRP panel
Manufacturer/Submitter:	Not Reported
Raw Data File Name:	Test A15 - FRP_Propane_50kW_1ft.txt
Reduced Data File Name:	Test A15 - FRP_Propane_50kW_1ft_reduced.xlsx
Date of Test:	2-Dec-2010
Tester:	W. Wong

Test Parameters

Ambient Temperature:	N/A
Relative Humidity:	N/A

Specimen Information

Specimen Initial Mass:	[kg]	8.5
Specimen Final Mass:	[kg]	6.8
Mass Lost:	[kg]	1.8
Heat Evolved (net):	[kJ]	0

Parameter	Unit	Value
Mass Loss		
Initial Mass	[kg]	8.5
Final Mass	[kg]	6.8
Mass Loss	[%]	20.66

LODS Test Run Data

Center for Firesafety Studies

100 Institute Road
Worcester, MA 01609
Phone: (508) 831-5628
Fax: (508) 831-5680

Test Notes

Test Number:	0
Date:	12/02/10
Material:	Class C FRP panel
Specimen Identification:	FRP 15, 50 kW initial Propane fire, 1 x 1 burner

Observations

Time	Observation
00:00	Start VI
05:30	Start Camera 1
09:45	Start Camera 2
13:19	Burner ignition
13:35	Reach target HRR @ 50 kW
14:05	Crackling noise
14:28	Panel ignition, mainly at area under TSC-2 to above burner
14:50	Burner off
15:30	Remote area smoking @ HFG-2 and on right edge @ y = 0.5 m
15:55	Flame hit ceiling
16:00	T-pattern starts
16:25	Burning hit edges
16:35	Rollover, flame layer about 50 cm thick under ceiling
17:50	Remote area ignition @ HFG-5, insignificant
28:00	Burner was on for 10 sec, human error, did not affect wall burning
32:00	Test terminated with little water application

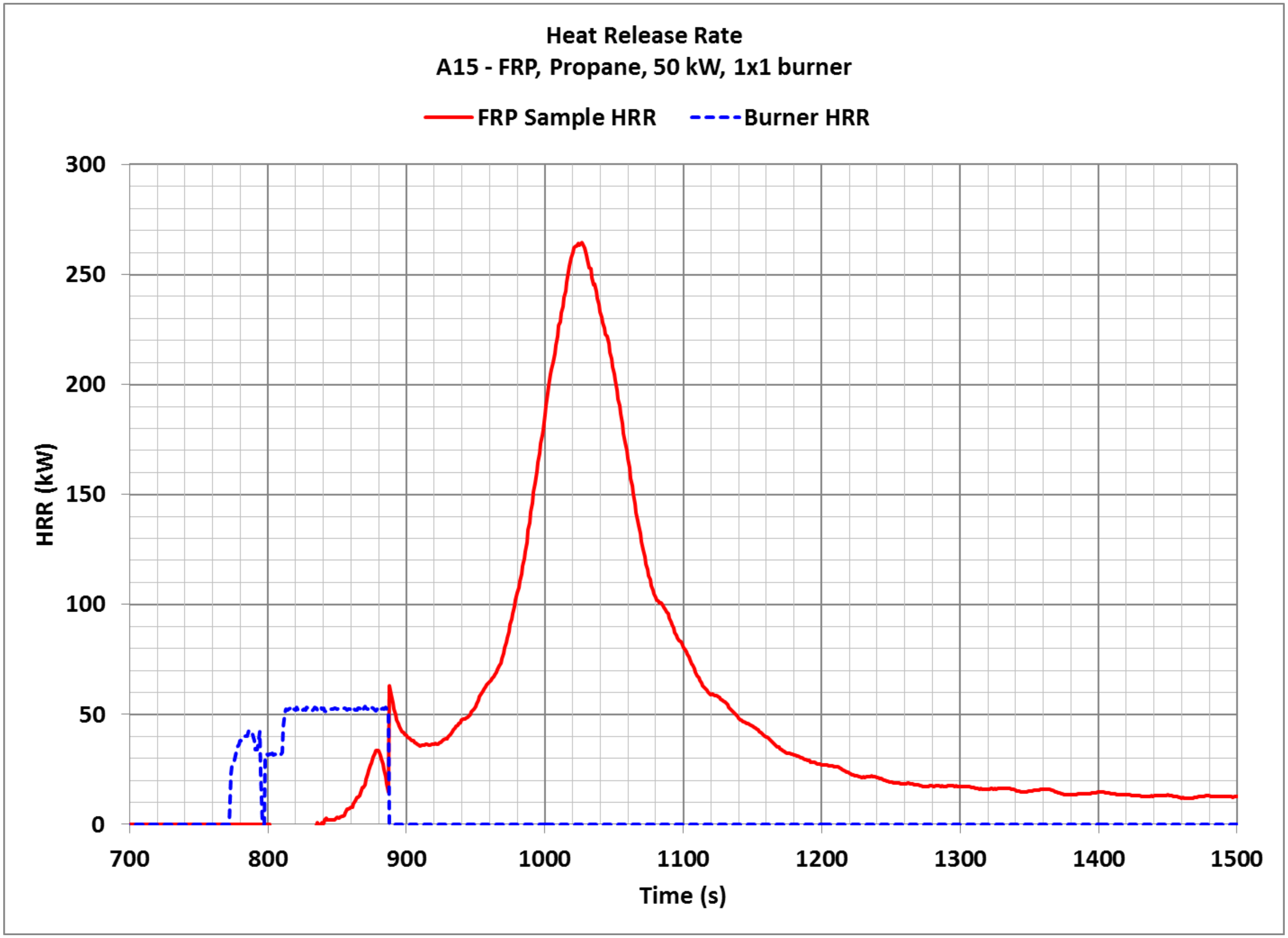

Heat release ratesof the source burner fire and of the specimen fire measured during test

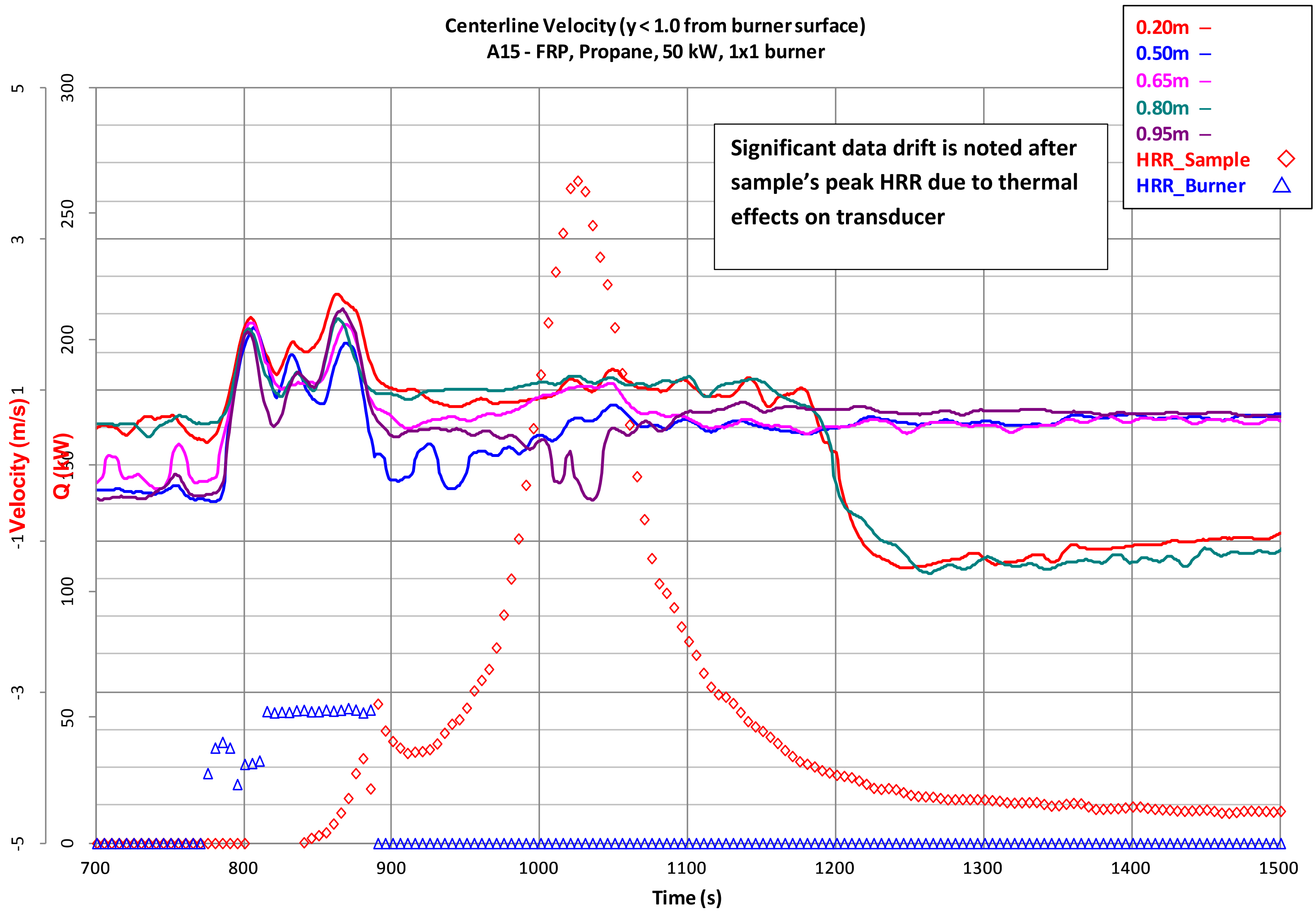

Centerline plume velocities measured from 0.2m to 0.95m above the burner surface

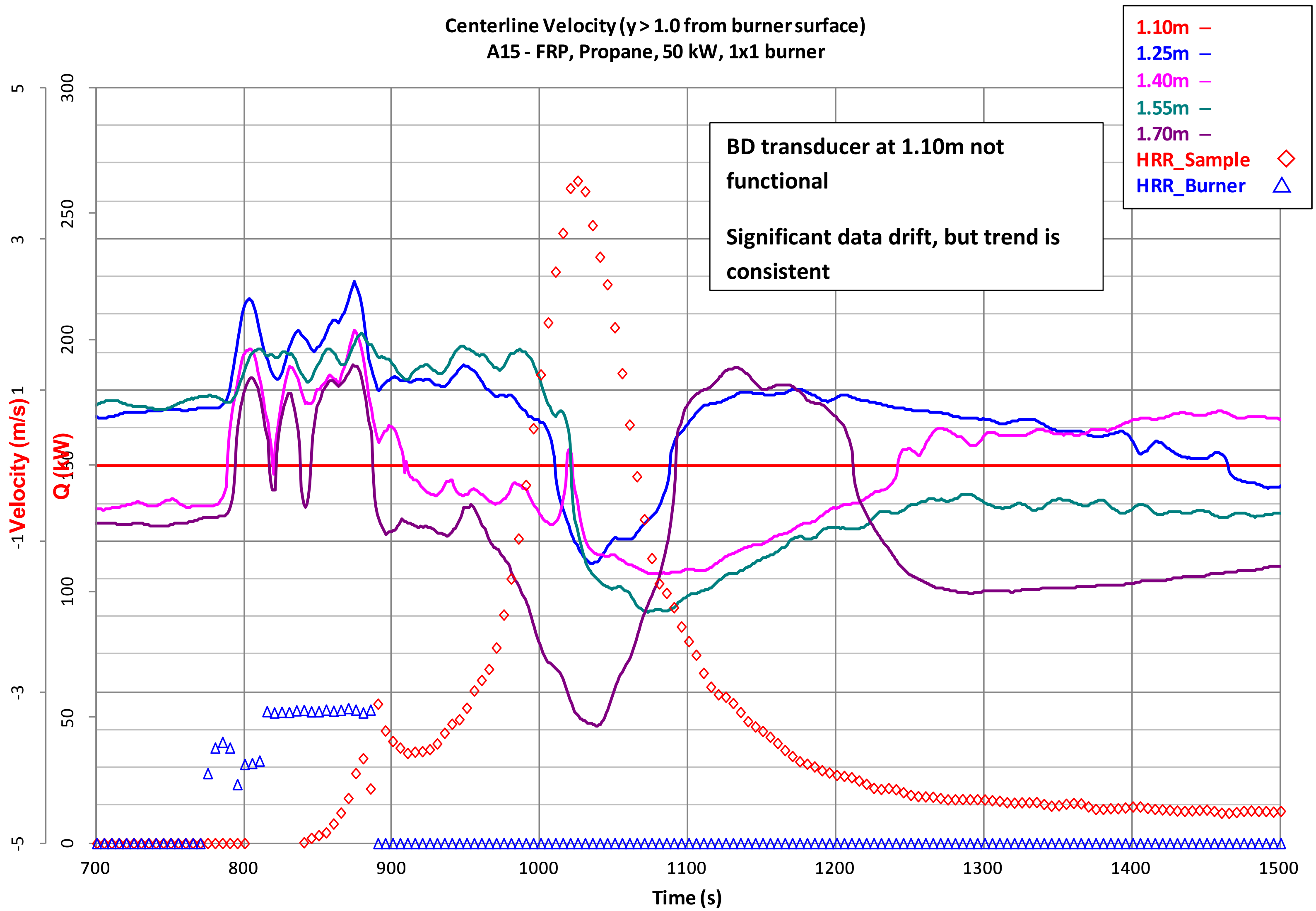

Centerline plume velocities measured from 1.1m to 1.7m above the burner surface

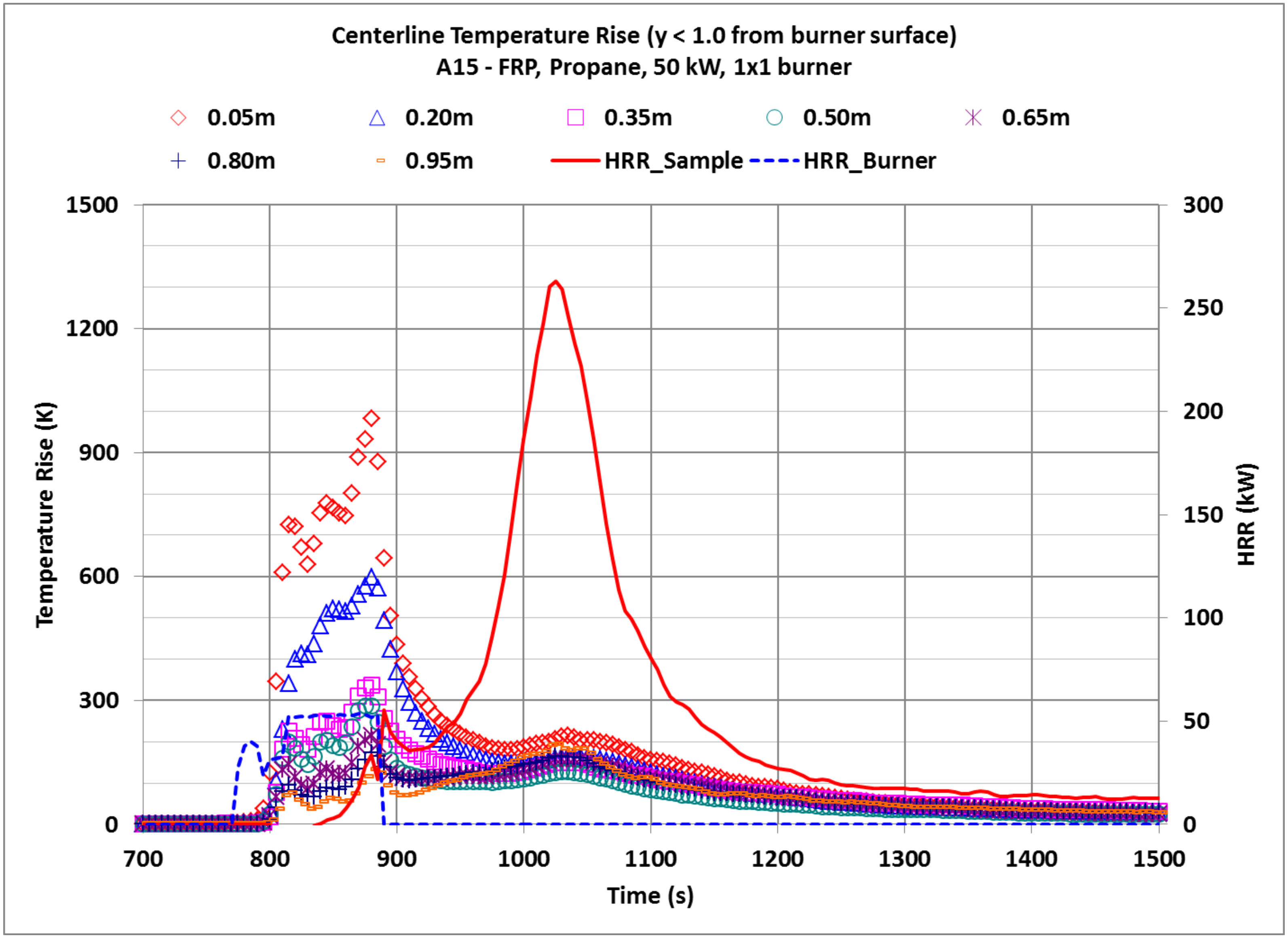

Centerline plume temperature rise measured from 0.05m to 0.95m above the burner surface

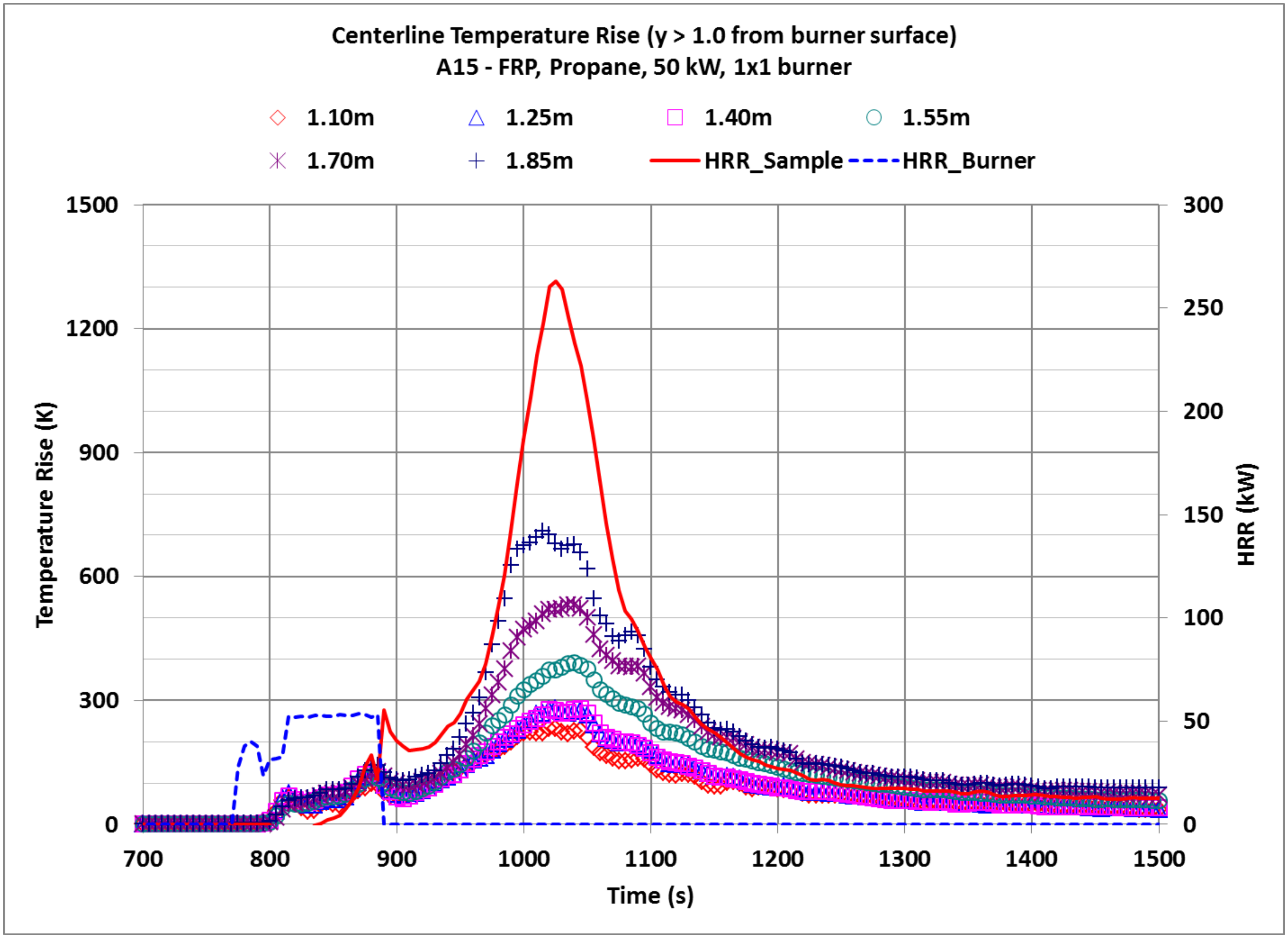

Centerline plume temperature rise measured from 1.10m to 1.85m above the burner surface

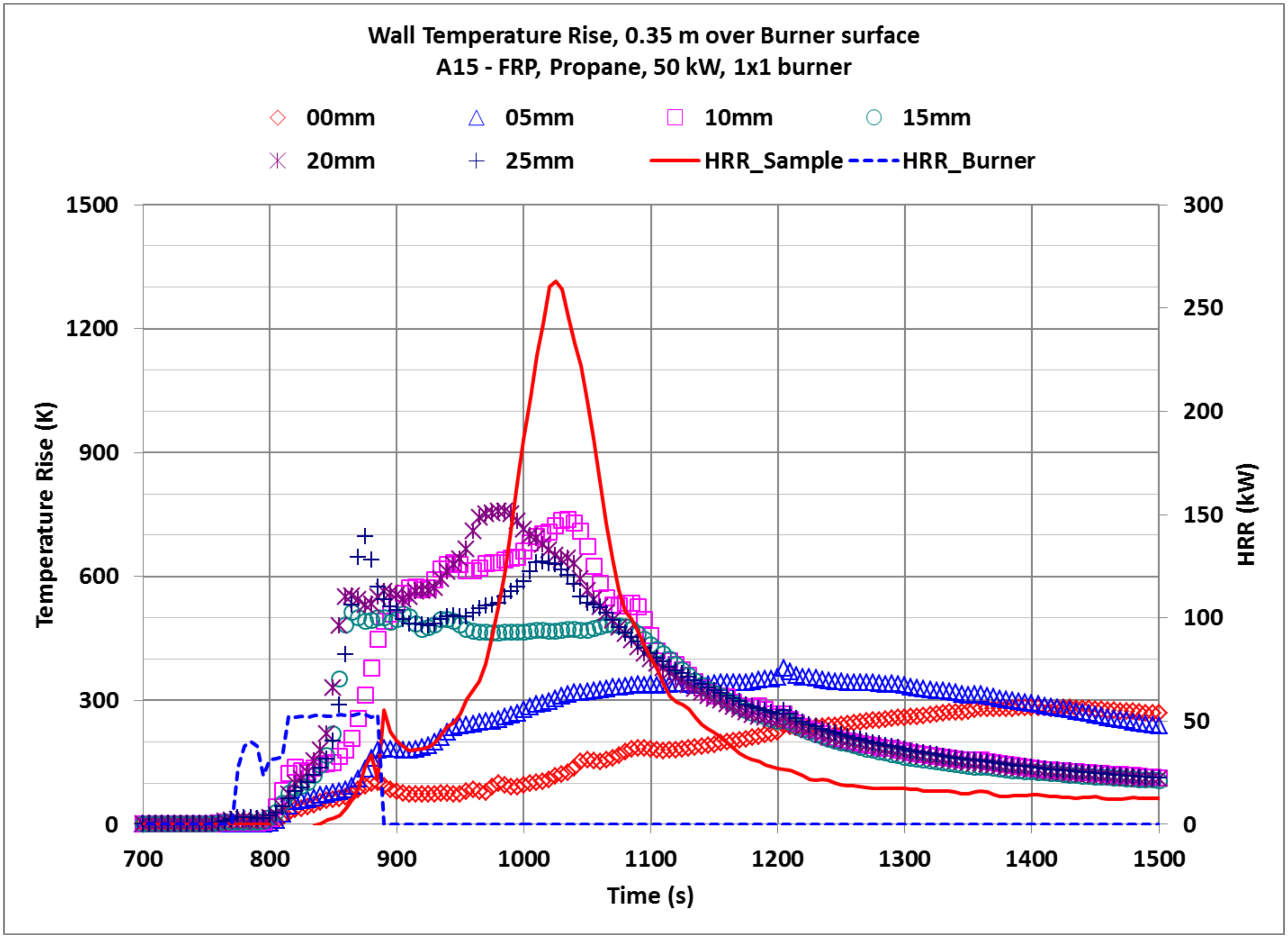

Temperature rise along the wall's centerline at 0.35m over the burner surface, measured at different perpendicular distances to as indicated

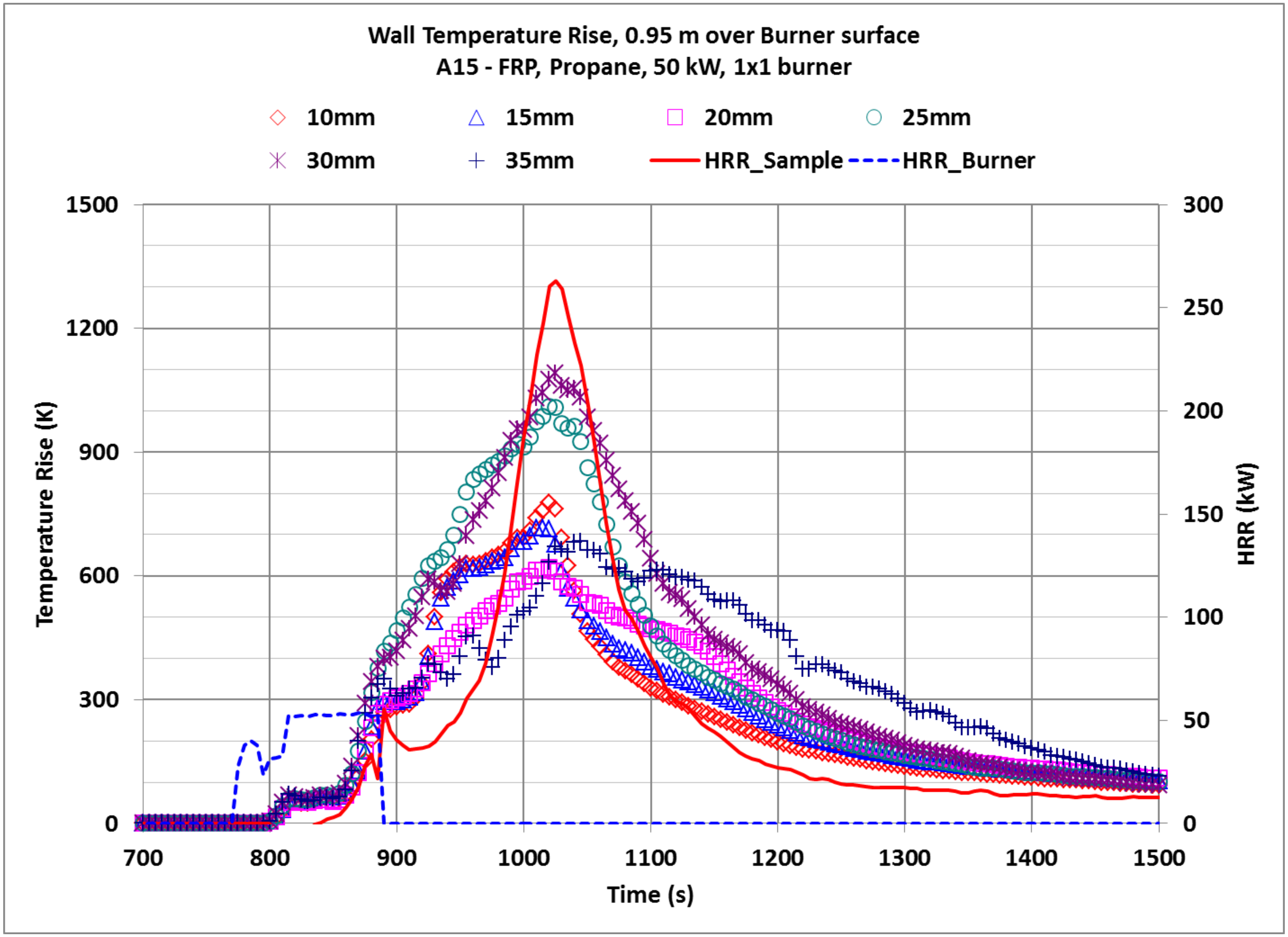

Temperature rise along the wall's centerline at 0.95m over the burner surface, measured at different perpendicular distances to as indicated

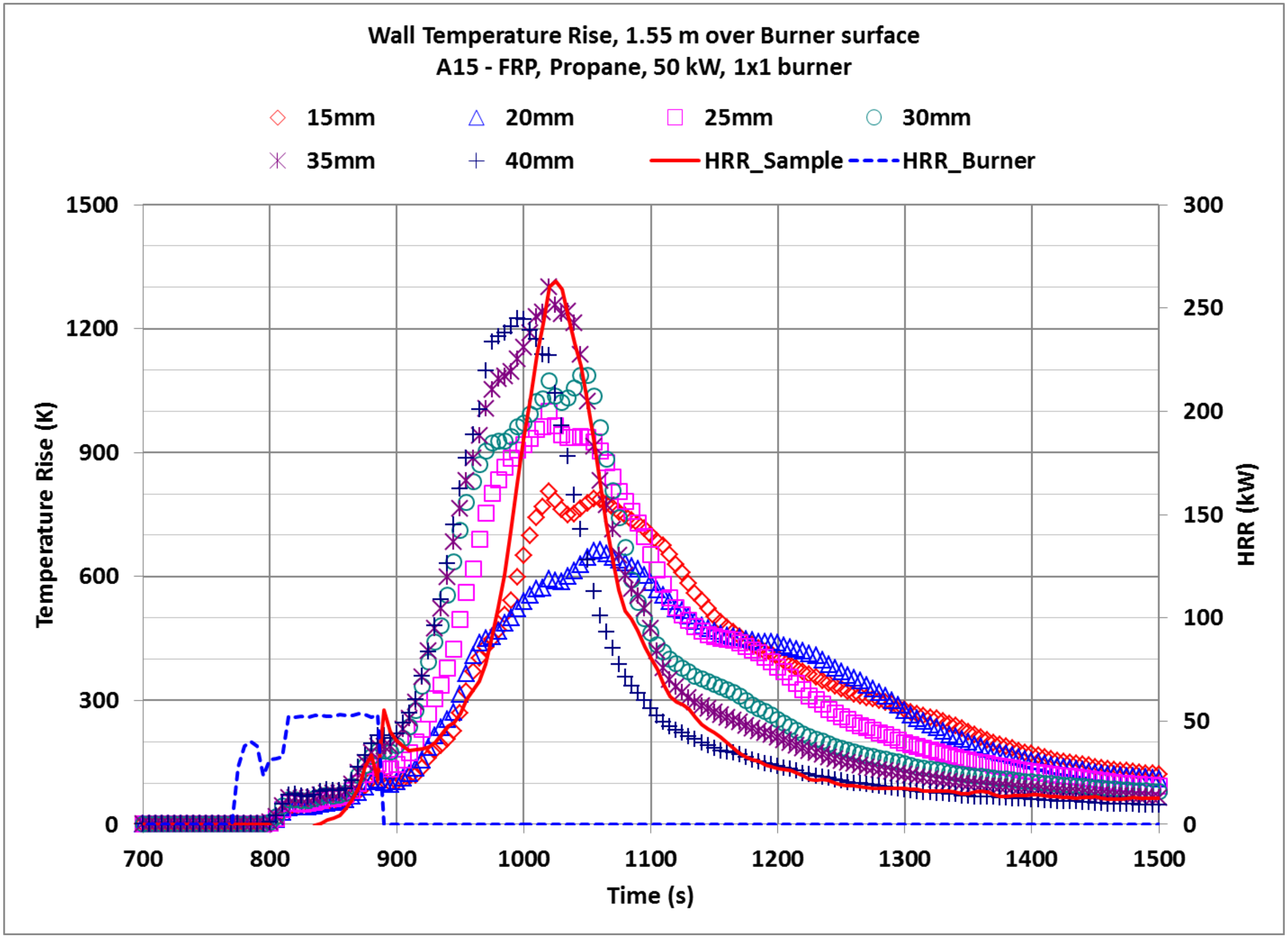

Temperature rise along the wall's centerline at 1.55m over the burner surface, measured at different perpendicular distances to as indicated

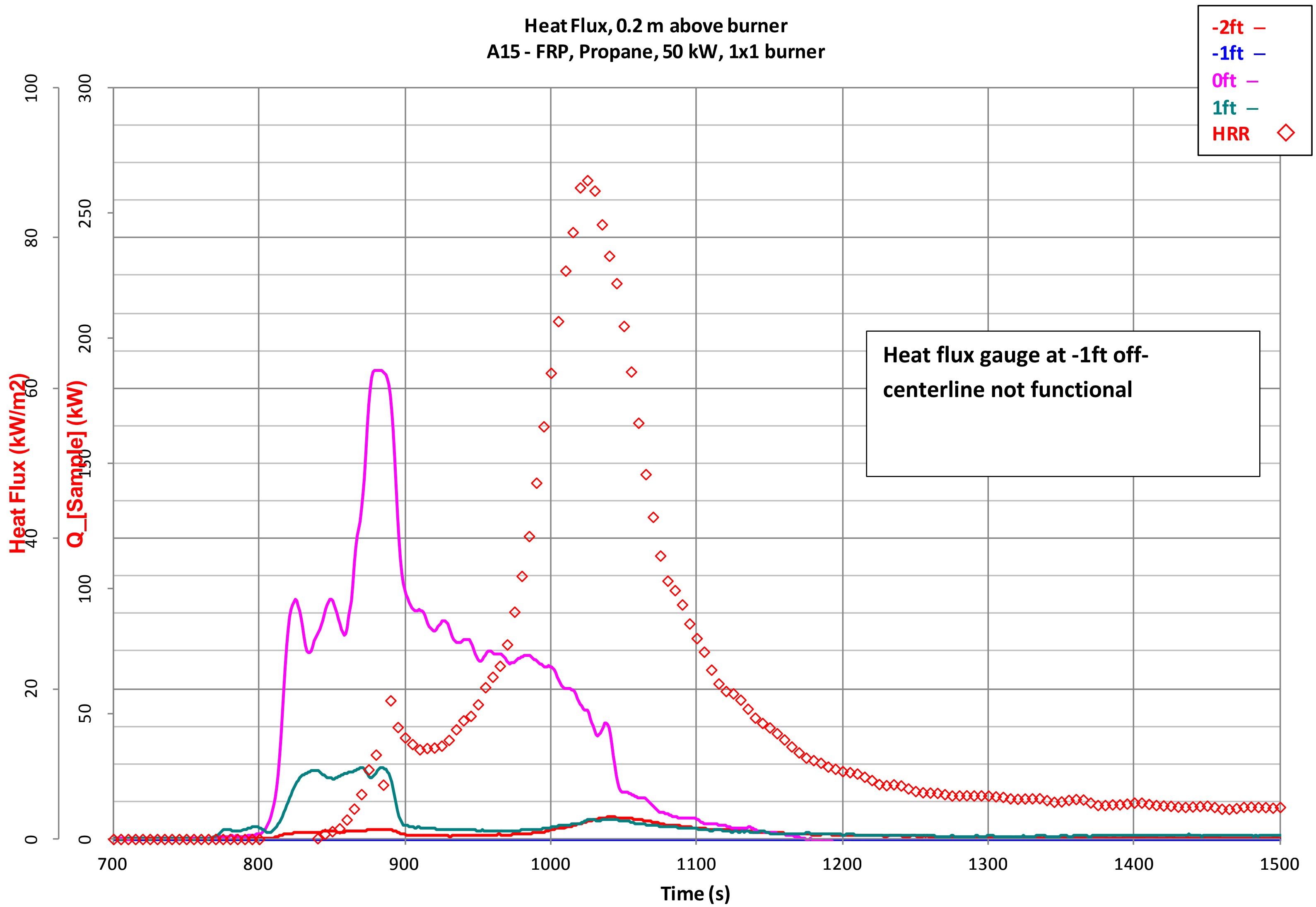

Heat flux measured at various distances from the centerline (negative indicates left of centerline), 0.2m vertically from burner surface

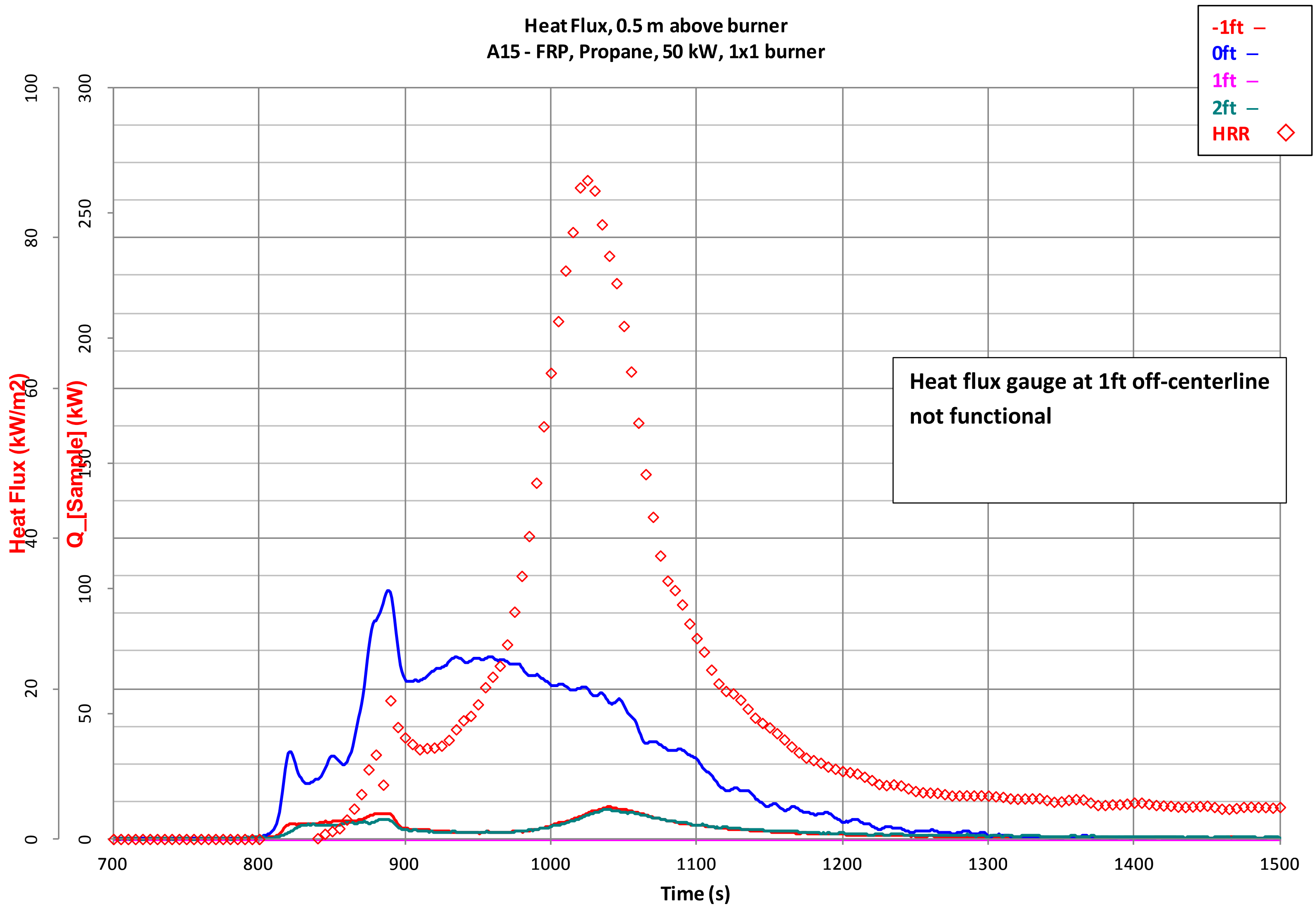

Heat flux measured at various distances from the centerline (negative indicates left of centerline), 0.5m vertically from burner surface

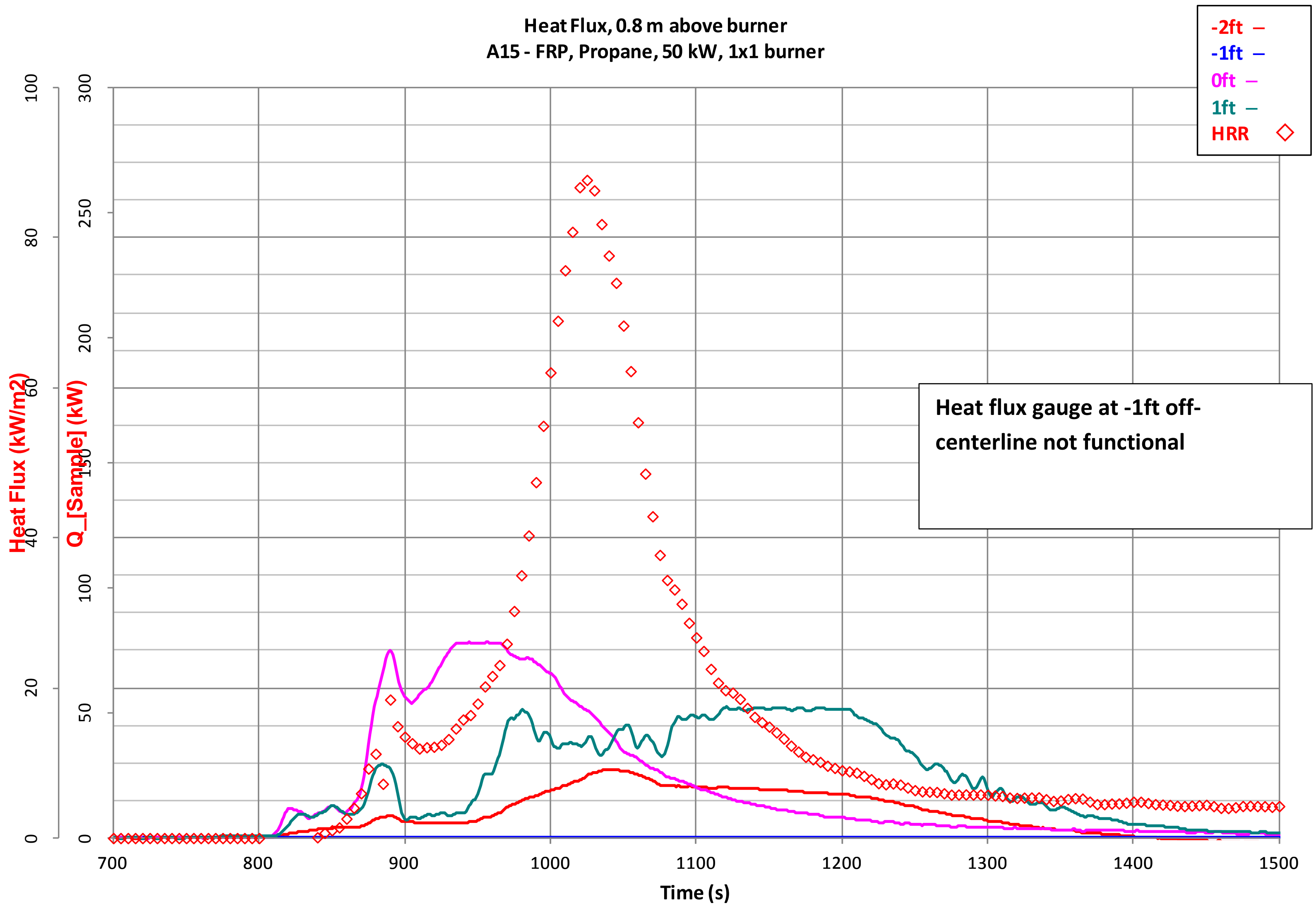

Heat flux measured at various distances from the centerline (negative indicates left of centerline), 0.8m vertically from burner surface

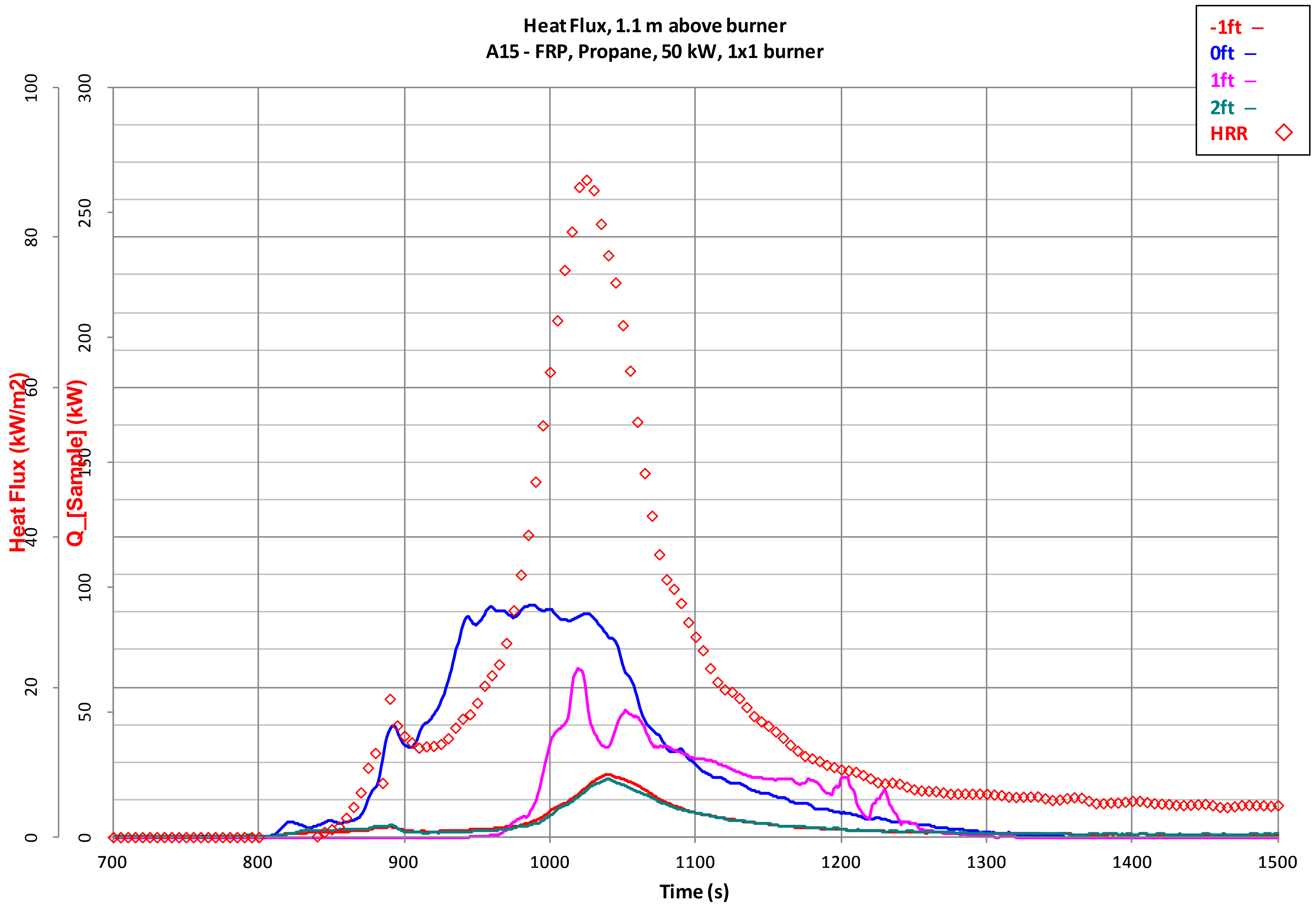

Heat flux measured at various distances from the centerline (negative indicates left of centerline), 1.1m vertically from burner surface

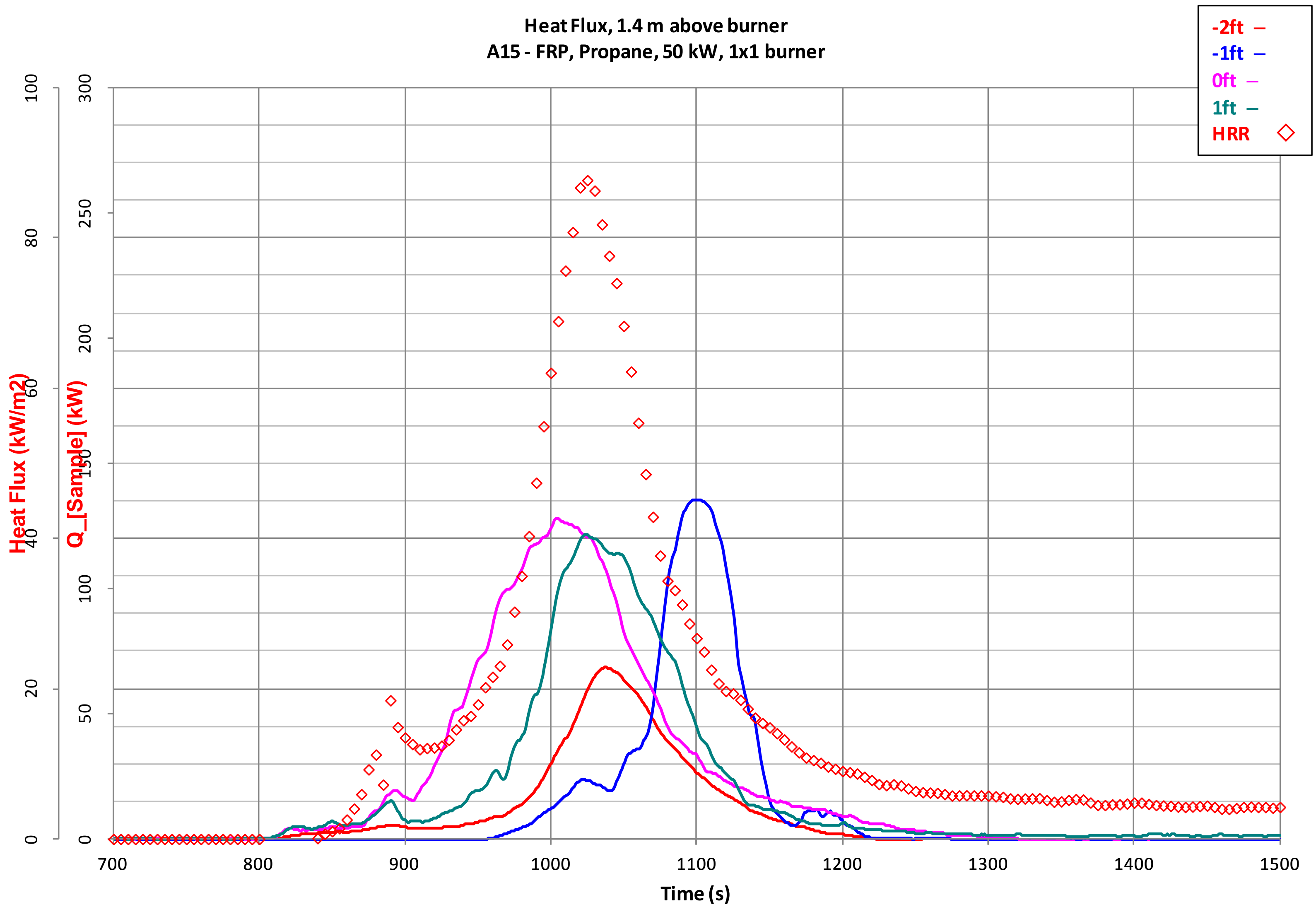

Heat flux measured at various distances from the centerline (negative indicates left of centerline), 1.4m vertically from burner surface

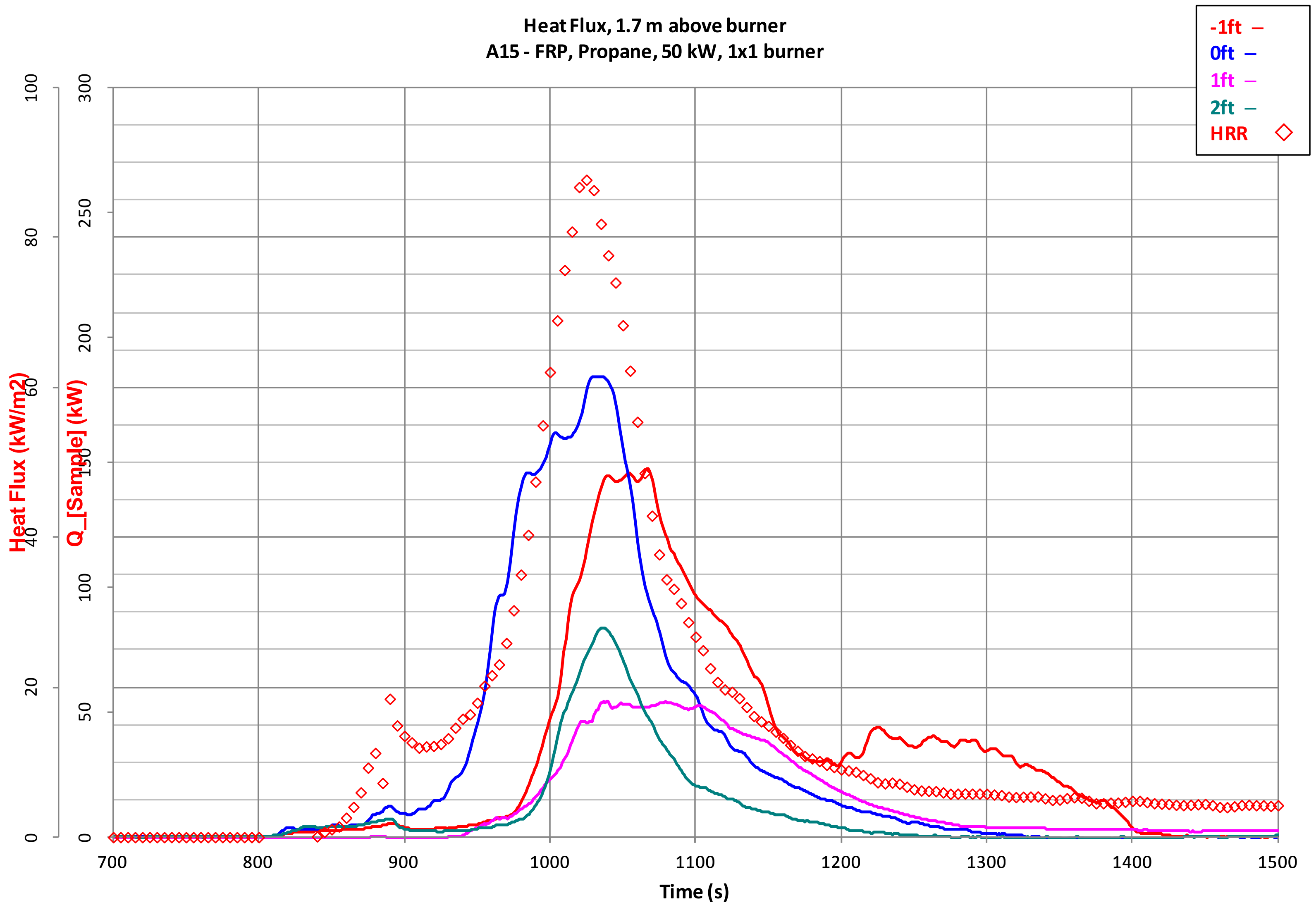

Heat flux measured at various distances from the centerline (negative indicates left of centerline), 1.7m vertically from burner surface

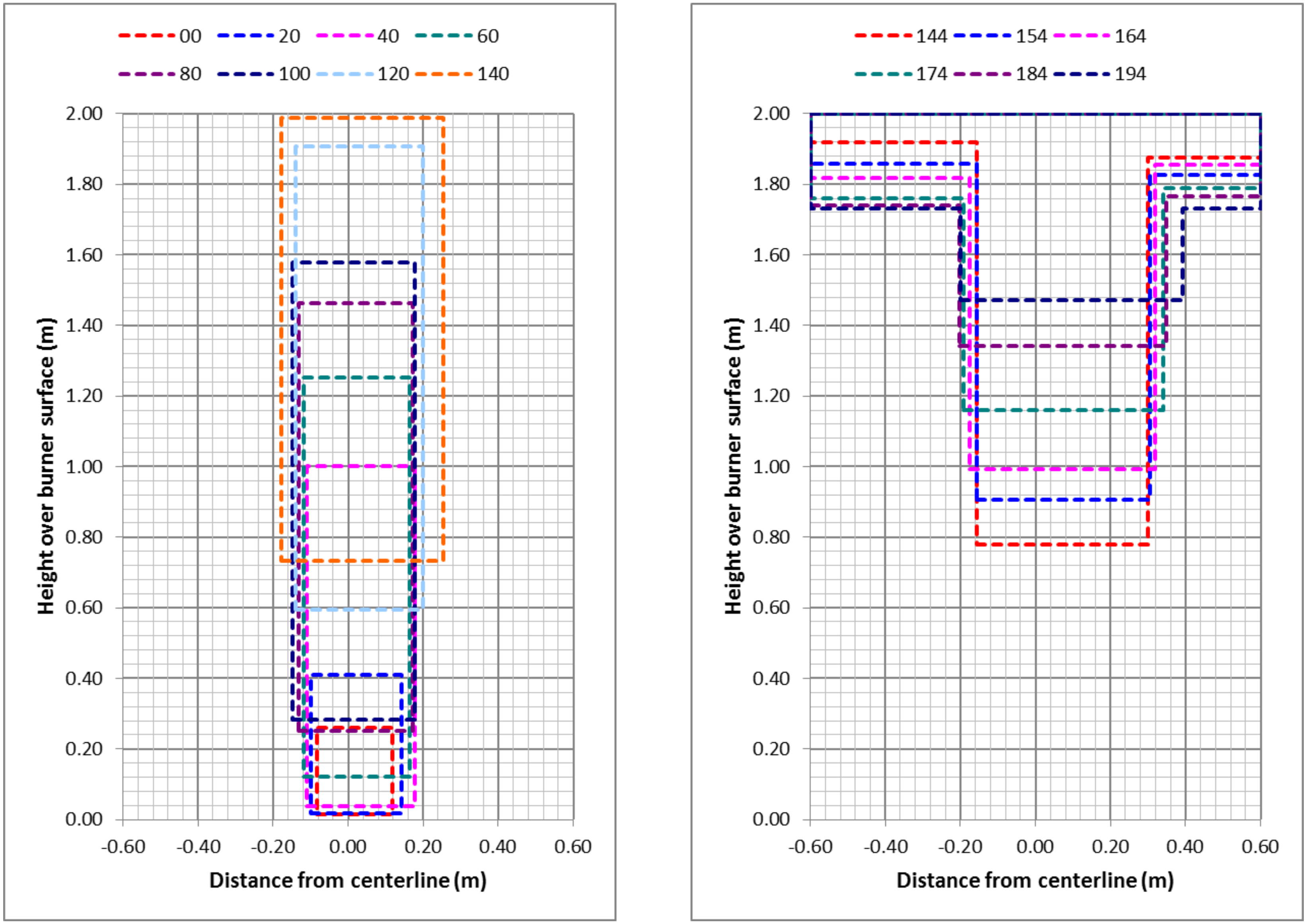

Stages 1 and 2 burning areas in Test A15 (1ft Square burner, Propane, 50 kW source)

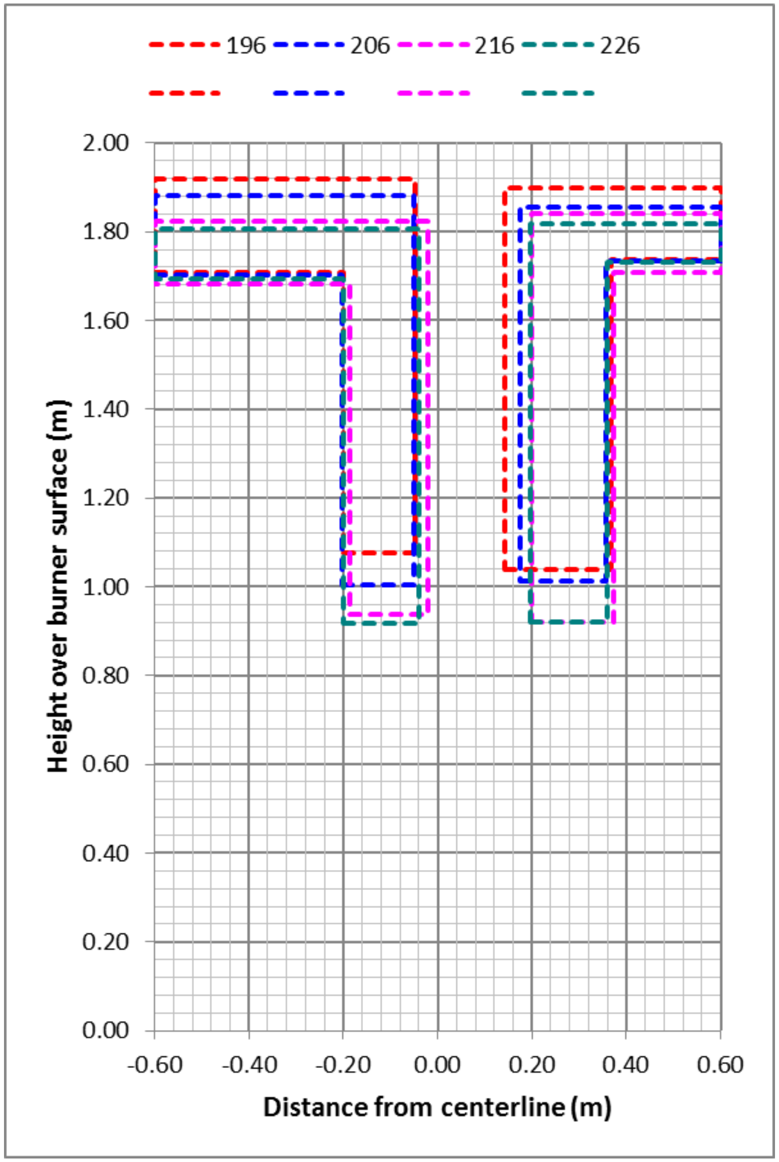

Stage 3 burn area and final damage chart of Test A15 (1ft Square burner, Propane, 50 kW source)

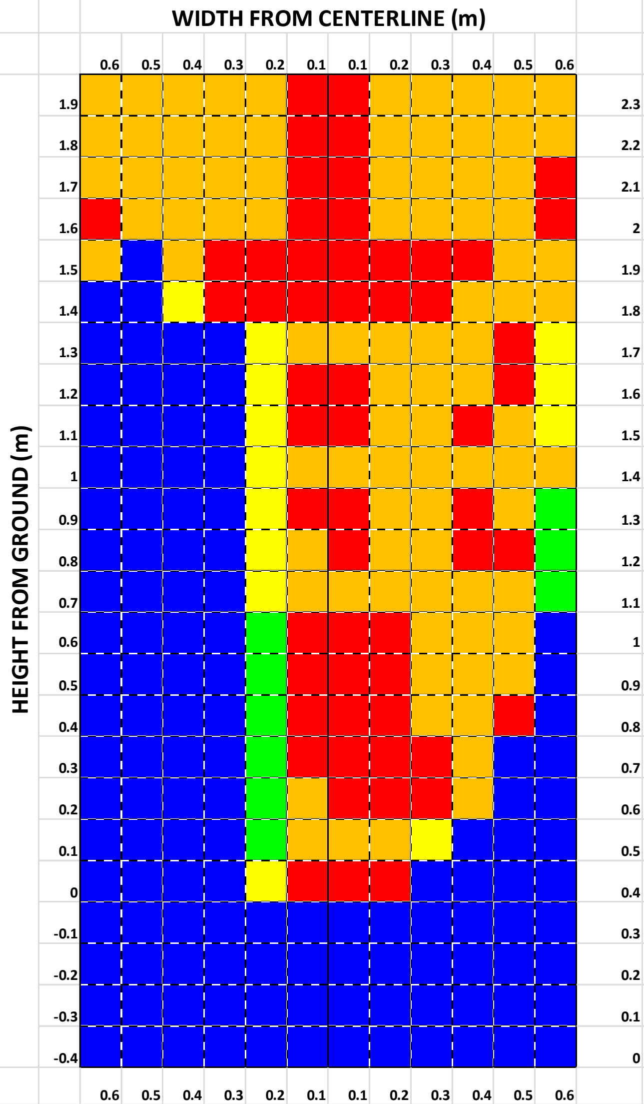

# of cell	Damage to Resin	Area (m2)
57	up to 100% damage	0.57
88	up to 75% damage	0.88
13	up to 50% damage	0.13
9	up to 25% damage	0.09
121	no damage	1.21

Initial mass:	8.52	kg
Final unburnt mass:	4.4	kg
Final burnt mass:	2.36	kg
Total mass loss during fire	1.76	kg

Burn damage pattern observed after fire test

F.3.16 Test A16

LODS Test Run Data

Center for Firesafety Studies

100 Institute Road
Worcester, MA 01609
Phone: (508) 831-5628
Fax: (508) 831-5680

Test Information

Test Number:	A16
Specimen Identification:	FRP 16, 75 kW continuous Propane fire, 1 x 1 burner
Material Name:	Class C FRP panel
Manufacturer/Submitter:	Not Reported
Raw Data File Name:	Test A16 - FRP_Propane_75kW_1ft.txt
Reduced Data File Name:	Test A16 - FRP_Propane_75kW_1ft_reduced.xlsx
Date of Test:	3-Dec-2010
Tester:	W. Wong

Test Parameters

Ambient Temperature:	N/A
Relative Humidity:	N/A

Specimen Information

Specimen Initial Mass:	[kg]	8.7
Specimen Final Mass:	[kg]	5.4
Mass Lost:	[kg]	3.3
Heat Evolved (net):	[kJ]	0

Parameter	Unit	Value
Mass Loss		
Initial Mass	[kg]	8.7
Final Mass	[kg]	5.4
Mass Loss	[%]	37.64

LODS Test Run Data

Center for Firesafety Studies

100 Institute Road
Worcester, MA 01609
Phone: (508) 831-5628
Fax: (508) 831-5680

Test Notes

Test Number:	0
Date:	12/03/10
Material:	Class C FRP panel
Specimen Identification:	FRP 16, 75 kW continuous Propane fire, 1 x 1 burner

Observations

Time	Observation
00:00	Start VI
04:00	Start Camera 1
04:15	Start Camera 2
08:00	Burner ignition
08:20	Reach target HRR @ 75 kW
08:45	Crackling noise
09:00	Panel ignition, mainly at area under TSC-2 to above burner
09:40	Flame hit ceiling
09:50	Burning reaches left and right sides as a T
10:12 to 12:0	Rollover under ceiling
	During rollover, remote area ignition at left edge from y = 1.5 to ceiling
11:30	this descended to y = 1.0 to ceiling
11:30	Remote area ignition at TSC-4
11:05	Some paper on sidewall burning
25:00	Line fires on the left side get disturbed by the burner fire plume
25:30	Remote ignition on left edge at y = 0.4, insignificant fire
29:30	Left side line fires regressing upward
31:00	Burner turned off
31:20	Terminated test by little water application

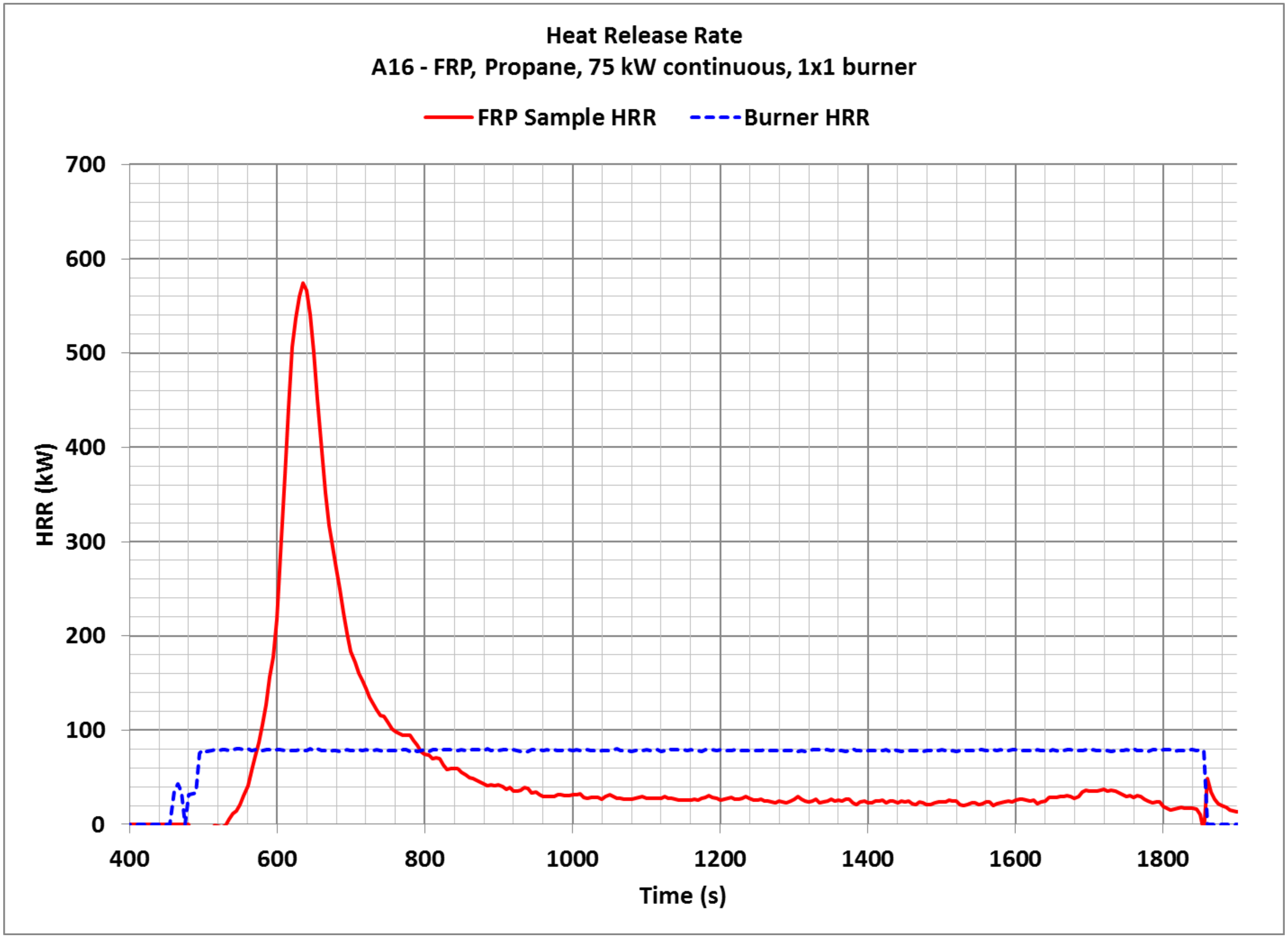

Heat release ratesof the source burner fire and of the specimen fire measured during test

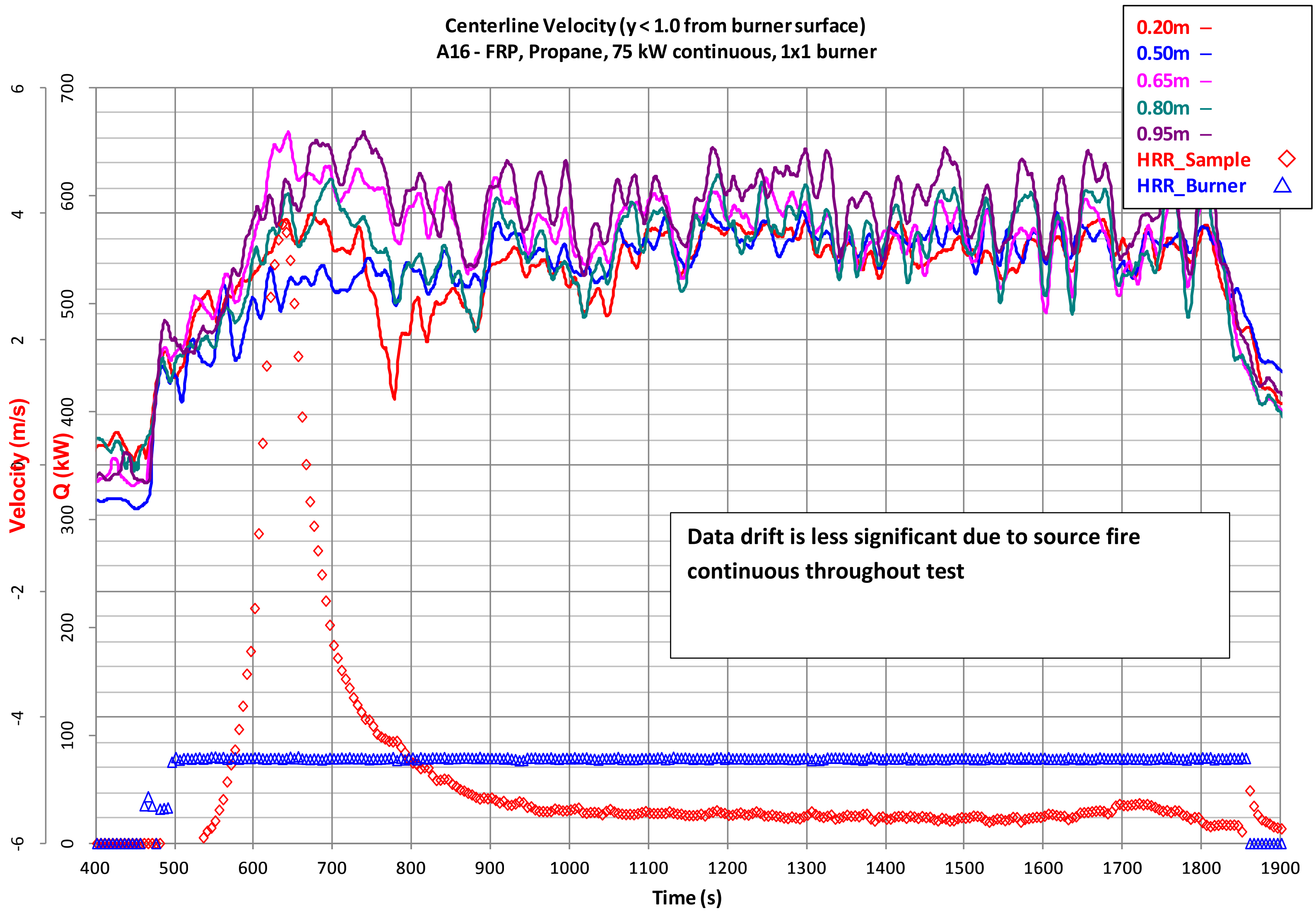

Centerline plume velocities measured from 0.2m to 0.95m above the burner surface

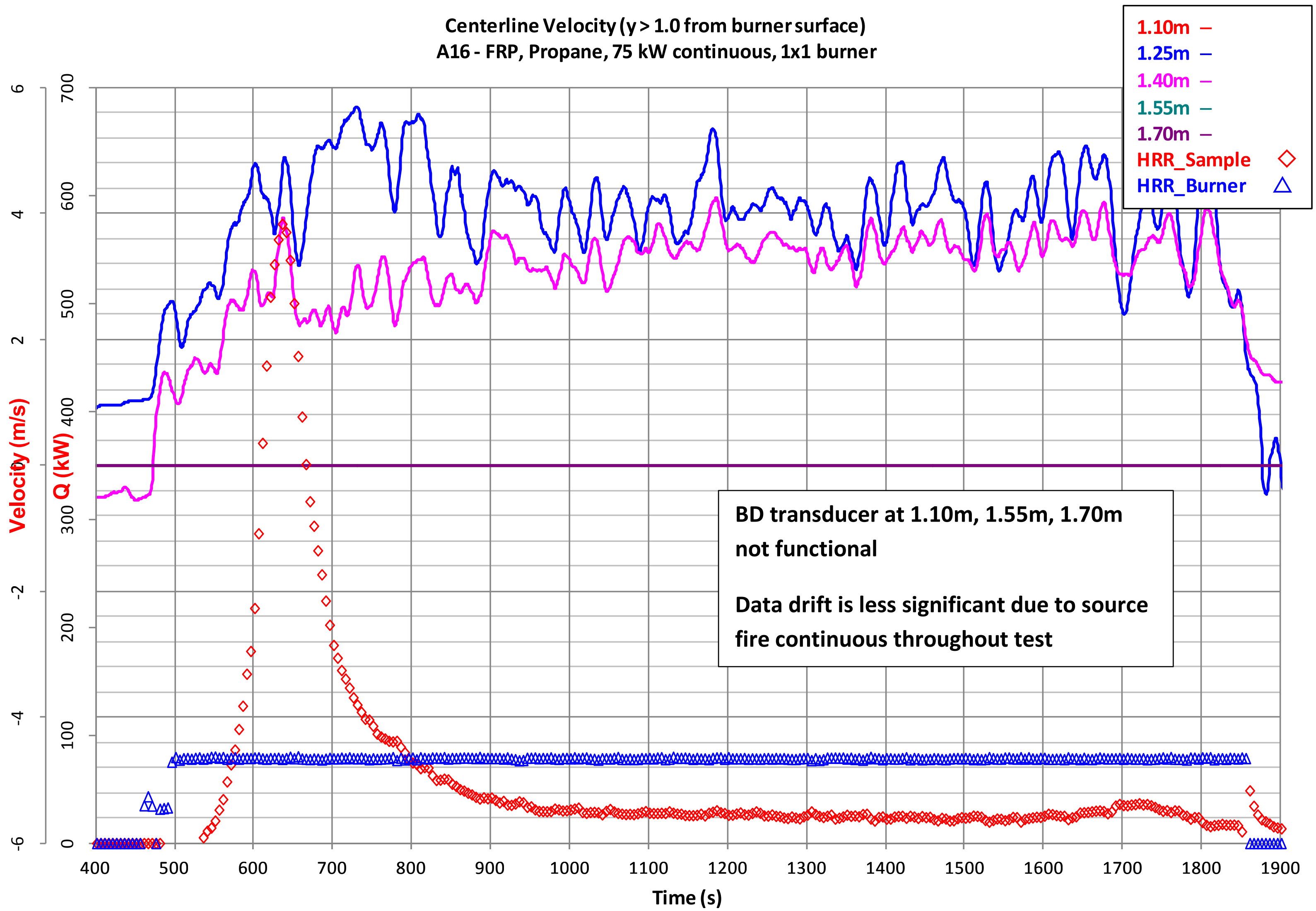

Centerline plume velocities measured from 1.1m to 1.7m above the burner surface

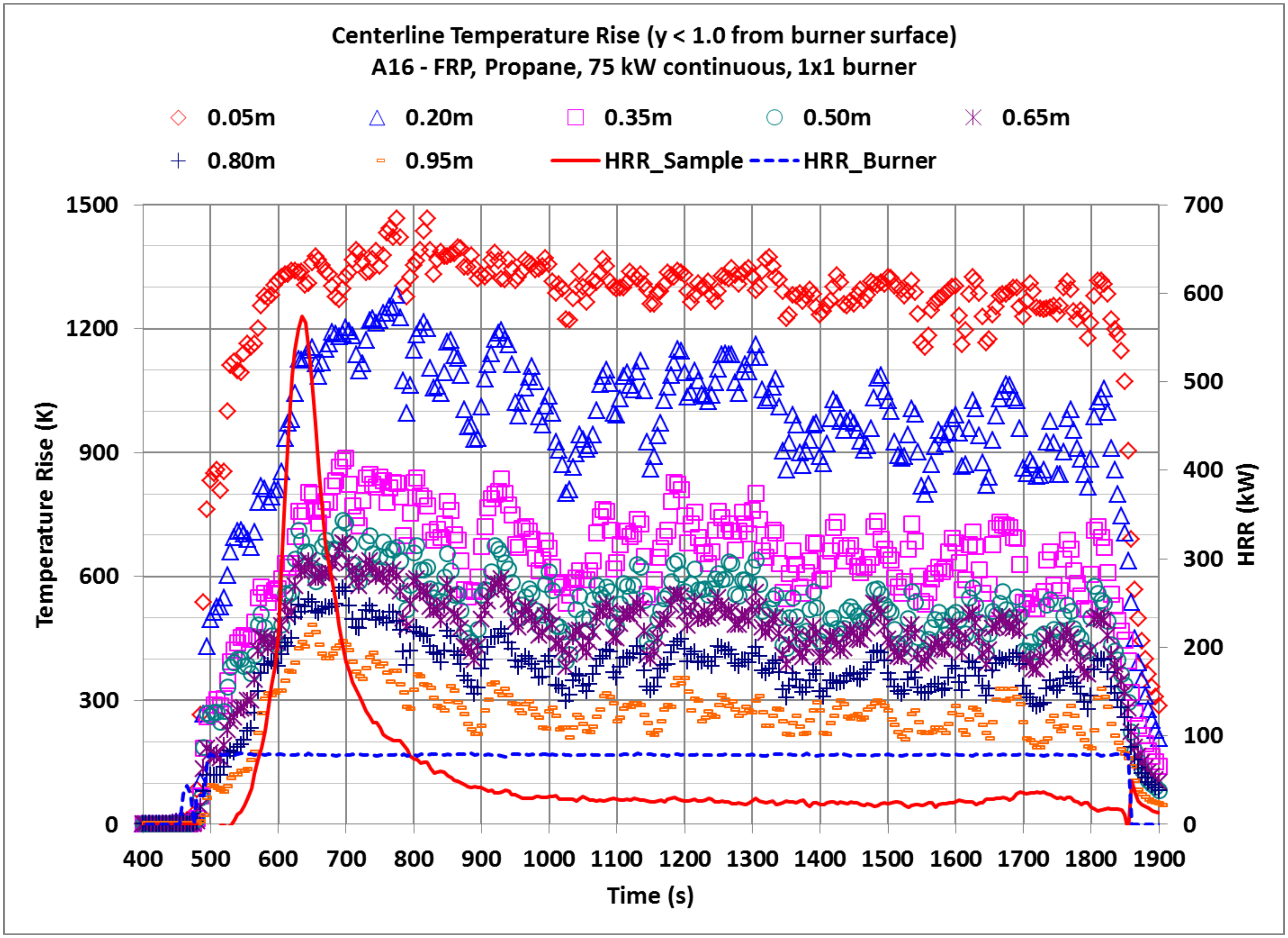

Centerline plume temperature rise measured from 0.05m to 0.95m above the burner surface

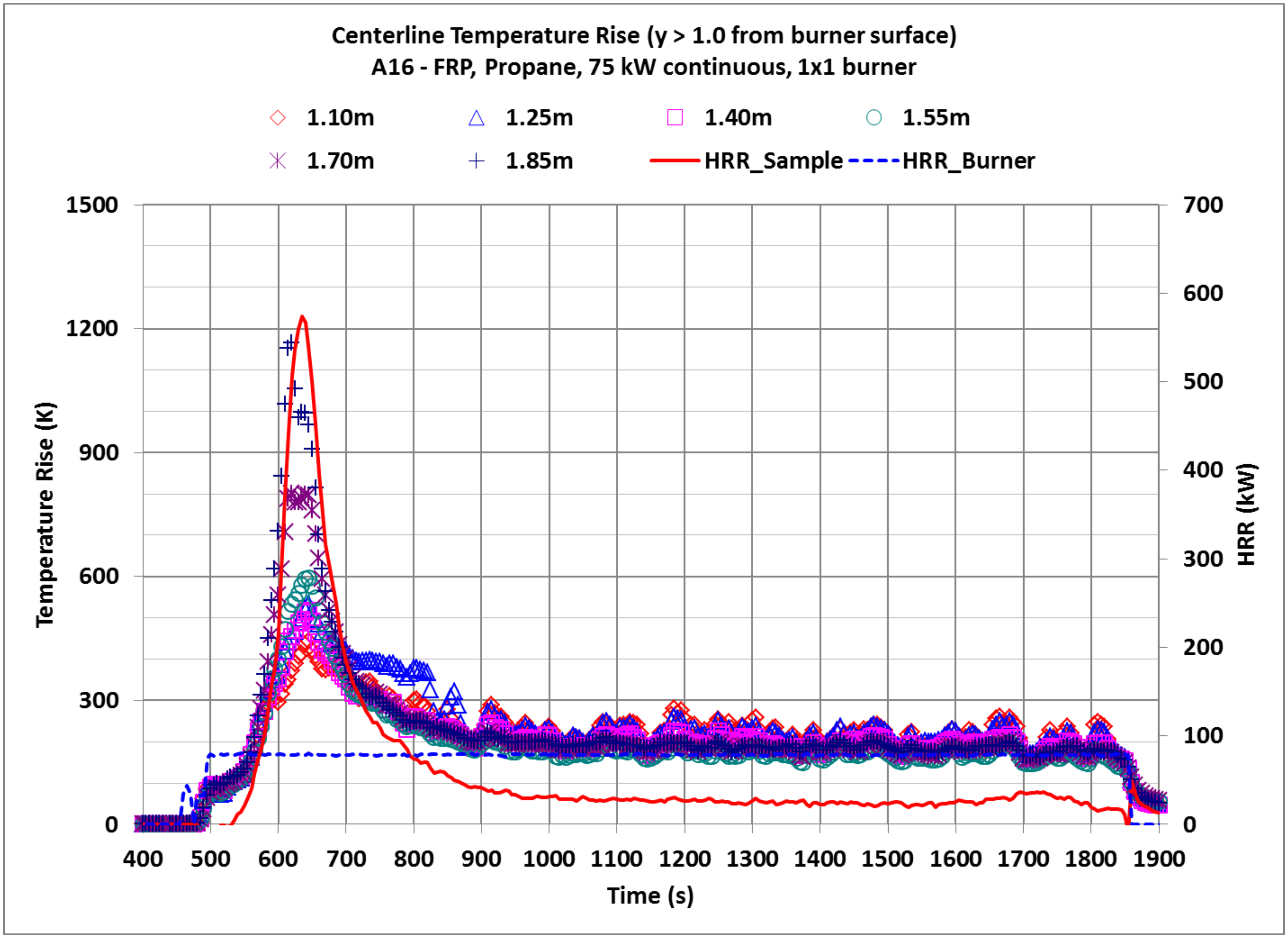

Centerline plume temperature rise measured from 1.10m to 1.85m above the burner surface

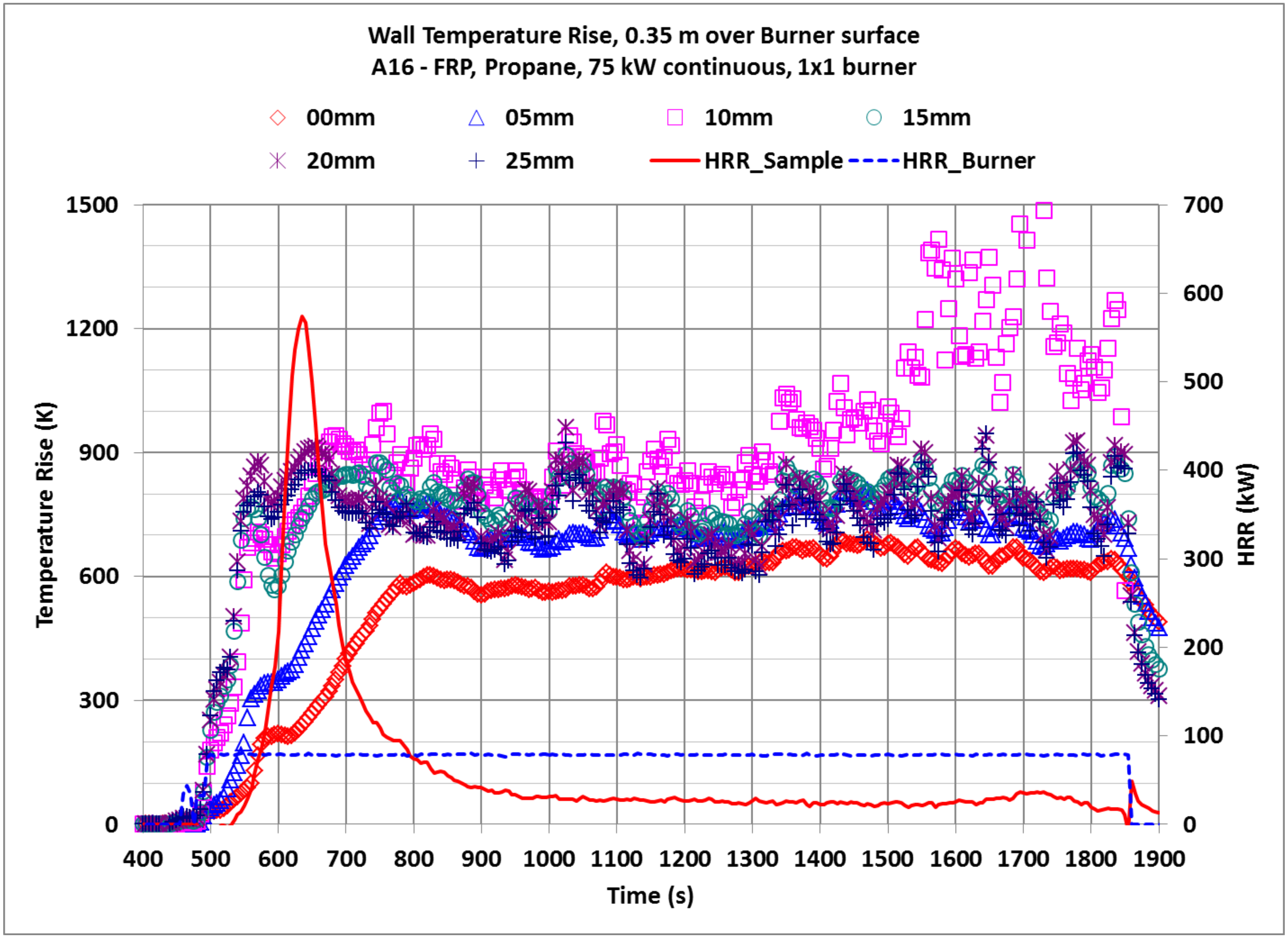

Temperature rise along the wall's centerline at 0.35m over the burner surface, measured at different perpendicular distances to as indicated

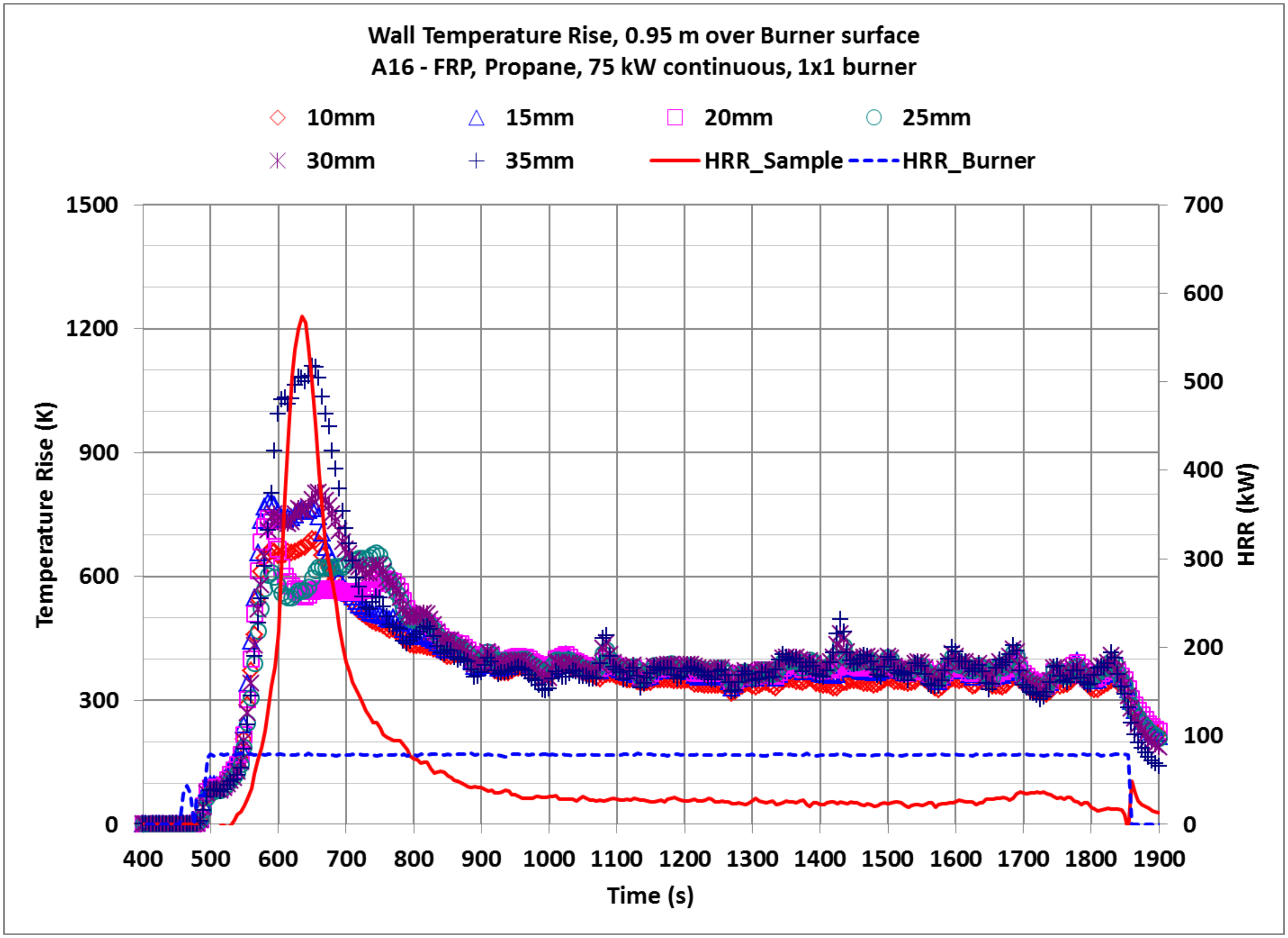

Temperature rise along the wall’s centerline at 0.95m over the burner surface, measured at different perpendicular distances to as indicated

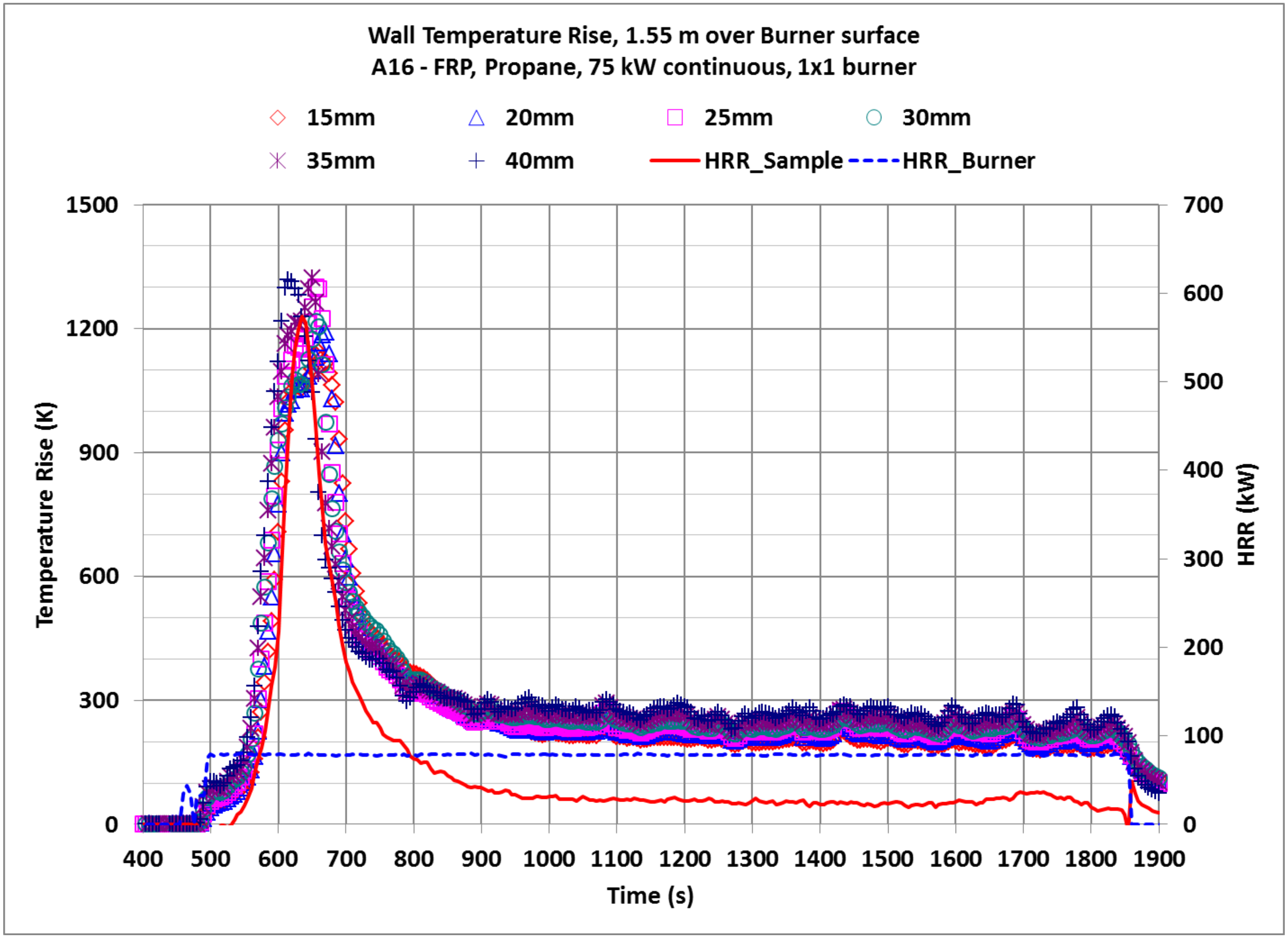

Temperature rise along the wall's centerline at 1.55m over the burner surface, measured at different perpendicular distances to as indicated

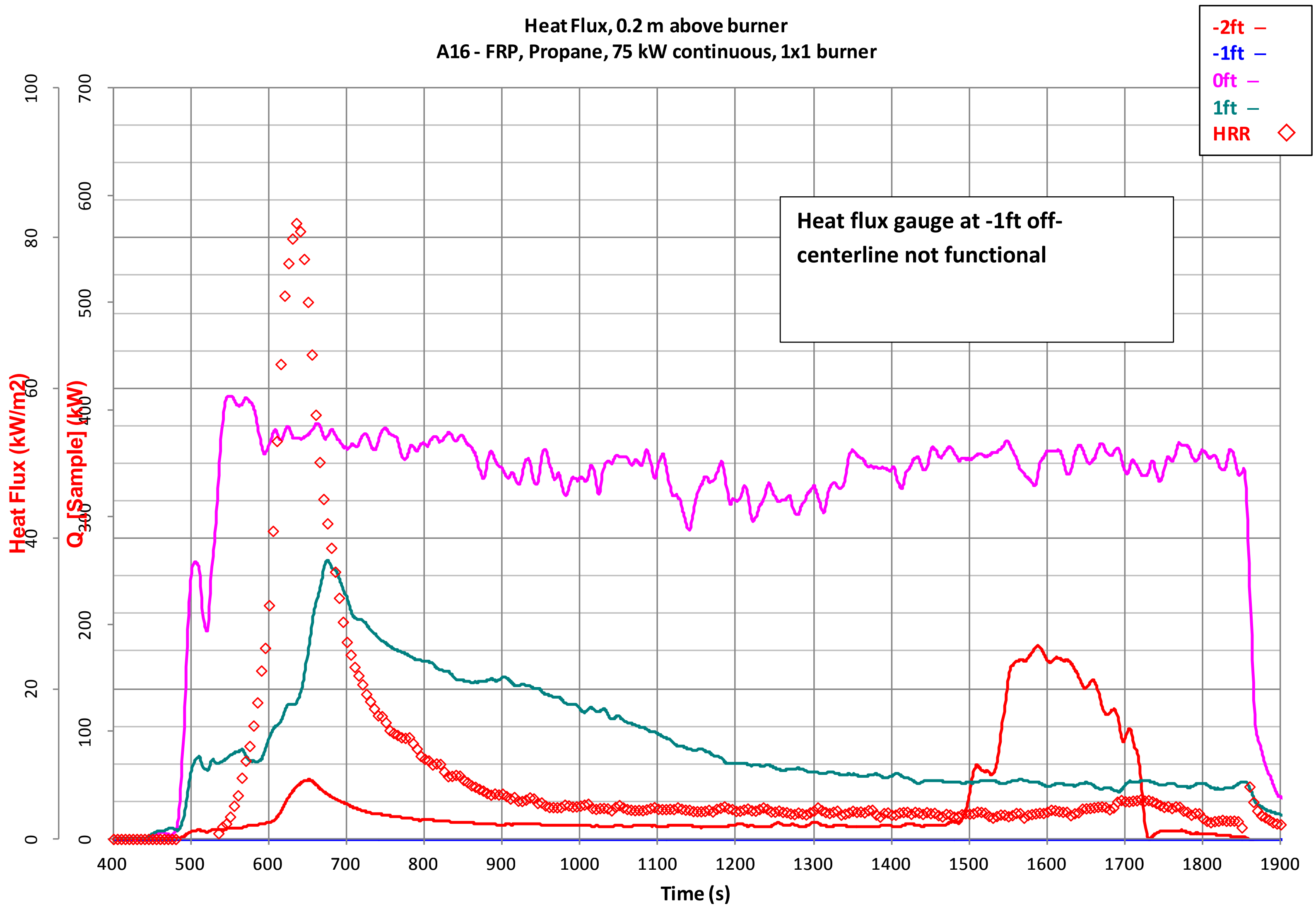

Heat flux measured at various distances from the centerline (negative indicates left of centerline), 0.2m vertically from burner surface

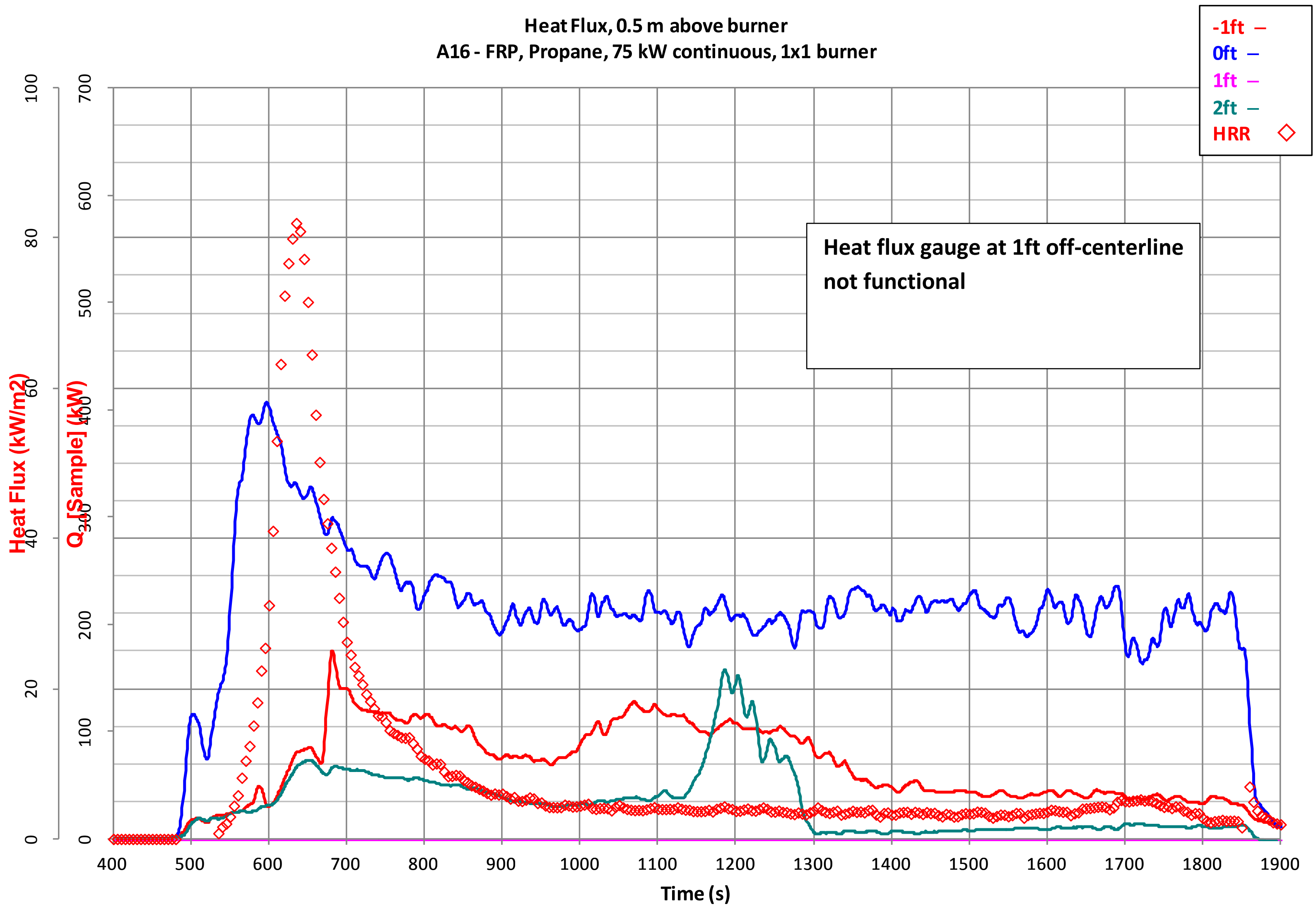

Heat flux measured at various distances from the centerline (negative indicates left of centerline), 0.5m vertically from burner surface

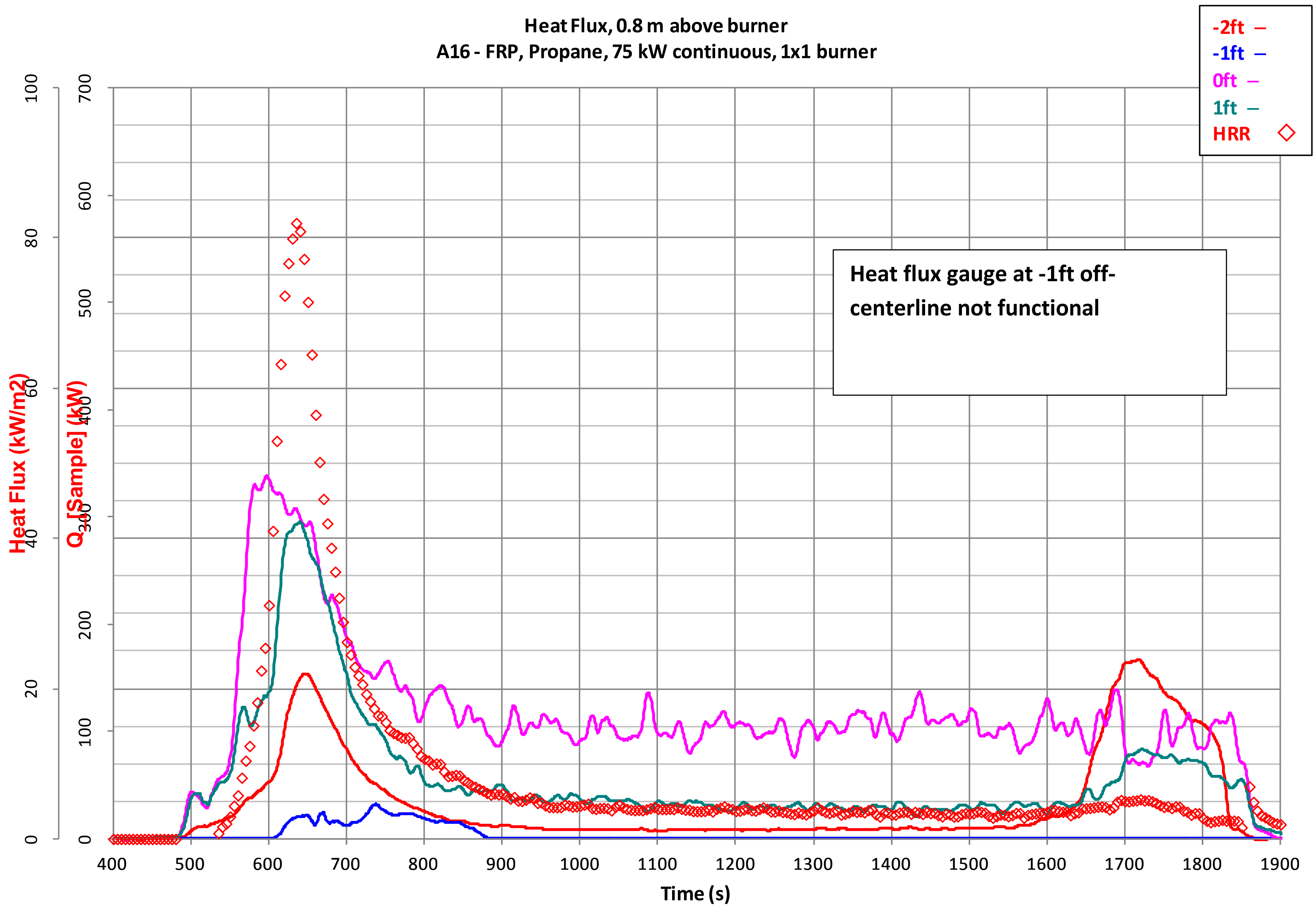

Heat flux measured at various distances from the centerline (negative indicates left of centerline), 0.8m vertically from burner surface

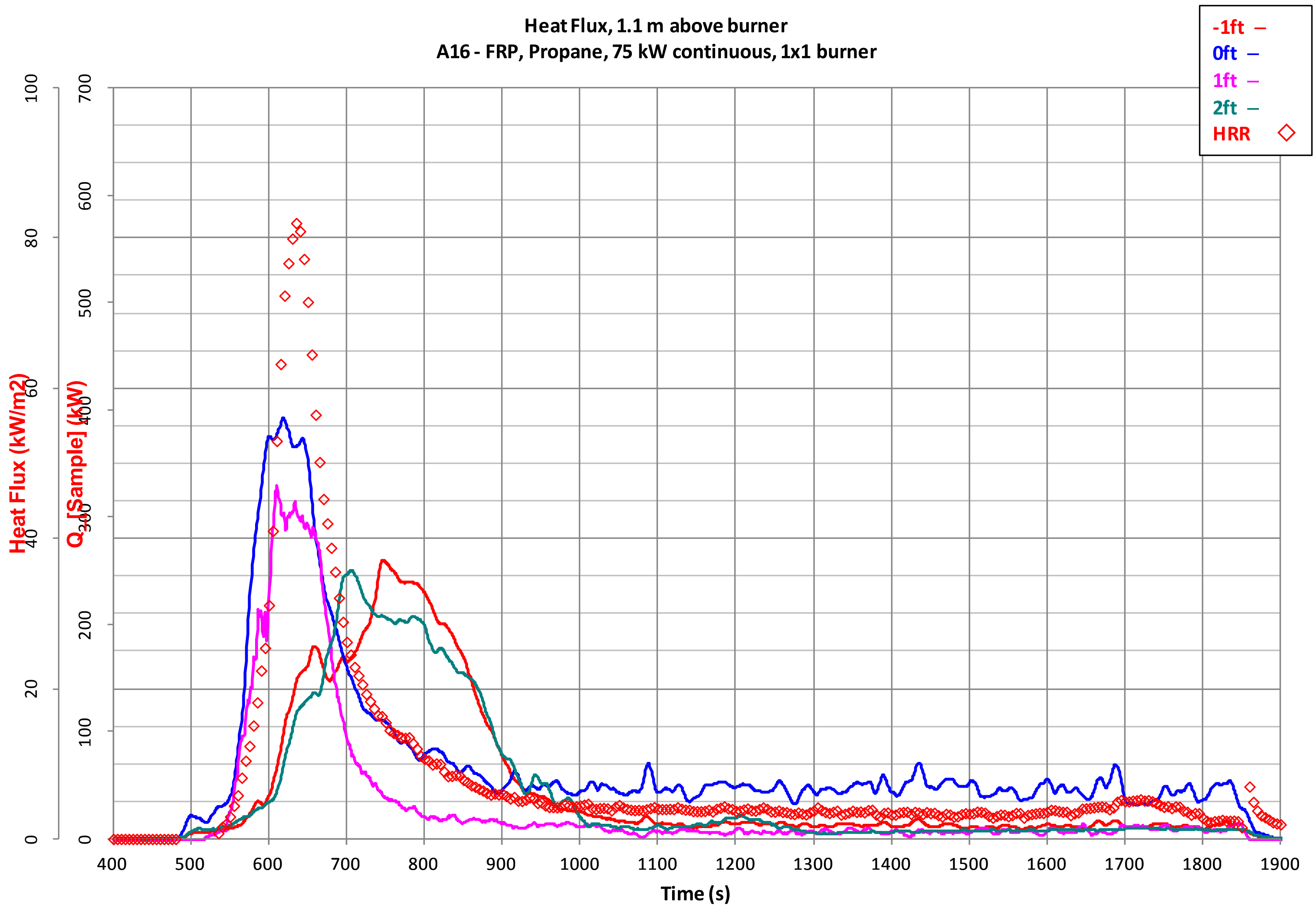

Heat flux measured at various distances from the centerline (negative indicates left of centerline), 1.1m vertically from burner surface

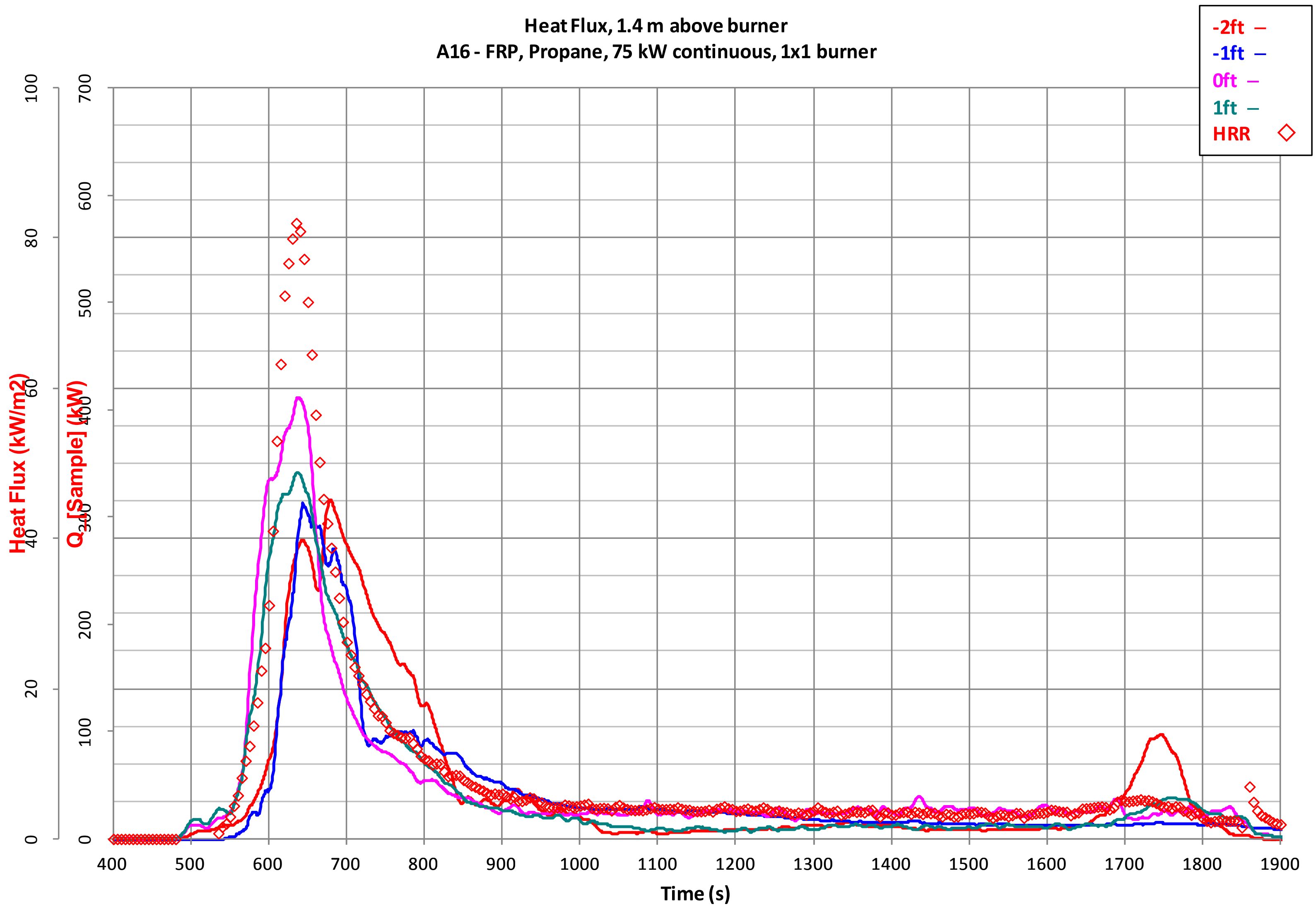

Heat flux measured at various distances from the centerline (negative indicates left of centerline), 1.4m vertically from burner surface

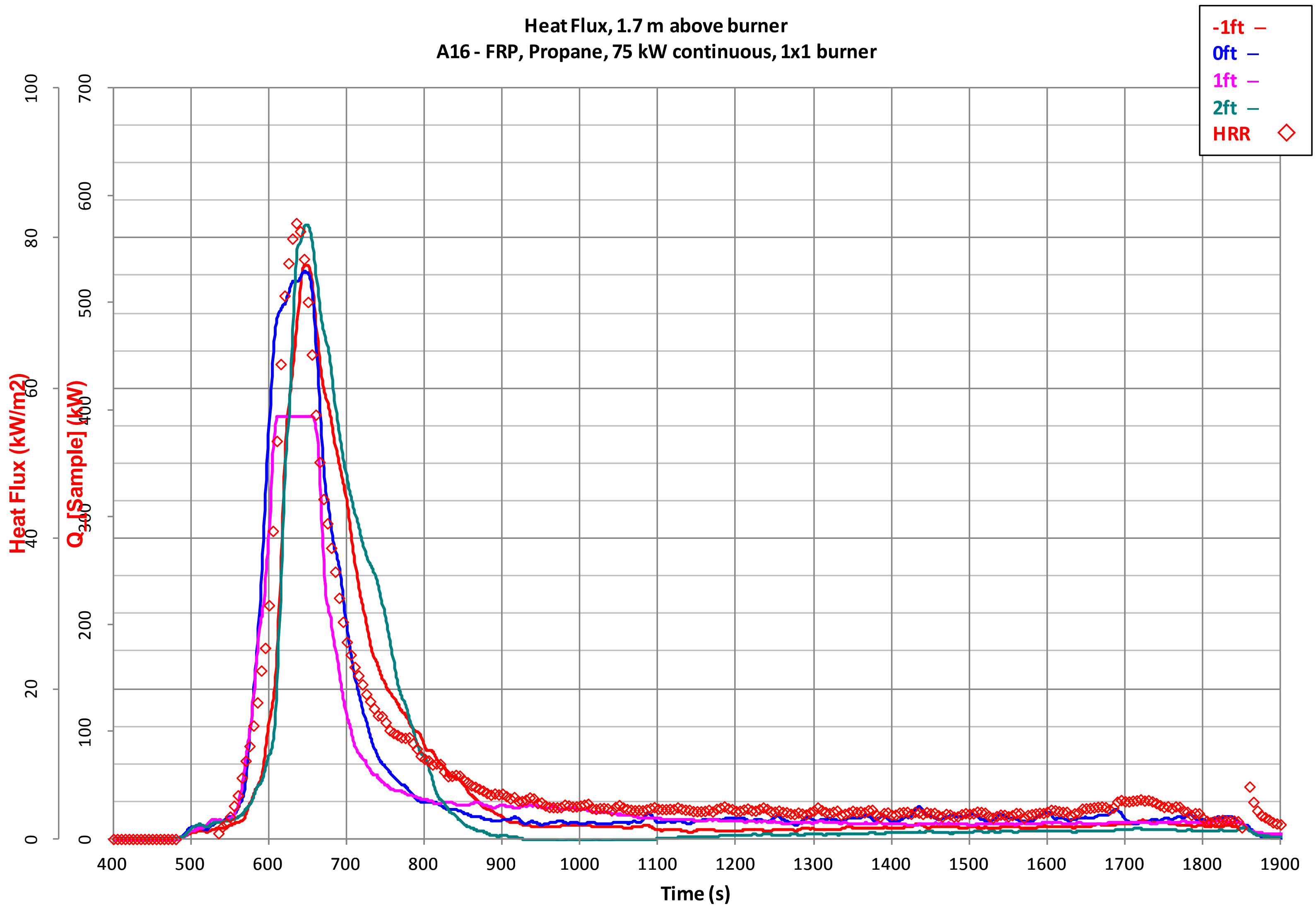

Heat flux measured at various distances from the centerline (negative indicates left of centerline), 1.7m vertically from burner surface

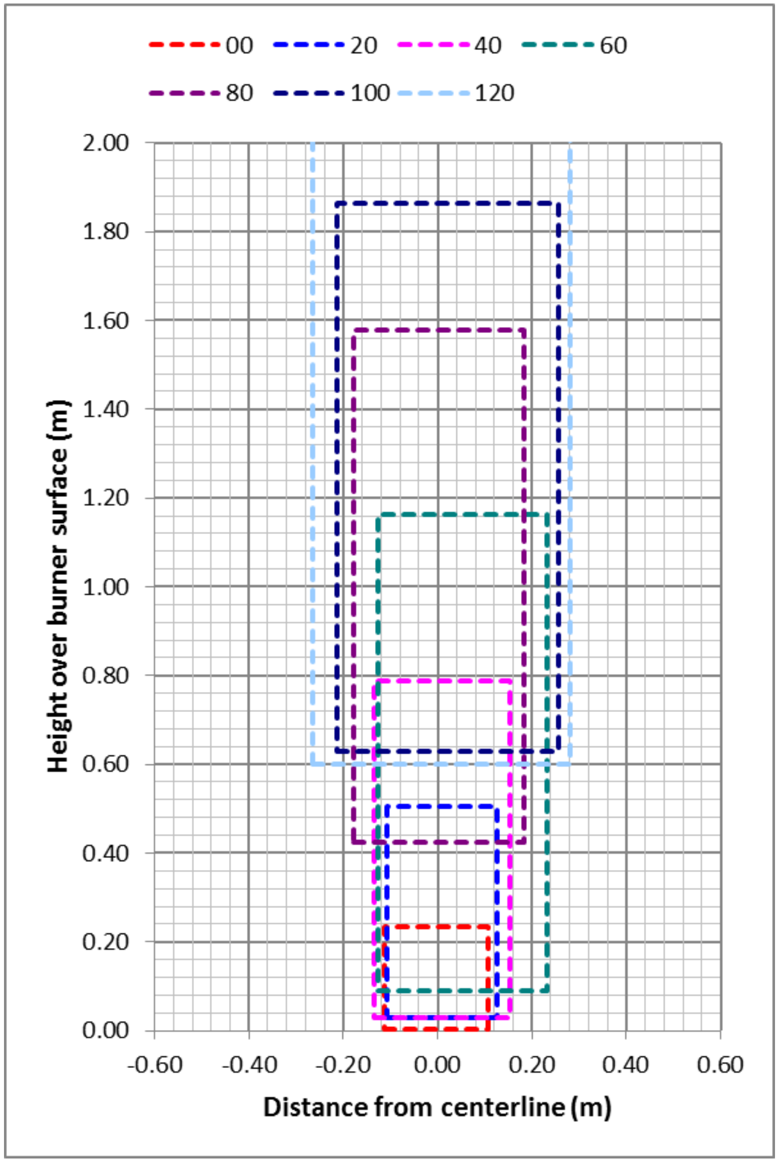

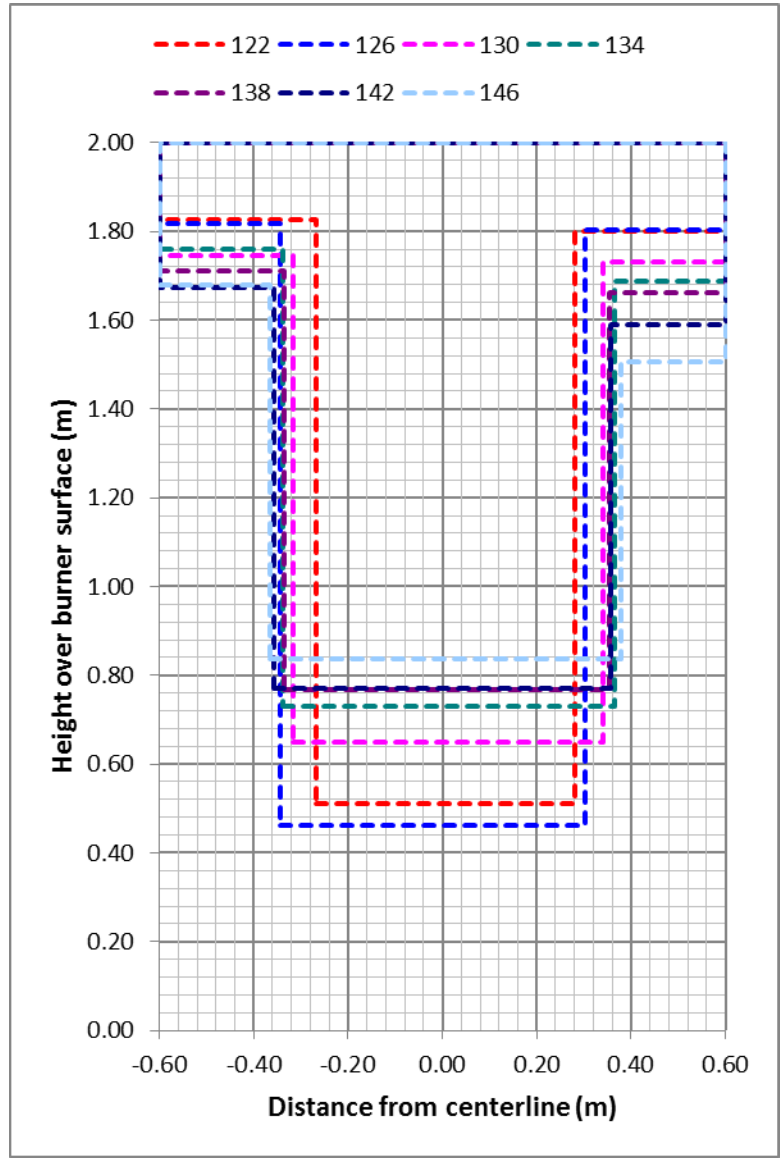

Stages 1 and 2 burning areas in Test A16 (1ft Square burner, Propane, 75 kW source on throughout test)

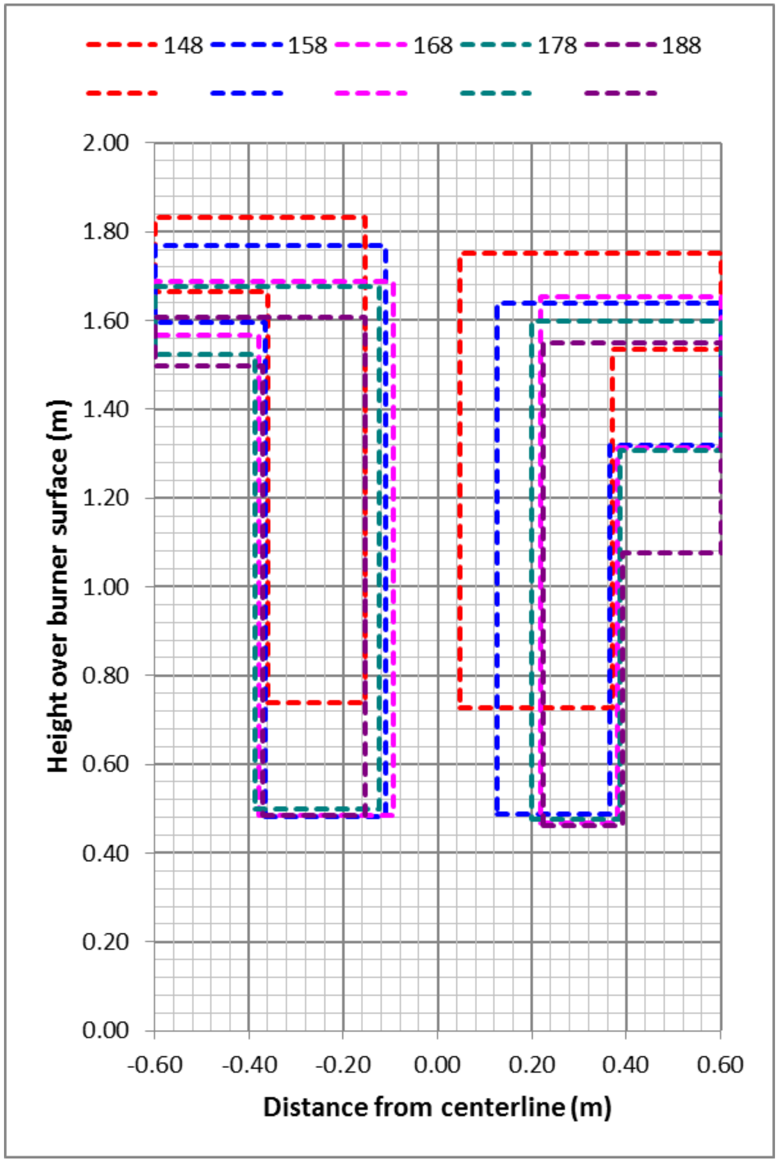

Stage 3 burn area and final damage chart of Test A16 (1ft Square burner, Propane, 75 kW source on throughout test)

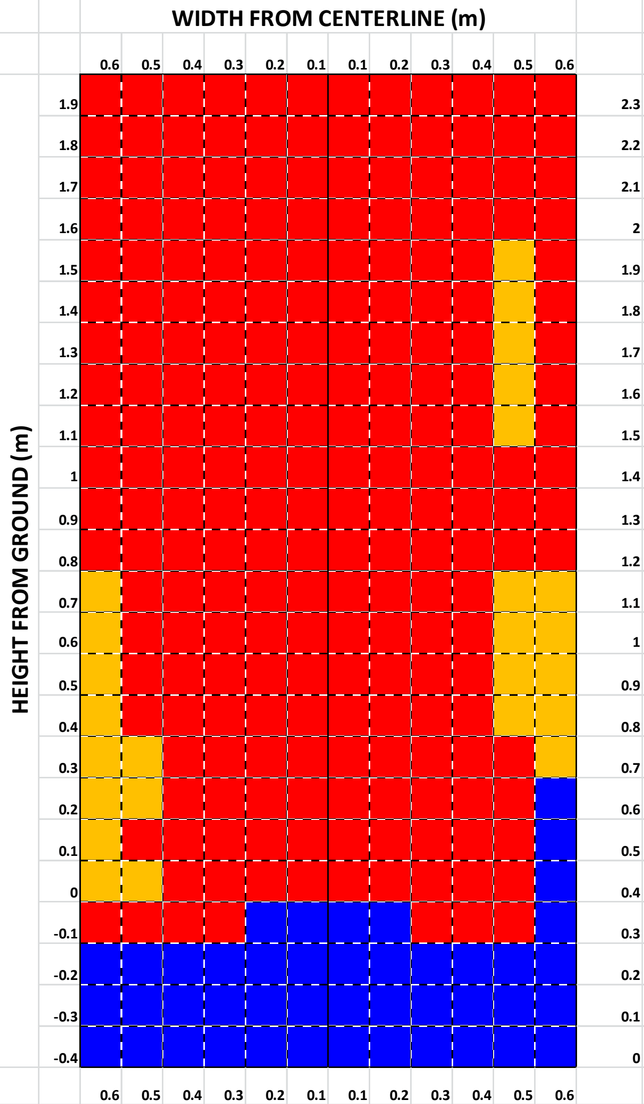

# of cell	Damage to Resin	Area (m2)
219	up to 100% damage	2.19
25	up to 75% damage	0.25
0	up to 50% damage	0
0	up to 25% damage	0
44	no damage	0.44

Initial mass:	8.66	kg
Final unburnt mass:	1.36	kg
Final burnt mass:	4.04	kg
Total mass loss during fire	3.26	kg

Burn damage pattern observed after fire test

F.3.17 Test A17

LODS Test Run Data

Center for Firesafety Studies

100 Institute Road
Worcester, MA 01609
Phone: (508) 831-5628
Fax: (508) 831-5680

Test Information

Test Number:	A17
Specimen Identification:	FRP 17, 75 kW continuous Propane fire, 1 x 2 burner
Material Name:	Class C FRP panel
Manufacturer/Submitter:	Not Reported
Raw Data File Name:	Test A17 - FRP_Propane_75kW_2ft.txt
Reduced Data File Name:	Test A17 - FRP_Propane_75kW_2ft_reduced.xlsx
Date of Test:	6-Dec-2010
Tester:	W. Wong

Test Parameters

Ambient Temperature:	N/A
Relative Humidity:	N/A

Specimen Information

Specimen Initial Mass:	[kg]	8.5
Specimen Final Mass:	[kg]	5.1
Mass Lost:	[kg]	3.4
Heat Evolved (net):	[kJ]	0
Specimen Identification:	FRP 17, 75 kW continuous Propane fire, 1 x 2 burner	

Parameter	Unit	Value
Mass Loss		
Initial Mass	[kg]	8.5
Final Mass	[kg]	5.1
Mass Loss	[%]	40.14

LODS Test Run Data

Center for Firesafety Studies

100 Institute Road
Worcester, MA 01609
Phone: (508) 831-5628
Fax: (508) 831-5680

Test Notes

Test Number:	0
Date:	12/06/10
Material:	Glasboard - Class C FRP panel
Specimen Identification:	FRP 17, 75 kW continuous Propane fire, 1 x 2 burner

Observations

Time	Observation
00:00	Start VI
04:45	Start Camera 1
05:00	Start Camera 2
06:45	Burner ignition
07:08	Reach target HRR @ 75 kW
07:30	Crackling noise
07:40	Panel ignition
08:00	Remote area smoking @ TSC-4, TSC-3
08:15	Insignificant remote area ignition @ TSC-4, TSC-3, HFG-2
	Ignition on right edge from y=0.7 m to 1.1 m until rollover
08:45	Burning reaches left and right edges
08:50 to 10:00	rollover under ceiling
20:35	Burner turned off
22:35	Terminated test by little water application
25:05	Terminate test by little water application

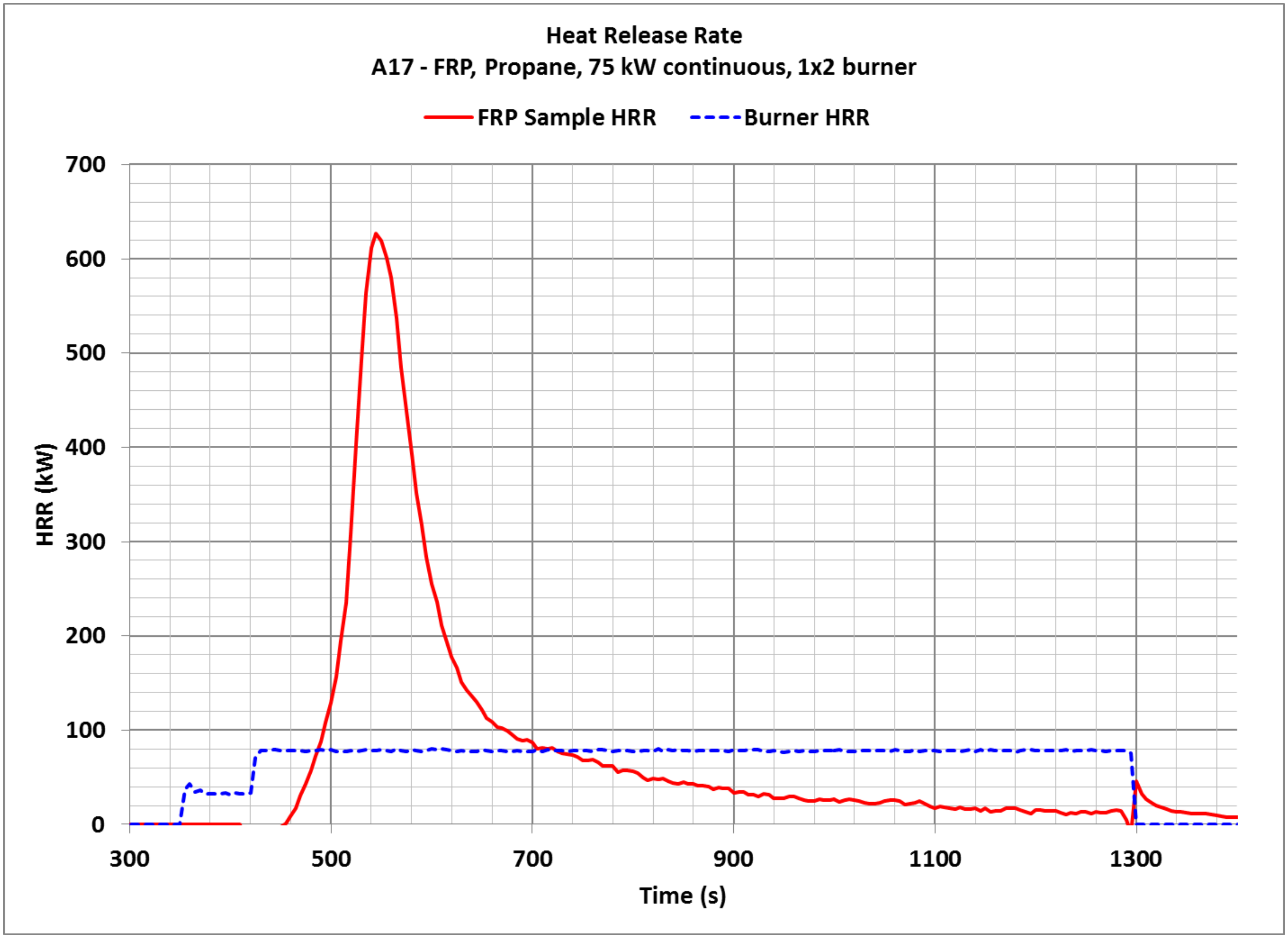

Heat release ratesof the source burner fire and of the specimen fire measured during test

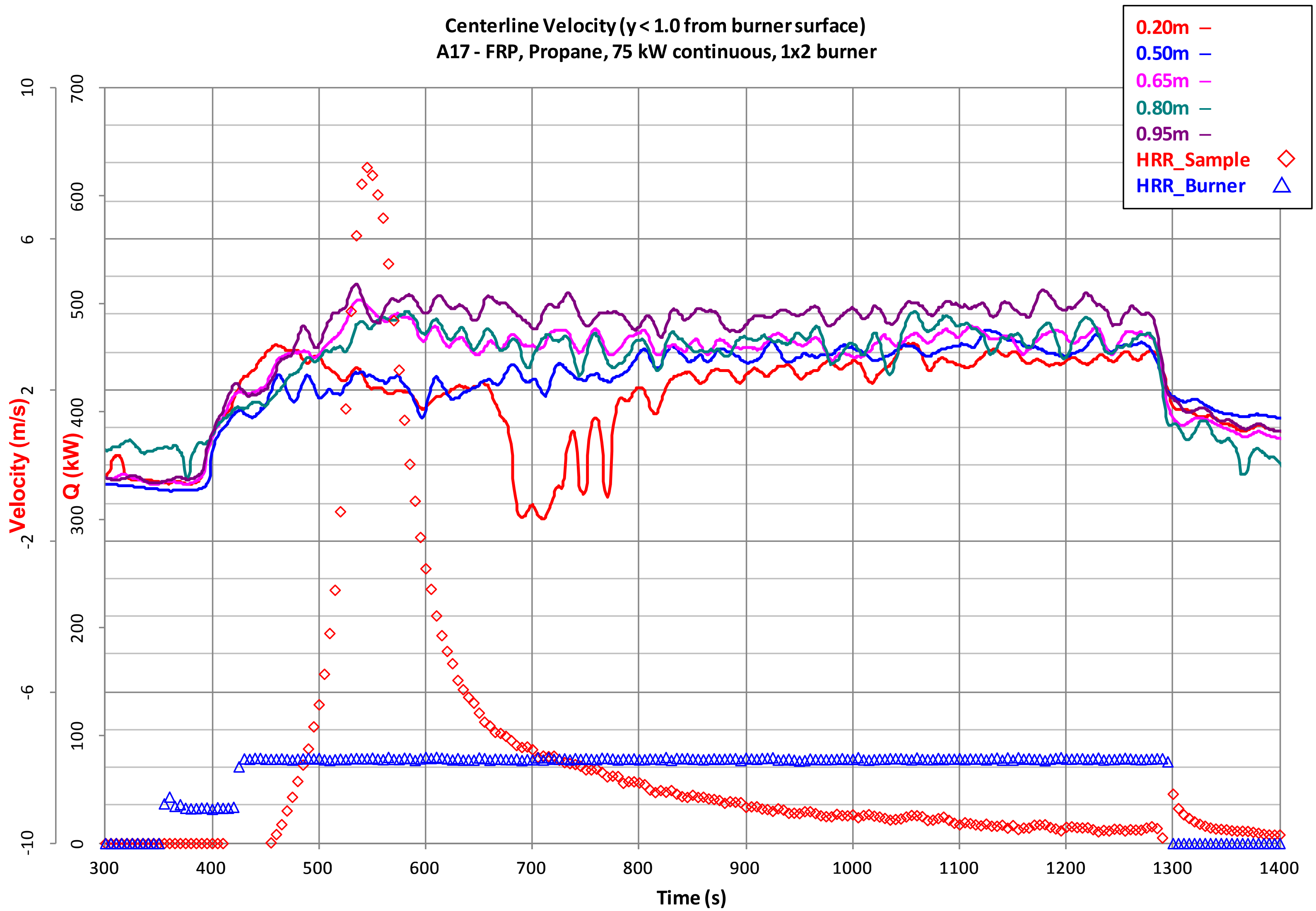

Centerline plume velocities measured from 0.2m to 0.95m above the burner surface

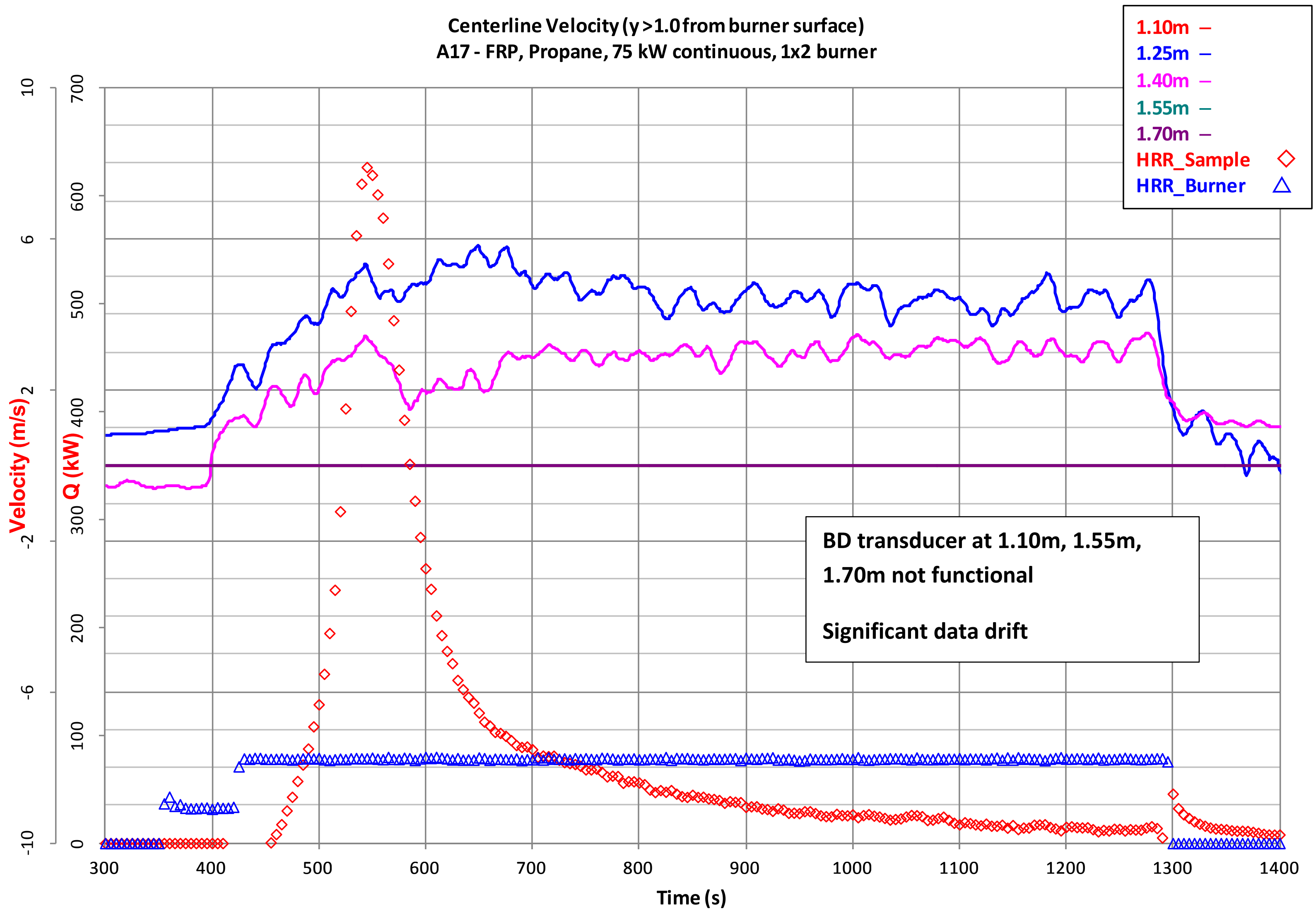

Centerline plume velocities measured from 1.1m to 1.7m above the burner surface

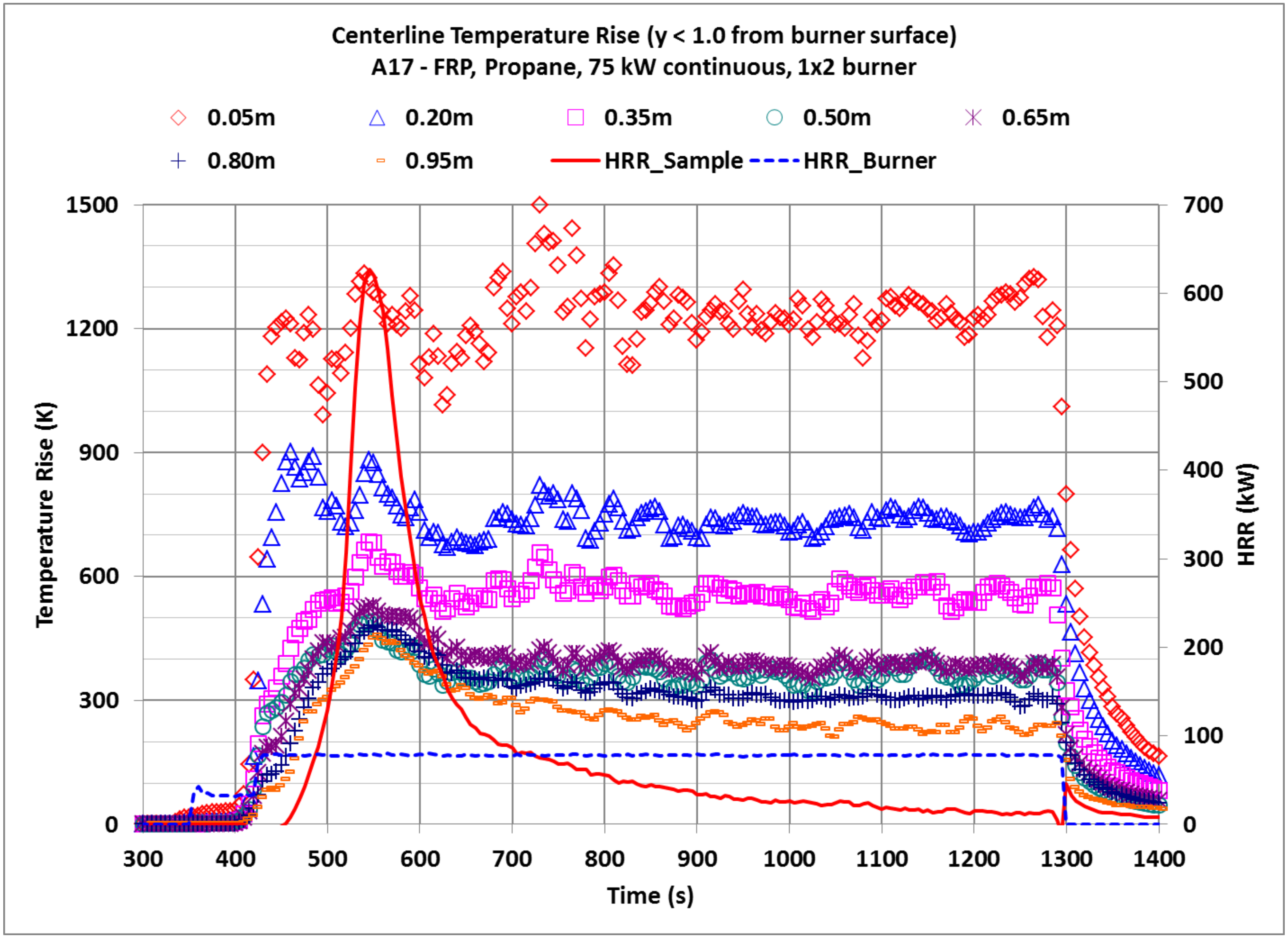

Centerline plume temperature rise measured from 0.05m to 0.95m above the burner surface

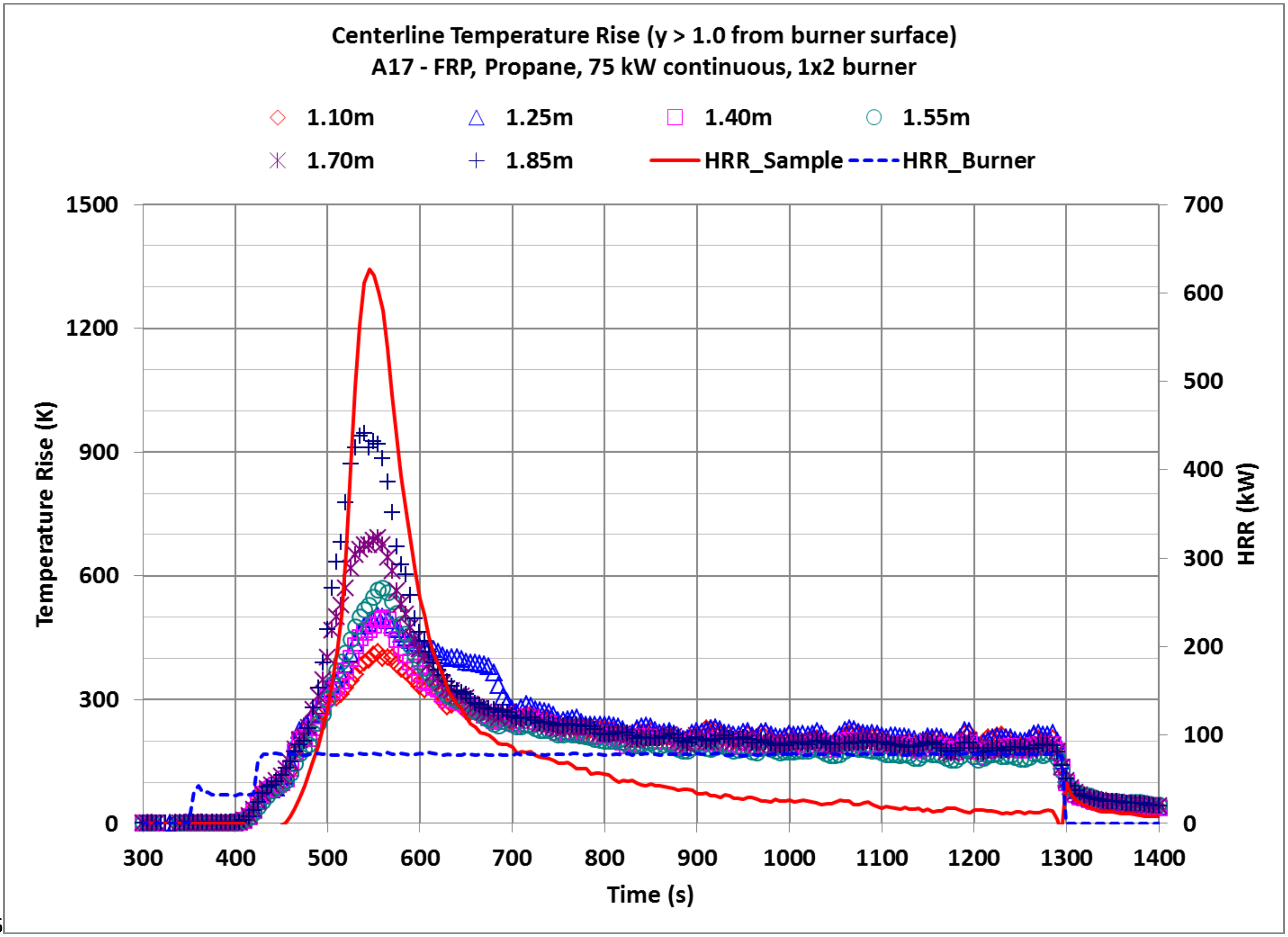

6

Centerline plume temperature rise measured from 1.10m to 1.85m above the burner surface

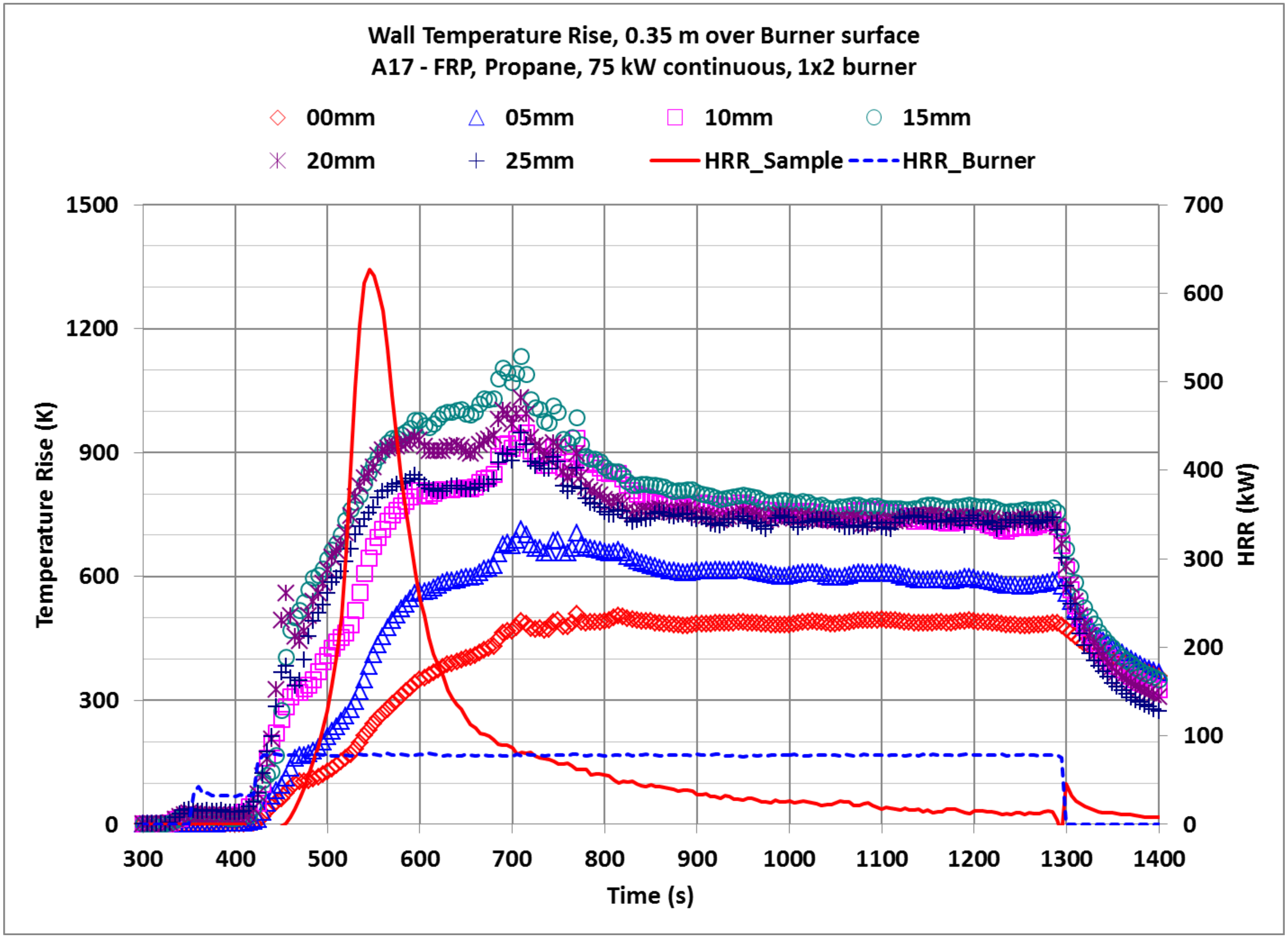

Temperature rise along the wall's centerline at 0.35m over the burner surface, measured at different perpendicular distances to as indicated

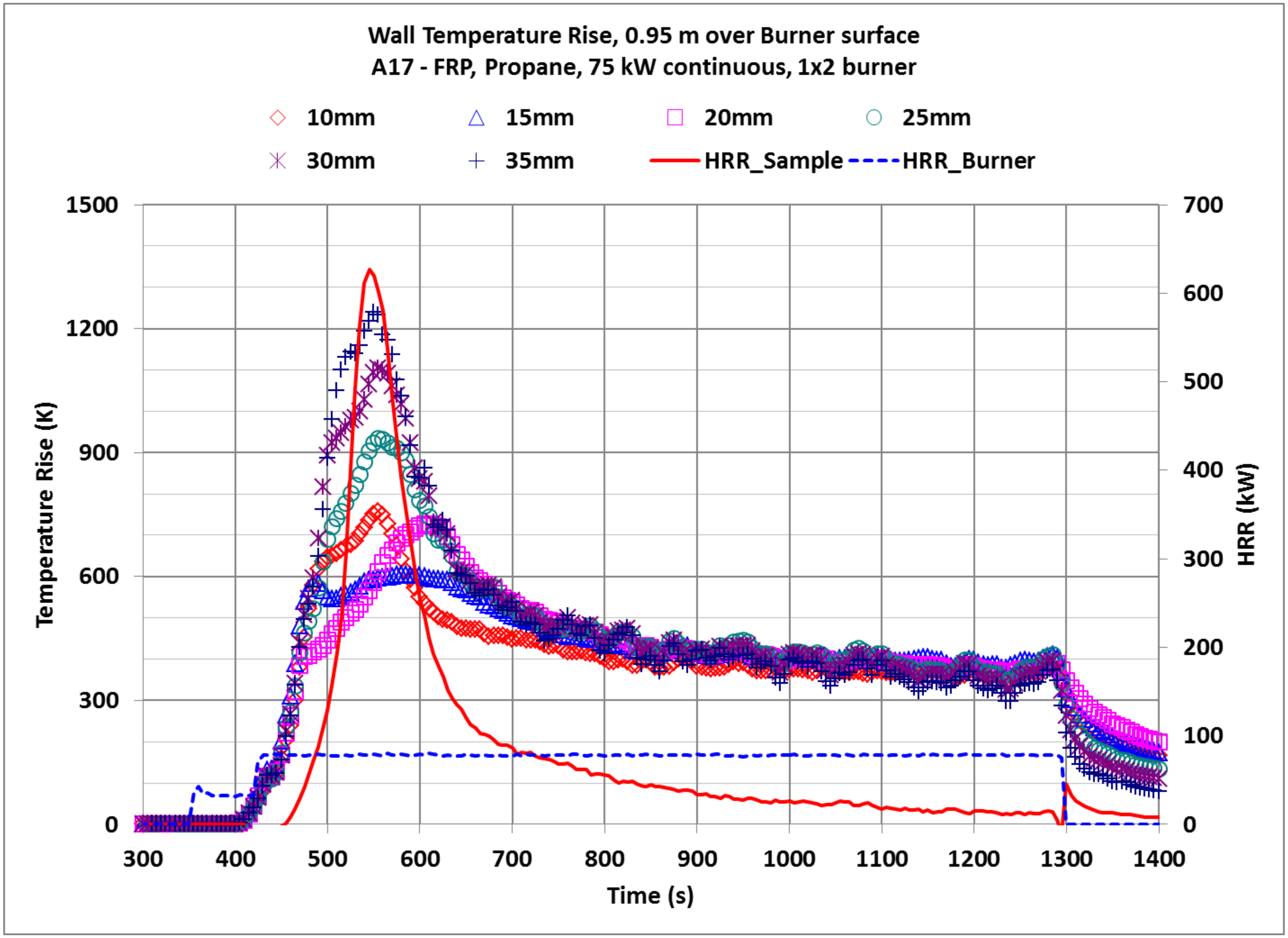

Temperature rise along the wall's centerline at 0.95m over the burner surface, measured at different perpendicular distances to as indicated

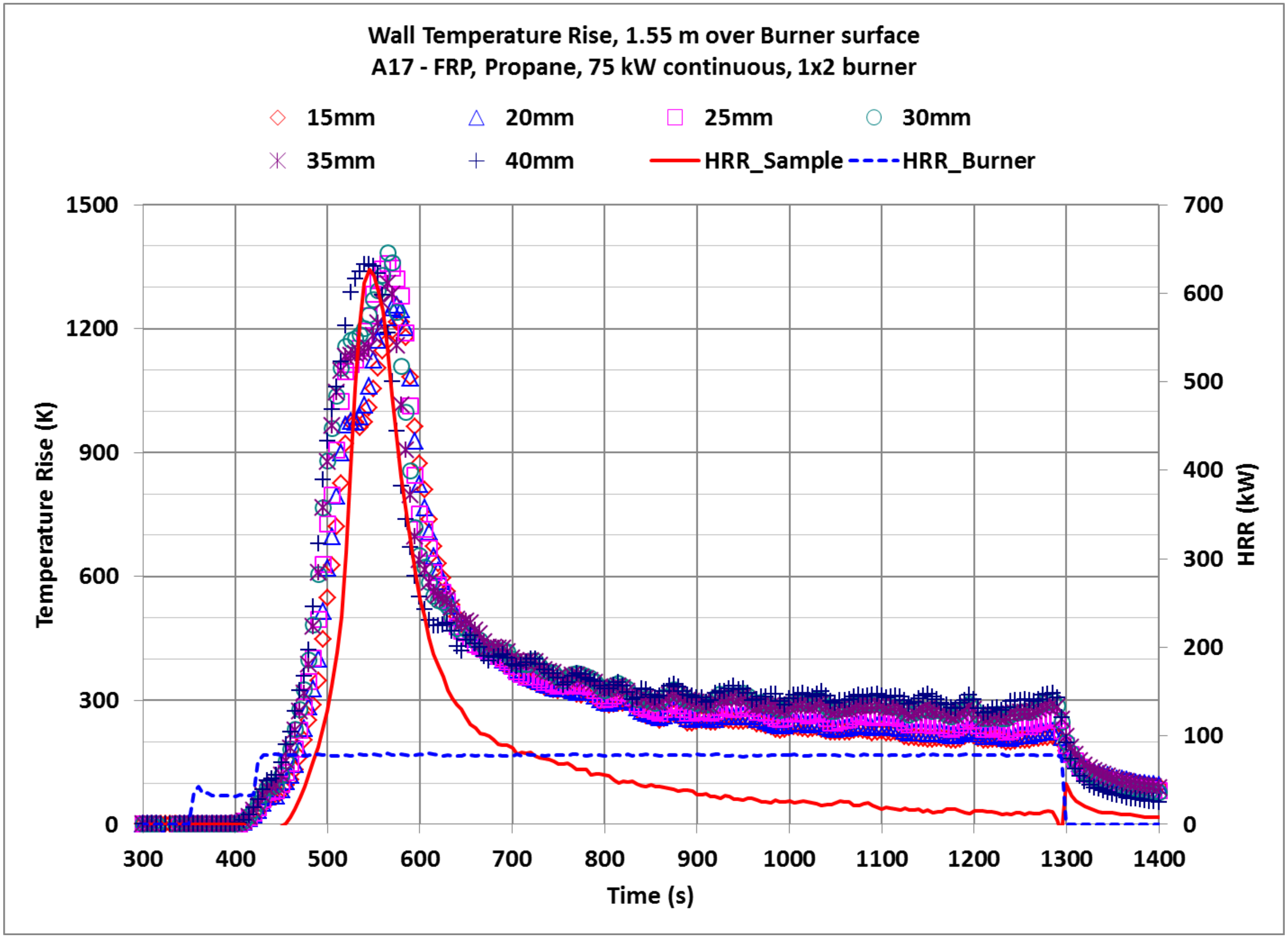

Temperature rise along the wall's centerline at 1.55m over the burner surface, measured at different perpendicular distances to as indicated

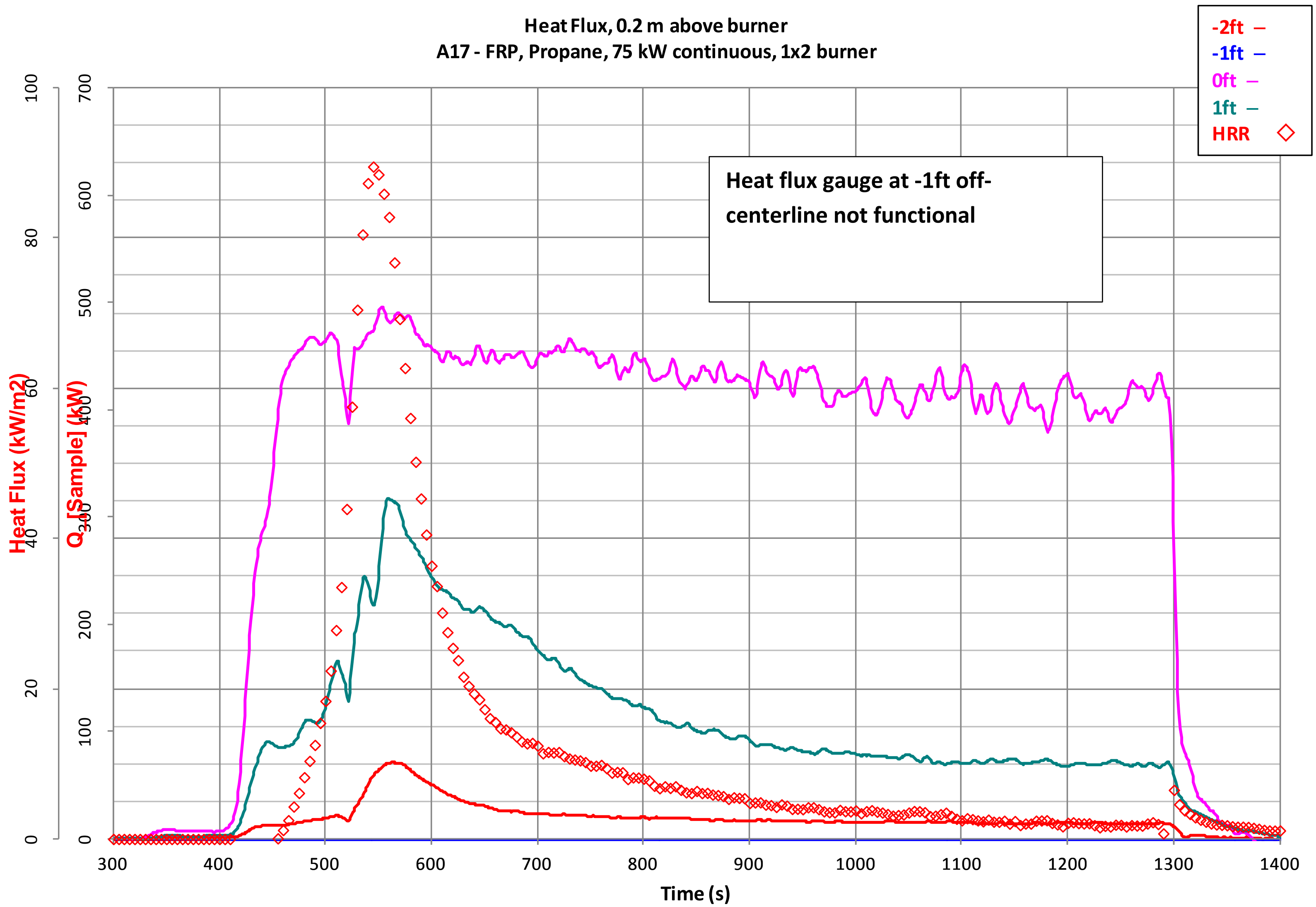

Heat flux measured at various distances from the centerline (negative indicates left of centerline), 0.2m vertically from burner surface

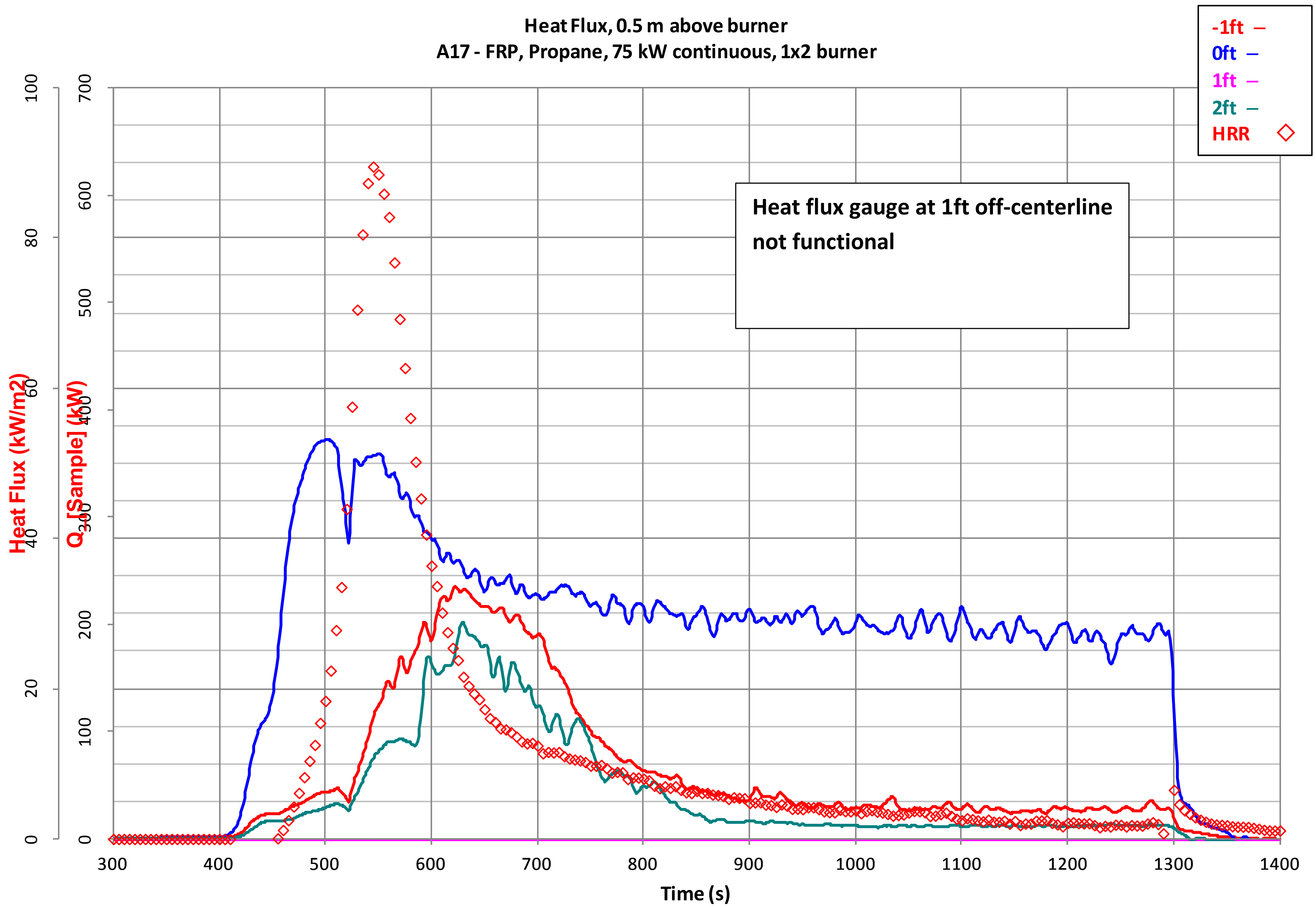

Heat flux measured at various distances from the centerline (negative indicates left of centerline), 0.5m vertically from burner surface

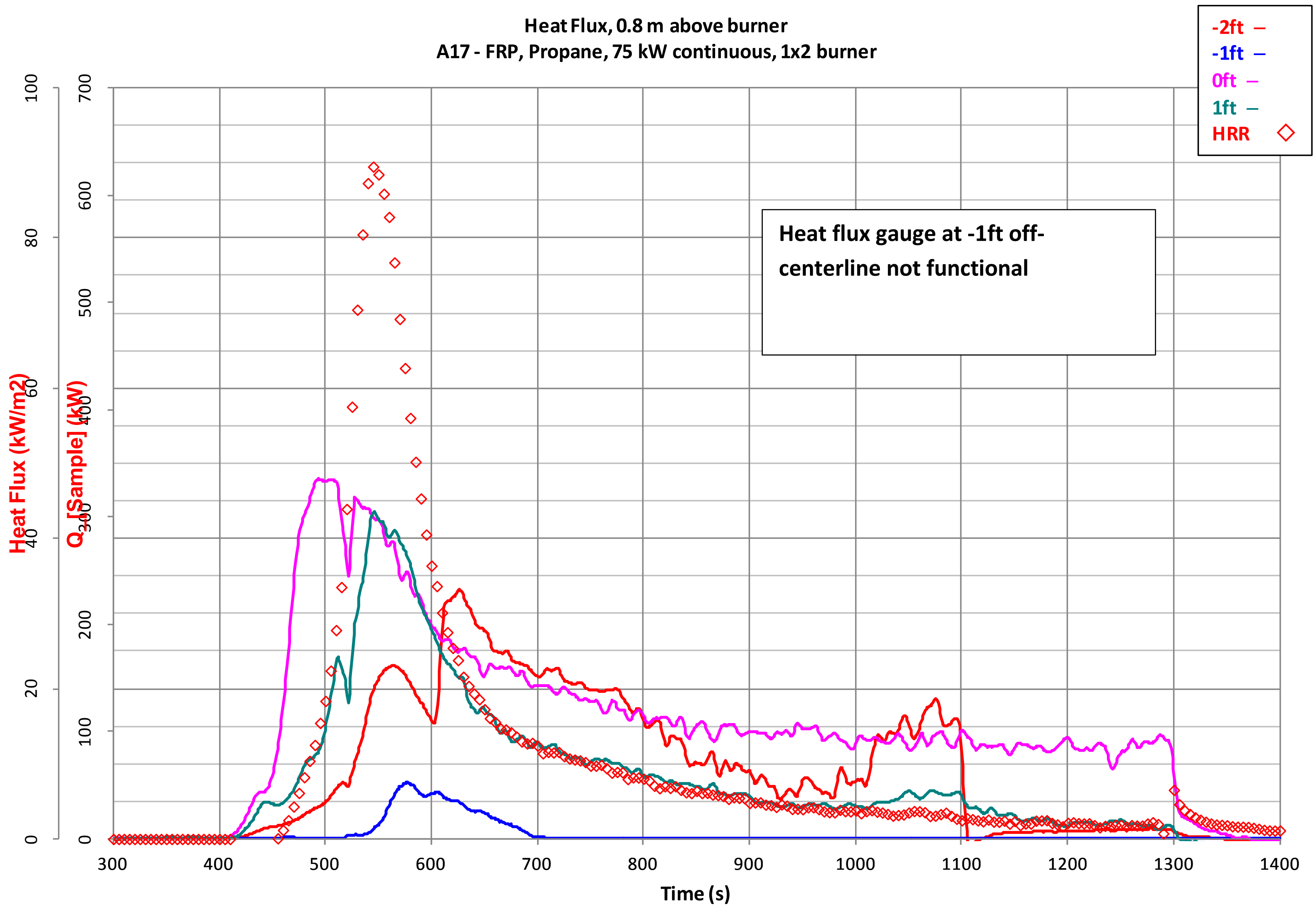

Heat flux measured at various distances from the centerline (negative indicates left of centerline), 0.8m vertically from burner surface

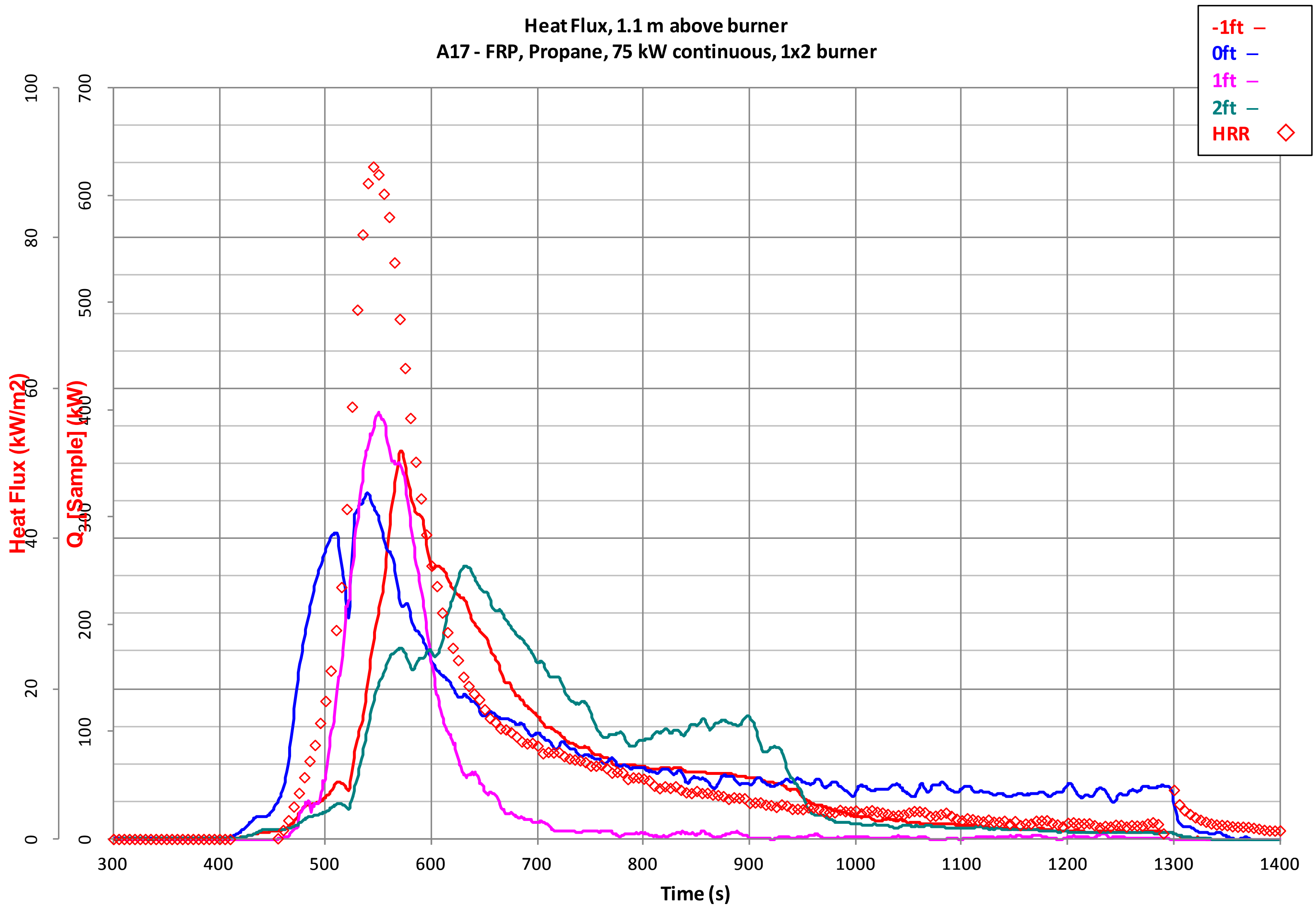

Heat flux measured at various distances from the centerline (negative indicates left of centerline), 1.1m vertically from burner surface

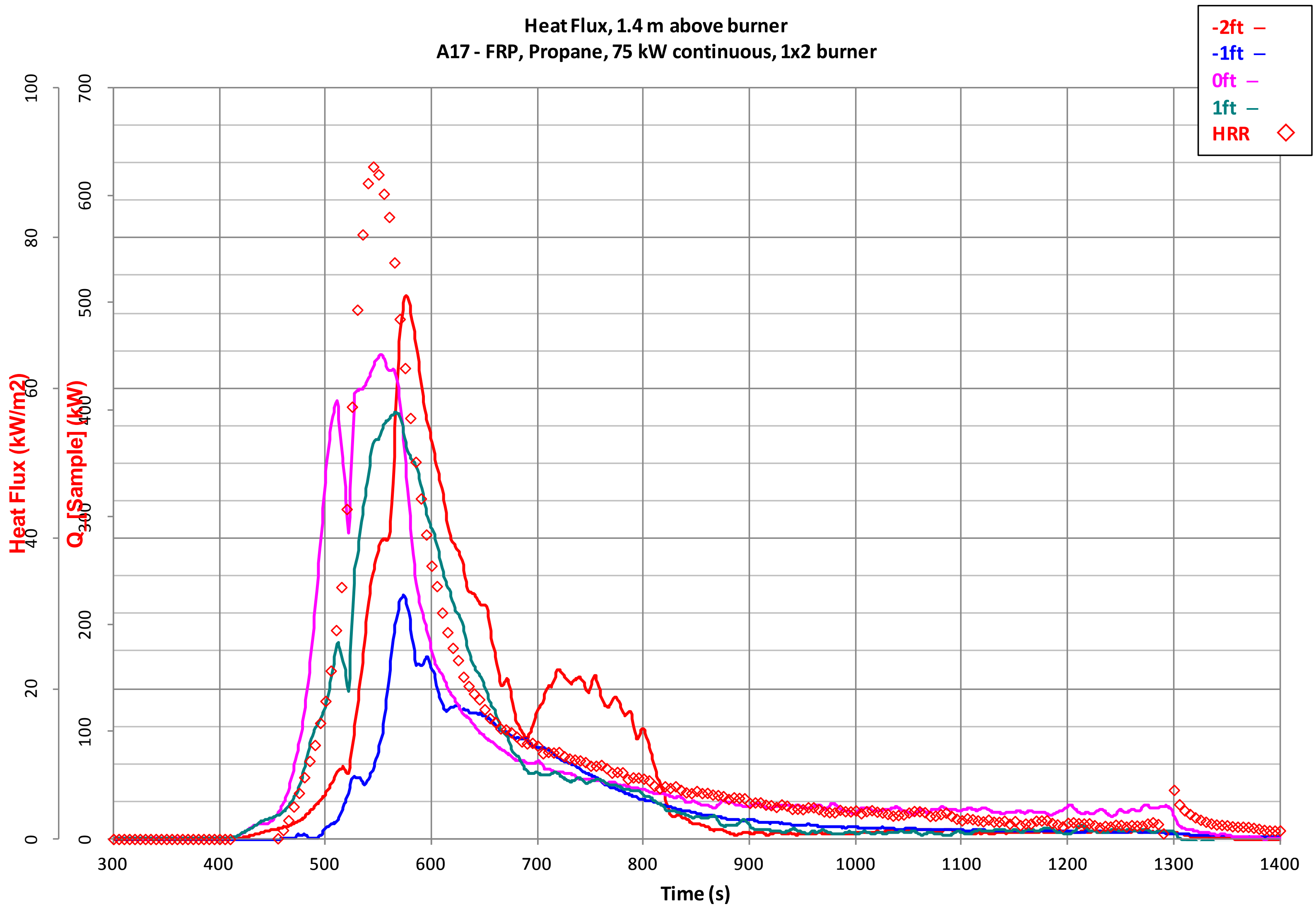

Heat flux measured at various distances from the centerline (negative indicates left of centerline), 1.4m vertically from burner surface

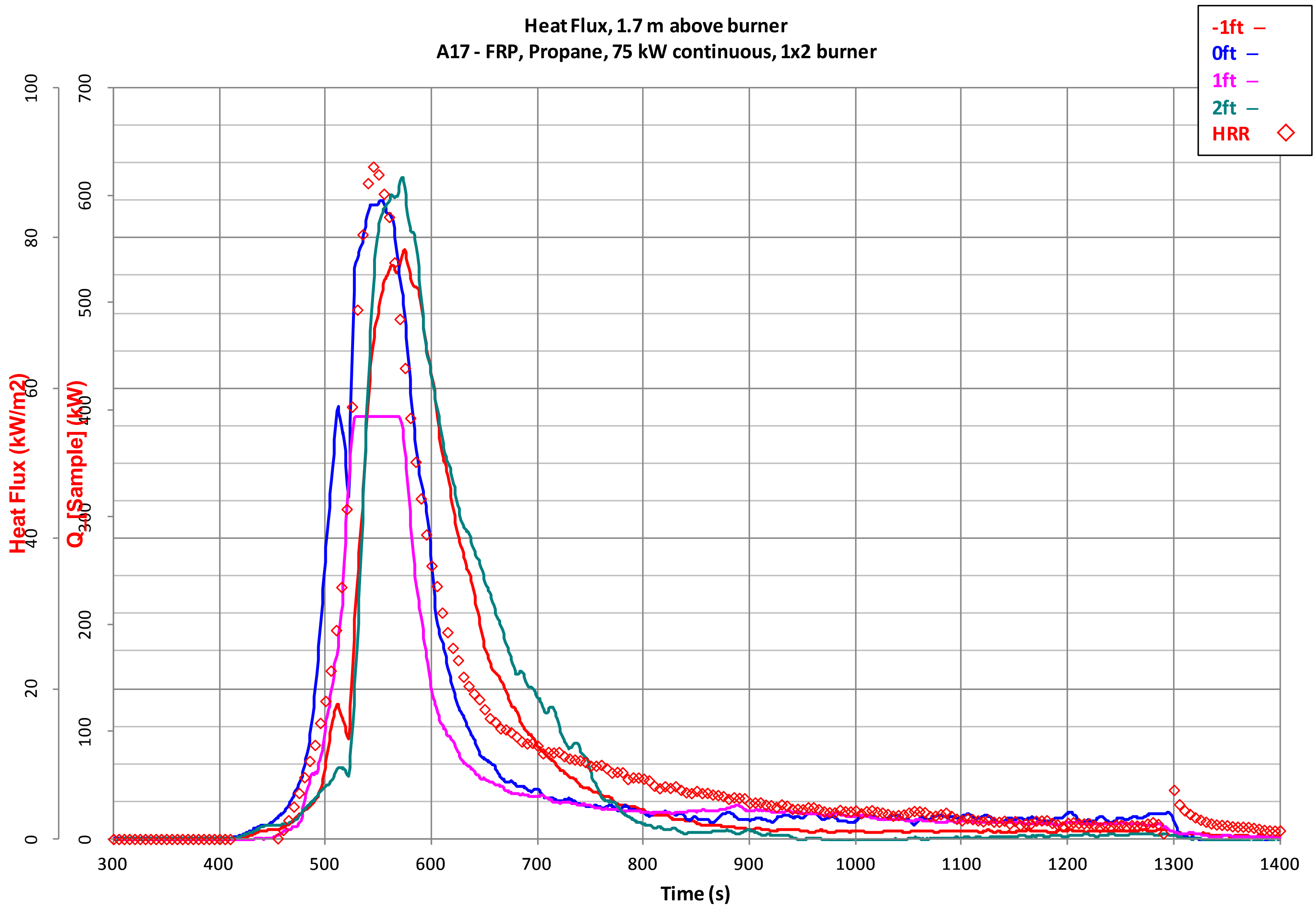

Heat flux measured at various distances from the centerline (negative indicates left of centerline), 1.7m vertically from burner surface

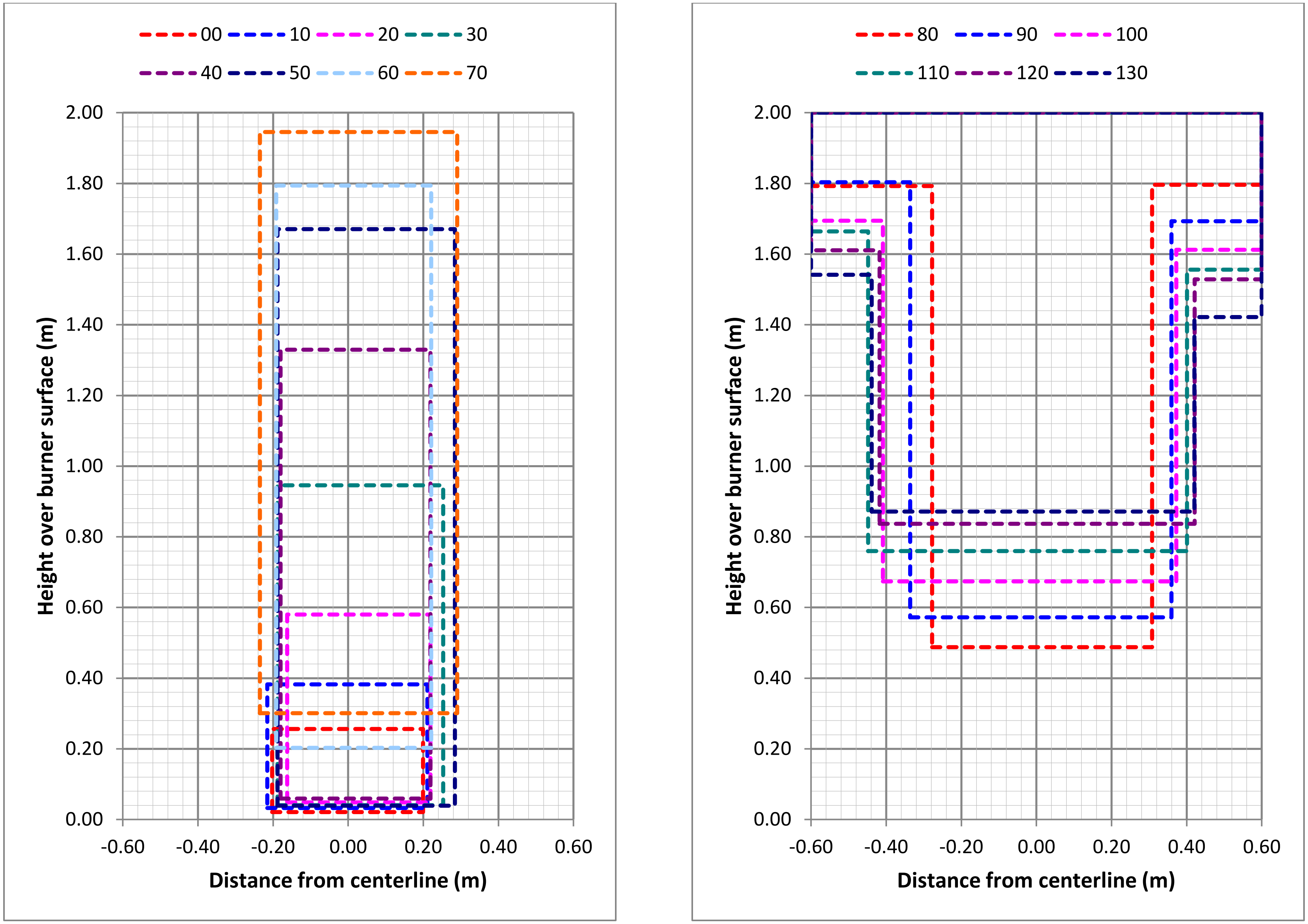

Stages 1 and 2 burning areas in Test A17 (2ft Rectangle burner, Propane, 75 kW source on throughout test)

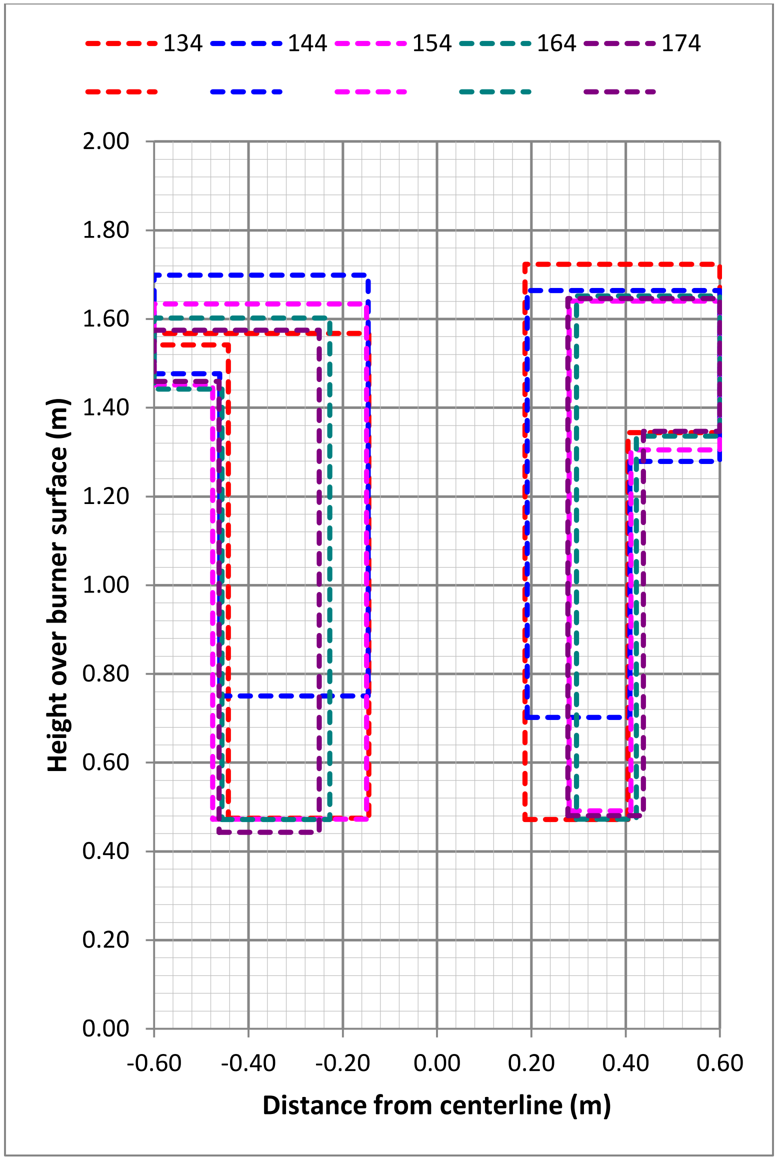

Stage 3 burn area and final damage chart of Test A17 (2ft Rectangle burner, Propane, 75 kW source on throughout test)

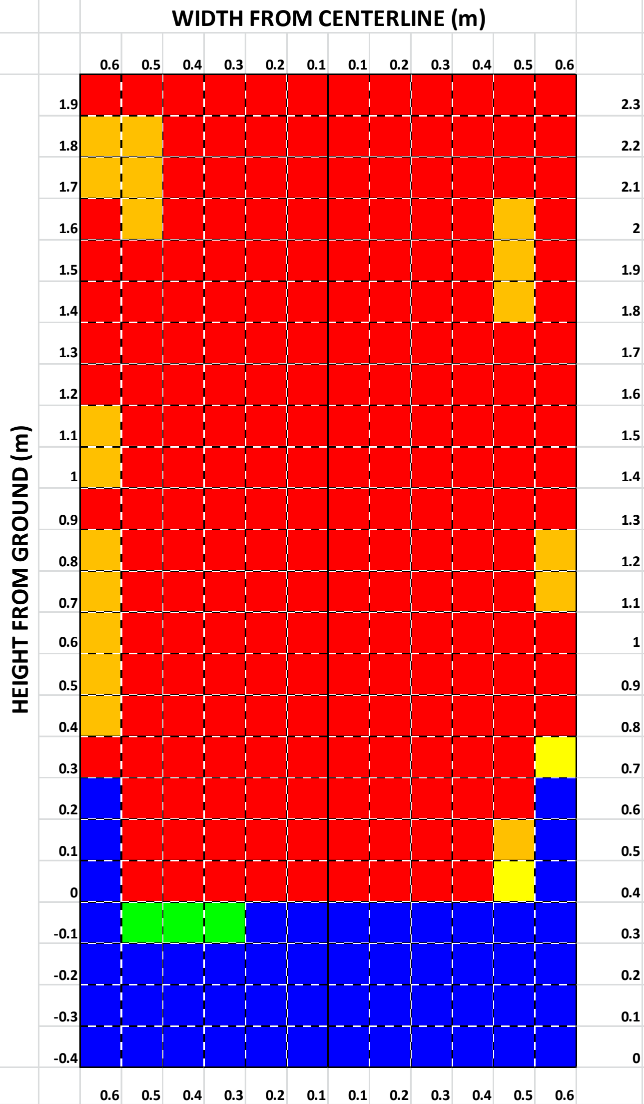

# of cell	Damage to Resin	Area (m2)
214	up to 100% damage	2.14
18	up to 75% damage	0.18
2	up to 50% damage	0.02
3	up to 25% damage	0.03
51	no damage	0.51

Initial mass:	8.52	kg
Final unburnt mass:	1.42	kg
Final burnt mass:	3.68	kg
Total mass loss during fire	3.42	kg

Burn damage pattern observed after fire test

F.3.18 Test A18

LODS Test Run Data

Center for Firesafety Studies

100 Institute Road
Worcester, MA 01609
Phone: (508) 831-5628
Fax: (508) 831-5680

Test Information

Test Number:	A18
Specimen Identification:	FRP 18, 50 kW initial Propane fire, 1 x 2 burner
Material Name:	Class C FRP panel
Manufacturer/Submitter:	Not Reported
Raw Data File Name:	Test A18 - FRP_Propane_50kW_2ft.txt
Reduced Data File Name:	Test A18 - FRP_Propane_50kW_2ft_reduced.xlsx
Date of Test:	7-Dec-2010
Tester:	W. Wong

Test Parameters

Ambient Temperature:	N/A
Relative Humidity:	N/A

Specimen Information

Specimen Initial Mass:	[kg]	8.1
Specimen Final Mass:	[kg]	6.2
Mass Lost:	[kg]	2.0
Heat Evolved (net):	[kJ]	0

Parameter	Unit	Value
Mass Loss		
Initial Mass	[kg]	8.1
Final Mass	[kg]	6.2
Mass Loss	[%]	24.32

LODS Test Run Data

Center for Firesafety Studies

100 Institute Road
Worcester, MA 01609
Phone: (508) 831-5628
Fax: (508) 831-5680

Test Notes

Test Number:	0
Date:	12/07/10
Material:	Class C FRP panel
Specimen Identification:	FRP 18, 50 kW initial Propane fire, 1 x 2 burner

Observations

Time	Observation
00:00	Start VI
04:00	Start Camera 1
04:15	Start Camera 2
07:15	Burner ignition
07:30	Reach target HRR @ 50 kW
08:08	Crackling noise
08:25	Panel ignition
08:42	Burner turned off
09:30	Remote area smoking @ TSC-4, HFG-2, and TSC-10
09:44	Flame hit ceiling
10:18	Burning reaches left and right edges, T burning starts
10:25	Rollover under ceiling, flame layer about 30 cm deep
	Flame spread down to y=2m on the left side, higher on the right side
12:30	Little ignition at TSC-10
25:05	Terminate test by little water application

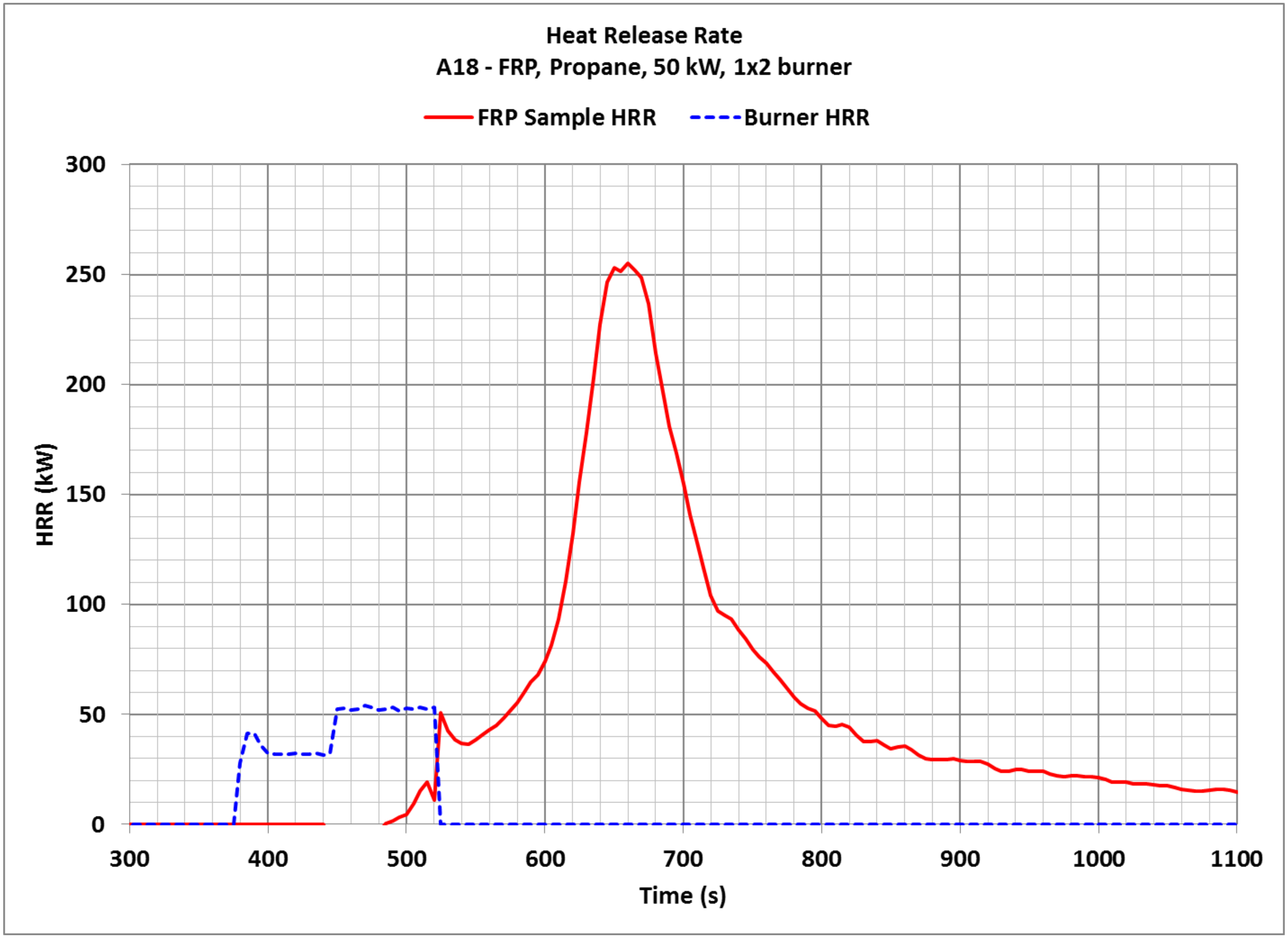

Heat release ratesof the source burner fire and of the specimen fire measured during test

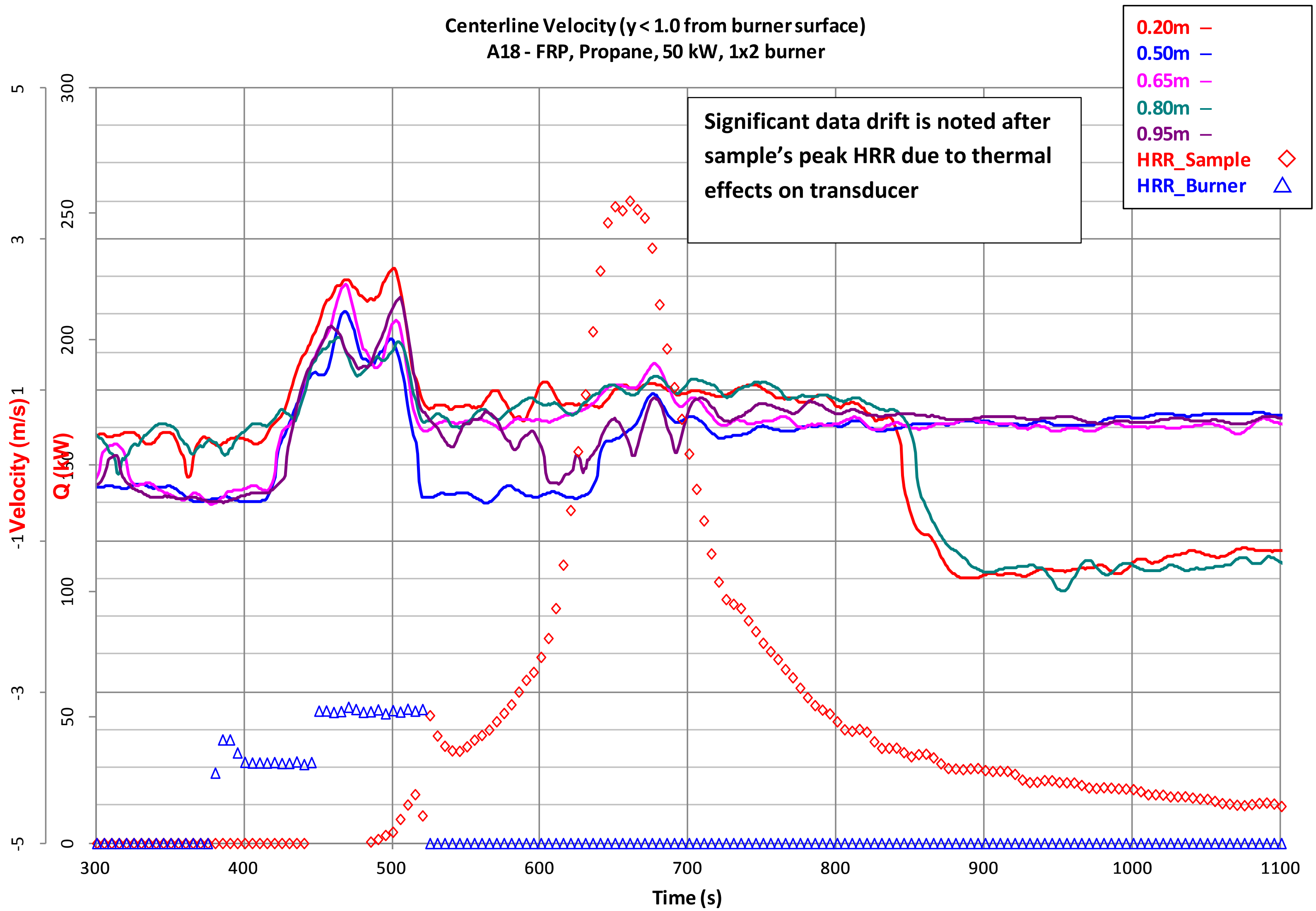

Centerline plume velocities measured from 0.2m to 0.95m above the burner surface

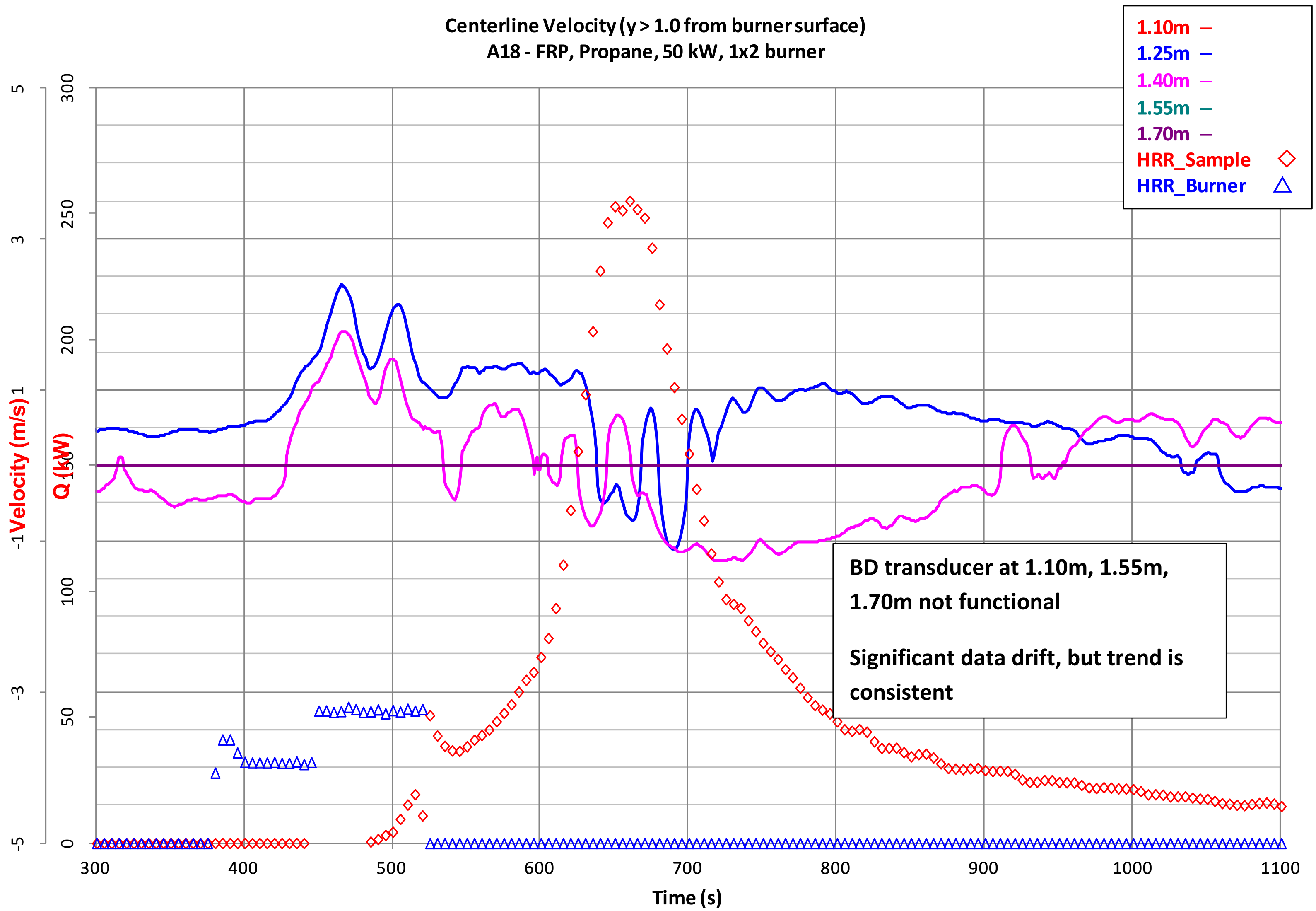

Centerline plume velocities measured from 1.1m to 1.7m above the burner surface

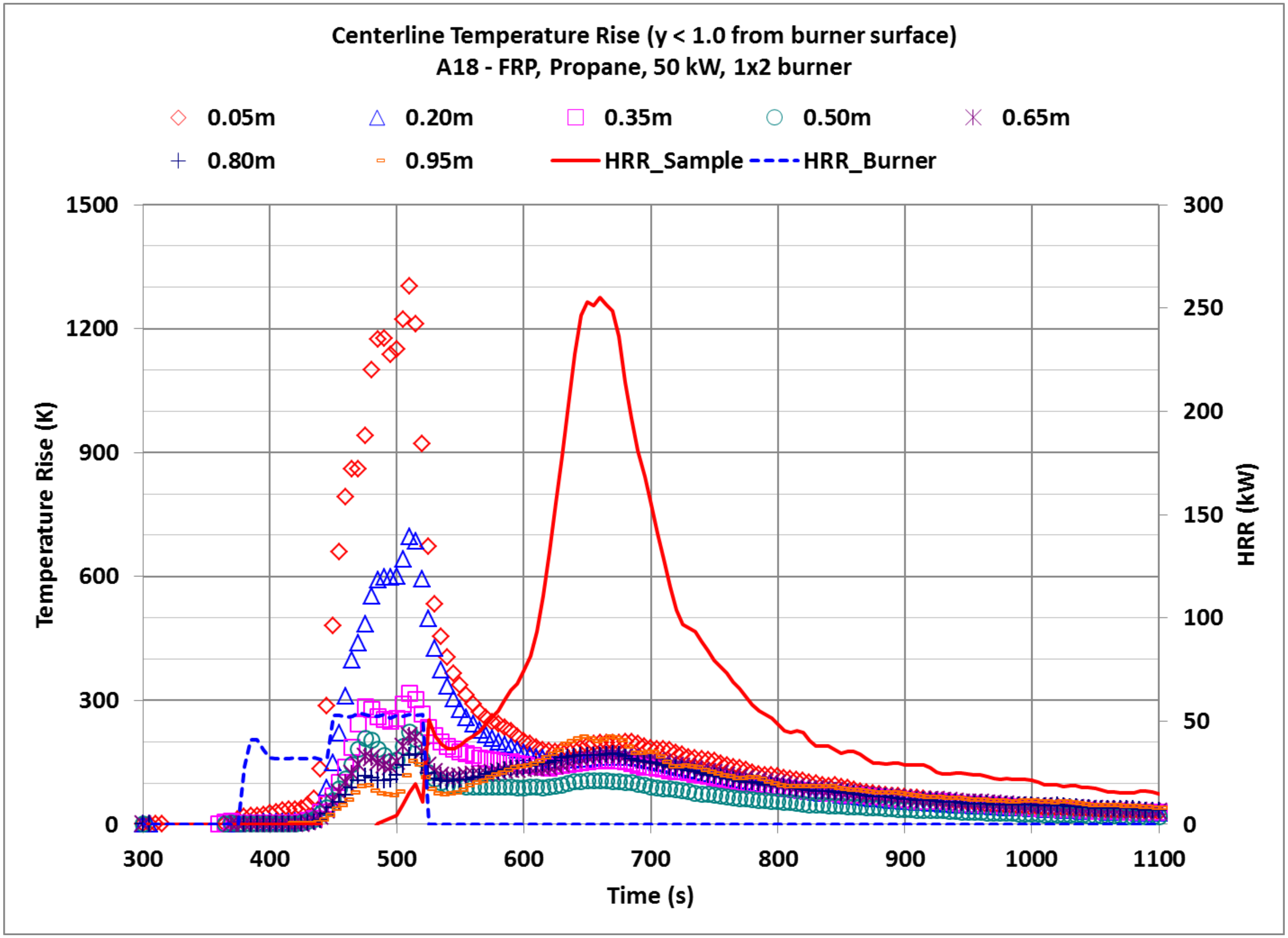

Centerline plume temperature rise measured from 0.05m to 0.95m above the burner surface

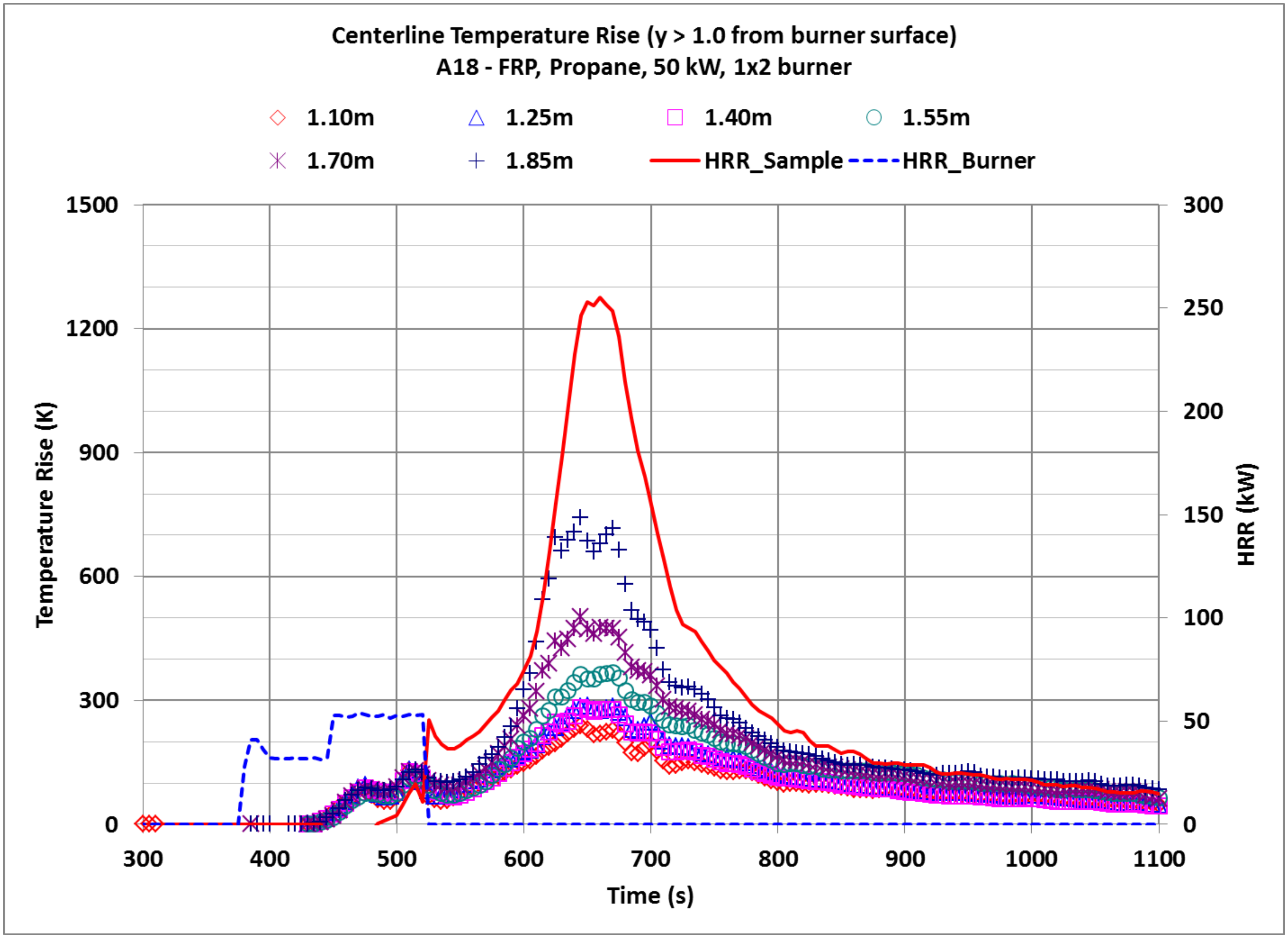

Centerline plume temperature rise measured from 1.10m to 1.85m above the burner surface

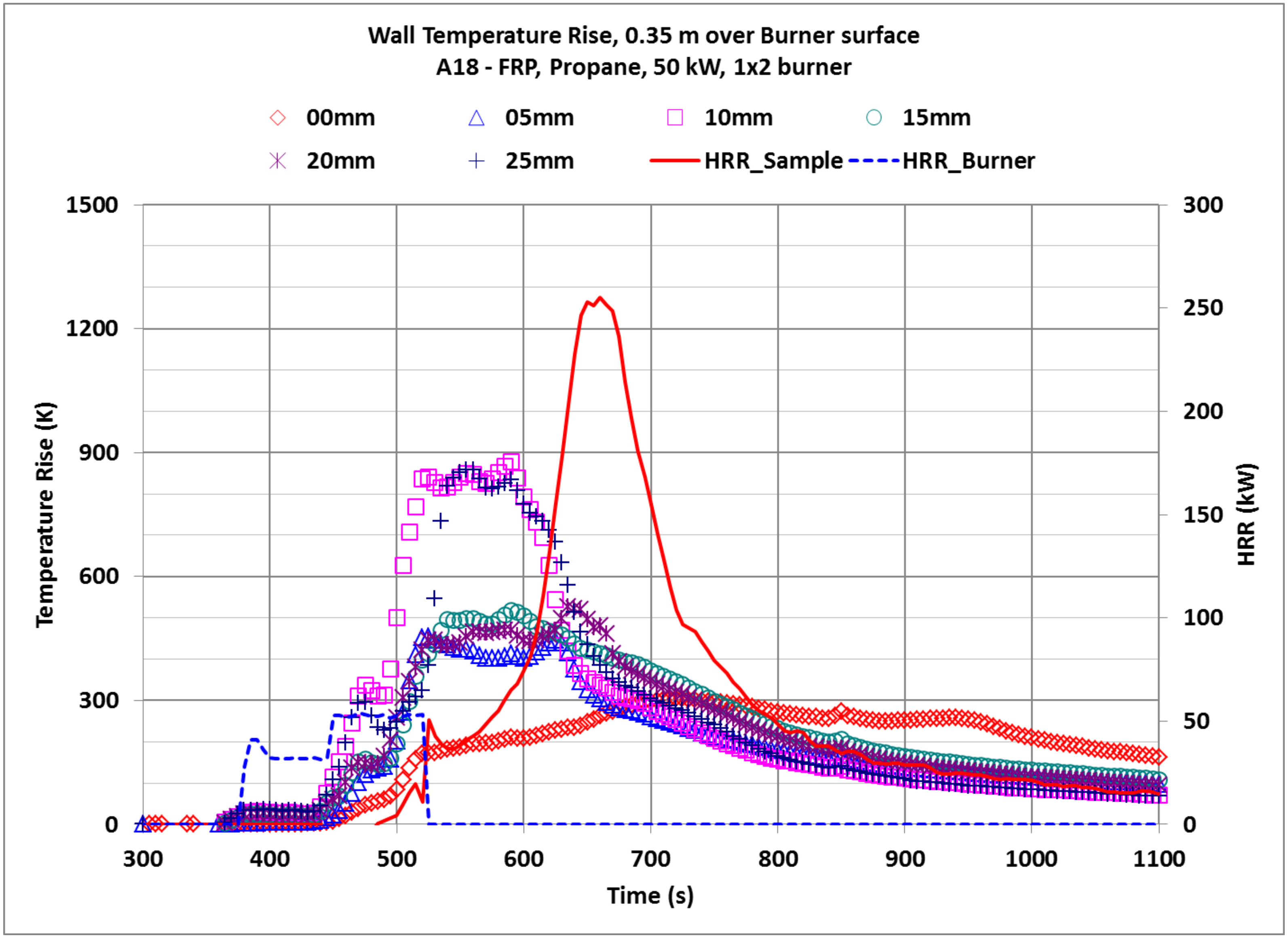

Temperature rise along the wall's centerline at 0.35m over the burner surface, measured at different perpendicular distances to as indicated

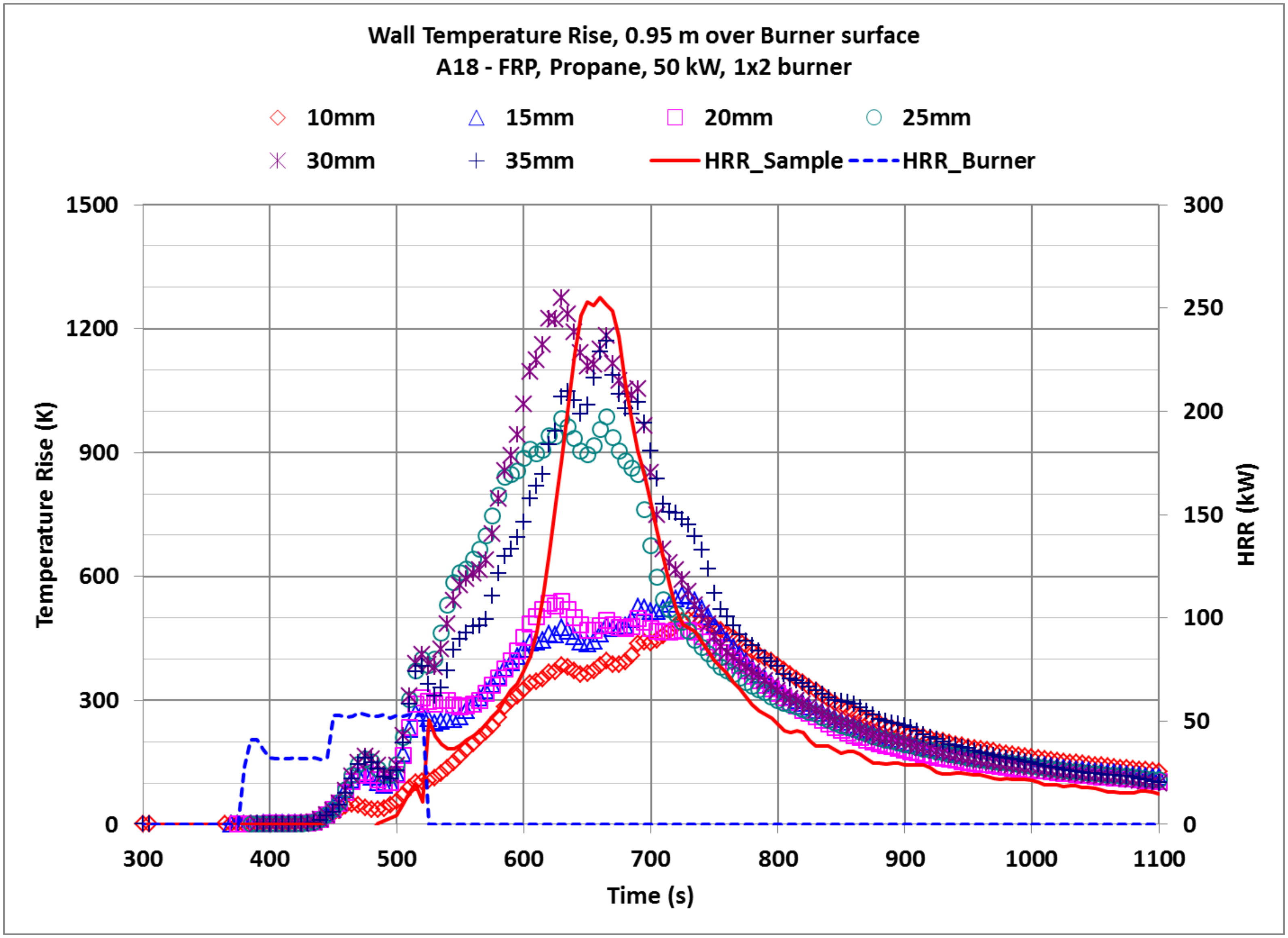

Temperature rise along the wall's centerline at 0.95m over the burner surface, measured at different perpendicular distances to as indicated

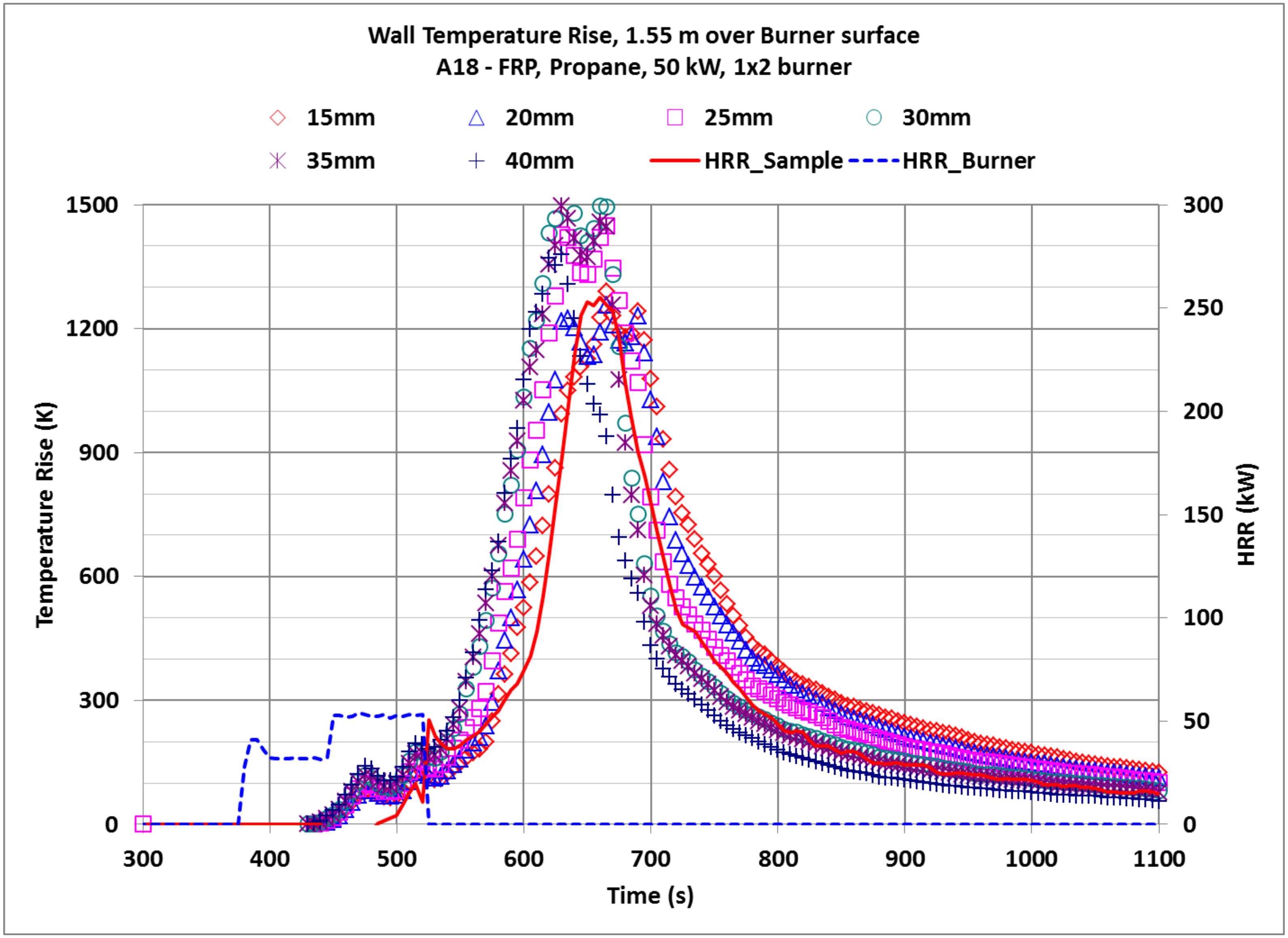

Temperature rise along the wall's centerline at 1.55m over the burner surface, measured at different perpendicular distances to as indicated

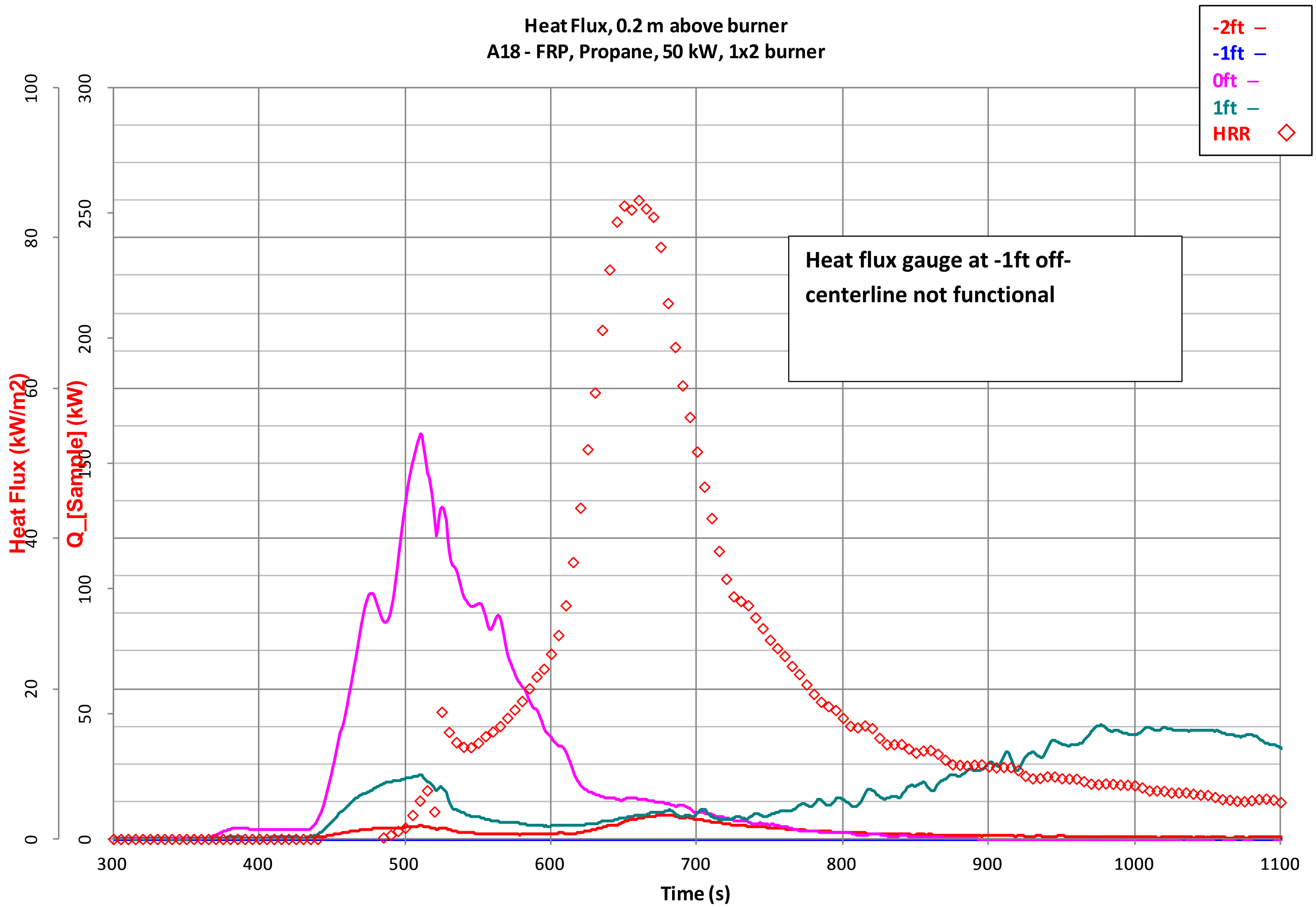

Heat flux measured at various distances from the centerline (negative indicates left of centerline), 0.2m vertically from burner surface

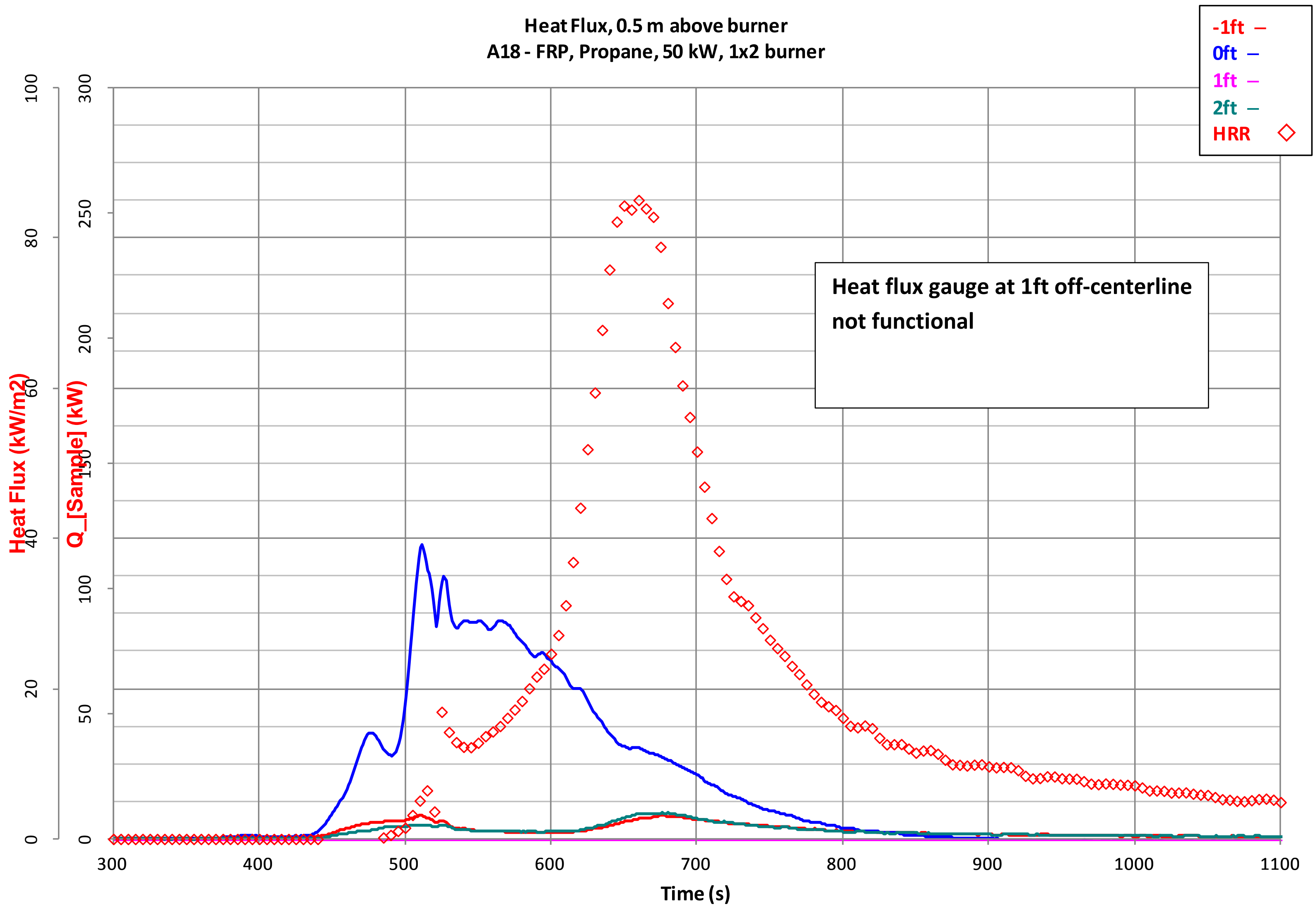

Heat flux measured at various distances from the centerline (negative indicates left of centerline), 0.5m vertically from burner surface

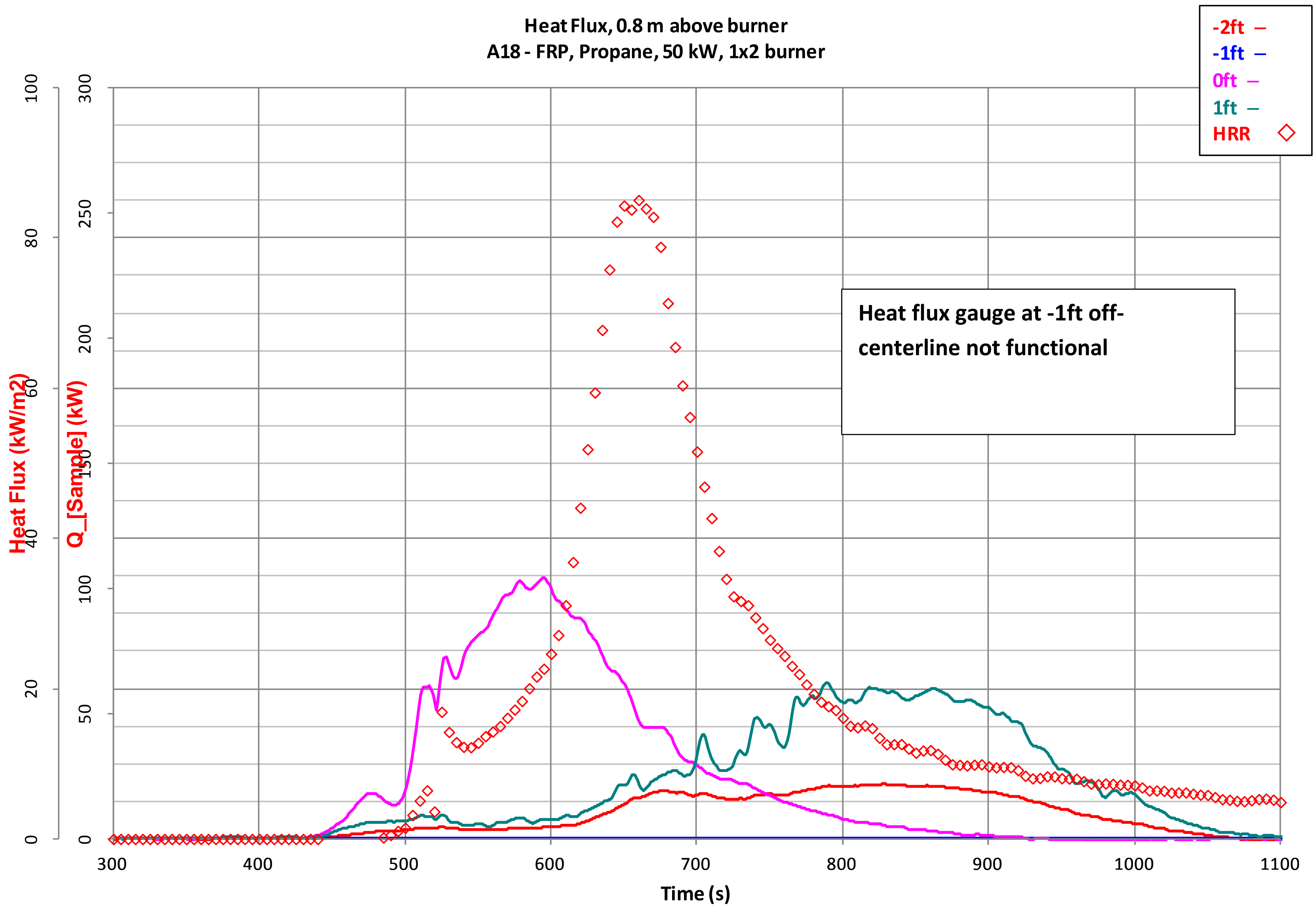

Heat flux measured at various distances from the centerline (negative indicates left of centerline), 0.8m vertically from burner surface

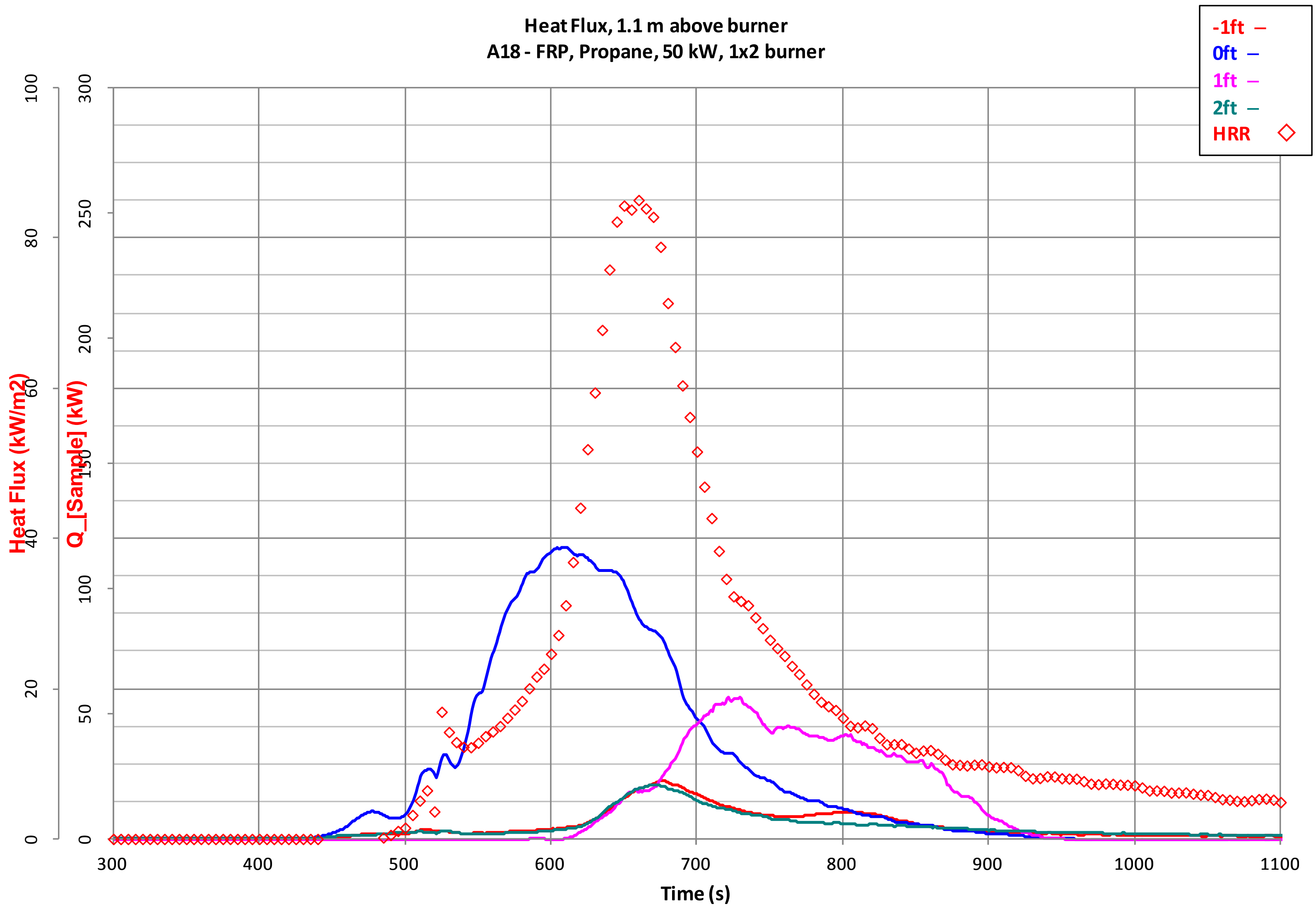

Heat flux measured at various distances from the centerline (negative indicates left of centerline), 1.1m vertically from burner surface

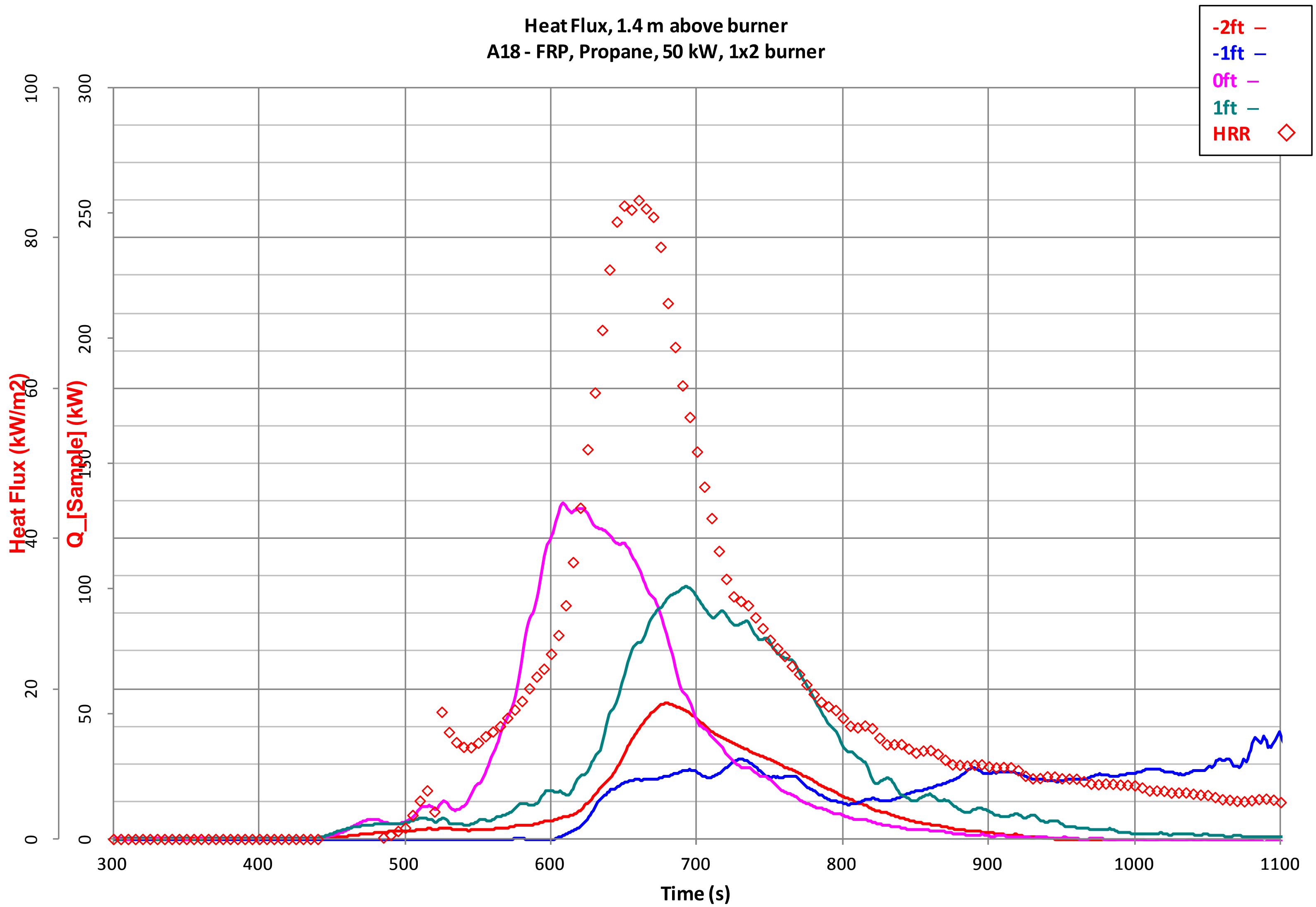

Heat flux measured at various distances from the centerline (negative indicates left of centerline), 1.4m vertically from burner surface

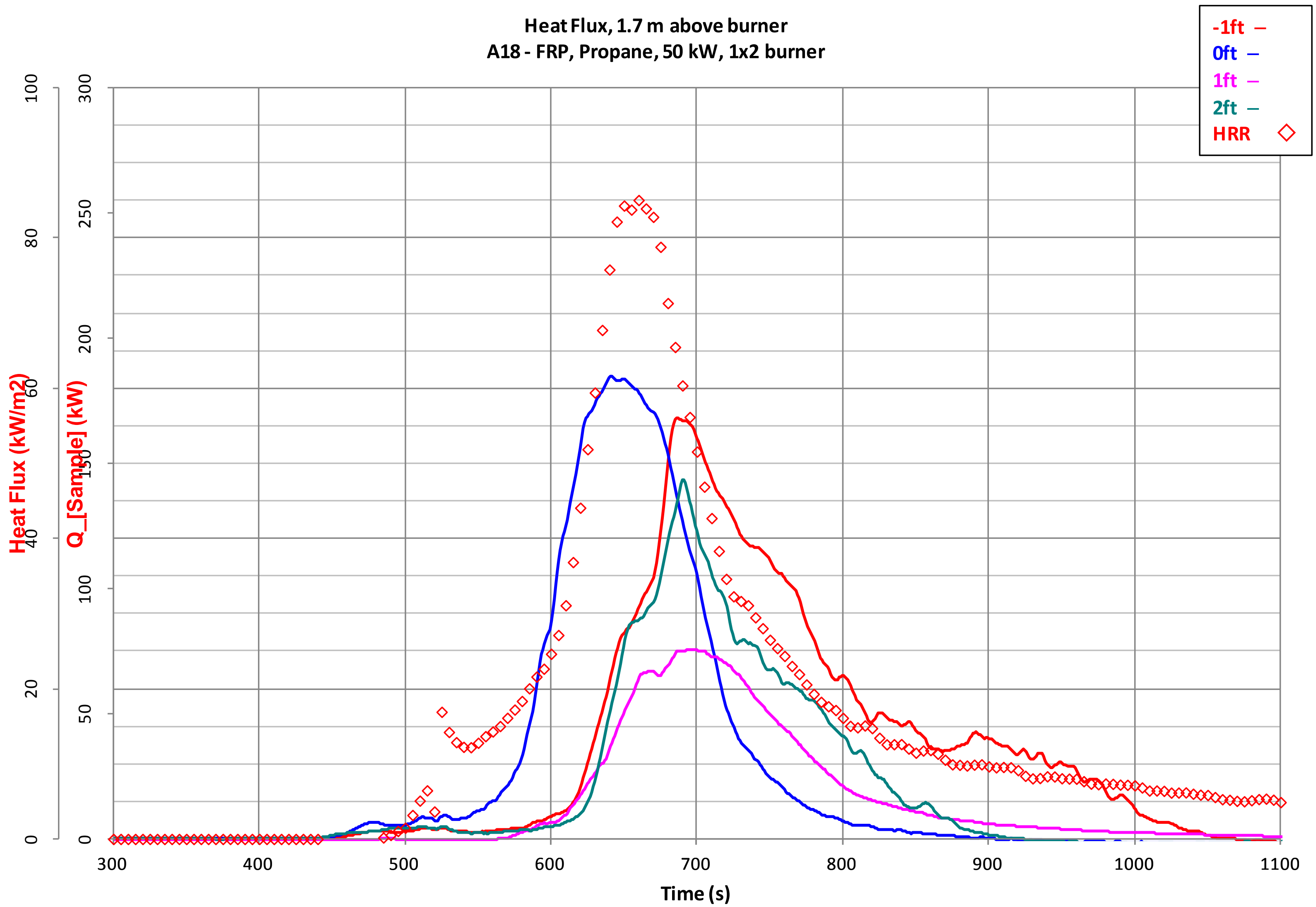

Heat flux measured at various distances from the centerline (negative indicates left of centerline), 1.7m vertically from burner surface

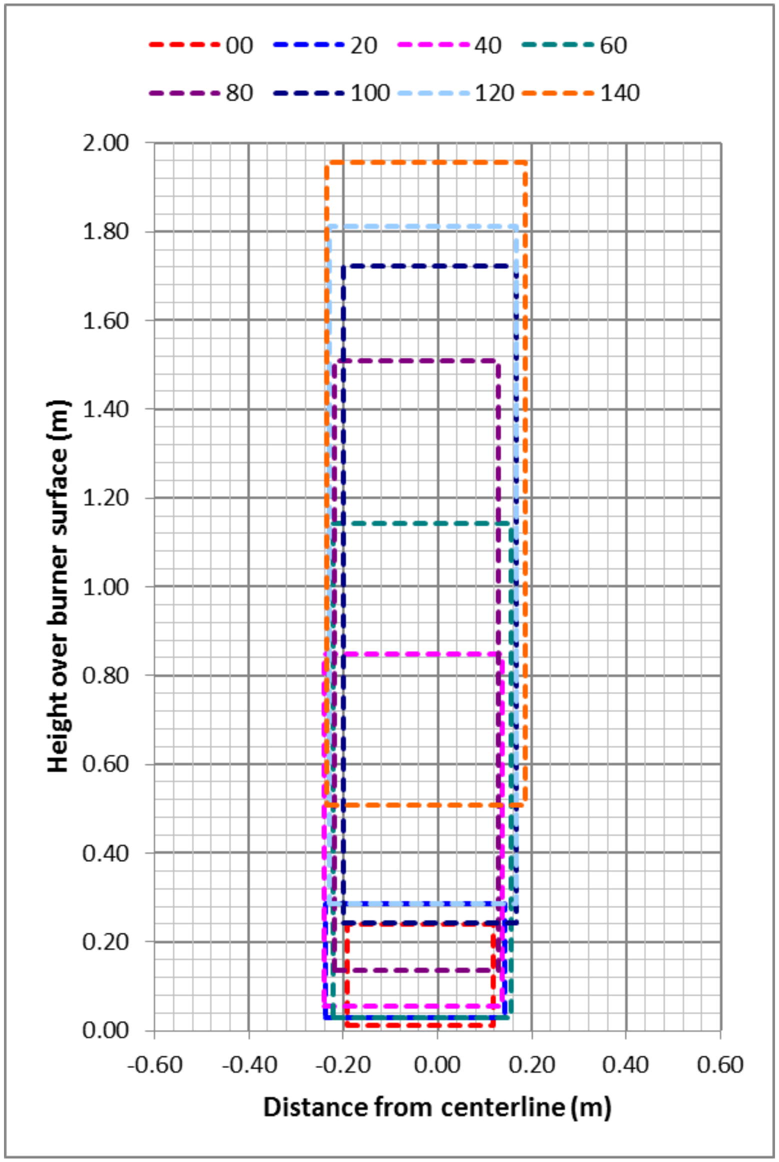

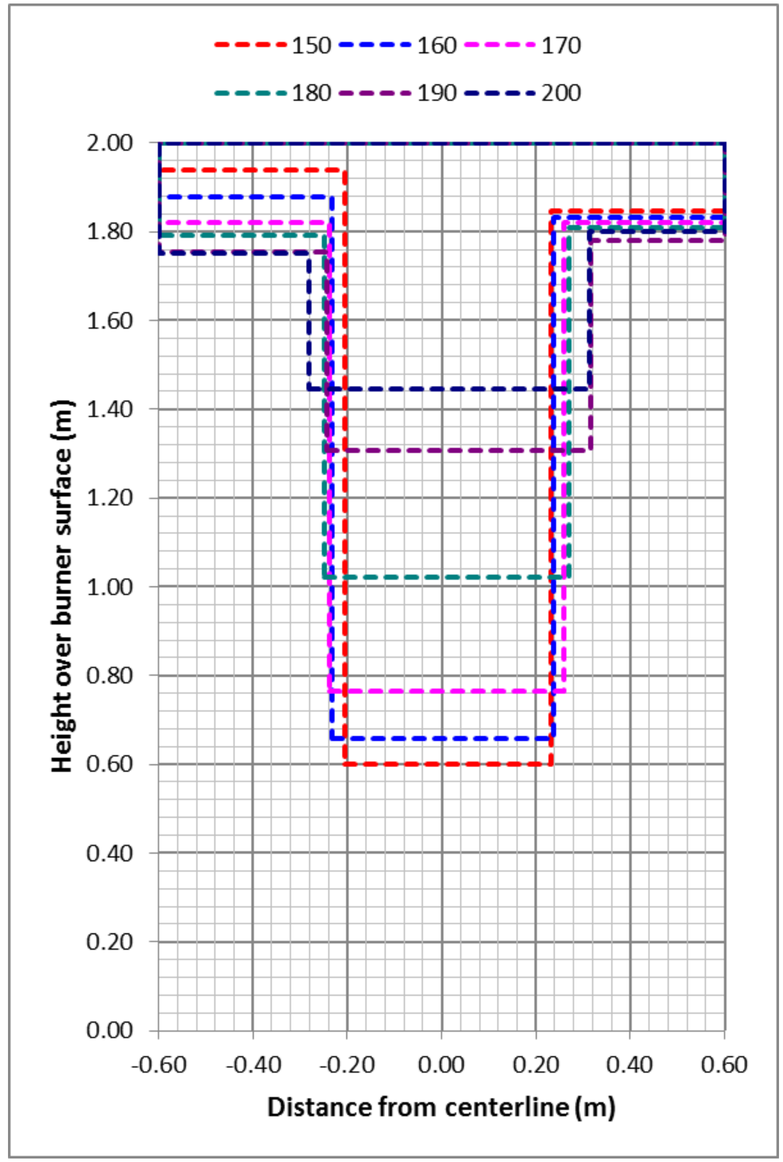

Stages 1 and 2 burning areas in Test A18 (2ft Rectangle burner, Propane, 50 kW source)

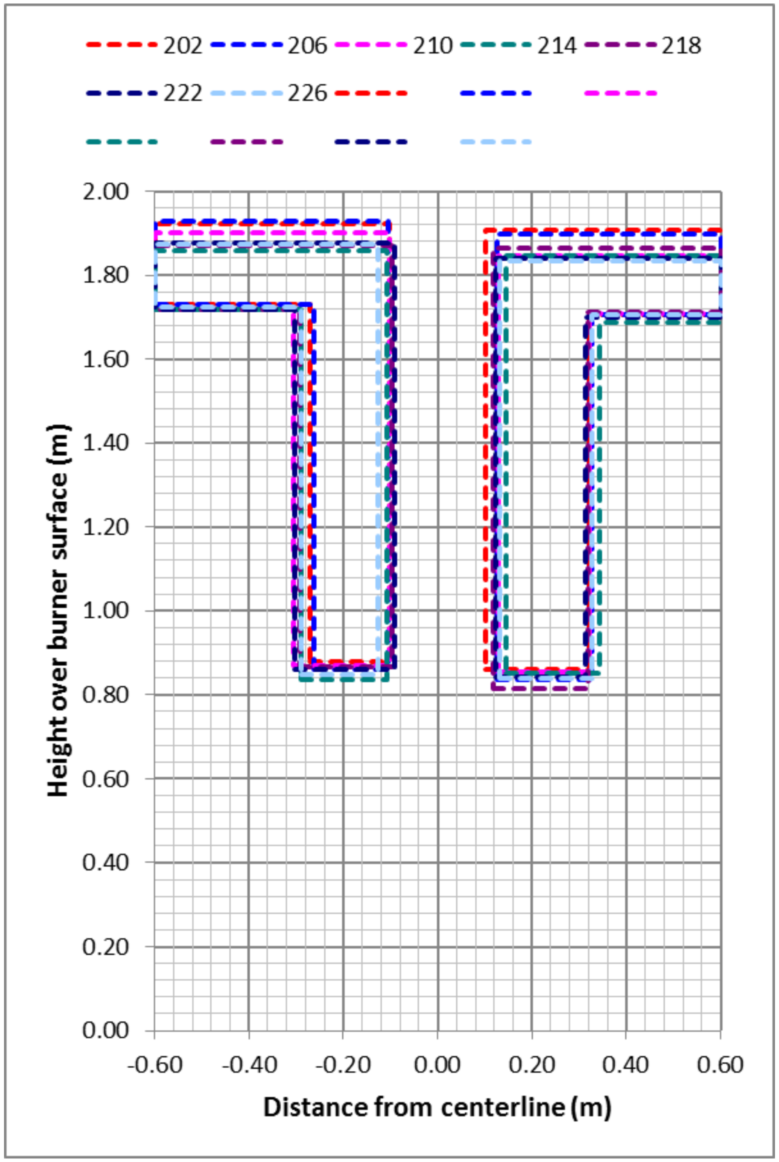

Stage 3 burn area and final damage chart of Test A18 (2ft Rectangle burner, Propane, 50 kW source)

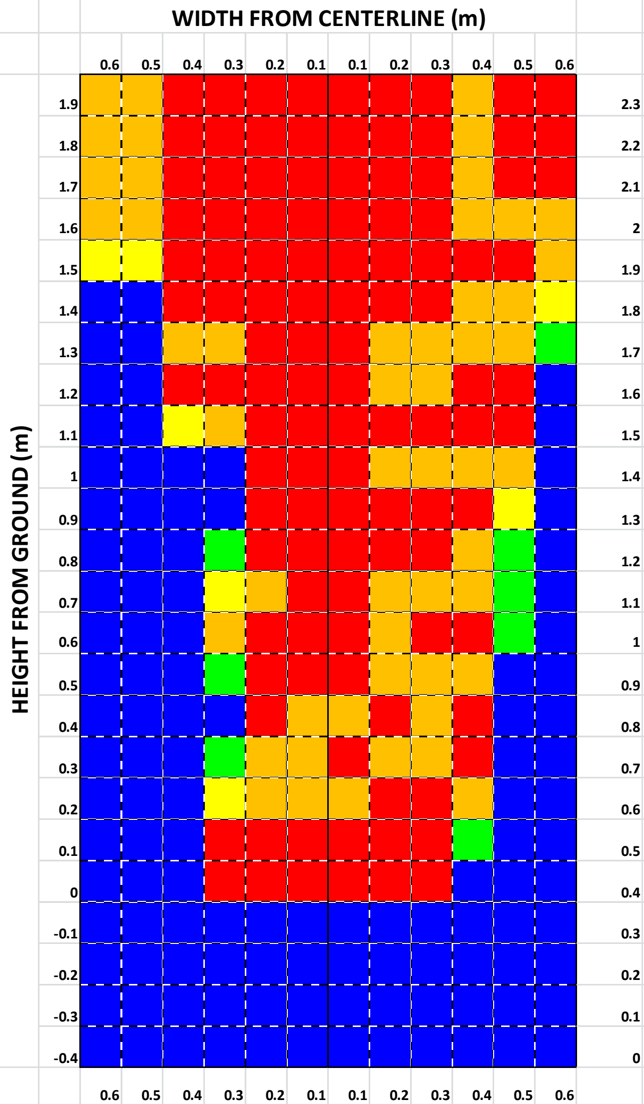

# of cell	Damage to Resin	Area (m2)
104	up to 100% damage	1.04
51	up to 75% damage	0.51
7	up to 50% damage	0.07
8	up to 25% damage	0.08
118	no damage	1.18

Initial mass:	8.14	kg
Final unburnt mass:	3.72	kg
Final burnt mass:	2.44	kg
Total mass loss during fire	1.98	kg

Burn damage pattern observed after fire test

Appendix G GPYRO Material Parameters Sensitivity Study

This section presents the two sets of material parameters sensitivity studies conducted to determine the validity of the material parameters used in the FRP FDS simulations.

G.1 GPYRO Material Parameters Sensitivity Study (Round 1)

In the parametric study regarding the GPYRO outputs for the FRP material, 11 parameters were varied in successive simulations in order to determine their effects on the heat release rate/flame spread simulation. The simulations were performed using 5 mm grid on a FRP fire simulation with a Square burner with a constant propane fire at 75 kW.

Material properties generated from a series of cone tests performed on the Class C FRP panel provided the initial inputs for the GPYRO algorithm in order to generate parameters useful in a FDS simulation. The 11 parameters of interested included the thermal conductivity, specific heat, and emissivity of the virgin and charred materials, the density of the char, the activation energy, order of reaction, heat of reaction, and the pre-exponential factor of the fuel.

The baseline of this series of simulations used all the optimal parameters generated by GPYRO. In each successive simulation, one of the parameter was changed to its maximum or minimum values produced by the GPYRO algorithm. A simulation with all average values of the parameters from the best GPYRO solutions was also executed for comparative purposes. Table 1 shows the order of simulations and the parameter used.

Table 1 - Parametric simulation run log

	Description	k_v	c_v	ε_v	k_c	c_c	r_c	ε_c	log A	E	n	log ΔH_v
Run 1	Optimal	0.423	2004.551	0.859	0.054	2109.081	853.842	0.936	10.524	140.429	1.439	6.023
Run 2	min kv	0.359										
Run 3	max kv	0.600										
Run 4	min cv		1564.691									
Run 5	max cv		2300.000									
Run 6	min ev			0.800								
Run 7	max ev			0.900								
Run 8	min kc				0.050							
Run 9	max kc				0.064							
Run 10	min cc					1537.234						
Run 11	max cc					2300.000						
Run 12	min rc						849.014					
Run 13	max rc						864.603					
Run 14	min ec							0.900				
Run 15	max ec							0.991				
Run 16	min log A								10.500			
Run 17	max log A								11.984			
Run 18	min E									140.429		
Run 19	max E									155.000		
Run 20	min n										0.813	
Run 21	max n										1.500	
Run 22	min log Hv											5.827
Run 23	max log Hv											6.094
Run 24	Average	0.454	1963.543	0.853	0.053	2049.385	856.620	0.923	11.022	148.964	1.224	5.956

In the following comparisons, the HRR curves are representative of the FRP burning only, the source 75 kW had been removed. Simulations were run for 900 seconds, but all models predicted little burning after 400 seconds.

G.1.1 Predicted HRRs from parametric study

A comparison was made between the resulting HRR curve from the runs with all optimized parameters, all average parameters, and the original parameters used in previous simulation efforts. The HRR curves shown in Figure 1 suggests that the previously used set of parameters and the current optimal sets of parameters generated similar HRR curves in terms of both timing of the peak and its magnitude. The average set of parameters also generated a HRR similar to the other two, but with a slightly higher HRR at peak.

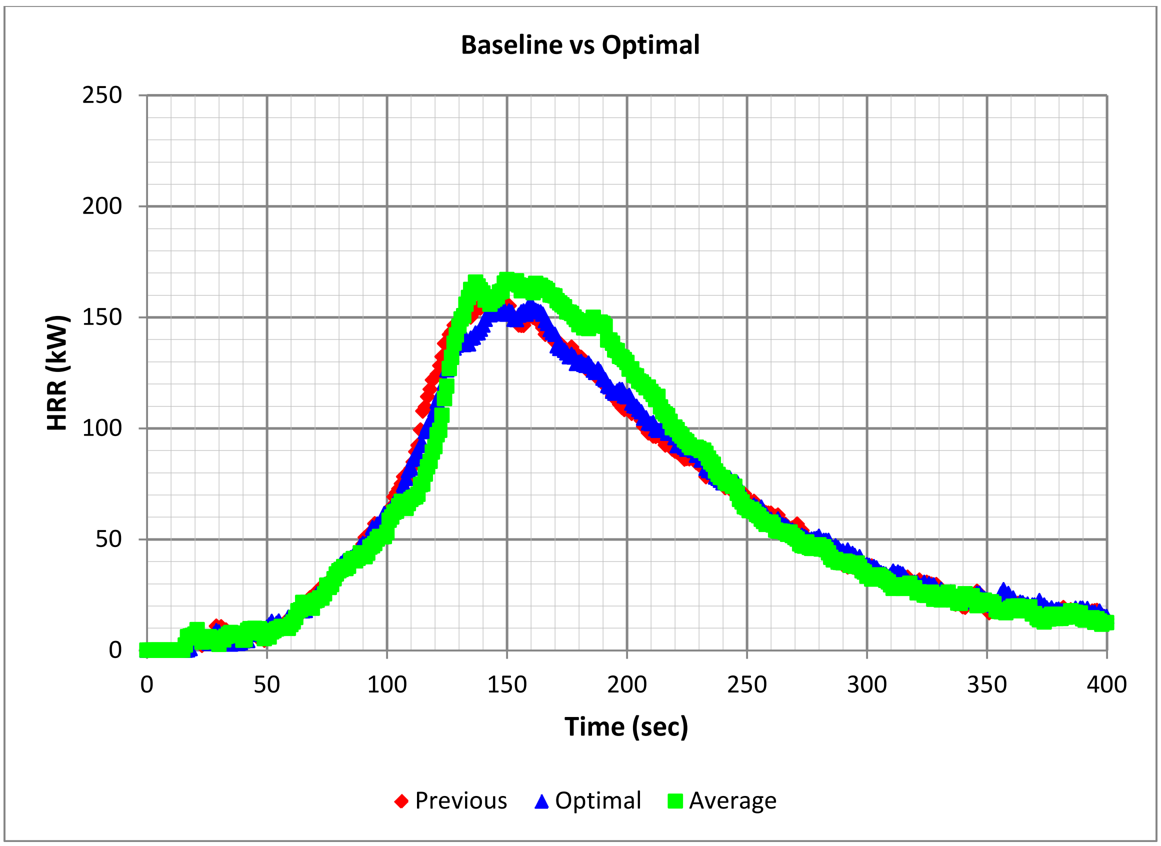

Figure 1 - HRR of FRP panel comparison between previous, optimal, and average sets of parameters

In Figure 2, the results from the simulations with a varied thermal conductivity value of the virgin material are presented. Increasing the thermal conductivity appears to increase the magnitude of the peak by 12.5% but also quicken the time to peak HRR. Decreasing the thermal conductivity appears to have the opposite effects, but the magnitude was only reduced by 6.25%. Since the thermal conductivity describes how well a material conducts heat, increasing its value would results in a quicker heating of the material and makes it easier to burn in the simulation, the results of the simulations are reasonable. Amending the thermal conductivity does not appear to have a significant effect on the HRR curve outside of the interval of the peak: the HRR predicted during the initial burning and decline after peaking are similar to the baseline simulation.

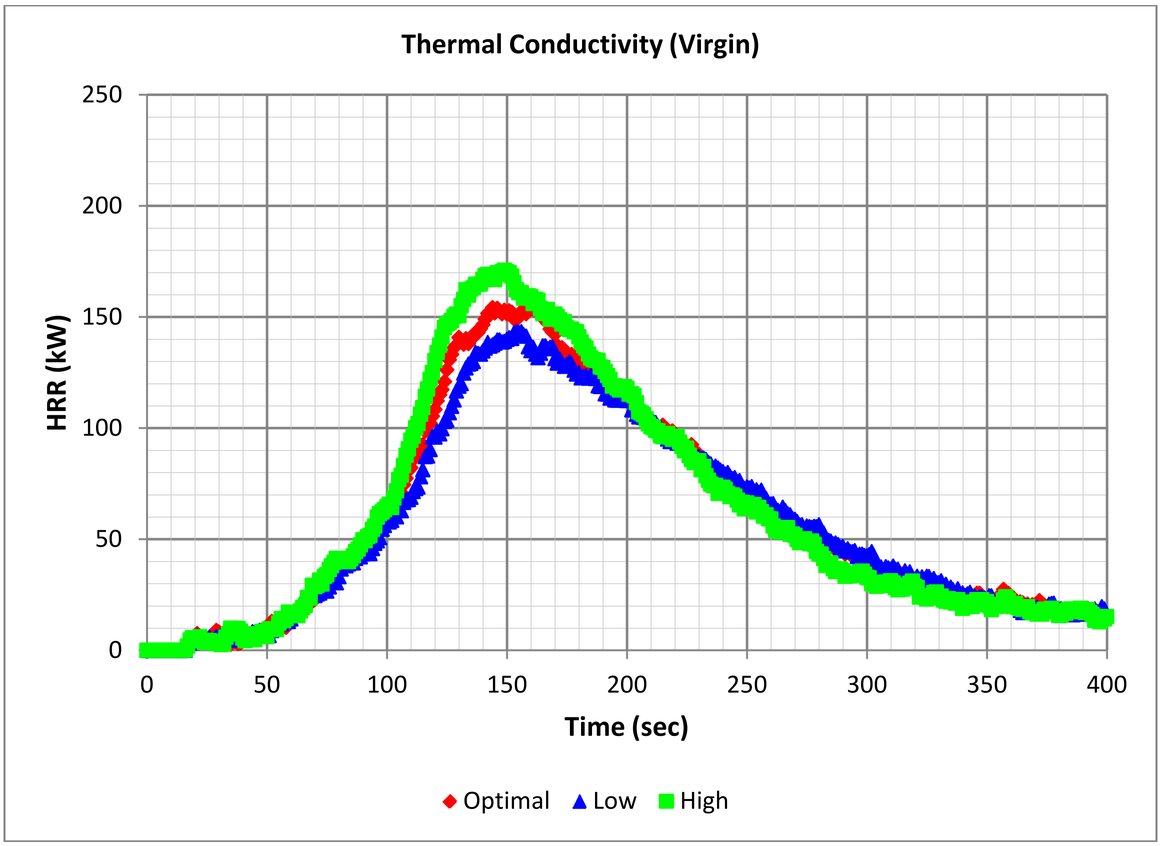

Figure 2 - HRR of FRP panel with varied thermal conductivity of virgin material

Changes in predicted HRR due to a variation of the virgin material's specific heat are reported in Figure 3. By increasing the specific heat, the material is "harder" to heat up, and results in a lower predicted HRR from initial burning to peak, and a slower peak, however, the predicted HRR is higher than baseline at the decline phase. Inversely, a decrease in the specific heat resulted in a higher HRR from initial burning to peak, and a lower HRR at the decline phase, along with a faster time to peak. The low specific heat value is -22%, and the high specific heat value is +14.7% over the optimal value.

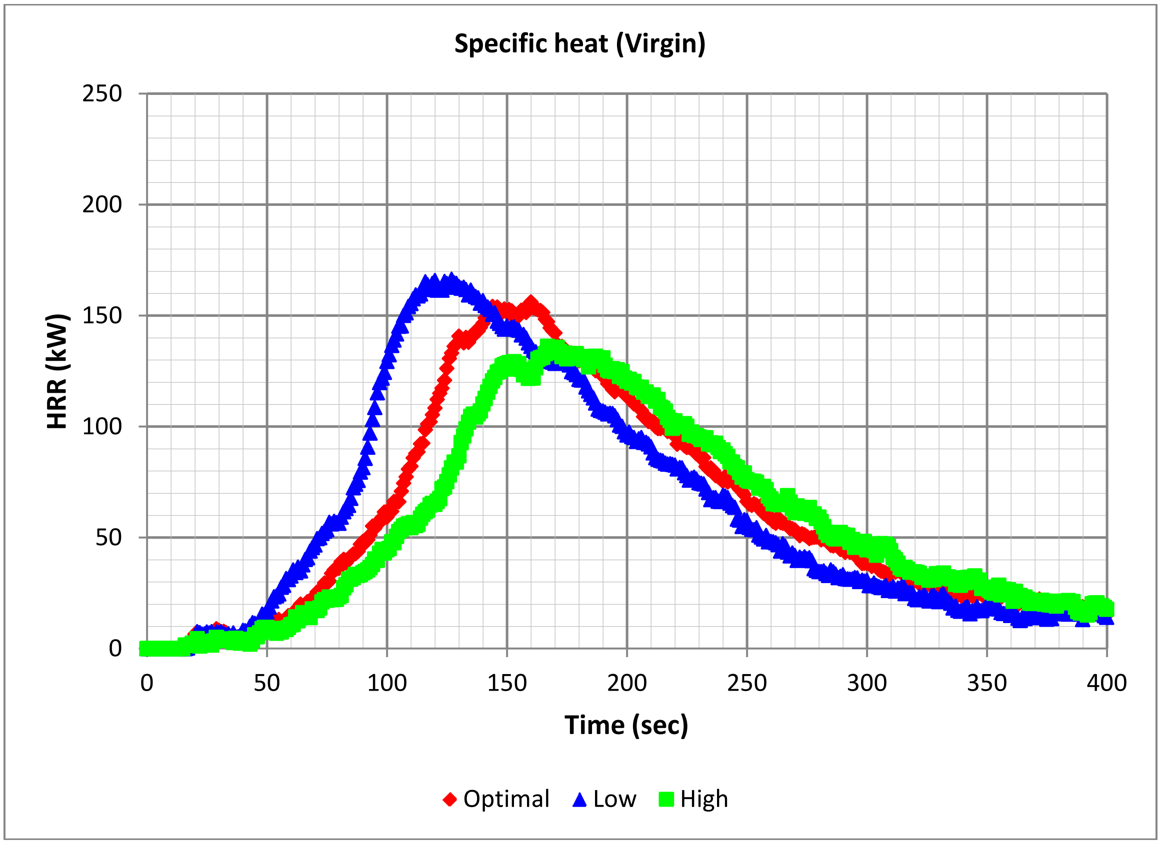

Figure 3 - HRR of FRP panel with varied specific heat of virgin material

Figure 4 presents the predicted HRR curve with varied emissivity of the virgin material. Overall, there are no significant changes to the magnitude or timing of the peak HRR. Reducing the emissivity appears to slightly reduce the HRR generated during the initial burning phase. Otherwise, the variations in emissivity did not incur much changed in the predicted HRR.

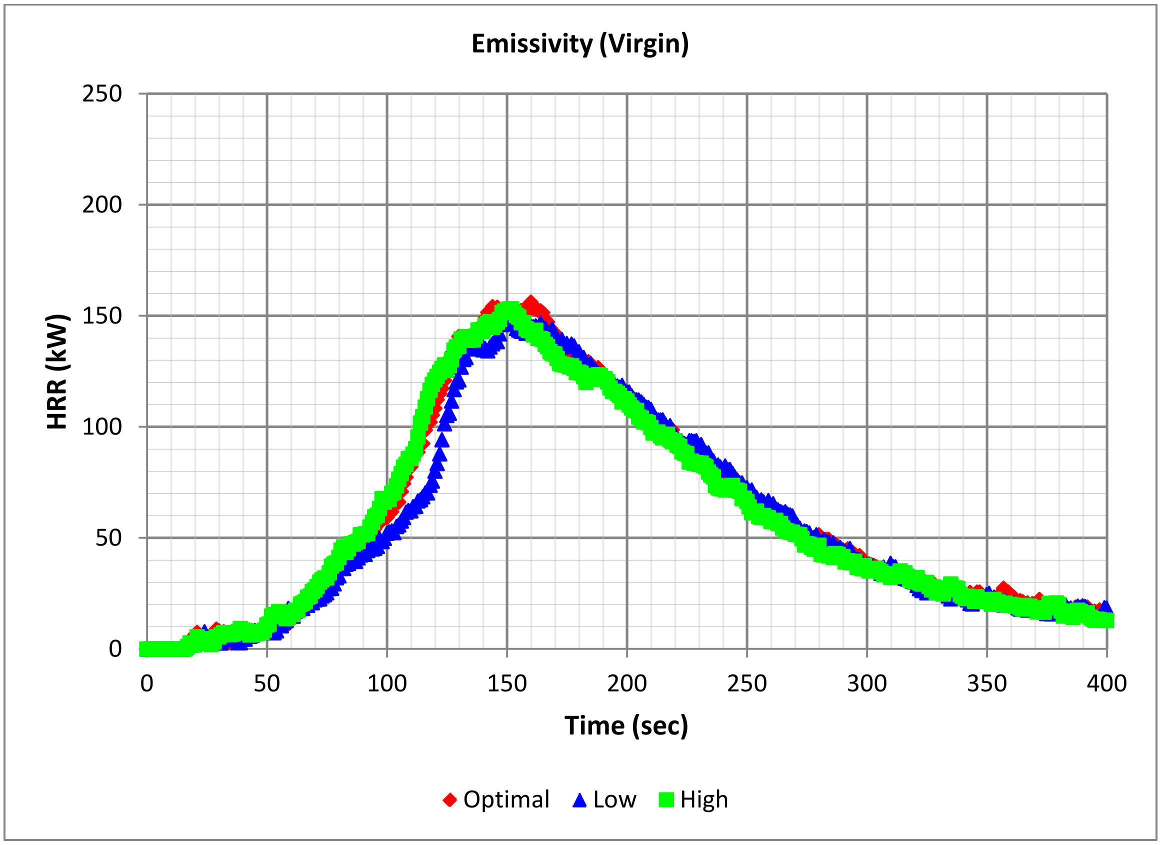

Figure 4 - HRR of FRP panel with varied emissivity of virgin material

The predicted HRR curves generated from varied thermal conductivity of the charred material are presented in Figure 5. Lowering the thermal diffusivity appears to slightly reduce the peak HRR by 6% without any change to the time to peak or to the magnitude of the HRR curve outside of the peak region. Increasing the thermal diffusivity does not appear to impact the HRR.

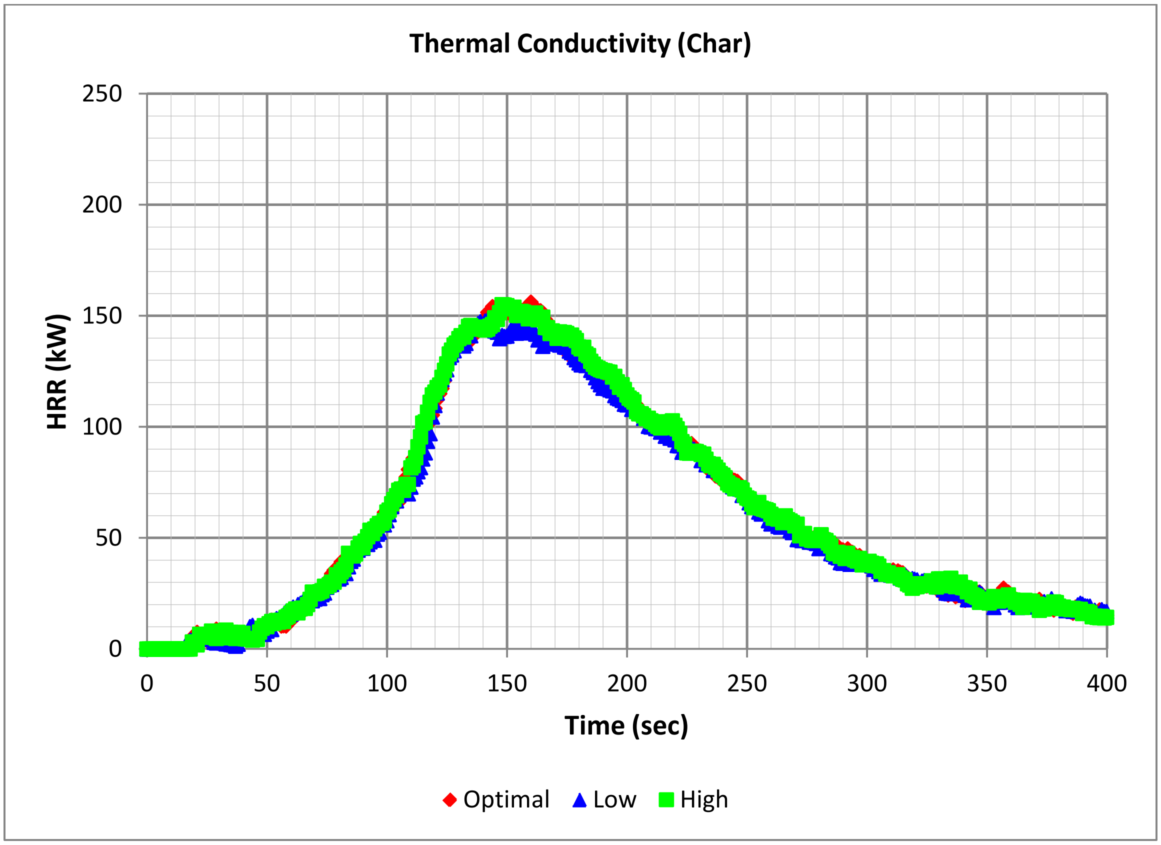

Figure 5 - HRR of FRP panel with varied thermal conductivity of charred material

Variations in the specific heat of the charred material appear to have negligible effects on the HRR curve as show in Figure 6. The shapes of the HRR curves from the three runs are similar to each other with only minimal differences at their peak values.

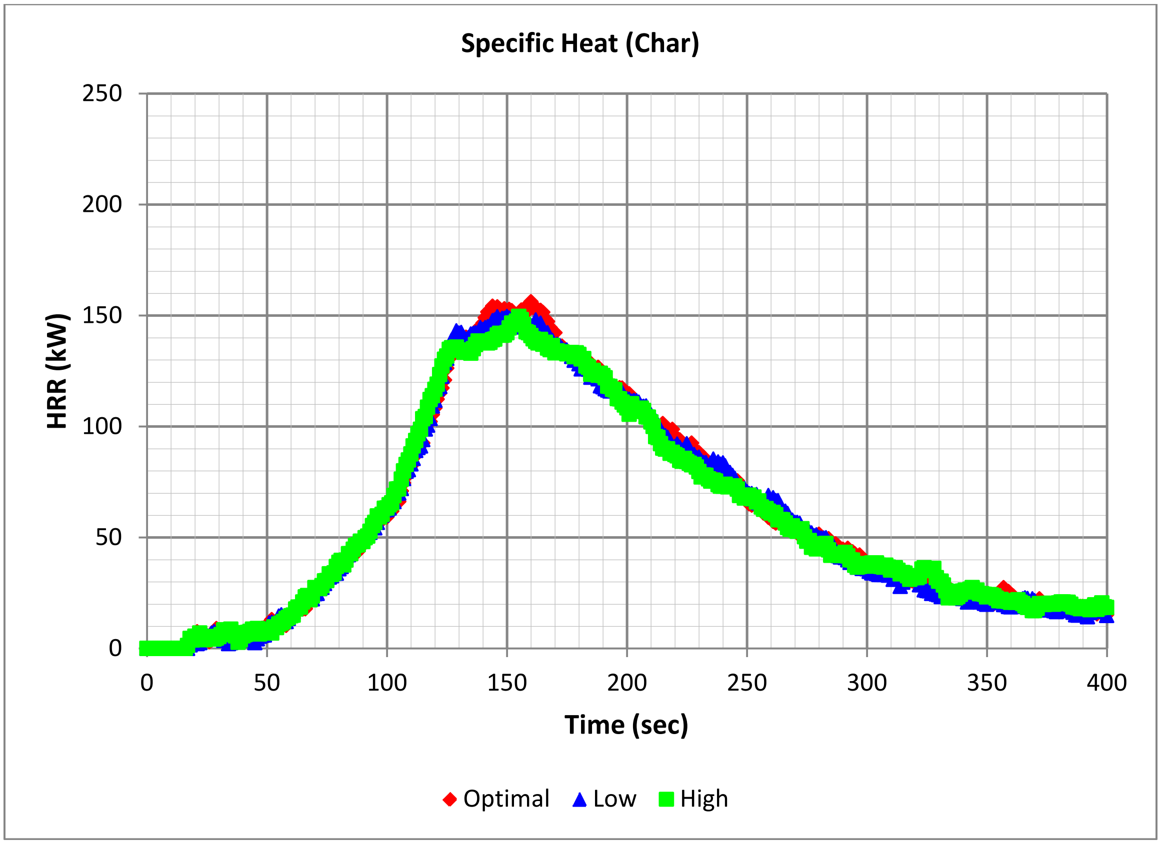

Figure 6 - HRR of FRP panel with varied specific heat of charred material

The density of the charred material was varied and the predicted HRR from the simulations are presented in Figure 7. The effects on HRR from the varied density are negligible: the shapes of the HRR curves from the three runs are similar to each other with only minimal differences at their peak values.

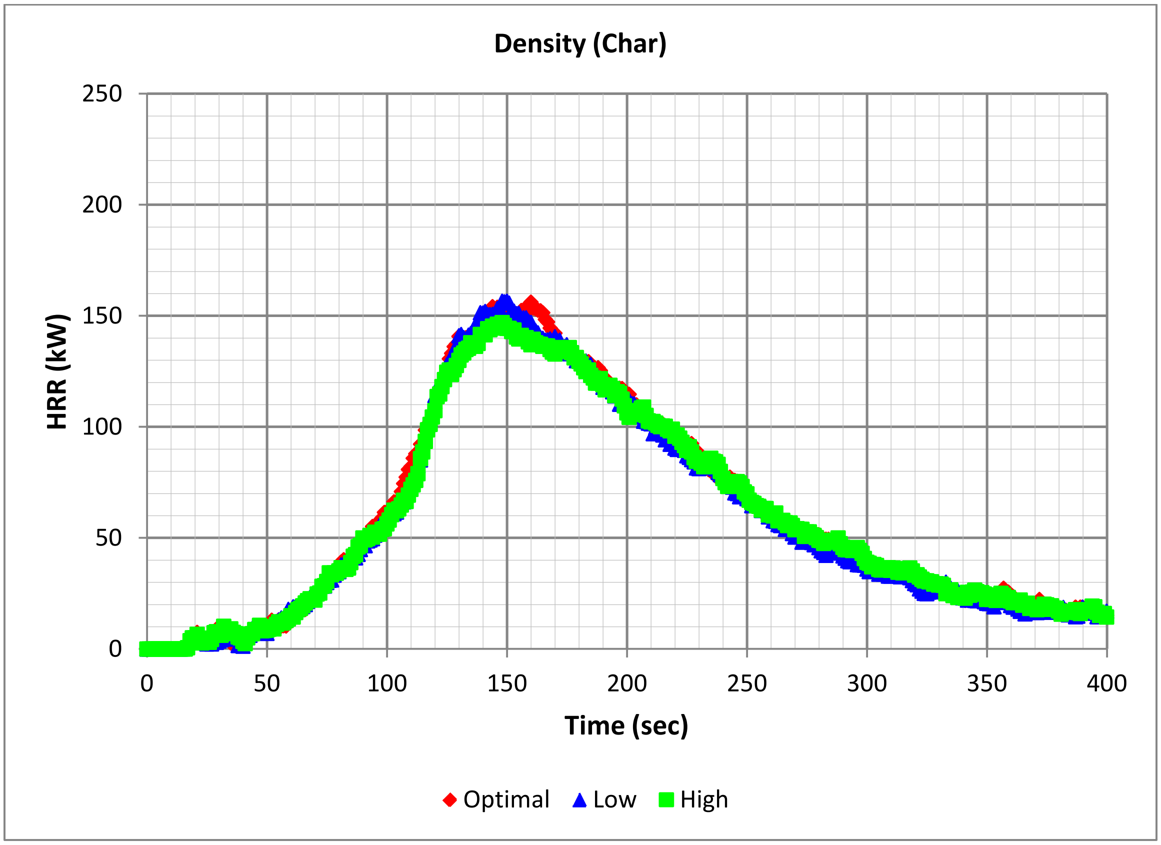

Figure 7 - HRR of FRP panel with varied density of charred material

The predicted HRR curves generated from varied emissivity of the charred material are presented in Figure 8. Lowering the emissivity appears to slightly reduce the peak HRR by 6% without any change to the time to peak or to the magnitude of the HRR curve outside of the peak region. Increasing the thermal diffusivity does not appear to impact the HRR.

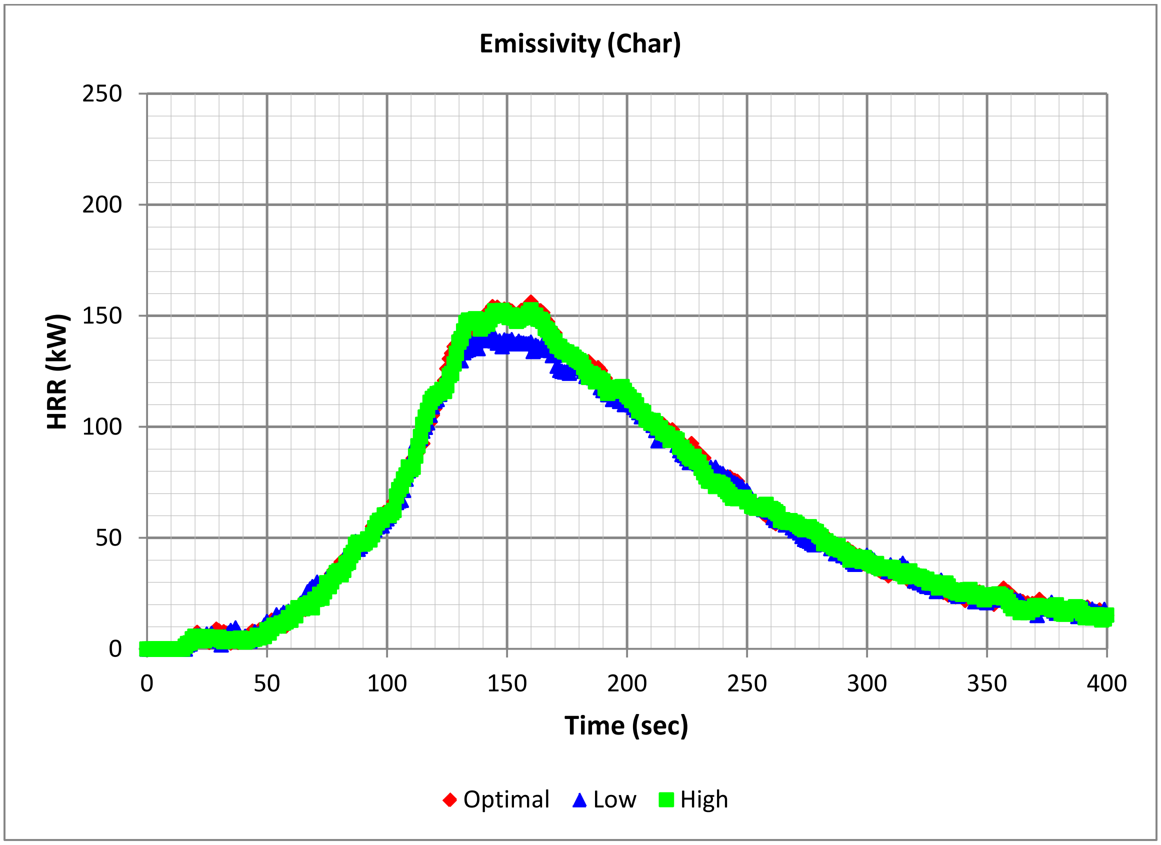

Figure 8 - HRR of FRP panel with varied emissivity of charred material

Figure 9 presents the HRR generated from varied pre-exponential factor (A factor). Using the higher value of the A factor drastically changed the pre-peaking behavior of the FRP fire by increasing the magnitude of the HRR and reducing the time to pea, whereas at the decline phase the HRR is mostly unchanged. The lower A factor value has negligible effects on the HRR curve. It should be noted that the higher A factor constitutes a 28% increase over the optimal value where the lower value only constitutes a 5% decrease.

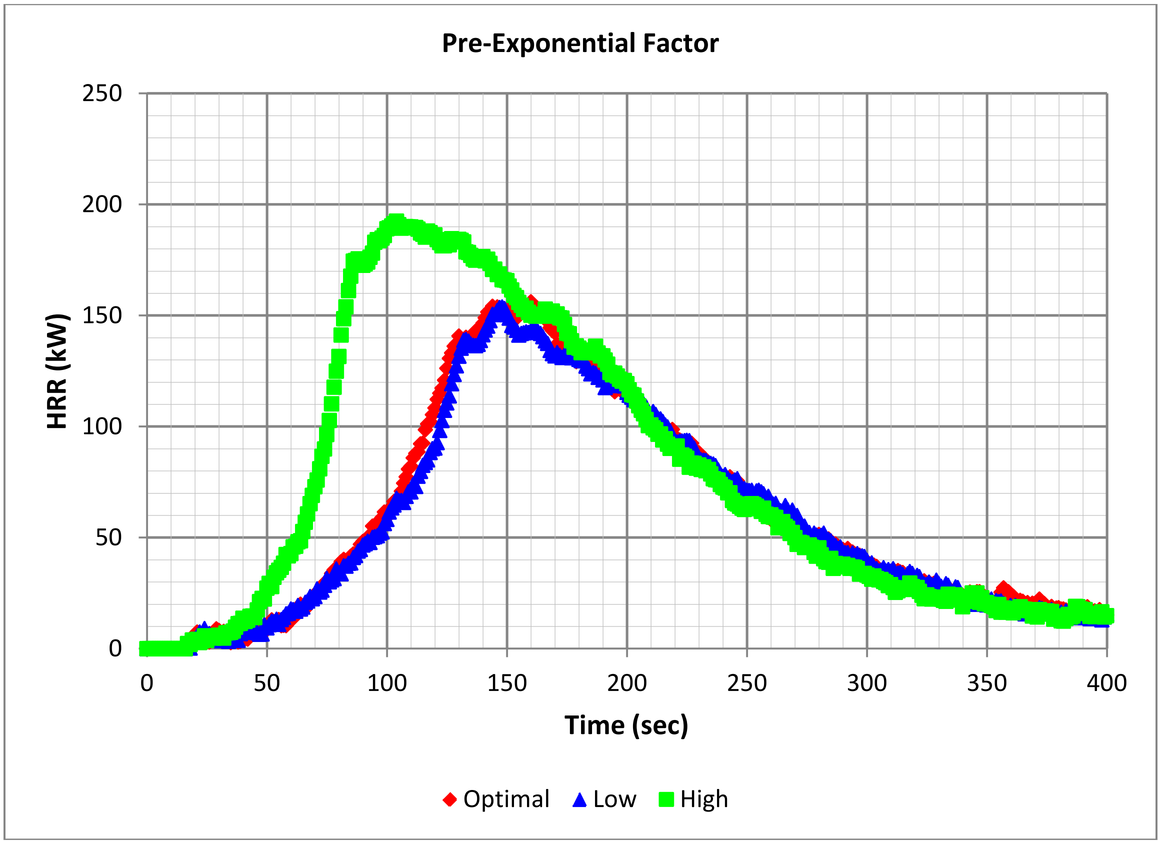

Figure 9 - HRR of FRP panel with varied pre-exponential factor

The optimal activation energy generated by the GPYRO algorithm is the same as the minimal value used, so in Figure 10, the comparison is only applicable between the optimal solution and the larger activation energy value. Increasing the activation energy is akin to increasing the amount of energy needed to be applied to a material so that combustion may be initiated. In the predicted HRR curve, an increase of activation energy increased the time to peak and reduced the peak magnitude; the overall heat released is also much lower than the baseline. These are indication that the FRP panel was essentially “harder” to burn. The low specific heat the same as, and the high specific heat value is +10.4% over the optimal value.

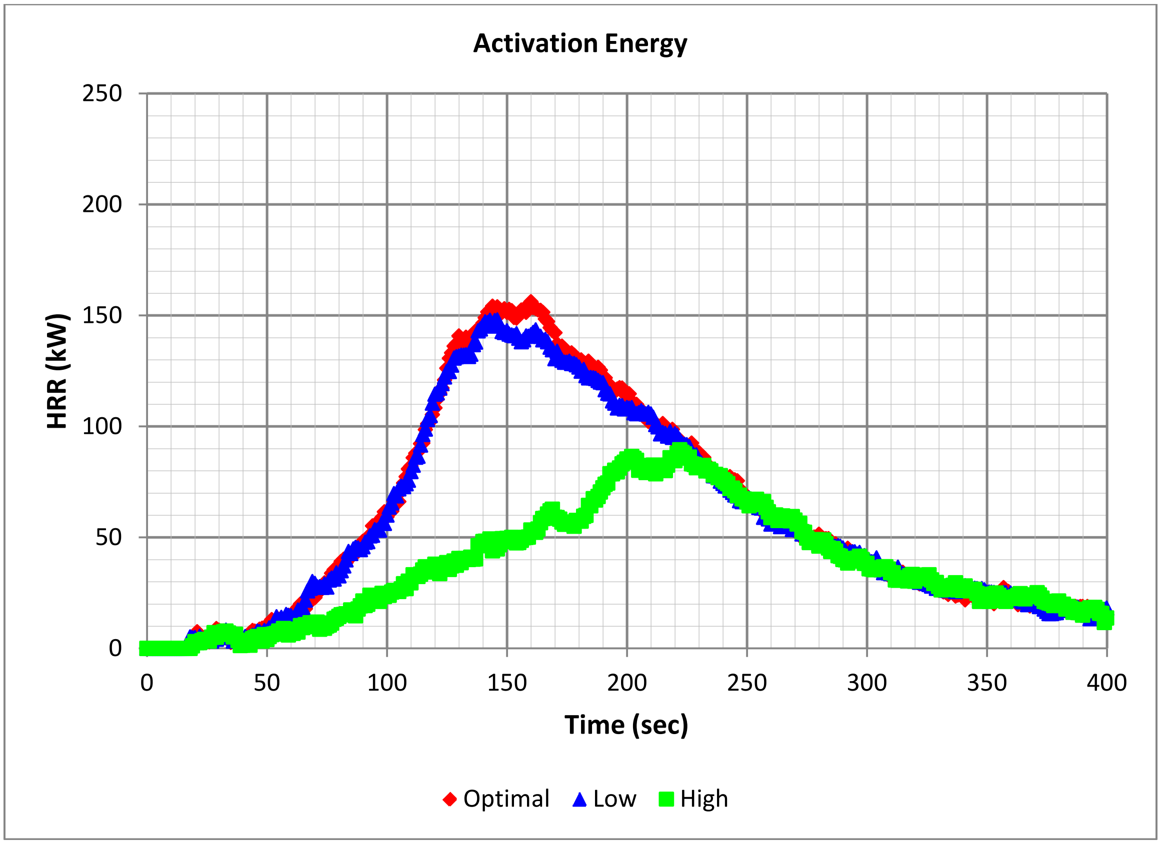

Figure 10 - HRR of FRP panel with varied activation energy

Variations of the reaction order, which may increase or decrease the rate of reaction of the FRP fuel, were made in the simulations with predicted HRR shown in Figure 11. The effects of the variation in reaction order are largely negligible. Effects of reaction orders in pyrolysis predictive capabilities are constantly being evaluated by combustion scientists, however, it should be noted that if the basic fluid dynamics and heat transfer phenomena are not accurate, the reaction order is irrelevant.

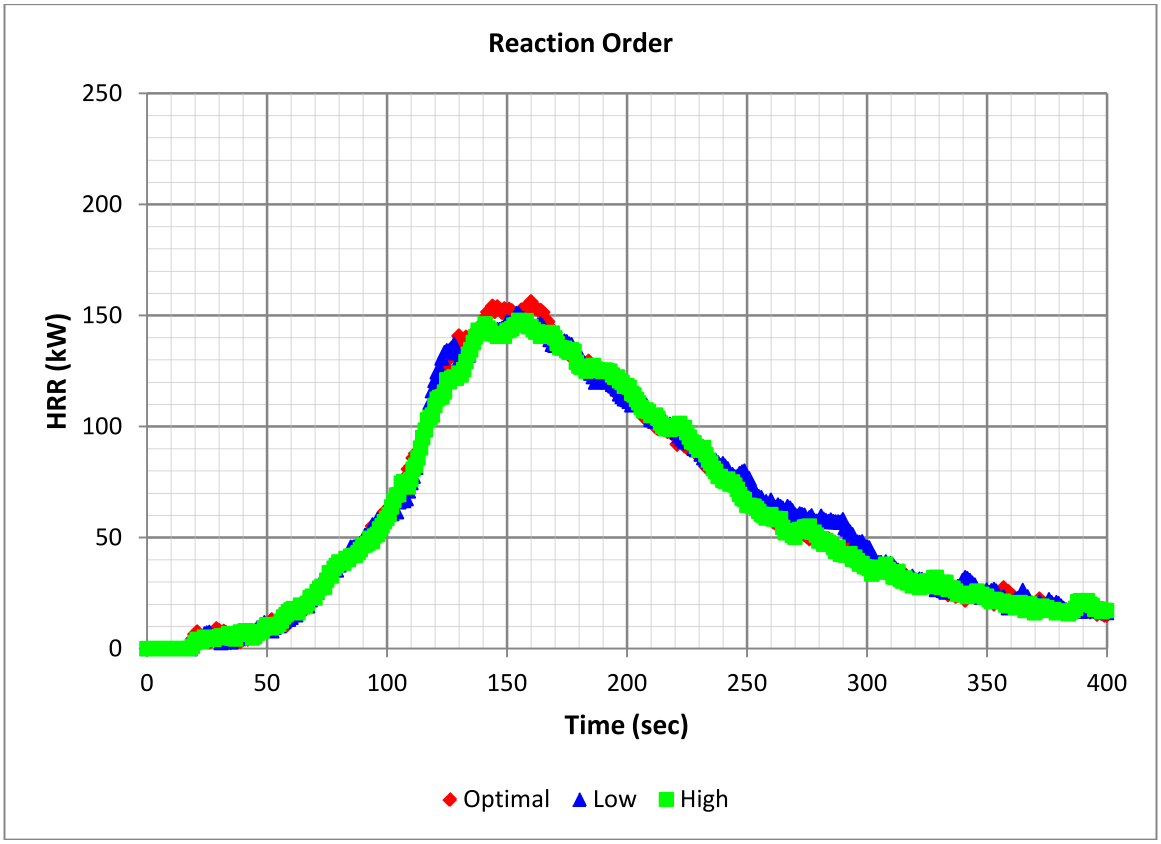

Figure 11 - HRR of FRP panel with varied reaction order

Figure 12 shows the HRR curves generated by varying the heat of reaction of the FRP fuel. The heat of reaction is the amount of energy per mass of reactant needed to convert the reactant to product. An increase of the heat of reaction causes the material to be “harder” to burn, and vice versa. In the simulations, an increase in the heat of reaction reduces the magnitude and slightly slows down the peak time, whereas the low in heat of reaction increases the magnitude of the HRR peak drastically. It is noted that the optimal heat of reaction generated by GPYRO is much closer to the maximum than the minimum. The low specific heat value is -36%, and the high specific heat value is +18% over the optimal value.

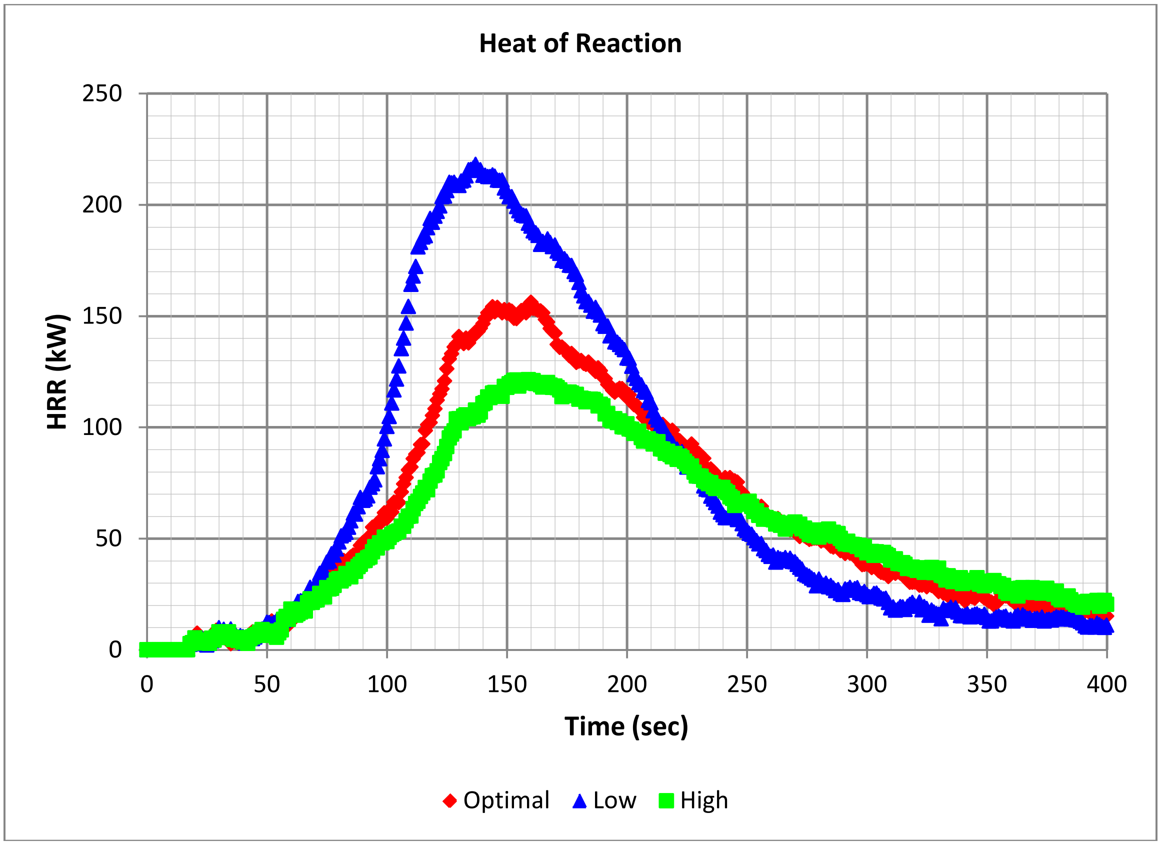

Figure 12 - HRR of FRP panel with varied heat of reaction

G.1.2 Variances on model prediction due to parameter change

In addition to the HRR time-history curve, the total heat released (THR), HRR at peak, and time to peak are also used as metrics to identify the significance of the parameter change. Figure 13 shows the variances of these quantities from the baseline for each simulation. It should be noted that for most simulations, the peak HRR and time to peak are reduced with a varied parameter, and that the three metrics usually trend in the same direction.

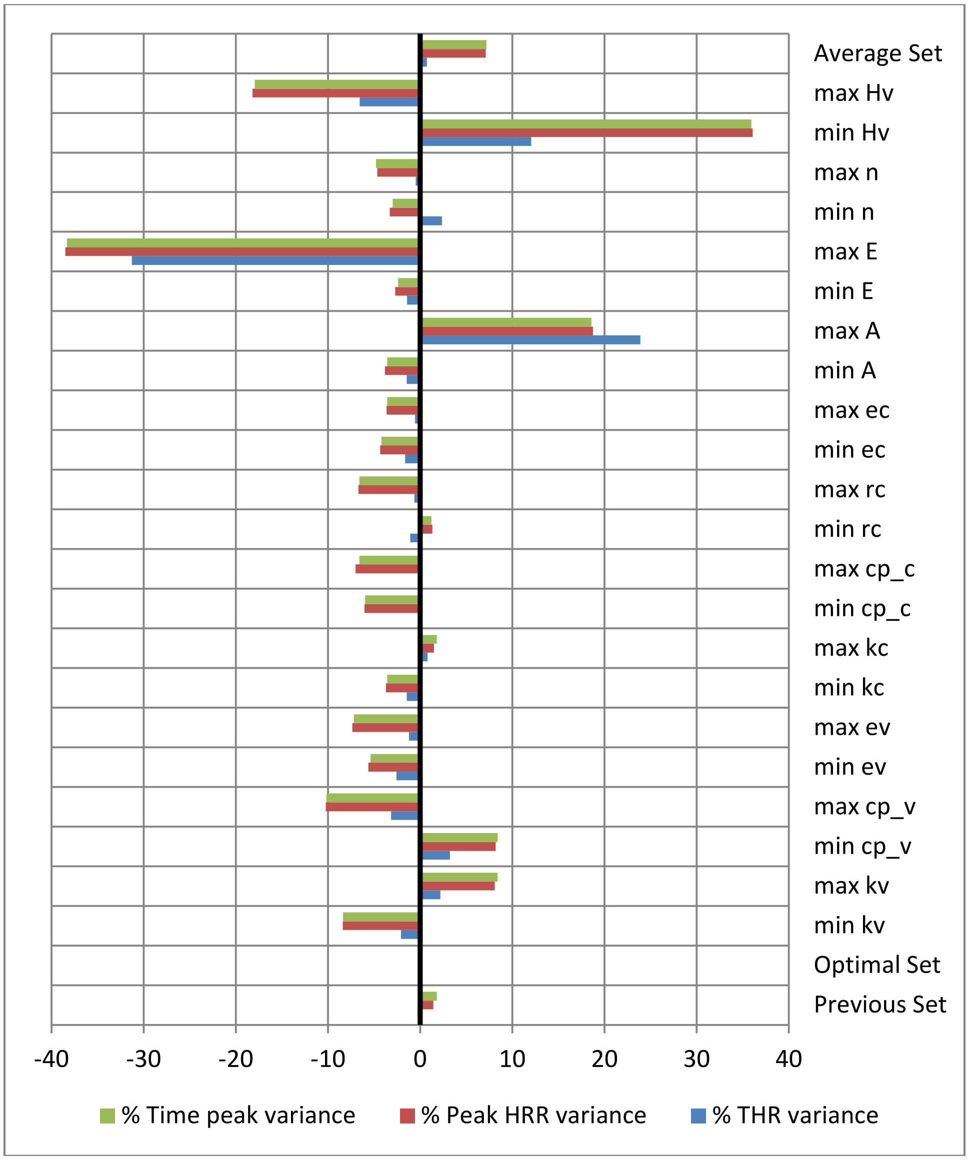

Figure 13 - Variances of time to peak, peak HRR, and THR

Figure 14 shows the differences in total heat released from each simulation over 900 seconds of simulation as compared to the total heat released predicted by the simulation using the optimal sets of parameters. In most simulations, the difference in total heat released is within 5% of the baseline (optimal). The simulations with predicted total heat released >±5% from baseline are:

- Max emissivity of virgin material

- Max pre-exponential factor
- Max activation energy
- Min heat of reaction
- Max heat of reaction

It should be noted that the direction of most parameter change has an inverse direction to the change in predicted total hat released: if a parameter raise increases the total heat released, then a parameter reduction will decrease the total heat released. Interestingly some parameters do not appear to follow this trend:

- Emissivity of virgin material
- Specific heat of charred material
- Density of charred material
- Emissivity of charred material

However, the simulation using the minimum of the activation energy (min E), which is the same as its optimal value, has a 1.4% lower total heat released predicted when compared to the identical baseline simulation. This suggests that the small differences in total heat released recorded may be due to the inherent uncertainty in the HRR prediction.

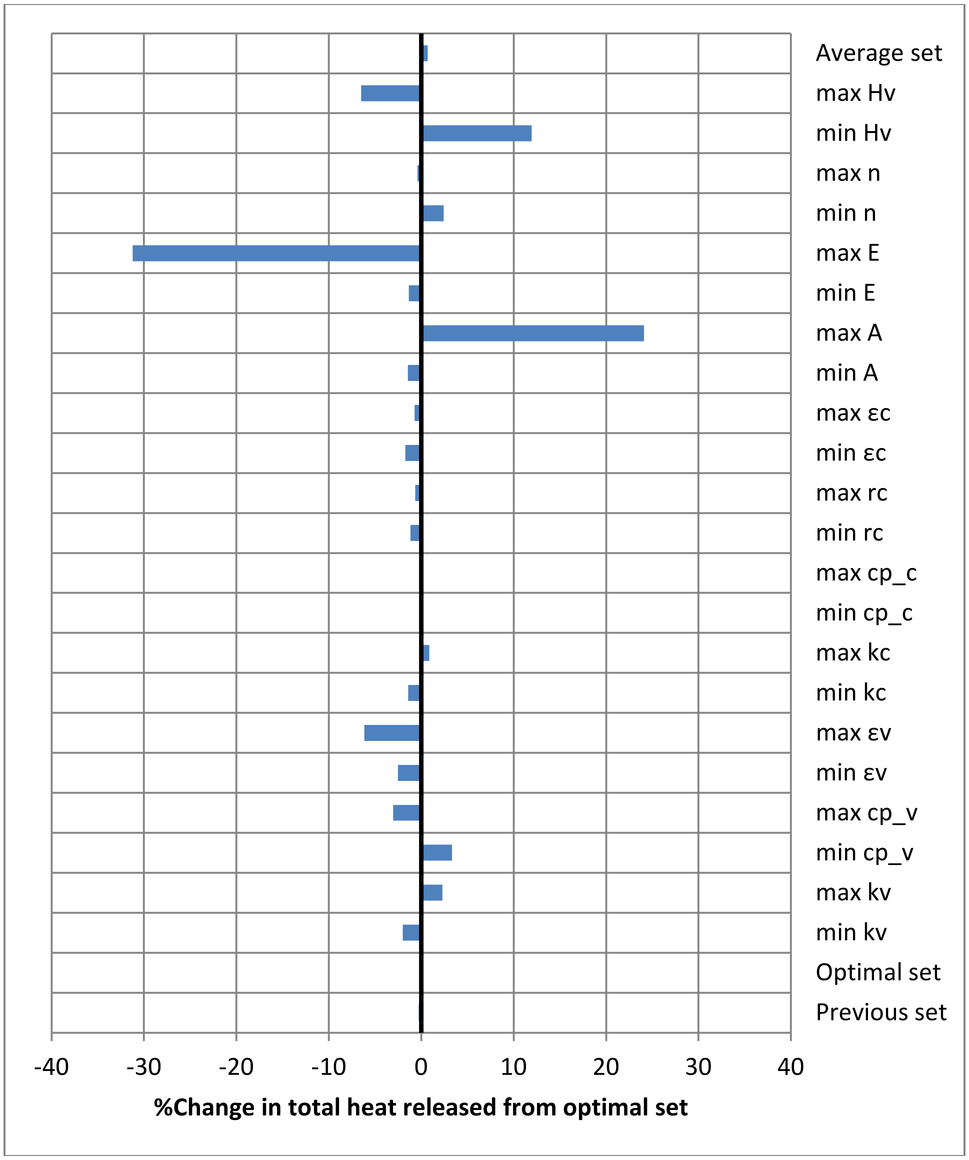

Figure 14 - Percentage change of total heat released, compared to simulation with optimal set of parameters

The variances found in the peak HRR and the time to peak in each simulation are larger than the variances in the total heat released, as shown in Figure 15 and . This is reasonable because the peak HRR and time to peak are instantaneous quantities, which would be affected by simulation uncertainty to a higher degree, as opposed to the total heat released quantity which is a global quantity. As seen in the variance for the simulation using the minimum activation energy (min E), which is the same as the default, optimal case, the uncertainty in these variances is at least 4%. In like of this fact, the parameters with significant effects on peak HRR are the same as those listed above.

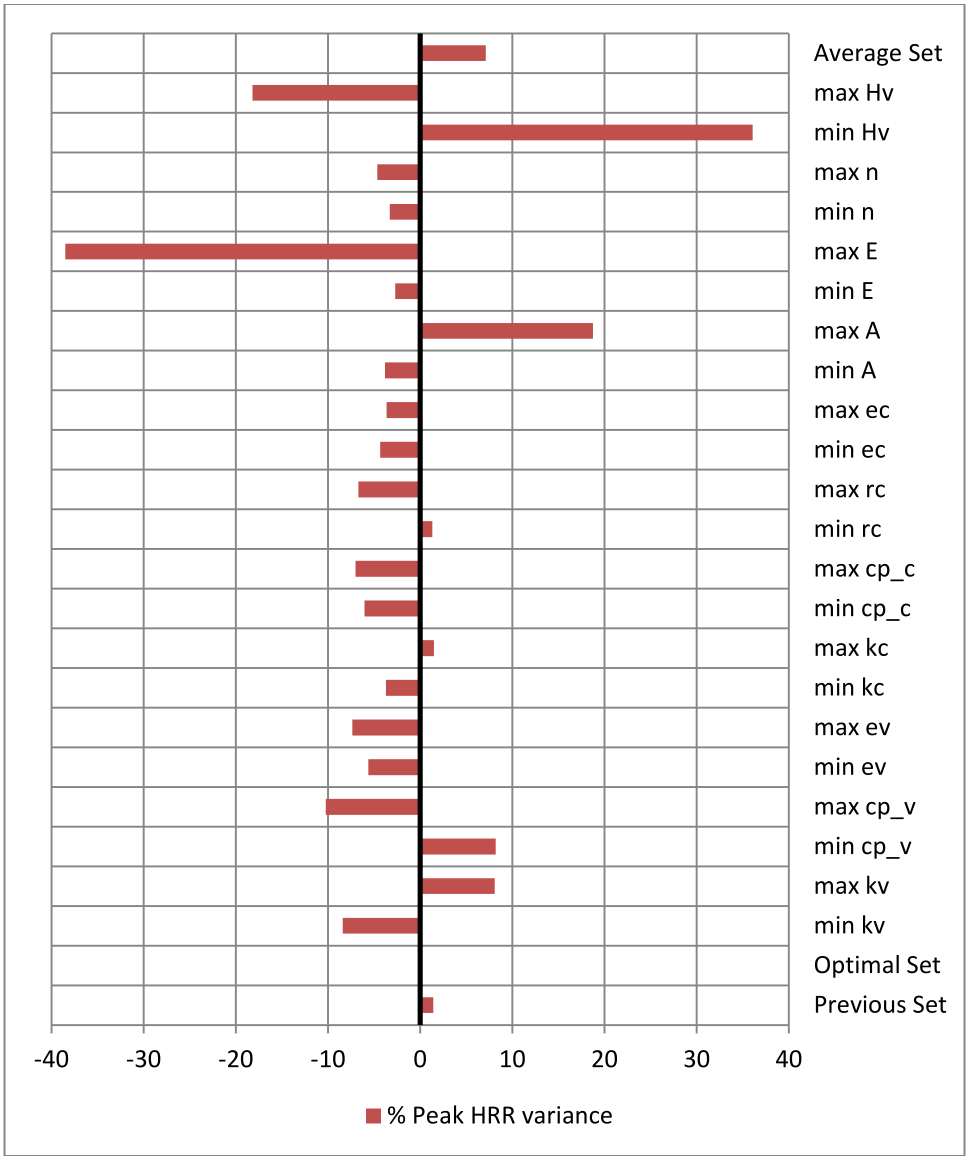

Figure 15 - Percentage change of HRR at peak, compared to simulation with optimal set of parameters

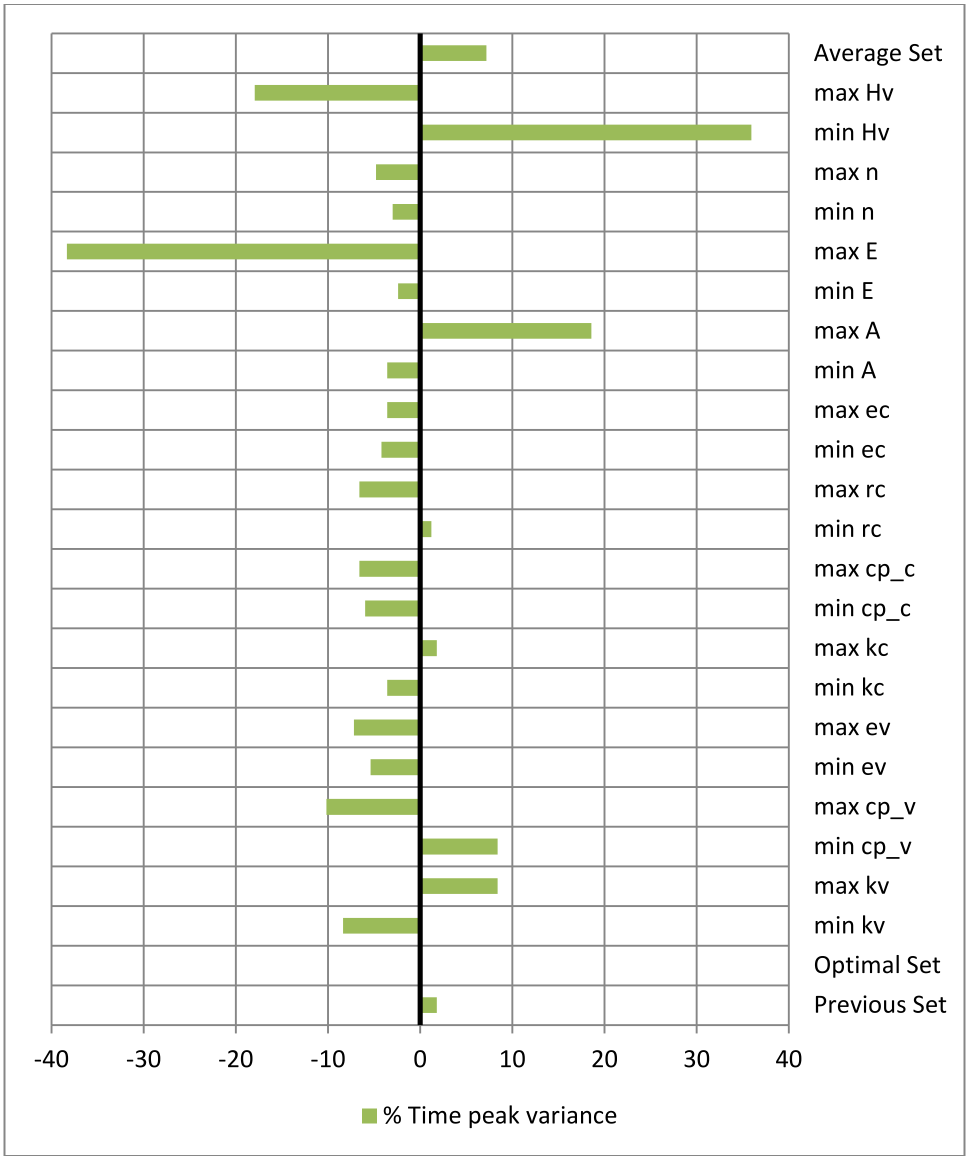

Figure 16 - Percentage change of time to peak, compared to simulation with optimal set of parameters

Figure 17 presents the sensitivity coefficients (SCs) of the various different parameters from the FRP material parameter study based on the three metrics. The coefficients are calculated by dividing the percentage difference between the quantities predicted by the current and optimal simulation, and the percentage difference between the current and optimal parameter value. They confirm that the parameters of special importance are the four listed above. The sign of the sensitivity coefficient denotes the relationship between the parameter change and the change in each predicted quantity; a positive SC means a direct correlation, but a negative SC means an inverse correlation. It is observed that for most of the parameters, the type of correlation between parameter and quantity change is consistent regardless if the parameter is increased or decreased. However, for the following parameters, the correlation behaves differently:

- Emissivity of virgin material
- Specific heat of charred material
- Density of charred material
- Emissivity of charred material

Also note the small SC values associated with these parameters, which suggests little effects on the predicted quantities by a change in the prescribed parameters. A review of the HRR curves created by these parameters show that they generally take the shape of the baseline HRR curve, which may suggest that these out-of-trend behaviors are residual from the uncertainty in the simulation.

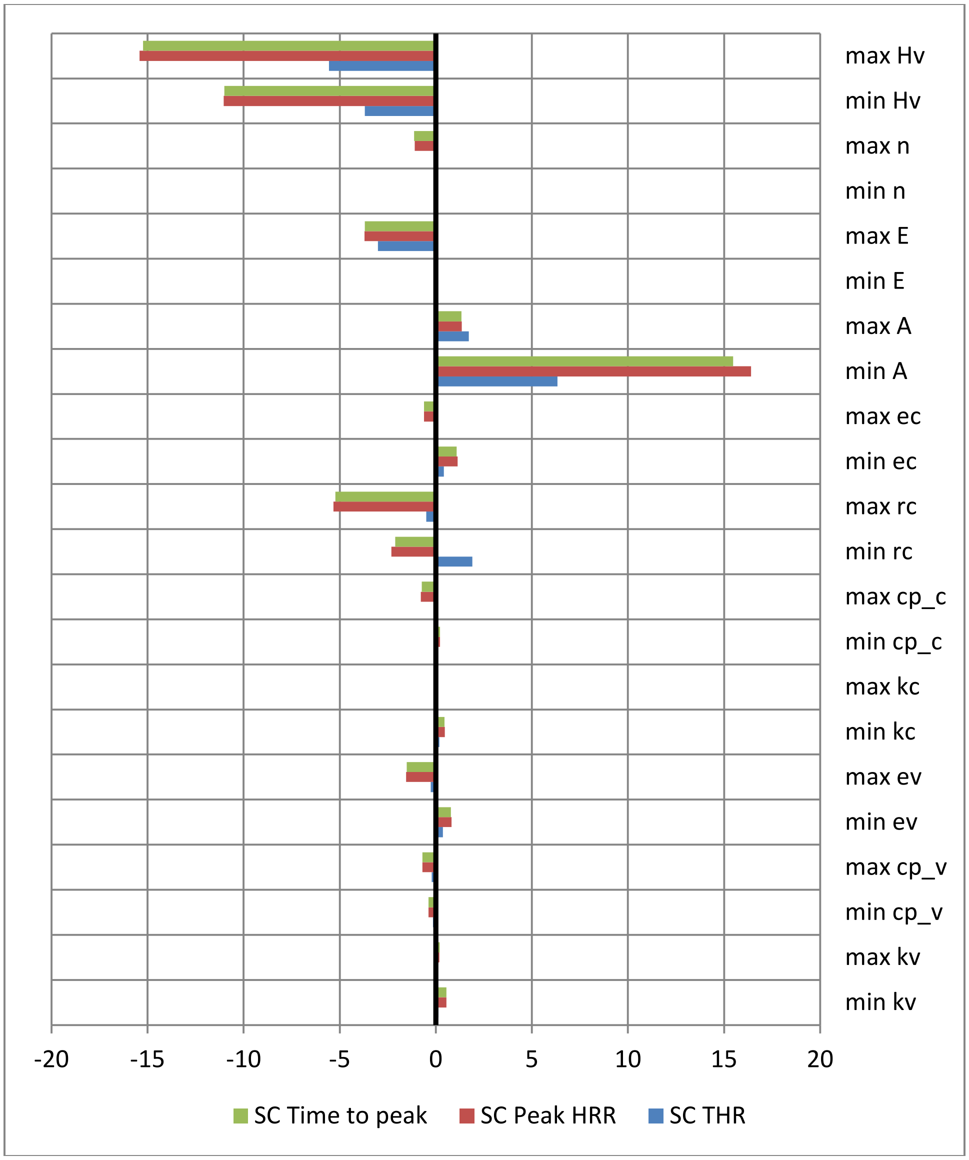

Figure 17 - Sensitivity coefficients of parameters

G.1.3 Discussion

The optimal values of the parameters generated by GPYRO appear to be consistent with those vales generated in previous simulation efforts and resulted in similar HRR curves. The average set of values, however, appears to create a HRR with a higher magnitude than the other two sets of parameter values.

Parameters describing the virgin material properties have a greater effect on the HRR and total heat released than those parameters for the charred material. This may be due to the fact that the thin nature of the material and the small amount of burning is less sensitive to the char that would form only if the material successfully burns.

The parameters with greatest effects are the pre-exponential factor, activation energy, and heat of reaction.

G.2 GPYRO Material Parameters Sensitivity Study (Round 2)

After the completion of the first series of GPYRO comparative FDS, it was determined to obtain a new set of FRP material fire properties using GPYRO, but this time using the converging trial solutions after additional generations of modeling.

The new (third) set of material parameters is presented in Table 2. As before, the material parameters tested in the baseline run include the optimal, maximum, minimum, and average values. The simulations were performed using 5 mm grid on a FRP fire simulation with a Square burner with a constant propane fire at 75 kW.

Table 2 - Parametric simulation run log for new parameters

	Description	k_v	c_v	ε_v	k_c	c_c	r_c	ε_c	log A	E	n	log ΔH_v
Run 31	Optimal	0.408	1759.970	0.906	0.057	2463.093	852.702	0.876	10.641	154.232	1.775	5.847
Run 32	min kv	0.311										
Run 33	max kv	0.484										
Run 34	min cv		1600.000									
Run 35	max cv		2037.631									
Run 36	min ev			0.832								
Run 37	max ev			0.920								
Run 38	min kc				0.037							
Run 39	max kc				0.066							
Run 40	min cc					1500.000						
Run 41	max cc					3000.000						
Run 42	min rc						843.486					
Run 43	max rc						869.837					
Run 44	min ec							0.809				
Run 45	max ec							0.954				
Run 46	min log A								10.200			
Run 47	max log A								11.342			
Run 48	min E									141.830		
Run 49	max E									160.000		
Run 50	min n										1.298	
Run 51	max n										2.000	
Run 52	min log Hv											5.700
Run 53	max log Hv											6.179
Run 54	Avg	0.415	1730.956	0.890	0.055	2410.536	851.702	0.879	10.602	154.614	1.753	5.830
Run 55	min A and E								10.200	141.830		
Run 56	max A and E								11.342	160.000		

In the following comparisons, the HRR curves are representative of the FRP burning only, the source 75 kW had been removed. Simulations were run for 900 seconds, but all models predicted little burning after 400 seconds. The comparisons between the results generated based on all three sets of GPYRO materials parameters are presented below with the following naming convention:

- "Previous" – Original set of parameters
- "Optimal, Average, High, Low" – Second set of parameters, presented above
- "New …" – Third set of parameters

G.2.1 Predicted HRRs from parametric study

A comparison was made between the resulting HRR curve from the two separate series of runs with all optimized parameters, all average parameters, and the original parameters used in the first simulation efforts. The HRR curves shown in Figure 18 suggests that the third set of optimal and average parameters resulted in similar HRR curve in terms of timing and magnitude, and they are both similar to the curve provided from the second-run optimal series.

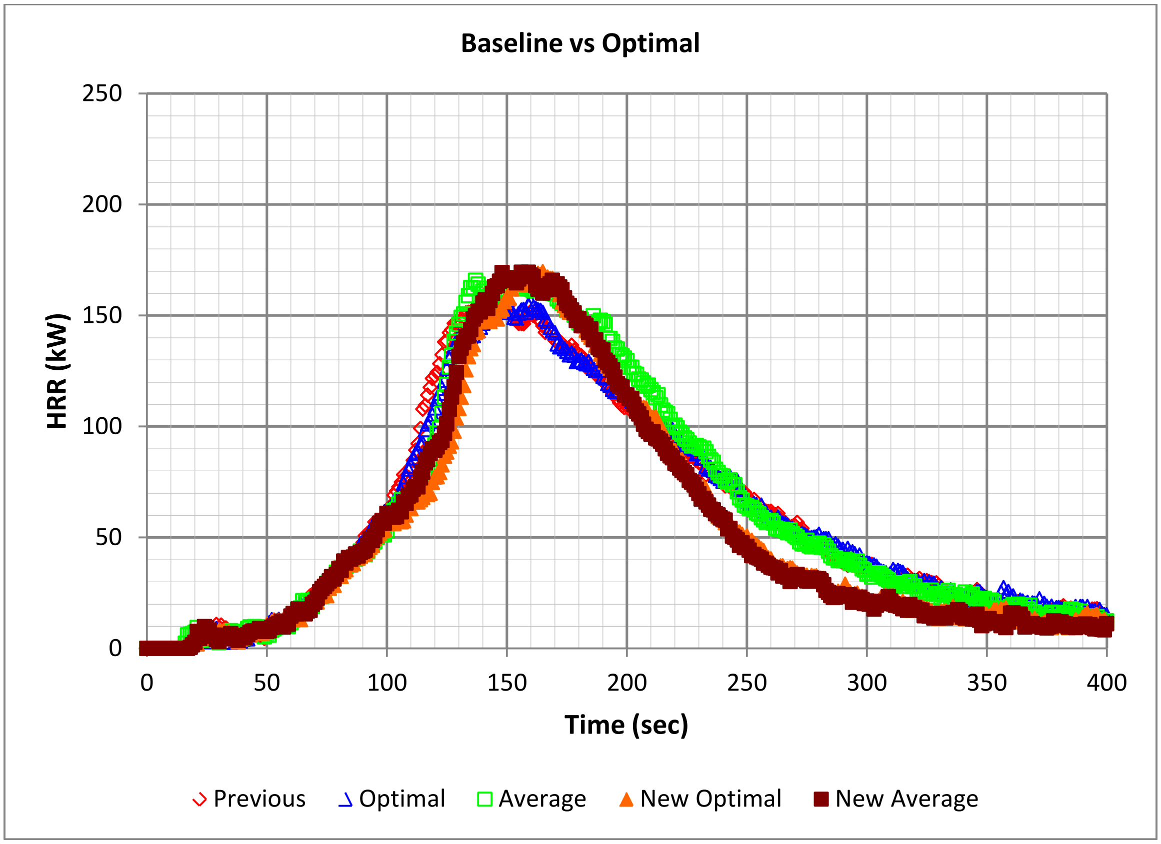

Figure 18 - HRR of FRP panel comparison between previous, optimal, and average sets of parameters [3 Series]

In Figure 19, the results from the simulations with a varied thermal conductivity value of the virgin material are presented. The results based on the third set of parameters follow the same trend observed previously. However, it is noted that the new set of results generally have a slower rate to peak, but higher peak HRR values, and drops off more sharply than the previous set of results. Since the difference between the thermal diffusivity values vary from the previous set at -3 to -20%, the differences in the predicted HRR time-history are reasonable.

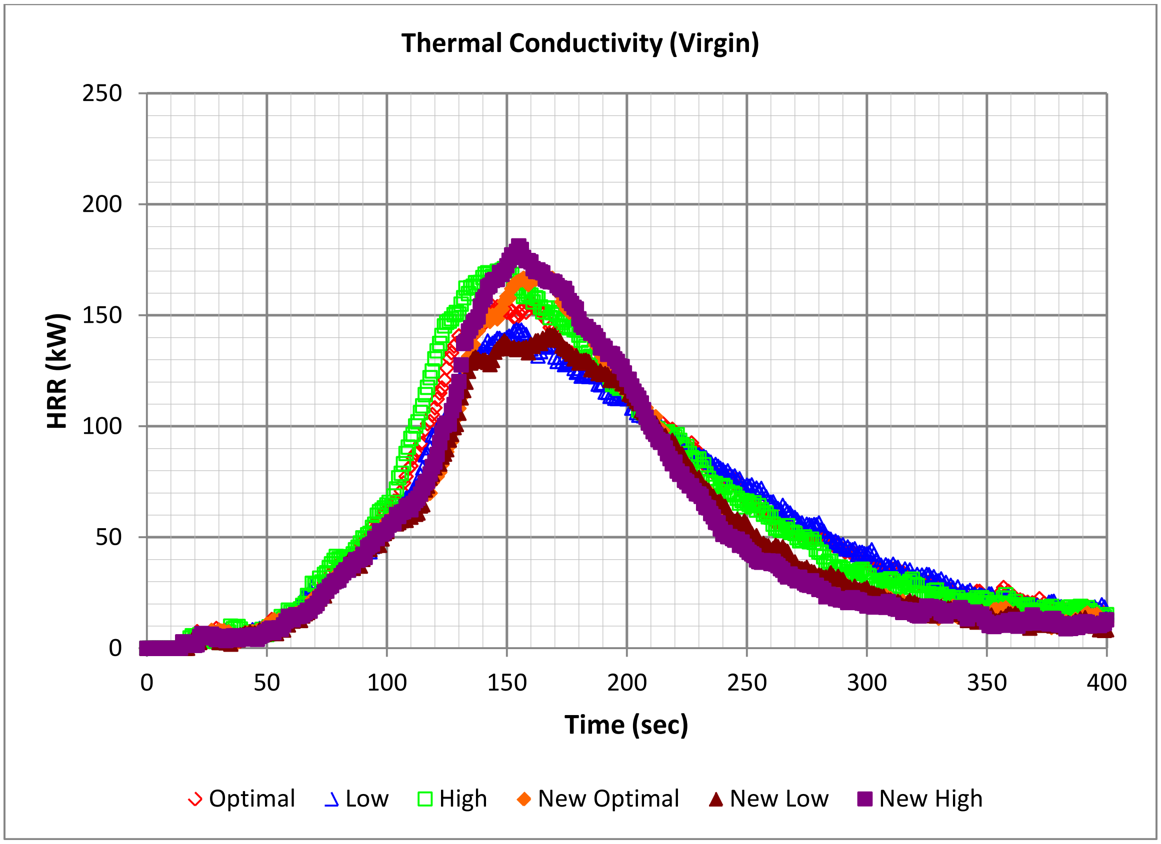

Figure 19 - HRR of FRP panel with varied thermal conductivity of virgin material [3 Series]

Changes in predicted HRR due to a variation of the virgin material's specific heat are reported in Figure 20. The results based on the third set of parameters follow the same trend observed previously. However, it is noted that the new set of results generally have a slower rate to peak, but higher peak HRR values, and drops off more sharply than the previous set of results. Since the difference between the specific heat values vary from the previous set at 2 to -12%, the differences in the predicted HRR time-history are reasonable.

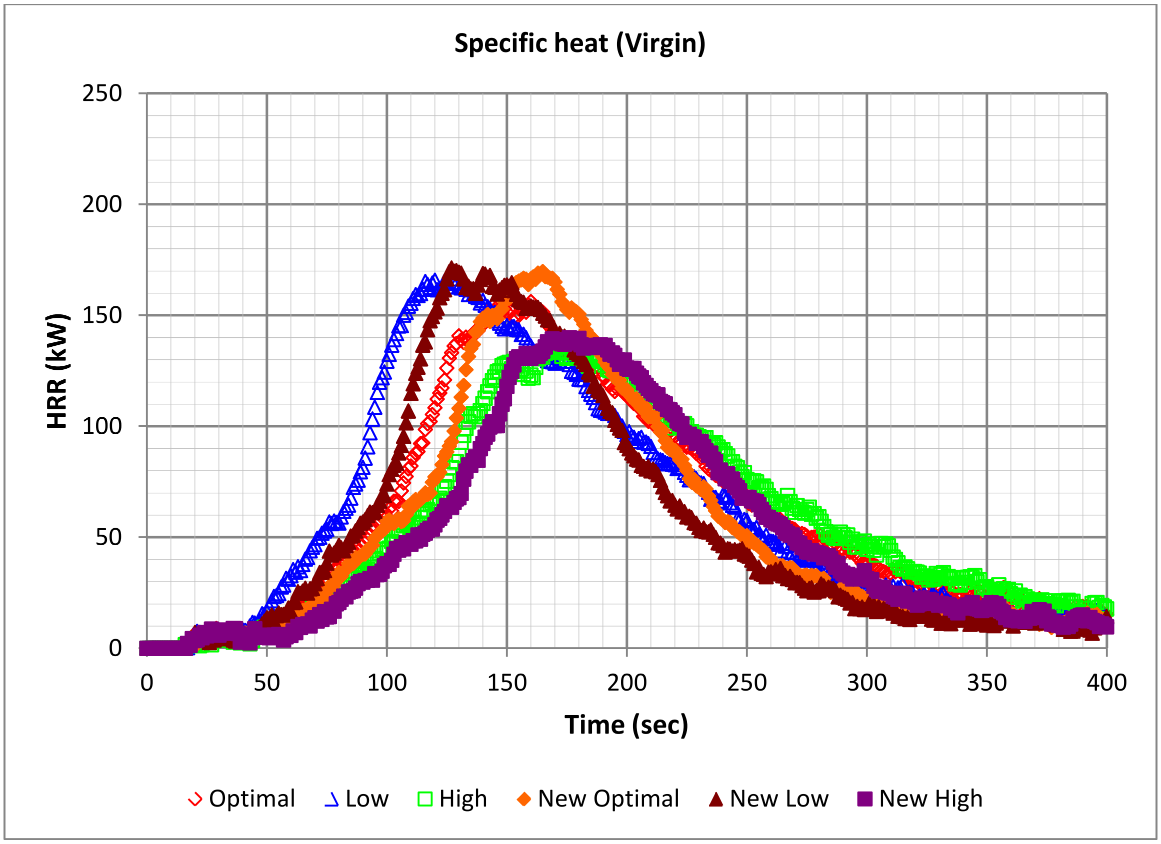

Figure 20 - HRR of FRP panel with varied specific heat of virgin material [3 Series]

Figure 21 presents the predicted HRR curve with varied emissivity of the virgin material. The results based on the third set of parameters follow the same trend observed previously. However, it is noted that the new set of results generally have a slower rate to peak, but higher peak HRR values, and drops off more sharply than the previous set of results. Since the difference between the emissivity values vary from the previous set at 2 to 5%, the differences in the predicted HRR time-history are reasonable. The similarity in the HRR time-history curves and o of the values between the two series of runs suggest that the emissivity of the virgin material does not vary significantly between GPYRO predictions.

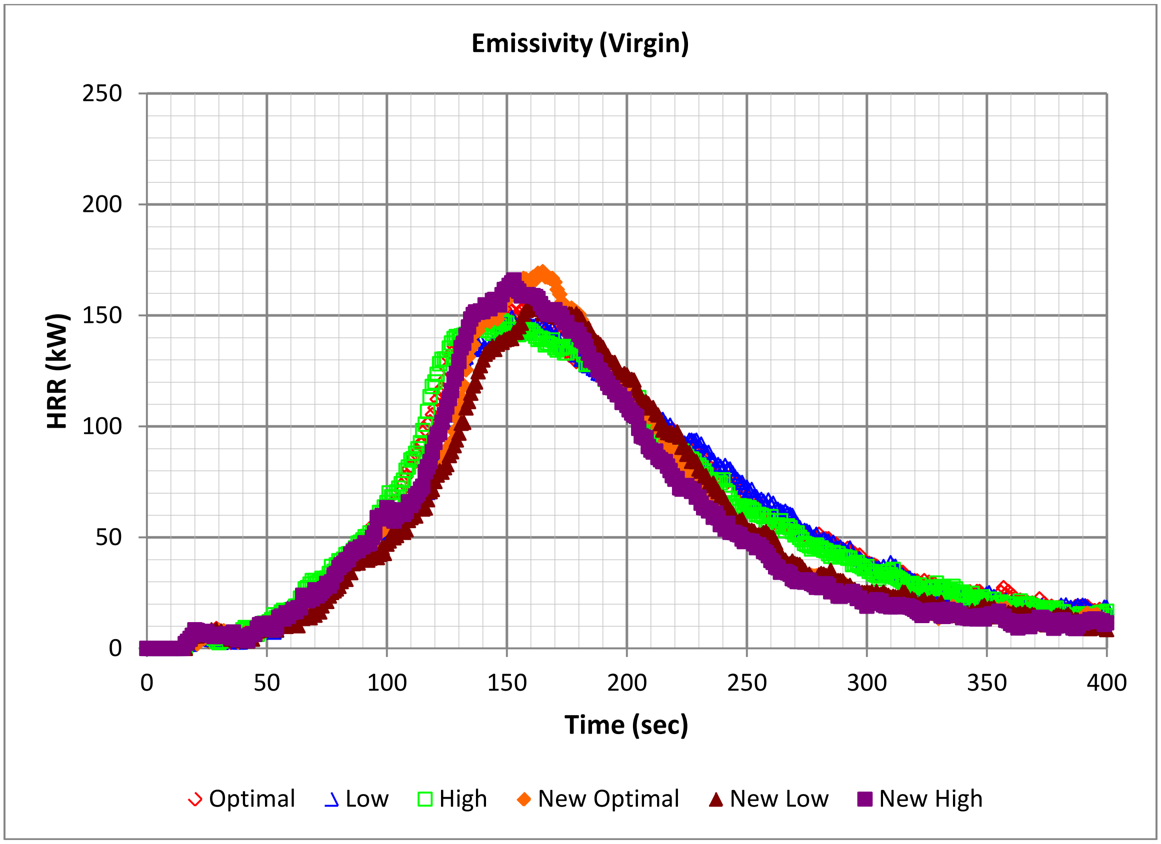

Figure 21 - HRR of FRP panel with varied emissivity of virgin material [3 Series]

The predicted HRR curves generated from varied thermal conductivity of the charred material are presented in Figure 22. The results based on the third set of parameters does not follow the same trend observed previously, for this parameter, the new Low value created a HRR curve with higher peak HRR than the other two limits, which is opposite of what was observed in the previous set of simulation. It is noted that the new series of results predicted similar rise to peak, but faster and deeper drop of HRR after peak. The difference between the thermal conductivity values vary from the previous set at -25% to 3%.

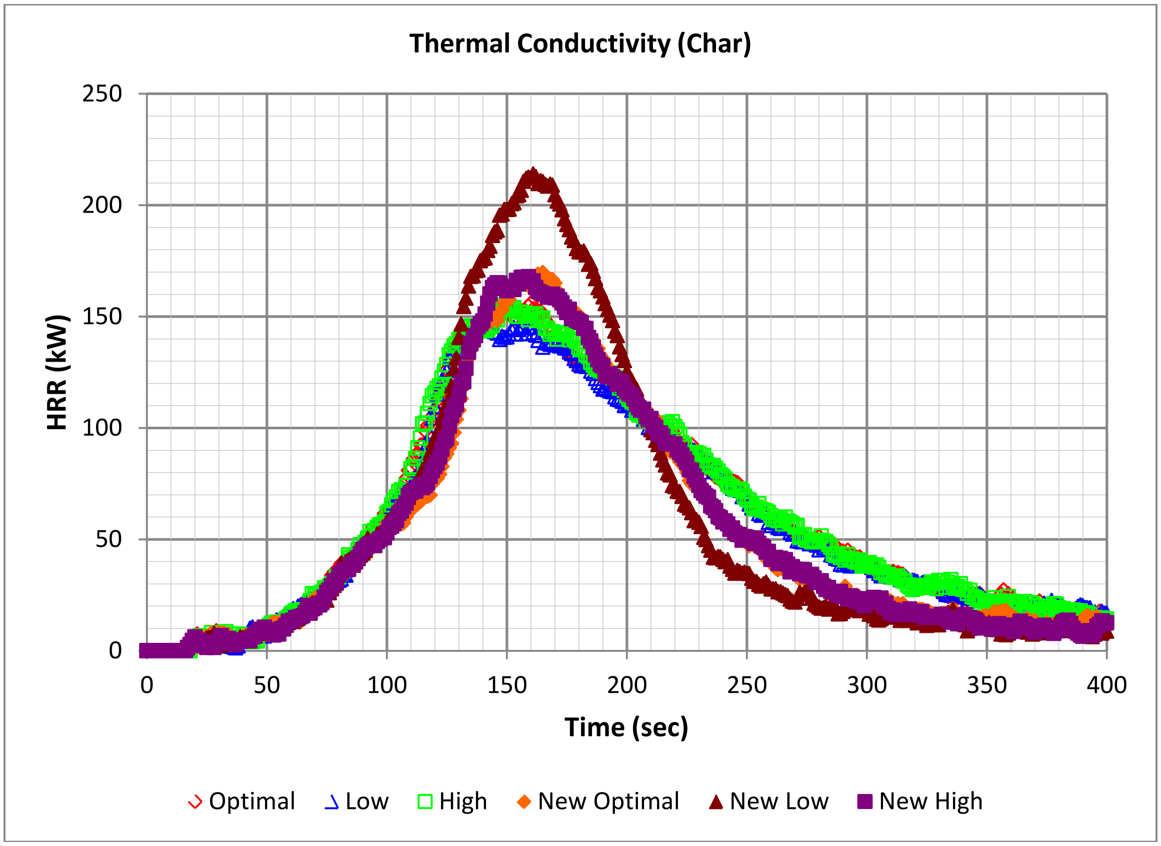

Figure 22 - HRR of FRP panel with varied thermal conductivity of charred material [3 Series]

Variations in the specific heat of the charred material appear to have negligible effects on the HRR curve as show in Figure 23. The results based on the third set of parameters follow the same trend observed previously. However, it is noted that the new set of results generally have a slower rate to peak, but higher peak HRR values, and drops off more sharply than the previous set of results. The difference between the specific heat values vary from the previous set at -2 to 30%, it shows that an increase in the specific heat of the char drives up the HRR predicted.

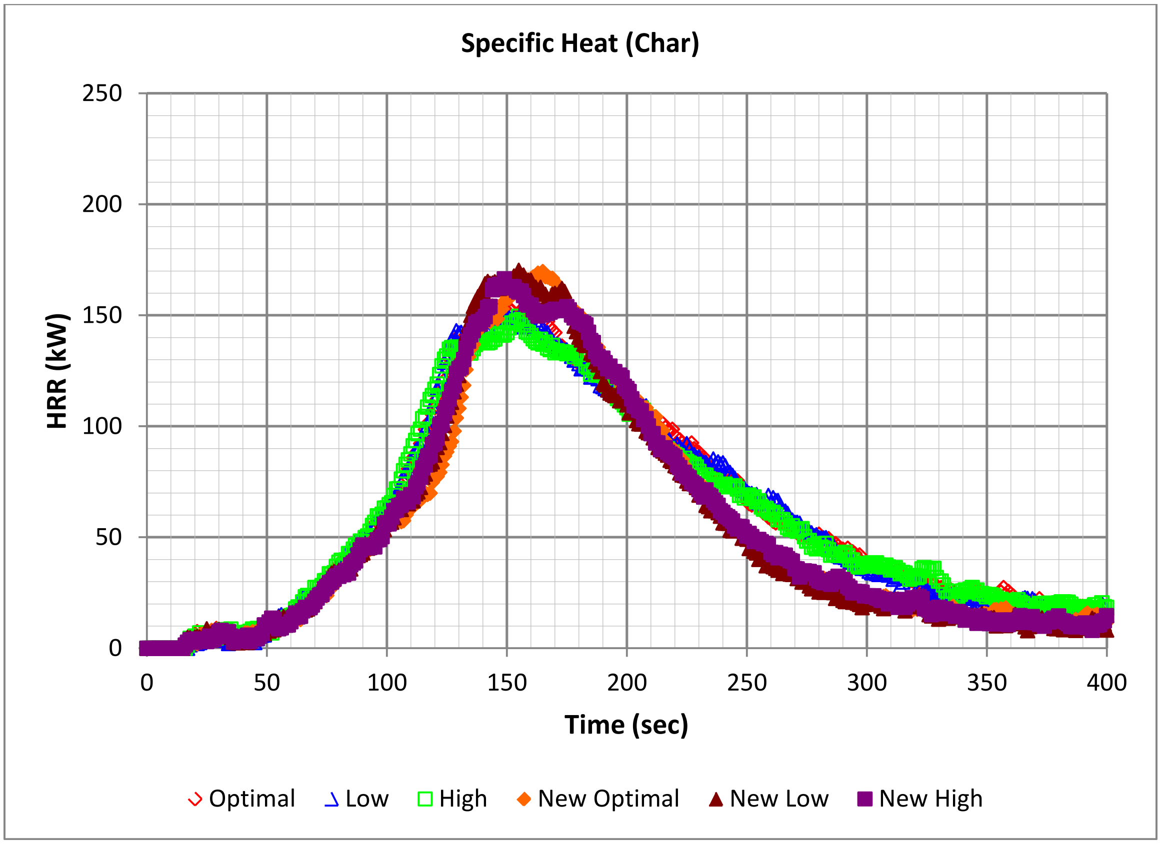

Figure 23 - HRR of FRP panel with varied specific heat of charred material [New+Old Comparison]

The density of the charred material was varied and the predicted HRR from the simulations are presented in Figure 24. The results based on the third set of parameters follow the same trend observed previously. However, it is noted that the new set of results generally have a slower rate to peak, but higher peak HRR values, and drops off more sharply than the previous set of results. Since the difference between the char density values vary slightly from the previous set at -0.6 to 0.6%, it appears that the predicted HRR is sensitive to the changes in density of the char.

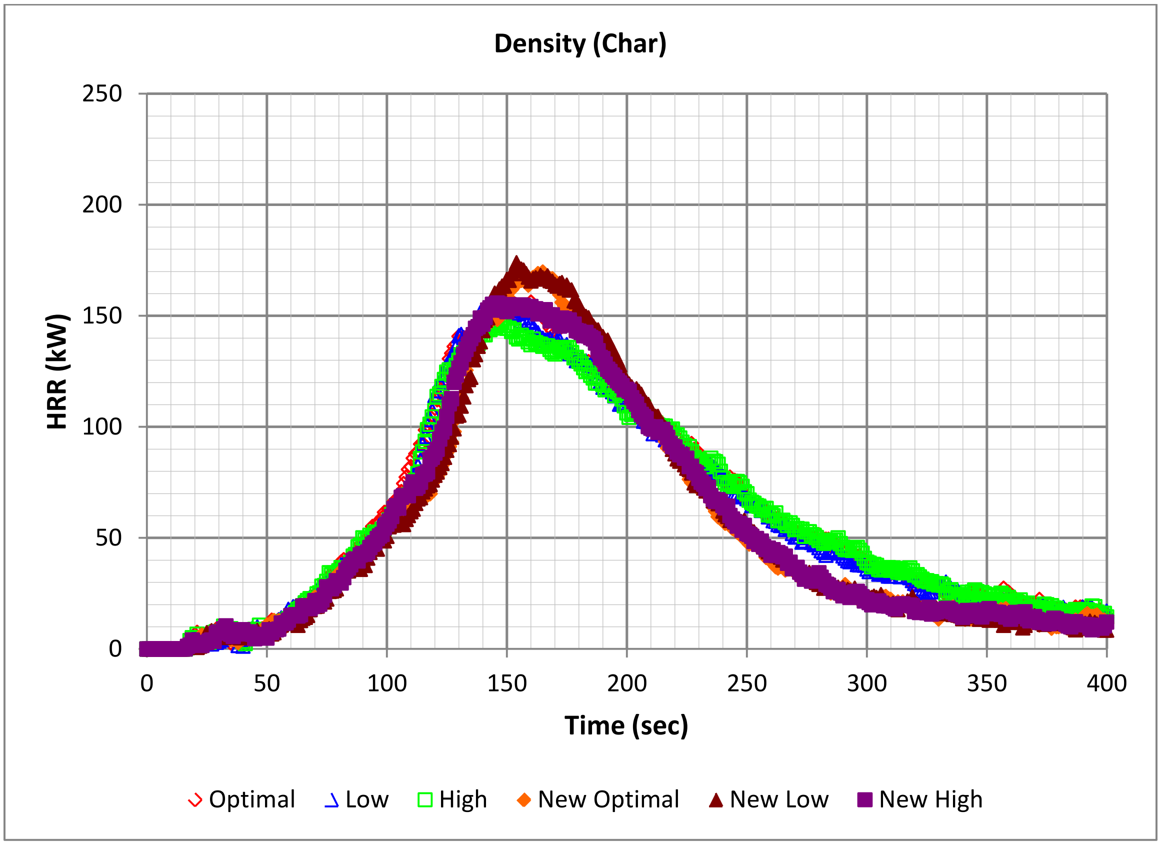

Figure 24 - HRR of FRP panel with varied density of charred material [New+Old Comparison]

The predicted HRR curves generated from varied emissivity of the charred material are presented in Figure 25. The results based on the third set of parameters follow the same trend observed previously. However, it is noted that the new set of results generally have a slower rate to peak, but higher peak HRR values, and drops off more sharply than the previous set of results. Since the difference between the emissivity values vary slightly from the previous set at -3 to -10%, it appears that the predicted HRR is sensitive to the changes in density of the char. The overall decrease in the char emissivity value in the new set of runs created a higher HRR than predicted using the previous set of values; however, this is the opposite effect when comparing the three values within one set of runs where the lowest emissivity value of the group generated the lowest HRR of the group.

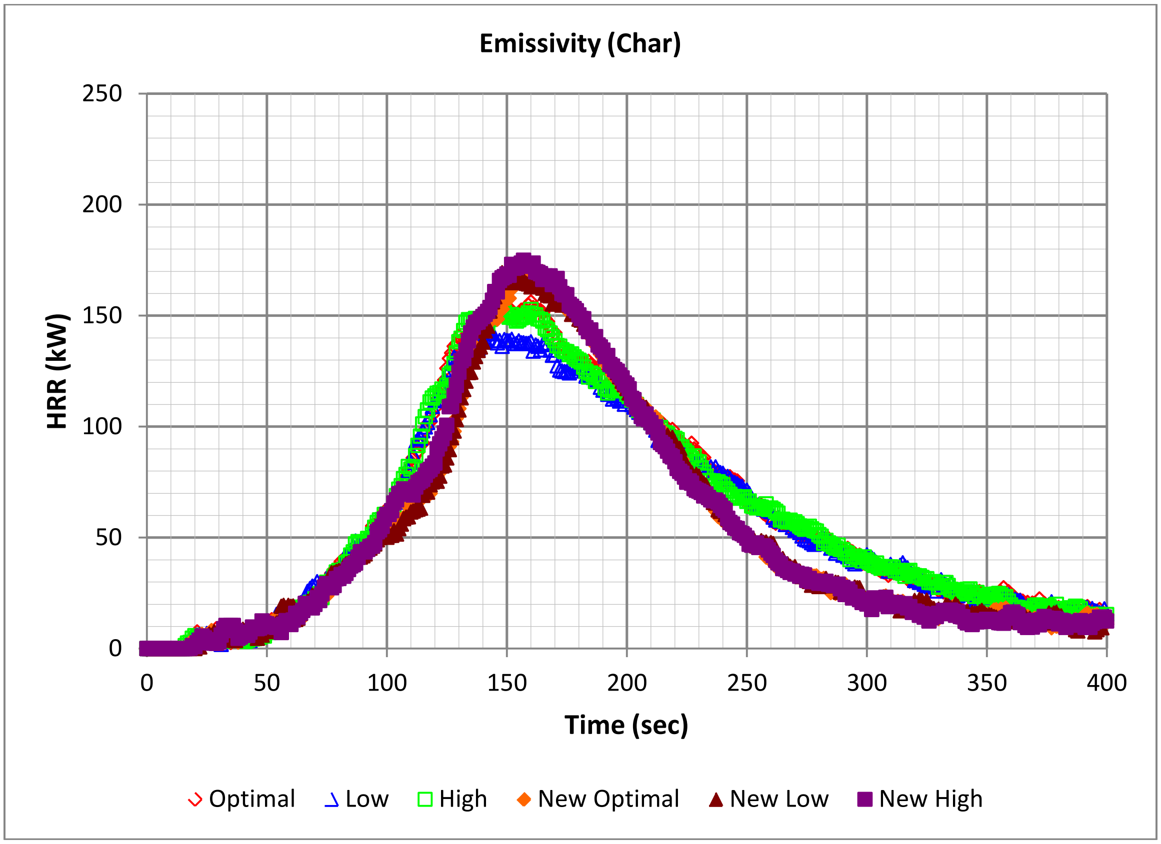

Figure 25 - HRR of FRP panel with varied emissivity of charred material [New+Old Comparison]

Figure 26 presents the HRR generated from varied pre-exponential factor (A factor). The results based on the new set of parameters predicted higher peak HRR values for the new optimal and high value in the A factor, but a lower peak HRR in the new low value in the A factor. It is noted that all of the new runs predicted slower time to reach the peak HRR and a faster drop-off after the peak. Since the difference between the A factor values vary slightly from the previous set at -5 to 1%, it appears that the predicted HRR is sensitive to the changes in the A factor.

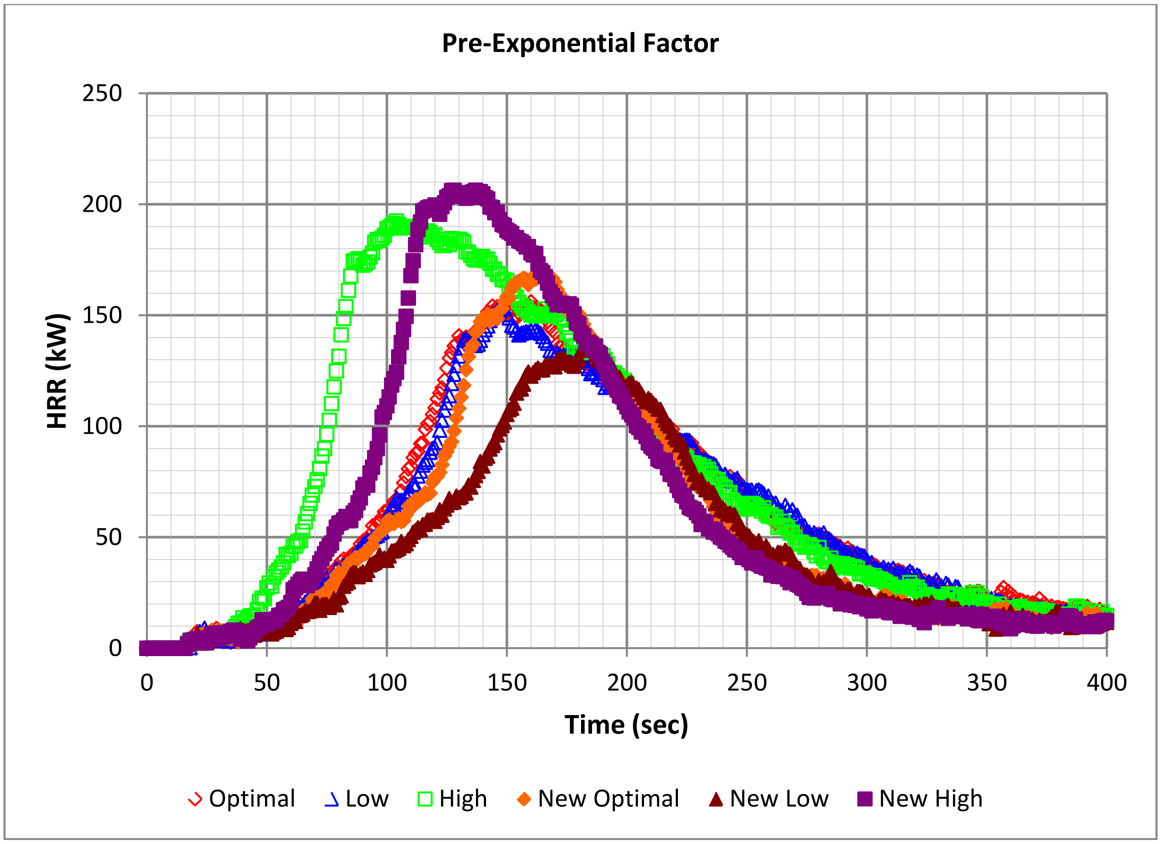

Figure 26 - HRR of FRP panel with varied pre-exponential factor [New+Old Comparison]

The optimal activation energy generated by the GPYRO algorithm is the same as the minimal value used, so in Figure 27, the comparison is only applicable between the optimal solution and the larger activation energy value. The results based on the new set of parameters predicted higher peak HRR values than their older counterparts. Additionally, it is noted that the trend established in the old results is not followed in the new results when the new Lower value led to a higher HRR than when the new optimal value is used.

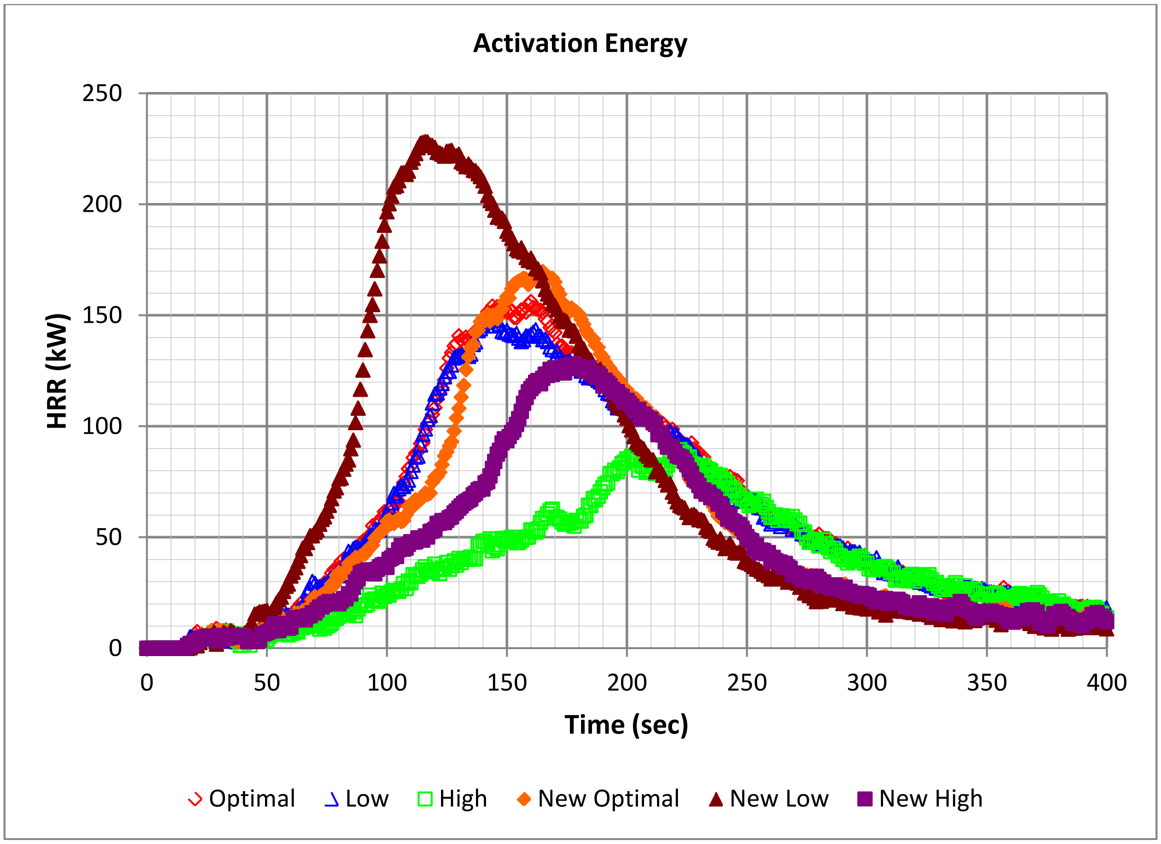

Figure 27 - HRR of FRP panel with varied activation energy [New+Old Comparison]

Variations of the reaction order, which may increase or decrease the rate of reaction of the FRP fuel, were made in the simulations with predicted HRR shown in Figure 28. The new sets of data generally raised and delayed the peak HRR predicted. Effects of reaction orders in pyrolysis predictive capabilities are constantly being evaluated by combustion scientists, however, it should be noted that if the basic fluid dynamics and heat transfer phenomena are not accurate, the reaction order is irrelevant.

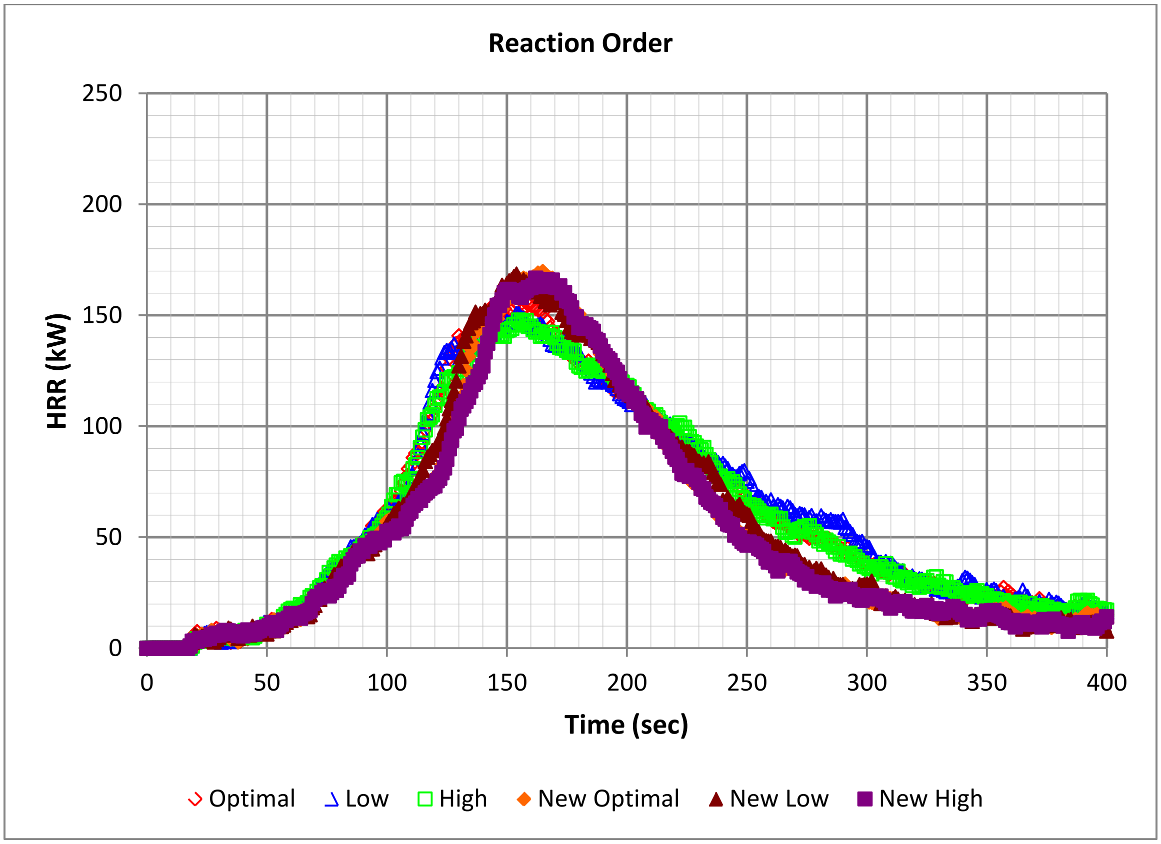

Figure 28 - HRR of FRP panel with varied reaction order [New+Old Comparison]

Figure 29 shows the HRR curves generated by varying the heat of reaction of the FRP fuel. There are little differences in the predicted HRR-time history curves between the ones generated by the new optimal and low values and their counterparts. However, the new high heat of reaction value severely depressed the HRR.

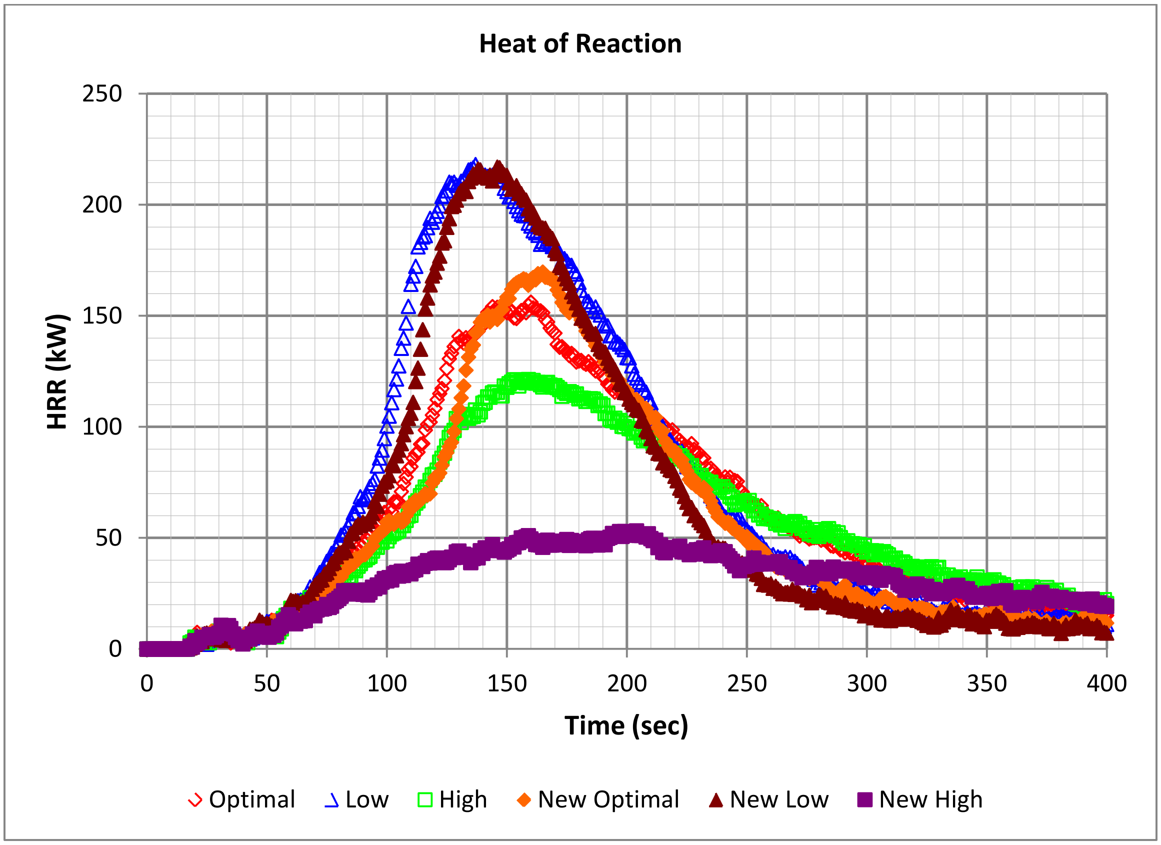

Figure 29 - HRR of FRP panel with varied heat of reaction [New+Old Comparison]

G.2.2 Discussion

The trends observed in the second GPYRO parametric study are similar to those noted in the first study. Additionally, the studies show that the original set of optimal parameter values are suitable since the final values obtained in three different GPYRO series are very similar.

G.3 Relationship between parameters, max HRR, and Max THR

To visualize the relationship between the HRR characteristics and the changes in the material parameter, the two quantities are plotted together in the section below. The quantities are based on the two set of optimal, low, and high values in FDS parameter and results. Before a comparison can be made, the quantities are normalized using the maximum value in each quantity.

The normalized HRR vs. virgin material thermal conductivity is presented in Figure 30. The datapoints are relatively spread out and has a positive trend, which indicates that the virgin material thermal conductivity has a positive effect on the peak HRR and THR.

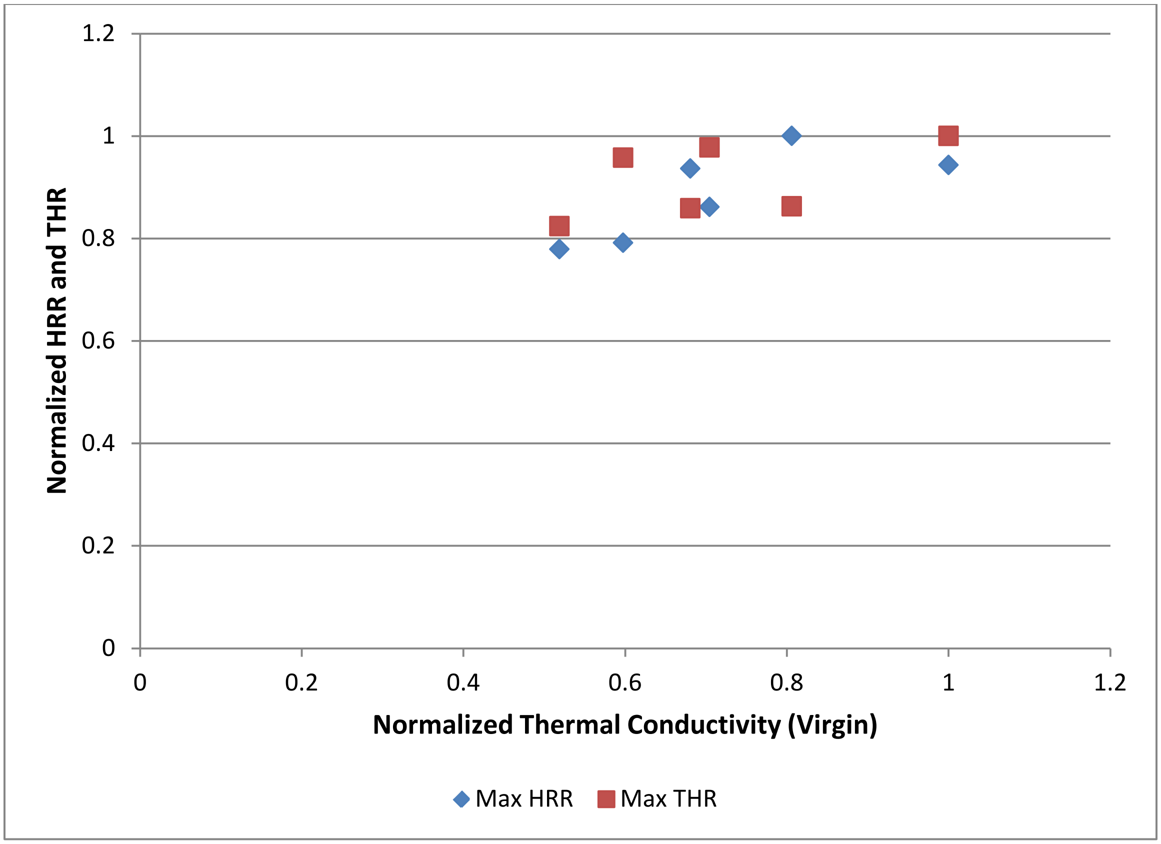

Figure 30 - HRR and THR vs. virgin material thermal conductivity

The normalized HRR vs. virgin material specific heat is presented in Figure 31. The datapoints are relatively spread out and has a negative trend, which indicates that the virgin material specific heat has a slightly negative effect on the peak HRR and THR.

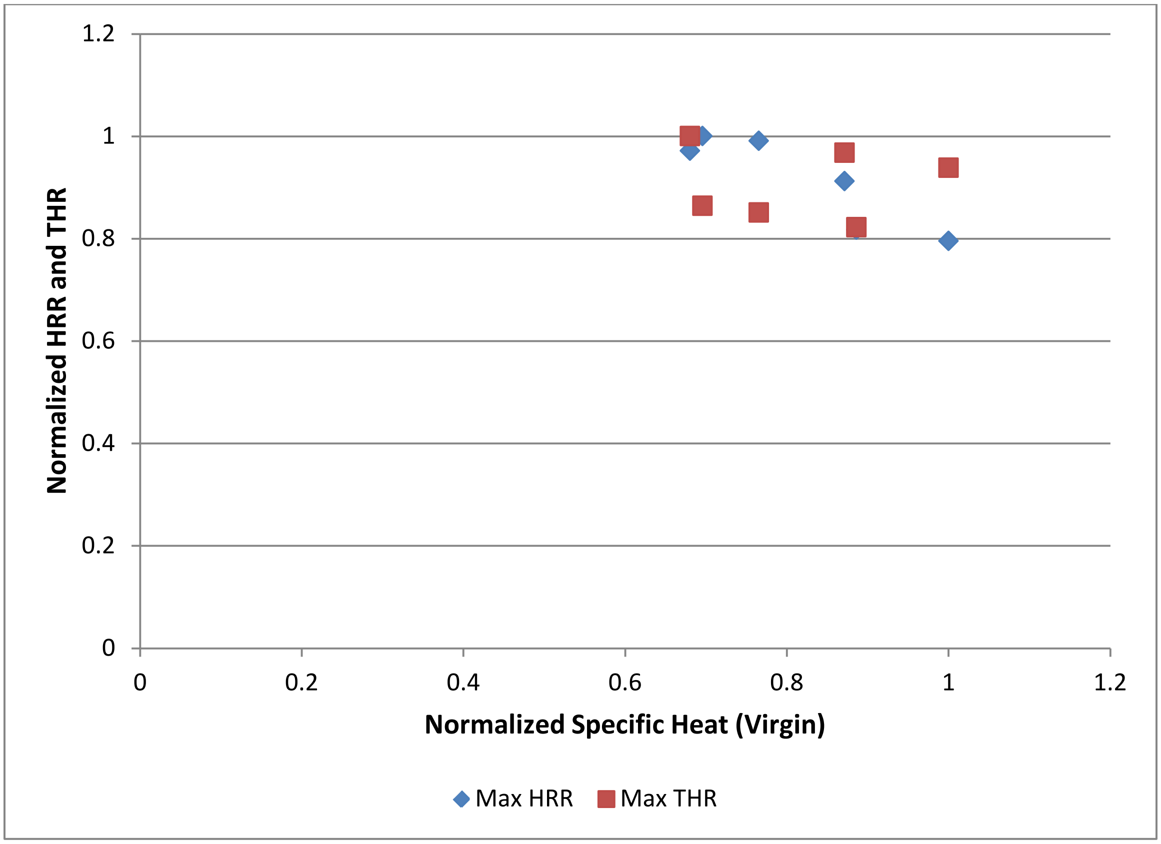

Figure 31 - HRR and THR vs. virgin material specific heat

The normalized HRR vs. virgin material emissivity is presented in Figure 32. The datapoints are tight together and without a clear positive or negative trend, so it appears that the virgin material emissivity has little effect on the peak HRR and the THR.

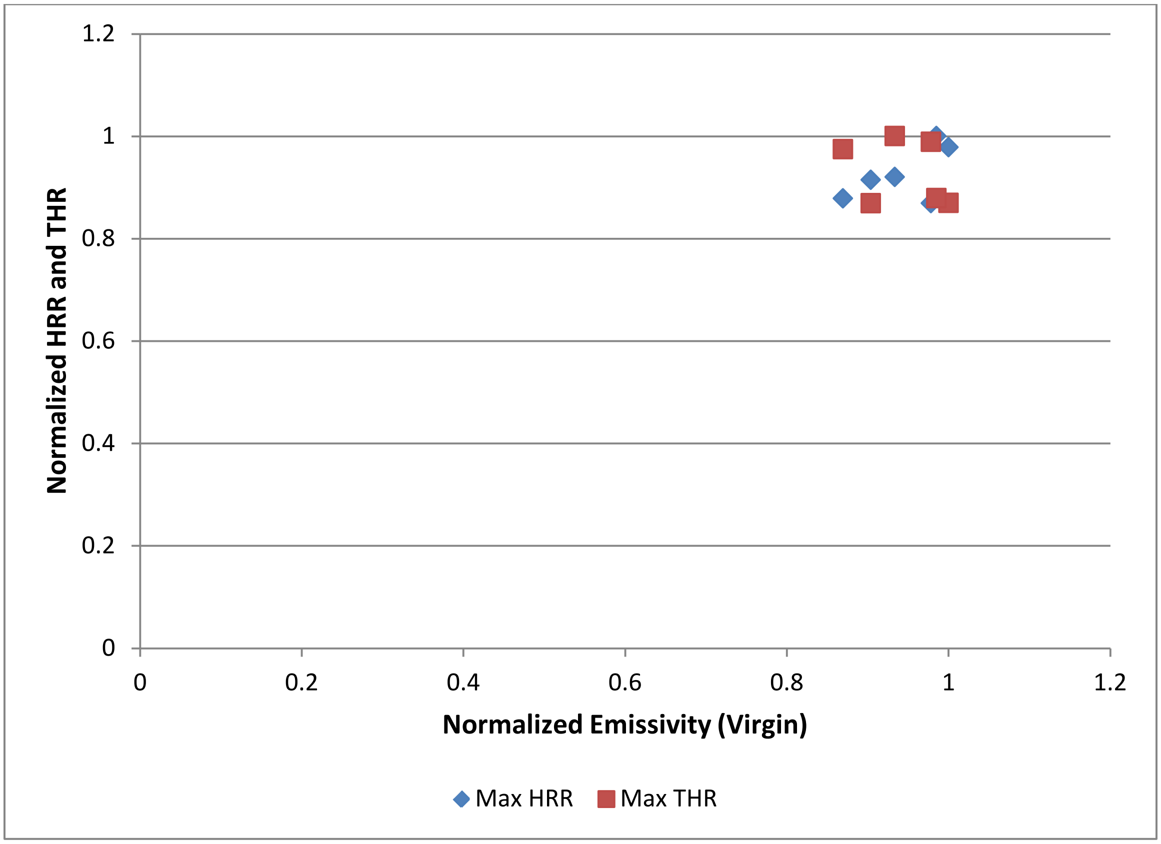

Figure 32 - HRR and THR vs. virgin material emissivity

The normalized HRR vs. char material thermal conductivity is presented in Figure 33. The datapoints are spread out with a slightly negative trend, so it appears that the char material thermal conductivity has a slightly negative effect on the peak HRR and the THR.

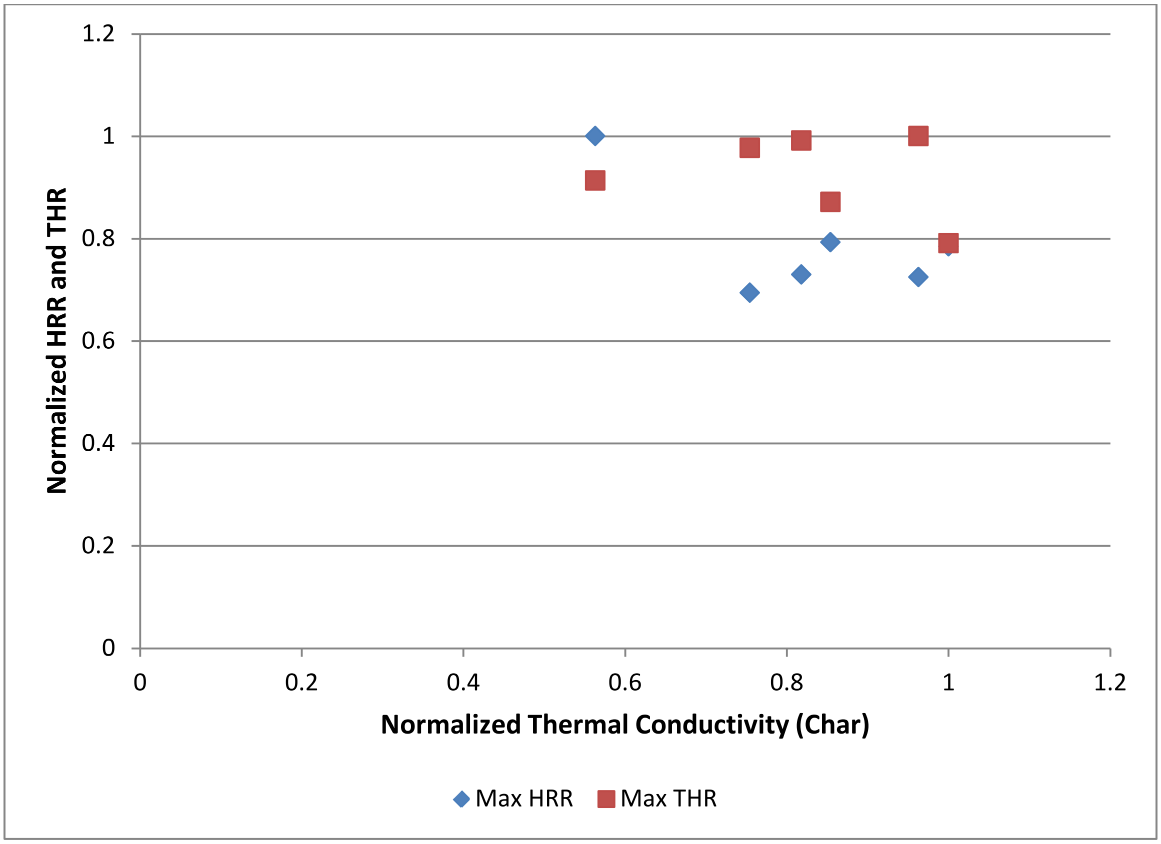

Figure 33 - HRR and THR vs. char material thermal conductivity

The normalized HRR vs. char material specific heat is presented in Figure 34. The datapoints are spread out with no definite positive or negative trend, so it appears that the char material specific heat has little effect on the peak HRR and the THR.

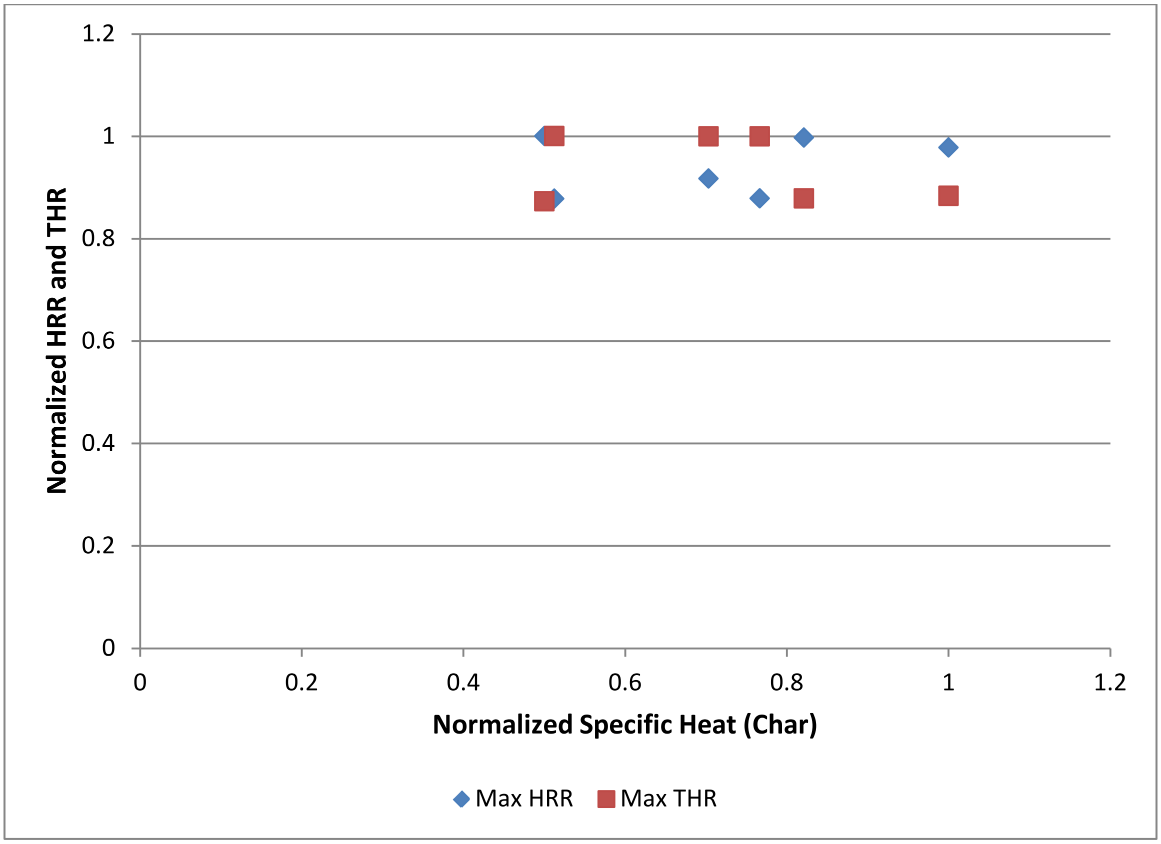

Figure 34 - HRR and THR vs. char material specific heat

The normalized HRR vs. char density is presented in Figure 35. The datapoints are tightly packed together, which indicates that the char density has little effect on the peak HRR or THR.

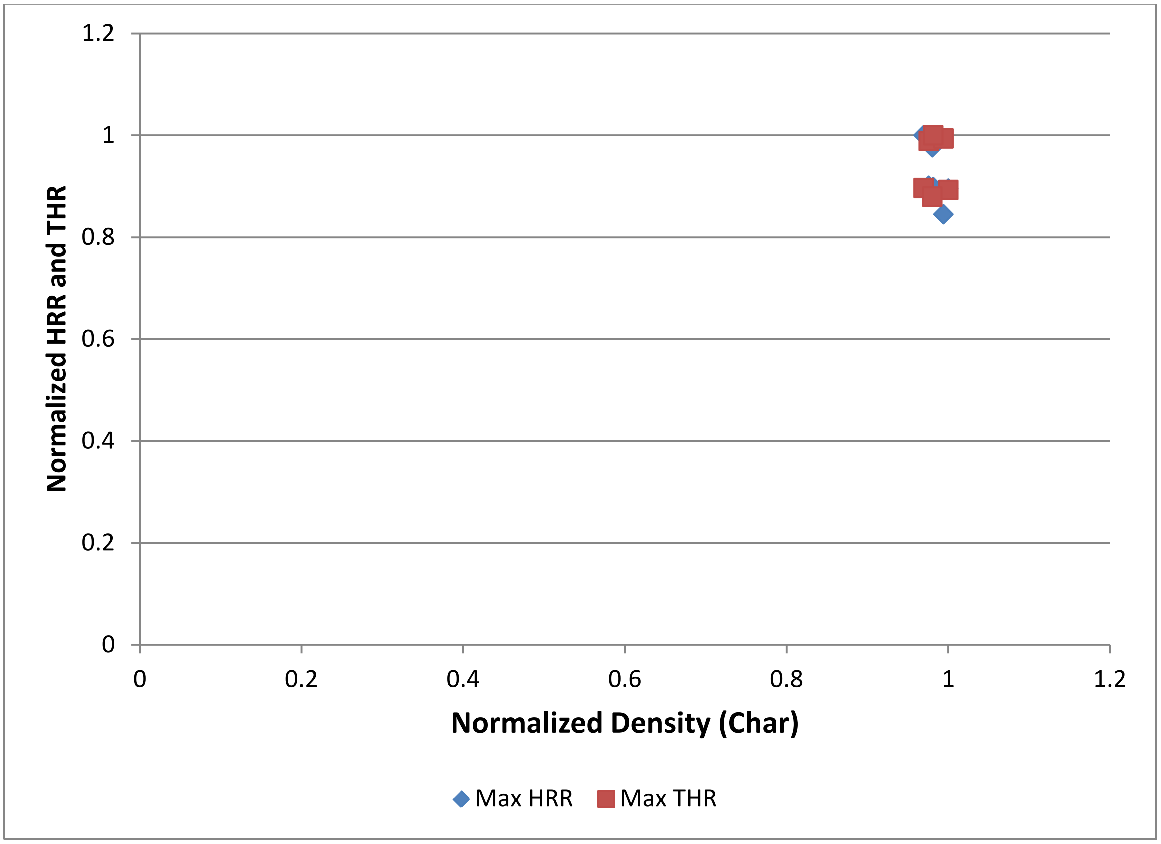

Figure 35 - HRR and THR vs. char material density

The normalized HRR vs. char material emissivity is presented in Figure 36. The datapoints are lightly spread out without a clear positive or negative trend, which indicates that the char density has little effect on the peak HRR or THR.

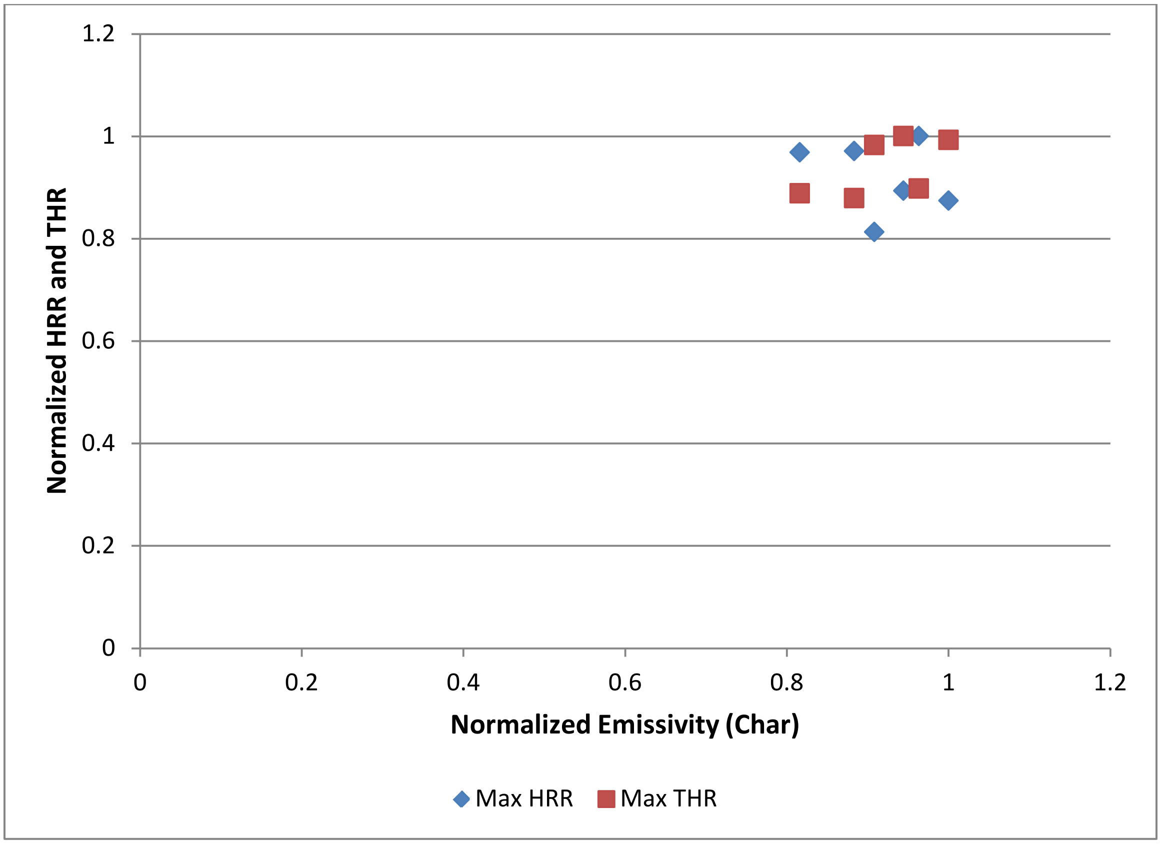

Figure 36 - HRR and THR vs. char material emissivity

The normalized HRR vs. fuel pre-exponential factor is presented in Figure 36. The datapoints are spreaded out with a strong positive correlation. This indicates that the fuel pre-exponential factor is related to the peak HRR and THR very positively.

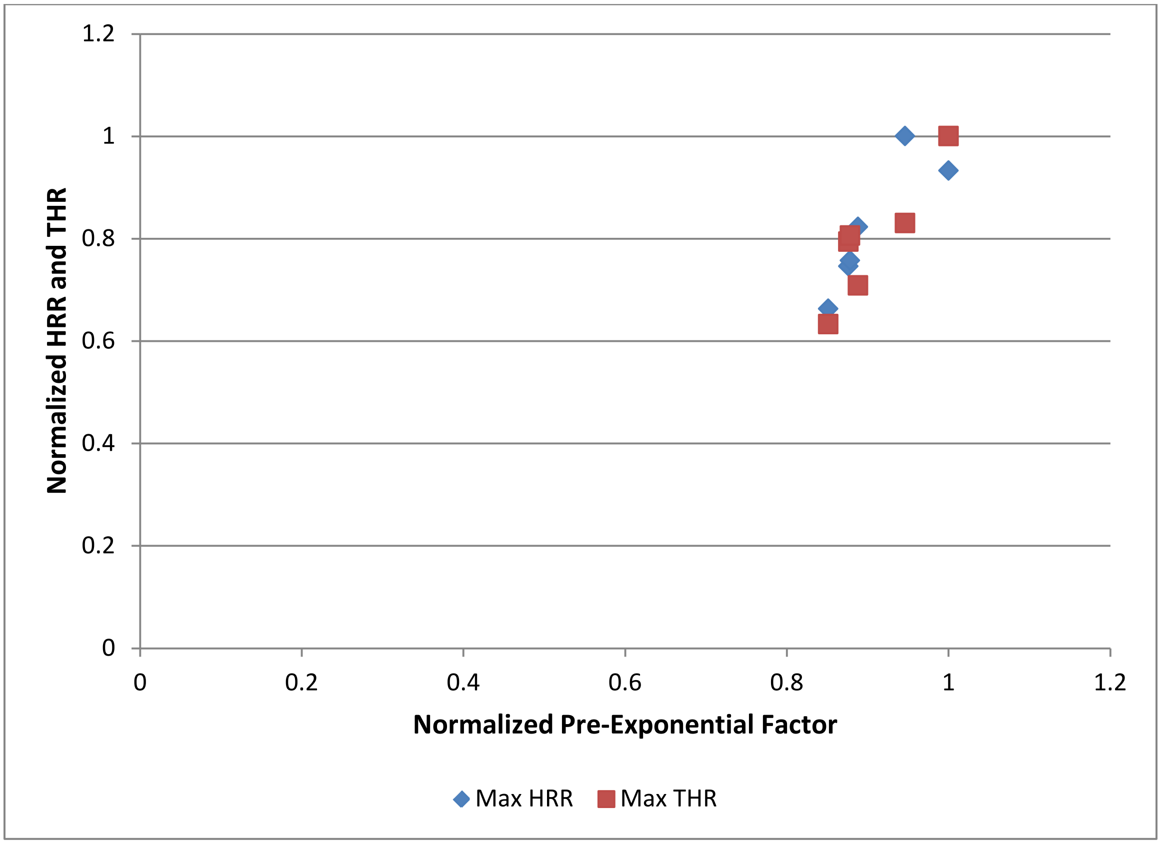

Figure 37 - HRR and THR vs. fuel pre-exponential factor

The normalized HRR vs. fuel activation energy is presented in Figure 38. The datapoints are more spread out with a strong negative correlation. This indicates that the fuel activation energy is related to the peak HRR and THR very inversely.

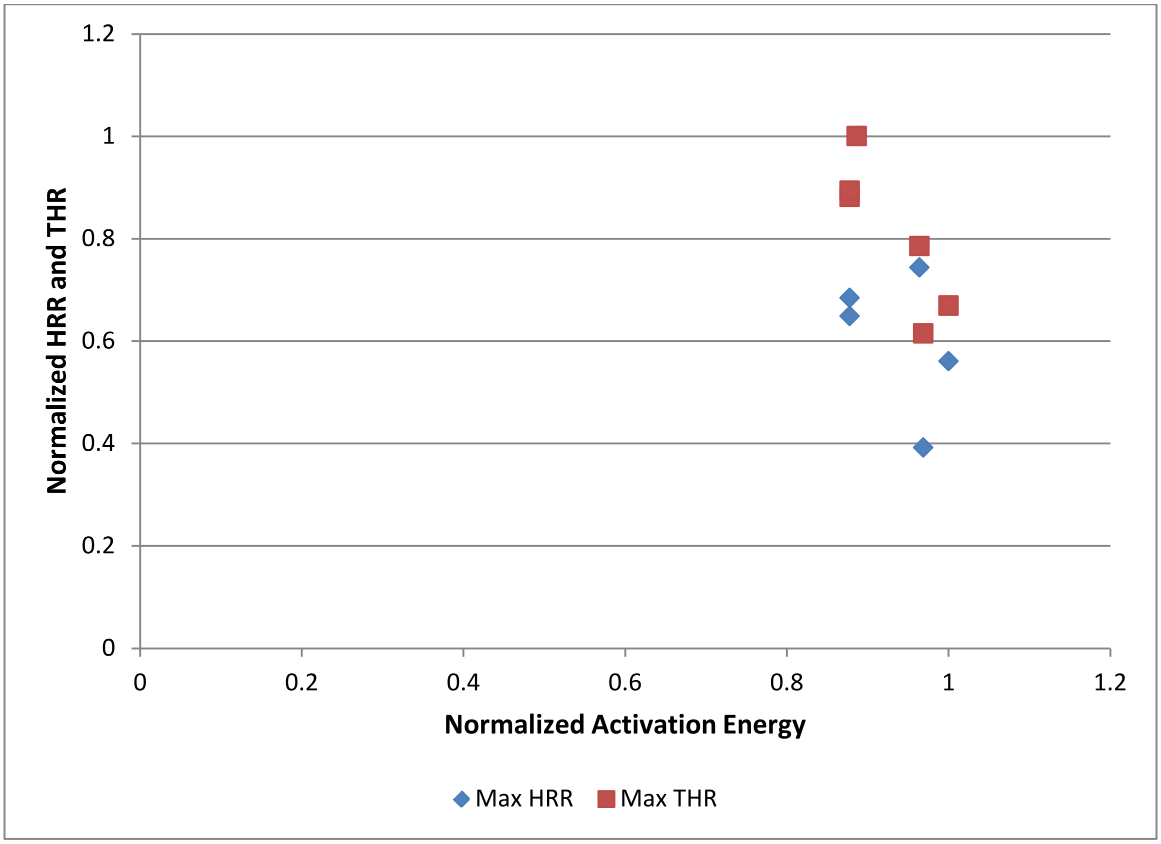

Figure 38 - HRR and THR vs. fuel activation energy

The normalized HRR vs. fuel reaction order is presented in Figure 39. The datapoints are spread out without a definitely positive or negative correlation. This indicates that the fuel reaction order is not likely to affect the peak HRR or the THR in a large degree.

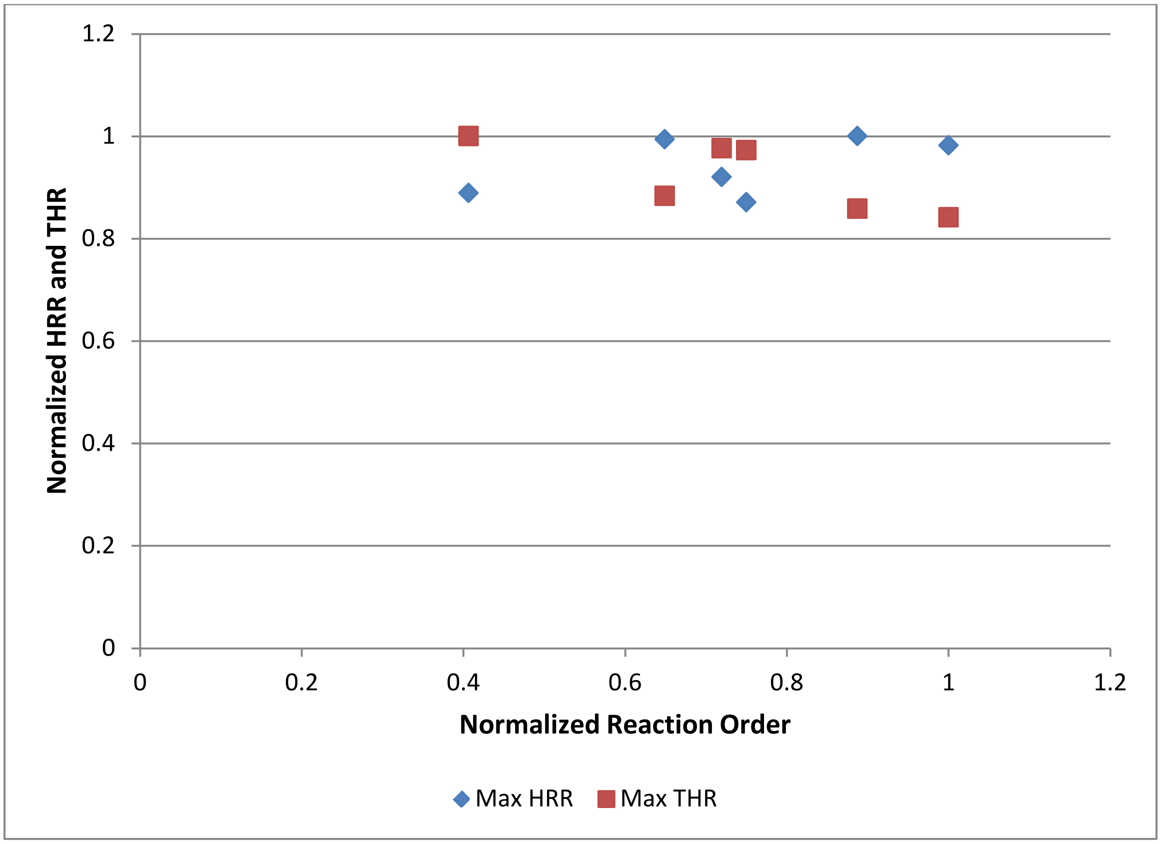

Figure 39 - HRR and THR vs. fuel reaction order

The normalized HRR vs. fuel heat of reaction is presented in Figure 40. The datapoints are spread out with a very strong negative trend. This indicates that the fuel heat of reaction is highly inversely related to the peak HRR and THR.

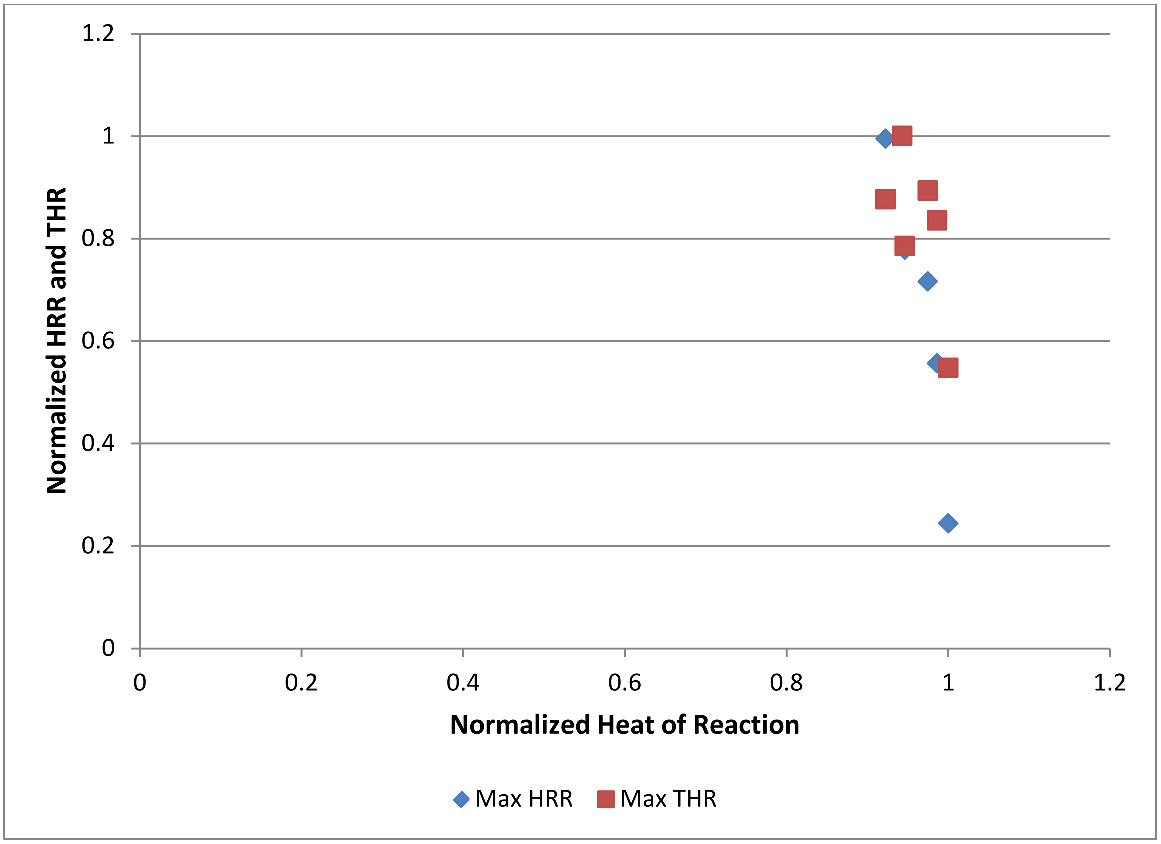

Figure 40 - HRR and THR vs. fuel heat of reaction

Appendix H FDS Grid Sensitivity Analysis on FRP Simulations

Separate series of Combustible Wall simulations of a FRP material were run at different grid sizes in order to perform a rudimentary grid sensitivity analysis. The grid sizes used were 2.5 cm cubes and 5.0 cm cubes. The number of grid cells in the models using the smaller grid size is 1,437,696 and for those using the larger grid size there are 179,712 cells in each model.

The doubling of the gird cell size and the subsequent reduction in cell number (by 87.5%) drastically reduced the time needed to complete the simulations by approximately 95% across all runs.

The initial fire shape, sizes, and timing are different in each model in order to simulate the FRP fire experiments, so in order to compare the FDS-predicted HRR, the HRR generated in the "burning" of the FRP lining material is needed instead. The FRP fire HRR is calculated by subtracting the source initial fire HRR from the total predicted HRR.

The following FRP fire HRR information are used to compare the results of each model at the two different grid sizes: peak HRR, time to peak HRR, and total heat released. The variances of these three quantities are based on the 5.0 cm grid models as found by the following equation:

$$\frac{Quantity_{2.5\text{cm}} - Quantity_{5.0cm}}{Quantity_{5.0cm}}$$

Since the baseline grid cell size chosen for the majority of the simulation in the related study is the larger grid size at 5.0 cm, the results from the 5.0 cm grid simulations are used as the baseline to which the other simulations are compared to.

All models in the grid analysis study used the default FDS variables where are the same as the ones used in the rest of the Series 1 simulations. The values used in the definition of the FRP material properties were created by the first (out of three) scenario of GPYRO models. The major difference between the 2.5 cm models and the 2.5 cm models are the grid size, number of cell, and the distance between the surface of the FRP and the burner's edge. In both sets of models there is a 1 cell gap between the wall surface and the burner edge, such that the distance of the gap is different by 2.5 cm.

In some of the following figures, the description of each model has been appreciated as follows:

- Pr: propane fuel
- PP: propylene fuel
- sb: Square burner
- lb: Rectangle burner
- 50: source fire peaks at 50 kW
- 75: source fire peaks at 75 kW

- Cont: source fire HRR is consistently at the prescribed HRR for the duration of the simulation (in all other simulations the source fire peaks then is shut down after approximately 1 min to mirror the experiments conducted)
- B: indicates a duplicate model with the same source fire parameters

Figure 1 provides a comprehensive summary of the variances for all models. It is evident that for the majority of the 2.5 cm grid models, the Total Heat Released (THR) and Peak HRR values are usually underpredicted (smaller) when compared to the baseline 5.0 cm models. However, the 2.5 cm grid models' predicted time to peak is consistently greater than that predicted by the 5.0 cm grid models except for two cases involving the Square burner at 50 kW. It is also noted that the undeprediction of the THR and the peak HRR are usually paired up, except for the few cases where the THR is over-predicted but with a (usual) underprediction of the peak HRR, or vice versa. Before the FDS results were analyzed, there was a notion that the 2.5 cm gird models would yield better prediction in the HRR and of the flame spread such that the predicted quantities are closer to the values measured during the experiments. However, based on the previously-made comparison between the FDS results and measured values, the basic 5.0 cm grid models predict much lower HRR and smaller flame spread.

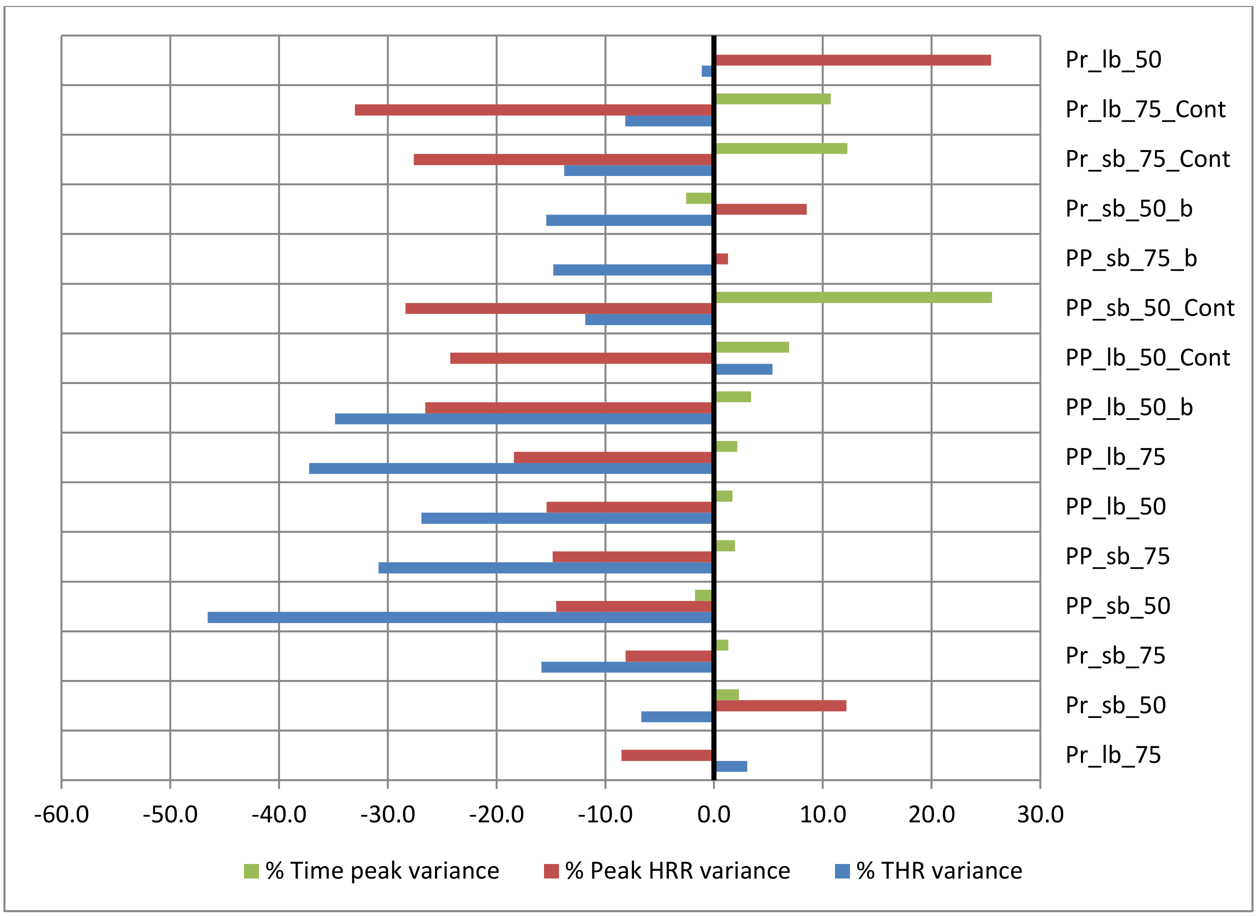

Figure 1 - All variances based on 2.5 cm grid models

The THR variance across all models is shown in Figure 2. The most negative variance has a value of approximately -45% and occurs at the propylene, Square burner at 50 kW comparisons. The most positive variance has a value of approximately 6% and occurs at the polypropylene, Rectangle burner at continuous50 kW comparison. Only in 2 instances are the variance positive (0.25 cm model predicts a higher THR than the 5.0 cm model), and both occurs when the Rectangle burner is simulated, but all other burner parameters are different. It is observed that the average THR variance is -17.1%.

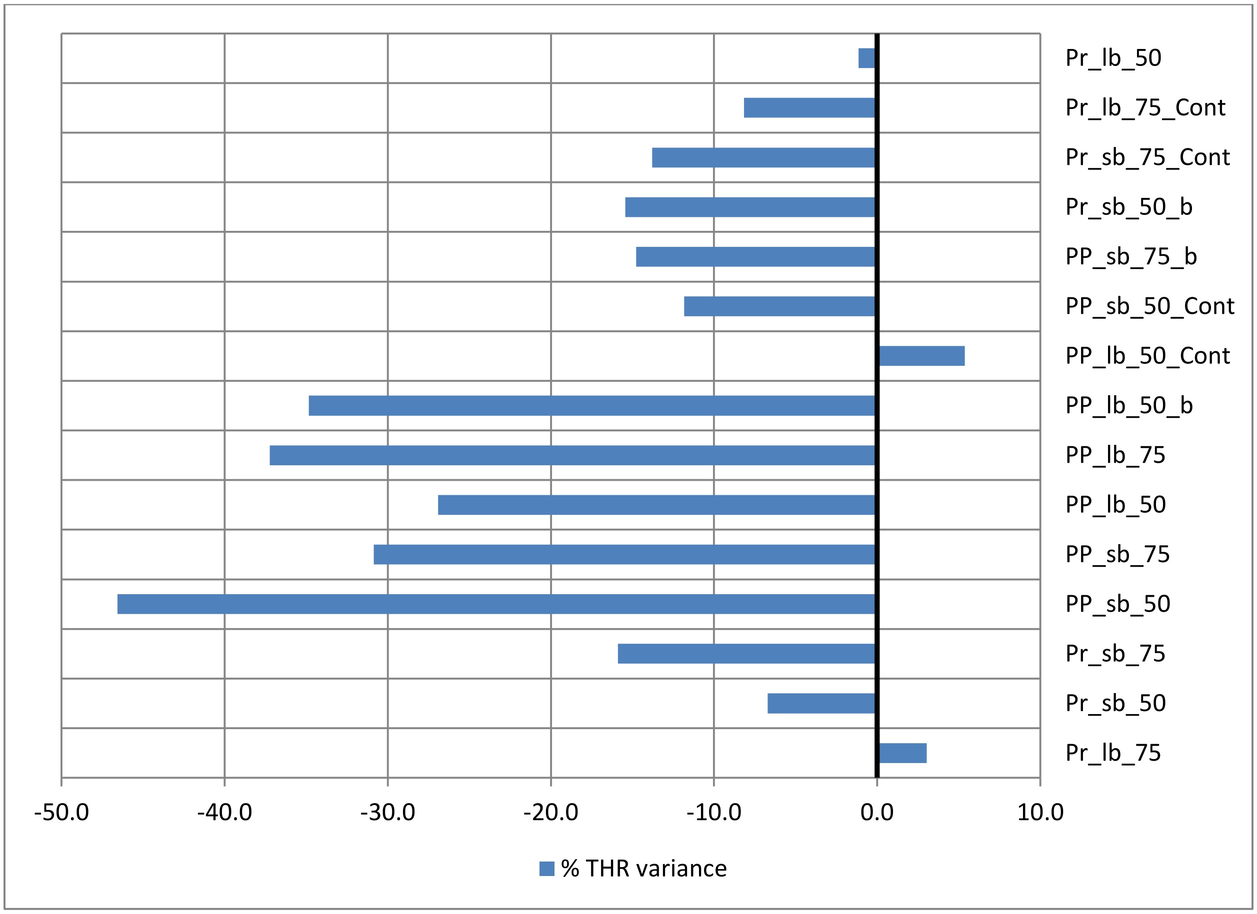

Figure 2 - THR variance across all models

The peak HRR variance across all models is shown in Figure 3. The majority of the values are negative, suggesting that the 2.5 cm grid models generally predict lower peak HRR than the 5.0 cm models. The most negative variance is approximately -33%, occurring in the propane, Rectangle burner, continuous 75 kW models comparison. The most positive variance is approximately 25% and occurring in the propane, Rectangle burner, and 50 kW models comparison. There are another 3 instances where the variance is positive: 2 models where propane, Square burner, and 50 kW were prescribed, and the model using propylene, Square burner, and 75 kW. It is noted that the variance values between the two identical models are similar. The average variance in peak HRR across all models is -11.5%.

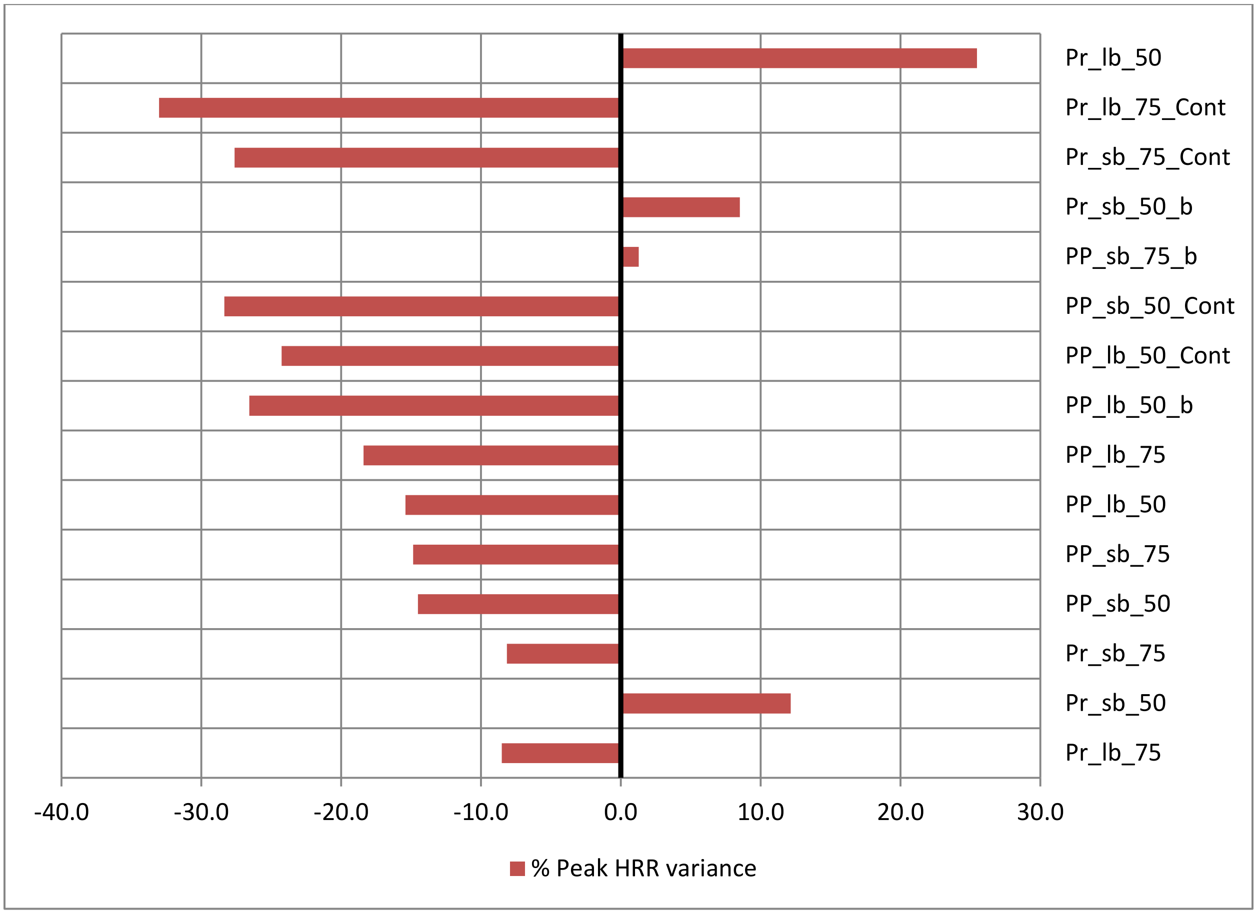

Figure 3 – Peak HRR variance across all models

Figure 4 presents the time to peak HRR variance across all models. The most negative variance is approximately -2.5% occurring in the propane, Square burner at 50 kW comparisons. The most positive variance is approximately 26% occurring at the propylene, Square burner, and continuous 50 kW comparisons. It is noted that the most positive variance is approximately twice the second most positive variance. There are two instances of negative variance, they both occur in the simulations using the Square burner at 50 kW, but different source fuel. The average time to peak HRR variance value is 4.3%.

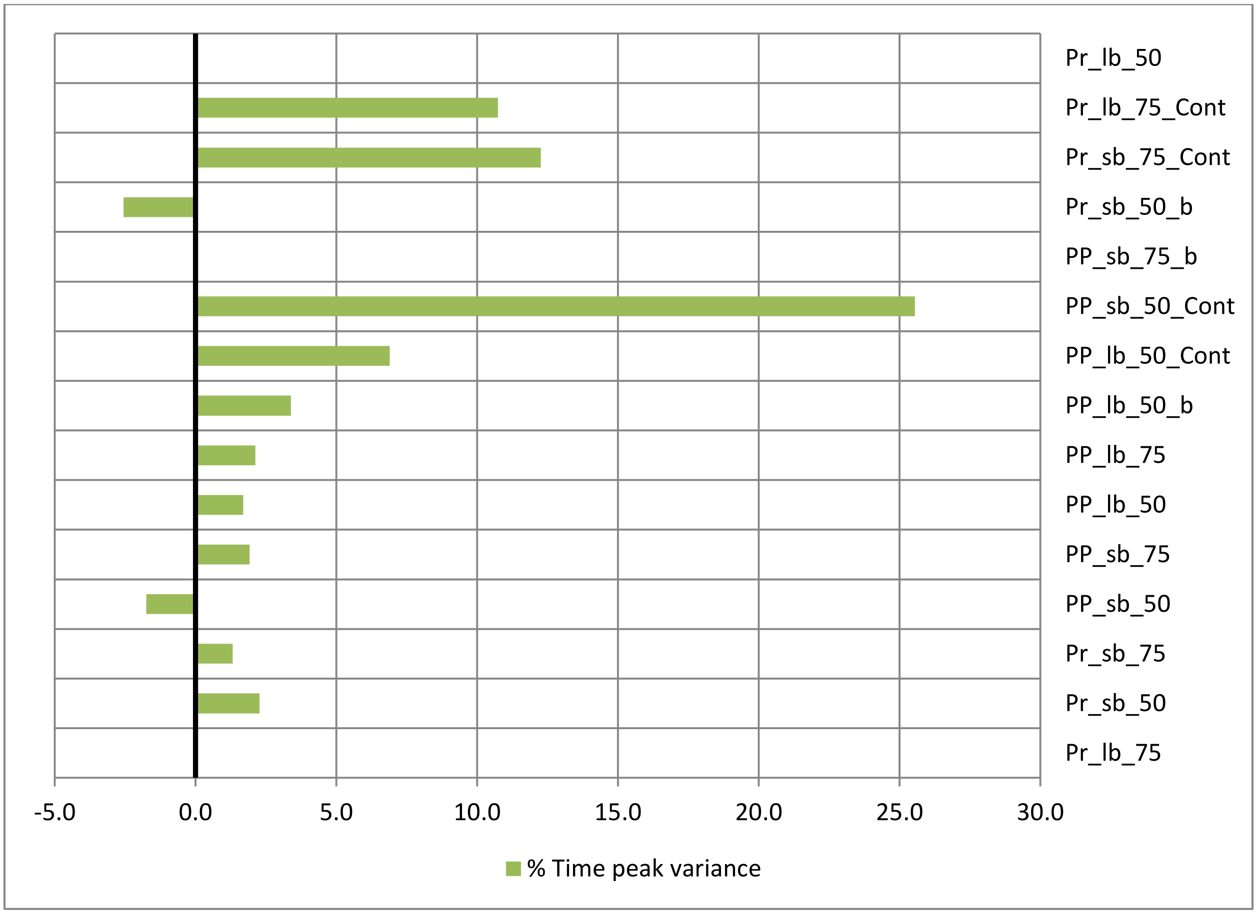

Figure 4 – Time to peak variance across all models

All three quantities' variances in the models using propane are presented in Figure 5. It appears that the sign of the variance values for the peak HRR and time to peak HRR are the most inconsistent. It appears that none of the burner parameter affects the magnitude or the direction of the variance significantly.

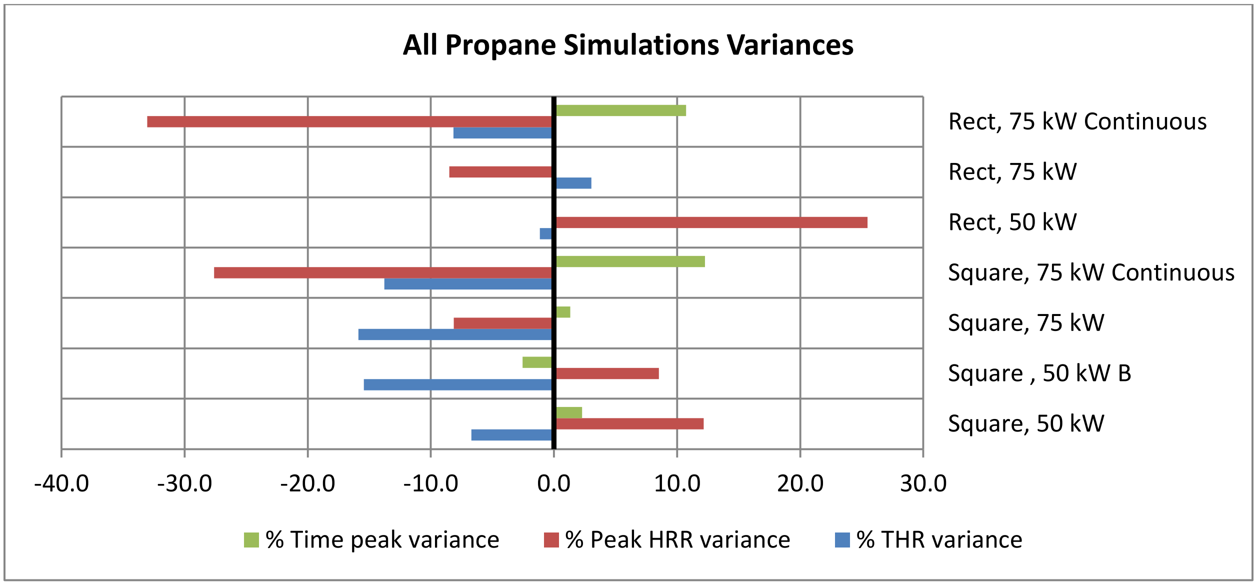

Figure 5 – Propane model variances

However, in the propylene models, the direction of the variances is mostly consistent, as shown in Figure 6. Comparing the propane models against the propylene models, it appears that the average variances of the three quantities are greater in the propylene models.

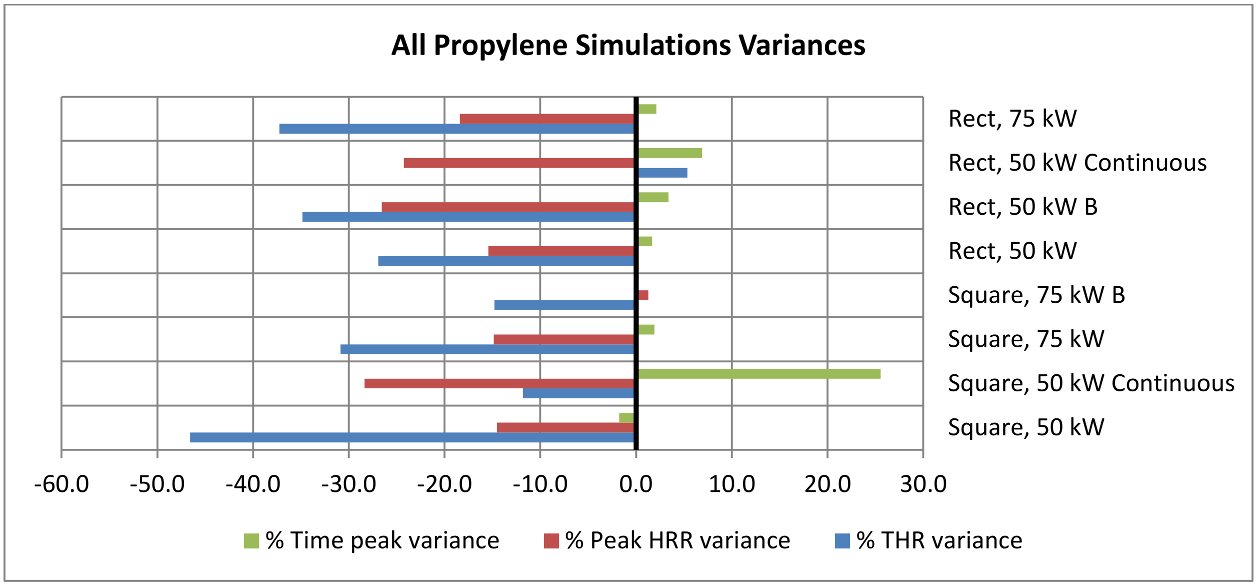

Figure 6 – Propylene model variances

Grouping the models by burner shape in Figure 7 and Figure 8 shows that the magnitude and the direction of the three types of variances are not consistent across the simulations. It appears that the magnitude of the average variances in time to peak and THR are greater for the Square burner models, whereas the average magnitude of the peak HRR variance is greater in the Rectangle burner models.

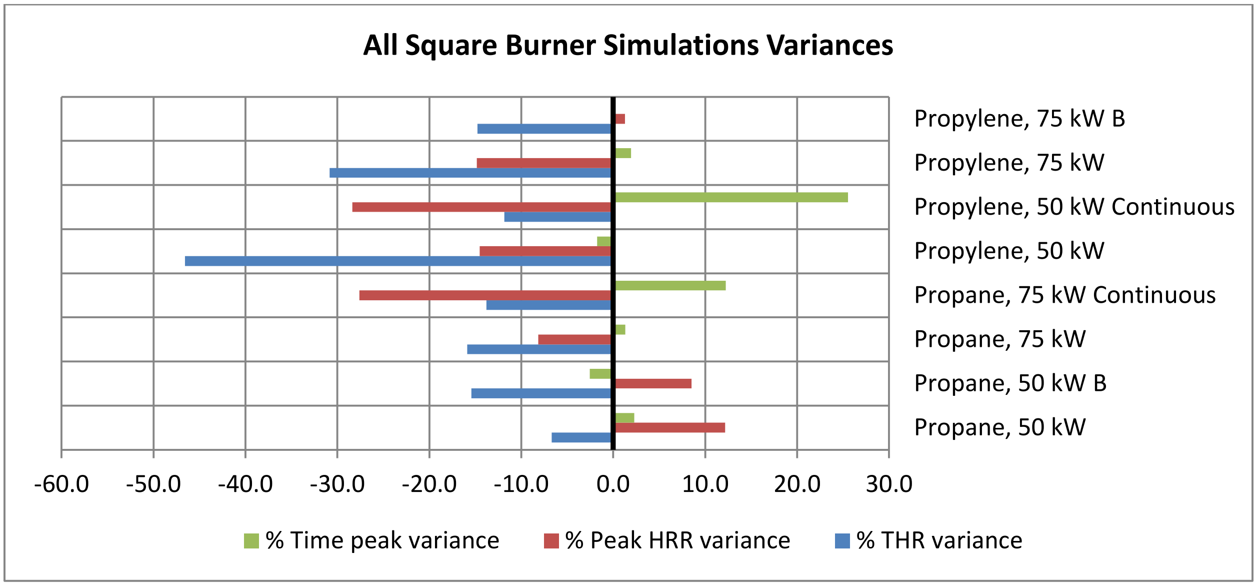

Figure 7 – Square burner model variances

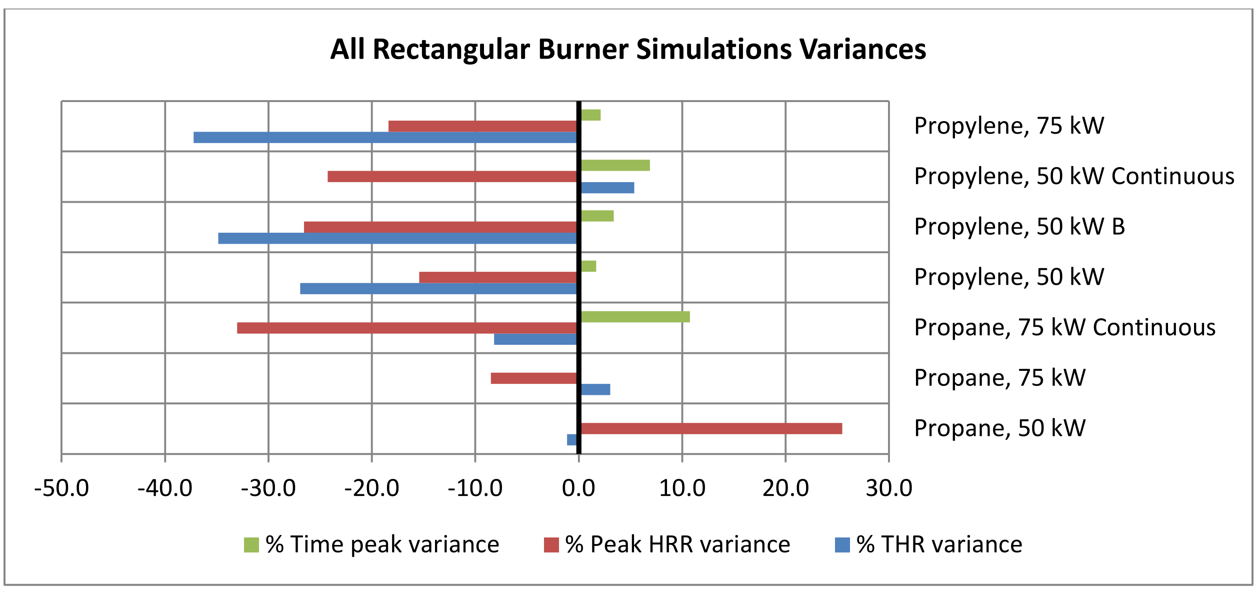

Figure 8 –Rectangle Burner model variances

Grouping the models by source fire HRR in Figure 9 and Figure 10 shows that the magnitude and the direction of the three types of variances are not consistent across the simulations. It appears that the magnitude of the average variances in time to peak and THR are greater for the 50 kW models, whereas the average magnitude of the peak HRR variance is greater in the 75 kW models. It should be noted that in the continuous 75 kW models using propane, the time to peak and peak HRR variances have the greatest magnitude.

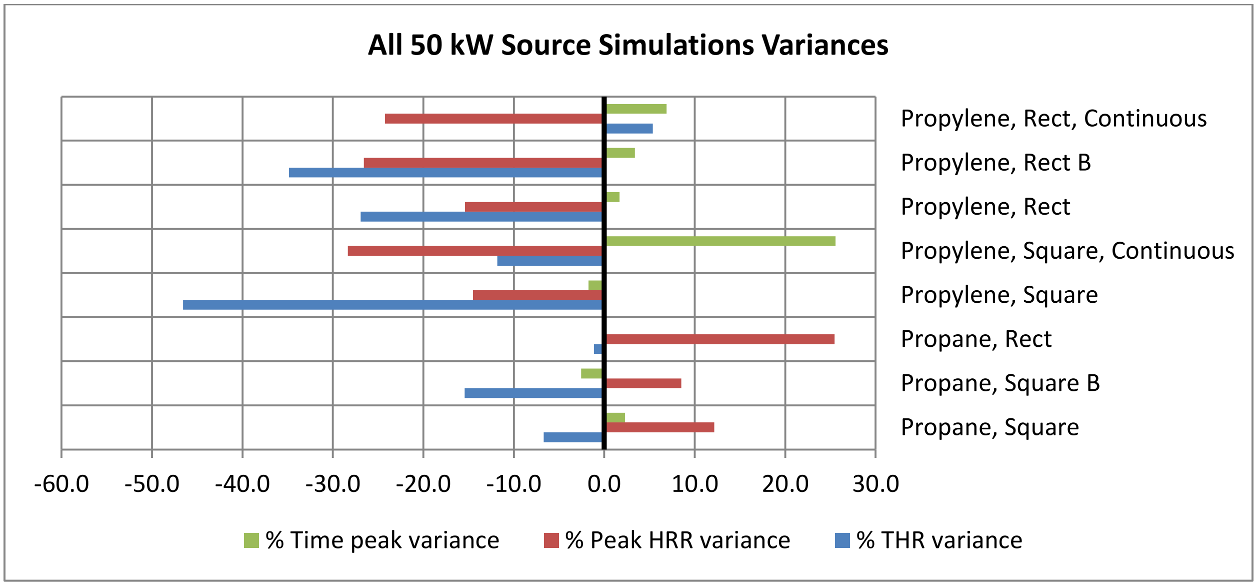

Figure 9 – 50 kW burner model variances

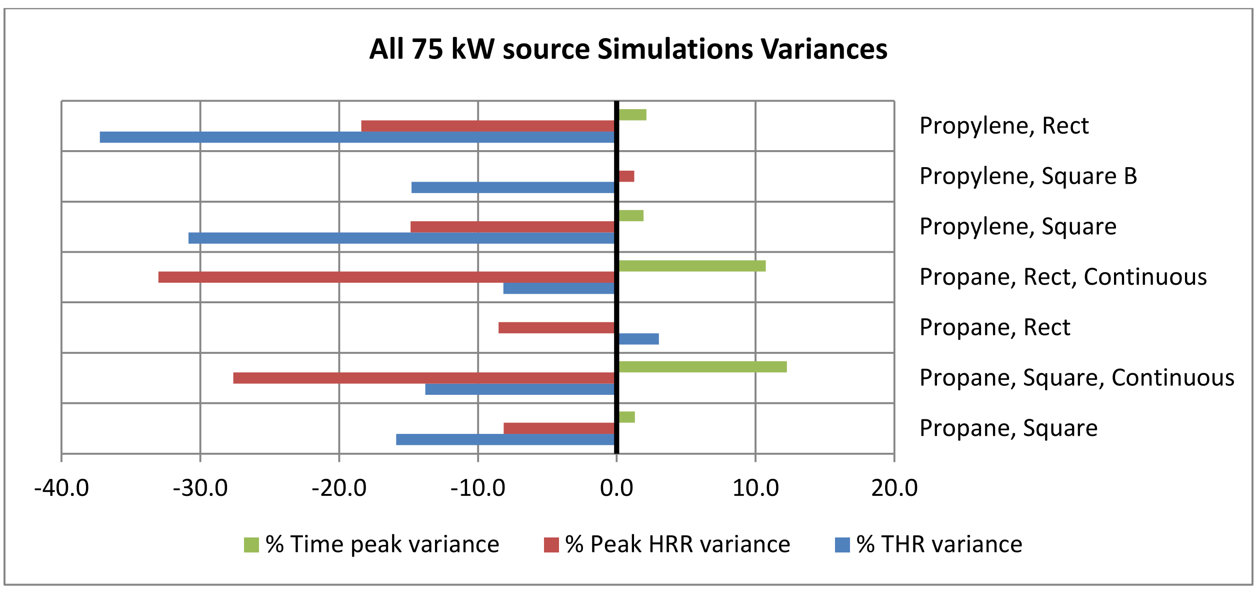

Figure 10 –75 kW Burner model variances

Based on the above comparison of the FDS results from the 2.5 cm and 5.0 cm models and the time needed to complete each runs, it appears that reducing the grid size does not aid the FDS predicts. Using the actual measured HRR data as a metric, it is shown that the smaller grid-cell models actually reduced the accuracy by predicting a smaller HRR and flame spread than the 5.0 cm models. Although it is not definitive, it appears that for the experiments in the current study, using the larger grid cells is more appropriate. Usually, a more refined computation space should represent reality better. However, in the current study to model the complex flame spread phenomenon, the accuracy of a model appears to depend more on factors other than the grid size.

In light of the results, executing additional simulations at a more refined grid size of 1.0 cm seems to be redundant and not economical.

Appendix I Effect on the HRR in FRP Simulations Due to the Heat of Reaction Parameter

After the initial comparisons between the FDS-predicted and the experimental HRR of the combustible wall experiments were made in Section 5, it was found that FDS significantly underpredicts the flame spread and heat release rate of the combustible wall fires. However, during the GPYRO sensitivity analysis (described in Appendix G), it was observed that the heat of reaction parameter of the FRP material can affect the predicted HRR significantly.

The heat of reaction of a material is the amount of energy per unit mass required to be applied to a reactant in order to cause a chemical reaction. Put simply, a material with a low heat of reaction is easier to be ignited than a similar material with a higher heat of reaction. Hence, to investigate the sensitivity of FRP HRR predictions to pyrolysis properties, additional series of simulations were run where the heat of reaction of the fuel properties was changed. The default heat of reaction used in previous simulations was 1000 kW/kg, so a lower estimate of 500 kW/kg and a higher estimate of 1500 kW/kg were used. HRR time-histories from the new simulations are compared to the experimental data and from the Series 1 simulations.

Not all of the test and simulation data are presented below, only those tests with repeated or similar conditions are presented herein so that comparisons of similar tests can also be shown. The results from the tests with more unique configurations and their corresponding simulations are consistent with those presented below.

The five test conditions that are repeated or are similar are shown in Table 1. The parameters considered for comparisons are the HRR and burning rate of the FRP fire.

Table 1 - Conditions of tests detailed in this report

Test Numbers	Burner size	Source HRR [kW]	Source HRR shut-off time [sec]	Source Fuel
A8, A14	Square	75	50 / 56	Propylene
A5, A15	Square	50	41 / 42	Propane
A9, A11	Rectangle	50	57 / 60	Propylene
A12, A13	Rectangle / Square*	50	879 / 680*	Propylene
A16, A17	Square / Rectangle*	75	1360 / 807*	Propane

*Note: Both burners are used in these tests where the source fire was not extinguished during testing.

I.1 Propylene, 75 kW, Square burner

Tests 8 and 14 were identical to each other except that the burner turn-off time was different. The source propylene fire was 75 kW with a Square burner. The HRRs of the burning panel in Tests 8 and 14, minus that of the source fire, are presented in Figure 1. Changing the heat of reaction did not have much effect to instigate flame spread in these simulations. Some initial burning was predicted when the source burner is on, but in all FDS models regardless of the heat of reaction, the fire on the FRP panel self-extinguished soon after the burner is turned off. Figure 1 shows the experimental vs. predicted HRRs.

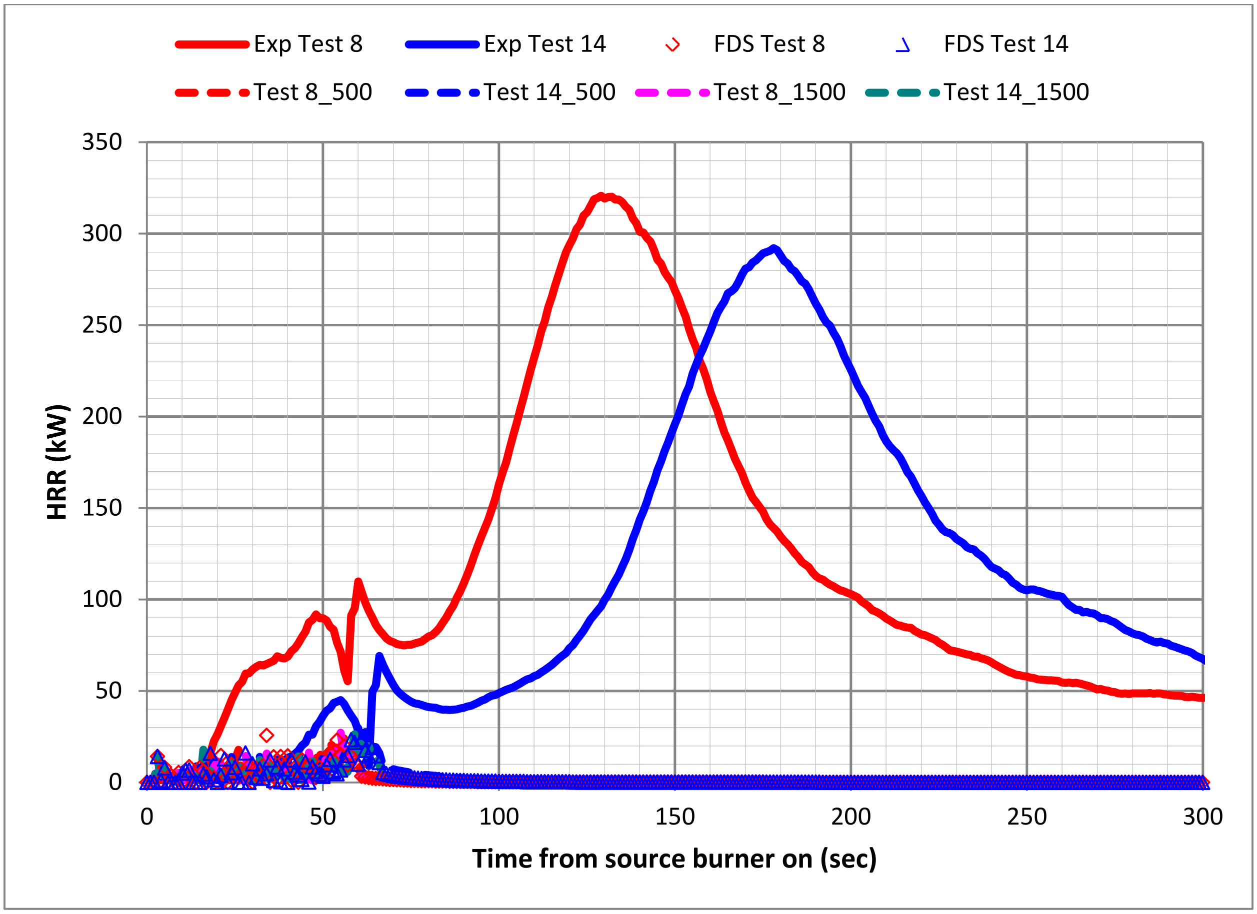

Figure 1 - HRRs of tests using propylene, 75 kW, Square burner

Figure 2 presents the burning rate of the FRP panel predicted by FDS. As expected, the runs with the lower heat of reaction created higher predicted burning rate, and the models with the highest heat of reaction created burning rate similar in magnitude to the ones predicted in the default simulations. It is also observed that the timing of all of predicted burning rate history, initial fire, growth, peak, and extinguished are essentially the same regardless of the heat of reaction value.

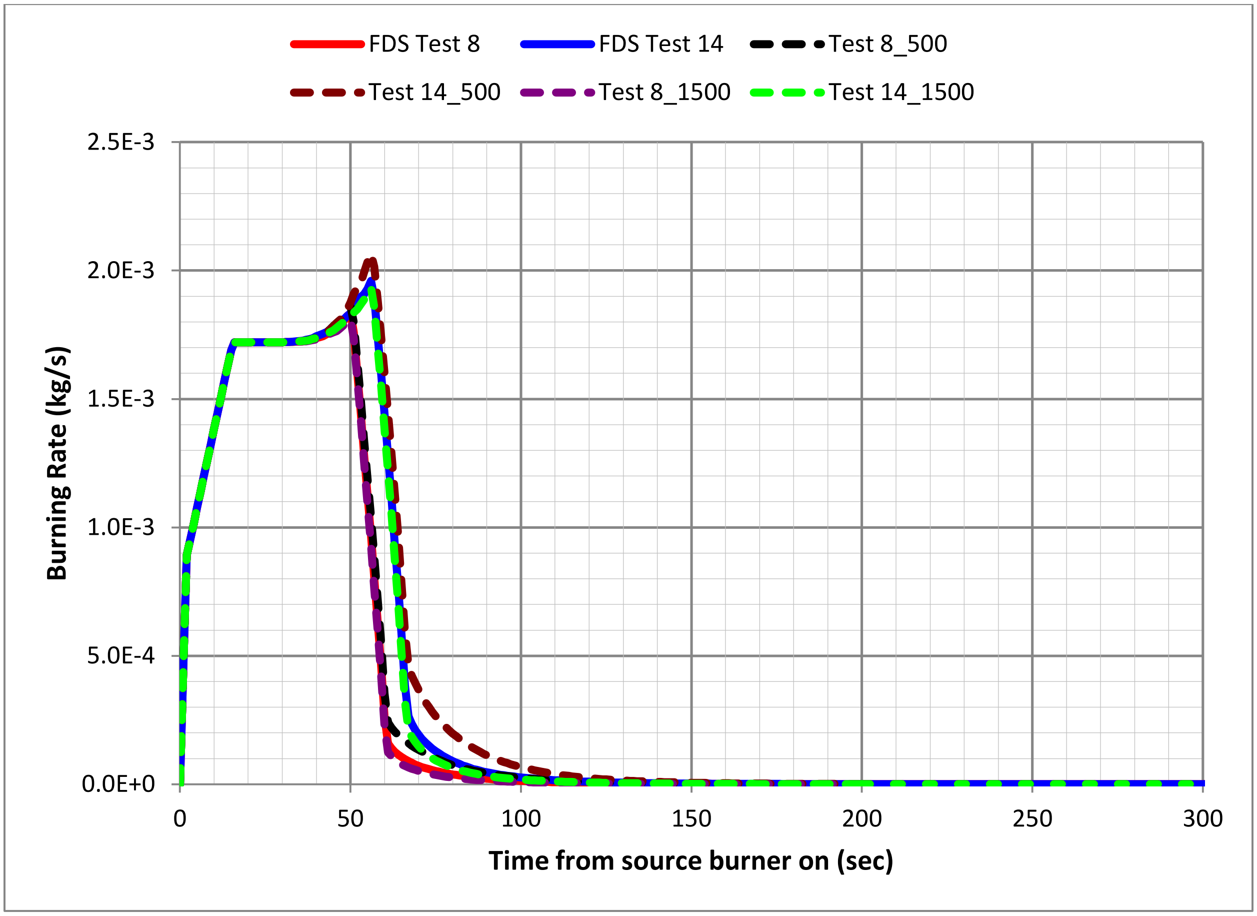

Figure 2 – Burning rates of tests using propylene, 75 kW, Square burner

I.2 Propane, 50 kW, Square burner

Tests 5 and 15 were identical to each other except that the burner turn-off time was different. The source propylene fire was 50 kW with a Square burner. The HRRs of the burning panel in Tests 5 and 15, minus that of the source fire, are presented in Figure 3. Again, changing the heat of reaction did not have much effect to instigate flame spread in these simulations. Some initial burning was predicted when the source burner is on, but in all FDS models regardless of the heat of reaction, the fire on the FRP panel self-extinguished soon after the burner is turned off. Figure 3 shows the experimental vs. predicted HRRs.

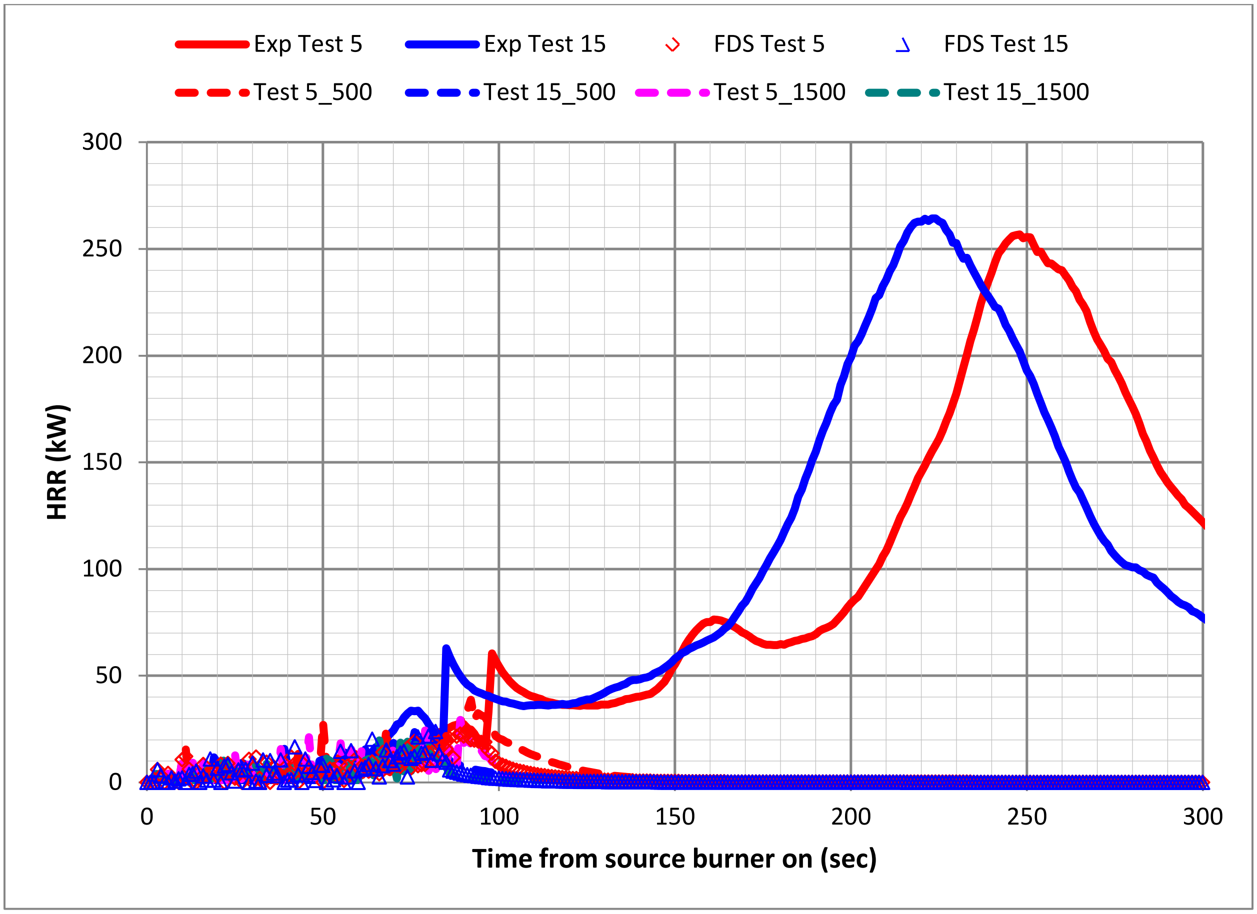

Figure 3 - HRRs of tests using propane, 50 kW, Square burner

Figure 4 presents the burning rate of the FRP panel predicted by FDS. As expected, the runs with the lower heat of reaction created higher predicted burning rate, and the models with the highest heat of reaction created burning rate similar in magnitude to the ones predicted in the default simulations. It is also observed that the timing of all of predicted burning rate history, initial fire, growth, peak, and extinguished are essentially the same regardless of the heat of reaction value. This is similar to what is noted in the previous section, but the magnitudes of the deviations are greater in this scenario.

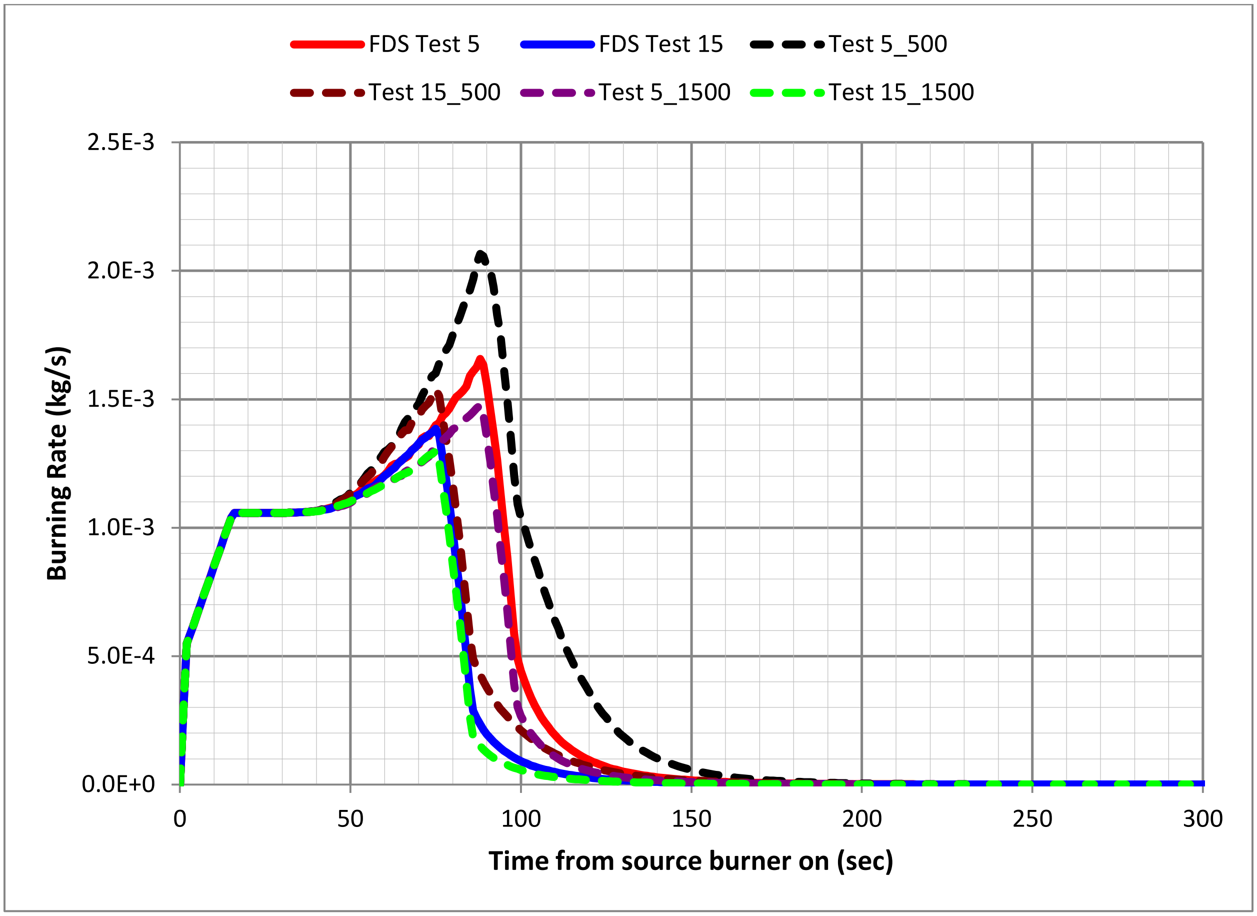

Figure 4 – Burning rates of tests using propane, 50 kW, Square burner

I.3 Propane, 50 kW, Rectangle burner

Tests 9 and 11 were identical to each other except that the burner turn-off time was different. The source propane fire was 50 kW with a Rectangle burner. The HRRs of the burning panel in Tests 9 and 11, minus that of the source fire, are presented in Figure 5. Again, changing the heat of reaction did not have much effect to instigate flame spread in these simulations. Some initial burning was predicted when the source burner is on, but in all FDS models regardless of the heat of reaction, the fire on the FRP panel self-extinguished soon after the burner is turned off. Figure 5 shows the experimental vs. predicted HRRs.

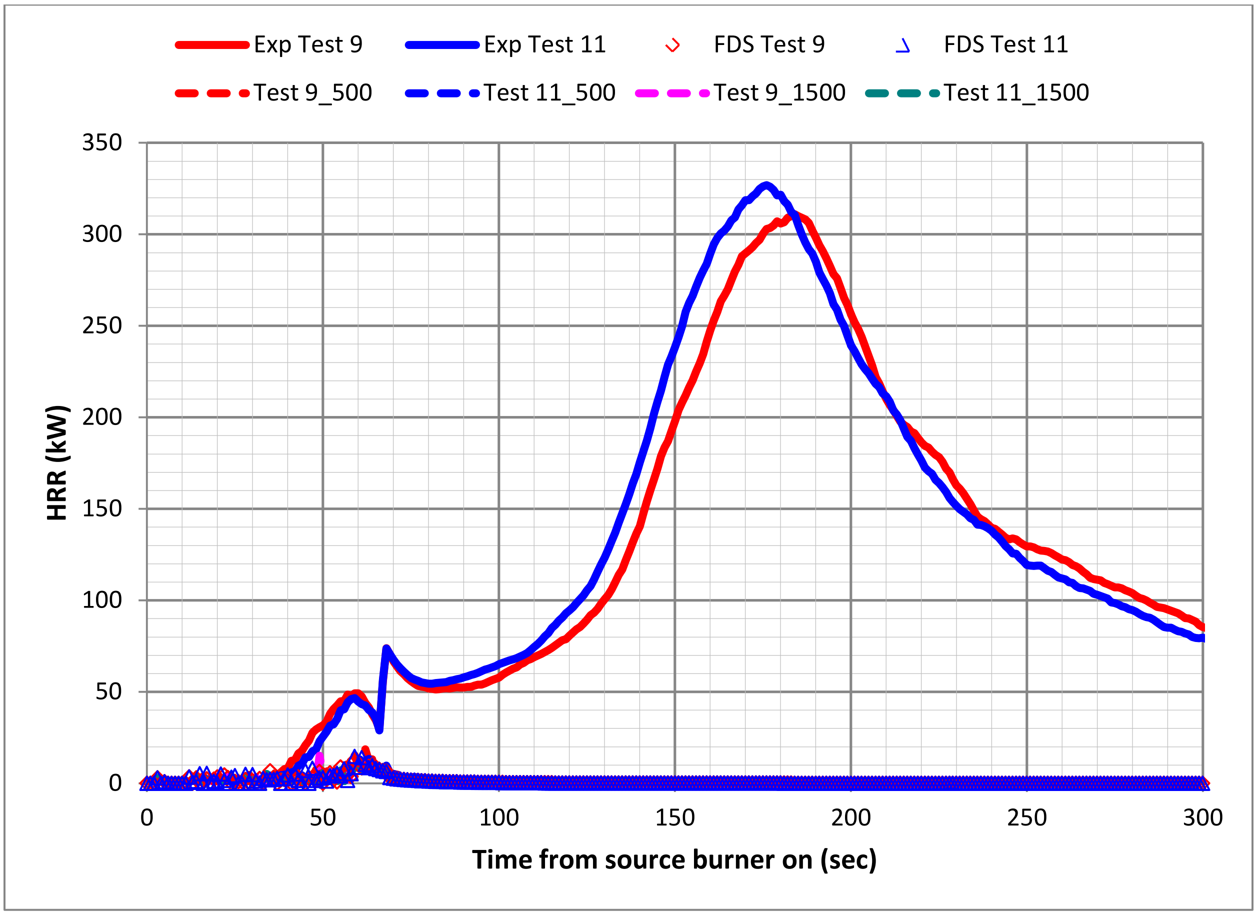

Figure 5 - HRRs of tests using propane, 50 kW, Rectangle burner

Figure 6 presents the burning rate of the FRP panel predicted by FDS. As expected, the runs with the lower heat of reaction created higher predicted burning rate, and the models with the highest heat of reaction created burning rate similar in magnitude to the ones predicted in the default simulations. It is also observed that the timing of all of predicted burning rate history, initial fire, growth, peak, and extinguished are essentially the same regardless of the heat of reaction value.

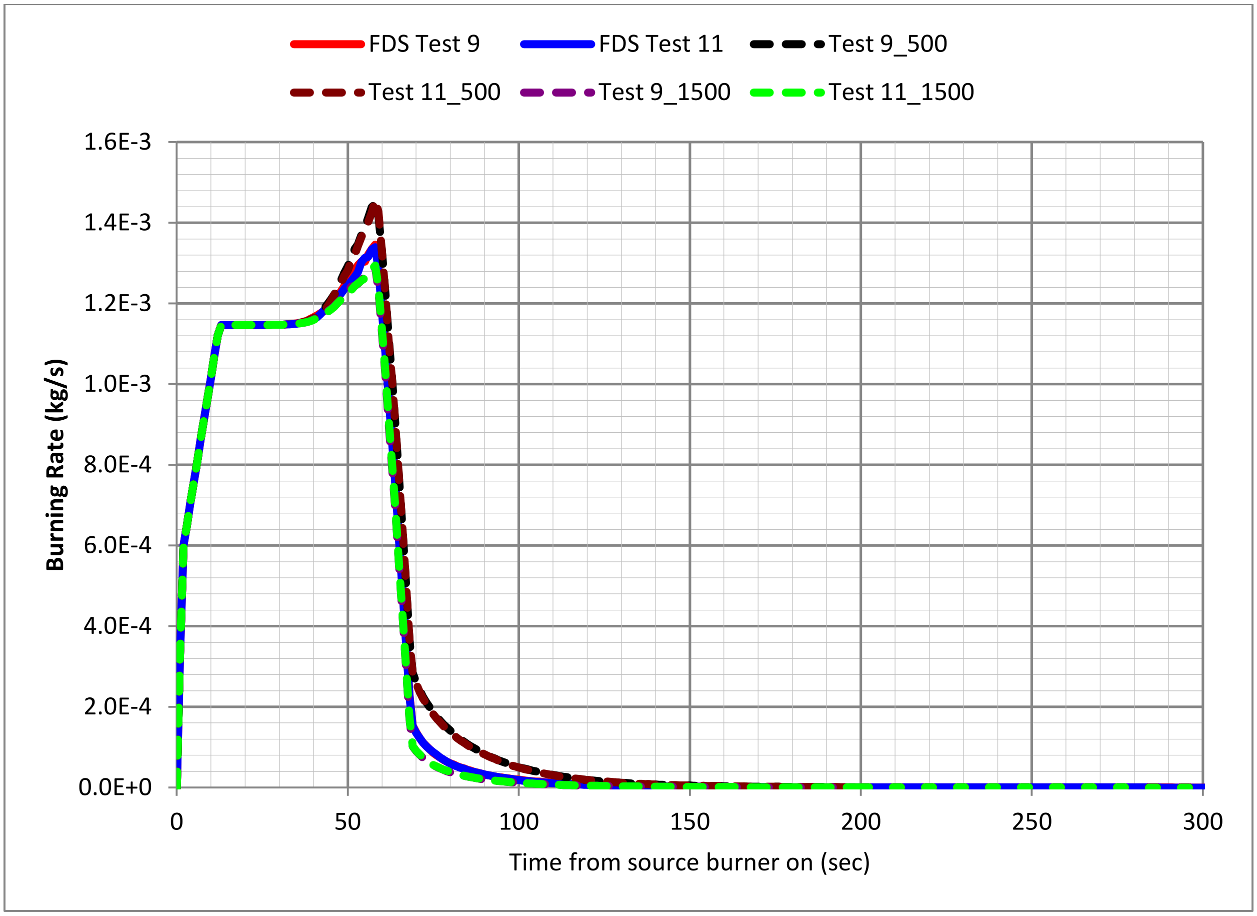

Figure 6 – Burning rates of tests using propane, 50 kW, Rectangle burner

I.4 Propylene, 50 kW continuous, both burners

Tests 12 and 13 were identical to each other except that both burners were used. The source propylene fire was 50 kW continuous through the tests. The HRRs of the burning panel in Tests 12 and 13, minus that of the source fire, are presented in Figure 7. In the FDS simulations where the upper estimate of heat of reaction at 500 kW/kg was applied, the HRR predicted was higher than the default simulation by about 150 kW at its peak, and the time to reach the peak of the HRR curve sped up. Using the lower estimate of heat of reaction at 1500 kW/kg, FDS predicted an overall lower HRR than the default. Figure 7 shows the experimental vs. predicted HRRs.

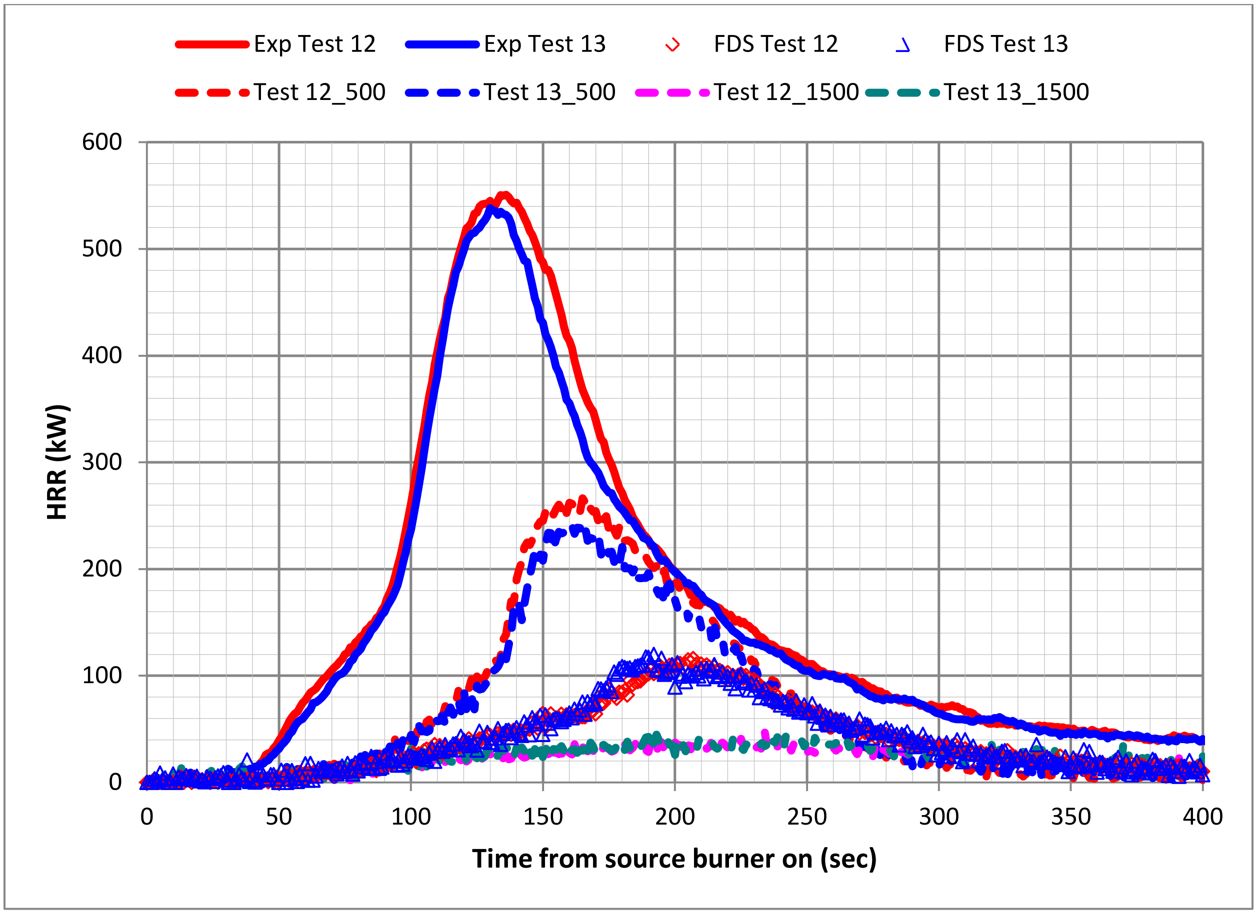

Figure 7 - HRRs of tests using propylene, 50 kW, both burners, but continuous souce fire

Figure 8 presents the burning rate of the FRP panel predicted by FDS. As expected, the runs with the lower heat of reaction created higher predicted burning rate, and the models with the highest heat of reaction created burning rate similar in magnitude to the ones predicted in the default simulations. It is notable that different from the other models where the source HRR was shut off early in the simulation, the burning rates predicted in the current models have different timing than the default simulations. In the simulations with the lower heat of reaction, the fire growth, peak, and extinguishment occurs before what is predicted in the default simulations, and vice versa for the simulations with the higher heat of reaction.

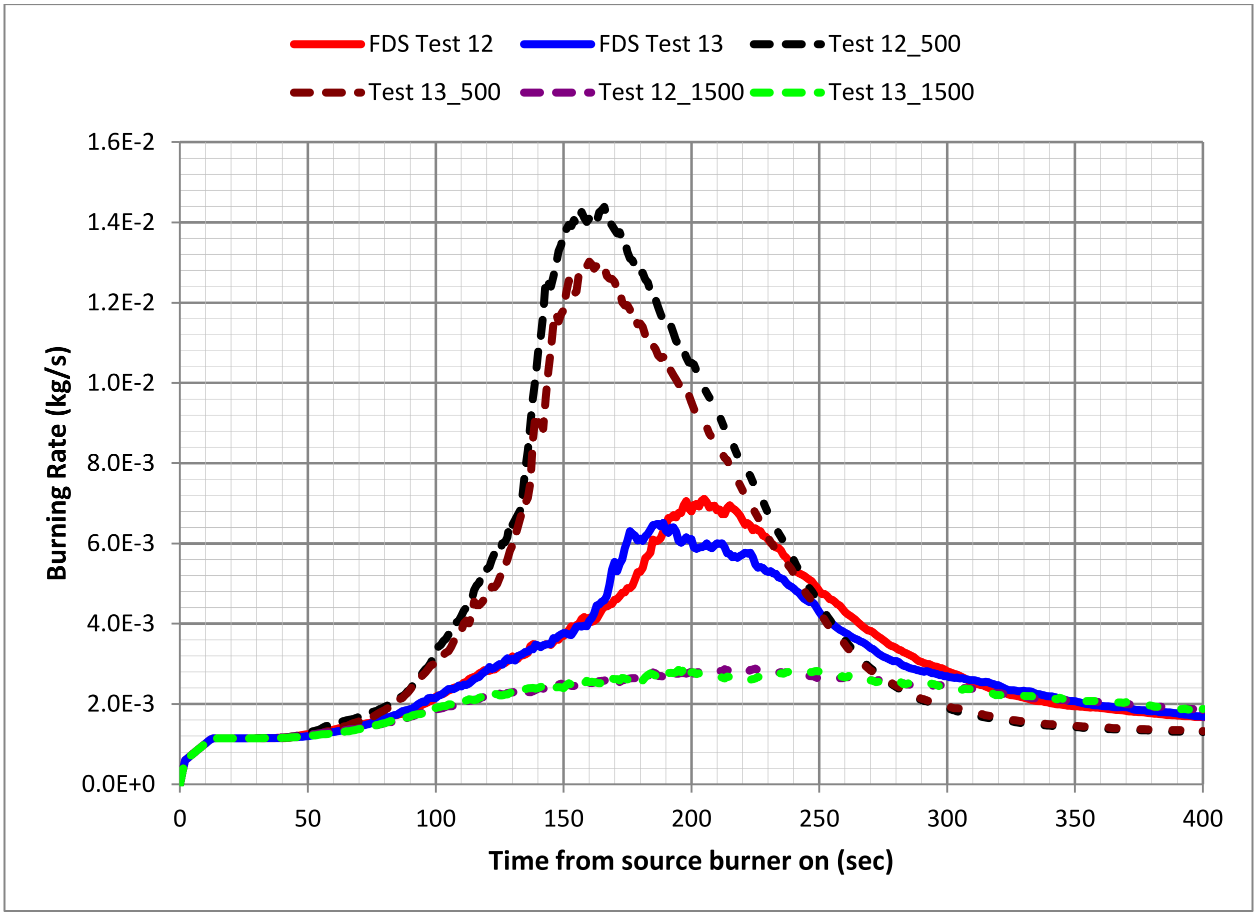

Figure 8 – Burning rates of tests using propylene, 50 kW, both burners, but continuous souce fire

I.5 Propane, 75 kW continuous, both burners

Tests 16 and 17 were identical to each other except that both burners were used. The source propane fire was 75 kW continuous throughout. The HRRs of the burning panel in Tests 16 and 17, minus that of the source fire, are presented in Figure 9. In the FDS simulations where the upper estimate of heat of reaction at 500 kW/kg was applied, the HRR predicted was higher than the default simulation by about 150 kW at its peak, and the time to reach the peak of the HRR curve sped up. Using the lower estimate of heat of reaction at 1500 kW/kg, FDS predicted an overall lower HRR than the default, and the time to reach its peak was delayed. Figure 9 shows the experimental vs. predicted HRRs.

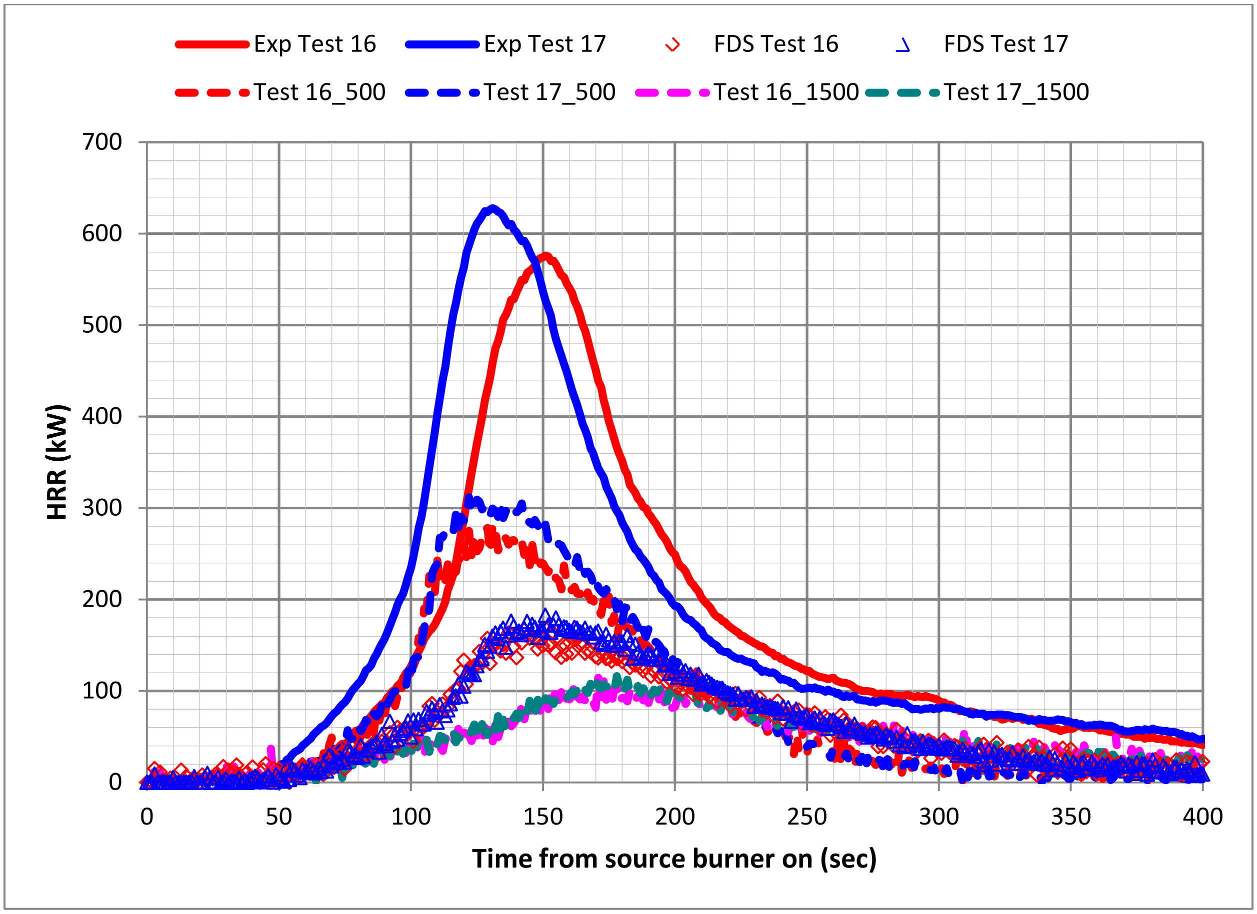

Figure 9 - HRRs of tests using propane, 75 kW, both burners, but continuous souce fire

Figure 8 presents the burning rate of the FRP panel predicted by FDS. As expected, the runs with the lower heat of reaction created higher predicted burning rate, and the models with the highest heat of reaction created burning rate similar in magnitude to the ones predicted in the default simulations. Similar to the other simulations with a constant source fire, it is notable that different from the other models where the source HRR was shut off early in the simulation, the burning rates predicted in the current models have different timing than the default simulations. In the simulations with the lower heat of reaction, the fire growth, peak, and extinguishment occurs before what is predicted in the default simulations, and vice versa for the simulations with the higher heat of reaction.

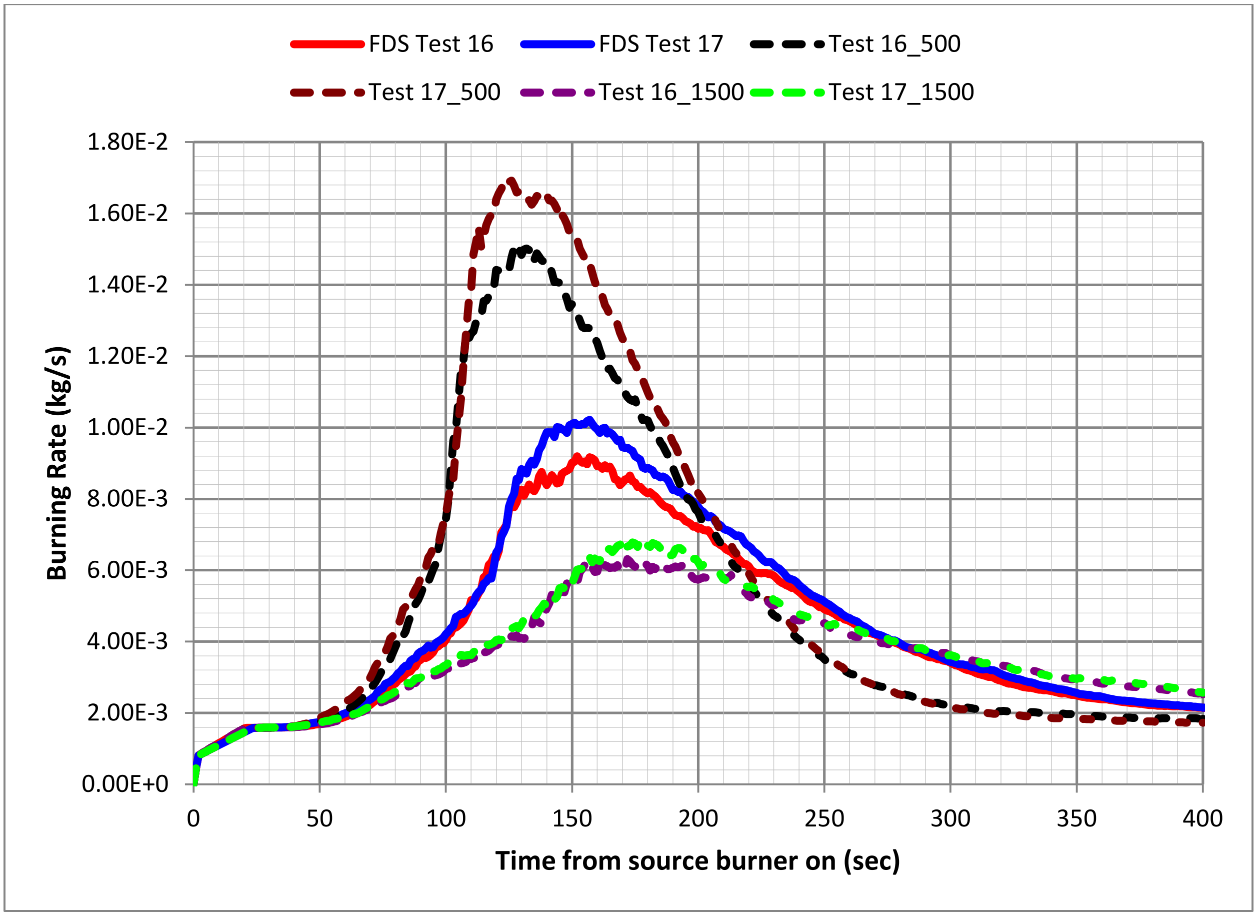

Figure 10 – Burning rates of tests using propane, 75 kW, both burners, but continuous souce fire

I.6 Discussion

Reducing the heat of reaction of the FRP material properties in FDS has the intended effect of increasing the HRR and flame spread, in essence making the FRP easily to "burn". The most significant effect on the HRR time history is that the time to peak HRR was also shortened and the magnitude of the peak has increased. The burning rate time history for simulations without a constant source fire is not significant affected by the change in the heat of reaction. The effects of the change in parameter is more significant in the burning rate prediction of the simulations with a constant source fire, where the burning rate is increased in magnitude and the time to peak burning rate has been reduced. Consequently, using a higher heat of reaction created the opposite effects. However, it is observed in the simulations of the tests where the source fire was not continuous, that changing the heat of reaction has little to no effects to the HRR or burning rate. This illustrates the importance of factors, other than the heat of reaction, on predicting flame spread using FDS.

Appendix J Representative FDS Input Files

This section reproduces a selection of the baseline series input files used in the FDS simulations. The grid resolution is 0.05 m. The source fuels of propane and propylene, the HRR sizes at 50 kW and 75 kW, and both burner shapes are presented in the plume and inert wall fire simulation files. Additionally, all 15 simulations of the FRP wall fires are also presented.

In the plume and inter wall simulations the source burner HRR is assumed to be constant throughout the simulation. In the FRP simulations, the source fire HRR mirror that used in each of the experiment.

J.1 Input File 1 – Plume scenario, Square burner, 50 kW, propane

```
Start Input File
&HEAD CHID='6_1_02-24-2011_Plume_Pr_sb_50kW' /

&TIME T_END =600, DT = 0.05, RESTRICT_TIME_STEP = .FALSE. /
&DUMP DT_BNDF=2.0, DT_DEVC=0.5, DT_HRR=1.0, DT_PL3D=5000.0, DT_SLCF=2.0, DT_RESTART=50 /

&MISC
      RESTART  = .FALSE.
      SURF_DEFAULT = 'INERT'
      TMPA  = 23
      FDS6  = .TRUE.
      DNS = .FALSE.
      DYNSMAG = .TRUE.
      CSMAG = 0.2
      PR = 0.5
      SC = 0.5
      H_EDDY = .TRUE.
      CFL_VELOCITY_NORM = 1
      FLUX_LIMITER = 2
      ISOTHERMAL = .FALSE.
      RADIATION = .TRUE.
      BAROCLINIC = .TRUE.
      CLIP_MASS_FRACTION   = .TRUE.
      CHECK_VN = .TRUE.
      NOBIAS = .TRUE.
      PROJECTION  = .FALSE.
      CHECK_KINETIC_ENERGY = .FALSE.
      /

&REAC
     ID = 'Propane'
     C = 3
     H = 8
     O = 0
     CO_YIELD = 0.024
     SOOT_YIELD = 0.005
     EDDY_DISSIPATION = .TRUE.
     C_EDC = 0.1
     HRRPUA_SHEET = 0
     HRRPUV_AVERAGE = 2500
      /

&RADI
    RADIATIVE_FRACTION = 0.3
    TIME_STEP_INCREMENT = 3
    ANGLE_INCREMENT = 5
    NUMBER_RADIATION_ANGLES = 104
    /

**** MESHES ****
 MESH IJK= 96, 156, 96, XB=-1.20, 1.20, 0.00, 3.90, 0.00, 2.40 / 2.50 cm grid,  1 mesh
```

```
&MESH ID= 'Mesh-1', IJK= 24, 26, 24, XB= -1.2, 0, 0, 1.3, 0, 1.2 / 0.025 cm grid 12 mesh
&MESH ID= 'Mesh-2', IJK= 24, 26, 24, XB= -1.2, 0, 1.3, 2.6, 0, 1.2 / 0.025 cm grid 12 mesh
&MESH ID= 'Mesh-3', IJK= 24, 26, 24, XB= -1.2, 0, 2.6, 3.9, 0, 1.2 / 0.025 cm grid 12 mesh
&MESH ID= 'Mesh-4', IJK= 24, 26, 24, XB= 0, 1.2, 0, 1.3, 0, 1.2 / 0.025 cm grid 12 mesh
&MESH ID= 'Mesh-5', IJK= 24, 26, 24, XB= 0, 1.2, 1.3, 2.6, 0, 1.2 / 0.025 cm grid 12 mesh
&MESH ID= 'Mesh-6', IJK= 24, 26, 24, XB= 0, 1.2, 2.6, 3.9, 0, 1.2 / 0.025 cm grid 12 mesh
&MESH ID= 'Mesh-7', IJK= 24, 26, 24, XB= -1.2, 0, 0, 1.3, 1.2, 2.4 / 0.025 cm grid 12 mesh
&MESH ID= 'Mesh-8', IJK= 24, 26, 24, XB= -1.2, 0, 1.3, 2.6, 1.2, 2.4 / 0.025 cm grid 12 mesh
&MESH ID= 'Mesh-9', IJK= 24, 26, 24, XB= -1.2, 0, 2.6, 3.9, 1.2, 2.4 / 0.025 cm grid 12 mesh
&MESH ID= 'Mesh-10', IJK= 24, 26, 24, XB= 0, 1.2, 0, 1.3, 1.2, 2.4 / 0.025 cm grid 12 mesh
&MESH ID= 'Mesh-11', IJK= 24, 26, 24, XB= 0, 1.2, 1.3, 2.6, 1.2, 2.4 / 0.025 cm grid 12 mesh
&MESH ID= 'Mesh-12', IJK= 24, 26, 24, XB= 0, 1.2, 2.6, 3.9, 1.2, 2.4 / 0.025 cm grid 12 mesh

****BURNER****
2 ft burner
OBST XB= -0.35, 0.35, 0.8, 1.2, 0, 0.4, SURF_ID = 'ADIABATIC' /
VENT XB= -0.3, 0.3, 0.85, 1.15, 0.4, 0.4, SURF_ID = 'BURNER' /

1 ft burner
&OBST XB= -0.20, 0.20, 0.8, 1.2, 0, 0.4, SURF_ID = 'ADIABATIC' /
&VENT XB= -0.15, 0.15, 0.85, 1.15, 0.4, 0.4, SURF_ID = 'BURNER' /

**** Burner Parameters*****
&SURF ID = 'BURNER'
      HRRPUA =555.6
      COLOR  = 'RED' /

**** MATERIAL PROPERTIES ****
&MATL ID            ='GYPSUM_MATL'
      SPECIFIC_HEAT = 0.84
      CONDUCTIVITY  = 0.48
      DENSITY       = 1440.0 /

&MATL ID            ='KAOWOOL_MATL'
      SPECIFIC_HEAT = 1.0
      CONDUCTIVITY  = 0.06
      DENSITY       = 320.0 /

&SURF ID        = 'ADIABATIC'
      ADIABATIC = .TRUE.
      RGB       = 0, 0, 0 /

&SURF ID                     = 'KAOWOOL'
      RGB                    = 51,102,255
      BACKING                = 'INSULATED'
      MATL_ID(1,1)           = 'KAOWOOL_MATL'
      MATL_MASS_FRACTION(1,1)= 1.0
      THICKNESS(1)           = 0.025
      CELL_SIZE_FACTOR       = 0.30
      STRETCH_FACTOR         = 1.0 /

&SURF ID                     = 'GYPSUM'
      RGB                    = 100,100,100
      BACKING                = 'INSULATED'
      MATL_ID(1,1)           = 'GYPSUM_MATL'
      MATL_MASS_FRACTION(1,1)= 1.0
      THICKNESS(1)           = 0.016
      CELL_SIZE_FACTOR       = 0.30
      STRETCH_FACTOR         = 1.0 /

&OBST XB=-1.200, 1.200, 0.000, 0.000, 0.000, 2.400, SURF_ID ='GYPSUM'  / Back wall
&OBST XB= 1.200, 1.200, 0.000, 2.700, 0.000, 2.400, SURF_ID ='GYPSUM'  / Right wall
&OBST XB=-1.200,-1.200, 0.000, 2.700, 0.000, 2.400, SURF_ID ='GYPSUM'  / Left wall
&OBST XB=-1.200, 1.200, 0.000, 2.700, 2.400, 2.400, SURF_ID ='GYPSUM'  / Ceiling
&OBST XB=-0.900, 0.900, 0.000, 0.025, 0.000, 2.400, SURF_ID ='KAOWOOL', PERMIT_HOLE = .TRUE. /
Kaowool on back wall

****OPEN VENTS****
&VENT XB=-1.20, 1.20, 3.90, 3.90, 0.00, 2.40, SURF_ID = 'OPEN' /
&VENT XB=-1.20,-1.20, 2.70, 3.90, 0.00, 2.40, SURF_ID = 'OPEN' /
&VENT XB= 1.20, 1.20, 2.70, 3.90, 0.00, 2.40, SURF_ID = 'OPEN' /
```

```
&VENT XB=-1.20, 1.20, 2.70, 3.90, 2.40, 2.40, SURF_ID = 'OPEN' /

**** OUTPUTS FILES ****
&SLCF PBX = 0.0, QUANTITY = 'TEMPERATURE' /
&SLCF PBX = 0.0, QUANTITY = 'HRRPUV' /

&BNDF QUANTITY='GAUGE HEAT FLUX' /
&BNDF QUANTITY='RADIATIVE HEAT FLUX' /
&BNDF QUANTITY='CONVECTIVE HEAT FLUX' /
&BNDF QUANTITY='NET HEAT FLUX' /
&BNDF QUANTITY='WALL TEMPERATURE' /
 BNDF QUANTITY='BURNING RATE' /

CENTERLINE RAKE
&DEVC XYZ=0, 1.0, 0.45, QUANTITY='TEMPERATURE', ID='CTC_1' /
&DEVC XYZ=0, 1.0, 0.60, QUANTITY='TEMPERATURE', ID='BDTC_1' /
&DEVC XYZ=0, 1.0, 0.75, QUANTITY='TEMPERATURE', ID='CTC_2' /
&DEVC XYZ=0, 1.0, 0.90, QUANTITY='TEMPERATURE', ID='BDTC_2' /
&DEVC XYZ=0, 1.0, 1.05, QUANTITY='TEMPERATURE', ID='CTC_3' /
&DEVC XYZ=0, 1.0, 1.20, QUANTITY='TEMPERATURE', ID='BDTC_3' /
&DEVC XYZ=0, 1.0, 1.35, QUANTITY='TEMPERATURE', ID='CTC_4' /
&DEVC XYZ=0, 1.0, 1.50, QUANTITY='TEMPERATURE', ID='BDTC_4' /
&DEVC XYZ=0, 1.0, 1.65, QUANTITY='TEMPERATURE', ID='CTC_5' /
&DEVC XYZ=0, 1.0, 1.80, QUANTITY='TEMPERATURE', ID='BDTC_5' /
&DEVC XYZ=0, 1.0, 1.95, QUANTITY='TEMPERATURE', ID='CTC_6' /
&DEVC XYZ=0, 1.0, 2.10, QUANTITY='TEMPERATURE', ID='BDTC_6' /
&DEVC XYZ=0, 1.0, 2.25, QUANTITY='TEMPERATURE', ID='CTC_7' /
&DEVC XYZ=0, 1.0, 0.60, QUANTITY='W-VELOCITY', ID='BD_1' /
&DEVC XYZ=0, 1.0, 0.90, QUANTITY='W-VELOCITY', ID='BD_2' /
&DEVC XYZ=0, 1.0, 1.20, QUANTITY='W-VELOCITY', ID='BD_3' /
&DEVC XYZ=0, 1.0, 1.50, QUANTITY='W-VELOCITY', ID='BD_4' /
&DEVC XYZ=0, 1.0, 1.80, QUANTITY='W-VELOCITY', ID='BD_5' /
&DEVC XYZ=0, 1.0, 2.10, QUANTITY='W-VELOCITY', ID='BD_6' /
&DEVC XYZ=0, 1.0, 1.05, QUANTITY='W-VELOCITY', ID='BD_7' /
&DEVC XYZ=0, 1.0, 1.35, QUANTITY='W-VELOCITY', ID='BD_8' /
&DEVC XYZ=0, 1.0, 1.65, QUANTITY='W-VELOCITY', ID='BD_9' /
&DEVC XYZ=0, 1.0, 1.95, QUANTITY='W-VELOCITY', ID='BD_10' /

MOVEABLE RAKE INSTRUMENTATION, POSITION CENTER FOR FLAME SPREAD
&DEVC XYZ=0, 1.0, 0.60, QUANTITY='TEMPERATURE', ID='PTC_1' /
&DEVC XYZ=0, 1.0, 0.75, QUANTITY='TEMPERATURE', ID='PTC_2' /
&DEVC XYZ=0, 1.0, 0.90, QUANTITY='TEMPERATURE', ID='PTC_3' /
&DEVC XYZ=0, 1.0, 1.05, QUANTITY='TEMPERATURE', ID='BDTC_7' /
&DEVC XYZ=0, 1.0, 1.20, QUANTITY='TEMPERATURE', ID='PTC_4' /
&DEVC XYZ=0, 1.0, 1.35, QUANTITY='TEMPERATURE', ID='BDTC_8' /
&DEVC XYZ=0, 1.0, 1.50, QUANTITY='TEMPERATURE', ID='PTC_5' /
&DEVC XYZ=0, 1.0, 1.65, QUANTITY='TEMPERATURE', ID='BDTC_9' /
&DEVC XYZ=0, 1.0, 1.80, QUANTITY='TEMPERATURE', ID='PTC_6' /
&DEVC XYZ=0, 1.0, 1.95, QUANTITY='TEMPERATURE', ID='BDTC_10' /
&DEVC XYZ=0, 1.0, 2.10, QUANTITY='TEMPERATURE', ID='PTC_7' /

&TAIL /
```

J.2 Input File 2 – Inert Wall scenario, Rectangle burner, 75 kW, propylene

```
Start Input File
&HEAD CHID='26_1_03-05-2011_Inert_Wall_PP_lb_75kW' /

&TIME T_END =300, DT = 0.05, RESTRICT_TIME_STEP = .FALSE. /
&DUMP DT_BNDF=2.0, DT_DEVC=0.5, DT_HRR=1.0, DT_PL3D=5000.0, DT_SLCF=2.0, DT_RESTART=50./

&MISC
      SURF_DEFAULT = 'INERT'
      TMPA  = 23
      FDS6  = .TRUE.
      DNS = .FALSE.
      DYNSMAG = .TRUE.
      CSMAG = 0.2
      PR = 0.5
      SC = 0.5
      H_EDDY = .TRUE.
      CFL_VELOCITY_NORM = 1
      FLUX_LIMITER = 2
      ISOTHERMAL = .FALSE.
      RADIATION = .TRUE.
      BAROCLINIC = .TRUE.
      CLIP_MASS_FRACTION   = .TRUE.
      CHECK_VN = .TRUE.
      NOBIAS = .TRUE.
      PROJECTION  = .FALSE.
      CHECK_KINETIC_ENERGY = .FALSE.
      /

&REAC
     ID = 'Propylene'
     C = 3
     H = 6
     O = 0
     CO_YIELD = 0.095
     SOOT_YIELD = 0.017
     EDDY_DISSIPATION = .TRUE.
     C_EDC = 0.1
     HRRPUA_SHEET = 0
     HRRPUV_AVERAGE = 2500
      /

&RADI
    RADIATIVE_FRACTION = 0.3
    TIME_STEP_INCREMENT = 3
    ANGLE_INCREMENT = 5
    NUMBER_RADIATION_ANGLES = 104
    /

**** MESHES ****
 MESH IJK= 96, 156, 96, XB=-1.20, 1.20, 0.00, 3.90, 0.00, 2.40 / 2.50 cm grid,  1 mesh

&MESH ID= 'Mesh-1', IJK= 24, 26, 24, XB= -1.2, 0, 0, 1.3, 0, 1.2 / 0.05 cm grid 12 mesh
&MESH ID= 'Mesh-2', IJK= 24, 26, 24, XB= -1.2, 0, 1.3, 2.6, 0, 1.2 / 0.05 cm grid 12 mesh
&MESH ID= 'Mesh-3', IJK= 24, 26, 24, XB= -1.2, 0, 2.6, 3.9, 0, 1.2 / 0.05 cm grid 12 mesh
&MESH ID= 'Mesh-4', IJK= 24, 26, 24, XB= 0, 1.2, 0, 1.3, 0, 1.2 / 0.05 cm grid 12 mesh
&MESH ID= 'Mesh-5', IJK= 24, 26, 24, XB= 0, 1.2, 1.3, 2.6, 0, 1.2 / 0.05 cm grid 12 mesh
&MESH ID= 'Mesh-6', IJK= 24, 26, 24, XB= 0, 1.2, 2.6, 3.9, 0, 1.2 / 0.05 cm grid 12 mesh
&MESH ID= 'Mesh-7', IJK= 24, 26, 24, XB= -1.2, 0, 0, 1.3, 1.2, 2.4 / 0.05 cm grid 12 mesh
&MESH ID= 'Mesh-8', IJK= 24, 26, 24, XB= -1.2, 0, 1.3, 2.6, 1.2, 2.4 / 0.05 cm grid 12 mesh
&MESH ID= 'Mesh-9', IJK= 24, 26, 24, XB= -1.2, 0, 2.6, 3.9, 1.2, 2.4 / 0.05 cm grid 12 mesh
&MESH ID= 'Mesh-10', IJK= 24, 26, 24, XB= 0, 1.2, 0, 1.3, 1.2, 2.4 / 0.05 cm grid 12 mesh
&MESH ID= 'Mesh-11', IJK= 24, 26, 24, XB= 0, 1.2, 1.3, 2.6, 1.2, 2.4 / 0.05 cm grid 12 mesh
&MESH ID= 'Mesh-12', IJK= 24, 26, 24, XB= 0, 1.2, 2.6, 3.9, 1.2, 2.4 / 0.05 cm grid 12 mesh

****BURNER****
2 ft burner
&OBST XB= -0.35, 0.35, 0.05, 0.45, 0, 0.4, SURF_ID = 'ADIABATIC' /
&VENT XB= -0.3, 0.3, 0.1, 0.4, 0.4, 0.4, SURF_ID = 'BURNER' /
```

```
1 ft burner
OBST XB= -0.2, 0.2, 0.05, 0.45, 0, 0.4, SURF_ID = 'ADIABATIC' /
VENT XB= -0.15, 0.15, 0.1, 0.4, 0.4, 0.4, SURF_ID = 'BURNER' /

**** Burner Parameters*****
&SURF ID = 'BURNER'
      HRRPUA =416.7
      COLOR  = 'RED' /

**** MATERIAL PROPERTIES ****
&MATL ID            ='GYPSUM_MATL'
      SPECIFIC_HEAT = 0.84
      CONDUCTIVITY  = 0.48
      DENSITY       = 1440.0 /

&MATL ID            ='KAOWOOL_MATL'
      SPECIFIC_HEAT = 1.0
      CONDUCTIVITY  = 0.06
      DENSITY       = 320.0 /

&SURF ID        = 'ADIABATIC'
      ADIABATIC = .TRUE.
      RGB       = 0, 0, 0 /

&SURF ID                     = 'KAOWOOL'
      RGB                    = 51,102,255
      BACKING                = 'INSULATED'
      MATL_ID(1,1)           = 'KAOWOOL_MATL'
      MATL_MASS_FRACTION(1,1)= 1.0
      THICKNESS(1)           = 0.025
      CELL_SIZE_FACTOR       = 0.30
      STRETCH_FACTOR         = 1.0 /

&SURF ID                     = 'GYPSUM'
      RGB                    = 100,100,100
      BACKING                = 'INSULATED'
      MATL_ID(1,1)           = 'GYPSUM_MATL'
      MATL_MASS_FRACTION(1,1)= 1.0
      THICKNESS(1)           = 0.016
      CELL_SIZE_FACTOR       = 0.30
      STRETCH_FACTOR         = 1.0 /

&OBST XB=-1.200, 1.200, 0.000, 0.000, 0.000, 2.400, SURF_ID ='GYPSUM'  / Back wall
&OBST XB= 1.200, 1.200, 0.000, 2.700, 0.000, 2.400, SURF_ID ='GYPSUM'  / Right wall
&OBST XB=-1.200,-1.200, 0.000, 2.700, 0.000, 2.400, SURF_ID ='GYPSUM'  / Left wall
&OBST XB=-1.200, 1.200, 0.000, 2.700, 2.400, 2.400, SURF_ID ='GYPSUM'  / Ceiling
&OBST XB=-0.900, 0.900, 0.000, 0.05, 0.000, 2.400, SURF_ID ='KAOWOOL', PERMIT_HOLE = .TRUE. /
Kaowool on back wall

****OPEN VENTS****
&VENT XB=-1.20, 1.20, 3.90, 3.90, 0.00, 2.40, SURF_ID = 'OPEN' /
&VENT XB=-1.20,-1.20, 2.70, 3.90, 0.00, 2.40, SURF_ID = 'OPEN' /
&VENT XB= 1.20, 1.20, 2.70, 3.90, 0.00, 2.40, SURF_ID = 'OPEN' /
&VENT XB=-1.20, 1.20, 2.70, 3.90, 2.40, 2.40, SURF_ID = 'OPEN' /

HOLES in panel for TSC's:
&HOLE XB= 0.55,  0.60, -0.010, 0.1, 0.55, 0.60 / HOLE 1
&HOLE XB= 0,  0.05, -0.010, 0.1, 0.55, 0.60 / HOLE 2
&HOLE XB= -0.3, -0.25, -0.010, 0.1, 0.55, 0.60 / HOLE 3
&HOLE XB= 0.25,  0.3, -0.010, 0.1, 0.85, 0.9 / HOLE 4
&HOLE XB= -0.05,  0, -0.010, 0.1, 0.85, 0.9 / HOLE 5
&HOLE XB= -0.60, -0.55, -0.010, 0.1, 0.85, 0.9 / HOLE 6
&HOLE XB= 0.55,  0.60, -0.010, 0.1, 1.15, 1.2 / HOLE 7
&HOLE XB= 0, 0.05, -0.010, 0.1, 1.15, 1.2 / HOLE 8
&HOLE XB= -0.3, -0.25, -0.010, 0.1, 1.15, 1.2 / HOLE 9
&HOLE XB= 0.25,  0.3, -0.010, 0.1, 1.45, 1.5 / HOLE 10
&HOLE XB= -0.05,  0, -0.010, 0.1, 1.45, 1.5 / HOLE 11
&HOLE XB=-0.60, -0.55, -0.010, 0.1, 1.45, 1.5 / HOLE 12
&HOLE XB= 0.55,  0.60, -0.010, 0.1, 1.75, 1.8 / HOLE 13
&HOLE XB= 0,  0.05, -0.010, 0.1, 1.75, 1.8 / HOLE 14
&HOLE XB=-0.3, -0.25, -0.010, 0.1, 1.75, 1.8 / HOLE 15
```

```
&HOLE XB= 0.25,  0.3, -0.010, 0.1, 2.05, 2.1 / HOLE 16
&HOLE XB= -0.05,  0, -0.010, 0.1, 2.05, 2.1 / HOLE 17
&HOLE XB=-0.60, -0.55, -0.010, 0.1, 2.05, 2.1 / HOLE 18

TSC'S:

&OBST XB= 0.55,  0.60, -0.010, 0.05, 0.55, 0.60, SURF_ID = 'ADIABATIC', PERMIT_HOLE = .FALSE. /
TSC 1
&OBST XB= 0,  0.05, -0.010, 0.05, 0.55, 0.60, SURF_ID = 'ADIABATIC', PERMIT_HOLE = .FALSE. / TSC
1
&OBST XB= -0.3, -0.25, -0.010, 0.05, 0.55, 0.60, SURF_ID = 'ADIABATIC', PERMIT_HOLE = .FALSE. /
TSC 1
&OBST XB= 0.25,  0.3, -0.010, 0.05, 0.85, 0.9, SURF_ID = 'ADIABATIC', PERMIT_HOLE = .FALSE. / TSC
1
&OBST XB= -0.05,  0, -0.010, 0.05, 0.85, 0.9, SURF_ID = 'ADIABATIC', PERMIT_HOLE = .FALSE. / TSC
1
&OBST XB= -0.60, -0.55, -0.010, 0.05, 0.85, 0.9, SURF_ID = 'ADIABATIC', PERMIT_HOLE = .FALSE. /
TSC 1
&OBST XB= 0.55,  0.60, -0.010, 0.05, 1.15, 1.2, SURF_ID = 'ADIABATIC', PERMIT_HOLE = .FALSE. /
TSC 1
&OBST XB= 0, 0.05, -0.010, 0.05, 1.15, 1.2, SURF_ID = 'ADIABATIC', PERMIT_HOLE = .FALSE. / TSC 1
&OBST XB= -0.3, -0.25, -0.010, 0.05, 1.15, 1.2, SURF_ID = 'ADIABATIC', PERMIT_HOLE = .FALSE. /
TSC 1
&OBST XB= 0.25,  0.3, -0.010, 0.05, 1.45, 1.5, SURF_ID = 'ADIABATIC', PERMIT_HOLE = .FALSE. / TSC
1
&OBST XB= -0.05,  0, -0.010, 0.05, 1.45, 1.5, SURF_ID = 'ADIABATIC', PERMIT_HOLE = .FALSE. / TSC
1
&OBST XB=-0.60, -0.55, -0.010, 0.05, 1.45, 1.5, SURF_ID = 'ADIABATIC', PERMIT_HOLE = .FALSE. /
TSC 1
&OBST XB= 0.55,  0.60, -0.010, 0.05, 1.75, 1.8, SURF_ID = 'ADIABATIC', PERMIT_HOLE = .FALSE. /
TSC 1
&OBST XB= 0,  0.05, -0.010, 0.05, 1.75, 1.8, SURF_ID = 'ADIABATIC', PERMIT_HOLE = .FALSE. / TSC 1
&OBST XB=-0.3, -0.25, -0.010, 0.05, 1.75, 1.8, SURF_ID = 'ADIABATIC', PERMIT_HOLE = .FALSE. / TSC
1
&OBST XB= 0.25,  0.3, -0.010, 0.05, 2.05, 2.1, SURF_ID = 'ADIABATIC', PERMIT_HOLE = .FALSE. / TSC
1
&OBST XB= -0.05,  0, -0.010, 0.05, 2.05, 2.1, SURF_ID = 'ADIABATIC', PERMIT_HOLE = .FALSE. / TSC
1
&OBST XB=-0.60, -0.55, -0.010, 0.05, 2.05, 2.1, SURF_ID = 'ADIABATIC', PERMIT_HOLE = .FALSE. /
TSC 1

**** OUTPUTS FILES ****
&SLCF PBX = 0.0, QUANTITY = 'TEMPERATURE' /
&SLCF PBX = 0.0, QUANTITY = 'HRRPUV' /

&BNDF QUANTITY='GAUGE HEAT FLUX' /
&BNDF QUANTITY='RADIATIVE HEAT FLUX' /
&BNDF QUANTITY='CONVECTIVE HEAT FLUX' /
&BNDF QUANTITY='NET HEAT FLUX' /
&BNDF QUANTITY='WALL TEMPERATURE' /
 BNDF QUANTITY='BURNING RATE' /

CENTERLINE RAKE
&DEVC XYZ=0, 0.25, 0.45, QUANTITY='TEMPERATURE', ID='CTC_1' /
&DEVC XYZ=0, 0.25, 0.60, QUANTITY='TEMPERATURE', ID='BDTC_1' /
&DEVC XYZ=0, 0.25, 0.75, QUANTITY='TEMPERATURE', ID='CTC_2' /
&DEVC XYZ=0, 0.25, 0.90, QUANTITY='TEMPERATURE', ID='BDTC_2' /
&DEVC XYZ=0, 0.25, 1.05, QUANTITY='TEMPERATURE', ID='CTC_3' /
&DEVC XYZ=0, 0.25, 1.20, QUANTITY='TEMPERATURE', ID='BDTC_3' /
&DEVC XYZ=0, 0.25, 1.35, QUANTITY='TEMPERATURE', ID='CTC_4' /
&DEVC XYZ=0, 0.25, 1.50, QUANTITY='TEMPERATURE', ID='BDTC_4' /
&DEVC XYZ=0, 0.25, 1.65, QUANTITY='TEMPERATURE', ID='CTC_5' /
&DEVC XYZ=0, 0.25, 1.80, QUANTITY='TEMPERATURE', ID='BDTC_5' /
&DEVC XYZ=0, 0.25, 1.95, QUANTITY='TEMPERATURE', ID='CTC_6' /
&DEVC XYZ=0, 0.25, 2.10, QUANTITY='TEMPERATURE', ID='BDTC_6' /
&DEVC XYZ=0, 0.25, 2.25, QUANTITY='TEMPERATURE', ID='CTC_7' /
&DEVC XYZ=0, 0.25, 0.60, QUANTITY='W-VELOCITY', ID='BD_1' /
&DEVC XYZ=0, 0.25, 0.90, QUANTITY='W-VELOCITY', ID='BD_2' /
&DEVC XYZ=0, 0.25, 1.20, QUANTITY='W-VELOCITY', ID='BD_3' /
&DEVC XYZ=0, 0.25, 1.50, QUANTITY='W-VELOCITY', ID='BD_4' /
&DEVC XYZ=0, 0.25, 1.80, QUANTITY='W-VELOCITY', ID='BD_5' /
```

```
&DEVC XYZ=0, 0.25, 2.10, QUANTITY='W-VELOCITY', ID='BD_6' /
&DEVC XYZ=0, 0.25, 1.05, QUANTITY='W-VELOCITY', ID='BD_7' /
&DEVC XYZ=0, 0.25, 1.35, QUANTITY='W-VELOCITY', ID='BD_8' /
&DEVC XYZ=0, 0.25, 1.65, QUANTITY='W-VELOCITY', ID='BD_9' /
&DEVC XYZ=0, 0.25, 1.95, QUANTITY='W-VELOCITY', ID='BD_10' /

WALL TEMPERATURE
&DEVC XYZ=0.0762, 0.05, 0.75, QUANTITY='TEMPERATURE', ID='WTC_1' /
&DEVC XYZ=0.0508, 0.055, 0.75, QUANTITY='TEMPERATURE', ID='WTC_2' /
&DEVC XYZ=0.0254, 0.060, 0.75, QUANTITY='TEMPERATURE', ID='WTC_3' /
&DEVC XYZ=-0.0254, 0.065, 0.75, QUANTITY='TEMPERATURE', ID='WTC_4' /
&DEVC XYZ=-0.0508, 0.070, 0.75, QUANTITY='TEMPERATURE', ID='WTC_5' /
&DEVC XYZ=-0.0762, 0.075, 0.75, QUANTITY='TEMPERATURE', ID='WTC_6' /
&DEVC XYZ=0.0762, 0.085, 1.35, QUANTITY='TEMPERATURE', ID='WTC_7' /
&DEVC XYZ=0.0508, 0.080, 1.35, QUANTITY='TEMPERATURE', ID='WTC_8' /
&DEVC XYZ=0.0254, 0.075, 1.35, QUANTITY='TEMPERATURE', ID='WTC_9' /
&DEVC XYZ=-0.0254, 0.070, 1.35, QUANTITY='TEMPERATURE', ID='WTC_10' /
&DEVC XYZ=-0.0508, 0.065, 1.35, QUANTITY='TEMPERATURE', ID='WTC_11' /
&DEVC XYZ=-0.0762, 0.060, 1.35, QUANTITY='TEMPERATURE', ID='WTC_12' /
&DEVC XYZ=0.0762, 0.065, 1.95, QUANTITY='TEMPERATURE', ID='WTC_13' /
&DEVC XYZ=0.0508, 0.070, 1.95, QUANTITY='TEMPERATURE', ID='WTC_14' /
&DEVC XYZ=0.0254, 0.075, 1.95, QUANTITY='TEMPERATURE', ID='WTC_15' /
&DEVC XYZ=-0.0254, 0.080, 1.95, QUANTITY='TEMPERATURE', ID='WTC_16' /
&DEVC XYZ=-0.0508, 0.085, 1.95, QUANTITY='TEMPERATURE', ID='WTC_17' /
&DEVC XYZ=-0.0762, 0.090, 1.95, QUANTITY='TEMPERATURE', ID='WTC_18' /

WALL HEAT FLUX MEASUREMENTS
&DEVC XYZ=  0.575, 0.050, 0.575, QUANTITY='GAUGE_HEAT_FLUX', ID='TS_1',  IOR = 2 /
&DEVC XYZ=  0.025, 0.050, 0.575, QUANTITY='GAUGE_HEAT_FLUX', ID='TS_2',  IOR = 2 /
&DEVC XYZ= -0.275, 0.050, 0.575, QUANTITY='GAUGE_HEAT_FLUX', ID='TS_3',  IOR = 2 /
&DEVC XYZ=  0.275, 0.050, 0.875, QUANTITY='GAUGE_HEAT_FLUX', ID='TS_4',  IOR = 2 /
&DEVC XYZ=  -0.025, 0.050, 0.875, QUANTITY='GAUGE_HEAT_FLUX', ID='TS_5',  IOR = 2 /
&DEVC XYZ= -0.575, 0.050, 0.875, QUANTITY='GAUGE_HEAT_FLUX', ID='TS_6',  IOR = 2 /
&DEVC XYZ=  0.575, 0.050, 1.175, QUANTITY='GAUGE_HEAT_FLUX', ID='TS_7',  IOR = 2 /
&DEVC XYZ=  0.025 0.050, 1.175, QUANTITY='GAUGE_HEAT_FLUX', ID='TS_8',  IOR = 2 /
&DEVC XYZ= -0.275, 0.050, 1.175, QUANTITY='GAUGE_HEAT_FLUX', ID='TS_9',  IOR = 2 /
&DEVC XYZ=  0.275, 0.050, 1.475, QUANTITY='GAUGE_HEAT_FLUX', ID='TS_10', IOR = 2 /
&DEVC XYZ=  -0.025, 0.050, 1.475, QUANTITY='GAUGE_HEAT_FLUX', ID='TS_11', IOR = 2 /
&DEVC XYZ= -0.575, 0.050, 1.475, QUANTITY='GAUGE_HEAT_FLUX', ID='TS_12', IOR = 2 /
&DEVC XYZ=  0.575, 0.050, 1.775, QUANTITY='GAUGE_HEAT_FLUX', ID='TS_13', IOR = 2 /
&DEVC XYZ=  0.025, 0.050, 1.775, QUANTITY='GAUGE_HEAT_FLUX', ID='TS_14', IOR = 2 /
&DEVC XYZ= -0.275, 0.050, 1.775, QUANTITY='GAUGE_HEAT_FLUX', ID='TS_15', IOR = 2 /
&DEVC XYZ=  0.275, 0.050, 2.075, QUANTITY='GAUGE_HEAT_FLUX', ID='TS_16', IOR = 2 /
&DEVC XYZ=  -0.025, 0.050, 2.075, QUANTITY='GAUGE_HEAT_FLUX', ID='TS_17', IOR = 2 /
&DEVC XYZ= -0.575, 0.050, 2.075, QUANTITY='GAUGE_HEAT_FLUX', ID='TS_18', IOR = 2 /

&DEVC XYZ=  0.275, 0.050, 0.60, QUANTITY='GAUGE_HEAT_FLUX', ID='HFG_1', IOR = 2 /
&DEVC XYZ= -0.275, 0.050, 0.875, QUANTITY='GAUGE_HEAT_FLUX', ID='HFG_2', IOR = 2 /
&DEVC XYZ=  0.275, 0.050, 1.175, QUANTITY='GAUGE_HEAT_FLUX', ID='HFG_3', IOR = 2 /
&DEVC XYZ= -0.275, 0.050, 1.475, QUANTITY='GAUGE_HEAT_FLUX', ID='HFG_4', IOR = 2 /
&DEVC XYZ=  0.275, 0.050, 1.775, QUANTITY='GAUGE_HEAT_FLUX', ID='HFG_5', IOR = 2 /
&DEVC XYZ= -0.275, 0.050, 2.075, QUANTITY='GAUGE_HEAT_FLUX', ID='HFG_6', IOR = 2 /

WALL NET HEAT FLUX
&DEVC XYZ=  0.575, 0.050, 0.575, QUANTITY='NET HEAT FLUX', ID='TS_1',  IOR = 2 /
&DEVC XYZ=  0.025, 0.050, 0.575, QUANTITY='NET HEAT FLUX', ID='TS_2',  IOR = 2 /
&DEVC XYZ= -0.275, 0.050, 0.575, QUANTITY='NET HEAT FLUX', ID='TS_3',  IOR = 2 /
&DEVC XYZ=  0.275, 0.050, 0.875, QUANTITY='NET HEAT FLUX', ID='TS_4',  IOR = 2 /
&DEVC XYZ=  -0.025, 0.050, 0.875, QUANTITY='NET HEAT FLUX', ID='TS_5',  IOR = 2 /
&DEVC XYZ= -0.575, 0.050, 0.875, QUANTITY='NET HEAT FLUX', ID='TS_6',  IOR = 2 /
&DEVC XYZ=  0.575, 0.050, 1.175, QUANTITY='NET HEAT FLUX', ID='TS_7',  IOR = 2 /
&DEVC XYZ=  0.025 0.050, 1.175, QUANTITY='NET HEAT FLUX', ID='TS_8',  IOR = 2 /
&DEVC XYZ= -0.275, 0.050, 1.175, QUANTITY='NET HEAT FLUX', ID='TS_9',  IOR = 2 /
&DEVC XYZ=  0.275, 0.050, 1.475, QUANTITY='NET HEAT FLUX', ID='TS_10', IOR = 2 /
&DEVC XYZ=  -0.025, 0.050, 1.475, QUANTITY='NET HEAT FLUX', ID='TS_11', IOR = 2 /
&DEVC XYZ= -0.575, 0.050, 1.475, QUANTITY='NET HEAT FLUX', ID='TS_12', IOR = 2 /
&DEVC XYZ=  0.575, 0.050, 1.775, QUANTITY='NET HEAT FLUX', ID='TS_13', IOR = 2 /
&DEVC XYZ=  0.025, 0.050, 1.775, QUANTITY='NET HEAT FLUX', ID='TS_14', IOR = 2 /
&DEVC XYZ= -0.275, 0.050, 1.775, QUANTITY='NET HEAT FLUX', ID='TS_15', IOR = 2 /
&DEVC XYZ=  0.275, 0.050, 2.075, QUANTITY='NET HEAT FLUX', ID='TS_16', IOR = 2 /
&DEVC XYZ=  -0.025, 0.050, 2.075, QUANTITY='NET HEAT FLUX', ID='TS_17', IOR = 2 /
```

```
&DEVC XYZ= -0.575, 0.050, 2.075, QUANTITY='NET HEAT FLUX', ID='TS_18', IOR = 2 /

WALL CONVECTIVE HEAT FLUX
&DEVC XYZ=  0.575, 0.050, 0.575, QUANTITY='CONVECTIVE HEAT FLUX', ID='TS_1',  IOR = 2 /
&DEVC XYZ=  0.025, 0.050, 0.575, QUANTITY='CONVECTIVE HEAT FLUX', ID='TS_2',  IOR = 2 /
&DEVC XYZ= -0.275, 0.050, 0.575, QUANTITY='CONVECTIVE HEAT FLUX', ID='TS_3',  IOR = 2 /
&DEVC XYZ=  0.275, 0.050, 0.875, QUANTITY='CONVECTIVE HEAT FLUX', ID='TS_4',  IOR = 2 /
&DEVC XYZ=  -0.025, 0.050, 0.875, QUANTITY='CONVECTIVE HEAT FLUX', ID='TS_5',  IOR = 2 /
&DEVC XYZ= -0.575, 0.050, 0.875, QUANTITY='CONVECTIVE HEAT FLUX', ID='TS_6',  IOR = 2 /
&DEVC XYZ=  0.575, 0.050, 1.175, QUANTITY='CONVECTIVE HEAT FLUX', ID='TS_7',  IOR = 2 /
&DEVC XYZ=  0.025 0.050, 1.175, QUANTITY='CONVECTIVE HEAT FLUX', ID='TS_8',  IOR = 2 /
&DEVC XYZ= -0.275, 0.050, 1.175, QUANTITY='CONVECTIVE HEAT FLUX', ID='TS_9',  IOR = 2 /
&DEVC XYZ=  0.275, 0.050, 1.475, QUANTITY='CONVECTIVE HEAT FLUX', ID='TS_10', IOR = 2 /
&DEVC XYZ=  -0.025, 0.050, 1.475, QUANTITY='CONVECTIVE HEAT FLUX', ID='TS_11', IOR = 2 /
&DEVC XYZ= -0.575, 0.050, 1.475, QUANTITY='CONVECTIVE HEAT FLUX', ID='TS_12', IOR = 2 /
&DEVC XYZ=  0.575, 0.050, 1.775, QUANTITY='CONVECTIVE HEAT FLUX', ID='TS_13', IOR = 2 /
&DEVC XYZ=  0.025, 0.050, 1.775, QUANTITY='CONVECTIVE HEAT FLUX', ID='TS_14', IOR = 2 /
&DEVC XYZ= -0.275, 0.050, 1.775, QUANTITY='CONVECTIVE HEAT FLUX', ID='TS_15', IOR = 2 /
&DEVC XYZ=  0.275, 0.050, 2.075, QUANTITY='CONVECTIVE HEAT FLUX', ID='TS_16', IOR = 2 /
&DEVC XYZ=  -0.025, 0.050, 2.075, QUANTITY='CONVECTIVE HEAT FLUX', ID='TS_17', IOR = 2 /
&DEVC XYZ= -0.575, 0.050, 2.075, QUANTITY='CONVECTIVE HEAT FLUX', ID='TS_18', IOR = 2 /

WALL RADIATIVE HEAT FLUX
&DEVC XYZ=  0.575, 0.050, 0.575, QUANTITY='RADIATIVE HEAT FLUX', ID='TS_1',  IOR = 2 /
&DEVC XYZ=  0.025, 0.050, 0.575, QUANTITY='RADIATIVE HEAT FLUX', ID='TS_2',  IOR = 2 /
&DEVC XYZ= -0.275, 0.050, 0.575, QUANTITY='RADIATIVE HEAT FLUX', ID='TS_3',  IOR = 2 /
&DEVC XYZ=  0.275, 0.050, 0.875, QUANTITY='RADIATIVE HEAT FLUX', ID='TS_4',  IOR = 2 /
&DEVC XYZ=  -0.025, 0.050, 0.875, QUANTITY='RADIATIVE HEAT FLUX', ID='TS_5',  IOR = 2 /
&DEVC XYZ= -0.575, 0.050, 0.875, QUANTITY='RADIATIVE HEAT FLUX', ID='TS_6',  IOR = 2 /
&DEVC XYZ=  0.575, 0.050, 1.175, QUANTITY='RADIATIVE HEAT FLUX', ID='TS_7',  IOR = 2 /
&DEVC XYZ=  0.025 0.050, 1.175, QUANTITY='RADIATIVE HEAT FLUX', ID='TS_8',  IOR = 2 /
&DEVC XYZ= -0.275, 0.050, 1.175, QUANTITY='RADIATIVE HEAT FLUX', ID='TS_9',  IOR = 2 /
&DEVC XYZ=  0.275, 0.050, 1.475, QUANTITY='RADIATIVE HEAT FLUX', ID='TS_10', IOR = 2 /
&DEVC XYZ=  -0.025, 0.050, 1.475, QUANTITY='RADIATIVE HEAT FLUX', ID='TS_11', IOR = 2 /
&DEVC XYZ= -0.575, 0.050, 1.475, QUANTITY='RADIATIVE HEAT FLUX', ID='TS_12', IOR = 2 /
&DEVC XYZ=  0.575, 0.050, 1.775, QUANTITY='RADIATIVE HEAT FLUX', ID='TS_13', IOR = 2 /
&DEVC XYZ=  0.025, 0.050, 1.775, QUANTITY='RADIATIVE HEAT FLUX', ID='TS_14', IOR = 2 /
&DEVC XYZ= -0.275, 0.050, 1.775, QUANTITY='RADIATIVE HEAT FLUX', ID='TS_15', IOR = 2 /
&DEVC XYZ=  0.275, 0.050, 2.075, QUANTITY='RADIATIVE HEAT FLUX', ID='TS_16', IOR = 2 /
&DEVC XYZ=  -0.025, 0.050, 2.075, QUANTITY='RADIATIVE HEAT FLUX', ID='TS_17', IOR = 2 /
&DEVC XYZ= -0.575, 0.050, 2.075, QUANTITY='RADIATIVE HEAT FLUX', ID='TS_18', IOR = 2 /

WALL INCIDENT HEAT FLUX
&DEVC XYZ=  0.575, 0.050, 0.575, QUANTITY='INCIDENT HEAT FLUX', ID='TS_1',  IOR = 2 /
&DEVC XYZ=  0.025, 0.050, 0.575, QUANTITY='INCIDENT HEAT FLUX', ID='TS_2',  IOR = 2 /
&DEVC XYZ= -0.275, 0.050, 0.575, QUANTITY='INCIDENT HEAT FLUX', ID='TS_3',  IOR = 2 /
&DEVC XYZ=  0.275, 0.050, 0.875, QUANTITY='INCIDENT HEAT FLUX', ID='TS_4',  IOR = 2 /
&DEVC XYZ=  -0.025, 0.050, 0.875, QUANTITY='INCIDENT HEAT FLUX', ID='TS_5',  IOR = 2 /
&DEVC XYZ= -0.575, 0.050, 0.875, QUANTITY='INCIDENT HEAT FLUX', ID='TS_6',  IOR = 2 /
&DEVC XYZ=  0.575, 0.050, 1.175, QUANTITY='INCIDENT HEAT FLUX', ID='TS_7',  IOR = 2 /
&DEVC XYZ=  0.025 0.050, 1.175, QUANTITY='INCIDENT HEAT FLUX', ID='TS_8',  IOR = 2 /
&DEVC XYZ= -0.275, 0.050, 1.175, QUANTITY='INCIDENT HEAT FLUX', ID='TS_9',  IOR = 2 /
&DEVC XYZ=  0.275, 0.050, 1.475, QUANTITY='INCIDENT HEAT FLUX', ID='TS_10', IOR = 2 /
&DEVC XYZ=  -0.025, 0.050, 1.475, QUANTITY='INCIDENT HEAT FLUX', ID='TS_11', IOR = 2 /
&DEVC XYZ= -0.575, 0.050, 1.475, QUANTITY='INCIDENT HEAT FLUX', ID='TS_12', IOR = 2 /
&DEVC XYZ=  0.575, 0.050, 1.775, QUANTITY='INCIDENT HEAT FLUX', ID='TS_13', IOR = 2 /
&DEVC XYZ=  0.025, 0.050, 1.775, QUANTITY='INCIDENT HEAT FLUX', ID='TS_14', IOR = 2 /
&DEVC XYZ= -0.275, 0.050, 1.775, QUANTITY='INCIDENT HEAT FLUX', ID='TS_15', IOR = 2 /
&DEVC XYZ=  0.275, 0.050, 2.075, QUANTITY='INCIDENT HEAT FLUX', ID='TS_16', IOR = 2 /
&DEVC XYZ=  -0.025, 0.050, 2.075, QUANTITY='INCIDENT HEAT FLUX', ID='TS_17', IOR = 2 /
&DEVC XYZ= -0.575, 0.050, 2.075, QUANTITY='INCIDENT HEAT FLUX', ID='TS_18', IOR = 2 /

WALL RADIOMETER
&DEVC XYZ=  0.575, 0.050, 0.575, QUANTITY='RADIOMETER', ID='TS_1',  IOR = 2 /
&DEVC XYZ=  0.025, 0.050, 0.575, QUANTITY='RADIOMETER', ID='TS_2',  IOR = 2 /
&DEVC XYZ= -0.275, 0.050, 0.575, QUANTITY='RADIOMETER', ID='TS_3',  IOR = 2 /
&DEVC XYZ=  0.275, 0.050, 0.875, QUANTITY='RADIOMETER', ID='TS_4',  IOR = 2 /
&DEVC XYZ=  -0.025, 0.050, 0.875, QUANTITY='RADIOMETER', ID='TS_5',  IOR = 2 /
&DEVC XYZ= -0.575, 0.050, 0.875, QUANTITY='RADIOMETER', ID='TS_6',  IOR = 2 /
&DEVC XYZ=  0.575, 0.050, 1.175, QUANTITY='RADIOMETER', ID='TS_7',  IOR = 2 /
&DEVC XYZ=  0.025 0.050, 1.175, QUANTITY='RADIOMETER', ID='TS_8',  IOR = 2 /
```

```
&DEVC XYZ= -0.275, 0.050, 1.175, QUANTITY='RADIOMETER', ID='TS_9',  IOR = 2 /
&DEVC XYZ=  0.275, 0.050, 1.475, QUANTITY='RADIOMETER', ID='TS_10', IOR = 2 /
&DEVC XYZ=  -0.025, 0.050, 1.475, QUANTITY='RADIOMETER', ID='TS_11', IOR = 2 /
&DEVC XYZ= -0.575, 0.050, 1.475, QUANTITY='RADIOMETER', ID='TS_12', IOR = 2 /
&DEVC XYZ=  0.575, 0.050, 1.775, QUANTITY='RADIOMETER', ID='TS_13', IOR = 2 /
&DEVC XYZ=  0.025, 0.050, 1.775, QUANTITY='RADIOMETER', ID='TS_14', IOR = 2 /
&DEVC XYZ= -0.275, 0.050, 1.775, QUANTITY='RADIOMETER', ID='TS_15', IOR = 2 /
&DEVC XYZ=  0.275, 0.050, 2.075, QUANTITY='RADIOMETER', ID='TS_16', IOR = 2 /
&DEVC XYZ=  -0.025, 0.050, 2.075, QUANTITY='RADIOMETER', ID='TS_17', IOR = 2 /
&DEVC XYZ= -0.575, 0.050, 2.075, QUANTITY='RADIOMETER', ID='TS_18', IOR = 2 /

&TAIL /
```

J.3 Input File 3 – FRP scenario, Rectangle burner, 75 kW, propane

```
Start Input File
&HEAD CHID='53_1_03-14-2011_FRP_Pr_lb_75kW' /

&TIME T_END = 900, DT = 0.05, RESTRICT_TIME_STEP = .FALSE. /
&DUMP DT_BNDF=2.0, DT_DEVC=0.5, DT_HRR=1.0, DT_PL3D=5000.0, DT_SLCF=2.0, DT_RESTART=50./

&MISC
      SURF_DEFAULT = 'INERT'
      TMPA  = 23
      FDS6  = .TRUE.
      DNS = .FALSE.
      DYNSMAG = .TRUE.
      CSMAG = 0.2
      PR = 0.5
      SC = 0.5
      H_EDDY = .TRUE.
      CFL_VELOCITY_NORM = 1
      FLUX_LIMITER = 2
      ISOTHERMAL = .FALSE.
      RADIATION = .TRUE.
      BAROCLINIC = .TRUE.
      CLIP_MASS_FRACTION   = .TRUE.
      CHECK_VN = .TRUE.
      NOBIAS = .TRUE.
      PROJECTION  = .FALSE.
      CHECK_KINETIC_ENERGY = .FALSE.
      /

&REAC
     ID = 'Propane'
     C = 3
     H = 8
     O = 0
     CO_YIELD = 0.024
     SOOT_YIELD = 0.005
     EDDY_DISSIPATION = .TRUE.
     C_EDC = 0.1
     HRRPUA_SHEET = 0
     HRRPUV_AVERAGE = 2500
      /

&RADI
    RADIATIVE_FRACTION = 0.3
    TIME_STEP_INCREMENT = 3
    ANGLE_INCREMENT = 5
    NUMBER_RADIATION_ANGLES = 104
    /

**** MESHES ****
 MESH IJK= 96, 156, 96, XB=-1.20, 1.20, 0.00, 3.90, 0.00, 2.40 / 2.50 cm grid,  1 mesh

&MESH ID= 'Mesh-1', IJK= 24, 26, 24, XB= -1.2, 0, 0, 1.3, 0, 1.2 / 0.05 cm grid 12 mesh
&MESH ID= 'Mesh-2', IJK= 24, 26, 24, XB= -1.2, 0, 1.3, 2.6, 0, 1.2 / 0.05 cm grid 12 mesh
&MESH ID= 'Mesh-3', IJK= 24, 26, 24, XB= -1.2, 0, 2.6, 3.9, 0, 1.2 / 0.05 cm grid 12 mesh
&MESH ID= 'Mesh-4', IJK= 24, 26, 24, XB= 0, 1.2, 0, 1.3, 0, 1.2 / 0.05 cm grid 12 mesh
&MESH ID= 'Mesh-5', IJK= 24, 26, 24, XB= 0, 1.2, 1.3, 2.6, 0, 1.2 / 0.05 cm grid 12 mesh
&MESH ID= 'Mesh-6', IJK= 24, 26, 24, XB= 0, 1.2, 2.6, 3.9, 0, 1.2 / 0.05 cm grid 12 mesh
&MESH ID= 'Mesh-7', IJK= 24, 26, 24, XB= -1.2, 0, 0, 1.3, 1.2, 2.4 / 0.05 cm grid 12 mesh
&MESH ID= 'Mesh-8', IJK= 24, 26, 24, XB= -1.2, 0, 1.3, 2.6, 1.2, 2.4 / 0.05 cm grid 12 mesh
&MESH ID= 'Mesh-9', IJK= 24, 26, 24, XB= -1.2, 0, 2.6, 3.9, 1.2, 2.4 / 0.05 cm grid 12 mesh
&MESH ID= 'Mesh-10', IJK= 24, 26, 24, XB= 0, 1.2, 0, 1.3, 1.2, 2.4 / 0.05 cm grid 12 mesh
&MESH ID= 'Mesh-11', IJK= 24, 26, 24, XB= 0, 1.2, 1.3, 2.6, 1.2, 2.4 / 0.05 cm grid 12 mesh
&MESH ID= 'Mesh-12', IJK= 24, 26, 24, XB= 0, 1.2, 2.6, 3.9, 1.2, 2.4 / 0.05 cm grid 12 mesh

****BURNER****
2 ft burner
&OBST XB= -0.35, 0.35, 0.05, 0.45, 0, 0.4, SURF_ID = 'ADIABATIC' /
&VENT XB= -0.3, 0.3, 0.1, 0.4, 0.4, 0.4, SURF_ID = 'BURNER' /
```

```
1 ft burner
OBST XB= -0.2, 0.2, 0.05, 0.45, 0, 0.4, SURF_ID = 'ADIABATIC' /
VENT XB= -0.15, 0.15, 0.1, 0.4, 0.4, 0.4, SURF_ID = 'BURNER' /

**** Burner Parameters*****
&SURF ID = 'BURNER'
      HRRPUA =416.7
      RAMP_Q = 'Burner_Ramp'
      COLOR  = 'RED' /

&RAMP ID = 'Burner_Ramp', T=0, F=0 /
&RAMP ID = 'Burner_Ramp', T=1, F=0.5 /
&RAMP ID = 'Burner_Ramp', T=15, F=1 /
&RAMP ID = 'Burner_Ramp', T=105, F=1 /
&RAMP ID = 'Burner_Ramp', T=115, F=0 /

**** MATERIAL PROPERTIES ****
&MATL ID            ='GYPSUM_MATL'
      SPECIFIC_HEAT = 0.84
      CONDUCTIVITY  = 0.48
      DENSITY       = 1440.0 /

&MATL ID            ='KAOWOOL_MATL'
      SPECIFIC_HEAT = 1.0
      CONDUCTIVITY  = 0.06
      DENSITY       = 320.0 /

&SURF ID        = 'ADIABATIC'
      ADIABATIC = .TRUE.
      RGB       = 0, 0, 0 /

&SURF ID                     = 'KAOWOOL'
      RGB                    = 51,102,255
      BACKING                = 'INSULATED'
      MATL_ID(1,1)           = 'KAOWOOL_MATL'
      MATL_MASS_FRACTION(1,1)= 1.0
      THICKNESS(1)           = 0.025
      CELL_SIZE_FACTOR       = 0.30
      STRETCH_FACTOR         = 1.0 /

&SURF ID                     = 'GYPSUM'
      RGB                    = 100,100,100
      BACKING                = 'INSULATED'
      MATL_ID(1,1)           = 'GYPSUM_MATL'
      MATL_MASS_FRACTION(1,1)= 1.0
      THICKNESS(1)           = 0.016
      CELL_SIZE_FACTOR       = 0.30
      STRETCH_FACTOR         = 1.0 /

&MATL ID                       = 'virgin'
      CONDUCTIVITY             =  0.480
      DENSITY                  = 1467.80
      SPECIFIC_HEAT            =    1.98
      EMISSIVITY               =  0.858
      ABSORPTION_COEFFICIENT   =  0.9000E+10
      RESIDUE(01)              = 'char'
      A(01)                    = 0.1139E+12
      E(01)                    = 0.1483E+06
      N_S(01)                  =   1.00
      THRESHOLD_TEMPERATURE(01)=   0.00
      HEAT_OF_REACTION(01)     =   996.67
      HEAT_OF_COMBUSTION       = 19700.
      NU_FUEL(01)              =   0.421
      NU_RESIDUE(01)           =   0.579
      NU_WATER(01)             =   0.000
      N_REACTIONS              = 01 /

&MATL ID                       = 'char'
      CONDUCTIVITY             =  0.050
      DENSITY                  =  850.56
      SPECIFIC_HEAT            =    2.12
```

```
      EMISSIVITY                =  0.943
      ABSORPTION_COEFFICIENT    =  0.9000E+10
      N_REACTIONS               = 00 /

&SURF ID                          = 'FRP'
      STRETCH_FACTOR              = 1.000
      CELL_SIZE_FACTOR            = 0.200
      THICKNESS(1)               = 0.0019
      MATL_ID(1,1)              = 'virgin'
      MATL_ID(1,2)              = 'char'
      MATL_MASS_FRACTION(1,1)   = 1.0000
      MATL_MASS_FRACTION(1,2)   = 0.0000
      BACKING                     = 'INSULATED'
      SHRINK                      = .TRUE.
      TMP_INNER                   = 27.0
      COLOR                       = 'WHITE' /


****OBSTRUCTIONS****
&OBST XB=-1.200, 1.200, 0.000, 0.000, 0.000, 2.400, SURF_ID ='GYPSUM'  / Back wall
&OBST XB= 1.200, 1.200, 0.000, 2.700, 0.000, 2.400, SURF_ID ='GYPSUM'  / Right wall
&OBST XB=-1.200,-1.200, 0.000, 2.700, 0.000, 2.400, SURF_ID ='GYPSUM'  / Left wall
&OBST XB=-1.200, 1.200, 0.000, 2.700, 2.400, 2.400, SURF_ID ='GYPSUM'  / Ceiling
&OBST XB=-0.900,-0.600, 0.000, 0.05, 0.000, 2.400, SURF_ID ='KAOWOOL' / Kaowool on back wall
&OBST XB= 0.600, 0.900, 0.000, 0.05, 0.000, 2.400, SURF_ID ='KAOWOOL' / Kaowool on back wall
&OBST XB=-0.600, 0.600, 0.000, 0.05, 0.000, 2.400, SURF_ID ='FRP', PERMIT_HOLE = .TRUE. / FRP
panel

****OPEN VENTS****
&VENT XB=-1.20, 1.20, 3.90, 3.90, 0.00, 2.40, SURF_ID = 'OPEN' / Back
&VENT XB=-1.20,-1.20, 2.70, 3.90, 0.00, 2.40, SURF_ID = 'OPEN' /
&VENT XB= 1.20, 1.20, 2.70, 3.90, 0.00, 2.40, SURF_ID = 'OPEN' /
&VENT XB=-1.20, 1.20, 2.70, 3.90, 2.40, 2.40, SURF_ID = 'OPEN' /

HOLES in panel for TSC's:
&HOLE XB= 0.55,  0.60, -0.010, 0.1, 0.55, 0.60 / HOLE 1
&HOLE XB= 0,  0.05, -0.010, 0.1, 0.55, 0.60 / HOLE 2
&HOLE XB= -0.3, -0.25, -0.010, 0.1, 0.55, 0.60 / HOLE 3
&HOLE XB= 0.25,  0.3, -0.010, 0.1, 0.85, 0.9 / HOLE 4
&HOLE XB= -0.05,  0, -0.010, 0.1, 0.85, 0.9 / HOLE 5
&HOLE XB= -0.60, -0.55, -0.010, 0.1, 0.85, 0.9 / HOLE 6
&HOLE XB= 0.55,  0.60, -0.010, 0.1, 1.15, 1.2 / HOLE 7
&HOLE XB= 0, 0.05, -0.010, 0.1, 1.15, 1.2 / HOLE 8
&HOLE XB= -0.3, -0.25, -0.010, 0.1, 1.15, 1.2 / HOLE 9
&HOLE XB= 0.25,  0.3, -0.010, 0.1, 1.45, 1.5 / HOLE 10
&HOLE XB= -0.05,  0, -0.010, 0.1, 1.45, 1.5 / HOLE 11
&HOLE XB=-0.60, -0.55, -0.010, 0.1, 1.45, 1.5 / HOLE 12
&HOLE XB= 0.55,  0.60, -0.010, 0.1, 1.75, 1.8 / HOLE 13
&HOLE XB= 0,  0.05, -0.010, 0.1, 1.75, 1.8 / HOLE 14
&HOLE XB=-0.3, -0.25, -0.010, 0.1, 1.75, 1.8 / HOLE 15
&HOLE XB= 0.25,  0.3, -0.010, 0.1, 2.05, 2.1 / HOLE 16
&HOLE XB= -0.05,  0, -0.010, 0.1, 2.05, 2.1 / HOLE 17
&HOLE XB=-0.60, -0.55, -0.010, 0.1, 2.05, 2.1 / HOLE 18

TSC'S:

&OBST XB= 0.55,  0.60, -0.010, 0.05, 0.55, 0.60, SURF_ID = 'ADIABATIC', PERMIT_HOLE = .FALSE. /
TSC 1
&OBST XB= 0,  0.05, -0.010, 0.05, 0.55, 0.60, SURF_ID = 'ADIABATIC', PERMIT_HOLE = .FALSE. / TSC
2
&OBST XB= -0.3, -0.25, -0.010, 0.05, 0.55, 0.60, SURF_ID = 'ADIABATIC', PERMIT_HOLE = .FALSE. /
TSC 3
&OBST XB= 0.25,  0.3, -0.010, 0.05, 0.85, 0.9, SURF_ID = 'ADIABATIC', PERMIT_HOLE = .FALSE. / TSC
4
&OBST XB= -0.05,  0, -0.010, 0.05, 0.85, 0.9, SURF_ID = 'ADIABATIC', PERMIT_HOLE = .FALSE. / TSC
5
&OBST XB= -0.60, -0.55, -0.010, 0.05, 0.85, 0.9, SURF_ID = 'ADIABATIC', PERMIT_HOLE = .FALSE. /
TSC 6
&OBST XB= 0.55,  0.60, -0.010, 0.05, 1.15, 1.2, SURF_ID = 'ADIABATIC', PERMIT_HOLE = .FALSE. /
TSC 7
&OBST XB= 0, 0.05, -0.010, 0.05, 1.15, 1.2, SURF_ID = 'ADIABATIC', PERMIT_HOLE = .FALSE. / TSC 8
```

```
&OBST XB= -0.3, -0.25, -0.010, 0.05, 1.15, 1.2, SURF_ID = 'ADIABATIC', PERMIT_HOLE = .FALSE. /
TSC 9
&OBST XB= 0.25,  0.3, -0.010, 0.05, 1.45, 1.5, SURF_ID = 'ADIABATIC', PERMIT_HOLE = .FALSE. / TSC
10
&OBST XB= -0.05,  0, -0.010, 0.05, 1.45, 1.5, SURF_ID = 'ADIABATIC', PERMIT_HOLE = .FALSE. / TSC
11
&OBST XB=-0.60, -0.55, -0.010, 0.05, 1.45, 1.5, SURF_ID = 'ADIABATIC', PERMIT_HOLE = .FALSE. /
TSC 12
&OBST XB= 0.55,  0.60, -0.010, 0.05, 1.75, 1.8, SURF_ID = 'ADIABATIC', PERMIT_HOLE = .FALSE. /
TSC 13
&OBST XB= 0,  0.05, -0.010, 0.05, 1.75, 1.8, SURF_ID = 'ADIABATIC', PERMIT_HOLE = .FALSE. / TSC
14
&OBST XB=-0.3, -0.25, -0.010, 0.05, 1.75, 1.8, SURF_ID = 'ADIABATIC', PERMIT_HOLE = .FALSE. / TSC
15
&OBST XB= 0.25,  0.3, -0.010, 0.05, 2.05, 2.1, SURF_ID = 'ADIABATIC', PERMIT_HOLE = .FALSE. / TSC
16
&OBST XB= -0.05,  0, -0.010, 0.05, 2.05, 2.1, SURF_ID = 'ADIABATIC', PERMIT_HOLE = .FALSE. / TSC
17
&OBST XB=-0.60, -0.55, -0.010, 0.05, 2.05, 2.1, SURF_ID = 'ADIABATIC', PERMIT_HOLE = .FALSE. /
TSC 18

&SLCF PBX = 0.0, QUANTITY = 'TEMPERATURE' /
&SLCF PBX = 0.0, QUANTITY = 'HRRPUV' /

&BNDF QUANTITY='GAUGE HEAT FLUX' /
&BNDF QUANTITY='RADIATIVE HEAT FLUX' /
&BNDF QUANTITY='CONVECTIVE HEAT FLUX' /
&BNDF QUANTITY='NET HEAT FLUX' /
&BNDF QUANTITY='WALL TEMPERATURE' /
&BNDF QUANTITY='BURNING RATE' /

CENTERLINE RAKE
&DEVC XYZ=0, 0.25, 0.45, QUANTITY='TEMPERATURE', ID='CTC_1' /
&DEVC XYZ=0, 0.25, 0.60, QUANTITY='TEMPERATURE', ID='BDTC_1' /
&DEVC XYZ=0, 0.25, 0.75, QUANTITY='TEMPERATURE', ID='CTC_2' /
&DEVC XYZ=0, 0.25, 0.90, QUANTITY='TEMPERATURE', ID='BDTC_2' /
&DEVC XYZ=0, 0.25, 1.05, QUANTITY='TEMPERATURE', ID='CTC_3' /
&DEVC XYZ=0, 0.25, 1.20, QUANTITY='TEMPERATURE', ID='BDTC_3' /
&DEVC XYZ=0, 0.25, 1.35, QUANTITY='TEMPERATURE', ID='CTC_4' /
&DEVC XYZ=0, 0.25, 1.50, QUANTITY='TEMPERATURE', ID='BDTC_4' /
&DEVC XYZ=0, 0.25, 1.65, QUANTITY='TEMPERATURE', ID='CTC_5' /
&DEVC XYZ=0, 0.25, 1.80, QUANTITY='TEMPERATURE', ID='BDTC_5' /
&DEVC XYZ=0, 0.25, 1.95, QUANTITY='TEMPERATURE', ID='CTC_6' /
&DEVC XYZ=0, 0.25, 2.10, QUANTITY='TEMPERATURE', ID='BDTC_6' /
&DEVC XYZ=0, 0.25, 2.25, QUANTITY='TEMPERATURE', ID='CTC_7' /
&DEVC XYZ=0, 0.25, 0.60, QUANTITY='W-VELOCITY', ID='BD_1' /
&DEVC XYZ=0, 0.25, 0.90, QUANTITY='W-VELOCITY', ID='BD_2' /
&DEVC XYZ=0, 0.25, 1.20, QUANTITY='W-VELOCITY', ID='BD_3' /
&DEVC XYZ=0, 0.25, 1.50, QUANTITY='W-VELOCITY', ID='BD_4' /
&DEVC XYZ=0, 0.25, 1.80, QUANTITY='W-VELOCITY', ID='BD_5' /
&DEVC XYZ=0, 0.25, 2.10, QUANTITY='W-VELOCITY', ID='BD_6' /
&DEVC XYZ=0, 0.25, 1.05, QUANTITY='W-VELOCITY', ID='BD_7' /
&DEVC XYZ=0, 0.25, 1.35, QUANTITY='W-VELOCITY', ID='BD_8' /
&DEVC XYZ=0, 0.25, 1.65, QUANTITY='W-VELOCITY', ID='BD_9' /
&DEVC XYZ=0, 0.25, 1.95, QUANTITY='W-VELOCITY', ID='BD_10' /

WALL TEMPERATURE
&DEVC XYZ=0.0762, 0.05, 0.75, QUANTITY='TEMPERATURE', ID='WTC_1' /
&DEVC XYZ=0.0508, 0.055, 0.75, QUANTITY='TEMPERATURE', ID='WTC_2' /
&DEVC XYZ=0.0254, 0.060, 0.75, QUANTITY='TEMPERATURE', ID='WTC_3' /
&DEVC XYZ=-0.0254, 0.065, 0.75, QUANTITY='TEMPERATURE', ID='WTC_4' /
&DEVC XYZ=-0.0508, 0.070, 0.75, QUANTITY='TEMPERATURE', ID='WTC_5' /
&DEVC XYZ=-0.0762, 0.075, 0.75, QUANTITY='TEMPERATURE', ID='WTC_6' /
&DEVC XYZ=0.0762, 0.085, 1.35, QUANTITY='TEMPERATURE', ID='WTC_7' /
&DEVC XYZ=0.0508, 0.080, 1.35, QUANTITY='TEMPERATURE', ID='WTC_8' /
&DEVC XYZ=0.0254, 0.075, 1.35, QUANTITY='TEMPERATURE', ID='WTC_9' /
&DEVC XYZ=-0.0254, 0.070, 1.35, QUANTITY='TEMPERATURE', ID='WTC_10' /
&DEVC XYZ=-0.0508, 0.065, 1.35, QUANTITY='TEMPERATURE', ID='WTC_11' /
&DEVC XYZ=-0.0762, 0.060, 1.35, QUANTITY='TEMPERATURE', ID='WTC_12' /
&DEVC XYZ=0.0762, 0.065, 1.95, QUANTITY='TEMPERATURE', ID='WTC_13' /
&DEVC XYZ=0.0508, 0.070, 1.95, QUANTITY='TEMPERATURE', ID='WTC_14' /
```

```
&DEVC XYZ=0.0254, 0.075, 1.95, QUANTITY='TEMPERATURE', ID='WTC_15' /
&DEVC XYZ=-0.0254, 0.080, 1.95, QUANTITY='TEMPERATURE', ID='WTC_16' /
&DEVC XYZ=-0.0508, 0.085, 1.95, QUANTITY='TEMPERATURE', ID='WTC_17' /
&DEVC XYZ=-0.0762, 0.090, 1.95, QUANTITY='TEMPERATURE', ID='WTC_18' /

WALL HEAT FLUX MEASUREMENTS
&DEVC XYZ=  0.575, 0.050, 0.575, QUANTITY='GAUGE_HEAT_FLUX', ID='TS_1',  IOR = 2 /
&DEVC XYZ=  0.025, 0.050, 0.575, QUANTITY='GAUGE_HEAT_FLUX', ID='TS_2',  IOR = 2 /
&DEVC XYZ= -0.275, 0.050, 0.575, QUANTITY='GAUGE_HEAT_FLUX', ID='TS_3',  IOR = 2 /
&DEVC XYZ=  0.275, 0.050, 0.875, QUANTITY='GAUGE_HEAT_FLUX', ID='TS_4',  IOR = 2 /
&DEVC XYZ=  -0.025, 0.050, 0.875, QUANTITY='GAUGE_HEAT_FLUX', ID='TS_5',  IOR = 2 /
&DEVC XYZ= -0.575, 0.050, 0.875, QUANTITY='GAUGE_HEAT_FLUX', ID='TS_6',  IOR = 2 /
&DEVC XYZ=  0.575, 0.050, 1.175, QUANTITY='GAUGE_HEAT_FLUX', ID='TS_7',  IOR = 2 /
&DEVC XYZ=  0.025 0.050, 1.175, QUANTITY='GAUGE_HEAT_FLUX', ID='TS_8',  IOR = 2 /
&DEVC XYZ= -0.275, 0.050, 1.175, QUANTITY='GAUGE_HEAT_FLUX', ID='TS_9',  IOR = 2 /
&DEVC XYZ=  0.275, 0.050, 1.475, QUANTITY='GAUGE_HEAT_FLUX', ID='TS_10', IOR = 2 /
&DEVC XYZ=  -0.025, 0.050, 1.475, QUANTITY='GAUGE_HEAT_FLUX', ID='TS_11', IOR = 2 /
&DEVC XYZ= -0.575, 0.050, 1.475, QUANTITY='GAUGE_HEAT_FLUX', ID='TS_12', IOR = 2 /
&DEVC XYZ=  0.575, 0.050, 1.775, QUANTITY='GAUGE_HEAT_FLUX', ID='TS_13', IOR = 2 /
&DEVC XYZ=  0.025, 0.050, 1.775, QUANTITY='GAUGE_HEAT_FLUX', ID='TS_14', IOR = 2 /
&DEVC XYZ= -0.275, 0.050, 1.775, QUANTITY='GAUGE_HEAT_FLUX', ID='TS_15', IOR = 2 /
&DEVC XYZ=  0.275, 0.050, 2.075, QUANTITY='GAUGE_HEAT_FLUX', ID='TS_16', IOR = 2 /
&DEVC XYZ=  -0.025, 0.050, 2.075, QUANTITY='GAUGE_HEAT_FLUX', ID='TS_17', IOR = 2 /
&DEVC XYZ= -0.575, 0.050, 2.075, QUANTITY='GAUGE_HEAT_FLUX', ID='TS_18', IOR = 2 /

&DEVC XYZ=  0.275, 0.050, 0.60, QUANTITY='GAUGE_HEAT_FLUX', ID='HFG_1', IOR = 2 /
&DEVC XYZ= -0.275, 0.050, 0.875, QUANTITY='GAUGE_HEAT_FLUX', ID='HFG_2', IOR = 2 /
&DEVC XYZ=  0.275, 0.050, 1.175, QUANTITY='GAUGE_HEAT_FLUX', ID='HFG_3', IOR = 2 /
&DEVC XYZ= -0.275, 0.050, 1.475, QUANTITY='GAUGE_HEAT_FLUX', ID='HFG_4', IOR = 2 /
&DEVC XYZ=  0.275, 0.050, 1.775, QUANTITY='GAUGE_HEAT_FLUX', ID='HFG_5', IOR = 2 /
&DEVC XYZ= -0.275, 0.050, 2.075, QUANTITY='GAUGE_HEAT_FLUX', ID='HFG_6', IOR = 2 /

WALL NET HEAT FLUX
&DEVC XYZ=  0.575, 0.050, 0.575, QUANTITY='NET HEAT FLUX', ID='TS_1',  IOR = 2 /
&DEVC XYZ=  0.025, 0.050, 0.575, QUANTITY='NET HEAT FLUX', ID='TS_2',  IOR = 2 /
&DEVC XYZ= -0.275, 0.050, 0.575, QUANTITY='NET HEAT FLUX', ID='TS_3',  IOR = 2 /
&DEVC XYZ=  0.275, 0.050, 0.875, QUANTITY='NET HEAT FLUX', ID='TS_4',  IOR = 2 /
&DEVC XYZ=  -0.025, 0.050, 0.875, QUANTITY='NET HEAT FLUX', ID='TS_5',  IOR = 2 /
&DEVC XYZ= -0.575, 0.050, 0.875, QUANTITY='NET HEAT FLUX', ID='TS_6',  IOR = 2 /
&DEVC XYZ=  0.575, 0.050, 1.175, QUANTITY='NET HEAT FLUX', ID='TS_7',  IOR = 2 /
&DEVC XYZ=  0.025 0.050, 1.175, QUANTITY='NET HEAT FLUX', ID='TS_8',  IOR = 2 /
&DEVC XYZ= -0.275, 0.050, 1.175, QUANTITY='NET HEAT FLUX', ID='TS_9',  IOR = 2 /
&DEVC XYZ=  0.275, 0.050, 1.475, QUANTITY='NET HEAT FLUX', ID='TS_10', IOR = 2 /
&DEVC XYZ=  -0.025, 0.050, 1.475, QUANTITY='NET HEAT FLUX', ID='TS_11', IOR = 2 /
&DEVC XYZ= -0.575, 0.050, 1.475, QUANTITY='NET HEAT FLUX', ID='TS_12', IOR = 2 /
&DEVC XYZ=  0.575, 0.050, 1.775, QUANTITY='NET HEAT FLUX', ID='TS_13', IOR = 2 /
&DEVC XYZ=  0.025, 0.050, 1.775, QUANTITY='NET HEAT FLUX', ID='TS_14', IOR = 2 /
&DEVC XYZ= -0.275, 0.050, 1.775, QUANTITY='NET HEAT FLUX', ID='TS_15', IOR = 2 /
```

J.4 Input File 4 – FRP scenario, Square burner, 50 kW, propane

```
Start Input File
&HEAD CHID='54_1_03-14-2011_FRP_Pr_sb_50kW' /

&TIME T_END = 900, DT = 0.05, RESTRICT_TIME_STEP = .FALSE. /
&DUMP DT_BNDF=2.0, DT_DEVC=0.5, DT_HRR=1.0, DT_PL3D=5000.0, DT_SLCF=2.0, DT_RESTART=50./

&MISC
      SURF_DEFAULT = 'INERT'
      TMPA  = 23
      FDS6  = .TRUE.
      DNS = .FALSE.
      DYNSMAG = .TRUE.
      CSMAG = 0.2
      PR = 0.5
      SC = 0.5
      H_EDDY = .TRUE.
      CFL_VELOCITY_NORM = 1
      FLUX_LIMITER = 2
      ISOTHERMAL = .FALSE.
      RADIATION = .TRUE.
      BAROCLINIC = .TRUE.
      CLIP_MASS_FRACTION   = .TRUE.
      CHECK_VN = .TRUE.
      NOBIAS = .TRUE.
      PROJECTION  = .FALSE.
      CHECK_KINETIC_ENERGY = .FALSE.
      /

&REAC
     ID = 'Propane'
     C = 3
     H = 8
     O = 0
     CO_YIELD = 0.024
     SOOT_YIELD = 0.005
     EDDY_DISSIPATION = .TRUE.
     C_EDC = 0.1
     HRRPUA_SHEET = 0
     HRRPUV_AVERAGE = 2500
      /

&RADI
    RADIATIVE_FRACTION = 0.3
    TIME_STEP_INCREMENT = 3
    ANGLE_INCREMENT = 5
    NUMBER_RADIATION_ANGLES = 104
    /

**** MESHES ****
 MESH IJK= 96, 156, 96, XB=-1.20, 1.20, 0.00, 3.90, 0.00, 2.40 / 2.50 cm grid,  1 mesh

&MESH ID= 'Mesh-1', IJK= 24, 26, 24, XB= -1.2, 0, 0, 1.3, 0, 1.2 / 0.05 cm grid 12 mesh
&MESH ID= 'Mesh-2', IJK= 24, 26, 24, XB= -1.2, 0, 1.3, 2.6, 0, 1.2 / 0.05 cm grid 12 mesh
&MESH ID= 'Mesh-3', IJK= 24, 26, 24, XB= -1.2, 0, 2.6, 3.9, 0, 1.2 / 0.05 cm grid 12 mesh
&MESH ID= 'Mesh-4', IJK= 24, 26, 24, XB= 0, 1.2, 0, 1.3, 0, 1.2 / 0.05 cm grid 12 mesh
&MESH ID= 'Mesh-5', IJK= 24, 26, 24, XB= 0, 1.2, 1.3, 2.6, 0, 1.2 / 0.05 cm grid 12 mesh
&MESH ID= 'Mesh-6', IJK= 24, 26, 24, XB= 0, 1.2, 2.6, 3.9, 0, 1.2 / 0.05 cm grid 12 mesh
&MESH ID= 'Mesh-7', IJK= 24, 26, 24, XB= -1.2, 0, 0, 1.3, 1.2, 2.4 / 0.05 cm grid 12 mesh
&MESH ID= 'Mesh-8', IJK= 24, 26, 24, XB= -1.2, 0, 1.3, 2.6, 1.2, 2.4 / 0.05 cm grid 12 mesh
&MESH ID= 'Mesh-9', IJK= 24, 26, 24, XB= -1.2, 0, 2.6, 3.9, 1.2, 2.4 / 0.05 cm grid 12 mesh
&MESH ID= 'Mesh-10', IJK= 24, 26, 24, XB= 0, 1.2, 0, 1.3, 1.2, 2.4 / 0.05 cm grid 12 mesh
&MESH ID= 'Mesh-11', IJK= 24, 26, 24, XB= 0, 1.2, 1.3, 2.6, 1.2, 2.4 / 0.05 cm grid 12 mesh
&MESH ID= 'Mesh-12', IJK= 24, 26, 24, XB= 0, 1.2, 2.6, 3.9, 1.2, 2.4 / 0.05 cm grid 12 mesh

****BURNER****
2 ft burner
OBST XB= -0.35, 0.35, 0.05, 0.45, 0, 0.4, SURF_ID = 'ADIABATIC' /
VENT XB= -0.3, 0.3, 0.1, 0.4, 0.4, 0.4, SURF_ID = 'BURNER' /
```

```
1 ft burner
&OBST XB= -0.2, 0.2, 0.05, 0.45, 0, 0.4, SURF_ID = 'ADIABATIC' /
&VENT XB= -0.15, 0.15, 0.1, 0.4, 0.4, 0.4, SURF_ID = 'BURNER' /

**** Burner Parameters*****
&SURF ID = 'BURNER'
      HRRPUA =555.6
      RAMP_Q = 'Burner_Ramp'
      COLOR  = 'RED' /

&RAMP ID = 'Burner_Ramp', T=0, F=0 /
&RAMP ID = 'Burner_Ramp', T=1, F=0.5 /
&RAMP ID = 'Burner_Ramp', T=15, F=1 /
&RAMP ID = 'Burner_Ramp', T=88, F=1 /
&RAMP ID = 'Burner_Ramp', T=98, F=0 /

**** MATERIAL PROPERTIES ****
&MATL ID            ='GYPSUM_MATL'
      SPECIFIC_HEAT = 0.84
      CONDUCTIVITY  = 0.48
      DENSITY       = 1440.0 /

&MATL ID            ='KAOWOOL_MATL'
      SPECIFIC_HEAT = 1.0
      CONDUCTIVITY  = 0.06
      DENSITY       = 320.0 /

&SURF ID        = 'ADIABATIC'
      ADIABATIC = .TRUE.
      RGB       = 0, 0, 0 /

&SURF ID                       = 'KAOWOOL'
      RGB                      = 51,102,255
      BACKING                  = 'INSULATED'
      MATL_ID(1,1)             = 'KAOWOOL_MATL'
      MATL_MASS_FRACTION(1,1)= 1.0
      THICKNESS(1)             = 0.025
      CELL_SIZE_FACTOR         = 0.30
      STRETCH_FACTOR           = 1.0 /

&SURF ID                       = 'GYPSUM'
      RGB                      = 100,100,100
      BACKING                  = 'INSULATED'
      MATL_ID(1,1)             = 'GYPSUM_MATL'
      MATL_MASS_FRACTION(1,1)= 1.0
      THICKNESS(1)             = 0.016
      CELL_SIZE_FACTOR         = 0.30
      STRETCH_FACTOR           = 1.0 /

&MATL ID                         = 'virgin'
      CONDUCTIVITY               =  0.480
      DENSITY                    = 1467.80
      SPECIFIC_HEAT              =    1.98
      EMISSIVITY                 =  0.858
      ABSORPTION_COEFFICIENT     =  0.9000E+10
      RESIDUE(01)                = 'char'
      A(01)                      = 0.1139E+12
      E(01)                      = 0.1483E+06
      N_S(01)                    =   1.00
      THRESHOLD_TEMPERATURE(01)=   0.00
      HEAT_OF_REACTION(01)       =   996.67
      HEAT_OF_COMBUSTION         = 19700.
      NU_FUEL(01)                =   0.421
      NU_RESIDUE(01)             =   0.579
      NU_WATER(01)               =   0.000
      N_REACTIONS                = 01 /

&MATL ID                         = 'char'
      CONDUCTIVITY               =  0.050
      DENSITY                    =  850.56
      SPECIFIC_HEAT              =    2.12
```

```
      EMISSIVITY               =  0.943
      ABSORPTION_COEFFICIENT   =  0.9000E+10
      N_REACTIONS              = 00 /

&SURF ID                         = 'FRP'
      STRETCH_FACTOR             = 1.000
      CELL_SIZE_FACTOR           = 0.200
      THICKNESS(1)              = 0.0019
      MATL_ID(1,1)             = 'virgin'
      MATL_ID(1,2)             = 'char'
      MATL_MASS_FRACTION(1,1)  = 1.0000
      MATL_MASS_FRACTION(1,2)  = 0.0000
      BACKING                    = 'INSULATED'
      SHRINK                     = .TRUE.
      TMP_INNER                  = 27.0
      COLOR                      = 'WHITE' /


****OBSTRUCTIONS****
&OBST XB=-1.200, 1.200, 0.000, 0.000, 0.000, 2.400, SURF_ID ='GYPSUM'  / Back wall
&OBST XB= 1.200, 1.200, 0.000, 2.700, 0.000, 2.400, SURF_ID ='GYPSUM'  / Right wall
&OBST XB=-1.200,-1.200, 0.000, 2.700, 0.000, 2.400, SURF_ID ='GYPSUM'  / Left wall
&OBST XB=-1.200, 1.200, 0.000, 2.700, 2.400, 2.400, SURF_ID ='GYPSUM'  / Ceiling
&OBST XB=-0.900,-0.600, 0.000, 0.05, 0.000, 2.400, SURF_ID ='KAOWOOL' / Kaowool on back wall
&OBST XB= 0.600, 0.900, 0.000, 0.05, 0.000, 2.400, SURF_ID ='KAOWOOL' / Kaowool on back wall
&OBST XB=-0.600, 0.600, 0.000, 0.05, 0.000, 2.400, SURF_ID ='FRP', PERMIT_HOLE = .TRUE. / FRP
panel

****OPEN VENTS****
&VENT XB=-1.20, 1.20, 3.90, 3.90, 0.00, 2.40, SURF_ID = 'OPEN' / Back
&VENT XB=-1.20,-1.20, 2.70, 3.90, 0.00, 2.40, SURF_ID = 'OPEN' /
&VENT XB= 1.20, 1.20, 2.70, 3.90, 0.00, 2.40, SURF_ID = 'OPEN' /
&VENT XB=-1.20, 1.20, 2.70, 3.90, 2.40, 2.40, SURF_ID = 'OPEN' /

HOLES in panel for TSC's:
&HOLE XB= 0.55,  0.60, -0.010, 0.1, 0.55, 0.60 / HOLE 1
&HOLE XB= 0,  0.05, -0.010, 0.1, 0.55, 0.60 / HOLE 2
&HOLE XB= -0.3, -0.25, -0.010, 0.1, 0.55, 0.60 / HOLE 3
&HOLE XB= 0.25,  0.3, -0.010, 0.1, 0.85, 0.9 / HOLE 4
&HOLE XB= -0.05,  0, -0.010, 0.1, 0.85, 0.9 / HOLE 5
&HOLE XB= -0.60, -0.55, -0.010, 0.1, 0.85, 0.9 / HOLE 6
&HOLE XB= 0.55,  0.60, -0.010, 0.1, 1.15, 1.2 / HOLE 7
&HOLE XB= 0, 0.05, -0.010, 0.1, 1.15, 1.2 / HOLE 8
&HOLE XB= -0.3, -0.25, -0.010, 0.1, 1.15, 1.2 / HOLE 9
&HOLE XB= 0.25,  0.3, -0.010, 0.1, 1.45, 1.5 / HOLE 10
&HOLE XB= -0.05,  0, -0.010, 0.1, 1.45, 1.5 / HOLE 11
&HOLE XB=-0.60, -0.55, -0.010, 0.1, 1.45, 1.5 / HOLE 12
&HOLE XB= 0.55,  0.60, -0.010, 0.1, 1.75, 1.8 / HOLE 13
&HOLE XB= 0,  0.05, -0.010, 0.1, 1.75, 1.8 / HOLE 14
&HOLE XB=-0.3, -0.25, -0.010, 0.1, 1.75, 1.8 / HOLE 15
&HOLE XB= 0.25,  0.3, -0.010, 0.1, 2.05, 2.1 / HOLE 16
&HOLE XB= -0.05,  0, -0.010, 0.1, 2.05, 2.1 / HOLE 17
&HOLE XB=-0.60, -0.55, -0.010, 0.1, 2.05, 2.1 / HOLE 18

TSC'S:

&OBST XB= 0.55,  0.60, -0.010, 0.05, 0.55, 0.60, SURF_ID = 'ADIABATIC', PERMIT_HOLE = .FALSE. /
TSC 1
&OBST XB= 0,  0.05, -0.010, 0.05, 0.55, 0.60, SURF_ID = 'ADIABATIC', PERMIT_HOLE = .FALSE. / TSC
2
&OBST XB= -0.3, -0.25, -0.010, 0.05, 0.55, 0.60, SURF_ID = 'ADIABATIC', PERMIT_HOLE = .FALSE. /
TSC 3
&OBST XB= 0.25,  0.3, -0.010, 0.05, 0.85, 0.9, SURF_ID = 'ADIABATIC', PERMIT_HOLE = .FALSE. / TSC
4
&OBST XB= -0.05,  0, -0.010, 0.05, 0.85, 0.9, SURF_ID = 'ADIABATIC', PERMIT_HOLE = .FALSE. / TSC
5
&OBST XB= -0.60, -0.55, -0.010, 0.05, 0.85, 0.9, SURF_ID = 'ADIABATIC', PERMIT_HOLE = .FALSE. /
TSC 6
&OBST XB= 0.55,  0.60, -0.010, 0.05, 1.15, 1.2, SURF_ID = 'ADIABATIC', PERMIT_HOLE = .FALSE. /
TSC 7
&OBST XB= 0, 0.05, -0.010, 0.05, 1.15, 1.2, SURF_ID = 'ADIABATIC', PERMIT_HOLE = .FALSE. / TSC 8
```

```
&OBST XB= -0.3, -0.25, -0.010, 0.05, 1.15, 1.2, SURF_ID = 'ADIABATIC', PERMIT_HOLE = .FALSE. /
TSC 9
&OBST XB= 0.25,  0.3, -0.010, 0.05, 1.45, 1.5, SURF_ID = 'ADIABATIC', PERMIT_HOLE = .FALSE. / TSC
10
&OBST XB= -0.05,  0, -0.010, 0.05, 1.45, 1.5, SURF_ID = 'ADIABATIC', PERMIT_HOLE = .FALSE. / TSC
11
&OBST XB=-0.60, -0.55, -0.010, 0.05, 1.45, 1.5, SURF_ID = 'ADIABATIC', PERMIT_HOLE = .FALSE. /
TSC 12
&OBST XB= 0.55,  0.60, -0.010, 0.05, 1.75, 1.8, SURF_ID = 'ADIABATIC', PERMIT_HOLE = .FALSE. /
TSC 13
&OBST XB= 0,  0.05, -0.010, 0.05, 1.75, 1.8, SURF_ID = 'ADIABATIC', PERMIT_HOLE = .FALSE. / TSC
14
&OBST XB=-0.3, -0.25, -0.010, 0.05, 1.75, 1.8, SURF_ID = 'ADIABATIC', PERMIT_HOLE = .FALSE. / TSC
15
&OBST XB= 0.25,  0.3, -0.010, 0.05, 2.05, 2.1, SURF_ID = 'ADIABATIC', PERMIT_HOLE = .FALSE. / TSC
16
&OBST XB= -0.05,  0, -0.010, 0.05, 2.05, 2.1, SURF_ID = 'ADIABATIC', PERMIT_HOLE = .FALSE. / TSC
17
&OBST XB=-0.60, -0.55, -0.010, 0.05, 2.05, 2.1, SURF_ID = 'ADIABATIC', PERMIT_HOLE = .FALSE. /
TSC 18

&SLCF PBX = 0.0, QUANTITY = 'TEMPERATURE' /
&SLCF PBX = 0.0, QUANTITY = 'HRRPUV' /

&BNDF QUANTITY='GAUGE HEAT FLUX' /
&BNDF QUANTITY='RADIATIVE HEAT FLUX' /
&BNDF QUANTITY='CONVECTIVE HEAT FLUX' /
&BNDF QUANTITY='NET HEAT FLUX' /
&BNDF QUANTITY='WALL TEMPERATURE' /
&BNDF QUANTITY='BURNING RATE' /

CENTERLINE RAKE
&DEVC XYZ=0, 0.25, 0.45, QUANTITY='TEMPERATURE', ID='CTC_1' /
&DEVC XYZ=0, 0.25, 0.60, QUANTITY='TEMPERATURE', ID='BDTC_1' /
&DEVC XYZ=0, 0.25, 0.75, QUANTITY='TEMPERATURE', ID='CTC_2' /
&DEVC XYZ=0, 0.25, 0.90, QUANTITY='TEMPERATURE', ID='BDTC_2' /
&DEVC XYZ=0, 0.25, 1.05, QUANTITY='TEMPERATURE', ID='CTC_3' /
&DEVC XYZ=0, 0.25, 1.20, QUANTITY='TEMPERATURE', ID='BDTC_3' /
&DEVC XYZ=0, 0.25, 1.35, QUANTITY='TEMPERATURE', ID='CTC_4' /
&DEVC XYZ=0, 0.25, 1.50, QUANTITY='TEMPERATURE', ID='BDTC_4' /
&DEVC XYZ=0, 0.25, 1.65, QUANTITY='TEMPERATURE', ID='CTC_5' /
&DEVC XYZ=0, 0.25, 1.80, QUANTITY='TEMPERATURE', ID='BDTC_5' /
&DEVC XYZ=0, 0.25, 1.95, QUANTITY='TEMPERATURE', ID='CTC_6' /
&DEVC XYZ=0, 0.25, 2.10, QUANTITY='TEMPERATURE', ID='BDTC_6' /
&DEVC XYZ=0, 0.25, 2.25, QUANTITY='TEMPERATURE', ID='CTC_7' /
&DEVC XYZ=0, 0.25, 0.60, QUANTITY='W-VELOCITY', ID='BD_1' /
&DEVC XYZ=0, 0.25, 0.90, QUANTITY='W-VELOCITY', ID='BD_2' /
&DEVC XYZ=0, 0.25, 1.20, QUANTITY='W-VELOCITY', ID='BD_3' /
&DEVC XYZ=0, 0.25, 1.50, QUANTITY='W-VELOCITY', ID='BD_4' /
&DEVC XYZ=0, 0.25, 1.80, QUANTITY='W-VELOCITY', ID='BD_5' /
&DEVC XYZ=0, 0.25, 2.10, QUANTITY='W-VELOCITY', ID='BD_6' /
&DEVC XYZ=0, 0.25, 1.05, QUANTITY='W-VELOCITY', ID='BD_7' /
&DEVC XYZ=0, 0.25, 1.35, QUANTITY='W-VELOCITY', ID='BD_8' /
&DEVC XYZ=0, 0.25, 1.65, QUANTITY='W-VELOCITY', ID='BD_9' /
&DEVC XYZ=0, 0.25, 1.95, QUANTITY='W-VELOCITY', ID='BD_10' /

WALL TEMPERATURE
&DEVC XYZ=0.0762, 0.05, 0.75, QUANTITY='TEMPERATURE', ID='WTC_1' /
&DEVC XYZ=0.0508, 0.055, 0.75, QUANTITY='TEMPERATURE', ID='WTC_2' /
&DEVC XYZ=0.0254, 0.060, 0.75, QUANTITY='TEMPERATURE', ID='WTC_3' /
&DEVC XYZ=-0.0254, 0.065, 0.75, QUANTITY='TEMPERATURE', ID='WTC_4' /
&DEVC XYZ=-0.0508, 0.070, 0.75, QUANTITY='TEMPERATURE', ID='WTC_5' /
&DEVC XYZ=-0.0762, 0.075, 0.75, QUANTITY='TEMPERATURE', ID='WTC_6' /
&DEVC XYZ=0.0762, 0.085, 1.35, QUANTITY='TEMPERATURE', ID='WTC_7' /
&DEVC XYZ=0.0508, 0.080, 1.35, QUANTITY='TEMPERATURE', ID='WTC_8' /
&DEVC XYZ=0.0254, 0.075, 1.35, QUANTITY='TEMPERATURE', ID='WTC_9' /
&DEVC XYZ=-0.0254, 0.070, 1.35, QUANTITY='TEMPERATURE', ID='WTC_10' /
&DEVC XYZ=-0.0508, 0.065, 1.35, QUANTITY='TEMPERATURE', ID='WTC_11' /
&DEVC XYZ=-0.0762, 0.060, 1.35, QUANTITY='TEMPERATURE', ID='WTC_12' /
&DEVC XYZ=0.0762, 0.065, 1.95, QUANTITY='TEMPERATURE', ID='WTC_13' /
&DEVC XYZ=0.0508, 0.070, 1.95, QUANTITY='TEMPERATURE', ID='WTC_14' /
```

```
&DEVC XYZ=0.0254, 0.075, 1.95, QUANTITY='TEMPERATURE', ID='WTC_15' /
&DEVC XYZ=-0.0254, 0.080, 1.95, QUANTITY='TEMPERATURE', ID='WTC_16' /
&DEVC XYZ=-0.0508, 0.085, 1.95, QUANTITY='TEMPERATURE', ID='WTC_17' /
&DEVC XYZ=-0.0762, 0.090, 1.95, QUANTITY='TEMPERATURE', ID='WTC_18' /

WALL HEAT FLUX MEASUREMENTS
&DEVC XYZ=  0.575, 0.050, 0.575, QUANTITY='GAUGE_HEAT_FLUX', ID='TS_1',  IOR = 2 /
&DEVC XYZ=  0.025, 0.050, 0.575, QUANTITY='GAUGE_HEAT_FLUX', ID='TS_2',  IOR = 2 /
&DEVC XYZ= -0.275, 0.050, 0.575, QUANTITY='GAUGE_HEAT_FLUX', ID='TS_3',  IOR = 2 /
&DEVC XYZ=  0.275, 0.050, 0.875, QUANTITY='GAUGE_HEAT_FLUX', ID='TS_4',  IOR = 2 /
&DEVC XYZ=  -0.025, 0.050, 0.875, QUANTITY='GAUGE_HEAT_FLUX', ID='TS_5',  IOR = 2 /
&DEVC XYZ= -0.575, 0.050, 0.875, QUANTITY='GAUGE_HEAT_FLUX', ID='TS_6',  IOR = 2 /
&DEVC XYZ=  0.575, 0.050, 1.175, QUANTITY='GAUGE_HEAT_FLUX', ID='TS_7',  IOR = 2 /
&DEVC XYZ=  0.025 0.050, 1.175, QUANTITY='GAUGE_HEAT_FLUX', ID='TS_8',  IOR = 2 /
&DEVC XYZ= -0.275, 0.050, 1.175, QUANTITY='GAUGE_HEAT_FLUX', ID='TS_9',  IOR = 2 /
&DEVC XYZ=  0.275, 0.050, 1.475, QUANTITY='GAUGE_HEAT_FLUX', ID='TS_10', IOR = 2 /
&DEVC XYZ=  -0.025, 0.050, 1.475, QUANTITY='GAUGE_HEAT_FLUX', ID='TS_11', IOR = 2 /
&DEVC XYZ= -0.575, 0.050, 1.475, QUANTITY='GAUGE_HEAT_FLUX', ID='TS_12', IOR = 2 /
&DEVC XYZ=  0.575, 0.050, 1.775, QUANTITY='GAUGE_HEAT_FLUX', ID='TS_13', IOR = 2 /
&DEVC XYZ=  0.025, 0.050, 1.775, QUANTITY='GAUGE_HEAT_FLUX', ID='TS_14', IOR = 2 /
&DEVC XYZ= -0.275, 0.050, 1.775, QUANTITY='GAUGE_HEAT_FLUX', ID='TS_15', IOR = 2 /
&DEVC XYZ=  0.275, 0.050, 2.075, QUANTITY='GAUGE_HEAT_FLUX', ID='TS_16', IOR = 2 /
&DEVC XYZ=  -0.025, 0.050, 2.075, QUANTITY='GAUGE_HEAT_FLUX', ID='TS_17', IOR = 2 /
&DEVC XYZ= -0.575, 0.050, 2.075, QUANTITY='GAUGE_HEAT_FLUX', ID='TS_18', IOR = 2 /

&DEVC XYZ=  0.275, 0.050, 0.60, QUANTITY='GAUGE_HEAT_FLUX', ID='HFG_1', IOR = 2 /
&DEVC XYZ= -0.275, 0.050, 0.875, QUANTITY='GAUGE_HEAT_FLUX', ID='HFG_2', IOR = 2 /
&DEVC XYZ=  0.275, 0.050, 1.175, QUANTITY='GAUGE_HEAT_FLUX', ID='HFG_3', IOR = 2 /
&DEVC XYZ= -0.275, 0.050, 1.475, QUANTITY='GAUGE_HEAT_FLUX', ID='HFG_4', IOR = 2 /
&DEVC XYZ=  0.275, 0.050, 1.775, QUANTITY='GAUGE_HEAT_FLUX', ID='HFG_5', IOR = 2 /
&DEVC XYZ= -0.275, 0.050, 2.075, QUANTITY='GAUGE_HEAT_FLUX', ID='HFG_6', IOR = 2 /

WALL NET HEAT FLUX
&DEVC XYZ=  0.575, 0.050, 0.575, QUANTITY='NET HEAT FLUX', ID='TS_1',  IOR = 2 /
&DEVC XYZ=  0.025, 0.050, 0.575, QUANTITY='NET HEAT FLUX', ID='TS_2',  IOR = 2 /
&DEVC XYZ= -0.275, 0.050, 0.575, QUANTITY='NET HEAT FLUX', ID='TS_3',  IOR = 2 /
&DEVC XYZ=  0.275, 0.050, 0.875, QUANTITY='NET HEAT FLUX', ID='TS_4',  IOR = 2 /
&DEVC XYZ=  -0.025, 0.050, 0.875, QUANTITY='NET HEAT FLUX', ID='TS_5',  IOR = 2 /
&DEVC XYZ= -0.575, 0.050, 0.875, QUANTITY='NET HEAT FLUX', ID='TS_6',  IOR = 2 /
&DEVC XYZ=  0.575, 0.050, 1.175, QUANTITY='NET HEAT FLUX', ID='TS_7',  IOR = 2 /
&DEVC XYZ=  0.025 0.050, 1.175, QUANTITY='NET HEAT FLUX', ID='TS_8',  IOR = 2 /
&DEVC XYZ= -0.275, 0.050, 1.175, QUANTITY='NET HEAT FLUX', ID='TS_9',  IOR = 2 /
&DEVC XYZ=  0.275, 0.050, 1.475, QUANTITY='NET HEAT FLUX', ID='TS_10', IOR = 2 /
&DEVC XYZ=  -0.025, 0.050, 1.475, QUANTITY='NET HEAT FLUX', ID='TS_11', IOR = 2 /
&DEVC XYZ= -0.575, 0.050, 1.475, QUANTITY='NET HEAT FLUX', ID='TS_12', IOR = 2 /
&DEVC XYZ=  0.575, 0.050, 1.775, QUANTITY='NET HEAT FLUX', ID='TS_13', IOR = 2 /
&DEVC XYZ=  0.025, 0.050, 1.775, QUANTITY='NET HEAT FLUX', ID='TS_14', IOR = 2 /
&DEVC XYZ= -0.275, 0.050, 1.775, QUANTITY='NET HEAT FLUX', ID='TS_15', IOR = 2 /
```

J.5 Input File 5 – FRP scenario, Square burner, 75 kW, propane

```
Start Input File
&HEAD CHID='55_1_03-14-2011_FRP_Pr_sb_75kW' /

&TIME T_END = 900, DT = 0.05, RESTRICT_TIME_STEP = .FALSE. /
&DUMP DT_BNDF=2.0, DT_DEVC=0.5, DT_HRR=1.0, DT_PL3D=5000.0, DT_SLCF=2.0, DT_RESTART=50./

&MISC
      SURF_DEFAULT = 'INERT'
      TMPA  = 23
      FDS6  = .TRUE.
      DNS = .FALSE.
      DYNSMAG = .TRUE.
      CSMAG = 0.2
      PR = 0.5
      SC = 0.5
      H_EDDY = .TRUE.
      CFL_VELOCITY_NORM = 1
      FLUX_LIMITER = 2
      ISOTHERMAL = .FALSE.
      RADIATION = .TRUE.
      BAROCLINIC = .TRUE.
      CLIP_MASS_FRACTION   = .TRUE.
      CHECK_VN = .TRUE.
      NOBIAS = .TRUE.
      PROJECTION  = .FALSE.
      CHECK_KINETIC_ENERGY = .FALSE.
      /

&REAC
     ID = 'Propane'
     C = 3
     H = 8
     O = 0
     CO_YIELD = 0.024
     SOOT_YIELD = 0.005
     EDDY_DISSIPATION = .TRUE.
     C_EDC = 0.1
     HRRPUA_SHEET = 0
     HRRPUV_AVERAGE = 2500
      /

&RADI
    RADIATIVE_FRACTION = 0.3
    TIME_STEP_INCREMENT = 3
    ANGLE_INCREMENT = 5
    NUMBER_RADIATION_ANGLES = 104
    /

**** MESHES ****
 MESH IJK= 96, 156, 96, XB=-1.20, 1.20, 0.00, 3.90, 0.00, 2.40 / 2.50 cm grid,  1 mesh

&MESH ID= 'Mesh-1', IJK= 24, 26, 24, XB= -1.2, 0, 0, 1.3, 0, 1.2 / 0.05 cm grid 12 mesh
&MESH ID= 'Mesh-2', IJK= 24, 26, 24, XB= -1.2, 0, 1.3, 2.6, 0, 1.2 / 0.05 cm grid 12 mesh
&MESH ID= 'Mesh-3', IJK= 24, 26, 24, XB= -1.2, 0, 2.6, 3.9, 0, 1.2 / 0.05 cm grid 12 mesh
&MESH ID= 'Mesh-4', IJK= 24, 26, 24, XB= 0, 1.2, 0, 1.3, 0, 1.2 / 0.05 cm grid 12 mesh
&MESH ID= 'Mesh-5', IJK= 24, 26, 24, XB= 0, 1.2, 1.3, 2.6, 0, 1.2 / 0.05 cm grid 12 mesh
&MESH ID= 'Mesh-6', IJK= 24, 26, 24, XB= 0, 1.2, 2.6, 3.9, 0, 1.2 / 0.05 cm grid 12 mesh
&MESH ID= 'Mesh-7', IJK= 24, 26, 24, XB= -1.2, 0, 0, 1.3, 1.2, 2.4 / 0.05 cm grid 12 mesh
&MESH ID= 'Mesh-8', IJK= 24, 26, 24, XB= -1.2, 0, 1.3, 2.6, 1.2, 2.4 / 0.05 cm grid 12 mesh
&MESH ID= 'Mesh-9', IJK= 24, 26, 24, XB= -1.2, 0, 2.6, 3.9, 1.2, 2.4 / 0.05 cm grid 12 mesh
&MESH ID= 'Mesh-10', IJK= 24, 26, 24, XB= 0, 1.2, 0, 1.3, 1.2, 2.4 / 0.05 cm grid 12 mesh
&MESH ID= 'Mesh-11', IJK= 24, 26, 24, XB= 0, 1.2, 1.3, 2.6, 1.2, 2.4 / 0.05 cm grid 12 mesh
&MESH ID= 'Mesh-12', IJK= 24, 26, 24, XB= 0, 1.2, 2.6, 3.9, 1.2, 2.4 / 0.05 cm grid 12 mesh

****BURNER****
2 ft burner
OBST XB= -0.35, 0.35, 0.05, 0.45, 0, 0.4, SURF_ID = 'ADIABATIC' /
VENT XB= -0.3, 0.3, 0.1, 0.4, 0.4, 0.4, SURF_ID = 'BURNER' /
```

```
1 ft burner
&OBST XB= -0.2, 0.2, 0.05, 0.45, 0, 0.4, SURF_ID = 'ADIABATIC' /
&VENT XB= -0.15, 0.15, 0.1, 0.4, 0.4, 0.4, SURF_ID = 'BURNER' /

**** Burner Parameters*****
&SURF ID = 'BURNER'
      HRRPUA =833.3
      RAMP_Q = 'Burner_Ramp'
      COLOR  = 'RED' /

&RAMP ID = 'Burner_Ramp', T=0, F=0 /
&RAMP ID = 'Burner_Ramp', T=1, F=0.5 /
&RAMP ID = 'Burner_Ramp', T=15, F=1 /
&RAMP ID = 'Burner_Ramp', T=74, F=1 /
&RAMP ID = 'Burner_Ramp', T=84, F=0 /

**** MATERIAL PROPERTIES ****
&MATL ID             ='GYPSUM_MATL'
      SPECIFIC_HEAT = 0.84
      CONDUCTIVITY  = 0.48
      DENSITY       = 1440.0 /

&MATL ID             ='KAOWOOL_MATL'
      SPECIFIC_HEAT = 1.0
      CONDUCTIVITY  = 0.06
      DENSITY       = 320.0 /

&SURF ID        = 'ADIABATIC'
      ADIABATIC = .TRUE.
      RGB       = 0, 0, 0 /

&SURF ID                     = 'KAOWOOL'
      RGB                     = 51,102,255
      BACKING                 = 'INSULATED'
      MATL_ID(1,1)            = 'KAOWOOL_MATL'
      MATL_MASS_FRACTION(1,1)= 1.0
      THICKNESS(1)            = 0.025
      CELL_SIZE_FACTOR        = 0.30
      STRETCH_FACTOR          = 1.0 /

&SURF ID                     = 'GYPSUM'
      RGB                     = 100,100,100
      BACKING                 = 'INSULATED'
      MATL_ID(1,1)            = 'GYPSUM_MATL'
      MATL_MASS_FRACTION(1,1)= 1.0
      THICKNESS(1)            = 0.016
      CELL_SIZE_FACTOR        = 0.30
      STRETCH_FACTOR          = 1.0 /

&MATL ID                       = 'virgin'
      CONDUCTIVITY              =  0.480
      DENSITY                   = 1467.80
      SPECIFIC_HEAT             =    1.98
      EMISSIVITY                =  0.858
      ABSORPTION_COEFFICIENT    =  0.9000E+10
      RESIDUE(01)               = 'char'
      A(01)                     = 0.1139E+12
      E(01)                     = 0.1483E+06
      N_S(01)                   =   1.00
      THRESHOLD_TEMPERATURE(01)=   0.00
      HEAT_OF_REACTION(01)      =   996.67
      HEAT_OF_COMBUSTION        = 19700.
      NU_FUEL(01)               =   0.421
      NU_RESIDUE(01)            =   0.579
      NU_WATER(01)              =   0.000
      N_REACTIONS               = 01 /

&MATL ID                       = 'char'
      CONDUCTIVITY              =  0.050
      DENSITY                   =  850.56
      SPECIFIC_HEAT             =    2.12
```

```
      EMISSIVITY               =  0.943
      ABSORPTION_COEFFICIENT   =  0.9000E+10
      N_REACTIONS              = 00 /

&SURF ID                        = 'FRP'
      STRETCH_FACTOR            = 1.000
      CELL_SIZE_FACTOR          = 0.200
      THICKNESS(1)             = 0.0019
      MATL_ID(1,1)             = 'virgin'
      MATL_ID(1,2)             = 'char'
      MATL_MASS_FRACTION(1,1)  = 1.0000
      MATL_MASS_FRACTION(1,2)  = 0.0000
      BACKING                   = 'INSULATED'
      SHRINK                    = .TRUE.
      TMP_INNER                 = 27.0
      COLOR                     = 'WHITE' /


****OBSTRUCTIONS****
&OBST XB=-1.200, 1.200, 0.000, 0.000, 0.000, 2.400, SURF_ID ='GYPSUM'  / Back wall
&OBST XB= 1.200, 1.200, 0.000, 2.700, 0.000, 2.400, SURF_ID ='GYPSUM'  / Right wall
&OBST XB=-1.200,-1.200, 0.000, 2.700, 0.000, 2.400, SURF_ID ='GYPSUM'  / Left wall
&OBST XB=-1.200, 1.200, 0.000, 2.700, 2.400, 2.400, SURF_ID ='GYPSUM'  / Ceiling
&OBST XB=-0.900,-0.600, 0.000, 0.05, 0.000, 2.400, SURF_ID ='KAOWOOL' / Kaowool on back wall
&OBST XB= 0.600, 0.900, 0.000, 0.05, 0.000, 2.400, SURF_ID ='KAOWOOL' / Kaowool on back wall
&OBST XB=-0.600, 0.600, 0.000, 0.05, 0.000, 2.400, SURF_ID ='FRP', PERMIT_HOLE = .TRUE. / FRP
panel

****OPEN VENTS****
&VENT XB=-1.20, 1.20, 3.90, 3.90, 0.00, 2.40, SURF_ID = 'OPEN' / Back
&VENT XB=-1.20,-1.20, 2.70, 3.90, 0.00, 2.40, SURF_ID = 'OPEN' /
&VENT XB= 1.20, 1.20, 2.70, 3.90, 0.00, 2.40, SURF_ID = 'OPEN' /
&VENT XB=-1.20, 1.20, 2.70, 3.90, 2.40, 2.40, SURF_ID = 'OPEN' /

HOLES in panel for TSC's:
&HOLE XB= 0.55,  0.60, -0.010, 0.1, 0.55, 0.60 / HOLE 1
&HOLE XB= 0,  0.05, -0.010, 0.1, 0.55, 0.60 / HOLE 2
&HOLE XB= -0.3, -0.25, -0.010, 0.1, 0.55, 0.60 / HOLE 3
&HOLE XB= 0.25,  0.3, -0.010, 0.1, 0.85, 0.9 / HOLE 4
&HOLE XB= -0.05,  0, -0.010, 0.1, 0.85, 0.9 / HOLE 5
&HOLE XB= -0.60, -0.55, -0.010, 0.1, 0.85, 0.9 / HOLE 6
&HOLE XB= 0.55,  0.60, -0.010, 0.1, 1.15, 1.2 / HOLE 7
&HOLE XB= 0, 0.05, -0.010, 0.1, 1.15, 1.2 / HOLE 8
&HOLE XB= -0.3, -0.25, -0.010, 0.1, 1.15, 1.2 / HOLE 9
&HOLE XB= 0.25,  0.3, -0.010, 0.1, 1.45, 1.5 / HOLE 10
&HOLE XB= -0.05,  0, -0.010, 0.1, 1.45, 1.5 / HOLE 11
&HOLE XB=-0.60, -0.55, -0.010, 0.1, 1.45, 1.5 / HOLE 12
&HOLE XB= 0.55,  0.60, -0.010, 0.1, 1.75, 1.8 / HOLE 13
&HOLE XB= 0,  0.05, -0.010, 0.1, 1.75, 1.8 / HOLE 14
&HOLE XB=-0.3, -0.25, -0.010, 0.1, 1.75, 1.8 / HOLE 15
&HOLE XB= 0.25,  0.3, -0.010, 0.1, 2.05, 2.1 / HOLE 16
&HOLE XB= -0.05,  0, -0.010, 0.1, 2.05, 2.1 / HOLE 17
&HOLE XB=-0.60, -0.55, -0.010, 0.1, 2.05, 2.1 / HOLE 18

TSC'S:

&OBST XB= 0.55,  0.60, -0.010, 0.05, 0.55, 0.60, SURF_ID = 'ADIABATIC', PERMIT_HOLE = .FALSE. /
TSC 1
&OBST XB= 0,  0.05, -0.010, 0.05, 0.55, 0.60, SURF_ID = 'ADIABATIC', PERMIT_HOLE = .FALSE. / TSC
2
&OBST XB= -0.3, -0.25, -0.010, 0.05, 0.55, 0.60, SURF_ID = 'ADIABATIC', PERMIT_HOLE = .FALSE. /
TSC 3
&OBST XB= 0.25,  0.3, -0.010, 0.05, 0.85, 0.9, SURF_ID = 'ADIABATIC', PERMIT_HOLE = .FALSE. / TSC
4
&OBST XB= -0.05,  0, -0.010, 0.05, 0.85, 0.9, SURF_ID = 'ADIABATIC', PERMIT_HOLE = .FALSE. / TSC
5
&OBST XB= -0.60, -0.55, -0.010, 0.05, 0.85, 0.9, SURF_ID = 'ADIABATIC', PERMIT_HOLE = .FALSE. /
TSC 6
&OBST XB= 0.55,  0.60, -0.010, 0.05, 1.15, 1.2, SURF_ID = 'ADIABATIC', PERMIT_HOLE = .FALSE. /
TSC 7
&OBST XB= 0, 0.05, -0.010, 0.05, 1.15, 1.2, SURF_ID = 'ADIABATIC', PERMIT_HOLE = .FALSE. / TSC 8
```

```
&OBST XB= -0.3, -0.25, -0.010, 0.05, 1.15, 1.2, SURF_ID = 'ADIABATIC', PERMIT_HOLE = .FALSE. /
TSC 9
&OBST XB= 0.25,  0.3, -0.010, 0.05, 1.45, 1.5, SURF_ID = 'ADIABATIC', PERMIT_HOLE = .FALSE. / TSC
10
&OBST XB= -0.05,  0, -0.010, 0.05, 1.45, 1.5, SURF_ID = 'ADIABATIC', PERMIT_HOLE = .FALSE. / TSC
11
&OBST XB=-0.60, -0.55, -0.010, 0.05, 1.45, 1.5, SURF_ID = 'ADIABATIC', PERMIT_HOLE = .FALSE. /
TSC 12
&OBST XB= 0.55,  0.60, -0.010, 0.05, 1.75, 1.8, SURF_ID = 'ADIABATIC', PERMIT_HOLE = .FALSE. /
TSC 13
&OBST XB= 0,  0.05, -0.010, 0.05, 1.75, 1.8, SURF_ID = 'ADIABATIC', PERMIT_HOLE = .FALSE. / TSC
14
&OBST XB=-0.3, -0.25, -0.010, 0.05, 1.75, 1.8, SURF_ID = 'ADIABATIC', PERMIT_HOLE = .FALSE. / TSC
15
&OBST XB= 0.25,  0.3, -0.010, 0.05, 2.05, 2.1, SURF_ID = 'ADIABATIC', PERMIT_HOLE = .FALSE. / TSC
16
&OBST XB= -0.05,  0, -0.010, 0.05, 2.05, 2.1, SURF_ID = 'ADIABATIC', PERMIT_HOLE = .FALSE. / TSC
17
&OBST XB=-0.60, -0.55, -0.010, 0.05, 2.05, 2.1, SURF_ID = 'ADIABATIC', PERMIT_HOLE = .FALSE. /
TSC 18

&SLCF PBX = 0.0, QUANTITY = 'TEMPERATURE' /
&SLCF PBX = 0.0, QUANTITY = 'HRRPUV' /

&BNDF QUANTITY='GAUGE HEAT FLUX' /
&BNDF QUANTITY='RADIATIVE HEAT FLUX' /
&BNDF QUANTITY='CONVECTIVE HEAT FLUX' /
&BNDF QUANTITY='NET HEAT FLUX' /
&BNDF QUANTITY='WALL TEMPERATURE' /
&BNDF QUANTITY='BURNING RATE' /

CENTERLINE RAKE
&DEVC XYZ=0, 0.25, 0.45, QUANTITY='TEMPERATURE', ID='CTC_1' /
&DEVC XYZ=0, 0.25, 0.60, QUANTITY='TEMPERATURE', ID='BDTC_1' /
&DEVC XYZ=0, 0.25, 0.75, QUANTITY='TEMPERATURE', ID='CTC_2' /
&DEVC XYZ=0, 0.25, 0.90, QUANTITY='TEMPERATURE', ID='BDTC_2' /
&DEVC XYZ=0, 0.25, 1.05, QUANTITY='TEMPERATURE', ID='CTC_3' /
&DEVC XYZ=0, 0.25, 1.20, QUANTITY='TEMPERATURE', ID='BDTC_3' /
&DEVC XYZ=0, 0.25, 1.35, QUANTITY='TEMPERATURE', ID='CTC_4' /
&DEVC XYZ=0, 0.25, 1.50, QUANTITY='TEMPERATURE', ID='BDTC_4' /
&DEVC XYZ=0, 0.25, 1.65, QUANTITY='TEMPERATURE', ID='CTC_5' /
&DEVC XYZ=0, 0.25, 1.80, QUANTITY='TEMPERATURE', ID='BDTC_5' /
&DEVC XYZ=0, 0.25, 1.95, QUANTITY='TEMPERATURE', ID='CTC_6' /
&DEVC XYZ=0, 0.25, 2.10, QUANTITY='TEMPERATURE', ID='BDTC_6' /
&DEVC XYZ=0, 0.25, 2.25, QUANTITY='TEMPERATURE', ID='CTC_7' /
&DEVC XYZ=0, 0.25, 0.60, QUANTITY='W-VELOCITY', ID='BD_1' /
&DEVC XYZ=0, 0.25, 0.90, QUANTITY='W-VELOCITY', ID='BD_2' /
&DEVC XYZ=0, 0.25, 1.20, QUANTITY='W-VELOCITY', ID='BD_3' /
&DEVC XYZ=0, 0.25, 1.50, QUANTITY='W-VELOCITY', ID='BD_4' /
&DEVC XYZ=0, 0.25, 1.80, QUANTITY='W-VELOCITY', ID='BD_5' /
&DEVC XYZ=0, 0.25, 2.10, QUANTITY='W-VELOCITY', ID='BD_6' /
&DEVC XYZ=0, 0.25, 1.05, QUANTITY='W-VELOCITY', ID='BD_7' /
&DEVC XYZ=0, 0.25, 1.35, QUANTITY='W-VELOCITY', ID='BD_8' /
&DEVC XYZ=0, 0.25, 1.65, QUANTITY='W-VELOCITY', ID='BD_9' /
&DEVC XYZ=0, 0.25, 1.95, QUANTITY='W-VELOCITY', ID='BD_10' /

WALL TEMPERATURE
&DEVC XYZ=0.0762, 0.05, 0.75, QUANTITY='TEMPERATURE', ID='WTC_1' /
&DEVC XYZ=0.0508, 0.055, 0.75, QUANTITY='TEMPERATURE', ID='WTC_2' /
&DEVC XYZ=0.0254, 0.060, 0.75, QUANTITY='TEMPERATURE', ID='WTC_3' /
&DEVC XYZ=-0.0254, 0.065, 0.75, QUANTITY='TEMPERATURE', ID='WTC_4' /
&DEVC XYZ=-0.0508, 0.070, 0.75, QUANTITY='TEMPERATURE', ID='WTC_5' /
&DEVC XYZ=-0.0762, 0.075, 0.75, QUANTITY='TEMPERATURE', ID='WTC_6' /
&DEVC XYZ=0.0762, 0.085, 1.35, QUANTITY='TEMPERATURE', ID='WTC_7' /
&DEVC XYZ=0.0508, 0.080, 1.35, QUANTITY='TEMPERATURE', ID='WTC_8' /
&DEVC XYZ=0.0254, 0.075, 1.35, QUANTITY='TEMPERATURE', ID='WTC_9' /
&DEVC XYZ=-0.0254, 0.070, 1.35, QUANTITY='TEMPERATURE', ID='WTC_10' /
&DEVC XYZ=-0.0508, 0.065, 1.35, QUANTITY='TEMPERATURE', ID='WTC_11' /
&DEVC XYZ=-0.0762, 0.060, 1.35, QUANTITY='TEMPERATURE', ID='WTC_12' /
&DEVC XYZ=0.0762, 0.065, 1.95, QUANTITY='TEMPERATURE', ID='WTC_13' /
&DEVC XYZ=0.0508, 0.070, 1.95, QUANTITY='TEMPERATURE', ID='WTC_14' /
```

```
&DEVC XYZ=0.0254, 0.075, 1.95, QUANTITY='TEMPERATURE', ID='WTC_15' /
&DEVC XYZ=-0.0254, 0.080, 1.95, QUANTITY='TEMPERATURE', ID='WTC_16' /
&DEVC XYZ=-0.0508, 0.085, 1.95, QUANTITY='TEMPERATURE', ID='WTC_17' /
&DEVC XYZ=-0.0762, 0.090, 1.95, QUANTITY='TEMPERATURE', ID='WTC_18' /

WALL HEAT FLUX MEASUREMENTS
&DEVC XYZ=  0.575, 0.050, 0.575, QUANTITY='GAUGE_HEAT_FLUX', ID='TS_1',  IOR = 2 /
&DEVC XYZ=  0.025, 0.050, 0.575, QUANTITY='GAUGE_HEAT_FLUX', ID='TS_2',  IOR = 2 /
&DEVC XYZ= -0.275, 0.050, 0.575, QUANTITY='GAUGE_HEAT_FLUX', ID='TS_3',  IOR = 2 /
&DEVC XYZ=  0.275, 0.050, 0.875, QUANTITY='GAUGE_HEAT_FLUX', ID='TS_4',  IOR = 2 /
&DEVC XYZ=  -0.025, 0.050, 0.875, QUANTITY='GAUGE_HEAT_FLUX', ID='TS_5',  IOR = 2 /
&DEVC XYZ= -0.575, 0.050, 0.875, QUANTITY='GAUGE_HEAT_FLUX', ID='TS_6',  IOR = 2 /
&DEVC XYZ=  0.575, 0.050, 1.175, QUANTITY='GAUGE_HEAT_FLUX', ID='TS_7',  IOR = 2 /
&DEVC XYZ=  0.025 0.050, 1.175, QUANTITY='GAUGE_HEAT_FLUX', ID='TS_8',  IOR = 2 /
&DEVC XYZ= -0.275, 0.050, 1.175, QUANTITY='GAUGE_HEAT_FLUX', ID='TS_9',  IOR = 2 /
&DEVC XYZ=  0.275, 0.050, 1.475, QUANTITY='GAUGE_HEAT_FLUX', ID='TS_10', IOR = 2 /
&DEVC XYZ=  -0.025, 0.050, 1.475, QUANTITY='GAUGE_HEAT_FLUX', ID='TS_11', IOR = 2 /
&DEVC XYZ= -0.575, 0.050, 1.475, QUANTITY='GAUGE_HEAT_FLUX', ID='TS_12', IOR = 2 /
&DEVC XYZ=  0.575, 0.050, 1.775, QUANTITY='GAUGE_HEAT_FLUX', ID='TS_13', IOR = 2 /
&DEVC XYZ=  0.025, 0.050, 1.775, QUANTITY='GAUGE_HEAT_FLUX', ID='TS_14', IOR = 2 /
&DEVC XYZ= -0.275, 0.050, 1.775, QUANTITY='GAUGE_HEAT_FLUX', ID='TS_15', IOR = 2 /
&DEVC XYZ=  0.275, 0.050, 2.075, QUANTITY='GAUGE_HEAT_FLUX', ID='TS_16', IOR = 2 /
&DEVC XYZ=  -0.025, 0.050, 2.075, QUANTITY='GAUGE_HEAT_FLUX', ID='TS_17', IOR = 2 /
&DEVC XYZ= -0.575, 0.050, 2.075, QUANTITY='GAUGE_HEAT_FLUX', ID='TS_18', IOR = 2 /

&DEVC XYZ=  0.275, 0.050, 0.60, QUANTITY='GAUGE_HEAT_FLUX', ID='HFG_1', IOR = 2 /
&DEVC XYZ= -0.275, 0.050, 0.875, QUANTITY='GAUGE_HEAT_FLUX', ID='HFG_2', IOR = 2 /
&DEVC XYZ=  0.275, 0.050, 1.175, QUANTITY='GAUGE_HEAT_FLUX', ID='HFG_3', IOR = 2 /
&DEVC XYZ= -0.275, 0.050, 1.475, QUANTITY='GAUGE_HEAT_FLUX', ID='HFG_4', IOR = 2 /
&DEVC XYZ=  0.275, 0.050, 1.775, QUANTITY='GAUGE_HEAT_FLUX', ID='HFG_5', IOR = 2 /
&DEVC XYZ= -0.275, 0.050, 2.075, QUANTITY='GAUGE_HEAT_FLUX', ID='HFG_6', IOR = 2 /

WALL NET HEAT FLUX
&DEVC XYZ=  0.575, 0.050, 0.575, QUANTITY='NET HEAT FLUX', ID='TS_1',  IOR = 2 /
&DEVC XYZ=  0.025, 0.050, 0.575, QUANTITY='NET HEAT FLUX', ID='TS_2',  IOR = 2 /
&DEVC XYZ= -0.275, 0.050, 0.575, QUANTITY='NET HEAT FLUX', ID='TS_3',  IOR = 2 /
&DEVC XYZ=  0.275, 0.050, 0.875, QUANTITY='NET HEAT FLUX', ID='TS_4',  IOR = 2 /
&DEVC XYZ=  -0.025, 0.050, 0.875, QUANTITY='NET HEAT FLUX', ID='TS_5',  IOR = 2 /
&DEVC XYZ= -0.575, 0.050, 0.875, QUANTITY='NET HEAT FLUX', ID='TS_6',  IOR = 2 /
&DEVC XYZ=  0.575, 0.050, 1.175, QUANTITY='NET HEAT FLUX', ID='TS_7',  IOR = 2 /
&DEVC XYZ=  0.025 0.050, 1.175, QUANTITY='NET HEAT FLUX', ID='TS_8',  IOR = 2 /
&DEVC XYZ= -0.275, 0.050, 1.175, QUANTITY='NET HEAT FLUX', ID='TS_9',  IOR = 2 /
&DEVC XYZ=  0.275, 0.050, 1.475, QUANTITY='NET HEAT FLUX', ID='TS_10', IOR = 2 /
&DEVC XYZ=  -0.025, 0.050, 1.475, QUANTITY='NET HEAT FLUX', ID='TS_11', IOR = 2 /
&DEVC XYZ= -0.575, 0.050, 1.475, QUANTITY='NET HEAT FLUX', ID='TS_12', IOR = 2 /
&DEVC XYZ=  0.575, 0.050, 1.775, QUANTITY='NET HEAT FLUX', ID='TS_13', IOR = 2 /
&DEVC XYZ=  0.025, 0.050, 1.775, QUANTITY='NET HEAT FLUX', ID='TS_14', IOR = 2 /
&DEVC XYZ= -0.275, 0.050, 1.775, QUANTITY='NET HEAT FLUX', ID='TS_15', IOR = 2 /
```

J.6 Input File 6 – FRP scenario, Square burner, 50 kW, propylene

```
Start Input File
&HEAD CHID='56_1_03-14-2011_FRP_PP_sb_50kW' /

&TIME T_END = 900, DT = 0.05, RESTRICT_TIME_STEP = .FALSE. /
&DUMP DT_BNDF=2.0, DT_DEVC=0.5, DT_HRR=1.0, DT_PL3D=5000.0, DT_SLCF=2.0, DT_RESTART=50./

&MISC
      SURF_DEFAULT = 'INERT'
      TMPA  = 23
      FDS6  = .TRUE.
      DNS = .FALSE.
      DYNSMAG = .TRUE.
      CSMAG = 0.2
      PR = 0.5
      SC = 0.5
      H_EDDY = .TRUE.
      CFL_VELOCITY_NORM = 1
      FLUX_LIMITER = 2
      ISOTHERMAL = .FALSE.
      RADIATION = .TRUE.
      BAROCLINIC = .TRUE.
      CLIP_MASS_FRACTION   = .TRUE.
      CHECK_VN = .TRUE.
      NOBIAS = .TRUE.
      PROJECTION  = .FALSE.
      CHECK_KINETIC_ENERGY = .FALSE.
      /

&REAC
     ID = 'Propylene'
     C = 3
     H = 6
     O = 0
     CO_YIELD = 0.095
     SOOT_YIELD = 0.017
     EDDY_DISSIPATION = .TRUE.
     C_EDC = 0.1
     HRRPUA_SHEET = 0
     HRRPUV_AVERAGE = 2500
      /

&RADI
    RADIATIVE_FRACTION = 0.3
    TIME_STEP_INCREMENT = 3
    ANGLE_INCREMENT = 5
    NUMBER_RADIATION_ANGLES = 104
    /

**** MESHES ****
 MESH IJK= 96, 156, 96, XB=-1.20, 1.20, 0.00, 3.90, 0.00, 2.40 / 2.50 cm grid,  1 mesh

&MESH ID= 'Mesh-1', IJK= 24, 26, 24, XB= -1.2, 0, 0, 1.3, 0, 1.2 / 0.05 cm grid 12 mesh
&MESH ID= 'Mesh-2', IJK= 24, 26, 24, XB= -1.2, 0, 1.3, 2.6, 0, 1.2 / 0.05 cm grid 12 mesh
&MESH ID= 'Mesh-3', IJK= 24, 26, 24, XB= -1.2, 0, 2.6, 3.9, 0, 1.2 / 0.05 cm grid 12 mesh
&MESH ID= 'Mesh-4', IJK= 24, 26, 24, XB= 0, 1.2, 0, 1.3, 0, 1.2 / 0.05 cm grid 12 mesh
&MESH ID= 'Mesh-5', IJK= 24, 26, 24, XB= 0, 1.2, 1.3, 2.6, 0, 1.2 / 0.05 cm grid 12 mesh
&MESH ID= 'Mesh-6', IJK= 24, 26, 24, XB= 0, 1.2, 2.6, 3.9, 0, 1.2 / 0.05 cm grid 12 mesh
&MESH ID= 'Mesh-7', IJK= 24, 26, 24, XB= -1.2, 0, 0, 1.3, 1.2, 2.4 / 0.05 cm grid 12 mesh
&MESH ID= 'Mesh-8', IJK= 24, 26, 24, XB= -1.2, 0, 1.3, 2.6, 1.2, 2.4 / 0.05 cm grid 12 mesh
&MESH ID= 'Mesh-9', IJK= 24, 26, 24, XB= -1.2, 0, 2.6, 3.9, 1.2, 2.4 / 0.05 cm grid 12 mesh
&MESH ID= 'Mesh-10', IJK= 24, 26, 24, XB= 0, 1.2, 0, 1.3, 1.2, 2.4 / 0.05 cm grid 12 mesh
&MESH ID= 'Mesh-11', IJK= 24, 26, 24, XB= 0, 1.2, 1.3, 2.6, 1.2, 2.4 / 0.05 cm grid 12 mesh
&MESH ID= 'Mesh-12', IJK= 24, 26, 24, XB= 0, 1.2, 2.6, 3.9, 1.2, 2.4 / 0.05 cm grid 12 mesh

****BURNER****
2 ft burner
OBST XB= -0.35, 0.35, 0.05, 0.45, 0, 0.4, SURF_ID = 'ADIABATIC' /
VENT XB= -0.3, 0.3, 0.1, 0.4, 0.4, 0.4, SURF_ID = 'BURNER' /
```

```
1 ft burner
&OBST XB= -0.2, 0.2, 0.05, 0.45, 0, 0.4, SURF_ID = 'ADIABATIC' /
&VENT XB= -0.15, 0.15, 0.1, 0.4, 0.4, 0.4, SURF_ID = 'BURNER' /

**** Burner Parameters*****
&SURF ID = 'BURNER'
      HRRPUA =555.6
      RAMP_Q = 'Burner_Ramp'
      COLOR  = 'RED' /

&RAMP ID = 'Burner_Ramp', T=0, F=0 /
&RAMP ID = 'Burner_Ramp', T=1, F=0.5 /
&RAMP ID = 'Burner_Ramp', T=15, F=1 /
&RAMP ID = 'Burner_Ramp', T=55, F=1 /
&RAMP ID = 'Burner_Ramp', T=65, F=0 /

**** MATERIAL PROPERTIES ****
&MATL ID            ='GYPSUM_MATL'
      SPECIFIC_HEAT = 0.84
      CONDUCTIVITY  = 0.48
      DENSITY       = 1440.0 /

&MATL ID            ='KAOWOOL_MATL'
      SPECIFIC_HEAT = 1.0
      CONDUCTIVITY  = 0.06
      DENSITY       = 320.0 /

&SURF ID        = 'ADIABATIC'
      ADIABATIC = .TRUE.
      RGB       = 0, 0, 0 /

&SURF ID                     = 'KAOWOOL'
      RGB                    = 51,102,255
      BACKING                = 'INSULATED'
      MATL_ID(1,1)           = 'KAOWOOL_MATL'
      MATL_MASS_FRACTION(1,1)= 1.0
      THICKNESS(1)           = 0.025
      CELL_SIZE_FACTOR       = 0.30
      STRETCH_FACTOR         = 1.0 /

&SURF ID                     = 'GYPSUM'
      RGB                    = 100,100,100
      BACKING                = 'INSULATED'
      MATL_ID(1,1)           = 'GYPSUM_MATL'
      MATL_MASS_FRACTION(1,1)= 1.0
      THICKNESS(1)           = 0.016
      CELL_SIZE_FACTOR       = 0.30
      STRETCH_FACTOR         = 1.0 /

&MATL ID                       = 'virgin'
      CONDUCTIVITY             =  0.480
      DENSITY                  = 1467.80
      SPECIFIC_HEAT            =    1.98
      EMISSIVITY               =  0.858
      ABSORPTION_COEFFICIENT   =  0.9000E+10
      RESIDUE(01)              = 'char'
      A(01)                    = 0.1139E+12
      E(01)                    = 0.1483E+06
      N_S(01)                  =   1.00
      THRESHOLD_TEMPERATURE(01)=   0.00
      HEAT_OF_REACTION(01)     =   996.67
      HEAT_OF_COMBUSTION       = 19700.
      NU_FUEL(01)              =   0.421
      NU_RESIDUE(01)           =   0.579
      NU_WATER(01)             =   0.000
      N_REACTIONS              = 01 /

&MATL ID                       = 'char'
      CONDUCTIVITY             =  0.050
      DENSITY                  =  850.56
      SPECIFIC_HEAT            =    2.12
```

```
      EMISSIVITY               =  0.943
      ABSORPTION_COEFFICIENT   =  0.9000E+10
      N_REACTIONS              = 00 /

&SURF ID                         = 'FRP'
      STRETCH_FACTOR             = 1.000
      CELL_SIZE_FACTOR           = 0.200
      THICKNESS(1)              = 0.0019
      MATL_ID(1,1)             = 'virgin'
      MATL_ID(1,2)             = 'char'
      MATL_MASS_FRACTION(1,1)  = 1.0000
      MATL_MASS_FRACTION(1,2)  = 0.0000
      BACKING                    = 'INSULATED'
      SHRINK                     = .TRUE.
      TMP_INNER                  = 27.0
      COLOR                      = 'WHITE' /


****OBSTRUCTIONS****
&OBST XB=-1.200, 1.200, 0.000, 0.000, 0.000, 2.400, SURF_ID ='GYPSUM'  / Back wall
&OBST XB= 1.200, 1.200, 0.000, 2.700, 0.000, 2.400, SURF_ID ='GYPSUM'  / Right wall
&OBST XB=-1.200,-1.200, 0.000, 2.700, 0.000, 2.400, SURF_ID ='GYPSUM'  / Left wall
&OBST XB=-1.200, 1.200, 0.000, 2.700, 2.400, 2.400, SURF_ID ='GYPSUM'  / Ceiling
&OBST XB=-0.900,-0.600, 0.000, 0.05, 0.000, 2.400, SURF_ID ='KAOWOOL' / Kaowool on back wall
&OBST XB= 0.600, 0.900, 0.000, 0.05, 0.000, 2.400, SURF_ID ='KAOWOOL' / Kaowool on back wall
&OBST XB=-0.600, 0.600, 0.000, 0.05, 0.000, 2.400, SURF_ID ='FRP', PERMIT_HOLE = .TRUE. / FRP
panel

****OPEN VENTS****
&VENT XB=-1.20, 1.20, 3.90, 3.90, 0.00, 2.40, SURF_ID = 'OPEN' / Back
&VENT XB=-1.20,-1.20, 2.70, 3.90, 0.00, 2.40, SURF_ID = 'OPEN' /
&VENT XB= 1.20, 1.20, 2.70, 3.90, 0.00, 2.40, SURF_ID = 'OPEN' /
&VENT XB=-1.20, 1.20, 2.70, 3.90, 2.40, 2.40, SURF_ID = 'OPEN' /

HOLES in panel for TSC's:
&HOLE XB= 0.55,  0.60, -0.010, 0.1, 0.55, 0.60 / HOLE 1
&HOLE XB= 0,  0.05, -0.010, 0.1, 0.55, 0.60 / HOLE 2
&HOLE XB= -0.3, -0.25, -0.010, 0.1, 0.55, 0.60 / HOLE 3
&HOLE XB= 0.25,  0.3, -0.010, 0.1, 0.85, 0.9 / HOLE 4
&HOLE XB= -0.05,  0, -0.010, 0.1, 0.85, 0.9 / HOLE 5
&HOLE XB= -0.60, -0.55, -0.010, 0.1, 0.85, 0.9 / HOLE 6
&HOLE XB= 0.55,  0.60, -0.010, 0.1, 1.15, 1.2 / HOLE 7
&HOLE XB= 0, 0.05, -0.010, 0.1, 1.15, 1.2 / HOLE 8
&HOLE XB= -0.3, -0.25, -0.010, 0.1, 1.15, 1.2 / HOLE 9
&HOLE XB= 0.25,  0.3, -0.010, 0.1, 1.45, 1.5 / HOLE 10
&HOLE XB= -0.05,  0, -0.010, 0.1, 1.45, 1.5 / HOLE 11
&HOLE XB=-0.60, -0.55, -0.010, 0.1, 1.45, 1.5 / HOLE 12
&HOLE XB= 0.55,  0.60, -0.010, 0.1, 1.75, 1.8 / HOLE 13
&HOLE XB= 0,  0.05, -0.010, 0.1, 1.75, 1.8 / HOLE 14
&HOLE XB=-0.3, -0.25, -0.010, 0.1, 1.75, 1.8 / HOLE 15
&HOLE XB= 0.25,  0.3, -0.010, 0.1, 2.05, 2.1 / HOLE 16
&HOLE XB= -0.05,  0, -0.010, 0.1, 2.05, 2.1 / HOLE 17
&HOLE XB=-0.60, -0.55, -0.010, 0.1, 2.05, 2.1 / HOLE 18

TSC'S:

&OBST XB= 0.55,  0.60, -0.010, 0.05, 0.55, 0.60, SURF_ID = 'ADIABATIC', PERMIT_HOLE = .FALSE. /
TSC 1
&OBST XB= 0,  0.05, -0.010, 0.05, 0.55, 0.60, SURF_ID = 'ADIABATIC', PERMIT_HOLE = .FALSE. / TSC
2
&OBST XB= -0.3, -0.25, -0.010, 0.05, 0.55, 0.60, SURF_ID = 'ADIABATIC', PERMIT_HOLE = .FALSE. /
TSC 3
&OBST XB= 0.25,  0.3, -0.010, 0.05, 0.85, 0.9, SURF_ID = 'ADIABATIC', PERMIT_HOLE = .FALSE. / TSC
4
&OBST XB= -0.05,  0, -0.010, 0.05, 0.85, 0.9, SURF_ID = 'ADIABATIC', PERMIT_HOLE = .FALSE. / TSC
5
&OBST XB= -0.60, -0.55, -0.010, 0.05, 0.85, 0.9, SURF_ID = 'ADIABATIC', PERMIT_HOLE = .FALSE. /
TSC 6
&OBST XB= 0.55,  0.60, -0.010, 0.05, 1.15, 1.2, SURF_ID = 'ADIABATIC', PERMIT_HOLE = .FALSE. /
TSC 7
&OBST XB= 0, 0.05, -0.010, 0.05, 1.15, 1.2, SURF_ID = 'ADIABATIC', PERMIT_HOLE = .FALSE. / TSC 8
```

```
&OBST XB= -0.3, -0.25, -0.010, 0.05, 1.15, 1.2, SURF_ID = 'ADIABATIC', PERMIT_HOLE = .FALSE. /
TSC 9
&OBST XB= 0.25,  0.3, -0.010, 0.05, 1.45, 1.5, SURF_ID = 'ADIABATIC', PERMIT_HOLE = .FALSE. / TSC
10
&OBST XB= -0.05,  0, -0.010, 0.05, 1.45, 1.5, SURF_ID = 'ADIABATIC', PERMIT_HOLE = .FALSE. / TSC
11
&OBST XB=-0.60, -0.55, -0.010, 0.05, 1.45, 1.5, SURF_ID = 'ADIABATIC', PERMIT_HOLE = .FALSE. /
TSC 12
&OBST XB= 0.55,  0.60, -0.010, 0.05, 1.75, 1.8, SURF_ID = 'ADIABATIC', PERMIT_HOLE = .FALSE. /
TSC 13
&OBST XB= 0,  0.05, -0.010, 0.05, 1.75, 1.8, SURF_ID = 'ADIABATIC', PERMIT_HOLE = .FALSE. / TSC
14
&OBST XB=-0.3, -0.25, -0.010, 0.05, 1.75, 1.8, SURF_ID = 'ADIABATIC', PERMIT_HOLE = .FALSE. / TSC
15
&OBST XB= 0.25,  0.3, -0.010, 0.05, 2.05, 2.1, SURF_ID = 'ADIABATIC', PERMIT_HOLE = .FALSE. / TSC
16
&OBST XB= -0.05,  0, -0.010, 0.05, 2.05, 2.1, SURF_ID = 'ADIABATIC', PERMIT_HOLE = .FALSE. / TSC
17
&OBST XB=-0.60, -0.55, -0.010, 0.05, 2.05, 2.1, SURF_ID = 'ADIABATIC', PERMIT_HOLE = .FALSE. /
TSC 18

&SLCF PBX = 0.0, QUANTITY = 'TEMPERATURE' /
&SLCF PBX = 0.0, QUANTITY = 'HRRPUV' /

&BNDF QUANTITY='GAUGE HEAT FLUX' /
&BNDF QUANTITY='RADIATIVE HEAT FLUX' /
&BNDF QUANTITY='CONVECTIVE HEAT FLUX' /
&BNDF QUANTITY='NET HEAT FLUX' /
&BNDF QUANTITY='WALL TEMPERATURE' /
&BNDF QUANTITY='BURNING RATE' /

CENTERLINE RAKE
&DEVC XYZ=0, 0.25, 0.45, QUANTITY='TEMPERATURE', ID='CTC_1' /
&DEVC XYZ=0, 0.25, 0.60, QUANTITY='TEMPERATURE', ID='BDTC_1' /
&DEVC XYZ=0, 0.25, 0.75, QUANTITY='TEMPERATURE', ID='CTC_2' /
&DEVC XYZ=0, 0.25, 0.90, QUANTITY='TEMPERATURE', ID='BDTC_2' /
&DEVC XYZ=0, 0.25, 1.05, QUANTITY='TEMPERATURE', ID='CTC_3' /
&DEVC XYZ=0, 0.25, 1.20, QUANTITY='TEMPERATURE', ID='BDTC_3' /
&DEVC XYZ=0, 0.25, 1.35, QUANTITY='TEMPERATURE', ID='CTC_4' /
&DEVC XYZ=0, 0.25, 1.50, QUANTITY='TEMPERATURE', ID='BDTC_4' /
&DEVC XYZ=0, 0.25, 1.65, QUANTITY='TEMPERATURE', ID='CTC_5' /
&DEVC XYZ=0, 0.25, 1.80, QUANTITY='TEMPERATURE', ID='BDTC_5' /
&DEVC XYZ=0, 0.25, 1.95, QUANTITY='TEMPERATURE', ID='CTC_6' /
&DEVC XYZ=0, 0.25, 2.10, QUANTITY='TEMPERATURE', ID='BDTC_6' /
&DEVC XYZ=0, 0.25, 2.25, QUANTITY='TEMPERATURE', ID='CTC_7' /
&DEVC XYZ=0, 0.25, 0.60, QUANTITY='W-VELOCITY', ID='BD_1' /
&DEVC XYZ=0, 0.25, 0.90, QUANTITY='W-VELOCITY', ID='BD_2' /
&DEVC XYZ=0, 0.25, 1.20, QUANTITY='W-VELOCITY', ID='BD_3' /
&DEVC XYZ=0, 0.25, 1.50, QUANTITY='W-VELOCITY', ID='BD_4' /
&DEVC XYZ=0, 0.25, 1.80, QUANTITY='W-VELOCITY', ID='BD_5' /
&DEVC XYZ=0, 0.25, 2.10, QUANTITY='W-VELOCITY', ID='BD_6' /
&DEVC XYZ=0, 0.25, 1.05, QUANTITY='W-VELOCITY', ID='BD_7' /
&DEVC XYZ=0, 0.25, 1.35, QUANTITY='W-VELOCITY', ID='BD_8' /
&DEVC XYZ=0, 0.25, 1.65, QUANTITY='W-VELOCITY', ID='BD_9' /
&DEVC XYZ=0, 0.25, 1.95, QUANTITY='W-VELOCITY', ID='BD_10' /

WALL TEMPERATURE
&DEVC XYZ=0.0762, 0.05, 0.75, QUANTITY='TEMPERATURE', ID='WTC_1' /
&DEVC XYZ=0.0508, 0.055, 0.75, QUANTITY='TEMPERATURE', ID='WTC_2' /
&DEVC XYZ=0.0254, 0.060, 0.75, QUANTITY='TEMPERATURE', ID='WTC_3' /
&DEVC XYZ=-0.0254, 0.065, 0.75, QUANTITY='TEMPERATURE', ID='WTC_4' /
&DEVC XYZ=-0.0508, 0.070, 0.75, QUANTITY='TEMPERATURE', ID='WTC_5' /
&DEVC XYZ=-0.0762, 0.075, 0.75, QUANTITY='TEMPERATURE', ID='WTC_6' /
&DEVC XYZ=0.0762, 0.085, 1.35, QUANTITY='TEMPERATURE', ID='WTC_7' /
&DEVC XYZ=0.0508, 0.080, 1.35, QUANTITY='TEMPERATURE', ID='WTC_8' /
&DEVC XYZ=0.0254, 0.075, 1.35, QUANTITY='TEMPERATURE', ID='WTC_9' /
&DEVC XYZ=-0.0254, 0.070, 1.35, QUANTITY='TEMPERATURE', ID='WTC_10' /
&DEVC XYZ=-0.0508, 0.065, 1.35, QUANTITY='TEMPERATURE', ID='WTC_11' /
&DEVC XYZ=-0.0762, 0.060, 1.35, QUANTITY='TEMPERATURE', ID='WTC_12' /
&DEVC XYZ=0.0762, 0.065, 1.95, QUANTITY='TEMPERATURE', ID='WTC_13' /
&DEVC XYZ=0.0508, 0.070, 1.95, QUANTITY='TEMPERATURE', ID='WTC_14' /
```

```
&DEVC XYZ=0.0254, 0.075, 1.95, QUANTITY='TEMPERATURE', ID='WTC_15' /
&DEVC XYZ=-0.0254, 0.080, 1.95, QUANTITY='TEMPERATURE', ID='WTC_16' /
&DEVC XYZ=-0.0508, 0.085, 1.95, QUANTITY='TEMPERATURE', ID='WTC_17' /
&DEVC XYZ=-0.0762, 0.090, 1.95, QUANTITY='TEMPERATURE', ID='WTC_18' /

WALL HEAT FLUX MEASUREMENTS
&DEVC XYZ=  0.575, 0.050, 0.575, QUANTITY='GAUGE_HEAT_FLUX', ID='TS_1',  IOR = 2 /
&DEVC XYZ=  0.025, 0.050, 0.575, QUANTITY='GAUGE_HEAT_FLUX', ID='TS_2',  IOR = 2 /
&DEVC XYZ= -0.275, 0.050, 0.575, QUANTITY='GAUGE_HEAT_FLUX', ID='TS_3',  IOR = 2 /
&DEVC XYZ=  0.275, 0.050, 0.875, QUANTITY='GAUGE_HEAT_FLUX', ID='TS_4',  IOR = 2 /
&DEVC XYZ=  -0.025, 0.050, 0.875, QUANTITY='GAUGE_HEAT_FLUX', ID='TS_5',  IOR = 2 /
&DEVC XYZ= -0.575, 0.050, 0.875, QUANTITY='GAUGE_HEAT_FLUX', ID='TS_6',  IOR = 2 /
&DEVC XYZ=  0.575, 0.050, 1.175, QUANTITY='GAUGE_HEAT_FLUX', ID='TS_7',  IOR = 2 /
&DEVC XYZ=  0.025 0.050, 1.175, QUANTITY='GAUGE_HEAT_FLUX', ID='TS_8',  IOR = 2 /
&DEVC XYZ= -0.275, 0.050, 1.175, QUANTITY='GAUGE_HEAT_FLUX', ID='TS_9',  IOR = 2 /
&DEVC XYZ=  0.275, 0.050, 1.475, QUANTITY='GAUGE_HEAT_FLUX', ID='TS_10', IOR = 2 /
&DEVC XYZ=  -0.025, 0.050, 1.475, QUANTITY='GAUGE_HEAT_FLUX', ID='TS_11', IOR = 2 /
&DEVC XYZ= -0.575, 0.050, 1.475, QUANTITY='GAUGE_HEAT_FLUX', ID='TS_12', IOR = 2 /
&DEVC XYZ=  0.575, 0.050, 1.775, QUANTITY='GAUGE_HEAT_FLUX', ID='TS_13', IOR = 2 /
&DEVC XYZ=  0.025, 0.050, 1.775, QUANTITY='GAUGE_HEAT_FLUX', ID='TS_14', IOR = 2 /
&DEVC XYZ= -0.275, 0.050, 1.775, QUANTITY='GAUGE_HEAT_FLUX', ID='TS_15', IOR = 2 /
&DEVC XYZ=  0.275, 0.050, 2.075, QUANTITY='GAUGE_HEAT_FLUX', ID='TS_16', IOR = 2 /
&DEVC XYZ=  -0.025, 0.050, 2.075, QUANTITY='GAUGE_HEAT_FLUX', ID='TS_17', IOR = 2 /
&DEVC XYZ= -0.575, 0.050, 2.075, QUANTITY='GAUGE_HEAT_FLUX', ID='TS_18', IOR = 2 /

&DEVC XYZ=  0.275, 0.050, 0.60, QUANTITY='GAUGE_HEAT_FLUX', ID='HFG_1', IOR = 2 /
&DEVC XYZ= -0.275, 0.050, 0.875, QUANTITY='GAUGE_HEAT_FLUX', ID='HFG_2', IOR = 2 /
&DEVC XYZ=  0.275, 0.050, 1.175, QUANTITY='GAUGE_HEAT_FLUX', ID='HFG_3', IOR = 2 /
&DEVC XYZ= -0.275, 0.050, 1.475, QUANTITY='GAUGE_HEAT_FLUX', ID='HFG_4', IOR = 2 /
&DEVC XYZ=  0.275, 0.050, 1.775, QUANTITY='GAUGE_HEAT_FLUX', ID='HFG_5', IOR = 2 /
&DEVC XYZ= -0.275, 0.050, 2.075, QUANTITY='GAUGE_HEAT_FLUX', ID='HFG_6', IOR = 2 /

WALL NET HEAT FLUX
&DEVC XYZ=  0.575, 0.050, 0.575, QUANTITY='NET HEAT FLUX', ID='TS_1',  IOR = 2 /
&DEVC XYZ=  0.025, 0.050, 0.575, QUANTITY='NET HEAT FLUX', ID='TS_2',  IOR = 2 /
&DEVC XYZ= -0.275, 0.050, 0.575, QUANTITY='NET HEAT FLUX', ID='TS_3',  IOR = 2 /
&DEVC XYZ=  0.275, 0.050, 0.875, QUANTITY='NET HEAT FLUX', ID='TS_4',  IOR = 2 /
&DEVC XYZ=  -0.025, 0.050, 0.875, QUANTITY='NET HEAT FLUX', ID='TS_5',  IOR = 2 /
&DEVC XYZ= -0.575, 0.050, 0.875, QUANTITY='NET HEAT FLUX', ID='TS_6',  IOR = 2 /
&DEVC XYZ=  0.575, 0.050, 1.175, QUANTITY='NET HEAT FLUX', ID='TS_7',  IOR = 2 /
&DEVC XYZ=  0.025 0.050, 1.175, QUANTITY='NET HEAT FLUX', ID='TS_8',  IOR = 2 /
&DEVC XYZ= -0.275, 0.050, 1.175, QUANTITY='NET HEAT FLUX', ID='TS_9',  IOR = 2 /
&DEVC XYZ=  0.275, 0.050, 1.475, QUANTITY='NET HEAT FLUX', ID='TS_10', IOR = 2 /
&DEVC XYZ=  -0.025, 0.050, 1.475, QUANTITY='NET HEAT FLUX', ID='TS_11', IOR = 2 /
&DEVC XYZ= -0.575, 0.050, 1.475, QUANTITY='NET HEAT FLUX', ID='TS_12', IOR = 2 /
&DEVC XYZ=  0.575, 0.050, 1.775, QUANTITY='NET HEAT FLUX', ID='TS_13', IOR = 2 /
&DEVC XYZ=  0.025, 0.050, 1.775, QUANTITY='NET HEAT FLUX', ID='TS_14', IOR = 2 /
&DEVC XYZ= -0.275, 0.050, 1.775, QUANTITY='NET HEAT FLUX', ID='TS_15', IOR = 2 /
```

J.7 Input File 7 – FRP scenario, Square burner, 75 kW, propylene

```
Start Input File
&HEAD CHID='57_1_03-14-2011_FRP_PP_sb_75kW' /

&TIME T_END = 900, DT = 0.05, RESTRICT_TIME_STEP = .FALSE. /
&DUMP DT_BNDF=2.0, DT_DEVC=0.5, DT_HRR=1.0, DT_PL3D=5000.0, DT_SLCF=2.0, DT_RESTART=50./

&MISC
      SURF_DEFAULT = 'INERT'
      TMPA  = 23
      FDS6  = .TRUE.
      DNS = .FALSE.
      DYNSMAG = .TRUE.
      CSMAG = 0.2
      PR = 0.5
      SC = 0.5
      H_EDDY = .TRUE.
      CFL_VELOCITY_NORM = 1
      FLUX_LIMITER = 2
      ISOTHERMAL = .FALSE.
      RADIATION = .TRUE.
      BAROCLINIC = .TRUE.
      CLIP_MASS_FRACTION   = .TRUE.
      CHECK_VN = .TRUE.
      NOBIAS = .TRUE.
      PROJECTION  = .FALSE.
      CHECK_KINETIC_ENERGY = .FALSE.
      /

&REAC
     ID = 'Propylene'
     C = 3
     H = 6
     O = 0
     CO_YIELD = 0.095
     SOOT_YIELD = 0.017
     EDDY_DISSIPATION = .TRUE.
     C_EDC = 0.1
     HRRPUA_SHEET = 0
     HRRPUV_AVERAGE = 2500
      /

&RADI
    RADIATIVE_FRACTION = 0.3
    TIME_STEP_INCREMENT = 3
    ANGLE_INCREMENT = 5
    NUMBER_RADIATION_ANGLES = 104
    /

**** MESHES ****
 MESH IJK= 96, 156, 96, XB=-1.20, 1.20, 0.00, 3.90, 0.00, 2.40 / 2.50 cm grid,  1 mesh

&MESH ID= 'Mesh-1', IJK= 24, 26, 24, XB= -1.2, 0, 0, 1.3, 0, 1.2 / 0.05 cm grid 12 mesh
&MESH ID= 'Mesh-2', IJK= 24, 26, 24, XB= -1.2, 0, 1.3, 2.6, 0, 1.2 / 0.05 cm grid 12 mesh
&MESH ID= 'Mesh-3', IJK= 24, 26, 24, XB= -1.2, 0, 2.6, 3.9, 0, 1.2 / 0.05 cm grid 12 mesh
&MESH ID= 'Mesh-4', IJK= 24, 26, 24, XB= 0, 1.2, 0, 1.3, 0, 1.2 / 0.05 cm grid 12 mesh
&MESH ID= 'Mesh-5', IJK= 24, 26, 24, XB= 0, 1.2, 1.3, 2.6, 0, 1.2 / 0.05 cm grid 12 mesh
&MESH ID= 'Mesh-6', IJK= 24, 26, 24, XB= 0, 1.2, 2.6, 3.9, 0, 1.2 / 0.05 cm grid 12 mesh
&MESH ID= 'Mesh-7', IJK= 24, 26, 24, XB= -1.2, 0, 0, 1.3, 1.2, 2.4 / 0.05 cm grid 12 mesh
&MESH ID= 'Mesh-8', IJK= 24, 26, 24, XB= -1.2, 0, 1.3, 2.6, 1.2, 2.4 / 0.05 cm grid 12 mesh
&MESH ID= 'Mesh-9', IJK= 24, 26, 24, XB= -1.2, 0, 2.6, 3.9, 1.2, 2.4 / 0.05 cm grid 12 mesh
&MESH ID= 'Mesh-10', IJK= 24, 26, 24, XB= 0, 1.2, 0, 1.3, 1.2, 2.4 / 0.05 cm grid 12 mesh
&MESH ID= 'Mesh-11', IJK= 24, 26, 24, XB= 0, 1.2, 1.3, 2.6, 1.2, 2.4 / 0.05 cm grid 12 mesh
&MESH ID= 'Mesh-12', IJK= 24, 26, 24, XB= 0, 1.2, 2.6, 3.9, 1.2, 2.4 / 0.05 cm grid 12 mesh

****BURNER****
2 ft burner
OBST XB= -0.35, 0.35, 0.05, 0.45, 0, 0.4, SURF_ID = 'ADIABATIC' /
VENT XB= -0.3, 0.3, 0.1, 0.4, 0.4, 0.4, SURF_ID = 'BURNER' /
```

```
1 ft burner
&OBST XB= -0.2, 0.2, 0.05, 0.45, 0, 0.4, SURF_ID = 'ADIABATIC' /
&VENT XB= -0.15, 0.15, 0.1, 0.4, 0.4, 0.4, SURF_ID = 'BURNER' /

**** Burner Parameters*****
&SURF ID = 'BURNER'
      HRRPUA =833.3
      RAMP_Q = 'Burner_Ramp'
      COLOR  = 'RED' /

&RAMP ID = 'Burner_Ramp', T=0, F=0 /
&RAMP ID = 'Burner_Ramp', T=1, F=0.5 /
&RAMP ID = 'Burner_Ramp', T=15, F=1 /
&RAMP ID = 'Burner_Ramp', T=50, F=1 /
&RAMP ID = 'Burner_Ramp', T=60, F=0 /

**** MATERIAL PROPERTIES ****
&MATL ID            ='GYPSUM_MATL'
      SPECIFIC_HEAT = 0.84
      CONDUCTIVITY  = 0.48
      DENSITY       = 1440.0 /

&MATL ID            ='KAOWOOL_MATL'
      SPECIFIC_HEAT = 1.0
      CONDUCTIVITY  = 0.06
      DENSITY       = 320.0 /

&SURF ID        = 'ADIABATIC'
      ADIABATIC = .TRUE.
      RGB       = 0, 0, 0 /

&SURF ID                       = 'KAOWOOL'
      RGB                      = 51,102,255
      BACKING                  = 'INSULATED'
      MATL_ID(1,1)             = 'KAOWOOL_MATL'
      MATL_MASS_FRACTION(1,1)= 1.0
      THICKNESS(1)             = 0.025
      CELL_SIZE_FACTOR         = 0.30
      STRETCH_FACTOR           = 1.0 /

&SURF ID                       = 'GYPSUM'
      RGB                      = 100,100,100
      BACKING                  = 'INSULATED'
      MATL_ID(1,1)             = 'GYPSUM_MATL'
      MATL_MASS_FRACTION(1,1)= 1.0
      THICKNESS(1)             = 0.016
      CELL_SIZE_FACTOR         = 0.30
      STRETCH_FACTOR           = 1.0 /

&MATL ID                         = 'virgin'
      CONDUCTIVITY               =  0.480
      DENSITY                    = 1467.80
      SPECIFIC_HEAT              =    1.98
      EMISSIVITY                 =  0.858
      ABSORPTION_COEFFICIENT     =  0.9000E+10
      RESIDUE(01)                = 'char'
      A(01)                      = 0.1139E+12
      E(01)                      = 0.1483E+06
      N_S(01)                    =   1.00
      THRESHOLD_TEMPERATURE(01)=   0.00
      HEAT_OF_REACTION(01)       =   996.67
      HEAT_OF_COMBUSTION         = 19700.
      NU_FUEL(01)                =   0.421
      NU_RESIDUE(01)             =   0.579
      NU_WATER(01)               =   0.000
      N_REACTIONS                = 01 /

&MATL ID                         = 'char'
      CONDUCTIVITY               =  0.050
      DENSITY                    =  850.56
      SPECIFIC_HEAT              =    2.12
```

```
      EMISSIVITY                = 0.943
      ABSORPTION_COEFFICIENT    = 0.9000E+10
      N_REACTIONS               = 00 /

&SURF ID                          = 'FRP'
      STRETCH_FACTOR              = 1.000
      CELL_SIZE_FACTOR            = 0.200
      THICKNESS(1)               = 0.0019
      MATL_ID(1,1)              = 'virgin'
      MATL_ID(1,2)              = 'char'
      MATL_MASS_FRACTION(1,1)   = 1.0000
      MATL_MASS_FRACTION(1,2)   = 0.0000
      BACKING                     = 'INSULATED'
      SHRINK                      = .TRUE.
      TMP_INNER                   = 27.0
      COLOR                       = 'WHITE' /


****OBSTRUCTIONS****
&OBST XB=-1.200, 1.200, 0.000, 0.000, 0.000, 2.400, SURF_ID ='GYPSUM'  / Back wall
&OBST XB= 1.200, 1.200, 0.000, 2.700, 0.000, 2.400, SURF_ID ='GYPSUM'  / Right wall
&OBST XB=-1.200,-1.200, 0.000, 2.700, 0.000, 2.400, SURF_ID ='GYPSUM'  / Left wall
&OBST XB=-1.200, 1.200, 0.000, 2.700, 2.400, 2.400, SURF_ID ='GYPSUM'  / Ceiling
&OBST XB=-0.900,-0.600, 0.000, 0.05, 0.000, 2.400, SURF_ID ='KAOWOOL' / Kaowool on back wall
&OBST XB= 0.600, 0.900, 0.000, 0.05, 0.000, 2.400, SURF_ID ='KAOWOOL' / Kaowool on back wall
&OBST XB=-0.600, 0.600, 0.000, 0.05, 0.000, 2.400, SURF_ID ='FRP', PERMIT_HOLE = .TRUE. / FRP
panel

****OPEN VENTS****
&VENT XB=-1.20, 1.20, 3.90, 3.90, 0.00, 2.40, SURF_ID = 'OPEN' / Back
&VENT XB=-1.20,-1.20, 2.70, 3.90, 0.00, 2.40, SURF_ID = 'OPEN' /
&VENT XB= 1.20, 1.20, 2.70, 3.90, 0.00, 2.40, SURF_ID = 'OPEN' /
&VENT XB=-1.20, 1.20, 2.70, 3.90, 2.40, 2.40, SURF_ID = 'OPEN' /

HOLES in panel for TSC's:
&HOLE XB= 0.55,  0.60, -0.010, 0.1, 0.55, 0.60 / HOLE 1
&HOLE XB= 0,  0.05, -0.010, 0.1, 0.55, 0.60 / HOLE 2
&HOLE XB= -0.3, -0.25, -0.010, 0.1, 0.55, 0.60 / HOLE 3
&HOLE XB= 0.25,  0.3, -0.010, 0.1, 0.85, 0.9 / HOLE 4
&HOLE XB= -0.05,  0, -0.010, 0.1, 0.85, 0.9 / HOLE 5
&HOLE XB= -0.60, -0.55, -0.010, 0.1, 0.85, 0.9 / HOLE 6
&HOLE XB= 0.55,  0.60, -0.010, 0.1, 1.15, 1.2 / HOLE 7
&HOLE XB= 0, 0.05, -0.010, 0.1, 1.15, 1.2 / HOLE 8
&HOLE XB= -0.3, -0.25, -0.010, 0.1, 1.15, 1.2 / HOLE 9
&HOLE XB= 0.25,  0.3, -0.010, 0.1, 1.45, 1.5 / HOLE 10
&HOLE XB= -0.05,  0, -0.010, 0.1, 1.45, 1.5 / HOLE 11
&HOLE XB=-0.60, -0.55, -0.010, 0.1, 1.45, 1.5 / HOLE 12
&HOLE XB= 0.55,  0.60, -0.010, 0.1, 1.75, 1.8 / HOLE 13
&HOLE XB= 0,  0.05, -0.010, 0.1, 1.75, 1.8 / HOLE 14
&HOLE XB=-0.3, -0.25, -0.010, 0.1, 1.75, 1.8 / HOLE 15
&HOLE XB= 0.25,  0.3, -0.010, 0.1, 2.05, 2.1 / HOLE 16
&HOLE XB= -0.05,  0, -0.010, 0.1, 2.05, 2.1 / HOLE 17
&HOLE XB=-0.60, -0.55, -0.010, 0.1, 2.05, 2.1 / HOLE 18

TSC'S:

&OBST XB= 0.55,  0.60, -0.010, 0.05, 0.55, 0.60, SURF_ID = 'ADIABATIC', PERMIT_HOLE = .FALSE. /
TSC 1
&OBST XB= 0,  0.05, -0.010, 0.05, 0.55, 0.60, SURF_ID = 'ADIABATIC', PERMIT_HOLE = .FALSE. / TSC
2
&OBST XB= -0.3, -0.25, -0.010, 0.05, 0.55, 0.60, SURF_ID = 'ADIABATIC', PERMIT_HOLE = .FALSE. /
TSC 3
&OBST XB= 0.25,  0.3, -0.010, 0.05, 0.85, 0.9, SURF_ID = 'ADIABATIC', PERMIT_HOLE = .FALSE. / TSC
4
&OBST XB= -0.05,  0, -0.010, 0.05, 0.85, 0.9, SURF_ID = 'ADIABATIC', PERMIT_HOLE = .FALSE. / TSC
5
&OBST XB= -0.60, -0.55, -0.010, 0.05, 0.85, 0.9, SURF_ID = 'ADIABATIC', PERMIT_HOLE = .FALSE. /
TSC 6
&OBST XB= 0.55,  0.60, -0.010, 0.05, 1.15, 1.2, SURF_ID = 'ADIABATIC', PERMIT_HOLE = .FALSE. /
TSC 7
&OBST XB= 0, 0.05, -0.010, 0.05, 1.15, 1.2, SURF_ID = 'ADIABATIC', PERMIT_HOLE = .FALSE. / TSC 8
```

```
&OBST XB= -0.3, -0.25, -0.010, 0.05, 1.15, 1.2, SURF_ID = 'ADIABATIC', PERMIT_HOLE = .FALSE. /
TSC 9
&OBST XB= 0.25,  0.3, -0.010, 0.05, 1.45, 1.5, SURF_ID = 'ADIABATIC', PERMIT_HOLE = .FALSE. / TSC
10
&OBST XB= -0.05,  0, -0.010, 0.05, 1.45, 1.5, SURF_ID = 'ADIABATIC', PERMIT_HOLE = .FALSE. / TSC
11
&OBST XB=-0.60, -0.55, -0.010, 0.05, 1.45, 1.5, SURF_ID = 'ADIABATIC', PERMIT_HOLE = .FALSE. /
TSC 12
&OBST XB= 0.55,  0.60, -0.010, 0.05, 1.75, 1.8, SURF_ID = 'ADIABATIC', PERMIT_HOLE = .FALSE. /
TSC 13
&OBST XB= 0,  0.05, -0.010, 0.05, 1.75, 1.8, SURF_ID = 'ADIABATIC', PERMIT_HOLE = .FALSE. / TSC
14
&OBST XB=-0.3, -0.25, -0.010, 0.05, 1.75, 1.8, SURF_ID = 'ADIABATIC', PERMIT_HOLE = .FALSE. / TSC
15
&OBST XB= 0.25,  0.3, -0.010, 0.05, 2.05, 2.1, SURF_ID = 'ADIABATIC', PERMIT_HOLE = .FALSE. / TSC
16
&OBST XB= -0.05,  0, -0.010, 0.05, 2.05, 2.1, SURF_ID = 'ADIABATIC', PERMIT_HOLE = .FALSE. / TSC
17
&OBST XB=-0.60, -0.55, -0.010, 0.05, 2.05, 2.1, SURF_ID = 'ADIABATIC', PERMIT_HOLE = .FALSE. /
TSC 18

&SLCF PBX = 0.0, QUANTITY = 'TEMPERATURE' /
&SLCF PBX = 0.0, QUANTITY = 'HRRPUV' /

&BNDF QUANTITY='GAUGE HEAT FLUX' /
&BNDF QUANTITY='RADIATIVE HEAT FLUX' /
&BNDF QUANTITY='CONVECTIVE HEAT FLUX' /
&BNDF QUANTITY='NET HEAT FLUX' /
&BNDF QUANTITY='WALL TEMPERATURE' /
&BNDF QUANTITY='BURNING RATE' /

CENTERLINE RAKE
&DEVC XYZ=0, 0.25, 0.45, QUANTITY='TEMPERATURE', ID='CTC_1' /
&DEVC XYZ=0, 0.25, 0.60, QUANTITY='TEMPERATURE', ID='BDTC_1' /
&DEVC XYZ=0, 0.25, 0.75, QUANTITY='TEMPERATURE', ID='CTC_2' /
&DEVC XYZ=0, 0.25, 0.90, QUANTITY='TEMPERATURE', ID='BDTC_2' /
&DEVC XYZ=0, 0.25, 1.05, QUANTITY='TEMPERATURE', ID='CTC_3' /
&DEVC XYZ=0, 0.25, 1.20, QUANTITY='TEMPERATURE', ID='BDTC_3' /
&DEVC XYZ=0, 0.25, 1.35, QUANTITY='TEMPERATURE', ID='CTC_4' /
&DEVC XYZ=0, 0.25, 1.50, QUANTITY='TEMPERATURE', ID='BDTC_4' /
&DEVC XYZ=0, 0.25, 1.65, QUANTITY='TEMPERATURE', ID='CTC_5' /
&DEVC XYZ=0, 0.25, 1.80, QUANTITY='TEMPERATURE', ID='BDTC_5' /
&DEVC XYZ=0, 0.25, 1.95, QUANTITY='TEMPERATURE', ID='CTC_6' /
&DEVC XYZ=0, 0.25, 2.10, QUANTITY='TEMPERATURE', ID='BDTC_6' /
&DEVC XYZ=0, 0.25, 2.25, QUANTITY='TEMPERATURE', ID='CTC_7' /
&DEVC XYZ=0, 0.25, 0.60, QUANTITY='W-VELOCITY', ID='BD_1' /
&DEVC XYZ=0, 0.25, 0.90, QUANTITY='W-VELOCITY', ID='BD_2' /
&DEVC XYZ=0, 0.25, 1.20, QUANTITY='W-VELOCITY', ID='BD_3' /
&DEVC XYZ=0, 0.25, 1.50, QUANTITY='W-VELOCITY', ID='BD_4' /
&DEVC XYZ=0, 0.25, 1.80, QUANTITY='W-VELOCITY', ID='BD_5' /
&DEVC XYZ=0, 0.25, 2.10, QUANTITY='W-VELOCITY', ID='BD_6' /
&DEVC XYZ=0, 0.25, 1.05, QUANTITY='W-VELOCITY', ID='BD_7' /
&DEVC XYZ=0, 0.25, 1.35, QUANTITY='W-VELOCITY', ID='BD_8' /
&DEVC XYZ=0, 0.25, 1.65, QUANTITY='W-VELOCITY', ID='BD_9' /
&DEVC XYZ=0, 0.25, 1.95, QUANTITY='W-VELOCITY', ID='BD_10' /

WALL TEMPERATURE
&DEVC XYZ=0.0762, 0.05, 0.75, QUANTITY='TEMPERATURE', ID='WTC_1' /
&DEVC XYZ=0.0508, 0.055, 0.75, QUANTITY='TEMPERATURE', ID='WTC_2' /
&DEVC XYZ=0.0254, 0.060, 0.75, QUANTITY='TEMPERATURE', ID='WTC_3' /
&DEVC XYZ=-0.0254, 0.065, 0.75, QUANTITY='TEMPERATURE', ID='WTC_4' /
&DEVC XYZ=-0.0508, 0.070, 0.75, QUANTITY='TEMPERATURE', ID='WTC_5' /
&DEVC XYZ=-0.0762, 0.075, 0.75, QUANTITY='TEMPERATURE', ID='WTC_6' /
&DEVC XYZ=0.0762, 0.085, 1.35, QUANTITY='TEMPERATURE', ID='WTC_7' /
&DEVC XYZ=0.0508, 0.080, 1.35, QUANTITY='TEMPERATURE', ID='WTC_8' /
&DEVC XYZ=0.0254, 0.075, 1.35, QUANTITY='TEMPERATURE', ID='WTC_9' /
&DEVC XYZ=-0.0254, 0.070, 1.35, QUANTITY='TEMPERATURE', ID='WTC_10' /
&DEVC XYZ=-0.0508, 0.065, 1.35, QUANTITY='TEMPERATURE', ID='WTC_11' /
&DEVC XYZ=-0.0762, 0.060, 1.35, QUANTITY='TEMPERATURE', ID='WTC_12' /
&DEVC XYZ=0.0762, 0.065, 1.95, QUANTITY='TEMPERATURE', ID='WTC_13' /
&DEVC XYZ=0.0508, 0.070, 1.95, QUANTITY='TEMPERATURE', ID='WTC_14' /
```

```
&DEVC XYZ=0.0254, 0.075, 1.95, QUANTITY='TEMPERATURE', ID='WTC_15' /
&DEVC XYZ=-0.0254, 0.080, 1.95, QUANTITY='TEMPERATURE', ID='WTC_16' /
&DEVC XYZ=-0.0508, 0.085, 1.95, QUANTITY='TEMPERATURE', ID='WTC_17' /
&DEVC XYZ=-0.0762, 0.090, 1.95, QUANTITY='TEMPERATURE', ID='WTC_18' /

WALL HEAT FLUX MEASUREMENTS
&DEVC XYZ=  0.575, 0.050, 0.575, QUANTITY='GAUGE_HEAT_FLUX', ID='TS_1',  IOR = 2 /
&DEVC XYZ=  0.025, 0.050, 0.575, QUANTITY='GAUGE_HEAT_FLUX', ID='TS_2',  IOR = 2 /
&DEVC XYZ= -0.275, 0.050, 0.575, QUANTITY='GAUGE_HEAT_FLUX', ID='TS_3',  IOR = 2 /
&DEVC XYZ=  0.275, 0.050, 0.875, QUANTITY='GAUGE_HEAT_FLUX', ID='TS_4',  IOR = 2 /
&DEVC XYZ=  -0.025, 0.050, 0.875, QUANTITY='GAUGE_HEAT_FLUX', ID='TS_5',  IOR = 2 /
&DEVC XYZ= -0.575, 0.050, 0.875, QUANTITY='GAUGE_HEAT_FLUX', ID='TS_6',  IOR = 2 /
&DEVC XYZ=  0.575, 0.050, 1.175, QUANTITY='GAUGE_HEAT_FLUX', ID='TS_7',  IOR = 2 /
&DEVC XYZ=  0.025 0.050, 1.175, QUANTITY='GAUGE_HEAT_FLUX', ID='TS_8',  IOR = 2 /
&DEVC XYZ= -0.275, 0.050, 1.175, QUANTITY='GAUGE_HEAT_FLUX', ID='TS_9',  IOR = 2 /
&DEVC XYZ=  0.275, 0.050, 1.475, QUANTITY='GAUGE_HEAT_FLUX', ID='TS_10', IOR = 2 /
&DEVC XYZ=  -0.025, 0.050, 1.475, QUANTITY='GAUGE_HEAT_FLUX', ID='TS_11', IOR = 2 /
&DEVC XYZ= -0.575, 0.050, 1.475, QUANTITY='GAUGE_HEAT_FLUX', ID='TS_12', IOR = 2 /
&DEVC XYZ=  0.575, 0.050, 1.775, QUANTITY='GAUGE_HEAT_FLUX', ID='TS_13', IOR = 2 /
&DEVC XYZ=  0.025, 0.050, 1.775, QUANTITY='GAUGE_HEAT_FLUX', ID='TS_14', IOR = 2 /
&DEVC XYZ= -0.275, 0.050, 1.775, QUANTITY='GAUGE_HEAT_FLUX', ID='TS_15', IOR = 2 /
&DEVC XYZ=  0.275, 0.050, 2.075, QUANTITY='GAUGE_HEAT_FLUX', ID='TS_16', IOR = 2 /
&DEVC XYZ=  -0.025, 0.050, 2.075, QUANTITY='GAUGE_HEAT_FLUX', ID='TS_17', IOR = 2 /
&DEVC XYZ= -0.575, 0.050, 2.075, QUANTITY='GAUGE_HEAT_FLUX', ID='TS_18', IOR = 2 /

&DEVC XYZ=  0.275, 0.050, 0.60, QUANTITY='GAUGE_HEAT_FLUX', ID='HFG_1', IOR = 2 /
&DEVC XYZ= -0.275, 0.050, 0.875, QUANTITY='GAUGE_HEAT_FLUX', ID='HFG_2', IOR = 2 /
&DEVC XYZ=  0.275, 0.050, 1.175, QUANTITY='GAUGE_HEAT_FLUX', ID='HFG_3', IOR = 2 /
&DEVC XYZ= -0.275, 0.050, 1.475, QUANTITY='GAUGE_HEAT_FLUX', ID='HFG_4', IOR = 2 /
&DEVC XYZ=  0.275, 0.050, 1.775, QUANTITY='GAUGE_HEAT_FLUX', ID='HFG_5', IOR = 2 /
&DEVC XYZ= -0.275, 0.050, 2.075, QUANTITY='GAUGE_HEAT_FLUX', ID='HFG_6', IOR = 2 /

WALL NET HEAT FLUX
&DEVC XYZ=  0.575, 0.050, 0.575, QUANTITY='NET HEAT FLUX', ID='TS_1',  IOR = 2 /
&DEVC XYZ=  0.025, 0.050, 0.575, QUANTITY='NET HEAT FLUX', ID='TS_2',  IOR = 2 /
&DEVC XYZ= -0.275, 0.050, 0.575, QUANTITY='NET HEAT FLUX', ID='TS_3',  IOR = 2 /
&DEVC XYZ=  0.275, 0.050, 0.875, QUANTITY='NET HEAT FLUX', ID='TS_4',  IOR = 2 /
&DEVC XYZ=  -0.025, 0.050, 0.875, QUANTITY='NET HEAT FLUX', ID='TS_5',  IOR = 2 /
&DEVC XYZ= -0.575, 0.050, 0.875, QUANTITY='NET HEAT FLUX', ID='TS_6',  IOR = 2 /
&DEVC XYZ=  0.575, 0.050, 1.175, QUANTITY='NET HEAT FLUX', ID='TS_7',  IOR = 2 /
&DEVC XYZ=  0.025 0.050, 1.175, QUANTITY='NET HEAT FLUX', ID='TS_8',  IOR = 2 /
&DEVC XYZ= -0.275, 0.050, 1.175, QUANTITY='NET HEAT FLUX', ID='TS_9',  IOR = 2 /
&DEVC XYZ=  0.275, 0.050, 1.475, QUANTITY='NET HEAT FLUX', ID='TS_10', IOR = 2 /
&DEVC XYZ=  -0.025, 0.050, 1.475, QUANTITY='NET HEAT FLUX', ID='TS_11', IOR = 2 /
&DEVC XYZ= -0.575, 0.050, 1.475, QUANTITY='NET HEAT FLUX', ID='TS_12', IOR = 2 /
&DEVC XYZ=  0.575, 0.050, 1.775, QUANTITY='NET HEAT FLUX', ID='TS_13', IOR = 2 /
&DEVC XYZ=  0.025, 0.050, 1.775, QUANTITY='NET HEAT FLUX', ID='TS_14', IOR = 2 /
&DEVC XYZ= -0.275, 0.050, 1.775, QUANTITY='NET HEAT FLUX', ID='TS_15', IOR = 2 /
```

J.8 Input File 8 – FRP scenario, Rectangle burner, 50 kW, propylene

General Comments

```
Start Input File
&HEAD CHID='58_1_03-14-2011_FRP_PP_lb_50kW' /

&TIME T_END = 900, DT = 0.05, RESTRICT_TIME_STEP = .FALSE. /
&DUMP DT_BNDF=2.0, DT_DEVC=0.5, DT_HRR=1.0, DT_PL3D=5000.0, DT_SLCF=2.0, DT_RESTART=50./

&MISC
      SURF_DEFAULT = 'INERT'
      TMPA  = 23
      FDS6  = .TRUE.
      DNS = .FALSE.
      DYNSMAG = .TRUE.
      CSMAG = 0.2
      PR = 0.5
      SC = 0.5
      H_EDDY = .TRUE.
      CFL_VELOCITY_NORM = 1
      FLUX_LIMITER = 2
      ISOTHERMAL = .FALSE.
      RADIATION = .TRUE.
      BAROCLINIC = .TRUE.
      CLIP_MASS_FRACTION   = .TRUE.
      CHECK_VN = .TRUE.
      NOBIAS = .TRUE.
      PROJECTION  = .FALSE.
      CHECK_KINETIC_ENERGY = .FALSE.
      /

&REAC
     ID = 'Propylene'
     C = 3
     H = 6
     O = 0
     CO_YIELD = 0.095
     SOOT_YIELD = 0.017
     EDDY_DISSIPATION = .TRUE.
     C_EDC = 0.1
     HRRPUA_SHEET = 0
     HRRPUV_AVERAGE = 2500
      /

&RADI
    RADIATIVE_FRACTION = 0.3
    TIME_STEP_INCREMENT = 3
    ANGLE_INCREMENT = 5
    NUMBER_RADIATION_ANGLES = 104
    /

**** MESHES ****
 MESH IJK= 96, 156, 96, XB=-1.20, 1.20, 0.00, 3.90, 0.00, 2.40 / 2.50 cm grid,  1 mesh

&MESH ID= 'Mesh-1', IJK= 24, 26, 24, XB= -1.2, 0, 0, 1.3, 0, 1.2 / 0.05 cm grid 12 mesh
&MESH ID= 'Mesh-2', IJK= 24, 26, 24, XB= -1.2, 0, 1.3, 2.6, 0, 1.2 / 0.05 cm grid 12 mesh
&MESH ID= 'Mesh-3', IJK= 24, 26, 24, XB= -1.2, 0, 2.6, 3.9, 0, 1.2 / 0.05 cm grid 12 mesh
&MESH ID= 'Mesh-4', IJK= 24, 26, 24, XB= 0, 1.2, 0, 1.3, 0, 1.2 / 0.05 cm grid 12 mesh
&MESH ID= 'Mesh-5', IJK= 24, 26, 24, XB= 0, 1.2, 1.3, 2.6, 0, 1.2 / 0.05 cm grid 12 mesh
&MESH ID= 'Mesh-6', IJK= 24, 26, 24, XB= 0, 1.2, 2.6, 3.9, 0, 1.2 / 0.05 cm grid 12 mesh
&MESH ID= 'Mesh-7', IJK= 24, 26, 24, XB= -1.2, 0, 0, 1.3, 1.2, 2.4 / 0.05 cm grid 12 mesh
&MESH ID= 'Mesh-8', IJK= 24, 26, 24, XB= -1.2, 0, 1.3, 2.6, 1.2, 2.4 / 0.05 cm grid 12 mesh
&MESH ID= 'Mesh-9', IJK= 24, 26, 24, XB= -1.2, 0, 2.6, 3.9, 1.2, 2.4 / 0.05 cm grid 12 mesh
&MESH ID= 'Mesh-10', IJK= 24, 26, 24, XB= 0, 1.2, 0, 1.3, 1.2, 2.4 / 0.05 cm grid 12 mesh
```

```
&MESH ID= 'Mesh-11', IJK= 24, 26, 24, XB= 0, 1.2, 1.3, 2.6, 1.2, 2.4 / 0.05 cm grid 12 mesh
&MESH ID= 'Mesh-12', IJK= 24, 26, 24, XB= 0, 1.2, 2.6, 3.9, 1.2, 2.4 / 0.05 cm grid 12 mesh

****BURNER****
2 ft burner
&OBST XB= -0.35, 0.35, 0.05, 0.45, 0, 0.4, SURF_ID = 'ADIABATIC' /
&VENT XB= -0.3, 0.3, 0.1, 0.4, 0.4, 0.4, SURF_ID = 'BURNER' /

1 ft burner
OBST XB= -0.2, 0.2, 0.05, 0.45, 0, 0.4, SURF_ID = 'ADIABATIC' /
VENT XB= -0.15, 0.15, 0.1, 0.4, 0.4, 0.4, SURF_ID = 'BURNER' /

**** Burner Parameters*****
&SURF ID = 'BURNER'
      HRRPUA =277.8
      RAMP_Q = 'Burner_Ramp'
      COLOR  = 'RED' /

&RAMP ID = 'Burner_Ramp', T=0, F=0 /
&RAMP ID = 'Burner_Ramp', T=1, F=0.5 /
&RAMP ID = 'Burner_Ramp', T=12, F=1 /
&RAMP ID = 'Burner_Ramp', T=58, F=1 /
&RAMP ID = 'Burner_Ramp', T=68, F=0 /

**** MATERIAL PROPERTIES ****
&MATL ID            ='GYPSUM_MATL'
      SPECIFIC_HEAT = 0.84
      CONDUCTIVITY  = 0.48
      DENSITY       = 1440.0 /

&MATL ID            ='KAOWOOL_MATL'
      SPECIFIC_HEAT = 1.0
      CONDUCTIVITY  = 0.06
      DENSITY       = 320.0 /

&SURF ID        = 'ADIABATIC'
      ADIABATIC = .TRUE.
      RGB       = 0, 0, 0 /

&SURF ID                     = 'KAOWOOL'
      RGB                    = 51,102,255
      BACKING                = 'INSULATED'
      MATL_ID(1,1)           = 'KAOWOOL_MATL'
      MATL_MASS_FRACTION(1,1)= 1.0
      THICKNESS(1)           = 0.025
      CELL_SIZE_FACTOR       = 0.30
      STRETCH_FACTOR         = 1.0 /

&SURF ID                     = 'GYPSUM'
      RGB                    = 100,100,100
      BACKING                = 'INSULATED'
      MATL_ID(1,1)           = 'GYPSUM_MATL'
      MATL_MASS_FRACTION(1,1)= 1.0
      THICKNESS(1)           = 0.016
      CELL_SIZE_FACTOR       = 0.30
      STRETCH_FACTOR         = 1.0 /

&MATL ID                       = 'virgin'
      CONDUCTIVITY             =  0.480
      DENSITY                  = 1467.80
      SPECIFIC_HEAT            =    1.98
      EMISSIVITY               =  0.858
      ABSORPTION_COEFFICIENT   =  0.9000E+10
      RESIDUE(01)              = 'char'
      A(01)                    = 0.1139E+12
      E(01)                    = 0.1483E+06
      N_S(01)                  =   1.00
      THRESHOLD_TEMPERATURE(01)=   0.00
      HEAT_OF_REACTION(01)     =   996.67
      HEAT_OF_COMBUSTION       = 19700.
      NU_FUEL(01)              =   0.421
```

```
      NU_RESIDUE(01)           =   0.579
      NU_WATER(01)             =   0.000
      N_REACTIONS              = 01 /

&MATL ID                       = 'char'
      CONDUCTIVITY             =  0.050
      DENSITY                  =  850.56
      SPECIFIC_HEAT            =    2.12
      EMISSIVITY               =  0.943
      ABSORPTION_COEFFICIENT   =  0.9000E+10
      N_REACTIONS              = 00 /

&SURF ID                         = 'FRP'
      STRETCH_FACTOR             = 1.000
      CELL_SIZE_FACTOR           = 0.200
      THICKNESS(1)              = 0.0019
      MATL_ID(1,1)             = 'virgin'
      MATL_ID(1,2)             = 'char'
      MATL_MASS_FRACTION(1,1)  = 1.0000
      MATL_MASS_FRACTION(1,2)  = 0.0000
      BACKING                    = 'INSULATED'
      SHRINK                     = .TRUE.
      TMP_INNER                  = 27.0
      COLOR                      = 'WHITE' /


****OBSTRUCTIONS****
&OBST XB=-1.200, 1.200, 0.000, 0.000, 0.000, 2.400, SURF_ID ='GYPSUM'  / Back wall
&OBST XB= 1.200, 1.200, 0.000, 2.700, 0.000, 2.400, SURF_ID ='GYPSUM'  / Right wall
&OBST XB=-1.200,-1.200, 0.000, 2.700, 0.000, 2.400, SURF_ID ='GYPSUM'  / Left wall
&OBST XB=-1.200, 1.200, 0.000, 2.700, 2.400, 2.400, SURF_ID ='GYPSUM'  / Ceiling
&OBST XB=-0.900,-0.600, 0.000, 0.05, 0.000, 2.400, SURF_ID ='KAOWOOL' / Kaowool on back wall
&OBST XB= 0.600, 0.900, 0.000, 0.05, 0.000, 2.400, SURF_ID ='KAOWOOL' / Kaowool on back wall
&OBST XB=-0.600, 0.600, 0.000, 0.05, 0.000, 2.400, SURF_ID ='FRP', PERMIT_HOLE = .TRUE. / FRP
panel

****OPEN VENTS****
&VENT XB=-1.20, 1.20, 3.90, 3.90, 0.00, 2.40, SURF_ID = 'OPEN' / Back
&VENT XB=-1.20,-1.20, 2.70, 3.90, 0.00, 2.40, SURF_ID = 'OPEN' /
&VENT XB= 1.20, 1.20, 2.70, 3.90, 0.00, 2.40, SURF_ID = 'OPEN' /
&VENT XB=-1.20, 1.20, 2.70, 3.90, 2.40, 2.40, SURF_ID = 'OPEN' /

HOLES in panel for TSC's:
&HOLE XB= 0.55,  0.60, -0.010, 0.1, 0.55, 0.60 / HOLE 1
&HOLE XB= 0,  0.05, -0.010, 0.1, 0.55, 0.60 / HOLE 2
&HOLE XB= -0.3, -0.25, -0.010, 0.1, 0.55, 0.60 / HOLE 3
&HOLE XB= 0.25,  0.3, -0.010, 0.1, 0.85, 0.9 / HOLE 4
&HOLE XB= -0.05,  0, -0.010, 0.1, 0.85, 0.9 / HOLE 5
&HOLE XB= -0.60, -0.55, -0.010, 0.1, 0.85, 0.9 / HOLE 6
&HOLE XB= 0.55,  0.60, -0.010, 0.1, 1.15, 1.2 / HOLE 7
&HOLE XB= 0, 0.05, -0.010, 0.1, 1.15, 1.2 / HOLE 8
&HOLE XB= -0.3, -0.25, -0.010, 0.1, 1.15, 1.2 / HOLE 9
&HOLE XB= 0.25,  0.3, -0.010, 0.1, 1.45, 1.5 / HOLE 10
&HOLE XB= -0.05,  0, -0.010, 0.1, 1.45, 1.5 / HOLE 11
&HOLE XB=-0.60, -0.55, -0.010, 0.1, 1.45, 1.5 / HOLE 12
&HOLE XB= 0.55,  0.60, -0.010, 0.1, 1.75, 1.8 / HOLE 13
&HOLE XB= 0,  0.05, -0.010, 0.1, 1.75, 1.8 / HOLE 14
&HOLE XB=-0.3, -0.25, -0.010, 0.1, 1.75, 1.8 / HOLE 15
&HOLE XB= 0.25,  0.3, -0.010, 0.1, 2.05, 2.1 / HOLE 16
&HOLE XB= -0.05,  0, -0.010, 0.1, 2.05, 2.1 / HOLE 17
&HOLE XB=-0.60, -0.55, -0.010, 0.1, 2.05, 2.1 / HOLE 18

TSC'S:

&OBST XB= 0.55,  0.60, -0.010, 0.05, 0.55, 0.60, SURF_ID = 'ADIABATIC', PERMIT_HOLE = .FALSE. /
TSC 1
&OBST XB= 0,  0.05, -0.010, 0.05, 0.55, 0.60, SURF_ID = 'ADIABATIC', PERMIT_HOLE = .FALSE. / TSC
2
&OBST XB= -0.3, -0.25, -0.010, 0.05, 0.55, 0.60, SURF_ID = 'ADIABATIC', PERMIT_HOLE = .FALSE. /
TSC 3
```

```
&OBST XB= 0.25,  0.3, -0.010, 0.05, 0.85, 0.9, SURF_ID = 'ADIABATIC', PERMIT_HOLE = .FALSE. / TSC
4
&OBST XB= -0.05,  0, -0.010, 0.05, 0.85, 0.9, SURF_ID = 'ADIABATIC', PERMIT_HOLE = .FALSE. / TSC
5
&OBST XB= -0.60, -0.55, -0.010, 0.05, 0.85, 0.9, SURF_ID = 'ADIABATIC', PERMIT_HOLE = .FALSE. /
TSC 6
&OBST XB= 0.55,  0.60, -0.010, 0.05, 1.15, 1.2, SURF_ID = 'ADIABATIC', PERMIT_HOLE = .FALSE. /
TSC 7
&OBST XB= 0, 0.05, -0.010, 0.05, 1.15, 1.2, SURF_ID = 'ADIABATIC', PERMIT_HOLE = .FALSE. / TSC 8
&OBST XB= -0.3, -0.25, -0.010, 0.05, 1.15, 1.2, SURF_ID = 'ADIABATIC', PERMIT_HOLE = .FALSE. /
TSC 9
&OBST XB= 0.25,  0.3, -0.010, 0.05, 1.45, 1.5, SURF_ID = 'ADIABATIC', PERMIT_HOLE = .FALSE. / TSC
10
&OBST XB= -0.05,  0, -0.010, 0.05, 1.45, 1.5, SURF_ID = 'ADIABATIC', PERMIT_HOLE = .FALSE. / TSC
11
&OBST XB=-0.60, -0.55, -0.010, 0.05, 1.45, 1.5, SURF_ID = 'ADIABATIC', PERMIT_HOLE = .FALSE. /
TSC 12
&OBST XB= 0.55,  0.60, -0.010, 0.05, 1.75, 1.8, SURF_ID = 'ADIABATIC', PERMIT_HOLE = .FALSE. /
TSC 13
&OBST XB= 0,  0.05, -0.010, 0.05, 1.75, 1.8, SURF_ID = 'ADIABATIC', PERMIT_HOLE = .FALSE. / TSC
14
&OBST XB=-0.3, -0.25, -0.010, 0.05, 1.75, 1.8, SURF_ID = 'ADIABATIC', PERMIT_HOLE = .FALSE. / TSC
15
&OBST XB= 0.25,  0.3, -0.010, 0.05, 2.05, 2.1, SURF_ID = 'ADIABATIC', PERMIT_HOLE = .FALSE. / TSC
16
&OBST XB= -0.05,  0, -0.010, 0.05, 2.05, 2.1, SURF_ID = 'ADIABATIC', PERMIT_HOLE = .FALSE. / TSC
17
&OBST XB=-0.60, -0.55, -0.010, 0.05, 2.05, 2.1, SURF_ID = 'ADIABATIC', PERMIT_HOLE = .FALSE. /
TSC 18

&SLCF PBX = 0.0, QUANTITY = 'TEMPERATURE' /
&SLCF PBX = 0.0, QUANTITY = 'HRRPUV' /

&BNDF QUANTITY='GAUGE HEAT FLUX' /
&BNDF QUANTITY='RADIATIVE HEAT FLUX' /
&BNDF QUANTITY='CONVECTIVE HEAT FLUX' /
&BNDF QUANTITY='NET HEAT FLUX' /
&BNDF QUANTITY='WALL TEMPERATURE' /
&BNDF QUANTITY='BURNING RATE' /

CENTERLINE RAKE
&DEVC XYZ=0, 0.25, 0.45, QUANTITY='TEMPERATURE', ID='CTC_1' /
&DEVC XYZ=0, 0.25, 0.60, QUANTITY='TEMPERATURE', ID='BDTC_1' /
&DEVC XYZ=0, 0.25, 0.75, QUANTITY='TEMPERATURE', ID='CTC_2' /
&DEVC XYZ=0, 0.25, 0.90, QUANTITY='TEMPERATURE', ID='BDTC_2' /
&DEVC XYZ=0, 0.25, 1.05, QUANTITY='TEMPERATURE', ID='CTC_3' /
&DEVC XYZ=0, 0.25, 1.20, QUANTITY='TEMPERATURE', ID='BDTC_3' /
&DEVC XYZ=0, 0.25, 1.35, QUANTITY='TEMPERATURE', ID='CTC_4' /
&DEVC XYZ=0, 0.25, 1.50, QUANTITY='TEMPERATURE', ID='BDTC_4' /
&DEVC XYZ=0, 0.25, 1.65, QUANTITY='TEMPERATURE', ID='CTC_5' /
&DEVC XYZ=0, 0.25, 1.80, QUANTITY='TEMPERATURE', ID='BDTC_5' /
&DEVC XYZ=0, 0.25, 1.95, QUANTITY='TEMPERATURE', ID='CTC_6' /
&DEVC XYZ=0, 0.25, 2.10, QUANTITY='TEMPERATURE', ID='BDTC_6' /
&DEVC XYZ=0, 0.25, 2.25, QUANTITY='TEMPERATURE', ID='CTC_7' /
&DEVC XYZ=0, 0.25, 0.60, QUANTITY='W-VELOCITY', ID='BD_1' /
&DEVC XYZ=0, 0.25, 0.90, QUANTITY='W-VELOCITY', ID='BD_2' /
&DEVC XYZ=0, 0.25, 1.20, QUANTITY='W-VELOCITY', ID='BD_3' /
&DEVC XYZ=0, 0.25, 1.50, QUANTITY='W-VELOCITY', ID='BD_4' /
&DEVC XYZ=0, 0.25, 1.80, QUANTITY='W-VELOCITY', ID='BD_5' /
&DEVC XYZ=0, 0.25, 2.10, QUANTITY='W-VELOCITY', ID='BD_6' /
&DEVC XYZ=0, 0.25, 1.05, QUANTITY='W-VELOCITY', ID='BD_7' /
&DEVC XYZ=0, 0.25, 1.35, QUANTITY='W-VELOCITY', ID='BD_8' /
&DEVC XYZ=0, 0.25, 1.65, QUANTITY='W-VELOCITY', ID='BD_9' /
&DEVC XYZ=0, 0.25, 1.95, QUANTITY='W-VELOCITY', ID='BD_10' /

WALL TEMPERATURE
&DEVC XYZ=0.0762, 0.05, 0.75, QUANTITY='TEMPERATURE', ID='WTC_1' /
&DEVC XYZ=0.0508, 0.055, 0.75, QUANTITY='TEMPERATURE', ID='WTC_2' /
&DEVC XYZ=0.0254, 0.060, 0.75, QUANTITY='TEMPERATURE', ID='WTC_3' /
&DEVC XYZ=-0.0254, 0.065, 0.75, QUANTITY='TEMPERATURE', ID='WTC_4' /
&DEVC XYZ=-0.0508, 0.070, 0.75, QUANTITY='TEMPERATURE', ID='WTC_5' /
```

```
&DEVC XYZ=-0.0762, 0.075, 0.75, QUANTITY='TEMPERATURE', ID='WTC_6' /
&DEVC XYZ=0.0762, 0.085, 1.35, QUANTITY='TEMPERATURE', ID='WTC_7' /
&DEVC XYZ=0.0508, 0.080, 1.35, QUANTITY='TEMPERATURE', ID='WTC_8' /
&DEVC XYZ=0.0254, 0.075, 1.35, QUANTITY='TEMPERATURE', ID='WTC_9' /
&DEVC XYZ=-0.0254, 0.070, 1.35, QUANTITY='TEMPERATURE', ID='WTC_10' /
&DEVC XYZ=-0.0508, 0.065, 1.35, QUANTITY='TEMPERATURE', ID='WTC_11' /
&DEVC XYZ=-0.0762, 0.060, 1.35, QUANTITY='TEMPERATURE', ID='WTC_12' /
&DEVC XYZ=0.0762, 0.065, 1.95, QUANTITY='TEMPERATURE', ID='WTC_13' /
&DEVC XYZ=0.0508, 0.070, 1.95, QUANTITY='TEMPERATURE', ID='WTC_14' /
&DEVC XYZ=0.0254, 0.075, 1.95, QUANTITY='TEMPERATURE', ID='WTC_15' /
&DEVC XYZ=-0.0254, 0.080, 1.95, QUANTITY='TEMPERATURE', ID='WTC_16' /
&DEVC XYZ=-0.0508, 0.085, 1.95, QUANTITY='TEMPERATURE', ID='WTC_17' /
&DEVC XYZ=-0.0762, 0.090, 1.95, QUANTITY='TEMPERATURE', ID='WTC_18' /

WALL HEAT FLUX MEASUREMENTS
&DEVC XYZ=  0.575, 0.050, 0.575, QUANTITY='GAUGE_HEAT_FLUX', ID='TS_1',  IOR = 2 /
&DEVC XYZ=  0.025, 0.050, 0.575, QUANTITY='GAUGE_HEAT_FLUX', ID='TS_2',  IOR = 2 /
&DEVC XYZ= -0.275, 0.050, 0.575, QUANTITY='GAUGE_HEAT_FLUX', ID='TS_3',  IOR = 2 /
&DEVC XYZ=  0.275, 0.050, 0.875, QUANTITY='GAUGE_HEAT_FLUX', ID='TS_4',  IOR = 2 /
&DEVC XYZ=  -0.025, 0.050, 0.875, QUANTITY='GAUGE_HEAT_FLUX', ID='TS_5',  IOR = 2 /
&DEVC XYZ= -0.575, 0.050, 0.875, QUANTITY='GAUGE_HEAT_FLUX', ID='TS_6',  IOR = 2 /
&DEVC XYZ=  0.575, 0.050, 1.175, QUANTITY='GAUGE_HEAT_FLUX', ID='TS_7',  IOR = 2 /
&DEVC XYZ=  0.025 0.050, 1.175, QUANTITY='GAUGE_HEAT_FLUX', ID='TS_8',  IOR = 2 /
&DEVC XYZ= -0.275, 0.050, 1.175, QUANTITY='GAUGE_HEAT_FLUX', ID='TS_9',  IOR = 2 /
&DEVC XYZ=  0.275, 0.050, 1.475, QUANTITY='GAUGE_HEAT_FLUX', ID='TS_10', IOR = 2 /
&DEVC XYZ=  -0.025, 0.050, 1.475, QUANTITY='GAUGE_HEAT_FLUX', ID='TS_11', IOR = 2 /
&DEVC XYZ= -0.575, 0.050, 1.475, QUANTITY='GAUGE_HEAT_FLUX', ID='TS_12', IOR = 2 /
&DEVC XYZ=  0.575, 0.050, 1.775, QUANTITY='GAUGE_HEAT_FLUX', ID='TS_13', IOR = 2 /
&DEVC XYZ=  0.025, 0.050, 1.775, QUANTITY='GAUGE_HEAT_FLUX', ID='TS_14', IOR = 2 /
&DEVC XYZ= -0.275, 0.050, 1.775, QUANTITY='GAUGE_HEAT_FLUX', ID='TS_15', IOR = 2 /
&DEVC XYZ=  0.275, 0.050, 2.075, QUANTITY='GAUGE_HEAT_FLUX', ID='TS_16', IOR = 2 /
&DEVC XYZ=  -0.025, 0.050, 2.075, QUANTITY='GAUGE_HEAT_FLUX', ID='TS_17', IOR = 2 /
&DEVC XYZ= -0.575, 0.050, 2.075, QUANTITY='GAUGE_HEAT_FLUX', ID='TS_18', IOR = 2 /

&DEVC XYZ=  0.275, 0.050, 0.60, QUANTITY='GAUGE_HEAT_FLUX', ID='HFG_1', IOR = 2 /
&DEVC XYZ= -0.275, 0.050, 0.875, QUANTITY='GAUGE_HEAT_FLUX', ID='HFG_2', IOR = 2 /
&DEVC XYZ=  0.275, 0.050, 1.175, QUANTITY='GAUGE_HEAT_FLUX', ID='HFG_3', IOR = 2 /
&DEVC XYZ= -0.275, 0.050, 1.475, QUANTITY='GAUGE_HEAT_FLUX', ID='HFG_4', IOR = 2 /
&DEVC XYZ=  0.275, 0.050, 1.775, QUANTITY='GAUGE_HEAT_FLUX', ID='HFG_5', IOR = 2 /
&DEVC XYZ= -0.275, 0.050, 2.075, QUANTITY='GAUGE_HEAT_FLUX', ID='HFG_6', IOR = 2 /

WALL NET HEAT FLUX
&DEVC XYZ=  0.575, 0.050, 0.575, QUANTITY='NET HEAT FLUX', ID='TS_1',  IOR = 2 /
&DEVC XYZ=  0.025, 0.050, 0.575, QUANTITY='NET HEAT FLUX', ID='TS_2',  IOR = 2 /
&DEVC XYZ= -0.275, 0.050, 0.575, QUANTITY='NET HEAT FLUX', ID='TS_3',  IOR = 2 /
&DEVC XYZ=  0.275, 0.050, 0.875, QUANTITY='NET HEAT FLUX', ID='TS_4',  IOR = 2 /
&DEVC XYZ=  -0.025, 0.050, 0.875, QUANTITY='NET HEAT FLUX', ID='TS_5',  IOR = 2 /
&DEVC XYZ= -0.575, 0.050, 0.875, QUANTITY='NET HEAT FLUX', ID='TS_6',  IOR = 2 /
&DEVC XYZ=  0.575, 0.050, 1.175, QUANTITY='NET HEAT FLUX', ID='TS_7',  IOR = 2 /
&DEVC XYZ=  0.025 0.050, 1.175, QUANTITY='NET HEAT FLUX', ID='TS_8',  IOR = 2 /
&DEVC XYZ= -0.275, 0.050, 1.175, QUANTITY='NET HEAT FLUX', ID='TS_9',  IOR = 2 /
&DEVC XYZ=  0.275, 0.050, 1.475, QUANTITY='NET HEAT FLUX', ID='TS_10', IOR = 2 /
&DEVC XYZ=  -0.025, 0.050, 1.475, QUANTITY='NET HEAT FLUX', ID='TS_11', IOR = 2 /
&DEVC XYZ= -0.575, 0.050, 1.475, QUANTITY='NET HEAT FLUX', ID='TS_12', IOR = 2 /
&DEVC XYZ=  0.575, 0.050, 1.775, QUANTITY='NET HEAT FLUX', ID='TS_13', IOR = 2 /
&DEVC XYZ=  0.025, 0.050, 1.775, QUANTITY='NET HEAT FLUX', ID='TS_14', IOR = 2 /
&DEVC XYZ= -0.275, 0.050, 1.775, QUANTITY='NET HEAT FLUX', ID='TS_15', IOR = 2 /
```

J.9 Input File 9 – FRP scenario, Rectangle burner, 75 kW, propylene

```
Start Input File
&HEAD CHID='59_1_03-14-2011_FRP_PP_lb_75kW' /

&TIME T_END = 900, DT = 0.05, RESTRICT_TIME_STEP = .FALSE. /
&DUMP DT_BNDF=2.0, DT_DEVC=0.5, DT_HRR=1.0, DT_PL3D=5000.0, DT_SLCF=2.0, DT_RESTART=50./

&MISC
      SURF_DEFAULT = 'INERT'
      TMPA  = 23
      FDS6  = .TRUE.
      DNS = .FALSE.
      DYNSMAG = .TRUE.
      CSMAG = 0.2
      PR = 0.5
      SC = 0.5
      H_EDDY = .TRUE.
      CFL_VELOCITY_NORM = 1
      FLUX_LIMITER = 2
      ISOTHERMAL = .FALSE.
      RADIATION = .TRUE.
      BAROCLINIC = .TRUE.
      CLIP_MASS_FRACTION   = .TRUE.
      CHECK_VN = .TRUE.
      NOBIAS = .TRUE.
      PROJECTION  = .FALSE.
      CHECK_KINETIC_ENERGY = .FALSE.
      /

&REAC
     ID = 'Propylene'
     C = 3
     H = 6
     O = 0
     CO_YIELD = 0.095
     SOOT_YIELD = 0.017
     EDDY_DISSIPATION = .TRUE.
     C_EDC = 0.1
     HRRPUA_SHEET = 0
     HRRPUV_AVERAGE = 2500
      /

&RADI
    RADIATIVE_FRACTION = 0.3
    TIME_STEP_INCREMENT = 3
    ANGLE_INCREMENT = 5
    NUMBER_RADIATION_ANGLES = 104
    /

**** MESHES ****
 MESH IJK= 96, 156, 96, XB=-1.20, 1.20, 0.00, 3.90, 0.00, 2.40 / 2.50 cm grid,  1 mesh

&MESH ID= 'Mesh-1', IJK= 24, 26, 24, XB= -1.2, 0, 0, 1.3, 0, 1.2 / 0.05 cm grid 12 mesh
&MESH ID= 'Mesh-2', IJK= 24, 26, 24, XB= -1.2, 0, 1.3, 2.6, 0, 1.2 / 0.05 cm grid 12 mesh
&MESH ID= 'Mesh-3', IJK= 24, 26, 24, XB= -1.2, 0, 2.6, 3.9, 0, 1.2 / 0.05 cm grid 12 mesh
&MESH ID= 'Mesh-4', IJK= 24, 26, 24, XB= 0, 1.2, 0, 1.3, 0, 1.2 / 0.05 cm grid 12 mesh
&MESH ID= 'Mesh-5', IJK= 24, 26, 24, XB= 0, 1.2, 1.3, 2.6, 0, 1.2 / 0.05 cm grid 12 mesh
&MESH ID= 'Mesh-6', IJK= 24, 26, 24, XB= 0, 1.2, 2.6, 3.9, 0, 1.2 / 0.05 cm grid 12 mesh
&MESH ID= 'Mesh-7', IJK= 24, 26, 24, XB= -1.2, 0, 0, 1.3, 1.2, 2.4 / 0.05 cm grid 12 mesh
&MESH ID= 'Mesh-8', IJK= 24, 26, 24, XB= -1.2, 0, 1.3, 2.6, 1.2, 2.4 / 0.05 cm grid 12 mesh
&MESH ID= 'Mesh-9', IJK= 24, 26, 24, XB= -1.2, 0, 2.6, 3.9, 1.2, 2.4 / 0.05 cm grid 12 mesh
&MESH ID= 'Mesh-10', IJK= 24, 26, 24, XB= 0, 1.2, 0, 1.3, 1.2, 2.4 / 0.05 cm grid 12 mesh
&MESH ID= 'Mesh-11', IJK= 24, 26, 24, XB= 0, 1.2, 1.3, 2.6, 1.2, 2.4 / 0.05 cm grid 12 mesh
&MESH ID= 'Mesh-12', IJK= 24, 26, 24, XB= 0, 1.2, 2.6, 3.9, 1.2, 2.4 / 0.05 cm grid 12 mesh

****BURNER****
2 ft burner
&OBST XB= -0.35, 0.35, 0.05, 0.45, 0, 0.4, SURF_ID = 'ADIABATIC' /
&VENT XB= -0.3, 0.3, 0.1, 0.4, 0.4, 0.4, SURF_ID = 'BURNER' /
```

```
1 ft burner
OBST XB= -0.2, 0.2, 0.05, 0.45, 0, 0.4, SURF_ID = 'ADIABATIC' /
VENT XB= -0.15, 0.15, 0.1, 0.4, 0.4, 0.4, SURF_ID = 'BURNER' /

**** Burner Parameters*****
&SURF ID = 'BURNER'
      HRRPUA =416.7
      RAMP_Q = 'Burner_Ramp'
      COLOR  = 'RED' /

&RAMP ID = 'Burner_Ramp', T=0, F=0 /
&RAMP ID = 'Burner_Ramp', T=1, F=0.5 /
&RAMP ID = 'Burner_Ramp', T=12, F=1 /
&RAMP ID = 'Burner_Ramp', T=45, F=1 /
&RAMP ID = 'Burner_Ramp', T=55, F=0 /

**** MATERIAL PROPERTIES ****
&MATL ID            ='GYPSUM_MATL'
      SPECIFIC_HEAT = 0.84
      CONDUCTIVITY  = 0.48
      DENSITY       = 1440.0 /

&MATL ID            ='KAOWOOL_MATL'
      SPECIFIC_HEAT = 1.0
      CONDUCTIVITY  = 0.06
      DENSITY       = 320.0 /

&SURF ID        = 'ADIABATIC'
      ADIABATIC = .TRUE.
      RGB       = 0, 0, 0 /

&SURF ID                     = 'KAOWOOL'
      RGB                    = 51,102,255
      BACKING                = 'INSULATED'
      MATL_ID(1,1)           = 'KAOWOOL_MATL'
      MATL_MASS_FRACTION(1,1)= 1.0
      THICKNESS(1)           = 0.025
      CELL_SIZE_FACTOR       = 0.30
      STRETCH_FACTOR         = 1.0 /

&SURF ID                     = 'GYPSUM'
      RGB                    = 100,100,100
      BACKING                = 'INSULATED'
      MATL_ID(1,1)           = 'GYPSUM_MATL'
      MATL_MASS_FRACTION(1,1)= 1.0
      THICKNESS(1)           = 0.016
      CELL_SIZE_FACTOR       = 0.30
      STRETCH_FACTOR         = 1.0 /

&MATL ID                       = 'virgin'
      CONDUCTIVITY             =  0.480
      DENSITY                  = 1467.80
      SPECIFIC_HEAT            =    1.98
      EMISSIVITY               =  0.858
      ABSORPTION_COEFFICIENT   =  0.9000E+10
      RESIDUE(01)              = 'char'
      A(01)                    = 0.1139E+12
      E(01)                    = 0.1483E+06
      N_S(01)                  =   1.00
      THRESHOLD_TEMPERATURE(01)=   0.00
      HEAT_OF_REACTION(01)     =   996.67
      HEAT_OF_COMBUSTION       = 19700.
      NU_FUEL(01)              =   0.421
      NU_RESIDUE(01)           =   0.579
      NU_WATER(01)             =   0.000
      N_REACTIONS              = 01 /

&MATL ID                       = 'char'
      CONDUCTIVITY             =  0.050
      DENSITY                  =  850.56
      SPECIFIC_HEAT            =    2.12
```

```
      EMISSIVITY               =  0.943
      ABSORPTION_COEFFICIENT   =  0.9000E+10
      N_REACTIONS              = 00 /

&SURF ID                         = 'FRP'
      STRETCH_FACTOR             = 1.000
      CELL_SIZE_FACTOR           = 0.200
      THICKNESS(1)              = 0.0019
      MATL_ID(1,1)             = 'virgin'
      MATL_ID(1,2)             = 'char'
      MATL_MASS_FRACTION(1,1)  = 1.0000
      MATL_MASS_FRACTION(1,2)  = 0.0000
      BACKING                    = 'INSULATED'
      SHRINK                     = .TRUE.
      TMP_INNER                  = 27.0
      COLOR                      = 'WHITE' /


****OBSTRUCTIONS****
&OBST XB=-1.200, 1.200, 0.000, 0.000, 0.000, 2.400, SURF_ID ='GYPSUM'  / Back wall
&OBST XB= 1.200, 1.200, 0.000, 2.700, 0.000, 2.400, SURF_ID ='GYPSUM'  / Right wall
&OBST XB=-1.200,-1.200, 0.000, 2.700, 0.000, 2.400, SURF_ID ='GYPSUM'  / Left wall
&OBST XB=-1.200, 1.200, 0.000, 2.700, 2.400, 2.400, SURF_ID ='GYPSUM'  / Ceiling
&OBST XB=-0.900,-0.600, 0.000, 0.05, 0.000, 2.400, SURF_ID ='KAOWOOL' / Kaowool on back wall
&OBST XB= 0.600, 0.900, 0.000, 0.05, 0.000, 2.400, SURF_ID ='KAOWOOL' / Kaowool on back wall
&OBST XB=-0.600, 0.600, 0.000, 0.05, 0.000, 2.400, SURF_ID ='FRP', PERMIT_HOLE = .TRUE. / FRP
panel

****OPEN VENTS****
&VENT XB=-1.20, 1.20, 3.90, 3.90, 0.00, 2.40, SURF_ID = 'OPEN' / Back
&VENT XB=-1.20,-1.20, 2.70, 3.90, 0.00, 2.40, SURF_ID = 'OPEN' /
&VENT XB= 1.20, 1.20, 2.70, 3.90, 0.00, 2.40, SURF_ID = 'OPEN' /
&VENT XB=-1.20, 1.20, 2.70, 3.90, 2.40, 2.40, SURF_ID = 'OPEN' /

HOLES in panel for TSC's:
&HOLE XB= 0.55,  0.60, -0.010, 0.1, 0.55, 0.60 / HOLE 1
&HOLE XB= 0,  0.05, -0.010, 0.1, 0.55, 0.60 / HOLE 2
&HOLE XB= -0.3, -0.25, -0.010, 0.1, 0.55, 0.60 / HOLE 3
&HOLE XB= 0.25,  0.3, -0.010, 0.1, 0.85, 0.9 / HOLE 4
&HOLE XB= -0.05,  0, -0.010, 0.1, 0.85, 0.9 / HOLE 5
&HOLE XB= -0.60, -0.55, -0.010, 0.1, 0.85, 0.9 / HOLE 6
&HOLE XB= 0.55,  0.60, -0.010, 0.1, 1.15, 1.2 / HOLE 7
&HOLE XB= 0, 0.05, -0.010, 0.1, 1.15, 1.2 / HOLE 8
&HOLE XB= -0.3, -0.25, -0.010, 0.1, 1.15, 1.2 / HOLE 9
&HOLE XB= 0.25,  0.3, -0.010, 0.1, 1.45, 1.5 / HOLE 10
&HOLE XB= -0.05,  0, -0.010, 0.1, 1.45, 1.5 / HOLE 11
&HOLE XB=-0.60, -0.55, -0.010, 0.1, 1.45, 1.5 / HOLE 12
&HOLE XB= 0.55,  0.60, -0.010, 0.1, 1.75, 1.8 / HOLE 13
&HOLE XB= 0,  0.05, -0.010, 0.1, 1.75, 1.8 / HOLE 14
&HOLE XB=-0.3, -0.25, -0.010, 0.1, 1.75, 1.8 / HOLE 15
&HOLE XB= 0.25,  0.3, -0.010, 0.1, 2.05, 2.1 / HOLE 16
&HOLE XB= -0.05,  0, -0.010, 0.1, 2.05, 2.1 / HOLE 17
&HOLE XB=-0.60, -0.55, -0.010, 0.1, 2.05, 2.1 / HOLE 18

TSC'S:

&OBST XB= 0.55,  0.60, -0.010, 0.05, 0.55, 0.60, SURF_ID = 'ADIABATIC', PERMIT_HOLE = .FALSE. /
TSC 1
&OBST XB= 0,  0.05, -0.010, 0.05, 0.55, 0.60, SURF_ID = 'ADIABATIC', PERMIT_HOLE = .FALSE. / TSC
2
&OBST XB= -0.3, -0.25, -0.010, 0.05, 0.55, 0.60, SURF_ID = 'ADIABATIC', PERMIT_HOLE = .FALSE. /
TSC 3
&OBST XB= 0.25,  0.3, -0.010, 0.05, 0.85, 0.9, SURF_ID = 'ADIABATIC', PERMIT_HOLE = .FALSE. / TSC
4
&OBST XB= -0.05,  0, -0.010, 0.05, 0.85, 0.9, SURF_ID = 'ADIABATIC', PERMIT_HOLE = .FALSE. / TSC
5
&OBST XB= -0.60, -0.55, -0.010, 0.05, 0.85, 0.9, SURF_ID = 'ADIABATIC', PERMIT_HOLE = .FALSE. /
TSC 6
&OBST XB= 0.55,  0.60, -0.010, 0.05, 1.15, 1.2, SURF_ID = 'ADIABATIC', PERMIT_HOLE = .FALSE. /
TSC 7
&OBST XB= 0, 0.05, -0.010, 0.05, 1.15, 1.2, SURF_ID = 'ADIABATIC', PERMIT_HOLE = .FALSE. / TSC 8
```

```
&OBST XB= -0.3, -0.25, -0.010, 0.05, 1.15, 1.2, SURF_ID = 'ADIABATIC', PERMIT_HOLE = .FALSE. /
TSC 9
&OBST XB= 0.25,  0.3, -0.010, 0.05, 1.45, 1.5, SURF_ID = 'ADIABATIC', PERMIT_HOLE = .FALSE. / TSC
10
&OBST XB= -0.05,  0, -0.010, 0.05, 1.45, 1.5, SURF_ID = 'ADIABATIC', PERMIT_HOLE = .FALSE. / TSC
11
&OBST XB=-0.60, -0.55, -0.010, 0.05, 1.45, 1.5, SURF_ID = 'ADIABATIC', PERMIT_HOLE = .FALSE. /
TSC 12
&OBST XB= 0.55,  0.60, -0.010, 0.05, 1.75, 1.8, SURF_ID = 'ADIABATIC', PERMIT_HOLE = .FALSE. /
TSC 13
&OBST XB= 0,  0.05, -0.010, 0.05, 1.75, 1.8, SURF_ID = 'ADIABATIC', PERMIT_HOLE = .FALSE. / TSC
14
&OBST XB=-0.3, -0.25, -0.010, 0.05, 1.75, 1.8, SURF_ID = 'ADIABATIC', PERMIT_HOLE = .FALSE. / TSC
15
&OBST XB= 0.25,  0.3, -0.010, 0.05, 2.05, 2.1, SURF_ID = 'ADIABATIC', PERMIT_HOLE = .FALSE. / TSC
16
&OBST XB= -0.05,  0, -0.010, 0.05, 2.05, 2.1, SURF_ID = 'ADIABATIC', PERMIT_HOLE = .FALSE. / TSC
17
&OBST XB=-0.60, -0.55, -0.010, 0.05, 2.05, 2.1, SURF_ID = 'ADIABATIC', PERMIT_HOLE = .FALSE. /
TSC 18

&SLCF PBX = 0.0, QUANTITY = 'TEMPERATURE' /
&SLCF PBX = 0.0, QUANTITY = 'HRRPUV' /

&BNDF QUANTITY='GAUGE HEAT FLUX' /
&BNDF QUANTITY='RADIATIVE HEAT FLUX' /
&BNDF QUANTITY='CONVECTIVE HEAT FLUX' /
&BNDF QUANTITY='NET HEAT FLUX' /
&BNDF QUANTITY='WALL TEMPERATURE' /
&BNDF QUANTITY='BURNING RATE' /

CENTERLINE RAKE
&DEVC XYZ=0, 0.25, 0.45, QUANTITY='TEMPERATURE', ID='CTC_1' /
&DEVC XYZ=0, 0.25, 0.60, QUANTITY='TEMPERATURE', ID='BDTC_1' /
&DEVC XYZ=0, 0.25, 0.75, QUANTITY='TEMPERATURE', ID='CTC_2' /
&DEVC XYZ=0, 0.25, 0.90, QUANTITY='TEMPERATURE', ID='BDTC_2' /
&DEVC XYZ=0, 0.25, 1.05, QUANTITY='TEMPERATURE', ID='CTC_3' /
&DEVC XYZ=0, 0.25, 1.20, QUANTITY='TEMPERATURE', ID='BDTC_3' /
&DEVC XYZ=0, 0.25, 1.35, QUANTITY='TEMPERATURE', ID='CTC_4' /
&DEVC XYZ=0, 0.25, 1.50, QUANTITY='TEMPERATURE', ID='BDTC_4' /
&DEVC XYZ=0, 0.25, 1.65, QUANTITY='TEMPERATURE', ID='CTC_5' /
&DEVC XYZ=0, 0.25, 1.80, QUANTITY='TEMPERATURE', ID='BDTC_5' /
&DEVC XYZ=0, 0.25, 1.95, QUANTITY='TEMPERATURE', ID='CTC_6' /
&DEVC XYZ=0, 0.25, 2.10, QUANTITY='TEMPERATURE', ID='BDTC_6' /
&DEVC XYZ=0, 0.25, 2.25, QUANTITY='TEMPERATURE', ID='CTC_7' /
&DEVC XYZ=0, 0.25, 0.60, QUANTITY='W-VELOCITY', ID='BD_1' /
&DEVC XYZ=0, 0.25, 0.90, QUANTITY='W-VELOCITY', ID='BD_2' /
&DEVC XYZ=0, 0.25, 1.20, QUANTITY='W-VELOCITY', ID='BD_3' /
&DEVC XYZ=0, 0.25, 1.50, QUANTITY='W-VELOCITY', ID='BD_4' /
&DEVC XYZ=0, 0.25, 1.80, QUANTITY='W-VELOCITY', ID='BD_5' /
&DEVC XYZ=0, 0.25, 2.10, QUANTITY='W-VELOCITY', ID='BD_6' /
&DEVC XYZ=0, 0.25, 1.05, QUANTITY='W-VELOCITY', ID='BD_7' /
&DEVC XYZ=0, 0.25, 1.35, QUANTITY='W-VELOCITY', ID='BD_8' /
&DEVC XYZ=0, 0.25, 1.65, QUANTITY='W-VELOCITY', ID='BD_9' /
&DEVC XYZ=0, 0.25, 1.95, QUANTITY='W-VELOCITY', ID='BD_10' /

WALL TEMPERATURE
&DEVC XYZ=0.0762, 0.05, 0.75, QUANTITY='TEMPERATURE', ID='WTC_1' /
&DEVC XYZ=0.0508, 0.055, 0.75, QUANTITY='TEMPERATURE', ID='WTC_2' /
&DEVC XYZ=0.0254, 0.060, 0.75, QUANTITY='TEMPERATURE', ID='WTC_3' /
&DEVC XYZ=-0.0254, 0.065, 0.75, QUANTITY='TEMPERATURE', ID='WTC_4' /
&DEVC XYZ=-0.0508, 0.070, 0.75, QUANTITY='TEMPERATURE', ID='WTC_5' /
&DEVC XYZ=-0.0762, 0.075, 0.75, QUANTITY='TEMPERATURE', ID='WTC_6' /
&DEVC XYZ=0.0762, 0.085, 1.35, QUANTITY='TEMPERATURE', ID='WTC_7' /
&DEVC XYZ=0.0508, 0.080, 1.35, QUANTITY='TEMPERATURE', ID='WTC_8' /
&DEVC XYZ=0.0254, 0.075, 1.35, QUANTITY='TEMPERATURE', ID='WTC_9' /
&DEVC XYZ=-0.0254, 0.070, 1.35, QUANTITY='TEMPERATURE', ID='WTC_10' /
&DEVC XYZ=-0.0508, 0.065, 1.35, QUANTITY='TEMPERATURE', ID='WTC_11' /
&DEVC XYZ=-0.0762, 0.060, 1.35, QUANTITY='TEMPERATURE', ID='WTC_12' /
&DEVC XYZ=0.0762, 0.065, 1.95, QUANTITY='TEMPERATURE', ID='WTC_13' /
&DEVC XYZ=0.0508, 0.070, 1.95, QUANTITY='TEMPERATURE', ID='WTC_14' /
```

```
&DEVC XYZ=0.0254, 0.075, 1.95, QUANTITY='TEMPERATURE', ID='WTC_15' /
&DEVC XYZ=-0.0254, 0.080, 1.95, QUANTITY='TEMPERATURE', ID='WTC_16' /
&DEVC XYZ=-0.0508, 0.085, 1.95, QUANTITY='TEMPERATURE', ID='WTC_17' /
&DEVC XYZ=-0.0762, 0.090, 1.95, QUANTITY='TEMPERATURE', ID='WTC_18' /

WALL HEAT FLUX MEASUREMENTS
&DEVC XYZ=  0.575, 0.050, 0.575, QUANTITY='GAUGE_HEAT_FLUX', ID='TS_1',  IOR = 2 /
&DEVC XYZ=  0.025, 0.050, 0.575, QUANTITY='GAUGE_HEAT_FLUX', ID='TS_2',  IOR = 2 /
&DEVC XYZ= -0.275, 0.050, 0.575, QUANTITY='GAUGE_HEAT_FLUX', ID='TS_3',  IOR = 2 /
&DEVC XYZ=  0.275, 0.050, 0.875, QUANTITY='GAUGE_HEAT_FLUX', ID='TS_4',  IOR = 2 /
&DEVC XYZ=  -0.025, 0.050, 0.875, QUANTITY='GAUGE_HEAT_FLUX', ID='TS_5',  IOR = 2 /
&DEVC XYZ= -0.575, 0.050, 0.875, QUANTITY='GAUGE_HEAT_FLUX', ID='TS_6',  IOR = 2 /
&DEVC XYZ=  0.575, 0.050, 1.175, QUANTITY='GAUGE_HEAT_FLUX', ID='TS_7',  IOR = 2 /
&DEVC XYZ=  0.025 0.050, 1.175, QUANTITY='GAUGE_HEAT_FLUX', ID='TS_8',  IOR = 2 /
&DEVC XYZ= -0.275, 0.050, 1.175, QUANTITY='GAUGE_HEAT_FLUX', ID='TS_9',  IOR = 2 /
&DEVC XYZ=  0.275, 0.050, 1.475, QUANTITY='GAUGE_HEAT_FLUX', ID='TS_10', IOR = 2 /
&DEVC XYZ=  -0.025, 0.050, 1.475, QUANTITY='GAUGE_HEAT_FLUX', ID='TS_11', IOR = 2 /
&DEVC XYZ= -0.575, 0.050, 1.475, QUANTITY='GAUGE_HEAT_FLUX', ID='TS_12', IOR = 2 /
&DEVC XYZ=  0.575, 0.050, 1.775, QUANTITY='GAUGE_HEAT_FLUX', ID='TS_13', IOR = 2 /
&DEVC XYZ=  0.025, 0.050, 1.775, QUANTITY='GAUGE_HEAT_FLUX', ID='TS_14', IOR = 2 /
&DEVC XYZ= -0.275, 0.050, 1.775, QUANTITY='GAUGE_HEAT_FLUX', ID='TS_15', IOR = 2 /
&DEVC XYZ=  0.275, 0.050, 2.075, QUANTITY='GAUGE_HEAT_FLUX', ID='TS_16', IOR = 2 /
&DEVC XYZ=  -0.025, 0.050, 2.075, QUANTITY='GAUGE_HEAT_FLUX', ID='TS_17', IOR = 2 /
&DEVC XYZ= -0.575, 0.050, 2.075, QUANTITY='GAUGE_HEAT_FLUX', ID='TS_18', IOR = 2 /

&DEVC XYZ=  0.275, 0.050, 0.60, QUANTITY='GAUGE_HEAT_FLUX', ID='HFG_1', IOR = 2 /
&DEVC XYZ= -0.275, 0.050, 0.875, QUANTITY='GAUGE_HEAT_FLUX', ID='HFG_2', IOR = 2 /
&DEVC XYZ=  0.275, 0.050, 1.175, QUANTITY='GAUGE_HEAT_FLUX', ID='HFG_3', IOR = 2 /
&DEVC XYZ= -0.275, 0.050, 1.475, QUANTITY='GAUGE_HEAT_FLUX', ID='HFG_4', IOR = 2 /
&DEVC XYZ=  0.275, 0.050, 1.775, QUANTITY='GAUGE_HEAT_FLUX', ID='HFG_5', IOR = 2 /
&DEVC XYZ= -0.275, 0.050, 2.075, QUANTITY='GAUGE_HEAT_FLUX', ID='HFG_6', IOR = 2 /

WALL NET HEAT FLUX
&DEVC XYZ=  0.575, 0.050, 0.575, QUANTITY='NET HEAT FLUX', ID='TS_1',  IOR = 2 /
&DEVC XYZ=  0.025, 0.050, 0.575, QUANTITY='NET HEAT FLUX', ID='TS_2',  IOR = 2 /
&DEVC XYZ= -0.275, 0.050, 0.575, QUANTITY='NET HEAT FLUX', ID='TS_3',  IOR = 2 /
&DEVC XYZ=  0.275, 0.050, 0.875, QUANTITY='NET HEAT FLUX', ID='TS_4',  IOR = 2 /
&DEVC XYZ=  -0.025, 0.050, 0.875, QUANTITY='NET HEAT FLUX', ID='TS_5',  IOR = 2 /
&DEVC XYZ= -0.575, 0.050, 0.875, QUANTITY='NET HEAT FLUX', ID='TS_6',  IOR = 2 /
&DEVC XYZ=  0.575, 0.050, 1.175, QUANTITY='NET HEAT FLUX', ID='TS_7',  IOR = 2 /
&DEVC XYZ=  0.025 0.050, 1.175, QUANTITY='NET HEAT FLUX', ID='TS_8',  IOR = 2 /
&DEVC XYZ= -0.275, 0.050, 1.175, QUANTITY='NET HEAT FLUX', ID='TS_9',  IOR = 2 /
&DEVC XYZ=  0.275, 0.050, 1.475, QUANTITY='NET HEAT FLUX', ID='TS_10', IOR = 2 /
&DEVC XYZ=  -0.025, 0.050, 1.475, QUANTITY='NET HEAT FLUX', ID='TS_11', IOR = 2 /
&DEVC XYZ= -0.575, 0.050, 1.475, QUANTITY='NET HEAT FLUX', ID='TS_12', IOR = 2 /
&DEVC XYZ=  0.575, 0.050, 1.775, QUANTITY='NET HEAT FLUX', ID='TS_13', IOR = 2 /
&DEVC XYZ=  0.025, 0.050, 1.775, QUANTITY='NET HEAT FLUX', ID='TS_14', IOR = 2 /
&DEVC XYZ= -0.275, 0.050, 1.775, QUANTITY='NET HEAT FLUX', ID='TS_15', IOR = 2 /
```

J.10 Input File 10 – FRP scenario, Rectangle burner, 50 kW, propylene

```
Start Input File
&HEAD CHID='60_1_03-14-2011_FRP_PP_lb_50kW' /

&TIME T_END = 900, DT = 0.05, RESTRICT_TIME_STEP = .FALSE. /
&DUMP DT_BNDF=2.0, DT_DEVC=0.5, DT_HRR=1.0, DT_PL3D=5000.0, DT_SLCF=2.0, DT_RESTART=50./

&MISC
      SURF_DEFAULT = 'INERT'
      TMPA  = 23
      FDS6  = .TRUE.
      DNS = .FALSE.
      DYNSMAG = .TRUE.
      CSMAG = 0.2
      PR = 0.5
      SC = 0.5
      H_EDDY = .TRUE.
      CFL_VELOCITY_NORM = 1
      FLUX_LIMITER = 2
      ISOTHERMAL = .FALSE.
      RADIATION = .TRUE.
      BAROCLINIC = .TRUE.
      CLIP_MASS_FRACTION   = .TRUE.
      CHECK_VN = .TRUE.
      NOBIAS = .TRUE.
      PROJECTION  = .FALSE.
      CHECK_KINETIC_ENERGY = .FALSE.
      /

&REAC
     ID = 'Propylene'
     C = 3
     H = 6
     O = 0
     CO_YIELD = 0.095
     SOOT_YIELD = 0.017
     EDDY_DISSIPATION = .TRUE.
     C_EDC = 0.1
     HRRPUA_SHEET = 0
     HRRPUV_AVERAGE = 2500
      /

&RADI
    RADIATIVE_FRACTION = 0.3
    TIME_STEP_INCREMENT = 3
    ANGLE_INCREMENT = 5
    NUMBER_RADIATION_ANGLES = 104
    /

**** MESHES ****
 MESH IJK= 96, 156, 96, XB=-1.20, 1.20, 0.00, 3.90, 0.00, 2.40 / 2.50 cm grid,  1 mesh

&MESH ID= 'Mesh-1', IJK= 24, 26, 24, XB= -1.2, 0, 0, 1.3, 0, 1.2 / 0.05 cm grid 12 mesh
&MESH ID= 'Mesh-2', IJK= 24, 26, 24, XB= -1.2, 0, 1.3, 2.6, 0, 1.2 / 0.05 cm grid 12 mesh
&MESH ID= 'Mesh-3', IJK= 24, 26, 24, XB= -1.2, 0, 2.6, 3.9, 0, 1.2 / 0.05 cm grid 12 mesh
&MESH ID= 'Mesh-4', IJK= 24, 26, 24, XB= 0, 1.2, 0, 1.3, 0, 1.2 / 0.05 cm grid 12 mesh
&MESH ID= 'Mesh-5', IJK= 24, 26, 24, XB= 0, 1.2, 1.3, 2.6, 0, 1.2 / 0.05 cm grid 12 mesh
&MESH ID= 'Mesh-6', IJK= 24, 26, 24, XB= 0, 1.2, 2.6, 3.9, 0, 1.2 / 0.05 cm grid 12 mesh
&MESH ID= 'Mesh-7', IJK= 24, 26, 24, XB= -1.2, 0, 0, 1.3, 1.2, 2.4 / 0.05 cm grid 12 mesh
&MESH ID= 'Mesh-8', IJK= 24, 26, 24, XB= -1.2, 0, 1.3, 2.6, 1.2, 2.4 / 0.05 cm grid 12 mesh
&MESH ID= 'Mesh-9', IJK= 24, 26, 24, XB= -1.2, 0, 2.6, 3.9, 1.2, 2.4 / 0.05 cm grid 12 mesh
&MESH ID= 'Mesh-10', IJK= 24, 26, 24, XB= 0, 1.2, 0, 1.3, 1.2, 2.4 / 0.05 cm grid 12 mesh
&MESH ID= 'Mesh-11', IJK= 24, 26, 24, XB= 0, 1.2, 1.3, 2.6, 1.2, 2.4 / 0.05 cm grid 12 mesh
&MESH ID= 'Mesh-12', IJK= 24, 26, 24, XB= 0, 1.2, 2.6, 3.9, 1.2, 2.4 / 0.05 cm grid 12 mesh

****BURNER****
2 ft burner
&OBST XB= -0.35, 0.35, 0.05, 0.45, 0, 0.4, SURF_ID = 'ADIABATIC' /
&VENT XB= -0.3, 0.3, 0.1, 0.4, 0.4, 0.4, SURF_ID = 'BURNER' /
```

```
1 ft burner
OBST XB= -0.2, 0.2, 0.05, 0.45, 0, 0.4, SURF_ID = 'ADIABATIC' /
VENT XB= -0.15, 0.15, 0.1, 0.4, 0.4, 0.4, SURF_ID = 'BURNER' /

**** Burner Parameters*****
&SURF ID = 'BURNER'
      HRRPUA =277.8
      RAMP_Q = 'Burner_Ramp'
      COLOR  = 'RED' /

&RAMP ID = 'Burner_Ramp', T=0, F=0 /
&RAMP ID = 'Burner_Ramp', T=1, F=0.5 /
&RAMP ID = 'Burner_Ramp', T=12, F=1 /
&RAMP ID = 'Burner_Ramp', T=58, F=1 /
&RAMP ID = 'Burner_Ramp', T=68, F=0 /

**** MATERIAL PROPERTIES ****
&MATL ID            ='GYPSUM_MATL'
      SPECIFIC_HEAT = 0.84
      CONDUCTIVITY  = 0.48
      DENSITY       = 1440.0 /

&MATL ID            ='KAOWOOL_MATL'
      SPECIFIC_HEAT = 1.0
      CONDUCTIVITY  = 0.06
      DENSITY       = 320.0 /

&SURF ID        = 'ADIABATIC'
      ADIABATIC = .TRUE.
      RGB       = 0, 0, 0 /

&SURF ID                    = 'KAOWOOL'
      RGB                   = 51,102,255
      BACKING               = 'INSULATED'
      MATL_ID(1,1)          = 'KAOWOOL_MATL'
      MATL_MASS_FRACTION(1,1)= 1.0
      THICKNESS(1)          = 0.025
      CELL_SIZE_FACTOR      = 0.30
      STRETCH_FACTOR        = 1.0 /

&SURF ID                    = 'GYPSUM'
      RGB                   = 100,100,100
      BACKING               = 'INSULATED'
      MATL_ID(1,1)          = 'GYPSUM_MATL'
      MATL_MASS_FRACTION(1,1)= 1.0
      THICKNESS(1)          = 0.016
      CELL_SIZE_FACTOR      = 0.30
      STRETCH_FACTOR        = 1.0 /

&MATL ID                      = 'virgin'
      CONDUCTIVITY            =  0.480
      DENSITY                 = 1467.80
      SPECIFIC_HEAT           =    1.98
      EMISSIVITY              =  0.858
      ABSORPTION_COEFFICIENT  =  0.9000E+10
      RESIDUE(01)             = 'char'
      A(01)                   = 0.1139E+12
      E(01)                   = 0.1483E+06
      N_S(01)                 =   1.00
      THRESHOLD_TEMPERATURE(01)=   0.00
      HEAT_OF_REACTION(01)    =   996.67
      HEAT_OF_COMBUSTION      = 19700.
      NU_FUEL(01)             =   0.421
      NU_RESIDUE(01)          =   0.579
      NU_WATER(01)            =   0.000
      N_REACTIONS             = 01 /

&MATL ID                      = 'char'
      CONDUCTIVITY            =  0.050
      DENSITY                 =  850.56
      SPECIFIC_HEAT           =    2.12
```

```
      EMISSIVITY               =  0.943
      ABSORPTION_COEFFICIENT   =  0.9000E+10
      N_REACTIONS              = 00 /

&SURF ID                         = 'FRP'
      STRETCH_FACTOR             = 1.000
      CELL_SIZE_FACTOR           = 0.200
      THICKNESS(1)              = 0.0019
      MATL_ID(1,1)             = 'virgin'
      MATL_ID(1,2)             = 'char'
      MATL_MASS_FRACTION(1,1)  = 1.0000
      MATL_MASS_FRACTION(1,2)  = 0.0000
      BACKING                    = 'INSULATED'
      SHRINK                     = .TRUE.
      TMP_INNER                  = 27.0
      COLOR                      = 'WHITE' /


****OBSTRUCTIONS****
&OBST XB=-1.200, 1.200, 0.000, 0.000, 0.000, 2.400, SURF_ID ='GYPSUM'  / Back wall
&OBST XB= 1.200, 1.200, 0.000, 2.700, 0.000, 2.400, SURF_ID ='GYPSUM'  / Right wall
&OBST XB=-1.200,-1.200, 0.000, 2.700, 0.000, 2.400, SURF_ID ='GYPSUM'  / Left wall
&OBST XB=-1.200, 1.200, 0.000, 2.700, 2.400, 2.400, SURF_ID ='GYPSUM'  / Ceiling
&OBST XB=-0.900,-0.600, 0.000, 0.05, 0.000, 2.400, SURF_ID ='KAOWOOL' / Kaowool on back wall
&OBST XB= 0.600, 0.900, 0.000, 0.05, 0.000, 2.400, SURF_ID ='KAOWOOL' / Kaowool on back wall
&OBST XB=-0.600, 0.600, 0.000, 0.05, 0.000, 2.400, SURF_ID ='FRP', PERMIT_HOLE = .TRUE. / FRP
panel

****OPEN VENTS****
&VENT XB=-1.20, 1.20, 3.90, 3.90, 0.00, 2.40, SURF_ID = 'OPEN' / Back
&VENT XB=-1.20,-1.20, 2.70, 3.90, 0.00, 2.40, SURF_ID = 'OPEN' /
&VENT XB= 1.20, 1.20, 2.70, 3.90, 0.00, 2.40, SURF_ID = 'OPEN' /
&VENT XB=-1.20, 1.20, 2.70, 3.90, 2.40, 2.40, SURF_ID = 'OPEN' /

HOLES in panel for TSC's:
&HOLE XB= 0.55,  0.60, -0.010, 0.1, 0.55, 0.60 / HOLE 1
&HOLE XB= 0,  0.05, -0.010, 0.1, 0.55, 0.60 / HOLE 2
&HOLE XB= -0.3, -0.25, -0.010, 0.1, 0.55, 0.60 / HOLE 3
&HOLE XB= 0.25,  0.3, -0.010, 0.1, 0.85, 0.9 / HOLE 4
&HOLE XB= -0.05,  0, -0.010, 0.1, 0.85, 0.9 / HOLE 5
&HOLE XB= -0.60, -0.55, -0.010, 0.1, 0.85, 0.9 / HOLE 6
&HOLE XB= 0.55,  0.60, -0.010, 0.1, 1.15, 1.2 / HOLE 7
&HOLE XB= 0, 0.05, -0.010, 0.1, 1.15, 1.2 / HOLE 8
&HOLE XB= -0.3, -0.25, -0.010, 0.1, 1.15, 1.2 / HOLE 9
&HOLE XB= 0.25,  0.3, -0.010, 0.1, 1.45, 1.5 / HOLE 10
&HOLE XB= -0.05,  0, -0.010, 0.1, 1.45, 1.5 / HOLE 11
&HOLE XB=-0.60, -0.55, -0.010, 0.1, 1.45, 1.5 / HOLE 12
&HOLE XB= 0.55,  0.60, -0.010, 0.1, 1.75, 1.8 / HOLE 13
&HOLE XB= 0,  0.05, -0.010, 0.1, 1.75, 1.8 / HOLE 14
&HOLE XB=-0.3, -0.25, -0.010, 0.1, 1.75, 1.8 / HOLE 15
&HOLE XB= 0.25,  0.3, -0.010, 0.1, 2.05, 2.1 / HOLE 16
&HOLE XB= -0.05,  0, -0.010, 0.1, 2.05, 2.1 / HOLE 17
&HOLE XB=-0.60, -0.55, -0.010, 0.1, 2.05, 2.1 / HOLE 18

TSC'S:

&OBST XB= 0.55,  0.60, -0.010, 0.05, 0.55, 0.60, SURF_ID = 'ADIABATIC', PERMIT_HOLE = .FALSE. /
TSC 1
&OBST XB= 0,  0.05, -0.010, 0.05, 0.55, 0.60, SURF_ID = 'ADIABATIC', PERMIT_HOLE = .FALSE. / TSC
2
&OBST XB= -0.3, -0.25, -0.010, 0.05, 0.55, 0.60, SURF_ID = 'ADIABATIC', PERMIT_HOLE = .FALSE. /
TSC 3
&OBST XB= 0.25,  0.3, -0.010, 0.05, 0.85, 0.9, SURF_ID = 'ADIABATIC', PERMIT_HOLE = .FALSE. / TSC
4
&OBST XB= -0.05,  0, -0.010, 0.05, 0.85, 0.9, SURF_ID = 'ADIABATIC', PERMIT_HOLE = .FALSE. / TSC
5
&OBST XB= -0.60, -0.55, -0.010, 0.05, 0.85, 0.9, SURF_ID = 'ADIABATIC', PERMIT_HOLE = .FALSE. /
TSC 6
&OBST XB= 0.55,  0.60, -0.010, 0.05, 1.15, 1.2, SURF_ID = 'ADIABATIC', PERMIT_HOLE = .FALSE. /
TSC 7
&OBST XB= 0, 0.05, -0.010, 0.05, 1.15, 1.2, SURF_ID = 'ADIABATIC', PERMIT_HOLE = .FALSE. / TSC 8
```

```
&OBST XB= -0.3, -0.25, -0.010, 0.05, 1.15, 1.2, SURF_ID = 'ADIABATIC', PERMIT_HOLE = .FALSE. /
TSC 9
&OBST XB= 0.25,  0.3, -0.010, 0.05, 1.45, 1.5, SURF_ID = 'ADIABATIC', PERMIT_HOLE = .FALSE. / TSC
10
&OBST XB= -0.05,  0, -0.010, 0.05, 1.45, 1.5, SURF_ID = 'ADIABATIC', PERMIT_HOLE = .FALSE. / TSC
11
&OBST XB=-0.60, -0.55, -0.010, 0.05, 1.45, 1.5, SURF_ID = 'ADIABATIC', PERMIT_HOLE = .FALSE. /
TSC 12
&OBST XB= 0.55,  0.60, -0.010, 0.05, 1.75, 1.8, SURF_ID = 'ADIABATIC', PERMIT_HOLE = .FALSE. /
TSC 13
&OBST XB= 0,  0.05, -0.010, 0.05, 1.75, 1.8, SURF_ID = 'ADIABATIC', PERMIT_HOLE = .FALSE. / TSC
14
&OBST XB=-0.3, -0.25, -0.010, 0.05, 1.75, 1.8, SURF_ID = 'ADIABATIC', PERMIT_HOLE = .FALSE. / TSC
15
&OBST XB= 0.25,  0.3, -0.010, 0.05, 2.05, 2.1, SURF_ID = 'ADIABATIC', PERMIT_HOLE = .FALSE. / TSC
16
&OBST XB= -0.05,  0, -0.010, 0.05, 2.05, 2.1, SURF_ID = 'ADIABATIC', PERMIT_HOLE = .FALSE. / TSC
17
&OBST XB=-0.60, -0.55, -0.010, 0.05, 2.05, 2.1, SURF_ID = 'ADIABATIC', PERMIT_HOLE = .FALSE. /
TSC 18

&SLCF PBX = 0.0, QUANTITY = 'TEMPERATURE' /
&SLCF PBX = 0.0, QUANTITY = 'HRRPUV' /

&BNDF QUANTITY='GAUGE HEAT FLUX' /
&BNDF QUANTITY='RADIATIVE HEAT FLUX' /
&BNDF QUANTITY='CONVECTIVE HEAT FLUX' /
&BNDF QUANTITY='NET HEAT FLUX' /
&BNDF QUANTITY='WALL TEMPERATURE' /
&BNDF QUANTITY='BURNING RATE' /

CENTERLINE RAKE
&DEVC XYZ=0, 0.25, 0.45, QUANTITY='TEMPERATURE', ID='CTC_1' /
&DEVC XYZ=0, 0.25, 0.60, QUANTITY='TEMPERATURE', ID='BDTC_1' /
&DEVC XYZ=0, 0.25, 0.75, QUANTITY='TEMPERATURE', ID='CTC_2' /
&DEVC XYZ=0, 0.25, 0.90, QUANTITY='TEMPERATURE', ID='BDTC_2' /
&DEVC XYZ=0, 0.25, 1.05, QUANTITY='TEMPERATURE', ID='CTC_3' /
&DEVC XYZ=0, 0.25, 1.20, QUANTITY='TEMPERATURE', ID='BDTC_3' /
&DEVC XYZ=0, 0.25, 1.35, QUANTITY='TEMPERATURE', ID='CTC_4' /
&DEVC XYZ=0, 0.25, 1.50, QUANTITY='TEMPERATURE', ID='BDTC_4' /
&DEVC XYZ=0, 0.25, 1.65, QUANTITY='TEMPERATURE', ID='CTC_5' /
&DEVC XYZ=0, 0.25, 1.80, QUANTITY='TEMPERATURE', ID='BDTC_5' /
&DEVC XYZ=0, 0.25, 1.95, QUANTITY='TEMPERATURE', ID='CTC_6' /
&DEVC XYZ=0, 0.25, 2.10, QUANTITY='TEMPERATURE', ID='BDTC_6' /
&DEVC XYZ=0, 0.25, 2.25, QUANTITY='TEMPERATURE', ID='CTC_7' /
&DEVC XYZ=0, 0.25, 0.60, QUANTITY='W-VELOCITY', ID='BD_1' /
&DEVC XYZ=0, 0.25, 0.90, QUANTITY='W-VELOCITY', ID='BD_2' /
&DEVC XYZ=0, 0.25, 1.20, QUANTITY='W-VELOCITY', ID='BD_3' /
&DEVC XYZ=0, 0.25, 1.50, QUANTITY='W-VELOCITY', ID='BD_4' /
&DEVC XYZ=0, 0.25, 1.80, QUANTITY='W-VELOCITY', ID='BD_5' /
&DEVC XYZ=0, 0.25, 2.10, QUANTITY='W-VELOCITY', ID='BD_6' /
&DEVC XYZ=0, 0.25, 1.05, QUANTITY='W-VELOCITY', ID='BD_7' /
&DEVC XYZ=0, 0.25, 1.35, QUANTITY='W-VELOCITY', ID='BD_8' /
&DEVC XYZ=0, 0.25, 1.65, QUANTITY='W-VELOCITY', ID='BD_9' /
&DEVC XYZ=0, 0.25, 1.95, QUANTITY='W-VELOCITY', ID='BD_10' /

WALL TEMPERATURE
&DEVC XYZ=0.0762, 0.05, 0.75, QUANTITY='TEMPERATURE', ID='WTC_1' /
&DEVC XYZ=0.0508, 0.055, 0.75, QUANTITY='TEMPERATURE', ID='WTC_2' /
&DEVC XYZ=0.0254, 0.060, 0.75, QUANTITY='TEMPERATURE', ID='WTC_3' /
&DEVC XYZ=-0.0254, 0.065, 0.75, QUANTITY='TEMPERATURE', ID='WTC_4' /
&DEVC XYZ=-0.0508, 0.070, 0.75, QUANTITY='TEMPERATURE', ID='WTC_5' /
&DEVC XYZ=-0.0762, 0.075, 0.75, QUANTITY='TEMPERATURE', ID='WTC_6' /
&DEVC XYZ=0.0762, 0.085, 1.35, QUANTITY='TEMPERATURE', ID='WTC_7' /
&DEVC XYZ=0.0508, 0.080, 1.35, QUANTITY='TEMPERATURE', ID='WTC_8' /
&DEVC XYZ=0.0254, 0.075, 1.35, QUANTITY='TEMPERATURE', ID='WTC_9' /
&DEVC XYZ=-0.0254, 0.070, 1.35, QUANTITY='TEMPERATURE', ID='WTC_10' /
&DEVC XYZ=-0.0508, 0.065, 1.35, QUANTITY='TEMPERATURE', ID='WTC_11' /
&DEVC XYZ=-0.0762, 0.060, 1.35, QUANTITY='TEMPERATURE', ID='WTC_12' /
&DEVC XYZ=0.0762, 0.065, 1.95, QUANTITY='TEMPERATURE', ID='WTC_13' /
&DEVC XYZ=0.0508, 0.070, 1.95, QUANTITY='TEMPERATURE', ID='WTC_14' /
```

```
&DEVC XYZ=0.0254, 0.075, 1.95, QUANTITY='TEMPERATURE', ID='WTC_15' /
&DEVC XYZ=-0.0254, 0.080, 1.95, QUANTITY='TEMPERATURE', ID='WTC_16' /
&DEVC XYZ=-0.0508, 0.085, 1.95, QUANTITY='TEMPERATURE', ID='WTC_17' /
&DEVC XYZ=-0.0762, 0.090, 1.95, QUANTITY='TEMPERATURE', ID='WTC_18' /

WALL HEAT FLUX MEASUREMENTS
&DEVC XYZ=  0.575, 0.050, 0.575, QUANTITY='GAUGE_HEAT_FLUX', ID='TS_1',  IOR = 2 /
&DEVC XYZ=  0.025, 0.050, 0.575, QUANTITY='GAUGE_HEAT_FLUX', ID='TS_2',  IOR = 2 /
&DEVC XYZ= -0.275, 0.050, 0.575, QUANTITY='GAUGE_HEAT_FLUX', ID='TS_3',  IOR = 2 /
&DEVC XYZ=  0.275, 0.050, 0.875, QUANTITY='GAUGE_HEAT_FLUX', ID='TS_4',  IOR = 2 /
&DEVC XYZ=  -0.025, 0.050, 0.875, QUANTITY='GAUGE_HEAT_FLUX', ID='TS_5',  IOR = 2 /
&DEVC XYZ= -0.575, 0.050, 0.875, QUANTITY='GAUGE_HEAT_FLUX', ID='TS_6',  IOR = 2 /
&DEVC XYZ=  0.575, 0.050, 1.175, QUANTITY='GAUGE_HEAT_FLUX', ID='TS_7',  IOR = 2 /
&DEVC XYZ=  0.025 0.050, 1.175, QUANTITY='GAUGE_HEAT_FLUX', ID='TS_8',  IOR = 2 /
&DEVC XYZ= -0.275, 0.050, 1.175, QUANTITY='GAUGE_HEAT_FLUX', ID='TS_9',  IOR = 2 /
&DEVC XYZ=  0.275, 0.050, 1.475, QUANTITY='GAUGE_HEAT_FLUX', ID='TS_10', IOR = 2 /
&DEVC XYZ=  -0.025, 0.050, 1.475, QUANTITY='GAUGE_HEAT_FLUX', ID='TS_11', IOR = 2 /
&DEVC XYZ= -0.575, 0.050, 1.475, QUANTITY='GAUGE_HEAT_FLUX', ID='TS_12', IOR = 2 /
&DEVC XYZ=  0.575, 0.050, 1.775, QUANTITY='GAUGE_HEAT_FLUX', ID='TS_13', IOR = 2 /
&DEVC XYZ=  0.025, 0.050, 1.775, QUANTITY='GAUGE_HEAT_FLUX', ID='TS_14', IOR = 2 /
&DEVC XYZ= -0.275, 0.050, 1.775, QUANTITY='GAUGE_HEAT_FLUX', ID='TS_15', IOR = 2 /
&DEVC XYZ=  0.275, 0.050, 2.075, QUANTITY='GAUGE_HEAT_FLUX', ID='TS_16', IOR = 2 /
&DEVC XYZ=  -0.025, 0.050, 2.075, QUANTITY='GAUGE_HEAT_FLUX', ID='TS_17', IOR = 2 /
&DEVC XYZ= -0.575, 0.050, 2.075, QUANTITY='GAUGE_HEAT_FLUX', ID='TS_18', IOR = 2 /

&DEVC XYZ=  0.275, 0.050, 0.60, QUANTITY='GAUGE_HEAT_FLUX', ID='HFG_1', IOR = 2 /
&DEVC XYZ= -0.275, 0.050, 0.875, QUANTITY='GAUGE_HEAT_FLUX', ID='HFG_2', IOR = 2 /
&DEVC XYZ=  0.275, 0.050, 1.175, QUANTITY='GAUGE_HEAT_FLUX', ID='HFG_3', IOR = 2 /
&DEVC XYZ= -0.275, 0.050, 1.475, QUANTITY='GAUGE_HEAT_FLUX', ID='HFG_4', IOR = 2 /
&DEVC XYZ=  0.275, 0.050, 1.775, QUANTITY='GAUGE_HEAT_FLUX', ID='HFG_5', IOR = 2 /
&DEVC XYZ= -0.275, 0.050, 2.075, QUANTITY='GAUGE_HEAT_FLUX', ID='HFG_6', IOR = 2 /

WALL NET HEAT FLUX
&DEVC XYZ=  0.575, 0.050, 0.575, QUANTITY='NET HEAT FLUX', ID='TS_1',  IOR = 2 /
&DEVC XYZ=  0.025, 0.050, 0.575, QUANTITY='NET HEAT FLUX', ID='TS_2',  IOR = 2 /
&DEVC XYZ= -0.275, 0.050, 0.575, QUANTITY='NET HEAT FLUX', ID='TS_3',  IOR = 2 /
&DEVC XYZ=  0.275, 0.050, 0.875, QUANTITY='NET HEAT FLUX', ID='TS_4',  IOR = 2 /
&DEVC XYZ=  -0.025, 0.050, 0.875, QUANTITY='NET HEAT FLUX', ID='TS_5',  IOR = 2 /
&DEVC XYZ= -0.575, 0.050, 0.875, QUANTITY='NET HEAT FLUX', ID='TS_6',  IOR = 2 /
&DEVC XYZ=  0.575, 0.050, 1.175, QUANTITY='NET HEAT FLUX', ID='TS_7',  IOR = 2 /
&DEVC XYZ=  0.025 0.050, 1.175, QUANTITY='NET HEAT FLUX', ID='TS_8',  IOR = 2 /
&DEVC XYZ= -0.275, 0.050, 1.175, QUANTITY='NET HEAT FLUX', ID='TS_9',  IOR = 2 /
&DEVC XYZ=  0.275, 0.050, 1.475, QUANTITY='NET HEAT FLUX', ID='TS_10', IOR = 2 /
&DEVC XYZ=  -0.025, 0.050, 1.475, QUANTITY='NET HEAT FLUX', ID='TS_11', IOR = 2 /
&DEVC XYZ= -0.575, 0.050, 1.475, QUANTITY='NET HEAT FLUX', ID='TS_12', IOR = 2 /
&DEVC XYZ=  0.575, 0.050, 1.775, QUANTITY='NET HEAT FLUX', ID='TS_13', IOR = 2 /
&DEVC XYZ=  0.025, 0.050, 1.775, QUANTITY='NET HEAT FLUX', ID='TS_14', IOR = 2 /
&DEVC XYZ= -0.275, 0.050, 1.775, QUANTITY='NET HEAT FLUX', ID='TS_15', IOR = 2 /
```

J.11 Input File 11 – FRP scenario, Rectangle burner, 50 kW continuous, propylene

```
Start Input File
&HEAD CHID='61_1_03-14-2011_FRP_PP_lb_50kW' /

&TIME T_END = 900, DT = 0.05, RESTRICT_TIME_STEP = .FALSE. /
&DUMP DT_BNDF=2.0, DT_DEVC=0.5, DT_HRR=1.0, DT_PL3D=5000.0, DT_SLCF=2.0, DT_RESTART=50./

&MISC
      SURF_DEFAULT = 'INERT'
      TMPA  = 23
      FDS6  = .TRUE.
      DNS = .FALSE.
      DYNSMAG = .TRUE.
      CSMAG = 0.2
      PR = 0.5
      SC = 0.5
      H_EDDY = .TRUE.
      CFL_VELOCITY_NORM = 1
      FLUX_LIMITER = 2
      ISOTHERMAL = .FALSE.
      RADIATION = .TRUE.
      BAROCLINIC = .TRUE.
      CLIP_MASS_FRACTION   = .TRUE.
      CHECK_VN = .TRUE.
      NOBIAS = .TRUE.
      PROJECTION  = .FALSE.
      CHECK_KINETIC_ENERGY = .FALSE.
      /

&REAC
     ID = 'Propylene'
     C = 3
     H = 6
     O = 0
     CO_YIELD = 0.095
     SOOT_YIELD = 0.017
     EDDY_DISSIPATION = .TRUE.
     C_EDC = 0.1
     HRRPUA_SHEET = 0
     HRRPUV_AVERAGE = 2500
      /

&RADI
    RADIATIVE_FRACTION = 0.3
    TIME_STEP_INCREMENT = 3
    ANGLE_INCREMENT = 5
    NUMBER_RADIATION_ANGLES = 104
    /

**** MESHES ****
 MESH IJK= 96, 156, 96, XB=-1.20, 1.20, 0.00, 3.90, 0.00, 2.40 / 2.50 cm grid,  1 mesh

&MESH ID= 'Mesh-1', IJK= 24, 26, 24, XB= -1.2, 0, 0, 1.3, 0, 1.2 / 0.05 cm grid 12 mesh
&MESH ID= 'Mesh-2', IJK= 24, 26, 24, XB= -1.2, 0, 1.3, 2.6, 0, 1.2 / 0.05 cm grid 12 mesh
&MESH ID= 'Mesh-3', IJK= 24, 26, 24, XB= -1.2, 0, 2.6, 3.9, 0, 1.2 / 0.05 cm grid 12 mesh
&MESH ID= 'Mesh-4', IJK= 24, 26, 24, XB= 0, 1.2, 0, 1.3, 0, 1.2 / 0.05 cm grid 12 mesh
&MESH ID= 'Mesh-5', IJK= 24, 26, 24, XB= 0, 1.2, 1.3, 2.6, 0, 1.2 / 0.05 cm grid 12 mesh
&MESH ID= 'Mesh-6', IJK= 24, 26, 24, XB= 0, 1.2, 2.6, 3.9, 0, 1.2 / 0.05 cm grid 12 mesh
&MESH ID= 'Mesh-7', IJK= 24, 26, 24, XB= -1.2, 0, 0, 1.3, 1.2, 2.4 / 0.05 cm grid 12 mesh
&MESH ID= 'Mesh-8', IJK= 24, 26, 24, XB= -1.2, 0, 1.3, 2.6, 1.2, 2.4 / 0.05 cm grid 12 mesh
&MESH ID= 'Mesh-9', IJK= 24, 26, 24, XB= -1.2, 0, 2.6, 3.9, 1.2, 2.4 / 0.05 cm grid 12 mesh
&MESH ID= 'Mesh-10', IJK= 24, 26, 24, XB= 0, 1.2, 0, 1.3, 1.2, 2.4 / 0.05 cm grid 12 mesh
&MESH ID= 'Mesh-11', IJK= 24, 26, 24, XB= 0, 1.2, 1.3, 2.6, 1.2, 2.4 / 0.05 cm grid 12 mesh
&MESH ID= 'Mesh-12', IJK= 24, 26, 24, XB= 0, 1.2, 2.6, 3.9, 1.2, 2.4 / 0.05 cm grid 12 mesh

****BURNER****
2 ft burner
&OBST XB= -0.35, 0.35, 0.05, 0.45, 0, 0.4, SURF_ID = 'ADIABATIC' /
```

```
&VENT XB= -0.3, 0.3, 0.1, 0.4, 0.4, 0.4, SURF_ID = 'BURNER' /

1 ft burner
OBST XB= -0.2, 0.2, 0.05, 0.45, 0, 0.4, SURF_ID = 'ADIABATIC' /
VENT XB= -0.15, 0.15, 0.1, 0.4, 0.4, 0.4, SURF_ID = 'BURNER' /

**** Burner Parameters*****
&SURF ID = 'BURNER'
      HRRPUA =277.8
      RAMP_Q = 'Burner_Ramp'
      COLOR  = 'RED' /

&RAMP ID = 'Burner_Ramp', T=0, F=0 /
&RAMP ID = 'Burner_Ramp', T=1, F=0.5 /
&RAMP ID = 'Burner_Ramp', T=12, F=1 /
&RAMP ID = 'Burner_Ramp', T=900, F=1 /


**** MATERIAL PROPERTIES ****
&MATL ID            ='GYPSUM_MATL'
      SPECIFIC_HEAT = 0.84
      CONDUCTIVITY  = 0.48
      DENSITY       = 1440.0 /

&MATL ID            ='KAOWOOL_MATL'
      SPECIFIC_HEAT = 1.0
      CONDUCTIVITY  = 0.06
      DENSITY       = 320.0 /

&SURF ID        = 'ADIABATIC'
      ADIABATIC = .TRUE.
      RGB       = 0, 0, 0 /

&SURF ID                    = 'KAOWOOL'
      RGB                   = 51,102,255
      BACKING               = 'INSULATED'
      MATL_ID(1,1)          = 'KAOWOOL_MATL'
      MATL_MASS_FRACTION(1,1)= 1.0
      THICKNESS(1)          = 0.025
      CELL_SIZE_FACTOR      = 0.30
      STRETCH_FACTOR        = 1.0 /

&SURF ID                    = 'GYPSUM'
      RGB                   = 100,100,100
      BACKING               = 'INSULATED'
      MATL_ID(1,1)          = 'GYPSUM_MATL'
      MATL_MASS_FRACTION(1,1)= 1.0
      THICKNESS(1)          = 0.016
      CELL_SIZE_FACTOR      = 0.30
      STRETCH_FACTOR        = 1.0 /

&MATL ID                      = 'virgin'
      CONDUCTIVITY            =  0.480
      DENSITY                 = 1467.80
      SPECIFIC_HEAT           =    1.98
      EMISSIVITY              =  0.858
      ABSORPTION_COEFFICIENT  =  0.9000E+10
      RESIDUE(01)             = 'char'
      A(01)                   = 0.1139E+12
      E(01)                   = 0.1483E+06
      N_S(01)                 =   1.00
      THRESHOLD_TEMPERATURE(01)=   0.00
      HEAT_OF_REACTION(01)    =   996.67
      HEAT_OF_COMBUSTION      = 19700.
      NU_FUEL(01)             =   0.421
      NU_RESIDUE(01)          =   0.579
      NU_WATER(01)            =   0.000
      N_REACTIONS             = 01 /

&MATL ID                      = 'char'
      CONDUCTIVITY            =  0.050
```

```
      DENSITY                   =  850.56
      SPECIFIC_HEAT             =    2.12
      EMISSIVITY                =  0.943
      ABSORPTION_COEFFICIENT    =  0.9000E+10
      N_REACTIONS               = 00 /

&SURF ID                          = 'FRP'
      STRETCH_FACTOR              = 1.000
      CELL_SIZE_FACTOR            = 0.200
      THICKNESS(1)               = 0.0019
      MATL_ID(1,1)              = 'virgin'
      MATL_ID(1,2)              = 'char'
      MATL_MASS_FRACTION(1,1)   = 1.0000
      MATL_MASS_FRACTION(1,2)   = 0.0000
      BACKING                     = 'INSULATED'
      SHRINK                      = .TRUE.
      TMP_INNER                   = 27.0
      COLOR                       = 'WHITE' /


****OBSTRUCTIONS****
&OBST XB=-1.200, 1.200, 0.000, 0.000, 0.000, 2.400, SURF_ID ='GYPSUM'  / Back wall
&OBST XB= 1.200, 1.200, 0.000, 2.700, 0.000, 2.400, SURF_ID ='GYPSUM'  / Right wall
&OBST XB=-1.200,-1.200, 0.000, 2.700, 0.000, 2.400, SURF_ID ='GYPSUM'  / Left wall
&OBST XB=-1.200, 1.200, 0.000, 2.700, 2.400, 2.400, SURF_ID ='GYPSUM'  / Ceiling
&OBST XB=-0.900,-0.600, 0.000, 0.05, 0.000, 2.400, SURF_ID ='KAOWOOL' / Kaowool on back wall
&OBST XB= 0.600, 0.900, 0.000, 0.05, 0.000, 2.400, SURF_ID ='KAOWOOL' / Kaowool on back wall
&OBST XB=-0.600, 0.600, 0.000, 0.05, 0.000, 2.400, SURF_ID ='FRP', PERMIT_HOLE = .TRUE. / FRP
panel

****OPEN VENTS****
&VENT XB=-1.20, 1.20, 3.90, 3.90, 0.00, 2.40, SURF_ID = 'OPEN' / Back
&VENT XB=-1.20,-1.20, 2.70, 3.90, 0.00, 2.40, SURF_ID = 'OPEN' /
&VENT XB= 1.20, 1.20, 2.70, 3.90, 0.00, 2.40, SURF_ID = 'OPEN' /
&VENT XB=-1.20, 1.20, 2.70, 3.90, 2.40, 2.40, SURF_ID = 'OPEN' /

HOLES in panel for TSC's:
&HOLE XB= 0.55,  0.60, -0.010, 0.1, 0.55, 0.60 / HOLE 1
&HOLE XB= 0,  0.05, -0.010, 0.1, 0.55, 0.60 / HOLE 2
&HOLE XB= -0.3, -0.25, -0.010, 0.1, 0.55, 0.60 / HOLE 3
&HOLE XB= 0.25,  0.3, -0.010, 0.1, 0.85, 0.9 / HOLE 4
&HOLE XB= -0.05,  0, -0.010, 0.1, 0.85, 0.9 / HOLE 5
&HOLE XB= -0.60, -0.55, -0.010, 0.1, 0.85, 0.9 / HOLE 6
&HOLE XB= 0.55,  0.60, -0.010, 0.1, 1.15, 1.2 / HOLE 7
&HOLE XB= 0, 0.05, -0.010, 0.1, 1.15, 1.2 / HOLE 8
&HOLE XB= -0.3, -0.25, -0.010, 0.1, 1.15, 1.2 / HOLE 9
&HOLE XB= 0.25,  0.3, -0.010, 0.1, 1.45, 1.5 / HOLE 10
&HOLE XB= -0.05,  0, -0.010, 0.1, 1.45, 1.5 / HOLE 11
&HOLE XB=-0.60, -0.55, -0.010, 0.1, 1.45, 1.5 / HOLE 12
&HOLE XB= 0.55,  0.60, -0.010, 0.1, 1.75, 1.8 / HOLE 13
&HOLE XB= 0,  0.05, -0.010, 0.1, 1.75, 1.8 / HOLE 14
&HOLE XB=-0.3, -0.25, -0.010, 0.1, 1.75, 1.8 / HOLE 15
&HOLE XB= 0.25,  0.3, -0.010, 0.1, 2.05, 2.1 / HOLE 16
&HOLE XB= -0.05,  0, -0.010, 0.1, 2.05, 2.1 / HOLE 17
&HOLE XB=-0.60, -0.55, -0.010, 0.1, 2.05, 2.1 / HOLE 18

TSC'S:

&OBST XB= 0.55,  0.60, -0.010, 0.05, 0.55, 0.60, SURF_ID = 'ADIABATIC', PERMIT_HOLE = .FALSE. /
TSC 1
&OBST XB= 0,  0.05, -0.010, 0.05, 0.55, 0.60, SURF_ID = 'ADIABATIC', PERMIT_HOLE = .FALSE. / TSC
2
&OBST XB= -0.3, -0.25, -0.010, 0.05, 0.55, 0.60, SURF_ID = 'ADIABATIC', PERMIT_HOLE = .FALSE. /
TSC 3
&OBST XB= 0.25,  0.3, -0.010, 0.05, 0.85, 0.9, SURF_ID = 'ADIABATIC', PERMIT_HOLE = .FALSE. / TSC
4
&OBST XB= -0.05,  0, -0.010, 0.05, 0.85, 0.9, SURF_ID = 'ADIABATIC', PERMIT_HOLE = .FALSE. / TSC
5
&OBST XB= -0.60, -0.55, -0.010, 0.05, 0.85, 0.9, SURF_ID = 'ADIABATIC', PERMIT_HOLE = .FALSE. /
TSC 6
```

```
&OBST XB= 0.55,  0.60, -0.010, 0.05, 1.15, 1.2, SURF_ID = 'ADIABATIC', PERMIT_HOLE = .FALSE. /
TSC 7
&OBST XB= 0, 0.05, -0.010, 0.05, 1.15, 1.2, SURF_ID = 'ADIABATIC', PERMIT_HOLE = .FALSE. / TSC 8
&OBST XB= -0.3, -0.25, -0.010, 0.05, 1.15, 1.2, SURF_ID = 'ADIABATIC', PERMIT_HOLE = .FALSE. /
TSC 9
&OBST XB= 0.25,  0.3, -0.010, 0.05, 1.45, 1.5, SURF_ID = 'ADIABATIC', PERMIT_HOLE = .FALSE. / TSC
10
&OBST XB= -0.05,  0, -0.010, 0.05, 1.45, 1.5, SURF_ID = 'ADIABATIC', PERMIT_HOLE = .FALSE. / TSC
11
&OBST XB=-0.60, -0.55, -0.010, 0.05, 1.45, 1.5, SURF_ID = 'ADIABATIC', PERMIT_HOLE = .FALSE. /
TSC 12
&OBST XB= 0.55,  0.60, -0.010, 0.05, 1.75, 1.8, SURF_ID = 'ADIABATIC', PERMIT_HOLE = .FALSE. /
TSC 13
&OBST XB= 0,  0.05, -0.010, 0.05, 1.75, 1.8, SURF_ID = 'ADIABATIC', PERMIT_HOLE = .FALSE. / TSC
14
&OBST XB=-0.3, -0.25, -0.010, 0.05, 1.75, 1.8, SURF_ID = 'ADIABATIC', PERMIT_HOLE = .FALSE. / TSC
15
&OBST XB= 0.25,  0.3, -0.010, 0.05, 2.05, 2.1, SURF_ID = 'ADIABATIC', PERMIT_HOLE = .FALSE. / TSC
16
&OBST XB= -0.05,  0, -0.010, 0.05, 2.05, 2.1, SURF_ID = 'ADIABATIC', PERMIT_HOLE = .FALSE. / TSC
17
&OBST XB=-0.60, -0.55, -0.010, 0.05, 2.05, 2.1, SURF_ID = 'ADIABATIC', PERMIT_HOLE = .FALSE. /
TSC 18

&SLCF PBX = 0.0, QUANTITY = 'TEMPERATURE' /
&SLCF PBX = 0.0, QUANTITY = 'HRRPUV' /

&BNDF QUANTITY='GAUGE HEAT FLUX' /
&BNDF QUANTITY='RADIATIVE HEAT FLUX' /
&BNDF QUANTITY='CONVECTIVE HEAT FLUX' /
&BNDF QUANTITY='NET HEAT FLUX' /
&BNDF QUANTITY='WALL TEMPERATURE' /
&BNDF QUANTITY='BURNING RATE' /

CENTERLINE RAKE
&DEVC XYZ=0, 0.25, 0.45, QUANTITY='TEMPERATURE', ID='CTC_1' /
&DEVC XYZ=0, 0.25, 0.60, QUANTITY='TEMPERATURE', ID='BDTC_1' /
&DEVC XYZ=0, 0.25, 0.75, QUANTITY='TEMPERATURE', ID='CTC_2' /
&DEVC XYZ=0, 0.25, 0.90, QUANTITY='TEMPERATURE', ID='BDTC_2' /
&DEVC XYZ=0, 0.25, 1.05, QUANTITY='TEMPERATURE', ID='CTC_3' /
&DEVC XYZ=0, 0.25, 1.20, QUANTITY='TEMPERATURE', ID='BDTC_3' /
&DEVC XYZ=0, 0.25, 1.35, QUANTITY='TEMPERATURE', ID='CTC_4' /
&DEVC XYZ=0, 0.25, 1.50, QUANTITY='TEMPERATURE', ID='BDTC_4' /
&DEVC XYZ=0, 0.25, 1.65, QUANTITY='TEMPERATURE', ID='CTC_5' /
&DEVC XYZ=0, 0.25, 1.80, QUANTITY='TEMPERATURE', ID='BDTC_5' /
&DEVC XYZ=0, 0.25, 1.95, QUANTITY='TEMPERATURE', ID='CTC_6' /
&DEVC XYZ=0, 0.25, 2.10, QUANTITY='TEMPERATURE', ID='BDTC_6' /
&DEVC XYZ=0, 0.25, 2.25, QUANTITY='TEMPERATURE', ID='CTC_7' /
&DEVC XYZ=0, 0.25, 0.60, QUANTITY='W-VELOCITY', ID='BD_1' /
&DEVC XYZ=0, 0.25, 0.90, QUANTITY='W-VELOCITY', ID='BD_2' /
&DEVC XYZ=0, 0.25, 1.20, QUANTITY='W-VELOCITY', ID='BD_3' /
&DEVC XYZ=0, 0.25, 1.50, QUANTITY='W-VELOCITY', ID='BD_4' /
&DEVC XYZ=0, 0.25, 1.80, QUANTITY='W-VELOCITY', ID='BD_5' /
&DEVC XYZ=0, 0.25, 2.10, QUANTITY='W-VELOCITY', ID='BD_6' /
&DEVC XYZ=0, 0.25, 1.05, QUANTITY='W-VELOCITY', ID='BD_7' /
&DEVC XYZ=0, 0.25, 1.35, QUANTITY='W-VELOCITY', ID='BD_8' /
&DEVC XYZ=0, 0.25, 1.65, QUANTITY='W-VELOCITY', ID='BD_9' /
&DEVC XYZ=0, 0.25, 1.95, QUANTITY='W-VELOCITY', ID='BD_10' /

WALL TEMPERATURE
&DEVC XYZ=0.0762, 0.05, 0.75, QUANTITY='TEMPERATURE', ID='WTC_1' /
&DEVC XYZ=0.0508, 0.055, 0.75, QUANTITY='TEMPERATURE', ID='WTC_2' /
&DEVC XYZ=0.0254, 0.060, 0.75, QUANTITY='TEMPERATURE', ID='WTC_3' /
&DEVC XYZ=-0.0254, 0.065, 0.75, QUANTITY='TEMPERATURE', ID='WTC_4' /
&DEVC XYZ=-0.0508, 0.070, 0.75, QUANTITY='TEMPERATURE', ID='WTC_5' /
&DEVC XYZ=-0.0762, 0.075, 0.75, QUANTITY='TEMPERATURE', ID='WTC_6' /
&DEVC XYZ=0.0762, 0.085, 1.35, QUANTITY='TEMPERATURE', ID='WTC_7' /
&DEVC XYZ=0.0508, 0.080, 1.35, QUANTITY='TEMPERATURE', ID='WTC_8' /
&DEVC XYZ=0.0254, 0.075, 1.35, QUANTITY='TEMPERATURE', ID='WTC_9' /
&DEVC XYZ=-0.0254, 0.070, 1.35, QUANTITY='TEMPERATURE', ID='WTC_10' /
&DEVC XYZ=-0.0508, 0.065, 1.35, QUANTITY='TEMPERATURE', ID='WTC_11' /
```

```
&DEVC XYZ=-0.0762, 0.060, 1.35, QUANTITY='TEMPERATURE', ID='WTC_12' /
&DEVC XYZ=0.0762, 0.065, 1.95, QUANTITY='TEMPERATURE', ID='WTC_13' /
&DEVC XYZ=0.0508, 0.070, 1.95, QUANTITY='TEMPERATURE', ID='WTC_14' /
&DEVC XYZ=0.0254, 0.075, 1.95, QUANTITY='TEMPERATURE', ID='WTC_15' /
&DEVC XYZ=-0.0254, 0.080, 1.95, QUANTITY='TEMPERATURE', ID='WTC_16' /
&DEVC XYZ=-0.0508, 0.085, 1.95, QUANTITY='TEMPERATURE', ID='WTC_17' /
&DEVC XYZ=-0.0762, 0.090, 1.95, QUANTITY='TEMPERATURE', ID='WTC_18' /

WALL HEAT FLUX MEASUREMENTS
&DEVC XYZ=  0.575, 0.050, 0.575, QUANTITY='GAUGE_HEAT_FLUX', ID='TS_1',  IOR = 2 /
&DEVC XYZ=  0.025, 0.050, 0.575, QUANTITY='GAUGE_HEAT_FLUX', ID='TS_2',  IOR = 2 /
&DEVC XYZ= -0.275, 0.050, 0.575, QUANTITY='GAUGE_HEAT_FLUX', ID='TS_3',  IOR = 2 /
&DEVC XYZ=  0.275, 0.050, 0.875, QUANTITY='GAUGE_HEAT_FLUX', ID='TS_4',  IOR = 2 /
&DEVC XYZ=  -0.025, 0.050, 0.875, QUANTITY='GAUGE_HEAT_FLUX', ID='TS_5',  IOR = 2 /
&DEVC XYZ= -0.575, 0.050, 0.875, QUANTITY='GAUGE_HEAT_FLUX', ID='TS_6',  IOR = 2 /
&DEVC XYZ=  0.575, 0.050, 1.175, QUANTITY='GAUGE_HEAT_FLUX', ID='TS_7',  IOR = 2 /
&DEVC XYZ=  0.025 0.050, 1.175, QUANTITY='GAUGE_HEAT_FLUX', ID='TS_8',  IOR = 2 /
&DEVC XYZ= -0.275, 0.050, 1.175, QUANTITY='GAUGE_HEAT_FLUX', ID='TS_9',  IOR = 2 /
&DEVC XYZ=  0.275, 0.050, 1.475, QUANTITY='GAUGE_HEAT_FLUX', ID='TS_10', IOR = 2 /
&DEVC XYZ=  -0.025, 0.050, 1.475, QUANTITY='GAUGE_HEAT_FLUX', ID='TS_11', IOR = 2 /
&DEVC XYZ= -0.575, 0.050, 1.475, QUANTITY='GAUGE_HEAT_FLUX', ID='TS_12', IOR = 2 /
&DEVC XYZ=  0.575, 0.050, 1.775, QUANTITY='GAUGE_HEAT_FLUX', ID='TS_13', IOR = 2 /
&DEVC XYZ=  0.025, 0.050, 1.775, QUANTITY='GAUGE_HEAT_FLUX', ID='TS_14', IOR = 2 /
&DEVC XYZ= -0.275, 0.050, 1.775, QUANTITY='GAUGE_HEAT_FLUX', ID='TS_15', IOR = 2 /
&DEVC XYZ=  0.275, 0.050, 2.075, QUANTITY='GAUGE_HEAT_FLUX', ID='TS_16', IOR = 2 /
&DEVC XYZ=  -0.025, 0.050, 2.075, QUANTITY='GAUGE_HEAT_FLUX', ID='TS_17', IOR = 2 /
&DEVC XYZ= -0.575, 0.050, 2.075, QUANTITY='GAUGE_HEAT_FLUX', ID='TS_18', IOR = 2 /

&DEVC XYZ=  0.275, 0.050, 0.60, QUANTITY='GAUGE_HEAT_FLUX', ID='HFG_1', IOR = 2 /
&DEVC XYZ= -0.275, 0.050, 0.875, QUANTITY='GAUGE_HEAT_FLUX', ID='HFG_2', IOR = 2 /
&DEVC XYZ=  0.275, 0.050, 1.175, QUANTITY='GAUGE_HEAT_FLUX', ID='HFG_3', IOR = 2 /
&DEVC XYZ= -0.275, 0.050, 1.475, QUANTITY='GAUGE_HEAT_FLUX', ID='HFG_4', IOR = 2 /
&DEVC XYZ=  0.275, 0.050, 1.775, QUANTITY='GAUGE_HEAT_FLUX', ID='HFG_5', IOR = 2 /
&DEVC XYZ= -0.275, 0.050, 2.075, QUANTITY='GAUGE_HEAT_FLUX', ID='HFG_6', IOR = 2 /

WALL NET HEAT FLUX
&DEVC XYZ=  0.575, 0.050, 0.575, QUANTITY='NET HEAT FLUX', ID='TS_1',  IOR = 2 /
&DEVC XYZ=  0.025, 0.050, 0.575, QUANTITY='NET HEAT FLUX', ID='TS_2',  IOR = 2 /
&DEVC XYZ= -0.275, 0.050, 0.575, QUANTITY='NET HEAT FLUX', ID='TS_3',  IOR = 2 /
&DEVC XYZ=  0.275, 0.050, 0.875, QUANTITY='NET HEAT FLUX', ID='TS_4',  IOR = 2 /
&DEVC XYZ=  -0.025, 0.050, 0.875, QUANTITY='NET HEAT FLUX', ID='TS_5',  IOR = 2 /
&DEVC XYZ= -0.575, 0.050, 0.875, QUANTITY='NET HEAT FLUX', ID='TS_6',  IOR = 2 /
&DEVC XYZ=  0.575, 0.050, 1.175, QUANTITY='NET HEAT FLUX', ID='TS_7',  IOR = 2 /
&DEVC XYZ=  0.025 0.050, 1.175, QUANTITY='NET HEAT FLUX', ID='TS_8',  IOR = 2 /
&DEVC XYZ= -0.275, 0.050, 1.175, QUANTITY='NET HEAT FLUX', ID='TS_9',  IOR = 2 /
&DEVC XYZ=  0.275, 0.050, 1.475, QUANTITY='NET HEAT FLUX', ID='TS_10', IOR = 2 /
&DEVC XYZ=  -0.025, 0.050, 1.475, QUANTITY='NET HEAT FLUX', ID='TS_11', IOR = 2 /
&DEVC XYZ= -0.575, 0.050, 1.475, QUANTITY='NET HEAT FLUX', ID='TS_12', IOR = 2 /
&DEVC XYZ=  0.575, 0.050, 1.775, QUANTITY='NET HEAT FLUX', ID='TS_13', IOR = 2 /
&DEVC XYZ=  0.025, 0.050, 1.775, QUANTITY='NET HEAT FLUX', ID='TS_14', IOR = 2 /
&DEVC XYZ= -0.275, 0.050, 1.775, QUANTITY='NET HEAT FLUX', ID='TS_15', IOR = 2 /
```

J.12 Input File 12 – FRP scenario, Square burner, 50 kW continuous, propylene

```
Start Input File
&HEAD CHID='62_1_03-14-2011_FRP_PP_lb_50kW' /

&TIME T_END = 900, DT = 0.05, RESTRICT_TIME_STEP = .FALSE. /
&DUMP DT_BNDF=2.0, DT_DEVC=0.5, DT_HRR=1.0, DT_PL3D=5000.0, DT_SLCF=2.0, DT_RESTART=50./

&MISC
      SURF_DEFAULT = 'INERT'
      TMPA  = 23
      FDS6  = .TRUE.
      DNS = .FALSE.
      DYNSMAG = .TRUE.
      CSMAG = 0.2
      PR = 0.5
      SC = 0.5
      H_EDDY = .TRUE.
      CFL_VELOCITY_NORM = 1
      FLUX_LIMITER = 2
      ISOTHERMAL = .FALSE.
      RADIATION = .TRUE.
      BAROCLINIC = .TRUE.
      CLIP_MASS_FRACTION   = .TRUE.
      CHECK_VN = .TRUE.
      NOBIAS = .TRUE.
      PROJECTION  = .FALSE.
      CHECK_KINETIC_ENERGY = .FALSE.
      /

&REAC
     ID = 'Propylene'
     C = 3
     H = 6
     O = 0
     CO_YIELD = 0.095
     SOOT_YIELD = 0.017
     EDDY_DISSIPATION = .TRUE.
     C_EDC = 0.1
     HRRPUA_SHEET = 0
     HRRPUV_AVERAGE = 2500
      /

&RADI
    RADIATIVE_FRACTION = 0.3
    TIME_STEP_INCREMENT = 3
    ANGLE_INCREMENT = 5
    NUMBER_RADIATION_ANGLES = 104
    /

**** MESHES ****
 MESH IJK= 96, 156, 96, XB=-1.20, 1.20, 0.00, 3.90, 0.00, 2.40 / 2.50 cm grid,  1 mesh

&MESH ID= 'Mesh-1', IJK= 24, 26, 24, XB= -1.2, 0, 0, 1.3, 0, 1.2 / 0.05 cm grid 12 mesh
&MESH ID= 'Mesh-2', IJK= 24, 26, 24, XB= -1.2, 0, 1.3, 2.6, 0, 1.2 / 0.05 cm grid 12 mesh
&MESH ID= 'Mesh-3', IJK= 24, 26, 24, XB= -1.2, 0, 2.6, 3.9, 0, 1.2 / 0.05 cm grid 12 mesh
&MESH ID= 'Mesh-4', IJK= 24, 26, 24, XB= 0, 1.2, 0, 1.3, 0, 1.2 / 0.05 cm grid 12 mesh
&MESH ID= 'Mesh-5', IJK= 24, 26, 24, XB= 0, 1.2, 1.3, 2.6, 0, 1.2 / 0.05 cm grid 12 mesh
&MESH ID= 'Mesh-6', IJK= 24, 26, 24, XB= 0, 1.2, 2.6, 3.9, 0, 1.2 / 0.05 cm grid 12 mesh
&MESH ID= 'Mesh-7', IJK= 24, 26, 24, XB= -1.2, 0, 0, 1.3, 1.2, 2.4 / 0.05 cm grid 12 mesh
&MESH ID= 'Mesh-8', IJK= 24, 26, 24, XB= -1.2, 0, 1.3, 2.6, 1.2, 2.4 / 0.05 cm grid 12 mesh
&MESH ID= 'Mesh-9', IJK= 24, 26, 24, XB= -1.2, 0, 2.6, 3.9, 1.2, 2.4 / 0.05 cm grid 12 mesh
&MESH ID= 'Mesh-10', IJK= 24, 26, 24, XB= 0, 1.2, 0, 1.3, 1.2, 2.4 / 0.05 cm grid 12 mesh
&MESH ID= 'Mesh-11', IJK= 24, 26, 24, XB= 0, 1.2, 1.3, 2.6, 1.2, 2.4 / 0.05 cm grid 12 mesh
&MESH ID= 'Mesh-12', IJK= 24, 26, 24, XB= 0, 1.2, 2.6, 3.9, 1.2, 2.4 / 0.05 cm grid 12 mesh

****BURNER****
2 ft burner
OBST XB= -0.35, 0.35, 0.05, 0.45, 0, 0.4, SURF_ID = 'ADIABATIC' /
```

```
VENT XB= -0.3, 0.3, 0.1, 0.4, 0.4, 0.4, SURF_ID = 'BURNER' /

1 ft burner
&OBST XB= -0.2, 0.2, 0.05, 0.45, 0, 0.4, SURF_ID = 'ADIABATIC' /
&VENT XB= -0.15, 0.15, 0.1, 0.4, 0.4, 0.4, SURF_ID = 'BURNER' /

**** Burner Parameters*****
&SURF ID = 'BURNER'
      HRRPUA =555.6
      RAMP_Q = 'Burner_Ramp'
      COLOR  = 'RED' /

&RAMP ID = 'Burner_Ramp', T=0, F=0 /
&RAMP ID = 'Burner_Ramp', T=1, F=0.5 /
&RAMP ID = 'Burner_Ramp', T=12, F=1 /
&RAMP ID = 'Burner_Ramp', T=900, F=1 /


**** MATERIAL PROPERTIES ****
&MATL ID            ='GYPSUM_MATL'
      SPECIFIC_HEAT = 0.84
      CONDUCTIVITY  = 0.48
      DENSITY       = 1440.0 /

&MATL ID            ='KAOWOOL_MATL'
      SPECIFIC_HEAT = 1.0
      CONDUCTIVITY  = 0.06
      DENSITY       = 320.0 /

&SURF ID        = 'ADIABATIC'
      ADIABATIC = .TRUE.
      RGB       = 0, 0, 0 /

&SURF ID                    = 'KAOWOOL'
      RGB                   = 51,102,255
      BACKING               = 'INSULATED'
      MATL_ID(1,1)          = 'KAOWOOL_MATL'
      MATL_MASS_FRACTION(1,1)= 1.0
      THICKNESS(1)          = 0.025
      CELL_SIZE_FACTOR      = 0.30
      STRETCH_FACTOR        = 1.0 /

&SURF ID                    = 'GYPSUM'
      RGB                   = 100,100,100
      BACKING               = 'INSULATED'
      MATL_ID(1,1)          = 'GYPSUM_MATL'
      MATL_MASS_FRACTION(1,1)= 1.0
      THICKNESS(1)          = 0.016
      CELL_SIZE_FACTOR      = 0.30
      STRETCH_FACTOR        = 1.0 /

&MATL ID                      = 'virgin'
      CONDUCTIVITY            =  0.480
      DENSITY                 = 1467.80
      SPECIFIC_HEAT           =    1.98
      EMISSIVITY              =  0.858
      ABSORPTION_COEFFICIENT  =  0.9000E+10
      RESIDUE(01)             = 'char'
      A(01)                   = 0.1139E+12
      E(01)                   = 0.1483E+06
      N_S(01)                 =   1.00
      THRESHOLD_TEMPERATURE(01)=   0.00
      HEAT_OF_REACTION(01)    =   996.67
      HEAT_OF_COMBUSTION      = 19700.
      NU_FUEL(01)             =   0.421
      NU_RESIDUE(01)          =   0.579
      NU_WATER(01)            =   0.000
      N_REACTIONS             = 01 /

&MATL ID                      = 'char'
      CONDUCTIVITY            =  0.050
```

```
      DENSITY                  =  850.56
      SPECIFIC_HEAT            =    2.12
      EMISSIVITY               =  0.943
      ABSORPTION_COEFFICIENT   =  0.9000E+10
      N_REACTIONS              = 00 /

&SURF ID                         = 'FRP'
      STRETCH_FACTOR             = 1.000
      CELL_SIZE_FACTOR           = 0.200
      THICKNESS(1)              = 0.0019
      MATL_ID(1,1)             = 'virgin'
      MATL_ID(1,2)             = 'char'
      MATL_MASS_FRACTION(1,1)  = 1.0000
      MATL_MASS_FRACTION(1,2)  = 0.0000
      BACKING                    = 'INSULATED'
      SHRINK                     = .TRUE.
      TMP_INNER                  = 27.0
      COLOR                      = 'WHITE' /


****OBSTRUCTIONS****
&OBST XB=-1.200, 1.200, 0.000, 0.000, 0.000, 2.400, SURF_ID ='GYPSUM'  / Back wall
&OBST XB= 1.200, 1.200, 0.000, 2.700, 0.000, 2.400, SURF_ID ='GYPSUM'  / Right wall
&OBST XB=-1.200,-1.200, 0.000, 2.700, 0.000, 2.400, SURF_ID ='GYPSUM'  / Left wall
&OBST XB=-1.200, 1.200, 0.000, 2.700, 2.400, 2.400, SURF_ID ='GYPSUM'  / Ceiling
&OBST XB=-0.900,-0.600, 0.000, 0.05, 0.000, 2.400, SURF_ID ='KAOWOOL' / Kaowool on back wall
&OBST XB= 0.600, 0.900, 0.000, 0.05, 0.000, 2.400, SURF_ID ='KAOWOOL' / Kaowool on back wall
&OBST XB=-0.600, 0.600, 0.000, 0.05, 0.000, 2.400, SURF_ID ='FRP', PERMIT_HOLE = .TRUE. / FRP
panel

****OPEN VENTS****
&VENT XB=-1.20, 1.20, 3.90, 3.90, 0.00, 2.40, SURF_ID = 'OPEN' / Back
&VENT XB=-1.20,-1.20, 2.70, 3.90, 0.00, 2.40, SURF_ID = 'OPEN' /
&VENT XB= 1.20, 1.20, 2.70, 3.90, 0.00, 2.40, SURF_ID = 'OPEN' /
&VENT XB=-1.20, 1.20, 2.70, 3.90, 2.40, 2.40, SURF_ID = 'OPEN' /

HOLES in panel for TSC's:
&HOLE XB= 0.55,  0.60, -0.010, 0.1, 0.55, 0.60 / HOLE 1
&HOLE XB= 0,  0.05, -0.010, 0.1, 0.55, 0.60 / HOLE 2
&HOLE XB= -0.3, -0.25, -0.010, 0.1, 0.55, 0.60 / HOLE 3
&HOLE XB= 0.25,  0.3, -0.010, 0.1, 0.85, 0.9 / HOLE 4
&HOLE XB= -0.05,  0, -0.010, 0.1, 0.85, 0.9 / HOLE 5
&HOLE XB= -0.60, -0.55, -0.010, 0.1, 0.85, 0.9 / HOLE 6
&HOLE XB= 0.55,  0.60, -0.010, 0.1, 1.15, 1.2 / HOLE 7
&HOLE XB= 0, 0.05, -0.010, 0.1, 1.15, 1.2 / HOLE 8
&HOLE XB= -0.3, -0.25, -0.010, 0.1, 1.15, 1.2 / HOLE 9
&HOLE XB= 0.25,  0.3, -0.010, 0.1, 1.45, 1.5 / HOLE 10
&HOLE XB= -0.05,  0, -0.010, 0.1, 1.45, 1.5 / HOLE 11
&HOLE XB=-0.60, -0.55, -0.010, 0.1, 1.45, 1.5 / HOLE 12
&HOLE XB= 0.55,  0.60, -0.010, 0.1, 1.75, 1.8 / HOLE 13
&HOLE XB= 0,  0.05, -0.010, 0.1, 1.75, 1.8 / HOLE 14
&HOLE XB=-0.3, -0.25, -0.010, 0.1, 1.75, 1.8 / HOLE 15
&HOLE XB= 0.25,  0.3, -0.010, 0.1, 2.05, 2.1 / HOLE 16
&HOLE XB= -0.05,  0, -0.010, 0.1, 2.05, 2.1 / HOLE 17
&HOLE XB=-0.60, -0.55, -0.010, 0.1, 2.05, 2.1 / HOLE 18

TSC'S:

&OBST XB= 0.55,  0.60, -0.010, 0.05, 0.55, 0.60, SURF_ID = 'ADIABATIC', PERMIT_HOLE = .FALSE. /
TSC 1
&OBST XB= 0,  0.05, -0.010, 0.05, 0.55, 0.60, SURF_ID = 'ADIABATIC', PERMIT_HOLE = .FALSE. / TSC
2
&OBST XB= -0.3, -0.25, -0.010, 0.05, 0.55, 0.60, SURF_ID = 'ADIABATIC', PERMIT_HOLE = .FALSE. /
TSC 3
&OBST XB= 0.25,  0.3, -0.010, 0.05, 0.85, 0.9, SURF_ID = 'ADIABATIC', PERMIT_HOLE = .FALSE. / TSC
4
&OBST XB= -0.05,  0, -0.010, 0.05, 0.85, 0.9, SURF_ID = 'ADIABATIC', PERMIT_HOLE = .FALSE. / TSC
5
&OBST XB= -0.60, -0.55, -0.010, 0.05, 0.85, 0.9, SURF_ID = 'ADIABATIC', PERMIT_HOLE = .FALSE. /
TSC 6
```

```
&OBST XB= 0.55,  0.60, -0.010, 0.05, 1.15, 1.2, SURF_ID = 'ADIABATIC', PERMIT_HOLE = .FALSE. /
TSC 7
&OBST XB= 0, 0.05, -0.010, 0.05, 1.15, 1.2, SURF_ID = 'ADIABATIC', PERMIT_HOLE = .FALSE. / TSC 8
&OBST XB= -0.3, -0.25, -0.010, 0.05, 1.15, 1.2, SURF_ID = 'ADIABATIC', PERMIT_HOLE = .FALSE. /
TSC 9
&OBST XB= 0.25,  0.3, -0.010, 0.05, 1.45, 1.5, SURF_ID = 'ADIABATIC', PERMIT_HOLE = .FALSE. / TSC
10
&OBST XB= -0.05,  0, -0.010, 0.05, 1.45, 1.5, SURF_ID = 'ADIABATIC', PERMIT_HOLE = .FALSE. / TSC
11
&OBST XB=-0.60, -0.55, -0.010, 0.05, 1.45, 1.5, SURF_ID = 'ADIABATIC', PERMIT_HOLE = .FALSE. /
TSC 12
&OBST XB= 0.55,  0.60, -0.010, 0.05, 1.75, 1.8, SURF_ID = 'ADIABATIC', PERMIT_HOLE = .FALSE. /
TSC 13
&OBST XB= 0,  0.05, -0.010, 0.05, 1.75, 1.8, SURF_ID = 'ADIABATIC', PERMIT_HOLE = .FALSE. / TSC
14
&OBST XB=-0.3, -0.25, -0.010, 0.05, 1.75, 1.8, SURF_ID = 'ADIABATIC', PERMIT_HOLE = .FALSE. / TSC
15
&OBST XB= 0.25,  0.3, -0.010, 0.05, 2.05, 2.1, SURF_ID = 'ADIABATIC', PERMIT_HOLE = .FALSE. / TSC
16
&OBST XB= -0.05,  0, -0.010, 0.05, 2.05, 2.1, SURF_ID = 'ADIABATIC', PERMIT_HOLE = .FALSE. / TSC
17
&OBST XB=-0.60, -0.55, -0.010, 0.05, 2.05, 2.1, SURF_ID = 'ADIABATIC', PERMIT_HOLE = .FALSE. /
TSC 18

&SLCF PBX = 0.0, QUANTITY = 'TEMPERATURE' /
&SLCF PBX = 0.0, QUANTITY = 'HRRPUV' /

&BNDF QUANTITY='GAUGE HEAT FLUX' /
&BNDF QUANTITY='RADIATIVE HEAT FLUX' /
&BNDF QUANTITY='CONVECTIVE HEAT FLUX' /
&BNDF QUANTITY='NET HEAT FLUX' /
&BNDF QUANTITY='WALL TEMPERATURE' /
&BNDF QUANTITY='BURNING RATE' /

CENTERLINE RAKE
&DEVC XYZ=0, 0.25, 0.45, QUANTITY='TEMPERATURE', ID='CTC_1' /
&DEVC XYZ=0, 0.25, 0.60, QUANTITY='TEMPERATURE', ID='BDTC_1' /
&DEVC XYZ=0, 0.25, 0.75, QUANTITY='TEMPERATURE', ID='CTC_2' /
&DEVC XYZ=0, 0.25, 0.90, QUANTITY='TEMPERATURE', ID='BDTC_2' /
&DEVC XYZ=0, 0.25, 1.05, QUANTITY='TEMPERATURE', ID='CTC_3' /
&DEVC XYZ=0, 0.25, 1.20, QUANTITY='TEMPERATURE', ID='BDTC_3' /
&DEVC XYZ=0, 0.25, 1.35, QUANTITY='TEMPERATURE', ID='CTC_4' /
&DEVC XYZ=0, 0.25, 1.50, QUANTITY='TEMPERATURE', ID='BDTC_4' /
&DEVC XYZ=0, 0.25, 1.65, QUANTITY='TEMPERATURE', ID='CTC_5' /
&DEVC XYZ=0, 0.25, 1.80, QUANTITY='TEMPERATURE', ID='BDTC_5' /
&DEVC XYZ=0, 0.25, 1.95, QUANTITY='TEMPERATURE', ID='CTC_6' /
&DEVC XYZ=0, 0.25, 2.10, QUANTITY='TEMPERATURE', ID='BDTC_6' /
&DEVC XYZ=0, 0.25, 2.25, QUANTITY='TEMPERATURE', ID='CTC_7' /
&DEVC XYZ=0, 0.25, 0.60, QUANTITY='W-VELOCITY', ID='BD_1' /
&DEVC XYZ=0, 0.25, 0.90, QUANTITY='W-VELOCITY', ID='BD_2' /
&DEVC XYZ=0, 0.25, 1.20, QUANTITY='W-VELOCITY', ID='BD_3' /
&DEVC XYZ=0, 0.25, 1.50, QUANTITY='W-VELOCITY', ID='BD_4' /
&DEVC XYZ=0, 0.25, 1.80, QUANTITY='W-VELOCITY', ID='BD_5' /
&DEVC XYZ=0, 0.25, 2.10, QUANTITY='W-VELOCITY', ID='BD_6' /
&DEVC XYZ=0, 0.25, 1.05, QUANTITY='W-VELOCITY', ID='BD_7' /
&DEVC XYZ=0, 0.25, 1.35, QUANTITY='W-VELOCITY', ID='BD_8' /
&DEVC XYZ=0, 0.25, 1.65, QUANTITY='W-VELOCITY', ID='BD_9' /
&DEVC XYZ=0, 0.25, 1.95, QUANTITY='W-VELOCITY', ID='BD_10' /

WALL TEMPERATURE
&DEVC XYZ=0.0762, 0.05, 0.75, QUANTITY='TEMPERATURE', ID='WTC_1' /
&DEVC XYZ=0.0508, 0.055, 0.75, QUANTITY='TEMPERATURE', ID='WTC_2' /
&DEVC XYZ=0.0254, 0.060, 0.75, QUANTITY='TEMPERATURE', ID='WTC_3' /
&DEVC XYZ=-0.0254, 0.065, 0.75, QUANTITY='TEMPERATURE', ID='WTC_4' /
&DEVC XYZ=-0.0508, 0.070, 0.75, QUANTITY='TEMPERATURE', ID='WTC_5' /
&DEVC XYZ=-0.0762, 0.075, 0.75, QUANTITY='TEMPERATURE', ID='WTC_6' /
&DEVC XYZ=0.0762, 0.085, 1.35, QUANTITY='TEMPERATURE', ID='WTC_7' /
&DEVC XYZ=0.0508, 0.080, 1.35, QUANTITY='TEMPERATURE', ID='WTC_8' /
&DEVC XYZ=0.0254, 0.075, 1.35, QUANTITY='TEMPERATURE', ID='WTC_9' /
&DEVC XYZ=-0.0254, 0.070, 1.35, QUANTITY='TEMPERATURE', ID='WTC_10' /
&DEVC XYZ=-0.0508, 0.065, 1.35, QUANTITY='TEMPERATURE', ID='WTC_11' /
```

```
&DEVC XYZ=-0.0762, 0.060, 1.35, QUANTITY='TEMPERATURE', ID='WTC_12' /
&DEVC XYZ=0.0762, 0.065, 1.95, QUANTITY='TEMPERATURE', ID='WTC_13' /
&DEVC XYZ=0.0508, 0.070, 1.95, QUANTITY='TEMPERATURE', ID='WTC_14' /
&DEVC XYZ=0.0254, 0.075, 1.95, QUANTITY='TEMPERATURE', ID='WTC_15' /
&DEVC XYZ=-0.0254, 0.080, 1.95, QUANTITY='TEMPERATURE', ID='WTC_16' /
&DEVC XYZ=-0.0508, 0.085, 1.95, QUANTITY='TEMPERATURE', ID='WTC_17' /
&DEVC XYZ=-0.0762, 0.090, 1.95, QUANTITY='TEMPERATURE', ID='WTC_18' /

WALL HEAT FLUX MEASUREMENTS
&DEVC XYZ=  0.575, 0.050, 0.575, QUANTITY='GAUGE_HEAT_FLUX', ID='TS_1',  IOR = 2 /
&DEVC XYZ=  0.025, 0.050, 0.575, QUANTITY='GAUGE_HEAT_FLUX', ID='TS_2',  IOR = 2 /
&DEVC XYZ= -0.275, 0.050, 0.575, QUANTITY='GAUGE_HEAT_FLUX', ID='TS_3',  IOR = 2 /
&DEVC XYZ=  0.275, 0.050, 0.875, QUANTITY='GAUGE_HEAT_FLUX', ID='TS_4',  IOR = 2 /
&DEVC XYZ=  -0.025, 0.050, 0.875, QUANTITY='GAUGE_HEAT_FLUX', ID='TS_5',  IOR = 2 /
&DEVC XYZ= -0.575, 0.050, 0.875, QUANTITY='GAUGE_HEAT_FLUX', ID='TS_6',  IOR = 2 /
&DEVC XYZ=  0.575, 0.050, 1.175, QUANTITY='GAUGE_HEAT_FLUX', ID='TS_7',  IOR = 2 /
&DEVC XYZ=  0.025 0.050, 1.175, QUANTITY='GAUGE_HEAT_FLUX', ID='TS_8',  IOR = 2 /
&DEVC XYZ= -0.275, 0.050, 1.175, QUANTITY='GAUGE_HEAT_FLUX', ID='TS_9',  IOR = 2 /
&DEVC XYZ=  0.275, 0.050, 1.475, QUANTITY='GAUGE_HEAT_FLUX', ID='TS_10', IOR = 2 /
&DEVC XYZ=  -0.025, 0.050, 1.475, QUANTITY='GAUGE_HEAT_FLUX', ID='TS_11', IOR = 2 /
&DEVC XYZ= -0.575, 0.050, 1.475, QUANTITY='GAUGE_HEAT_FLUX', ID='TS_12', IOR = 2 /
&DEVC XYZ=  0.575, 0.050, 1.775, QUANTITY='GAUGE_HEAT_FLUX', ID='TS_13', IOR = 2 /
&DEVC XYZ=  0.025, 0.050, 1.775, QUANTITY='GAUGE_HEAT_FLUX', ID='TS_14', IOR = 2 /
&DEVC XYZ= -0.275, 0.050, 1.775, QUANTITY='GAUGE_HEAT_FLUX', ID='TS_15', IOR = 2 /
&DEVC XYZ=  0.275, 0.050, 2.075, QUANTITY='GAUGE_HEAT_FLUX', ID='TS_16', IOR = 2 /
&DEVC XYZ=  -0.025, 0.050, 2.075, QUANTITY='GAUGE_HEAT_FLUX', ID='TS_17', IOR = 2 /
&DEVC XYZ= -0.575, 0.050, 2.075, QUANTITY='GAUGE_HEAT_FLUX', ID='TS_18', IOR = 2 /

&DEVC XYZ=  0.275, 0.050, 0.60, QUANTITY='GAUGE_HEAT_FLUX', ID='HFG_1', IOR = 2 /
&DEVC XYZ= -0.275, 0.050, 0.875, QUANTITY='GAUGE_HEAT_FLUX', ID='HFG_2', IOR = 2 /
&DEVC XYZ=  0.275, 0.050, 1.175, QUANTITY='GAUGE_HEAT_FLUX', ID='HFG_3', IOR = 2 /
&DEVC XYZ= -0.275, 0.050, 1.475, QUANTITY='GAUGE_HEAT_FLUX', ID='HFG_4', IOR = 2 /
&DEVC XYZ=  0.275, 0.050, 1.775, QUANTITY='GAUGE_HEAT_FLUX', ID='HFG_5', IOR = 2 /
&DEVC XYZ= -0.275, 0.050, 2.075, QUANTITY='GAUGE_HEAT_FLUX', ID='HFG_6', IOR = 2 /

WALL NET HEAT FLUX
&DEVC XYZ=  0.575, 0.050, 0.575, QUANTITY='NET HEAT FLUX', ID='TS_1',  IOR = 2 /
&DEVC XYZ=  0.025, 0.050, 0.575, QUANTITY='NET HEAT FLUX', ID='TS_2',  IOR = 2 /
&DEVC XYZ= -0.275, 0.050, 0.575, QUANTITY='NET HEAT FLUX', ID='TS_3',  IOR = 2 /
&DEVC XYZ=  0.275, 0.050, 0.875, QUANTITY='NET HEAT FLUX', ID='TS_4',  IOR = 2 /
&DEVC XYZ=  -0.025, 0.050, 0.875, QUANTITY='NET HEAT FLUX', ID='TS_5',  IOR = 2 /
&DEVC XYZ= -0.575, 0.050, 0.875, QUANTITY='NET HEAT FLUX', ID='TS_6',  IOR = 2 /
&DEVC XYZ=  0.575, 0.050, 1.175, QUANTITY='NET HEAT FLUX', ID='TS_7',  IOR = 2 /
&DEVC XYZ=  0.025 0.050, 1.175, QUANTITY='NET HEAT FLUX', ID='TS_8',  IOR = 2 /
&DEVC XYZ= -0.275, 0.050, 1.175, QUANTITY='NET HEAT FLUX', ID='TS_9',  IOR = 2 /
&DEVC XYZ=  0.275, 0.050, 1.475, QUANTITY='NET HEAT FLUX', ID='TS_10', IOR = 2 /
&DEVC XYZ=  -0.025, 0.050, 1.475, QUANTITY='NET HEAT FLUX', ID='TS_11', IOR = 2 /
&DEVC XYZ= -0.575, 0.050, 1.475, QUANTITY='NET HEAT FLUX', ID='TS_12', IOR = 2 /
&DEVC XYZ=  0.575, 0.050, 1.775, QUANTITY='NET HEAT FLUX', ID='TS_13', IOR = 2 /
&DEVC XYZ=  0.025, 0.050, 1.775, QUANTITY='NET HEAT FLUX', ID='TS_14', IOR = 2 /
&DEVC XYZ= -0.275, 0.050, 1.775, QUANTITY='NET HEAT FLUX', ID='TS_15', IOR = 2 /
```

J.13 Input File 13 – FRP scenario, Square burner, 75 kW, propylene

```
Start Input File
&HEAD CHID='63_1_03-14-2011_FRP_PP_sb_75kW' /

&TIME T_END = 900, DT = 0.05, RESTRICT_TIME_STEP = .FALSE. /
&DUMP DT_BNDF=2.0, DT_DEVC=0.5, DT_HRR=1.0, DT_PL3D=5000.0, DT_SLCF=2.0, DT_RESTART=50./

&MISC
      SURF_DEFAULT = 'INERT'
      TMPA  = 23
      FDS6  = .TRUE.
      DNS = .FALSE.
      DYNSMAG = .TRUE.
      CSMAG = 0.2
      PR = 0.5
      SC = 0.5
      H_EDDY = .TRUE.
      CFL_VELOCITY_NORM = 1
      FLUX_LIMITER = 2
      ISOTHERMAL = .FALSE.
      RADIATION = .TRUE.
      BAROCLINIC = .TRUE.
      CLIP_MASS_FRACTION   = .TRUE.
      CHECK_VN = .TRUE.
      NOBIAS = .TRUE.
      PROJECTION  = .FALSE.
      CHECK_KINETIC_ENERGY = .FALSE.
      /

&REAC
     ID = 'Propylene'
     C = 3
     H = 6
     O = 0
     CO_YIELD = 0.095
     SOOT_YIELD = 0.017
     EDDY_DISSIPATION = .TRUE.
     C_EDC = 0.1
     HRRPUA_SHEET = 0
     HRRPUV_AVERAGE = 2500
      /

&RADI
    RADIATIVE_FRACTION = 0.3
    TIME_STEP_INCREMENT = 3
    ANGLE_INCREMENT = 5
    NUMBER_RADIATION_ANGLES = 104
    /

**** MESHES ****
 MESH IJK= 96, 156, 96, XB=-1.20, 1.20, 0.00, 3.90, 0.00, 2.40 / 2.50 cm grid,  1 mesh

&MESH ID= 'Mesh-1', IJK= 24, 26, 24, XB= -1.2, 0, 0, 1.3, 0, 1.2 / 0.05 cm grid 12 mesh
&MESH ID= 'Mesh-2', IJK= 24, 26, 24, XB= -1.2, 0, 1.3, 2.6, 0, 1.2 / 0.05 cm grid 12 mesh
&MESH ID= 'Mesh-3', IJK= 24, 26, 24, XB= -1.2, 0, 2.6, 3.9, 0, 1.2 / 0.05 cm grid 12 mesh
&MESH ID= 'Mesh-4', IJK= 24, 26, 24, XB= 0, 1.2, 0, 1.3, 0, 1.2 / 0.05 cm grid 12 mesh
&MESH ID= 'Mesh-5', IJK= 24, 26, 24, XB= 0, 1.2, 1.3, 2.6, 0, 1.2 / 0.05 cm grid 12 mesh
&MESH ID= 'Mesh-6', IJK= 24, 26, 24, XB= 0, 1.2, 2.6, 3.9, 0, 1.2 / 0.05 cm grid 12 mesh
&MESH ID= 'Mesh-7', IJK= 24, 26, 24, XB= -1.2, 0, 0, 1.3, 1.2, 2.4 / 0.05 cm grid 12 mesh
&MESH ID= 'Mesh-8', IJK= 24, 26, 24, XB= -1.2, 0, 1.3, 2.6, 1.2, 2.4 / 0.05 cm grid 12 mesh
&MESH ID= 'Mesh-9', IJK= 24, 26, 24, XB= -1.2, 0, 2.6, 3.9, 1.2, 2.4 / 0.05 cm grid 12 mesh
&MESH ID= 'Mesh-10', IJK= 24, 26, 24, XB= 0, 1.2, 0, 1.3, 1.2, 2.4 / 0.05 cm grid 12 mesh
&MESH ID= 'Mesh-11', IJK= 24, 26, 24, XB= 0, 1.2, 1.3, 2.6, 1.2, 2.4 / 0.05 cm grid 12 mesh
&MESH ID= 'Mesh-12', IJK= 24, 26, 24, XB= 0, 1.2, 2.6, 3.9, 1.2, 2.4 / 0.05 cm grid 12 mesh

****BURNER****
2 ft burner
OBST XB= -0.35, 0.35, 0.05, 0.45, 0, 0.4, SURF_ID = 'ADIABATIC' /
VENT XB= -0.3, 0.3, 0.1, 0.4, 0.4, 0.4, SURF_ID = 'BURNER' /
```

```
1 ft burner
&OBST XB= -0.2, 0.2, 0.05, 0.45, 0, 0.4, SURF_ID = 'ADIABATIC' /
&VENT XB= -0.15, 0.15, 0.1, 0.4, 0.4, 0.4, SURF_ID = 'BURNER' /

**** Burner Parameters*****
&SURF ID = 'BURNER'
      HRRPUA =833.3
      RAMP_Q = 'Burner_Ramp'
      COLOR  = 'RED' /

&RAMP ID = 'Burner_Ramp', T=0, F=0 /
&RAMP ID = 'Burner_Ramp', T=1, F=0.5 /
&RAMP ID = 'Burner_Ramp', T=15, F=1 /
&RAMP ID = 'Burner_Ramp', T=56, F=1 /
&RAMP ID = 'Burner_Ramp', T=66, F=0 /

**** MATERIAL PROPERTIES ****
&MATL ID            ='GYPSUM_MATL'
      SPECIFIC_HEAT = 0.84
      CONDUCTIVITY  = 0.48
      DENSITY       = 1440.0 /

&MATL ID            ='KAOWOOL_MATL'
      SPECIFIC_HEAT = 1.0
      CONDUCTIVITY  = 0.06
      DENSITY       = 320.0 /

&SURF ID        = 'ADIABATIC'
      ADIABATIC = .TRUE.
      RGB       = 0, 0, 0 /

&SURF ID                      = 'KAOWOOL'
      RGB                     = 51,102,255
      BACKING                 = 'INSULATED'
      MATL_ID(1,1)            = 'KAOWOOL_MATL'
      MATL_MASS_FRACTION(1,1)= 1.0
      THICKNESS(1)            = 0.025
      CELL_SIZE_FACTOR        = 0.30
      STRETCH_FACTOR          = 1.0 /

&SURF ID                      = 'GYPSUM'
      RGB                     = 100,100,100
      BACKING                 = 'INSULATED'
      MATL_ID(1,1)            = 'GYPSUM_MATL'
      MATL_MASS_FRACTION(1,1)= 1.0
      THICKNESS(1)            = 0.016
      CELL_SIZE_FACTOR        = 0.30
      STRETCH_FACTOR          = 1.0 /

&MATL ID                        = 'virgin'
      CONDUCTIVITY              =  0.480
      DENSITY                   = 1467.80
      SPECIFIC_HEAT             =    1.98
      EMISSIVITY                =  0.858
      ABSORPTION_COEFFICIENT    =  0.9000E+10
      RESIDUE(01)               = 'char'
      A(01)                     = 0.1139E+12
      E(01)                     = 0.1483E+06
      N_S(01)                   =   1.00
      THRESHOLD_TEMPERATURE(01)=   0.00
      HEAT_OF_REACTION(01)      =   996.67
      HEAT_OF_COMBUSTION        = 19700.
      NU_FUEL(01)               =   0.421
      NU_RESIDUE(01)            =   0.579
      NU_WATER(01)              =   0.000
      N_REACTIONS               = 01 /

&MATL ID                        = 'char'
      CONDUCTIVITY              =  0.050
      DENSITY                   =  850.56
      SPECIFIC_HEAT             =    2.12
```

```
      EMISSIVITY               =  0.943
      ABSORPTION_COEFFICIENT   =  0.9000E+10
      N_REACTIONS              = 00 /

&SURF ID                         = 'FRP'
      STRETCH_FACTOR             = 1.000
      CELL_SIZE_FACTOR           = 0.200
      THICKNESS(1)              = 0.0019
      MATL_ID(1,1)             = 'virgin'
      MATL_ID(1,2)             = 'char'
      MATL_MASS_FRACTION(1,1)  = 1.0000
      MATL_MASS_FRACTION(1,2)  = 0.0000
      BACKING                    = 'INSULATED'
      SHRINK                     = .TRUE.
      TMP_INNER                  = 27.0
      COLOR                      = 'WHITE' /


****OBSTRUCTIONS****
&OBST XB=-1.200, 1.200, 0.000, 0.000, 0.000, 2.400, SURF_ID ='GYPSUM'  / Back wall
&OBST XB= 1.200, 1.200, 0.000, 2.700, 0.000, 2.400, SURF_ID ='GYPSUM'  / Right wall
&OBST XB=-1.200,-1.200, 0.000, 2.700, 0.000, 2.400, SURF_ID ='GYPSUM'  / Left wall
&OBST XB=-1.200, 1.200, 0.000, 2.700, 2.400, 2.400, SURF_ID ='GYPSUM'  / Ceiling
&OBST XB=-0.900,-0.600, 0.000, 0.05, 0.000, 2.400, SURF_ID ='KAOWOOL' / Kaowool on back wall
&OBST XB= 0.600, 0.900, 0.000, 0.05, 0.000, 2.400, SURF_ID ='KAOWOOL' / Kaowool on back wall
&OBST XB=-0.600, 0.600, 0.000, 0.05, 0.000, 2.400, SURF_ID ='FRP', PERMIT_HOLE = .TRUE. / FRP
panel

****OPEN VENTS****
&VENT XB=-1.20, 1.20, 3.90, 3.90, 0.00, 2.40, SURF_ID = 'OPEN' / Back
&VENT XB=-1.20,-1.20, 2.70, 3.90, 0.00, 2.40, SURF_ID = 'OPEN' /
&VENT XB= 1.20, 1.20, 2.70, 3.90, 0.00, 2.40, SURF_ID = 'OPEN' /
&VENT XB=-1.20, 1.20, 2.70, 3.90, 2.40, 2.40, SURF_ID = 'OPEN' /

HOLES in panel for TSC's:
&HOLE XB= 0.55,  0.60, -0.010, 0.1, 0.55, 0.60 / HOLE 1
&HOLE XB= 0,  0.05, -0.010, 0.1, 0.55, 0.60 / HOLE 2
&HOLE XB= -0.3, -0.25, -0.010, 0.1, 0.55, 0.60 / HOLE 3
&HOLE XB= 0.25,  0.3, -0.010, 0.1, 0.85, 0.9 / HOLE 4
&HOLE XB= -0.05,  0, -0.010, 0.1, 0.85, 0.9 / HOLE 5
&HOLE XB= -0.60, -0.55, -0.010, 0.1, 0.85, 0.9 / HOLE 6
&HOLE XB= 0.55,  0.60, -0.010, 0.1, 1.15, 1.2 / HOLE 7
&HOLE XB= 0, 0.05, -0.010, 0.1, 1.15, 1.2 / HOLE 8
&HOLE XB= -0.3, -0.25, -0.010, 0.1, 1.15, 1.2 / HOLE 9
&HOLE XB= 0.25,  0.3, -0.010, 0.1, 1.45, 1.5 / HOLE 10
&HOLE XB= -0.05,  0, -0.010, 0.1, 1.45, 1.5 / HOLE 11
&HOLE XB=-0.60, -0.55, -0.010, 0.1, 1.45, 1.5 / HOLE 12
&HOLE XB= 0.55,  0.60, -0.010, 0.1, 1.75, 1.8 / HOLE 13
&HOLE XB= 0,  0.05, -0.010, 0.1, 1.75, 1.8 / HOLE 14
&HOLE XB=-0.3, -0.25, -0.010, 0.1, 1.75, 1.8 / HOLE 15
&HOLE XB= 0.25,  0.3, -0.010, 0.1, 2.05, 2.1 / HOLE 16
&HOLE XB= -0.05,  0, -0.010, 0.1, 2.05, 2.1 / HOLE 17
&HOLE XB=-0.60, -0.55, -0.010, 0.1, 2.05, 2.1 / HOLE 18

TSC'S:

&OBST XB= 0.55,  0.60, -0.010, 0.05, 0.55, 0.60, SURF_ID = 'ADIABATIC', PERMIT_HOLE = .FALSE. /
TSC 1
&OBST XB= 0,  0.05, -0.010, 0.05, 0.55, 0.60, SURF_ID = 'ADIABATIC', PERMIT_HOLE = .FALSE. / TSC
2
&OBST XB= -0.3, -0.25, -0.010, 0.05, 0.55, 0.60, SURF_ID = 'ADIABATIC', PERMIT_HOLE = .FALSE. /
TSC 3
&OBST XB= 0.25,  0.3, -0.010, 0.05, 0.85, 0.9, SURF_ID = 'ADIABATIC', PERMIT_HOLE = .FALSE. / TSC
4
&OBST XB= -0.05,  0, -0.010, 0.05, 0.85, 0.9, SURF_ID = 'ADIABATIC', PERMIT_HOLE = .FALSE. / TSC
5
&OBST XB= -0.60, -0.55, -0.010, 0.05, 0.85, 0.9, SURF_ID = 'ADIABATIC', PERMIT_HOLE = .FALSE. /
TSC 6
&OBST XB= 0.55,  0.60, -0.010, 0.05, 1.15, 1.2, SURF_ID = 'ADIABATIC', PERMIT_HOLE = .FALSE. /
TSC 7
&OBST XB= 0, 0.05, -0.010, 0.05, 1.15, 1.2, SURF_ID = 'ADIABATIC', PERMIT_HOLE = .FALSE. / TSC 8
```

```
&OBST XB= -0.3, -0.25, -0.010, 0.05, 1.15, 1.2, SURF_ID = 'ADIABATIC', PERMIT_HOLE = .FALSE. /
TSC 9
&OBST XB= 0.25,  0.3, -0.010, 0.05, 1.45, 1.5, SURF_ID = 'ADIABATIC', PERMIT_HOLE = .FALSE. / TSC
10
&OBST XB= -0.05,  0, -0.010, 0.05, 1.45, 1.5, SURF_ID = 'ADIABATIC', PERMIT_HOLE = .FALSE. / TSC
11
&OBST XB=-0.60, -0.55, -0.010, 0.05, 1.45, 1.5, SURF_ID = 'ADIABATIC', PERMIT_HOLE = .FALSE. /
TSC 12
&OBST XB= 0.55,  0.60, -0.010, 0.05, 1.75, 1.8, SURF_ID = 'ADIABATIC', PERMIT_HOLE = .FALSE. /
TSC 13
&OBST XB= 0,  0.05, -0.010, 0.05, 1.75, 1.8, SURF_ID = 'ADIABATIC', PERMIT_HOLE = .FALSE. / TSC
14
&OBST XB=-0.3, -0.25, -0.010, 0.05, 1.75, 1.8, SURF_ID = 'ADIABATIC', PERMIT_HOLE = .FALSE. / TSC
15
&OBST XB= 0.25,  0.3, -0.010, 0.05, 2.05, 2.1, SURF_ID = 'ADIABATIC', PERMIT_HOLE = .FALSE. / TSC
16
&OBST XB= -0.05,  0, -0.010, 0.05, 2.05, 2.1, SURF_ID = 'ADIABATIC', PERMIT_HOLE = .FALSE. / TSC
17
&OBST XB=-0.60, -0.55, -0.010, 0.05, 2.05, 2.1, SURF_ID = 'ADIABATIC', PERMIT_HOLE = .FALSE. /
TSC 18

&SLCF PBX = 0.0, QUANTITY = 'TEMPERATURE' /
&SLCF PBX = 0.0, QUANTITY = 'HRRPUV' /

&BNDF QUANTITY='GAUGE HEAT FLUX' /
&BNDF QUANTITY='RADIATIVE HEAT FLUX' /
&BNDF QUANTITY='CONVECTIVE HEAT FLUX' /
&BNDF QUANTITY='NET HEAT FLUX' /
&BNDF QUANTITY='WALL TEMPERATURE' /
&BNDF QUANTITY='BURNING RATE' /

CENTERLINE RAKE
&DEVC XYZ=0, 0.25, 0.45, QUANTITY='TEMPERATURE', ID='CTC_1' /
&DEVC XYZ=0, 0.25, 0.60, QUANTITY='TEMPERATURE', ID='BDTC_1' /
&DEVC XYZ=0, 0.25, 0.75, QUANTITY='TEMPERATURE', ID='CTC_2' /
&DEVC XYZ=0, 0.25, 0.90, QUANTITY='TEMPERATURE', ID='BDTC_2' /
&DEVC XYZ=0, 0.25, 1.05, QUANTITY='TEMPERATURE', ID='CTC_3' /
&DEVC XYZ=0, 0.25, 1.20, QUANTITY='TEMPERATURE', ID='BDTC_3' /
&DEVC XYZ=0, 0.25, 1.35, QUANTITY='TEMPERATURE', ID='CTC_4' /
&DEVC XYZ=0, 0.25, 1.50, QUANTITY='TEMPERATURE', ID='BDTC_4' /
&DEVC XYZ=0, 0.25, 1.65, QUANTITY='TEMPERATURE', ID='CTC_5' /
&DEVC XYZ=0, 0.25, 1.80, QUANTITY='TEMPERATURE', ID='BDTC_5' /
&DEVC XYZ=0, 0.25, 1.95, QUANTITY='TEMPERATURE', ID='CTC_6' /
&DEVC XYZ=0, 0.25, 2.10, QUANTITY='TEMPERATURE', ID='BDTC_6' /
&DEVC XYZ=0, 0.25, 2.25, QUANTITY='TEMPERATURE', ID='CTC_7' /
&DEVC XYZ=0, 0.25, 0.60, QUANTITY='W-VELOCITY', ID='BD_1' /
&DEVC XYZ=0, 0.25, 0.90, QUANTITY='W-VELOCITY', ID='BD_2' /
&DEVC XYZ=0, 0.25, 1.20, QUANTITY='W-VELOCITY', ID='BD_3' /
&DEVC XYZ=0, 0.25, 1.50, QUANTITY='W-VELOCITY', ID='BD_4' /
&DEVC XYZ=0, 0.25, 1.80, QUANTITY='W-VELOCITY', ID='BD_5' /
&DEVC XYZ=0, 0.25, 2.10, QUANTITY='W-VELOCITY', ID='BD_6' /
&DEVC XYZ=0, 0.25, 1.05, QUANTITY='W-VELOCITY', ID='BD_7' /
&DEVC XYZ=0, 0.25, 1.35, QUANTITY='W-VELOCITY', ID='BD_8' /
&DEVC XYZ=0, 0.25, 1.65, QUANTITY='W-VELOCITY', ID='BD_9' /
&DEVC XYZ=0, 0.25, 1.95, QUANTITY='W-VELOCITY', ID='BD_10' /

WALL TEMPERATURE
&DEVC XYZ=0.0762, 0.05, 0.75, QUANTITY='TEMPERATURE', ID='WTC_1' /
&DEVC XYZ=0.0508, 0.055, 0.75, QUANTITY='TEMPERATURE', ID='WTC_2' /
&DEVC XYZ=0.0254, 0.060, 0.75, QUANTITY='TEMPERATURE', ID='WTC_3' /
&DEVC XYZ=-0.0254, 0.065, 0.75, QUANTITY='TEMPERATURE', ID='WTC_4' /
&DEVC XYZ=-0.0508, 0.070, 0.75, QUANTITY='TEMPERATURE', ID='WTC_5' /
&DEVC XYZ=-0.0762, 0.075, 0.75, QUANTITY='TEMPERATURE', ID='WTC_6' /
&DEVC XYZ=0.0762, 0.085, 1.35, QUANTITY='TEMPERATURE', ID='WTC_7' /
&DEVC XYZ=0.0508, 0.080, 1.35, QUANTITY='TEMPERATURE', ID='WTC_8' /
&DEVC XYZ=0.0254, 0.075, 1.35, QUANTITY='TEMPERATURE', ID='WTC_9' /
&DEVC XYZ=-0.0254, 0.070, 1.35, QUANTITY='TEMPERATURE', ID='WTC_10' /
&DEVC XYZ=-0.0508, 0.065, 1.35, QUANTITY='TEMPERATURE', ID='WTC_11' /
&DEVC XYZ=-0.0762, 0.060, 1.35, QUANTITY='TEMPERATURE', ID='WTC_12' /
&DEVC XYZ=0.0762, 0.065, 1.95, QUANTITY='TEMPERATURE', ID='WTC_13' /
&DEVC XYZ=0.0508, 0.070, 1.95, QUANTITY='TEMPERATURE', ID='WTC_14' /
```

```
&DEVC XYZ=0.0254, 0.075, 1.95, QUANTITY='TEMPERATURE', ID='WTC_15' /
&DEVC XYZ=-0.0254, 0.080, 1.95, QUANTITY='TEMPERATURE', ID='WTC_16' /
&DEVC XYZ=-0.0508, 0.085, 1.95, QUANTITY='TEMPERATURE', ID='WTC_17' /
&DEVC XYZ=-0.0762, 0.090, 1.95, QUANTITY='TEMPERATURE', ID='WTC_18' /

WALL HEAT FLUX MEASUREMENTS
&DEVC XYZ=  0.575, 0.050, 0.575, QUANTITY='GAUGE_HEAT_FLUX', ID='TS_1',  IOR = 2 /
&DEVC XYZ=  0.025, 0.050, 0.575, QUANTITY='GAUGE_HEAT_FLUX', ID='TS_2',  IOR = 2 /
&DEVC XYZ= -0.275, 0.050, 0.575, QUANTITY='GAUGE_HEAT_FLUX', ID='TS_3',  IOR = 2 /
&DEVC XYZ=  0.275, 0.050, 0.875, QUANTITY='GAUGE_HEAT_FLUX', ID='TS_4',  IOR = 2 /
&DEVC XYZ=  -0.025, 0.050, 0.875, QUANTITY='GAUGE_HEAT_FLUX', ID='TS_5',  IOR = 2 /
&DEVC XYZ= -0.575, 0.050, 0.875, QUANTITY='GAUGE_HEAT_FLUX', ID='TS_6',  IOR = 2 /
&DEVC XYZ=  0.575, 0.050, 1.175, QUANTITY='GAUGE_HEAT_FLUX', ID='TS_7',  IOR = 2 /
&DEVC XYZ=  0.025 0.050, 1.175, QUANTITY='GAUGE_HEAT_FLUX', ID='TS_8',  IOR = 2 /
&DEVC XYZ= -0.275, 0.050, 1.175, QUANTITY='GAUGE_HEAT_FLUX', ID='TS_9',  IOR = 2 /
&DEVC XYZ=  0.275, 0.050, 1.475, QUANTITY='GAUGE_HEAT_FLUX', ID='TS_10', IOR = 2 /
&DEVC XYZ=  -0.025, 0.050, 1.475, QUANTITY='GAUGE_HEAT_FLUX', ID='TS_11', IOR = 2 /
&DEVC XYZ= -0.575, 0.050, 1.475, QUANTITY='GAUGE_HEAT_FLUX', ID='TS_12', IOR = 2 /
&DEVC XYZ=  0.575, 0.050, 1.775, QUANTITY='GAUGE_HEAT_FLUX', ID='TS_13', IOR = 2 /
&DEVC XYZ=  0.025, 0.050, 1.775, QUANTITY='GAUGE_HEAT_FLUX', ID='TS_14', IOR = 2 /
&DEVC XYZ= -0.275, 0.050, 1.775, QUANTITY='GAUGE_HEAT_FLUX', ID='TS_15', IOR = 2 /
&DEVC XYZ=  0.275, 0.050, 2.075, QUANTITY='GAUGE_HEAT_FLUX', ID='TS_16', IOR = 2 /
&DEVC XYZ=  -0.025, 0.050, 2.075, QUANTITY='GAUGE_HEAT_FLUX', ID='TS_17', IOR = 2 /
&DEVC XYZ= -0.575, 0.050, 2.075, QUANTITY='GAUGE_HEAT_FLUX', ID='TS_18', IOR = 2 /

&DEVC XYZ=  0.275, 0.050, 0.60, QUANTITY='GAUGE_HEAT_FLUX', ID='HFG_1', IOR = 2 /
&DEVC XYZ= -0.275, 0.050, 0.875, QUANTITY='GAUGE_HEAT_FLUX', ID='HFG_2', IOR = 2 /
&DEVC XYZ=  0.275, 0.050, 1.175, QUANTITY='GAUGE_HEAT_FLUX', ID='HFG_3', IOR = 2 /
&DEVC XYZ= -0.275, 0.050, 1.475, QUANTITY='GAUGE_HEAT_FLUX', ID='HFG_4', IOR = 2 /
&DEVC XYZ=  0.275, 0.050, 1.775, QUANTITY='GAUGE_HEAT_FLUX', ID='HFG_5', IOR = 2 /
&DEVC XYZ= -0.275, 0.050, 2.075, QUANTITY='GAUGE_HEAT_FLUX', ID='HFG_6', IOR = 2 /

WALL NET HEAT FLUX
&DEVC XYZ=  0.575, 0.050, 0.575, QUANTITY='NET HEAT FLUX', ID='TS_1',  IOR = 2 /
&DEVC XYZ=  0.025, 0.050, 0.575, QUANTITY='NET HEAT FLUX', ID='TS_2',  IOR = 2 /
&DEVC XYZ= -0.275, 0.050, 0.575, QUANTITY='NET HEAT FLUX', ID='TS_3',  IOR = 2 /
&DEVC XYZ=  0.275, 0.050, 0.875, QUANTITY='NET HEAT FLUX', ID='TS_4',  IOR = 2 /
&DEVC XYZ=  -0.025, 0.050, 0.875, QUANTITY='NET HEAT FLUX', ID='TS_5',  IOR = 2 /
&DEVC XYZ= -0.575, 0.050, 0.875, QUANTITY='NET HEAT FLUX', ID='TS_6',  IOR = 2 /
&DEVC XYZ=  0.575, 0.050, 1.175, QUANTITY='NET HEAT FLUX', ID='TS_7',  IOR = 2 /
&DEVC XYZ=  0.025 0.050, 1.175, QUANTITY='NET HEAT FLUX', ID='TS_8',  IOR = 2 /
&DEVC XYZ= -0.275, 0.050, 1.175, QUANTITY='NET HEAT FLUX', ID='TS_9',  IOR = 2 /
&DEVC XYZ=  0.275, 0.050, 1.475, QUANTITY='NET HEAT FLUX', ID='TS_10', IOR = 2 /
&DEVC XYZ=  -0.025, 0.050, 1.475, QUANTITY='NET HEAT FLUX', ID='TS_11', IOR = 2 /
&DEVC XYZ= -0.575, 0.050, 1.475, QUANTITY='NET HEAT FLUX', ID='TS_12', IOR = 2 /
&DEVC XYZ=  0.575, 0.050, 1.775, QUANTITY='NET HEAT FLUX', ID='TS_13', IOR = 2 /
&DEVC XYZ=  0.025, 0.050, 1.775, QUANTITY='NET HEAT FLUX', ID='TS_14', IOR = 2 /
&DEVC XYZ= -0.275, 0.050, 1.775, QUANTITY='NET HEAT FLUX', ID='TS_15', IOR = 2 /
```

J.14 Input File 14 – FRP scenario, Square burner, 50 kW, propane

```
Start Input File
&HEAD CHID='64_1_03-14-2011_FRP_Pr_sb_50kW' /

&TIME T_END = 900, DT = 0.05, RESTRICT_TIME_STEP = .FALSE. /
&DUMP DT_BNDF=2.0, DT_DEVC=0.5, DT_HRR=1.0, DT_PL3D=5000.0, DT_SLCF=2.0, DT_RESTART=50./

&MISC
      SURF_DEFAULT = 'INERT'
      TMPA  = 23
      FDS6  = .TRUE.
      DNS = .FALSE.
      DYNSMAG = .TRUE.
      CSMAG = 0.2
      PR = 0.5
      SC = 0.5
      H_EDDY = .TRUE.
      CFL_VELOCITY_NORM = 1
      FLUX_LIMITER = 2
      ISOTHERMAL = .FALSE.
      RADIATION = .TRUE.
      BAROCLINIC = .TRUE.
      CLIP_MASS_FRACTION   = .TRUE.
      CHECK_VN = .TRUE.
      NOBIAS = .TRUE.
      PROJECTION  = .FALSE.
      CHECK_KINETIC_ENERGY = .FALSE.
      /

&REAC
     ID = 'Propane'
     C = 3
     H = 8
     O = 0
     CO_YIELD = 0.024
     SOOT_YIELD = 0.005
     EDDY_DISSIPATION = .TRUE.
     C_EDC = 0.1
     HRRPUA_SHEET = 0
     HRRPUV_AVERAGE = 2500
      /

&RADI
    RADIATIVE_FRACTION = 0.3
    TIME_STEP_INCREMENT = 3
    ANGLE_INCREMENT = 5
    NUMBER_RADIATION_ANGLES = 104
    /

**** MESHES ****
 MESH IJK= 96, 156, 96, XB=-1.20, 1.20, 0.00, 3.90, 0.00, 2.40 / 2.50 cm grid,  1 mesh

&MESH ID= 'Mesh-1', IJK= 24, 26, 24, XB= -1.2, 0, 0, 1.3, 0, 1.2 / 0.05 cm grid 12 mesh
&MESH ID= 'Mesh-2', IJK= 24, 26, 24, XB= -1.2, 0, 1.3, 2.6, 0, 1.2 / 0.05 cm grid 12 mesh
&MESH ID= 'Mesh-3', IJK= 24, 26, 24, XB= -1.2, 0, 2.6, 3.9, 0, 1.2 / 0.05 cm grid 12 mesh
&MESH ID= 'Mesh-4', IJK= 24, 26, 24, XB= 0, 1.2, 0, 1.3, 0, 1.2 / 0.05 cm grid 12 mesh
&MESH ID= 'Mesh-5', IJK= 24, 26, 24, XB= 0, 1.2, 1.3, 2.6, 0, 1.2 / 0.05 cm grid 12 mesh
&MESH ID= 'Mesh-6', IJK= 24, 26, 24, XB= 0, 1.2, 2.6, 3.9, 0, 1.2 / 0.05 cm grid 12 mesh
&MESH ID= 'Mesh-7', IJK= 24, 26, 24, XB= -1.2, 0, 0, 1.3, 1.2, 2.4 / 0.05 cm grid 12 mesh
&MESH ID= 'Mesh-8', IJK= 24, 26, 24, XB= -1.2, 0, 1.3, 2.6, 1.2, 2.4 / 0.05 cm grid 12 mesh
&MESH ID= 'Mesh-9', IJK= 24, 26, 24, XB= -1.2, 0, 2.6, 3.9, 1.2, 2.4 / 0.05 cm grid 12 mesh
&MESH ID= 'Mesh-10', IJK= 24, 26, 24, XB= 0, 1.2, 0, 1.3, 1.2, 2.4 / 0.05 cm grid 12 mesh
&MESH ID= 'Mesh-11', IJK= 24, 26, 24, XB= 0, 1.2, 1.3, 2.6, 1.2, 2.4 / 0.05 cm grid 12 mesh
&MESH ID= 'Mesh-12', IJK= 24, 26, 24, XB= 0, 1.2, 2.6, 3.9, 1.2, 2.4 / 0.05 cm grid 12 mesh

****BURNER****
2 ft burner
OBST XB= -0.35, 0.35, 0.05, 0.45, 0, 0.4, SURF_ID = 'ADIABATIC' /
VENT XB= -0.3, 0.3, 0.1, 0.4, 0.4, 0.4, SURF_ID = 'BURNER' /
```

```
1 ft burner
&OBST XB= -0.2, 0.2, 0.05, 0.45, 0, 0.4, SURF_ID = 'ADIABATIC' /
&VENT XB= -0.15, 0.15, 0.1, 0.4, 0.4, 0.4, SURF_ID = 'BURNER' /

**** Burner Parameters*****
&SURF ID = 'BURNER'
      HRRPUA =555.6
      RAMP_Q = 'Burner_Ramp'
      COLOR  = 'RED' /

&RAMP ID = 'Burner_Ramp', T=0, F=0 /
&RAMP ID = 'Burner_Ramp', T=1, F=0.5 /
&RAMP ID = 'Burner_Ramp', T=15, F=1 /
&RAMP ID = 'Burner_Ramp', T=75, F=1 /
&RAMP ID = 'Burner_Ramp', T=85, F=0 /

**** MATERIAL PROPERTIES ****
&MATL ID            ='GYPSUM_MATL'
      SPECIFIC_HEAT = 0.84
      CONDUCTIVITY  = 0.48
      DENSITY       = 1440.0 /

&MATL ID            ='KAOWOOL_MATL'
      SPECIFIC_HEAT = 1.0
      CONDUCTIVITY  = 0.06
      DENSITY       = 320.0 /

&SURF ID        = 'ADIABATIC'
      ADIABATIC = .TRUE.
      RGB       = 0, 0, 0 /

&SURF ID                     = 'KAOWOOL'
      RGB                    = 51,102,255
      BACKING                = 'INSULATED'
      MATL_ID(1,1)           = 'KAOWOOL_MATL'
      MATL_MASS_FRACTION(1,1)= 1.0
      THICKNESS(1)           = 0.025
      CELL_SIZE_FACTOR       = 0.30
      STRETCH_FACTOR         = 1.0 /

&SURF ID                     = 'GYPSUM'
      RGB                    = 100,100,100
      BACKING                = 'INSULATED'
      MATL_ID(1,1)           = 'GYPSUM_MATL'
      MATL_MASS_FRACTION(1,1)= 1.0
      THICKNESS(1)           = 0.016
      CELL_SIZE_FACTOR       = 0.30
      STRETCH_FACTOR         = 1.0 /

&MATL ID                       = 'virgin'
      CONDUCTIVITY             =  0.480
      DENSITY                  = 1467.80
      SPECIFIC_HEAT            =    1.98
      EMISSIVITY               =  0.858
      ABSORPTION_COEFFICIENT   =  0.9000E+10
      RESIDUE(01)              = 'char'
      A(01)                    = 0.1139E+12
      E(01)                    = 0.1483E+06
      N_S(01)                  =   1.00
      THRESHOLD_TEMPERATURE(01)=   0.00
      HEAT_OF_REACTION(01)     =   996.67
      HEAT_OF_COMBUSTION       = 19700.
      NU_FUEL(01)              =   0.421
      NU_RESIDUE(01)           =   0.579
      NU_WATER(01)             =   0.000
      N_REACTIONS              = 01 /

&MATL ID                       = 'char'
      CONDUCTIVITY             =  0.050
      DENSITY                  =  850.56
      SPECIFIC_HEAT            =    2.12
```

```
      EMISSIVITY               =  0.943
      ABSORPTION_COEFFICIENT   =  0.9000E+10
      N_REACTIONS              = 00 /

&SURF ID                        = 'FRP'
      STRETCH_FACTOR            = 1.000
      CELL_SIZE_FACTOR          = 0.200
      THICKNESS(1)             = 0.0019
      MATL_ID(1,1)             = 'virgin'
      MATL_ID(1,2)             = 'char'
      MATL_MASS_FRACTION(1,1)  = 1.0000
      MATL_MASS_FRACTION(1,2)  = 0.0000
      BACKING                   = 'INSULATED'
      SHRINK                    = .TRUE.
      TMP_INNER                 = 27.0
      COLOR                     = 'WHITE' /


****OBSTRUCTIONS****
&OBST XB=-1.200, 1.200, 0.000, 0.000, 0.000, 2.400, SURF_ID ='GYPSUM'  / Back wall
&OBST XB= 1.200, 1.200, 0.000, 2.700, 0.000, 2.400, SURF_ID ='GYPSUM'  / Right wall
&OBST XB=-1.200,-1.200, 0.000, 2.700, 0.000, 2.400, SURF_ID ='GYPSUM'  / Left wall
&OBST XB=-1.200, 1.200, 0.000, 2.700, 2.400, 2.400, SURF_ID ='GYPSUM'  / Ceiling
&OBST XB=-0.900,-0.600, 0.000, 0.05, 0.000, 2.400, SURF_ID ='KAOWOOL' / Kaowool on back wall
&OBST XB= 0.600, 0.900, 0.000, 0.05, 0.000, 2.400, SURF_ID ='KAOWOOL' / Kaowool on back wall
&OBST XB=-0.600, 0.600, 0.000, 0.05, 0.000, 2.400, SURF_ID ='FRP', PERMIT_HOLE = .TRUE. / FRP
panel

****OPEN VENTS****
&VENT XB=-1.20, 1.20, 3.90, 3.90, 0.00, 2.40, SURF_ID = 'OPEN' / Back
&VENT XB=-1.20,-1.20, 2.70, 3.90, 0.00, 2.40, SURF_ID = 'OPEN' /
&VENT XB= 1.20, 1.20, 2.70, 3.90, 0.00, 2.40, SURF_ID = 'OPEN' /
&VENT XB=-1.20, 1.20, 2.70, 3.90, 2.40, 2.40, SURF_ID = 'OPEN' /

HOLES in panel for TSC's:
&HOLE XB= 0.55,  0.60, -0.010, 0.1, 0.55, 0.60 / HOLE 1
&HOLE XB= 0,  0.05, -0.010, 0.1, 0.55, 0.60 / HOLE 2
&HOLE XB= -0.3, -0.25, -0.010, 0.1, 0.55, 0.60 / HOLE 3
&HOLE XB= 0.25,  0.3, -0.010, 0.1, 0.85, 0.9 / HOLE 4
&HOLE XB= -0.05,  0, -0.010, 0.1, 0.85, 0.9 / HOLE 5
&HOLE XB= -0.60, -0.55, -0.010, 0.1, 0.85, 0.9 / HOLE 6
&HOLE XB= 0.55,  0.60, -0.010, 0.1, 1.15, 1.2 / HOLE 7
&HOLE XB= 0, 0.05, -0.010, 0.1, 1.15, 1.2 / HOLE 8
&HOLE XB= -0.3, -0.25, -0.010, 0.1, 1.15, 1.2 / HOLE 9
&HOLE XB= 0.25,  0.3, -0.010, 0.1, 1.45, 1.5 / HOLE 10
&HOLE XB= -0.05,  0, -0.010, 0.1, 1.45, 1.5 / HOLE 11
&HOLE XB=-0.60, -0.55, -0.010, 0.1, 1.45, 1.5 / HOLE 12
&HOLE XB= 0.55,  0.60, -0.010, 0.1, 1.75, 1.8 / HOLE 13
&HOLE XB= 0,  0.05, -0.010, 0.1, 1.75, 1.8 / HOLE 14
&HOLE XB=-0.3, -0.25, -0.010, 0.1, 1.75, 1.8 / HOLE 15
&HOLE XB= 0.25,  0.3, -0.010, 0.1, 2.05, 2.1 / HOLE 16
&HOLE XB= -0.05,  0, -0.010, 0.1, 2.05, 2.1 / HOLE 17
&HOLE XB=-0.60, -0.55, -0.010, 0.1, 2.05, 2.1 / HOLE 18

TSC'S:

&OBST XB= 0.55,  0.60, -0.010, 0.05, 0.55, 0.60, SURF_ID = 'ADIABATIC', PERMIT_HOLE = .FALSE. /
TSC 1
&OBST XB= 0,  0.05, -0.010, 0.05, 0.55, 0.60, SURF_ID = 'ADIABATIC', PERMIT_HOLE = .FALSE. / TSC
2
&OBST XB= -0.3, -0.25, -0.010, 0.05, 0.55, 0.60, SURF_ID = 'ADIABATIC', PERMIT_HOLE = .FALSE. /
TSC 3
&OBST XB= 0.25,  0.3, -0.010, 0.05, 0.85, 0.9, SURF_ID = 'ADIABATIC', PERMIT_HOLE = .FALSE. / TSC
4
&OBST XB= -0.05,  0, -0.010, 0.05, 0.85, 0.9, SURF_ID = 'ADIABATIC', PERMIT_HOLE = .FALSE. / TSC
5
&OBST XB= -0.60, -0.55, -0.010, 0.05, 0.85, 0.9, SURF_ID = 'ADIABATIC', PERMIT_HOLE = .FALSE. /
TSC 6
&OBST XB= 0.55,  0.60, -0.010, 0.05, 1.15, 1.2, SURF_ID = 'ADIABATIC', PERMIT_HOLE = .FALSE. /
TSC 7
&OBST XB= 0, 0.05, -0.010, 0.05, 1.15, 1.2, SURF_ID = 'ADIABATIC', PERMIT_HOLE = .FALSE. / TSC 8
```

```
&OBST XB= -0.3, -0.25, -0.010, 0.05, 1.15, 1.2, SURF_ID = 'ADIABATIC', PERMIT_HOLE = .FALSE. /
TSC 9
&OBST XB= 0.25,  0.3, -0.010, 0.05, 1.45, 1.5, SURF_ID = 'ADIABATIC', PERMIT_HOLE = .FALSE. / TSC
10
&OBST XB= -0.05,  0, -0.010, 0.05, 1.45, 1.5, SURF_ID = 'ADIABATIC', PERMIT_HOLE = .FALSE. / TSC
11
&OBST XB=-0.60, -0.55, -0.010, 0.05, 1.45, 1.5, SURF_ID = 'ADIABATIC', PERMIT_HOLE = .FALSE. /
TSC 12
&OBST XB= 0.55,  0.60, -0.010, 0.05, 1.75, 1.8, SURF_ID = 'ADIABATIC', PERMIT_HOLE = .FALSE. /
TSC 13
&OBST XB= 0,  0.05, -0.010, 0.05, 1.75, 1.8, SURF_ID = 'ADIABATIC', PERMIT_HOLE = .FALSE. / TSC
14
&OBST XB=-0.3, -0.25, -0.010, 0.05, 1.75, 1.8, SURF_ID = 'ADIABATIC', PERMIT_HOLE = .FALSE. / TSC
15
&OBST XB= 0.25,  0.3, -0.010, 0.05, 2.05, 2.1, SURF_ID = 'ADIABATIC', PERMIT_HOLE = .FALSE. / TSC
16
&OBST XB= -0.05,  0, -0.010, 0.05, 2.05, 2.1, SURF_ID = 'ADIABATIC', PERMIT_HOLE = .FALSE. / TSC
17
&OBST XB=-0.60, -0.55, -0.010, 0.05, 2.05, 2.1, SURF_ID = 'ADIABATIC', PERMIT_HOLE = .FALSE. /
TSC 18

&SLCF PBX = 0.0, QUANTITY = 'TEMPERATURE' /
&SLCF PBX = 0.0, QUANTITY = 'HRRPUV' /

&BNDF QUANTITY='GAUGE HEAT FLUX' /
&BNDF QUANTITY='RADIATIVE HEAT FLUX' /
&BNDF QUANTITY='CONVECTIVE HEAT FLUX' /
&BNDF QUANTITY='NET HEAT FLUX' /
&BNDF QUANTITY='WALL TEMPERATURE' /
&BNDF QUANTITY='BURNING RATE' /

CENTERLINE RAKE
&DEVC XYZ=0, 0.25, 0.45, QUANTITY='TEMPERATURE', ID='CTC_1' /
&DEVC XYZ=0, 0.25, 0.60, QUANTITY='TEMPERATURE', ID='BDTC_1' /
&DEVC XYZ=0, 0.25, 0.75, QUANTITY='TEMPERATURE', ID='CTC_2' /
&DEVC XYZ=0, 0.25, 0.90, QUANTITY='TEMPERATURE', ID='BDTC_2' /
&DEVC XYZ=0, 0.25, 1.05, QUANTITY='TEMPERATURE', ID='CTC_3' /
&DEVC XYZ=0, 0.25, 1.20, QUANTITY='TEMPERATURE', ID='BDTC_3' /
&DEVC XYZ=0, 0.25, 1.35, QUANTITY='TEMPERATURE', ID='CTC_4' /
&DEVC XYZ=0, 0.25, 1.50, QUANTITY='TEMPERATURE', ID='BDTC_4' /
&DEVC XYZ=0, 0.25, 1.65, QUANTITY='TEMPERATURE', ID='CTC_5' /
&DEVC XYZ=0, 0.25, 1.80, QUANTITY='TEMPERATURE', ID='BDTC_5' /
&DEVC XYZ=0, 0.25, 1.95, QUANTITY='TEMPERATURE', ID='CTC_6' /
&DEVC XYZ=0, 0.25, 2.10, QUANTITY='TEMPERATURE', ID='BDTC_6' /
&DEVC XYZ=0, 0.25, 2.25, QUANTITY='TEMPERATURE', ID='CTC_7' /
&DEVC XYZ=0, 0.25, 0.60, QUANTITY='W-VELOCITY', ID='BD_1' /
&DEVC XYZ=0, 0.25, 0.90, QUANTITY='W-VELOCITY', ID='BD_2' /
&DEVC XYZ=0, 0.25, 1.20, QUANTITY='W-VELOCITY', ID='BD_3' /
&DEVC XYZ=0, 0.25, 1.50, QUANTITY='W-VELOCITY', ID='BD_4' /
&DEVC XYZ=0, 0.25, 1.80, QUANTITY='W-VELOCITY', ID='BD_5' /
&DEVC XYZ=0, 0.25, 2.10, QUANTITY='W-VELOCITY', ID='BD_6' /
&DEVC XYZ=0, 0.25, 1.05, QUANTITY='W-VELOCITY', ID='BD_7' /
&DEVC XYZ=0, 0.25, 1.35, QUANTITY='W-VELOCITY', ID='BD_8' /
&DEVC XYZ=0, 0.25, 1.65, QUANTITY='W-VELOCITY', ID='BD_9' /
&DEVC XYZ=0, 0.25, 1.95, QUANTITY='W-VELOCITY', ID='BD_10' /

WALL TEMPERATURE
&DEVC XYZ=0.0762, 0.05, 0.75, QUANTITY='TEMPERATURE', ID='WTC_1' /
&DEVC XYZ=0.0508, 0.055, 0.75, QUANTITY='TEMPERATURE', ID='WTC_2' /
&DEVC XYZ=0.0254, 0.060, 0.75, QUANTITY='TEMPERATURE', ID='WTC_3' /
&DEVC XYZ=-0.0254, 0.065, 0.75, QUANTITY='TEMPERATURE', ID='WTC_4' /
&DEVC XYZ=-0.0508, 0.070, 0.75, QUANTITY='TEMPERATURE', ID='WTC_5' /
&DEVC XYZ=-0.0762, 0.075, 0.75, QUANTITY='TEMPERATURE', ID='WTC_6' /
&DEVC XYZ=0.0762, 0.085, 1.35, QUANTITY='TEMPERATURE', ID='WTC_7' /
&DEVC XYZ=0.0508, 0.080, 1.35, QUANTITY='TEMPERATURE', ID='WTC_8' /
&DEVC XYZ=0.0254, 0.075, 1.35, QUANTITY='TEMPERATURE', ID='WTC_9' /
&DEVC XYZ=-0.0254, 0.070, 1.35, QUANTITY='TEMPERATURE', ID='WTC_10' /
&DEVC XYZ=-0.0508, 0.065, 1.35, QUANTITY='TEMPERATURE', ID='WTC_11' /
&DEVC XYZ=-0.0762, 0.060, 1.35, QUANTITY='TEMPERATURE', ID='WTC_12' /
&DEVC XYZ=0.0762, 0.065, 1.95, QUANTITY='TEMPERATURE', ID='WTC_13' /
&DEVC XYZ=0.0508, 0.070, 1.95, QUANTITY='TEMPERATURE', ID='WTC_14' /
```

```
&DEVC XYZ=0.0254, 0.075, 1.95, QUANTITY='TEMPERATURE', ID='WTC_15' /
&DEVC XYZ=-0.0254, 0.080, 1.95, QUANTITY='TEMPERATURE', ID='WTC_16' /
&DEVC XYZ=-0.0508, 0.085, 1.95, QUANTITY='TEMPERATURE', ID='WTC_17' /
&DEVC XYZ=-0.0762, 0.090, 1.95, QUANTITY='TEMPERATURE', ID='WTC_18' /

WALL HEAT FLUX MEASUREMENTS
&DEVC XYZ=  0.575, 0.050, 0.575, QUANTITY='GAUGE_HEAT_FLUX', ID='TS_1',  IOR = 2 /
&DEVC XYZ=  0.025, 0.050, 0.575, QUANTITY='GAUGE_HEAT_FLUX', ID='TS_2',  IOR = 2 /
&DEVC XYZ= -0.275, 0.050, 0.575, QUANTITY='GAUGE_HEAT_FLUX', ID='TS_3',  IOR = 2 /
&DEVC XYZ=  0.275, 0.050, 0.875, QUANTITY='GAUGE_HEAT_FLUX', ID='TS_4',  IOR = 2 /
&DEVC XYZ=  -0.025, 0.050, 0.875, QUANTITY='GAUGE_HEAT_FLUX', ID='TS_5',  IOR = 2 /
&DEVC XYZ= -0.575, 0.050, 0.875, QUANTITY='GAUGE_HEAT_FLUX', ID='TS_6',  IOR = 2 /
&DEVC XYZ=  0.575, 0.050, 1.175, QUANTITY='GAUGE_HEAT_FLUX', ID='TS_7',  IOR = 2 /
&DEVC XYZ=  0.025 0.050, 1.175, QUANTITY='GAUGE_HEAT_FLUX', ID='TS_8',  IOR = 2 /
&DEVC XYZ= -0.275, 0.050, 1.175, QUANTITY='GAUGE_HEAT_FLUX', ID='TS_9',  IOR = 2 /
&DEVC XYZ=  0.275, 0.050, 1.475, QUANTITY='GAUGE_HEAT_FLUX', ID='TS_10', IOR = 2 /
&DEVC XYZ=  -0.025, 0.050, 1.475, QUANTITY='GAUGE_HEAT_FLUX', ID='TS_11', IOR = 2 /
&DEVC XYZ= -0.575, 0.050, 1.475, QUANTITY='GAUGE_HEAT_FLUX', ID='TS_12', IOR = 2 /
&DEVC XYZ=  0.575, 0.050, 1.775, QUANTITY='GAUGE_HEAT_FLUX', ID='TS_13', IOR = 2 /
&DEVC XYZ=  0.025, 0.050, 1.775, QUANTITY='GAUGE_HEAT_FLUX', ID='TS_14', IOR = 2 /
&DEVC XYZ= -0.275, 0.050, 1.775, QUANTITY='GAUGE_HEAT_FLUX', ID='TS_15', IOR = 2 /
&DEVC XYZ=  0.275, 0.050, 2.075, QUANTITY='GAUGE_HEAT_FLUX', ID='TS_16', IOR = 2 /
&DEVC XYZ=  -0.025, 0.050, 2.075, QUANTITY='GAUGE_HEAT_FLUX', ID='TS_17', IOR = 2 /
&DEVC XYZ= -0.575, 0.050, 2.075, QUANTITY='GAUGE_HEAT_FLUX', ID='TS_18', IOR = 2 /

&DEVC XYZ=  0.275, 0.050, 0.60, QUANTITY='GAUGE_HEAT_FLUX', ID='HFG_1', IOR = 2 /
&DEVC XYZ= -0.275, 0.050, 0.875, QUANTITY='GAUGE_HEAT_FLUX', ID='HFG_2', IOR = 2 /
&DEVC XYZ=  0.275, 0.050, 1.175, QUANTITY='GAUGE_HEAT_FLUX', ID='HFG_3', IOR = 2 /
&DEVC XYZ= -0.275, 0.050, 1.475, QUANTITY='GAUGE_HEAT_FLUX', ID='HFG_4', IOR = 2 /
&DEVC XYZ=  0.275, 0.050, 1.775, QUANTITY='GAUGE_HEAT_FLUX', ID='HFG_5', IOR = 2 /
&DEVC XYZ= -0.275, 0.050, 2.075, QUANTITY='GAUGE_HEAT_FLUX', ID='HFG_6', IOR = 2 /

WALL NET HEAT FLUX
&DEVC XYZ=  0.575, 0.050, 0.575, QUANTITY='NET HEAT FLUX', ID='TS_1',  IOR = 2 /
&DEVC XYZ=  0.025, 0.050, 0.575, QUANTITY='NET HEAT FLUX', ID='TS_2',  IOR = 2 /
&DEVC XYZ= -0.275, 0.050, 0.575, QUANTITY='NET HEAT FLUX', ID='TS_3',  IOR = 2 /
&DEVC XYZ=  0.275, 0.050, 0.875, QUANTITY='NET HEAT FLUX', ID='TS_4',  IOR = 2 /
&DEVC XYZ=  -0.025, 0.050, 0.875, QUANTITY='NET HEAT FLUX', ID='TS_5',  IOR = 2 /
&DEVC XYZ= -0.575, 0.050, 0.875, QUANTITY='NET HEAT FLUX', ID='TS_6',  IOR = 2 /
&DEVC XYZ=  0.575, 0.050, 1.175, QUANTITY='NET HEAT FLUX', ID='TS_7',  IOR = 2 /
&DEVC XYZ=  0.025 0.050, 1.175, QUANTITY='NET HEAT FLUX', ID='TS_8',  IOR = 2 /
&DEVC XYZ= -0.275, 0.050, 1.175, QUANTITY='NET HEAT FLUX', ID='TS_9',  IOR = 2 /
&DEVC XYZ=  0.275, 0.050, 1.475, QUANTITY='NET HEAT FLUX', ID='TS_10', IOR = 2 /
&DEVC XYZ=  -0.025, 0.050, 1.475, QUANTITY='NET HEAT FLUX', ID='TS_11', IOR = 2 /
&DEVC XYZ= -0.575, 0.050, 1.475, QUANTITY='NET HEAT FLUX', ID='TS_12', IOR = 2 /
&DEVC XYZ=  0.575, 0.050, 1.775, QUANTITY='NET HEAT FLUX', ID='TS_13', IOR = 2 /
&DEVC XYZ=  0.025, 0.050, 1.775, QUANTITY='NET HEAT FLUX', ID='TS_14', IOR = 2 /
&DEVC XYZ= -0.275, 0.050, 1.775, QUANTITY='NET HEAT FLUX', ID='TS_15', IOR = 2 /
```

J.15 Input File 15 – FRP scenario, Square burner, 75 kW continuous, propane

```
Start Input File
&HEAD CHID='65_1_03-14-2011_FRP_Pr_sb_75kW' /

&TIME T_END = 900, DT = 0.05, RESTRICT_TIME_STEP = .FALSE. /
&DUMP DT_BNDF=2.0, DT_DEVC=0.5, DT_HRR=1.0, DT_PL3D=5000.0, DT_SLCF=2.0, DT_RESTART=50./

&MISC
      SURF_DEFAULT = 'INERT'
      TMPA  = 23
      FDS6  = .TRUE.
      DNS = .FALSE.
      DYNSMAG = .TRUE.
      CSMAG = 0.2
      PR = 0.5
      SC = 0.5
      H_EDDY = .TRUE.
      CFL_VELOCITY_NORM = 1
      FLUX_LIMITER = 2
      ISOTHERMAL = .FALSE.
      RADIATION = .TRUE.
      BAROCLINIC = .TRUE.
      CLIP_MASS_FRACTION   = .TRUE.
      CHECK_VN = .TRUE.
      NOBIAS = .TRUE.
      PROJECTION  = .FALSE.
      CHECK_KINETIC_ENERGY = .FALSE.
      /

&REAC
     ID = 'Propane'
     C = 3
     H = 8
     O = 0
     CO_YIELD = 0.024
     SOOT_YIELD = 0.005
     EDDY_DISSIPATION = .TRUE.
     C_EDC = 0.1
     HRRPUA_SHEET = 0
     HRRPUV_AVERAGE = 2500
      /

&RADI
    RADIATIVE_FRACTION = 0.3
    TIME_STEP_INCREMENT = 3
    ANGLE_INCREMENT = 5
    NUMBER_RADIATION_ANGLES = 104
    /

**** MESHES ****
 MESH IJK= 96, 156, 96, XB=-1.20, 1.20, 0.00, 3.90, 0.00, 2.40 / 2.50 cm grid,  1 mesh

&MESH ID= 'Mesh-1', IJK= 24, 26, 24, XB= -1.2, 0, 0, 1.3, 0, 1.2 / 0.05 cm grid 12 mesh
&MESH ID= 'Mesh-2', IJK= 24, 26, 24, XB= -1.2, 0, 1.3, 2.6, 0, 1.2 / 0.05 cm grid 12 mesh
&MESH ID= 'Mesh-3', IJK= 24, 26, 24, XB= -1.2, 0, 2.6, 3.9, 0, 1.2 / 0.05 cm grid 12 mesh
&MESH ID= 'Mesh-4', IJK= 24, 26, 24, XB= 0, 1.2, 0, 1.3, 0, 1.2 / 0.05 cm grid 12 mesh
&MESH ID= 'Mesh-5', IJK= 24, 26, 24, XB= 0, 1.2, 1.3, 2.6, 0, 1.2 / 0.05 cm grid 12 mesh
&MESH ID= 'Mesh-6', IJK= 24, 26, 24, XB= 0, 1.2, 2.6, 3.9, 0, 1.2 / 0.05 cm grid 12 mesh
&MESH ID= 'Mesh-7', IJK= 24, 26, 24, XB= -1.2, 0, 0, 1.3, 1.2, 2.4 / 0.05 cm grid 12 mesh
&MESH ID= 'Mesh-8', IJK= 24, 26, 24, XB= -1.2, 0, 1.3, 2.6, 1.2, 2.4 / 0.05 cm grid 12 mesh
&MESH ID= 'Mesh-9', IJK= 24, 26, 24, XB= -1.2, 0, 2.6, 3.9, 1.2, 2.4 / 0.05 cm grid 12 mesh
&MESH ID= 'Mesh-10', IJK= 24, 26, 24, XB= 0, 1.2, 0, 1.3, 1.2, 2.4 / 0.05 cm grid 12 mesh
&MESH ID= 'Mesh-11', IJK= 24, 26, 24, XB= 0, 1.2, 1.3, 2.6, 1.2, 2.4 / 0.05 cm grid 12 mesh
&MESH ID= 'Mesh-12', IJK= 24, 26, 24, XB= 0, 1.2, 2.6, 3.9, 1.2, 2.4 / 0.05 cm grid 12 mesh

****BURNER****
2 ft burner
OBST XB= -0.35, 0.35, 0.05, 0.45, 0, 0.4, SURF_ID = 'ADIABATIC' /
VENT XB= -0.3, 0.3, 0.1, 0.4, 0.4, 0.4, SURF_ID = 'BURNER' /
```

```
1 ft burner
&OBST XB= -0.2, 0.2, 0.05, 0.45, 0, 0.4, SURF_ID = 'ADIABATIC' /
&VENT XB= -0.15, 0.15, 0.1, 0.4, 0.4, 0.4, SURF_ID = 'BURNER' /

**** Burner Parameters*****
&SURF ID = 'BURNER'
      HRRPUA =833.3
      RAMP_Q = 'Burner_Ramp'
      COLOR  = 'RED' /

&RAMP ID = 'Burner_Ramp', T=0, F=0 /
&RAMP ID = 'Burner_Ramp', T=1, F=0.5 /
&RAMP ID = 'Burner_Ramp', T=20, F=1 /
&RAMP ID = 'Burner_Ramp', T=900, F=1 /


**** MATERIAL PROPERTIES ****
&MATL ID            ='GYPSUM_MATL'
      SPECIFIC_HEAT = 0.84
      CONDUCTIVITY  = 0.48
      DENSITY       = 1440.0 /

&MATL ID            ='KAOWOOL_MATL'
      SPECIFIC_HEAT = 1.0
      CONDUCTIVITY  = 0.06
      DENSITY       = 320.0 /

&SURF ID        = 'ADIABATIC'
      ADIABATIC = .TRUE.
      RGB       = 0, 0, 0 /

&SURF ID                      = 'KAOWOOL'
      RGB                     = 51,102,255
      BACKING                 = 'INSULATED'
      MATL_ID(1,1)            = 'KAOWOOL_MATL'
      MATL_MASS_FRACTION(1,1)= 1.0
      THICKNESS(1)            = 0.025
      CELL_SIZE_FACTOR        = 0.30
      STRETCH_FACTOR          = 1.0 /

&SURF ID                      = 'GYPSUM'
      RGB                     = 100,100,100
      BACKING                 = 'INSULATED'
      MATL_ID(1,1)            = 'GYPSUM_MATL'
      MATL_MASS_FRACTION(1,1)= 1.0
      THICKNESS(1)            = 0.016
      CELL_SIZE_FACTOR        = 0.30
      STRETCH_FACTOR          = 1.0 /

&MATL ID                        = 'virgin'
      CONDUCTIVITY              =  0.480
      DENSITY                   = 1467.80
      SPECIFIC_HEAT             =    1.98
      EMISSIVITY                =  0.858
      ABSORPTION_COEFFICIENT    =  0.9000E+10
      RESIDUE(01)               = 'char'
      A(01)                     = 0.1139E+12
      E(01)                     = 0.1483E+06
      N_S(01)                   =   1.00
      THRESHOLD_TEMPERATURE(01)=   0.00
      HEAT_OF_REACTION(01)      =   996.67
      HEAT_OF_COMBUSTION        = 19700.
      NU_FUEL(01)               =   0.421
      NU_RESIDUE(01)            =   0.579
      NU_WATER(01)              =   0.000
      N_REACTIONS               = 01 /

&MATL ID                        = 'char'
      CONDUCTIVITY              =  0.050
      DENSITY                   =  850.56
      SPECIFIC_HEAT             =    2.12
```

```
      EMISSIVITY               =  0.943
      ABSORPTION_COEFFICIENT   =  0.9000E+10
      N_REACTIONS              = 00 /

&SURF ID                         = 'FRP'
      STRETCH_FACTOR             = 1.000
      CELL_SIZE_FACTOR           = 0.200
      THICKNESS(1)              = 0.0019
      MATL_ID(1,1)              = 'virgin'
      MATL_ID(1,2)              = 'char'
      MATL_MASS_FRACTION(1,1)  = 1.0000
      MATL_MASS_FRACTION(1,2)  = 0.0000
      BACKING                    = 'INSULATED'
      SHRINK                     = .TRUE.
      TMP_INNER                  = 27.0
      COLOR                      = 'WHITE' /


****OBSTRUCTIONS****
&OBST XB=-1.200, 1.200, 0.000, 0.000, 0.000, 2.400, SURF_ID ='GYPSUM'  / Back wall
&OBST XB= 1.200, 1.200, 0.000, 2.700, 0.000, 2.400, SURF_ID ='GYPSUM'  / Right wall
&OBST XB=-1.200,-1.200, 0.000, 2.700, 0.000, 2.400, SURF_ID ='GYPSUM'  / Left wall
&OBST XB=-1.200, 1.200, 0.000, 2.700, 2.400, 2.400, SURF_ID ='GYPSUM'  / Ceiling
&OBST XB=-0.900,-0.600, 0.000, 0.05, 0.000, 2.400, SURF_ID ='KAOWOOL' / Kaowool on back wall
&OBST XB= 0.600, 0.900, 0.000, 0.05, 0.000, 2.400, SURF_ID ='KAOWOOL' / Kaowool on back wall
&OBST XB=-0.600, 0.600, 0.000, 0.05, 0.000, 2.400, SURF_ID ='FRP', PERMIT_HOLE = .TRUE. / FRP
panel

****OPEN VENTS****
&VENT XB=-1.20, 1.20, 3.90, 3.90, 0.00, 2.40, SURF_ID = 'OPEN' / Back
&VENT XB=-1.20,-1.20, 2.70, 3.90, 0.00, 2.40, SURF_ID = 'OPEN' /
&VENT XB= 1.20, 1.20, 2.70, 3.90, 0.00, 2.40, SURF_ID = 'OPEN' /
&VENT XB=-1.20, 1.20, 2.70, 3.90, 2.40, 2.40, SURF_ID = 'OPEN' /

HOLES in panel for TSC's:
&HOLE XB= 0.55,  0.60, -0.010, 0.1, 0.55, 0.60 / HOLE 1
&HOLE XB= 0,  0.05, -0.010, 0.1, 0.55, 0.60 / HOLE 2
&HOLE XB= -0.3, -0.25, -0.010, 0.1, 0.55, 0.60 / HOLE 3
&HOLE XB= 0.25,  0.3, -0.010, 0.1, 0.85, 0.9 / HOLE 4
&HOLE XB= -0.05,  0, -0.010, 0.1, 0.85, 0.9 / HOLE 5
&HOLE XB= -0.60, -0.55, -0.010, 0.1, 0.85, 0.9 / HOLE 6
&HOLE XB= 0.55,  0.60, -0.010, 0.1, 1.15, 1.2 / HOLE 7
&HOLE XB= 0, 0.05, -0.010, 0.1, 1.15, 1.2 / HOLE 8
&HOLE XB= -0.3, -0.25, -0.010, 0.1, 1.15, 1.2 / HOLE 9
&HOLE XB= 0.25,  0.3, -0.010, 0.1, 1.45, 1.5 / HOLE 10
&HOLE XB= -0.05,  0, -0.010, 0.1, 1.45, 1.5 / HOLE 11
&HOLE XB=-0.60, -0.55, -0.010, 0.1, 1.45, 1.5 / HOLE 12
&HOLE XB= 0.55,  0.60, -0.010, 0.1, 1.75, 1.8 / HOLE 13
&HOLE XB= 0,  0.05, -0.010, 0.1, 1.75, 1.8 / HOLE 14
&HOLE XB=-0.3, -0.25, -0.010, 0.1, 1.75, 1.8 / HOLE 15
&HOLE XB= 0.25,  0.3, -0.010, 0.1, 2.05, 2.1 / HOLE 16
&HOLE XB= -0.05,  0, -0.010, 0.1, 2.05, 2.1 / HOLE 17
&HOLE XB=-0.60, -0.55, -0.010, 0.1, 2.05, 2.1 / HOLE 18

TSC'S:

&OBST XB= 0.55,  0.60, -0.010, 0.05, 0.55, 0.60, SURF_ID = 'ADIABATIC', PERMIT_HOLE = .FALSE. /
TSC 1
&OBST XB= 0,  0.05, -0.010, 0.05, 0.55, 0.60, SURF_ID = 'ADIABATIC', PERMIT_HOLE = .FALSE. / TSC
2
&OBST XB= -0.3, -0.25, -0.010, 0.05, 0.55, 0.60, SURF_ID = 'ADIABATIC', PERMIT_HOLE = .FALSE. /
TSC 3
&OBST XB= 0.25,  0.3, -0.010, 0.05, 0.85, 0.9, SURF_ID = 'ADIABATIC', PERMIT_HOLE = .FALSE. / TSC
4
&OBST XB= -0.05,  0, -0.010, 0.05, 0.85, 0.9, SURF_ID = 'ADIABATIC', PERMIT_HOLE = .FALSE. / TSC
5
&OBST XB= -0.60, -0.55, -0.010, 0.05, 0.85, 0.9, SURF_ID = 'ADIABATIC', PERMIT_HOLE = .FALSE. /
TSC 6
&OBST XB= 0.55,  0.60, -0.010, 0.05, 1.15, 1.2, SURF_ID = 'ADIABATIC', PERMIT_HOLE = .FALSE. /
TSC 7
&OBST XB= 0, 0.05, -0.010, 0.05, 1.15, 1.2, SURF_ID = 'ADIABATIC', PERMIT_HOLE = .FALSE. / TSC 8
```

```
&OBST XB= -0.3, -0.25, -0.010, 0.05, 1.15, 1.2, SURF_ID = 'ADIABATIC', PERMIT_HOLE = .FALSE. /
TSC 9
&OBST XB= 0.25,  0.3, -0.010, 0.05, 1.45, 1.5, SURF_ID = 'ADIABATIC', PERMIT_HOLE = .FALSE. / TSC
10
&OBST XB= -0.05,  0, -0.010, 0.05, 1.45, 1.5, SURF_ID = 'ADIABATIC', PERMIT_HOLE = .FALSE. / TSC
11
&OBST XB=-0.60, -0.55, -0.010, 0.05, 1.45, 1.5, SURF_ID = 'ADIABATIC', PERMIT_HOLE = .FALSE. /
TSC 12
&OBST XB= 0.55,  0.60, -0.010, 0.05, 1.75, 1.8, SURF_ID = 'ADIABATIC', PERMIT_HOLE = .FALSE. /
TSC 13
&OBST XB= 0,  0.05, -0.010, 0.05, 1.75, 1.8, SURF_ID = 'ADIABATIC', PERMIT_HOLE = .FALSE. / TSC
14
&OBST XB=-0.3, -0.25, -0.010, 0.05, 1.75, 1.8, SURF_ID = 'ADIABATIC', PERMIT_HOLE = .FALSE. / TSC
15
&OBST XB= 0.25,  0.3, -0.010, 0.05, 2.05, 2.1, SURF_ID = 'ADIABATIC', PERMIT_HOLE = .FALSE. / TSC
16
&OBST XB= -0.05,  0, -0.010, 0.05, 2.05, 2.1, SURF_ID = 'ADIABATIC', PERMIT_HOLE = .FALSE. / TSC
17
&OBST XB=-0.60, -0.55, -0.010, 0.05, 2.05, 2.1, SURF_ID = 'ADIABATIC', PERMIT_HOLE = .FALSE. /
TSC 18

&SLCF PBX = 0.0, QUANTITY = 'TEMPERATURE' /
&SLCF PBX = 0.0, QUANTITY = 'HRRPUV' /

&BNDF QUANTITY='GAUGE HEAT FLUX' /
&BNDF QUANTITY='RADIATIVE HEAT FLUX' /
&BNDF QUANTITY='CONVECTIVE HEAT FLUX' /
&BNDF QUANTITY='NET HEAT FLUX' /
&BNDF QUANTITY='WALL TEMPERATURE' /
&BNDF QUANTITY='BURNING RATE' /

CENTERLINE RAKE
&DEVC XYZ=0, 0.25, 0.45, QUANTITY='TEMPERATURE', ID='CTC_1' /
&DEVC XYZ=0, 0.25, 0.60, QUANTITY='TEMPERATURE', ID='BDTC_1' /
&DEVC XYZ=0, 0.25, 0.75, QUANTITY='TEMPERATURE', ID='CTC_2' /
&DEVC XYZ=0, 0.25, 0.90, QUANTITY='TEMPERATURE', ID='BDTC_2' /
&DEVC XYZ=0, 0.25, 1.05, QUANTITY='TEMPERATURE', ID='CTC_3' /
&DEVC XYZ=0, 0.25, 1.20, QUANTITY='TEMPERATURE', ID='BDTC_3' /
&DEVC XYZ=0, 0.25, 1.35, QUANTITY='TEMPERATURE', ID='CTC_4' /
&DEVC XYZ=0, 0.25, 1.50, QUANTITY='TEMPERATURE', ID='BDTC_4' /
&DEVC XYZ=0, 0.25, 1.65, QUANTITY='TEMPERATURE', ID='CTC_5' /
&DEVC XYZ=0, 0.25, 1.80, QUANTITY='TEMPERATURE', ID='BDTC_5' /
&DEVC XYZ=0, 0.25, 1.95, QUANTITY='TEMPERATURE', ID='CTC_6' /
&DEVC XYZ=0, 0.25, 2.10, QUANTITY='TEMPERATURE', ID='BDTC_6' /
&DEVC XYZ=0, 0.25, 2.25, QUANTITY='TEMPERATURE', ID='CTC_7' /
&DEVC XYZ=0, 0.25, 0.60, QUANTITY='W-VELOCITY', ID='BD_1' /
&DEVC XYZ=0, 0.25, 0.90, QUANTITY='W-VELOCITY', ID='BD_2' /
&DEVC XYZ=0, 0.25, 1.20, QUANTITY='W-VELOCITY', ID='BD_3' /
&DEVC XYZ=0, 0.25, 1.50, QUANTITY='W-VELOCITY', ID='BD_4' /
&DEVC XYZ=0, 0.25, 1.80, QUANTITY='W-VELOCITY', ID='BD_5' /
&DEVC XYZ=0, 0.25, 2.10, QUANTITY='W-VELOCITY', ID='BD_6' /
&DEVC XYZ=0, 0.25, 1.05, QUANTITY='W-VELOCITY', ID='BD_7' /
&DEVC XYZ=0, 0.25, 1.35, QUANTITY='W-VELOCITY', ID='BD_8' /
&DEVC XYZ=0, 0.25, 1.65, QUANTITY='W-VELOCITY', ID='BD_9' /
&DEVC XYZ=0, 0.25, 1.95, QUANTITY='W-VELOCITY', ID='BD_10' /

WALL TEMPERATURE
&DEVC XYZ=0.0762, 0.05, 0.75, QUANTITY='TEMPERATURE', ID='WTC_1' /
&DEVC XYZ=0.0508, 0.055, 0.75, QUANTITY='TEMPERATURE', ID='WTC_2' /
&DEVC XYZ=0.0254, 0.060, 0.75, QUANTITY='TEMPERATURE', ID='WTC_3' /
&DEVC XYZ=-0.0254, 0.065, 0.75, QUANTITY='TEMPERATURE', ID='WTC_4' /
&DEVC XYZ=-0.0508, 0.070, 0.75, QUANTITY='TEMPERATURE', ID='WTC_5' /
&DEVC XYZ=-0.0762, 0.075, 0.75, QUANTITY='TEMPERATURE', ID='WTC_6' /
&DEVC XYZ=0.0762, 0.085, 1.35, QUANTITY='TEMPERATURE', ID='WTC_7' /
&DEVC XYZ=0.0508, 0.080, 1.35, QUANTITY='TEMPERATURE', ID='WTC_8' /
&DEVC XYZ=0.0254, 0.075, 1.35, QUANTITY='TEMPERATURE', ID='WTC_9' /
&DEVC XYZ=-0.0254, 0.070, 1.35, QUANTITY='TEMPERATURE', ID='WTC_10' /
&DEVC XYZ=-0.0508, 0.065, 1.35, QUANTITY='TEMPERATURE', ID='WTC_11' /
&DEVC XYZ=-0.0762, 0.060, 1.35, QUANTITY='TEMPERATURE', ID='WTC_12' /
&DEVC XYZ=0.0762, 0.065, 1.95, QUANTITY='TEMPERATURE', ID='WTC_13' /
&DEVC XYZ=0.0508, 0.070, 1.95, QUANTITY='TEMPERATURE', ID='WTC_14' /
```

```
&DEVC XYZ=0.0254, 0.075, 1.95, QUANTITY='TEMPERATURE', ID='WTC_15' /
&DEVC XYZ=-0.0254, 0.080, 1.95, QUANTITY='TEMPERATURE', ID='WTC_16' /
&DEVC XYZ=-0.0508, 0.085, 1.95, QUANTITY='TEMPERATURE', ID='WTC_17' /
&DEVC XYZ=-0.0762, 0.090, 1.95, QUANTITY='TEMPERATURE', ID='WTC_18' /

WALL HEAT FLUX MEASUREMENTS
&DEVC XYZ=  0.575, 0.050, 0.575, QUANTITY='GAUGE_HEAT_FLUX', ID='TS_1',  IOR = 2 /
&DEVC XYZ=  0.025, 0.050, 0.575, QUANTITY='GAUGE_HEAT_FLUX', ID='TS_2',  IOR = 2 /
&DEVC XYZ= -0.275, 0.050, 0.575, QUANTITY='GAUGE_HEAT_FLUX', ID='TS_3',  IOR = 2 /
&DEVC XYZ=  0.275, 0.050, 0.875, QUANTITY='GAUGE_HEAT_FLUX', ID='TS_4',  IOR = 2 /
&DEVC XYZ=  -0.025, 0.050, 0.875, QUANTITY='GAUGE_HEAT_FLUX', ID='TS_5',  IOR = 2 /
&DEVC XYZ= -0.575, 0.050, 0.875, QUANTITY='GAUGE_HEAT_FLUX', ID='TS_6',  IOR = 2 /
&DEVC XYZ=  0.575, 0.050, 1.175, QUANTITY='GAUGE_HEAT_FLUX', ID='TS_7',  IOR = 2 /
&DEVC XYZ=  0.025 0.050, 1.175, QUANTITY='GAUGE_HEAT_FLUX', ID='TS_8',  IOR = 2 /
&DEVC XYZ= -0.275, 0.050, 1.175, QUANTITY='GAUGE_HEAT_FLUX', ID='TS_9',  IOR = 2 /
&DEVC XYZ=  0.275, 0.050, 1.475, QUANTITY='GAUGE_HEAT_FLUX', ID='TS_10', IOR = 2 /
&DEVC XYZ=  -0.025, 0.050, 1.475, QUANTITY='GAUGE_HEAT_FLUX', ID='TS_11', IOR = 2 /
&DEVC XYZ= -0.575, 0.050, 1.475, QUANTITY='GAUGE_HEAT_FLUX', ID='TS_12', IOR = 2 /
&DEVC XYZ=  0.575, 0.050, 1.775, QUANTITY='GAUGE_HEAT_FLUX', ID='TS_13', IOR = 2 /
&DEVC XYZ=  0.025, 0.050, 1.775, QUANTITY='GAUGE_HEAT_FLUX', ID='TS_14', IOR = 2 /
&DEVC XYZ= -0.275, 0.050, 1.775, QUANTITY='GAUGE_HEAT_FLUX', ID='TS_15', IOR = 2 /
&DEVC XYZ=  0.275, 0.050, 2.075, QUANTITY='GAUGE_HEAT_FLUX', ID='TS_16', IOR = 2 /
&DEVC XYZ=  -0.025, 0.050, 2.075, QUANTITY='GAUGE_HEAT_FLUX', ID='TS_17', IOR = 2 /
&DEVC XYZ= -0.575, 0.050, 2.075, QUANTITY='GAUGE_HEAT_FLUX', ID='TS_18', IOR = 2 /

&DEVC XYZ=  0.275, 0.050, 0.60, QUANTITY='GAUGE_HEAT_FLUX', ID='HFG_1', IOR = 2 /
&DEVC XYZ= -0.275, 0.050, 0.875, QUANTITY='GAUGE_HEAT_FLUX', ID='HFG_2', IOR = 2 /
&DEVC XYZ=  0.275, 0.050, 1.175, QUANTITY='GAUGE_HEAT_FLUX', ID='HFG_3', IOR = 2 /
&DEVC XYZ= -0.275, 0.050, 1.475, QUANTITY='GAUGE_HEAT_FLUX', ID='HFG_4', IOR = 2 /
&DEVC XYZ=  0.275, 0.050, 1.775, QUANTITY='GAUGE_HEAT_FLUX', ID='HFG_5', IOR = 2 /
&DEVC XYZ= -0.275, 0.050, 2.075, QUANTITY='GAUGE_HEAT_FLUX', ID='HFG_6', IOR = 2 /

WALL NET HEAT FLUX
&DEVC XYZ=  0.575, 0.050, 0.575, QUANTITY='NET HEAT FLUX', ID='TS_1',  IOR = 2 /
&DEVC XYZ=  0.025, 0.050, 0.575, QUANTITY='NET HEAT FLUX', ID='TS_2',  IOR = 2 /
&DEVC XYZ= -0.275, 0.050, 0.575, QUANTITY='NET HEAT FLUX', ID='TS_3',  IOR = 2 /
&DEVC XYZ=  0.275, 0.050, 0.875, QUANTITY='NET HEAT FLUX', ID='TS_4',  IOR = 2 /
&DEVC XYZ=  -0.025, 0.050, 0.875, QUANTITY='NET HEAT FLUX', ID='TS_5',  IOR = 2 /
&DEVC XYZ= -0.575, 0.050, 0.875, QUANTITY='NET HEAT FLUX', ID='TS_6',  IOR = 2 /
&DEVC XYZ=  0.575, 0.050, 1.175, QUANTITY='NET HEAT FLUX', ID='TS_7',  IOR = 2 /
&DEVC XYZ=  0.025 0.050, 1.175, QUANTITY='NET HEAT FLUX', ID='TS_8',  IOR = 2 /
&DEVC XYZ= -0.275, 0.050, 1.175, QUANTITY='NET HEAT FLUX', ID='TS_9',  IOR = 2 /
&DEVC XYZ=  0.275, 0.050, 1.475, QUANTITY='NET HEAT FLUX', ID='TS_10', IOR = 2 /
&DEVC XYZ=  -0.025, 0.050, 1.475, QUANTITY='NET HEAT FLUX', ID='TS_11', IOR = 2 /
&DEVC XYZ= -0.575, 0.050, 1.475, QUANTITY='NET HEAT FLUX', ID='TS_12', IOR = 2 /
&DEVC XYZ=  0.575, 0.050, 1.775, QUANTITY='NET HEAT FLUX', ID='TS_13', IOR = 2 /
&DEVC XYZ=  0.025, 0.050, 1.775, QUANTITY='NET HEAT FLUX', ID='TS_14', IOR = 2 /
&DEVC XYZ= -0.275, 0.050, 1.775, QUANTITY='NET HEAT FLUX', ID='TS_15', IOR = 2 /
```

J.16 Input File 16 – FRP scenario, Rectangle burner, 75 kW continuous, propane

```
Start Input File
&HEAD CHID='66_1_03-14-2011_FRP_Pr_lb_75kW' /

&TIME T_END = 900, DT = 0.05, RESTRICT_TIME_STEP = .FALSE. /
&DUMP DT_BNDF=2.0, DT_DEVC=0.5, DT_HRR=1.0, DT_PL3D=5000.0, DT_SLCF=2.0, DT_RESTART=50./

&MISC
      SURF_DEFAULT = 'INERT'
      TMPA  = 23
      FDS6  = .TRUE.
      DNS = .FALSE.
      DYNSMAG = .TRUE.
      CSMAG = 0.2
      PR = 0.5
      SC = 0.5
      H_EDDY = .TRUE.
      CFL_VELOCITY_NORM = 1
      FLUX_LIMITER = 2
      ISOTHERMAL = .FALSE.
      RADIATION = .TRUE.
      BAROCLINIC = .TRUE.
      CLIP_MASS_FRACTION   = .TRUE.
      CHECK_VN = .TRUE.
      NOBIAS = .TRUE.
      PROJECTION  = .FALSE.
      CHECK_KINETIC_ENERGY = .FALSE.
      /

&REAC
     ID = 'Propane'
     C = 3
     H = 8
     O = 0
     CO_YIELD = 0.024
     SOOT_YIELD = 0.005
     EDDY_DISSIPATION = .TRUE.
     C_EDC = 0.1
     HRRPUA_SHEET = 0
     HRRPUV_AVERAGE = 2500
      /

&RADI
    RADIATIVE_FRACTION = 0.3
    TIME_STEP_INCREMENT = 3
    ANGLE_INCREMENT = 5
    NUMBER_RADIATION_ANGLES = 104
    /

**** MESHES ****
 MESH IJK= 96, 156, 96, XB=-1.20, 1.20, 0.00, 3.90, 0.00, 2.40 / 2.50 cm grid,  1 mesh

&MESH ID= 'Mesh-1', IJK= 24, 26, 24, XB= -1.2, 0, 0, 1.3, 0, 1.2 / 0.05 cm grid 12 mesh
&MESH ID= 'Mesh-2', IJK= 24, 26, 24, XB= -1.2, 0, 1.3, 2.6, 0, 1.2 / 0.05 cm grid 12 mesh
&MESH ID= 'Mesh-3', IJK= 24, 26, 24, XB= -1.2, 0, 2.6, 3.9, 0, 1.2 / 0.05 cm grid 12 mesh
&MESH ID= 'Mesh-4', IJK= 24, 26, 24, XB= 0, 1.2, 0, 1.3, 0, 1.2 / 0.05 cm grid 12 mesh
&MESH ID= 'Mesh-5', IJK= 24, 26, 24, XB= 0, 1.2, 1.3, 2.6, 0, 1.2 / 0.05 cm grid 12 mesh
&MESH ID= 'Mesh-6', IJK= 24, 26, 24, XB= 0, 1.2, 2.6, 3.9, 0, 1.2 / 0.05 cm grid 12 mesh
&MESH ID= 'Mesh-7', IJK= 24, 26, 24, XB= -1.2, 0, 0, 1.3, 1.2, 2.4 / 0.05 cm grid 12 mesh
&MESH ID= 'Mesh-8', IJK= 24, 26, 24, XB= -1.2, 0, 1.3, 2.6, 1.2, 2.4 / 0.05 cm grid 12 mesh
&MESH ID= 'Mesh-9', IJK= 24, 26, 24, XB= -1.2, 0, 2.6, 3.9, 1.2, 2.4 / 0.05 cm grid 12 mesh
&MESH ID= 'Mesh-10', IJK= 24, 26, 24, XB= 0, 1.2, 0, 1.3, 1.2, 2.4 / 0.05 cm grid 12 mesh
&MESH ID= 'Mesh-11', IJK= 24, 26, 24, XB= 0, 1.2, 1.3, 2.6, 1.2, 2.4 / 0.05 cm grid 12 mesh
&MESH ID= 'Mesh-12', IJK= 24, 26, 24, XB= 0, 1.2, 2.6, 3.9, 1.2, 2.4 / 0.05 cm grid 12 mesh

****BURNER****
2 ft burner
&OBST XB= -0.35, 0.35, 0.05, 0.45, 0, 0.4, SURF_ID = 'ADIABATIC' /
```

```
&VENT XB= -0.3, 0.3, 0.1, 0.4, 0.4, 0.4, SURF_ID = 'BURNER' /

1 ft burner
OBST XB= -0.2, 0.2, 0.05, 0.45, 0, 0.4, SURF_ID = 'ADIABATIC' /
VENT XB= -0.15, 0.15, 0.1, 0.4, 0.4, 0.4, SURF_ID = 'BURNER' /

**** Burner Parameters*****
&SURF ID = 'BURNER'
      HRRPUA =416.7
      RAMP_Q = 'Burner_Ramp'
      COLOR  = 'RED' /

&RAMP ID = 'Burner_Ramp', T=0, F=0 /
&RAMP ID = 'Burner_Ramp', T=1, F=0.5 /
&RAMP ID = 'Burner_Ramp', T=23, F=1 /
&RAMP ID = 'Burner_Ramp', T=900, F=1 /


**** MATERIAL PROPERTIES ****
&MATL ID            ='GYPSUM_MATL'
      SPECIFIC_HEAT = 0.84
      CONDUCTIVITY  = 0.48
      DENSITY       = 1440.0 /

&MATL ID            ='KAOWOOL_MATL'
      SPECIFIC_HEAT = 1.0
      CONDUCTIVITY  = 0.06
      DENSITY       = 320.0 /

&SURF ID        = 'ADIABATIC'
      ADIABATIC = .TRUE.
      RGB       = 0, 0, 0 /

&SURF ID                     = 'KAOWOOL'
      RGB                    = 51,102,255
      BACKING                = 'INSULATED'
      MATL_ID(1,1)           = 'KAOWOOL_MATL'
      MATL_MASS_FRACTION(1,1)= 1.0
      THICKNESS(1)           = 0.025
      CELL_SIZE_FACTOR       = 0.30
      STRETCH_FACTOR         = 1.0 /

&SURF ID                     = 'GYPSUM'
      RGB                    = 100,100,100
      BACKING                = 'INSULATED'
      MATL_ID(1,1)           = 'GYPSUM_MATL'
      MATL_MASS_FRACTION(1,1)= 1.0
      THICKNESS(1)           = 0.016
      CELL_SIZE_FACTOR       = 0.30
      STRETCH_FACTOR         = 1.0 /

&MATL ID                       = 'virgin'
      CONDUCTIVITY             =  0.480
      DENSITY                  = 1467.80
      SPECIFIC_HEAT            =    1.98
      EMISSIVITY               =  0.858
      ABSORPTION_COEFFICIENT   =  0.9000E+10
      RESIDUE(01)              = 'char'
      A(01)                    = 0.1139E+12
      E(01)                    = 0.1483E+06
      N_S(01)                  =   1.00
      THRESHOLD_TEMPERATURE(01)=   0.00
      HEAT_OF_REACTION(01)     =   996.67
      HEAT_OF_COMBUSTION       = 19700.
      NU_FUEL(01)              =   0.421
      NU_RESIDUE(01)           =   0.579
      NU_WATER(01)             =   0.000
      N_REACTIONS              = 01 /

&MATL ID                       = 'char'
      CONDUCTIVITY             =  0.050
```

```
      DENSITY                   =  850.56
      SPECIFIC_HEAT             =    2.12
      EMISSIVITY                =  0.943
      ABSORPTION_COEFFICIENT    =  0.9000E+10
      N_REACTIONS               = 00 /

&SURF ID                          = 'FRP'
      STRETCH_FACTOR              = 1.000
      CELL_SIZE_FACTOR            = 0.200
      THICKNESS(1)               = 0.0019
      MATL_ID(1,1)              = 'virgin'
      MATL_ID(1,2)              = 'char'
      MATL_MASS_FRACTION(1,1)   = 1.0000
      MATL_MASS_FRACTION(1,2)   = 0.0000
      BACKING                     = 'INSULATED'
      SHRINK                      = .TRUE.
      TMP_INNER                   = 27.0
      COLOR                       = 'WHITE' /


****OBSTRUCTIONS****
&OBST XB=-1.200, 1.200, 0.000, 0.000, 0.000, 2.400, SURF_ID ='GYPSUM'  / Back wall
&OBST XB= 1.200, 1.200, 0.000, 2.700, 0.000, 2.400, SURF_ID ='GYPSUM'  / Right wall
&OBST XB=-1.200,-1.200, 0.000, 2.700, 0.000, 2.400, SURF_ID ='GYPSUM'  / Left wall
&OBST XB=-1.200, 1.200, 0.000, 2.700, 2.400, 2.400, SURF_ID ='GYPSUM'  / Ceiling
&OBST XB=-0.900,-0.600, 0.000, 0.05, 0.000, 2.400, SURF_ID ='KAOWOOL' / Kaowool on back wall
&OBST XB= 0.600, 0.900, 0.000, 0.05, 0.000, 2.400, SURF_ID ='KAOWOOL' / Kaowool on back wall
&OBST XB=-0.600, 0.600, 0.000, 0.05, 0.000, 2.400, SURF_ID ='FRP', PERMIT_HOLE = .TRUE. / FRP
panel

****OPEN VENTS****
&VENT XB=-1.20, 1.20, 3.90, 3.90, 0.00, 2.40, SURF_ID = 'OPEN' / Back
&VENT XB=-1.20,-1.20, 2.70, 3.90, 0.00, 2.40, SURF_ID = 'OPEN' /
&VENT XB= 1.20, 1.20, 2.70, 3.90, 0.00, 2.40, SURF_ID = 'OPEN' /
&VENT XB=-1.20, 1.20, 2.70, 3.90, 2.40, 2.40, SURF_ID = 'OPEN' /

HOLES in panel for TSC's:
&HOLE XB= 0.55,  0.60, -0.010, 0.1, 0.55, 0.60 / HOLE 1
&HOLE XB= 0,  0.05, -0.010, 0.1, 0.55, 0.60 / HOLE 2
&HOLE XB= -0.3, -0.25, -0.010, 0.1, 0.55, 0.60 / HOLE 3
&HOLE XB= 0.25,  0.3, -0.010, 0.1, 0.85, 0.9 / HOLE 4
&HOLE XB= -0.05,  0, -0.010, 0.1, 0.85, 0.9 / HOLE 5
&HOLE XB= -0.60, -0.55, -0.010, 0.1, 0.85, 0.9 / HOLE 6
&HOLE XB= 0.55,  0.60, -0.010, 0.1, 1.15, 1.2 / HOLE 7
&HOLE XB= 0, 0.05, -0.010, 0.1, 1.15, 1.2 / HOLE 8
&HOLE XB= -0.3, -0.25, -0.010, 0.1, 1.15, 1.2 / HOLE 9
&HOLE XB= 0.25,  0.3, -0.010, 0.1, 1.45, 1.5 / HOLE 10
&HOLE XB= -0.05,  0, -0.010, 0.1, 1.45, 1.5 / HOLE 11
&HOLE XB=-0.60, -0.55, -0.010, 0.1, 1.45, 1.5 / HOLE 12
&HOLE XB= 0.55,  0.60, -0.010, 0.1, 1.75, 1.8 / HOLE 13
&HOLE XB= 0,  0.05, -0.010, 0.1, 1.75, 1.8 / HOLE 14
&HOLE XB=-0.3, -0.25, -0.010, 0.1, 1.75, 1.8 / HOLE 15
&HOLE XB= 0.25,  0.3, -0.010, 0.1, 2.05, 2.1 / HOLE 16
&HOLE XB= -0.05,  0, -0.010, 0.1, 2.05, 2.1 / HOLE 17
&HOLE XB=-0.60, -0.55, -0.010, 0.1, 2.05, 2.1 / HOLE 18

TSC'S:

&OBST XB= 0.55,  0.60, -0.010, 0.05, 0.55, 0.60, SURF_ID = 'ADIABATIC', PERMIT_HOLE = .FALSE. /
TSC 1
&OBST XB= 0,  0.05, -0.010, 0.05, 0.55, 0.60, SURF_ID = 'ADIABATIC', PERMIT_HOLE = .FALSE. / TSC
2
&OBST XB= -0.3, -0.25, -0.010, 0.05, 0.55, 0.60, SURF_ID = 'ADIABATIC', PERMIT_HOLE = .FALSE. /
TSC 3
&OBST XB= 0.25,  0.3, -0.010, 0.05, 0.85, 0.9, SURF_ID = 'ADIABATIC', PERMIT_HOLE = .FALSE. / TSC
4
&OBST XB= -0.05,  0, -0.010, 0.05, 0.85, 0.9, SURF_ID = 'ADIABATIC', PERMIT_HOLE = .FALSE. / TSC
5
&OBST XB= -0.60, -0.55, -0.010, 0.05, 0.85, 0.9, SURF_ID = 'ADIABATIC', PERMIT_HOLE = .FALSE. /
TSC 6
```

```
&OBST XB= 0.55,  0.60, -0.010, 0.05, 1.15, 1.2, SURF_ID = 'ADIABATIC', PERMIT_HOLE = .FALSE. /
TSC 7
&OBST XB= 0, 0.05, -0.010, 0.05, 1.15, 1.2, SURF_ID = 'ADIABATIC', PERMIT_HOLE = .FALSE. / TSC 8
&OBST XB= -0.3, -0.25, -0.010, 0.05, 1.15, 1.2, SURF_ID = 'ADIABATIC', PERMIT_HOLE = .FALSE. /
TSC 9
&OBST XB= 0.25,  0.3, -0.010, 0.05, 1.45, 1.5, SURF_ID = 'ADIABATIC', PERMIT_HOLE = .FALSE. / TSC
10
&OBST XB= -0.05,  0, -0.010, 0.05, 1.45, 1.5, SURF_ID = 'ADIABATIC', PERMIT_HOLE = .FALSE. / TSC
11
&OBST XB=-0.60, -0.55, -0.010, 0.05, 1.45, 1.5, SURF_ID = 'ADIABATIC', PERMIT_HOLE = .FALSE. /
TSC 12
&OBST XB= 0.55,  0.60, -0.010, 0.05, 1.75, 1.8, SURF_ID = 'ADIABATIC', PERMIT_HOLE = .FALSE. /
TSC 13
&OBST XB= 0,  0.05, -0.010, 0.05, 1.75, 1.8, SURF_ID = 'ADIABATIC', PERMIT_HOLE = .FALSE. / TSC
14
&OBST XB=-0.3, -0.25, -0.010, 0.05, 1.75, 1.8, SURF_ID = 'ADIABATIC', PERMIT_HOLE = .FALSE. / TSC
15
&OBST XB= 0.25,  0.3, -0.010, 0.05, 2.05, 2.1, SURF_ID = 'ADIABATIC', PERMIT_HOLE = .FALSE. / TSC
16
&OBST XB= -0.05,  0, -0.010, 0.05, 2.05, 2.1, SURF_ID = 'ADIABATIC', PERMIT_HOLE = .FALSE. / TSC
17
&OBST XB=-0.60, -0.55, -0.010, 0.05, 2.05, 2.1, SURF_ID = 'ADIABATIC', PERMIT_HOLE = .FALSE. /
TSC 18

&SLCF PBX = 0.0, QUANTITY = 'TEMPERATURE' /
&SLCF PBX = 0.0, QUANTITY = 'HRRPUV' /

&BNDF QUANTITY='GAUGE HEAT FLUX' /
&BNDF QUANTITY='RADIATIVE HEAT FLUX' /
&BNDF QUANTITY='CONVECTIVE HEAT FLUX' /
&BNDF QUANTITY='NET HEAT FLUX' /
&BNDF QUANTITY='WALL TEMPERATURE' /
&BNDF QUANTITY='BURNING RATE' /

CENTERLINE RAKE
&DEVC XYZ=0, 0.25, 0.45, QUANTITY='TEMPERATURE', ID='CTC_1' /
&DEVC XYZ=0, 0.25, 0.60, QUANTITY='TEMPERATURE', ID='BDTC_1' /
&DEVC XYZ=0, 0.25, 0.75, QUANTITY='TEMPERATURE', ID='CTC_2' /
&DEVC XYZ=0, 0.25, 0.90, QUANTITY='TEMPERATURE', ID='BDTC_2' /
&DEVC XYZ=0, 0.25, 1.05, QUANTITY='TEMPERATURE', ID='CTC_3' /
&DEVC XYZ=0, 0.25, 1.20, QUANTITY='TEMPERATURE', ID='BDTC_3' /
&DEVC XYZ=0, 0.25, 1.35, QUANTITY='TEMPERATURE', ID='CTC_4' /
&DEVC XYZ=0, 0.25, 1.50, QUANTITY='TEMPERATURE', ID='BDTC_4' /
&DEVC XYZ=0, 0.25, 1.65, QUANTITY='TEMPERATURE', ID='CTC_5' /
&DEVC XYZ=0, 0.25, 1.80, QUANTITY='TEMPERATURE', ID='BDTC_5' /
&DEVC XYZ=0, 0.25, 1.95, QUANTITY='TEMPERATURE', ID='CTC_6' /
&DEVC XYZ=0, 0.25, 2.10, QUANTITY='TEMPERATURE', ID='BDTC_6' /
&DEVC XYZ=0, 0.25, 2.25, QUANTITY='TEMPERATURE', ID='CTC_7' /
&DEVC XYZ=0, 0.25, 0.60, QUANTITY='W-VELOCITY', ID='BD_1' /
&DEVC XYZ=0, 0.25, 0.90, QUANTITY='W-VELOCITY', ID='BD_2' /
&DEVC XYZ=0, 0.25, 1.20, QUANTITY='W-VELOCITY', ID='BD_3' /
&DEVC XYZ=0, 0.25, 1.50, QUANTITY='W-VELOCITY', ID='BD_4' /
&DEVC XYZ=0, 0.25, 1.80, QUANTITY='W-VELOCITY', ID='BD_5' /
&DEVC XYZ=0, 0.25, 2.10, QUANTITY='W-VELOCITY', ID='BD_6' /
&DEVC XYZ=0, 0.25, 1.05, QUANTITY='W-VELOCITY', ID='BD_7' /
&DEVC XYZ=0, 0.25, 1.35, QUANTITY='W-VELOCITY', ID='BD_8' /
&DEVC XYZ=0, 0.25, 1.65, QUANTITY='W-VELOCITY', ID='BD_9' /
&DEVC XYZ=0, 0.25, 1.95, QUANTITY='W-VELOCITY', ID='BD_10' /

WALL TEMPERATURE
&DEVC XYZ=0.0762, 0.05, 0.75, QUANTITY='TEMPERATURE', ID='WTC_1' /
&DEVC XYZ=0.0508, 0.055, 0.75, QUANTITY='TEMPERATURE', ID='WTC_2' /
&DEVC XYZ=0.0254, 0.060, 0.75, QUANTITY='TEMPERATURE', ID='WTC_3' /
&DEVC XYZ=-0.0254, 0.065, 0.75, QUANTITY='TEMPERATURE', ID='WTC_4' /
&DEVC XYZ=-0.0508, 0.070, 0.75, QUANTITY='TEMPERATURE', ID='WTC_5' /
&DEVC XYZ=-0.0762, 0.075, 0.75, QUANTITY='TEMPERATURE', ID='WTC_6' /
&DEVC XYZ=0.0762, 0.085, 1.35, QUANTITY='TEMPERATURE', ID='WTC_7' /
&DEVC XYZ=0.0508, 0.080, 1.35, QUANTITY='TEMPERATURE', ID='WTC_8' /
&DEVC XYZ=0.0254, 0.075, 1.35, QUANTITY='TEMPERATURE', ID='WTC_9' /
&DEVC XYZ=-0.0254, 0.070, 1.35, QUANTITY='TEMPERATURE', ID='WTC_10' /
&DEVC XYZ=-0.0508, 0.065, 1.35, QUANTITY='TEMPERATURE', ID='WTC_11' /
```

```
&DEVC XYZ=-0.0762, 0.060, 1.35, QUANTITY='TEMPERATURE', ID='WTC_12' /
&DEVC XYZ=0.0762, 0.065, 1.95, QUANTITY='TEMPERATURE', ID='WTC_13' /
&DEVC XYZ=0.0508, 0.070, 1.95, QUANTITY='TEMPERATURE', ID='WTC_14' /
&DEVC XYZ=0.0254, 0.075, 1.95, QUANTITY='TEMPERATURE', ID='WTC_15' /
&DEVC XYZ=-0.0254, 0.080, 1.95, QUANTITY='TEMPERATURE', ID='WTC_16' /
&DEVC XYZ=-0.0508, 0.085, 1.95, QUANTITY='TEMPERATURE', ID='WTC_17' /
&DEVC XYZ=-0.0762, 0.090, 1.95, QUANTITY='TEMPERATURE', ID='WTC_18' /

WALL HEAT FLUX MEASUREMENTS
&DEVC XYZ=  0.575, 0.050, 0.575, QUANTITY='GAUGE_HEAT_FLUX', ID='TS_1',  IOR = 2 /
&DEVC XYZ=  0.025, 0.050, 0.575, QUANTITY='GAUGE_HEAT_FLUX', ID='TS_2',  IOR = 2 /
&DEVC XYZ= -0.275, 0.050, 0.575, QUANTITY='GAUGE_HEAT_FLUX', ID='TS_3',  IOR = 2 /
&DEVC XYZ=  0.275, 0.050, 0.875, QUANTITY='GAUGE_HEAT_FLUX', ID='TS_4',  IOR = 2 /
&DEVC XYZ=  -0.025, 0.050, 0.875, QUANTITY='GAUGE_HEAT_FLUX', ID='TS_5',  IOR = 2 /
&DEVC XYZ= -0.575, 0.050, 0.875, QUANTITY='GAUGE_HEAT_FLUX', ID='TS_6',  IOR = 2 /
&DEVC XYZ=  0.575, 0.050, 1.175, QUANTITY='GAUGE_HEAT_FLUX', ID='TS_7',  IOR = 2 /
&DEVC XYZ=  0.025 0.050, 1.175, QUANTITY='GAUGE_HEAT_FLUX', ID='TS_8',  IOR = 2 /
&DEVC XYZ= -0.275, 0.050, 1.175, QUANTITY='GAUGE_HEAT_FLUX', ID='TS_9',  IOR = 2 /
&DEVC XYZ=  0.275, 0.050, 1.475, QUANTITY='GAUGE_HEAT_FLUX', ID='TS_10', IOR = 2 /
&DEVC XYZ=  -0.025, 0.050, 1.475, QUANTITY='GAUGE_HEAT_FLUX', ID='TS_11', IOR = 2 /
&DEVC XYZ= -0.575, 0.050, 1.475, QUANTITY='GAUGE_HEAT_FLUX', ID='TS_12', IOR = 2 /
&DEVC XYZ=  0.575, 0.050, 1.775, QUANTITY='GAUGE_HEAT_FLUX', ID='TS_13', IOR = 2 /
&DEVC XYZ=  0.025, 0.050, 1.775, QUANTITY='GAUGE_HEAT_FLUX', ID='TS_14', IOR = 2 /
&DEVC XYZ= -0.275, 0.050, 1.775, QUANTITY='GAUGE_HEAT_FLUX', ID='TS_15', IOR = 2 /
&DEVC XYZ=  0.275, 0.050, 2.075, QUANTITY='GAUGE_HEAT_FLUX', ID='TS_16', IOR = 2 /
&DEVC XYZ=  -0.025, 0.050, 2.075, QUANTITY='GAUGE_HEAT_FLUX', ID='TS_17', IOR = 2 /
&DEVC XYZ= -0.575, 0.050, 2.075, QUANTITY='GAUGE_HEAT_FLUX', ID='TS_18', IOR = 2 /

&DEVC XYZ=  0.275, 0.050, 0.60, QUANTITY='GAUGE_HEAT_FLUX', ID='HFG_1', IOR = 2 /
&DEVC XYZ= -0.275, 0.050, 0.875, QUANTITY='GAUGE_HEAT_FLUX', ID='HFG_2', IOR = 2 /
&DEVC XYZ=  0.275, 0.050, 1.175, QUANTITY='GAUGE_HEAT_FLUX', ID='HFG_3', IOR = 2 /
&DEVC XYZ= -0.275, 0.050, 1.475, QUANTITY='GAUGE_HEAT_FLUX', ID='HFG_4', IOR = 2 /
&DEVC XYZ=  0.275, 0.050, 1.775, QUANTITY='GAUGE_HEAT_FLUX', ID='HFG_5', IOR = 2 /
&DEVC XYZ= -0.275, 0.050, 2.075, QUANTITY='GAUGE_HEAT_FLUX', ID='HFG_6', IOR = 2 /

WALL NET HEAT FLUX
&DEVC XYZ=  0.575, 0.050, 0.575, QUANTITY='NET HEAT FLUX', ID='TS_1',  IOR = 2 /
&DEVC XYZ=  0.025, 0.050, 0.575, QUANTITY='NET HEAT FLUX', ID='TS_2',  IOR = 2 /
&DEVC XYZ= -0.275, 0.050, 0.575, QUANTITY='NET HEAT FLUX', ID='TS_3',  IOR = 2 /
&DEVC XYZ=  0.275, 0.050, 0.875, QUANTITY='NET HEAT FLUX', ID='TS_4',  IOR = 2 /
&DEVC XYZ=  -0.025, 0.050, 0.875, QUANTITY='NET HEAT FLUX', ID='TS_5',  IOR = 2 /
&DEVC XYZ= -0.575, 0.050, 0.875, QUANTITY='NET HEAT FLUX', ID='TS_6',  IOR = 2 /
&DEVC XYZ=  0.575, 0.050, 1.175, QUANTITY='NET HEAT FLUX', ID='TS_7',  IOR = 2 /
&DEVC XYZ=  0.025 0.050, 1.175, QUANTITY='NET HEAT FLUX', ID='TS_8',  IOR = 2 /
&DEVC XYZ= -0.275, 0.050, 1.175, QUANTITY='NET HEAT FLUX', ID='TS_9',  IOR = 2 /
&DEVC XYZ=  0.275, 0.050, 1.475, QUANTITY='NET HEAT FLUX', ID='TS_10', IOR = 2 /
&DEVC XYZ=  -0.025, 0.050, 1.475, QUANTITY='NET HEAT FLUX', ID='TS_11', IOR = 2 /
&DEVC XYZ= -0.575, 0.050, 1.475, QUANTITY='NET HEAT FLUX', ID='TS_12', IOR = 2 /
&DEVC XYZ=  0.575, 0.050, 1.775, QUANTITY='NET HEAT FLUX', ID='TS_13', IOR = 2 /
&DEVC XYZ=  0.025, 0.050, 1.775, QUANTITY='NET HEAT FLUX', ID='TS_14', IOR = 2 /
&DEVC XYZ= -0.275, 0.050, 1.775, QUANTITY='NET HEAT FLUX', ID='TS_15', IOR = 2 /
```

J.17 Input File 17 – FRP scenario, Rectangle burner, 50 kW, propane

```
Start Input File
&HEAD CHID='67_1_03-14-2011_FRP_Pr_lb_50kW' /

&TIME T_END = 900, DT = 0.05, RESTRICT_TIME_STEP = .FALSE. /
&DUMP DT_BNDF=2.0, DT_DEVC=0.5, DT_HRR=1.0, DT_PL3D=5000.0, DT_SLCF=2.0, DT_RESTART=50./

&MISC
      SURF_DEFAULT = 'INERT'
      TMPA  = 23
      FDS6  = .TRUE.
      DNS = .FALSE.
      DYNSMAG = .TRUE.
      CSMAG = 0.2
      PR = 0.5
      SC = 0.5
      H_EDDY = .TRUE.
      CFL_VELOCITY_NORM = 1
      FLUX_LIMITER = 2
      ISOTHERMAL = .FALSE.
      RADIATION = .TRUE.
      BAROCLINIC = .TRUE.
      CLIP_MASS_FRACTION   = .TRUE.
      CHECK_VN = .TRUE.
      NOBIAS = .TRUE.
      PROJECTION  = .FALSE.
      CHECK_KINETIC_ENERGY = .FALSE.
      /

&REAC
     ID = 'Propane'
     C = 3
     H = 8
     O = 0
     CO_YIELD = 0.024
     SOOT_YIELD = 0.005
     EDDY_DISSIPATION = .TRUE.
     C_EDC = 0.1
     HRRPUA_SHEET = 0
     HRRPUV_AVERAGE = 2500
      /

&RADI
    RADIATIVE_FRACTION = 0.3
    TIME_STEP_INCREMENT = 3
    ANGLE_INCREMENT = 5
    NUMBER_RADIATION_ANGLES = 104
    /

**** MESHES ****
 MESH IJK= 96, 156, 96, XB=-1.20, 1.20, 0.00, 3.90, 0.00, 2.40 / 2.50 cm grid,  1 mesh

&MESH ID= 'Mesh-1', IJK= 24, 26, 24, XB= -1.2, 0, 0, 1.3, 0, 1.2 / 0.05 cm grid 12 mesh
&MESH ID= 'Mesh-2', IJK= 24, 26, 24, XB= -1.2, 0, 1.3, 2.6, 0, 1.2 / 0.05 cm grid 12 mesh
&MESH ID= 'Mesh-3', IJK= 24, 26, 24, XB= -1.2, 0, 2.6, 3.9, 0, 1.2 / 0.05 cm grid 12 mesh
&MESH ID= 'Mesh-4', IJK= 24, 26, 24, XB= 0, 1.2, 0, 1.3, 0, 1.2 / 0.05 cm grid 12 mesh
&MESH ID= 'Mesh-5', IJK= 24, 26, 24, XB= 0, 1.2, 1.3, 2.6, 0, 1.2 / 0.05 cm grid 12 mesh
&MESH ID= 'Mesh-6', IJK= 24, 26, 24, XB= 0, 1.2, 2.6, 3.9, 0, 1.2 / 0.05 cm grid 12 mesh
&MESH ID= 'Mesh-7', IJK= 24, 26, 24, XB= -1.2, 0, 0, 1.3, 1.2, 2.4 / 0.05 cm grid 12 mesh
&MESH ID= 'Mesh-8', IJK= 24, 26, 24, XB= -1.2, 0, 1.3, 2.6, 1.2, 2.4 / 0.05 cm grid 12 mesh
&MESH ID= 'Mesh-9', IJK= 24, 26, 24, XB= -1.2, 0, 2.6, 3.9, 1.2, 2.4 / 0.05 cm grid 12 mesh
&MESH ID= 'Mesh-10', IJK= 24, 26, 24, XB= 0, 1.2, 0, 1.3, 1.2, 2.4 / 0.05 cm grid 12 mesh
&MESH ID= 'Mesh-11', IJK= 24, 26, 24, XB= 0, 1.2, 1.3, 2.6, 1.2, 2.4 / 0.05 cm grid 12 mesh
&MESH ID= 'Mesh-12', IJK= 24, 26, 24, XB= 0, 1.2, 2.6, 3.9, 1.2, 2.4 / 0.05 cm grid 12 mesh

****BURNER****
2 ft burner
&OBST XB= -0.35, 0.35, 0.05, 0.45, 0, 0.4, SURF_ID = 'ADIABATIC' /
&VENT XB= -0.3, 0.3, 0.1, 0.4, 0.4, 0.4, SURF_ID = 'BURNER' /
```

```
1 ft burner
OBST XB= -0.2, 0.2, 0.05, 0.45, 0, 0.4, SURF_ID = 'ADIABATIC' /
VENT XB= -0.15, 0.15, 0.1, 0.4, 0.4, 0.4, SURF_ID = 'BURNER' /

**** Burner Parameters*****
&SURF ID = 'BURNER'
      HRRPUA =277.8
      RAMP_Q = 'Burner_Ramp'
      COLOR  = 'RED' /

&RAMP ID = 'Burner_Ramp', T=0, F=0 /
&RAMP ID = 'Burner_Ramp', T=1, F=0.5 /
&RAMP ID = 'Burner_Ramp', T=15, F=1 /
&RAMP ID = 'Burner_Ramp', T=72, F=1 /
&RAMP ID = 'Burner_Ramp', T=82, F=0 /

**** MATERIAL PROPERTIES ****
&MATL ID            ='GYPSUM_MATL'
      SPECIFIC_HEAT = 0.84
      CONDUCTIVITY  = 0.48
      DENSITY       = 1440.0 /

&MATL ID            ='KAOWOOL_MATL'
      SPECIFIC_HEAT = 1.0
      CONDUCTIVITY  = 0.06
      DENSITY       = 320.0 /

&SURF ID        = 'ADIABATIC'
      ADIABATIC = .TRUE.
      RGB       = 0, 0, 0 /

&SURF ID                     = 'KAOWOOL'
      RGB                    = 51,102,255
      BACKING                = 'INSULATED'
      MATL_ID(1,1)           = 'KAOWOOL_MATL'
      MATL_MASS_FRACTION(1,1)= 1.0
      THICKNESS(1)           = 0.025
      CELL_SIZE_FACTOR       = 0.30
      STRETCH_FACTOR         = 1.0 /

&SURF ID                     = 'GYPSUM'
      RGB                    = 100,100,100
      BACKING                = 'INSULATED'
      MATL_ID(1,1)           = 'GYPSUM_MATL'
      MATL_MASS_FRACTION(1,1)= 1.0
      THICKNESS(1)           = 0.016
      CELL_SIZE_FACTOR       = 0.30
      STRETCH_FACTOR         = 1.0 /

&MATL ID                       = 'virgin'
      CONDUCTIVITY             =  0.480
      DENSITY                  = 1467.80
      SPECIFIC_HEAT            =    1.98
      EMISSIVITY               =  0.858
      ABSORPTION_COEFFICIENT   =  0.9000E+10
      RESIDUE(01)              = 'char'
      A(01)                    = 0.1139E+12
      E(01)                    = 0.1483E+06
      N_S(01)                  =   1.00
      THRESHOLD_TEMPERATURE(01)=   0.00
      HEAT_OF_REACTION(01)     =   996.67
      HEAT_OF_COMBUSTION       = 19700.
      NU_FUEL(01)              =   0.421
      NU_RESIDUE(01)           =   0.579
      NU_WATER(01)             =   0.000
      N_REACTIONS              = 01 /

&MATL ID                       = 'char'
      CONDUCTIVITY             =  0.050
      DENSITY                  =  850.56
      SPECIFIC_HEAT            =    2.12
```

```
      EMISSIVITY                =  0.943
      ABSORPTION_COEFFICIENT    =  0.9000E+10
      N_REACTIONS               = 00 /

&SURF ID                          = 'FRP'
      STRETCH_FACTOR              = 1.000
      CELL_SIZE_FACTOR            = 0.200
      THICKNESS(1)               = 0.0019
      MATL_ID(1,1)              = 'virgin'
      MATL_ID(1,2)              = 'char'
      MATL_MASS_FRACTION(1,1)   = 1.0000
      MATL_MASS_FRACTION(1,2)   = 0.0000
      BACKING                     = 'INSULATED'
      SHRINK                      = .TRUE.
      TMP_INNER                   = 27.0
      COLOR                       = 'WHITE' /


****OBSTRUCTIONS****
&OBST XB=-1.200, 1.200, 0.000, 0.000, 0.000, 2.400, SURF_ID ='GYPSUM'  / Back wall
&OBST XB= 1.200, 1.200, 0.000, 2.700, 0.000, 2.400, SURF_ID ='GYPSUM'  / Right wall
&OBST XB=-1.200,-1.200, 0.000, 2.700, 0.000, 2.400, SURF_ID ='GYPSUM'  / Left wall
&OBST XB=-1.200, 1.200, 0.000, 2.700, 2.400, 2.400, SURF_ID ='GYPSUM'  / Ceiling
&OBST XB=-0.900,-0.600, 0.000, 0.05, 0.000, 2.400, SURF_ID ='KAOWOOL' / Kaowool on back wall
&OBST XB= 0.600, 0.900, 0.000, 0.05, 0.000, 2.400, SURF_ID ='KAOWOOL' / Kaowool on back wall
&OBST XB=-0.600, 0.600, 0.000, 0.05, 0.000, 2.400, SURF_ID ='FRP', PERMIT_HOLE = .TRUE. / FRP
panel

****OPEN VENTS****
&VENT XB=-1.20, 1.20, 3.90, 3.90, 0.00, 2.40, SURF_ID = 'OPEN' / Back
&VENT XB=-1.20,-1.20, 2.70, 3.90, 0.00, 2.40, SURF_ID = 'OPEN' /
&VENT XB= 1.20, 1.20, 2.70, 3.90, 0.00, 2.40, SURF_ID = 'OPEN' /
&VENT XB=-1.20, 1.20, 2.70, 3.90, 2.40, 2.40, SURF_ID = 'OPEN' /

HOLES in panel for TSC's:
&HOLE XB= 0.55,  0.60, -0.010, 0.1, 0.55, 0.60 / HOLE 1
&HOLE XB= 0,  0.05, -0.010, 0.1, 0.55, 0.60 / HOLE 2
&HOLE XB= -0.3, -0.25, -0.010, 0.1, 0.55, 0.60 / HOLE 3
&HOLE XB= 0.25,  0.3, -0.010, 0.1, 0.85, 0.9 / HOLE 4
&HOLE XB= -0.05,  0, -0.010, 0.1, 0.85, 0.9 / HOLE 5
&HOLE XB= -0.60, -0.55, -0.010, 0.1, 0.85, 0.9 / HOLE 6
&HOLE XB= 0.55,  0.60, -0.010, 0.1, 1.15, 1.2 / HOLE 7
&HOLE XB= 0, 0.05, -0.010, 0.1, 1.15, 1.2 / HOLE 8
&HOLE XB= -0.3, -0.25, -0.010, 0.1, 1.15, 1.2 / HOLE 9
&HOLE XB= 0.25,  0.3, -0.010, 0.1, 1.45, 1.5 / HOLE 10
&HOLE XB= -0.05,  0, -0.010, 0.1, 1.45, 1.5 / HOLE 11
&HOLE XB=-0.60, -0.55, -0.010, 0.1, 1.45, 1.5 / HOLE 12
&HOLE XB= 0.55,  0.60, -0.010, 0.1, 1.75, 1.8 / HOLE 13
&HOLE XB= 0,  0.05, -0.010, 0.1, 1.75, 1.8 / HOLE 14
&HOLE XB=-0.3, -0.25, -0.010, 0.1, 1.75, 1.8 / HOLE 15
&HOLE XB= 0.25,  0.3, -0.010, 0.1, 2.05, 2.1 / HOLE 16
&HOLE XB= -0.05,  0, -0.010, 0.1, 2.05, 2.1 / HOLE 17
&HOLE XB=-0.60, -0.55, -0.010, 0.1, 2.05, 2.1 / HOLE 18

TSC'S:

&OBST XB= 0.55,  0.60, -0.010, 0.05, 0.55, 0.60, SURF_ID = 'ADIABATIC', PERMIT_HOLE = .FALSE. /
TSC 1
&OBST XB= 0,  0.05, -0.010, 0.05, 0.55, 0.60, SURF_ID = 'ADIABATIC', PERMIT_HOLE = .FALSE. / TSC
2
&OBST XB= -0.3, -0.25, -0.010, 0.05, 0.55, 0.60, SURF_ID = 'ADIABATIC', PERMIT_HOLE = .FALSE. /
TSC 3
&OBST XB= 0.25,  0.3, -0.010, 0.05, 0.85, 0.9, SURF_ID = 'ADIABATIC', PERMIT_HOLE = .FALSE. / TSC
4
&OBST XB= -0.05,  0, -0.010, 0.05, 0.85, 0.9, SURF_ID = 'ADIABATIC', PERMIT_HOLE = .FALSE. / TSC
5
&OBST XB= -0.60, -0.55, -0.010, 0.05, 0.85, 0.9, SURF_ID = 'ADIABATIC', PERMIT_HOLE = .FALSE. /
TSC 6
&OBST XB= 0.55,  0.60, -0.010, 0.05, 1.15, 1.2, SURF_ID = 'ADIABATIC', PERMIT_HOLE = .FALSE. /
TSC 7
&OBST XB= 0, 0.05, -0.010, 0.05, 1.15, 1.2, SURF_ID = 'ADIABATIC', PERMIT_HOLE = .FALSE. / TSC 8
```

```
&OBST XB= -0.3, -0.25, -0.010, 0.05, 1.15, 1.2, SURF_ID = 'ADIABATIC', PERMIT_HOLE = .FALSE. /
TSC 9
&OBST XB= 0.25,  0.3, -0.010, 0.05, 1.45, 1.5, SURF_ID = 'ADIABATIC', PERMIT_HOLE = .FALSE. / TSC
10
&OBST XB= -0.05,  0, -0.010, 0.05, 1.45, 1.5, SURF_ID = 'ADIABATIC', PERMIT_HOLE = .FALSE. / TSC
11
&OBST XB=-0.60, -0.55, -0.010, 0.05, 1.45, 1.5, SURF_ID = 'ADIABATIC', PERMIT_HOLE = .FALSE. /
TSC 12
&OBST XB= 0.55,  0.60, -0.010, 0.05, 1.75, 1.8, SURF_ID = 'ADIABATIC', PERMIT_HOLE = .FALSE. /
TSC 13
&OBST XB= 0,  0.05, -0.010, 0.05, 1.75, 1.8, SURF_ID = 'ADIABATIC', PERMIT_HOLE = .FALSE. / TSC
14
&OBST XB=-0.3, -0.25, -0.010, 0.05, 1.75, 1.8, SURF_ID = 'ADIABATIC', PERMIT_HOLE = .FALSE. / TSC
15
&OBST XB= 0.25,  0.3, -0.010, 0.05, 2.05, 2.1, SURF_ID = 'ADIABATIC', PERMIT_HOLE = .FALSE. / TSC
16
&OBST XB= -0.05,  0, -0.010, 0.05, 2.05, 2.1, SURF_ID = 'ADIABATIC', PERMIT_HOLE = .FALSE. / TSC
17
&OBST XB=-0.60, -0.55, -0.010, 0.05, 2.05, 2.1, SURF_ID = 'ADIABATIC', PERMIT_HOLE = .FALSE. /
TSC 18

&SLCF PBX = 0.0, QUANTITY = 'TEMPERATURE' /
&SLCF PBX = 0.0, QUANTITY = 'HRRPUV' /

&BNDF QUANTITY='GAUGE HEAT FLUX' /
&BNDF QUANTITY='RADIATIVE HEAT FLUX' /
&BNDF QUANTITY='CONVECTIVE HEAT FLUX' /
&BNDF QUANTITY='NET HEAT FLUX' /
&BNDF QUANTITY='WALL TEMPERATURE' /
&BNDF QUANTITY='BURNING RATE' /

CENTERLINE RAKE
&DEVC XYZ=0, 0.25, 0.45, QUANTITY='TEMPERATURE', ID='CTC_1' /
&DEVC XYZ=0, 0.25, 0.60, QUANTITY='TEMPERATURE', ID='BDTC_1' /
&DEVC XYZ=0, 0.25, 0.75, QUANTITY='TEMPERATURE', ID='CTC_2' /
&DEVC XYZ=0, 0.25, 0.90, QUANTITY='TEMPERATURE', ID='BDTC_2' /
&DEVC XYZ=0, 0.25, 1.05, QUANTITY='TEMPERATURE', ID='CTC_3' /
&DEVC XYZ=0, 0.25, 1.20, QUANTITY='TEMPERATURE', ID='BDTC_3' /
&DEVC XYZ=0, 0.25, 1.35, QUANTITY='TEMPERATURE', ID='CTC_4' /
&DEVC XYZ=0, 0.25, 1.50, QUANTITY='TEMPERATURE', ID='BDTC_4' /
&DEVC XYZ=0, 0.25, 1.65, QUANTITY='TEMPERATURE', ID='CTC_5' /
&DEVC XYZ=0, 0.25, 1.80, QUANTITY='TEMPERATURE', ID='BDTC_5' /
&DEVC XYZ=0, 0.25, 1.95, QUANTITY='TEMPERATURE', ID='CTC_6' /
&DEVC XYZ=0, 0.25, 2.10, QUANTITY='TEMPERATURE', ID='BDTC_6' /
&DEVC XYZ=0, 0.25, 2.25, QUANTITY='TEMPERATURE', ID='CTC_7' /
&DEVC XYZ=0, 0.25, 0.60, QUANTITY='W-VELOCITY', ID='BD_1' /
&DEVC XYZ=0, 0.25, 0.90, QUANTITY='W-VELOCITY', ID='BD_2' /
&DEVC XYZ=0, 0.25, 1.20, QUANTITY='W-VELOCITY', ID='BD_3' /
&DEVC XYZ=0, 0.25, 1.50, QUANTITY='W-VELOCITY', ID='BD_4' /
&DEVC XYZ=0, 0.25, 1.80, QUANTITY='W-VELOCITY', ID='BD_5' /
&DEVC XYZ=0, 0.25, 2.10, QUANTITY='W-VELOCITY', ID='BD_6' /
&DEVC XYZ=0, 0.25, 1.05, QUANTITY='W-VELOCITY', ID='BD_7' /
&DEVC XYZ=0, 0.25, 1.35, QUANTITY='W-VELOCITY', ID='BD_8' /
&DEVC XYZ=0, 0.25, 1.65, QUANTITY='W-VELOCITY', ID='BD_9' /
&DEVC XYZ=0, 0.25, 1.95, QUANTITY='W-VELOCITY', ID='BD_10' /

WALL TEMPERATURE
&DEVC XYZ=0.0762, 0.05, 0.75, QUANTITY='TEMPERATURE', ID='WTC_1' /
&DEVC XYZ=0.0508, 0.055, 0.75, QUANTITY='TEMPERATURE', ID='WTC_2' /
&DEVC XYZ=0.0254, 0.060, 0.75, QUANTITY='TEMPERATURE', ID='WTC_3' /
&DEVC XYZ=-0.0254, 0.065, 0.75, QUANTITY='TEMPERATURE', ID='WTC_4' /
&DEVC XYZ=-0.0508, 0.070, 0.75, QUANTITY='TEMPERATURE', ID='WTC_5' /
&DEVC XYZ=-0.0762, 0.075, 0.75, QUANTITY='TEMPERATURE', ID='WTC_6' /
&DEVC XYZ=0.0762, 0.085, 1.35, QUANTITY='TEMPERATURE', ID='WTC_7' /
&DEVC XYZ=0.0508, 0.080, 1.35, QUANTITY='TEMPERATURE', ID='WTC_8' /
&DEVC XYZ=0.0254, 0.075, 1.35, QUANTITY='TEMPERATURE', ID='WTC_9' /
&DEVC XYZ=-0.0254, 0.070, 1.35, QUANTITY='TEMPERATURE', ID='WTC_10' /
&DEVC XYZ=-0.0508, 0.065, 1.35, QUANTITY='TEMPERATURE', ID='WTC_11' /
&DEVC XYZ=-0.0762, 0.060, 1.35, QUANTITY='TEMPERATURE', ID='WTC_12' /
&DEVC XYZ=0.0762, 0.065, 1.95, QUANTITY='TEMPERATURE', ID='WTC_13' /
&DEVC XYZ=0.0508, 0.070, 1.95, QUANTITY='TEMPERATURE', ID='WTC_14' /
```

```
&DEVC XYZ=0.0254, 0.075, 1.95, QUANTITY='TEMPERATURE', ID='WTC_15' /
&DEVC XYZ=-0.0254, 0.080, 1.95, QUANTITY='TEMPERATURE', ID='WTC_16' /
&DEVC XYZ=-0.0508, 0.085, 1.95, QUANTITY='TEMPERATURE', ID='WTC_17' /
&DEVC XYZ=-0.0762, 0.090, 1.95, QUANTITY='TEMPERATURE', ID='WTC_18' /

WALL HEAT FLUX MEASUREMENTS
&DEVC XYZ=  0.575, 0.050, 0.575, QUANTITY='GAUGE_HEAT_FLUX', ID='TS_1',  IOR = 2 /
&DEVC XYZ=  0.025, 0.050, 0.575, QUANTITY='GAUGE_HEAT_FLUX', ID='TS_2',  IOR = 2 /
&DEVC XYZ= -0.275, 0.050, 0.575, QUANTITY='GAUGE_HEAT_FLUX', ID='TS_3',  IOR = 2 /
&DEVC XYZ=  0.275, 0.050, 0.875, QUANTITY='GAUGE_HEAT_FLUX', ID='TS_4',  IOR = 2 /
&DEVC XYZ=  -0.025, 0.050, 0.875, QUANTITY='GAUGE_HEAT_FLUX', ID='TS_5',  IOR = 2 /
&DEVC XYZ= -0.575, 0.050, 0.875, QUANTITY='GAUGE_HEAT_FLUX', ID='TS_6',  IOR = 2 /
&DEVC XYZ=  0.575, 0.050, 1.175, QUANTITY='GAUGE_HEAT_FLUX', ID='TS_7',  IOR = 2 /
&DEVC XYZ=  0.025 0.050, 1.175, QUANTITY='GAUGE_HEAT_FLUX', ID='TS_8',  IOR = 2 /
&DEVC XYZ= -0.275, 0.050, 1.175, QUANTITY='GAUGE_HEAT_FLUX', ID='TS_9',  IOR = 2 /
&DEVC XYZ=  0.275, 0.050, 1.475, QUANTITY='GAUGE_HEAT_FLUX', ID='TS_10', IOR = 2 /
&DEVC XYZ=  -0.025, 0.050, 1.475, QUANTITY='GAUGE_HEAT_FLUX', ID='TS_11', IOR = 2 /
&DEVC XYZ= -0.575, 0.050, 1.475, QUANTITY='GAUGE_HEAT_FLUX', ID='TS_12', IOR = 2 /
&DEVC XYZ=  0.575, 0.050, 1.775, QUANTITY='GAUGE_HEAT_FLUX', ID='TS_13', IOR = 2 /
&DEVC XYZ=  0.025, 0.050, 1.775, QUANTITY='GAUGE_HEAT_FLUX', ID='TS_14', IOR = 2 /
&DEVC XYZ= -0.275, 0.050, 1.775, QUANTITY='GAUGE_HEAT_FLUX', ID='TS_15', IOR = 2 /
&DEVC XYZ=  0.275, 0.050, 2.075, QUANTITY='GAUGE_HEAT_FLUX', ID='TS_16', IOR = 2 /
&DEVC XYZ=  -0.025, 0.050, 2.075, QUANTITY='GAUGE_HEAT_FLUX', ID='TS_17', IOR = 2 /
&DEVC XYZ= -0.575, 0.050, 2.075, QUANTITY='GAUGE_HEAT_FLUX', ID='TS_18', IOR = 2 /

&DEVC XYZ=  0.275, 0.050, 0.60, QUANTITY='GAUGE_HEAT_FLUX', ID='HFG_1', IOR = 2 /
&DEVC XYZ= -0.275, 0.050, 0.875, QUANTITY='GAUGE_HEAT_FLUX', ID='HFG_2', IOR = 2 /
&DEVC XYZ=  0.275, 0.050, 1.175, QUANTITY='GAUGE_HEAT_FLUX', ID='HFG_3', IOR = 2 /
&DEVC XYZ= -0.275, 0.050, 1.475, QUANTITY='GAUGE_HEAT_FLUX', ID='HFG_4', IOR = 2 /
&DEVC XYZ=  0.275, 0.050, 1.775, QUANTITY='GAUGE_HEAT_FLUX', ID='HFG_5', IOR = 2 /
&DEVC XYZ= -0.275, 0.050, 2.075, QUANTITY='GAUGE_HEAT_FLUX', ID='HFG_6', IOR = 2 /

WALL NET HEAT FLUX
&DEVC XYZ=  0.575, 0.050, 0.575, QUANTITY='NET HEAT FLUX', ID='TS_1',  IOR = 2 /
&DEVC XYZ=  0.025, 0.050, 0.575, QUANTITY='NET HEAT FLUX', ID='TS_2',  IOR = 2 /
&DEVC XYZ= -0.275, 0.050, 0.575, QUANTITY='NET HEAT FLUX', ID='TS_3',  IOR = 2 /
&DEVC XYZ=  0.275, 0.050, 0.875, QUANTITY='NET HEAT FLUX', ID='TS_4',  IOR = 2 /
&DEVC XYZ=  -0.025, 0.050, 0.875, QUANTITY='NET HEAT FLUX', ID='TS_5',  IOR = 2 /
&DEVC XYZ= -0.575, 0.050, 0.875, QUANTITY='NET HEAT FLUX', ID='TS_6',  IOR = 2 /
&DEVC XYZ=  0.575, 0.050, 1.175, QUANTITY='NET HEAT FLUX', ID='TS_7',  IOR = 2 /
&DEVC XYZ=  0.025 0.050, 1.175, QUANTITY='NET HEAT FLUX', ID='TS_8',  IOR = 2 /
&DEVC XYZ= -0.275, 0.050, 1.175, QUANTITY='NET HEAT FLUX', ID='TS_9',  IOR = 2 /
&DEVC XYZ=  0.275, 0.050, 1.475, QUANTITY='NET HEAT FLUX', ID='TS_10', IOR = 2 /
&DEVC XYZ=  -0.025, 0.050, 1.475, QUANTITY='NET HEAT FLUX', ID='TS_11', IOR = 2 /
&DEVC XYZ= -0.575, 0.050, 1.475, QUANTITY='NET HEAT FLUX', ID='TS_12', IOR = 2 /
&DEVC XYZ=  0.575, 0.050, 1.775, QUANTITY='NET HEAT FLUX', ID='TS_13', IOR = 2 /
&DEVC XYZ=  0.025, 0.050, 1.775, QUANTITY='NET HEAT FLUX', ID='TS_14', IOR = 2 /
&DEVC XYZ= -0.275, 0.050, 1.775, QUANTITY='NET HEAT FLUX', ID='TS_15', IOR = 2 /
```

Appendix K FDS Parametric Study Results [Free Plume]

Varying the FDS parameters that govern the CFD simulation characteristics changed the behaviors of the model to different degrees. The predictive capabilities and the performance of the model are both affected by parameter changes; and to understand the relationships between the cause (parameter change) and the results (predictions and performance) is of great importance to end-users so that simulations can be conducted effectively and efficiently. A systemic approach to varying some notable parameters in FDS individually was undertaken using all three configurations of fire models in this study. The default cases used mostly FDS default parameters, and in each iteration only one parameter was varied from the default. Some parameters from the MISC, RADI, REAC, and TIME groups were changed during this exercise. Comparisons of the outputs and performance of successive series of models were made against the default cases. The list of parameters changed in the study is presented in Table 1.

Table 1 - Variable simulation parameters

Series	Parameter Group	Parameter change	Default Value	New value in simulation	Change from default
0	FDS6	DYNSMAG	.TRUE.	.FALSE.	x
1	N/A	No change, Default situation using default FDS6 options			
2	MISC	RADIATION	.TRUE.	.FALSE.	x
3	RADI	RADIATIVE FRACTION	0.30	Source fire specific	varies
4	RADI	RADIATIVE FRACTION	0.30	0.1	~33%
5	RADI	RADIATIVE FRACTION	0.30	0.2	~50%
6	RADI	RADIATIVE FRACTION	0.30	0.5	~160%
7	RADI	WIDE_BAND_MODEL	.FALSE.	.TRUE	x
8	RADI	NUMBER_RADIATION_ANGLES	104	52	50%
9	RADI	NUMBER_RADIATION_ANGLES	104	208	200%
10	RADI	ANGLE_INCREMENT	5	2	50%
11	RADI	ANGLE_INCREMENT	5	10	200%
12	RADI	TIME_STEP_INCREMENT	3	1	50%
13	RADI	TIME_STEP_INCREMENT	3	6	200%
~~14~~	~~Skipped~~				
15	REAC	C_EDC	0.1	0.2	50%
16	REAC	C_EDC	0.1	0.05	200%
17	REAC	EDDY_DISSIPATION	.TRUE.	.FALSE.	x
18	REAC	HRRPUA_SHEET	0	400	40000%
19	REAC	HRRPUA_SHEET	0	100	10000%
20	REAC	HRRPUV_AVERAGE	3000	1200	40%
21	MISC	ISOTHERMAL	.FALSE.	.TRUE	x
22	MISC	CSMAG	0.2	0.1	50%
23	MISC	CSMAG	0.2	0.4	200%

Series	Parameter Group	Parameter change	Default Value	New value in simulation	Change from default
24	MISC	PR	0.5	0.25	50%
25	MISC	PR	0.5	1	200%
26	MISC	SC	0.5	0.25	50%
27	MISC	SC	0.5	1	200%
28	MISC	BAROCLINIC	.TRUE.	.FALSE.	x
29	MISC	CFL_MAX	1	2	200%
30	MISC	CFL_MIN	0.8	0.4	50%
31	MISC	CFL_MAX and CFL_MIN	1 / 0.8	2 / 0.4	x
32	FDS6	FLUX_LIMITER	2	-1	x
33	FDS6	CFL_VELOCITY_NORM	1	2	x
34	FDS6	CFL_VELOCITY_NORM	1	0	x
35	FDS6	H_EDDY	.TRUE.	.FALSE.	x

The variable parameters and their functions are described in this section. Many of the parameters have an effect on the stability and the performance of the model by changing the amount or complexity of the calculations performed by the FDS software. Moreover, some of the parameters can also affect the predicted fire behaviors and change the various quantities predicted by FDS.

1) RADI parameters
   - **a) RADIATIVE_FRACTION**
     - i) Determines the fraction of combustion energy released in the model as thermal radiation
     - ii) Default simulations used a value of 0.30
     - iii) Parametric study used the radiative fraction values of the fuel modeled: methane at 0.141, propane at 0.286, and propylene at 0.368
   - **b) WIDE_BAND_MODEL**
     - i) Determine whether the six band wide band gray gas model is assumed and used in the simulation
     - ii) Default simulations disables the six band model method
     - iii) Parametric study simulations had the six band model enabled
   - **c) NUMBER_RADIATION_ANGLES**
     - i) Number of solid angles used in radiation calculations, not compatible if radiation transport calculations are disabled elsewhere in the input file
     - ii) Default simulations used 104 solid angles for calculations
     - iii) Parametric study simulations used 52 and 208 solid angles
   - **d) ANGLE_INCREMENT**
     - i) Number of solid angles skipped per update of radiation calculations
     - ii) Default simulations used the default FDS value of 5
     - iii) Parametric study simulations used values of 2 and 10
   - **e) TIME_STEP_INCREMENT**

i) Number of time steps skip per update of radiation calculations
ii) Default simulations used the default FDS value of 3
iii) Parametric study simulations used values of 1 and 6

2) REAC parameters

a) C_EDC

i) Coefficient to calculate mixing time scale of fuel and oxygen within the grid cells used in the turbulent combustion calculations
ii) Default simulations used a value of 0.1 for the coefficient, determined based on comparison to flame height correlations[*6*]
iii) Parametric study simulations used 0.05 and 0.2 solid angles

b) EDDY_DISSIPATION

i) Determines whether the default heat release rate calculation model based on the default mixture time scale method is used
ii) Default simulations enabled the eddy dissipation to be determined
iii) Parametric study enabled the eddy dissipation

c) HRRPUA_SHEET

i) Max HRRPUA of a flame sheet, acts as a bound of local HRRPU-volume
ii) Default simulations used a default value of 0kW/m^2 for LES
iii) Parametric study used values at 100 kW/m^2 and 400 kW/m^2, these are chosen based on the value of 200 kW/m^2 as default for the DNS mode (not used in these simulations)

d) HRRPUV_AVERAGE

i) Average volumetric HRR of a fire, bounds local HRRPU-volume value
ii) Default simulations used a default value of 3000 kW/m^3
iii) Parametric study used values at 1200 kW/m^3, as suggested by Orloff and De Ris[*6*]

3) MISC parameters

a) CFL_MAX and CFL_MIN

i) Numerical stability parameters that limit the time step sizing by imposing limits on the Courant-Friedrichs-Lewy (CFL) number that is calculated within each timestep: if the number is outside of the range, then the time step size is adjusted
ii) Default simulations set the max value at 1 and the min value at 0.8
iii) Several combinations of CFL limits are tested in the parametric study as follow: [2, 0.8], [1, 0.4], and [2, 0.4]

b) ISOTHERMAL

i) Set the calculations to ignore any changes in temperature or radiation heat transfer, also automatically turn off radiation transport model as well
ii) Default simulations disabled the isothermal option
iii) Parametric study enabled the isothermal option

c) CSMAG

i) Smagorinsky constant used to calculate the viscosity, usually more stable if a small value is used
ii) Default simulations used a default value of 0.2, justified through comparisons with experimental data[*7*]
iii) Parametric study used values at 0.1 and 0.4

d) **PR**
   i) Turbulent Prandtl number, a ratio of momentum diffusivity to thermal diffusivity, related to turbulent viscosity in LES simulations
   ii) Default simulations used FDS's default value of 0.5, justified through comparisons with experimental data[*7*]
   iii) Parametric study used values at 0.25 and 1

e) **SC**
   i) Turbulent Schmidt number, a ratio of momentum diffusivity to mass diffusivity, related to turbulent viscosity in LES simulations
   ii) Default simulations used FDS's default value of 0.5, justified through comparisons with experimental data[*7*]
   iii) Parametric study used values at 0.25 and 1

f) **BAROCLINIC**
   i) Enables the baroclinic vorticity correction calculations that can changes the properties in the turbulence calculations and may affect the plume shape significantly
   ii) Default simulations enables the baroclinic correction
   iii) Parametric study disabled the correction calculations

g) **RADIATION**
   i) Turns On or Off radiation transport calculations in the simulations
   ii) Default simulation use the radiation transport model, as in real life
   iii) Parametric study disabled the radiation transport calculations

4) FDS6 parameters

a) **FLUX_LIMITER**
   i) Changes the finite volume discretization scheme used in simulations
   ii) Default simulations use the Superbee scheme, suitable for LES simulations
   iii) Parametric study used a central differencing scheme with boundedness correction applied

b) **DYNSMAG**
   i) Turns on/off variable density formulation of dynamic Smagorinsky model
   ii) Default simulation use the dynamic Smagorinsky model
   iii) Parametric study disabled the dynamic Smagorinsky model

c) **CFL_VELOCITY_NORM**
   i) Normalization of CFL velocity, controls the time step sizing within a simulation
   ii) FDS default uses a moderate time step sizing control
   iii) Parametric study tested for the effects due to an increase and decrease of the time step sizing control

d) **H_EDDY**
   i) Enables the eddy-diffusivity model to use a turbulent convective heat transfer model
   ii) Default simulations has the eddy diffusivity model enabled
   iii) Parametric study disabled eddy diffusivity model

K.1 Sensitivity Coefficients

To identify the parameters that yield significant changes to specific predicted quantities, the concept of "sensitivity coefficients" was employed. Each coefficient was determined based on the changes in one of the three recorded quantities (plume centerline temperature, plume centerline velocity, and centerline gauge heat flux) and of the FDS parameter over their baseline values. The coefficient is based on the ratios of change, and is found using equation [1.1]:

$$\left(\frac{Quantity_{new} - Quantity_{baseline}}{Quantity_{baseline}}\right) \Bigg/ \left(\frac{Parameter_{new} - Parameter_{baseline}}{Parameter_{baseline}}\right) \qquad [0.1]$$

Where "Quantity" denotes the recorded quantities in the model (velocity, temperature, gauge heat flux), and the "Parameter" denotes the model inputs (RADIATIVE_FRACTION, SC, etc)

Equation [1.1] was applied to the steady-state, time-averaged FDS results of plume centerline temperature and velocity at different heights of the free plume fire simulations. For the "toggle" parameters, if a parameter is turned "ON" or "TRUE", the nondimensional parameter change is assumed to be "+1", and if the parameter is turned "OFF" or "FALSE", then the nondimensional parameter change is assumed to be "-1", this is necessary for the sensitivity coefficients be calculated for the "toggle" parameters since they do not have any numerical values.. Regardless of the parameter type, a sensitivity coefficient is calculated for each quantity at each "measuring" location, then they are averaged. The coefficients can then be used to represent the significance and effects of the parameter change for each of the predicted quantities.

Non-toggle parameters such as radiative fraction, Prandtl number, and the maximum and minimum CFL range dominate the changes of the measured temperature and velocity along the plume centerline in the simulations. These parameters contribute to the resolution of the flow field and the stability of the plume and of the simulations. And because the plume velocity and temperature are both closely related to the plume's structure, they are especially affected by these parameters.

For the toggled parameter studied, the ones with the greatest changes include: isothermal model, CFL velocity normalization, eddy diffusivity model, and the dynamic Smagorinsky model. All these parameter contributes to the stability and structure of the flow field. The flux limiter, which controls the calculations scheme used in the calculations, is consistently one of the greatest contributors to quantity changes because the simulations all crashed due to numerical instability.

Additionally, the results from the parametric study show that characteristics of the simulations such as propane fuel, Rectangle burner, and the lower HRR at 50 kW are more greatly affected by the parameter changes than their counterparts.

K.1.1 Fuel Type

This section presents the sensitivity coefficients generated from the various simulations as grouped by the fuel type: methane, propane, or propylene. The parameters and their variances that generated sensitivity coefficients ≥ 0.1 are considered significant. Each sensitivity coefficient was based on one of the predicted quantities, and was averaged over height and across those simulations using identical fuel types regardless of the scenario, burner shape, and base HRR. The results from the toggle parameters are located at the bottom of the charts, and the parameter change that correlates with the overall maximum sensitivity coefficients are presented first.

Figure 1 shows the sensitivity coefficients based on the predicted plume centerline velocity averaged over free plume simulations using the same fuel type. The parameters that created the most significant changes to the plume velocity are the radiative fraction and the Prandtl number, as well as the when the isothermal mode was used, and which calculation scheme used based on the value of the flux limiter.

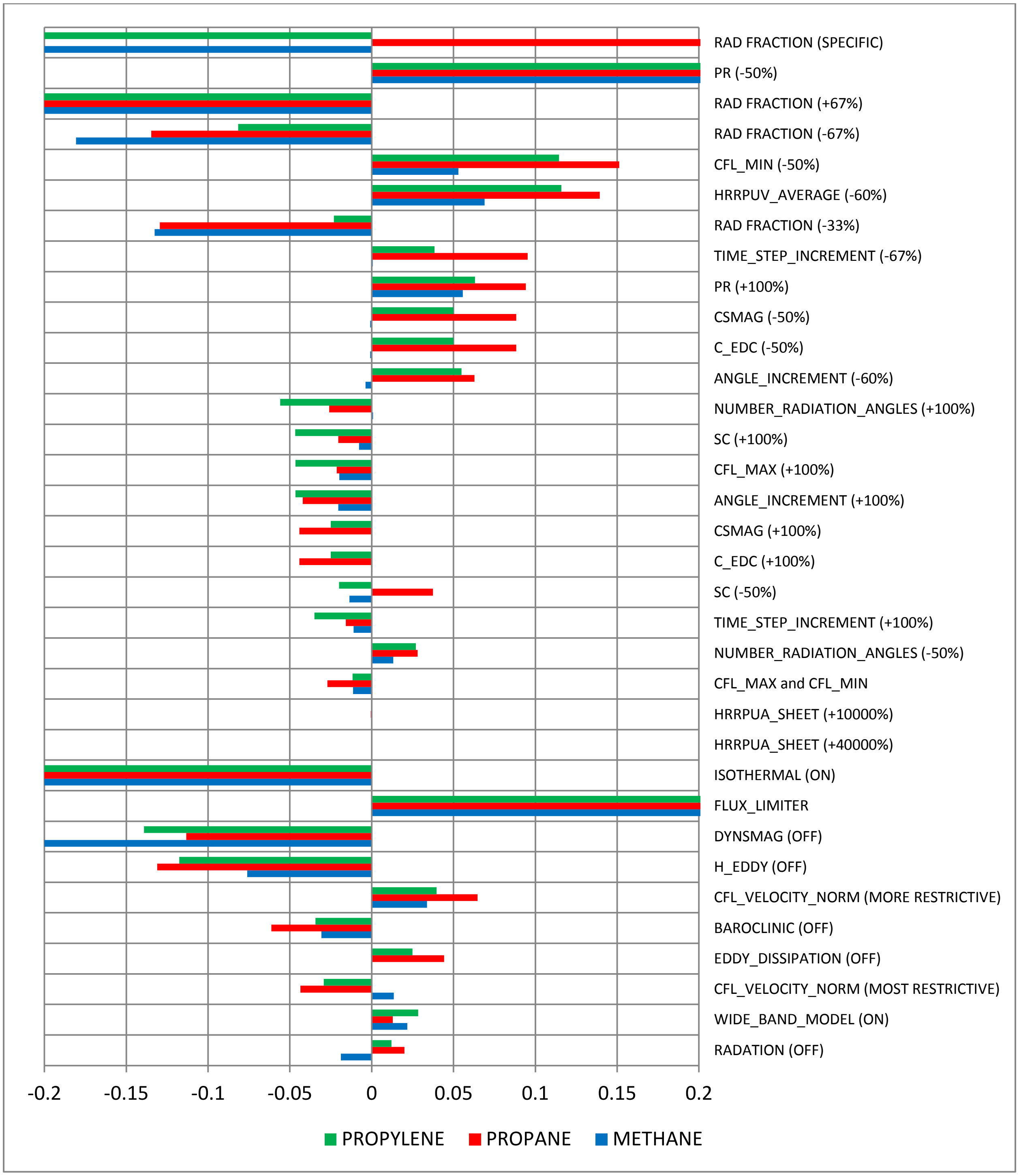

Figure 1 – Plume velocity sensitivity coefficients, grouped by fuel type

Figure 2 shows the sensitivity coefficients based on the predicted plume centerline velocity averaged over simulations with consistent fuel type. The values of the CFL parameters, the Schmidt number, the CFL_velocity_norm parameter, and whether the eddy diffusivity model was utilized contributed most significant to the change in plume temperature.

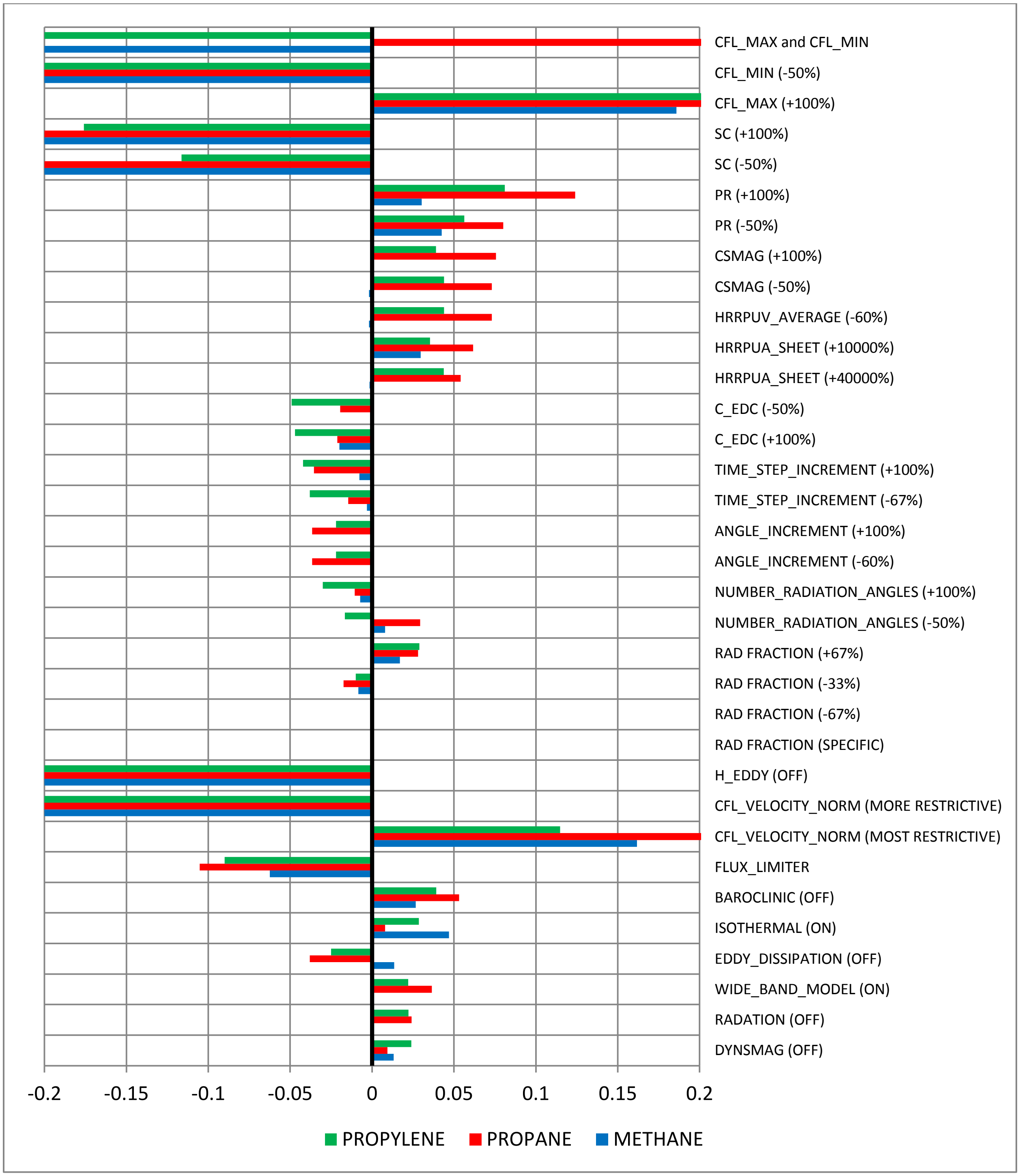

Figure 2 – Plume temperature sensitivity coefficients, grouped by fuel type

Table 2 - Sensitivity coefficients based on source fuel type

Parameter change	Default Value	New Value	METHANE Velocity	METHANE Temp	PROPANE Velocity	PROPANE Temp	PROPYLENE Velocity	PROPYLENE Temp
DYNSMAG (OFF)	.TRUE.	.FALSE.	-0.2721	-0.6751	-0.1133	-0.3310	-0.1392	-0.3606
RADATION (OFF)	.TRUE.	.FALSE.	-0.0189	-0.0011	0.0200	0.0241	0.0122	0.0223
WIDE_BAND_MODEL (ON)	.FALSE.	.TRUE	0.0218	0.0132	0.0129	0.0094	0.0284	0.0240
EDDY_DISSIPATION (OFF)	.TRUE.	.FALSE.	-0.0004	-0.0009	0.0442	0.0366	0.0249	0.0220
ISOTHERMAL (ON)	.FALSE.	.TRUE	-0.7439	-0.8447	-0.9570	-0.8144	-0.9601	-0.8142
BAROCLINIC (OFF)	.TRUE.	.FALSE.	-0.0307	0.0469	-0.0613	0.0079	-0.0343	0.0286
FLUX_LIMITER	2	-1	0.2887	0.1617	0.4056	0.2339	0.2496	0.1149
CFL_VELOCITY_NORM (MOST RESTRICTIVE)	1	2	0.0135	0.0135	-0.0435	-0.0381	-0.0294	-0.0250
CFL_VELOCITY_NORM (MORE RESTRICTIVE)	1	0	0.0338	0.0267	0.0647	0.0532	0.0397	0.0392
H_EDDY (OFF)	.FALSE.	.TRUE.	-0.0761	-0.0625	-0.1310	-0.1052	-0.1175	-0.0901
RAD FRACTION (SPECIFIC)	0.3	Source fire specific	-0.2015	-0.2936	1.2019	0.9672	-0.3846	-0.4534
RAD FRACTION (-67%)	0.3	0.1	-0.1807	-0.2770	-0.1346	-0.2275	-0.0815	-0.1759
RAD FRACTION (-33%)	0.3	0.2	-0.1326	-0.2289	-0.1295	-0.2124	-0.0231	-0.1163
RAD FRACTION (+67%)	0.3	0.5	-0.2510	-0.3231	-0.2910	-0.3422	-0.2445	-0.3033
NUMBER_RADIATION_ANGLES (-50%)	104	52	0.0132	0.0170	0.0281	0.0281	0.0270	0.0288
NUMBER_RADIATION_ANGLES (+100%)	104	208	0.0008	0.0000	-0.0259	-0.0195	-0.0560	-0.0492
ANGLE_INCREMENT (-60%)	5	2	-0.0038	-0.0016	0.0628	0.0541	0.0548	0.0438
ANGLE_INCREMENT (+100%)	5	10	-0.0204	-0.0077	-0.0421	-0.0355	-0.0465	-0.0421
TIME_STEP_INCREMENT (-67%)	3	1	0.0007	-0.0009	0.0952	0.0757	0.0384	0.0390
TIME_STEP_INCREMENT (+100%)	3	6	-0.0111	-0.0073	-0.0159	-0.0105	-0.0350	-0.0301
C_EDC (+100%)	0.1	0.2	0.0004	0.0009	-0.0442	-0.0366	-0.0249	-0.0220
C_EDC (-50%)	0.1	0.05	-0.0009	-0.0019	0.0884	0.0731	0.0499	0.0440
HRRPUA_SHEET (+40000%)	0	400	-0.0001	-0.0001	-0.0001	-0.0001	-0.0001	-0.0002
HRRPUA_SHEET (+10000%)	0	100	0.0000	-0.0001	-0.0006	-0.0007	-0.0001	-0.0003
HRRPUV_AVERAGE (-60%)	3000	1200	0.0690	0.0425	0.1394	0.0800	0.1159	0.0563
CSMAG (-50%)	0.2	0.1	-0.0009	-0.0019	0.0884	0.0731	0.0499	0.0440
CSMAG (+100%)	0.2	0.4	0.0004	0.0009	-0.0442	-0.0366	-0.0249	-0.0220
PR (-50%)	0.5	0.25	0.2591	0.1858	0.3572	0.2775	0.3536	0.2764
PR (+100%)	0.5	1	0.0556	0.0296	0.0942	0.0616	0.0631	0.0354
SC (-50%)	0.5	0.25	-0.0136	0.0079	0.0375	0.0294	-0.0200	-0.0166
SC (+100%)	0.5	1	-0.0078	-0.0032	-0.0205	-0.0146	-0.0468	-0.0381
CFL_MAX (+100%)	1	2	-0.0198	-0.0199	-0.0214	-0.0212	-0.0466	-0.0470
CFL_MIN (-50%)	0.8	0.4	0.0529	0.0303	0.1513	0.1240	0.1145	0.0811
CFL_MAX and CFL_MIN	1 / 0.8	2 / 0.4	-0.0114	-0.0083	-0.0271	-0.0174	-0.0117	-0.0100

K.1.2 Burner Shape

This section presents the sensitivity coefficients generated from the various simulations as grouped by the burner shape: Square or Rectangle. Figure 4 shows the sensitivity coefficients based on the predicted plume centerline velocity averaged over simulations using the same source fire burner. The parameter changes that caused the most significant velocity change are the radiative fraction, Prandtl number, the CFL limits, the isothermal mode was used, which calculation scheme used based on the value of the flux limiter, and whether the dynamic Smagorinsky model is turned off.

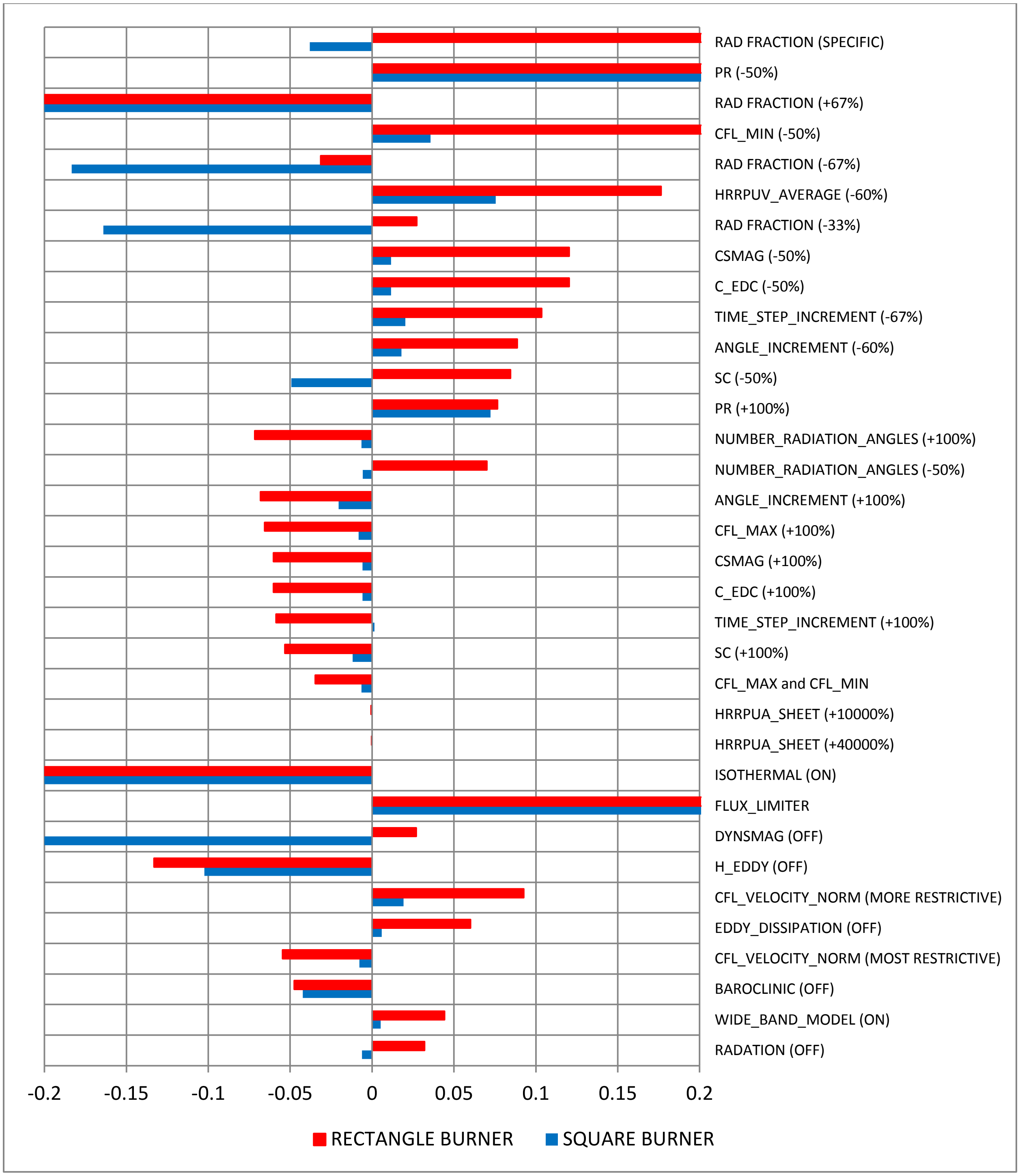

Figure 3 – Plume velocity sensitivity coefficients, grouped by burner shape

Figure 5 shows the sensitivity coefficients based on the predicted plume centerline temperature averaged over simulations using the same source fire burner. The parameter changes that caused the most significant plume temperature change are the radiative fraction, Prandtl number, the isothermal mode was used, and whether the dynamic Smagorinsky model is turned off.

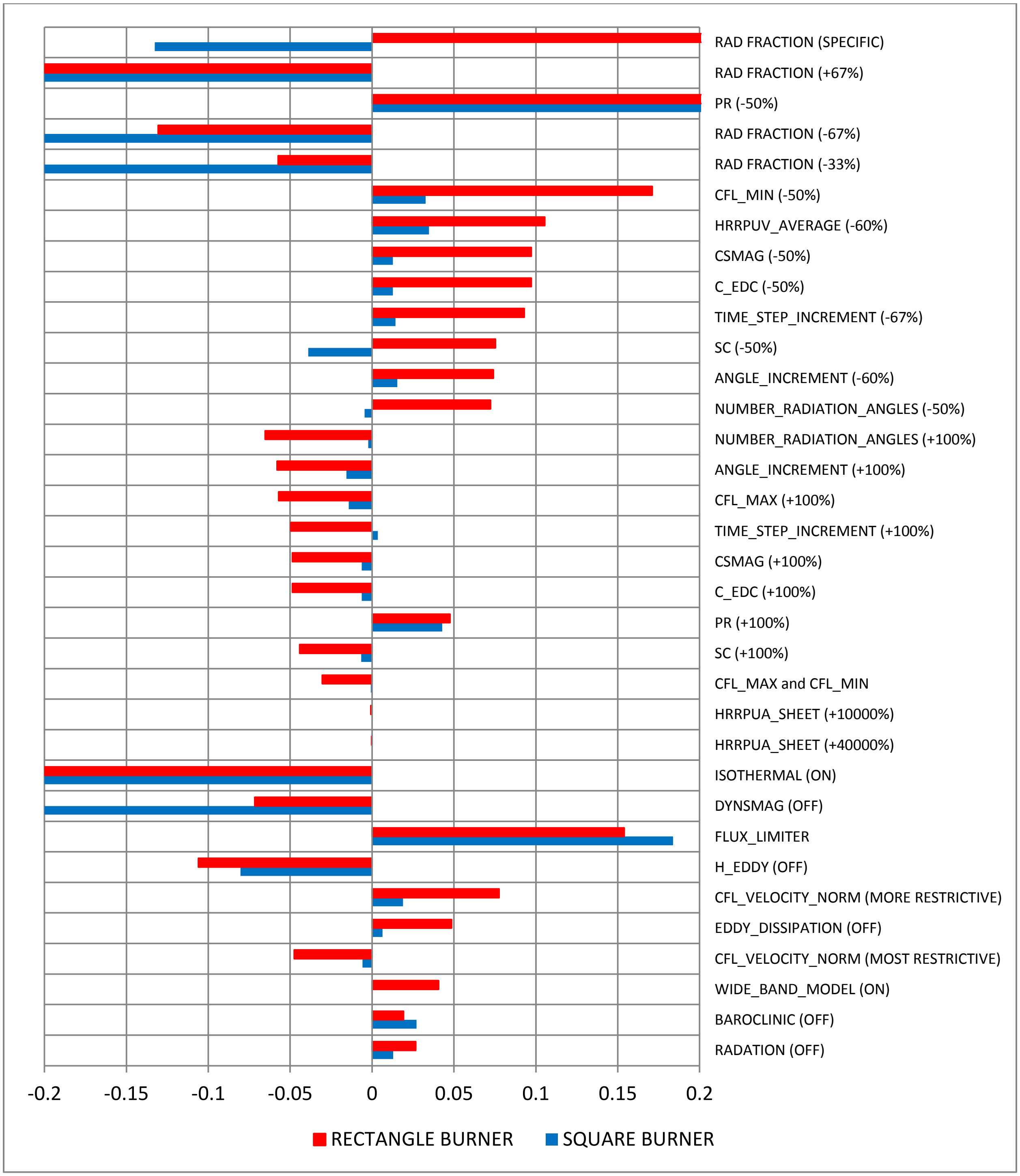

Figure 4 – Plume temperature sensitivity coefficients, grouped by burner shape

Table 3 - Sensitivity coefficients based on source burner shape

Parameter change	Default Value	New Value	SQUARE BURNER Velocity	SQUARE BURNER Temp	RECTANGLE BURNER Velocity	RECTANGLE BURNER Temp
DYNSMAG (OFF)	.TRUE.	.FALSE.	-0.2770	-0.6383	0.0270	-0.0716
RADATION (OFF)	.TRUE.	.FALSE.	-0.0062	0.0128	0.0320	0.0266
WIDE_BAND_MODEL (ON)	.FALSE.	.TRUE	0.0053	-0.0004	0.0443	0.0405
EDDY_DISSIPATION (OFF)	.TRUE.	.FALSE.	0.0058	0.0063	0.0602	0.0486
ISOTHERMAL (ON)	.FALSE.	.TRUE	-0.8888	-0.8390	-0.9560	-0.7925
BAROCLINIC (OFF)	.TRUE.	.FALSE.	-0.0423	0.0271	-0.0475	0.0193
FLUX_LIMITER	2	-1	0.3394	0.1838	0.2904	0.1540
CFL_VELOCITY_NORM (MOST RESTRICTIVE)	1	2	-0.0077	-0.0059	-0.0546	-0.0475
CFL_VELOCITY_NORM (MORE RESTRICTIVE)	1	0	0.0191	0.0189	0.0926	0.0775
H_EDDY (OFF)	.FALSE.	.TRUE.	-0.1023	-0.0804	-0.1331	-0.1060
RAD FRACTION (SPECIFIC)	0.3	Source fire specific	-0.0380	-0.1327	0.7736	0.5661
RAD FRACTION (-67%)	0.3	0.1	-0.1835	-0.2742	-0.0313	-0.1306
RAD FRACTION (-33%)	0.3	0.2	-0.1641	-0.2571	0.0272	-0.0574
RAD FRACTION (+67%)	0.3	0.5	-0.2518	-0.3193	-0.2833	-0.3281
NUMBER_RADIATION_ANGLES (-50%)	104	52	-0.0057	-0.0046	0.0701	0.0723
NUMBER_RADIATION_ANGLES (+100%)	104	208	-0.0065	-0.0023	-0.0717	-0.0653
ANGLE_INCREMENT (-60%)	5	2	0.0180	0.0154	0.0886	0.0740
ANGLE_INCREMENT (+100%)	5	10	-0.0205	-0.0156	-0.0681	-0.0580
TIME_STEP_INCREMENT (-67%)	3	1	0.0203	0.0142	0.1035	0.0929
TIME_STEP_INCREMENT (+100%)	3	6	0.0015	0.0036	-0.0586	-0.0497
C_EDC (+100%)	0.1	0.2	-0.0058	-0.0063	-0.0602	-0.0486
C_EDC (-50%)	0.1	0.05	0.0117	0.0127	0.1204	0.0971
HRRPUA_SHEET (+40000%)	0	400	0.0000	-0.0001	-0.0002	-0.0002
HRRPUA_SHEET (+10000%)	0	100	0.0000	-0.0001	-0.0007	-0.0007
HRRPUV_AVERAGE (-60%)	3000	1200	0.0755	0.0348	0.1765	0.1054
CSMAG (-50%)	0.2	0.1	0.0117	0.0127	0.1204	0.0971
CSMAG (+100%)	0.2	0.4	-0.0058	-0.0063	-0.0602	-0.0486
PR (-50%)	0.5	0.25	0.2992	0.2264	0.3916	0.3073
PR (+100%)	0.5	1	0.0723	0.0428	0.0766	0.0476
SC (-50%)	0.5	0.25	-0.0492	-0.0390	0.0845	0.0753
SC (+100%)	0.5	1	-0.0119	-0.0067	-0.0533	-0.0442
CFL_MAX (+100%)	1	2	-0.0082	-0.0142	-0.0656	-0.0570
CFL_MIN (-50%)	0.8	0.4	0.0357	0.0327	0.2387	0.1711
CFL_MAX and CFL_MIN	1 / 0.8	2 / 0.4	-0.0065	-0.0008	-0.0347	-0.0303

K.1.3 Heat Release Rate

This section presents the sensitivity coefficients generated from the various simulations as grouped by the base burner HRR: 50 kW or 75 kW. Figure 7 shows the sensitivity coefficients based on the predicted plume centerline velocity averaged over simulations using the same source fire HRR. The parameter changes that caused the most significant velocity change are the radiative fraction, Prandtl number, the isothermal mode was used, and which calculation scheme used based on the value of the flux limiter.

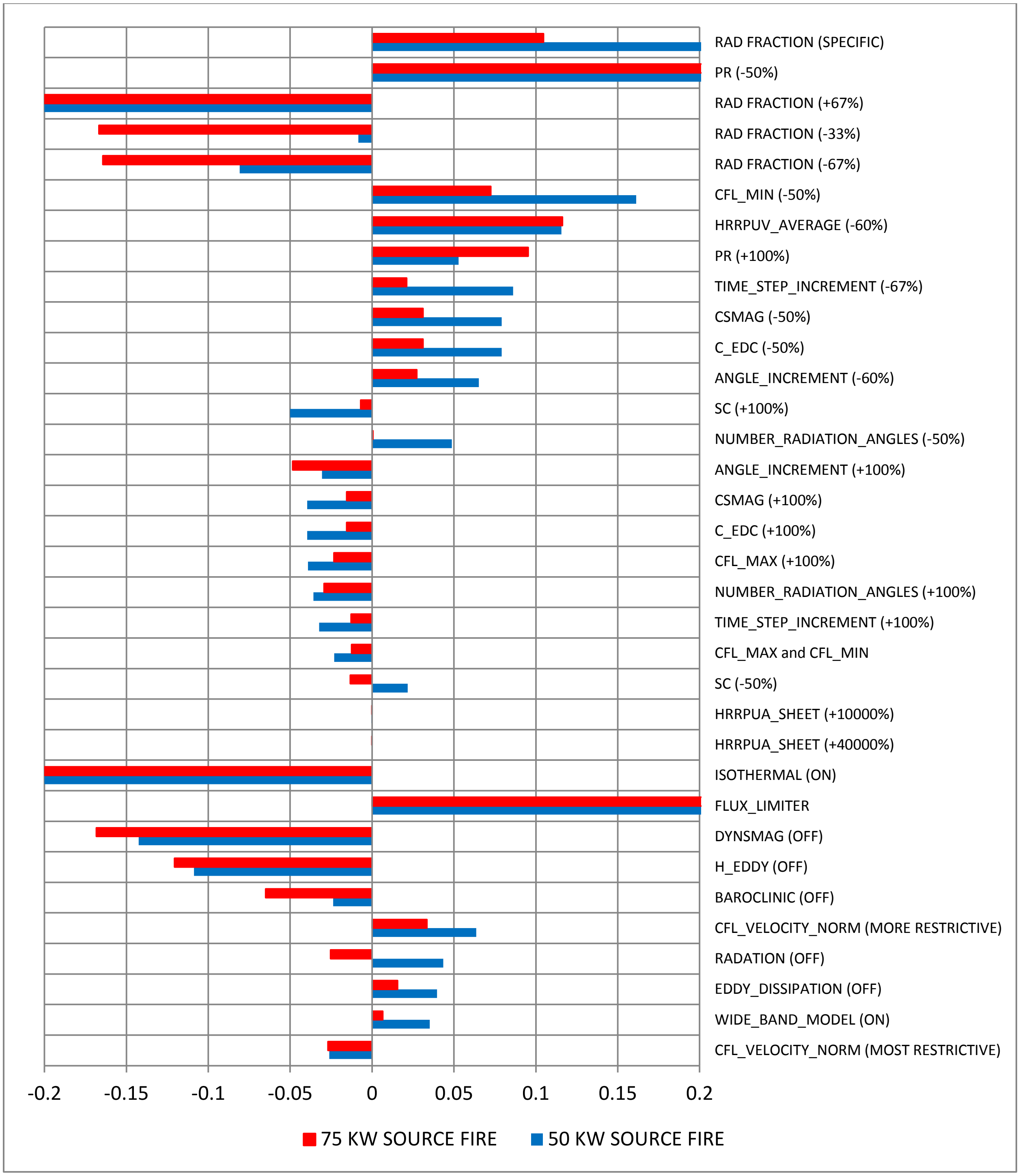

Figure 5 – Plume velocity sensitivity coefficients, grouped by HRR

Figure 8 shows the sensitivity coefficients based on the predicted plume centerline temperature averaged over simulations using the same source fire HRR. The parameter changes that caused the most significant plume temperature change are the radiative fraction, Prandtl number, the isothermal mode was used, which calculation scheme used based on the value of the flux limiter, and whether the dynamic Smagorinsky model is turned off.

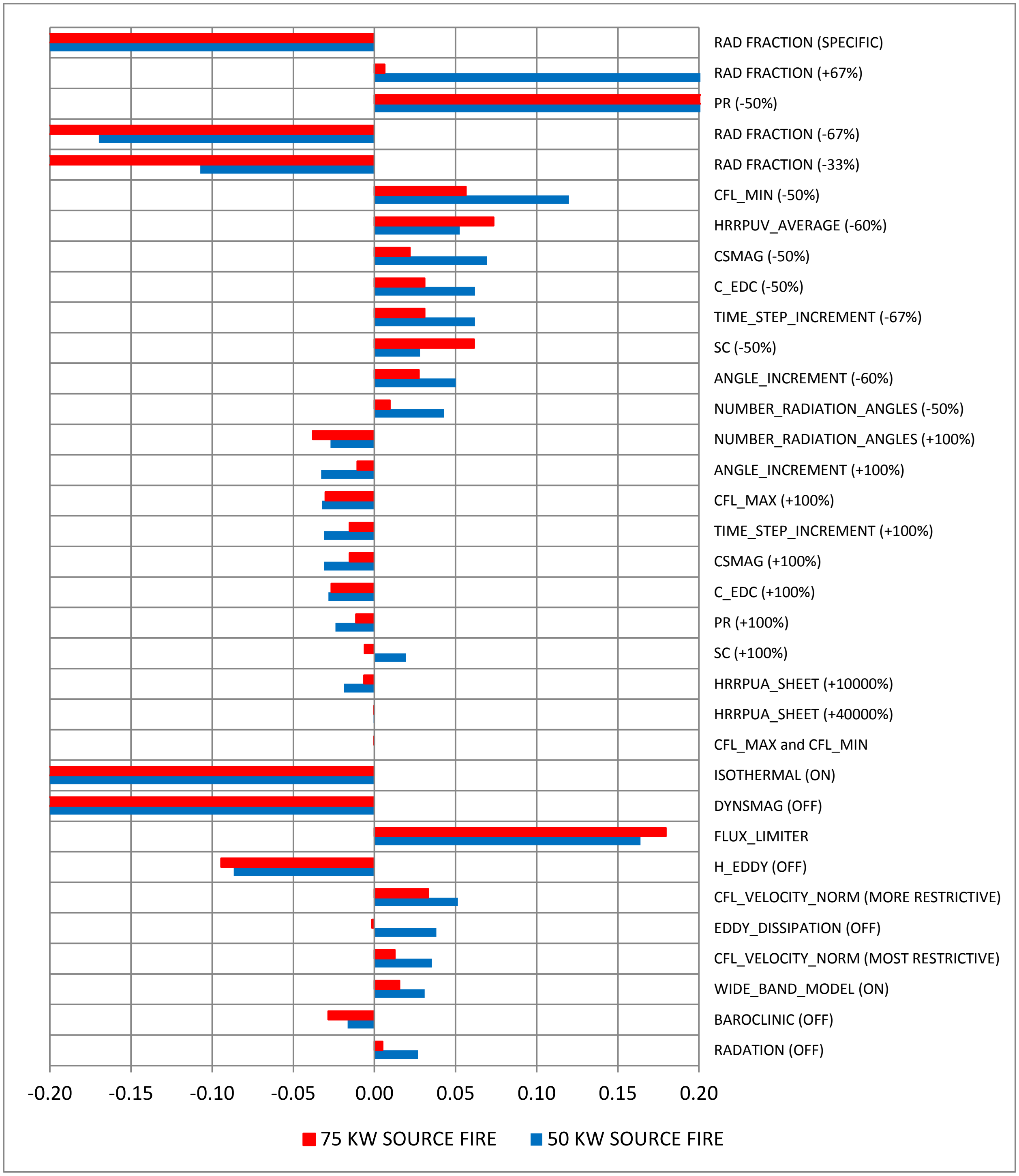

Figure 6 – Plume temperature sensitivity coefficients, grouped by HRR

Table 4 - Sensitivity coefficients based on source fire HRR

			50 KW SOURCE FIRE		75 KW SOURCE FIRE	
Parameter change	**Default Value**	**New Value**	**Velocity**	**Temp**	**Velocity**	**Temp**
DYNSMAG (OFF)	.TRUE.	.FALSE.	-0.1425	-0.3913	-0.1683	-0.4320
RADATION (OFF)	.TRUE.	.FALSE.	0.0434	0.0381	-0.0253	-0.0015
WIDE_BAND_MODEL (ON)	.FALSE.	.TRUE	0.0353	0.0270	0.0065	0.0050
EDDY_DISSIPATION (OFF)	.TRUE.	.FALSE.	0.0396	0.0310	0.0155	0.0155
ISOTHERMAL (ON)	.FALSE.	.TRUE	-0.9154	-0.8010	-0.9159	-0.8397
BAROCLINIC (OFF)	.TRUE.	.FALSE.	-0.0238	0.0354	-0.0650	0.0125
FLUX_LIMITER	2	-1	0.3499	0.1640	0.2897	0.1797
CFL_VELOCITY_NORM (MOST RESTRICTIVE)	1	2	-0.0261	-0.0165	-0.0269	-0.0285
CFL_VELOCITY_NORM (MORE RESTRICTIVE)	1	0	0.0636	0.0514	0.0335	0.0332
H_EDDY (OFF)	.FALSE.	.TRUE.	-0.1087	-0.0867	-0.1205	-0.0946
RAD FRACTION (SPECIFIC)	0.3	Source fire specific	0.4686	0.2874	0.1047	0.0063
RAD FRACTION (-67%)	0.3	0.1	-0.0809	-0.1698	-0.1643	-0.2636
RAD FRACTION (-33%)	0.3	0.2	-0.0084	-0.1073	-0.1667	-0.2472
RAD FRACTION (+67%)	0.3	0.5	-0.2609	-0.3090	-0.2679	-0.3366
NUMBER_RADIATION_ANGLES (-50%)	104	52	0.0488	0.0427	0.0005	0.0096
NUMBER_RADIATION_ANGLES (+100%)	104	208	-0.0359	-0.0284	-0.0293	-0.0266
ANGLE_INCREMENT (-60%)	5	2	0.0652	0.0502	0.0274	0.0275
ANGLE_INCREMENT (+100%)	5	10	-0.0306	-0.0270	-0.0485	-0.0381
TIME_STEP_INCREMENT (-67%)	3	1	0.0861	0.0695	0.0211	0.0219
TIME_STEP_INCREMENT (+100%)	3	6	-0.0323	-0.0240	-0.0128	-0.0115
C_EDC (+100%)	0.1	0.2	-0.0396	-0.0310	-0.0155	-0.0155
C_EDC (-50%)	0.1	0.05	0.0792	0.0620	0.0311	0.0309
HRRPUA_SHEET (+40000%)	0	400	-0.0002	-0.0002	-0.0001	-0.0001
HRRPUA_SHEET (+10000%)	0	100	-0.0004	-0.0005	-0.0001	-0.0003
HRRPUV_AVERAGE (-60%)	3000	1200	0.1155	0.0526	0.1163	0.0734
CSMAG (-50%)	0.2	0.1	0.0792	0.0620	0.0311	0.0309
CSMAG (+100%)	0.2	0.4	-0.0396	-0.0310	-0.0155	-0.0155
PR (-50%)	0.5	0.25	0.3635	0.2781	0.3088	0.2394
PR (+100%)	0.5	1	0.0528	0.0280	0.0953	0.0615
SC (-50%)	0.5	0.25	0.0218	0.0195	-0.0132	-0.0061
SC (+100%)	0.5	1	-0.0501	-0.0329	-0.0069	-0.0105
CFL_MAX (+100%)	1	2	-0.0391	-0.0323	-0.0232	-0.0303
CFL_MIN (-50%)	0.8	0.4	0.1613	0.1198	0.0725	0.0563
CFL_MAX and CFL_MIN	1 / 0.8	2 / 0.4	-0.0231	-0.0188	-0.0125	-0.0065

K.2 Ratios of Quantity Change

Since the sensitivity coefficients are averaged regardless of the height of the "measurement" locations, the changes in the quantities due to parametric variation that are height-depended are omitted. To show the height-dependent effects, the ratios of change for the centerline plume temperature and velocity are plotted against the height of measurement locations. The ratio is calculated in equation [1.2]:

$$\left(\frac{Quantity_{new} - Quantity_{baseline}}{Quantity_{baseline}} \right) \quad [0.2]$$

The ratios for all simulations are plotted for each parametric series in the following section. This allows the effects of the parametric change on simulations with different source fuel, source burner size, and HRR be observed.

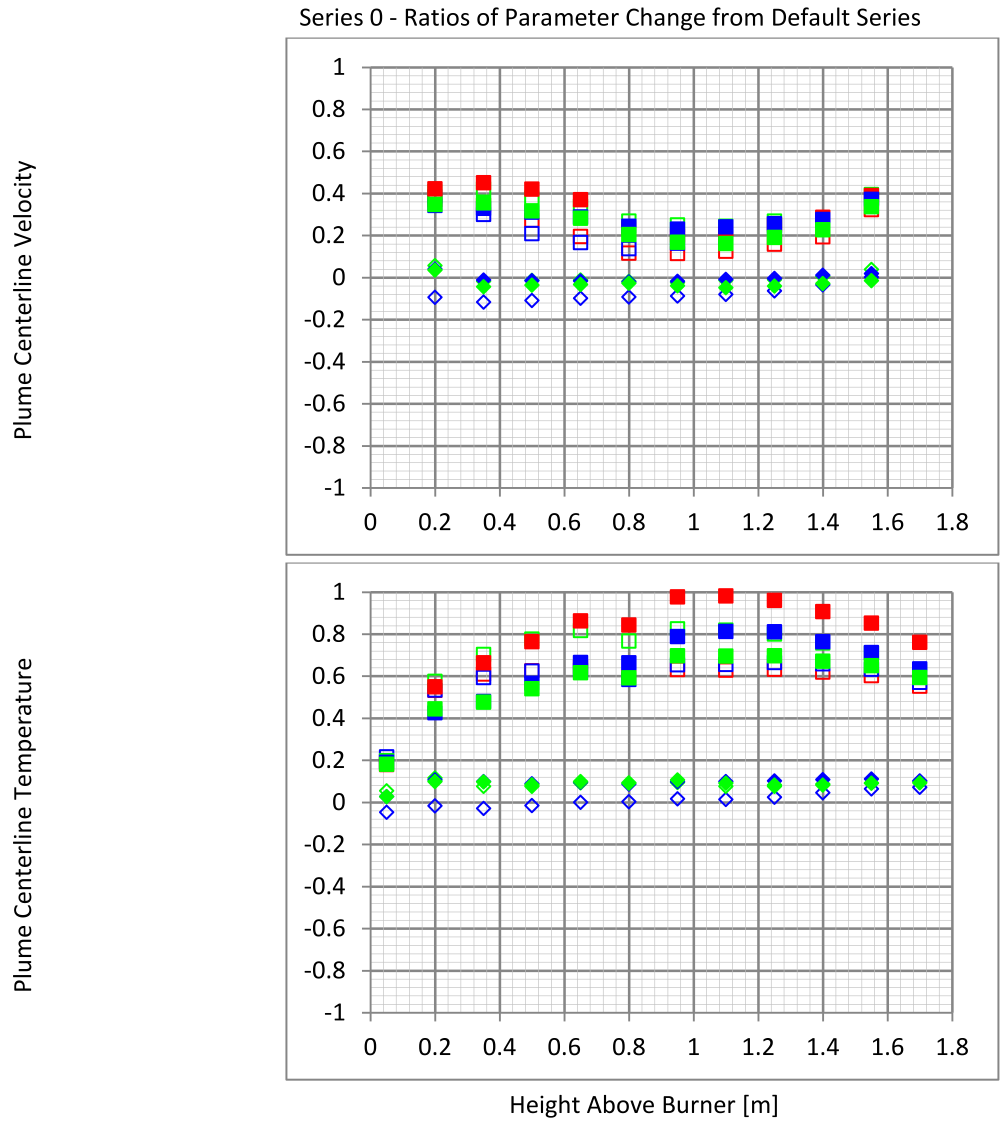

Legend

Propane-Sq-50 ✓	Propane-Sq-75 ✓	Propane-Re-50 ✓	Propane-Re-75 ✓
Propylene-Sq-50 ✓	Propylene-Sq-75 ✓	Propylene-Re-50 ✓	Propylene-Re-75 ✓
Methane-Sq-50 ✓	Methane-Sq-75 ✓	Methane-Re-50 ×	Methane-Re-75 ×

Observations

In Series 0, the dynamics Smagorinsky model was turned off in the FDS models, which resulted in a more disordered flow field inside the computational domain. The parameter change increased the centerline velocity and temperature in the models using the Square burner but in models where the Rectangle burner was used at 50 kW, the temperature was not changed but the velocity predicted was reduced.

It is observed that the computation time of Series 0 about the same as that of the default series (average 4 hrs).

Series 2 - Ratios of Parameter Change from Default Series

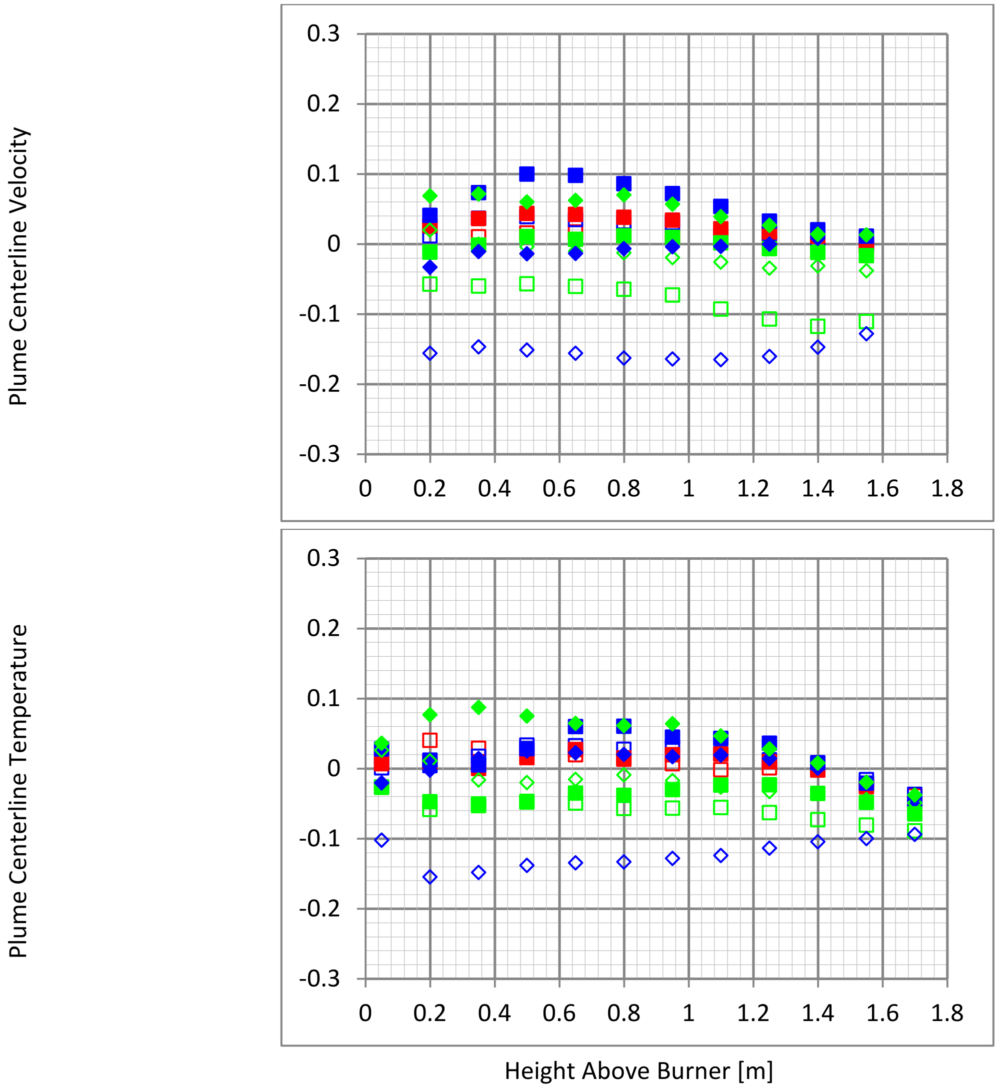

Legend

Propane-Sq-50 ✓	Propane-Sq-75 ✓	Propane-Re-50 ✓	Propane-Re-75 ✓
Propylene-Sq-50 ✓	Propylene-Sq-75 ✓	Propylene-Re-50 ✓	Propylene-Re-75 ✓
Methane-Sq-50 ✓	Methane-Sq-75 ✓	Methane-Re-50 ×	Methane-Re-75 ×

Observations

With radiation solver disabled in FDS in the Series 2 simulations, across the two sets of free plume fire simulations, a comparison between the predicted centerline plume velocity and temperature shows minor differences driven more by the fuel type, burner shape and HRR value: in some cases turning off radiation decreases the predicted centerline velocity while in others the velocity was over predicted. However, the discrepancy was consistent in that an over-prediction in velocity generally accompanies with an over-prediction of temperature as well and vice versa.

However, it was observed that the computation time of Series 2 is half (average 2 hrs) that of the default series (average 4 hrs), suggesting that the model significantly speeds up if radiation is turned off.

Series 3 - Ratios of Parameter Change from Default Series

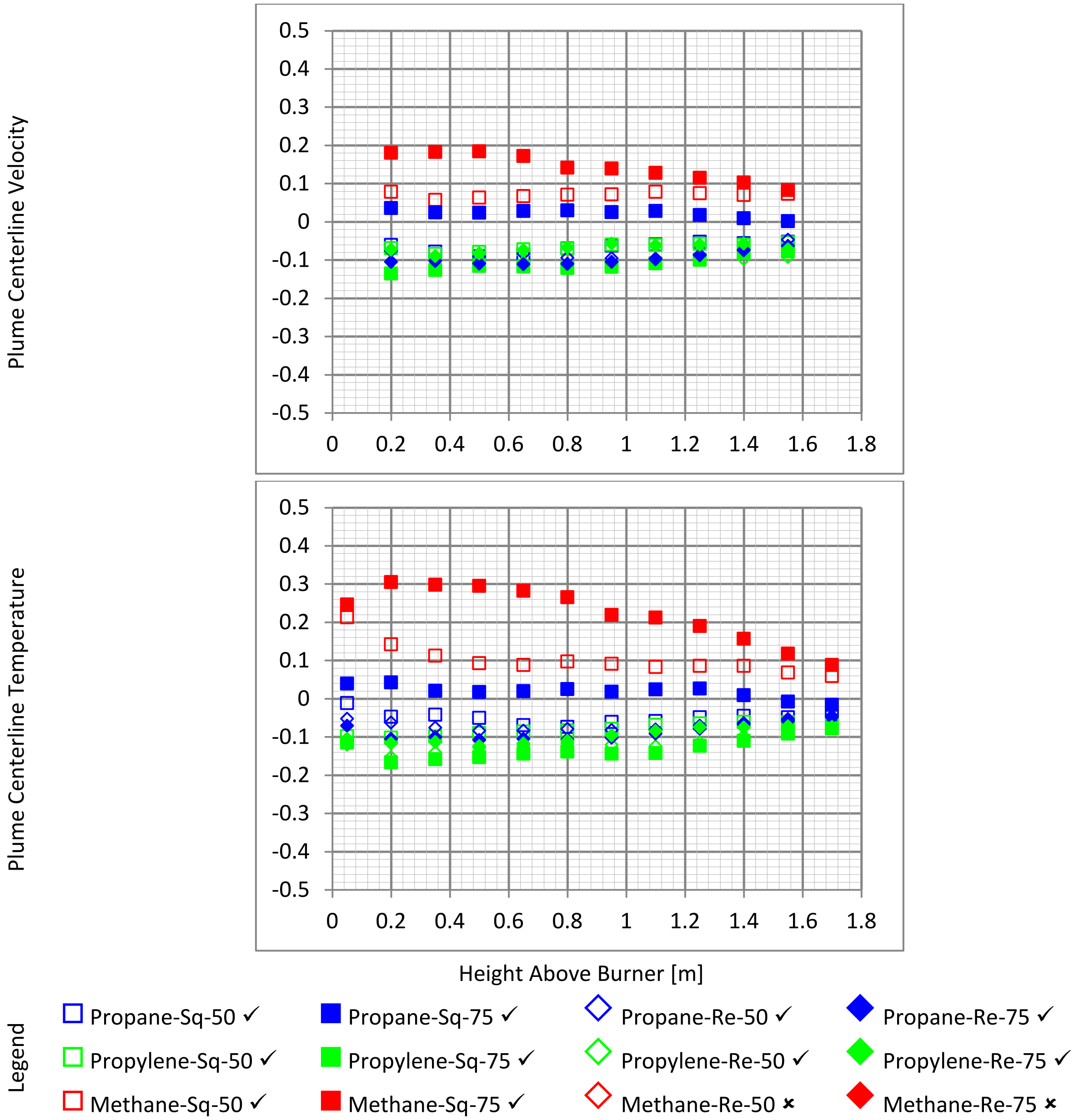

In Series 3, the radiative fraction used in each of the simulations was changed from the default 0.30 to suit the fuels' specific radiative fractions. For methane, a value of 0.141 was used; for propane, 0.286; and for propylene, 0.368.

Observations

In the plume test simulations, reducing the radiative fraction increased the velocity and temperature while increasing the radiative fraction has the opposite effects. The amount of increase in velocity or temperature was also governed by the HRR of the source fire as well, where a larger fire size corresponds with a larger rise/drop in the predicted temperature/velocity. Although it should also be noted that the temperature change away from the burner surface is lower in magnitude than at locations close to the burner surface. Regardless, the predicted temperatures are lower than those recorded in the experiments in the current studies and by McCaffrey.

The change in radiative fraction does not affect the computational performance of the models.

Series 4 - Ratios of Parameter Change from Default Series

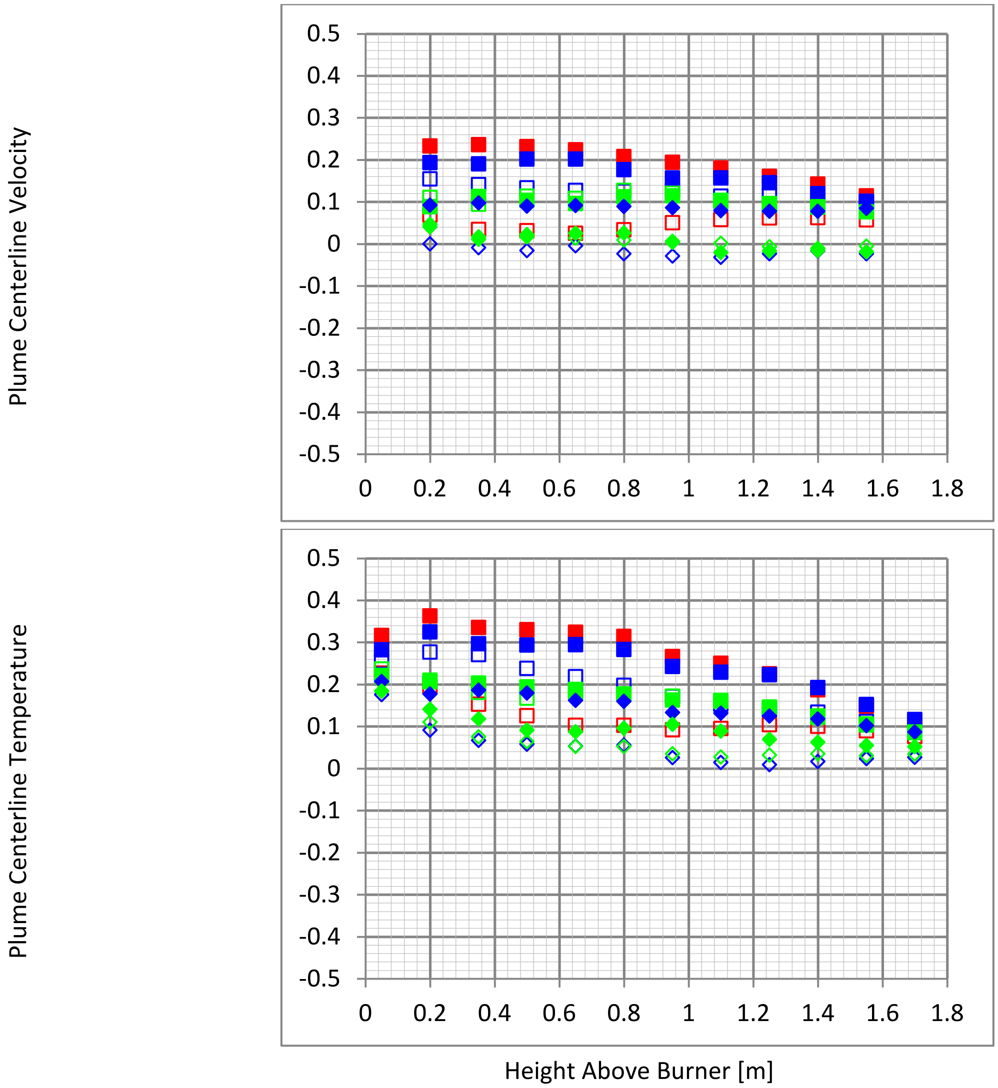

Legend

□ Propane-Sq-50 ✓	■ Propane-Sq-75 ✓	◇ Propane-Re-50 ✓	◆ Propane-Re-75 ✓
□ Propylene-Sq-50 ✓	■ Propylene-Sq-75 ✓	◇ Propylene-Re-50 ✓	◆ Propylene-Re-75 ✓
□ Methane-Sq-50 ✓	■ Methane-Sq-75 ✓	◇ Methane-Re-50 ×	◆ Methane-Re-75 ×

In Series 4, the radiative fraction of all simulations was lowered 66% from the default 0.30 to 0.1.

Observations

This change increased the velocity and temperature along the centerline plume. This is consistent with the results for the methane fire simulations in Series 3. The centerline velocity was increased from the default simulations with positive correlation to the increase of the fire's HRR. The centerline temperature predictions comparison between Series 4 and the default series shows that reducing the radiative fraction universally increase the temperature by a larger amount at locations near the burner surface than at locations further up along the plume.

Again, the change in radiative fraction does not affect the computational performance of the models.

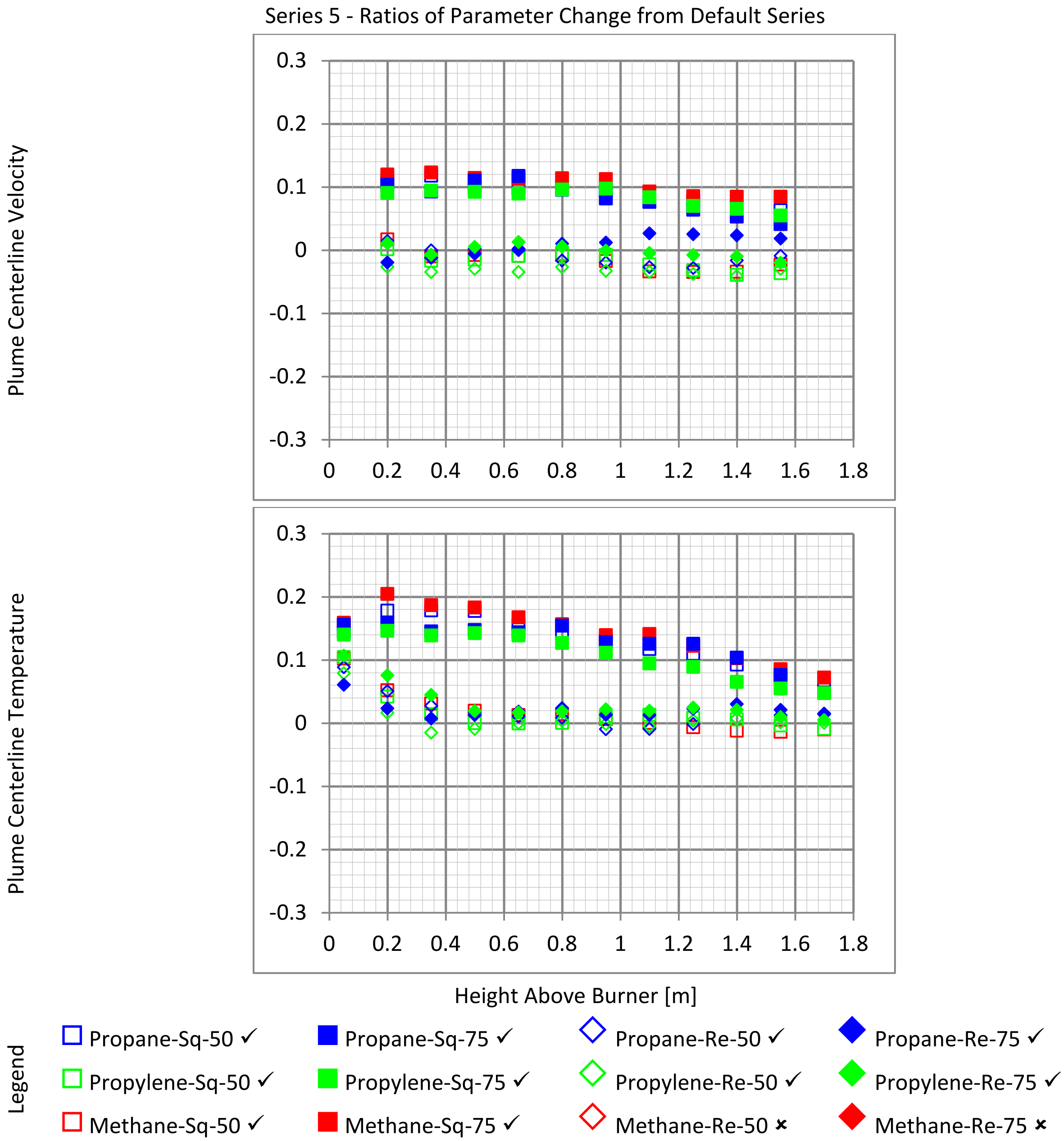

In Series 5, the radiative fraction of all simulations was reduced 33% from the default 0.30 to 0.2.

Observations

This change increased the velocity and temperature along the centerline plume. This is consistent with the results for the methane and propane fire simulations in Series 3. The centerline velocity was increased from the default simulations with positive correlation to the increase of the fire's HRR. The centerline temperature predictions comparison between Series 5 and the default series shows that reducing the radiative fraction universally increase the temperature by a larger amount at locations near the burner surface than at locations further up along the plume. Overall the rise in centerline velocity and temperature is less that that as shown in Series 4 where the reduction in radiative fraction was greater.

Again, the change in radiative fraction does not affect the computational performance of the models.

Series 6 - Ratios of Parameter Change from Default Series

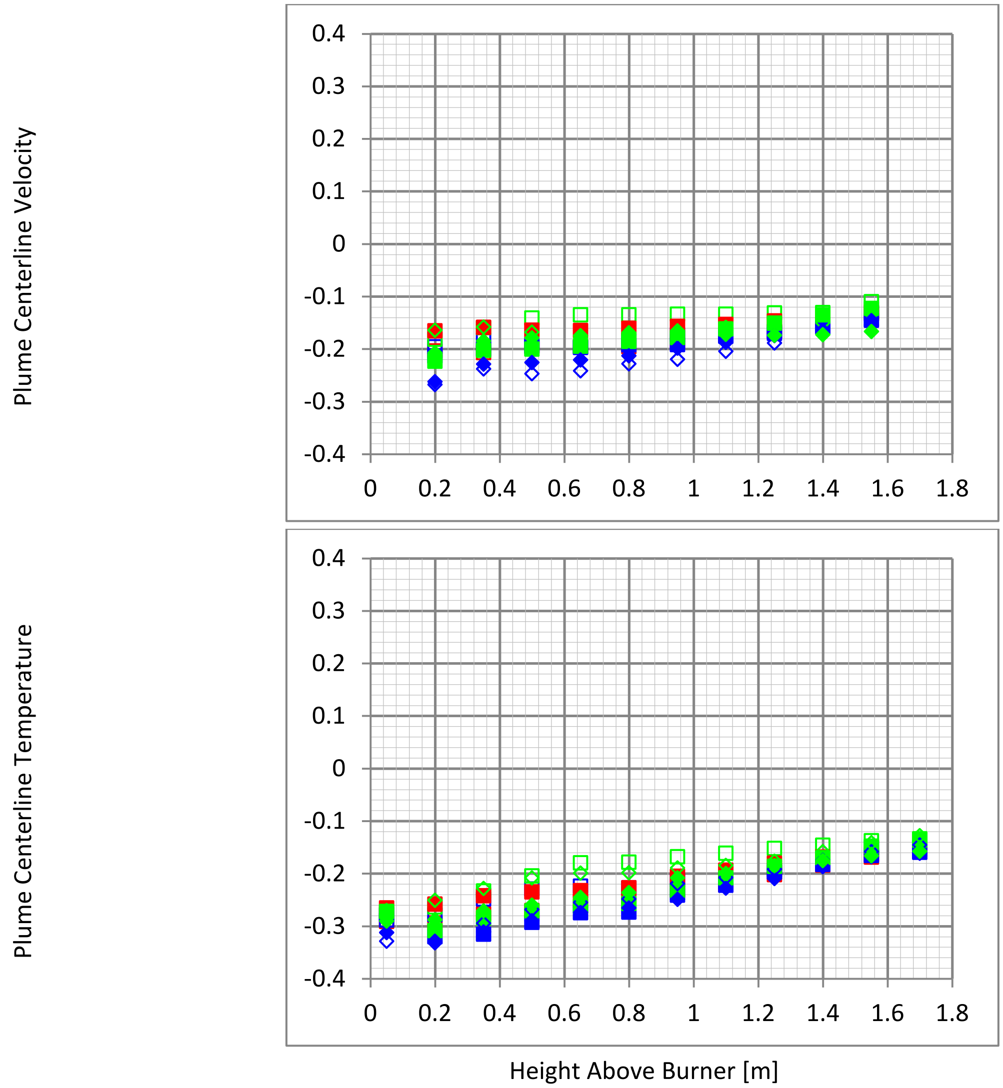

Legend

Propane-Sq-50 ✓	Propane-Sq-75 ✓	Propane-Re-50 ✓	Propane-Re-75 ✓
Propylene-Sq-50 ✓	Propylene-Sq-75 ✓	Propylene-Re-50 ✓	Propylene-Re-75 ✓
Methane-Sq-50 ✓	Methane-Sq-75 ✓	Methane-Re-50 ×	Methane-Re-75 ×

In Series 6, the radiative fraction of all simulations was increased 66% from the default 0.30 to 0.5.

Observations

This change reduced the velocity and temperature along the centerline plume. This is consistent with the results for the propylene fire simulations in Series 3. The centerline velocity was reduced from the default simulations with positive correlation to the increase of the fire's HRR. The centerline temperature predictions comparison between Series 6 and the default series shows that increasing the radiative fraction universally decreases the temperature by a larger amount at locations near the burner surface than at locations further up along the plume.

Again, the change in radiative fraction does not affect the computational performance of the models.

Series 7 - Ratios of Parameter Change from Default Series

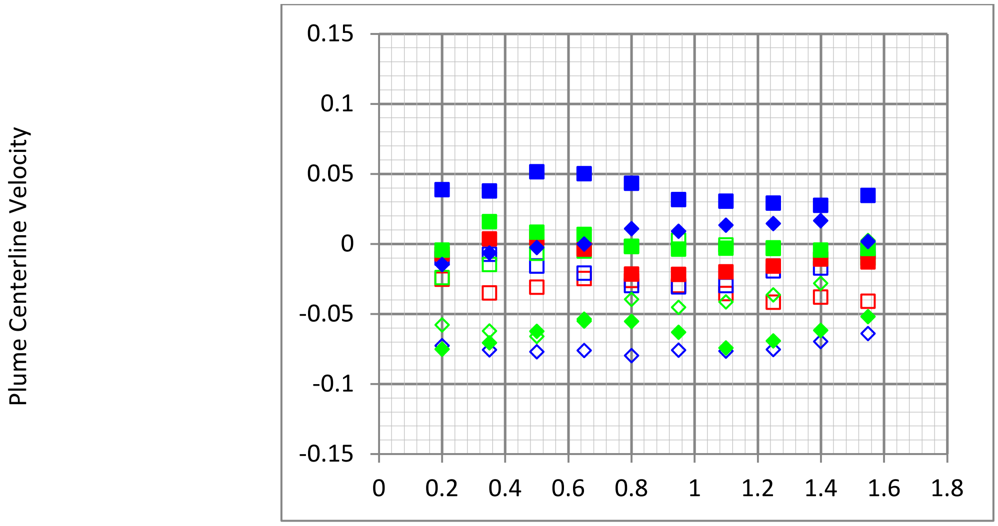

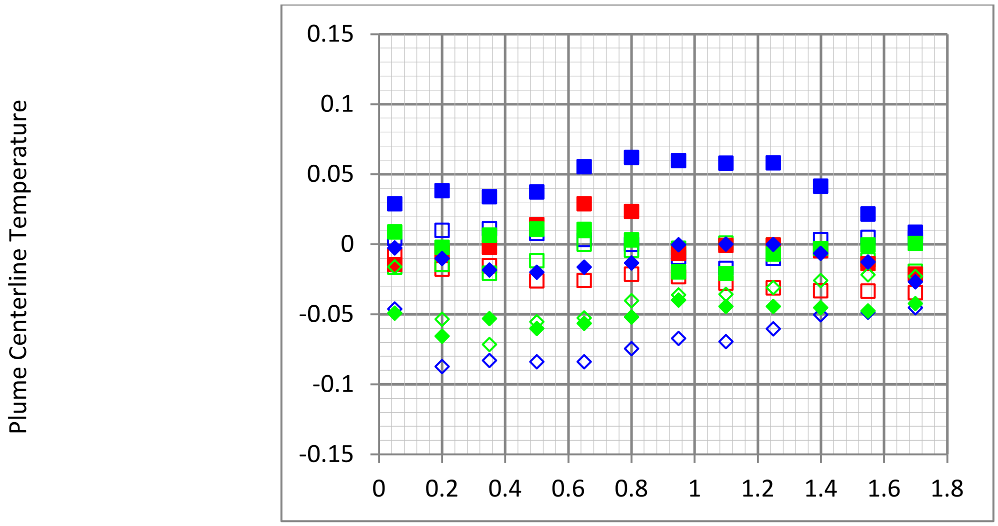

Height Above Burner [m]

Legend

□ Propane-Sq-50 ✓	■ Propane-Sq-75 ✓	◇ Propane-Re-50 ✓	◆ Propane-Re-75 ✓
□ Propylene-Sq-50 ✓	■ Propylene-Sq-75 ✓	◇ Propylene-Re-50 ✓	◆ Propylene-Re-75 ✓
□ Methane-Sq-50 ✓	■ Methane-Sq-75 ✓	◇ Methane-Re-50 ×	◆ Methane-Re-75 ×

In the Series 7 simulations, the wide band model mode to calculate radiation transports was enabled.

Observations

Results from the plume fire simulations show little changes in centerline velocity and temperature prediction due to enabling of the wide band model. It should be noted that the simulations with the higher HRR (@ 75 kW) typically correspond with a larger change in the predicted quantities for models with the same configuration, but at a lower HRR.

The computational performance of the Series 7 simulations is reduced, they took on average 10 hours to execute as compared to the average 4 hours runtime of the default series with the wide band model disabled.

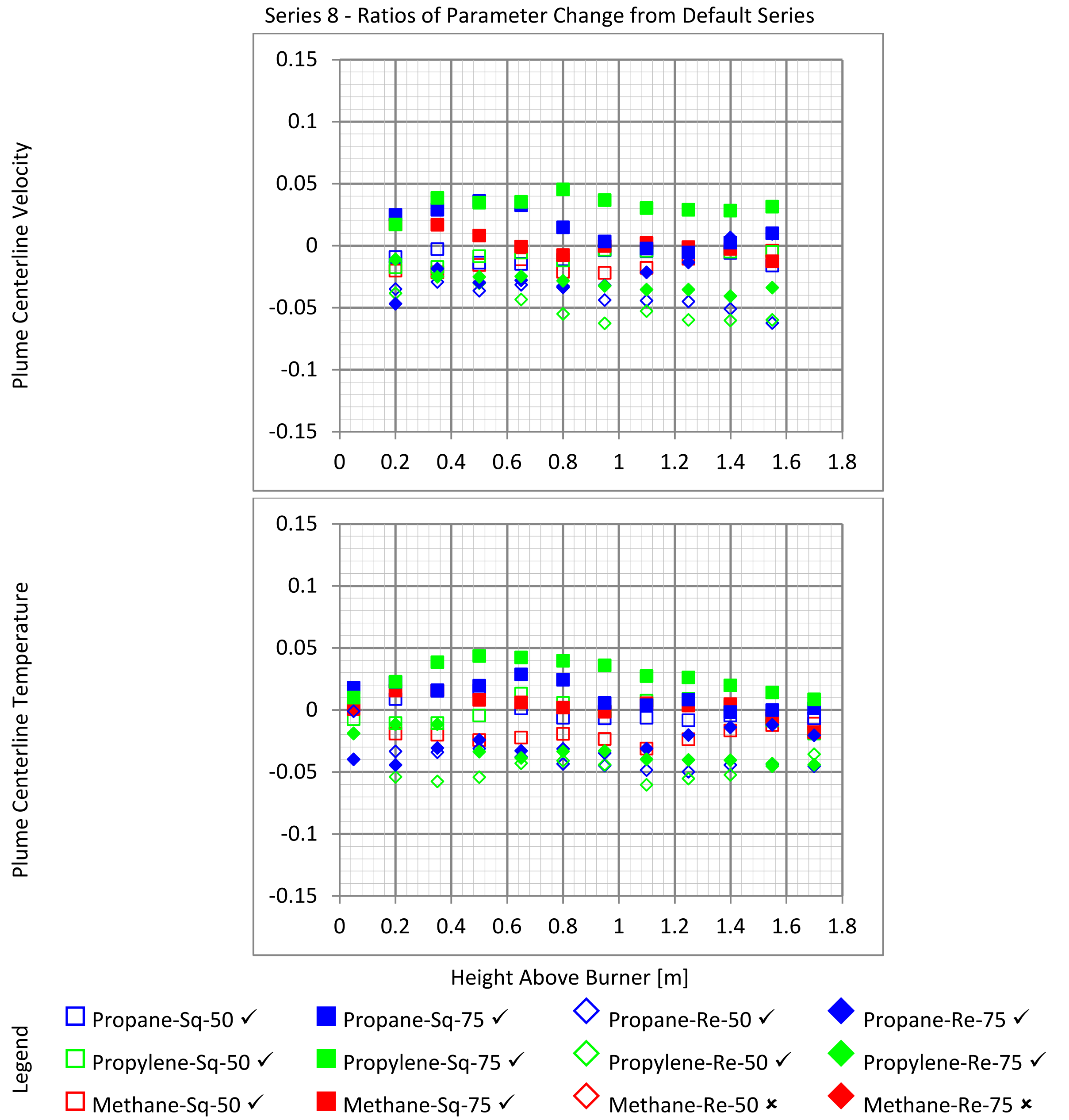

The Series 8 simulations were conducted with a 50% reduction of the default number of radiation angles to be accounted for in the calculations.

Observations

Results from the plume fire simulations show some small increases in centerline velocity and temperature prediction due to the change in radiation angles considered. It is observed that the models with the Square burner generally correspond with an increase of temperature and velocity vs. the default, but the models with the Rectangle burner correspond with a decrease of the two predicted quantities. The average runtime of the Series 8 simulations was about 3 hours, as compared to the default series' average 4 hours runtime.

The reduction in radiation angles by 50% appears to slightly increase the computational performance with minimal effects to the precision of the predictions.

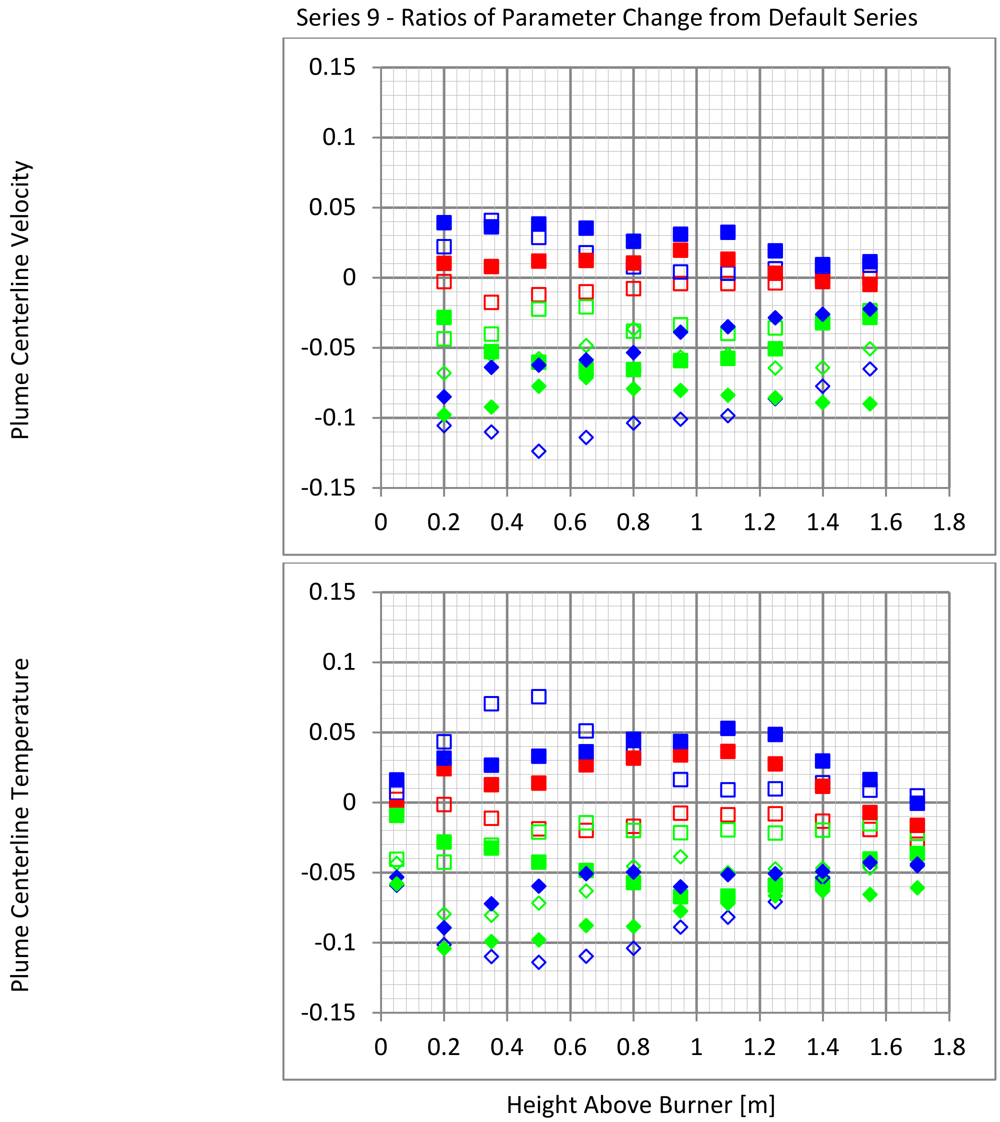

Legend

Propane-Sq-50 ✓	Propane-Sq-75 ✓	Propane-Re-50 ✓	Propane-Re-75 ✓
Propylene-Sq-50 ✓	Propylene-Sq-75 ✓	Propylene-Re-50 ✓	Propylene-Re-75 ✓
Methane-Sq-50 ✓	Methane-Sq-75 ✓	Methane-Re-50 ×	Methane-Re-75 ×

The Series 9 simulations were conducted with a 100% increase of the number of radiation angles to be calculated for in the models.

Observations

Results from the plume fire simulations show that the parameter change decreased the velocity and temperature prediction for the methane and propylene fire plume but increased these two quantities for the propane fire plume models. It should be noted that the simulations with the higher HRR (@ 75 kW) correspond with a change with a greater magnitude than those from the lower HRR models. Changes in the models using the Rectangle burner were generally higher and more negative regardless or fire size or fuel type, except for propylene where the changes are negative regardless of the burner being modeled.

The computational performance was not greatly affected by the increase in the radiation angles to be calculated.

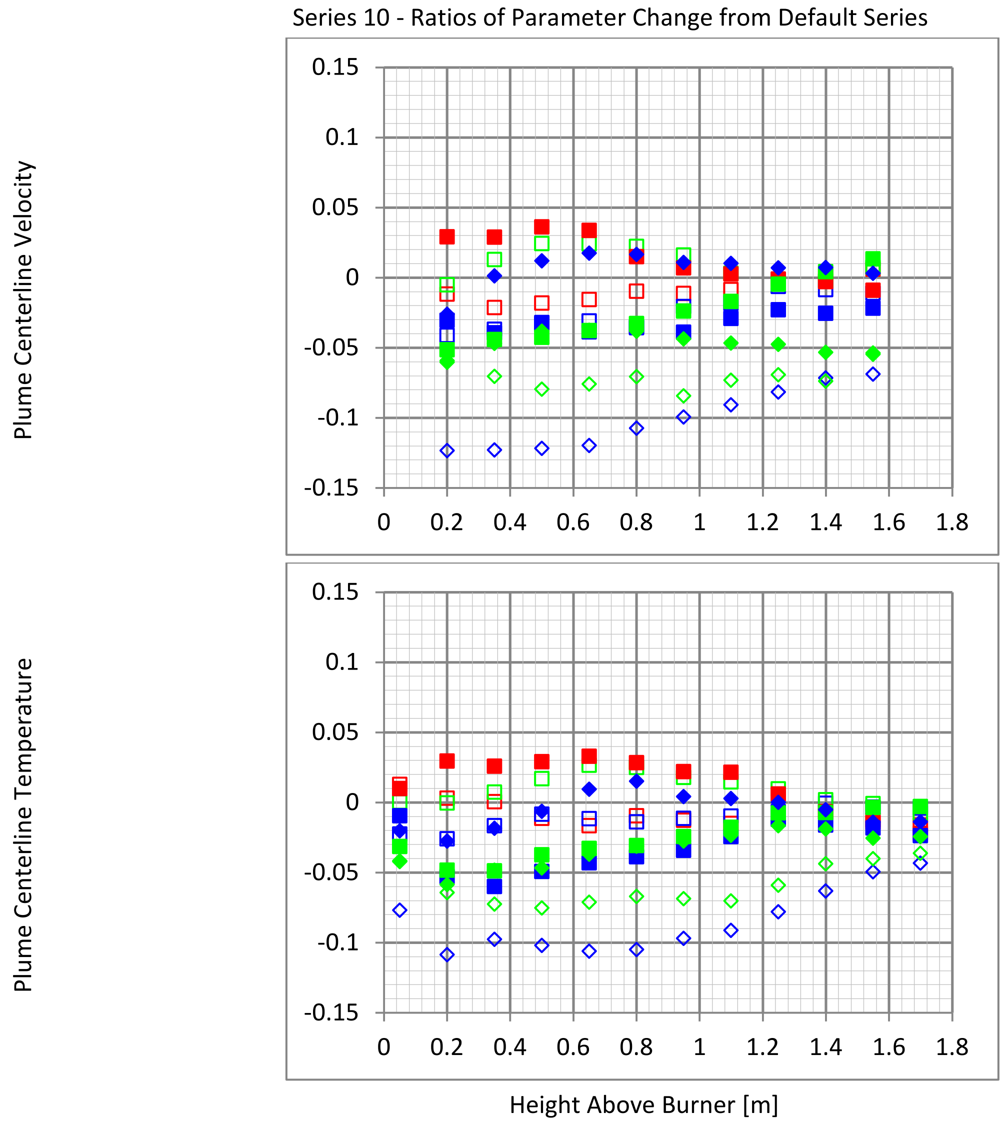

Legend

Propane-Sq-50 ✓	Propane-Sq-75 ✓	Propane-Re-50 ✓	Propane-Re-75 ✓
Propylene-Sq-50 ✓	Propylene-Sq-75 ✓	Propylene-Re-50 ✓	Propylene-Re-75 ✓
Methane-Sq-50 ☐	Methane-Sq-75 ✓	Methane-Re-50 ×	Methane-Re-75 ×

The radiation angle increment, which determine how often FDS updates the radiation solution, was reduced from 5 to 2 in the Series 10 simulations.

Observations

Results from the plume fire simulations show that the parameter change slightly decreased the velocity and temperature prediction for the propane and propylene fire plume while increasing these two quantities for the methane fire plume models for the Square burner fire at 75 kW. However, this trend does not hold true in other situation with a different burner and alower HRR where the deviation from the default models appears to be random. However, the changes found in the models using the Rectangle burner were generally more negative than the deviations noted for models using the Square burner.

The average runtime of the Series 10 simulations was about 3 hours, as compared to the default series' average 4 hours runtime.

Series 11 - Ratios of Parameter Change from Default Series

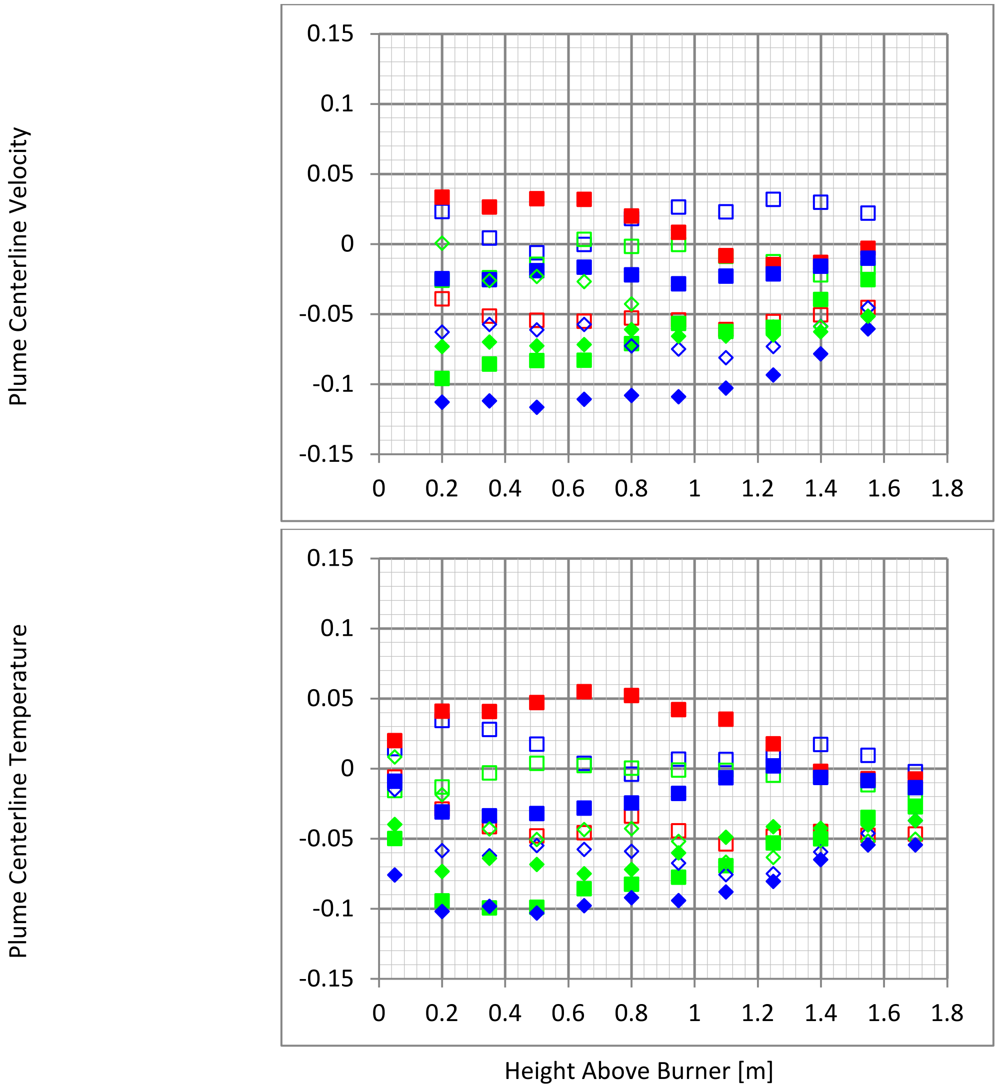

Legend

□ Propane-Sq-50 ✓	■ Propane-Sq-75 ✓	◇ Propane-Re-50 ✓	◆ Propane-Re-75 ✓
□ Propylene-Sq-50 ✓	■ Propylene-Sq-75 ✓	◇ Propylene-Re-50 ✓	◆ Propylene-Re-75 ✓
□ Methane-Sq-50 ☐	■ Methane-Sq-75 ✓	◇ Methane-Re-50 ×	◆ Methane-Re-75 ×

The radiation angle increment, which determine how often FDS updates the radiation solution, was increased from 5 to 10 in the Series 11 simulations, essentially halving the rate at which the radiation angles were updated.

Observations

Results from the plume fire simulations show that the parameter change slightly decreased the velocity and temperature prediction for the propane and propylene fire plume while increasing these 2 quantities for the methane fire plume models for the Square burner fire at 75 kW. However, this trend does not hold true in other situation with a different burner with a lower HRR where the deviation from the default models appears to be random. The changes found in the models using the Rectangle burner were generally higher and negative regardless or fire size or fuel type. The results are similar to that observed in Series 10.

The average runtime of the Series 11 simulations was about 2 hours, as compared to the default series' average 4 hours runtime, which indicates an increase in computational performance.

Series 12 - Ratios of Parameter Change from Default Series

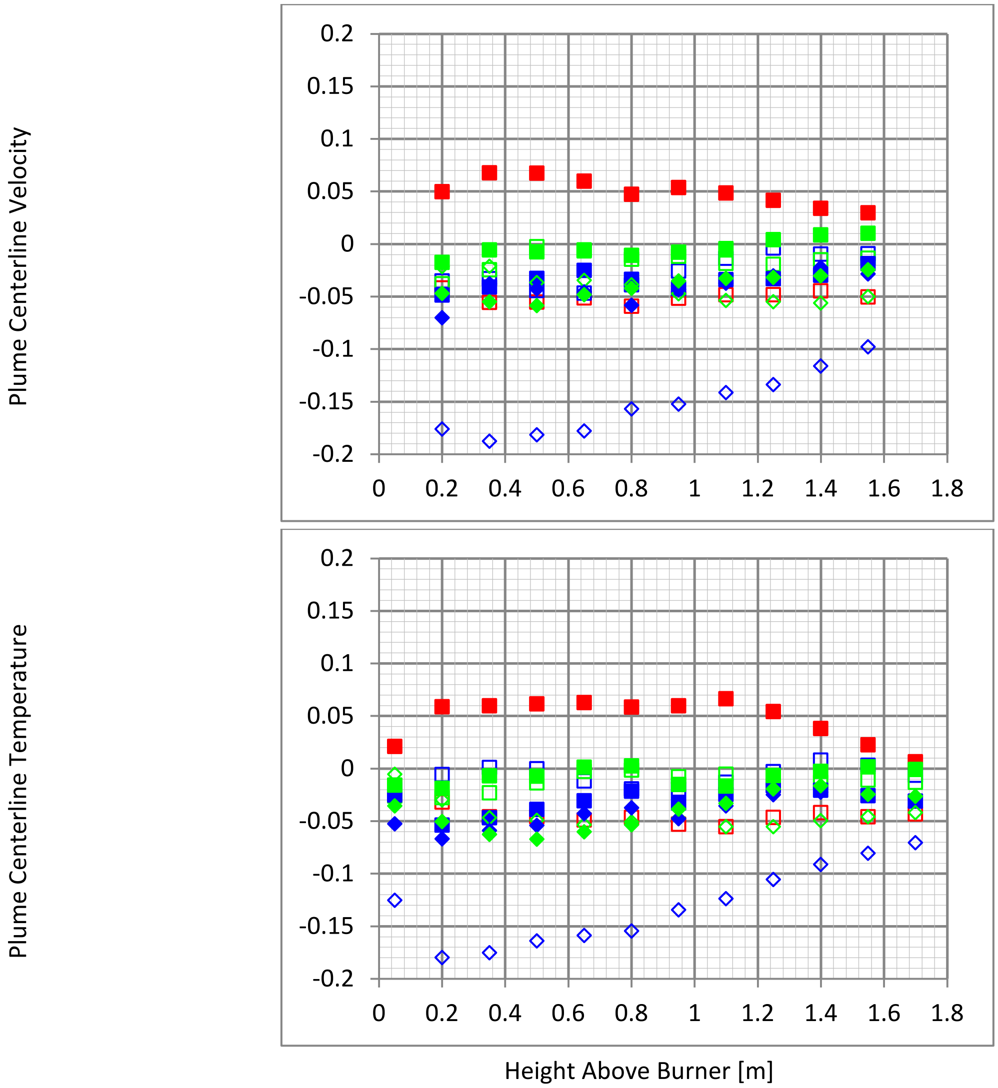

Legend

□ Propane-Sq-50 ✓	■ Propane-Sq-75 ✓	◇ Propane-Re-50 ✓	◆ Propane-Re-75 ✓
□ Propylene-Sq-50 ✓	■ Propylene-Sq-75 ✓	◇ Propylene-Re-50 ✓	◆ Propylene-Re-75 ✓
□ Methane-Sq-50 □	■ Methane-Sq-75 ✓	◇ Methane-Re-50 ×	◆ Methane-Re-75 ×

The time step increment of the radiation solver was reduced from 3 to 1 in the Series 12 simulations, essentially increasing the update rate of the radiation solver in every time step.

Observations

Results from the plume fire simulations show that the parameter change slightly decreased the velocity and temperature prediction for the propane fire plume, slightly increased these predicted quantities for the methane plume, and had no significant change for the propylene plume modeled with the Square burner at 75 kW. It should be noted that the predicted temperature and velocity for the propane plume using the Rectangle burner with 75 kW is greatly reduced.

The changes found in the models using the Rectangle burner were generally higher and negative regardless or fire size or fuel type.

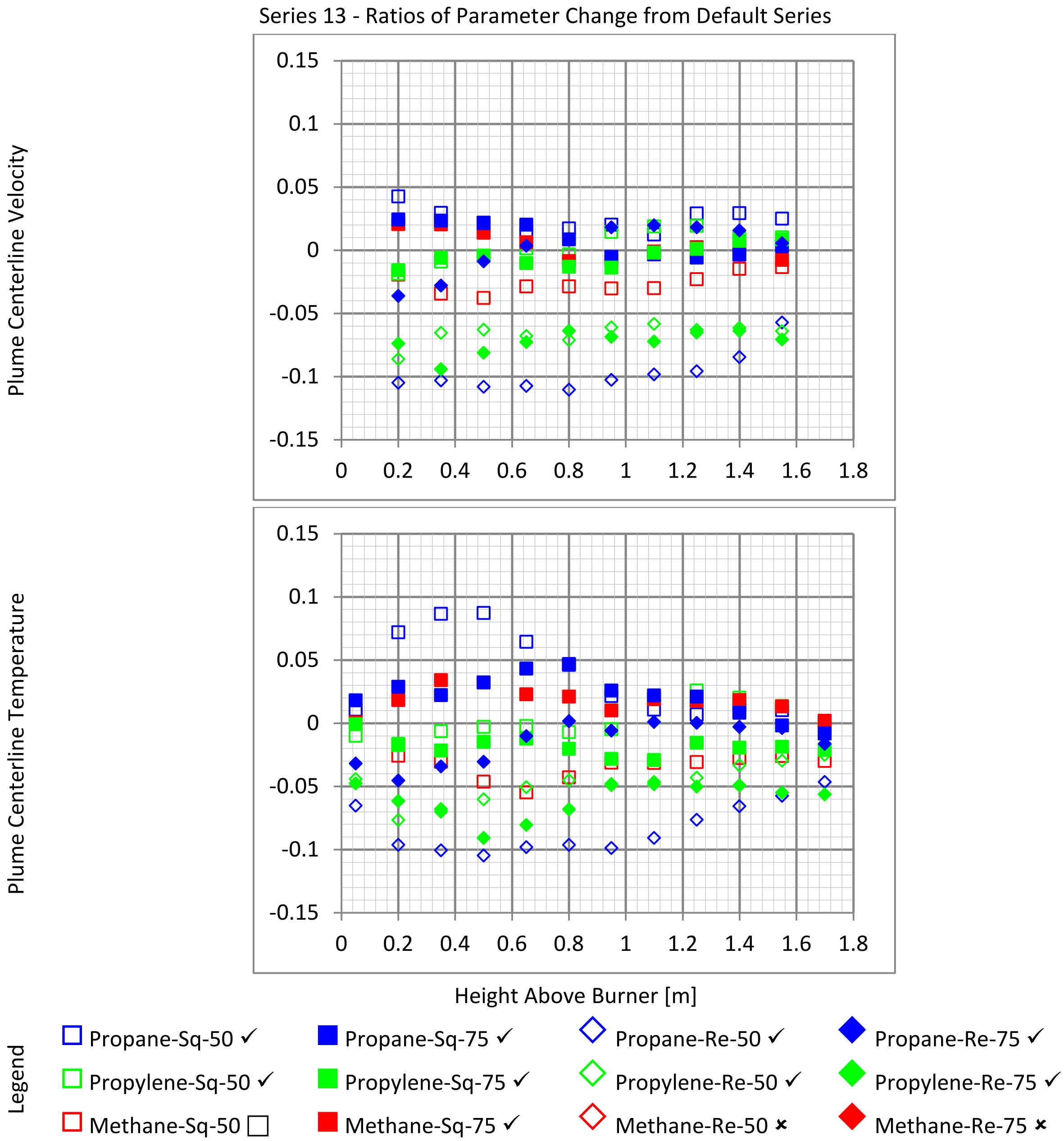

The time step increment was increased from 3 to 6 in the Series 13 simulations, essentially reducing the rate at which the radiation solver was updated by half.

Observations

Generally the predicted velocity and temperature for the models with a rectangle burner are decreased to a more significant amount than models using the Square burner. The models with the Square burner with the propane fuel have increased velocity and temperature, whereas the other Square burner models experienced both an increase and a decrease.

The average runtime of the Series 13 simulations was about 2 hours, essentially half that of the default series' runtime, suggesting that reducing the rate of update to the radiation solution increased the computational performance.

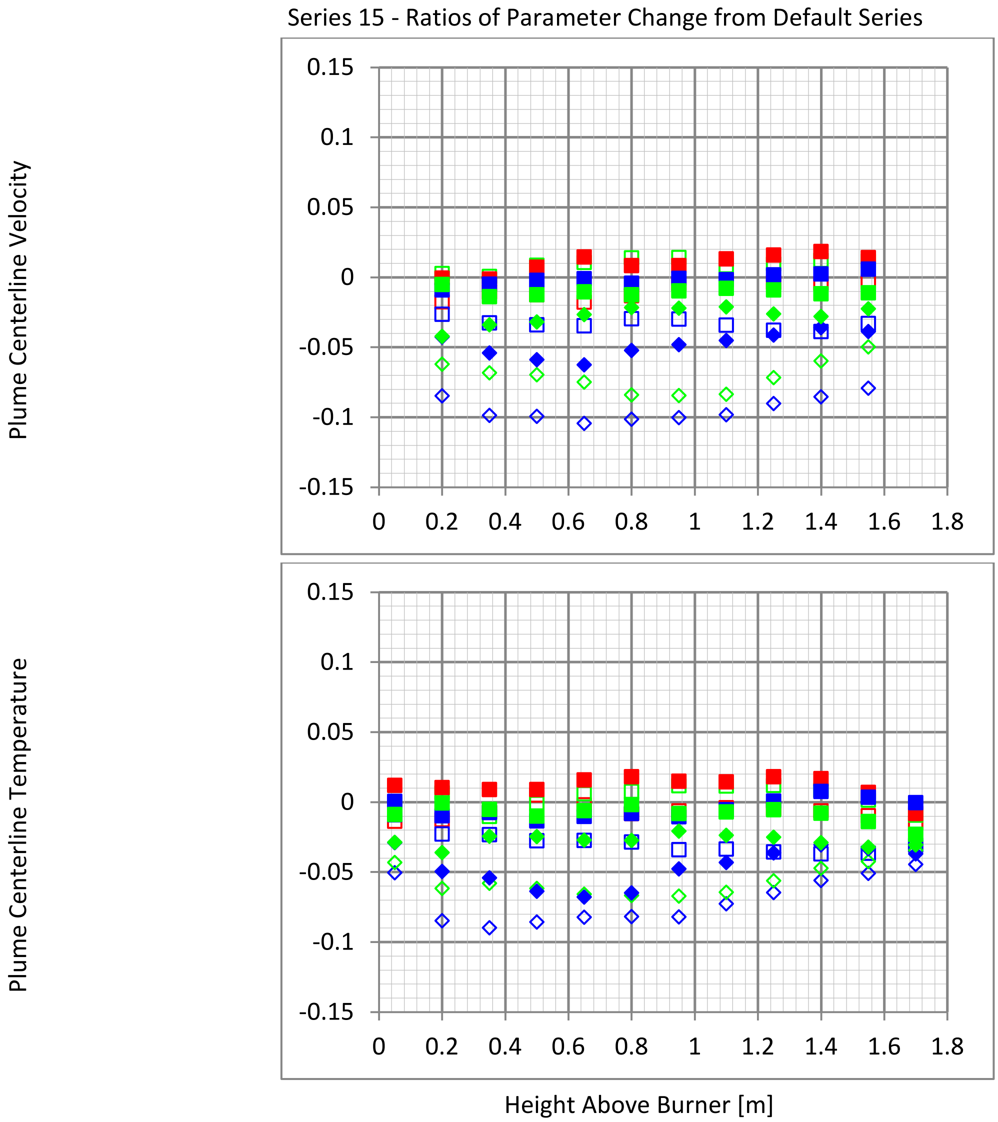

Legend

Propane-Sq-50 ✓ | Propane-Sq-75 ✓ | Propane-Re-50 ✓ | Propane-Re-75 ✓

Propylene-Sq-50 ✓ | Propylene-Sq-75 ✓ | Propylene-Re-50 ✓ | Propylene-Re-75 ✓

Methane-Sq-50 ☐ | Methane-Sq-75 ✓ | Methane-Re-50 × | Methane-Re-75 ×

Observations

The parameter C_EDC which is a constant used to determine the mixing time scale used in the turbulent combustion calculations was increased from 0.1 to 0.2 in the Series 15 simulations thereby doubling the mixing time scale.

The parameter change generally caused a decrease in both the temperature and velocity predicted, or very slightly increase in models using the Square burner.

The average runtime of the Series 15 simulations was about 2 hours, essentially half that of the default series' runtime, suggesting an increase in computational performance.

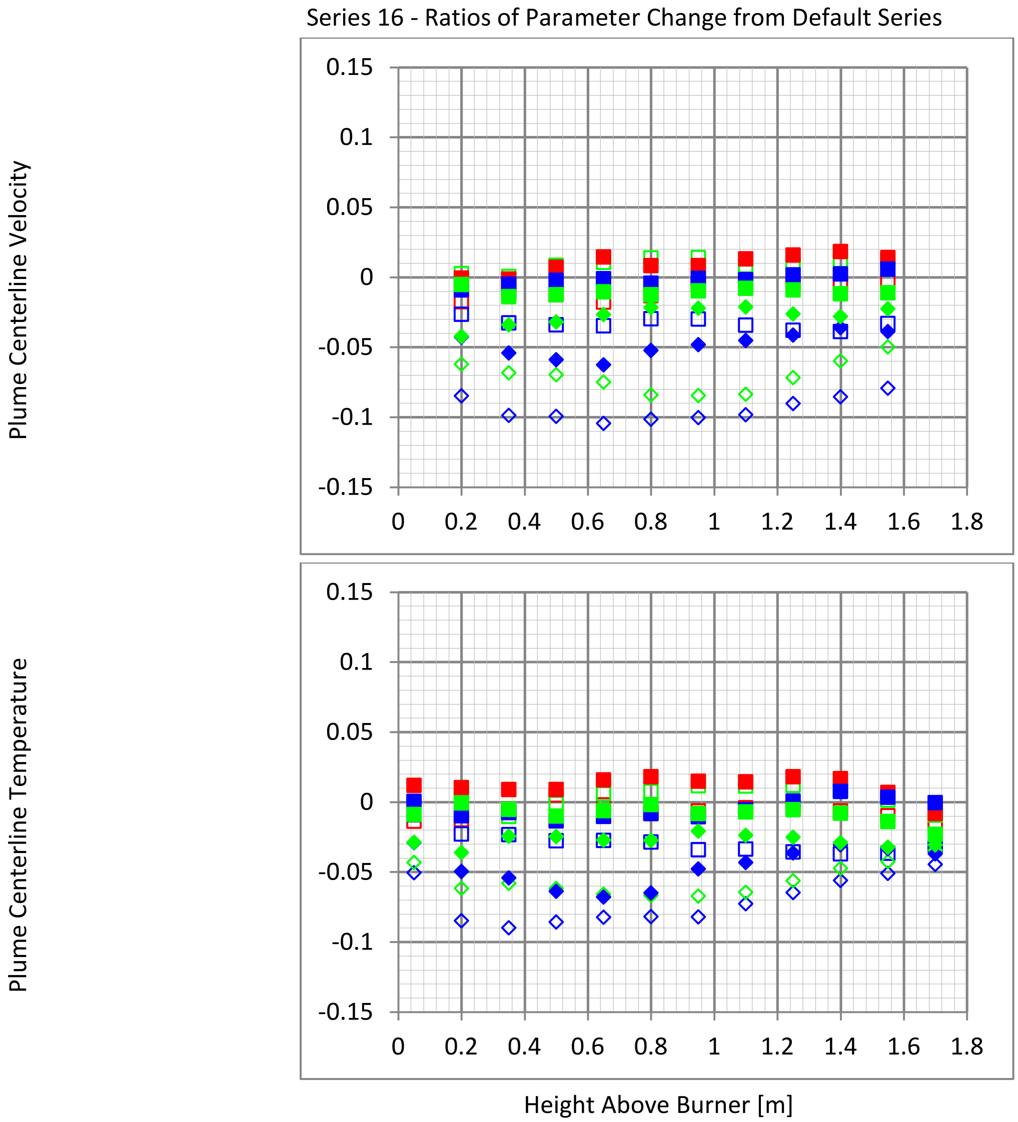

Legend

□ Propane-Sq-50 ✓	■ Propane-Sq-75 ✓	◇ Propane-Re-50 ✓	◆ Propane-Re-75 ✓
□ Propylene-Sq-50 ✓	■ Propylene-Sq-75 ✓	◇ Propylene-Re-50 ✓	◆ Propylene-Re-75 ✓
□ Methane-Sq-50 □	■ Methane-Sq-75 ✓	◇ Methane-Re-50 ✗	◆ Methane-Re-75 ✗

Observations

The parameter C_EDC which is a constant used to determine the mixing time scale used in the turbulent combustion calculations was reduced to 0.05 from 0.1 in the Series 16 simulations thereby halving the mixing time scale.

The parameter change generally caused a decrease in both the temperature and velocity predicted, or very slightly increase in models using the Square burner. This is similar to the results from the Series 15 simulations.

The average runtime of the Series 16 simulations was about 2 hours, essentially half that of the default series' runtime, suggesting an increase in computational performance.

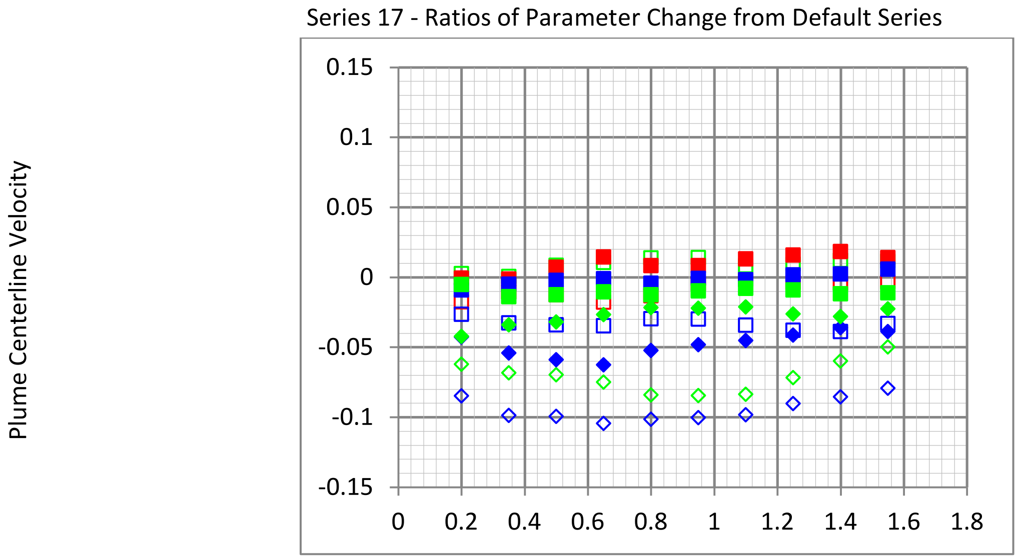

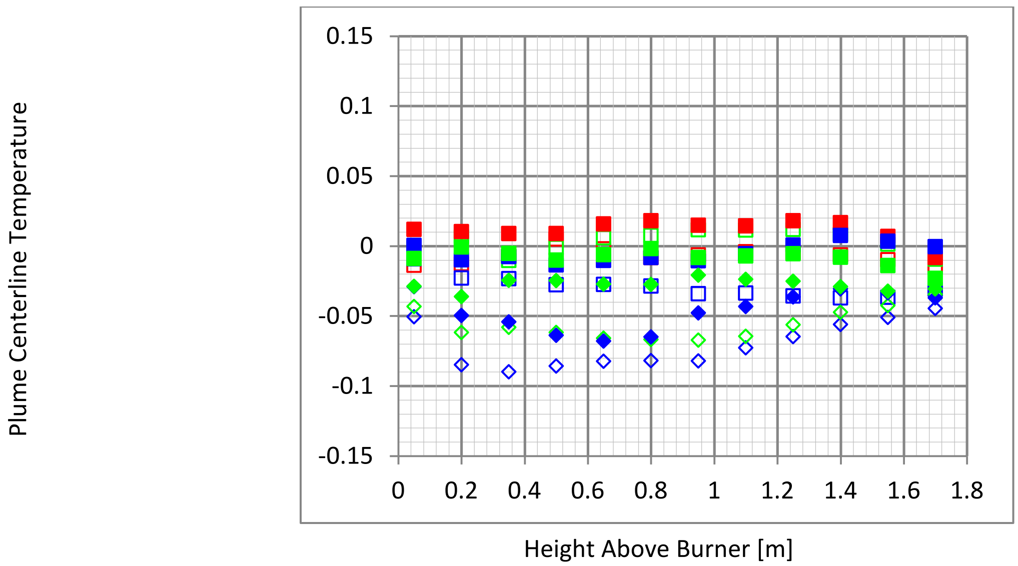

Legend

Propane-Sq-50 ✓	Propane-Sq-75 ✓	Propane-Re-50 ✓	Propane-Re-75 ✓
Propylene-Sq-50 ✓	Propylene-Sq-75 ✓	Propylene-Re-50 ✓	Propylene-Re-75 ✓
Methane-Sq-50 ☐	Methane-Sq-75 ✓	Methane-Re-50 ×	Methane-Re-75 ×

Eddy dissipation mode is usually enabled in the large eddy simulations, but disabling it, the mixing time scale of the turbulent combustion becomes the time step of the simulation.

Observations

The parameter change generally caused a decrease in both the temperature and velocity predicted, or very slightly increase in models using the Square burner. This is similar to the results from the Series 15 and Series 16 simulations.

The average runtime of the Series 17 simulations was about 2 hours, essentially half that of the default series' runtime, suggesting an increase in computational performance.

Series 18 - Ratios of Parameter Change from Default Series

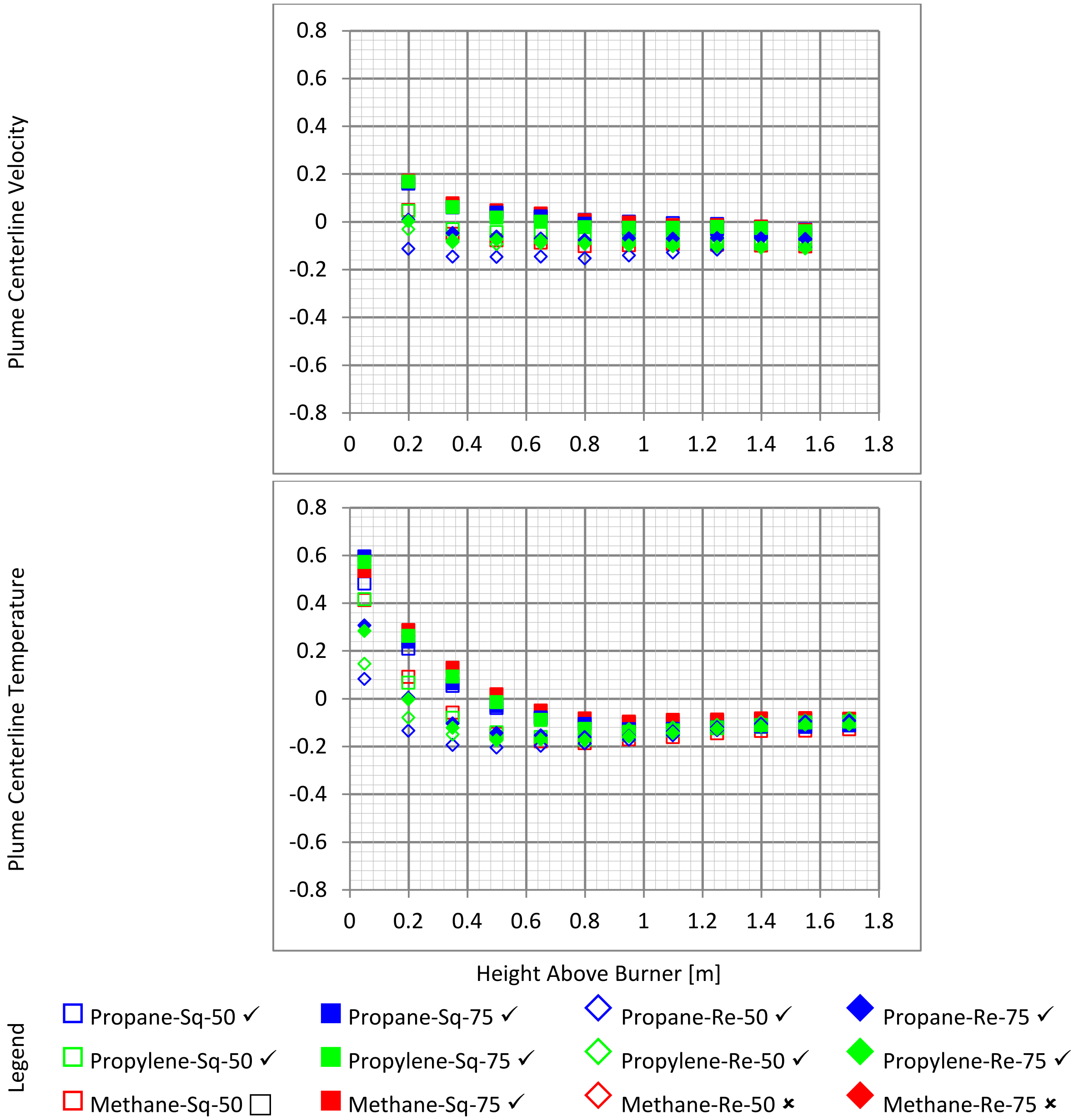

In the Series 18 simulations, the heat release rate per unit area of the flame sheet was increased from 0 kW/m^2 to 400 kW/m^2 for LES simulations.

Observations

In the plume simulations, this parameter change resulted in an increase of the centerline velocity and temperature essentially up to the flame tip in the Square burner models. In the models using the Rectangle burner, however, the temperature was raised by a small amount but the velocity was decreased. It is noted that the temperature predicted in Series 18's Square burner models was closer to the temperature predicted using McCaffrey's theory.

The average runtime of the Series 18 simulations was about 3 hours, showing a slight reduction from the default simulations.

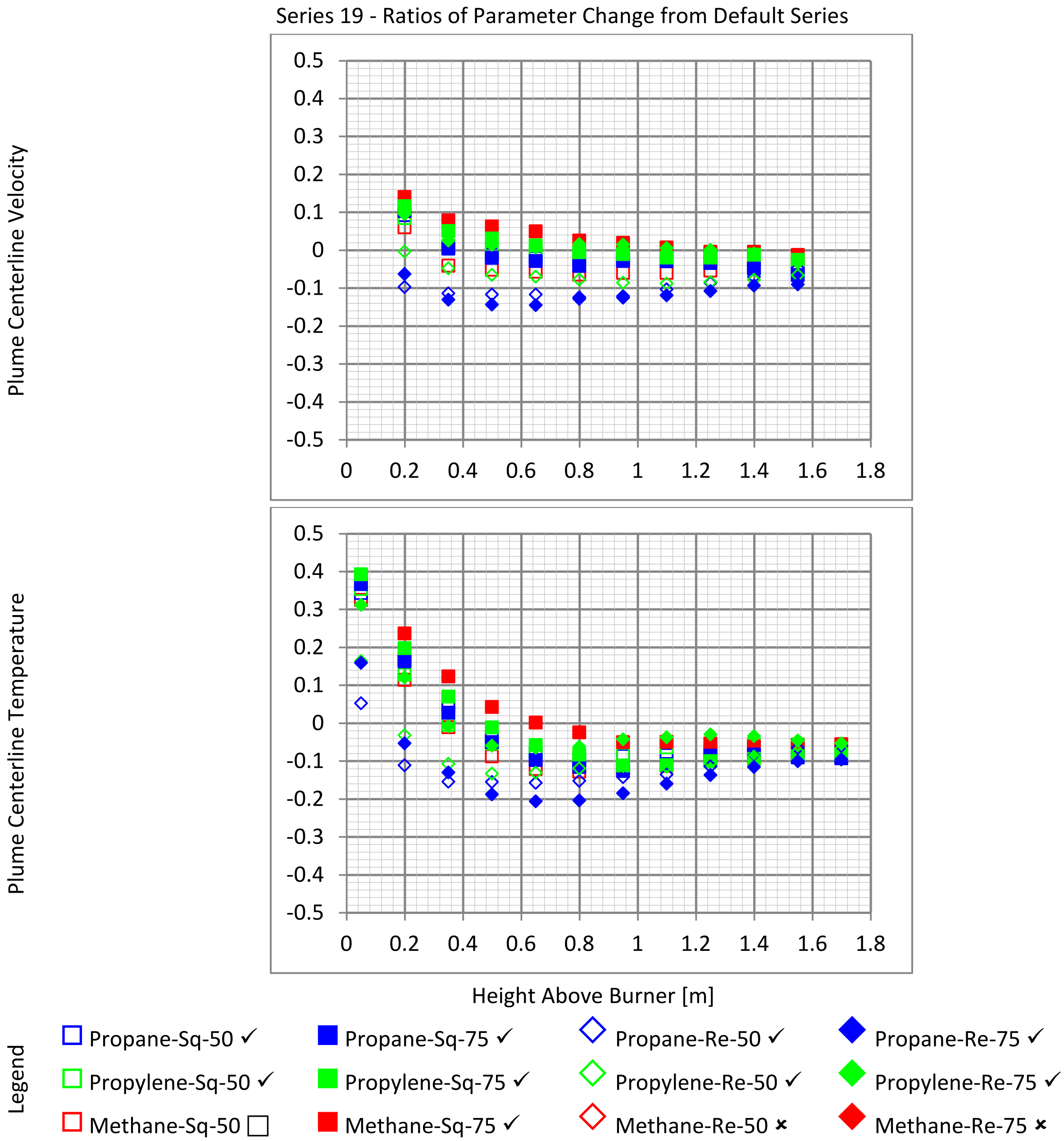

In Series 19 simulations, the heat release rate per unit area of the flame sheet was increased to 100 kW/m^2 from 0 kW/m^2 for LES simulations.

Observations

An increase in centerline plume temperature was noted near the burner's surface, but to a less degree that that observed in Series 18. The velocity near the burner surface was increased in the Square burner cases using methane and propylene, however, the velocity away from the burner surface in the cases modeling propane was decreased. Again, the models with a Rectangle burner generally experienced a decrease in velocity.

The average runtime of the Series 19 simulations was about 2 hours; when compared to the default series' average or 4 hours, it shows an increase in computational performance from the decrease of the HRRPUA_SHEET parameter.

Series 20 - Ratios of Parameter Change from Default Series

Plume Centerline Velocity

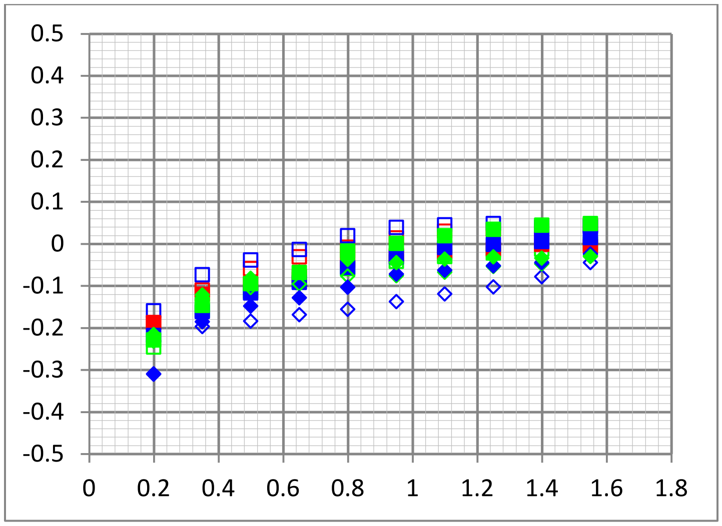

Plume Centerline Temperature

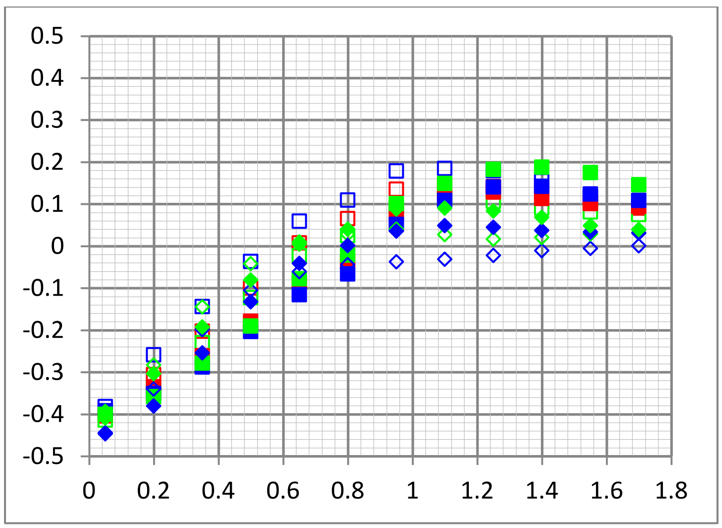

Height Above Burner [m]

Legend

□ Propane-Sq-50 ✓	■ Propane-Sq-75 ✓	◇ Propane-Re-50 ✓	◆ Propane-Re-75 ✓
□ Propylene-Sq-50 ✓	■ Propylene-Sq-75 ✓	◇ Propylene-Re-50 ✓	◆ Propylene-Re-75 ✓
□ Methane-Sq-50 □	■ Methane-Sq-75 ✓	◇ Methane-Re-50 ×	◆ Methane-Re-75 ×

In Series 20 simulations, the average local heat release rate per unit volume was reduced from the default 2500 kW/m3 to a value of 1200 kW/m3 as suggested by Orloff and De Ris for the entire fire.

Observations

In all of the free plume simulation, regardless of burner size or HRR, the velocity and temperature were reduced from the default at locations closest to the fire in the flame zones, but there was minimal to no change in the region above that for velocity, but a slight increase in temperature.

The average runtime of the Series 19 simulations was about 2 hours; when compared to the default series' average or 4 hours, it shows an increase in computational performance from the decrease of the HRRPUV_AVERAGE parameter.

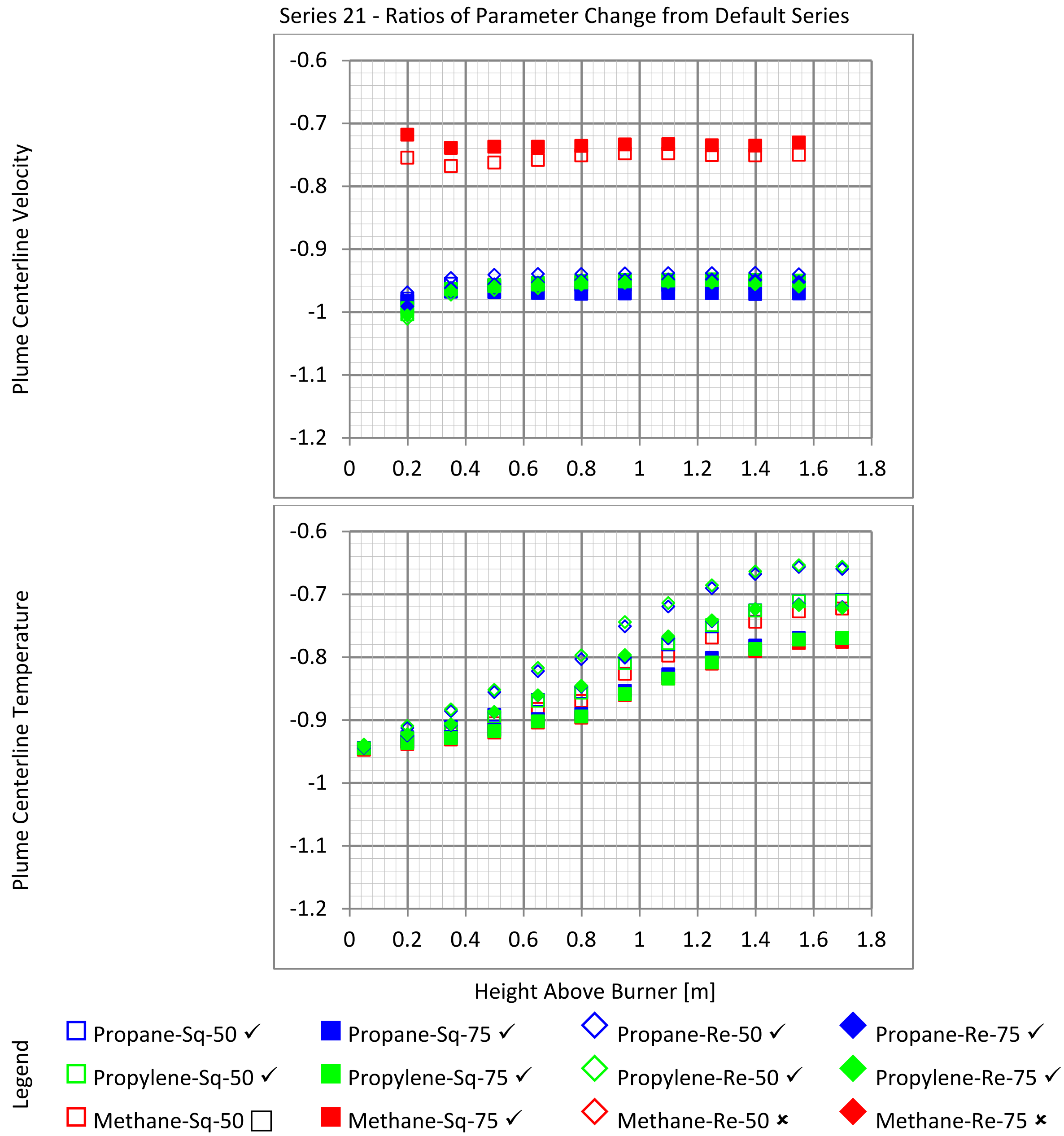

Observations

The isothermal model was enabled in the Series 21 simulations to test the effects of a fire simulation in which the temperature was forced to not changed. It was intended to show whether a mistake in writing the FDS file would result in a simulation with some salvageable and meaningful data.

The plume simulations predicted that the centerline velocity of an isothermal methane fire plume is about 0.5 m/s throughout, but the velocity of the isothermal propane and propylene plume is about 0.1 m/s throughout. The centerline temperature was found to be set to the ambient. These results are expected, and it shows that an isothermal fire simulation would be ineffective and entirely erroneous.

On average, the isothermal fire models took about 15 minutes to complete.

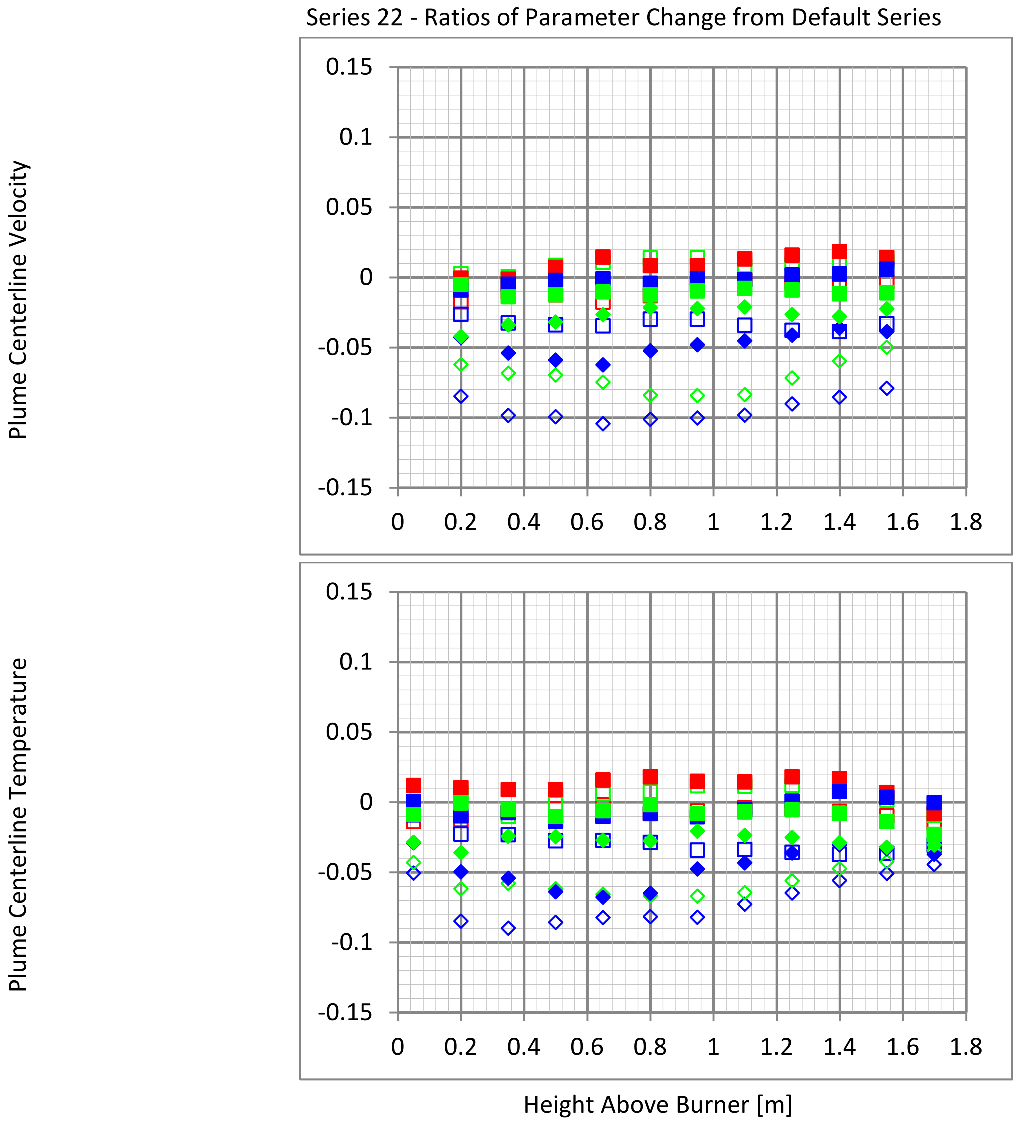

Legend

Propane-Sq-50 ✓	Propane-Sq-75 ✓	Propane-Re-50 ✓	Propane-Re-75 ✓
Propylene-Sq-50 ✓	Propylene-Sq-75 ✓	Propylene-Re-50 ✓	Propylene-Re-75 ✓
Methane-Sq-50 ☐	Methane-Sq-75 ✓	Methane-Re-50 ✗	Methane-Re-75 ✗

In Series 22, the Smagorinsky constant was reduced from 0.2 to 0.1, it was used to calculate the viscosity of the fluid and to model the subgrid-scale turbulence in the models.

Observations

Generally, the parameter change generated little to no effect on the overall temperature and velocity prediction for the Square burner model, but these two quantities are predicted to be lower in the models using the Rectangle burner.

On average, the Series 22 models took about 2.5 hours to run, showing small increase in computational performance over the default series.

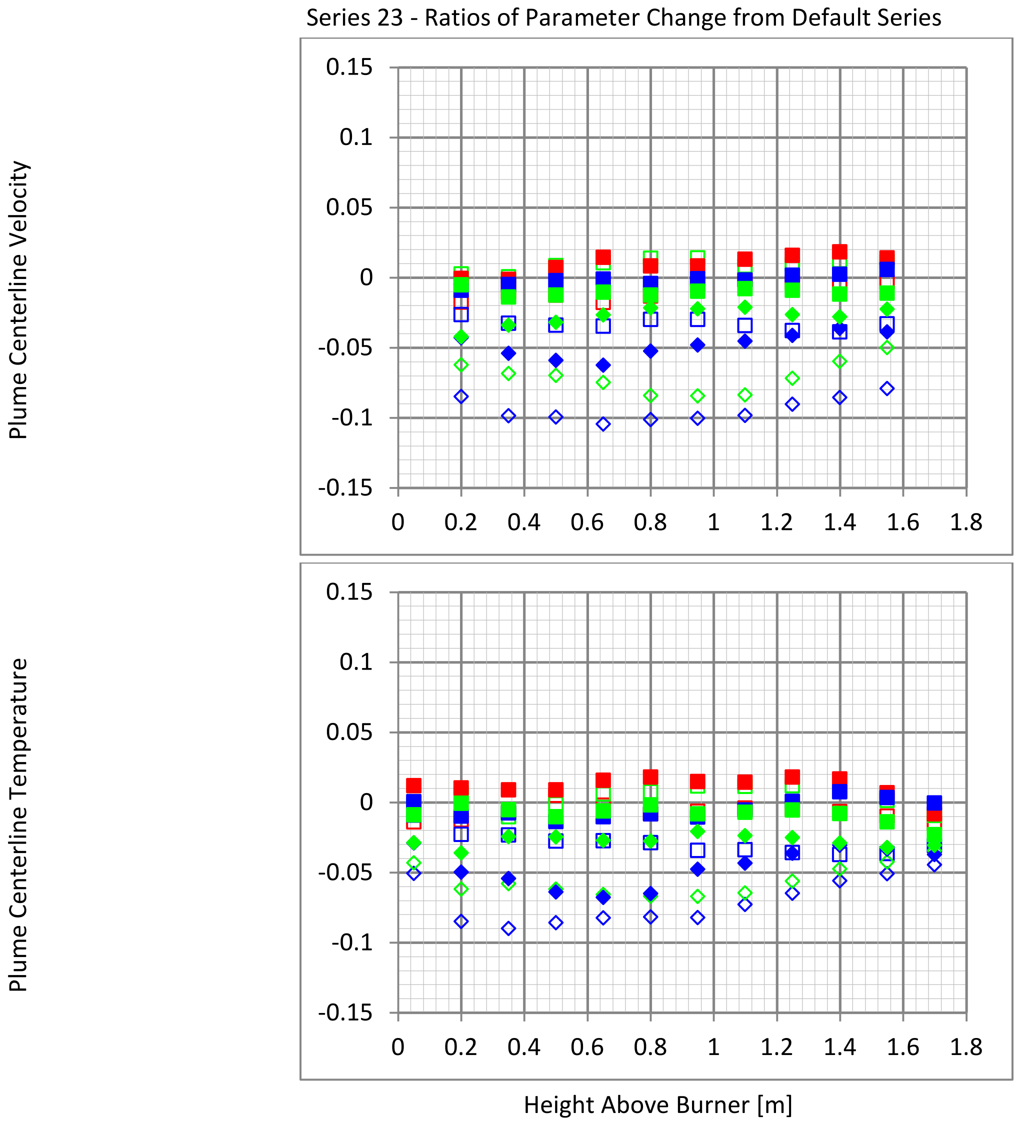

Legend

Propane-Sq-50 ✓	Propane-Sq-75 ✓	Propane-Re-50 ✓	Propane-Re-75 ✓
Propylene-Sq-50 ✓	Propylene-Sq-75 ✓	Propylene-Re-50 ✓	Propylene-Re-75 ✓
Methane-Sq-50 ☐	Methane-Sq-75 ✓	Methane-Re-50 ×	Methane-Re-75 ×

In Series 23, the Smagorinsky constant was increased from 0.2 to 0.4, it was used to calculate the viscosity of the fluid and to model the subgrid-scale turbulence in the models.

Observations

Similar to the results from Series 22 simulations, increasing the Smagorinsky constant by 200% generated little to no effect on the overall temperature and velocity prediction for the Square burner model, but these two quantities are lower in the cases using the Rectangle burner. Additionally, the results from the Series 23 simulations are almost identical to the Series 22 simulations This suggests that a Smagorinsky constant within the range of 0.1 to 0.4 does not significantly affect the FDS results in plume configuration.

On average, the Series 23 models took about 2.5 hours to run, showing small increase in computational performance over the default series.

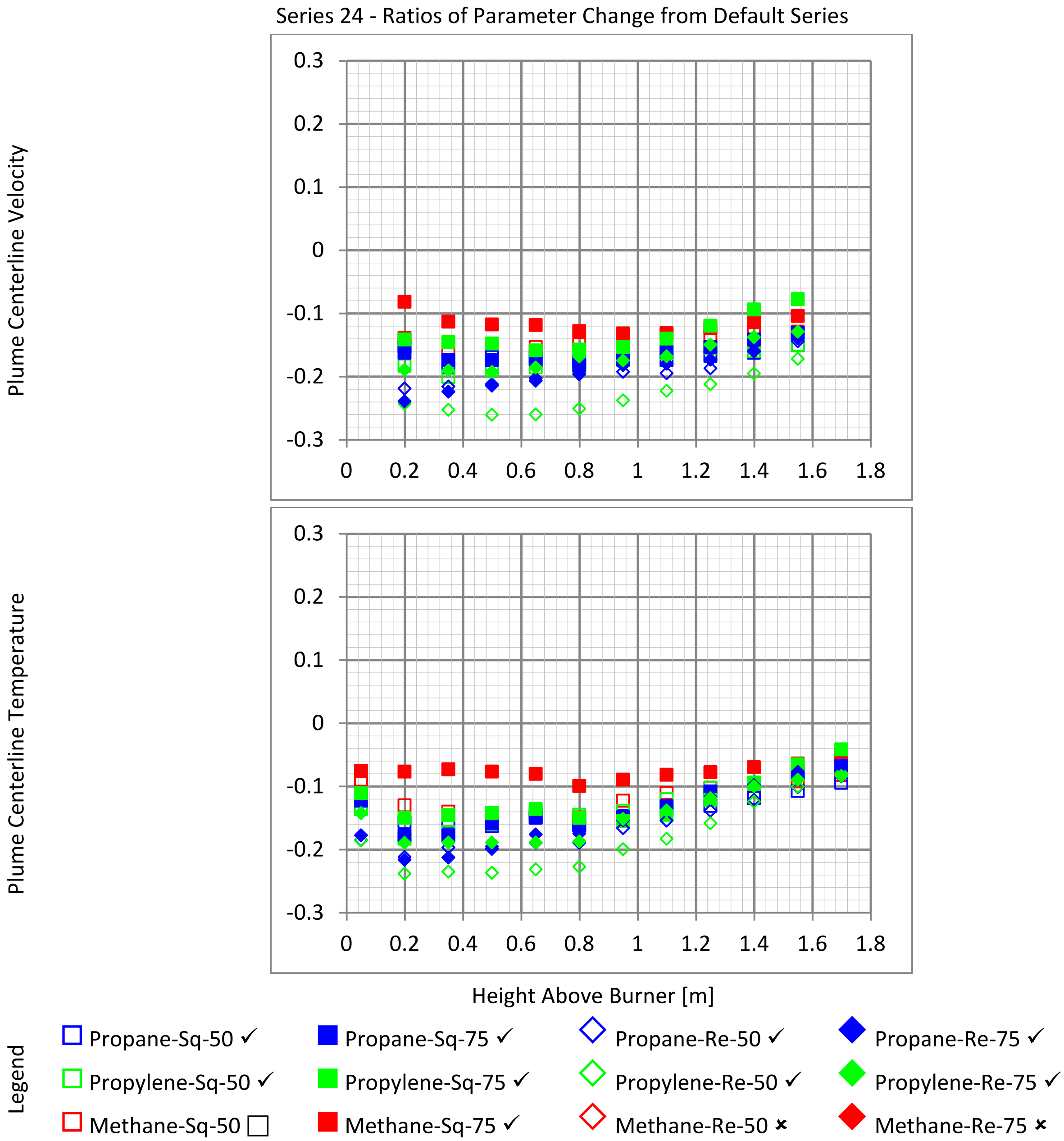

Observations

In Series 24, the turbulent Prandtl number was decreased to 0.25 from 0.5, the Prandtl number is a ratio of the momentum diffusivity to thermal diffusivity, so this parameter change had the potential to change the flow characteristics in the simulations.

Both the centerline temperature and velocity are reduced when compared to the default Series results, regardless of burner shape, HRR, or fuel.

On average, the Series 24 models took about 2 hours to run, showing some increase in computational performance over the default series.

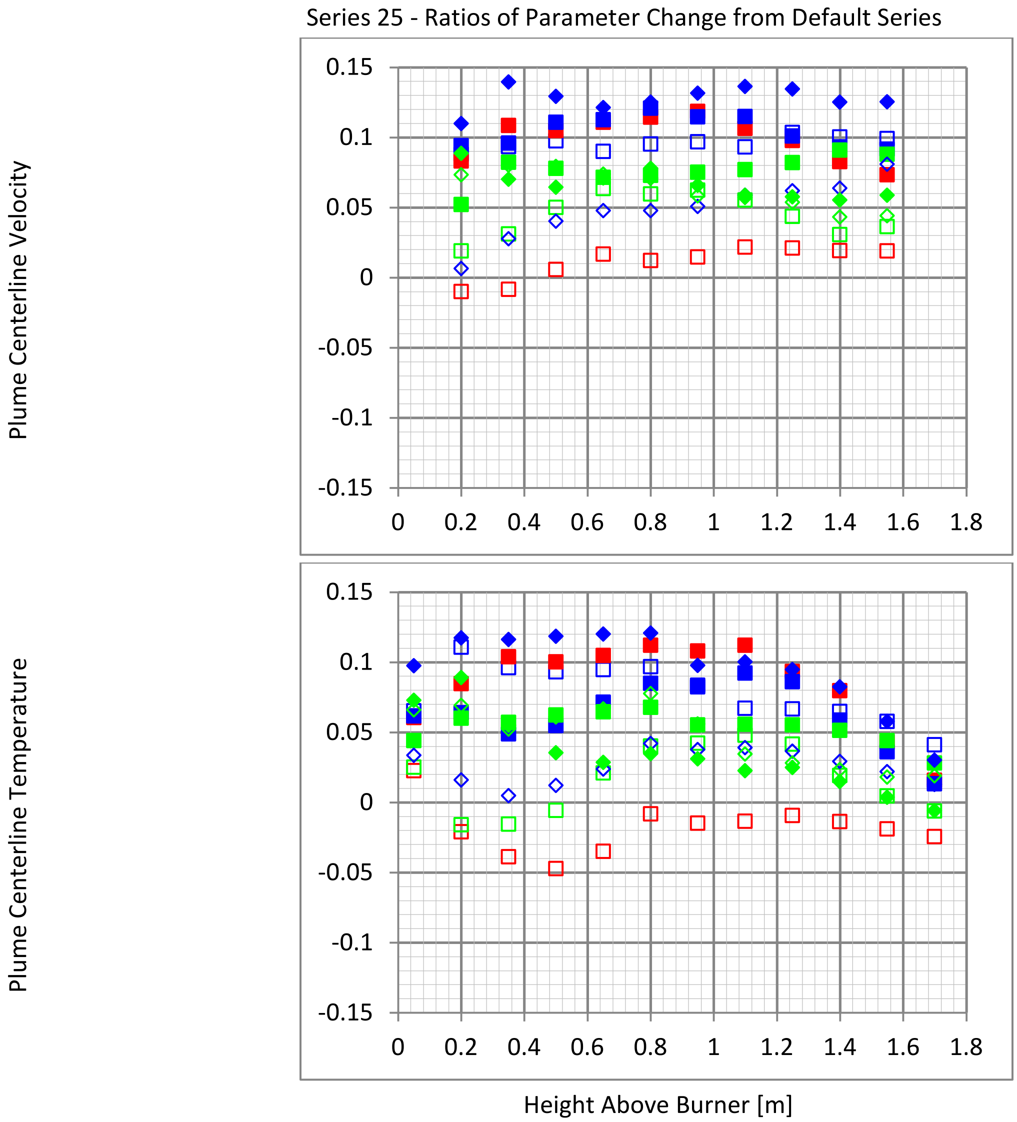

Legend

Propane-Sq-50 ✓	Propane-Sq-75 ✓	Propane-Re-50 ✓	Propane-Re-75 ✓
Propylene-Sq-50 ✓	Propylene-Sq-75 ✓	Propylene-Re-50 ✓	Propylene-Re-75 ✓
Methane-Sq-50 □	Methane-Sq-75 ✓	Methane-Re-50 ×	Methane-Re-75 ×

Observations

In Series 25, the turbulent Prandtl number was increased from 0.5 to 1, the Prandtl number is a ratio of the momentum diffusivity to thermal diffusivity, so this parameter change had the potential to change the flow characteristics in the simulations.

Both the centerline temperature and velocity are increased when compared to the default Series results, with the larger increase corresponding to the models with a higher HRR. The results from this Series are opposite of that from Series 24 where the Prandtl number was decreased instead of increased. Compared to the results from other parametric study series, the effects of the Prandtl number change appears to be significant.

On average, the Series 25 models took about 2 hours to run, showing small increase in computational performance over the default series.

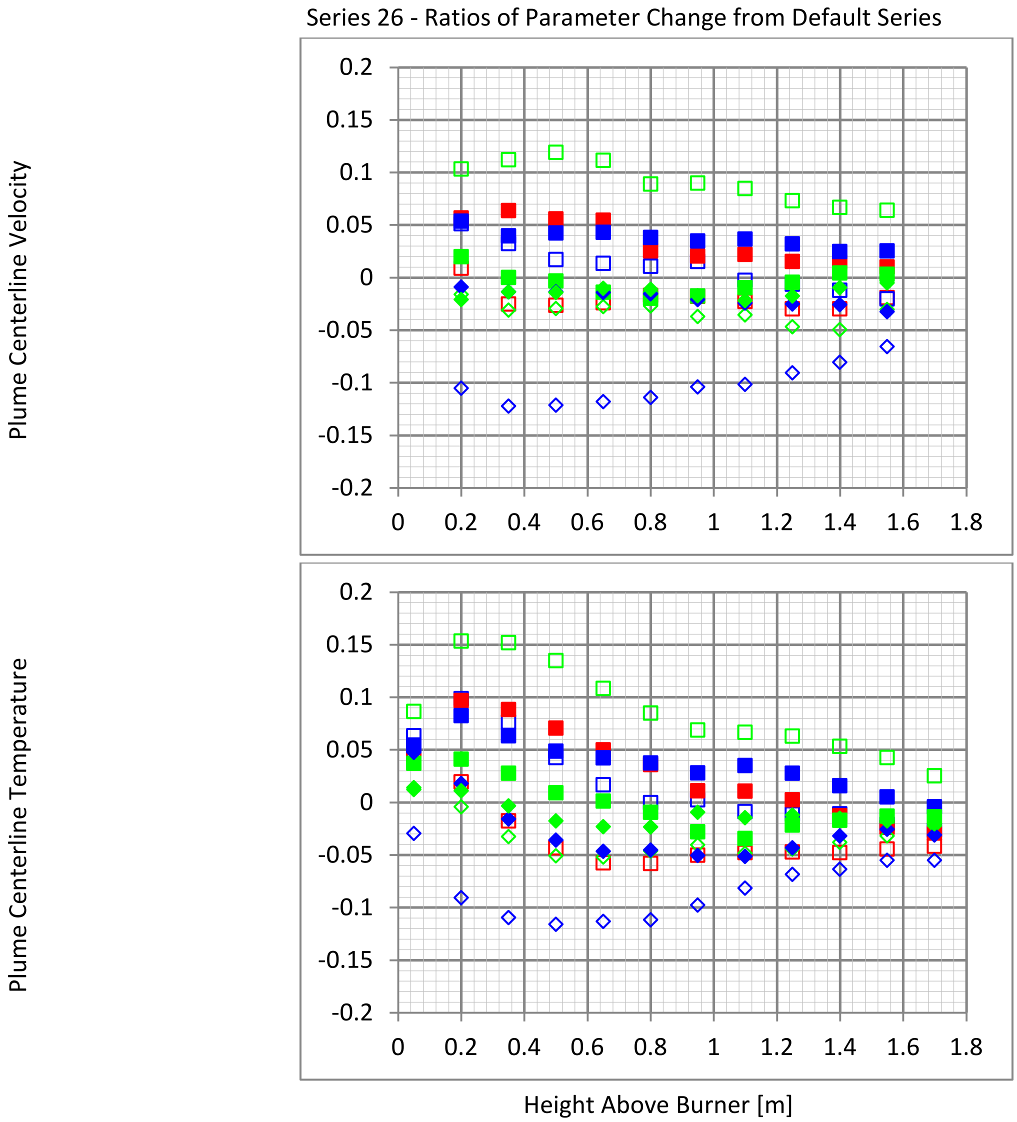

Legend

Propane-Sq-50 ✓	Propane-Sq-75 ✓	Propane-Re-50 ✓	Propane-Re-75 ✓
Propylene-Sq-50 ✓	Propylene-Sq-75 ✓	Propylene-Re-50 ✓	Propylene-Re-75 ✓
Methane-Sq-50 ☐	Methane-Sq-75 ✓	Methane-Re-50 ✗	Methane-Re-75 ✗

In Series 26, the turbulent Schmidt number was decreased from 0.5 to 0.25, the Schmidt number is a ratio of the momentum diffusivity to mass diffusivity, so this parameter change had the potential to change the flow characteristics in the simulations.

Observations

For the models with a Square burner, the velocity and temperature near the burner surface was slightly increased, but for the Rectangle burner models, the predicted velocity and temperature had negative were lowered or had no change from the parameter change.

On average, the Series 26 models took about 2 hours to run, showing small increase in computational performance over the default series.

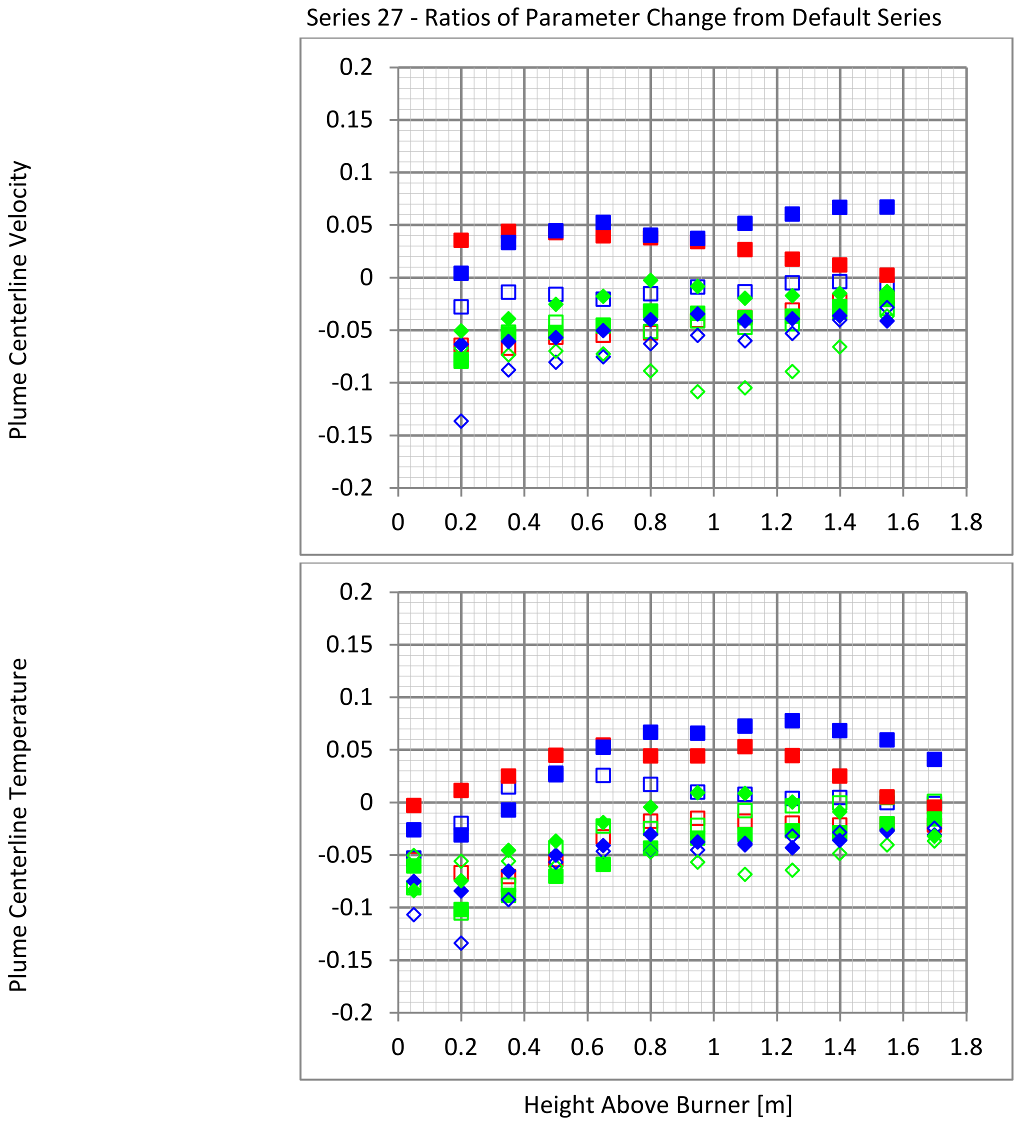

Legend

□ Propane-Sq-50 ✓	■ Propane-Sq-75 ✓	◇ Propane-Re-50 ✓	◆ Propane-Re-75 ✓
□ Propylene-Sq-50 ✓	■ Propylene-Sq-75 ✓	◇ Propylene-Re-50 ✓	◆ Propylene-Re-75 ✓
□ Methane-Sq-50 ☐	■ Methane-Sq-75 ✓	◇ Methane-Re-50 ×	◆ Methane-Re-75 ×

Observations

In Series 27, the turbulent Schmidt number was increased from 0.5 to 1, the Schmidt number is a ratio of the momentum diffusivity to mass diffusivity, so this parameter change had the potential to change the flow characteristics in the simulations.

The effects of increasing the Schmidt number appear to be quite random, but the changes are small, suggesting that the FDS prediction on centerline velocity and temperature are insensitive to the Schmidt number in the range tested.

On average, the Series 27 models took about 2 hours to run, showing small increase in computational performance over the default series.

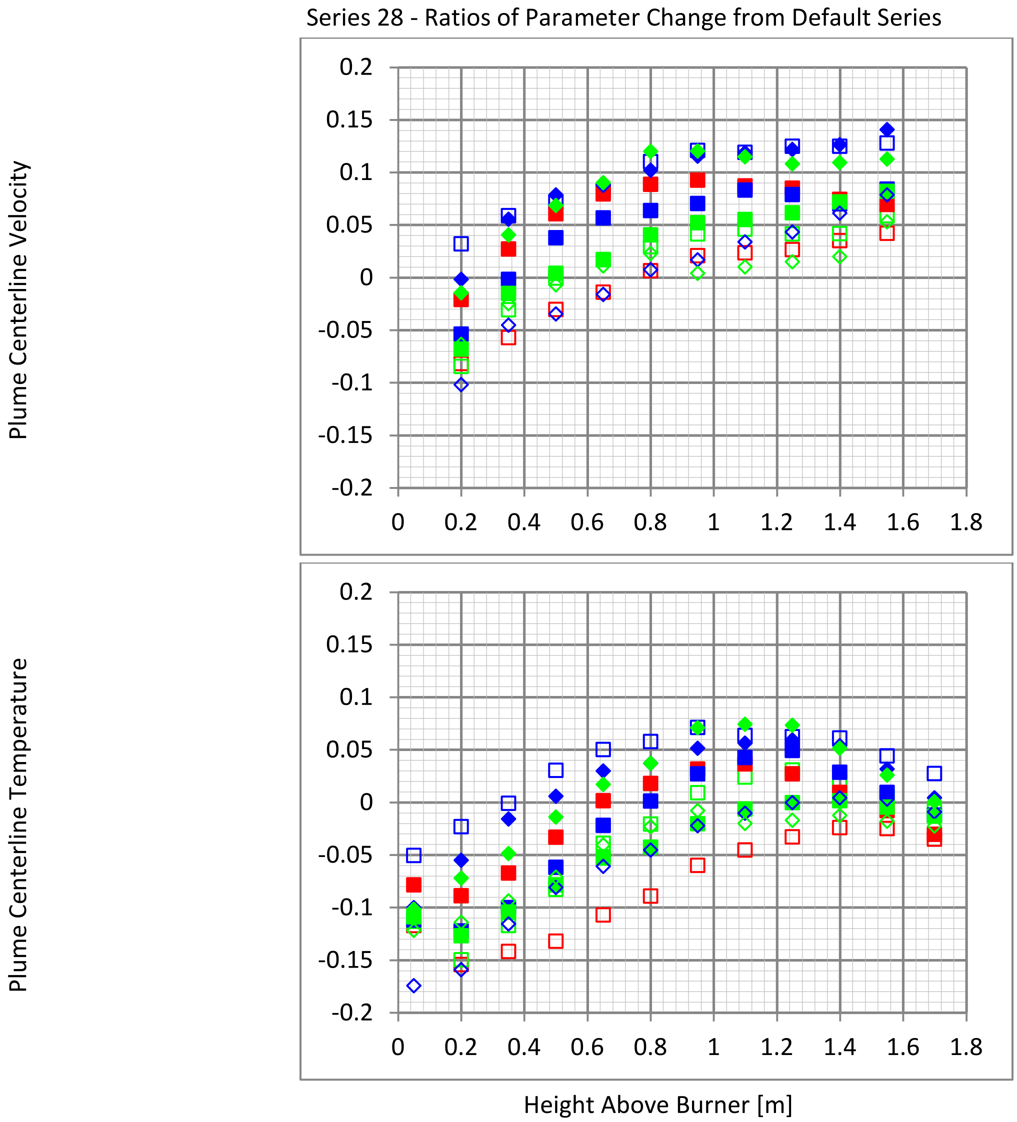

Legend

□ Propane-Sq-50 ✓	■ Propane-Sq-75 ✓	◇ Propane-Re-50 ✓	◆ Propane-Re-75 ✓
□ Propylene-Sq-50 ✓	■ Propylene-Sq-75 ✓	◇ Propylene-Re-50 ✓	◆ Propylene-Re-75 ✓
□ Methane-Sq-50 ☐	■ Methane-Sq-75 ✓	◇ Methane-Re-50 ×	◆ Methane-Re-75 ×

Observations

The baroclinic torque correction was disabled in the Series 28 models, this parameter determines properties of the vorticity in the flow calculations.

The change in velocity and temperature due to the disabled baroclinic torque correction model appear to be quite random, the changes occurred both positively and negatively across all models.

On average, the Series 28 models took about 2.5 hours to run, showing small increase in computational performance over the default series.

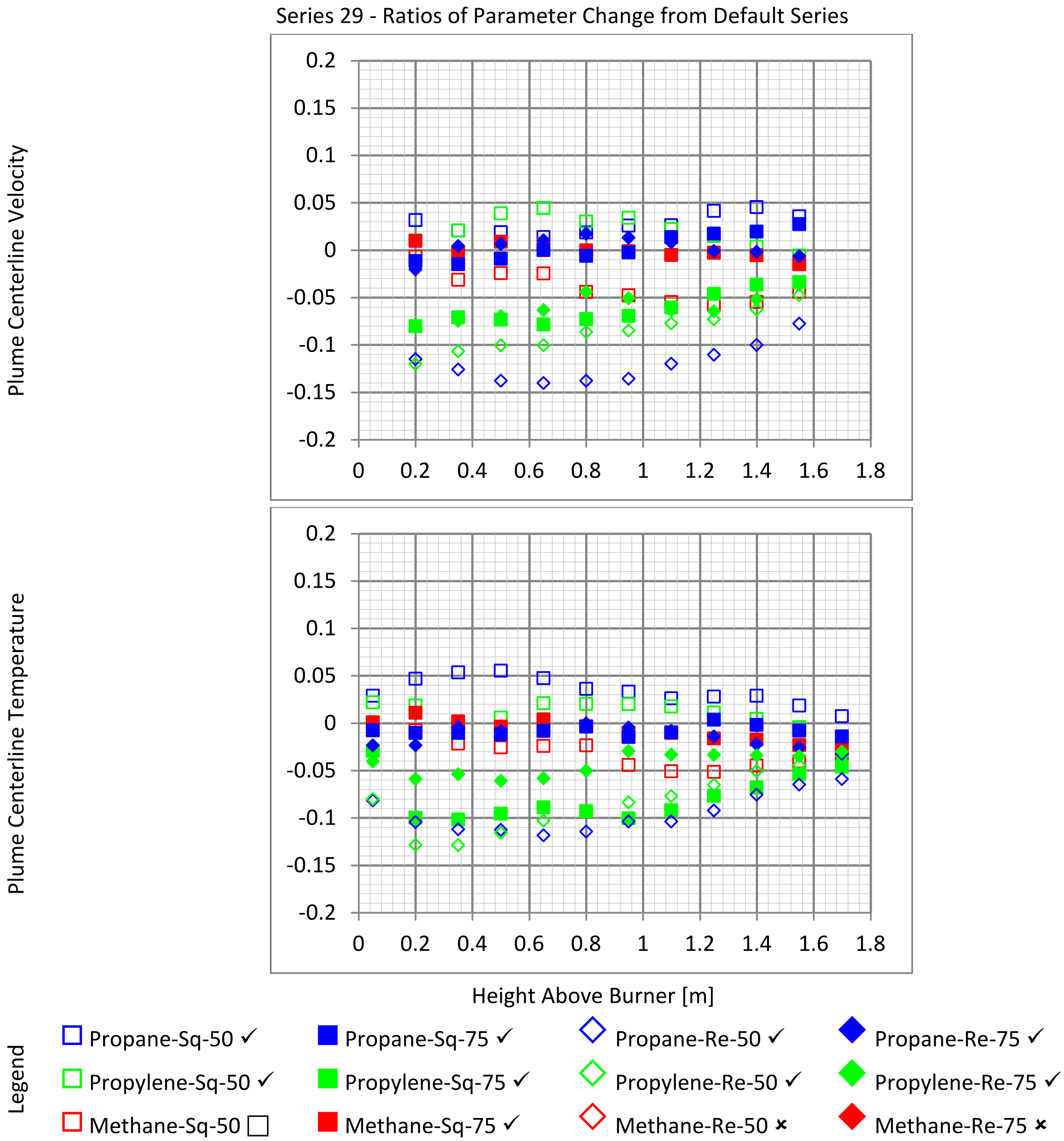

Observations

The CFL_MAX parameter controls the time step size used in a FDS simulation, at each time step, a CFL (Courant-Friedrichs-Lewy) number was calculated, and if the number is outside of the range set forth by the minimum and the maximum CFL constraints, then the time step size is adjusted. By increasing the CFL_MAX parameter from 1 to 2, the range was increased, allowing more flexibility in the time step size calculation, but might increase the chances for numerical instability.

Generally, increasing the CFL_MAX value has little effect to the predicted velocity and temperature values except for the cases involving the Rectangle burner or propylene. In these cases, the two predicted quantities were generally lowered.

On average, the Series 29 models took about 2hours to run, showing some increase in computational performance over the default series. The additional flexibility afforded in the time step sizing did not drastically increase the computational efficiency of FDS.

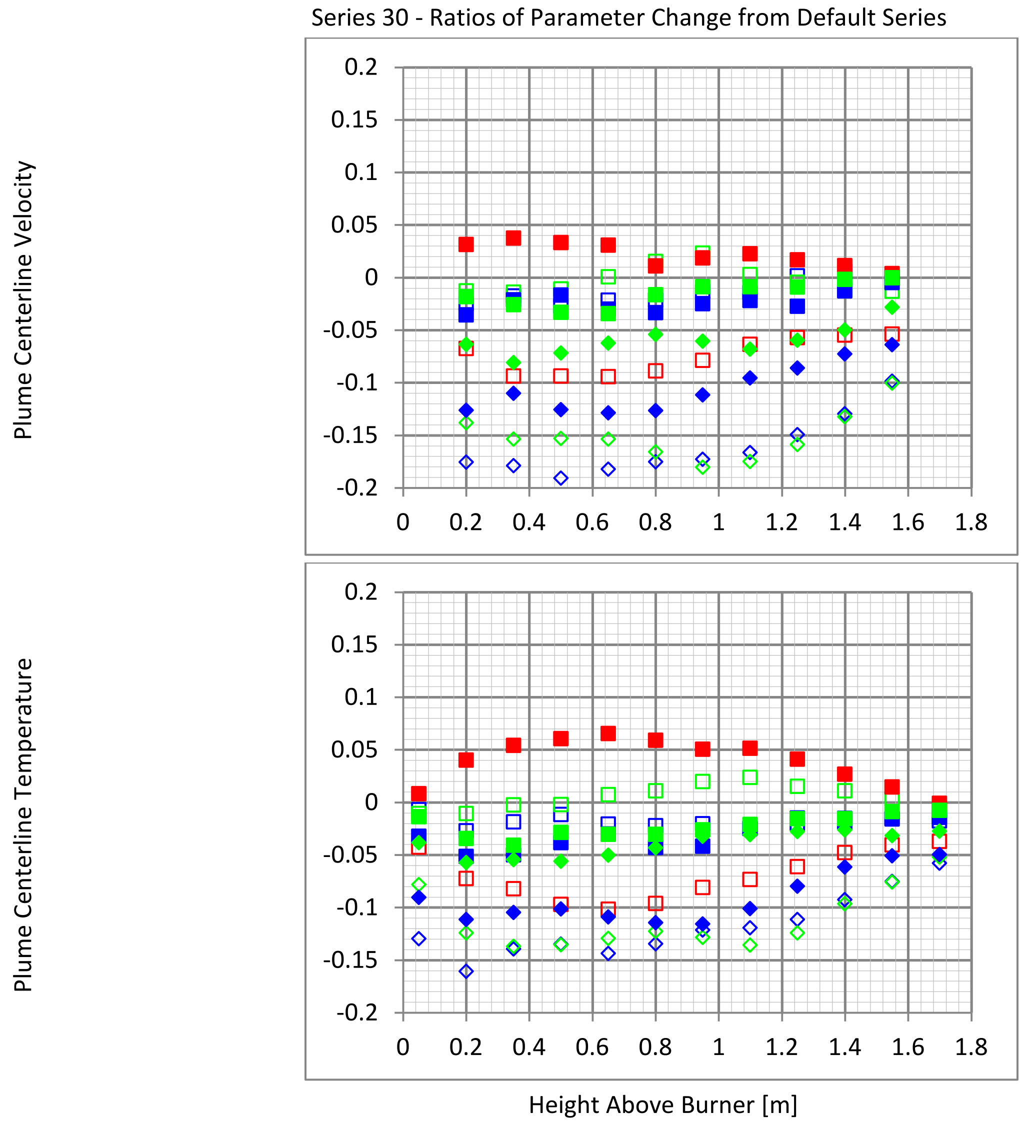

Legend

Propane-Sq-50 ✓	Propane-Sq-75 ✓	Propane-Re-50 ✓	Propane-Re-75 ✓
Propylene-Sq-50 ✓	Propylene-Sq-75 ✓	Propylene-Re-50 ✓	Propylene-Re-75 ✓
Methane-Sq-50 ☐	Methane-Sq-75 ✓	Methane-Re-50 ×	Methane-Re-75 ×

Observations

By decreasing the CFL_MIN parameter from 0.8 to 0.4, the range was increased, allowing more flexibility in the time step size calculation, but might increase the chances for numerical instability.

Generally, decreasing the CFL_MIN value has little effect to the predicted velocity and temperature values except for the cases involving the Rectangle burner or methane. In these cases, the two quantities were generally lowered, except for the methane Square burner at 75 kW model.

On average, the Series 30 models took about 3 hours to run, showing very little increase in computational performance over the default series. The additional flexibility afforded in the time step sizing did not drastically increase the computational efficiency of FDS.

Compared to Series 29, decreasing the CFL_MIN constraint appears to slow down the simulation.

Series 31 - Ratios of Parameter Change from Default Series

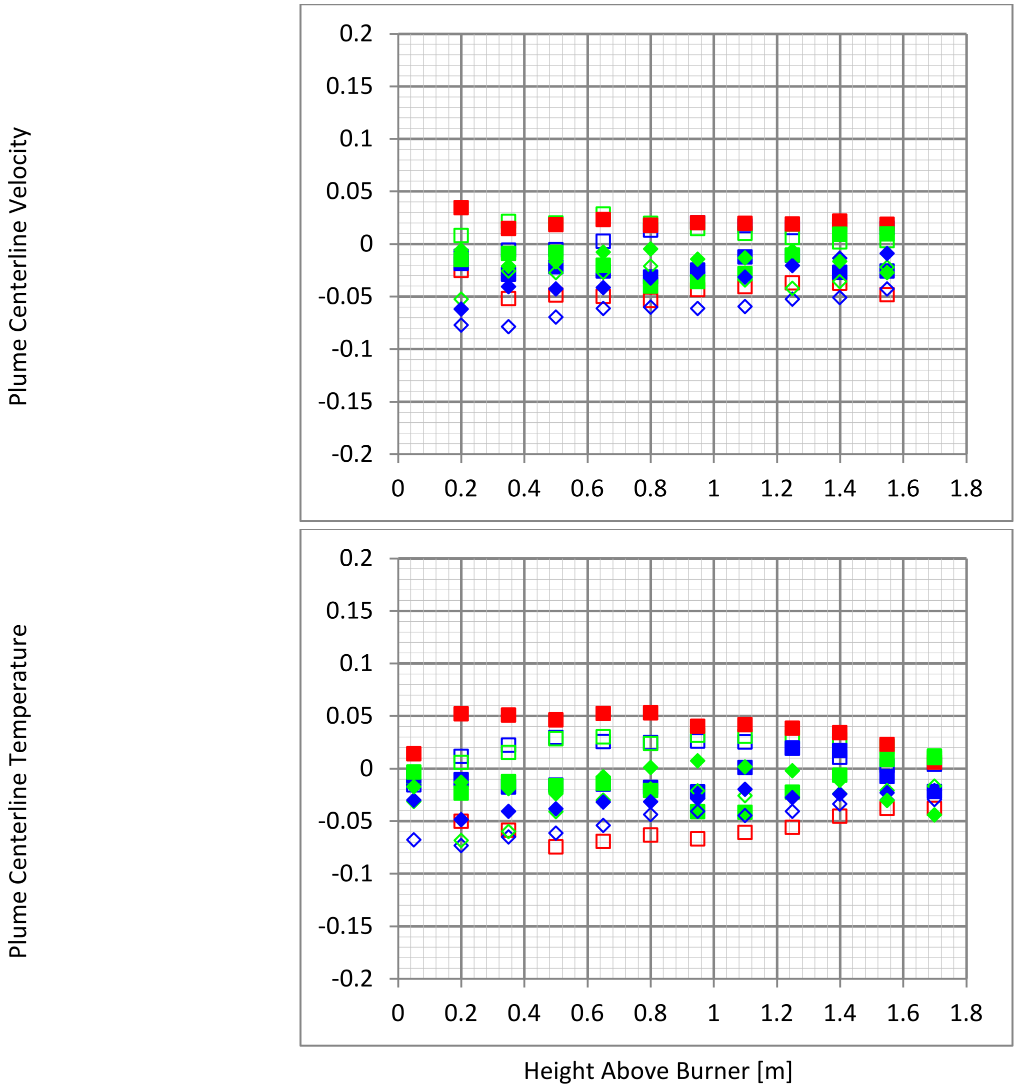

Legend

Propane-Sq-50 ✓	Propane-Sq-75 ✓	Propane-Re-50 ✓	Propane-Re-75 ✓
Propylene-Sq-50 ✓	Propylene-Sq-75 ✓	Propylene-Re-50 ✓	Propylene-Re-75 ✓
Methane-Sq-50 ☐	Methane-Sq-75 ✓	Methane-Re-50 ×	Methane-Re-75 ×

In Series 31, the range between the max and min CFL was further increased to 2 and 0.4, respectively, to test their effects.

Observations

The deviation predicted in the Series 31 models appears to be smaller than those found in the Series 29 and 30 models where the range of CFL was increased to one side only. This shows that increasing the CFL range does not drastically increase the deviation unless the change to the CFL parameters is biased.

On average, the Series 31 models took about 4 hours to run, basically no improvement on computational performance the default series. The additional flexibility afforded in the time step sizing did not drastically increase the computational efficiency of FDS.

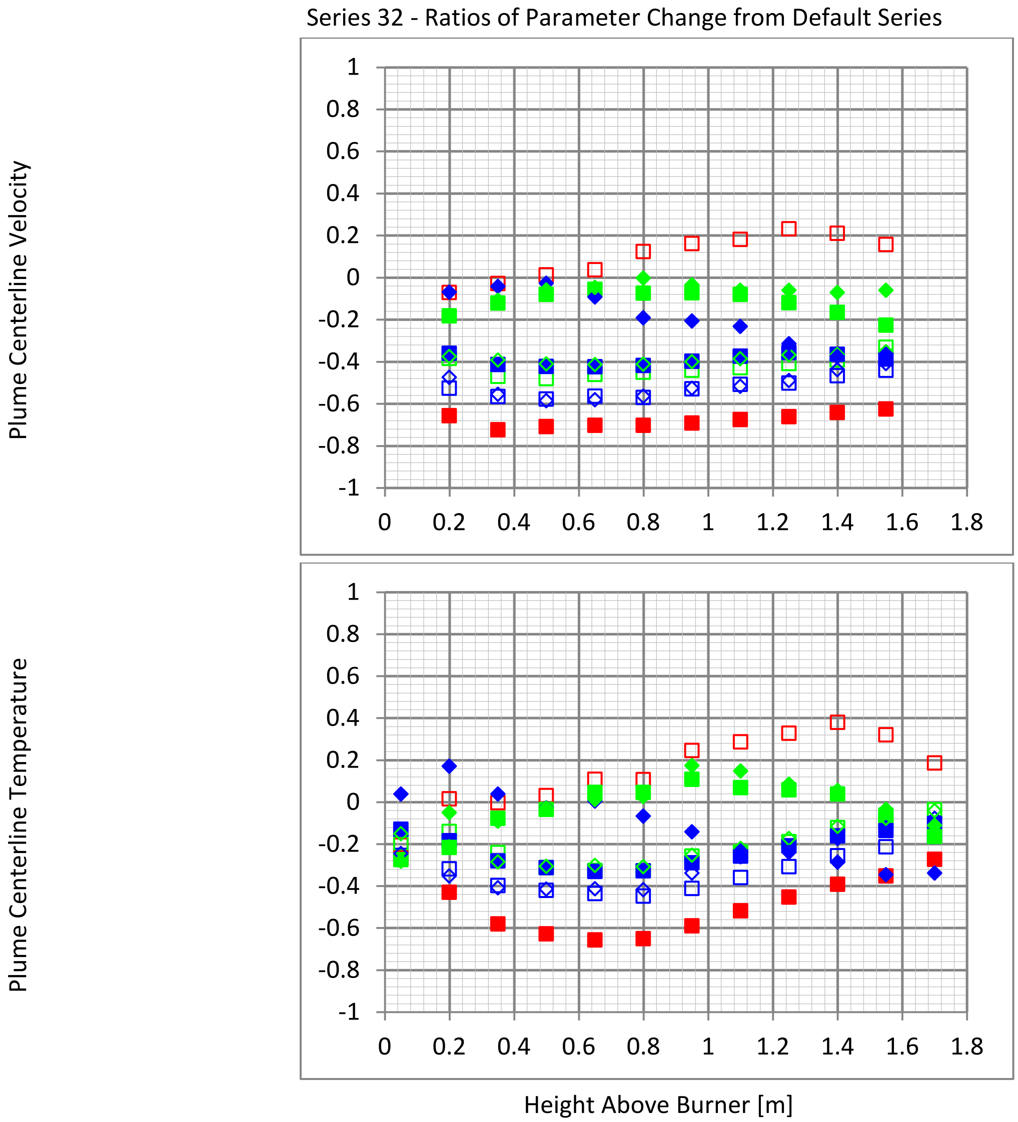

Legend

Propane-Sq-50 ✓	Propane-Sq-75 ✓	Propane-Re-50 ✓	Propane-Re-75 ✓
Propylene-Sq-50 ✓	Propylene-Sq-75 ✓	Propylene-Re-50 ✓	Propylene-Re-75 ✓
Methane-Sq-50 ☐	Methane-Sq-75 ✓	Methane-Re-50 ✗	Methane-Re-75 ✗

Observations

The FLUX_LIMITER parameter is a FDS6 parameter that changes the way the finite difference calculations are set up. The FDS default is to use a central differencing method with boundedness correction applied if the scalar goes out of the range between 0 and 1. In Series 32, flux limiter is set to 2, which uses the Superbee scheme, suitable for LES simulations.

The deviations predicted in Series 32 are very random and large in magnitude. However, 9 out of 10 of the plume fire simulations in Series 32 crashed due to numerical instability, suggesting that the FDS's default setting for the FLUX_LIMITER parameter may be more appropriate for the current application.

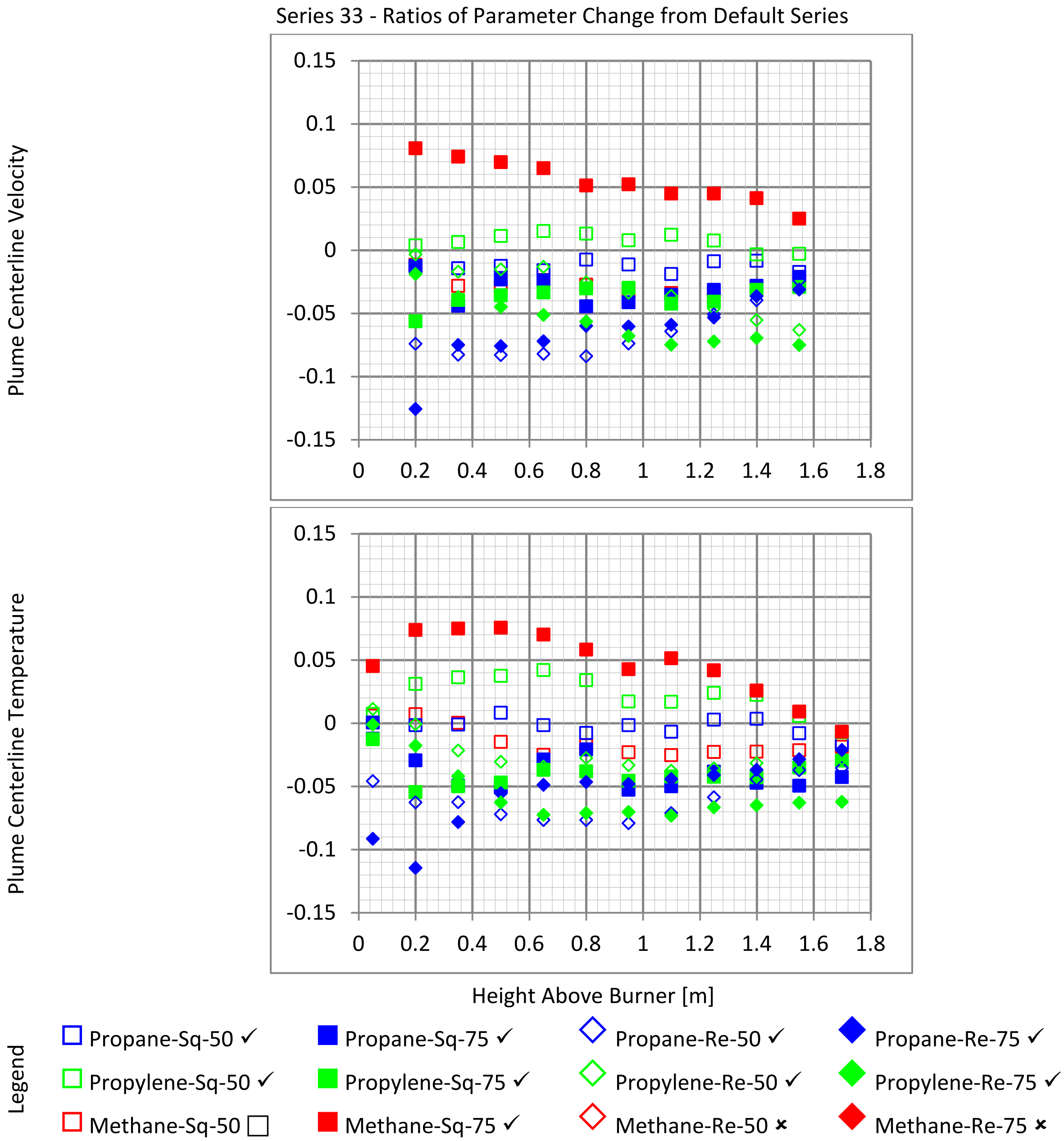

Observations

The CFL_VELOCITY_NORM parameter is a FDS6 parameter that controls the time step sizing. The use of CFL_VELOCITY_NORM=2 in the Series 33 simulations makes the time step sizing more restrictive than the default.

The results from Series 33 show that the parameter change created deviation in the predicted temperature and velocity in quite a random fashion, but mostly decreasing both quantities except for the methane with Square burner at 75 kW model.

On average, the Series 33 models took about 2 hours to run, showing an increase in computational efficiency.

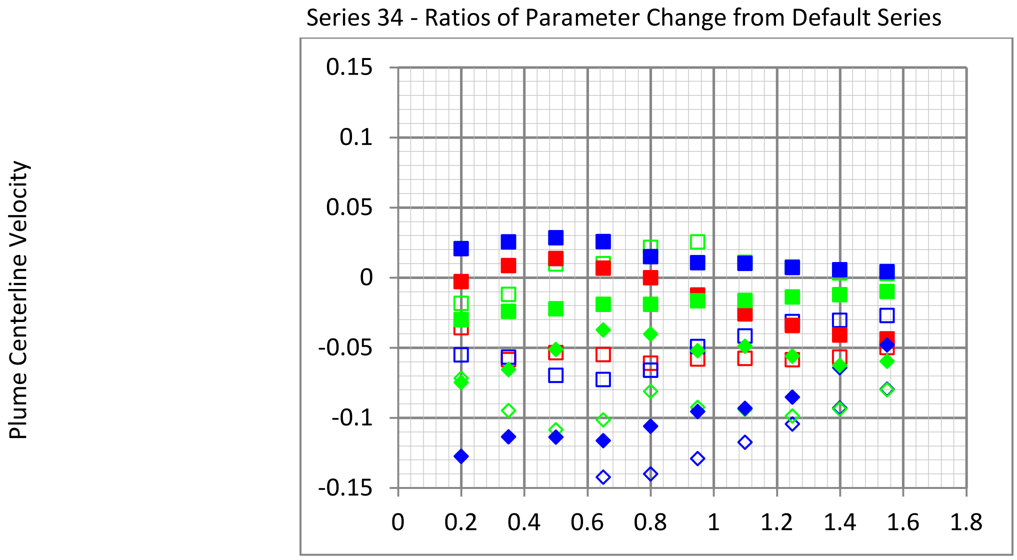

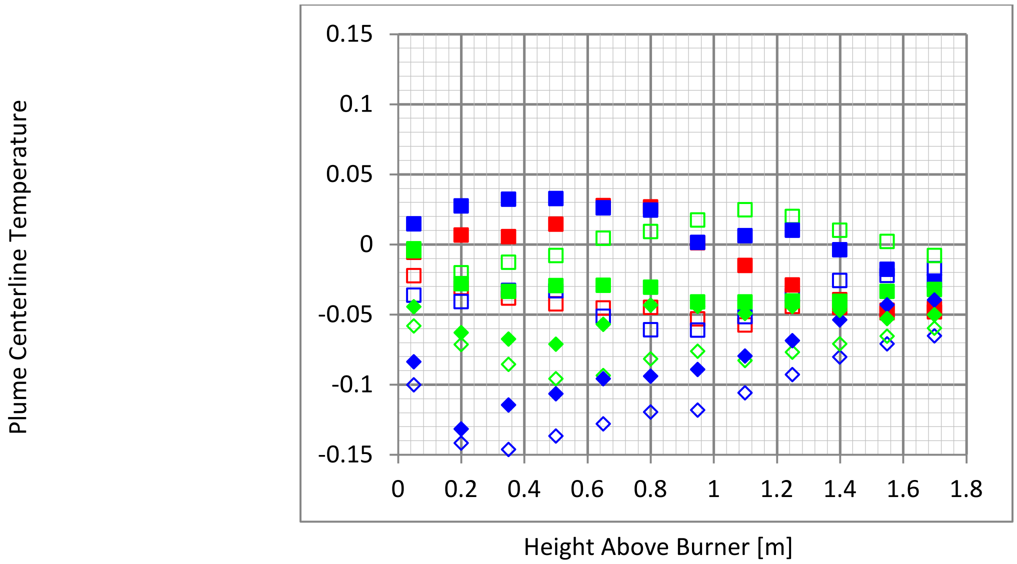

Legend

Propane-Sq-50 ✓	Propane-Sq-75 ✓	Propane-Re-50 ✓	Propane-Re-75 ✓
Propylene-Sq-50 ✓	Propylene-Sq-75 ✓	Propylene-Re-50 ✓	Propylene-Re-75 ✓
Methane-Sq-50 ☐	Methane-Sq-75 ✓	Methane-Re-50 ✗	Methane-Re-75 ✗

Observations

The CFL_VELOCITY_NORM parameter is a FDS6 parameter that controls the time step sizing. The Use of CFL_VELOCITY_NORM=0 makes the time step sizing less restrictive than the default.

The results from Series 34 show that the parameter change generally has a larger impact on fire with a lower HRR, opposite from that of Series 33. However, the deviations generated still seem to be quite random.

On average, the Series 34 models took about 2 hours to run, showing an increase in computational efficiency.

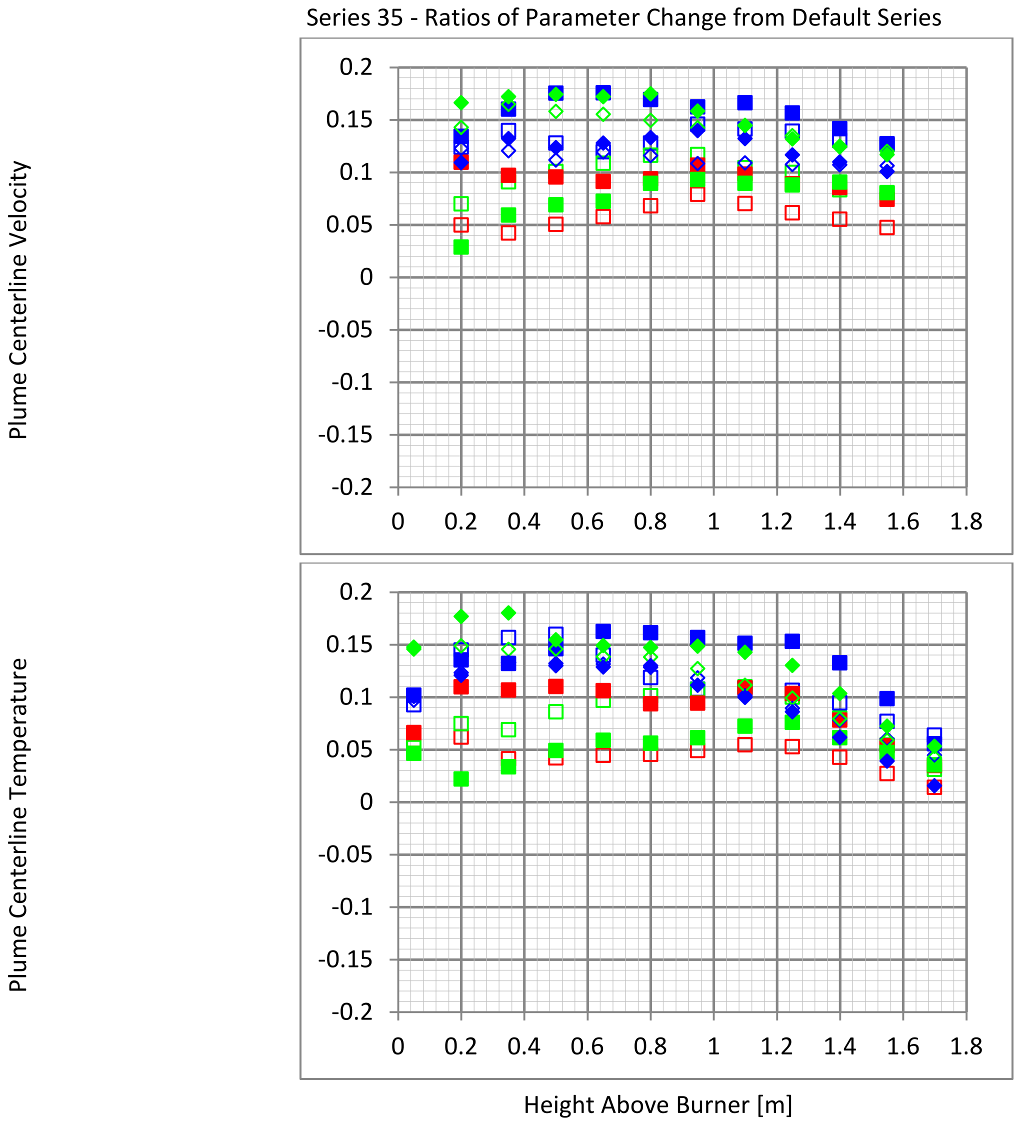

Legend

Propane-Sq-50 ✓	Propane-Sq-75 ✓	Propane-Re-50 ✓	Propane-Re-75 ✓
Propylene-Sq-50 ✓	Propylene-Sq-75 ✓	Propylene-Re-50 ✓	Propylene-Re-75 ✓
Methane-Sq-50 ☐	Methane-Sq-75 ✓	Methane-Re-50 ×	Methane-Re-75 ×

Observations

When the H_EDDY parameter is disabled in Series 35 simulations, the FDS default convective heat transfer model is used instead of the turbulent convective heat transfer model.

The results from Series 35 show that using the FDS default convective heat transfer model, the plume centerline temperature and velocity are raised.

On average, the Series 35 models took about 2.5 hours to run, showing an increase in computational efficiency.

Appendix L FDS Parametric Study Results [Inert Wall]

Varying the FDS parameters that govern the CFD simulation characteristics changed the behaviors of the model to different degrees. The predictive capabilities and the performance of the model are both affected by parameter changes; and to understand the relationships between the cause (parameter change) and the results (predictions and performance) is of great importance to end-users so that simulations can be conducted effectively and efficiently. A systemic approach to varying some notable parameters in FDS individually was undertaken using all three configurations of fire models in this study. The default cases used mostly FDS default parameters, and in each iteration, only one parameter was varied from the default set. Some parameters from the MISC, RADI, REAC, and TIME groups were changed during this exercise. Comparisons of the outputs and performance of successive series of models were made against the default cases. The list of parameters changed in the study is presented in Table 1.

Table 1 - Variable simulation parameters

Series	Parameter Group	Parameter change	Default Value	New value in simulation	Change from default
0	FDS6	DYNSMAG	.TRUE.	.FALSE.	x
1	N/A	No change, Default situation using default FDS6 options			
2	MISC	RADATION	.TRUE.	.FALSE.	x
3	RADI	RADIATIVE FRACTION	0.30	Source fire specific	varies
4	RADI	RADIATIVE FRACTION	0.30	0.1	~33%
5	RADI	RADIATIVE FRACTION	0.30	0.2	~50%
6	RADI	RADIATIVE FRACTION	0.30	0.5	~160%
7	RADI	WIDE_BAND_MODEL	.FALSE.	.TRUE	x
8	RADI	NUMBER_RADIATION_ANGLES	104	52	50%
9	RADI	NUMBER_RADIATION_ANGLES	104	208	200%
10	RADI	ANGLE_INCREMENT	5	2	50%
11	RADI	ANGLE_INCREMENT	5	10	200%
12	RADI	TIME_STEP_INCREMENT	3	1	50%
13	RADI	TIME_STEP_INCREMENT	3	6	200%
~~14~~	~~Skipped~~				
15	REAC	C_EDC	0.1	0.2	50%
16	REAC	C_EDC	0.1	0.05	200%
17	REAC	EDDY_DISSIPATION	.TRUE.	.FALSE.	x
18	REAC	HRRPUA_SHEET	0	400	40000%
19	REAC	HRRPUA_SHEET	0	100	10000%
20	REAC	HRRPUV_AVERAGE	3000	1200	40%
21	MISC	ISOTHERMAL	.FALSE.	.TRUE	x
22	MISC	CSMAG	0.2	0.1	50%
23	MISC	CSMAG	0.2	0.4	200%
24	MISC	PR	0.5	0.25	50%

Series	Parameter Group	Parameter change	Default Value	New value in simulation	Change from default
25	MISC	PR	0.5	1	200%
26	MISC	SC	0.5	0.25	50%
27	MISC	SC	0.5	1	200%
28	MISC	BAROCLINIC	.TRUE.	.FALSE.	x
29	MISC	CFL_MAX	1	2	200%
30	MISC	CFL_MIN	0.8	0.4	50%
31	MISC	CFL_MAX and CFL_MIN	1 / 0.8	2 / 0.4	x
32	FDS6	FLUX_LIMITER	2	-1	x
33	FDS6	CFL_VELOCITY_NORM	1	2	x
34	FDS6	CFL_VELOCITY_NORM	1	0	x
35	FDS6	H_EDDY	.TRUE.	.FALSE.	x

The variable parameters and their functions are described in this section. Many of the parameters have an effect on the stability and the performance of the model by changing the amount or complexity of the calculations performed by the FDS software. Moreover, some of the parameters can also affect the predicted fire behaviors and change the various quantities predicted by FDS.

1) RADI parameters
   a) **RADIATIVE_FRACTION**
      i) Determines the fraction of combustion energy released in the model as thermal radiation
      ii) Default simulations used a value of 0.30
      iii) Parametric study used the radiative fraction values of the fuel modeled: methane at 0.141, propane at 0.286, and propylene at 0.368
   b) **WIDE_BAND_MODEL**
      i) Determine whether the six band wide band gray gas model is assumed and used in the simulation
      ii) Default simulations disables the six band model method
      iii) Parametric study simulations had the six band model enabled
   c) **NUMBER_RADIATION_ANGLES**
      i) Number of solid angles used in radiation calculations, not compatible if radiation transport calculations are disabled elsewhere in the input file
      ii) Default simulations used 104 solid angles for calculations
      iii) Parametric study simulations used 52 and 208 solid angles
   d) **ANGLE_INCREMENT**
      i) Number of solid angles skipped per update of radiation calculations
      ii) Default simulations used the default FDS value of 5
      iii) Parametric study simulations used values of 2 and 10
   e) **TIME_STEP_INCREMENT**
      i) Number of time steps skip per update of radiation calculations
      ii) Default simulations used the default FDS value of 3
      iii) Parametric study simulations used values of 1 and 6

2) REAC parameters
   a) **C_EDC**
      i) Coefficient to calculate mixing time scale of fuel and oxygen within the grid cells used in the turbulent combustion calculations
      ii) Default simulations used a value of 0.1 for the coefficient, determined based on comparison to flame height correlations[*6*]
      iii) Parametric study simulations used 0.05 and 0.2 solid angles
   b) **EDDY_DISSIPATION**
      i) Determines whether the default heat release rate calculation model based on the default mixture time scale method is used
      ii) Default simulations enabled the eddy dissipation to be determined
      iii) Parametric study enabled the eddy dissipation
   c) **HRRPUA_SHEET**
      i) Max HRRPUA of a flame sheet, acts as a bound of local HRRPU-volume
      ii) Default simulations used a default value of 0kW/m^2 for LES
      iii) Parametric study used values at 100 kW/m^2 and 400 kW/m^2, these are chosen based on the value of 200 kW/m^2 as default for the DNS mode (not used in these simulations)
   d) **HRRPUV_AVERAGE**
      i) Average volumetric HRR of a fire, bounds local HRRPU-volume value
      ii) Default simulations used a default value of 3000 kW/m^3
      iii) Parametric study used values at 1200 kW/m^3, as suggested by Orloff and De Ris[*6*]
3) MISC parameters
   a) **CFL_MAX and CFL_MIN**
      i) Numerical stability parameters that limit the time step sizing by imposing limits on the Courant-Friedrichs-Lewy (CFL) number that is calculated within each timestep: if the number is outside of the range, then the time step size is adjusted
      ii) Default simulations set the max value at 1 and the min value at 0.8
      iii) Several combinations of CFL limits are tested in the parametric study as follow: [2, 0.8], [1, 0.4], and [2, 0.4]
   b) **ISOTHERMAL**
      i) Set the calculations to ignore any changes in temperature or radiation heat transfer, also automatically turn off radiation transport model as well
      ii) Default simulations disabled the isothermal option
      iii) Parametric study enabled the isothermal option
   c) **CSMAG**
      i) Smagorinsky constant used to calculate the viscosity, usually more stable if a small value is used
      ii) Default simulations used a default value of 0.2, justified through comparisons with experimental data[*7*]
      iii) Parametric study used values at 0.1 and 0.4
   d) **PR**
      i) Turbulent Prandtl number, a ratio of momentum diffusivity to thermal diffusivity, related to turbulent viscosity in LES simulations

ii) Default simulations used FDS's default value of 0.5, justified through comparisons with experimental data[7]
iii) Parametric study used values at 0.25 and 1

e) SC

i) Turbulent Schmidt number, a ratio of momentum diffusivity to mass diffusivity, related to turbulent viscosity in LES simulations
ii) Default simulations used FDS's default value of 0.5, justified through comparisons with experimental data[7]
iii) Parametric study used values at 0.25 and 1

f) BAROCLINIC

i) Enables the baroclinic vorticity correction calculations that can changes the properties in the turbulence calculations and may affect the plume shape significantly
ii) Default simulations enables the baroclinic correction
iii) Parametric study disabled the correction calculations

g) RADIATION

i) Turns On or Off radiation transport calculations in the simulations
ii) Default simulation use the radiation transport model, as in real life
iii) Parametric study disabled the radiation transport calculations

4) FDS6 parameters

a) FLUX_LIMITER

i) Changes the finite volume discretization scheme used in simulations
ii) Default simulations use the Superbee scheme, suitable for LES simulations
iii) Parametric study used a central differencing scheme with boundedness correction applied

b) DYNSMAG

i) Turns on/off variable density formulation of dynamic Smagorinsky model
ii) Default simulation use the dynamic Smagorinsky model
iii) Parametric study disabled the dynamic Smagorinsky model

c) CFL_VELOCITY_NORM

i) Normalization of CFL velocity, controls the time step sizing within a simulation
ii) FDS default uses a moderate time step sizing control
iii) Parametric study tested for the effects due to an increase and decrease of the time step sizing control

d) H_EDDY

i) Enables the eddy-diffusivity model to use a turbulent convective heat transfer model
ii) Default simulations has the eddy diffusivity model enabled
iii) Parametric study disabled eddy diffusivity model

L.1 Sensitivity Coefficients

To identify the parameters that yield significant changes to specific predicted quantities, the concept of "sensitivity coefficients" was employed. Each coefficient was determined based on the changes in one of the three recorded quantities (plume centerline temperature, plume centerline velocity, and centerline gauge heat flux) and of the FDS parameter over their baseline values. The coefficient is based on the ratios of change, and is found using equation [1.1]:

$$\left(\frac{Quantity_{new} - Quantity_{baseline}}{Quantity_{baseline}}\right) \bigg/ \left(\frac{Parameter_{new} - Parameter_{baseline}}{Parameter_{baseline}}\right) \qquad [0.1]$$

Where "Quantity" denotes the recorded quantities in the model (velocity, temperature, gauge heat flux), and the "Parameter" denotes the model inputs (RADIATIVE_FRACTION, SC, etc)

Equation [1.1] was applied to the steady-state, time-averaged FDS results of plume centerline temperature, velocity, and gauge heat flux at different heights from the inert wall fire simulations. For the "toggle" parameters, if a parameter is turned "ON" or "TRUE", the nondimensional parameter change is assumed to be "+1", and if the parameter is turned "OFF" or "FALSE", then the nondimensional parameter change is assumed to be "-1", this is necessary for the sensitivity coefficients be calculated for the "toggle" parameters since they do not have any numerical values.. Regardless of the parameter type, a sensitivity coefficient is calculated for each quantity at each "measuring" location, and then they are averaged. The coefficients can then be used to represent the significance and effects of the parameter change for each of the predicted quantities.

Non-toggle parameters such as radiative fraction, Prandtl number, and the average HRRPUV of the fire dominate the changes of the measured temperature, velocity, and gauge heat flux to wall along the plume centerline in the simulations. These parameters contribute to the structure of the plume, and the amount of heat output of the fire, all related to the plume characteristics and the heat flux to wall.

For the toggled parameter studied, the ones with the greatest changes include: isothermal model, CFL velocity normalization, eddy diffusivity model, the dynamic Smagorinsky model, and the baroclinic vorticity calculations. All these parameter contributes to the stability and structure of the flow field, which are especially important factors that describe the interaction between the plume and the solid wall. Isothermal simulations forces the no temperature change within the model, and turning off the radiation model prevents radiative heat transfer, both limiting changes in the plume temperature and heat flux to the wall to be properly calculated. The flux limiter, which controls the calculations scheme used in the calculations, is consistently one of the greatest contributors to quantity changes because the simulations all crashed due to numerical instability.

Additionally, the results from the parametric study show that simulations with Square burner or the higher HRR at 75 kW are more greatly affected by the parameter changes than their counterparts, which is opposite to the trend from the plume simulations. Effects on the three different source fuels appear to be relatively similar.

L.1.1 Fuel Type

This section presents the sensitivity coefficients generated from the various simulations as grouped by the fuel type: methane, propane, or propylene. The parameters and their variances that generated sensitivity coefficients ≥ 0.1 are considered significant. Each sensitivity coefficient was based on one of the predicted quantities, and was averaged over height and across those simulations using identical fuel types regardless of the scenario, burner shape, and base HRR. The results from the toggle parameters are located at the bottom of the charts, and the parameter change that correlates with the overall maximum sensitivity coefficients are presented first.

Figure 1 shows the sensitivity coefficients based on the predicted plume centerline velocity averaged over inert wall simulations using the same fuel type. The parameters that created the most significant changes to the plume velocity are the radiative fraction, as well as the when the isothermal mode was used, which calculation scheme used based on the value of the flux limiter, and whether the radiation model is activated.

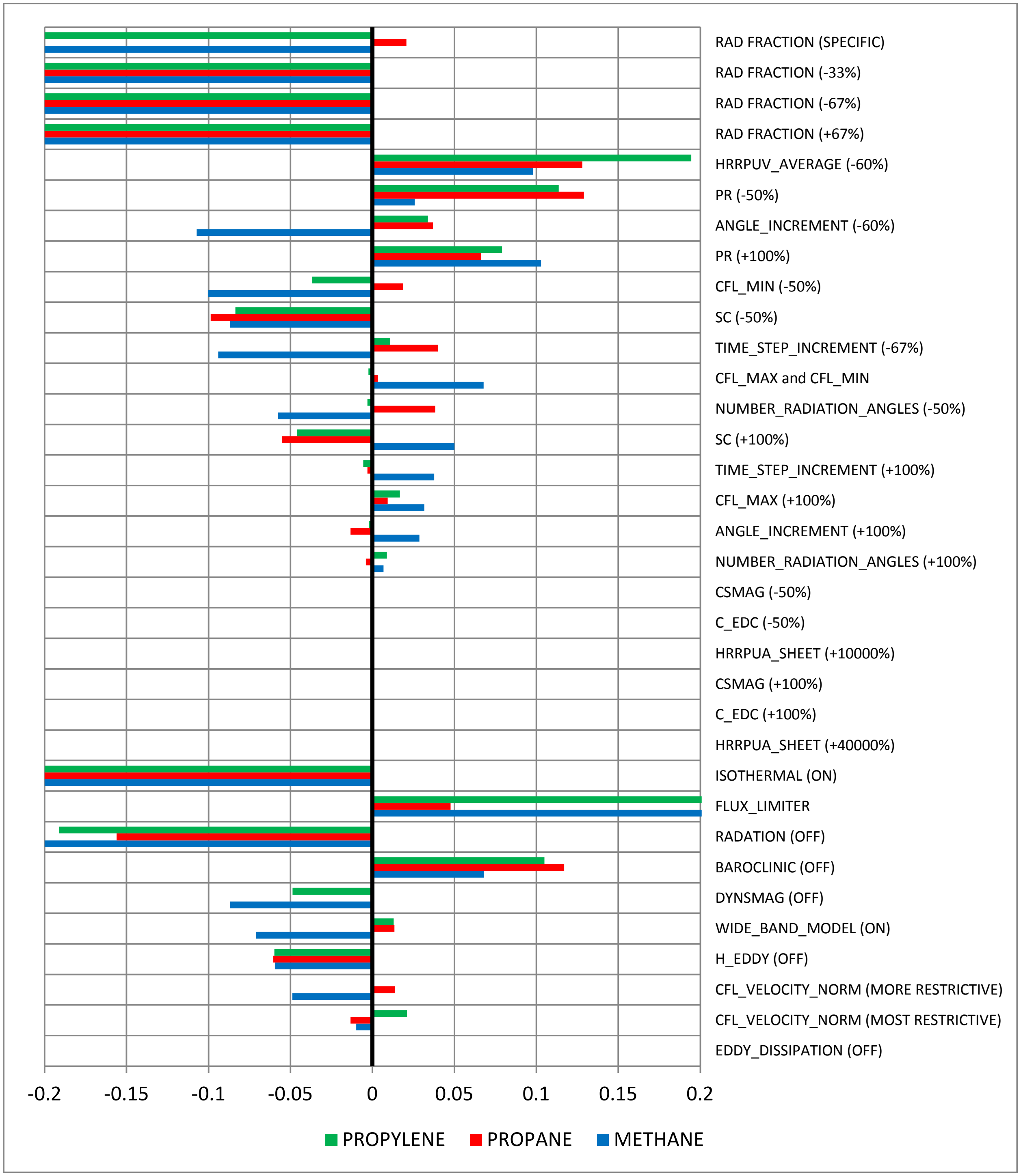

Figure 1 – Plume velocity sensitivity coefficients, grouped by fuel type

Figure 2 shows the sensitivity coefficients based on the predicted plume centerline velocity averaged over simulations with consistent fuel type. The parameters that created the most significant changes to the plume temperature are the radiative fraction, as well as the when the isothermal mode was used, which calculation scheme used based on the value of the flux limiter, and whether the dynamic Smagorinsky model is activated.

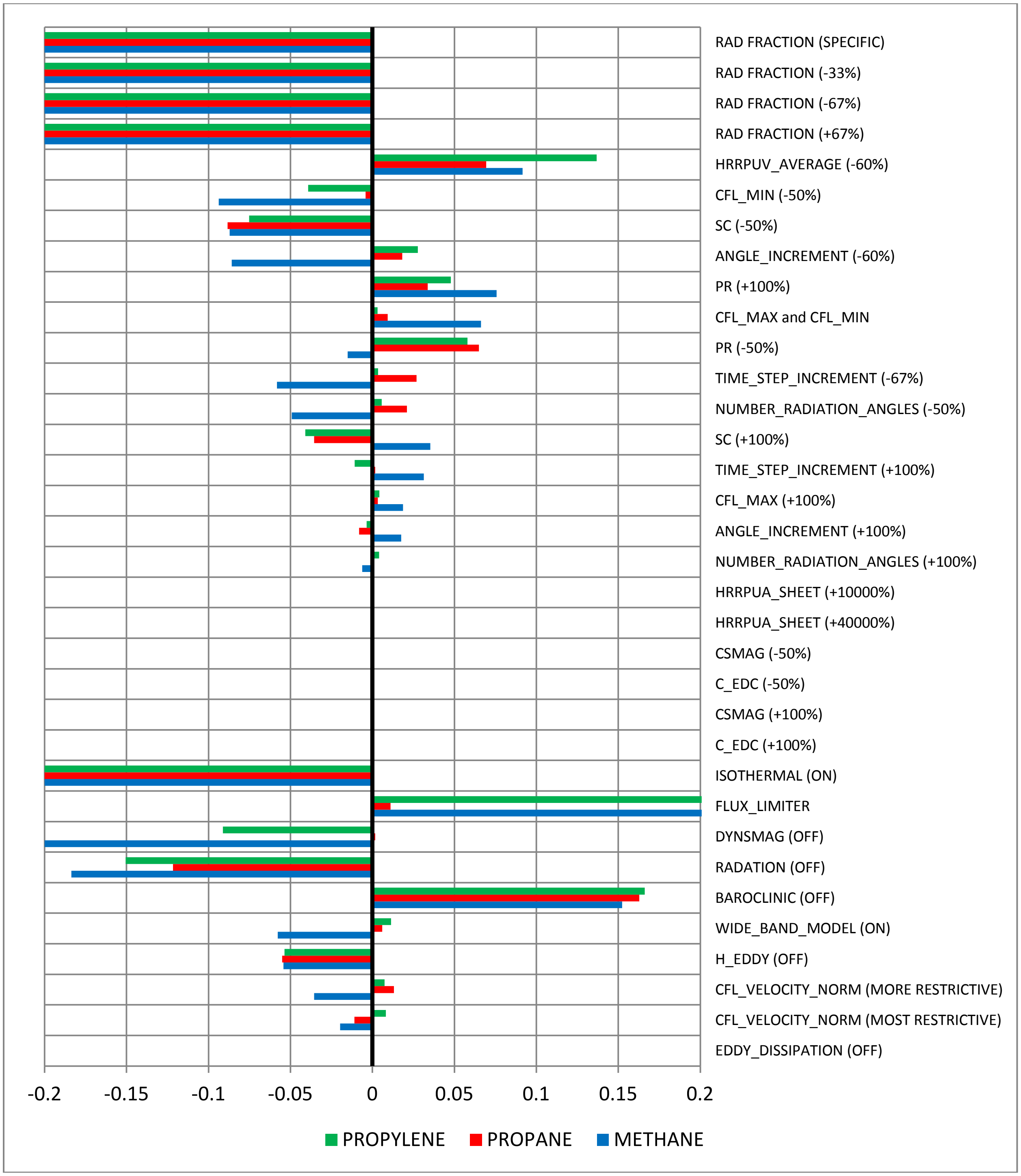

Figure 2 – Plume temperature sensitivity coefficients, grouped by fuel type

Figure 3 shows the sensitivity coefficients based on the predicted centerline gauge heat flux to wall averaged over simulations with consistent fuel type. The parameters that contributed to the most significant changes to the gauge heat flux are the Prandtl number, the radiative fraction, the decrease of the HRRPUV of the fire, whether the dynamic Smagorinsky model is activated, when the isothermal mode was used, which calculation scheme used based on the value of the flux limiter, if the eddy diffusivity model is turned off, and whether the radiation model is activated.

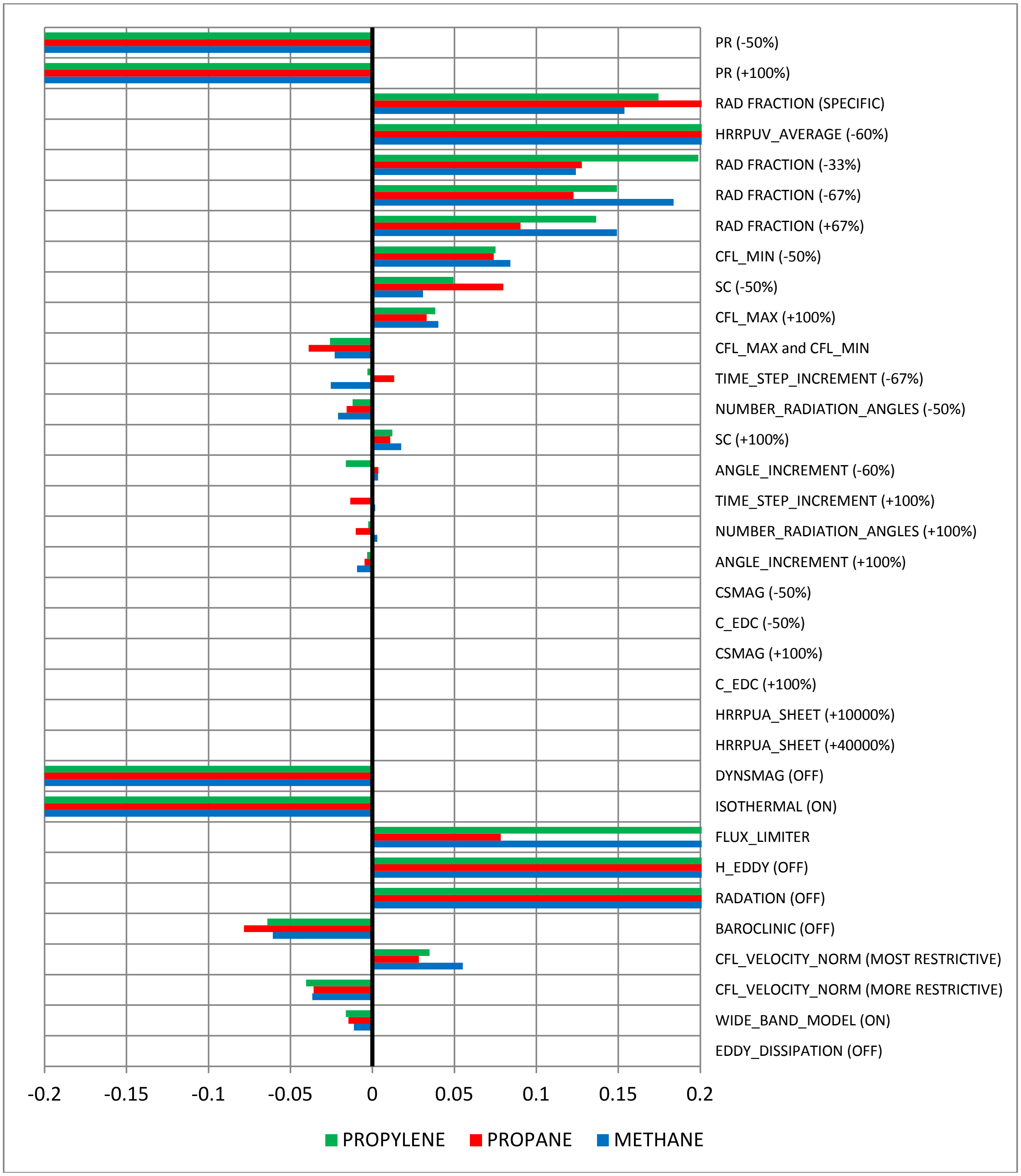

Figure 3 – Centerline gauge heat flux to wall sensitivity coefficients, grouped by fuel type

Table 2 - Sensitivity coefficients based on source fuel type

Parameter change	Default Value	New Value	METHANE			PROPANE			PROPYLENE		
			Velocity	Temp	GHF	Velocity	Temp	GHF	Velocity	Temp	GHF
DYNSMAG (OFF)	.TRUE.	.FALSE.	-0.0868	-0.2020	-2.8653	-0.0005	0.0017	-2.8738	-0.0487	-0.0912	-2.8490
RADIATION (OFF)	.TRUE.	.FALSE.	-0.2210	-0.1837	0.4409	-0.1561	-0.1216	0.3557	-0.1912	-0.1505	0.4054
WIDE_BAND_MODEL (ON)	.FALSE.	.TRUE	-0.0709	-0.0577	-0.0114	0.0134	0.0060	-0.0147	0.0129	0.0114	-0.0163
EDDY_DISSIPATION (OFF)	.TRUE.	.FALSE.	0.0000	0.0000	0.0000	0.0000	0.0000	-0.0001	0.0000	0.0000	-0.0001
ISOTHERMAL (ON)	.FALSE.	.TRUE	-0.7919	-0.8509	-0.9987	-0.9353	-0.7815	-0.9984	-0.9644	-0.8144	-0.9985
BAROCLINIC (OFF)	.TRUE.	.FALSE.	0.0679	0.1523	-0.0608	0.1170	0.1628	-0.0784	0.1048	0.1662	-0.0641
FLUX_LIMITER	2	-1	0.9582	0.7708	0.9576	0.0477	0.0110	0.0783	0.3461	0.2173	0.2964
CFL_VELOCITY_NORM (MOST RESTRICTIVE)	1	2	-0.0099	-0.0198	0.0551	-0.0134	-0.0110	0.0283	0.0210	0.0081	0.0348
CFL_VELOCITY_NORM (MORE RESTRICTIVE)	1	0	-0.0490	-0.0355	-0.0367	0.0137	0.0131	-0.0359	0.0001	0.0074	-0.0405
H_EDDY (OFF)	.FALSE.	.TRUE.	-0.0595	-0.0543	0.5853	-0.0605	-0.0551	0.6277	-0.0598	-0.0536	0.5978
RAD FRACTION (SPECIFIC)	0.3	Source fire specific	-0.4237	-0.5055	0.1537	0.0207	-0.2645	0.3014	-0.5716	-0.5673	0.1745
RAD FRACTION (-67%)	0.3	0.1	-0.3377	-0.4220	0.1837	-0.3154	-0.3633	0.1226	-0.3541	-0.3920	0.1492
RAD FRACTION (-33%)	0.3	0.2	-0.4481	-0.5157	0.1240	-0.2995	-0.3555	0.1278	-0.2950	-0.3250	0.1988
RAD FRACTION (+67%)	0.3	0.5	-0.2401	-0.3124	0.1492	-0.3293	-0.3281	0.0904	-0.3008	-0.3287	0.1365
NUMBER_RADIATION_ANGLES (-50%)	104	52	-0.0577	-0.0492	-0.0211	0.0383	0.0211	-0.0158	-0.0031	0.0056	-0.0121
NUMBER_RADIATION_ANGLES (+100%)	104	208	0.0068	-0.0063	0.0030	-0.0040	-0.0002	-0.0102	0.0089	0.0040	-0.0026
ANGLE_INCREMENT (-60%)	5	2	-0.1073	-0.0859	0.0035	0.0369	0.0181	0.0036	0.0339	0.0277	-0.0163
ANGLE_INCREMENT (+100%)	5	10	0.0287	0.0176	-0.0094	-0.0133	-0.0082	-0.0048	-0.0022	-0.0036	-0.0032
TIME_STEP_INCREMENT (-67%)	3	1	-0.0941	-0.0583	-0.0255	0.0399	0.0268	0.0133	0.0109	0.0034	-0.0030
TIME_STEP_INCREMENT (+100%)	3	6	0.0376	0.0314	0.0017	-0.0031	0.0017	-0.0135	-0.0056	-0.0109	-0.0007
C_EDC (+100%)	0.1	0.2	0.0000	0.0000	0.0000	0.0000	0.0000	0.0001	0.0000	0.0000	0.0001
C_EDC (-50%)	0.1	0.05	0.0000	0.0000	0.0000	0.0000	0.0000	-0.0003	0.0000	0.0000	-0.0003
HRRPUA_SHEET (+40000%)	0	400	0.0000	0.0000	0.0000	0.0000	0.0000	0.0000	0.0000	0.0000	0.0000
HRRPUA_SHEET (+100000%)	0	100	0.0000	0.0000	0.0000	0.0000	0.0000	0.0000	0.0000	0.0000	0.0000
HRRPUV_AVERAGE (-60%)	3000	1200	0.0980	0.0916	0.2541	0.1280	0.0693	0.2558	0.1945	0.1368	0.2537
CSMAG (-50%)	0.2	0.1	0.0000	0.0000	0.0000	0.0000	0.0000	-0.0003	0.0000	0.0000	-0.0003
CSMAG (+100%)	0.2	0.4	0.0000	0.0000	0.0000	0.0000	0.0000	0.0001	0.0000	0.0000	0.0001
PR (-50%)	0.5	0.25	0.0257	-0.0152	-1.2831	0.1290	0.0649	-1.3264	0.1136	0.0580	-1.2804
PR (+100%)	0.5	1	0.1029	0.0757	-0.3429	0.0664	0.0338	-0.3656	0.0791	0.0478	-0.3485
SC (-50%)	0.5	0.25	-0.0869	-0.0871	0.0308	-0.0987	-0.0884	0.0799	-0.0837	-0.0753	0.0494
SC (+100%)	0.5	1	0.0501	0.0354	0.0175	-0.0552	-0.0356	0.0108	-0.0459	-0.0410	0.0122
CFL_MAX (+100%)	1	2	0.0316	0.0187	0.0402	0.0093	0.0032	0.0331	0.0167	0.0042	0.0383
CFL_MIN (-50%)	0.8	0.4	-0.1002	-0.0938	0.0841	0.0188	-0.0043	0.0740	-0.0368	-0.0392	0.0751
CFL_MAX and CFL_MIN	1 / 0.8	2 / 0.4	0.0678	0.0662	-0.0231	0.0034	0.0093	-0.0389	-0.0024	0.0031	-0.0259

L.1.2 Burner Shape

This section presents the sensitivity coefficients generated from the various simulations as grouped by the burner shape: Square or Rectangle. Figure 4 shows the sensitivity coefficients based on the predicted plume centerline velocity averaged over simulations using the same source fire burner. The parameters that created the most significant changes to the plume velocity are the radiative fraction, decreased in the heat release rate per unit volume of the flame, as well as the when the isothermal mode was used, which calculation scheme used based on the value of the flux limiter, and whether the radiation model is activated.

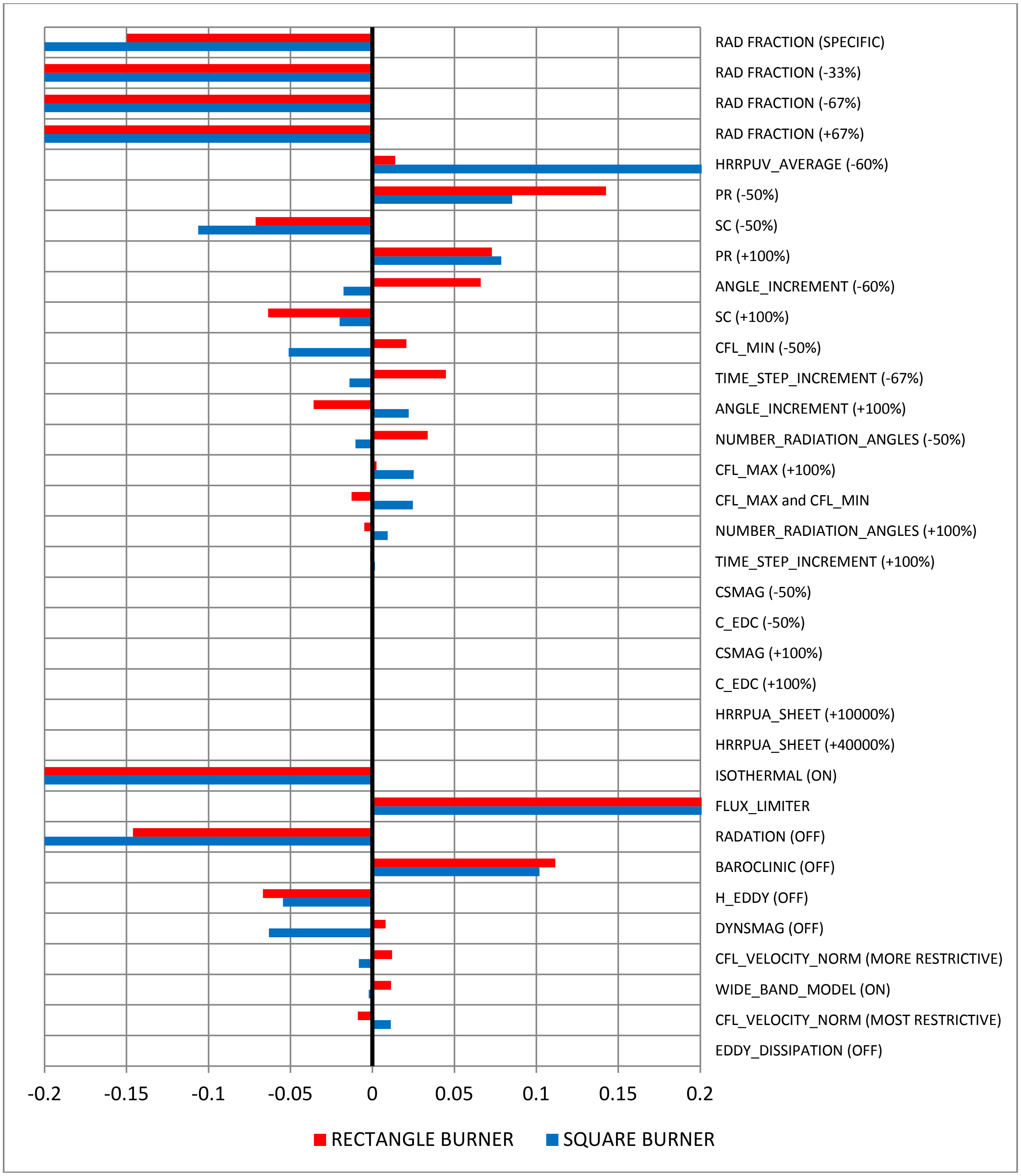

Figure 4 – Plume velocity sensitivity coefficients, grouped by burner shape

Figure 5 shows the sensitivity coefficients based on the predicted plume centerline temperature averaged over simulations using the same source fire burner. The parameters that contributed to the most significant changes to the plume temperature are the radiative fraction, the decrease of the HRRPUV of the fire, when the isothermal mode was used, and which calculation scheme used based on the value of the flux limiter

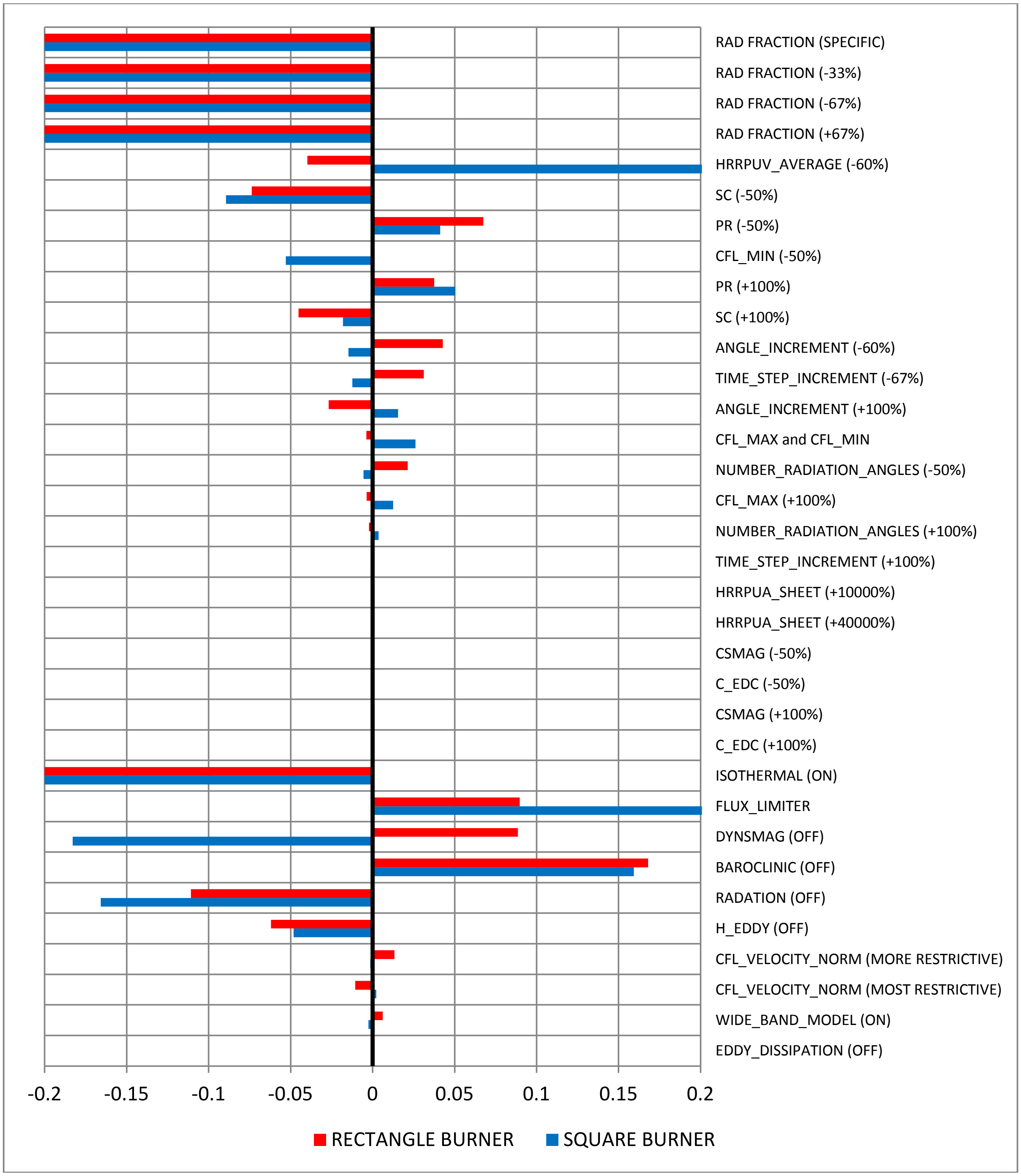

Figure 5 – Plume temperature sensitivity coefficients, grouped by burner shape

Figure 6 shows the sensitivity coefficients based on the predicted centerline gauge heat flux to wall averaged over simulations using the same source fire burner. The parameter changes that caused the most significant gauge heat flux change are the Prandtl number, the radiative fraction, a decrease of the HRRPUV of the fire, when the dynamic Smagorinsky model is turned off, whether the isothermal mode was used, when the eddy diffusivity model was activated, if the radiation transport model was turned off, and which calculation scheme used based on the value of the flux limiter.

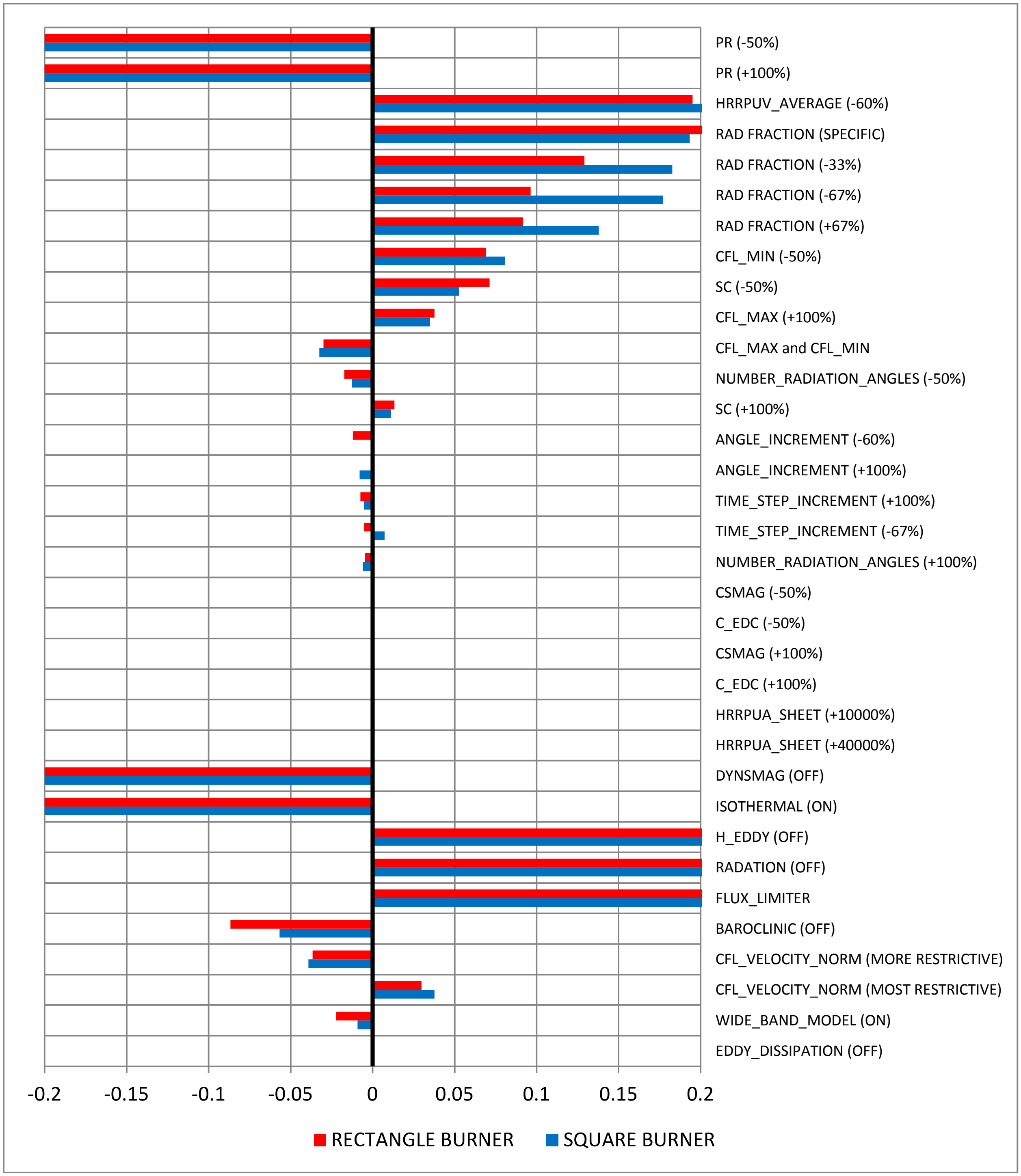

Figure 6 – Centerline gauge heat flux to wall sensitivity coefficients, grouped by burner shape

Table 3 - Sensitivity coefficients based on source burner shape

			SQUARE BURNER			RECTANGLE BURNER		
Parameter change	**Default Value**	**New Value**	**Velocity**	**Temp**	**GHF**	**Velocity**	**Temp**	**GHF**
DYNSMAG (OFF)	.TRUE.	.FALSE.	-0.0631	-0.1829	-2.8138	0.0080	0.0886	-2.9218
RADIATION (OFF)	.TRUE.	.FALSE.	-0.2052	-0.1658	0.4271	-0.1461	-0.1108	0.3374
WIDE_BAND_MODEL (ON)	.FALSE.	.TRUE	-0.0023	-0.0025	-0.0093	0.0114	0.0061	-0.0222
EDDY_DISSIPATION (OFF)	.TRUE.	.FALSE.	0.0000	0.0000	-0.0001	0.0000	0.0000	-0.0001
ISOTHERMAL (ON)	.FALSE.	.TRUE	-0.9242	-0.8257	-0.9985	-0.9424	-0.7765	-0.9985
BAROCLINIC (OFF)	.TRUE.	.FALSE.	0.1018	0.1592	-0.0568	0.1115	0.1680	-0.0868
FLUX_LIMITER	2	-1	0.3364	0.2650	0.2501	0.2129	0.0897	0.3015
CFL_VELOCITY_NORM (MOST RESTRICTIVE)	1	2	0.0113	0.0022	0.0377	-0.0090	-0.0107	0.0298
CFL_VELOCITY_NORM (MORE RESTRICTIVE)	1	0	-0.0084	-0.0014	-0.0392	0.0120	0.0133	-0.0366
H_EDDY (OFF)	.FALSE.	.TRUE.	-0.0547	-0.0483	0.5964	-0.0669	-0.0620	0.6263
RAD FRACTION (SPECIFIC)	0.3	Source fire specific	-0.4056	-0.4886	0.1934	-0.1499	-0.3474	0.2725
RAD FRACTION (-67%)	0.3	0.1	-0.3546	-0.4097	0.1770	-0.3106	-0.3487	0.0964
RAD FRACTION (-33%)	0.3	0.2	-0.3680	-0.4138	0.1828	-0.2464	-0.2921	0.1291
RAD FRACTION (+67%)	0.3	0.5	-0.2870	-0.3273	0.1379	-0.3314	-0.3258	0.0918
NUMBER_RADIATION_ANGLES (-50%)	104	52	-0.0104	-0.0056	-0.0127	0.0337	0.0214	-0.0173
NUMBER_RADIATION_ANGLES (+100%)	104	208	0.0092	0.0036	-0.0059	-0.0050	-0.0023	-0.0046
ANGLE_INCREMENT (-60%)	5	2	-0.0176	-0.0148	0.0001	0.0661	0.0428	-0.0120
ANGLE_INCREMENT (+100%)	5	10	0.0221	0.0155	-0.0079	-0.0360	-0.0268	-0.0005
TIME_STEP_INCREMENT (-67%)	3	1	-0.0140	-0.0124	0.0073	0.0447	0.0312	-0.0052
TIME_STEP_INCREMENT (+100%)	3	6	0.0016	-0.0007	-0.0050	-0.0013	-0.0005	-0.0074
C_EDC (+100%)	0.1	0.2	0.0000	0.0000	0.0001	0.0000	0.0000	0.0001
C_EDC (-50%)	0.1	0.05	0.0000	0.0000	-0.0002	0.0000	0.0000	-0.0003
HRRPUA_SHEET (+40000%)	0	400	0.0000	0.0000	0.0000	0.0000	0.0000	0.0000
HRRPUA_SHEET (+10000%)	0	100	0.0000	0.0000	0.0000	0.0000	0.0000	0.0000
HRRPUV_AVERAGE (-60%)	3000	1200	0.2665	0.2150	0.3023	0.0139	-0.0397	0.1952
CSMAG (-50%)	0.2	0.1	0.0000	0.0000	-0.0002	0.0000	0.0000	-0.0003
CSMAG (+100%)	0.2	0.4	0.0000	0.0000	0.0001	0.0000	0.0000	0.0001
PR (-50%)	0.5	0.25	0.0852	0.0412	-1.2665	0.1425	0.0676	-1.3443
PR (+100%)	0.5	1	0.0786	0.0504	-0.3495	0.0729	0.0375	-0.3629
SC (-50%)	0.5	0.25	-0.1063	-0.0894	0.0526	-0.0712	-0.0737	0.0713
SC (+100%)	0.5	1	-0.0200	-0.0181	0.0113	-0.0636	-0.0451	0.0133
CFL_MAX (+100%)	1	2	0.0252	0.0125	0.0350	0.0025	-0.0036	0.0378
CFL_MIN (-50%)	0.8	0.4	-0.0511	-0.0530	0.0809	0.0207	-0.0007	0.0691
CFL_MAX and CFL_MIN	1 / 0.8	2 / 0.4	0.0246	0.0261	-0.0325	-0.0128	-0.0037	-0.0299

L.1.3 Heat Release Rate

This section presents the sensitivity coefficients generated from the various simulations as grouped by the source fire HRR: 50 kW or 75 kW. Figure 7 shows the sensitivity coefficients based on the predicted plume centerline velocity averaged over simulations using the same source fire HRR. The parameter changes that caused the most significant velocity change are the radiative fraction, a decrease of the HRRPUV of the fire, whether the isothermal mode was used, and which calculation scheme used based on the value of the flux limiter.

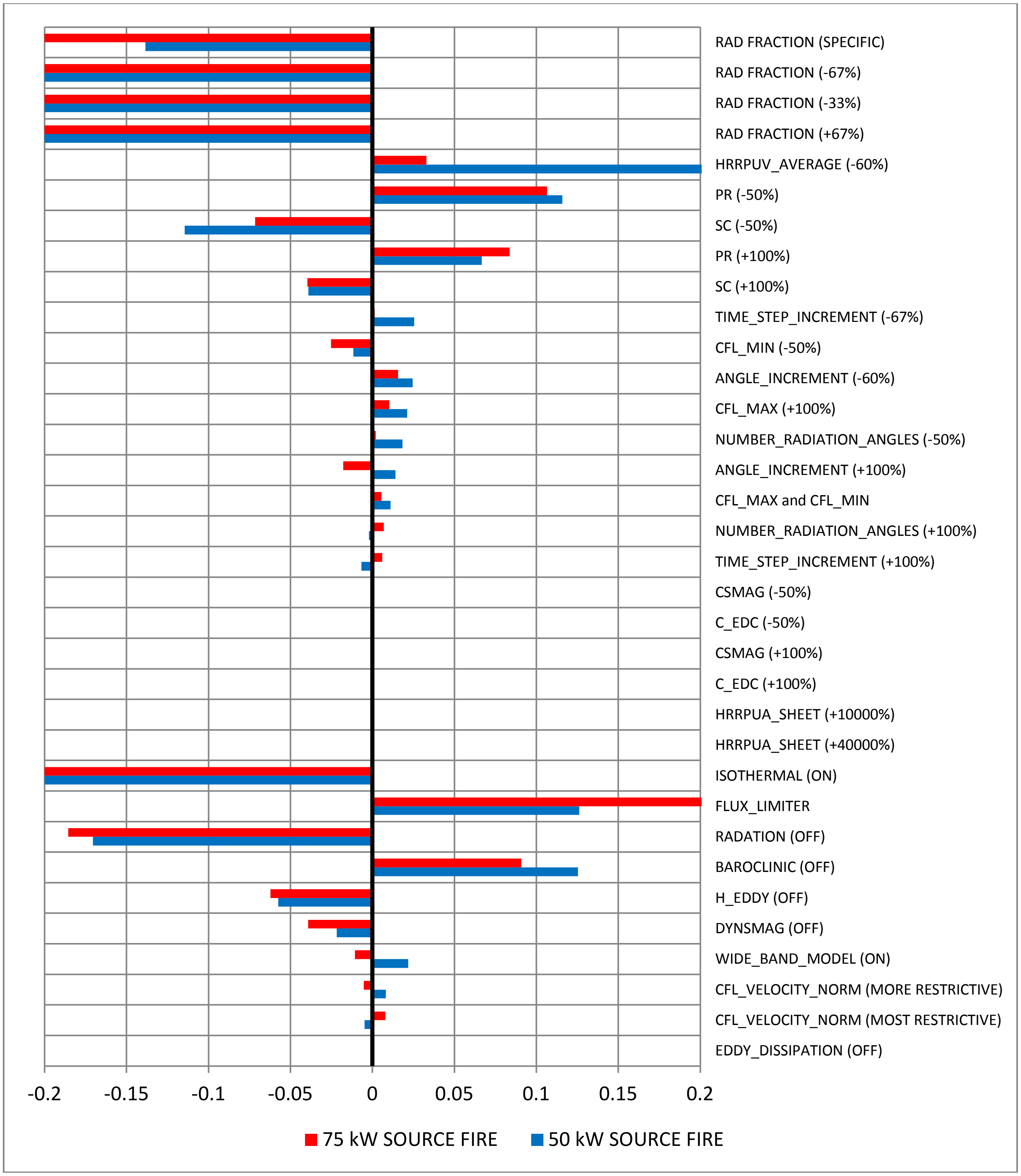

Figure 7 – Plume velocity sensitivity coefficients, grouped by HRR

Figure 8 shows the sensitivity coefficients based on the predicted plume centerline temperature averaged over simulations using the same source fire HRR. The parameters that contributed to the most significant changes to the plume temperature are the radiative fraction, the decrease of the HRRPUV of the fire, when the isothermal mode was used, and which calculation scheme used based on the value of the flux limiter

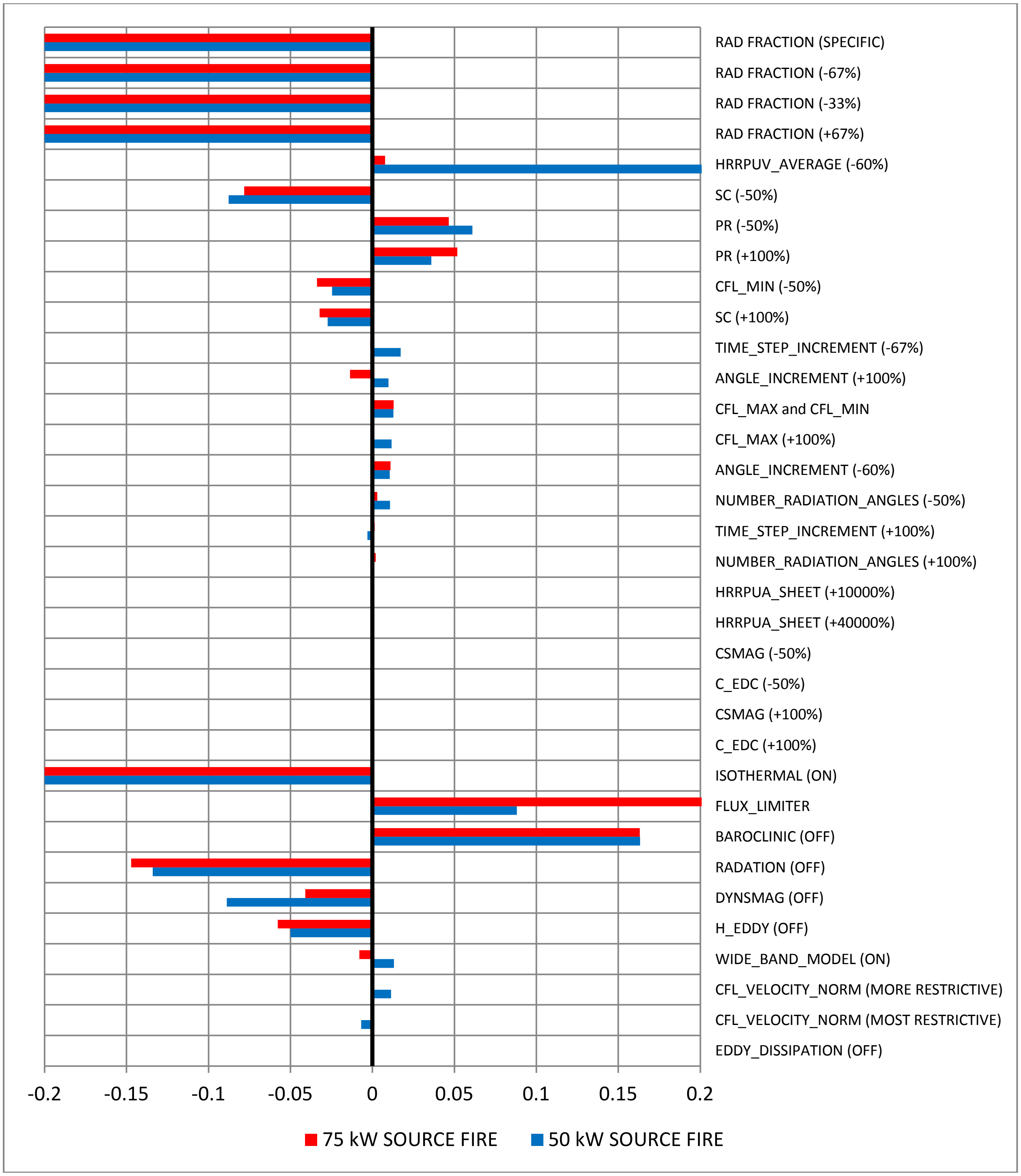

Figure 8 – Plume temperature sensitivity coefficients, grouped by HRR

Figure 9 shows the sensitivity coefficients based on the predicted centerline gauge heat flux to wall averaged over simulations using the same source fire HRR. The parameter changes that caused the most significant gauge heat flux change are the Prandtl number, the radiative fraction, a decrease of the HRRPUV of the fire, when the dynamic Smagorinsky model is turned off, whether the isothermal mode was used, when the eddy diffusivity model was activated, if the radiation transport model was turned off, and which calculation scheme used based on the value of the flux limiter.

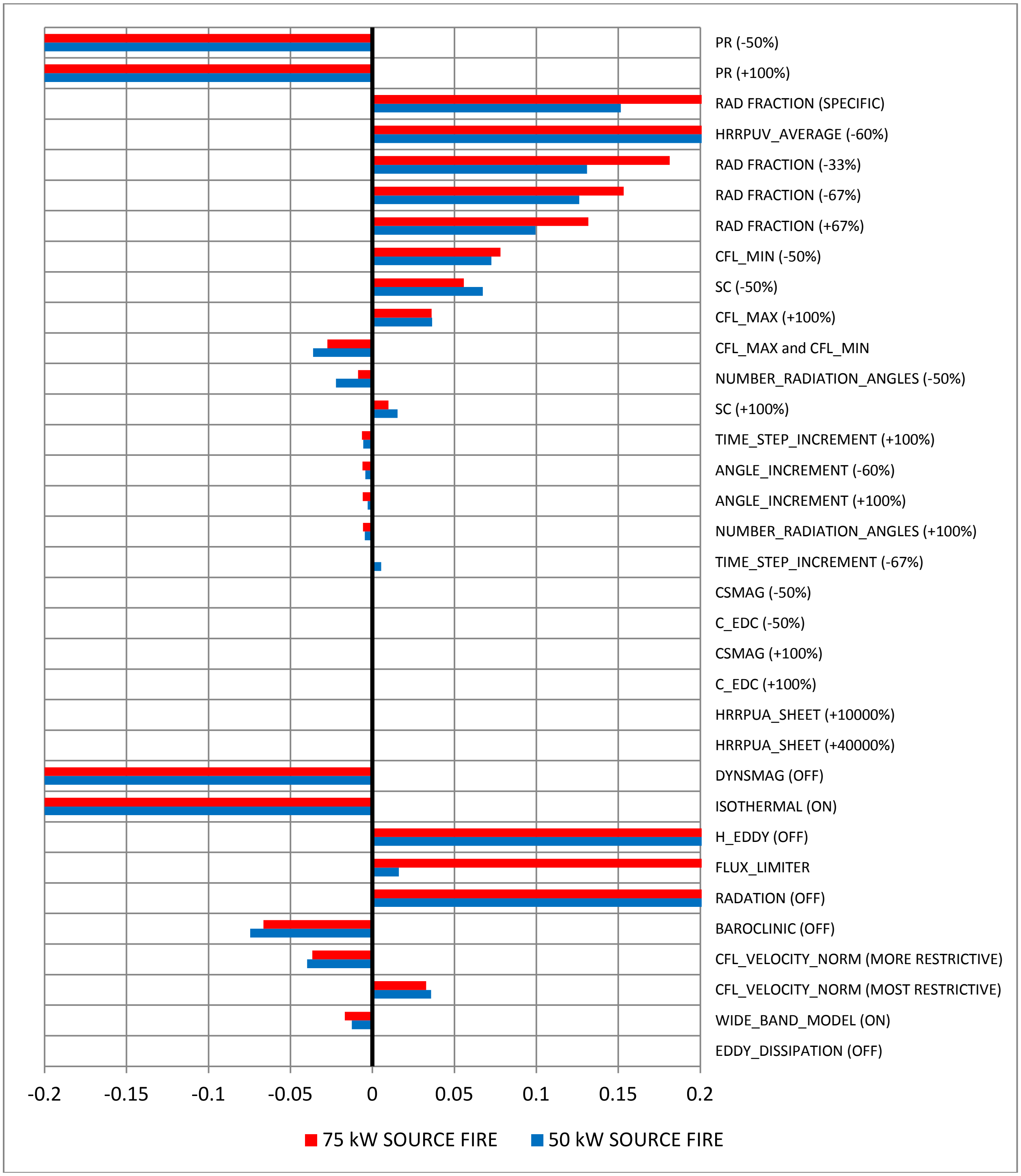

Figure 9 – Centerline gauge heat flux to wall sensitivity coefficients, grouped by HRR

Table 4 - Sensitivity coefficients based on source fire HRR

			SOURCE FIRE 50 KW			SOURCE FIRE 75 KW		
Parameter change	**Default Value**	**New Value**	**Velocity**	**Temp**	**GHF**	**Velocity**	**Temp**	**GHF**
DYNSMAG (OFF)	.TRUE.	.FALSE.	-0.0218	-0.0888	-2.8687	-0.0393	-0.0409	-2.8564
RADATION (OFF)	.TRUE.	.FALSE.	-0.1705	-0.1340	0.3750	-0.1856	-0.1472	0.3971
WIDE_BAND_MODEL (ON)	.FALSE.	.TRUE	0.0219	0.0130	-0.0126	-0.0107	-0.0080	-0.0169
EDDY_DISSIPATION (OFF)	.TRUE.	.FALSE.	0.0000	0.0000	-0.0001	0.0000	0.0000	-0.0001
ISOTHERMAL (ON)	.FALSE.	.TRUE	-0.9366	-0.7865	-0.9982	-0.9289	-0.8176	-0.9986
BAROCLINIC (OFF)	.TRUE.	.FALSE.	0.1253	0.1632	-0.0745	0.0908	0.1631	-0.0666
FLUX_LIMITER	2	-1	0.1262	0.0882	0.0161	0.4058	0.2663	0.4784
CFL_VELOCITY_NORM (MOST RESTRICTIVE)	1	2	-0.0048	-0.0069	0.0358	0.0079	-0.0008	0.0328
CFL_VELOCITY_NORM (MORE RESTRICTIVE)	1	0	0.0082	0.0113	-0.0398	-0.0053	0.0002	-0.0367
H_EDDY (OFF)	.FALSE.	.TRUE.	-0.0575	-0.0501	0.6265	-0.0622	-0.0578	0.5962
RAD FRACTION (SPECIFIC)	0.3	Source fire specific	-0.1385	-0.3097	0.1515	-0.4147	-0.5188	0.2902
RAD FRACTION (-67%)	0.3	0.1	-0.3307	-0.3773	0.1262	-0.3386	-0.3869	0.1532
RAD FRACTION (-33%)	0.3	0.2	-0.3092	-0.3563	0.1310	-0.3178	-0.3624	0.1813
RAD FRACTION (+67%)	0.3	0.5	-0.3141	-0.3225	0.0996	-0.3008	-0.3299	0.1317
NUMBER_RADIATION_ANGLES (-50%)	104	52	0.0183	0.0106	-0.0223	0.0019	0.0030	-0.0088
NUMBER_RADIATION_ANGLES (+100%)	104	208	-0.0021	-0.0003	-0.0047	0.0069	0.0021	-0.0058
ANGLE_INCREMENT (-60%)	5	2	0.0245	0.0105	-0.0043	0.0157	0.0111	-0.0061
ANGLE_INCREMENT (+100%)	5	10	0.0140	0.0097	-0.0030	-0.0179	-0.0136	-0.0059
TIME_STEP_INCREMENT (-67%)	3	1	0.0255	0.0173	0.0053	0.0014	-0.0013	-0.0011
TIME_STEP_INCREMENT (+100%)	3	6	-0.0067	-0.0031	-0.0057	0.0059	0.0014	-0.0064
C_EDC (+100%)	0.1	0.2	0.0000	0.0000	0.0001	0.0000	0.0000	0.0001
C_EDC (-50%)	0.1	0.05	0.0000	0.0000	-0.0003	0.0000	0.0000	-0.0002
HRRPUA_SHEET (+40000%)	0	400	0.0000	0.0000	0.0000	0.0000	0.0000	0.0000
HRRPUA_SHEET (+10000%)	0	100	0.0000	0.0000	0.0000	0.0000	0.0000	0.0000
HRRPUV_AVERAGE (-60%)	3000	1200	0.3058	0.2193	0.2566	0.0330	0.0077	0.2532
CSMAG (-50%)	0.2	0.1	0.0000	0.0000	-0.0003	0.0000	0.0000	-0.0002
CSMAG (+100%)	0.2	0.4	0.0000	0.0000	0.0001	0.0000	0.0000	0.0001
PR (-50%)	0.5	0.25	0.1159	0.0610	-1.3345	0.1065	0.0465	-1.2744
PR (+100%)	0.5	1	0.0666	0.0359	-0.3630	0.0836	0.0517	-0.3494
SC (-50%)	0.5	0.25	-0.1145	-0.0877	0.0673	-0.0716	-0.0782	0.0558
SC (+100%)	0.5	1	-0.0390	-0.0274	0.0152	-0.0397	-0.0323	0.0098
CFL_MAX (+100%)	1	2	0.0211	0.0116	0.0364	0.0103	0.0004	0.0361
CFL_MIN (-50%)	0.8	0.4	-0.0116	-0.0246	0.0726	-0.0252	-0.0338	0.0781
CFL_MAX and CFL_MIN	1 / 0.8	2 / 0.4	0.0111	0.0128	-0.0362	0.0055	0.0129	-0.0275

L.2 Ratios of Quantity Change

Since the sensitivity coefficients are averaged regardless of the height of the “measurement” locations, the changes in the quantities due to parametric variation that are height-depended are omitted. To show the height-dependent effects, the ratios of change for the centerline plume temperature and velocity are plotted against the height of measurement locations. The ratio is calculated in equation [1.2]:

$$\left(\frac{Quantity_{new} - Quantity_{baseline}}{Quantity_{baseline}} \right) \quad [0.2]$$

The ratios for all simulations are plotted for each parametric series in the following section. This allows the effects of the parametric change on simulations with different source fuel, source burner size, and HRR be observed.

Series 0 - Ratios of Parameter Change from Default Series

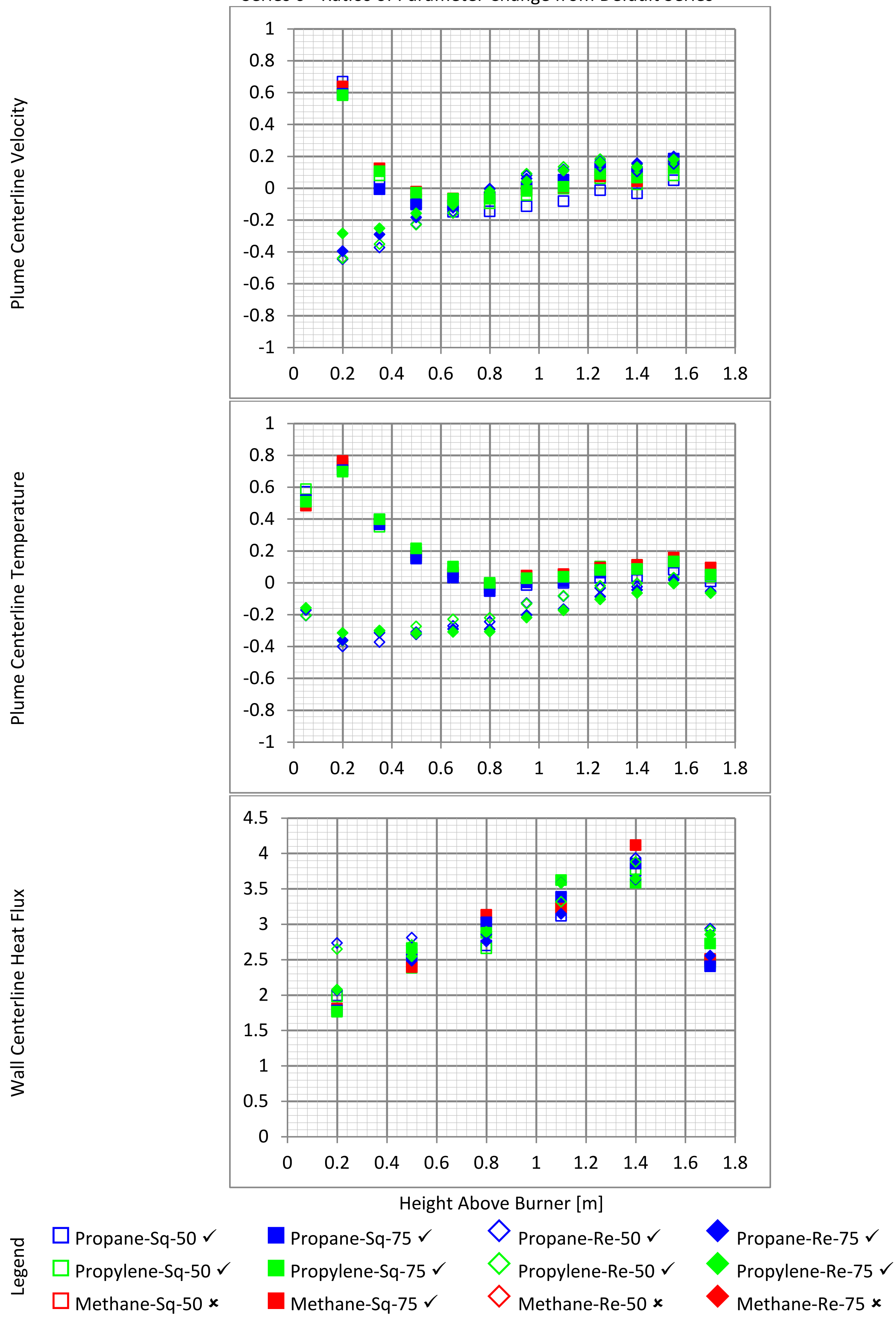

In Series 0, the dynamics Smagorinsky model was turned off in the FDS models, which resulted in a more disordered flow field inside the computational domain. An increase in centerline velocity is noted for the Square burner simulations at the elevation of 0.2 m and 0.4 m, but at the same range, a decrease in velocity is observed in the Rectangle burner simulations. Past 0.4 m, velocity is underpredicted versus the default up to 1 m over the burner, but generally experienced in another increase at the elevations above.

For the centerline plume temperature, all Square burner simulations had an increased temperature that is inversely proportional to the elevation, whereas the opposite is true for the Rectangle burner, which generally predicted a decrease in temperature.

The centerline wall gauge heat flux is sharply increased in all simulations at an elevation from 0.2 m to 1.4 m above the burner. However, at 1.7 m above the burner, the heat flux's ratio of change dropped off into the same level as from 0.5 m over the burner.

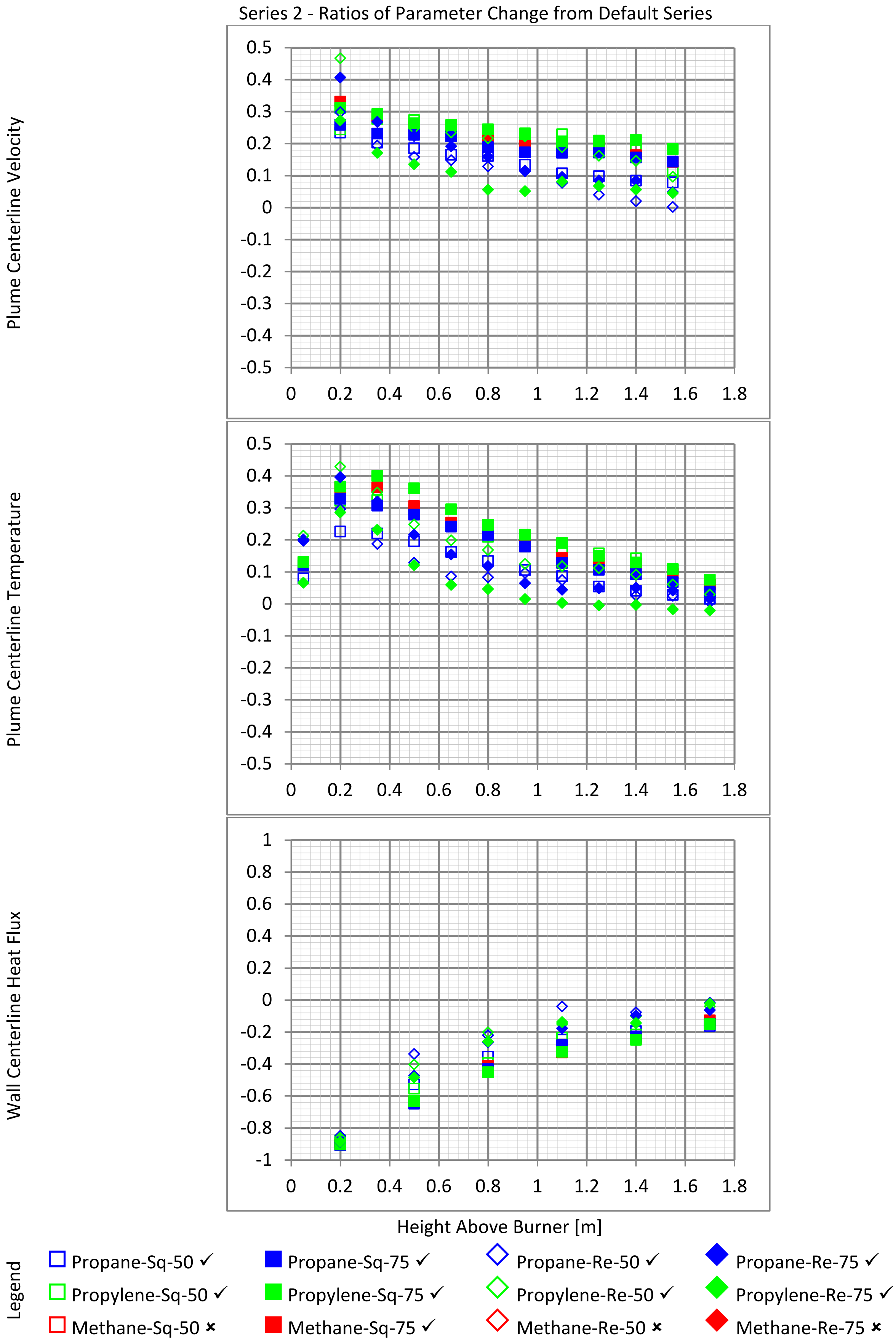

Series 2 - Ratios of Parameter Change from Default Series
Plume Centerline Velocity
Plume Centerline Temperature
Wall Centerline Heat Flux
Height Above Burner [m]
Legend
Propane-Sq-50 ✓
Propane-Sq-75 ✓
Propane-Re-50 ✓
Propane-Re-75 ✓
Propylene-Sq-50 ✓
Propylene-Sq-75 ✓
Propylene-Re-50 ✓
Propylene-Re-75 ✓
Methane-Sq-50 ×
Methane-Sq-75 ✓
Methane-Re-50 ×
Methane-Re-75 ×

Observations

With radiation solver disabled in FDS in the Series 2 simulations, the effects from the source fire size and fuel type are more pronounced in the centerline temperature and velocity predictions, evident in the wide spread of the datapoints at each elevation. For both the velocity and temperature, an increase in velocity that is inversely proportional to the elevation is observed.

The wall centerline heat flux is greatly decreased due to the parametric change, due to the fact that the heat flux in the inert wall environment is largely driven by the radiative component.

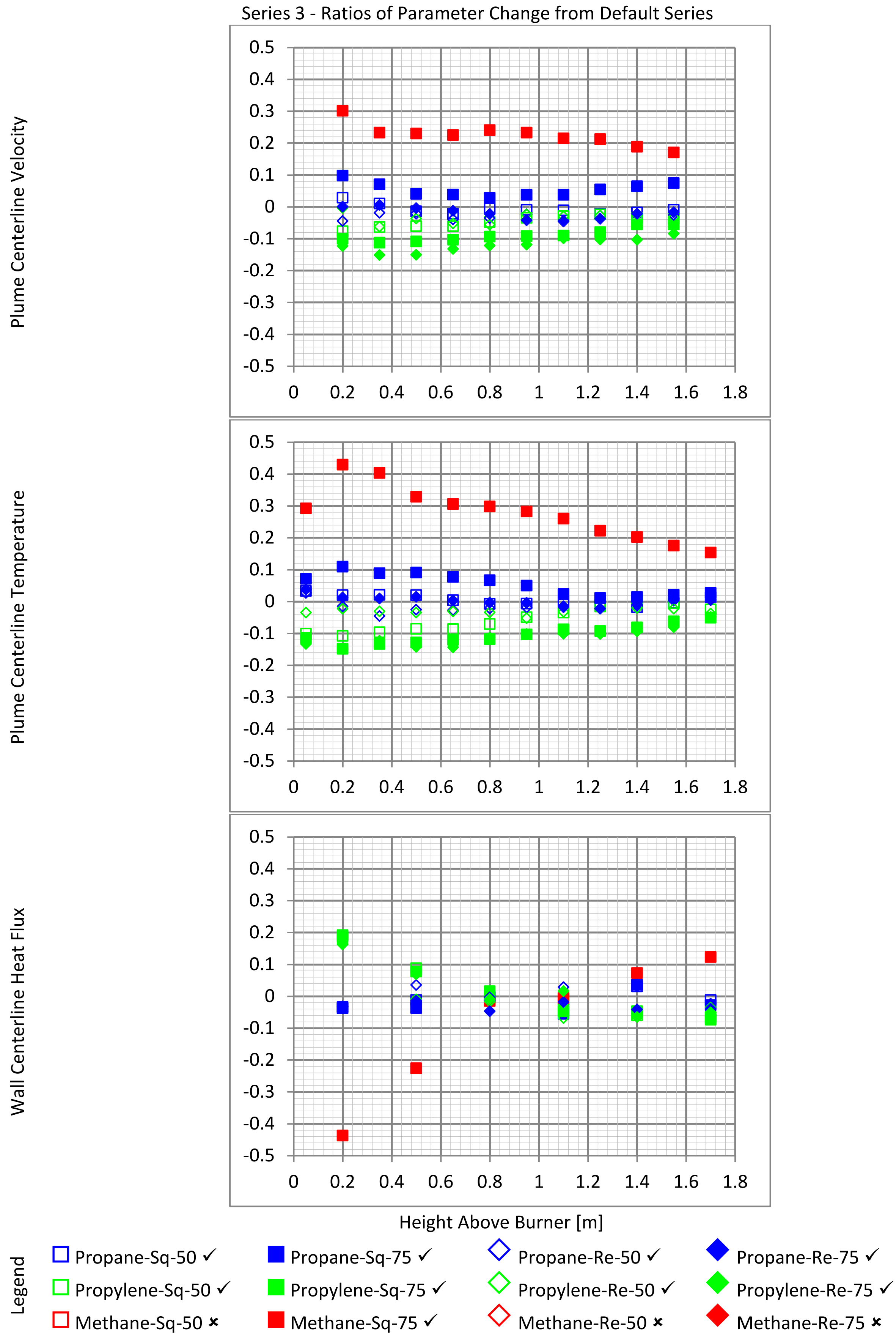
Series 3 - Ratios of Parameter Change from Default Series
Plume Centerline Velocity
Plume Centerline Temperature
Wall Centerline Heat Flux
0.5
0.4
0.3
0.2
0.1
0
-0.1
-0.2
-0.3
-0.4
-0.5
0
0.2
0.4
0.6
0.8
1
1.2
1.4
1.6
1.8
Height Above Burner [m]
Legend
Propane-Sq-50 ✓
Propane-Sq-75 ✓
Propane-Re-50 ✓
Propane-Re-75 ✓
Propylene-Sq-50 ✓
Propylene-Sq-75 ✓
Propylene-Re-50 ✓
Propylene-Re-75 ✓
Methane-Sq-50 ×
Methane-Sq-75 ✓
Methane-Re-50 ×
Methane-Re-75 ×

Observations

In Series 3, the radiative fraction used in each of the simulations was changed from the default 0.30 to suit the fuels' specific radiative fractions. For methane, a value of 0.141 was used; for propane, 0.286; and for propylene, 0.368.

The change caused significant effects on all three quantities that is closely related to the fuel type. For methane, the parameter change created an increased velocty and temperautre, yet the gauge heat flux is reduced significantly at low elevation but increased with elevation.

For propane, the change in velocity, the velocity and temperature are slightly increased up to 1.2 m above the burner, then remained largely unchanged at higher elevation. The magnitude of the changes has bee noted to be more pronouned for Square burner tests and for source fires with higher HRR. The change to the guage heat flux is minmial.

The preidcted velocity and temperature for propylene fires are slightly depressed, again, the magnitude of change is larger for Square burner than Rectangle and for 75 kW than 50 kW source fires. In the gauge heat flux, however, at the loweer elevation the heat flux is increased but beomes slightly decreased at the highest elevation.

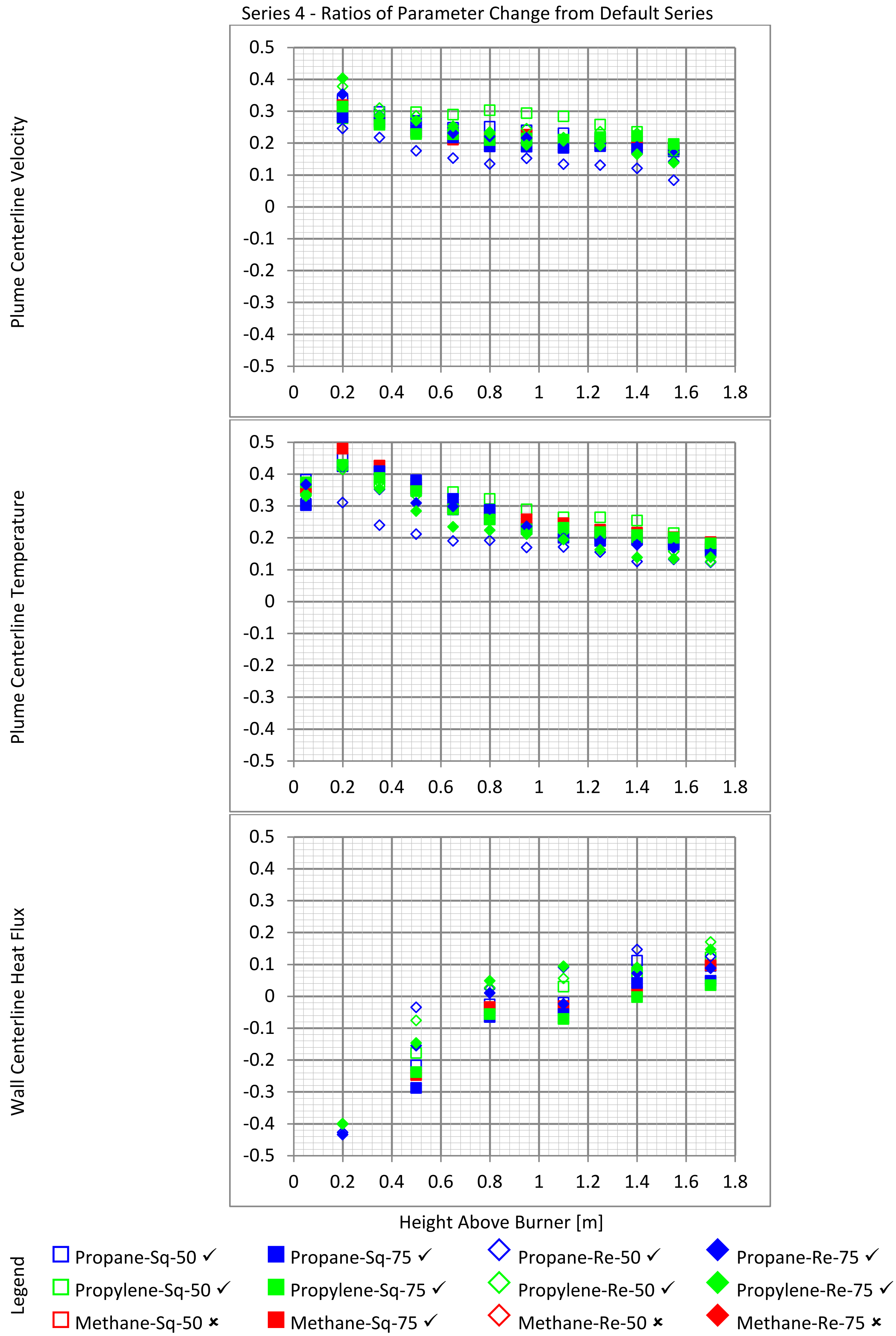
Series 4 - Ratios of Parameter Change from Default Series
Plume Centerline Velocity
Plume Centerline Temperature
Wall Centerline Heat Flux
0.5
0.4
0.3
0.2
0.1
0
-0.1
-0.2
-0.3
-0.4
-0.5
0
0.2
0.4
0.6
0.8
1
1.2
1.4
1.6
1.8
Height Above Burner [m]
Legend
Propane-Sq-50 ✓
Propane-Sq-75 ✓
Propane-Re-50 ✓
Propane-Re-75 ✓
Propylene-Sq-50 ✓
Propylene-Sq-75 ✓
Propylene-Re-50 ✓
Propylene-Re-75 ✓
Methane-Sq-50 ×
Methane-Sq-75 ✓
Methane-Re-50 ×
Methane-Re-75 ×

Observations

In Series 4, the radiative fraction of all simulations was lowered 66% from the default 0.30 to 0.1.

The parameter change caused an increase in the velocity and temperature that is inversely proportional to the elevation. The effects on the propane fires appears to be more prominent for fires with either the Square burner or at 75 kW, howevr, for the propylene fires, the change is more significant for Rectangle burner and 50 kW. The predicted gaue heat flux is decreased at elevations close to the burner surface but becomes slightly increased at the locations furthest away from the burner surface.

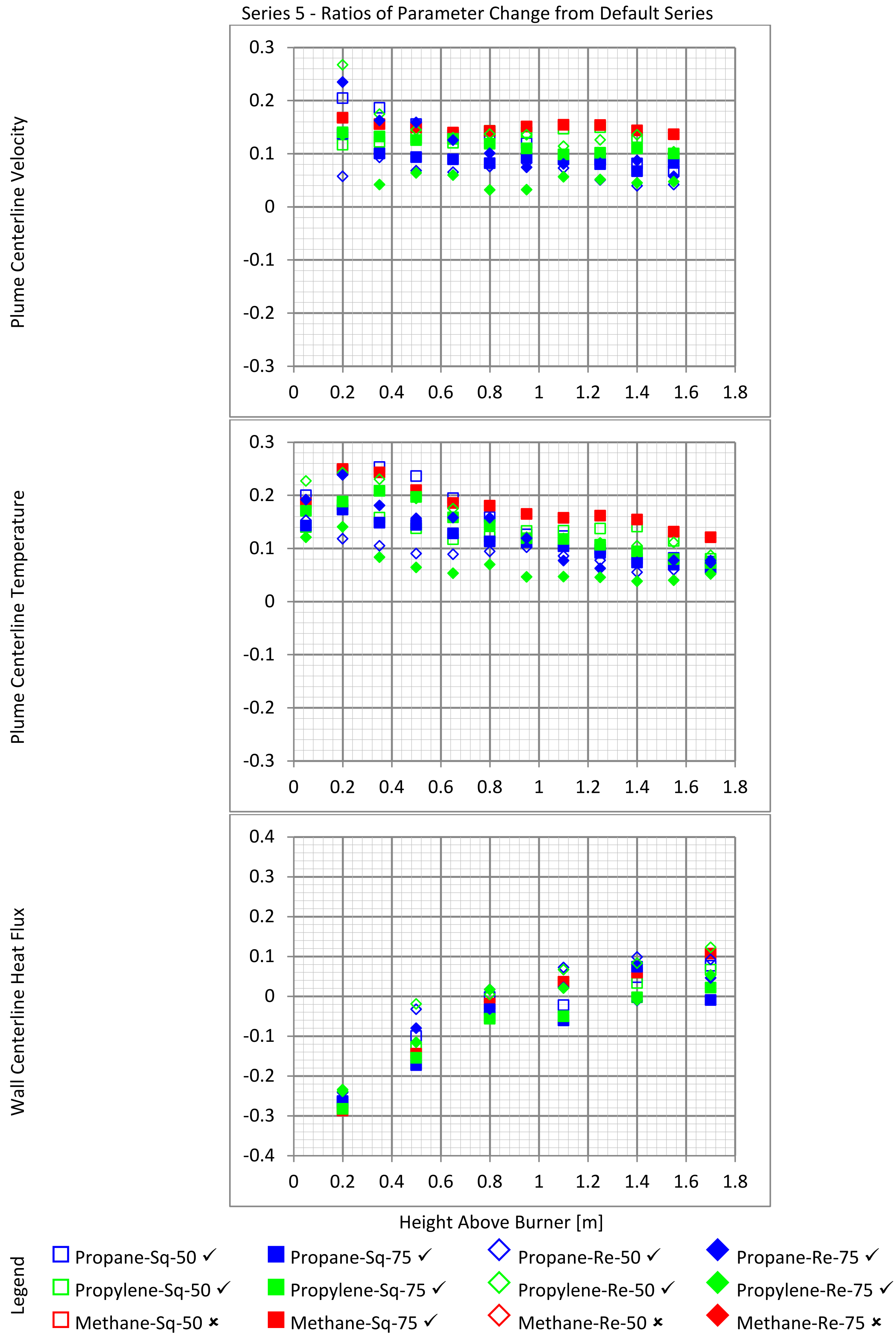
Series 5 - Ratios of Parameter Change from Default Series
Plume Centerline Velocity
Plume Centerline Temperature
Wall Centerline Heat Flux
0.4
0.3
0.2
0.1
0
-0.1
-0.2
-0.3
-0.4
0
0.2
0.4
0.6
0.8
1
1.2
1.4
1.6
1.8
Height Above Burner [m]
Legend
Propane-Sq-50 ✓
Propane-Sq-75 ✓
Propane-Re-50 ✓
Propane-Re-75 ✓
Propylene-Sq-50 ✓
Propylene-Sq-75 ✓
Propylene-Re-50 ✓
Propylene-Re-75 ✓
Methane-Sq-50 ×
Methane-Sq-75 ✓
Methane-Re-50 ×
Methane-Re-75 ×

Observations

In Series 5, the radiative fraction of all simulations was reduced 33% from the default 0.30 to 0.2.

Similar to the effects of Series 4, the parameter change caused an increase in the velocity and temperature that is inversely proportional to the elevation. The effects on the propane fires appears to be more prominent for fires with either the Square burner or at 50 kW, howevr, for the propylene fires, the change is more significant for Rectangle burner and 50 kW. The predicted gaue heat flux is decreased at elevations close to the burner surface but becomes slightly increased at the locations furthest away from the burner surface, similar to the changes noted in Series 4.

It should be noted that the magnitude of the change is less significant than that noted from Series 4.

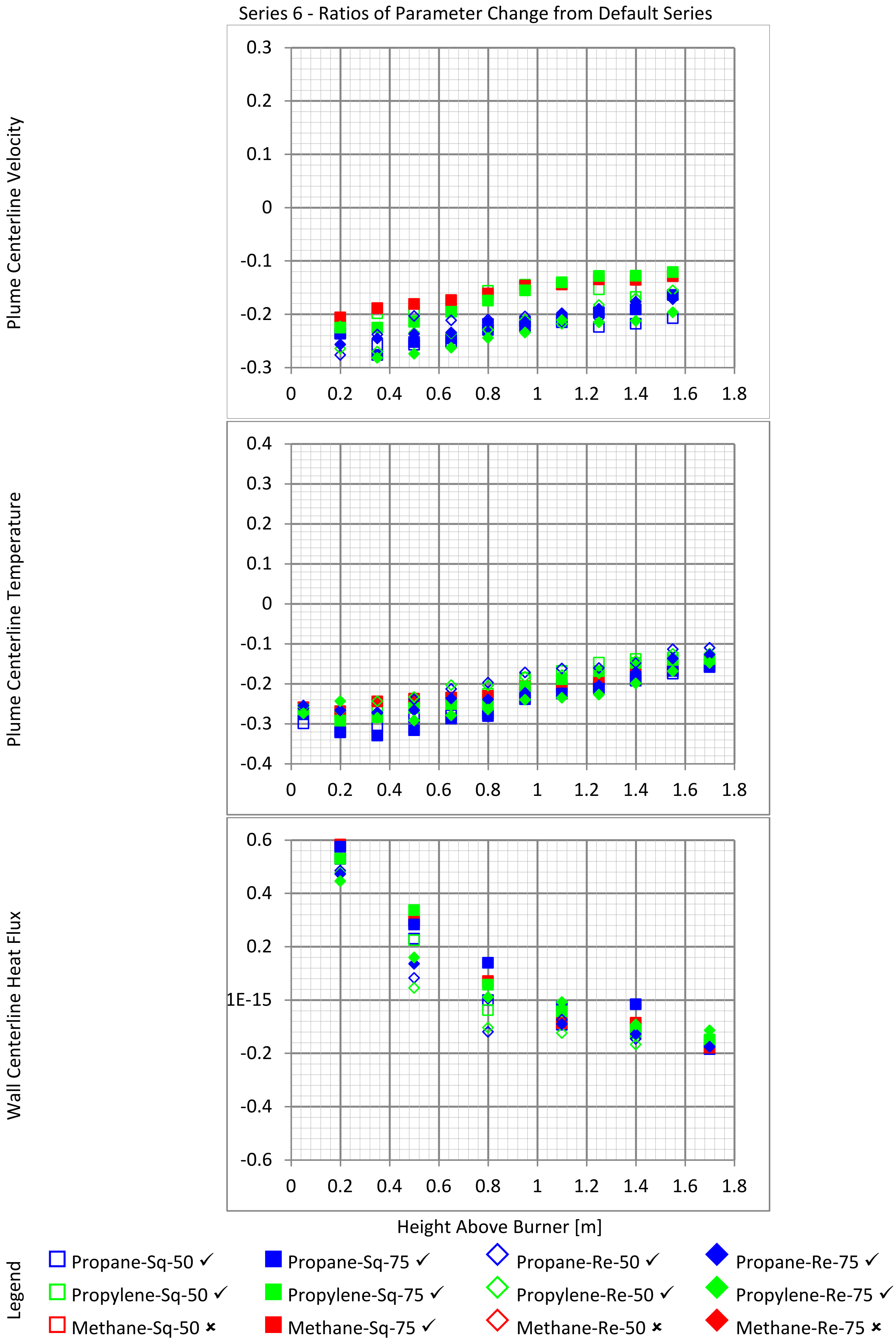
Series 6 - Ratios of Parameter Change from Default Series
Plume Centerline Velocity
0.3
0.2
0.1
0
-0.1
-0.2
-0.3
Plume Centerline Temperature
0.4
0.3
0.2
0.1
0
-0.1
-0.2
-0.3
-0.4
Wall Centerline Heat Flux
0.6
0.4
0.2
1E-15
-0.2
-0.4
-0.6
0
0.2
0.4
0.6
0.8
1
1.2
1.4
1.6
1.8
Height Above Burner [m]
Legend
Propane-Sq-50 ✓
Propane-Sq-75 ✓
Propane-Re-50 ✓
Propane-Re-75 ✓
Propylene-Sq-50 ✓
Propylene-Sq-75 ✓
Propylene-Re-50 ✓
Propylene-Re-75 ✓
Methane-Sq-50 ×
Methane-Sq-75 ✓
Methane-Re-50 ×
Methane-Re-75 ×

Observations

In Series 6, the radiative fraction of all simulations was increased 66% from the default 0.30 to 0.5.

The parameter change caused a decrease in the velocity and temperature that is inversely proportional to the elevation. The predicted gaue heat flux is increased at the lowest elevation but gradually decreased with an increase of the elevation.

The changes in Series 6 are opposite to those shown in Series 4 and 5, which is consistent with the changes in the radiative farction parameter.

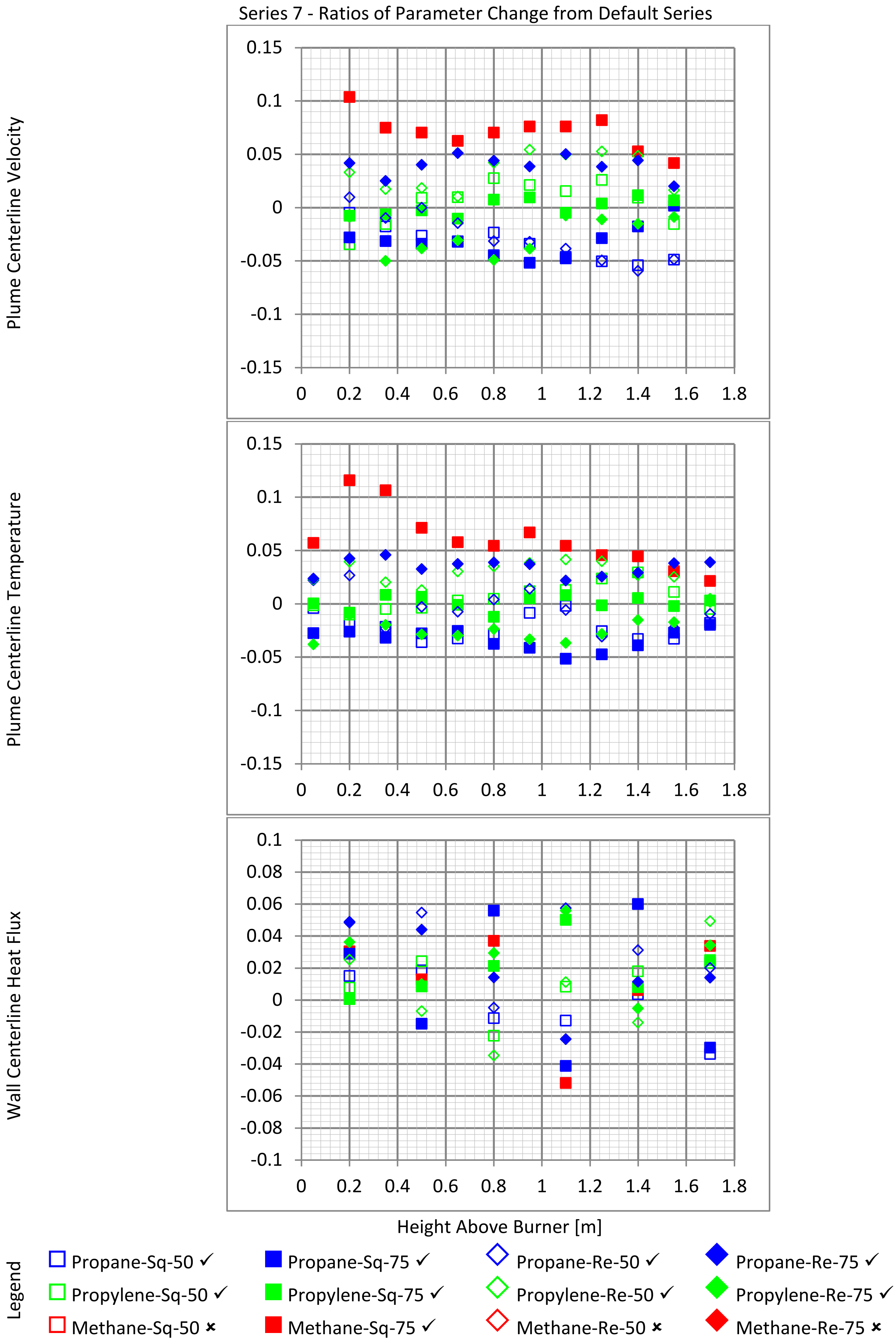

Series 7 - Ratios of Parameter Change from Default Series
Plume Centerline Velocity
Plume Centerline Temperature
Wall Centerline Heat Flux
Height Above Burner [m]
Legend
Propane-Sq-50 ✓
Propane-Sq-75 ✓
Propane-Re-50 ✓
Propane-Re-75 ✓
Propylene-Sq-50 ✓
Propylene-Sq-75 ✓
Propylene-Re-50 ✓
Propylene-Re-75 ✓
Methane-Sq-50 ×
Methane-Sq-75 ✓
Methane-Re-50 ×
Methane-Re-75 ×

In the Series 7 simulations, the wide band model mode to calculate radiation transports was enabled.

Observations

The changes in the velocity and temperature are the most pronounced for the methane fire, but overall, the changes are relatively insignificant. For the propane fire simulations, the changes are mostly negative, except for the Rectangle burner with 75 kW. Compared to the other simulations, the effects on the propylene fires' velocity and temperature are small. The changes on the gauge heat flux are less organized, but the magnitude of change is very insignificant, but seems to increase with elevation.

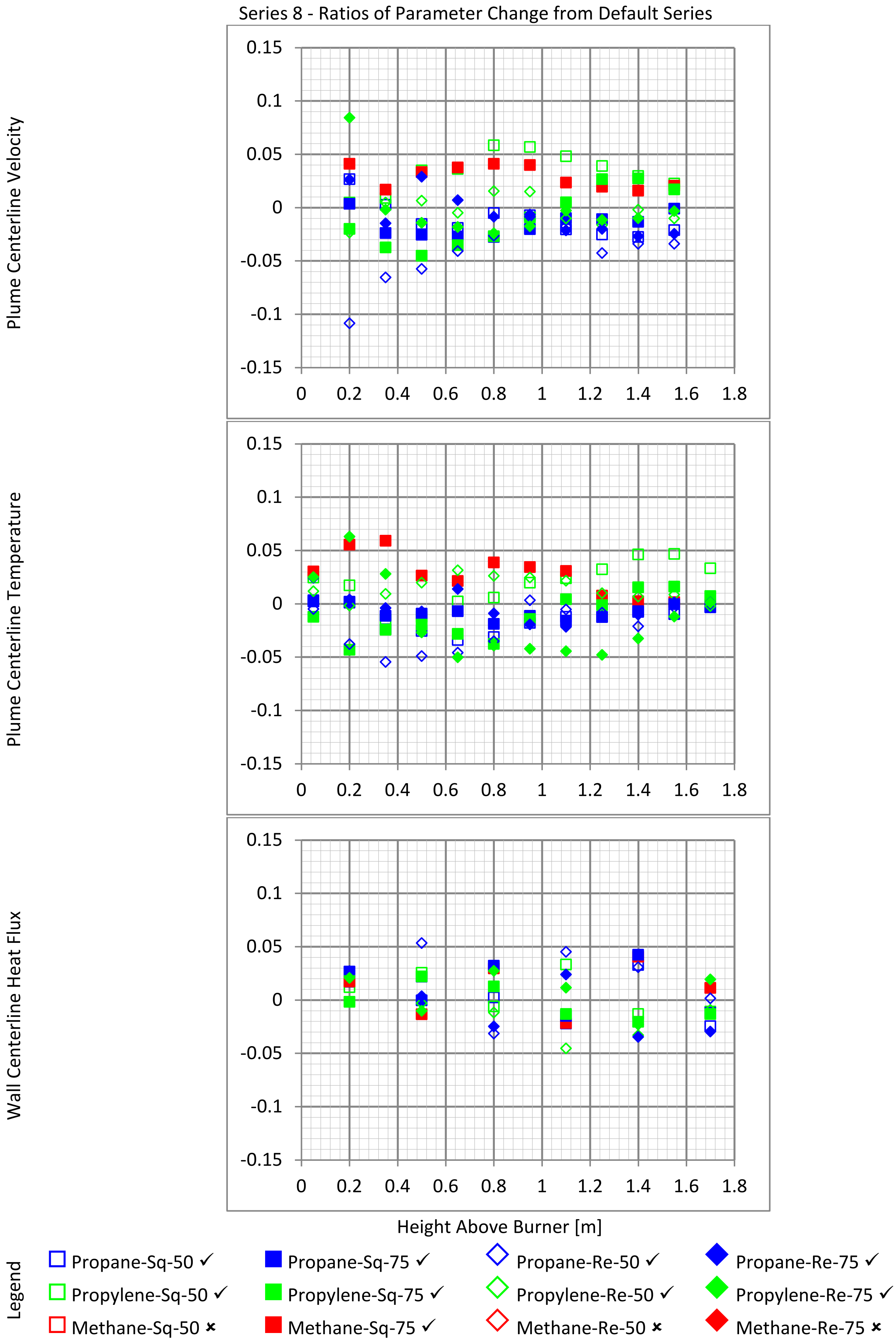

Series 8 - Ratios of Parameter Change from Default Series
Plume Centerline Velocity
Plume Centerline Temperature
Wall Centerline Heat Flux
0.15
0.1
0.05
0
-0.05
-0.1
-0.15
0
0.2
0.4
0.6
0.8
1
1.2
1.4
1.6
1.8
Height Above Burner [m]
Legend
Propane-Sq-50 ✓
Propane-Sq-75 ✓
Propane-Re-50 ✓
Propane-Re-75 ✓
Propylene-Sq-50 ✓
Propylene-Sq-75 ✓
Propylene-Re-50 ✓
Propylene-Re-75 ✓
Methane-Sq-50 ×
Methane-Sq-75 ✓
Methane-Re-50 ×
Methane-Re-75 ×

The Series 8 simulations were conducted with a 50% reduction of the default number of radiation angles to be accounted for in the calculations.

Observations

The parameter change caused a slight increase in velocity and temperature for the methane fire simulation, but for the propane and propylene fire simulations, both increase and decrease in the quantities are observed. It is noted that the magnitude of the change is most significant for the Rectangle burner simulations. Changes to the gauge heat flux are small and not consistent with the trends noted for the simulation type as shown in the temperature and velocity, however, the magnitude of the change appears to be proportional to the elevation.

Series 9 - Ratios of Parameter Change from Default Series

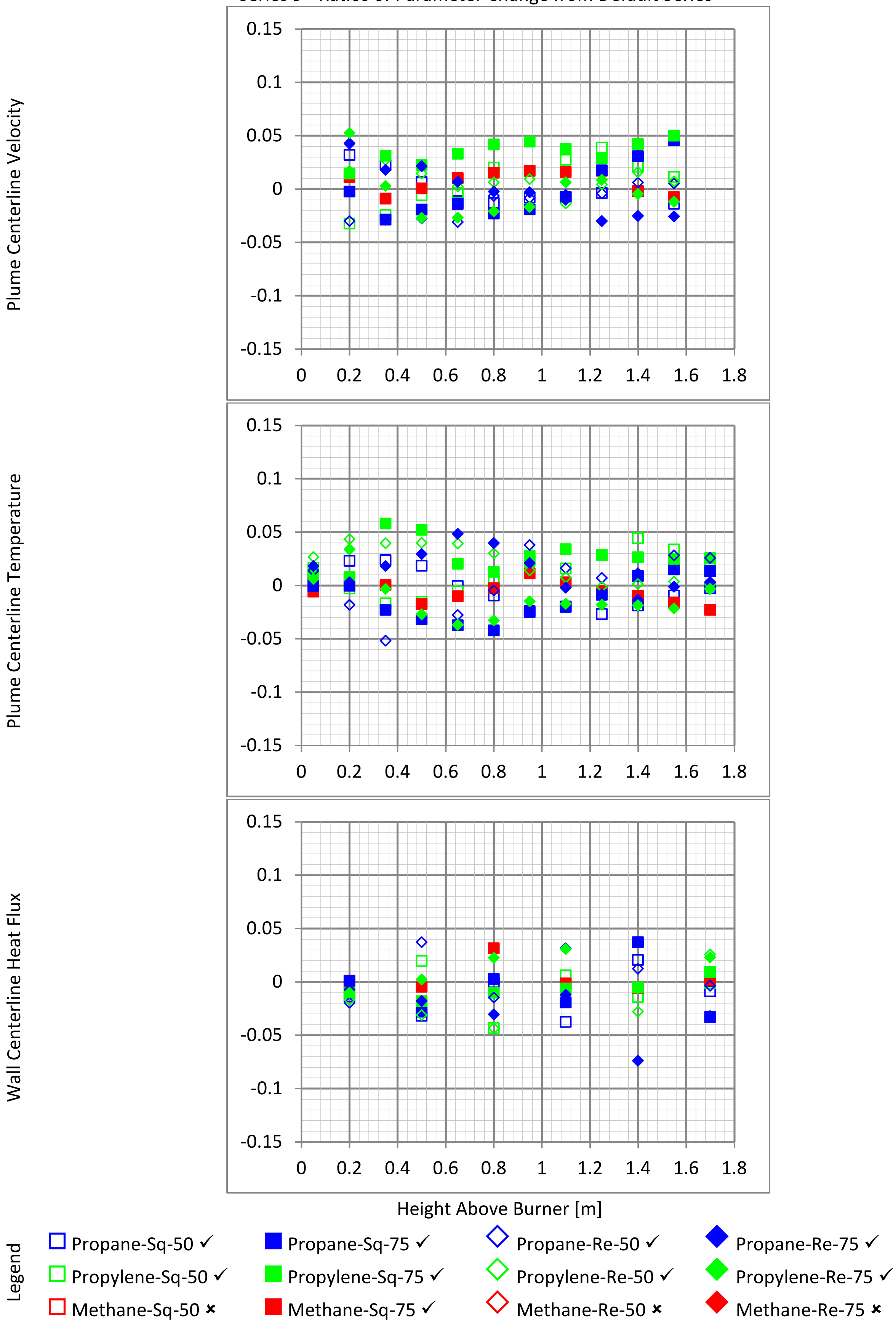

Observations

The Series 9 simulations were conducted with a 100% increase of the number of radiation angles to be calculated for in the models.

For all simulations, the parameter change created very slight changes in magnitude and direction for all three quantities that appears to be relatively random. In addition, the magnitude of the gauge heat flux change appears to be proportional to the elevation.

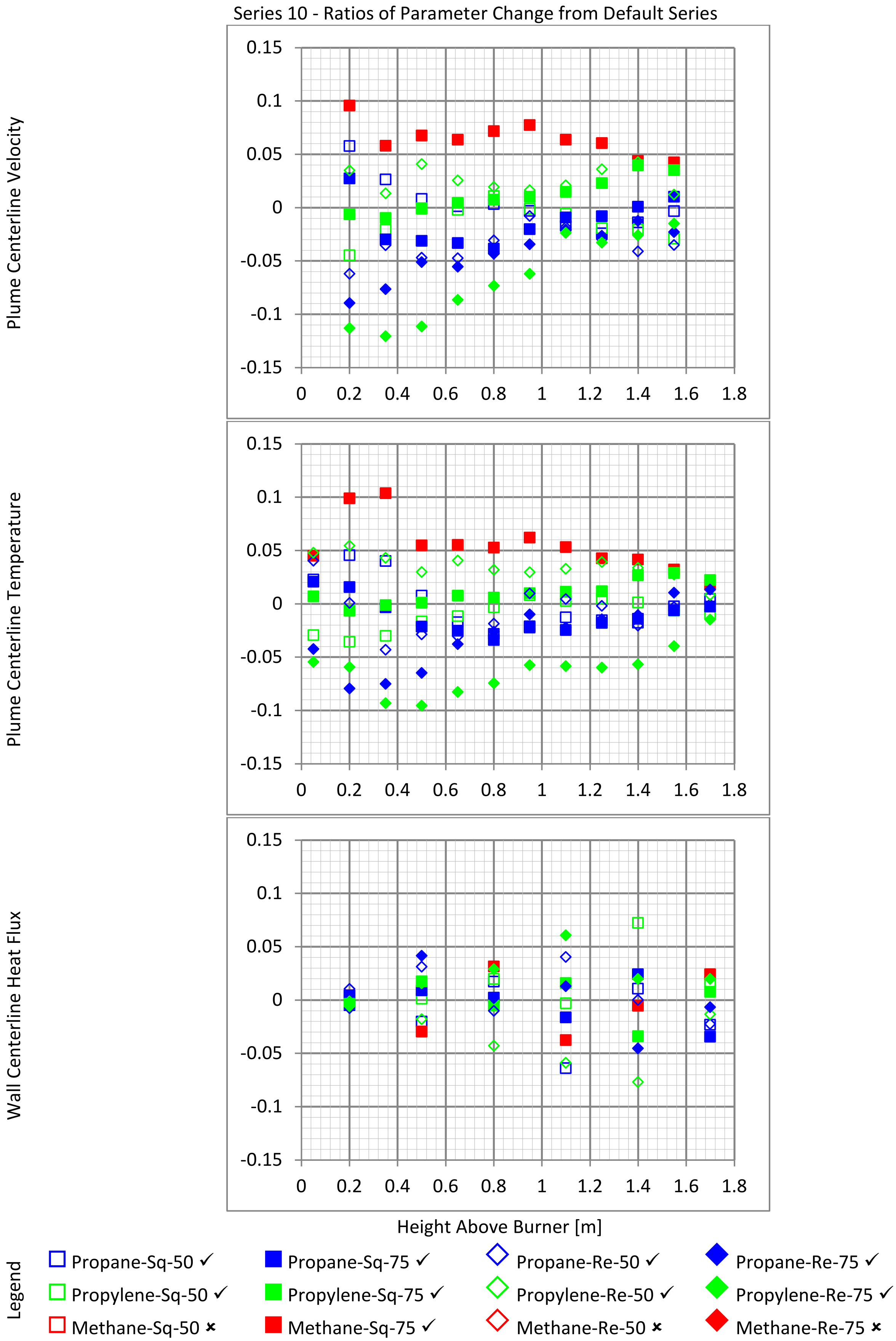

Series 10 - Ratios of Parameter Change from Default Series
Plume Centerline Velocity
Plume Centerline Temperature
Wall Centerline Heat Flux
0.15
0.1
0.05
0
-0.05
-0.1
-0.15
0
0.2
0.4
0.6
0.8
1
1.2
1.4
1.6
1.8
Height Above Burner [m]
Legend
Propane-Sq-50 ✓
Propane-Sq-75 ✓
Propane-Re-50 ✓
Propane-Re-75 ✓
Propylene-Sq-50 ✓
Propylene-Sq-75 ✓
Propylene-Re-50 ✓
Propylene-Re-75 ✓
Methane-Sq-50 ×
Methane-Sq-75 ✓
Methane-Re-50 ×
Methane-Re-75 ×

Observations

The radiation angle increment, which determine how often FDS updates the radiation solution, was reduced from 5 to 2 in the Series 10 simulations.

The parameter change caused in increase in the velocity and temperature for the methane simulation that is inversely proportional to the elevation. For the propane and propylene simulations, the changes occurred in both the positive and negative directions, but it appears that the changes for the cases with the Rectangle burner at 75 kW are the most prominent. In addition, the gauge heat flux's change is random in direction but its magnitude appears to be proportional to the elevation, but still very insignificant in the order of ±5%.

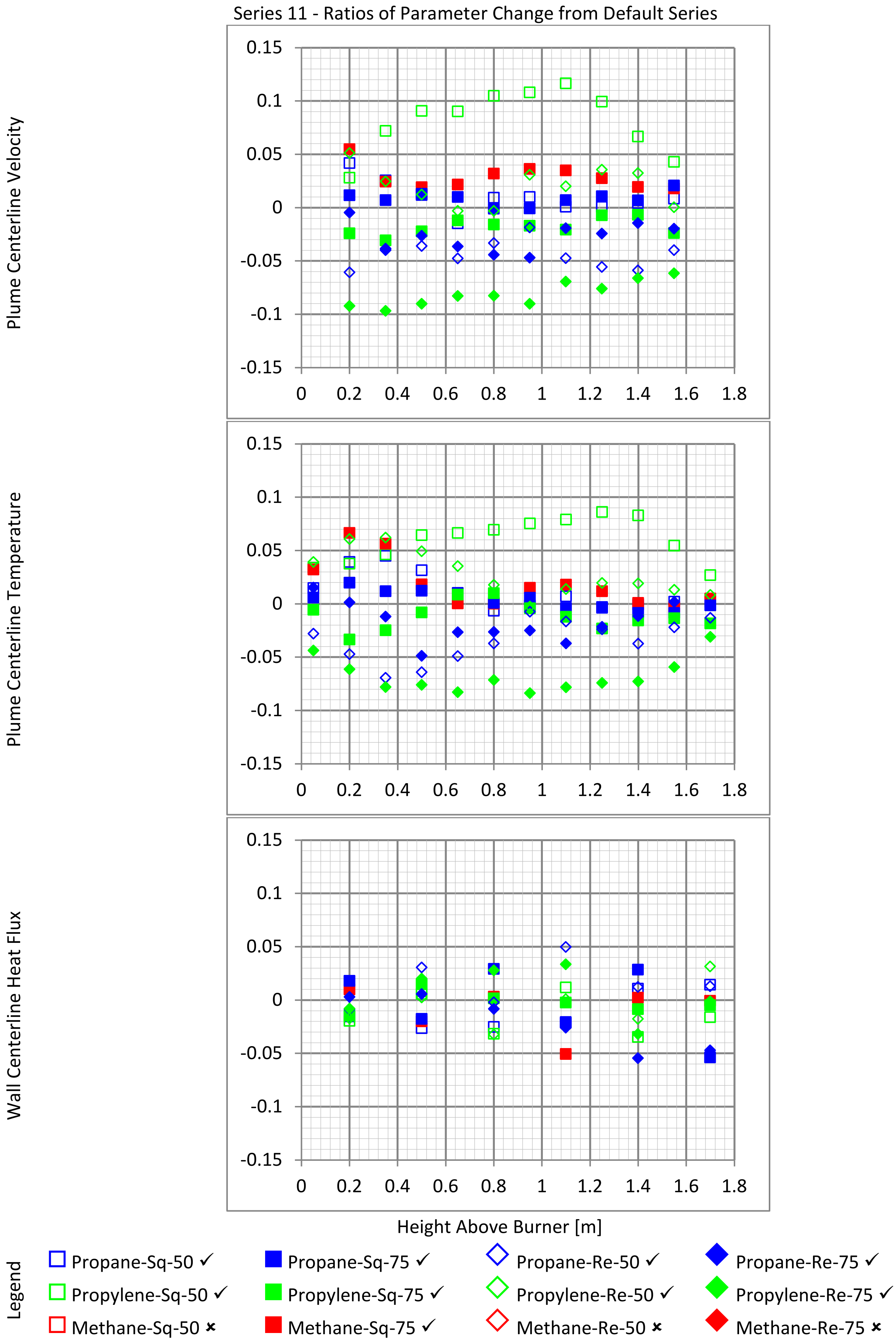
Series 11 - Ratios of Parameter Change from Default Series
Plume Centerline Velocity
Plume Centerline Temperature
Wall Centerline Heat Flux
0.15
0.1
0.05
0
-0.05
-0.1
-0.15
0 0.2 0.4 0.6 0.8 1 1.2 1.4 1.6 1.8
Height Above Burner [m]
Legend
Propane-Sq-50 ✓
Propane-Sq-75 ✓
Propane-Re-50 ✓
Propane-Re-75 ✓
Propylene-Sq-50 ✓
Propylene-Sq-75 ✓
Propylene-Re-50 ✓
Propylene-Re-75 ✓
Methane-Sq-50 ×
Methane-Sq-75 ✓
Methane-Re-50 ×
Methane-Re-75 ×

The radiation angle increment, which determine how often FDS updates the radiation solution, was increased from 5 to 10 in the Series 11 simulations, essentially halving the rate at which the radiation angles were updated.

Observations

Velocity and temperature for the methane fire simulation have been slightly increased due to the parameter change. The changes to the propane fire simulations are less significant, but in the negative direction. However, for the propylene simulations, the most positive change occurred to the Square burner at 50 kW but the most negative for the Rectangle burner at 75 kW. In addition, the gauge heat flux's change is random in direction but its magnitude appears to be proportional to the elevation, but still very insignificant in the order of ±5%.

Series 12 - Ratios of Parameter Change from Default Series

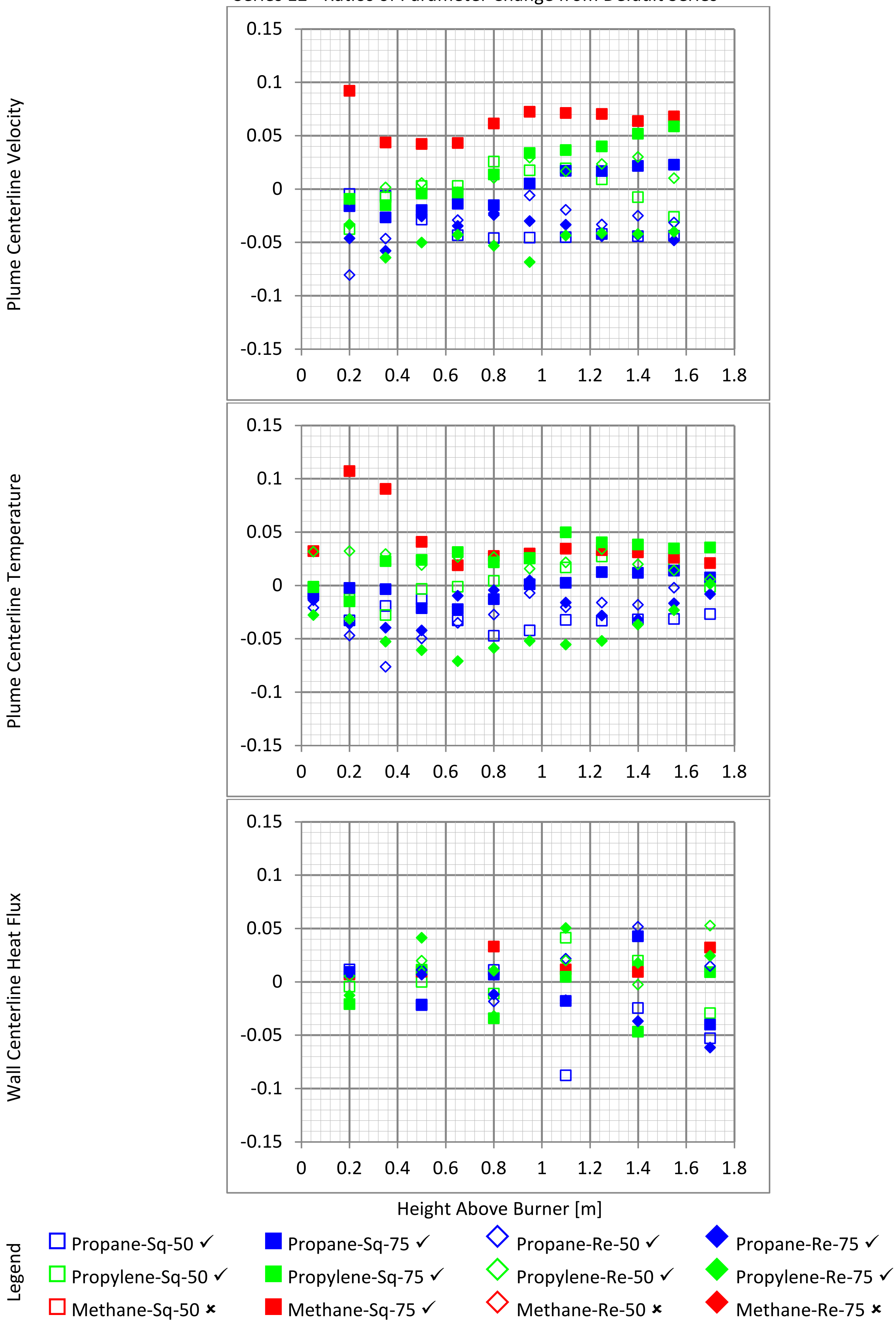

The time step increment of the radiation solver was reduced from 3 to 1 in the Series 12 simulations, essentially increasing the update rate of the radiation solver in every time step.

Observations

The changes in the velocity and temperature are the most significant to the methane fire simulation. The centerline plume velocity for the other simulations appears to have generally been decreased, except for a few cases where the velocity had increased from elevation at 0.6 m and above. The centerline plume temperature of the simulations other than the methane fire had generally been decreased, except for several of the propylene simulations. In addition, the gauge heat flux's change is random in direction but its magnitude appears to be proportional to the elevation, but within the range of ±10% over the different elevations.

Series 13 - Ratios of Parameter Change from Default Series

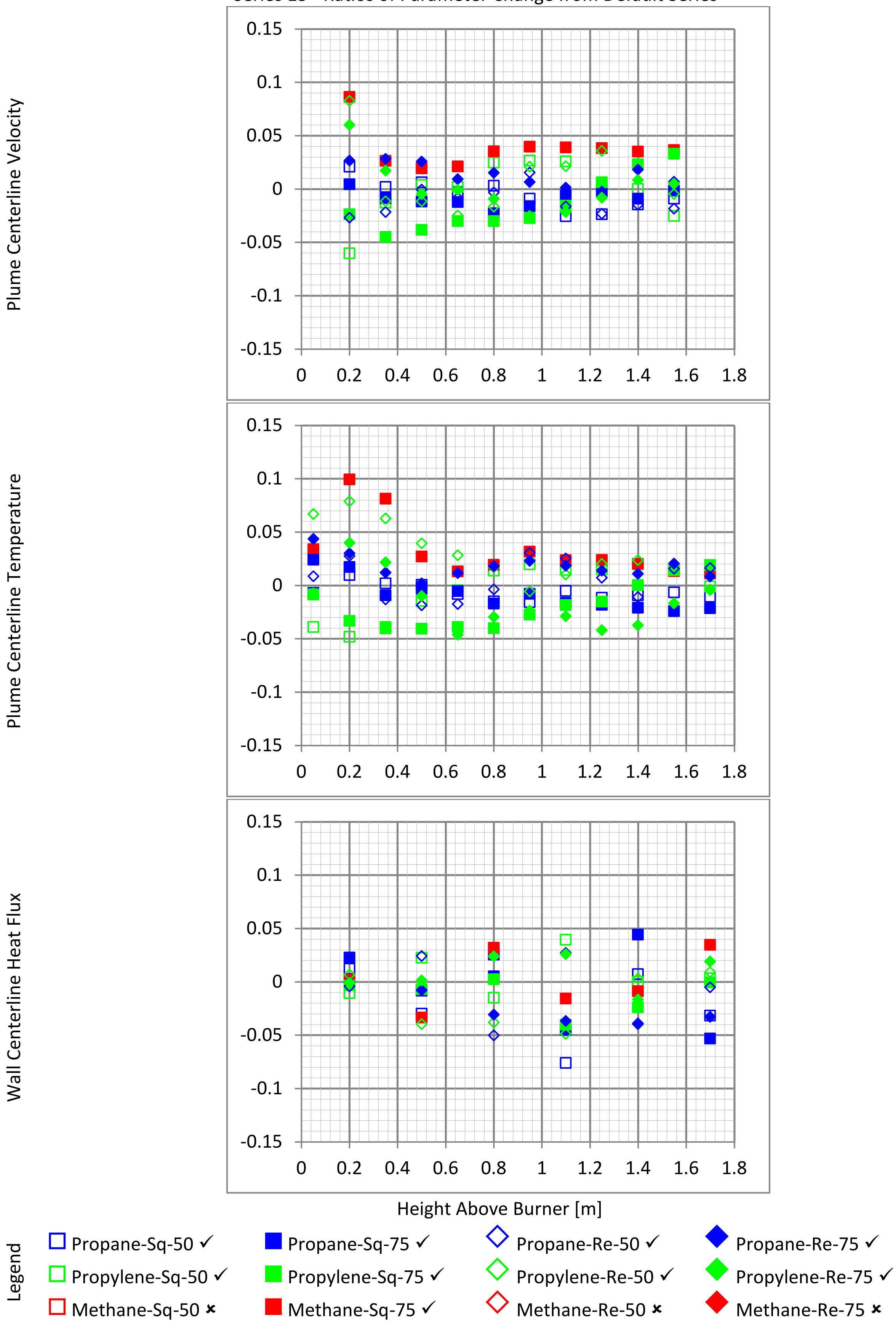

Observations

The time step increment was increased from 3 to 6 in the Series 13 simulations, essentially reducing the rate at which the radiation solver was updated by half.

The most significant change in the centerline plume velociyt occurrs at the lower elevation of 0.2 m for all simulations, then the magnitude of the change, regardless of the direction is within ±5%. In general, the velcoity of the propane simulations isincreased for the lower elevations but increased further away from the burner surface, for the propylene simulations, the inverse has been observed. In terms of temperature, the methane simulation again has the most significant changes in the positive direction. For all simulations, the magnitude change is small at the lowest elevation but increased at elevation of 0.2 to 0.4 m, but decreased to the previous level from 0.5 m and above. For the propane simulations, the Rectangle burner fires generally has an increase, where as the Square burner generally has a decrease from the elevation of 0.5 m and above. In propylene simulations, the Square burner fires have generally a decrease in temerature, whereas an increase in temperature is noted for the Rectangle burner fires. In addition, the gauge heat flux's change is random in direction but its magnitude appears to be proportional to the elevation, but within the range of ±10% over the different elevations.

Series 15 - Ratios of Parameter Change from Default Series

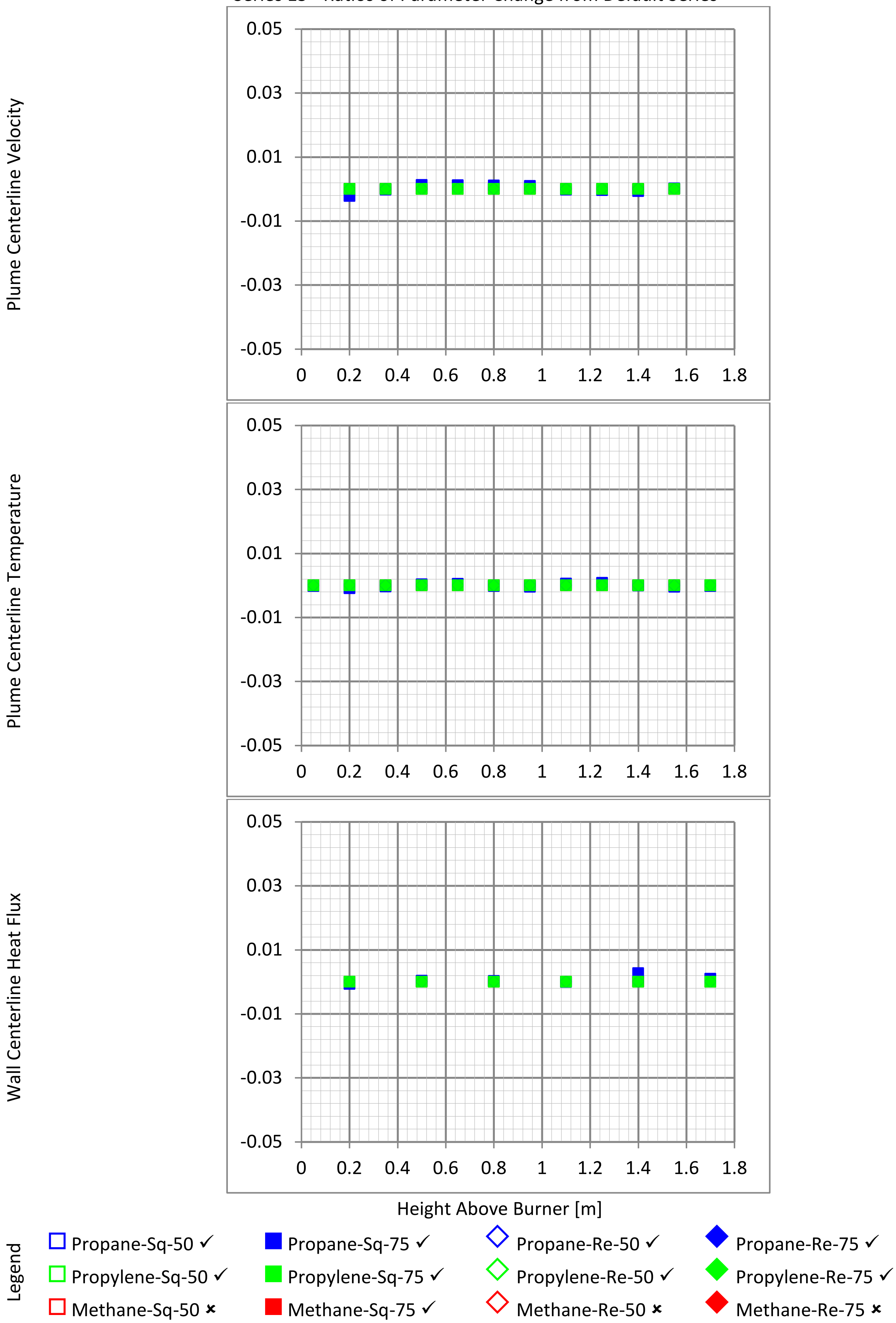

Observations

The parameter C_EDC which is a constant used to determine the mixing time scale used in the turbulent combustion calculations was increased from 0.1 to 0.2 in the Series 15 simulations thereby doubling the mixing time scale.

The changes for the velocity, temperature, and heat flux are almost non-existent for due to the change in the C_EDC parameter for the inert wall fire simulation series. This is different to the plume series where some changes, although quite insignificant, have been observed.

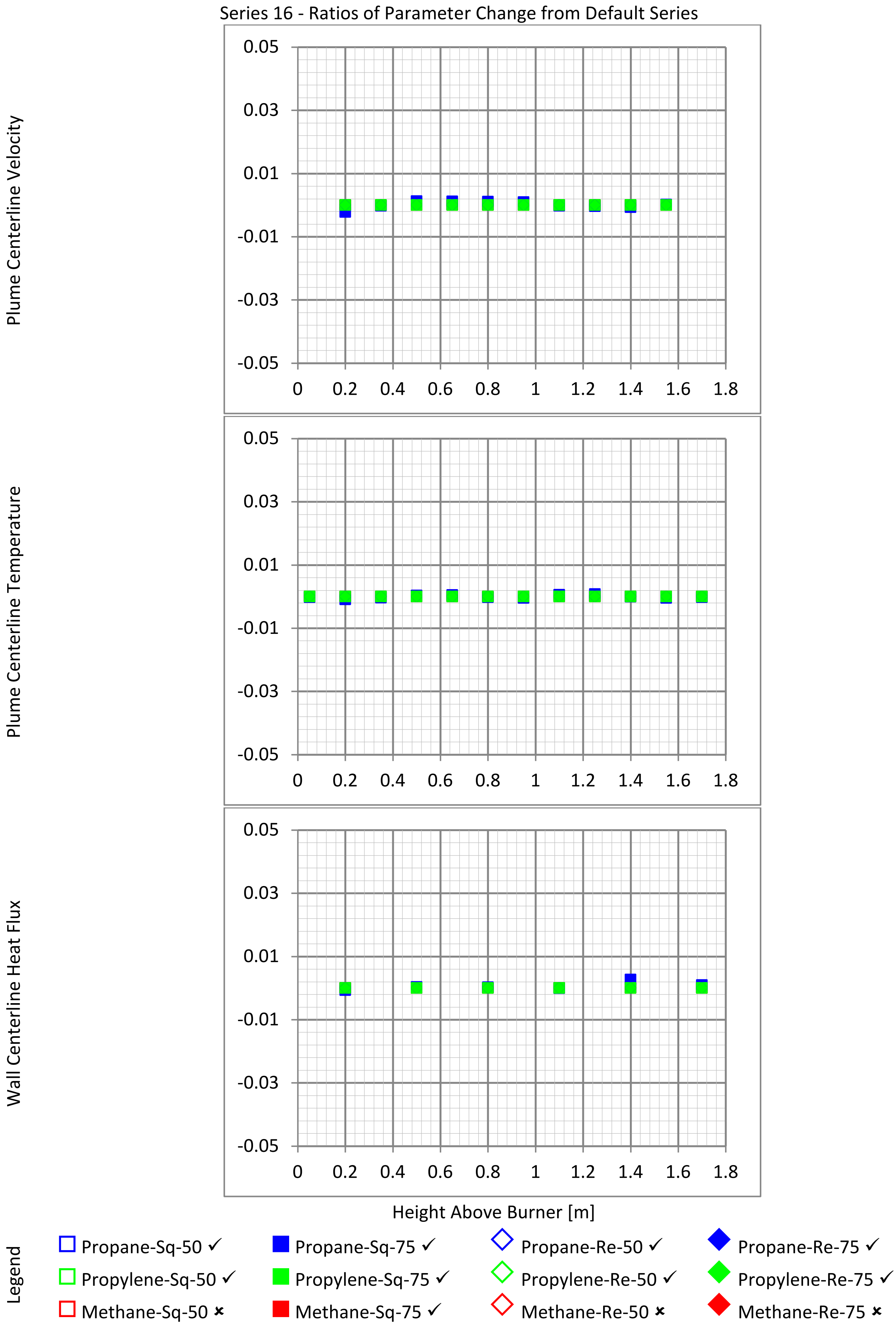

Series 16 - Ratios of Parameter Change from Default Series
Plume Centerline Velocity
Plume Centerline Temperature
Wall Centerline Heat Flux
0.05
0.03
0.01
-0.01
-0.03
-0.05
0
0.2
0.4
0.6
0.8
1
1.2
1.4
1.6
1.8
Height Above Burner [m]
Legend
Propane-Sq-50 ✓
Propane-Sq-75 ✓
Propane-Re-50 ✓
Propane-Re-75 ✓
Propylene-Sq-50 ✓
Propylene-Sq-75 ✓
Propylene-Re-50 ✓
Propylene-Re-75 ✓
Methane-Sq-50 ×
Methane-Sq-75 ✓
Methane-Re-50 ×
Methane-Re-75 ×

Observations

The parameter C_EDC which is a constant used to determine the mixing time scale used in the turbulent combustion calculations was reduced to 0.05 from 0.1 in the Series 16 simulations thereby halving the mixing time scale.

The changes for the velocity, temperature, and heat flux are almost non-existent for due to the change in the C_EDC parameter for the inert wall fire simulation series. This is different to the plume series where some changes, although quite insignificant, have been observed.

Series 17 - Ratios of Parameter Change from Default Series

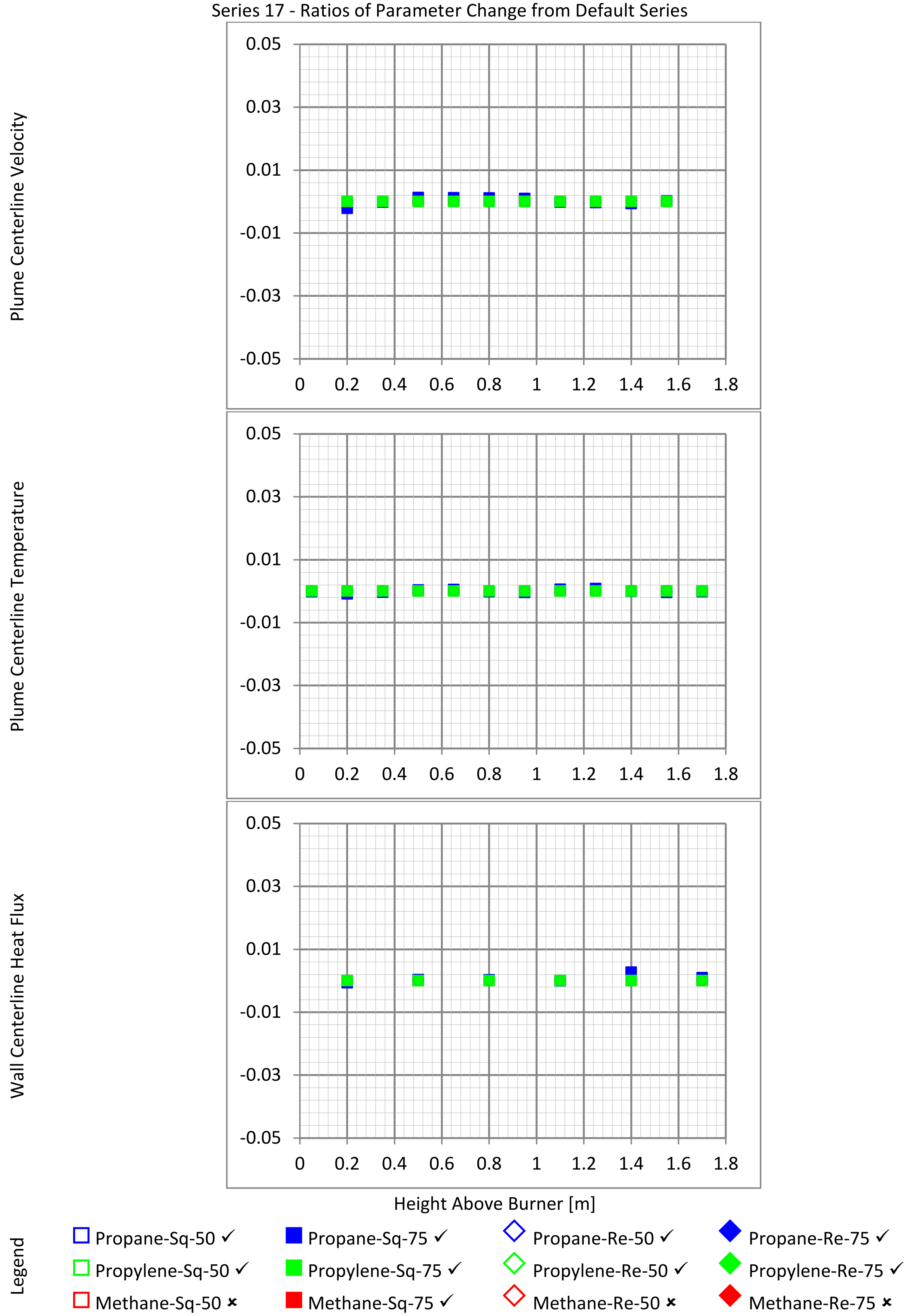

Observations

Eddy dissipation mode is usually enabled in the large eddy simulations, but disabling it, the mixing time scale of the turbulent combustion becomes the time step of the simulation.

The changes for the velocity, temperature, and heat flux are almost non-existent for due to disabling of the eddy dissipation simulation mode for the inert wall fire simulation series. This is different to the plume series where some changes, although quite insignificant, have been observed.

Series 18 - Ratios of Parameter Change from Default Series

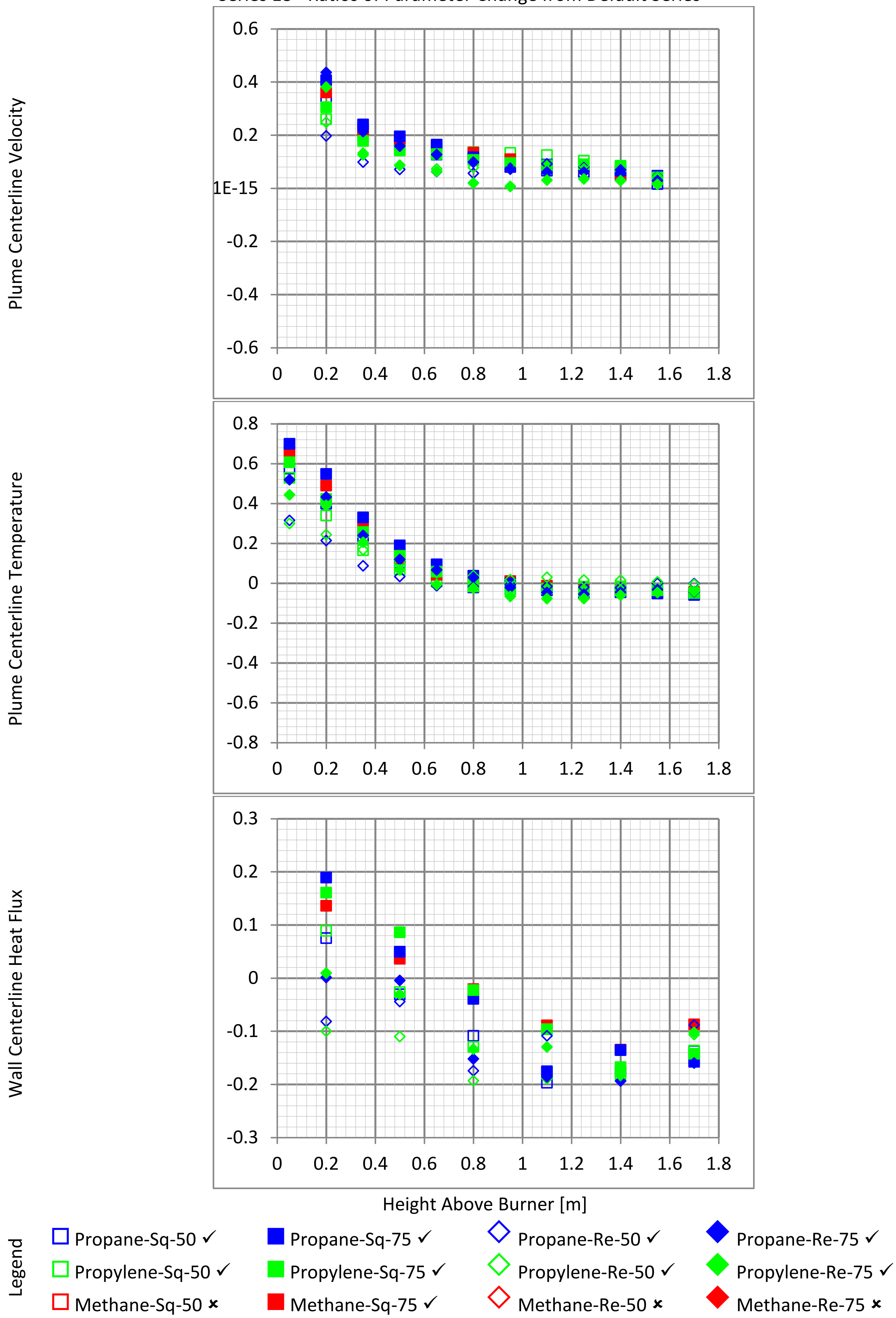

In Series 18 simulations, the heat release rate per unit area of the flame sheet was increased from 0 kW/m^2 to 400 kW/m^2 for LES simulations.

Observations

A significant increase is noted in the velocity for all of the simulations regardless of the set up. For the centerline plume temperature, however, the increase is significant for the locations up to 0.8 m, where the changes becomes in significant fo rthe elevations above. In term of the centerline gauge heat flux, the changes are positive for all tests except for the simulations of the Rectangle burner at 50 kW at the lowest location at 0.2 m. The change then becomes more negative with an increase in elevation.

Series 19 - Ratios of Parameter Change from Default Series

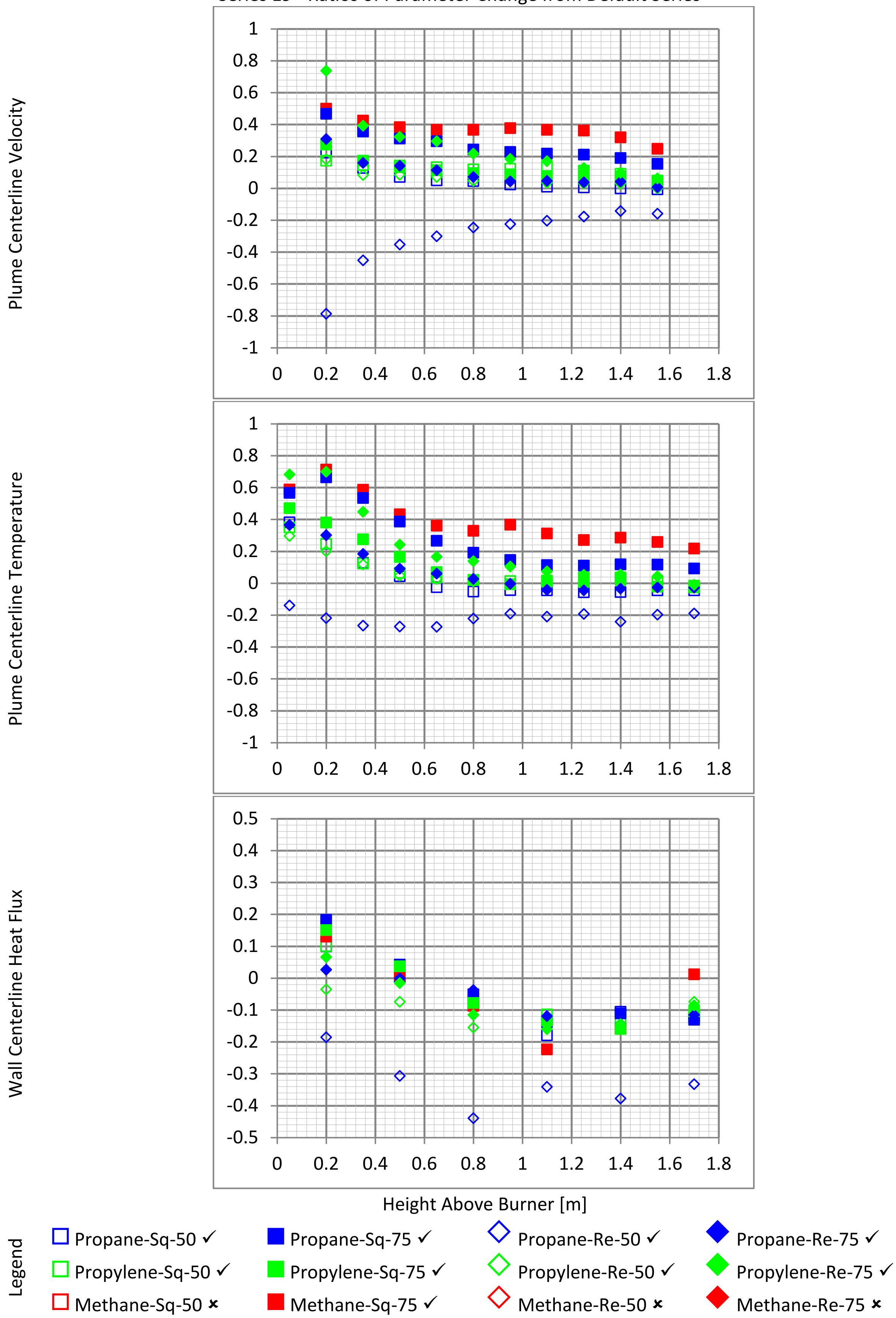

In Series 19 simulations, the heat release rate per unit area of the flame sheet was increased to 100 kW/m^2 from 0 kW/m^2 for LES simulations.

Observations

For all simulations except for the propane fire with the Square burner at 50 kW, the changes in velocity and temperature are drasticlally positive. This discrepency is noted in the centerline heat flux as well in that the changes in the propane Squre burner at 50 kW simulations are more negative than the other simulations. Although the input files had been investigated, no erros had been found there but it is likely that the predictions was due to software/hardware errors and should be considered an anomaly. Similar to the results of Series 18, the centerline gauge heat flux, the changes are mostly positive at the lower elevation at 0.2 and 0.5 m, but become significantly more negative with increase in elevation.

Series 20 - Ratios of Parameter Change from Default Series

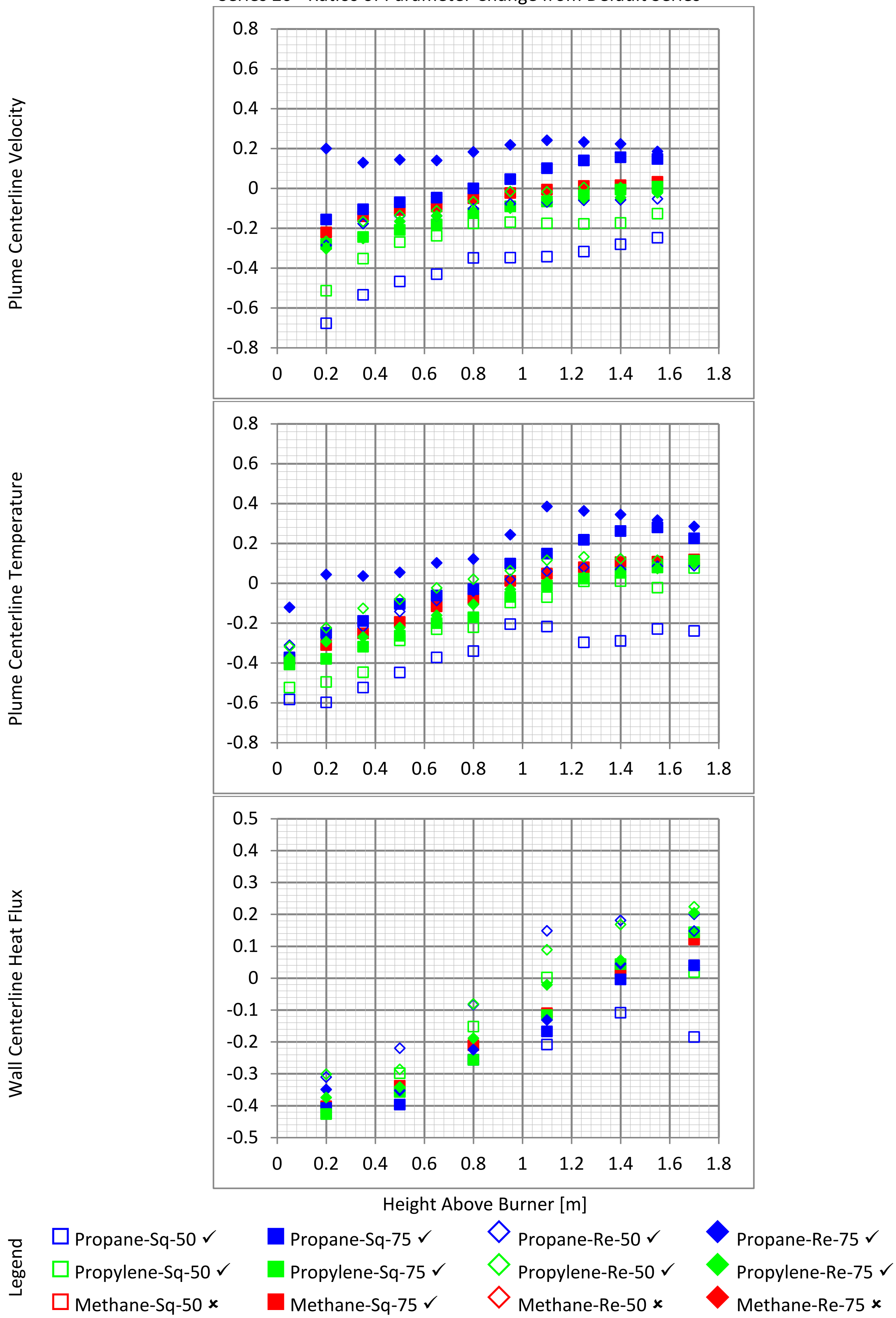

Observations

In Series 20 simulations, the average local heat release rate per unit volume was reduced from the default 2500 kW/m^3 to a value of 1200 kW/m^3 as suggested by Orloff and De Ris for the entire fire.

For veocity, temperature, and gauge heat flux, the parameter change generally caused a decrease in the predicted quantity that is inversely proportional to the elevation, casusing some increase after 1 m in elevation. The propane Rectangle burner at 75 kW fire simulation does not follow this trend however, and has generally positive changes for velocity and temperature. The simulation with the overall greatest magnitude (in negative) is for the propane fire at 50 kW using the Square burner.

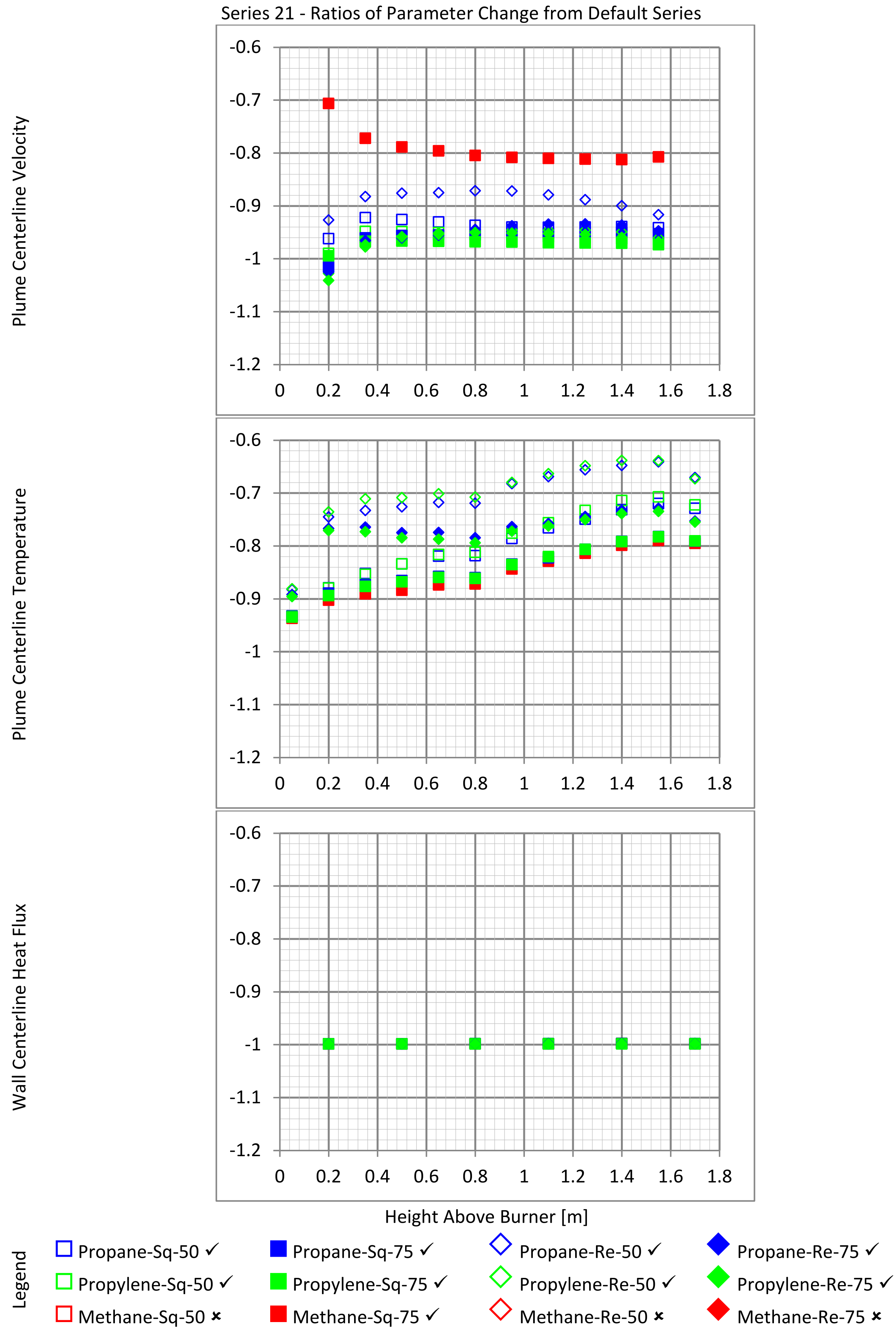

Series 21 - Ratios of Parameter Change from Default Series
Plume Centerline Velocity
Plume Centerline Temperature
Wall Centerline Heat Flux
-0.6
-0.7
-0.8
-0.9
-1
-1.1
-1.2
0
0.2
0.4
0.6
0.8
1
1.2
1.4
1.6
1.8
Height Above Burner [m]
Legend
Propane-Sq-50 ✓
Propane-Sq-75 ✓
Propane-Re-50 ✓
Propane-Re-75 ✓
Propylene-Sq-50 ✓
Propylene-Sq-75 ✓
Propylene-Re-50 ✓
Propylene-Re-75 ✓
Methane-Sq-50 ×
Methane-Sq-75 ✓
Methane-Re-50 ×
Methane-Re-75 ×

Observations

The isothermal model was enabled in the Series 21 simulations to test the effects of a fire simulation in which the temperature was forced to not changed. It was intended to show whether a mistake in writing the FDS file would result in a simulation with some salvageable and meaningful data.

As espected, the velocity and temperature are severely depressed in this series of simulations, furthermore, the heat fluxes are reduced to zero. It is noted that the methane simulation had the smallest drop in velocity but the greatest decrease in velocity comapred to the default.

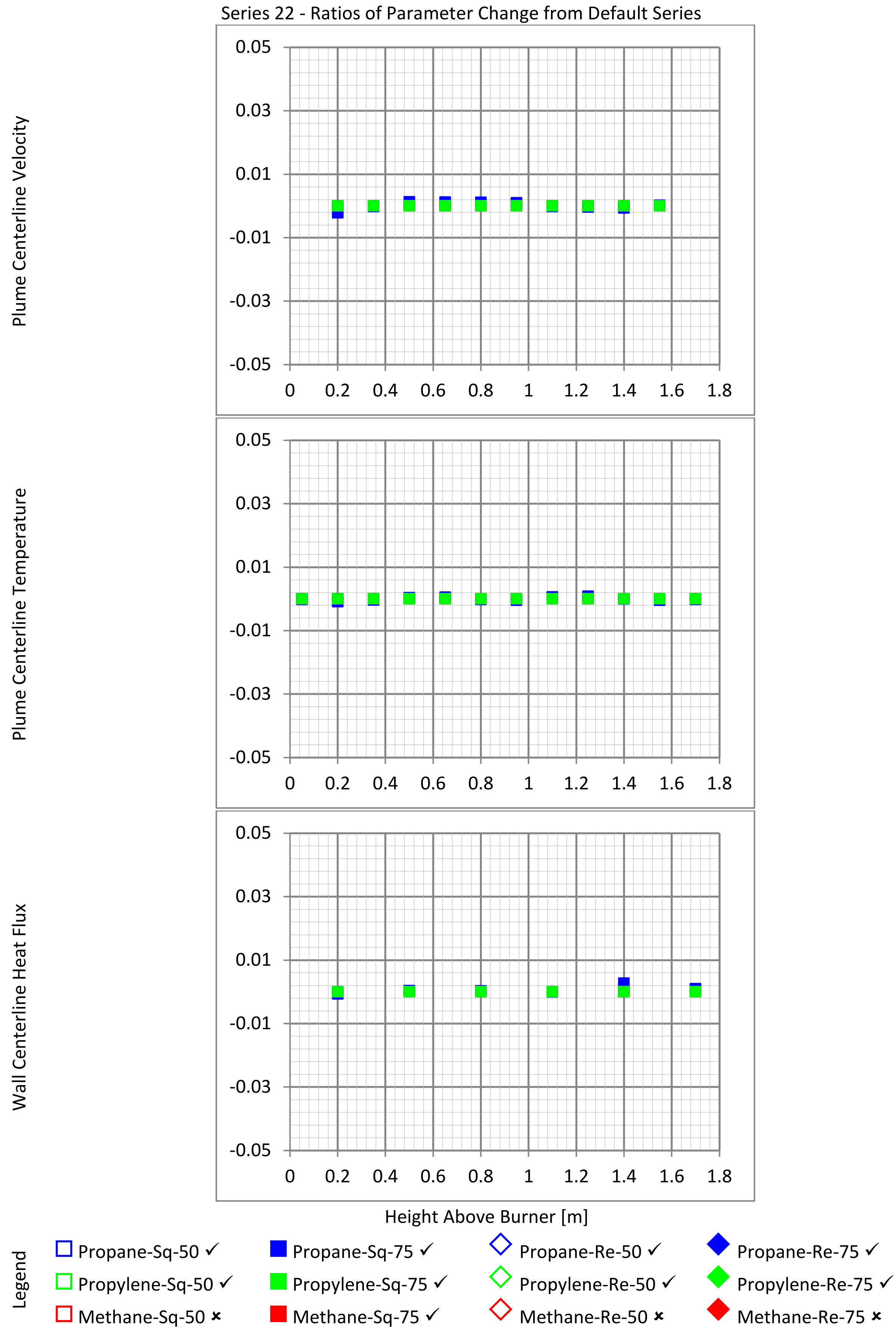
Series 22 - Ratios of Parameter Change from Default Series
Plume Centerline Velocity
Plume Centerline Temperature
Wall Centerline Heat Flux
0.05
0.03
0.01
-0.01
-0.03
-0.05
0
0.2
0.4
0.6
0.8
1
1.2
1.4
1.6
1.8
Height Above Burner [m]
Legend
Propane-Sq-50 ✓
Propane-Sq-75 ✓
Propane-Re-50 ✓
Propane-Re-75 ✓
Propylene-Sq-50 ✓
Propylene-Sq-75 ✓
Propylene-Re-50 ✓
Propylene-Re-75 ✓
Methane-Sq-50 ×
Methane-Sq-75 ✓
Methane-Re-50 ×
Methane-Re-75 ×

Observations

In Series 22, the Smagorinsky constant was reduced from 0.2 to 0.1, it was used to calculate the viscosity of the fluid and to model the subgrid-scale turbulence in the models.

The changes for the velocity, temperature, and heat flux are almost non-existent for due to the change in the Smagorinsky constant for the inert wall fire simulation series. This is different to the plume series where some changes, although quite insignificant, have been observed.

Series 23 - Ratios of Parameter Change from Default Series

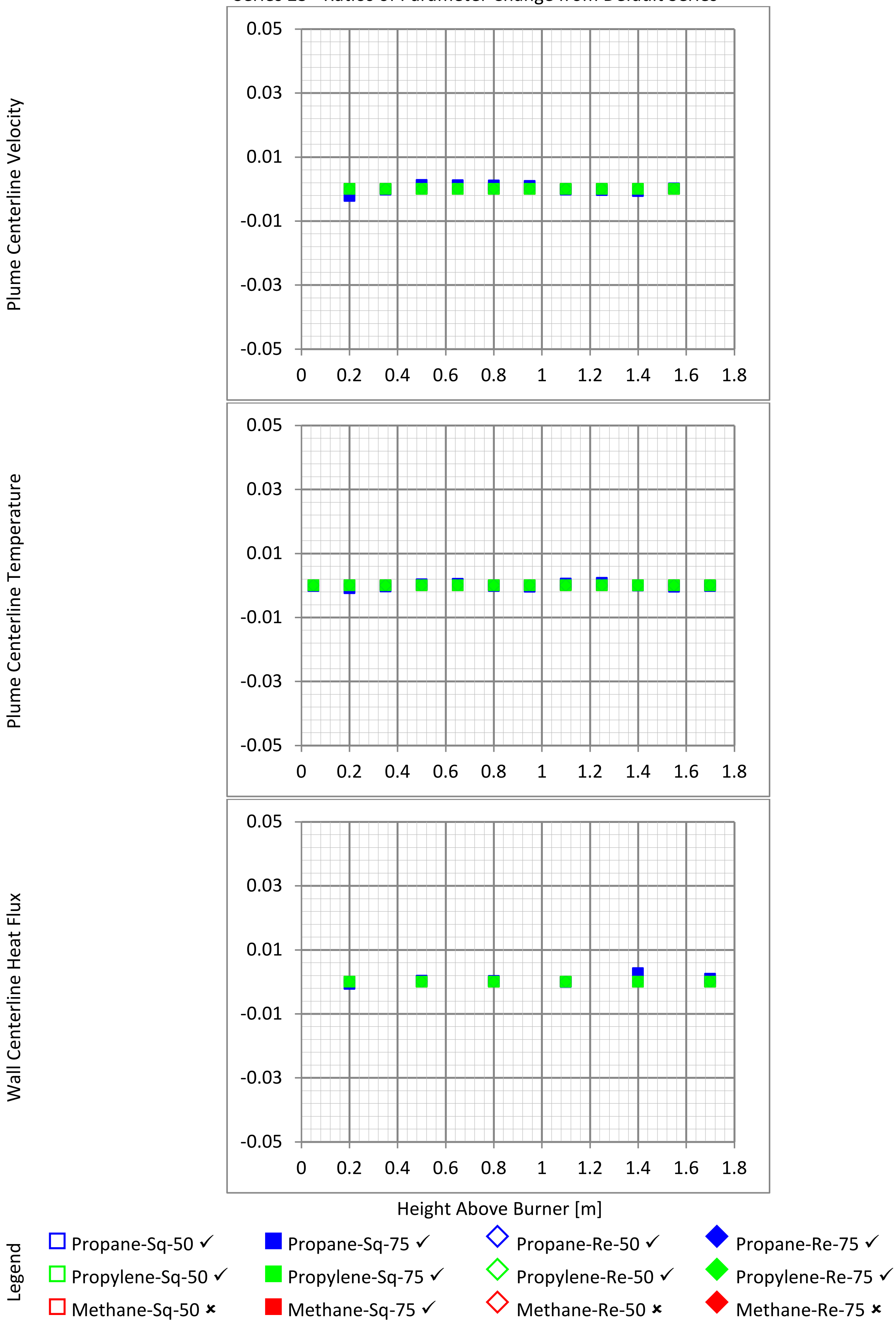

Observations

In Series 23, the Smagorinsky constant was increased from 0.2 to 0.4, it was used to calculate the viscosity of the fluid and to model the subgrid-scale turbulence in the models.

The changes for the velocity, temperature, and heat flux are almost non-existent for due to the change in the Smagorinsky constant for the inert wall fire simulation series. This is different to the plume series where some changes, although quite insignificant, have been observed.

Series 24 - Ratios of Parameter Change from Default Series

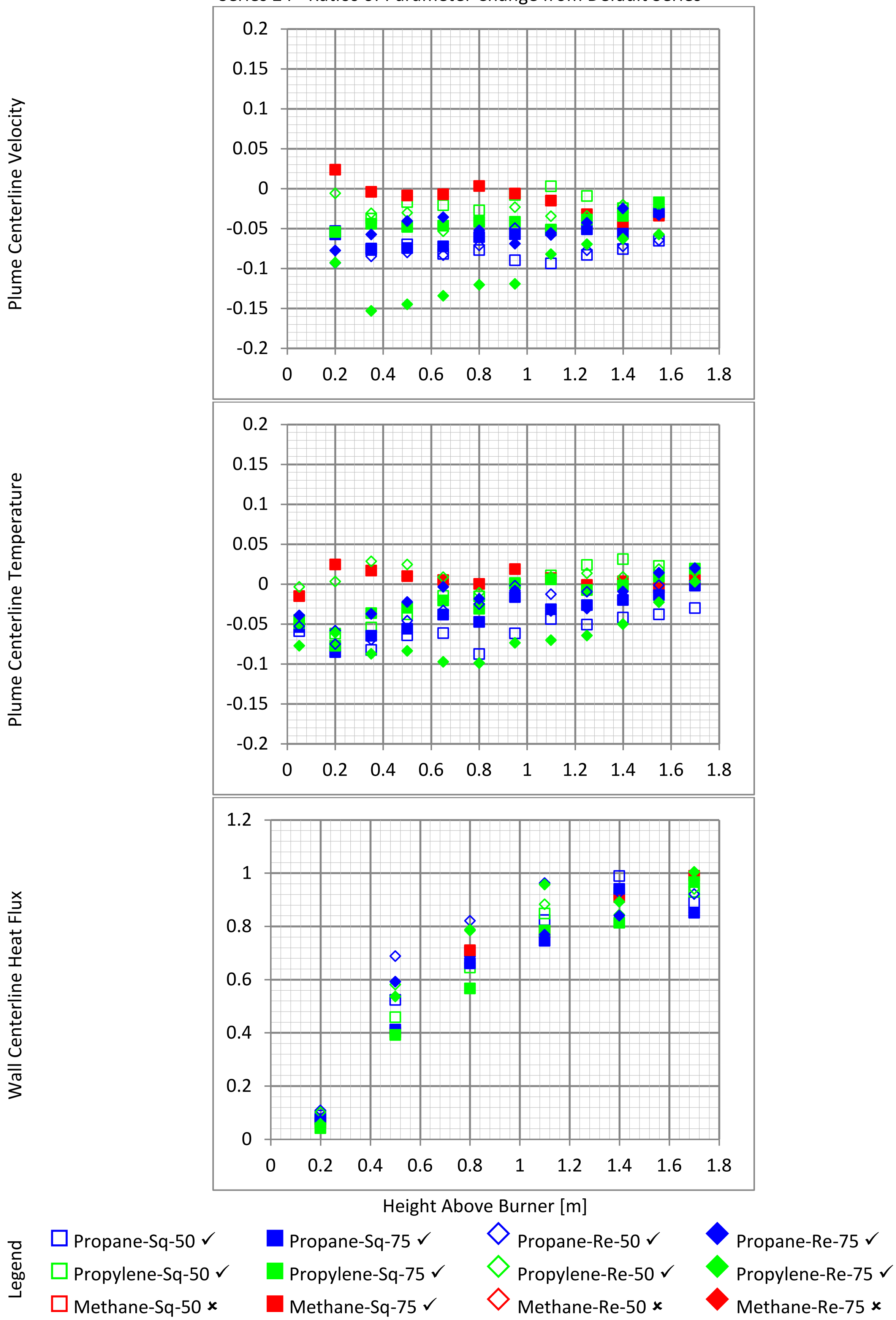

Observations

In Series 24, the turbulent Prandtl number was decreased to 0.25 from 0.5, the Prandtl number is a ratio of the momentum diffusivity to thermal diffusivity, so this parameter change had the potential to change the flow characteristics in the simulations.

The parameter change generally created a decrease in the predicted centerline pume velocity and temperature for all fire simulations, with the least changes recorded for the methane fire siulation, and the largest change in both these quantities occurred for the propylene fire with Rectangle burner at 75 kW. In term of the centerline gauge heat flux, the parameter change caused a significant increase that is proportional to the elevation.

Series 25 - Ratios of Parameter Change from Default Series

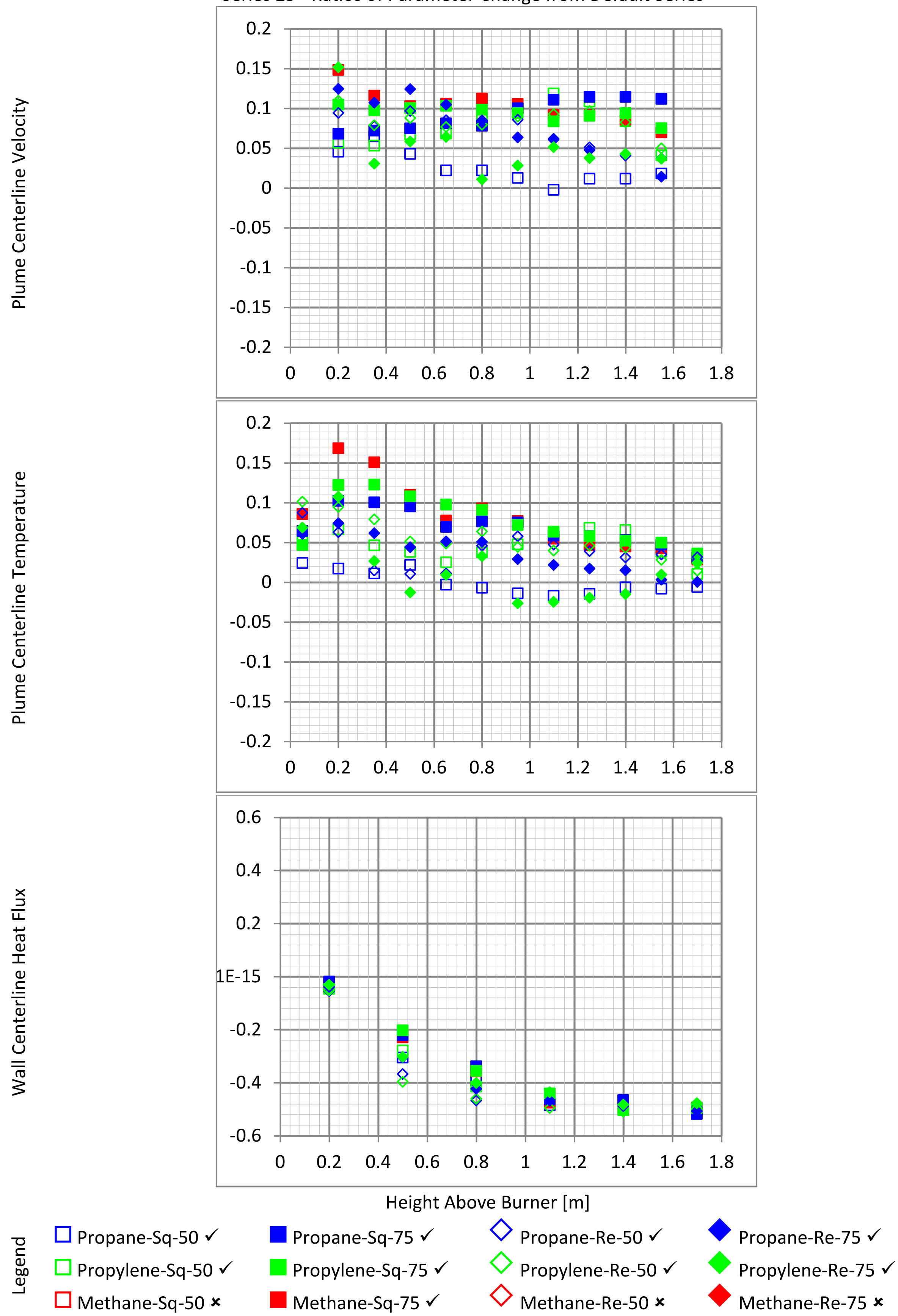

Observations

In Series 25, the turbulent Prandtl number was increased from 0.5 to 1, the Prandtl number is a ratio of the momentum diffusivity to thermal diffusivity, so this parameter change had the potential to change the flow characteristics in the simulations.

Increases to the velocity and temperature are noted due to the parameter change, the changes are relatively consistent for the velocity over the elevation, but the increases are inversely proportional to the elevation for the plume temperature. For the gauge heat flux, the parameter change affected a negative change that is proportional to elevation.

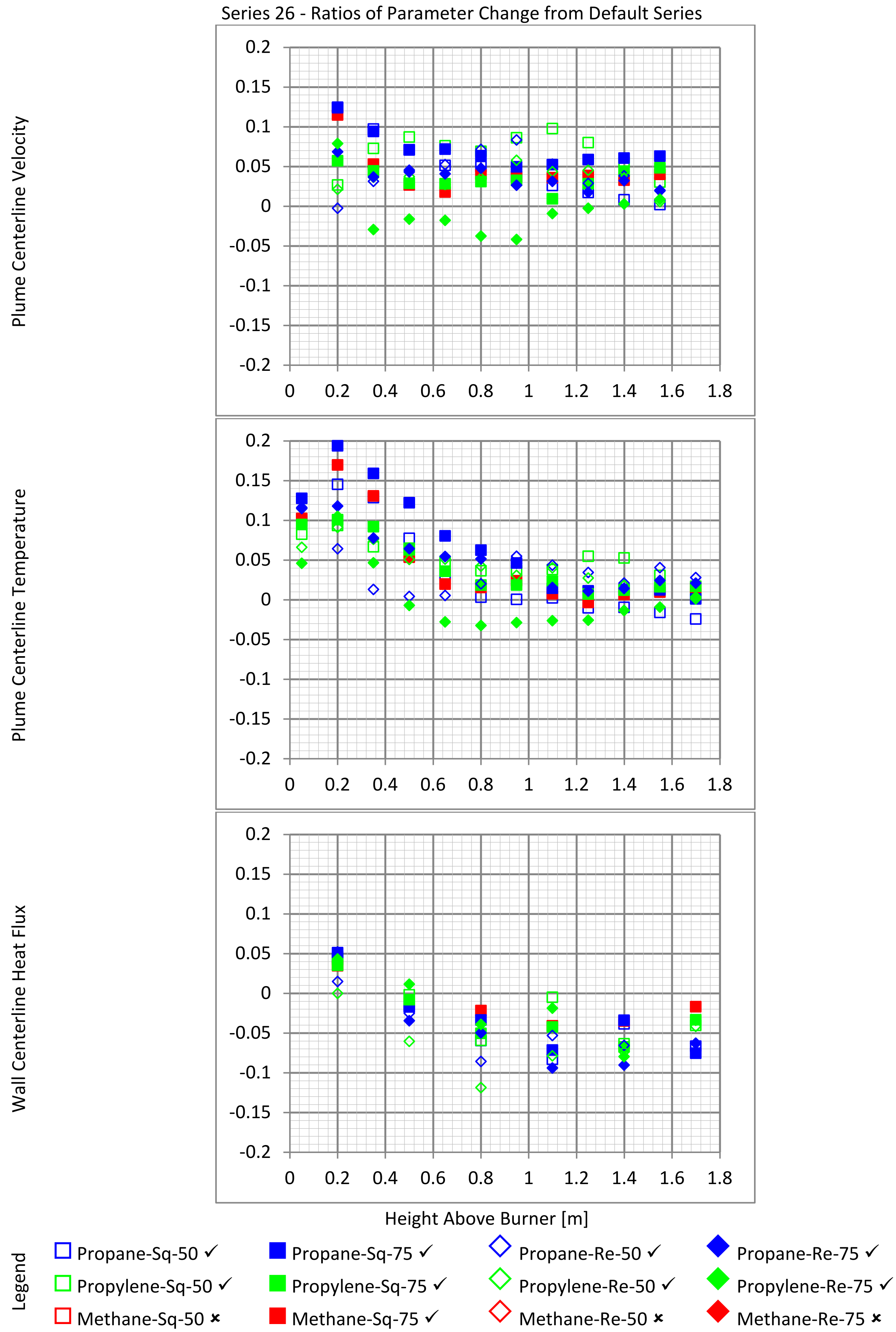

Series 26 - Ratios of Parameter Change from Default Series
Plume Centerline Velocity
Plume Centerline Temperature
Wall Centerline Heat Flux
0.2
0.15
0.1
0.05
0
-0.05
-0.1
-0.15
-0.2
0
0.2
0.4
0.6
0.8
1
1.2
1.4
1.6
1.8
Height Above Burner [m]
Legend
Propane-Sq-50 ✓
Propane-Sq-75 ✓
Propane-Re-50 ✓
Propane-Re-75 ✓
Propylene-Sq-50 ✓
Propylene-Sq-75 ✓
Propylene-Re-50 ✓
Propylene-Re-75 ✓
Methane-Sq-50 ×
Methane-Sq-75 ✓
Methane-Re-50 ×
Methane-Re-75 ×

Observations

In Series 26, the turbulent Schmidt number was decreased from 0.5 to 0.25, the Schmidt number is a ratio of the momentum diffusivity to mass diffusivity, so this parameter change had the potential to change the flow characteristics in the simulations.

Increases to the velocity and temperature are noted due to the parameter change, the changes are relatively consistent for the velocity over the elevation, but the increases are inversely proportional to the elevation for the plume temperature. This is similar to the Series 25 results except for the magnitude and trends of the simulations with the different fuel. For the gauge heat flux, the parameter change created a positive change for the lowest elevation at 0.2m and a negative change that is proportional to elevation.

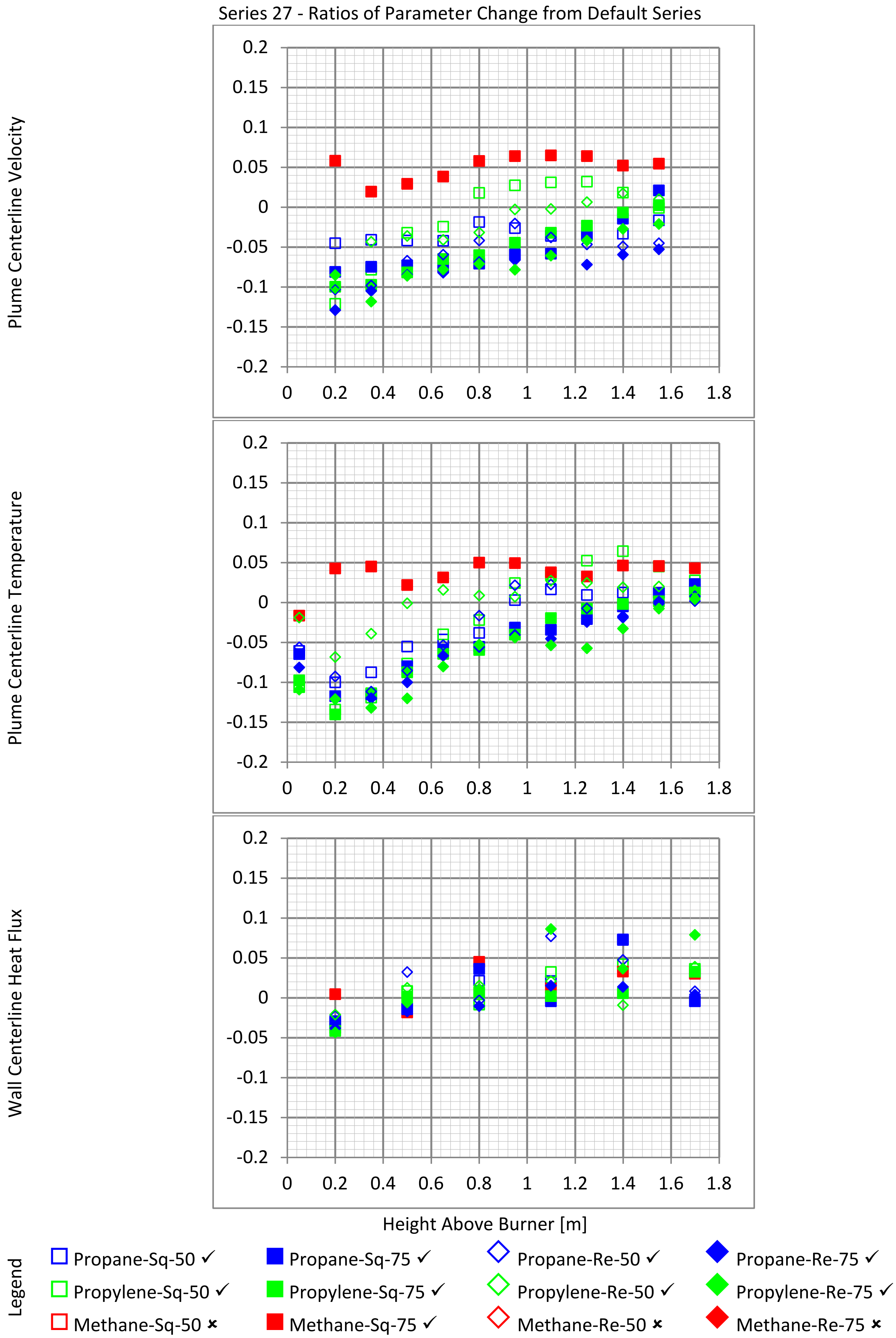

Series 27 - Ratios of Parameter Change from Default Series
Plume Centerline Velocity
Plume Centerline Temperature
Wall Centerline Heat Flux
0.2
0.15
0.1
0.05
0
-0.05
-0.1
-0.15
-0.2
0 0.2 0.4 0.6 0.8 1 1.2 1.4 1.6 1.8
Height Above Burner [m]
Legend
Propane-Sq-50 ✓
Propane-Sq-75 ✓
Propane-Re-50 ✓
Propane-Re-75 ✓
Propylene-Sq-50 ✓
Propylene-Sq-75 ✓
Propylene-Re-50 ✓
Propylene-Re-75 ✓
Methane-Sq-50 ×
Methane-Sq-75 ✓
Methane-Re-50 ×
Methane-Re-75 ×

Observations

In Series 27, the turbulent Schmidt number was increased from 0.5 to 1, the Schmidt number is a ratio of the momentum diffusivity to mass diffusivity, so this parameter change had the potential to change the flow characteristics in the simulations.

The changes in centerline velocity and temperature are similar: the changes for the methane siulation are slightly positive, whereas for the other simulations the changes are mostly in the negative direction. The simulations with the greatest magnitude in the change are the simulations with a HRR at 75 kW. For the centerline gauge heat flux, the changes are slightly negative at the lowest elevation at 0.2 m but becomes positive with magnitude proportional to the elevation.

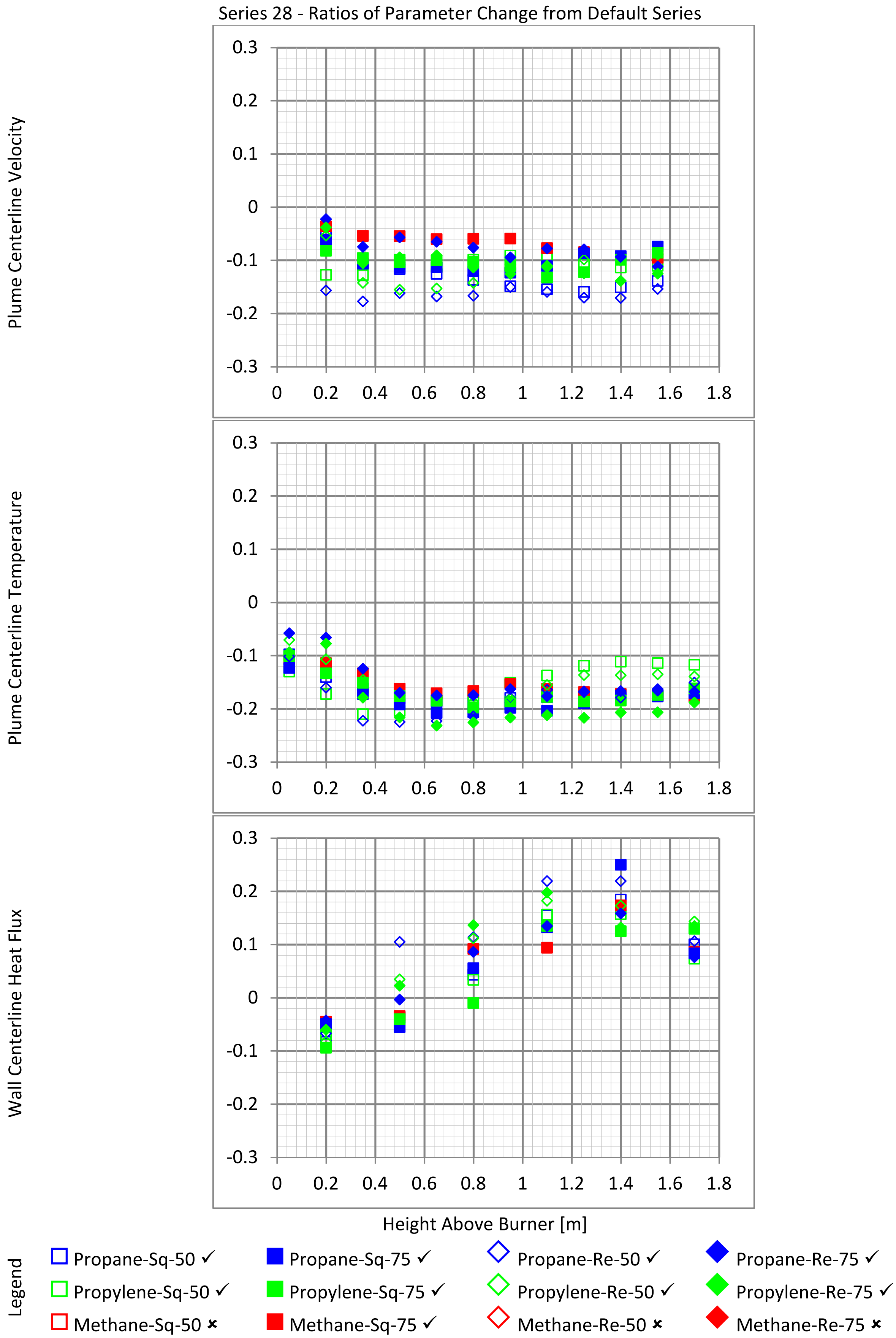
Series 28 - Ratios of Parameter Change from Default Series
Plume Centerline Velocity
Plume Centerline Temperature
Wall Centerline Heat Flux
0.3
0.2
0.1
0
-0.1
-0.2
-0.3
0
0.2
0.4
0.6
0.8
1
1.2
1.4
1.6
1.8
Height Above Burner [m]
Legend
Propane-Sq-50 ✓
Propane-Sq-75 ✓
Propane-Re-50 ✓
Propane-Re-75 ✓
Propylene-Sq-50 ✓
Propylene-Sq-75 ✓
Propylene-Re-50 ✓
Propylene-Re-75 ✓
Methane-Sq-50 ×
Methane-Sq-75 ✓
Methane-Re-50 ×
Methane-Re-75 ×

The baroclinic torque correction was disabled in the Series 28 models, this parameter determines properties of the vorticity in the flow calculations.

Observations

The changes in the plume centerline velocity are negative for all of the fire simulations, and the magnitude of the change is consistent over the whole range of the elevation. The parameter change decreased the plume temperature from 10% up to 0.2 m above the burner and then consistently at 20% for the higher elevation. The heat flux is decreased at the elevation from 0.2 to 0.5 m, but an increas was observed for all simulation at the higher elevations. Based on the spreads of the datapoints, the changes in velocity and temperature are less affected by fuel type, burner size, and HRR than the heat flux, as evident in the larger spread for the heat flux..

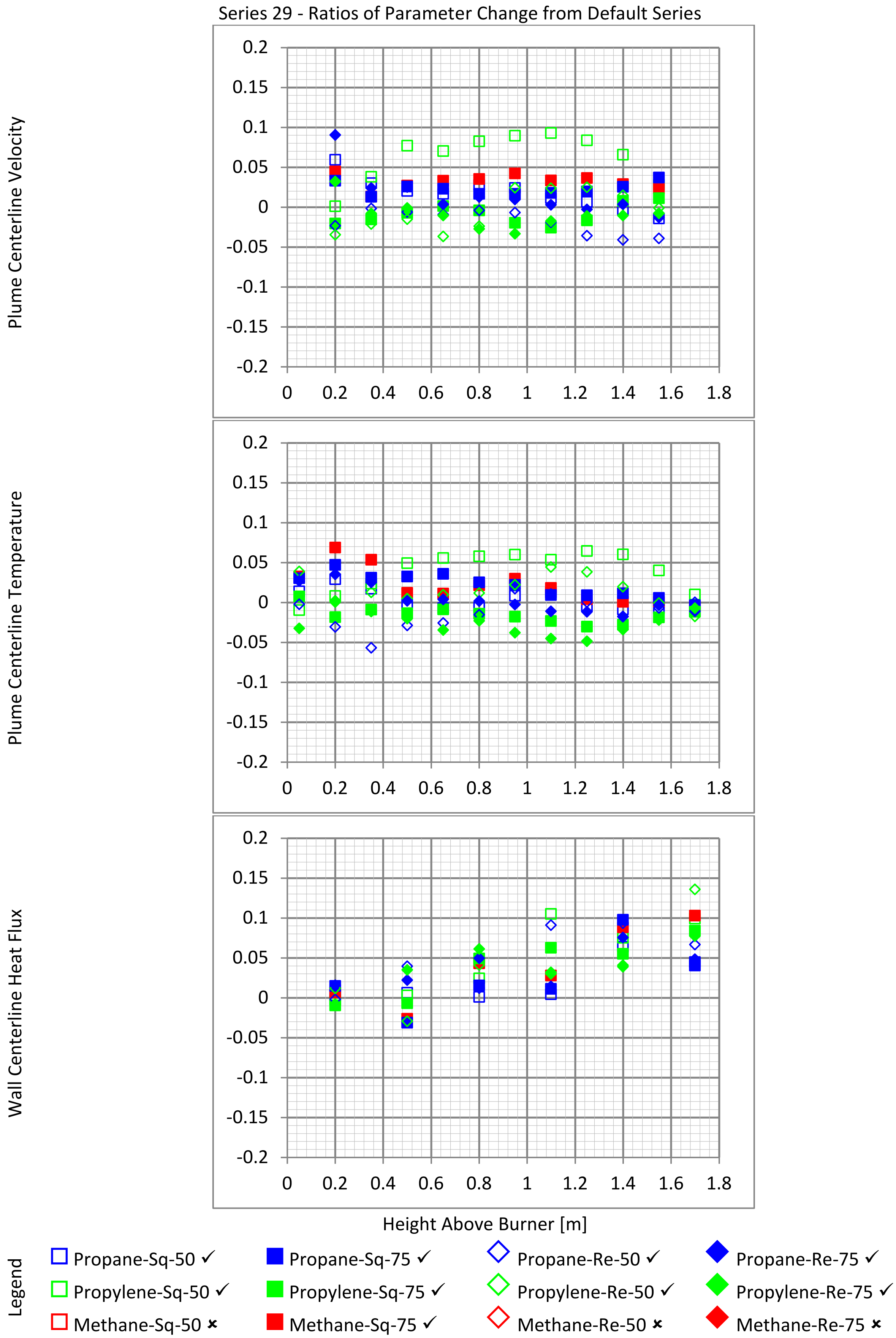

Series 29 - Ratios of Parameter Change from Default Series
Plume Centerline Velocity
Plume Centerline Temperature
Wall Centerline Heat Flux
0.2
0.15
0.1
0.05
0
-0.05
-0.1
-0.15
-0.2
0
0.2
0.4
0.6
0.8
1
1.2
1.4
1.6
1.8
Height Above Burner [m]
Legend
Propane-Sq-50 ✓
Propane-Sq-75 ✓
Propane-Re-50 ✓
Propane-Re-75 ✓
Propylene-Sq-50 ✓
Propylene-Sq-75 ✓
Propylene-Re-50 ✓
Propylene-Re-75 ✓
Methane-Sq-50 ×
Methane-Sq-75 ✓
Methane-Re-50 ×
Methane-Re-75 ×

The CFL_MAX parameter controls the time step size used in a FDS simulation, at each time step, a CFL (Courant-Friedrichs-Lewy) number was calculated, and if the number is outside of the range set forth by the minimum and the maximum CFL constraints, then the time step size is adjusted. By increasing the CFL_MAX parameter from 1 to 2, the range was increased, allowing more flexibility in the time step size calculation, but might increase the chances for numerical instability.

Increases to the velocity are noted due to the parameter change, where they are relatively consistent over the range of elevation. It is observed that the simulations with the Square burner are mostly positve whereas the Rectangle burner simulations most incurred negative changes. Temperature change are relatively positive for most of the simulations, whereas the negative changes are observed for the 75 kW propylene fires. For the gauge heat flux, the changes are positive from 0.5 to 1.7 m, and the magnitude of the change is proportional to the elevation.

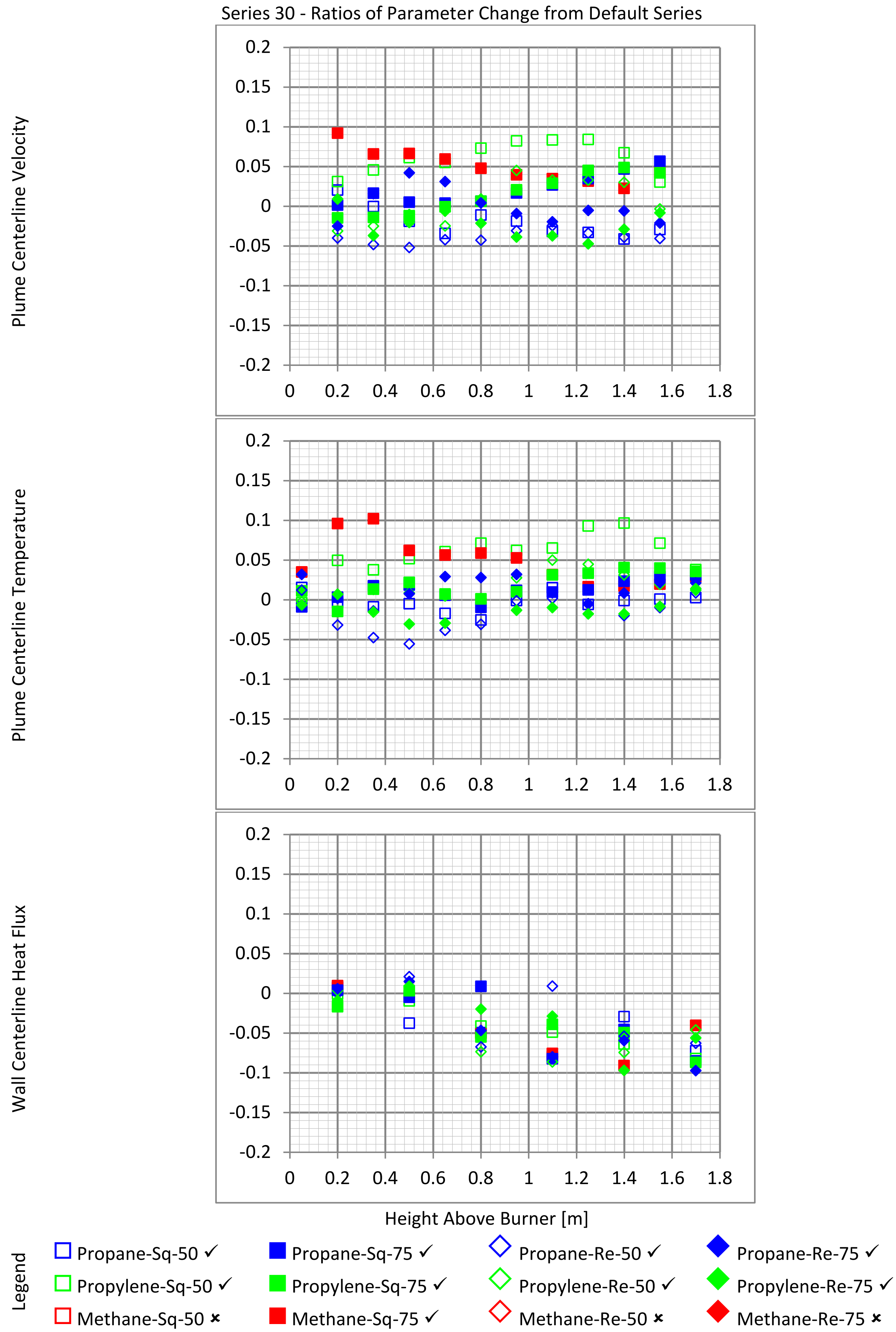

Series 30 - Ratios of Parameter Change from Default Series
Plume Centerline Velocity
Plume Centerline Temperature
Wall Centerline Heat Flux
0.2
0.15
0.1
0.05
0
-0.05
-0.1
-0.15
-0.2
0 0.2 0.4 0.6 0.8 1 1.2 1.4 1.6 1.8
Height Above Burner [m]
Legend
Propane-Sq-50 ✓
Propane-Sq-75 ✓
Propane-Re-50 ✓
Propane-Re-75 ✓
Propylene-Sq-50 ✓
Propylene-Sq-75 ✓
Propylene-Re-50 ✓
Propylene-Re-75 ✓
Methane-Sq-50 ×
Methane-Sq-75 ✓
Methane-Re-50 ×
Methane-Re-75 ×

Observations

By decreasing the CFL_MIN parameter from 0.8 to 0.4, the range was increased, allowing more flexibility in the time step size calculation, but might increase the chances for numerical instability.

Increases to the velocity and temperature are noted due to the parameter change, the changes are relatively consistent for the velocity over the elevation, but the increases are more inversely proportional to the elevation for the plume temperature. For the gauge heat flux, the changes are mostly negative with magnitude proportional to the elevation.

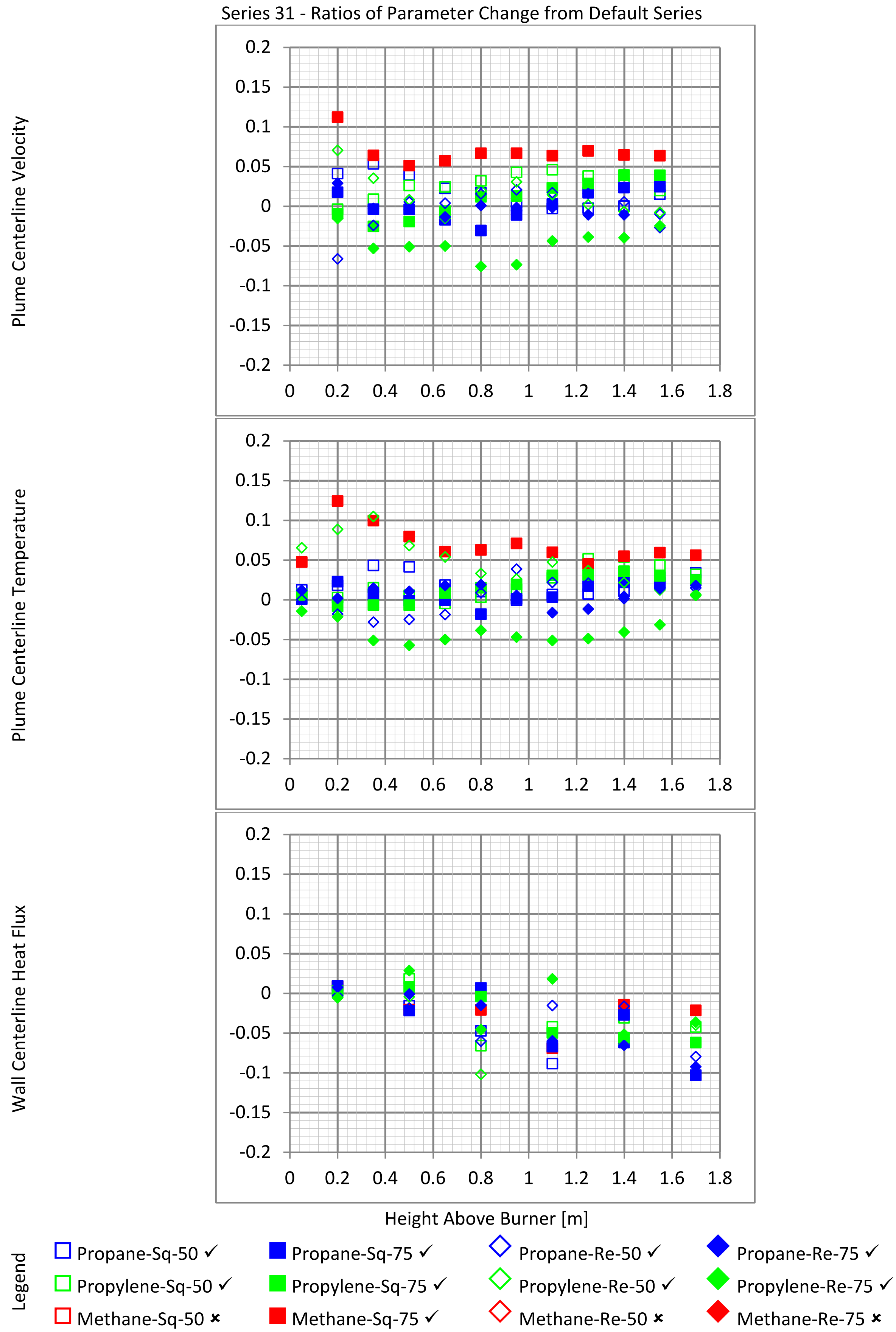

Series 31 - Ratios of Parameter Change from Default Series
Plume Centerline Velocity
Plume Centerline Temperature
Wall Centerline Heat Flux
0.2
0.15
0.1
0.05
0
-0.05
-0.1
-0.15
-0.2
0
0.2
0.4
0.6
0.8
1
1.2
1.4
1.6
1.8
Height Above Burner [m]
Legend
Propane-Sq-50 ✓
Propane-Sq-75 ✓
Propane-Re-50 ✓
Propane-Re-75 ✓
Propylene-Sq-50 ✓
Propylene-Sq-75 ✓
Propylene-Re-50 ✓
Propylene-Re-75 ✓
Methane-Sq-50 ×
Methane-Sq-75 ✓
Methane-Re-50 ×
Methane-Re-75 ×

Observations

In Series 31, the range between the max and min CFL was further increased to 2 and 0.4, respectively, to test their effects.

Increases to the velocity and temperature are noted due to the parameter change, the changes are relatively consistent for the velocity over the elevation, but the increases are more inversely proportional to the elevation for the plume temperature. For the gauge heat flux, the changes are mostly negative with magnitude proportional to the elevation. The changes are similar to those observed in the Series 30 parametric simulations.

Series 32 - Ratios of Parameter Change from Default Series

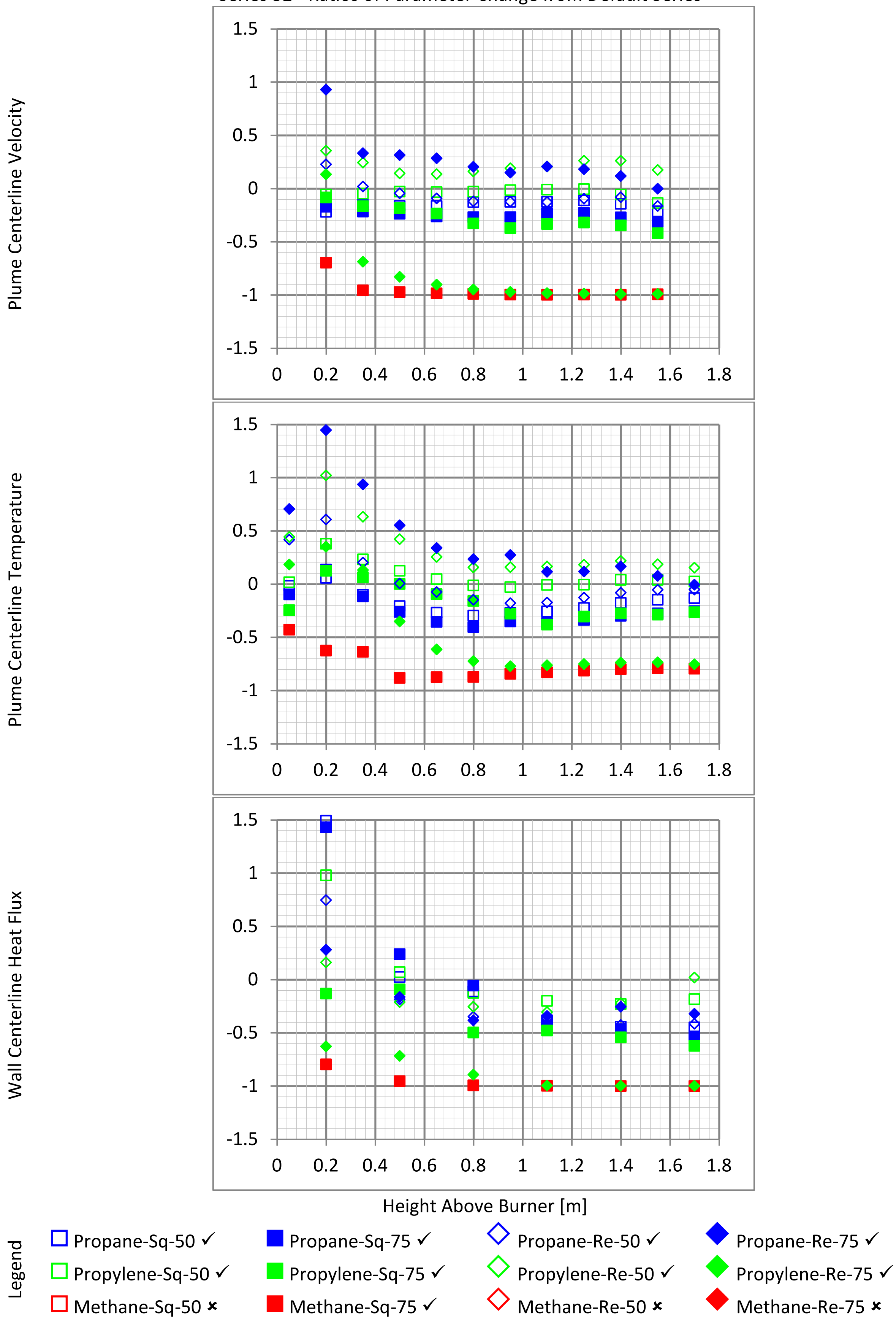

The FLUX_LIMITER parameter is a FDS6 parameter that changes the way the finite difference calculations are set up. The FDS default is to use a central differencing method with boundedness correction applied if the scalar goes out of the range between 0 and 1. In Series 32, flux limiter is set to 2, which uses the Superbee scheme, suitable for LES simulations.

The deviations predicted in Series 32 are very random and large in magnitude. However, most of the inert wall simulations in Series 32 crashed due to numerical instability, suggesting that the FDS's default setting for the FLUX_LIMITER parameter may be more appropriate for the current application.

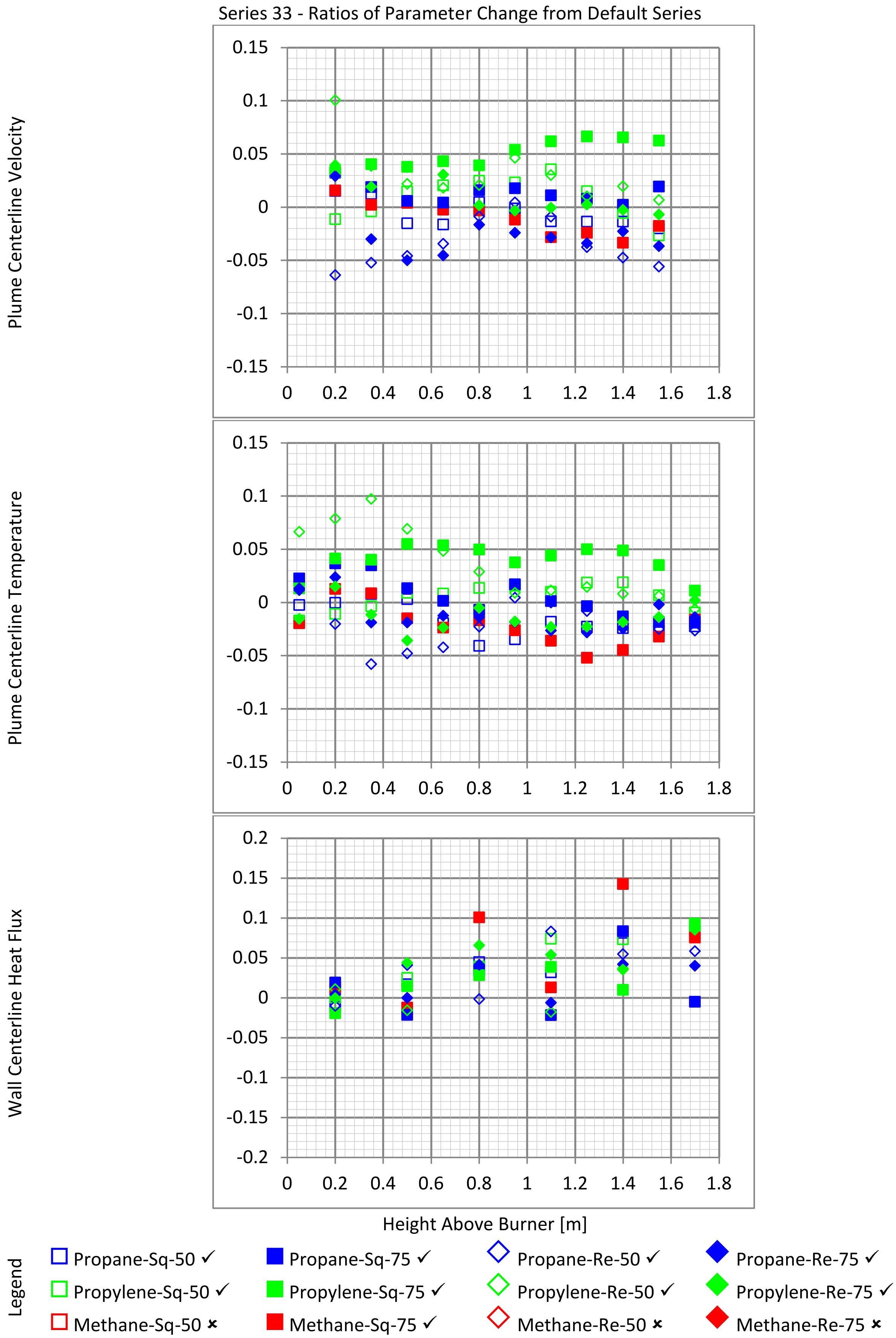

Series 33 - Ratios of Parameter Change from Default Series
Plume Centerline Velocity
Plume Centerline Temperature
Wall Centerline Heat Flux
0.2
0.15
0.1
0.05
0
-0.05
-0.1
-0.15
-0.2
0
0.2
0.4
0.6
0.8
1
1.2
1.4
1.6
1.8
Height Above Burner [m]
Legend
Propane-Sq-50 ✓
Propane-Sq-75 ✓
Propane-Re-50 ✓
Propane-Re-75 ✓
Propylene-Sq-50 ✓
Propylene-Sq-75 ✓
Propylene-Re-50 ✓
Propylene-Re-75 ✓
Methane-Sq-50 ×
Methane-Sq-75 ✓
Methane-Re-50 ×
Methane-Re-75 ×

Observations

The CFL_VELOCITY_NORM parameter is a FDS6 parameter that controls the time step sizing. The use of CFL_VELOCITY_NORM=2 in the Series 33 simulations makes the time step sizing more restrictive than the default.

The results from Series 33 show that the parameter change created deviation in the predicted temperature and velocity in quite a random fashion. For the guage heat flux, the changes at the lowest elevation at 0.2 m are slight, but the changes become more positive proportional to the elevation.

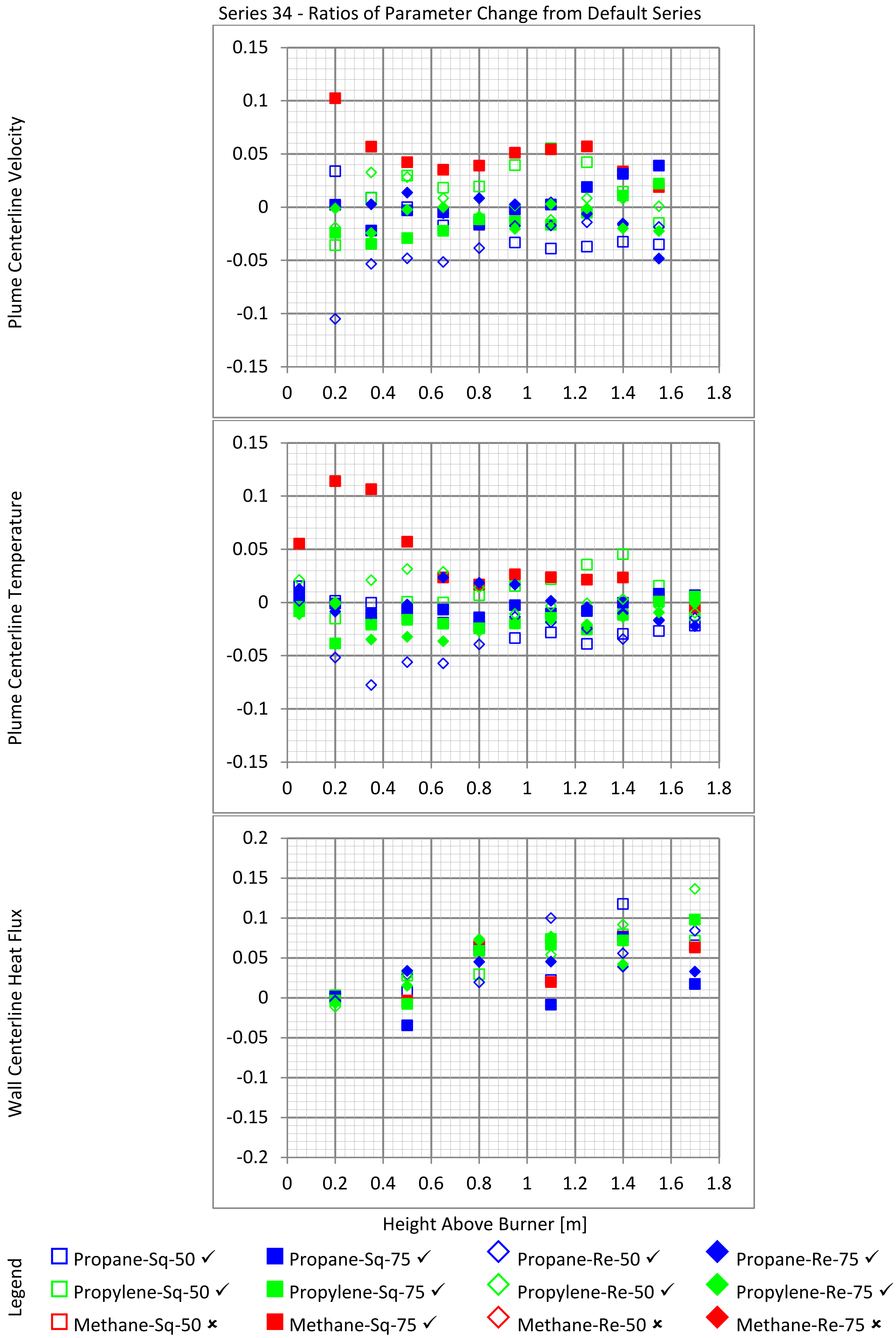
Series 34 - Ratios of Parameter Change from Default Series
Plume Centerline Velocity
Plume Centerline Temperature
Wall Centerline Heat Flux
Height Above Burner [m]
Legend
Propane-Sq-50 ✓
Propane-Sq-75 ✓
Propane-Re-50 ✓
Propane-Re-75 ✓
Propylene-Sq-50 ✓
Propylene-Sq-75 ✓
Propylene-Re-50 ✓
Propylene-Re-75 ✓
Methane-Sq-50 ×
Methane-Sq-75 ✓
Methane-Re-50 ×
Methane-Re-75 ×

Observations

The CFL_VELOCITY_NORM parameter is a FDS6 parameter that controls the time step sizing. The Use of CFL_VELOCITY_NORM=0 makes the time step sizing less restrictive than the default.

The parameter change appears to have greater changes in velocity and temperature for the fire simulations with the lower HRR, except for the methane fire at 75 kW simulation. For the guage heat flux, the changes at the lowest elevation at 0.2 m are slight, but the changes become more positive proportional to the elevation.

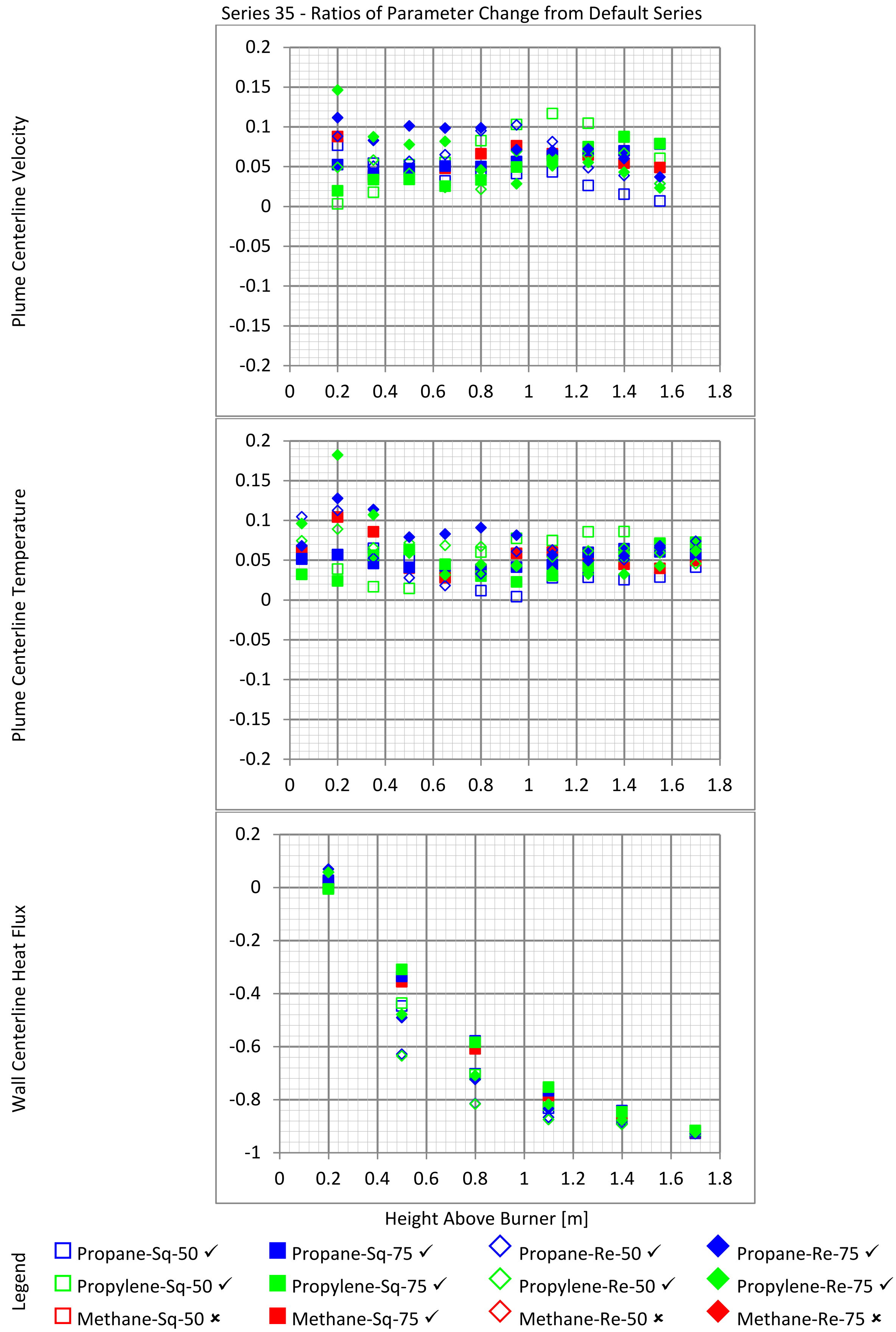
Series 35 - Ratios of Parameter Change from Default Series
Plume Centerline Velocity
Plume Centerline Temperature
Wall Centerline Heat Flux
0.2
0.15
0.1
0.05
0
-0.05
-0.1
-0.15
-0.2
-0.4
-0.6
-0.8
-1
0 0.2 0.4 0.6 0.8 1 1.2 1.4 1.6 1.8
Height Above Burner [m]
Legend
Propane-Sq-50 ✓
Propane-Sq-75 ✓
Propane-Re-50 ✓
Propane-Re-75 ✓
Propylene-Sq-50 ✓
Propylene-Sq-75 ✓
Propylene-Re-50 ✓
Propylene-Re-75 ✓
Methane-Sq-50 ×
Methane-Sq-75 ✓
Methane-Re-50 ×
Methane-Re-75 ×

Observations

When the H_EDDY parameter is disabled in Series 35 simulations, the FDS default convective heat transfer model is used instead of the turbulent convective heat transfer model.

The plume centerline velocity and temperature had been increased due to the paramter change, additionally, the changes are relatively consisten over the range of the elevation. For the centerline heat flux, however, the changes are negative with the magnitude proportional to the elevation.

Appendix M FDS Parametric Study Results [Combustible Wall]

Varying the FDS parameters that govern the CFD simulation characteristics changed the behaviors of the model to different degrees. The predictive capabilities and the performance of the model are both affected by parameter changes; and to understand the relationships between the cause (parameter change) and the results (predictions and performance) is of great importance to end-users so that simulations can be conducted effectively and efficiently. A systemic approach to varying some notable parameters in FDS individually was undertaken using all three configurations of fire models in this study. The default cases used mostly FDS default parameters, and in each iteration, only one parameter was varied from the default set. Some parameters from the MISC, RADI, REAC, and TIME groups were changed during this exercise. Comparisons of the outputs and performance of successive series of models were made against the default cases. The list of parameters changed in the study is presented in Table 1.

Table 1 - Variable simulation parameters

Series	Parameter Group	Parameter change	Default Value	New value in simulation	Change from default
0	FDS6	DYNSMAG	.TRUE.	.FALSE.	x
1	**N/A**	**No change, Default situation using default FDS6 options**			
2	MISC	RADATION	.TRUE.	.FALSE.	x
3	RADI	RADIATIVE FRACTION	0.30	Source fire specific	varies
4	RADI	RADIATIVE FRACTION	0.30	0.1	~33%
5	RADI	RADIATIVE FRACTION	0.30	0.2	~50%
6	RADI	RADIATIVE FRACTION	0.30	0.5	~160%
7	RADI	WIDE_BAND_MODEL	.FALSE.	.TRUE	x
8	RADI	NUMBER_RADIATION_ANGLES	104	52	50%
9	RADI	NUMBER_RADIATION_ANGLES	104	208	200%
10	RADI	ANGLE_INCREMENT	5	2	50%
11	RADI	ANGLE_INCREMENT	5	10	200%
12	RADI	TIME_STEP_INCREMENT	3	1	50%
13	RADI	TIME_STEP_INCREMENT	3	6	200%
~~14~~	~~Skipped~~				
15	REAC	C_EDC	0.1	0.2	50%
16	REAC	C_EDC	0.1	0.05	200%
17	REAC	EDDY_DISSIPATION	.TRUE.	.FALSE.	x
18	REAC	HRRPUA_SHEET	0	400	40000%
19	REAC	HRRPUA_SHEET	0	100	10000%
20	REAC	HRRPUV_AVERAGE	3000	1200	40%
21	MISC	ISOTHERMAL	.FALSE.	.TRUE	x
22	MISC	CSMAG	0.2	0.1	50%
23	MISC	CSMAG	0.2	0.4	200%
24	MISC	PR	0.5	0.25	50%
25	MISC	PR	0.5	1	200%

Series	Parameter Group	Parameter change	Default Value	New value in simulation	Change from default
26	MISC	SC	0.5	0.25	50%
27	MISC	SC	0.5	1	200%
28	MISC	BAROCLINIC	.TRUE.	.FALSE.	x
29	MISC	CFL_MAX	1	2	200%
30	MISC	CFL_MIN	0.8	0.4	50%
31	MISC	CFL_MAX and CFL_MIN	1 / 0.8	2 / 0.4	x
32	FDS6	FLUX_LIMITER	2	-1	x
33	FDS6	CFL_VELOCITY_NORM	1	2	x
34	FDS6	CFL_VELOCITY_NORM	1	0	x
35	FDS6	H_EDDY	.TRUE.	.FALSE.	x

The variable parameters and their functions are described in this section. Many of the parameters have an effect on the stability and the performance of the model by changing the amount or complexity of the calculations performed by the FDS software. Moreover, some of the parameters can also affect the predicted fire behaviors and change the various quantities predicted by FDS.

1) RADI parameters
   a) **RADIATIVE_FRACTION**
      i) Determines the fraction of combustion energy released in the model as thermal radiation
      ii) Default simulations used a value of 0.30
      iii) Parametric study used the radiative fraction values of the fuel modeled: methane at 0.141, propane at 0.286, and propylene at 0.368
   b) **WIDE_BAND_MODEL**
      i) Determine whether the six band wide band gray gas model is assumed and used in the simulation
      ii) Default simulations disables the six band model method
      iii) Parametric study simulations had the six band model enabled
   c) **NUMBER_RADIATION_ANGLES**
      i) Number of solid angles used in radiation calculations, not compatible if radiation transport calculations are disabled elsewhere in the input file
      ii) Default simulations used 104 solid angles for calculations
      iii) Parametric study simulations used 52 and 208 solid angles
   d) **ANGLE_INCREMENT**
      i) Number of solid angles skipped per update of radiation calculations
      ii) Default simulations used the default FDS value of 5
      iii) Parametric study simulations used values of 2 and 10
   e) **TIME_STEP_INCREMENT**
      i) Number of time steps skip per update of radiation calculations
      ii) Default simulations used the default FDS value of 3
      iii) Parametric study simulations used values of 1 and 6
2) REAC parameters
   a) **C_EDC**

  i) Coefficient to calculate mixing time scale of fuel and oxygen within the grid cells used in the turbulent combustion calculations
  ii) Default simulations used a value of 0.1 for the coefficient, determined based on comparison to flame height correlations[*6*]
  iii) Parametric study simulations used 0.05 and 0.2 solid angles

b) EDDY_DISSIPATION

  i) Determines whether the default heat release rate calculation model based on the default mixture time scale method is used
  ii) Default simulations enabled the eddy dissipation to be determined
  iii) Parametric study enabled the eddy dissipation

c) HRRPUA_SHEET

  i) Max HRRPUA of a flame sheet, acts as a bound of local HRRPU-volume
  ii) Default simulations used a default value of 0kW/m^2 for LES
  iii) Parametric study used values at 100 kW/m^2 and 400 kW/m^2, these are chosen based on the value of 200 kW/m^2 as default for the DNS mode (not used in these simulations)

d) HRRPUV_AVERAGE

  i) Average volumetric HRR of a fire, bounds local HRRPU-volume value
  ii) Default simulations used a default value of 3000 kW/m^3
  iii) Parametric study used values at 1200 kW/m^3, as suggested by Orloff and De Ris[*6*]

3) MISC parameters

a) CFL_MAX and CFL_MIN

  i) Numerical stability parameters that limit the time step sizing by imposing limits on the Courant-Friedrichs-Lewy (CFL) number that is calculated within each timestep: if the number is outside of the range, then the time step size is adjusted
  ii) Default simulations set the max value at 1 and the min value at 0.8
  iii) Several combinations of CFL limits are tested in the parametric study as follow: [2, 0.8], [1, 0.4], and [2, 0.4]

b) ISOTHERMAL

  i) Set the calculations to ignore any changes in temperature or radiation heat transfer, also automatically turn off radiation transport model as well
  ii) Default simulations disabled the isothermal option
  iii) Parametric study enabled the isothermal option

c) CSMAG

  i) Smagorinsky constant used to calculate the viscosity, usually more stable if a small value is used
  ii) Default simulations used a default value of 0.2, justified through comparisons with experimental data[*7*]
  iii) Parametric study used values at 0.1 and 0.4

d) PR

  i) Turbulent Prandtl number, a ratio of momentum diffusivity to thermal diffusivity, related to turbulent viscosity in LES simulations
  ii) Default simulations used FDS's default value of 0.5, justified through comparisons with experimental data[*7*]
  iii) Parametric study used values at 0.25 and 1

e) SC

i) Turbulent Schmidt number, a ratio of momentum diffusivity to mass diffusivity, related to turbulent viscosity in LES simulations

ii) Default simulations used FDS's default value of 0.5, justified through comparisons with experimental data[*7*]

iii) Parametric study used values at 0.25 and 1

f) BAROCLINIC

i) Enables the baroclinic vorticity correction calculations that can changes the properties in the turbulence calculations and may affect the plume shape significantly

ii) Default simulations enables the baroclinic correction

iii) Parametric study disabled the correction calculations

g) RADIATION

i) Turns On or Off radiation transport calculations in the simulations

ii) Default simulation use the radiation transport model, as in real life

iii) Parametric study disabled the radiation transport calculations

4) FDS6 parameters

a) FLUX_LIMITER

i) Changes the finite volume discretization scheme used in simulations

ii) Default simulations use the Superbee scheme, suitable for LES simulations

iii) Parametric study used a central differencing scheme with boundedness correction applied

b) DYNSMAG

i) Turns on/off variable density formulation of dynamic Smagorinsky model

ii) Default simulation use the dynamic Smagorinsky model

iii) Parametric study disabled the dynamic Smagorinsky model

c) CFL_VELOCITY_NORM

i) Normalization of CFL velocity, controls the time step sizing within a simulation

ii) FDS default uses a moderate time step sizing control

iii) Parametric study tested for the effects due to an increase and decrease of the time step sizing control

d) H_EDDY

i) Enables the eddy-diffusivity model to use a turbulent convective heat transfer model

ii) Default simulations has the eddy diffusivity model enabled

iii) Parametric study disabled eddy diffusivity model

K.1 Sensitivity Coefficients

To identify the parameters that yield significant changes to specific predicted quantities, the concept of "sensitivity coefficients" was employed. Each coefficient was determined based on the changes in one of the three recorded quantities (plume centerline temperature, plume centerline velocity, and centerline gauge heat flux) and of the FDS parameter over their baseline values. The coefficient is based on the ratios of change, and is found using equation [1.1]:

$$\left(\frac{Quantity_{new} - Quantity_{baseline}}{Quantity_{baseline}}\right) \Big/ \left(\frac{Parameter_{new} - Parameter_{baseline}}{Parameter_{baseline}}\right) \qquad [0.1]$$

Where "Quantity" denotes the recorded quantities in the model (velocity, temperature, gauge heat flux), and the "Parameter" denotes the model inputs (RADIATIVE_FRACTION, SC, etc)

Equation [1.1] was applied to the overall modeled results of total mass loss, peak HRR, time to peak HRR, and total heat released. For the "toggle" parameters, if a parameter is turned "ON" or "TRUE", the nondimensional parameter change is assumed to be "+1", and if the parameter is turned "OFF" or "FALSE", then the nondimensional parameter change is assumed to be "-1", this is necessary for the sensitivity coefficients be calculated for the "toggle" parameters since they do not have any numerical values.. Regardless of the parameter type, a sensitivity coefficient is calculated for each quantity at each "measuring" location, then they are averaged. The coefficients can then be used to represent the significance and effects of the parameter change for each of the predicted quantities.

Sensitivity coefficients are presented as grouped by the source fuel, burner size, source fire HRR, and whether the simulations were of a terminated source fire or a continuous source fire were used in the simulations.

Continuous parameters such as radiative fraction, Prandtl number, and the average HRRPUV of the fire dominate the changes of the total mass lost, peak HRR, time to peak HRR, and total heat released predicted in the various simulations. These are the same parameters that affected the plume and inert wall simulations, suggesting a relationship between these parameters and their importance. The significance of plume characteristics and flame heat transfer behaviors are also highlighted through these parameters.

For the toggled parameter studied, the ones with the greatest changes include: isothermal model, CFL velocity normalization, eddy diffusivity model, the dynamic Smagorinsky model, and the baroclinic vorticity calculations. Again, all parameters of import identified from the inert wall fire parametric study. All these parameter contributes to the stability and structure of the flow field, which are especially important factors that describe the interaction between the plume and the solid wall. Isothermal simulation forces the no temperature change within the model, and turning off the radiation model prevents radiative heat transfer, both limiting changes in the environment and kill any flame spread. Since flame spread is greatly dependent on the source fire and its intereaction with the environment, especially the external solid fuel on the wall, if the interactions are not modeled correctly, flame spread will not be predicted, hence the much greater discrepancy between the baseline models and the parametric runs in the combustible wall simulations than those found in the inert wall or plume simulations. Clearly the discrepancy is propagated through the successively complex simulations runs from plume to inert wall to combustible wall fire modeling.

Additionally, the results from the parametric study generally show that the parametric changes have the greatest effects on simulations where a continuous source fire is used. This may be biased because of the very low flame spread predicted by all of the simulations with a terminated source fire, which suggest a contributing factor from another level of the modeling calculation schemes.

K.1.1 Fuel Type

This section presents the sensitivity coefficients generated from the various simulations as grouped by the fuel type. The parameters and their variances that generated sensitivity coefficients ≥ 0.5 are considered significant. Each sensitivity coefficient was based on one of the predicted quantities, and was averaged over height and across those simulations using identical fuel types regardless of the scenario, burner shape, and base HRR. The results from the toggle parameters are located at the bottom of the charts, and the parameter change that correlates with the overall maximum sensitivity coefficients are presented first.

Figure 1 shows the sensitivity coefficients based on the total mass loss averaged over combustible wall simulations using the same fuel type. The parameters that created the most significant changes to the mass loss are changes in the radiative fraction and Prandtl number, as well as whether the dynamic Smagorinsky model is deactivated, and which calculation scheme was used based on the value of the flux limiter. It is noted that an isothermal does not have the most drastic changes to the total mass loss. Changes to the simulations with a Continuous source fire appear to be greater. It is noted that the simulations with change to the FLUX_LIMITER value crashed due to numerical instability.

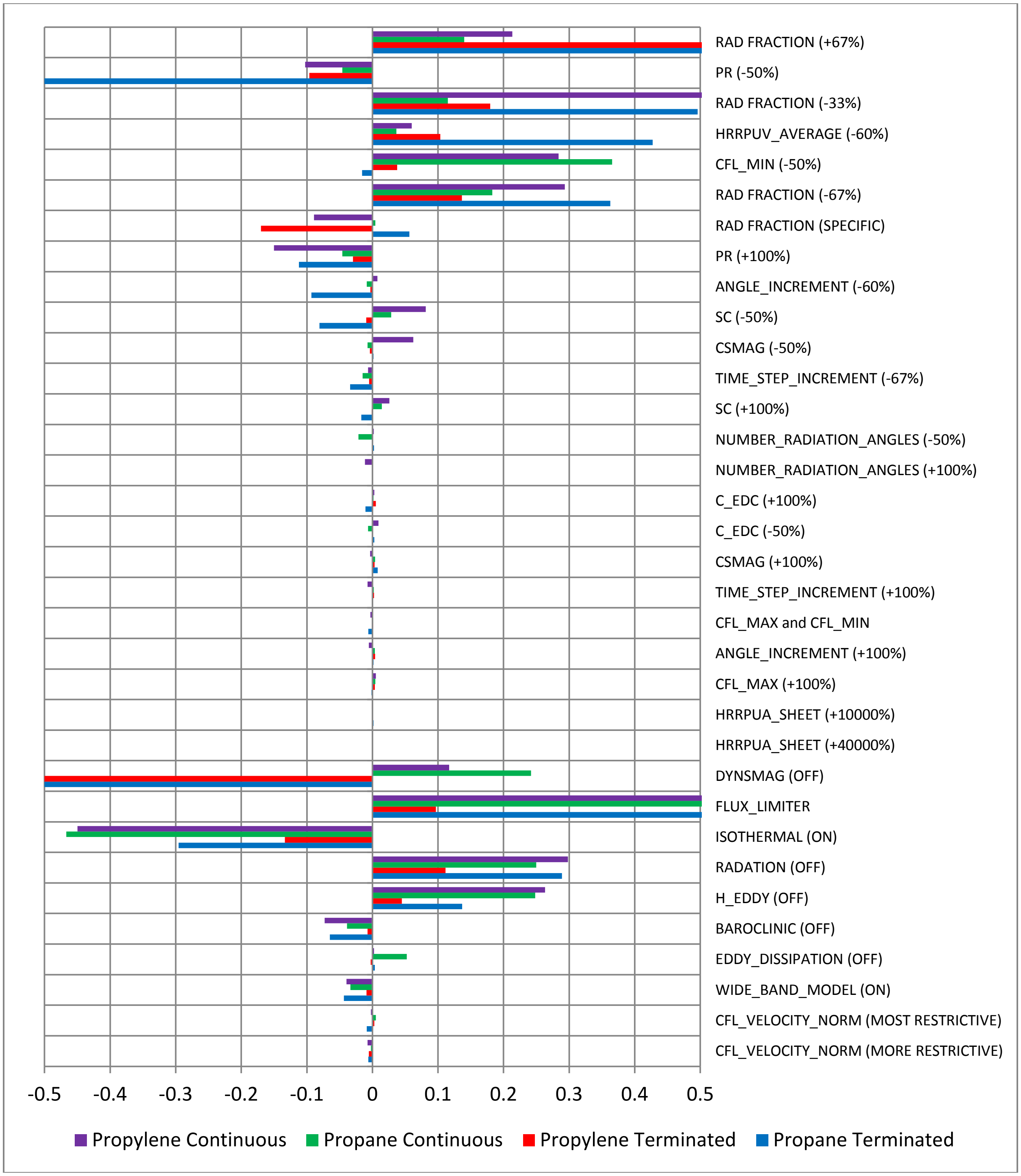

Figure 1 – Total mass loss sensitivity coefficients, grouped by fuel type

Figure 2 shows the sensitivity coefficients based on the peak HRR value averaged over simulations with consistent fuel type. The parameters that created the most significant changes to the time to peak HRR are changes in the radiative fraction, Prandtl number, and the average HRRPUV of the flame. For the "toggled" parameters, changes are most significant when the dynamic Smagorinsky model is deactivated, the isothermal model is used, the radiation solver is turned off, and when the eddy diffusivity model is deactivated. The flux limiter value that controls the calculation scheme also contributes greatly to the peak HRR value. It is noted that the simulations with change to the FLUX_LIMITER value crashed due to numerical instability. Changes to the simulations with the terminated source fire are usually greater.

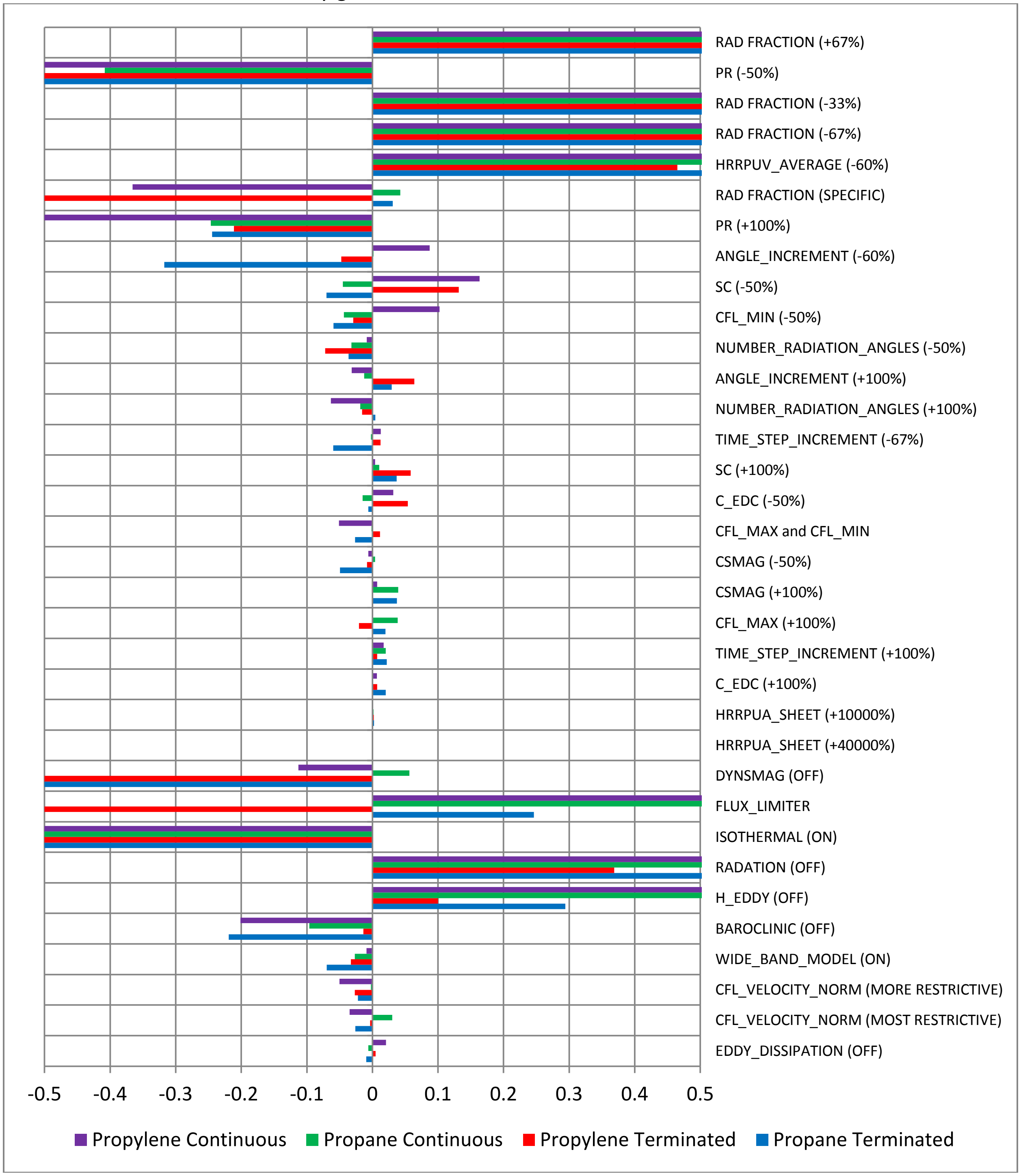

Figure 2 – Peak HRR sensitivity coefficients, grouped by fuel type

Figure 3 shows the sensitivity coefficients based on the predicted time to peak HRR averaged over simulations with consistent fuel type. The parameters that created the most significant changes to the time to peak are changes in the radiative fraction. For the "toggled" parameters, changes are most significant when the dynamic Smagorinsky model is deactivated, the isothermal model is used, the radiation solver is turned off, and when the eddy diffusivity model is deactivated. The flux limiter value that controls the calculation scheme also contributes greatly to the peak HRR value. It is noted that the simulations with change to the FLUX_LIMITER value crashed due to numerical instability. Changes to the simulations with a Continuous source fire appear to be greater.

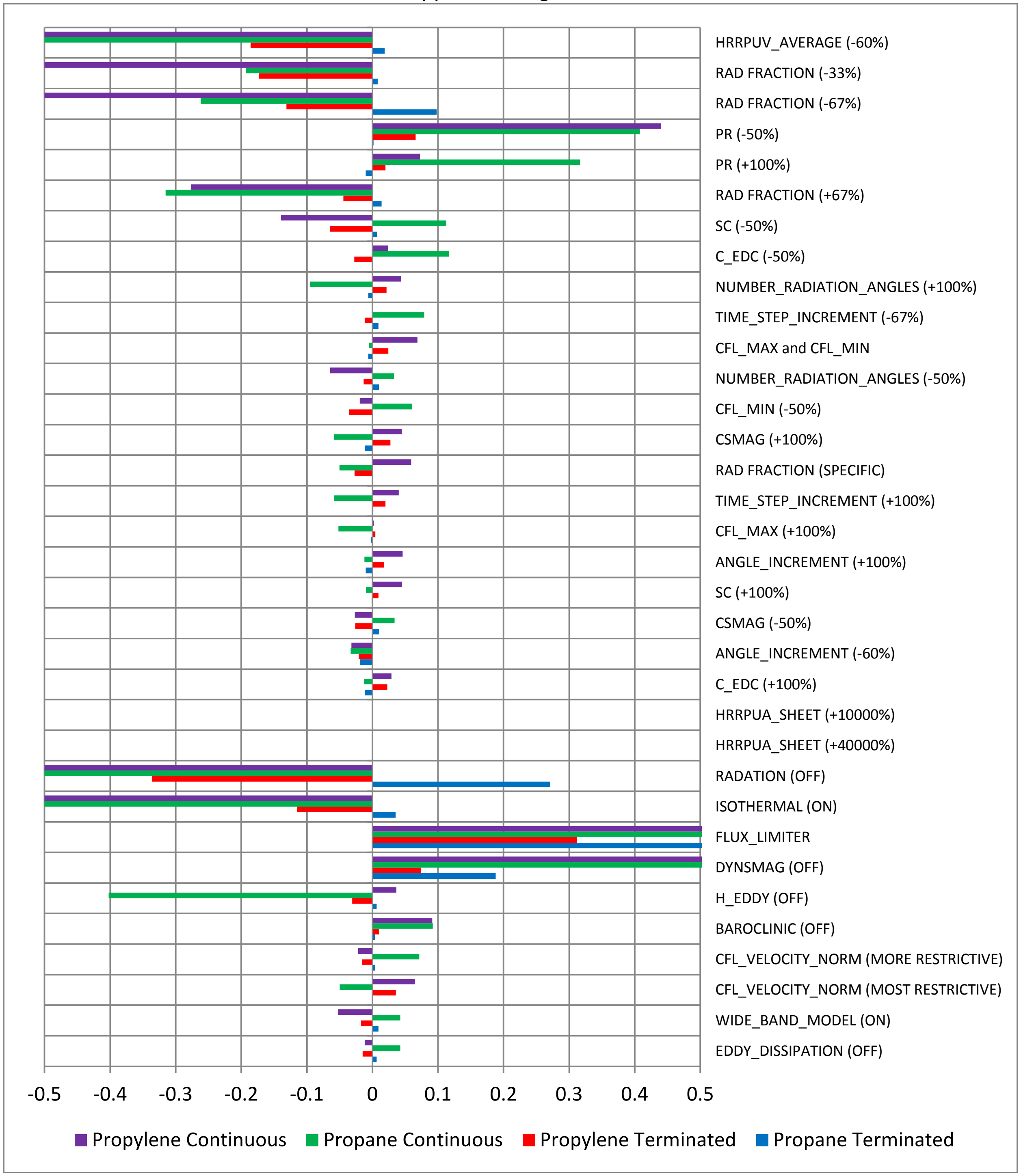

Figure 3 – Time to peak HRR sensitivity coefficients, grouped by fuel type

Figure 4 shows the sensitivity coefficients based on the predicted total heat released averaged over simulations with consistent fuel type. The parameters that created the most significant changes to the time to peak HRR are changes in the radiative fraction, Prandtl number, and the average HRRPUV of the flame. For the "toggled" parameters, changes are most significant when the dynamic Smagorinsky model is deactivated, the isothermal model is used, the radiation solver is turned off, and when the eddy diffusivity model is deactivated. The flux limiter value that controls the calculation scheme also contributes greatly to the peak HRR value, although these simulations all crashed due to numerical instability. Changes to the simulations with the terminated source fire are generally greater. The trends here are similar to the trends noted for the peak HRR changes.

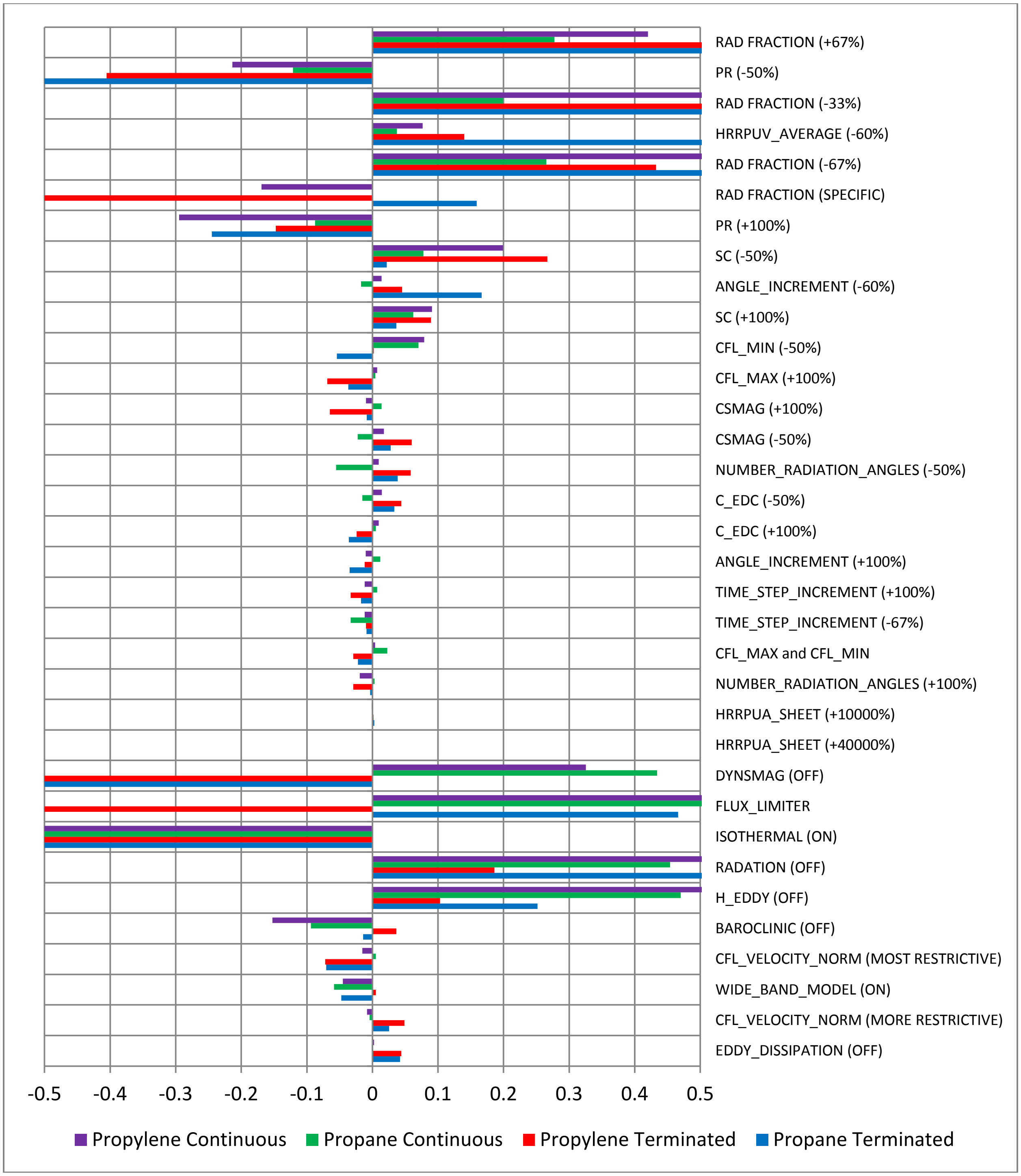

Figure 4 – Total heat Released sensitivity coefficients, grouped by fuel type

Table 2 - Sensitivity coefficients based on source fuel type

			Propane fuel, terminated source fire				Propylene fuel, terminated source fire				Propane fuel, continuous source fire				Propylene fuel, continuous source fire			
Parameter change	**Default Value**	**New Value**	**Total Mass Lost**	**Peak HRR**	**Time@ Peak**	**Heat Releas ed**	**Total Mass Lost**	**Peak HRR**	**Time@ Peak**	**Heat Releas ed**	**Total Mass Lost**	**Peak HRR**	**Time@ Peak**	**Heat Releas ed**	**Total Mass Lost**	**Peak HRR**	**Time@ Peak**	**Heat Releas ed**
DYNSMAG (OFF)	.TRUE.	.FALSE.	-1.7665	-3.4528	0.1878	-4.8966	-1.7869	-7.0926	0.0742	-7.0624	0.2418	0.0562	0.5754	0.4339	0.1168	-0.1127	0.6003	0.3255
RADIATION (OFF)	.TRUE.	.FALSE.	0.2888	0.6468	0.2712	0.5834	0.1115	0.3688	-0.3366	0.1861	0.2498	0.7837	-1.0274	0.4539	0.2983	0.8516	-1.8803	0.5575
WIDE_BAND_MODEL (ON)	.FALSE.	.TRUE	-0.0435	-0.0695	0.0090	-0.0473	-0.0090	-0.0329	-0.0173	0.0054	-0.0336	-0.0270	0.0425	-0.0585	-0.0396	-0.0090	-0.0523	-0.0453
EDDY_DISSIPATION (OFF)	.TRUE.	.FALSE.	0.0038	-0.0096	0.0062	0.0420	-0.0027	0.0049	-0.0150	0.0442	0.0523	-0.0063	0.0425	-0.0012	0.0023	0.0209	-0.0117	0.0024
ISOTHERMAL (ON)	.FALSE.	.TRUE	-0.2958	-0.9409	0.0352	-0.9895	-0.1333	-0.8067	-0.1152	-0.9504	-0.4669	-1.0000	-1.0000	-1.0000	-0.4498	-1.0000	-1.0000	-1.0000
BAROCLINIC (OFF)	.TRUE.	.FALSE.	-0.0650	-0.2190	0.0040	-0.0141	-0.0076	-0.0137	0.0098	0.0367	-0.0388	-0.0964	0.0921	-0.0940	-0.0728	-0.2014	0.0912	-0.1527
FLUX_LIMITER	2	-1	0.7818	0.2464	0.8159	0.4662	0.0966	-1.4638	0.3121	-2.3787	0.9393	0.7194	0.6513	0.9122	0.9650	0.7274	0.7846	0.9524
CFL_VELOCITY_NORM (MOST RESTRICTIVE)	1	2	-0.0088	-0.0260	0.0000	-0.0704	0.0027	-0.0037	0.0359	-0.0719	0.0052	0.0303	-0.0498	0.0053	-0.0024	-0.0349	0.0650	-0.0155
CFL_VELOCITY_NORM (MORE RESTRICTIVE)	1	0	-0.0061	-0.0220	0.0041	0.0254	-0.0056	-0.0269	-0.0163	0.0487	-0.0022	-0.0022	0.0714	-0.0044	-0.0073	-0.0505	-0.0218	-0.0084
H_EDDY (OFF)	.FALSE.	.TRUE.	0.1369	0.2940	0.0063	0.2516	0.0450	0.1001	-0.0307	0.1030	0.2481	0.7534	-0.4021	0.4700	0.2631	0.7961	0.0365	0.5162
RAD FRACTION (SPECIFIC)	0.3	Source specific	0.0564	0.0312	-0.0003	0.1589	-0.1700	-0.6919	-0.0272	-0.5428	0.0046	0.0425	-0.0504	0.0003	-0.0891	-0.3659	0.0590	-0.1692
RAD FRACTION (-67%)	0.3	0.1	0.3626	0.8115	0.0980	0.7743	0.1365	0.6934	-0.1311	0.4326	0.1828	0.5250	-0.2617	0.2652	0.2935	1.0751	-0.6958	0.5685
RAD FRACTION (-33%)	0.3	0.2	0.4957	1.0931	0.0079	1.1685	0.1797	0.9250	-0.1729	0.7272	0.1149	0.5964	-0.1928	0.1991	0.5477	0.9024	-0.8173	0.5838
RAD FRACTION (+67%)	0.3	0.5	1.2177	2.1598	0.0139	2.1886	0.5473	2.0059	-0.0443	1.8514	0.1399	0.5885	-0.3153	0.2775	0.2133	0.7927	-0.2771	0.4201
NUMBER_RADIATION_ANGLES (-50%)	104	52	0.0026	-0.0362	0.0100	0.0384	-0.0003	-0.0720	-0.0134	0.0584	-0.0212	-0.0319	0.0328	-0.0554	0.0020	-0.0085	-0.0647	0.0094
NUMBER_RADIATION_ANGLES (+100%)	104	208	0.0006	0.0045	-0.0063	-0.0034	-0.0003	-0.0160	0.0216	-0.0293	0.0002	-0.0187	-0.0952	0.0031	-0.0113	-0.0632	0.0435	-0.0193
ANGLE_INCREMENT (-60%)	5	2	-0.0932	-0.3172	-0.0188	0.1666	-0.0031	-0.0476	-0.0208	0.0454	-0.0086	0.0015	-0.0331	-0.0175	0.0074	0.0873	-0.0321	0.0140
ANGLE_INCREMENT (+100%)	5	10	0.0017	0.0293	-0.0103	-0.0349	0.0040	0.0639	0.0177	-0.0118	0.0036	-0.0128	-0.0121	0.0118	-0.0055	-0.0316	0.0459	-0.0101
TIME_STEP_INCREMENT (-67%)	3	1	-0.0341	-0.0598	0.0094	-0.0091	-0.0053	0.0122	-0.0117	-0.0099	-0.0149	-0.0024	0.0788	-0.0331	-0.0067	0.0129	0.0003	-0.0120
TIME_STEP_INCREMENT (+100%)	3	6	0.0009	0.0218	0.0012	-0.0175	0.0024	0.0073	0.0199	-0.0333	0.0019	0.0204	-0.0581	0.0073	-0.0074	0.0172	0.0403	-0.0118
C_EDC (+100%)	0.1	0.2	-0.0108	0.0203	-0.0114	-0.0360	0.0051	0.0071	0.0225	-0.0242	0.0016	0.0007	-0.0130	0.0053	0.0029	0.0070	0.0291	0.0097
C_EDC (-50%)	0.1	0.05	0.0029	-0.0064	0.0001	0.0332	-0.0006	0.0541	-0.0277	0.0441	-0.0068	-0.0151	0.1164	-0.0155	0.0093	0.0318	0.0240	0.0142
HRRPUA_SHEET (+40000%)	0	400	0.0004	0.0006	0.0000	0.0006	0.0002	0.0004	0.0000	0.0005	-0.0001	0.0006	-0.0003	-0.0001	-0.0003	-0.0003	0.0001	-0.0006
HRRPUA_SHEET (+10000%)	0	100	0.0017	0.0024	-0.0001	0.0027	0.0006	0.0021	0.0000	0.0016	-0.0002	0.0018	-0.0009	-0.0003	-0.0005	0.0007	-0.0005	-0.0012
HRRPUV_AVERAGE (-60%)	3000	1200	0.4272	0.8064	0.0189	0.8266	0.1036	0.4649	-0.1859	0.1400	0.0367	0.7522	-0.8263	0.0375	0.0598	0.8853	-1.1059	0.0766
CSMAG (-50%)	0.2	0.1	0.0018	-0.0494	0.0099	0.0277	-0.0040	-0.0081	-0.0260	0.0598	-0.0076	0.0041	0.0336	-0.0224	0.0623	-0.0064	-0.0268	0.0174
CSMAG (+100%)	0.2	0.4	0.0078	0.0372	-0.0118	-0.0087	0.0032	0.0005	0.0275	-0.0648	0.0041	0.0393	-0.0591	0.0141	-0.0036	0.0071	0.0447	-0.0099
PR (-50%)	0.5	0.25	-0.7189	-1.9578	0.0017	-1.3888	-0.0961	-0.7084	0.0658	-0.4055	-0.0459	-0.4081	0.4081	-0.1211	-0.1027	-0.6649	0.4399	-0.2134
PR (+100%)	0.5	1	-0.1119	-0.2446	-0.0103	-0.2448	-0.0297	-0.2112	0.0200	-0.1473	-0.0460	-0.2464	0.3168	-0.0875	-0.1503	-0.6038	0.0728	-0.2949
SC (-50%)	0.5	0.25	-0.0806	-0.0700	0.0071	0.0220	-0.0095	0.1316	-0.0648	0.2668	0.0287	-0.0453	0.1128	0.0779	0.0813	0.1635	-0.1393	0.1990
SC (+100%)	0.5	1	-0.0171	0.0368	-0.0011	0.0364	-0.0013	0.0582	0.0093	0.0891	0.0143	0.0103	-0.0097	0.0623	0.0259	0.0042	0.0452	0.0907
CFL_MAX (+100%)	1	2	-0.0014	0.0200	-0.0024	-0.0368	0.0037	-0.0204	0.0044	-0.0688	0.0044	0.0387	-0.0520	0.0045	0.0052	0.0002	0.0020	0.0073
CFL_MIN (-50%)	0.8	0.4	-0.0159	-0.0596	-0.0002	-0.0543	0.0377	-0.0291	-0.0355	0.0021	0.3654	-0.0434	0.0604	0.0700	0.2839	0.1024	-0.0194	0.0789
CFL_MAX and CFL_MIN	1 / 0.8	2 / 0.4	-0.0063	-0.0267	-0.0062	-0.0223	0.0011	0.0114	0.0243	-0.0294	0.0013	-0.0017	-0.0055	0.0227	-0.0031	-0.0511	0.0687	0.0040

K.1.2 Burner Shape

This section presents the sensitivity coefficients generated from the various simulations as grouped by the burner shape: Square or Rectangle. Figure 5 shows the sensitivity coefficients based on the total mass loss averaged over simulations using the same source fire burner. The parameters with significant changes are changes in the radiative fraction and a decrease of the Prandtl number, when the dynamic Smagorinsky model is deactivated, and which calculation scheme was used based on the FLUX_LIMITER value. All simulations with change to the FLUX_LIMITER value crashed. Effects on the simulations with a terminated source fire were greatest for the non-toggle parameter changes, whereas the effects of the toggled parameters are greater for simulations with a continuous source fire.

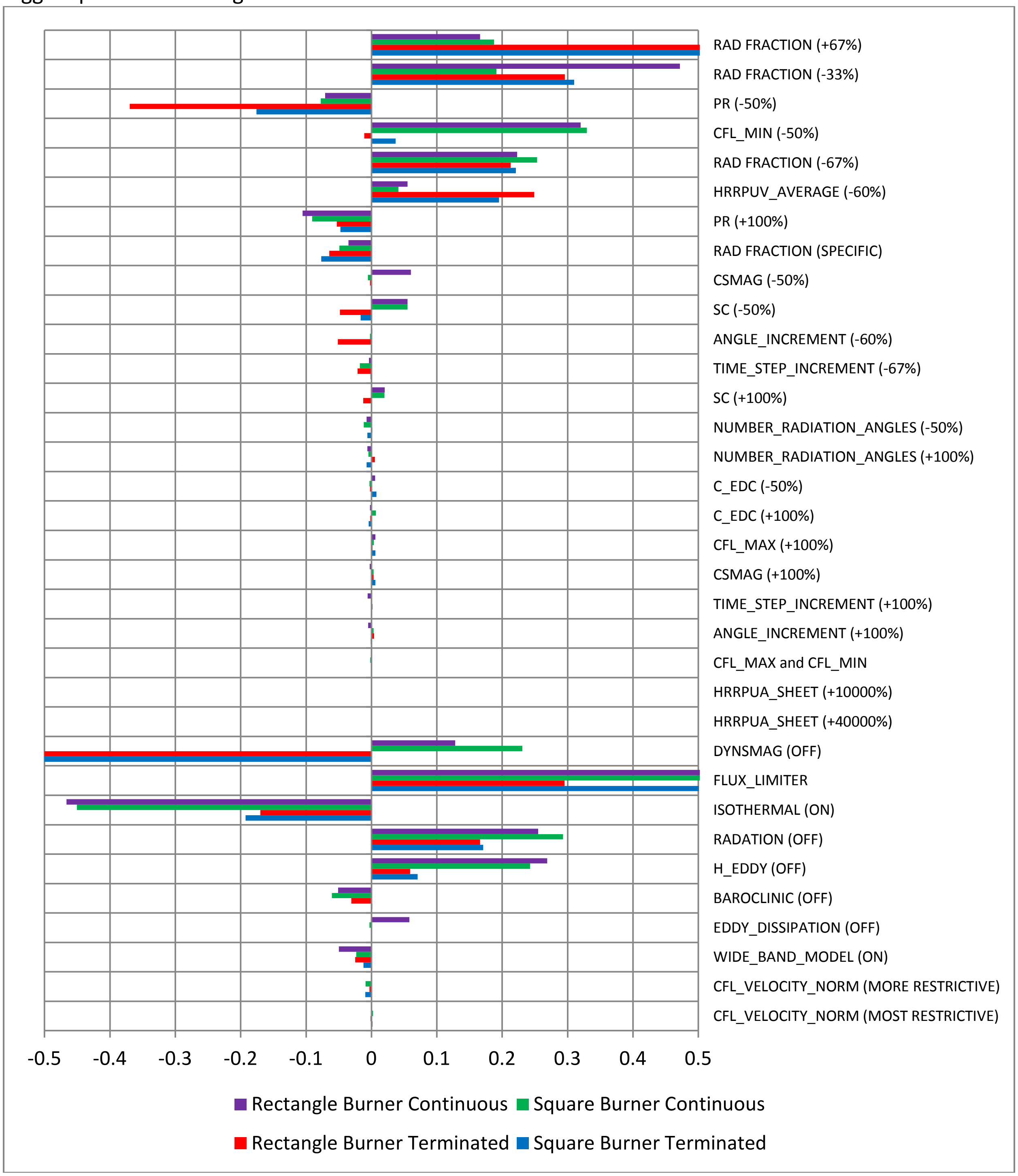

Figure 5 – Total mass loss sensitivity coefficients, grouped by burner shape

Figure 6 shows the sensitivity coefficients based on the peak HRR magnitude averaged over simulations using the same source fire burner. The parameters with significant changes are changes in the radiative fraction, a decrease of the Prandtl number, a decrease of the average HRRPUV, when the dynamic Smagorinsky model is deactivated, or when the isothermal model is turned on, when the radiation transport mode was turned off, which calculation scheme was used based on the FLUX_LIMITER value, and whether the eddy diffusivity model was not used. It is noted that the simulations with change to the FLUX_LIMITER value crashed due to numerical instability. Compared to the total mass loss, changes to the peak HRR magnitude appear to be much greater.

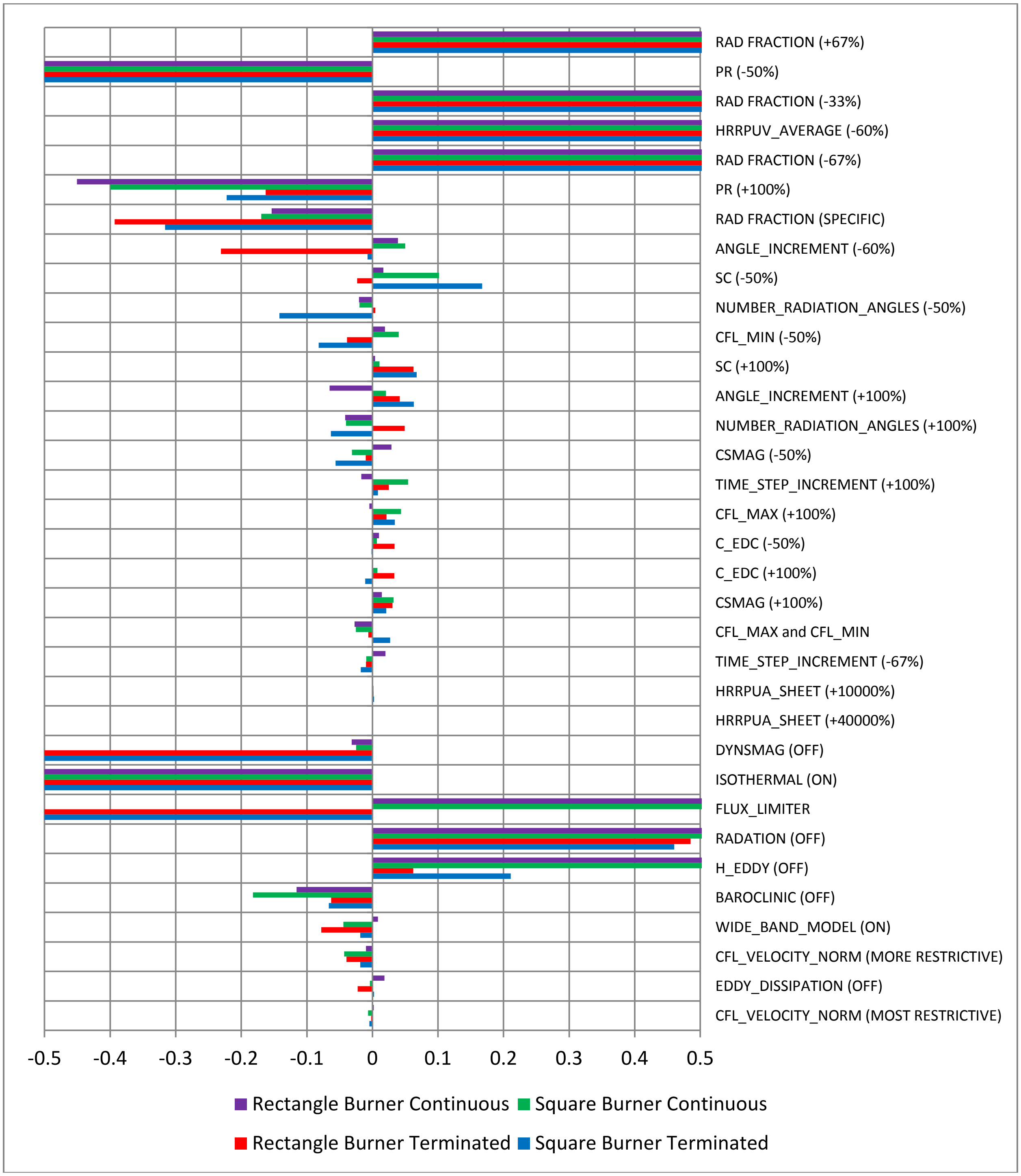

Figure 6 – Peak HRR sensitivity coefficients, grouped by burner shape

Figure 7 shows the sensitivity coefficients based on the predicted time to peak HRR averaged over simulations using the same source fire burner. The parameters with significant changes are changes in the radiative fraction, a decrease of the Prandtl number, a decrease of the average HRRPUV, when the dynamic Smagorinsky model is deactivated, or when the isothermal model is turned on, when the radiation transport mode was turned off, and which calculation scheme was used based on the FLUX_LIMITER value. It is noted that the simulations with change to the FLUX_LIMITER value crashed due to numerical instability. The effects on the simulations with a continuous source fire are generally greater than the effect on the simulations with a terminated source fire.

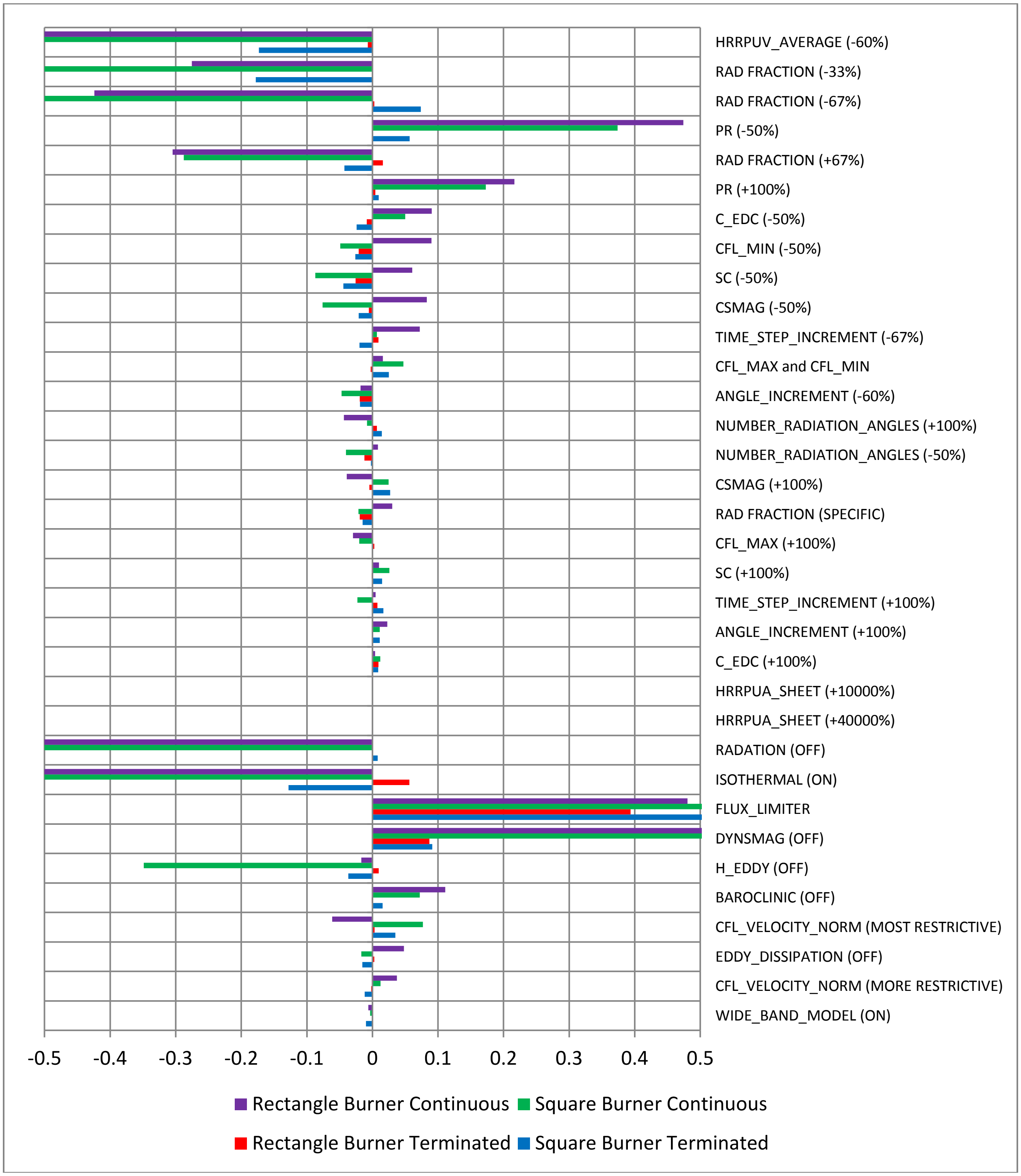

Figure 7 – Time to peak HRR sensitivity coefficients, grouped by burner shape

Figure 8 shows the sensitivity coefficients based on the predicted total mass loss averaged over simulations using the same source fire burner. The parameters with significant changes are changes in the radiative fraction, a decrease of the Prandtl number, a decrease of the average HRRPUV, when the dynamic Smagorinsky model is deactivated, or when the isothermal model is turned on, when the radiation transport mode was turned off, when the eddy diffusivity model is turned off, and which calculation scheme was used based on the FLUX_LIMITER value. It is noted that the simulations with change to the FLUX_LIMITER value crashed due to numerical instability. The effects on the simulations with a terminated source fire are generally greater than the effect on the simulations with a continuous source fire.

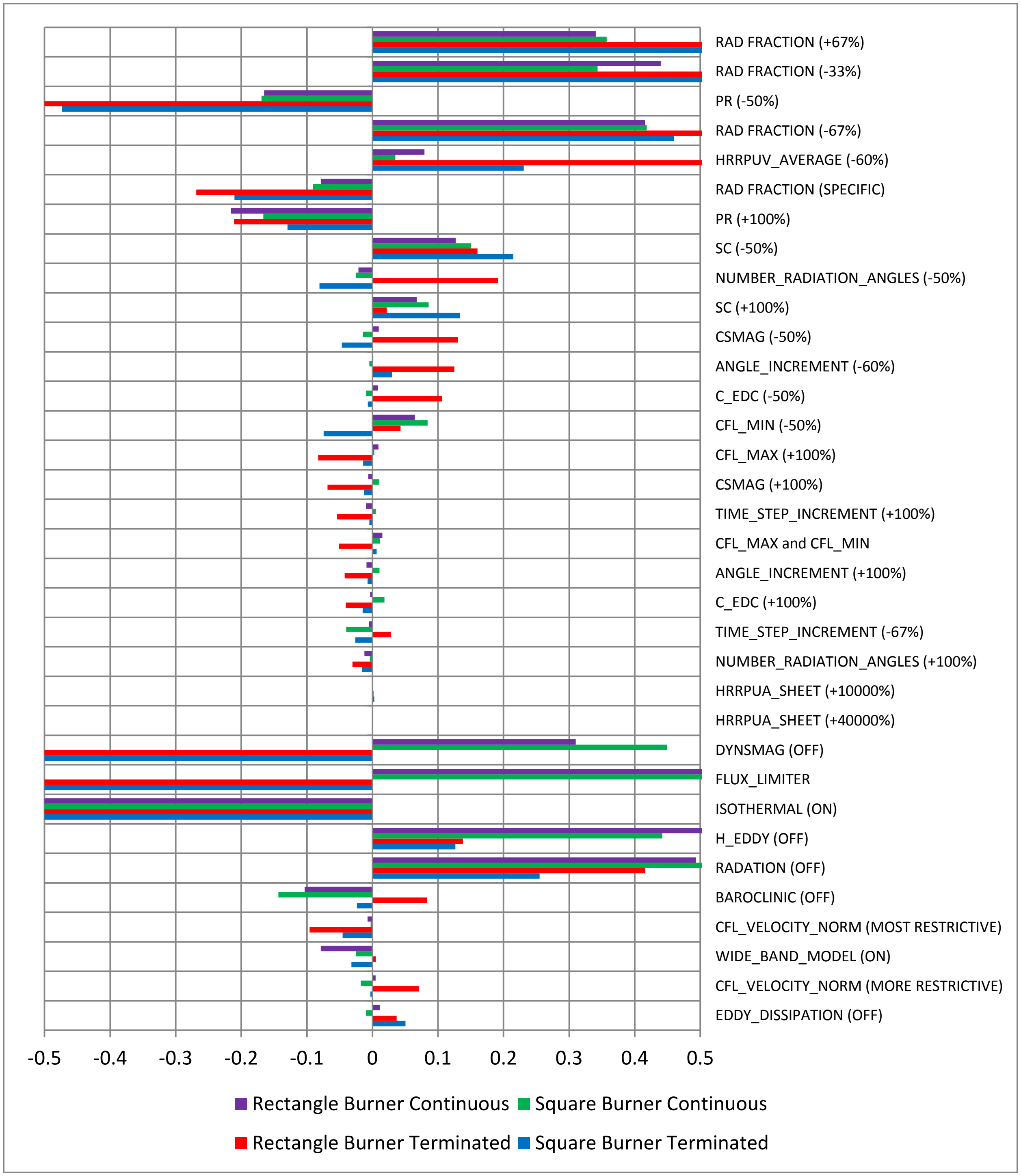

Figure 8 – Total heat released sensitivity coefficients, grouped by burner shape

Table 3 - Sensitivity coefficients based on source burner shape

			Square burner, terminated source fire				Rect. burner, terminated source fire				Square burner, continuous source fire				Rect. burner, continuous source fire			
Parameter change	Default Value	New Value	Total Mass Lost	Peak HRR	Time@ Peak	Heat Releas ed	Total Mass Lost	Peak HRR	Time@ Peak	Heat Releas ed	Total Mass Lost	Peak HRR	Time@ Peak	Heat Releas ed	Total Mass Lost	Peak HRR	Time@ Peak	Heat Releas ed
DYNSMAG (OFF)	.TRUE.	.FALSE.	-1.4548	-3.7111	0.0913	-3.6563	-2.2579	-8.1836	0.0868	-9.2007	0.2305	-0.0249	0.5490	0.4496	0.1280	-0.0315	0.6267	0.3098
RADIATION (OFF)	.TRUE.	.FALSE.	0.1708	0.4601	0.0079	0.2548	0.1661	0.4853	-0.0009	0.4159	0.2930	0.8175	-1.8132	0.5181	0.2551	0.8178	-1.0945	0.4933
WIDE_BAND_MODEL (ON)	.FALSE.	.TRUE	-0.0120	-0.0185	-0.0097	-0.0321	-0.0248	-0.0780	0.0004	0.0052	-0.0233	-0.0442	-0.0036	-0.0248	-0.0499	0.0082	-0.0063	-0.0789
EDDY_DISSIPATION (OFF)	.TRUE.	.FALSE.	-0.0008	0.0026	-0.0155	0.0505	-0.0007	-0.0226	0.0027	0.0368	-0.0032	-0.0037	-0.0172	-0.0099	0.0578	0.0182	0.0479	0.0112
ISOTHERMAL (ON)	.FALSE.	.TRUE	-0.1924	-0.9204	-0.1281	-0.9836	-0.1701	-0.8012	0.0565	-0.9492	-0.4505	-1.0000	-1.0000	-1.0000	-0.4662	-1.0000	-1.0000	-1.0000
BAROCLINIC (OFF)	.TRUE.	.FALSE.	0.0012	-0.0665	0.0155	-0.0236	-0.0307	-0.0630	-0.0010	0.0835	-0.0607	-0.1822	0.0723	-0.1435	-0.0509	-0.1156	0.1110	-0.1032
FLUX_LIMITER	2	-1	0.5008	-0.8254	0.6500	-0.8177	0.2951	-0.6811	0.3935	-1.4464	0.9945	0.8313	0.9555	0.9905	0.9098	0.6155	0.4804	0.8741
CFL_VELOCITY_NORM (MOST RESTRICTIVE)	1	2	0.0018	-0.0046	0.0350	-0.0454	-0.0013	-0.0018	0.0034	-0.0957	0.0026	-0.0067	0.0768	-0.0029	0.0002	0.0021	-0.0615	-0.0074
CFL_VELOCITY_NORM (MORE RESTRICTIVE)	1	0	-0.0095	-0.0186	-0.0117	-0.0030	-0.0032	-0.0395	-0.0019	0.0711	-0.0089	-0.0430	0.0124	-0.0177	-0.0005	-0.0096	0.0372	0.0049
H_EDDY (OFF)	.FALSE.	.TRUE.	0.0708	0.2108	-0.0368	0.1264	0.0589	0.0623	0.0095	0.1378	0.2426	0.7453	-0.3488	0.4421	0.2686	0.8041	-0.0169	0.5440
RAD FRACTION (SPECIFIC)	0.3	Source specific	-0.0770	-0.3160	-0.0150	-0.2102	-0.0647	-0.3930	-0.0192	-0.2686	-0.0493	-0.1695	-0.0215	-0.0907	-0.0352	-0.1539	0.0300	-0.0782
RAD FRACTION (-67%)	0.3	0.1	0.2209	0.7450	0.0738	0.4597	0.2128	0.7351	0.0028	0.6631	0.2535	0.8028	-0.5334	0.4180	0.2229	0.7974	-0.4241	0.4157
RAD FRACTION (-33%)	0.3	0.2	0.3101	1.0490	-0.1777	0.7677	0.2956	1.0155	0.0000	1.0960	0.1909	0.6839	-0.7346	0.3434	0.4716	0.8150	-0.2754	0.4395
RAD FRACTION (+67%)	0.3	0.5	0.8119	2.0789	-0.0428	1.9412	0.7885	2.0312	0.0161	2.1218	0.1873	0.7175	-0.2876	0.3571	0.1659	0.6638	-0.3048	0.3405
NUMBER_RADIATION_ANGLES (-50%)	104	52	-0.0064	-0.1417	-0.0024	-0.0809	0.0013	0.0044	-0.0123	0.1916	-0.0117	-0.0199	-0.0404	-0.0247	-0.0075	-0.0205	0.0085	-0.0213
NUMBER_RADIATION_ANGLES (+100%)	104	208	-0.0076	-0.0633	0.0142	-0.0161	0.0053	0.0493	0.0066	-0.0304	-0.0046	-0.0405	-0.0081	-0.0040	-0.0065	-0.0415	-0.0436	-0.0121
ANGLE_INCREMENT (-60%)	5	2	0.0002	-0.0076	-0.0190	0.0297	-0.0514	-0.2310	-0.0192	0.1249	-0.0025	0.0500	-0.0470	-0.0049	0.0013	0.0388	-0.0183	0.0013
ANGLE_INCREMENT (+100%)	5	10	-0.0013	0.0632	0.0110	-0.0074	0.0040	0.0419	0.0000	-0.0422	0.0032	0.0208	0.0112	0.0107	-0.0051	-0.0653	0.0226	-0.0090
TIME_STEP_INCREMENT (-67%)	3	1	-0.0016	-0.0178	-0.0196	-0.0261	-0.0214	-0.0097	0.0092	0.0281	-0.0177	-0.0094	0.0069	-0.0399	-0.0039	0.0198	0.0722	-0.0052
TIME_STEP_INCREMENT (+100%)	3	6	-0.0008	0.0083	0.0166	-0.0045	0.0015	0.0249	0.0078	-0.0540	0.0005	0.0545	-0.0227	0.0054	-0.0059	-0.0170	0.0049	-0.0098
C_EDC (+100%)	0.1	0.2	-0.0042	-0.0110	0.0088	-0.0151	-0.0018	0.0333	0.0092	-0.0409	0.0070	0.0074	0.0121	0.0184	-0.0024	0.0003	0.0040	-0.0033
C_EDC (-50%)	0.1	0.05	0.0075	-0.0016	-0.0243	-0.0072	-0.0023	0.0338	-0.0085	0.1058	-0.0032	0.0069	0.0499	-0.0098	0.0056	0.0098	0.0905	0.0084
HRRPUA_SHEET (+40000%)	0	400	0.0003	0.0005	0.0000	0.0007	0.0003	0.0004	0.0000	0.0004	-0.0002	0.0001	0.0000	-0.0003	-0.0001	0.0002	-0.0002	-0.0003
HRRPUA_SHEET (+10000%)	0	100	0.0010	0.0026	-0.0001	0.0027	0.0009	0.0017	0.0000	0.0015	-0.0003	0.0016	-0.0008	-0.0007	-0.0003	0.0009	-0.0005	-0.0008
HRRPUV_AVERAGE (-60%)	3000	1200	0.1949	0.5964	-0.1731	0.2308	0.2489	0.5825	-0.0071	0.5918	0.0412	0.7604	-0.9951	0.0348	0.0552	0.8771	-0.9371	0.0792
CSMAG (-50%)	0.2	0.1	-0.0013	-0.0563	-0.0208	-0.0469	-0.0024	-0.0103	-0.0055	0.1305	-0.0056	-0.0312	-0.0761	-0.0146	0.0602	0.0289	0.0828	0.0096
CSMAG (+100%)	0.2	0.4	0.0062	0.0210	0.0271	-0.0127	0.0031	0.0304	-0.0048	-0.0683	0.0033	0.0322	0.0248	0.0104	-0.0028	0.0143	-0.0392	-0.0063
PR (-50%)	0.5	0.25	-0.1761	-0.7420	0.0566	-0.4730	-0.3697	-1.3974	0.0000	-0.9017	-0.0777	-0.5648	0.3739	-0.1692	-0.0710	-0.5083	0.4741	-0.1654
PR (+100%)	0.5	1	-0.0476	-0.2223	0.0098	-0.1296	-0.0532	-0.1627	0.0043	-0.2109	-0.0908	-0.3995	0.1730	-0.1666	-0.1055	-0.4506	0.2166	-0.2158
SC (-50%)	0.5	0.25	-0.0164	0.1671	-0.0445	0.2151	-0.0481	-0.0231	-0.0255	0.1601	0.0550	0.1015	-0.0873	0.1500	0.0551	0.0167	0.0608	0.1269
SC (+100%)	0.5	1	-0.0009	0.0672	0.0146	0.1333	-0.0128	0.0628	-0.0010	0.0220	0.0201	0.0107	0.0256	0.0856	0.0201	0.0039	0.0099	0.0674
CFL_MAX (+100%)	1	2	0.0062	0.0343	0.0001	-0.0141	0.0016	0.0213	0.0027	-0.0826	0.0037	0.0435	-0.0202	0.0028	0.0059	-0.0047	-0.0298	0.0090
CFL_MIN (-50%)	0.8	0.4	0.0369	-0.0819	-0.0259	-0.0746	-0.0109	-0.0387	-0.0208	0.0427	0.3293	0.0399	-0.0489	0.0842	0.3200	0.0191	0.0900	0.0647
CFL_MAX and CFL_MIN	1 / 0.8	2 / 0.4	0.0000	0.0272	0.0248	0.0063	-0.0007	-0.0062	-0.0027	-0.0512	-0.0018	-0.0254	0.0471	0.0115	0.0000	-0.0274	0.0161	0.0152

K.1.3 Heat Release Rate

This section presents the sensitivity coefficients generated from the various simulations as grouped by the base burner HRR: 50 kW or 75 kW. Figure 9 shows the sensitivity coefficients based on the total mass loss averaged over simulations using the same source fire burner. The parameters with significant changes are changes in the radiative fraction and a decrease of the Prandtl number, when the dynamic Smagorinsky model is deactivated, and which calculation scheme was used based on the FLUX_LIMITER value. All simulations with change to the FLUX_LIMITER value crashed. Effects on the simulations with a terminated source fire were greatest for the non-toggle parameter changes, whereas the effects of the toggled parameters are greater for simulations with a continuous source fire.

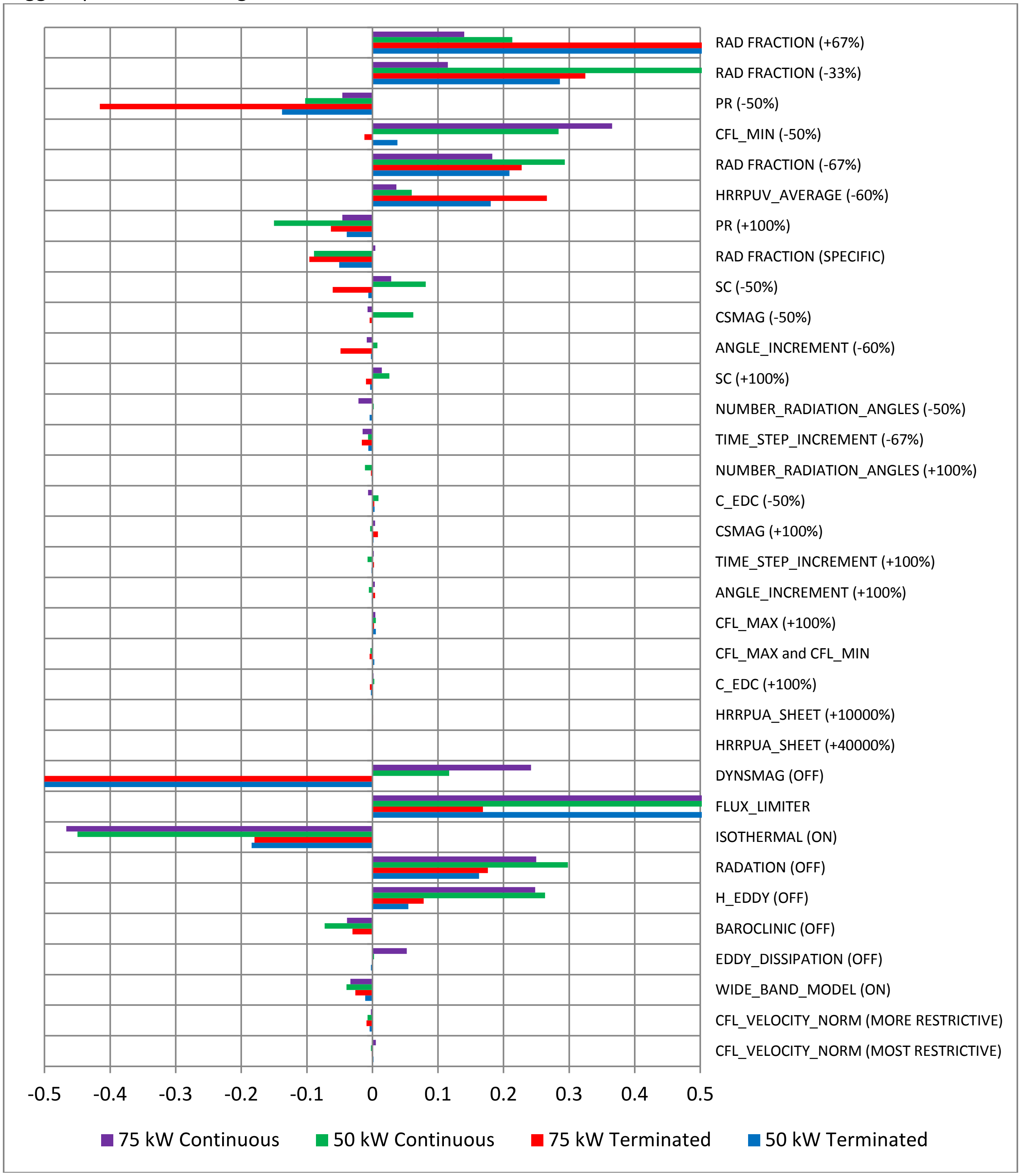

Figure 9 – Total mass loss sensitivity coefficients, grouped by HRR

Figure 10 shows the shows the sensitivity coefficients based on the peak HRR magnitude averaged over simulations using the same source fire burner. The parameters with significant changes are changes in the radiative fraction, a decrease of the Prandtl number, a decrease of the average HRRPUV, when the dynamic Smagorinsky model is deactivated, or when the isothermal model is turned on, when the radiation transport mode was turned off, which calculation scheme was used based on the FLUX_LIMITER value, and whether the eddy diffusivity model was not used. It is noted that the simulations with change to the FLUX_LIMITER value crashed due to numerical instability. Effects on the simulations with a terminated source fire appear to be more significant than simulations with a continuous source fire.

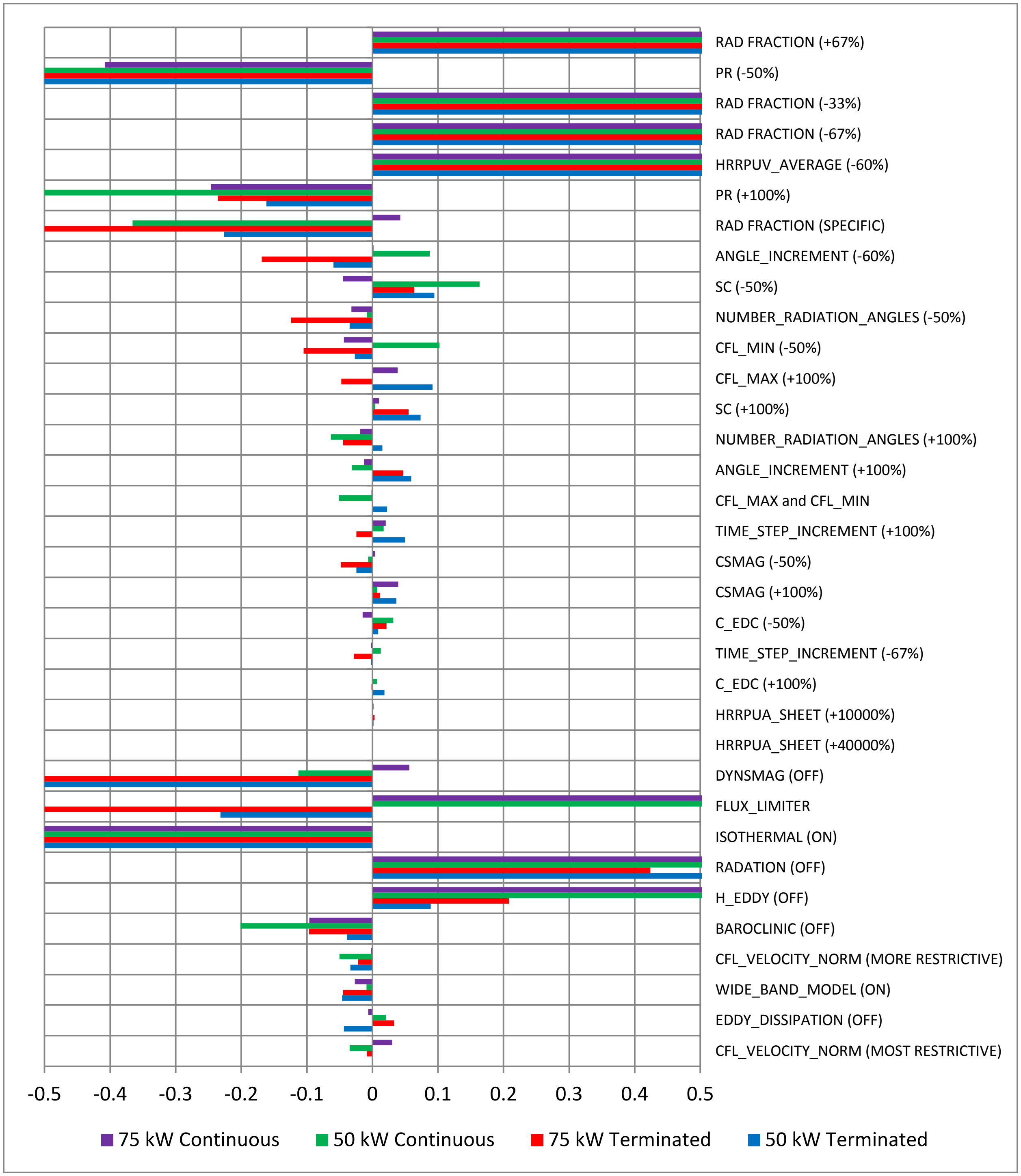

Figure 10 – Peak HRR sensitivity coefficients, grouped by HRR

Figure 11 shows the sensitivity coefficients based on the predicted time to peak HRR averaged over simulations using the same source fire burner. The parameters with significant changes are a decrease of the average HRRPUV, changes in the radiative fraction, , when the dynamic Smagorinsky model is deactivated, or when the isothermal model is turned on, when the radiation transport mode was turned off, and which calculation scheme was used based on the FLUX_LIMITER value. It is noted that the simulations with change to the FLUX_LIMITER value crashed due to numerical instability. The effects on the simulations with a continuous source fire are generally greater than the effect on the simulations with a terminated source fire.

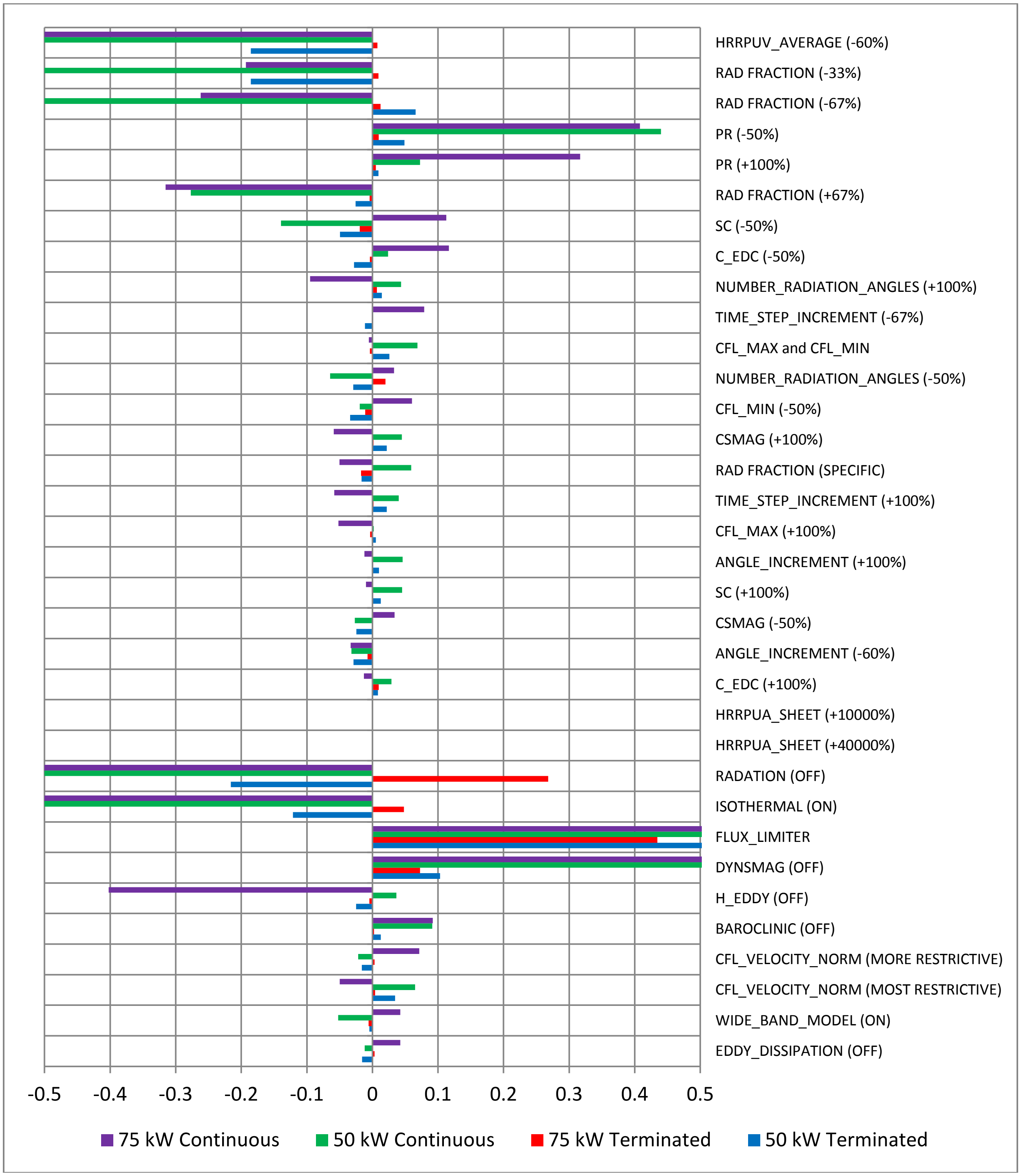

Figure 11 – Time to peak HRR sensitivity coefficients, grouped by HRR

Figure 12 shows the sensitivity coefficients based on the predicted total heat released averaged over simulations using the same source fire burner. The parameters with significant changes are changes in the radiative fraction, a decrease of the Prandtl number, when the dynamic Smagorinsky model is deactivated, or when the isothermal model is turned on, when the radiation transport mode was turned off, when the eddy diffusivity model is turned off, and which calculation scheme was used based on the FLUX_LIMITER value. It is noted that the simulations with change to the FLUX_LIMITER value crashed due to numerical instability. The effects on the simulations with a terminated source fire are generally greater than the effect on the simulations with a continuous source fire.

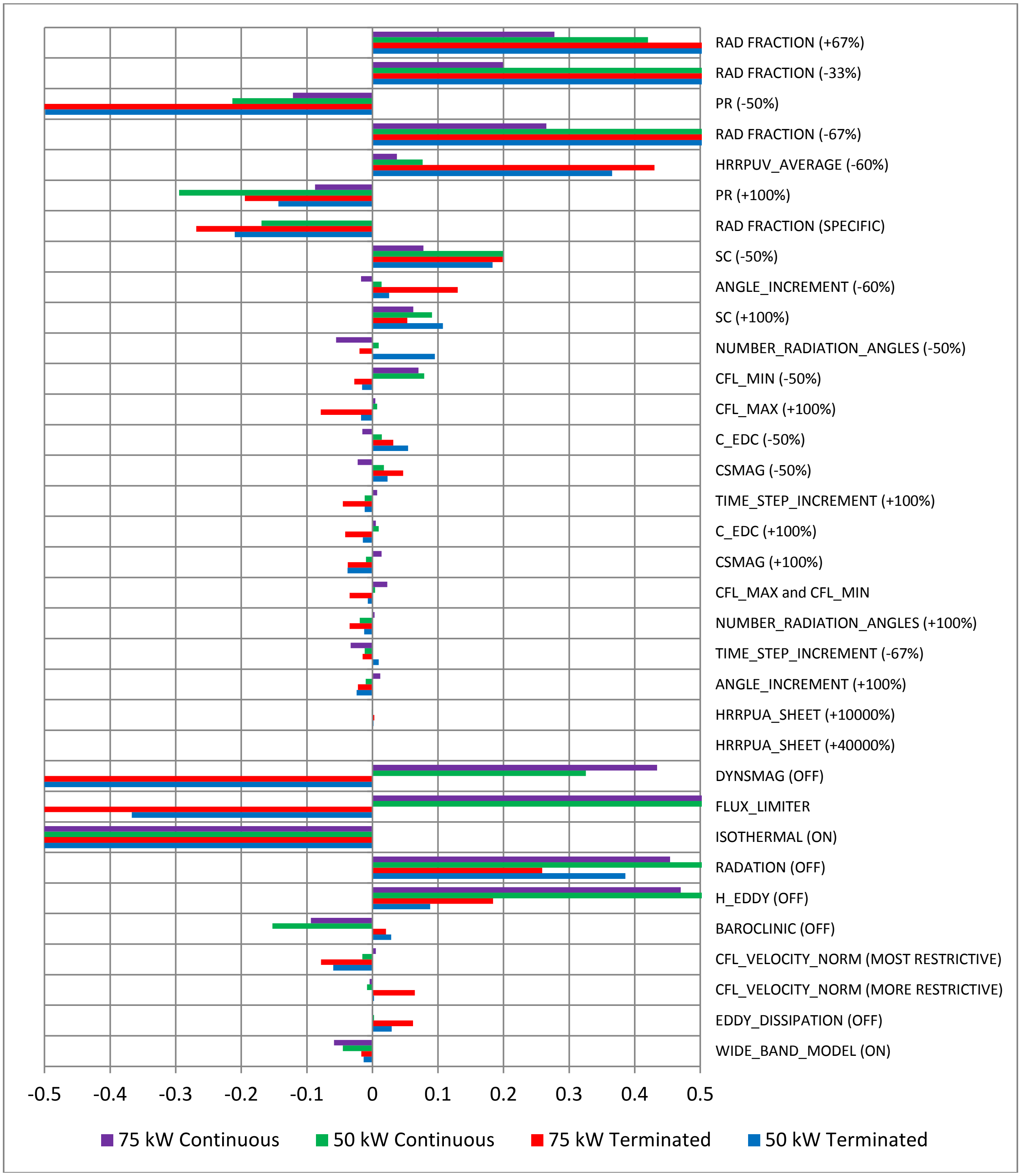

Figure 12 – Total heat released sensitivity coefficients, grouped by burner shape

Table 4 - Sensitivity coefficients based on source fire HRR

			HRR = 50 kW, terminated source fire				HRR = 75 kW, terminated source fire				HRR = 50 kW, continuous source fire				HRR = 75 kW, continuous source fire			
Parameter change	**Default Value**	**New Value**	-1.7680	-6.3772	0.1033	-6.6594	-1.8820	-4.9843	0.0725	-5.5970	0.1168	-0.1127	0.6003	0.3255	0.2418	0.0562	0.5754	0.4339
DYNSMAG (OFF)	.TRUE.	.FALSE.	0.1626	0.5116	-0.2160	0.3856	0.1759	0.4236	0.2679	0.2589	0.2983	0.8516	-1.8803	0.5575	0.2498	0.7837	-1.0274	0.4539
RADATION (OFF)	.TRUE.	.FALSE.	-0.0110	-0.0464	-0.0046	-0.0136	-0.0260	-0.0445	-0.0058	-0.0171	-0.0396	-0.0090	-0.0523	-0.0453	-0.0336	-0.0270	0.0425	-0.0585
WIDE_BAND_MODEL (ON)	.FALSE.	.TRUE	-0.0021	-0.0436	-0.0158	0.0296	0.0008	0.0329	0.0031	0.0619	0.0023	0.0209	-0.0117	0.0024	0.0523	-0.0063	0.0425	-0.0012
EDDY_DISSIPATION (OFF)	.TRUE.	.FALSE.	-0.1843	-0.8701	-0.1212	-0.9695	-0.1797	-0.8616	0.0482	-0.9661	-0.4498	-1.0000	-1.0000	-1.0000	-0.4669	-1.0000	-1.0000	-1.0000
ISOTHERMAL (ON)	.FALSE.	.TRUE	0.0010	-0.0386	0.0126	0.0286	-0.0305	-0.0965	0.0024	0.0208	-0.0728	-0.2014	0.0912	-0.1527	-0.0388	-0.0964	0.0921	-0.0940
BAROCLINIC (OFF)	.TRUE.	.FALSE.	0.6065	-0.2319	0.6160	-0.3667	0.1683	-1.3933	0.4343	-1.9876	0.9650	0.7274	0.7846	0.9524	0.9393	0.7194	0.6513	0.9122
FLUX_LIMITER	2	-1	0.0016	0.0010	0.0346	-0.0597	-0.0010	-0.0086	0.0038	-0.0786	-0.0024	-0.0349	0.0650	-0.0155	0.0052	0.0303	-0.0498	0.0053
CFL_VELOCITY_NORM (MOST RESTRICTIVE)	1	2	-0.0045	-0.0334	-0.0161	0.0023	-0.0092	-0.0217	0.0034	0.0648	-0.0073	-0.0505	-0.0218	-0.0084	-0.0022	-0.0022	0.0714	-0.0044
CFL_VELOCITY_NORM (MORE RESTRICTIVE)	1	0	0.0548	0.0890	-0.0250	0.0879	0.0781	0.2086	-0.0046	0.1840	0.2631	0.7961	0.0365	0.5162	0.2481	0.7534	-0.4021	0.4700
H_EDDY (OFF)	.FALSE.	.TRUE.	-0.0507	-0.2262	-0.0166	-0.2101	-0.0961	-0.5008	-0.0172	-0.2688	-0.0891	-0.3659	0.0590	-0.1692	0.0046	0.0425	-0.0504	0.0003
RAD FRACTION (SPECIFIC)	0.3	Source specific	0.2088	0.7939	0.0657	0.5858	0.2274	0.6764	0.0125	0.5117	0.2935	1.0751	-0.6958	0.5685	0.1828	0.5250	-0.2617	0.2652
RAD FRACTION (-67%)	0.3	0.1	0.2859	1.0781	-0.1853	0.9806	0.3248	0.9806	0.0091	0.8405	0.5477	0.9024	-0.8173	0.5838	0.1149	0.5964	-0.1928	0.1991
RAD FRACTION (-33%)	0.3	0.2	0.6716	1.8216	-0.0258	1.9612	0.9569	2.3400	-0.0042	2.0978	0.2133	0.7927	-0.2771	0.4201	0.1399	0.5885	-0.3153	0.2775
RAD FRACTION (+67%)	0.3	0.5	-0.0044	-0.0348	-0.0292	0.0950	-0.0010	-0.1238	0.0199	-0.0196	0.0020	-0.0085	-0.0647	0.0094	-0.0212	-0.0319	0.0328	-0.0554
NUMBER_RADIATION_ANGLES (-50%)	104	52	-0.0013	0.0151	0.0142	-0.0125	-0.0022	-0.0448	0.0066	-0.0347	-0.0113	-0.0632	0.0435	-0.0193	0.0002	-0.0187	-0.0952	0.0031
NUMBER_RADIATION_ANGLES (+100%)	104	208	-0.0021	-0.0594	-0.0290	0.0255	-0.0486	-0.1688	-0.0073	0.1300	0.0074	0.0873	-0.0321	0.0140	-0.0086	0.0015	-0.0331	-0.0175
ANGLE_INCREMENT (-60%)	5	2	-0.0012	0.0590	0.0100	-0.0240	0.0040	0.0469	0.0012	-0.0222	-0.0055	-0.0316	0.0459	-0.0101	0.0036	-0.0128	-0.0121	0.0118
ANGLE_INCREMENT (+100%)	5	10	-0.0062	-0.0021	-0.0115	0.0097	-0.0160	-0.0285	-0.0005	-0.0148	-0.0067	0.0129	0.0003	-0.0120	-0.0149	-0.0024	0.0788	-0.0331
TIME_STEP_INCREMENT (-67%)	3	1	-0.0015	0.0494	0.0219	-0.0120	0.0023	-0.0244	0.0015	-0.0451	-0.0074	0.0172	0.0403	-0.0118	0.0019	0.0204	-0.0581	0.0073
TIME_STEP_INCREMENT (+100%)	3	6	-0.0024	0.0182	0.0084	-0.0146	-0.0040	-0.0017	0.0097	-0.0416	0.0029	0.0070	0.0291	0.0097	0.0016	0.0007	-0.0130	0.0053
C_EDC (+100%)	0.1	0.2	0.0032	0.0088	-0.0280	0.0543	0.0028	0.0213	-0.0040	0.0319	0.0093	0.0318	0.0240	0.0142	-0.0068	-0.0151	0.1164	-0.0155
C_EDC (-50%)	0.1	0.05	0.0001	0.0001	0.0000	0.0002	0.0004	0.0009	0.0000	0.0010	-0.0003	-0.0003	0.0001	-0.0006	-0.0001	0.0006	-0.0003	-0.0001
HRRPUA_SHEET (+40000%)	0	400	0.0007	0.0015	-0.0001	0.0015	0.0014	0.0031	0.0000	0.0030	-0.0005	0.0007	-0.0005	-0.0012	-0.0002	0.0018	-0.0009	-0.0003
HRRPUA_SHEET (+10000%)	0	100	0.1806	0.6005	-0.1853	0.3655	0.2662	0.5776	0.0075	0.4302	0.0598	0.8853	-1.1059	0.0766	0.0367	0.7522	-0.8263	0.0375
HRRPUV_AVERAGE (-60%)	3000	1200	0.0004	-0.0246	-0.0247	0.0229	-0.0044	-0.0483	-0.0008	0.0468	0.0623	-0.0064	-0.0268	0.0174	-0.0076	0.0041	0.0336	-0.0224
CSMAG (-50%)	0.2	0.1	0.0018	0.0367	0.0218	-0.0382	0.0084	0.0116	0.0016	-0.0377	-0.0036	0.0071	0.0447	-0.0099	0.0041	0.0393	-0.0591	0.0141
CSMAG (+100%)	0.2	0.4	-0.1379	-0.8190	0.0487	-0.4989	-0.4155	-1.3050	0.0094	-0.8706	-0.1027	-0.6649	0.4399	-0.2134	-0.0459	-0.4081	0.4081	-0.1211
PR (-50%)	0.5	0.25	-0.0390	-0.1615	0.0091	-0.1432	-0.0635	-0.2357	0.0051	-0.1946	-0.1503	-0.6038	0.0728	-0.2949	-0.0460	-0.2464	0.3168	-0.0875
PR (+100%)	0.5	1	-0.0061	0.0945	-0.0496	0.1830	-0.0606	0.0641	-0.0194	0.1986	0.0813	0.1635	-0.1393	0.1990	0.0287	-0.0453	0.1128	0.0779
SC (-50%)	0.5	0.25	-0.0035	0.0735	0.0127	0.1074	-0.0097	0.0553	0.0012	0.0530	0.0259	0.0042	0.0452	0.0907	0.0143	0.0103	-0.0097	0.0623
SC (+100%)	0.5	1	0.0053	0.0918	0.0053	-0.0174	0.0026	-0.0476	-0.0034	-0.0787	0.0052	0.0002	0.0020	0.0073	0.0044	0.0387	-0.0520	0.0045
CFL_MAX (+100%)	1	2	0.0379	-0.0268	-0.0341	-0.0159	-0.0121	-0.1048	-0.0109	-0.0277	0.2839	0.1024	-0.0194	0.0789	0.3654	-0.0434	0.0604	0.0700
CFL_MIN (-50%)	0.8	0.4	0.0030	0.0223	0.0258	-0.0072	-0.0044	-0.0004	-0.0039	-0.0350	-0.0031	-0.0511	0.0687	0.0040	0.0013	-0.0017	-0.0055	0.0227
CFL_MAX and CFL_MIN	1 / 0.8	2 / 0.4	-1.7680	-6.3772	0.1033	-6.6594	-1.8820	-4.9843	0.0725	-5.5970	0.1168	-0.1127	0.6003	0.3255	0.2418	0.0562	0.5754	0.4339

K.2 Ratios of Quantity Change

Since the sensitivity coefficients are averaged regardless of the height of the “measurement” locations, the changes in the quantities due to parametric variation that are height-depended are omitted. To show the height-dependent effects, the ratios of change for the centerline plume temperature and velocity are plotted against the height of measurement locations. The ratio is calculated in equation [1.2]:

$$\left(\frac{Quantity_{new} - Quantity_{baseline}}{Quantity_{baseline}}\right) \qquad [0.2]$$

The ratios for all simulations are plotted for each parametric series in the following section. This allows the effects of the parametric change on simulations with different source fuel, source burner size, and HRR be observed.

Based on the changes in the total mass loss, peak HRR, time to peak HRR, and total heat released, the simulations most affected by a change in the FDS parameters are the simulations with a continuous source fire and the simulation of a terminated propane source fire with a Rectangle burner at 75 kW.

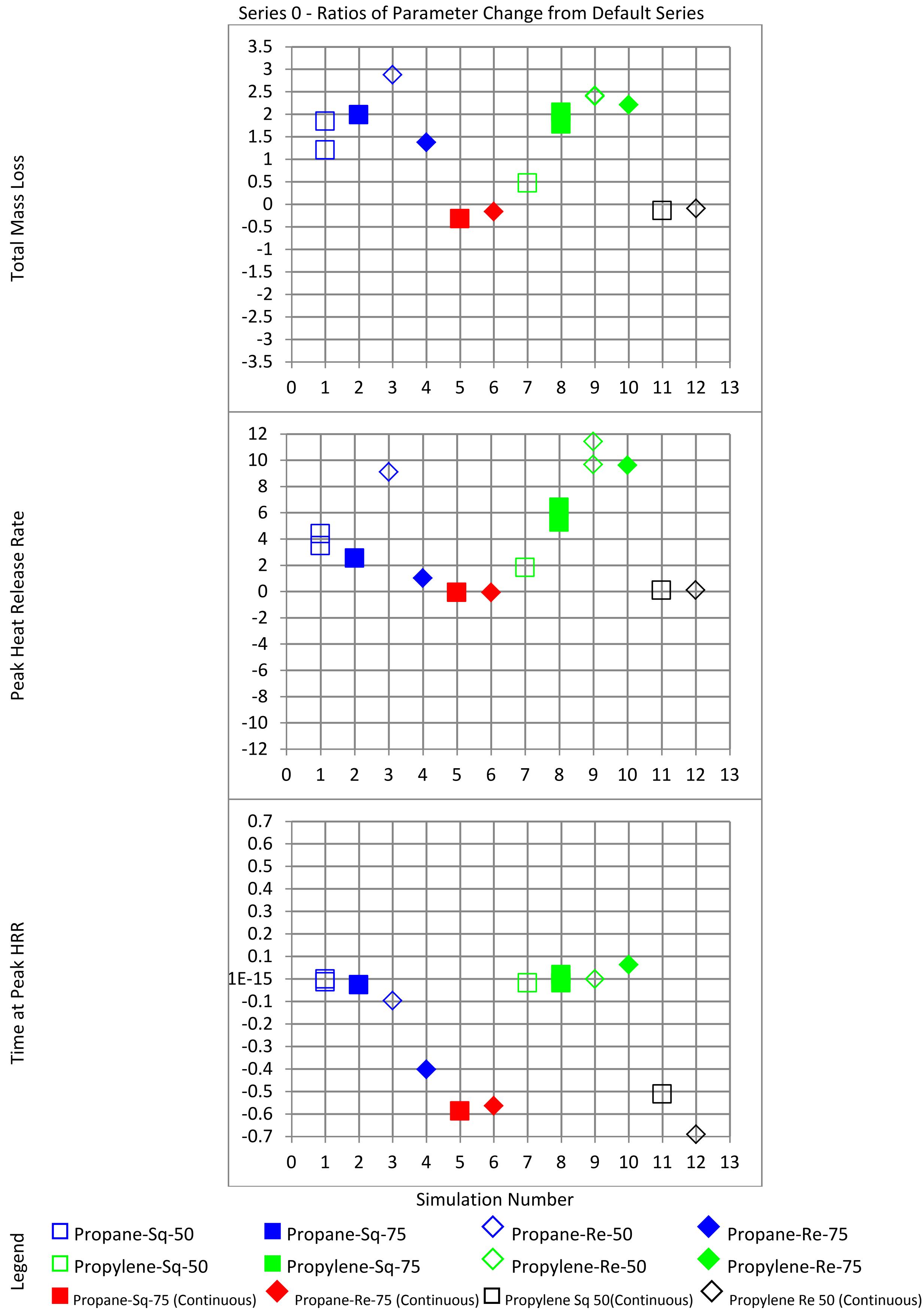

Series 0 - Ratios of Parameter Change from Default Series
Total Mass Loss
Peak Heat Release Rate
Time at Peak HRR
Simulation Number
Legend
Propane-Sq-50
Propane-Sq-75
Propane-Re-50
Propane-Re-75
Propylene-Sq-50
Propylene-Sq-75
Propylene-Re-50
Propylene-Re-75
Propane-Sq-75 (Continuous)
Propane-Re-75 (Continuous)
Propylene Sq 50(Continuous)
Propylene Re 50 (Continuous)

Total Heat Released

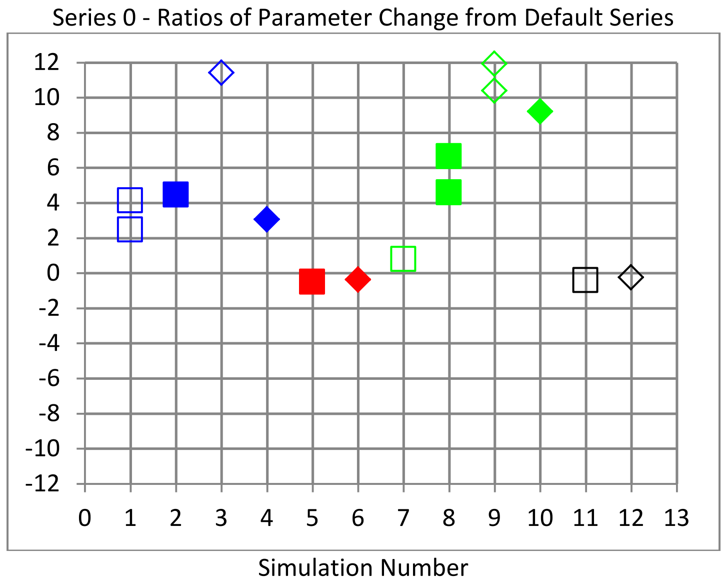

Legend

Propane-Sq-50 | Propane-Sq-75 | Propane-Re-50 | Propane-Re-75
Propylene-Sq-50 | Propylene-Sq-75 | Propylene-Re-50 | Propylene-Re-75
Propane-Sq-75 (Continuous) | Propane-Re-75 (Continuous) | Propylene Sq 50(Continuous) | Propylene Re 50 (Continuous)

Observations

In Series 0, the dynamics Smagorinsky model was turned off in the FDS models, which resulted in a more disordered flow field inside the computational domain.

In the total mass lost preiction, the parameter change incurred an increase for all simulations with a terminated source fire, whereas little change was observed for the simulations with a continousou source fire. The totall mass loss was essentially doubled for all cases, except for the propylene, Square, 50 kW simulation.

Similar to the total mass lost, the peak HRR of simulations with a terinated source fire all experience a drastic increase. The increase is especially significant for the simulation with the Rectangle burner at 50 kW, where there was essentially no flame spread on the combustible wall material predicted in the default simulations. The increase in all of the peak HRR indiciated flame spread on the panel. The peak HRR predicted in the simulations with a continuous source fire was changed only slightly.

The time to peak HRR was shorted in the simulations with a continuous source fire, but not for most of the other simulations except the one with propane at 75 kW with a Rectangle burner.

The predicted THR correlates well with the peak HRR, where the increases were drastic for the simulations with a terminated source fire, and very slightly decreases for those with a continuous source fire.

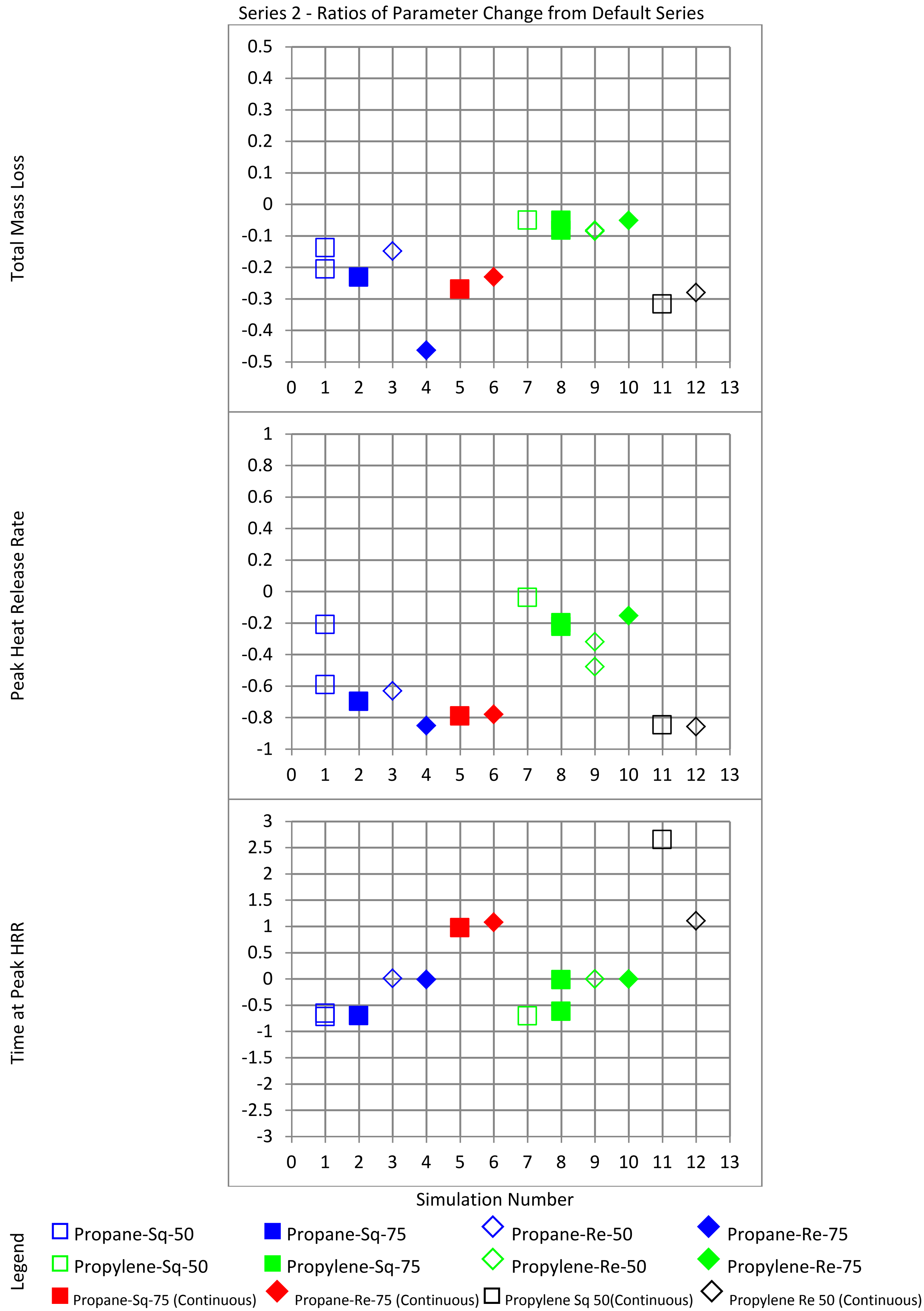
Series 2 - Ratios of Parameter Change from Default Series
Total Mass Loss
Peak Heat Release Rate
Time at Peak HRR
Simulation Number
Legend
Propane-Sq-50
Propane-Sq-75
Propane-Re-50
Propane-Re-75
Propylene-Sq-50
Propylene-Sq-75
Propylene-Re-50
Propylene-Re-75
Propane-Sq-75 (Continuous)
Propane-Re-75 (Continuous)
Propylene Sq 50(Continuous)
Propylene Re 50 (Continuous)

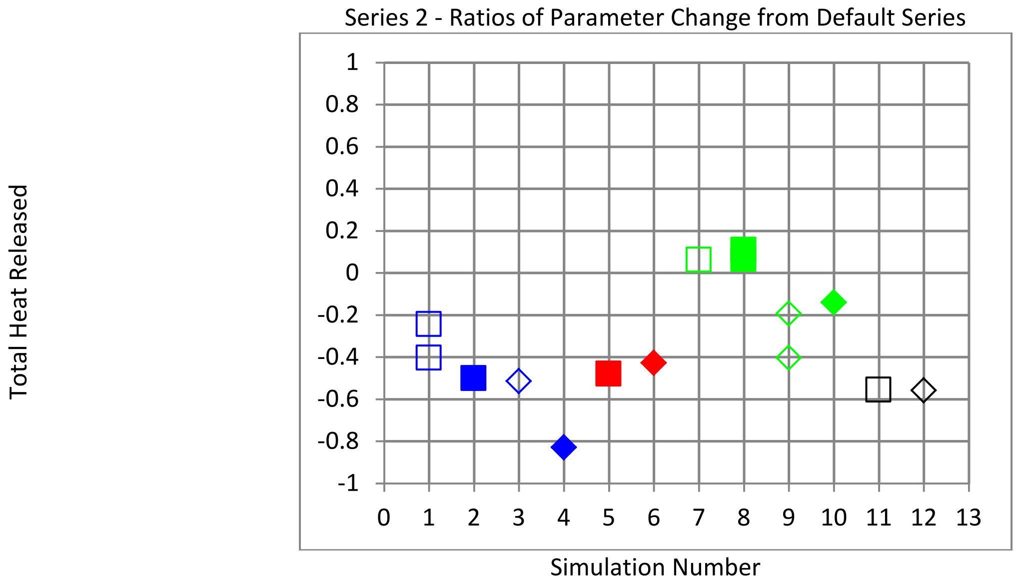

Legend

Propane-Sq-50 | Propane-Sq-75 | Propane-Re-50 | Propane-Re-75

Propylene-Sq-50 | Propylene-Sq-75 | Propylene-Re-50 | Propylene-Re-75

Propane-Sq-75 (Continuous) | Propane-Re-75 (Continuous) | Propylene Sq 50(Continuous) | Propylene Re 50 (Continuous)

Observations

The radiation solver of FDS is disabled in the Series 2 simulations.

The total mass lost was decreased for all simulations, its effect is more prominent for the ones with the continuous source fire, and the ones simulating propane source fuel.

The changes in the peak HRR is similar to the total mass lost where the changes are more prominent for the ones with the continuous source fire, and the ones simulating propane source fuel.

Generally, the parameter change affected slightly negatively on the time to peak HRR for the simulations with a terminated source fire; the time is shortened especially for the cases with the Square burner. However, the time was lengthened for the simulations with a continuous source fire.

The changes in the THR is similar to the total mass lost and peak HRR magnitude where the changes are most prominent for the ones with the continuous source fire, and the ones simulating propane source fuel.

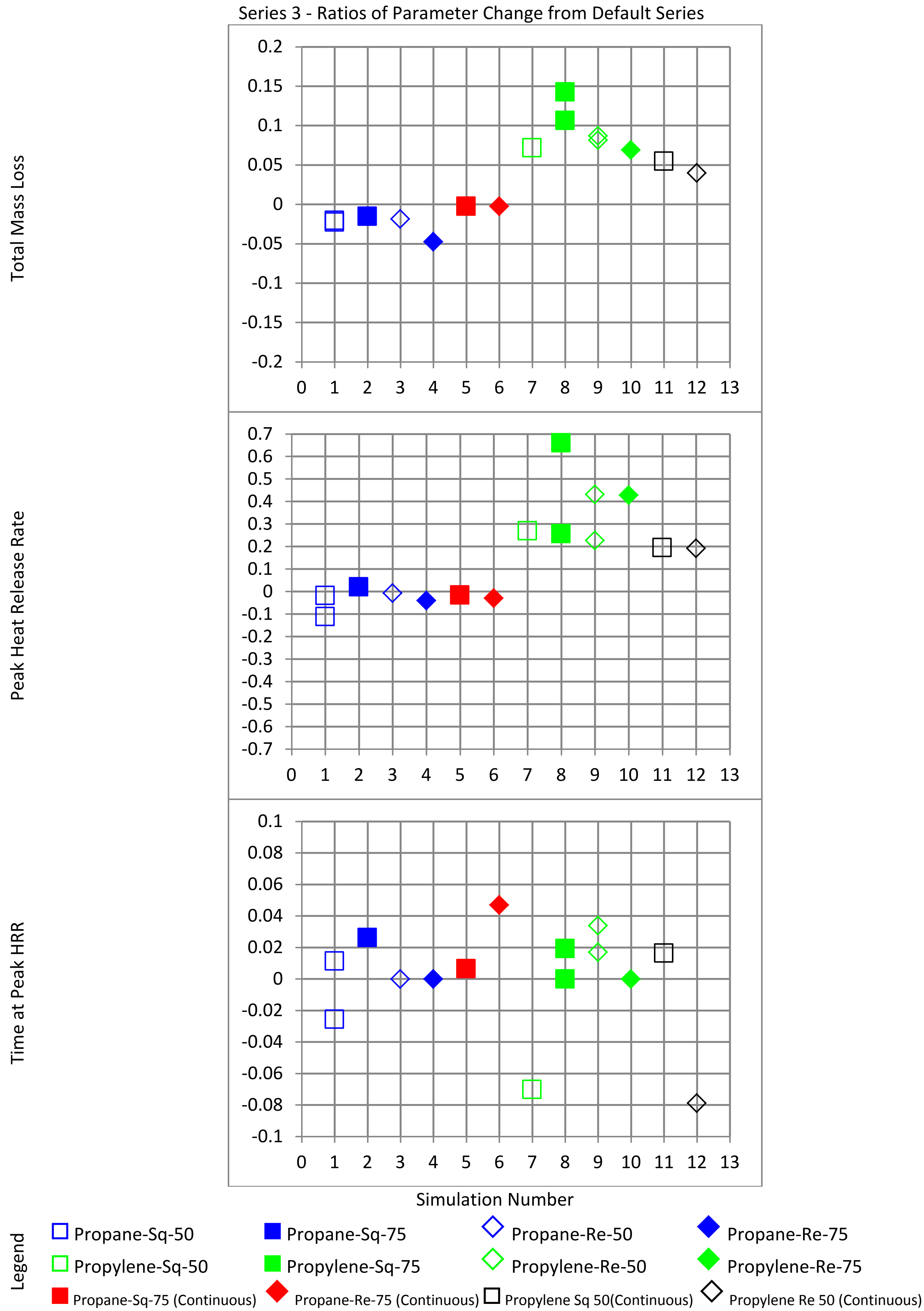

Series 3 - Ratios of Parameter Change from Default Series
Total Mass Loss
Peak Heat Release Rate
Time at Peak HRR
Simulation Number
Legend
Propane-Sq-50
Propane-Sq-75
Propane-Re-50
Propane-Re-75
Propylene-Sq-50
Propylene-Sq-75
Propylene-Re-50
Propylene-Re-75
Propane-Sq-75 (Continuous)
Propane-Re-75 (Continuous)
Propylene Sq 50(Continuous)
Propylene Re 50 (Continuous)

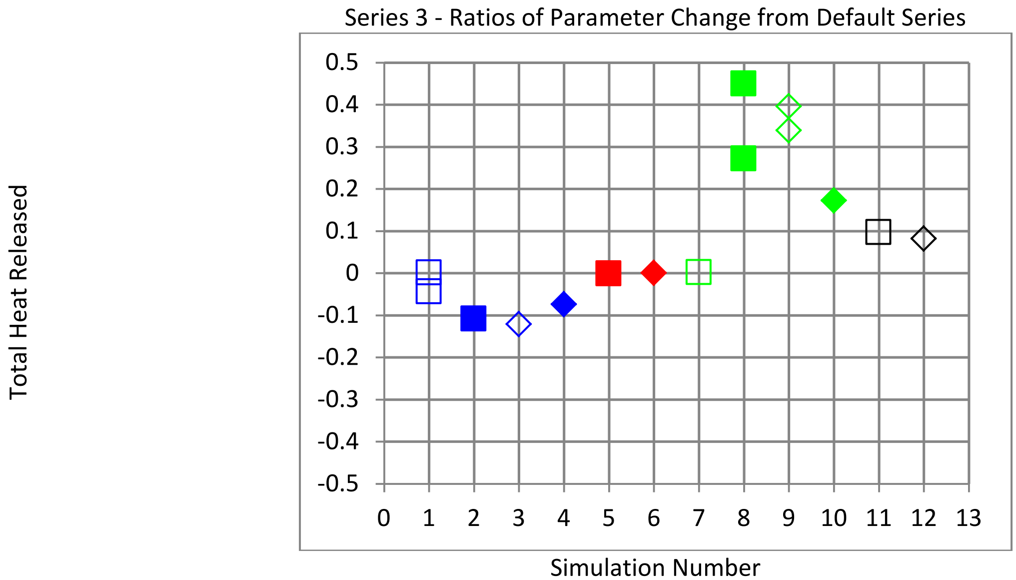

Legend

Propane-Sq-50 | Propane-Sq-75 | Propane-Re-50 | Propane-Re-75
Propylene-Sq-50 | Propylene-Sq-75 | Propylene-Re-50 | Propylene-Re-75
Propane-Sq-75 (Continuous) | Propane-Re-75 (Continuous) | Propylene Sq 50(Continuous) | Propylene Re 50 (Continuous)

Observations

In Series 3, the radiative fraction used in each of the simulations was changed from the default 0.30 to suit the fuels' specific radiative fractions. For propane, 0.286; and for propylene, 0.368.

The total mass lost predicted was not changed significantly for the tests using propane as source fuel, but for the simulations with propylene source fire, the mass lost increased in the simulations. The effect is most prominent for the cases with the Square burner at 75 kW.

Changes to the peak HRR were similar to the total mass lost, except more significant.

The time to peak HRR was only changed slightly due to the difference in the radiative fraction, generally within the range of ±2%, except for two propylene simulations at 50 kW where the difference approached -8%

The changes to the THR is similar to changes in both the mass loss and peak HRR where the simulations with propane source fuel was slightly changed but the simulations with propylene with Square burner at 75 kW was most significantly increased.

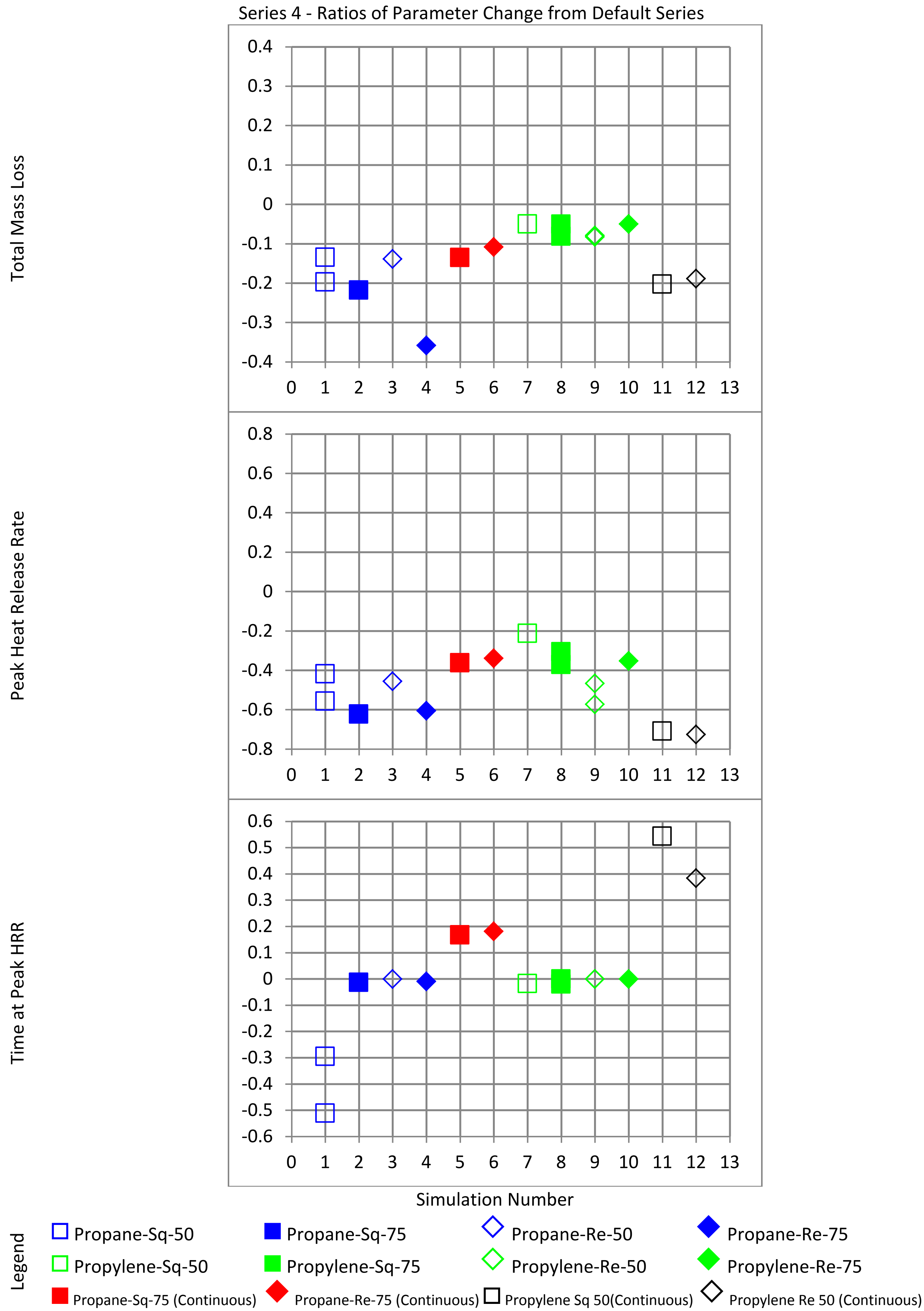
Series 4 - Ratios of Parameter Change from Default Series
Total Mass Loss
Peak Heat Release Rate
Time at Peak HRR
0.4
0.3
0.2
0.1
0
-0.1
-0.2
-0.3
-0.4
0.8
0.6
0.4
0.2
0
-0.2
-0.4
-0.6
-0.8
0.6
0.5
0.4
0.3
0.2
0.1
0
-0.1
-0.2
-0.3
-0.4
-0.5
-0.6
0 1 2 3 4 5 6 7 8 9 10 11 12 13
Simulation Number
Legend
Propane-Sq-50
Propane-Sq-75
Propane-Re-50
Propane-Re-75
Propylene-Sq-50
Propylene-Sq-75
Propylene-Re-50
Propylene-Re-75
Propane-Sq-75 (Continuous)
Propane-Re-75 (Continuous)
Propylene Sq 50(Continuous)
Propylene Re 50 (Continuous)

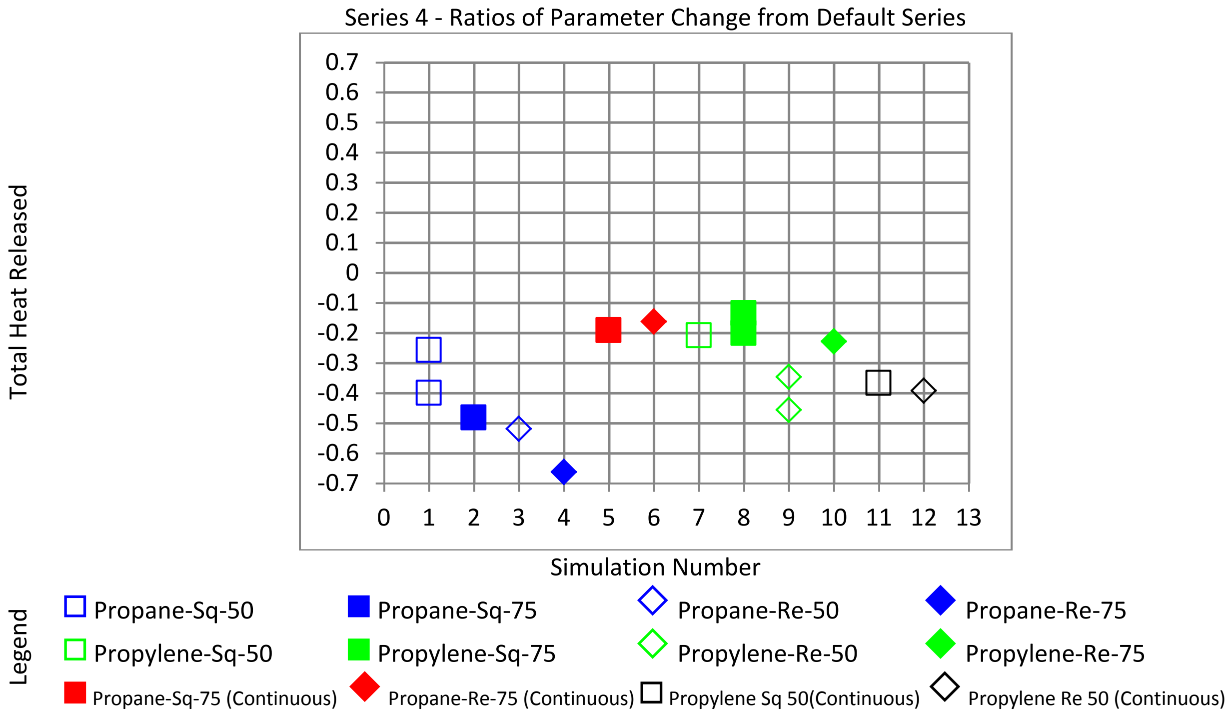

Observations

In Series 4, the radiative fraction of all simulations was lowered 66% from the default 0.30 to 0.1.

The total mass lost for all simulations were reduced, and the effects on the propane simulations appear to be more prominent for the equivalent simulations using propylene. The mass loss for both simulations with a continuous fire for propylene was the most repressed of all simulations.

The peak HRR was also reduced for all simulations, similar to the mass loss prediction where the propane simulations appear to be more greatly affected, but the most repressed peak HRR occurred for the propylene simulations with continuous source fire.

Time to peak HRR was changed differently from the other quantities, for most simulations with a terminated source fire, the time was not changed. However, the simulations with propane and a Square burner at 50 kW has a faster peak time. The time to peak for the simulations with a continuous source fire was increased, more significant for the propylene source fuel than for the propane.

Generally, the mass loss for all simulations was reduced. The effect was most significant for the propane simulations without a continuous source fire.

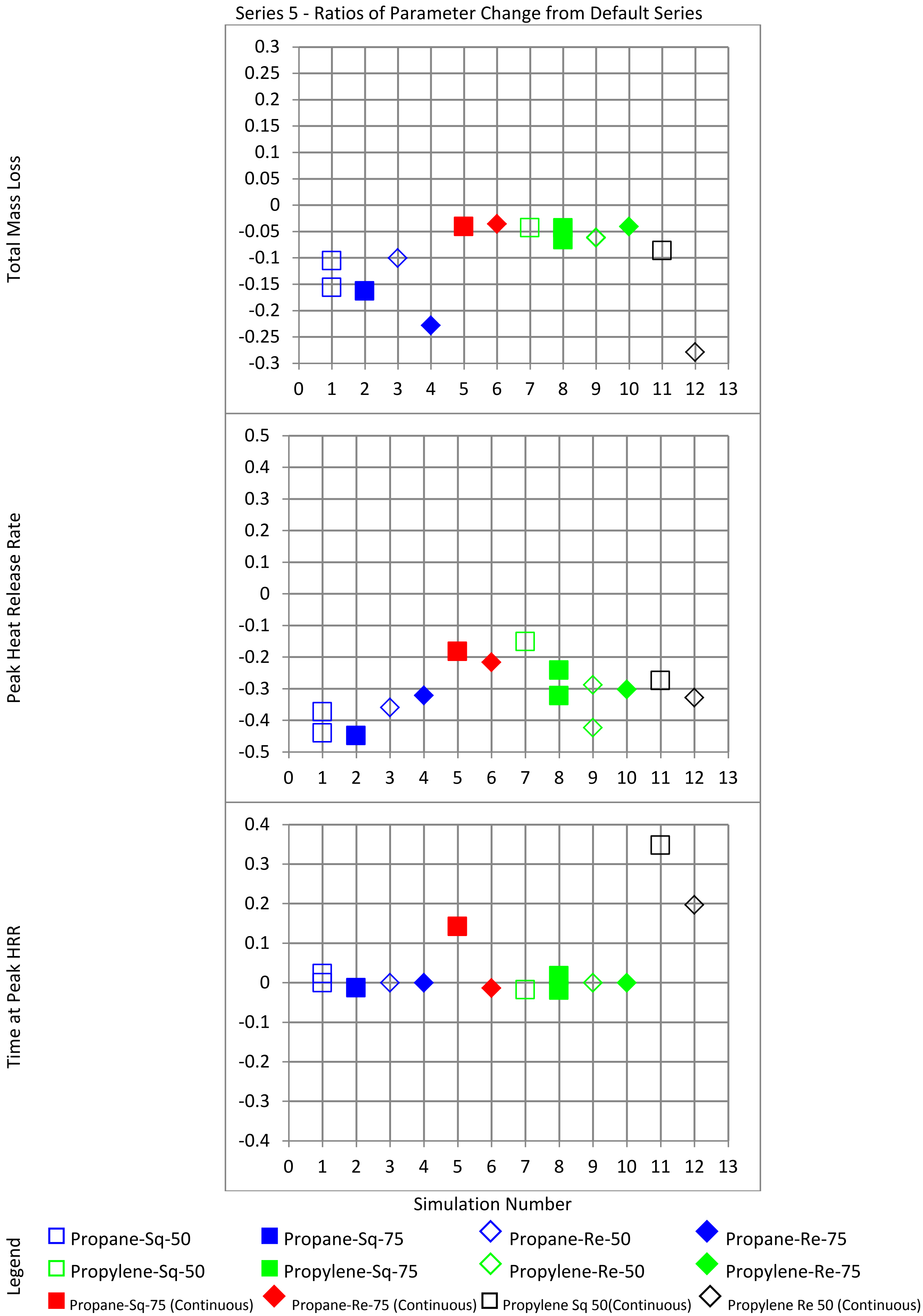
Series 5 - Ratios of Parameter Change from Default Series
Total Mass Loss
Peak Heat Release Rate
Time at Peak HRR
Simulation Number
Legend
Propane-Sq-50
Propane-Sq-75
Propane-Re-50
Propane-Re-75
Propylene-Sq-50
Propylene-Sq-75
Propylene-Re-50
Propylene-Re-75
Propane-Sq-75 (Continuous)
Propane-Re-75 (Continuous)
Propylene Sq 50(Continuous)
Propylene Re 50 (Continuous)

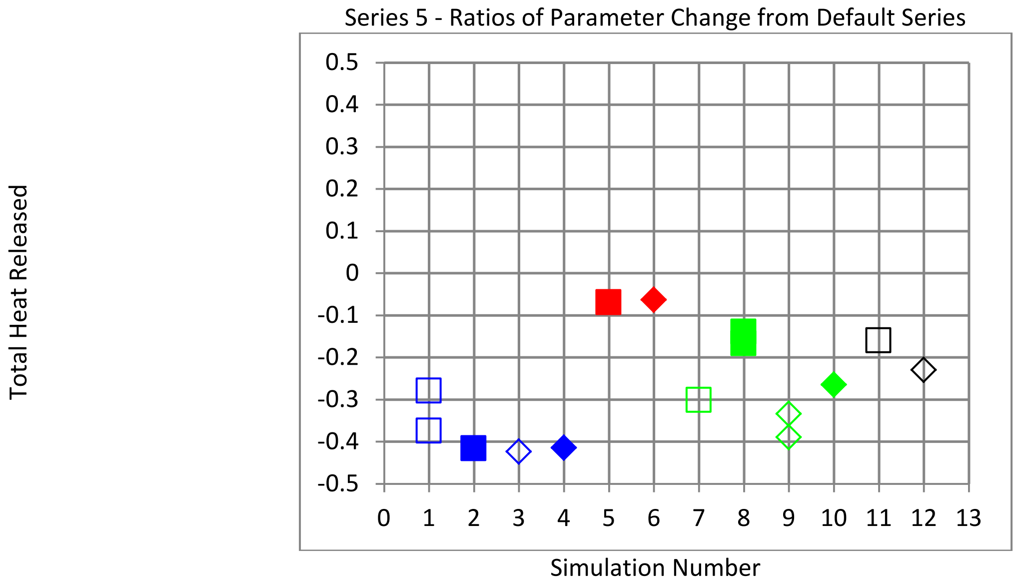

Legend

Propane-Sq-50 | Propane-Sq-75 | Propane-Re-50 | Propane-Re-75

Propylene-Sq-50 | Propylene-Sq-75 | Propylene-Re-50 | Propylene-Re-75

Propane-Sq-75 (Continuous) | Propane-Re-75 (Continuous) | Propylene Sq 50(Continuous) | Propylene Re 50 (Continuous)

Observations

In Series 5, the radiative fraction of all simulations was reduced 33% from the default 0.30 to 0.2.

The behaviors of all the quantity changes share the same trends based on source fuel, burner type, and source fire sizes as in Series 4 where the radiative fraction was also reduced from the default value. It is also noted that the changes incurred in Series 5 are less prominent than in Series 4, which is reasonable because the parameter change in Series 5 is less than in Series 4.

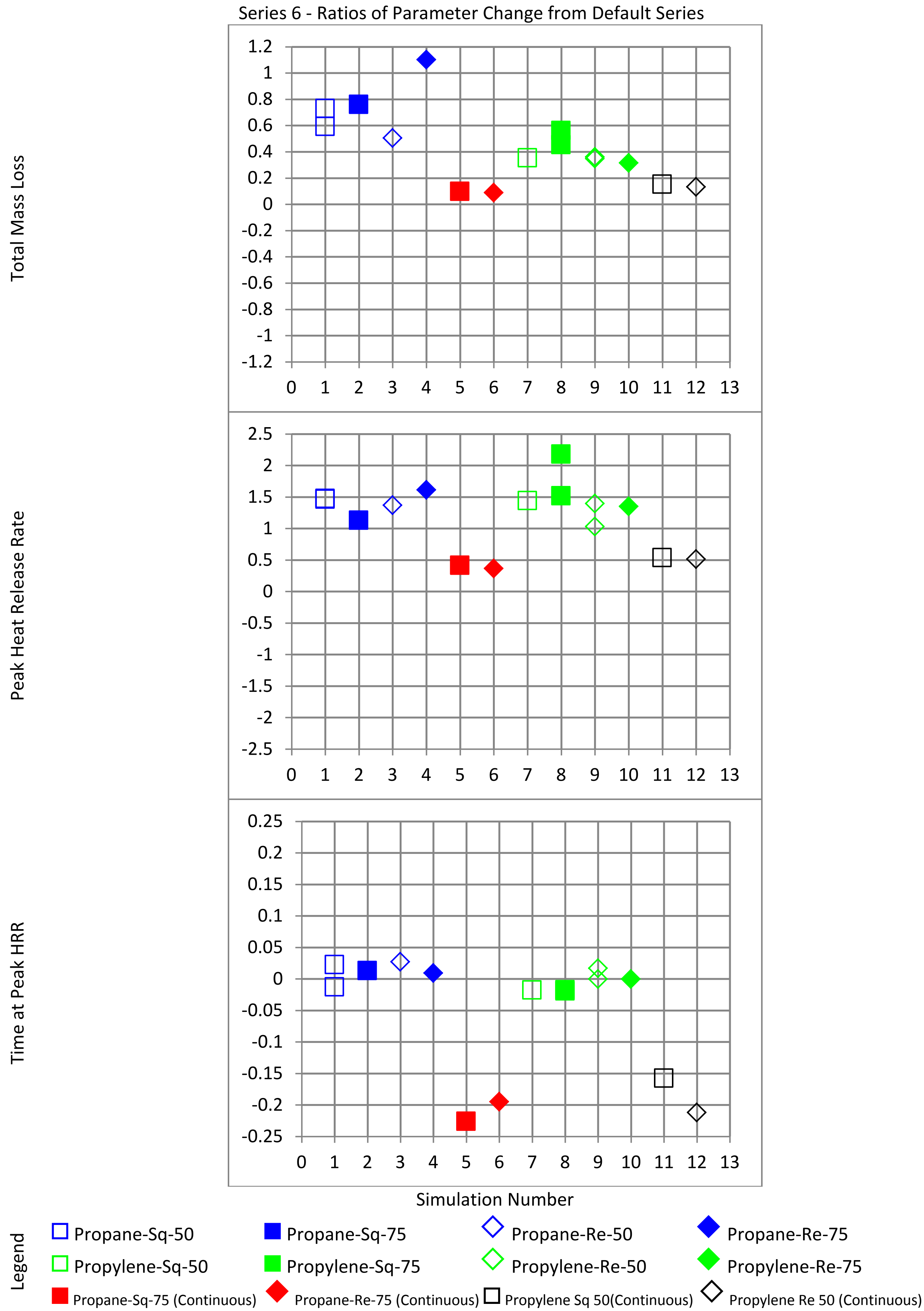

Series 6 - Ratios of Parameter Change from Default Series
Total Mass Loss
Peak Heat Release Rate
Time at Peak HRR
Simulation Number
Legend
Propane-Sq-50
Propane-Sq-75
Propane-Re-50
Propane-Re-75
Propylene-Sq-50
Propylene-Sq-75
Propylene-Re-50
Propylene-Re-75
Propane-Sq-75 (Continuous)
Propane-Re-75 (Continuous)
Propylene Sq 50(Continuous)
Propylene Re 50 (Continuous)

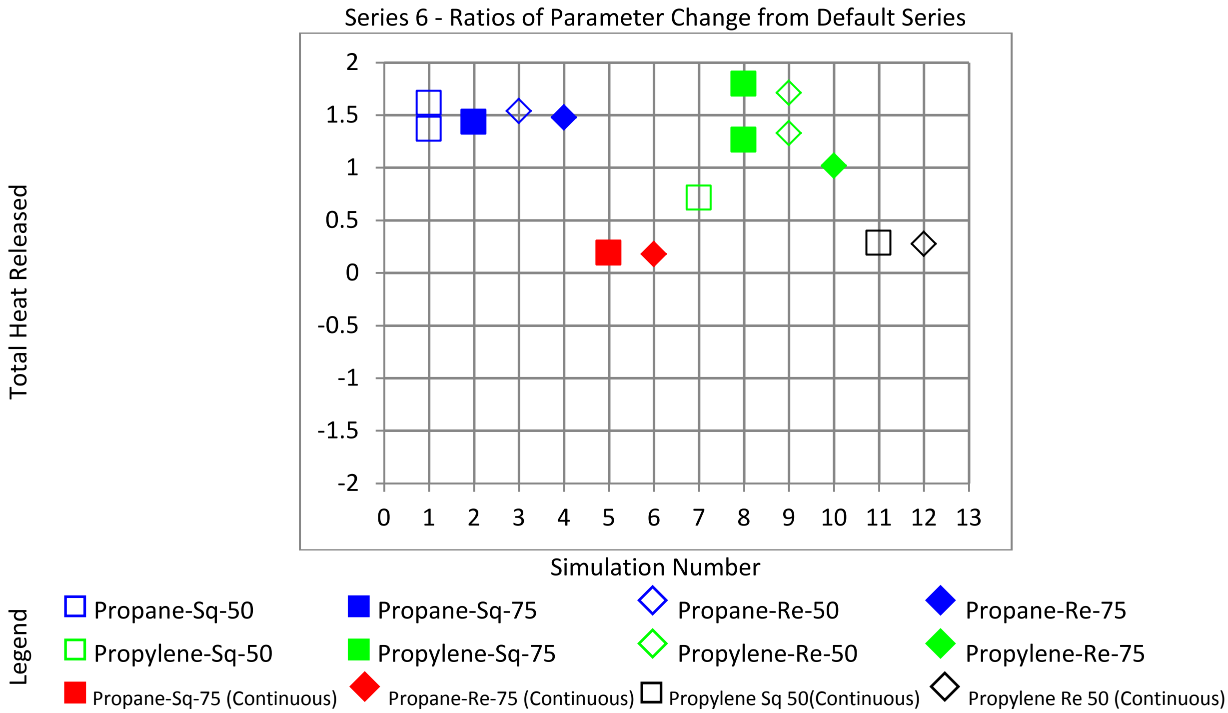

Observations

In Series 6, the radiative fraction of all simulations was increased 66% from the default 0.30 to 0.5.

Changes in the measured quantities appear to have increased in magnitude to what was observed in the results from the Series 4 and 5 simulations.

The total mass lost for all simulations were increased, and the effects on the propane simulations appear to be more prominent for the equivalent simulations using propylene. The mass loss for simulations with a continuous fire was the least changed.

The peak HRR was greatly increased for all simulations, the changes are similar for simulations using both source fuels. Again, the changes in the simulations with the continuous source fire were the smallest.

Time to peak HRR was changed differently from the other quantities, for most simulations with a terminated source fire, the time was not changed. However, the time to peak for the simulations with a continuous source fire was decreased similarly regardless of the source fire size and fuel type.

Generally, the mass loss for all simulations was increased regardless of the source fuel type and source fire HRR. However, the changes in the simulations with a continuous source fire were again the smallest.

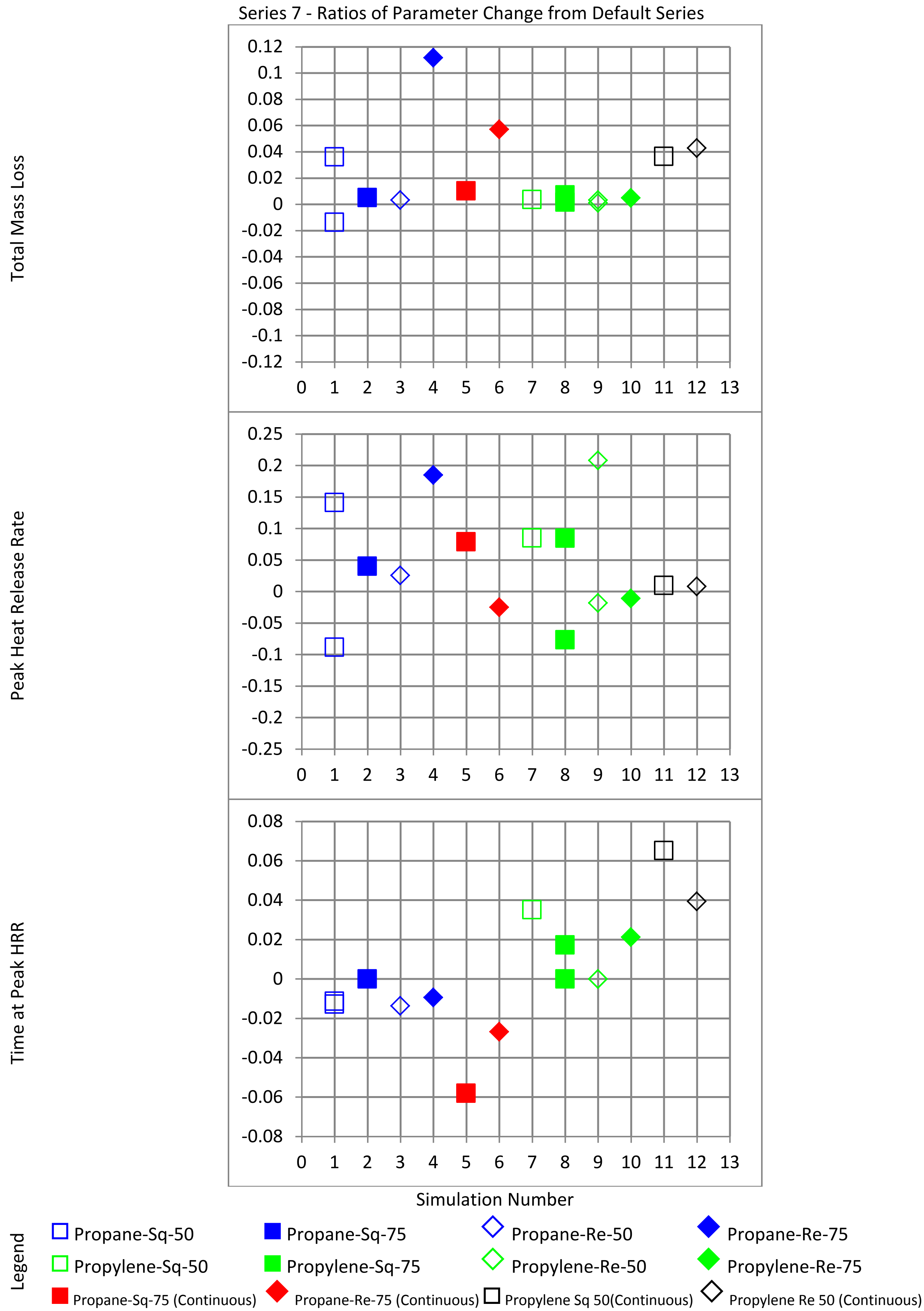

Series 7 - Ratios of Parameter Change from Default Series
Total Mass Loss
Peak Heat Release Rate
Time at Peak HRR
Simulation Number
Legend
Propane-Sq-50
Propane-Sq-75
Propane-Re-50
Propane-Re-75
Propylene-Sq-50
Propylene-Sq-75
Propylene-Re-50
Propylene-Re-75
Propane-Sq-75 (Continuous)
Propane-Re-75 (Continuous)
Propylene Sq 50(Continuous)
Propylene Re 50 (Continuous)

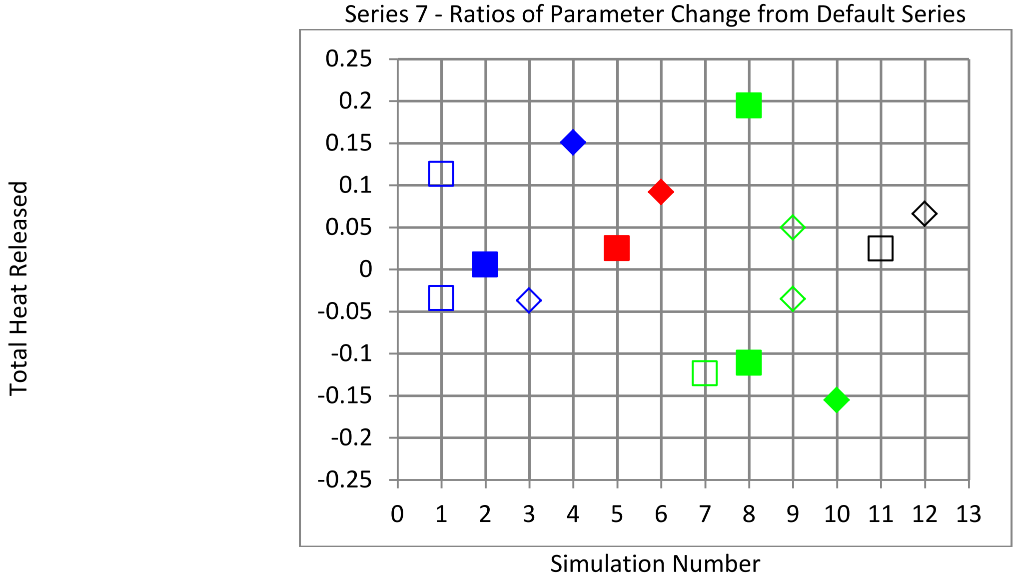

Legend

Propane-Sq-50	Propane-Sq-75	Propane-Re-50	Propane-Re-75
Propylene-Sq-50	Propylene-Sq-75	Propylene-Re-50	Propylene-Re-75
Propane-Sq-75 (Continuous)	Propane-Re-75 (Continuous)	Propylene Sq 50(Continuous)	Propylene Re 50 (Continuous)

Observations

In the Series 7 simulations, the wide band model mode to calculate radiation transports was enabled.

For most simulations, the total mass loss was unchanged, except for the simulations with a continuous source fire where the mass loss was slightly increased. The greatest change occurred in the simulation of the case using propane with a Rectangle burner at 75 kW.

The peak HRR for all simulations were slightly changed in this series, however, the changes appear to be quite random, evident in large difference in the change ratios for simulations with identical scenarios.

Time to peak HRR decreased for simulations with the propane source fire, but it was increased for the simulations with the propylene source fire. The effects on the simulations with the continuous fire were the most prominent.

Similar to the peak HRR changes, the changes to the THR appear to be quite random with no observed trends for different source fuel, burner size, and source fire HRR.

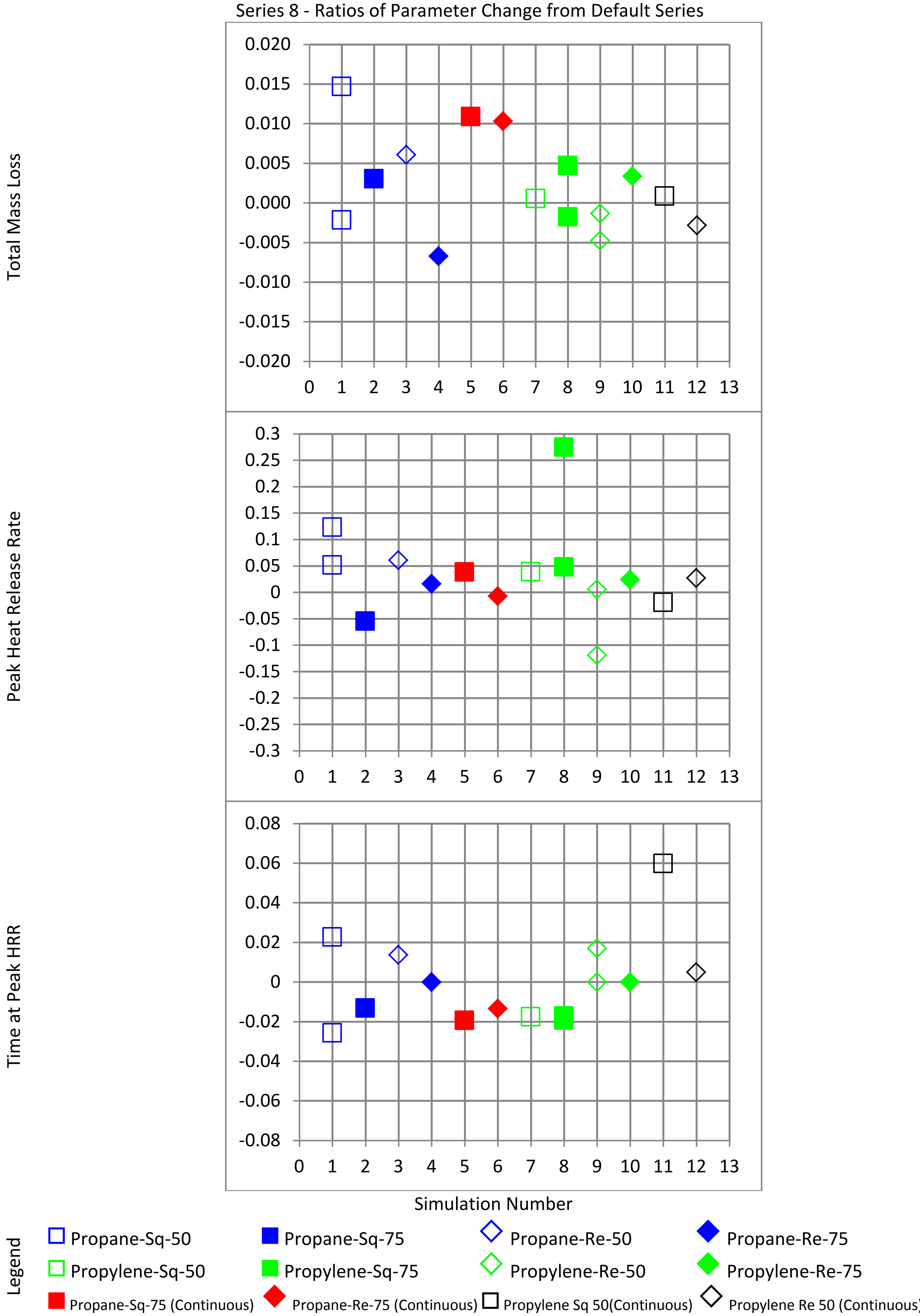
Series 8 - Ratios of Parameter Change from Default Series
Total Mass Loss
0.020
0.015
0.010
0.005
0.000
-0.005
-0.010
-0.015
-0.020
Peak Heat Release Rate
0.3
0.25
0.2
0.15
0.1
0.05
0
-0.05
-0.1
-0.15
-0.2
-0.25
-0.3
Time at Peak HRR
0.08
0.06
0.04
0.02
0
-0.02
-0.04
-0.06
-0.08
0 1 2 3 4 5 6 7 8 9 10 11 12 13
Simulation Number
Legend
Propane-Sq-50
Propane-Sq-75
Propane-Re-50
Propane-Re-75
Propylene-Sq-50
Propylene-Sq-75
Propylene-Re-50
Propylene-Re-75
Propane-Sq-75 (Continuous)
Propane-Re-75 (Continuous)
Propylene Sq 50(Continuous)
Propylene Re 50 (Continuous)

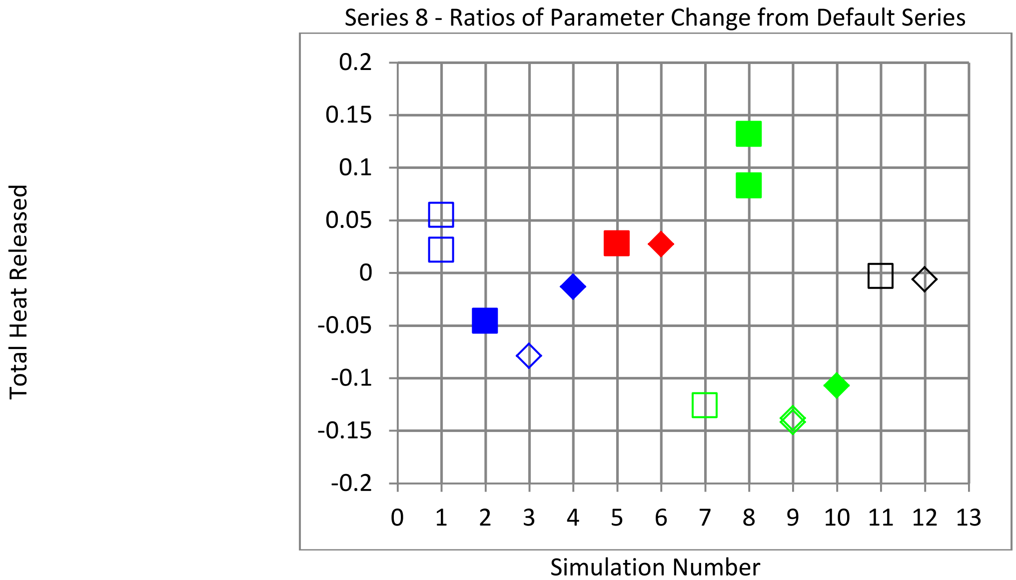

Legend

Propane-Sq-50 | Propane-Sq-75 | Propane-Re-50 | Propane-Re-75
Propylene-Sq-50 | Propylene-Sq-75 | Propylene-Re-50 | Propylene-Re-75
Propane-Sq-75 (Continuous) | Propane-Re-75 (Continuous) | Propylene Sq 50(Continuous) | Propylene Re 50 (Continuous)

Observations

The Series 8 simulations were conducted with a 50% reduction of the default number of radiation angles to be accounted for in the calculations.

Changes in total mass loss due to a decrease in the number of radiation angles used were extremely small, within a range of ±1.5%, and random.

The peak HRR magnitudes were also slightly changed, but the changes appear to be random, as seen from the large difference in the change ratio for simulations with identical configurations. However, it is noted that the effects on simulations with the propylene source fuel are more prominent than for the propane simulations.

The time to peak and the THR changes due to the decrease in the number of radiation angle used both appear to be random but more prominent for the propylene simulations than the propane simulations.

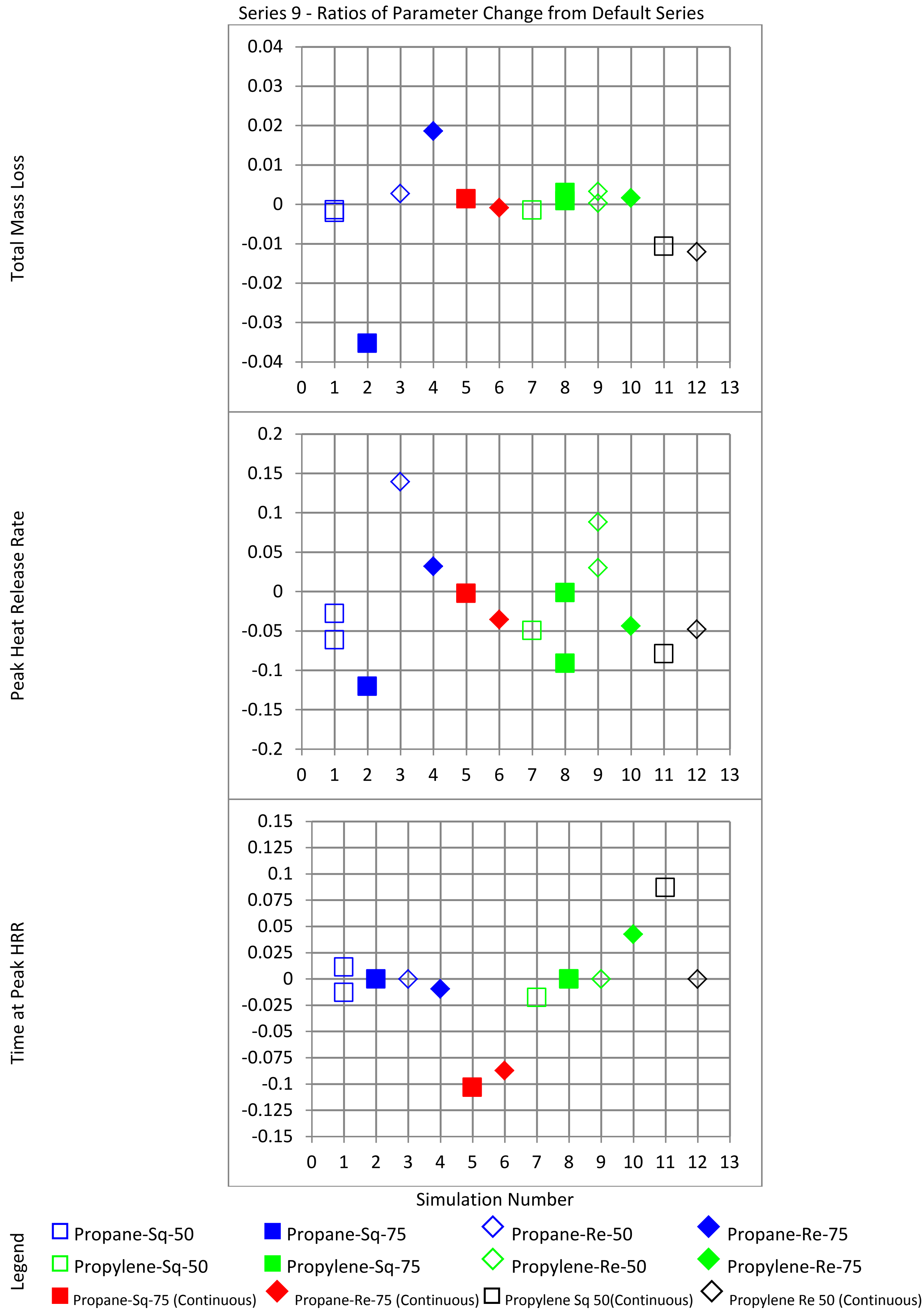
Series 9 - Ratios of Parameter Change from Default Series
Total Mass Loss
0.04
0.03
0.02
0.01
0
-0.01
-0.02
-0.03
-0.04
Peak Heat Release Rate
0.2
0.15
0.1
0.05
0
-0.05
-0.1
-0.15
-0.2
Time at Peak HRR
0.15
0.125
0.1
0.075
0.05
0.025
0
-0.025
-0.05
-0.075
-0.1
-0.125
-0.15
0 1 2 3 4 5 6 7 8 9 10 11 12 13
Simulation Number
Legend
Propane-Sq-50
Propane-Sq-75
Propane-Re-50
Propane-Re-75
Propylene-Sq-50
Propylene-Sq-75
Propylene-Re-50
Propylene-Re-75
Propane-Sq-75 (Continuous)
Propane-Re-75 (Continuous)
Propylene Sq 50(Continuous)
Propylene Re 50 (Continuous)

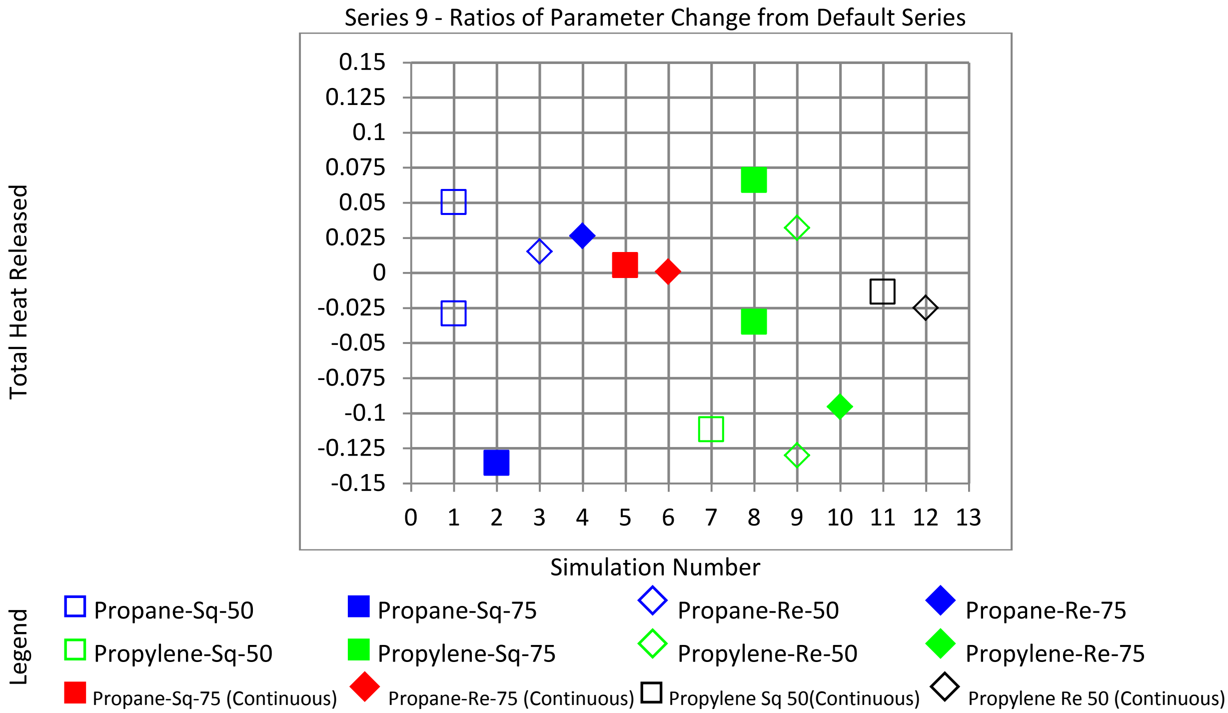

Observations

The Series 9 simulations were conducted with a 100% increase of the number of radiation angles to be calculated for in the models.

The behaviors of all the quantity changes appear to be quite random, which is similar to what were observed for Series 8 where the number of radiation angles was decreased. However, the changes noted in the Series 9 simulations are of greater magnitudes, but still more prominent for the propylene than the propane simulations.

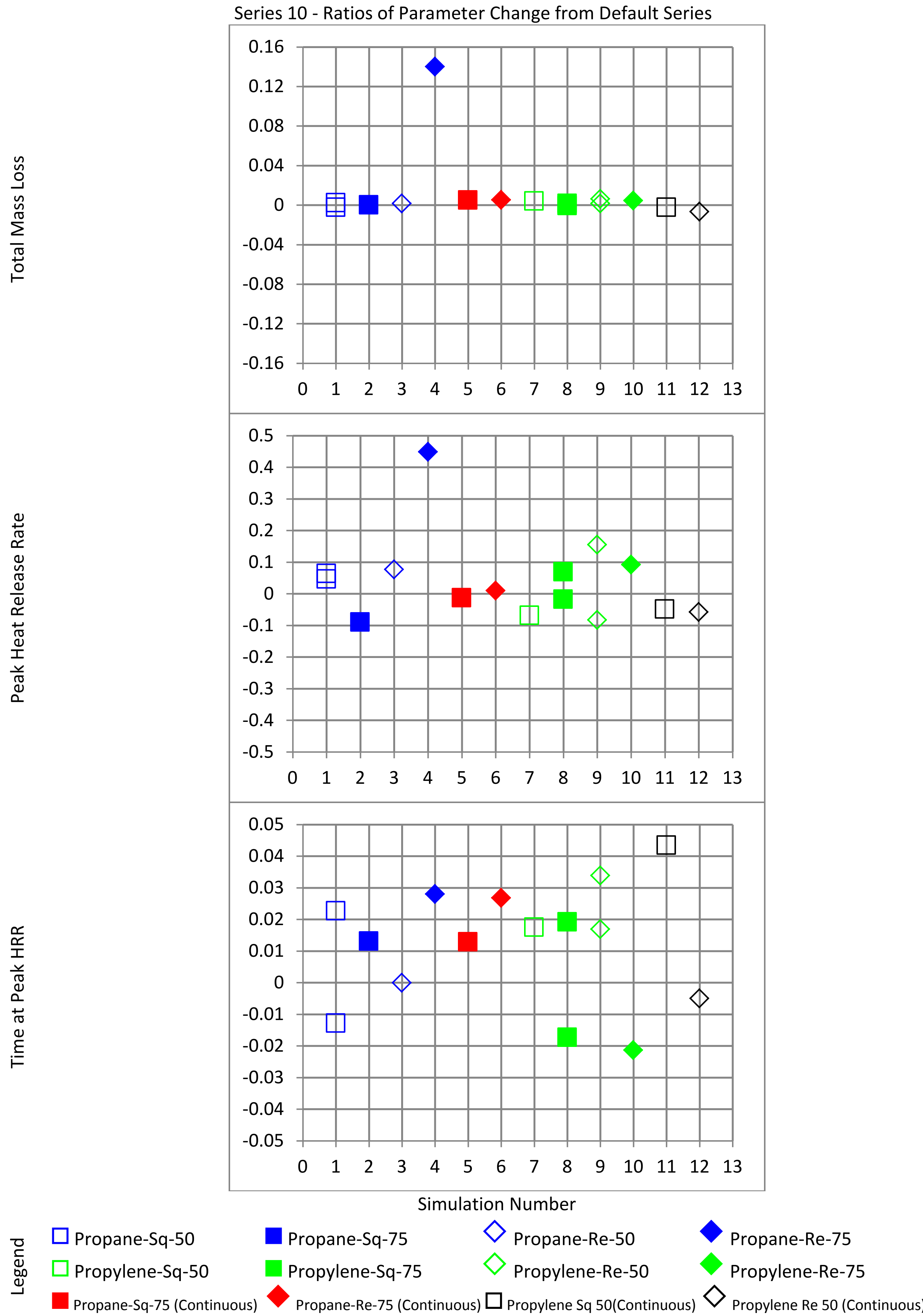

Series 10 - Ratios of Parameter Change from Default Series
Total Mass Loss
0.16
0.12
0.08
0.04
0
-0.04
-0.08
-0.12
-0.16
Peak Heat Release Rate
0.5
0.4
0.3
0.2
0.1
0
-0.1
-0.2
-0.3
-0.4
-0.5
Time at Peak HRR
0.05
0.04
0.03
0.02
0.01
0
-0.01
-0.02
-0.03
-0.04
-0.05
0 1 2 3 4 5 6 7 8 9 10 11 12 13
Simulation Number
Legend
Propane-Sq-50
Propane-Sq-75
Propane-Re-50
Propane-Re-75
Propylene-Sq-50
Propylene-Sq-75
Propylene-Re-50
Propylene-Re-75
Propane-Sq-75 (Continuous)
Propane-Re-75 (Continuous)
Propylene Sq 50(Continuous)
Propylene Re 50 (Continuous)

Series 10 - Ratios of Parameter Change from Default Series

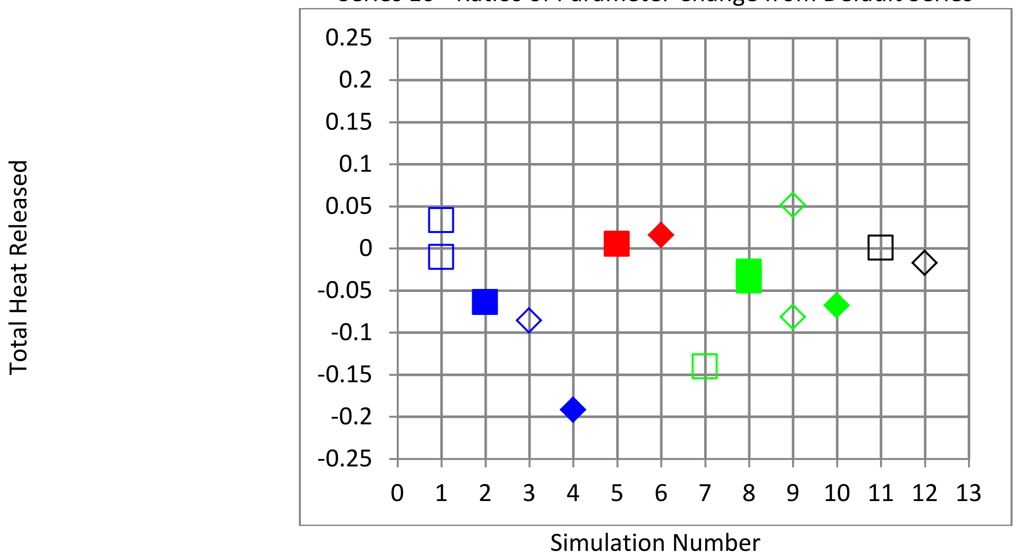

Legend

Propane-Sq-50	Propane-Sq-75	Propane-Re-50	Propane-Re-75
Propylene-Sq-50	Propylene-Sq-75	Propylene-Re-50	Propylene-Re-75
Propane-Sq-75 (Continuous)	Propane-Re-75 (Continuous)	Propylene Sq 50(Continuous)	Propylene Re 50 (Continuous)

Observations

The radiation angle increment, which determine how often FDS updates the radiation solution, was reduced from 5 to 2 in the Series 10 simulations.

There was essentially no change on the total mass loss observed for all simulations, except for the one of propane with a Rectangle burner at 75 kW where the mass loss had increased by approximately 14%.

Similar to the changes in predicted mass loss, the peak HRR was increased by 50% for the single simulation of propane with a Rectangle burner at 75 kW. For the other simulations, the magnitude of change was within ±10% and does not appear to follow any trend.

As expected, the time to peak HRR for all simulations were only slightly increased.

The THR for most simulations have been reduced, this is especially prominent for the single simulation of propane with a Rectangle burner at 75 kW.

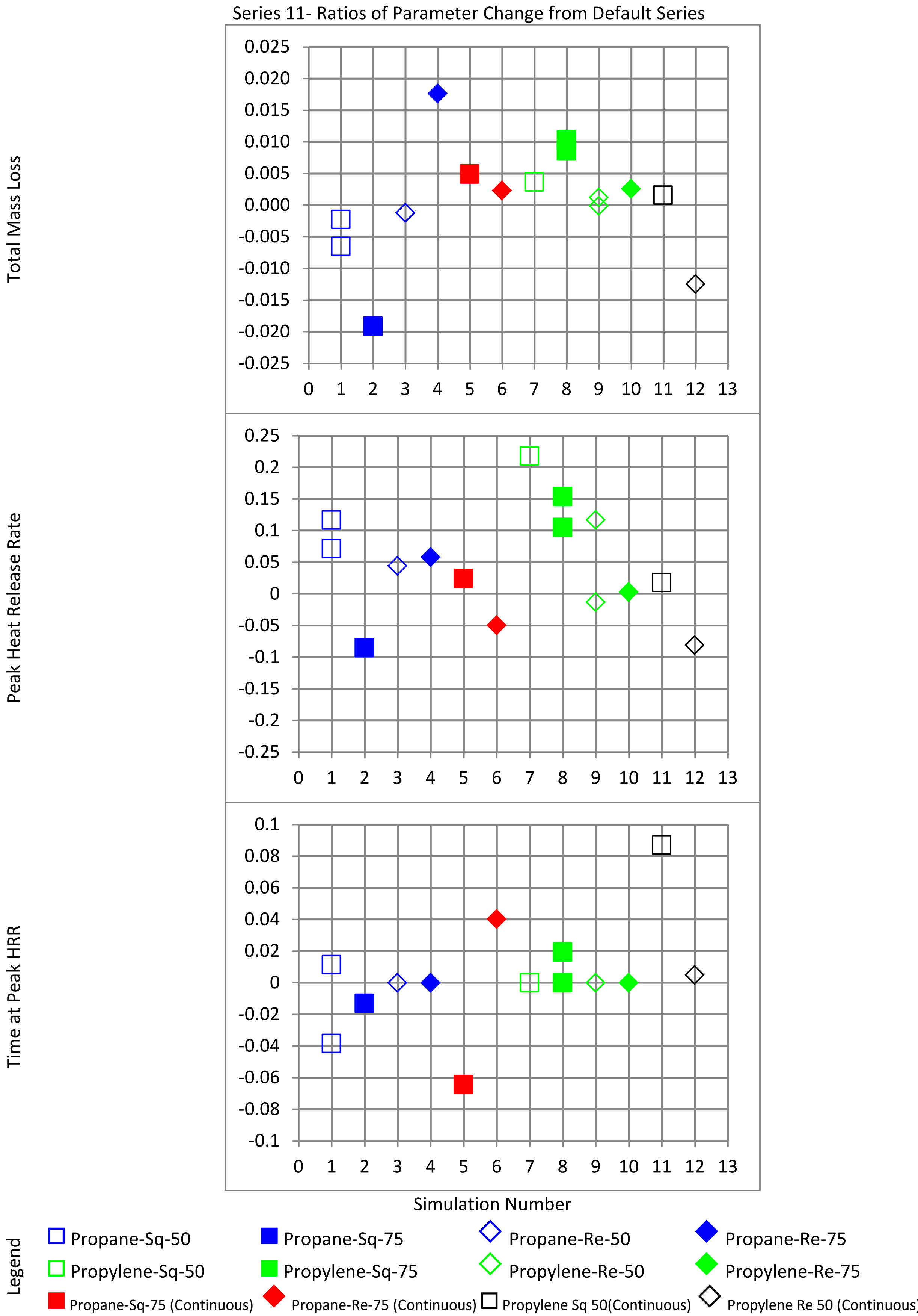

Series 11- Ratios of Parameter Change from Default Series
Total Mass Loss
0.025
0.020
0.015
0.010
0.005
0.000
-0.005
-0.010
-0.015
-0.020
-0.025
0 1 2 3 4 5 6 7 8 9 10 11 12 13
Peak Heat Release Rate
0.25
0.2
0.15
0.1
0.05
0
-0.05
-0.1
-0.15
-0.2
-0.25
0 1 2 3 4 5 6 7 8 9 10 11 12 13
Time at Peak HRR
0.1
0.08
0.06
0.04
0.02
0
-0.02
-0.04
-0.06
-0.08
-0.1
0 1 2 3 4 5 6 7 8 9 10 11 12 13
Simulation Number
Legend
Propane-Sq-50
Propane-Sq-75
Propane-Re-50
Propane-Re-75
Propylene-Sq-50
Propylene-Sq-75
Propylene-Re-50
Propylene-Re-75
Propane-Sq-75 (Continuous)
Propane-Re-75 (Continuous)
Propylene Sq 50(Continuous)
Propylene Re 50 (Continuous)

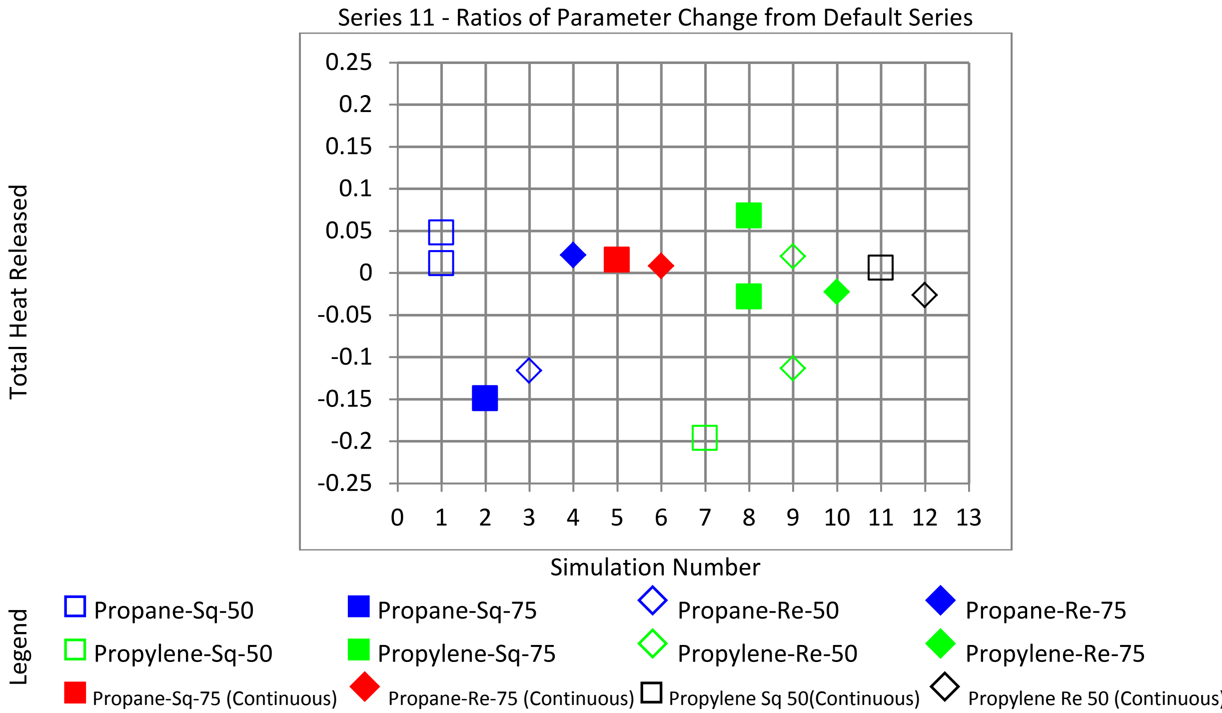

Observations

The radiation angle increment, which determine how often FDS updates the radiation solution, was increased from 5 to 10 in the Series 11 simulations, essentially halving the rate at which the radiation angles were updated.

With some exceptions, the changes in the total mass loss are generally very small, and are negative for the simulations using propane as source fuel, and positive for the simulations using propylene.

Changes in the peak HRR are mostly positive, except for the simulations with a continuous fire with a Rectangle burner, and the propane terminated fire with Square burner at 75 kW, where the changes are negative instead.

The time to peak HRR was not changed for most of the simulations. However, it is noted that the simulations with a continuous source fire with the Square burner incurred opposite change from each other: the propane at 75 kW simulation has a shortened time to peak, but the one with propylene at 50 kW had an increased time to peak.

Changes in the THR are small for most of the simulations, except for a few cases with terminated source fire, such as the propane simulation with the Square burner at 75 kW, the propylene simulation with the Square burner at 50 kW, and the ones with the Rectangle burner at 50 kW for both fuels.

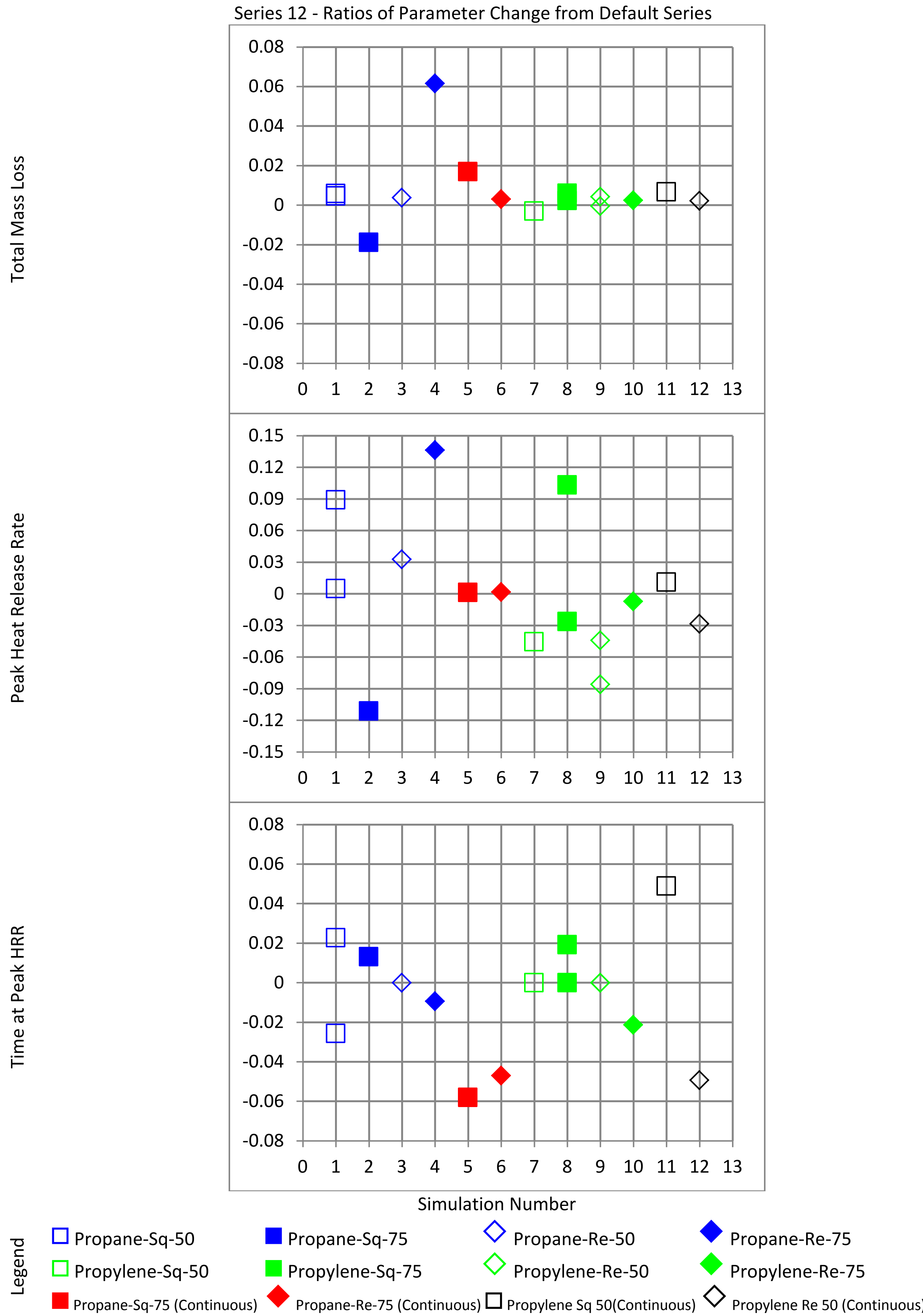

Series 12 - Ratios of Parameter Change from Default Series
Total Mass Loss
Peak Heat Release Rate
Time at Peak HRR
Simulation Number
Legend
Propane-Sq-50
Propane-Sq-75
Propane-Re-50
Propane-Re-75
Propylene-Sq-50
Propylene-Sq-75
Propylene-Re-50
Propylene-Re-75
Propane-Sq-75 (Continuous)
Propane-Re-75 (Continuous)
Propylene Sq 50(Continuous)
Propylene Re 50 (Continuous)

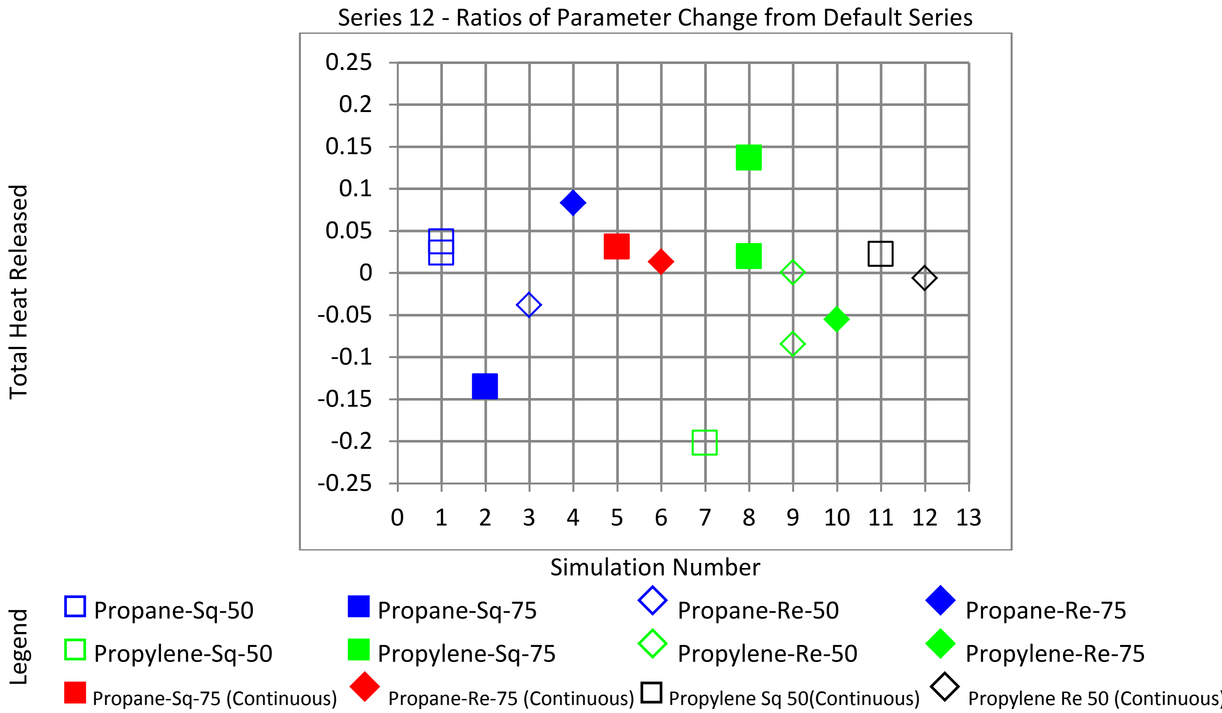

Observations

The time step increment of the radiation solver was reduced from 3 to 1 in the Series 12 simulations, essentially increasing the update rate of the radiation solver in every time step.

There was essentially no change on the total mass loss observed for all simulations, except for the one of propane with a Rectangle burner at 75 kW where the mass loss had increased by approximately 6%.

For the Peak HRR magnitude, the changes to simulations using propane fuel were quite random, but the changes to simulations with propylene fuel were mostly negative. It is noted that the changes recorded for simulations with a continuous source fire were the smallest.

The time to peak HRR was reduced for most simulations, except for the one with a continuous propylene fire with a Square burner at 50 kW. For the simulations with a terminated source fire, the negative change is more prominent for Rectangle burner and source fire at 75 kW than for Square burner and source fire at 50 kW.

The THR changes appear to be mostly random, and more prominent for the simulations with a terminated source fire than for the simulations with a continuous source fire.

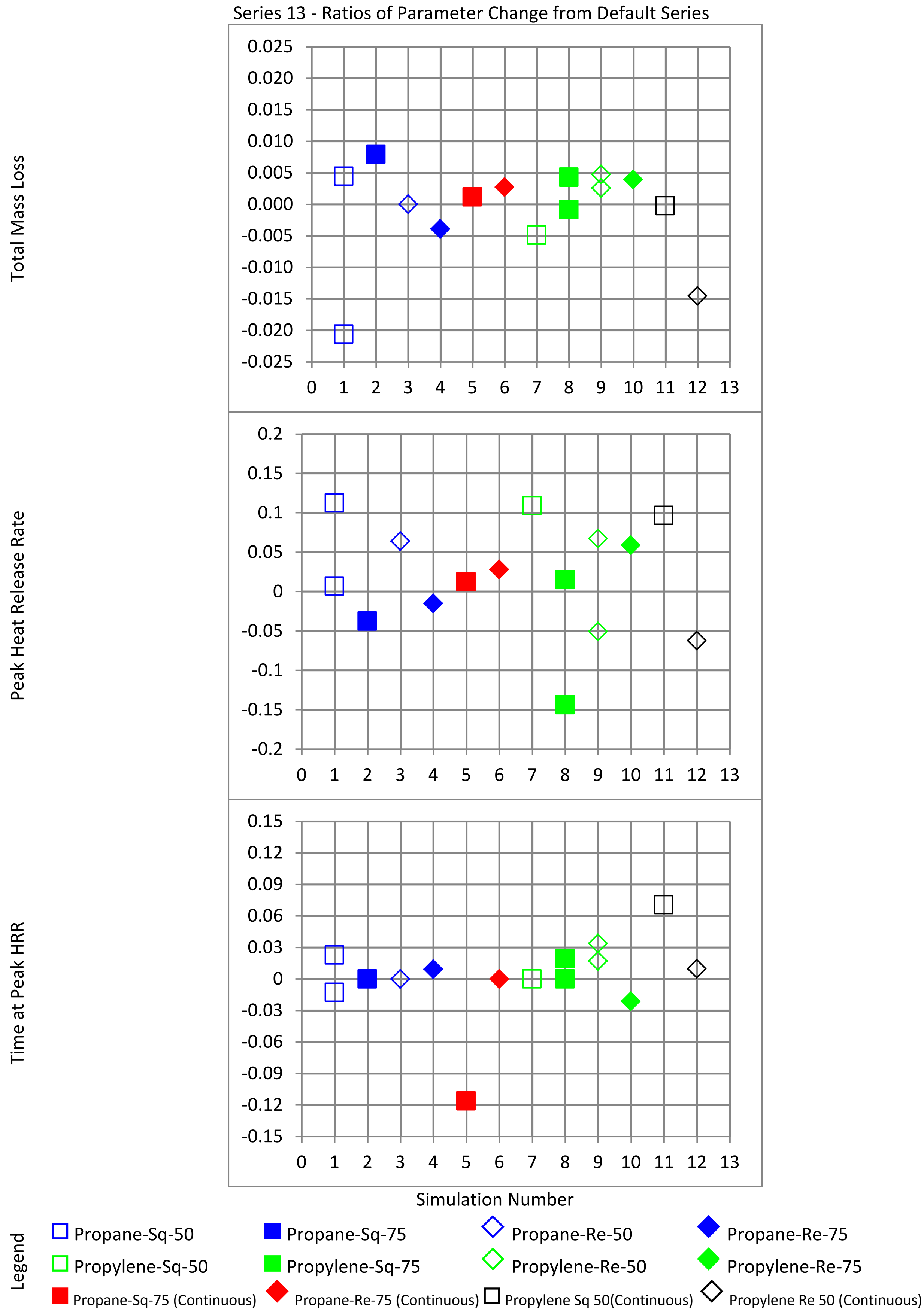

Series 13 - Ratios of Parameter Change from Default Series
Total Mass Loss
Peak Heat Release Rate
Time at Peak HRR
Simulation Number
Legend
Propane-Sq-50
Propane-Sq-75
Propane-Re-50
Propane-Re-75
Propylene-Sq-50
Propylene-Sq-75
Propylene-Re-50
Propylene-Re-75
Propane-Sq-75 (Continuous)
Propane-Re-75 (Continuous)
Propylene Sq 50(Continuous)
Propylene Re 50 (Continuous)

Series 13 - Ratios of Parameter Change from Default Series

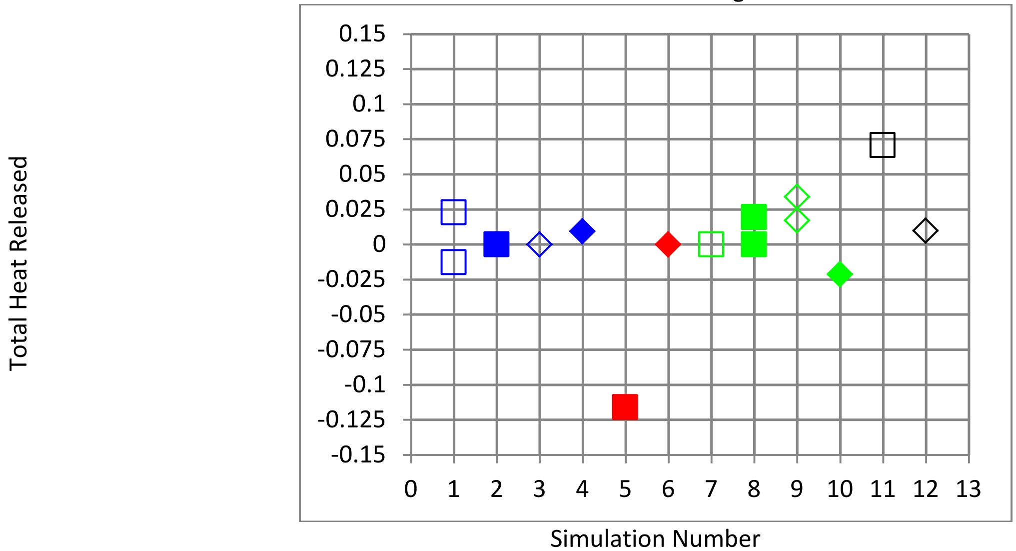

Legend

Propane-Sq-50 | Propane-Sq-75 | Propane-Re-50 | Propane-Re-75
Propylene-Sq-50 | Propylene-Sq-75 | Propylene-Re-50 | Propylene-Re-75
Propane-Sq-75 (Continuous) | Propane-Re-75 (Continuous) | Propylene Sq 50(Continuous) | Propylene Re 50 (Continuous)

Observations

The time step increment was increased from 3 to 6 in the Series 13 simulations, essentially reducing the rate at which the radiation solver was updated by half.

The changes in the total mass loss due to the parametric change are very small, with the greatest change recorded at -2% for the simulation with a terminated propane fire with the Square burner at 50 kW.

Changes to the peak HRR magnitude were relatively random for all simulations, all within the range of ±15%. The change magnitude for the simulations using a propylene source fire is generally larger than for the propane ones.

The changes to the time to peak HRR were slight, mostly within ±3%, except for the simulations of the continuous source fire with the Square burner. For the propane at 75 kW, the time to peak was shortened, whereas for propylene at 50 kW, the time to peak was delayed.

Interestingly, the changes for the THR are similar to those in the time to peak HRR, both in magnitude and trends.

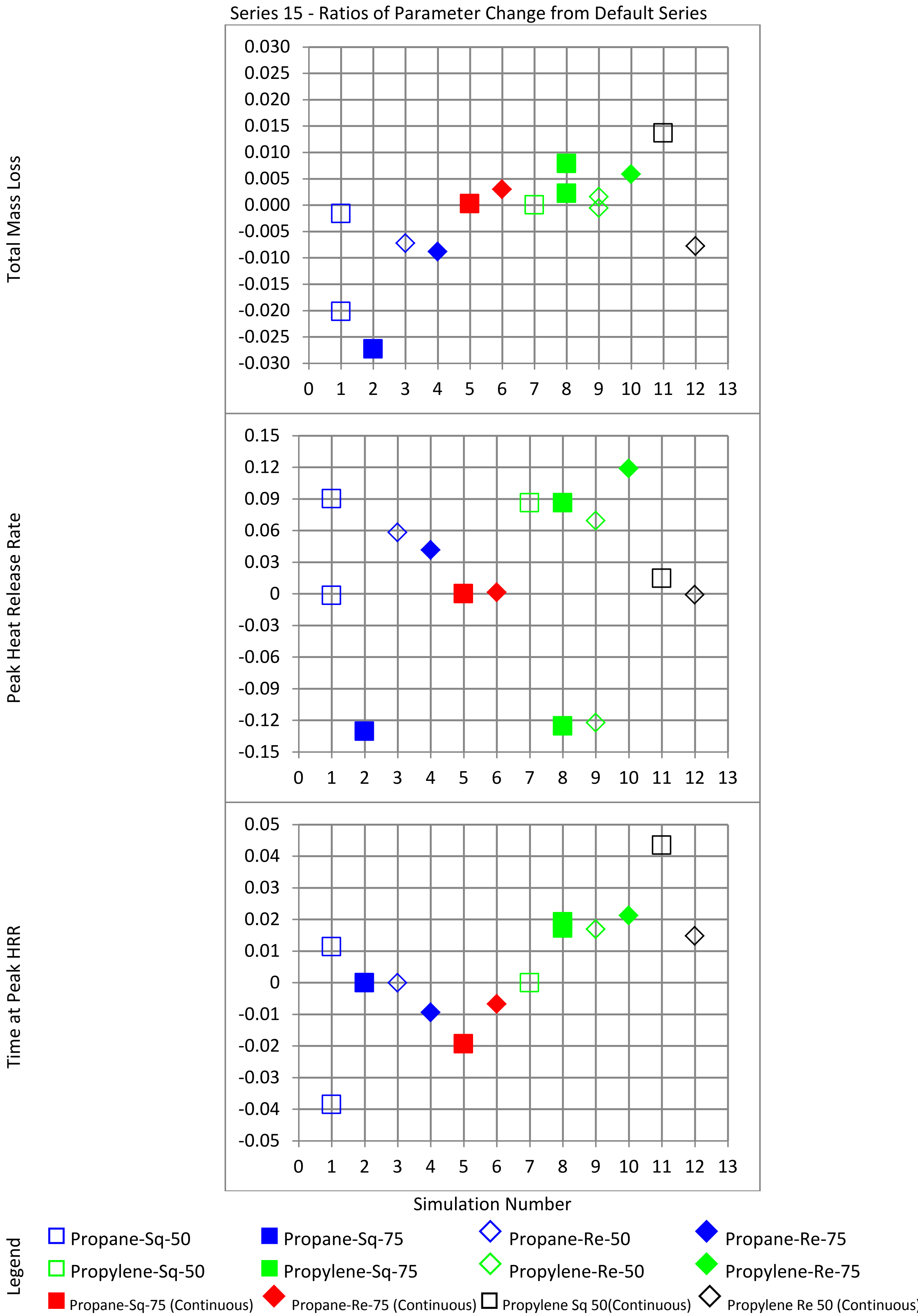

Series 15 - Ratios of Parameter Change from Default Series
Total Mass Loss
Peak Heat Release Rate
Time at Peak HRR
Simulation Number
Legend
Propane-Sq-50
Propane-Sq-75
Propane-Re-50
Propane-Re-75
Propylene-Sq-50
Propylene-Sq-75
Propylene-Re-50
Propylene-Re-75
Propane-Sq-75 (Continuous)
Propane-Re-75 (Continuous)
Propylene Sq 50(Continuous)
Propylene Re 50 (Continuous)

Series 15 - Ratios of Parameter Change from Default Series

Total Heat Released

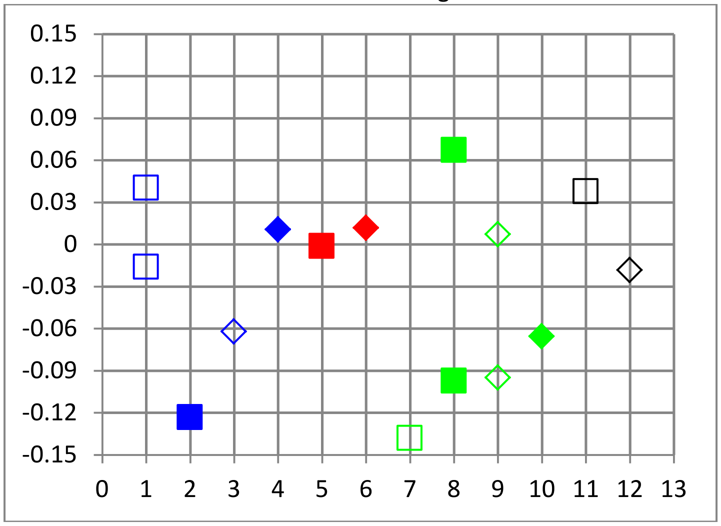

Simulation Number

Legend

Propane-Sq-50 | Propane-Sq-75 | Propane-Re-50 | Propane-Re-75
Propylene-Sq-50 | Propylene-Sq-75 | Propylene-Re-50 | Propylene-Re-75
Propane-Sq-75 (Continuous) | Propane-Re-75 (Continuous) | Propylene Sq 50(Continuous) | Propylene Re 50 (Continuous)

Observations

The parameter C_EDC which is a constant used to determine the mixing time scale used in the turbulent combustion calculations was increased from 0.1 to 0.2 in the Series 15 simulations thereby doubling the mixing time scale.

The changes to the total mass loss were mostly insignificant. For the propane simulations, the total mass loss were lowered whereas for the propylene simulations the changes were slightly positive.

For the simulations with a continous source fire, the changes to the peak HRR were insignificant. However, for the other simultions, both increaes and decreases to the peak HRR were recorded, and appear to be qutie random, as evident by the large difference between the change ratio for simulations with the same configurations.

Changes in the time to peak HRR for the simulations of temrinated source fire using propane were mostly negative, with the changes for Rectangle burner and higher HRR more prominent. For the propylene simulaitons, however, the changes were postive, but the correlations between burner shape and HRR with magnitude of the change were conserved, regardless of the direction of the change. It is also noted that these trends appear to be the reverse for the tests with continuous source fire.

The THR changes were mostly negative for this series of simulations. It may be observed that the magnitude of change is greater for Square burner and lower HRR than for Rectangle burner and higher HRR for the simultions with a terminated propylene source fire. However, this trend is not noted for simulations with the other configurations.

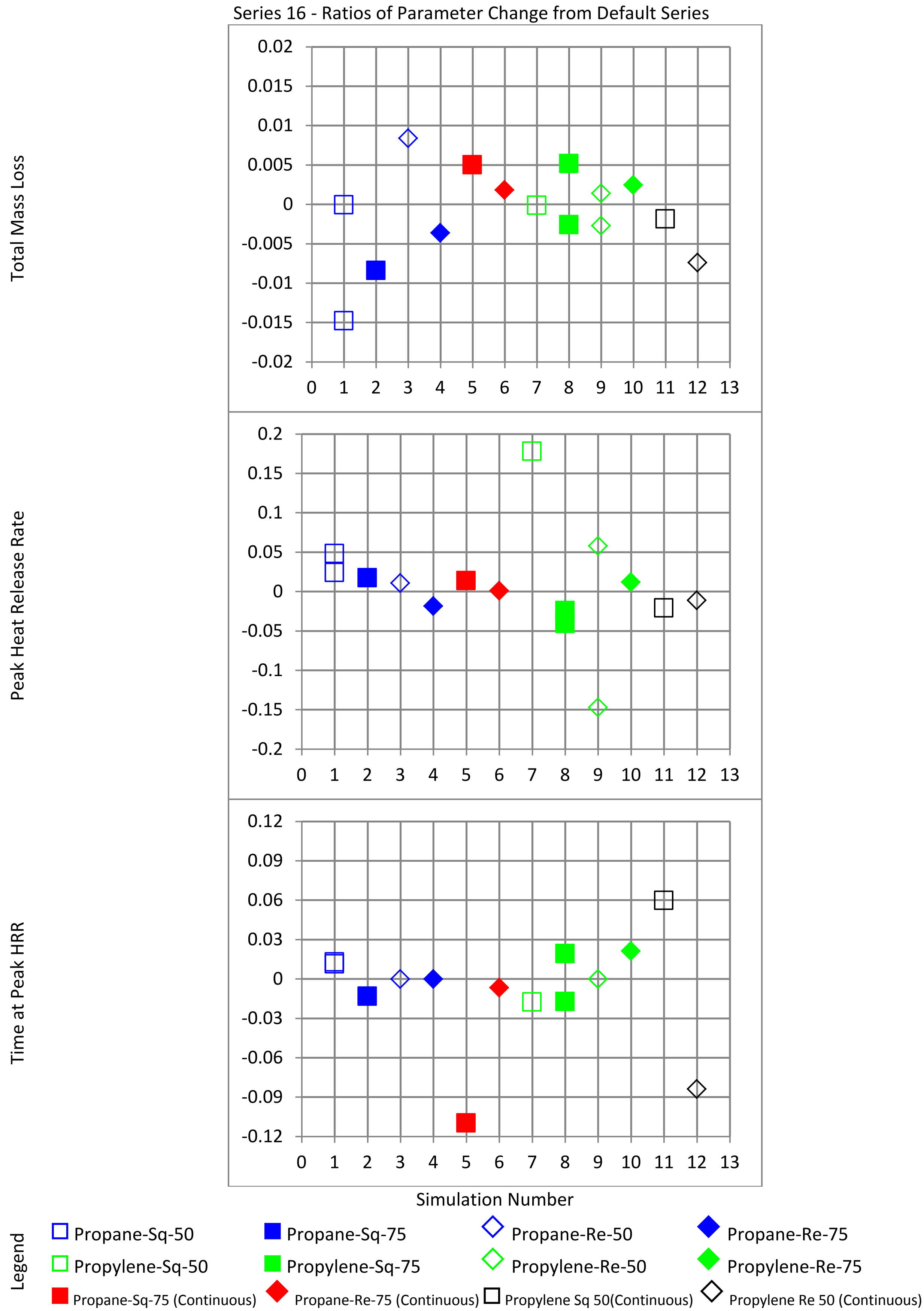
Series 16 - Ratios of Parameter Change from Default Series
Total Mass Loss
Peak Heat Release Rate
Time at Peak HRR
Simulation Number
Legend
Propane-Sq-50
Propane-Sq-75
Propane-Re-50
Propane-Re-75
Propylene-Sq-50
Propylene-Sq-75
Propylene-Re-50
Propylene-Re-75
Propane-Sq-75 (Continuous)
Propane-Re-75 (Continuous)
Propylene Sq 50(Continuous)
Propylene Re 50 (Continuous)

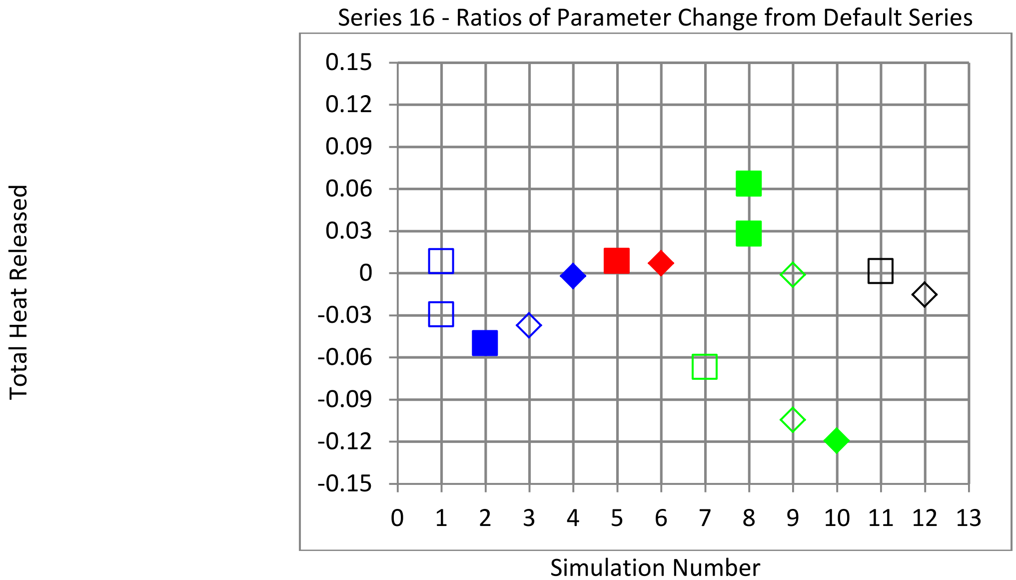

Legend

- Propane-Sq-50
- Propane-Sq-75
- Propane-Re-50
- Propane-Re-75
- Propylene-Sq-50
- Propylene-Sq-75
- Propylene-Re-50
- Propylene-Re-75
- Propane-Sq-75 (Continuous)
- Propane-Re-75 (Continuous)
- Propylene Sq 50(Continuous)
- Propylene Re 50 (Continuous)

Observations

The parameter C_EDC which is a constant used to determine the mixing time scale used in the turbulent combustion calculations was reduced to 0.05 from 0.1 in the Series 16 simulations thereby halving the mixing time scale.

The changes in the total mass loss for simulations with propane source fire are generally greater in magnitude than those for the propylene simulations. Additionally, the changes for propane simulations are mostly negative, but all total mass loss deviations are quite small.

For the peak HRR, the changes for the propane simulations are generally positive and much smaller in magnitude than those recorded for the propylene simulations. Changes for the propylene simulations are both included both increases and decreases with no trends based on test scenario. It is noted that the changes for the simulations with a continuous propane fire are slightly positive whereas the changes for the simulations with a continuous propylene fire are slightly negative.

The time to peak HRR changes are generally insignificant for most simulations, however the simulations with the greatest changes are those with the continuous source fire regardless of the source fuel type.

For the THR, the changes for the propane simulations are generally negative and much smaller in magnitude than those recorded for the propylene simulations. Changes for the propylene simulations are both included both increases and decreases with no trends based on test scenario. It is noted that the changes for the simulations with a continuous propane fire are slightly positive whereas the changes for the simulations with a continuous propylene fire are slightly negative.

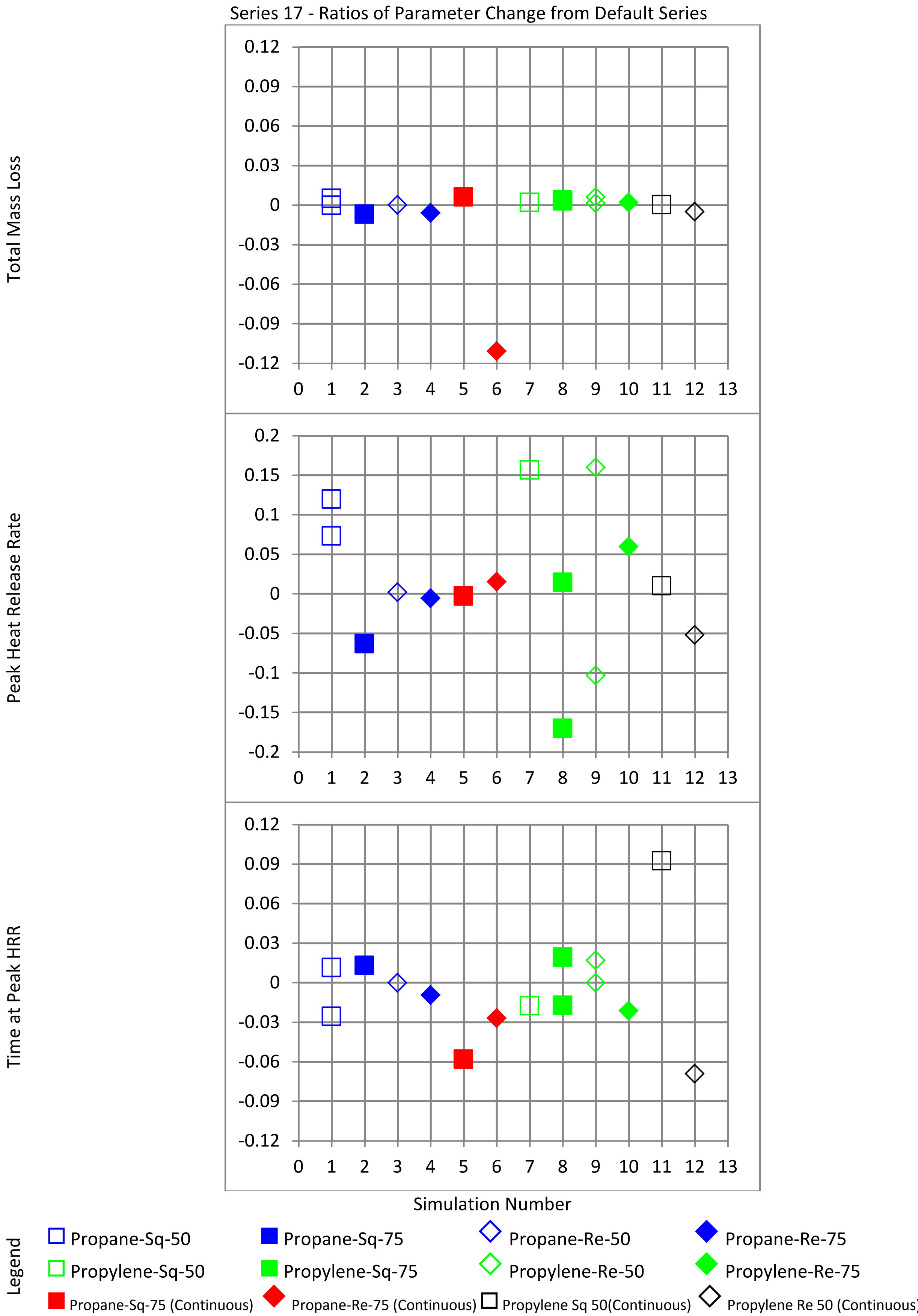

Series 17 - Ratios of Parameter Change from Default Series
Total Mass Loss
Peak Heat Release Rate
Time at Peak HRR
Simulation Number
Legend
Propane-Sq-50
Propane-Sq-75
Propane-Re-50
Propane-Re-75
Propylene-Sq-50
Propylene-Sq-75
Propylene-Re-50
Propylene-Re-75
Propane-Sq-75 (Continuous)
Propane-Re-75 (Continuous)
Propylene Sq 50(Continuous)
Propylene Re 50 (Continuous)

Series 17 - Ratios of Parameter Change from Default Series

Total Heat Released

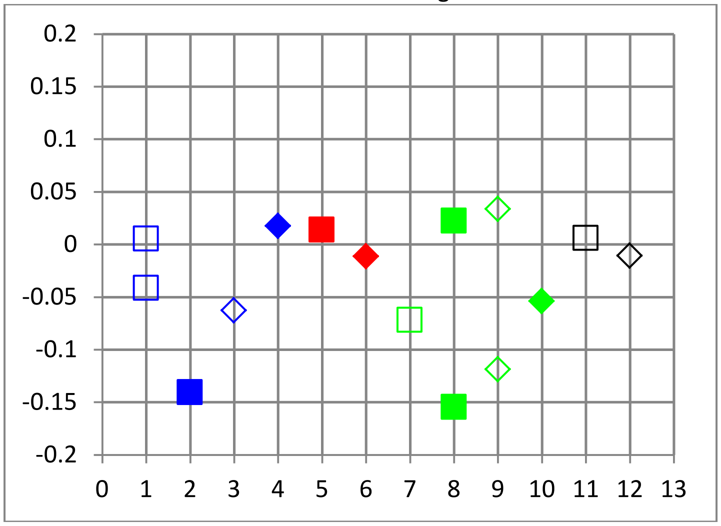

Simulation Number

Legend

- Propane-Sq-50
- Propane-Sq-75
- Propane-Re-50
- Propane-Re-75
- Propylene-Sq-50
- Propylene-Sq-75
- Propylene-Re-50
- Propylene-Re-75
- Propane-Sq-75 (Continuous)
- Propane-Re-75 (Continuous)
- Propylene Sq 50(Continuous)
- Propylene Re 50 (Continuous)

Observations

Eddy dissipation mode is usually enabled in the large eddy simulations, but disabling it, the mixing time scale of the turbulent combustion becomes the time step of the simulation.

Minimal changes to the total mass loss were recorded for all of the simulations except for the one with a continuous propane source fire at 75 kW with the Square burner.

Changes to the peak HRR appear to be quite random without clearly defined trends. Changes recorded for similar simulations had a wide range of difference.

Generally the changes to the time at peak recorded for simulations with a terminated source fire were small at ±3%. However, for the simulations with a continuous fire regardless of the source fuel, the changes from default were greater.

The THR changes for all simulations are generally negative, with the greatest reduction for the simulations with the Square burner at 75 kW. The changes for the simulations with a continuous fire with a Square burner were slightly positive whereas the simulations with a continuous fire using a Rectangle burner were slightly negative.

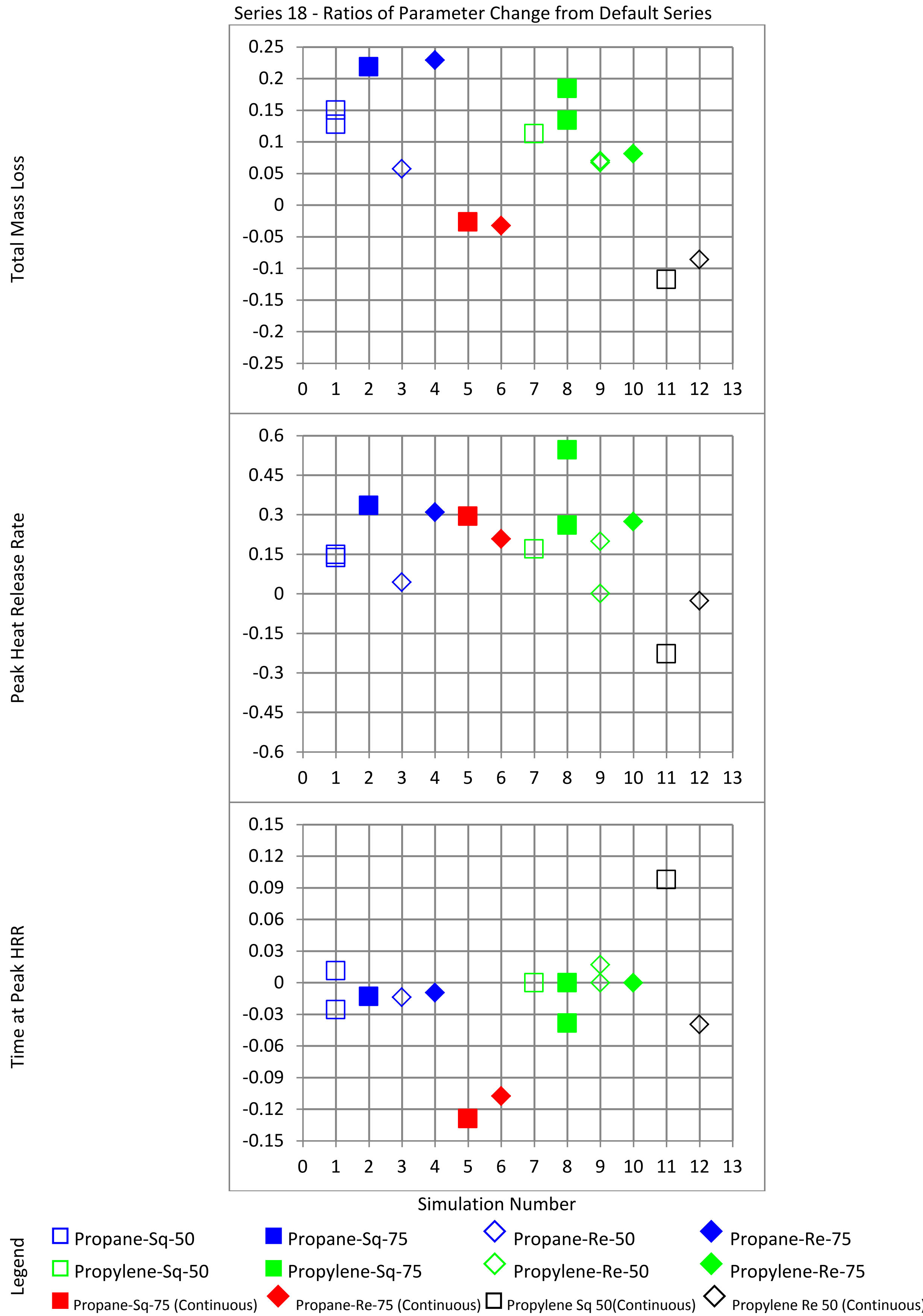
Series 18 - Ratios of Parameter Change from Default Series
Total Mass Loss
Peak Heat Release Rate
Time at Peak HRR
0.25
0.2
0.15
0.1
0.05
0
-0.05
-0.1
-0.15
-0.2
-0.25
0.6
0.45
0.3
0.15
-0.15
-0.3
-0.45
-0.6
0.12
0.09
0.06
0.03
-0.03
-0.06
-0.09
-0.12
0 1 2 3 4 5 6 7 8 9 10 11 12 13
Simulation Number
Legend
Propane-Sq-50
Propane-Sq-75
Propane-Re-50
Propane-Re-75
Propylene-Sq-50
Propylene-Sq-75
Propylene-Re-50
Propylene-Re-75
Propane-Sq-75 (Continuous)
Propane-Re-75 (Continuous)
Propylene Sq 50(Continuous)
Propylene Re 50 (Continuous)

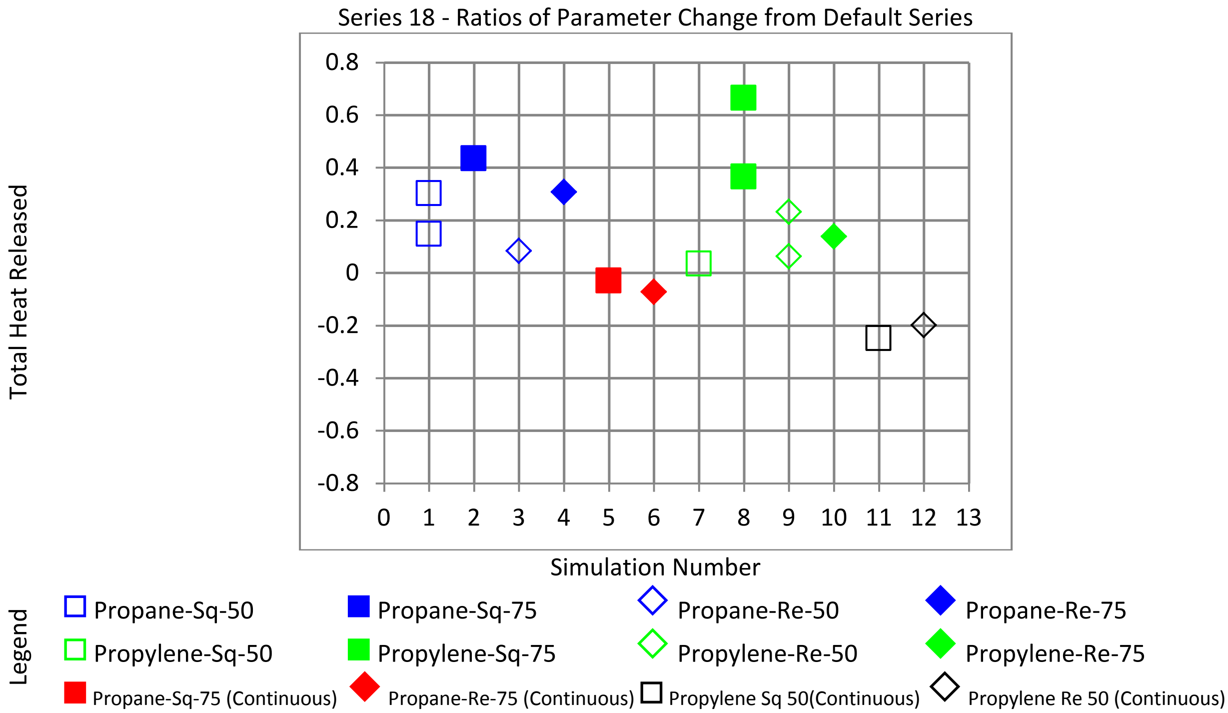

Observations

In the Series 18 simulations, the heat release rate per unit area of the flame sheet was increased from 0 kW/m^2 to 400 kW/m^2 for LES simulations.

The total mass loss predicted was increased for all simultions where a termianted source fire was used, however, but reductions were noted for the simulations wit a continuous source fire. Generally the mass loss changes for the simulations with a higher source fire are more positive.

Changes to the peak HRR were positive and significant for all simulations, except for the cases with a continuous propylene source fire, where the peak HRR were reduced. It is noted that simulations with a higher source HR generally had a greater increase than the cases with the lower HRR at 50 kW.

Time to peak HRR changes were minimal for most of the simulaitons except for the cases with a continuous propane source fire. The only case with a large increase in the time to peak was the simulation with a continuous propylene fire with a Square burner at 50 kW.

Changes to the THR correlate well with the changes observed for the peak HRR, except for the simulations with a continuous propane fire where the changes to the THR were minimal compared to the others.

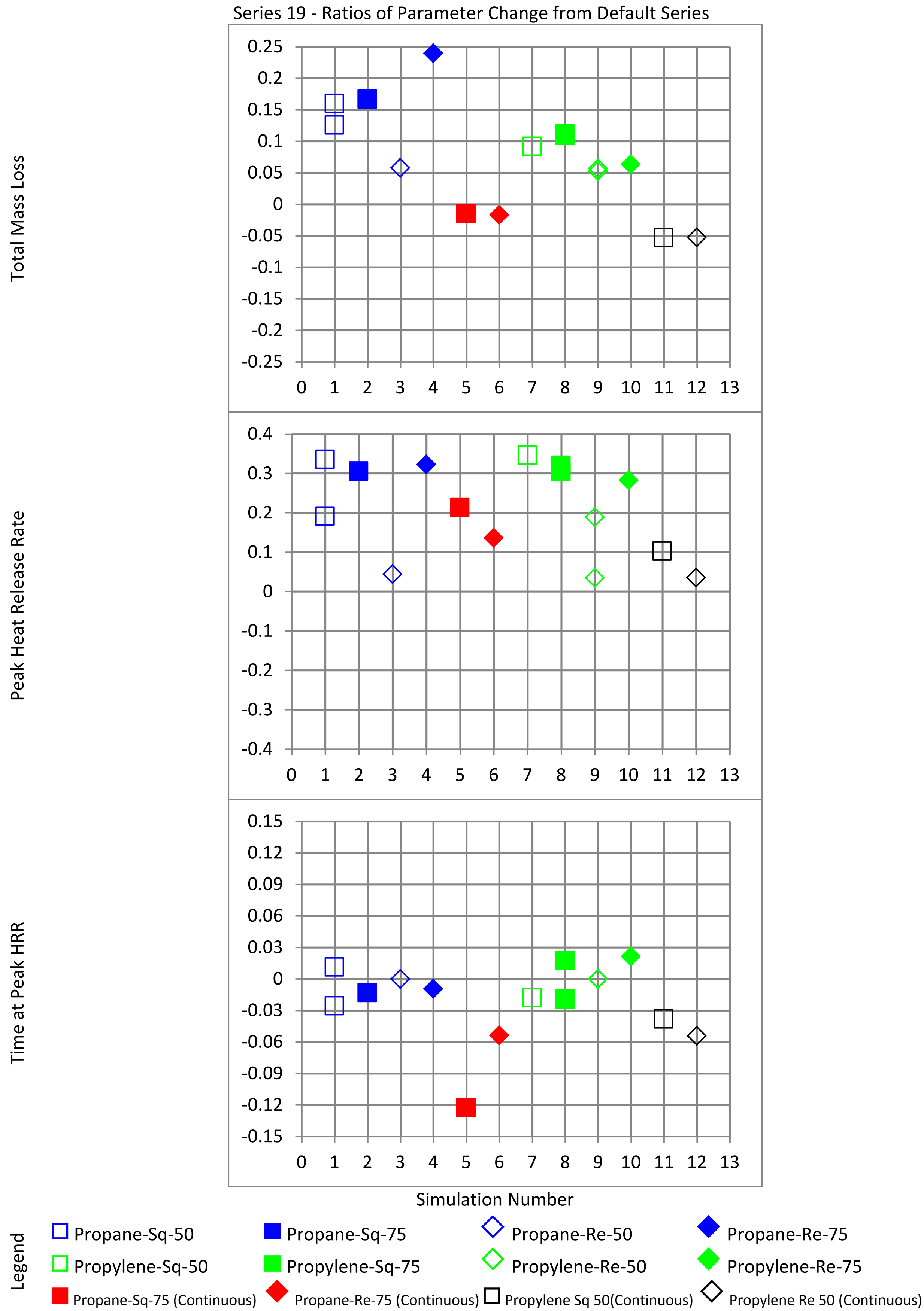
Series 19 - Ratios of Parameter Change from Default Series
Total Mass Loss
Peak Heat Release Rate
Time at Peak HRR
Simulation Number
Legend
Propane-Sq-50
Propane-Sq-75
Propane-Re-50
Propane-Re-75
Propylene-Sq-50
Propylene-Sq-75
Propylene-Re-50
Propylene-Re-75
Propane-Sq-75 (Continuous)
Propane-Re-75 (Continuous)
Propylene Sq 50(Continuous)
Propylene Re 50 (Continuous)

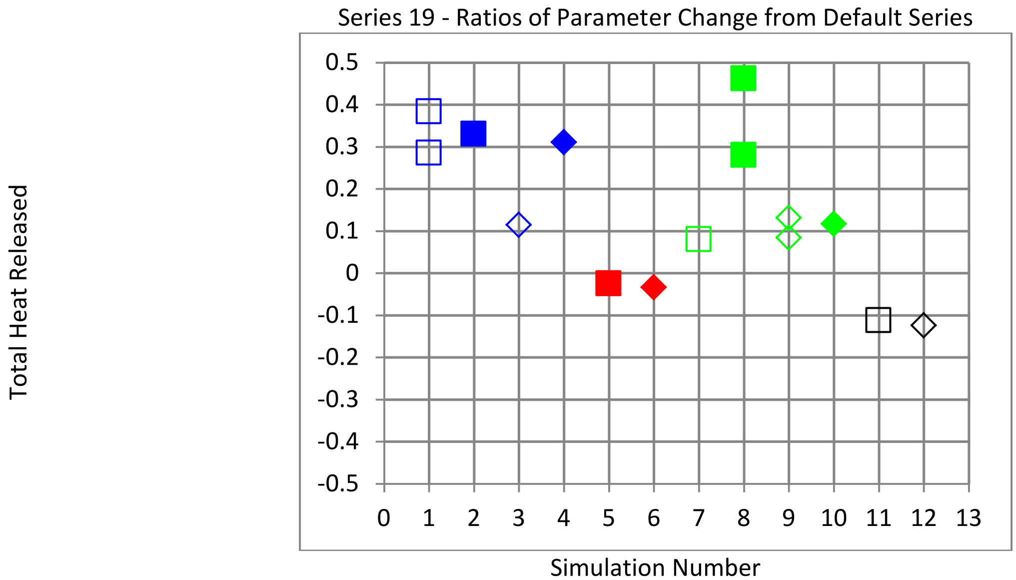

Legend

Propane-Sq-50 | Propane-Sq-75 | Propane-Re-50 | Propane-Re-75
Propylene-Sq-50 | Propylene-Sq-75 | Propylene-Re-50 | Propylene-Re-75
Propane-Sq-75 (Continuous) | Propane-Re-75 (Continuous) | Propylene Sq 50(Continuous) | Propylene Re 50 (Continuous)

Observations

In Series 19 simulations, the heat release rate per unit area of the flame sheet was increased to 100 kW/m^2 from 0 kW/m^2 for LES simulations.

It is noted that the changes to the total mass loss and the time at peak HRR were similar to those noted in the Series 18 simulations, whereas the changes to the peak HRR and THR were smaller in magnitude to those in Series 18. The trends based on the different fire scenarios are preseved between both set of simulations. The similarities in the results between Series 18 and 19 are reasonable because the same parameter was changed in both simulations, with the parametric change smaller in Series 19 than in Series 18, which correlate with the smaller changes in the quantities.

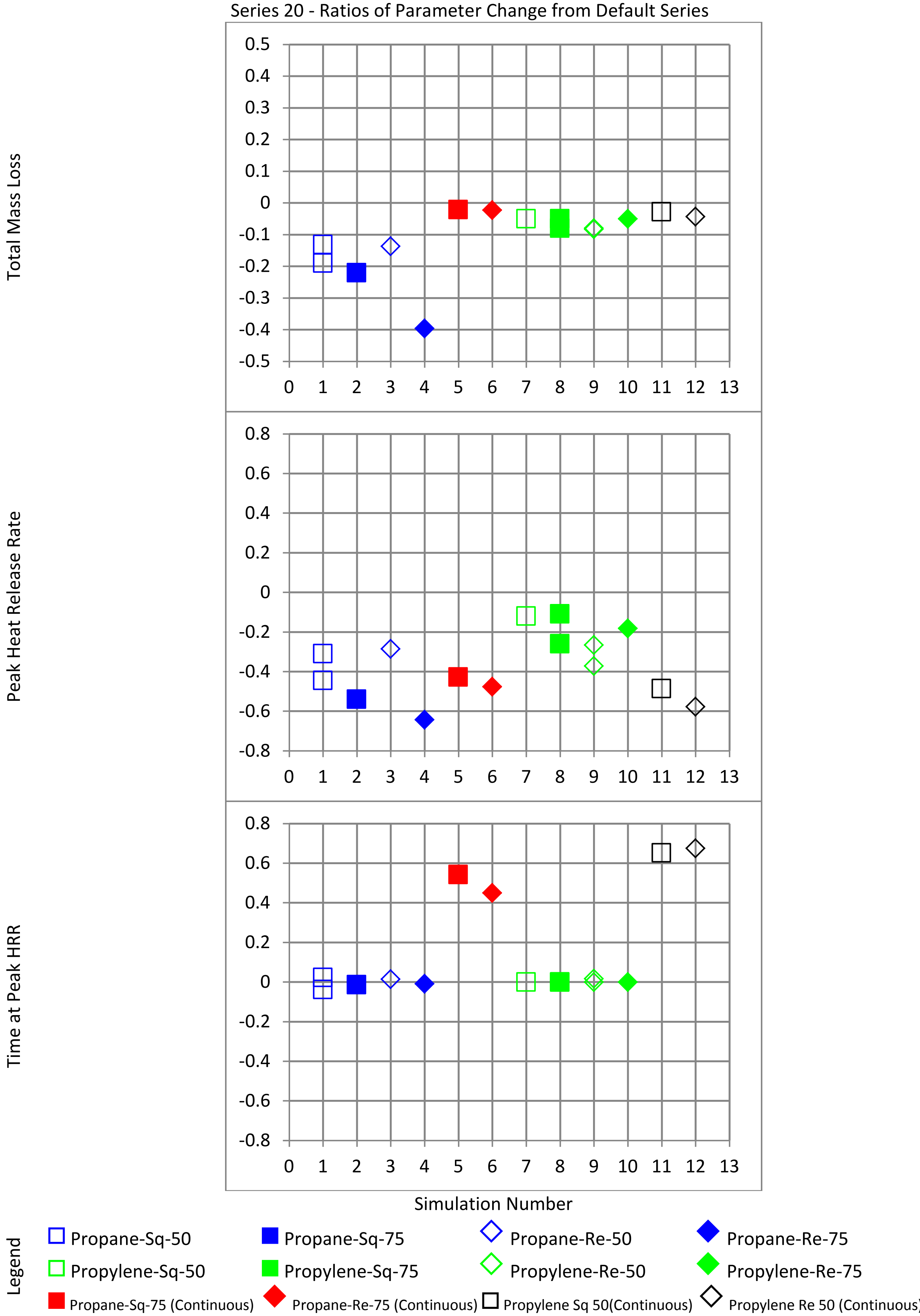

Series 20 - Ratios of Parameter Change from Default Series
Total Mass Loss
Peak Heat Release Rate
Time at Peak HRR
0.5
0.4
0.3
0.2
0.1
0
-0.1
-0.2
-0.3
-0.4
-0.5
0.8
0.6
0.4
0.2
0
-0.2
-0.4
-0.6
-0.8
0 1 2 3 4 5 6 7 8 9 10 11 12 13
Simulation Number
Legend
Propane-Sq-50
Propane-Sq-75
Propane-Re-50
Propane-Re-75
Propylene-Sq-50
Propylene-Sq-75
Propylene-Re-50
Propylene-Re-75
Propane-Sq-75 (Continuous)
Propane-Re-75 (Continuous)
Propylene Sq 50(Continuous)
Propylene Re 50 (Continuous)

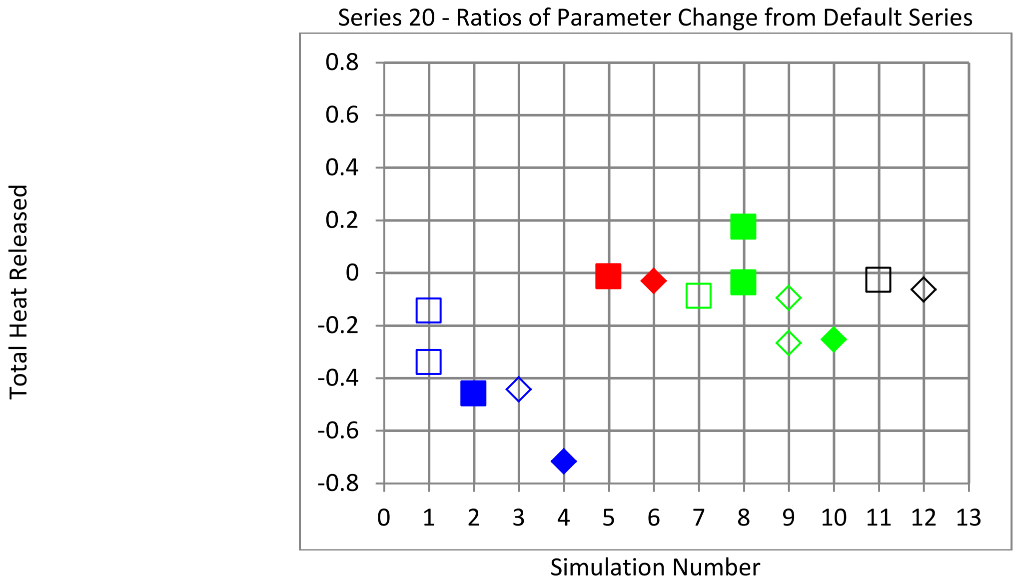

Legend

Propane-Sq-50 | Propane-Sq-75 | Propane-Re-50 | Propane-Re-75
Propylene-Sq-50 | Propylene-Sq-75 | Propylene-Re-50 | Propylene-Re-75
Propane-Sq-75 (Continuous) | Propane-Re-75 (Continuous) | Propylene Sq 50(Continuous) | Propylene Re 50 (Continuous)

Observations

In Series 20 simulations, the average local heat release rate per unit volume was reduced from the default 2500 kW/m^3 to a value of 1200 kW/m^3 as suggested by Orloff and De Ris for the entire fire.

Changes to the total mass loss were essentially negative for all simulations, for the simulations with a continuous source fire and all simulations with a propylene fire, the changes were slight. The changes to the simulaitons with a terminated propane fire were more prominent, especially for the simulations with a greater source HRR.

The peak HRR for all simulations were also lowered in this Series of simulation. The effect is more pronouced for thesimulations with a propane source fire than for the simulations with a propylene source fire. Additionally, it is noted that the changes to the simulations with a continuous source fire were more prominent.

There were essentially no chang in the time at peak HRR for all simulations with a terminated source fire. However, the time to peak HRR had been increased for the simulations with a continuous source fire. The magnitude of the increases was greater for the propylene cource fire simulations.

Changes to the THR share the same trend as those for the total mass loss, except that the magnitude of change to the smulations with a terminated propylene source firewas greater than for propane. Again, there is indications that the magnitude of change was direcly related to the size of the source fire.

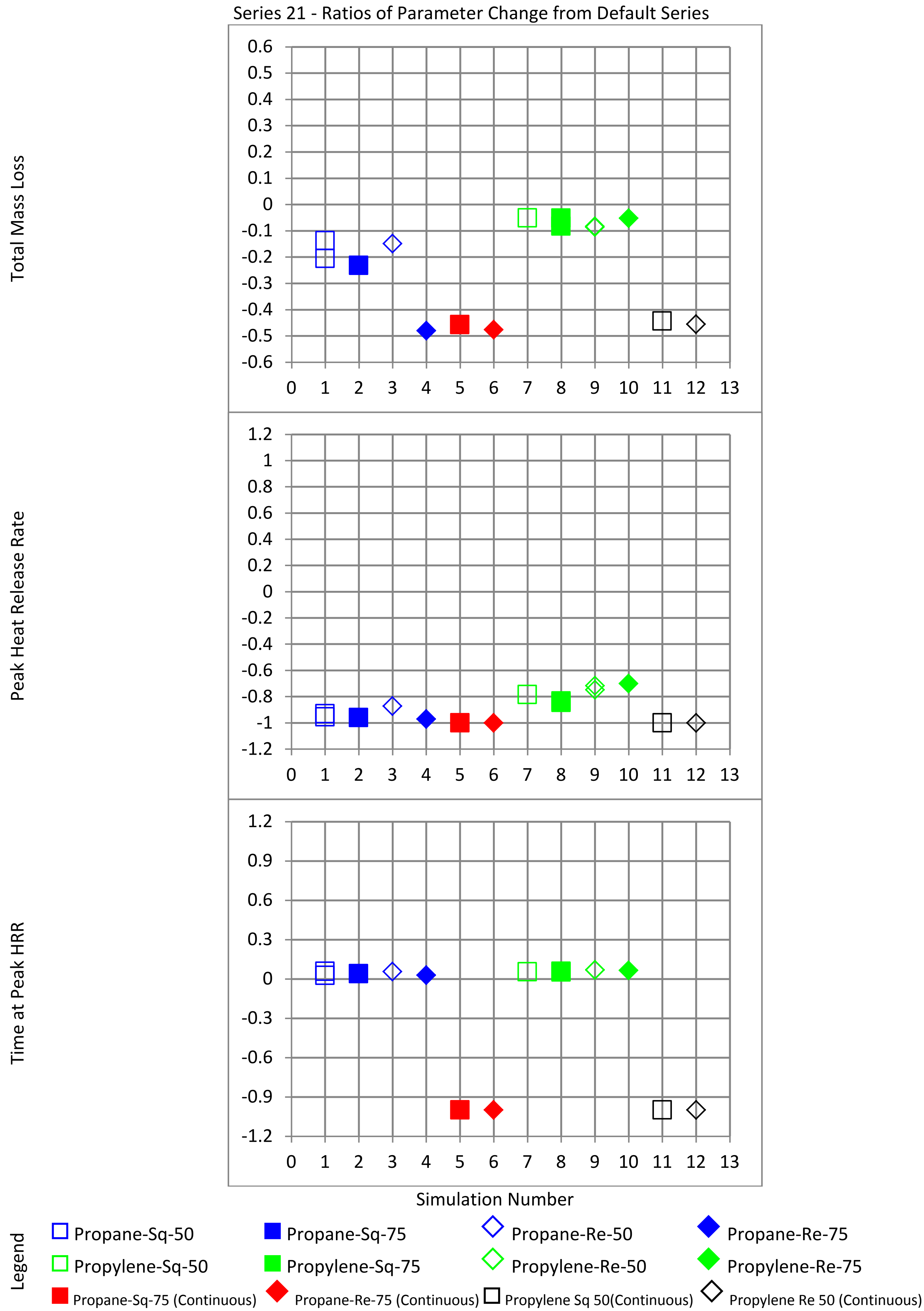
Series 21 - Ratios of Parameter Change from Default Series
Total Mass Loss
Peak Heat Release Rate
Time at Peak HRR
Simulation Number
Legend
Propane-Sq-50
Propane-Sq-75
Propane-Re-50
Propane-Re-75
Propylene-Sq-50
Propylene-Sq-75
Propylene-Re-50
Propylene-Re-75
Propane-Sq-75 (Continuous)
Propane-Re-75 (Continuous)
Propylene Sq 50(Continuous)
Propylene Re 50 (Continuous)

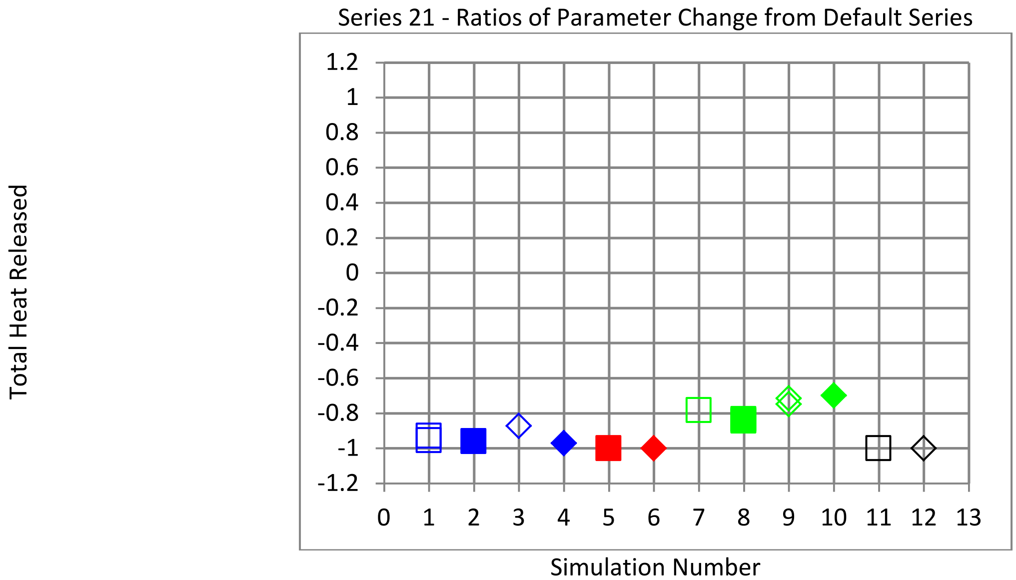

Legend

Propane-Sq-50	Propane-Sq-75	Propane-Re-50	Propane-Re-75
Propylene-Sq-50	Propylene-Sq-75	Propylene-Re-50	Propylene-Re-75
Propane-Sq-75 (Continuous)	Propane-Re-75 (Continuous)	Propylene Sq 50(Continuous)	Propylene Re 50 (Continuous)

Observations

The isothermal model was enabled in the Series 21 simulations to test the effects of a fire simulation in which the temperature was forced to not changed. It was intended to show whether a mistake in writing the FDS file would result in a simulation with some salvageable and meaningful data.

Since the simulations are forced to have no temperature change, fire spread on the combustible wall material was essentially unachievable. Hence, the simulations in this series of simulations experienced greatly repressed mass loss, HRR, and THR. Although

An isothermal condition should not be used if modeling flame spread.

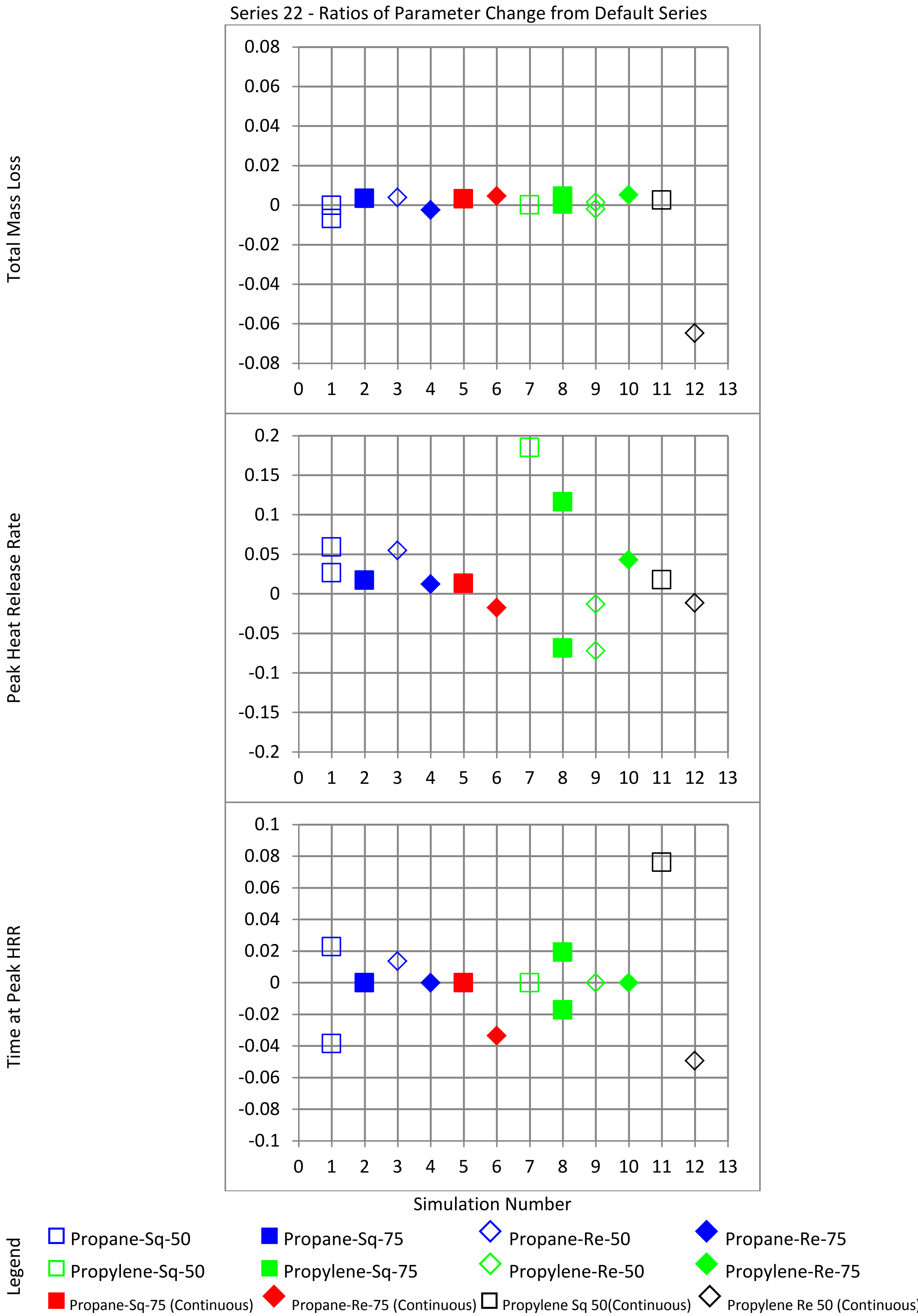

Series 22 - Ratios of Parameter Change from Default Series
Total Mass Loss
0.08
0.06
0.04
0.02
0
-0.02
-0.04
-0.06
-0.08
Peak Heat Release Rate
0.2
0.15
0.1
0.05
0
-0.05
-0.1
-0.15
-0.2
Time at Peak HRR
0.1
0.08
0.06
0.04
0.02
0
-0.02
-0.04
-0.06
-0.08
-0.1
0 1 2 3 4 5 6 7 8 9 10 11 12 13
Simulation Number
Legend
Propane-Sq-50
Propane-Sq-75
Propane-Re-50
Propane-Re-75
Propylene-Sq-50
Propylene-Sq-75
Propylene-Re-50
Propylene-Re-75
Propane-Sq-75 (Continuous)
Propane-Re-75 (Continuous)
Propylene Sq 50(Continuous)
Propylene Re 50 (Continuous)

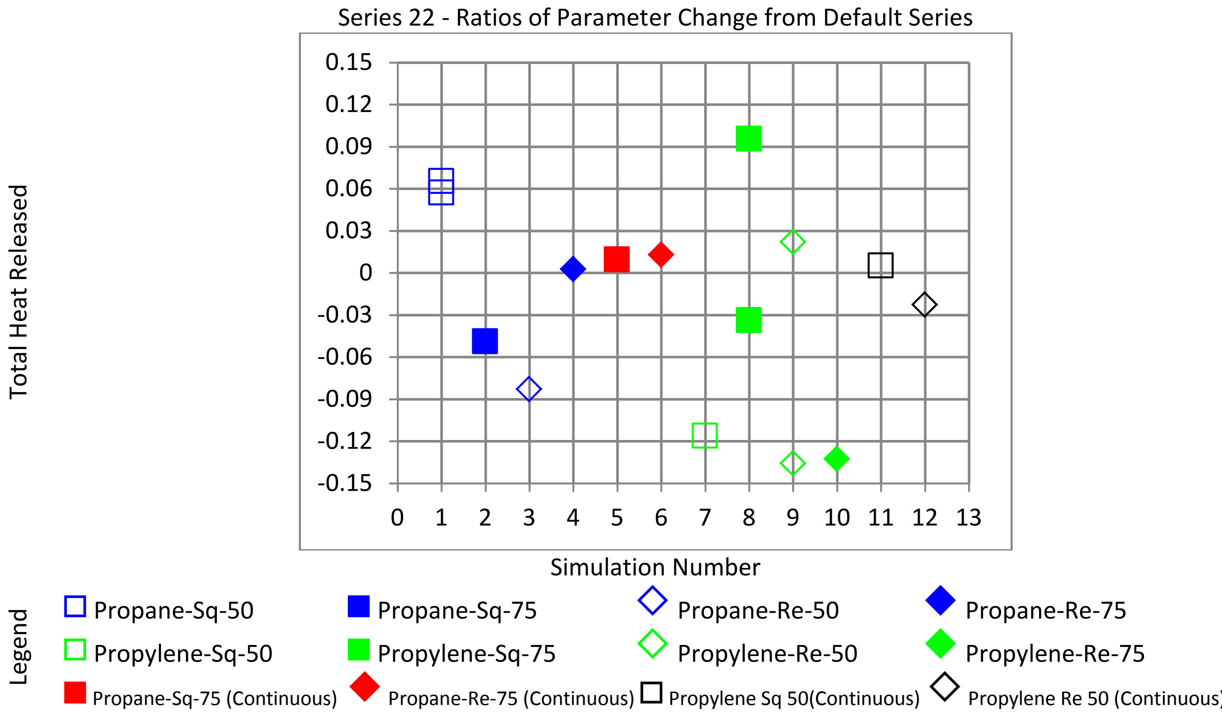

Observations

In Series 22, the Smagorinsky constant was reduced from 0.2 to 0.1, it was used to calculate the viscosity of the fluid and to model the subgrid-scale turbulence in the models.

There were insignificant changes to the total mass loss for all of the simulaitons except for thecase with a continuous propylene Rectangle fire at 75 kW.

Changes to the peak HRR appear to be positive for most of the simulations except for several propylene source fire simulations and the simulations with a continuous source fire with a Rectangle burner. The changes to the simulations with a propylene source fire were more prominent for changes for propane source fire combustible wall simulations.

For the time at peak HRR, changes were more prominent for the simulaitons using propylene as the source fuel. It also appears that the magnitude of change is greatest for simulations with a continuous source fire.

In terms of THR, changes were more significant for the simulations with a terminated source fire than those with a continuous source fire, but effects on propylen still appear to be more prominent than on propane.

Series 23 - Ratios of Parameter Change from Default Series

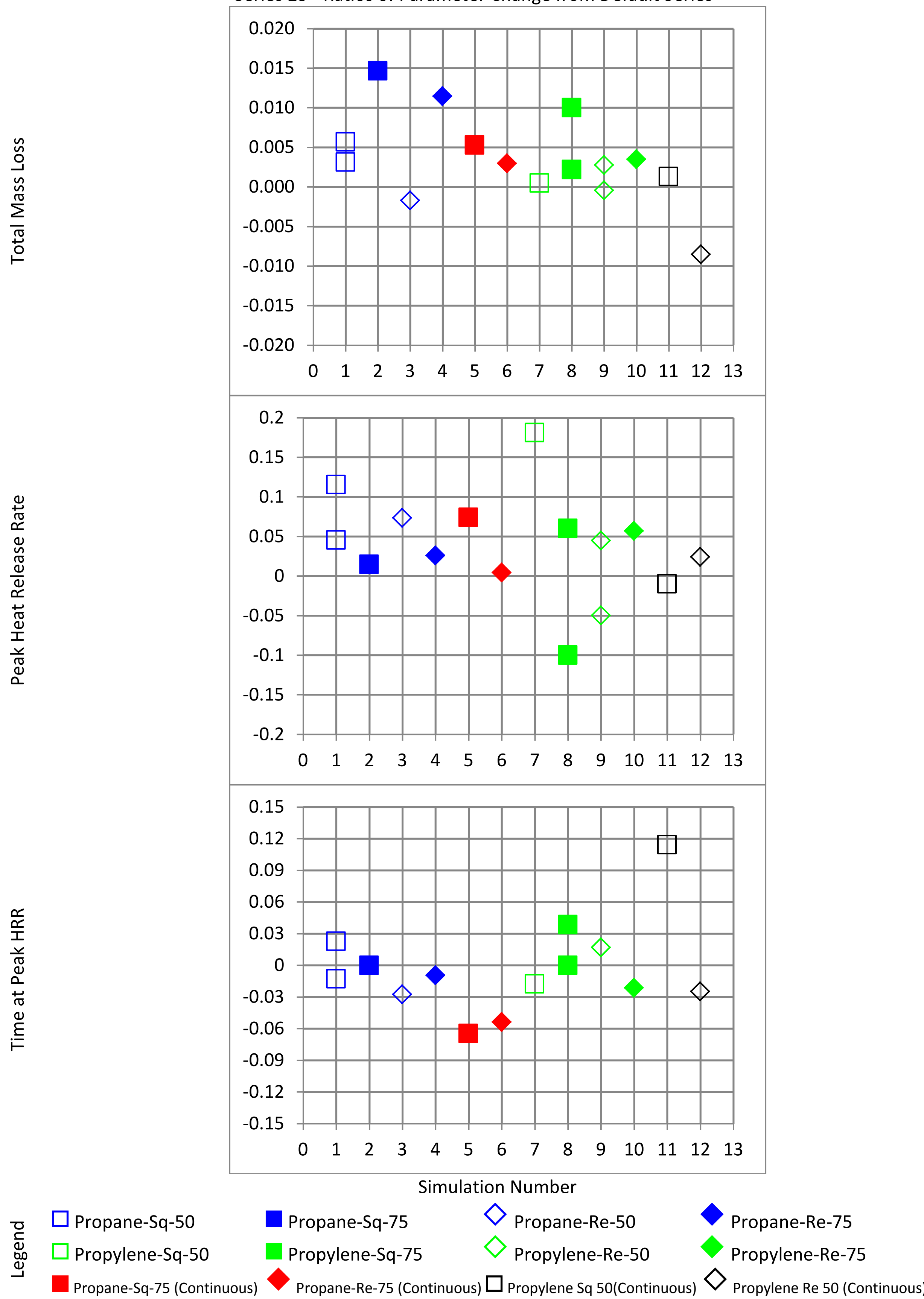

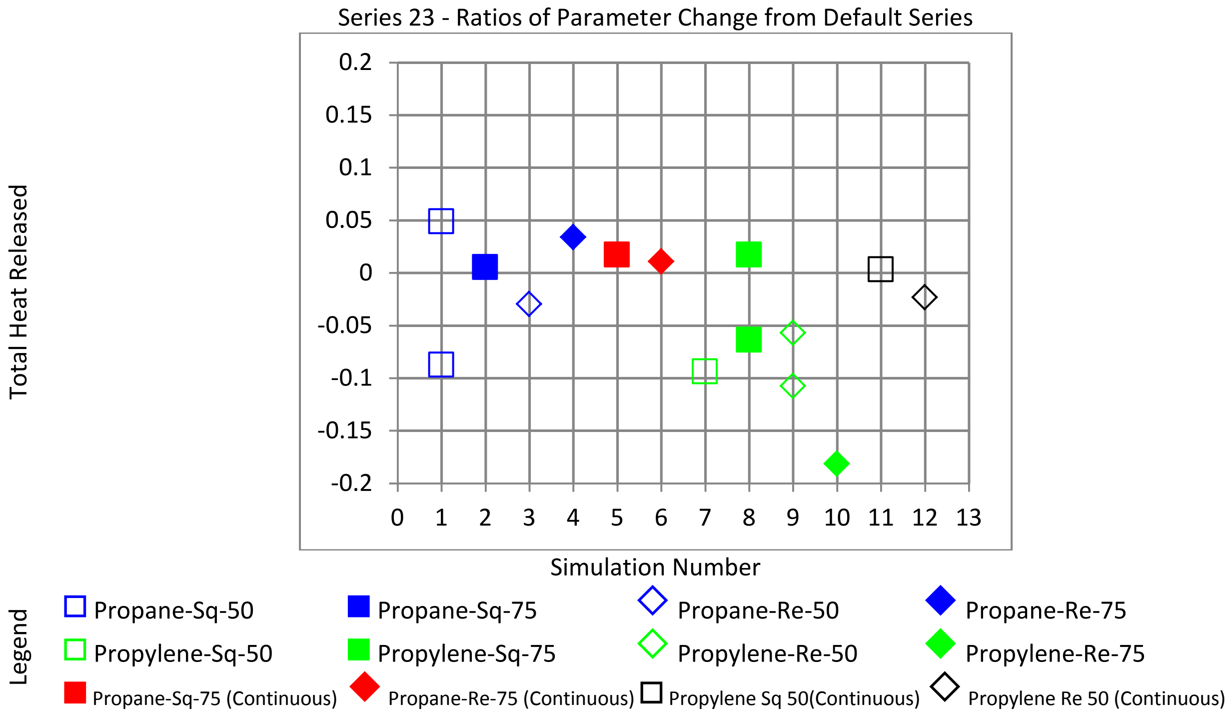

Observations

In Series 23, the Smagorinsky constant was increased from 0.2 to 0.4, it was used to calculate the viscosity of the fluid and to model the subgrid-scale turbulence in the models.

Changes to the total mass loss were mostly positive, but quite insignificant in their magnitude. The most negative change occurred to the simulation with a continuous propylene source fire with a Rectangle burner at 50 kW.

For the peak HRR, the changes were positive for the simulations using apropane source fire, and it is observed that the changes are more significant for Square burner and lower HRR. However, for the propylene source fire simulaitons, the changes lie both in the positive and the negative, without a definite trend between the changes in the quantity with burner size and size of the source fire HRR.

Chagnes to the time to peak HRR were small for all of the simulaitons which range from ±6%, except for the simulaiton with a continuous propylene source fire with a Square burner at 50 kW.

The parameter change created mostly positive changes to the simulations using a propane source fire, but mostly negative changes to the simulations with a propylen source fire. The greatest change occurred to the simulation of a terminated propylene source fire with a Rectangle fire at 75 kW. Changes to the simulations using a continuous fire were small.

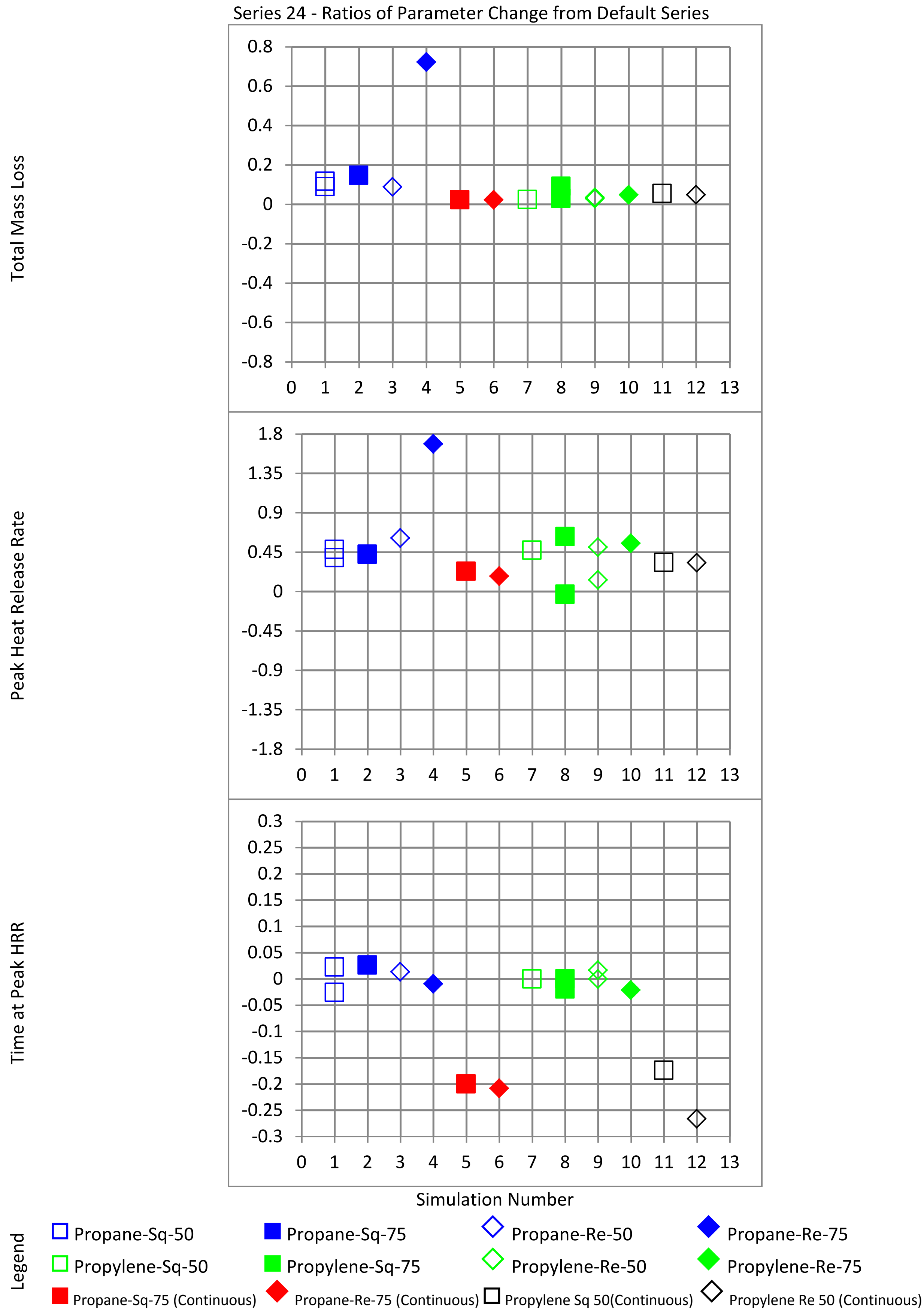

Series 24 - Ratios of Parameter Change from Default Series
Total Mass Loss
Peak Heat Release Rate
Time at Peak HRR
Simulation Number
Legend
Propane-Sq-50
Propane-Sq-75
Propane-Re-50
Propane-Re-75
Propylene-Sq-50
Propylene-Sq-75
Propylene-Re-50
Propylene-Re-75
Propane-Sq-75 (Continuous)
Propane-Re-75 (Continuous)
Propylene Sq 50(Continuous)
Propylene Re 50 (Continuous)

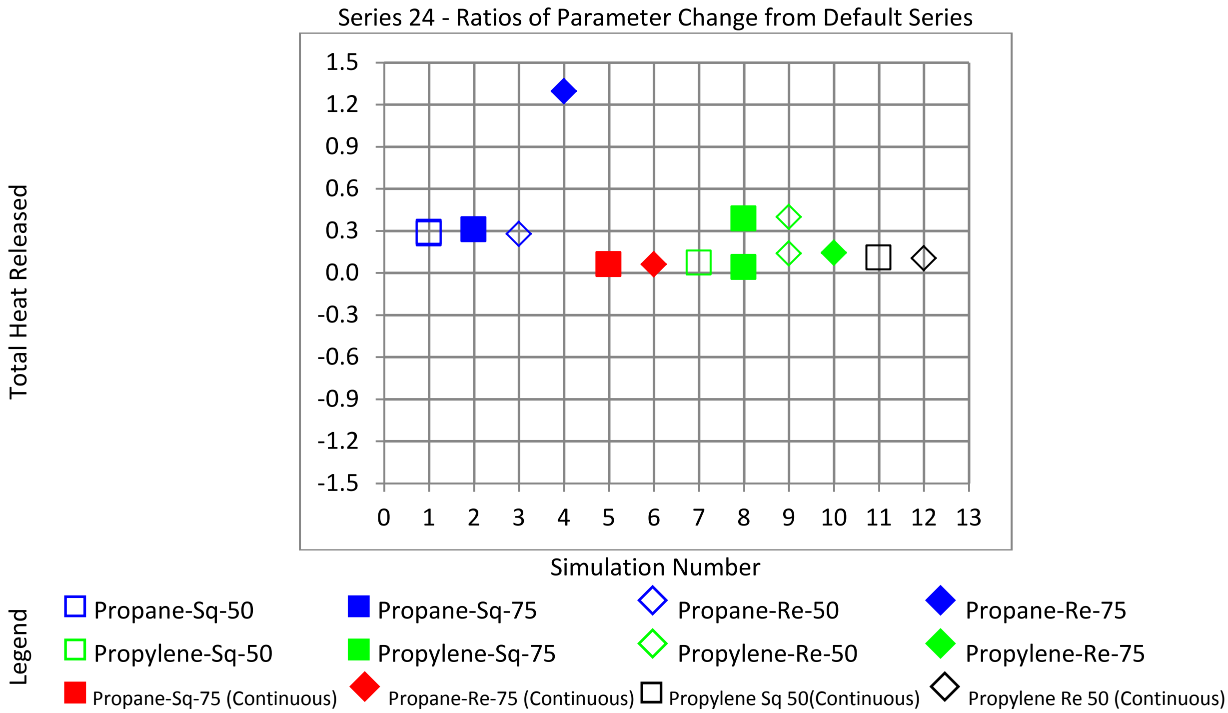

Observations

In Series 24, the turbulent Prandtl number was decreased to 0.25 from 0.5, the Prandtl number is a ratio of the momentum diffusivity to thermal diffusivity, so this parameter change had the potential to change the flow characteristics in the simulations.

In terms of the total mass loss, the changes were all within a range of 0 to 20% for all simulations except for the single case of a terminated propane source fire with a Rectangle burner at 75 kW. The change for the single case was approximately an increase of 70%

The behaviors of the peak HRR changes are similar to those observed for the total mass loss, excpet that the magnitude of the changes were much greater for the peak HRR.

Changes to the time to peak HRR were within a range of ±5% for all simulations with a termianted source fire. For the simulations with a continous source fire, however, the time to peak were reduced to approximately 25%.

For the THR, the changes correlate well with the changes to the peak HRR, except the magnitude of the changes were smaller.

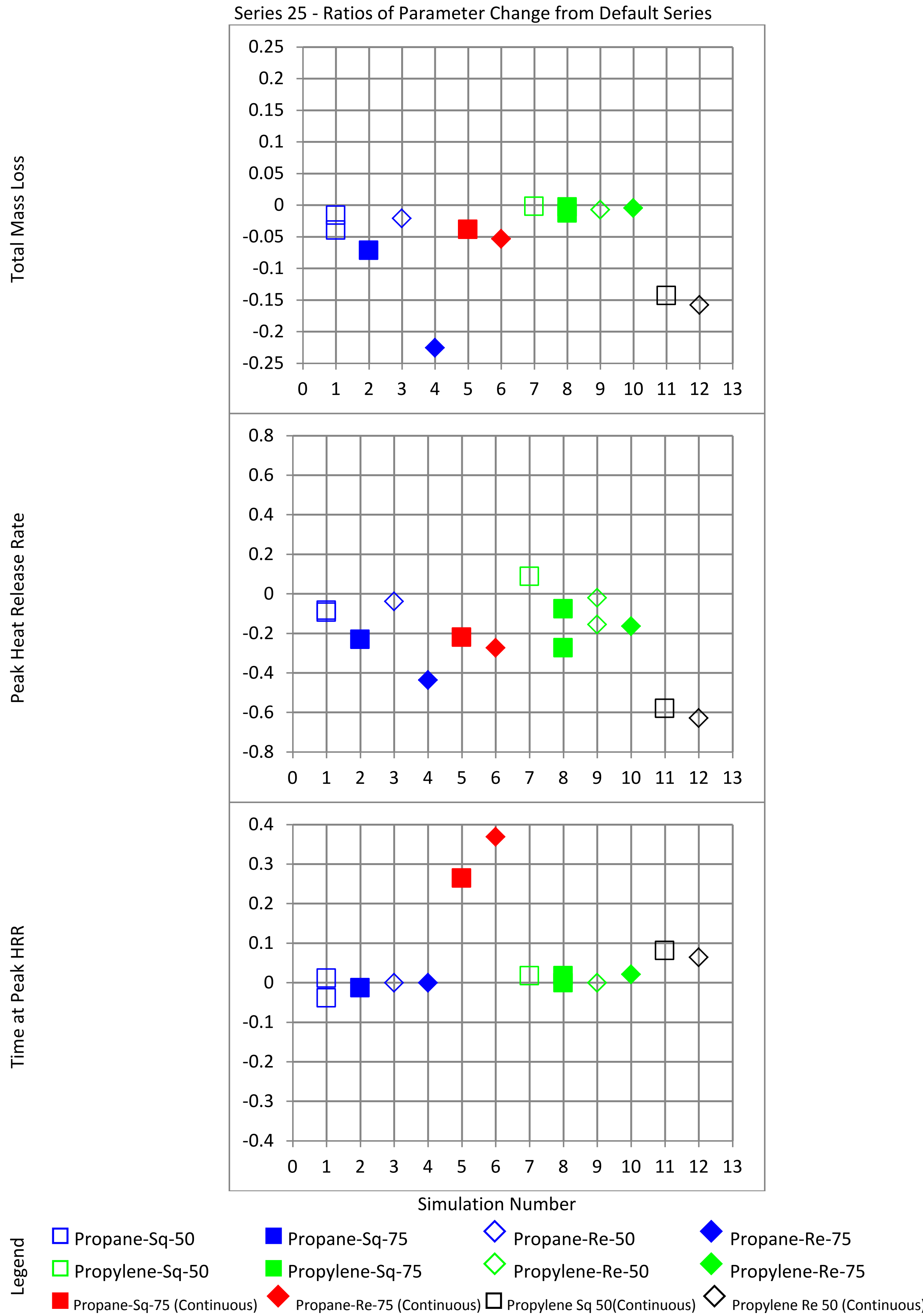

Series 25 - Ratios of Parameter Change from Default Series
Total Mass Loss
Peak Heat Release Rate
Time at Peak HRR
Simulation Number
Legend
Propane-Sq-50
Propane-Sq-75
Propane-Re-50
Propane-Re-75
Propylene-Sq-50
Propylene-Sq-75
Propylene-Re-50
Propylene-Re-75
Propane-Sq-75 (Continuous)
Propane-Re-75 (Continuous)
Propylene Sq 50(Continuous)
Propylene Re 50 (Continuous)

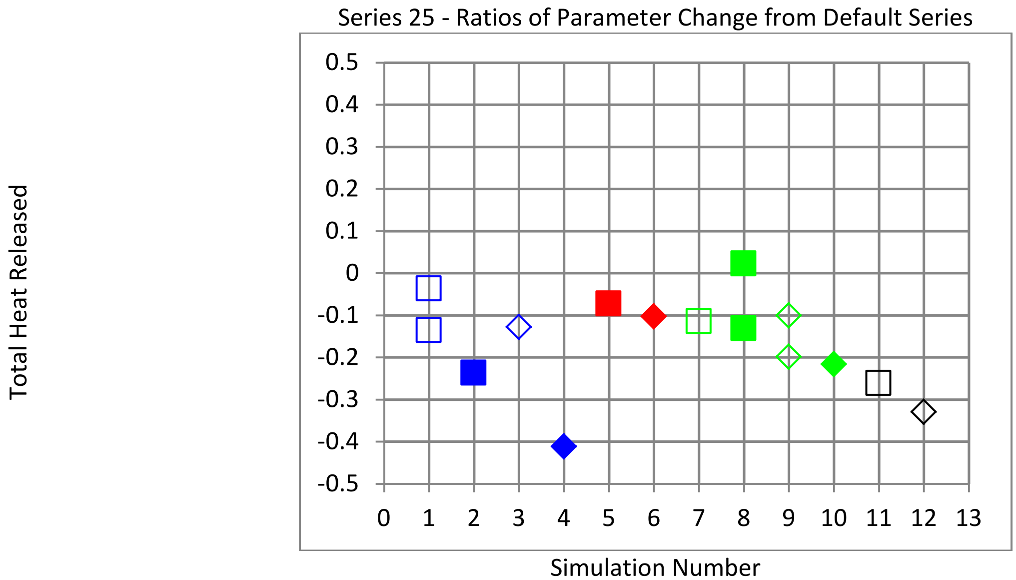

Legend

□ Propane-Sq-50 ■ Propane-Sq-75 ◇ Propane-Re-50 ◆ Propane-Re-75
□ Propylene-Sq-50 ■ Propylene-Sq-75 ◇ Propylene-Re-50 ◆ Propylene-Re-75
■ Propane-Sq-75 (Continuous) ◆ Propane-Re-75 (Continuous) □ Propylene Sq 50(Continuous) ◇ Propylene Re 50 (Continuous)

Observations

In Series 25, the turbulent Prandtl number was increased from 0.5 to 1, the Prandtl number is a ratio of the momentum diffusivity to thermal diffusivity, so this parameter change had the potential to change the flow characteristics in the simulations.

The total mass loss was generally reduced due to the parameter change for all simulations. The changes were most significant for the simulations with a continuous propylene source fire and for the simulation with a terminated propane source fire with a Rectangle burner at 75 kW.

Changes to the peak HRR were mostly negative a well. The greatest reduction in peak HRR occurred in the simulations with a continuous propylene source fire. It is also noted that the magnitude of change was greater for the Rectangle burner and the higher HRR at 75 kW.

For the time to peak HRR, the changes were generally small, except for the cases with a continuous propane source fire.

Changes to the THR have similar trends to the changes in peak HRR, but at a slightly smaller magnitude.

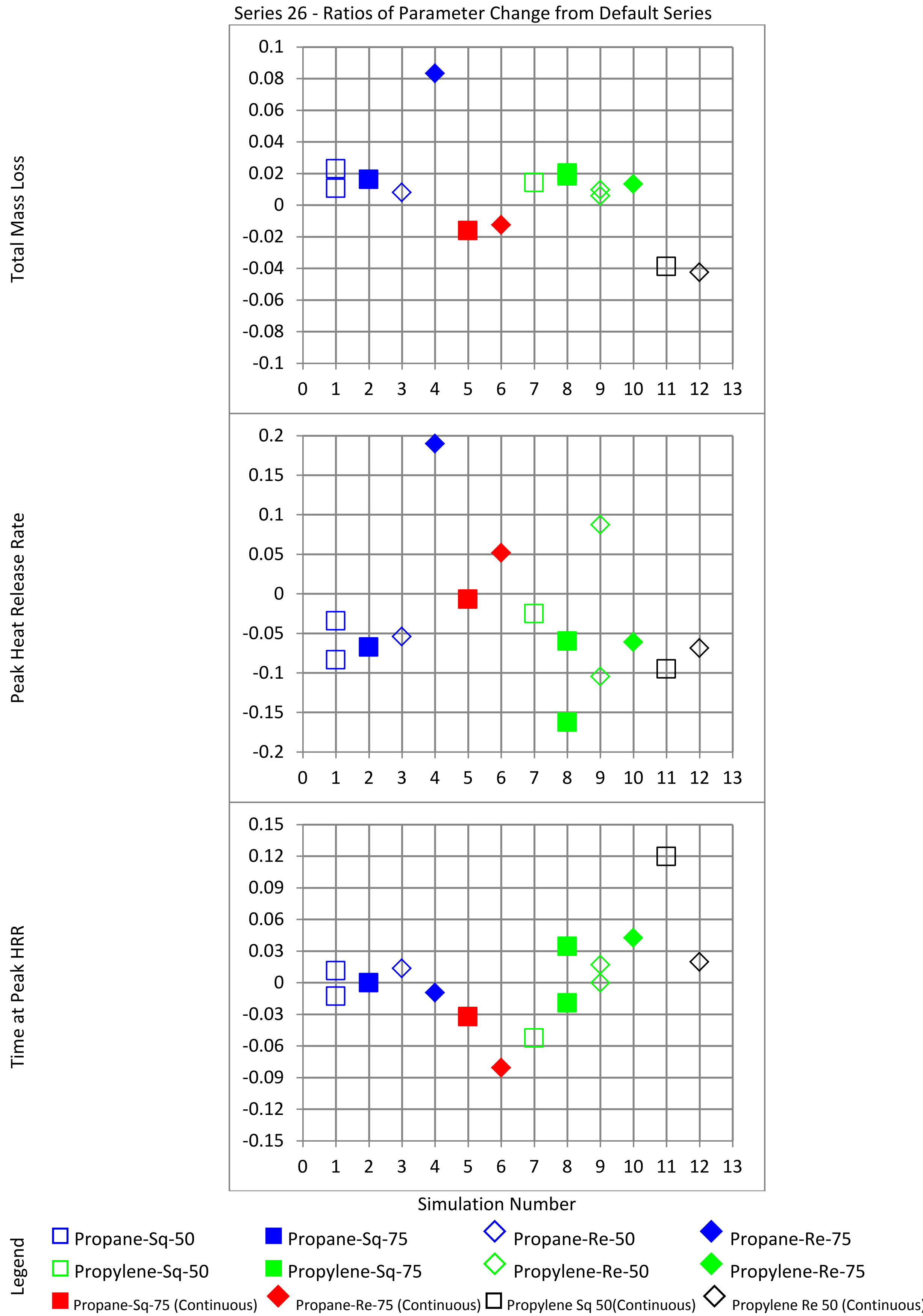

Series 26 - Ratios of Parameter Change from Default Series
Total Mass Loss
Peak Heat Release Rate
Time at Peak HRR
Simulation Number
Legend
Propane-Sq-50
Propane-Sq-75
Propane-Re-50
Propane-Re-75
Propylene-Sq-50
Propylene-Sq-75
Propylene-Re-50
Propylene-Re-75
Propane-Sq-75 (Continuous)
Propane-Re-75 (Continuous)
Propylene Sq 50(Continuous)
Propylene Re 50 (Continuous)

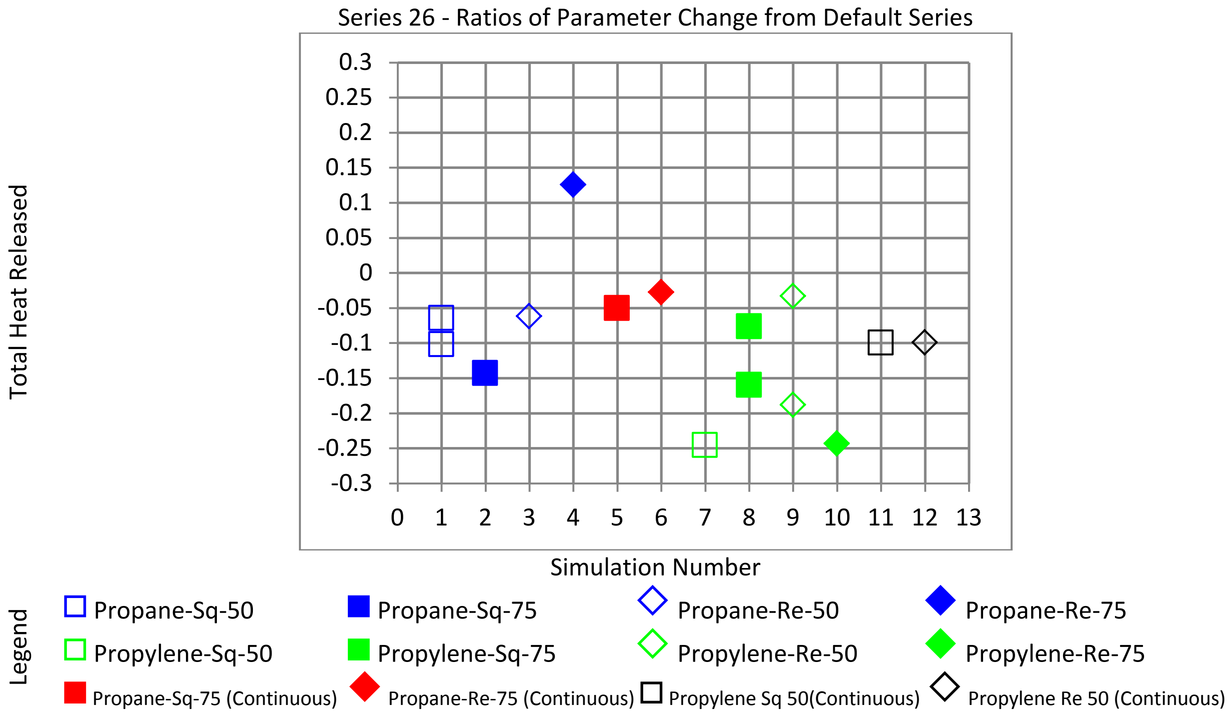

Observations

In Series 26, the turbulent Schmidt number was decreased from 0.5 to 0.25, the Schmidt number is a ratio of the momentum diffusivity to mass diffusivity, so this parameter change had the potential to change the flow characteristics in the simulations.

Deviations of the total mass loss due to the parameter change were positive for all simulations with a termainted source fire. Most of the changes were within 3%, excpet for the change in the simulation with a propane source fire with the Rectangle burner at 75 kW at +8%. However, the changes for the simulations with a continuous source fire were negative, regardless of the source fuel used.

For the peak HRR, the changes were mostly negative, and at greater magnitude for the simulations with a propylen source fire. Again, the simulation with a terminated propane source fire with a Rectanlge burner at 75 kW had a greatly positive change. It is noted that the changes for the simulations with a continuous propane fire were slightly positive whereas the changes were negative for the propylene continuous fire.

Changes in the time to peak HRR were more random, but it is observed that the changes for the simulations using a propane source fire was mostly negative whereas it ws mostly postiive for the propylene source fire simulations.

Again changes to the THR collerate well with the changes to the peak HRR.

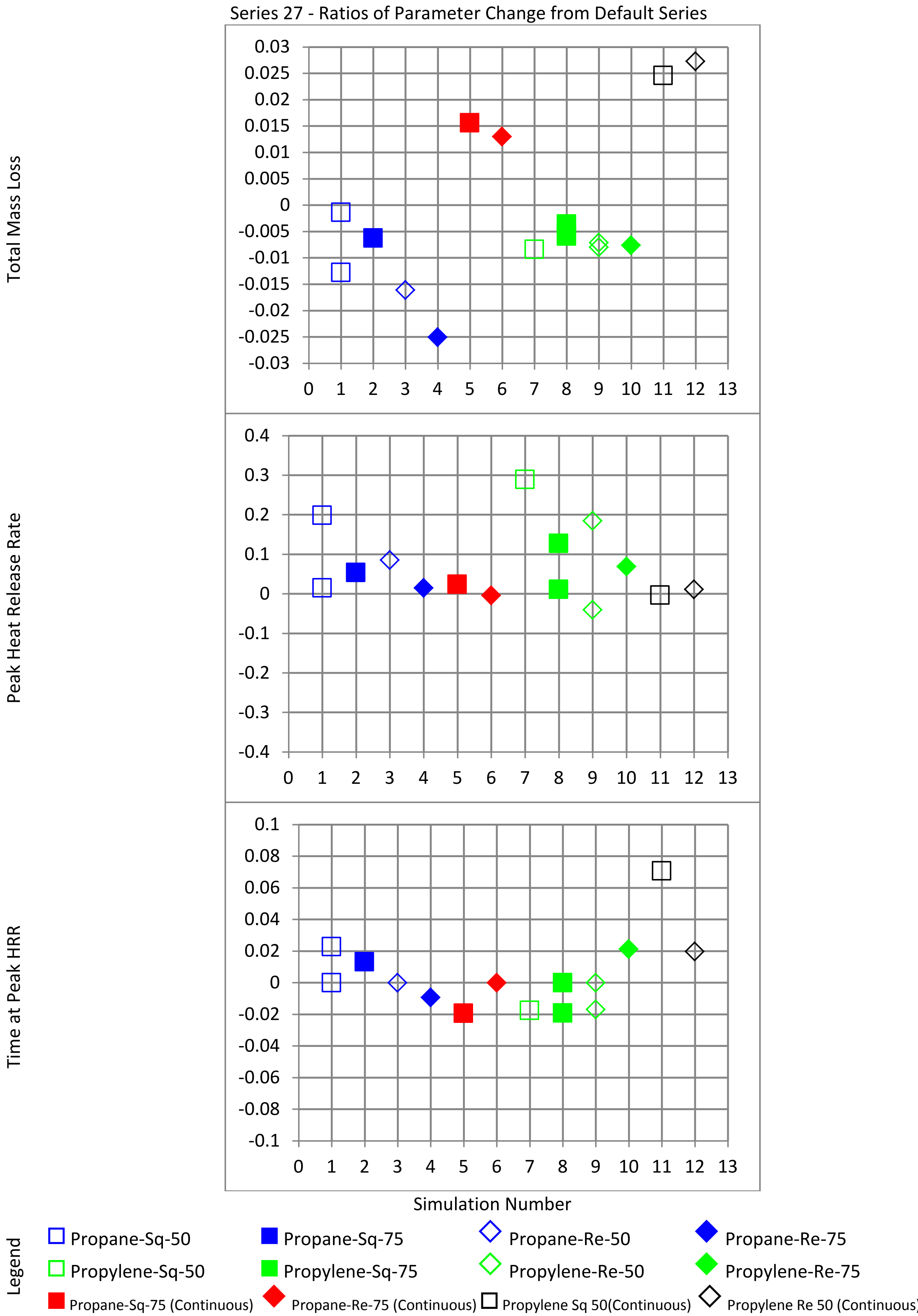

Series 27 - Ratios of Parameter Change from Default Series
Total Mass Loss
0.03
0.025
0.02
0.015
0.01
0.005
0
-0.005
-0.01
-0.015
-0.02
-0.025
-0.03
Peak Heat Release Rate
0.4
0.3
0.2
0.1
0
-0.1
-0.2
-0.3
-0.4
Time at Peak HRR
0.1
0.08
0.06
0.04
0.02
0
-0.02
-0.04
-0.06
-0.08
-0.1
0 1 2 3 4 5 6 7 8 9 10 11 12 13
Simulation Number
Legend
Propane-Sq-50
Propane-Sq-75
Propane-Re-50
Propane-Re-75
Propylene-Sq-50
Propylene-Sq-75
Propylene-Re-50
Propylene-Re-75
Propane-Sq-75 (Continuous)
Propane-Re-75 (Continuous)
Propylene Sq 50(Continuous)
Propylene Re 50 (Continuous)

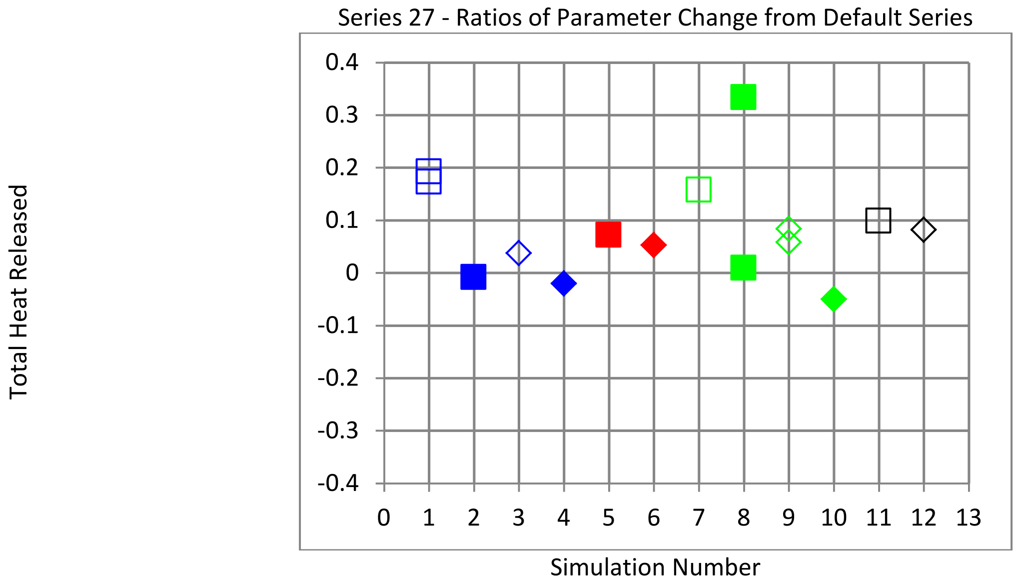

Legend

Propane-Sq-50 | Propane-Sq-75 | Propane-Re-50 | Propane-Re-75
Propylene-Sq-50 | Propylene-Sq-75 | Propylene-Re-50 | Propylene-Re-75
Propane-Sq-75 (Continuous) | Propane-Re-75 (Continuous) | Propylene Sq 50(Continuous) | Propylene Re 50 (Continuous)

Observations

In Series 27, the turbulent Schmidt number was increased from 0.5 to 1, the Schmidt number is a ratio of the momentum diffusivity to mass diffusivity, so this parameter change had the potential to change the flow characteristics in the simulations.

For the total mass loss, the changes were mostly opposite to those noted in the Series 27 where the Schmidt number was changed in the opposite direction.

In term of the peak HRR, the changes were positive for most of the simulations. And it appears that the magnitude of change was greater for simulaiton susing the Square burner and at a lower HRR. it should benoted that the changes for the simulations with a continuous source fire were the smallest.

Changes in the time to peak HRR were more random, but it is observed that the changes for the simulations using a propane source fire was mostly negative whereas it ws mostly postiive for the propylene source fire simulations.

Again changes to the THR collerate well with the changes to the peak HRR.

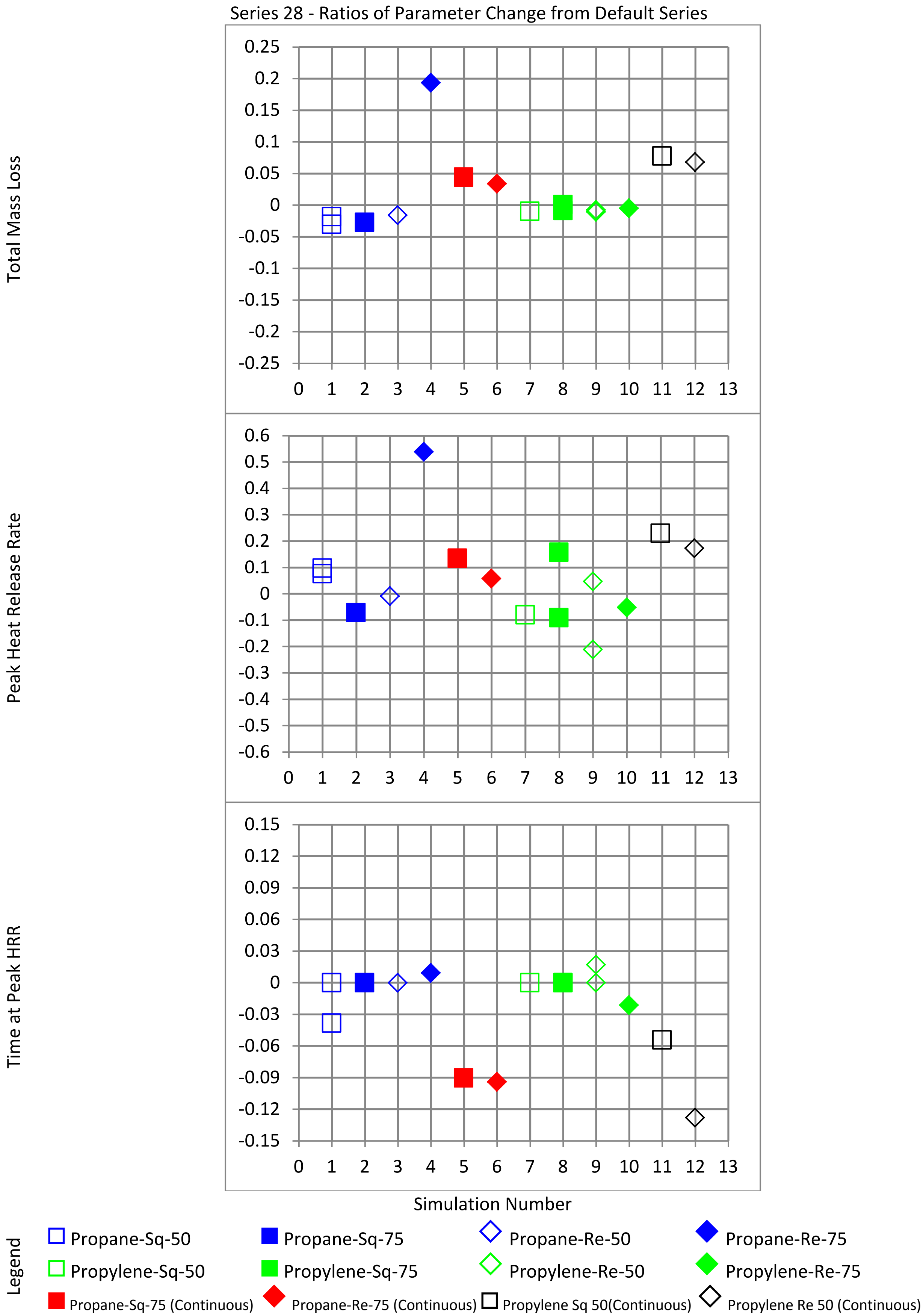

Series 28 - Ratios of Parameter Change from Default Series
Total Mass Loss
Peak Heat Release Rate
Time at Peak HRR
Simulation Number
Legend
Propane-Sq-50
Propane-Sq-75
Propane-Re-50
Propane-Re-75
Propylene-Sq-50
Propylene-Sq-75
Propylene-Re-50
Propylene-Re-75
Propane-Sq-75 (Continuous)
Propane-Re-75 (Continuous)
Propylene Sq 50(Continuous)
Propylene Re 50 (Continuous)

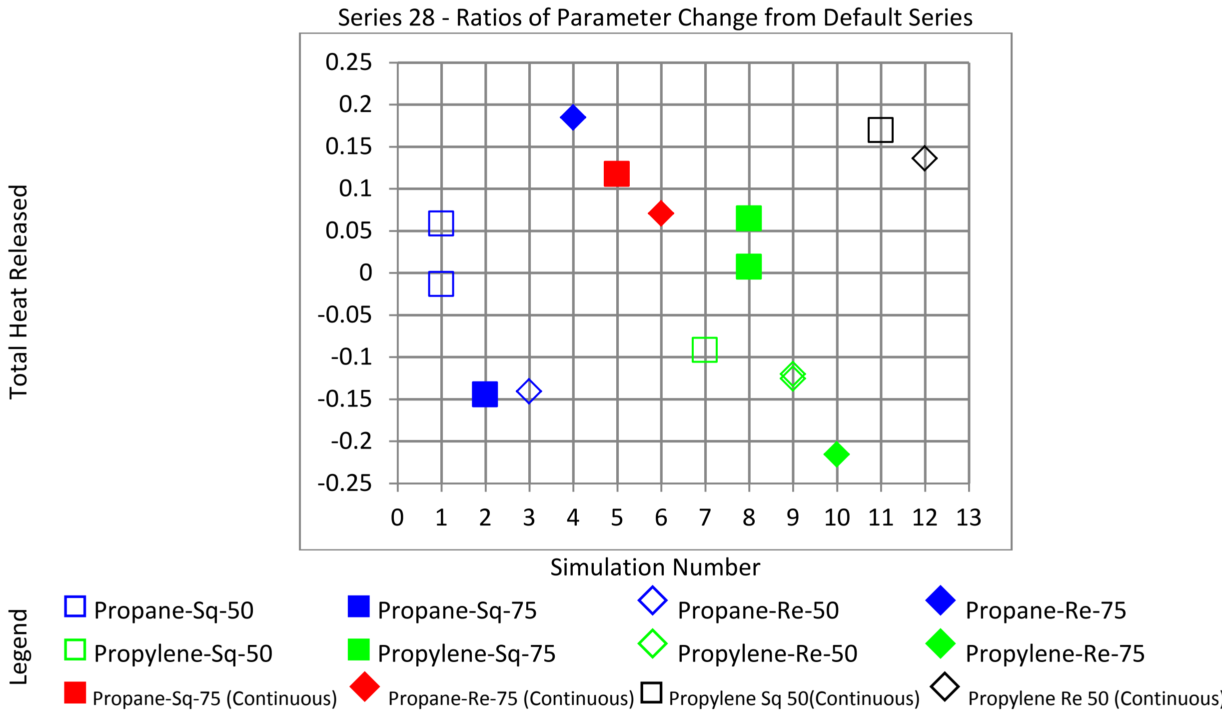

Observations

The baroclinic torque correction was disabled in the Series 28 models, this parameter determines properties of the vorticity in the flow calculations.

Changes to the simulations with a terminated source fire were mostly slightly negative, exept for the simulation with a a propane source fire with a Rectangle burner at 75 kW. The simulations with a continuous source fire had slightly positive changes.

In term of peak HRR, the magnitude of the changes were more significant than for the total mass loss, although the changes occurred in both the negative and the positive direction. The simulations with a continuous source fire had slightly positive changes.

The time to peak HRR were shortened for the simulations with a continuous source fire, but the chagnes were small for the cases with a terminated source fire.

The trends of the THR change correlate well with those found in the peak HRR,b ut generally with a smaller magnitude.

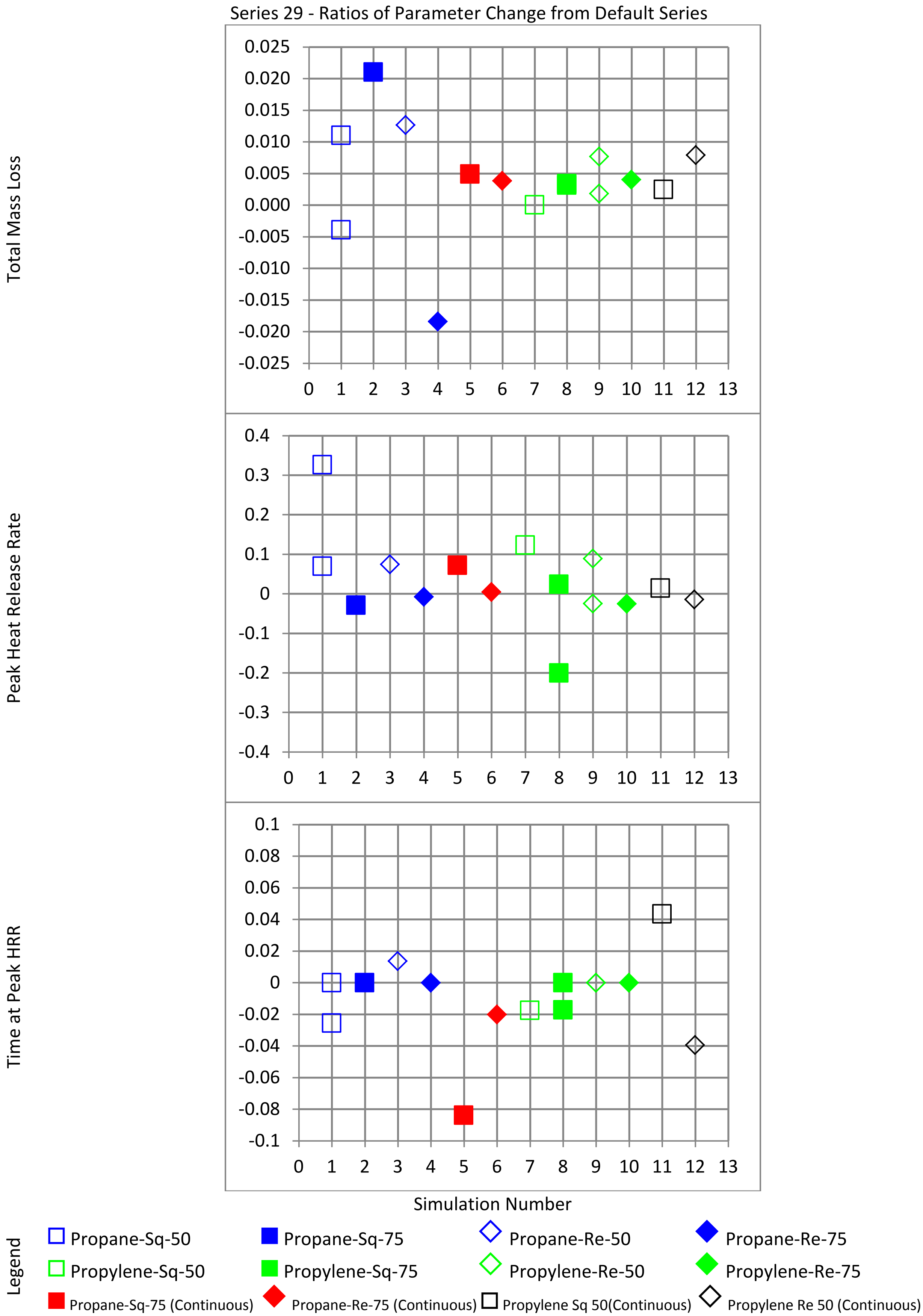
Series 29 - Ratios of Parameter Change from Default Series
Total Mass Loss
Peak Heat Release Rate
Time at Peak HRR
Simulation Number
Legend
Propane-Sq-50
Propane-Sq-75
Propane-Re-50
Propane-Re-75
Propylene-Sq-50
Propylene-Sq-75
Propylene-Re-50
Propylene-Re-75
Propane-Sq-75 (Continuous)
Propane-Re-75 (Continuous)
Propylene Sq 50(Continuous)
Propylene Re 50 (Continuous)

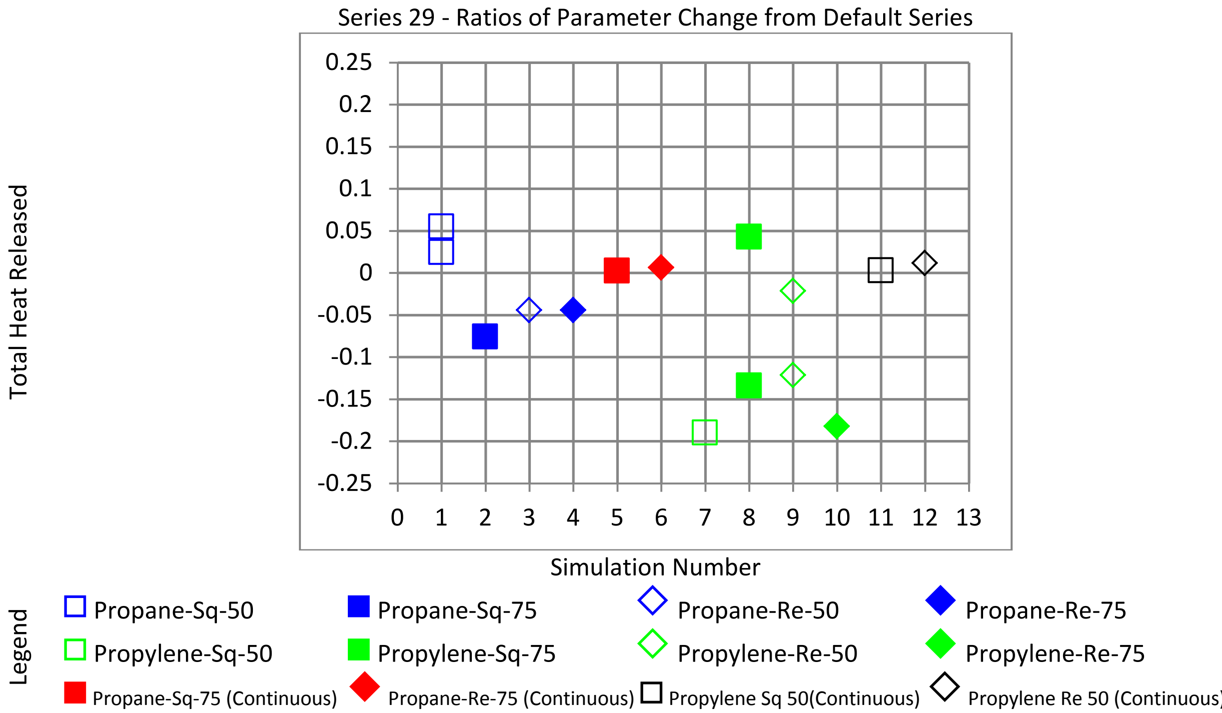

The CFL_MAX parameter controls the time step size used in a FDS simulation, at each time step, a CFL (Courant-Friedrichs-Lewy) number was calculated, and if the number is outside of the range set forth by the minimum and the maximum CFL constraints, then the time step size is adjusted. By increasing the CFL_MAX parameter from 1 to 2, the range was increased, allowing more flexibility in the time step size calculation, but might increase the chances for numerical instability.

Observations

Total mass loss changes were mostly positive, except for two cases simulating a propane source fire. There appears to be a large difference in quantity change based on burner shape for propane at the higher source fire HRR, where the Square burner case had a positive change but a negative change for the case with a Rectangle burner.

For the peak HRR, it is shown that most of the changes were positive, and that the magnitude of change is greater for the simulations using Squre burner and the lower HRR at 50 kW.

Changes in the time to peak HRR weresmall for all of the simulaitons with a terminatedsource fire. The changes recorded in the cases with a continuous fire where largest for the ones using the Square burner. However, the changes where opposite based on the source fuel used.

In term of THR, the changes for the simulations with a continuous source fire were the smallest, and it appears that the magnitude of changes were more significatn for all simultions using a propylene source fire than those using a propane source fire.

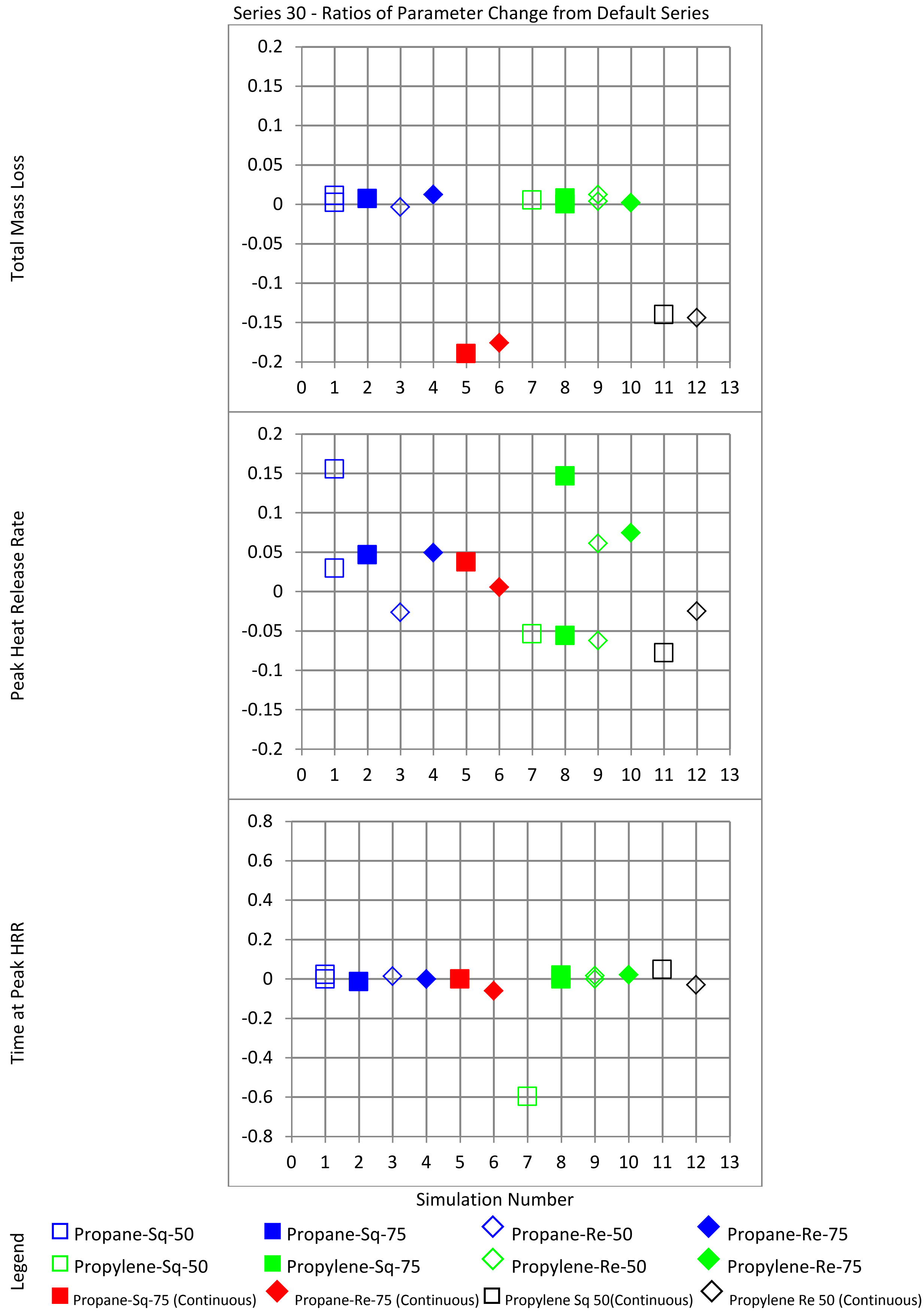
Series 30 - Ratios of Parameter Change from Default Series
Total Mass Loss
Peak Heat Release Rate
Time at Peak HRR
Simulation Number
Legend
Propane-Sq-50
Propane-Sq-75
Propane-Re-50
Propane-Re-75
Propylene-Sq-50
Propylene-Sq-75
Propylene-Re-50
Propylene-Re-75
Propane-Sq-75 (Continuous)
Propane-Re-75 (Continuous)
Propylene Sq 50(Continuous)
Propylene Re 50 (Continuous)

Series 30 - Ratios of Parameter Change from Default Series

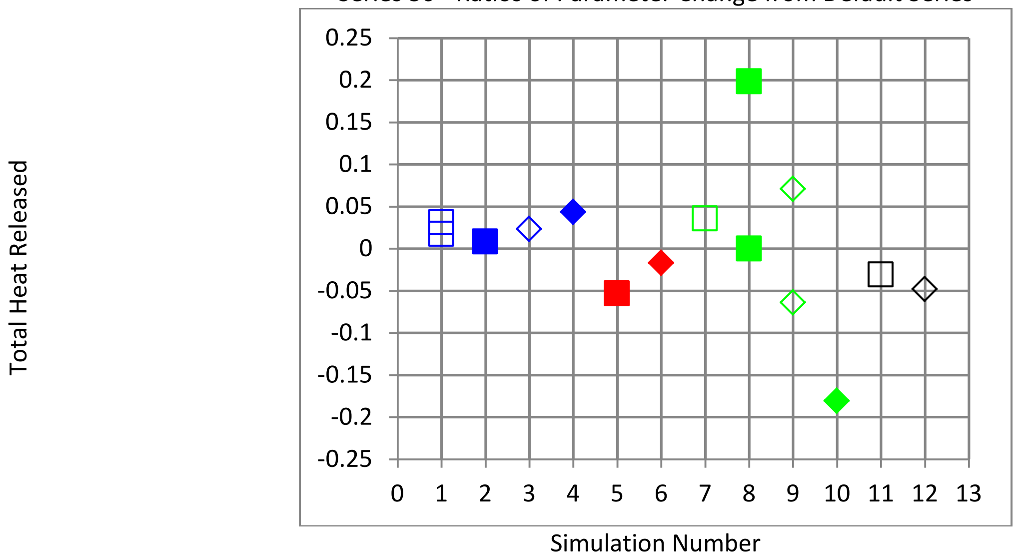

Legend

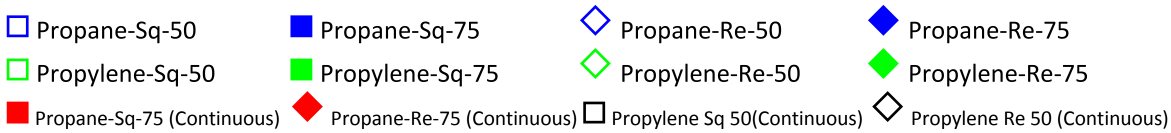

Observations

By decreasing the CFL_MIN parameter from 0.8 to 0.4, the range was increased, allowing more flexibility in the time step size calculation, but might increase the chances for numerical instability.

The parameter changed had little effects on the total mass loss for the simulations using a termainted source fire, but it reduced the mass loss for the simulations with a continuous source fire. The magnitude of the changes appear to more significant at the higher HRR of 75 kW.

Changes in the peak HRR appear to be quite random, as evident by the large differences in the changes for the simultions with similar scenarios. Simulations with the propane source fires were mostly positive whereas the changes for the propylene were in both directions.

The time to peak HRR were not changed significantly for all of the simulations except for the simulation with a terminated propylene source fire with a Square burner at 50 kW where the time to peak was reduced by 60% from the default.

For the THR, the changes to the simulations with propane were smaller than the cases for the propylene source fire. For propane simultions with a termianted source fire, the changes were slightly positve, where as for propylene the changes were in both directions, and more significant than the porpane changes. Changes for the simulations with a continuous source fire were slightly negative at approximately -5%.

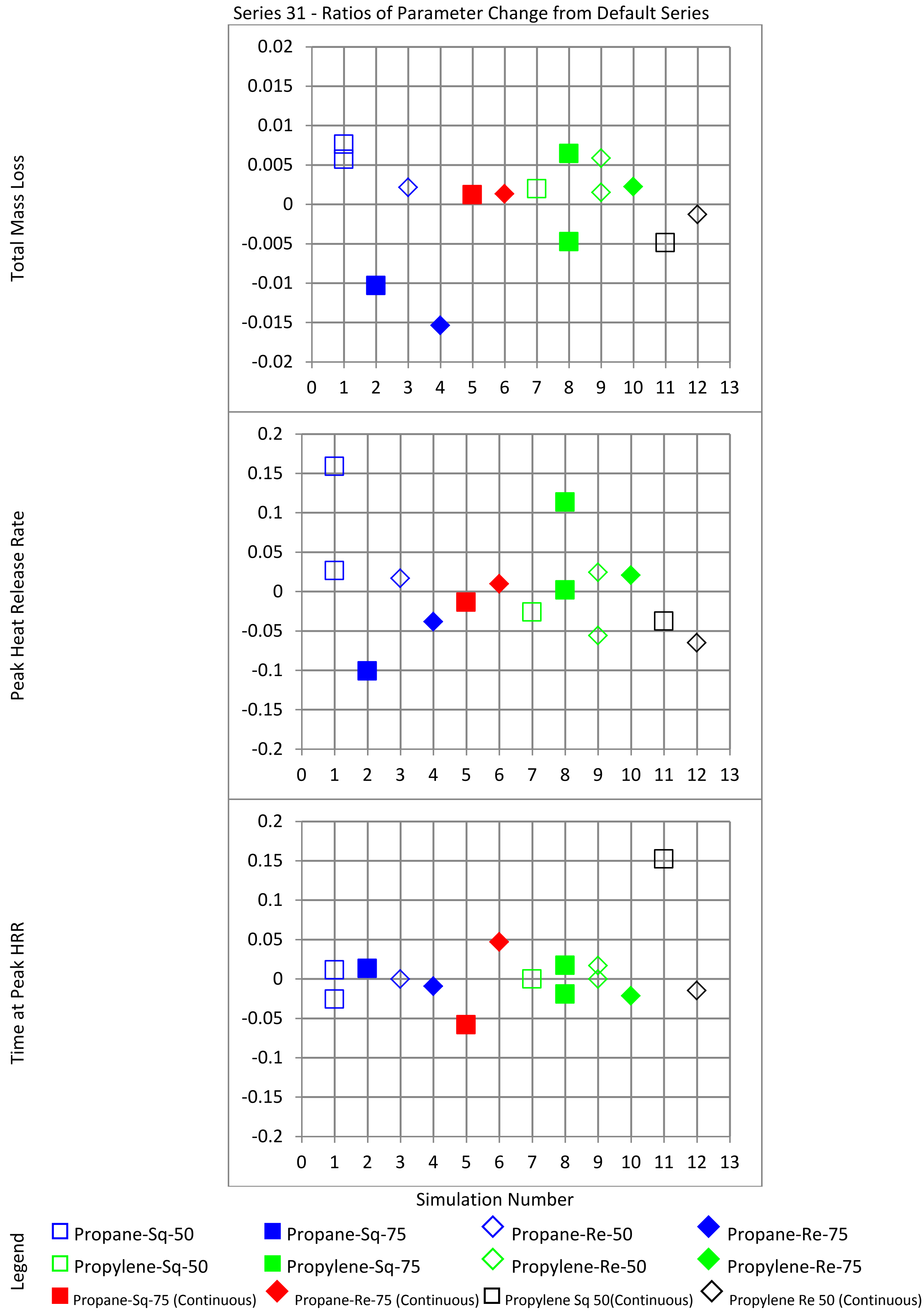
Series 31 - Ratios of Parameter Change from Default Series
Total Mass Loss
Peak Heat Release Rate
Time at Peak HRR
Simulation Number
Legend
Propane-Sq-50
Propane-Sq-75
Propane-Re-50
Propane-Re-75
Propylene-Sq-50
Propylene-Sq-75
Propylene-Re-50
Propylene-Re-75
Propane-Sq-75 (Continuous)
Propane-Re-75 (Continuous)
Propylene Sq 50(Continuous)
Propylene Re 50 (Continuous)

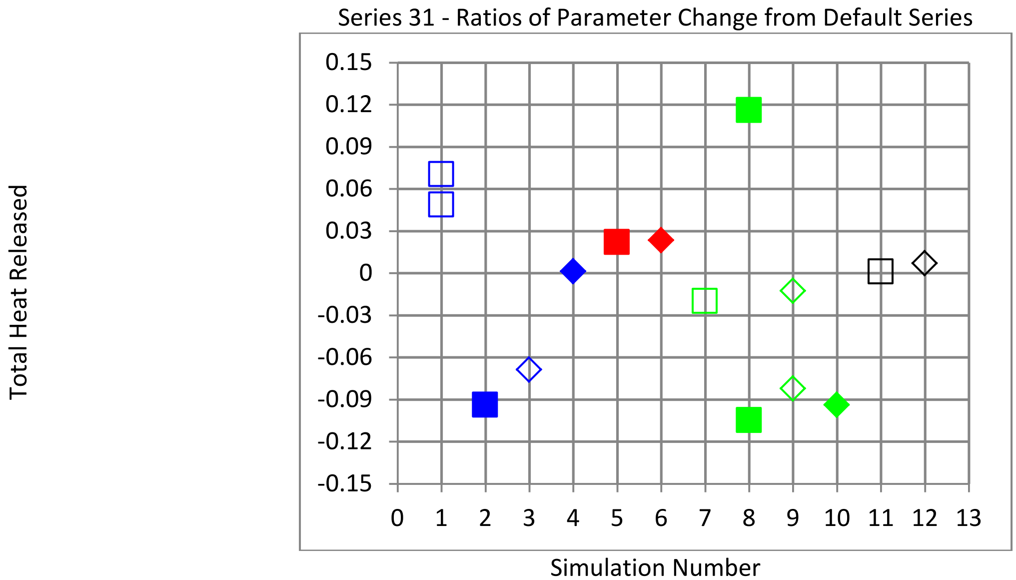

Legend

Propane-Sq-50 | Propane-Sq-75 | Propane-Re-50 | Propane-Re-75
Propylene-Sq-50 | Propylene-Sq-75 | Propylene-Re-50 | Propylene-Re-75
Propane-Sq-75 (Continuous) | Propane-Re-75 (Continuous) | Propylene Sq 50(Continuous) | Propylene Re 50 (Continuous)

Observations

In Series 31, the range between the max and min CFL was further increased to 2 and 0.4, respectively, to test their effects.

Changes for the simulations with a termianted propane fire were slightly positive for the lower HRR source fire, but negative for the higher HRR source fire. For the terminated propylene fire simulations, however, the changes were in both direction and less significant in magnitude than the propane cases. It is observed that the simulations with a continuous propane source fire had slightly positive changes, but slightly negative changes for the continuous propylene source fire.

For the peak HRR, the changes for the simulations with a termianted propane fire were slightly positive for the lower HRR source fire, but negative for the higher HRR source fire. For the terminated propylene fire simulations, however, the changes were mostly positive and less significant in magnitude than the propane cases. It is observed that the simulations with a continuous propane source fire had slight changes from the default values.

Time to peak HRR changes were small for the all of the simulations with a terminated source fire regardless of the source fuel used. For the simulations with a continuous proapane source fire, the change was negative where a propane burner was used, and negative when a Rectangle burner was used. However, the opposite was true for the simulations with a continuous propylenesource fire.

THR changes were more random , and mostly negative for all combustible wall simultions.

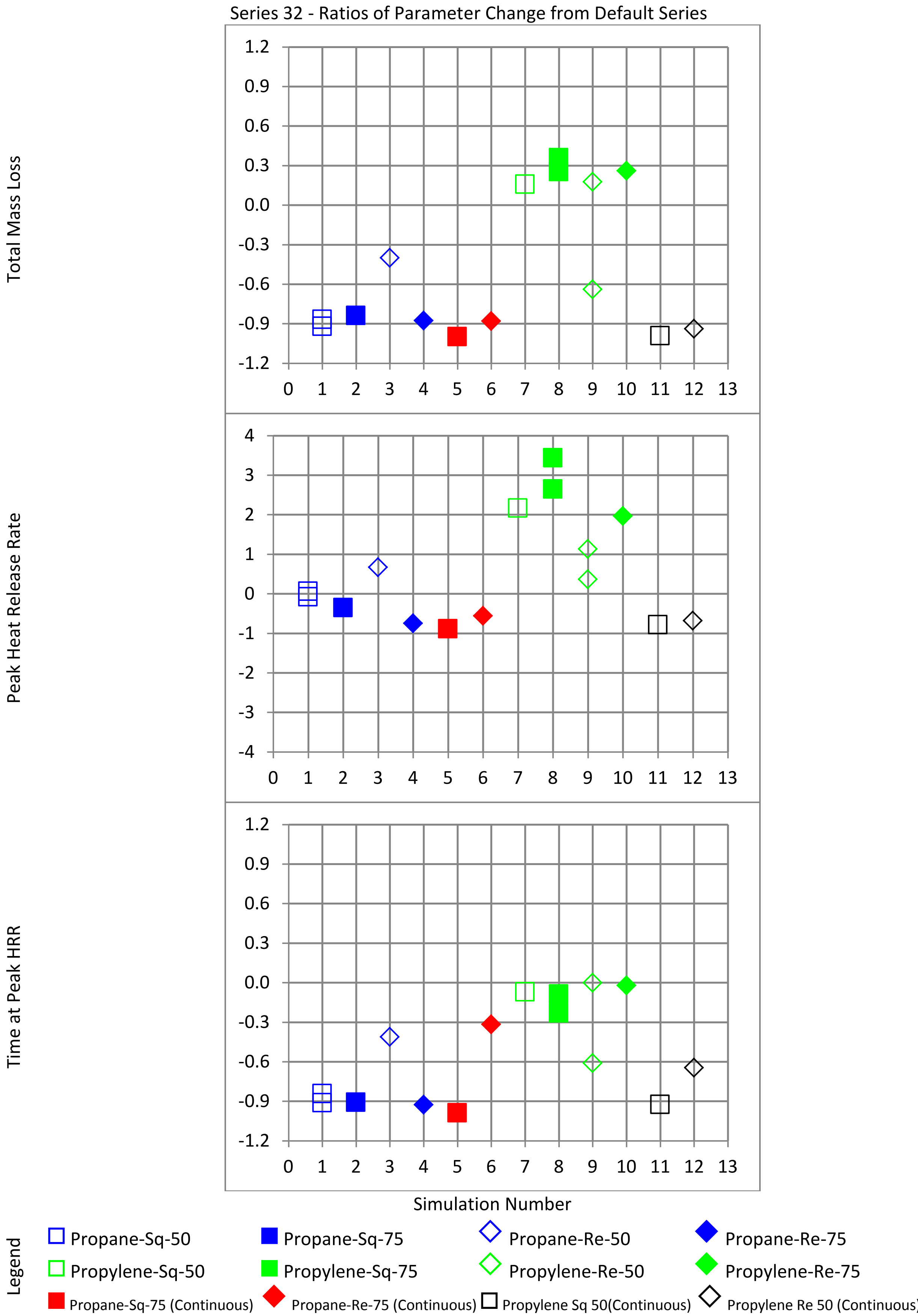
Series 32 - Ratios of Parameter Change from Default Series
Total Mass Loss
Peak Heat Release Rate
Time at Peak HRR
Simulation Number
Legend
Propane-Sq-50
Propane-Sq-75
Propane-Re-50
Propane-Re-75
Propylene-Sq-50
Propylene-Sq-75
Propylene-Re-50
Propylene-Re-75
Propane-Sq-75 (Continuous)
Propane-Re-75 (Continuous)
Propylene Sq 50(Continuous)
Propylene Re 50 (Continuous)

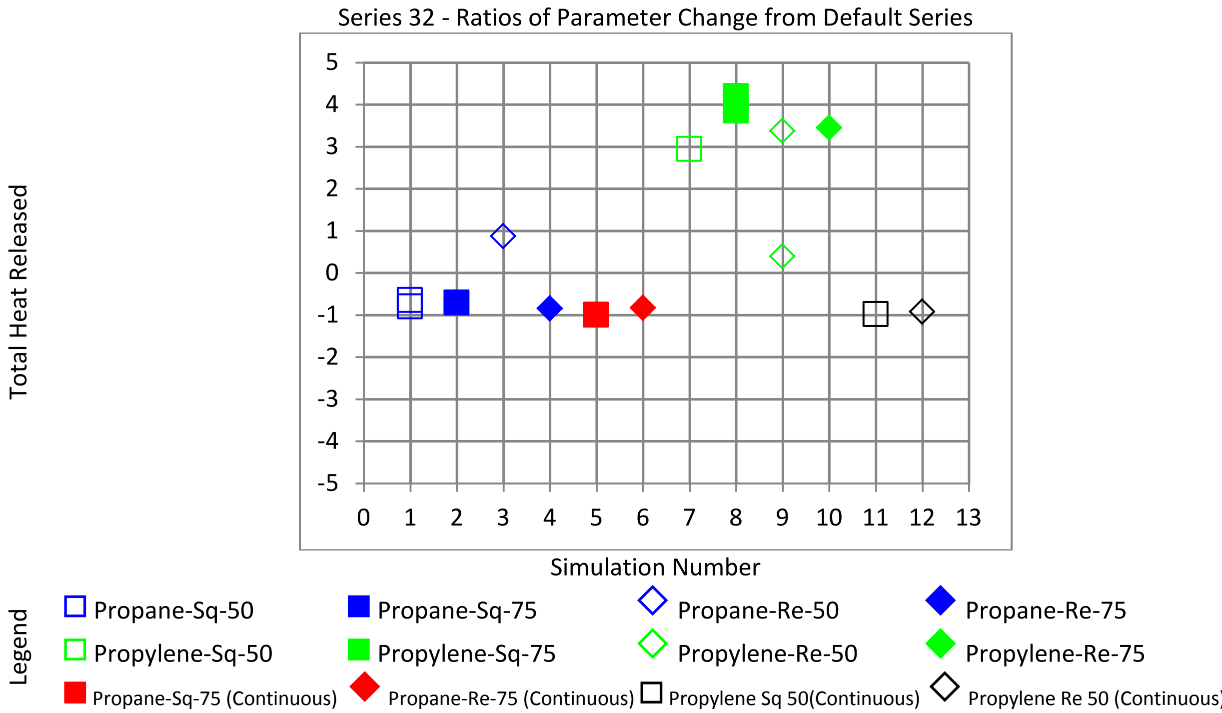

Observations

The FLUX_LIMITER parameter is a FDS6 parameter that changes the way the finite difference calculations are set up. The FDS default is to use a central differencing method with boundedness correction applied if the scalar goes out of the range between 0 and 1. In Series 32, flux limiter is set to 2, which uses the Superbee scheme, suitable for LES simulations.

The simulations in this series of parametric study all crashed due to numercial instability, so the changes recorded were mostly futile. The simulation crashes suggest that the FDS's default setting for the FLUX_LIMITER paramer may be more appropriate.

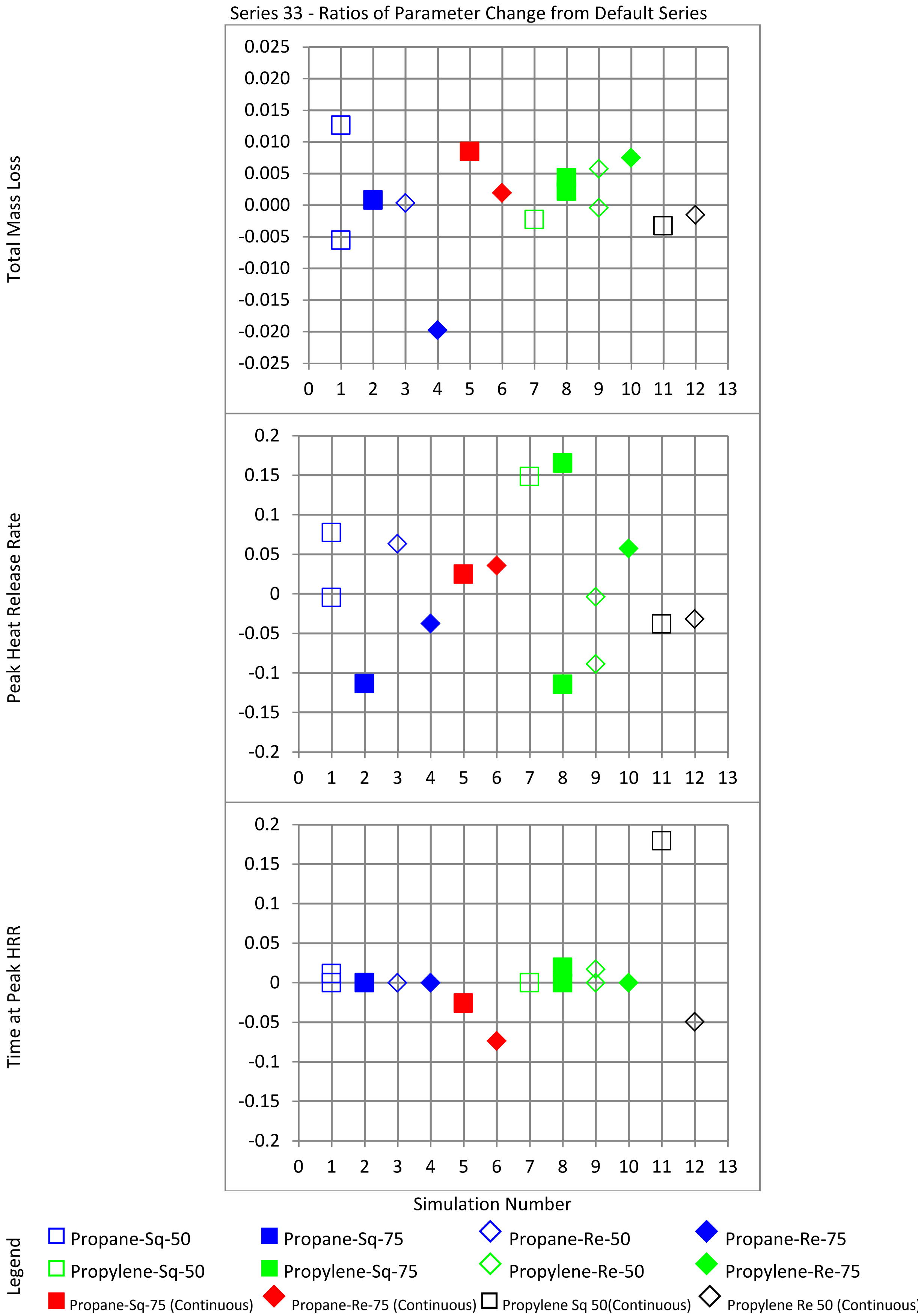
Series 33 - Ratios of Parameter Change from Default Series
Total Mass Loss
0.025
0.020
0.015
0.010
0.005
0.000
-0.005
-0.010
-0.015
-0.020
-0.025
0 1 2 3 4 5 6 7 8 9 10 11 12 13
Peak Heat Release Rate
0.2
0.15
0.1
0.05
0
-0.05
-0.1
-0.15
-0.2
0 1 2 3 4 5 6 7 8 9 10 11 12 13
Time at Peak HRR
0.2
0.15
0.1
0.05
0
-0.05
-0.1
-0.15
-0.2
0 1 2 3 4 5 6 7 8 9 10 11 12 13
Simulation Number
Legend
Propane-Sq-50
Propane-Sq-75
Propane-Re-50
Propane-Re-75
Propylene-Sq-50
Propylene-Sq-75
Propylene-Re-50
Propylene-Re-75
Propane-Sq-75 (Continuous)
Propane-Re-75 (Continuous)
Propylene Sq 50(Continuous)
Propylene Re 50 (Continuous)

Series 33 - Ratios of Parameter Change from Default Series

Total Heat Released

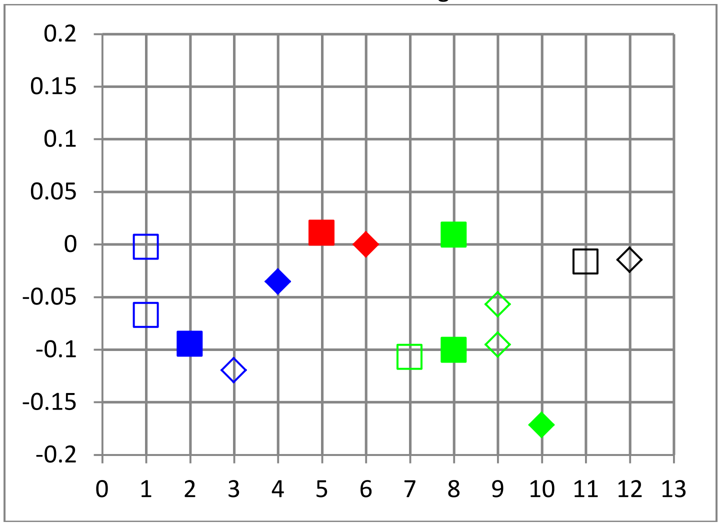

Simulation Number

Legend

Propane-Sq-50 | Propane-Sq-75 | Propane-Re-50 | Propane-Re-75
Propylene-Sq-50 | Propylene-Sq-75 | Propylene-Re-50 | Propylene-Re-75
Propane-Sq-75 (Continuous) | Propane-Re-75 (Continuous) | Propylene Sq 50(Continuous) | Propylene Re 50 (Continuous)

The CFL_VELOCITY_NORM parameter is a FDS6 parameter that controls the time step sizing. The use of CFL_VELOCITY_NORM=2 in the Series 33 simulations makes the time step sizing more restrictive than the default.

Observations

Simultions of the termainted propane fire incurred random changes in the total mass loss, however, the changes were positive for simulations with the propylene source fire. The trends were different for the simulations with the continuous source fire, with positive changes for the continuous propane simulations, and negative for the continuous propylene simulations. It is also noted that the changes for simulations for propane source fire were generally greater in magnitude than the for propylene.

For the peak HRR, the changes were positive for the lower HRR and negative for the higher HRR in simulations of terminated propane sourc fire. Changes for the simulations with terminated propylene source fire were higher in magnitude and in both directions. Changes observed in the continuous propane source fire were positive, but negative for propylene source fire.

Changes in the time to peak HRR were insignificant for all simulations with a terminated source fore. For the simulations with a continuous soruce fire, the changes were negative, excpet for the case with a propylene source fire with a Square burner at 50 kW.

THR was generlaly reduced due to the parameter change., with the magnitude of change greater for the propylene than for the propane simulations with a temrinated source fire. Simulations with the continuous source fire had very slight changes in THR.

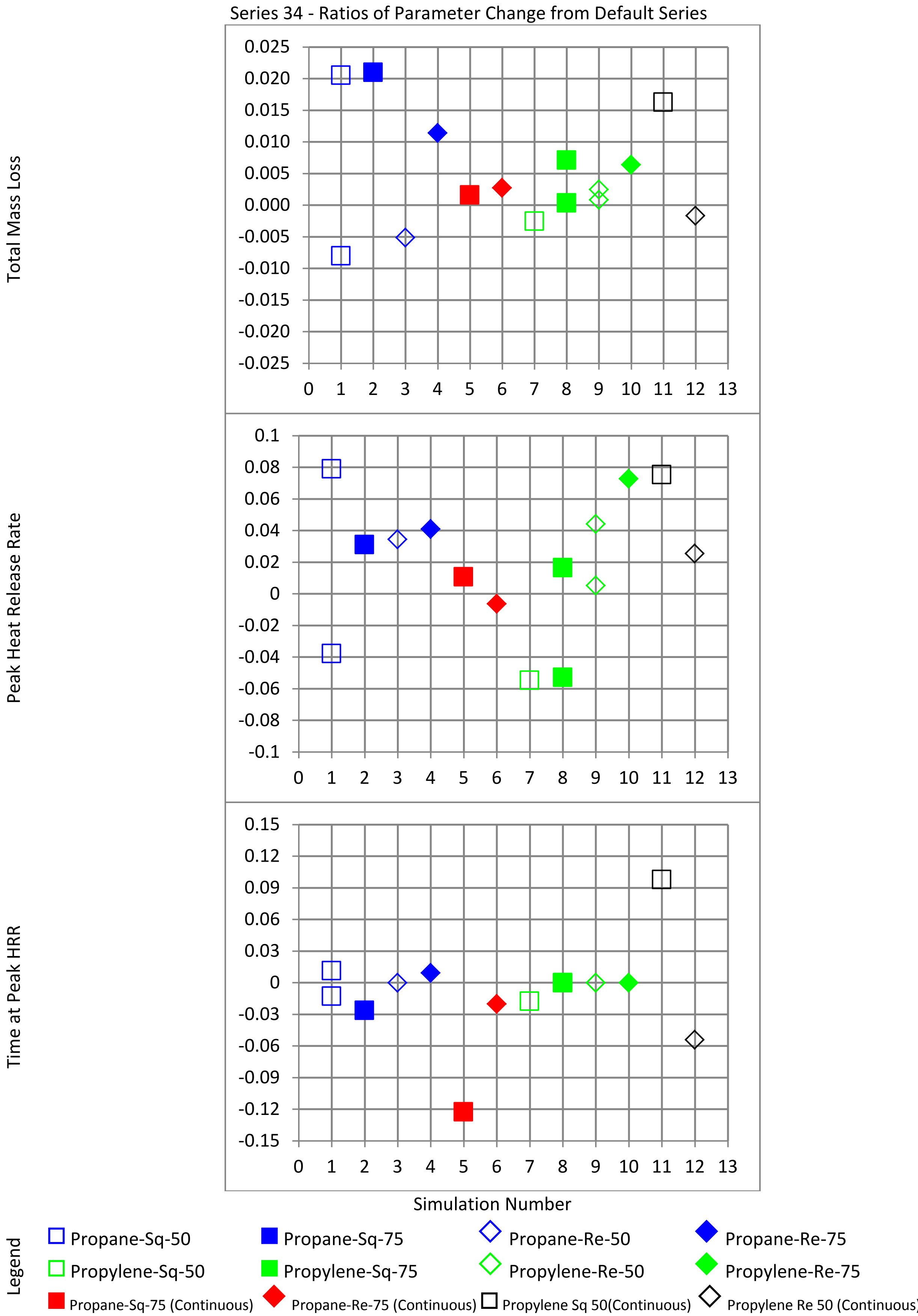
Series 34 - Ratios of Parameter Change from Default Series
Total Mass Loss
0.025
0.020
0.015
0.010
0.005
0.000
-0.005
-0.010
-0.015
-0.020
-0.025
Peak Heat Release Rate
0.1
0.08
0.06
0.04
0.02
0
-0.02
-0.04
-0.06
-0.08
-0.1
Time at Peak HRR
0.15
0.12
0.09
0.06
0.03
0
-0.03
-0.06
-0.09
-0.12
-0.15
0 1 2 3 4 5 6 7 8 9 10 11 12 13
Simulation Number
Legend
Propane-Sq-50
Propane-Sq-75
Propane-Re-50
Propane-Re-75
Propylene-Sq-50
Propylene-Sq-75
Propylene-Re-50
Propylene-Re-75
Propane-Sq-75 (Continuous)
Propane-Re-75 (Continuous)
Propylene Sq 50(Continuous)
Propylene Re 50 (Continuous)

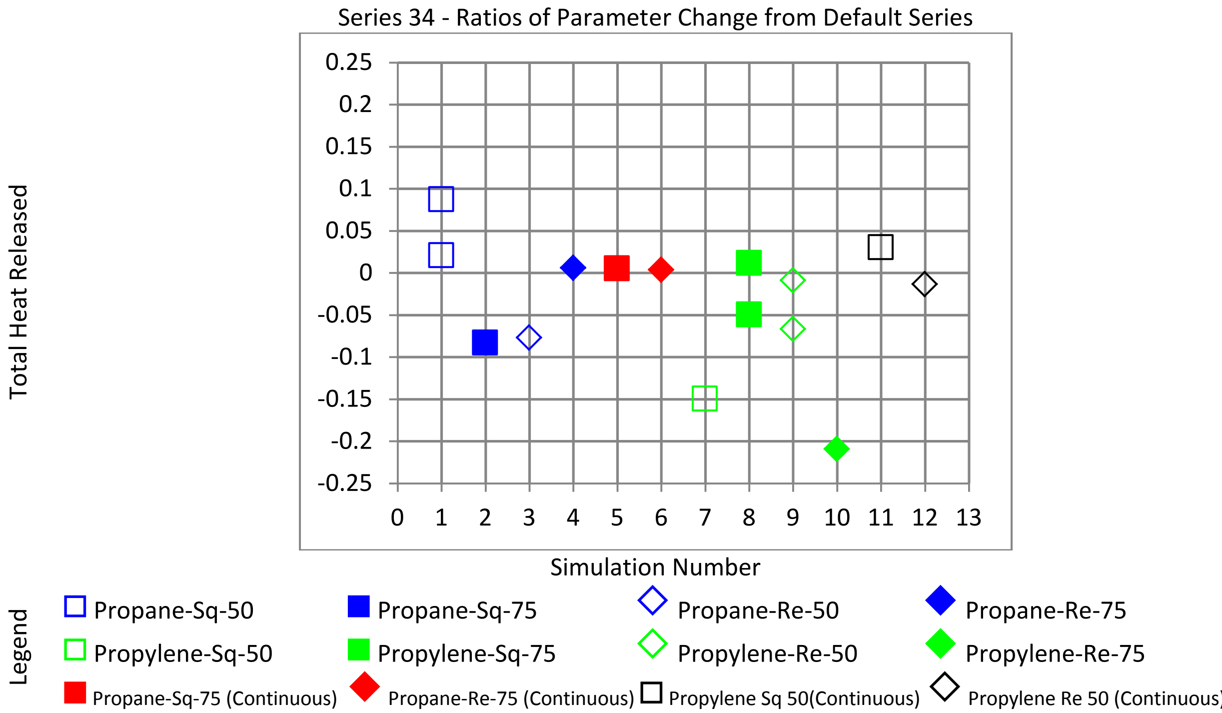

Observations

The CFL_VELOCITY_NORM parameter is a FDS6 parameter that controls the time step sizing. The Use of CFL_VELOCITY_NORM=0 makes the time step sizing less restrictive than the default.

Changes in the total mass loss appear to be mostly positive, but highly random in the simulations of this series, as evident by the large range of values between changes recorded in tests of identical scenarios. It may be observed that the changes were grater in magnitude for simulations using propane as source fuel than propylene. Although the magnitude of the greatest changes was still small at approximately 2%, so quite insignificant.

For the peak HRR, the changes were highly random, but mostly positive for simulations of propane source fuel, whereas the changes were both postivie and negative when tests with propylene source fuel were simulated. The mangnitude of changes were not affected by fuel type significantly.

In term of the time to peak HRR, the changes were small for the simulations using a terminated source fire. However, for the simulations with a continuous source fire, the changes were greater in magnitude.

Changes in the THR predicted were mostly negative or for alll simulations except those with a terminated propane fire with a Square burner at 50 kW., the magnitude of changes were greater in propylene simualtions than in propane simulations.

Series 35 - Ratios of Parameter Change from Default Series

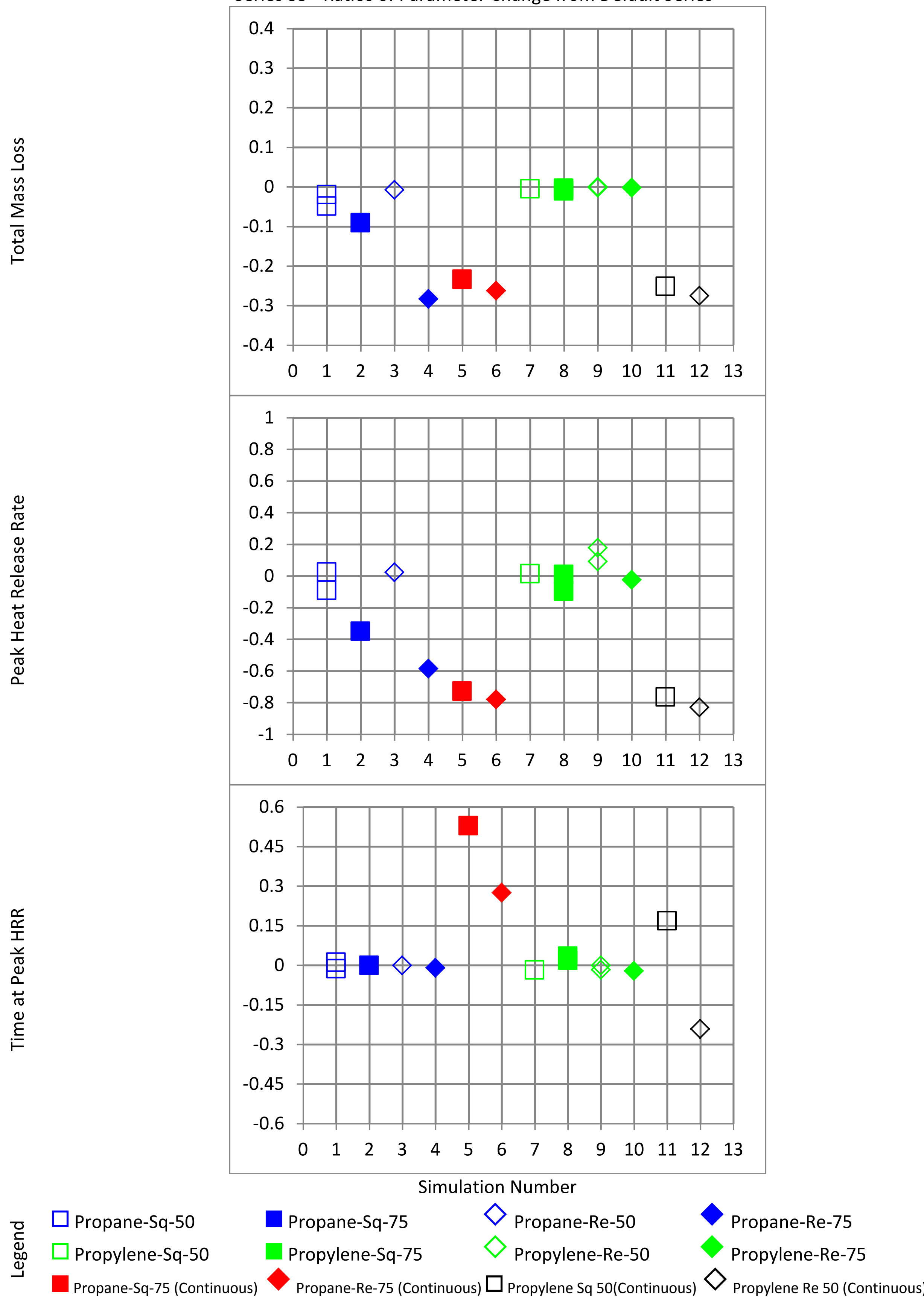

Total Heat Released

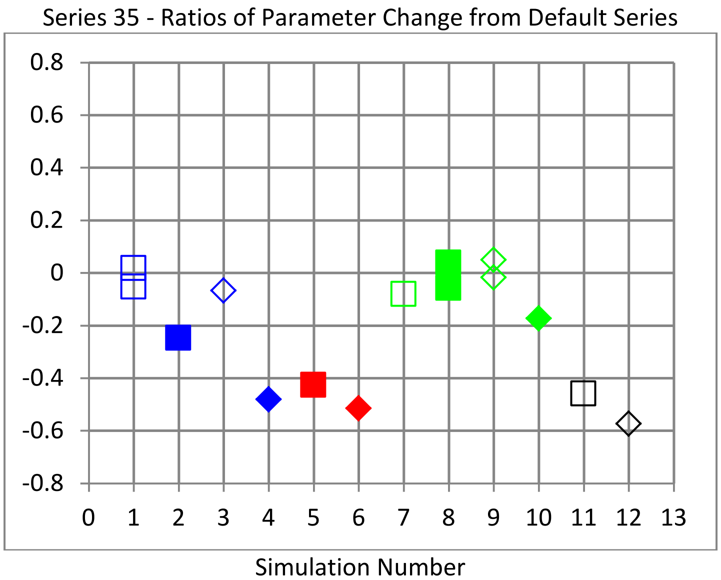

Legend

Propane-Sq-50 | Propane-Sq-75 | Propane-Re-50 | Propane-Re-75
Propylene-Sq-50 | Propylene-Sq-75 | Propylene-Re-50 | Propylene-Re-75
Propane-Sq-75 (Continuous) | Propane-Re-75 (Continuous) | Propylene Sq 50(Continuous) | Propylene Re 50 (Continuous)

Observations

When the H_EDDY parameter is disabled in Series 35 simulations, the FDS default convective heat transfer model is used instead of the turbulent convective heat transfer model.

Changes in the total mass loss for most of the simulations of a termianted source fire were quite small. Greater reduction in the mass loss was noted for all simulations of a continuous source fire regardless of source fuel, burner size, and source HRR.

Trends similar to those in the total mass loss deviaitons were noted in the changes in the peak HRR, except that the magnitude of changes were significantly higher.

The parameter change had little effect on the time at peak HRR for simulations where the source fire was termianted during test. For simulations of a continuous fire with propane, and for propylene with a Square burner, the time to peak was lengthened, whereas the time to peak was shortened in the simulation of a continuous propylene fire with a Rectangle burner at 50 kW.

The THR changes correlate well with those noted for the peak HRR.

Appendix N Expanded thesis report

This appendix contains the thesis in an expanded format where additional information and analysis are presented.

Table of Contents of Appendix N

List of Tables

List of Figures

N.1. Introduction

Over the years, fire modeling as a means to investigate material and environmental behaviors in a fire situation has become a necessary tool in the academy and in the industry. Historically, fire testing of materials and products has been the norm for many industries as manufacturers devise new ways to enhance their products while meeting stringent regulations imposed by the government. All manners of materials are tested, and testing protocols range from the bench-scale to the full-scale depending on the end uses. However, fire tests can be cost-prohibitive, especially during research and development when tests of multiple permutations of the products are often needed. Hence, with the advances in computational capabilities brought forth by new software and hardware, manufacturers and engineers are increasingly focusing on fire modeling tools as the replacement for fire tests.

Computational Fluid Dynamics (CFD) fire modeling has been used to simulate large-scale fire development since the mid 1990's. A recent review of the literature suggests that even now there remains considerable uncertainty associated with CFD-based large scale fire development (fire growth) modeling[1]. Comparisons between experimental data and model calculations have been shown to exhibit various amount of discrepancy between different researches.

Traditionally, experimentally-measured heat release rate (HRR) is used by various researchers and engineers as the primary metric against which a fire model's predictive capabilities are judged. However, due to compensating effects, a good correlation between a modeled heat release rate curve and its experimental counterpart does not necessarily mean that the model accurately simulated the physics of fire growth; other parameters must also be considered. A simulation wherein the pyrolysis area is over-estimated but the burning rate is under-estimated could conceivably match the experimental heat release rate if the errors cancel out.

Due to the many coupled factors that contribute to fire growth, it is difficult to identify from fire growth simulations the causes for the varying degree of compatibility between experimental data and simulated results. There are at least four main physical phenomena that contribute to fire development:

1. Turbulent buoyant fluid flow
2. Gas phase kinetics
3. Flame heat transfer to burning and unburned fuel
4. Condensed-phase pyrolysis

These four components of fire development are described in greater details in Section 1.1.1 to Section 1.1.4.

There are some overlap and interactions between these four categories, and they could certainly be expanded, refined, and clarified. However, the salient point is that there exist several isolatable phenomena that together control the fire growth process. The degree to which a CFD model can accurately portray each of these four components individually and cohesively contributes greatly to the accuracy of the modeled results.

In order to understand the effects and interactions of the four components of flame development, data from published fire experiments dealing with the various areas of interest to flame spread were gathered and the experiments were modeled using the CFD software Fire Dynamics Simulator (FDS). FDS was developed by NIST with focus on fire research and engineering applications. These data-mining and preliminary modeling efforts for the preliminary simulations led to the conclusion that there is a lack of comprehensive fire research data in the literature[2]. While the datasets available in the literature are usually of good quality, most experiments only deal with one or two specific components to fire development. There is a wealth of information pertinent to fire plume related data such as plume temperature and velocity; heat flux on wall data that deals with heat transfer, and flame spread data such as burning rate and heat release rate. One may study flame spread by using different sets of research data available in the literature, but this method requires many assumptions and contains some discrepancies. A comprehensive set of data covering all four flame spread components from experiments with different permutations can mitigate these obstacles. Hence, to adequately determine FDS's capabilities for flame spread, there is a need to conduct a series of experiments with a focus on data relevant to all four components of flame spread, and then construct FDS models to test out various faucets of the modeling software and compare the experimental data against simulated results to determine their compatibility.

1.1 Flame spread

Flame spread is a physical phenomenon defined as the process where the fire front advances in air, along surfaces, or through porous solids[3]. It is controlled by a large variety of physical characteristics, constraints, and complex interactions between a fuel and its environment. Some important factors that determine flame spread include the orientation of the fuel, the direction of propagation, dimensions of the fuel, and the thermochemical properties of the fuel[4]. CFD modeling of flame spread have the added obstacles such as computational limitations and the necessary simplification when applying the relevant theories. Because of the complex nature of the fire growth, it is difficult to study this process as a whole using CFD modeling. However, since the theories behind the basic physical phenomena that drive the spread process are well developed individually, it is possible to deconstruct the problem of flame spread into the basic components for in-depth examinations. Four major physical phenomena are identified: fire plume turbulence, gas phase kinetics flame heat transfer, and condensed phase pyrolysis.

Although these components of flame spread can be further reduced into smaller subsets, the four major processes have been intensely studied and are built into the algorithms used in fire modleing. By decoupling these physical phenomena from each other and studying them separately, one could investigate their interactions and improve the accuracy of simulations by making more informed modeling choices.

1.1.1 Turbulent buoyant fluid flow

The fluid flow component of flame spread considers the characteristics of the fire plume and flow field around the plume: such as the velocity, temperature, entrainment, flame height, and dimensions. The fire plume is consisted of the flame zone, the intermittent zone, and the heated buoyant plume[4]. In flame spread, the gravitational and wind properties are important factors that affect the buoyancy of the plume and can determine the direction and velocity of the spread[3]. In a combustible wall situation, the fire plume from the source area burner was changed from its free plume behaviors and shape because of the presence of the wall. The temperature and velocity of the plume, along with its flame height, can affect the flow on the combustible wall and control the flame spread rate and direction.

1.1.2 Gas phase kinetics

Inside the flame and the intermittent zones of the fire plume, combustible gases are mixed with oxygen and undergo chemical reactions that results in combustion and flame sheets. This creates a region with high temperature that provides the energy needed to preheat unburned fuel, ignite pyrolyzed fuel particles, and support further combustion. Gas phase kinetics are characterized by the combustion properties and flame temperature of a fire are intimately related to the thermochemical properties of the burning fuel, such as its heat of combustion, chemical makeup, density, specific, radiative fraction, etc. These properties control the energy stored within the fuel and how it is released during pyrolysis that affect the overall heat transfer.

1.1.3 Flame heat transfer to burning and unburned fuel

During the heating phase, the fuel is heated by the flame mainly through convective and radiative means, although some preheating was driven by the buoyant plume as well, but at a much slower rate due to its lower temperature. The heat transfer between a fire and the fuel also takes into consideration their respective geometries and orientations, which affect greatly the rate and way the fuel is heated. For example, the flame spread in the combustible wall scenario where the burner is placed next the wall will be different in a scenario where the burner is located away from the wall, in the corner, or where the combustible wall cover is concave or convex. With enough energy transferred from a fire to the unburned fuel, pyrolysis and ignition may occur to initiate flame spread.

1.1.4 Condensed phase pyrolysis

The study of condensed phase pyrolysis considers how a solid fuel is pyrolyzed, and then subsequently achieving ignition and spread. In pyrolysis, the high temperature of the fuel causes chemical decompositions of its materials that produce combustion gases and char. The combustible gases are energized by flame and ignited, and as more fuel is consumed, the flame spread to new region of the fuel. As the virgin material is converted to char, the char layer became an insulating layer that protects the virgin layer beneath by slowing the heat insult to the virgin material imposed by the flames. In FDS, these processes are controlled by the pyrolysis models.

1.2 Review of datasets available from the literature

This section presents a short review of datasets available in the literature that contain information on flame spread or its four components. The various datasets have varying amount and types of data that can be categorized and used in the validation of fire and flame spread models. Experiments that generated these data range from the small scale to the large scale. In theory, data from different, but similar experiments may be combined together into a coherent dataset; however, this requires much interpretation and interpolation between the data, which may reduce its accuracy. This highlights the value of a dataset that contains various types of data dealing with the four component of flame spread collected together from a single experiment.

Data presented in scientific papers on flame spread generally consist of information describing two or three components of flame spread. A review of the literature found that researcher generally focused on turbulence and flame heat transfer together, or flame heat transfer together with condensed phase pyrolysis. Some of the turbulence- and flame heat transfer-oriented flame spread experiments are performed by Yan and Holmstedt[5], Peacock et al[6], Shields et al[7], and the USNRC[8]. All of these experiments collected velocity and temperature data around the test compartment and wall surface temperature distribution, while some collected heat flux distribution or flame height data as well. Wu et al[9], Consalvi[10] et al, Mitler and Steckler[11], Ohlemiller et al[12], Ohlemiller and Cleary[13], Brehob et al[14], and Qian et al[15] all reported experimental results dealing with flame heat transfer and condensed phase pyrolysis in the form of heat flux distribution and pyrolysis progression, some of these works also presented wall surface temperature data. Gas phase kinetics data is not widely collected, some works that include flame temperature data include Kokkala et al[16, 17], and Wu et al[18]. Experiments that report three of the four component of flame spread are rarer, with one example being Walmerdahl and Werling's[19] series of flame spread experiments in a model-scale compartment where the interior surfaces are lined with medium density fiberboards and reported temperature and velocity in the room, heat flux distribution and surface temperature, as well as mass loss data. Subsequently, Carlsson[20] reproduced these experiments using CFD modeling. Other flame spread research in the literature has various amounts of data useful for model validation[21-26]. It is noted that PMMA was used in a large percentage of these experiments, most likely due to their availability and well documented burning behaviors. Many of the test configurations used in the aforementioned studies are of that of room lined with combustible wall paneling or a single combustible wall, but in various scales.

Experiments that do not directly report condensed phase pyrolysis usually deal with one component of flame spread, whereas the others collected data of interest in two areas. Turbulence experiments were conducted by researchers[27-36] using both inert and fire plumes, data reported include, to varying degrees, plume temperature and velocity, fluid mixture mass fraction, turbulent kinetic energy contour or profiles, and other turbulent energy information. Experiments that deal with gas phase kinetics, or flame temperature, exclusively include those by Blevins et al[37], de Ris[38], and Hamins et al[39], some other data collected by these researchers include flame velocity, CH chemiluminescence, soot depth, mass loss, and flame heat flux. Flame heat transfer to wall are represented by experiments that characterize a fire's effects on its surroundings, which reports the heat flux to the interior surfaces and the vicinity around a flame; flame height, gas temperature and velocity in the compartment are also recorded in several instances[40-46].

Pierce and Moss[47], and Nowlen[48] conducted experiments and reported turbulence and flame heat transfer in terms of gas temperature and velocity, as well as heat fluxes to surfaces. Some of the datasets dealing with the two components of flame spread in gas phase kinetics and turbulence include the works by McCaffrey[49], Cox and Chitty[50], as well as Hasemi and Tokunaga[51]; Quintiere and Grove[52] collected data from other researches and derived correlations for fire plumes. These datasets reported flame and plume velocity and temperature as well as velocity and flame height. Of special interest is Tran and Janssens'[53] experiments to model the effects of the burner used in ASTM room fire tests that collected temperature and velocity in the plume and the flame region, as well as wall temperature and heat flux, which covered three components of flame spread sans condensed phased pyrolysis.

1.3 Scope of research

The current flame spread research focuses on a combustible vertical wall scenario where ignition of the wall is achieved with an area burner. This is similar to an upward flame spread test that limits the flame to only spread in one direction/dimension[9]. However, in the current experiments, the combustible wall material was installed on a wall in a compartment with a ceiling, and area burners with a width up to 50% of the combustible wall panel's width were used. Under this configuration, the fire would initially spread upward and outward, then downward upon ceiling impingement, thus achieving a two-dimensional flame spread. This scenario has a basis in reality such as when a trash bin against combustible wall is set on fire, which can ignite the wall material as the fire progresses. In order to study this scenario using the four components of flame spread identified previously, it is necessary to deconstruct the scenario into its fuel: a combustible and thermally-thin wall covering; its environment: a compartment; and its source: an area burner. By analyzing these three elements one by one and in relationship to each other, the underlying flame spread problem can be simplified and studied.

Flame spread is defined by Quintiere as the process where the fire front advances in air, along surfaces, or through porous solids[3]. A solid or liquid fuel must be present and assaulted with enough energy in order to pyrolyze, ignite, and spread. In the current scenario, the combustible wall covering mounted on a vertical wall inside a compartment is heated by a fire and subsequently ignite and spread. The process in which the fuel breaks down and burns is described as a condensed phase pyrolysis. If the fuel is subtracted from this situation, it becomes an inert wall scenario where a fire is transferring its energy onto the wall and raising the wall's temperature. The means and degree to which the wall is energized forms the basis of the flame heat transfer study; and the interaction between the wall and the fire plume can be described by fluid mechanics. Furthermore, if the wall is absent, the fire can be visualized as a free fire plume that burns and projects its energy into an empty surrounding. The behaviors of the fire plume can be defined through its fluid turbulence and combustion characteristics. The deconstruction of a complicated combustible wall fire scenario into these three different sets of experimental configurations will allows in-depth examination of the components of flame spread and collection of a comprehensive set of data.

From simple free fire plume tests to full-scale combustible wall tests, three progressively comprehensive series of tests were designed and carried out. The three series of tests can be viewed as a natural evolution from a free fire plume test with a burner inside a compartment, to an inert wall fire test where the burner was placed against an inert wall, and finally to a combustible wall fire test where the inert wall was covered with a combustible wall panel and ignited with a source fire. Each series of tests deals with certain components of fire development but also expanded upon the last. This tactic allows data relevant for the four specific components of fire development to be collected and then analyzed separately and cohesively, such that their interactions can be isolated and studied. The details of the experimental setup and procedure are presented in Section 2 of this report.

In order to provide comparable datasets, the three series of experiments were conducted using similar configurations that included three fuels (methane, propane, and propylene), two differently shaped and sized burners, and a small range of source fire heat release rates (HRRs). The material used in the combustible wall test series was a commercially available fiber-reinforced plastic. Fire-related quantities such as plume centerline temperature and velocity (turbulent buoyant fluid flow and gas phase kinetics), heat flux to the wall (flame heat transfer to fuel), and HRR were measured at identical locations across all tests. These data were coupled with flame spread specific quantities such as burning area and mass loss (condensed-phase pyrolysis) of the FRP combustible wall panel to provide a complete look at flame spread across all four components of fire development. The complete dataset, which is available as a CSV format, may serve as a basis to which CFD fire simulations can be validated. An analysis of the various experimental data is presented in Section 4.

CFD simulations of the experiments were performed with FDS version 5.7031 on a Linux cluster with parallel processing with OpenMPI 1.5.1 protocol. 12 grids were used in the discretization of the computational space to maximize the speed and performance of the simulations. The models' results were compared with the experimental data collected. In the baseline models, most simulation parameters were set to their program-default values, including the options for FDS6-specific parameters. Detailed descriptions of the FDS simulations are available in Section 3, while comparisons between experimental data and FDS simulation results are presented in Section 5 of this report.

Before the FRP panel was selected as the testing material in the combustible wall fire tests, several different plastic sheets were tested for their compatibility with the current experimental design. The material selection tests are detailed in Appendix A of this report. The procedure to improve velocity measurement in the various fire tests is presented in Appendix B. Methods of radiation correction for the thermocouple readings are detailed in Appendix C. Additional analysis of the data from the plume and inert wall tests are presented in Appendix D. Cone calorimeter test data of all of the thermoplastic and FRP specimens is presented in Appendix E. Summary of the combustible wall test data are presented in Appendix F.

Material properties of the FRP panel reduced from the cone test data were used as inputs in the GPYRO algorithm in order to generate material parameters suitable for use in the FDS simulations; a sensitivity study was carried out to determine the various parameters' effects on the fire simulations, as detailed in Appendix G. A grid sensitivity analysis was also performed on the three types of FDS simulations to determine the effects grid cell sizes have on the simulated quantities, the results are presented in Appendix H. The effects of the predicted HRR based on the heat of reaction parameter used in FDS material specification were examined in a separate study and is presented in Appendix I.

A selection of FDS parameters were systematically changed in order to determine their effect on the different configuration of the simulations, each series of simulated results were compared with the results from the baseline models to investigate the effects form the FDS parameter change. The goal of the simulations was to document a process in which FDS predictions on flame spread related quantities can be improved without changes made to the source code itself. The sample baseline case FDS files are presented in Appendix J, and the FDS parametric studies are presented in Appendices K to M.

N.2. Experimental Setup and Procedure

Three different series of experiments were conducted with the intent to collect various data related to the four components of fire spread. The three series were the fire plume tests, inert wall fire tests, and combustible wall fire tests. Although the three experimental configurations differed significantly, some similarities, such as the source fire HRRs, burner sizes, and measurement locations were preserved across the test series so that data obtained could be compared.

2.1 Test environment and primary conditions

All tests were conducted inside the standard room-testing compartment at WPI's Fire Safety Laboratory with dimensions of 2.4 m wide by 3.6 m long by 2.4 m high. A large scale hood (2.4 m x 2.4 m) was located next to the test compartment and was connected to the Large Oxygen Depletion System (LODS) via a gas sampling line, through which the heat release rate of a fire could be determined using two different methods.

2.1.1 Source fuel gases and delivery system

Three fuels were used in the study: natural gas (methane), propane, and propylene. The natural gas was routed to the lab via a dedicated connection, and is about 90-95% methane. Propane and propylene used in the tests were from vapor-draw bottles provided by an external vender, they were assumed to be at least 99% pure. Although the provided fuel gases had inherent impurities, in subsequent data analysis, it was assumed that the fuel gases were made up of 100% of the primary gases, regardless of their true purity ratings.

Table 1 – Methane (natural gas) fuel gas properties

Methane Property	Value for Methane (CH_4) (CAS Registry 74-82-8)
Molecular weight (MW)	16.04 kg/kmol
Density* (ρ)	0.668 kg/m³
Chemical heat of combustion ΔH_{ch}	49.6 kJ/g
Lower Flammable Limit (LFL)	5.0% Vol.
Upper Flammable Limit (UFL)	15% Vol.
*Measured at NTP, pressure at 1 atm and temperature at 20°C	

Table 2 - Propane fuel gas properties

Propane Property	Value for Propane (C_3H_8) (CAS Registry 74-98-6)
Molecular weight (MW)	44.11 kg/kmol
Density* (ρ)	1.882 kg/m³
Chemical heat of combustion ΔH_{ch}	43.7 kJ/g
Lower Flammable Limit (LFL)	2.1% Vol.
Upper Flammable Limit (UFL)	9.5% Vol.
*Measured at NTP, pressure at 1 atm and temperature at 20°C	

Table 3 - Propylene fuel gas properties

Propylene Property	Value for Propylene (C_3H_6) (CAS Registry 115-07-1)
Molecular weight (MW)	42.08 kg/kmol
Density* (ρ)	1.748 kg/m³
Chemical heat of combustion ΔH_{ch}	40.5 kJ/g
Lower Flammable Limit (LFL)	2.4% Vol.
Upper Flammable Limit (UFL)	11% Vol.
*Measured at NTP, pressure at 1 atm and temperature at 20°C	

For propane and propylene, the gas cylinders were connected to a fuel vaporizer, originally intended for liquefied propane. The vaporizer has a nitrogen gas flush and over-pressure prevention devices. The outlet of the vaporizer is connected to a mass flow controller leading to the burner. The mass flow controller has a range of 0 slpm to 875 slpm also was used to control the source fire size. The flowmeter used by the flow controller also measured and outputted the flow rate to a data acquisition (DAC) system.

For methane, the fuel gas was directly routed from the city line to the burner without passing through the flow controller hence the methane fuel flow rate was not recorded during a test.

2.1.2 Source burners

Two different burners were used in the study: an 1-ft Square and a 2-ft by 1-ft Rectangle burner. Both of the burners were constructed of 6mm welded steel, they were designed with a baffle over the fuel gas inlet on the bottom of the burners to smooth out the flow by providing a low-Reynolds number condition inside the burner volume. An 1 in wide flange made of the same 6 mm steel was welded around the top edges of both burners.

An ½ in thick ceramic fiber blanket (Cerablanket®), manufactured by Thermal Ceramics[57], was installed over each burner's top surface as a diffuser that allowed the fuel gas to flow out evenly at the burner surface. The edges of the ceramic blanket were clamped down by a 6 mm thick frame screwed into the burner's flange. The Cerablanket® blanket was also supported on the bottom by a web made out of some thin galvanized steel wires. During a test, the burner was placed on top of cement blocks, where the top surface of the burner was set to be at 0.4 m above the floor.

2.2 Fire plume experimental setup and procedure

Fire plume experiments were designed to provide data relevant to the fluid dynamics/turbulence and combustion/gas phase kinetics characteristics of fire plumes. Data collected during these experiments include plume centerline temperature, plume centerline velocity, HRR, and flame height. The collected information was adequate for characterization of a fire plume based on established theories and correlations.

All three fuels (methane, propane, and propylene) and both burners were used in the free fire plume tests. In these tests, the burners were located in the room test compartment with at least 1 m to the back wall and about 1.2 m to the walls on the left and right. Plume velocity and temperature measuring probes were mounted on two support rakes made from 80/20 aluminum erectors. Velocity was measured using 10 bi-directional probes and temperature was measured using multiple different sized welded thermocouple wires. The instruments were positioned along the centerline of the burner by long, thin metal strips to allow the rakes to locate sufficiently far away to mitigate their effects on plume entrainment.

Previous experience indicated that adverse flow conditions inside the test compartment can cause the fire plume to be significantly tilted or offseted from the centerline of the burner. To combat this effect, a layer of aluminum bug-screen mesh was installed around the rakes to the front of the burner, and another mesh was installed at the compartment's front opening to the exhaust hood. The meshes sufficiently diffused the flow in and out of the compartment which resulted in more stabilized flame structures.

Figure 1 shows a schematic of the free plume fire test configuration

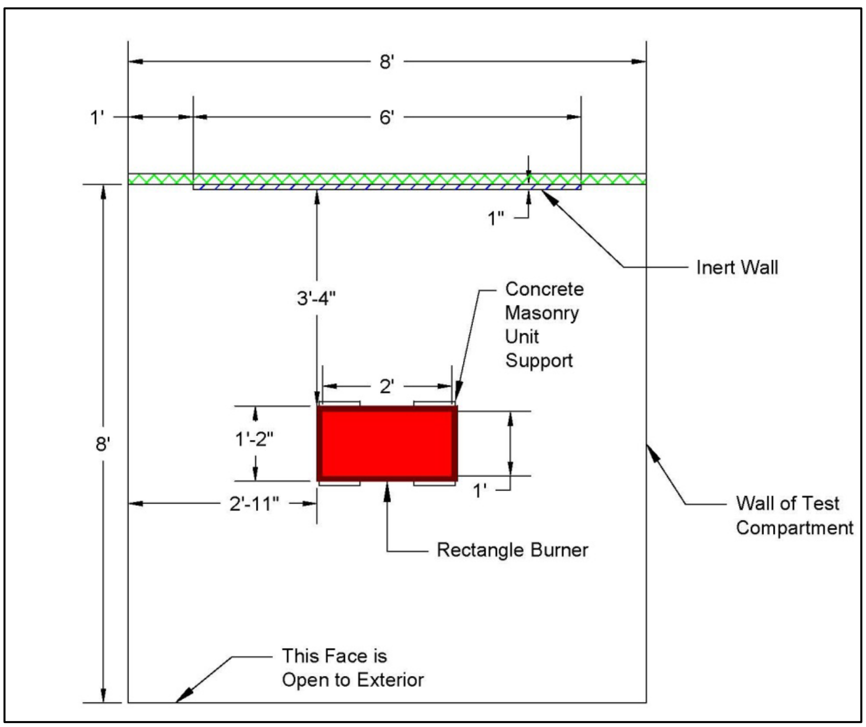

Figure 1 - Free plume fire test configuration - plan view

After burner ignition, each test continued for at least 5 minutes of steady fuel flow so that a quasi-steady state environment may be achieved for data collection. A total of 27 tests were run, and most conditions were repeated at least once. For methane, several tests with HRRs under 100 kW was conducted. For propane and propylene tests, the fires were set to be at either 50 or 75 kW based on fuel flow rates. These HRRs for the propane and propylene tests were chosen based on the Critical Ignition Source Strength (CISS) concept[58, 59], as applied to the FRP specimen used in the combustible wall fire experiments. This is discussed in more detailed in Section 2.4. Table 4 shows the different permutations of the fire plume experiments.

Table 4 - Free plume fire test specifications

Test Name	Source Fire Fuel	Source Fire HRR (kW)	Source Burner Size (ft x ft)
1	Methane	30	1 x 1
2	Methane	50	1 x 1
3	Methane	60	1 x 1
4	Methane	70	1 x 1
5	Methane	75	1 x 1
6	Propane	50	1 x 1
7	Propane	75	1 x 1
8	Propane	50	2 x 1
9	Propane	75	2 x 1
10	Propylene	50	1 x 1
11	Propylene	75	1 x 1
12	Propylene	50	2 x 1
13	Propylene	75	2 x 1

2.2.1 Fire plume temperature measurements

The majority of the centerline temperature measurements were made via 24-AWG thermocouple wires with welded bead-ends at 15 cm intervals. Six Isotherm stations, consisting of three welded thermocouple wires using 20 AWG, 28 AWG, and 30 AWG wires were installed at varying intervals alongside with the 24-AWG thermocouples. The isotherm stations were designed to allow calculations for the radiation correction of the thermocouples. Some of the thermocouples located below a height of 0.8 m over the burner were consisted of pre-fabricated 24-AWG thermocouple with a slightly larger diameter than the welded 24-AWG thermocouple wires. These pre-fabricated thermocouples were protected with a ceramic fiber weave against fire damage; the thermocouple wires elsewhere on the rakes were coated with a fiberglass weave that provides less protection against fire. All thermocouples were manufactured by Omega Engineering, Inc. Figure 2 shows the instrumentation locations on the two rakes.

CENTERLINE RAKE 1 INSTRUMENTATION

	Height above Ground (m)	Height above Burner (m)	Thermocouple	Isotherm
•	2.25	1.85	CTC-7	
•	2.1	1.7	BDTC-6	
•	1.95	1.55	CTC-6	CISO-3
•	1.8	1.4	BDTC-5	
•	1.65	1.25	CTC-5	
•	1.5	1.1	BDTC-4	
•	1.35	0.95	CTC-4	CISO-2
•	1.2	0.8	BDTC-3	
•	1.05	0.65	CTC-3	
•	0.9	0.5	BDTC-2	
•	0.75	0.35	CTC-2	CISO-1
•	0.6	0.2	BDTC-1	
•	0.45	0.05	CTC-1	

CENTERLINE RAKE 2 INSTRUMENTATION

	Height above Ground (m)	Height above Burner (m)	Thermocouple	Isotherm
•	2.1	1.7	PTC-7	PISO-3
•	1.95	1.55	BDTC-10	
•	1.8	1.4	PTC-6	
•	1.65	1.25	BDTC-9	
•	1.5	1.1	PTC-5	PISO-2
•	1.35	0.95	BDTC-8	
•	1.2	0.8	PTC-4	
•	1.05	0.65	BDTC-7	
•	0.9	0.5	PTC-3	PISO-1
•	0.75	0.35	PTC-2	
•	0.6	0.2	PTC-1	

Figure 2 - Rake Instrumentations

All of the thermocouple wires were of K type with Special Limits of Error (SLE) with an uncertainty of ±1°C or 0.4% full scale. The operable range of the K type thermocouples is between 0°C to 1250°C, and given our application to locate the thermocouples inside the hot fire plume, it is assumed that the uncertainty of the thermocouples will be at the higher limit, at 0.4% = 5°C.

2.2.1.1 Radiation correction of thermocouple measurement

The temperature reported by thermocouples in close proximity to a fire may differs from the true gas temperature because they have an actual body and are subjected to radiative and convective heat transfers that are not easily quantified. In this case correction to the temperature measurements should be made. This is achieved by comparing and combining the temperature recorded by the regular 24 AWG thermocouples and the different-sized thermocouples at the six isotherm stations along the plume centerline.

A number of different radiation correction principles had been developed by researchers over the year, such as the one developed by Young, but it was found that Blevins and Pitts' methodology[61] was most suitable for current use. The correction method is described in greater details in Section 4.2.2.1 and in Appendix C.

2.2.2 Plume velocity measurements

One of the simplest and reliable methods of measuring flow velocity inside a fire plume was to use bi-directional probes, originally designed by Heskestad[62]. A total of 10 bi-directional probes were used in the study, they were located from 0.2 m to 1.7 m above the burner at 0.15 m intervals.

In the current study bi-directional probe's design was based on Newman's[63], which was in turn based on Heskestad's design. The design calls for a short, 1" metal pipe (0.5" OD) with a diaphragm that bisects the tube over a circular plane in the middle. A pair of long pipes (12") with small diameter (1/8" OD) were attached and opened to the two halves of the larger cylinder. The bi-directional probes were made out of stainless steel 303 has the dimensions shown in Figure 3. The probe was positioned with an open end perpendicular to the flow; in the current research, the probes were oriented vertically along the centerline of the plume, and the lower section of a probe was designated the front end where the other section was referred to as the back end. The back end of the velocity probe was assumed to remain close to static pressure. When flow was introduced into the front end, it resulted in a pressure difference between the two tail ends of the thinner pipes that was measured with a pressure transducer.

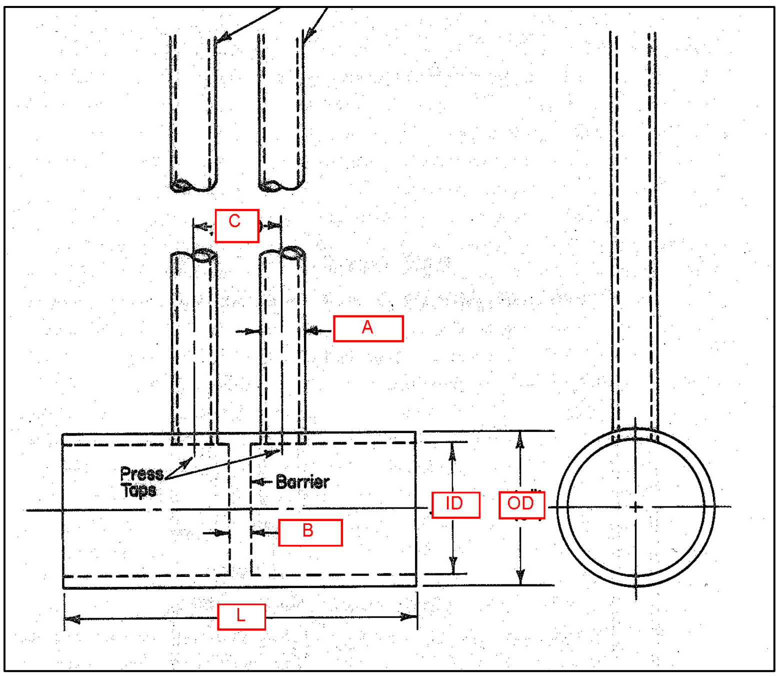

Designation	Dimension	Distance (in)
OD	Outer Diameter	0.5
ID	Inner Diameter	0.428
L	Length	1
B	Barrier thickness	0.071
A	Tube Diameter	0.125
C	Separation	0.286

Figure 3 - Dimensions of a bi-directional probe

The transducers used in the current research were manufactured by Omega Engineering, Inc. and had a range of ±12.5 Pa and a sensitivity of ±1% over 10 V, about 0.1 V[64, 65]. A voltage change from ambient value indicated a flow and a pressure differential. The transducer was connected to the bi-directional probe via a short length of copper tubing (< 1') and Swagelok connectors. Although the instruments were well insulated inside metal casings, high temperature generated during a fire test would offset the transducers. Hence, the ambient pressures before and after a fire tests were averaged over 3 minutes and used to scale the readings during each test. The transducers were connected in series and powered by a variable power supply. Data output from the transducers was provided to the DAC system via shielded wires wrapped in ceramic paper and a ceramic weave sleeve to protect against high temperature.

Heskestad developed a formula to reduce the velocity measurements from pressure data by using equation (1).

$$U = C * \sqrt{2\Delta P / \rho} \quad (1)$$

Where:

$U = Velocity\ [m/s]$
$C = Calibration\ constant$
$\Delta P = Pressure\ differential\ [Pa]$
$\rho = Fluid\ density\ [kg/m^3]$

The calibration constant for Newman's design of the bi-directional probe was determined to be 1.18 during its development. The flow inside the fire plume was assumed to be made up of air only, and the fluid density was determined based on the temperature of the thermocouple installed in the proximity of the bi-directional probe.

The evolution of the velocity measurement method is documented in Appendix B.

2.2.3 Heat release rate measurement

The HRR of the fire in each test was determined in several different ways. In the tests using propane and propylene, since the fuel gases passed through a series of mass flow controller and flowmeter, the flow rates were recorded, and from there the HRR was determined through calculations based on the chemical heat of combustion of the fuel. The HRR could also be determined through oxygen consumption calorimetry based on the oxygen content of the gas sample collected during each test[66-68]. The gas sampling system at the LODS also accounts for carbon monoxide and carbon dioxide (CO/CO_2), which was used to determine HRR based on CO/CO_2 generation rate[67, 68]. The LODS's gas sampling equipment was calibrated prior to a day's tests to ensure the accuracy of the heat release measurements. In the tests using methane fuel, the HRR was determined using the oxygen consumption calorimetry and CO/CO_2 generation calorimetry only since the flow rate of the fuel gas was not recorded. Appendix D shows the derivation of the various HRR methods in more details.

2.2.4 Flame height measurement

Digital video recording of the fire test was recorded by a camcorder located outside of the test compartment. The video was taken at 30 frames per second (fps). In order to analyze the flame height of each test fire efficiently, images were exported from the videos at one image per second and then imported into a motion tracking software. The positions of the flame tips were then tracked manually and the 0%, 10%, 50%, 90% and 100% intermittency flame heights were found; the mean flame height of the fire was recognized at the 50% intermittency flame height. Appendix D contains a detailed summary of the method form flame height tracking.

Table 5 – Fire plume test measurements

Measurement	Instruments used	Locations
Plume centerline velocity	• Bi-directional probes/transducers and thermocouples	10 locations along burner centerline, from 0.2 m, 0.5 to 1.7 m above burner
Plume centerline temperature	• Different gauged thermocouple wires, mostly 24 AWG (20 to 30 AWG wires for radiation correction	13 locations along burner centerline, from 0.05 m to 1.85 m above burner
Source fire heat release rate	• Flow controller (propane/propylene only) • LODS's oxygen consumption (all 3 fuels) • LODS's CO/CO_2 generation (all 3 fuels)	N/A
Flame height	• Digital video camcorder	N/A

2.3 Inert wall experimental setup and procedure

Evolving from the simple free plume fire tests, the inert wall tests dealt with three out of four components of flame spread: fluid dynamics/turbulence, combustion/gas phase kinetics, and heat transfer to environment. The inert wall experiments were very similar to the free plume experiments except that one side of the burner was positioned flush (2 ft side of the Rectangle burner) against the instrumented inert wall rather than located in the middle of the compartment. The same burners, HRR sizes, and fuels from the free plume scenario were used in the inert wall test series, as shown in Table 6. Under this scenario, heat flux to the wall and near-wall temperature measurements were made in addition to the plume-specific and HRR-related measurements.

Table 6 - Inert wall fire test specifications

Test Name	Source Fire Fuel	Source Fire HRR (kW)	Source Burner Size (ft x ft)
1	Methane	70	1 x 1
2	Methane	75	1 x 1
3	Methane	80	1 x 1
4	Propylene	50	1 x 1
5	Propylene	75	1 x 1
6	Propylene	50	2 x 1
7	Propylene	75	2 x 1
8	Propane	50	1 x 1
9	Propane	75	1 x 1
10	Propane	50	2 x 1
11	Propane	75	2 x 1

The inert wall used in the test was constructed of two layers of ½" thick Kaowool®HT ceramic fiberboards [69], two layers of ½" drywalls, and a layer of ½" plywood. The Kaowool® fiberboards were mounted 6' wide by 8' high centered on the 8' wide by 8' high drywall and plywood wall structure at the end of the test compartment. The centerline of the wall aligns with the center of the room and also with the source burner. Heat flux and temperature measuring instruments were installed on the front of the wall through the back.

Figure 4 and Figure 5 show the orientation of the burner in relation to the back wall in the inert wall test configuration.

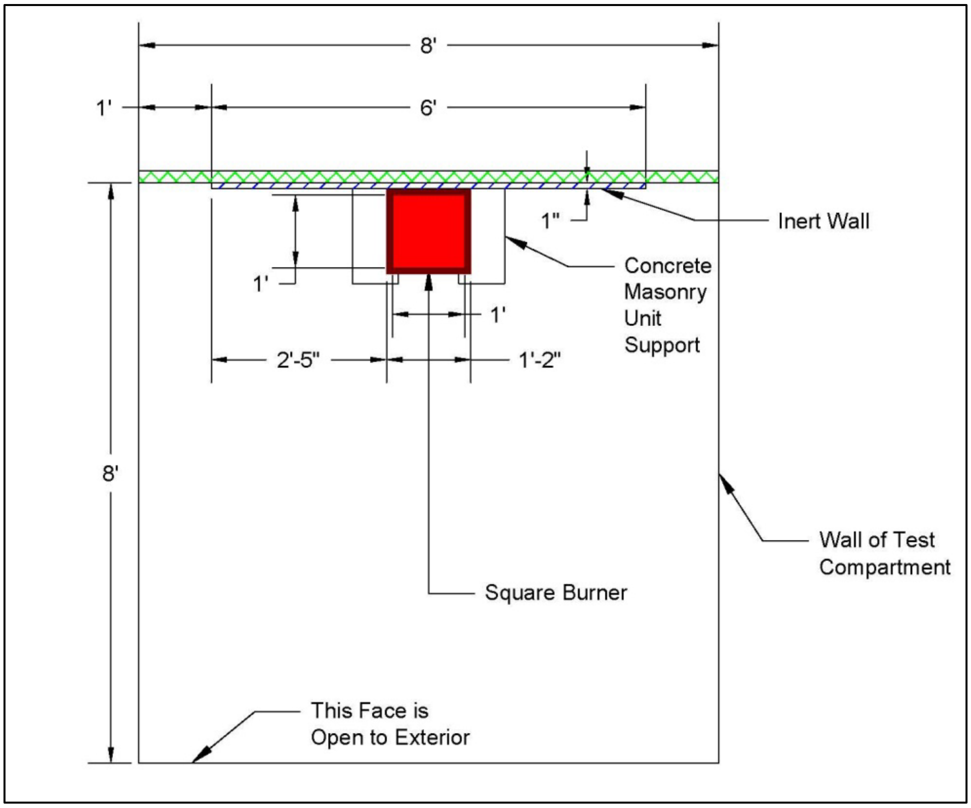

Figure 4 – Inert wall fire test configuration - plan view

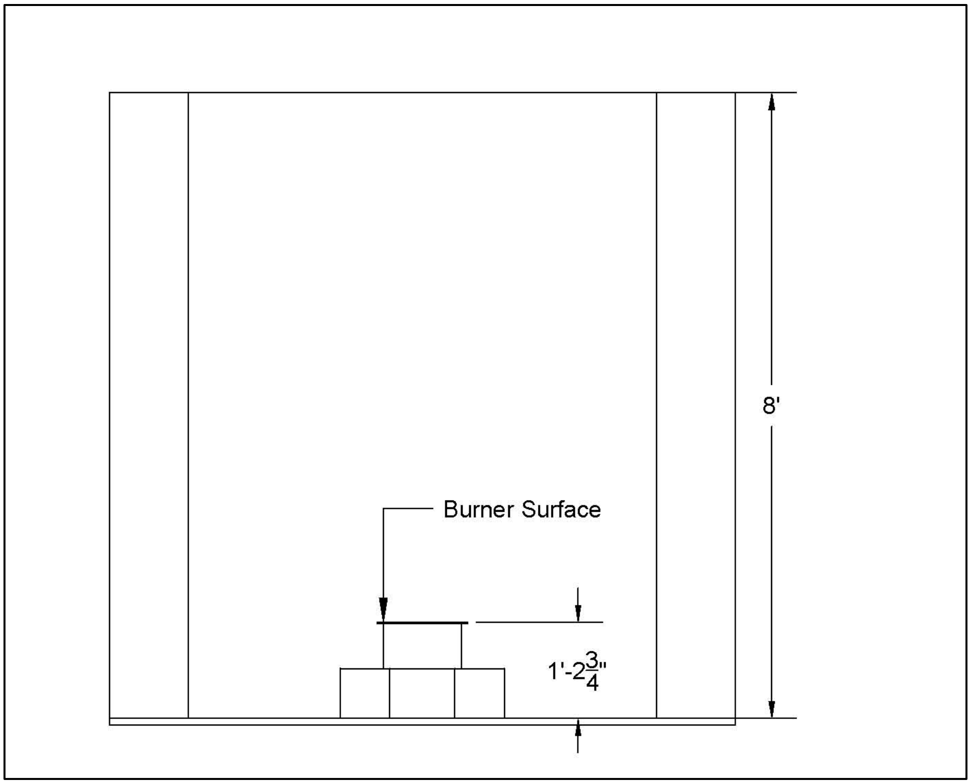

Figure 5 – Inert Wall fire test configuration - front view

Similar to the free plume experiments, the inert wall experiments were allowed to run for at least 5 minutes so that quasi-steady-state conditions may be achieved. Aluminum meshes were kept in place for the inert wall fire tests in order to stabilize the flame structure.

2.3.1 Wall heat flux measurement

Heat flux on the wall was measured using 18 thin-skin calorimeters (TSCs) installed along the centerline, and at 1 ft and 2 ft away on both side of the centerline at 6 different heights. The locations of the TSCs are presented in Figure 6.

Height above Ground (m)	Height above Burner (m)
2.25	1.85
2.1	1.7
1.95	1.55
1.8	1.4
1.65	1.25
1.5	1.1
1.35	0.95
1.2	0.8
1.05	0.65
0.9	0.5
0.75	0.35
0.6	0.2
0.45	0.05

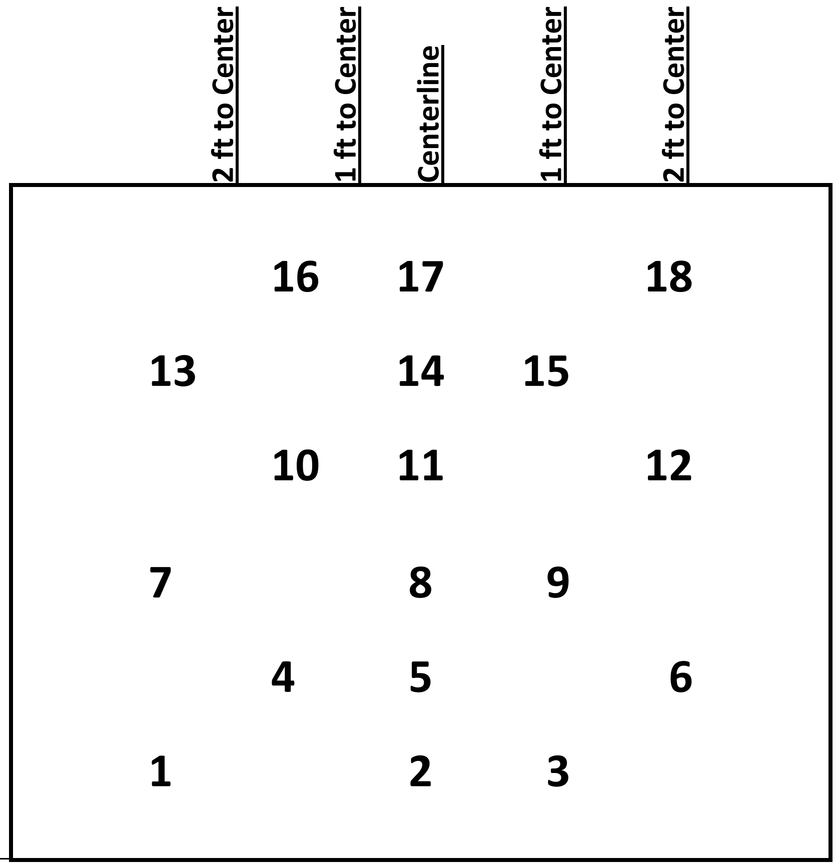

Figure 6 - Thin skin calorimeter locations on wall

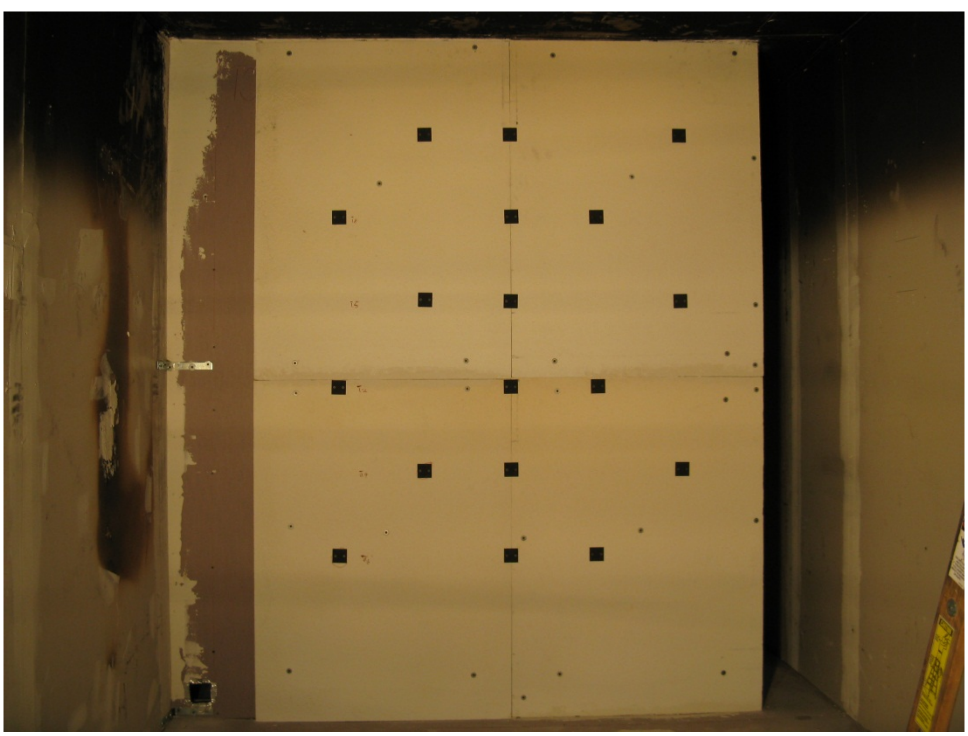

Figure 7 - Inert wall construction showing TSCs and void behind the wall

Each TSC was consisted of a metal plate on top of two insulating substrates, and two AWG 20 thermocouples. The TSCs were constructed in accordance with ASTM E459[70], but instead of separate units, they were installed as part of the inert wall directly, using the wall's top two layers of ½" thick refractory ceramic fiberboards as the substrates.

A nickel based super-alloy, Inconel 718 was used as the "thin skin" of the calorimeter. Inconel 718 is precipitation-hardened and has an eutectoid temperature at about 1000°C, and shows high yield and tensile properties. The properties of the Inconel 718 alloy are presented in Table 7. Each plate was a 5 cm x 5 cm square with two holes for coarse drywall screws to mount the plates onto the surface of the inert wall. A high-temperature rated black paint was applied to the top, exposed surface of the plate, such that the absorptivity of the plate can be assumed to equal to 1. The paint was rated to be resilient against flame and high temperature up to 600°C, it was manufactured by Rustoleum.

Table 7 - Inconel 718 compositions and properties

Alloy	Composition		Applications	Thermal Properties	
Inconel 718	Aluminum	0.2 - 0.8	Gas turbine hot section components and cryogenic storage tanks	Density	8190 kg/m³
	Boron	0.006 max			
Source: [71]	Carbon	0.08 max			
	Chromium	17 - 21		Thickness	1.6 mm
	Cobalt	1 max			
	Copper	0.3 max			
	Iron	Balance			
	Manganese	0.35 max		Specific heat	435 J/kg-K
	Molybdenum	2.8 - 3.3			
	Nickel	50 – 55			
	Niobium	4.75 - 5.5			
	Phosphorus	0.015 max		Thermal Conductivity	11.4 W/m-K
	Silicon	0.35 max			
	Sulfur	0.015 max			
	Titanium	0.65 - 1.15			

An AWG 20 thermocouple wire was welded intrinsically to the center-back of the Inconel plate so that an open thermocouple reading would result for any detachment, rather than false data. Another thermocouple was sandwiched between the two layers of fiberboard insulation substrates. The temperature measured by the two thermocouples was used to calculate the heat flux at the calorimeter's location imposed by the source fire. Figure 8 shows the cross-sectional view of a TSC assembly.

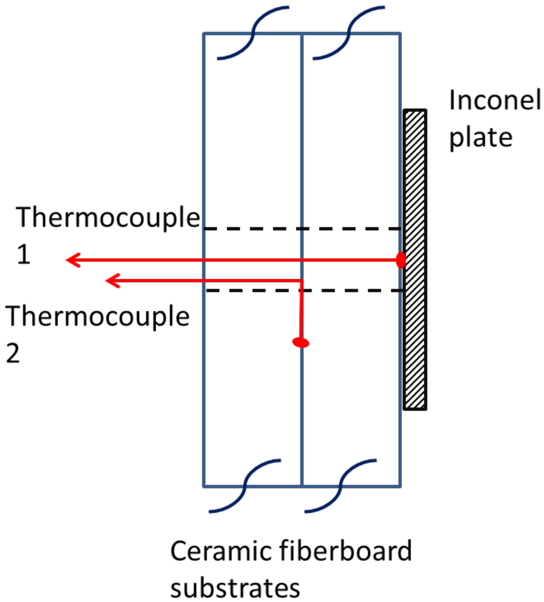

Figure 8 - Cross sectional view of a thin skin calorimeter

2.3.2 Near-wall temperature measurement

Near-wall temperature was measured by welded 20 AWG (0.81 mm) thermocouple wires; they were installed through the back of the inert wall and offseted from the wall's front surface at various distances from 0 mm to 40 mm perpendicular to the wall. A series of 18 thermocouples were used, grouped into 3 groups of six and installed at different heights at 0.35 m, 0.95 m, and 1.55 m from the burner surface. The thermocouples were located at 2.5 cm, 5 cm, and 7.5 cm away from the centerline horizontally and on both side of the center. Table 20 shows the positions of the near-wall thermocouples.

Table 8 - Locations of near-wall thermocouples

		Distance from centerline					
		-7.5 cm	**-5.0 cm**	**-2.5 cm**	**2.5 cm**	**5.0 cm**	**7.5 cm**
		Perpendicular distance from wall [mm]					
Height above burner	**155 cm**	15	20	25	30	35	40
	95 cm	35	30	25	20	15	10
	35 cm	0	5	10	15	20	25

2.3.3 Other inert wall fire test measurements

In addition to the inert wall-related test measurements, during each test, the fuel flow rate was measured by the mass flow controller and recorded (except for methane fuel), gas samples were collected for HRR measurement using oxygen consumption and CO/CO_2 generation methodology, and digital video was taken for flame height analysis.

Table 9 – Inert wall fire test measurements

Measurement	Instruments used	Locations
Plume centerline velocity	• Bi-directional probes/transducers and thermocouples	10 locations along burner centerline, from 0.2 m, 0.5 to 1.7 m above burner
Plume centerline temperature	• Different gauged thermocouple wires, mostly 24 AWG (20 to 30 AWG wires for radiation correction	13 locations along burner centerline, from 0.05 m to 1.85 m above burner
Heat flux to wall	• Thin skin calorimeter, constructed with Inconel plate and a pair of 20 AWG thermocouples	6 at different heights along centerline, 3 at 1-ft , 3 at 2-ft left of centerline, 3 at 1-ft , 3 at 2-ft right of centerline
Near-wall temperature	• Welded 20 AWG thermocouple wire	18 total, in three groups of 6 at three different heights and within 7.5 cm of the centerline
Source fire heat release rate	• Flow controller (propane/propylene only) • LODS's oxygen consumption (all 3 fuels) • LODS's CO/CO_2 generation (all 3 fuels)	N/A
Flame height	• Digital video camcorder	N/A

2.4 Combustible wall experimental setup and procedure

The combustible wall fire test series was the final progression from the simple free plume and inert wall fires test; it allowed a chance to measure data relevant of all four components of flame spread: fluid dynamics/turbulence, combustion/gas phase kinetics, heat transfer to environment, and solid state pyrolysis. The combustible wall experiments were similar to the inert wall experiments except that a piece of combustible wall finish material was installed over the inert wall and subjected to an igniting fire from the source burner. The experiment was designed to maximize measurements most relevant to flame spread along with data describing the initiating fire plume and the associated flame heat transfer process to the combustible material.

The aluminum meshes used in inert wall and free plume tests to smooth out the adverse ambient flow conditions of the test compartment were not used in the combustible wall tests due to safety reasons. As such, the initial fire plumes were not necessary straight and the flame spread may be driven, to a small degree, by this adverse flow.

Only propane and propylene were used as the source fire fuel for the source fires. Both the 1ft Square and the 2ft Rectangle burners were used. A similar concept of Critical Ignition Source Strength (CISS) was used to as a basis to determine the suitable source fire sizes for the combustible wall tests. The CISS is defined as the lowest source fire size that causes flame spared on a combustible material at a rate that would lead to flashover conditions in the compartment[4], which is not desirable in a test environment. To estimate the "CISS" of the FRP specimen, an initial test was conducted using propylene at 100 kW. In this test, the FRP panel was quickly ignited, causing fast flame spread leading to the brink of flashover of the test compartment. In addition to the danger that a flashover poses to the test personnel, it was determined that the short flame spread time, meaning an inadequate amount of data collected, was not advantageous to the goal of this study. So to slow down the initial flame spread, a lower HRR during the initial fire was needed, and HRR at 50 kW and 75 kW were chosen. These HRRs were high enough to ignite the FRP panel readily, but lower than the CISS and provided adequate flame spread time.

Figure 9 presents a schematic of the combustible wall fire test configuration.

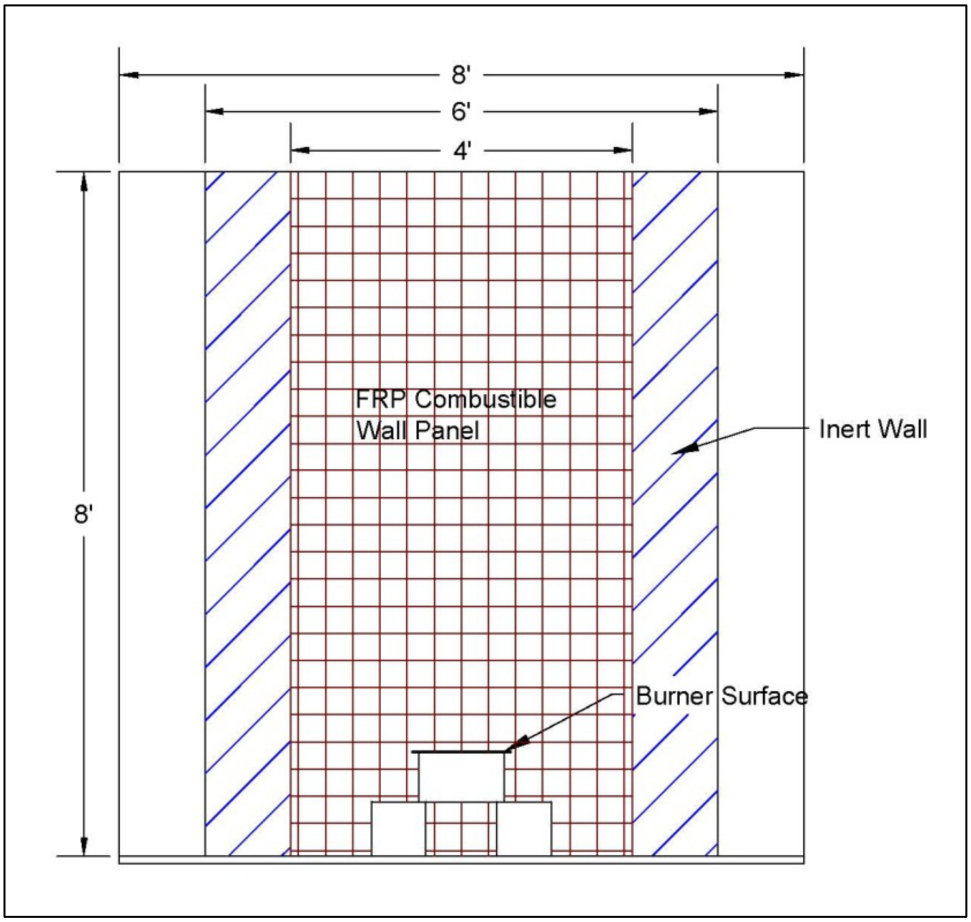

Figure 9 – Combustible wall fire test configuration - front view

Two different types of tests were run, one where the initiating fire was snuffed upon panel ignition, and another type where the initial fire had a constant HRR throughout the test, as shown in Table 10. The first test configuration (type 1) imitated a small source fire that was put out soon after discovery, and the second test configuration (type 2) was similar to a situation where the source fire was unattended for a short period of time. Major differences in flame spread progression were expected between the two test types.

Table 10 - FRP combustible wall fire test specifications

Test Name	Source Fire Fuel	Source Fire HRR (kW)	Source Burner Size (ft x ft)	Constant Source HRR
A1	Propylene	100	2 x 1	
A2	Propylene	75	2 x 1	
A3	Propane	50	2 x 1	
A4	Propane	75	2 x 1	
A5	Propane	50	1 x 1	
A6	Propane	75	1 x 1	
A7	Propylene	50	1 x 1	
A8	Propylene	75	1 x 1	
A9	Propylene	50	2 x 1	
A10	Propylene	75	2 x 1	
A11	Propylene	50	2 x 1	
A12	Propylene	50	2 x 1	✓
A13	Propylene	50	1 x 1	✓
A14	Propylene	75	1 x 1	
A15	Propane	50	1 x 1	
A16	Propane	75	1 x 1	✓
A17	Propane	75	2 x 1	✓
A18	Propane	50	2 x 1	

Upon ignition of the burner, the source fire was kept at a constant HRR; special attentions were paid to note the time when flame attachment and a definite ignition area was achieved on the wall panel. For type 1 tests, the burner would then be turned off and data collection would last until most burning had stopped. For type 2 tests, the burner was left on until the panel was mostly burnt out. At the end of the test, any flame left on the wall panel was put out with application of small amount of water spray.

All tests were conducted at an ambient temperature of 23 ± 5°C and low relative humidity.

2.4.1 Combustible wall paneling

The combustible wall specimen used in the tests was a commercially available fiber-reinforced-plastic (FRP) sheet that has a Class C (ASTM E84) flame spread rating. The FRP sheet consisted of modified polyester copolymer and inorganic fillers as the resin base and reinforced with a weave of random chopped fiberglass. Similar products are commonly used in construction projects where moisture and mold protection on walls or ceilings are desired. The panel's thickness is 0.09" (2 mm) nominal, with a smooth backface and a pebbled, embossed white front surface. The width of the panel was 1.2 m and its height was 2.4 m.

A 0.1 m by 0.1 m grid was drawn on the panel to aid in flame and burning area tracking. Small openings were cut into the FRP panel to expose the thin skin calorimeters, the water-cooled heat flux gauges, and the near wall thermocouples that were located on the inert wall surface. Although these openings had the potential to alter the natural flame spread progression because heated gases could escape from these locations and ignite remotely, they were essential for measurements to be collected that can aid in burning area tracking. Special care was taken during the installation of each test panel to ensure all gaps between the inert wall and the panel was minimized. All specimen panels were fastened onto the inert wall with about 30 screws; there was no fixed pattern in the screws' locations.

Prior to choosing the FRP as a combustible wall test specimen, several 1/2" thick thermoplastics panels of polypropylene and high-density polyethylene (HDPE) were considered. However, half-scale wall and bench-scale cone tests on these panels resulting in excessively high heat released and mass loss due to melting. Since FDS cannot model melting and pooling plastic fires, these panels were not considered further. A summary of these thermal plastic wall panel tests is available in Appendix A.

2.4.2 Combustible wall test measurements

The data collected in the combustible wall tests were identical to those from the inert wall tests, including HRR, plume centerline temperature and velocity, heat flux to wall, near-wall temperature with new data directly describing flame spread such as total mass loss, final burn pattern, and burning area tracking. Since mass loss during burn was not measurable, mass loss was calculated based on the initial and final mass of the panel. Final mass was measured as the sum of the mass of the unburned portion of the panel and the mass of the burnt residue (mostly glass fiber). The final burn pattern was recorded based on the grid, and four categories were used to describe each sector: 100% burnt (no resin left), 75% burnt (some resin left), 50% burnt (half resin half fiber-base), 25% burnt (mostly resin), and no burn. The damage chart can be used to validate or compliment the mass loss data. Two cameras were used to collect video data of the tests for burn area tracking purposes. One camera was located directly in front of the burning wall and the second camera was positioned at the compartment opening at a diagonal to the wall. The test videos were digitalized and one image was extracted per two seconds for manual flame tracking with special analysis on the pyrolysis front position. When used together with the HRR, mass loss, and burnt area data, the burning area rate can be estimated. Manual observations regarding burning area were also made during each test and incorporated with the other flame spread data where needed.

Table 11 – Combustible wall fire test measurements

Measurement	Instruments used	Locations
Plume centerline velocity	• Bi-directional probes/transducers and thermocouples	10 locations along burner centerline, from 0.2 m, 0.5 to 1.7 m above burner
Plume centerline temperature	• Different gauged thermocouple wires, mostly 24 AWG (20 to 30 AWG wires for radiation correction	13 locations along burner centerline, from 0.05 m to 1.85 m above burner
Heat flux to wall	• Thin skin calorimeter, constructed with Inconel plate and a pair of 20 AWG thermocouples	6 at different heights along centerline, 3 at 1-ft , 3 at 2-ft left of centerline, 3 at 1-ft , 3 at 2-ft right of centerline
Near-wall temperature	• Welded 20 AWG thermocouple wire	18 total, in three groups of 6 at three different heights and within 7.5 cm of the centerline
Heat release rate	• Flow controller (for source fire only) • LODS's oxygen consumption • LODS's CO/CO_2 generation	N/A
Flame spread	• Digital video camcorders • Damage index • Mass load cell	A video was filmed head on outside of the compartment (View A) Another video was filmed from the corner of the compartment (View B)

2.5 FRP specimen cone calorimeter test setup

A series of bench-scale cone calorimetry (ASTM E1354 [67], ISO 5660 [72]) testing were conducted with the Class C FRP specimen. A cone calorimeter imposes a uniform heat flux across the surface of a sample material to determine the ignition and burning characteristics of the test sample.

In the current research, the sample, cut into a 10 cm by 10 cm square, was oriented horizontally with its surface located at 1" below the cone shaped heating coil. Each sample was wrapped in aluminum foil and placed in a metal sample holder over a load cell that collected mass loss data.

A water-cooled metal shield was placed between the sample and the cone heater; it opened upon start-of-test to allow heat insult on the sample. A high-voltage electric sparker was located over the central of the sample, which provided the ignition source if the test sample was combustible. During each test, the FRP sample ignited and burned, giving out hot gases that were collected by an exhaust hood above the cone heater. The gases were sampled continuously for oxygen, CO, and CO_2 contents that were then translated into HRR data.

To simulate a range of heat flux from typical source fires, the heat flux levels used in the cone calorimetry testing were 25 kW/m^2, 50 kW/m^2, and 75 kW/m^2. In some of the tests, thermocouples were attached to the front-center and back-center surfaces of the sample using thermal paste to collect information such as surface temperature at ignition and heating time-time history.

GPYRO, a material property estimation algorithm developed by Lautenberger, was utilized to convert the results from the cone tests to generate the core material parameters of the FRP panel for use in the FDS simulations of the combustible wall fires.

N.3. CFD Modeling using FDS

Flame spread is a major factor in determining the severity and survivability of fires in the built environment. The recognition of this fact by the authority, designers, and scientific communities led to the development of various flame spread test methods and standards starting in early 20th century. These tests were developed originally for typical building materials of the last century; today, many researchers believe that the tests are obsolete for testing innovative materials, such as composites and plastics, for their flame spread properties. One way to rectify this problem is to develop new test methods targeted for these new building materials, and another way is to utilize computer simulations to predict flame spread in realistic scenarios.

One of the most widely accepted fire simulation tools in the industry is the Fire Dynamics Simulator (FDS) developed by NIST, now in its 5th version. The program utilizes various scientific principles correlation in the areas of combustion, fluid mechanics, and radiation transport to simulate a large variety of hydrodynamics and fire-related scenarios using method common to computational fluid dynamics modeling.

Flame spread is a complicated physical phenomenon that can only be accurately described through coupling some simpler phenomena, such as fluid mechanics, gas phase kinetics, flame heat flux, and pyrolysis. To tackle “flame spread” simulation by itself is unrealistic, so in this research, the larger problem will be broken down into these four areas and they will be analyzed individually through computer simulations using FDS. Insights gained during these simulations will be employed to create an accurate flame spread simulation model in FDS.

3.1 Computational environment

All simulations were conducted using on a Linux cluster. An FDS executable was compiled based on the 64bit-FDS Linux source code release 5.7031. Since parallel processing on the simulations was desired because of the multi-mesh nature of the simulations, an Open MPI-based complier was used along with the Intel 64-bit complier. An individual CPU, or node, was assigned for each mesh to maximize the efficiency of the models.

3.2 Baseline FDS modeling scenarios

The goal of a fire dynamics model is to predict the changes to an environment caused by the presence of a fire. In FDS, this is achieved by replicating the real world in a finite “control volume” in the computational environment, applying various physical parameters, and then allowing the software to solve a series of Navier-Stokes equations. As with any other type of simulation efforts, the calculation environment and parameters must be well defined and sufficiently represent the real world situations. In the current research all three test scenarios: plume, inert wall, and combustible walls, had been reproduced in the FDS environment. Each of the three simulation scenarios are described in the following sections, but refer to Appendix J for the baseline FDS model input files.

All baseline models had the same mesh size at 0.05 m x 0.05 m x 0.05 m (or 5.0 cm cubes).

3.2.1 Free plume FDS simulation model

The free plume simulations can be described as the simplest form of simulation out of the three. The basic model has a 2.4 m wide x 3.9 m long x 2.4 m high computational space occupied by twelve 1.2 m x 1.3 m x 1.2 m meshes. The source burner was replicated as a solid obstruction in the middle of the "room" with a surface specified with a constant heat release rate per unit area (HRRPUA) output. The &REAC lines, which describe the chemical reaction in the calculation, were specified as a reaction of one of the three different test fuels used (methane, propane, or propylene). Figure 10 presents the setup of the free plume fire simulation in FDS using a 2 ft Rectangle burner and also shows the discrete data measurement locations along the centerline of the burner. All simulations were executed for a 300 seconds period.

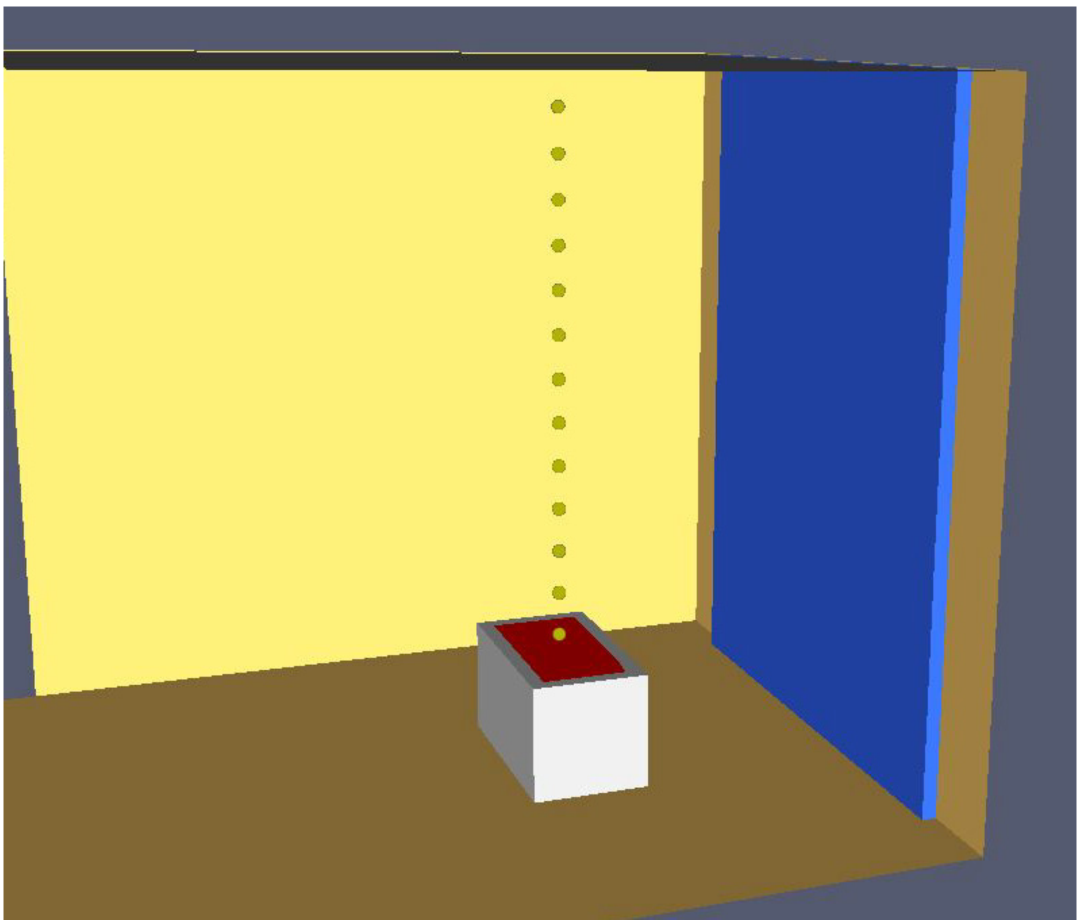

Figure 10 - FDS simulation space of a free plume test scenario

Over the burner, the vertical velocity and temperature along the plume centerline was measured via "W-VELOCITY" and "TEMPERATURE" in the &DEVC lines. The positions of these virtual devices corresponded to their real life counterparts. Section 1 in Appendix J presents an exemplar FDS input file for the plume fire simulation.

Table 12 - List of FDS simulations of the free plume scenario

Source Fuel	Source Fire HRR [kW]	Burner Size [ft x ft]
Methane	50	1 x 1
Methane	75	1 x 1
Propane	50	1 x 1
Propane	75	1 x 1
Propane	50	2 x 1
Propane	75	2 x 1
Propylene	50	1 x 1
Propylene	75	1 x 1
Propylene	50	2 x 1
Propylene	75	2 x 1

3.2.2 Inert wall fire FDS simulation model

The inert wall FDS models share the same mesh specifications as the free plume models. The source burner was replicated with a surface specified with a constant heat release rate per unit area (HRRPUA) output and placed against the inert wall, which was prescribed with the thermal characteristics of the Kaowool® insulation board. The &REAC line, which describes the chemical reaction in the calculation, was specified as a reaction of one of the three different test fuels used (methane, propane, and propylene). Figure 11 presents the setup of the inert wall fire simulation in FDS using a 1 ft Square burner and also shows the discrete data measurement locations along the centerline of the burner and on the wall. . All simulations were executed for a 300 seconds period.

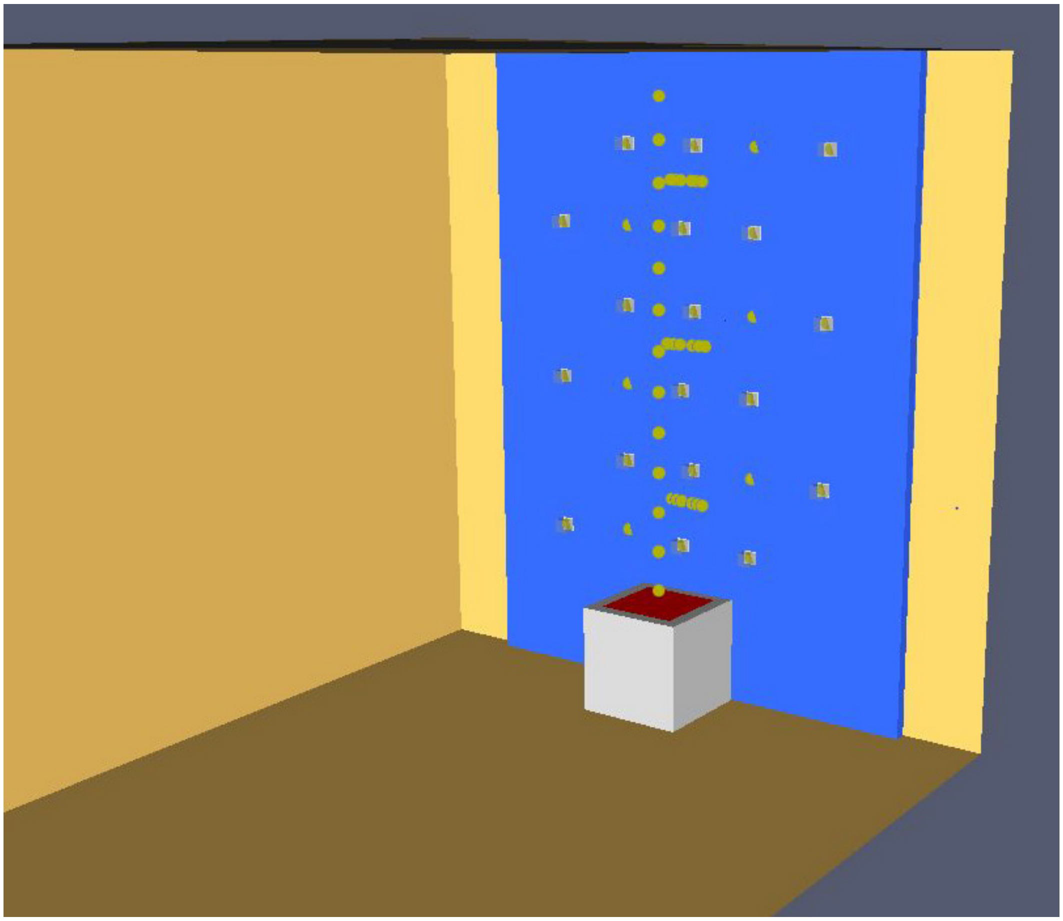

Figure 11 - FDS simulation space of a inert wall test scenario

Similar to the free plume models, the vertical velocity and temperature along the plume centerline were "measured". Devices specified as GAUGE_HEAT_FLUX, CONVECTIVE_HEAT_FLUX, RADIATIVE_HEAT_FLUX, INCIDENT_HEAT_FLUX, and RADIOMETER were used to replicate the real-life thin skin calorimeters (TSCs) on the inert wall. Adiabatic obstructions were used to simulate the assumed adiabatic surface of the TSCs. TEMPERATURE devices were also used at the near wall positions to simulate the near-wall thermocouples. Section 2 in Appendix J presents an exemplar FDS input file for the inert wall fire simulation.

Table 13 - List of FDS simulations of the inert wall scenario

Source Fuel	Source Fire HRR [kW]	Burner Size [ft x ft]
Methane	75	1 x 1
Methane	80	1 x 1
Propylene	75	1 x 1
Propylene	50	2 x 1
Propylene	75	2 x 1
Propane	50	1 x 1
Propane	75	1 x 1
Propane	50	2 x 1
Propane	75	2 x 1

3.2.3 Combustible wall fire FDS simulation model

The combustible wall fire models are essentially identical to their inert wall counterparts except that the combustible FRP panel was specific in place alongside the Kaowool® inert wall. The FRP wall was specified as one cell thick, but made of two layers of materials: with the 19 mm thick top layer backed by an inert insulating layer. In the FDS environment, the FRP material contains an initial “virgin”, unburned stage, which is replaced by an insulating “char” and burnt stage. The properties of the FRP materials were generated by the material properties estimation algorithm, GPYRO provided by Dr. Lautenberger form University of California, Berkeley based on test data of from cone calorimeter tests of the FRP material, available in Appendix E.

The source fire HRR time histories used in the simulations are unique for each simulation, which follow those established in the actual experiments. Additionally, it is assumed that the source burner HRR ramps up to 50% of the full range within 1 second, and up to 100% in approximately 15 to 25 seconds, the same as in the experiments. Figure 12 presents the setup of the combustible wall fire simulation in FDS using a 1 ft Square burner and also shows the discrete data measurement locations along the centerline of the burner and on the wall. The entire combustible wall simulation series was executed for 900 seconds, which sufficiently cover the major burning progress observed in all of the tests.

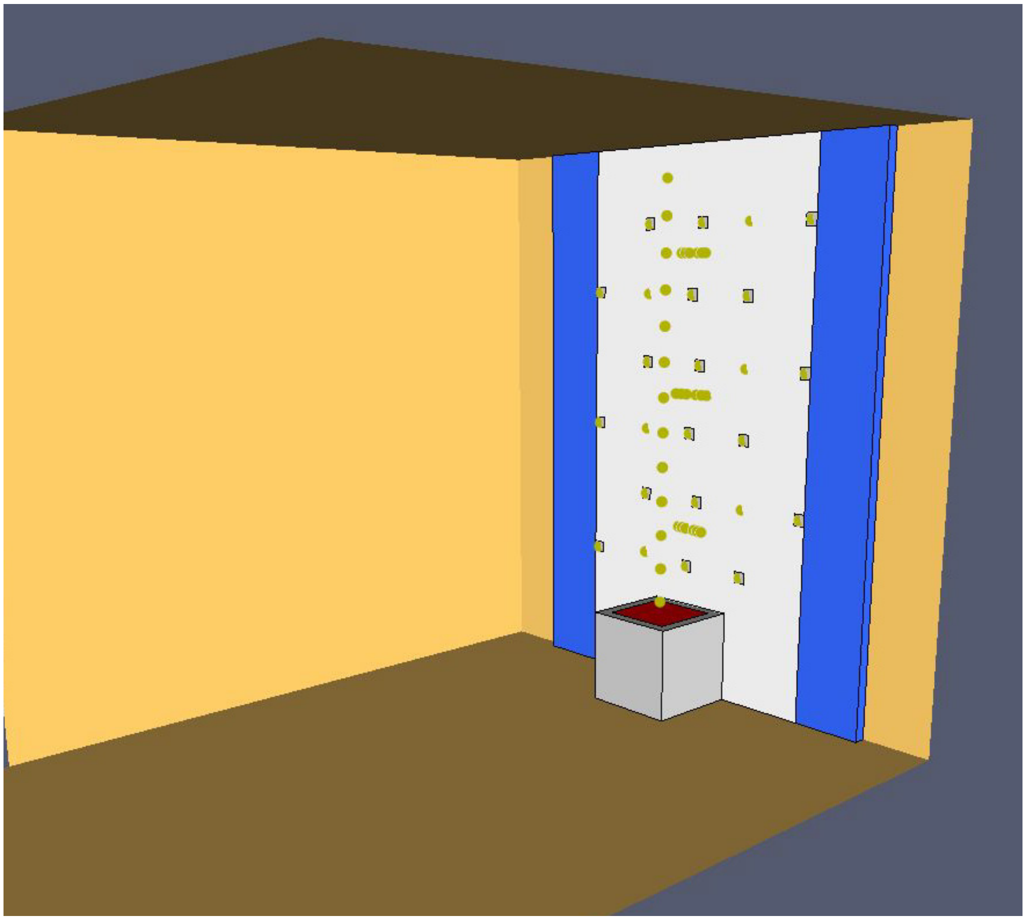

Figure 12 - FDS simulation space of a combustible wall test scenario

The various “measurement devices” in the combustible wall tests were identical to the ones in the inert wall tests. Section 3 in Appendix J presents an exemplar FDS input file for the combustible wall fire simulation.

Table 14 - List of FDS simulations of the combustible wall scenario

Source Fuel	Source Fire HRR [kW]	Burner Size [ft x ft]	Source Fire Reaches 100% time [sec]	Source Fire Duration [sec]
Propane	75	2 x 1	15	115
Propane	50	1 x 1	15	98
Propane	75	1 x 1	15	84
Propylene	50	1 x 1	15	65
Propylene	75	1 x 1	15	60
Propylene	50	2 x 1	12	68
Propylene	75	2 x 1	12	55
Propylene	50	2 x 1	12	68
Propylene	50	2 x 1	12	900
Propylene	50	1 x 1	12	900
Propylene	75	1 x 1	15	66
Propane	50	1 x 1	15	85
Propane	75	1 x 1	20	900
Propane	75	2 x 1	23	900
Propane	50	2 x 1	15	82

3.3 FDS grid sensitivity analysis

In any computational fluid dynamic model, the grid size of the calculation domain (mesh) plays an important role in determining the accuracy and the performance of the simulation. Researchers had linked a FDS simulation's grid resolution to the software's capability to model the features of the fluid flow and combustion characteristics, both of which are important factor in flame spread simulation[74-77]. A smaller grid size is generally preferred for its tendency to give more accurate results; however, the generally larger computational cost associated with such a grid size may be prohibitive for many applications. To identify the effects of grid resolution size, simulations of the fire plume simulation series were conducted using the default FDS parameters and grid sizes at 5.0 cm (baseline), and 2.5 cm. The results of these simulations were compared against each other to identify trends in fire behavior predictions from due to grid differences and are presented in Appendix H.

3.4 Parametric study for flame spread modeling in FDS

The default parameters that govern the various calculations in FDS were established through vigorous verification and validation exercises by the developers at NIST and many other fire researchers. These default values would work sufficiently well for most simple fire scenarios. However, the real life is much more complicated than any reasonable model, and oftentimes, the various parameters must be changed to accommodate a given situation so that the prediction may be accurate. This is especially true for flame spread modeling because of its complexity that leads to unpredictability in the simulation environment.

By comparing the experimental data from the current research to the baseline simulation data of those tests, one found that FDS often under-predicts some conditions of the test while over-predicting others. There was certainly a need to identify how changes in the various simulation parameters will affect the simulated results, and yet, this process must proceed methodically, so that the interactions of the parameters can be pinpointed. Also, any parameter change must be reasonable; otherwise the simulation would be unrealistic and thus inaccurate.

In this research, aside from those directly related to the geometries and the material descriptions, the following FDS parameters in Table 15 were changed systemically in succeeding simulation series in order to record the change in model behaviors. Each parameter change was applied a whole series of simulations that may be consisted of a single scenario to all three scenarios (plume, inert wall, and combustible wall). Across each series all variables are the same, so that any different in the results to previous series may be attributed only to the changed parameter. The ranges of the variable parameters had been determined to be justifiable and are presented in Table 15.

Table 15 - Variable simulation parameters

Series	Parameter Group	Parameter change	Default Value	New value in simulation	Change from default
0	FDS6	DYNSMAG	.TRUE.	.FALSE.	x
1	N/A	No change, Default situation using default FDS6 options			
2	MISC	RADATION	.TRUE.	.FALSE.	x
3	RADI	RADIATIVE FRACTION	0.30	Source fire specific	varies
4	RADI	RADIATIVE FRACTION	0.30	0.1	~33%
5	RADI	RADIATIVE FRACTION	0.30	0.2	~50%
6	RADI	RADIATIVE FRACTION	0.30	0.5	~160%
7	RADI	WIDE_BAND_MODEL	.FALSE.	.TRUE	x
8	RADI	NUMBER_RADIATION_ANGLES	104	52	50%
9	RADI	NUMBER_RADIATION_ANGLES	104	208	200%
10	RADI	ANGLE_INCREMENT	5	2	50%
11	RADI	ANGLE_INCREMENT	5	10	200%
12	RADI	TIME_STEP_INCREMENT	3	1	50%
13	RADI	TIME_STEP_INCREMENT	3	6	200%
~~14~~	~~Skipped~~				
15	REAC	C_EDC	0.1	0.2	50%
16	REAC	C_EDC	0.1	0.05	200%
17	REAC	EDDY_DISSIPATION	.TRUE.	.FALSE.	x
18	REAC	HRRPUA_SHEET	0	400	50%
19	REAC	HRRPUA_SHEET	0	100	200%
20	REAC	HRRPUV_AVERAGE	3000	1200	40%
21	MISC	ISOTHERMAL	.FALSE.	.TRUE	x
22	MISC	CSMAG	0.2	0.1	50%
23	MISC	CSMAG	0.2	0.4	200%
24	MISC	PR	0.5	0.25	50%
25	MISC	PR	0.5	1	200%
26	MISC	SC	0.5	0.25	50%
27	MISC	SC	0.5	1	200%
28	MISC	BAROCLINIC	.TRUE.	.FALSE.	x
29	MISC	CFL_MAX	1	2	200%
30	MISC	CFL_MIN	0.8	0.4	50%
31	MISC	CFL_MAX and CFL_MIN	1 / 0.8	2 / 0.4	x
32	FDS6	FLUX_LIMITER	2	-1	x
33	FDS6	CFL_VELOCITY_NORM	1	2	x
34	FDS6	CFL_VELOCITY_NORM	1	0	x
35	FDS6	H_EDDY	.TRUE.	.FALSE.	x

3.4.1 Variable parameters properties

The variable parameters and their functions are described in this section. Many of the parameters have an effect on the stability and the performance of the model by changing the amount or complexity of the calculations performed by the FDS software. Moreover, some of the parameters can also affect the predicted fire behaviors and change the various quantities predicted by FDS.

1) RADI parameters
   a) **RADIATIVE_FRACTION**
      i) Determines the fraction of combustion energy released in the model as thermal radiation
      ii) Default simulations used a value of 0.30
      iii) Parametric study used the radiative fraction values of the fuel modeled: methane at 0.141, propane at 0.286, and propylene at 0.368
   b) **WIDE_BAND_MODEL**
      i) Determine whether the six band wide band gray gas model is assumed and used in the simulation
      ii) Default simulations disables the six band model method
      iii) Parametric study simulations had the six band model enabled
   c) **NUMBER_RADIATION_ANGLES**
      i) Number of solid angles used in radiation calculations, not compatible if radiation transport calculations are disabled elsewhere in the input file
      ii) Default simulations used 104 solid angles for calculations
      iii) Parametric study simulations used 52 and 208 solid angles
   d) **ANGLE_INCREMENT**
      i) Number of solid angles skipped per update of radiation calculations
      ii) Default simulations used the default FDS value of 5
      iii) Parametric study simulations used values of 2 and 10
   e) **TIME_STEP_INCREMENT**
      i) Number of time steps skip per update of radiation calculations
      ii) Default simulations used the default FDS value of 3
      iii) Parametric study simulations used values of 1 and 6
2) REAC parameters
   a) **C_EDC**
      i) Coefficient to calculate mixing time scale of fuel and oxygen within the grid cells used in the turbulent combustion calculations
      ii) Default simulations used a value of 0.1 for the coefficient, determined based on comparison to flame height correlations[78]
      iii) Parametric study simulations used 0.05 and 0.2 solid angles
   b) **EDDY_DISSIPATION**
      i) Determines whether the default heat release rate calculation model based on the default mixture time scale method is used
      ii) Default simulations enabled the eddy dissipation to be determined
      iii) Parametric study enabled the eddy dissipation
   c) **HRRPUA_SHEET**

i) Max HRRPUA of a flame sheet, acts as a bound of local HRRPU-volume
ii) Default simulations used a default value of $0 kW/m^2$ for LES
iii) Parametric study used values at $100\ kW/m^2$ and $400\ kW/m^2$

d) HRRPUV_AVERAGE

i) Average volumetric HRR of a fire, bounds local HRRPU-volume value
ii) Default simulations used a default value of $3000\ kW/m^3$
iii) Parametric study used values at $1200\ kW/m^3$, as suggested by Orloff and De Ris[78]

3) MISC parameters

a) CFL_MAX and CFL_MIN (only test for inert wall/plume simulations)

i) Numerical stability parameters that limit the time step sizing by imposing limits on the Courant-Friedrichs-Lewy (CFL) number that is calculated within each timestep: if the number is outside of the range, then the time step size is adjusted
ii) Default simulations set the max value at 1 and the min value at 0.8
iii) Several combinations of CFL limits are tested in the parametric study as follow: [2, 0.8], [1, 0.4], and [2, 0.4]

b) ISOTHERMAL (only test for inert wall/free plume simulations)

i) Set the calculations to ignore any changes in temperature or radiation heat transfer, also automatically turn off radiation transport model as well
ii) Default simulations disabled the isothermal option
iii) Parametric study enabled the isothermal option

c) CSMAG

i) Smagorinsky constant used to calculate the viscosity, usually more stable if a small value is used
ii) Default simulations used a default value of 0.2, justified through comparisons with experimental data[79]
iii) Parametric study used values at 0.1 and 0.4

d) PR

i) Turbulent Prandtl number, a ratio of momentum diffusivity to thermal diffusivity, related to turbulent viscosity in LES simulations
ii) Default simulations used FDS's default value of 0.5, justified through comparisons with experimental data[79]
iii) Parametric study used values at 0.25 and 1

e) SC

i) Turbulent Schmidt number, a ratio of momentum diffusivity to mass diffusivity, related to turbulent viscosity in LES simulations
ii) Default simulations used FDS's default value of 0.5, justified through comparisons with experimental data[79]
iii) Parametric study used values at 0.25 and 1

f) BAROCLINIC

i) Enables the baroclinic vorticity correction calculations that can changes the properties in the turbulence calculations and may affect the plume shape significantly
ii) Default simulations enables the baroclinic correction

iii) Parametric study disabled the correction calculations

g) RADIATION (only for inert wall/plume simulations)

i) Turns On or Off radiation transport calculations in the simulations

ii) Default simulation use the radiation transport model, as in real life

iii) Parametric study disabled the radiation transport calculations

4) FDS6 parameters

a) FLUX_LIMITER

i) Changes the finite volume discretization scheme used in simulations

ii) Default simulations use the Superbee scheme, suitable for LES simulations

iii) Parametric study used a central differencing scheme with boundedness correction applied

b) DYNSMAG

i) Turns on/off variable density formulation of dynamic Smagorinsky model

ii) Default simulation use the dynamic Smagorinsky model

iii) Parametric study disabled the dynamic Smagorinsky model

c) CFL_VELOCITY_NORM

i) Normalization of CFL velocity, controls the time step sizing within a simulation

ii) FDS default uses a moderate time step sizing control

iii) Parametric study tested for the effects due to an increase and decrease of the time step sizing control

d) H_EDDY

i) Enables the eddy-diffusivity model to use a turbulent convective heat transfer model

ii) Default simulations has the eddy diffusivity model enabled

iii) Parametric study disabled eddy diffusivity model

The results of the parametric study are presented in Appendices K to M.

3.5 GPYRO material properties sensitivity study

In addition to the grid resolution and simulation environment parameters, the material property parameters of the FRP panel in the combustible wall FDS simulations may contribute to the validity of the predicted results. GPYRO uses the cone test results to predict the optimal set of material properties to be used in FDS.

The material property estimation process of GPYRO utilizes a set of estimated maximum and minimum possible values for each of the material property in order to generate the optimal values. The max and min values are user-inputs, and may contribute to the optimal values. In order to determine the validity of the optimal material property values, a sensitivity study was carried out by using the different GPYRO-generated values.

The baseline of this series of simulations used all the 11 optimal parameters generated by GPYRO. In each successive simulation, one of the parameter was changed to its maximum or minimum values predicted by the GPYRO algorithm. The total heat released (THR), the time to peak, and the peak HRR predicted in each simulation were compared in order to determine the effects of varying the parameters. The details of the sensitivity study are presented in Appendix G.

N.4. Experimental data analysis

Full scale tests were conducted based on the three progressive scenarios set out in Section 2: free plume, inert wall, and combustible wall fire tests. A large amount of tests were conducted within each series and in each test there were over 130 data streams for measurements.

The data presented in this Section are only snippets from the complete dataset. The full dataset is found is available as CSV files in Appendix N. Complete combustible wall test data are presented in Appendix F. Alternate analysis of the data can be found in Appendix D.

4.1 Experimental data uncertainty

Every measurement has an inherent uncertainty stemming from the limitations of the instrument that made the measurement, variations in the environments, and simplifications in the theories and calculations used to deriver same measurement[80]. The experimental uncertainty, or errors, of any measurement must be identified and reported for the data to have real meanings and support its analysis.

Errors are unavoidable in any measurement procedure: every instrument manufactured is inherently uncertain to a degree; usually the quality of the instrument and how it was used determine how large or small the uncertainty is. Conditions of the environment may also be attributed to measurement errors. Although special care may be taken to conduct an experiment "perfectly", one can only minimize the errors but not totally eliminate them. Measurement uncertainty can be broken down into two different categories: systematic and random[81]. Systematic errors usually create bias in the measurements; it is easily identified when all measurements of a single quantity are skewed to one side of the scale. Systematic errors are usually caused by faulty equipment, badly calibrated instruments, or wrongful use of the instruments. Conversely, random errors are closely related to the sensitivity and uncertainty of the equipment, they result in a scattering of measured data, and can usually be minimized by using instruments with smaller uncertainties.

Uncertainty in direct measurements makes up the majority of the experimental uncertainty and is based on the sensitivity of the instruments. Experimental uncertainties are categorized as two components: "Type A" if they are determined from data using statistical methods, such as the mean and standard deviation of a series of measured data, or "Type B" if they are determined based on a research's own scientific judgment, experience, and manufacturer's specifications[82]. Experimental measurements usually include both components of measurement uncertainty.

In most complex experiments, the physical quantities of interest aren't measured directly, but derived from a series of calculations based on other direct measurements. In this case, the errors in the different direct measurements will propagate through the calculations and at last combined to represent the uncertainty of the derived quantity. This is of special importance to the current study because most quantities reported in each fire experiment are calculated from two or more measurements of other quantities, with the exception being plume or near-wall temperature. For example, the chemical oxygen consumption-based HRR was calculated with the temperature, pressure, and O2 content of the gas sample; the heat flux was calculated based on two temperature readings and various thermal parameters; and the plume velocity was based on pressure and temperature measurements made along the plume's centerline. Hence, to identify the uncertainty in the derived quantities, one must first determine the uncertainties of the direct measurements, then identify the "propagation" of the individual errors that results in the representative uncertainty of the derived quantity.

The propagation of the individual uncertainties depends on the relationship of the final, derived quantity, and the directly measured quantities. Partial differentiation of the formula with respect to each of the measured quantities were used of determine the "weight" the measured quantities affect the derived quantity since different variable contribute in different amount to the value of the derived quantity. The general form of error propagation is shown in equation (1).

$$\delta u = \sqrt{\left(\frac{\delta u}{\delta x}\delta x\right)^2 + \left(\frac{\delta u}{\delta y}\delta y\right)^2 + \ldots + \left(\frac{\delta u}{\delta z}\delta z\right)^2} \tag{2}$$

Where the variable, u represents the derived quantity of interest, and the variables x, y, and z represent the different measurements used to calculate u.

4.2 Experimental data reduction

This section examines each subset of data collected during a fire test in details and explores the methods in which direct measurements are converted into derived quantities of interest. The uncertainty associated with each significant measurement is also determined.

4.2.1 Heat release rate

Although not belong to any of the four components of flame spread, the heat release rate is the main driving force behind the mechanics of all four of the components. HRR of each fire was measured with several methods: oxygen consumption calorimetry, CO/CO_2 generation calorimetry (CDG), and except for methane, estimation of the source fire is mainly based on the fuel flow rate recorded by the mass flow controller. Additional derivations and explanations of the various HRR measurements are presented in a previous section

4.2.1.1 Fuel flow rate based heat release rate

The flowmeter used for the propane and propylene gases reports the fuel flow at standard liter per minute (slpm), it was calibrated at standard temperate and pressure (STP) conditions at 0°C and 1 atm. To determine the HRR from the gas flow rate, the following equation was used:

$$HRR_{flow} = q_{fuel} * \rho_{fuel} * \Delta H_{ch} \tag{3}$$

Where $HRR_{flow} = HRR\ based\ on\ flow\ rate\ [kW]$
$q_{fuel} = fuel\ gas\ flow\ rate\ [m^3/s]$
$\rho_{fuel} = fuel\ gas\ density\ [kg/m\text{^}3]$
$\Delta H_{ch} = fuel\ gas\ chemical\ heat\ of\ combustion\ [kJ/kg]$

The flowmeter, manufactured by Teledyne-Hastings has a range of 0 slpm to 875 slpm with a manufacturer reported uncertainty of 1%, or 8.75 slpm. Propane was used by the manufacturer to calibrate the flowmeter and it was found that 33 slpm of propane gas corresponds to a fire at 50 kW, and 50 slpm of propane gas corresponds to a fire at 75 kW based on experimental results from mass loss data and the Oxygen consumption calorimetry data. Since a fuel's flow rate and the fire's HRR are related linearly, the ratio was calculated to be 1.5 kW/slpm and this suggests that the uncertainty of the flow-based HRR can be expressed in HRR term as about 13 kW.

4.2.1.2 Oxygen consumption based heat release rate

The overall HRR of a test was calculated was based on oxygen consumption calorimetry in line with ASTM E-1354[67] using the LODS. The LODS is consisted of the exhaust hood and ductworks that serve to both exhaust the heated combustion gases for safety reasons and to carry the gases to be sampled. A sample line with a small flow rate compared to the exhaust rate is hooked up to the exhaust ductworks. A series of filters, intended to remove soot, other particulates, and moisture found in the sample gas before it is analyzed were installed along the sample line. Afterward, the "cleaned" sample gas is transported into a paramagnetic oxygen analyzer and a CO/CO_2 analyzer that measures the oxygen and CO/CO_2 contents. At the oxygen analyzer, filters were used to scrub CO and CO_2 from the flow.

The system collects all the combustion products from a fire test and then at a location in the duct sufficiently downstream for adequate mixing of the gases, the flow rate is measured via a bi-directional probe and thermocouple, and the gases' compositions are sampled. Based on the oxygen content of the sampled gas mixture and other flow quantities, the HRR can then be calculated. In order to ensure the accuracy of the measurements during an experiment, each component of the LODS was calibrated and the filters were changed out if necessary prior to a day's tests.

Along with most other measurements made in the experiments, all instruments of the LODS are connected to the data acquisition (DAC) system. The DAC system converts and scales the voltage output from the instruments into actual measurements. It was found that delay times of the various measurements related to the oxygen consumption calorimetry must be accounted for before calculations of the HRR can proceed. This and the subsequent data reduction are achieved using a specialized Microsoft Excel spreadsheet.

Parker and Janssens[68] provided a series of equations to calculate the HRR based on the various measurements from the LODS based only on oxygen contents, they are modified and simplified for use in the WPI's LODS. First, the oxygen depletion factor that relates the ratio of measured O_2 content to ambient air O_2 content must be found using equation (3):

$$\phi = \frac{X_{O2}^{e} - X_{O2}^{A}}{(1 - X_{O2}^{A}) X_{O2}^{e}} \tag{4}$$

Where $\phi = oxygen\ depletion\ factor$

$X_{O2}^{e} = measured\ mole\ fraction\ of\ oxygen\ in\ combustion\ gases$

$X_{O2}^{A} = measured\ mole\ fraction\ of\ oxygen\ in\ ambient\ air$

It is noted that the mole fraction of oxygen in ambient air was determined and scaled from the values measured during the three minutes before a test commenced and the three minutes after all the test compartment was clear of smoke. The value was typically around 0.209.

Then, the gas velocity in the duct was found through the bi-directional probe's pressure differential readings and the temperature of the gas flow in the proximity of the probe. The volumetric flow rate is found using equation (4):

$$\dot{V}_S = 22.4\,jkA\left(\frac{\Delta P}{T_e}\right)^{0.5} \tag{5}$$

Where $\dot{V}_S = volumetric\ flow\ rate\ in\ the\ duct$

$j = correction\ factor\ for\ bi - direcitonal\ probe\ used, 0.926$

$k = C - factor\ of\ the\ duct, 0.975$

$A = cross - sectional\ area\ of\ duct\ [0.126\ m^2]$

$T_e = gas\ temperature\ in\ duct\ [K]$

$\Delta P = pressure\ differential\ [Pa]$

The C-factors for the bi-directional probe and the duct was previously determined based on manufacturers' specifications and old calibration experiments conducted using the LODS.

The gas volumetric flow rate is converted to the volumetric flow rate of air into the system by equation (5).

$$\dot{V}_A = \frac{\dot{V}_S}{(1+(\alpha-1)\phi)} \tag{6}$$

Where $\dot{V}_A = volumetric\ flow\ rate\ of\ air\ in\ the\ duct$
$\alpha = molar\ expansion\ (typically\ 1.1)$

The heat release rate is then calculated using equation (6):

$$\dot{Q} = E\left(\frac{M_{O2}}{M_{air}}\right)\rho_{air}\dot{V}_A\left(\frac{X_{O2}^{e} - X_{O2}^{A}}{1 - X_{O2}^{A}}\right) \tag{7}$$

Where $M_{O2} = molecular\ mass\ of\ oxygen\ [28\ g/mol]$
$M_{air} = molecular\ mass\ of\ the\ combustion\ air\ [29\ g/mol\ for\ dry\ air]$
$\rho_{air} = density\ of\ air\ [kg/m^3]$
$E = fuel's\ heat\ released\ per\ unit\ mass\ of\ oxygen\ [kJ/g_{(O_2)}]$

In equation (6), the parameter E was found to be approximately 13.1 kJ/g, ±5% of oxygen by Huggett for organic solids, it implies that for most combustible organic liquids and gases, a relatively constant amount of heat is released. However, since the E values for the specific fuels are known, as listed in Table 16, this generic E value was used in the calculations of the HRR during combustible walls only. For the free plume and inert wall fire tests using methane, propane, and propylene, the fuel specific E value was used for HRR determination.

Table 16 - Heat release per unit mass O_2 for different fuels

Fuel type	Heat released per unit mass oxygen, E [kJ/g(O_2)]
Methane	12.54
Propane	12.80
Propylene	13.40
FRP and others	13.1

The use of Parker and Janssens' formulation assumes complete combustion and ignores the formation of carbon monoxide. Different tests with natural gas (methane) at known HRRs based on an analog rotary flowmeter where conducted in order to calibrate the O_2-based HRR calculation method. These calibration tests were conducted periodically in between the three main series of the plume, inert wall, and combustible wall fire tests. It was found that the methane HRR based on rotary flowmeter is consistently higher than the O_2-based HRR in the same test. The ratio between the actual and calculated HRRs is found to be $C = HRR_{O2}/HRR_{actual}$, where c is the correction factor that describes the bias of the LODS in calculating HRR. This bias most likely resulted from the specific instruments used as parts of LODS and the interaction and relationships between instruments and the measured data. The bias was found to be consistent throughout the two-year period of time that experiments were being conducted, it has a value of 0.77 ±0.05, suggesting that the O_2 based HRR is about 77% lower than the actual HRR of any fire test. This discrepancy between the true HRR of a fire and the O_2 based HRR was also observed when comparing the HRR_{flow} and the HRR_{o2}, The analysis between the different HRR calculation methods may be found in Appendix D.

The uncertainty of the oxygen consumption calorimetry of the LODS at WPI was established to be approximately 25 kW based on the manufacture specifications of the O2 analyzer and the standard deviation from the statistical analysis of the various fire tests conducted. Given the larger uncertainty associated with the O_2-based HRR vs. the flow-based HRR, the HRR_{flow} is deemed more accurate and used in the final reporting of the HRR for free plume and inert wall fires where propane and propylene are used. For all plume and inert wall fires with methane, the O_2-based HRRs are reported. In the case of combustible wall fire tests, the source fire HRRs were characterized based on the flow-based HRR, but the global HRR of the test reports the O_2-based HRRs calculated.

As suggested previously, Parker and Janssens' O_2-based HRR formulation assumes a complete combustion (all carbon is converted to CO_2). However, this is typically not realistic since carbon in a fire can also form CO or soot. Since the CO and CO_2 contents are also measured in each test, a more comprehensive HRR determination method was developed that also accounts for CO and CO_2 generation rates in a fire and is presented in Section 4.2.1.3.

4.2.1.3 CO/CO_2 generation based heat release rate

Along with the O_2 content measured with the oxygen analyzer in the LODS, an analyzer for CO and CO_2 was also installed and the CO/CO_2 content measurements can be used for HRR calculation. Unlike the oxygen consumption method that is based on the reduction of oxygen, the CO and CO_2 generation (CDG) calorimetry is based solely on the generation of CO and CO_2, two by-products of a fire, to account for the incomplete combustion nature of most fires. The CDG HRR measures the chemical HRR of a fire and was developed by Tewarson[83] and reproduced in ASTM E2058[84]. Due to some difference in hardware settings, the formulas presented in ASTM E2508 for CDG HRR calculations were modified to the current state so that the mass flow rate at the duct assuming the exhaust flow has a density of that of ambient air in equation (7):

$$\dot{m}_d = \dot{V}_S * \rho_{air} \tag{8}$$

Where $\dot{m}_d = mass\ flow\ rate\ of\ the\ duct\ [kg/s]$

Then, the mole fraction of CO_2 was modified from its measured value based on the chemical formula of the fuel:

$$X_{CO2} = X_{CO2}^{A}\left(\frac{1}{\left(1+\frac{a}{2b}\right)X_{CO2}^{A}}\right) \tag{9}$$

Where $X_{CO2} = modified\ CO_2\ mole\ fraction$
$X_{CO2}^{A} = measured\ CO_2\ mole\ fraction$
$a = number\ of\ carbon\ atoms\ in\ a\ fuel\ molecule$
$b = number\ of\ hydrogen\ atoms\ in\ a\ fuel\ molecule$

The a and b values of methane, propane, and propylene are listed in Table 17.

Table 17 - Hydrocarbon fuel chemical formulas

Fuel type	Formula	a (carbon atom)	b (hydrogen atom)
Methane	CH_4	1	4
Propane	C_3H_8	3	8
Propylene	C_3H_6	3	6

The generation rates of the CO and CO_2 gases are then found by equations (9) and (10):

$$\dot{G}_{CO}^{"} = SG_{CO}X_{CO}\dot{m}_d \tag{10}$$

$$\dot{G}_{CO2}^{"} = SG_{CO2}X_{CO2}\dot{m}_d \tag{11}$$

Where $\dot{G}_{CO}'' = generation\ rate\ of\ carbon\ monoxide\ [g/s]$
$\dot{G}_{CO2}'' = generation\ rate\ of\ carbon\ dioxide\ [g/s]$
$SG_{CO} = specific\ gravity\ of\ carbon\ monoxide, 0.967$
$SG_{CO2} = specific\ gravity\ of\ carbon\ dioxide, 1.52$
$X_{CO} = measured\ CO\ mole\ fraction$

Finally, the HRR is found using equation (11)

$$\dot{Q}_{CDG}^{"} = \Delta H_{CO}^{*}\dot{G}_{CO}^{"} = \Delta H_{CO2}^{*}\dot{G}_{CO2}^{"} \tag{12}$$

Where $\dot{Q}_{CDG}'' = CO/CO2\ \ based\ chemical\ heat\ release\ rate\ [kW]$
$H_{co}^{*} = fuel\ net\ heat\ of\ complete\ combustion\ per\ unit\ mass\ of\ CO\ generated\ [kJ/kg]$
$H_{co2}^{*} = fuel\ net\ heat\ of\ complete\ combustion\ per\ unit\ mass\ of\ CO_2\ generated\ [kJ/kg]$

Table 18 - Heat release per unit mass CO and CO_2 generated for different fuels

Fuel type	Heat released per unit mass CO generated, [kJ/kg]	Heat released per unit mass CO_2 generated, [kJ/kg]
Methane	18600	18200
Propane	14000	15300
Propylene	12900	14600
Average	11100 ±11%	13300 ±11%

The results of the various tests have shown that the CDG-based HRR calculated usually falls slightly below the corrected O_2-based HRR value. This suggests that the bias of the O_2 based HRR applies to the CDG-based HRR as well, although the true extent of the bias was not fully investigated. The uncertainty of the CDG-based HRR was found to be approximately 30 kW, slight higher than the O_2-based HRR. Given the less common approach to the HRR calculation and the higher uncertainty, the CDG-based HRR was generally used as a validation for the other two methods of HRR determination. The comparison between the various HRR calculation methods are detailed in Appendix D.

4.2.2 Plume temperature

The majority of the centerline temperature measurements were made via 24-AWG thermocouple wires with welded bead-ends at 15 cm intervals. Six Isotherm stations, consisting of three welded thermocouple wires using 20 AWG, 28 AWG, and 30 AWG wires were installed at varying intervals alongside with the 24-AWG thermocouples. Some of the thermocouples located below a height of 0.8 m over the burner were consisted of pre-made 24-AWG thermocouple with a larger diameter than the welded 24-AWG thermocouple wires. These wires were protected with a ceramic fiber weave against fire damage; the thermocouple wires elsewhere on the rakes were coated with a fiberglass weave that provides less protection against fire. The isotherm stations were intended to allow radiation correction of the temperature data.

All of the thermocouple wires were of K type with Special Limits of Error (SLE) with an uncertainty of ±1°C or 0.4% full scale. The operable range of the K type thermocouples is between 0°C to 1250°C, and given our application to locate the thermocouples inside the hot fire plume, it is assumed that the uncertainty of the thermocouples will be at the higher limit, at 0.4% = 5°C. Data analysis of the centerline plume temperature data has shown that this inherent uncertainty is insignificant when the thermocouples were measuring temperature inside the fire plume with large temperature variations.

4.2.2.1 Radiation correction methods

Bare-bead thermocouples are widely used in fire studies because they are cheap and easy to set up, however, the temperature reported by thermocouples in close proximity to a fire may differs from the true gas temperature because they have an actual body and are subjected to radiative and convective heat transfers that are not easily quantified.

In a fire situation, radiation is exchanged between a thermocouple and the enclosure walls, the hot gases, and the ambient environment. Heat can also be exchanged via convection to and from the thermocouples. Additionally, the heating time lag of a thermocouple can also cause misrepresentation of the true temperature. These effects are extremely hard to be addressed during a fire test, so a temperature correction may be performed after data have been collected in order to determine the true gas temperature from the bead temperature. The experimental setup had been designed with this in mind, allowing the plume velocity measurements to be used as part of the convective heat transfer correction for the plume temperature.

Two methods of correction, developed separated by Blevins and Pitts[85], and by Young[60] have been tested with some minor variations to determine the applicable corrective method for the current tests data, see Appendix C. It was found that for the thermocouples used in extreme-close proximity to a fire, such as for the centerline plume temperature measurement during steady-state conditions of the free plume and inert wall fires, the Blevins and Pitts' method of thermocouple compensation works better than Young's method for radiation correction. However, Young's method works well in situation where the thermocouples were located away from the fire where the temperature change is less chaotic[86, 87].

Blevins and Pitts' method is summarized below, and the Young's method is summarized in Appendix C.

Blevins and Pitts' method[85] of thermocouple compensation assumes a steady state heat transfer between the thermocouple and its environment. The enclosure was assumed to be a graybody, where all surfaces are surfaces opaque and isothermal, with abosroptivities and emissivities independent of wavelength and temperature. Additionally, it is assumed that all transferred radiation has the same intensity in all directions. Moreover, for the idealized form of heat transfer equation to hold true, the surrounding environment is assumed to have a constant temperature.

The model used by Blevins and Pitts assumes that heat is transferred to and from the bare-bead thermocouple through convection and radiation only. The energy balance equation is reported in equation (12).

$$T_b^{\ 4}[\varepsilon_{TC}\sigma]+\mathrm{T}_b[h_{bU}]-[\varepsilon_{TC}\sigma T_\infty^{\ 4}+h_{bU}T_g]=0 \tag{13}$$

Where:

$T_b = bare - bead\ thermocouple\ temperature\ [K]$
$T_g = true\ gas\ temperature\ [K]$
$T_\infty = surrounding\ environment\ (radiating) temperature[K]$
$h_{bU} = average\ convective\ heat\ transfer\ coefficient\ over\ the\ thermocouple\ [W/m^2K]$
$\epsilon_{TC} = emissivity\ of\ thermocouple$
$\sigma = Stefan - Boltzmann\ constant\ [5.67 \times 10^{-8}\ \ W/m^2K^4]$

The bare-bead thermocouple temperature is the temperature recorded by the thermocouple; the surrounding temperature is the graybody enclosure temperature, assumed to be the ambient temperature of the test compartment ~25°C. The emissivity of the thermocouple is assumed to be 0.80, typical for a dull, oxidized metal. The convective heat transfer coefficient is calculated using equation (13).

$$h_{bU} = \frac{Nu_D k}{D} \qquad (14)$$

Where:

$Nu_D = Nusselt\ number\ of\ external\ flow\ over\ sphere$
$k = thermal\ conductivity\ of\ air\ at\ thermocouple\ [W/mK]$
$D = bead\ diameter\ [m]$

The Nusselt number takes into consideration of the external flow's turbulence (Reynolds number) and thermal diffusivity (Prandtl number), as suggested by Whitaker's correlation [88] in equation (14).

$$\overline{Nu_D} = 2 + (0.4\,\mathrm{Re}_D{}^{0.5} + 0.06\,\mathrm{Re}_D{}^{2/3})\,\mathrm{Pr}^{0.4}\left(\frac{\mu_\infty}{\mu_\omega}\right)^{0.25} \qquad (15)$$

Where:

$\mu_\infty = visocity\ evalucated\ at\ the\ free\ stream\ temperature\ [kg/s\ m]$
$\mu_w = visocity\ evaluated\ at\ the\ thermocouple\ surface\ [kg/s\ m]$

In Whitaker's correlation, physical properties are evaluated at the true gas temperature, except for μ_w. However, since the true gas temperature is not known, the physical properties are evaluated at the bare-bead thermocouple temperature instead by assuming that the thermocouple temperature is sufficiently close to the true gas temperature.

For the free plume and inert wall fire tests, assuming a steady state condition, the thermocouple correction under Blevins and Pitts' method was carried out using the recorded time-averaged temperature for T_b. The Reynolds number was calculated using the velocity recorded by the bi-directional probes at the corresponding heights, or interpolated with neighboring measurements. The physical properties needed were calculated or interpolated from published correlations.

For the combustible wall tests, since the conditions are decidedly not in steady state, temperature correction of the temperature data (plume centerline and near-wall) was carried out using Young's method.

A comparison between the two methods of radiation correction showed that the Blevins and Pitt's method yields more consistent and reasonable results. It has been observed that at the isotherm stations nearest to the burner base, the temperature variations over the 4 different-sized thermocouples differ greatly from under 50K to over 100K; these variations were much decreased at locations away from the burner. The corrected temperature appears to rise significantly near the burner where the thermocouples had direct contact with the flames, but the difference decreased and became similar to the recorded temperature further away along the centerline.

4.2.3 Plume velocity

Velocity measurements were made at ten locations at 0.2 m, and from 0.5 to 1.7 m above the burner at 0.15 m intervals along the centerline of the plume. The velocity at each point was derived from the pressure differential measurement made with a bi-directional probe and the temperature measurement made with a thermocouple.

A bi-directional probe measures the pressure differential at a particular point; since the probes were oriented vertically, a positive differential is resulted from an upward flow and a downward flow results in a negative differential. The pressure change was measured with a transducer with a range of ±12.5 Pa and output of ±5 V with the ambient condition represented by a nominal ~5 V reading, this means that that the transducer output has a ratio of 2.5 Pa/V and the data received is in terms of voltage. It was found that the transducer's output drifts in away from ambient over time and especially during a test, most likely due to heating and cooling of the transducer during a fire test. Before the calculation of the velocity, the voltage time history output was smoothed using a running average over 10 seconds in order to reduce the noise in the data. To correct for this, for 3 minutes before and after a test, the average voltage was averaged and the drift ratio was found, and then retroactively applied to the voltage history over time, forcing the "after test" ambient voltage to the "before test" ambient value in order to reduce the drift effect. The differential pressure due to a flow was then determined based on the corrected ambient voltage value in equation (15) :

$$\Delta P = 2.5 * (V - V_{amb}) \tag{16}$$

Where:

$V = voltage\ measured\ during\ test\ [V]$
$V_{amb} = ambient\ voltage\ measured\ outside\ of\ test\ [V]$
$\Delta P = pressure\ differential\ calculated\ [Pa]$

To convert the pressure differential information, Heskestad developed a formula to reduce the velocity measurements from pressure differential measurement by using equation (16).

$$U = \frac{C}{\sqrt{2\Delta P / \rho}} \tag{17}$$

Where:

$U = velocity\ [m/s]$
$C = calibration\ constant$
$\rho = fluid\ density\ [kg/m^3]$

The calibration constant for Newman's design of the bi-directional probe was determined to be 1.18 during its development. The flow inside the fire plume was assumed to be made up of air only, and conforms to the ideal gas law. Hence, the fluid density was determined from the ideal gas law based on the temperature measured by the thermocouple installed in the proximity of the bi-directional probe. Furthermore, in the free plume and inert wall fire tests, the velocity history at each probe was averaged over the time when the fire was at steady state, recognized by a long period of near-constant HRR. In the combustible wall tests, such reduction was not applied because the situation was inherently not steady.

4.2.4 Flame height

Video data of each fire test was captured using a Canon digital camcorder at a rate of 30 frames per second in the high-definition MTS format. The videos were then converted into jpeg images using Virtualdub-1.9.9 at default resolution. Each sequence of images was decimated by 30 frames so that one image extraction was taken per second. Finally, 300 frames/images over 300 seconds from each test were then imported into Tracker 3.10, a software designed for motion tracking[89]. Tracker allows a user-defined set of axis, scale, and origin to be superimposed on a series of images or video, and allowed the tracking of objects' positions over time. In the current study, positions of the flame tips in each image were manually tracked in relation to the center of the burner surface. The position data was then exported to Excel for further analysis. The 0%, 10%, 50%, 90% and 100% intermittency flame heights were found with statistical methods. Although the different intermittency flame heights were calculated based on flame tip heights above the burner, the mean flame height is defined at the 50% intermittency flame height.

Based on the distance of the digital camcorder from the flame, the resolution of the video recording, the sensitivity of the tracking software, and the human errors in the manual flame tip tracking procedure, the uncertainty associated with the native flame height data is estimated to be ±0.05 m.

Previous works by researchers such as Zukoski[90], Heskestad[91], Quintiere and Grove[52], and Alston and Dembsey [92] presented their experimental mean flame height data as normalized by the burner's dimension vs. a non-dimensional heat release rate, defined differently. This is an appropriate and necessary procedure to reduce the flame height data such that data from different source fire scenarios (fuel type, HRR, and burner size) can be compared adequately. Note that the previous flame height data are conducted using a free fire plume centrally in a room and not near a compartment wall or corner.

The non-dimensional HRR Q* is commonly found by using equation (17)

$$Q^{*}=\frac{\dot{q}}{\rho_{\infty}c_{p}T_{\infty}g^{0.5}D^{2.5}} \tag{18}$$

Where $\dot{q}$ is the total heat release rate of the fire and D is the hydraulic diameter of the source burner. It has been reported by Alston and Dembsey[92] and Anderson[93] that Zukoski's method of normalization uses the total heat release rate, although Drysdale[4] suggests that the convective HRR was used in Zukoski's reporting of flame height data. However, the convective HRR was used to the normalization of the current data because it appears to provide better correlation to established theories and data.

Zukoski suggests that the non-dimensional flame height, z_f correlates to the non-dimensional HRR Q* as shown in equation (18)

$$\frac{z_f}{D_h} = \gamma Q^{*n} \tag{19}$$

Where γ=3.3, and n=2/3 for Q*≤1 and n=2/5 for Q*>1. The non-dimensional Q* parameter is calculated using the hydraulic diameter of the fire, D_h where D_h=4A/P (A=area and P=perimeter of the burner) and using the total heat release rate of the fuel. A similar correlation was developed by Anderson [93] using propane and a square burner, with a modification to γ=2.5, which resulted in a 25% decrease of flame height. This can be explained by the different fuel (propane) and different burner shape (circular) used in Zukoski's study.

Alston and Dembsey[92] conducted experiments very similar to the current research using methane, propane, and propylene and 0.3 m Square and 0.3 m Circle burners. The flame heights were normalized with the burner's hydraulic diameter and the HRR was normalized with total HRR.

Heskestad[91] developed his flame height correlation based on a wide range of experiments of different fuels as shown in equation (19) and equation (20)

$$\frac{Z_{50}}{D_e} = -1.02 + 15.6 N^{\frac{1}{5}} \tag{20}$$

$$N = \left[\frac{c_p T_\infty}{\frac{H_T}{r}} \right]^3 Q^{*2} \tag{21}$$

In this case, the length the flame height is normalized to is the equivalent fire diameter, $D_e=(4A/\pi)^{0.5}$, and the HRR is reduced to the non-dimensional parameter N.

Quintiere and Grove[52] developed a flame height correlation based on the convective fraction of the heat release rate, thereby taking combustion efficiency and plume buoyance into consideration. The original Quintiere and Grove flame height correlation, which uses the chemical heat of combustion in the calculation of Q*, was modified by Alston to use the total heat of combustion in its formulation so that comparison can be made. The modified flame height correlation is show in equation (21)

$$Q^* = 0.00590 \frac{\Psi^{\frac{3}{2}}}{\left(\chi_{ch} - \chi_{rad}\right)} \left(\frac{z_f}{D}\right)^{\frac{1}{2}} \left(1 + C_1\left(\frac{z_f}{D}\right)\right)^m \left(1 + C_1 a\left(\frac{z_f}{D}\right)\right)^n \tag{22}$$

$$where\ \Psi = \frac{(\chi_{ch} - \chi_{rad})\left(\frac{H_T}{r}\right)}{c_p T_\infty}$$

Where shape aspect ratio, a, is the burner's short dimension divided by the long, D is the fire characteristic dimension, and C_1, m, and n are coefficients based on burner shape as shown in Table 19.

Table 19 - Quintiere and Grove flame height correlation coefficients

Source Type	C_1	m	n	D
Axisymmetric	0.357	1	1	Hydraulic diameter
Rectangle	0.398	1	1	Short side
Infinite line	0.888	1	0	Line width

For the Square burner, D=0.304m (hydraulic diameter = edge length), and for the Rectangle burner D=0.304m (short side length).

The correlation is produced by predetermining a series of Z_f/D ratios and calculating the corresponding Q*. To allow comparison with this correlation, the current data's HRRs were corrected to a convective HRR then non-dimensional zed. This is achieved by using (22) and the D value prescribed in Table 19.

$$Q_c = Q*\left(\frac{H_{Tot}}{H_{ch}}\right)*\left(\frac{H_{cov}}{H_{Tot}}\right) \tag{23}$$

$$Q^* = \frac{Q_c}{\rho_\infty c_p T_\infty g^{0.5} D^{2.5}}$$

4.2.5 Near wall temperature

The near-wall temperatures were measured with 18 welded 20 AWG thermocouple wires situated near the vertical surface of the inert wall at different heights and perpendicular distances according to Table 20. The goal was to deduce the thermal and turbulent boundary layer on the wall created by the fire plumes. The temperature measurements had been radiation-corrected based on the test type, so the uncertainty of the true gas temperature measurement is within the upper and lower bounds created by the corrected and uncorrected temperatures, respectively.

Table 20 - Locations of near-wall thermocouples

		Distance from centerline					
		-7.5 cm	**-5.0 cm**	**-2.5 cm**	**2.5 cm**	**5.0 cm**	**7.5 cm**
		Perpendicular distance from wall [mm]					
Height above burner	**155 cm**	15	20	25	30	35	40
	95 cm	35	30	25	20	15	10
	35 cm	0	5	10	15	20	25

With this thermocouple grid, a partial map of the wall boundary layer may be obtained based on temperature readings. An upward thermal boundary layer is created on the inert wall by the fire plume adjacent to the wall. The plume and boundary layer differs in size, temperature, and velocity based on the burning area and fire size, which are all properties that drives the flame spread process on a vertical wall. The boundary layer is assumed to be one-dimensional and points vertically upward, and its thickness is defined as the interface where the temperature is the highest. By tracking the highest temperature from each group of six thermocouples at different heights, the boundary layer thickness at each height is approximated as the thermocouple's distance from centerline. The temperature history at each station is reduced to a time-averaged reading over the steady-state period of the inert wall fire tests; however, this procedure was not applied to the combustible wall test data as the situation positivity did not approach steady state.

All of the thermocouple wires were of K type with Special Limits of Error (SLE) with an uncertainty of ±1°C or 0.4% full scale. Since the operable range of the K type thermocouples is between 0°C to 1250°C, and given our application to locate the thermocouples inside the hot fire plume, it is assumed that the uncertainty of the thermocouples will be at the higher limit, at 0.4% full scale or ±5°C. However, the uncertainty of the measurement is dominated by the difference between the corrected and uncorrected temperatures.

The Blevins and Pitts' method of thermocouple radiation correction was applied to the near-wall temperature data for the inert wall fire tests. But for the combustible wall pane fire tests, Young's method of correction was used instead. Similar to the plume thermocouple correction, for the near wall data, the temperature increase due to the correction was on the order of 400 K for thermocouples near the source burner surface to 10 K for the thermocouples inside the buoyant plume at the top of the rakes.

4.2.6 Incident heat flux to wall

Thin skin calorimeters (TSCs) were used to measured heat flux on the wall at different locations, the design of the TSC was based on ASTM E459[70] and previous research at the WPI Fire Lab[86, 87]. The use of TSC assumes a one-dimensional heat transfer process. Additionally, since the metal calorimeter plate of the TSC is thin, and that the calorimeter plate is of a metal with known properties and thickness, a lumped thermal capacity analysis was employed in determining the net heat flux. Also known as the hot wall heat flux, the net heat flux represents the rate at which energy is transferred in and stored within the plate material, and is found using equation (23):

$$\dot{q}''_{net} = \rho_{TS} c_{TS} \delta_{TS} \frac{dT_s}{dt} \tag{24}$$

Where $\dot{q}''_{net} = net\ heat\ flux\ [kW/m^2]$

$\rho_{TS} = density\ of\ metal\ calorimeter\ [kg/m^3]$

$c_{TS} = specific\ heat\ of\ metal\ clorimeter\ [J/kg\ K]$

$\delta_{TS} = thickness\ of\ metal\ claorimeter\ [m]$

$\frac{dT_s}{dt} = temperature\ change\ rate\ at\ the\ back\ face\ of\ the\ metal\ calorimeter\ [K/s]$

Equation (23) shows that the net heat flux is calculated based on the temperature change measured by the thermocouple per second at the back of the plate, and the term $\rho c \delta$, which is dubbed the "thermal capacitance" of the plate material. In the experiments, the metal calorimeters were made of Inconel and its properties are detailed in Table 7. The backface temperature was measured with the thermocouple wire welded at the back-center of the Inconel plate.

To deduce the incident, or cold wall, heat flux from the net heat flux measurements, the heat transfer losses from the plate calorimeter to its environment must be accounted for by expanding equation (23) into equation (24):

$$\dot{q}_{net}^{"} = \rho_{TS} c_{TS} \delta_{TS} \frac{dT_s}{dt} = \alpha_s \dot{q}_i^{"} - \varepsilon_s \sigma (T_s^4 - T_0^4) - h_{conv}(T_s - T_g) - (4\varepsilon_b \sigma T_s^3 + h_{cr})(T_s - T_1) \qquad (25)$$

Where $\dot{q}_i'' = incident\ heat\ flux\ [kW/m^2]$

$\dot{q}_{lat}'' = lateral\ conduction\ (loss)\ rate\ [kW/m^2]$

$\alpha_s = absorpivity\ of\ plate\ calorimeter$

$\epsilon_s = emissivity\ of\ plate\ calorimeter$

$T_s = temperature\ recorded\ at\ plate\ calorimeter\ [K]$

$T_0 = ambient\ temperature\ [K]$

$h_{conv} = convective\ heat\ transfer\ coefficient\ [W/m^2K]$

$T_g = gas\ temperature\ in\ front\ of\ plate\ calorimeter\ [K]$

$\sigma = Stefan - Boltzmann\ constant\ [5.67 \times 10^{-8}\ \ W/m^2K^4]$

$T_0 = ambient\ temperature\ [K]$

$\epsilon_b = emissivity\ of\ plate\ calorimeter's\ back\ surface$

$T_1 = substrate\ front\ surface\ temperature\ [K]$

$h_{cr} = contact\ resistance\ heat\ transfer\ coefficient\ [W/m^2K]$

The various heat transfer routes are shown in Figure 13, and the incident heat flux can be found by rearranging equation (24) into equation (25):

$$\dot{q}_i^{"} = \frac{\rho_{TS} c_{TS} \delta_{TS} \frac{dT_s}{dt} + \varepsilon_s \sigma (T_s^4 - T_0^4) + h_{conv}(T_s - T_g) + (4\varepsilon_b \sigma T_s^3 + h_{cr})(T_s - T_1)}{\alpha_s} \qquad (26)$$

Where the various tem in the equation can be described as the following:

$\rho c \delta \frac{dT_s}{dt} =$ Net heat flux, store within the plate calorimeter

$\varepsilon_s \sigma (T_s^4 - T_0^4) =$ Irradiative loss from plate surface

$h_{conv}(T_s - T_g) =$ Convective loss from plate surface

$(4\varepsilon_b \sigma T_s^3 + h_{cr})(T_s - T_1) =$ Conductive and radiative loss into the substrate from back of plate

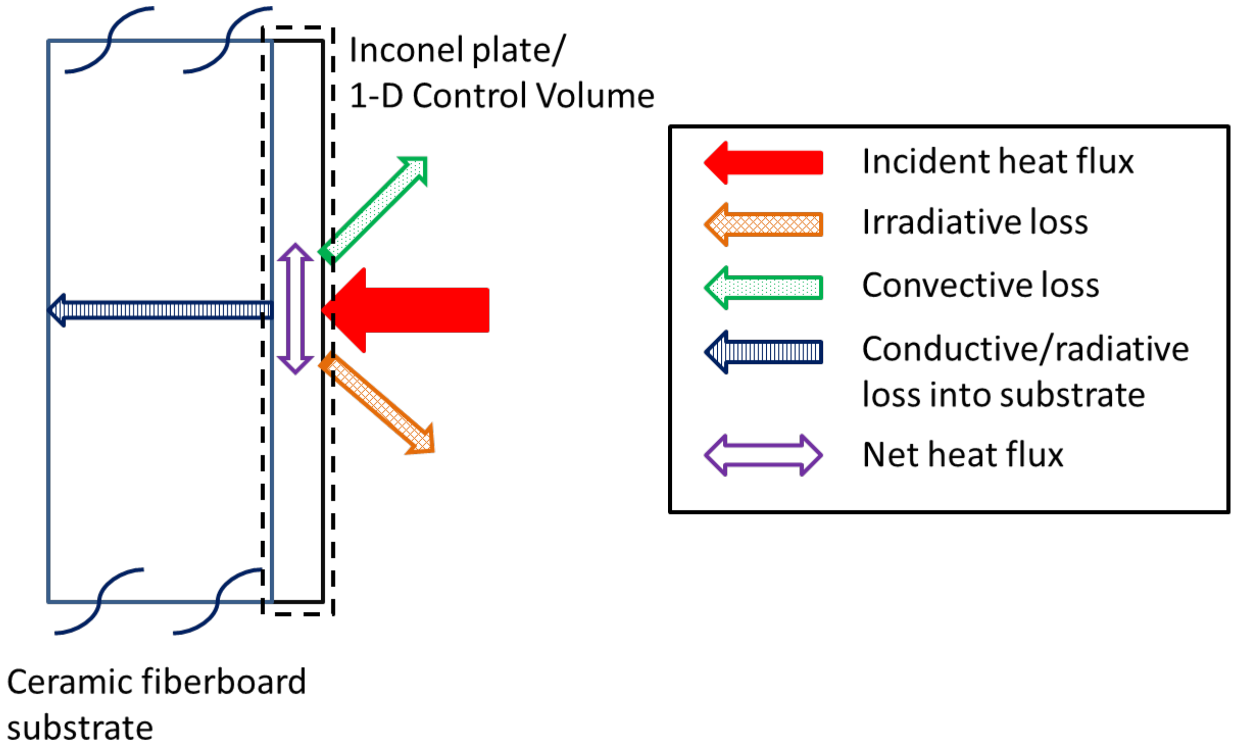

Figure 13 - Heat transfer balance of TSC

Equation (24) shows that the net heat flux is made up of the incident heat flux and a series of heat losses to the environment. The first term on the right $\alpha_s \dot{q}_i^{"}$, represents the fraction of the incident heat absorbed by the plate. The recorded temperature of the plate T_s was assumed to be constant throughout the thickness of the plate because of its thermally-thin characteristics, meaning that the thermocouple's measurement was the same as the temperature at the surface of the plate. The second term on the right $\varepsilon_s \sigma (T_s^4 - T_0^4)$, represents the re-radiative heat transfer from the plate into the ambient environment, which is assumed to be at room temperature at 300 K. Black spray paint was applied to the top surface of the plate to increase the absorptivity and the emissivity of the Inconel surface, these two parameters were determined to be 0.92 from previous research on at WPI[86, 87].

The term $h_{conv}(T_s - T_g)$ represents the convective heat loss from the surface of the plate to the environment. The convection over the plate was assumed to be from a flow moving over the vertical direction. In the inert wall experiments, the convective heat transfer coefficient was determined in two different ways depending on the location of the TSC: for those along the centerline of the burner/plume, forced convection was assumed, for those located 2 ft away from the centerline, free convection was assumed, as shown in Table 21. Assuming that the width of the plume at the wall widen as the height increases, For the TSCs located 1 ft away from the centerline, a forced flow was assumed when the 2 ft Rectangle burner was used, and a free flow was assumed when the 1 ft Square burner was used. The convective heat coefficients were calculated based on a series of non-dimensional numbers such as the

Nusselt number (Nu), the Reynolds number (Re), the Prandtl number (Pr), and the Rayleigh number (Ra), the correlations between these non-dimensional values of a flow are presented in Table 22.

Table 21 - Velocity levels for convective heat transfer coefficient calculation for heat flux

	Velocity at TSCs		
	TSCs on centerline	TSCs 1 ft away	TSCs 2 ft away
Square	Forced Conv.	Free Conv.	Free Conv.
Rectangle	Forced Conv.	Forced Conv.	Free Conv.

Table 22 - Correlations of Nusselt number for use on the thin skin calorimeter

Flow Type	**Location**	**Equation**	**Restrictions**
Forced	Inside plume	$\overline{Nu_l} = 0.664\,\mathrm{Re}_l^{1/2}\,\mathrm{Pr}^{1/3}$	0.6 ≤ Pr ≤ 50
Free/Natural	Outside plume	$\overline{Nu_l} = \left\{0.825 + \frac{0.387 Ra_l^{1/6}}{\left[1+\left(0.492/\mathrm{Pr}\right)^{9/16}\right]^{8/27}}\right\}^2$	None

To find the h_{conv} at the TSC, a series of flow parameters presented in Table 22 must first be calculated in equations (26) to (28). The film temperature is defined as the average between the plate temperature T_s and the flow temperature T_g. Furthermore, the gas temperature measured at the centerline of the plume was used as T_g for forced convection cases, and the ambient temperature was used as T_g for free convection cases.

$$\mathrm{Pr} = \frac{\nu}{\alpha} \tag{27}$$

$$Ra_l = \frac{g\beta(T_s - T_g)l^3}{\alpha\nu} \tag{28}$$

$$\mathrm{Re}_l = \frac{Ul}{\nu} \tag{29}$$

Where $Pr = Prandtl\ number$

$Ra_l = Rayleigh\ number$

$Re_l = Reynolds\ number$

$\nu = kinematic\ viscosity\ of\ air, determined\ at\ T_f\ [m^2/s]$

$\alpha = thermal\ diffusivity\ of\ air, determined\ at\ T_f\ [m^2/s]$

$g = gravity\ [m/s^2]$

$\beta = coefficient\ of\ volumetric\ thermal\ expansion\ [1/K]$

$l = length\ of\ plate\ [m]$

The coefficient of volumetric thermal expansion β was calculated as $\frac{1}{T_f}$, and was used to describe the buoyancy of a hot gas along with the Rayleigh number. The Prandtl number describes the ratio between the momentum diffusivity to thermal diffusivity of a flow. In the calculations, the properties of air at the film temperature were used. The length of the plate is taken as 0.05 m, same as the TSC plate dimensions.

For forced convection, the velocity was assumed to be constant throughout the test and is based on the time-averaged velocity value measured via the bi-directional probe at the same height: plume centerline velocities were used for the flow over the TSC along the center. In some fire tests using the Rectangle burner, the velocity at the TSCs 1 ft away from the centerline was measured about 2.5 cm away from the wall surface, these velocity data was used for the h_{conv} calculation of these TSCs. For plates with specified with free convection, the flow was assumed to be at 0.5 m/s, which is a velocity generally regarded as typical on walls in a compartment fire. Regardless of the location of the TSC or the velocity of the flow over the plate, it was assumed that given the short length and width of the plate (0.05 m x 0.05 m), the flow over the plate was laminar.

The Nusselt number of the flow over plate was found differently for free flow or forced flow condition, as shown by equations (29) and (30), respectively.

Free flow:
$$\overline{Nu_l} = \left\{ 0.825 + \frac{0.387 Ra_l^{1/6}}{\left[1 + \left(0.492/\Pr\right)^{9/16}\right]^{8/27}} \right\}^2 \qquad (30)$$

Forced flow:
$$\overline{Nu_l} = 0.664 \mathrm{Re}_l^{1/2} \Pr^{1/3} \qquad (31)$$

The convective heat transfer coefficient h_{conv} was found based on the Nusselt number using equation (31):

$$h_{conv} = \frac{\overline{Nu_l} k}{l} \qquad (32)$$

The fourth term on the right $(4\varepsilon_b \sigma T_s^3 + h_{cr})(T_s - T_1)$, represents the heat loss into the inert substrate from the back of the plate. The temperature T_1 is the temperature of the ceramic-fiberboard substrate at the surface at the interface with the Inconel plate. According to the theory developed by de Ris and Khan[94], the loss has a radiative component represented by $(4\varepsilon_b \sigma T_s^3)(T_s - T_1)$ and a conductive component represented by $h_{cr}(T_s - T_1)$. The contact resistance (interfacial conductance), h_{cr} was previously determined to have an value of approximately 340 W/m^2K via bench scale validation tests[86]. Due to the interface between the plate and the substrate and the presence of the contact resistance, the temperature T_1 was not the same as T_s, and it was found using an implicit finite difference method based on the boundary conditions imposed by the temperature of the plate T_s and the temperature at the backface of the substrate. The substrate backface temperature was measured by the second thermocouple in a TSC unit. Since both the radiative component and the conductive component of the heat loss depends on both T_s and T_1, a heat transfer coefficient that summarized both the radiative component and the interfacial conductance can be presented in a simpler form as $h = (4\varepsilon_b \sigma T_s^3 + h_{cr})$. It was found that the heat loss into the substrate usually was the most significant out of all of the losses.

For the inert wall fire tests, the incident heat flux measurements are averaged over the time when the HRR was consistent. However, the incident heat flux recorded during the combustible wall fire tests were not averaged due to the non-steady state nature of the experiments. Furthermore, since the flame spread over the wall panel created flow over the TSCs at different intensity and at different time and that the velocity was not explicitly measured at each TSC, the convective heat transfer component of equation (24): $h_{conv}(T_s - T_g)$, was not considered in the combustible wall fire heat flux data.

In series of validation tests of the TSCs using the cone calorimeter, the uncertainty of the heat flux measurement was found to be approximately 2.6 kW/m^2. In a cone test setting, however, the TSCs were only subjected under radiative heat flux insult, there was no flame impingement or forced flow over the plate. It is reasonable to deduce that the uncertainty of the TSC heat flux measurements in an actual fire test should be greater, at least by twice the amount found during cone validation test, so at about 5.2 kW/m^2. Earlier research suggested that the uncertainty may be as great as 10% of the measurement[86]. With this information, it is conservation to estimate the uncertainty of the TSCs to be at least 5.2 kW/m^2, or 10% of the measurements, whichever is greater.

4.2.7 Flame spread rate

The flame spread rate is one of the more difficult quantities to be properly measured during a fire test. For a combustible solid, it is generally defined as a velocity term that describes the speed of the pyrolysis front's movement. Quintiere[3] defines the flame spread velocity of a material through a balance between the rate of energy required for its ignition vs. the rate of energy supplied to the material in equation (32):

$$\rho V_{FS} A c_p (T_{ig} - T_s) = \dot{q} \qquad (33)$$

Where $\rho = fuel\ density\ [kg/m^3]$

$c_p = fuel\ specific\ heat\ [J/kgK]$

$A = cross\ sectional\ area\ of\ fuel\ [m^2]$

$T_{ig} = fuel\ ignition\ temperature\ [K]$

$T_s = fuel\ tempreature\ before\ heating\ [K]$

$V_{FS} = flame\ spread\ velocity\ [m/s]$

The energy balance equation can be rearranged to form the equation for flame spread rate as equation (33):

$$V_{FS} = \frac{\dot{q}}{\rho c_p A (T_{ig} - T_s)} \qquad (34)$$

The flame spread rate as a velocity term works well if the flame spread on a material is essentially one dimensional. However, this is not the case in the combustible wall tests conducted using FRP, since the pyrolysis fronts moved at different direction during different stages of the fire. Hence there is a need to modify the flame spread rate as an area construct to capture the fire movement details. Two methods of flame spread rate determination based on area had been investigated and the results are summarized below.

4.2.7.1 Flame spread rate based on HRR time history

Since the heat release rate of the burning FRP panel is closely related to the flame spread, the HRR can be used to approximate the flame spread area rate by utilizing the material's heat release rate per unit area (HRRPUA) value.

A burning area time-history could be determined from the full-scale FRP panel tests with a constant HRRUPA using equation (34).

$$A_{burning}(t) = \frac{HRR(t)}{HRRPUA} \tag{35}$$

Where $A_{burning}(t) = combustible\ material\ burning\ time\ history$
$HRR(t) = heat\ release\ rate\ of\ fire\ (minus\ source\ burner\ HRR)\ [kW]$
$HRRPUA = average\ combustible\ material's\ heat\ release\ rate\ per\ unit\ area\ [kW/m^2]$

The HRRPUA of the material was previously determined in the cone calorimeter tests of the FRP; however, the cone experimental data shows that the HRRPUA changes over time so its average was used in the full scale test flame spread rate calculations.

Assuming that flame spread rate (FSR) takes the form of area per unit time, its calculation needs to take into the consideration that it is not physically possible to have negative flame spread. So the flame spread rate is of the FRP panel is represented in equation (35).

$$FSR(t) = A_{burning}(t) - A_{burning}(t-1) \quad \text{,only positive, otherwise, zero} \tag{36}$$

A way to ground the FSR calculations was to utilize the final burnt area as an upper bound: total burning area cannot be larger than the final burnt area. The final burnt area of each FRP panel specimen was measured using the 0.1m x 0.1m grid drawn on the panel as a guide to gauge the fire damage to the cell. A rod was used to poke the various cells and the damage to the cell could be determined by observation of the amount of resin left. 100% damage means all resin burnt off, only fiberglass weave left behind, 75% damage suggests only some resin left, mostly fiberglass, 50% damage is where half of the cell's resin remains, 25% damage means most resin survives, and 0% means no fire damage, as shown in Table 23. All cells were assigned a damage index, and the subtotals for each damage range were found, with the total area set to the area of the panel.

Table 23 – Sample of fire damage summary

# of cell	Damage to Resin	Area (m2)
109	**up to 100% damage**	1.09
78	**up to 75% damage**	0.78
9	**up to 50% damage**	0.09
0	**up to 25% damage**	0
92	**no damage**	0.92

It was found that this derivation method for flame spread rate works sufficient well to provide burning area data for 1-D spread case. But since in the current research the flame spread is decidedly two-dimensional at different directions, this method does not provide a sense of the direction of the burn (straight up or skewed), nor the shape of the burning areas, which are important quantities for validation of FDS predictions. Hence another flame spread rate derivation method was investigated and summarized in Section 4.2.7.2. Additional details for this flame spread rate derivation method based on cone-determined HRRPUA is available in Appendix D.

4.2.7.2 Flame spread rate based on video evidence and manual observation

Another method to determine flame spread of the FRP wall panel used the video recordings for analysis. Each burn test was filmed with two digital video cameras usually, head-on, and at an angle to the side of the burn compartment. It was determined that the angled video camera captured the better footage since smoke often obscured the top of the burning panel in the footage by the head-on camera. As such, the footage from the angled video camera was used as the primary source for the flame spread analysis with the other footage and notes made during the test as complimentary sources only.

The angled camera's output was converted from MiniDV format into Windows Media Video (WMV) format, whereas the head-on camera's output was recorded in the high-definition MTS format; both cameras recorded at 30 frames per seconds (fps). Similar to the flame height recordings, Virtualdub-1.9.9 (with plug-ins) was used to extract image sequences from the videos at 1 fps. The images were then imported into the software Tracker-3.10 to track the flame spread by pinpointing the outline of burning areas. Due to the amount of images and limitation of software, the process was performed for every 2 seconds from the video; moreover, it was found that tracking the burning areas every 2 seconds was sufficient because of the relatively slow spread rate.

In order to track the flame spread using video data, it was assumed that the burning areas may be approximated by rectangular shapes and the progression was separated into 3 phases as shown in Figure 14 from left to right. In the early phase of the wall panel fires, the burning area may be summarized as a centered rectangle A that was bounded at the burner's edge at the bottom with an upper bound (pyrolysis front) that progressed upward; but as the panel burn, the lower bound of the rectangular area also moved up.

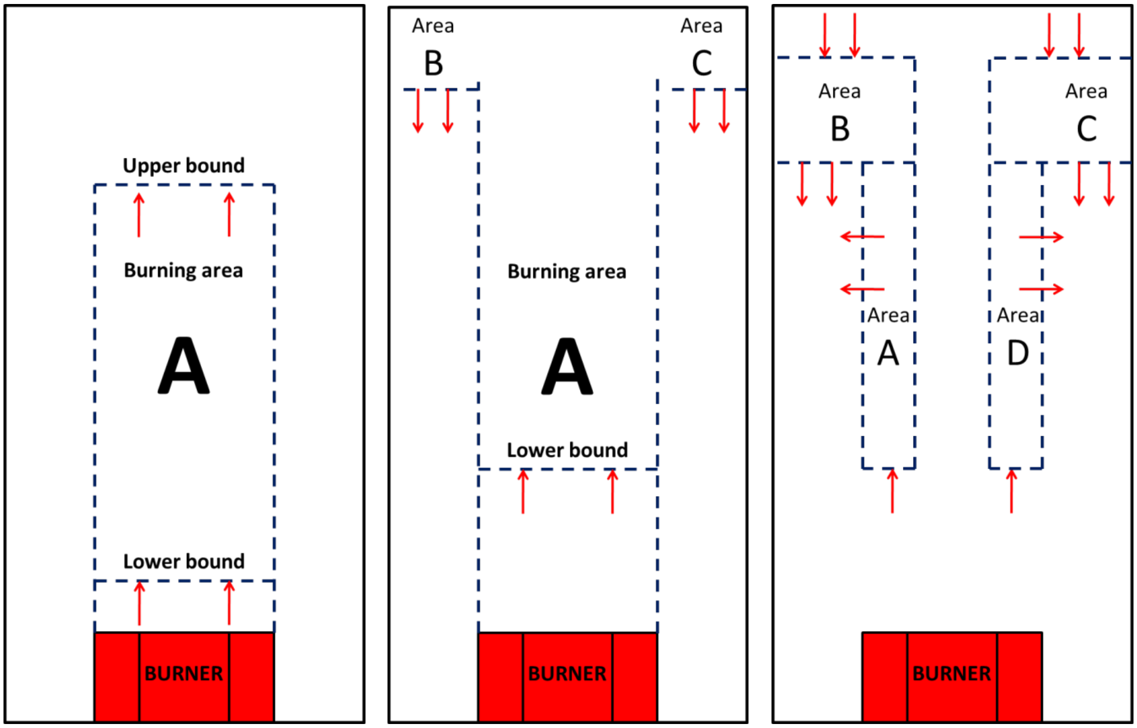

Figure 14 - Burning area progression, from left to right (early to late stages)

After the initial burn period, flames reached and became bent at the ceiling and the fire spread to the edges of the wall panel and the burning area, obtaining a "T" shape with a downward-moving horizontal top-bar. At this stage the burning area may be approximated by three rectangles A, B and C, all bounded at the top by the top edge of the wall panel. The central rectangle A shrink from the bottom edge up, but the flange rectangles B and C's bottom edge (pyrolysis front) progressed downward. During this time there was usually little lateral spread to the vertical sides of rectangle A.

At the later stage of major flame progression, the area along the center was burnt out and the burning area could be described by Areas A, B, C and D. The Areas A and D regressed upward and outward, whereas the horizontal edges (pyrolysis fronts) of Areas B and C continued moving downward. After this stage of flame spread, the burning that remained was in the form of line fires where the burning area cannot be accurately measured given the resolution of the video footage.

In the tracking process, the positions of the corners of the fire were recorded using Tracker. Since the edges of the fire were not straight, some post-processing, such as averaging the x- or y- coordinates at certain points, was performed to the location data to create straight rectangular shapes that conform to those presented in Figure 14.

Although this method of flame spread measurement was reasonably accurate and may be used to compliment the HRRPUA method, however, there are some limitations to this analysis. First of all, the quality of the video footage dictated the quality of the base data. The high-definition video data recorded high quality image but the top of the wall panel image was obscured by smoke; the standard-definition video from the angled camera recorded more details, such as flame attachment, that made burn area tracking easier in the SD video than from the front-view HD video, although at a much lower resolution. The 0.1m x 0.1m square grid drawn on the wall panel sufficiently aided in the tracking process, and the resulting largest uncertainty could be estimated to be two grid length 0.2 m or four grid area 0.04 m^2, based on the drawn grid, the manual tracking process, the position of the camcorder, and the resolution of the images.

The burning area time-history was developed from the total burning areas based on the rectangle area estimation method over a minimum of 180 seconds, starting from the point when flame attachment was visible on the FRP panel. The burning area was found to increase from Stage 1 until the end of Stage 2, then decreased in Stage 3 and the subsequent line burning. There were some scatters in the data mainly due to the sensitivity of the manual tracking method. Nevertheless, this method presents a more illustrative view of the flame spread progress than the other method by showing the actual burning areas' movement and progression.

4.3 Free plume fire experimental data

The free plume fire tests were the simplest scenario with the least amount of data collected: HRR, centerline plume temperature, centerline plume velocity, and flame height. These measurements are related to the fluid dynamics/turbulence and gas phase kinetics components of flame spread.

4.3.1 Heat release rate

The time-averaged heat release rate measured in each of the propane and propylene free plume fire test is presented in Figure 15. All of these tests used either a 75 kW or a 50 kW source fire. As discussed in Section 4.2.1, HRR was calculated at each test using the flow rate method and oxygen calorimetry. The O_2-based HRR has an uncertainty of 25 kW, the flow-based HRR has an uncertainty of 13 kW, and both values are within each other's uncertainty. Additionally, the uncertainties of all HRRs fall within their intended HRR level. The difference between the two HRR methods appears to increase from about 6 kW in for the 50 kW fires to about 20 kW for the 75 kW fires.

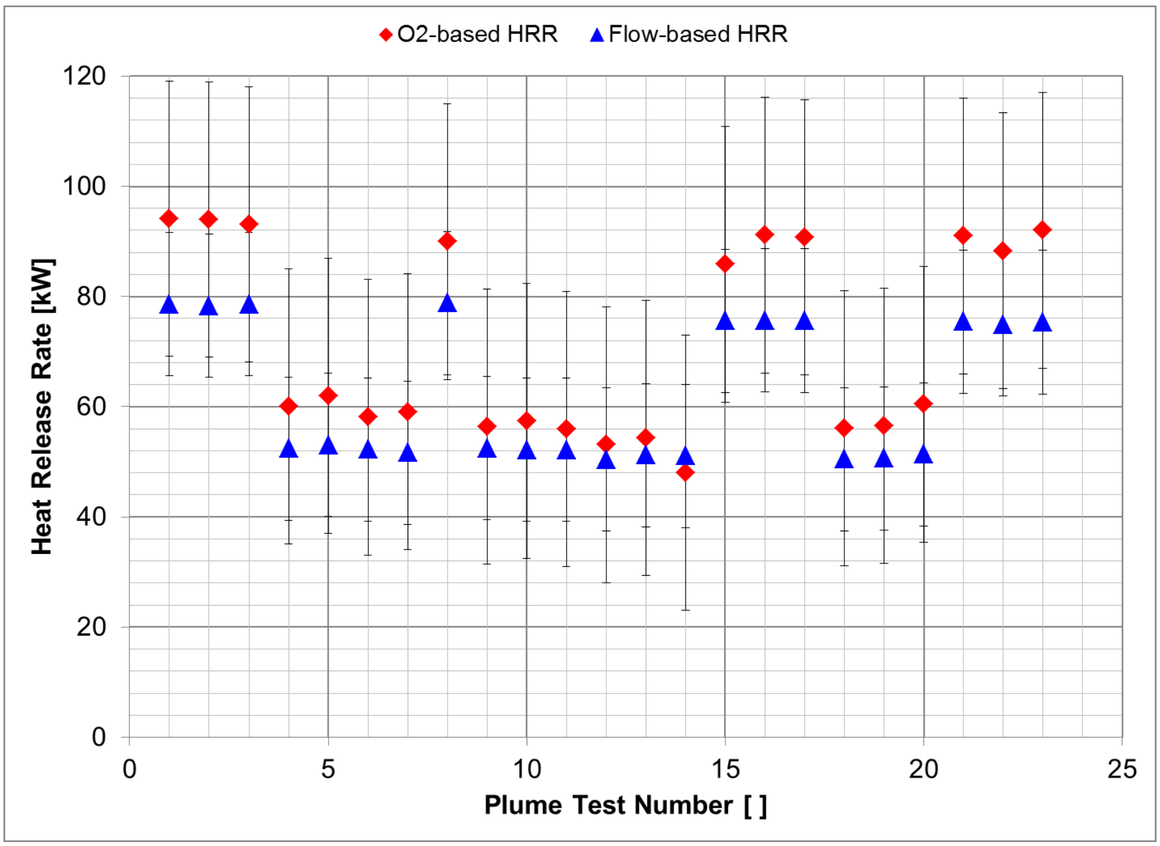

Figure 15 - Heat Release Rate from Free Plume Fire Tests

Figure 15 also shows that even though the O_2-based HRR was corrected with a C-factor of 0.77, the spread of the data away from the intended HRR levels is greater than the flow-based HRR values. Hence, the flow-based HRR values are more consistent and used in the other analyses as a normalizing agent where needed.

4.3.2 Centerline temperature

The corrected and uncorrected centerline temperature of the plume and inert wall fires are presented in this section. The correction method used was developed by Blevins and Pitts, and it was applied to the time-averaged centerline temperature data measured during the tests. It is expected that the uncertainty in the temperature measurement is represented by the range between the corrected and uncorrected temperature measurements, and the actual plume temperature lays within the ranged with the upper limit at the corrected values and the lower limit at the uncorrected values.

Figure 16 shows the temperature of methane free plume fires from the 1 ft Square burner as compared to the McCaffrey's methane plume data and theory[49]. The comparison here is made between fires using the same fuel type and sized burners. The height over the burner had been normalized with the convective HRR. For the region close to the burner surface up to 0.05, the measured and corrected temperature were greater McCaffrey's data and theory, however between the normalized height value of 0.05 and 0.15, the corrected temperature were in line with McCaffrey's data and theory. After 0.15, the corrected temperature is within the distribution of the McCaffrey data although the uncorrected temperature is lower.

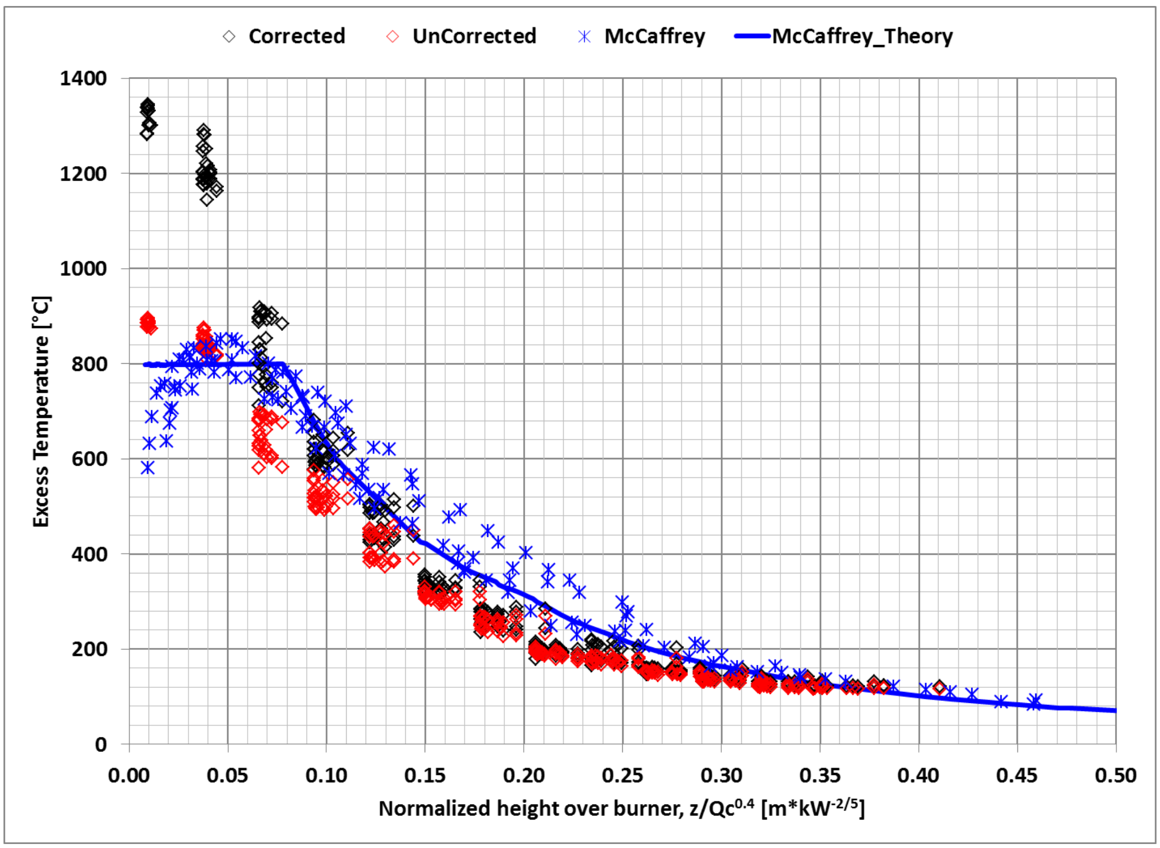

Figure 16 – Centerline temperature of methane fires using 1 ft Square burner, normalized with convective HRR

A comparison between the 1 ft Square methane free plume fire centerline temperature and McCaffrey's data normalized against the flame heights is presented in Figure 17. The same trends are noted as in the comparison using the other normalization method using the convective HRR.

This suggests that the current methane centerline temperature data relates well with McCaffrey's data within a reasonable range.

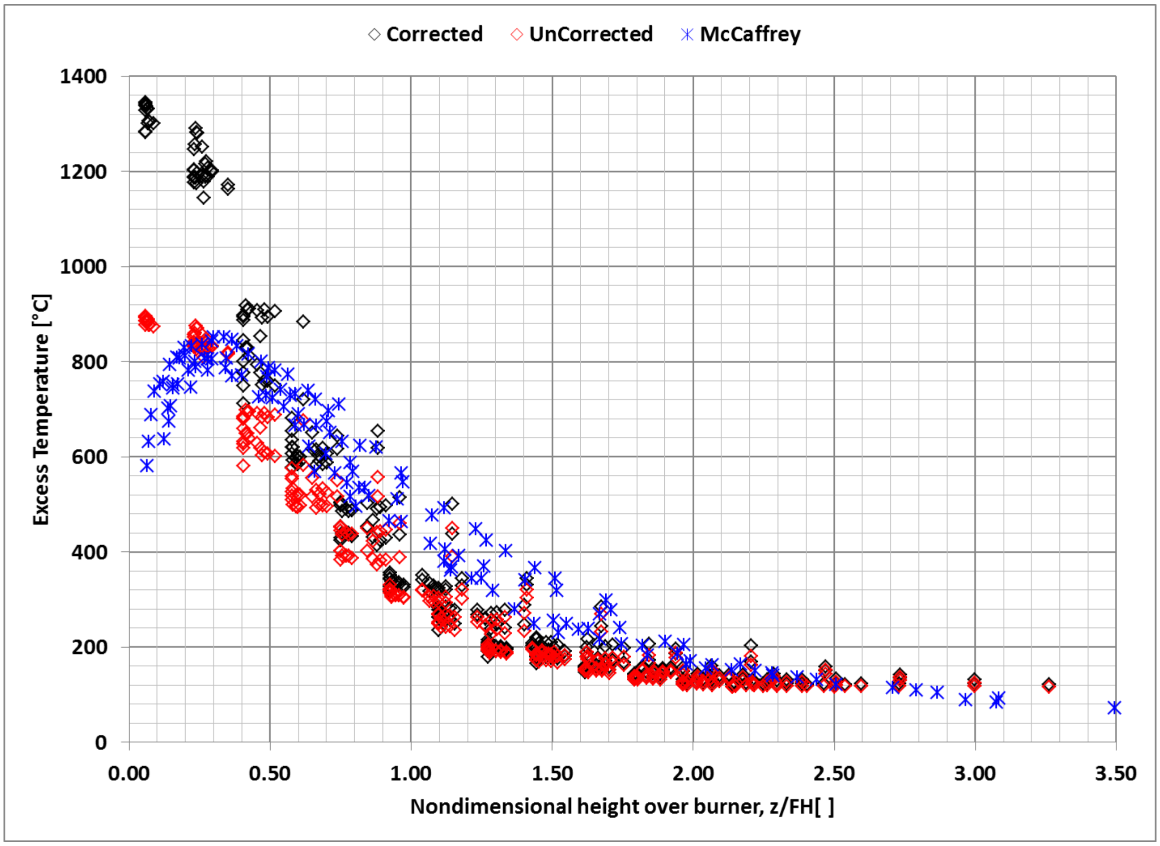

Figure 17 - Centerline temperature of methane fires using 1 ft Square burner, normalized with mean flame height

Figure 18 shows the centerline temperature of all free plume fires using the 1 ft Square burner normalized with convective HRR. Both corrected and uncorrected temperatures are plotted, and the real gas temperature should be within these two sets of values. The correction often increased the measured temperature by 50% for normalized height < 0.05, but it significantly decreases as z increased. It can be observed that the McCaffrey's theory cut between the two bands of data. The relatively tight grouping of the data across the different fire fuel type shows the effectiveness of the normalization method.

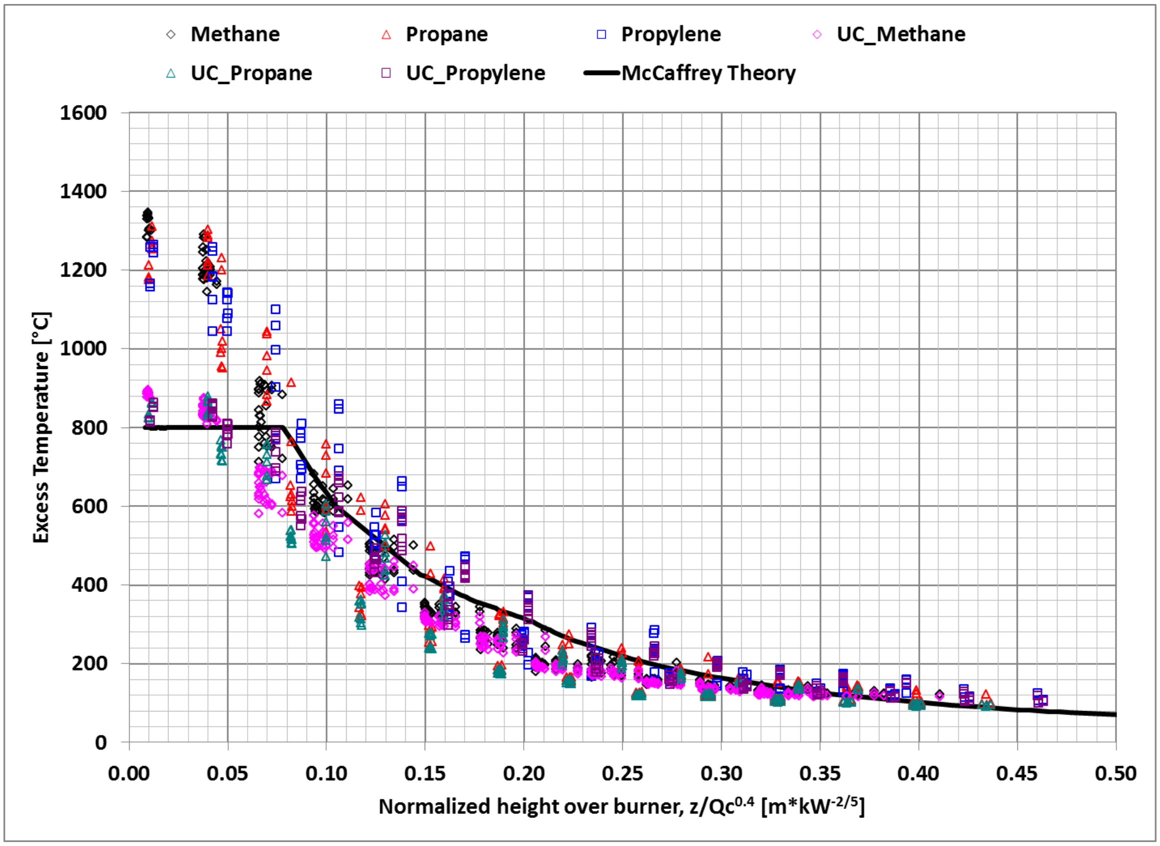

Figure 18 - Centerline temperature of all free plume fires using 1 ft Square burner, normalized with convective HRR

Figure 19 shows the centerline temperature of all free plume fires using the 2 ft Rectangle burner normalized with convective HRR. Both corrected and uncorrected temperatures are plotted, and the real gas temperature should be within these two sets of values. The correction often increased the measured temperature by 50% for normalized height < 0.05, but it significantly decreases as z increased. It is observed that compared to the centerline temperature of the 1 ft Square burner fires and McCaffrey's theory, the temperature generated using the 2 ft Rectangle burner was much lower starting from normalized height = 0.05. This is reasonable because of the shorter flames from the Rectangle burner.

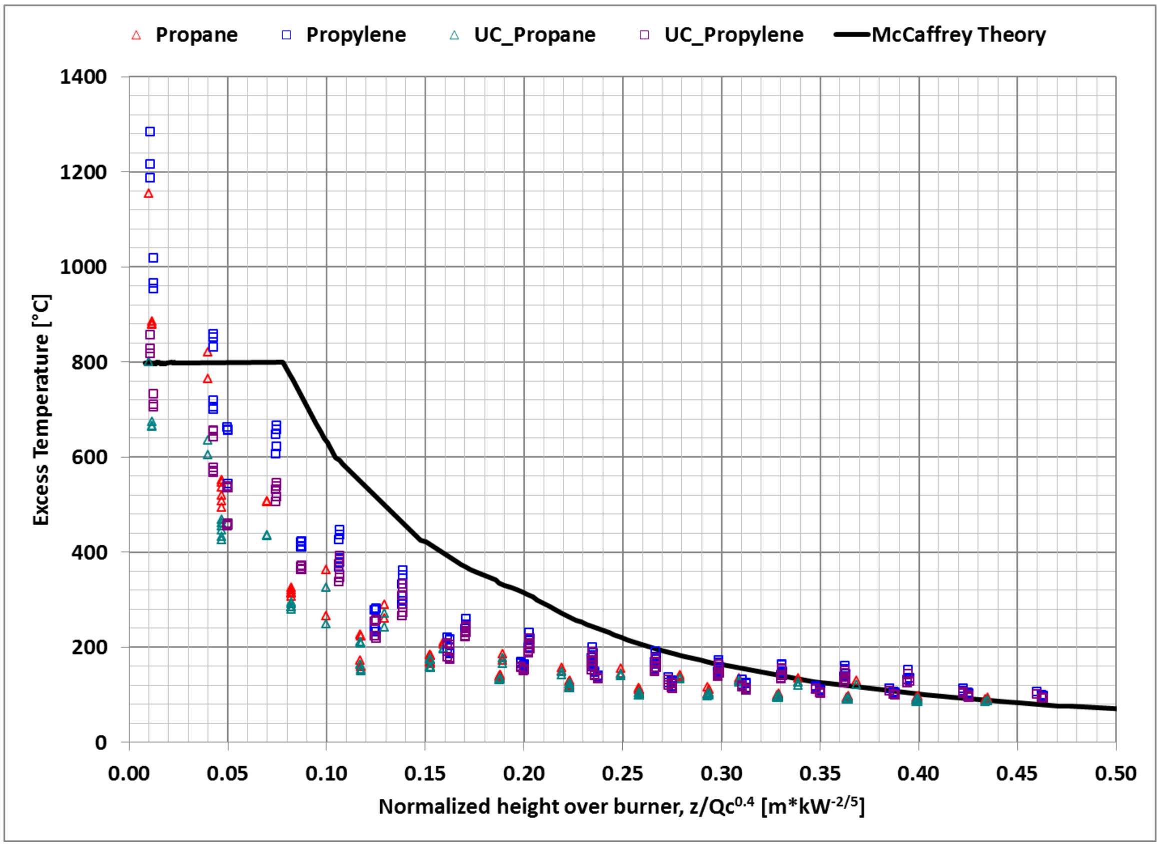

Figure 19 - Centerline temperature of all free plume fires using 2 ft Rectangle burner, normalized with convective HRR

The free plume temperature data is normalized using the mean flame height and presented in Figure 20 to Figure 21. The two different sets of corrected and uncorrected data still formed two bands of temperature "limits" but overall the temperature distribution is tighter when normalized against mean flame height than when normalized with the convective HRR. The tight grouping of the data across the different fire fuel type shows the effectiveness of the normalization method.

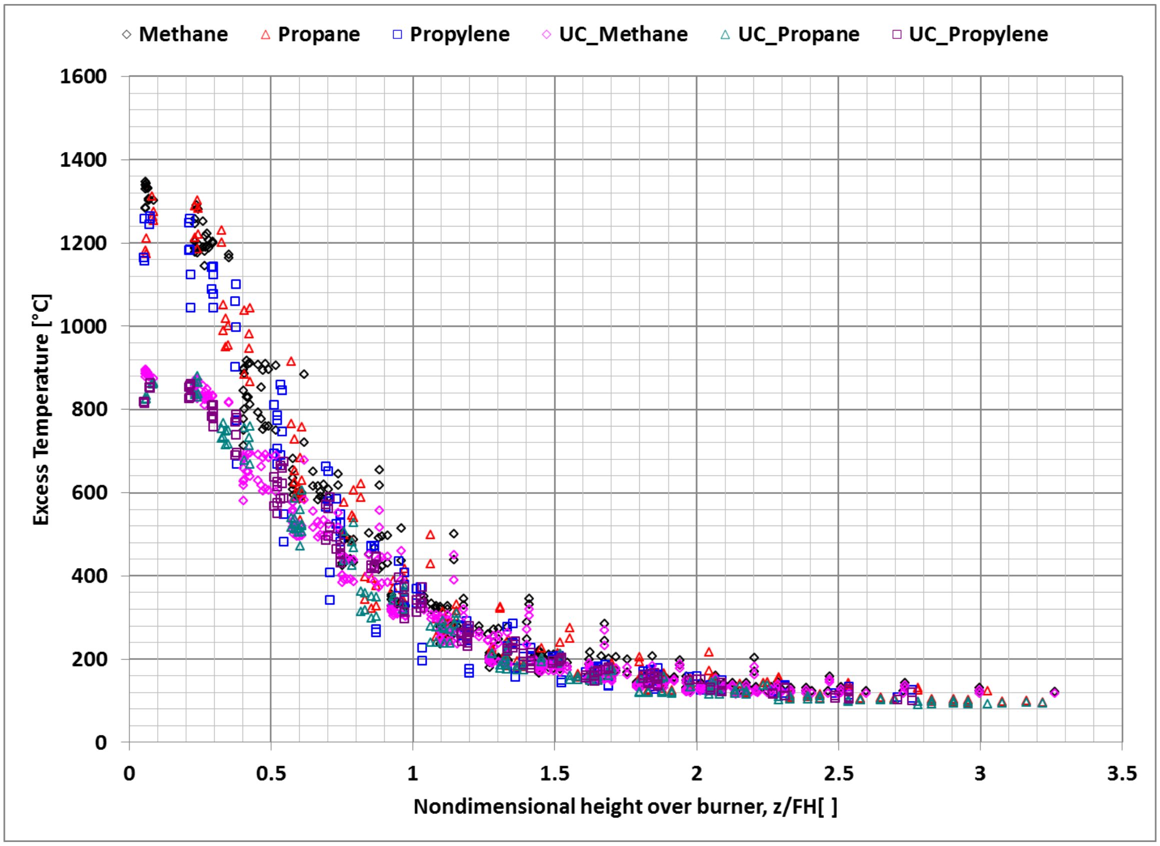

Figure 20 - Centerline temperature of all free plume fires using 1 ft Square burner, normalized with mean flame height

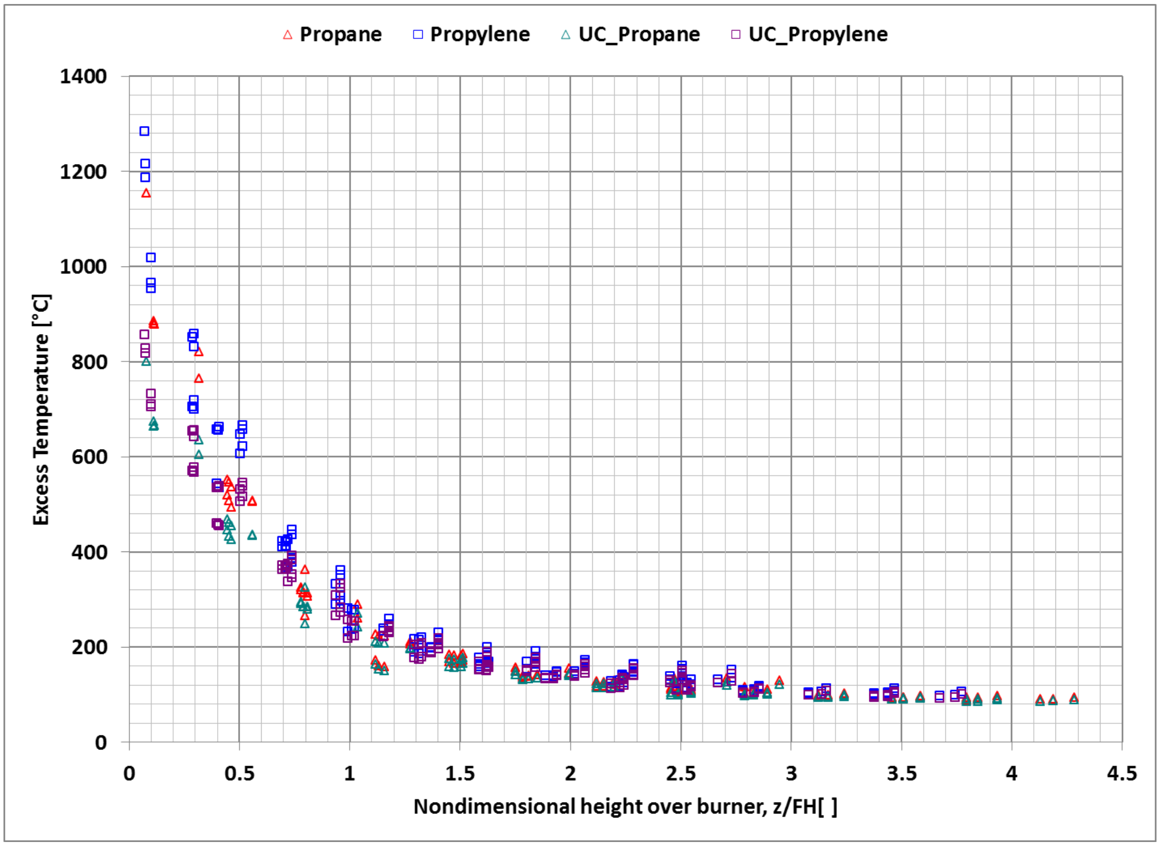

Figure 21 - Centerline temperature of all free plume fires using 2 ft Rectangle burner, normalized with mean flame height

4.3.3 Centerline velocity

In the current study, normalization has been applied to the data in the two different ways used by McCaffrey and by Hesemi. They are of similar format, but with McCaffrey relying on the measured HRR, where Hasemi used a characteristic HRR, the hydraulic diameter of the burner, and the virtual origin. Both methods had been applied to the current data, McCaffrey's data, and some of Hasemi's data where possible. (In his article, Hasemi had reported data under both normalization methods; however, some of the data were reported without the necessary information to deconstruct the data to be transformed for different ways of comparisons).

A drawback to directly compare the current dataset with McCaffrey's and Hasemi's is that the fuels of the source fire were different: McCaffrey used methane and Hasemi used propane exclusively, and loose correlation between the datasets could be due to fuel effects. To combat this, an equalization method was applied to the data by finding the convective HRR from each test and from the dataset (where possible) and back-calculating the reported normalizations through the use of the convective HRR. By using this method, the most significant differing feature of the fire based on the fuels, which is the radiative heat output, was taken out of consideration and the data can be compared on equal grounds. Note that the McCaffrey's data is from a series of tests using a 1' x 1' Square burner; Hasemi's data is from tests using a diameter=0.2 m, 0.3 m, 0.5 m circular burner and square burner with sides at 0.2 m, .3 m, and .5 m.

Since McCaffrey also reported the mean flame height recorded during his fire tests along with the velocity data, an attempt was made to use the mean flame height as a means for normalization. In this method, the heights of the bi-directional probe were normalized against the mean flame heights. The non-dimensional height was found using equation (36):

$$Z_{FH} = Z / FH \tag{37}$$

Where:

$Z_{FH} = Non-dimensional\ height$
$Z = Height\ of\ bi-directional\ probe\ above\ burner$
$FH = mean\ flame\ height\ of\ source\ fire$

In this normalization, the velocity was not non-dimensionalized, but is reported in unit of m/s. Both the current data and McCaffrey's data were normalized using this method for comparison. Similar to the normalizing of McCaffrey's data to account for the convective heat released, his plume centerline velocity data from fires with different HRR was back-calculated to instrument height [m] and velocity [m/s], then equation (36) was used to normalize the height.

To find the uncertainty in McCaffrey's dataset normalized with the convective HRR, velocity data at similar normalized height (0.01 m/kW$^{0.4}$) were grouped together and the standard deviation within each group was found. A similar approach was used to find the uncertainty in the flame height normalized dataset, but an interval of the nondimensional height at 0.05 was used instead. It is assumed that the largest standard deviation value should sufficiently represent the uncertainty in McCaffrey's data. The uncertainty in McCaffrey's velocity, normalized with the convective HRR was found to be about 0.13 $m\ s^{-1}\ kW^{1/5}$, and is about 0.72 m/s when normalized with the mean flame height.

The uncertainties in the current dataset were found using the above methods; an uncertainty is associated with each burner size and test type and shown in Table 24.

Table 24 - Velocity data uncertainties based on different factors

Burner Size	Test Type	Uncertainty in velocity
Convective HRR Normalization		
1 ft Square	Free plume	0.28 $m\ s^{-1}\ kW^{1/5}$
2 ft Rectangle	Free plume	0.28 $m\ s^{-1}\ kW^{1/5}$
1 ft Square	Inert wall	0.23 $m\ s^{-1}\ kW^{1/5}$
2 ft Rectangle	Inert wall	0.40 $m\ s^{-1}\ kW^{1/5}$
Flame Height normalization		
1 ft Square	Free plume	0.84 m/s
2 ft Rectangle	Free plume	0.94 m/s
1 ft Square	Inert wall	1.33 m/s
2 ft Rectangle	Inert wall	1.42 m/s

Centerline velocity of the free plume fire tests conducted with the 1 ft Square burner, with the mean flame height normalization is presented in Figure 22. The current data falls mostly within the uncertainty of McCaffrey's data for the velocity measured up to 2.5 times the mean flame height. At 1.5 to 3 times of the mean flame height, velocity of the propane and propylene fires falls out of the uncertain range of McCaffrey's data. It is noted that the current data from methane fires correlate quite well with McCaffrey's data from methane fires since both study used same-sized burner and fuel.

The uncertainty of the measured data is about 0.84 m/s.

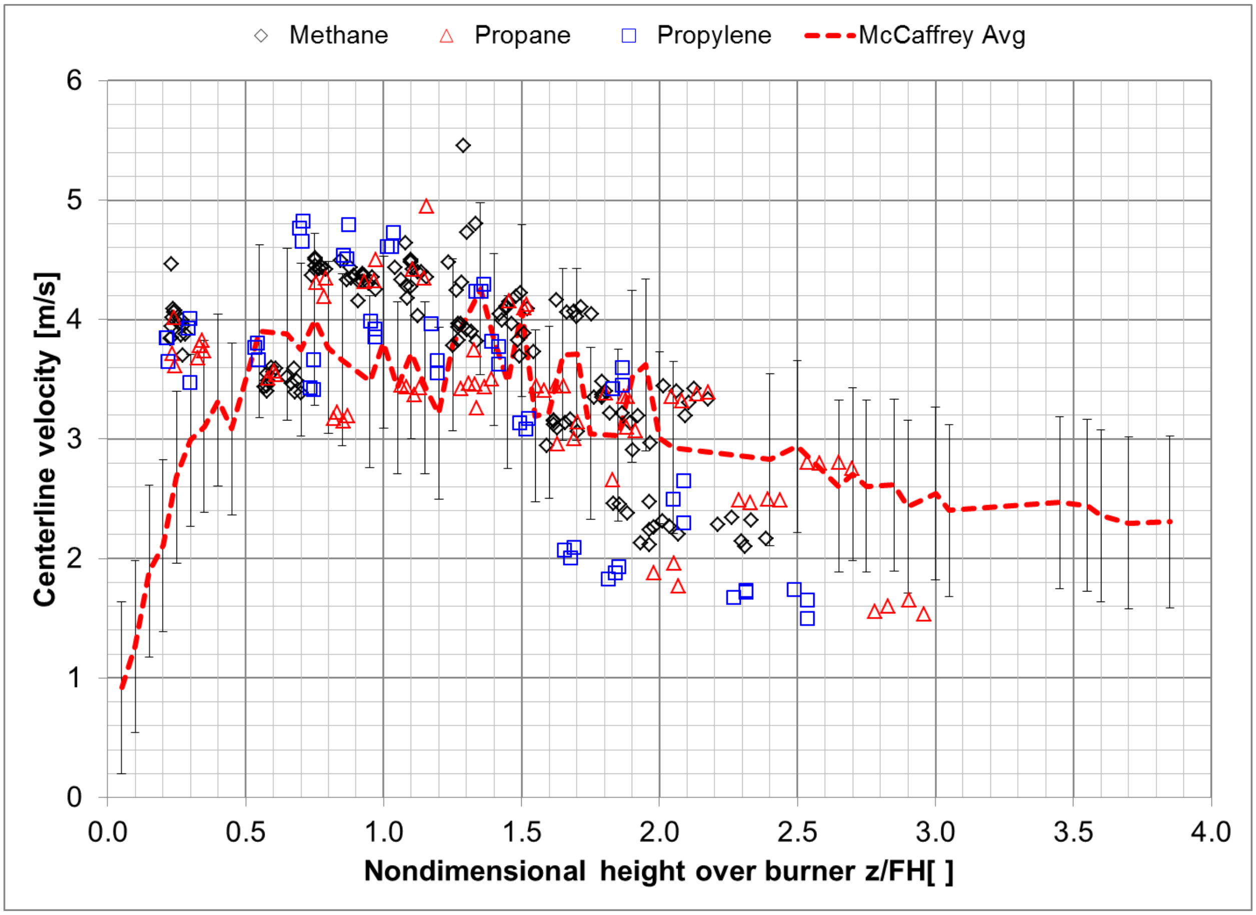

Figure 22 – Free plume fire test centerline velocity, 1 ft Square burner, normalized with mean flame height

Centerline velocity of the free plume fire tests conducted with the 1 ft Square burner, normalized with the convective HRR is presented in Figure 23. The current data generally falls out of the range of McCaffrey's data with uncertainty, although some good correlation is observed in the methane test data. At the normalized height above 2.5, the measured velocity falls below that of McCaffrey's data. The uncertainty of the measured data is about 0.28 m s^{-1} $kW^{1/5}$, more than twice that of McCaffrey's.

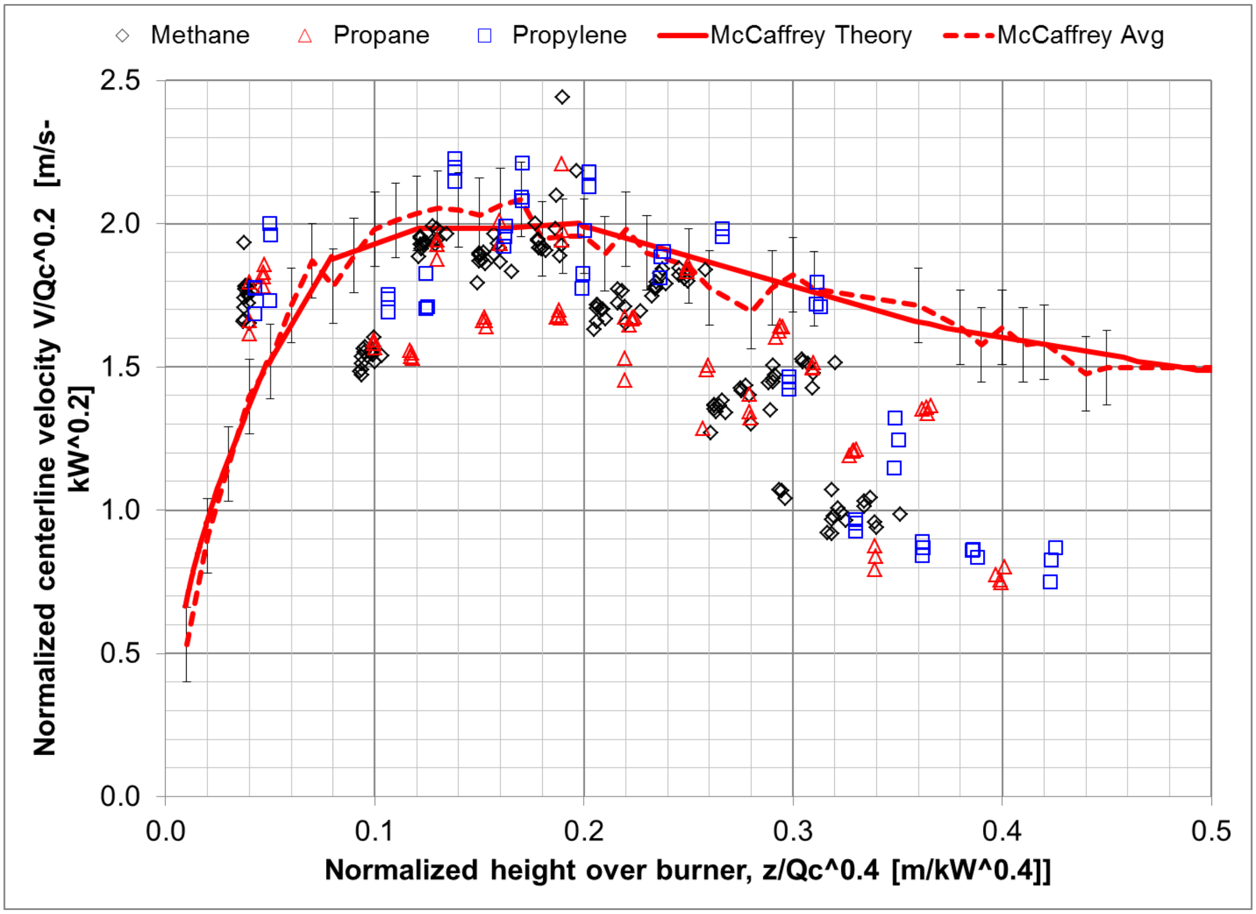

Figure 23 – Free plume fire test centerline velocity, 1 ft Square burner, normalized with convective HRR

Figure 24 presents the centerline velocity from the free plume tests conducted with the 2 ft Rectangle burner, as normalized with mean flame height. The current data falls mostly within the uncertainty of McCaffrey's data. But at over 2 times the mean flame height, some of the measured velocity falls below McCaffrey's uncertainty.

The uncertainty of the measured data is about 0.94 m/s, higher than that of the free plume using 1 ft Square burner. This is reasonable since the plume above the Rectangle burner was observed to fluctuate more.

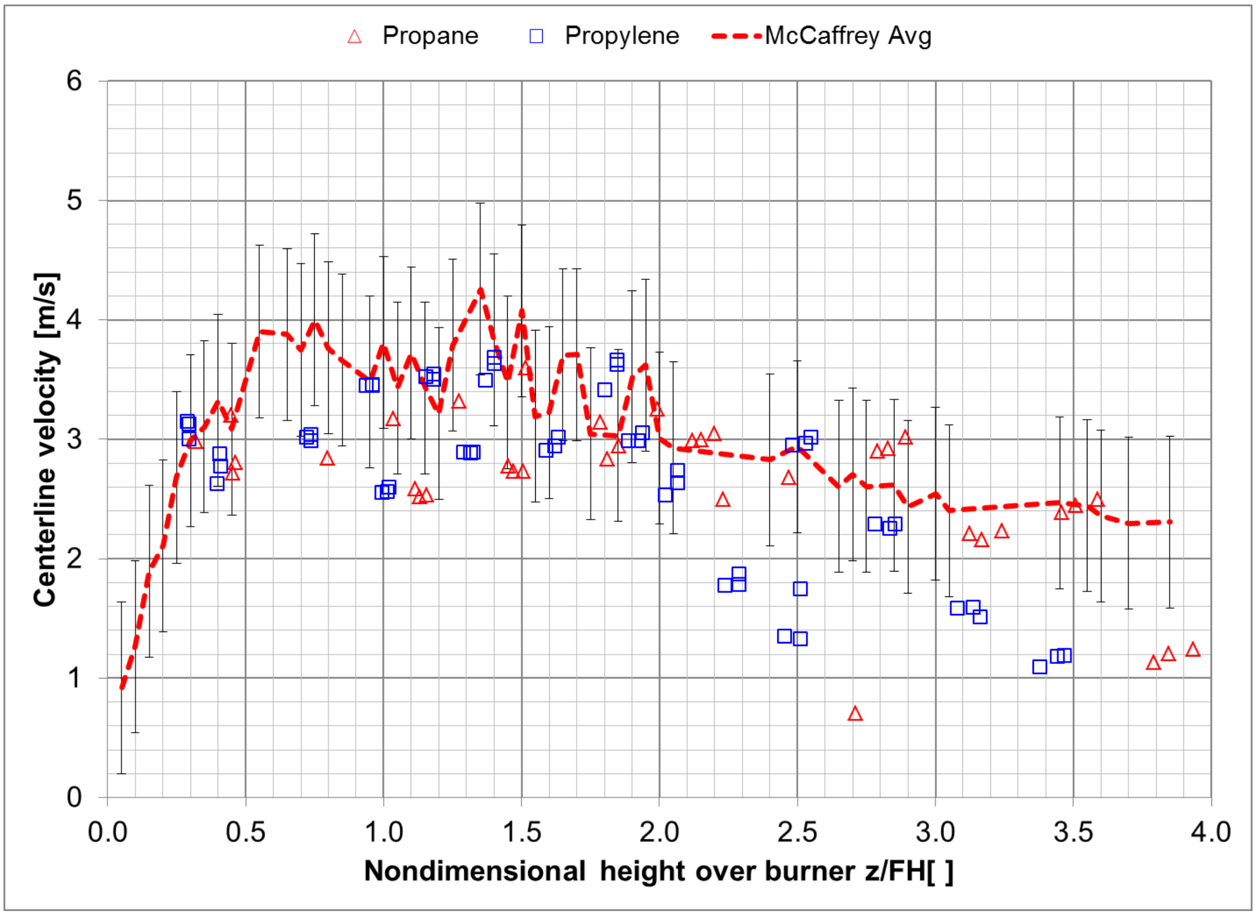

Figure 24 - Free plume fire test centerline velocity, 2 ft Rectangle burner, normalized with mean flame height

Figure 25 presents the centerline velocity from the free plume tests conducted with the 2 ft Rectangle burner, as normalized with the convective HRR. The current data falls mostly below the uncertainty of McCaffrey's data except for the velocity measured at normalized height at 0.05 m/kW$^{0.4}$.

The uncertainty of the measured data is about 0.28 m s^{-1} kW$^{1/5}$, more than twice that of McCaffrey's.

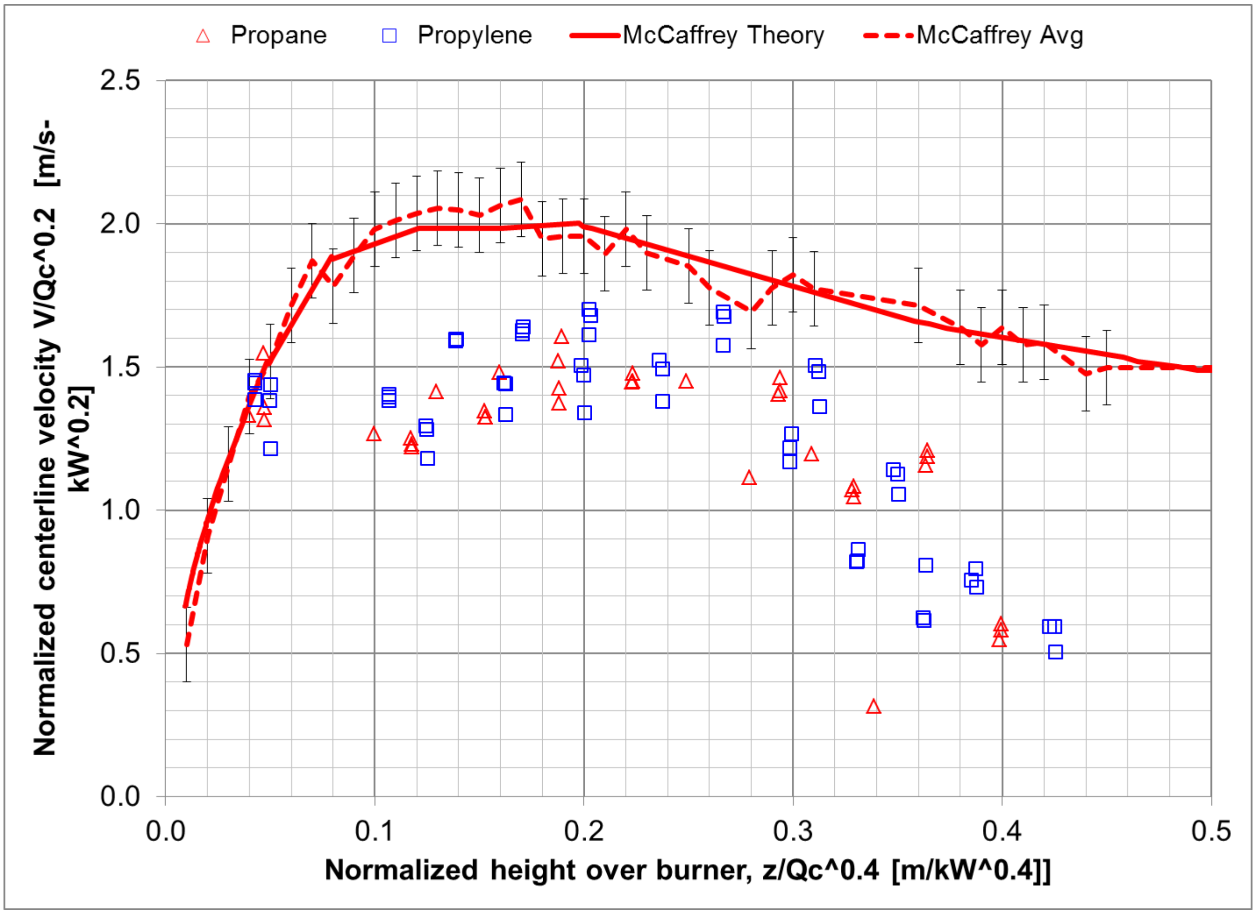

Figure 25 - Free plume fire test centerline velocity, 2 ft Rectangle burner, normalized with convective HRR

4.3.4 Flame height

The comparison between current data normalized to the method used by Zukoski to his and Anderson's correlation is presented in Figure 26. Current data falls between Anderson's and Zukoski's correlations and it is shown that Propylene fires seem to have a higher non-dimensional flame height than propane fires, which is in turn higher than methane fires. This is expected because of the varying fuels' properties.

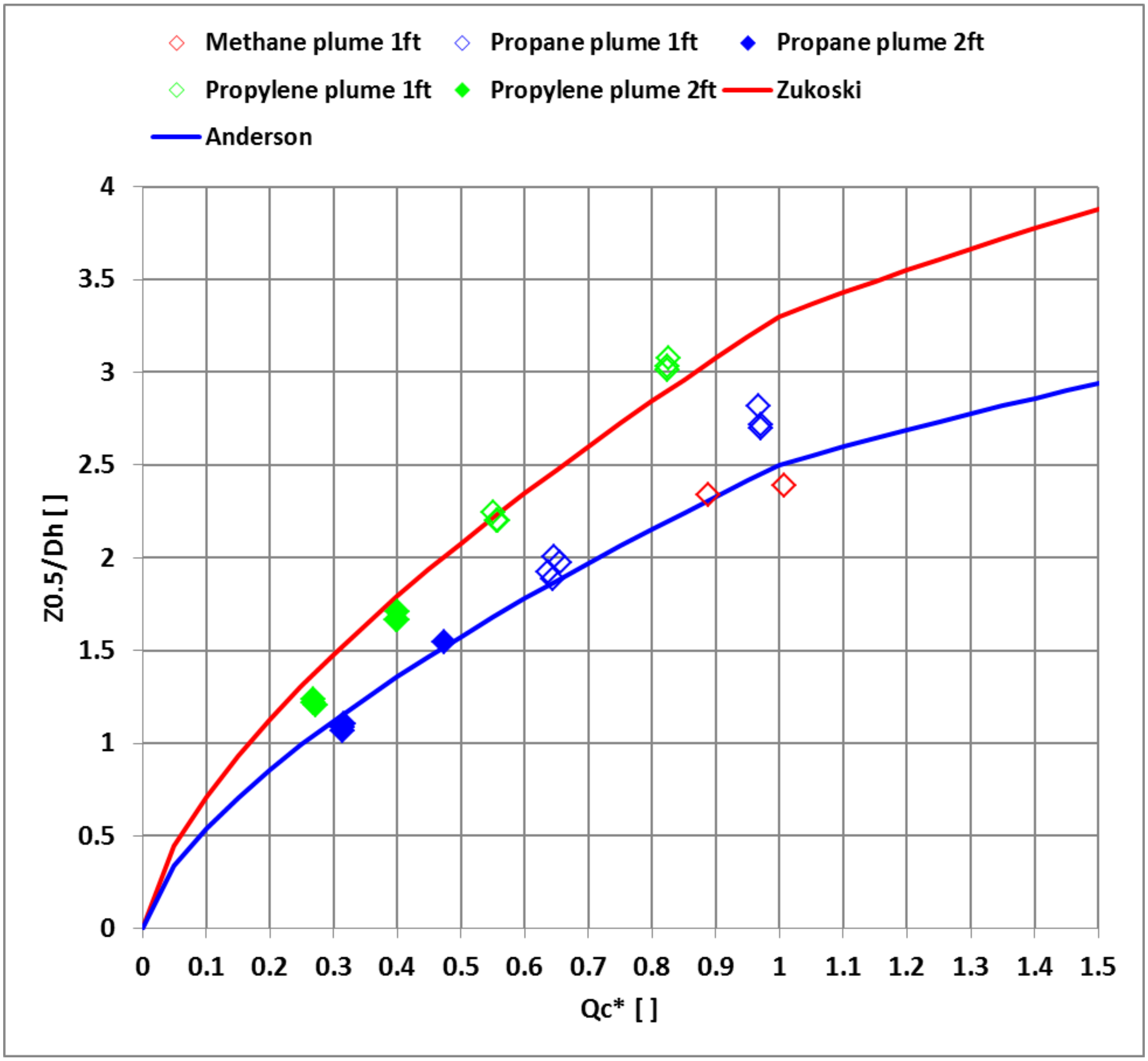

Figure 26 - Comparison of current free plume flame height data with Zukoski's and Anderson's correlations

Alston and Dembsey's data suggested that there is little distinction in flame height between similar sized square and circle burner, but propane fires had taller flame than propylene fires which are similar to methane fires, as shown in Figure 27. The uncertainty of their data is reported to be about ±5 cm or ± 0.2 in non-dimensional term, which overlaps the current data (with normalized convective HRR) for Q* < 0.6 only, for propane and propylene. Past Q*>0.6, the observed flame heights are lower than that predicted using Alston and Dembsey's data. However, it should be noted that the geometric effects of the source burner appear to have been normalized successfully since the observed flame heights using the Rectangle fall within the uncertainty of the correlations, which were generated using a square and a circular burner.

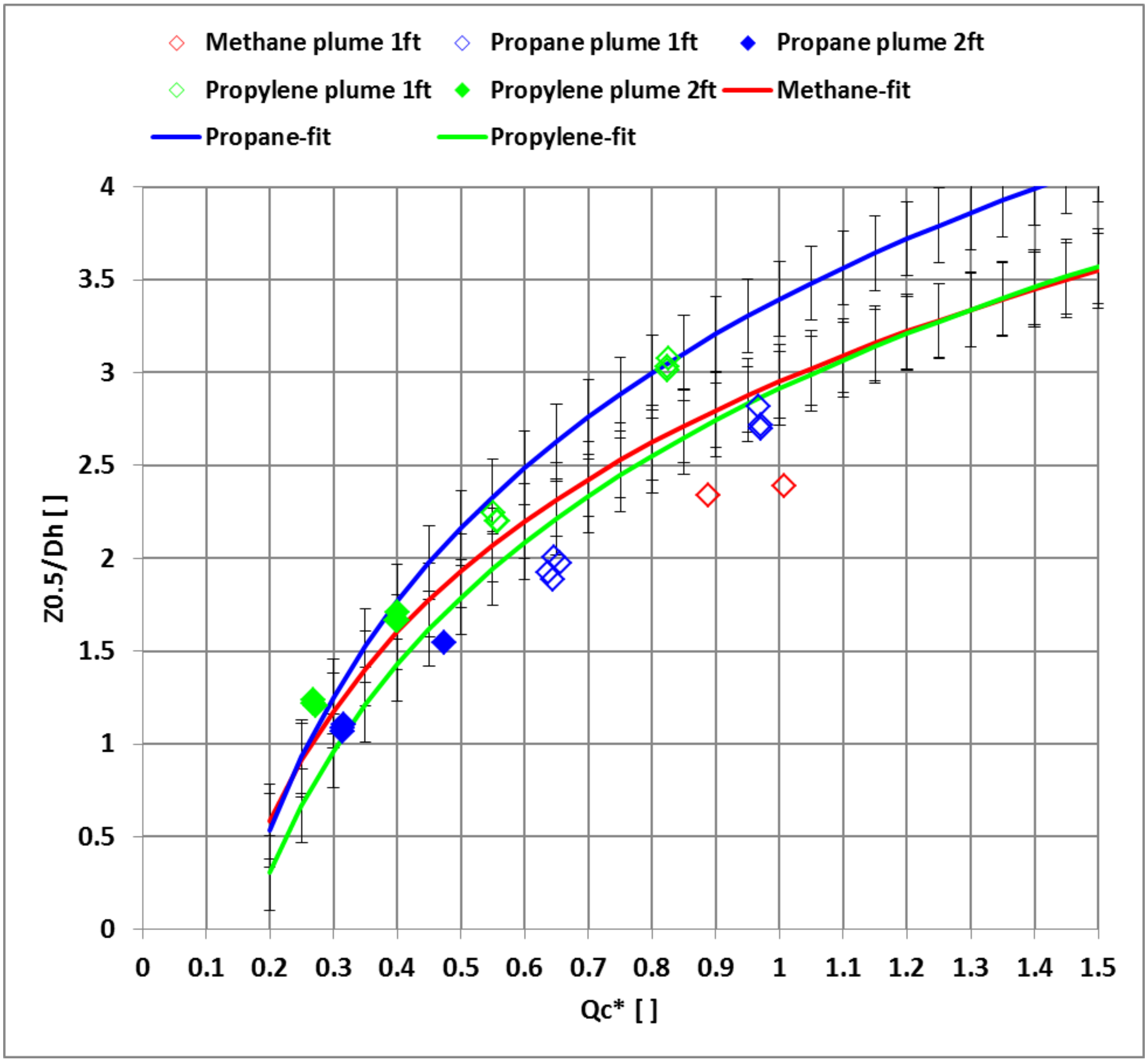

Figure 27 - Comparison of current free plume flame height data with Alston and Dembsey's data-fitted lines

The non-dimensional parameter N (based on the convective HRR) was determined for the current data to be plotted against the measured flame height in Figure 28. Using the total heat release rates of methane, propane, and propylene, Heskestad's correlation suggests that the propylene flame height is taller than the propane and the methane flame heights, which is also observed in the current dataset. The uncertainty of the Heskestad's correlation is reported by Anderson to be about 15-20%, making the current data falls within range of the uncertainties, except for the measured methane test flame height.

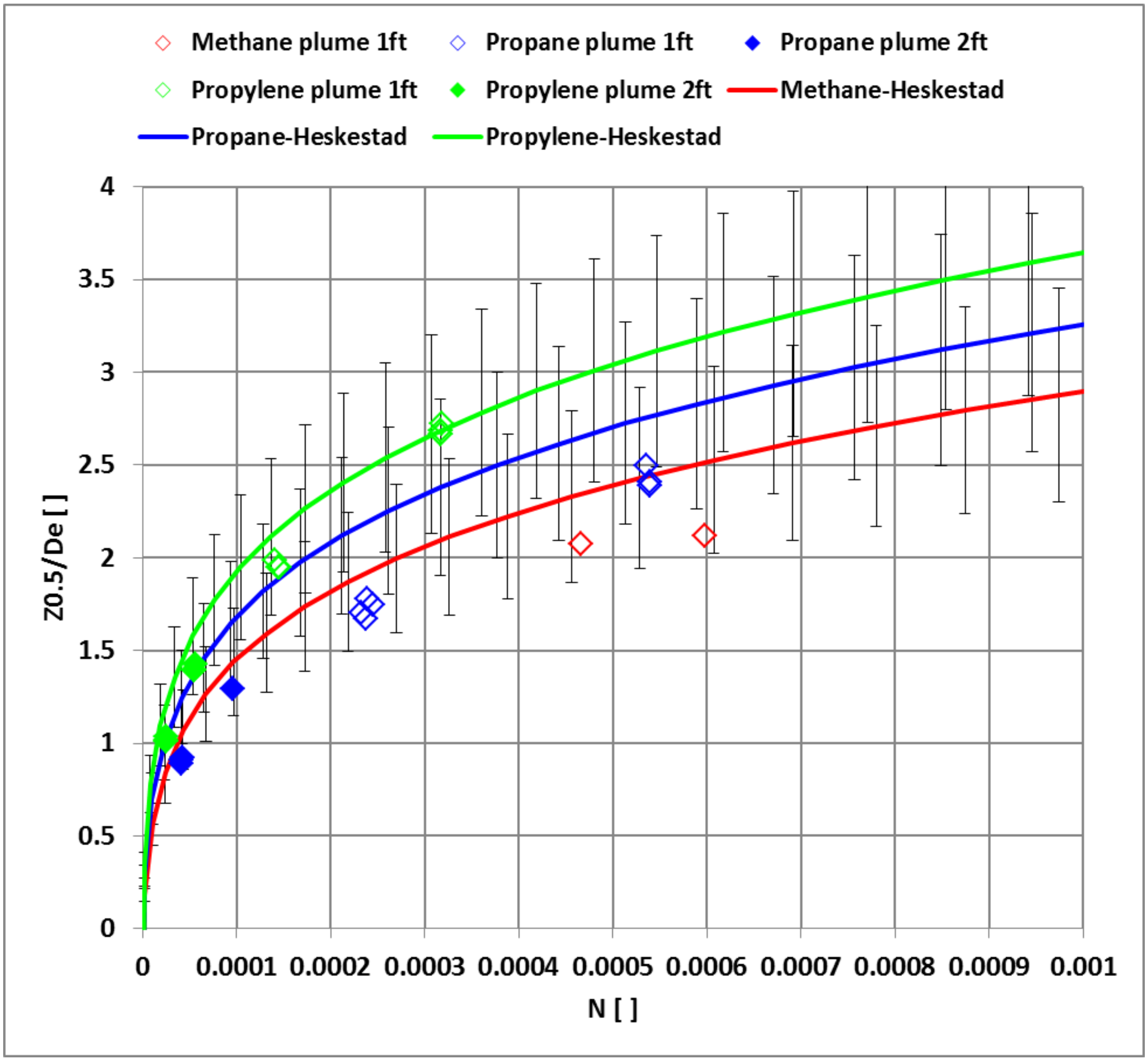

Figure 28 - Comparison of current free plume flame height data with Heskestad's correlation

Figure 29 shows that Quintiere and Grove's correlation makes no distinction between the flame heights of a propane or propylene fire and that curiously the flame height from the Rectangle burner is higher than the Square burner. The correlation for the Rectangle was generated from data from Hasemi and Nishihata[95].

However, contrary to the correlation, in the current data the propylene fires had taller flame heights than propane fires and so did the Square burner over Rectangle burner fires. It should be noted that the propane Square burner flame heights correlate very well with the Q+G correlation for propane and propylene fires whereas the flame heights measured from the Rectangle source fires fall outside the correlation by a large margin.

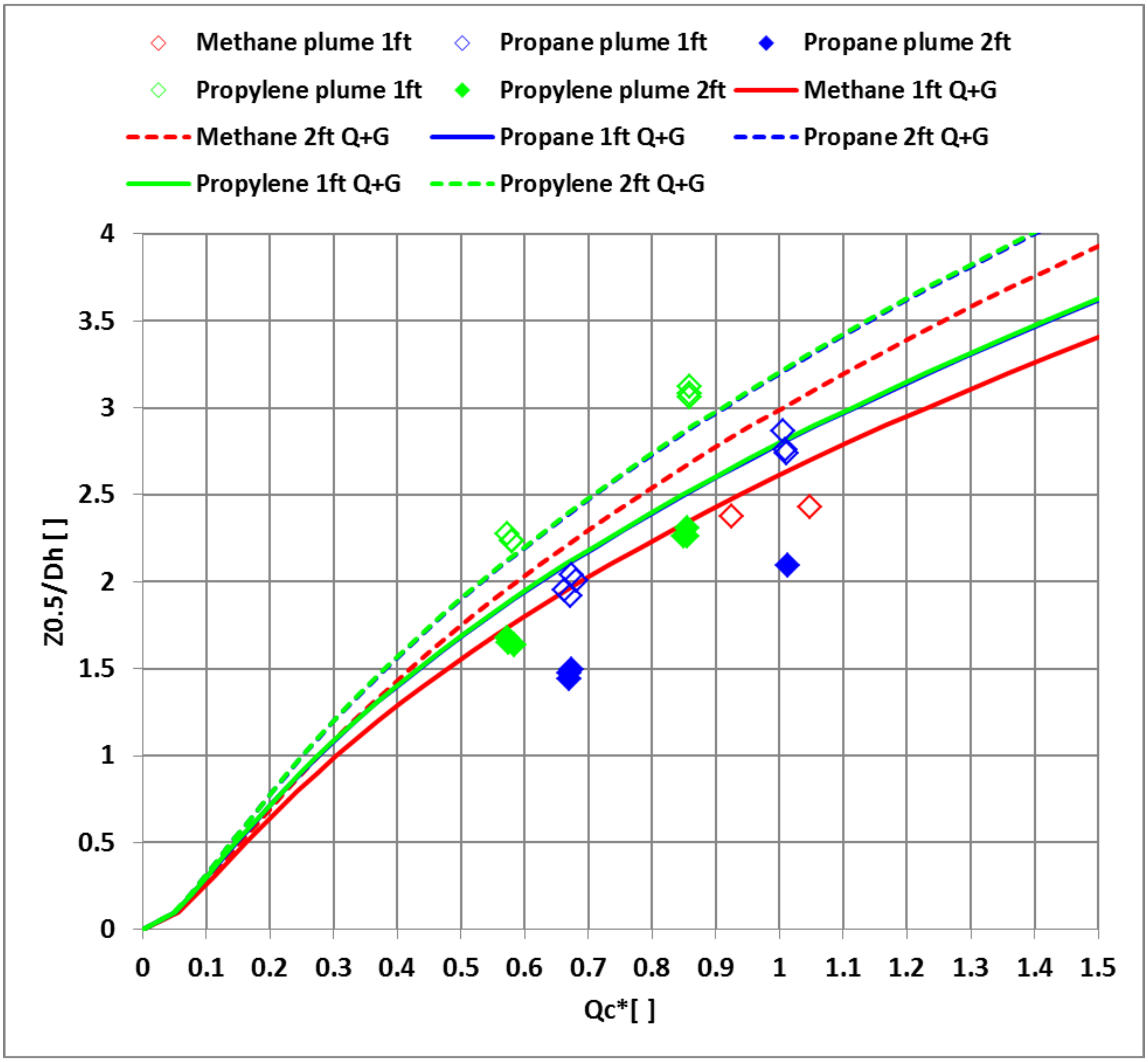

Figure 29 - Comparison of current free plume flame height data with Quintiere and Grove's correlation

4.4 Inert wall fire experimental data

Measurements made in the inert wall fire scenario of the full-scale tests are related to the fluid dynamics/turbulence, gas phase kinetics, and heat transfer to environment components of flame spread. The data collected in these tests include: HRR, centerline plume temperature, centerline plume velocity, flame height, heat flux to inert wall, and near-wall temperature.

4.4.1 Heat release rate

The time-averaged heat release rate measured in each of the propane and propylene inert wall fire test is presented in Figure 30. All of these tests used either a 75 kW or a 50 kW source fire. As discussed in Section 4.2.1, HRR was calculated at each test using the flow rate method and oxygen calorimetry. The O_2-based HRR has an uncertainty of 25 kW, the flow-based HRR has an uncertainty of 13 kW, and both values are within each other's uncertainty. Additionally, the uncertainties of all HRRs fall within their intended HRR level. The difference between the two HRR methods appears to be smaller for the 50 kW fires.

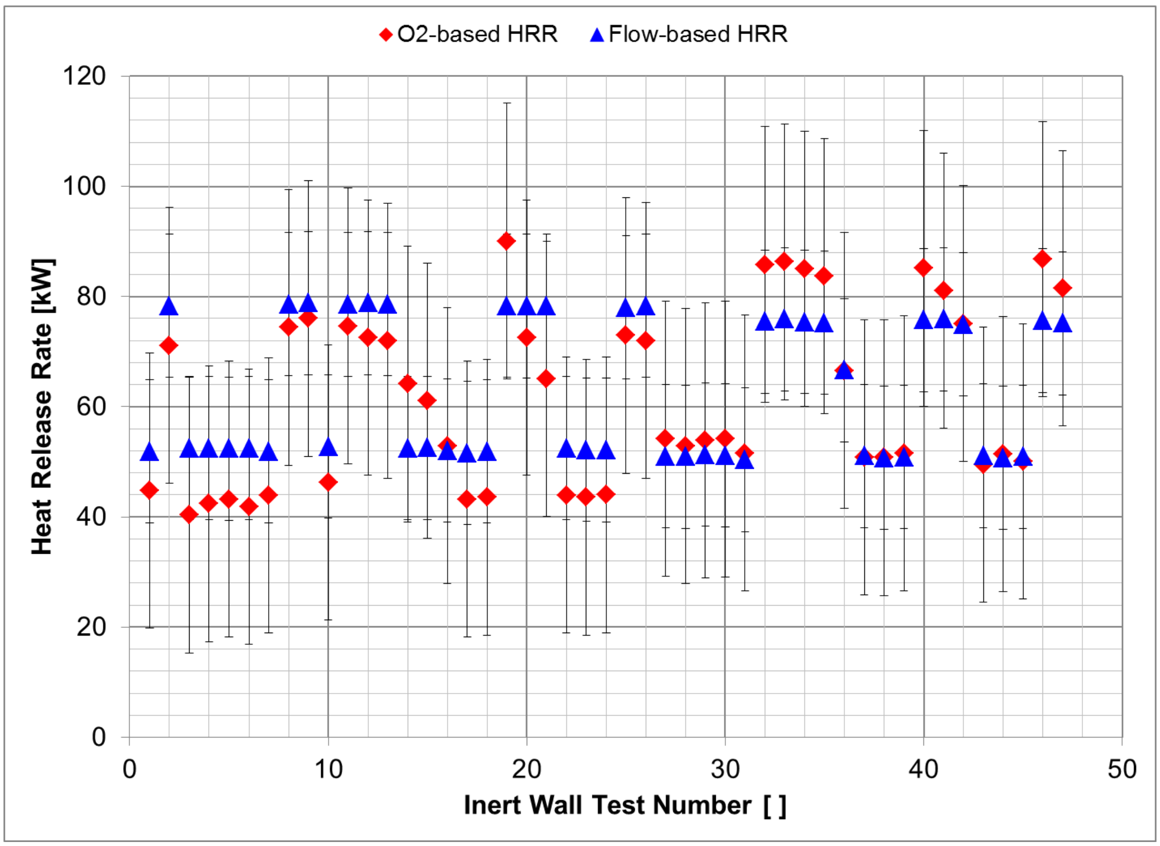

Figure 30 - Heat Release Rate from Inert Wall Fire Tests

Figure 30 also shows that even though the O_2-based HRR was corrected with a C-factor of 77%, the spread of the data away from the intended HRR levels is greater than the flow-based HRR values. Hence, the flow-based HRR values are more consistent and used in the other analyses as a normalizing agent where needed.

4.4.2 Centerline temperature

Figure 31 shows the centerline temperature of all inert wall fires using the 1 ft Square burner normalized with convective HRR. Both corrected and uncorrected temperatures are plotted, and the real gas temperature should be within these two sets of values. Compared to the temperature from the comparable free plume fires, the centerline temperature of the inert wall fire is lower, most likely due to the fact that the fire plume leans against the inert wall, tilting the axis of the plume centerline. Since the rakes are not tilted during the test, as the height increases, the locations where the temperature was measured become more off-centered. The temperature correction often increased the measured temperature by 50% for the normalized height < 0.05, but it significantly decreases as the normalized height increased. It can be observed that the McCaffrey's theory still fits reasonable well in the inert wall data.

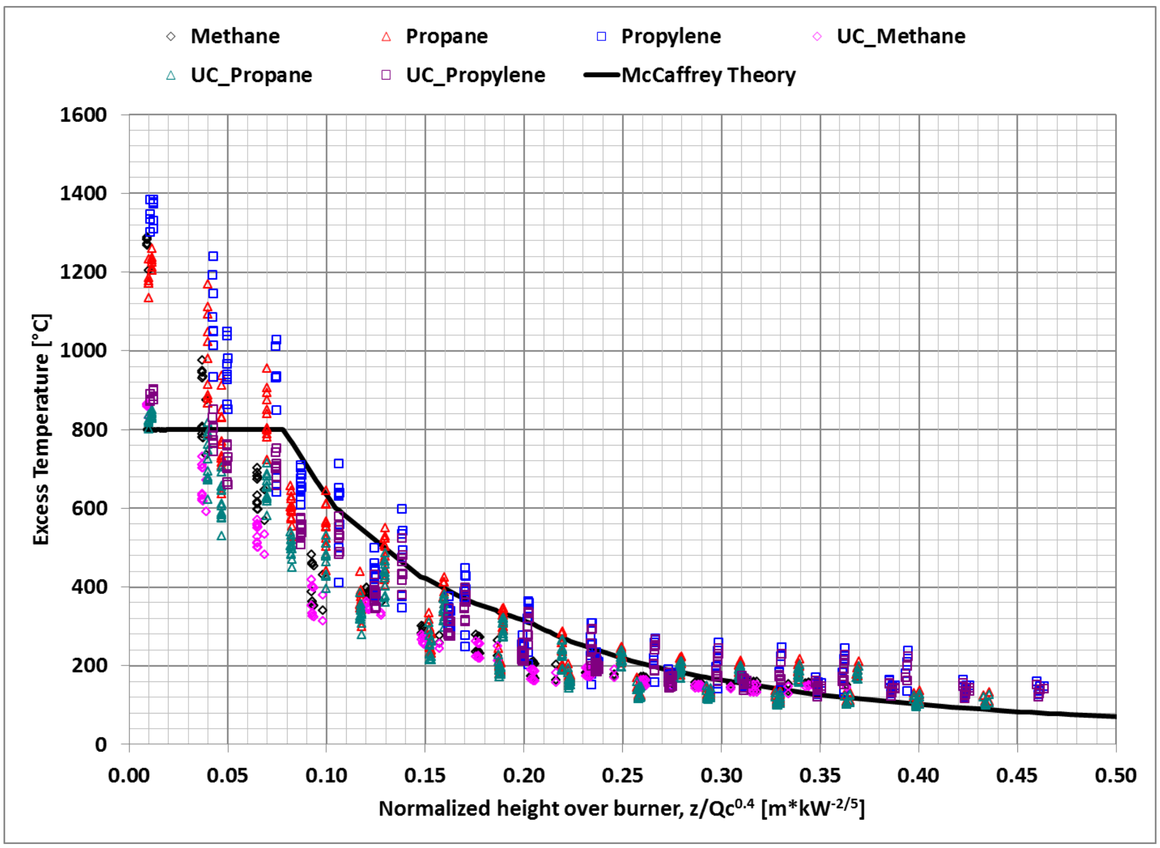

Figure 31 - Centerline temperature of all inert wall fires using 1 ft Square burner, normalized with convective HRR

Figure 32 shows the centerline temperature of all inert wall fires using the 2 ft Rectangle burner normalized with convective HRR. Both corrected and uncorrected temperatures are plotted, and the real gas temperature should be within these two sets of values. The correction often increased the measured temperature by 50% for normalized height < 0.05, but it significantly decreases as z increased. It is observed that compared to the centerline temperature of the 1 ft Square burner inert wall fires and McCaffrey's theory, the temperature generated using the 2 ft Rectangle burner was much lower starting from z = 0.05. This is reasonable because of the shorter flames from the Rectangle burner. The temperature here is also lower than that recorded during the free plume 2 ft burner fires, most likely due to flame lean against the wall.

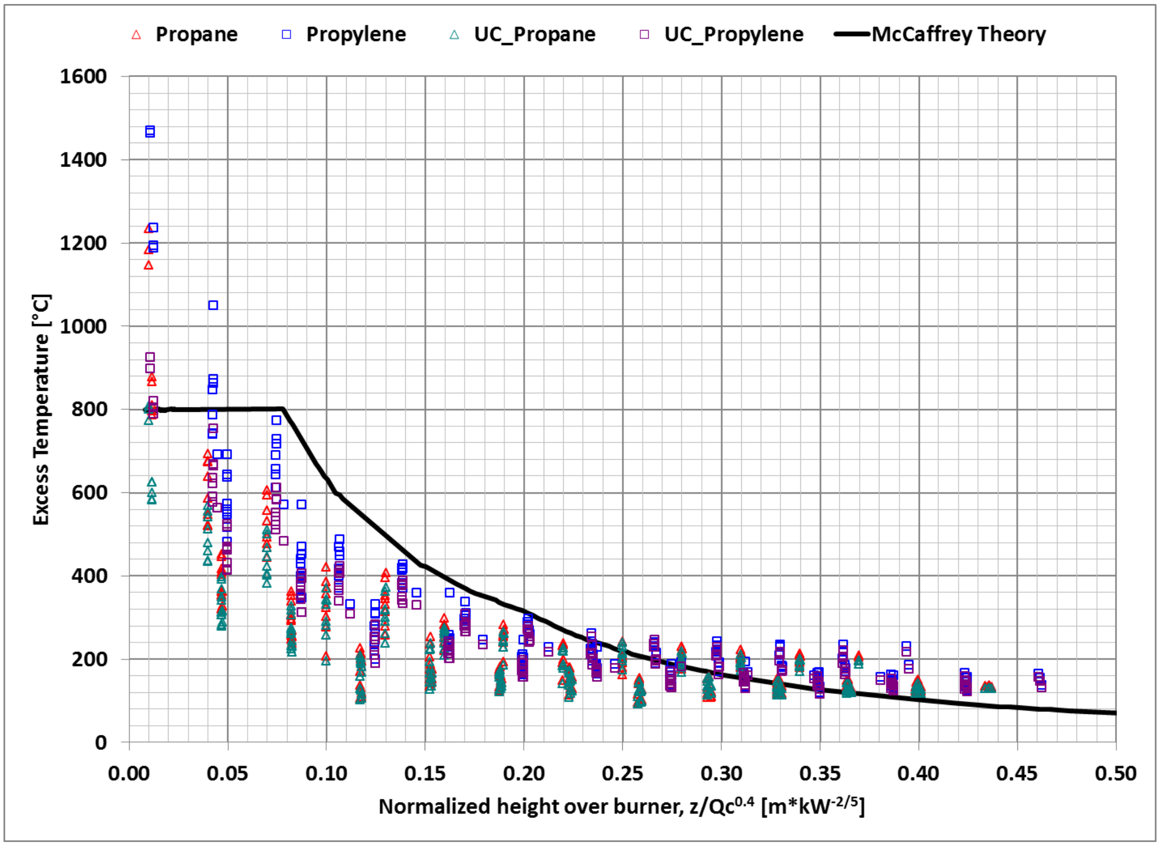

Figure 32 - Centerline temperature of all inert wall fires using 2 ft Rectangle burner, normalized with convective HRR

The free plume temperature data is normalized using the mean flame height and presented in Figure 59 to Figure 60. The two different sets of corrected and uncorrected data still formed two bands of temperature "limits" but overall the temperature distribution is tighter when normalized against mean flame height than when normalized with the convective HRR. The tight grouping of the data across the different fire fuel type shows the effectiveness of the normalization method.

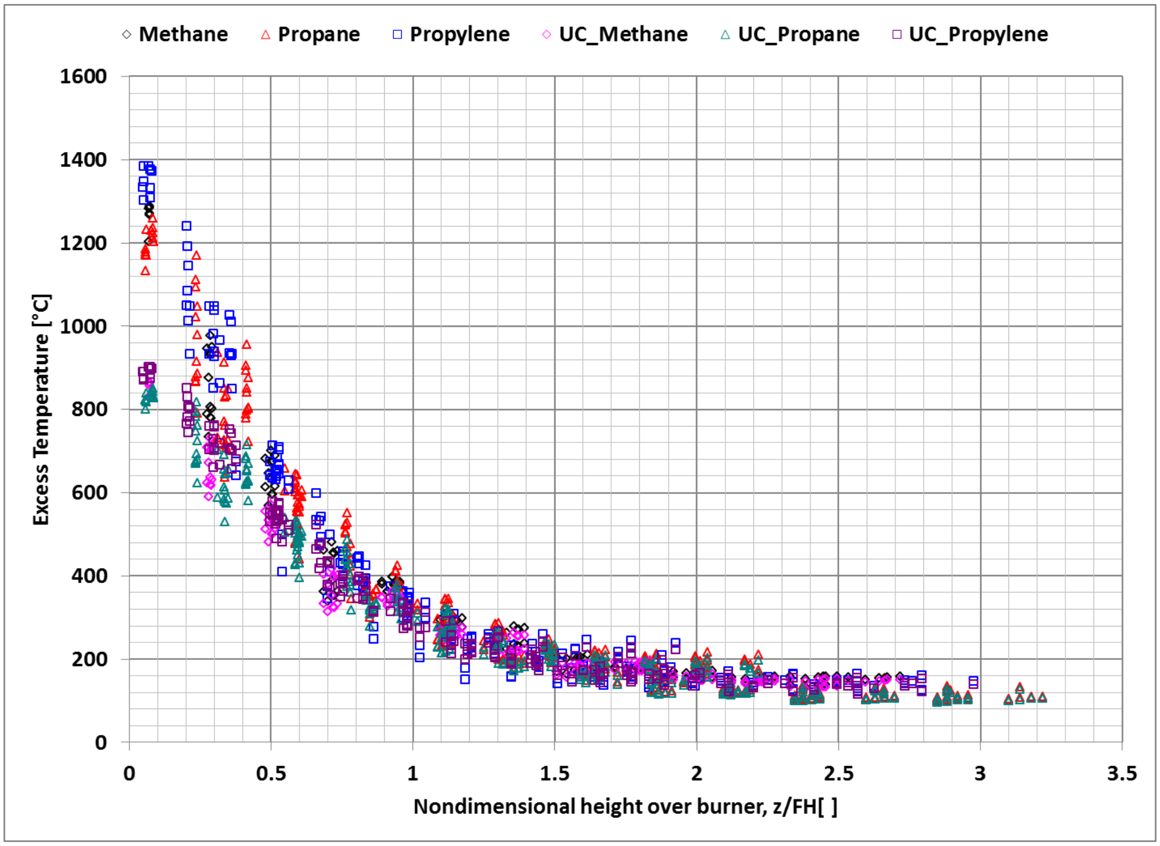

Figure 33 - Centerline temperature of all inert wall fires using 1 ft Square burner, normalized with mean flame height

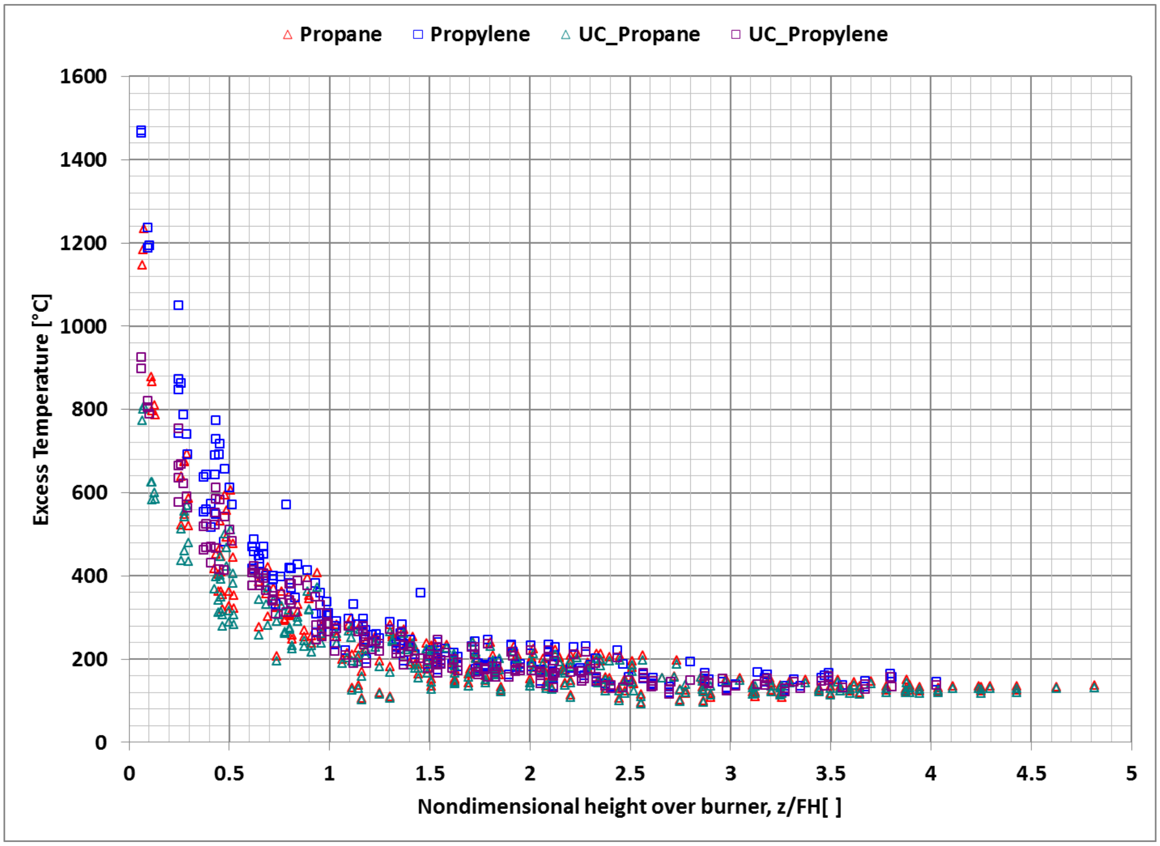

Figure 34 - Centerline temperature of all inert wall fires using 2 ft Rectangle burner, normalized with mean flame height

4.4.3 Centerline velocity

Centerline velocity of the inert wall fire tests conducted with the 1 ft Square burner, with the mean flame height normalization is presented in Figure 35. The current data falls mostly within the uncertainty of McCaffrey's data for the velocity measured up to 1.5 times the mean flame height. At 1.5 to 3 times of the mean flame height, velocity of the propane and propylene fires falls out of the uncertain range of McCaffrey's data. It is noted that the current data from methane fires correlate quite well with McCaffrey's data from methane fires since both study used same-sized burner and fuel. The measured velocity in the inert wall tests is generally lower than that from the free plume tests, most likely due to the fact that the plume leans against the inert wall and its centerline no longer corresponds to the bi-directional probes' centerline.

The uncertainty of the measured data is about 1.33 m/s, greater than that from the free plume tests, most likely due to the plume's leaning tendency as previously mentioned.

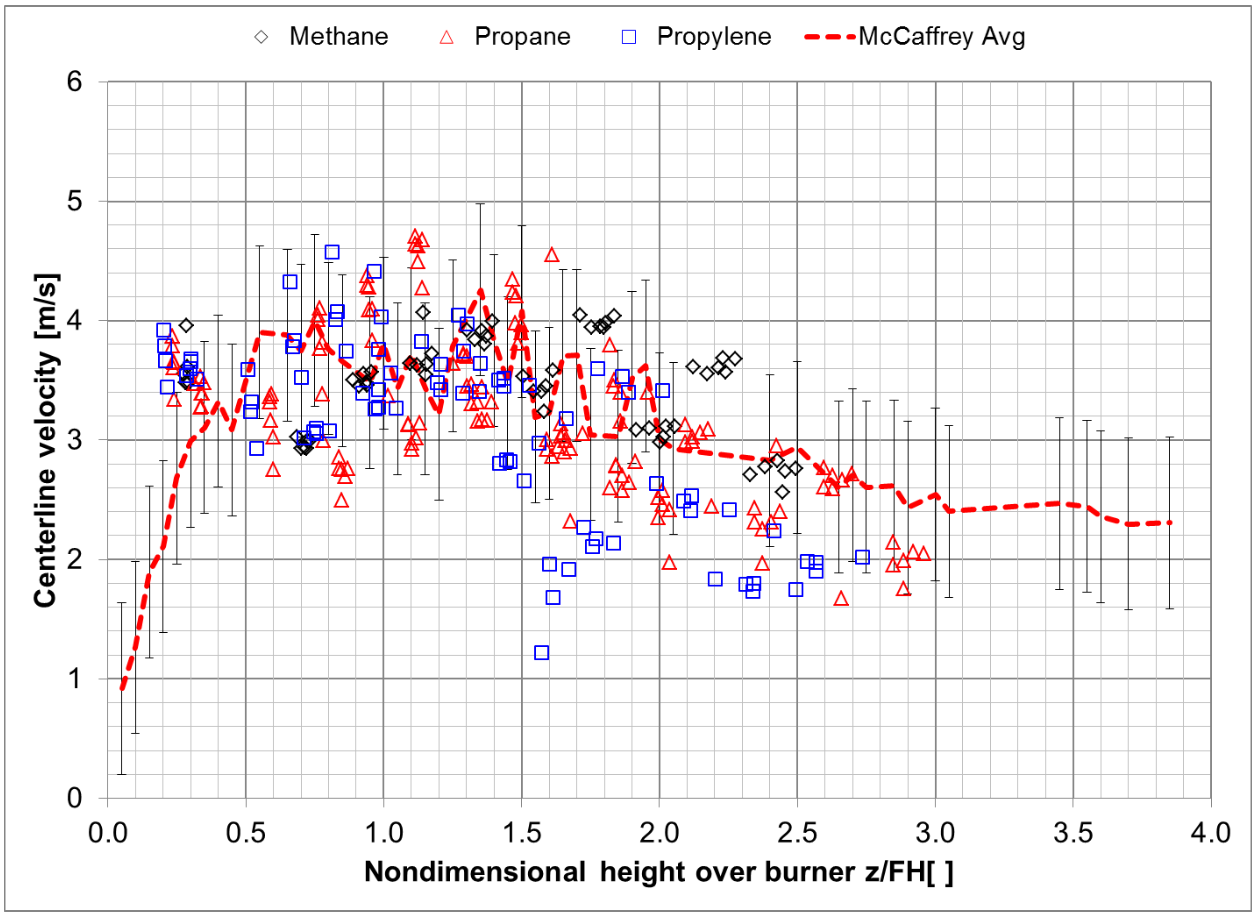

Figure 35 – Inert wall fire test centerline velocity, 1 ft Square burner, normalized with mean flame height

Centerline velocity of the inert wall fire tests conducted with the 1 ft Square burner, with the convective HRR normalization is presented in Figure 36. The current data generally falls out of the range of McCaffrey's data with uncertainty, which is to be expected due to the plume's leaning against the wall and out of the centerline.

The uncertainty of the measured data is about 0.22 m s^{-1} $kW^{1/5}$, about twice that of McCaffrey's.

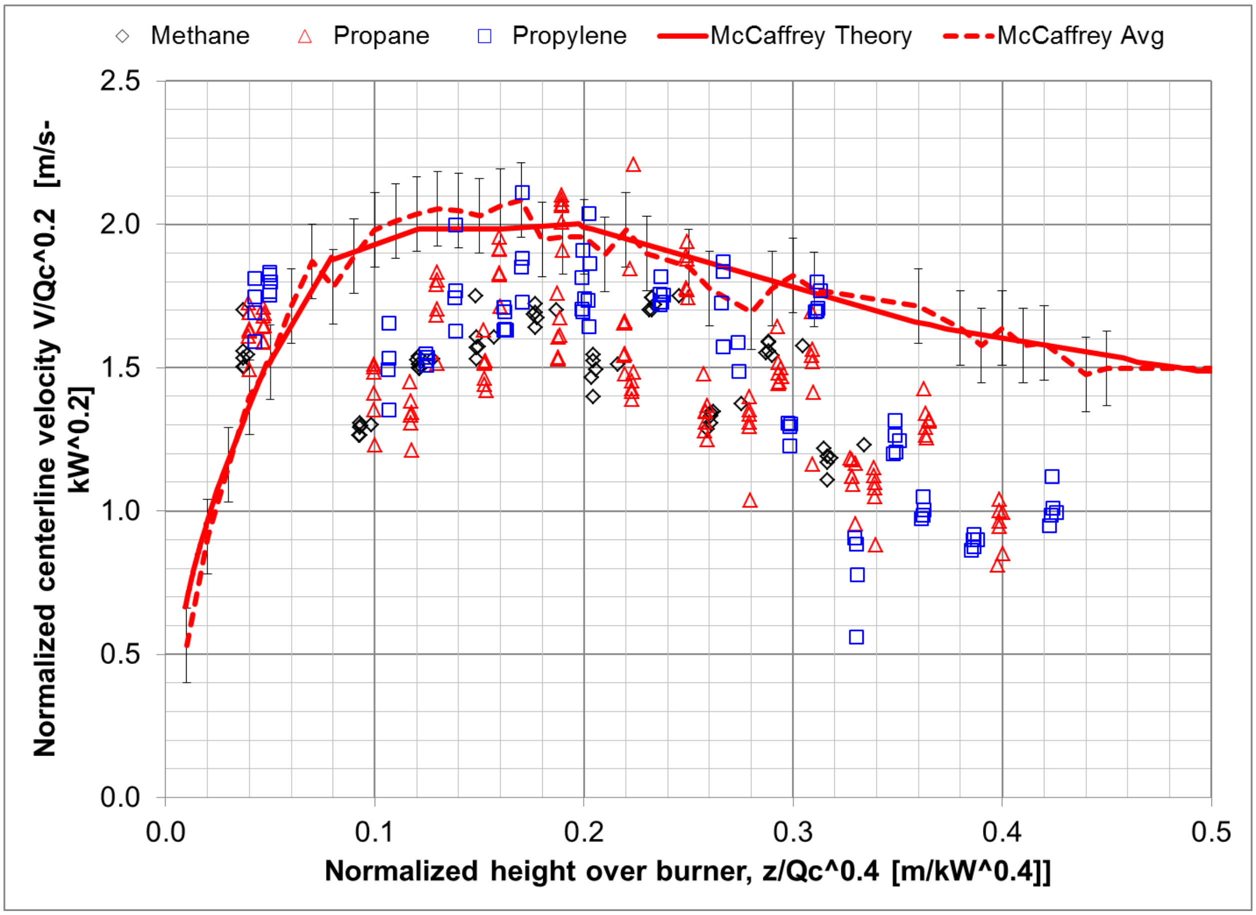

Figure 36 – Inert wall fire test centerline velocity, 1 ft Square burner, normalized with convective HRR

Figure 37 presents the centerline velocity from the inert wall tests conducted with the 2 ft Rectangle burner, as normalized with mean flame height. There is significantly greater scatter in this data than the velocity data generated in other test configurations, due to the larger burner used and the wall leaning tendencies common in inert wall fire tests.

The uncertainty of the measured data is about 1.42 m/s, highest of all.

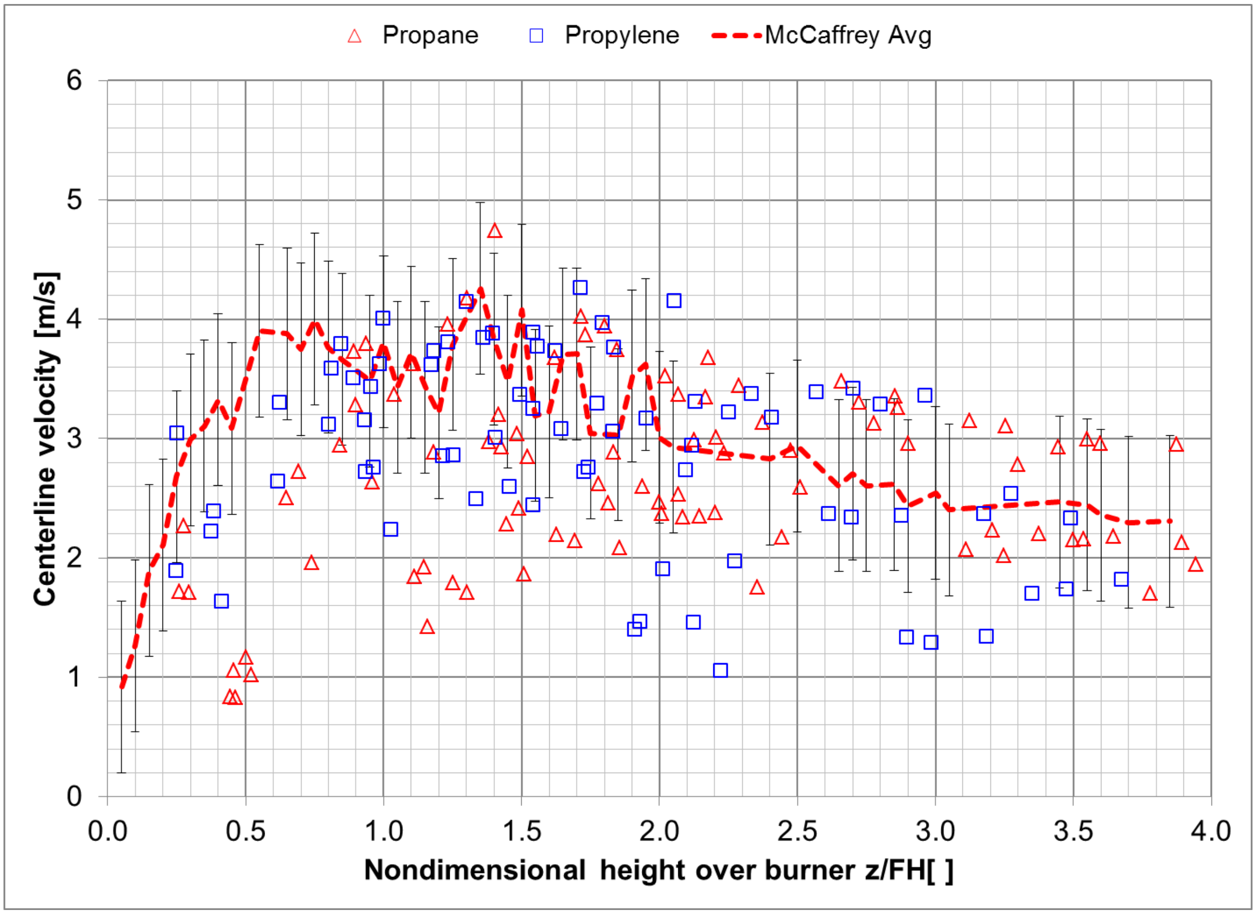

Figure 37 – Inert wall fire test centerline velocity, 2 ft Rectangle burner, normalized with mean flame height

Centerline velocity of the inert wall fire tests conducted with the 2 ft Rectangle burner, with the convective HRR normalization is presented in Figure 38. The current data generally falls out of the range of McCaffrey's data with uncertainty, which is to be expected due to the larger burner used and the fire plume's leaning against the wall and out of the centerline.

The uncertainty of the measured data is about 0.40 m s^{-1} $kW^{1/5}$, about three times that of McCaffrey's.

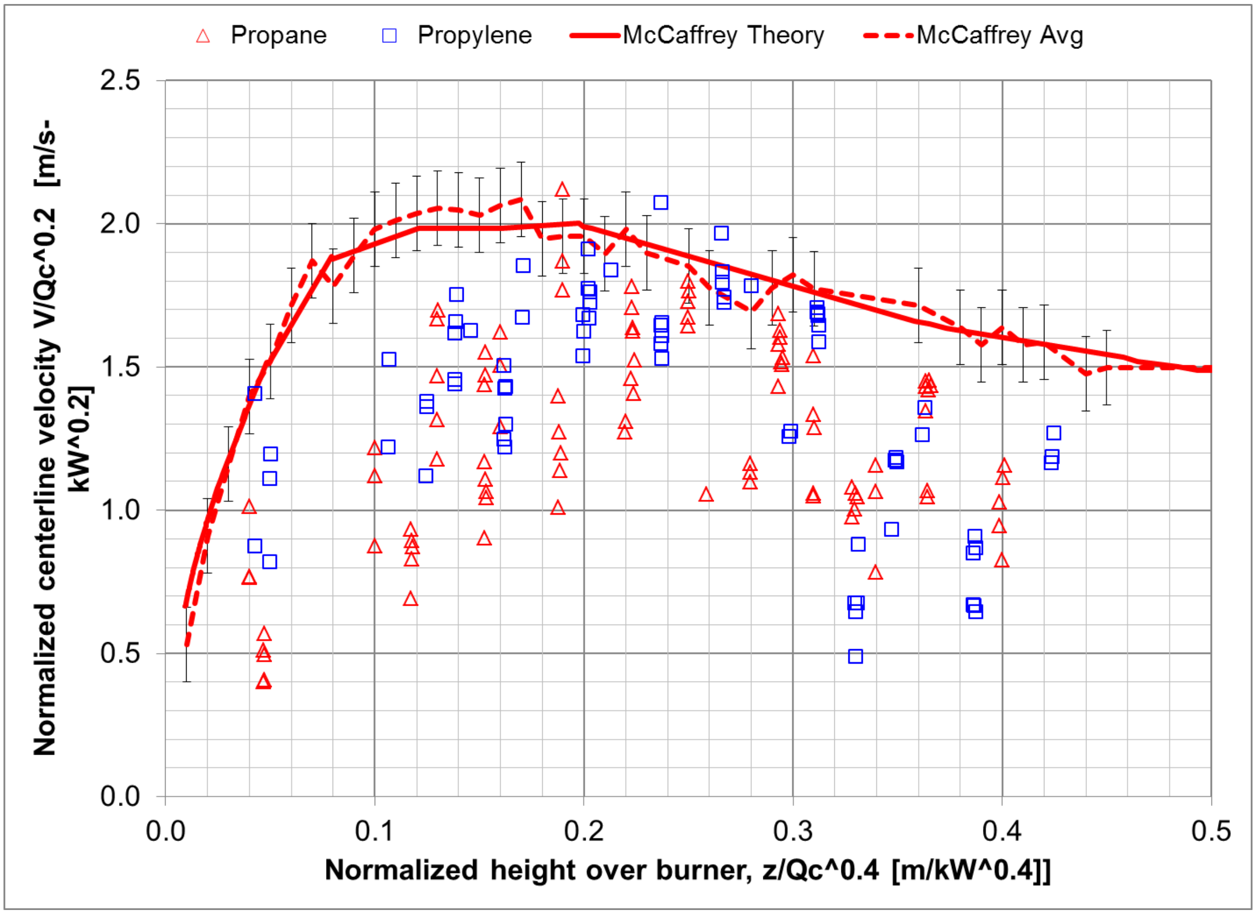

Figure 38 – Inert wall fire test centerline velocity, 2 ft Rectangle burner, normalized with convective HRR

It was found that generally the centerline velocity measured in the inert wall fire tests was lower that the velocity measured in the free plume fire tests. This is caused by the fire plume leaning against the wall next to the burner, where the plume is shifted out of the centerline of the burner as it was the case in the free plume tests. The plume's lean also caused additional scatter in the data reflected in the greater uncertainty in the 2 ft burner with inert wall tests.

4.4.4 Flame height

The comparison between current data normalized to the method used by Zukoski to his and Anderson's correlation is presented in Figure 39. Current data from propane and propylene source fires falls between Anderson's and Zukoski's correlations quite well and it is shown that Propylene fires seem to have a higher non-dimensional flame height than propane fires, which is in turn higher than methane fires. This is expected because of the varying fuels' properties. The flame heights of the fires using methane as the source fuel fall outside of the margins created by correlations. There does not seem to be a difference between plume and wall effect on flame height, however, it is noted that in inert wall tests, the flame plume tends to lean back and hug the wall regardless of burner size or HRR.

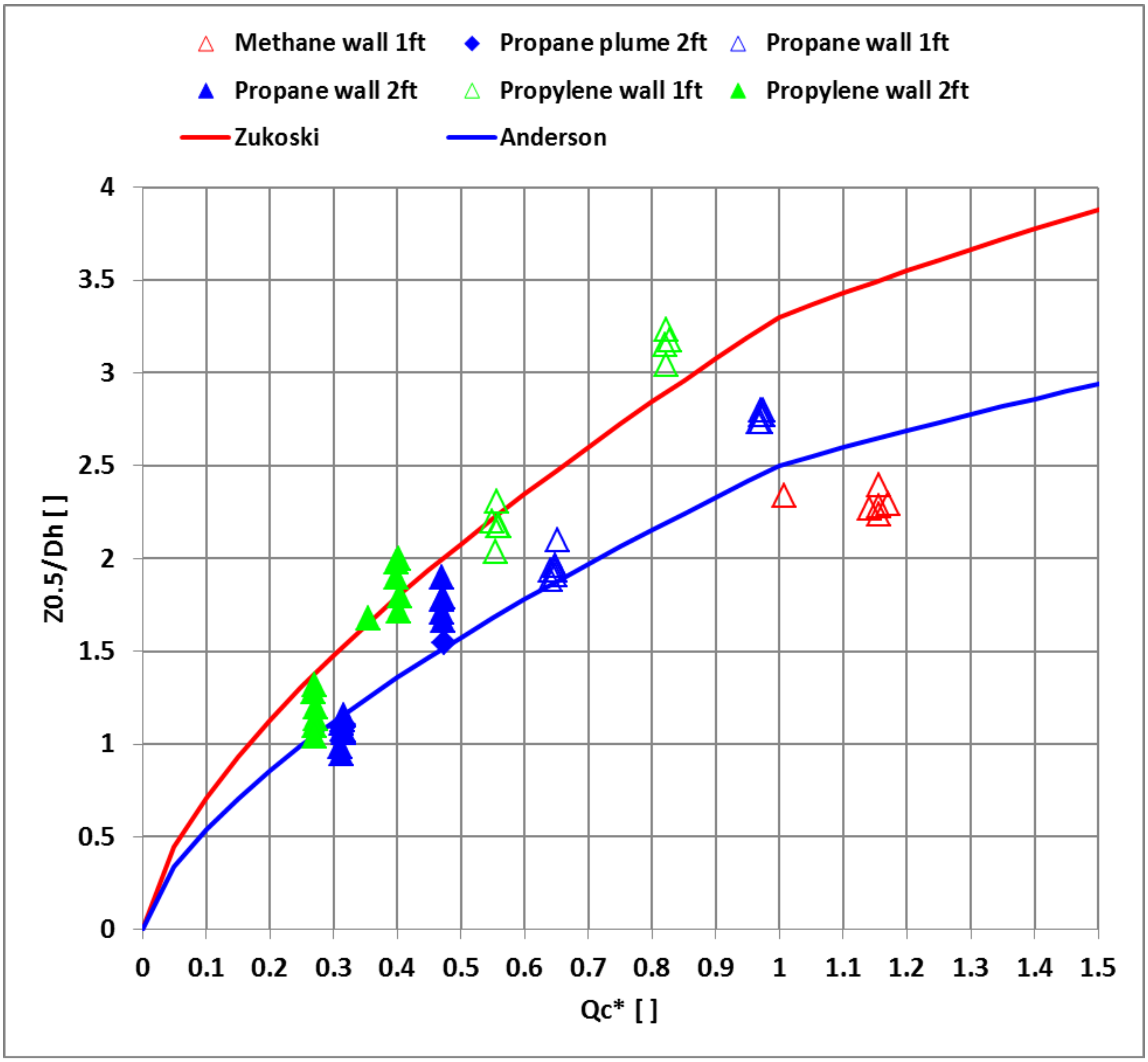

Figure 39 - Comparison of current inert wall flame height data with Zukoski's and Anderson's correlations

Alston and Dembsey's data suggested that there is little distinction in flame height between similar sized square and circle burner, but propane fires had taller flame than propylene fires and methane fires, as shown in Figure 40. The uncertainty of their data is reported to be about ±5 cm or ± 0.2 in non-dimensional term, which overlaps the current data (with normalized convective HRR) for Q* < 0.6 only, for propane and propylene. Past Q*>0.6, the observed flame heights are significantly lower than that predicted using Alston and Dembsey's data. However, it should be noted that the geometric effects of the source burner appear to have been normalized successfully since the observed flame heights using the Rectangle fall within the uncertainty of the correlations, which were generated using a square and a circular burner. It may be observed that the presence of the inert wall does not alter the flame heights significantly.

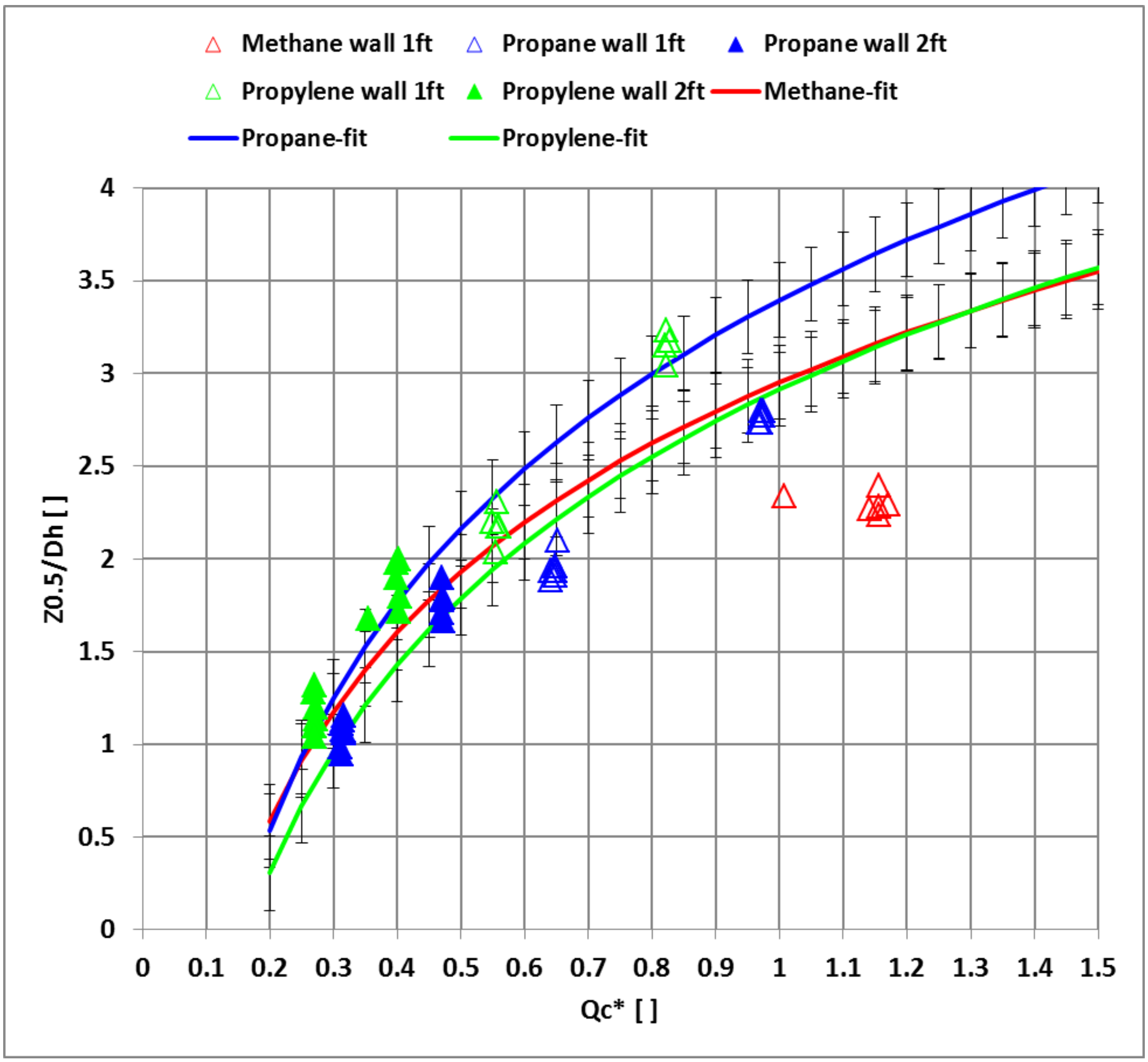

Figure 40 - Comparison of current inert wall flame height data with Alston and Dembsey's data-fitted lines

The non-dimensional parameter N (based on the convective HRR) was determined for the current data to be plotted against the measured flame height and compared to Heskestad's correlation in Figure 41. Using the total heat release rates of methane, propane, and propylene, Heskestad's correlation suggests that the propylene flame height is taller than the propane and the methane flame heights, which is also observed in the current dataset. The uncertainty of the Heskestad's correlation is reported by Anderson to be about 15-20%, making the current data falls within range of the uncertainties, except for the measured methane test flame height. It may be observed that the presence of the inert wall does not alter the flame heights significantly.

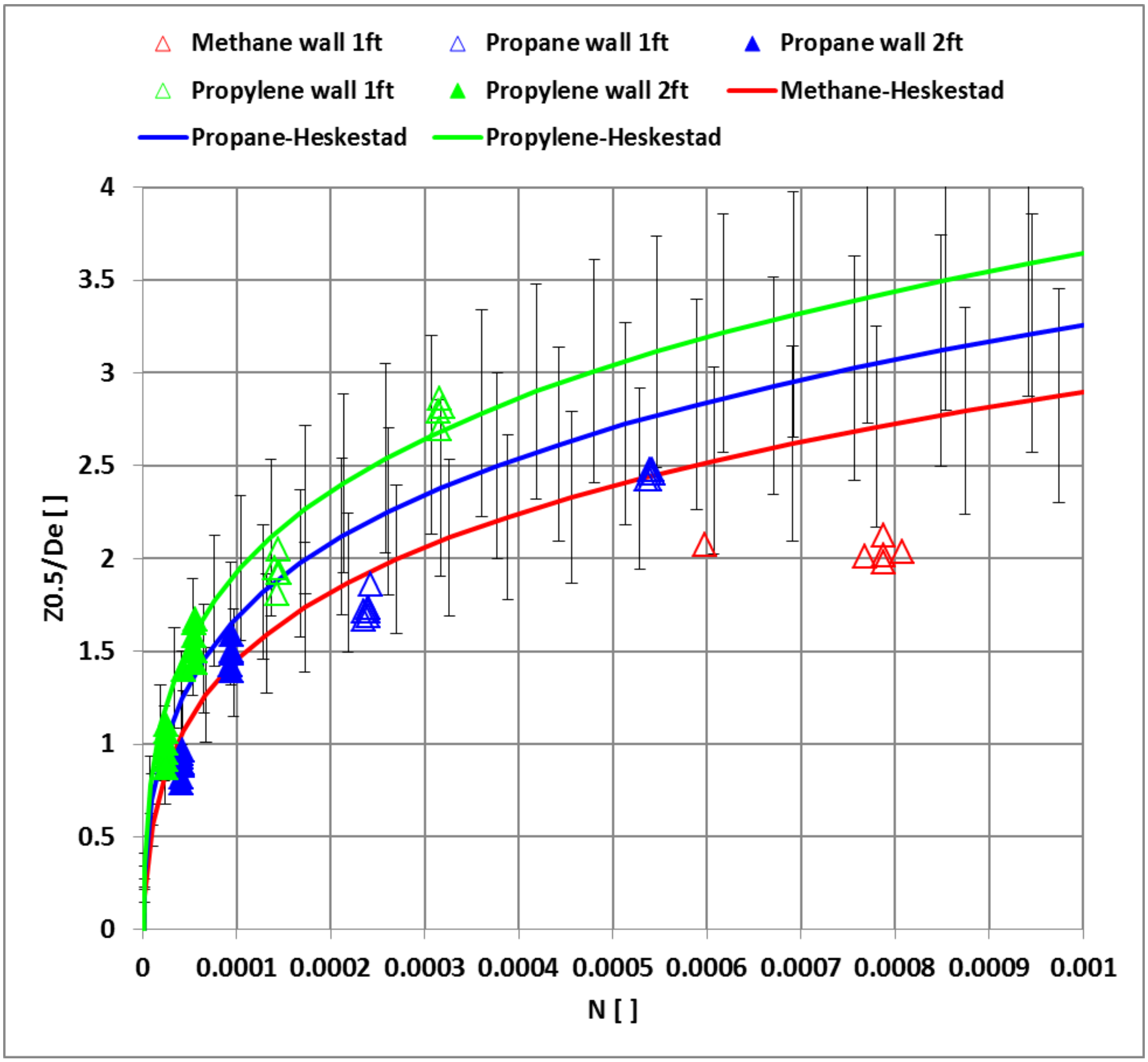

Figure 41 - Comparison of current inert wall flame height data with Heskestad's correlation

Figure 42 shows that the Quintiere and Grove's correlation makes no distinction between the flame heights of a propane or propylene fire and that curiously the flame height from the Rectangle burner is higher than the Square burner. The correlation for the Rectangle was generated from data from Hasemi and Nishihata[95].

However, contrary to the correlation, in the current data the propylene fires had taller flame heights than propane fires and so did the Square burner over Rectangle burner fires. It should be noted that the propane Square burner flame heights correlate very well with the Q+G correlation for propane and propylene fires whereas the flame heights measured from the Rectangle source fires fall outside the correlation by a large margin. It may be observed that the presence of the inert wall does not alter the flame heights significantly.

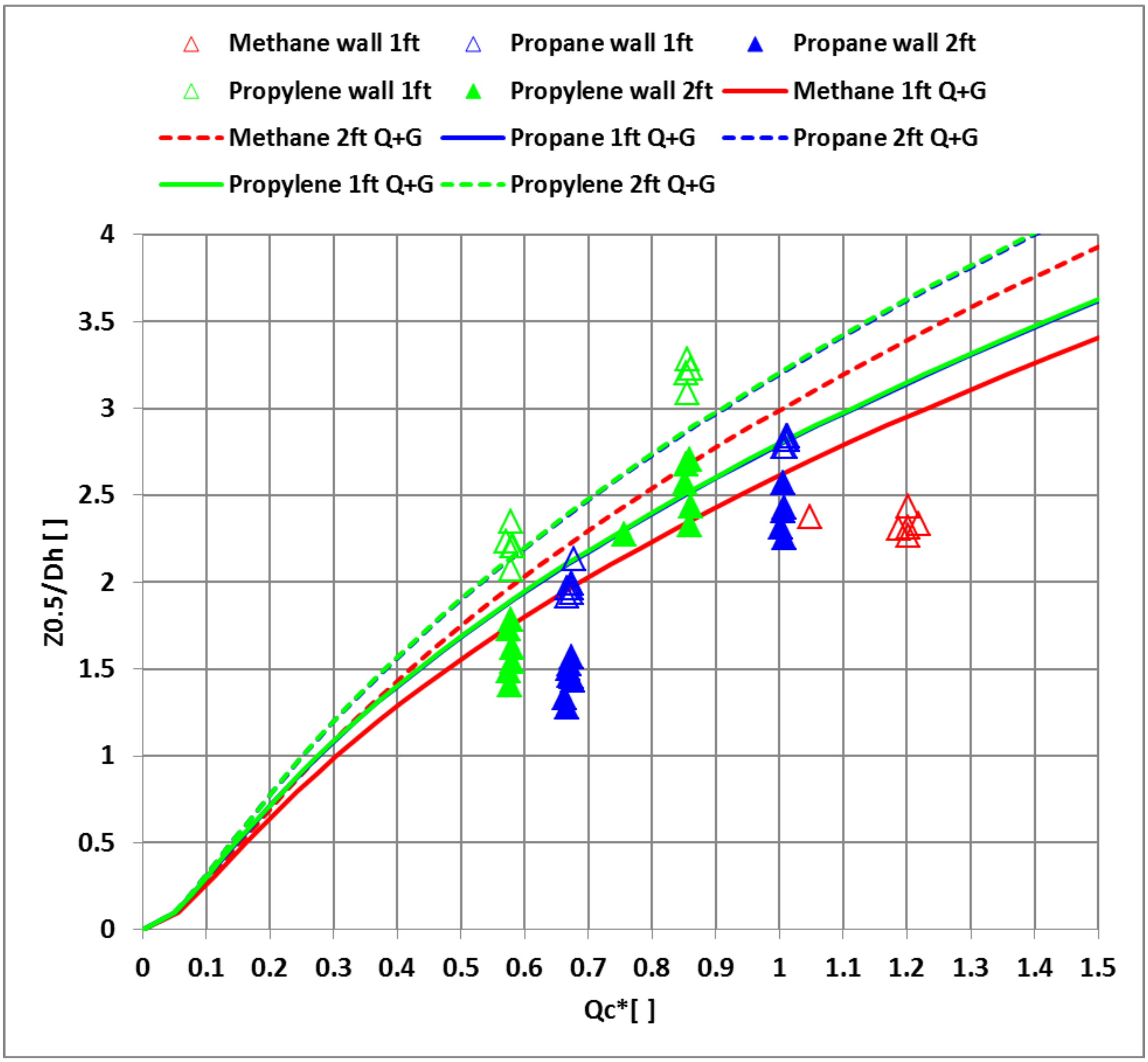

Figure 42 - Comparison of current inert wall flame height data with Quintiere and Grove's correlation

4.4.5 Heat flux to inert wall

Heat flux to the wall measured by the TSCs was normalized using the 100% intermittency flame height and the radiative HRR of the fire. It was assumed that the fire may be represented by a cylinder with a surface that output a constant heat release rate per unit area (HRRPUA). The diameter of the cylindrical fire was assumed to be the hydraulic diameter of the source burner, and the 100% intermittency flame height was used as the cylinder's height. The 100% intermittency flame height was calculated as 6/10 of the 50% intermittency mean flame height, it represents the maximum height where there was a constant presence of flames during the test. The surface area of the cylinder does not consider the circular faces, and is calculated with equation (37):

$$A_{fire} = \pi D_h H_f \tag{38}$$

Where D_h is the hydraulic diameter of the burner, and H_f is the 100% intermittency flame height.
The HRRUPA on the surface of the cylindrical fire can then be determined using equation (38):

$$HRRPUA_{fire} = \frac{HRR_{rad}}{A_{fire}} \tag{39}$$

Where the HRR_{rad} represents the radiative component of the heat released, found based on the radiative fraction of the fuel and the measured HRR of the fire. This allows the effects from the different fuel properties to be neutralized.
Finally the incident heat flux measured at the TSCs was normalized against the HRRPUA of the fire cylinder using equation (39):

$$HF = \frac{\dot{q}_i''}{HRRPUA_{fire}} \tag{40}$$

Where HF is the non-dimensional heat flux. It was assumed that the fires were symmetrical so that heat flux measured on both sides of the centerline was would be equal. This method of normalization was used primarily to collapse the data recorded at all of the TSCs at different height and horizontal distance from the source burner centerline regardless of the size of the burner.
Figure 43 shows the normalized incident heat flux measured in all of the inert wall fire tests, regardless of fire size, fuel type, and burner size. As expected, the heat flux along the centerline was larger than the heat flux recorded 1 ft and 2 ft away from the centerline. Ideally, the normalized heat flux would not be greater than 1 because the incident heat flux measured at a point cannot be greater than the HRRPUA at the source due to energy balance. However, the approximation of the shape and dimensions of the fire cylinder caused some distortion to this rule, as shown by the heat flux value higher than 1 in Figure 43. In this case, using the hydraulic diameter of the burner as the fire cylinder's diameter may be reasonable but unsuitable due to the different shapes of the Square and Rectangle burners.

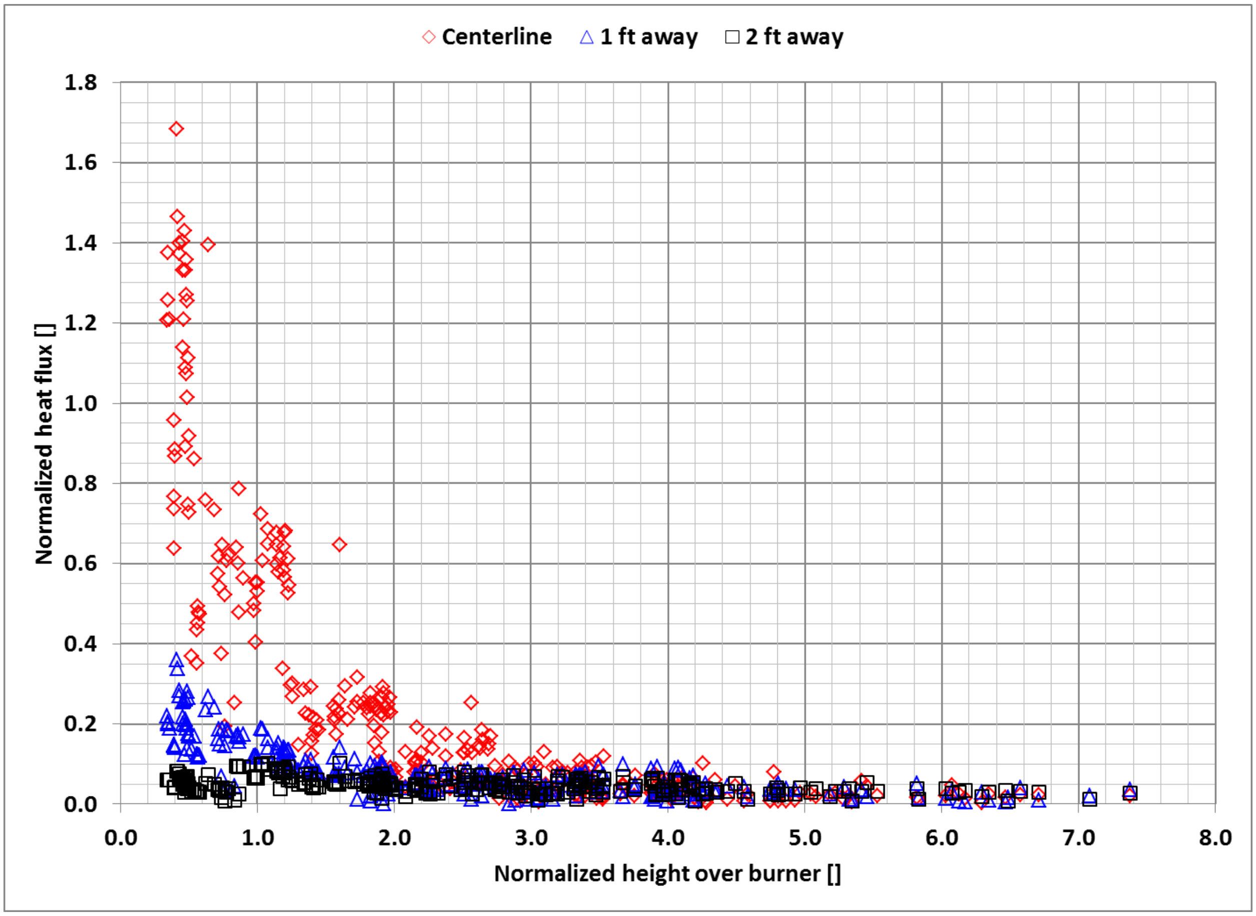

Figure 43 - Normalized heat flux of all inert wall fire tests

Figure 44 shows the heat flux recorded at the tests using the 1 ft Square burner. The highest heat flux again was measured along the center. It is also shown that the heat flux measured 1 ft away from centerline was greater than the heat flux measured at 2 ft away from centerline.

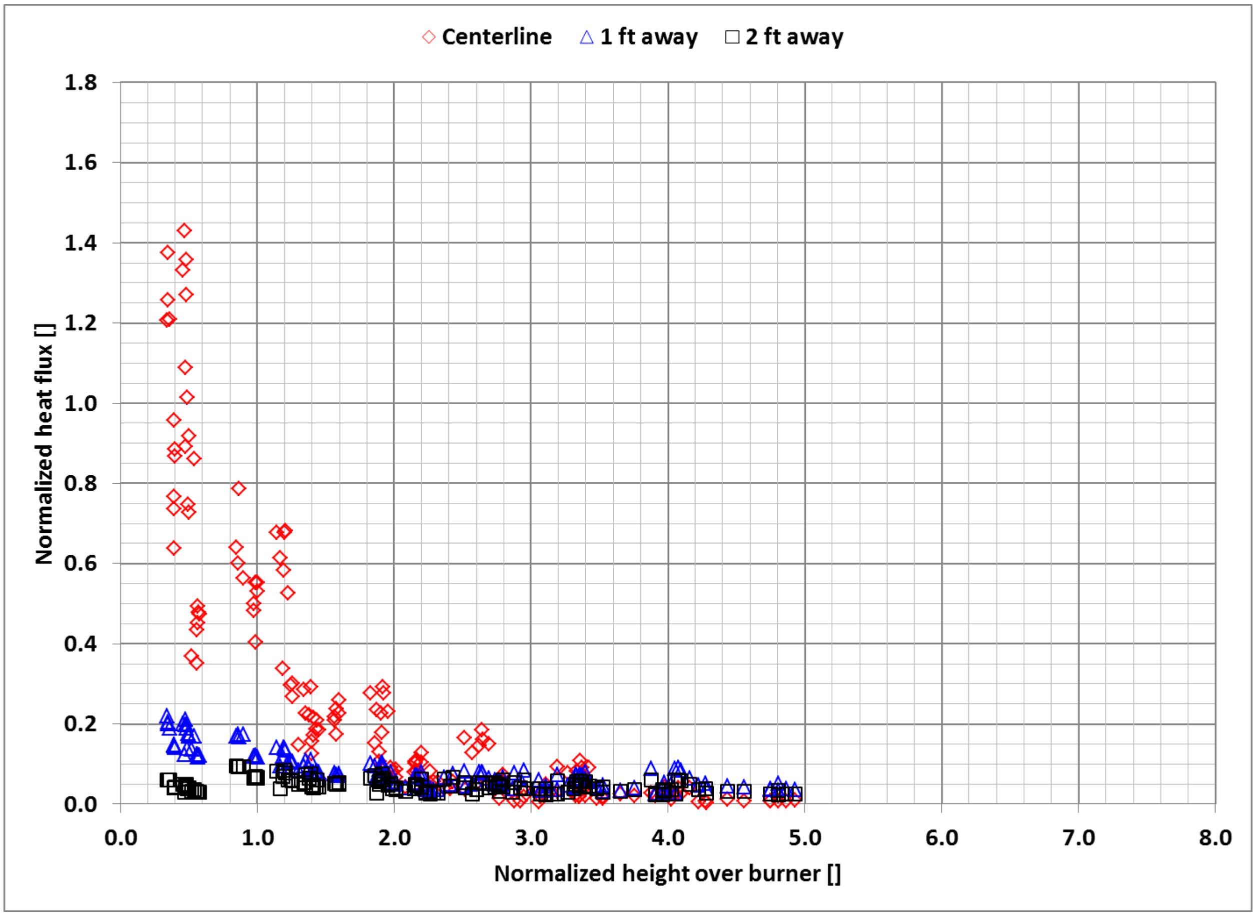

Figure 44 - Normalized heat flux of all 1 ft Square burner tests

Figure 45 shows the heat flux measured at the 2 ft Rectangle burner tests. Compared to the 1 ft burner case, the heat flux measured at the center near the burner surface was greater. However, there was little variation in the heat flux measured at the TSCs 1 ft and 2 ft away from the centerline.

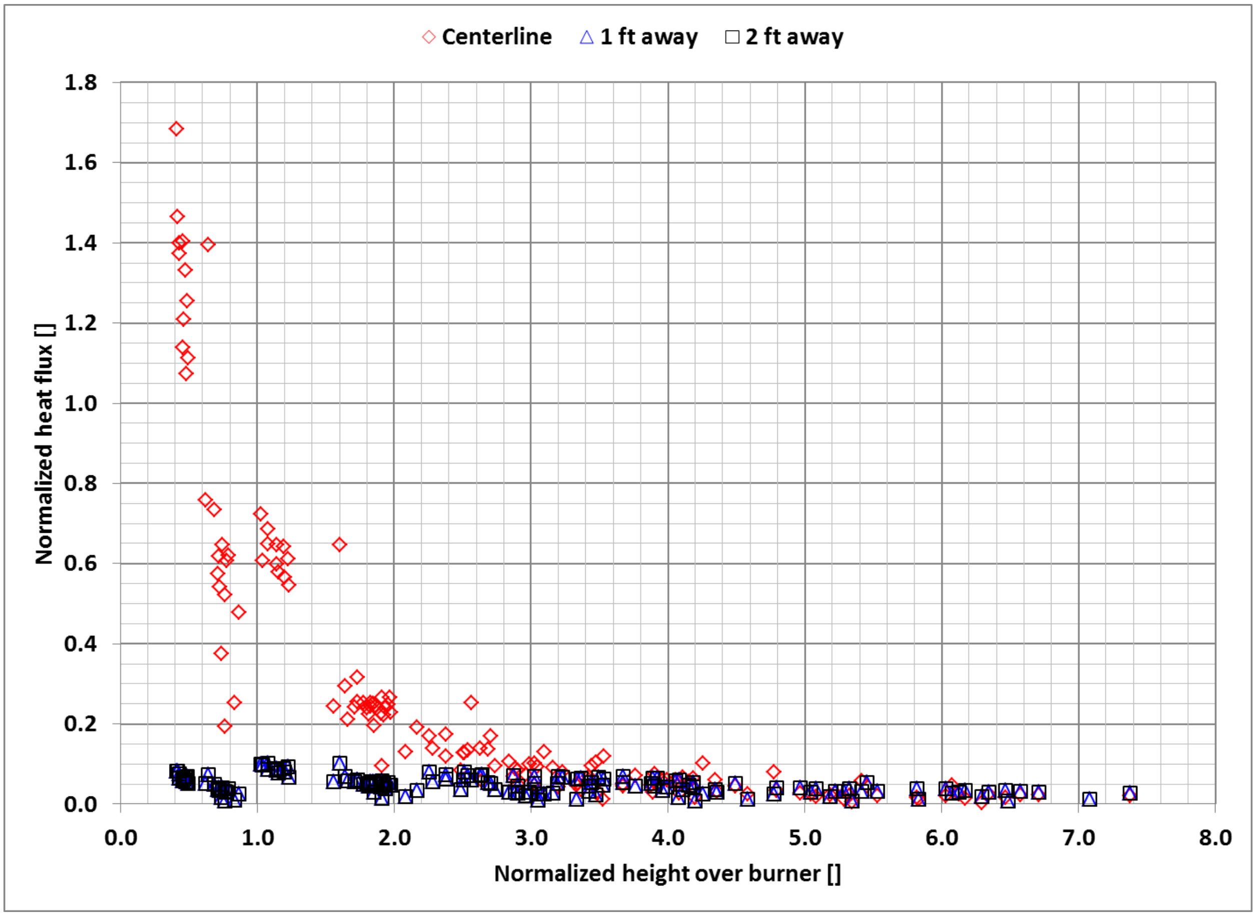

Figure 45 - Normalized heat flux of all 2 ft Rectangle burner

4.4.6 Near wall temperature

In the current inert and combustible wall experiments, near-wall temperature was measured by thermocouples installed on the wall at regular intervals close to the centerline.

A series of 18 thermocouples were used, grouped into 3 groups of six and installed at 0.35 m, 0.95 m, and 1.55 m from the burner surface. The thermocouples are located at 2.5 cm, 5 cm, and 7.5 cm away from the centerline. Table 25 shows the locations of the thermocouples.

Table 25 - Locations of near-wall thermocouples

		Distance from centerline					
		-7.5 cm	**-5.0 cm**	**-2.5 cm**	**2.5 cm**	**5.0 cm**	**7.5 cm**
		Perpendicular distance from wall [mm]					
Height above burner	**155 cm**	15	20	25	30	35	40
	95 cm	35	30	25	20	15	10
	35 cm	0	5	10	15	20	25

This section presents the temperature measured during the inert wall tests as grouped by source burner size and source fire HRR. Although the HRR of each test differs slightly, they are all based on either 50 kW or 75 kW and are grouped as such.

The measurements had been corrected using Blevins and Pitts' method of thermocouple correction based on the time-averaged velocity measured at nearby stations. The measurements presented have been time-averaged, over the period when the source fire was at constant HRR. In each of the charts, the datapoints represent the corrected temperature and the lines represent the averaged uncorrected temperature from tests of the same configuration using the same fuel.

Near-wall temperature rise measured 0.35 m above burner surface during tests using the Square burner at 50 kW is presented in Figure 46. It is shown that generally the spread of the temperature data from tests using propylene is greater those from the propane tests, but the maximum spread for both fuel types approach 80°C. It should also be noted that the data spread is relatively consistent for the propylene tests, but for propane tests the magnitude of the data spread increases with distance from the wall surface. The correction for the propane test data is also found to be smaller than for the propylene test data.

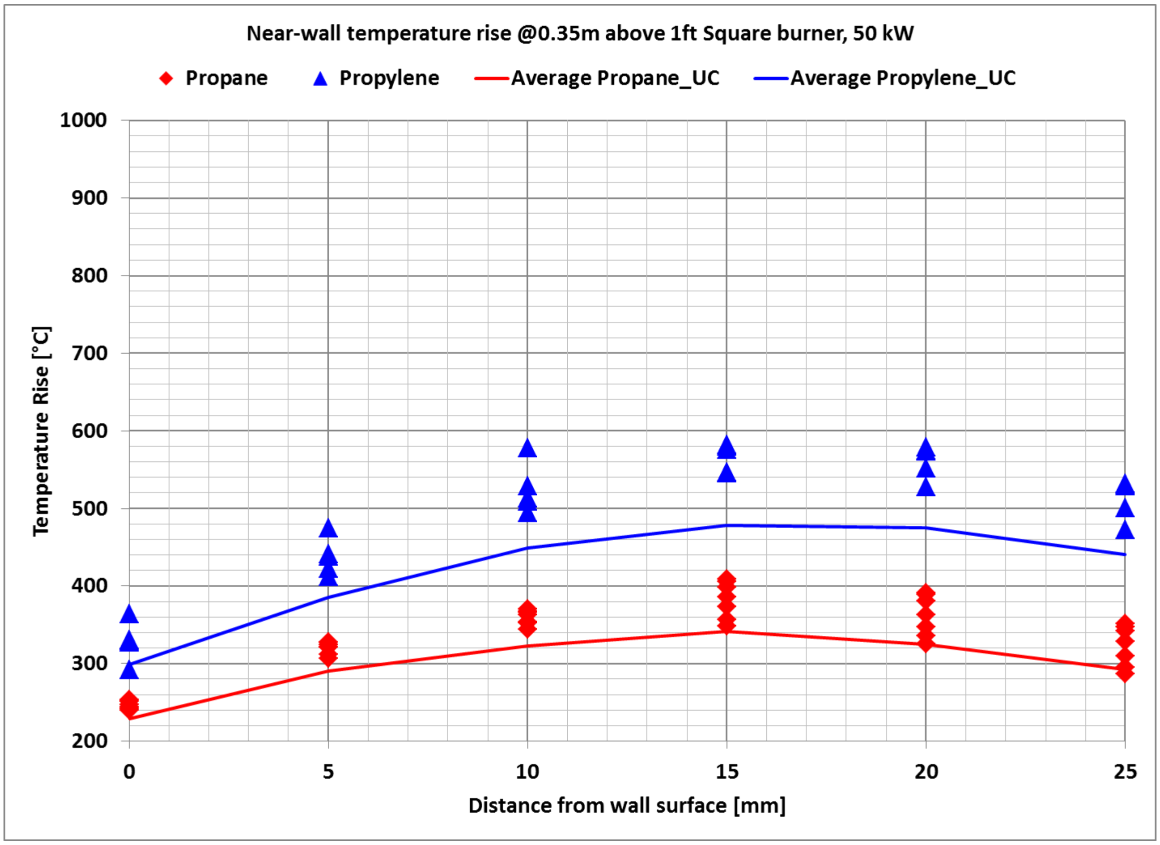

Figure 46 - Near-wall temperature, Square burner, 50 kW, @ 0.35m

Figure 47 shows the temperature recorded at 0.35 m over the burner surface in tests using the Square burner at 75 kW. The spread for the propylene data for the same thermocouple location is especially large, reaching 200°C for the thermocouples at 10 mm and 15 mm away from the wall surface. The data spread for propane and methane both approach 100°C. The magnitude of the data spread for each location appears to increase with the distance from the wall surface. The correction temperature magnitude for the propylene tests is also much greater than the correction for the tests using the other two fuels.

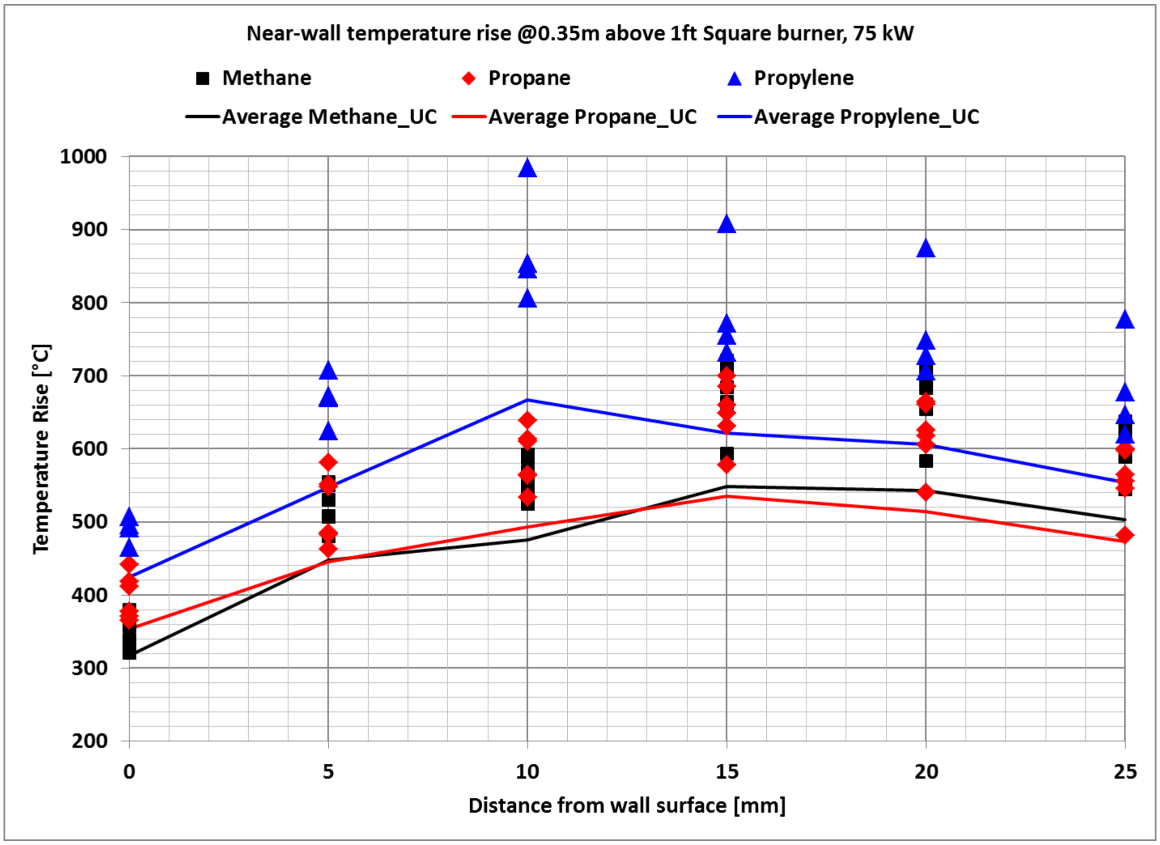

Figure 47 - Near-wall temperature, Square burner, 75 kW, @ 0.35m

Near-wall temperature rise measured 0.35 m above burner surface during tests using the Rectangle burner at 50 kW is presented in Figure 48. It is shown that generally the spread of the temperature data from tests using propylene is greater those from the propane tests, with the maximum data spread for propylene at 200°C for thermocouples at 5 to 20 mm away from the wall. For the propane tests, the data spread near the wall was small, but increases to approximately 160°C at 20 mm and 25 mm away from the wall. The magnitude of the data correction for propylene tests is much greater than the correction for the propane tests.

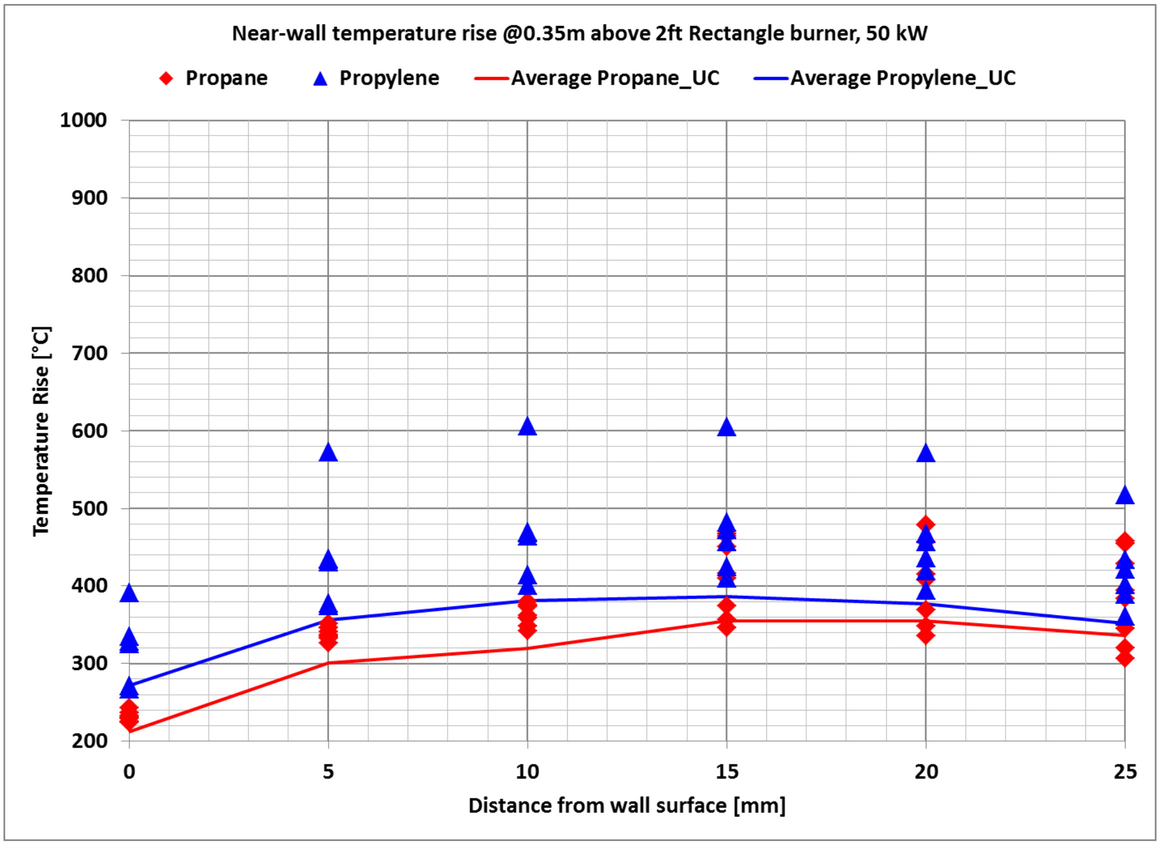

Figure 48 - Near-wall temperature, Rectangle burner, 50 kW, @ 0.35m

Near-wall temperature rise measured 0.35 m above burner surface during tests using the Rectangle burner at 75 kW is presented in Figure 49. It is shown that generally the spread of the temperature data from tests using propylene is greater those from the propane tests, with the maximum data spread for propylene at 240°C for thermocouples at 15 to 20 mm away from the wall. For the propane tests, the data spread near the wall was small, but increases to approximately 180°C at 25 mm away from the wall. The magnitude of the data correction for propylene tests is generally much greater than the correction for the propane tests.

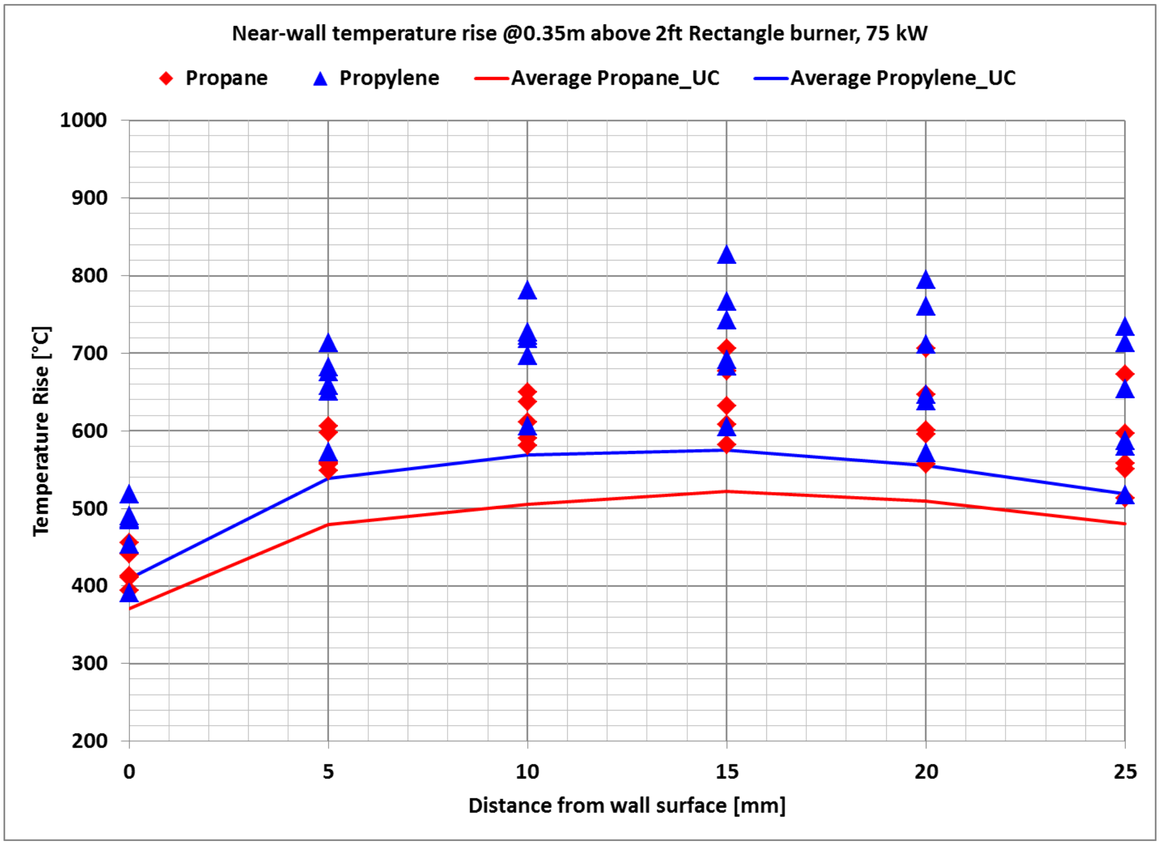

Figure 49 - Near-wall temperature, Rectangle burner, 75 kW, @ 0.35m

Near-wall temperature rise measured 0.95 m above burner surface during tests using the Square burner at 50 kW is presented in Figure 50. The spread of the data for tests using both source fuels is considerably smaller than at 0.35 m above the burner surface. This may suggest a less turbulent flow region near the thermocouples than at below. The data spread for the propylene tests is relatively consistent at 50°C, where as it is approximately 40°C for propane. The correction for these thermocouples is on the order of approximately +10°C.

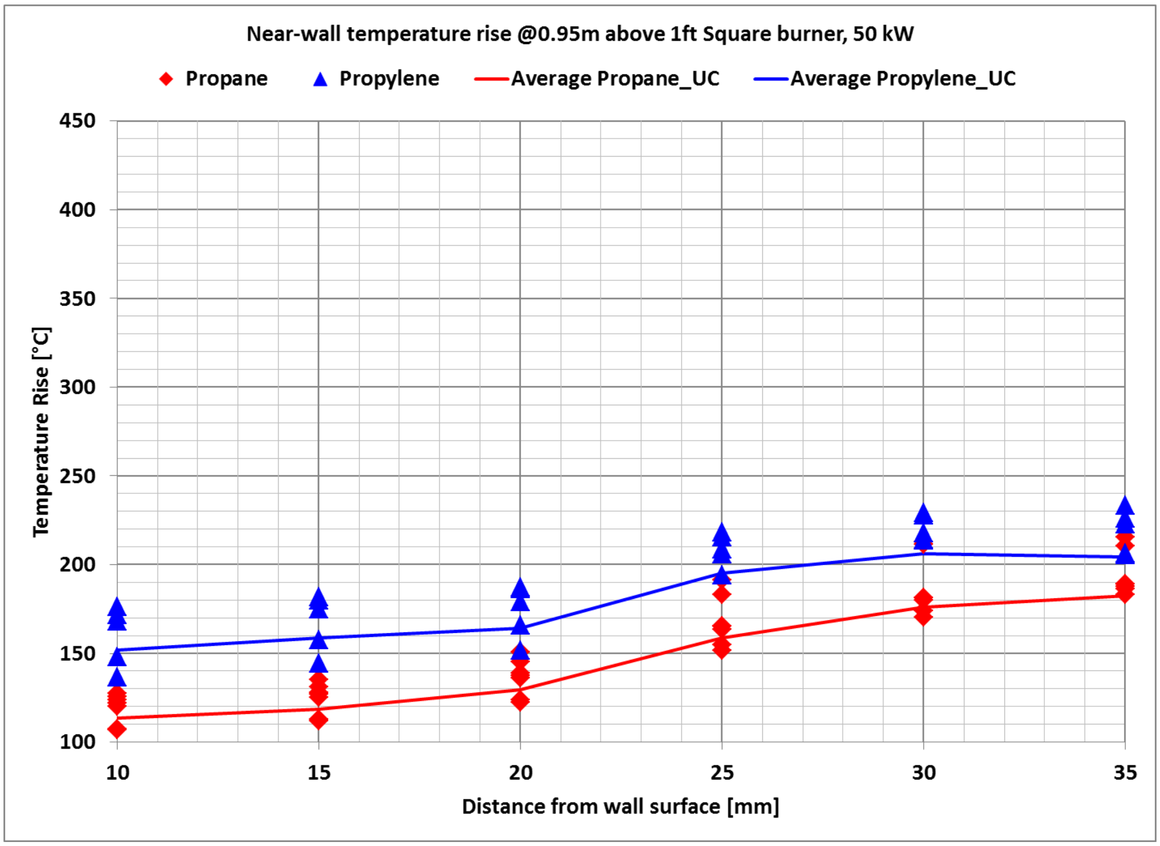

Figure 50 - Near-wall temperature, Square burner, 50 kW, @ 0.95m

Figure 51 shows the temperature recorded at 0.95 m over the burner surface in tests using the Square burner at 75 kW. The data spread for the propylene tests is the largest at 90°C, whereas the spread for the propane data is approximately 50°C and 40°C for the methane. The spread are all relatively consistent for at distances away from the wall surface. The tests where the highest near-wall temperature recorded were conducted using propylene, then propane and methane. The correction is also greatest for the propylene tests, but similar for the propane and methane tests.

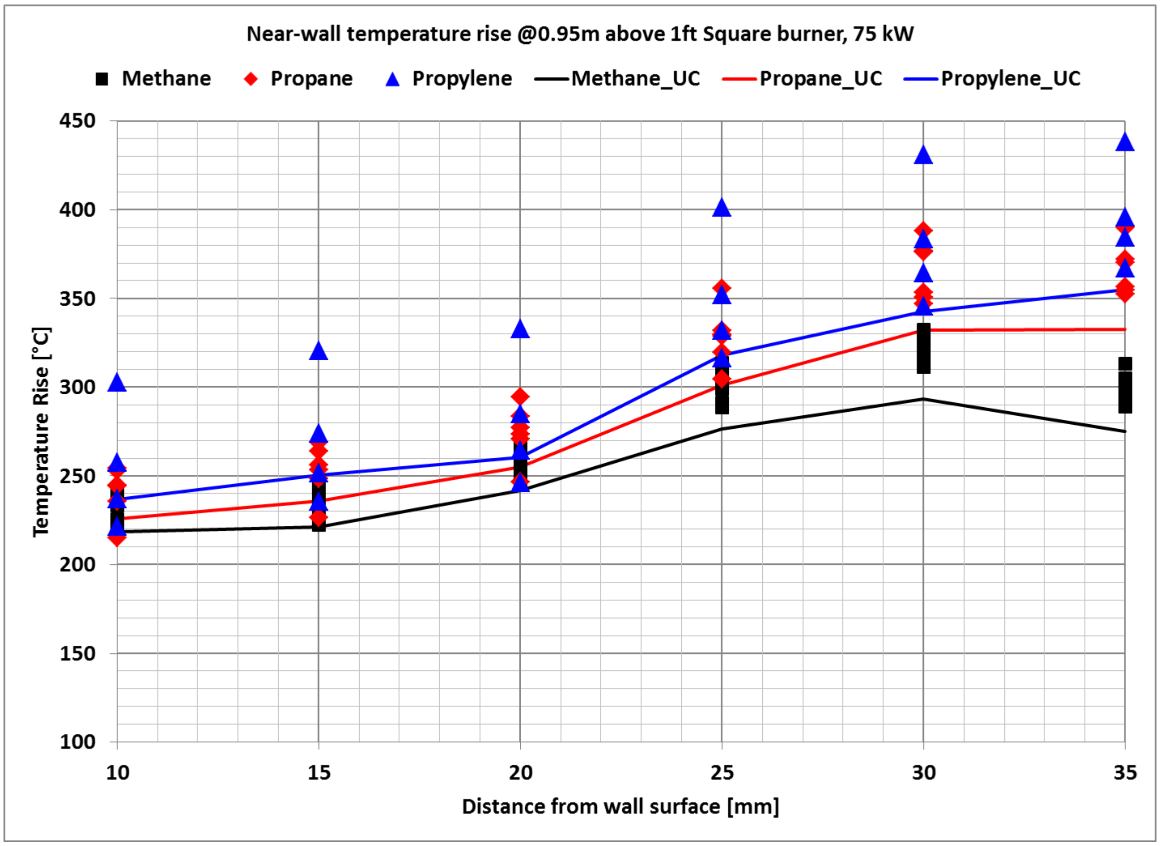

Figure 51 - Near-wall temperature, Square burner, 75 kW, @ 0.95m

Near-wall temperature rise measured 0.95 m above burner surface during tests using the Rectangle burner at 50 kW is presented in Figure 52. For the propane test temperature data, the data spread appears to decrease from 60°C at 10 mm away from the wall surface to 30°C at 35 mm away. However, in the propylene tests, the spread increased from 70°C to over 110°C over the same range. Again, the temperature correction for the propylene is much greater than the correction for the propane test data.

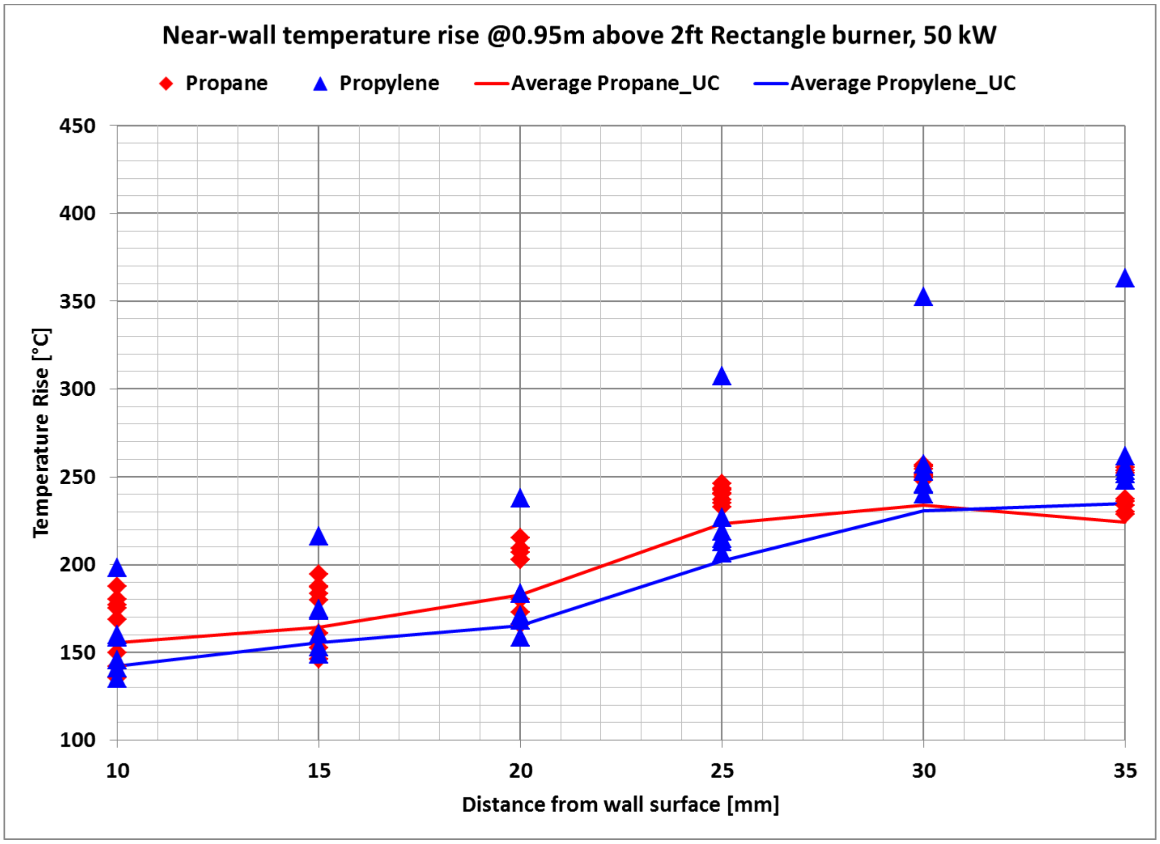

Figure 52 - Near-wall temperature, Rectangle burner, 50 kW, @ 0.95m

Near-wall temperature rise measured 0.95 m above burner surface during tests using the Rectangle burner at 75 kW is presented in Figure 62. At this elevation the wall temperature for both the propylene and propane tests is similar. The data spread for both sets of tests is also similar, decreasing from 80°C to 50°C from 10 mm to 35 mm from wall surface. This is different from the other data where the propylene near-wall temperature is generally greater than the propane source fire near-wall temperature for the same location.

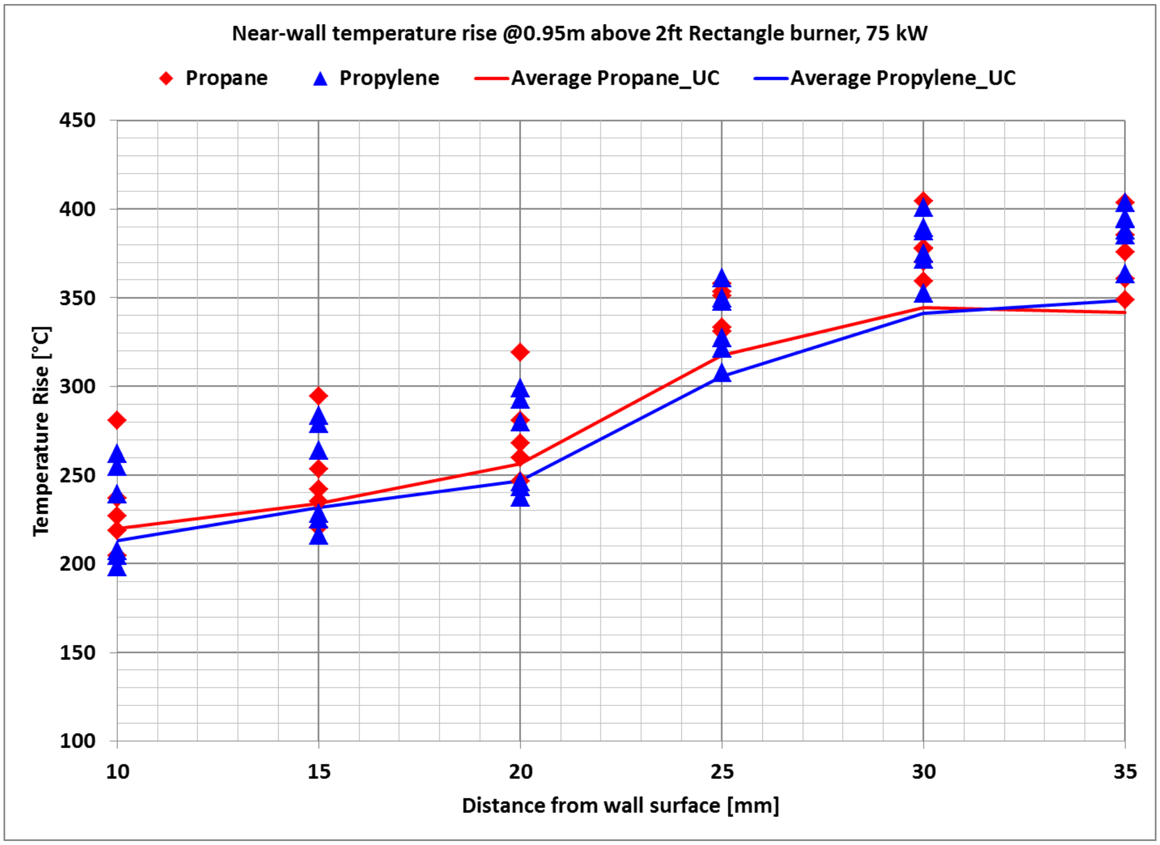

Figure 53 - Near-wall temperature, Rectangle burner, 75 kW, @ 0.95m

Near-wall temperature rise measured 0.95 m above burner surface during tests using the Square burner at 50 kW is presented in Figure 54. The data spread for the both test series is relatively consistent at 40°C. Overall, the propylene tests near-wall temperature data is higher than for the propane tests. The thermocouple correction for both test series is also small.

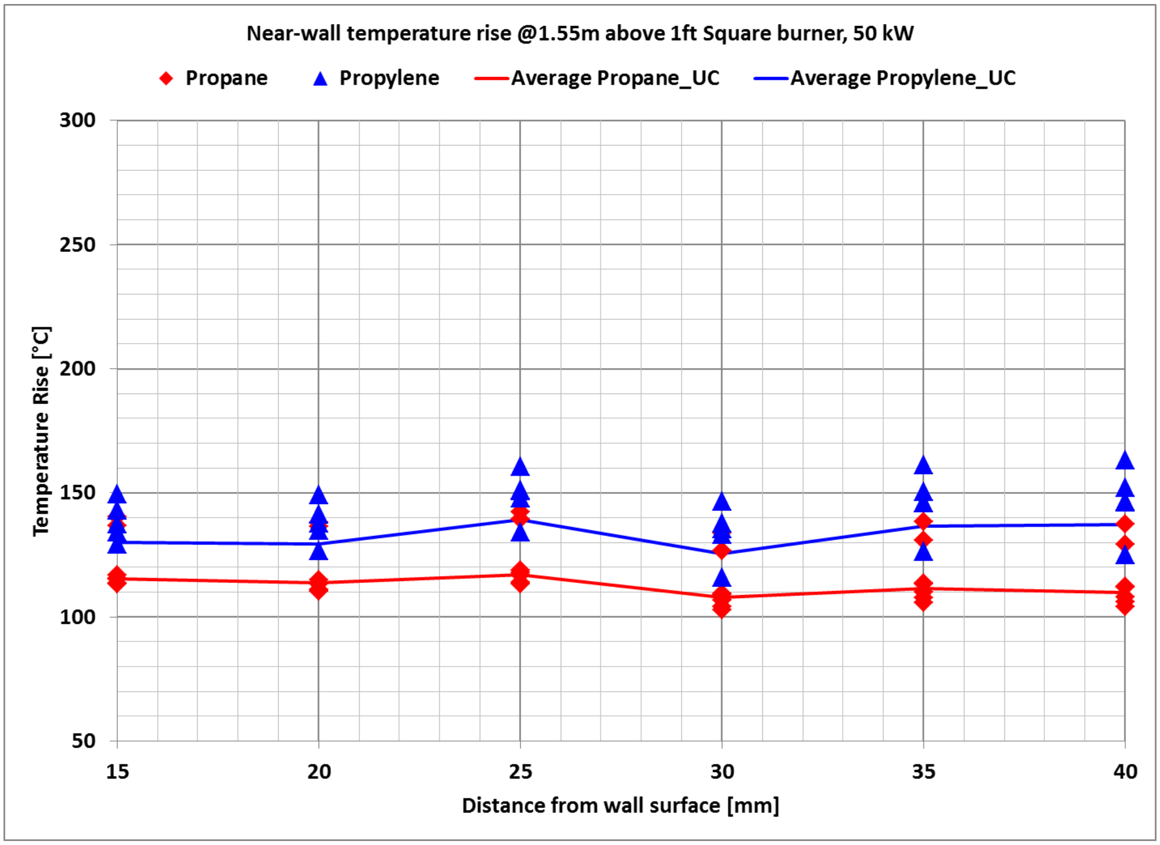

Figure 54 - Near-wall temperature, Square burner, 50 kW, @ 1.55m

Figure 55 shows the temperature recorded at 1.55 m over the burner surface in tests using the Square burner at 75 kW. The data spread for the propylene tests is the largest at 80°C, whereas the spread for the propane data is approximately 40°C and 20°C for the methane. The spread are all relatively consistent for at distances away from the wall surface. The tests where the highest near-wall temperature recorded were conducted using propylene, then propane and methane. The correction is also greatest for the propylene tests, but similar for the propane and methane tests.

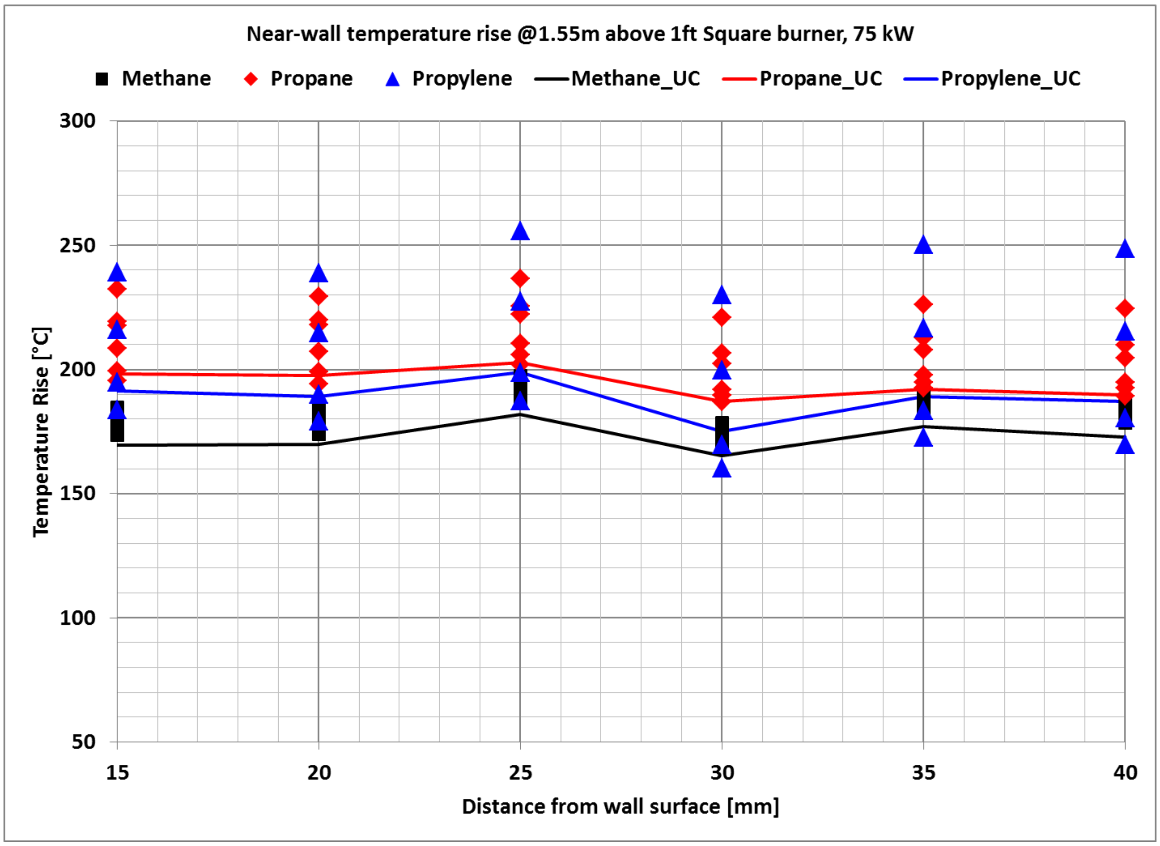

Figure 55 - Near-wall temperature, Square burner, 75 kW, @ 1.55m

Near-wall temperature rise measured 1.55 m above burner surface during tests using the Rectangle burner at 50 kW is presented in Figure 56. For the propane test temperature data, the data spread is relatively consistent at 30°C. However, in the propylene tests, the spread is about 50°C. Again, the temperature correction for the propylene is much greater than the correction for the propane test data. However, at this location, the near-wall temperature measured in both propane and propylene tests are similar.

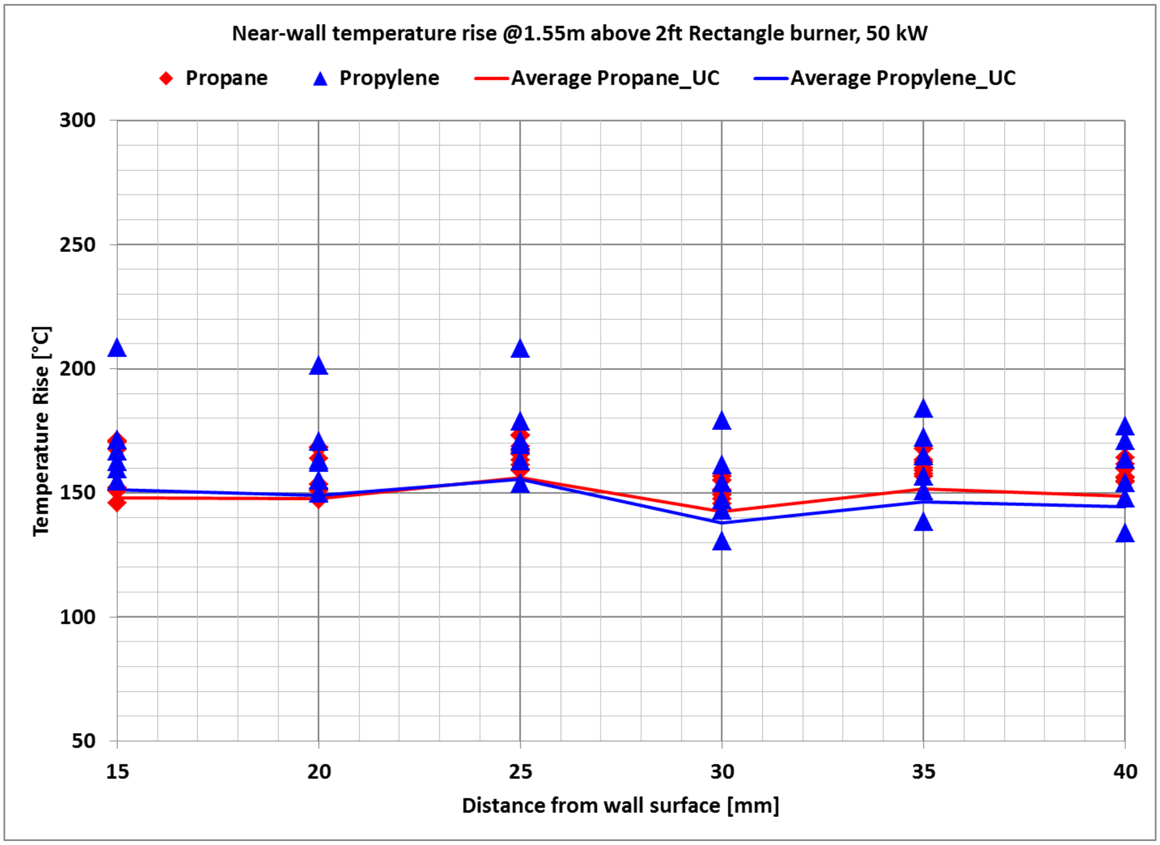

Figure 56 - Near-wall temperature, Rectangle burner, 50 kW, @ 1.55m

Near-wall temperature rise measured 1.55 m above burner surface during tests using the Rectangle burner at 75 kW is presented in Figure 57. The data spread for propylene increases from approximately 40°C to 70°C from 15 mm to 40 mm away from the surface of the wall. For the propane tests, the data spread is approximately 30°C overall. The correction is also greater for the propylene tests than for the propane tests.

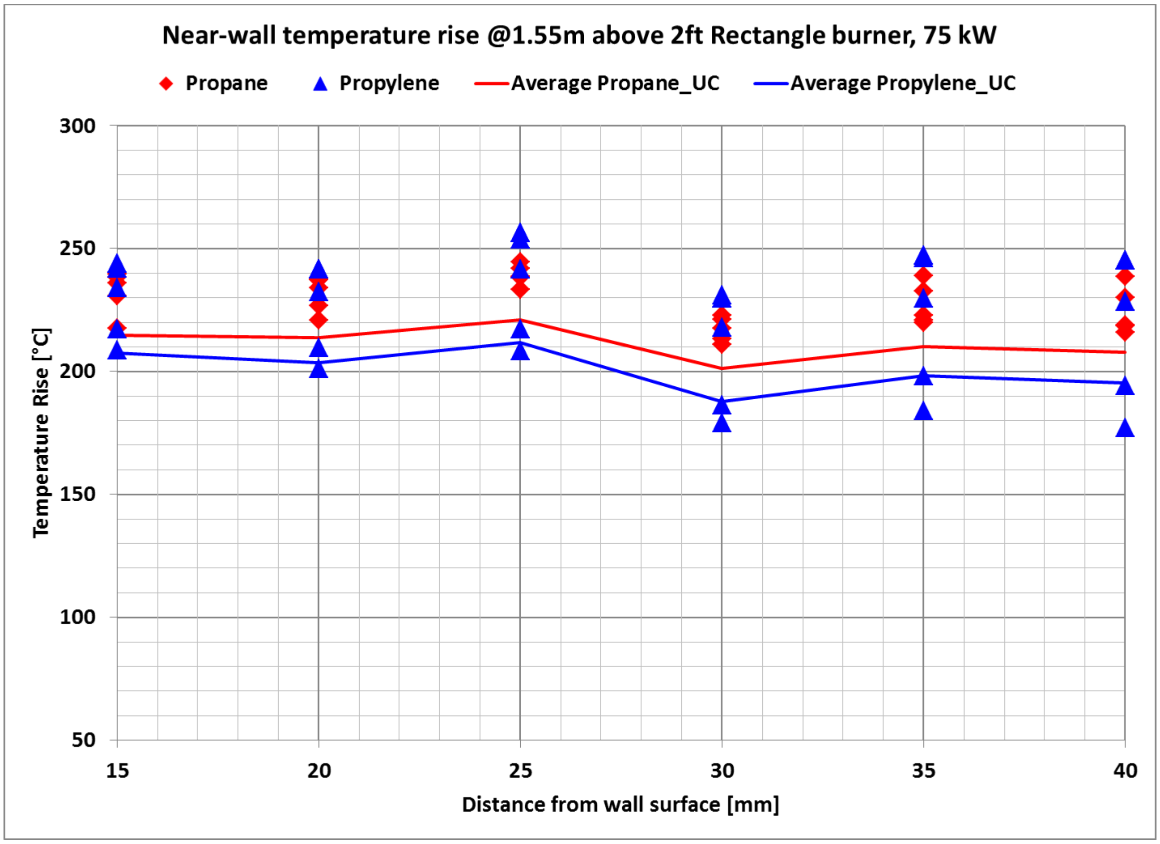

Figure 57 - Near-wall temperature, Rectangle burner, 75 kW, @ 1.55m

The near-wall temperature data for the various inert wall tests show that for fires of the same HRRs, propylene generally generate higher temperatures, and methane generated the lowest temperatures. As expected, at the lowest elevation of 0.35 m, the temperature measured is generally higher than the temperature measured at the higher elevations of 0.95 m and 1.55 m. At 0.35 m, the highest near-wall temperature is measured at the thermocouples at 10 mm and 15 mm from the wall surface. At 0.95 m, the highest temperature is generally recorded at 35 mm away from the wall surface, and at 1.55, the temperature measured at thermocouples from 15 mm to 40 mm away from the wall surface is generally similar.

Based on the principles of fluid dynamics, the source fire creates a flow over the inert wall that also forms a thermal boundary layer, and the interface is at the distance where the temperature is the highest. From the data, it can be inferred that the boundary layer interface is approximately 10 mm to 15 mm thick at 0.35 m above the source burner’s surface, and at over 35 mm at 0.95 m above the burner's surface. At the highest elevation of 1.55 m, the boundary layer is ill-defined using the temperature data because the measured temperatures are similar.

4.5 Combustible wall fire experimental data

Measurements in the combustible wall experiments consisted of HRR, centerline plume temperature, centerline plume velocity, heat flux to inert wall, and near-wall temperature, and flame spread. These data are related to all four components of flame spread: fluid dynamics/turbulence, gas phase kinetics, heat transfer to environment, and solid state pyrolysis. Data from Tests A4 and A13 are presented in details in the following sections.

Settings of the combustible wall fire tests are presented in Table 26.

Table 26 - Combustible wall fire test settings

Test Number	Fuel Type	Source Burner	Source Fire HRR [kW]	Burner Shut-Down time [sec]
A1*	Propylene	Rectangle	100	Not Recorded
A2*	Propylene	Rectangle	75	5
A3	Propane	Rectangle	50	91
A4	Propane	Rectangle	75	105
A5	Propane	Square	50	88
A6	Propane	Square	75	74
A7	Propylene	Square	50	55
A8	Propylene	Square	75	50
A9	Propylene	Rectangle	50	58
A10	Propylene	Rectangle	75	45
A11	Propylene	Rectangle	50	58
A12	Propylene	Rectangle	50	879**
A13	Propylene	Square	50	680**
A14	Propylene	Square	75	56
A15	Propane	Square	50	75
A16	Propane	Square	75	1360**
A17	Propane	Rectangle	75	807**
A18	Propane	Rectangle	50	72

* Tests A1 and A2 required water stream against fire growth during burn for safety reasons

** In these tests the source fire was on for the whole duration of the fire test

4.5.1 Heat release rate

The HRR from the combustible fire test was based on both the O_2 calorimetry and the flow rate calculations. The O_2 based HRR measures the global HRR and accounts for both the source burner fire and the fire on the FRP panel, whereas the flow-based HRR only accounts for the source fire. It is noted that since the source fire HRR was calculated from the flow measurements, the initial rise of to the consistent HRR at approximately 30 kW describes the time needed for the fuel gas to reach the burner. As the source fire is ignited, the fire is immediately turned up to the requisite levels at 75 kW and 50 kW.

Figure 58 shows an HRR time-history curve of Test A6, ignited with a 75 kW propane fire using the Square burner where the source fire was shut off after about 100 sec; Figure 59 shows the HRR curves of another experiment where the burner remained on the whole duration of the test. Using the total HRR obtained from O_2 calorimetry, the source fire HRR from flow rate calculations was subtracted to obtain the HRR history of the FRP fire only:

$$HRR_{FRP} = HRR_{Total} - HRR_{Source} \tag{41}$$

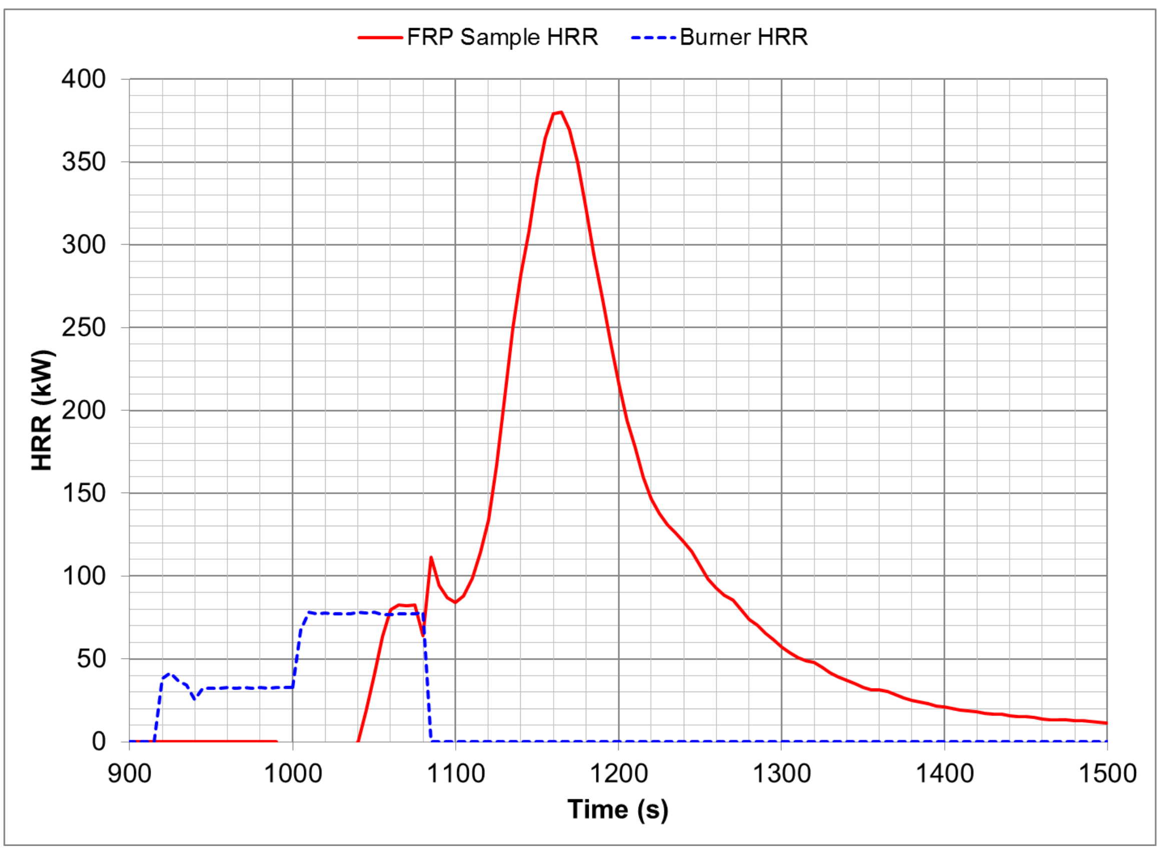

Figure 58 – Test A4 HRRs of source fire and FRP sample (Propane fuel, 75 kW source, Rectangle burner)

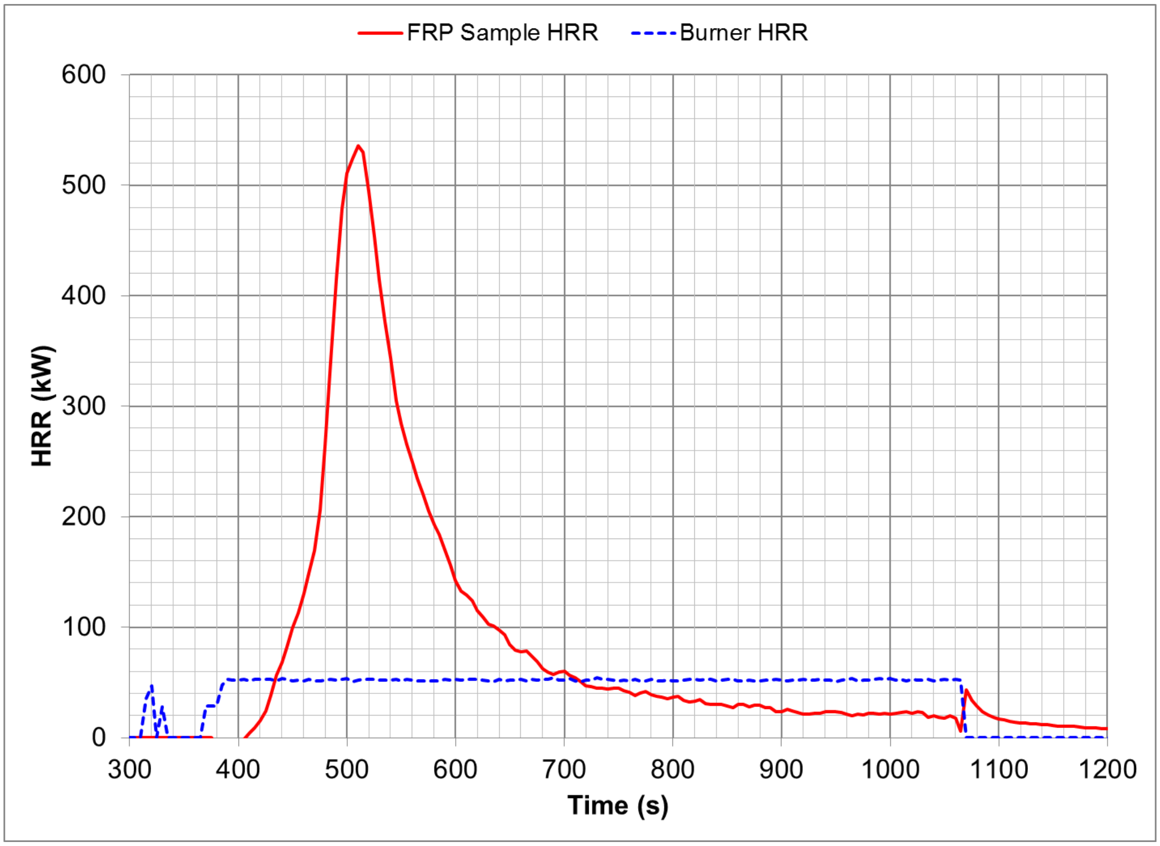

Figure 59 – Test A13 HRRs of source fire and FRP sample (Propylene fuel, 50 kW continuous source, Square burner)

The following figures have been time-shifted making the time zero equals to the time when the burner was ignited. Although the FRP panel generally burns for more than 20 minutes, the HRR during first 10 minutes of test was reported since most flame spread occurred in this period. The source burner HRR was subtracted from the global O_2-based HRR, so only the FRP HRR data is reported in Figure 60 to Figure 64. A discrepancy in the HRR curve is noted in most tests soon after ignition, this reflects the time when the fuel gas flow to the burner was terminated, where the burning panel's fire usually decreased in size momentarily then increases until rollover. The tests are grouped by the source burner types (Square vs. Rectangle) and source HRRs (50 kW vs. 75 kW).

Based on equation (1), the uncertainty of the FRP panel fire HRR can be calculated as to be about ±28 kW using equation (41). This higher uncertainty in the HRR stems from the contribution of both the O_2-based HRR uncertainty and the flow-based HRR uncertainty.

$$\delta_{HRR-FRP} = \sqrt{\delta^2{}_{HRR-O2} + \delta^2{}_{HRR-Flow}} \tag{42}$$

Where $\delta_{HRR-FRP} = uncertainty\ in\ the\ HRR\ of\ the\ FRP\ fire$

$\delta_{HRR-O2} = uncertainty\ in\ the\ HRR\ using\ O_2\ calorimetry\ [25\ kW]$

$\delta_{HRR-Flow} = uncertainty\ in\ the\ HRR\ using\ flow\ measurements\ [13\ kW]$

Figure 60 shows the HRR time histories from the tests using the Square burner with a 50 kW source fire. The propylene tests had overall quicker times to peak (rollover under ceiling) than the propane test at the same source fire size. However, the test where the propylene source fire was kept on for the whole test had the quickest time to peak, and also the most heat generated.

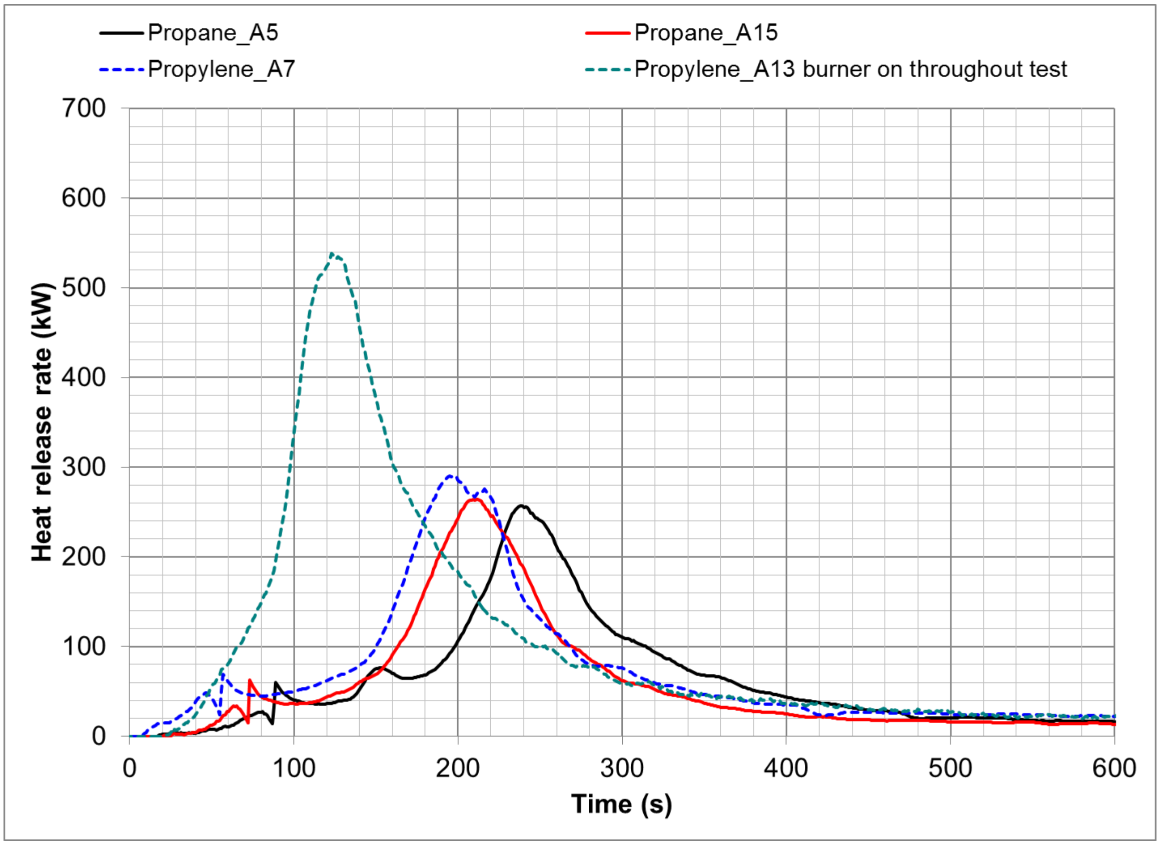

Figure 60 - HRR time histories for 1ft Square burner with 50 kW source fire

Figure 61 shows the HRR time histories from the experiments using the Square burner with a 75 kW source fire. The propylene tests had overall quicker times to peak (rollover under ceiling) than the propane test at the same source fire size. In test where the source fire was kept on for the whole test the highest HRR was generated. Compared to the cases using the same burner but at 50 kW source fire size, the times to peak was quicker in the 75 kW tests where the burner fuel was shut off.

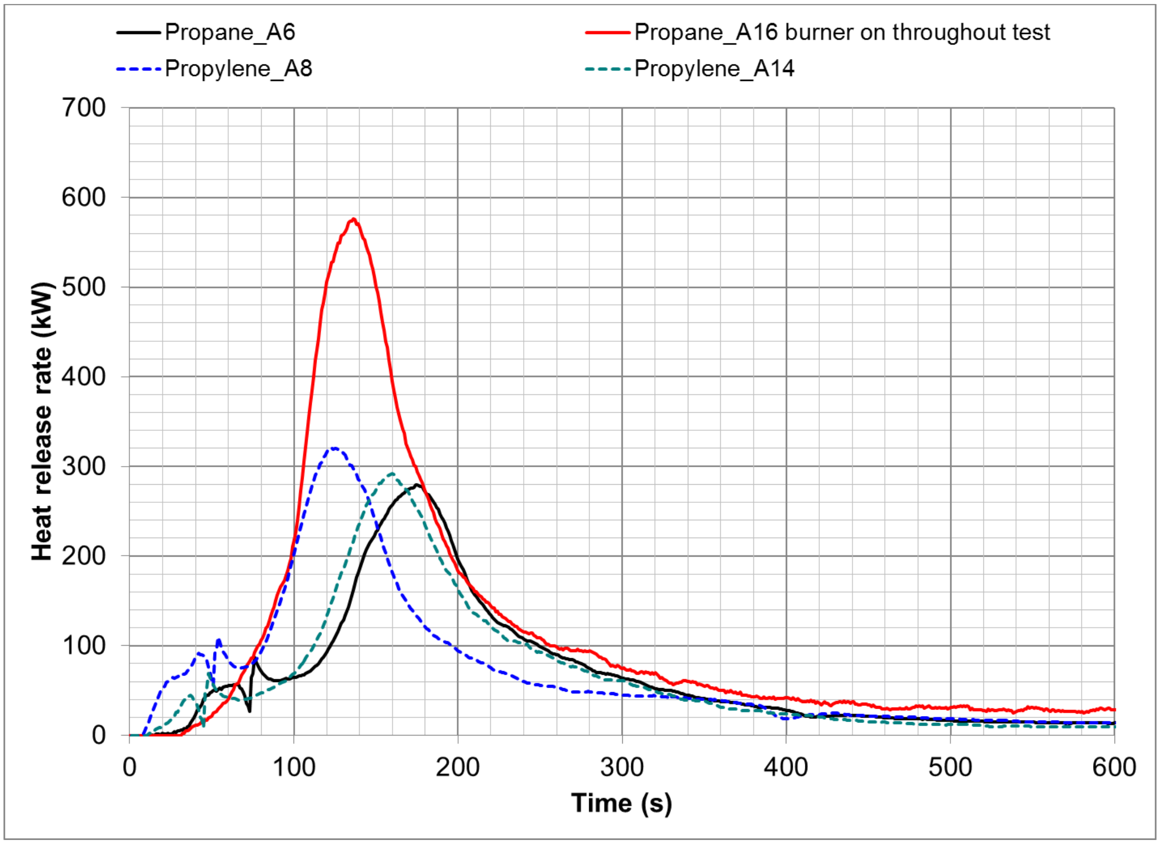

Figure 61 - HRR time histories for 1ft Square burner with 75 kW source fire

Figure 62 shows the HRR time histories from the experiments using the Rectangle burner with a 50 kW source fire. The propylene tests had quicker times to peak (rollover under ceiling) than the propane test at the same source fire size. However, the test where the source fire was kept on for the whole test had the quickest time to peak, and also the most heat generated. These trends are similar to the 50 kW cases with the 1 ft Square burner.

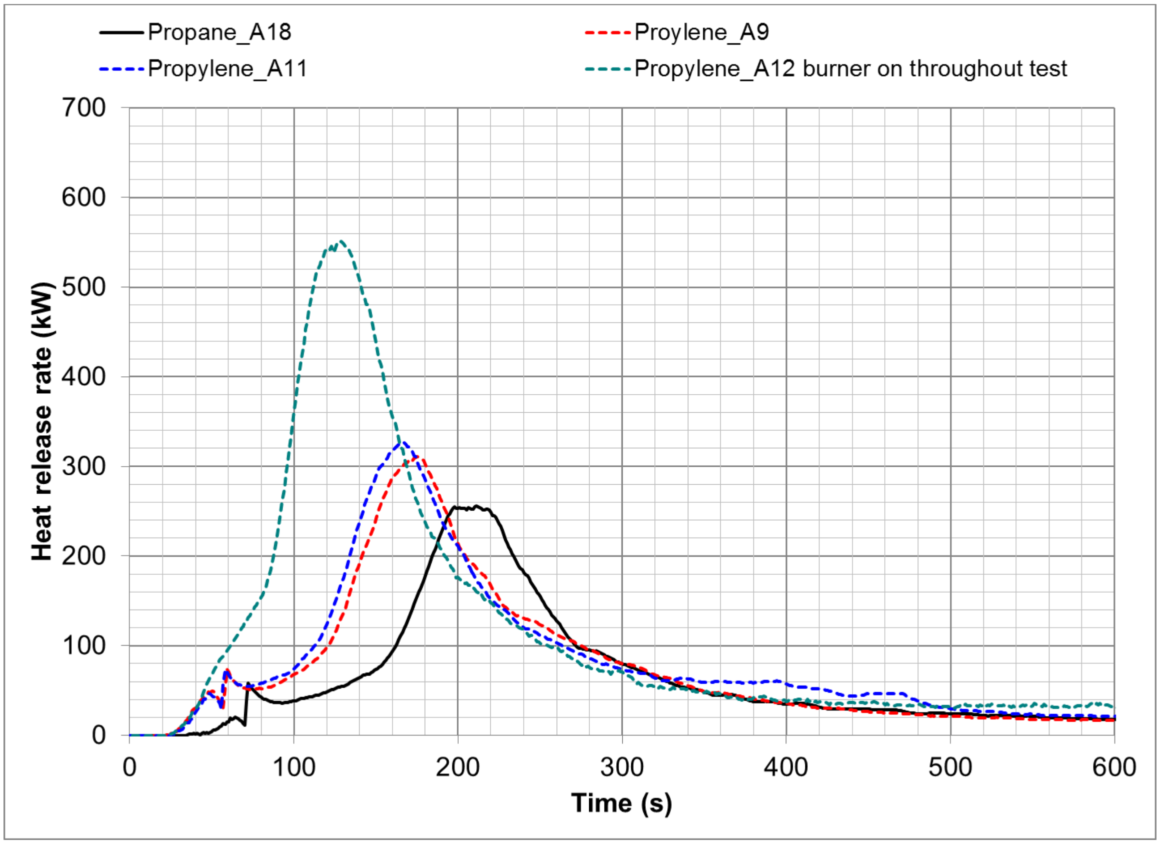

Figure 62 - HRR time histories for 2ft Rectangle burner with 50 kW source fire

Figure 63 shows the HRR time histories from the tests using the Rectangle burner with a 75 kW source fire. The propylene tests had faster times to peak (rollover under ceiling) than the propane test at the same source fire size. In the test where the source fire was kept on for the whole test the most heat was generated. Compared to the experiments using the same Rectangle burner but with a 50 kW source fire size, the times to peak was shorter in the 75 kW cases.

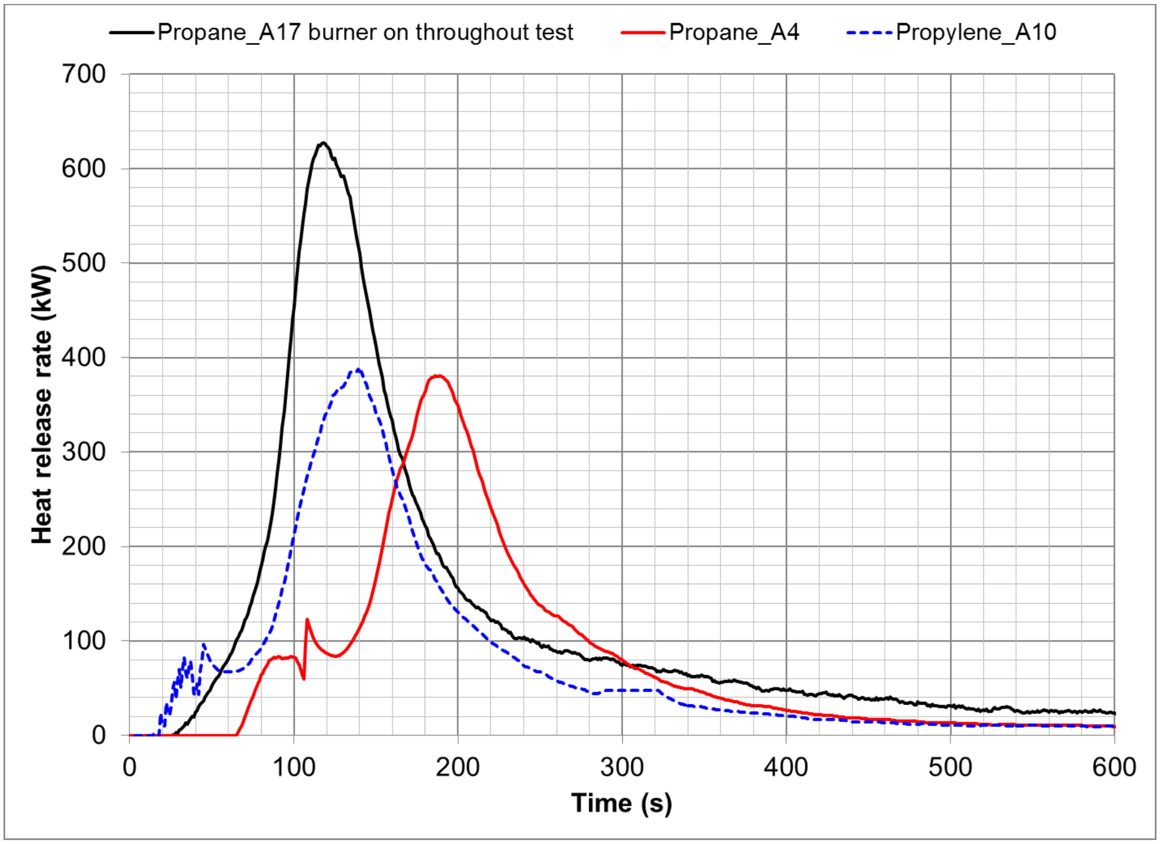

Figure 63 - FRP fire HRRs using Rectangle burner at 75 kW

From the data shown in Figure 60 to Figure 63, it is evident that the peak HRR measured was about 300 kW ±40 kW for the cases where the source fire was extinguished upon flame attachment on the FRP. For the cases where the source fire was at a constant HRR, the FRP's HRR peaked at 580 kW ±50 kW. The difference in the peak HRR may be attributed to the fact that the source burner continuously drives the flame spread on the FRP so that more area was involved through the presence of the plume and the radiation from the source flame. It is also found that for the same source burner type and same source HRR, a propylene fire would lead to a faster HRR peak time vs. a propane fire.

Figure 64 shows the HRR time histories from the tests using the Rectangle burner with different source fire HRRs. Streams of water were applied to these tests in order to cool the fire and prevent flashover as the side walls and ceiling was burning from the rollover. Additionally, in Tests A1 and A2 the source propylene fire flared up over the desired constant source HRR due to equipment malfunctions, creating a less than optimal situation and accelerated the flame spread process. Since the goal of the research is to record a sufficient amount of data relevant to flame spread, the situations created by these flare-ups were prohibitive to the goal and the data form these tests are not presented in the rest of this Section, but they are available in Appendix F.

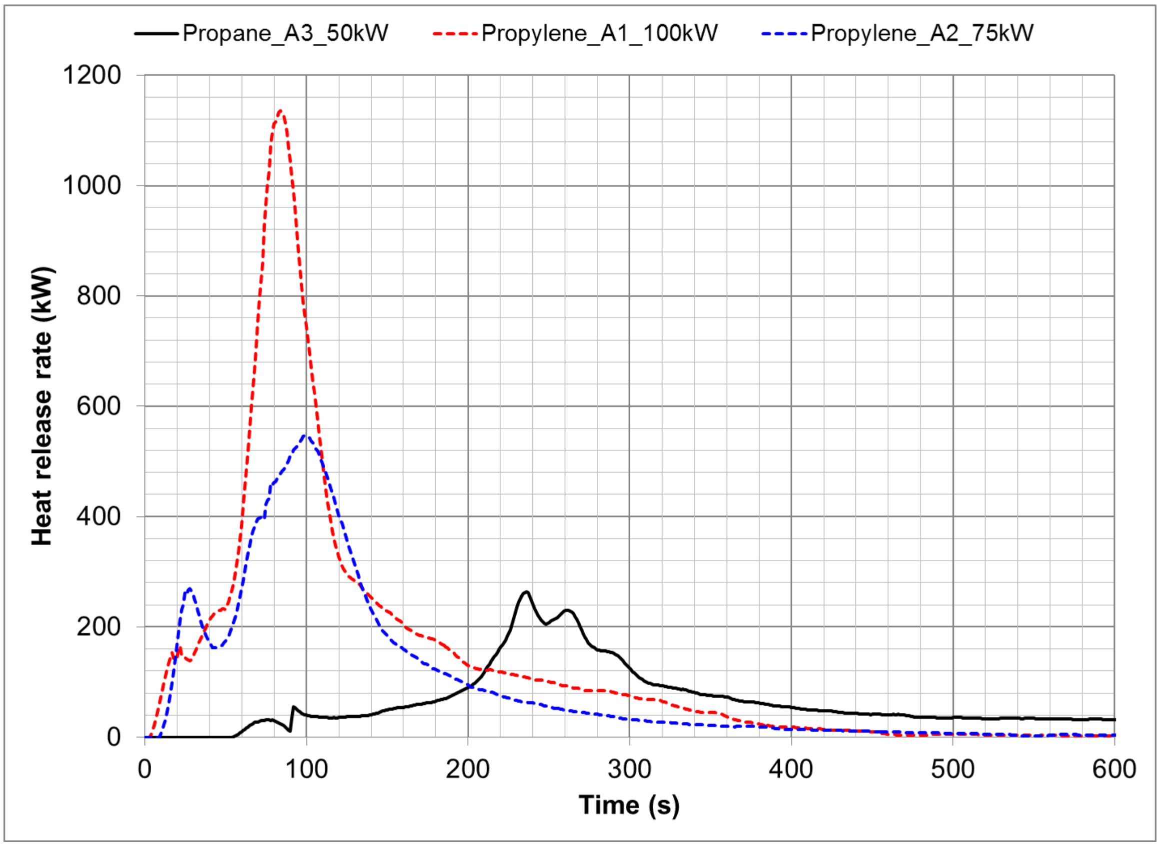

Figure 64 - HRR time histories for 2ft Rectangle burner with various source fires

4.5.2 Centerline temperature

Temperature along the centerline of the burner and the FRP panel was measured at different heights during the combustible wall fire tests. The thermocouples are about 13" away from the wall. Compared to the time-averaged temperature value presented in Section 0 and 4.4.2, the temperature in the combustible wall experiment is presented as temperature time history to show the un-steady state natural of these fires. As described in Section 4.2.2.1, the temperature correction method used for the combustible wall panel fire tests was based on Young's method.

Due to the amount of data collected in each experiments and the number of combustible wall experiments, the data from only two representative experiments are presented from this point forth. The parameters of these 2 tests are shown in Table 27. The two tests chosen had the opposite configurations in terms of source fuel, source HRR, burner size, and source burner operation time; these tests are shown to reflect the change in data due to change in configurations.

Table 27 - Configurations of combustible wall tests with data presented in this Section

Test	Source Fuel	Source HRR	Burner size	Source HRR constant throughout test?
A4	Propane	75 kW	Rectangle	No
A6	Propylene	50 kW	Square	Yes

The uncorrected centerline temperature rise over ambient, measured in Test A4 was superimposed on the Test's HRR history and presented in Figure 65 and Figure 66. The temperature at heights from 0.05 m to 0.95 m over the burner is presented in Figure 65. It is shown that the temperature rises are largest when the source burner was outputting a constant HRR at 75 kW, then the temperature reduces as the source burner was turned off and the FRP began to burn. This suggests that the thermocouples measured the plume and not actually affected by the wall fire.

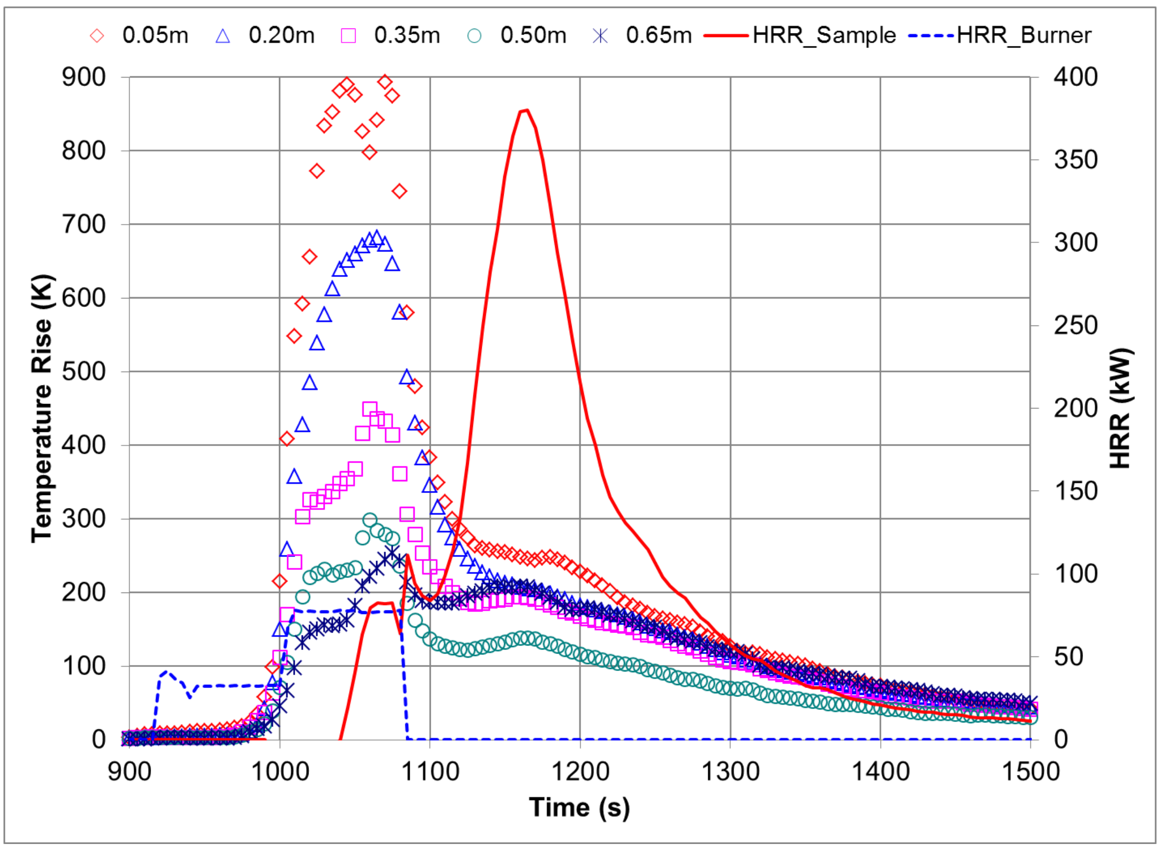

Figure 65 - UNCORRECTED Centerline temperature rise (< 1 m over burner) in Test A4 (Propane fuel, 75 kW source, Rectangle burner)

The uncorrected temperature rise at heights from 1.10 m to 1.85 m over the burner in Test A4 is presented in Figure 66. Since these thermocouples are above the source fire's flame region, it is shown that the temperature rises were low before the FRP started to burn. However, as the fire spread along the center of the panel, the temperature along this portion of the centerline rapidly increased until the FRP's HRR peaked. At the peak, the highest centerline temperature was registered at the thermocouple 1.85 m above the burner's surface due to the rollover under the ceiling.

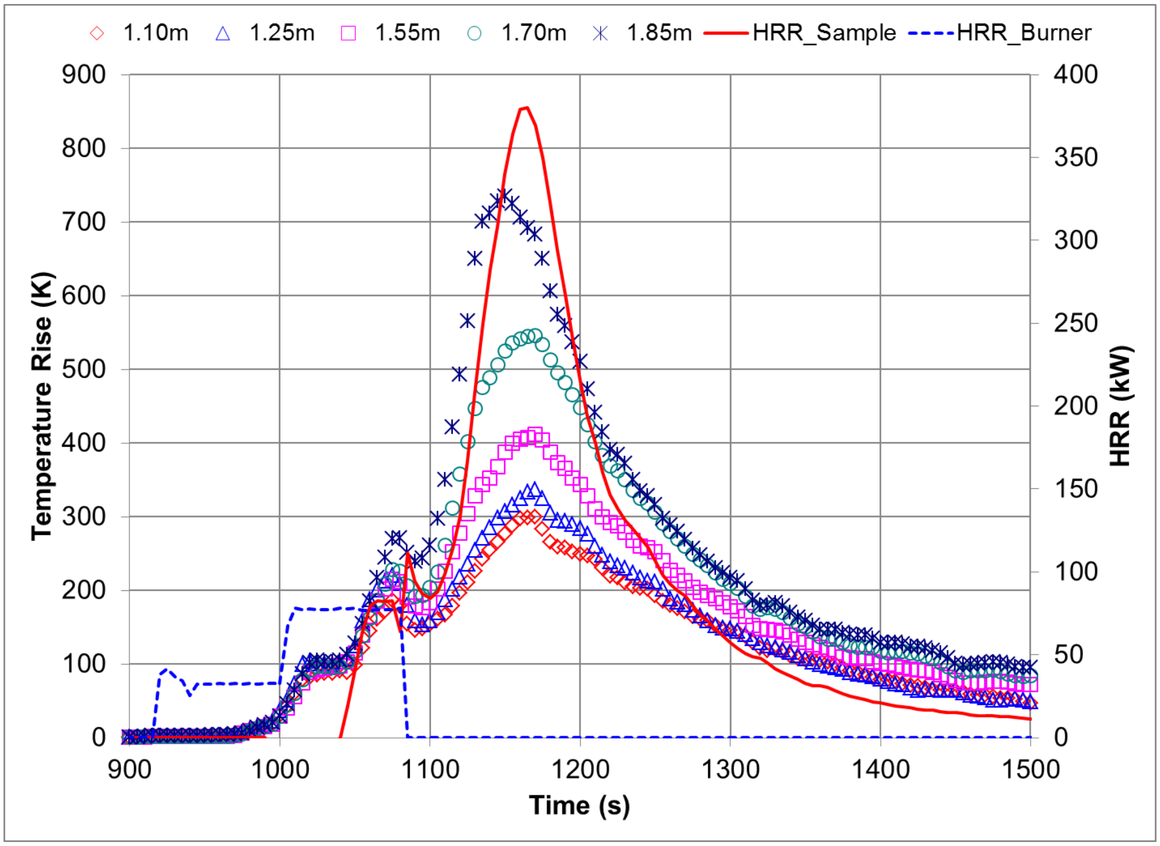

Figure 66 – <u>UNCORRECTED</u> Centerline temperature rise (> 1 m over burner) in Test A4 (Propane fuel, 75 kW source, Rectangle burner)

The <u>corrected</u> centerline temperature rise over ambient, measured in Test A4 was superimposed on the Test's HRR history and presented in Figure 67 and Figure 68. The temperature at heights from 0.05 m to 0.95 m over the burner is presented in Figure 67. The correction accounts for the heat loss via convection and radiation from the surface of the thermocouple; the resulting true gas temperature is an increase of the recorded temperature. For the thermocouples near the burner surface, the corrected temperature shows an increase of about 400 K to 500 K. The large correction was due to the flame surrounding the thermocouples and when flow velocities at the thermocouples were higher. At the thermocouples further up the centerline from 0.35 m to 0.65 m away from the burner surface, the temperature increase due to correction drastically dropped off to the order of 100 K.

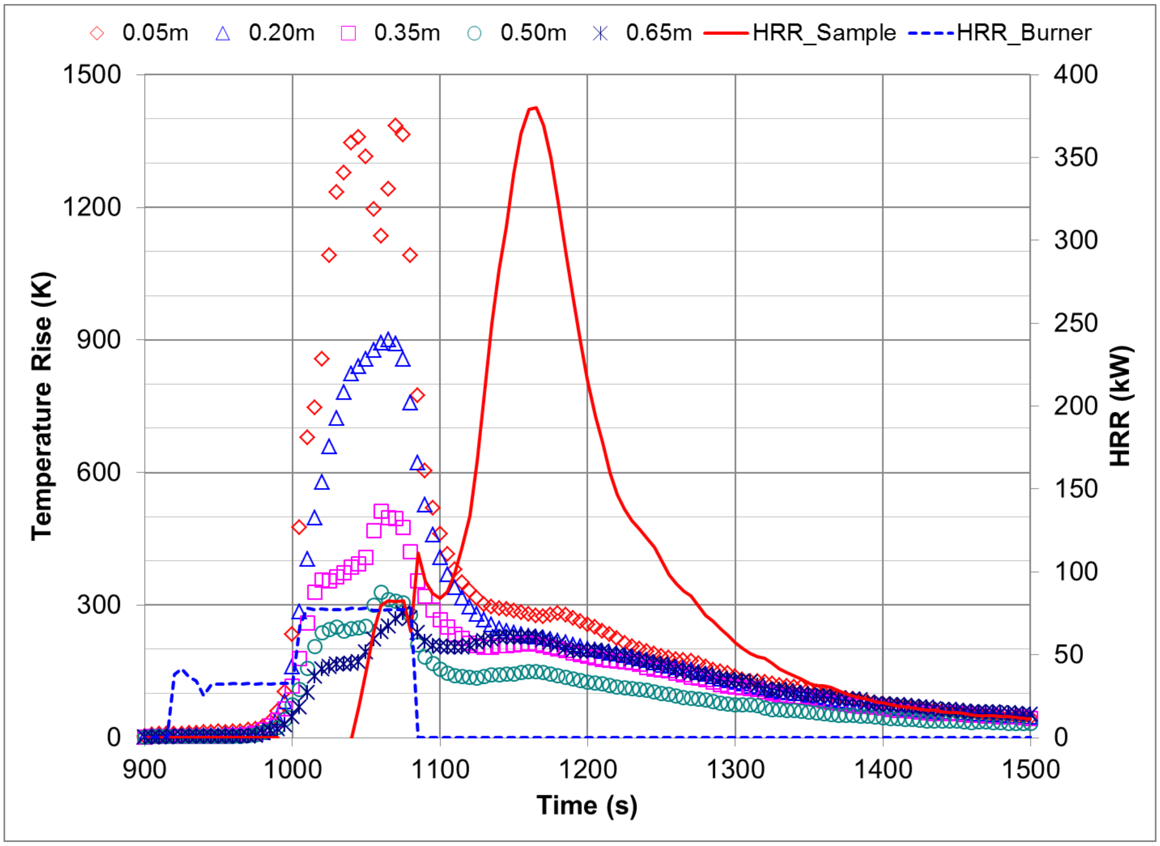

Figure 67 – CORRECTED centerline temperature rise (< 1 m over burner) in Test A4 (Propane fuel, 75 kW source, Rectangle burner)

The data shown in Figure 68 corresponds to the corrected temperature measured at those thermocouples from 1.10 m to 1.85 m away from the burner surface. These thermocouples were in the buoyant plume above the flame and had relative small correction on the order of 50 K to 100 K. However, the correction at the highest thermocouple was larger at around 200 K when the HRR of the FRP fire was at its peak where the thermocouple was surrounded by flames under the ceiling and the flow velocities at the thermocouples were higher.

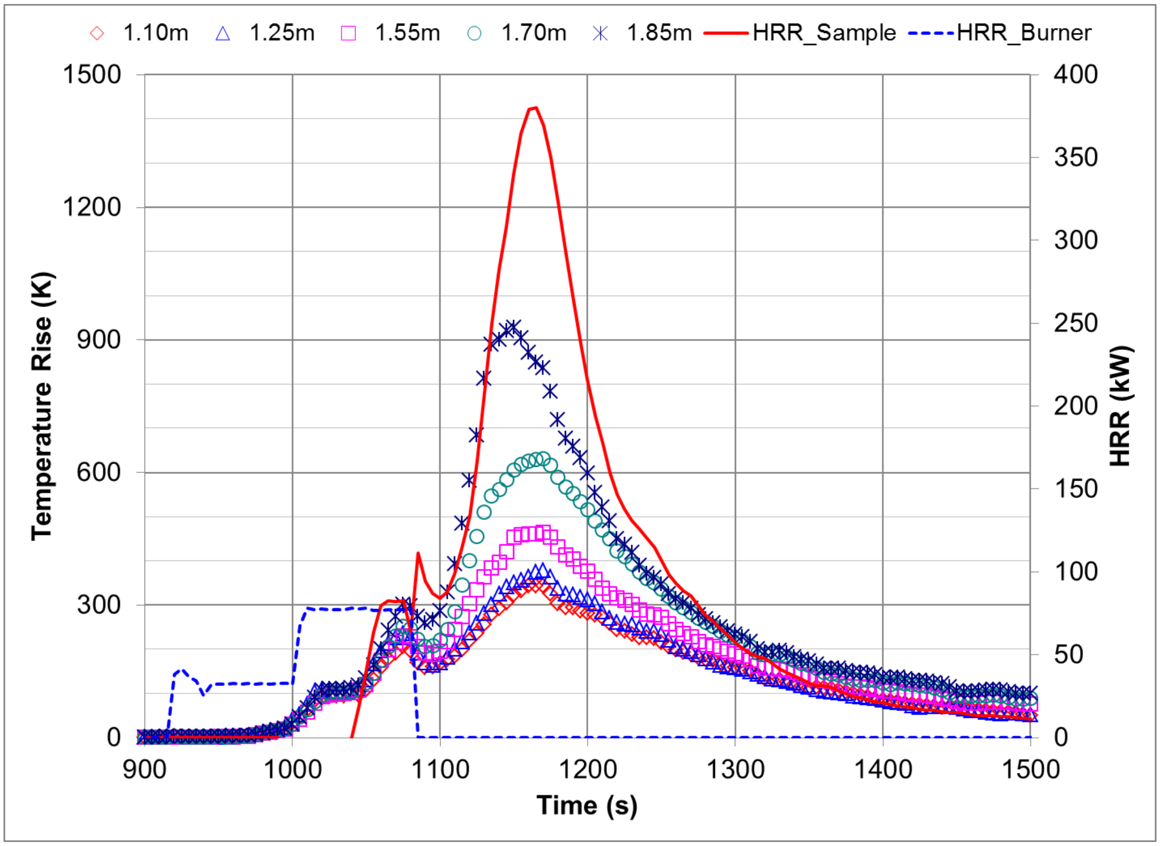

Figure 68 - <u>CORRECTED</u> centerline temperature rise (> 1 m over burner) in Test A4 (Propane fuel, 75 kW source, Rectangle burner)

Taken together, the uncorrected and corrected plume centerline temperature values represent the lower and upper bounds, respectively, of the uncertainty of the temperature measurements. The uncertainty was greatest when the thermocouple was bathed in flames, and lower if it was in the buoyant plume. Compared to the thermocouple compensation, the inherent uncertainty of the thermocouples was insignificant.

Uncorrected centerline temperature rise over ambient, measured in Test A13 was superimposed on the Test's HRR history and presented in Figure 69 and Figure 70. The temperature at heights from 0.05 m to 0.95 m over the burner is presented in Figure 69. The temperature rises at these thermocouples were quite constant during the experiment since the burner was on throughout the test. However, an increase in temperature was noted at these thermocouples when the HRR peaked, one can also observe that the centerline plume temperatures at this lower region were affected by the fire when it rollover.

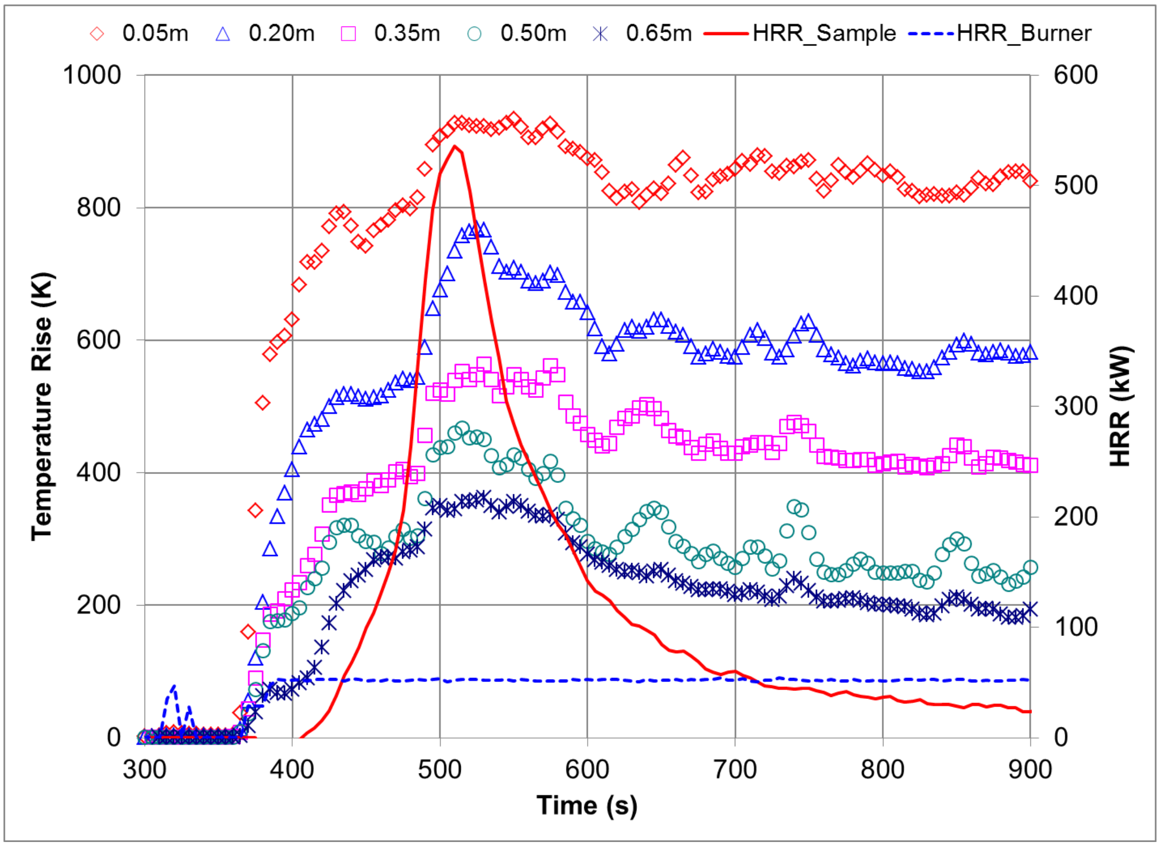

Figure 69 – UNCORRECTED Centerline temperature rise (< 1 m over burner) in Test A13 (Propylene fuel, 50 kW continuous source, Square burner)

Test A13's <u>uncorrected</u> temperature rise at heights from 1.10 m to 1.85 m over the burner is presented in Figure 70. Since these thermocouples are above the source fire's flame region, it is shown that the temperature rises were low before the FRP started to burn. However, as the fire spread along the center of the panel, the temperature along this portion of the centerline rapidly increased until the FRP's HRR peaked. At the peak, the highest centerline temperature was registered at the thermocouple 1.85 m above the burner's surface due to the rollover under the ceiling; similar to the Test A4 where the burner was turned off.

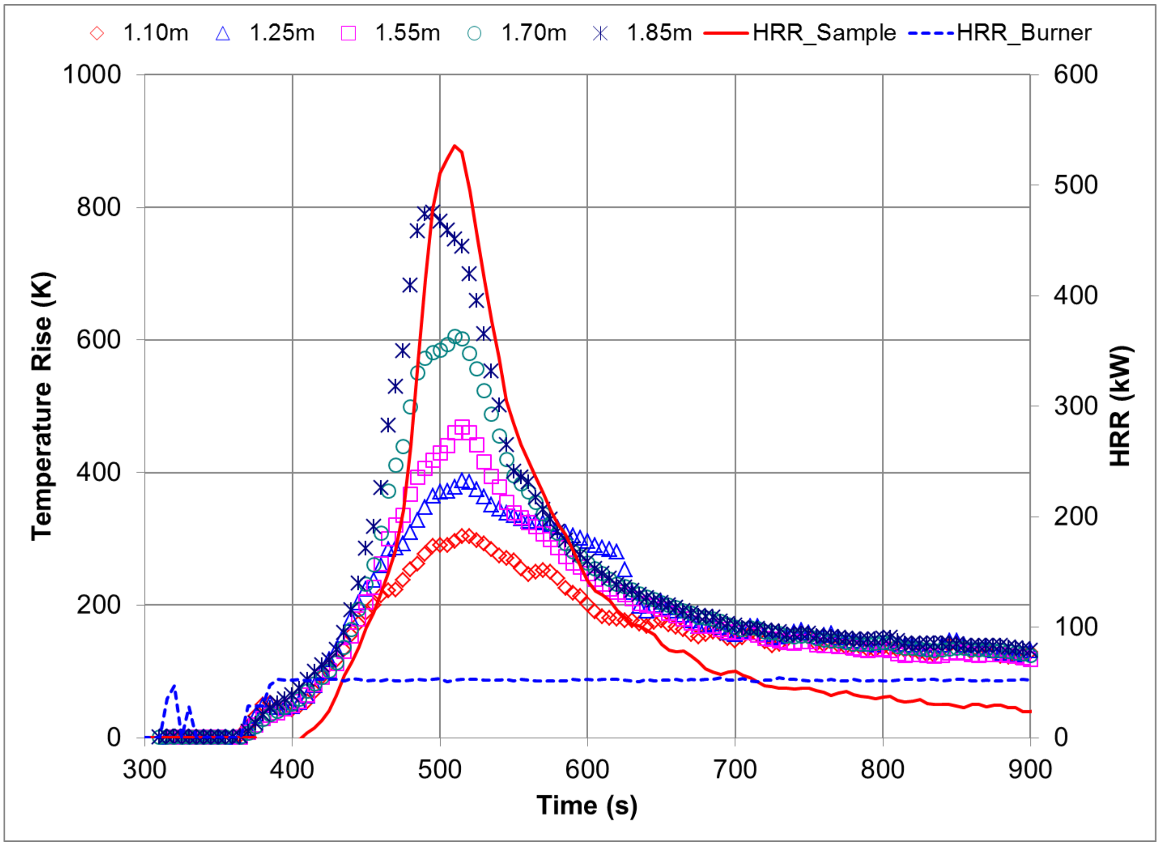

Figure 70 - <u>UNCORRECTED</u> Centerline temperature rise (> 1 m over burner) in Test A13 (Propylene fuel, 50 kW continuous source, Square burner)

The <u>corrected</u> centerline temperature rise over ambient, measured in Test A13 was superimposed on the Test's HRR history and presented in Figure 71 and Figure 72. The correction accounts for the heat loss via convection and radiation from the surface of the thermocouple; the resulting true gas temperature is an increase of the recorded temperature. For the thermocouples near the burner surface, the corrected temperature shows an increase of about 400 K to 600 K. The large correction was due to the flame surrounding the thermocouples. At the thermocouples further up the centerline from 0.35 m to 0.65 m away from the burner surface, the temperature increase due to correction drastically dropped off to the order of 100 K.

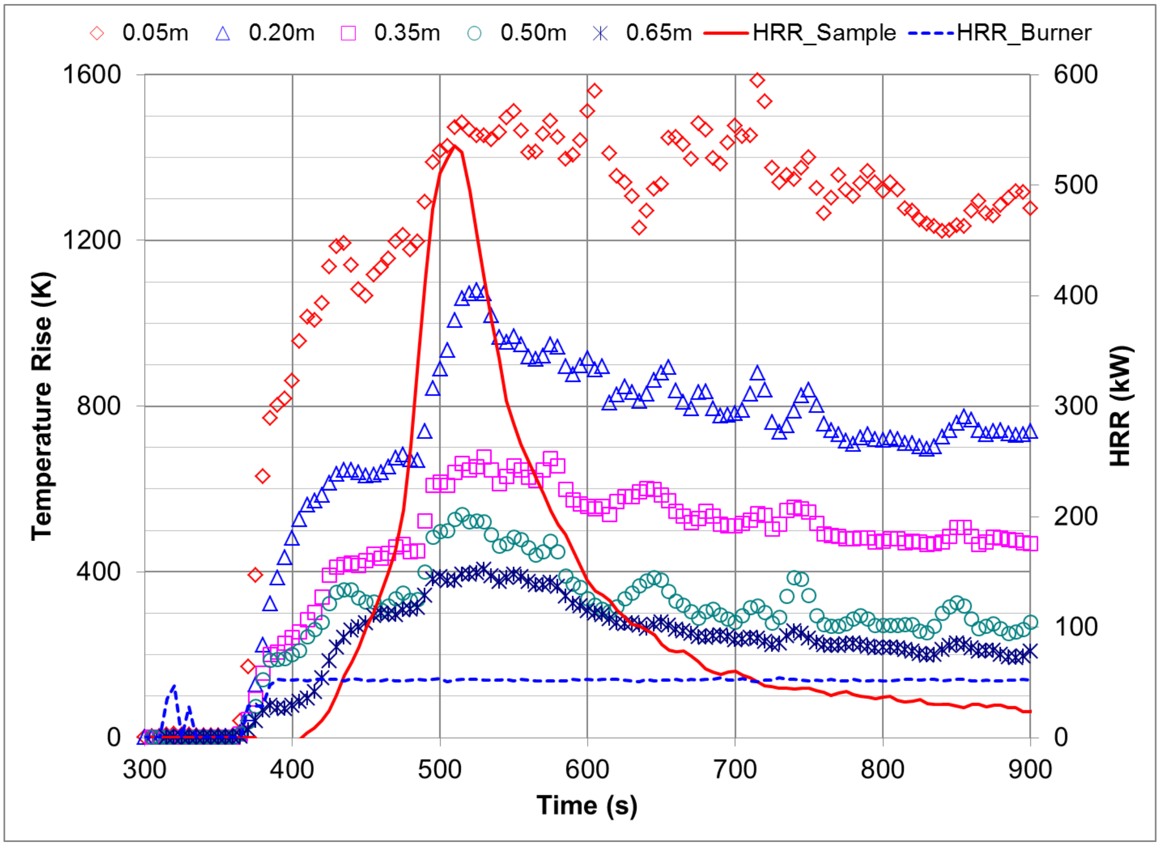

Figure 71 – <u>CORRECTED</u> Centerline temperature rise (< 1 m over burner) in Test A13 (Propylene fuel, 50 kW continuous source, Square burner)

The data shown in Figure 72 corresponds to the <u>corrected</u> temperature measured at those thermocouples from 1.10 m to 1.85 m away from the burner surface. These thermocouples were in the buoyant plume above the flame and had relative small correction on the order of 50 K to 100 K. However, the correction at the highest thermocouple was larger at around 300 K when the HRR of the FRP fire was at its peak where the thermocouple was surrounded by flames under the ceiling.

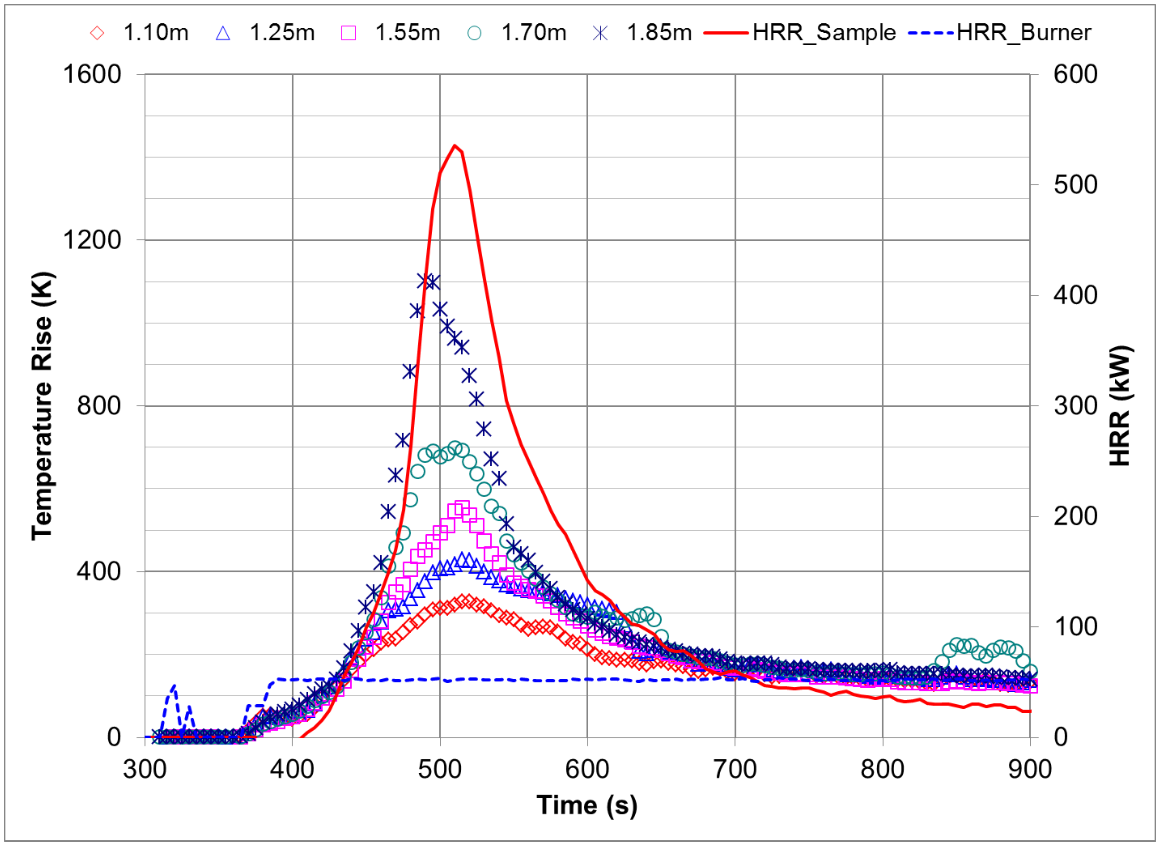

Figure 72 - <u>CORRECTED</u> Centerline temperature rise (> 1 m over burner) in Test A13 (Propylene fuel, 50 kW continuous source, Square burner)

Taken together, the uncorrected and corrected plume centerline temperature values represent the lower and upper bounds, respectively, of the uncertainty of the temperature measurements. The uncertainty was greatest when the thermocouple was bathed in flames, and lower if it was in the buoyant plume. Compared to the thermocouple compensation, the inherent uncertainty of the thermocouples was insignificant.

4.5.3 Centerline velocity

Centerline velocity measured during the combustible wall panel fire tests are presented in this section. The bi-directional probes were oriented inside the compartment at the centerline of the burner, similar to the inert wall scenario. However, due to the nature of the test type, the velocity was very transient and is greatly affected by the source fire and the burning of the combustible wall panel.

Since the bi-directional probes, the Swagelok connections, the copper tubings, the pressure transducers, and the wirings were all located in the compartment close to the burning wall, the thermal effects on these components were greatly increased than from the small HRR free plume and inert wall source fires. The transducers were found to be extremely sensitive to the temperature change of their environment and can greatly affect the pressure change measurements. Due to the limitations of the equipment, the uncertainty of the velocity data is large, greater than that defined for the free plume and inert wall fire tests.

Most importantly, it had been observed once the sample fire peaked in HRR, an unfavorable thermal environments where the equipment were rapidly heated and cooled was created, which essentially rendered the velocity data mostly erroneous at that point. Hence it is cautioned that the velocity data be ignored after the sample peaked in HRR. However, although the velocity measurements are inaccurate, the trends of the flow's direction were found to still be valid.

Due to data drift and the characteristics of the velocity sensing equipment, the uncertainty of the velocity measurements for the period of times before the sample HRR peaked is approximately 0.7 m/s for probe locations less than 1.0 m above the source burner surface, and 1 m/s for probe locations at least 1.0 m above the burner surface.

Figure 73 presents the upward vertical velocity recorded in Test A4 at elevations from 0.20 m to 0.95 m above the source burner surface. The velocity in this range was driven mostly by the source fire plume as from the large increase to the highest and relatively constant velocity value when the source burner HRR is at 75 kW. After the source fire was extinguished, the velocity sharply reduced to the ambient level. As the sample fire peaked, the velocity increased at the locations between 0.20 m to 0.80 m above the burner surface, however, the probe located at 0.95 m registered a negative flow over the same period of time. The largely negative flows measured by the 0.20 m and 0.80 m probes at approximately 1400 sec when the burning was almost extinguished are effects of data drift caused by the heating and cooling of the transducers.

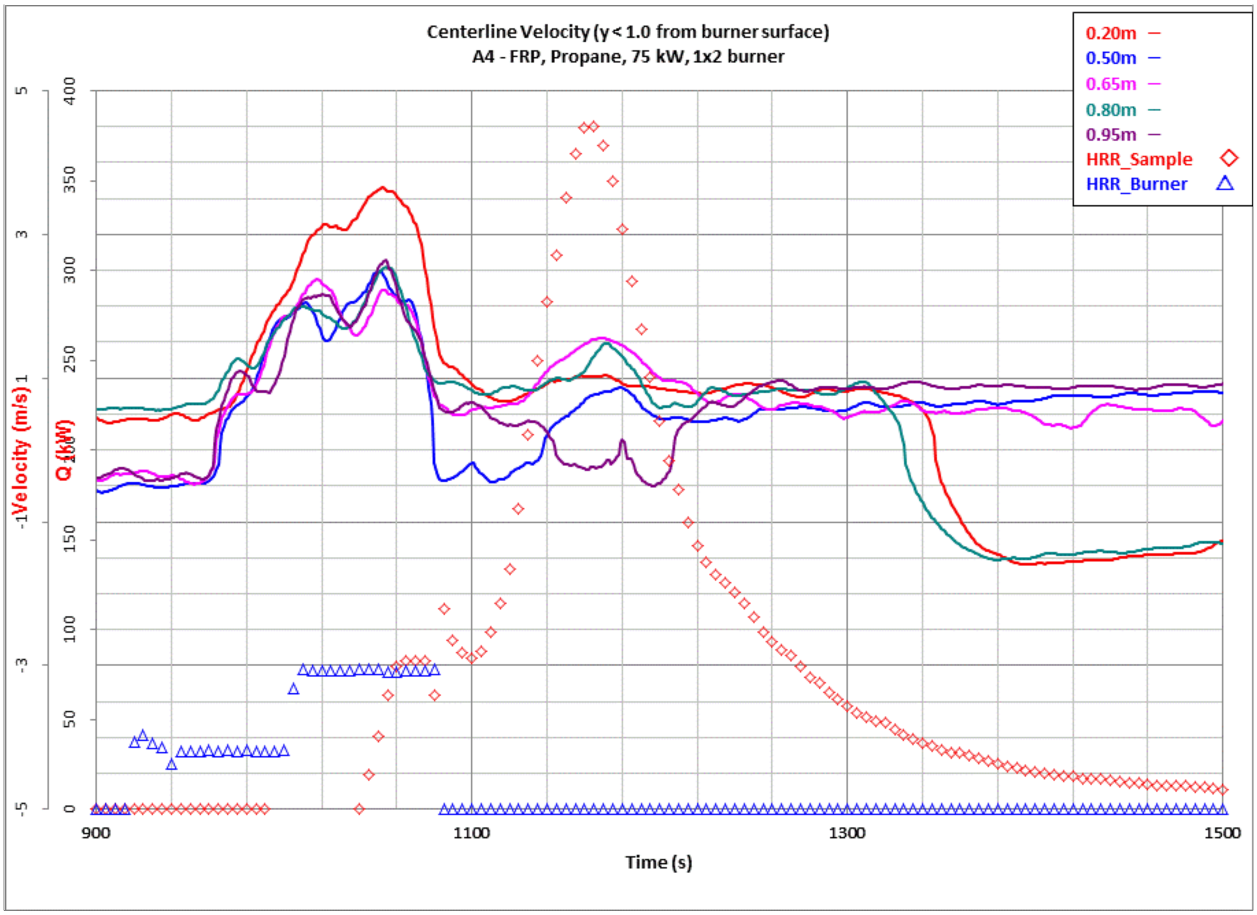

Figure 73 – Velocity measurements made at elevations below 1 m away from source burner's surface in Test A4

Velocity measurements at probe locations from 1.10 m to 1.70 m from Test A4 are presented in Figure 74. The probes at 1.25 m to 1.70 m registered an increase when the source fire was at 75 kW, but once the source fire extinguished, the velocity reduced to the ambient level. However, as the sample HRR peaked, the velocity became negative due to the flow and smoke layer descending due to the ceiling. The magnitude of the downward flow was largest at the highest probe and decreased for the probes at the lower elevations. Significant drifts are observed for all the probes after the sample HRR's decrease after its peak.

Note that the velocity probe at 1.10 m malfunctioned during this test.

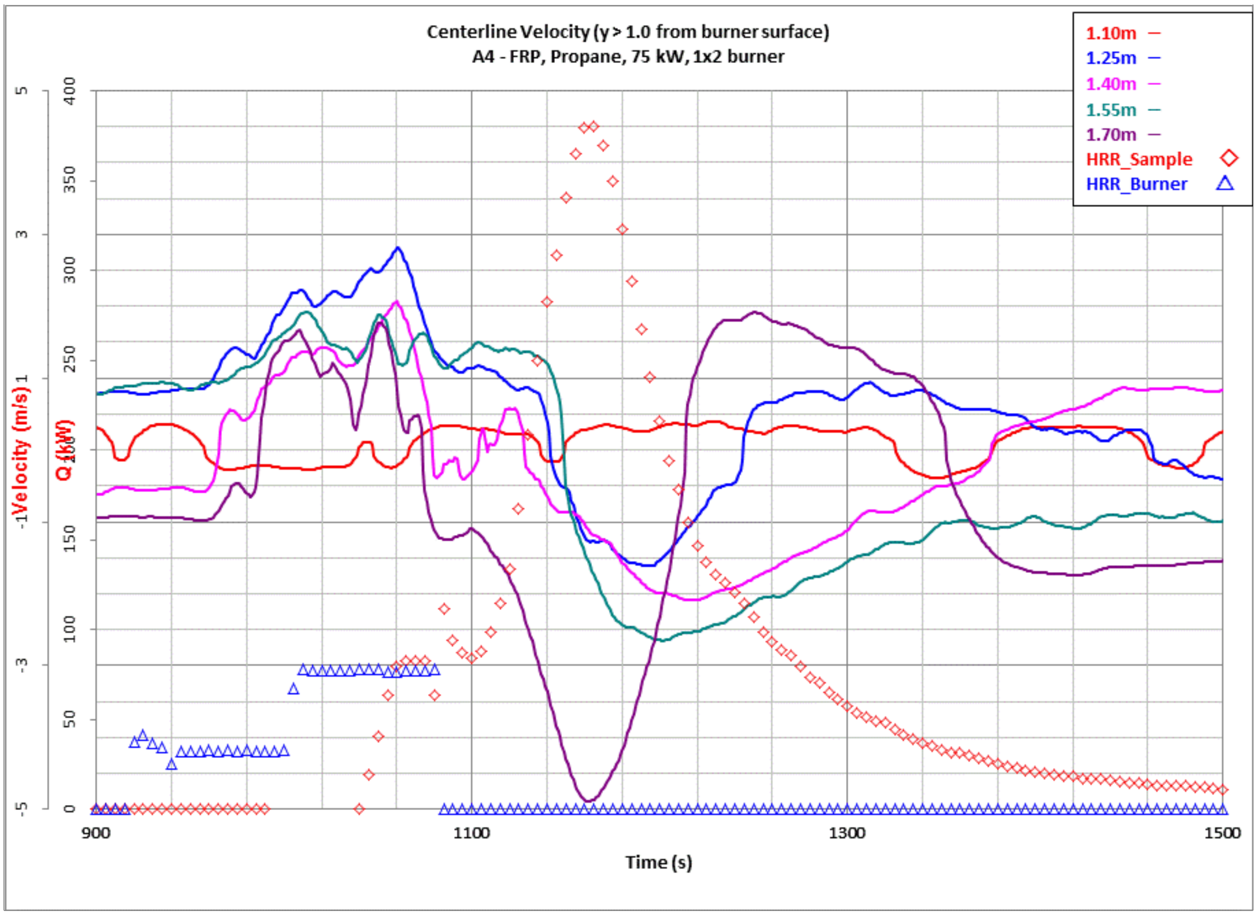

Figure 74 - Velocity measurements made at elevations above 1 m away from source burner's surface in Test A4

Test A13's velocity measurements for probe locations from 0.2 m to 0.95 m above the source burner surface. The velocity increased as the source fire was ignited and remained at positive value for the duration of the test because the source fire was continuous. At the point when the sample HRR peaked, the velocity at these probe locations also increased. The sudden drops for the probe at 0.2 m from 600 to 700 sec were data drift due to thermal effects.

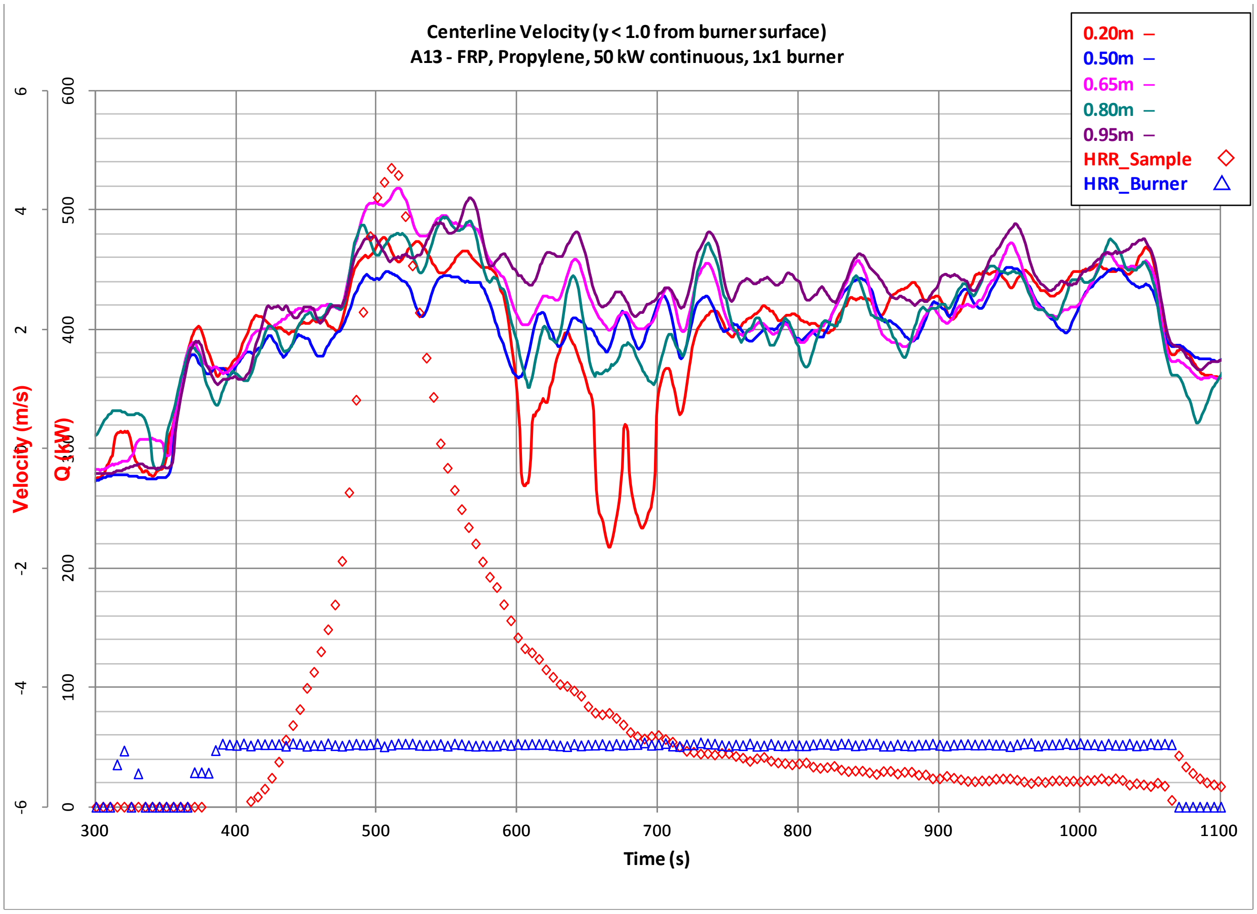

Figure 75 - Velocity measurements made at elevations below 1 m away from source burner's surface in Test A13

Velocity measurements at probe locations from 1.10 m to 1.70 m from Test A13 are presented in Figure 76. The probes at 1.25 m to 1.70 m registered an increase when the source fire was at 75 kW, and remain mostly positive due to the continuous source fire for the whole duration of the test. However, as the sample HRR peaked, the velocity became negative for probes at 1.55 m and 1.7 m due to the flow and smoke layer descending due to the ceiling. The probes at 1.25 m and 1.4 m behaved differently, which increased ahead of the peak sample HRR but reduced back to the previous level at the peak HRR. The data drift is less significant for the period of time after the peak HRR to the test termination, most likely due to the fact that the source fire was continuous and the heating and cooling thermal effects were less substantial.

Note that the velocity probe at 1.10 m malfunctioned during this test.

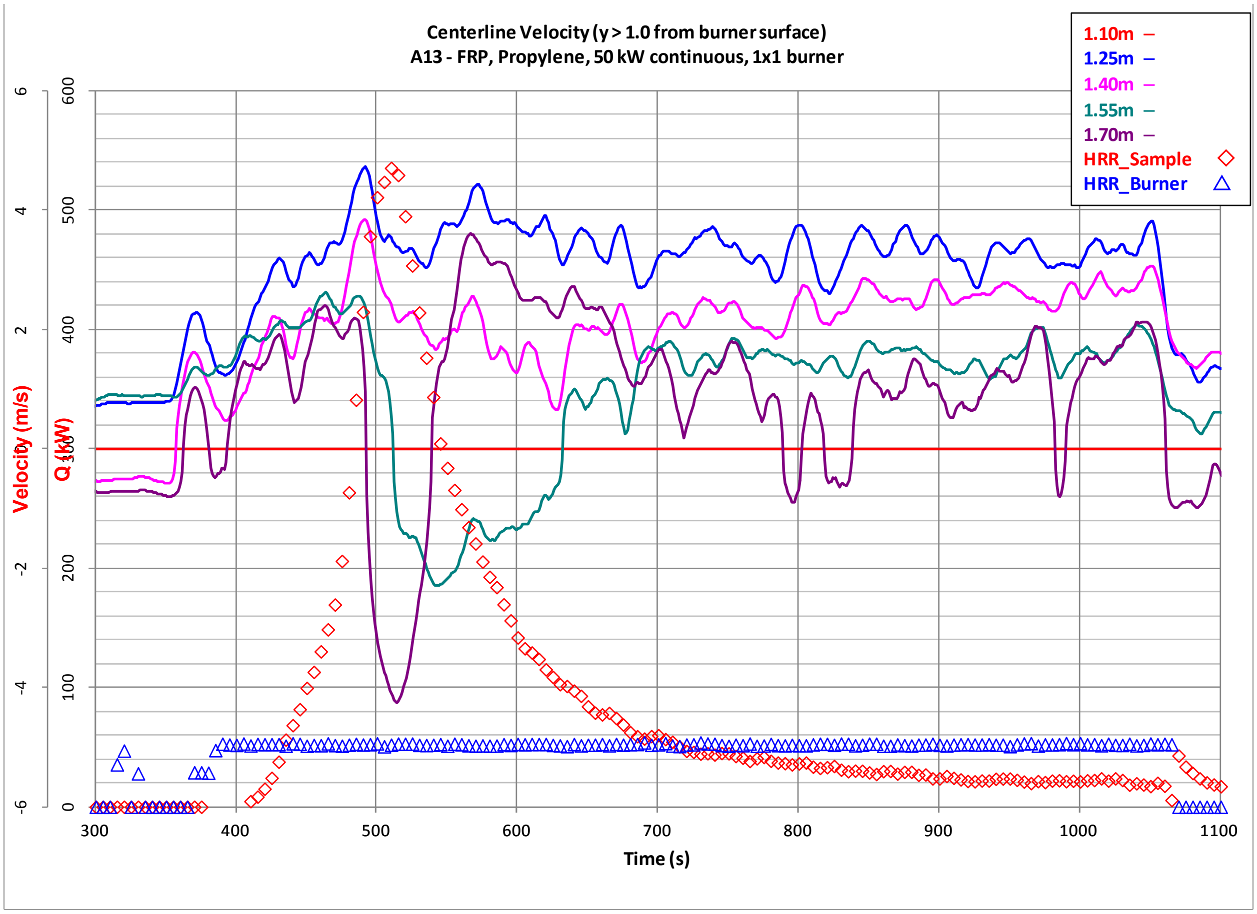

Figure 76 - Velocity measurements made at elevations above 1 m away from source burner's surface in Test A13

4.5.4 Heat flux to wall

The heat flux measured during the combustible wall test A4 superimposed with the sample and burner HRRs are presented in Figure 77 to Figure 82. The data are grouped by different heights above the burner surface, as they were measured along the centerline and at 1 ft and 2 ft away on both sides. Some of the instruments malfunctioned during the tests and not reporting measurements; they are noted in the caption of each chart. The heat flux history at each gauge may be used as a guide to track the flame spread over the FRP panel.

At 0.2 m above the burner surface, the centerline heat flux reached 40 kW/m^2 during the time when the source fire first started, and then rose to 70 kW/m^2 when the panel was ignited. Before the specimen's HRR peaked, the centerline heat flux at this height sharply reduced, indicating that the fire on the panel had moved away from this location. It is also noted that at 1 ft to the right of the centerline, the heat flux measured averages at approximately 15 kW/m^2 regardless whether the source fire was present or not.

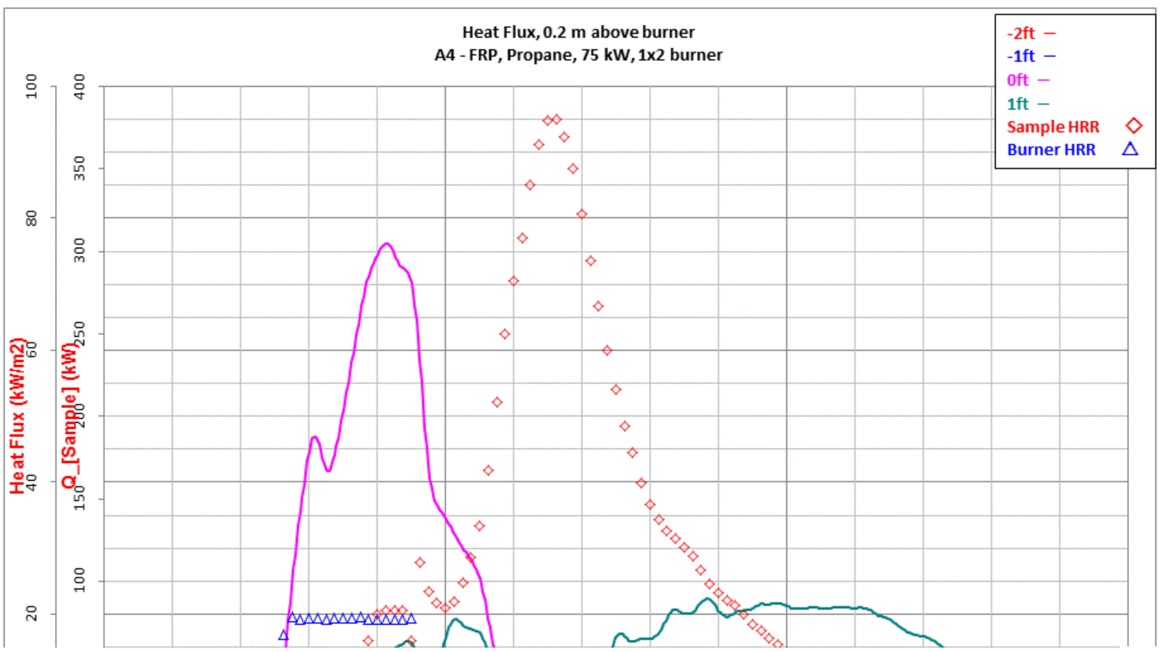

Figure 77 – Heat flux (0.2 m over burner) in Test A4 (Propane fuel, 75 kW source, Rectangle burner), note that heat flux gauge at -1 ft off centerline was not reporting data.

The heat flux measured at 0.5 m above the burner surface at Test A4 is presented in Figure 78. Similar to the heat flux measured at 0.2 m above the burner, the highest heat flux at this height was measured at the centerline. Before the FRP panel was ignited, the heat flux measured was approximately 20 kW/m^2, then reaching 50 kW/m^2 when the burner was on and the panel was just ignited. Again, the centerline heat flux sharply reduced just as the FRP's HRR peaked. The heat flux measured at 1 ft to the left and at 2 ft to the right of the centerline averaged approximately at 5 kW/m^2 during majority of the panel's burning.

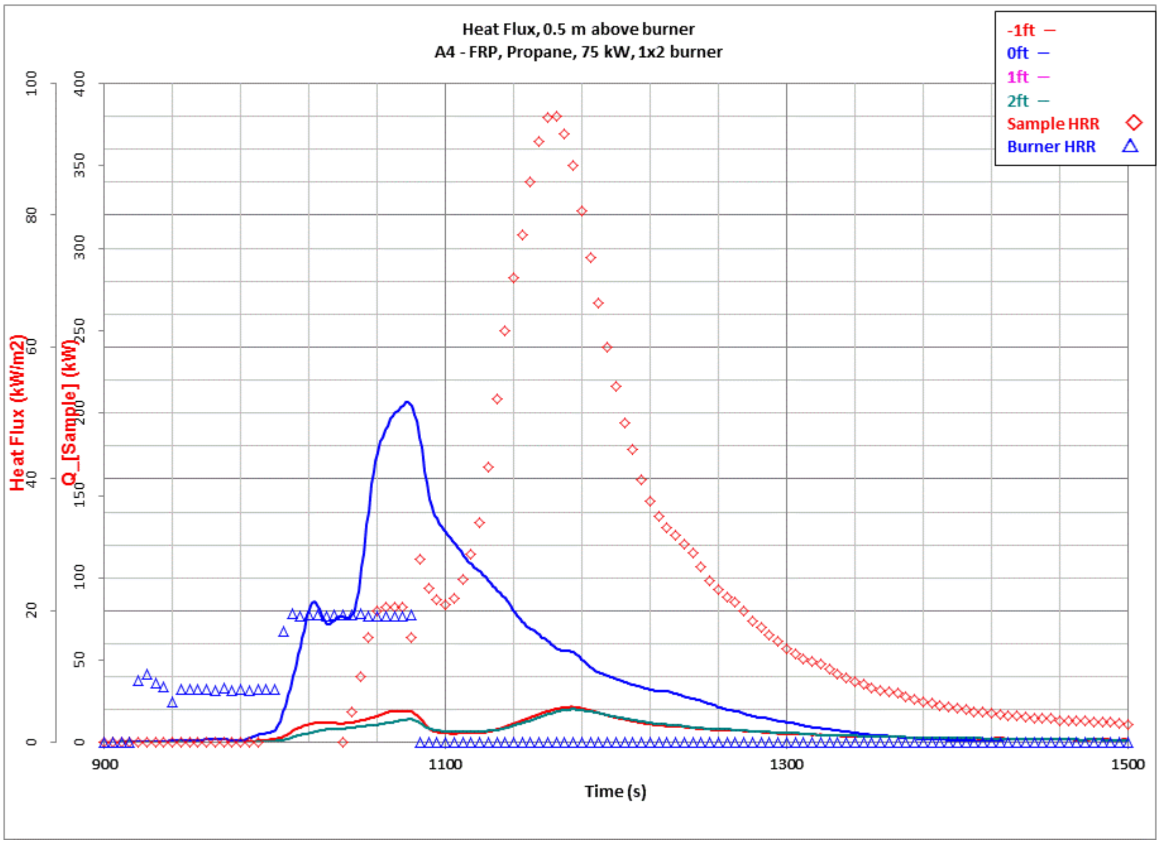

Figure 78 - Heat flux (0.5 m over burner) in Test A4 (Propane fuel, 75 kW source, Rectangle burner), note that heat flux gauge at 1 ft off centerline was not reporting data.

The heat flux measured at 0.8 m above the burner surface at Test A4 is presented in Figure 79. Again, the highest heat flux at this height was measured at the centerline. Before the FRP panel was ignited, the heat flux measured was approximately 15 kW/m^2, then reaching 40 kW/m^2 when the burner was on and the panel was just ignited. Again, the centerline heat flux reduced as the FRP's HRR peaked. However, for the TSC at 2 ft to the left and 1 ft to the right of the centerline, the peak occurs at the peak HRR., this sharp rise corresponds with the sharp increase in flame spread measured at the peak HRR, and may also be affected by the hot ceiling layer.

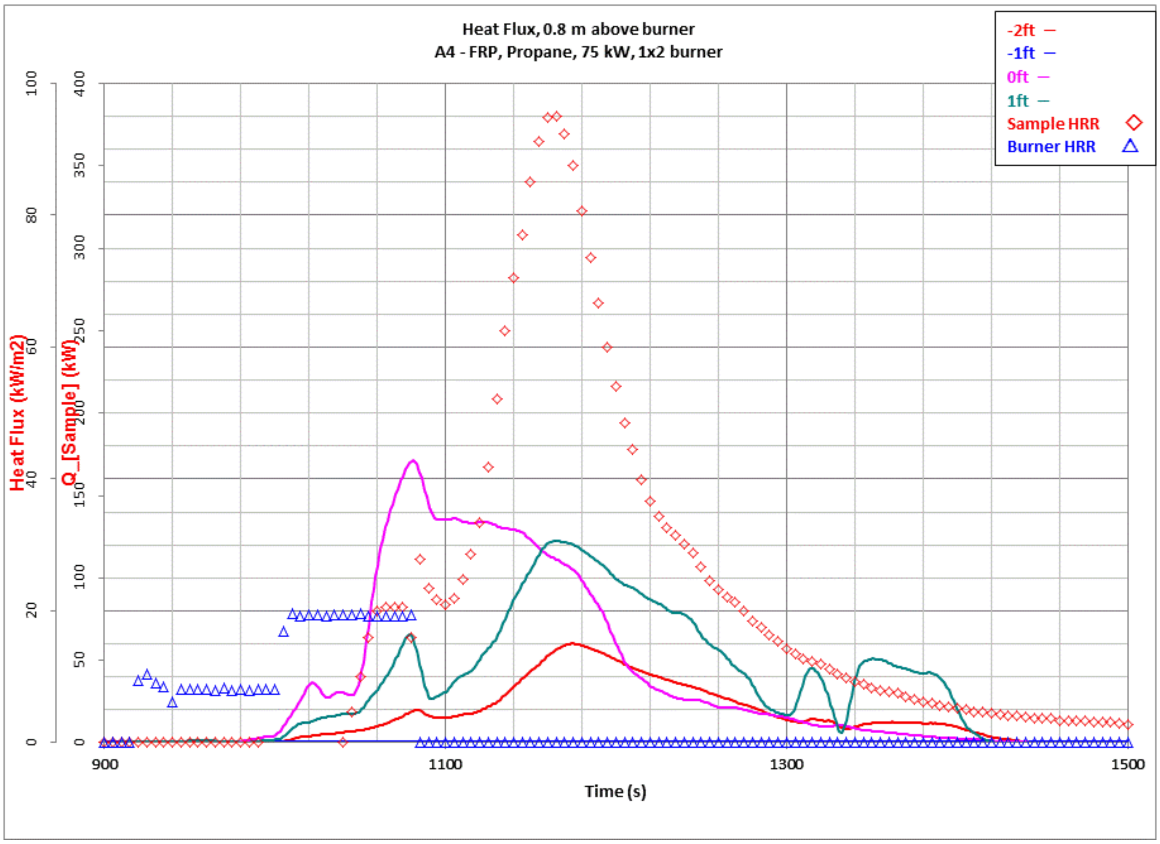

Figure 79 - Heat flux (0.8 m over burner) in Test A4 (Propane fuel, 75 kW source, Rectangle burner), note that heat flux gauge at -1 ft off centerline was not reporting data.

The heat flux measured at 1.1 m above the burner surface at Test A4 is presented in Figure 80. Again, the highest heat flux at this height was measured at the centerline. Before the FRP panel was ignited, the heat flux measured was approximately 5 kW/m^2, then reaching 40 kW/m^2 when the burner was on and the panel was just ignited. Again, the centerline heat flux reduced as the FRP's HRR peaked. However, for the other heat flux measurements at this level, their peaks correspond with the HRR peak. It is also noted that at 1 ft to the left and 2 ft to the right of the centerline, the heat flux measured are almost identical in its magnitude and timing. The effects of the hot ceiling layer would be more prominent at this elevation than on the gauges below.

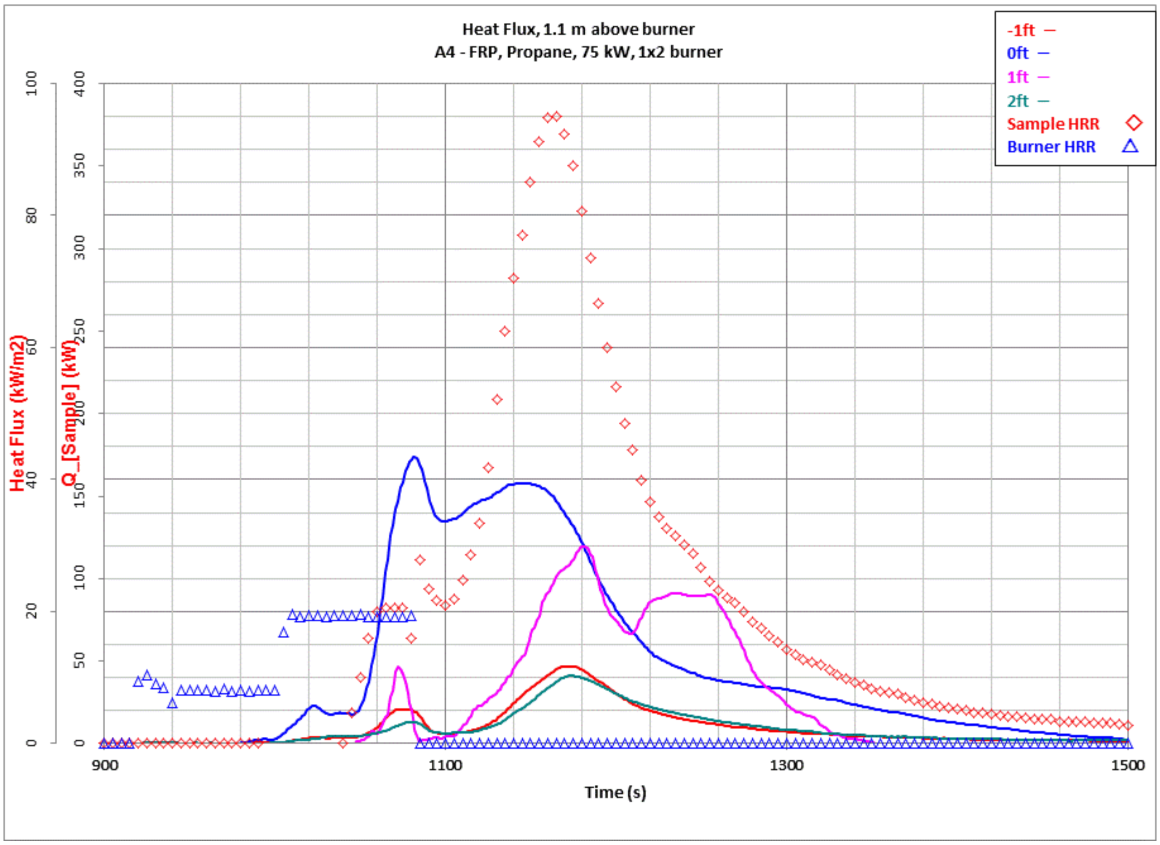

Figure 80 - Heat flux (1.1 m over burner) in Test A4 (Propane fuel, 75 kW source, Rectangle burner)

The heat flux measured at 1.4 m above the burner surface at Test A4 is presented in Figure 81. Again, the highest heat flux at this height was measured at the centerline. Before the FRP panel was ignited, the heat flux measured was approximately 5 kW/m^2, then reaching 40 kW/m^2 when the burner was on and the panel was just ignited, and finally peaking at 45 kW/m^2 when the fire reached its peak HRR. It is also observed that the other heat flux gauges peaked at approximately the same time, with the highest of that registering at 40 kW/m^2 at 1 ft to the right of the centerline. For the gauge at 1 ft to the left of the centerline, a peak was noted after the majority of the FRP panel had been burnt, this is due to a small fire at that location, but also may be extravagated by malfunctioning at the gauge due to directly flame impingement.

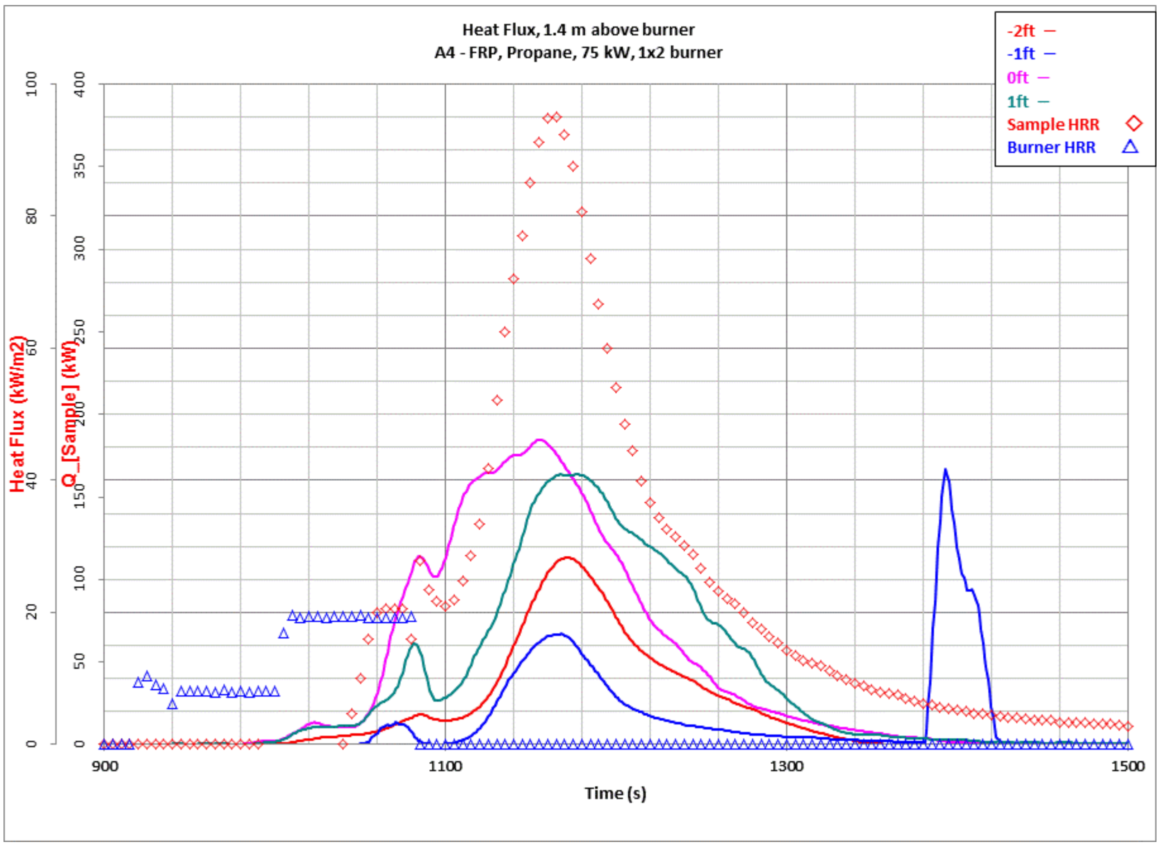

Figure 81 - Heat flux (1.4 m over burner) in Test A4 (Propane fuel, 75 kW source, Rectangle burner)

At 1.7 m above the burner surface, the heat flux measured before the FRP specimen ignited was under 5 kW/m^2. The peak heat flux measured at all location corresponds with the peak HRR, except for the gauge located 2 ft to the right of the centerline, which occurred as the HRR reduced. The peak heat flux measured ranged from 55 to 65 kW/m^2 at this elevation, suggesting that the flame spread at this elevation occurred almost simultaneously across the width of the FRP panel, and that the effects of the hot layer under the ceiling is most prominent.

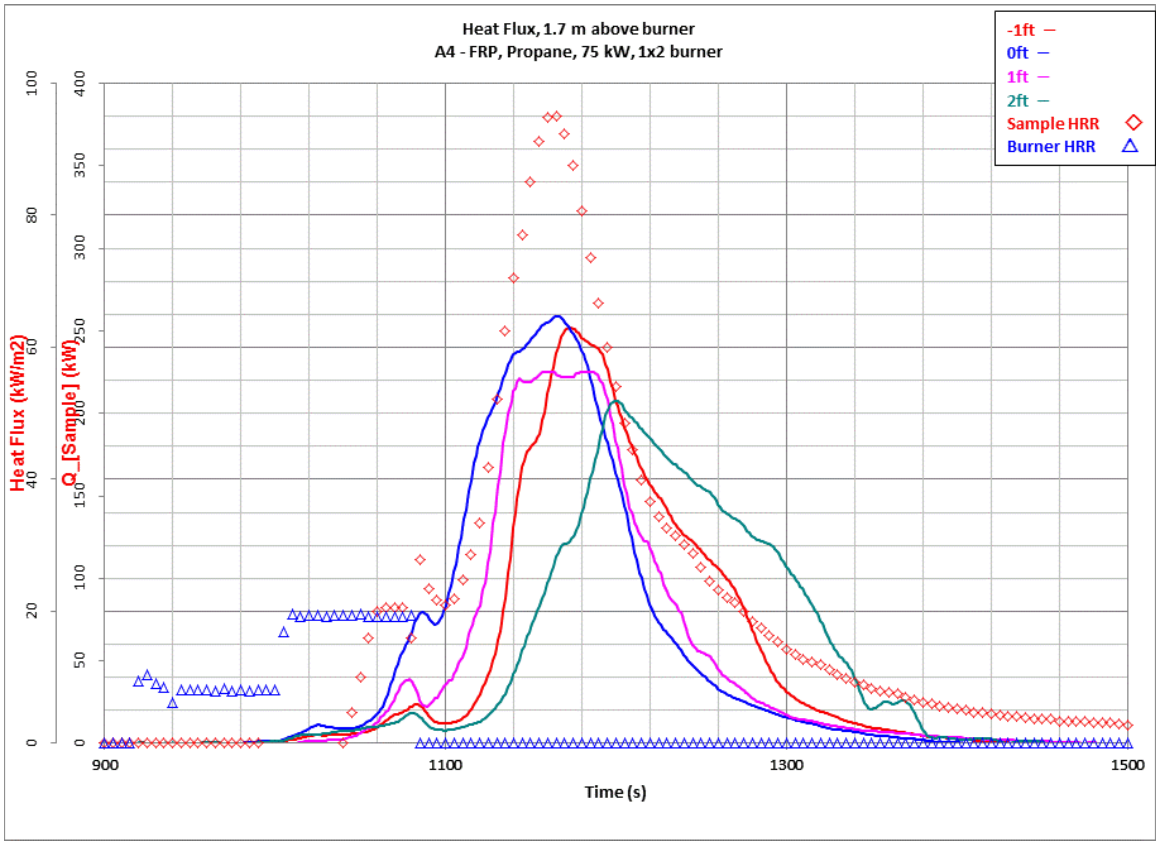

Figure 82 - Heat flux (1.7 m over burner) in Test A4 (Propane fuel, 75 kW source, Rectangle burner)

The heat flux measured during the combustible wall test A13 superimposed with the sample and burner HRRs are presented in Figure 83 to Figure 88. The data are grouped by different heights above the burner surface, as they were measured along the centerline and at 1 ft and 2 ft away on both sides. Some of the instruments malfunctioned during the tests and not reporting measurements; they are noted in the caption of each chart. The heat flux history at each gauge may be used as a guide to track the flame spread over the FRP panel.

The centerline heat flux averaged at 60 kW/m^2 regardless if the sample panel was burning, suggesting that the heat flux at this location is driven mostly by the source fire. The heat flux at 1 ft to the right of the centerline averages at approximately 10 kW/m^2, but increased to 45 kW/m^2 at the peak sample HRR. At 2 ft to the left of the centerline, the heat flux measured ranged from 7.5 to 2.5 kW/m^2. The flat heat flux time histories are driven mostly by the source fire.

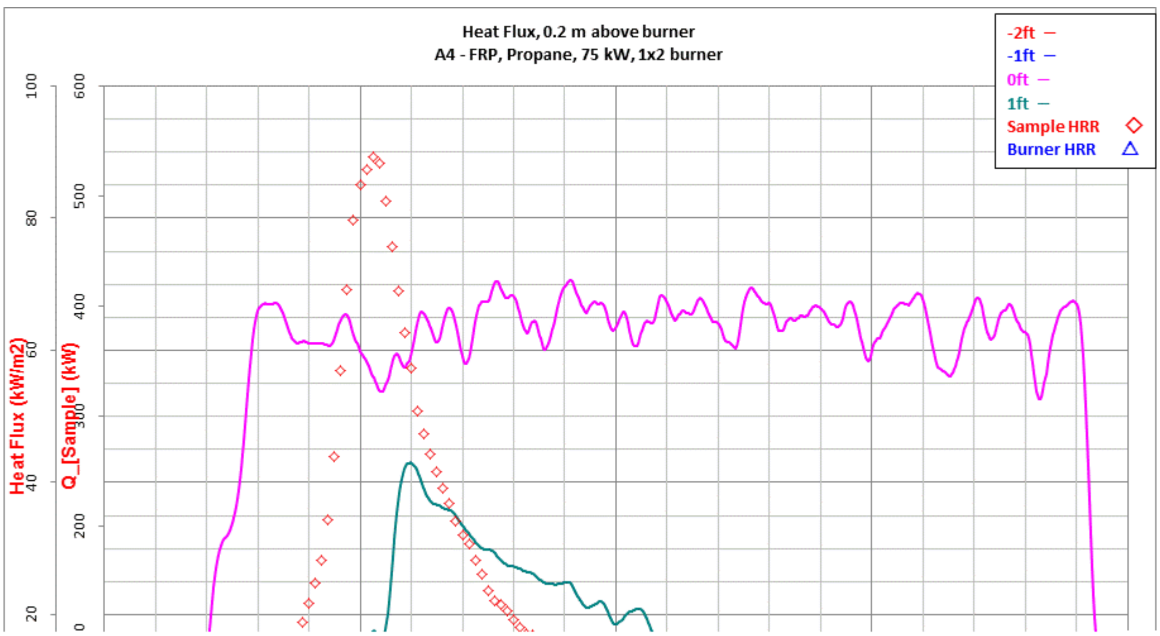

Figure 83 – Heat flux (0.2 m over burner) in Test A13 (Propylene fuel, 50 kW continuous source, Square burner), note that heat flux gauge at -1 ft off centerline was not reporting data.

The heat flux measured at 0.5 m above the burner surface at Test A13 is presented in Figure 84. The centerline heat flux peaked at 60 kW/m^2 before the peak HRR occurred, and then dropped off to an average of 30 kW/m^2 for the rest of the test. The heat flux at 1 ft to the left and at 2 ft to the right of the centerline rose to the peak value at approximately the same rate and peaked at the same time when the sample HRR peaked. At both locations, the heat flux remained relatively constant at their peaks during the majority of the sample's burn, and then dropped off along with the reduction of the sample HRR. The flat heat flux time histories are driven mostly by the source fire.

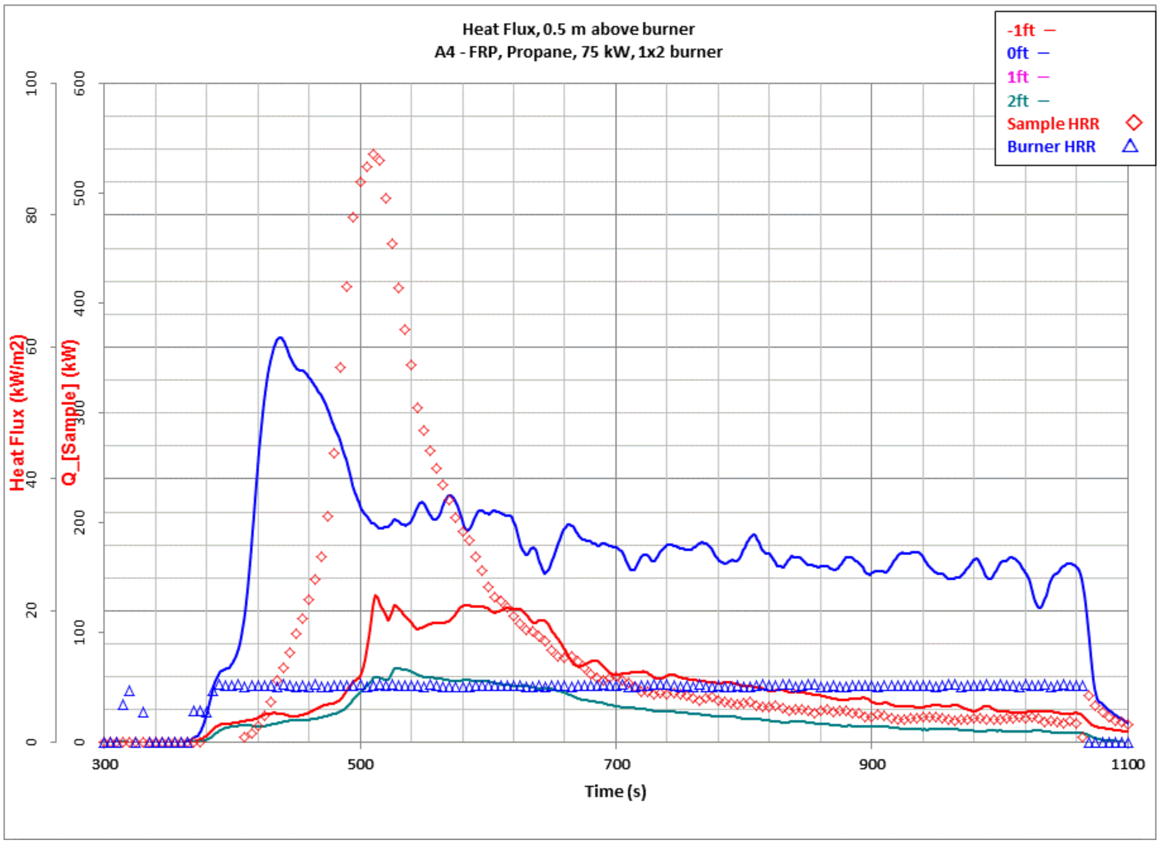

Figure 84 - Heat flux (0.5m above burner) in Test A13 (Propylene fuel, 50 kW continuous source, Square burner), note that heat flux gauge at 1 ft off centerline was not reporting data.

The heat flux measured at 0.8 m above the burner surface at Test A13 is presented in Figure 85. Again, the centerline heat flux peaked before the peak sample HRR at approximately 40 kW/m^2, then dropping off to a constant average level of 10 kW/m^2. Heat flux measured at the location 1 ft to the right and 2 ft to the left of center both peaked at 40 kW/m^2 and 20 kW/m^2 respectively, and correspond with the peak sample HRR. The flat heat flux time histories are driven mostly by the source fire. The low heat flux measured away from the centerline after the majority of the sample HRR had been burnt suggests that the source fire has small effects on the magnitude of heat flux away from the centerline at this elevation.

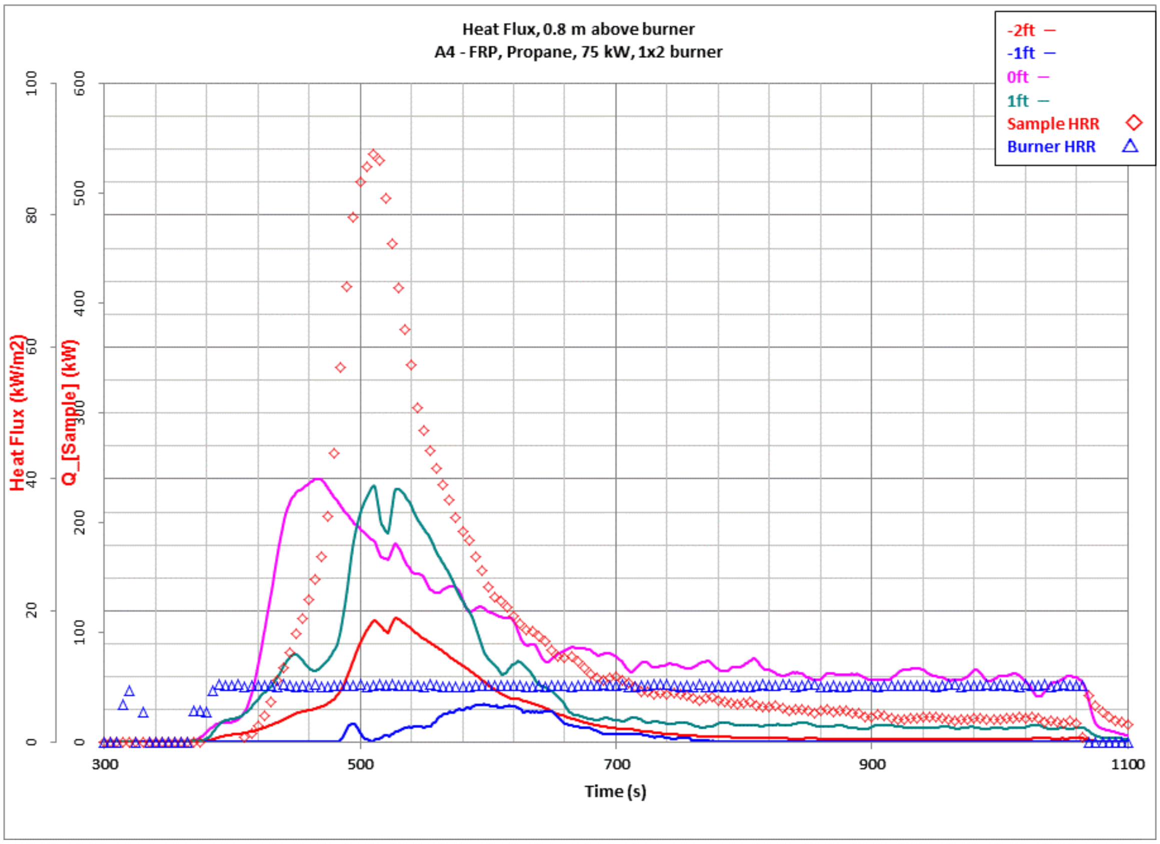

Figure 85 - Heat flux (0.8 m above burner) in Test A13 (Propylene fuel, 50 kW continuous source, Square burner), note that heat flux gauge at -1 ft off centerline was not reporting data.

The heat flux measured at 1.1 m above the burner surface at Test A13 is presented in Figure 86. The centerline heat flux remained close to zero until the FRP panel started burning, then rising and peaking just ahead of the peak HRR, afterward, it reduced sharply to about 5 kW/m^2 for the remainder of the burn. At both locations 1 ft to the left and right of center, the peak heat flux occurred at 35 kW/m^2, but with a different timing. The heat flux measured at 2 ft to the right of center peaked the latest after the sample HRR had already reduced, and reaching 25 kW/m^2. The source fire appears to have little effects on the heat flux at this elevation except for the centerline location.

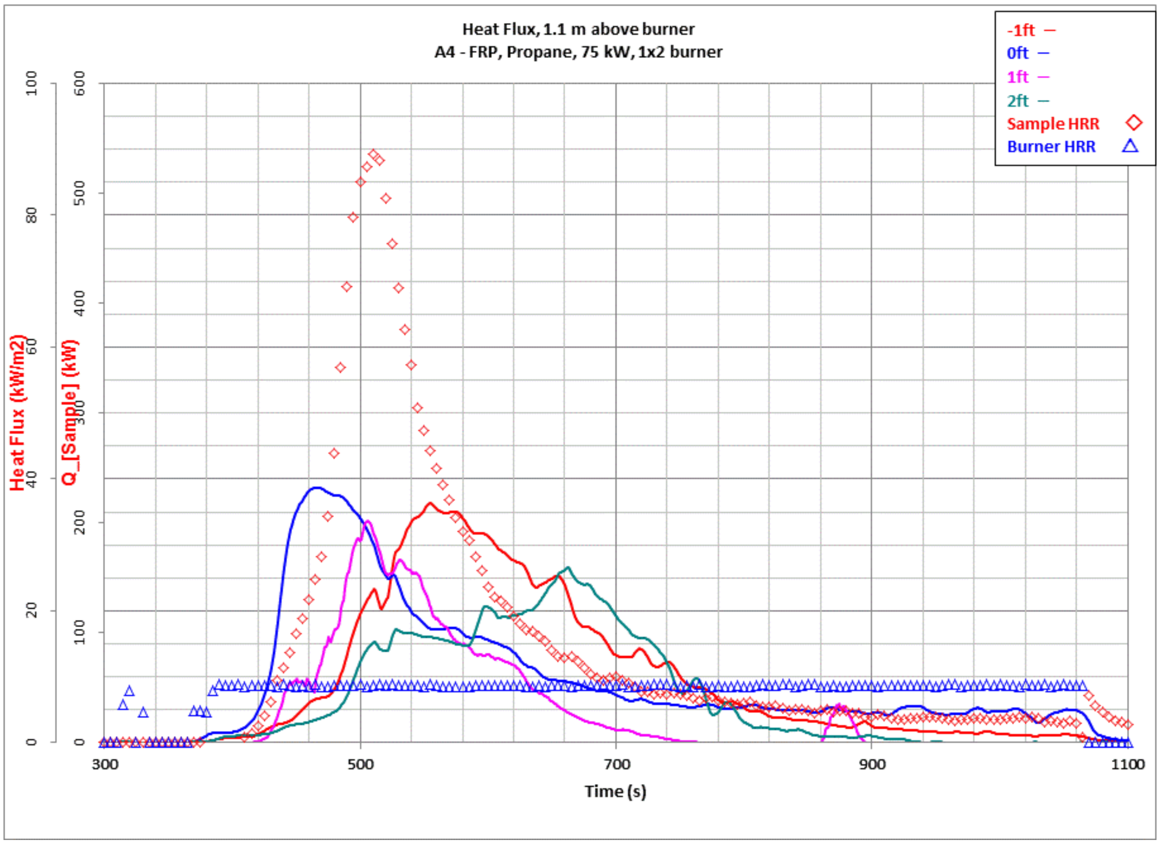

Figure 86 - Heat flux (1.1 m over burner) in Test A13 (Propylene fuel, 50 kW continuous source, Square burner)

The heat flux measured at 1.4 m above the burner surface at Test A13 is presented in Figure 87. All heat flux measured at this elevation peaked during the peak of the sample HRR. It is notable that the peak centerline heat flux does not have the highest magnitude; rather the highest heat flux measured was at 2 ft to the left and 1 ft to the right of the centerline at approximately 50 kW/m^2. The timing of the peaks is indicative that the flame spread during the peak of the sample HRR is rapid and widespread. In comparison, the heat flux recorded at 1 ft to the left was the lowest; however, this may be misleading because the heat flux gauge is probe to malfunctions. Additionally, it may be observed that the source fire has almost no effects on the heat flux measured at this elevation.

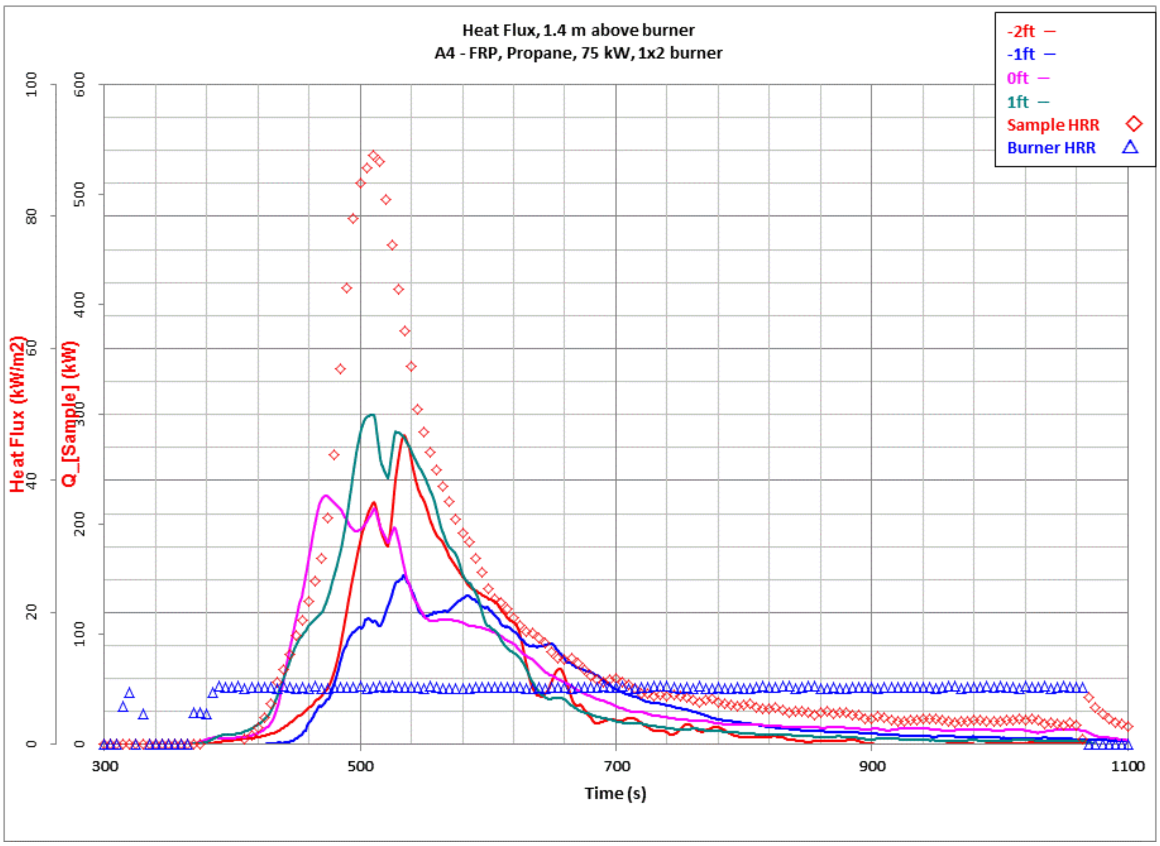

Figure 87 - Heat flux (1.4 m over burner) in Test A13 (Propylene fuel, 50 kW continuous source, Square burner)

Figure 88 shows the heat flux measured at 1.7 m above the burner surface. Again, the peak heat fluxes all correspond with the peak HRR, reaching the highest level recorded with a range of 55 to 75 kW/m^2. At this elevation, the source burner has virtually no effect on the heat flux, suggesting that the high heat flux is due only to the burning FRP panel. Additionally, since all the heat flux rose and fell at around the same time, this suggests that the flame spread at this elevation occurred almost instantaneously across the width of the panel.

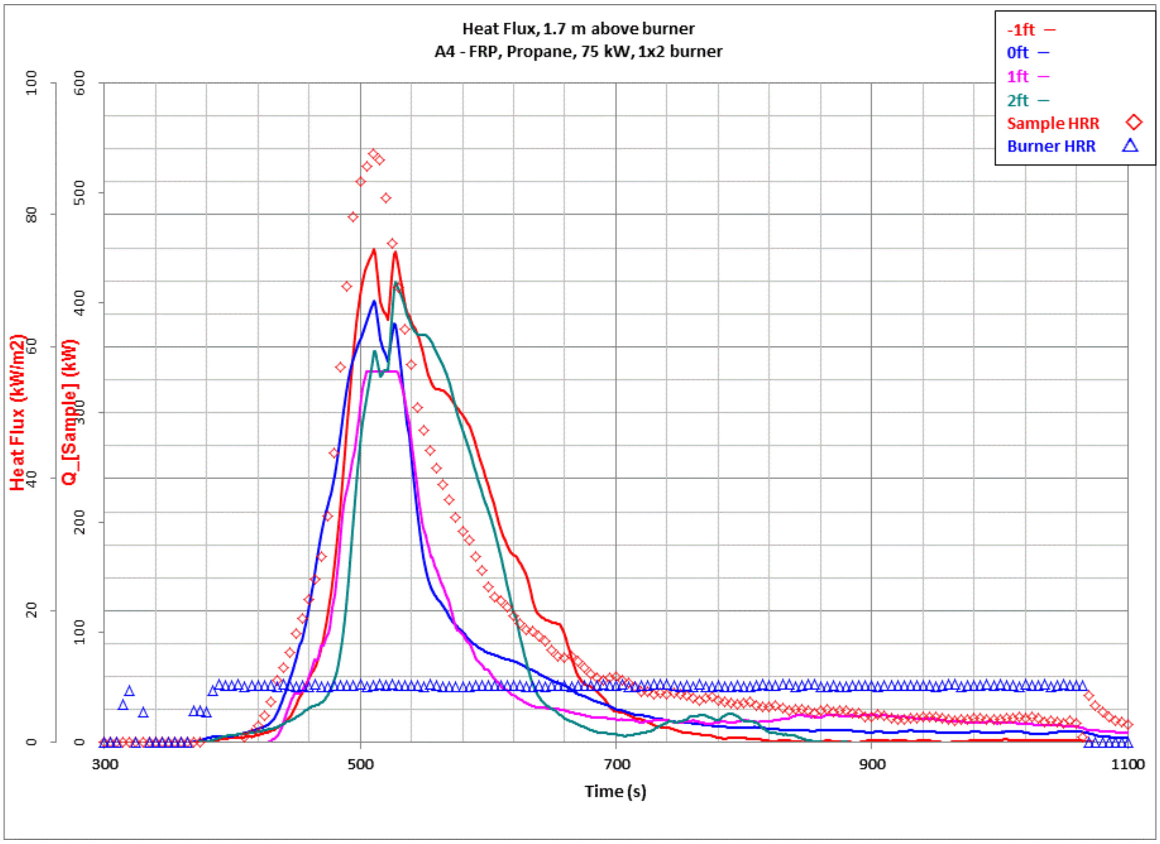

Figure 88 - Heat flux (1.7 m over burner) in Test A13 (Propylene fuel, 50 kW continuous source, Square burner)

4.5.5 Near-wall temperature

The uncorrected near-wall temperature measurements made in Test A4 are presented in Figure 89 to Figure 91, and the corrected temperatures are presented in Figure 92 to Figure 94. The thermocouples had different heights over the burner and also were offseted perpendicularly to the wall at different distances; their locations are shown in Table 28.

Table 28 - Locations of near-wall thermocouples

		Distance from centerline					
		-7.5 cm	**-5.0 cm**	**-2.5 cm**	**2.5 cm**	**5.0 cm**	**7.5 cm**
		Perpendicular distance from wall [mm]					
Height above burner	**155 cm**	15	20	25	30	35	40
	95 cm	35	30	25	20	15	10
	35 cm	0	5	10	15	20	25

The temperature measured by the six thermocouples at 0.35 m in Test A4 above the burner surface is presented in Figure 89. The highest temperature were recorded generally when the source burner was outputting a constant HRR and when the FRP started to burn in the lower region. However, for the thermocouple on with 0mm offset to the wall, the temperature measured tracked the HRR of the burning FRP panel but were not significantly affected by the source fire.

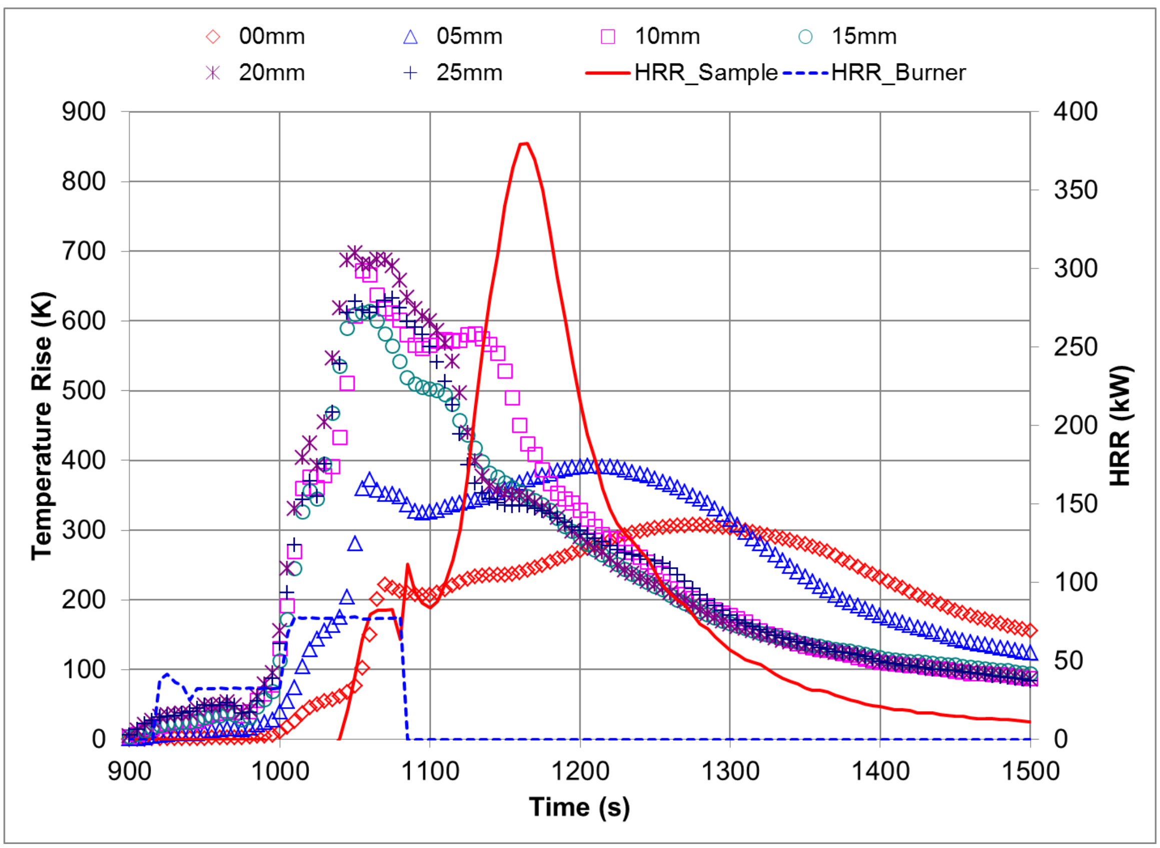

Figure 89 - UNCORRECTED Near-wall temperature rise (0.35 m over burner) in Test A4 (Propane fuel, 75 kW source, Rectangle burner)

At 0.95 m over the burner surface, the temperature rise near the wall during the source fire phase was at around 200 K above ambient. As the FRP started to burn, the temperature rise increased and peaked when the HRR of the FRP fire peaked also, as shown in Figure 90. The highest temperature was recorded by the thermocouple at 35mm offseted to the wall. As the FRP fire spread away from the center, the near-wall temperature also decreased to about 100 K over ambient.

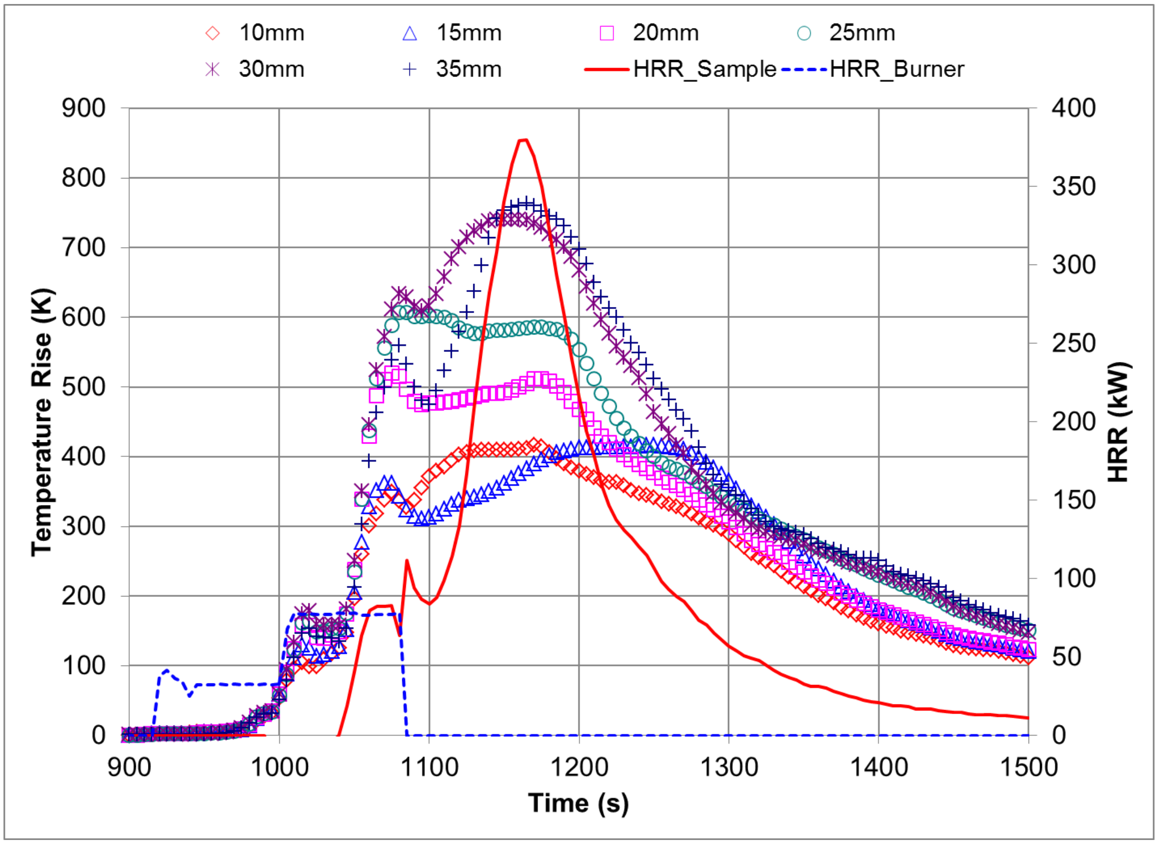

Figure 90 - UNCORRECTED Near-wall temperature rise (0.95 m over burner) in Test A4 (Propane fuel, 75 kW source, Rectangle burner)

At 1.55 m over the burner surface, the temperature rise near the wall during the source fire phase was at around 100 K above ambient, which is lower than the temperature recorded at 0.95 m over the burner. As the FRP started to burn and spread up the wall, the temperature rise increased and peaked when the HRR of the FRP fire peaked also, as shown in Figure 91. The highest temperature was recorded by the thermocouple at 35mm offseted to the wall. As the FRP fire spread away from the center, the near-wall temperature also decreased to about 100 K over ambient.

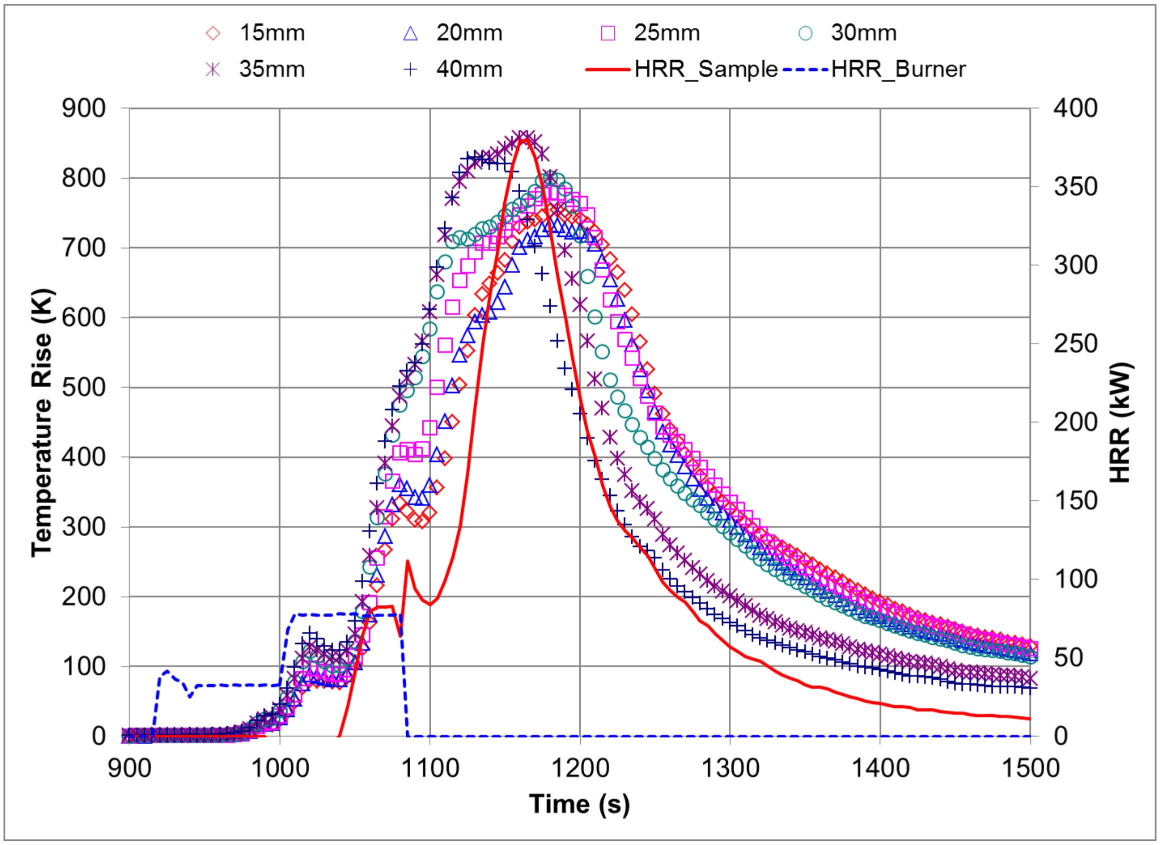

Figure 91 - UNCORRECTED Near-wall temperature rise (1.55 m over burner) in Test A4 (Propane fuel, 75 kW source, Rectangle burner)

The corrected near-wall temperature in Test A4 is presented in Figure 92 to Figure 94. Overall, the amount of correction was consistent, where the peak temperatures were corrected upward about 400K-500K. This occurred usually when the thermocouples were surrounded by flames or when the flow over the thermocouple had a higher velocity. The correction amounted to about a 50% increase of the recorded temperature.

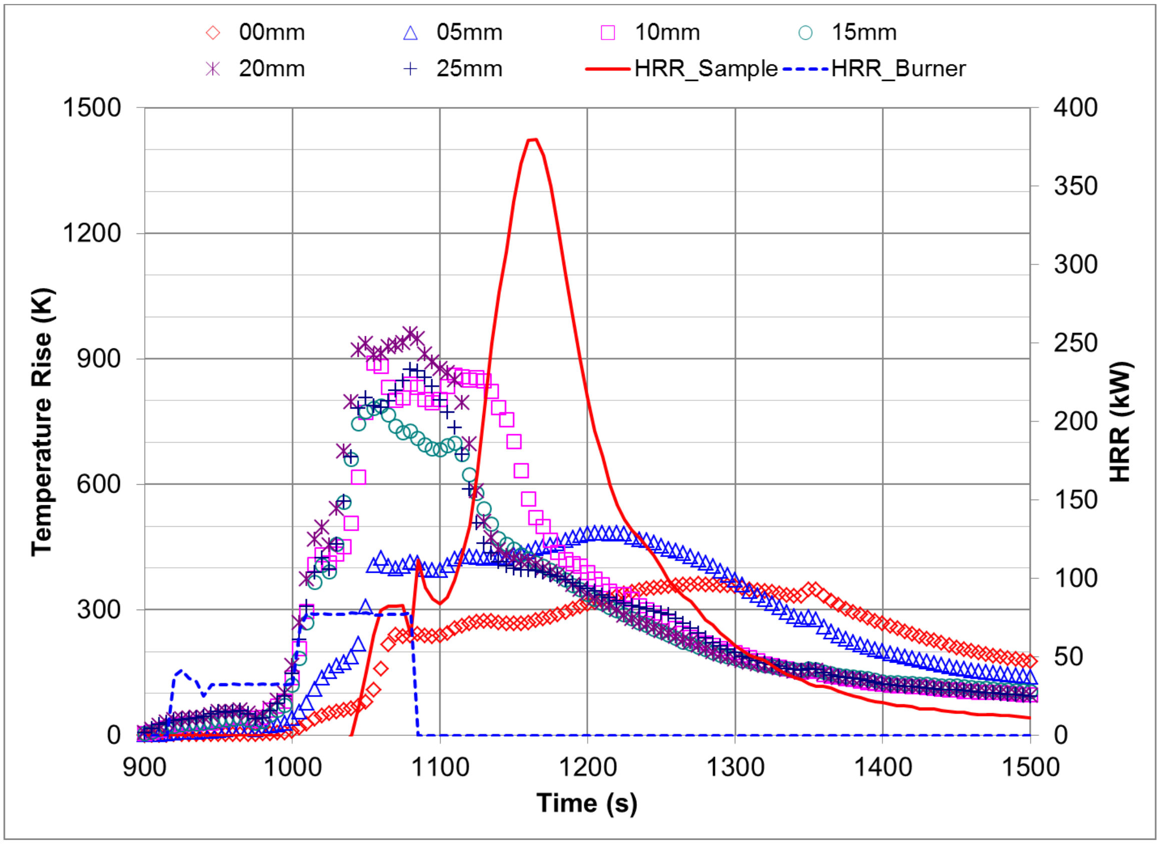

Figure 92 - CORRECTED Near-wall temperature rise (0.35 m over burner) in Test A4 (Propane fuel, 75 kW source, Rectangle burner)

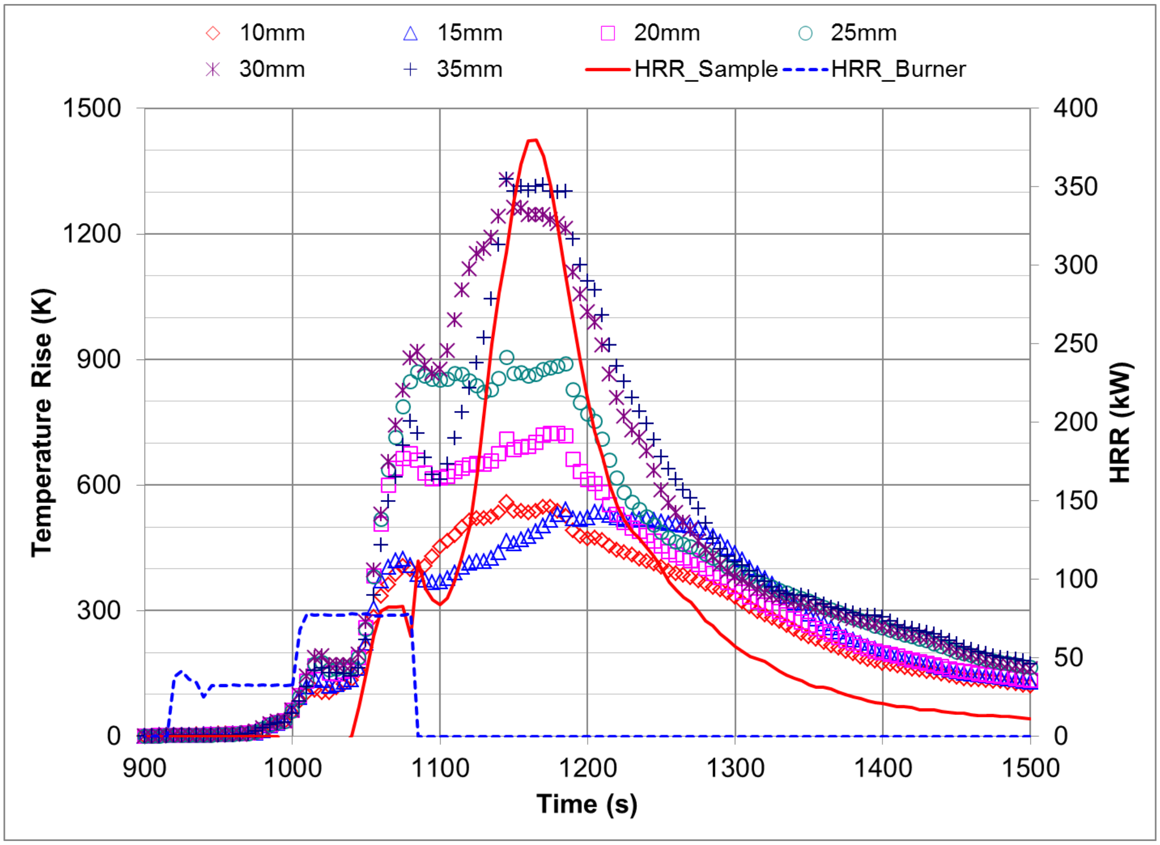

Figure 93 - CORRECTED Near-wall temperature rise (0.95 m over burner) in Test A4 (Propane fuel, 75 kW source, Rectangle burner)

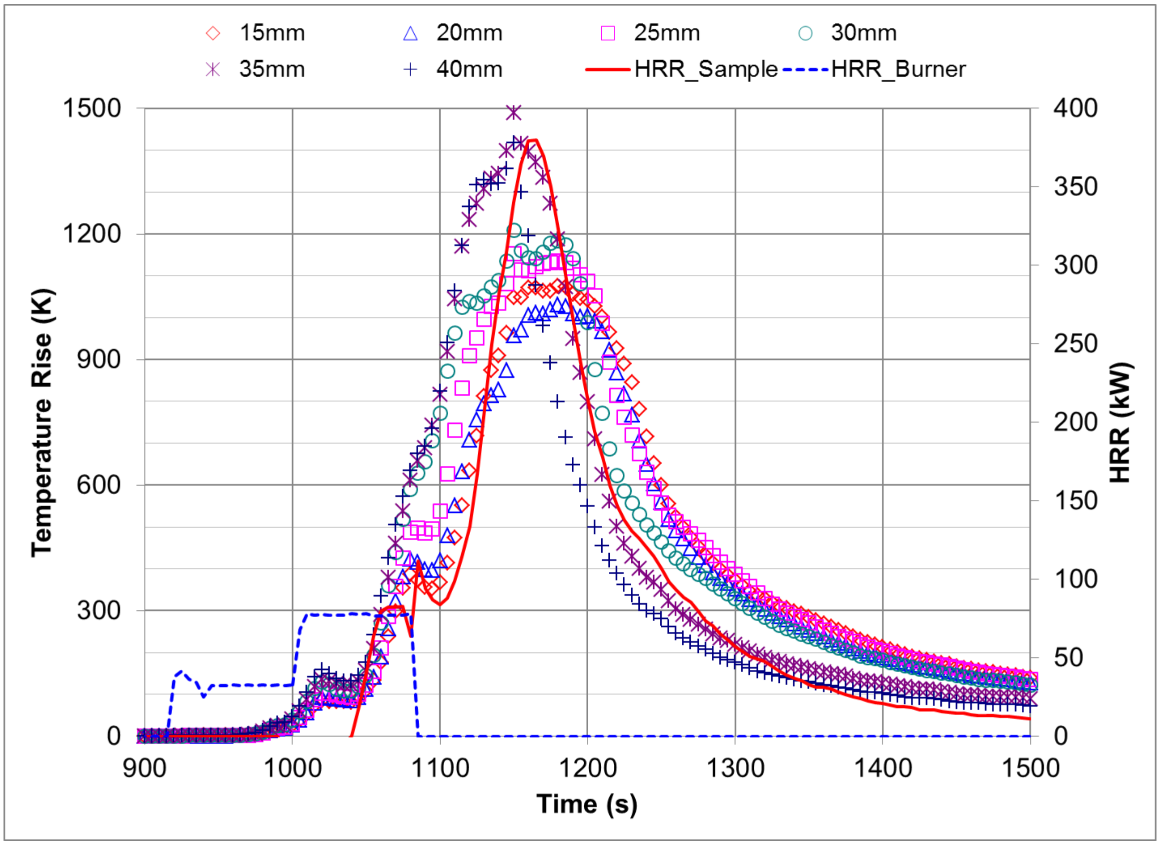

Figure 94 - CORRECTED Near-wall temperature rise (1.55 m over burner) in Test A4 (Propane fuel, 75 kW source, Rectangle burner)

The temperature measured by the six thermocouples in Test A13 at 0.35 m above the burner surface is presented in Figure 95. The highest temperatures were recorded by the thermocouples from 15 mm to 25 mm away from the wall during the initial burn period of the FRP before the FRP fire reached its peak. However, the thermocouples at 00 mm to 10 mm offseted from the wall recorded a steady temperature rise during the initial and peak of the FRP fire. After the fire peaked, the wall temperature was consistent as the thermocouples were heated by the source fire.

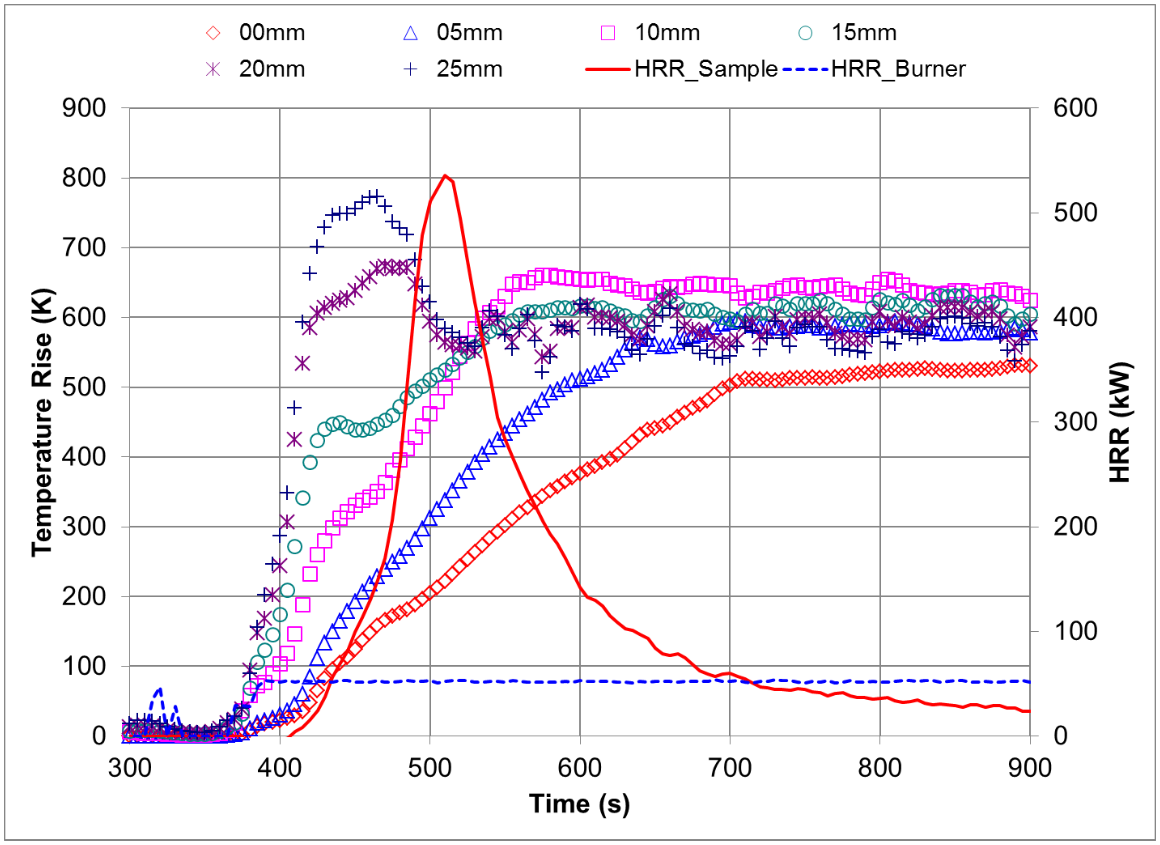

Figure 95 - UNCORRECTED Near-wall temperature rise (0.35 m over burner) in Test A13 (Propylene fuel, 50 kW continuous source, Square burner)

At 0.95 m over the burner surface, the temperature rise near the wall after the burner was turned on but before the FRP started to burn was at around 50 K above ambient. As the FRP started to burn, the temperature rise drastically increased and peaked just prior to the FRP HRR's peak, as shown in Figure 96. The highest temperature was recorded by the thermocouple at 35mm offseted to the wall. As the FRP fire spread away from the center, the near-wall temperature also decreased to about 300 K over ambient, typical as the source fire was outputting at 75 kW.

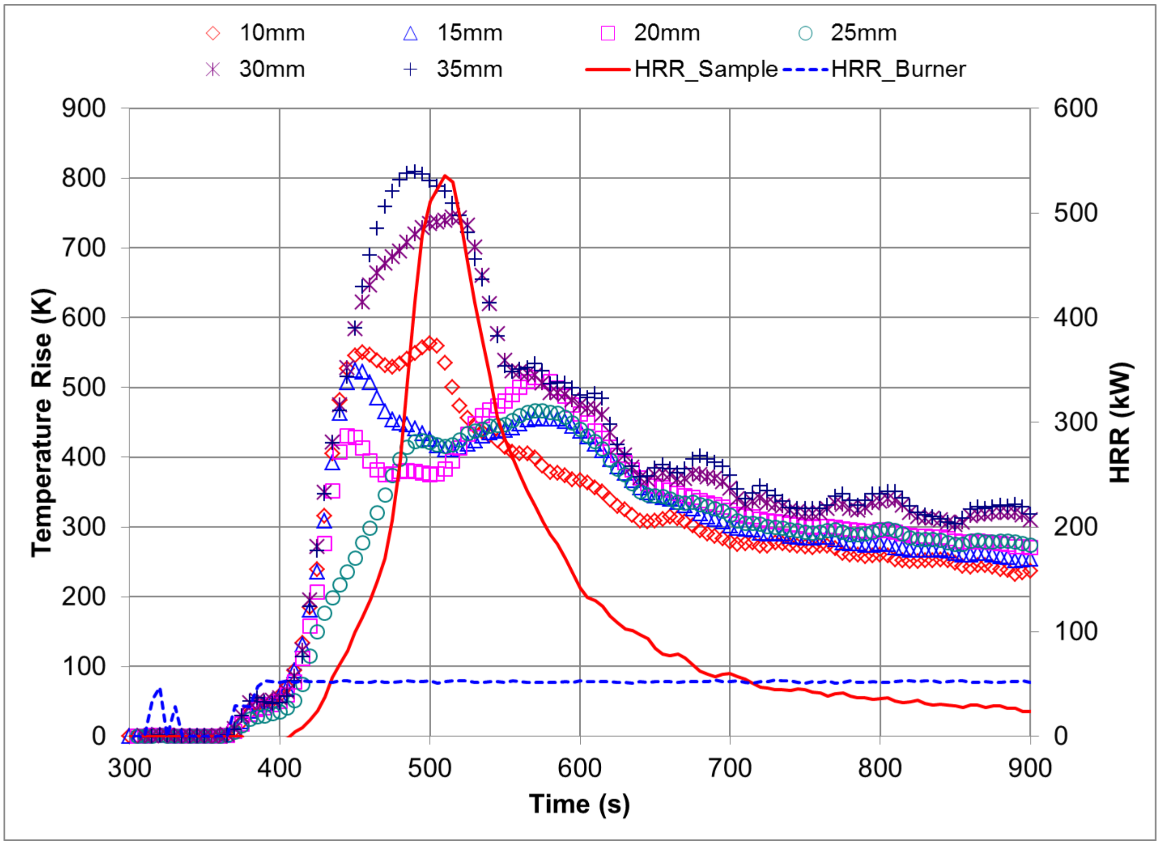

Figure 96 - UNCORRECTED Near-wall temperature rise (0.95 m over burner) in Test A13 (Propylene fuel, 50 kW continuous source, Square burner)

At 1.55 m over the burner surface, the temperature rise near the wall after the burner was turned on but before the FRP started to burn was at around 50 K above ambient. As the FRP started to burn, the temperature rise drastically increased and peaked close to the FRP HRR's peak, as shown in Figure 97. The highest temperature was recorded by the thermocouple at 40 mm offseted to the wall. As the FRP fire spread away from the center, the near-wall temperature also decreased to about 200 K over ambient, typical as the source fire was outputting at 75 kW.

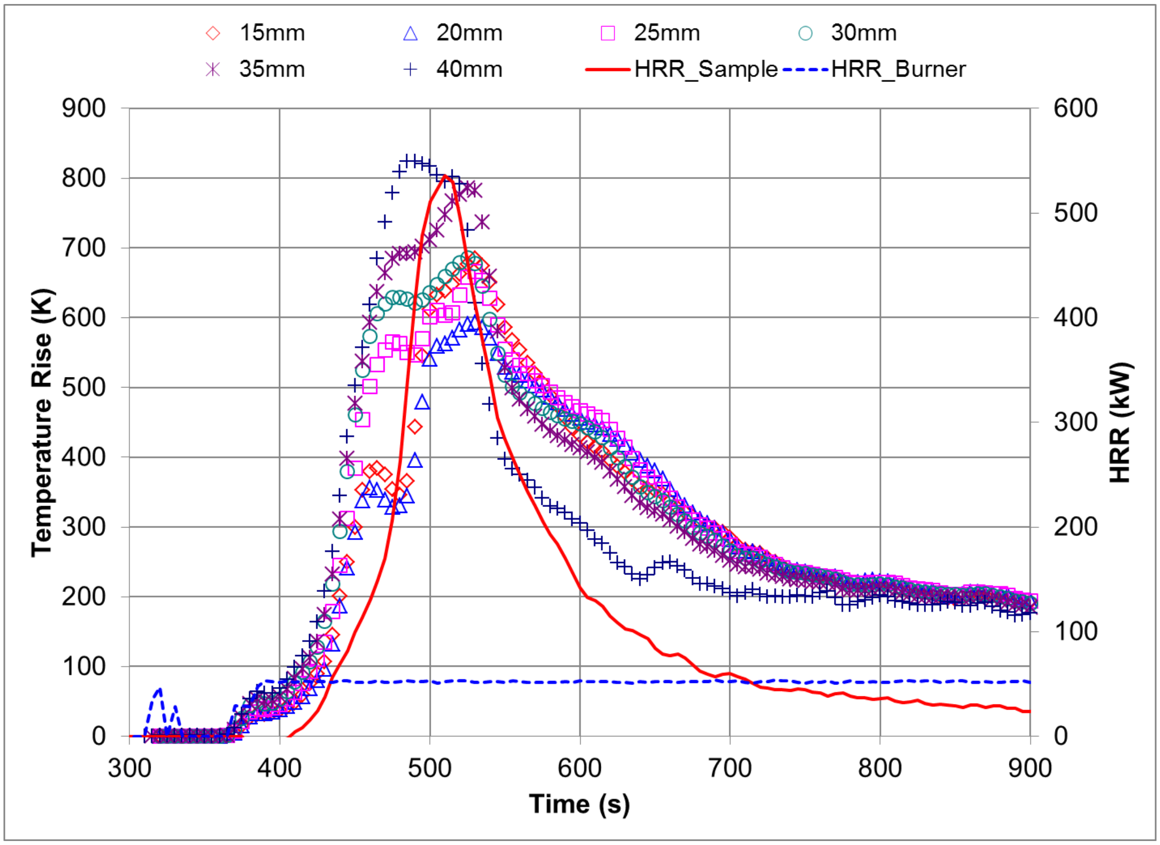

Figure 97 - UNCORRECTED Near-wall temperature rise (1.55 m over burner) in Test A13 (Propylene fuel, 50 kW continuous source, Square burner)

The corrected near-wall temperature in Test A13 is presented in Figure 98 to Figure 100. Overall, the amount of correction was consistent, where the peak temperatures were corrected upward about 200K-300K. This occurred usually when the thermocouples were surrounded by flames or when the flow over the thermocouple had a higher velocity. The correction amounted to about a 50% increase of the recorded temperature.

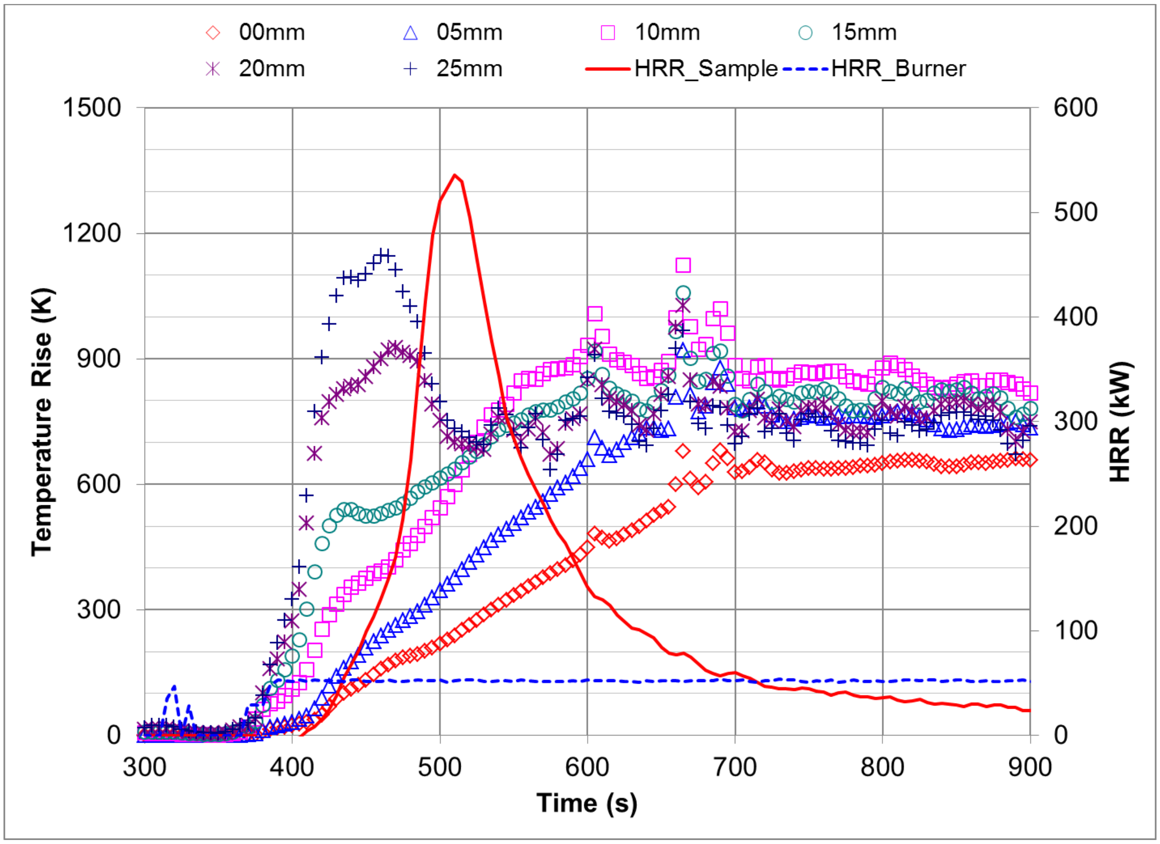

Figure 98 - CORRECTED Near-wall temperature rise (0.35 m over burner) in Test A13 (Propylene fuel, 50 kW continuous source, Square burner)

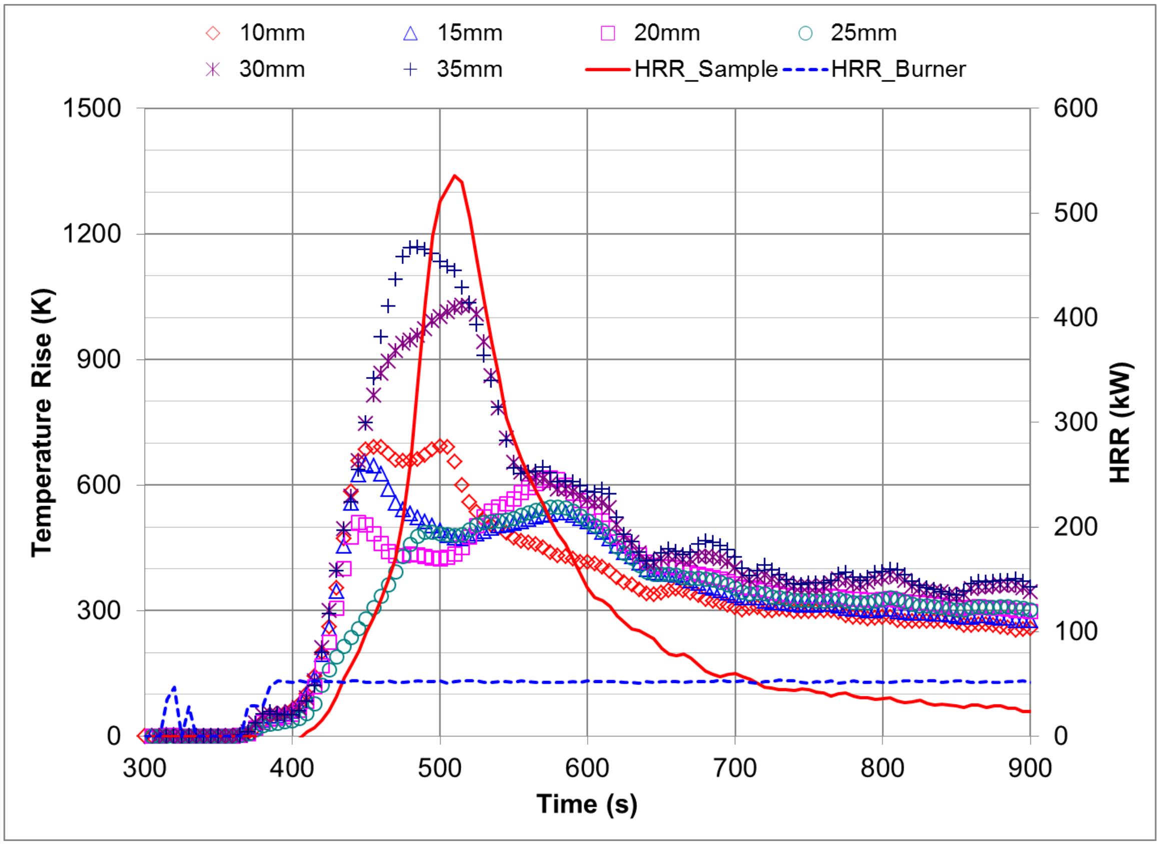

Figure 99 - CORRECTED Near-wall temperature rise (0.95 m over burner) in Test A13 (Propylene fuel, 50 kW continuous source, Square burner)

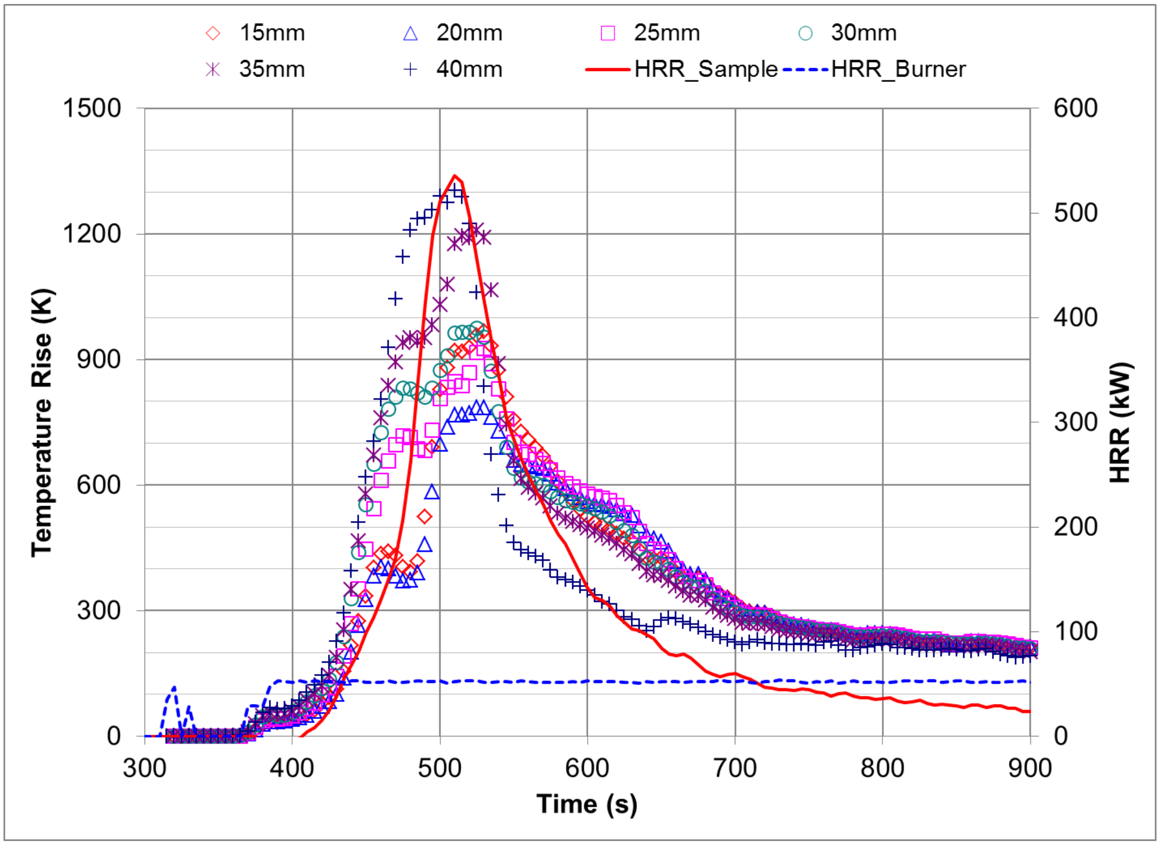

Figure 100 - CORRECTED Near-wall temperature rise (1.55 m over burner) in Test A13 (Propylene fuel, 50 kW continuous source, Square burner)

4.5.6 Flame spread

The FRP burning area history of Test A4 is presented in Figure 101 to Figure 103, the progress of the fire essentially followed the three-stage vertical wall flame spread process described in Section 4.2.7.2. The time history chart had been time-shifted to begin at the time when the source burner was turned off. In Test A4 the Rectangle burner was used, and the initial burning area's width in series "00" in Figure 101 had approximately the same dimension as the burner's width. The width for the burning area stays relatively constant as it moved upward until after 70 sec and the fire became impinged at the ceiling.

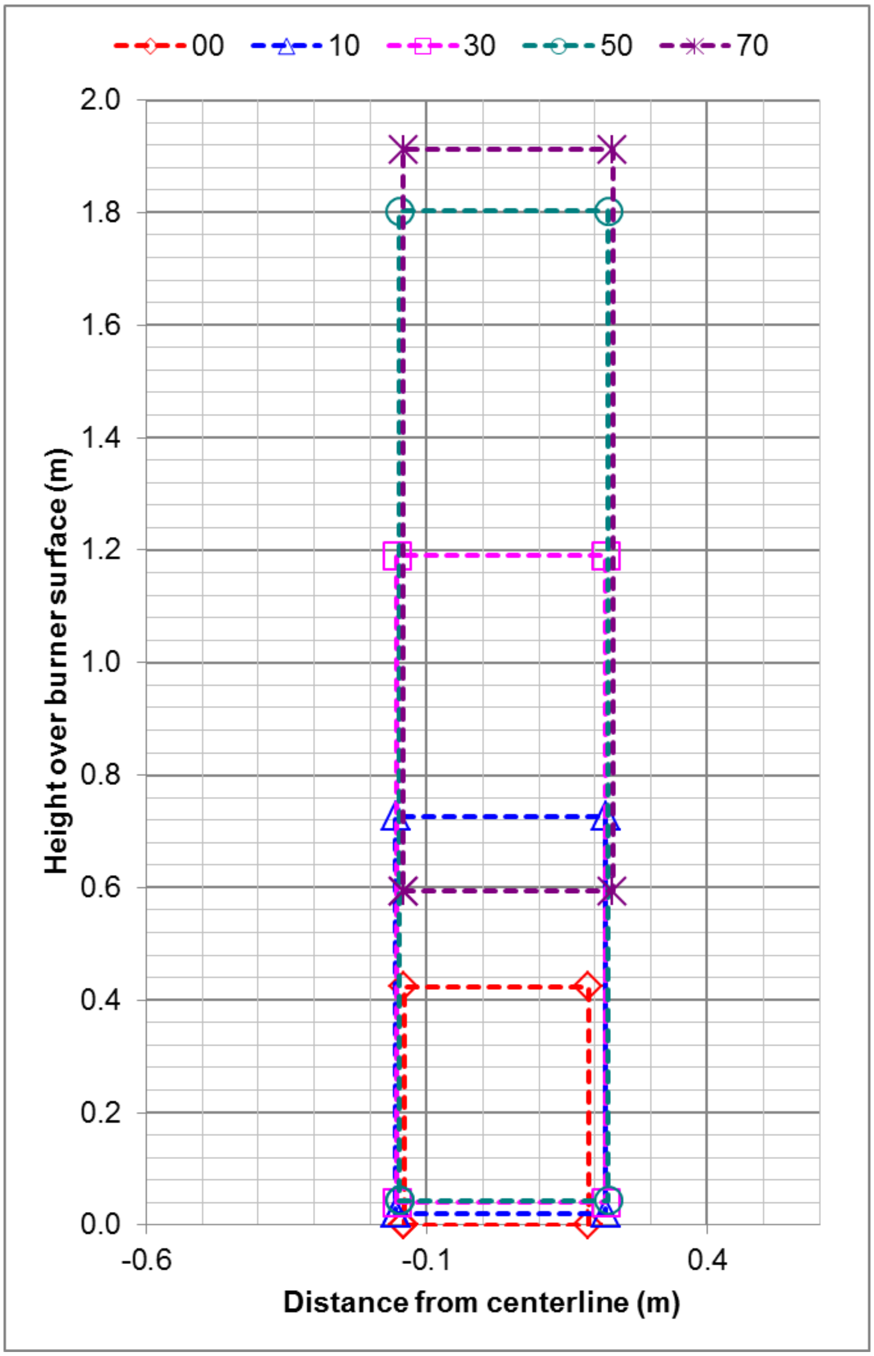

Figure 101 - Stage 1 flame spread in Test A4 (Propane fuel, 75 kW source, Rectangle burner)

Figure 102 shows the "T pattern" burning area in Stage 2 of the vertical wall fire spread. This phase lasted about 40 seconds where the burning area progressed downward at the areas of the panel away from the center and continued to shrink from the bottom. The downward spread was caused mainly by the flame under the ceiling. The peak of the FRP fire HRR happened at this stage when the burning area was largest.

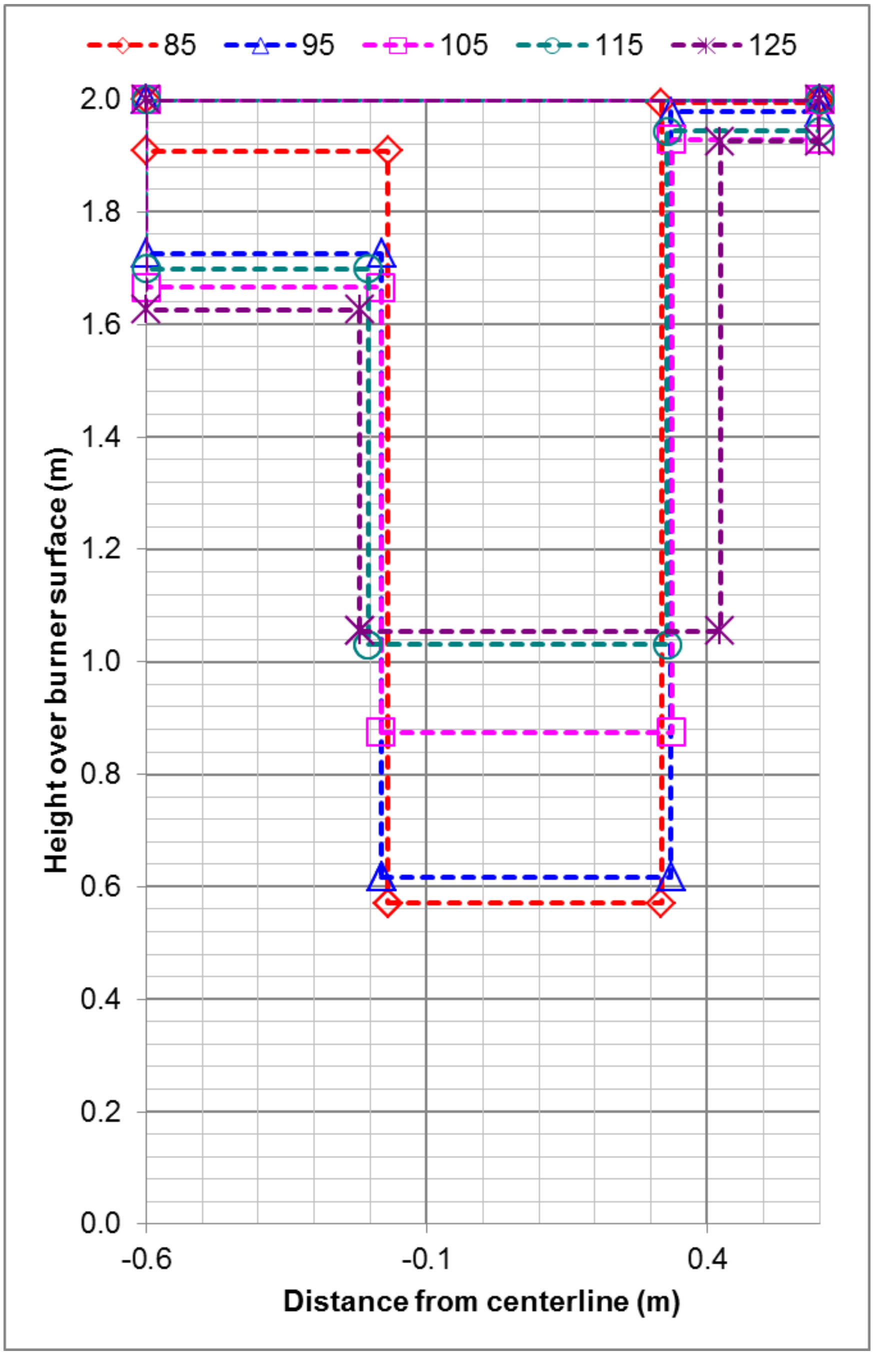

Figure 102 – Stage 2 flame spread in Test A4 (Propane fuel, 75 kW source, Rectangle burner)

At Stage 3, shown in Figure 103, the central area of the panel was burnt out, and the burning area was spilt into two. Both burn areas progressed downward and also toward the outside edge of the panel until total burnout. After this stage of burning, only small line fires remained on the panel.

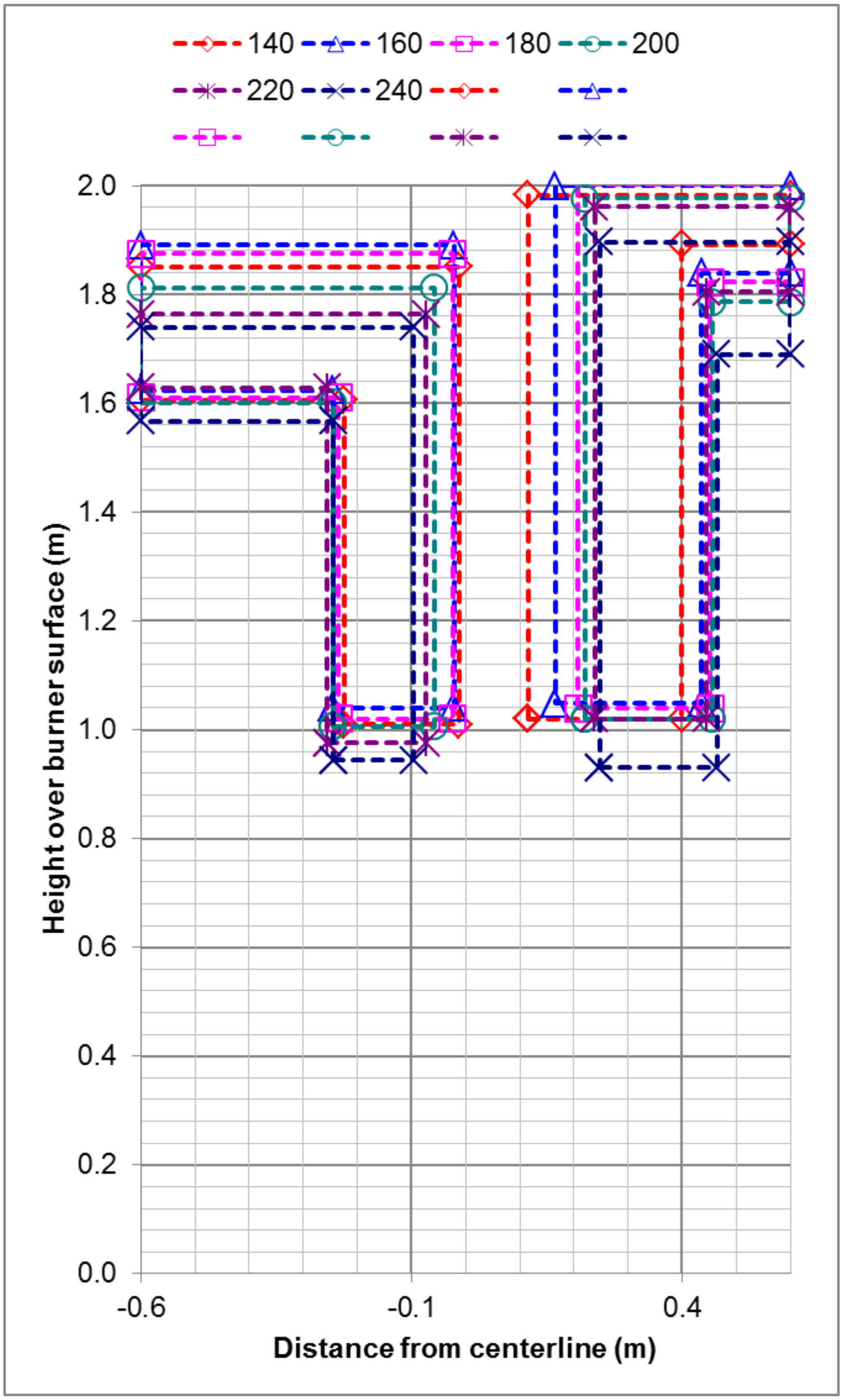

Figure 103 – Stage 3 flame spread in Test A4 (Propane fuel, 75 kW source, Rectangle burner)

The final fire damage analysis of the Test A4 FRP sample shows that the majority of the panel on the right side was consumed. However, an area at a height up to 1.4 m above the burner on the left edge and about 30 cm width was undamaged during the fire, as shown in Figure 104. This was due to the source fire plume being skewed to the right due to adverse flow conditions in the test compartment. And although a large portion of the panel was damaged in the fire, a lot of the resin and the entire fiberglass weave were still present at the end. The total mass loss was about 2.20 kg, or 25.3% of total mass.

Table 29 – Fire damage assessment of Test A4

# of cell	Damage to Resin	Area (m2)
109	**up to 100% damage**	1.09
78	**up to 75% damage**	0.78
9	**up to 50% damage**	0.09
0	**up to 25% damage**	0
92	**no damage**	0.92

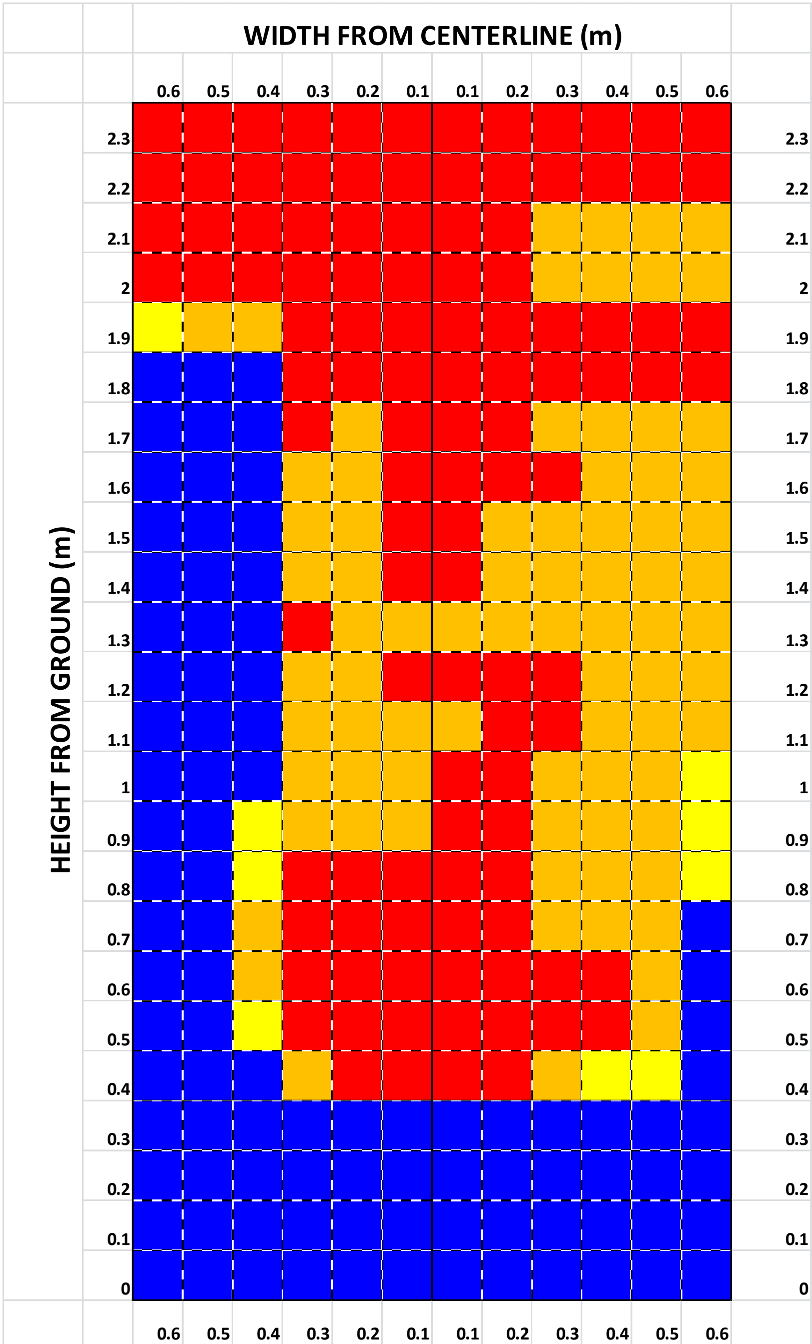

Figure 104 - Test A4 FRP specimen final burn area

The FRP burning area history of Test A13 is presented in Figure 105 to Figure 107. The time history chart had been time-shifted to begin at the time when flame attachment on the panel was observed In Test A13 the Square burner was used and the source burner HRR was constant throughout the whole test, and the initial burning area's width in series "00" in Figure 105 had approximately the same dimension as the burner's width. The width then steadily increased from the center outward as the flame spread upward toward the ceiling.

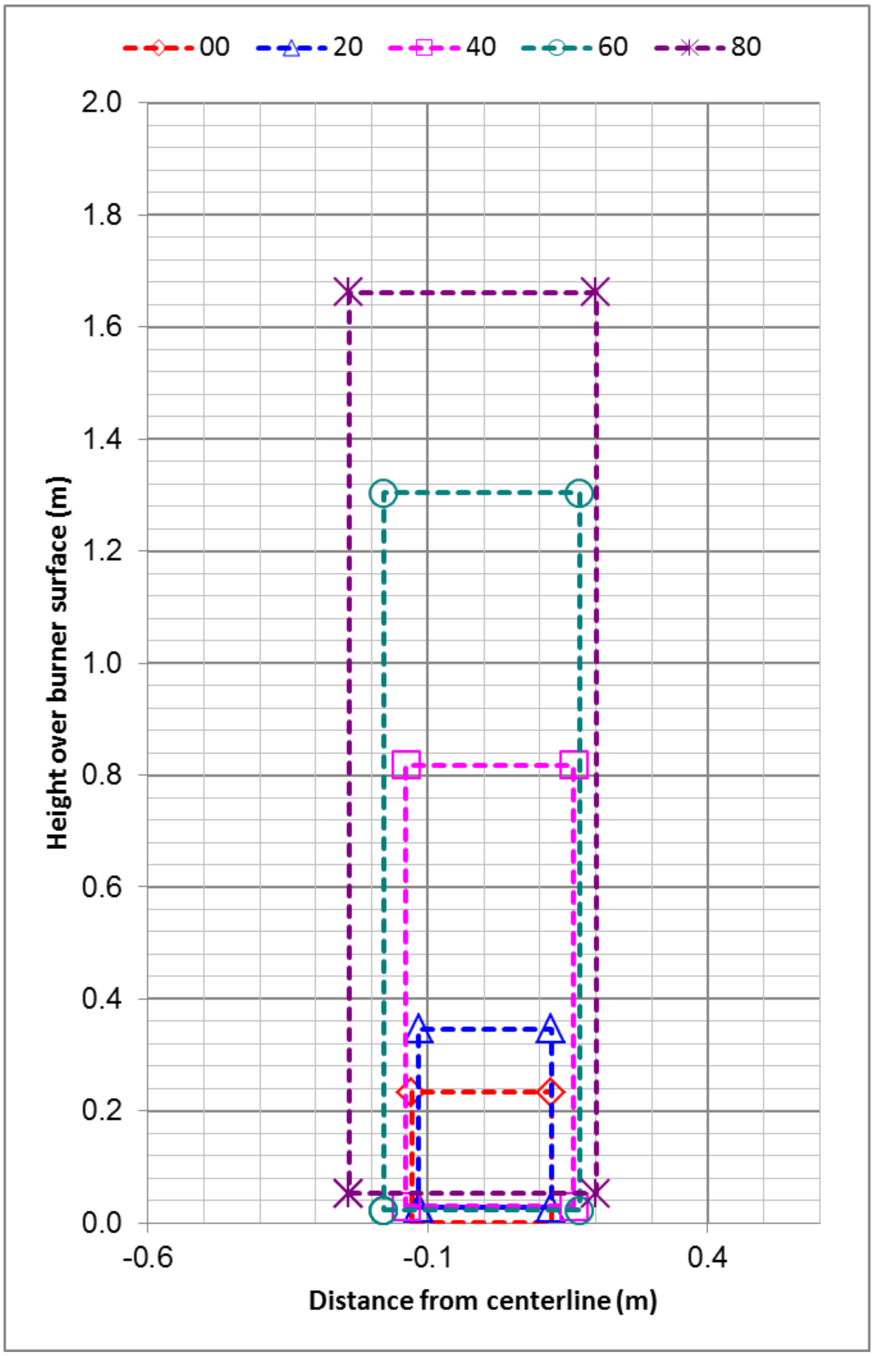

Figure 105 – Stage 1 flame spread in Test A13 (Propylene fuel, 50 kW continuous source, Square burner)

Figure 106 shows the “T pattern” burning area in Stage 2 of the vertical wall fire spread. This phase lasted about 50 seconds where the burning area progressed downward at the areas of the panel away from the center and continued to shrink from the bottom. The central area of burning also steadily increased in width. The downward spread was caused mainly by the flame under the ceiling. The peak of the FRP fire HRR happened at this stage when the burning area was largest.

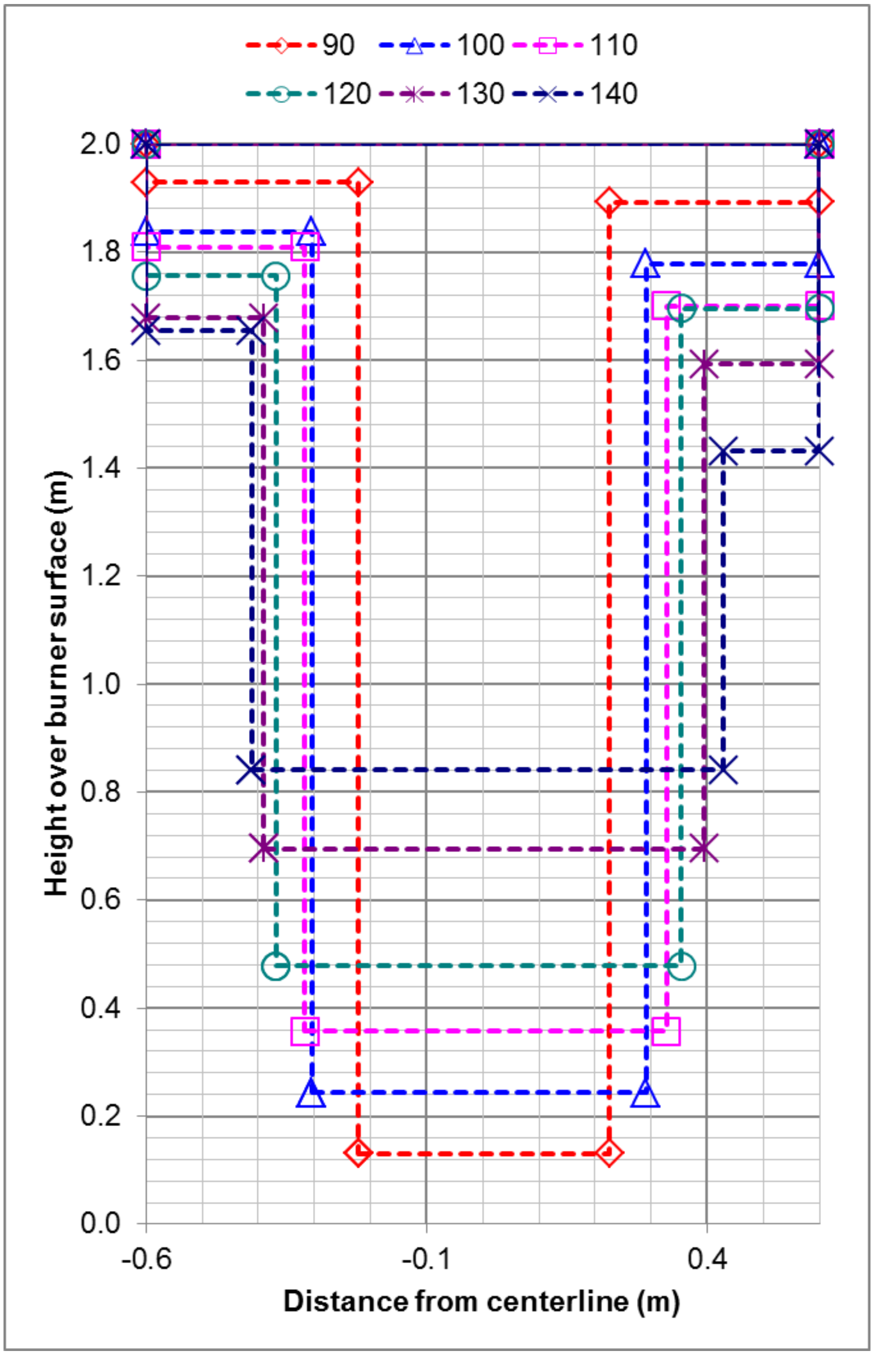

Figure 106 - Stage 2 flame spread in Test A13 (Propylene fuel, 50 kW continuous source, Square burner)

At Stage 3 flame spread in Test A13, shown in Figure 107, the central area of the panel was burnt out, and the burning area was spilt into two. Both areas progressed downward and also toward the outside edge of the panel. After this stage of burning, only small line fires remained on the panel.

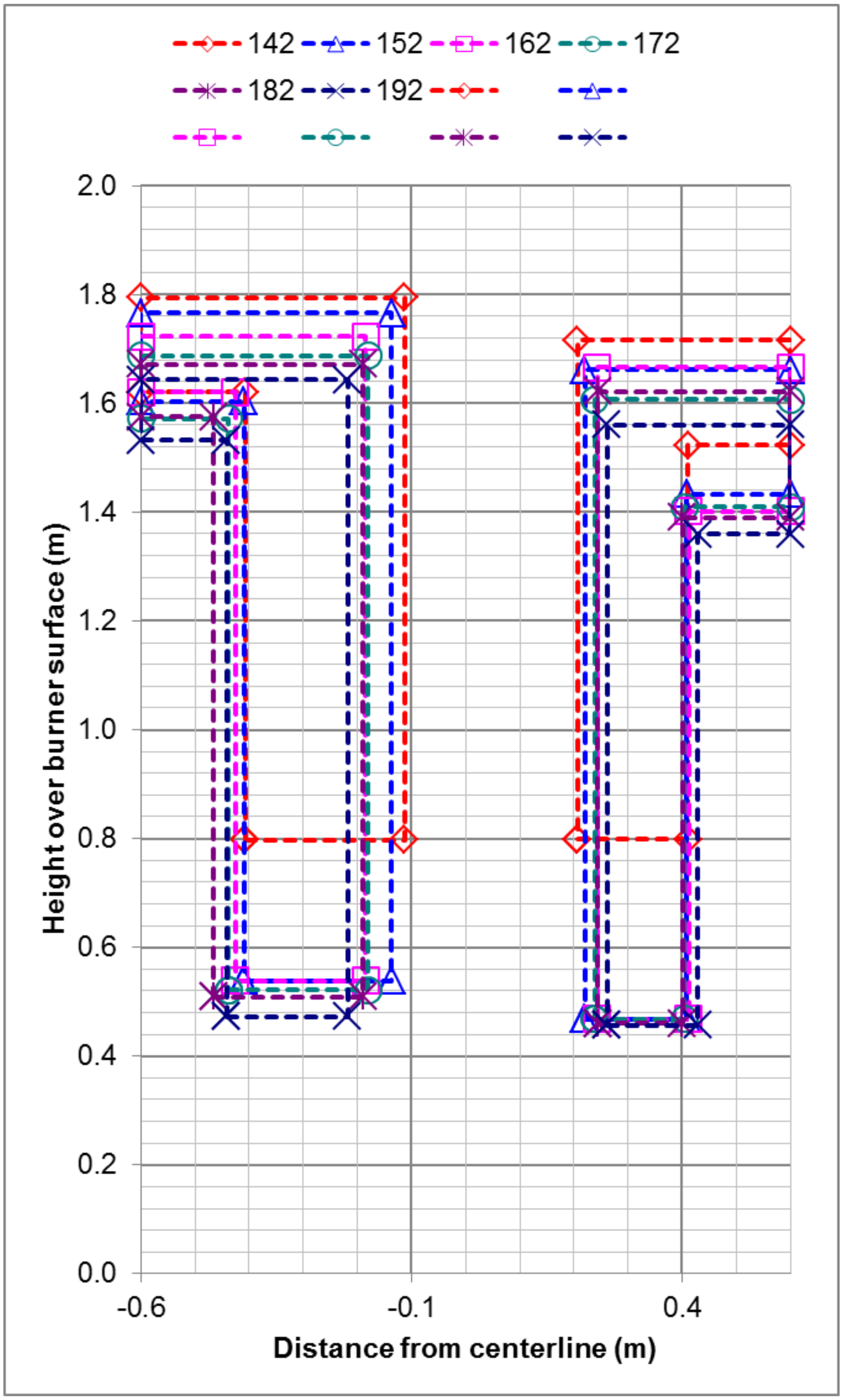

Figure 107 - Stage 3 flame spread in Test A13 (Propylene fuel, 50 kW continuous source, Square burner)

The final fire damage analysis of the Test A13 FRP sample shows that most of the panel above the level of the source burner surface was consumed in the fire. A large portion of the panel was burnout with little to no resin left. The total mass loss was about 2.78kg, or 34.1% of total mass.

Table 30 – Fire damage assessment of Test A13

# of cell	Damage to Resin	Area (m2)
173	up to 100% damage	1.73
37	up to 75% damage	0.37
18	up to 50% damage	0.18
3	up to 25% damage	0.03
57	no damage	0.57

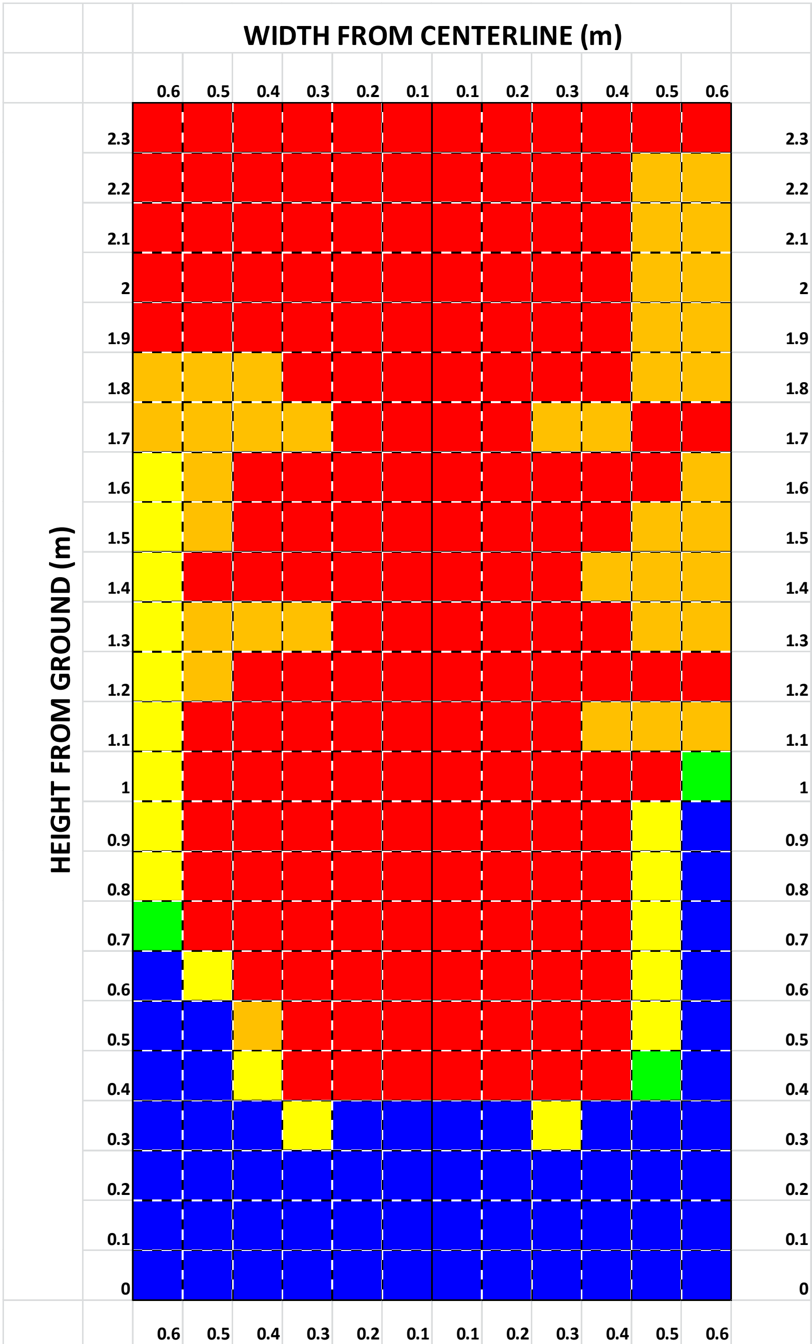

Figure 108 - Test A13 FRP specimen final burn area

4.5.7 Summary of combustible wall fire test results

For the tests where the source fire was extinguished during the test, it is observed that propylene and the higher HRR at 75 kW contributes to shorter times at crackling noise, panel ignition, and peak HRR (shown in Figure 109 to Figure 111). Conversely, propylene and the higher HRR appears to contribute to a higher peak HRR and total mass lost ratio on the panel than propane (shown in Figure 112Figure 113).

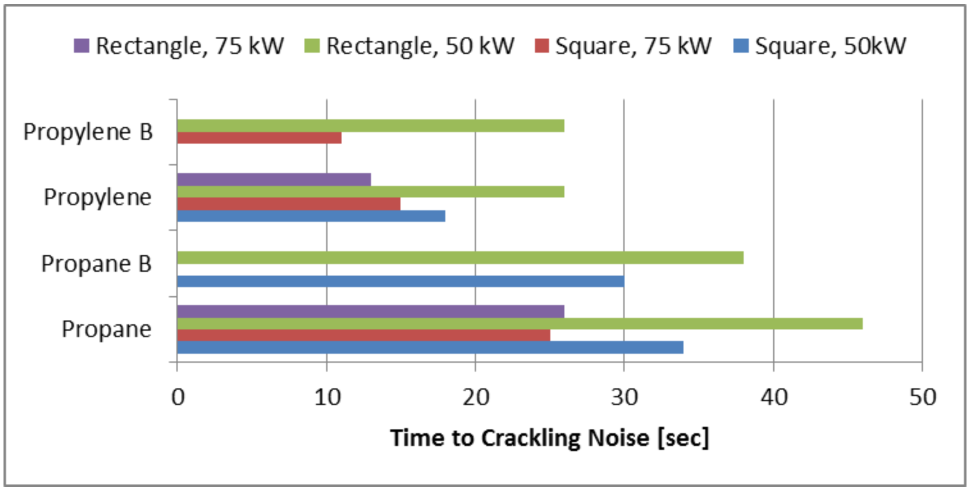

Figure 109 - Time to Crackling Noise Comparison [Fuel type]

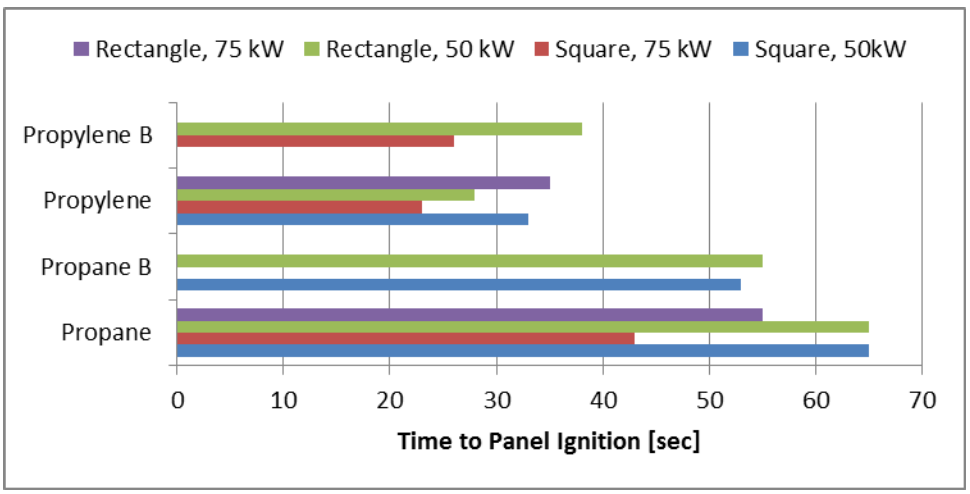

Figure 110 - Time to Panel Ignition Comparison [Fuel type]

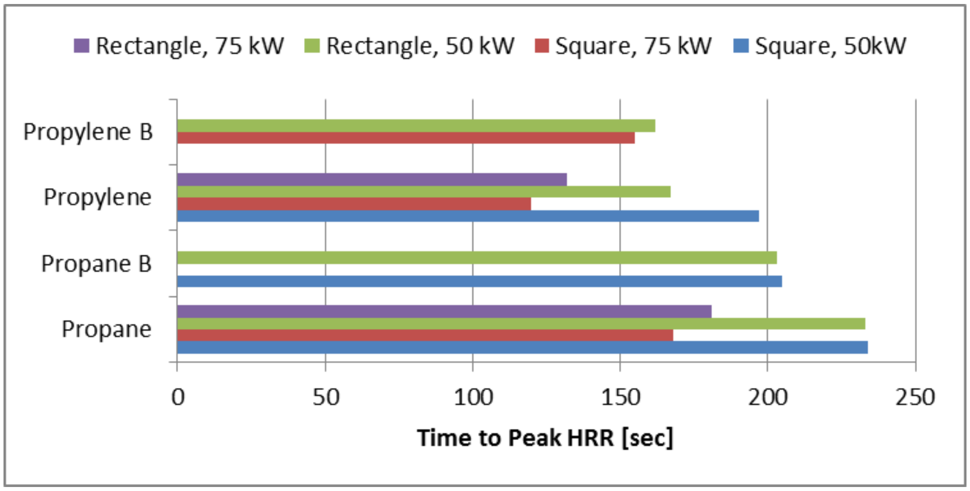

Figure 111 - Time to Peak HRR Comparison [Fuel type]

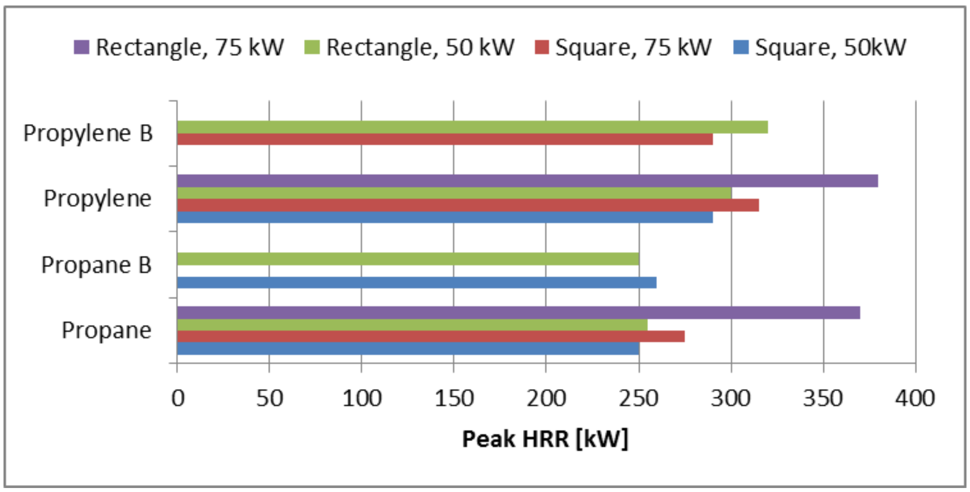

Figure 112 - Peak HRR Comparison [Fuel type]

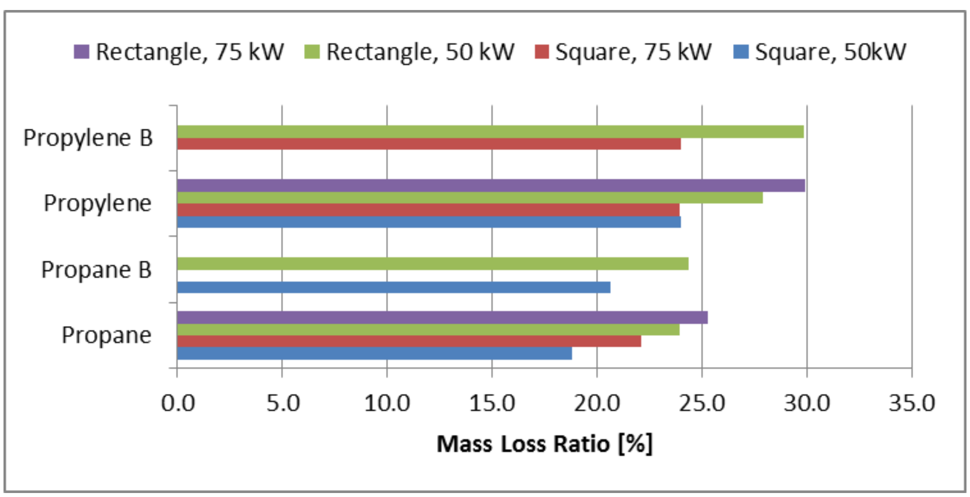

Figure 113 - Specimen Mass Loss Ratio Comparison [Fuel type]

Comparing the different tests using the same source fuel at the same source HRR but different sized burner, it is shown that the Rectangle burner contributes to a greater time to panel emitting crackling noise as well as the time to panel ignition (shown in Figure 114 and Figure 115). The effect of burner size to the peak HRR time is less significant, as shown in Figure 116. However, Figure 117 and Figure 118 show that the Rectangle burner generally contribute a higher peak HRR, and greater mass loss ratio.

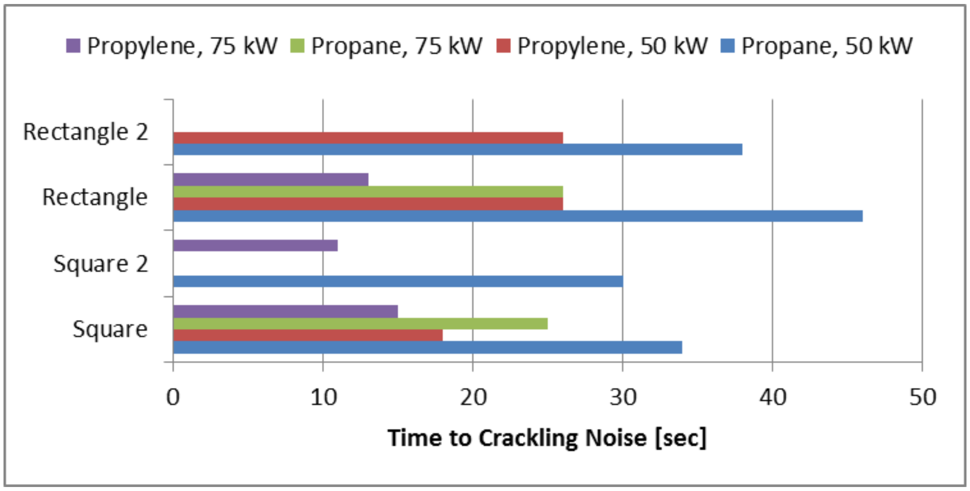

Figure 114 - Time to Crackling Noise Comparison [Burner size]

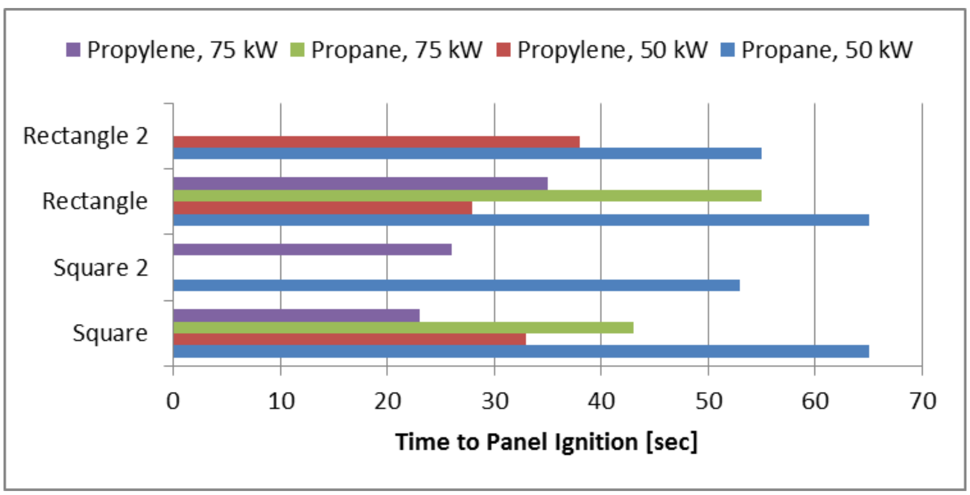

Figure 115 - Time to Panel Ignition Comparison [Burner size]

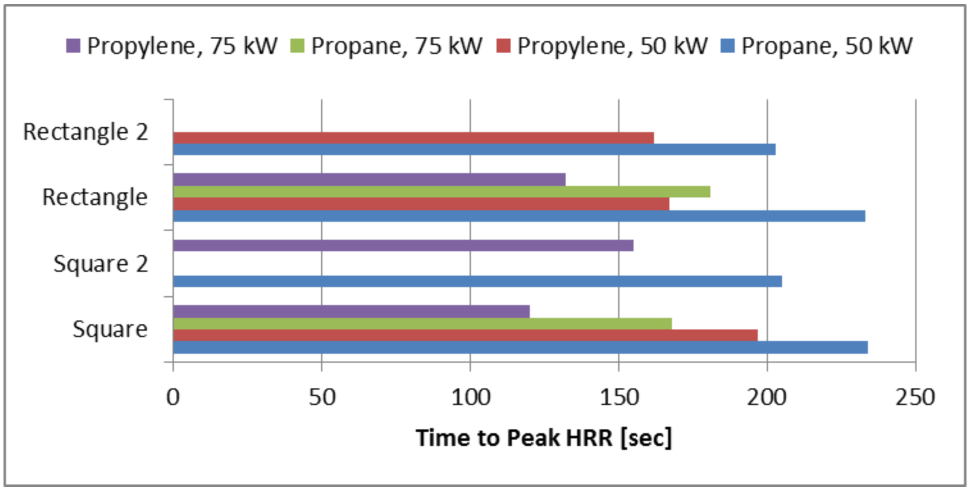

Figure 116 - Time to Peak HRR [Burner size]

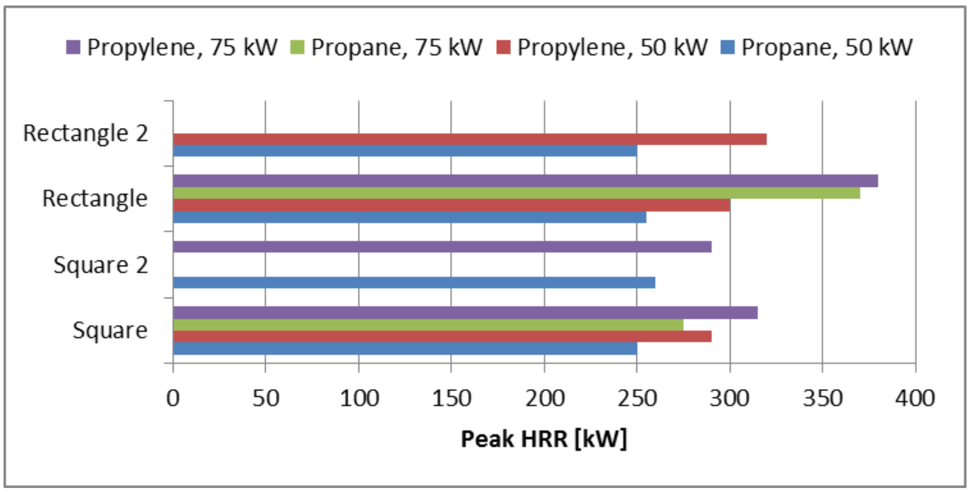

Figure 117 - Peak HRR Comparison [Burner Size]

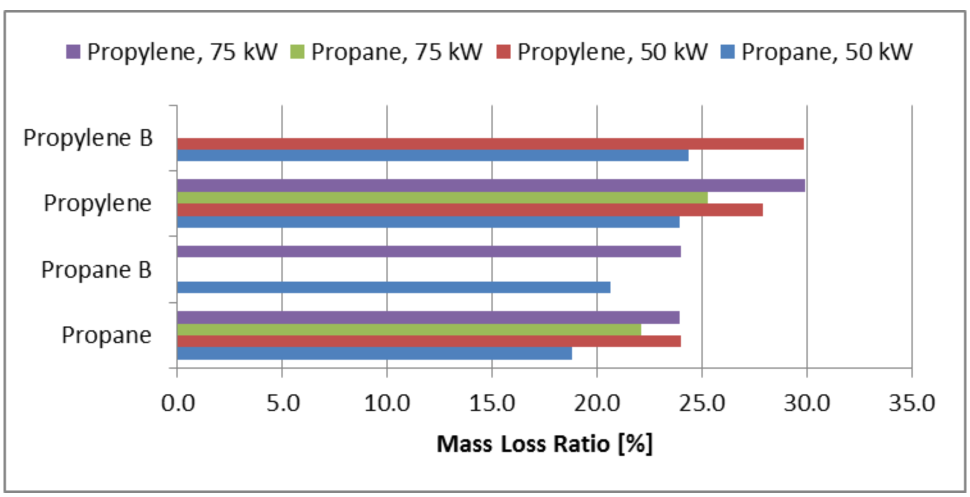

Figure 118 - Specimen Mass Loss Ratio Comparison [Burner Size]

4.5.8 Flame spread rate

Although flame spread was not directly measurable in the full scale combustible wall experiment, the flame spread rate can be estimated from the HRR, wall temperature, heat flux, and video footage data from a test.

In the cone calorimeter tests of the FRP panel material under different external heat fluxes, the HRRPUA was determined as a function of time, and its time-averaged value was found. It was observed that the HRRPUA of the FRP specimens had a range of values as determined from the different tests. Table 31 shows the average, and as well as the 50% to 100% percentile, of the time-averaged HRRPUA from the tests, averaged with all 6 tests in the first column, and averaged between tests with similar heat flux levels in the second to fourth column.

Table 31 - Time-averaged HRRPUA values from cone tests

	Overall	25kW Avg	50kW Avg	75kW Avg
Average	110.1	96.5	95.6	138.2
50%	84.7	63.6	76.8	113.7
60%	104.4	80.8	97.2	135.1
70%	132.3	120.2	102.4	174.2
80%	203.7	184.2	161.7	265.3
90%	267.8	219.3	261.6	322.5
100%	295.5	238.3	286.8	361.4

According to Table 31, the measured HRRPUA of the FRP appears to increase with the imposed heat flux. The average value across all six tests was found to be about 110 kW/m^2, with a low at about 96 kW/m^2 determined at the imposed 25 kW/m^2 and 50 kW/m^2 heat fluxes, and a high at 138 kW/m^2 determined at imposed 75 kW/m^2 heat flux. The time-averaged HRRPUA may be misleading because the typical HRRPUA curves of the sample had a high peak soon after ignition but tail off for a long duration during subsequent burning. Since the major flame spread of the full-sized FRP panels occurred quickly after ignition, the representative HRRPUA of the sample should be higher than the time-based averages, and more likely in the 70-80 percentiles of the value, which ranges from 100 kW/m^2 for imposed heat flux at 50 kW/m^2 to 270 kW/m^2 for imposed heat flux at 75 kW/m^2.

Based on the wall heat flux measurements made during the full-scale FRP tests, the centerline heat flux reached up to 80 kW/m^2 to 100 kW/m^2, hence it may be assumed that the specimen's HRRPUAs in these cases could be upward of the 270 kW/m^2 found previously in the cone tests (80 percentiles of the 75 kW/m^2 tests). It must be cautioned that using a constant HRRPUA served only as an approximation since the FRP panel's HRRUPA can vary with time and imposed heat flux.

A burning area time-history could be determined from the full-scale FRP panel tests using a constant HRRUPA using (42).

$$A_{burning}(t) = \frac{HRR(t)}{HRRPUA} \tag{43}$$

The burning area change history would then be calculated as the change in the burning area using (43).

$$\frac{dA_{burning}}{dt} = A_{burning}(t) - A_{burning}(t-1) \tag{44}$$

Assuming that flame spread rate (FSR) takes the form of area per unit time, its calculation is the same as (43), but only with consideration to the positive or zero values since it is not physically possible to have negative flame spread. So the flame spread rate is of the FRP panel is represented in (35).

$$FSR(t) = A_{burning}(t) - A_{burning}(t-1) \quad \text{,only positive, otherwise, zero} \tag{45}$$

A way to ground the FSR calculations was to utilize the final burnt area as an upper bound: total burning area cannot be larger than the final burnt area. The final burnt area of each FRP panel specimen was measured using the 0.1m x 0.1m grid drawn on the panel as a guide to gauge the fire damage to the cell. A metal rod was used to prod each grid cell and the damage to the cell inspected for amount of resin left. 100% damage means all resin burnt off, only fiberglass weave left behind, 75% damage suggests only some resin left, mostly fiberglass, 50% damage is where half of the cell's resin remains, 25% damage means most resin survives, and 0% means no fire damage. All cells were assigned a damage index, and the subtotals for each damage range were found, and the total is always 2.88 m^2. Table 32 shows a sample damage index summary.

Table 32 - Sample damage summary from Test A5

# of cell	Damage to Resin	Area (m2)
56	up to 100% damage	0.56
77	up to 75% damage	0.77
15	up to 50% damage	0.15
4	up to 25% damage	0.04
136	no damage	1.36

The total burnt area is assumed to be the summation of the product of the percentage damage and the damage area, as shown in (45).

$$\text{Total burnt area} = \sum(\text{Burn area} * \%damage) \tag{46}$$

Since the definition of flame spread means that only spreads to new area were counted ((35)), the summation of the FSR equates to adding up the new spread area over time until the total burnt area was reached. So, in terms of flame spread, the total burnt area also equals to the summation of the products between FSR per unit time, as shown in (46).

$$\text{Total burnt area} = \sum(\text{FSR}(t)) \tag{47}$$

Using (46) and a constant HRRPUAs found as the overall average between all cone tests (110 kW/m^2), average between cone tests with at 25 kW/m^2 heat flux (96.5 110kW/m^2), and average between cone tests with heat flux at 75 kW/m^2 (138.2 kW/m^2), it was determined that these HRRPUA values were too low and produces a calculated total burnt area much larger than the actual burnt area found using (45). This holds true for all FRP panel tests, hence, these time-averaged HRRPUA values from the cone tests were most likely too low to be of use for flame spread calculations.

In light of the discrepancy with the low HRRPUA values, an iterative method to find an assumed constant HRRPUA value for each FRP full scale test that equates both (45) and (46) into (47) was created.

$$\sum(\mathrm{FSR}(t)) = \sum(\mathrm{Burn\ area} * \%damage) \tag{48}$$

$$HRRPUA_{Iterative} = \frac{\sum(\mathrm{FSR}(t))}{\sum(\mathrm{HRR}(t))}$$

The resulting, corrected HRRPUA values for the full-scale tests were all larger than the time-averaged values, and were plotted in Figure 119. The similar trend of increasing heat flux to the wall (increasing HRR of burner fire) leading to an increase in the assumed constant HRRPUA is evident.

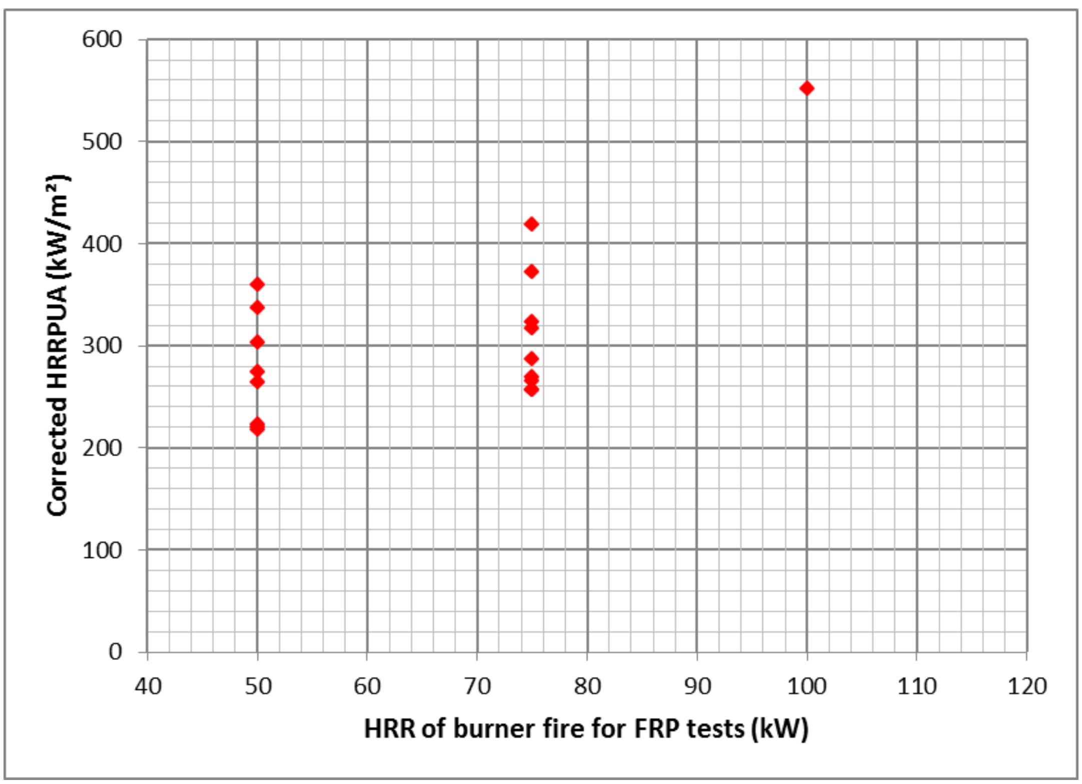

Figure 119 - Corrected HRRPUA for all 18 full-scale FRP panel tests

Compared to the average cone HRRPUA, the iterative HRRPUA from the wall tests were higher. However, as stated previously, the average cone HRRPUA would be an estimate on the low end since heat fluxes to the wall during the fire reaches upward of 80 kW/m^2 to 100 kW/m^2. A more reasonable comparison should be made with the 80th to 90th percentiles cone HRRPUA data from the cone tests with 75 kW/m^2 heat flux insult cases. The ratio between the cone HRRPUA and the iterative HRRPUA values are plotted in Figure 120, which shows the comparison with the 75 kW/m^2 heat flux tests' average, 70 percentile, 80th percentile, and 90th percentile HRRPUA values. The ratios were calculated using (48).

$$Ratio\_difference = \frac{\text{Iterative HRRPUA - Cone HRRPUA}}{\text{Cone HRRPUA}} \quad (49)$$

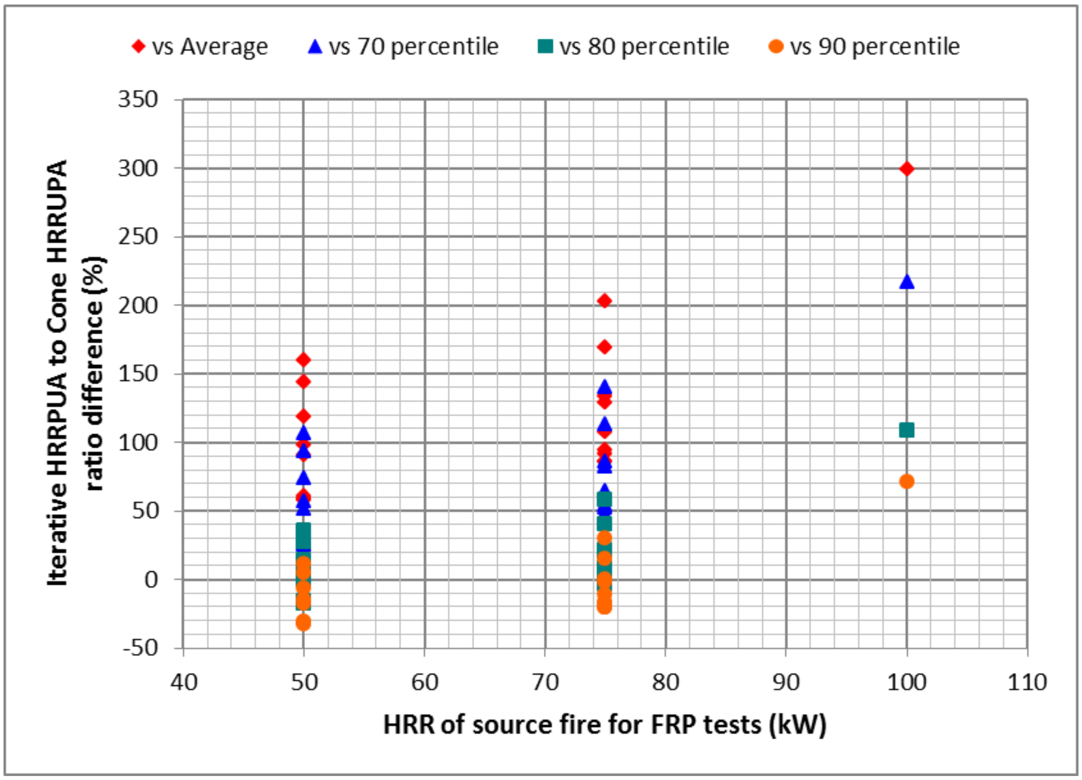

Figure 120 - Iterative HRRPUA vs. Cone HRRPUA ratios

It is shown that the iterative HRRPUA values correspond well with the cone HRRPUA value at 75 kW/m^2 incident heat fluxes at the 90th percentile, as evident by the lower magnitude of the ratio difference. The differences were at most at +15%/-50% for the FRP tests with 50 kW source fire, and at +30%/-20% for those tests using a 75 kW source fire, which are reasonable. The iterative HRRPUA from the 100 kW source fire test should be considered an outlier since that corresponding FRP test had a faulty ignition fire and had to be suppressed with water spray.

This method of estimating flame spread rate appears to be reasonable and the flame spread rate time histories for the 18 tests are plotted in Figure 121 to Figure 125 - Flame spread rate of tests conducted with 2ft Rectangle burner at 75 kW, separated into different groups based on burner size and burner

HRR. It should be noted that the time zero in the following charts was set to the time when the source burner reached the designated HRRs.

Figure 121 shows the 5-sec running average flame spread rates measured in tests using the 1 ft Square burner at 50 kW source fire. All of the curves show a gradual increase in FSR, then three of the four FSR curves have a large spike, which correspond to the point where rollover occurred under the ceiling. At this point there was a rapid increase of the flame spread rate due to increase in lateral spread and downward spread. The Test A13 using Propylene did not have such a spike because the source fire was burning throughout the test and the peak flame did not spike instantaneously. After the peaking/spiking, the FSR gradually increases again into a higher peak then decreases and becomes insignificant for the remaining of the test.

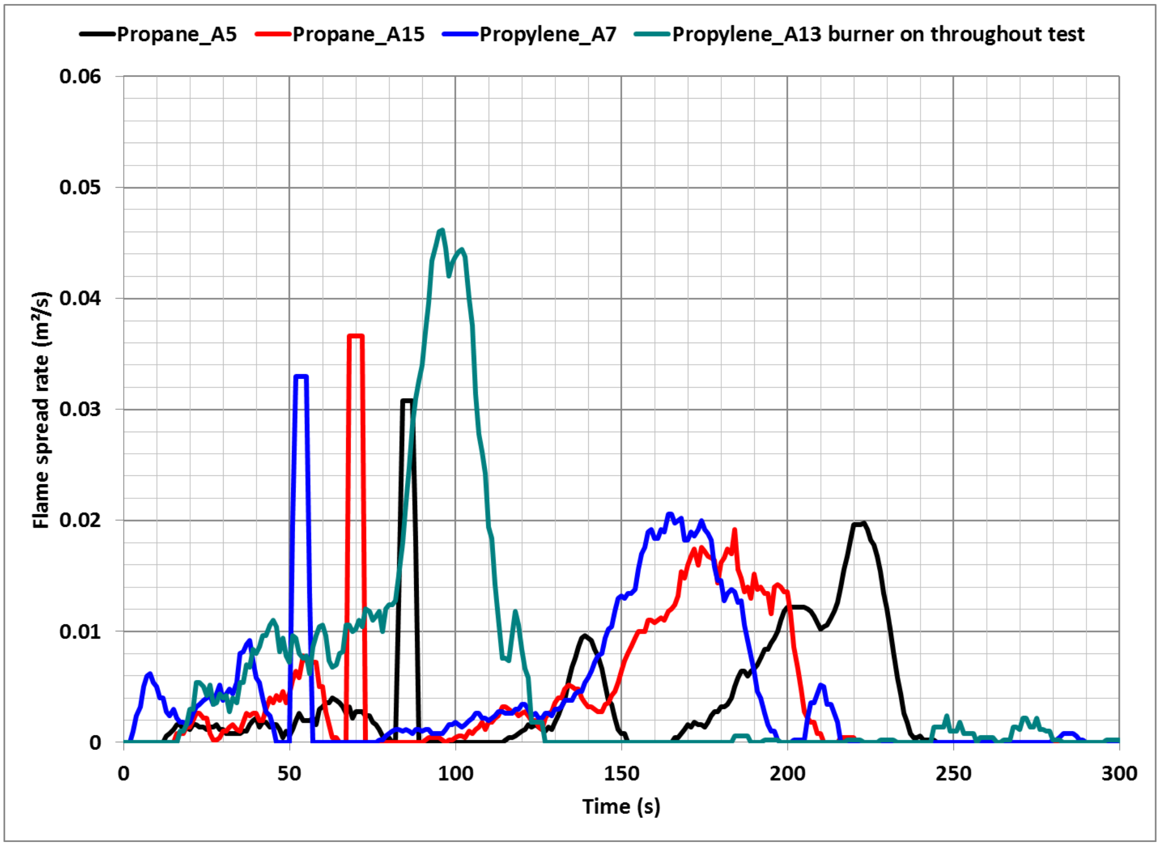

Figure 121 - Flame spread rate of tests conducted with 1ft Square burner at 50 kW

Figure 122 shows the 5-sec running average flame spread rate of tests using the 1 ft Square burner at 75 kW source fire. All of the curves show a gradual increase in FSR, then three of the four FSR curves have a large spike, which correspond to the point where rollover occurred under the ceiling. At this point there was a rapid increase of the flame spread rate due to increase in lateral spread and downward spread. The Test A16 using Propane did not have such a spike because the source fire was burning throughout the test and the peak flame did not spike instantaneously. After the peaking/spiking, the FSR gradually increases again into a peak then decreases and becomes insignificant for the remaining of the test. This is similar to the Square burner with 50 kW cases, but the calculated FSRs here were generally higher, and the total burn times are shorter.

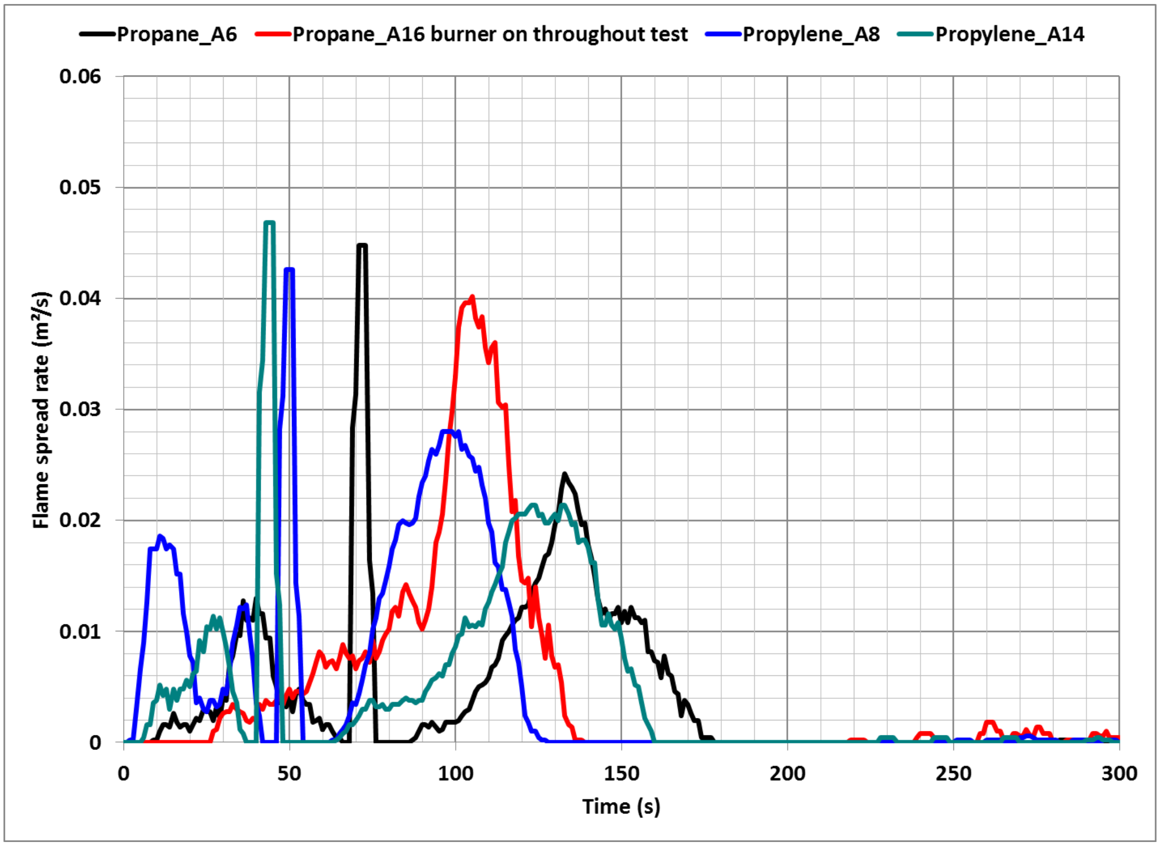

Figure 122 - Flame spread rate of tests conducted with 1ft Square burner at 75 kW

Figure 123 shows the 5-sec running average flame spread rate of tests using the 2 ft Rectangle burner at 50 kW source fire. All of the curves show a gradual increase in FSR, then three of the four FSR curves have a large spike, which correspond to the point where rollover occurred under the ceiling. At this point there was a rapid increase of the flame spread rate due to increase in lateral spread and downward spread. The Test A12 using Propylene did not have such a spike because the source fire was burning during the entire. After the peaking/spiking, the FSR gradually increases again into a peak then decreases and becomes insignificant for the remaining of the test.

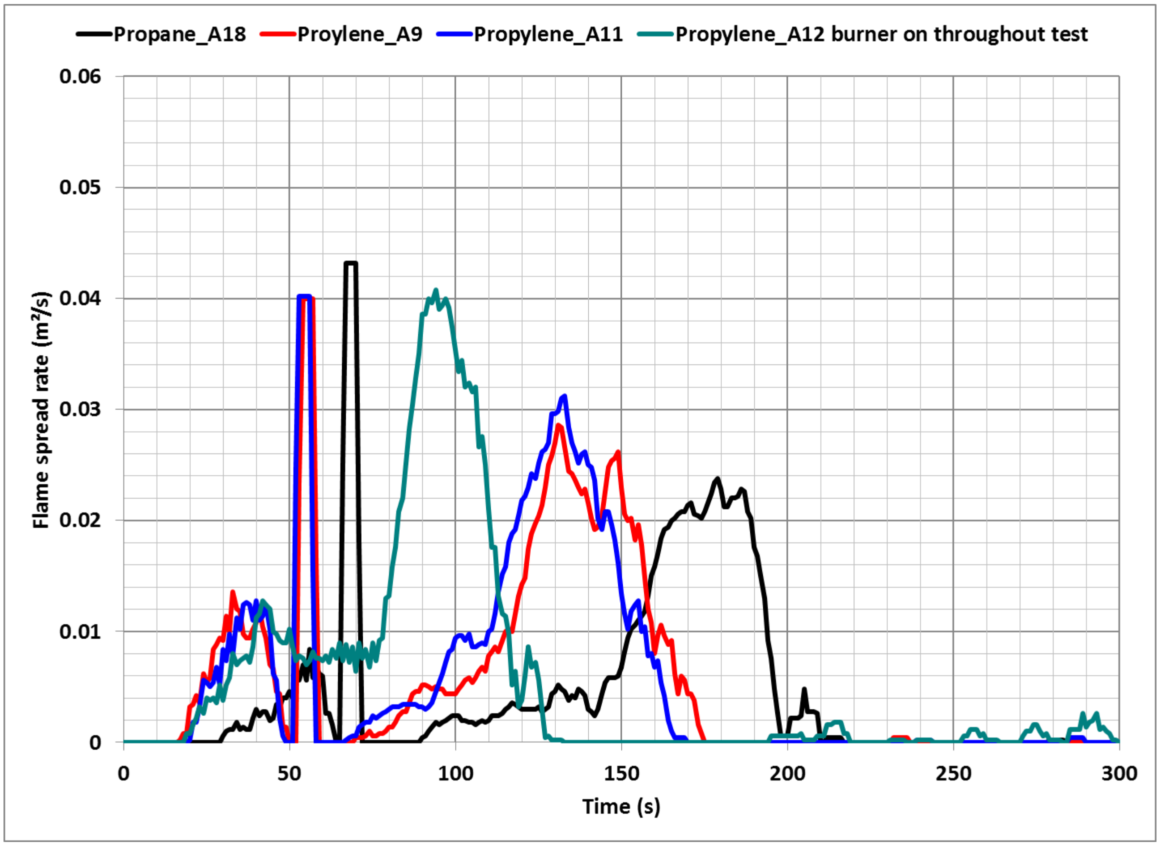

Figure 123 - Flame spread rate of tests conducted with 2ft Rectangle burner at 50 kW

Figure 124 shows the 5-sec running average flame spread rate of tests using the 2 ft Rectangle burner at 75 kW source fire. All of the curves show a gradual increase in FSR, then three of the four FSR curves have a large spike, which correspond to the point where rollover occurred under the ceiling. At this point there was a rapid increase of the flame spread rate due to increase in lateral spread and downward spread. The Test A17 using Propane did not have such a spike because the burner was on throughout the test. Also, the Propylene A10 test had a series of chaotic spikes early in the test, most likely due to sensitivity in the HRR curve. After the peaking/spiking, the FSR gradually increases again into a peak then decreases and becomes insignificant for the remaining of the test. This is similar to the Rectangle burner with 50 kW source fire cases.

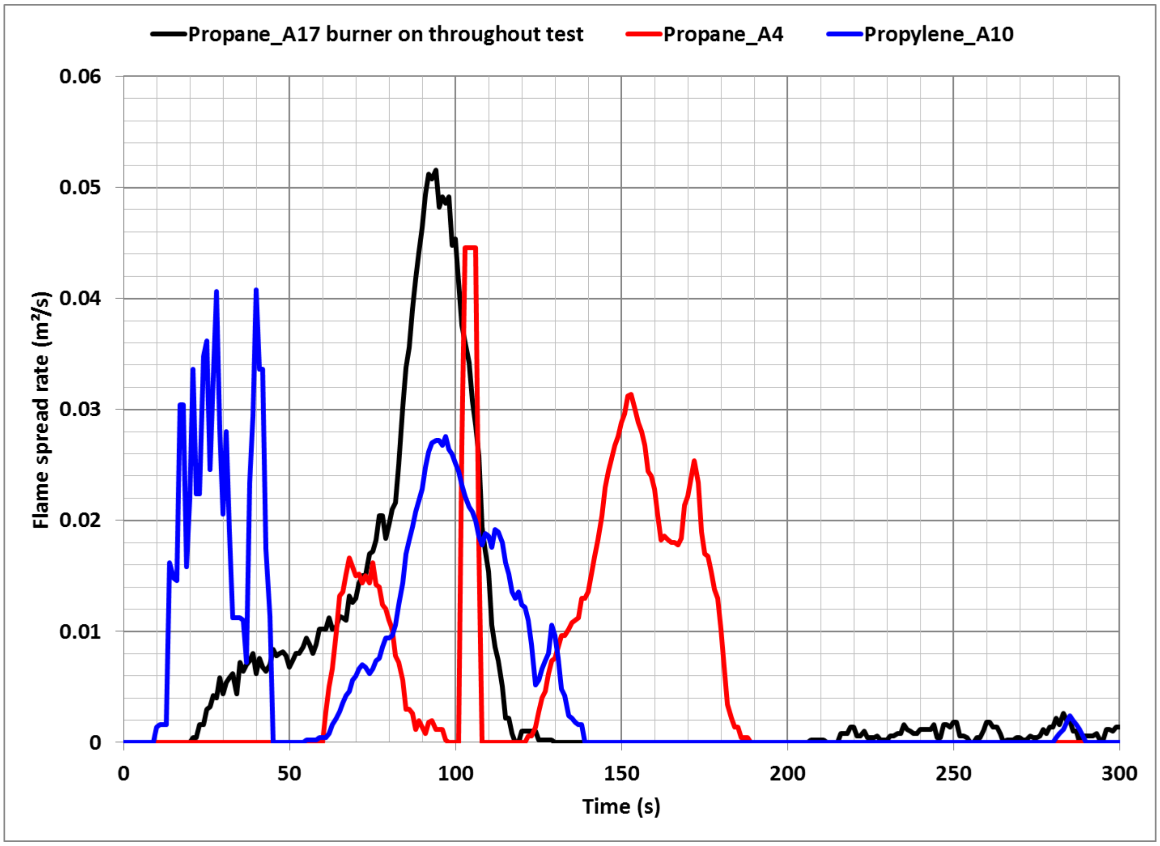

Figure 124 - Flame spread rate of tests conducted with 2ft Rectangle burner at 75 kW

Figure 125 shows the flame spread rate of tests using the 2 ft Rectangle burner at different source fire sizes. These tests are singled out because water was applied during the all three tests and they have more unique source heat release rate (source fire in Tests A1 and A2 had flare-ups above 100 kW and 75 kW at the beginning of the test). These resulted in more chaotic heat release curve that translated into chaotic FSR curves.

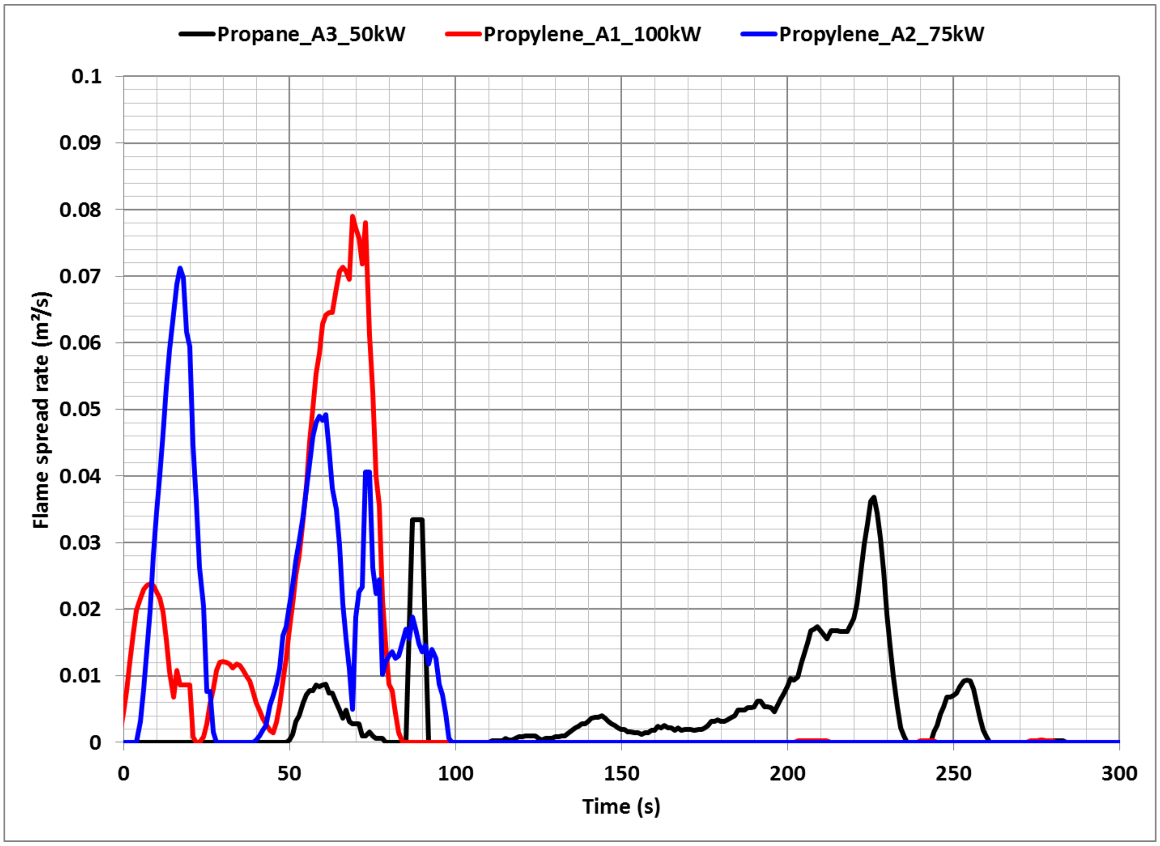

Figure 125 - Flame spread rate of tests conducted with 2ft Rectangle burner at 75 kW

The tests using propane as the source fire fuel appear to ignite the panel slower than the propylene cases at the same source HRRs. The differences in total burn time appear to be related to burner source fire HRR, where the higher HRR relates to a shorter burn time.

4.5.9 Velocity, temperature, and heat flux from similar combustible wall panel fire tests

Comparison of the velocity, plume temperature, near-wall temperature, and centerline heat flux was made between tests with identical experimental configurations and between tests where the configurations are identical except where the source fire was in one case extinguished and in the other case continuous throughout the test. It must be noted that in tests where the configurations are identical, the source fire extinguishment times are different.

Two different periods of time during the fire tests of special importance where the measured quantities exhibited major differences are the time when the source fire has reached its designated HRR level, but before the sample wall panel was ignited, and at the time when the sample HRR peaked. In the following analysis, the measured quantities were averaged over the time between source fire reaching full HRR and the sample's ignition, and the time between 5 seconds before and after the peak sample HRR.

Centerline plume temperature from tests with identical configurations is presented in Figure 126 to Figure 129. Generally, the measurements are very consistent between different tests.

Centerline plume temperature from tests where the source fuel, burner shape, and HRR are the same, but where the source fire was extinguished and continuous is presented in Figure 130 to Figure 132. The measurements from the sampling period before the panels' ignitions are very consistent. However, for the tests where the source fire was continuously for the whole test, the plume centerline temperature was greater than from the other test, which was due to the presence of the source fire.

Centerline plume velocity from tests with identical configurations is presented in Figure 133 to Figure 136. The velocity measurement from before the panel's ignition is consistent. However, for the period at the peak sample HRR, the measurements between identical tests are less consistent, but it is cautioned again that the uncertainty in the data is high at this period in time due to the fire's thermal effects on the equipment.

Centerline plume velocity from tests where the source fuel, burner shape, and HRR are the same, but where the source fire was extinguished and continuous is presented in Figure 137 to Figure 139. It is shown that the velocity is consistent for the period before the panel's ignition. At the peak HRR period, for the tests where the source fire was extinguished, the velocity became negative for the probes at the higher elevation. Conversely, for the tests where the source fire was continuous, the velocity at the peak HRR period is greater than what had been measured during the earlier period.

Near-wall temperature from Test A4 (propane, Rectangle burner, 75 kW) and Test A17 (propane, Rectangle burner, 75 kW continuous throughout) at the three elevations of 0.35 m, 0.95 m, and 1.55 m are presented in Figure 140 to Figure 142. The temperature before the panel's ignition is not consistent for several thermocouples at 0.35 m above the burner, but very consistent for the thermocouples at 0.95 and 1.55 m above the burner. Near-wall temperature at 0.35 m above the source burner during the period of the peak HRR for tests where the source fire was continuous is greater than that measured during the tests without the continuous source fire, as expected. However for the thermocouples at the other elevations, the differences are less consistent between the tests.

Near-wall temperature from Test A6 (propane, Square burner, 75 kW) and Test A16 (propane, Square burner, 75 kW continuous throughout) at the three elevations of 0.35 m, 0.95 m, and 1.55 m are presented in Figure 143 to Figure 145. The temperature before the panel's ignition is very consistent for all near-wall thermocouples. Near-wall temperature at all elevations during the period of the peak HRR for tests where the source fire was continuous is greater than that measured during the tests without the continuous source fire, as expected. However for the thermocouples at the other elevations, the differences are less consistent between the tests.

Near-wall temperature from Test A7 (propylene, Square burner, 50 kW) and Test A13 (propylene, Square burner, 55 kW continuous throughout) at the three elevations of 0.35 m, 0.95 m, and 1.55 m are presented in Figure 143 to Figure 145. The temperature before the panel's ignition is very consistent for all near-wall thermocouples. Near-wall temperature at all elevations during the period of the peak HRR for tests where the source fire was continuous is greater than that measured during the tests without the continuous source fire, as expected. However for the thermocouples at the other elevations, the differences are less consistent between the tests.

The centerline heat flux from Tests A4 and A17 is presented in Figure 149, heat flux from Tests A6 and A16 is presented in Figure 150, and the heat flux from Tests A7 and A13 is presented in Figure 151. For all cases, the heat flux measured in the period of time before the panel's ignition is consistent between the tests. For the peak HRR period, the heat flux measured in tests with the continuous source fire is generally higher than from that measured in the tests without the continuous source flame.

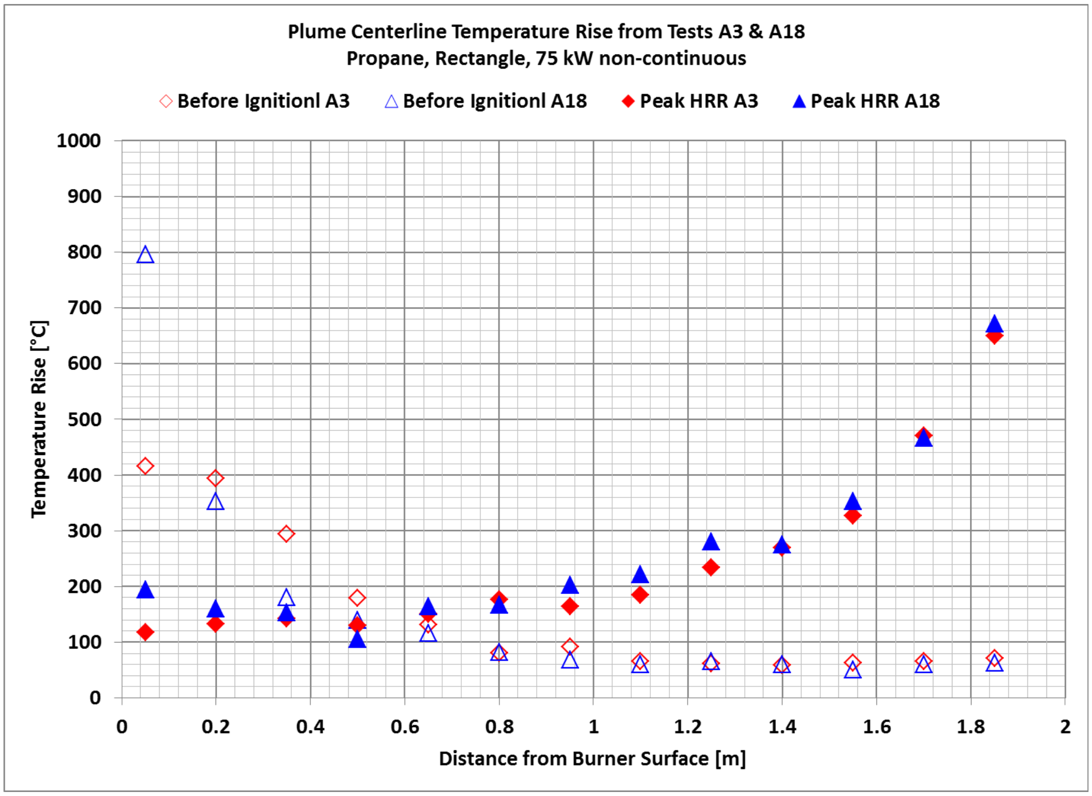

Figure 126 - Centerline Temperature of Tests A3 and A18

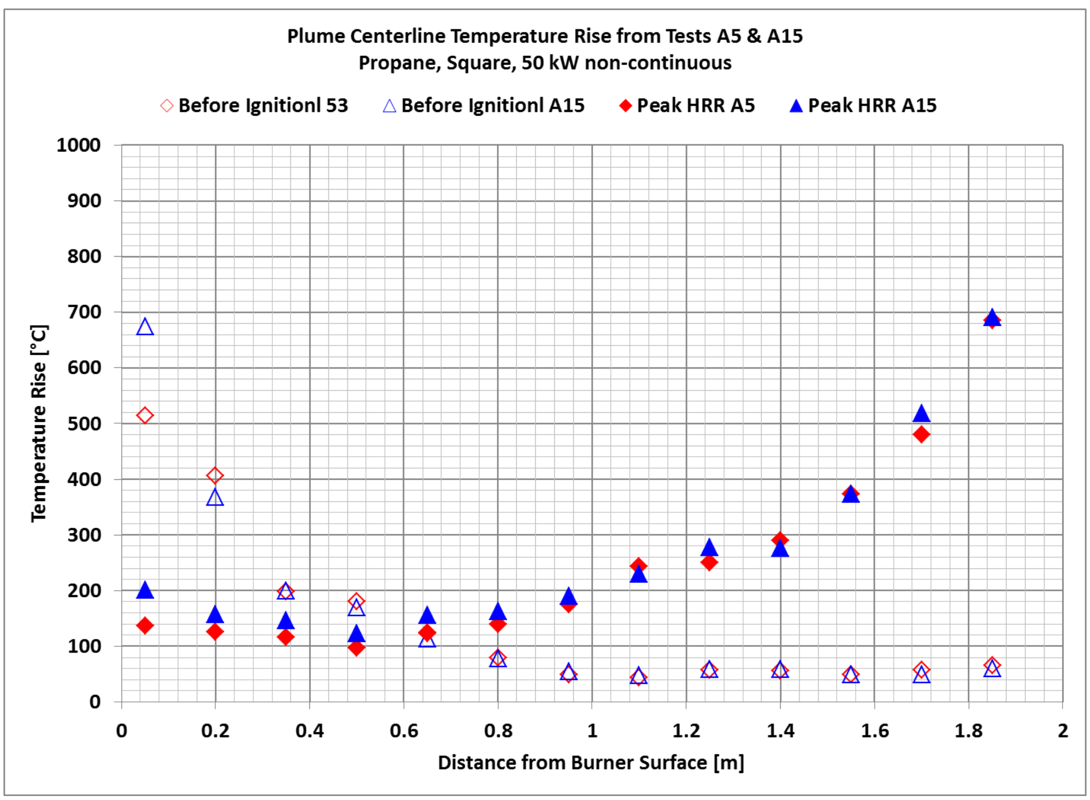

Figure 127 - Centerline Temperature of Tests A5 and A15

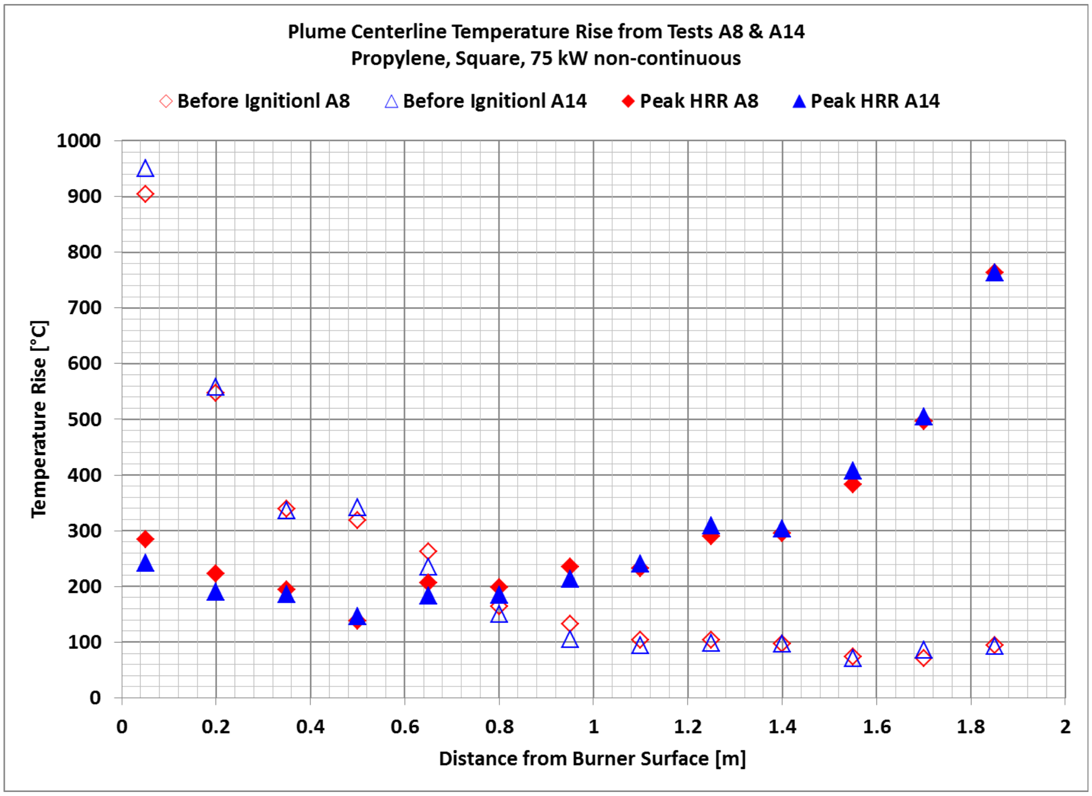

Figure 128 - Centerline Temperature of Tests A8 and A14

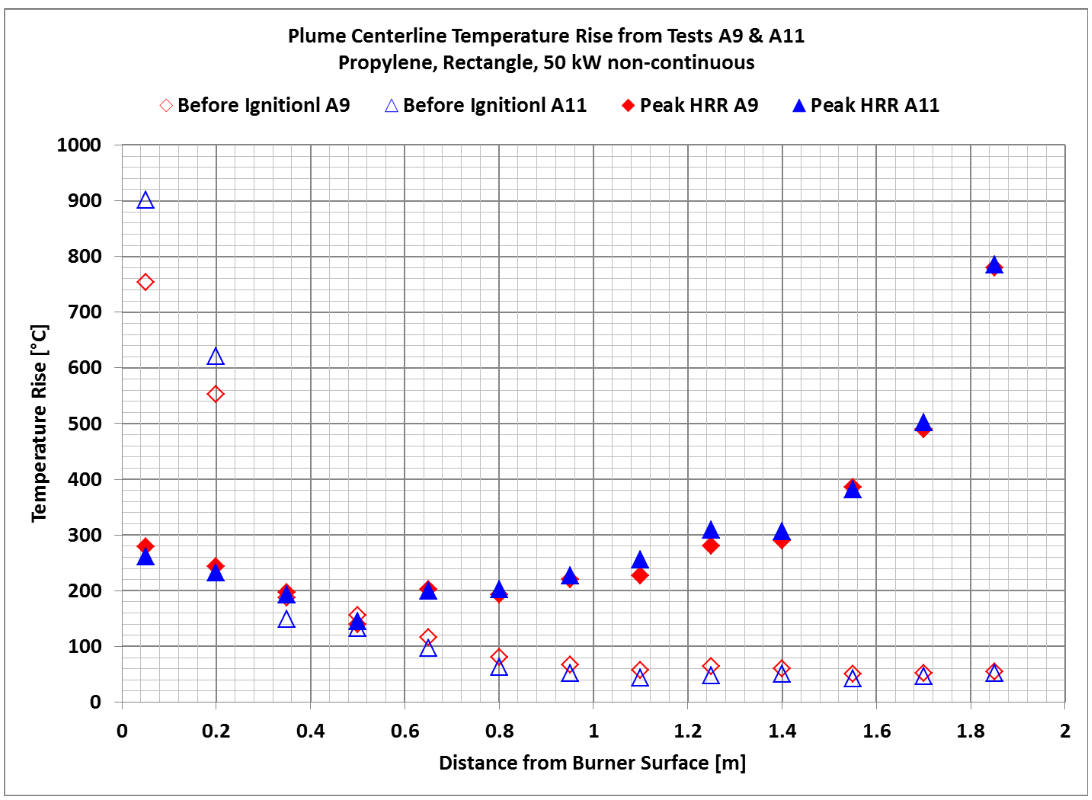

Figure 129 - Centerline Temperature of Tests A9 and A11

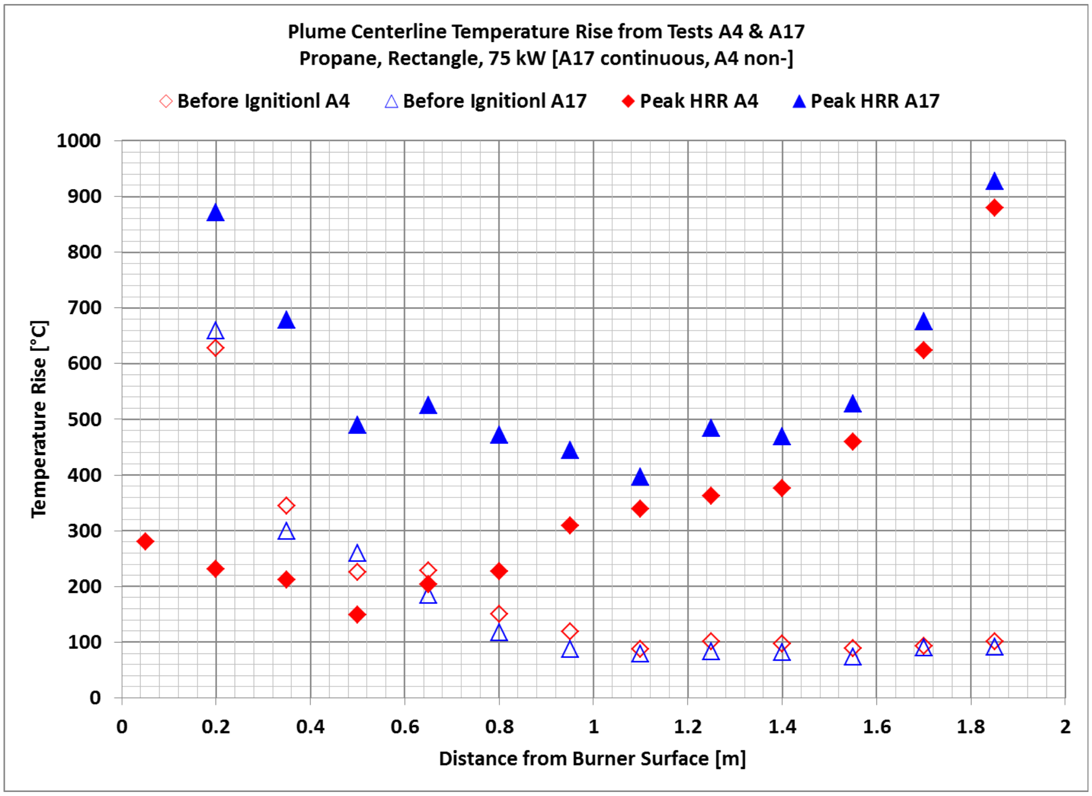

Figure 130 - Centerline Temperature of Tests A4 and A17

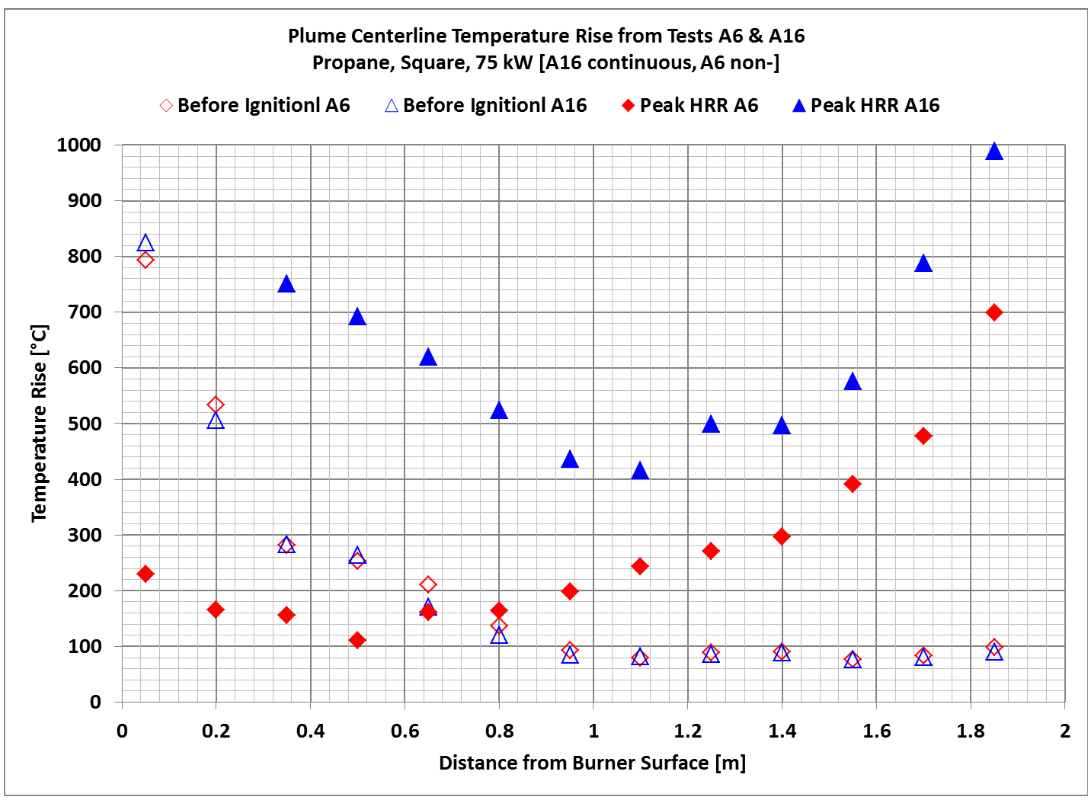

Figure 131 - Centerline Temperature of Tests A6 and A16

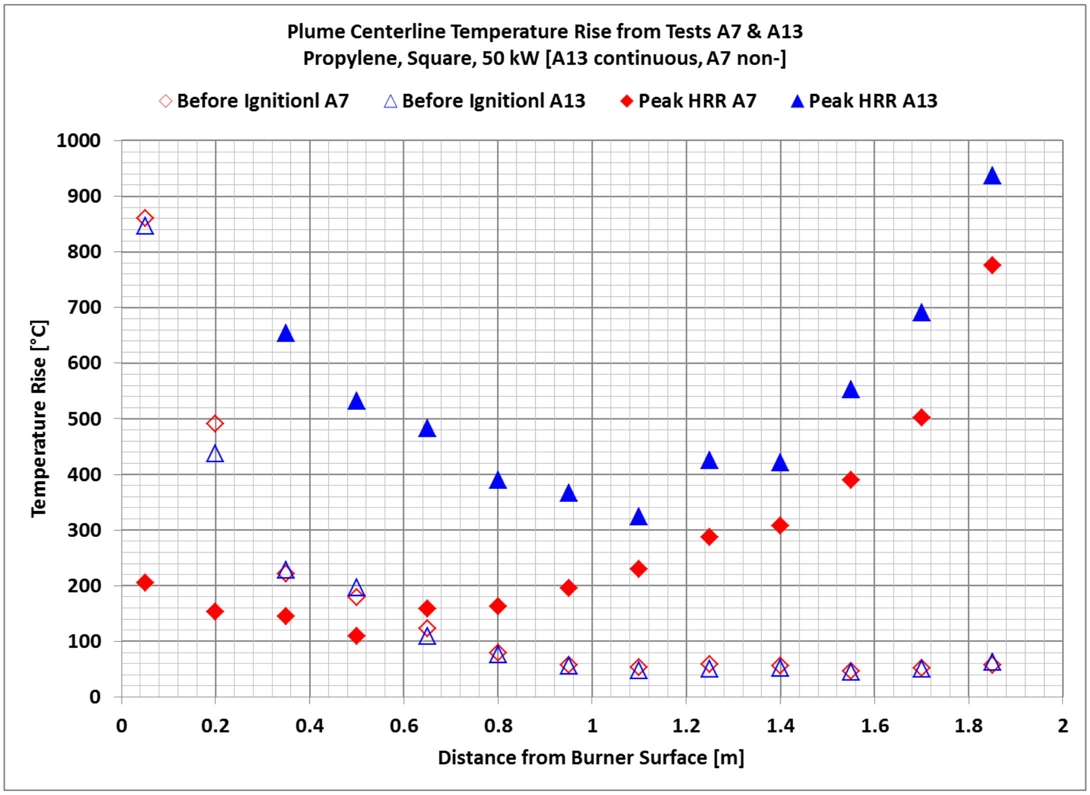

Figure 132 - Centerline Temperature of Tests A7 and A13

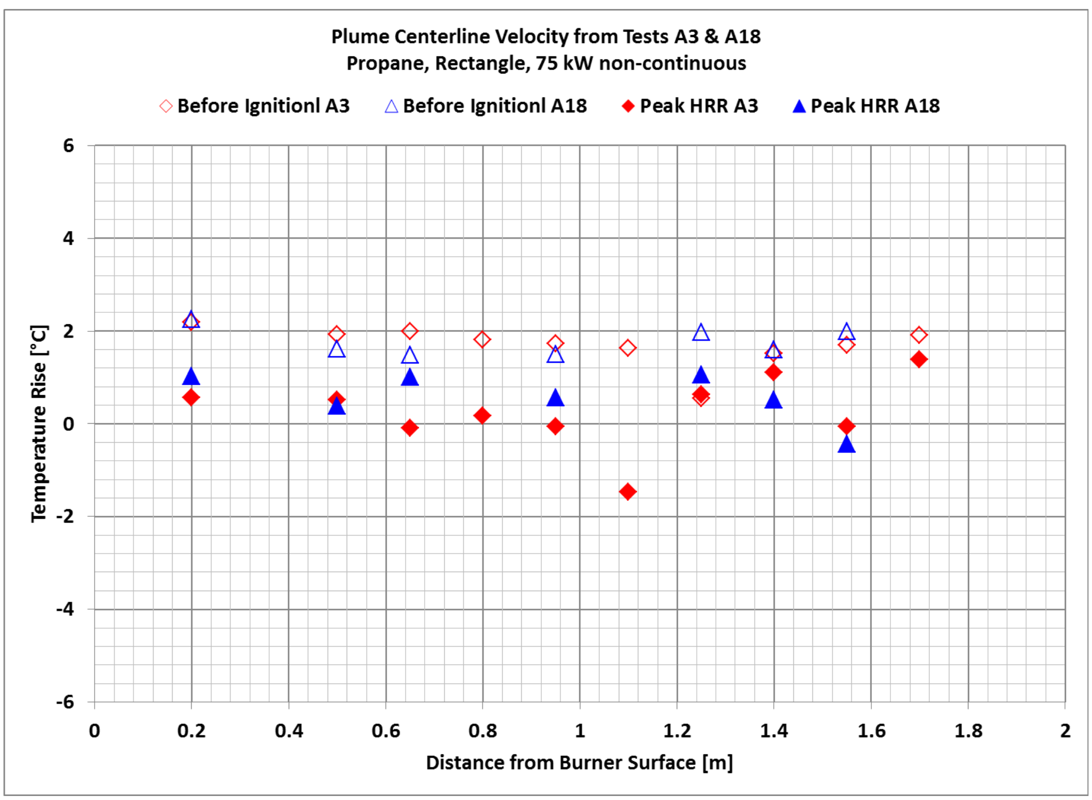

Figure 133 - Centerline Velocity of Tests A3 and A18

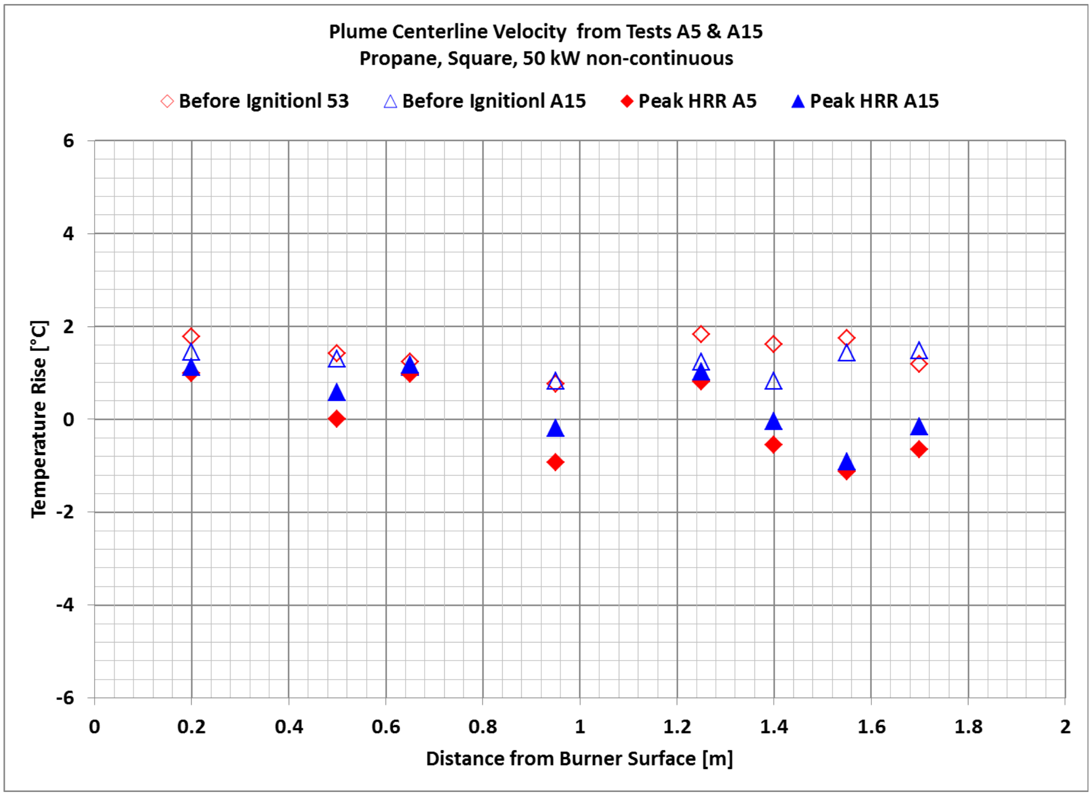

Figure 134 - Centerline Velocity of Tests A5 and A15

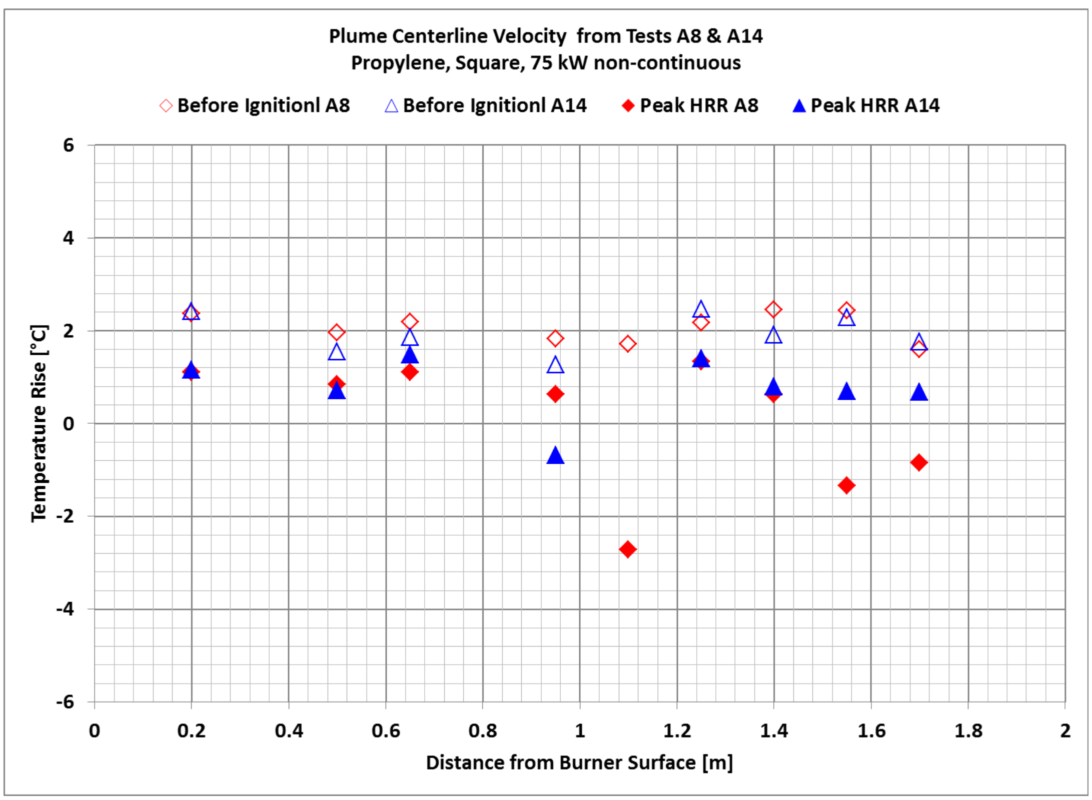

Figure 135 - Centerline Velocity of Tests A8 and A14

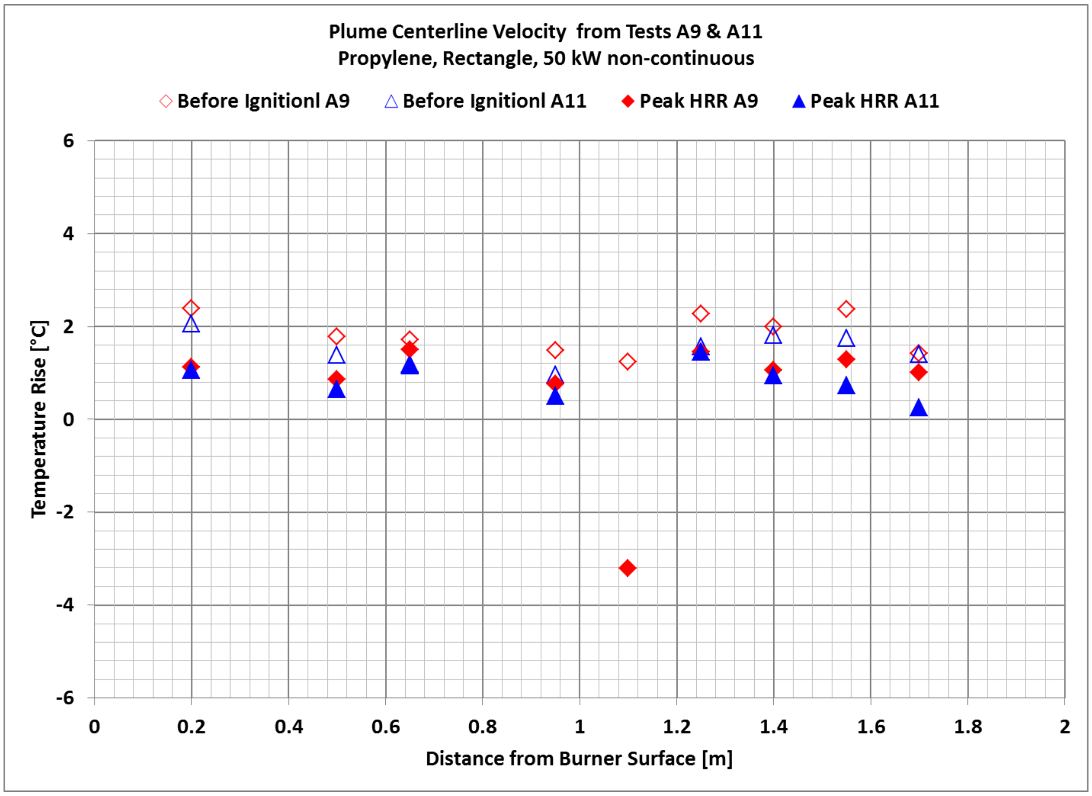

Figure 136 - Centerline Velocity of Tests A9 and A11

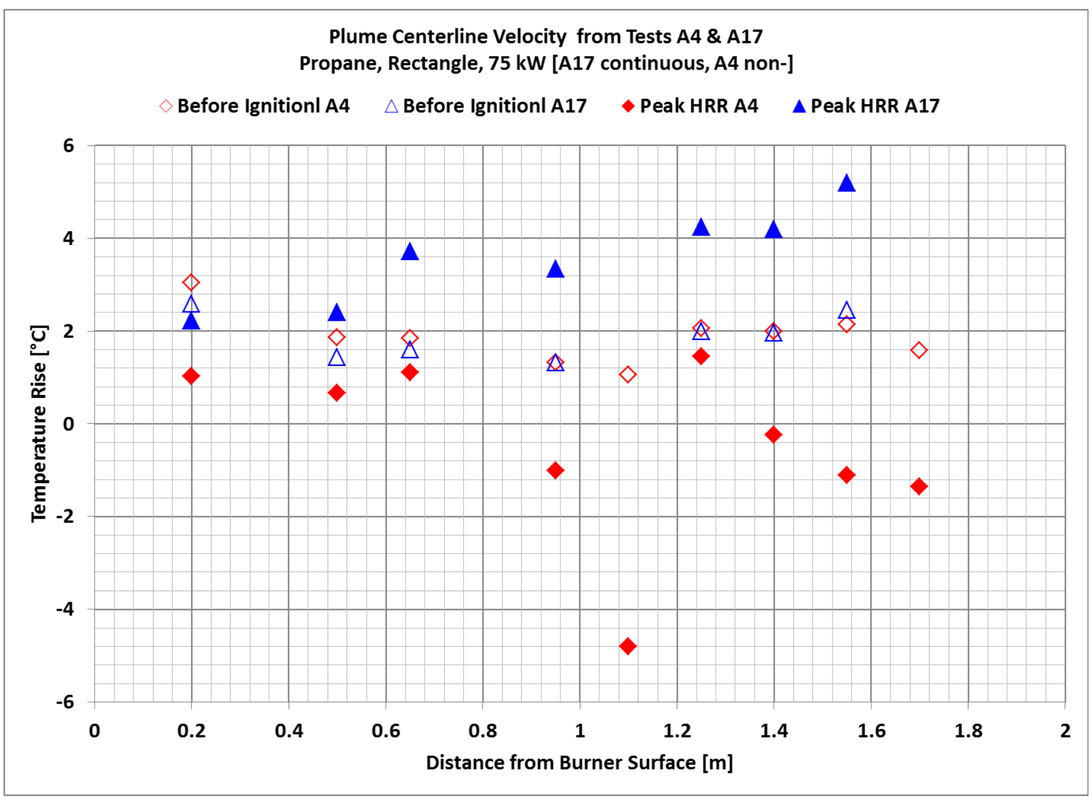

Figure 137 - Centerline Velocity of Tests A4 and A17

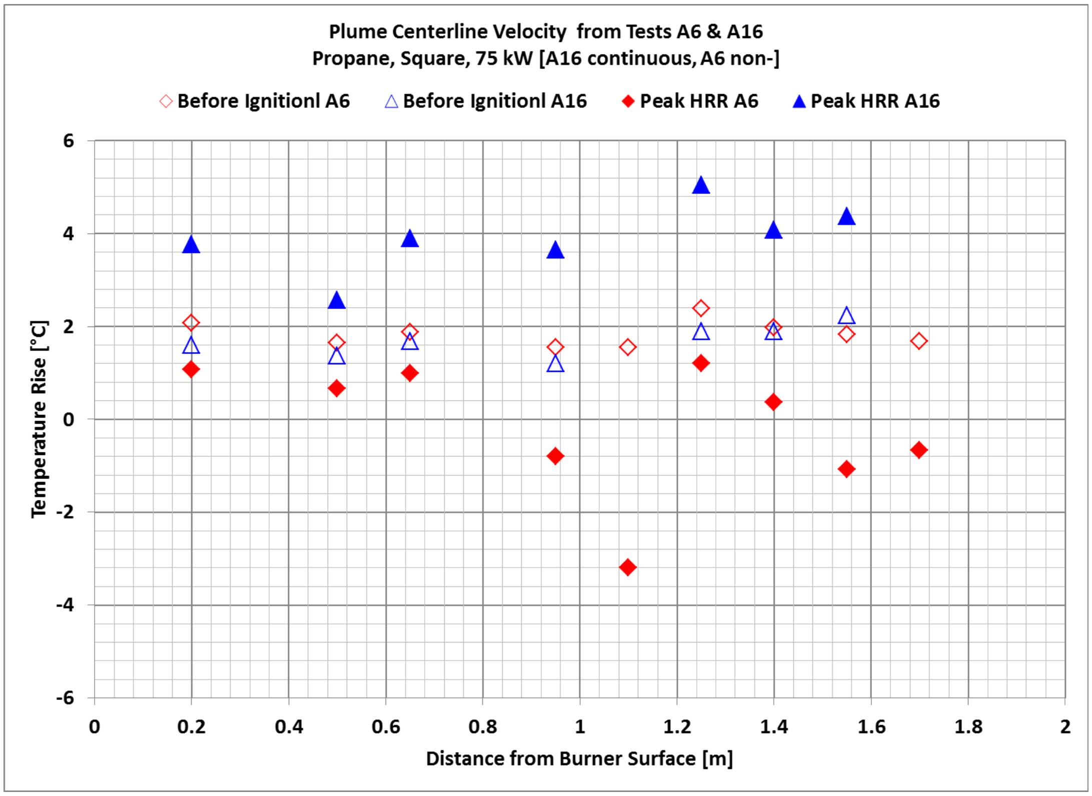

Figure 138 - Centerline Velocity of Tests A6 and A16

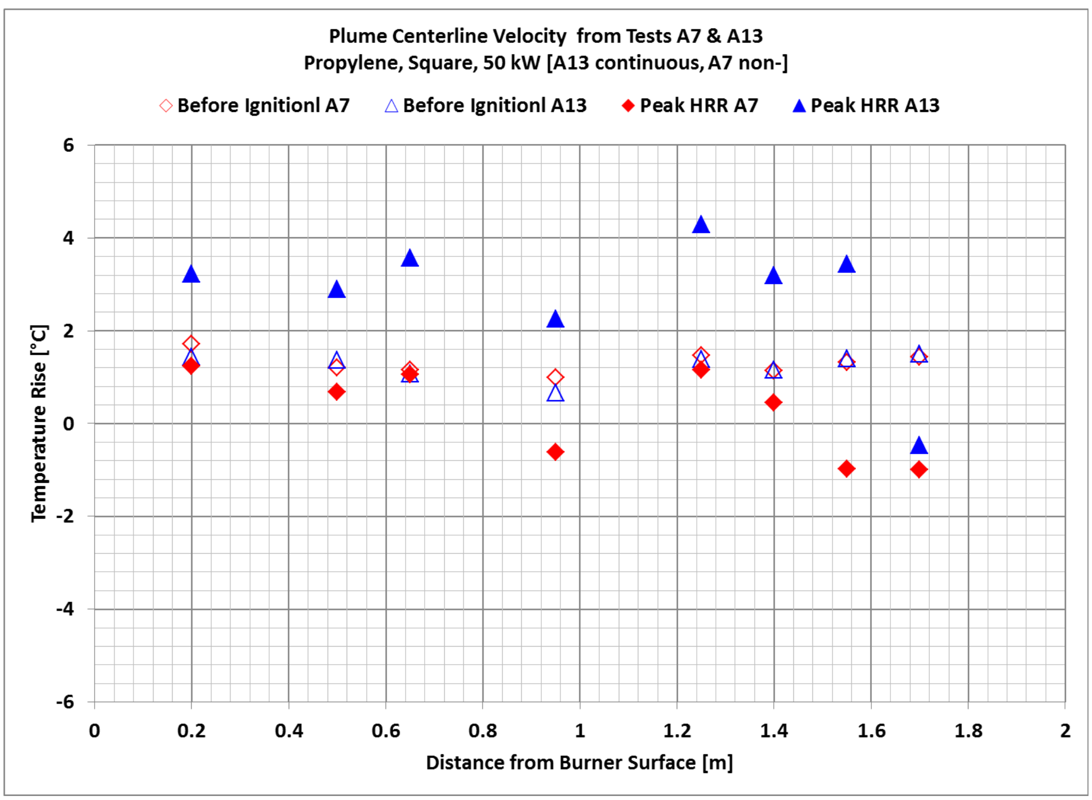

Figure 139 - Centerline Velocity of Tests A7 and A13

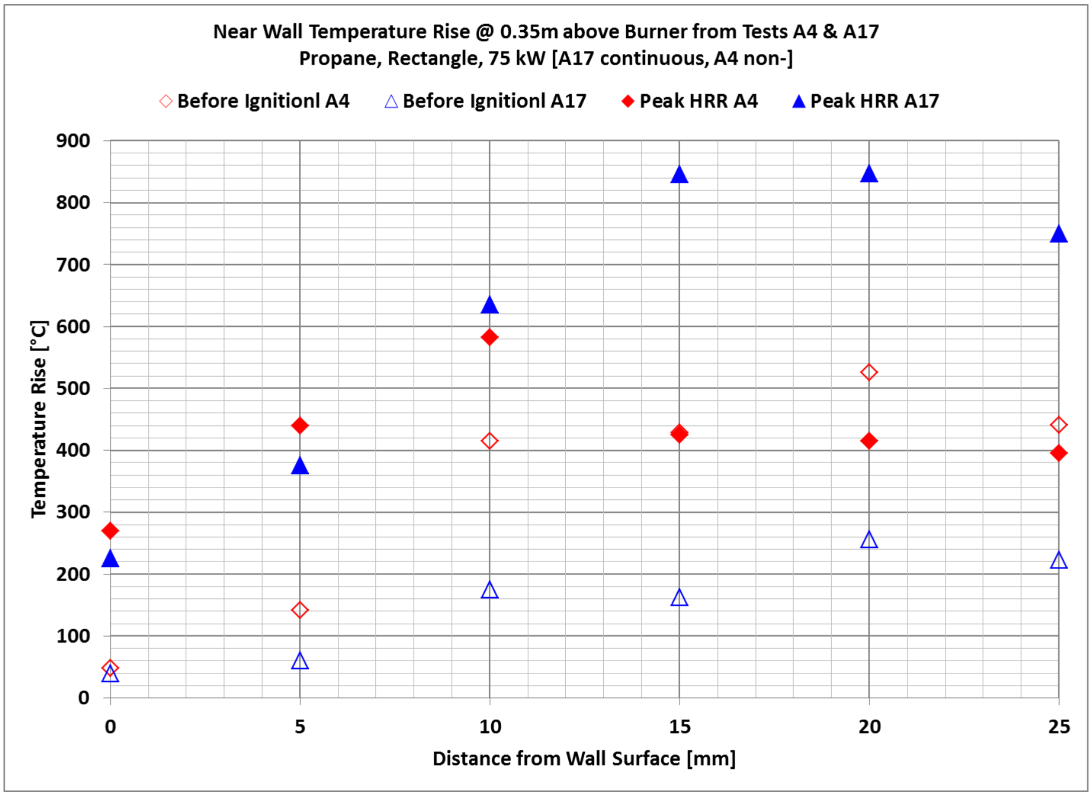

Figure 140 - Near-wall Temperature 0.35 m from Burner Surface in Tests A4 & A17

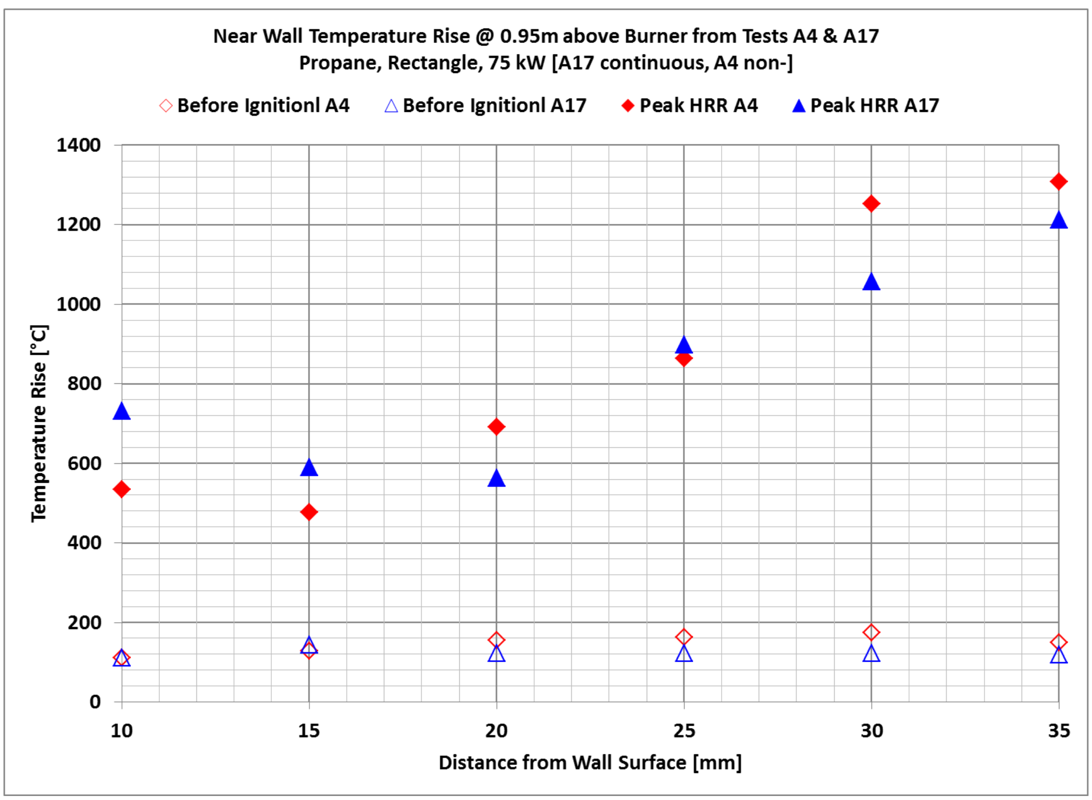

Figure 141 - Near-wall Temperature 0.95 m from Burner Surface in Tests A4 & A17

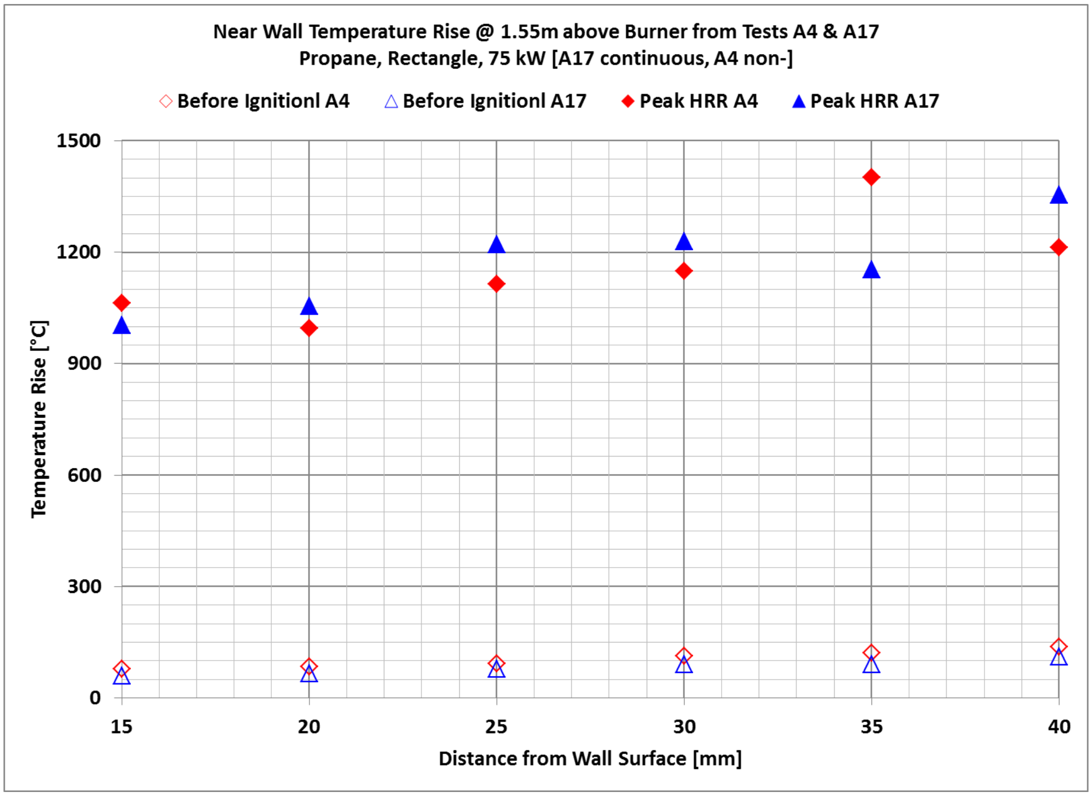

Figure 142 - Near-wall Temperature 1.55 m from Burner Surface in Tests A4 & A17

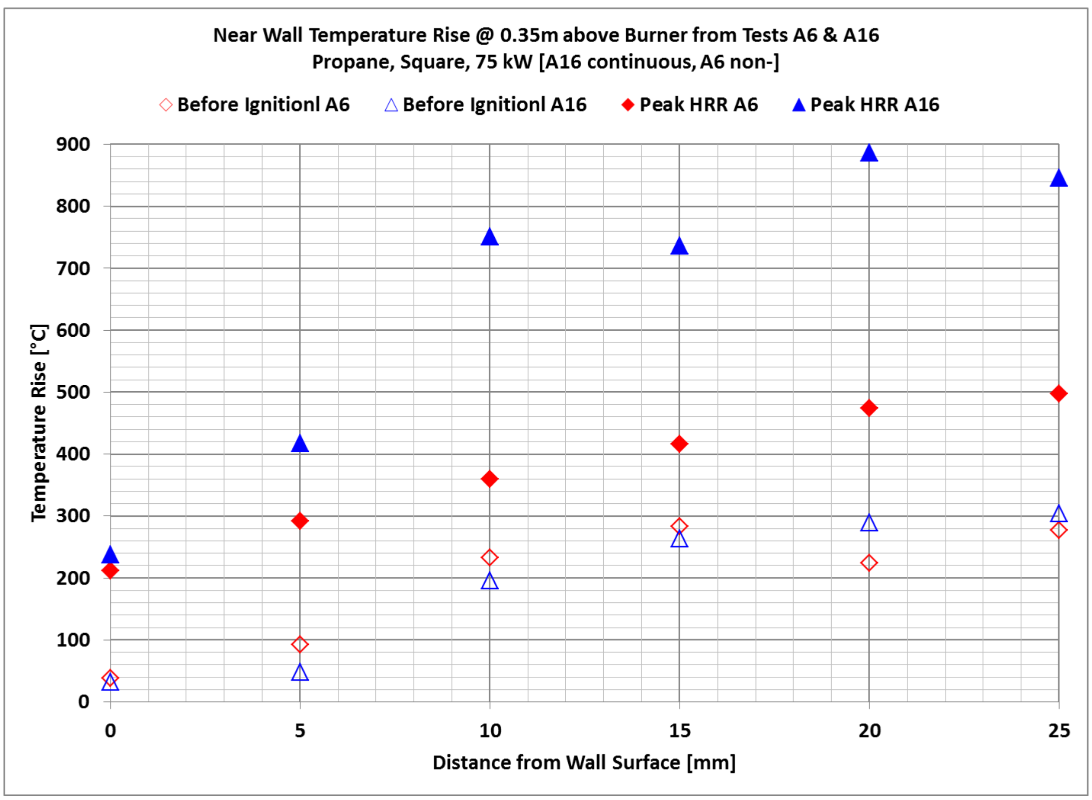

Figure 143 - Near-wall Temperature 0.35 m from Burner Surface in Tests A6 & A16

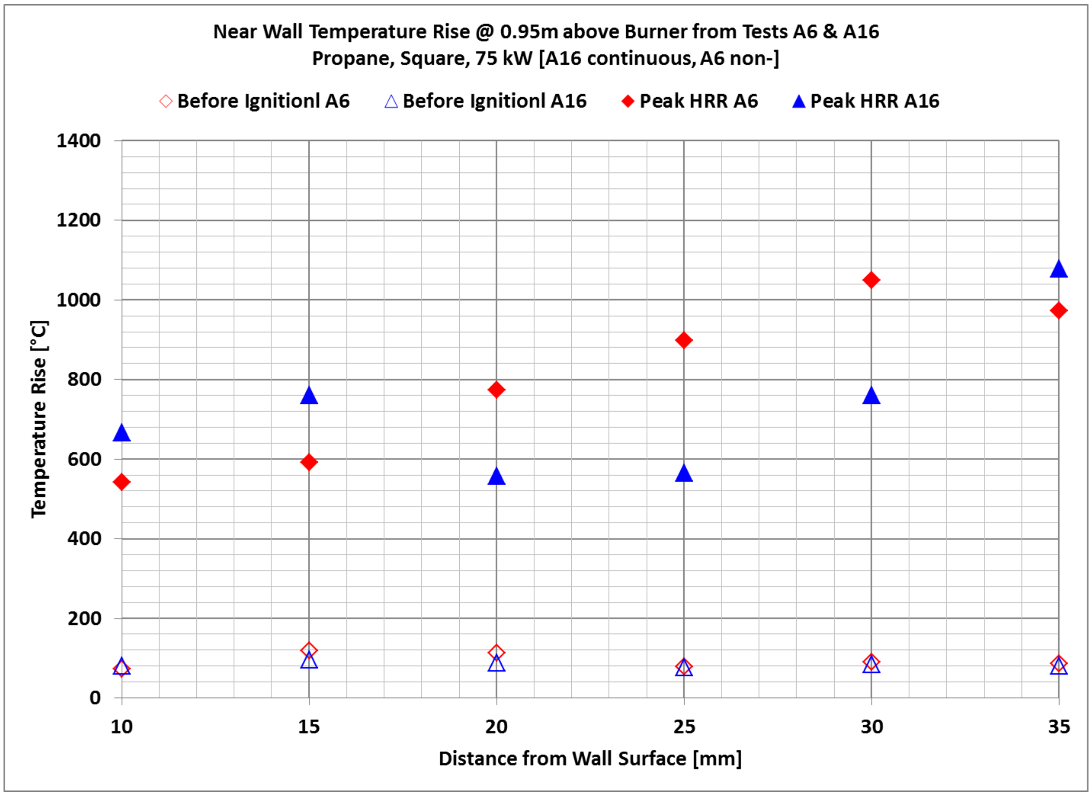

Figure 144 - Near-wall Temperature 0.95 m from Burner Surface in Tests A6 & A16

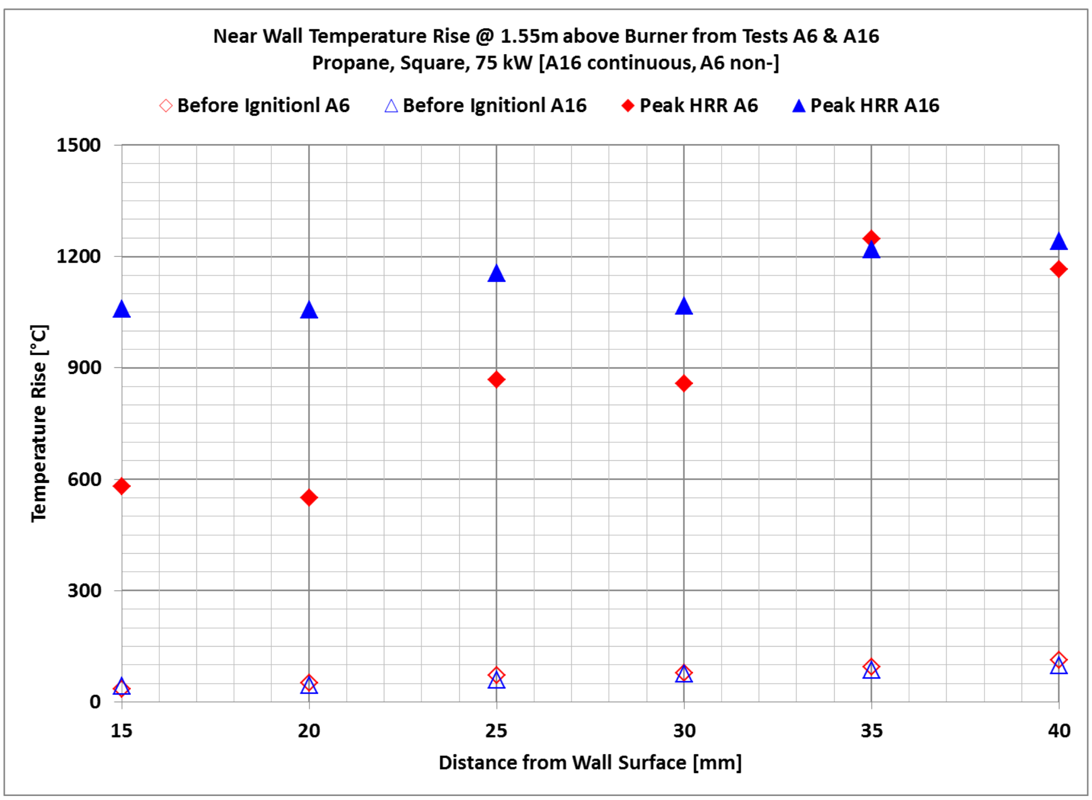

Figure 145 - Near-wall Temperature 1.55 m from Burner Surface in Tests A6 & A16

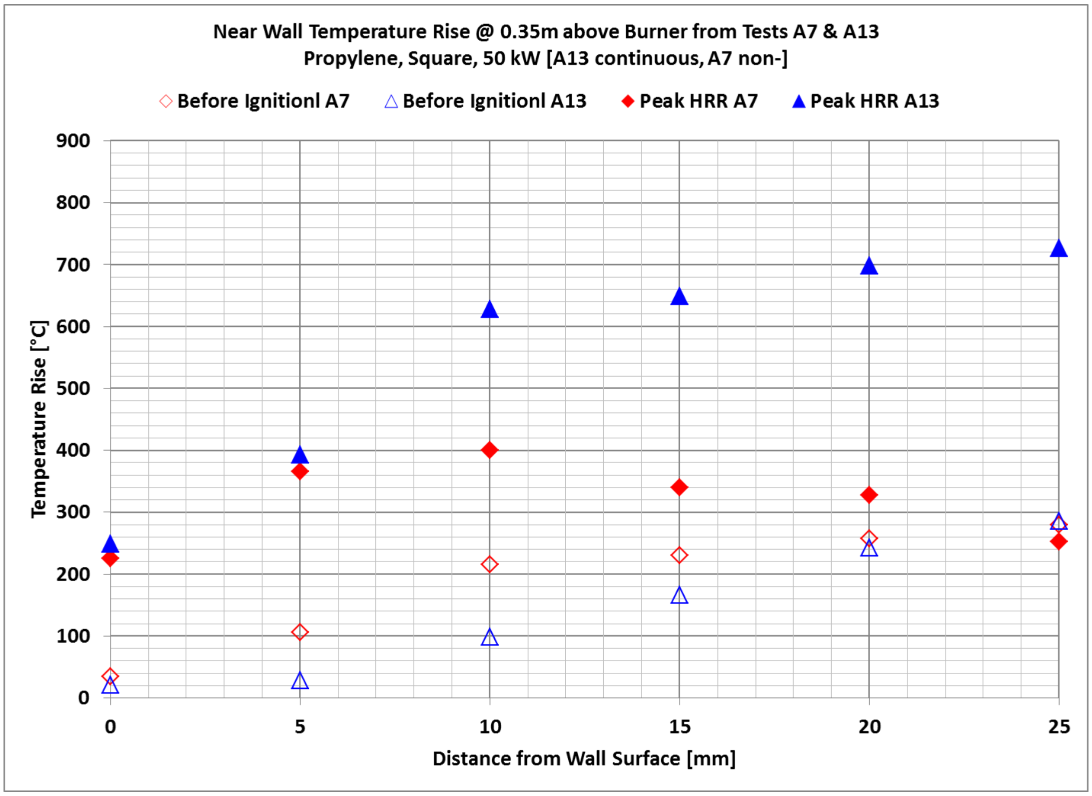

Figure 146 - Near-wall Temperature 0.35 m from Burner Surface in Tests A7 & A13

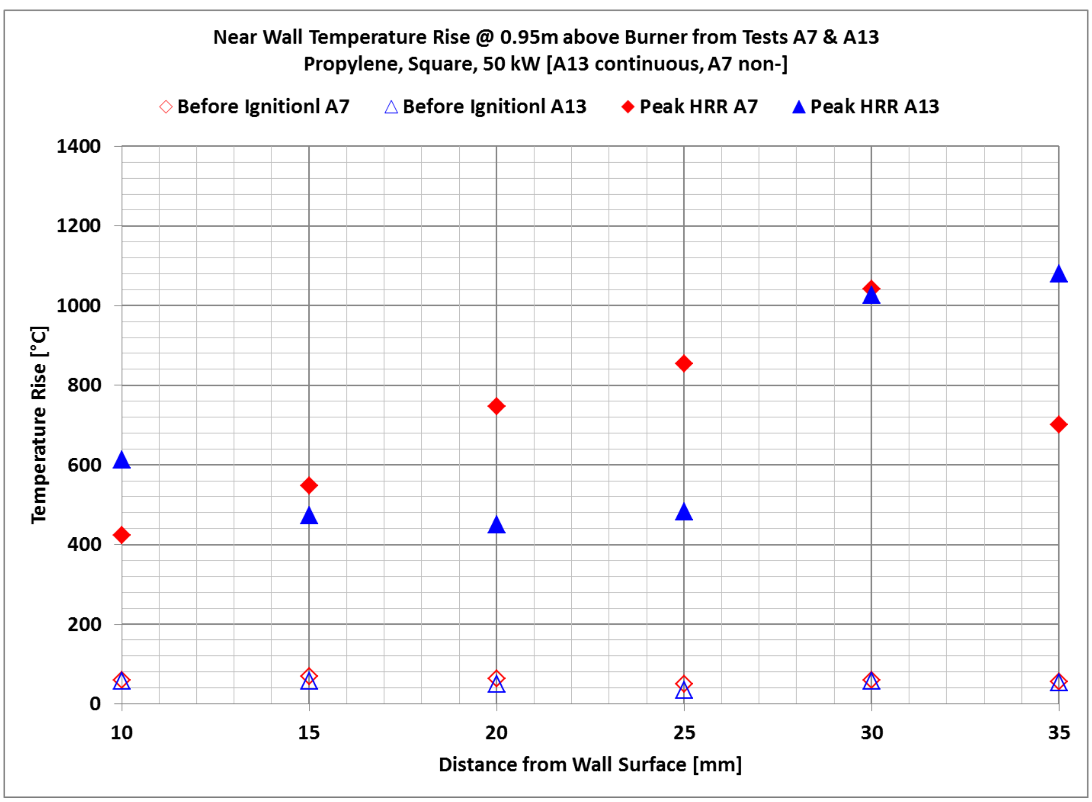

Figure 147 - Near-wall Temperature 0.95 m from Burner Surface in Tests A7 & A13

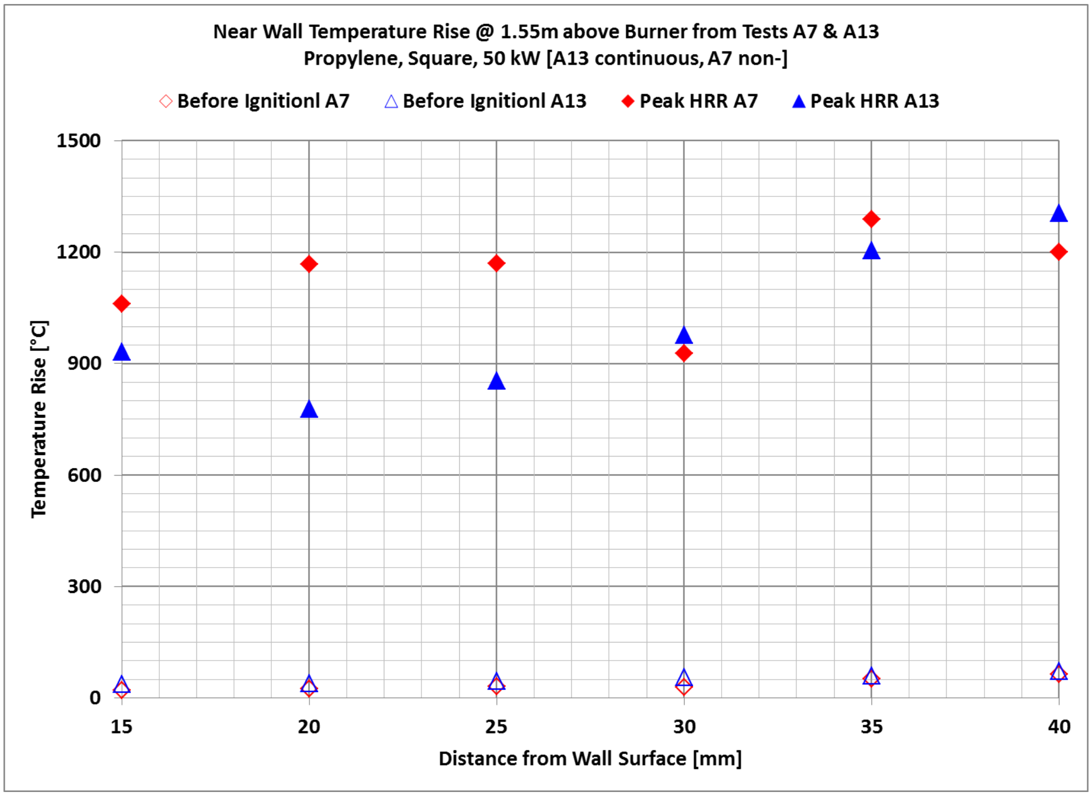

Figure 148 - Near-wall Temperature 1.55 m from Burner Surface in Tests A7 & A13

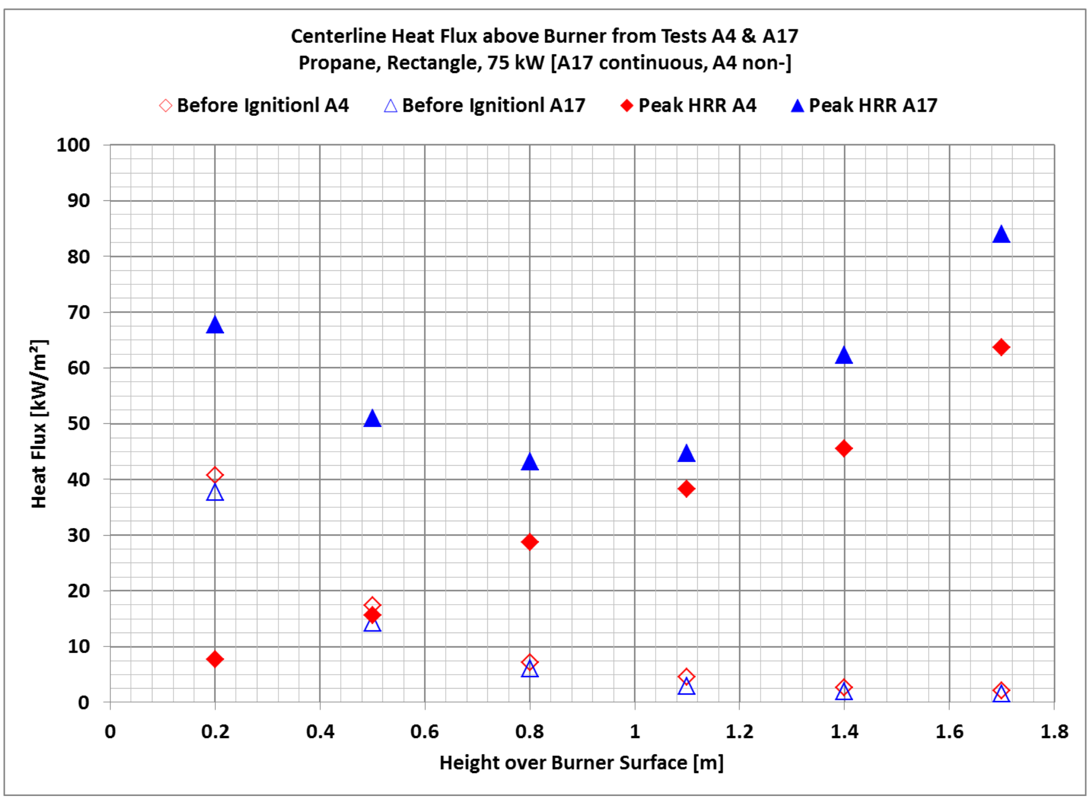

Figure 149 - Centerline Heat Flux of Tests A4 and A17

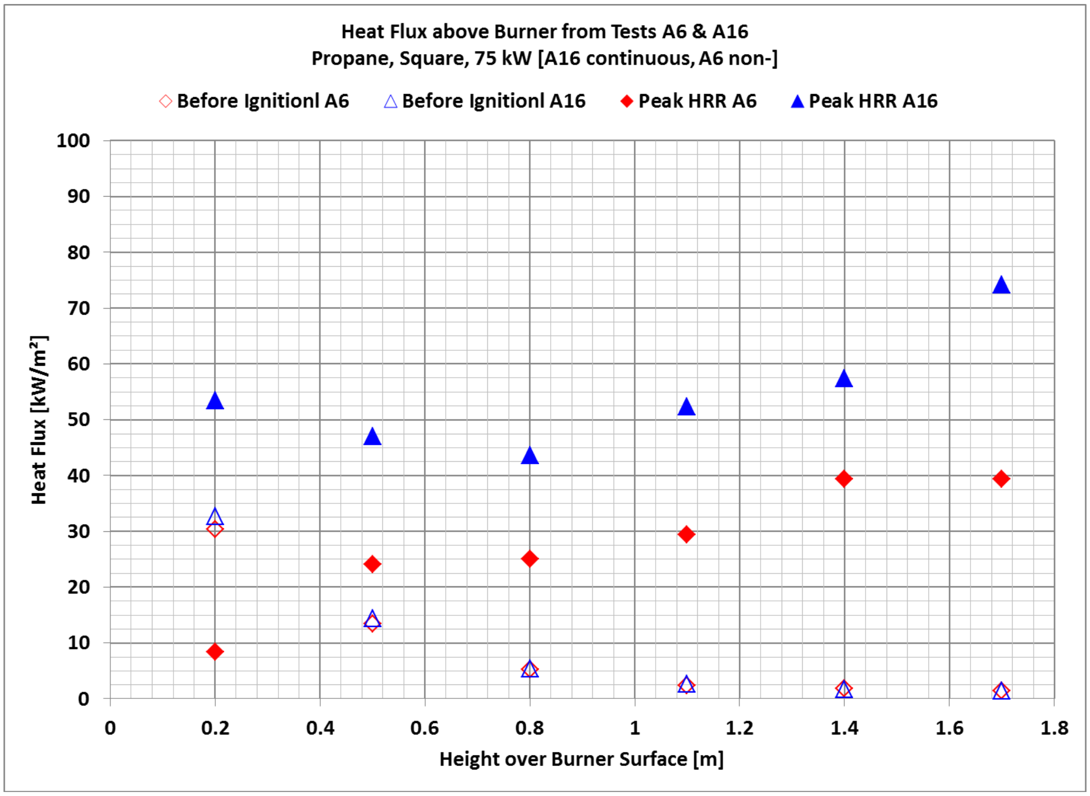

Figure 150 - Centerline Heat Flux of Tests A6 and A16

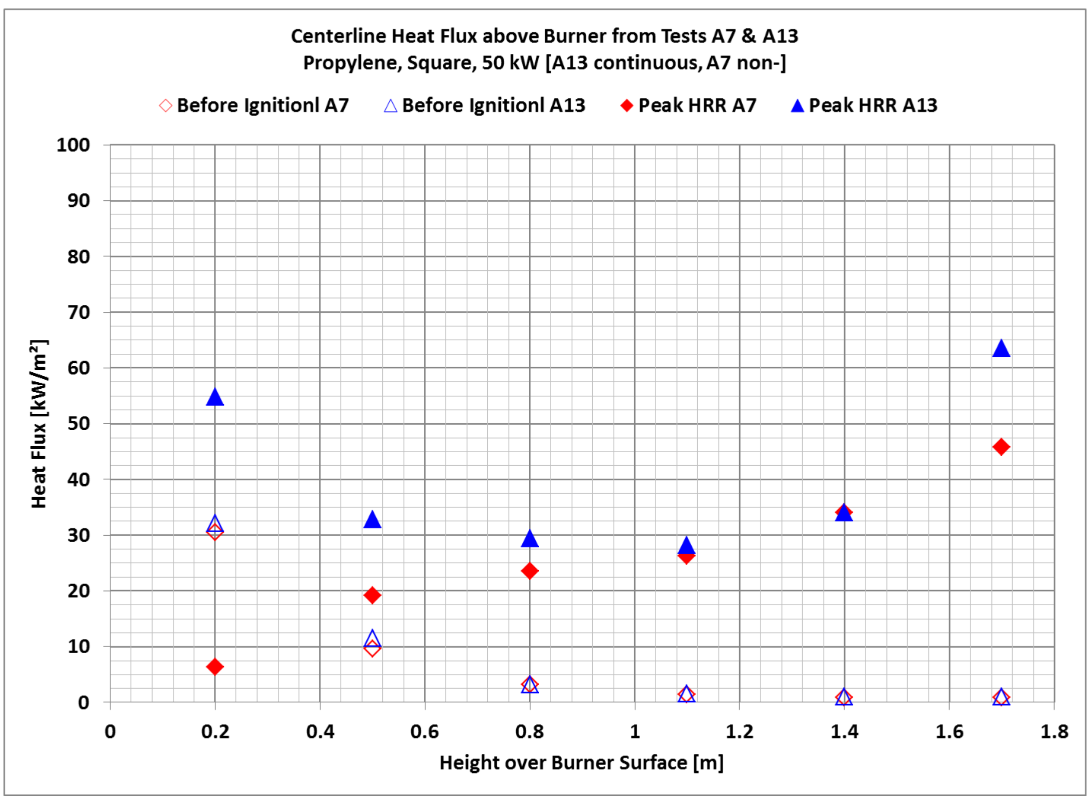

Figure 151 - Centerline Heat Flux of Tests A7 and A13

The characteristics of the combustible wall fires are summarized in Table 33, and the characteristics of the test specimen are presented in Table 34.

Table 33 - Combustible wall test fire characteristics

Combustible Wall Test	Time at Crackling Noise [sec]	Time at Panel Ignition [sec]	Time at Burner Shutoff [sec]	HRR at Burner Shutoff [kW]	Initial Burn Area at Source Shutoff [m x m]	Time at Peak HRR [sec]	Peak HRR [kW]	End Test Time [sec]
A3	46	65	91	40	0.4 x 0.6 / Triangular	233	255	3215
A4	26	55	105	92	0.4 x 1.5 / Rectangular	181	370	2120
A5	34	65	88	41	0.2 x 0.8 / Rectangular	234	250	1685
A6	25	43	74	67	0.2 x 0.8 / Rectangular	168	275	1390
A7	18	33	55	50	0.2 x 1.3 / Rectangular	190 - 204	290	1845
A8	15	23	50	80	0.2 x 1.3 / Rectangular	120	315	1195
A9	26	28	58	57	0.4 x 0.6 / Triangular	167	300	1488
A10	13	35	45	75	0.4 x 1.0 / Triangular	132	380	1225
A11	26	38	58	60	0.2 x 0.4 / Triangular	162	320	1288
A12	25	34	879	N/A	N/A	119	540	1092
A13	15	40	680	N/A	N/A	121	530	710
A14	11	26	56	45	0.2 x 0.8 / Rectangular	155	290	1131
A15	30	53	75	42	0.2 x 0.8 / Rectangular	205	260	1105
A16	25	40	1360	N/A	N/A	131	565	1380
A17	28	38	807	N/A	N/A	113	615	942
A18	38	55	72	41	0.4 x 0.8 / Rectangular	196 - 210	250	1055

*All "TIME AT" data were measured from the time the burner starts to output the target HRR, which is about 15 seconds after burner ignition
**”Time at Panel Ignition” is determined when the panel shows flame attachments

Table 34 presents the combustible wall test specimens' pre-burn and post-burn characteristic.

Table 34 - Combustible wall test specimen characteristics

Combustible Wall Test	Specimen Initial Mass [kg]	Burnt Panel Mass (kg)	Burnt Panel Mass Ratio [%]	Unburned Panel mass (kg)	Unburned Panel Mass Ratio [%]	Total Mass Loss [kg]	Mass Loss Ratio [%]
A3	8.73	3.26	37.3	3.4	38.7	2.09	23.9
A4	8.70	3.26	37.5	3.2	37.2	2.20	25.3
A5	8.72	2.26	25.9	4.8	55.3	1.64	18.8
A6	8.32	2.54	30.5	3.9	47.4	1.84	22.1
A7	8.18	2.78	34.0	3.4	42.1	1.96	24.0
A8	8.10	2.6	32.1	3.6	44.0	1.94	24.0
A9	8.32	2.92	35.1	3.1	37.0	2.32	27.9
A10	8.30	3.1	37.3	2.7	32.8	2.48	29.9
A11	8.38	2.92	34.8	3.0	35.3	2.50	29.8
A12	8.12	3.58	44.1	1.5	18.2	3.06	37.7
A13	8.16	3.22	39.5	2.2	26.5	2.78	34.1
A14	8.50	2.46	28.9	4.0	47.1	2.04	24.0
A15	8.52	2.36	27.7	4.4	51.6	1.76	20.7
A16	8.66	4.04	46.7	1.4	15.7	3.26	37.6
A17	8.52	3.68	43.2	1.4	16.7	3.42	40.1
A18	8.14	2.44	30.0	3.7	45.7	1.98	24.3

*Burnt panel means the residual left behind by fire, which is mostly glass fiber

**Unburned panel is the part where the panel was not damaged by fire, which contains both polyester resin and glass fiber

N.5. FDS fire test simulation results

The fire tests conducted under the various configurations were replicated in a number of FDS simulations (see Section 3 for details) and comparisons were made between the experimental data and the FDS predicted results. Considerable discrepancies between the data and the simulated results have been observed, though it must be stressed that the objective of this area of research is to assess FDS's initial capabilities using default simulation parameters. In addition, series of simulations where a FDS parameter is changed one at a time were executed in order to complete a parametric study where the effects of the FDS parameters are examined in details (see Appendices K to M).

5.1 Free plume experiment and simulation comparisons

Comparisons of the plume centerline temperature and velocity are made between the FDS predictions and the actual data measured during the free plume fire tests conducted as part of the current research. Assuming that the conditions of the tests and the simulations are reaches steady state, the data and the predictions are both time-averaged over the period where source fire was at a relatively consistent HRR.

Only the default series simulations (Series 1) were used in the comparison with the actual data. The other simulations where various FDS parameters were changed are used in the parametric study only.

5.1.1 Centerline temperature

Figure 152 and Figure 153 show the FDS-predicted corrected, time-averaged centerline plume temperature rise vs. the time-average measured temperature rise from the current experiments superimposed over McCaffrey's correlation, both with normalization of the height similar to McCaffrey's correlation using the convective HRR.

Although the trends between them are similar, FDS vastly under predicts the centerline plume temperature of the fires using the square source burner for the range of normalized height of 0 to 0.25 $m/kW^{2/5}$, and for the rectangle burner over the range of 0 to 0.1 $m/kW^{2/5}$. For the other locations, FDS's predictions are similar to the lower-bound values of the measured temperature. It is likely that the particular set of FDS parameters used in the default series of simulations and the relatively coarse grid size at 5 mm both contributed to the low predictions. Additionally, the FDS predictions for the various fire sizes and source fuel are collapsed into a very tight cluster, showing that that height normalization method is valid.

The corrected and uncorrected experimental centerline plume excess temperatures are compared to FDS's predictions are presented in Figure 154 to Figure 163, in these charts the height is not normalized. It can be shown that the FDS predictions fall below both the corrected and uncorrected experimental data for all cases. The predictions are closer to the uncorrected measurements, but the maximum difference ranges from 40°C far away from the burner surface to 500°C at 5 mm over the burner surface.

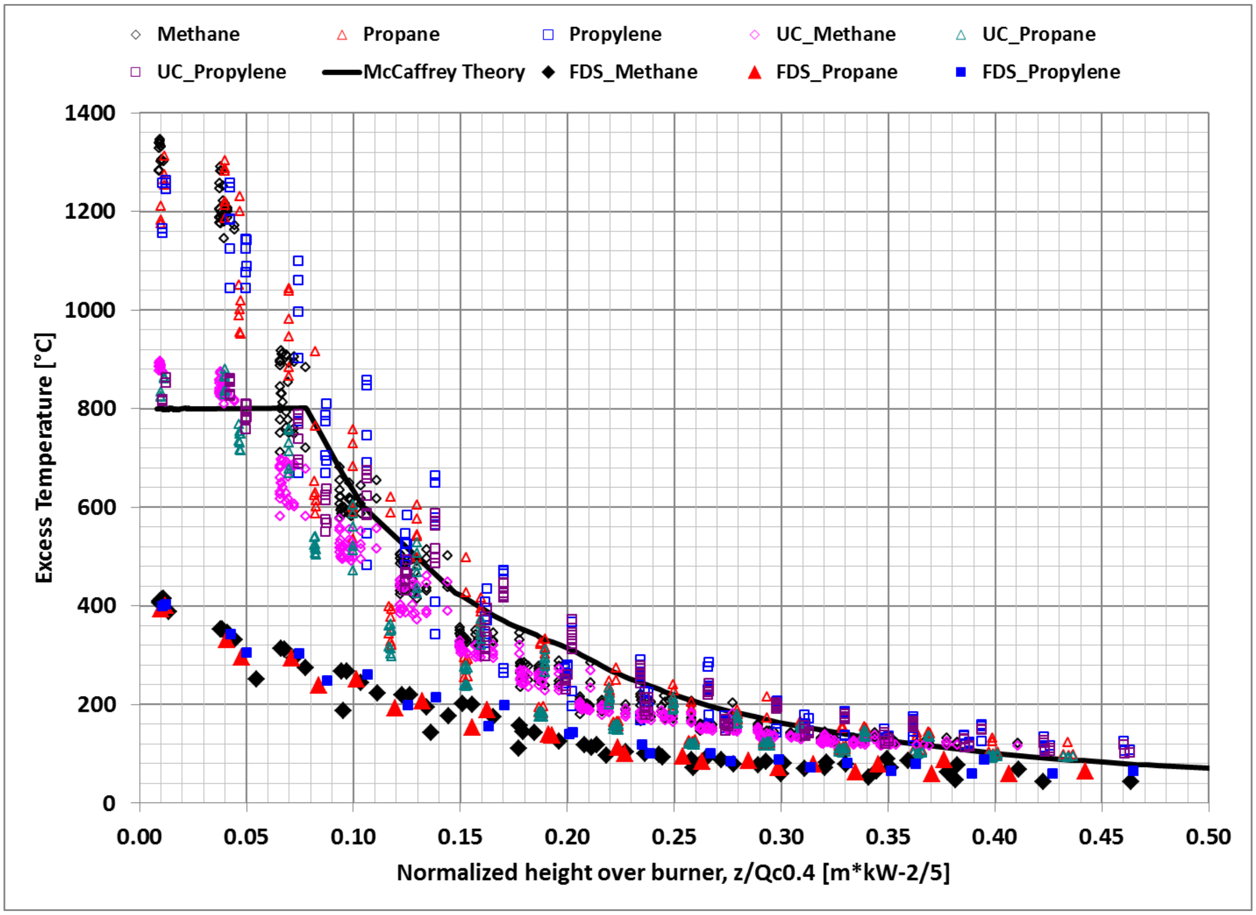

Figure 152 - Plume Centerline Temperature Rise Experimental vs. FDS data, Square Burner, with McCaffrey's Correlation

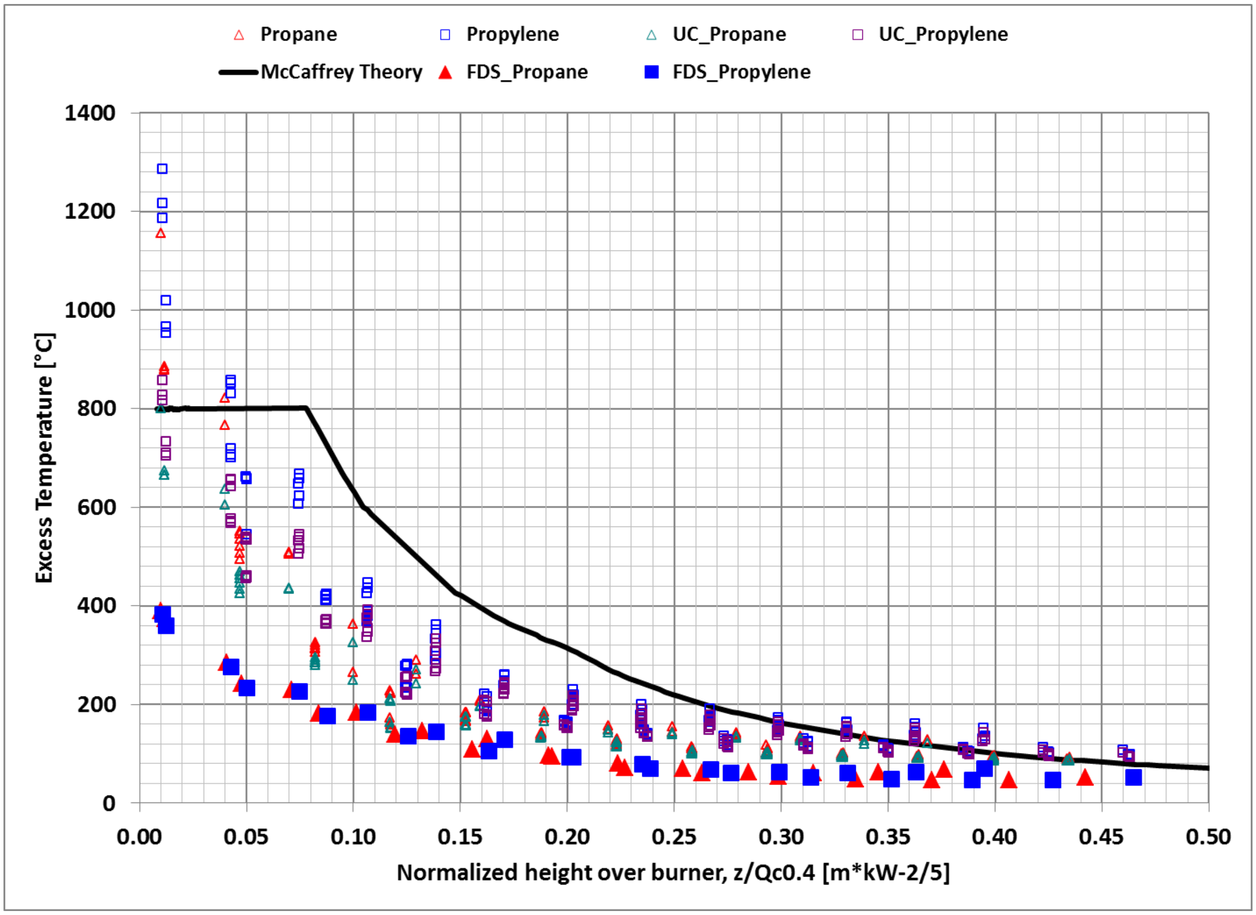

Figure 153 - Plume Centerline Temperature Rise Experimental vs. FDS data, Rectangle Burner, with McCaffrey's Correlation

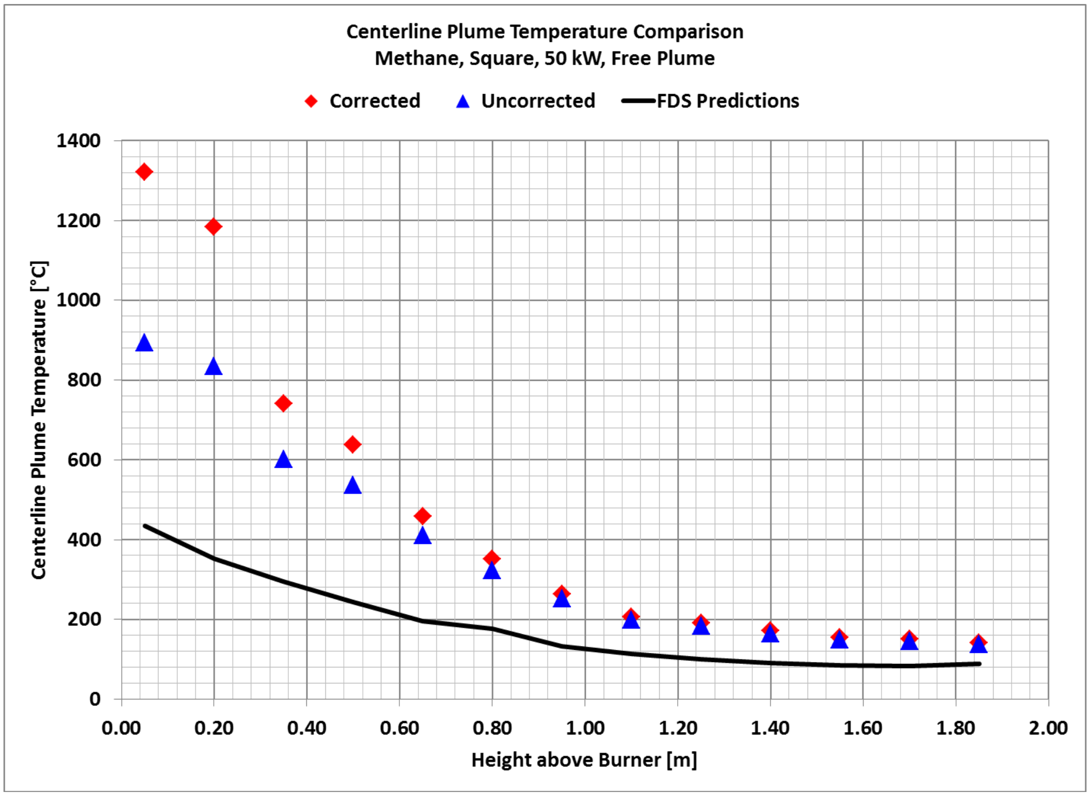

Figure 154 - Plume Temperature, Methane, Square, 50kW

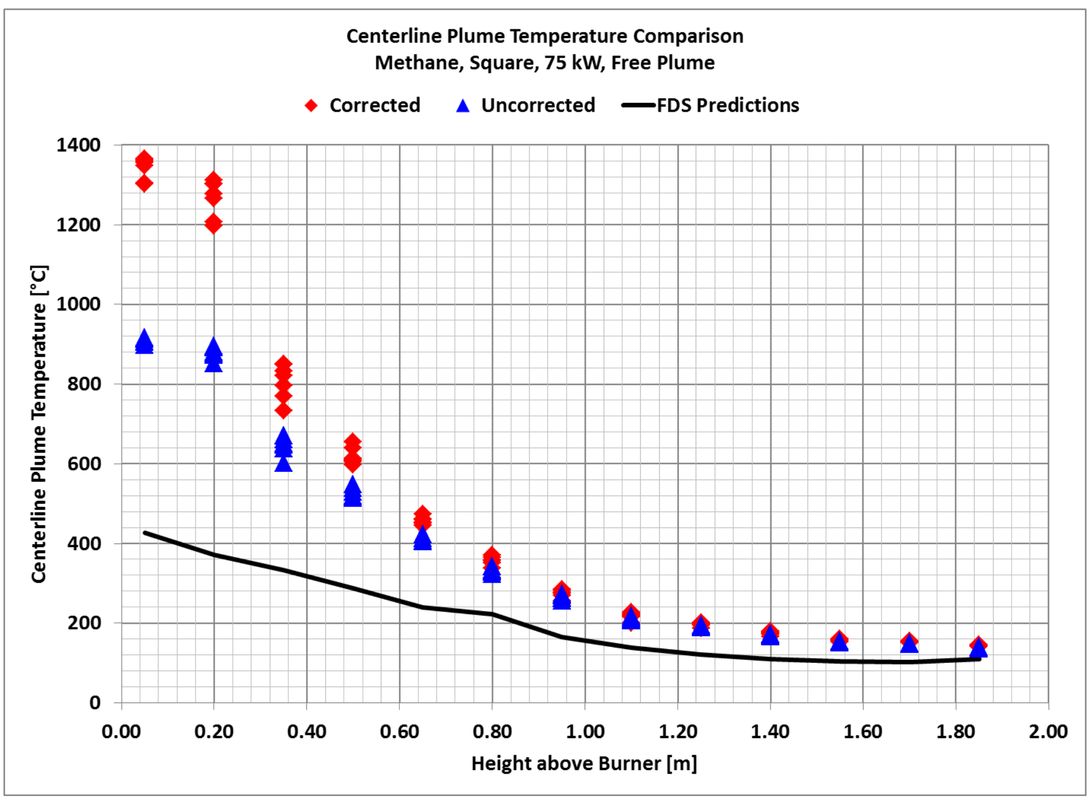

Figure 155 - Plume Temperature, Methane, Square, 75kW

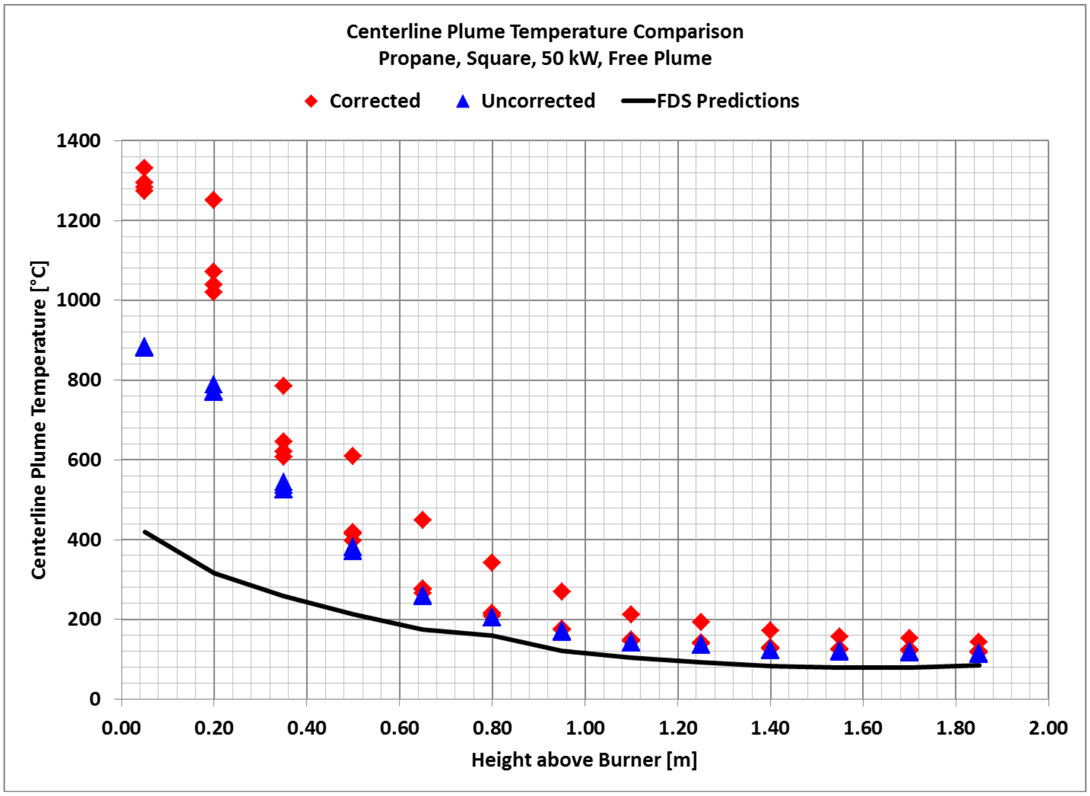

Figure 156 - Plume Temperature, Propane, Square, 50kW

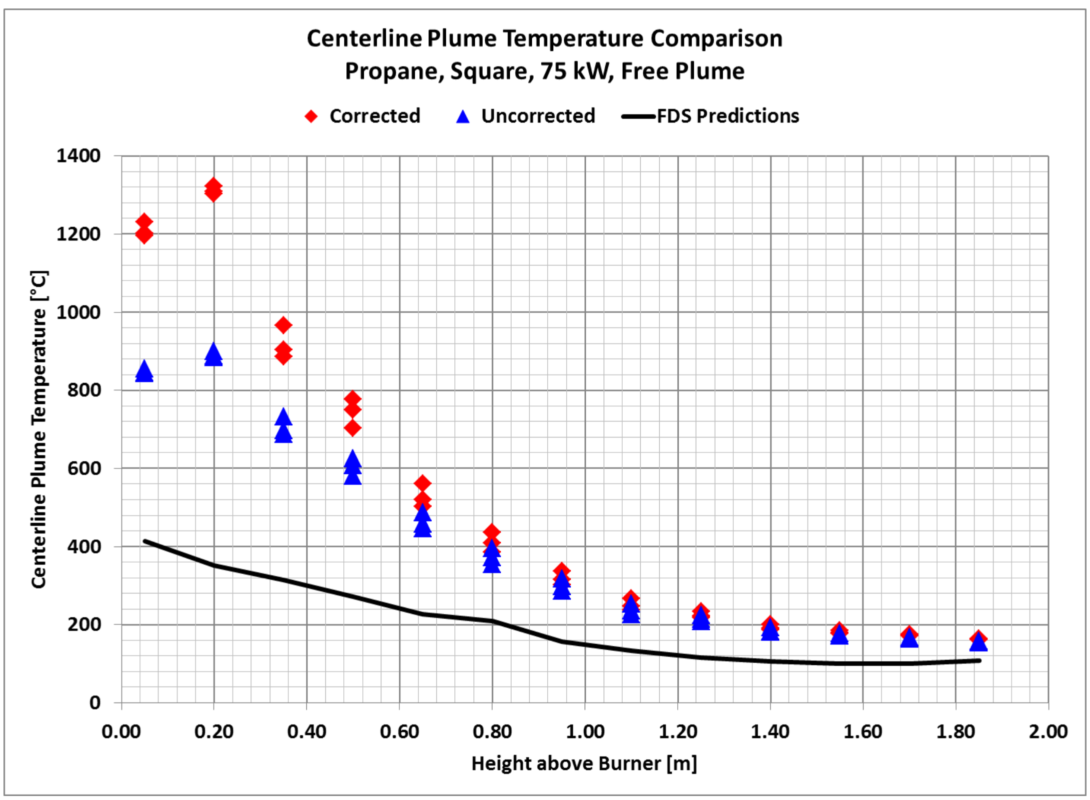

Figure 157 - Plume Temperature, Propane, Square, 75kW

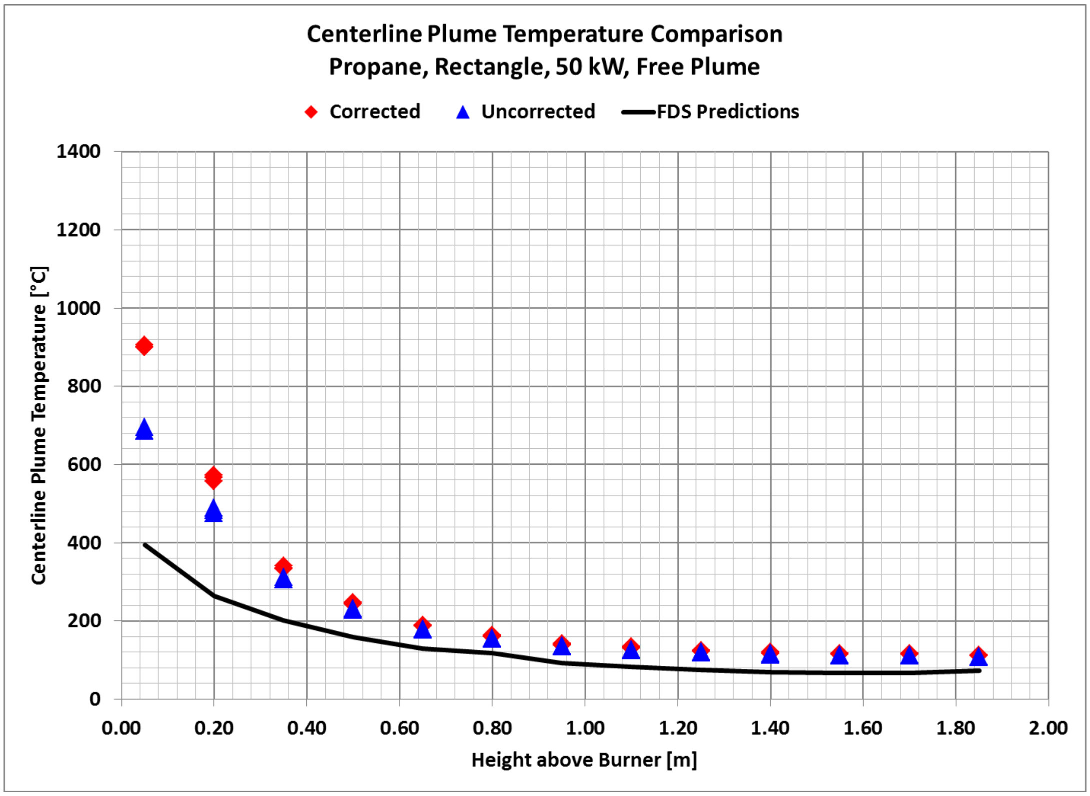

Figure 158 - Plume Temperature, Propane, Rectangle, 50kW

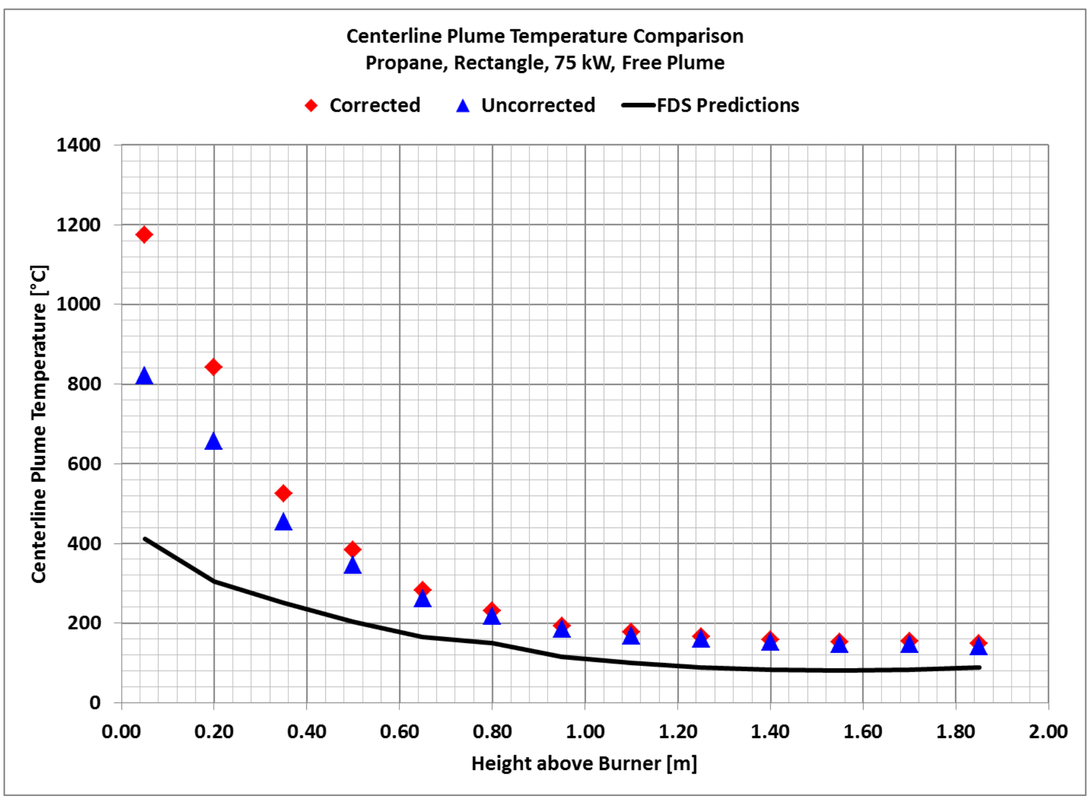

Figure 159 - Plume Temperature, Propane, Rectangle, 75kW

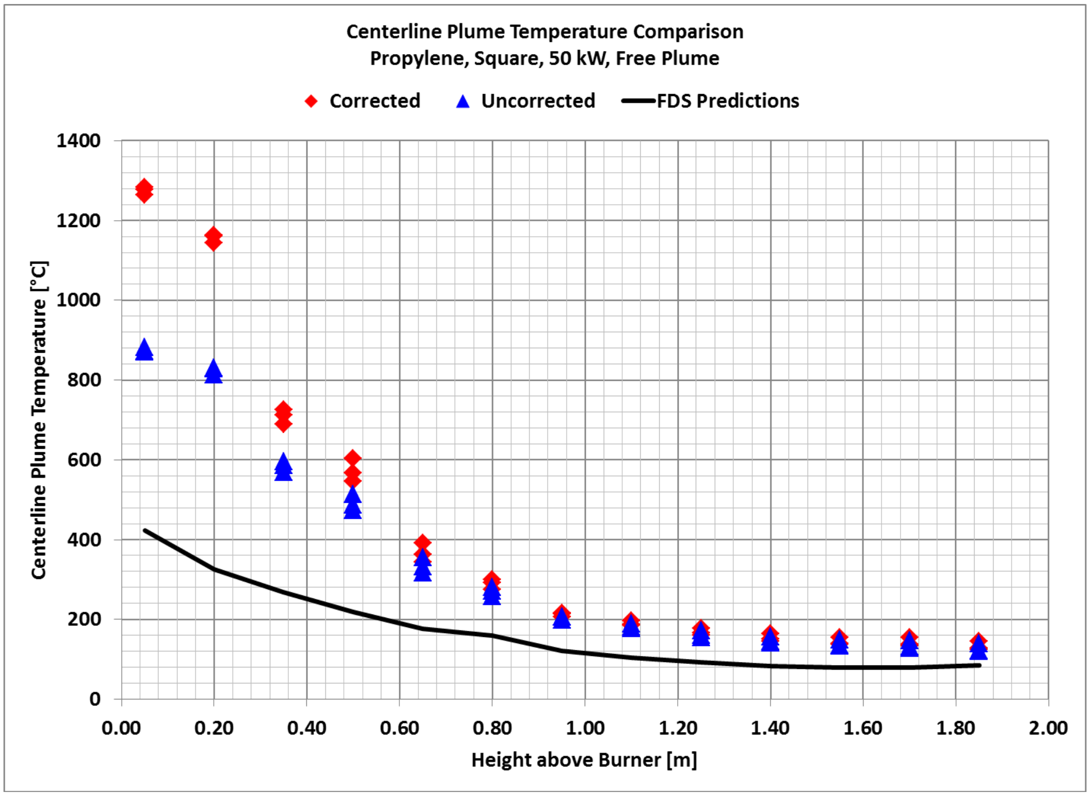

Figure 160 - Plume Temperature, Propylene, Square, 50kW

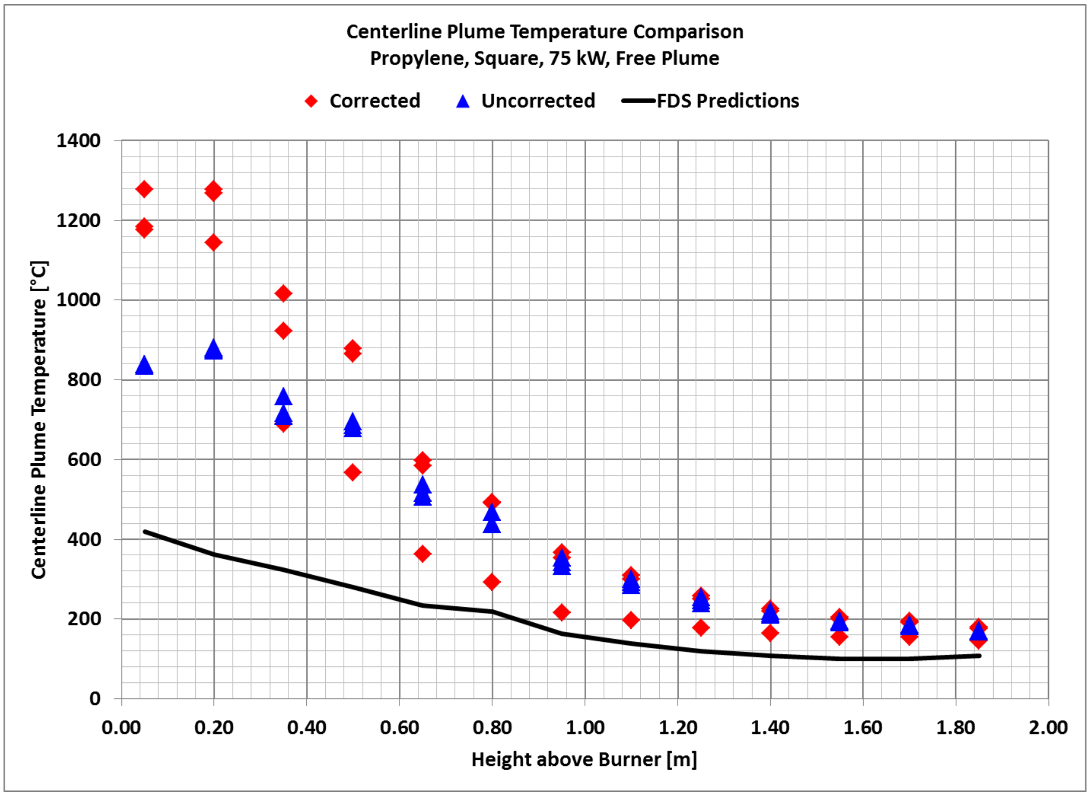

Figure 161 - Plume Temperature, Propylene, Square, 75kW

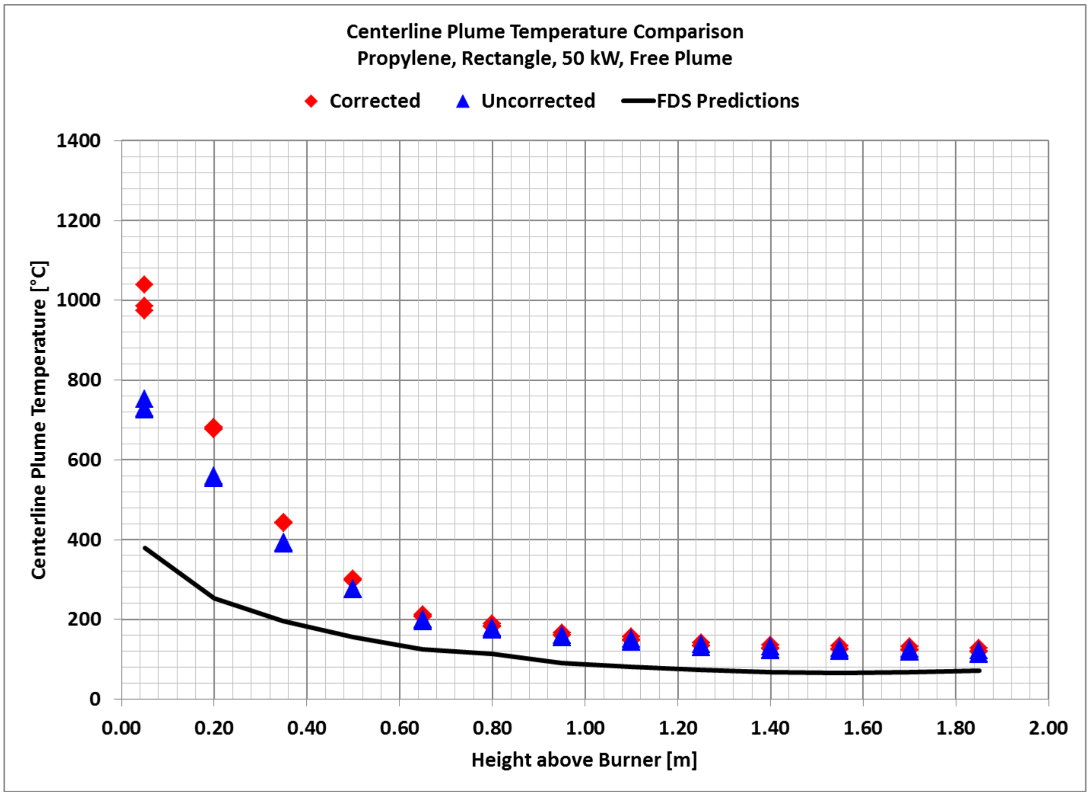

Figure 162 - Plume Temperature, Propylene, Rectangle, 50kW

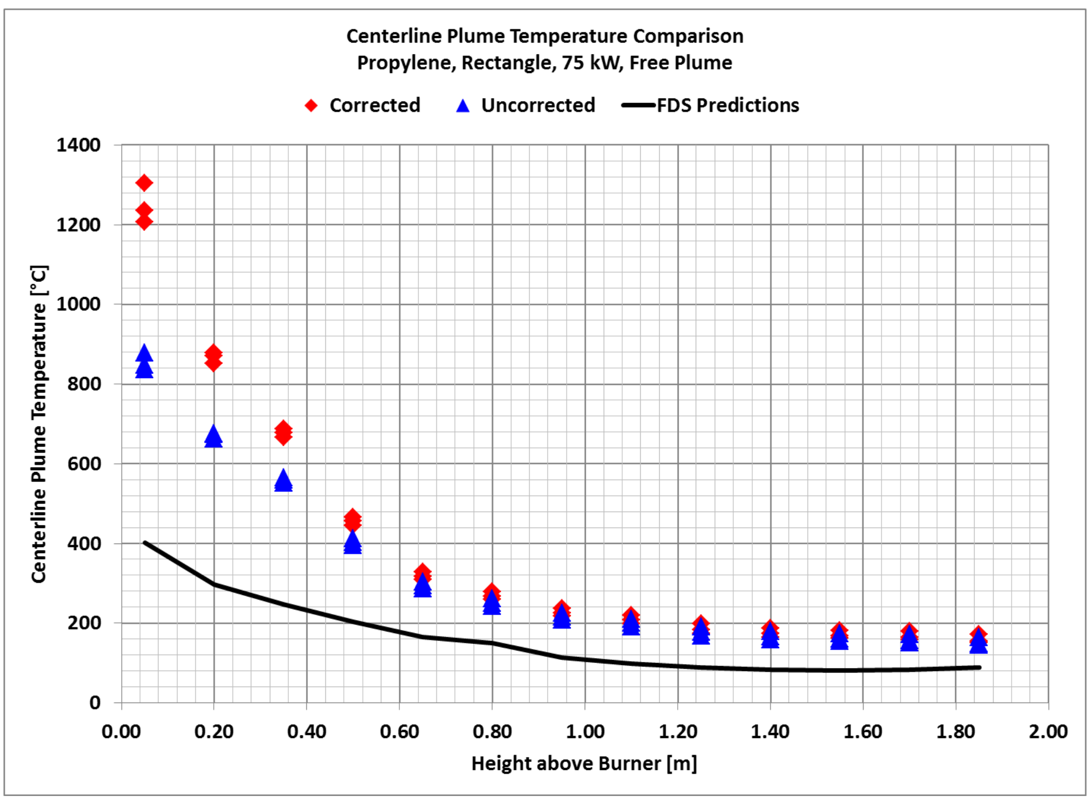

Figure 163 - Plume Temperature, Propylene, Rectangle, 75kW

5.1.2 Centerline velocity

Figure 164 and Figure 165 show the FDS-predicted time-averaged centerline plume velocity and the experimental data from the current experiments. McCaffrey's correlation is also presented in the charts for comparisons. Again, the FDS predictions are lower than the experimental data and McCaffrey's correlation, but the normalization using the convective HRR collapsed the data into a trend similar to the correlation. This suggests that that FDS is predicting the physics in a reasonable manner similar to the extensive experimental data by McCaffrey, but the magnitude of the velocity appears to have been scaled down due to other reasons, most likely from the set of FDS modeling parameters chosen for the simulations and the coarse gird being used.

However, FDS predicted the trends correctly in that the velocity for the fires with the Square burner was greater than that predicted in the fires using the Rectangle burner.

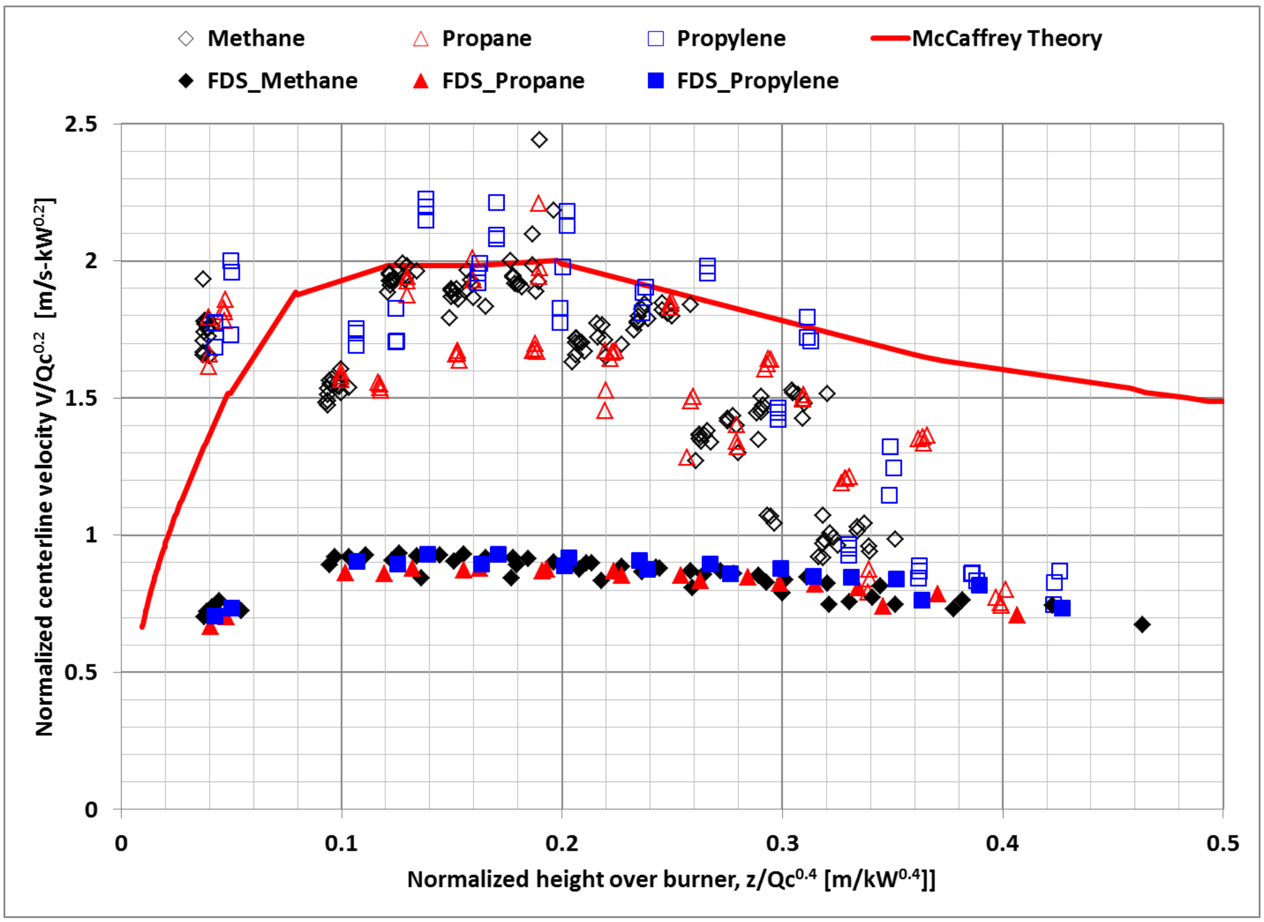

Figure 164 – Plume Centerline Velocity Experimental vs. FDS data, Square Burner, with McCaffrey's Correlation

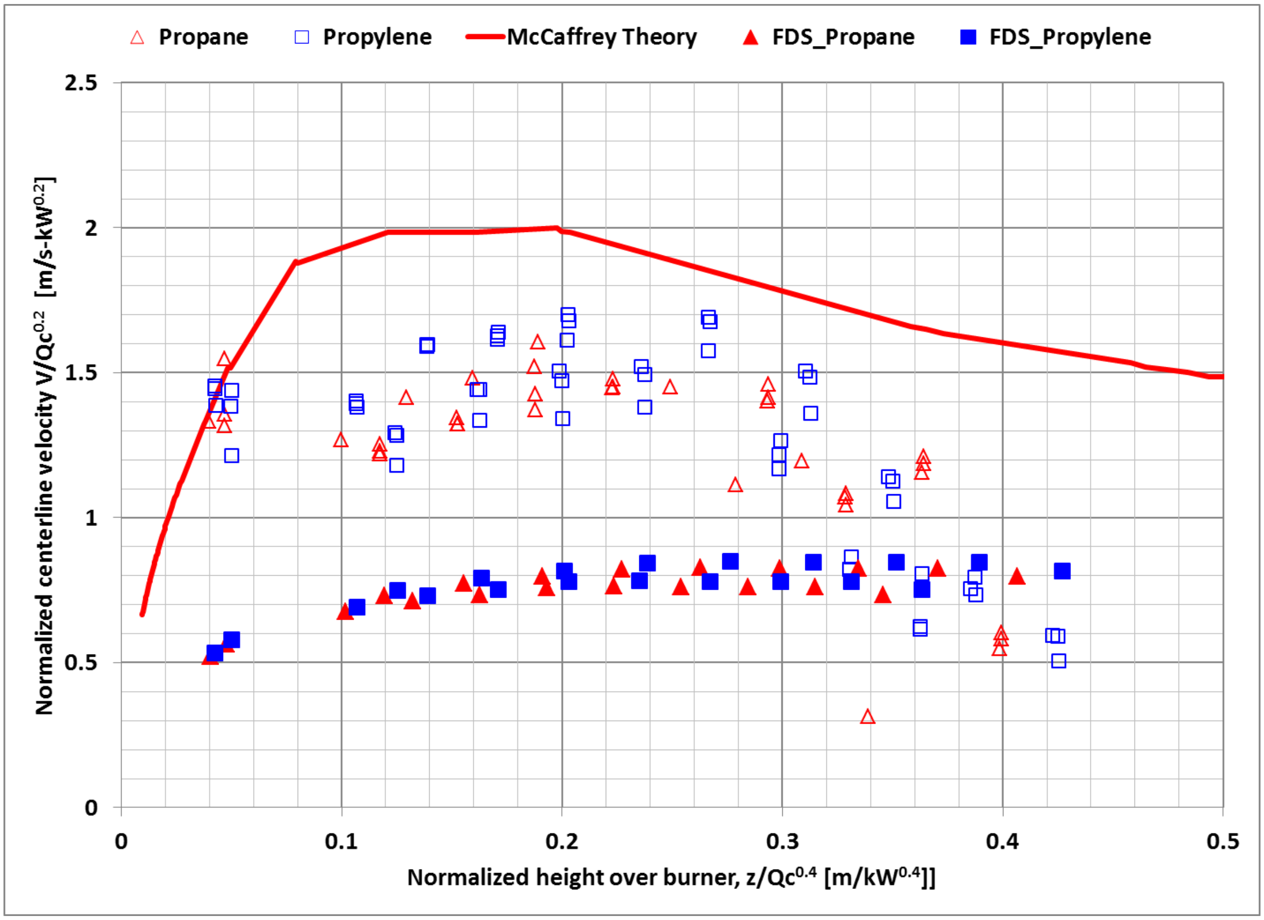

Figure 165 - Plume Centerline Velocity Experimental vs. FDS data, Rectangle Burner, with McCaffrey's Correlation

5.2 Inert wall experiment and simulation comparisons

Comparisons of the plume centerline temperature, velocity, and heat flux are made between the FDS predictions and the actual data measured during the inert wall fire tests conducted as part of the current research. Assuming that the conditions of the tests and the simulations have reached steady state, the data and the predictions are both time-averaged over the period where source fire was at a relatively consistent HRR.

Only the default series simulations (Series 1) were used in the comparison with the actual data. The other simulations where various FDS parameters were changed are used in the parametric study only.

5.2.1 Centerline temperature

Figure 166 and Figure 167 show the FDS-predicted corrected, time-averaged centerline plume temperature rise vs. the time-average measured temperature rise from the current experiments superimposed over McCaffrey's correlation, both with normalization of the height similar to McCaffrey's correlation using the convective HRR.

Although the trends between them are similar, FDS vastly underpredicts the centerline plume temperature of the fires using the square source burner for the range of normalized height of 0 to 0.20 $m/kW^{2/5}$, and for the rectangle burner at 0.01 $m/kW^{2/5}$. For the other locations, FDS's predictions are similar to the lower-bound values of the measured temperature, especially for the simulations of the source fires using the Rectangle burner. It is likely that the particular set of FDS parameters used in the default series of simulations and the relatively coarse grid size at 5 mm both contributed to the low predictions. Additionally, the FDS predictions for the various fire sizes and source fuel are collapsed into a very tight cluster, showing that that height normalization method is valid.

The corrected and uncorrected experimental centerline plume excess temperatures are compared to FDS's predictions are presented in Figure 168 to Figure 176, in these charts the height is not normalized. It can be shown that the FDS predictions fall below both the corrected and uncorrected experimental data for all cases. The predictions are closer to the uncorrected measurements, but the difference ranges from 40°C far away from the burner surface to 700°C at 5 mm over the burner surface.

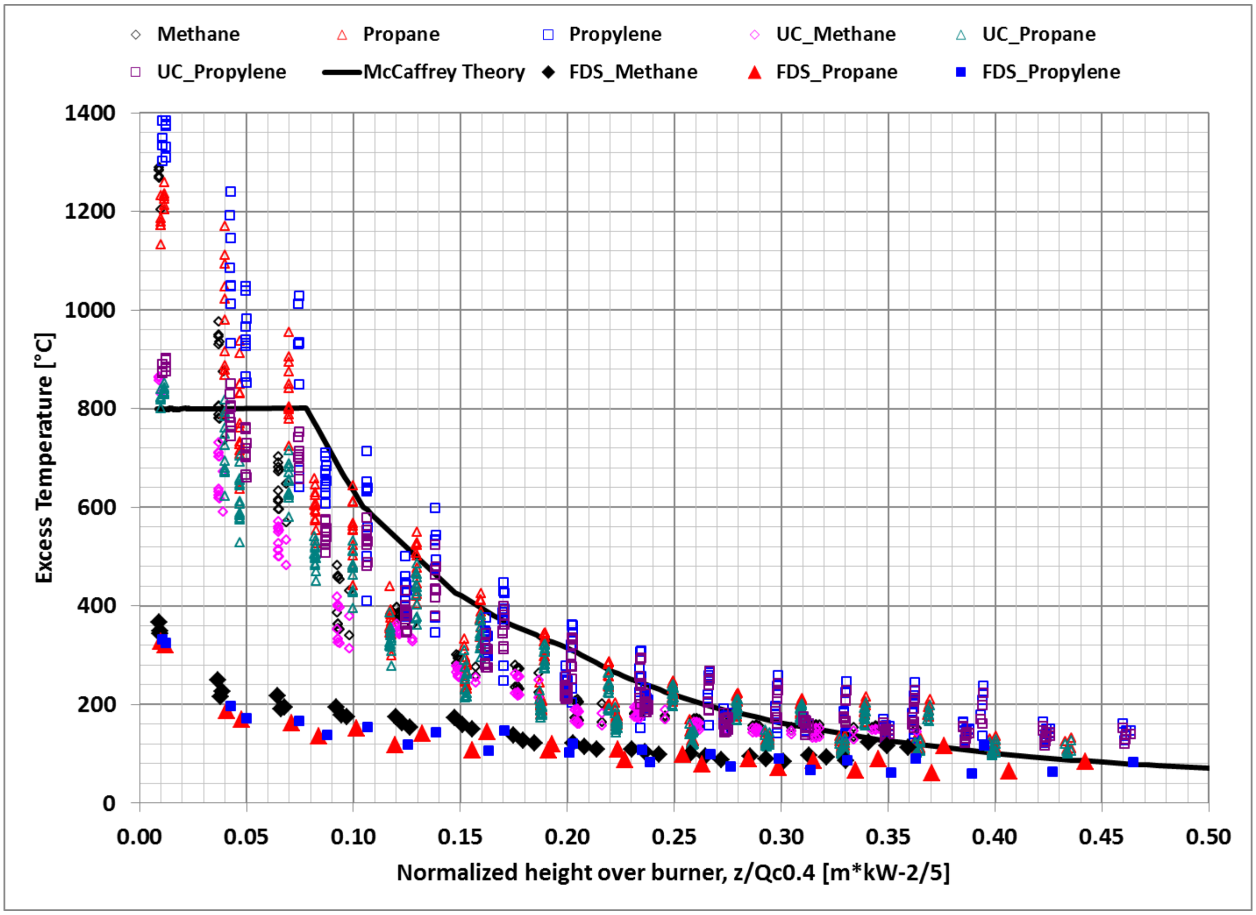

Figure 166 - Plume Centerline Temperature Rise Experimental vs. FDS data, Rectangle Burner, with McCaffrey's Correlation

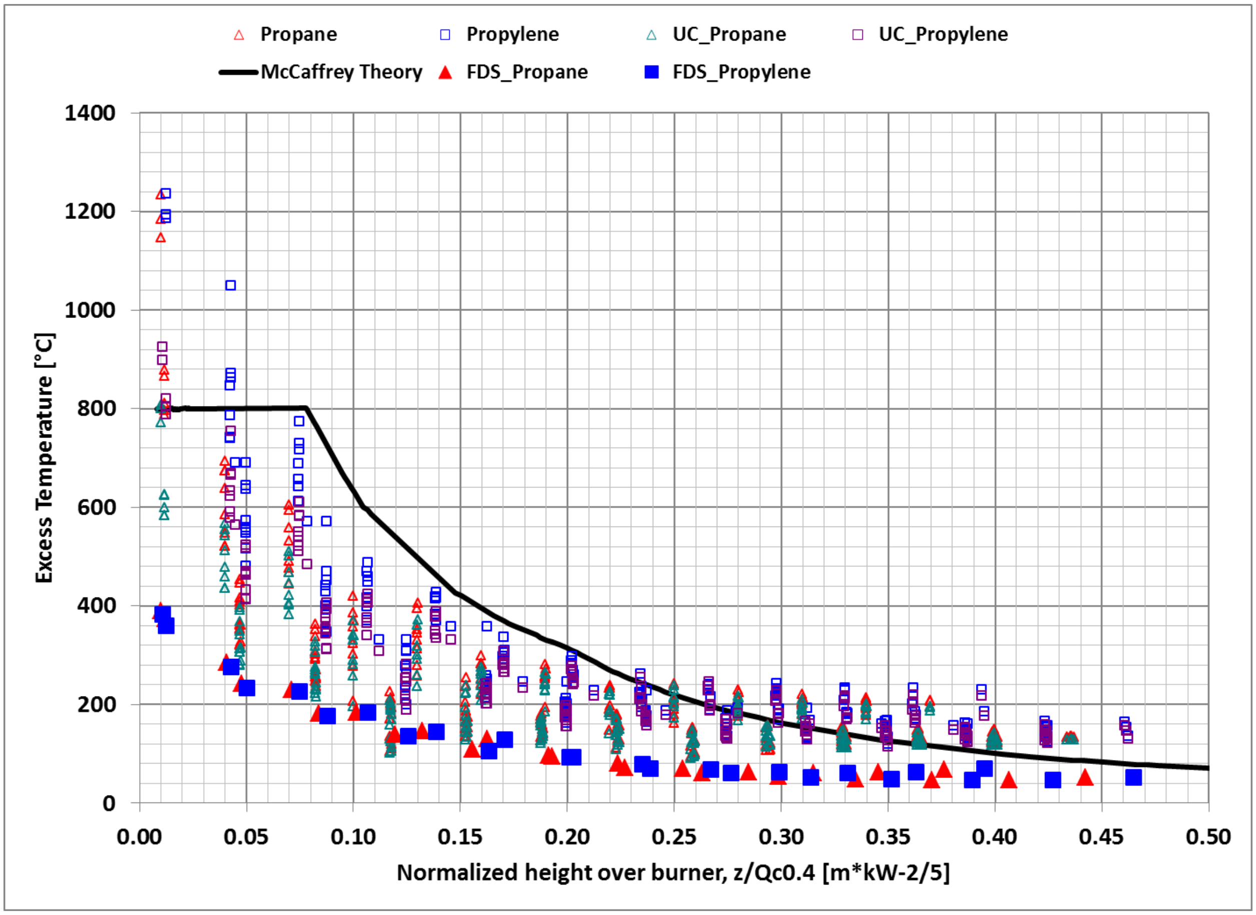

Figure 167 - Plume Centerline Temperature Rise Experimental vs. FDS data, Rectangle Burner, with McCaffrey's Correlation

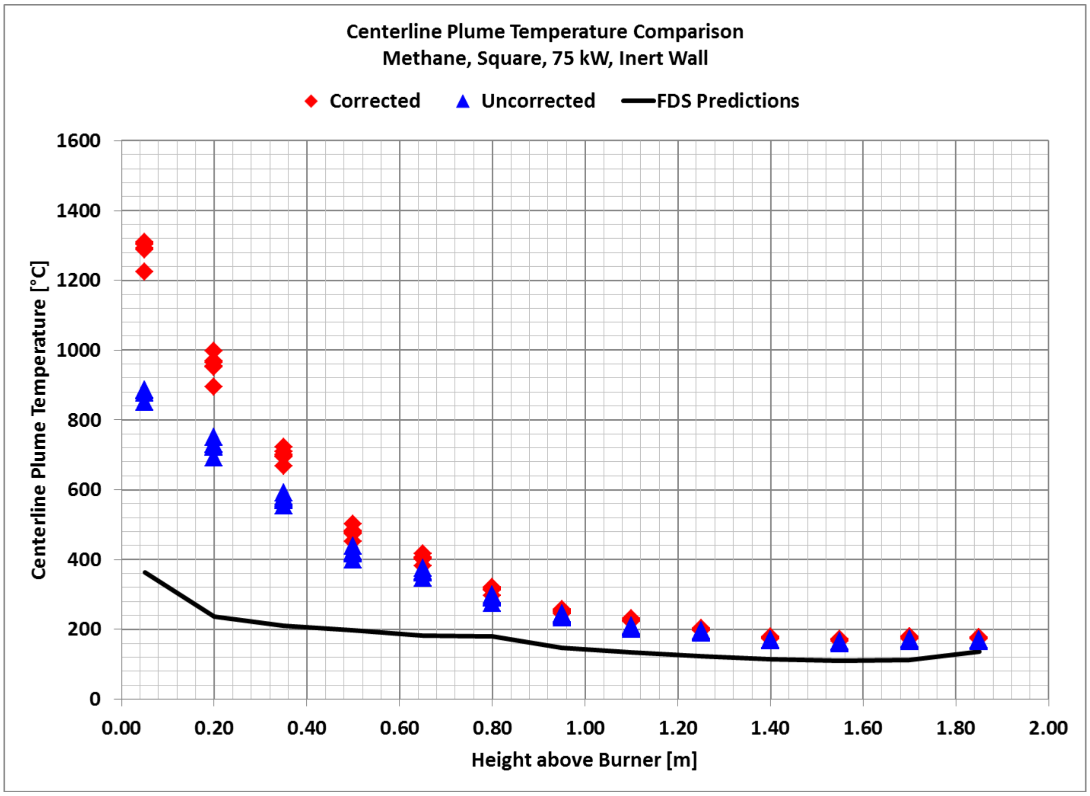

Figure 168 - Plume Temperature, Methane, Square, 75kW

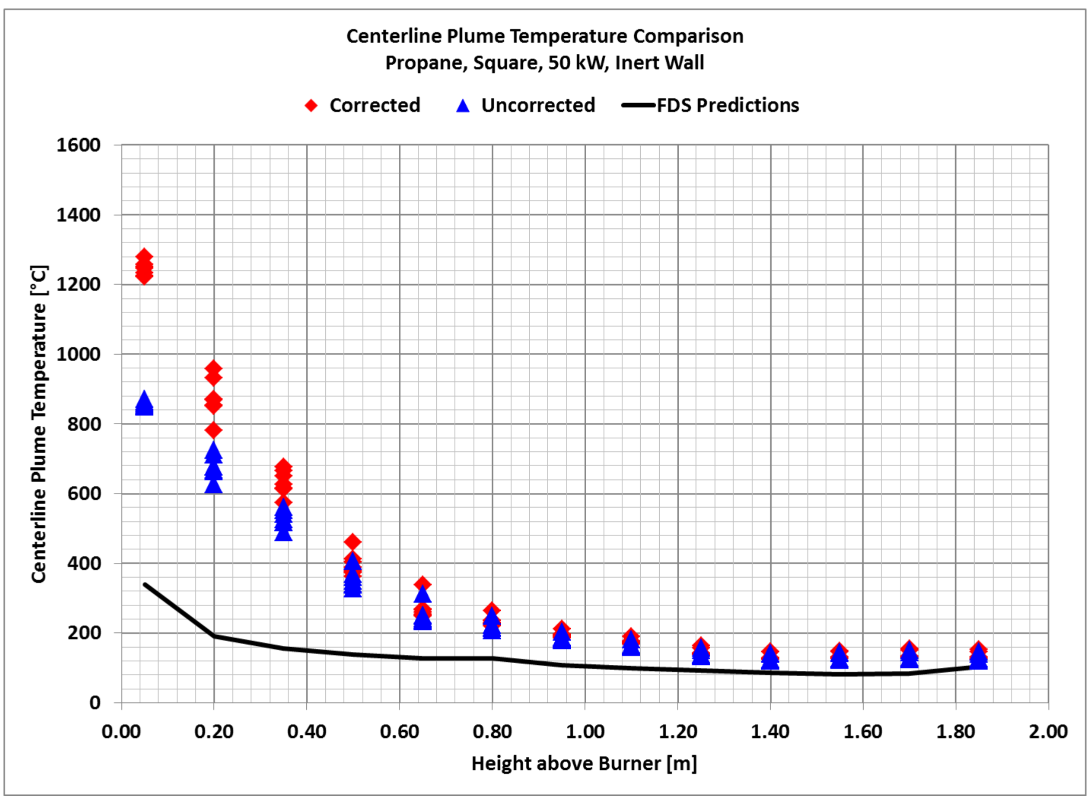

Figure 169 - Plume Temperature, Propane, Square, 50kW

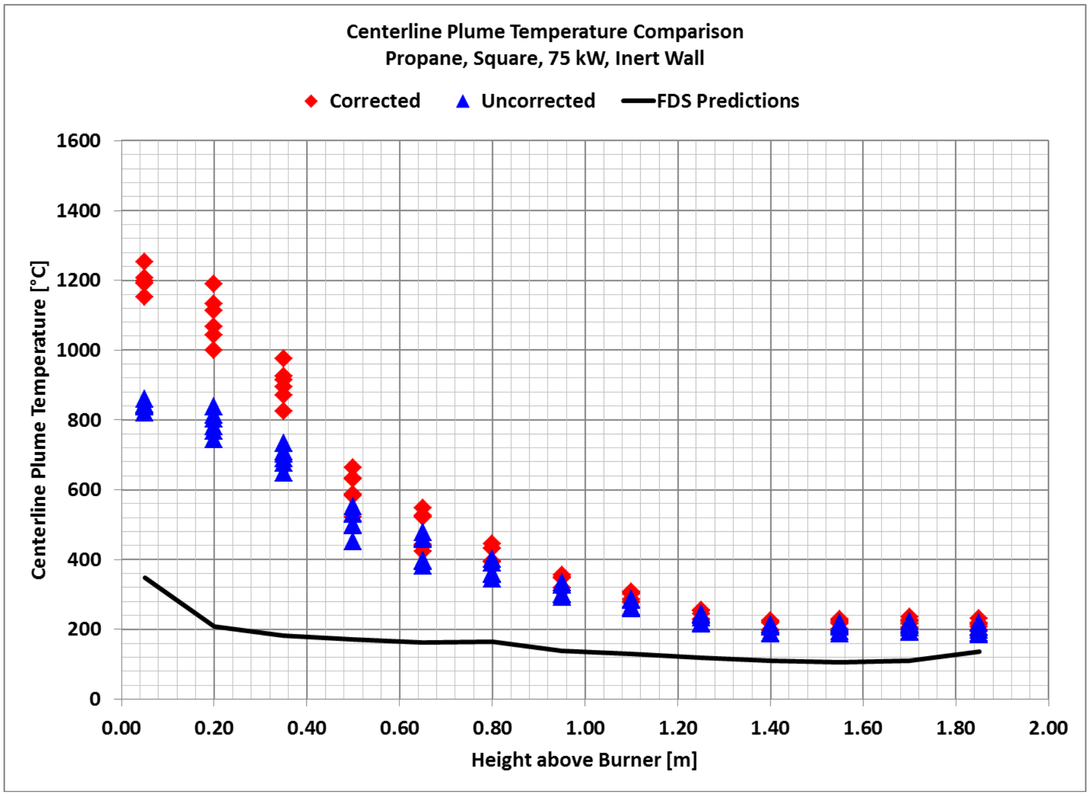

Figure 170 - Plume Temperature, Propane, Square, 75kW

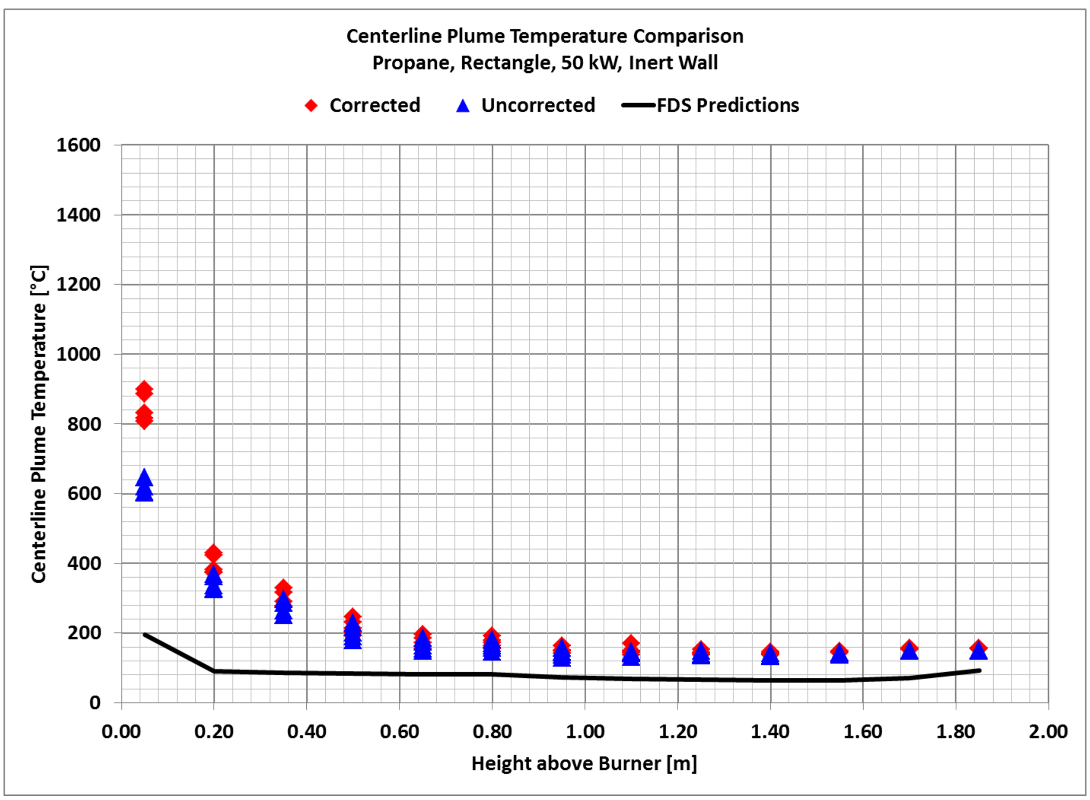

Figure 171 - Plume Temperature, Propane, Rectangle, 50kW

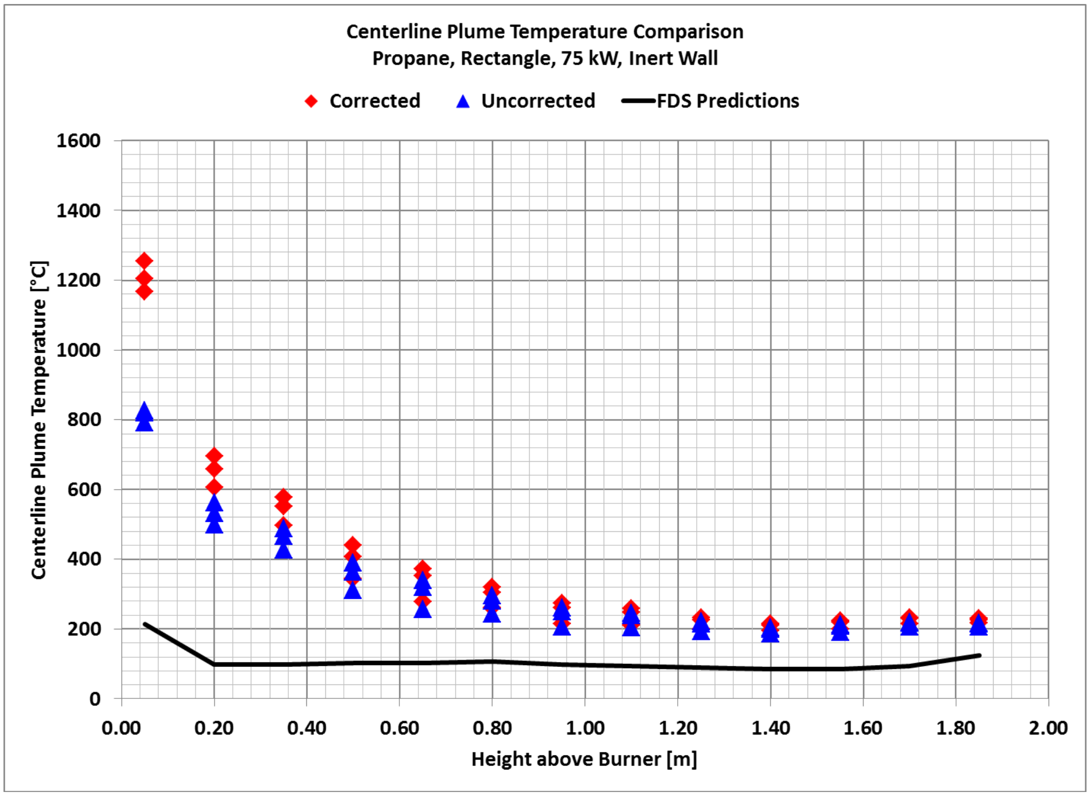

Figure 172 - Plume Temperature, Propane, Rectangle, 75kW

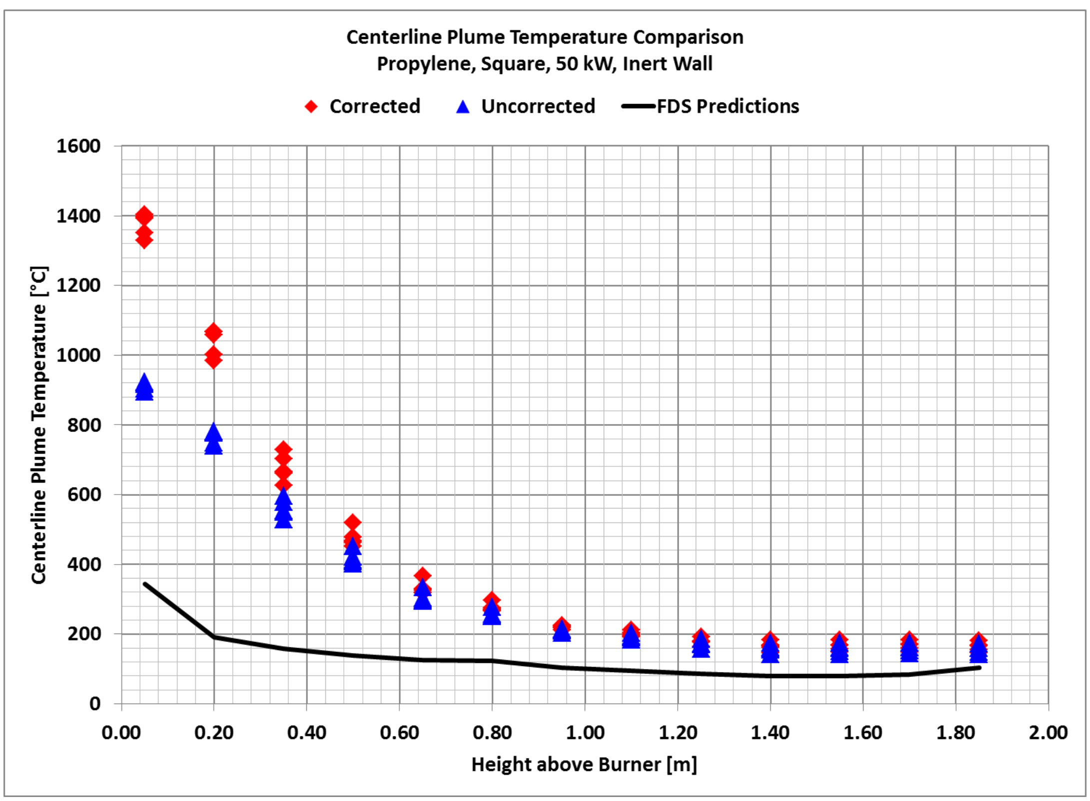

Figure 173 - Plume Temperature, Propylene, Square, 50kW

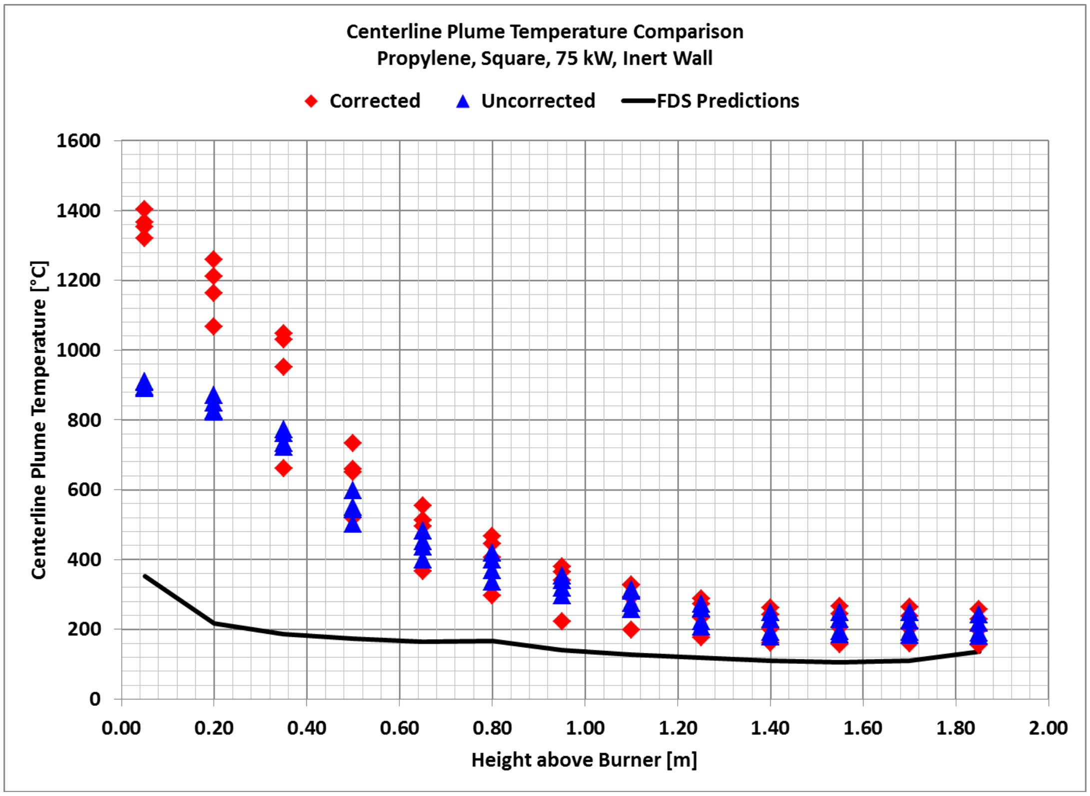

Figure 174 - Plume Temperature, Propylene, Square, 75kW

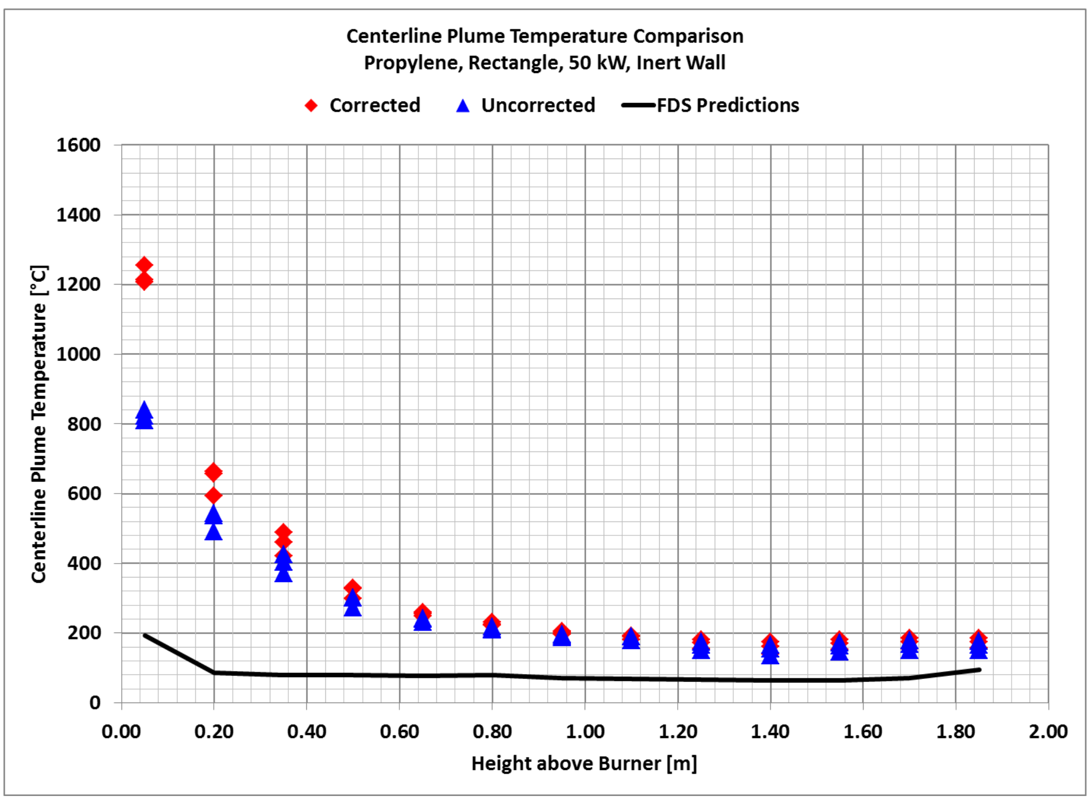

Figure 175 - Plume Temperature, Propylene, Rectangle, 50kW

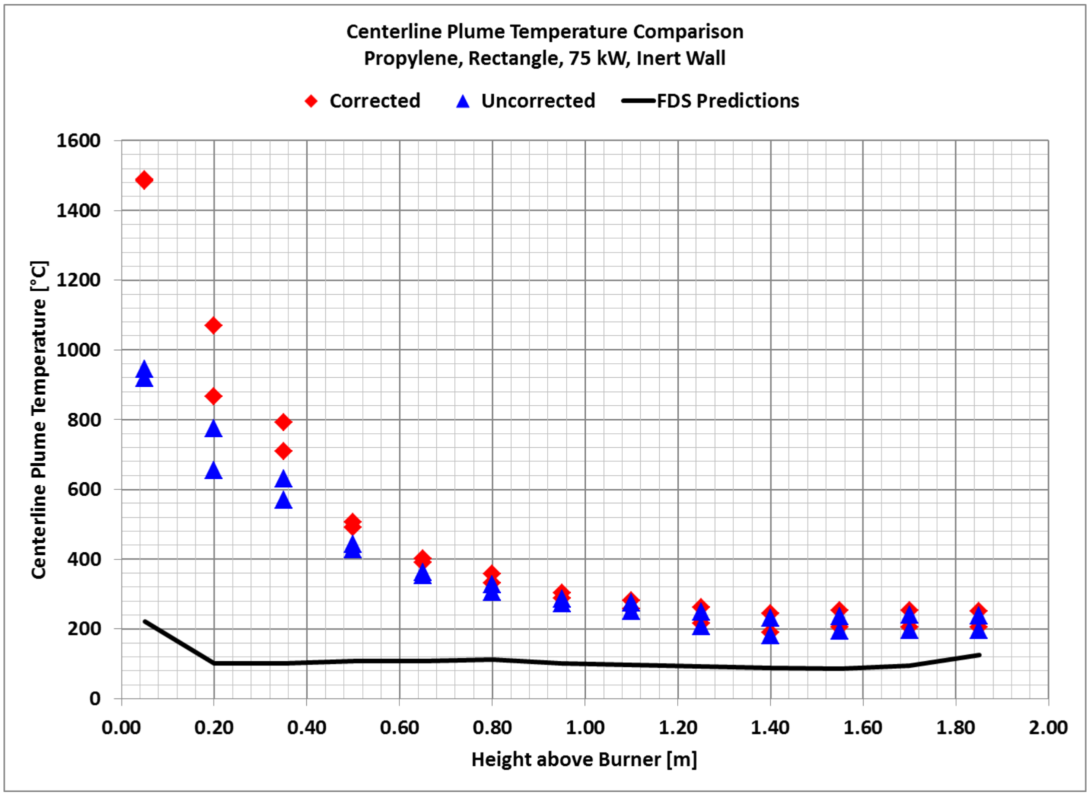

Figure 176 - Plume Temperature, Propylene, Rectangle, 75kW

5.2.2 Centerline velocity

Figure 177 and Figure 178 show the FDS-predicted time-averaged centerline plume velocity and the experimental data from the current experiments. McCaffrey's correlation is also presented in the charts for comparisons. Again, the FDS predictions are lower than the experimental data and McCaffrey's correlation, but the normalization using the convective HRR collapsed the data into a trend similar to the correlation. This suggests that that FDS is predicting the physics in a reasonable manner similar to the extensive experimental data by McCaffrey, but the magnitude of the velocity appears to have been scaled down due to other reasons, most likely from the set of FDS modeling parameters chosen for the simulations and the coarse gird being used.

It is noted that the FDS prediction for the plume centerline velocity are very similar regardless of the size of the source burner simulated. Although the spread of the experimental data is significant in the inert wall experiments, the experiments show that the centerline velocity measured in the Square burner tests are greater than that measured in the Rectangle burner tests.

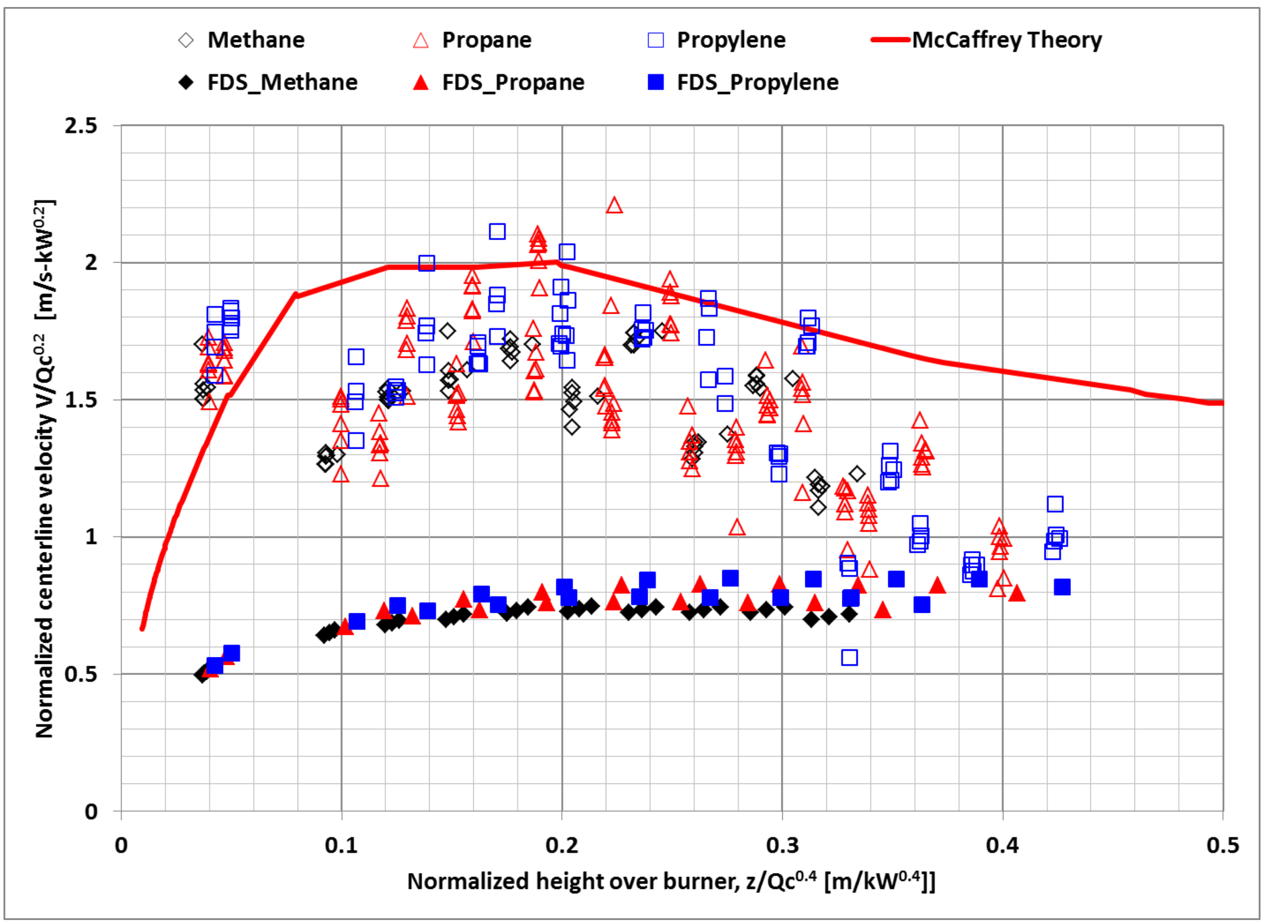

Figure 177 – Inert Wall Plume Centerline Velocity Experimental vs. FDS data, Square Burner, with McCaffrey's Correlation

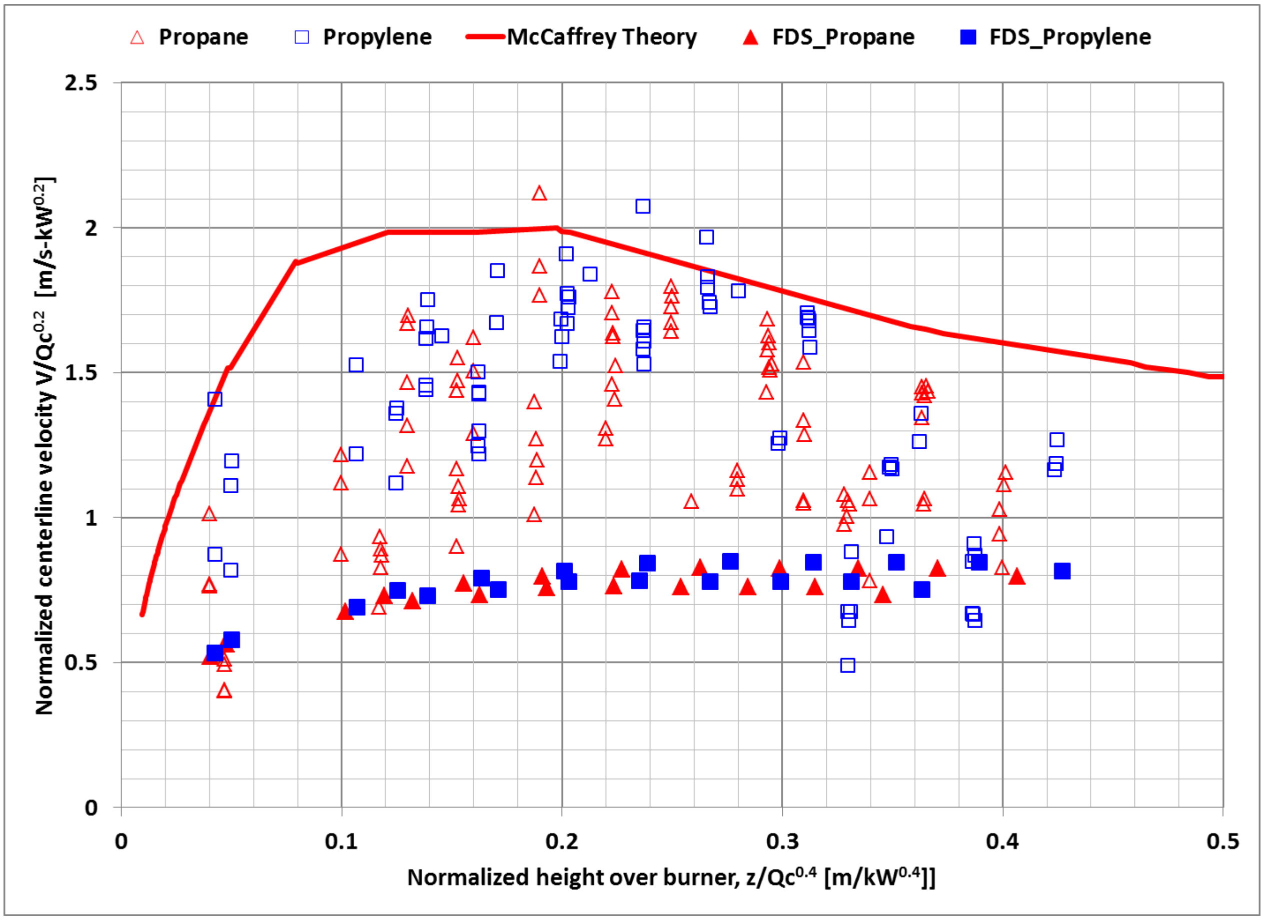

Figure 178 – Inert Wall Plume Centerline Velocity Experimental vs. FDS data, Rectangle Burner, with McCaffrey's Correlation

5.2.3 Near-wall temperature

Experimental near-wall excess temperature comparisons with the FDS predictions at 0.35 m above the burner surface are presented in Figure 179 to Figure 182. The predicted temperature at the same locations between the different fuels are very similar, with difference in the range of 10°C, however, in the experiments, the near-wall temperature rise are different between the fuels, regardless if it has been corrected or not. Also, in the experimental data, the propylene fires generated the highest near-wall temperature, followed with propane and methane, however, the FDS simulations did not show such trends.

For the Square burner at 50 kW and the Rectangle burner at 75 kW fires, the predicted near-wall temperature is generally within the range established with the experimental data. However, FDS generally underpredicted the near-wall temperature for the Square burner at 75 kW simulations, whereas for the Rectangle burner at 50 kW, the FDS predictions are similar to the corrected temperatures.

It is noted that the temperature predicted at the middle two locations are always higher than the predictions made at the two locations closest to and furthest away from the wall.

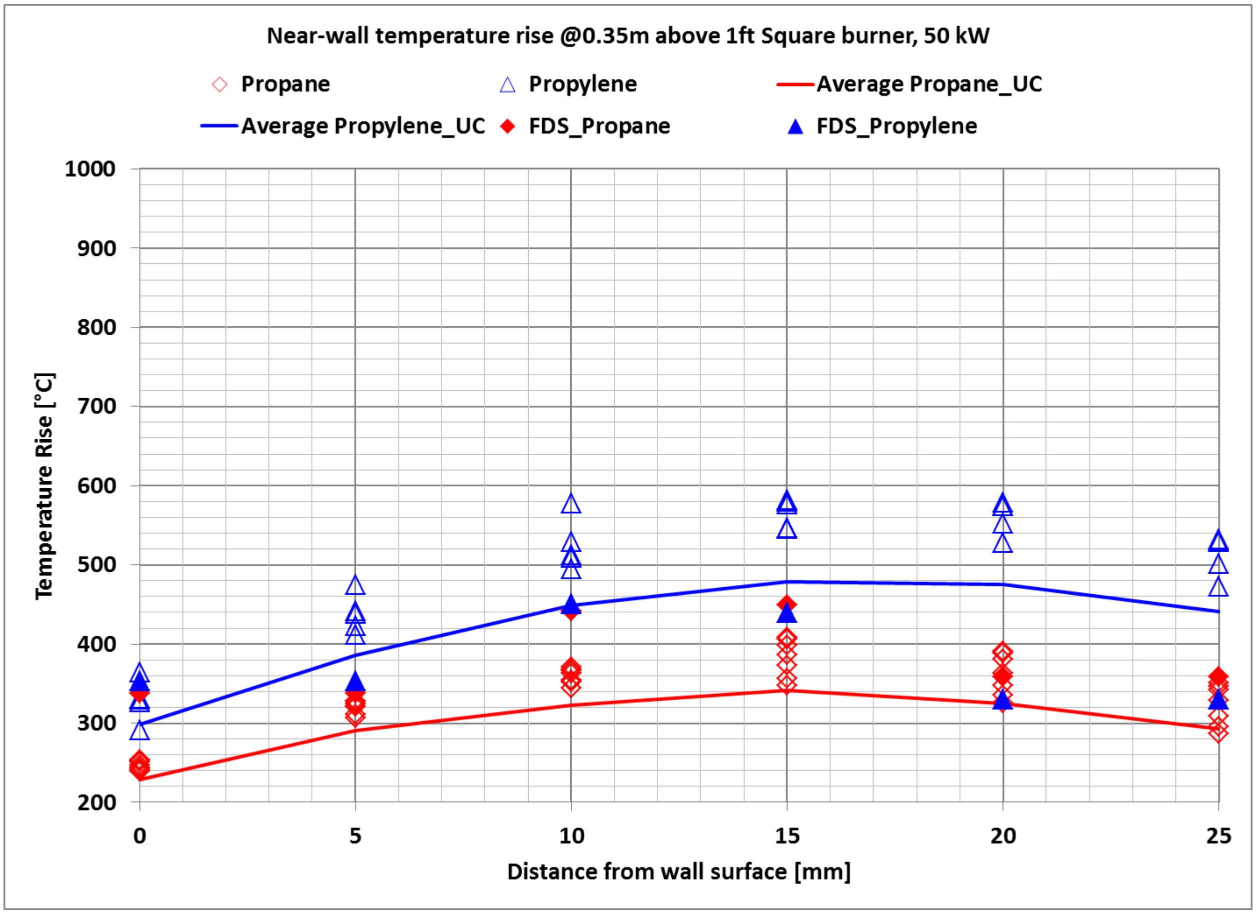

Figure 179 - Near-Wall Temperature Rise Experimental vs. FDS data @ 0.35m Above Burner, Square, 50 kW

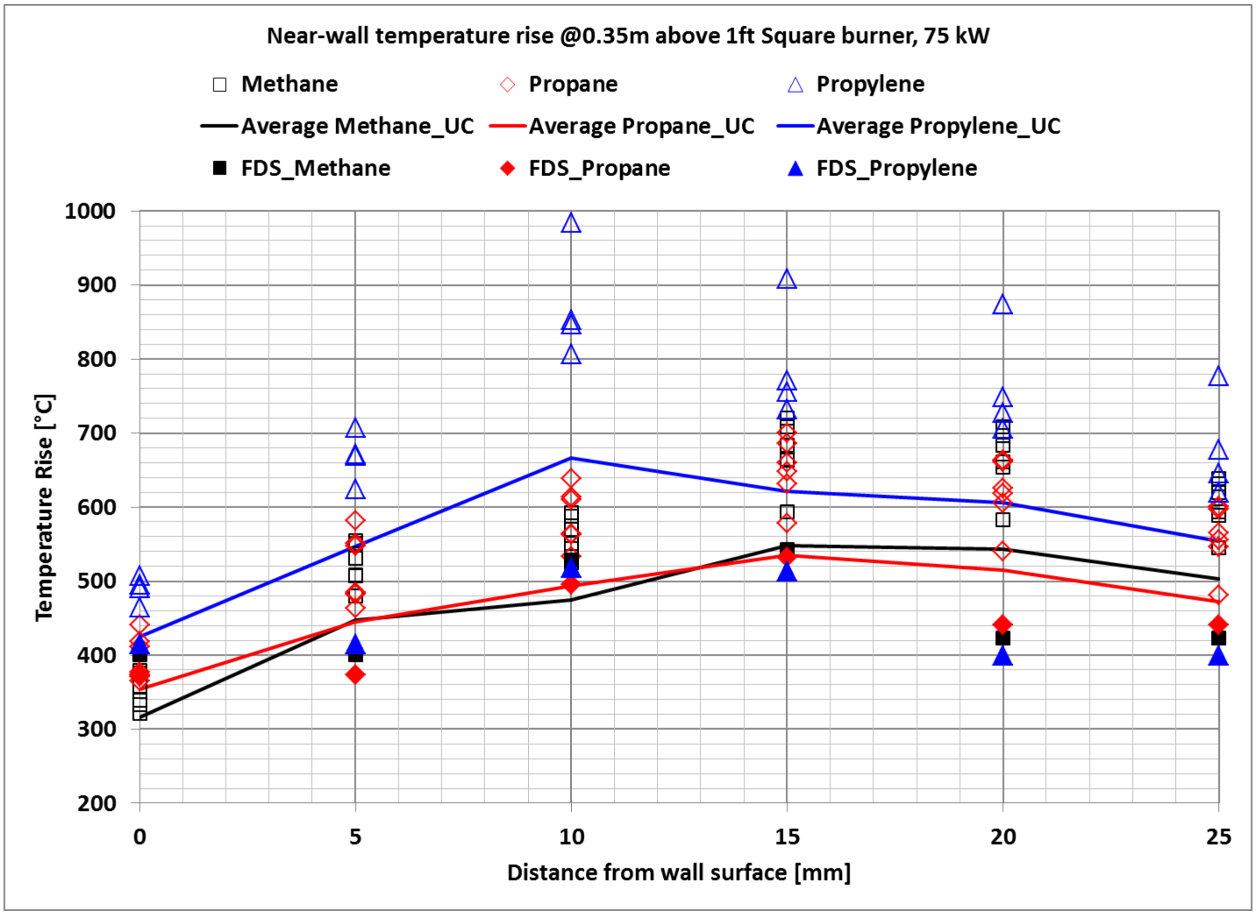

Figure 180 - Near-Wall Temperature Rise Experimental vs. FDS data @ 0.35m Above Burner, Square, 75 kW

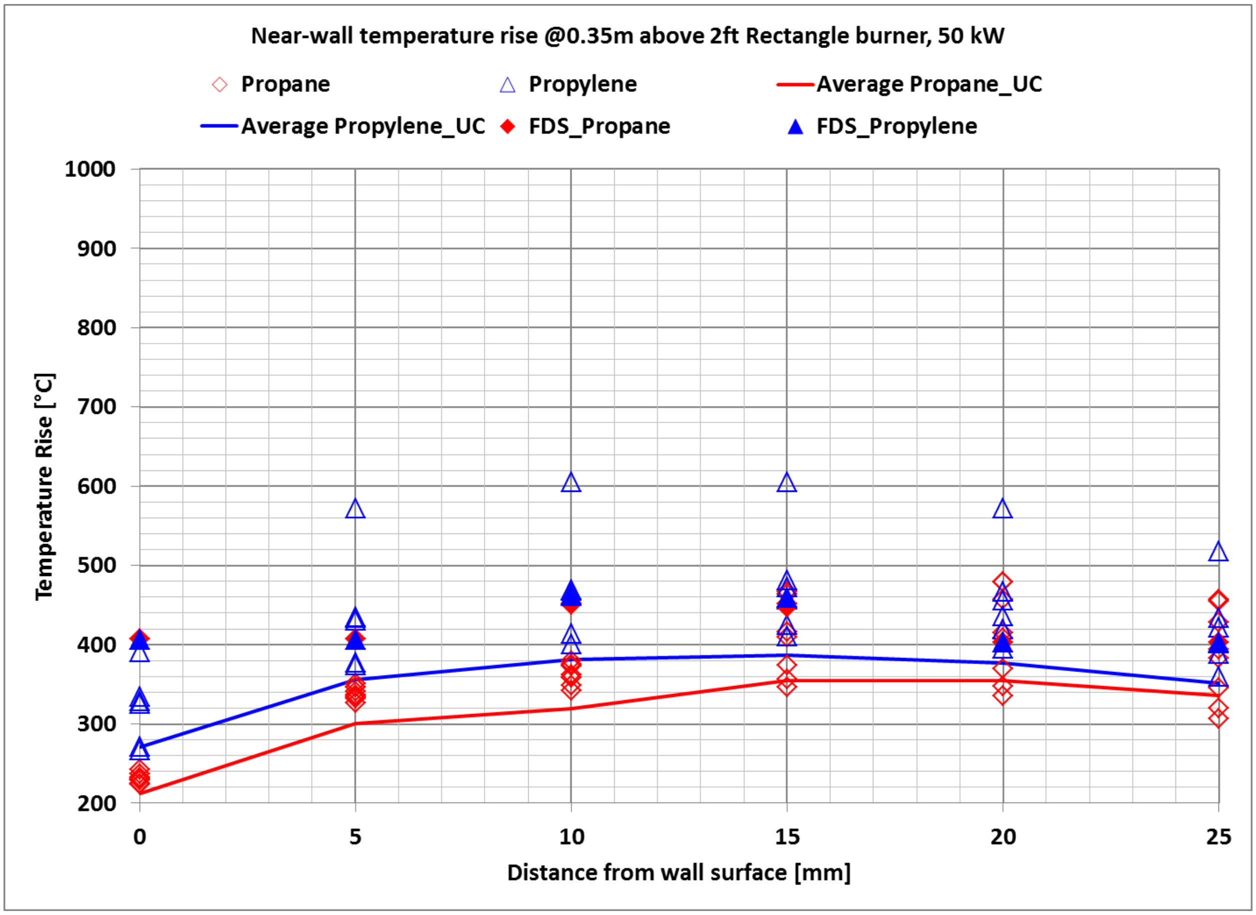

Figure 181 - Near-Wall Temperature Rise Experimental vs. FDS data @ 0.35m Above Burner, Rectangle, 50 kW

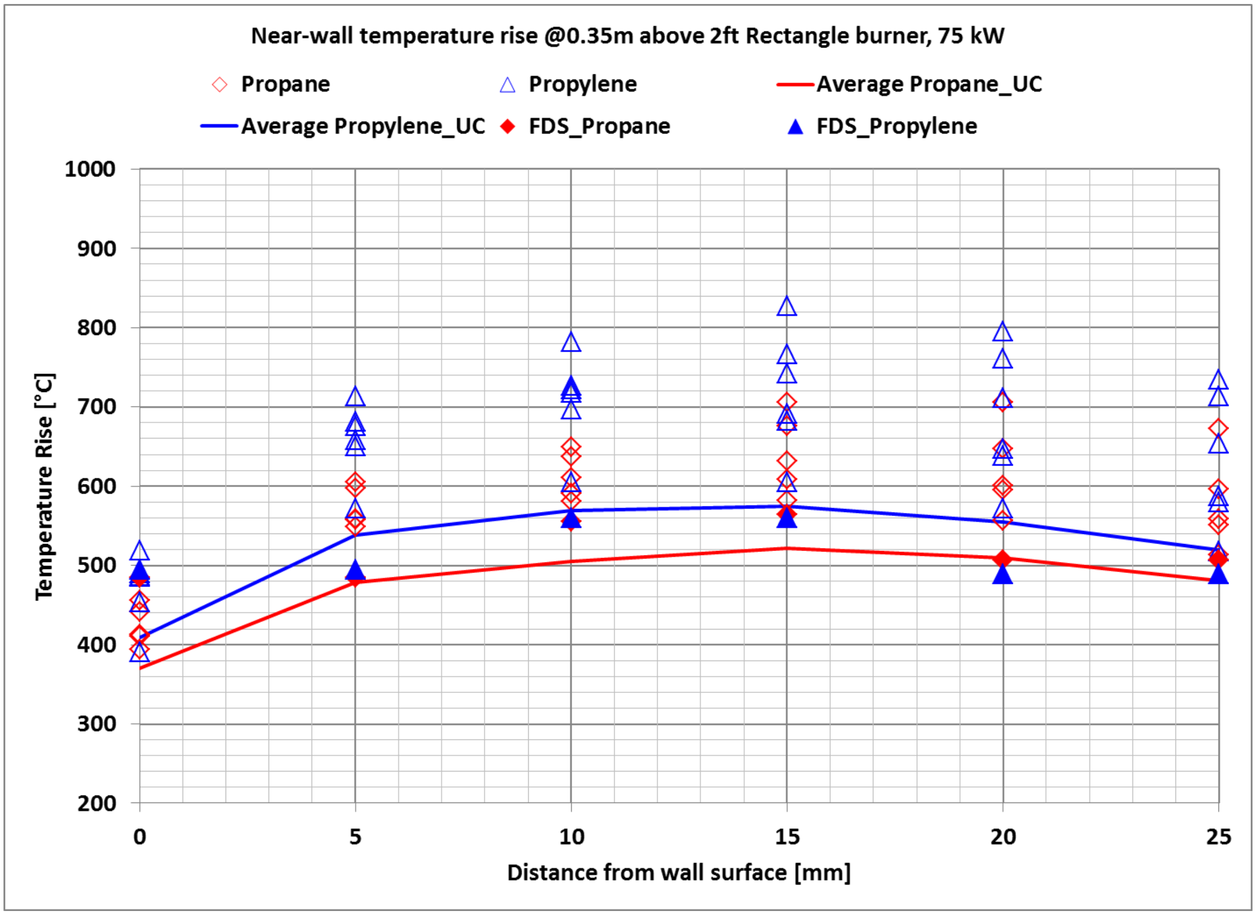

Figure 182 - Near-Wall Temperature Rise Experimental vs. FDS data @ 0.35m Above Burner, Rectangle, 75 kW

Experimental near-wall excess temperature comparisons with the FDS predictions at 0.95 m above the burner surface are presented in Figure 183 to Figure 186. Again, the predicted temperature at the same locations between the different fuels are very similar, with difference in the range of 10°C, however, in the experiments, the near-wall temperature rise are different between the fuels, regardless if it has been corrected or not. Also, in the experimental data, the propylene fires generated the highest near-wall temperature, followed with propane and methane, however, the FDS simulations did not show such trends.

FDS predicted very similar temperature at the six locations each set of tests; they are all within a 40°C range. Again, the temperatures predicted at the middle two locations are always higher than the predictions made at the two locations closest to and furthest away from the wall.

In the simulations of the Square burner at 50 kW fire, the near-wall temperature for 10 to 25 mm away from the wall is greater than the measured temperature, whereas at 30 to 35 mm the predictions are similar to the measured corrected temperature. For the Square burner at 75 kW simulations, overprediction was noted from 10 to 20 mm, but the temperature at 30 and 35 mm is lower than the experimental data. For the Rectangle burner simulations, regardless of the source HRR, FDS predicted temperature similar to the corrected temperature from 10 to 20 mm, but underpredicted from 25 to 35 mm.

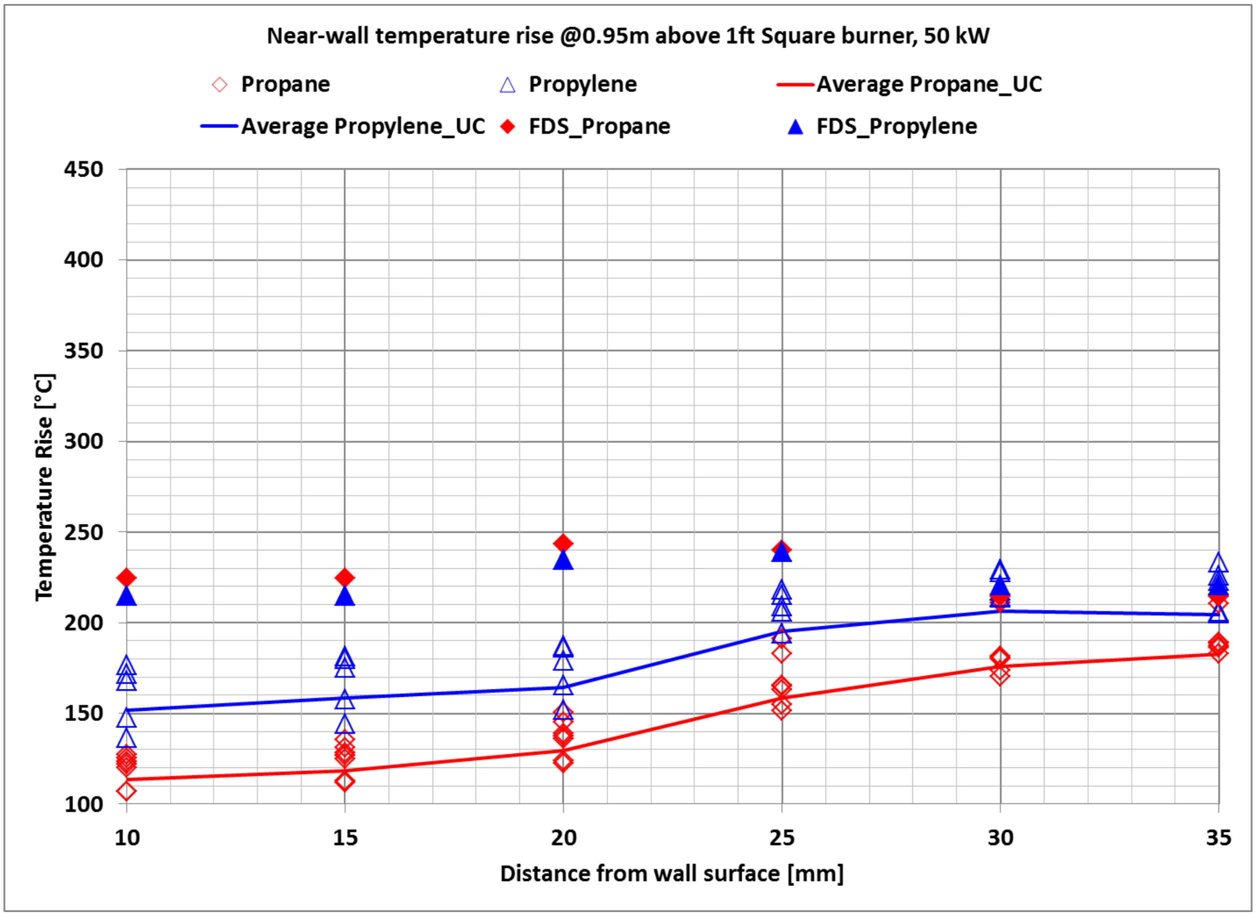

Figure 183 - Near-Wall Temperature Rise Experimental vs. FDS data @ 0.95m Above Burner, Square, 50 kW

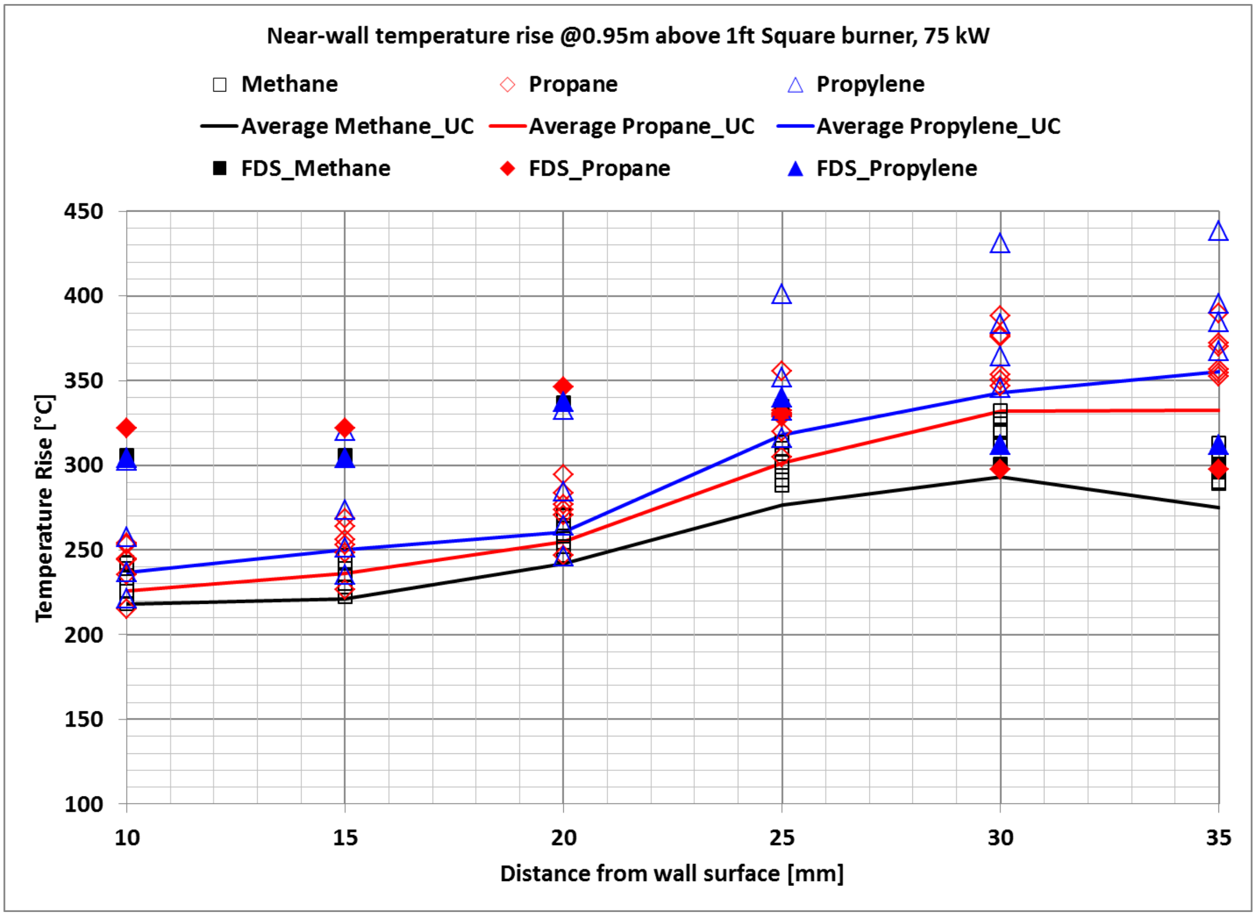

Figure 184 - Near-Wall Temperature Rise Experimental vs. FDS data @ 0.95m Above Burner, Square, 75 kW

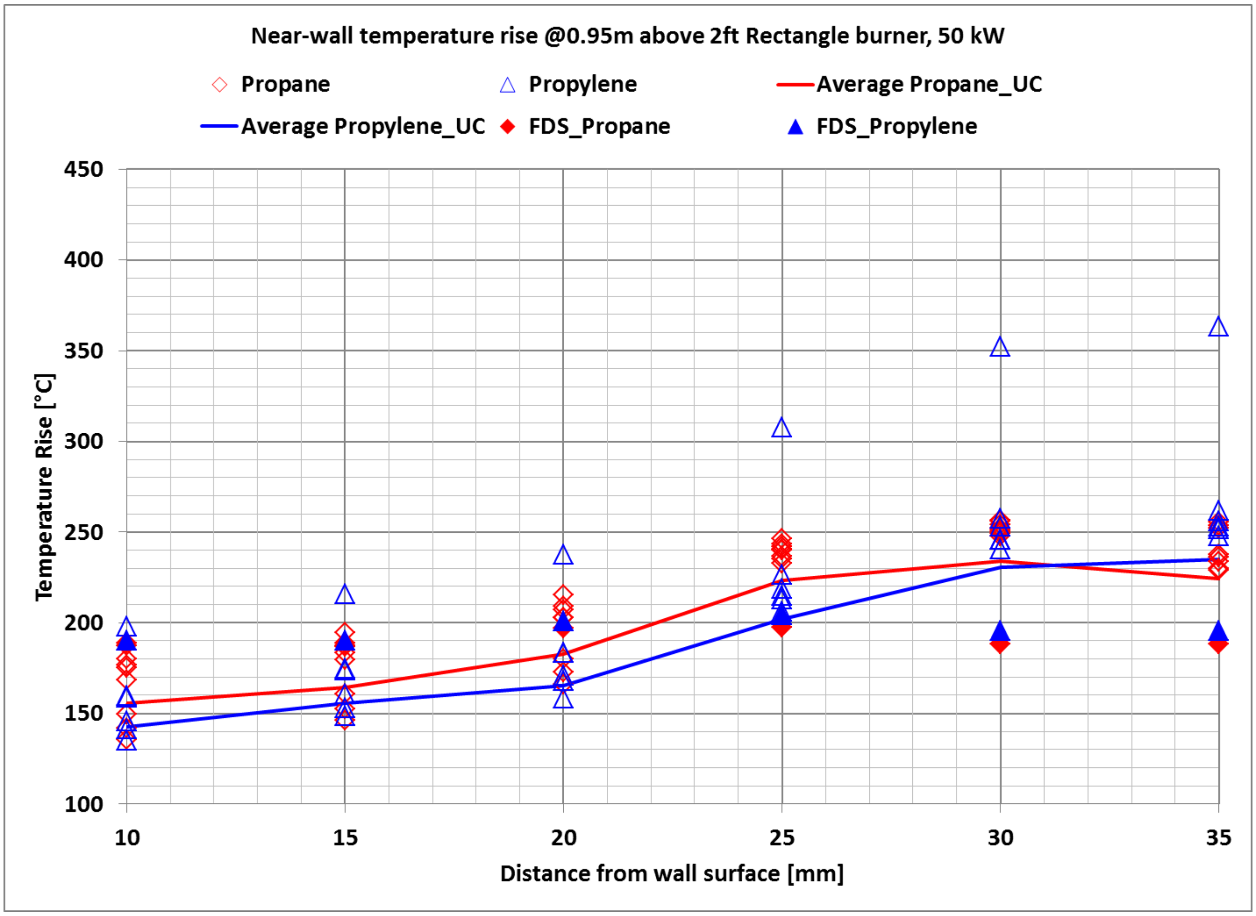

Figure 185 - Near-Wall Temperature Rise Experimental vs. FDS data @ 0.95m Above Burner, Rectangle, 50 kW

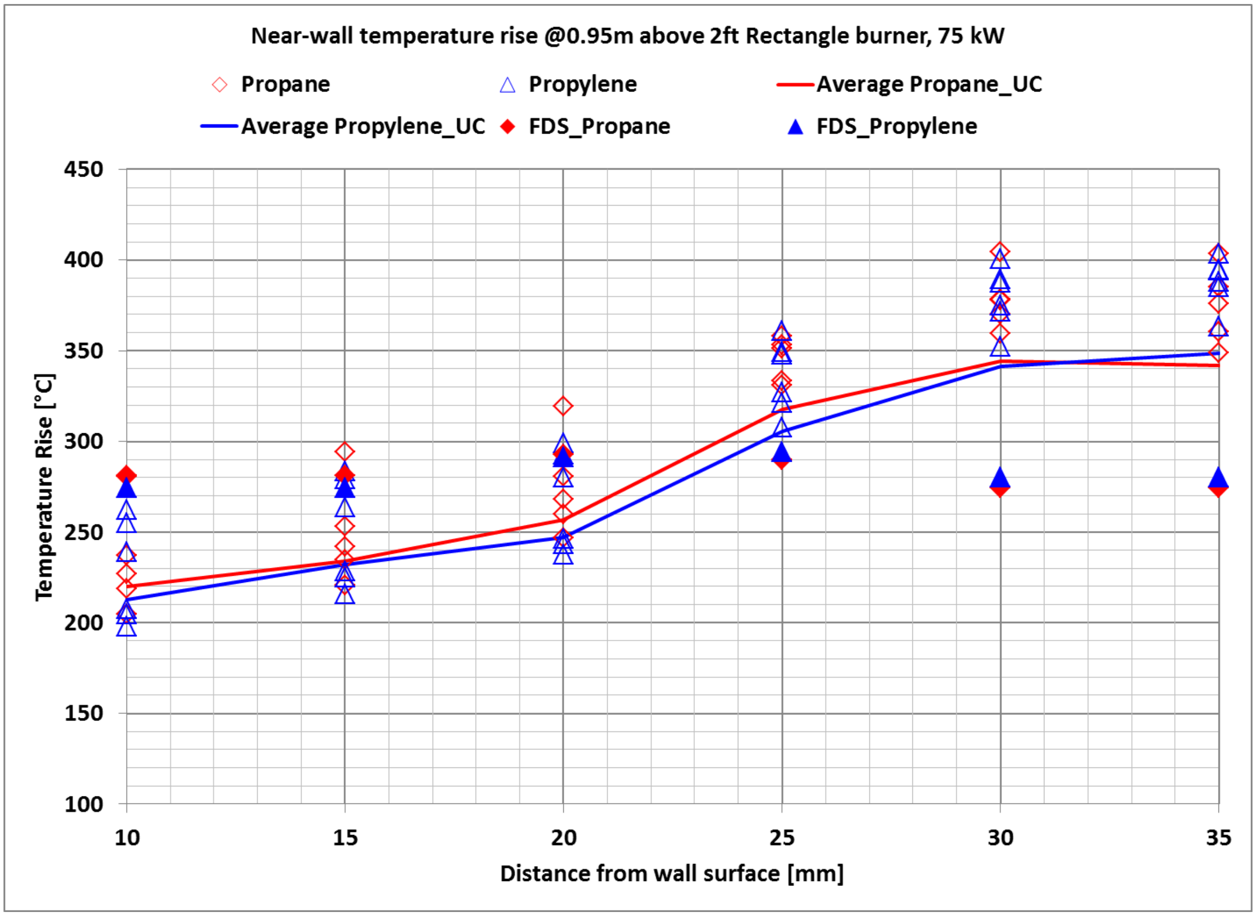

Figure 186 - Near-Wall Temperature Rise Experimental vs. FDS data @ 0.95m Above Burner, Rectangle, 75 kW

Experimental near-wall excess temperature comparisons with the FDS predictions at 1.55 m above the burner surface are presented in Figure 187 to Figure 190. Again, the predicted temperature at the same locations between the different fuels are very similar, with difference in the range of 10°C, however, in the experiments, the near-wall temperature rise are different between the fuels, regardless if it has been corrected or not. Also, in the experimental data, the propylene fires generated the highest near-wall temperature, followed with propane and methane, however, the FDS simulations did not show such trends.

FDS predicted extremely similar temperature at the six locations each set of tests; they are all within a 10°C range. At this elevation, the temperature predicted for all six locations are almost identical.

For the Square burner simulations, regardless of the source HRR, FDS predicted temperature similar to the corrected temperature from the experiments. However, for the Rectangle burner simulations, FDS underpredicted at all six locations.

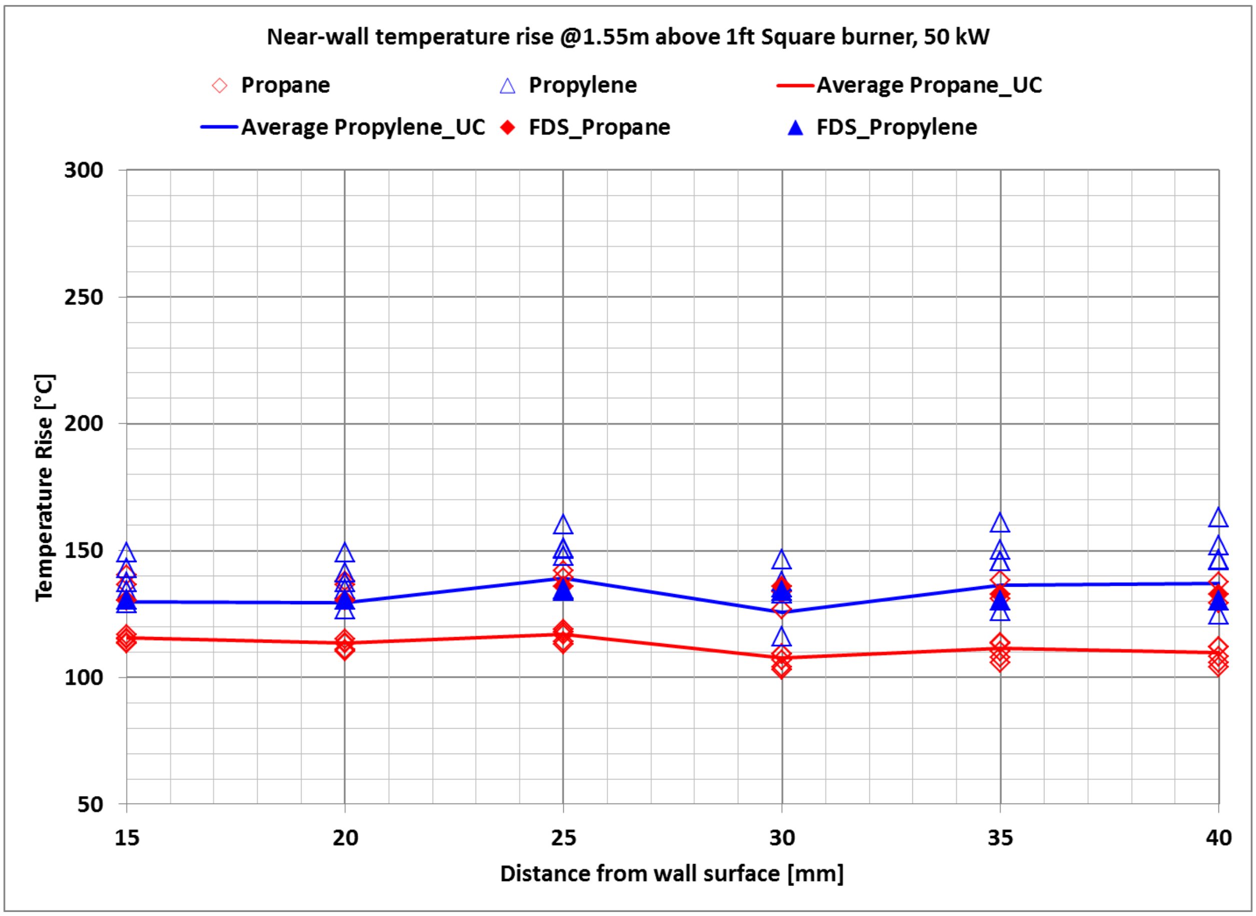

Figure 187 - Near-Wall Temperature Rise Experimental vs. FDS data @ 1.55m Above Burner, Square, 50 kW

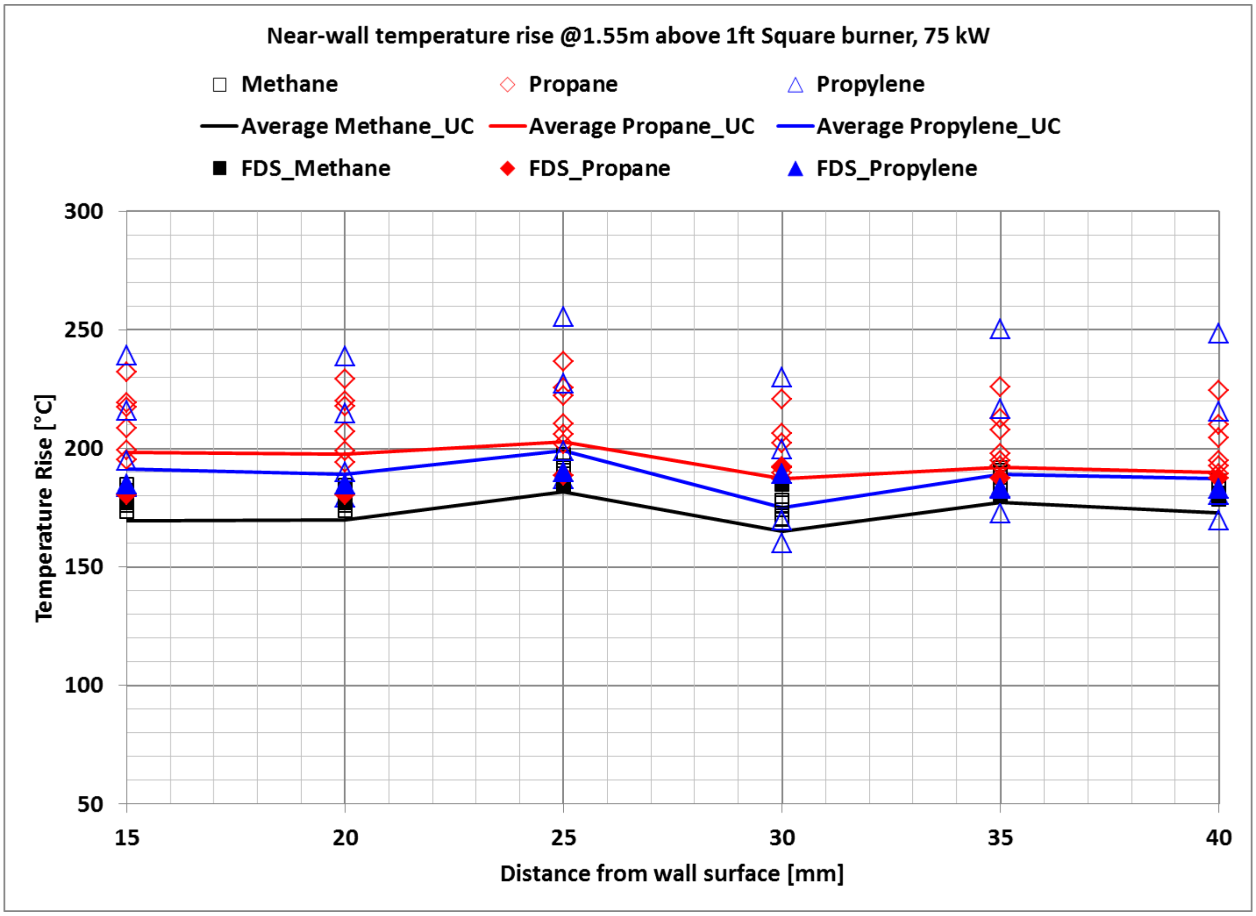

Figure 188 - Near-Wall Temperature Rise Experimental vs. FDS data @ 1.55m Above Burner, Square, 75 kW

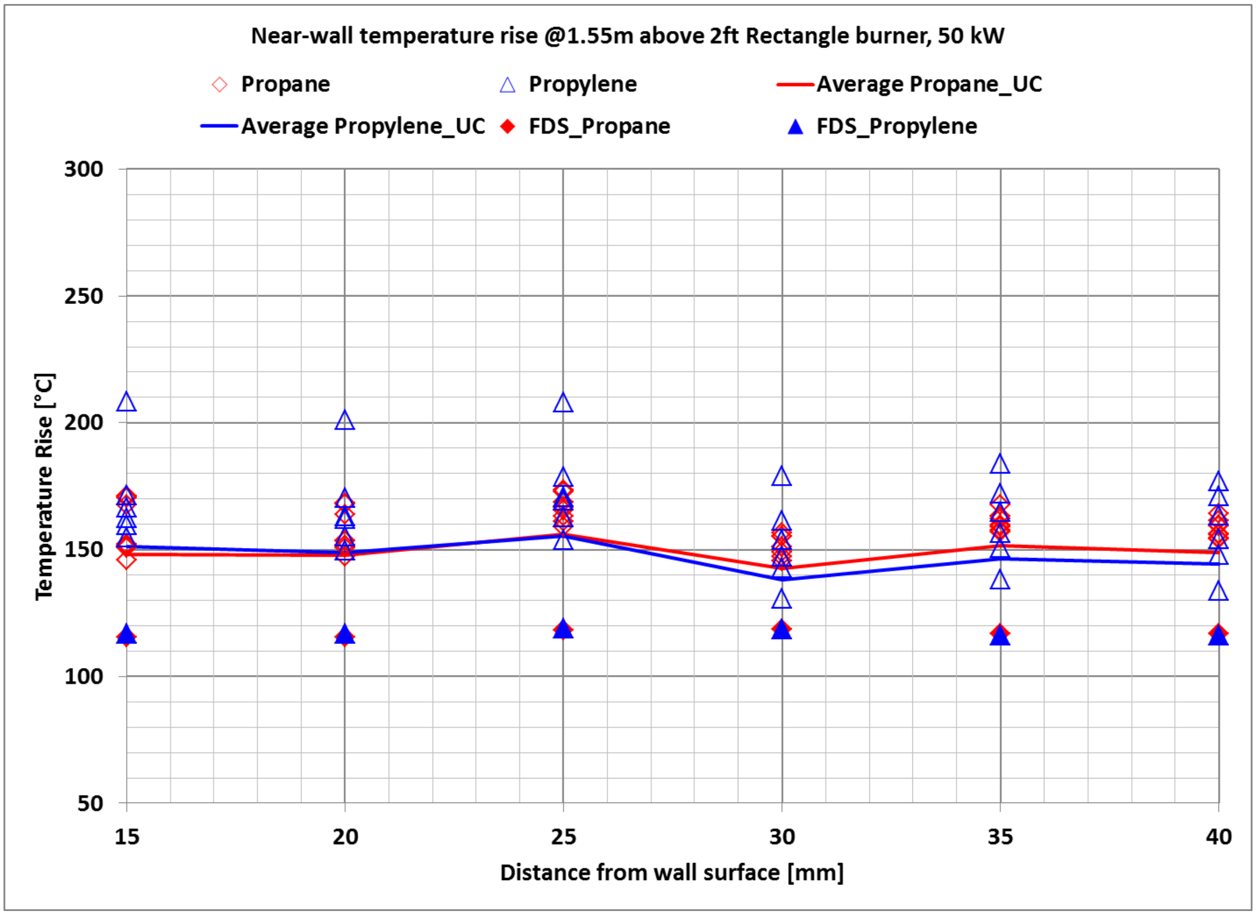

Figure 189 - Near-Wall Temperature Rise Experimental vs. FDS data @ 1.55m Above Burner, Rectangle, 50 kW

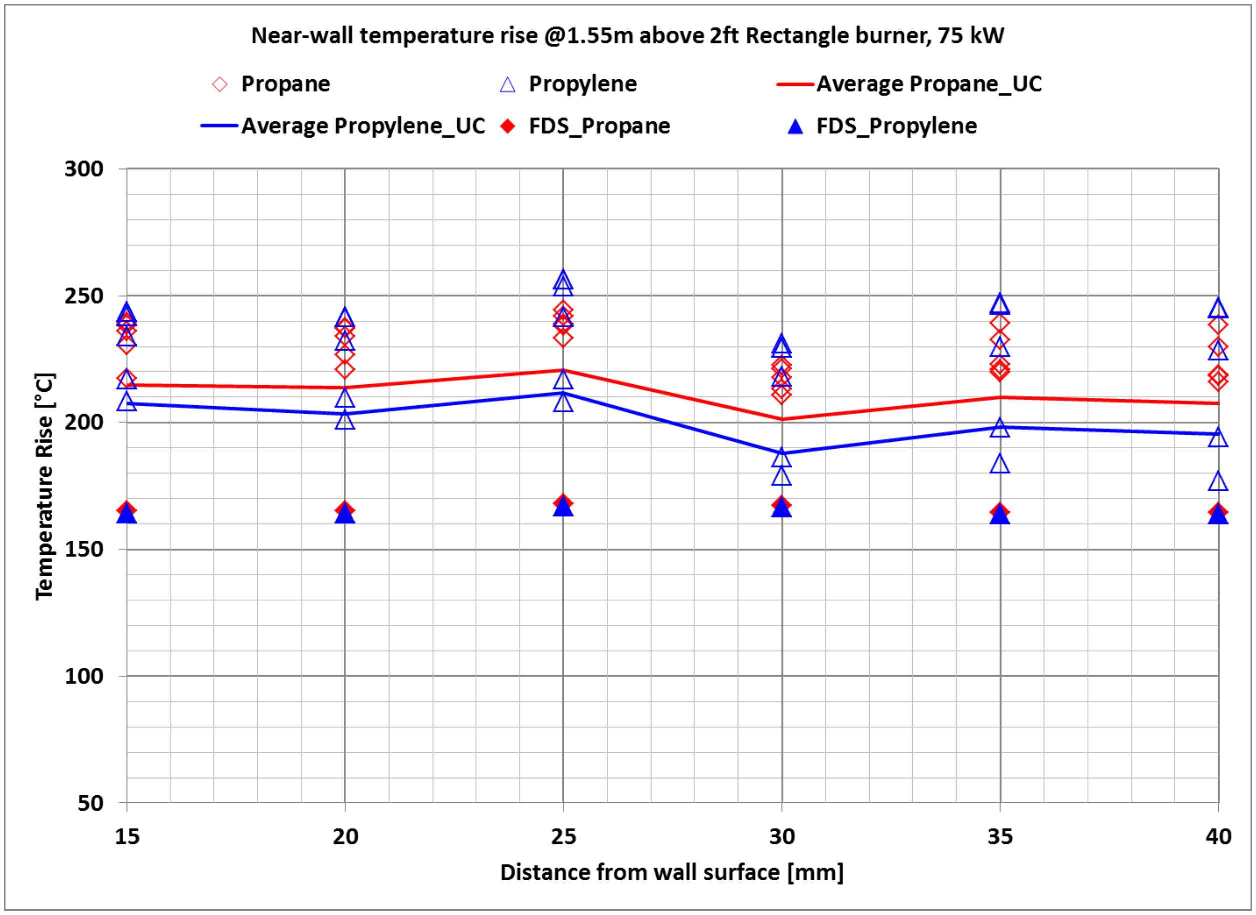

Figure 190 - Near-Wall Temperature Rise Experimental vs. FDS data @ 1.55m Above Burner, Rectangle, 75 kW

5.2.4 Wall heat flux

Gauge wall heat flux comparisons between experimental data and predictions, as grouped by fuel type and burner size, are presented in Figure 191 to Figure 195. The elevation of the probes had been normalized by the 50% intermittency flame height.

For all cases, the predicted heat flux at 2 ft away from the centerline correlates well with the measurements. The prediction of the heat flux at 1 ft away from the centerline correlates with the experimental data well up to a normalized height of 0.5, but over that height, the heat flux is greatly over-predicted by FDS. For the centerline heat flux, FDS underpredicted up to a normalized height of 0.5, but correlates well from the normalized height of 0.5 to 1.0, and vastly over-predicted from normalized height of 1.0 and above.

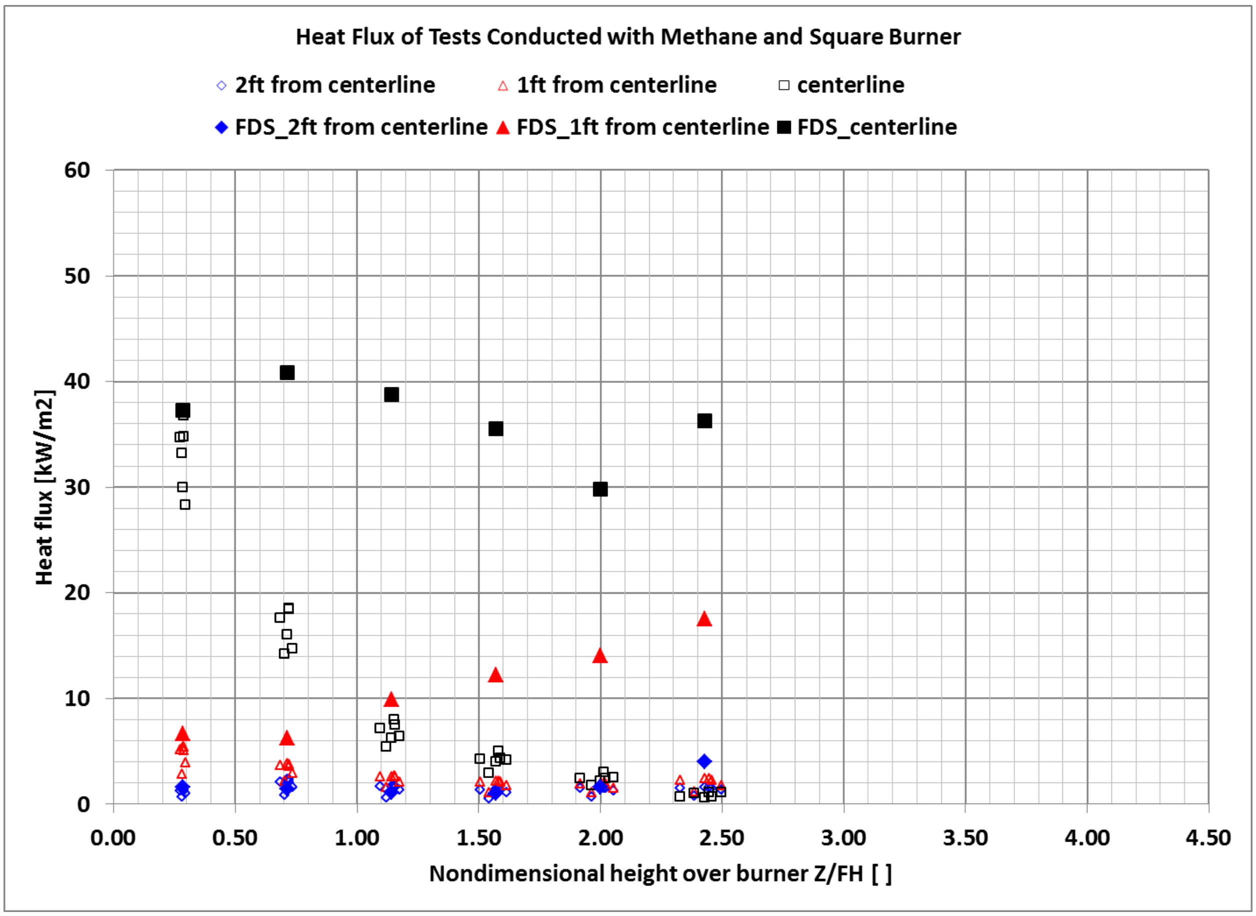

Figure 191 - Wall Heat Flux with Methane Source Fire Using the Square Burner

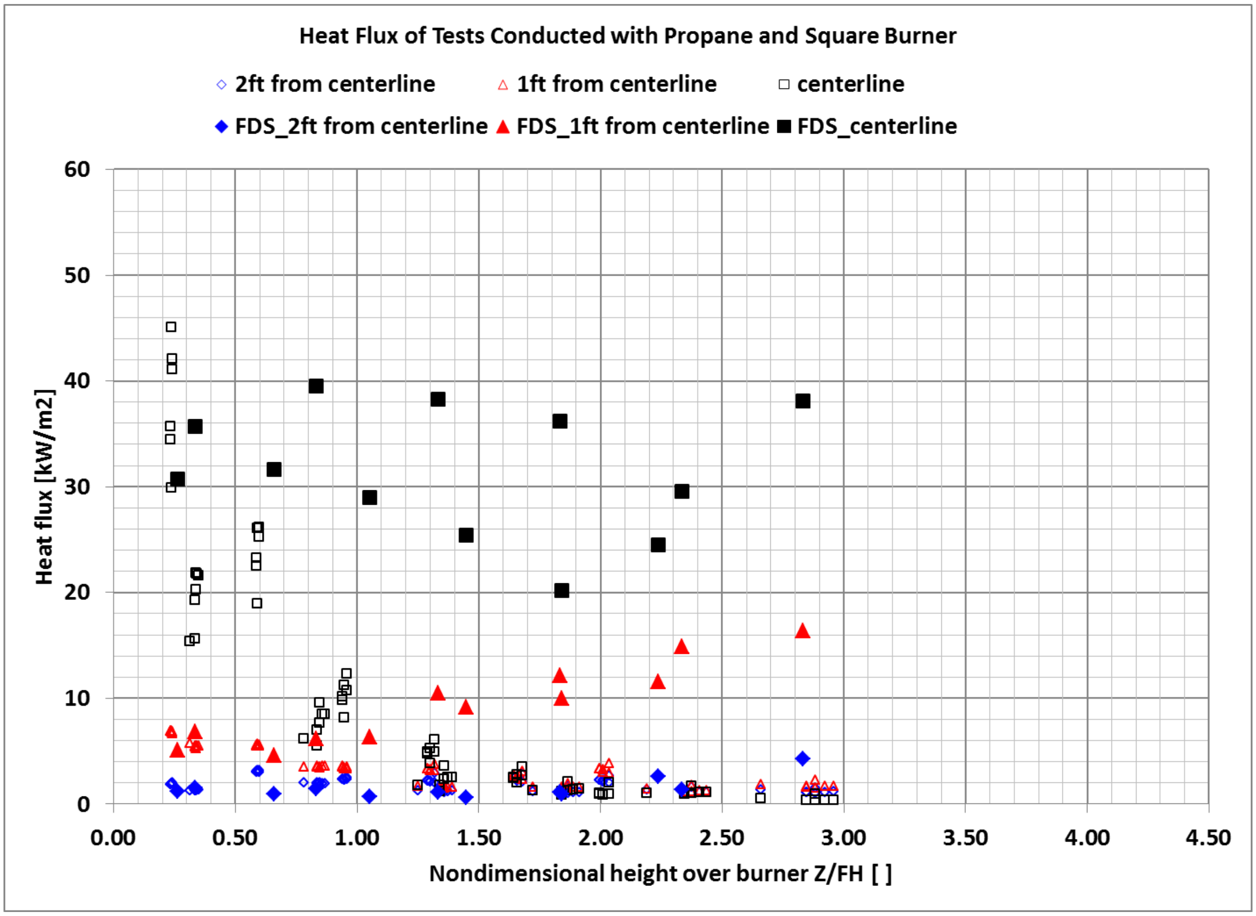

Figure 192 - Wall Heat Flux with Propane Source Fire Using the Square Burner

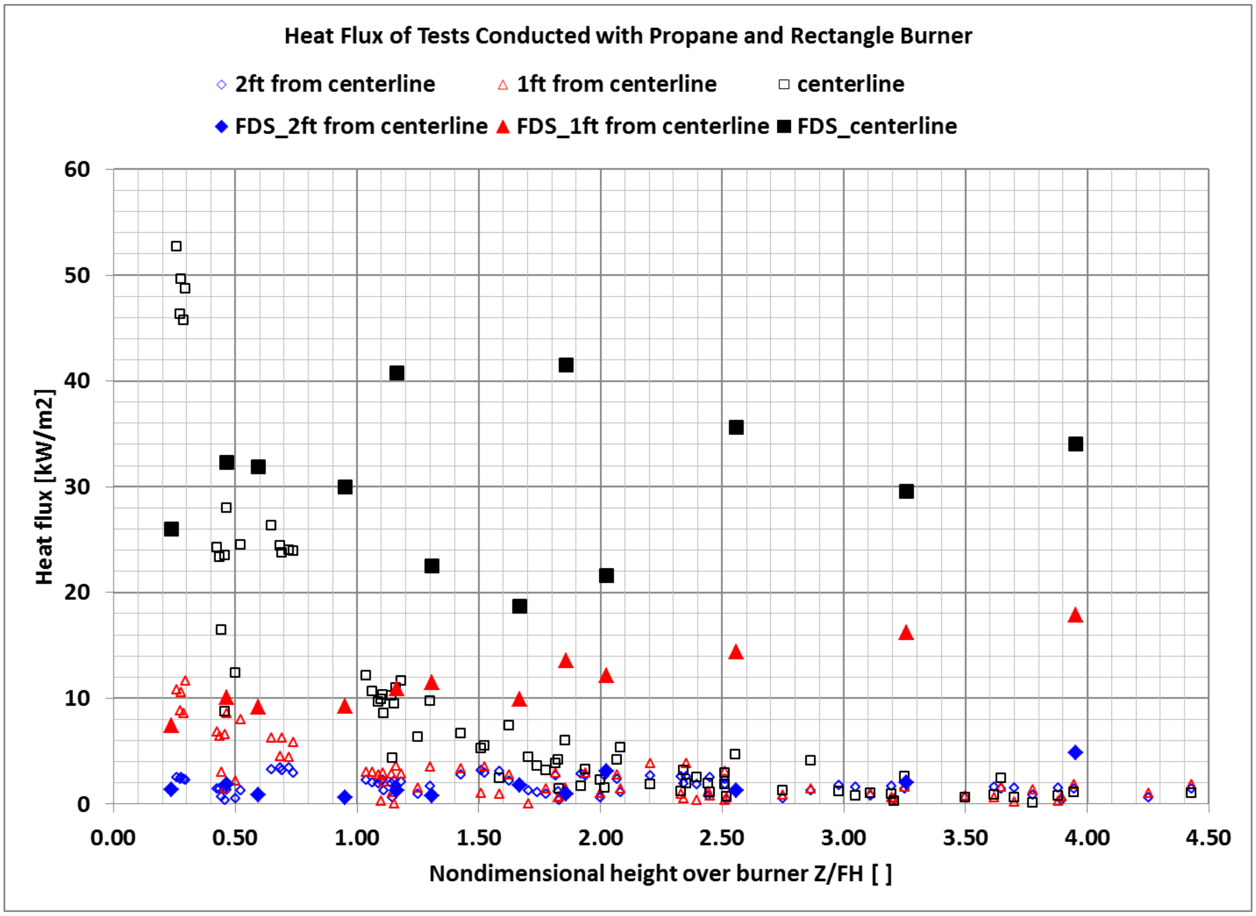

Figure 193 - Wall Heat Flux with Propane Source Fire Using the Rectangle Burner

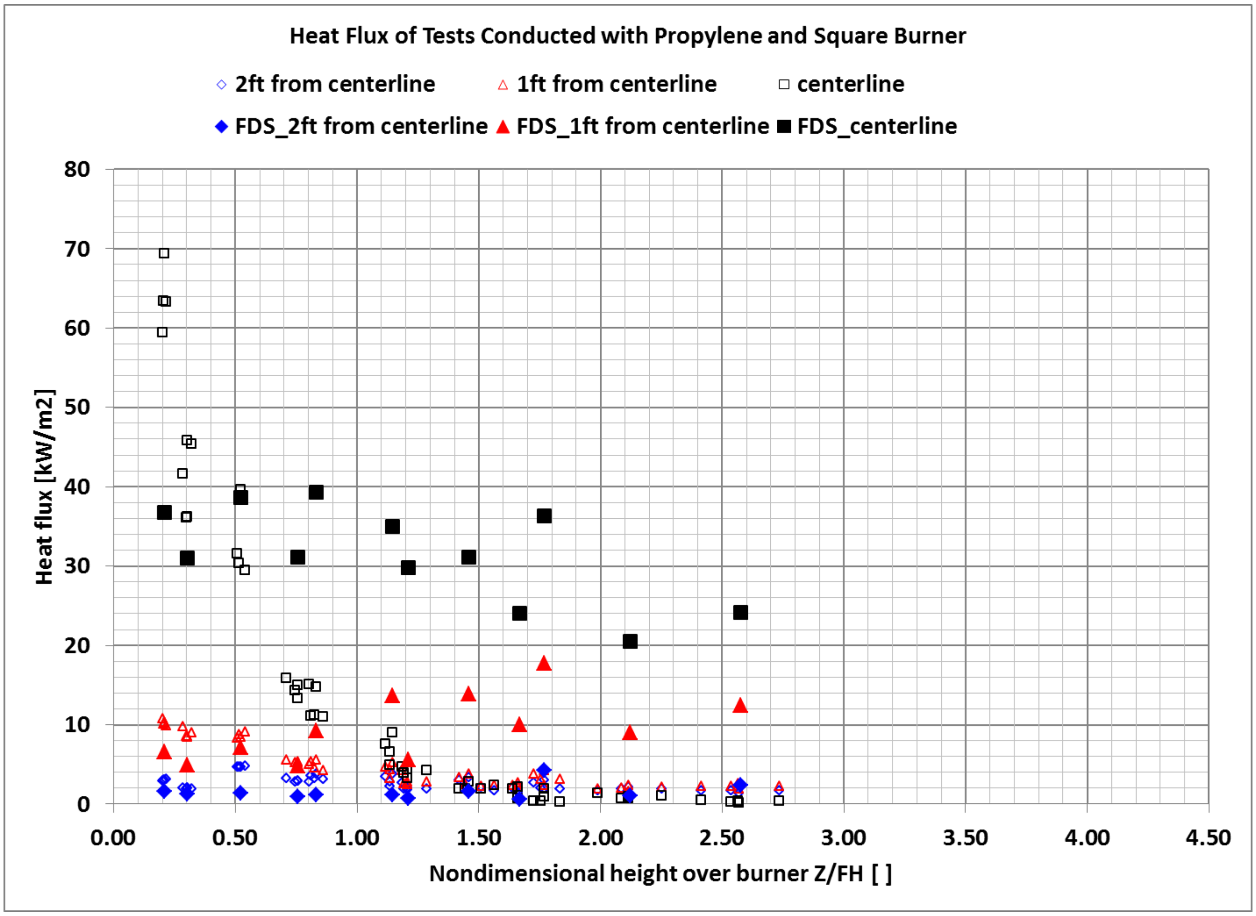

Figure 194 - Wall Heat Flux with Propylene Source Fire Using the Square Burner

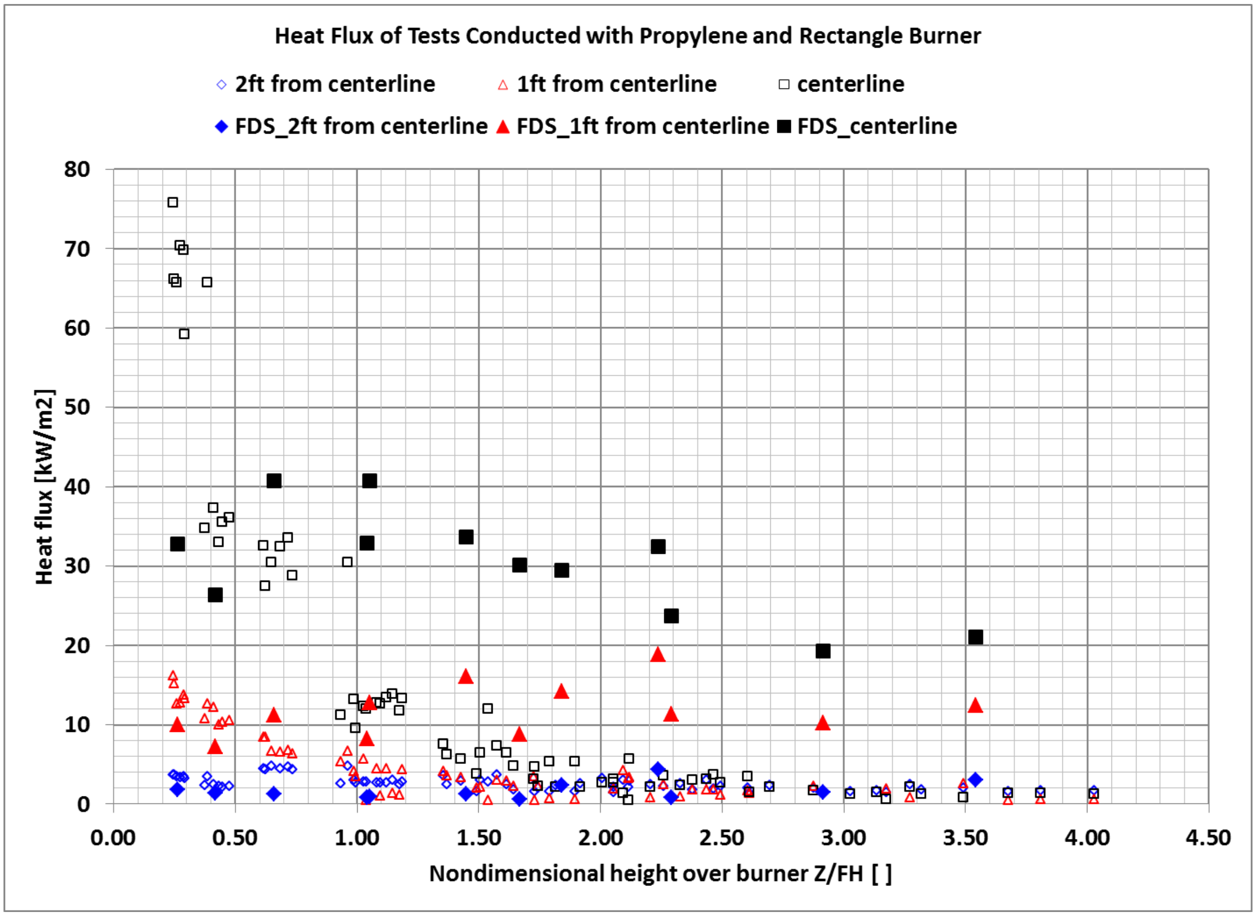

Figure 195 - Wall Heat Flux with Propylene Source Fire Using the Rectangle Burner

5.3 Combustible wall experiment and simulation comparisons

This section summarizes the comparison between the combustible wall experiments and the FDS results of the experiments. Not all of the data are presented, for now, only those test with a repeat or similar conditions are presented herein so that comparisons of similar tests can also be shown. The five test conditions that are repeated or similar are shown in Table 35.

Table 35 - Conditions of tests detailed in this report

Test Numbers	Burner size	Source HRR	Source Fuel
A8, A14	Square	75 kW	Propylene
A5, A15	Square	50 kW	Propane
A9, A11	Rectangle	50 kW	Propylene
A12, A13	Both	50 kW, continuous	Propylene
A16, A17	Both	75 kW, continuous	Propane

The combustible wall tests were conducted with a FRP wall material where the source fire was put against for ignition. The aluminum mesh used in the inert and plume tests were not used in the combustible wall tests and the initial fire plumes were observed to have skewed to the left or right by about 5° to 10°, this caused the subsequent flame spread over the panel to be skewed also. However, the final burn pattern revealed that the flame spread would be mostly symmetric if the skewed part of the burnt area was pasted to the opposite side. Also, due to the construction of the compartment, some of the hot gases from burning were trapped under the ceiling and developed a hot layer. These 2 effects are not modeled in the FDS simulations.

The FDS simulations presented in this report used mesh size at 0.05 m and all default FDS parameters except those needed to define the geometry and material properties of the FRP panel, which were provided by GPYRO. The HRR, centerline velocity, and centerline wall gauge heat flux are presented of the simulated tests are presented below.

5.3.1 Propylene, 75 kW, Square burner

Tests 8 and 14 were identical to each other except that the burner turn-off time was different. The source propylene fire was 75 kW with a Square burner. The HRRs of the burning panel in Tests 8 and 14, minus that of the source fire, are presented in Figure 196. The two FDS simulations were not able to predict flame spread adequately. During the first 60 to 70 sec when the source fire was on, the simulations predicted little ignition of the panel; then when the burner was “shut off” in the simulations, the fire on the panel did not sustain and spread as it would in the real tests.

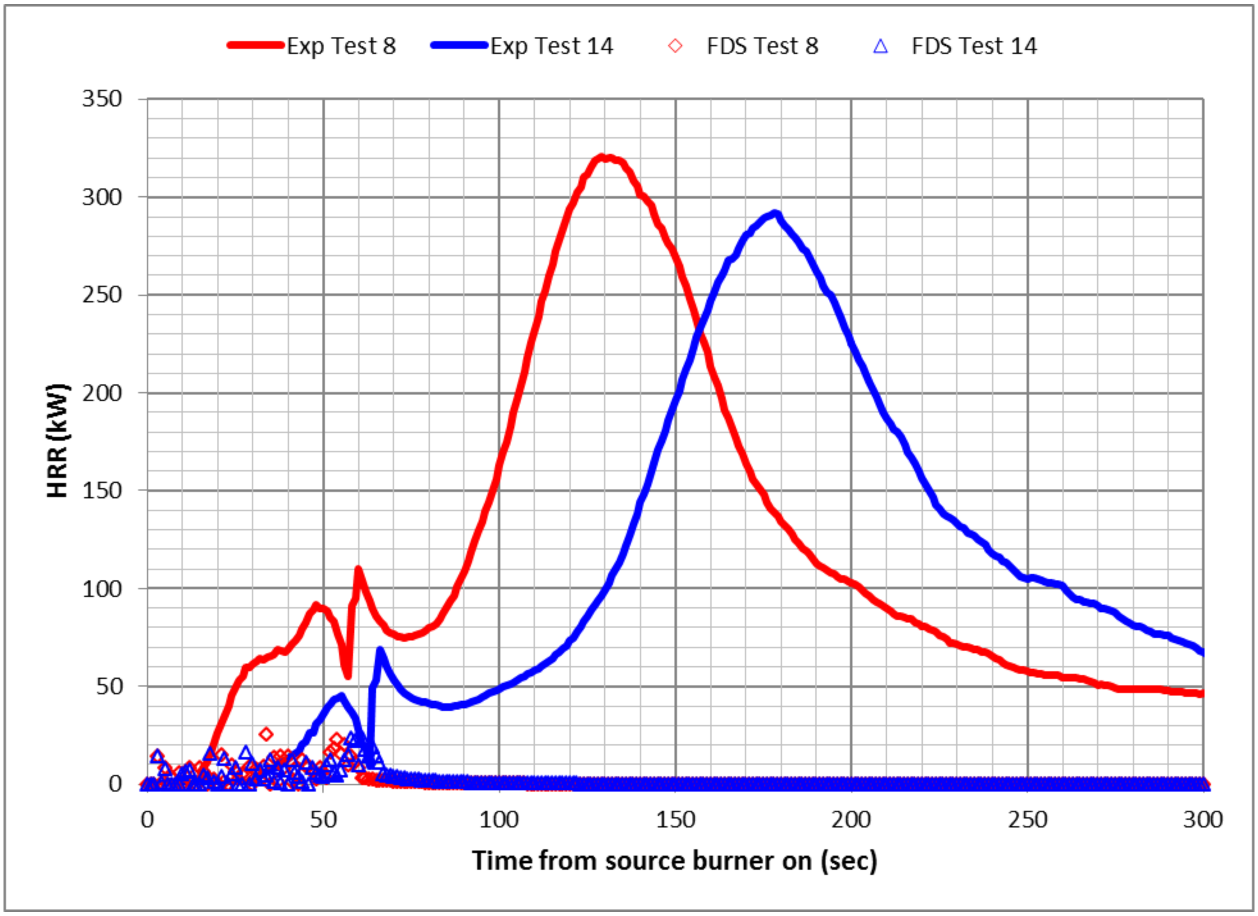

Figure 196 - HRRs of tests using propylene, 75 kW, Square burner

The velocity measured at 0.2 m, 0.8 m, and 1.4 m over the burner along the center is presented in Figure 197 to Figure 199. It is noted that the velocity measurement during the tests may be inaccurate after the instruments were exposed to fire for a short period of time, where the resulting velocity measurement is shifted due to thermal exposure. At 0.2 m above the burner, the velocity was under predicted, however at 0.8 m and 1.4 m FDS generally underpredicts but to a lesser degree. The velocity prediction was especially well done for Test 14 at 1.4 m above the burner, where the prediction tracks the centerline velocity during source fire activation and deactivation well.

Given the lack of flame spread and locations of the thermocouples in the FDS, the “devices” were not expected to pick up the changes in centerline velocity generated due to the real flame spread such as when the upper layer descended and created a negative-Z flow.

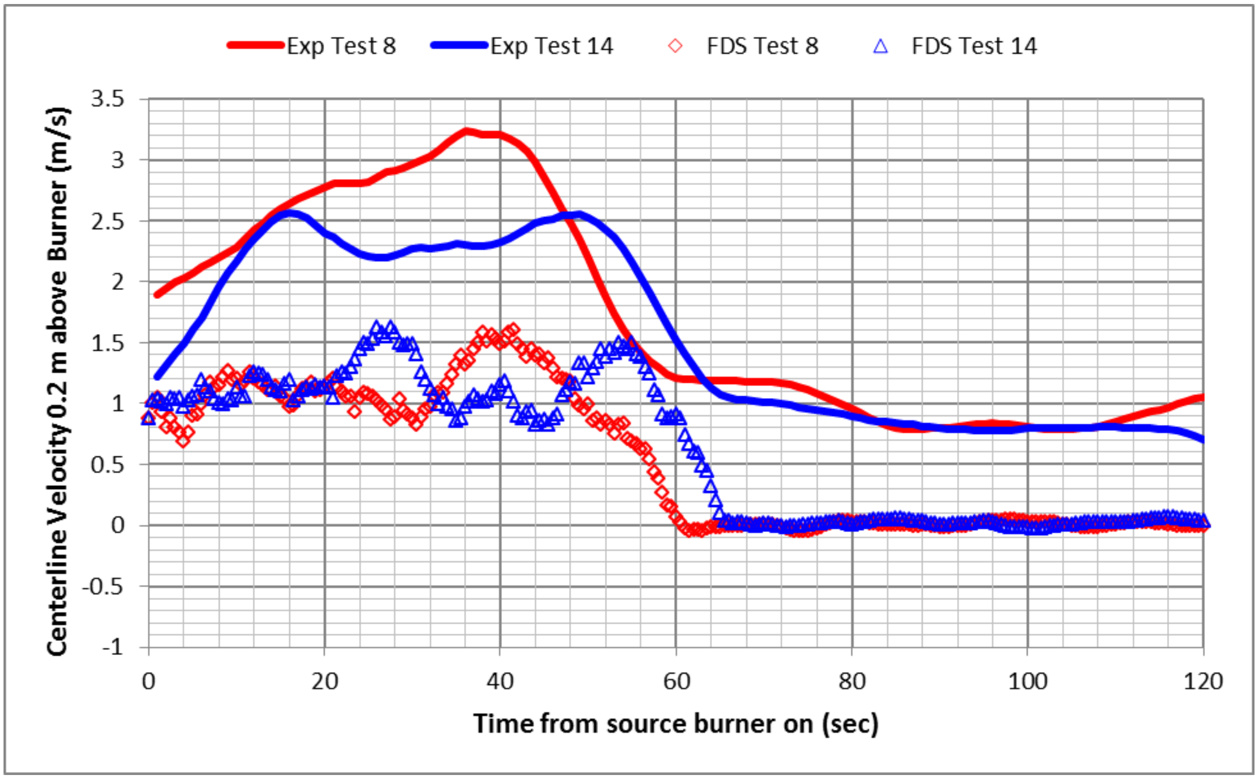

Figure 197 – Centerline temperature at 0.2 m above burner of tests using propylene, 75 kW, Square burner

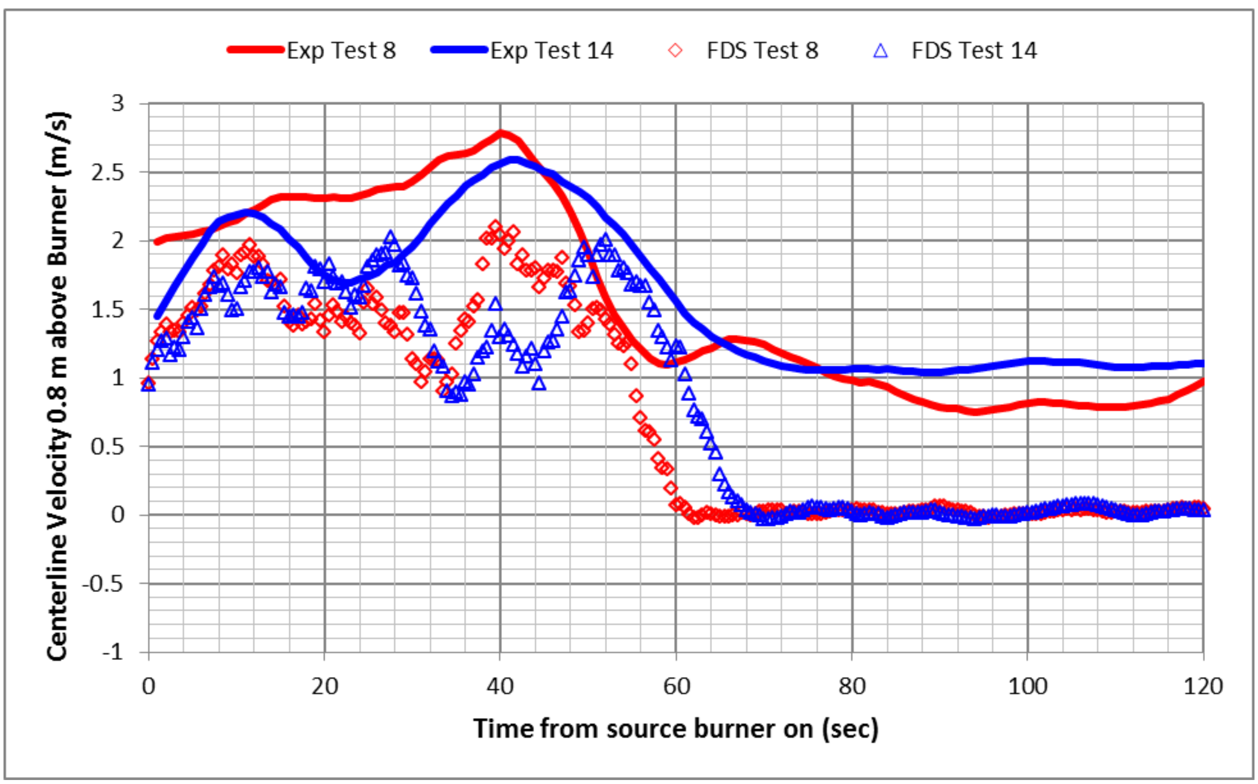

Figure 198 - Centerline temperature at 0.8 m above burner of tests using propylene, 75 kW, Square burner

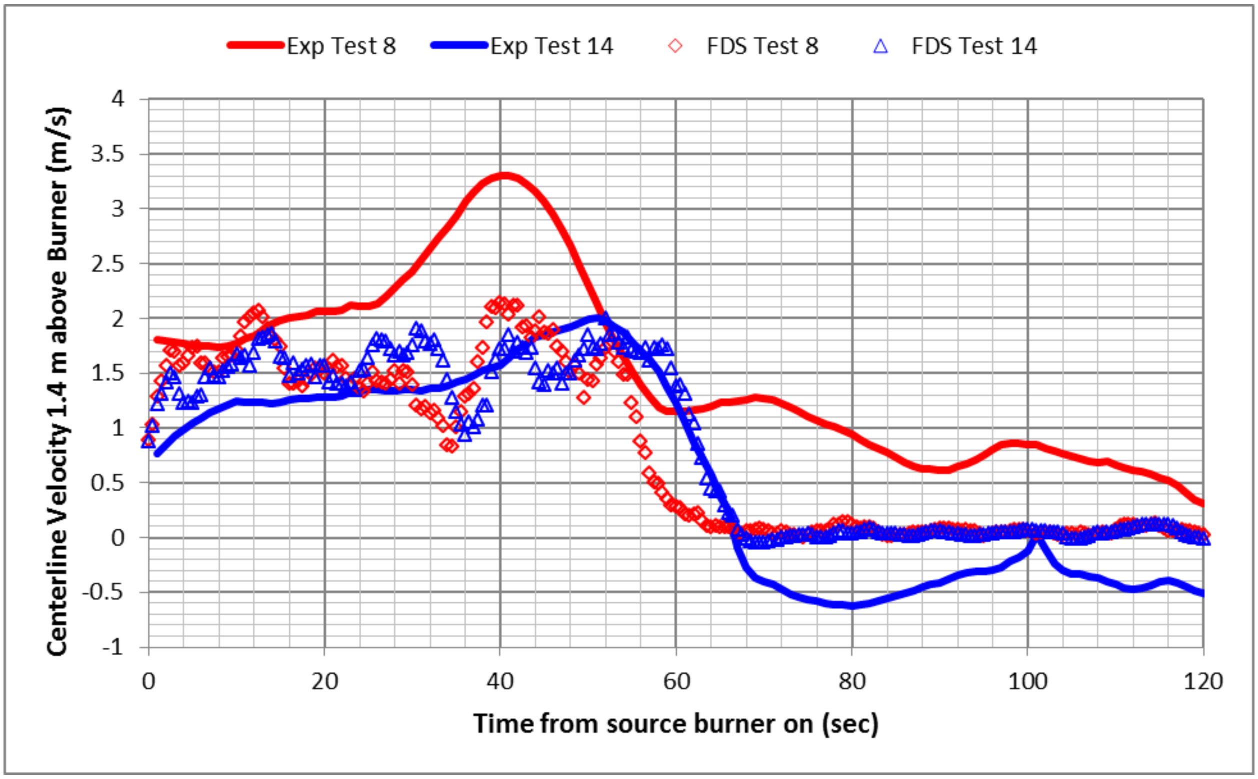

Figure 199 - Centerline temperature at 1.4 m above burner of tests using propylene, 75 kW, Square burner

The heat flux measured along the centerline was not corrected for convection. The comparison between the measured heat flux to the predicted gauge heat flux at 0.2 m, 0.5 m, 1.1 m, and 1.7 m over the burner surface are shown in Figure 200 to Figure 203. FDS appears to over-predict the heat flux at these locations except for the one located at 0.2 m. However, due to the lack of flame spread predicted, the modeled heat flux only accounts for that generated by the source fire, whereas in the experiments, the heat flux measured was from the source fire and from the FRP panel fire, as well as from the upper layer.

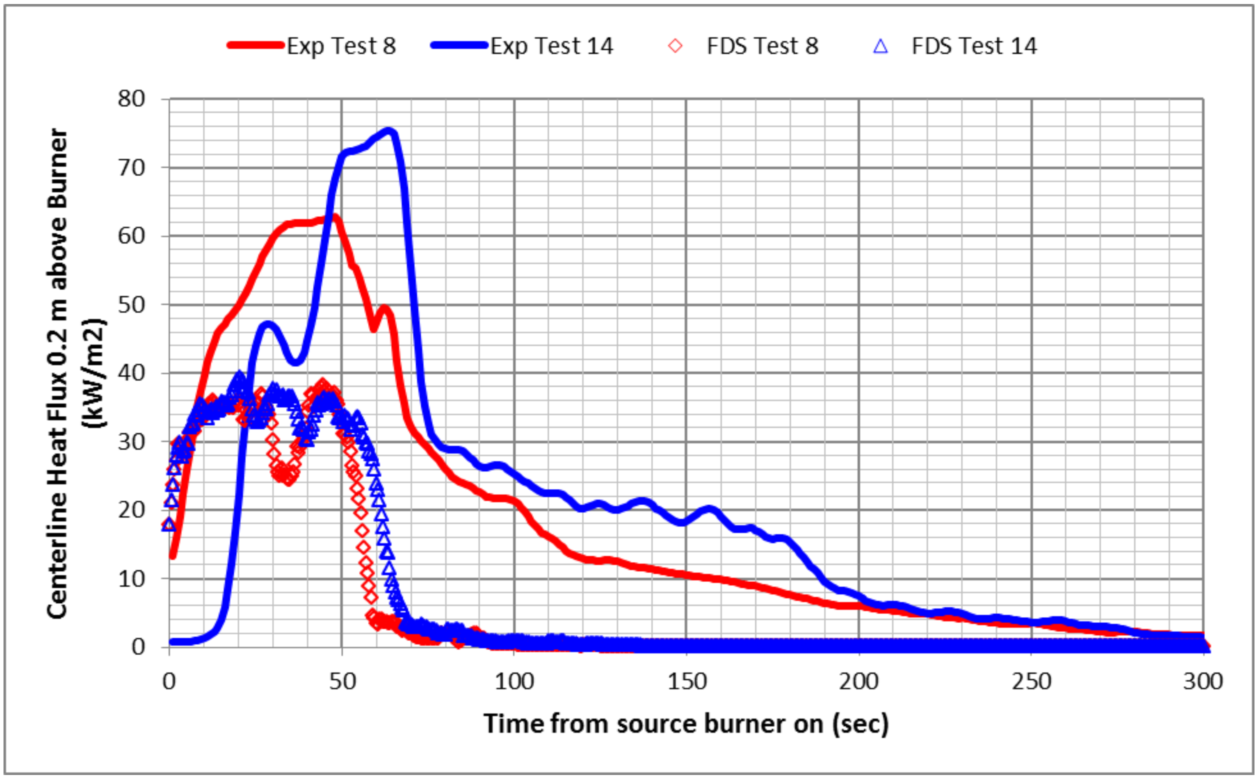

Figure 200 - Centerline heat flux at 0.2 m above burner of tests using propylene, 75 kW, Square burner

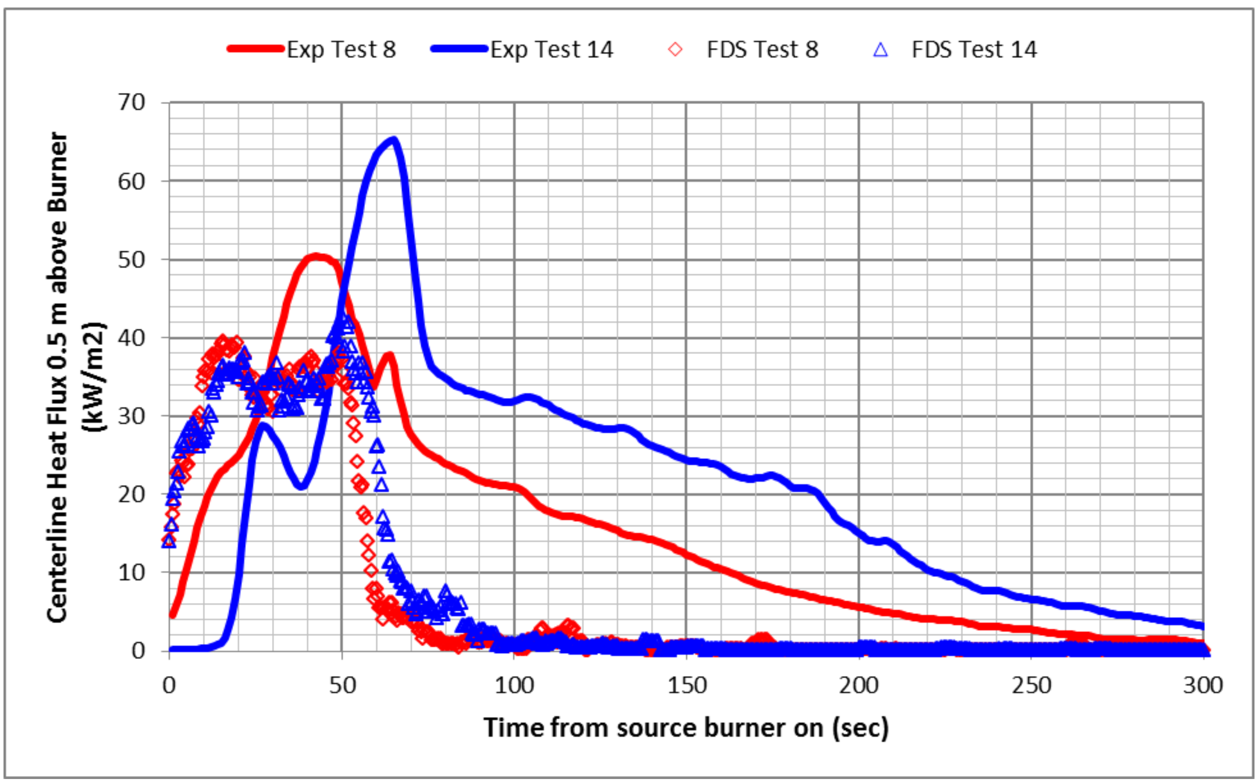

Figure 201 – Centerline heat flux at 0.5 m above burner of tests using propylene, 75 kW, Square burner

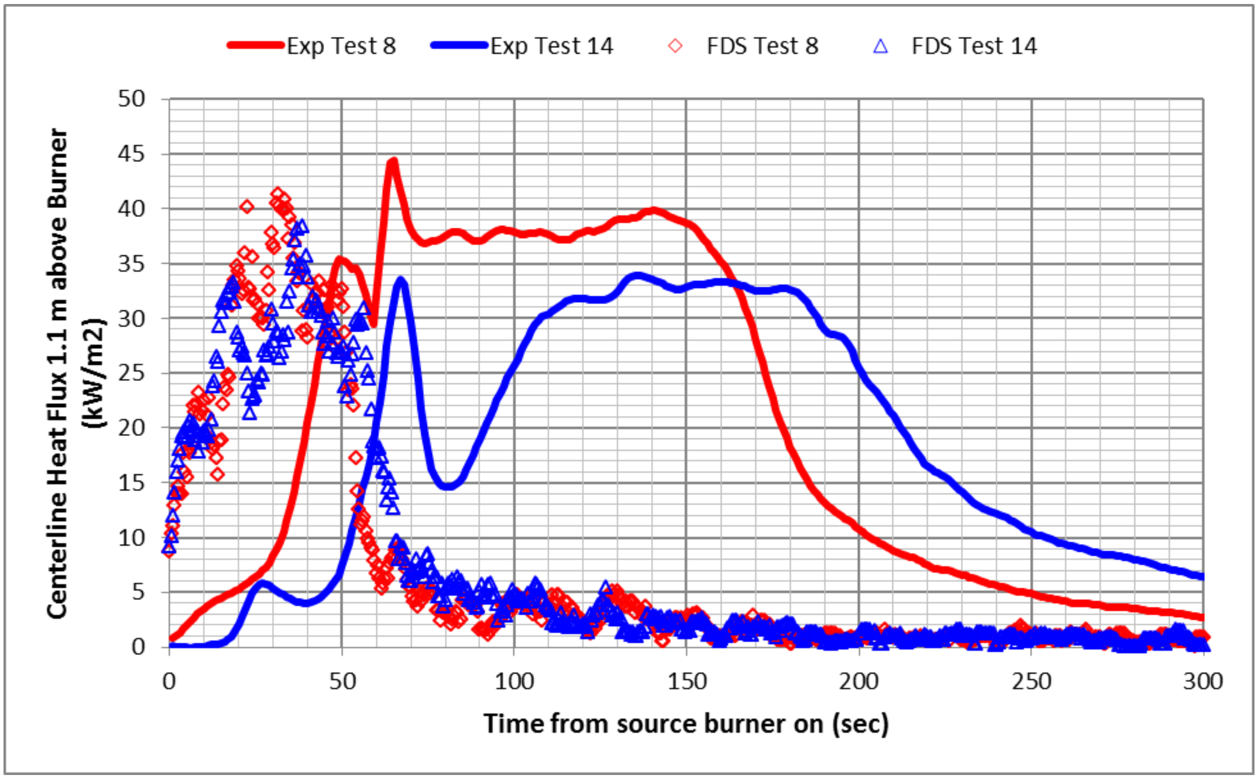

Figure 202 - Centerline heat flux at 1.1 m above burner of tests using propylene, 75 kW, Square burner

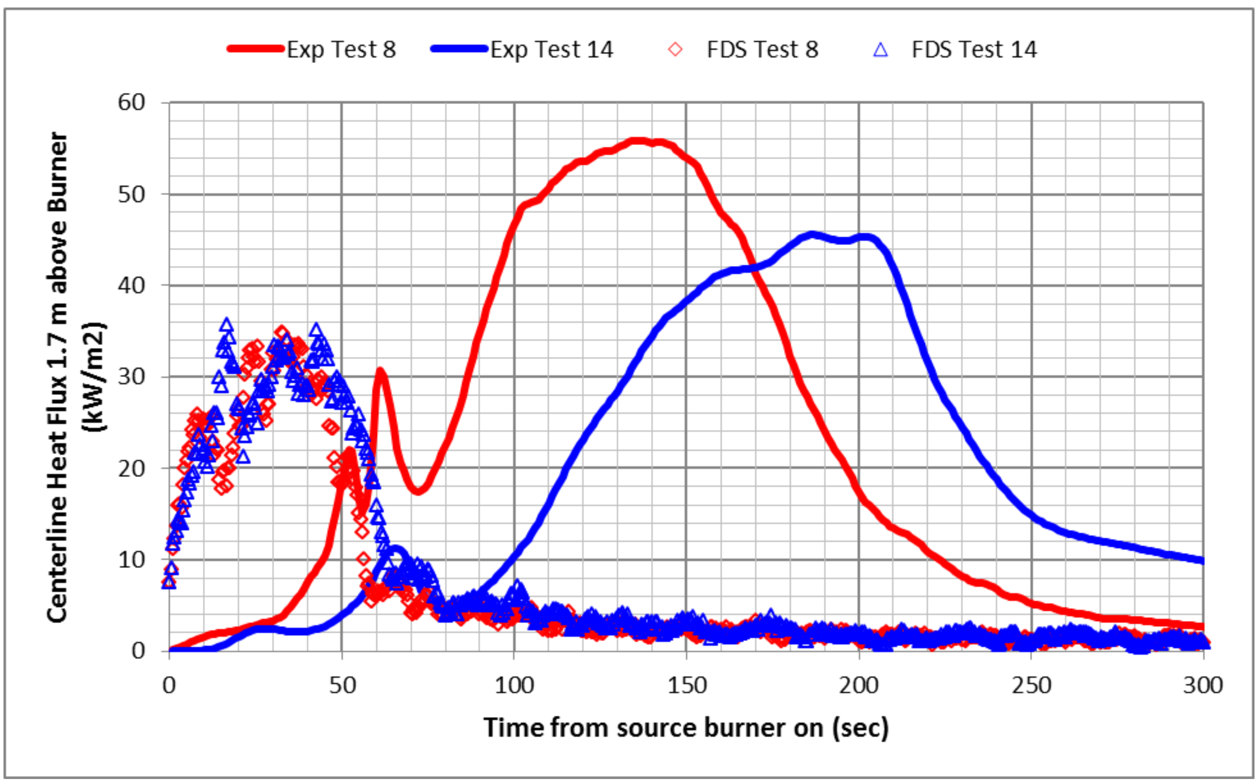

Figure 203 - Centerline heat flux at 1.7 m above burner of tests using propylene, 75 kW, Square burner

5.3.2 Propane, 50 kW, Square burner

Tests 5 and 15 were identical to each other except that the burner turn-off time was different. The source propylene fire was 50 kW with a Square burner. The HRRs of the burning panel in Tests 5 and 15, minus that of the source fire, are presented in Figure 204. The two FDS simulations were not able to predict flame spread adequately. During the first 70 to 90 sec when the source fire was on, the simulations predicted little ignition of the panel; then when the burner was "shut off" in the simulations, the fire on the panel did not sustain and spread as it would in the real tests. It should be noted that both simulations appeared to track the initial FRP burning quite well until the burner was turned off (shown by the "discontinuity" of the HRR curve).

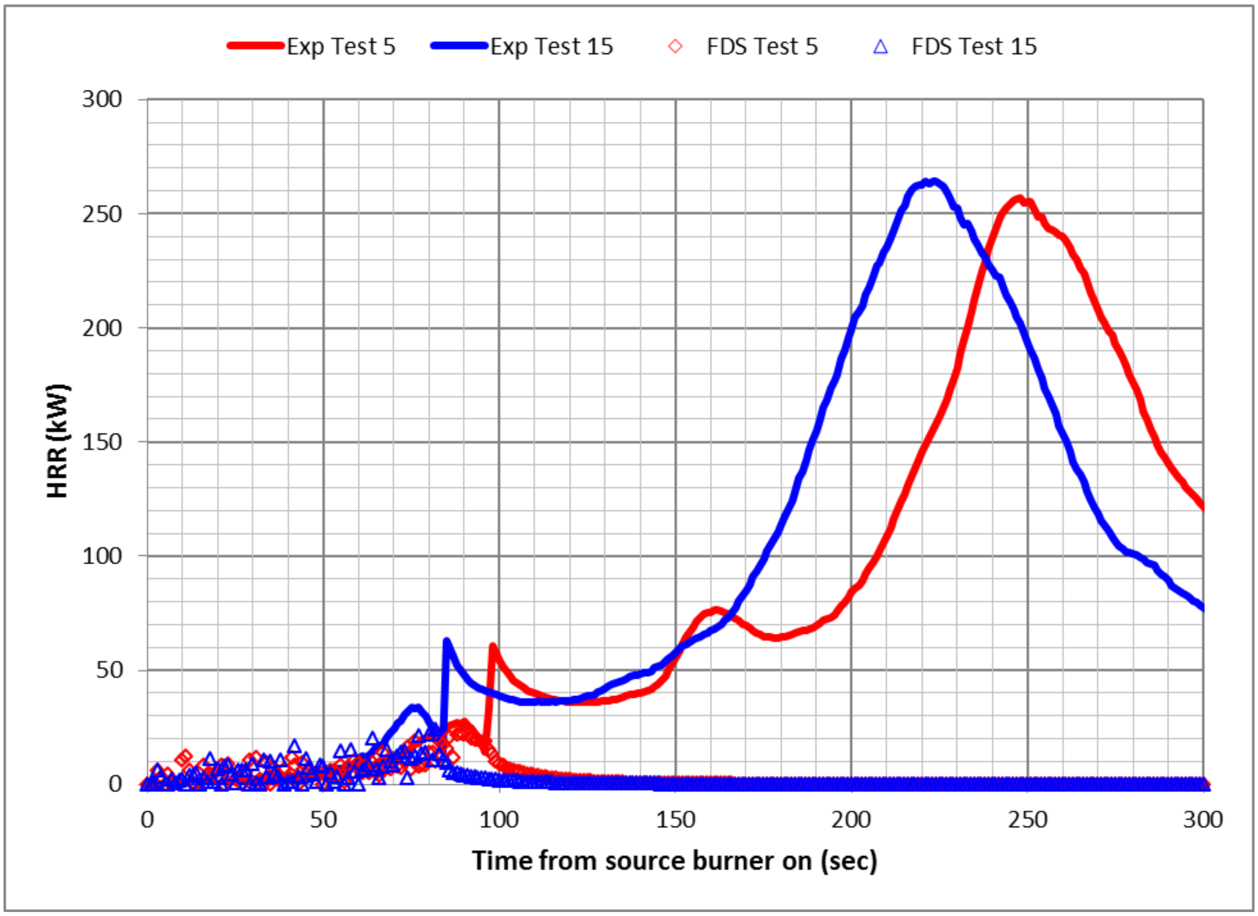

Figure 204 - HRRs of tests using propane, 50 kW, Square burner

The velocity measured at 0.2 m, 0.8 m, and 1.4 m over the burner along the center is presented in Figure 205 to Figure 207. It is noted that the velocity measurement during the tests may be inaccurate after the instruments were exposed to fire for a short period of time, where the resulting velocity measurement is shifted due to thermal exposure. At 0.2 m above the burner, the velocity was under predicted; however at 0.8 m and 1.4 m FDS generally tracks the measured velocity quite well.

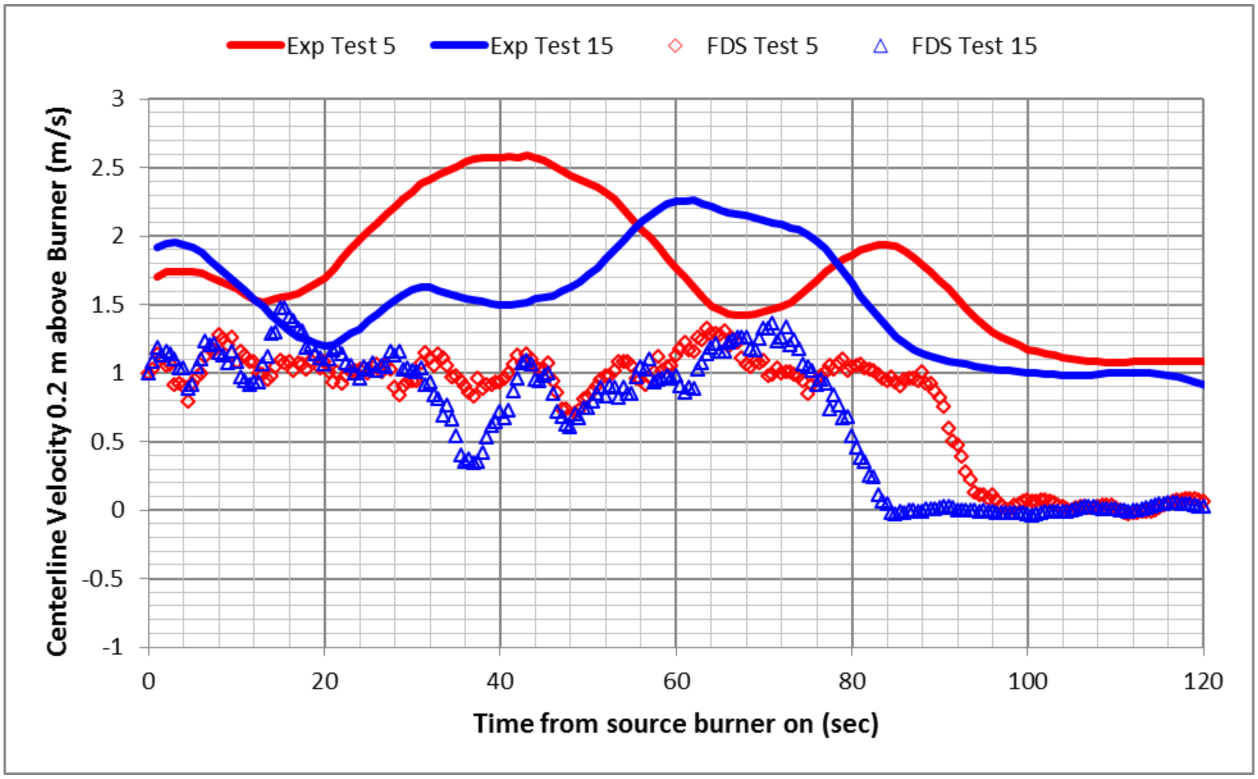

Figure 205 – Centerline temperature at 0.2 m above burner of tests using propane, 50 kW, Square burner

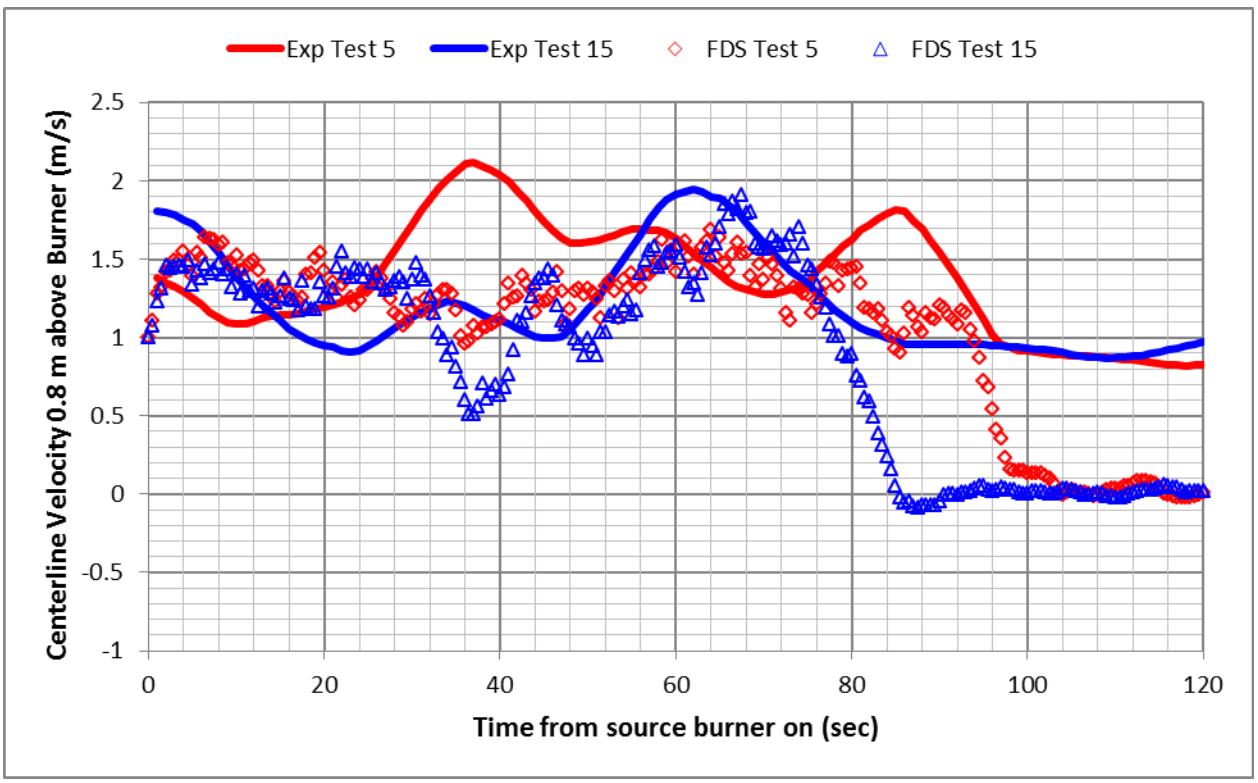

Figure 206 - Centerline temperature at 0.8 m above burner of tests using propane, 50 kW, Square burner

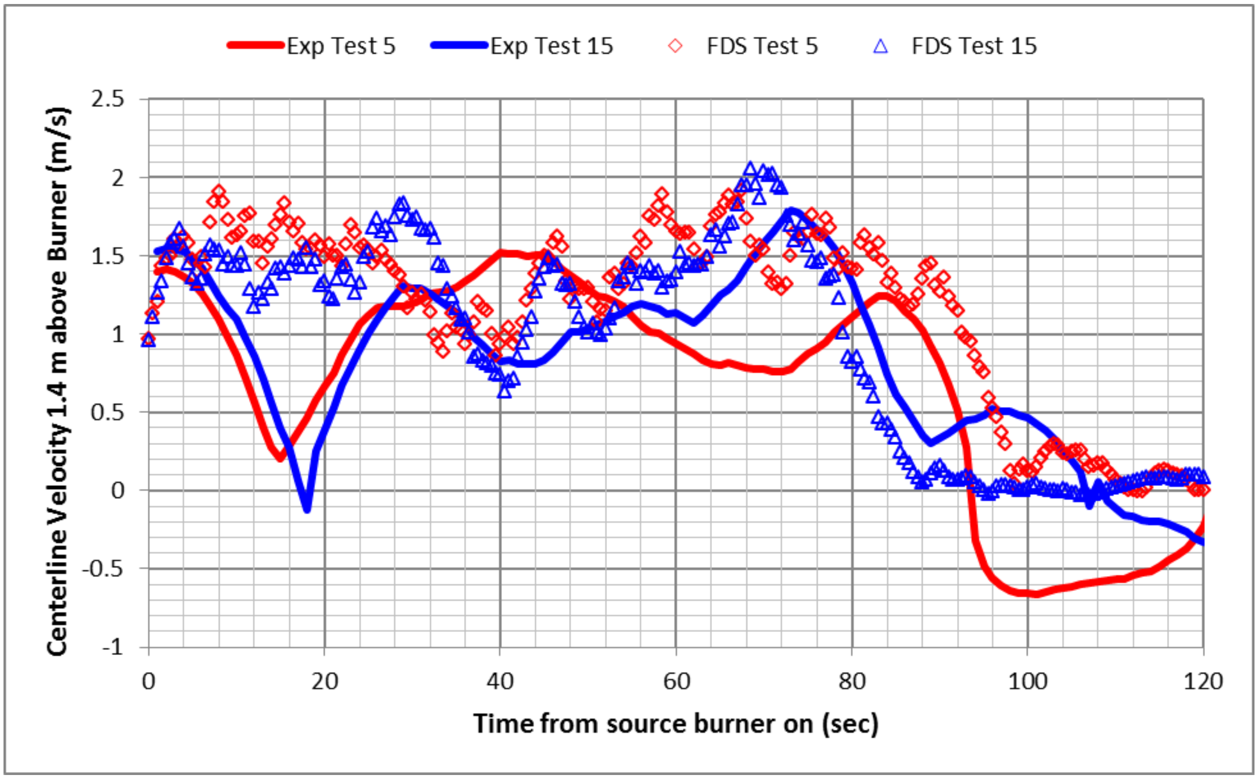

Figure 207 - Centerline temperature at 1.4 m above burner of tests using propane, 50 kW, Square burner

The heat flux measured along the centerline was not corrected for convection. The comparison between the measured heat flux to the predicted gauge heat flux at 0.2 m, 0.5 m, 1.1 m, and 1.7 m over the burner surface are shown in Figure 208 to Figure 211. FDS appears to over-predict the heat flux at these locations except for the one located at 0.2 m, where the predicted and measured heat flux was on par with each other. However, due to the lack of flame spread predicted, the modeled heat flux only accounts for that generated by the source fire, whereas in the experiments, the heat flux measured was from the source fire and from the FRP panel fire, as well as from the upper layer.

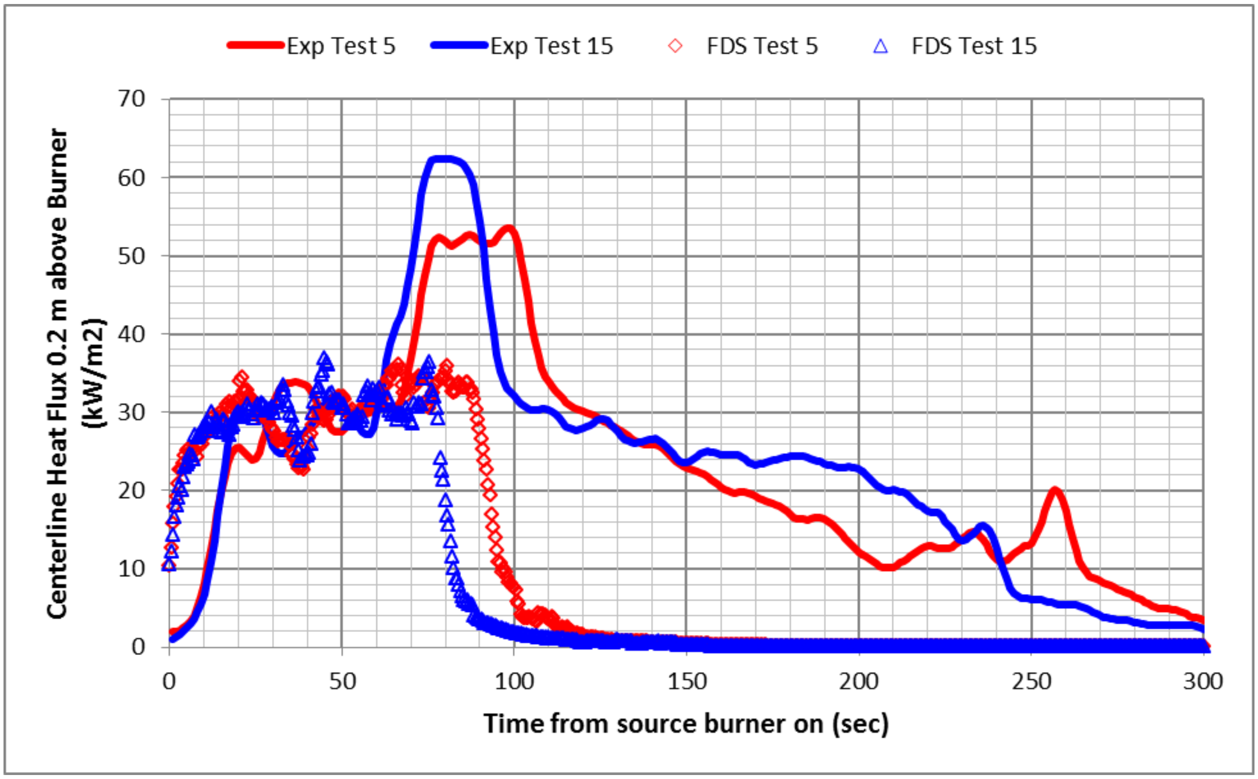

Figure 208 - Centerline heat flux at 0.2 m above burner of tests using propane, 50 kW, Square burner

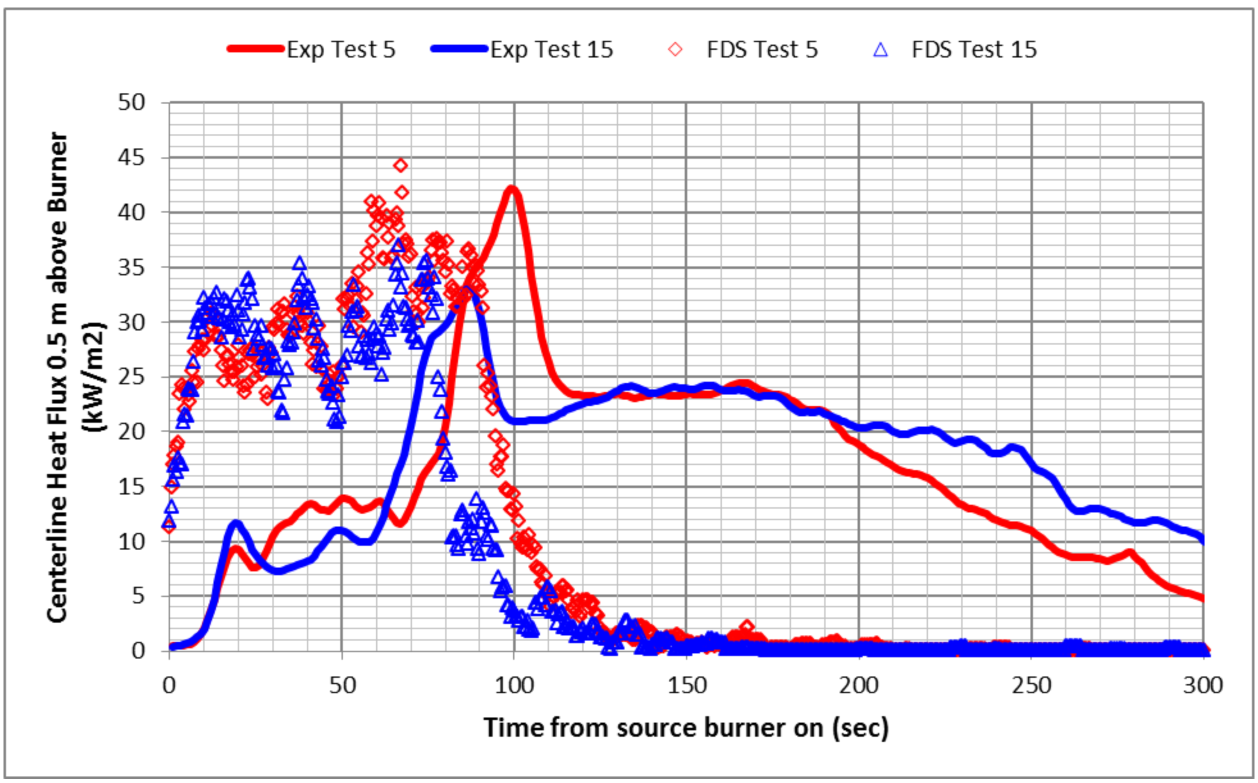

Figure 209 – Centerline heat flux at 0.5 m above burner of tests using propane, 50 kW, Square burner

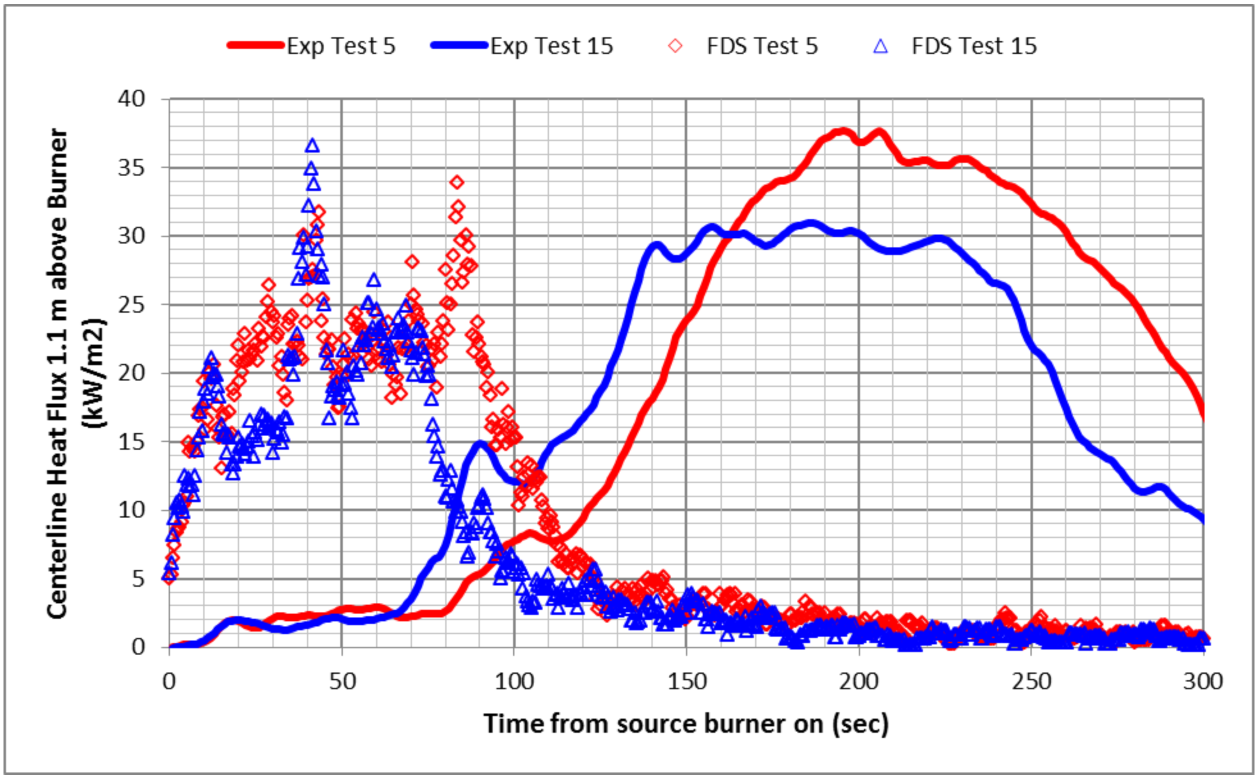

Figure 210 - Centerline heat flux at 1.1 m above burner of tests using propane, 50 kW, Square burner

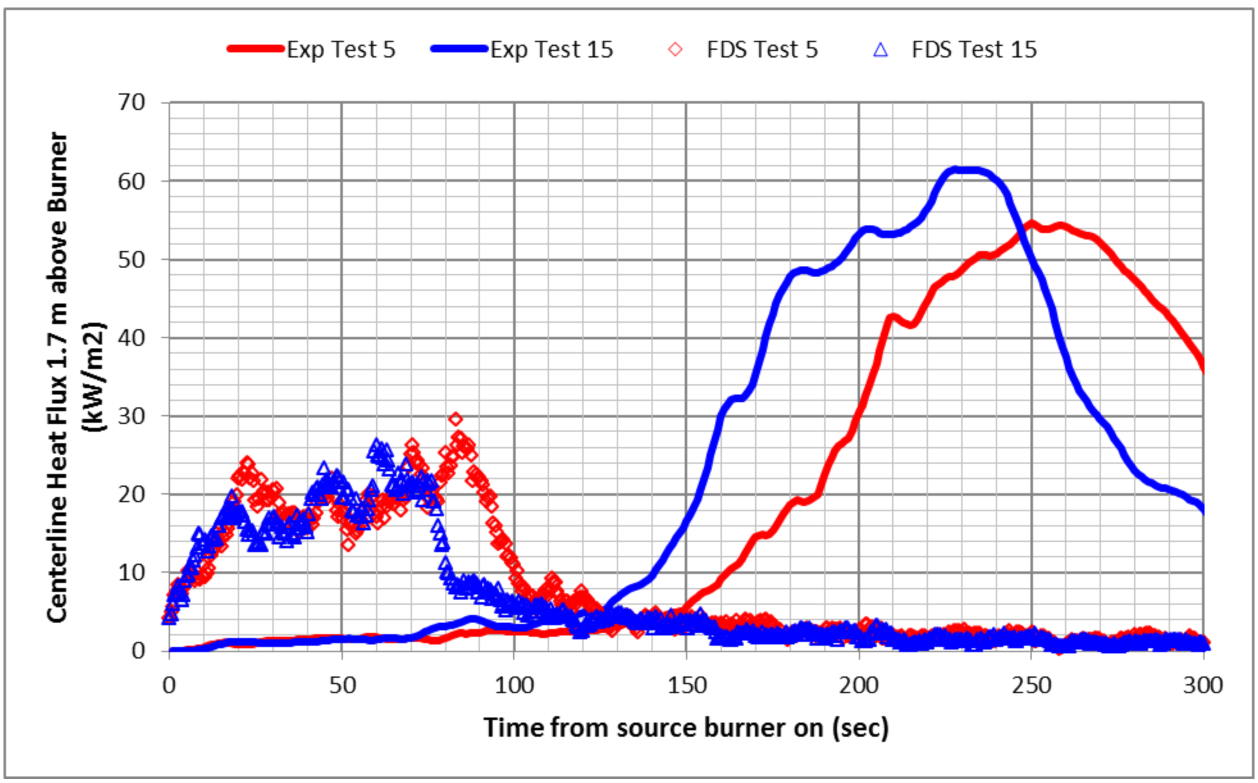

Figure 211 - Centerline heat flux at 1.7 m above burner of tests using propane, 50 kW, Square burner

5.3.3 Propane, 50 kW, Rectangle burner

Tests 9 and 11 were identical to each other except that the burner turn-off time was different. The source propane fire was 50 kW with a Rectangle burner. The HRRs of the burning panel in Tests 9 and 11, minus that of the source fire, are presented in Figure 212. The two FDS simulations were not able to predict flame spread adequately. During the first 60 to 70 sec when the source fire was on, the simulations predicted little ignition of the panel; then when the burner was “shut off” in the simulations, the fire on the panel did not sustain and spread as it would in the real tests.

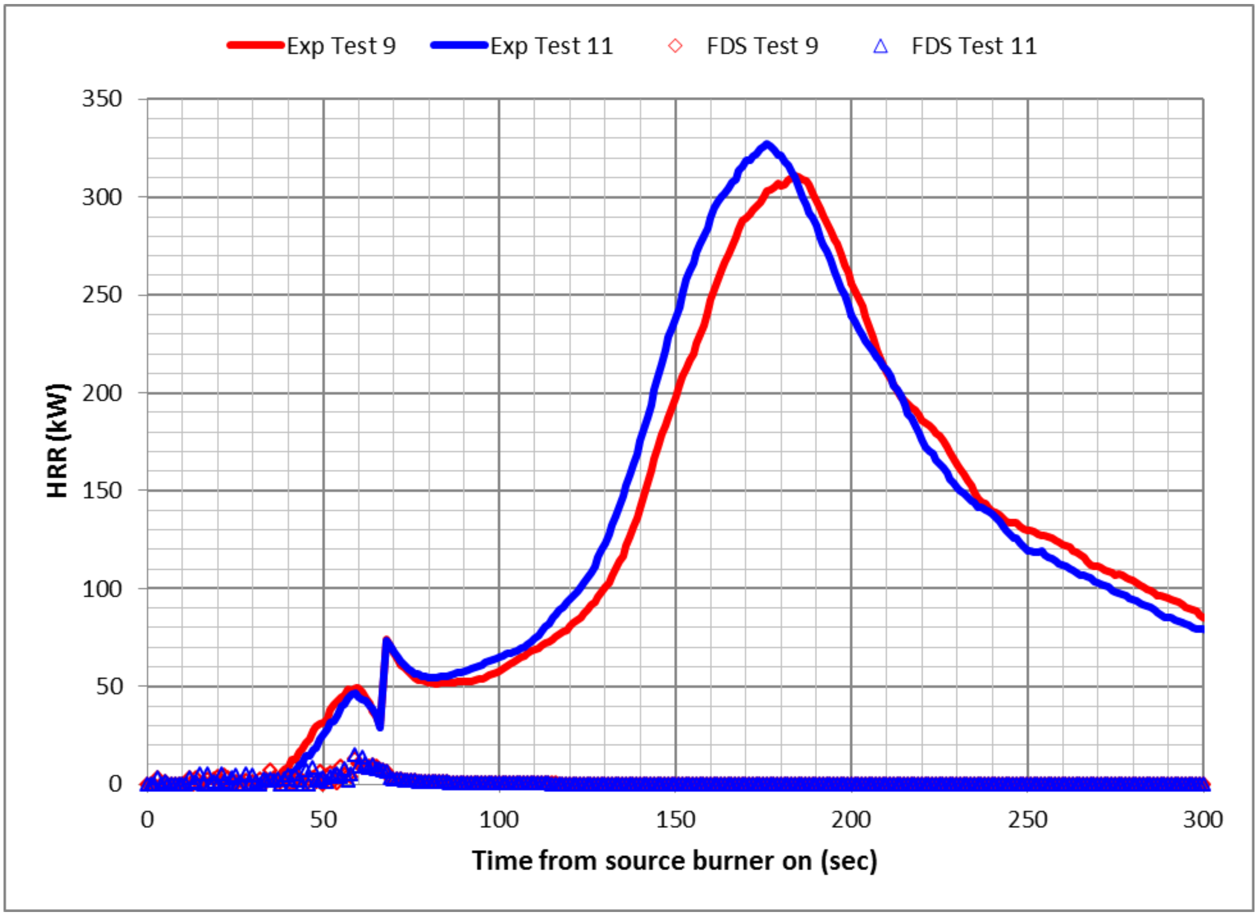

Figure 212 - HRRs of tests using propane, 50 kW, Rectangle burner

The velocity measured at 0.2 m, 0.8 m, and 1.4 m over the burner along the center is presented in Figure 213 to Figure 215. It is noted that the velocity measurement during the tests may be inaccurate after the instruments were exposed to fire for a short period of time, where the resulting velocity measurement is shifted due to thermal exposure. Generally, FDS under predicts the velocity at these points as compared to the experimental data.

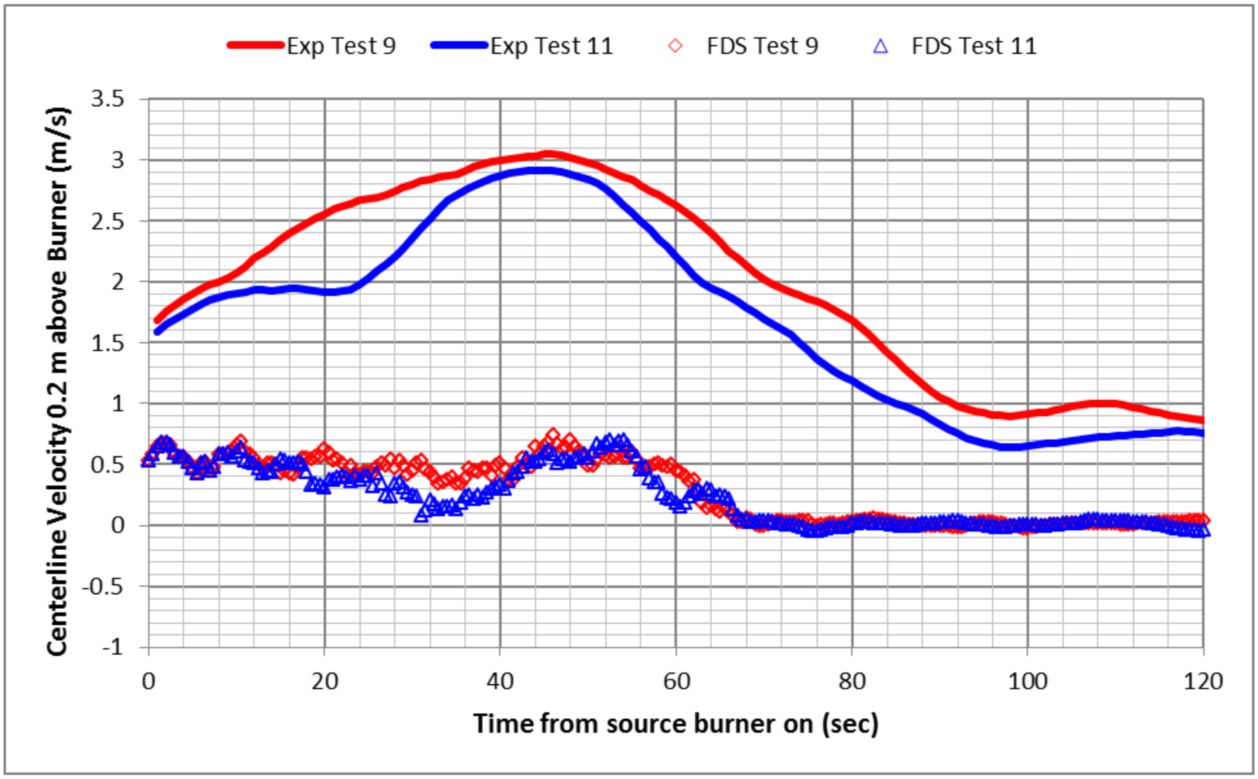

Figure 213 – Centerline temperature at 0.2 m above burner of tests using propane, 50 kW, Rectangle burner

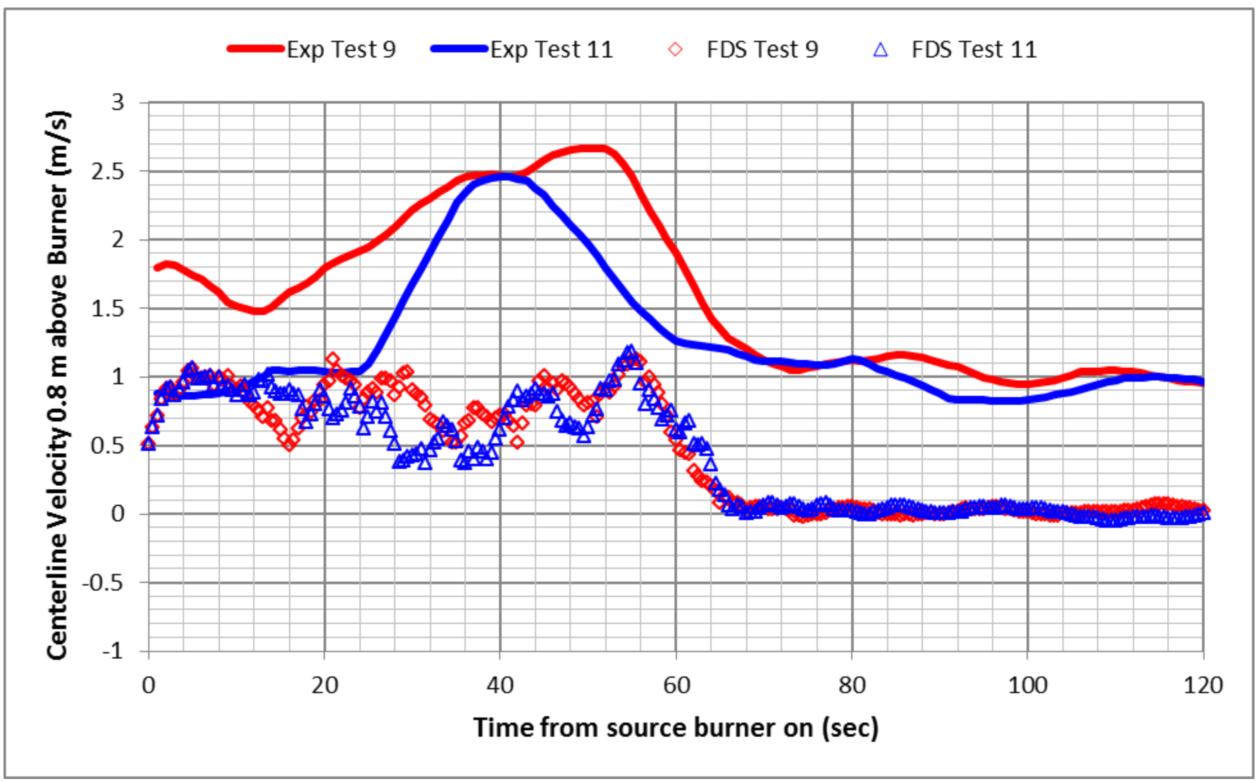

Figure 214 - Centerline temperature at 0.8 m above burner of tests using propane, 50 kW, Rectangle burner

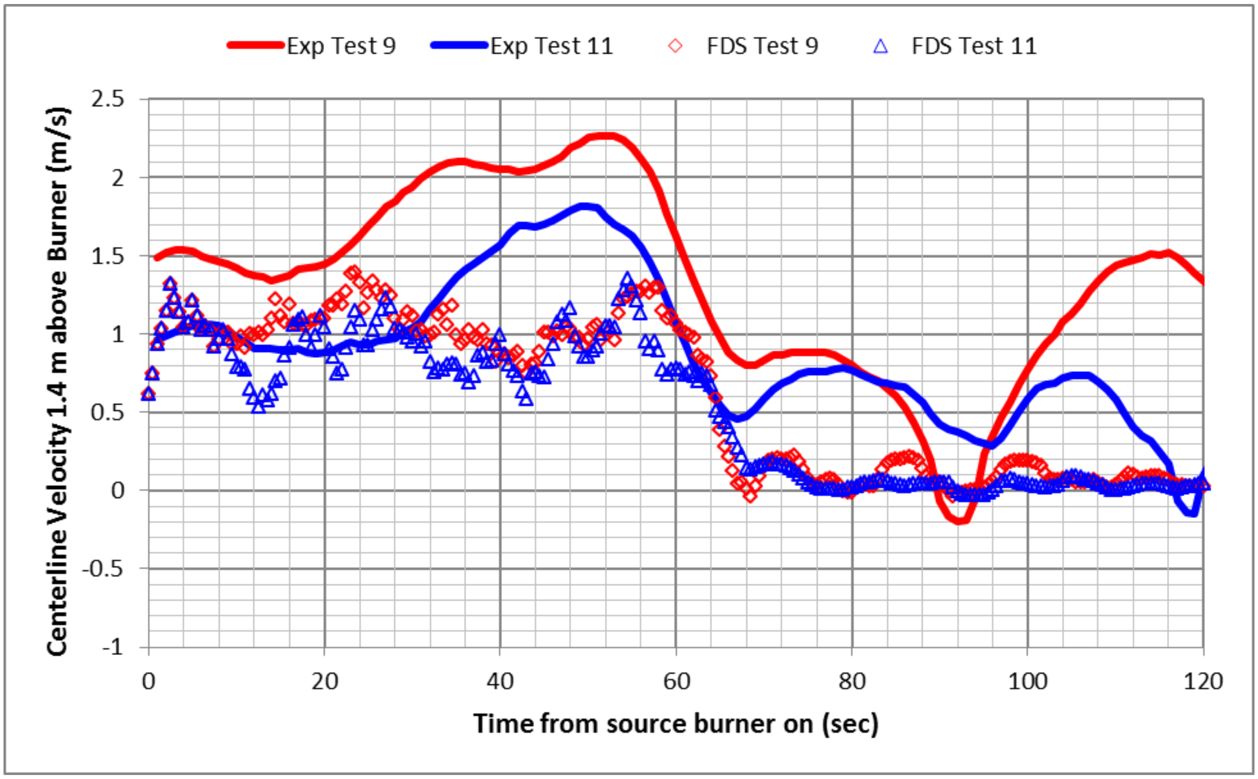

Figure 215 - Centerline temperature at 1.4 m above burner of tests using propane, 50 kW, Rectangle burner

The heat flux measured along the centerline was not corrected for convection. The comparison between the measured heat flux to the predicted gauge heat flux at 0.2 m, 0.5 m, 1.1 m, and 1.7 m over the burner surface are shown in Figure 216 to Figure 219. FDS appears to over-predict the heat flux at these locations except for the one located at 0.2 m. However, due to the lack of flame spread predicted, the modeled heat flux only accounts for that generated by the source fire, whereas in the experiments, the heat flux measured was from the source fire and from the FRP panel fire, as well as from the upper layer.

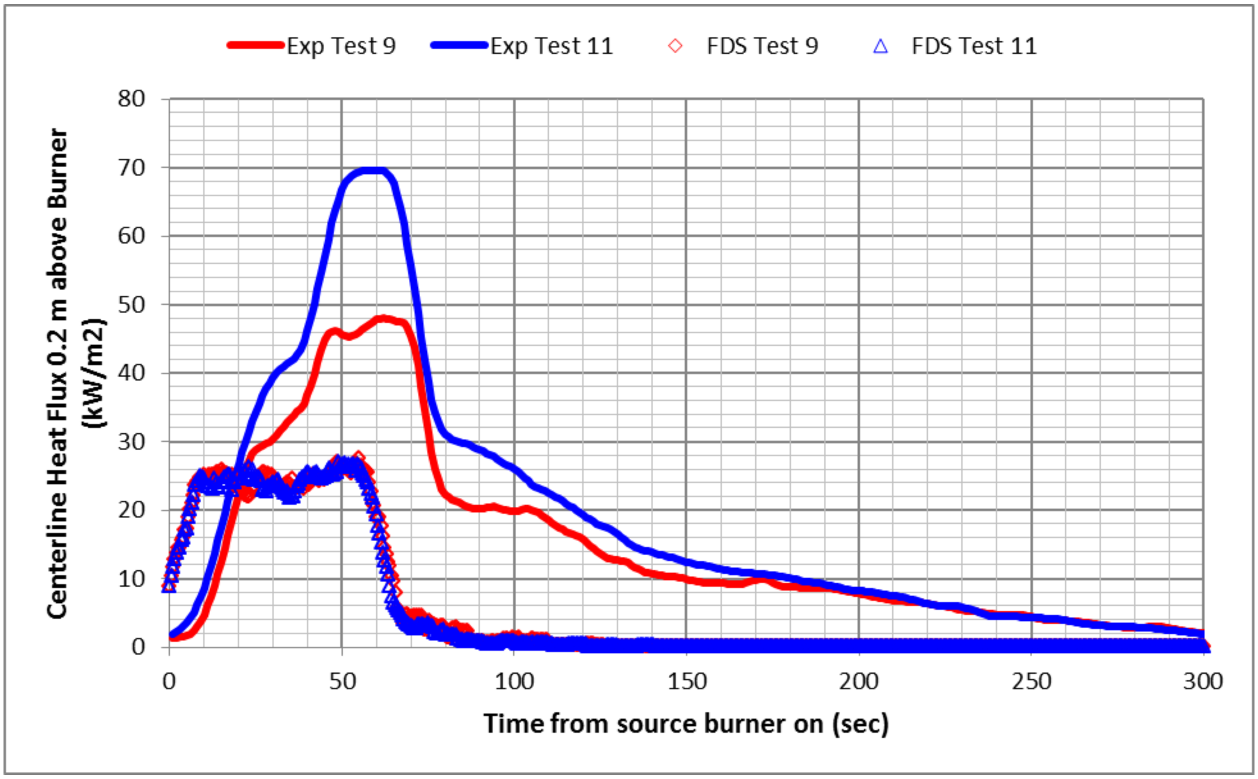

Figure 216 - Centerline heat flux at 0.2 m above burner of tests using propane, 50 kW, Rectangle burner

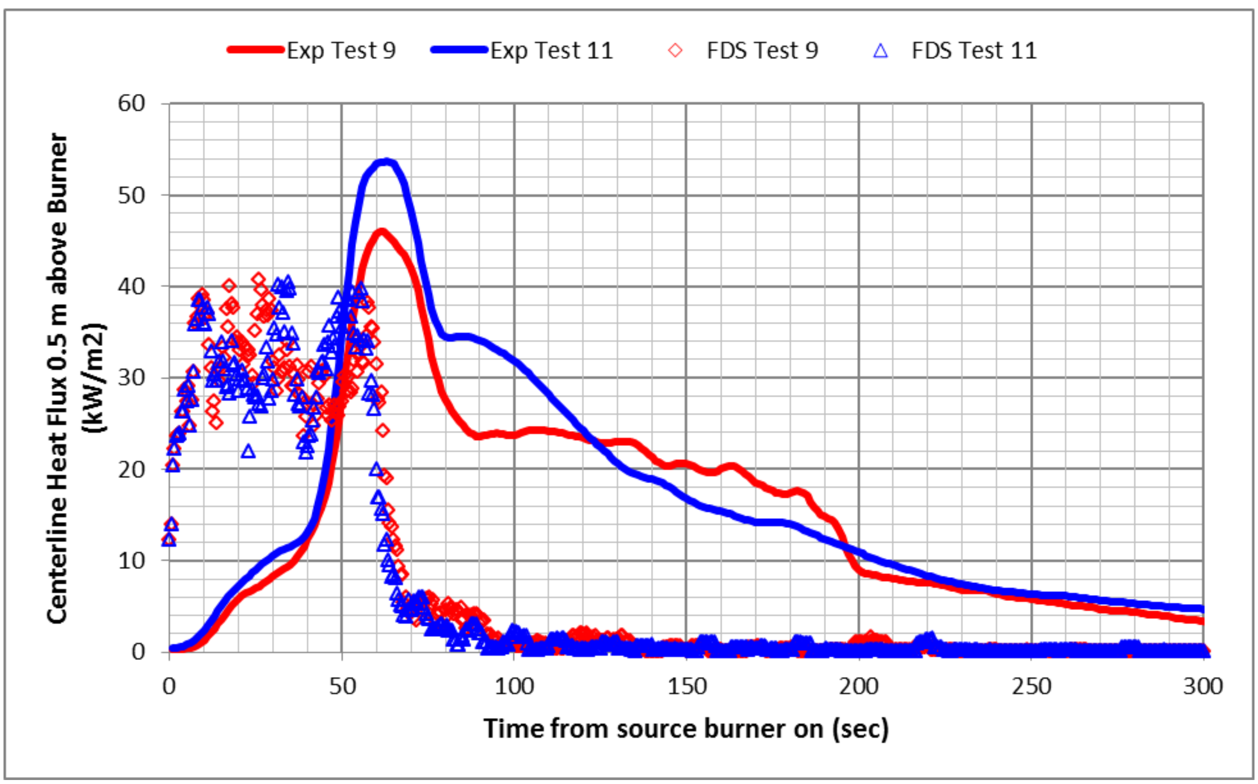

Figure 217 – Centerline heat flux at 0.5 m above burner of tests using propane, 50 kW, Rectangle burner

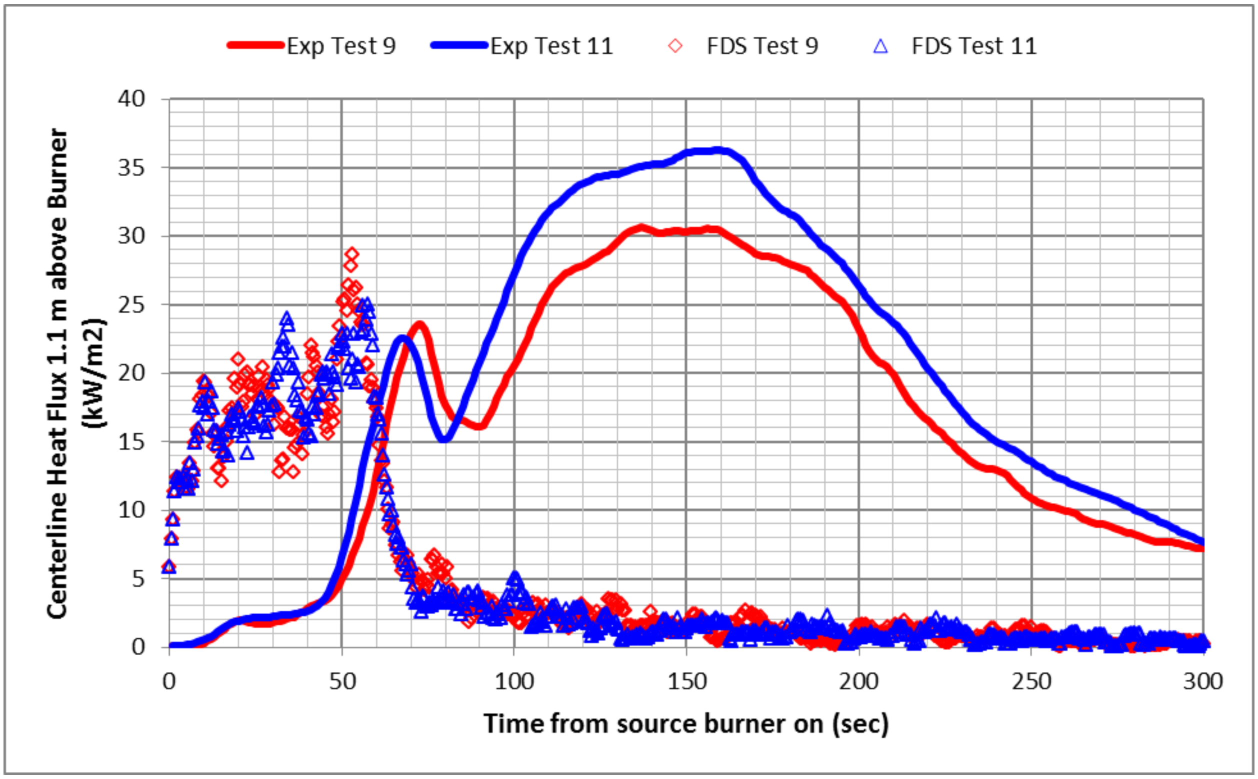

Figure 218 - Centerline heat flux at 1.1 m above burner of tests using propane, 50 kW, Rectangle burner

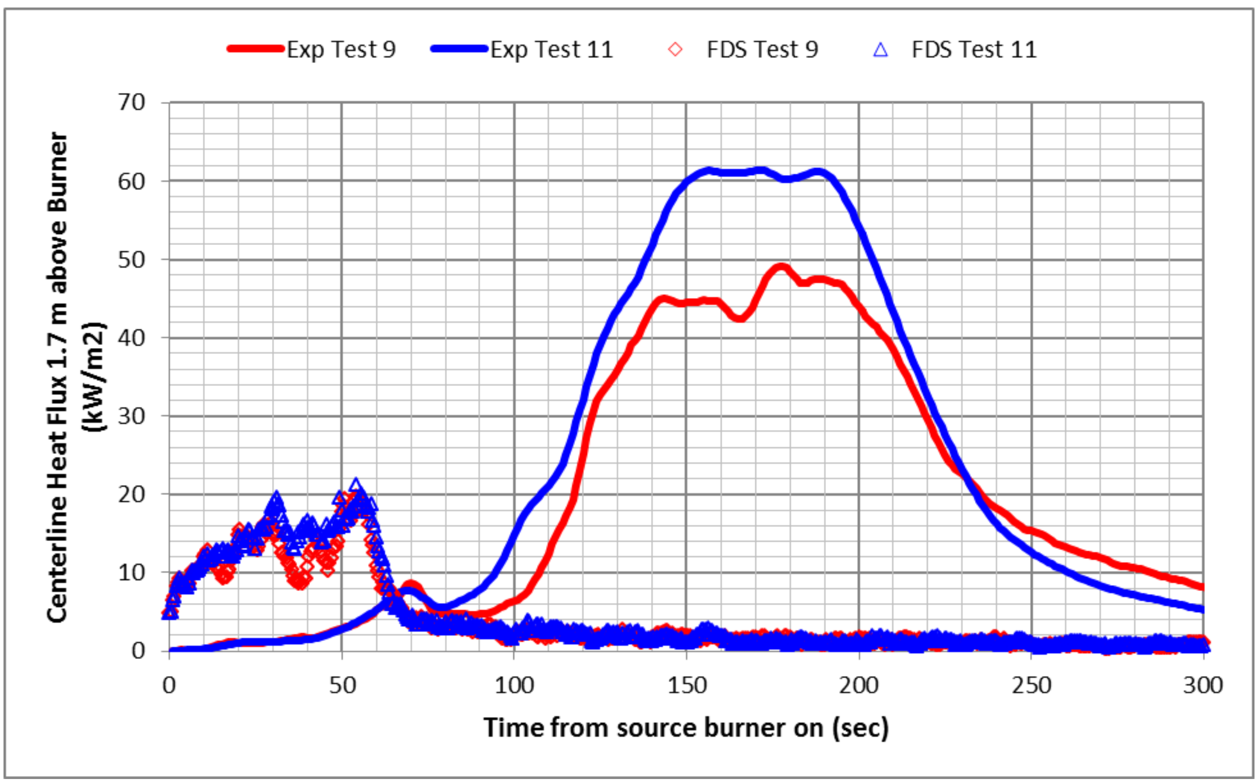

Figure 219 - Centerline heat flux at 1.7 m above burner of tests using propane, 50 kW, Rectangle burner

5.3.4 Propylene, 50 kW continuous, both burners

Tests 12 and 13 were identical to each other except that both burners were used. The source propylene fire was 50 kW continuous through the tests. The HRRs of the burning panel in Tests 12 and 13, minus that of the source fire, are presented in Figure 220. The two FDS simulations were not able to predict flame spread adequately. It is interesting to note that although both burners were used, both panel peaked at around the same time in the experiments. Although FDS does predict some flame spread, the HRR peaks were delayed, and the HRR of the burning FRP was greatly under-predicted.

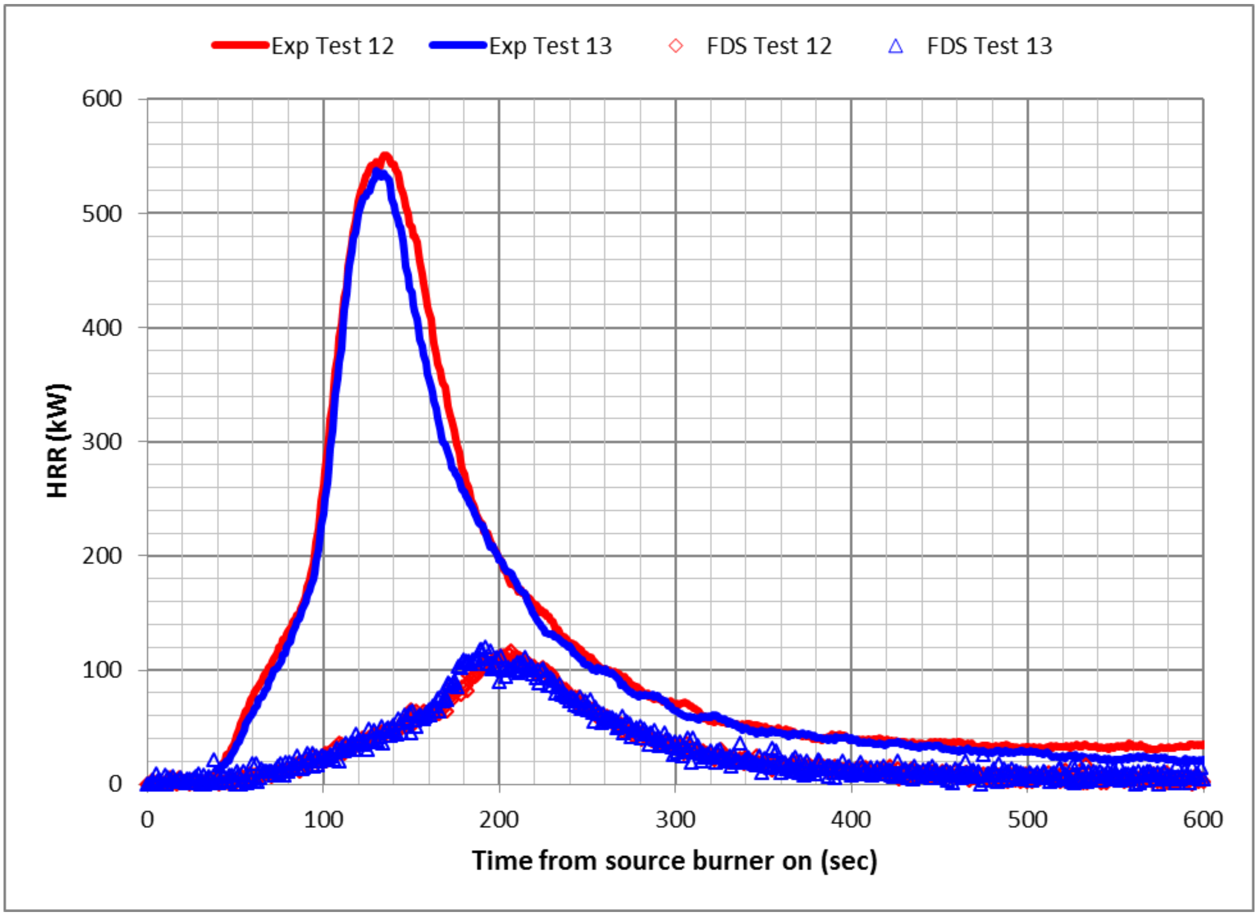

Figure 220 - HRRs of tests using propylene, 50 kW, both burners, but continuous souce fire

The velocity measured at 0.2 m, 0.8 m, and 1.4 m over the burner along the center is presented in Figure 221 to Figure 223. It is noted that the velocity measurement during the tests may be inaccurate after the instruments were exposed to fire for a short period of time, where the resulting velocity measurement is shifted due to thermal exposure. Generally, FDS under predicts the velocity at these points as compared to the experimental data.

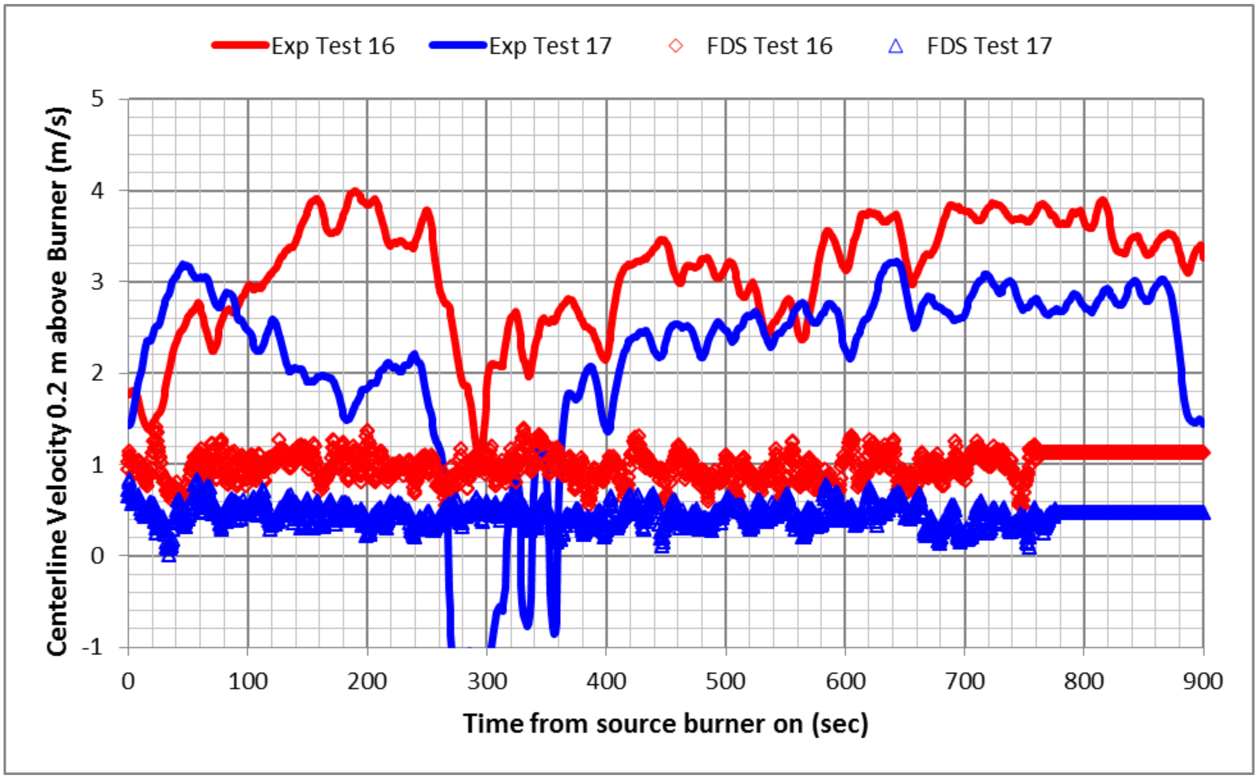

Figure 221 – Centerline temperature at 0.2 m above burner of tests using propylene, 50 kW, both burners, but continuous

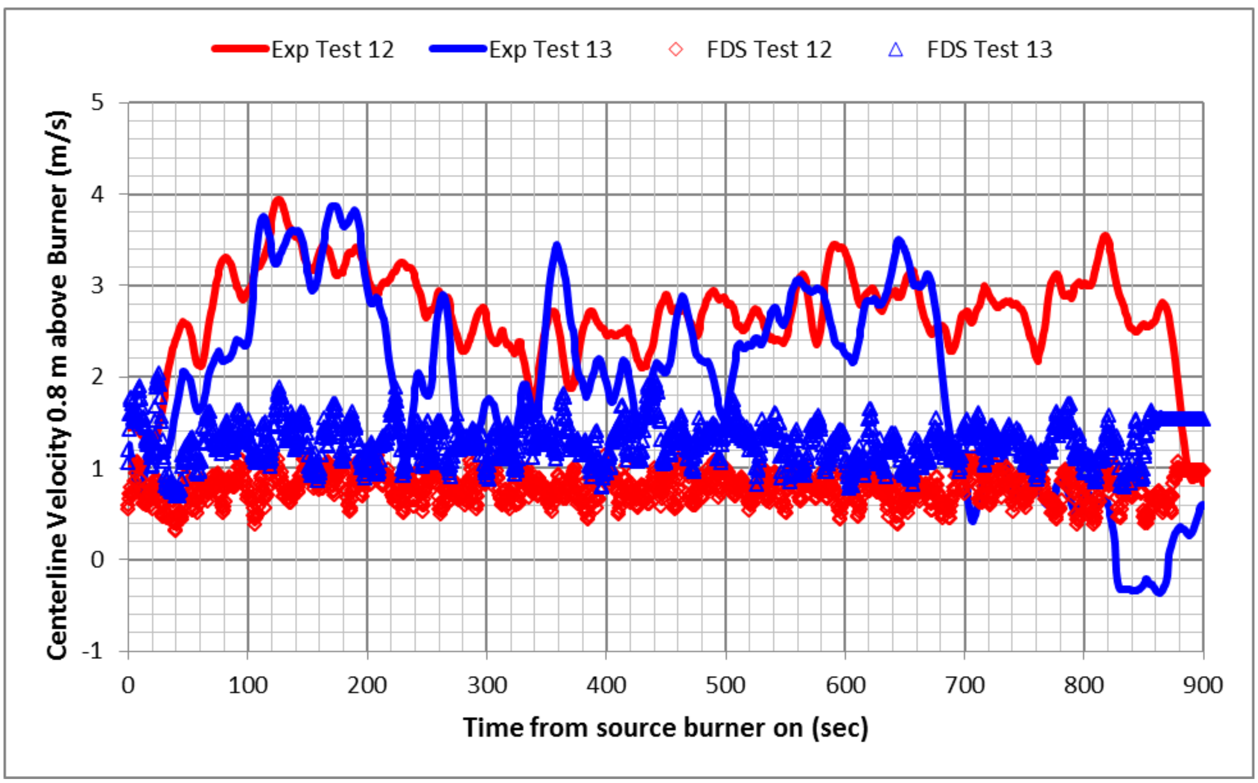

Figure 222 - Centerline temperature at 0.8 m above burner of tests using propylene, 50 kW, both burners, but continuous

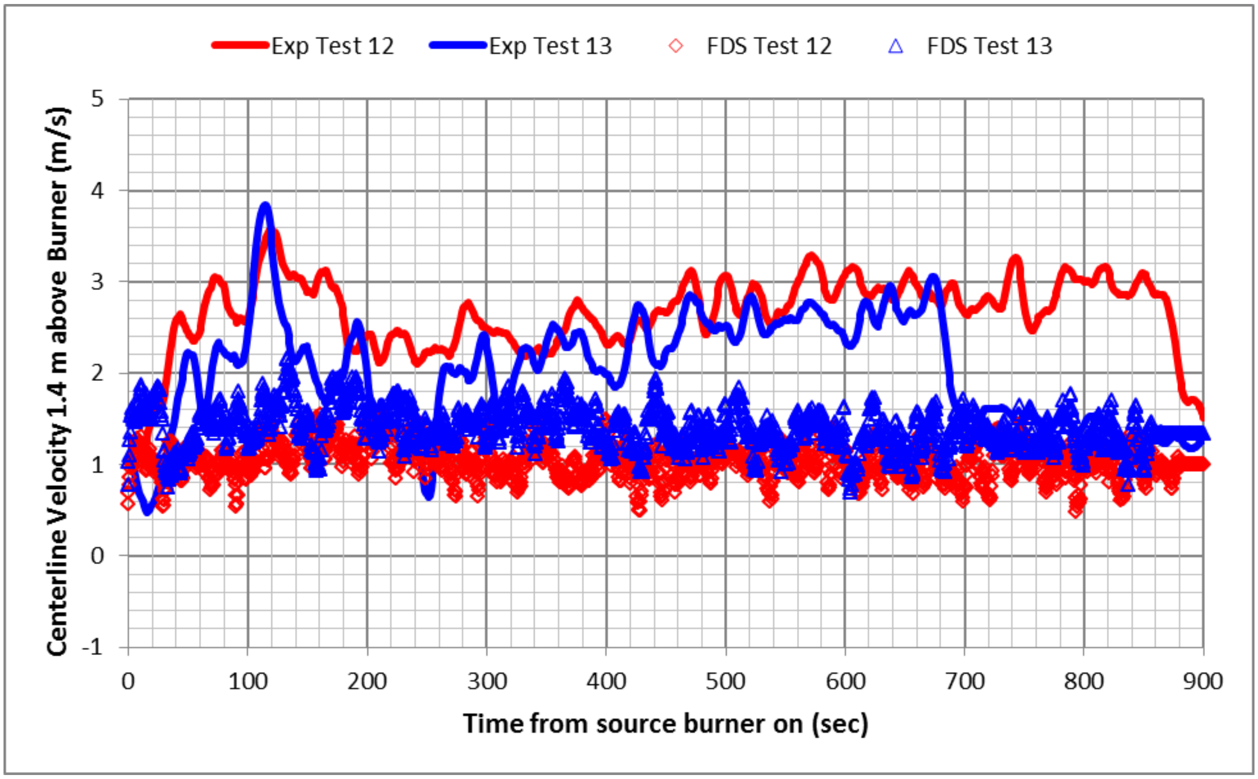

Figure 223 - Centerline temperature at 1.4 m above burner of tests using propylene, 50 kW, both burners, but continuous

The heat flux measured along the centerline was not corrected for convection. The comparison between the measured heat flux to the predicted gauge heat flux at 0.2 m, 0.5 m, 1.1 m, and 1.7 m over the burner surface are shown in Figure 224 to Figure 227. FDS appears to over-predict the heat flux at these locations except for the one located at 0.2 m. Even though the flame spread predicted by FDS was much smaller than that observed in the experiments, the heat flux predicted was still higher than that measured.

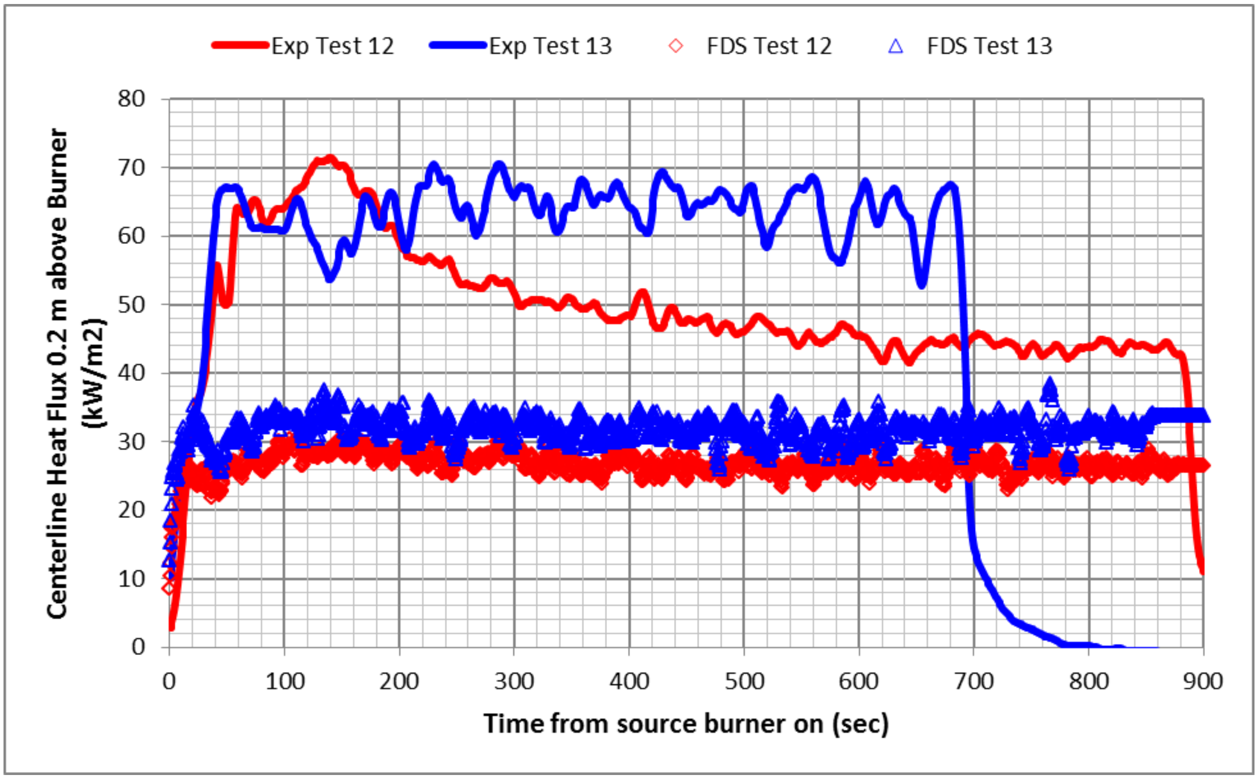

Figure 224 - Centerline heat flux at 0.2 m above burner of tests using propylene, 50 kW, both burners, but continuous

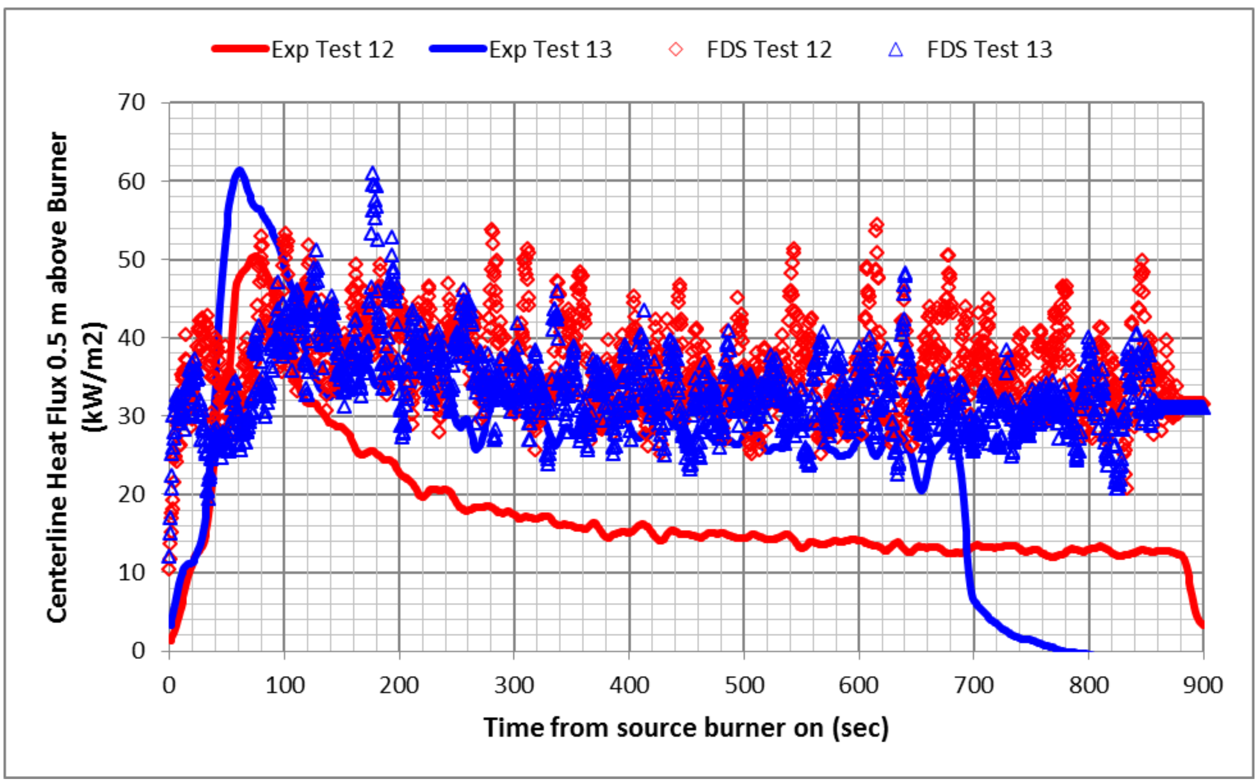

Figure 225 – Centerline heat flux at 0.5 m above burner of tests using propylene, 50 kW, both burners, but continuous

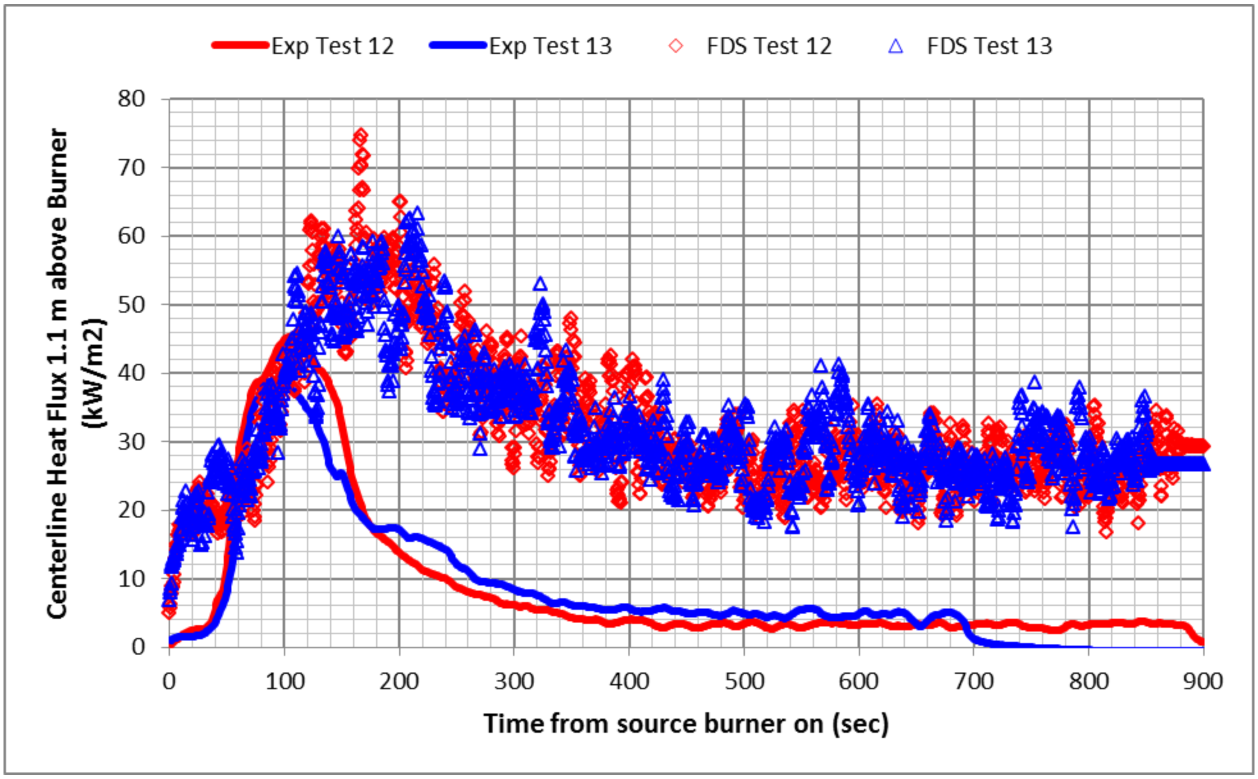

Figure 226 - Centerline heat flux at 1.1 m above burner of tests using propylene, 50 kW, both burners, but continuous

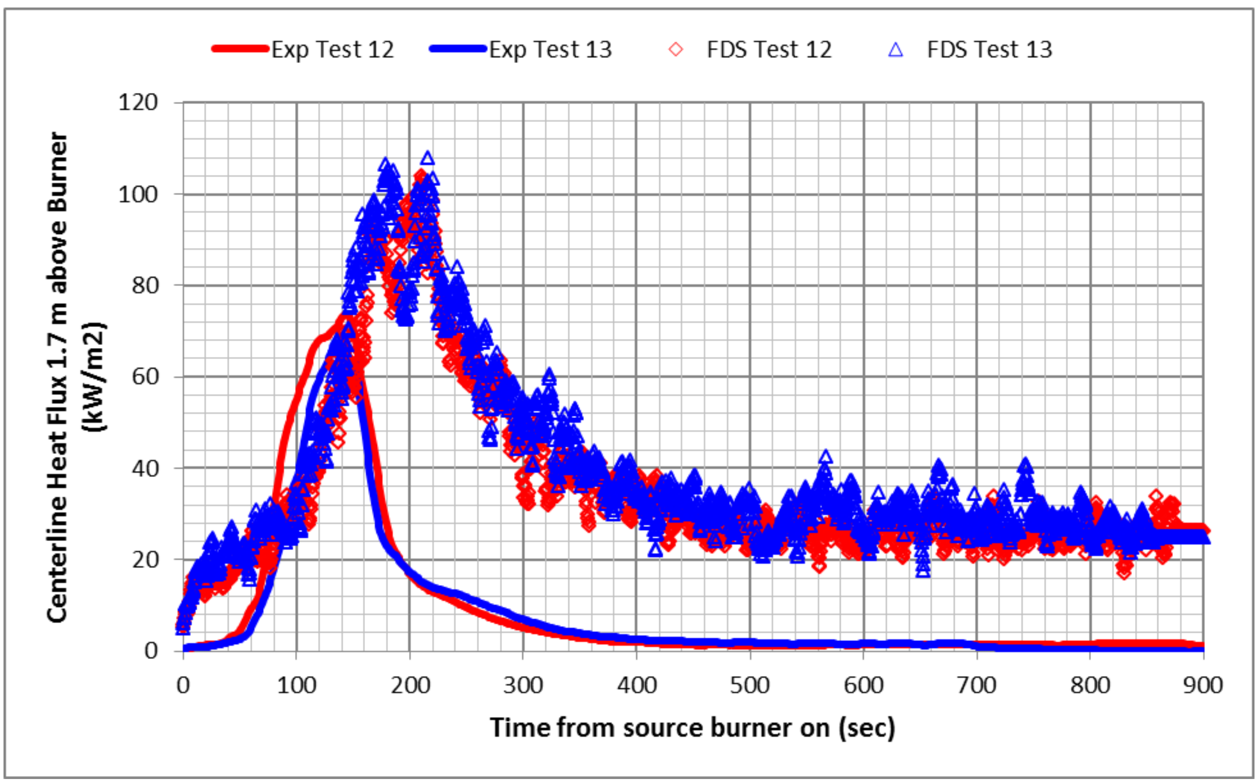

Figure 227 - Centerline heat flux at 1.7 m above burner of tests using propylene, 50 kW, both burners, but continuous

5.3.5 Propane, 75 kW continuous, both burners

Tests 16 and 17 were identical to each other except that both burners were used. The source propane fire was 75 kW continuous throughout. The HRRs of the burning panel in Tests 16 and 17, minus that of the source fire, are presented in Figure 228. The two FDS simulations were not able to predict flame spread adequately. In the experiments, the HRR of the panel peaked within 20 seconds of each other at similar value. The test with the Square burner created an earlier peak and higher HRR. Although FDS does predict some flame spread, the HRR was greatly under predicted at around 30% of the experiments, but the modeled peak times were similar to the experimental peak times.

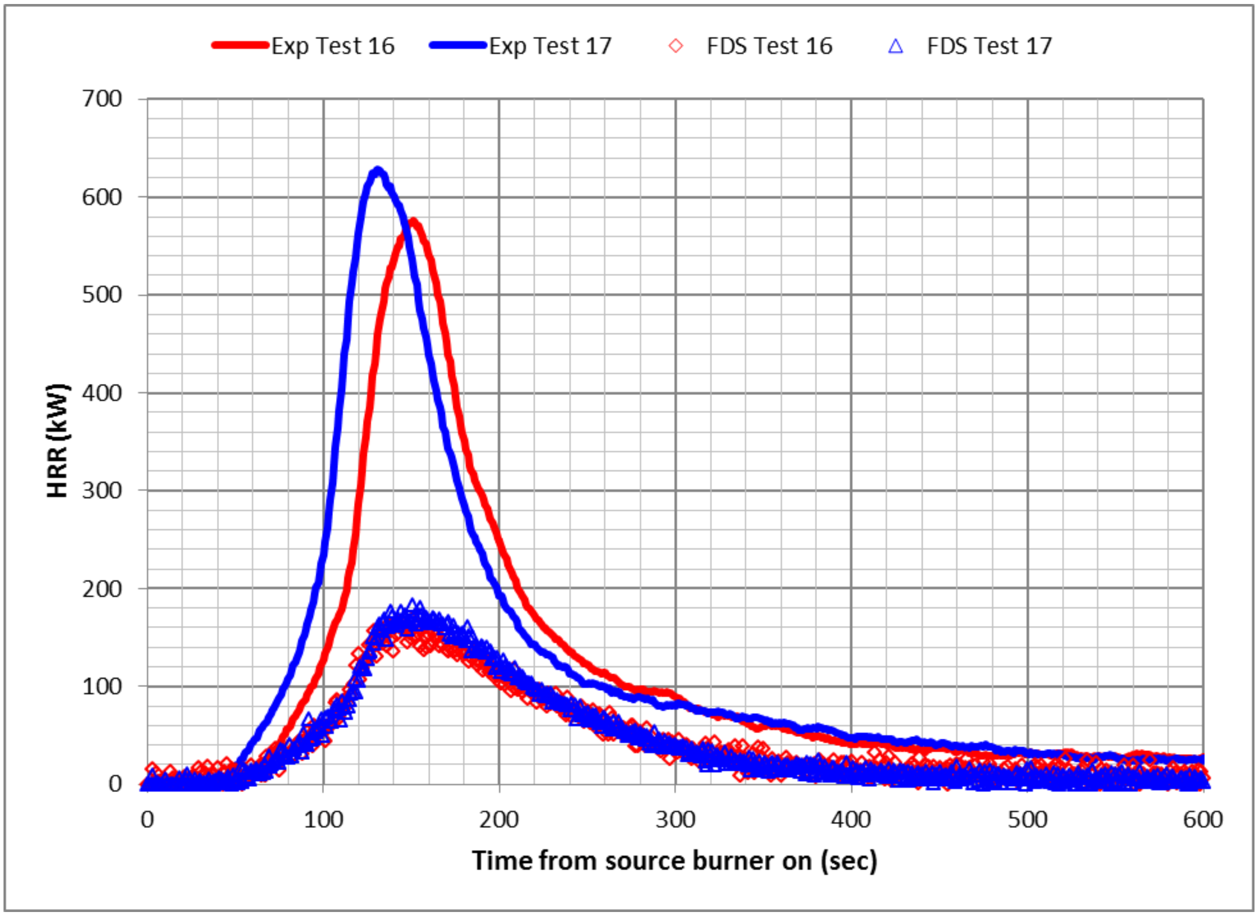

Figure 228 - HRRs of tests using propane, 75 kW, both burners, but continuous souce fire

The velocity measured at 0.2 m, 0.8 m, and 1.4 m over the burner along the center is presented in Figure 229 to Figure 231. It is noted that the velocity measurement during the tests may be inaccurate after the instruments were exposed to fire for a short period of time, where the resulting velocity measurement is shifted due to thermal exposure. Generally, FDS under predicts the velocity at these points as compared to the experimental data.

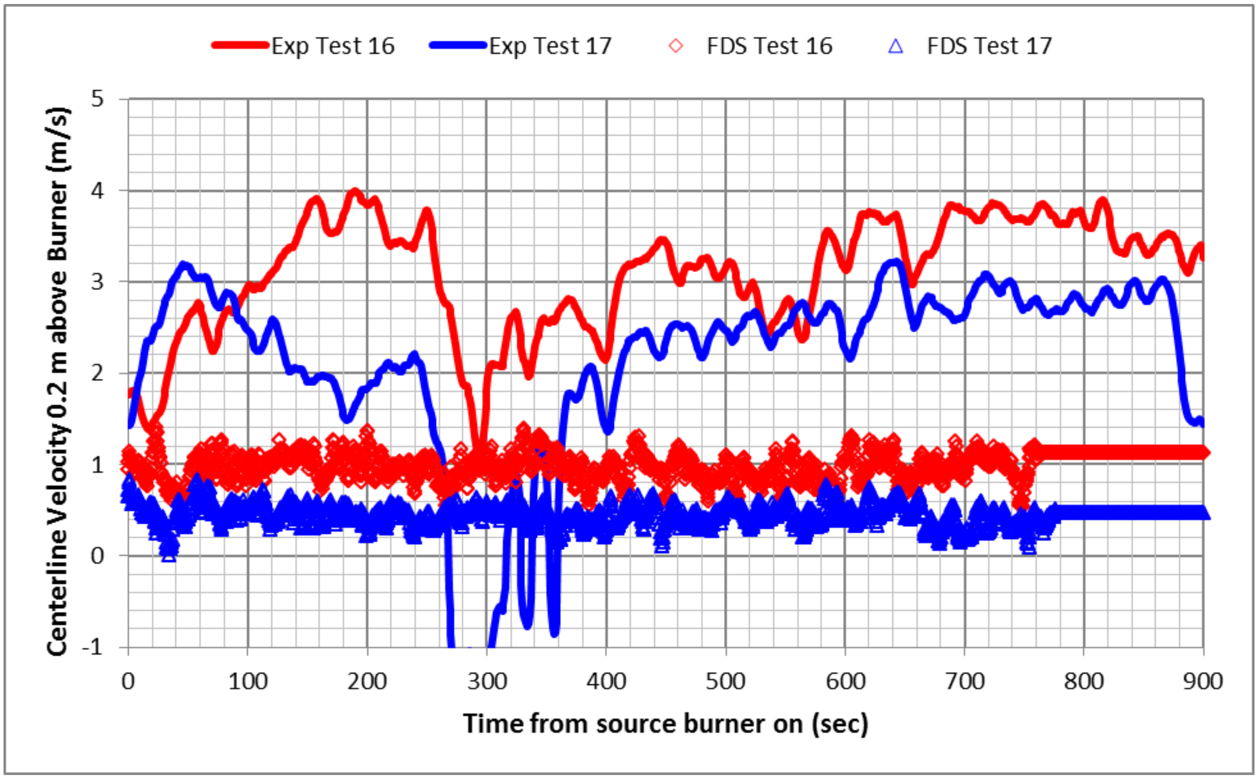

Figure 229 – Centerline temperature at 0.2 m above burner of tests using propane, 75 kW, both burners, but continuous

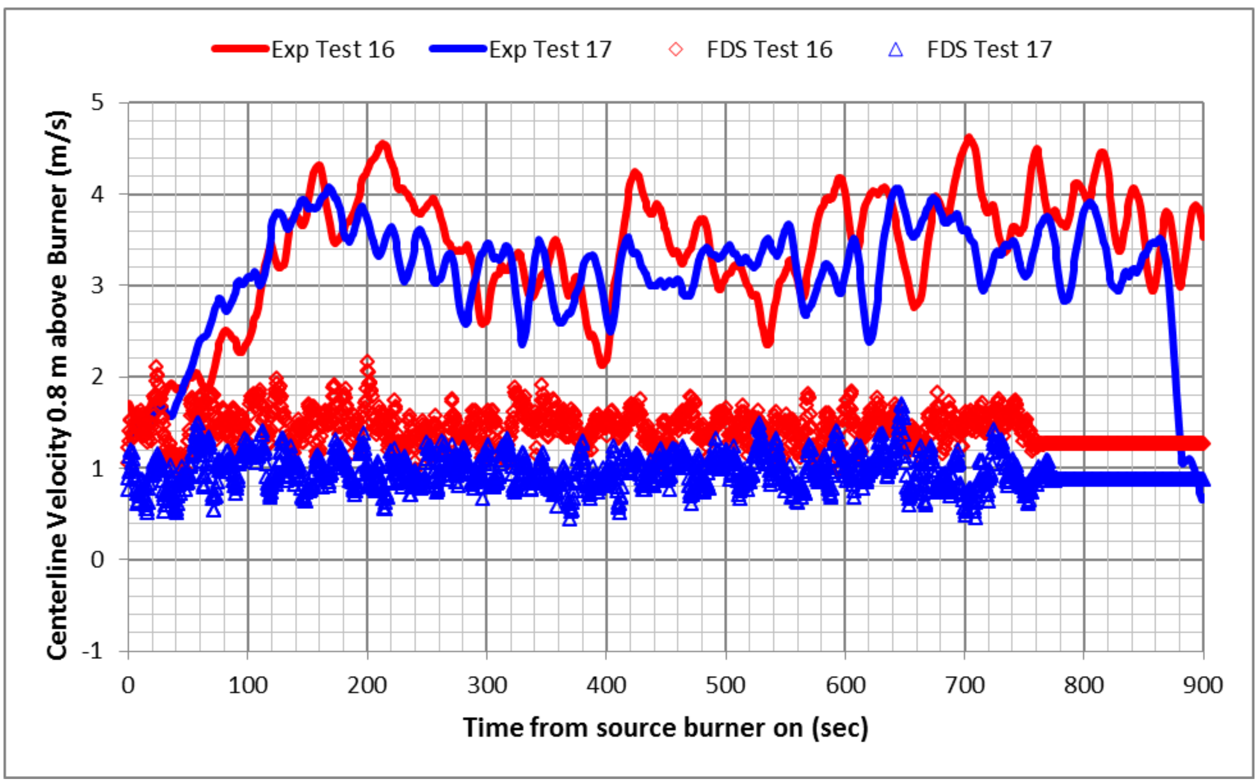

Figure 230 - Centerline temperature at 0.8 m above burner of tests using propane, 75 kW, both burners, but continuous

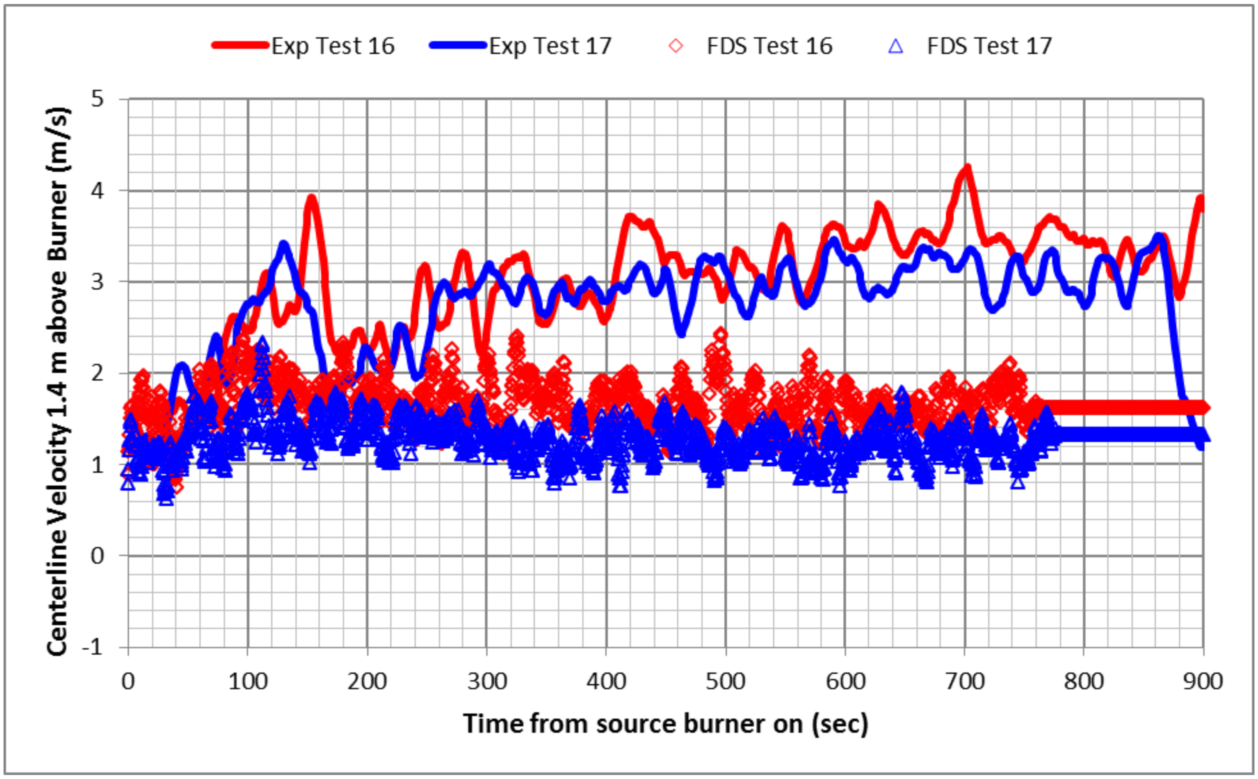

Figure 231 - Centerline temperature at 1.4 m above burner of tests using propane, 75 kW, both burners, but continuous

The heat flux measured along the centerline was not corrected for convection. The comparison between the measured heat flux to the predicted gauge heat flux at 0.2 m, 0.5 m, 1.1 m, and 1.7 m over the burner surface are shown in Figure 232 to Figure 235. FDS appears to over-predict the heat flux at these locations except for the one located at 0.2 m. Even though the flame spread predicted by FDS was much smaller than that observed in the experiments, the heat flux predicted was still higher than that measured. It is noted that the timing of the peak heat flux was predicted quite well, just like at of the peak HRR.

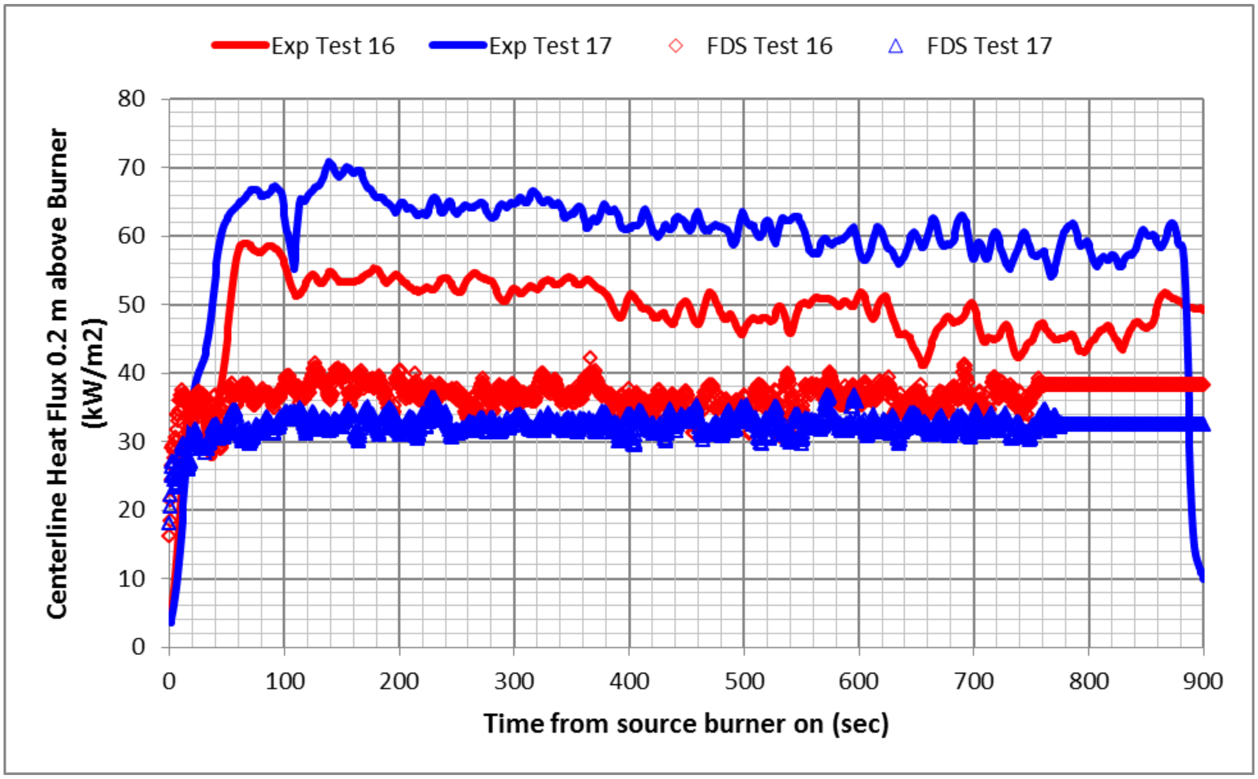

Figure 232 - Centerline heat flux at 0.2 m above burner of tests using propane, 75 kW, both burners, but continuous

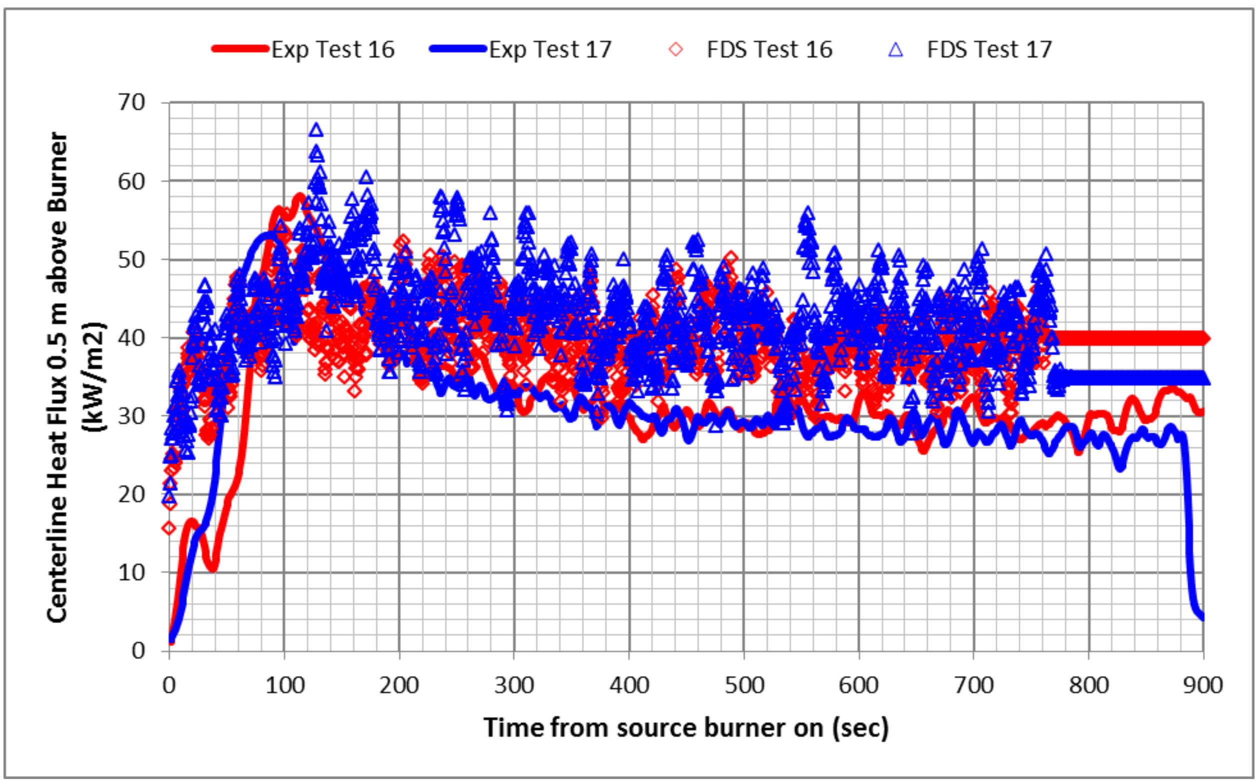

Figure 233 – Centerline heat flux at 0.5 m above burner of tests using propane, 75 kW, both burners, but continuous

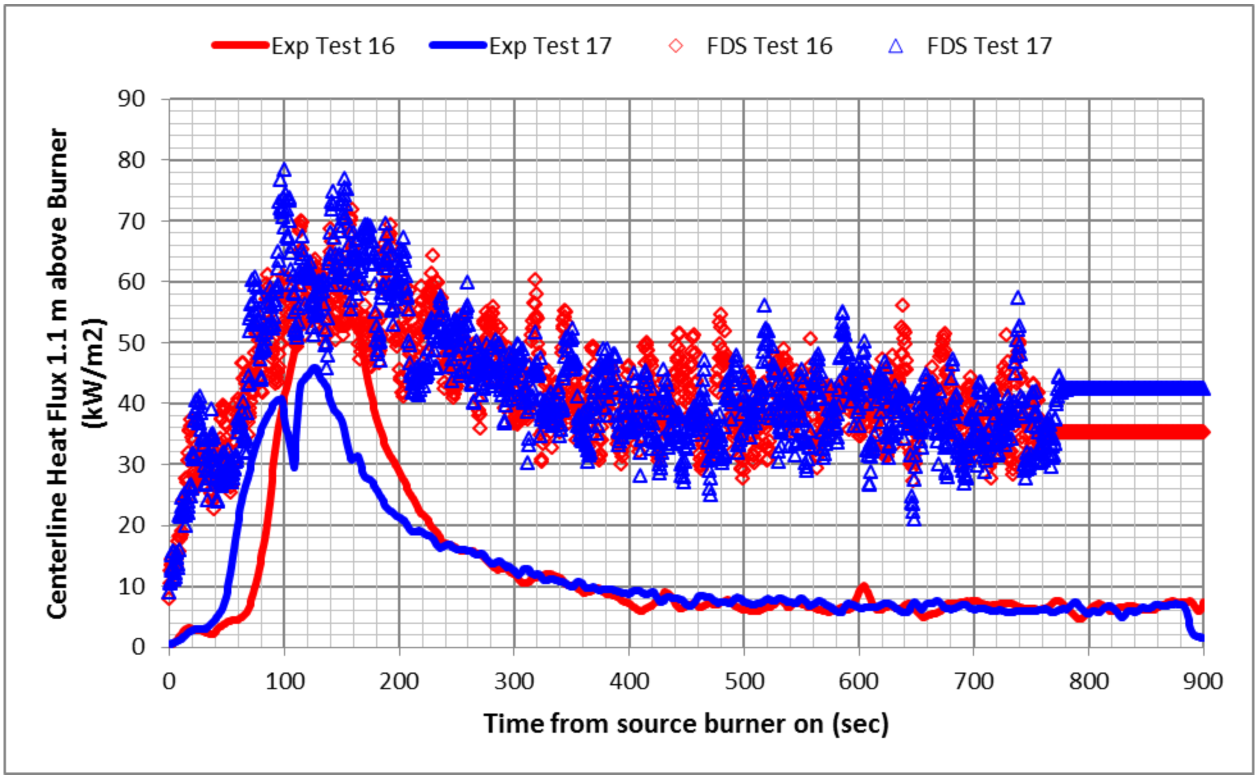

Figure 234 - Centerline heat flux at 1.1 m above burner of tests using propane, 75 kW, both burners, but continuous

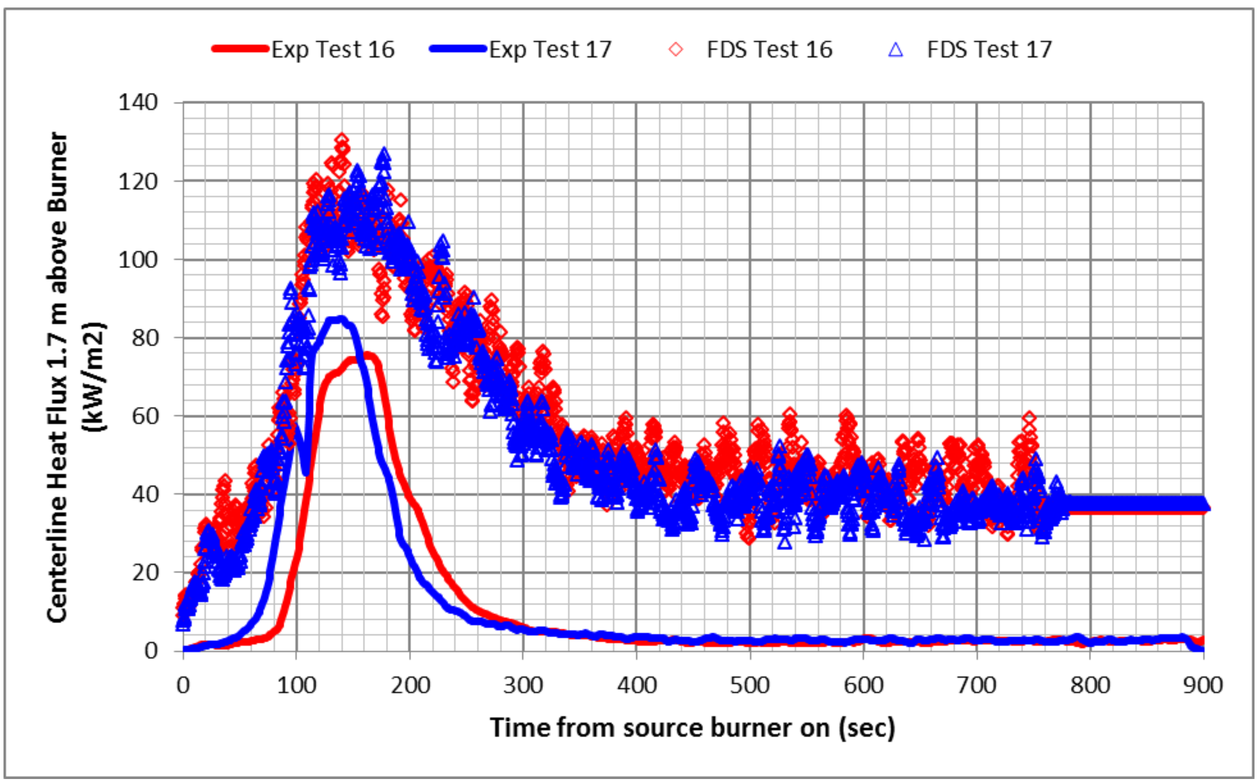

Figure 235 - Centerline heat flux at 1.7 m above burner of tests using propane, 75 kW, both burners, but continuous

5.4 FDS variable parameters modeling results

Varying the FDS parameters that govern the CFD simulation characteristics change the behaviors of the model to different degrees. The predictive capabilities and the performance of the model are both affected by parameter changes; and the understanding of the relationships between the cause (parameter change) and the results (predictions and performance) is of great importance to end-users so that simulations can be conducted effectively and efficiently.

A systemic approach to vary some notable parameters in FDS individually was undertaken as described in Section 3.4 utilizing all three configurations of fire models in this study. The default cases used mostly FDS's default parameters, but in each successive iteration, only one parameter was varied from the default set of parameters. Some parameters from the MISC, RADI, REAC, and TIME groups were changed during this modeling exercise. Various values of the parameters used in the study are shown in Table 36.

Table 36 – Values of parameters utilized in FDS parametric study

Series	Parameter Group	Parameter change	Default Value	New value in simulation	Change from default
0	FDS6	DYNSMAG	.TRUE.	.FALSE.	x
1	**N/A**	**No change, Default situation using default FDS6 options**			
2	MISC	RADIATION	.TRUE.	.FALSE.	x
3	RADI	RADIATIVE FRACTION	0.30	Source fire specific	varies
4	RADI	RADIATIVE FRACTION	0.30	0.1	~33%
5	RADI	RADIATIVE FRACTION	0.30	0.2	~50%
6	RADI	RADIATIVE FRACTION	0.30	0.5	~160%
7	RADI	WIDE_BAND_MODEL	.FALSE.	.TRUE	x
8	RADI	NUMBER_RADIATION_ANGLES	104	52	50%
9	RADI	NUMBER_RADIATION_ANGLES	104	208	200%
10	RADI	ANGLE_INCREMENT	5	2	50%
11	RADI	ANGLE_INCREMENT	5	10	200%
12	RADI	TIME_STEP_INCREMENT	3	1	50%
13	RADI	TIME_STEP_INCREMENT	3	6	200%
~~14~~	~~Skipped~~				
15	REAC	C_EDC	0.1	0.2	50%
16	REAC	C_EDC	0.1	0.05	200%
17	REAC	EDDY_DISSIPATION	.TRUE.	.FALSE.	x
18	REAC	HRRPUA_SHEET	0	400	40000%
19	REAC	HRRPUA_SHEET	0	100	10000%
20	REAC	HRRPUV_AVERAGE	3000	1200	40%
21	MISC	ISOTHERMAL	.FALSE.	.TRUE	x
22	MISC	CSMAG	0.2	0.1	50%

Series	Parameter Group	Parameter change	Default Value	New value in simulation	Change from default
23	MISC	CSMAG	0.2	0.4	200%
24	MISC	PR	0.5	0.25	50%
25	MISC	PR	0.5	1	200%
26	MISC	SC	0.5	0.25	50%
27	MISC	SC	0.5	1	200%
28	MISC	BAROCLINIC	.TRUE.	.FALSE.	x
29	MISC	CFL_MAX	1	2	200%
30	MISC	CFL_MIN	0.8	0.4	50%
31	MISC	CFL_MAX and CFL_MIN	1 / 0.8	2 / 0.4	x
32	FDS6	FLUX_LIMITER	2	-1	x
33	FDS6	CFL_VELOCITY_NORM	1	2	x
34	FDS6	CFL_VELOCITY_NORM	1	0	x
35	FDS6	H_EDDY	.TRUE.	.FALSE.	x

Comparison of different set of predicted fire quantities was made between successive series of parametric models vs. the default cases. The fire quantities comparisons made between models are different for each model configuration, as shown in Table 37.

Table 37 - Quantities utilized in parametric study comparison

Simulation Configuration	Quantities Compared
Plume	Time-averaged centerline plume temperature Time-averaged centerline plume velocity
Inert wall	Time-averaged centerline plume temperature Time-averaged centerline plume velocity Time-averaged centerline heat flux to wall
Combustible wall	Total mass loss (Mass) Peak heat release rate (HRR) Time to peak heat release rate (Time) Total heat released (THR)

Appendices K to M present the complete analysis of the parametric simulation runs. The parameter changes with the most significant effects on the quantities are described in the following sections.

To identify the parameters that yield significant changes to specific predicted quantities, the concept of "sensitivity coefficients" was employed. Each coefficient was determined based on the changes in one of the quantities under consideration, and of the FDS parameter over their baseline values. The coefficient is based on the ratios of change, and is found using equation (1):

$$\left(\frac{Quantity_{new} - Quantity_{baseline}}{Quantity_{baseline}}\right) \Bigg/ \left(\frac{Parameter_{new} - Parameter_{baseline}}{Parameter_{baseline}}\right) \qquad (50)$$

Where “Quantity” denotes the recorded quantities in the model (velocity, temperature, gauge heat flux), and the “Parameter” denotes the model inputs (RADIATIVE_FRACTION, SC, etc.)

Equation (1) was applied to the steady-state, time-averaged FDS results of plume centerline temperature, velocity, and gauge heat flux at different heights from the plume and inert wall fire simulations, and the total mass loss, peak HRR, time to peak HRR, and total heat released for simulations of the combustible wall fires. For the “toggle” parameters, if a parameter is turned “ON” or “TRUE”, the nondimensional parameter change is assumed to be “+1”, and if the parameter is turned “OFF” or “FALSE”, then the nondimensional parameter change is assumed to be “-1”, this is necessary for the sensitivity coefficients be calculated for the “toggle” parameters since they do not have any numerical values.. Regardless of the parameter type, a sensitivity coefficient is calculated for each quantity at each “measuring” location, and then they are averaged. The coefficients can then be used to represent the significance and effects of the parameter change for each of the predicted quantities.

5.4.1 FDS parameters with significant effects on plume fire simulations

This section presents the sensitivity coefficients generated from the various simulations as grouped by the fuel type, burner shape, and source fire HRR. The parameters and their variances that generated sensitivity coefficients ≥ 0.1 are considered significant. Each sensitivity coefficient was based on one of the predicted quantities, and was averaged over height and across those simulations using identical fuel types regardless of the scenario, burner shape, and base HRR. The results from the toggle parameters are located at the bottom of the charts, and the parameter change that correlates with the overall maximum sensitivity coefficients are presented first.

Non-toggle parameters such as radiative fraction, Prandtl number, and the maximum and minimum CFL range dominate the changes of the measured temperature and velocity along the plume centerline in the simulations. These parameters contribute to the resolution of the flow field and the stability of the plume and of the simulations. And because the plume velocity and temperature are both closely related to the plume’s structure, they are especially affected by these parameters.

For the toggled parameter studied, the ones with the greatest changes include: isothermal model, CFL velocity normalization, eddy diffusivity model, and the dynamic Smagorinsky model. All these parameter contributes to the stability and structure of the flow field. The flux limiter, which controls the calculations scheme used in the calculations, is consistently one of the greatest contributors to quantity changes because the simulations all crashed due to numerical instability.

Additionally, the results from the parametric study show that characteristics of the simulations such as propane fuel, Rectangle burner, and the lower HRR at 50 kW are more greatly affected by the parameter changes than their counterparts.

Figure 236 shows the sensitivity coefficients based on the predicted plume centerline velocity averaged over free plume simulations using the same fuel type. The parameters that created the most significant changes to the plume velocity are the radiative fraction and the Prandtl number, as well as the when the isothermal mode was used, and which calculation scheme used based on the value of the flux limiter.

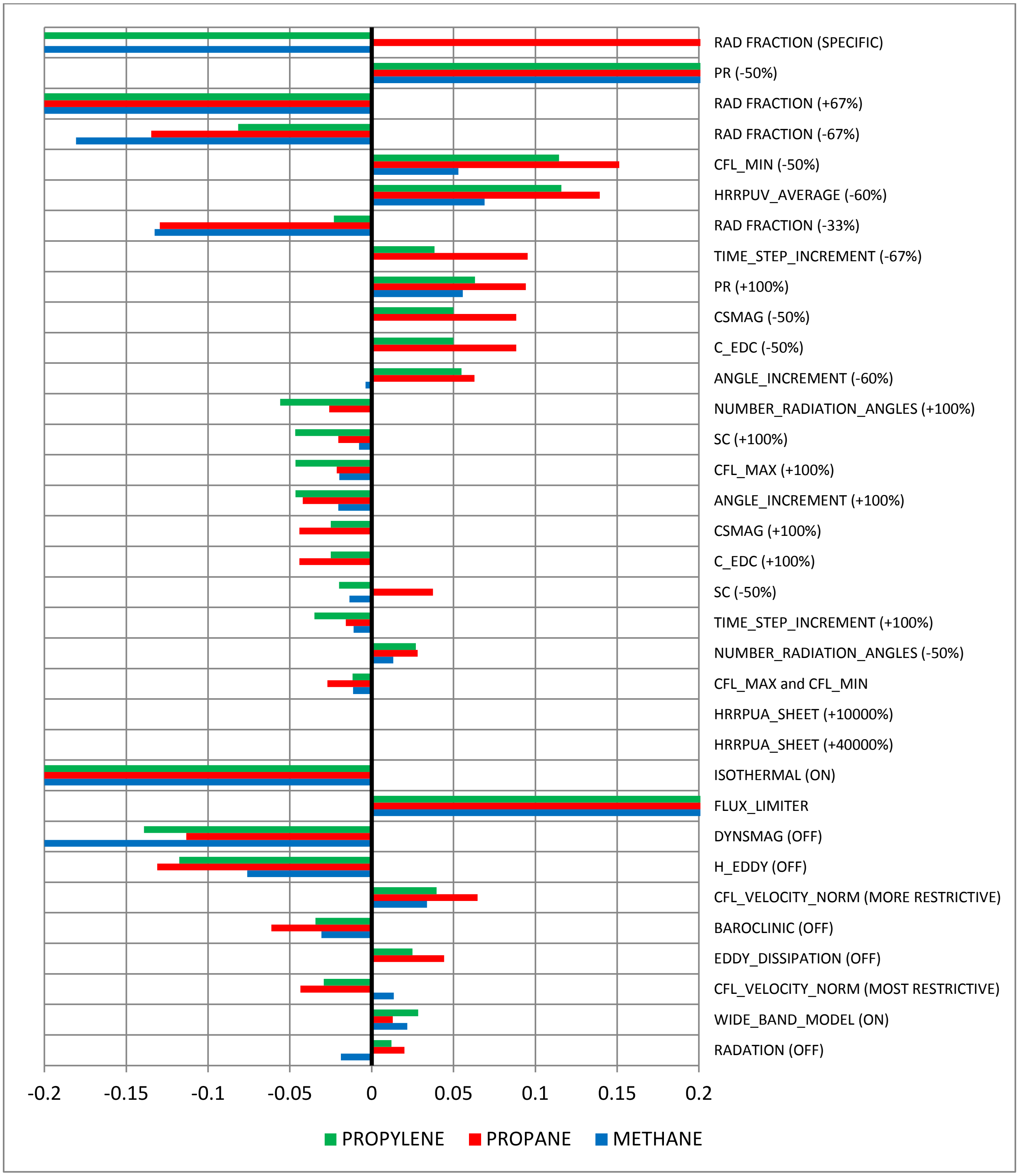

Figure 236 – Plume velocity sensitivity coefficients, grouped by fuel type

Figure 237 shows the sensitivity coefficients based on the predicted plume centerline velocity averaged over simulations with consistent fuel type. The values of the CFL parameters, the Schmidt number, the CFL_velocity_norm parameter, and whether the eddy diffusivity model was utilized contributed most significant to the change in plume temperature.

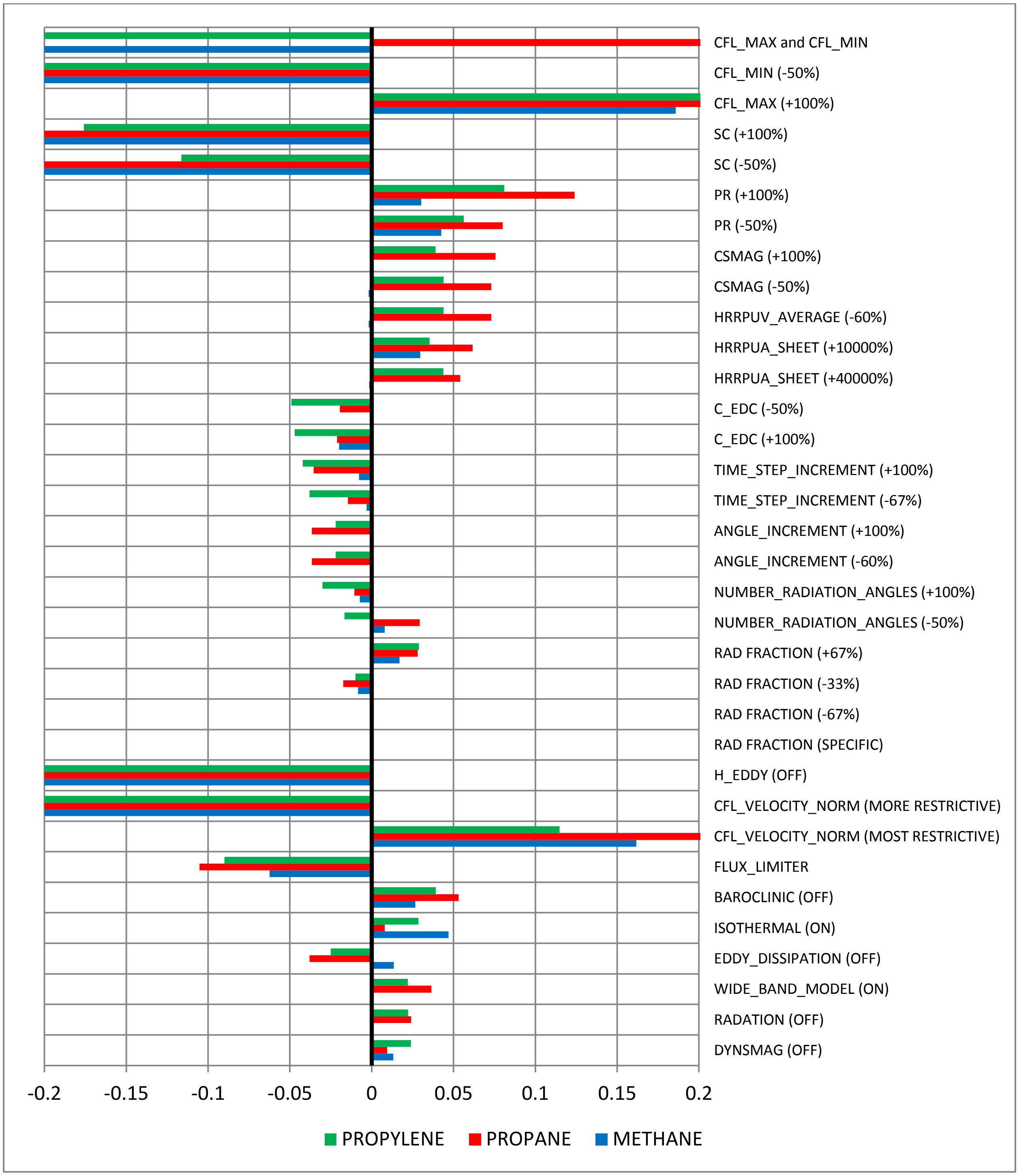

Figure 237 – Plume temperature sensitivity coefficients, grouped by fuel type

Figure 238 shows the sensitivity coefficients based on the predicted plume centerline velocity averaged over simulations using the same source fire burner. The parameter changes that caused the most significant velocity change are the radiative fraction, Prandtl number, the CFL limits, the isothermal mode was used, which calculation scheme used based on the value of the flux limiter, and whether the dynamic Smagorinsky model is turned off.

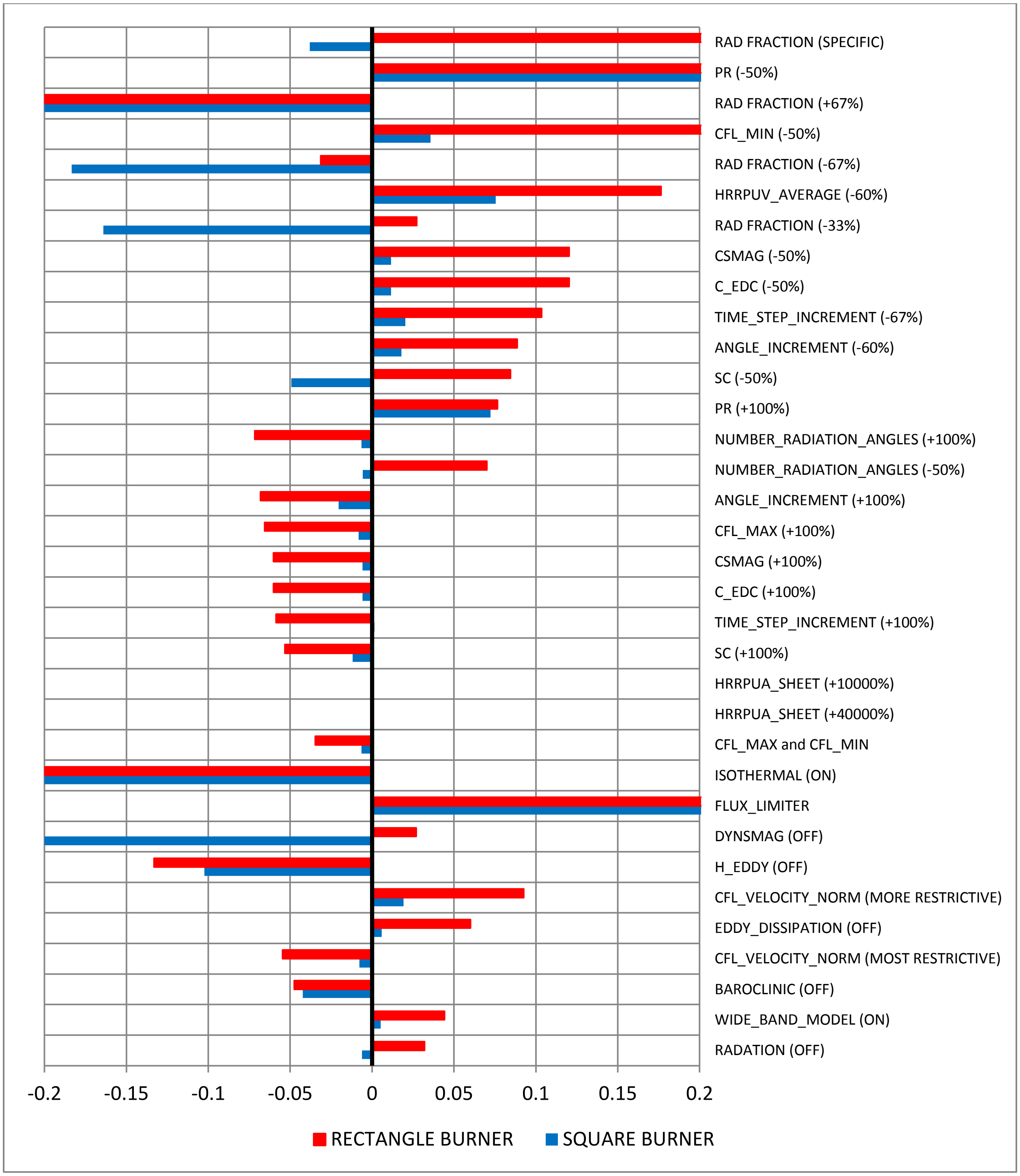

Figure 238 – Plume velocity sensitivity coefficients, grouped by burner shape

Figure 239 shows the sensitivity coefficients based on the predicted plume centerline temperature averaged over simulations using the same source fire burner. The parameter changes that caused the most significant plume temperature change are the radiative fraction, Prandtl number, the isothermal mode was used, and whether the dynamic Smagorinsky model is turned off.

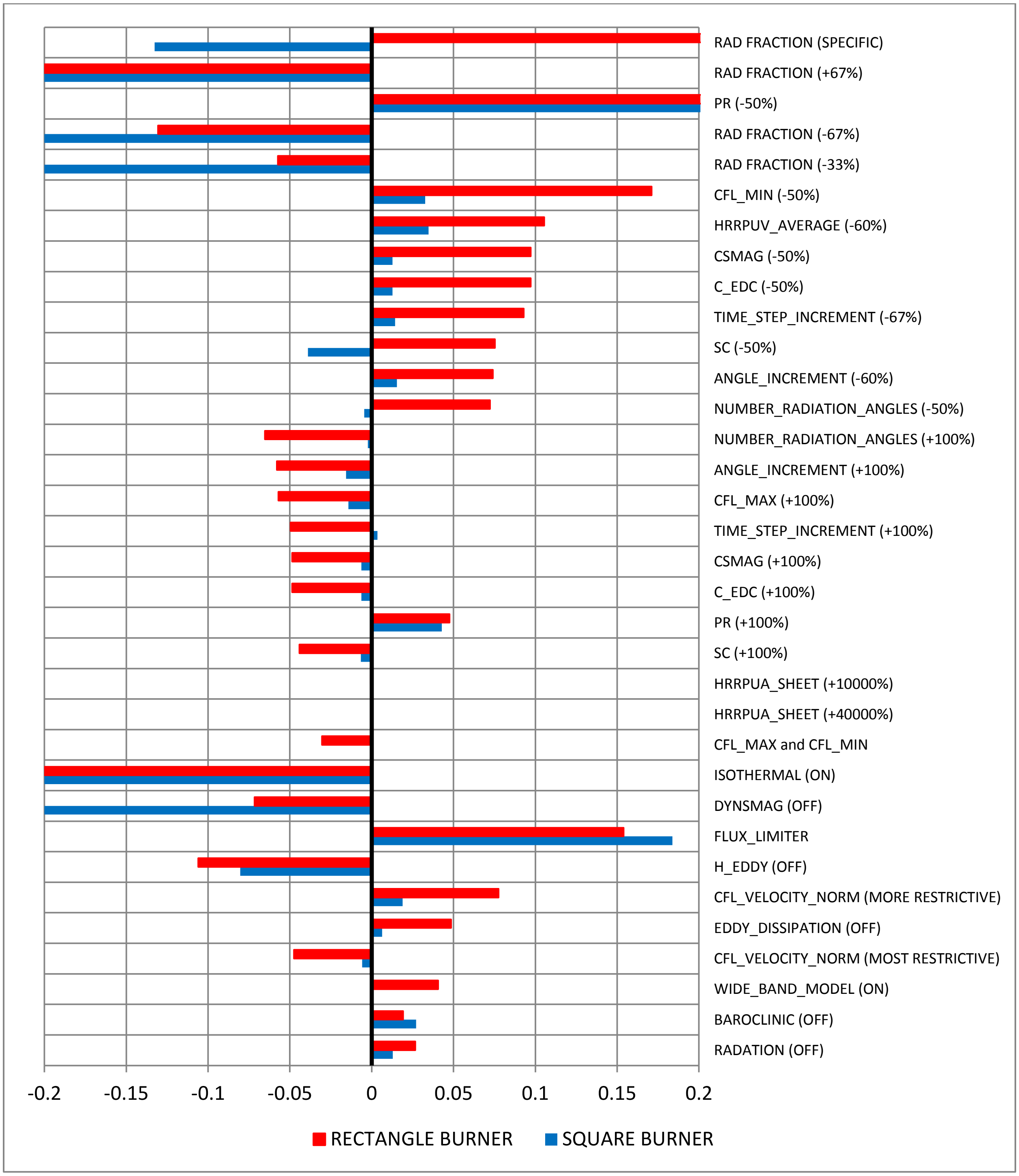

Figure 239 – Plume temperature sensitivity coefficients, grouped by burner shape

This section presents the sensitivity coefficients generated from the various simulations as grouped by the base burner HRR: 50 kW or 75 kW. Figure 240 shows the sensitivity coefficients based on the predicted plume centerline velocity averaged over simulations using the same source fire HRR. The parameter changes that caused the most significant velocity change are the radiative fraction, Prandtl number, the isothermal mode was used, and which calculation scheme used based on the value of the flux limiter.

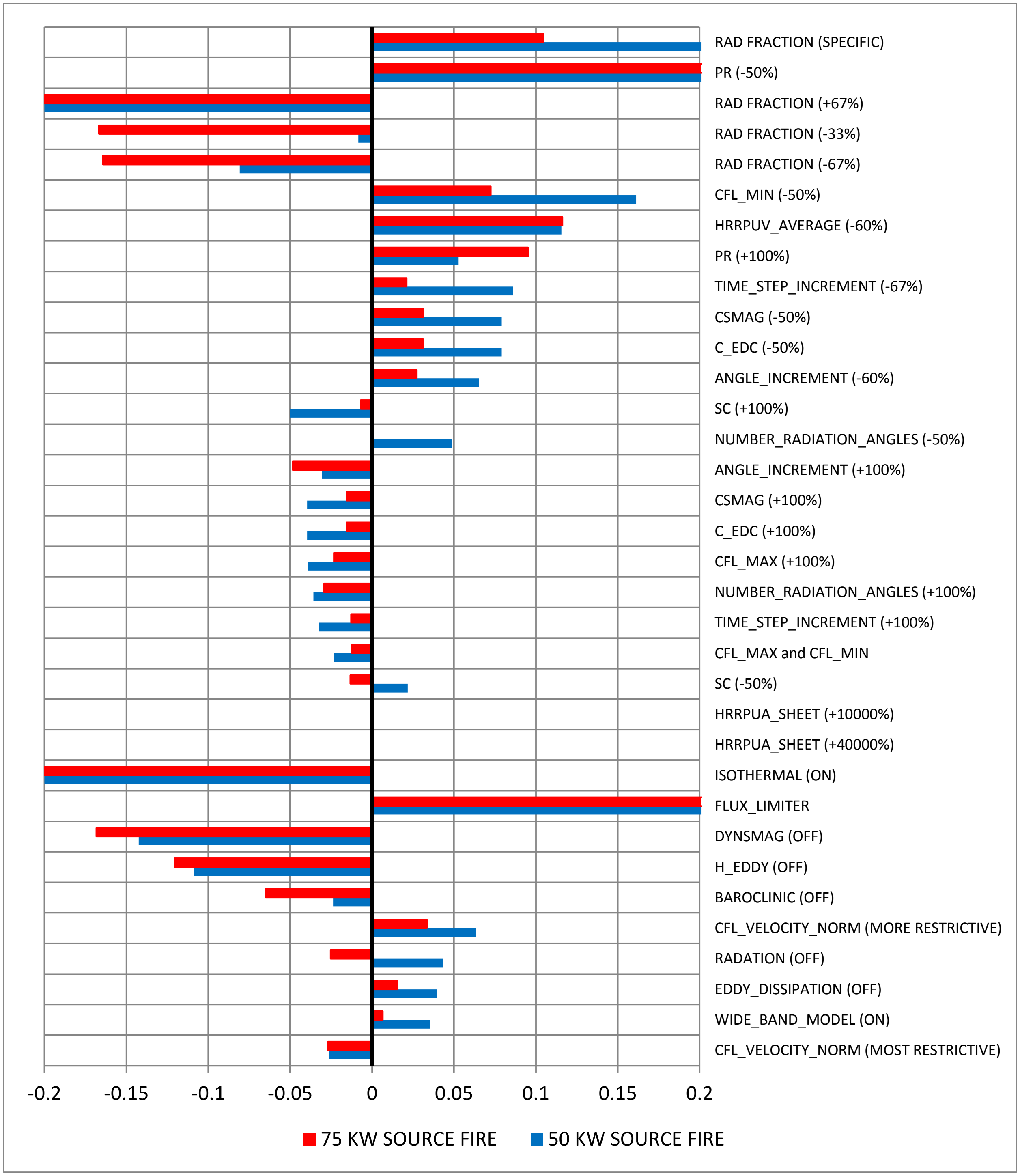

Figure 240 – Plume velocity sensitivity coefficients, grouped by HRR

Figure 241 shows the sensitivity coefficients based on the predicted plume centerline temperature averaged over simulations using the same source fire HRR. The parameter changes that caused the most significant plume temperature change are the radiative fraction, Prandtl number, the isothermal mode was used, which calculation scheme used based on the value of the flux limiter, and whether the dynamic Smagorinsky model is turned off.

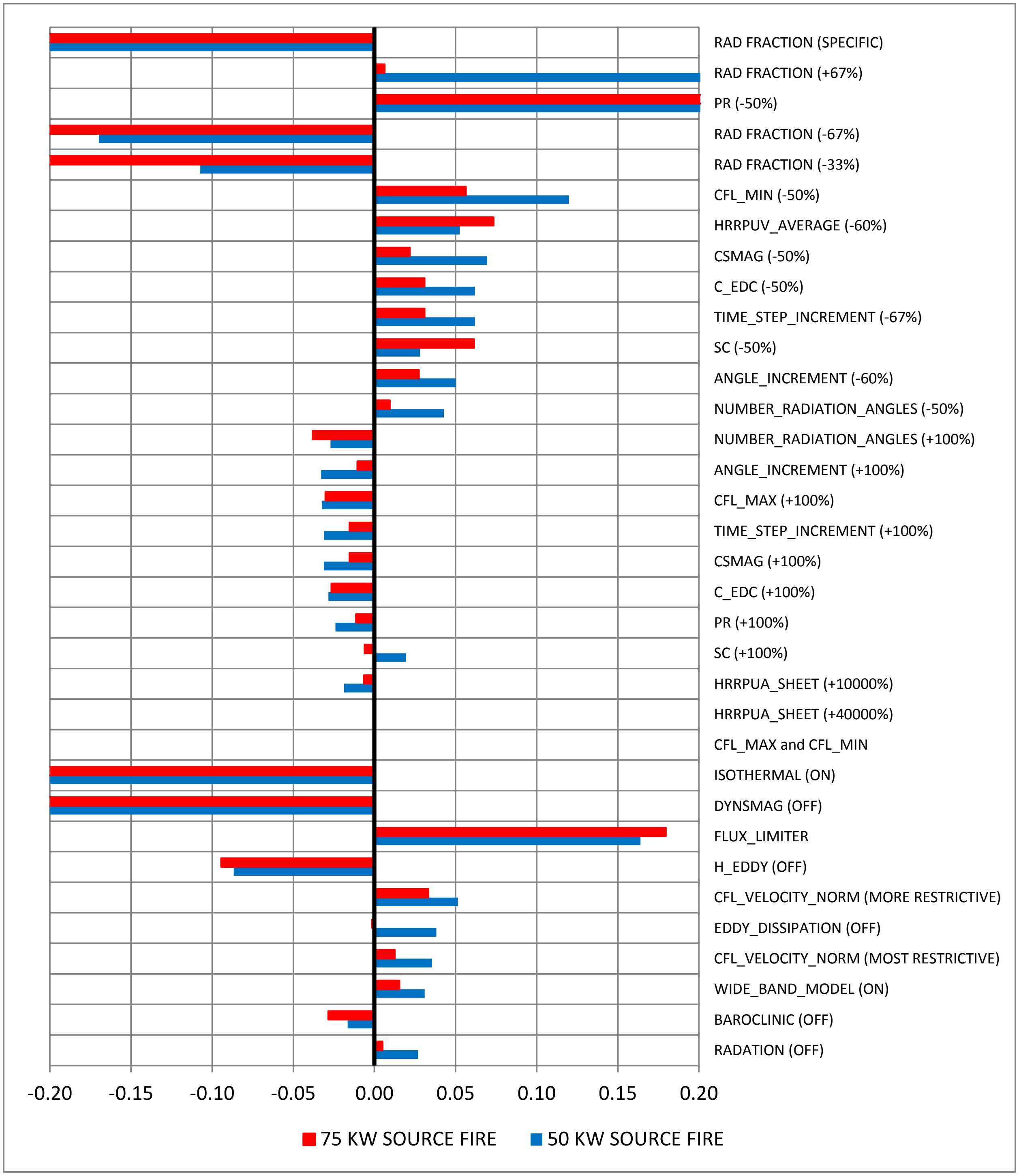

Figure 241 - Plume temperature sensitivity coefficients, grouped by HRR

5.4.2 FDS parameters with significant effects on inert wall fire simulations

This section presents the sensitivity coefficients generated from the various simulations as grouped by the fuel type, burner shape, and source fire HRR. The parameters and their variances that generated sensitivity coefficients ≥ 0.1 are considered significant. Each sensitivity coefficient was based on one of the predicted quantities, and was averaged over height and across those simulations using identical fuel types regardless of the scenario, burner shape, and base HRR. The results from the toggle parameters are located at the bottom of the charts, and the parameter change that correlates with the overall maximum sensitivity coefficients are presented first.

Non-toggle parameters such as radiative fraction, Prandtl number, and the average HRRPUV of the fire dominate the changes of the measured temperature, velocity, and gauge heat flux to wall along the plume centerline in the simulations. These parameters contribute to the structure of the plume, and the amount of heat output of the fire, all related to the plume characteristics and the heat flux to wall.

For the toggled parameter studied, the ones with the greatest changes include: isothermal model, CFL velocity normalization, eddy diffusivity model, the dynamic Smagorinsky model, and the baroclinic vorticity calculations. All these parameter contributes to the stability and structure of the flow field, which are especially important factors that describe the interaction between the plume and the solid wall. Isothermal simulations forces the no temperature change within the model, and turning off the radiation model prevents radiative heat transfer, both limiting changes in the plume temperature and heat flux to the wall to be properly calculated. The flux limiter, which controls the calculations scheme used in the calculations, is consistently one of the greatest contributors to quantity changes because the simulations all crashed due to numerical instability.

Additionally, the results from the parametric study show that simulations with Square burner or the higher HRR at 75 kW are more greatly affected by the parameter changes than their counterparts, which is opposite to the trend from the plume simulations. Effects on the three different source fuels appear to be relatively similar.

Figure 242 shows the sensitivity coefficients based on the predicted plume centerline velocity averaged over inert wall simulations using the same fuel type. The parameters that created the most significant changes to the plume velocity are the radiative fraction, as well as the when the isothermal mode was used, which calculation scheme used based on the value of the flux limiter, and whether the radiation model is activated.

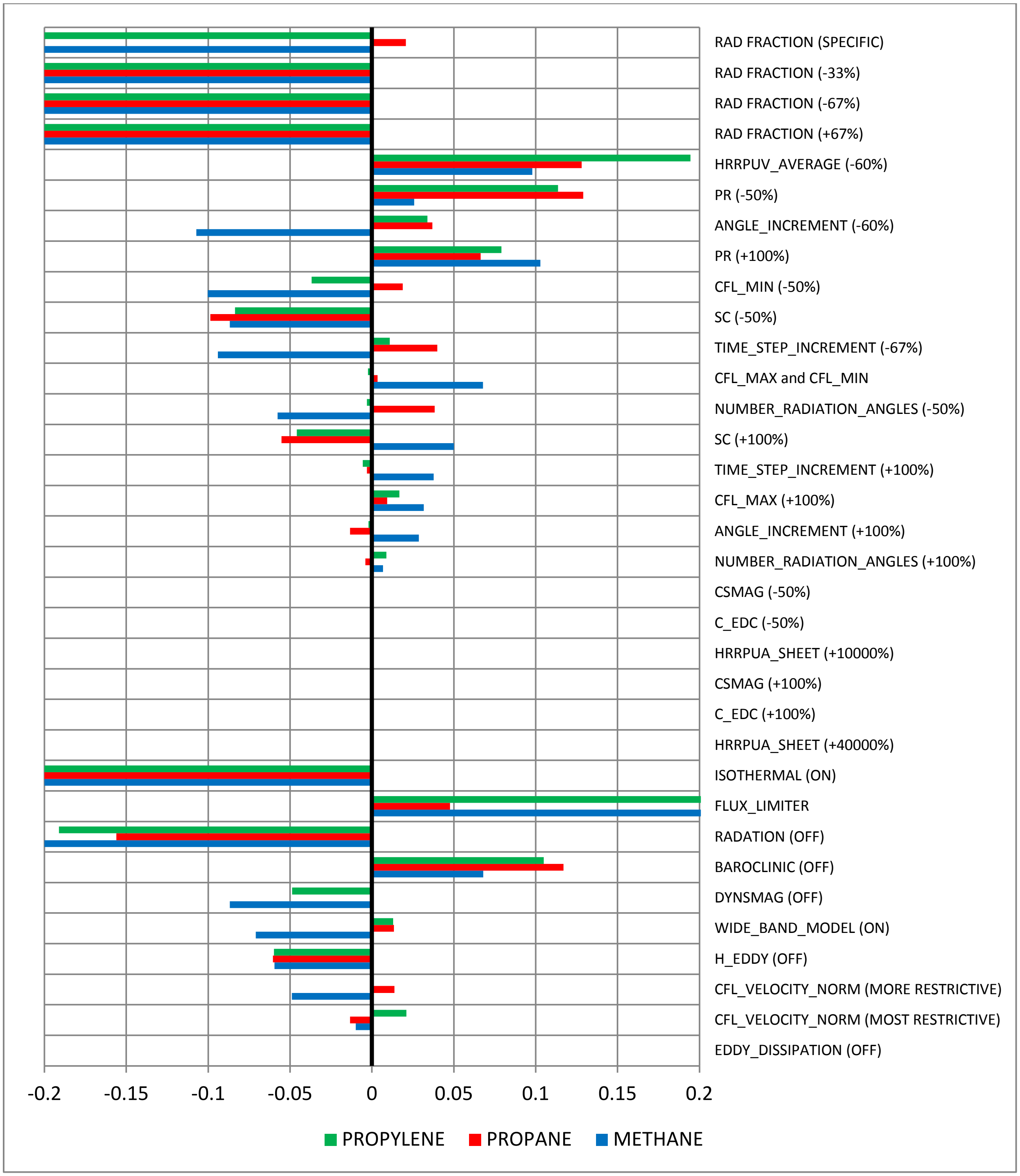

Figure 242 – Plume velocity sensitivity coefficients, grouped by fuel type

Figure 243 shows the sensitivity coefficients based on the predicted plume centerline velocity averaged over simulations with consistent fuel type. The parameters that created the most significant changes to the plume temperature are the radiative fraction, as well as the when the isothermal mode was used, which calculation scheme used based on the value of the flux limiter, and whether the dynamic Smagorinsky model is activated.

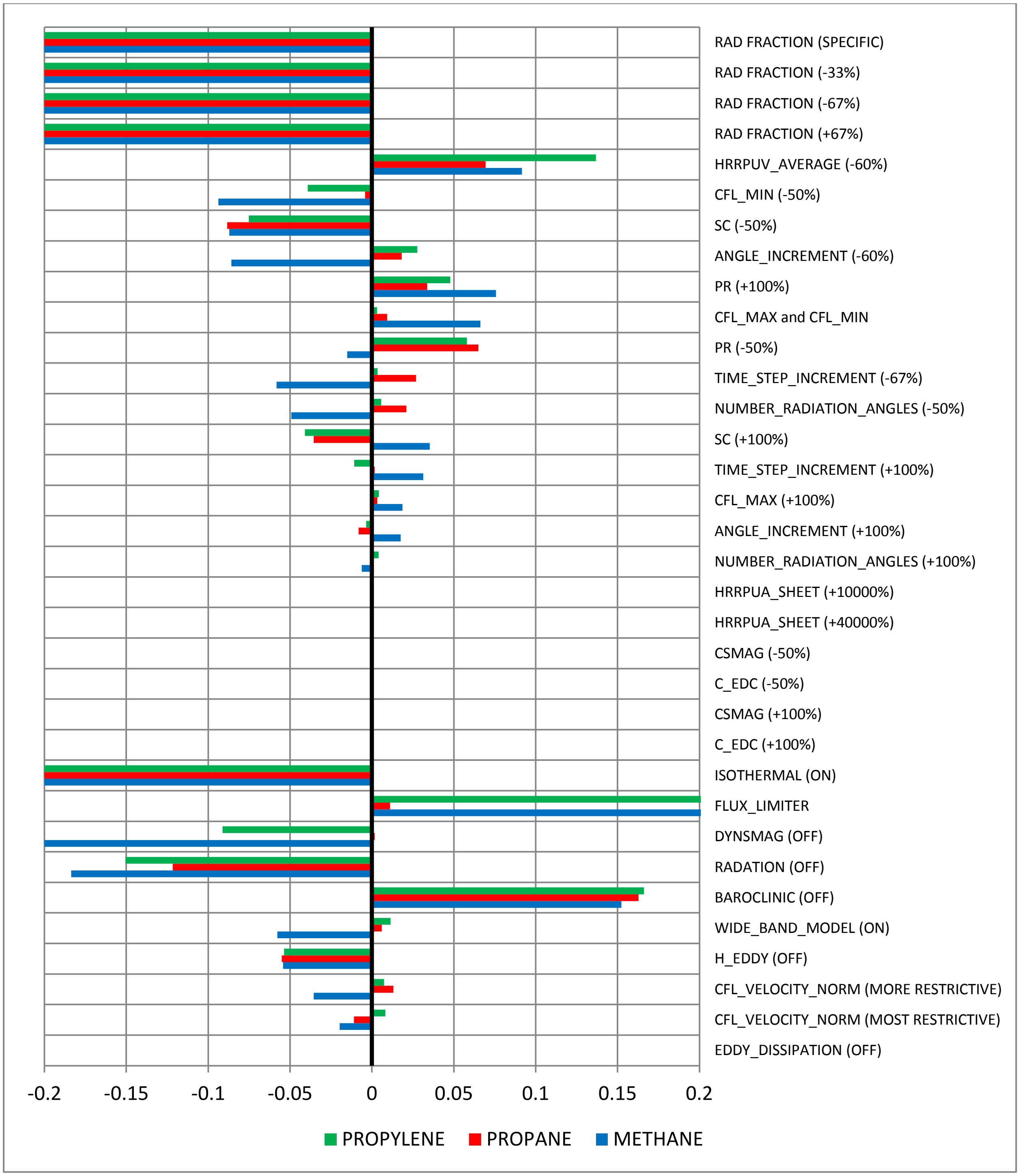

Figure 243 – Plume temperature sensitivity coefficients, grouped by fuel type

Figure 244 shows the sensitivity coefficients based on the predicted centerline gauge heat flux to wall averaged over simulations with consistent fuel type. The parameters that contributed to the most significant changes to the gauge heat flux are the Prandtl number, the radiative fraction, the decrease of the HRRPUV of the fire, whether the dynamic Smagorinsky model is activated, when the isothermal mode was used, which calculation scheme used based on the value of the flux limiter, if the eddy diffusivity model is turned off, and whether the radiation model is activated.

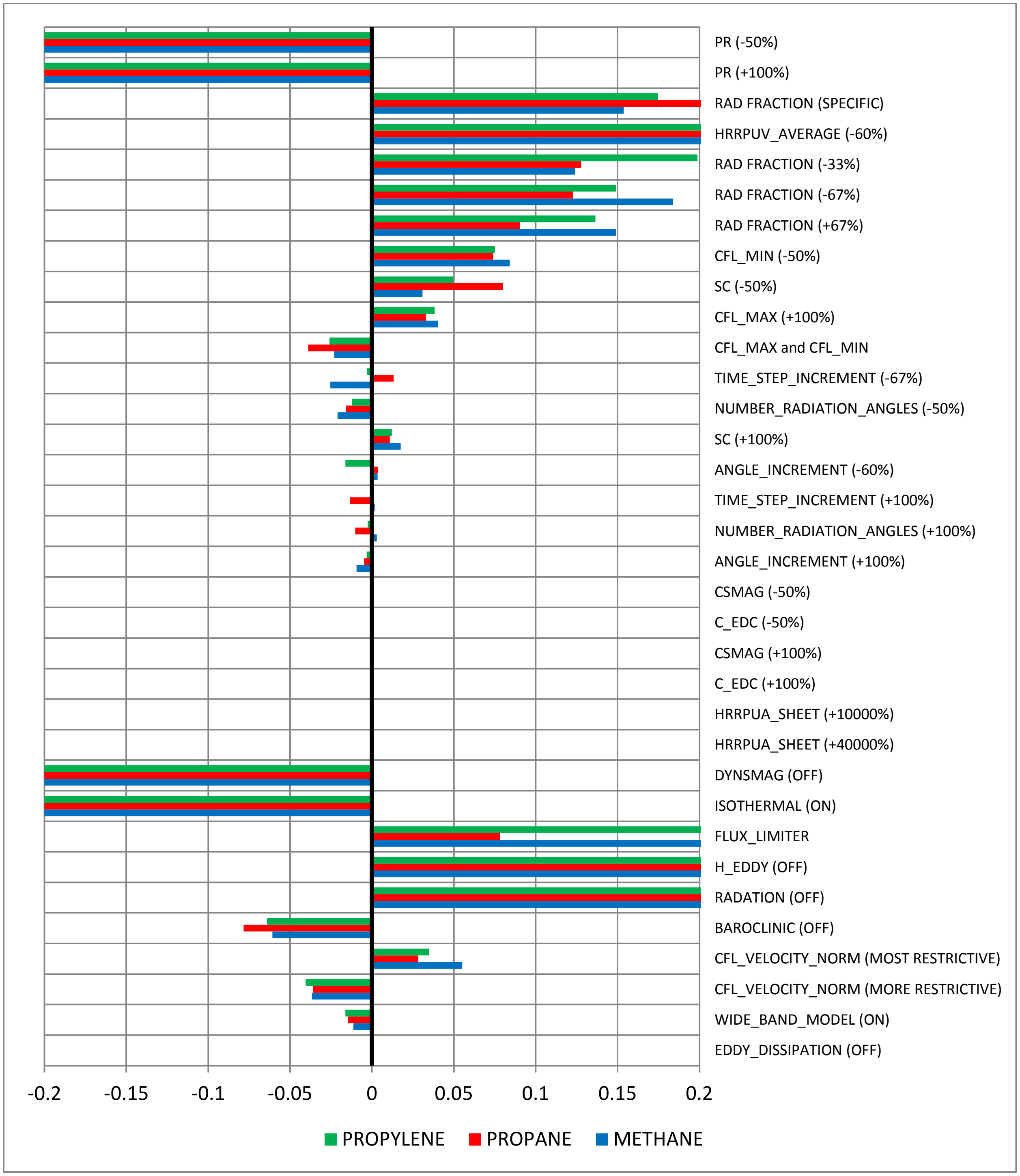

Figure 244 – Centerline gauge heat flux to wall sensitivity coefficients, grouped by fuel type

Figure 245 shows the sensitivity coefficients based on the predicted plume centerline velocity averaged over simulations using the same source fire burner. The parameters that created the most significant changes to the plume velocity are the radiative fraction, decreased in the heat release rate per unit volume of the flame, as well as the when the isothermal mode was used, which calculation scheme used based on the value of the flux limiter, and whether the radiation model is activated.

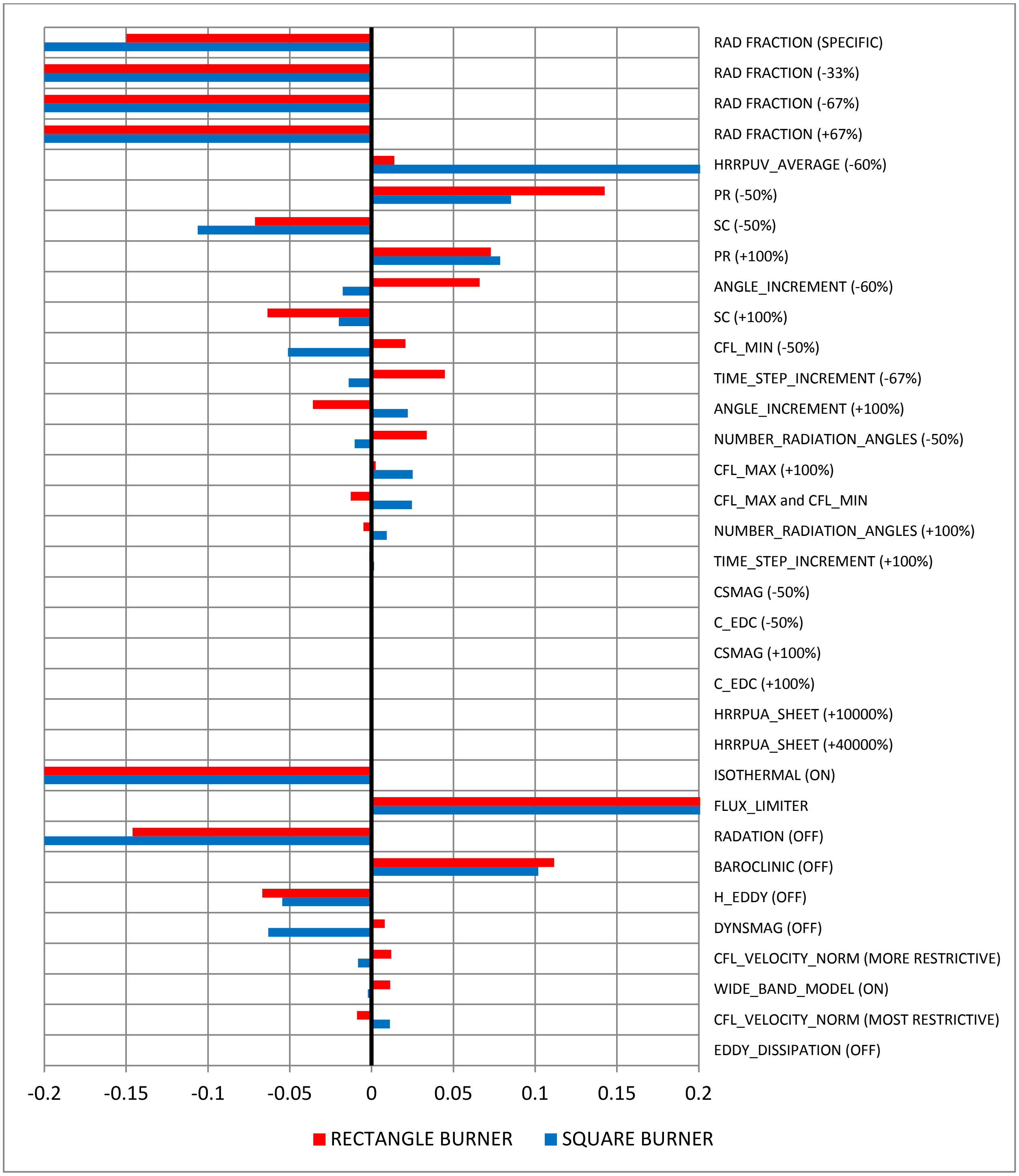

Figure 245 – Plume velocity sensitivity coefficients, grouped by burner shape

Figure 246 shows the sensitivity coefficients based on the predicted plume centerline temperature averaged over simulations using the same source fire burner. The parameters that contributed to the most significant changes to the plume temperature are the radiative fraction, the decrease of the HRRPUV of the fire, when the isothermal mode was used, and which calculation scheme used based on the value of the flux limiter

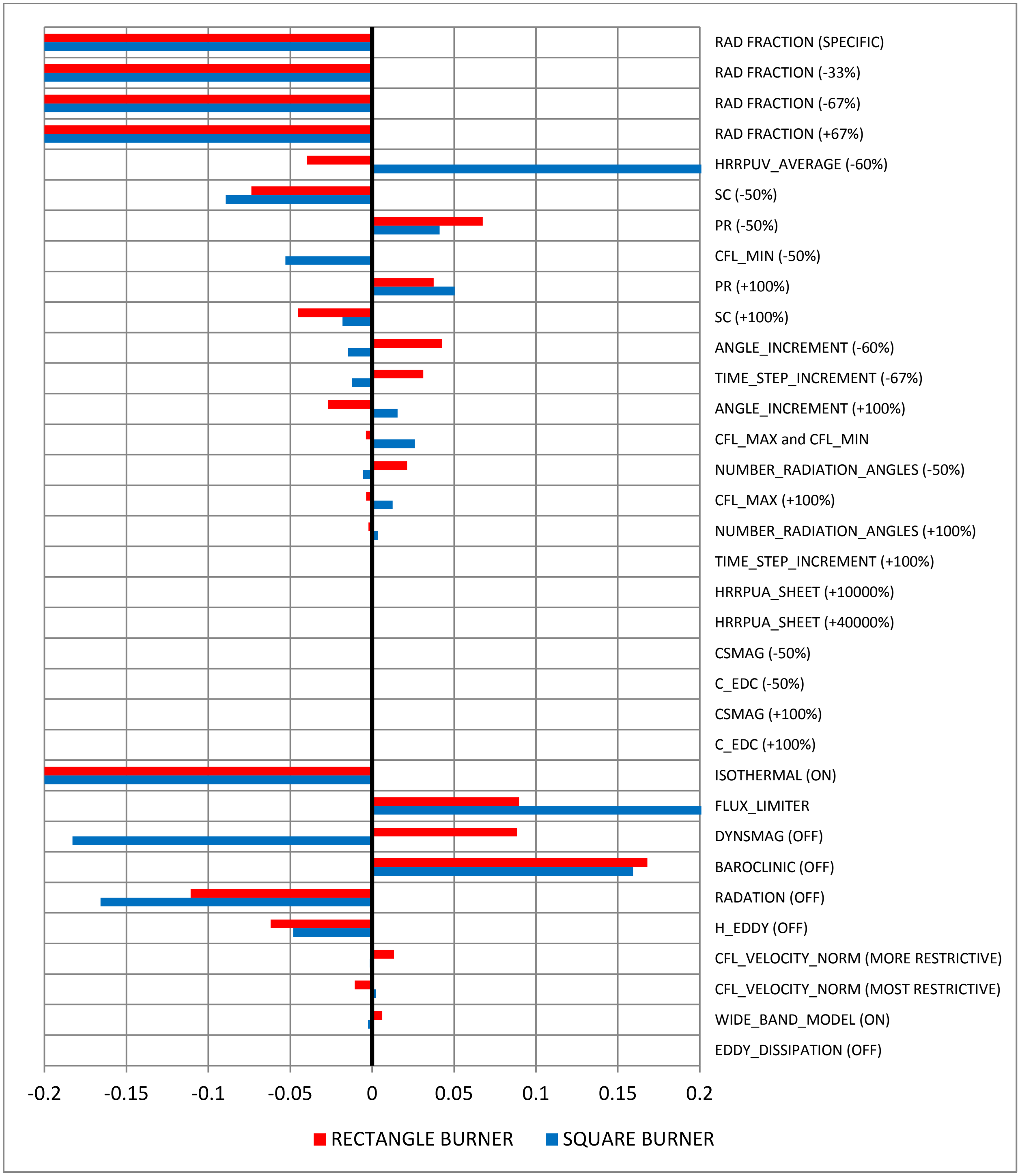

Figure 246 – Plume temperature sensitivity coefficients, grouped by burner shape

Figure 247 shows the sensitivity coefficients based on the predicted centerline gauge heat flux to wall averaged over simulations using the same source fire burner. The parameter changes that caused the most significant gauge heat flux change are the Prandtl number, the radiative fraction, a decrease of the HRRPUV of the fire, when the dynamic Smagorinsky model is turned off, whether the isothermal mode was used, when the eddy diffusivity model was activated, if the radiation transport model was turned off, and which calculation scheme used based on the value of the flux limiter.

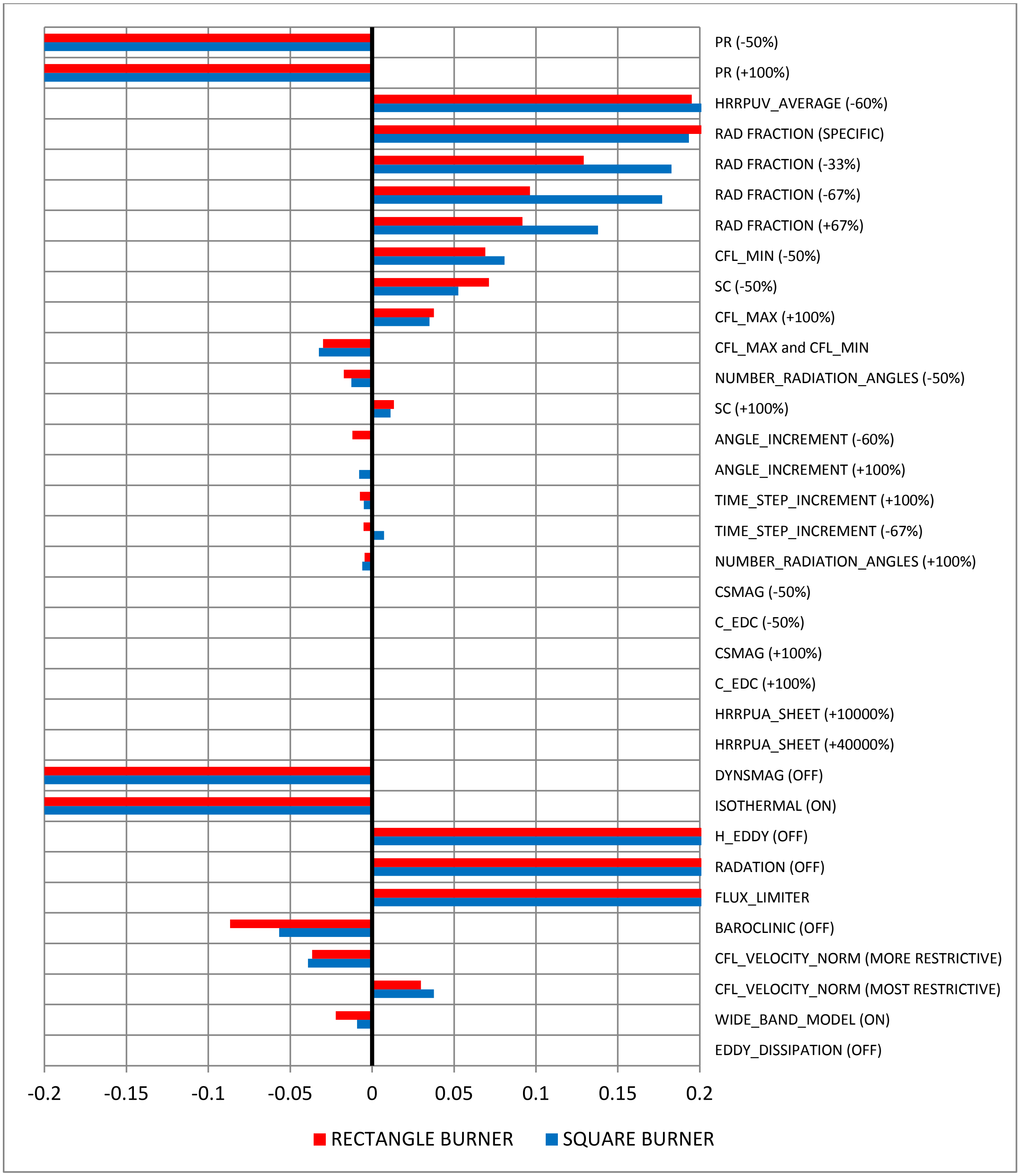

Figure 247 – Centerline gauge heat flux to wall sensitivity coefficients, grouped by burner shape

Figure 248 shows the sensitivity coefficients based on the predicted plume centerline velocity averaged over simulations using the same source fire HRR. The parameter changes that caused the most significant velocity change are the radiative fraction, a decrease of the HRRPUV of the fire, whether the isothermal mode was used, and which calculation scheme used based on the value of the flux limiter.

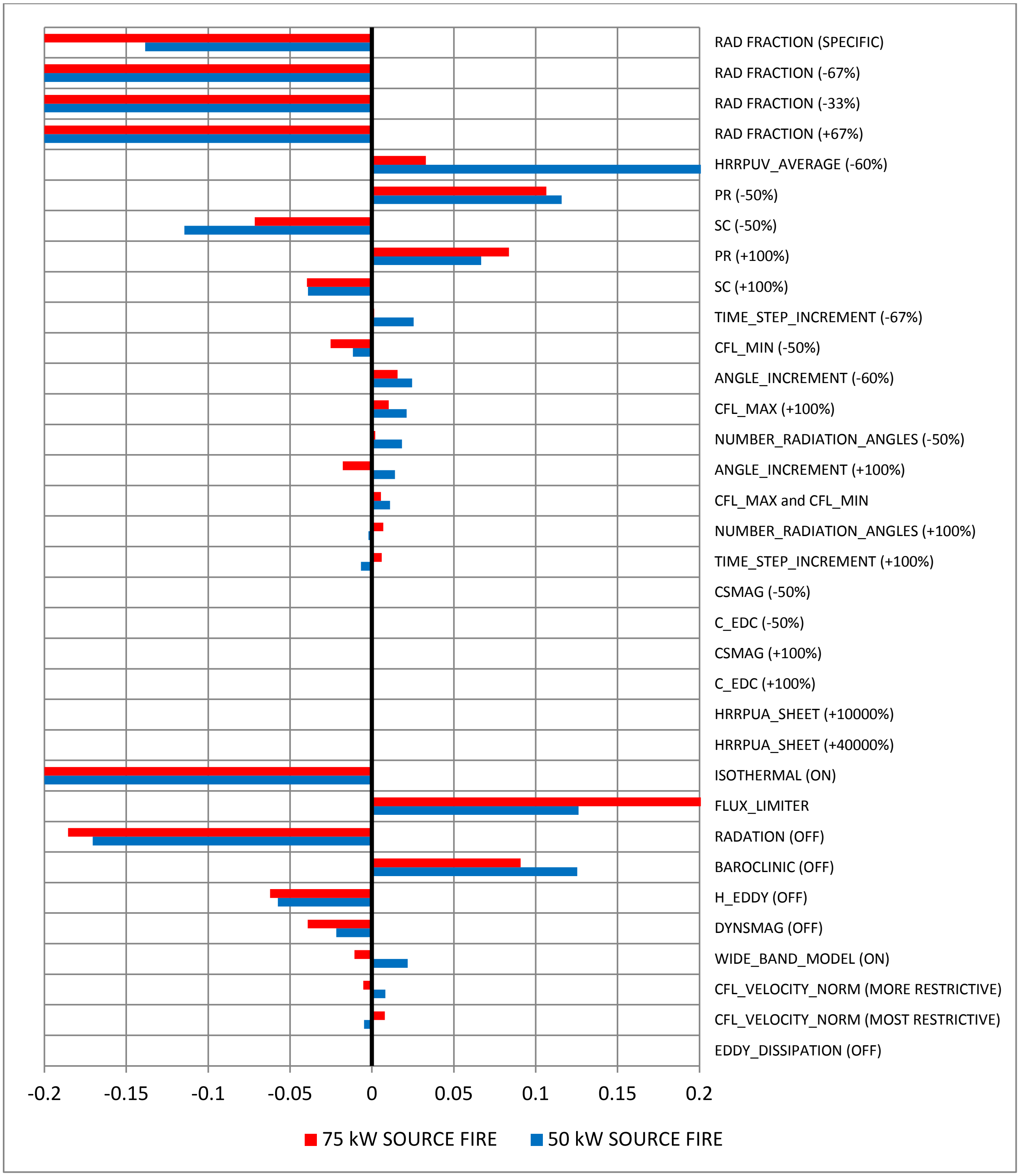

Figure 248 – Plume velocity sensitivity coefficients, grouped by HRR

Figure 249 shows the sensitivity coefficients based on the predicted plume centerline temperature averaged over simulations using the same source fire HRR. The parameters that contributed to the most significant changes to the plume temperature are the radiative fraction, the decrease of the HRRPUV of the fire, when the isothermal mode was used, and which calculation scheme used based on the value of the flux limiter

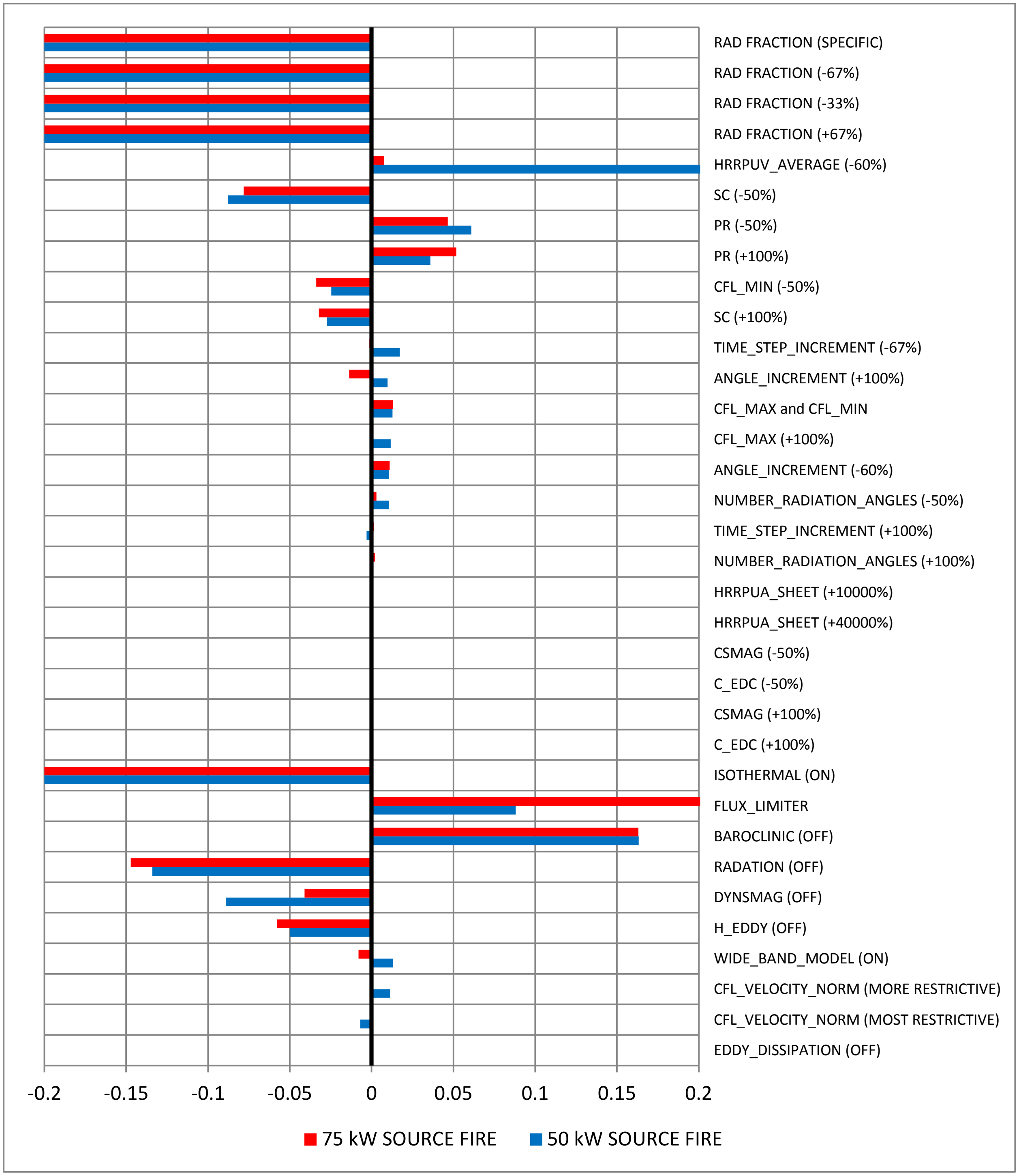

Figure 249 – Plume temperature sensitivity coefficients, grouped by HRR

Figure 250 shows the sensitivity coefficients based on the predicted centerline gauge heat flux to wall averaged over simulations using the same source fire HRR. The parameter changes that caused the most significant gauge heat flux change are the Prandtl number, the radiative fraction, a decrease of the HRRPUV of the fire, when the dynamic Smagorinsky model is turned off, whether the isothermal mode was used, when the eddy diffusivity model was activated, if the radiation transport model was turned off, and which calculation scheme used based on the value of the flux limiter.

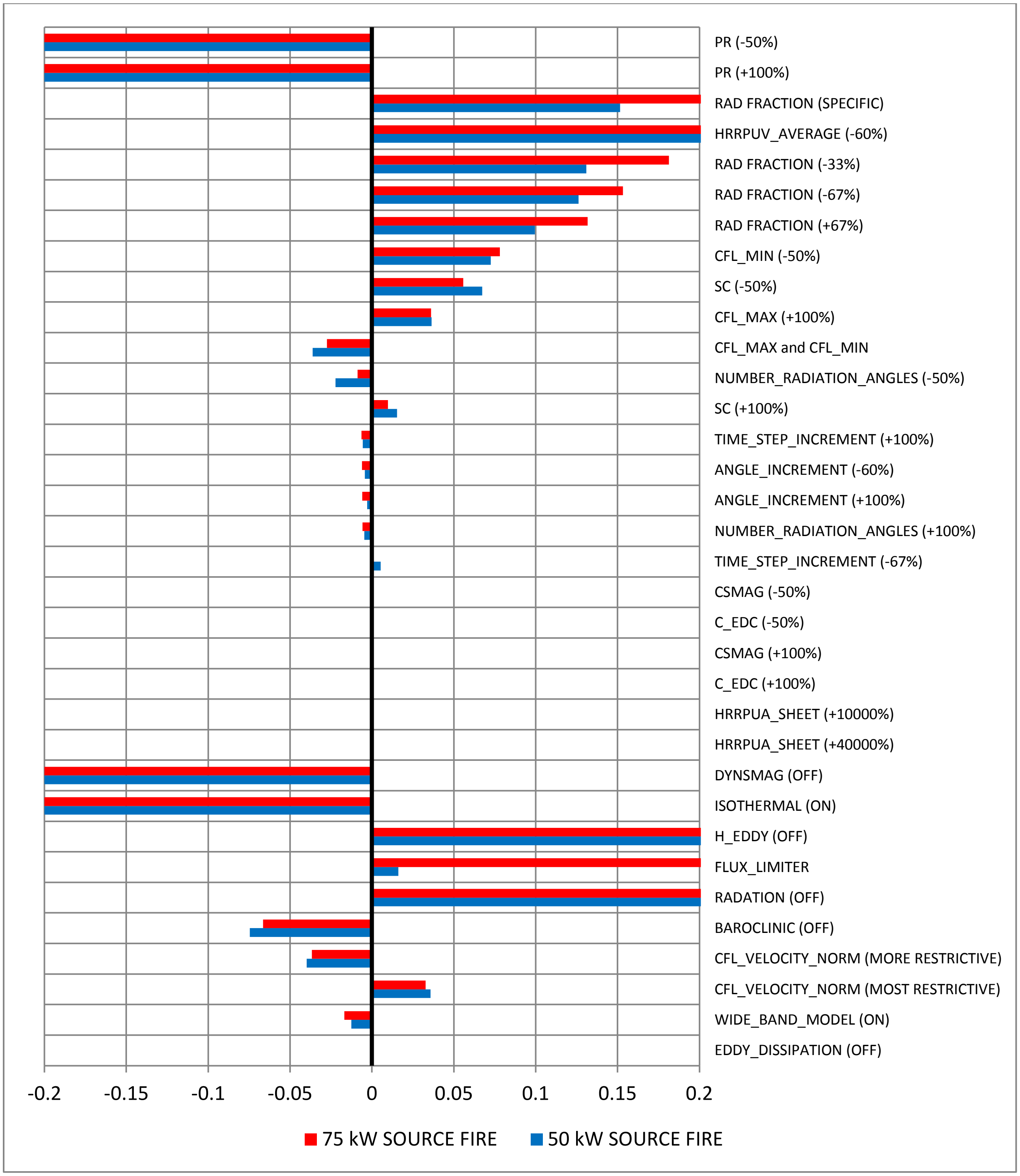

Figure 250 – Centerline gauge heat flux to wall sensitivity coefficients, grouped by HRR

5.4.3 FDS parameters with significant effects on combustible wall fire simulations

This section presents the sensitivity coefficients generated from the various simulations as grouped by the fuel type, source burner size, and source fire HRR. Additionally, the simulations are also grouped based on whether the source fire was terminated during the simulation or continuous throughout. The parameters and their variances that generated sensitivity coefficients ≥ 0.5 are considered significant. Each sensitivity coefficient was based on one of the predicted quantities, and was averaged over height and across those simulations using identical fuel types regardless of the scenario, burner shape, and base HRR. The results from the toggle parameters are located at the bottom of the charts, and the parameter change that correlates with the overall maximum sensitivity coefficients are presented first.

Continuous parameters such as radiative fraction, Prandtl number, and the average HRRPUV of the fire dominate the changes of the total mass lost, peak HRR, time to peak HRR, and total heat released predicted in the various simulations. These are the same parameters that affected the plume and inert wall simulations, suggesting a relationship between these parameters and their importance. The significance of plume characteristics and flame heat transfer behaviors are also highlighted through these parameters.

For the toggled parameter studied, the ones with the greatest changes include: isothermal model, CFL velocity normalization, eddy diffusivity model, the dynamic Smagorinsky model, and the baroclinic vorticity calculations. Again, all parameters of import identified from the inert wall fire parametric study. All these parameter contributes to the stability and structure of the flow field, which are especially important factors that describe the interaction between the plume and the solid wall. Isothermal simulation forces the no temperature change within the model, and turning off the radiation model prevents radiative heat transfer, both limiting changes in the environment and kill any flame spread. Since flame spread is greatly dependent on the source fire and its interaction with the environment, especially the external solid fuel on the wall, if the interactions are not modeled correctly, flame spread will not be predicted, hence the much greater discrepancy between the baseline models and the parametric runs in the combustible wall simulations than those found in the inert wall or plume simulations. Clearly the discrepancy is propagated through the successively complex simulations runs from plume to inert wall to combustible wall fire modeling.

Additionally, the results from the parametric study generally show that the parametric changes have the greatest effects on simulations where a continuous source fire is used. This may be biased because of the very low flame spread predicted by all of the simulations with a terminated source fire, which suggest a contributing factor from another level of the modeling calculation schemes.

Figure 251 shows the sensitivity coefficients based on the total mass loss averaged over combustible wall simulations using the same fuel type. The parameters that created the most significant changes to the mass loss are changes in the radiative fraction and Prandtl number, as well as whether the dynamic Smagorinsky model is deactivated, and which calculation scheme was used based on the value of the flux limiter. It is noted that an isothermal does not have the most drastic changes to the total mass loss.

Changes to the simulations with a Continuous source fire appear to be greater. It is noted that the simulations with change to the FLUX_LIMITER value crashed due to numerical instability.

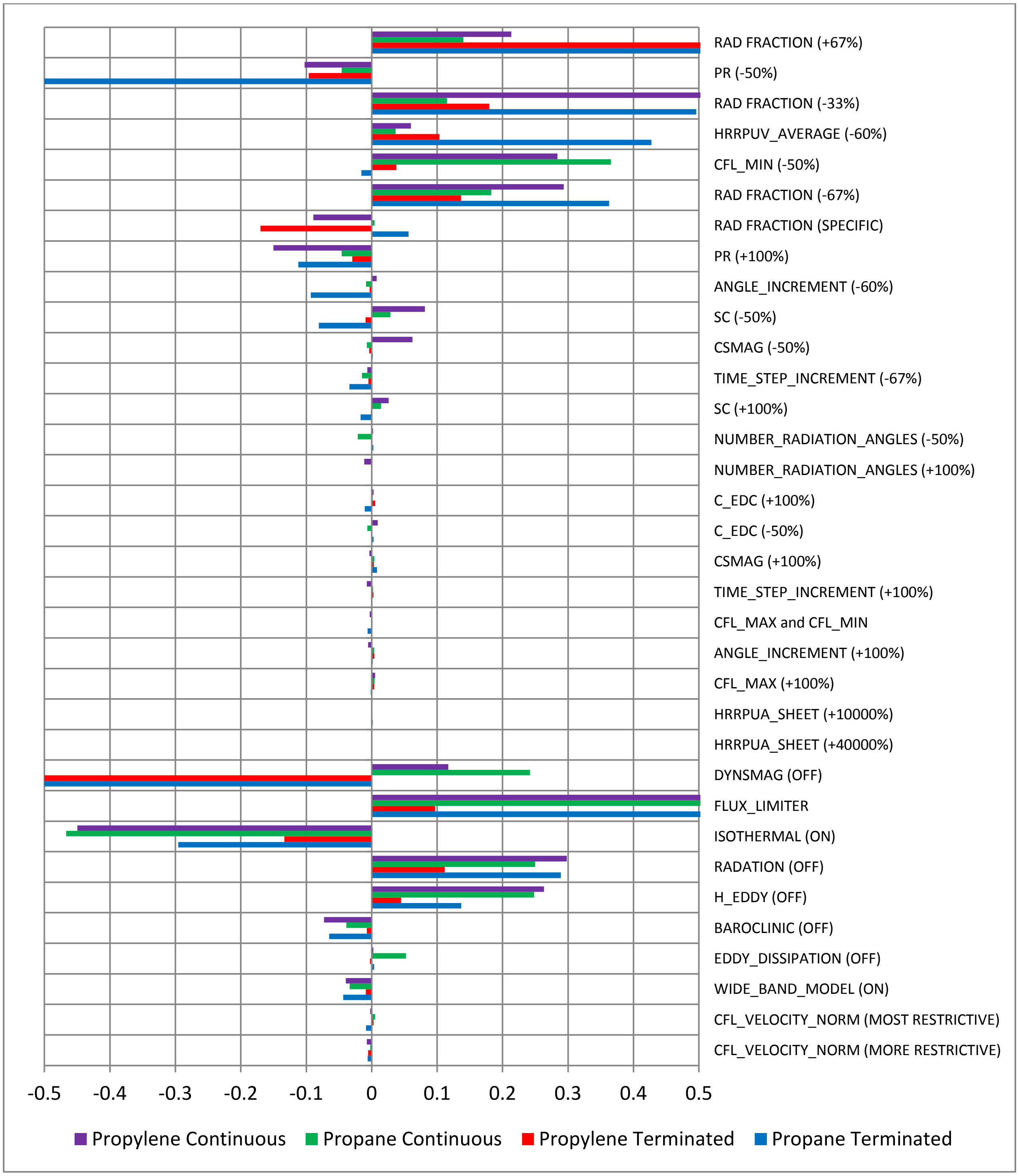

Figure 251 – Total mass loss sensitivity coefficients, grouped by fuel type

Figure 252 shows the sensitivity coefficients based on the peak HRR value averaged over simulations with consistent fuel type. The parameters that created the most significant changes to the time to peak HRR are changes in the radiative fraction, Prandtl number, and the average HRRPUV of the flame. For the “toggled” parameters, changes are most significant when the dynamic Smagorinsky model is deactivated, the isothermal model is used, the radiation solver is turned off, and when the eddy diffusivity model is deactivated. The flux limiter value that controls the calculation scheme also contributes greatly to the peak HRR value. It is noted that the simulations with change to the FLUX_LIMITER value crashed due to numerical instability. Changes to the simulations with the terminated source fire are usually greater.

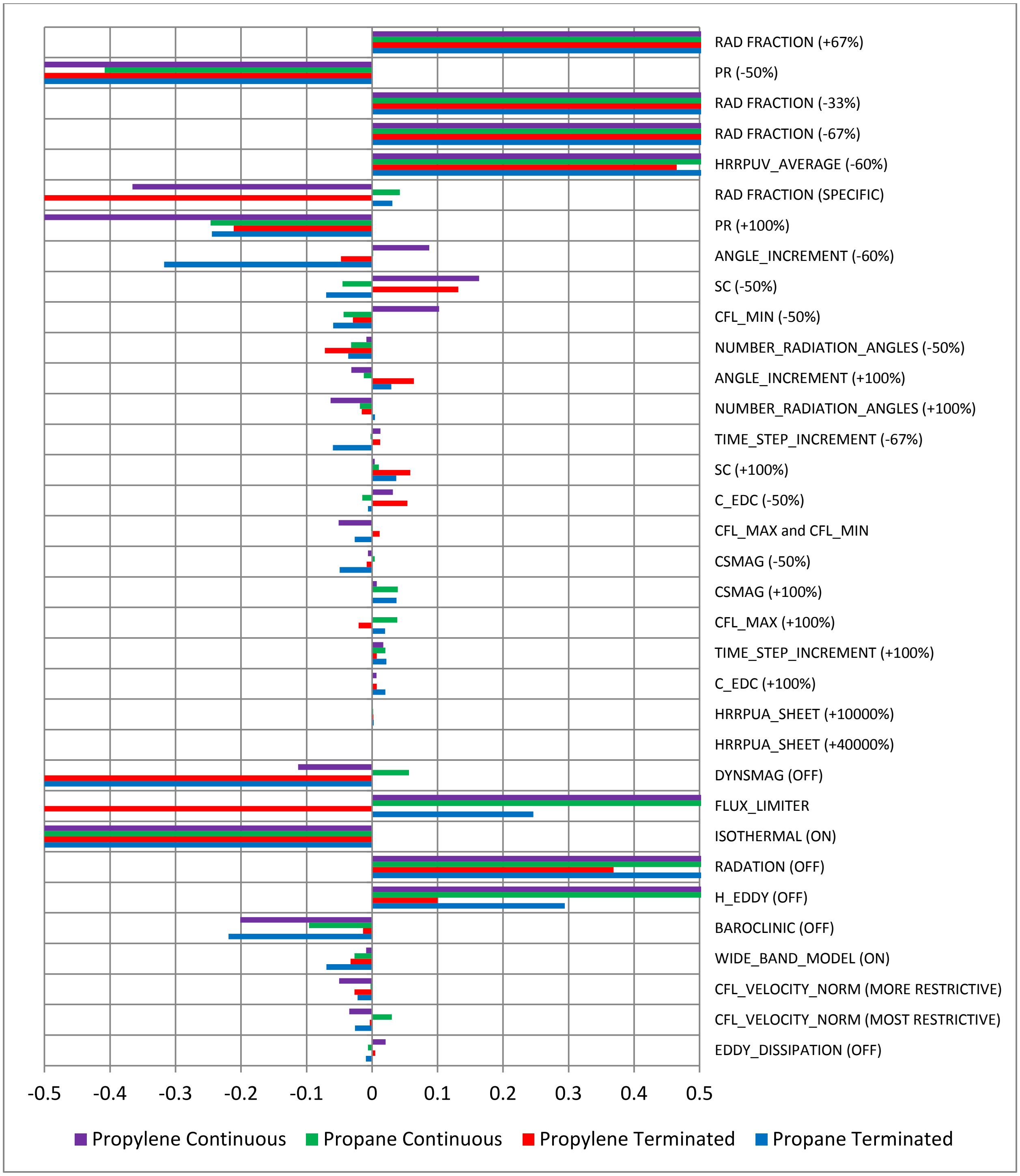

Figure 252 – Peak HRR sensitivity coefficients, grouped by fuel type

Figure 253 shows the sensitivity coefficients based on the predicted time to peak HRR averaged over simulations with consistent fuel type. The parameters that created the most significant changes to the time to peak are changes in the radiative fraction. For the “toggled” parameters, changes are most significant when the dynamic Smagorinsky model is deactivated, the isothermal model is used, the radiation solver is turned off, and when the eddy diffusivity model is deactivated. The flux limiter value that controls the calculation scheme also contributes greatly to the peak HRR value. It is noted that the simulations with change to the FLUX_LIMITER value crashed due to numerical instability. Changes to the simulations with a Continuous source fire appear to be greater.

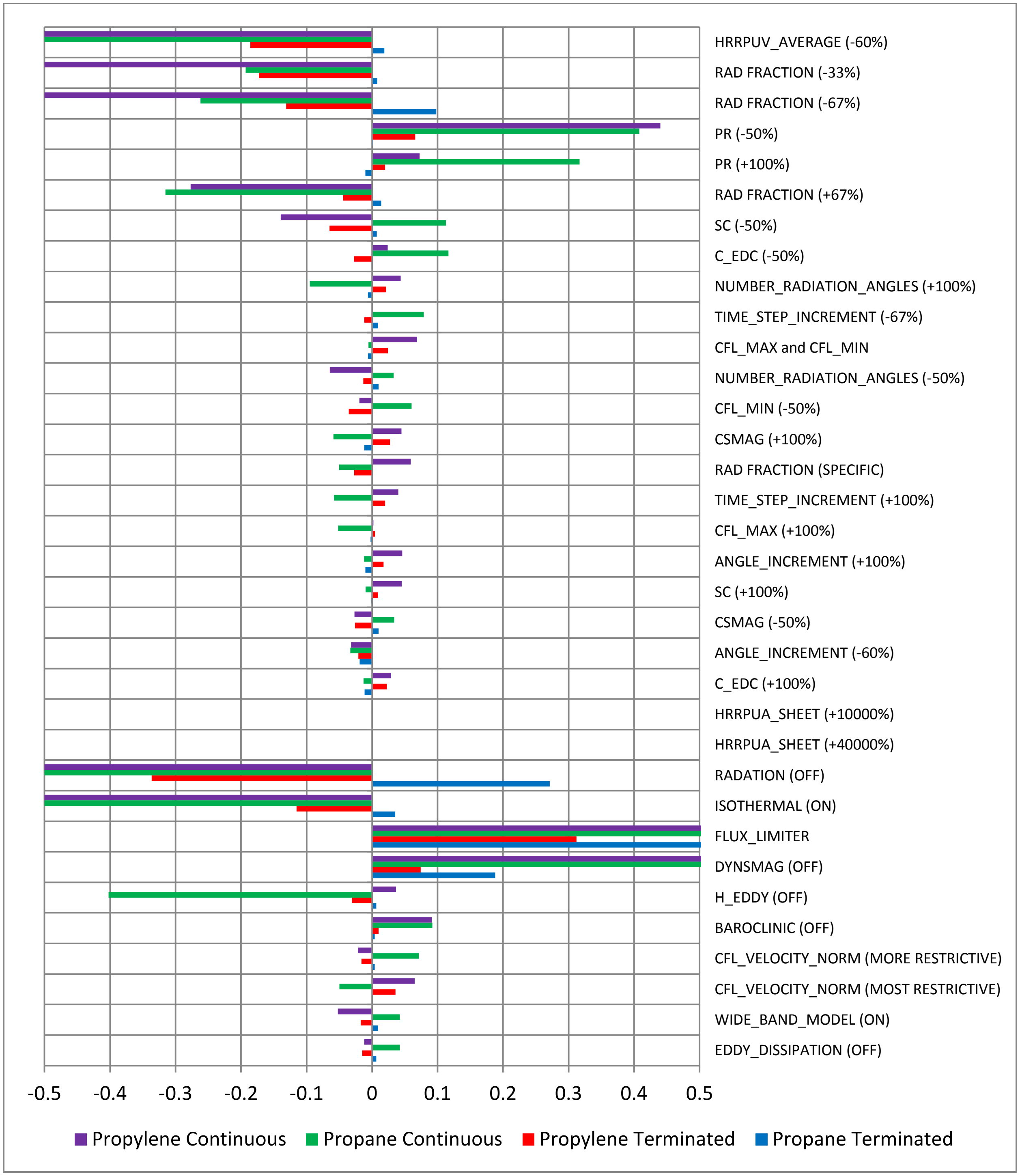

Figure 253 – Time to peak HRR sensitivity coefficients, grouped by fuel type

Figure 254 shows the sensitivity coefficients based on the predicted total heat released averaged over simulations with consistent fuel type. The parameters that created the most significant changes to the time to peak HRR are changes in the radiative fraction, Prandtl number, and the average HRRPUV of the flame. For the “toggled” parameters, changes are most significant when the dynamic Smagorinsky model is deactivated, the isothermal model is used, the radiation solver is turned off, and when the eddy diffusivity model is deactivated. The flux limiter value that controls the calculation scheme also contributes greatly to the peak HRR value, although these simulations all crashed due to numerical instability. Changes to the simulations with the terminated source fire are generally greater. The trends here are similar to the trends noted for the peak HRR changes.

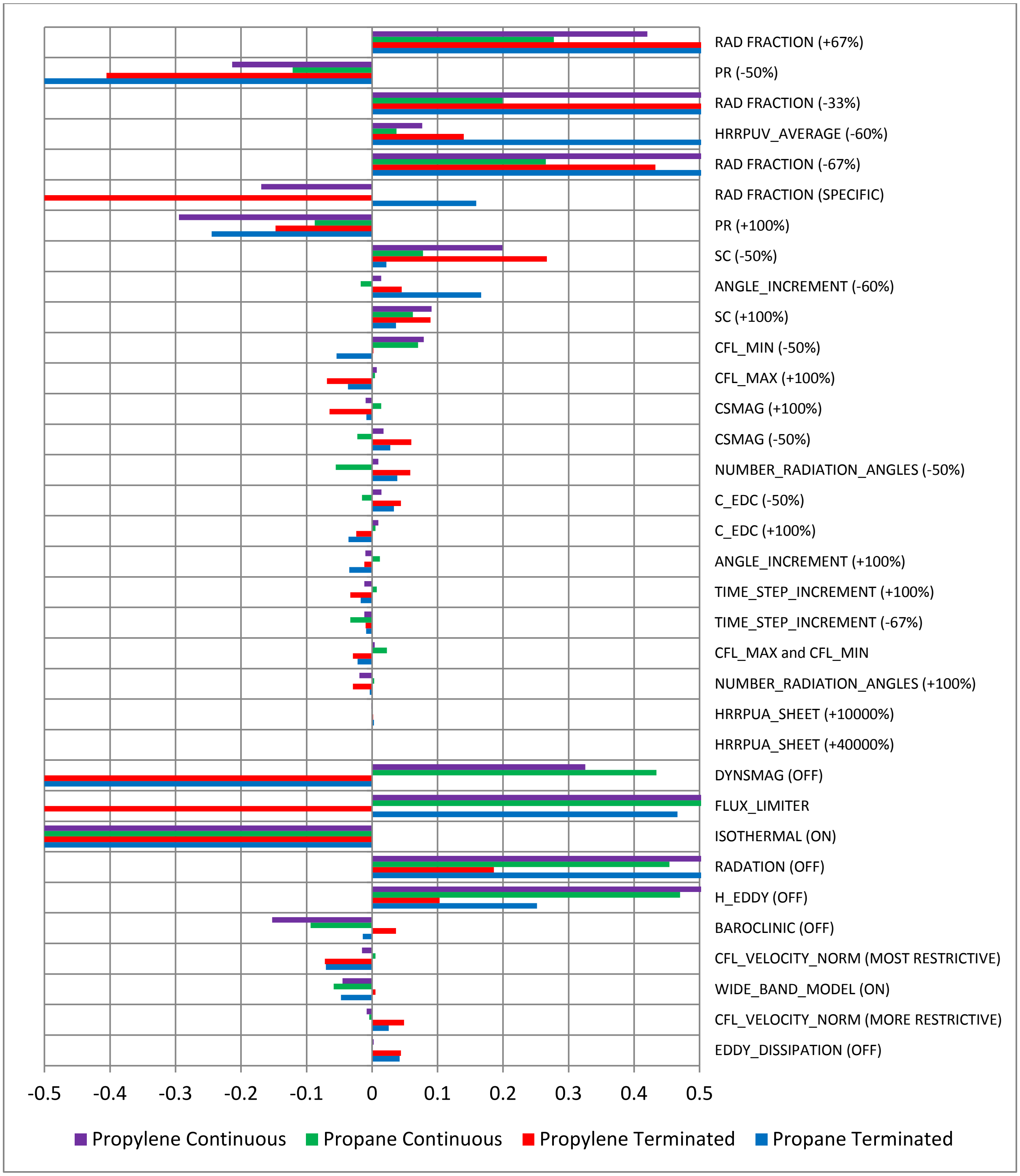

Figure 254 – Total heat Released sensitivity coefficients, grouped by fuel type

Figure 255 shows the sensitivity coefficients based on the total mass loss averaged over simulations using the same source fire burner. The parameters with significant changes are changes in the radiative fraction and a decrease of the Prandtl number, when the dynamic Smagorinsky model is deactivated, and which calculation scheme was used based on the FLUX_LIMITER value. All simulations with change to the FLUX_LIMITER value crashed. Effects on the simulations with a terminated source fire were greatest for the non-toggle parameter changes, whereas the effects of the toggled parameters are greater for simulations with a continuous source fire.

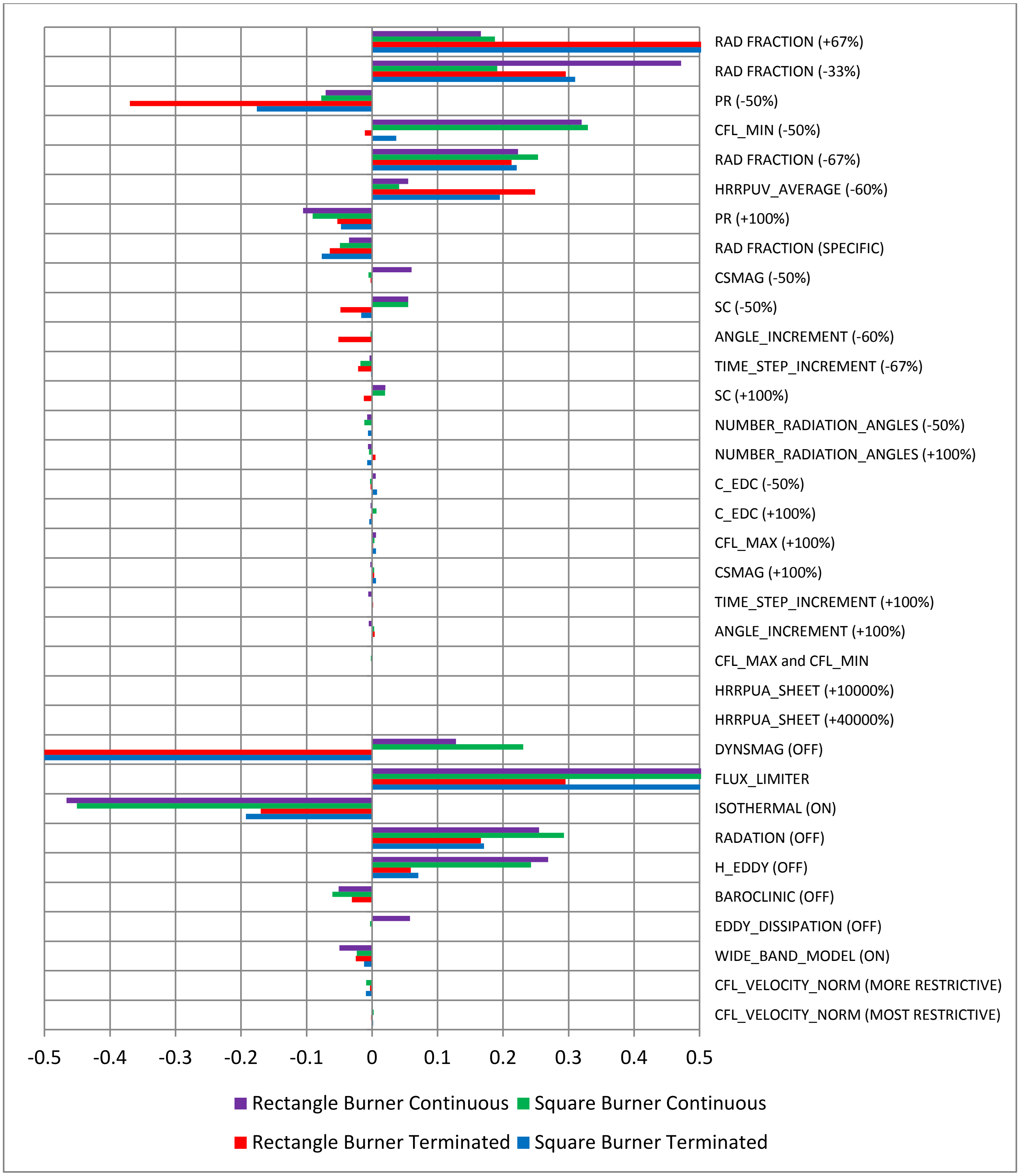

Figure 255 – Total mass loss sensitivity coefficients, grouped by burner shape

Figure 256 shows the sensitivity coefficients based on the peak HRR magnitude averaged over simulations using the same source fire burner. The parameters with significant changes are changes in the radiative fraction, a decrease of the Prandtl number, a decrease of the average HRRPUV, when the dynamic Smagorinsky model is deactivated, or when the isothermal model is turned on, when the radiation transport mode was turned off, which calculation scheme was used based on the FLUX_LIMITER value, and whether the eddy diffusivity model was not used. It is noted that the simulations with change to the FLUX_LIMITER value crashed due to numerical instability. Compared to the total mass loss, changes to the peak HRR magnitude appear to be much greater.

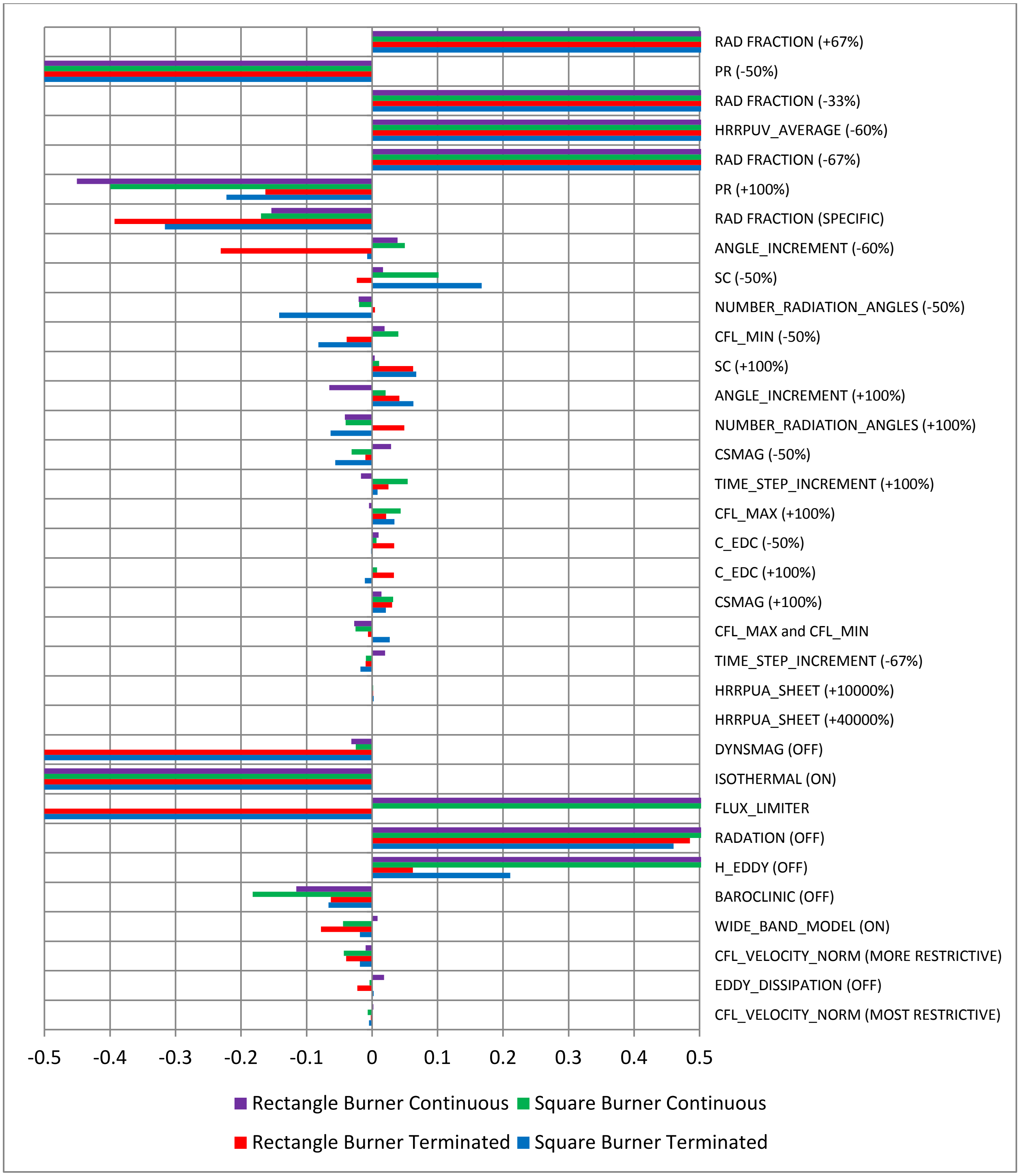

Figure 256 – Peak HRR sensitivity coefficients, grouped by burner shape

Figure 257 shows the sensitivity coefficients based on the predicted time to peak HRR averaged over simulations using the same source fire burner. The parameters with significant changes are changes in the radiative fraction, a decrease of the Prandtl number, a decrease of the average HRRPUV, when the dynamic Smagorinsky model is deactivated, or when the isothermal model is turned on, when the radiation transport mode was turned off, and which calculation scheme was used based on the FLUX_LIMITER value. It is noted that the simulations with change to the FLUX_LIMITER value crashed due to numerical instability. The effects on the simulations with a continuous source fire are generally greater than the effect on the simulations with a terminated source fire.

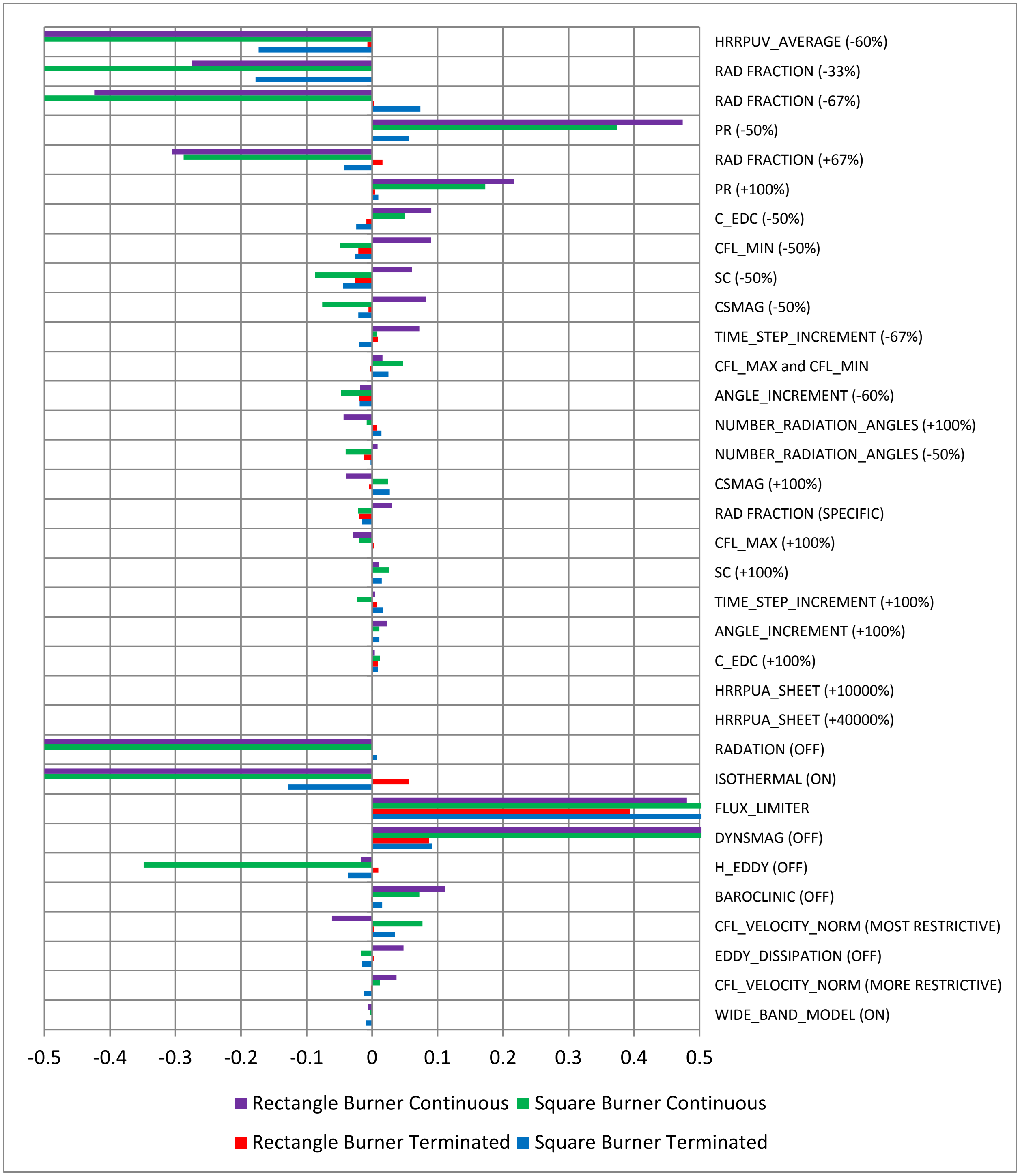

Figure 257 – Time to peak HRR sensitivity coefficients, grouped by burner shape

Figure 258 shows the sensitivity coefficients based on the predicted total mass loss averaged over simulations using the same source fire burner. The parameters with significant changes are changes in the radiative fraction, a decrease of the Prandtl number, a decrease of the average HRRPUV, when the dynamic Smagorinsky model is deactivated, or when the isothermal model is turned on, when the radiation transport mode was turned off, when the eddy diffusivity model is turned off, and which calculation scheme was used based on the FLUX_LIMITER value. The effects on the simulations with a terminated source fire are generally greater than the effect on the simulations with a continuous source fire.

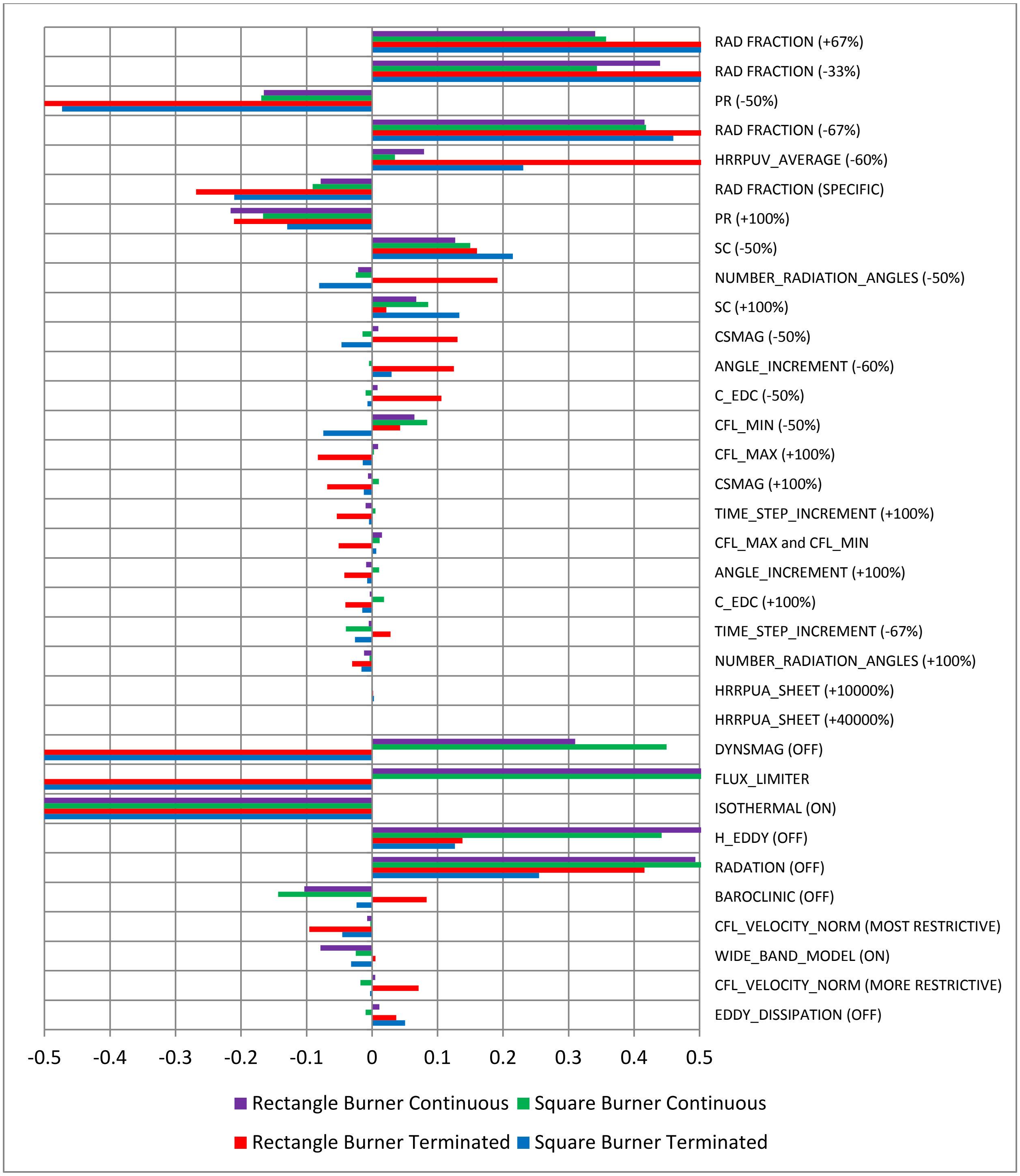

Figure 258 – Total heat released sensitivity coefficients, grouped by burner shape

Figure 259 shows the sensitivity coefficients based on the total mass loss averaged over simulations using the same source fire HRR. The parameters with significant changes are changes in the radiative fraction and a decrease of the Prandtl number, when the dynamic Smagorinsky model is deactivated, and which calculation scheme was used based on the FLUX_LIMITER value. All simulations with change to the FLUX_LIMITER value crashed. Effects on the simulations with a terminated source fire were greatest for the non-toggle parameter changes, whereas the effects of the toggled parameters are greater for simulations with a continuous source fire.

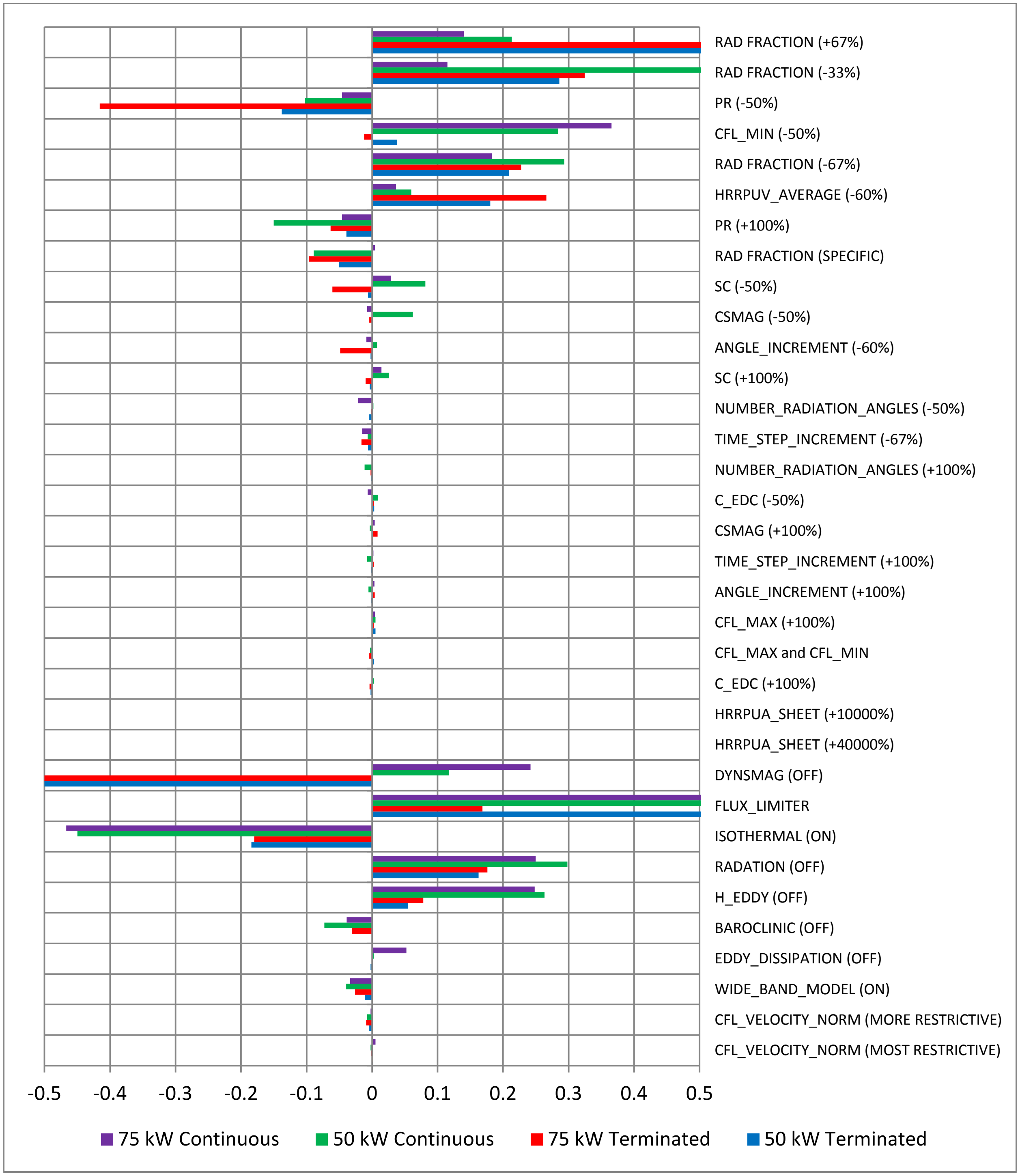

Figure 259 – Total mass loss sensitivity coefficients, grouped by HRR

Figure 260 shows the shows the sensitivity coefficients based on the peak HRR magnitude averaged over simulations using the same source fire HRR. The parameters with significant changes are changes in the radiative fraction, a decrease of the Prandtl number, a decrease of the average HRRPUV, when the dynamic Smagorinsky model is deactivated, or when the isothermal model is turned on, when the radiation transport mode was turned off, which calculation scheme was used based on the FLUX_LIMITER value, and whether the eddy diffusivity model was not used. Effects on the simulations with a terminated source fire appear to be more significant than simulations with a continuous source fire.

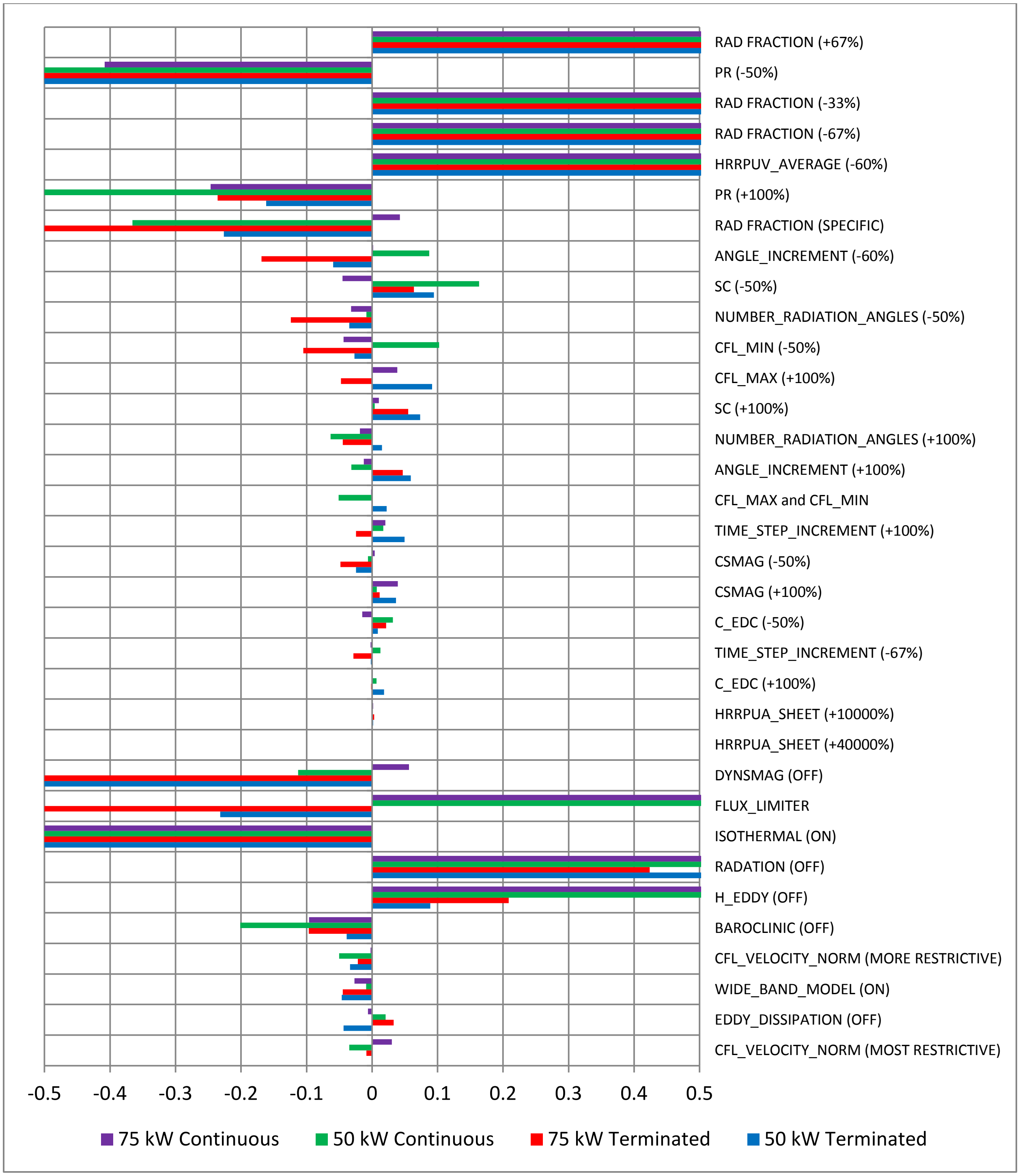

Figure 260 – Peak HRR sensitivity coefficients, grouped by HRR

Figure 261 shows the sensitivity coefficients based on the predicted time to peak HRR averaged over simulations using the same source fire HRR. The parameters with significant changes are a decrease of the average HRRPUV, changes in the radiative fraction, , when the dynamic Smagorinsky model is deactivated, or when the isothermal model is turned on, when the radiation transport mode was turned off, and which calculation scheme was used based on the FLUX_LIMITER value. It is noted that the simulations with change to the FLUX_LIMITER value crashed due to numerical instability. The effects on the simulations with a continuous source fire are generally greater than the effect on the simulations with a terminated source fire.

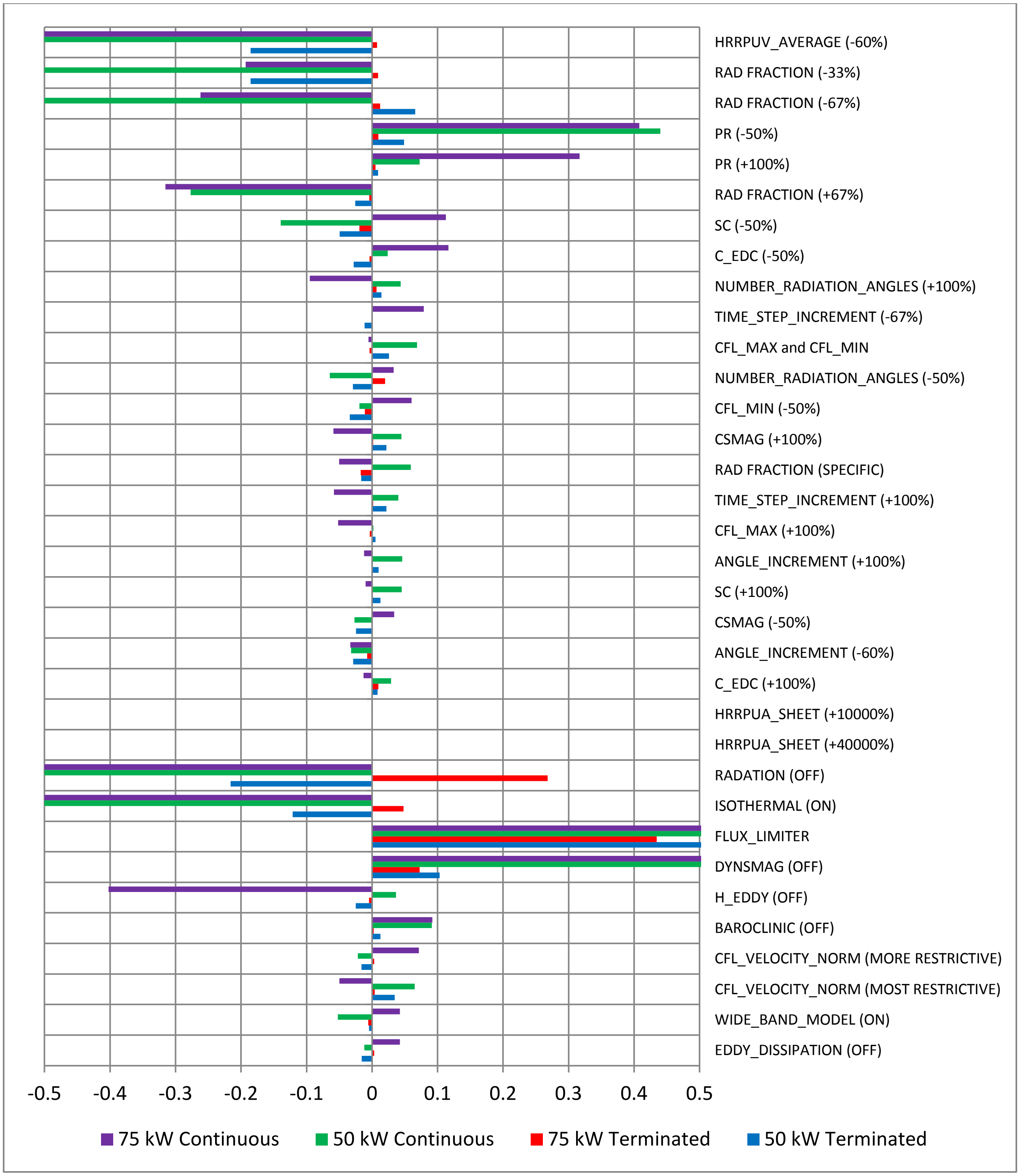

Figure 261 – Time to peak HRR sensitivity coefficients, grouped by HRR

Figure 262 shows the sensitivity coefficients based on the predicted total mass loss averaged over simulations using the same source fire HRR. The parameters with significant changes are changes in the radiative fraction, a decrease of the Prandtl number, when the dynamic Smagorinsky model is deactivated, or when the isothermal model is turned on, when the radiation transport mode was turned off, when the eddy diffusivity model is turned off, and which calculation scheme was used based on the FLUX_LIMITER value. It is noted that the simulations with change to the FLUX_LIMITER value crashed due to numerical instability. The effects on the simulations with a terminated source fire are generally greater than the effect on the simulations with a continuous source fire.

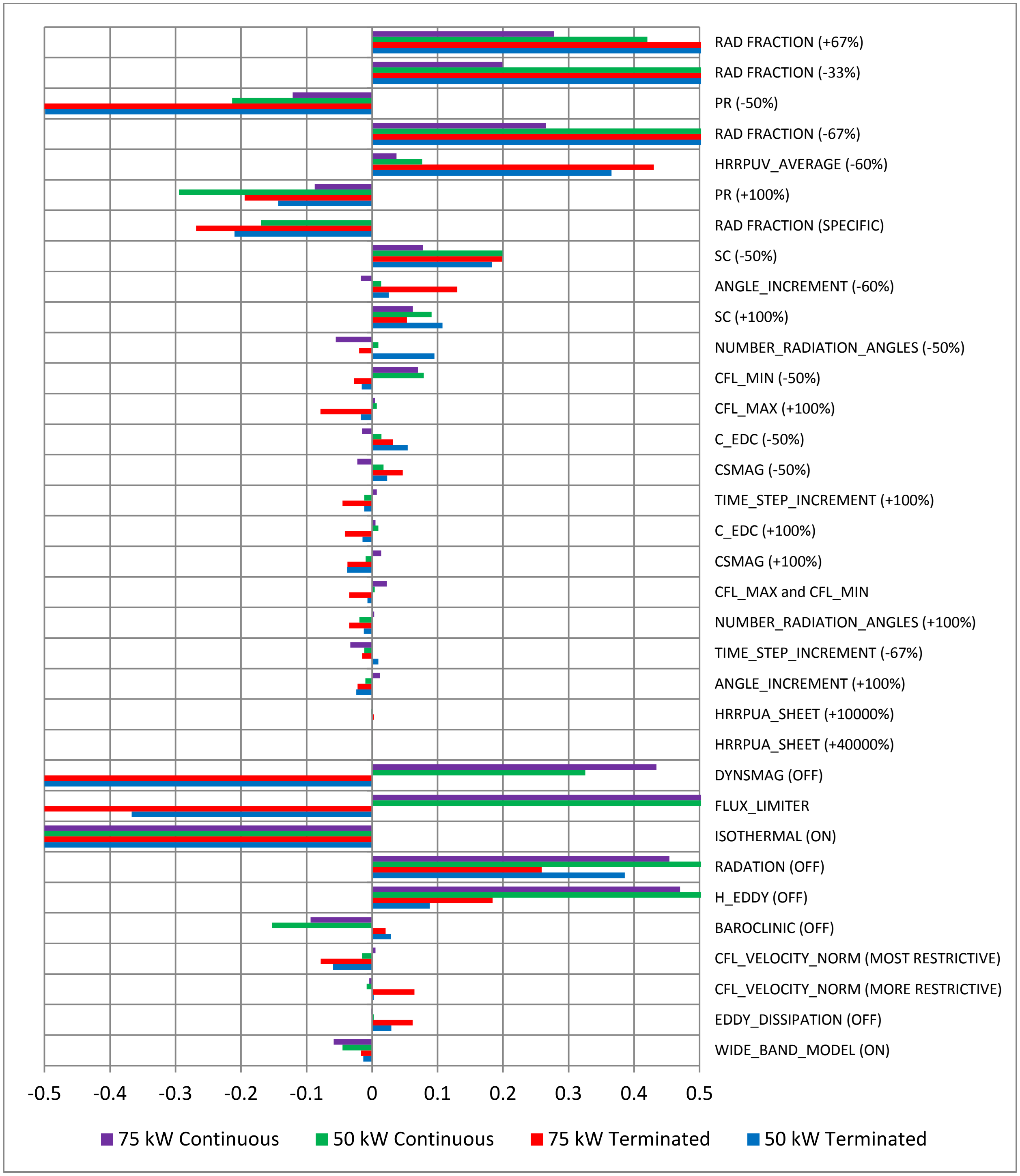

Figure 262 – Total heat released sensitivity coefficients, grouped by burner shape

N.6. Future Work and Recommendations

A comprehensive set of fire test data aimed to provide measurements dealing with the four phenomena that contribute to flame spread was collected from three different series of experiments. From free plume fires, to inert wall fires, to the combustible wall fires, each series of experiments was a more complex than the last, but the base elements of the experiments are kept consistent throughout the different series. In order to cover a wide range of possible ignition scenarios, different fuels, burner shapes, and source fire HRRs were utilized in the experiments. The various measurements in the experiments include plume centerline temperature and velocity, heat flux to wall, near-wall temperature, flame height, flame spread progression, mass loss, and burn pattern.

Collected data are intended to be used in future research for the validation and verification of fire models. A user of the dataset can choose different fire experiments to model and compare with the real experimental data, or use the current data with other researchers' results to deduce correlations that describe free fire plumes, inert wall fires, and combustible wall fires.

Review of the collected data shows that there are large uncertainties in plume velocity and temperature. The data measurement was limited, in part, by the equipment available. Although bi-directional probes have been proved to be extremely reliable in many different research projects, the associated pressure transducers needed to accurately measure the relatively small pressure differential in a low-HRR fire plume can be cost-prohibitive. Thermal effects from the fire on the gas sampling lines, and on the transducers they were connected to, were also difficult to overcome. Other methods of measuring fire plume velocity that may reduce the uncertainty should be considered, such as using the laser Doppler technique or transducers with higher sensitivity, and different mounting options for the equipment. Thermocouples measurements of the plume temperature may also be complimented by other temperature measurement methods such as infrared sensing of the test compartment. In addition, video camera with a higher resolution can also improve the accuracy of the flame height and flame spread progression measurements.

Some supplementary quantities that can expand the dataset may include additional wall-surface and near-wall temperatures embedded on the wall in additional locations, as well as wall cooling measured using thermocouples or with a high-resolution infrared camera, both quantities will aid in the understanding of the flame heat transfer to its surrounding, as well as provide another mean to track the progression of flame spread. Temperature and velocity away from the centerline can also be measured to better describe the environment within and around the fire plume.

Expansion of the dataset may also include more configurations of the source fire such as additional fuels, burner sizes, and HRRs. Additional HRRs was not considered in the current research because the sensitivity of the transducers would not allow accurate measurement of the lower plume velocity at the smaller-HRR, nor the velocity generated by a fire with a high-HRR because of negative thermal effects on the equipment. The materials used in the combustible wall fire tests may also be expanded to include materials of different characteristics as well, such as different types of plastic and wood paneling commonly used in the built environment. However, it is cautioned that the critical source fire HRR should be found that correlates with the minimal heat flux needed to ignite the paneling.

FDS simulations conducted in the current study had shown that the predictive capabilities of the software are in need of improvement, especially for complex situations such as flame spread on a wall. Discrepancies between collected experimental data and FDS fires simulation results were found in the simpler plume configurations and also in the complex FRP combustible wall configurations when default FDS parameters were used. It must be stressed that the experiments and simulations conducted were of small fire sizes within a very specific range, assessment of FDS using larger fires was not performed in this research. In the literature, however, FDS simulations with larger fire sizes (200-300 kW range) were found to achieve better correlation with experimental data. Limited by time constraints and available computing resources, the majority of the simulations were executed using a grid size of 0.05 m, with limited simulations repeated using a grid size of 0.10 m and 0.025 m for grid sensitivity analysis. Based on the results of the sensitivity analysis, a finer grid at 0.025 m may show improvement on the correlation between the experimental data and the predicted results. If conditions permitted, FDS simulations of the current tests shall be re-executed at grid cell size finer at 0.025 m.

A parametric study that utilized different values of over 20 FDS parameters revealed that the effects on the predicted quantities (plume temperature, velocity, and heat flux to wall) vary greatly due to parameter change. The results showed that clear trends in prediction changes were not easily established and the interactions between various parameters are very complicated. To expand the FDS parametric study, additional FDS parameters and values may be used.

Although a modeler may change the various parameters in order to force the FDS predictions to correlate with the collected data, this practice is not recommended. Unless there are very sound and justifiable reasons to change the parameters, the FDS parameters are not recommended to be changed, additionally, the process can be laborious and the model's behaviors may be unrealistic and outside of the true capabilities and limitations of the software and the underlying physics.

To construct more accurate models and to produce better results, it may not be enough to just vary the various parameters that FDS uses for calculations. There seem to be a need to modify how the calculations are conducted at a deeper level: changes may be needed in the source code of the FDS software so that more accurate fire simulations of different complexities are possible.

N.7. Conclusion

The process of flame spread was analyzed by decomposing the complex phenomenon into four inter-related components: fluid dynamics/turbulence, gas phase kinetics, heat transfer to environment, and solid state pyrolysis. Each component of flame spread is governed by basic physical interactions that are easily studied. Based on this concept, three different series of experiments, ranging from the free plume fires, to inert wall fires, to combustible wall fires were designed and executed to collect data relevant to each component of flame spread. Similar configurations of the fire tests were carried from series to series in order to show the evolution of the tests and the interconnectivity of the components of flame spread. This resulted in a comprehensive set of data useful for future fire analysis.

Data from the four component of flame spread including plume temperature and velocity, flame heat flux to wall, flame height, and flame spread progression were measured in the various experiments. Different configurations tested in the three series of experiments included various source fuel, burner size, and HRR, allowing many variations to the setup. For the combustible materials, only a commercially available FRP paneling was used as the wall material. Error analysis was applied to measured quantities according to standard practices and statistical principles. Comparisons of current data were made against published data and FDS predictions based on modeling using best practices and default simulation parameters.

Series of FDS models were built to simulate the fire tests using a standard grid size of 0.025 m; additional models using other grid sizes were also performed for a grid sensitivity analysis. Moreover, a parametric study of over 20 FDS parameters was conducted using the baseline FDS model where one parameter was changed at a time. Comparisons were then made on the predicted quantities and performance between the default series and the parametric series of simulations. The analysis of the results show some trends between parameter changes and their effects on the predicted results, however, usually the trends were unpredictable. Extrapolating from this, it is reasonable to suggest that changing FDS simulation parameters should be undertaken with utmost caution and justifiable reasons. Since the interactions of the parameters are extremely intricate, the default FDS parameters should be used except for very specialized cases.

N.8. References

1. Lautenberger C and Hostikka S. Large Scale Fire Modeling. In: Wilkie CA, Morgan AB and Dekker M, (eds.). *Flame Retardancy of Polymeric Materials, 2nd ed*. Boca Raton, FL: Taylor and Francis, 2009.
2. Lautenberger C, Wong W, N. Dembsey, Coles A and Fernadez-Pello C. Large-Scale Turbulent Flame Spread Modeling with FDS5 on Charring and Noncharring Materials. In: *Fire and Materials 2009*, San Francisco, CA, 2009. London, UK: Interscience Communications, Ltd.
3. Quintiere JG. Flame Spread. *Principles of Fire Behavior*. Albany, NY: Delmar, 1998.
4. Drysdale D. *An Introduction to Fire dynamics*. New York, NY: John Wiley and Sons, 1985.
5. Yan Z and Holmstedt G. CFD and Experimental Studies of Room Fire Growth on Wall Lining Materials. *Fire Safety Journal*. 1996; 27: pp.201-38.
6. Peacock RD, Davis S and Babrauskas V. Data for Room Fire Model Comparisons. *Journal of Research of the National Institute of Standards and Technolog*. 1991; 96: pp.411-62.
7. Shields TJ, Silcock GWH, Moghaddam AZ and Azhakesan MAZ, J. A Comparison of Fire Retarded and Non-Fire Retarded Wood-Based Wall Linings Exposed to Fire in an Enclosure. *Fire and Materials*. 1999; 23: pp.17-25.
8. Verification and Validation of Selected Fire Models for Nuclear Power Plant Applications. NUREG-1824. Washington, DC: U.S. Nuclear Regulatory Commission, 2006.
9. Wu PK, Orloff L and Tewarson A. Assessment of Material Flammability with the FSG Propagation Model and Laboratory Test Methods. In: *Thirteenth Joint Panel Meeting of the UJNR Panel of Fire Research and Safety*, Gaithersburg, MD, 1996. Gaithersburg, MD: NIST.
10. Consalvi JL, Pizzo Y and Porterie B. Numerical Analysis of the Heating Process in Upward Flame Spread Over Thick PMMA Slabs. *Fire Safety Journal*. 2008; 43: pp.351-62.
11. Mitler HE and Steckler KD. Comparison of Wall-Fire Behavior with and without a Ceiling. NISTIR 5380. Gaithersburg, MD: National Institute of Standards and Technology, 1993.
12. Ohlemiller T, Cleary T and Shields J. Effect of Ignition Conditions on Upward Flame Spread on a Composite Material in a Corner Configuration. *Fire Safety Journal*. 1998; 31: pp.331-44.
13. Ohlemiller TJ and Cleary TG. Upward Flame Spread on Composite Materials. In: *Fire and Polymers II: Materials and Test for Hazard Prevention, American Chemical Society, ACS Symposium Series 599*, Washington, DC, 1994.
14. Brehob EG, Kim CI and Kulkarni AK. Numerical Model of Upward Flame Spread on Practical Wall Materials. *Fire Safety Journal*. 2006; 36: pp.225-40.
15. Qian C, Ishida H and Saito K. Upward Flame Spread Along the Vertical Corner Walls. NIST-GCR-94-648. Gaithersburg, MD: National Institute of Standards and Technology, 1993.
16. Kokkala M, Goransson U and Soderbom J. EUREFIC - Large Scale Fire Experiments in a Room with Combustible Linings. SP Report 1990:41. Boras: Swedish National Testing and Research Institute, 1990.
17. Kokkala M, Goransson U and Soderbom J. Five Large_Scale Room Fire Experiments: Project 3 of the EUREFIC Fire Research Programee. Espoo: Technical Research Centre of Finland, 1992.
18. Wu KK, Fan WF, Chen CH, Liou TM and Pan IJ. Downward Flame Spread Over a Thick PMMA Slab in an Opposed Flow Environment: Experiment and Modeling. *Combustion and Flame* 2003; 132: pp.697-707.
19. Walmerdahl P and Werling P. Fire Growth and Spread - An Experimental Study in Model-Scale. FOI-R--0907--SE. Stockholm: Swedish Defence Research Agency, 2003.
20. Carlsson J. Flame Spread and Fire Growth – Modelling Capabilities in Various Room Configurations. FOI-R--1579--SE. Tumba, Sweden: Swedish Defence Research Agency, 2005.
21. Wu PK and Bill RG. Laboratory Tests for Flammability Using Enhanced Oxygen. *Fire Safety Journal*. 2003; 38: pp.203-17.

22. Rangwala AS, Buckley SG and and Torero JL. Upward Flame Spread on a Vertically Oriented Fuel Surface: The Effect of Finite Width. *Proceedings of the Combustion Institute*. 2007; 31: pp.2607-15.
23. Hietaniemi J, Hostikka S and Vaari J. FDS Simulation of Fire Spread - Comparison of Model Results with Experimental Data. VTT Working Papers 1459-7683. Finland: VTT Building and Transport, 2004.
24. Hostikka S and McGrattan KB. Large Eddy Simulation of Wood Combustion. In: *International Interflam Conference*, Edinburgh, Scotland, 2001. London, UK: Interscience Communications, Ltd.
25. Stroup DW, Delauter L, Lee J and Roadarmel G. Upholstered Chair Fire Tests Using a California Technical Bulletin 133 Burner Ignition Source. Gaithersburg, MD: National Institute of Standards and Technology, 2001.
26. Lattimer BY, Hunt SP, Wright M and Sorathia U. Modeling Fire Growth in a Combustible Corner. *Fire Safety Journal*. 2003; 38: pp.771-96.
27. Poreh M and Garrad G. A Study of Wall and Corner Fire Plumes. *Fire Safety Journal*. 2000; 34: pp.81-98.
28. O'Hern TJ, Weckman EJ, Gerhart AL, Tieszen SR and Schefer RW. Experimental Study of a Turublent Buoyant Helium Plume. *Journal of Fluid Mechanics*. 2005; 544: pp.143-71.
29. DesJardin PE, O'Hern TJ and Tieszen SR. Large Eddy Simulation and Experimental Measurements of the Near-Field of a Large Turbulent Helium Plume. *Physics of Fluids*. 2004; 16: pp.1866-83.
30. Tieszen SR, O'Hern TJ, Weckman EJ and Schefer RW. Experimental Study of the Effect of Fuel Mass Flux on a 1-m-Diameter Methane Fire and Comparison with a Hydrogen Fire. *Combustion and Flame*. 2004; 139: pp.126-41.
31. Tieszen SR, O'Hern TJ, Schefer RW, Weckman EJ and Blanchat TK. Experimental Study of the Flow Field In and Around a One Meter Diameter Methane Fire. *Combustion and Flame*. 2002; 129: pp.378-91.
32. Gengembre E, Cambray P, Karmed D and Bellet JC. Turbulent Diffusion Flames with Large Buoyancy Effects. *Combustion Science and Technology*. 1984; 41: pp.55-67.
33. Evans G, Greif R, Siebers D and Tieszen SR. Turbulent Mixed Convection from a Large, High Temperature, Vertical Flat Surface. *International Journal of Heat and Fluid Flow*. 2005; 26: pp.1-11.
34. Zhou XC and Gore JP. Air Entrainment Flow Field Induced by a Pool Fire. *Combustion and Flame*. 1995; 100: pp.52-60.
35. Zhou XC and Gore JP. Experimental Estimation of Thermal Expansions and Vorticity Distribution in a Buoyant Diffusion Flame. *Twenty-Seventh Symposium (International) on Combustion*. 1998: pp.2767-73.
36. Sheppard D and Meacham BJ. Acquistion, Analysis, and Reporting of Fire Plume Data for Fire Safety Engineering. In: *Sixth (6th) International Symposium International Association for Fire Safety Science*, Boston, MA, 1999. London, UK: Interscience Communications Ltd.
37. Blevins LR, M.W., Lyle KH, Laurendeau NM and Gore JP. Experimental Study of Temperature and CH Radical Location in Partically Premized CH_4/air Coflow Flames. *Combustion and Flame*. 1999; 118: pp.684-96.
38. de Ris JL. Experiments Establishing the Similarity of Wall Fire Combusstion. NISTIR 6588. Gaithersburg, MD: National Institute of Standards and Technology, 2000.
39. Hamins A, Bundy M and Dillon SE. Characterization of Candle Flames. *Journal of Fire Protection Engineering*. 2005; 15: pp.265-85.
40. Dillon SE. Analysis of the ISO 9705 Room/Corner Test: Simulations, Correlations and Heat Flux Measurements. NIST-GCR-98-756. Gaithersburg, MD: National Institute of Standard and Technology, 1998.

41. Floyd J and Lattimer B. Validation of FDS V4 Boundary Heat Flux Predictions for a Corner Fire. In: *Interflam 2004 International Interflam Conference, 10th Proceedings*, London, 2004. London, UK: Interscience Communications, Ltd.
42. Hasemi Y. Experimental Wall Flame Heat Transfer Correlations for the Analysis of Upward Wall Flame Spread. *Fire Science and Technology*. 1984; 4: pp.75-90.
43. Hostikka S, McGrattan KB and Hamins A. Numerical Modeling of Pool Fires Using LES and Finite Volume Method for Radiation. In: *Fire Safety Science--Proceedings of the Seventh International Symposium*, Worcester, MA, 2002. Interscience Communications, Ltd.
44. Lattimer BY and Sorathia U. Thermal Characteristics of Fires in a Noncombustible Corner. *Fire Safety Journal*. 2003; 38: pp.771-96.
45. Lock A, Bundy M, Johnsson EL, et al. Experimental Study of Effects of Fuel Type, Fuel Distribution, and Vent Size on Full Scale Underventilated Compartment Fires in an ISO 8705 Room. NIST Technical Note 1603. Gaithersburg, MD: National Institute of Standards and Technology, 2008.
46. Quintiere J, Harkleroad M and Hasemi Y. Wall Flames and Implications for Upward Flame Spread. *Combustion Science and Technology*. 1986; 48: pp.191-222.
47. Pierce JBM and Moss JB. Smoke Production, Radiation Heat Transfer and Fire Growth in a Liquid-Fuelled Compartment Fire. *Fire Safety Journal*. 2007; 42: pp.310-20.
48. Nowlen SP. Enclosure Environment Characterization Testing for the Base Line Validation of Computer Fire Simulation Codes. NUREG/CR-4681. Albuquerque, NM: U.S. Nuclear Regulartory Commission, 1987.
49. McCaffrey BJ. Purely Buoyant Diffusion Flames: Some Experimental Results. NBSIR 79-1910. Washington, D.C.: Center for Fire Research, National Engineering Laboratory, 1979.
50. Cox G and Chitty R. Some Source-Dependent Effects of Unbounded Fires. *Combustion and Flame*. 1985; 60: pp.219-32.
51. Hasemi Y and Tokunaga T. Flame Geometry Effects on the Buoyant Plumes from Turbulent Diffusion Flames. *Fire Science and Technology*. 1984; 4: pp.15-6.
52. Quintiere J and Grove B. Correlations for Fire Plumes. NIST-GCR-98-744. Gaithersburg, MD: National Institute for Standards and Technology, 1998.
53. Tran HC and Janssens M. Modeling the Burner Source Used in the ASTM Room Fire Test. *Journal of Fire Protection Engineering*. 1993; 5: pp.53-66.
54. OSHA, United States Department of Labor. Methane. Safety and Health Topics, http://www.osha.gov/dts/chemicalsampling/data/CH_250700.html (2003, accessed March 9, 2011).
55. OSHA, United States Department of Labor. Propane. Safety and Health Topics, http://www.osha.gov/dts/chemicalsampling/data/CH_264000.html (2003, accessed March 9, 2011).
56. OSHA, United States Department of Labor. Propylene. Safety and Health Topics, http://www.osha.gov/dts/chemicalsampling/data/CH_264442.html (2003, accessed March 9, 2011).
57. Blanket Products Product Information. Product Literature No: 01.07/5 14-205.
58. Dembsey N and Williamson R. Coupling the Fire Behavior of Contents and Interior Finishes for Performance Fire Codes: Evaluation of a Fire Spread Model. *Journal of Fire Protection Engineering*. 1997; 8: pp.119-32.
59. Dembsey N and Williamson R. The Effect of Ignition Source Exposure and Specimen Configuration on the Fire Growth Characteristics of a Combustible Interior Finish Material. *Fire Safety Journal*. 1993; 21: pp.313-30.
60. Young CN. *Thermocouple Compensation.* MS Thesis, University of Waterloo, Waterloo, ON, 1998.
61. Blevins L and Pitts W. Modeling of Bare and Aspirated Thermocouples in Compartment Fires. NISTIR 6310. Gaithersburg, MD: National Institute of Standards and Technology, 1999.

62. Heskestad G. Bidirectional Flow Tube for Fire-Induced Vent Flows. FMRC Serial Number 21011.4. Factory Mutual Research Corporation, 1974.
63. Newman JS. Multi-Directional Flow Probe Assembly for Fire Application. *Journal of Fire Sciences*. 1987; 5: pp.50-6.
64. Omega Engineering, Inc. Differential Pressure Transducer with Field Selectable Range, PX277. http://www.omega.com/Pressure/pdf/PX277.pdf (2012, accessed July 15, 2012).
65. Low Pressure Transducer PX274, PX275, PX277, and PX278 Instruction Sheet. Product Literature No: M2759-0305.
66. Parker W. Calculations of the Heat Release Rate by Oxygen Consumption for Various Applications. NBSIR 81-2427-1. Washington, DC: National Bureau of Standards, Center for Fire Research, 1982.
67. ASTM Standard E1354-04a, "Standard Test Method for Heat and Visible Smoke Release Rates for Materials and Products Using an Oxygen Consumption Calorimeter". West Conshochocken, PA: ASTM International, 2004.
68. Janssens M. Calorimetry. *The SFPE Handbook of Fire Protection Engineering, 3rd ed*. Quincy, MA: NFPA, 2002.
69. Kaowool High Temperature Boards Product Information. Product Literature No: 06.06/5 14-715.
70. ASTM Standard E459-05, "Standard Test Method for Measuring Heat Transfer Rate using a Thin-Skin Calorimeter". West Conshochocken, PA: ASTM International, 2005.
71. High Temp Metals. Inconel 718 Technical Data. http://www.hightempmetals.com/techdata/hitempInconel718data.php (2011, accessed March 9, 2011).
72. ISO 5660-1:2002 "Reaction-to-fire tests -- Heat release, smoke production and mass loss rate -- Part 1: Heat release rate (cone calorimeter method)". Geneva Switzerland: International Organization for Standardization, 2002.
73. Grosshandler WL, Bryner NP, Madrzykowski D and Kuntz K. Report of the Technical Investigation of the Station Night Club Fire. NIST NCSTAR 2: Vol 1. Gaithersburg, MD: National Institute of Standards and Technology, 2005.
74. McGrattan KB, Floyd JE, Forney GP, Baum HR and Hostikka S. Improved Radiation and Combustion Routines for a Large Eddy Simulation Fire Model. In: *7th International IAFSS Symposium*, Worcester, MA, 2002. London, UK: Interscience Communications, Ltd.
75. Ma T. *Numerical Simulation of Axi-symmetric Fire Plumes: Accuracy and Limitations.* MS Thesis, University of Maryland, College Park, MD, 2001.
76. Friday P and Mowrer FW. Comparison of FDS Model Predictions with FM/SNL Fire Test Data. NIST GCR 01-810. Gaithersburg, MD: National Institute of Standards and Technology, 2001.
77. Bounagui A, Kashef A and Benichou N. Simulation of the Fire for a Section of the L.H. - La Fortaine Tunnel. IRC-RR-140. Ottawa, Ontario: National Research Council Canada, 2003.
78. McGrattan KB, McDermott R, Hostikka S and Floyd JE. Fire Dynamics Simulator (Version 5) User's Guide. NIST Special Publication 1019-5. Gaithersburg, MD: National Institute of Standards and Technology, 2010.
79. McGrattan KB, Hostikka S, Floyd JE, et al. Fire Dynamics Simulator (Version 5) Technical Reference Guide Volume 1: Mathematical Model. NIST Special Publication 1018-5. Gaithersburg, MD: National Institute of Standards and Technology, 2010.
80. Taylor JR. *An Introduction to Error Analysis The study of Uncertainties in Physical Measurements*. 2nd ed. Sausalito, CA: University Science Books, 1997.
81. Mandel J. *The Statistical Analysis of Experimental Data*. New York, NY: Dovers Publications, Inc., 1984.

82. Physical Measurement Laboratory of NIST. Uncertainty of Measurement Results - Evaluating uncertainty components: Type B. The NIST Reference on Constants, Units, and Uncertainty, http://physics.nist.gov/cuu/Uncertainty/typeb.html (2011, accessed Mar 14, 2011).
83. Tewarson A. Generation of Heat and Chemical Compounds in Fires. *The SFPE Handbook of Fire Protection Engineering, 3rd ed*. Quincy, MA: NFPA, 2002.
84. ASTM Standard E2058-03 "Standard Test Methods for Measurement of Synthetic Polymer Material Flammability Using a Fire Propagation Apparatus (FPA). West Conshochocken, PA: ASTM International, 2003.
85. Blevins LG and Pitts WM. Modeling of Bare and Aspirated Thermocouples in Compartment Fires. NISTIR 6310. Gaithersburg, MD: National Institute of Standards and Technology, 1999.
86. Alston J. *Room/Corner Fire Calibration Data: Marine Composite Screening Specimens.* MS Thesis, Worcester Polytechnic Institute, Worcester, MA, 2004.
87. Kwon JW. *Evaluating FDSv4 Upward Flame Spread.* M.S. Thesis, Worcester Polytechnic Insitute, Worcester, MA, 2006.
88. Bejan A. *Heat Transfer*. New York, NY: John Wiley & Sons, Inc., 1993.
89. Douglas Brown. Tracker Help. Tracker Video Analysis and Modeling Tool, http://www.cabrillo.edu/~dbrown/tracker/help/frameset.html (2011, accessed Mar 15, 2011).
90. Zukoski E, T. Kubota and B. Cetegen. Entrainment in Fire Plumes. *Fire Safety Journal*. 1981; 3: pp.107-22.
91. Heskestad G. On Q* and the Dynamics of Turbulent Diffusion Flames. *Fire Safety Journal*. 1998; 30: pp.215-27.
92. Alston J and Dembsey N. Evaluation of Dimensionless Flame Height Parameters to Account for Fuel Source Effects. In: *Fire Safety Science-Proceedings of the Seventh International Symposium*, Worcester, MA, 2002. London, UK: Interscience Communications, Ltd.
93. Anderson SK. *Qualitative Study of the Effect of a Compartment Enclosure on Fire Plume Entrainment.* MS Thesis, Worcester Polytechnic Institute, Worcester, MA, 1998.
94. De-Ris J and Khan M. A Sample Holder for Determining Material Properties. *Fire and Materials*. 2000; 24: pp.219-26.
95. Hasemi YaMN. Fuel Shape Effect on the Deterministic Properties of Turbulent Diffusion Flames. In: *Fire Safety Science - Proceedings of the Second International Symposium, International Association for Fire Safety Science*, New York, 1988. Washington, DC: Hemisphere Publishing Corporation.